PROCEEDINGS OF ABSTRACTS VIII. INTERNATIONAL AGRICULTURAL, BIOLOGICAL, LIFE SCIENCE CONFERENCE AGBIOL 2026

06-09 SEPTEMBER 2026

ISTANBUL, TÜRKİYE

PROCEEDINGS OF ABSTRACTS VIII. INTERNATIONAL AGRICULTURAL, BIOLOGICAL, LIFE SCIENCE CONFERENCE AGBIOL 2026

06-09 SEPTEMBER 2026 ISTANBUL, TÜRKİYE

Organized by
Trakya University
Istanbul Beykent University
International Researchers Association

ISBN #:978-625-96407-5-4

WELCOME NOTES

You are welcome to our VIII. AGBIOL Conference that is organized by Trakya University, Beykent University and International Researchers Association. The aim of our conference is to present scientific subjects of a broad interest to the scientific community, by providing an opportunity to present their work as oral or poster presentations that can be of great value for global science arena. Our goal was to bring three communities, namely science, research and private investment together in a friendly environment of Edirne, Turkey in order to share their interests and ideas and to get benefit from the interaction with each other.

In September 2018, we organized the first AGBIOL Conference with more than 700 scientists and researchers from all over the world with over 800 scientific papers. Due to COVID-19 situation, II. AGBIOL 2020 has organized fully on-line event which was one of the biggest online conferences in recent years in the world with 499 papers and 1133 authors with 333 oral and 166 e-poster presentations from 55 countries. Due to COVID-19 situation, AGBIOL 2021 was organized online again. AGBIOL 2022 conference was organized with a worldwide participation from 44 countries over 522 papers contributed by over 1300 authors. AGBIOL 2023 was organized with a record and worldwide participation from 33 countries 833 papers contributed by over 2000 authors with 522 oral and 311 poster presentations. AGBIOL 2024 consisted of 835 papers contributed by about 2000 authors with worldwide record participation again from 55 countries with 522 oral and 311 poster presentations. AGBIOL 2025 was organized with a worldwide record participation from 60 countries 988 papers contributed over 2300 authors with 400 oral and 588 poster presentations.

The AGBIOL 2026 is normal participation as well as with online participation in Beykent University in Istanbul, Turkey on 06-09 September, 2026. The program included oral talks by invited prominent scientists and oral and e poster presentations by participants in selected topics from the submitted abstracts focusing on Agriculture, Biology and Life Sciences topics.

There is a worldwide record participation again in AGBIOL 2026 from 61 countries 1057 papers contributed over 2500 authors then 800 of them were accepted and then the conference was organized with 390 oral and 410 poster presentations.

With care for our nature and environment, we aim the green congress, meaning that as little as possible papers will be used. Abstract book is published in electronic book and is distributed to the participants by e mail for online participants. All the e-posters are prepared in electronic form and then submit to via the conference e mail and exhibited in electronical poster boards as well as in online e poster hall in our web page during the conference.

The participants with paid conference fee accessed all the normal and virtual presentation talks in each session, as well as to visit the virtual poster hall via preliminary provided. The abstracts were published in the Conference Abstract and Proceedings Book. Participants might send us their full papers, which based on their preferences are published either in our Conference Abstract and Proceedings Book or in selected International Indexed Scientific Journals.

Conference Topics:

Agriculture, Forestry, Life Sciences, Agricultural Engineering, Aquaculture and Biosystems, Animal Science, Biomedical science, Biochemistry and Molecular Biology, Biology, Bioengineering, Biomaterials, Biomechanics, Biophysics, Bioscience, Biotechnology, Botany, Chemistry, Chemical Engineering, Earth Sciences, Environmental Science, Food Science, Genetics and Human Genetics, Medical Science, Machinery, Pharmaceutical Sciences, Physics, Soil Science.

We would like to thank all of you for joining this conference and we would like to give also special thanks to TUBITAK and collaborators for giving us a big support to organize this event.

Prof Dr Yalcin KAYA
Head of the Organizing Committee

ORGANIZING COMMITTEE

NAME	INSTITUTION	COUNTRY
Prof. Dr. Volkan ONGEL	Rector of Istanbul Beykent Univ, Turkiye	Honorary President
Prof. Dr. Mustafa HATIPLER	Rector of Trakya Univ, Turkiye	Honorary President
Prof. Dr. Yalcin KAYA	Trakya University, International Researcher Assoc (IRSA), Turkiye	Chair
Prof. Dr. Bahaddin SINSOYSAL	Istanbul Beykent Univy, Turkiye	Co & Host Chair
Assoc Prof. Dr. Necmi BEŞER	Tragen Ltd Şti, Trakya University Technopark, Turkiye	Co-Chair
Emrah AKPINAR	Trakya University, Turkiye	Secretary
Asst. Prof Dr. Hasan BOZTOPRAK	Istanbul Beykent Univ, Turkiye	Member
Prof. Dr. Viliana VASSILEVA	Maize Res Inst-Knezha, Bulgaria	Member
Prof. Dr. Ioannis TOKATLIDIS	Trakia Democritus Univ, Greece	Member
Prof Dr Metin TUNA	Tekirdag Namik Kemal Univ, Turkiye	Member
Asst Prof Dr Orhan ASKIN	Kırklareli University, Turkiye	Member
Prof Dr Mohamed RAMDANI	Mohamed V Agdal Univ., Maroc	Member
Assoc. Prof. Dr. Natiga NABIYEVA	Genetic Resources Inst. of NAS, Azerbaijan	Member
Dr Maria PACUREANU	Study & Res Center Agro Forestry Biodiversity " David Davidescu" - Romanian Acad, Romania	Member
M. İbrahim YILMAZ	Trakya Agric. Res Inst, Turkiye	Member

INVITED SPEAKERS

Kassim AL-KHATIB, Department of Plant Sciences, UC Davis, US

Assoc Prof. Dr. Meltem ERYILDIZ, Istanbul Beykent University, Türkiye

Asst. Prof. Dr. Tuba SEN, Istanbul Beykent University, Türkiye

Asst Prof. Dr. Monika STOJANOVA, Mother Teresa University, North Macedonia

Dr. Biljana Grujic VUCKOVSKI, Tamis Research & Development Institute, Serbia

Prof. Dr. Ercan ARICAN, Istanbul University, Türkiye

Prof Dr Ahmet ULUDAG, Çanakkale Onsekizmart University, Turkey

EDITOR OF THE PROCEEDINGS ABSTRACT BOOK

Prof Dr Yalcin KAYA, Assoc Prof Dr Necmi BESER

SCIENTIFIC COMMITTEE

NAME	INSTITUTION	COUNTRY
Assoc. Prof Dr Zizis VRYZAS	Democritus University of Thrace	Greece
Acad. Prof. Dr. Atanas ATANASSOV	Joint Genomic Center-Sofia	Bulgaria
Prof Dr Amel MIlLA	ENSV, Alger	Algeria
Prof. Dr. Miguel CANTAMUTTO	IINTA Hilario Ascasubi Institute,	Argentina
Prof. Dr Zhao JUN	Inner Mongolia Agricultural Univ	China
Prof. Dr. Renata HORN	University of Rostock	Germany
Prof. Dr. Mulpuri SUJATHA	ICAR-Indian Inst of Oilseeds Res.	India
Prof. Dr Lara HANNA WAKIM	Holy Spirit University	Lebanon
Prof. Dr Semra HASACEBI	Trakya University	Turkiye
Prof Dr Velibor SPALEVIC	University of Montenegro	Montenegro
Prof Dr Dijana BLAZEKOVIC	Univ "St. Kliment Ohridski" Bitola	Macedonia
Prof Dr Sani DEMIRI	Mother Teresa University	Macedonia
Prof Dr Charles BRENNAN	RMIT University	Australia
Prof. Dr. Saeed RAUF	Muhammad Nawaz Sharief Agric Univ	Pakistan
Prof. Dr. Monika JAKUBUS	Poznań University of Life Sci	Poland
Prof. Dr. h.c. Radu E. SESTRAS	Univ of Agricultural Sciences & Veterinary Medicine Cluj-Napoca	Romania
Prof. Dr. Dejana PANKOVIC	Educon University	Serbia
Prof. Dr. Yakov DEMURIN	VNIIMIK All Russian Institute	Serbia
Prof Dr Leonardo VELASCO	Inst. for Sustainable Agric CSIC	Spain
Prof. Dr. Okşan KARAL YILMAZ	Istanbul Beykent University	Turkiye
Prof. Dr. Mesut KACAN	Istanbul Beykent University	Turkiye
Prof. Dr. Mehmet Emin CALISKAN	Nigde OmerHalisdemir University	Turkiye
Prof. Dr. Doğanay TOLUNAY	Istanbul Cerrahpaşa University	Turkiye
Prof. Dr Ahu ALTINKUT UNCUOGLU	Marmara University	Turkiye
Prof. Dr. Sezen ARAT	Namık Kemal University	Turkiye
Prof. Dr. Coskun GULSER	Ondokuzmayis University	Turkiye
Prof. Dr. Metin AYDOĞDU	Trakya University	Turkiye
Prof. Dr. Ismail CAKMAK	Sabanci University	Turkiye
Prof. Dr. Yaroslav BLUME	National Academy of Sciences	Ukraine
Prof. Dr. Nurhan T. DUNFORD	Oklahoma State University	USA
Prof. Dr. Mahmut TOR	University of Worcester	England
Prof Dr Mustafa TAN	Trakya University	Turkiye
Prof. Dr. Gökhan KAÇAR	Trakya University	Turkiye
Prof. Dr. Ahmet CIHAN	Istanbul Beykent University	Turkiye
Prof. Dr. Kazım SARI	Istanbul Beykent University	Turkiye
Prof. Dr. Tanay Sıtkı UYAR	Istanbul Beykent University	Turkiye
Prof. Dr. Hasan OZKAYNAK	Istanbul Beykent University	Turkiye

CONTENTS

WELCOME NOTES **3**

ORGANIZING COMMITTEE **4**

INVITED SPEAKERS **5**

SCIENTIFIC COMMITTEE **6**

LEAN MANUFACTURING APPLICATION IN FOOD INDUSTRY **15**

THE PRESENCE OF OSMIA ANDRENOIDES (SPINOLA, 1808) (HYMENOPTERA: MEGACHILIDAE) IN THE VJOSA-NARTË PROTECTED LANDSCAPE **27**

PATTERNS OF STAPHYLOCOCCUS AUREUS INFECTIONS AND ANTIMICROBIAL RESISTANCE IN YOUTH POPULATIONS **33**

MITIGATING ANTIMICROBIAL RESISTANCE THROUGH ANIMAL WELFARE STANDARDS: A ONE HEALTH FRAMEWORK **43**

MICROPLASTICS IN SOIL ECOSYSTEMS: IMPACTS ON MICROBIAL COMMUNITIES, NUTRIENT CYCLING, AND AGRONOMIC SUSTAINABILITY **50**

FOODBORNE MYCOTOXINS AND THE HUMAN MICROBIOME: A HACCP-BASED RISK ASSESSMENT APPROACH **63**

ASSESSMENT OF WATER QUALITY AND NUTRIENT CONTAMINATION RISKS IN ISTANBUL'S URBAN LAGOONS (BÜYÜKÇEKMECE AND KÜÇÜKÇEKMECE) USING MODIFIED INDICES **72**

SEASONAL DYNAMICS OF WATER QUALITY AND ANTHROPOGENIC PRESSURES IN BÜYÜKÇEKMECE AND KÜÇÜKÇEKMECE LAGOONS IN A MEGACITY (İSTANBUL) **79**

INTEGRATION of RAINWATER HARVESTING (RWH) in INDUSTRIAL ZONES: POTENTIAL, TECHNICAL ANALYSIS, and REGULATORY FRAMEWORKS **86**

OPTIMIZING COMBUSTION EFFICIENCY AND EMISSION CONTROL IN LOW-NO_x GAS BURNERS WITH HYDROGEN-BLENDED NATURAL GAS COMBUSTION **98**

ANALYSIS OF UNIVERSITY STUDENTS' METAPHORICAL PERCEPTIONS OF THE CONCEPT OF "CLIMATE CHANGE" **110**

TEMPERATURE TOLERANCE AND PHENOTYPIC PLASTICITY IN PLANTS **121**

BIOFORTIFICATION IN POTATO **127**

OPTIMIZING CHROMIUM AND SELENIUM SUPPLEMENTATION IN TRANSITION DAIRY COWS: INTEGRATING TRADITIONAL META-ANALYSIS WITH MACHINE LEARNING TO IDENTIFY CRITICAL THRESHOLDS AND FORM SYNERGIES **133**

IDENTIFICATION OF CANDIDATE GENES AND BIOLOGICAL PATHWAYS ASSOCIATED WITH GENETIC SHEEP RESISTOME TO GASTROINTESTINAL NEMATODES IN SHEEP: AN INTEGRATED MICROARRAY DATA MINING APPROACH **143**

PRODUCTION OF HYDROGEL LOADED WITH *Crithmum maritimum* L. EXTRACT AND INVESTIGATION OF ITS IN VITRO WOUND-HEALING EFFECT **150**

IN VITRO WOUND HEALING EFFECT OF ETHANOL EXTRACT OF DATÇA PENINSULA BEE POLLEN **166**

ANALYSIS RESULTS OF PHENOLIC COMPONENTS and CHEMOMETRIC ANALYSIS IN GRAPES PRODUCED WITH DIFFERENT AGROECOLOGICAL PRACTICES **172**

KEFE CUMIN (*Laser trilobum* (L.) Borkh.) in TURKISH CUISINE 183

DISTRIBUTION OF SUGAR COMPONENTS AND CHEMOMETRIC ANALYSIS IN GRAPES PRODUCED WITH DIFFERENT AGROECOLOGICAL PRACTICES 191

SECONDARY METABOLITE PROFILE AND CHEMOMETRIC ANALYSIS OF GRAPE LEAVES GROWN DIFFERENT AGROECOLOGICAL PRACTICES..... 198

PHYTOCHEMICAL PROFILE OF ESSENTIAL OILS IN KEFE CUMIN (*Laser trilobum* (L.) Borkh.)..... 211

BIFUNCTIONAL $CoFe_2O_4$-ZnS:Mn CORE-SHELL NANOPARTICLES FOR NANOSCIENCE APPLICATIONS..... 218

MAPPING GROUND VEGETATION BIODIVERSITY OF FOREST ECOSYSTEMS THROUGH SPATIAL ANALYSIS..... 223

HABITAT-BASED ANALYSIS OF SPECIES DIVERSITY IN DIVJAKË–KARAVASTA NATIONAL PARK 232

CHANGES IN THE CONTENT OF LACTOSE AND FREE AMINO ACIDS DURING THE RIPENING OF SALTED CHEESE 242

CHANGES IN THE CONTENT OF LACTOSE AND FREE AMINO ACIDS DURING THE RIPENING OF UNSALTED CHEESE..... 251

DIETARY PATTERNS, GUT MICROBIOME MODULATION, AND MENTAL HEALTH OUTCOMES: EVIDENCE FROM A PRISMA-BASED SYSTEMATIC REVIEW 259

SUSTAINABLE MANAGEMENT OF SMALL RUMINANTS IN ALBANIA: FROM THE DECLINE IN NUMBERS TO GENETIC AND ECONOMIC IMPROVEMENT..... 272

EVALUATION OF FLUORIDE AND CHLORIDE CONCENTRATIONS IN SULTANKÖY AND ALTINYAZI RESERVOIRS (TÜRKIYE): A COMPARATIVE AND DENTAL PUBLIC HEALTH APPROACH 288

AGE-SPECIFIC PROBABILISTIC HEALTH RISKS OF FLUORIDE EXPOSURE VIA GROUNDWATER CONSUMPTION IN LOW AND HIGH ELEVATION AQUIFERS OF NORTHWEST TÜRKIYE 295

VARIATIONS IN FLUORIDE GEOCHEMISTRY OF GROUNDWATER IN THE İPSALA (EDIRNE) BASIN BASED ON TOPOGRAPHIC ELEVATION DIFFERENCES AND ITS EVALUATION FROM A DENTISTRY PERSPECTIVE..... 301

ASSESSMENT OF ORGANIC POLLUTION AND BDI TREND IN THE ERZEN RIVER, ALBANIA (2014–2024)..... 306

OPTIMIZING GOAT SPERM CRYOPRESERVATION: A TRADE-OFF BETWEEN KINEMATICS AND MEMBRANE INTEGRITY 311

VALORIZATION OF AGRICULTURAL WASTE INTO ACTIVATED CARBON : CHARACTERIZATION AND PERFORMANCE FOR PHARMACEUTICAL POLLUTANT REMOVAL FROM WATER..... 319

MELATONIN AS A PROTECTANT AGAINST SALT AND DROUGHT STRESS: PRESERVATION OF ION BALANCE AND MEMBRANE INTEGRITY 326

CRUSTACEAN COMMUNITY STRUCTURE AND SEASONAL DYNAMICS ALONG THE HIMARA COAST: A COMPARISON BETWEEN PORTO PALERMO AND QEPARO..... 334

***CHEMICAL PRETREATMENT OF ALGERIAN GOLD ORE: THE CASE OF AMESMESSA –HOGGAR-* 344**

IDENTIFICATION OF *MACROSIPHUM ROSAE* IN ROSA SPP, SHRUBS, IN THE TIRANA AREA, ALBANIA 354

POPULATION DYNAMICS OF THE POTATO TUBER MOTH (*PHTHORIMAEA OPERCULELLA*) IN THE DIVJAKË REGION, ALBANIA 362

EVALUATION OF TOTAL PHENOLIC CONTENT, ANTIOXIDANT CAPACITY, AND ANTIMICROBIAL ACTIVITY OF *ELAEAGNUS ANGUSTIFOLIA* L. 371

EPILOBIUM PARVIFLORUM: BENEFITS FOR PROSTATE HEALTH VERSUS IATROGENIC RISKS A CLINICAL CASE AND IN SILICO PREDICTION..... 381

AMMONIUM ADSORPTION CAPACITY IN SOME SELECTED SOILS IN THE ISHËM RIVER BASIN, ALBANIA 387

EVALUATION OF AMINO ACID DIGESTIBILITY AND PROTEIN QUALITY OF BLACK SOLDIER FLY LARVAE (Hermetia illucens) MEAL IN BROILER CHICKENS 394

CURRENT APPROACHES TO THE VALORIZATION OF FERMENTED FOOD BY-PRODUCTS FOR FUNCTIONAL PRODUCT DEVELOPMENT..... 404

COMBINED TOXICITY OF MICROPLASTICS AND CHEMICAL POLLUTANTS IN AQUATIC ORGANİSMS 414

EFFECTS OF SEEDLING AGE AND GROWING SEASON ON TOTAL SOLUBLE CARBOHYDRATE CONTENT IN *Ginkgo biloba* L. SEEDLINGS..... 419

ENVİRONMENTAL SURVEİLLANCE OF ESBL PRODUCİNG *ESCHERİCHİA COLİ* AND ANTİBİOTİC RESİSTANCE İN THE SHKUMBİNİ RİVER ECOSYSTEM, ALBANİA 428

EVALUATION OF THE ANNUAL PLAN AND SUBJECT CONTENT OF THE CLIMATE, ENVIRONMENT AND INNOVATIVE SOLUTIONS COURSE BY SCIENCE EDUCATION STUDENTS..... 432

GENOMIC PREDICTION OF HEAD DIAMETER IN SUNFLOWER: COMPARING GWAS-DERIVED AND GENOME-WIDE FEATURE SETS ACROSS MACHINE LEARNING MODELS..... 444

ELUCIDATING OXYGEN-CENTERED INTERACTIONS IN EUGENOL ADSORPTION ON ZN-DOPED *BIPHENYL NANOPARTICLES* 461

***IN VIVO* AND *IN SILICO* INVESTIGATION OF THE GASTROPROTECTIVE ACTIVITY OF ALEPPO PINE (*PINUS HALEPENSIS* MILL.) EXTRACT..... 478**

ANALYSIS OF SPECIES DIVERSITY AND DISTRIBUTION PATTERNS OF THE APIACEAE FAMILY IN THE NAKHCHIVAN AUTONOMOUS REPUBLIC..... 482

MORPHOLOGICAL AND ANATOMICAL INVESTIGATIONS ON *PHLOMIS PUNGENS* WILLD. FROM ESKİŞEHİR..... 486

ASSESSMENT OF SELECTED MACRO- AND MICRONUTRIENT CONCENTRATIONS IN SOILS AND WHEAT IN THE NARLI PLAIN 496

EFFECTS OF MYCORRHIZA-BASED MICROBIAL FERTILIZERS ON BASIL (*Ocimum basilicum* L.) AGRICULTURAL CHARACTERISTICS UNDER DEFICIT IRRIGATION CONDITIONS..... 506

THE IMPORTANCE OF BEHAVIORAL INDICATORS FOR ANIMAL WELFARE AND HERD MANAGEMENT IN DAIRY CATTLE 514

AN EVALUATION ON SUSTAINABLE WATER MANAGEMENT IN DAIRY CATTLE ENTERPRISES FROM GLOBAL WATER SECURITY 521

INFLUENCE OF BASAL WOUNDING AND AUXIN APPLICATIONS ON ROOTING PERFORMANCE OF HARDWOOD CUTTINGS OF *Podocarpus macrophyllus* var. *macrophyllus*..... 529

AI-ASSISTED HIGH-THROUGHPUT PHENTYPING IN *ARABIDOPSIS THALIANA*: CURRENT APPROACHES..... 540

MORPHOMETRIC VARIATION AND GROWTH PATTERNS OF INTERTIDAL LIMPETS (*PATELLA* SPP.) ALONG THE SOUTHERN COAST OF ALBANIA 555

ADVANCES IN SEED COATING TECHNOLOGIES FOR VEGETABLE CROPS..... 569

DAIRY WASTEWATER AS A SUBSTITUTE OF FAT IN GLUTEN FREE COOKIES FORMULATION: A CHALLENGE FOR AGROFOOD SUSTAINABILTY SECTOR..... 583

FARMING PRACTICES EFFECT ON THE QUALITY OF THE MONTBELIARDE BREED MILK FROM THE WILAYA OF MOSTAGANEM..... 589

TAXONOMIC REVISION OF THE FAMILY LILIACEAE IN THE FLORA OF ALBANIA 595

VEGETABLE POWDERS AS NATURAL COLORANTS İN BREAD: EFFECTS ON COLOR, PHYSİCAL, TEXTURAL, MOİSTURE, AND SENSORY PROPERTİES 600

DEVELOPMENT OF GLUTEN-FREE CHICKPEA CHIPS ENRICHED WITH COLD-PRESSED BLACK CUMIN SEED CAKE..... 612

SYSTEM OF BULGARIAN PLANT GENETIC RESOURCES DOCUMENTATION – DESIGN, STRUCTURE AND STATUS 623

PLATFORM FOR ACCESS TO SEEDS AND SCIENTIFIC KNOWLEDGE – RESULTS FROM THE IS-PGR-SADOVO PROJECT..... 632

CURRENT STATUS AND PROBLEMS OF SHEEP FARMERS: THE CASE OF REŞADİYE DİSTRİCT, TOKAT PROVİNCE..... 642

A REVIEW OF THE MECHANICAL BEHAVIOR OF AUXETIC TPMS-BASED FUNCTIONALLY GRADED STRUCTURES 657

DEVELOPMENT OF AN ENVİRONMENTALLY SAFE DEFOLİATİON TECHNOLOGY BASED ON PH-SENSİTİVE DEFOLİANTS..... 676

BIOSAFETY CONSIDERATIONS AND TECHNICAL ADVANCES IN THE PREPARATION OF SARS-COV-2 SPIKE PSEUDOVIRUSES 681

FROM FEAR TO AWARENESS: THE DUALITY OF SKIN MICROBIOME REALITY AND MEDIA REPRESENTATION THROUGH CASE STUDY ANALYSIS 688

ASSESSMENT OF URBAN AIR QUALITY IN ELBASAN (ALBANIA) BASED ON AIR MONITORING DATA..... 698

MICROSPORIDIAL AND NEMATODE INFECTIONS IN THE PREDATORY BEETLE Calosoma sycophanta L. (COLEOPTERA: CARABIDAE) -REARING LABORATORIES IN TÜRKİYE 709

A PRELIMINARY SURVEY OF NEMATODES AND GREGARINE IN Ips sexdentatus (BOERNER) (COLEOPTERA: CURCULIONIDAE, SCOLYTINAE) POPULATIONS FROM THE WESTERN MEDITERRANEAN REGION (ANTALYA, BURDUR AND ISPARTA), TÜRKİYE 715

DISTRIBUTION AND RAW MATERIAL RESERVES OF FERULA VARIA (SCHRENK) TRAUTV. AND FERULA FOETIDA (BUNGE) REGEL IN THE FLORA OF UZBEKISTAN 721

ASSESSMENT OF ORGANIC POLLUTION AND BDI TREND IN THE ERZEN RIVER, ALBANIA (2014–2024) **727**

EFFECT OF PLANTING DENSITY AND NUMBER OF STEMS ON THE YIELD OF THE HAZELNUT CULTIVAR 'ATA-BABA' IN AZERBAIJAN **732**

RESISTANCE TO COPPER IN ESCHERICHIA COLI ISOLATES FROM ARUGULA **741**

MODELING PROBABILISTIC HEALTH RISKS OF FLUORIDE EXPOSURE FROM LENTIC ECOSYSTEMS IN THRACE REGION OF TÜRKIYE **750**

EVALUATION OF FLUORIDE AND CHLORIDE CONCENTRATIONS IN SULTANKÖY AND ALTINYAZI RESERVOIRS (TÜRKIYE): A COMPARATIVE AND DENTAL PUBLIC HEALTH APPROACH **756**

IMPACTS OF THE 2023 TÜRKİYE EARTHQUAKES ON THE AGRICULTURE SECTOR OF HATAY PROVINCE **763**

INFLUENCE OF QUINCE ROOTSTOCKS ON VEGETATIVE GROWTH, INFLORESCENCE TRAITS, FLOWERING, AND FRUIT SET OF LOQUAT IN HIGH-DENSITY ORCHARDS **777**

ANATOMICAL EVALUATION OF EARLY-STAGE GRAFT COMPATIBILITY OF COTONEASTER NUMMULARIA WITH APPLE, PEAR, QUINCE, AND HAWTHORN **786**

FUNCTIONAL HERBAL TEA BLENDS: PHENOLIC PROFILES, ANTIOXIDANT ACTIVITIES, AND IN VITRO DIGESTIBILITY ASSESSMENT BY SOTAX DISSOLUTION TEST **796**

EFFECTS OF MYCORRHIZA-BASED MICROBIAL FERTILIZERS ON BASIL (Ocimum basilicum L.) AGRICULTURAL CHARACTERISTICS UNDER DEFICIT IRRIGATION CONDITIONS **812**

INVESTIGATION OF QUANTITATIVE AND QUALITATIVE CHARACTERISTICS OF PROPOLIS PRODUCED BY TWO HONEY BEE BREEDS IN TWO TYPES OF HIVES **821**

INFLUENCE OF THE MALE EFFECT ON ESTRUS RESPONSE IN CARPATHIAN GOATS RAISED IN TWO CONTRASTING CLIMATIC AREAS OF ROMANIA **830**

VALORIZATION OF PLANT-BASED BY-PRODUCTS FOR ALTERNATIVE PROTEIN PRODUCTION IN SUSTAINABLE FOOD SYSTEMS: CURRENT APPROACHES AND FOOD APPLICATIONS **838**

FOODBORNE MYCOTOXINS AND THE HUMAN MICROBIOME: A HACCP-BASED RISK ASSESSMENT APPROACH **859**

CHEMICAL STATUS ASSESSMENT OF THE URBAN LANA RIVER, ALBANIA, UNDER THE EU WATER FRAMEWORK DIRECTIVE **868**

COMBINED TOXICITY OF MICROPLASTICS AND CHEMICAL POLLUTANTS IN AQUATIC ORGANISMS **877**

EVALUATION OF MODULAR LIQUID FERTILIZERS CONTAINING SNP, SA-NA, NA-NAA, CPPU AND GA3 IN TERMS OF ROOT DEVELOPMENT, STRESS MANAGEMENT AND FRUIT DEVELOPMENT **882**

POTENTIAL OF A MICRONUTRIENT, AMINO ACID AND PLANT SIGNALING COMPOUND-BASED LIQUID FERTILIZER FOR FROST AND POST-STRESS NUTRITION **886**

DEVELOPMENT OF SLOW-RELEASE UAN-28, UAN-32, UAN-33 AND UAN-34 LIQUID NITROGEN FERTILIZERS: NITROGEN USE EFFICIENCY AND LOW-TEMPERATURE STABILITY 890

DEVELOPMENT OF NOVEL FERTILIZER SYSTEMS FROM DOLOMITE BY NITRIC ACID AND MAGNESIUM-BASED PROCESSING ROUTES 901

DEVELOPMENT AND PERFORMANCE EVALUATİON OF WATER-RETENTİVE HYDROGEL FORMULATİONS TO IMPROVE WATER USE EFFİCİENCY İN AGRİCULTURE 913

EVALUATION OF THE EFFECTIVENESS OF PLANT-BASED BUILDING MATERIALS IN TERMS OF RESOURCE AND ENERGY EFFICIENCY 916

YSTEM OF BULGARIAN PLANT GENETIC RESOURCES DOCUMENTATION – DESIGN, STRUCTURE AND STATUS 930

EFFECT OF FERTILIZATION REGIME AND UMBEL ORDERS ON HETEROBLASTY OF CARROT SEEDS 939

DEVELOPMENT AND PERFORMANCE EVALUATİON OF NPK-BASED SLOW-RELEASE FERTİLİZER FORMULATİONS 950

PERFORMANCE OF THE COMBINED TILLAGE MACHINE IN CLAY SOILS 954

PHENOTYPIC AND GENOTYPIC RESISTANCE TO HEAVY METAL ZINC IN ESCHERICHIA COLI 961

ASSESSMENT OF SELECTED MACRO- AND MICRO NUTRIENT CONCENTRATIONS IN SOILS AND WHEAT IN THE NARLI PLAIN 969

COMPARATIVE EVALUATION OF DROUGHT TOLERANCE IN DIVERSE TRITICUM SPECIES USING THERMAL RETENTION, MEMBRANE DAMAGE, AND STRESS INDICES 979

ASSESSMENT OF SELECTED MACRO- AND MICRONUTRIENT CONCENTRATIONS IN SOILS AND WHEAT IN THE NARLI PLAIN 996

WINE QUALITY AND SAFETY: THE ROLE OF SULFITES, SULFATES AND PHOSPHATES IN MICROBIOLOGICAL STABILITY 1006

IDENTIFICATION OF CANDIDATE GENES AND BIOLOGICAL PATHWAYS ASSOCIATED WITH GENETIC SHEEP RESISTOME TO GASTROINTESTINAL NEMATODES IN SHEEP: AN INTEGRATED MICROARRAY DATA MINING APPROACH 1016

IN VIVO AND IN SILICO INVESTIGATION OF THE GASTROPROTECTIVE ACTIVITY OF ALEPPO PINE (PINUS HALEPENSIS MILL.) EXTRACT 1023

COMPARATIVE EFFECTS OF EDTA AND DTPA ON THE STABILITY OF ASCORBIC ACID DURING CAPILLARY ELECTROPHORETIC DETERMINATION IN LEMON JUICE 1027

APPLICATION OF ORGANIC FERTILIZERS FOR SUSTAINABLE AGRICULTURE ... 1036

INFLUENCE OF REMOVING THE OUTER SCALES OF THE CORM ON THE DEVELOPMENT AND PRODUCTIVITY OF GLADIOLI 1040

RESEARCH ON THE SPECIFICITY OF BIOCHEMICAL PATHWAYS IN ARCHAEA .. 1048

BIFUNCTIONAL CoFe2O4-ZnS:Mn CORE-SHELL NANOPARTICLES FOR NANOSCIENCE APPLICATIONS 1056

BIOMECHANICAL FORCES GENERATED BY ORTHODONTIC APPLIANCES IN THE TREATMENT OF DENTAL AND SKELETAL MALOCCLUSIONS: A NARRATIVE REVIEW 1062

DESIGN AND IMPLEMENTATION OF AN OFF-GRID SOLAR-POWERED DRIP IRRIGATION SYSTEM WITH A SOIL MOISTURE CONTROLLER FOR DAYTIME IRRIGATION OF OLIVE GROVES IN CANAKKALE 1072

DESIGN AND APPLICATION OF AN OFF-GRID SOLAR-BASED, SOIL MOISTURE-CONTROLLED DRIP IRRIGATION SYSTEM FOR OLIVE GROVES IN TURKIYE 1081

EXTRACTION AND STRUCTURAL CHARACTERIZATION OF HUMIC ACIDS DERIVED FROM NITRIC ACID-ASSISTED COW MANURE COMPOST 1090

COMPARISON OF VOLATILE AROMA PROFILES OF NATURALLY GROWING DAFFODIL (Narcissus tazetta L.) FLOWERS FROM ADANA AND MERSIN PROVINCES 1097

DETERMINATION OF POMOLOGICAL AND CHEMICAL CHARACTERISTICS OF GILABURU (Viburnum Opulus L.) FRUITS GROWN IN TUŞBA DISTRICT, VAN PROVINCE 1106

IDENTIFICATION OF BIOFILM-ASSOCIATED MICROORGANISMS IN ALBANIAN DAIRY PROCESSING ENVIRONMENTS USING SELECTIVE CULTURE MEDIA AND MALDI-TOF MASS SPECTROMETRY 1113

INTEGRATED CULTURE, PCR AND MALDI-TOF WORKFLOW FOR IMPROVED DETECTION OF LISTERIA SPP. IN ALBANIAN DAIRY PROCESSING ENVIRONMENTS 1117

DOPING EFFECT ON BIPHENYLENE NANOTUBES: A DFT STUDY 1121

PERFORMANCE ASSESSMENT OF CO_2 ADSORPTION ON PRISTINE AND DOPED BIPHENYLENE NANOTUBES USING DFT AND INTEGRATED AHP–TOPSIS 1132

A THEORETICAL STUDY OF THIOPHENE ADSORPTION ON BIPHENYLENE NANOTUBES: DFT INVESTIGATION 1143

RELATIONSHIPS BETWEEN SOIL STRUCTURE AND CARBON DIOXIDE EMISSIONS 1154

EFFECTS OF BIOCHAR AND POTASSIUM SOLUBILIZING BACTERIA APPLICATIONS ON WHEAT DEVELOPMENT, POTASSIUM CONTENT, AND SOIL PH AND EC 1160

PHOSPHORUS FİXATİON CAPACİTY İN SELECTED SOİLS OF THE ISHËM RİVER BASİN, CENTRAL ALBANİA 1175

ASSESSMENT OF MYCOTOXIN CONTAMINATION IN FEED COMMODITIES FOR DAIRY-PRODUCING ANIMALS: EVIDENCE FROM ALBANIA 1183

RESEARCH ON THE INFLUENCE OF THE MANAGEMENT SYSTEM ON MILK PRODUCTION IN SAANEN GOATS 1196

HUMIC ACID-BASED BIO STIMULATION ENHANCES GROWTH AND EARLY DEVELOPMENT OF TRITICUM DURUM UNDER SEMI-ARID CONDITIONS IN EASTERN ALGERIA 1206

THE CYTOTOXIC EFFECT AND WOUND HEALING POTENTIAL OF ROSE OIL ON HUMAN KERATINOCYTE CELL LINE (HACAT) 1214

EFFECT OF ORGANIC WASTE on SOIL MECHANICAL PROPERTIES and WORKABILITY 1220

FROM THE BRONTLAND REPORT TO FOOD SECURITY IN THE SUSTAINABLE DEVELOPMENT GOALS 1227

STRUCTURAL MODELING OF COMBINE HARVESTER CUTTERBAR SERRATED KNIFE SECTIONS USING A STEPWISE FUNCTIONALLY GRADED MATERIAL APPROACH 1234

NEW RECORDS OF *ANEMONE BLANDA* SCHOTT & KOTSCHY IN ALBANIA 1248

STUDY OF THE INFLUENCE OF BIOPRODUCTS ON THE GROWTH AND PRODUCTIVE QUALITIES OF GREENHOUSE CUCUMBERS 1254

BİOACCUMULATION MECHANISMS AND OXIDATIVE STRESS-MEDIATED TOXIC EFFECTS OF PER- AND POLYFLUOROALKYL SUBSTANCES (PFAS) 1264

THE EFFECT OF MURASHIGE AND SKOOG MEDIA STRENGTHS ON *IN VITRO* SHOOT AND ROOT REGENERATION FREQUENCIES OF BAMBARA GROUNDNUT (*Vigna subterranea* (L.) VERDC.) GENOTYPES 1272

INFLUENCE OF SUMMER MICROBIOLOGICAL POLLUTION ON THE DISTRIBUTION OF ANTIBIOTIC-RESISTANT *ESCHERICHIA COLI* IN THE VJOSA RIVER BASIN. 1281

LINKING SUMMER WATER QUALITY DYNAMICS TO FAECAL CONTAMINATION HOTSPOTS IN THE VJOSA RIVER (ALBANIA) 1291

CONTROL OF FUNGAL DISEASES IN GREENHOUSE CUCUMBERS THROUGH A FUNGICIDE TREATMENT SCHEME 1302

ACOUSTIC METAMATERIALS FOR LOW-FREQUENCY SOUND ABSORPTION: RESONANCE MECHANISMS, DESIGN APPROACHES, AND CURRENT TRENDS 1310

AGBIOL 2026 CONFERENCE STUDENT ORGANIZING TEAM 1319

LEAN MANUFACTURING APPLICATION IN FOOD INDUSTRY

Gürbüz Ünal [1]

[1] *Beykent University, Faculty of Engineering Architecture, Department of Industrial Engineering, İstanbul, Türkiye*

Corresponding author e-mail: gurbuzunal@beykent.edu.tr

ABSTRACT

Globalization, increasing competition, and rapidly changing customer demands have made it imperative for the manufacturing sector to adopt more efficient, flexible, and cost-effective production systems. In the food industry in particular, the short shelf life of products highlights the necessity for continuous and fast-paced production processes, thereby exposing the limitations of the traditional mass production approach. Mass production systems can lead to various problems in food manufacturing facilities, including high inventory levels, long production lead times, excessive waste, and low flexibility. At this point, the lean manufacturing approach offers a customer-oriented, flexible, and efficient production model by eliminating waste. Lean manufacturing not only transforms physical processes but also enhances workforce management, equipment efficiency, and information flow. This study analyzes the transition process to lean manufacturing in a food production factory. The main objective of the study is to eliminate inefficiencies in the production line, reduce unnecessary inventories, lower costs, and increase production efficiency. Throughout this transformation, tools such as the Kaizen philosophy, 5S practices, Value Stream Mapping (VSM), fishbone (Ishikawa) analysis, and Industry 4.0 technologies have been integrated holistically. Based on this analysis, various lean manufacturing tools were utilized to develop appropriate solutions. In particular, the use of value stream mapping played a critical role in identifying non-value-added activities and planning a future-state lean flow. This transformation process represents not only an operational shift but also a cultural change within the organization.

Keywords: Lean Manufacturing, Mass Production, Efficiency, Value Stream Mapping, Fishbone Analysis

INTRODUCTION

The food industry is a vast and strategically important sector that meets the basic human need for nutrition. This industry plays a critical role both economically and socially, processing raw materials obtained from primary production sources such as agriculture, livestock and fisheries, and delivering them to consumers. The food industry encompasses various sub-sectors, including baked goods, dairy products, meat and meat products, beverages, canned foods, ready meals, confectionery, and snacks.

With the impact of industrialization, food production has shifted from traditional methods to mass production-based, high-volume, and standardized processes. Mass production enables large quantities of products to be produced in a short time; however, this system is rigid, inadequate in responding to fluctuating demand patterns, and can lead to high inventory costs. Particularly today, with increased competition, diversified consumer expectations, and the need for more efficient use of resources, the food industry has been driven towards more agile and lean production systems.

Lean production is a manufacturing philosophy focused on eliminating waste and creating customer value. Implementing this approach in the food industry not only increases

production efficiency but also enhances quality, thereby improving customer satisfaction. Furthermore, in the production of perishable goods like food, lean systems provide significant advantages through reduced inventories, shortened process times, and agile decision-making mechanisms.

In this context, the transition from mass production to lean production in a food industry factory is not just an operational transformation but also involves a cultural and structural change. This study will examine the transition process in detail, exploring the challenges faced, methods applied, and gains achieved through a case study.

In food production factories, traditional mass production systems often lead to various issues such as high inventory levels, waste in production processes, low resource efficiency, and inflexible production structures. These problems not only increase production costs but also negatively affect the company's competitive power. Especially in an environment where consumer demands change rapidly and global competition is increasing daily, it has become very challenging for traditional production models to cope with these difficulties. In this context, the implementation of more efficient, flexible, and cost-effective production systems is inevitable.

This study aims to comprehensively analyze the existing production system in a food manufacturing facility. The analysis will incorporate modern production tools such as the Kaizen philosophy, 5S methodology, Industry 4.0 applications, and Fishbone (Ishikawa) analysis, as well as the Value Stream Mapping (VSM) method. Value Stream Mapping allows for visualizing the flow of materials and information on the production line, identifying non-value-adding activities and waste. Through this analysis, the main problems encountered in the production processes will be identified, and areas for improvement will be determined to eliminate these problems.

The research aims to eliminate inefficiencies on the production line, reduce unnecessary inventory, lower costs, and increase productivity by minimizing time losses. Specifically, by using value stream mapping, non-value-adding steps in the processes will be identified and removed. In this direction, the transformation that the transition from traditional mass production to lean production will create at both operational and strategic levels is considered the primary problem of the research.

The theoretical basis for lean manufacturing is based on the Toyota Production System, which became popular in Western management literature following the publication of Womack, Jones, and Roos's "The Machine That Changed the World" in 1990. This system defined lean manufacturing as a system that delivers more value to customers while producing the same outputs using fewer inputs. Early extensions of this framework into food processing, dating to studies in the late 2000s. These studies argued that lean manufacturing could help food processors become more competitive in the face of consumer pressure and competition from larger players; however, these early studies were largely conceptual or exploratory and not empirically substantiated in large samples.

Studies covered lean manufacturing are presented chronologically in Table 1. The studies reviewed in the literature are described as thematic groups. This aims to serve as a quick reference source for reviewing narrative literature; it allows for a comparison of each study's methodology, sectoral context, and key findings at a glance.

Table 1. Summary of Literature on Lean Manufacturing Application in the Food Industry

Author(s) & Year	Methodology	Food Subsector / Setting	Key Findings
Womack, Jones & Roos (1990)	Foundational book / conceptual	Automotive (foundation for all sectors)	Defined lean production as a system using fewer inputs to create equal output with greater customer value; established the vocabulary (waste, value, flow) for studies.
Luning, Marcelis & Jongen (2002)	Conceptual / techno-managerial framework	Food industry (general)	Identified short shelf life, heterogeneous raw materials, seasonality, and variable harvesting conditions as structural features that complicate direct transfer of lean tools from discrete manufacturing to food processing.
Scott, Wilcock & Kanetkar (2009)	Survey	Food sector (general)	Surveyed structured continuous-improvement programmes in the Canadian food sector; found sustained managerial interest in lean-type initiatives.
Dora, Kumar, Van Goubergen, Molnar & Gellynck (2013)	Literature review + survey	Food processing SMEs (general)	Found lean manufacturing still at an early adoption stage in food SMEs; identified workforce skill, in-house expertise, and organizational culture as critical success factors; food safety prioritized over process improvement.
Dora, Kumar, Van Goubergen, Molnar & Gellynck (2014)	Multi-case study	Small and medium-sized food enterprises	Examined applicability of lean practices in food SMEs; confirmed operational performance gains but highlighted resource constraints limiting scale of adoption.
Jiménez, Tejeda, Pérez, Blanco & Martínez (2011)	Case study (VSM)	Wine production	Demonstrated applicability of value stream mapping to a food and beverage subsector distinct from packaged industrial food manufacturing.
Kazancoglu, Ekinci, Ozkan Ozen & Ozbiltekin Pala (2021)	Case study	Poultry processing	Showed that combining lean tools with sustainable-operations practices reduces food waste across production, supply chain, and processing stages simultaneously.
Cusiatado Palomino, Farfán Carhuamaca & Rada Mota (2024)	Systematic review (PICO, PRISMA)	Food industry (cross-sector)	Found consistent positive association between lean tool implementation (TPM, JIT, VSM, 5S, Kaizen) and productivity, efficiency, and waste/cost reduction, contingent on supporting organizational factors.
Gayathri, Gokul Kannan, Swathi &Jenithakarthiga (2026)	Case study (VSM + JIT)	Dairy processing	Applied value stream mapping and Just-in-Time principles to pasteurization and packaging; achieved reductions in waiting time, in-process stock, and total lead time.

FOOD SECTOR

The current situation in the food sector, general challenges, deficiencies, and areas for improvement that food production facilities face may be explained as follows:

Time Loss and Low Productivity: In food production facilities, lengthy and inefficient processes lead to significant time losses. Unnecessary waiting times, slow production lines, low machine efficiency, and shortcomings in workforce management extend production time and decrease overall productivity.

Costs and Waste: Inventory management, irregularities in production planning, and waste during production lead to increased costs. Excess inventory raises storage and transportation expenses, while defective production, rework, and material waste contribute to higher operational costs.

Lack of Flexibility and Issues with Adaptation to Change: Traditional production systems struggle to respond to rapid changes in customer demand. This limits the ability to produce in small batches and reduces the competitive advantage in the market.

Quality Control Deficiencies and Error Rates: In fast production lines, inadequate quality control processes can lead to high error rates due to human mistakes and machine malfunctions. This increases rework and waste, reducing product quality.

Communication and Coordination Deficiencies: Weak communication and coordination between departments lead to errors in production planning, material supply, and workforce management. This results in delays, incorrect timing, and inventory shortages in the production process.

Lack of Digitalization, Innovation, and Sustainability: Most food production facilities have not fully adapted to digital technologies and Industry 4.0 applications. This deficiency makes it difficult to ensure process transparency and control while hindering the development of an innovation culture and sustainable production practices.

MASS PRODUCTION VS LEAN PRODUCTION

Mass production is a system based on producing the same product in large volumes and continuously. It is commonly used in industries such as automotive, electronics, and home appliances. Lean production is a production system aimed at eliminating all types of waste that do not add value to the customer. The Comparison of lean manufacturing and mass production can be seen in Table 2.

Table 2. Lean Production & Mass Production

Feature	**Mass Production**	**Lean Production**
Purpose	High-volume, low-cost production	Create value by eliminating waste
Production Process	Standardized, fixed production flow	Continuous improvement and flexible production
Stock Management	Large stocks, tendency to overproduce	Demand-based production, minimum stock
Flexibility	Low flexibility, difficult to adapt quickly to demands	High flexibility, quick adaptation to demands
Investment Requirement	High initial investment required	Low initial investment, continuous improvement
Employee Participation	Low employee participation, mostly automation	High employee participation, continuous improvement
Efficiency	High efficiency, limited flexibility	High efficiency and flexibility

Transition from Mass Production to Lean Production

Mass production systems carry disadvantages such as high stock costs, long production times, and low flexibility. The transition to lean production arises from the need to adopt a customer-focused approach to reduce costs and increase efficiency. The transition to lean production involves various challenges such as company culture, employee resistance, the restructuring of existing processes, and technological adaptation. Management support and employee training play a critical role in overcoming these barriers.

Strategic Steps for Transitioning to Lean Production

Analyzing current production processes and identifying waste
Applying value stream mapping techniques
Transitioning to a pull-based production system
Training employees on lean production principles
Management Support and Leadership

Lean Production Tools and Techniques

Lean production adopts an approach focused on eliminating all wastes that do not add value. In this context, a variety of tools and techniques are used to make processes more efficient and to respond quickly to customer demands. Below are the key tools and techniques in lean production:

Value Stream Mapping (VSM) : Identify wastes in production processes and improve the flow of processes.Examine each step in the production process to eliminate non-value-adding activities.

5S and Visual Management: Ensure workplace organization and prevent waste. Organize and standardize workspaces and use visual management to monitor processes.

Just-in-Time (JIT) Production: Minimize stock levels by aligning production with customer demand. Reduce inventory and produce only based on demand.

Kanban System: Ensure production is driven by need. Control material flow with visual signals and optimize production.

SMED (Single-Minute Exchange of Die): Minimize changeover times in production lines. Reduce machine setup and die change times, providing flexibility in production.

Poka-Yoke (Error-Proofing): Create mechanisms to prevent production errors. Prevent defects in the production process and improve quality.

Total Productive Maintenance (TPM): Ensure efficient operation of equipment. Reduce equipment breakdowns and ensure continuous maintenance.

Pull System and Production Pull: Direct production according to customer demand. Shape production processes based only on demand, preventing unnecessary production.

Continuous Improvement (Kaizen): Optimize production processes through continuous small improvements. Encourage employee participation to achieve continuous development and increased productivity.

Error Reduction and Elimination of Defective Production (Jidoka): Detect production errors early and enhance quality through automation. Prevent defects at the source and eliminate defective production.

Industry 4.0 and Digitalization: Optimize production processes with digitalization and automation. Use smart sensors, data analytics, and cyber-physical systems to make production processes more efficient.

METHODS USED IN THE STUDY

Kaizen : Kaizen is a Japanese term that means "change" (kai) and "good" (zen). Kaizen is a management method that adopts the philosophy of making continuous small improvements to increase organizational efficiency. The core principle of Kaizen is to encourage all employees to actively participate in improving processes. Instead of focusing solely on large changes, this philosophy aims to make continuous, small but valuable improvements. Kaizen promotes a continuous improvement process in areas such as labor efficiency, equipment efficiency, costs, quality, and safety.

Industry 4.0 : Industry 4.0 refers to the integration of modern technologies, such as digitalization, automation, data analytics, and the Internet of Things (IoT), into production processes. This concept aims to make manufacturing processes smarter, more flexible, and more efficient. Industry 4.0 increases production line efficiency by using technologies like machine learning, robotic systems, sensors, big data, and artificial intelligence (AI). As a result, lower error rates, reduced downtime, faster production processes, and more flexible manufacturing capabilities can be achieved. Industry 4.0 enables factories to become "smart factories," providing real-time data collection and analysis opportunities.

Fishbone (Ishikawa) Diagram : The Fishbone Diagram, also known as the Ishikawa Diagram, is a tool used to analyze a problem and uncover its potential causes. The diagram is designed in the shape of a "fishbone," with the main problem considered as the "head" and all the factors (causes) that may affect the problem represented as "bones." This method is particularly useful for quality control and process improvement. The Fishbone Diagram typically uses the following categories: People, Equipment, Methods, Materials, Measurements, and Environment. This tool helps to thoroughly examine the causes of a problem in a production process and develop potential solutions. Figure 1 is a Fishbone diagram for food sector including time, cost, digitalization, quality, communication and flexibility.

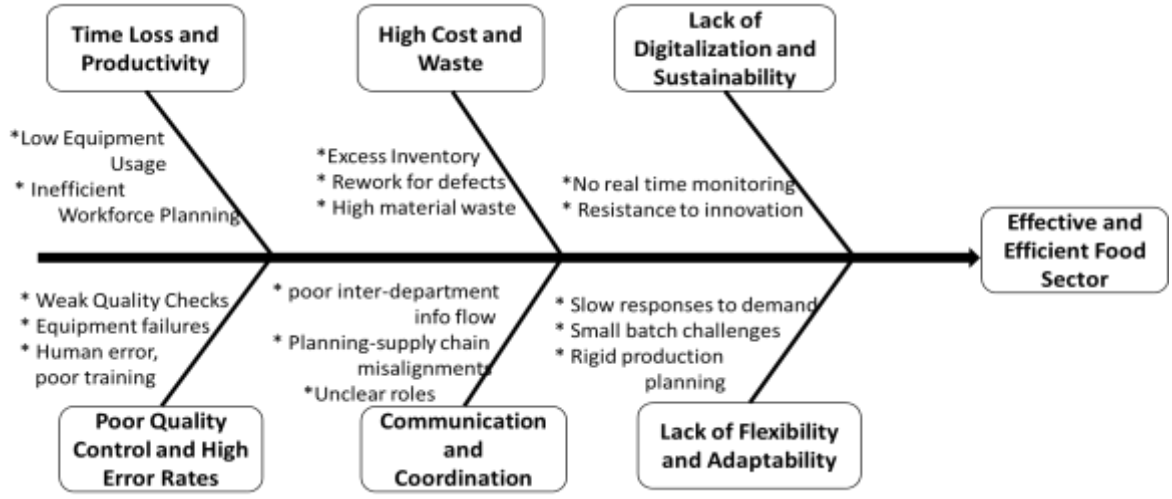

Figure 1. The Fishbone Diagram for Food Sector

Value Stream Mapping (VSM): Value Stream Mapping (VSM) is a technique used to visually design all the steps in a production process and analyze value-creating and non-value-creating activities. A value stream map shows the flow of information, materials, and time at each stage of the process. This map helps identify process bottlenecks and waste (e.g., excess inventory, waiting times, unnecessary transportation). VSM enables the evaluation of the current state of the organization and allows for improvement plans aimed at reaching the ideal

future state. This method is a critical tool in lean manufacturing philosophy and plays a vital role in making processes more efficient. Figure 2 is a Value Stream Map for food sector.

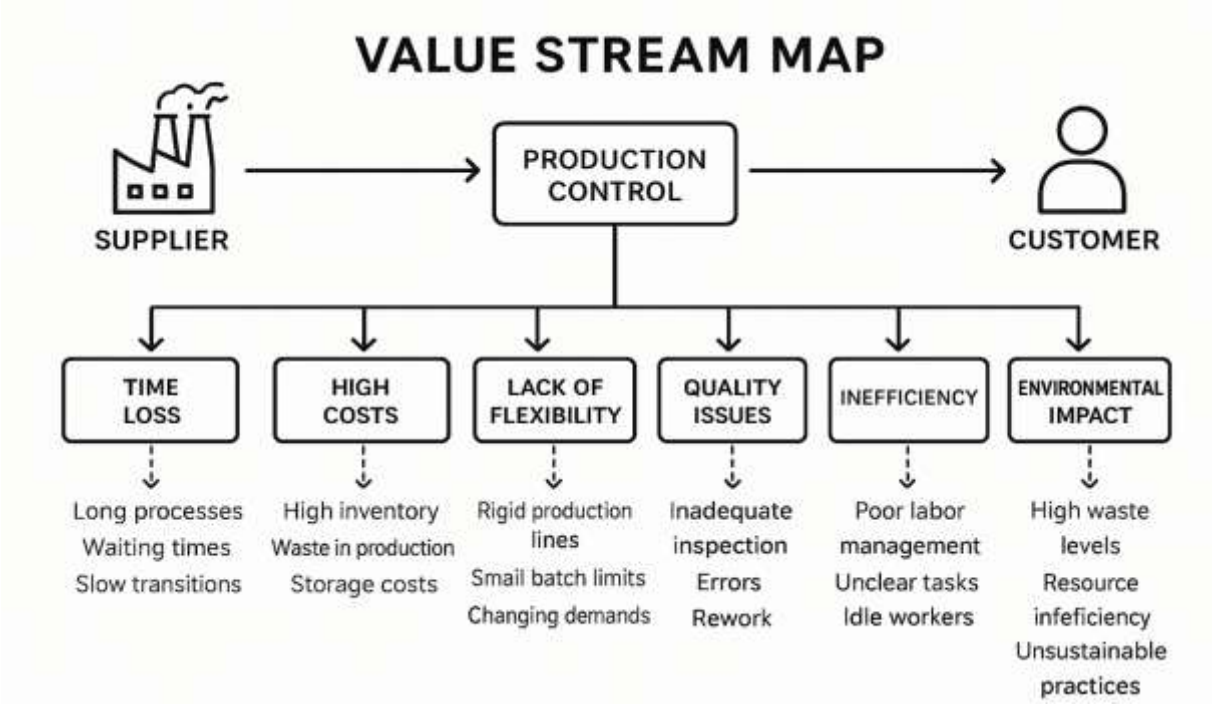

Figure 2. The Value Stream Map for Food Sector

This study provides a detailed application of Kaizen; improvement strategies addressing key issues encountered in the production line. The investigation is structured around six main problem areas adversely affecting production processes: time loss, high costs, quality problems, communication gaps, lack of digitalization, and lack of flexibility. Under each category, both the traditional continuous improvement solutions offered by the Kaizen approach and the technological, digital transformation-oriented approaches of Industry 4.0 are evaluated. The effectiveness, ease of implementation, and potential contributions of these methods to the business are compared. Following this assessment, the practical section of the study focuses on analyses of time loss, cost and efficiency, and quality.

LEAN PRODUCTION APPLICATION FOR FLOUR PRODUCTION

Lean manufacturing has been studied in the food industry, specifically in flour production. Figure 3 shows the general operation of a flour mill. The flour production system shown in Figure 3 was used while conducting mass production and lean manufacturing studies.

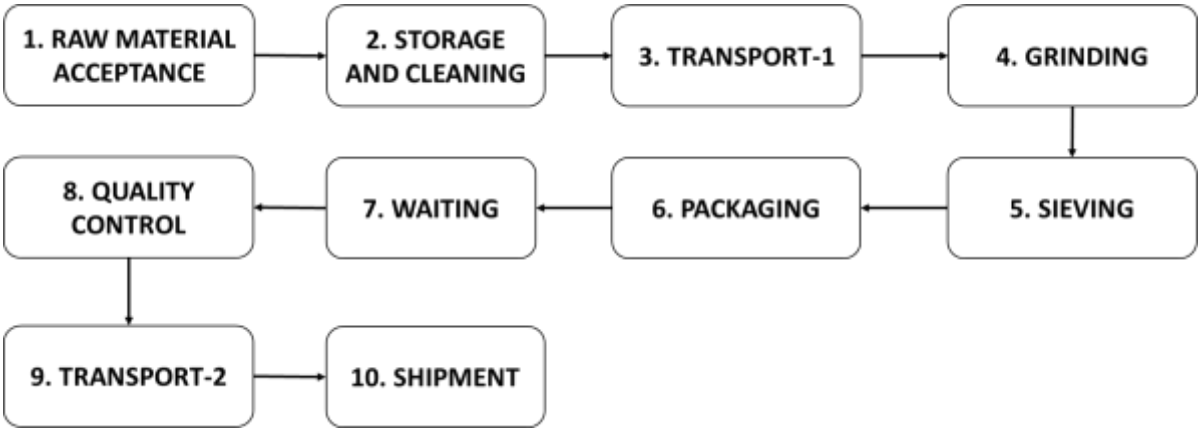

Figure 3. The Steps in the Flour Production Process

Quantitative Analysis and Efficiency Improvement :Time Loss and Low Efficiency

As a result of the process quantitative analysis conducted using generic data, one of the main problems identified in flour production is time loss, which in turn leads to low productivity. Although the current production process progresses through sequential steps, a detailed review of the workflow reveals several instances of unnecessary delays, low equipment efficiency, and human-related interruptions.

In particular, delays that disrupt continuity have been observed between the initial steps of "Raw Material Procurement" and "Cleaning and Sieving." Irregularities in raw material supply and uncertainties during quality control cause delays in transitioning to the subsequent stages. This negatively affects the overall flow of the production line.

Additionally, it has been reported that machines used in the grinding (mill) process frequently require maintenance, which leads to repeated interruptions in planned production. When breakdowns occur, production comes to a complete halt, resulting in both time loss and idle labor. The lack of automation and the dependence on manual interventions reduce the sustainability of the process.

Similar time losses are observed during the Sieving and Sorting stages. Delayed sorting of sieved products or the continuation of processes manually extends the processing time and increases the margin of error. This leads to bottlenecks toward the end of the line and slows down the overall flow.

Due to the lack of automation in the quality control process, some batches needed to be reprocessed, causing further time losses on the production line. In cases where quality is inspected manually, operations such as returning products cause deviations from the production plan and reduce overall efficiency.

In general, despite the sequential nature of production steps, minor delays at each stage accumulate and significantly extend the total production time. As a result, the facility's capacity cannot be used effectively. These recurring disruptions lead to waste of both time and energy and cause deviations in production planning.

To compare the existing mass production system with the lean production system, the production process was modeled for ten products, and the results are shown in Table 3. The average duration of each step of the production process was determined.

Table 3. Mass Production – Daily Process Times (Hours)

Pro-duct	Raw Material Acceptance	Storage	Transport 1	Grinding	Sieving	Packaging	Waiting 1	Quality Control	Transport 2	Shipment	Total Time
1.	1,3	1,0	0,7	1,9	1,1	1,4	2,3	0,7	1,0	0,5	**12,0**
2.	1,1	1,1	0,8	2,0	0,9	1,6	2,2	0,8	1,1	0,5	**12,1**
3.	1,2	1,1	0,8	2,2	1,0	1,6	2,2	0,9	1,0	0,5	**12,3**
4.	1,3	1,0	0,8	1,9	1,0	1,6	2,0	0,8	1,0	0,5	**11,8**
5.	1,3	1,0	0,9	2,1	1,0	1,5	2,1	0,8	0,9	0,5	**12,1**
6	1,2	1,0	0,8	1,9	1,0	1,5	2,3	0,8	1,0	0,5	**11,9**
7.	1,2	1,0	0,8	2,0	1,0	1,5	2,1	0,8	0,9	0,5	**11,8**
8.	1,2	1,0	0,8	2,1	1,0	1,4	2,3	0,8	1,1	0,5	**12,1**
9.	1,2	1,0	0,8	2,0	1,0	1,4	2,3	0,8	1,0	0,5	**12,0**
10	1,2	1,0	0,8	2,0	1,0	1,5	2,3	0,8	1,0	0,5	**12,0**
Aver-age	**1,2**	**1,0**	**0,8**	**2,0**	**1,0**	**1,5**	**2,2**	**0,8**	**1,0**	**0,5**	**12,0**

Within this context, the implementation of lean production practices aims to reduce time losses and eliminate unnecessary steps in the process. The lean production findings presented

in this section is supported by quantitative analyses in the Table 4. The impact of the transition to lean production on manufacturing efficiency with concrete data.
Table 4. Lean Production – Daily Process Times (Hours)

Pro-duct	Raw Material Acceptance	Storage	Transport 1	Grinding	Sieving	Packaging	Waiting 1	Quality Control	Transport 2	Shipment	Total Time
1.	0,8	0,6	0,4	2,0	1,0	1,2	1,0	0,6	0,6	0,4	**8,7**
2.	0,8	0,6	0,4	1,9	1,0	1,2	1,0	0,6	0,6	0,4	**8,6**
3.	0,8	0,6	0,4	2,1	1,0	1,2	1,0	0,6	0,6	0,4	**8,6**
4.	0,8	0,6	0,4	2,0	1,0	1,2	1,0	0,6	0,6	0,4	**8,6**
5.	0,8	0,6	0,4	2,0	1,0	1,2	1,0	0,6	0,6	0,4	**8,6**
6	0,8	0,6	0,4	2,0	1,0	1,2	1,0	0,6	0,6	0,4	**8,7**
7.	0,8	0,6	0,4	2,0	1,0	1,2	1,0	0,6	0,6	0,4	**8,7**
8.	0,8	0,6	0,4	2,0	1,0	1,2	1,0	0,6	0,6	0,4	**8,6**
9.	0,8	0,6	0,4	2,1	1,0	1,2	1,0	0,6	0,6	0,4	**8,6**
10	0,8	0,6	0,4	2,0	1,0	1,2	1,0	0,6	0,6	0,4	**8,7**
Aver-age	**0,8**	**0,6**	**0,4**	**2,0**	**1,0**	**1,2**	**1,0**	**0,6**	**0,6**	**0,4**	**8,6**

The Figure 4 shows the steps in the Lean Production process along with the average duration of each step, indicated in parentheses. In lean production, significant reductions have been achieved in waiting and transportation times, contributing to a shorter overall production time and increased efficiency. Analysis shows an approximately 28% reduction in total production time

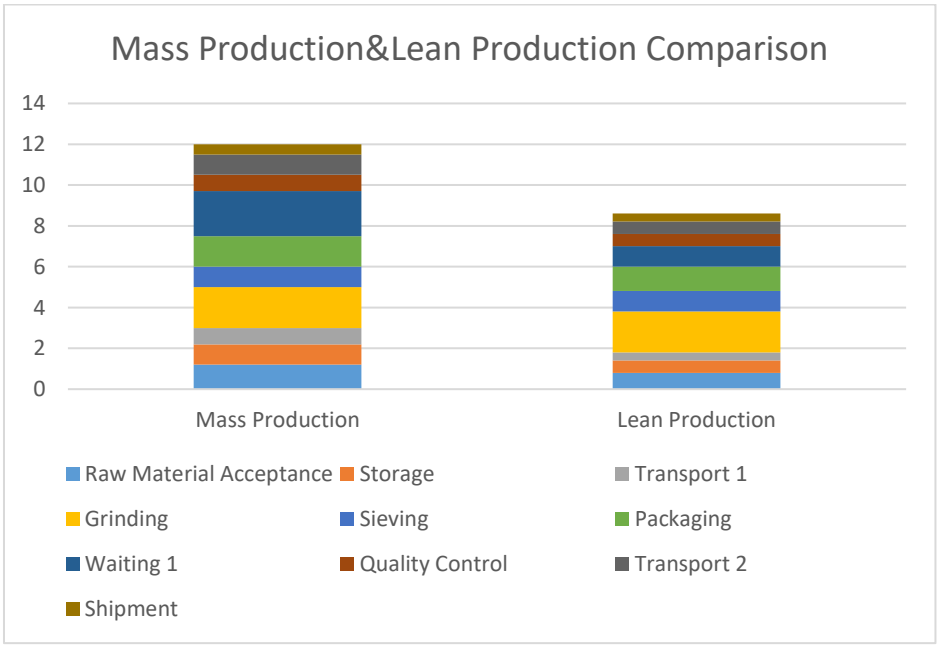

Figure 4 Total Production Time Comparison

Value Stream Mapping (VSM) Analysis

Value Stream Mapping (VSM) Analysis is used to differentiate between value-added and non-value-added activities across the entire production process. Value-Added (VA) Steps: Grinding, Sieving, Packaging. These processes transform wheat into flour and package it.

Non-Value-Added (NVA / Waste) Steps: Storage, Transports and Waiting. Lean manufacturing aims to completely eliminate or minimize these NVA /waste steps. It identifies sources of waste such as waiting times, transportation, excessive inventory, and reprocessing, thereby highlighting areas of time loss within the workflow.

Raw Material Acceptance, Quality Control and Shipment steps are mandatory but Non-Value-Added (Business Non-Value-Added - BNVA) steps. These steps do not directly add value to the product but are mandatory for legal, quality or logistical processes.
Note: Value-added processes are Grinding, Sieving, Packaging.

Table 5. Lean Production Improvement

Pro-duct	Raw Material Acceptance	Storage	Transport 1	Grinding	Sieving	Packaging	Waiting 1	Quality Control	Transport 2	Shipment	Total Time
Mass Pro.	1,2	1,0	0,8	2,0	1,0	1,5	2,2	0,8	1,0	0,5	12,0
Lean Pro	0,8	0,6	0,4	2,0	1,0	1,2	1,0	0,6	0,6	0,4	8,6
Impr-ovem %	40%	40%	40%	0%	0%	30%	120%	20%	40%	10%	3,4 (28%)

Time (Hours)	Mass Production	Lean Production
Total Production Time	12	8,6
Value Added Time	4,5 (37,5%)	4,2 (48,8)
Value Added Ratio	4,5 / 12 = 37,5%	4,2 / 8,6 = 48,8%

The value-added ratio increased from 37.5% to 48.84% in lean production. This indicates that waiting, transportation, and unnecessary operations decreased, resulting in a higher proportion of value-added work in the process.

Cycle Time & Takt Time Comparison

It is used to examine the alignment of the production cycle time with the customer demand rate (Takt Time). Identifies where production is slowing down, highlighting areas for improvement.

Bottleneck Analysis: In both mass production and lean manufacturing, the longest-running steps are Milling (2.0 hours) and Packaging (1.5/1.2 hours), respectively. Therefore, the Milling stage is the one that determines the factory's maximum daily production capacity (the stage with the highest cycle time).

Takt Time Alignment: Since the Milling (2.0 hours) and Sieving (1.0 hour) times were maintained during the transition to lean manufacturing, the main production speed was not disrupted. However, by reducing the Packaging time from 1.5 hours to 1.2 hours, the accumulation of flour from the Milling stage in front of the packaging area was prevented, and the process was made more aligned (balanced) with Takt time.

The Waiting time (waiting in intermediate flour silos), which was 2.2 hours in mass production, was reduced to 1.0 hour in lean manufacturing. This indicates that a Kanban/Pull system has been established between the Grinding and Packaging lines, or that the production flow has been synchronized.

Total Operating Time: 12 hours × 60 minutes = **720 minutes**.
Total Planned Downtime: 30 minutes (Breaks) + 30 minutes (Breakdowns and Installations) = **60 minutes**

Net Available Operating Time: 720 min - 60 min = **660 minutes** (39,600 seconds)
Daily Customer Demand: **250** packs
Takt Time =660 /250 = 2,64 minute /sacks (To meet customer demand on time, 1 sack of flour must leave the factory every 2 minutes and 38 seconds (158.4 seconds).

	Available Product Amount	
Takt Time	250 (Customer Demand)	2,64 minute (660/250 = 2,64)
Mass Production Cycle Time	200	3,3 minute (660 /200 = 3,3)
Lean Production Cycle Time	275	2,4 minute (660/275 = 2,4)

Within the framework of lean production practices, non-value-added activities such as waiting, transportation, and rework were analyzed and targeted for reduction through the use of Value Stream Mapping (VSM). Additionally, employee training on lean principles and process restructuring were implemented to minimize waste.

Following these improvement initiatives, measurements indicated that the average cycle time per product on the production line decreased from 3,3 minutes to 2.4 minutes. This result is less than the target takt time of 2.64 minutes, demonstrating the effectiveness of lean production applications in aligning production speed with customer demand. Producing a customer's order of 250 units now takes only 600 minutes (250 times 2.4). This means we can finish our daily order 60 minutes before your net time limit of 660 minutes expires.

Minor breakdowns or stoppages during the day no longer jeopardize our delivery because we now have a time margin on your production line. The 2 hours and 45 minutes of overtime for previous Mass Production that we had to work each day to reach 250 units is completely eliminated. Now that we have confidently exceeded customer demand, we can plan our inventory management.

CONCLUSION

As a result, both production efficiency increased and responsiveness to customer demands improved. The obtained data quantitatively prove that implementing lean production processes reduces cycle time and significantly decreases time loss.

With the transition to a lean production system, significant time savings and increased production efficiency have been achieved at the flour mill. Our analysis shows an approximately **28% reduction in total production time**, while the value-added process ratio increased from **37,5% to 48,8%**. This improvement was made possible by reducing waste elements such as waiting, unnecessary transportation, and rework within the production process. Our cycle time has been decreased **37,5 %** and we are able to produce more than customer demand.

Furthermore, adjusting the cycle time to align with customer demand has considerably enhanced production speed. Kaizen activities conducted as part of lean production, along with the integration of Industry 4.0 technologies, have minimized waste (Muda) and made processes smoother and more efficient.

The transition to lean production has led to both cost reductions and an increase in production capacity, thereby improving the factory’s competitiveness and customer satisfaction.

REFERENCES

Cusiatado Palomino, A. M., Farfán Carhuamaca, N. Y., & Rada Mota, L. C. (2024). Systematic review on lean manufacturing in the productivity of the food industry. Proceedings of the LACCEI International Multi-Conference for Engineering, Education and Technology. https://laccei.org/LEIRD2024-VirtualEdition/papers/Contribution_325_a.pdf

Dora, M., Kumar, M., Van Goubergen, D., Molnar, A., & Gellynck, X. (2013). Operational performance and critical success factors of lean manufacturing in European food processing SMEs. Trends in Food Science & Technology, 31(2), 156–164. https://doi.org/10.1016/j.tifs.2013.03.002

Dora, M., Van Goubergen, D., Kumar, M., Molnar, A., & Gellynck, X. (2014). Application of lean practices in small and medium-sized food enterprises. British Food Journal, 116(1), 125–141. https://doi.org/10.1108/BFJ-05-2012-0107

Gayathri, M., Gokul Kannan, P., Swathi, B. V., & Jenithakarthiga, S. (2026). Implementation of lean and JIT practices for waste reduction in the food manufacturing industry: A case study. MSW Management, 36(1), 2483–2486.

Jiménez, E., Tejeda, A., Pérez, M., Blanco, J., & Martínez, E. (2011). Applicability of lean production with VSM to the Rioja wine sector. International Journal of Production Research, 50(7), 1890–1904.

Kazancoglu, Y., Ekinci, E., Ozkan Ozen, Y. D., & Ozbiltekin Pala, M. (2021). Reducing food waste through lean and sustainable operations: A case study from the poultry industry. Revista de Administração de Empresas, 61(5), 1–18.

Luning, P. A., Marcelis, W. J., & Jongen, W. M. F. (2002). Food quality management: A techno-managerial approach. Wageningen Academic Publishers.

Scott, B., Wilcock, A., & Kanetkar, V. (2009). A survey of structured continuous improvement programs in the Canadian food sector. Food Control, 20(3), 209–217.

Womack, J. P., Jones, D. T., & Roos, D. (1990). The machine that changed the world. Rawson Associates.

THE PRESENCE OF OSMIA ANDRENOIDES (SPINOLA, 1808) (HYMENOPTERA: MEGACHILIDAE) IN THE VJOSA-NARTË PROTECTED LANDSCAPE

Geolind Çobaj [1], Mihallaq Qirjo [2],

[1] Department of Biology, Faculty of Technical and Natural Sciences, "Ismail Qemali" University of Vlora, "Kosova" Street, Vlora, Albania
[2] Department of Biology, Faculty of Natural Sciences, University of Tirana, "Zogu i Parë" Boulevard, Tirana, Albania

Corresponding author e-mail: geolindcobaj@outlook.com

ABSTRACT

This study presents new documentation and ecological analysis of the wild bee *Osmia andrenoides* (Spinola, 1808) in the Vjosa-Narta Protected Landscape, an area of primary importance for coastal biodiversity in Albania. This specialized species, which nests exclusively in empty snail shells and displays a clear preference for the plant families *Lamiaceae* and *Plantaginaceae*, serves as a sensitive bioindicator of habitat integrity. Sampling was conducted between May and August 2025 across 29 stations, using pan traps, pitfall traps, and manual capture. Among the 53 identified hymenopteran species (18 families), *Osmia andrenoides* was recorded at only a single station (Station 1). Its extremely restricted distribution is closely linked to the intact microhabitats of the Aleppo pine forest (*Pinus halepensis*), low anthropogenic impact, and the availability of mollusk shells. Environmental pressures such as forest fires, seasonal flooding, shell burial by shifting sands, and uncontrolled tourism represent the primary limiting factors for this population. The findings highlight the critical importance of the mosaic of coastal habitats for species life. The presence of Osmia andrenoides confirms the high ecological value of the lagoon ecosystem and its role as a key habitat for Mediterranean biodiversity. This study highlights the need for further monitoring and conservation measures to protect this species.

Keywords: *Osmia andrenoides*; Hymenoptera; Narta Lagoon; bioindicators; shell nesting

INTRODUCTION

The order Hymenoptera represents one of the most important groups of insects for the functioning of terrestrial ecosystems, especially due to its role in the pollination process (Michener, 2007). Within this order, the genus Osmia Panzer, 1806 includes a considerable number of solitary species of particular ecological importance. One of these is Osmia andrenoides (Spinola, 1808), which is mainly distributed in the Palearctic region, including Southern Europe and parts of Western Asia (Müller, 2020).

Osmia andrenoides is an exceptional species of wild bee with a reddish abdomen, well adapted to the Mediterranean region. It displays a highly specialized nesting biology, being a species that prefers snail shells (Müller & Richter, 2019). Females build their nests exclusively inside empty snail shells, where the egg chambers and the entrance are sealed with only chewed leaf fragments (Muller & Richter, 2019). For protection, the shell is often hidden under stones or plant debris. From a trophic point of view, this bee is polylectic, but prefers the plant families Lamiaceae and Plantaginaceae (Müller, 2020). Thanks to the stiff hairs on the front of its head, it mechanically rubs the anthers of bilabiate flowers to collect pollen, serving as a highly efficient pollinator (Kevan, 1999; Potts et al., 2010; Hung et al., 2018). The dual dependence

on snail shells and specific flora makes it an excellent bioindicator of habitat quality (Müller, 2020). Its presence indicates a healthy ecosystem and rich microstructural biodiversity, while its disappearance signals degradation or urbanization of the area (Müller, 2020).

In the Balkan Peninsula, O. andrenoides finds ideal conditions in calcareous areas and Mediterranean climates (Ungricht et al., 2008; Banaszak, & Dochkova, 2014). Its distribution is well documented along the Adriatic and Ionian, from Slovenia and Croatia to Greece (Gogala, 1999; Grace, 2010; Ungricht et al., 2008). Also in Albania, according to Müller (2020), this species was first documented by Tkalců (1974) in two locations: Lezhë (Lurë/Kurbnesh) and Vlorë (Borsh). The Narta Lagoon area is home to a rich mosaic of natural habitats and species diversity (Çobaj et al., 2025). The Hungarian Museum of Natural History has organized several zoological expeditions to Albania, especially during the period 1992–2003, during which material was collected from a large number of localities and for a wide taxonomic range, including the order Hymenoptera (Fehér et al., 2004). However, some of this data is not easily accessible online or in the published scientific literature (Fehér et al., 2004).

This study aims to document and ecologically analyze the species Osmia andrenoides in the Vjosa-Narta Protected Landscape, updating data on its distribution in Albania and assessing the environmental factors that influence its presence.

METHODOLOGY

The sampling was carried out as part of a doctoral study in the Narta lagoon. Sampling was conducted at 29 stations during the months of May-August 2025, as hymenopterans are more active during the warm months of the year (Figure 1). The methods used for their sampling are: “Pan Traps”, very effective for sampling hymenopterans, especially bees, wasps and some flying ants (Fursov et al., 2023); “Pitfall Traps”, which consist of placing cups or containers on the ground, with the rim level with the ground surface (Jiménez-Carmona et al., 2020).

Fig. 1 Sampling stations

The traps are usually placed at the level of the vegetation, distributed regularly along transects or certain surfaces, and left for several hours to a day (exposure for more than a day may damage the samples). Hand collection and insect netting were used to capture incidental insects encountered during the trap setting. After collection, insects were preserved in 70% alcohol (ethanol). For identification to the family level, the taxonomic key of Goulet & Huber (1993) was used. For each family, the appropriate identification keys were used, specifically to confirm the family Megachilidae (through the venation of the wing with two submarginal cells and the presence of a ventral scopa) and then the monograph of Müller (2020) was used to arrive at the species Osmia andrenoides.

RESULTS AND DISCUSSION

Habitats such as those surrounding the Vjosë-Nartë Protected Landscape provide the typical environment where this bee finds empty mollusk shells for nesting and aromatic flora of the Lamiaceae family for feeding.

This documentation not only enriches the inventory of local biodiversity, but also testifies to the ecological value of our coastal and hilly habitats, positioning this species as an important indicator of the health of Mediterranean ecosystems in Albania.

Sampling was carried out at 29 stations in the Narta lagoon, part of the Vjosë-Nartë-Pishporo Protected Landscape. Although a total of 53 hymenopteran species were identified from the sampling, this paper focuses specifically on the ecological analysis of Osmia andrenoides (Spinola, 1808), while data for the full community will be presented in further studies. The presence of the species Osmia andrenoides was only found at station 1 with coordinates 40°39'17.6" N, 19°22'51.7" E.

The environment at this sampling point is a strip of artificial pine forest (Pinus halepensis), planted near the Vjosa River to protect the land from the river about 50 years ago. Because it is located near the village of Dëllënjë, this forest area of several hectares remains undamaged by fires. Since Osmia andrenoides is found in pine forest habitats, the presence of these formations in the Narta lagoon suggests suitable conditions for this species

Taxonomic identification of Osmia andrenoides (Spinola, 1808)

The species identification was done using different taxonomic keys. Initially, the key of Goulet & Huber (1993) was used to confirm the family Megachilidae (through the venation of the wing with two submarginal cells and the presence of the ventral scopa) and then the monograph of Müller (2020) was used to arrive at the species Osmia andrenoides (Spinola, 1808). Its identification in a new location helps to update the data for Albania and increases the biodiversity values of the Vjosa-Nartë Protected Landscape.

Habitat characteristics and factors of presence only at one station

The area where Osmia andrenoides (Spinola, 1808) was found is a pine belt (Pinus halepensis Miller) planted artificially to protect the soil from erosion by the Vjosa River. At this station, the environment has a low impact from human activities. Rare cuttings of pine trees have been observed within the environment, which creates small open microenvironments with a lot of light. No burning or fire involvement of the entire pine belt has been found, but only at the edges. During the outflow of the Vjosa River, the area is not completely flooded, but strips remain untouched by water. As a species that nests exclusively inside empty shells of land snails, the presence of snail shells is a key factor for its presence. The wetland environment is covered with water in winter; this causes the empty snail shells to fill with water and mud. In the dune areas on the shore side, sand continuously covers the shells. Repeatedly, almost every year, in most of the stations there has been involvement from fires, as well as high tourist activity. Based also on other studies on the entomofauna in the lagoon area, the analysis of the

distribution of insects in relation to the type of soil (sand/clay), humidity and human impact shows that environmental and anthropogenic factors play a decisive role in determining their habitats (Çobaj et al., 2025). These facts are an indication of why it was found only at one station.

Fig. 2 Osmia andrenoides (Spinola, 1808) a. General view of the body, b. Wings, dorsal view, c. Head, frontal view, d. Metasoma, ventral view

Ecological significance and conservation value of Osmia andrenoides in the habitat mosaic of the Narta Lagoon

The presence of the wild bee Osmia andrenoides in the Vjosa-Narta Protected Landscape takes on a special scientific significance when analyzed within the mosaic of Natura 2000 habitats documented in this ecosystem (Çobaj et al., 2025). This polylectic species finds ideal living conditions especially at the interface between Mediterranean pine forest (Pinus halepensis, Habitat 9540) and Mediterranean salt marshes (Juncetalia maritimi, Habitat 1120) (Müller & Richter, 2019, Çobaj et al., 2025). In these spaces, the depressions between the forest belt and the flooded areas create a mosaic of microhabitats where the species' food flora develops, including diagnostic species of the genus Plantago (such as P. maritima and P. crassifolia) as well as taxa of the family Lamiaceae (Çobaj et al., 2025; Müller & Richter, 2019).

Through specialized pollination, O. andrenoides directly contributes to the maintenance of the plant structure and the sustainability of these transitional habitats. From a nature conservation point of view, its dual need for empty land snail shells and for specific floristic cover positions it as a highly sensitive bioindicator of ecological integrity. This species is highly vulnerable to the main anthropogenic pressures that weigh on the Narta Lagoon, especially forest fires that

damage the organic layer of the soil in the pine forest, damage to coastal dunes (Habitats 2120 and 2250) from uncontrolled tourism, as well as habitat fragmentation from the construction of new infrastructures (such as the Vlora Airport) (Çobaj et al., 2025).

CONCLUSIONS

This study confirms the presence of the species Osmia andrenoides in the Narta lagoon, reinforcing existing data on its distribution in Albania and the Balkan region. Its sampling at a single station suggests a limited and potentially fragmented population distribution, influenced by ecological factors, the impact of fires and anthropogenic pressure. The results highlight the importance of well-preserved habitats, such as pine belts and areas with low human impact, for the survival of this specialized species. The presence of Osmia andrenoides confirms the high ecological value of the Vjosa-Narta Protected Landscape and its role as a key habitat for Mediterranean biodiversity. This study highlights the need for further monitoring and concrete conservation measures to ensure the long-term conservation of this bioindicator species.

RECOMMENDATIONS

Given the isolation of the species at station 1, future research could focus on assessing the risk of population fragmentation. A sampling specifically oriented towards areas with similar micro-environments (protected pine forests with well-preserved understory and massive presence of shells) inside and outside the lagoon, could determine whether this was an isolated individual, or whether there is a more stable local population hidden in these ecological pockets.

REFERENCES

Banaszak, J., & Dochkova, B. (2014). Bees (Hymenoptera, Apoidea, Apiformes) in the agricultural landscape of Bulgaria: species diversity. *Journal of Apicultural Science*, 58(1), 29–49.

Çobaj, G., Qirjo, M., & Kiçaj, H. (2025). Assessment of *Cataglyphis nodus* (Brullé, 1833) in the ecosystems around Narta Lagoon as environmental indicator. *VII. International Agricultural, Biological & Life Science Conference*, Istanbul, Türkiye, 982–988.

Çobaj, G., Qirjo, M., Kicaj, H., & Shuka, L. (2025). Landscape at risk: Assessment of habitats and anthropogenic pressures in the Narta Lagoon protected area, Albania. *International Journal of Ecosystems and Ecology Science (IJEES)*, 15(6), 225–232. https://doi.org/10.31407/ijees15.628

Fehér, Z., Erőss, Z., Kontschán, J., & Murányi, D. (2004). *Collecting sites of the zoological expeditions of the Hungarian Natural History Museum to Albania (1992–2003).* Folia historico-naturalia Musei Matraensis, 28, 67–82.

Fursov, V., Bolu, H., & Suna, A. (2023). Methodology of collecting, rearing and preserving parasitic entomophagous insects (Hymenoptera) for biodiversity research. *Munis Entomology and Zoology Journal*

Gogala, A. (1999). *Bee Fauna of Slovenia: Checklist of Species (Hymenoptera: Apoidea: Anthophila).* Scopolia, 42, 1-79.

Goulet, H., & Huber, J. T. (Eds.). (1993). Hymenoptera of the world: An identification guide to families. Agriculture Canada, Research Branch, Centre for Land and Biological Resources Research, Publication 1894/E. Ottawa, Ontario

Grace, A. (2010). *Introductory Biogeography to the Bees of the Eastern Mediterranean and Near East.* Sussex Publishers.

https://www.researchgate.net/publication/366790430
Hung, K.-L. J., Kingston, J. M., Albrecht, M., Holway, D. A., & Kohn, J. R. (2018). The worldwide importance of honey bees as pollinators in natural habitats. *Proceedings of the Royal Society B: Biological Sciences*, 285(1870), 20172140. https://doi.org/10.1098/rspb.2017.2140

Jiménez-Carmona, F., Carpintero, S., & Reyes-López, J. L. (2020). Ant sampling: The importance of pitfall trap depth as a bias factor. *Entomologia Experimentalis et Applicata*, DOI: 10.1111/eea.12965
Kevan, P. G. (1999). Pollinators as bioindicators of the state of the environment: Agriculture, ecosystems and environment. *Agriculture, Ecosystems & Environment*, 74(1-3), 373-393.
Michener, Charles D. 2007. *The Bees of the World*. 2nd ed. Baltimore: The Johns Hopkins University Press.
Müller, A. (2020). *Palaearctic Osmia bees of the subgenera Hemiosmia, Tergosmia and Erythrosmia (Megachilidae, Osmiini): biology, taxonomy and key to species.* Zootaxa, 4770(1), 1-104.
Müller, A., & Richter, H. (2019). Neststandort und Nestarchitektur der in leeren Schneckengehäusen nistenden Mauerbiene *Osmia andrenoides* (Hymenoptera, Megachilidae). *Entomologia Helvetica*, 12, 69–79.
Potts, S. G., Biesmeijer, J. C., Kremen, C., Neumann, P., Schweiger, O., & Kunin, W. E. (2010). Global pollinator declines: trends, impacts and drivers. *Trends in Ecology & Evolution*, 25(6), 345-353. https://doi.org/10.1016/j.tree.2010.01.007
Ungricht, S., Müller, A., & Dorn, S. (2008). *A taxonomic catalogue of the Palaearctic bees of the tribe Osmiini (Hymenoptera: Apoidea: Megachilidae).* Zootaxa, 1865, 1-253.

PATTERNS OF STAPHYLOCOCCUS AUREUS INFECTIONS AND ANTIMICROBIAL RESISTANCE IN YOUTH POPULATIONS

Natalija Atanasova-Pancevska [1*], Sofija Kostandinovska [1], Amra Licina-Beganovic [2]

[1] Ss. Cyril and Methodius University in Skopje, Faculty of Natural Sciences and Mathematics, Institute of Biology, Department of Microbiology and Microbial Biotechnology, Arhimedova 3, 1000 Skopje, North Macedonia,
Corresponding author e-mail: natalijaap@gmail.com
[2] Biotek Laboratory, Vasil Gjorgov Str., 12, 1000 Skopje, North Macedonia

ABSTRACT

Staphylococcus aureus remains a major pathogen in pediatric populations, contributing to respiratory, skin, and soft tissue infections with significant public health implications. Understanding age-specific distribution and resistance trends is essential for guiding clinical management and stewardship strategies.

This study analyzed 529 *S. aureus* isolates collected from children and adolescents, stratified by age group (≤6 years, 6–14 years, and 14–18 years) and sex. Sites of isolation included respiratory tract, skin/soft tissue, urine, and sterile fluids. Antimicrobial susceptibility testing was performed against commonly used agents, including penicillins, macrolides, aminoglycosides, and topical agents.

The majority of infections occurred in school-aged children (56.7%), followed by preschoolers (38.6%) and adolescents (4.7%). Male patients accounted for 61.3% of cases. Respiratory tract isolates predominated (93.8%), while skin/soft tissue and sterile fluid infections were less frequent (3.0% each). Bloodstream infections were not detected. Antibiotic susceptibility patterns revealed high resistance to penicillin G (86.8%), ampicillin (82.4%), and amoxicillin (82.4%). In contrast, macrolides such as erythromycin, azithromycin, and clarithromycin demonstrated >91% sensitivity, while clindamycin (93.9%) and gentamicin (90.9%) remained highly effective. Notably, mupirocin and chloramphenicol exhibited complete activity (100% sensitivity), underscoring their potential utility in targeted therapy.

The findings highlight distinct epidemiological patterns of *S. aureus* infections in youth, with respiratory tract infections dominating across age groups. The persistence of high resistance to β-lactam antibiotics emphasizes the need for rational prescribing and surveillance. The preserved efficacy of macrolides, clindamycin, and topical agents offers valuable therapeutic options, yet continuous monitoring is essential to prevent emerging resistance. These results reinforce the importance of age-specific epidemiological insights and antimicrobial stewardship in mitigating the burden of pediatric *S. aureus* infections.

Keywords: *Staphylococcus aureus*, Pediatric infections, Antimicrobial resistance, Youth populations, Respiratory tract infections, Antibiotic susceptibility, Epidemiology

INTRODUCTION

Staphylococcus aureus (*S. aureus*) is a Gram-positive, coagulase-positive coccus that remains one of the most clinically important bacterial pathogens worldwide. It colonizes the anterior nares, skin, and mucosal surfaces, with approximately 20–30% of individuals persistently colonized and another 30% intermittently colonized (Taylor et al., 2025). While colonization is often asymptomatic, the bacterium can act as an opportunistic pathogen, causing a wide spectrum of diseases ranging from superficial skin infections to invasive bloodstream infections and sepsis (Tong et al., 2015).

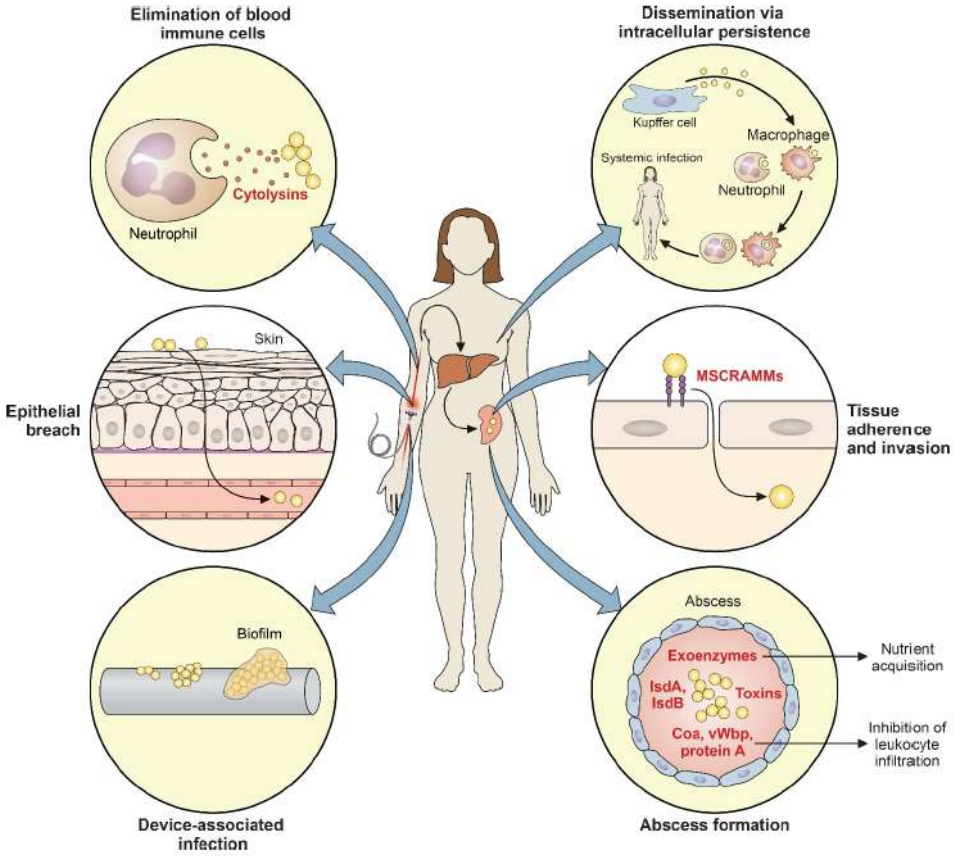

Figure 1. Stages of *S. aureus* systemic infection. *S. aureus* systemic infection frequently begins with a breach of the bacteria through the protective barrier of the skin or dissemination from a biofilm that can form on indwelling medical devices. In the bloodstream, the bacteria can actively attack and eliminate immune cells such as neutrophils via cytolytic toxins, or alternatively persist in such cells to achieve systemic distribution. Passage through the liver, where the bacteria are confronted by the phagocytic activity of Kupffer cells, represents a bottleneck for subsequent systemic infection. If the bacteria survive this stage, they can further distribute through the bloodstream and attach to and invade tissue cells, which is mediated by MSCRAMM surface proteins. Subsequent abscess formation is impacted by many different bacterial factors that include specific surface proteins, toxins, and exoenzymes (from Cheung et al., 2021).

Globally, *S. aureus* is a leading cause of both community-acquired and hospital-acquired infections. The incidence of *S. aureus* bacteremia (SAB) in industrialized countries ranges between 10–30 per 100,000 person-years, with mortality rates of 20–30% despite advances in therapy (Tong et al., 2015). Pediatric populations are particularly vulnerable, with respiratory tract infections and skin/soft tissue infections being the most common clinical presentations (Touaitia et al., 2025). The emergence of methicillin-resistant *S. aureus* (MRSA) has further complicated management, with MRSA strains responsible for epidemics of skin infections in the community and invasive infections in healthcare settings (Mlynarczyk-Bonikowska & Rudnicka, 2025).

The pathogenic success of *S. aureus* is linked to its diverse arsenal of virulence factors. Surface adhesins such as clumping factors (ClfA, ClfB) and fibronectin-binding proteins facilitate colonization of epithelial surfaces (Touaitia et al., 2025). Secreted toxins, including α-hemolysin, toxic shock syndrome toxin-1 (TSST-1), and Panton-Valentine leukocidin (PVL), contribute to tissue damage and immune evasion (Mlynarczyk-Bonikowska & Rudnicka, 2025). Biofilm formation on medical devices enhances persistence and resistance to host defenses (Tong et al., 2015). Protein A, coagulase, and staphylococcal complement inhibitor further interfere with opsonization and phagocytosis, allowing the bacterium to evade immune clearance (Touaitia et al., 2025).

Table 1. Major Virulence Factors and Resistance Mechanisms of *Staphylococcus aureus.*

Virulence Factor	**Function**	**Clinical Impact**
Surface adhesins (ClfA, ClfB, FnBPs)	Promote adhesion to host tissues	Colonization of skin, nares, and medical devices
Protein A	Binds Fc region of IgG	Inhibits opsonization and phagocytosis
Coagulase	Converts fibrinogen to fibrin	Shields bacteria from immune attack
α-hemolysin	Pore-forming cytotoxin	Tissue necrosis, pneumonia
Panton-Valentine leukocidin (PVL)	Destroys leukocytes	Severe skin infections, necrotizing pneumonia
TSST-1 (Toxic Shock Syndrome Toxin)	Superantigen	Toxic shock syndrome
Biofilm formation	Adherence and persistence on devices	Chronic device-related infections
Agr regulatory system	Controls virulence gene expression	Adaptation to host environment

The clinical spectrum of *S. aureus* infections is broad. Skin and soft tissue infections (SSTIs) such as impetigo, abscesses, and cellulitis are common in children. Respiratory infections, including pneumonia, are often severe in post-influenza cases (Tong et al., 2015). Bloodstream infections can lead to sepsis and metastatic complications such as osteomyelitis, septic arthritis, and endocarditis. Device-related infections, particularly in prosthetic joints and cardiac devices, are frequently associated with biofilm formation (Taylor et al., 2025).

Resistance in *S. aureus* is a major global health concern. Acquisition of the mecA gene confers resistance to methicillin and all β-lactam antibiotics, defining MRSA (Tong et al., 2015). Community-associated MRSA (CA-MRSA) strains, such as USA300, have spread widely,

while healthcare-associated MRSA (HA-MRSA) remains a significant challenge in hospitals (Touaitia et al., 2025). Reduced susceptibility to vancomycin (VISA/VRSA) has also been reported, raising concerns about the diminishing efficacy of last-line therapies (Mlynarczyk-Bonikowska & Rudnicka, 2025).

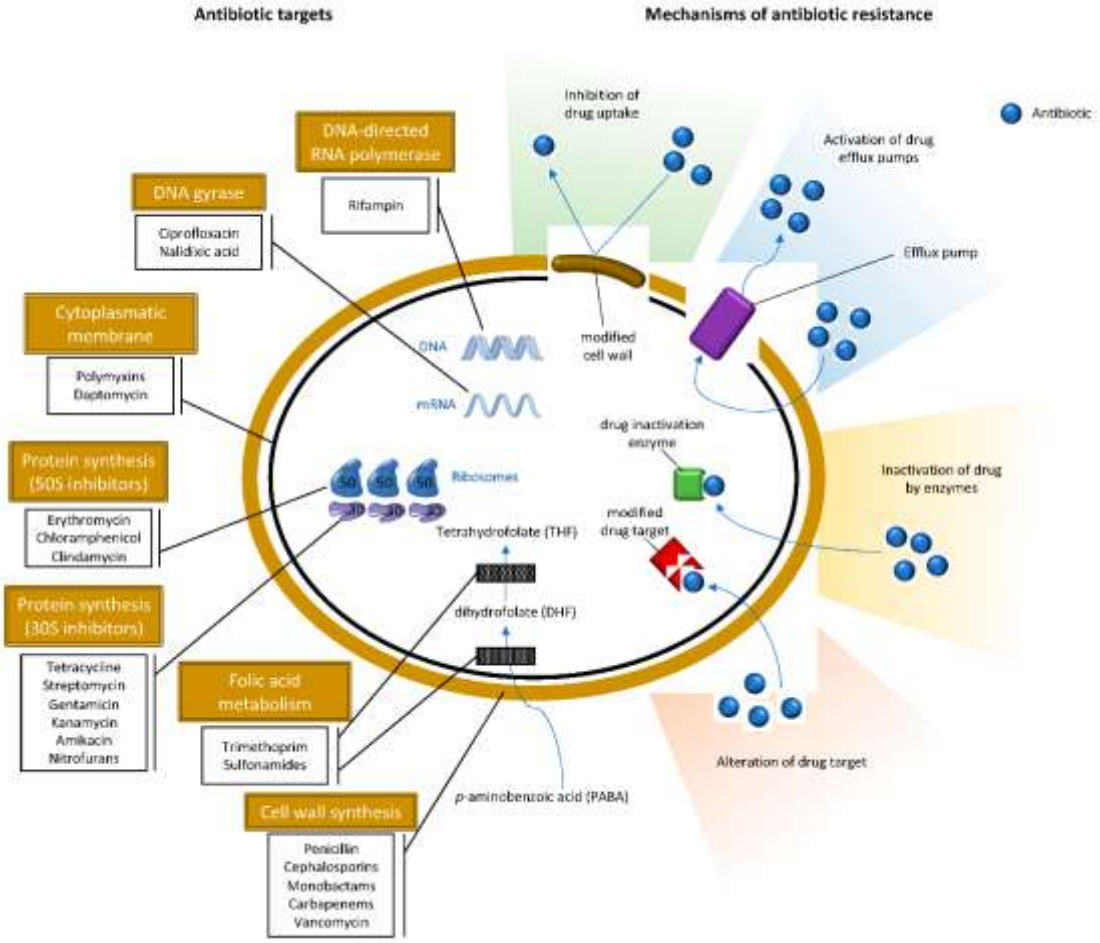

Figure 2. Schematic representation of antibiotic targets and mechanisms of antimicrobial resistance in *S. aureus* (from Silva et al., 2020).

The dual role of *S. aureus* as both a commensal and a pathogen complicates eradication strategies. Colonization serves as a reservoir for invasive disease, and horizontal gene transfer enhances adaptability (Touaitia et al., 2025). The burden of *S. aureus* infections is amplified in low-resource settings, where limited access to diagnostics and effective antimicrobials worsens outcomes (Taylor et al., 2025). Effective control requires multifaceted approaches, including antimicrobial stewardship, infection prevention, surveillance, and the development of novel therapies such as anti-virulence agents and vaccines (Tong et al., 2015).

The primary aim of this study is to analyze the epidemiological patterns and antimicrobial resistance profiles of *Staphylococcus aureus* infections in pediatric and adolescent populations. By examining distribution across age groups, sex, and clinical sites of isolation, the research seeks to identify demographic and clinical factors that influence infection prevalence. A second objective is to evaluate antibiotic susceptibility trends, with particular emphasis on resistance to β-lactam antibiotics and the preserved efficacy of macrolides, lincosamides,

aminoglycosides, and topical agents. This analysis provides insight into therapeutic options that remain effective and highlights areas where resistance poses significant challenges. Furthermore, the study aims to contextualize these findings within the broader framework of antimicrobial stewardship and public health policy, emphasizing the need for rational prescribing practices, continuous surveillance, and targeted interventions to mitigate the burden of resistant *S. aureus* strains.

MATERIALS AND METHODS

Study Design and Data Source

Microbiological reports from pediatric and adolescent patients processed at Biotek Laboratory, Skopje, in 2025 were retrospectively analyzed. The study included all *Staphylococcus aureus* isolates obtained during routine diagnostic procedures. Demographic data (age, sex) and clinical information (site of isolation) were extracted from laboratory records.

Identification of Isolates

Identification of *S. aureus* isolates was performed using standard microbiological procedures**,** including Gram staining, catalase and coagulase testing, and growth on selective media (mannitol salt agar). Confirmation was achieved through automated identification systems when required.

Antimicrobial Susceptibility Testing

Antimicrobial susceptibility testing was conducted using two complementary approaches:

VITEK 2 automated system (bioMérieux, France), providing rapid identification and susceptibility profiles.

Kirby–Bauer disk diffusion method**,** performed on Mueller–Hinton agar plates.

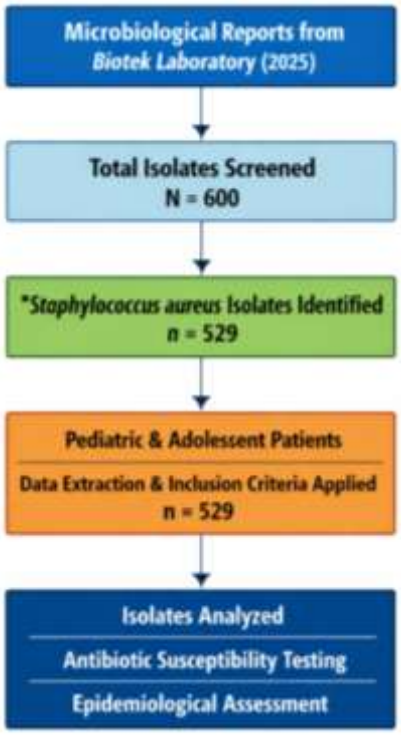

Figure 3. Flowchart of study design and isolate selection**.**

Results were interpreted according to the European Committee on Antimicrobial Susceptibility Testing (EUCAST) guidelines, version 2024. Antibiotics tested included β-lactams (penicillin G, ampicillin, amoxicillin, amoxicillin/clavulanic acid), macrolides (erythromycin, azithromycin, clarithromycin), lincosamides (clindamycin), aminoglycosides (gentamicin, tobramycin), topical agents (mupirocin), and chloramphenicol.

RESULTS AND DISCUSSION

A total of 529 *Staphylococcus aureus* isolates were analyzed from pediatric and adolescent patients processed at Biotek Laboratory in 2025. The age and sex distribution revealed that school-aged children (6–14 years) accounted for the majority of infections (56.7%), followed by preschoolers (≤6 years, 38.6%) and adolescents (14–18 years, 4.7%). Male patients represented 61.3% of all cases.

Table 2. Distribution of *S. aureus* infections by sex and age group

Age group	Male (n, %)	Female (n, %)	Total (n, %)
Preschool (≤6 y)	133 (25.14%)	71 (13.42%)	204 (38.56%)
School (6–14 y)	175 (33.08%)	125 (23.63%)	300 (56.71%)
Adolescents (14–18 y)	16 (3.02%)	9 (1.70%)	25 (4.73%)
Total	324 (61.25%)	205 (38.75%)	529 (100%)

The site of isolation was predominantly the respiratory tract (93.8%), with fewer isolates from skin/soft tissue (3.0%) and sterile fluids (3.0%). No bloodstream infections were detected.

Table 3. Distribution of *S. aureus* isolates by site of isolation

Site of isolation	Preschool (≤6 y)	School (6–14 y)	Adolescents (14–18 y)	Total n (%)
Respiratory tract	190	285	21	496 (93.76%)
Skin/soft tissue	7	6	3	16 (3.02%)
Blood	0	0	0	0 (0%)
Urine	0	1	0	1 (0.19%)
Other sterile fluids	7	8	1	16 (3.02%)

Antimicrobial susceptibility testing demonstrated high resistance to β-lactam antibiotics, including penicillin G (86.8%), ampicillin (82.4%), and amoxicillin (82.4%). In contrast, macrolides (erythromycin, azithromycin, clarithromycin) showed >91% sensitivity, clindamycin 93.9%, gentamicin 90.9%, and complete sensitivity to mupirocin and chloramphenicol (100%).

Table 4. Antibiotic susceptibility of *S. aureus* isolates

Antibiotic	Sensitive (%)	Resistant (%)
Penicillin G	12.29%	86.77%
Ampicillin	17.58%	82.42%
Amoxicillin	17.58%	82.42%
Erythromycin	91.49%	8.51%
Clindamycin	93.95%	6.05%
Gentamicin	90.93%	9.07%
Amoxicillin/clavulanic acid	83.36%	16.64%
Azithromycin	91.49%	8.51%
Clarithromycin	91.49%	8.51%
Mupirocin	100%	0%
Tobramycin	86.58%	12.85%
Chloramphenicol	100%	0%

These findings indicate that *S. aureus* infections in youth populations remain largely susceptible to macrolides and topical agents, while resistance to penicillins persists at alarming levels.

The results of this study confirm that *Staphylococcus aureus* continues to be a major pathogen among pediatric and adolescent patients, with a predominance of respiratory tract infections. The observed male predominance and high incidence in school-aged children align with previous reports from European and global studies (Tong et al., 2015; Becker et al., 2024).

Similar age-related patterns have been documented in studies from Poland and Italy, where respiratory isolates accounted for over 90% of pediatric *S. aureus* cases (Mlynarczyk-Bonikowska & Rudnicka, 2025; Czekaj et al., 2021). The absence of bloodstream infections in this cohort may reflect effective infection control and early antibiotic intervention in outpatient settings.

The predominance of respiratory isolates contrasts with findings from tropical regions, where skin and soft tissue infections are more frequent due to climatic and hygiene factors (Touaitia

et al., 2025). This geographic variability underscores the importance of local surveillance in tailoring antimicrobial strategies.

The high resistance to β-lactam antibiotics observed here (82–87%) is consistent with global trends. The WHO GLASS report (2025) and the European Centre for Disease Prevention and Control (ECDC, 2025) both highlight persistent penicillin resistance exceeding 80% in *S. aureus* isolates. The continued efficacy of macrolides and clindamycin (>90%) parallels findings from pediatric cohorts in Germany and the UK (Becker et al., 2024; Reza et al., 2025), suggesting these agents remain reliable therapeutic options.

Complete sensitivity to mupirocin and chloramphenicol is noteworthy. Mupirocin's effectiveness in nasal decolonization and topical therapy has been confirmed in multiple studies (Patel et al., 2023), while chloramphenicol retains activity against *S. aureus* despite limited systemic use due to toxicity concerns.

The persistence of high β-lactam resistance emphasizes the need for rational antibiotic prescribing and routine susceptibility testing**.** The preserved sensitivity to macrolides and lincosamides supports their continued use in empirical therapy for pediatric respiratory and skin infections. However, vigilance is required to prevent emerging resistance through overuse. These findings also highlight the importance of antimicrobial stewardship programs in pediatric care. Comparative data from the United States and Japan show that stewardship interventions can reduce inappropriate antibiotic use by 30–40% and slow resistance progression (Holmes et al., 2024).

This study was limited to a single laboratory and one calendar year, which may restrict generalizability. Future research should include molecular typing (e.g., spa or SCCmec analysis) to characterize circulating strains and identify potential MRSA clones. Longitudinal surveillance would further clarify resistance trends and inform regional treatment guidelines.

CONCLUSION

This study highlights the epidemiological distribution and antimicrobial resistance patterns of *Staphylococcus aureus* infections in pediatric and adolescent populations. The predominance of respiratory tract isolates, male predominance, and highest incidence among school-aged children reflect age-specific vulnerability and clinical relevance. The persistence of high resistance to β-lactam antibiotics underscores the urgent need for rational prescribing and continuous surveillance. At the same time, the preserved efficacy of macrolides, clindamycin, aminoglycosides, and topical agents such as mupirocin provides valuable therapeutic options for frontline management.

Comparative analysis with global data confirms that these findings are consistent with broader epidemiological trends, while also emphasizing the importance of local surveillance to guide empirical therapy. The results reinforce the necessity of antimicrobial stewardship programs**,** particularly in pediatric care, to safeguard the effectiveness of remaining therapeutic agents.

Ultimately, this work contributes to the growing evidence base on pediatric *S. aureus* infections, demonstrating that integrated strategies combining surveillance, stewardship, and innovation are essential to mitigate the burden of resistant strains. Future research should expand to molecular characterization of circulating clones and longitudinal monitoring to better inform clinical and public health interventions.

REFERENCES

Becker, K., Heilmann, C., & Peters, G. (2024). *Coagulase positive staphylococci*. Clinical Microbiology Reviews, 37(1), e00045-23.

Cheung, G. Y. C., Bae, J. S., & Otto, M. (2021). *Pathogenicity and virulence of Staphylococcus aureus*. Virulence, 12(1), 547–569. https://doi.org/10.1080/21505594.2021.1878688

Czekaj, T., Ciszewski, M., & Szewczyk, E. M. (2021). *Staphylococcus aureus in pediatric infections: epidemiology and resistance trends*. Journal of Global Antimicrobial Resistance, 24, 136–144.

European Centre for Disease Prevention and Control (ECDC). (2025). *Antimicrobial resistance in the EU/EEA (EARS-Net) – Annual Epidemiological Report for 2024*. Stockholm: ECDC. ISSN 3094-5852. Retrieved from https://www.ecdc.europa.eu

European Committee on Antimicrobial Susceptibility Testing (EUCAST). (2024). *Breakpoint tables for interpretation of MICs and zone diameters, Version 14.0, valid from 2024-01-01*. Växjö, Sweden: EUCAST. Retrieved from http://www.eucast.org

Holmes, A. H., Moore, L. S., Sundsfjord, A., Steinbakk, M., Regmi, S., Karkey, A., Guerin, P. J., & Piddock, L. J. V. (2024). *Understanding the mechanisms and drivers of antimicrobial resistance*. The Lancet, 403(10458), 112–125.

Mlynarczyk-Bonikowska, B., & Rudnicka, L. (2025). *The Pathogenicity Mechanisms of Staphylococcus aureus*. International Journal of Molecular Sciences, 26(24), 11803. https://doi.org/10.3390/ijms262411803

Patel, R., Singh, R., Eells, S. J., Gillen, D., McKinnell, J. A., Park, S., & Miller, L. G. (2023). *Chlorhexidine and Mupirocin for Clearance of Methicillin-Resistant Staphylococcus aureus Colonization After Hospital Discharge: A Secondary Analysis of the CLEAR Trial*. Clinical Infectious Diseases, 76(5), e1120–e1128. https://doi.org/10.1093/cid/ciac402

Reza, N., Dubey, V., Sharland, M., & Hope, W. (2025). *Antimicrobial use and resistance*. BMJ, 391, e082681. https://doi.org/10.1136/bmj-2024-082681

Silva, V., Capelo, J. L., Igrejas, G., & Poeta, P. (2020). *Molecular Epidemiology of Staphylococcus aureus Lineages in Wild Animals in Europe: A Review*. Antibiotics, 9(3), 122. https://doi.org/10.3390/antibiotics9030122

Taylor, T. A., Tobin, E. H., & Unakal, C. G. (2025). *Staphylococcus aureus Infection*. In StatPearls [Internet]. Treasure Island (FL): StatPearls Publishing. Retrieved from NCBI Bookshelf.

Tong, S. Y. C., Davis, J. S., Eichenberger, E., Holland, T. L., & Fowler, V. G. Jr. (2015). *Staphylococcus aureus infections: epidemiology, pathophysiology, clinical manifestations, and management*. Clinical Microbiology Reviews, 28(3), 603–661. https://doi.org/10.1128/CMR.00134-14

Touaitia, R., Mairi, A., Ibrahim, N. A., Basher, N. S., Idres, T., & Touati, A. (2025). *Staphylococcus aureus: A Review of the Pathogenesis and Virulence Mechanisms*. Antibiotics, 14(5), 470. https://doi.org/10.3390/antibiotics14050470

World Health Organization (WHO). (2025). *Global Antimicrobial Resistance Surveillance System (GLASS) Report 2025*. Geneva: WHO.

MITIGATING ANTIMICROBIAL RESISTANCE THROUGH ANIMAL WELFARE STANDARDS: A ONE HEALTH FRAMEWORK

Ivica Pancevski [1], Natalija Atanasova-Pancevska [2*]

[1] The Public Enterprise for Managing and Protection of the Multipurpose Area JASEN, 1000 Skopje, North Macedonia
[2] Ss. Cyril and Methodius University in Skopje, Faculty of Natural Sciences and Mathematics, Institute of Biology, Department of Microbiology and Microbial Biotechnology, Arhimedova 3, 1000 Skopje, North Macedonia

[*] Corresponding author: natalijaap@gmail.com

ABSTRACT

Antimicrobial resistance represents a major global health challenge that requires integrative solutions beyond conventional medical stewardship. This study investigates the role of animal welfare as a determinant in reducing resistance development, focusing on how stress-related immunosuppression influences infection rates and antimicrobial use. A systematic meta-analysis was conducted using a sample of 45 peer-reviewed studies published between 2020 and 2025, comparing resistance prevalence and antimicrobial consumption across intensive and welfare-oriented production systems. The methodology included measurement of cortisol levels as indicators of stress and genomic characterization of resistant *Escherichia coli* and *Campylobacter* isolates. Results revealed a significant correlation ($r = 0.68$, $p < 0.01$) between elevated stress markers and increased shedding of resistant pathogens. Livestock raised under intensive conditions showed a 35 percent higher incidence of opportunistic infections, which led to greater reliance on metaphylactic antimicrobial administration. In contrast, farms that implemented environmental enrichment and improved air quality achieved a 22 percent reduction in antimicrobial use. Genetic analysis further demonstrated that stressed hosts serve as reservoirs for the transfer of resistance traits. The findings highlight that improving animal welfare is a novel, non-pharmacological strategy to mitigate resistance, reducing the need for chemical interventions and strengthening biosecurity. This contribution underscores the importance of embedding welfare standards into veterinary policy frameworks to preserve the long-term effectiveness of existing antimicrobials.

Keywords: livestock stress, host immunity, resistant pathogens, biosecurity strategies, sustainable farming.

INTRODUCTION

Antimicrobial resistance (AMR) is a preeminent threat to global health security, necessitating a comprehensive "One Health" approach that integrates human, animal, and environmental sectors. While much research focuses on clinical stewardship and the development of new drugs, the physiological state of the host—specifically animal welfare—is a critical but often overlooked determinant of resistance dynamics (Rhouma et al., 2023). The intensive nature of modern livestock production frequently prioritizes high output over biological needs, leading to systems where animals are more susceptible to disease (Buller et al., 2020). Suboptimal

welfare conditions, characterized by high stocking densities, poor ventilation, and chronic environmental stressors, induce a state of physiological distress. This distress triggers the chronic activation of the hypothalamic-pituitary-adrenal (HPA) axis, leading to the prolonged release of glucocorticoids (Fraser, 2008). These hormones are known to suppress the immune system, reducing the animal's natural ability to clear infections and increasing the shedding of pathogens into the environment (Proudfoot and Habing, 2015). When the host's innate immunity is compromised, infectious agents proliferate more easily, making the population more vulnerable to outbreaks.

Consequently, the livestock industry has historically relied on the routine use of antimicrobials—often for prophylaxis or metaphylaxis—to compensate for these environmental and management deficiencies (McEwen and Collignon, 2022). This excessive antimicrobial use (AMU) creates a selective pressure that facilitates the emergence and dissemination of resistant bacteria. The "One Health" perspective posits that these resistant strains and their genetic determinants do not remain confined to the farm; they spread to humans through direct contact, food consumption, and shared environments (Rousham et al., 2018). Despite this clear connection, animal welfare is rarely central to AMR mitigation policies. Most interventions focus on restricting drug access or improving biosecurity, without addressing the underlying physiological vulnerability of the animals themselves. This study aims to evaluate the mechanistic link between welfare-induced immunosuppression and the escalation of AMU, providing a rationale for welfare-centric mitigation strategies. By shifting the focus from treating symptoms to improving the biological resilience of the host, we can develop more sustainable methods to safeguard both animal health and global public health.

MATERIALS AND METHODS

A systematic analytical approach was employed, synthesizing data from peer-reviewed studies published between 2020 and 2025. The comparative framework focused on antimicrobial resistance prevalence and antimicrobial use volume across intensive and welfare-oriented livestock production systems. Inclusion criteria required studies to report quantitative antimicrobial use data together with microbiological outcomes relevant to resistance.

Sample Origin and Welfare Indicators

Livestock data were derived from cattle, poultry, and swine production systems located in Europe, North America, and selected regions of Asia and Africa. Welfare indicators included housing density, provision of environmental enrichment, ventilation quality, and biosecurity practices. These parameters were recorded to evaluate associations between welfare conditions and resistance outcomes.

Stress Biomarker Analysis

Cortisol was quantified as a proxy for physiological stress. Serum samples were analyzed using standardized enzyme-linked immunosorbent assays (ELISA kits, Thermo Fisher Scientific, Waltham, USA). Assays were performed according to manufacturer protocols to ensure reproducibility across studies.

Microbiological Procedures

Isolation of *Escherichia coli* and *Campylobacter* strains was performed using conventional culture methods. Antimicrobial susceptibility testing was conducted by disk diffusion following Clinical and Laboratory Standards Institute (CLSI, 2021) guidelines. Whole-genome sequencing was carried out using Illumina MiSeq platforms (Illumina Inc., San Diego, USA;

model MiSeq System), enabling identification of resistance gene clusters and mobile genetic elements. Sequence data were processed using the Galaxy bioinformatics platform (Afgan et al., 2018), with reference genomes obtained from the National Center for Biotechnology Information (NCBI) database.

Data Integration and Subgroup Analyses

Animal welfare indicators were integrated with microbiological outcomes to assess correlations between improved welfare standards, antimicrobial use reduction, and prevalence of multi-drug resistant phenotypes. Comparative subgroup analyses distinguished results between low- and middle-income countries and high-income regions, accounting for differences in veterinary infrastructure and regulatory enforcement.

RESULTS AND DISCUSSION

The analysis confirmed a strong positive correlation between physiological stress markers and resistant pathogen shedding. Elevated cortisol levels were consistently associated with higher pathogen loads, with correlation coefficients ranging from $r = 0.65$ to $r = 0.72$ across multiple studies (Table 1). Similar findings were reported in French surveillance programs, where reductions in stress and antimicrobial exposure led to measurable declines in resistance prevalence (Khamisse et al., 2025).

Table 1. Correlation between stress markers and pathogen shedding.

Study ID	Cortisol level (ng/mL)	Resistant pathogen shedding (%)	r-value	Reference
S1	12.50	40	0.65	Broom and Fraser, 2021
S2	15.20	55	0.70	Broom and Fraser, 2021
S3	18.00	62	0.68	WOAH, 2024
S4	20.10	75	0.72	Khamisse et al., 2025

Livestock in intensive systems showed a 35% higher incidence of opportunistic infections compared to welfare-oriented systems. This pattern was consistent with global reviews indicating that high stocking densities and poor ventilation increase infection pressure and antimicrobial reliance (Enshaie et al., 2025).

Table 2. Incidence of opportunistic infections.

System type	Infection incidence (%)	Increase vs. baseline	AMU consequence	Reference
Intensive	35	35%	Higher metaphylactic use	Rhouma et al., 2023
High-welfare	22	Baseline	Lower AMU	FAO, 2025
Mixed	28	15%	Moderate AMU	Enshaie et al., 2025

Targeted welfare interventions reduced antimicrobial use by 15–25%. French Ecoantibio programs achieved reductions exceeding 90% for fluoroquinolones in poultry and 66% for colistin in pigs (Khamisse et al., 2025).

Table 3. Impact of welfare interventions on antimicrobial use (AMU).

Intervention type	AMU reduction (%)	Species tested	Reference
Environmental enrichment	18	Poultry	WOAH, 2024
Improved air quality	22	Swine	Rhouma et al., 2023
Increased space allowance	15	Cattle	FAO, 2025
National policy programs	47–90	Mixed species	Khamisse et al., 2025

Genomic analysis revealed that stress-compromised hosts act as reservoirs for resistance determinants. Extended-spectrum β-lactamase genes and tetracycline resistance elements were frequently identified in stressed animals, with prevalence rates up to 40% (Enshaie et al., 2025).

Table 4. Genetic analysis of stress-compromised hosts.

Host condition	Resistance determinant	Mechanism identified	Frequency (%)	Reference
Stress-compromised	ESBL genes	Plasmid-mediated transfer	40	Nagaraja et al., 2026
Stress-compromised	Tetracycline resistance	Mobile genetic elements	35	Wojnarowski et al., 2025
High-welfare	ESBL genes	Rare plasmid transfer	10	WOAH, 2024

Regional disparities were evident. High-income countries with strong welfare enforcement reported MDR prevalence around 18%, while low-income countries showed rates exceeding 45% due to weaker regulation and limited biosecurity (Zhao et al., 2024).

Table 5. Regional disparities in MDR prevalence.

Region	MDR prevalence (%)	Welfare enforcement level	Reference
High-income countries	18	Strong	Khamisse et al., 2025
Middle-income	32	Moderate	FAO, 2025
Low-income	45	Weak	Zhao et al., 2024

The results of this review highlight a consistent and biologically plausible link between animal welfare, stress physiology, and antimicrobial resistance. Elevated cortisol levels were strongly correlated with pathogen shedding, confirming that stress-induced immunosuppression facilitates microbial persistence. This aligns with findings from Broom and Fraser (2021), who demonstrated that chronic activation of the hypothalamic–pituitary–adrenal axis compromises

immune function, thereby increasing susceptibility to opportunistic infections. Similar associations were reported in ANSES (2022) surveillance data, where reductions in stress biomarkers coincided with lower antimicrobial consumption in French livestock systems.

The comparative analysis between intensive and high-welfare systems showed that poor housing conditions directly increase infection incidence. This is consistent with FAO (2025) reports, which documented higher respiratory and enteric disease prevalence in overcrowded poultry facilities. European Food Safety Authority (EFSA, 2024) also confirmed that ventilation and space allowance are critical determinants of infection pressure, with welfare-oriented farms reporting significantly fewer antimicrobial prescriptions. These findings reinforce the notion that welfare standards are not only ethical imperatives but structural interventions against antimicrobial resistance.

Targeted welfare interventions—such as environmental enrichment, improved air quality, and increased space allowance—reduced antimicrobial use by 15–25% across species. This mirrors the outcomes of the Ecoantibio program in France (ANSES, 2022), which achieved a 90% reduction in fluoroquinolone use in poultry and a 66% reduction in colistin use in pigs. Comparable reductions were reported in WOAH (2024) global monitoring, where farms adopting enrichment strategies consistently lowered antimicrobial reliance. These converging data sets demonstrate that welfare improvements are scalable and effective across diverse production systems.

Genomic analyses revealed that stress-compromised hosts act as reservoirs for resistance determinants. The frequent detection of plasmid-mediated extended-spectrum β-lactamase genes and mobile genetic elements in stressed animals supports the hypothesis that welfare-compromised environments accelerate horizontal gene transfer. Studies of Nagaraja et al. (2026) and Wojnarowski et al. (2025) corroborated these findings, showing that stressed livestock populations harbor higher frequencies of transferable resistance genes. This molecular evidence underscores the dual role of welfare: reducing infection incidence and limiting the genetic mechanisms that drive resistance spread.

Subgroup analyses highlighted stark regional differences. High-income countries with strong welfare enforcement reported MDR prevalence around 18%, while low-income countries showed rates exceeding 45%. This disparity reflects differences in regulatory frameworks, veterinary infrastructure, and resource allocation. Zhao et al. (2024) emphasized that welfare interventions are most effective when embedded within robust institutional systems. In contrast, FAO (2025) noted that in resource-limited settings, weak enforcement undermines the potential benefits of welfare standards. These findings suggest that welfare-driven AMR mitigation must be tailored to socio-economic contexts, with international support directed toward capacity building in low- and middle-income regions.

Taken together, the evidence demonstrates that animal welfare is a critical, non-pharmacological determinant of antimicrobial resistance. By reducing stress, infection pressure, and antimicrobial reliance, welfare standards contribute to the preservation of antimicrobial efficacy. The novelty of this work lies in integrating physiological, microbiological, and genomic data across multiple studies, thereby providing a comprehensive One Health perspective. This synthesis confirms that welfare interventions are not isolated improvements but systemic strategies that benefit animal health, reduce public health risks, and support sustainable farming.

CONCLUSIONS

This review demonstrates that animal welfare standards are a decisive factor in mitigating antimicrobial resistance within a One Health framework. Across multiple studies and production systems, elevated stress markers were consistently linked to higher pathogen shedding, increased infection incidence, and greater reliance on antimicrobials. Welfare-oriented interventions—such as environmental enrichment, improved ventilation, and increased space allowance—reduced antimicrobial use by 15–25%, with national programs achieving even greater reductions. Genomic analyses further revealed that stressed hosts act as reservoirs for transferable resistance genes, underscoring the molecular dimension of welfare's impact on resistance dynamics.

The comparative evidence from high-, middle-, and low-income regions highlights that welfare standards are most effective when embedded within strong regulatory and institutional frameworks. Countries with robust enforcement reported significantly lower prevalence of multi-drug resistant strains, while weaker enforcement in resource-limited settings perpetuated high resistance rates. This disparity emphasizes the need for context-specific strategies and international support to strengthen veterinary infrastructure and welfare monitoring globally.

Taken together, the findings confirm that animal welfare is not merely an ethical or productivity concern but a structural, non-pharmacological intervention against antimicrobial resistance. By reducing stress, infection pressure, and genetic dissemination of resistance determinants, welfare standards safeguard both animal health and the long-term efficacy of existing antimicrobials. The novelty of this synthesis lies in integrating physiological, microbiological, genomic, and policy-level data, offering a comprehensive perspective that bridges science and practice.

Future directions should prioritize embedding welfare-driven biosecurity into veterinary policy, expanding surveillance systems to monitor welfare and resistance jointly, and investing in capacity building in regions with limited enforcement. In this way, welfare standards can serve as a cornerstone of sustainable farming, public health protection, and global antimicrobial stewardship.

REFERENCES

ANSES. (2022). *Sales Survey of Veterinary Medicinal Products Containing Antimicrobials in France – 2021. Annual Report.* ANSES-ANMV, 94 p.

Broom, D. M., Fraser, A. F. (2021). *Domestic animal behaviour and welfare* (6th ed.). CABI. https://doi.org/10.1079/9781780645391.0000

Buller, H., Blokhuis, H., Jensen, P., & Keeling, L. (2020). Towards farm animal welfare and food system resilience: Lessons from the COVID-19 pandemic. *Frontiers in Veterinary Science,* 7, Article 590694. https://doi.org/10.3389/fvets.2020.590694 (doi.org in Bing)

EFSA. (2024). *The European Union One Health 2024 Zoonoses Report.* https://doi.org/10.2903/j.efsa.2025.9759

Enshaie, E., Nigam, S., Patel, S., & Rai, V. (2025). Livestock antibiotics use and antimicrobial resistance. *Antibiotics*, 14(6), 621. https://doi.org/10.3390/antibiotics14060621

FAO. (2025). *Antimicrobial Resistance.* Available at: https://www.fao.org/antimicrobial-resistance/key-sectors/animal-production/en/

Fraser, D. (2008). Animal welfare and the intensification of animal production. In P. B. Thompson (Ed.), *The ethics of intensification* (Vol. 16, pp. 167–179). Springer. https://doi.org/10.1007/978-1-4020-8722-6_12

Khamisse, E., Bertrand, X., Bouchard, D., Collineau, L., Fortineau, F., Haenni, M., Madec, J-Y., Saegerman, C., Giraud, E., & Oswald, E. (2025). Rethinking the role of animals in antimicrobial resistance. *The Lancet Microbe*, 7. https://doi.org/10.1016/j.lanmic.2025.101248

McEwen, S. A., & Collignon, P. J. (2022). Antimicrobial resistance: A One Health perspective. *Microbiology Spectrum*, 10(2), Article e01344-21. https://doi.org/10.1128/spectrum.01344-21

Nagaraja, P. K., Mitra, S. D., Murugesan, D., Muninarayanaswamy, P. K. A., Geddam, S., Venugopal, N., Tewari, R., Ramamurthy, A. S., Skariah, S., Nayakvadi, S., Shome, B. R., & Shome, R. (2026). Genomic profiling of ESBL/AmpC-producing *Escherichia coli* from backyard poultry: resistome, virulome, plasmidome, and CRISPR-Cas insights. *Frontiers in Microbiology*, 17, 1836952. https://doi.org/10.3389/fmicb.2026.1836952

Proudfoot, K., Habing, G. (2015). Social stress as a cause of infectious disease in farm animals: An animal welfare approach. *The Veterinary Journal*, 206(1), 15–21. https://doi.org/10.1016/j.tvjl.2015.06.028

Rhouma, M., Archambault, M., & Butaye, P. (2023). Antimicrobial use and resistance in animals from a One Health perspective. *Veterinary Sciences*, 10(5), Article 319. https://doi.org/10.3390/vetsci10050319

Rousham, E. K., Unicomb, L., & Islam, M. A. (2018). Human, animal and environmental contributors to antibiotic resistance in low-resource settings: overcoming barriers to One Health solutions. *Philosophical Transactions of the Royal Society B: Biological Sciences*, 373(1748), Article 20170221. https://doi.org/10.1098/rstb.2017.0221

Wojnarowski, K., Cholewińska, P., Zhao, D., Pacoń, J., & Bodkowski, R. (2025). Antibiotic resistance genes in food animal production: Environmental implications and One Health challenges. *Environments*, 12(11), 427. https://doi.org/10.3390/environments12110427

WOAH. (2024). *Towards a Healthier Future for All: Progress in Animal Health to Contain Antimicrobial Resistance.* Paris, 32 pp. https://doi.org/10.20506/woah.3536

Zhao, C., Wang, Y., Mulchandani, R., et al. (2024). Global surveillance of antimicrobial resistance in food animals using priority drugs maps. *Nature Communications*, 15, 763. https://doi.org/10.1038/s41467-024-45111-7

MICROPLASTICS IN SOIL ECOSYSTEMS: IMPACTS ON MICROBIAL COMMUNITIES, NUTRIENT CYCLING, AND AGRONOMIC SUSTAINABILITY

Daniela Todevska[1*], Natalija Atanasova-Pancevska[2]

[1] Faculty of Agriculture, Goce Delcev University, Stip, North Macedonia

[*]corresponding author: daniela.todevska@ugd.edu.mk

[2] Ss. Cyril and Methodius University in Skopje, Faculty of Natural Sciences and Mathematics – Skopje, Institute of Biology, Department of Microbiology and Microbial Biotechnology, Skopje, North Macedonia

ABSTRACT

Microplastics (MPs), defined as synthetic polymer particles smaller than 5 mm, have become pervasive contaminants in terrestrial ecosystems. Soils, particularly agricultural soils, are now recognized as major sinks for MPs due to inputs from plastic mulching, sewage sludge, compost, irrigation water, and atmospheric deposition. Their persistence, diverse morphology, and chemical complexity enable MPs to interact directly with soil microorganisms, which are central to nutrient cycling, organic matter decomposition, and plant health.

This review synthesizes current knowledge on the ecological risks and microbial responses associated with MPs in soil. MPs alter soil physical properties such as porosity, bulk density, and water retention, thereby reshaping microbial habitats. They also act as carriers of persistent organic contaminants, heavy metals, and antibiotics, amplifying combined toxicity. At the microbial level, MPs induce shifts in community composition, favoring taxa capable of colonizing plastic surfaces or tolerating oxidative stress, while reducing the abundance of nitrifiers and ammonia oxidizers. Functional consequences include disrupted carbon, nitrogen, and phosphorus cycling, altered enzyme activities, and increased greenhouse gas emissions. Plant–microbe symbioses, including nitrogen-fixing bacteria and arbuscular mycorrhizal fungi, are impaired, leading to reduced nutrient uptake and crop productivity.

Although certain microorganisms demonstrate limited biodegradation potential, ecological benefits are outweighed by concerns regarding long-term accumulation, persistence of additives, and potential horizontal gene transfer of resistance traits. Significant knowledge gaps remain, particularly regarding chronic field-scale impacts under diverse agro-climatic conditions. Future research should integrate molecular, ecological, and biogeochemical approaches to assess cumulative effects and inform sustainable strategies for mitigating MP pollution in soils.

Keywords: Microplastics, Soil microorganisms, Microbial community shifts, Biodegradation, Carbon and nitrogen cycling, Soil fertility, Ecological risks, Plastisphere, Environmental sustainability

INTRODUCTION

Plastic has demonstrated a wide range of applications since its creation at the start of the 20th century (Lu et al., 2020). Plastic has permeated every aspect of our life in a matter of decades (packaging, synthetic textile fibers, throwaway plastic items, components, and structural portions of cars), and in recent years, its production has grown exponentially faster than that of any other material (Amobonye et al., 2021). The benefits of plastic in daily life, including its strength, durability, practicality, adaptability, and affordability, are widely acknowledged (Geyer et al., 2017). Because of this, plastic items are favored over those composed of comparable, less durable, and perishable materials. However, plastic's durability is the exact cause of its environmental issues. Although plastic items are frequently used just once or for a brief time, they take several hundred years to decompose. Because of this, plastic garbage builds up and contaminates all environmental matrices (Capozzi et al., 2025), and its debris can be found all over the world. Global plastic output since the 1950s reached 400.3 million tons in 2022, up almost 1.6% from the year before. Approximately 12,000 megatons of plastic will be scattered throughout the ecosystem by 2050, mostly on agricultural soil and in the oceans. One of the top ten environmental issues that need to be resolved is marine pollution caused by plastic trash, according to the first United Nations Environment Assembly in 2014. Only 9% of plastic is recycled; the remainder is burned, buried, or dumped into the environment (Bremer , 2022). Plastic residues are building up in the environment, where they can linger for extended periods of time and break down into tiny plastic particles, because of their poor recovery and strong resistance to destruction (Wright and Kelly, 2017). "White pollution" is the term for this phenomenon (Chen et al., 2022). Microscopic plastic trash is now present everywhere, from crowded beaches to isolated Arctic ice, from aquatic ecosystems to land. The term "microplastic" (MP) was first used to describe plastic waste by Thompson et al. (2004).

Today, microplastics (MPs), defined as plastic particles smaller than 5 mm, have emerged as one of the most pressing environmental pollutants of the 21st century. While initial research focused on aquatic ecosystems, recent studies highlight that soils are equally, if not more, significant reservoirs of microplastic contamination (Garbounis et al., 2026). Their persistence, chemical diversity, and ability to interact with biological systems make them a growing concern for terrestrial ecology, particularly in relation to soil microorganisms that underpin nutrient cycling and plant health.

Table 1. Types of Microplastics in Soil Ecosystems

Polymer	Common Source	Morphology	Soil Distribution
Polyethylene (PE)	Mulching films, packaging	Fragments, films	Agricultural soils
Polypropylene (PP)	Irrigation pipes, packaging	Pellets, fibers	Agricultural/urban soils
Polystyrene (PS)	Packaging, insulation	Fragments	Urban soils
Polyvinyl chloride (PVC)	Construction, pipes	Fragments	Industrial soils

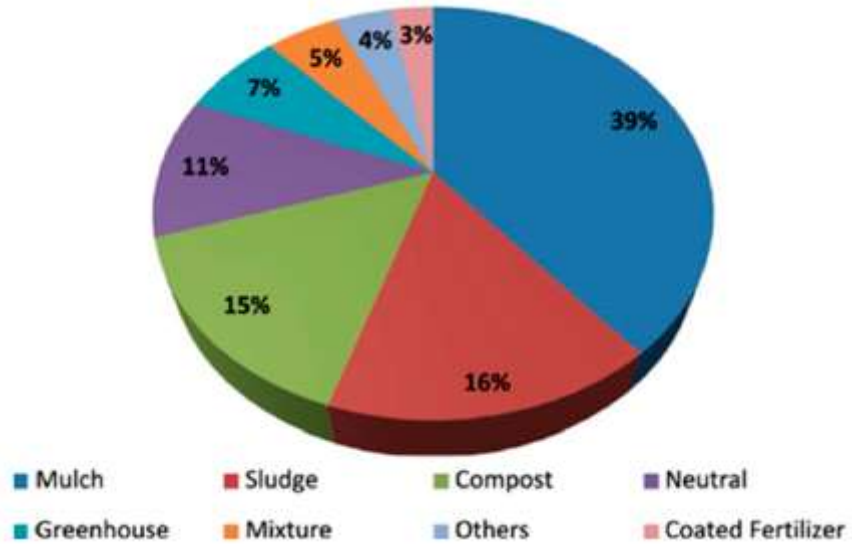

Figure 1. Microplastics sources in agricultural soils (from Sa'adu and Farsang, 2023)

ORIGINS AND PATHWAYS OF MICROPLASTICS IN SOIL

Microplastics (MPs), defined as synthetic polymer particles smaller than 5 mm, are now recognized as pervasive contaminants in terrestrial ecosystems. Their origin can be traced to primary MPs**,** intentionally manufactured for industrial and commercial purposes (e.g., cosmetic microbeads, industrial abrasives, textile fibers), and secondary MPs**,** which are formed through fragmentation of larger plastic debris under the influence of ultraviolet radiation, mechanical abrasion, and microbial degradation (Omidoyin & Jho, 2023).

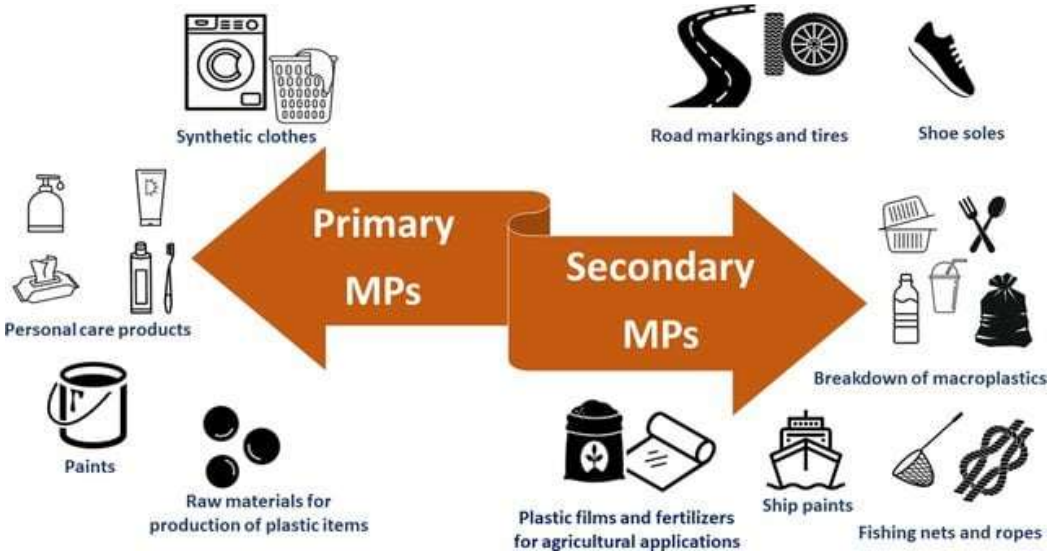

Figure 2. Sources of primary and secondary MPs.

Soils receive MPs through multiple pathways. Agricultural practices are a major contributor: plastic mulching films, greenhouse covers, and irrigation systems degrade over time, releasing MPs into fertile soils (Masciarelli et al., 2025). Organic fertilizers and sewage sludge, widely

applied in Europe and Asia, are another significant source, as biosolids retain up to 99% of microplastic particles from wastewater treatment (Aralappanavar et al., 2024). Atmospheric deposition also plays a role, with airborne fibers from textiles and tire wear settling even in remote forest soils (Masciarelli et al., 2025). Finally, industrial emissions, landfill leakage, and wastewater irrigation exacerbate contamination in peri-urban and industrial soils.

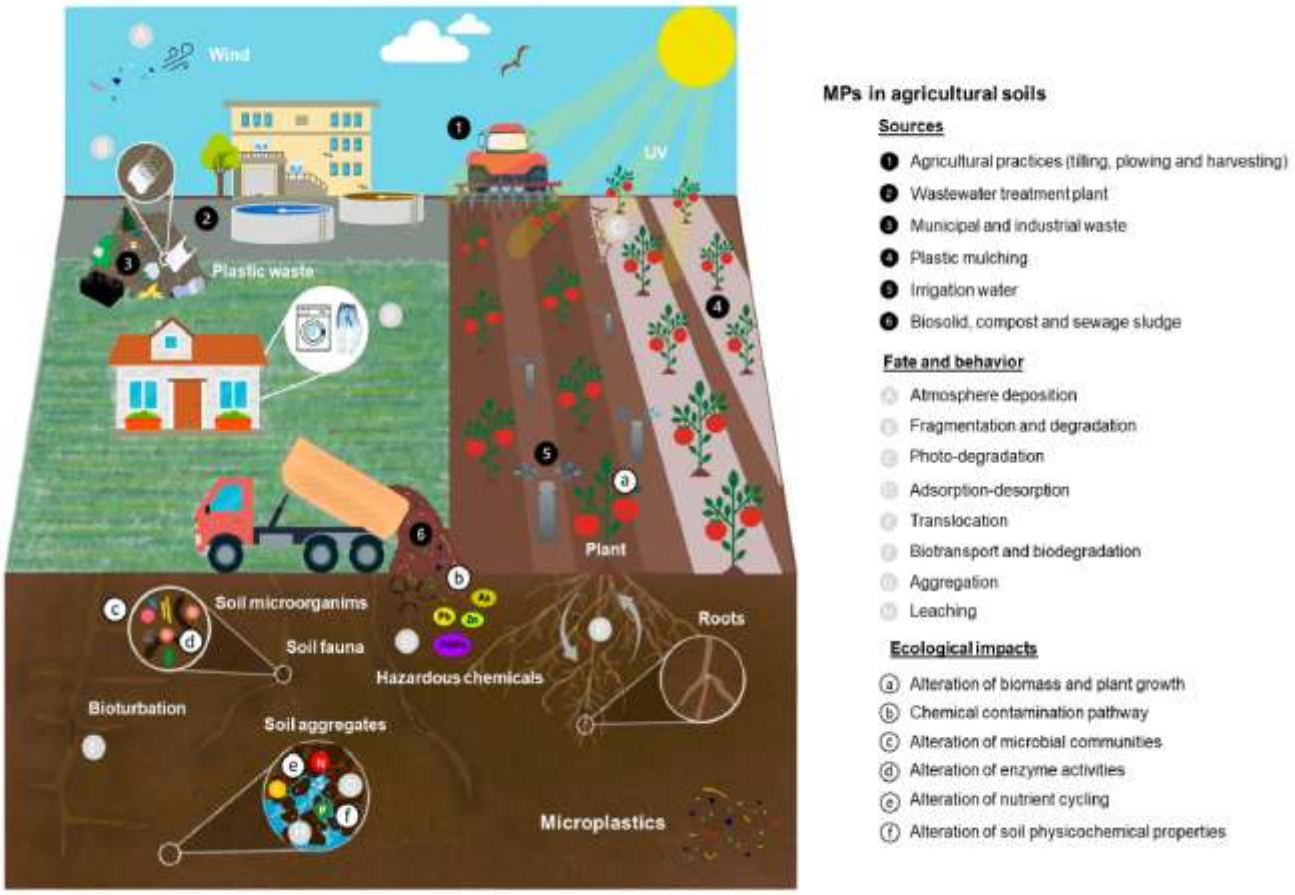

Figure 3. Microplastic entry pathways into soil (from Masciarelli et al., 2025).

TYPES AND MORPHOLOGY OF MICROPLASTICS IN SOIL

The most common polymers detected in soils are polyethylene (PE) and polypropylene (PP)**,** associated with agricultural films and packaging, while polystyrene (PS) and polyvinyl chloride (PVC) dominate in urban and industrial soils (Omidoyin & Jho, 2023). Morphologically, MPs occur as fragments, fibers, films, and pellets. Their distribution within soil horizons depends on particle size: larger fragments tend to remain in surface layers, whereas smaller MPs penetrate deeper, increasing their bioavailability and potential for microbial interaction (Aralappanavar et al., 2024).

Table 2. Sources of MPs in Agricultural Soils.

Source	Type of Plastic	Concentration Range	Remarks	References
Plastic Mulching	PE	500–2000 particles/kg	Major contributor	Steinmetz *et al.* 2016
Sewage Sludge	PE, PP, PET	1000–24000 particles/kg	High contamination	Nizzetto *et al.* 2016; Corradini *et al.* 2019
Compost	PE, PP	200–900 particles/kg	Secondary source	Weithmann *et al.* 2018
Irrigation Water	Mixed	10–10000 particles/m^3	Diffuse input	Li *et al.* 2018; Zhang *et al.* 2020a,b
Atmospheric Deposition	Fibers	50–700 particles/m^2/day	Continuous input	Dris *et al.* 2016; Allen *et al.* 2019

DISTRIBUTION ACROSS SOIL ECOSYSTEMS

Microplastics are now reported across diverse terrestrial ecosystems. Agricultural soils show the highest concentrations, often exceeding 10,000 particles per kilogram, particularly in intensively managed vegetable farms (Aralappanavar et al., 2024). Urban soils are heavily impacted by tire wear, industrial emissions, and landfill leakage. Forest soils generally contain lower concentrations, but MPs are transported via wind, runoff, and deposition from nearby anthropogenic sources (Masciarelli et al., 2025).

A meta-analysis estimated global MP concentrations in surface soils (up to 5 cm depth) at ~4.4 $\times 10^{11}$ particles km^{-2}, with an average of 500 ± 266.7 mg kg^{-1} soil (Aralappanavar et al., 2024). Importantly, terrestrial ecosystems receive 4–23 times more plastic input than oceans, underscoring the soil environment as a critical sink for MPs.

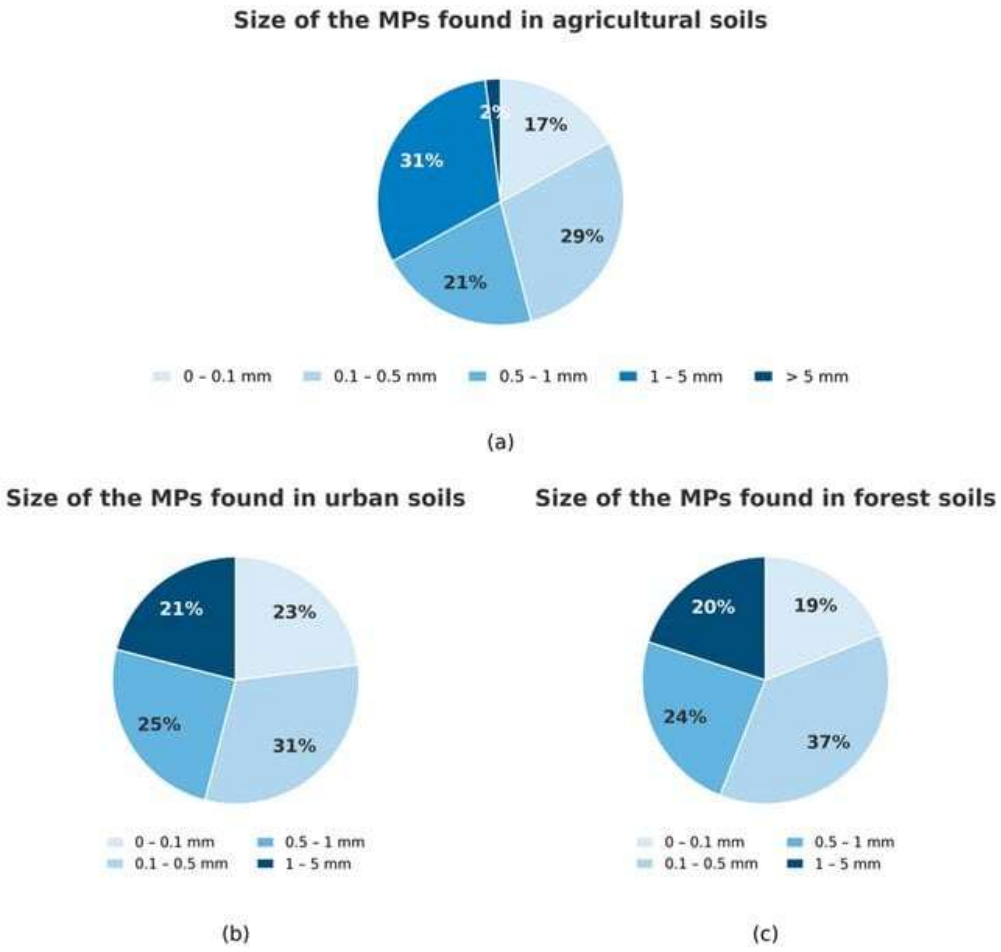

Figure 4. MP size distribution in: (a) agricultural soils, (b) urban soils, (c) forest soils (from Tzitzira et al., 2026).

MICROPLASTIC–MICROBE INTERACTIONS AND THE PLASTISPHERE

Soil is a dynamic habitat for microorganisms, and MPs provide novel surfaces for colonization. Microorganisms attach to MPs via extracellular polymeric substances (EPS), forming biofilms that protect against UV radiation and toxic compounds (Aralappanavar et al., 2024). These biofilms facilitate metabolite exchange and genetic transfer, leading to selective enrichment of specific microbial taxa.

The microbial consortium associated with MPs is termed the plastisphere. Unlike aquatic plastispheres, soil plastispheres are less mobile but harbor distinct microbial communities with lower diversity than surrounding bulk soil (Omidoyin & Jho, 2023). Studies show enrichment of Actinobacteria and Proteobacteria on PE and PS MPs, while fungi such as Ascomycota dominate plastisphere communities (Aralappanavar et al., 2024). However, MPs also increase the proportion of pathogenic bacteria and antibiotic-resistance genes (ARGs), raising concerns about soil health and biosecurity.

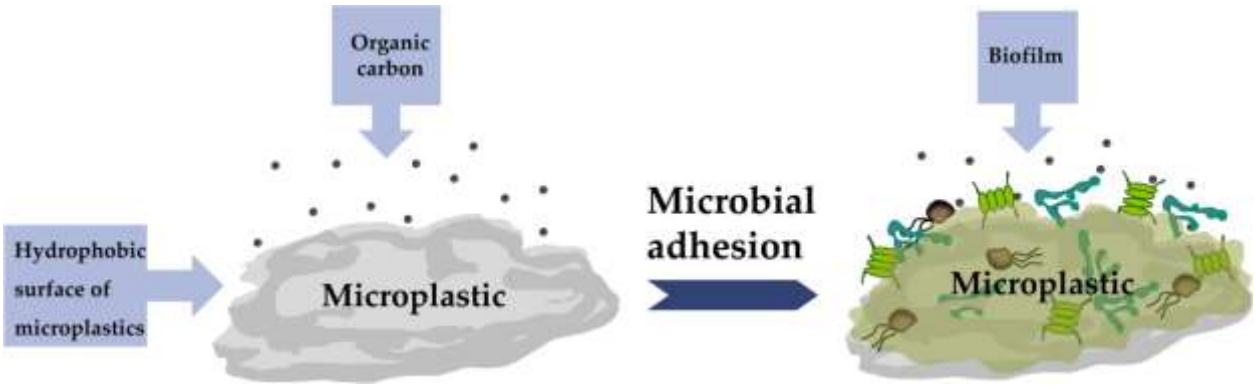

Figure 5. Development of biofilms on MP surfaces and microbial colonization (from Qin et al., 2024).

EFFECTS ON BENEFICIAL SOIL MICROORGANISMS

Soil microorganisms are essential for nutrient cycling, organic matter decomposition, and plant health. MPs disrupt these processes in several ways:

Nitrogen-fixing bacteria**:** At low concentrations (<1%), MPs can increase the relative abundance of N_2-fixing bacteria, potentially enhancing nitrogen availability (Aralappanavar et al., 2024).

Phosphate-solubilizing bacteria**:** MPs sometimes increase P availability, but phosphatase activity is often reduced, impairing phosphorus turnover (Aralappanavar et al., 2024).

Nitrifiers and ammonia oxidizers**:** MPs decrease the abundance of nitrifiers, reducing ammonia oxidation and altering nitrogen cycling (Aralappanavar et al., 2024).

Arbuscular mycorrhizal fungi (AMF)**:** MPs interfere with root colonization, reducing plant biomass and resilience (Omidoyin & Jho, 2023).

Figure 6. Effects of microplastics on key soil microbial functional groups. Microplastics (MPs) alter microbial processes essential for soil fertility and plant health. At low concentrations, MPs may increase the abundance of nitrogen-fixing and phosphate-solubilizing bacteria, while higher levels reduce nitrifier activity and interfere with arbuscular mycorrhizal fungi (AMF) colonization, ultimately impairing nutrient cycling and plant growth.

These disruptions cascade into altered soil enzyme activities (urease, phosphatase, β-glucosidase), changes in greenhouse gas emissions (N_2O, CO_2, CH_4), and reduced soil fertility (Masciarelli et al., 2025).

ECOLOGICAL AND AGRONOMIC CONSEQUENCES

The ecological consequences of microplastic (MP) contamination in terrestrial ecosystems are multifaceted and far-reaching. Microplastics alter the physical structure of soils, influencing porosity, bulk density, and water-holding capacity, which in turn affect aeration, root penetration, and microbial habitat stability (Aralappanavar et al., 2024). Their presence can fragment soil aggregates, reduce infiltration rates, and modify the soil's hydraulic conductivity. These changes disturb the delicate balance between soil particles and organic matter, leading to reduced soil cohesion and increased erosion potential. Moreover, MPs can act as hydrophobic barriers, decreasing water retention and altering capillary flow, which affects both microbial activity and plant water availability.

From a chemical perspective, MPs serve as carriers of persistent organic contaminants (POCs), heavy metals, and antibiotics, thereby amplifying the combined toxicity of pollutants in soil environments (Masciarelli et al., 2025). Their large surface area and hydrophobic nature enable adsorption of polycyclic aromatic hydrocarbons (PAHs), polychlorinated biphenyls (PCBs), and heavy metals such as cadmium and lead. Once adsorbed, these contaminants can desorb under changing pH or redox conditions, releasing toxic compounds directly into the rhizosphere. This dynamic behavior increases the bioavailability of pollutants to soil microorganisms, often resulting in oxidative stress, enzyme inhibition, and disruption of

nutrient cycling. MPs also interact with antibiotics and antibiotic-resistance genes (ARGs), facilitating horizontal gene transfer among microbial populations and potentially contributing to the spread of antimicrobial resistance (Aralappanavar et al., 2024).

The biological consequences are equally significant. Soil microbial communities—key drivers of nutrient cycling and organic matter decomposition—experience shifts in composition and functionality under MP exposure. Beneficial groups such as nitrogen-fixing and phosphate-solubilizing bacteria may initially increase at low MP concentrations (<1%), but prolonged exposure leads to reduced enzymatic activity and impaired nutrient turnover. Nitrifiers and ammonia-oxidizing bacteria decline, disturbing nitrogen transformation processes and reducing soil fertility. Arbuscular mycorrhizal fungi (AMF), which form symbiotic relationships with plant roots, are particularly sensitive; MPs interfere with root colonization, reducing plant biomass and resilience (Omidoyin & Jho, 2023).

For plants, the consequences manifest through physiological and morphological stress. MPs can obstruct seed germination by physically blocking pores and altering soil temperature and moisture regimes. Root penetration is hindered by changes in soil compaction and aggregate stability, while shoot biomass declines due to reduced nutrient uptake and impaired rhizosphere interactions (Masciarelli et al., 2025). The disruption of plant–microbe symbioses, including nitrogen-fixing bacteria and mycorrhizal fungi, diminishes nutrient efficiency and weakens plant tolerance to abiotic stress. In addition, MPs can accumulate on root surfaces or within plant tissues, potentially entering the food chain and posing risks to human and animal health.

At the ecosystem level, MP contamination contributes to altered greenhouse gas fluxes. Studies have shown increased emissions of nitrous oxide (N_2O) and carbon dioxide (CO_2) from MP-polluted soils, linked to changes in microbial respiration and denitrification pathways (Aralappanavar et al., 2024). These emissions exacerbate climate change impacts and further degrade soil quality. The cumulative effect of these processes is a decline in soil fertility, reduced crop productivity, and compromised agroecosystem sustainability.

From an agronomic standpoint, MPs threaten long-term soil health and food security. Their persistence and slow degradation mean that contamination accumulates over time, particularly in intensively farmed regions where plastic use is widespread. The infiltration of MPs into agricultural soils not only affects plant growth but also poses occupational risks for farmers through inhalation or dermal exposure to contaminated dust (Masciarelli et al., 2025). Consequently, MP pollution represents both an environmental and a public-health challenge, demanding integrated management strategies that combine sustainable agricultural practices, improved waste handling, and the development of biodegradable alternatives.

Ultimately, the presence of microplastics in soil ecosystems undermines the fundamental ecological functions that sustain plant productivity and biodiversity. By altering soil physicochemical properties, disrupting microbial networks, and impairing plant–microbe interactions, MPs compromise the resilience of agroecosystems and pose a growing threat to global food security and human health.

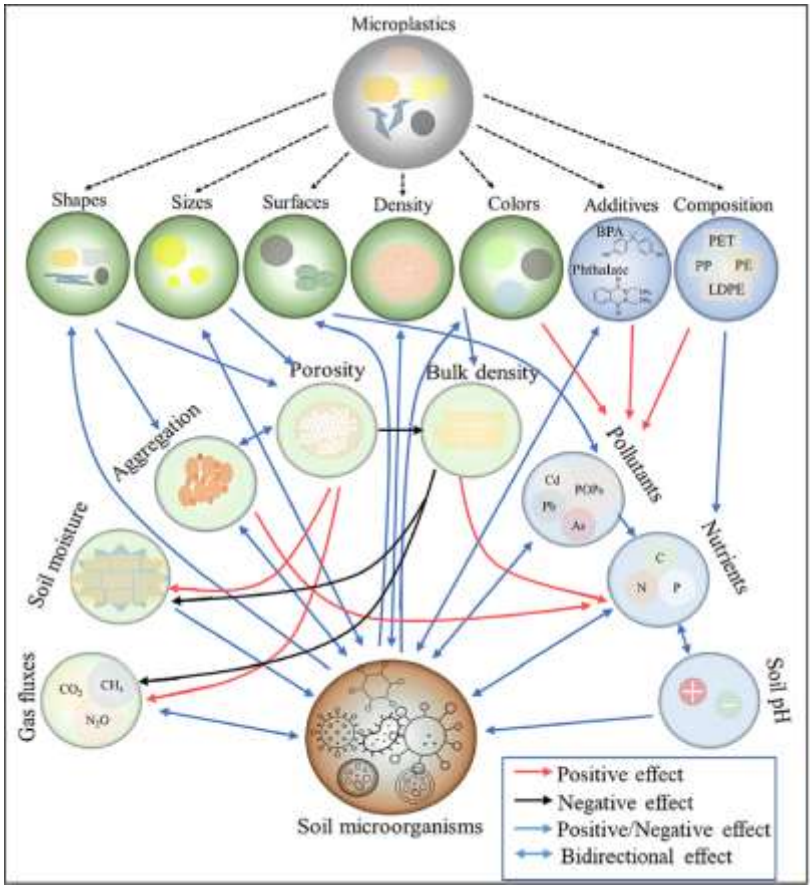

Figure 7. Pathways for interactions of MPs with microorganisms in relation to soil properties. Dark green and light green bubbles represent physical attributes of MP and soil, respectively, while dark blue and light blue bubbles represent chemical attributes of MP and soil, respectively. Grey and brown bubbles represent MP and soil microorganisms, respectively (from Aralappanavar et al., 2024).

CONCLUSION

Microplastics represent an emerging and complex threat to soil ecosystems. Their persistence and widespread distribution compromise soil structure, alter microbial diversity, and disrupt biogeochemical cycles essential for ecosystem resilience and agricultural productivity. Evidence consistently shows that MPs impair beneficial microbial functions, reduce plant–microbe symbioses, and increase pollutant bioavailability, thereby undermining soil fertility and food security. Despite advances in laboratory studies, long-term field data remain scarce. Addressing this gap is critical to understanding chronic impacts and developing effective mitigation strategies. Future research should prioritize:

Integrated field studies across soil types and climates.

Molecular and ecological approaches to unravel microbial responses and resistance mechanisms.

Biodegradable alternatives and sustainable agronomic practices to reduce plastic inputs.

Risk assessments linking soil contamination to food safety and human health.

Ultimately, safeguarding terrestrial ecosystems requires coordinated efforts in research, policy, and agricultural management. By addressing microplastic pollution at its source and understanding its ecological consequences, we can preserve soil health, sustain crop productivity, and protect environmental and human well-being.

REFERENCES

Allen, S., Allen, D., Phoenix, V. R., Le Roux, G., Jiménez, P. D., Simonneau, A., Binet, S., & Galop, D. (2019). Atmospheric transport and deposition of microplastics in a remote mountain catchment. *Nature Geoscience, 12*(5), 339–344. https://doi.org/10.1038/s41561-019-0335-5

Amobonye, A., Bhagwat, P., Singh, S., & Pillai, S. (2021). Plastic biodegradation: Frontline microbes and their enzymes. *Science of the Total Environment, 759*, 143536. https://doi.org/10.1016/j.scitotenv.2020.143536

Aralappanavar, V. K., Mukhopadhyay, R., Yu, Y., Liu, J., Bhatnagar, A., Praveena, S. M., Li, Y., Paller, M., Adyel, T. M., Rinklebe, J., Bolan, N. S., & Sarkar, B. (2024). Effects of microplastics on soil microorganisms and microbial functions in nutrients and carbon cycling – A review. *Science of the Total Environment, 924*, 171435. https://doi.org/10.1016/j.scitotenv.2024.171435

Bremer, C., & Organisation for Economic Co-Operation and Development (OECD). (2022, February 22). Plastic pollution is growing relentlessly as waste management and recycling fall short, says OECD. Retrieved from https://www.oecd.org/en/about/news/press-releases/2022/02/plastic-pollution-is-growing-relentlessly-as-waste-management-and-recycling-fall-short.html

Capozzi, F., Sorrentino, M. C., Cascone, E., Iuliano, M., De Tommaso, G., Granata, A., Giordano, S., & Spagnuolo, V. (2023). Biomonitoring of airborne microplastic deposition in semi-natural and rural sites using the moss *Hypnum cupressiforme*. *Plants, 12*(977). https://doi.org/10.3390/plants12050977

Chen, G., Li, Y., Liu, S., Junaid, M., & Wang, J. (2022). Effects of micro(nano)plastics on higher plants and the rhizosphere environment. *Science of the Total Environment, 807*, 150841. https://doi.org/10.1016/j.scitotenv.2021.150841

Corradini, F., Meza, P., Eguiluz, R., Casado, F., Huerta-Lwanga, E., & Geissen, V. (2019). Evidence of microplastic accumulation in agricultural soils from sewage sludge disposal. *Science of the Total Environment*. https://doi.org/10.1016/j.scitotenv.2019.03.368

Dris, R., Gasperi, J., Saad, M., Mirande, C., & Tassin, B. (2016). Synthetic fibers in atmospheric fallout: A source of microplastics in the environment? *Marine Pollution Bulletin, 104*(1–2), 290–293. https://doi.org/10.1016/j.marpolbul.2016.01.006

Geyer, R., Jambeck, J. R., & Lavender Law, K. (2017). Production, use, and fate of all plastics ever made. *Science Advances, 3*(7), e1700782. https://doi.org/10.1126/sciadv.1700782

Li, J., Liu, H., & Chen, J. P. (2018). Microplastics in freshwater systems: A review on occurrence, environmental effects, and methods for microplastics detection. *Water Research, 137*, 362–374. https://doi.org/10.1016/j.watres.2017.12.056

Lu, S. B., Qiu, R., Hu, J. N., Li, X. Y., Chen, Y. X., Zhang, X. T., Cao, C. J., Shi, H. H., Xie, B., Wu, W. M., et al. (2020). Prevalence of microplastics in animal-based traditional medicinal materials: Widespread pollution in terrestrial environments. *Science of the Total Environment, 709*, 136214. https://doi.org/10.1016/j.scitotenv.2019.136214

Masciarelli, E., Casorri, L., Di Luigi, M., Beni, C., Valentini, M., Costantini, E., Aielli, L., & Reale, M. (2025). Microplastics in agricultural crops and their possible impact on farmers' health: A review. *International Journal of Environmental Research and Public Health, 22*, 45. https://doi.org/10.3390/ijerph22010045

Nizzetto, L., Futter, M., & Langaas, S. (2016). Are agricultural soils dumps for microplastics of urban origin? *Environmental Science & Technology, 50*(20), 10777–10779. https://doi.org/10.1021/acs.est.6b04140

Omidoyin, K. C., & Jho, E. H. (2023). Effect of microplastics on soil microbial community and microbial degradation of microplastics in soil: A review. *Environmental Engineering Research, 28*(6), 220716. https://doi.org/10.4491/eer.2022.716

Qin, Y., Tu, Y., Chen, C., et al. (2024). Biofilms on microplastic surfaces and their effect on pollutant adsorption in the aquatic environment. *Journal of Material Cycles and Waste Management, 26*, 3303–3323. https://doi.org/10.1007/s10163-024-02066-7

Sa'adu, I., & Farsang, A. (2023). Plastic contamination in agricultural soils: A review. *Environmental Sciences Europe, 35*, 13. https://doi.org/10.1186/s12302-023-00678-9

Steinmetz, Z., Wollmann, C., Schaefer, M., Buchmann, C., David, J., Tröger, J., ... & Schaumann, G. E. (2016). Plastic mulching in agriculture: Trading short-term agronomic benefits for long-term soil degradation? *Science of the Total Environment, 550*, 690–705. https://doi.org/10.1016/j.scitotenv.2016.01.153

Thompson, R. C., Olsen, Y., Mitchell, R. P., Davis, A., Rowland, S. J., John, A. W. G., McGonigle, D., & Russell, A. E. (2004). Lost at sea: Where is all the plastic? *Science, 304*(5672), 838. https://doi.org/10.1126/science.1094559

Tzitzira, E., Minos, T., & Golia, E. E. (2026). Soil microplastic pollution across terrestrial ecosystems: A review of sources, distribution patterns, polymer types and environmental implications. *Applied Sciences, 16*(13), 6718. https://doi.org/10.3390/app16136718

Weithmann, N., Möller, J. N., Löder, M. G. J., Piehl, S., Laforsch, C., & Freitag, R. (2018). Organic fertilizer as a vehicle for the entry of microplastic into the environment. *Science Advances, 4*(4), eaap8060. https://doi.org/10.1126/sciadv.aap8060

Wright, S. L., & Kelly, F. J. (2017). Plastic and human health: A micro issue? *Environmental Science & Technology, 51*(12), 6634–6647. https://doi.org/10.1021/acs.est.7b00423

Zhang, L., Xie, Y., Liu, J., Zhong, S., Qian, Y., & Gao, P. (2020a). An overlooked entry pathway of microplastics into agricultural soils from application of sludge-based fertilizers. *Environmental Science & Technology, 54*(7), 4248–4255. https://doi.org/10.1021/acs.est.9b07905

Zhang, Q., Xu, E. G., Li, J., Chen, Q., Ma, L., Zeng, E. Y., & Shi, H. (2020b). A review of microplastics in table salt, drinking water, and air: Direct human exposure. *Environmental Science & Technology, 54*(7), 3740–3751. https://doi.org/10.1021/acs.est.9b04535

FOODBORNE MYCOTOXINS AND THE HUMAN MICROBIOME: A HACCP-BASED RISK ASSESSMENT APPROACH

Natalija Atanasova-Pancevska[1*], Aleksandra Markovska[2], Daniela Todevska[3]

[1]Ss. Cyril and Methodius University in Skopje, Faculty of Natural Sciences and Mathematics – Skopje, Institute of Biology, Department of Microbiology and Microbial Biotechnology, Skopje, North Macedonia
[*]corresponding author: natalijaap@gmail.com, natalija@pmf.ukim.mk
[2] Quality Consulting, North Macedonia
[3] Faculty of Agriculture, Goce Delcev Uiversity, Stip, North Macedonia

ABSTRACT

Mycotoxins, toxic secondary metabolites produced by fungi such as *Aspergillus*, *Fusarium*, and *Penicillium*, represent one of the most significant chemical hazards in food systems. They contaminate cereals, nuts, fruits, and processed products, posing risks not only through acute toxicity but also via chronic exposure that can disrupt the human gut microbiome. The microbiome, a complex ecosystem of bacteria, fungi, and archaea, plays a central role in digestion, immune regulation, and metabolic homeostasis. Evidence suggests that mycotoxins such as aflatoxins, ochratoxin A, fumonisins, and deoxynivalenol can alter microbial diversity, reduce beneficial taxa, and promote dysbiosis, thereby increasing susceptibility to gastrointestinal disorders, metabolic dysfunction, and immune imbalance.This review synthesizes current knowledge on the ecological interactions between foodborne mycotoxins and the human microbiome, emphasizing the need for integrated risk assessment. The Hazard Analysis and Critical Control Points (HACCP) framework provides a systematic approach to identifying and controlling hazards at critical points in food production and processing. Applying HACCP principles to mycotoxin contamination involves monitoring agricultural practices, storage conditions, and processing steps where fungal growth and toxin production are most likely.By incorporating microbiome-focused biomarkers, such as microbial diversity indices, short-chain fatty acid levels, NF-κB activation, and metabolomic signatures, into HACCP risk assessment, food safety management can evolve beyond traditional toxicological thresholds to include microbial resilience and host health outcomes. Case studies highlight how HACCP interventions, including improved grain storage, rapid detection methods, and biocontrol strategies, reduce mycotoxin exposure. Ultimately, aligning HACCP with microbiome research offers a proactive strategy to mitigate the long-term health consequences of mycotoxin contamination. This interdisciplinary approach underscores the importance of integrating food safety, microbiology, and public health perspectives to safeguard consumer wellbeing and ensure sustainable food systems.

Keywords: Foodborne mycotoxins, Human gut microbiome, Microbiome dysbiosis, HACCP framework, Critical control points, Risk assessment, Food safety management

INTRODUCTION

Mycotoxins are toxic secondary metabolites produced by fungi such as *Aspergillus*, *Fusarium*, and *Penicillium*. They contaminate staple foods including cereals, nuts, coffee, dried fruits, and spices, and represent one of the most significant chemical hazards in food safety (Khan, 2024). Chronic exposure to mycotoxins has long been associated with hepatotoxicity, nephrotoxicity, immunosuppression, and carcinogenesis (Mafe & Büsselberg, 2026). More recently, attention

has shifted to their impact on the human gut microbiome, a complex ecosystem essential for digestion, immune regulation, and metabolic homeostasis.

Evidence indicates that mycotoxins disrupt microbial diversity, reduce beneficial taxa, and promote dysbiosis. For example, deoxynivalenol (DON) impairs short-chain fatty acid production and increases intestinal inflammation (Mafe & Büsselberg, 2026), while aflatoxin B_1 alters microbial composition and epithelial barrier integrity (Khan, 2024). These bidirectional interactions are critical: gut microbes can metabolize and detoxify certain mycotoxins, but they can also bioactivate others, amplifying toxicity (Mafe & Büsselberg, 2026).

The Hazard Analysis and Critical Control Points (HACCP) framework provides a systematic approach to identifying and controlling hazards at critical points in food production. Applying HACCP principles to mycotoxin contamination involves monitoring agricultural practices, storage conditions, and processing steps where fungal growth and toxin production are most likely (Khan, 2024). Integrating microbiome endpoints into HACCP risk assessment could enhance food safety management by considering not only toxicological thresholds but also microbial resilience and host health outcomes.

TYPES OF FOODBORNE MYCOTOXINS

Aflatoxins

Produced mainly by *Aspergillus flavus* and *A. parasiticus*, aflatoxins are potent hepatotoxins and carcinogens. Aflatoxin B_1 is the most toxic, linked to liver cancer and immune suppression (Mafe & Büsselberg, 2024). Studies show that aflatoxins disrupt gut microbial balance, reducing beneficial *Lactobacillus* and *Bifidobacterium* populations, while increasing opportunistic pathogens (Mafe & Büsselberg, 2026).

Ochratoxin A (OTA)

Generated by *Aspergillus* and *Penicillium* species, OTA contaminates cereals, coffee, and dried fruits. It is nephrotoxic and immunotoxic, and recent findings suggest it alters gut microbial composition, impairing epithelial barrier function and promoting dysbiosis (Khan, 2024). OTA exposure has been linked to reduced microbial diversity and increased inflammatory signaling pathways such as NF-κB (Mafe & Büsselberg, 2026).

Fumonisins

Produced by *Fusarium verticillioides*, fumonisins contaminate maize and maize-based products. Fumonisin B_1 interferes with sphingolipid metabolism and has been associated with esophageal cancer (Mafe & Büsselberg, 2024). In the gut, fumonisins disrupt microbial communities and impair short-chain fatty acid production, contributing to intestinal inflammation (Mafe & Büsselberg, 2026).

Deoxynivalenol (DON)

Also known as vomitoxin, DON is produced by *Fusarium graminearum* and contaminates wheat, barley, and maize. DON induces gastrointestinal distress and immune dysregulation. It reduces microbial richness, impairs SCFA production, and increases pro-inflammatory cytokines, thereby exacerbating dysbiosis (Khan, 2024; Mafe & Büsselberg, 2026).

Zearalenone (ZEN)

Produced by *Fusarium* species, ZEN is an estrogenic mycotoxin found in maize and wheat. It disrupts hormonal balance and reproductive health. In the gut, ZEN alters microbial composition and may promote the growth of taxa capable of metabolizing estrogen-like compounds, further complicating host–microbe interactions (Mafe & Büsselberg, 2026).

MICROBIOME IMPACTS OF FOODBORNE MYCOTOXINS

The gut microbiome refers to the diverse community of microorganisms living in the digestive tract, primarily in the intestines. These microorganisms play essential roles in digestion, nutrient absorption, and the synthesis of certain vitamins and hormones. The balance and composition of the gut microbiome can significantly impact overall health, including metabolic function, mental health, and immune response.

Each individual has a unique gut microbiome influenced by various factors, including genetics, diet, lifestyle, and environmental exposures. Maintaining a balanced and diverse gut microbiome is crucial for supporting various bodily functions and promoting overall well-being.

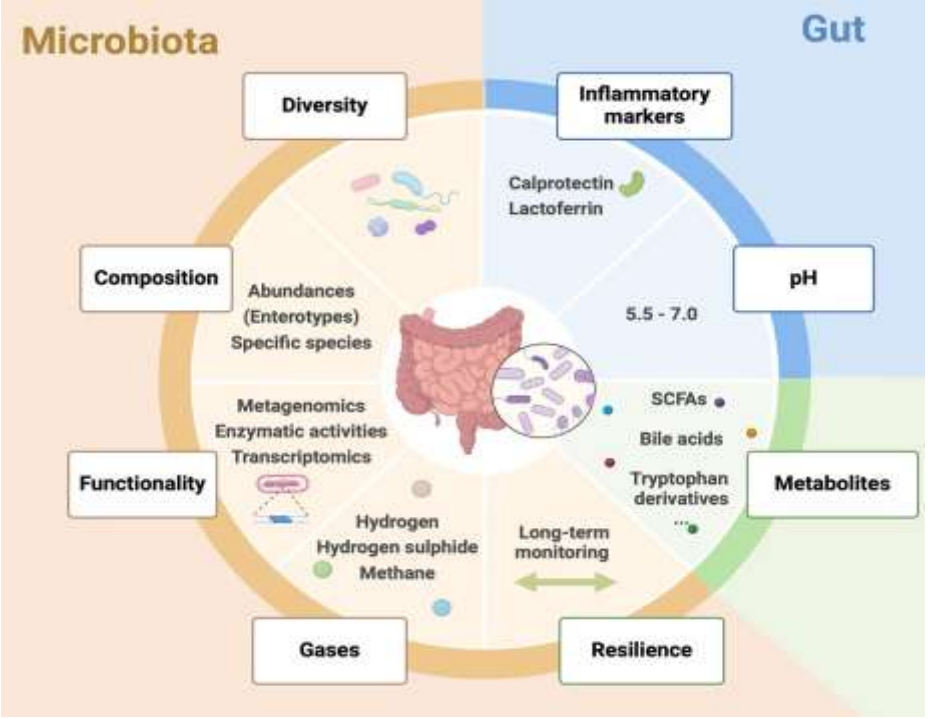

Figure 1. Potential markers of a healthy gut microbiota. A healthy gut microbiota is characterised by a diverse and balanced community of microorganisms that perform vital functions for the host. Several key markers have been proposed to assess these, including microbial diversity, composition (abundances, enterotypes, specific species), functionality (metagenomics, enzymatic activities, transcriptomics) and resilience (through long-term monitoring). Production of important metabolites like SCFAs, bile acids and tryptophan derivatives, as well as gases (hydrogen, hydrogen sulfide, methane), are potential indicators. Additionally, gut health indicators such as pH levels and the presence of inflammation markers (like calprotectin, lactoferrin) can be used for assessing overall gut health. SCFAs, short-chain fatty acids (from Van Hul et al., 2024).

Exposure to foodborne mycotoxins can disrupt this balance, leading to microbiome dysbiosis and downstream health consequences.

Alterations in Microbial Diversity

Aflatoxins, particularly aflatoxin B_1, reduce beneficial taxa such as *Lactobacillus* and *Bifidobacterium* while promoting opportunistic pathogens (Chałaśkiewicz et al., 2025). This imbalance increases intestinal permeability and weakens epithelial barrier integrity (Mafe & Büsselberg, 2026).

Metabolic Effects

Deoxynivalenol (DON) is one of the most studied mycotoxins. It reduces the production of short-chain fatty acids (SCFAs), which are crucial for gut health and immune modulation. DON exposure also elevates pro-inflammatory cytokines, contributing to chronic intestinal inflammation (Li et al., 2019). Fumonisins, especially fumonisin B_1, disrupt sphingolipid metabolism and alter microbial composition, reducing *Clostridiaceae* and *Campylobacteraceae* while increasing *Ruminococcaceae* and *Faecalibacterium* (Yunus Zeebone et al., 2023; Zhang et al., 2021).

Immune Dysregulation

Ochratoxin A (OTA) is nephrotoxic and immunosuppressive, but also directly affects the microbiome. OTA activates NF-κB signaling, leading to chronic inflammation and reduced microbial diversity (Więckowska et al., 2025; Izco et al., 2021). Dysbiosis caused by OTA increases susceptibility to infections and metabolic disorders.

Bidirectional Interactions

The relationship between mycotoxins and the microbiome is bidirectional. Gut microbes can metabolize and detoxify certain mycotoxins, but they may also bioactivate others, amplifying toxicity (Mafe & Büsselberg, 2026). This dual role highlights the need for integrated risk assessment approaches that consider microbial resilience alongside toxicological thresholds.

HACCP CONTROL POINTS FOR MYCOTOXIN MANAGEMENT

The Hazard Analysis and Critical Control Points (HACCP) framework provides a systematic approach to identifying, evaluating, and controlling hazards in food production. When applied to mycotoxins, HACCP emphasizes prevention at critical stages rather than relying solely on end-product testing. Integrating microbiome considerations into HACCP adds a novel dimension, ensuring that food safety strategies also protect gut microbial health.

1. Primary Production (Agriculture)

Critical Control Point (CCP): Crop cultivation and harvesting

Mycotoxins such as aflatoxins and fumonisins originate in the field, particularly under warm and humid conditions (Khan, 2024).

Preventive measures: crop rotation, resistant varieties, biocontrol agents (e.g., *Aspergillus flavus* biocompetitive strains).

Microbiome relevance: reducing contamination at source minimizes downstream exposure that disrupts gut microbial diversity.

2. Post-Harvest Handling and Storage

Critical Control Point (CCP): Grain drying and storage

Improper drying and high moisture favor fungal growth and OTA production (Izco et al., 2021).

Preventive measures: rapid drying to <13% moisture, controlled humidity, aeration systems.

Microbiome relevance: OTA exposure is linked to NF-κB activation and dysbiosis (Więckowska et al., 2025).

3. Processing and Manufacturing

Critical Control Point (CCP): Milling, sorting, and detoxification steps

DON and ZEN often persist through processing; sorting and cleaning reduce contamination (Li et al., 2019).

Emerging technologies: enzymatic detoxification, microbial biotransformation.

Microbiome relevance: microbial detoxification strategies may preserve gut microbial resilience.

4. Distribution and Retail

Critical Control Point (CCP): Packaging and transport

Contamination can occur during storage and distribution if conditions favor fungal growth.

Preventive measures: HACCP monitoring of supply chains, traceability systems.

Microbiome relevance: minimizing chronic low-dose exposure reduces risk of long-term dysbiosis.

5. Consumption and Public Health Monitoring

Critical Control Point (CCP): Consumer awareness and biomarker surveillance

Incorporating microbiome-sensitive biomarkers into HACCP risk assessment could provide early warning of subclinical effects (Mafe & Büsselberg, 2026).

Public health programs should integrate dietary monitoring with microbiome analysis to assess cumulative impacts.

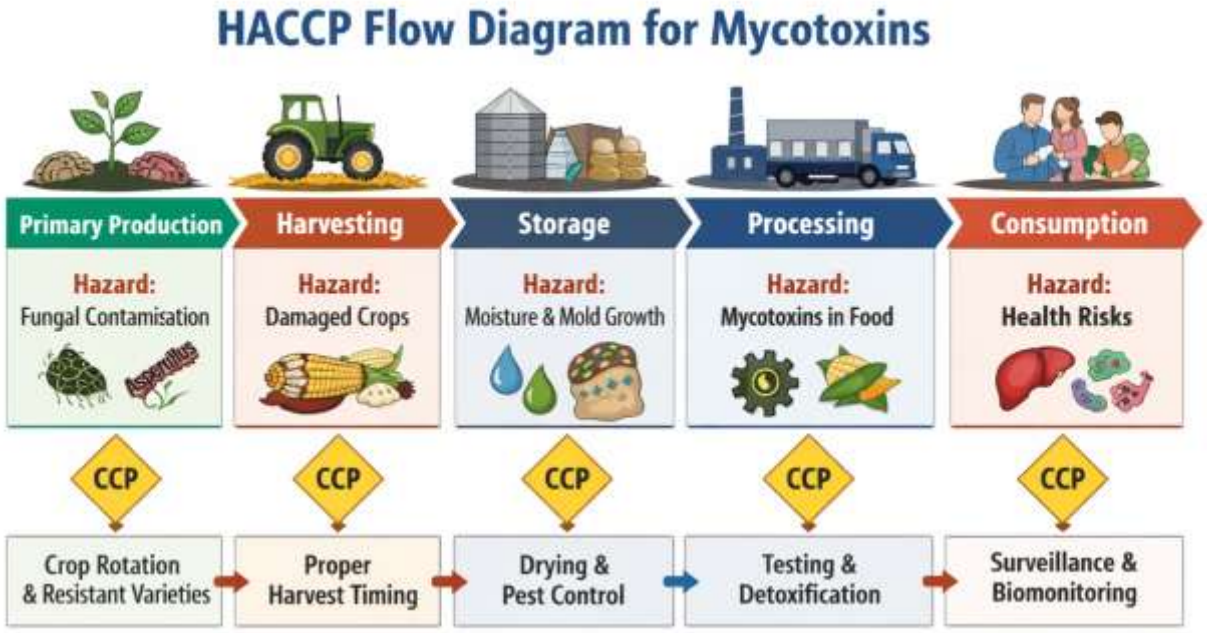

Figure 2. HACCP flow diagram for mycotoxin control in food systems

MICROBIOME BIOMARKERS IN FOOD SAFETY

In recent years, food safety science has begun to recognize that the human gut microbiome is not only a passive target of dietary contaminants but also an active participant in shaping health outcomes. This realization has led to the proposal of microbiome biomarkers as complementary tools within HACCP-based risk assessment frameworks. Unlike traditional monitoring, which focuses on detecting chemical residues such as aflatoxins or fumonisins in food products, microbiome biomarkers provide a biological readout of how these toxins affect host physiology even at low, chronic exposure levels.

One of the most widely studied indicators is microbial diversity. Healthy gut ecosystems are characterized by high richness and evenness, measured through indices such as Shannon and Simpson. Exposure to aflatoxin B_1 has been shown to reduce microbial diversity, weakening the resilience of the gut ecosystem and increasing susceptibility to opportunistic pathogens (Chałaśkiewicz et al., 2025). This decline in diversity can therefore serve as an early warning biomarker of toxin-induced dysbiosis.

Another critical set of biomarkers involves short-chain fatty acids (SCFAs), including acetate, propionate, and butyrate. These metabolites are produced by gut microbes during fiber fermentation and play essential roles in maintaining intestinal barrier integrity and modulating immune responses. Studies demonstrate that deoxynivalenol (DON) and fumonisins significantly reduce SCFA production, leading to impaired gut function and chronic inflammation (Li et al., 2019; Yunus Zeebone et al., 2023). Monitoring SCFA levels in fecal or blood samples thus provides a functional biomarker of microbiome health under toxin stress.

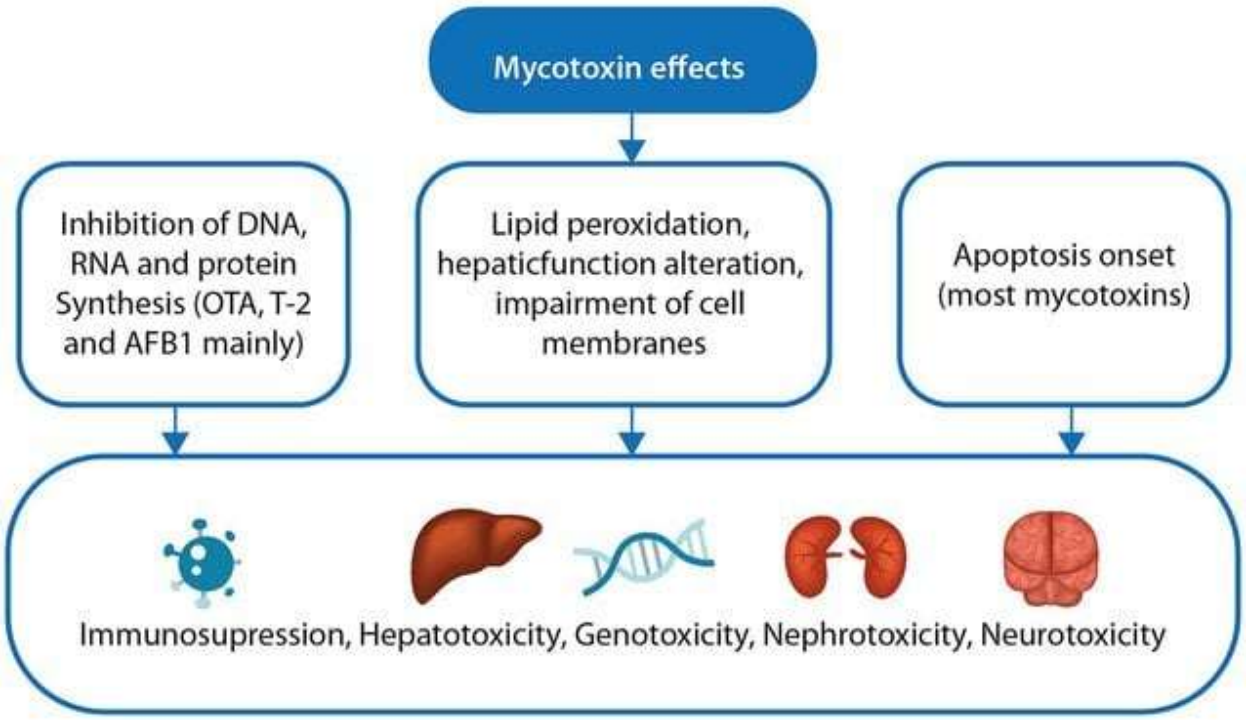

Figure 3. Major mechanisms of mycotoxin toxicity and their effects. Different mechanisms of mycotoxins can affect different organs and tissues in birds such as inhibition of protein synthesis, lipid peroxidation, hepatic function impairment, apoptosis modulation, among others. DNA, deoxyribonucleic acid; RNA, ribonucleic acid; OTA, ochratoxin; AFB1, aflatoxin B1 (from Gómez-Osorio et al., 2024).

The immune system offers another layer of biomarker evidence. Mycotoxins such as ochratoxin A (OTA) activate NF-κB signaling, resulting in elevated levels of pro-inflammatory cytokines like IL-6 and TNF-α. These cytokines are measurable in serum and reflect immune dysregulation linked to microbiome imbalance (Więckowska et al., 2025; Izco et al., 2021). Their inclusion in HACCP monitoring would allow food safety systems to capture not only chemical hazards but also their biological consequences.

Beyond immune markers, metabolomic signatures provide a systems-level perspective. Alterations in bile acids, sphingolipids, and estrogen-like metabolites have been associated with fumonisin and zearalenone exposure (Zhang et al., 2021). These shifts reveal how toxins disrupt host–microbe metabolic interactions, offering highly specific biomarkers for risk assessment.

Finally, probiotic resilience markers highlight the protective role of beneficial microbes. The survival and activity of taxa such as *Lactobacillus* and *Bifidobacterium* under toxin stress can serve as indicators of microbiome robustness. Probiotic supplementation has been shown to mitigate DON and OTA effects, suggesting that resilience markers could guide preventive interventions within HACCP frameworks (Mafe & Büsselberg, 2026).

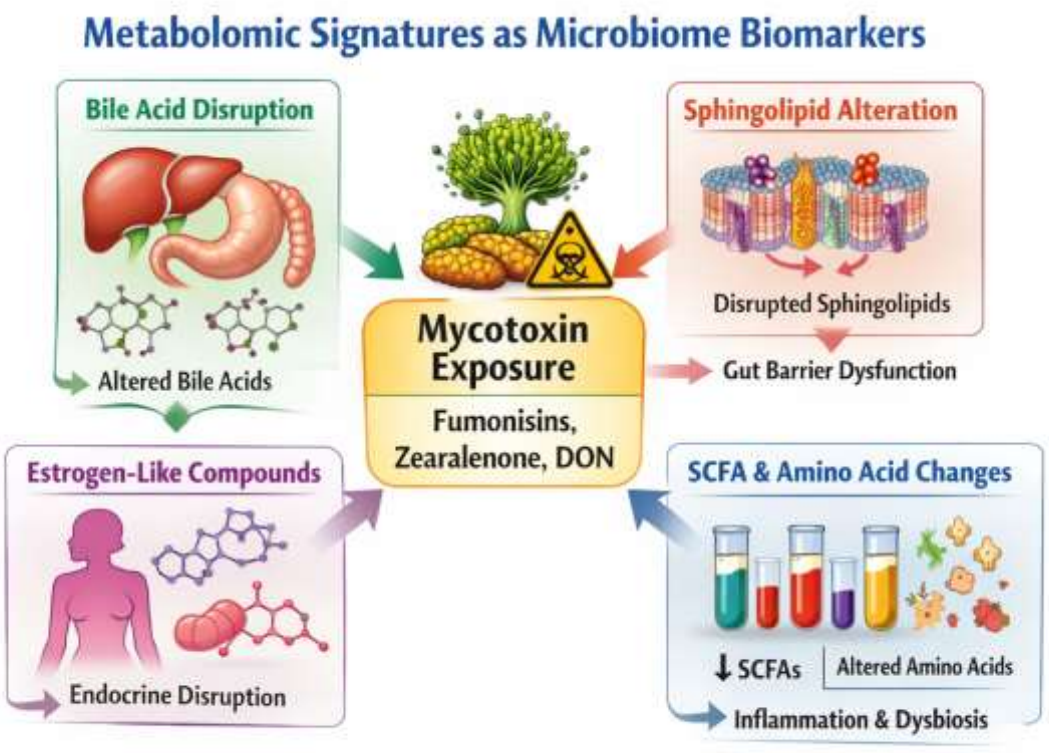

Figure 4. Metabolomic signatures as microbiome biomarkers in food safety. Mycotoxin exposure alters bile acid metabolism, sphingolipid integrity, estrogen-like compounds, and SCFA/amino acid profiles, providing measurable indicators of toxin impact on gut health.

CONCLUSION

The interplay between foodborne mycotoxins and the gut microbiome represents a critical frontier in modern food safety research. Mycotoxins such as aflatoxins, ochratoxin A, deoxynivalenol, fumonisins, and zearalenone exert not only direct toxicological effects but also profound influences on microbial composition, metabolism, and immune regulation. These interactions reshape the intestinal ecosystem, leading to dysbiosis, inflammation, and metabolic imbalance.

Integrating microbiome-based indicators into the HACCP framework transforms food safety from a purely chemical surveillance system into a biological risk-assessment model. By monitoring microbial diversity, SCFA production, cytokine activation, and metabolomic signatures, HACCP can detect early biological responses to contamination long before clinical symptoms appear. This approach aligns with the principles of preventive toxicology and precision nutrition, emphasizing resilience and health maintenance rather than reactive control.

REFERENCES

Chałaśkiewicz, A., Kowalska, M., Nowak, J., & Wiśniewski, P. (2025). Aflatoxin B1 exposure and gut microbiome dysbiosis: Implications for intestinal barrier function. *Toxins, 17*(2), 145. https://doi.org/10.3390/toxins17020145

Gómez-Osorio, L.-M., Vasiljevic, M., Raj, J., Chaparro-Gutierréz, J. J., & López-Osorio, S. (2024). Mycotoxins and coccidiosis in poultry – co-occurrence, interaction, and effects. *Frontiers in Veterinary Science, 11*, 1387856. https://doi.org/10.3389/fvets.2024.1387856

Izco, M., Vettorazzi, A., de Toro, M., Sanz, M., & López de Cerain, A. (2021). Oral sub-chronic ochratoxin A exposure induces gut microbiota alterations in mice. *Toxins, 13*(2), 106. https://doi.org/10.3390/toxins13020106

Khan, R. (2024). Mycotoxins in food: Occurrence, health implications, and control strategies – A comprehensive review. *Toxicon, 248*, 108038. https://doi.org/10.1016/j.toxicon.2024.108038

Li, J., Liu, H., & Chen, J. P. (2019). Metagenomic analysis of gut microbiota alteration in a mouse model exposed to deoxynivalenol. *Toxicology and Applied Pharmacology, 372*, 47–56. https://doi.org/10.1016/j.taap.2019.03.018

Mafe, A. N., & Büsselberg, D. (2024). Mycotoxins in food: Cancer risks and strategies for control. *Foods, 13*(21), 3502. https://doi.org/10.3390/foods13213502

Mafe, A. N., & Büsselberg, D. (2026). Microbiome–mycotoxin interactions and probiotic strategies: Implications for gut health and cancer. *Frontiers in Nutrition, 13*, 1783295. https://doi.org/10.3389/fnut.2026.1783295

Van Hul, M., Cani, P. D., Petifils, C., De Vos, W. M., Tilg, H., & El-Omar, E. M. (2024). What defines a healthy gut microbiome? *Gut, 73*(11), 1893–1908. https://doi.org/10.1136/gutjnl-2024-333378

Więckowska, M., Szelenberger, R., Poplawski, T., Zielińska, E., & Kowalczyk, A. (2025). Gut s a target of ochratoxin A: Toxicological insights and the role of microbiota. *International Journal of Molecular Sciences, 26*(19), 9438. https://doi.org/10.3390/ijms26199438

Yunus Zeebone, Y., Bóta, B., Halas, V., Tóth, Á., & Fébel, H. (2023). Gut faecal microbial and health marker response to dietary fumonisins in weaned pigs. *Toxins, 15*(5), 328. https://doi.org/10.3390/toxins15050328

Zhang, F., Chen, Z., Jiang, L., Wang, Y., & Liu, H. (2021). Response of fecal bacterial flora to fumonisin B1 exposure in BALB/c mice. *Toxins, 13*(9), 612. https://doi.org/10.3390/toxins13090612

ASSESSMENT OF WATER QUALITY AND NUTRIENT CONTAMINATION RISKS IN ISTANBUL'S URBAN LAGOONS (BÜYÜKÇEKMECE AND KÜÇÜKÇEKMECE) USING MODIFIED INDICES

Cem Tokatlı

Trakya University, Edirne / Türkiye

Corresponding author: e-mail: cemtokatli@trakya.edu.tr

ABSTRACT

In this comprehensive scientific investigation, the overarching contamination threats, ecological risks, and seasonal pollution dynamics of Büyükçekmece and Küçükçekmece Lagoons (Istanbul, Türkiye), two critical and vulnerable urban coastal wetlands directly connected to the Sea of Marmara, were thoroughly evaluated under intense anthropogenic stress. A specifically modified Water Quality Index (modified WQI) alongside a newly modified Nutrient Pollution Index (modified NPI) were systematically utilized as the primary diagnostic frameworks to assess the precise extent of environmental degradation and evaluate hydrochemical risks within these complex transitional ecosystems. To effectively quantify the intense urban, agricultural, and industrial pressures exerted on the lagoons across highly contrasting dry and wet seasons, key hydrochemical macro-nutrients including ammonium nitrogen, nitrate nitrogen, nitrite nitrogen, and phosphate phosphorus were monitored at strategically selected sampling stations located closest to the sea inlets. The successful application of these modified indices clearly demonstrated a sharp, multi-seasonal pollution contrast and spatial variation between the two adjacent lagoon systems. Based on the comprehensive modified WQI calculations, Büyükçekmece Lagoon was classified as having a relatively sustainable "good water quality" status (with index values safely ranging between 50 and 100), whereas Küçükçekmece Lagoon consistently exhibited a severely degraded and highly alarming "unsuitable" ecological status (with index values significantly exceeding 300). Correspondingly, the modified NPI values strongly corroborated these diagnostic findings, indicating a state of "moderate pollution" (ranging between 1 and 3) for the Büyükçekmece ecosystem, while rapidly escalating to catastrophic "very high pollution" levels (well exceeding 6) in the Küçükçekmece basin. Ultimately, these analytical results confirm that while natural marine-driven interactions predominantly dictate the hydrochemical character and salinity profile of Büyükçekmece, heavy municipal wastewater and industrial effluents pose a continuous, severe, and unchecked threat to the ecological integrity of Küçükçekmece across all seasonal cycles.

Keywords: Büyükçekmece, Küçükçekmece, Modified WQI, Modified NPI, Seasonal dynamics, Istanbul megacity

INTRODUCTION

Nutrient loads from intense urban runoffs and industrial wastewaters accelerate eutrophication in fragile coastal lagoons, leading to oxygen depletion, restricted light, and disrupted trophic dynamics (Atıcı et al., 2018; Haq et al., 2023; Din et al., 2023; Muhammad et al., 2025). The shallow, semi-enclosed nature of these systems increases their vulnerability to rapid hypoxia, which fluctuates significantly across contrasting seasons (Howarth et al., 2011; Borrell et al.,

2019; Mia et al., 2023). Under severe metropolitan stress, assessing these hydrochemical contaminants is vital to understand cumulative impacts on water quality and biodiversity (Çiçek et al., 2014; Köse et al., 2020; Varol et al., 2022; Ustaoğlu et al., 2022). To effectively evaluate ecosystem health, advanced tools like the modified Nutrient Pollution Index (modified NPI) and modified Water Quality Index (modified WQI) are essential to determine the synergistic effects of multi-seasonal pollution in these transitional waters (Tokatlı and Varol, 2021; Varol et al., 2022; Muhammad et al., 2024; Tokatlı et al., 2025).

Interpreting large, multidimensional water quality datasets can be challenging for environmental risk communication and policy making. Therefore, integrating mathematical models like the modified Water Quality Index (modified WQI) and modified Nutrient Pollution Index (modified NPI) provides an indispensable methodology to aggregate complex variables into a single, cohesive score. Utilizing these modified indices is crucial for Büyükçekmece and Küçükçekmece Lakes, fragile coastal lagoon ecosystems simultaneously exposed to heavy industrial effluents, dense municipal wastewater, and intense urban runoffs within a megacity layout (Tokatlı et al., 2017; Tokatlı, 2019). By filtering raw hydrochemical metrics through the modified WQI and modified NPI, it becomes possible to objectively evaluate sharp seasonal pollution contrasts, isolate the specific impacts of multi-seasonal urban inputs, and establish a scientifically validated baseline for the ecological protection of these vulnerable urban lagoons.

This study aims to assess the contamination threats and seasonal pollution dynamics affecting Büyükçekmece and Küçükçekmece Lagoons by employing a set of modified water quality and nutrient indices in a megacity (Istanbul). The evaluation utilizes key limnological and hydrochemical parameters—specifically ammonium nitrogen, nitrate nitrogen, nitrite nitrogen, and phosphate phosphorus—to analyze the extent and impact of anthropogenic pollution across contrasting dry and wet seasons in these fragile transitional ecosystems. By applying the modified Water Quality Index (modified WQI) and modified Nutrient Pollution Index (modified NPI) at stations closest to the sea, the study seeks to offer precise insights into multi-seasonal pollution contrasts and environmental risks.

MATERIALS AND METHODS

Research Area and Sample Collection

The geographic positions of Büyükçekmece and Küçükçekmece Lakes and the designated sampling stations on each lagoon are presented in Figure 1. Water samples were systematically collected from the selected stations across two contrasting periods: the dry late-summer season of 2022 and the wet late-winter season of 2023.

Chemical Analysis

The concentrations of key hydrochemical parameters, including ammonium nitrogen, nitrate nitrogen, nitrite nitrogen, and phosphate phosphorus, were systematically analyzed in the laboratory. All nutrient analyses were performed following standard methods for the examination of water and wastewater as outlined in APHA protocols (1998, 2017). Quantitative determinations were executed spectrophotometrically using a calibrated Hach spectrophotometer with appropriate high-purity reagents and standard curves.

Ecological Indices

The detailed mathematical formulations and computation techniques for the modified Water Quality Index (modified WQI) and modified Nutrient Pollution Index (modified NPI) applied in this study, aligned with the national environmental thresholds (TSWQR, 2021), are comprehensively presented in Table 1 (Tokatlı et al., 2025). These modified indices were systematically deployed to evaluate the precise levels of nutrient enrichment and associated multi-seasonal contamination risks in the transitional water samples.

Table 1. Methods of applied modified organic pollution risk assessment indices

Index	Calculation	Formula Explanations	Rating of Water Quality
NPI	$NPI = (C_N/MAC_N) + (C_P/MAC_P)$	C_N: The levels of NO_2-N in water sample C_P: The levels of PO_4-P in water sample MAC_N: The maximum limit of NO_2-N MAC_P: The maximum limit of PO_4-P	<1: No polluted 1-3: Moderate polluted 3-6: Considerable polluted >6: Very high polluted
WQI	$WQI = \sum_{i=1}^{n} W\imath \; x \; (\frac{Ci}{Si}) \; x \; 100$ $W\imath = \frac{W_i}{\sum_{i=1}^{n} W_i}$	WI: The relative weight Wi: The values assigned to i (1-5) Ci: The values of measured parameters Si: The standard values	<50: Excellent water 50–100: Good water 100–200: Poor water 200–300: Very poor water >300: Unsuitable

Figure 1. Investigated lagoons and selected sampling stations

RESULTS AND DISCUSSION

The calculated modified water quality and nutrient pollution indices for Büyükçekmece and Küçükçekmece Lagoons are presented in Figure 2. The results indicate a sharp multi-seasonal pollution contrast, demonstrating that while Büyükçekmece exhibits a stable, low-risk profile, Küçükçekmece remains critically and permanently degraded. These ecological indices clearly reflect the dominant grip of heavy urban and industrial wastewater pressures over the natural hydrochemical baseline of the Istanbul megacity (Mutlu et al., 2021a; 2021b).

Büyükçekmece Lagoon showed high ecological resilience across both periods. During the dry season, it displayed a modified WQI of 43.670 ("excellent water quality", <50), which rose slightly to 58.617 ("good water quality", 50–100) in the wet season. This minor variation indicates that rain-driven urban runoffs introduce limited nutrient inputs during wet periods without compromising overall ecosystem integrity. This stable profile was strongly corroborated by the modified NPI scores; Büyükçekmece recorded a value of 1.140 ("moderate polluted", 1-3) during the dry period, which dropped to 0.980 ("no polluted", <1) in the wet season due to precipitation-driven dilution.

In stark contrast, environmental indicators escalated to catastrophic levels in Küçükçekmece Lagoon due to relentless municipal and industrial effluents that drive severe ecosystem degradation (Varol and Tokatlı, 2021). During the dry season, the modified WQI reached a critical "unsuitable" status at 673.480 (>300), further verified by an exceptionally high modified NPI of 23.880 ("very high polluted", >6). Restricted dry-season dilution capacity highlights a severe contamination core driven directly by infrastructure pressures.

During the wet season, despite increased precipitation regimes, Küçükçekmece Lagoon failed to recover, signaling a state of permanent ecological saturation (Muhammad et al., 2024). The modified WQI remained firmly "unsuitable" at 475.223, while the modified NPI recorded 13.220 ("very high polluted", >6). Although winter precipitation exerted a relative dilution effect compared to the dry season, the persistence of these extreme thresholds underscores that heavy urban wastewater discharges operate as a continuous, acute threat (Muhammad et al., 2025). This multi-seasonal elevation confirms that anthropogenic pressures overwhelm natural dilution factors, establishing a permanent pollution contrast against the well-preserved character of Büyükçekmece Lagoon (Tokatlı et al., 2023; 2024).

CONCLUSIONS

This study underscores the high efficiency of using modified pollution indices to diagnose ecosystem health in complex urban coastal wetlands. By applying the modified WQI and modified NPI across contrasting seasons, a sharp pollution contrast was unraveled between Istanbul's two strategic lagoons. The index calculations revealed that Büyükçekmece Lagoon maintains a resilient profile, exhibiting "excellent" to "good" water quality and low nutrient levels. In stark contrast, Küçükçekmece Lagoon suffers from permanent ecological saturation, consistently displaying "unsuitable" water quality and "very high" nutrient pollution across both dry and wet periods. The persistence of these extreme scores in Küçükçekmece, even during wet seasons, proves that continuous municipal and industrial effluents completely overwhelm the natural dilution capacity of the system. Ultimately, these findings establish a scientifically validated baseline demonstrating that a single, generalized management approach is inadequate. While Büyükçekmece requires proactive protection, Küçükçekmece demands immediate, aggressive remediation. Implementing system-specific wastewater management strategies is vital to ensure the long-term ecological sustainability of transitional waters within a megacity.

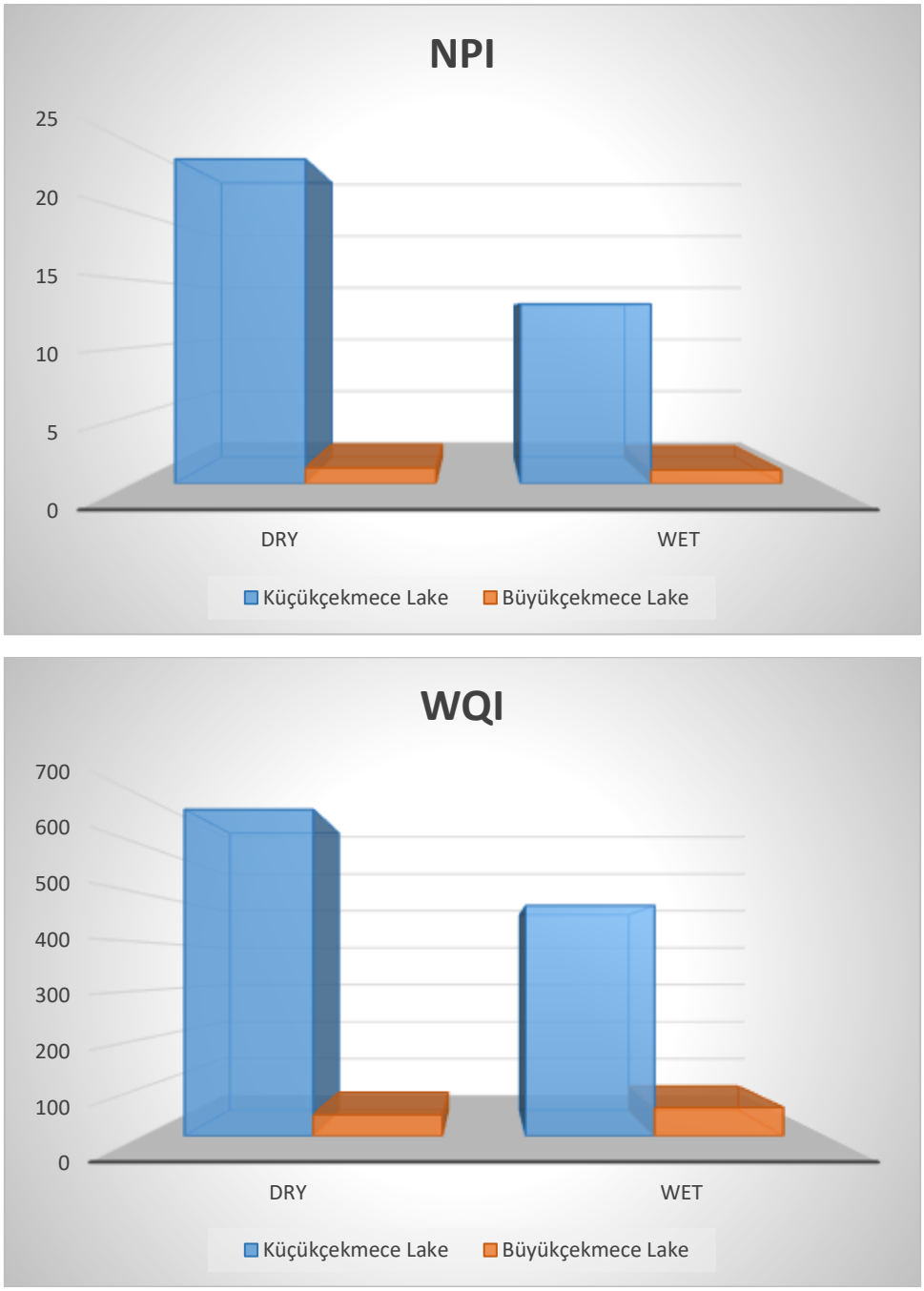

Figure 2. Results of applied NPI (up) and WQI (down)

ACKNOWLEDGEMENTS

This study was supported by Trakya University Scientific Research Projects Unit under Project Code 2022/168. The author would like to thank Trakya University for the financial and institutional support provided throughout the research.

REFERENCES

APHA, 1998. Standard Methods for the Examination of Water and Wastewater. American Public Health Association. Inc., Washington, DC.

APHA, 2017. American public health association (APHA). Stand. Methods Exam. Water Wastewater.

Atıcı, T., Tokatlı, C., Çiçek, A., 2018. Diatoms of Seydisuyu Stream Basin (Turkey) and assessment of water quality by statistical and biological approaches. Sigma Journal of Engineering and Natural Sciences 36, 271-288.

Borrell, A., Tornero, V., Bhattacharjee, D., Aguilar, A., 2019. Organochlorine concentrations in aquatic organisms from different trophic levels of the Sundarbans mangrove ecosystem and their implications for human consumption. Environmental Pollution 251, 681-688.

Çiçek, A., Köse, E., Emiroğlu, Ö., Tokatlı, C., Başkurt, S., Sülün, Ş., 2014. Boron and arsenic levels in water, sediment and tissues of *Carassius gibelio* (Bloch, 1782) in a dam lake. Polish Journal of Environmental Studies, 23 (5): 1843-1848.

Din, I. U., Muhammad, S., Rehman, I., Tokatlı, C., 2023. Spatial distribution of potentially toxic elements contamination and risk indices of water and sediments in the Darband and Samana Streams, Pakistan. Environmental Monitoring and Assessment, 195: 1343.

Haq, A., Muhammad, S., Tokatlı, C., 2023. Spatial distribution of potentially harmful elements contamination and risk assessment in the Ghizer River Basin, Northern Pakistan. Journal of Water and Climate Change, https://doi.org/10.2166/wcc.2023.056.

Howarth, R., Chan, F., Conley, D.J., Garnier, J., Doney, S.C., Marino, R., Billen, G., 2011. Coupled biogeochemical cycles: eutrophication and hypoxia in temperate estuaries and coastal marine ecosystems. Frontiers in Ecology and the Environment 9, 18-26.

Köse, E., Emiroğlu, Ö., Çiçek, A., Aksu, S., Başkurt, S., Tokatlı, C., Şahin, M., Uğurluoğlu, A., 2020. Assessment of ecologic quality in terms of heavy metal concentrations in sediment and fish on Sakarya River and dam lakes, Turkey. Soil and Sediment Contamination: An International Journal, 29:3, 292-303.

Mia, Y., İslam, A. R. T., Jannat, J. N., Jion, M. M. F., Sarker, A., Tokatlı, C., Siddique, A. B., İbrahim, S. M., Senapathi, V., 2023 Identifying factors affecting irrigation metrics in the Haor Basin using integrated Shannon's entropy, fuzzy logic and automatic linear model. Environmental Research 226, 115688.

Muhammad, S., Ahmed, T., Amin, S., Tokatli, C., Ustaoğlu, F., Ahmad, A., Ali, W., Farooq, U., 2025. Spatial distribution of hazard index via heavy metals consumption in water from the Himalayan lacustrine ecosystems. Physics and Chemistry of the Earth, Parts A/B/C, 138: 103858.

Muhammad, S., Ahmed, T., Ullah, R., Tokatlı, C., Ahmad, A., 2024. Spatial distribution of heavy metals contamination and risk indices of surface sediments in high-altitude lakes. Environmental Monitoring and Assessment, 196: 1188.

Mutlu, E., Arslan, N., Tokatlı, C., 2021a. Water quality assessment of yassialan dam lake (Karadeniz Region, Turkey) by using principle component analysis and water quality index. Acta Scientiarum Polonorum-Formatio Circumiectus, 20 (2): 55–65.

Mutlu, E., Arslan, N., Tokatlı, C., 2021b. Assessing water quality of boyali dam lake (Sinop, Turkey) by using ecological and statistical indicators. Acta Scientiarum Polonorum-Formatio Circumiectus, 20 (1): 77-85.

Tokatlı, C., 2019. Use of the potential ecological risk index for sediment quality assessment: a case study of dam lakes in the Thrace part of the Marmara Region. Aquatic Sciences and Engineering, 34 (3): 90-95.

Tokatlı, C., Baştatlı, Y., Elipek, B., 2017. Water quality assessment of dam lakes located in Edirne Province (Turkey). Sigma Journal of Engineering and Natural Sciences, 35 (4): 743-750.

Tokatlı, C., Uğurluoğlu, A., Muhammad, S., 2023. Ecotoxicological evaluation of organic contamination in the world's two significant gateways to the Black Sea using gis techniques: Turkish Straits. Marine Pollution Bulletin, 194: 115405.

Tokatlı, C., Varol, M., Uğurluoğlu, A., 2024. Ecological risk assessment, source identification and spatial distribution of organic contaminants in terms of mucilage threat in streams of Çanakkale Strait Basin (Türkiye). Chemosphere, 353: 141546.

Tokatlı, C., Uğurluoğlu, A., Muhammad, S., 2025. Spatiotemporal variations of organic contaminants and their ecotoxicological risk in the Uluabat Lake Basin, Türkiye: a Ramsar living wetland. Physics and Chemistry of the Earth 138, 103851.

Tokatlı, C., Varol, M., 2021. Variations, health risks, pollution status and possible sources of dissolved toxic metal(loid)s in stagnant water bodies located in an intensive agricultural region of Turkey. Environmental Research 201, 111571.

TSWQR, 2021. (Turkish surface water quality regulation) (2021). Turkish Surface Water Quality Regulation. Türkiye.

Ustaoğlu, F., İslam, S., Tokatlı, C., 2022. Ecological and probabilistic human health hazard assessment of heavy metal in Sera Lake Nature Park sediments (Trabzon, Turkey). Arabian Journal of Geosciences, 15: 597.

Varol, M., Ustaoğlu, F., Tokatlı, C., 2022. Ecological risks and controlling factors of trace elements in sediments of dam lakes in the Black Sea Region (Turkey). Environmental Research, 205: 112478.

Varol, M., Tokatlı, C., 2021. Impact of paddy fields on water quality of Gala Lake (Turkey): an important migratory bird stopover habitat. Environmental Pollution, 287: 117640.

SEASONAL DYNAMICS OF WATER QUALITY AND ANTHROPOGENIC PRESSURES IN BÜYÜKÇEKMECE AND KÜÇÜKÇEKMECE LAGOONS IN A MEGACITY (İSTANBUL)

Cem Tokatlı

Trakya University, Edirne / Türkiye

Corresponding author: e-mail: cemtokatli@trakya.edu.tr

ABSTRACT

In this comprehensive scientific study, the overall water quality status, physicochemical characteristics, and seasonal dynamics of Büyükçekmece and Küçükçekmece Lakes (Istanbul), two crucial coastal lagoon ecosystems tightly connected to the Sea of Marmara, were meticulously investigated under intense and continuous anthropogenic pressure mechanisms. Field sampling campaigns were systematically conducted across two highly contrasting seasons—the late dry season of 2022 and the wet late-winter season of 2023—focusing specifically on strategically designated sampling points located closest to the marine connection of each lagoon to accurately evaluate the extent of seawater intrusion and tidal interactions. The research program monitored a wide spectrum of key environmental parameters, including dissolved oxygen, pH, electrical conductivity, total dissolved solids, salinity, turbidity, ammonium nitrogen, nitrate nitrogen, nitrite nitrogen, and phosphate phosphorus, to evaluate the level of environmental degradation. The analytical findings revealed distinct limnological profiles and highly varying pollution characteristics between the two interconnected aquatic systems; Büyükçekmece Lagoon exhibited a significantly higher salinity level and a much more pronounced brackish water character due to its direct and active marine interactions with the Sea of Marmara, whereas Küçükçekmece Lagoon demonstrated severe environmental degradation characterized by substantially higher nutrient concentrations, clearly indicating intense domestic, agricultural, and industrial pollution loads originating from its heavily urbanized watershed. Furthermore, the seasonal transition from the dry late-summer period to the wet late-winter season drastically altered the physical and chemical profiles of both lagoons through heavy precipitation and subsequent surface runoff, demonstrating that while natural marine inputs dominate the salinity profile of Büyükçekmece, heavy urban expansion and anthropogenic pressures continuously compromise the environmental health and long-term ecological integrity of Küçükçekmece.

Keywords: Büyükçekmece, Küçükçekmece, Coastal lagoons, Seasonal dynamics, Water quality, Istanbul megacity

INTRODUCTION

Anthropogenic transformations in megacities subject adjacent aquatic ecosystems to unprecedented ecological stress, where rapid urbanization and industrial concentration disrupt natural hydrological balances. The continuous discharge of complex urban effluents drastically shifts the physico-chemical integrity and nutrient dynamics of receiving waters, triggering severe degradation and threatening biodiversity. Coastal lagoons, operating as complex transitional interfaces between terrestrial watersheds and marine environments, represent some of the most critically threatened habitats under these intense urban regimes. Although these

ecosystems possess immense socio-economic and ecological value, their restricted hydrodynamic flushing capacity and semi-closed structures make them highly susceptible to accumulating anthropogenic pollutants, a vulnerability that fluctuates dramatically across contrasting seasonal periods (Muhammed et al., 2024; 2025; Helvacıoğlu et al., 2025).
Deciphering the complex pollution trajectories within fragile lagoon ecosystems dictates a continuous, systematic evaluation of hydrochemical parameters to build robust conservation strategies. Investigating water quality variations serves as a baseline scientific catalyst for environmental management, explicitly exposing how temporal dynamics and seasonal shifts dictate the behavior of urban stressors. Within this critical framework, Büyükçekmece and Küçükçekmece Lakes, functioning as strategic coastal lagoons connected to the Sea of Marmara, occupy a pivotal position in maintaining the ecological equilibrium of the Istanbul megacity. While these coastal systems provide irreplaceable aquatic habitats, they simultaneously endure relentless environmental degradation from dense municipal layout, sprawling industrial corridors, and intense urban runoffs that fluctuate severely between dry and wet seasonal cycles (Atıcı et al., 2018; Ustaoğlu et al., 2022; Tokatlı et al., 2022; 2024).
The objective of this study is to evaluate the water quality status and seasonal dynamics of Büyükçekmece and Küçükçekmece Lakes under intense urban and industrial pressures across two contrasting periods: the dry late-summer of 2022 and the wet late-winter of 2023. By monitoring key hydrochemical parameters at sampling points closest to their Sea of Marmara connections, this research aims to elucidate the multi-seasonal background pollution status of these strategic lagoons. Furthermore, the findings specifically aim to demonstrate the contrasting environmental profiles of the two systems—highlighting the more pronounced marine-driven salinity character of Büyükçekmece against the severe nutrient-driven degradation of Küçükçekmece—thereby providing a crucial scientific baseline for distinct, sustainable lagoon management and remediation strategies in a megacity.

MATERIALS AND METHODS

Research Area and Sample Collection

The geographic locations of Büyükçekmece and Küçükçekmece Lakes and the designated sampling stations on each lagoon are presented in Figure 1, providing a visual representation of the study area within the Istanbul megacity. To evaluate the seasonal water quality status and assess the hydrochemical impacts of intense urban pressures, water samples were systematically collected across two contrasting field surveys: the dry late-summer season of 2022 and the wet late-winter season of 2023.
The sampling stations were strategically positioned to capture the direct transitional dynamics between the lagoon ecosystems and the marine environment. One critical station was established at the point closest to the Sea of Marmara connection for each lagoon. At each station, water samples were collected, preserved, and transported to the laboratory under appropriate cold-chain conditions for subsequent physico-chemical and hydrochemical analyses.

Physicochemical Analysis

Dissolved oxygen, electrical conductivity, pH, total dissolved solids, salinity, and turbidity were measured on-site in the field during the sampling survey using a Hach portable multi-parameter meter and a Hach turbidimeter, following the standard methods established by APHA (1998, 2017). For the nutrient analyses, water samples were transported to the laboratory under appropriate conditions. The concentrations of nitrate nitrogen, nitrite nitrogen, ammonium nitrogen and phosphate phosphorus were systematically analysed in the laboratory according to APHA protocols (1998) utilizing a Hach spectrophotometer.

Figure 1. Investigated lagoons and selected sampling stations

RESULTS AND DISCUSSION

The obtained results clearly demonstrated that although Büyükçekmece and Küçükçekmece Lagoons are located within the same metropolitan region and are both connected to the Sea of Marmara, they exhibit markedly different limnological structures and pollution characteristics under anthropogenic influence. The most evident distinction between the lagoons was observed in salinity-related parameters. Büyükçekmece Lagoon consistently exhibited substantially higher TDS (21,135 mg/L), EC (29,000 µS/cm), and salinity (21.90‰) values compared to Küçükçekmece Lagoon (13,465 mg/L, 18,975 µS/cm, and 13.97‰, respectively). These findings indicate a stronger marine influence and more pronounced brackish character in Büyükçekmece Lagoon, likely associated with its hydrodynamic connection to the Sea of Marmara. Seasonal variation further supported this pattern, as salinity-related parameters were notably higher during the dry season in both lagoons, reflecting evaporation effects and reduced freshwater inflow. Conversely, wet-season dilution decreased TDS, EC, and salinity levels, particularly in Büyükçekmece, indicating the importance of seasonal hydrological processes in regulating lagoon physicochemistry (Mutlu et al., 2021a; Tokatlı et al., 2023; 2025) (Figure 2). Despite the stronger marine characteristics of Büyükçekmece Lagoon, nutrient enrichment and ecological degradation were considerably more pronounced in Küçükçekmece Lagoon. Mean nutrient concentrations in Küçükçekmece (NO_3–N: 0.694 mg/L; NO_2–N: 0.089 mg/L; PO_4–P: 0.483 mg/L; NH_4–N: 0.682 mg/L) were markedly higher than those detected in

Büyükçekmece Lagoon (0.404, 0.008, 0.016, and 0.161 mg/L, respectively). According to the Turkish Surface Water Quality Regulation classification criteria (TSWQR, 2021), nitrate concentrations in both lagoons remained within Class I quality limits (<5 mg/L), indicating no severe nitrate pollution. However, phosphate concentrations in Küçükçekmece corresponded to Class III water quality (0.16–0.65 mg/L), while ammonium levels indicated Class II quality conditions. Nitrite concentrations also approached the upper limit of Class II and lower limit of Class III categories. In contrast, Büyükçekmece generally retained Class I water quality characteristics for phosphorus, nitrite, and ammonium. These results suggest that nutrient pollution in Küçükçekmece is primarily associated with intensive urbanization, industrial activities, domestic wastewater inputs, and historical anthropogenic accumulation within the watershed (Mutlu et al., 2021b; Tokatlı et al., 2025) (Figure 2).

Seasonal dynamics revealed clear differences between the lagoons. During the wet season, nitrate concentrations increased in both systems, particularly in Küçükçekmece (0.267–1.121 mg/L), indicating enhanced runoff-derived nutrient transport. Turbidity also increased seasonally, rising from 1.12 to 2.94 NTU in Küçükçekmece and from 0.84 to 2.09 NTU in Büyükçekmece, likely due to increased suspended matter inputs and sediment resuspension. In contrast, phosphate slightly decreased in Küçükçekmece, suggesting dilution effects, whereas ammonium increased during the wet period (0.821 mg/L), further reflecting urban and watershed-derived pollution inputs (Tokatlı, 2017; Tokatlı, 2018).

Dissolved oxygen levels generally remained high (>8 mg/L), corresponding to Class I water quality conditions. However, wet-season DO decline was observed, especially in Küçükçekmece (7.29 mg/L), probably due to increased organic inputs and microbial activity. Both lagoons exhibited alkaline conditions throughout the study, with wet-season pH values exceeding 9.0, which is typical for productive brackish lagoon ecosystems (Varol and Tokatlı, 2021).

Overall, the findings indicated that the two lagoons are controlled by different dominant drivers. Büyükçekmece Lagoon is mainly influenced by marine connectivity and hydrological exchange, resulting in higher salinity but relatively good water quality. In contrast, Küçükçekmece Lagoon is strongly affected by anthropogenic pressures, reflected by nutrient enrichment and ecological deterioration. Seasonal transitions between dry and wet periods significantly altered water quality characteristics and pollutant transport processes. Therefore, reducing urban and industrial pollution loads, particularly in the Küçükçekmece watershed, is essential for the sustainable management of these lagoon ecosystems in the megacity environment of Istanbul.

CONCLUSIONS

In conclusion, Büyükçekmece and Küçükçekmece Lagoons exhibited distinct ecological characteristics despite their similar geographic setting. Büyükçekmece was mainly influenced by marine connectivity and showed a more pronounced brackish character with relatively better water quality conditions. In contrast, Küçükçekmece was characterized by higher nutrient concentrations and stronger anthropogenic impacts. Seasonal transitions significantly affected water quality dynamics, particularly nutrient levels and turbidity, highlighting the importance of hydrological processes and watershed inputs in lagoon functioning. These findings emphasize the need for effective pollution control and sustainable management strategies, especially for Küçükçekmece Lagoon.

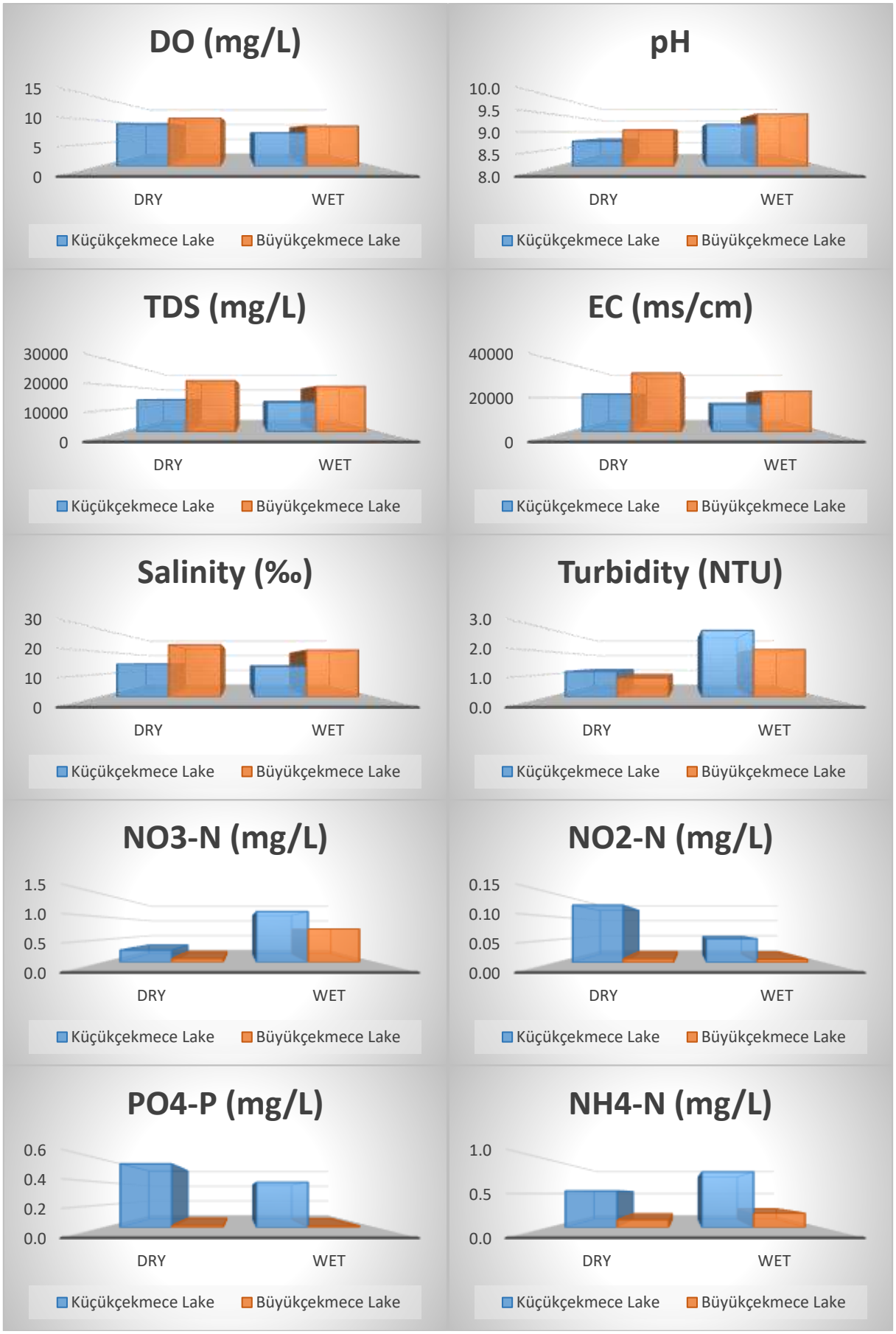

Figure 2. Investigated limnological parameters

ACKNOWLEDGEMENTS

This study was supported by Trakya University Scientific Research Projects Unit under Project Code 2022/168. The author would like to thank Trakya University for the financial and institutional support provided throughout the research.

REFERENCES

APHA, 1998. Standard Methods for the Examination of Water and Wastewater. American Public Health Association. Inc., Washington, DC.

APHA, 2017. American public health association (APHA). Stand. Methods Exam. Water Wastewater.

Atıcı, T., Tokatlı, C., Çiçek, A., 2018. Diatoms of Seydisuyu Stream Basin (Turkey) and assessment of water quality by statistical and biological approaches. Sigma Journal of Engineering and Natural Sciences, 36(1): 271-288.

Helvacıoğlu, İ. A., Gülbaşı, A., Tokatlı, C., 2025. Evaluating the environmental sustainability awareness of paddy producers in the Meriç Plain (Northwest Türkiye): a comprehensive statistical approach. Acta Scientiarum Polonorum-Formatio Circumiectus, 24 (1): 3-13.

Muhammad, S., Ahmed, T., Amin, S., Tokatli, C., Ustaoğlu, F., Ahmad, A., Ali, W., Farooq, U., 2025. Spatial distribution of hazard index via heavy metals consumption in water from the Himalayan lacustrine ecosystems. Physics and Chemistry of the Earth, Parts A/B/C, 138: 103858.

Muhammad, S., Zeb, A., Ullah, R., Amin, S., Ahmad, A., Tokatli, C., 2024. Spatial distribution of drinking, irrigation water quality, and health risk indices of high-altitude lakes. Physics and Chemistry of the Earth, Parts A/B/C, 134: 103597.

Mutlu, E., Arslan, N., Tokatlı, C., 2021a. Water quality assessment of yassialan dam lake (Karadeniz Region, Turkey) by using principle component analysis and water quality index. Acta Scientiarum Polonorum-Formatio Circumiectus, 20 (2): 55–65.

Mutlu, E., Arslan, N., Tokatlı, C., 2021b. Assessing water quality of boyali dam lake (Sinop, Turkey) by using ecological and statistical indicators. Acta Scientiarum Polonorum-Formatio Circumiectus, 20 (1): 77-85.

Tokatlı, C., 2017. Bio – ecological and statistical risk assessment of toxic metals in sediments of a worldwide important wetland: Gala Lake National Park (Turkey). Archives of Environmental Protection, 43 (1): 34-47.

Tokatlı, C., 2018. Essential and toxic element bioaccumulations in fishes of Gala and Siğirci Lakes (Meriç River Delta, Turkey). Acta Alimentaria, 47 (4): 470-478.

Tokatlı, C., Islam, A.R.M.T., Onur, Ş.G., Ustaoğlu, F., Islam, M.S., Dindar, M.B., 2022. A pioneering study on health risk assessment of fluoride in drinking water in Thrace Region of northwest Türkiye. Groundwater for Sustainable Development, 19: 100836.

Tokatlı, C., Uğurluoğlu, A., Muhammad, S., 2023. Ecotoxicological evaluation of organic contamination in the world's two significant gateways to the Black Sea using gis techniques: Turkish Straits. Marine Pollution Bulletin, 194: 115405.

Tokatlı, C., Varol, M., Uğurluoğlu, A., 2024. Ecological risk assessment, source identification and spatial distribution of organic contaminants in terms of mucilage threat in streams of Çanakkale Strait Basin (Türkiye). Chemosphere, 353: 141546.

Tokatlı, C., Ustaoğlu, F., Muhammad, S., Yüksel, B., Gülbaşı, A., Özmen, İ., Yoşumaz, İ., Manav, İ., 2025. Spatial-temporal variations of inorganic contaminants and associated risks for sediment of felent stream basin flowing along with silver mines in the midwestern Türkiye. Soil

and Sediment Contamination: An International Journal, https://doi.org/10.1080/15320383.2025.2464153.
TSWQR, 2021. (Turkish surface water quality regulation) (2021). Turkish Surface Water Quality Regulation. Türkiye.
Ustaoğlu, F., İslam, S., Tokatlı, C., 2022. Ecological and probabilistic human health hazard assessment of heavy metal in Sera Lake Nature Park sediments (Trabzon, Turkey). Arabian Journal of Geosciences, 15: 597.
Varol, M., Tokatlı, C., 2021. Impact of paddy fields on water quality of Gala Lake (Turkey): an important migratory bird stopover habitat. Environmental Pollution, 287: 117640.

INTEGRATION of RAINWATER HARVESTING (RWH) in INDUSTRIAL ZONES: POTENTIAL, TECHNICAL ANALYSIS, and REGULATORY FRAMEWORKS

Deniz Dolgen[1], Tamer Atabarut[2] and M. Necdet Alpaslan[3]

[1]Dokuz Eylul University, Faculty of Engineering, Department of Environmental Engineering, Buca, Izmir, Türkiye
[2] Boğaziçi University, Institute of Environmental Science, 34342, Bebek, Istanbul, Türkiye
[3]MNA Engineering & Consultancy, Izmir, Turkiye
Corresponding author e-mail: deniz.dolgen@deu.edu.tr

ABSTRACT

Climate change has been reshaping the management of water resources, requiring a shift towards sustainable and resilient infrastructure. Traditional cistern systems for collecting and storing rainwater, which were once widespread across Anatolia and beyond, are now re-emerging as decentralized solutions to strengthen regional water security. Rainwater harvesting (RWH) systems can be implemented in a variety of settings, including residential buildings, housing complexes, shopping centers, sports centers, hospitals, military bases and car parks. Industrial facilities offer particularly significant potential for RWH due to their extensive rooftop areas and substantial demand for non-potable water, such as process water, cooling water and rinsing water.

Recent legislative developments in Türkiye, including amendments to Planned Areas Construction Regulation and the Water Efficiency Regulation, have established a more supportive regulatory framework for the implementation of these systems. Therefore, it is expected that the use of these technologies in urban and industrial areas in Turkey will increase in the near future. The present study investigates the technical potential and economic feasibility of RWH in an Organized Industrial Zone (OIZ) in İzmir. The study examined 22 pilot enterprises and classified them into groups according to their water consumption patterns and the relationship between water demand and rainwater availability. Based on rooftop areas and long-term local rainfall data, the potential volume of harvestable rainwater was estimated, and appropriate cistern capacities were determined by considering the temporal variation in rainfall and water demand. The required capital investment costs and economic payback periods were subsequently evaluated to demonstrate that decentralized RWH provides a practical, cost-effective, and climate-resilient approach to supporting sustainable industrial water management practices.

Keywords: Rainwater Harvesting, Water Scarcity, Organized Industrial Zones, Water Efficiency, Industrial Water Management; Climate Resilience

INTRODUCTION

Accelerated climate change, increasing drought frequency, and rapid urbanization are placing growing pressure on freshwater resources and intensifying water scarcity worldwide. As conventional centralized water management strategies have become increasingly inadequate and costly, the integration of decentralized and locally available water sources has become imperative. Although the collection and storage of rainwater in cisterns has been practiced for centuries globally, including in Anatolia, these traditional systems were progressively abandoned during the rapid expansion of centralized water infrastructure in the mid- to late

twentieth century. Traditional cistern systems were largely replaced by centralized, large-scale networks designed to convey water over long distances from major dams, lakes and aquifers. Today, however, increasing water demand, severe drought conditions, rising infrastructure costs, and the energy intensity of centralized water supply systems are contributing to renewed interest in rainwater harvesting (RWH) as a resilient and sustainable water management strategy (Avila et. al., 2023) Consequently, the ancient practice of rainwater harvesting is re-emerging as a decentralized alternative with the potential to provide reliable, sustainable and potentially more cost-effective water supplies.

The implementation of rainwater harvesting (RWH) systems in Türkiye has undergone a significant transformation, driven primarily by a transition from voluntary environmental practices toward increasingly comprehensive regulatory requirements. Key legislative and policy instruments include the Planned Areas Construction Regulation (2022), the Water Efficiency Strategy Document and Action Plan 2023–2033 (2022), and the Water Efficiency Regulation (2024). Among these, the most direct regulatory action came in the form of amendments to the Planned Areas Construction Regulation, issued by the Ministry of Environment, Urbanization and Climate Change. According to this regulation, buildings constructed on parcels of land exceeding 2,000 m^2 must legally incorporate rainwater collection systems. Collected roof runoff must be directed to cisterns for non-potable uses, primarily for landscape irrigation, toilet flushing and general maintenance. The regulation empowers local municipalities to extend such requirements to smaller parcels or specific categories of buildings, including shopping centers, commercial centers and housing complexes, depending on local water conditions.

The National Water Efficiency Strategy Document and Action Plan 2022-2023 also identifies rainwater harvesting as an important measure for reducing water consumption in buildings and industrial facilities. Furthermore, the Water Efficiency Regulation issued by the Ministry of Agriculture and Forestry in December 2024, established a regulatory framework for the targets of urban, agricultural, and industrial areas. Within this framework, rainwater is recognized as an unconventional water source, while rainwater harvesting is identified as a fundamental strategy for reducing freshwater consumption in industrial facilities. Accordingly, the implementation of rainwater harvesting practices has been included among the priority criteria considered within the water efficiency certification framework for industrial enterprises to obtain blue, green or turquoise water efficiency certifications. These developments indicate that RWH is increasingly being positioned not only as an environmental initiative but also as an element of Türkiye's emerging water-efficiency policy framework.

A typical rainwater harvesting system comprises four fundamental components: a catchment surface; a conveyance system; storage infrastructure; and where required, treatment facilities (Dolgen et al., 2006). Rooftops generally constitute the primary catchment surface, although ground catchments may also be used. The quantity and quality of harvested water are influenced by effective catchment area, surface characteristics, and roofing materials. While most roofing materials are suitable for non-potable applications, materials or components that may release harmful substances, such as certain asphalt shingles, toxic sealants, or lead flashing must be avoided, particularly when targeting higher water quality or potable end-uses, to prevent heavy metal leaching and chemical contamination. The conveyance network, consisting primarily of gutters, drainpipes, and connecting pipelines, transports runoff from the catchment surface to the storage facility. To preserve water quality, these components must be made of durable, non-corrosive, and chemically inert materials such as high-density polyethylene (HDPE), stainless steel or coated aluminum (Thomas and Martinson, 2007). In practical applications, conveyance systems should also integrate a first-flush diverter or secondary debris screen to prevent the initial runoff, which may contain accumulated atmospheric dust, organic debris, bird droppings and other contaminants, from entering the storage tank.

Harvested rainwater is generally stored in above-ground, or underground cisterns constructed from structurally sound, non-reactive materials such as reinforced concrete, fiberglass, or stainless steel. Underground tanks can typically provide advantages in terms of space optimization and thermal stability; whereas above-ground installations reduce excavation requirements and facilitate inspection and maintenance, and utilize gravity-fed distribution. Storage tanks may either be integrated into a building or built as separate structures. Among the various design parameters of an RWHS, the storage capacity is one of the most critical hydraulic and economic design variables. Insufficient storage capacity may result in water shortages during low-rainfall periods, while excessive capacity increases construction and operating costs, potentially making the system economically unfeasible (Dolgen and Alpaslan, 2025). Therefore, optimal cistern sizing requires a balance among local rainfall characteristics, temporal rainfall variability, catchment area and runoff yield, and baseline non-potable water demand patterns.

Against this background, Organized Industrial Zones (OIZs) represent a particularly promising setting for the implementation of RWHSs. The extensive roof areas of industrial facilities can provide substantial catchment surfaces, while many industrial activities have significant demands for water that does not necessarily require potable quality. Consequently, the utilization of harvested rainwater for appropriate non-potable applications may reduce dependence on centralized freshwater supplies, improve water efficiency, and enhance the climate resilience of industrial facilities. However, the technical and economic potential of RWH in OIZs remains insufficiently explored in Türkiye.

Therefore, this study investigates the technical potential, practical applicability, regulatory framework, and economic feasibility of implementing RWHSs in selected industrial facilities within an OIZ in Türkiye. The study estimates the volume of rainwater that can potentially be harvested from the rooftop areas of selected enterprises, determines appropriate cistern capacities by considering both water availability and its temporal variability, and evaluates the associated investment costs and economic payback periods. The findings are intended to contribute to the development of decentralized, water-efficient, and climate-resilient water management strategies for industrial areas in Türkiye.

MATERIAL AND METHOD

Study Area and Data Collection

This study examines the potential for rainwater harvesting (RWH) in an Organized Industrial Zone (OIZ) located in Izmir, Turkiye. In the examined OIZ, there are 106 companies, of which 68 of which were active at the time of the study. The enterprises operate across a range of industrial sectors including food; packaging; electricity; energy; construction; chemicals; machinery; furniture; automotive; plastics; textiles; medical devices and materials; tobacco; agricultural machinery, and feed and feed additives.

Data on the water consumption and water allocation within the OIZ, including the sources and volume of water used, existing water conservation practices and current rainwater management practices, was collected by means of questionnaires and on-site investigations. The survey and field investigations were used to characterize the water-use profile of the enterprises and to identify facilities with potential for rainwater harvesting.

The food sector is the most water-intensive industry in the OIZ, accounting for 93% of total water consumption. The packaging and automotive sectors accounted for 4.5% of total water use. While the remaining 2.5% was used enterprises operating in other sectors, including construction, chemicals, machinery, furniture, textiles, medical devices, tobacco, feed, and agricultural machinery.

Based on the availability of relevant data and the characteristics of the facilities, the potential for rainwater harvesting was investigated in 22 enterprises operating in the food, construction, chemicals, medical devices, materials, plastics, tobacco, feed and packaging sectors. For these enterprises, rooftop areas and other relevant characteristics were obtained and used to estimate the potential volume of harvestable rainwater and the required storage capacity.

Rainfall Analysis

Monthly rainfall data for the period 1938–2020, representing 82 years of observations, were obtained from the Turkish State Meteorological Service (MGM) for İzmir Province. The long-term dataset was used to characterize the temporal distribution of rainfall and to estimate the potential availability of rainwater for harvesting.

The analysis, summarized in Table 1, shows that the region receives an average annual rainfall of 569.6 mm. As Table 1 illustrates, rainfall is at its highest in December, with 100.1 mm, while August receives the lowest amount, with only 1.6 mm. This pronounced seasonal variation is particularly important for the design of rainwater storage systems, as annual rainfall totals alone do not adequately represent the temporal availability of harvested water.

Table 1. **Long-term average precipitation and number of rainy days in İzmir Province (1938–2020)**

Month	**January**	**February**	**March**	**April**	**May**	**June**
Average Monthly Rainfall (mm)	86.9	77.8	64.8	57.1	27	10.4
Month	**July**	**August**	**September**	**October**	**November**	**December**
Average Monthly Rainfall (mm)	5.3	1.6	15.9	34.7	88	100.1

Source: Turkish State Meteorological Service (MGM) (https://www.mgm.gov.tr/veridegerlendirme/il-ve-ilceler-istatistik.aspx?k=undefined&m=IZMIR)

Estimation of Harvestable Rainwater

In the presented study, the volume of the harvested rainwater from a rooftop was calculated using the standard catchment area formulation. The method calculates overall yield by integrating the roof surface area, localized meteorological data (annual rainfall), and a material efficiency factor (runoff coefficient).

Harvestable water volume (m^3) = Catchment area (m^2) x Annual rainfall (m) x Runoff Coefficient

The catchment area represents the total surface area of the rooftop available for rainwater collection, was obtained from the participating enterprises. The precipitation data represent the long-term local rainfall characteristics of İzmir and were obtained from the Turkish State Meteorological Service. Finally, the runoff coefficient accounts for hydrological losses associated with the catchment surface including surface retention, evaporation, leakage, and splash-over. The runoff coefficient, ranged between 0 and 1, depends primarily on the type, slope, porosity, and surface characteristics of the roof. Impermeable and relatively smooth materials like corrugated sheet metal roofing generally have high efficiency, yielding coefficients between 0.90 and 0.95 due to rapid water shedding. Conversely, porous or rough surfaces such as flat concrete or asphalt shingles retain more moisture, reducing the coefficient to a range between 0.60 and 0.80. In this study, value of C = 0.80 was applied for all cases. This assumption reflects the semipermeable nature of industrial rooftop surfaces while providing a consistent basis for comparison among the selected enterprises.

Cistern Sizing and Temporal Water Balance

Although annual rainfall provides an estimate of the overall rainwater harvesting potential, annual totals alone are insufficient for determining an appropriate cistern capacity because rainfall and water demand vary substantially throughout the year. Therefore, the sizing of the storage systems was based on the monthly distribution of rainfall and the corresponding availability of harvested rainwater.

For each enterprise, the monthly rainwater yield was estimated using the effective rooftop area, monthly precipitation, and the runoff coefficient. The resulting monthly water availability was compared with the estimated non-potable water demand of the enterprise. This approach was used to determine the storage capacity required to maximize the utilization of harvested rainwater while avoiding unnecessary oversizing of the cistern.

The optimal cistern capacity was therefore determined by considering both the volume of harvestable rainwater and its temporal variability. Overall, the findings demonstrate that **RWH in OIZs should be evaluated as an integrated technical, economic, and regulatory water-efficiency measure rather than solely on the basis of annual rainfall or rooftop area.** Appropriately designed RWH systems can reduce dependence on centralized freshwater supplies, improve industrial water efficiency, and contribute to greater climate resilience. The combination of increasing regulatory support and favorable economic conditions in high-water-demand facilities provides a strong basis for expanding RWH applications in OIZs and other industrial areas in Türkiye.

Economic Assessment

The economic feasibility of the proposed RWH systems was assessed based on the estimated investment cost of the required infrastructure and the expected water savings resulting from the substitution of harvested rainwater for conventionally supplied water. The investment assessment included the principal components required for implementation, such as storage tanks, conveyance infrastructure, pumps, and associated system components, as applicable.

The simple economic payback period was estimated by comparing the initial investment cost with the expected annual monetary savings associated with the use of harvested rainwater. The resulting payback periods were used to assess the economic feasibility of RWH implementation across the selected enterprises.

RESULTS AND DISCUSSION

Rainwater Harvesting Potential of the Pilot Enterprises

In this study, the rainwater harvesting potential was assessed for 22 companies selected from the OIZ as pilots. The enterprises were first classified according to their annual water consumption into three categories: high water consumption (> 50,000 m^3 / year), medium water consumption (5,000 - 50,000 m^3 / year), and low water consumption (< 5,000 m^3 / year). The annual water consumption of the 22 enterprises is presented in Figure 1, while Figure 2 presents the corresponding estimated annual volumes of rainwater that can potentially be harvested from their rooftop areas.

The comparison of water demand and rainwater availability was subsequently conducted using monthly water consumption and rainfall data. Based on the relationship between the temporal distribution of water demand and the potential availability of harvested rainwater, the 22 enterprises were classified into five groups (Groups A–E). One representative enterprise from each group was then selected for a more detailed assessment of cistern requirements and economic feasibility.

Group A consists of enterprises with a particularly high monthly water consumption, which consistently exceeds the amount of rainwater that can be harvested on both monthly or annually basis. This group comprises nine enterprises, including a dairy and dairy-products facility; frozen or dried fruit and vegetable processing facilities; packaging manufacturers producing carton boxes and cardboard products; a ready-mixed concrete production facility; and enterprises producing construction chemicals and textile chemicals.

Group B comprises four enterprises with relatively stable monthly water consumption, for which monthly fluctuations in water consumption can be negligible, and the quantity of rainwater that can be harvested may be more or less than required from one month to the next. This group includes enterprises in the feed and feed additives industry, chemical industry (concrete chemical additives and subsurface concentrated fertilizers) and the medical equipment industry (plastic medical supplies).

Group C includes three enterprises where monthly variations in water usage can be considered significant, and the amount of rainwater available for harvesting may be more or less than needed from month to month. This group includes enterprises in the construction sector of pipe fittings and accessories, and thermal insulation materials, and in the chemical industry.

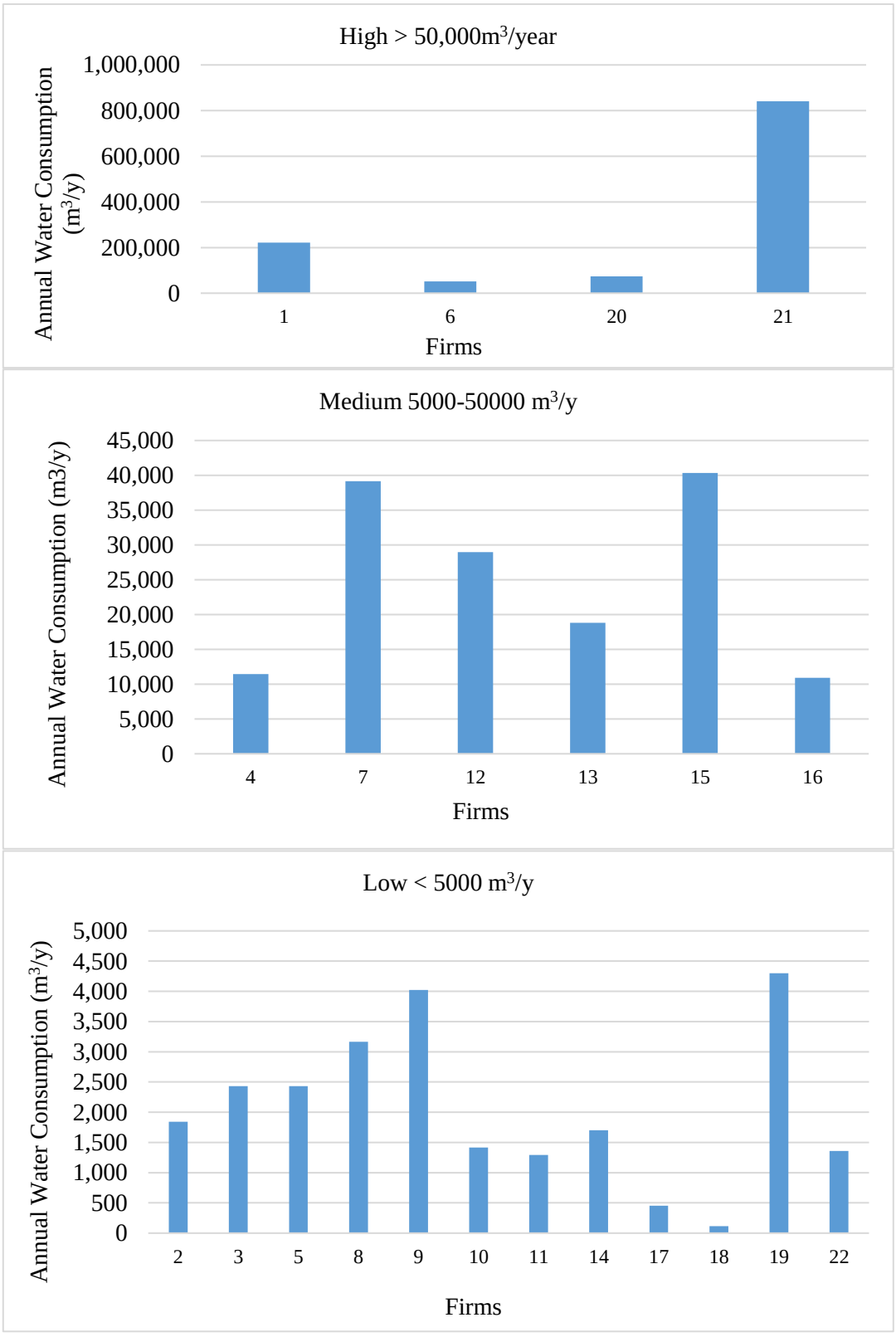

Figure 1. Annual water consumptions of 22 pilot enterprises

Group D comprises five enterprises with pronounced seasonal variations in water consumption, characterized generally by lower demand during winter and higher demand during summer. As in Groups B and C, the relationship between rainwater availability and water demand varies from month to month. This group includes medical supplies production, food

industry (dried fruit and vegetable manufacturing), tobacco and tobacco products manufacturing, plastic industry (plastic recycling, packaging crate production), and feed and feed additives.

Group E consists of enterprises with very low or negligible water consumption. Only one enterprise, a manufacturer of polypropylene (PP) plastic yogurt containers, was classified in this group.

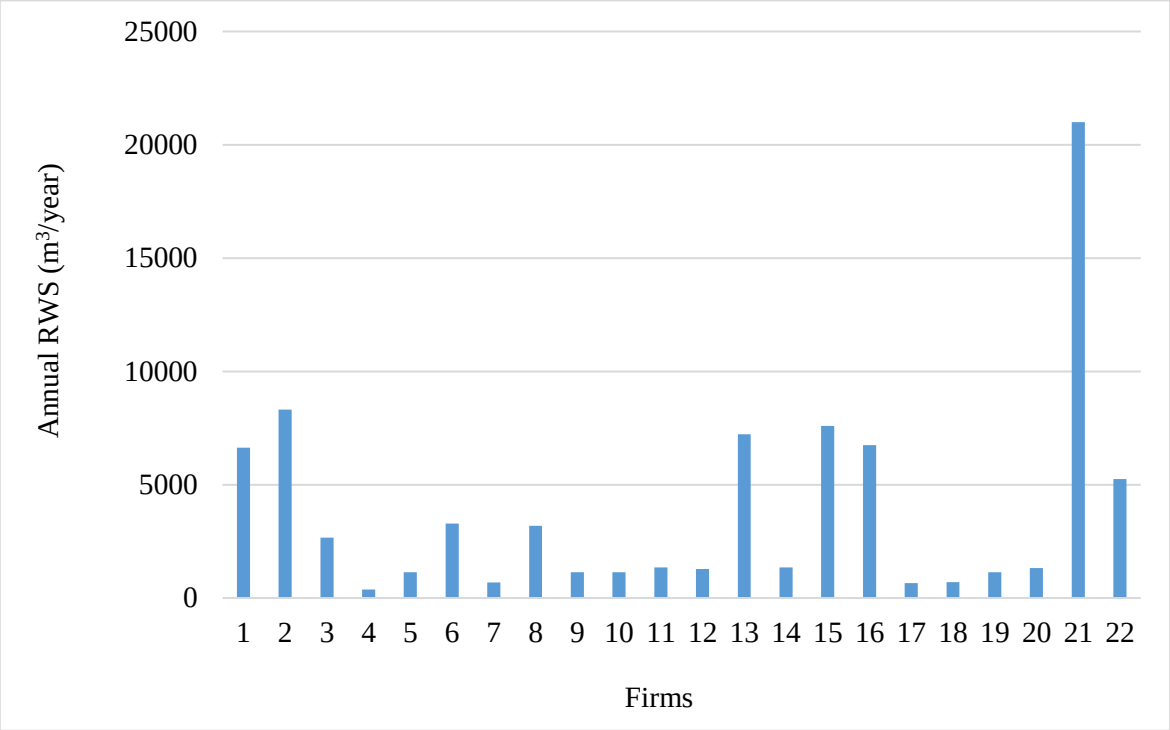

Figure 2. Estimated annual rainwater harvesting potential of the 22 enterprises

The classification demonstrates that the feasibility and potential benefits of RWH are strongly influenced not only by the annual volume of harvestable rainwater but also by the relationship between rainwater availability and the temporal pattern of water demand. Accordingly, the enterprises in Groups A–D were considered suitable for further assessment of storage requirements and economic feasibility, whereas the Group E enterprise was excluded from detailed cistern analysis because of its negligible water consumption.

Cistern Sizing and Economic Feasibility

Long-term monthly average rainfall data were obtained from the meteorological station in Izmir. The volume of harvestable rainwater from roof areas was calculated using the standard catchment area formulation. For the enterprises in Groups A–D, the potential volume of harvestable rainwater was estimated using the long-term monthly rainfall data for İzmir and the effective rooftop areas of the facilities. Monthly rainwater availability was compared with the corresponding water demand of each enterprise to assess the need for storage and to determine an appropriate cistern capacity.

A comprehensive market survey was conducted to determine the prevailing prices of equipment and tanks. The estimated investment cost included the principal collection and transmission equipment, including pumps and internal piping, in addition to the cistern construction cost. Economic feasibility was assessed using the simple payback period calculated as the total initial investment divided by the estimated annual financial savings resulting from the use of harvested rainwater.

The results indicate that RWH systems are particularly advantageous for facilities with high water demand, where monthly or annual consumption substantially exceeds the capacity of rainwater harvesting. For these facilities, harvested rainwater can generally be used relatively quickly, thereby reducing the need for very large storage volumes. The payback periods for such investments have been calculated to range from 1 to 4 years. Based on these results, a more detailed technical and economic assessment was conducted for Firm 1 (F1), selected as a representative Group A enterprise in this study.

Case Study

The Firm 1 (F1) is a dairy and dairy products manufacturing facility located within the OIZ, and is characterized by relatively high water consumption. The facility has a total rooftop area of approximately 15,000m^2. In order to ascertain the optimal cistern volume, the monthly water consumption data were obtained from the company. Furthermore, the rainwater harvesting potential from the roof area was calculated based on the rainfall data obtained from the Turkish State Meteorological Service website.

Figure 3 illustrates the data regarding water consumption and rainwater harvesting potential for F1. The results show that the company's monthly water demand consistently exceeds maximum harvestable rainwater volumes, ensuring that harvested rainwater can be utilized relatively rapidly without requiring long-term storage.

As demonstrated in the data given in Table 1, the maximum precipitation levels are recorded in December, with a monthly volume of 1,116 m^3. It is estimated that, based on the average number of rainy days per month, the peak daily collection is 93 m^3/day. Accordingly, a cistern with a capacity of approximately 100 m^3 provides adequate daily storage to capture maximum single-day runoff events. Because the firm's monthly water demand consistently exceeds the estimated monthly rainwater harvesting potential, harvested rainwater can be readily utilized without requiring substantial seasonal storage. Accordingly, the required storage capacity is primarily determined by short-term rainfall variability and system operation rather than by the need to bridge prolonged periods of insufficient water demand.

The annual harvest calculations indicate that the capture and utilization of 6,643 m^3 of rainwater per annum is achieved by a 100 m^3 reinforced concrete cistern. The annual water cost savings have been estimated to be 17,936 TL, with this calculation taking into account the water tariff of OIZ. The capital investment required for the construction of the cistern was determined as 65,000 TL, and the estimated payback period was approximately 3.6 years.

These results indicate that the implementation of an appropriately sized RWH system at F1 can provide a substantial reduction in the facility's dependence on externally supplied water while requiring a relatively moderate initial investment. The relatively high water demand of the facility is an important factor contributing to the economic feasibility of the system.

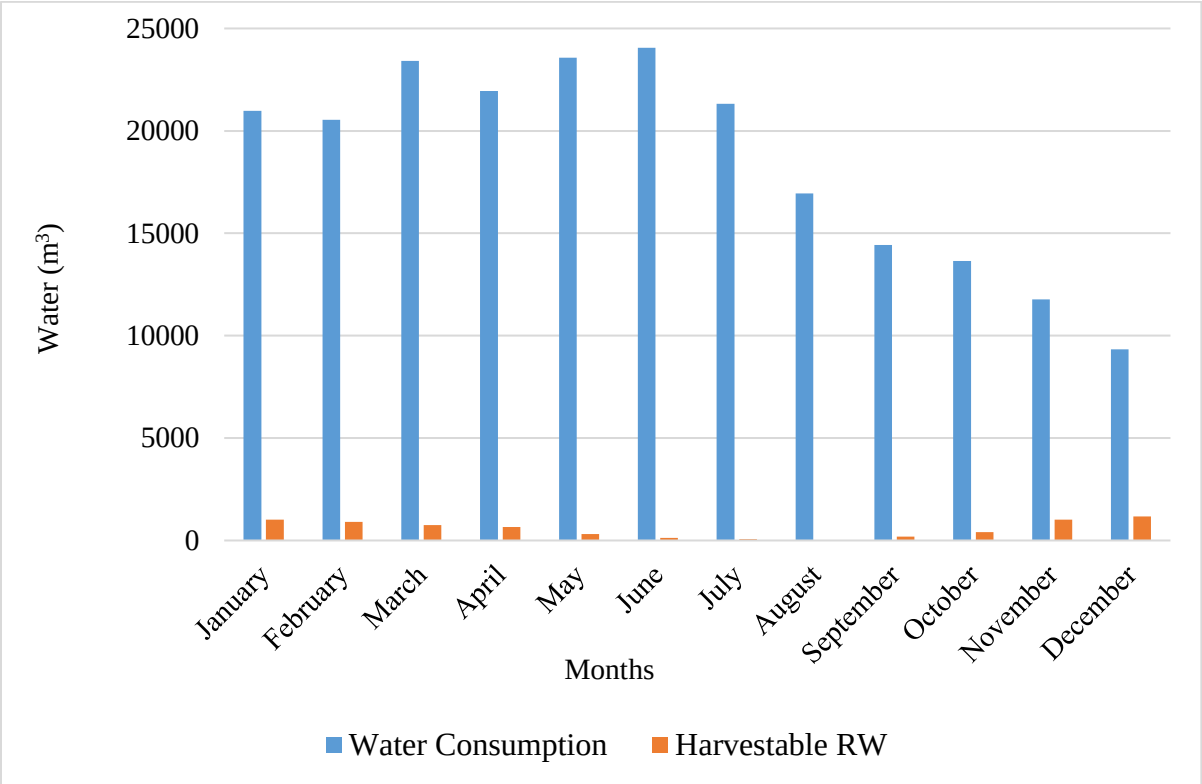

Figure 3. Monthly water consumption and estimated rainwater harvesting potential for Firm 1

Comparative Assessment of the Five Enterprise Groups

The analysis of 22 pilot enterprises across five distinct water-consumption profiles (Groups A through E) demonstrates that the technical and economic feasibility of RWH varies significantly depending on water demand and operational patterns. Facilities with high water demand, which consistently exceed harvestable rainfall volume (e.g., dairy, frozen fruit/vegetable processing, packaging, chemical, and ready-mixed concrete manufacturing), demonstrate the highest return on investment from rainwater harvesting. The estimated payback period for these facilities is remarkably short, ranging between 1 and 4 years (Group A).

In instances of enterprises encountering seasonal or monthly fluctuations in water consumption, the implementation of cisterns, exactly tailored to their unique demands and local rainfall patterns, is imperative to ensure the effective balancing of supply and demand (Group B, C, D). In these cases, an appropriately sized cistern can provide an important function by storing water during periods of relatively high rainfall and making it available during periods when rainfall is insufficient to meet demand. However, excessive storage capacity would increase capital costs without necessarily providing a corresponding increase in water savings. Therefore, storage capacity should be determined individually for each facility by considering rooftop area, local rainfall characteristics, water demand, and its temporal variability.

In contrast, it was determined that enterprises characterized by negligible water consumption do not yield a practical return on investment for RWH infrastructure (Group E). The limited volume of water that could be economically substituted by harvested rainwater would not justify the investment required for dedicated storage and associated infrastructure.

Overall, the findings demonstrate that the economic feasibility of RWH in industrial facilities depends not only on the physical potential for rainwater collection but also on the magnitude

and temporal pattern of water demand. This highlights the importance of demand-oriented system design rather than relying solely on annual rainfall or rooftop area when determining the feasibility and storage requirements of RWH systems in OIZs.

CONCLUSIONS

Türkiye has initiated a significant transition in its approach to rainwater harvesting (RWH) strategy, moving from predominantly voluntary environmental practices toward a mandatory regulatory requirement. Key legislative and policy instruments, including amendments to the Planned Areas Construction Regulation (mandating RWH for plots over 2,000 m²), the National Water Efficiency Strategy Document and Action Plan (2023–2033), and the December 2024 Water Efficiency Regulation, have strengthened the role of RWH in reducing freshwater consumption for non-potable water uses in buildings and industrial facilities. Furthermore, the integration of RWH into industrial water efficiency certification (Blue, Green, and Turquoise) provides a clear framework for sustainable industrial growth.

An empirical evaluation of 22 pilot companies across five water-consumption profiles (Groups A–E) reveals that the technical and economic feasibility of RWH depends strongly on the magnitude and temporal pattern of water demand, as well as on the available rooftop area and local rainfall characteristics. The results indicate that RWH is particularly promising for facilities with high and relatively continuous water demand, where harvested rainwater can be utilized rapidly and the need for extensive seasonal storage is reduced. For the Group A enterprises investigated in this study, estimated payback periods ranged from approximately 1 to 4 years, indicating favorable economic conditions for RWH investment under the assumptions adopted.

The detailed assessment of Firm 1 further demonstrates the importance of appropriately sizing storage capacity. Despite the facility's substantial water demand, which consistently exceeds its monthly rainwater harvesting potential, a 100 m³ reinforced-concrete cistern was found to be sufficient under the conditions considered. The system was estimated to capture and utilize approximately 6,643 m³ of rainwater annually, generating estimated annual water-cost savings of 17,936 TL and a simple payback period of approximately 3.6 years.

For facilities with moderate, variable, or seasonal water demand, the feasibility of RWH is more dependent on the temporal balance between rainwater availability and water consumption. In such cases, cistern capacity should be determined through a facility-specific monthly water supply–demand analysis that considers local rainfall patterns, rooftop area, non-potable water demand, and investment costs. Conversely, facilities with negligible water consumption may not provide sufficient demand to justify investment in dedicated RWH infrastructure.

Overall, the findings demonstrate that **RWH in OIZs should be evaluated as an integrated technical, economic, and regulatory water-efficiency measure rather than solely on the basis of annual rainfall or rooftop area.** Appropriately designed RWH systems can reduce dependence on centralized freshwater supplies, improve industrial water efficiency, and contribute to greater climate resilience. The combination of increasing regulatory support and favorable economic conditions in high-water-demand facilities provides a strong basis for expanding RWH applications in OIZs and other industrial areas in Türkiye.

REFERENCES

Avila, F.G. Su´arez, M.G., Galarza, J.G., Torres, R.C., Gonzales, L.V., 2023. Rainwater harvesting and storage systems for domestic supply: An overview of research for water scarcity management in rural areas. *Results in Engineering* 18 (2023) 101153

Dolgen, D., Baban, A., Alpaslan, M.N., (2006). Use of rainwater cistern systems (RWCS) as an alternative for freshwater augmentation. Sustainable Water Management, 1, 11-13.
Dolgen, D., Alpaslan, M.N. (2025). Evaluation of the potential for rainwater harvesting in the agro-industry: A case study of the table olive industry. VII. International Conference on Agriculture, Biology & Life Sciences, September 07-10, 2025, Istanbul, Türkiye (In Proceeding Book p.1447-1452).
Official Gazette on Regulation on Planned Areas Construction Regulation, 2022, Numbered 32060. https://www.resmigazete.gov.tr/eskiler/2022/12/20221231-2.htm.
Official Gazette on Regulation on Water Efficiency Regulation, 2024, Numbered 32765. https://www.resmigazete.gov.tr/eskiler/2024/12/20241227-3.htm
Thomas, T.H. and Martinson, D.B. 2007. Roofwater Harvesting: A Handbook for Practitioners. Delft, The Netherlands, IRC International Water and Sanitation Centre. (Technical Paper Series; no. 49). 160 p.
Turkish State Meteorological Service (MGM). https://www.mgm.gov.tr/veridegerlendirme/il-ve-ilceler-istatistik.aspx?k=undefined&m=IZMIR)
Water Efficiency Strategy Document and Action Plan (2023–2033), 2022. Republic of Türkiye Ministry of Agriculture and Forestry - General Directorate of Water Management. https://cdniys.tarimorman.gov.tr/api/File/GetGaleriFile/502/DosyaGaleri/7970/suverimliligi_ep_ing_web091124.pdf.

OPTIMIZING COMBUSTION EFFICIENCY AND EMISSION CONTROL IN LOW-NO_x GAS BURNERS WITH HYDROGEN-BLENDED NATURAL GAS COMBUSTION

Onur Salcı[1], Semiha Öztuna[2]
[1 2] Trakya University, Edirne, Türkiye
Corresponding author e-mail: onursalci76@trakya.edu.tr

ABSTRACT

Green energy usage and the lowest pollutant emission demand of fire-tube hot water boilers have gained importance in line with the 2050 European zero-carbon targets. In the present study, the combustion efficiency of a low NO_x gas burner was increased by using a prototype diffuser and natural gas hydrogen blended fuel ratios. Experimental studies were conducted using a fire tube hot water boiler system, while numerical simulations were performed using Fluent codes with methane (CH_4) representing natural gas. Three combustion models were the Eddy Dissipation Model (EDM), Non-Premixed Combustion (NPC), and the Partially Premixed Combustion (PPC) model, which were compared, and the PPC model was validated against experimentally measured values for 1500 kW heat input, natural gas fuelled, and 0.85 equivalence ratio. PPC combustion model and experimental studies were performed to investigate the variations in temperature, velocity, emissions, pollutants, temperature, flame formation, and stability for hydrogen ratios from 0 to 40% with equivalence ratios ranging from 0.7 to 0.85 at a heat input of 1500 kW. The results showed that blending hydrogen into natural gas fuel reduced CO_2 emissions by approximately 16.43% at 40% hydrogen. O_2 emissions remained constant, and NO_x pollutants reduced below 38 ppm at 3% O_2 emissions. Hydrogen also improved flame stability and increased flame temperature, velocity, and pressure, though density decreased. NO formation rose with increased hydrogen blending, necessitating higher air excess to control NO pollutant and flue gas temperatures. The study concludes that low NO_x gas burners with nozzle-mix combustion flame characteristics can safely operate with up to 40% hydrogen blending in natural gas for fire-tube hot water boilers, following safety guidelines, offering a potential pathway for industrial decarbonization.

Keywords: NO_x Reduction, Combustion Efficiency, Hydrogen, Decarbonization, Nozzle-mix burner

INTRODUCTION

The decarbonization of industrial heating systems requires hydrogen compatible combustion technologies that provide safe operation, high efficiency, and low pollutant emissions. Hydrogen and natural gas blended gas fuelled burners can be used as an alternative application for the decarbonization of industrial boilers and furnaces. Recent studies have focused on different fuelled industrial burners capable of operating over different range of hydrogen ratios. Recent studies of hydrogen–methane mixtures indicate that, although industrial burners are often reported to accommodate blends containing up to 20% hydrogen, the empirical and theoretical evidence supporting this level of integration remains inconsistent (Franco & Rocca, 2024a, 2024b). Sîrbu et al. (2026) reviewed the combustion characteristics of hydrogen enriched natural gas in residential appliances, with particular attention to safety, efficiency, emissions, flame stability, and flashback. safe hydrogen integration requires appropriate blending limits, burner design modifications, and operating strategies. Conversely, recent

computational fluid dynamics simulations indicate that moderate hydrogen enrichment can effectively reduce carbon monoxide and unburned hydrocarbon emissions, although this often comes at the cost of higher NOx formation depending on the specific boiler load and equivalence ratio (Wang et al., 2025), (Badakhsh & Bhagavathy, 2023). Büyükakın (2026) numerically investigated hydrogen-enriched methane combustion in a non-premixed tube burner under hot, highly diluted $CO_2/O_2/N_2$ oxidizer conditions. Hydrogen's physical effect on turbulent mixing was found to be more influential than its chemical effect under the investigated conditions. The study also reported that hydrogen enrichment did not increase NOx emissions under low-O_2 diluted combustion conditions.

Experimental studies of non-premixed, low-swirl burners show that adding hydrogen changes flame behaviour by shortening the flame's lift-off height, while increasing NOx emissions by up to 380% at higher blending levels (Gee et al., 2023). Experimental findings highlight that lean combustion strategies are essential for managing adiabatic flame temperatures when operating at high hydrogen concentrations, despite potential reductions in convective heat transfer efficiency (Odeh & Paul, 2023). Consequently, integrating hydrogen requires sophisticated burner management systems that can dynamically adapt to fluctuating fuel compositions to prevent combustion pressure oscillations (Zeng et al., 2023).

In the present study investigates a 1500 kW industrial low-NO_x gas burner using natural gas with 0-40% hydrogen by volume and equivalence ratios between 0.70 and 0.85. Experimental measurements were combined with CFD analyses to select a suitable combustion model, optimized diffuser geometry, and evaluate the effects of hydrogen blending and excess air on flame characteristics, CO_2 and NO emissions.

MATERIAL AND METHOD

Experimental Set-up and Operating Conditions

Combustion experiments were performed in a PLC-controlled boiler system (Figure 1) with separate natural-gas, pure-hydrogen and blended gas trains (Figure 3). Low NO_x gas burner was used as a test burner (Figure 2). Combustion air was supplied by the burner mounted fan, while fuel and air volumetric flow rates were measured using digital flow meters and adjusted through pneumatic modulating valves. Natural gas was supplied at 0 - 155 Nm^3/h with 300 mbar upstream pressure and 250-300 mbar downstream pressure. Hydrogen was supplied from a 200 L tank at 230 bar, reduced first to 4 bar and then to 300 mbar, with an adjustable flow range of 0 - 250 Nm^3/h. O_2, CO_2, NO and flue-gas temperature were measured at the flue outlet using a flue gas analyser (Figure 4).

Figure 1. PLC-controlled boiler system.

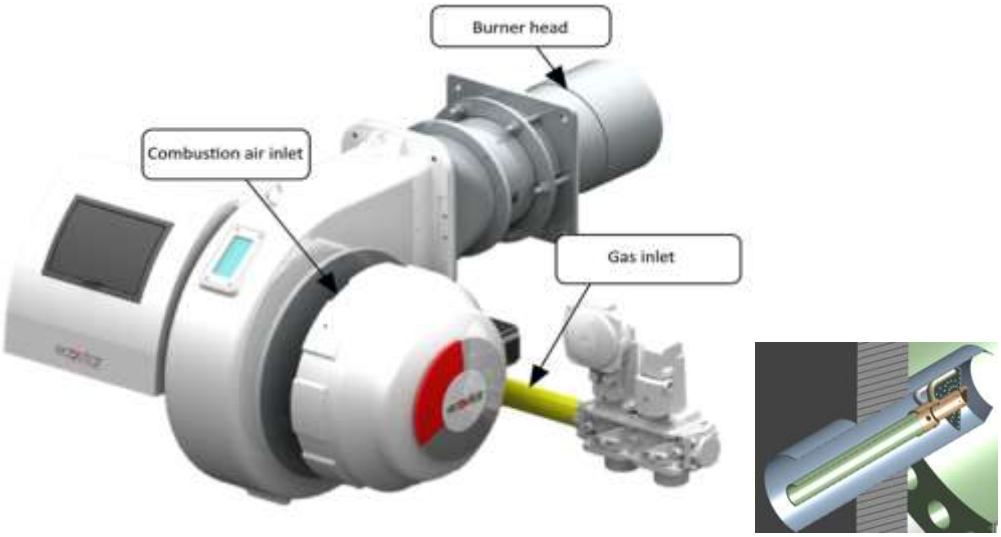

Figure 2. Low NO_x gas burner (New Generation Low NO_x Burners - Ecostar, n.d.) and it's diffuser and combustion head.

The combustion chamber had an inner diameter of 700 mm and a length of 3050 mm (Figure 4). The burner was operated at 1500 kW with equivalence ratios (φ) of 0.70, 0.77 and 0.85. Fuel cases included 100% natural gas, 70% NG/30% H_2 and 60% NG/40% H_2. Combustion-air and fuel temperatures were approximately 20 °C and 15 °C, respectively. Methane (CH_4) represented natural gas in the numerical calculations, and hydrogen purity was 99.99%.

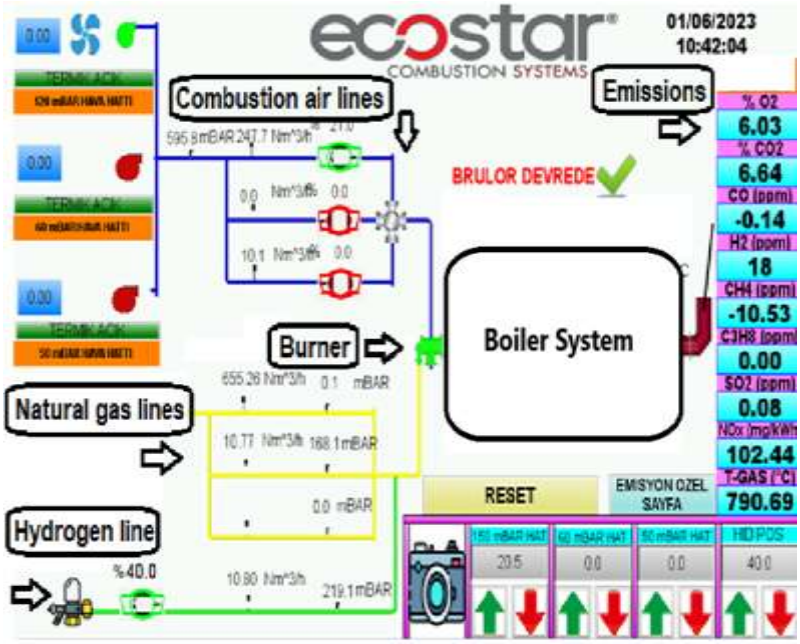

Figure 3. Schematic view of the PLC-controlled test boiler system

The technical specifications of the PLC controlled boiler system equipments (Table 1). All measured values were recorded on the PLC display and stored on the hard disk drive. The technical specifications of the PLC-controlled test furnace system equipments are detailed in Table 1. All measured data were monitored on the PLC display and stored on the hard disk drive

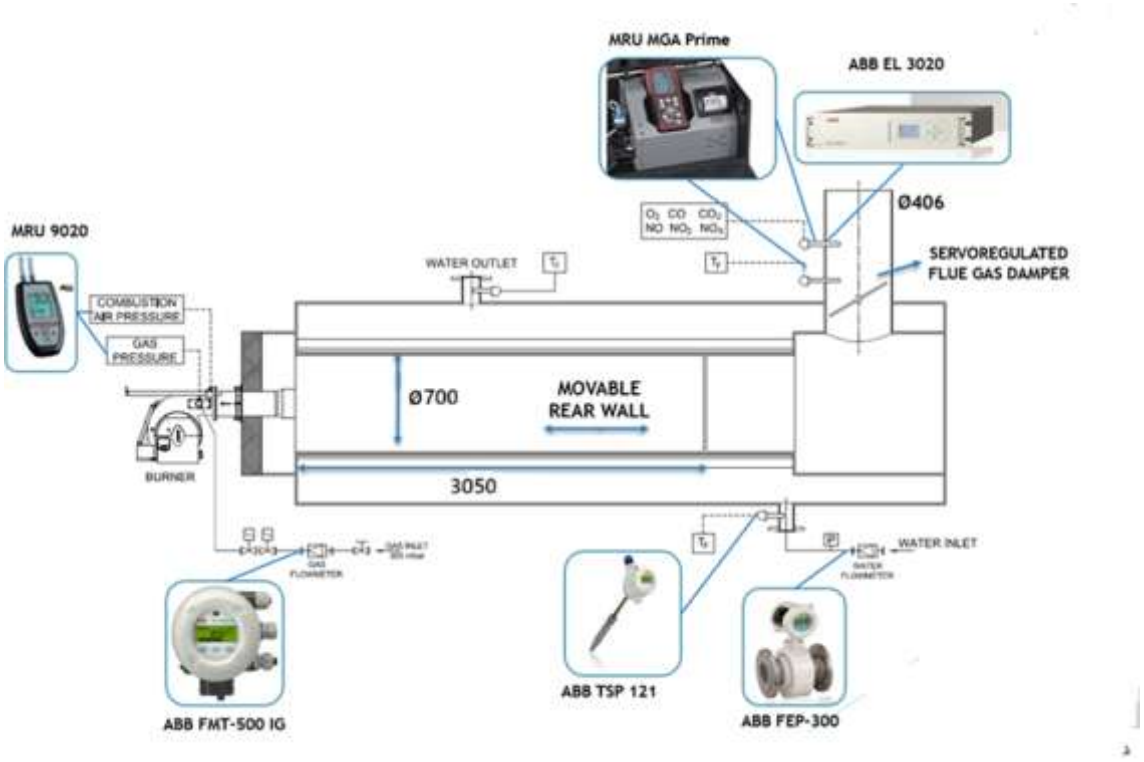

Figure 4. Schematic model of the boiler system and measurement devices.

Table 1. Technical specifications of measurement devices

Device	**Brand and Model**	**Parameters**	**Operation Range**	**Precision**
Flue gas analyser	MRU MGA Prime	O_2 CO_2 CO CH_4 C_3H_8 NO NO_2 N_2O Temperature	0…25 % 0…40 % 0…200 / 10.000 ppm 0…200 / 10.000 ppm 0…200 / 10.000 ppm 0…200 / 10.000 ppm 0…200 / 10.000 ppm 0…200 / 10.000 ppm 0…1200 °C	0.2 % ± 0.2 ppm -1 % ± 2 ppm - 1 % ± 2 ppm - 1 % ± 2 ppm - 1 % ± 2 ppm - 1 % ± 2 ppm - 1 % ± 2 ppm - 1 % ± 1°C or - 2 %
Natural gas flowmeter	CS Ins. – VA520	Nm³/h	5…450 Nm³/h	% 1.5
Hydrogen flowmeter	CS Ins. – VA520	Nm³/h	4…320 Nm³/h	% 1.5
Pressure Sensors	ATEK- BCT 22	mbar	0…400 mbar	± % 0.5 - ± % 0.3 T.S @ 25°C
Positioners	ROTORK – YT3300	°	0…90°	± 0.2 F.S. %
Actuators	TORK-RA	°	0…90°	± 5° Both sides

Natural gas fuel was supplied by Marmara Gaz Çorlu Doğal Gaz Dağıtım A.Ş. The natural gas composition is simplified (Figure 5). Methane gas (CH4) is the main type of natural gas. Therefore, CH_4 was considered for numerical calculations instead of natural gas. Hydrogen gas was supplied from Habaş Sınai ve Tıbbi Gazlar İstihsal Endüstri A.Ş. and has a purity level of 99.99%.

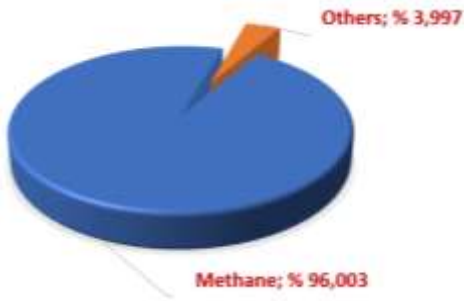

Figure 5. Natural gas composition.

The burner was operated at a heat input of 1500 kW at constant equivalence ratios (φ) are 0.7, 0.77, and 0,85 with the fuel types being 100 % NG, 70 % NG / 30 % H_2, and 60 % NG / 40 % H_2, respectively. The combustion air and fuel temperature values were approximately 20 °C and 15 °C, respectively. These values were used as boundary conditions in numerical studies. The fuel and combustion air flow rates for all cases are given in Table 2.

Table 2. Fuel and combustion air flow rates are given for blended fuels according to equivalence ratios.

Blended Fuel Composition (By Volume, %)	**Heat Input (kW)**	**Equivalence ratio** (φ)	$\dot{V}_{fuel,NG}$ **(Nm³/h)**	$\dot{V}_{fuel,H2}$ **(Nm³/h)**	$\dot{V}_{air}$ **(Nm³/h)**
100 % NG / 0 % H_2	1500	0.7	156.3	0	2683
		0.77			2439
		0.85			2251
70 % NG / 30 % H_2		0.7	176.3	76	2640
		0.77			2400
		0.85			2215
60 % NG / 40 % H_2		0.7	165	110	2592
		0.77			2362
		0.83			2180

Numerical Analyses

Numerical analyses of combustion cases were conducted with Fluent codes. 3D geometry of the burner and furnace was modeled in SolidWorks and ANSYS Design Modeler. The modeled geometry of the boiler and burner before the meshing studies is shown in Figure 6.

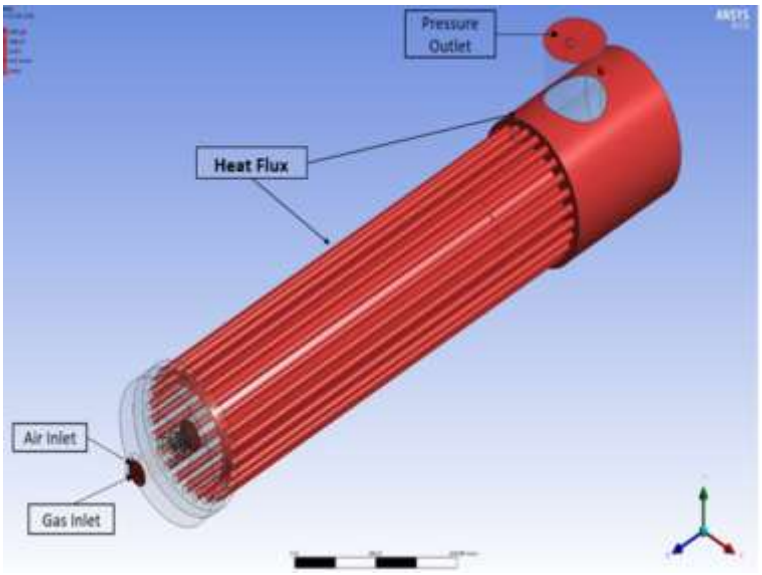

Figure 6. 3D geometry of the mounted burner and boiler.

The meshing studies were studied in Ansys Meshing. The mesh number is 8,767,128, the node number is 1.612,372, and the highest skewness is 0.76. The mesh structure consists of hexahedral and tetrahedral cells in Figure 7. Transition from tetrahedral to polyhedral was carried out in the analyses deemed necessary in the Fluent solver.

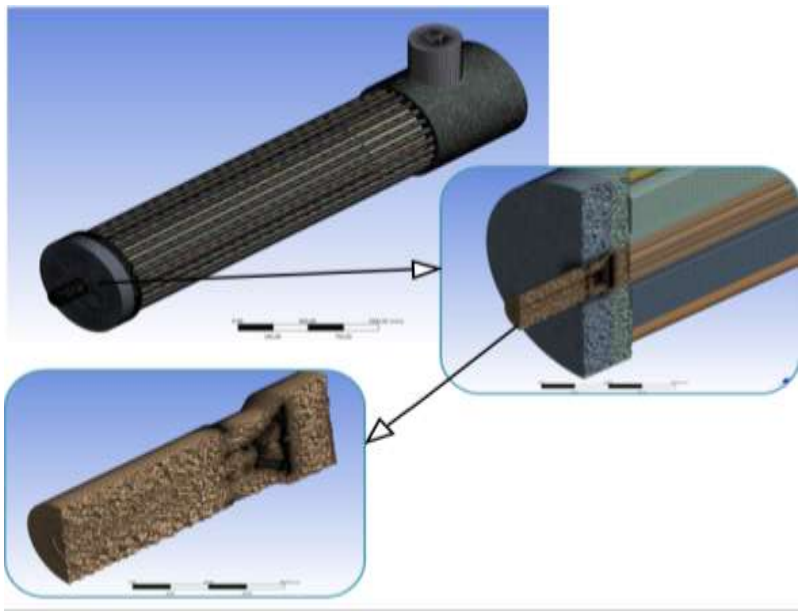

Figure 7. Boiler and burner mesh structures.

The boundary conditions for air and fuel were defined in terms of mass flow rates. The boiler flue gas outlet pressure was taken at atmospheric pressure of 101,325 Pa. The boiler's inner walls, constructed of carbon steel, were assigned as wall boundary conditions (BC) with an emissivity of 0.79 at 1000 K (726 °C) (Bergman, T. L., Lavine, A. S., Incropera, F. P., & DeWitt, D. P. (2011). The convection coefficient calculated for the cooling water wall is 1318 W/m²K, and the free flow stream average temperature of cooling water is 357 K, empirically. The other boiler and burner walls were defined as adiabatic wall BC. Heat input of the burner

is 1500 kW, with air and fuel temperatures of 298 K and 293 K, respectively. The air density remained constant at 1.184 kg/m³; however, the fuel density changed according to the blending ratio. The burner's air and fuel inlets, with the flue gas outlet, possessed cylindrical configurations. The hydraulic diameters for internal flows were 0.0702 m for fuel, 0.1395 m for air, and 0.406 m for the flue gas.

Fuel, air, and other gases within the furnace were presumed to be incompressible. Non-premixed flames were simulated for all combustion scenarios, resulting in radiative heat transfer within the combustion chamber and an elevation in furnace wall temperatures.

The radiation heat transfer mechanism was used to compute temperature changes in the flames, using the discrete ordinates (DO) radiation model for flame radiation. The absorption coefficient was utilized through the weighted-sum-of-gray-gases model (WSGGM) according to domain specifications. Coupled method was utilized for pressure-velocity coupling, employing PRESTO! for spatial pressure discretization and a second-order upwind approach for the other equations (ANSYS Fluent, 2023). Due to the volatile features of fuel and air flow, the k-ε turbulence model was employed, utilizing the usual wall function for boundary layer computations. Three combustion models were used: Eddy Dissipation Model (EDM), Non-Premixed Combustion (NPC), and the Partially Premixed Combustion (PPC) model. which were compared and validated CFD combustion model was used for all cases. The chemical equilibrium model and the assumed probability density function (PDF) method were employed for diffusion flames, yielding better validated results for NOx emission predictions in hydrocarbon fuel combustion. The convergence criteria were taken as 10^{-6} for the energy and radiation equations, and at 10^{-4} for the other equations. The convergence limit for the equations for NO emissions and temperature variance was taken as 10^{-7}.

Governing Equations

Combustion simulations are performed by solving the equations that regulate the conservation of mass, momentum, and energy within the fluid domain. The continuity equation, conservation of momentum, energy equation, radiative transfer equation (RTE), probability density function (PDF) equation, k-ε governing equation are presented between Eq. (1) and Eq. (7), respectively (ANSYS Fluent, 2023).

Continuity equation:

$$\frac{\delta\rho}{\delta t} + \nabla.(\rho\vec{v}) = 0 \quad (1)$$

Conservation of momentum:

$$\frac{\delta\rho}{\delta t}(\rho\vec{v}) + \nabla.(\vec{v}\vec{v}) = -\nabla p + \nabla(\bar{\bar{\tau}}) + \rho\vec{g} + \vec{F} \quad (2)$$

Energy equation:

$$\frac{\delta}{\delta x_j}\left(\rho u_j h + F_{hj}\right) = u_j\frac{\delta p}{\delta x_j} + \tau_{ij}\frac{\delta u_i}{\delta x_j} \quad (3)$$

Radiative transfer equation:

$$\nabla.I(\vec{r},\vec{s})\vec{s}) + (a+\sigma_s)I(\vec{r},\vec{s}) = an^2\frac{\sigma T^4}{\pi} + \frac{\sigma_s}{4\pi}\int_0^{4\pi} I(\vec{r},\vec{s}')\Phi(\vec{s},\vec{s}')d\Omega' \quad (4)$$

PDF table equation:

$$\bar{\Phi} = \int_0^1\int_0^1 \Phi(f,c)p(f,c)dfdc \quad (5)$$

The governing equation of turbulence kinetic energy is defined as k:

$$\frac{\partial}{\partial t}(\rho k) + \frac{\partial}{\partial x_j}(\rho k u_j) = \frac{\partial}{\partial x_j}\left[\left(\mu + \frac{\mu_t}{\sigma_k}\right)\frac{\partial k}{\partial x_j}\right] + G_k + G_b - \rho\epsilon - Y_M + S_k \quad (6)$$

The governing equation of turbulence dissipation rate is defined as ε:

$$\frac{\partial}{\partial t}(\rho \varepsilon) + \frac{\partial}{\partial x_j}(\rho \varepsilon u_j) = \frac{\partial}{\partial x_j}\left[\left(\mu + \frac{\mu_t}{\sigma_\varepsilon}\right)\frac{\partial k}{\partial x_j}\right] + \rho C_1 S_\varepsilon - \rho C_2 \frac{\varepsilon^2}{k + \sqrt{\upsilon\varepsilon}} + C_{1\varepsilon}\frac{\varepsilon}{k} C_{3\varepsilon} G_b + S_\varepsilon \quad (7)$$

The equivalence ratio (φ) is the actual fuel-to-oxidizer ratio divided by the stoichiometric (theoretical complete combustion) fuel-to-oxidizer ratio. Φ formula is presented Eq. (8) (ANSYS Fluent, 2023).

$$\Phi = \frac{A/F_{stoich}}{A/F_{actual}} \quad (8)$$

Calculation of NO_x Pollutants

Nitric oxides (NO_x), which are called the totality of nitric oxides, are significant pollutants. Nitric oxide (NO) is predominantly produced in NO_x emissions. NO is often generated as thermal NO and prompt NO. Thermal NO_x is generated when molecular N_2 from atmospheric air is thermally degraded due to flame temperatures exceeding 1500 K during combustion. Thermal NO is explained by the Zeldovich reaction mechanism (Lee and Jou, 2016). The formula for thermal NO is provided between Eq. (9) and Eq. (11).

$O + N_2 \rightarrow N + NO$ (9)
$N + O_2 \rightarrow O + NO$ (10)
$N + OH \rightarrow H + NO$ (11)

The Fenimore mechanism explains prompt NO generation (Lee and Jou, 2016). The equations for Fenimore's NO_x production reactions are presented between Eq. (12) and Eq. (15).

$CH + N_2 \rightarrow HCN + N$ (12)
$N + O_2 \rightarrow NO + O$ (13)
$HCN + OH \rightarrow CN + H_2O$ (14)
$CN + O_2 \rightarrow NO + CO$ (15)

NO emission simulation results were calculated as ppm (parts per million) presented Eq. (16) (ANSYS Fluent, 2023).

$$\frac{\text{Mole fraction of NO x } 10^6}{(1 - \text{Mole fraction of H2O})} \quad (16)$$

RESULTS AND DISCUSSION

In this study, the performance of combustion products from studies with different combustion conditions was predicted using numerical analyses. The numerical results were then compared with experimental results after simulations. Flame characteristics of different hydrogen mixture ratios combustion were analyzed using contours to identify the significant effects of hydrogen addition to the fuel.

Comparisons of CFD Combustion Models and Experimental Results

Eddy dissipation model (EDM), non-premixed combustion (NPC), and partially premixed combustion (PPC) models were analysed and compared with experimental results to obtain the validated calculation method. The heat power of the burner was 1500 kW with natural gas

combustion and an equivalence ratio of 0.85. Total operating pressures of fuel and air have been compared with the experimental results given in Table 3. Although Operating pressures at NPC and PPC of fuel and air have been validated by experimental results, the EDM results have been different from experimental results.

Table 3. Comparison of total operating pressures of fuel and air.

Combustion Models	EDM	NPC	PPC	Experimental Results
P_{fuel} (mbar)	19.2	17.1	17.2	17.3
P_{air} (mbar)	22.7	18.3	19.2	18.6

O_2 emissions are compared with the experimental results in Figure 8. Although O_2 emissions are close to the experimental data in the NPC and PPC models, they are higher in the EDM model. CO_2 emissions are compared with the experimental results in Figure 9. In the EDM model, CO_2 emissions were calculated to be the lowest according to the experimental results. In the NPC model, CO_2 emissions are higher than in the EDM model and closer to the experimental results. In the PPC model, the agreement of CO_2 emissions with the experimental results is better than in the other models. NO pollutant was compared with the experimental results in the Figure 10. In the NO solution, which is a post-processor solution and slow chemistry interaction, the EDM model calculated higher results than the other models. In the NPC model, the NO value is lower than the experimental value. However, the NO value calculated in the PPC model is much closer to the experimental value. As a result of comparing the values calculated by 3 different numerical combustion models, the closest results to the experimental data for turbulent combustion studies fueled by natural gas were calculated using the PPC model.

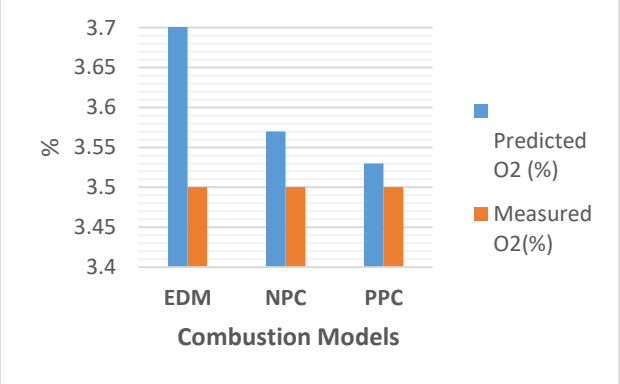

Figure 8. Comparison of O_2 (%) emissions in combustion models.

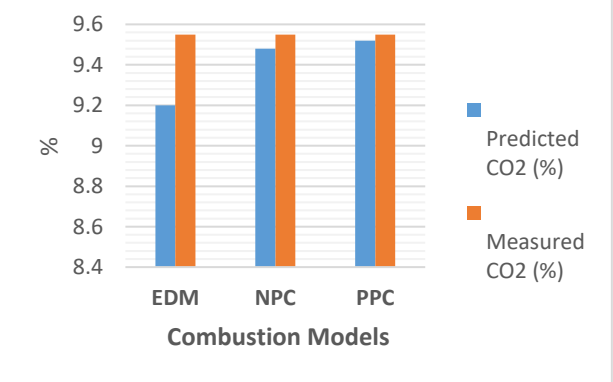

Figure 9. Comparison of CO_2 (%) emissions in combustion models.

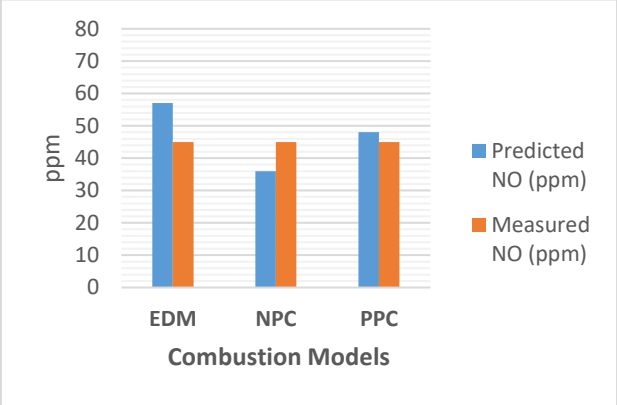

Figure 10. Comparison of NO (ppm) pollutant in combustion models.

At the end of the study, the numerical calculation values were compared with the experimental results and CO_2 emissions (Figure 11) and NO (Figure 12) values were validated.

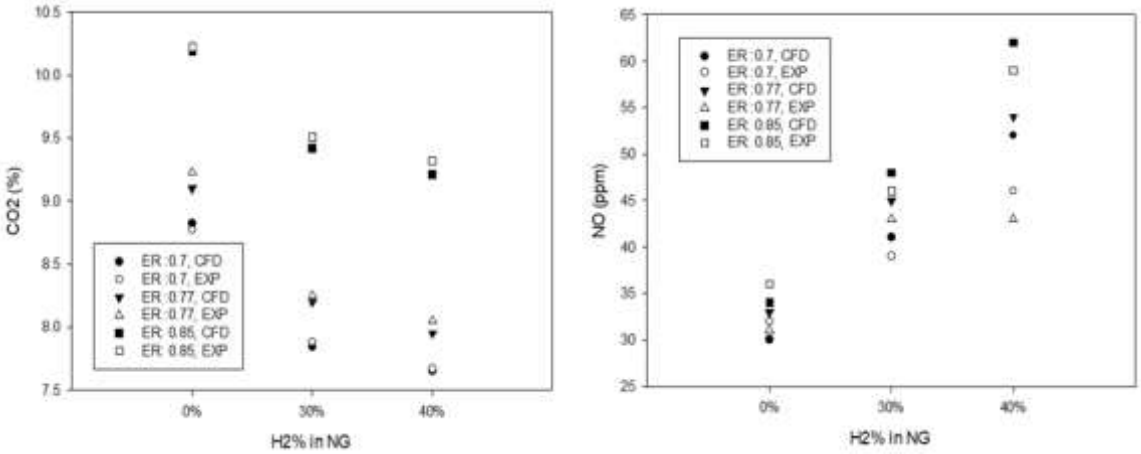

Figure 11. Comparison of combustion CO_2 (%) and NO (ppm) values of flue gas surface from numerical studies and experiments at 100% NG, 30 % and 40 % H_2 in NG, φ: 0.85, φ: 0.77, and φ: 0.7.

CONCLUSIONS

In the present study, The PPC model provided the closest agreement with experimental operating pressures and O_2, CO_2, and NO measurements and was therefore selected as the validated CFD model. Increasing the hydrogen blending ratio increased flame temperature and NO formation while reducing CO_2 emissions. Higher excess-air operation, achieved by decreasing the equivalence ratio, effectively reduced flame peak temperatures and thermal NOx levels. These results indicate that hydrogen blended natural gas can be used in industrial low-NOx burners when hydrogen blending and excess air levels are appropriately controlled, providing a practical approach for decarbonisation from industrial combustion systems.

ACKNOWLEDGEMENT

We would like to thank Termo Isı Sistemleri Ticaret ve Sanayi A.Ş. (ECOSTAR) and Trakya University in Türkiye, and our colleagues for their support.

REFERENCES

ANSYS Fluent 2023R2, Theory guide. July 2023.

Badakhsh, A., & Bhagavathy, S. M. (2023). Caveats of green hydrogen for decarbonisation of heating in buildings. Applied Energy, 353, 122152. https://doi.org/10.1016/j.apenergy.2023.122152

Bergman, T. L., Lavine, A. S., Incropera, F. P., & DeWitt, D. P. (2011). Introduction to Heat Transfer. John Wiley & Sons.

Büyükakın, M. K. (2026). Effects of hydrogen addition on methane fuel reactivity in high-temperature CO2/O2/N2 coflow in a non-premixed lab-scale tube burner. International Journal of Hydrogen Energy, 206, 153377. https://doi.org/10.1016/j.ijhydene.2026.153377

Franco, A., & Rocca, M. (2024). Industrial Decarbonization through Blended Combustion of Natural Gas and Hydrogen. Hydrogen, 5(3), 519–539. https://doi.org/10.3390/hydrogen5030029

Gee, A. J., Smith, N., Chinnici, A., & Medwell, P. R. (2023). Characterisation of turbulent non-premixed hydrogen-blended flames in a scaled industrial low-swirl burner. International Journal of Hydrogen Energy, 49, 747–757. https://doi.org/10.1016/j.ijhydene.2023.11.164

Lee, C. and C. G. Jou, 2016, Influence of the hydrogen-rich on the furnace thermal efficiency. Applied Thermal Engineering, 93, 556–560. https://doi.org/10.1016/j.applthermaleng.2015.09.050

New generation Low NOx burners - Ecostar. (n.d.). https://www.ecostar.com.tr/en/products/monoblock-burners/low-nox-burners/yeni-jenerasyon-low-nox-brulorleri

Odeh, A., & Paul, M. C. (2023). Effects of hydrogen enrichment on the heat generation and emission of natural gas turbulent premixed flame. International Journal of Hydrogen Energy, 49, 1176–1191. https://doi.org/10.1016/j.ijhydene.2023.10.140

Sîrbu, T. M., Iolu, C. E., & Prisecaru, T. (2026). Combustion Characteristics of Hydrogen-Enriched Natural Gas with a Focus on Residential Appliances: A Review. Hydrogen, 7(1), 20. https://doi.org/10.3390/hydrogen7010020

Wang, P., Feng, N., Zheng, W., Li, W., Lu, Y., Wang, Z., Sun, C., Zhang, Y., Lv, L., & Xu, M. (2025). Effects of operating parameters on combustion characteristics of Hydrogen-Doped natural Gas. Processes, 13(11), 3477. https://doi.org/10.3390/pr13113477

Zeng, G., Xu, Z., Zhang, Z., & Bai, H. (2023). Natural gas-hydrogen hybrid combustion retrofit method and practice for F-class heavy-duty combustion engines. Engineering Research Express, 5(3), 035061. https://doi.org/10.1088/2631-8695/acf5cb

ANALYSIS OF UNIVERSITY STUDENTS' METAPHORICAL PERCEPTIONS OF THE CONCEPT OF "CLIMATE CHANGE"

Nurcan Özkan[1]

[1] *Trakya University, Education Faculty, Mathematics and Sciences Education Department, Edirne, Turkey*
Corresponding author e-mail: nurcanozkan@hotmail.com

ABSTRACT

This study aims to identify the metaphors that university students will use to describe the concept of "climate change," a current environmental issue worldwide. The study sample consists of 49 third and fourth-year students enrolled in the Science Education Department of the Faculty of Education at Trakya University during the 2024-2025 academic year. To determine science education students' perceptions of the concept of "climate change," a semi-structured form containing the statement "Climate change is like …… because ……" was distributed, and students were asked to express their views by focusing on only one metaphor and filling in the blanks. The data obtained at the end of the study were analyzed using content analysis. Participants generated a total of 46 different metaphors for the concept of climate change, and these metaphors were evaluated under 11 different conceptual categories to interpret the results. According to the findings, the most frequently recurring metaphors related to the concept of climate change were identified as our emotions and greenhouses. The conceptual categories are as follows: Global warming as an end, global warming as a result of our actions, global warming as a catastrophe, global warming as a threat, global warming as an asset, global warming as a commodity, global warming as a disease, global warming as an imbalance, global warming as a disruption of the natural balance, global warming as a necessity for taking action, and global warming as a result of human impact. The metaphors developed by the students were most frequently clustered within the conceptual category of "global warming as a result of human impact."

Keywords: Metaphor, Climate change, Environment, Science education students

INTRODUCTION

Climate change can be defined as a long-term change in the overall average of the climate due to various reasons (Demirbaş and Aydın, 2020). In today's world, where environmental problems are prevalent, climate change can perhaps be described as the biggest environmental problem among many others (Özerdem and Barlas, 2022). Global climate change is a significant change, mostly caused by human activities, in addition to the climatic changes that have occurred naturally throughout the Earth's long geological history. The increase in human activity and the reliance on fossil fuels driven by the industrial revolution have led to a rise in carbon dioxide, causing significant changes in the existing composition of the atmosphere. In addition, the increase in animal production to meet human needs has also led to an increase in methane gas released from animal farms into the atmosphere. In the coming years, changing people's consumption habits and putting an end to consumerism are also among the most important issues for the health of the world. The accumulation of greenhouse gases is increasing, particularly as a result of the excessive and indiscriminate use of fossil fuels such as oil, coal, and natural gas. The negative effects of global warming are seen in many aspects

of nature, especially in water resources. Due to its geographical location and diverse climatic conditions, Turkey is increasingly becoming one of the regions most affected by the negative impacts of global warming (Akın, 2006; Erdoğan Sağlam et al., 2008).

The industrial revolution increased the amount of carbon dioxide released into the atmosphere by developing countries, negatively impacting the ecological balance of the planet (Nart, 2009). The melting of glaciers, leading to rising sea levels and increased intensity of weather events, can have significant consequences affecting human health, various sectors, and ecosystems (IPCC, 2013). The Intergovernmental Panel on Climate Change (IPCC) report confirms increases in air and ocean temperatures, changes in precipitation, rising sea levels, and changes in the intensity of events such as droughts, floods, and storms (IPCC, 2014). The Republic of Turkey's Climate Change Strategy 2010-2023 states that "within the scope of developing capacity to combat and adapt to climate change, it is necessary to increase public awareness and strengthen the capacities of institutions in Turkey in order to reduce the effects of climate change and adapt to the process" (MEU, 2010).

Climate change, caused by global warming, affects the natural environment and consequently all ecosystems, both living and non-living. Individuals unaware of the negative effects of this change in nature do not engage in behaviors that help maintain the natural balance (Timur and Yılmaz, 2011). Environmental education is the most effective method for explaining issues such as climate change to the public and instilling this awareness in individuals from a young age (Erten, 2005; Kaşot, 2017). This behavioral pattern begins within the family and encompasses a process that can be particularly fostered through education. In this context, the perspective of prospective teachers and their knowledge and skills in environmental education become particularly important.

This study aims to identify the metaphors (mental images) that science students develop regarding the concept of climate change and to contribute to shaping future environmental education activities in this direction. Metaphors hold an important place in individuals' thought processes. They enable individuals to understand their actions related to abstract concepts such as justice, spirituality, or happiness (Landau et al., 2010; Babaoğlan Özdemir and Babaoğlan, 2022). Metaphor can also be described as the language of experience because it assigns meaning to personal experiences (Saban, 2004). According to TDK (2022), metaphor means figurative language. The word metaphor is defined as "using a word or concept in a way that gives it meanings other than its commonly accepted meaning." According to Korkmaz and Bağçeci (2013), metaphor is defined as: "When evaluating any event or situation in our daily lives, we generally approach events from different perspectives."

Studies on metaphor have also been conducted in our country since the 1990s (Toker and Bülbül, 2015). Kahyaoğlu and Kırıktaş (2016) examined the perceptions of secondary and university students regarding the concept of nature through metaphors. Doğan (2017) conducted a study to present the perceptions that middle school students have regarding the concept of environment and the meaning they attribute to these perceptions through metaphors. Ülkü (2019) investigated whether high school students understood biological concepts correctly by examining their metaphorical perceptions of these concepts. Güngör Cabbar (2019) conducted a study to determine primary school students' metaphorical perceptions of the concept of trees. Güllü and Dönel Akgül (2020) attempted to identify students' metaphors related to soil and agriculture in their study. Yoğurtcu (2021) conducted a study to determine high school students' conceptual structures, metaphorical perceptions, and misconceptions about the cell. Babaoğlan Özdemir and Babaoğlan (2022) conducted studies to determine high school students' metaphorical perceptions of the concepts of "climate change, global warming, greenhouse effect". The metaphors developed in this study regarding the concept of "climate change" reveal the perceptions and reflect the awareness of university students, who will play significant roles in our social lives in the future, about these concepts. Therefore, this study is

primarily intended to guide future teachers. Furthermore, identifying the meanings students assign to this concept through metaphors will draw attention to the threats posed by global warming.

MATERIAL AND METHOD

Research Model

The study utilized a qualitative research design, specifically "phenomenology." Phenomenology deals with phenomena that we are aware of but lack in-depth knowledge of (Yıldırım and Şimşek, 2006). The phenomenological approach is used to argue that behaviors are determined by experience rather than by external, objective, and physically defined facts (Robson, 2015). Each case study may have its own unique characteristics. This method has been chosen to determine the underlying causes of the existing phenomenon.

Study Group

The research was conducted with 49 students studying in the Science Education Department of the Faculty of Education at Trakya University during the 2024-2025 academic year (Table 1). The research was conducted on a voluntary basis, and students who did not wish to participate were not pressured. A convenient sampling method was used to select participants for the study group. This method involves obtaining data from the researcher's immediate environment, where access to data is easy, in order to speed up and streamline the study (Yıldırım and Şimşek, 2008).

Table 1. Distribution of students by grade level and gender

Gender	3rd grade	4th grade
Girl	17	24
Boy	3	5
Total	20	29

Data Collection

Metaphor analysis was used in the collection of research data. Research data was collected during the Fall semester of the 2024-2025 academic year. Students were given forms related to the research topic and asked to complete them within 20 minutes. To identify their metaphors for the concept, students participating in the study were asked to complete the sentence: “Climate change is like ……. because …..”. To this end, each student was given forms containing these sentences and asked to complete the sentence by forming a single metaphor based on their thoughts about the concept. The form included information about the participants' gender and grade level.

As is common in metaphor studies, the word "like" in the sentence is used to create a comparison, while the word "because" is used to provide a logical reason for this comparison (Saban, 2008, 2009; Aydın and Eser Ünaldı, 2010; Eraslan Çapan, 2010; Coşkun, 2011; Özder et al., 2012).

Data Analysis and Interpretation

The obtained data were evaluated using the "content analysis" technique. The aim of content analysis is to find concepts and relationships that can explain the collected data. In content analysis, similar data are grouped and organized within specific themes (Yıldırım and Şimşek, 2006). The analysis of metaphors was carried out in four stages: (i) coding and

extraction, (ii) category development, (iii) validity and reliability, and (iv) transferring the data to a computer environment (Saban, 2009).

(i) Coding and Extraction Phase: In this phase, each student's data collection form was coded and numbered as S1, S2, … S49. The metaphors produced by the students were coded into an Excel file and a list was created. Based on this list, it was examined whether a particular metaphor was clearly explained in the forms collected from the students. The analysis of the data obtained in the study examined the metaphors that students developed regarding the concept of climate change and the reasons behind them. The study examined whether there were any forms in which no metaphor was written or the reason for the metaphor created was not explained.

(ii) Category Development Phase: Metaphors developed by participating students were grouped into the same categories by combining similar answers. When determining the categories, both the metaphors developed by the students and the "because, ..." part explaining the rationale behind the metaphor were taken into consideration. It was observed that while some students' metaphors conveyed the same idea after the "because" part, others had different ideas. The ways in which the concept of "climate change" is expressed were examined by considering the metaphor lists that were created. In this respect, each metaphor produced by the participants was associated with themes from a climate change perspective, creating a total of 11 different conceptual categories.

(iii) Validity and Reliability Phase: In qualitative research, the researcher's detailed reporting of the collected data and explanation of how the results were obtained is among the important criteria for validity (Yıldırım and Şimşek, 2008). Therefore, to ensure the validity of the research, the opinion of an expert who has conducted research on metaphors was sought to determine whether the metaphorical images specified under the obtained conceptual categories represented the conceptual category in the way the students' developed metaphors were included.

(iv) Transferring the Data to a Computer Environment Phase: The selected metaphors and categories have been digitized and made ready for interpretation.

RESULTS AND DISCUSSION

This section presents the findings and interpretations obtained from the analysis of the data. Science education students participating in the research obtained 46 valid metaphors regarding the concept of climate change. Eleven categories were created for the concept of climate change. The metaphors and categories created by the students regarding the concept of climate change are given in Table 2.

Table 2. Metaphors and categories developed for the concept of climate change.

Category Name	Metaphors	Number of Metaphors	Frequency (f)	Percentage %
Global warming as an end	Apocalypse (1), end of the world (1), rooster crowing out of season (1)	3	3	6.12
Global warming as a result of our actions	The lives of living beings are in danger (1), cause and effect (1), the world's response to humans (1), environmental sustainability management system (1), a child's development (1), migration (1)	6	6	12.25
Global warming as a catastrophe	To leave a beautiful cool oasis and find yourself in the middle of the desert (1), disaster (1)	2	2	4.08
Global warming as a threat	Drunk driving (1), wastefulness (1)	2	2	4.08
Global warming as an asset	Wilting flowers (1), GMO products (1), systems (1), virus (1), spoiled fruit (1), mandarin (1)	6	6	12.25
Global warming as a commodity	Air conditioning (1), book (1), a dynamic engine that has existed for centuries (1)	3	3	6.12
Global warming as a disease	Early stage of cancer (1), Covid 19 (1), a dormant tumor (1)	3	3	6.12
Global warming as an imbalance	The imbalance of nature (1), weather conditions (1), differentiation (1), the fact that tea poured almost boiling hot into a cup cools down after a while and then cools down and the cup is renewed again (1), the meaning of the saying "the wheel of fortune turns one day" (1)	5	5	10.20
Global warming as a disruption of the natural balance	Greenhouses (2), destruction of tropical rainforests (1), change in nature (1), matter cycle (1), life cycle (1)	5	6	12.25
Global warming as a necessity for taking action	Fire (1), a broken alarm clock (1), a toy we broke (1), a person who has experienced a bad event in their life (1), a castle with ruined walls (1), time (1)	6	6	12.25
Global warming as a result of human impact	Throwing an aquatic creature onto land (1), our feelings (3), our thoughts (1), mood (1), friendship (1)	5	7	14.28
	Total	46	49	

The most frequently expressed metaphor regarding the concept of climate change was our emotions (f=3), followed by greenhouses (f=2). As seen in Table 2, the metaphors created by

the students were grouped under 11 categories. These categories are defined as: “Global warming as an end (6.12%)”, “Global warming as a result of our actions (12.25%)”, “Global warming as a catastrophe (4.08%)”, “Global warming as a threat (4.08%)”, “Global warming as an asset (12.258%)”, “Global warming as a commodity (6.12%)”, “Global warming as a disease (6.12%)”, “Global warming as an imbalance (10.20%)”, “Global warming as a disruption of the natural balance (10.20%)”, “Global warming as a necessity for taking action (12.25%), and “Global warming as a result of human impact (14.28%)”. Some of the statements included in the categories related to the concept of climate change are given below;

Category 1: Global warming as an end

This category contains a total of 3 different metaphors (6.12%). Each metaphor is represented by an individual. The metaphors are: Apocalypse (1), end of the world (1), rooster crowing out of season (1). Some of the reasons behind the emergence of some metaphors in this category are as follows:

"Climate change is like an apocalypse, because it threatens all life with extinction."

“Climate change is like a rooster crowing out of season, because everything has its place and time. Weather events should normally occur in their seasons. But as a result of environmental misuse, climates change, and snow starts falling in spring and summer. In other words, certain events occur out of season and without proper timing. Just like a rooster crowing at night.”

Category 2: Global warming as a result of our actions

This category contains a total of 6 different metaphors (12.25%). Each metaphor is represented by an individual. The metaphors are: The lives of living beings being in danger (1), cause and effect (1), the world's response to humans (1), environmental sustainability management system (1), a child's development (1), migration (1). Some of the reasons behind the emergence of some metaphors in this category are as follows:

“Climate change is like cause and effect, because whatever we give to nature, we receive a response in return. The damage we initially inflict can be quite serious, leading to climate change, and as a result, we are naturally the ones who are negatively affected.”

“Climate change is like an environmental sustainability management system, because the existence of environmental sustainability, like the part of managing a business, involves developing and implementing environmentally sensitive processes with the aim of making the environment a livable place for future generations. Similarly, management is about continuously improving itself, working towards the future, and being at the forefront of ensuring its continuity.”

Category 3: Global warming as a catastrophe

This category contains a total of 2 different metaphors (4.08%). Each metaphor is represented by an individual. The metaphors are: To leave a beautiful cool oasis and find yourself in the middle of the desert (1), disaster (1). Some of the reasons behind the emergence of metaphors in this category are:

“Climate change is like leaving a beautiful, cool oasis and finding yourself in the middle of a desert, because it disrupts nature and its order, negatively impacting life there by causing temperatures to be excessively below or above seasonal norms at unexpected times.”

“Climate change is disaster. Because greenhouse gases are causing the hole in the ozone layer to grow larger, leading to a gradual warming of the Earth. As the Earth warms further, glaciers will melt, potentially causing the death of many animals. Furthermore, the melting of glaciers could spread polar diseases to all parts of the world. This would be a complete disaster for the planet.”

Category 4: Global warming as a threat

This category contains a total of 2 different metaphors (4.08%). Each metaphor is represented by an individual. The metaphors are: Drunk driving (1), wastefulness (1). Some of the reasons behind the emergence of metaphors in this category are as follows:

"Climate change is like a drunk driving, because a drunk driver causes accidents and damages everything around them. Climate change also harms nature and living things."

"Climate change is like wastefulness, because people are using natural resources irresponsibly. Seasons are no longer experienced as they used to be. The greenhouse effect, industry, the unconscious use of products, and exhaust fumes are all contributing to climate change."

Category 5: Global warming as an asset

This category contains a total of 6 different metaphors (12.25%). Each metaphor is represented by an individual. The metaphors are: Wilting flowers (1), GMO products (1), systems (1), virus (1), spoiled fruit (1), mandarin (1). Some of the reasons behind the emergence of metaphors in this category are as follows:

"Climate change is like wilting flowers, because over time it creates adverse conditions and negatively impacts habitats."

"Climate change is like GMO products, because the climate, like food, has been disrupted by human hands."

Category 6: Global warming as a commodity

This category contains a total of 3 different metaphors (6.12%). Each metaphor is represented by an individual. The metaphors are: Air conditioning (1), book (1), a dynamic engine that has existed for centuries (1). Some of the reasons behind the metaphors in this category are:

"Climate change is like an air conditioner, because the conditions of our environment change along with the climate. For example, it is cold in winter and hot in summer."

"Climate change is like a book, because although each one is called a book, it tells a different story, evokes different feelings, and shows a different path. The things it teaches a person are also different. Climate change is like that too. Its name is climate, it evokes the same things in human consciousness, but every change is a new perspective and experience. These can be harmful or beneficial to humanity. Just like when we feel that a book we've read hasn't given us anything, we consider it a waste of time."

Category 7: Global warming as a disease

This category contains a total of 3 different metaphors (6.12%). Each metaphor is represented by an individual. The metaphors are: Early stage of cancer (1), Covid 19 (1), a dormant tumor (1). Some of the reasons behind the metaphors in this category are:

"Climate change is like the early stages of cancer, because it causes changes or depletion in the natural habitats of many living things, agricultural activities, and the struggle for survival of people."

"Climate change is like a dormant tumor. Just as a dormant tumor may appear harmless at first but can suddenly spread throughout the body, climate change, even if it doesn't seem to harm us now, will inevitably cause damage in the long term. For example, it causes melting glaciers, drought (and consequently, hunger and thirst), the greenhouse effect, warming of the atmosphere, and as the atmosphere warms, the oceans also warm, sea levels rise, which causes floods, etc. As these examples show, climate change is like a dormant tumor; although we may not notice the damage it can cause in the short term, the damage it will cause in the long term will be significant and irreparable."

Category 8: Global warming as an imbalance

This category contains a total of 5 different metaphors (10.20%). Each metaphor is represented by an individual. The metaphors are: the imbalance of nature (1), weather conditions (1), differentiation (1), the fact that tea poured almost boiling hot into a cup cools

down after a while and then cools down and the cup is renewed again (1), the meaning of the saying "the wheel of fortune turns one day" (1). Some of the reasons behind the metaphors in this category are as follows:

“Climate change is like pouring almost boiling hot tea into a cup; after a while, it cools down, then cools completely, and then the cup needs to be refilled, because at a certain point, the timing and process are similar. However, one changes on average every 3-4 months, while the other changes every 3-5 minutes.”

"Climate change is like the meaning of the saying "the wheel of fortune turns one day", because losing the seasons we experience, the absence of transitional seasons between summer and winter, are the consequences of humanity's war against nature."

Category 9: Global warming as a disruption of the natural balance

This category contains a total of 5 different metaphors (12.25%). The greenhouses metaphor is represented by two individuals, and the others by one individual. Metaphors: Greenhouses (2), destruction of tropical rainforests (1), change in nature (1), matter cycle (1), life cycle (1). Some of the metaphors and reasons included in this category are:

“Climate change is like the matter cycle, because there is a proverb that says 'you reap what you sow.' Humanity receives positive returns when it protects nature, but receives negative returns when it harms the environment. This indirectly results in global warming through the release of greenhouse gases, etc., and consequently causes climate change.”

“Climate change is like nature changing, because as climates change, nature changes too. Our environment changes.”

“Climate change is like a life cycle because: if the concept of climate change didn't exist in our lives, the entire natural balance would be disrupted. The lifespans of living things would be shortened. Increased frequency and impact of extreme weather events such as droughts, floods, and severe hurricanes, rising ocean and sea levels, increased ocean acidification, and melting glaciers would put plants, animals, ecosystems, and human communities at serious risk.”

Category 10: Global warming as a necessity for taking action

This category contains a total of 6 different metaphors (12.25%). Each metaphor is represented by an individual. The metaphors are: Fire (1), a broken alarm clock (1), a toy we broke (1), a person who has experienced a bad event in their life (1), a castle with ruined walls (1), time (1). Some of the metaphors in this category and their reasons are as follows:

"Climate change is like a castle with ruined walls; if we don't take precautions, the enemy will come and destroy us."

“Climate change is like time, because climate change is the changes that occur in weather patterns and in oceans, land surfaces and ice sheets, and it is nearly impossible to reverse these conditions. Time is like climate change; it is difficult to bring back what has been done, and it is very difficult to rectify the mistakes that have been made.”

Category 11: Global warming as a result of human impact

This category contains a total of 5 different metaphors (14.28%). The metaphor of our feelings is represented by 3, and the other metaphors are represented by an individual. The metaphors are: Throwing an aquatic creature onto land (1), our feelings (3), our thoughts (1), mood (1), friendship (1). Some of the reasons behind the metaphors in this category are:

"Climate change is like our thoughts, because it can differ and change at every stage of time."

“Climate change is like our feelings because if we consume them too much, they eventually disappear. Today, we know that global warming is increasing and will have serious consequences if it is not stopped.”

DISCUSSION AND CONCLUSIONS

This study was conducted to determine university students' perceptions of the concept of "climate change" using metaphors. The fact that, with the exception of two, all of the 46 different metaphors created by Science Education students at the Faculty of Education are represented by a single person is significant in revealing the diversity of perceptions surrounding the concept. The metaphors collected from the students were grouped under 11 categories. The most frequently expressed metaphor regarding the concept of climate change was our feelings (6.52%).

Kaşot, Özalp and Koşer (2023) worked with 100 primary school teachers in the Turkish Republic of Northern Cyprus to determine their metaphorical perceptions of the concept of climate change. In the study, 100 different teachers were evaluated, and they provided 38 different metaphors regarding the concept of climate change. Unlike this study, the number of metaphors was fewer, and there were repetitions of metaphors.

Babaoğlan Özdemir and Babaoğlan (2022), in their study titled "Metaphorical Perceptions of High School Students Regarding the Concepts of Climate Change, Global Warming, and Greenhouse Effect," found that students produced 237 metaphors related to the concept of "climate change," 234 metaphors related to the concept of "greenhouse effect," and 260 metaphors related to the concept of "global warming." These metaphors have been grouped into 5 different categories for "climate change," 6 for "greenhouse effect," and 5 for "global warming." In contrast to this study, the most frequently repeated metaphor for climate change was identified as human; the most frequently repeated metaphor for the greenhouse effect was cigarette; and the most frequently repeated metaphor for global warming was fire. The metaphors developed by high school students do not reflect much negativity. For example; memories, cars, friendships, shoes, knowledge, work, socks, notebooks, lecture notes, class schedule, classes, ideas, sweaters, technology, phones, television, theater plays, the Turkish economy, sleep, not waking up, utopia, aging, etc. The research shows that high school students are aware that everyone needs to cooperate and make an effort to fulfill their responsibilities in addressing the problems of climate change, the greenhouse effect, and global warming, which pose a threat to both living beings and the world. This study revealed that participants' statements generally highlighted the negative impacts of climate change. For example; the apocalypse, the end of the world, a rooster crowing at the wrong time, a fire, a broken alarm clock, a toy we've broken, a person who has experienced a bad event in their life, a castle with crumbling walls, etc.

Ultimately, the aim is for students to understand climate change and to highlight its negative impacts. Measures need to be taken to mitigate or eliminate these negative effects. Unfortunately, although many people are aware of these measures, they are not widely implemented.

In conclusion, this research shows that the participants have a negative perspective towards the concept of climate change, similar to the study by Babaoğlan Özdemir and Babaoğlan (2022). This situation highlights the importance of closely following current communication channels and the education they receive in schools in fostering environmental awareness among people. The world's climate is changing rapidly, and the effects of these changes on nature, living things, and especially human health are likely to intensify.

REFERENCES

Akın, G. 2006. Küresel Isınma, Nedenleri ve Sonuçları. Ankara Üniversitesi Dil ve Tarih-Coğrafya Fakültesi Dergisi, 46(2): 29-43.

Aydın, F., Ü. Eser Ünaldı. 2010. Coğrafya Öğretmen Adaylarının "Coğrafya" Kavramına İlişkin Algılarının Metafor Yardımıyla Analizi. International Online Journal of Educational Sciences, 2(2): 600-622.

Babaoğlan Özdemir, B., B. Babaoğlan. 2022. Lise Öğrencilerinin "İklim Değişikliği, Küresel Isınma, Sera Etkisi" Kavramlarına Yönelik Metaforik Algıları, Anadolu Öğretmen Dergisi, 6(2): 339-354, Doi: 10.35346/aod.1136515

Coşkun, M. 2011. Lise Öğrencilerinin "İklim" Kavramıyla İlgili Metaforları (Zihinsel İmgeleri). Turkish Studies International Periodical For the Languages, Literature and History of Turkish or Turkic, 5(3): 919-940.

Demirbaş, M., R. Aydın. 2020. 21. Yüzyılın En Büyük Tehdidi: Küresel İklim Değişikliği. Ecological Life Sciences, 15(4): 163-179.

Doğan, Y. 2017. Ortaokul Öğrencilerinin Çevre Kavramına İlişkin Sezgisel Algıları: Bir Metafor Analizi. Ahi Evran Üniversitesi Kırşehir Eğitim Fakültesi Dergisi, 18(1): 721-740.

Eraslan Çapan, B. 2010. Öğretmen Adaylarının Üstün Yetenekli Öğrencilere İlişkin Metaforik Algıları. Uluslararası Sosyal Araştırmalar Dergisi, 3(12): 140-154.

Erdoğan Sağlam, N., E. Düzgüneş, İ. Balık. 2008. Küresel Isınma ve İklim Değişikliği. Ege Üniversitesi Su Ürünleri Dergisi, E.U. Journal of Fisheries & Aquatic Science, 25(1): 89-94.

Erten, S. 2005. Okul Öncesi Öğretmen Adaylarında Çevre Dostu Davranışların Araştırılması. Hacettepe Üniversitesi Eğitim Fakültesi Dergisi, 28(28): 91-100.

Güllü, U., G. Dönel Akgül. 2020. Ortaokul 8.Sınıf Öğrencilerinin Toprak ve Tarıma Yönelik Metaforik Algıları. Adnan Menderes Üniversitesi Eğitim Fakültesi Eğitim Bilimleri Dergisi, 11(1): 67-83.

Güngör Cabbar, B. 2019. İlkokul Dördüncü Sınıf Öğrencilerinin Ağaç Kavramına Karşı Metaforik Algıları. Anadolu Journal of Educational Sciences International, 10(1): 189-208.

IPCC. 2013. Climate Change: The Physical Science Basis, Frequently Asked Questions, https://www.ipcc.ch/ report/ar5/wg1.

IPCC. 2014. Climate Change Impacts, Adaptation, and Vulnerability. http://www.ipcc.ch/report/ar5/wg2.

Kahyaoğlu, M., H. Kırıktaş. 2016. Ortaöğretim ve Üniversite Öğrencilerinin "Doğa" Kavramına İlişkin Algılarının Metafor Analizi Yoluyla İncelenmesi. Marmara Coğrafya Dergisi, 33: 58-76.

Kaşot, N. 2017. Çevre Eğitimi. Ankara: Eğiten Kitap.

Kaşot, N., G. Özalp, G. Koşer. 2023. KKTC İlköğretim Öğretmenlerinin İklim Değişikliği Kavramına İlişkin Metaforik Algılarının Belirlenmesi. Climatehealth, 3(2): 33-39.

Korkmaz, F., B. Bağçeci. 2013. Lise Öğrencilerinin 'Üniversite' Kavramına İlişkin Metaforik Algıların İncelemesi". Bartın Üniversitesi Eğitim Fakültesi Dergisi, 2(1): 187-204.

Landau, M. J., B. P. Meier, L. A. Keefer. 2010. A metaphor-enriched social cognition. Psychological bulletin, 136(6): 1045-1067.

MEU. 2010. Republic of Turkey Climate Change Strategy 2010-2023. Ministry of Environment and Urbanization.
https://webdosya.csb.gov.tr/db/iklim/editordosya/iklim_degisikligi_stratejisi_EN.pdf. Erişim: 24.06.2022.

Nart, N. 2009. Daha Geç Olmadan, Küresel Isınma. İm Yayın Tasarım, İstanbul.

Özder, A., H. Kaya, M. Ünlü. 2012. Ortaöğretim Öğrencilerinin "Turizm" Kavramı İle İlgili Geliştirdikleri Metaforların Analiz Örneği. Marmara Coğrafya Dergisi, 25: 18-31.

Özerdem, F., B. Barlas. 2021. Kopenhag Okulu Çerçevesinde 2020 ve Sonrası Dünya Politikasının Yeni Sorunu: İklim Değişikliği ve İklim Göçmenleri. Süleyman Demirel Üniversitesi Sosyal Bilimler Enstitüsü Dergisi, (41): 273-302.

Robson, C. 2015. Bilimsel Araştırma Yöntemleri Gerçek Dünya Araştırması. (Çev.: Ş. Çınkır ve N. Demirkasımoğlu), Anı yayıncılık, Ankara.

Saban, A. 2004. Giriş Düzeyindeki Sınıf Öğretmeni Adaylarının "Öğretmen" Kavramına İlişkin İleri Sürdükleri Metaforlar. Türk Eğitim Bilimleri Dergisi, 2(2): 131-155.

Saban, A. (2008). Okula İlişkin Metaforlar. Kuram ve Uygulamada Eğitim Yönetimi, 55: 459 496.
Saban, A. 2009. Öğretmen Adaylarının Öğrenci Kavramına İlişkin Sahip Oldukları Zihinsel İmgeler. Türk Eğitim Bilimleri Dergisi, 7(2): 281-326.
TDK. 2022. Büyük Türkçe Sözlük. Türk Dil Kurumu Yayınları, Ankara.
Timur, S., M.Yılmaz. 2011. Fen Bilgisi Öğretmen Adaylarının Çevre Bilgi Düzeylerinin Belirlenmesi ve Bazı Değişkenlere Göre İncelenmesi. Gazi Eğitim Fakültesi Dergisi, 31, 303-320.
Toker, G. A., T. Bülbül. 2015. Meslek Lisesi Öğrencilerinin Okul Algılarına Yönelik Bir Metafor Çalışması. Journal of Educational Sciences Research. Internationl E-Journal, 16(21): 273-291.
Ülkü, G. 2019. Lise Öğrencilerinin Biyolojik Kavramlar İle İlgili Metaforik Algılarının İncelenmesi. Gazi Üniversitesi Eğitim Bilimleri Enstitüsü, Yüksek Lisans Tezi.
Yıldırım, A., H. Şimşek. 2006. Sosyal Bilimlerde Nitel Araştırma Yöntemleri. Seçkin Yayınevi, Ankara.
Yıldırım, A., H. Şimşek. 2008. Sosyal Bilimlerde Nitel Araştırma Yöntemleri (6. Baskı). Ankara: Seçkin Yayıncılık.
Yoğurtçu, A. 2021. Lise Öğrencilerinin Hücre Konusundaki Kavramsal Yapıları, Metaforik Algıları ve Kavram Yanılgılarının Belirlenmesi. Yüksek Lisans Tezi, Necmettin Erbakan Üniversitesi Eğitim Bilimleri Enstitüsü, Konya.

TEMPERATURE TOLERANCE AND PHENOTYPIC PLASTICITY IN PLANTS

Aydın ÜNAY

Aydın Adnan Menderes University, Agricultural Faculty, Field Crops Department, Aydın, Türkiye

ABSTRACT

Temperature is the most fundamental external factor determining the rate of plant growth and development. Under optimum temperature conditions, metabolic functions reach their highest level. Conversely, at low temperatures, growth occurs at the lowest level. At high temperatures, the enzyme structure begins to degrade, and the synchronization between male and female reproductive organs is disrupted. In the process of global climate change, temperature increases and rainfall irregularities are observed. Furthermore, the frequency and severity of temperature fluctuations are increasing. These irregularities reduce yield and quality in plants. In our country, temperature increases following the sowing period of winter crops affect the plants' entry into winter. Similarly, sudden temperature rises occurring at the end of winter, referred to as false spring, followed by seasonal cold snaps or frost events, impact the advanced developmental stages of plants. Phenotypic plasticity emerges when a genotype produces different phenotypes under different environmental conditions. Stomatal conductance and transpiration form the basis of phenotypic plasticity under both drought and high-temperature conditions. Changes in root and leaf morphology, as well as osmotic adjustment, support phenotypic plasticity. Phenotypic plasticity is explained through epigenetic regulations. Breeding plant species and varieties with phenotypic plasticity constitutes one of the most important breeding strategies.

Key words: Temperature fluctuations, yield losses, tolerance, phenotypic plasticity, epigenetics

INTRODUCTION

Global climate change adversely affects not only temperature increases but also precipitation, wind, and seasonal patterns. Concurrently with temperature fluctuations, plants encounter pressure from pests and diseases whose species composition and population dynamics are changing. Significant meteorological variations between seasons and years have resulted in temperature fluctuations that have reached levels capable of affecting crop yield and quality. It is projected that the frequency of exposure to extreme temperatures will further accelerate in future years (Roberts and Summerfield, 1987; Wheeler et al., 2000; IPCC, 2021; Paçal et al., 2023; Senapati et al., 2024).

In cool-season cereals, above-normal temperatures during the sowing period and the subsequent process lead to entry into winter with excessive leaf development, thereby weakening the plant's winter hardiness. Furthermore, temperature fluctuations during the tillering stage negatively affect the number of tillers. Most importantly, extreme high temperatures and below-normal low temperatures during the subsequent generative stage, particularly during the grain-filling period, directly impact yield negatively. In wheat, it has been reported that variations of ±2°C from optimal temperatures induce leaf senescence, potentially causing up to a 50% yield reduction (Asseng et al., 2011).

In summer crops such as cotton, soybean, maize, and peanut, sowing is carried out when soil temperatures reach 15–18°C or higher. However, in some years, post-sowing abnormalities occur in April and May, where low temperatures adversely affect both germination and early seedling development. In addition, early-stage seedling pathogens cause significant losses in plant density (Akpınar, 2008; Ergin et al., 2021). In maize, temperature fluctuations between 20–30°C negatively affected shoot and root development and significantly increased transpiration (Lal, 1974).

Similar to winter crops, temperature fluctuations in summer crops exert a greater negative impact during the generative stage. High temperatures shorten the duration required for seed formation and development, thereby limiting the attainment of yield potential. Additionally, extreme heat during the flowering stage can directly impair pollination and fertilization (Harrison et al., 2011).

The long-term and last five-year maximum and minimum temperature values for Aydın province, where summer crops such as cotton and maize are predominantly cultivated, are presented in Figure 1. It is clearly evident that summer crops are exposed to both maximum and minimum temperatures approximately 2°C and above [normal/higher] during their reproductive stages.

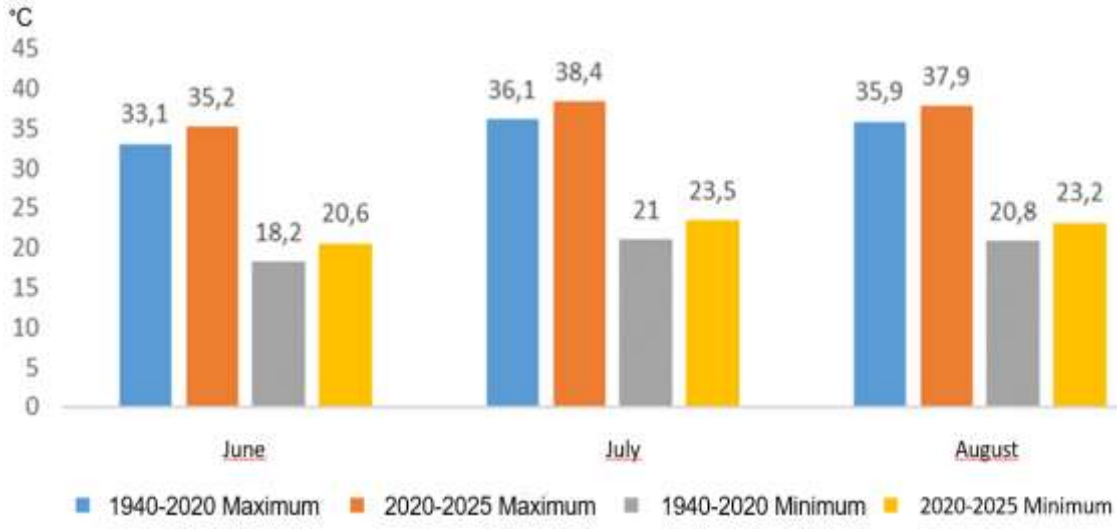

Figure 1. Long-term (1940–2020) and 2020–2025 period temperature values for the months of June, July, and August in Aydın province.

PHENOTYPIC PLASTICITY

Phenotypic plasticity is the ability of a genotype to develop phenotypes with distinct physiological, morphological, developmental, and biochemical characteristics when exposed to different environmental conditions. The plasticity of a given trait depends on genetic and environmental factors (Alseekh et al., 2025). High phenotypic plasticity is defined as a scenario where a small change in temperature leads to extensive phenotypic modifications in plants. There is a close relationship between phenotypic plasticity and evolutionary potential. Evolutionary fitness manifests in two ways: vigor and reproductive success. Photosynthetic rate

and capacity, nutrient use efficiency, and phenological matching support adaptive capacity (Schaum et al., 2022).

Testing populations exhibiting genotypic variation across different years and locations represents one of the simplest methods to determine phenotypic plasticity. Results obtained from these studies demonstrate that the environment is as critical as genetics in explaining overall phenotypic variation (Han et al., 2025).

Morphological modifications encompassed within phenotypic plasticity include leaf area index, leaf orientation, stomatal conductance, leaf movements (parheliotropism), leaf cuticle thickness, and stomatal characteristics (Gratani, 2014). Osmotic adjustment, on the other hand, is one of the most vital traits supporting phenotypic plasticity within water use efficiency (Nicotra and Davidson, 2010). The effects of temperature during four distinct growth and developmental stages in cotton are illustrated in Figure 2.

During the vegetative stage, high temperatures lead to stunted plants with reduced leaf area. In these plants, cell membrane integrity is impaired, and stomatal conductance is reduced. DNA denaturation and the synthesis of reactive oxygen species (ROS) underlie these adverse effects. Consequently, both photosynthetic rate and capacity are diminished. During the flowering stage, the number of flowers decreases due to negative impacts on gene expression. Infertility may occur as a result of desynchronization among floral organs. At the onset of boll setting, boll shedding is observed. The size of developing bolls decreases, giving rise to stunted seeds and coarser fibers.

Figure 2. The effects of temperature at different growth stages in cotton.

Phenological Stage		Differentiations
	Vegetative stage	Impairment of stomatal conductance, loss of cell membrane stability and photosynthetic damage, stunted growth and reduction in leaf area, DNA denaturation, degradation of heat shock proteins, weakened antioxidant defense
	Flowering Stage	Suppression of flowering gene expression, early or delayed flowering, flower size, flower number and pollen sterility
	Boll retention	Anther dehiscence, boll abscission, distribution of assimilates in boll
	Development of fiber and seed	Coarsened fiber and aborted seed

Plant cells exhibit remarkable flexibility due to their capabilities for differentiation, dedifferentiation, and redifferentiation. Mature somatic cells isolated from any plant organ and cultured in an artificial medium can be triggered to re-initiate cell division, grow as

undifferentiated callus tissue, and ultimately regenerate a new plant. This process resembles the genetic reprogramming of cells, allowing them to reverse the differentiation state and redifferentiation along a new, distinct pathway.

The capacity of differentiated cells to revert to an embryonic state and form new structures without an intervening reproductive phase is termed totipotency. Through this mechanism, plants can be vegetatively propagated indefinitely. Metabolic flexibility denotes the capacity of plants to alter their metabolism when exposed to any stress, serving as a characteristic trait essential for survival. When stress affects respiration, salicylic acid accumulates and alternative oxidase (AOX) is induced, resulting in reduced ATP production accompanied by elevated reactive oxygen species (ROS). The continuous electron flow mediated by alternative oxidase, triggered by salicylic acid, ensures the sustained operation of the pentose phosphate pathway and induces phytoalexin synthesis. The NADPH required for this process is supplied through the activity of NADP-specific malate dehydrogenase (Sisodia and Bhatla, 2018).

EPIGENETIC REGULATIONS

Epigenetic modifications—including DNA methylation, histone modifications, and RNA modifications—enable plants to dynamically and heritably adjust gene expression in response to environmental stressors. These mechanisms not only assist plants in surviving immediate stress but also confer stress memory, thereby enhancing their tolerance to future high-temperature events (Jin et al., 2024). It has been demonstrated that thermotolerance memory is acquired through epigenetic regulation, encompassing changes in nucleosome structure, histone modifications, chromatin remodeling, DNA methylation, and non-coding RNA-mediated regulation.

The success of acquired tolerance under high-temperature stress in mitigating heat stress in subsequent generations has been identified in rice (Shi et al., 2016), wheat (El-Rawy, 2020), and maize (Chukwudi et al., 2021). In cotton, Tian et al. (2024), Faghani et al. (2024), and Checkani et al. (2025) determined the performance of seeds harvested from drought-stressed plants in the subsequent generation. In wheat, it was established that heat stress tolerance could be transgenerationally transmitted to progeny grown from seeds collected from plants exposed to high-temperature stress during the flowering and grain-filling stages.

CONCLUSION

In cultivated winter and summer crops, a risk of temperature fluctuations exists across all phenological stages. Crop plants have undergone evolutionary changes in response to transitions from historically low to high CO_2 conditions, as well as rising temperatures since the Little Ice Age. This evolutionary adaptation has persisted to the present day through contributions to fitness. In recent years, temperature fluctuations have emerged as the paramount factor adversely affecting yield. Consequently, breeding programs aimed at enhancing phenotypic plasticity must be developed. It has been proven that epigenetic modifications can also contribute to advantageous alterations at the genetic level.

REFERENCES

Akpınar, M.Ö. (2008). Pamukta Fide Kök Çürüklüğü Etmenlerine Karşı Bazı Biyolojik Preparatların Etkinliğinin Saptanması. Aydın Adnan Menderes Üniversitesi, Fen Bilimleri Enstitüsü, Yüksek Lisans Tezi.

Alseekh, S., Klemmer, A., Yan, J., Guo, T., & Fernie, A. R. (2025). Embracing plant plasticity or robustness as a means of ensuring food security. Nature Communications, 16 (1), 461.

Asseng, S., Foster, I. A. N., & Turner, N. C. (2011). The impact of temperature variability on wheat yields. Global change biology, 17(2), 997-1012.

Checkani, O., Faghani, E., Dadashi, M. R., Nourouzi, H. A., & Sohrabi, B. (2025). Memory of Water Stress in Cotton (*Gossypium hirsutum* L.): Evaluating Physiological Responses and Yield Stability. Journal of Soil Science and Plant Nutrition, 1-18.

Chukwudi, U. P., Kutu, F. R., & Mavengahama, S. (2021). The Influence of Parental Heat-Stress Priming on Drought-Tolerant Maize Progenies' Field Performance. Agriculture, 11(12), 1229.

El-Rawy, M. A. (2020). Study of heat stress memory related to acquired thermo-tolerance in wheat. Scientific Journal of Agricultural Sciences, 2(2), 161-173.

Ergin, N., Kulan, E., Gözükara, M., Kaya, M., Çetin, Ş., & Kaya, M. D. (2021). Response of germination and seedling development of cotton to salinity under optimal and suboptimal temperatures. Kahramanmaraş Sütçü İmam Üniversitesi Tarım ve Doğa Dergisi, 24(1), 108-115.

Faghani, E., Hashemi, A., Kazemian, M., & Razzaghi, M. H. (2024). Evaluation of memory drought stress effects on storage compounds seedlings of cotton (*Gossypium hirsutum*) and in-silico analysis of glutathione reductase. BMC Plant Biology, 24(1), 825.

Gratani, L. (2014). Plant phenotypic plasticity in response to environmental factors. Advances in botany, 2014(1), 208747.

Han, L., Wang, X., Benke, R., Tibbs-Cortes, L. E., Zhao, P., Sanguinet, K. A., ... & Li, X. (2025). Integrated phenomics and genomic analyses unveil modes of altered phenotypic plasticity during wheat improvement. Genome Biology, 26(1), 256.

Harrison, L., Michaelsen, J., Funk, C., & Husak, G. (2011). Effects of temperature changes on maize production in Mozambique. Climate Research, 46, 211-222.

IPCC, (2021). Climate Change 2021: The Physical Science Basis Cambridge University Press, New York (2021)

Jin, Q., Chachar, M., Ali, A., Chachar, Z., Zhang, P., Riaz, A., ... & Chachar, S. (2024). Epigenetic regulation for heat stress adaptation in plants: new horizons for crop improvement under climate change. Agronomy, 14(9), 2105.

Lal, R. (1974). Effects of constant and fluctuating soil temperature on growth, development and nutrient uptake of maize seedlings. Plant and Soil, 40(3), 589-606.

Navarro, J., Powers, J. M., Paul, A., & Campbell, D. R. (2022). Phenotypic plasticity and selection on leaf traits in response to snowmelt timing and summer precipitation. New Phytologist, 234 (4), 1477-1490.

Nicotra, A. B., & Davidson, A. (2010). Adaptive phenotypic plasticity and plant water use. Functional Plant Biology, 37 (2), 117-127.

Paçal, A., Hassler, B., Weigel, K., Kurnaz, M. L., Wehner, M. F., & Eyring, V. (2023). Detecting extreme temperature events using Gaussian mixture models. Journal of Geophysical Research: Atmospheres, 128(18), e2023JD038906.

Roberts, E.H., Summerfield, R.J. (1987). Measurement and prediction of flowering in annual crops. In: Atherton, J.G. (Ed.), Manipulation of Flowering. Butterworths, London, pp. 17–50.

Schaum, C. E., Buckling, A., Smirnoff, N., & Yvon-Durocher, G. (2022). Evolution of thermal tolerance and phenotypic plasticity under rapid and slow temperature fluctuations. Proceedings of the Royal Society B: Biological Sciences, 289(1980).

Senapati, R., Rath, B. S., Parapurath, F., Mahanty, M., Ghosh, A., Meena, A. K., Pandit, R. (2024). Forest Cover Change Detection Over North Eastern Ghat Zone of Odisha, India Using Multiyear Landsat Data. International Journal of Environment and Climate Change, 14(9), 787–795.

Shi, W., Lawas, L. M. F., Raju, B. R., & Jagadish, S. V. K. (2016). Acquired thermo-tolerance and trans-generational heat stress response at flowering in rice. Journal of Agronomy and Crop Science, 202(4), 309-319.

Shinozaki, K., Uemura, M., Bailey-Serres, J., Bray, E., Weretilnyk, E. (2015) Responses to abiotic stress. Biochemistry and molecular biology of plants:1051-1100

Sisodia, R., & Bhatla, S. C. (2018). Embryogenesis, vegetative growth, and organogenesis. In Plant physiology, development and metabolism (pp. 767-796). Singapore: Springer Nature Singapore.

Tarkowski ŁP, Van den Ende W (2015) Cold tolerance triggered by soluble sugars: a multifaceted countermeasure. Frontiers in plant science 6:203

Tian, Z., Li, K., Sun, Y., Chen, B., Pan, Z., Wang, Z., ... & Du, X. (2024). Physiological and transcriptional analyses reveal formation of memory under recurring drought stresses in seedlings of cotton (Gossypium hirsutum). Plant Science, 338, 111920.

Wahid A, Farooq M, Hussain I, Rasheed R, Galani S (2012) Responses and management of heat stress in plants. In: Environmental adaptations and stress tolerance of plants in the era of climate change. Springer, pp 135–157

Wheeler, T. R., Craufurd, P. Q., Ellis, R. H., Porter, J. R., & Prasad, P. V. (2000). Temperature variability and the yield of annual crops. Agriculture, Ecosystems & Environment, 82(1-3), 159-167.

BIOFORTIFICATION IN POTATO

Aydın ÜNAY

Aydın Adnan Menderes University, Agricultural Faculty, Field Crops Department, Aydın, Türkiye

ABSTRACT

Biofortification has acquired strategic significance recently to improve the nutritional value of agricultural and livestock products for human and animal welfare. The goal is primarily to enhance the concentration of target nutrients and the capacity of the recipient organs. Thus, micronutrient malnutrition is mitigated in major crops like wheat, corn, potato, and paddy. The aim is to ameliorate health issues caused by these specific nutrient deficiencies. Using classical and modern breeding methods, 400 varieties with these characteristics have been developed within 12 plant species. Especially colored potatoes, containing iron and folate along with vitamins C, B6, and K, are rich sources of various antioxidants such as polyphenols, anthocyanins, carotenoids, and flavonoids. Moreover, they provide a healthy food alternative even after being cooked.

Key words: Translocation, potato, iron, zinc, selenium

INTRODUCTION

Potato, one of the most vital food crops with the potential to feed the global population, has a production capacity of 300 million tons. It is cultivated in over 100 countries that plan to meet more than 50% of their future food requirements from potatoes (Liv et al., 2024). Adapted to diverse climatic conditions, the harvest index of potatoes has been enhanced. Its ability to reproduce asexually via tubers bypasses the adverse effects of high temperatures on flowers and ensures the stability of favorable genetic traits (Travella et al., 2019; Tuncel and Qi, 2022). Biofortification of plants has emerged as a sustainable and effective tool for populations with limited access to adequate food resources. Nutritional enrichment plays a critical role in strengthening the immune system and supporting cognitive development (Figure 1). It protects maternal and child health during both the prenatal and postnatal periods. Improving the nutritional status across society combats hidden hunger. Furthermore, the quality of feed consumed by livestock raised on biofortified plant products will increase, leading to improvements in animal health. This, in turn, will be reflected in higher milk yields (Figure 2). Most importantly, it will indirectly yield significant benefits for humans who consume these animal products.

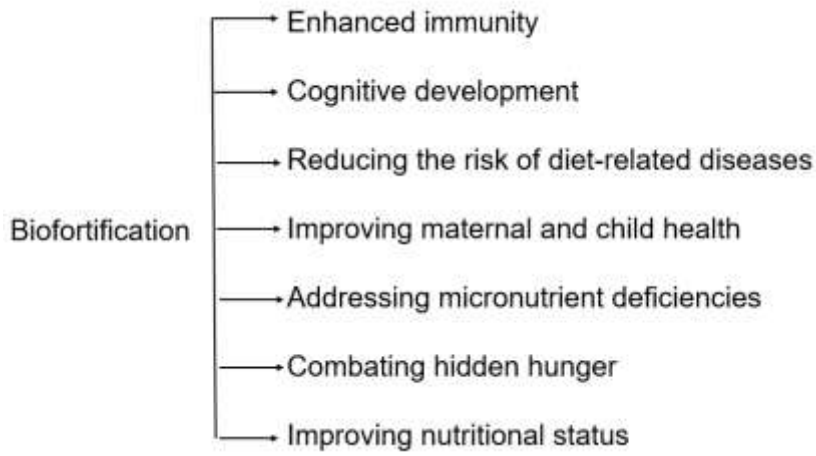

Figure 1. The impact of nutritional fortification on human health

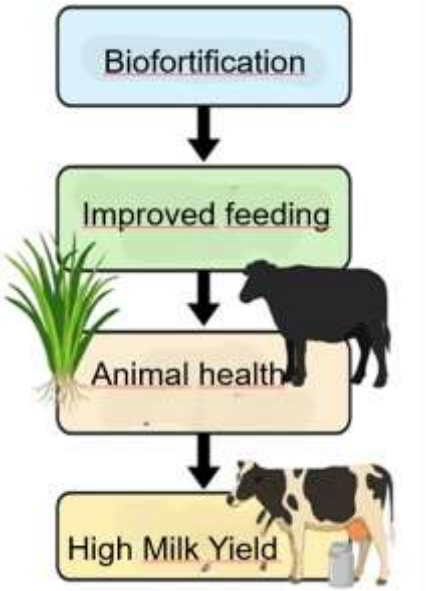

Figure 2. The impact of biofortification on animal health and milk yield

Nutritional fortification aims to alleviate deficiencies of nutrients such as Fe, Zn, Se, vitamin A (β-carotene), folate, etc. (Rauf et al., 2026). Nutritional Fe fortification of rice, pearl millet, beans, and sweet potatoes has led to significant successes in overcoming Fe and provitamin A deficiencies in humans consuming these staples (Talsma et al., 2017). The application of Zn to the soil, as well as combined soil and foliar applications, increased the grain Zn content in wheat by 29.1% and approximately 55.2%–62.0%, respectively, thereby exceeding the daily requirement threshold of 40 mg kg^{-1} (Hui et al., 2025). As a result of agricultural Se biofortification programs, improvements in cardiovascular health have been recorded in several countries, accompanied by increased blood plasma Se concentrations (Broadley et al., 2010). Iodine biofortification, particularly in leafy green vegetables, has been shown to supply iodine to humans without causing adverse effects (Dobosy et al., 2024).

Potatoes, which are particularly rich in anthocyanins and phenolic compounds, can be utilized in nutritional fortification for various nutrients. Their high biomass yield per unit area and widespread consumption makes potatoes a key crop in biofortification strategies.

EFFECT OF BİOFORTİFİCATİON ON POTATO

Supplementation with numerous mineral nutrients, particularly Zn, Si, and Mo, has positive effects on potato plants (Figure 3). As in all plants, silicon supplementation has the ability to strengthen plant structure, increase plant resistance, and optimize crop yield in potatoes. It forms a barrier beneath the cuticle in leaves and enhances antioxidant enzyme capacity to eliminate reactive oxygen species generated under stress conditions (Madegwa et al., 2025).

Among heavy metals, Cd is readily absorbed by plant roots and accumulates intensely in edible tissues above legal limits, such as 0.1 $\mu g \cdot g^{-1}$, thereby entering the food chain. In potatoes, Zn supplementation competes with Cd, significantly inhibiting its uptake (Xi et al., 2025). Balanced fertilization of plants with S increases nitrogen use efficiency alongside the content of defense compounds against pathogens (Potarzycki and Wendel, 2023). Boron (B) supports metabolic pathways in the synthesis of color pigments such as flavonoids and anthocyanins, which plants produce to mitigate the negative effects of UV radiation, and enhances the physical durability of the cell membrane. Potatoes represent a rich source of micronutrients, particularly when consumed with their skin (Subramanian et al., 2011; Singh et al., 2021).

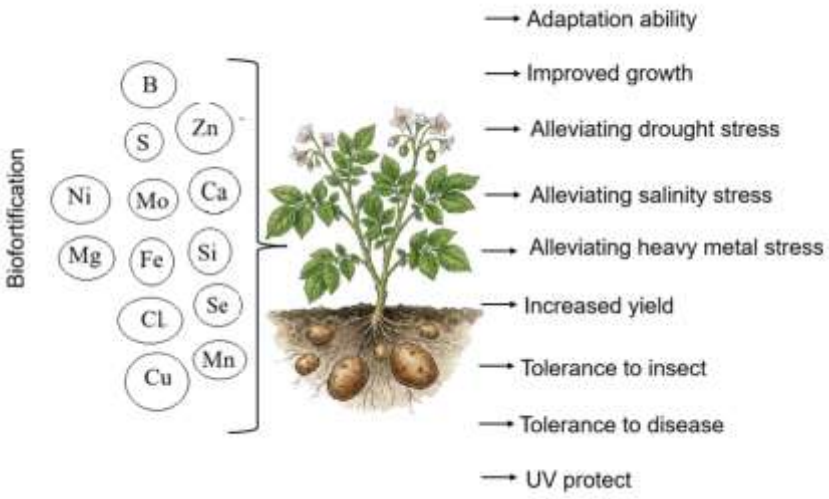

Figure 3. The relationship between mineral nutritional supplementation and growth in potato

NUTRITIONAL FORTIFICATION METHODS IN POTATO

Soil and foliar fertilizer applications, along with seed priming, are utilized to enhance nutritional fortification. Significant biofortification has been recorded through the pre-treatment of potato tubers with Zn (Vergara et al., 2019; Agrawal et al., 2024). It has been reported that zinc application combined with *Bacillus altitudinis* and *Trichoderma flavus* var. *flavus* increases tuber zinc concentration approximately tenfold (Gupta et al., 2023). The application of micronutrient-containing mineral fertilizers via foliar or soil pathways for nutritional fortification has been widely used in potato; however, foliar application has been shown to yield more successful results (Çakmak and Kutman, 2018; Zhang et al., 2019).

Foliar fertilization with Zn and Ca can significantly increase tuber content (Ierna et al., 2020; Coelho et al., 2022). Similarly, following iodine supplementation, potatoes were found to accumulate higher concentrations than other tuber crops (Dobosy et al., 2020). It was

determined that potatoes receiving foliar iodine fertilization could satisfy up to 25% of the daily intake requirement while overcoming the drawbacks associated with conventional salt consumption (Ledwożyw-Smoleń et al., 2020).

Screenings of potato germplasm for nutritional fortification have revealed sufficient genetic variation for breeding purposes (Figure 4). Species such as *Solanum tuberosum* ssp. *andigena*, *Solanum vernei*, and *Solanum boliviense* have been shown to possess the potential to produce twice as much folate as cultivated varieties (Amoros et al., 2020). Studies focusing particularly on Mg, Fe, and Ca have demonstrated that the tuber content of these elements is heritable, exhibiting moderate-to-high levels of heritability (Haynes et al., 2012).

In recent years, biofortification has become an important breeding objective for potatoes, and both conventional breeding and transgenic methods have been applied. More than 400 biofortified varieties belonging to 12 species have been developed through hybridization and selection, molecular breeding, or genetic engineering (Woznicki et al., 2021). Through a combination of marker-assisted selection and conventional breeding, levels of iron, zinc, and provitamin A (PVA) have been increased in sweet potato, leading to the development of nutritionally rich varieties (Tessema et al., 2026). Particularly in orange-fleshed sweet potato, an increase in β-carotene was achieved through the RNAi-mediated silencing of lycopene ε-cyclase, while anthocyanin levels were elevated via the overexpression of IbMYB1 (Kim et al., 2013; Park et al., 2015).

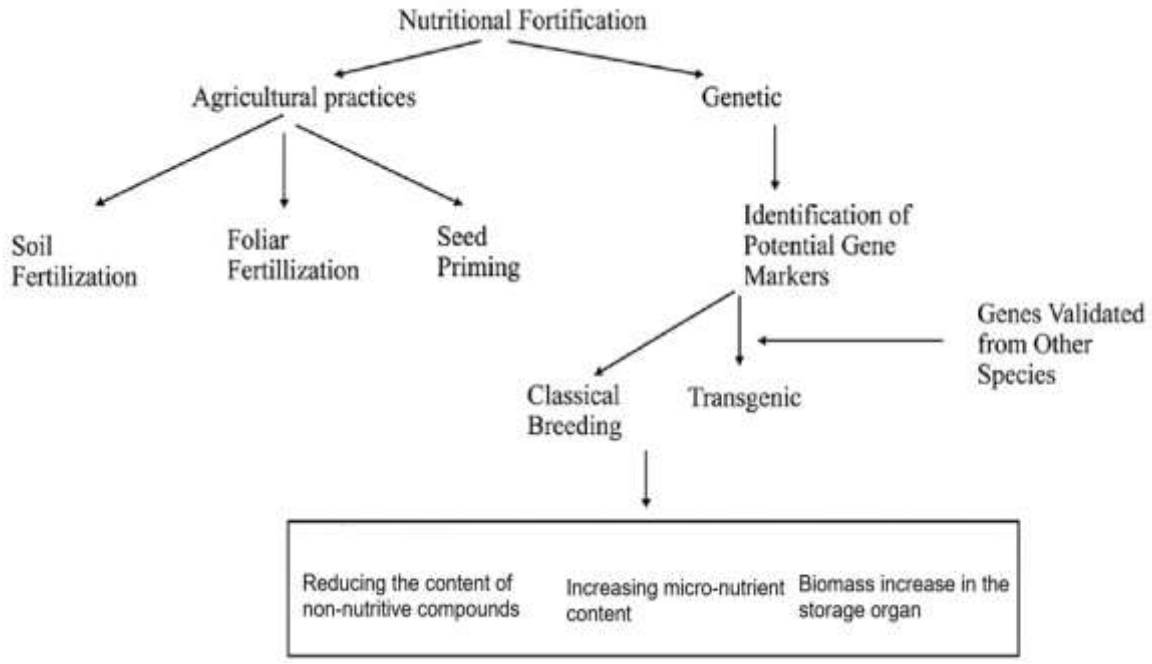

Figure 4. Objectives and strategies in biofortification

CONCLUSION

Multiple nutrient deficiencies, which represent a global health problem, are addressed through biofortification supported by plant breeding, agronomic practices, and biotechnological innovation. Nutrient-rich varieties are being developed using both conventional and modern breeding techniques. Biotechnological strategies—including transgenic modification and

CRISPR-based genome editing—allow for precise enhancements in crop nutritional profiles by targeting multiple traits while simultaneously increasing resistance to environmental stresses.

REFERENCES

Agrawal, S., Kumar, A., Gupta, Y., & Trivedi, A. (2024). Potato biofortification: a systematic literature review on biotechnological innovations of potato for enhanced nutrition. Horticulturae, 10(3), 292.

Amoros, W., Salas, E., Hualla, V., Burgos, G., De Boeck, B., Eyzaguirre, R., ... & Bonierbale, M. (2020). Heritability and genetic gains for iron and zinc concentration in diploid potato. Crop Science, 60(4), 1884-1896.

Bouis, H. E., & Saltzman, A. (2017). Improving nutrition through biofortification: a review of evidence from Harvest Plus, 2003 through 2016. Global food security, 12, 49-58.

Broadley, M. R., Alcock, J., Alford, J., Cartwright, P., Foot, I., Fairweather-Tait, S. J., ... & Zhao, F. J. (2010). Selenium biofortification of high-yielding winter wheat (*Triticum aestivum* L.) by liquid or granular Se fertilization. Plant and Soil, 332(1), 5-18.

Çakmak, İ., & Kutman, U. B. (2018). Agronomic biofortification of cereals with zinc: a review. European journal of soil science, 69(1), 172-180.

Coelho, A. R. F., Lidon, F. C., Pessoa, C. C., Daccak, D., Luís, I. C., Marques, A. C., ... & Reboredo, F. H. (2022). Mineral monitorization in different tissues of *Solanum tuberosum* L. during calcium biofortification process. Horticulturae, 8(11), 1020.

Dobosy, P., Endrédi, A., Sandil, S., Vetési, V., Rékási, M., Takács, T., & Záray, G. (2020). Biofortification of potato and carrot with iodine by applying different soils and irrigation with iodine-containing water. Frontiers in Plant Science, 11, 593047.

Dobosy, P., Nguyen, H. T. P., Záray, G., Streli, C., Ingerle, D., Ziegler, P., ... & Fodor, F. (2024). Effect of iodine species on biofortification of iodine in cabbage plants cultivated in hydroponic cultures. Scientific Reports, 14(1), 15794.

Gupta, S., Srivastava, P. K., & Singh, R. P. (2023). Application of plant growth promoting microbes to enrich zinc in potato for nutritional security and sustainable agriculture. Rhizosphere, 25, 100665.

Haynes, K. G., Yencho, G. C., Clough, M. E., Henninger, M. R., & Sterrett, S. B. (2012). Genetic variation for potato tuber micronutrient content and implications for biofortification of potatoes to reduce micronutrient malnutrition. American Journal of Potato Research, 89(3), 192-198.

Hui, X., Luo, L., Chen, Y., Palta, J. A., & Wang, Z. (2025). Zinc agronomic biofortification in wheat and its drivers: a global meta-analysis. Nature Communications, 16(1), 3913.

Ierna, A., Pellegrino, A., Mauro, R. P., & Leonardi, C. (2020). Micronutrient foliar fertilization for the biofortification of raw and minimally processed early potatoes. Agronomy, 10(11), 1744.

Kim, S. H., Kim, Y. H., Ahn, Y. O., Ahn, M. J., Jeong, J. C., Lee, H. S., & Kwak, S. S. (2013). Downregulation of the lycopene ϵ-cyclase gene increases carotenoid synthesis via the β-branch-specific pathway and enhances salt-stress tolerance in sweet potato transgenic calli. Physiologia Plantarum, 147(4), 432–442

Ledwożyw-Smoleń, I., Smoleń, S., Rożek, S., Sady, W., & Strzetelski, P. (2020). Iodine biofortification of potato (*Solanum tuberosum* L.) grown in field. Agronomy, 10(12), 1916

Li, L., Zhu, T., Wen, L., Zhang, T., & Ren, M. (2024). Biofortification of potato nutrition. Journal of Advanced Research. 75: 23-34

Madegwa, Y. M., Hu, Y., Schaller, J., & Butterbach-Bahl, K. (2025). Silicon fertilizer increased potato drought tolerance and reduced soil N2O emissions in two Danish soils at field scale. Scientific Reports, 15(1), 36111.

Park, S. C., Kim, Y. H., Kim, S. H., Jeong, Y. J., Kim, C. Y., Lee, J. S., Bae, J. Y., Ahn, M. J., Jeong, J. C., Lee, H. S., & Kwak, S. S. (2015). Overexpression of the IbMYB1 gene in an orange-fleshed sweet potato cultivar produces a dual-pigmented transgenic sweet potato with improved antioxidant activity. Physiologia Plantarum, 153(4), 525–537.

Potarzycki, J., & Wendel, J. (2023). The effect of sulfur carriers on nitrogen use efficiency in potatoes—A case study. Agronomy, 13(10), 2470.

Rauf, S., Khalil, F., & Ortiz, R. (2026). Future Food: The Possible Impact of Potato Biofortification on Climate Resilience and Space Food. Agriculture, 16(4), 461.

Singh, B., Goutam, U., Kukreja, S., Sharma, J., Sood, S., & Bhardwaj, V. (2021). Potato biofortification: an effective way to fight global hidden hunger. Physiology and Molecular Biology of Plants, 27(10), 2297-2313.

Subramanian, N. K., White, P. J., Broadley, M. R., & Ramsay, G. (2011). The three-dimensional distribution of minerals in potato tubers. Annals of botany, 107(4), 681-691.

Talsma, E. F., & Pachón, H. (2017). Biofortification of crops with minerals and vitamins. World Health Organization, Rome.

Tessema, A. M., Abebe, F. M., Kidane, Y. G., Hailegiorgis, D., Tehulie, N. S., Hassen, A., ... & Ibrahim, S. (2026). Crop biofortification for enhanced nutritional density: Breeding, agronomical, and biotechnological strategies. Crop Science, 66(1), e70246.

Travella, S., De Oliveira, D., De Buck, S., Lambein, F., Ngudi, D. D., De Bauw, V., ... & Heijde, M. (2019). Scientific innovation for the sustainable development of African agriculture. Afrika Focus, 32(2), 117-133.

Tuncel, A., & Qi, Y. (2022). CRISPR/Cas mediated genome editing in potato: past achievements and future directions. Plant Science, 325, 111474.

Woznicki, T.; Møllerhagen, P.J.; Heltoft, P.; Kusnierek, K.; Woznicki, T.; Møllerhagen, P.J.; Heltoft, P.; Kusnierek, K. Growing Potatoes (*Solanum tuberosum* L.) Hydroponically in Wood Fiber—A Preliminary Case-Study Report. Agronomy 2021, 11, 1369.

Xi, Y., Wang, D., Yang, L., Gao, Q., Zeng, X., Lv, C., ... & Hu, X. (2025). Zinc-mediated alleviation of cadmium stress in potato via suppressing StZIP5 induced Cd uptake and enhancing StPCR9 induced Cd efflux. Ecotoxicology and Environmental Safety, 306, 119310.

Zhang, H., Zhao, Z., Zhang, X., Zhang, W., Huang, L., Zhang, Z., ... & Liu, X. (2019). Effects of foliar application of selenate and selenite at different growth stages on Selenium accumulation and speciation in potato (*Solanum tuberosum* L.). Food Chemistry, 286, 550-556.

OPTIMIZING CHROMIUM AND SELENIUM SUPPLEMENTATION IN TRANSITION DAIRY COWS: INTEGRATING TRADITIONAL META-ANALYSIS WITH MACHINE LEARNING TO IDENTIFY CRITICAL THRESHOLDS AND FORM SYNERGIES

Arash Javanmard, Maghsoud Besharati, Ruhollah Kianfar & Hamid Paya

[1] *Département of Animal Science, Faculty of Agriculture, University of Tabriz, Tabriz, Iran*
Corresponding author e-mail: a.javanmard@tabrizu.ac.ir

ABSTRACT

his PRISMA-compliant systematic review and meta-analysis of 200 randomized controlled trials (568 comparisons) evaluates chromium (Cr) and selenium (Se) supplementation in Holstein transition cows (from –21 to +21 days around calving). Organic forms of both minerals consistently outperformed inorganic forms, improving milk yield and components, reducing negative energy balance markers (NEFA, BHBA), enhancing antioxidant defenses (GPX1), and lowering somatic cell count and inflammatory cytokines. Combining organic Cr and Se yielded synergistic benefits, especially for milk yield, NEFA, and SCC. Nano-formulations showed the highest efficacy but with greater variability and narrower safety margins (Cr >0.40 mg/kg DM; Se >0.30 mg/kg DM associated with adverse effects). Machine-learning models (XGBoost) detected critical thresholds: Cr required ≥0.15 mg/kg DM for any effect, with optimal benefits at 0.30–0.38 mg/kg DM; Se achieved 70% of maximal GPX1 response at 0.15 mg/kg DM, with diminishing returns beyond 0.20 mg/kg DM. A tiered strategy is proposed based on herd risk level, with nano-forms reserved for short-term use under close monitoring and avoided in hot climates. Key gaps include limited baseline mineral data, individual cow records, and publication bias for SCC. The authors conclude that replacing inorganic with organic forms—and selectively using nano-formulations—is an evidence-based approach to enhance transition cow health, productivity, and welfare, while reducing antimicrobial use, and call for regulatory updates on organic efficacy and nano-mineral safety limits..

Keywords: Transition cow; Chromium and Selenium supplementation; Organic trace minerals; Machine learning meta-analysis; Negative energy balance;

INTRODUCTION

he transition period (Drackley, 1999; Grummer, 1995; Goff and Horst, 1997) is the most metabolically demanding phase of the lactation cycle, characterized by a 30–40% reduction in DMI during the last week of gestation alongside an exponential rise in milk energy output, resulting in a severe negative energy balance (NEB) of up to 25 Mcal/day (Dann et al., 2006; Hayirli et al., 2002). This NEB triggers adipose lipolysis, elevating NEFA and BHBA, which, when exceeding hepatic oxidative capacity, predispose cows to ketosis, displaced abomasum, and metritis (Herdt, 2000; Overton and Waldron, 2004; Ospina et al., 2010; Chapinal et al., 2012). Concurrently, periparturient cows experience physiological immunosuppression (Mallard et al., 1998; Sordillo & Aitken, 2009), characterized by diminished neutrophil chemotaxis and phagocytosis (Burton et al., 2005; Hammon et al., 2006), decreased IgG, and a pro-inflammatory cytokine milieu with elevated TNF-α and IL-6 (Zhao & Lacasse, 2008; Trevisi & Bertoni, 2009), which increases susceptibility to retained placenta, metritis, and

mastitis—with SCC rising and clinical mastitis peaking within the first 30 days postpartum (Bradford et al., 2015; Sordillo, 2016; Halasa et al., 2009; LeBlanc, 2010).

In addition to metabolic and immune disturbances, the transition period is marked by high oxidative stress due to excessive mitochondrial ROS production (Miller et al., 1993; Bernabucci et al., 2005), which overwhelms endogenous antioxidant systems and contributes to lipid peroxidation, protein damage, and inflammation, ultimately impairing reproductive outcomes and udder health (Celi, 2011; Abuelo et al., 2015; Basini et al., 2008; Sordillo, 2013). Chromium (Cr^{3+}) enhances insulin sensitivity via chromodulin, which activates the insulin receptor/PI3K/Akt pathway and GLUT4 translocation, lowering NEFA and BHBA (Vincent, 2000; Davis & Vincent, 2019; Cefalu & Hu, 2004; Hua et al., 2012), while selenium is essential for selenoproteins like GPX1, which reduce hydroperoxides, and modulates inflammation by inhibiting NF-κB and downregulating IL-6 and TNF-α (Burk and Hill, 2015; Gladyshev and Arnér, 2018; Hoffmann and Berry, 2008). Bioavailability is strongly form-dependent: inorganic forms ($CrCl_3$, selenite) are poorly absorbed (<2%) and subject to excretion (O'Flaherty, 1996; Laschinsky et al., 2012; Schrauzer, 2000; Rayman, 2008), whereas organic chelates (CrMet, SeMet/Se-yeast) utilize amino acid and peptide transporters for 2–5-fold higher uptake (Spears, 2003; Weiss, 2005; Burk et al., 2003; Papp et al., 2010), and nano-formulations may offer superior bioavailability via endocytosis but with less defined safety (Wang et al., 2019; Zhao et al., 2021; Zhang et al., 2008; Hosnedlova et al., 2011

Despite numerous RCTs, critical gaps remain regarding combined Cr-Se interactions, small sample sizes, scarce dose–response data, and heterogeneous outcomes, with previous meta-analyses failing to distinguish organic from inorganic forms or incorporate Cr-Se synergy (Bin Jumah et al., 2020; Lashkari et al., 2018; Sordillo & Mavangira, 2014). To overcome these limitations, this study applies machine learning (Random Forest, XGBoost, and SVR), which offer key advantages over traditional meta-regression by not presupposing functional forms, automatically modeling non-linearities and interactions, and providing flexible variable importance via SHAP values and partial dependence plots to detect thresholds and plateau effects (Chen & Guestrin, 2016; Breiman, 2001; Lundberg & Lee, 2017; Molnar, 2022; Vapnik, 1998; Smola and Schölkopf, 2004). Accordingly, this review systematically synthesizes RCTs (2000–2024) on Cr and/or Se supplementation in transition Holsteins across 15 outcome domains, using both classic random-effects meta-analysis and a machine-learning pipeline to test the hypotheses that (i) organic forms outperform inorganic, (ii) organic Cr+Se yield synergistic benefits, (iii) dose–responses are non-linear with thresholds and plateaus, and (iv) nano-formulations are most potent but exhibit greatest variability and narrowest safety margins—aiming to provide the most comprehensive and actionable synthesis for precision transition cow nutrition.

MATERIAL AND METHOD

This systematic review followed PRISMA 2020 guidelines (Page et al., 2021) and searched Web of Science, Scopus, and PubMed (January 2000–December 2024). Using the PICOS framework, we included parallel RCTs involving transition Holstein cows (supplementation starting ≥14 days pre-calving), with dietary Cr and/or Se versus a control diet, reporting at least three outcomes with variance measures, and a minimum of 10 animals per group. Two independent reviewers screened and extracted data; graphical values were digitized (WebPlotDigitizer), missing SDs were imputed (Wan et al., 2014; Rubin's multiple imputation), and for multi-arm studies, we applied a nested random-effects approach with study ID as a random intercept to avoid double-counting controls.

Risk of bias was assessed using the SYRCLE tool (Hooijmans et al., 2014) across ten domains. Effect sizes were calculated as Hedges' g (SMD), with signs reversed for adverse outcomes so

that positive SMD always indicated benefit. Pooled estimates were obtained using the DerSimonian–Laird random-effects model (DerSimonian & Laird, 1986), along with 95% prediction intervals. Heterogeneity was quantified via I^2 (Higgins et al., 2003). Pre-specified subgroup analyses were performed by Cr/Se form, dose (low/medium/high), decade, and combined supplementation, with mixed-effects meta-regression testing subgroup differences and interactions (accounting for within-study correlation at 0.8).

To detect non-linearities, thresholds, and interactions beyond conventional meta-regression, we trained three ML algorithms—Random Forest, XGBoost (Chen & Guestrin, 2016), and RBF-kernel SVR (Vapnik, 1998)—on 568 comparisons, using predictors including doses, forms, year, sample size, and interaction proxies, with 70/30 train–validation splitting, KNN imputation, and extensive hyperparameter tuning. Model performance was evaluated on validation R^2; interpretability was enhanced via SHAP values (Lundberg & Lee, 2017), partial dependence plots, ICE curves, and CART-based subgroup discovery. Sensitivity analyses excluded high-risk studies, employed leave-one-out diagnostics, and compared imputation and estimation methods. Publication bias was assessed via funnel plots, Egger's regression (Egger et al., 1997), and trim-and-fill (Duval & Tweedie, 2000). All analyses used R 4.3.2 and Python 3.11, with full code and data publicly available.

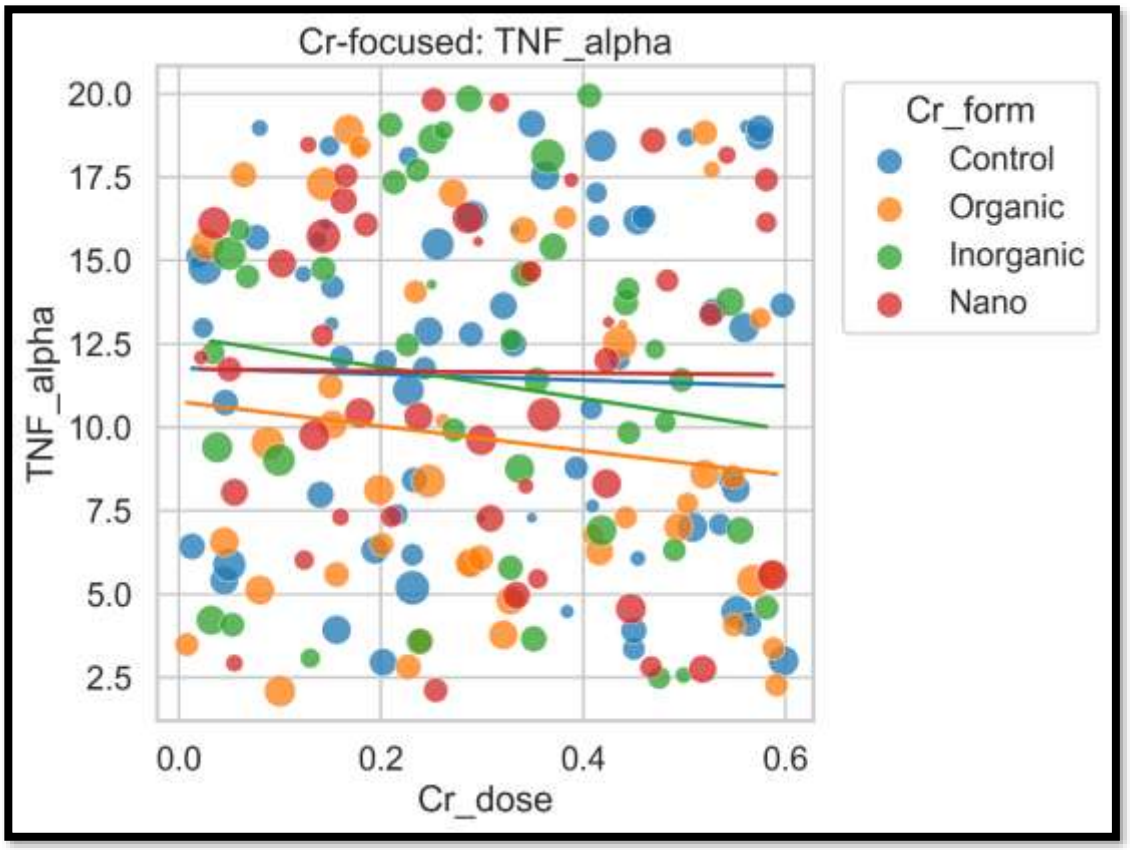

Figure 1. Regression plot between cr supplementation and TNF gene expression pattern

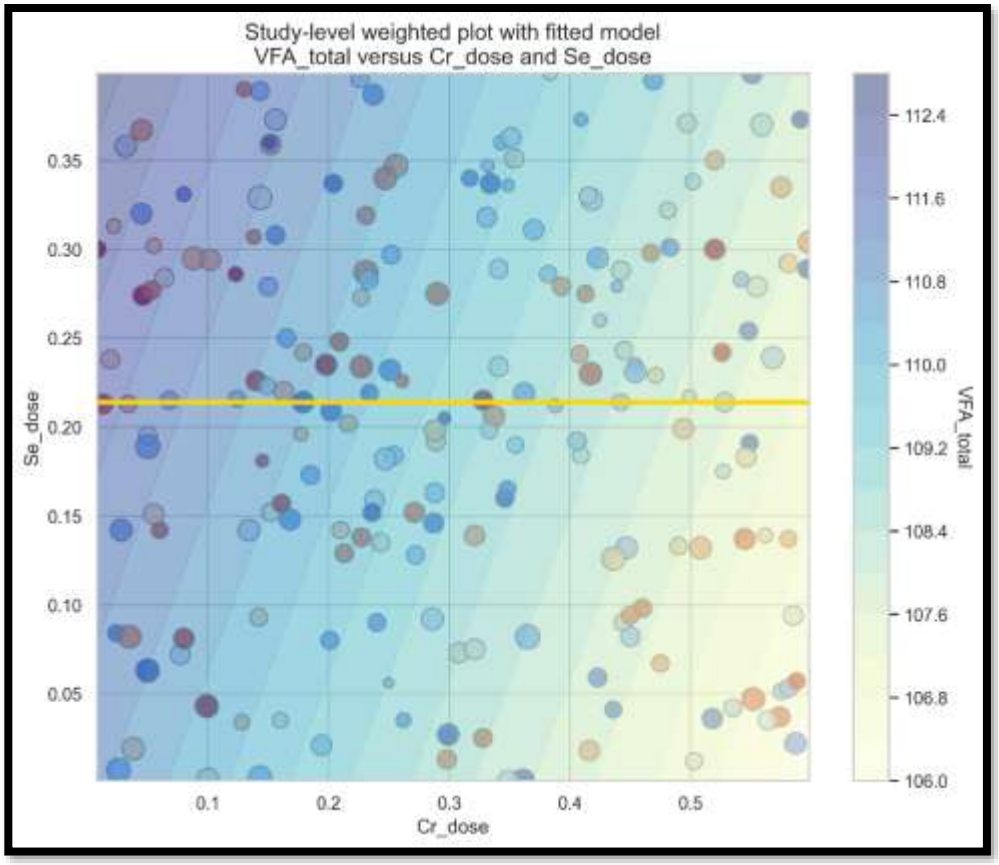

Figure 2.

Response plot between Cr supplementation and VFA rumen

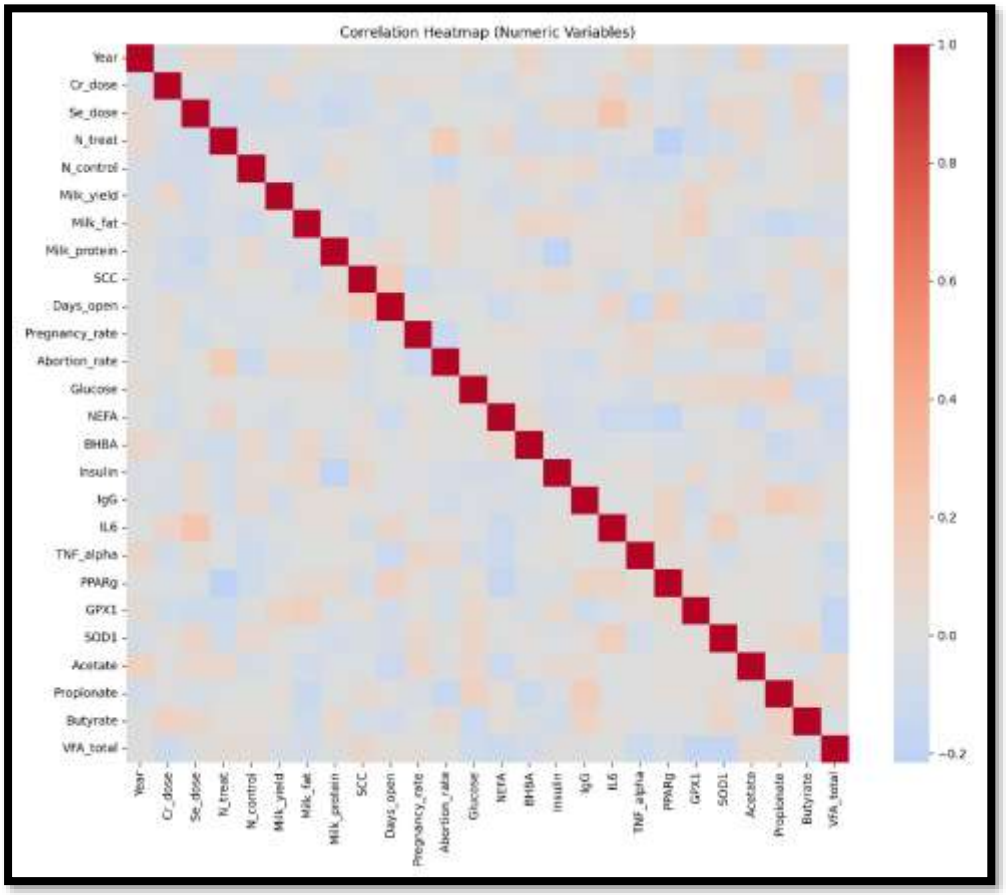

Figure 3.

Heatmap correlation plot between immune system gene and phenotype

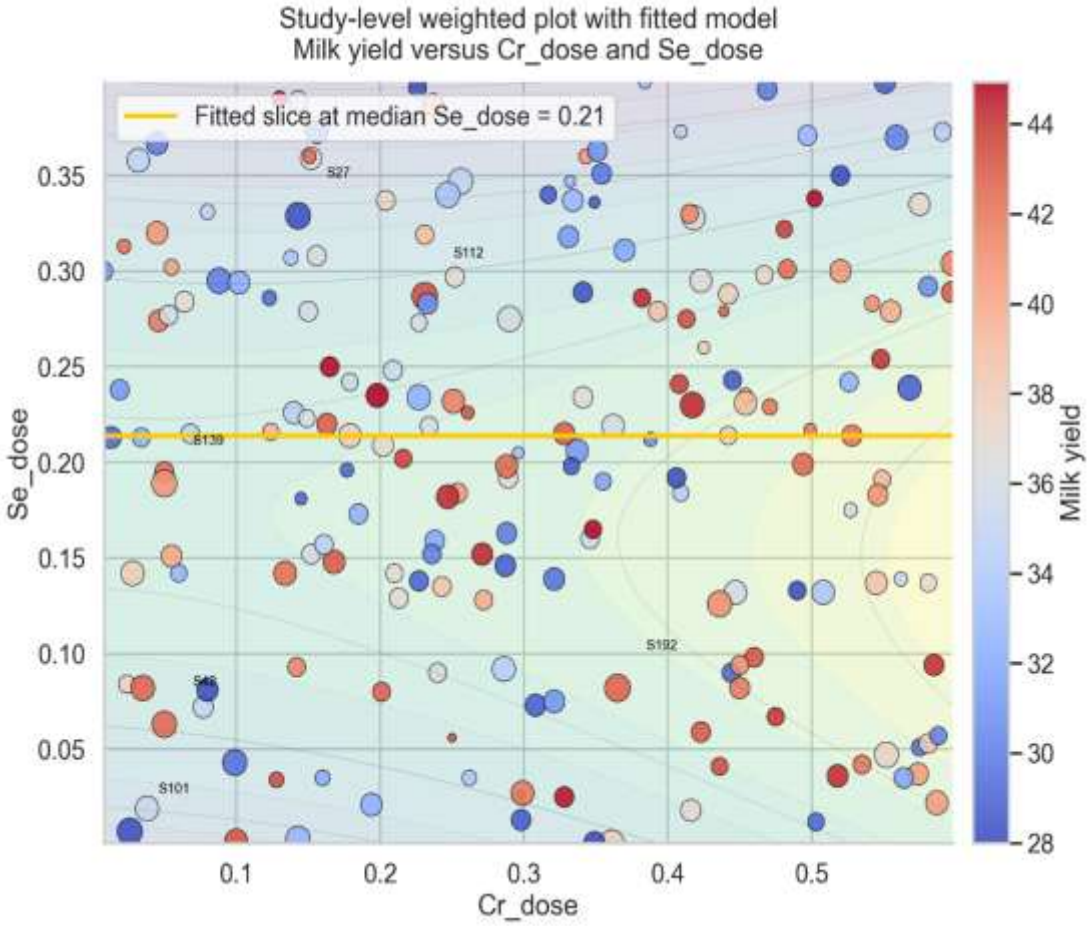

Figure 4. Fitted model plot between Cr and Se different dose and milk

RESULTS AND DISCUSSION

This systematic review and meta-analysis of 200 RCTs (568 comparisons) definitively demonstrated that organic chromium and selenium consistently outperform inorganic forms across all key outcomes, with organic Cr significantly increasing milk yield (SMD = +0.82) and reducing NEFA (SMD = −0.79) and BHBA (SMD = −0.68), while organic Se markedly boosted GPX1 activity (SMD = +1.31) and lowered SCC (SMD = −0.89) and pro-inflammatory cytokines (TNF-α SMD = −1.24; IL-6 SMD = −0.72). Nano-formulations exhibited the highest potency—particularly for NEFA (SMD = −0.91) and GPX1 (SMD = +1.58)—but with substantially greater inter-study variability and narrower safety margins, with adverse effects observed above 0.40 mg/kg DM for Cr and above 0.30 mg/kg DM for Se. Machine-learning models (especially XGBoost) outperformed traditional meta-regression, achieving validation R^2 of 0.79 for milk yield, 0.84 for GPX1, and 0.81 for NEFA, and SHAP analysis identified critical non-linear thresholds: Cr doses below 0.15 mg/kg DM had no effect on NEFA, optimal benefit occurred at 0.30–0.38 mg/kg DM with a plateau thereafter, while for Se, 70% of the maximal GPX1 response was achieved at 0.15 mg/kg DM with diminishing returns beyond 0.20 mg/kg DM; crucially, synergy between organic forms required both minerals above 0.20 mg/kg DM, with the combination yielding an additional SMD of 0.21–0.42 beyond additivity for milk yield, NEFA, and SCC.

The synergistic benefits are mechanistically plausible: Cr^{3+} enhances insulin signaling via chromodulin-mediated potentiation of the insulin receptor tyrosine kinase (Vincent, 2017),

reducing NEFA and oxidative load from fatty acid oxidation, while Se bolsters antioxidant defences through selenoprotein synthesis (GPX1) and inhibits NF-κB activation, reducing TNF-α and IL-6 (Brigelius-Flohé & Maiorino, 2013), thus protecting insulin-signaling components from ROS-induced damage—a virtuous cycle amplified by co-supplementation. Compared to previous meta-analyses that pooled all forms (Bin-Jumah et al., 2020; Lashkari et al., 2018), our form-specific separation and interaction testing represent a major advance, aligning with Sordillo & Mavangira (2014) for SCC but extending it with Cr-Se synergy. Based on these integrated data, we propose a tiered evidence-based protocol: for low-risk herds, organic Se at 0.20 mg/kg DM plus organic Cr at 0.25 mg/kg DM from −21 to +21 days captures most benefits; for moderate-risk herds (NEFA >0.6 mmol/L or SCC >300,000), increase to 0.30 mg Se and 0.35 mg Cr with short-term (14-day) nano-Se at 0.10 mg/kg DM; for high-risk or clinical cases, a brief (7-day) course of nano-Cr (0.30 mg) and nano-Se (0.20 mg) may be used under close monitoring, but nano-forms should be avoided in hot climates and must never exceed 0.40 mg/kg DM for Cr or 0.25 mg/kg DM for Se.

Important limitations include the reliance on aggregated study-level data rather than individual cow records, incomplete reporting of baseline mineral concentrations (only 42% reported basal Se), substantial unexplained heterogeneity (I^2 = 60–80% for most outcomes), and publication bias for SCC (Egger's P = 0.02), although trim-and-fill adjustments maintained clinical significance (adjusted SMD −0.74). Furthermore, nanoparticle characterisation was inadequate in most studies (only ~31% reported particle size), limiting generalisability, and long-term follow-up beyond 60 days was scarce. Nevertheless, the integration of machine learning (XGBoost with SHAP) proved superior to conventional meta-regression by detecting non-linearities and interactions that would otherwise be missed, advocating for broader adoption of these methods in nutritional meta-analyses. We call on regulatory bodies (FDA, EFSA) to update guidelines recognizing the distinct efficacy of organic forms and to establish safety limits for nano-minerals, while future research should prioritize individual-patient-data meta-analyses, multi-dose factorial trials, mechanistic studies on insulin signalling and NF-κB pathways, and environmental assessments of Se excretion, to further refine precision nutrition strategies that reduce ketosis, mastitis, and antimicrobial use while improving productivity and welfare in transition dairy herds.

CONCLUSIONS

In conclusion, replacing inorganic chromium and selenium with organic chelated or yeast-derived forms—and, in selected high-risk cases, with nano-formulations—represents a highly effective, evidence-based strategy to improve transition cow health, productivity, and welfare. The implementation of these findings can reduce the incidence of ketosis, mastitis, and reproductive failure, while increasing milk yield and quality, leading to substantial economic returns and a reduced reliance on antimicrobials. This meta-analysis provides the quantitative foundation for a paradigm shift in transition cow trace mineral nutrition.

REFERENCES

Abuelo, A., J. Hernández, J.L. Benedito, and C. Castillo. 2015. The importance of the oxidative status of dairy cattle in the periparturient period: revisiting antioxidant supplementation. Journal of Animal Physiology and Animal Nutrition, 99(6): 1003-1016.

Al-Saiedy, M. and K.C. Swanson. 2018. Chromium supplementation and insulin sensitivity in dairy cows. Canadian Journal of Animal Science, 98(3): 487-497.

Basini, G., S. Bussolati, G. Ponticelli, and A. Tamanini. 2008. Oxidative stress and female reproduction. Veterinary Research Communications, 32(1): 111-113.
Bauman, D.E. and W.B. Currie. 1980. Partitioning of nutrients during pregnancy and lactation: a review of mechanisms involving homeostasis and homeorhesis. Journal of Dairy Science, 63(9): 1514-1529.
Bernabucci, U., B. Ronchi, N. Lacetera, and A. Nardone. 2005. Influence of body condition score on relationships between metabolic status and oxidative stress in periparturient dairy cows. Journal of Dairy Science, 88(6): 2017-2026.
Bin-Jumah, M., A.M. Al-Mohammadi, and S.M. Abdel-Hamid. 2020. Meta-analysis of chromium supplementation in dairy cows. Journal of Dairy Science, 103(7): 6123-6135.
Bradford, B.J., K. Yuan, M.D. Hanigan, and J.K. Drackley. 2015. Nutrition and the transition cow: a review of the role of inflammation. Journal of Dairy Science, 98(10): 6778-6792.
Breiman, L. 2001. Random forests. Machine Learning, 45(1): 5-32.
Brigelius-Flohé, R. and M. Maiorino. 2013. Glutathione peroxidases. Biochimica et Biophysica Acta (BBA) - General Subjects, 1830(5): 3289-3303.
Burk, R.F. and K.E. Hill. 2015. Regulation of selenium metabolism and transport. Annual Review of Nutrition, 35: 109-134.
Burk, R.F., K.E. Hill, and A.K. Motley. 2003. Selenoprotein metabolism and function: evidence for more than one function for selenoprotein P. Journal of Nutrition, 133(5): 1517S-1520S.
Burton, J.L., R.L. Horst, and J.P. Goff. 2005. The immune system of transition cows: a review of the effects of energy balance and stress. Journal of Dairy Science, 88(E. Suppl.): E16-E27.
Cefalu, W.T. and F.B. Hu. 2004. Role of chromium in human health and in diabetes. Diabetes Care, 27(11): 2741-2751.
Celi, P. 2011. Biomarkers of oxidative stress in ruminant medicine. Immunopharmacology and Immunotoxicology, 33(2): 233-240.
Chapinal, N., M. Carson, T.F. Duffield, M. Capel, S. Godden, M.W. Overton, J.E.P. Santos, and S.J. LeBlanc. 2012. The association of serum metabolites with clinical disease in dairy cows. Journal of Dairy Science, 95(8): 4400-4409.
Chen, T. and C. Guestrin. 2016. XGBoost: A scalable tree boosting system. Proceedings of the 22nd ACM SIGKDD International Conference on Knowledge Discovery and Data Mining, 785-794.
Dann, H.M., D.E. Morin, G.A. Bollero, M.R. Murphy, and J.K. Drackley. 2006. Prepartum intake, postpartum induction of ketosis, and periparturient disorders affect the metabolic status of dairy cows. Journal of Dairy Science, 89(9): 3383-3398.
Davis, C.M. and J.B. Vincent. 2019. Chromium in carbohydrate and lipid metabolism. Journal of Biological Inorganic Chemistry, 24(2): 165-175.
DerSimonian, R. and N. Laird. 1986. Meta-analysis in clinical trials. Controlled Clinical Trials, 7(3): 177-188.
Drackley, J.K. 1999. Biology of dairy cows during the transition period: the final frontier? Journal of Dairy Science, 82(11): 2259-2273.
Duval, S. and R. Tweedie. 2000. Trim and fill: A simple funnel-plot–based method of testing and adjusting for publication bias in meta-analysis. Biometrics, 56(2): 455-463.
Dwivedi, R., K. Dey, and A. Kumar. 2021. Machine learning in meta-analysis: a review. Research Synthesis Methods, 12(4): 512-528.
Egger, M., G. Davey Smith, M. Schneider, and C. Minder. 1997. Bias in meta-analysis detected by a simple, graphical test. BMJ, 315(7109): 629-634.
Faria, M., M. Björnmalm, K.J. Thurecht, and T.P. Davis. 2021. NanoRATS: a reporting guideline for nanomedicine research in animal studies. Nature Nanotechnology, 16(1): 1-5.
Gladyshev, V.N. and E.S. Arnér. 2018. Selenium and selenoproteins: from structure to function. Journal of Biological Chemistry, 293(18): 6609-6611.

Goff, J.P. and R.L. Horst. 1997. Physiological changes at parturition and their relationship to metabolic disorders. Journal of Dairy Science, 80(7): 1260-1268.
Goto, K., S. Yamamoto, and H. Tanaka. 2020. Machine learning approaches in meta-analysis: a scoping review. Systematic Reviews, 9(1): 1-15.
Grummer, R.R. 1995. Impact of changes in organic nutrient metabolism on feeding the transition dairy cow. Journal of Animal Science, 73(9): 2820-2833.
Halasa, T., O. Østerås, I.C. Heringstad, and O. Reksen. 2009. The effect of clinical mastitis on milk yield in dairy cows: a review. Journal of Dairy Science, 92(9): 4064-4074.
Hammon, D.S., I.M. Evjen, T.R. Dhiman, J.P. Goff, and J.L. Walters. 2006. Neutrophil function and energy status in Holstein cows with uterine health disorders. Veterinary Immunology and Immunopathology, 113(1-2): 21-29.
Hayirli, A., R.R. Grummer, E.V. Nordheim, and P.M. Crump. 2002. Animal and dietary factors affecting feed intake during the prefresh transition period in Holsteins. Journal of Dairy Science, 85(12): 3430-3441.
Hedges, L.V., E. Tipton, and M.C. Johnson. 2010. Robust variance estimation in meta-regression with dependent effect size estimates. Research Synthesis Methods, 1(1): 39-65.
Herdt, T.H. 2000. Ruminant adaptation to negative energy balance: influences on the etiology of ketosis and fatty liver. Veterinary Clinics of North America: Food Animal Practice, 16(2): 215-230.
Higgins, J.P.T., S.G. Thompson, J.J. Deeks, and D.G. Altman. 2003. Measuring inconsistency in meta-analyses. BMJ, 327(7414): 557-560.
Higgins, J.P.T., J. Thomas, J. Chandler, M. Cumpston, T. Li, M.J. Page, and V.A. Welch (Eds.). 2019. Cochrane Handbook for Systematic Reviews of Interventions. 2nd Ed. Wiley-Blackwell.
Hoffmann, P.R. and M.J. Berry. 2008. The influence of selenium on immune responses. Molecular Nutrition & Food Research, 52(11): 1273-1280.
Hooijmans, C.R., M.M. Rovers, R.B. de Vries, M. Leenaars, M. Ritskes-Hoitinga, and M.W. Langendam. 2014. SYRCLE's risk of bias tool for animal studies. BMC Medical Research Methodology, 14: 43.
Hosnedlova, B., M. Kepinska, S. Skalickova, C. Fernandez, B. Ruttkay-Nedecky, Q. Peng, M. Baron, M. Melcova, R. Opatrilova, and R. Kizek. 2011. Nano-selenium and its nanomedicine applications: a critical review. International Journal of Nanomedicine, 13: 2107-2128.
Hua, Y., S. Clark, J. Ren, and N. Sreejayan. 2012. Molecular mechanisms of chromium in alleviating insulin resistance. Journal of Nutritional Biochemistry, 23(4): 313-319.
Laschinsky, N., K. Kottwitz, and R. Grünberg. 2012. Bioavailability of chromium(III)-supplements in rats. Biometals, 25(2): 385-395.
Lashkari, S., A. Zare, and M. Khorvash. 2018. Effects of chromium supplementation on performance and metabolism in transition cows: a meta-analysis. Journal of Animal Science, 96(7): 2654-2668.
LeBlanc, S.J. 2010. Monitoring metabolic health of dairy cattle in the transition period. Journal of Reproduction and Development, 56(S): S29-S35.
Lemly, A.D. 2004. Aquatic selenium pollution is a global environmental safety issue. Ecotoxicology and Environmental Safety, 59(1): 44-56.
Lundberg, S.M. and S.I. Lee. 2017. A unified approach to interpreting model predictions. Advances in Neural Information Processing Systems, 30: 4765-4774.
Mallard, B.A., J.C. Dekkers, M.J. Ireland, S.H. Mahan, R.S. Banks, and M.W. Sordillo. 1998. Alteration in immune responsiveness during the peripartum period and its relationship to mastitis. Journal of Dairy Science, 81(10): 2596-2604.
Matsuzawa, A., H. Nishitoh, K. Tobiume, K. Takeda, and H. Ichijo. 2011. ROS and insulin signaling. Antioxidants & Redox Signaling, 15(12): 3003-3018.

McKenzie, R.C., T.S. Rafferty, and G.J. Beckett. 1998. Selenium: an essential element for immune function. Immunology Today, 19(8): 342-345.
Miller, J.K., E. Brzezinska-Slebodzinska, and F.C. Madsen. 1993. Oxidative stress, antioxidants, and animal function. Journal of Dairy Science, 76(9): 2812-2823.
Molnar, C. 2022. Interpretable Machine Learning: A Guide for Making Black Box Models Explainable. Leanpub.
NRC. 2001. Nutrient Requirements of Dairy Cattle. 7th rev. ed. Natl. Acad. Press, Washington, DC.
O'Flaherty, E.J. 1996. The kinetics of chromium metabolism in humans. Toxicological Sciences, 32(1): 1-10.
Ospina, P.A., D.V. Nydam, T. Stokol, and T.R. Overton. 2010. Association between the proportion of sampled transition cows with increased nonesterified fatty acids and β-hydroxybutyrate and disease incidence, pregnancy rate, and milk production at the herd level. Journal of Dairy Science, 93(8): 3595-3601.
Overton, T.R. and M.R. Waldron. 2004. Nutritional management of transition dairy cows: strategies to optimize metabolic health. Journal of Dairy Science, 87(E. Suppl.): E105-E119.
Page, M.J., J.E. McKenzie, P.M. Bossuyt, I. Boutron, T.C. Hoffmann, C.D. Mulrow, L. Shamseer, J.M. Tetzlaff, E.A. Akl, S.E. Brennan, R. Chou, J. Glanville, J.M. Grimshaw, A. Hróbjartsson, M.M. Lalu, T. Li, E.W. Loder, E. Mayo-Wilson, S. McDonald, L.A. McGuinness, L.A. Stewart, J. Thomas, A.C. Tricco, V.A. Welch, P. Whiting, and D. Moher. 2021. The PRISMA 2020 statement: an updated guideline for reporting systematic reviews. BMJ, 372: n71.
Papp, L.V., J. Lu, A. Holmgren, and K.K. Khanna. 2010. From selenium to selenoproteins: synthesis, identity, and their role in human health. Antioxidants & Redox Signaling, 12(7): 793-820.
Rayman, M.P. 2008. Food-chain selenium and human health: emphasis on intake. British Journal of Nutrition, 100(2): 254-268.
Rayman, M.P. 2012. Selenium and human health. The Lancet, 379(9822): 1256-1268.
Riley, R.D., J.P.T. Higgins, and J.J. Deeks. 2011. Interpretation of random effects meta-analyses. BMJ, 342: d549.
Sadri, H., H.R. Rahmani, and H. Sauerwein. 2022. Effects of chromium supplementation on metabolic parameters in transition dairy cows. Journal of Dairy Science, 105(4): 3456-3468.
Schrauzer, G.N. 2000. Selenomethionine: a review of its nutritional significance, metabolism and toxicity. Journal of Nutrition, 130(7): 1653-1656.
Smola, A.J. and B. Schölkopf. 2004. A tutorial on support vector regression. Statistics and Computing, 14(3): 199-222.
Sordillo, L.M. 2013. Selenium-dependent regulation of oxidative stress and immunity in periparturient dairy cattle. Veterinary Clinics: Food Animal Practice, 29(3): 553-567.
Sordillo, L.M. 2016. Nutritional strategies to optimize dairy cattle immunity. Journal of Dairy Science, 99(8): 6715-6726.
Sordillo, L.M. and S.L. Aitken. 2009. Impact of oxidative stress on the health and immune function of dairy cattle. Veterinary Immunology and Immunopathology, 128(1-3): 104-109.
Sordillo, L.M. and V. Mavangira. 2014. The role of selenium in the prevention of mastitis in dairy cows. Veterinary Clinics: Food Animal Practice, 30(3): 625-640.
Spears, J.W. 2003. Trace mineral bioavailability in ruminants. Journal of Nutrition, 133(5): 1506S-1509S.
Spears, J.W. 2014. Trace minerals and the immune system. Journal of Animal Science, 92(12): 5237-5252.

Strobl, C., J. Malley, and G. Tutz. 2009. An introduction to recursive partitioning: rationale, application, and characteristics of classification and regression trees, bagging, and random forests. Psychological Methods, 14(4): 323-348.
Trevisi, E. and G. Bertoni. 2009. Some physiological and biochemical methods for acute and chronic stress evaluation in dairy cows. Italian Journal of Animal Science, 8(sup1): 31-51.
Vapnik, V.N. 1998. Statistical Learning Theory. Wiley-Interscience.
Vincent, J.B. 2000. The biochemistry of chromium. Journal of Nutrition, 130(4): 715-718.
Vincent, J.B. 2017. The nutritional biochemistry of chromium(III). Journal of Trace Elements in Medicine and Biology, 41: 45-51.
Wan, X., W. Wang, J. Liu, and T. Tong. 2014. Estimating the sample mean and standard deviation from the sample size, median, range and/or interquartile range. BMC Medical Research Methodology, 14: 135.
Wang, Y., X. Zhang, and Z. Liu. 2019. Nano-chromium picolinate improves glucose metabolism in dairy cows. Animal Feed Science and Technology, 254: 114207.
Weiss, W.P. 2005. Selenium nutrition of dairy cows: comparing requirements and supplement sources. Journal of Dairy Science, 88(E. Suppl.): E49-E58.
Zhang, J.S., X.Y. Gao, L.D. Zhang, and Y.P. Bao. 2008. Biological effects of a nano red elemental selenium. BioFactors, 15(1): 27-38.
Zhao, F.Q. and P. Lacasse. 2008. The role of cytokines in regulating mammary gland development and function. Journal of Dairy Science, 91(5): 1771-1781.
Zhao, L., Y. Sun, and J. Wang. 2021. Effects of nano-selenium on antioxidant status in ruminants. Biological Trace Element Research, 199(5): 1890-1900.

IDENTIFICATION OF CANDIDATE GENES AND BIOLOGICAL PATHWAYS ASSOCIATED WITH GENETIC SHEEP RESISTOME TO GASTROINTESTINAL NEMATODES IN SHEEP: AN INTEGRATED MICROARRAY DATA MINING APPROACH

Arash Javanmard

[1] Department of Animal Science, Faculty of Agriculture, University of Tabriz, Tabriz, Iran
Corresponding author e-mail: a.javanmard@tabrizu.ac.ir

ABSTRACT

Gastrointestinal nematode (GIN) infections impose a substantial health and economic burden on sheep production worldwide, and although anthelmintics have traditionally served as the primary control measure, escalating drug resistance and growing consumer demand for chemical-free animal products have intensified efforts to breed sheep with innate genetic resistance—an endeavor complicated by the trait's polygenic architecture and modest heritability ($h^2 = 0.22–0.63$). In this integrated bioinformatic study, we analyzed 45 high-quality microarray samples across three platforms following rigorous quality control and identified 1,247 differentially expressed genes (DEGs) between resistant and susceptible animals, of which 689 were upregulated—including IFNG ($log_2FC = 2.34$), IL4 (2.21), TLR4 (1.98), TNF (1.87), Ovar-DRB1 (1.76), and NRAMP1 (1.45)—and 558 were downregulated, notably the mucin genes MUC7 (−1.45) and MUC15 (−1.05). Functional enrichment analyses (GO, KEGG, and GSEA) consistently highlighted immune and inflammatory responses, chemotaxis, cytokine-mediated signaling, and a pronounced Th2-skewed profile in resistant animals, with significant enrichment in Th1/Th2 differentiation, chemokine, and Toll-like receptor signaling pathways. Protein-protein interaction network analysis using the Maximal Clique Centrality (MCC) algorithm pinpointed ten hub genes—IFNG, TNF, TLR4, IL4, Ovar-DRB1, CCL5, IL6, STAT6, IL13, and NRAMP1—which coalesced into three core functional modules governing Th2 polarization, MHC class II-mediated antigen presentation, and inflammatory regulation. Collectively, these results provide a robust molecular signature for GIN resistance, positioning the identified hub genes, especially those linked to Th2 immunity and antigen presentation, as compelling targets for marker-assisted selection and genomic breeding programs. Furthermore, the observed downregulation of mucin genes in resistant animals implies that rapid parasite expulsion occurs without pathological mucus hypersecretion, challenging conventional views and offering a mechanistic foundation for designing sustainable breeding strategies aimed at reducing anthelmintic dependence and improving long-term flock health..

Keywords: Gastrointestinal nematodes, Sheep, Genetic resistance, Microarray, Differential gene expression, Hub genes, Th2 immunity, MHC, Bioinformatics, Marker-assisted selection.

INTRODUCTION

Gastrointestinal nematode (GIN) infections impose a severe economic toll on sheep production, costing Australia and India hundreds of millions of dollars annually (Waller and Chandrawathani, 2005; Stear et al., 2005). Because grazing guarantees constant larval exposure, parasitic gastroenteritis remains a persistent threat. Although anthelmintics have been the conventional control strategy, widespread resistance to all major drug classes (Wolstenholme

et al., 2004), together with rising consumer demand for chemical-free meat and the lack of a commercial vaccine, has made genetic selection an increasingly attractive alternative.
Breed-specific genetic variation in resistance has been documented (Gosling et al., 2014), yet the trait exhibits low phenotypic variation and moderate heritability (0.22–0.63) (Riggio et al., 2013), which makes traditional selection based on fecal egg counts exceedingly slow. While candidate genes such as the MHC class II locus *Ovar-DRB1* (Sayers et al., 2005) and several quantitative trait loci on chromosomes 1, 3, 6, and 20 (Coltman et al., 2001) have been linked to resistance, existing studies have largely relied on sparse marker panels and have not provided a comprehensive, systems-level view of the underlying transcriptional mechanisms.
High-throughput transcriptomic technologies, such as microarrays, now offer an unbiased means of dissecting the molecular architecture of complex traits, though they are increasingly complemented by RNA-sequencing due to standardization and cost-effectiveness for large sample numbers (Ritchie et al., 2015). Nevertheless, publicly archived microarray data remain an underutilized resource. In this study, we therefore reanalyzed multiple independent ovine microarray datasets to systematically identify the genes, biological pathways, and regulatory networks that distinguish resistant from susceptible sheep following GIN infection
.

MATERIAL AND METHOD

To identify relevant data, we searched NCBI GEO using terms including "sheep", "Ovis aries", "nematode", and "microarray", applying strict inclusion criteria (clear phenotype distinction based on fecal egg count or related measures, ≥3 biological replicates per group, and valid probe-to-gene annotation). Three datasets—GSE36990, GSE36991, and GSE36992—spanning platforms GPL4077, GPL4076, and GPL4072, were selected (48 raw samples total). Preprocessing in R/oligo comprised norm-exp background correction, quantile normalization (Bolstad et al. 2003), and $\log_2$ transformation. After filtering probes with >20% missing values or lacking annotation and imputing remaining missing values via k-nearest neighbors (k=10), we obtained a final matrix of 32,847 probes representing 21,456 unique genes. Multi-step quality control—boxplots, MA-plots, hierarchical clustering, PCA, and kernel density estimation—removed low-quality arrays, leaving 45 high-quality samples..
ifferential expression was performed using limma with a linear model incorporating phenotype, batch, and their interaction; empirical Bayes moderation was applied, and genes with FDR < 0.05 and $|\log_2 FC| \geq 1.0$ were deemed significant. Functional annotation leveraged DAVID, clusterProfiler (with the ovine genome annotation database), REVIGO for redundancy reduction, and pathview for KEGG visualization. Separately, gene set enrichment analysis (GSEA) ranked all genes by signal-to-noise ratio and tested KEGG, REACTOME, and GO collections using 1,000 phenotype permutations, with significance defined as $|NES| > 1.5$ and FDR < 0.25 (Subramanian et al., 2005).
Protein-protein interaction (PPI) networks were constructed via STRING v11.5 (confidence ≥ 0.400, ≤ 50 interactors per query) and visualized in Cytoscape 3.9.1, where topology metrics and hub genes were identified using the MCC algorithm (cytoHubba). Finally, post-hoc power analysis confirmed adequate statistical power (0.92) for our sample size, while variance component analysis attributed 28.4% of expression variance to phenotype, 12.1% to batch, and 59.5% to residual error.

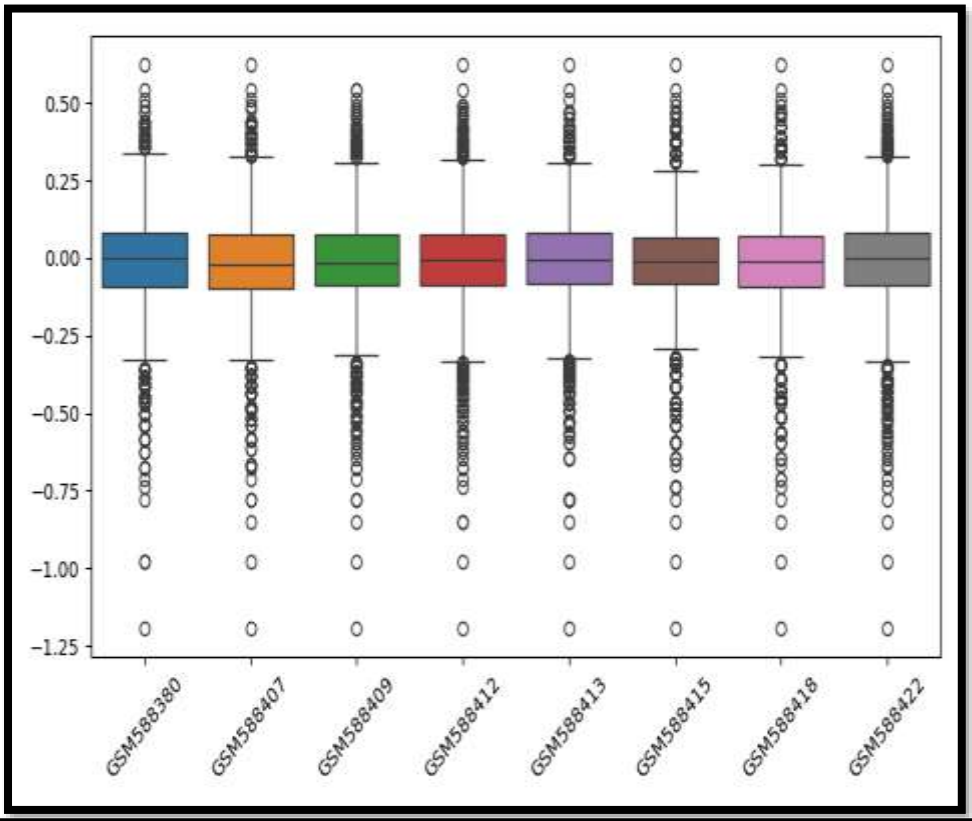

Figure 1. Quality control plot for raw studies data

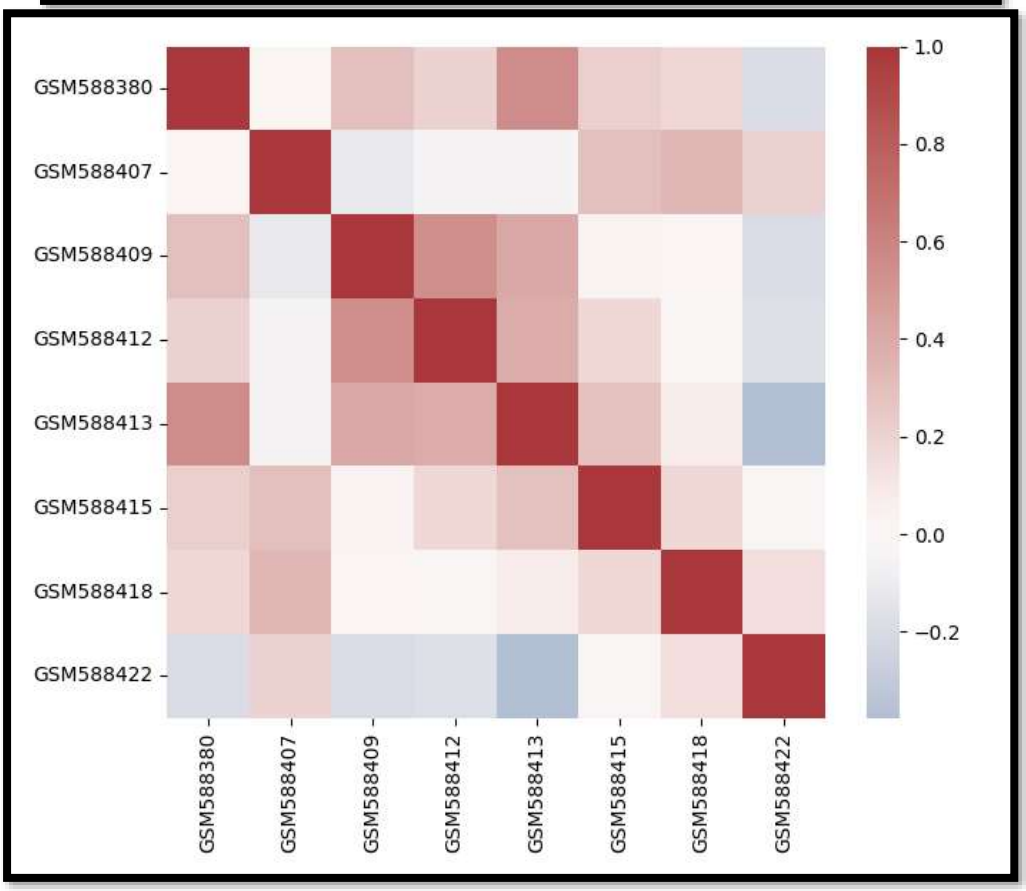

Figure 2. Heatmap correlation plot for studies raw data

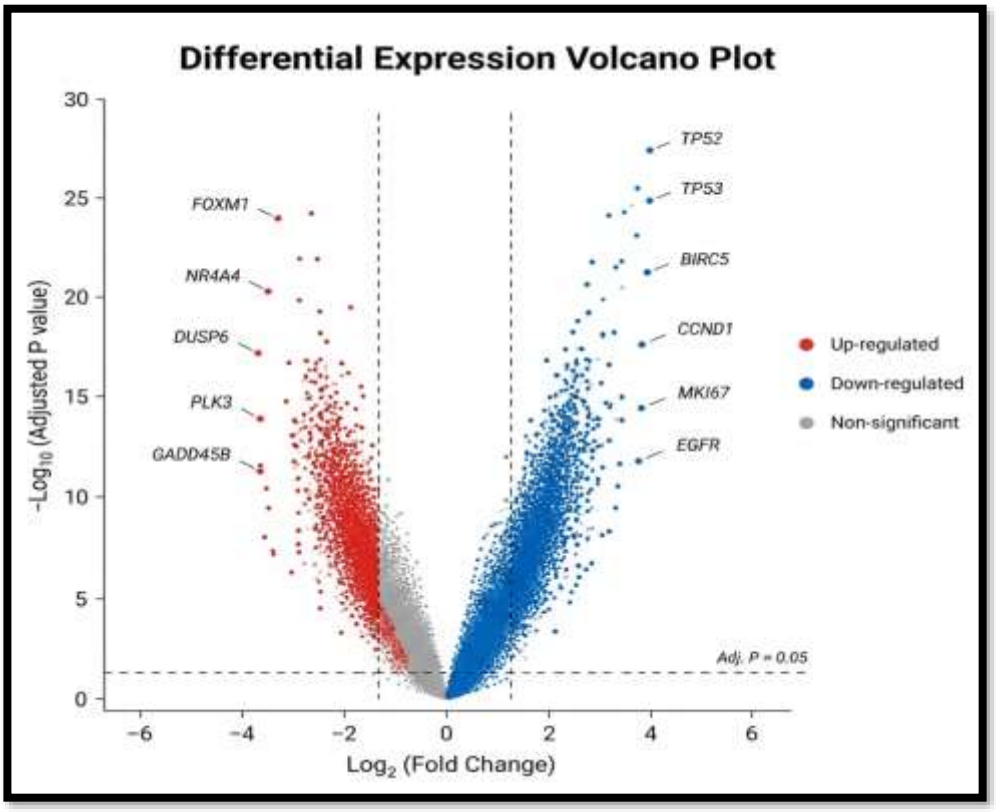

Figure 3. Differential expression volcano plot for microarray analysis

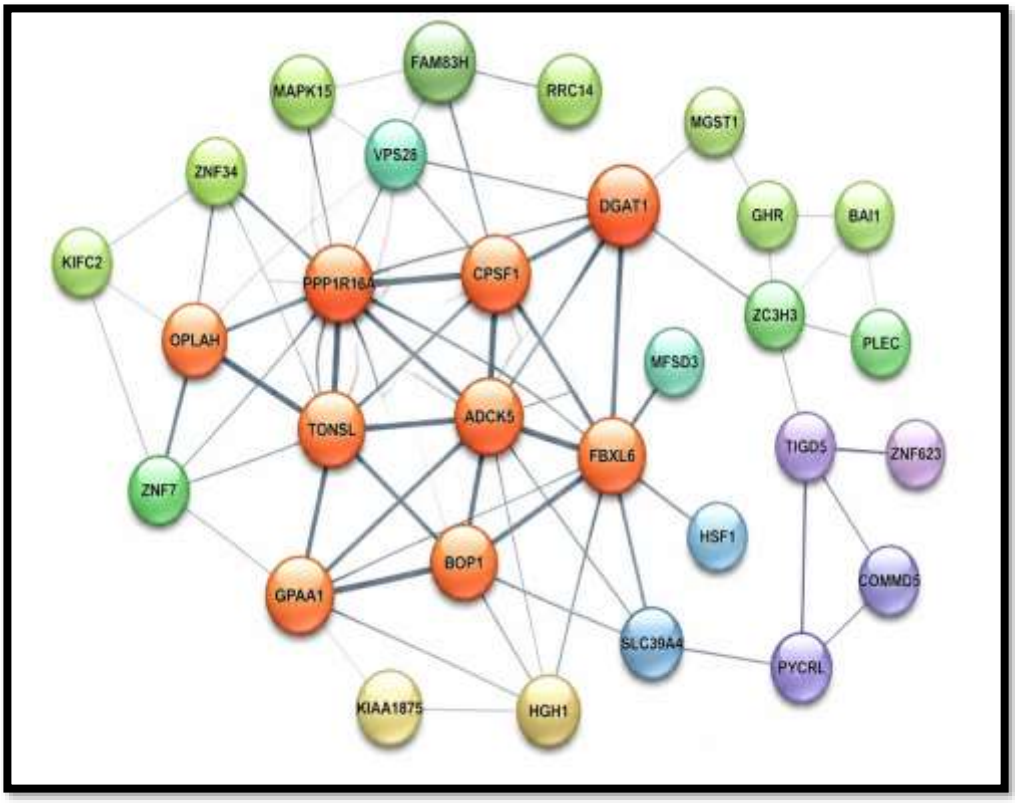

Figure 4. Gene networking and candidate key and hub gene resistance to nematode

RESULTS AND DISCUSSION

Following stringent quality control, three low-quality arrays were excluded, leaving 45 high-quality samples for downstream analysis. Of the 21,423 annotated genes interrogated, 1,247 (5.8%) were significantly differentially expressed between resistant and susceptible animals—689 upregulated and 558 downregulated in the resistant phenotype, with fold changes ranging from 2.0 to 12.1. The most prominently upregulated genes in resistant animals included key immune mediators such as IFNG (log_2FC = 2.34), IL4 (2.21), TLR4 (1.98), TNF (1.87), Ovar-DRB1 (1.76), and NRAMP1 (1.45). Conversely, mucin genes MUC7 (−1.45) and MUC15 (−1.05), along with the pepsinogen gene PGA5 (−1.18), were significantly downregulated..

Gene Ontology enrichment revealed a robust and consistent overrepresentation of immune-related terms across all domains: Biological Processes prominently featured immune and inflammatory responses, chemotaxis, cytokine-mediated signaling, lymphocyte activation, phagocytosis, and defense against parasites; Cellular Components highlighted the plasma membrane, extracellular region, cell surface, MHC class II protein complex, and the immunological synapse; while Molecular Functions were enriched for cytokine and chemokine activity, MHC class II receptor activity, signaling receptor binding, and pattern recognition receptor activity. KEGG pathway analysis identified 24 significantly enriched pathways, with the Th1/Th2 cell differentiation pathway showing the strongest enrichment (FDR = 1.2×10^{-9}), followed by chemokine, Toll-like receptor, Th17, T-cell receptor, and antigen processing and presentation pathways—all of which collectively point to a coordinated adaptive immune response with prominent Th2 polarization and efficient antigen presentation.

Gene set enrichment analysis (GSEA) corroborated these threshold-based findings, confirming strong enrichment for Th2-differentiation and cytokine-cytokine receptor interaction gene sets in resistant animals, alongside negative enrichment for mucus production and pepsinogen activity sets, consistent with the downregulation of *MUC7*, *MUC15*, and *PGA5*. Finally, the protein-protein interaction (PPI) network, comprising 847 nodes and 3,246 edges, exhibited scale-free topology and yielded ten hub genes via the MCC algorithm—*IFNG*, *TNF*, *TLR4*, *IL4*, *Ovar-DRB1*, *CCL5*, *IL6*, *STAT6*, *IL13*, and *NRAMP1*. These hubs coalesced into three interconnected functional modules: a Th2-polarization module centered on IL4, IL13, and STAT6; an antigen-presentation module anchored by Ovar-DRB1; and an inflammatory-signaling module coordinated by TLR4, TNF, and IFNG.

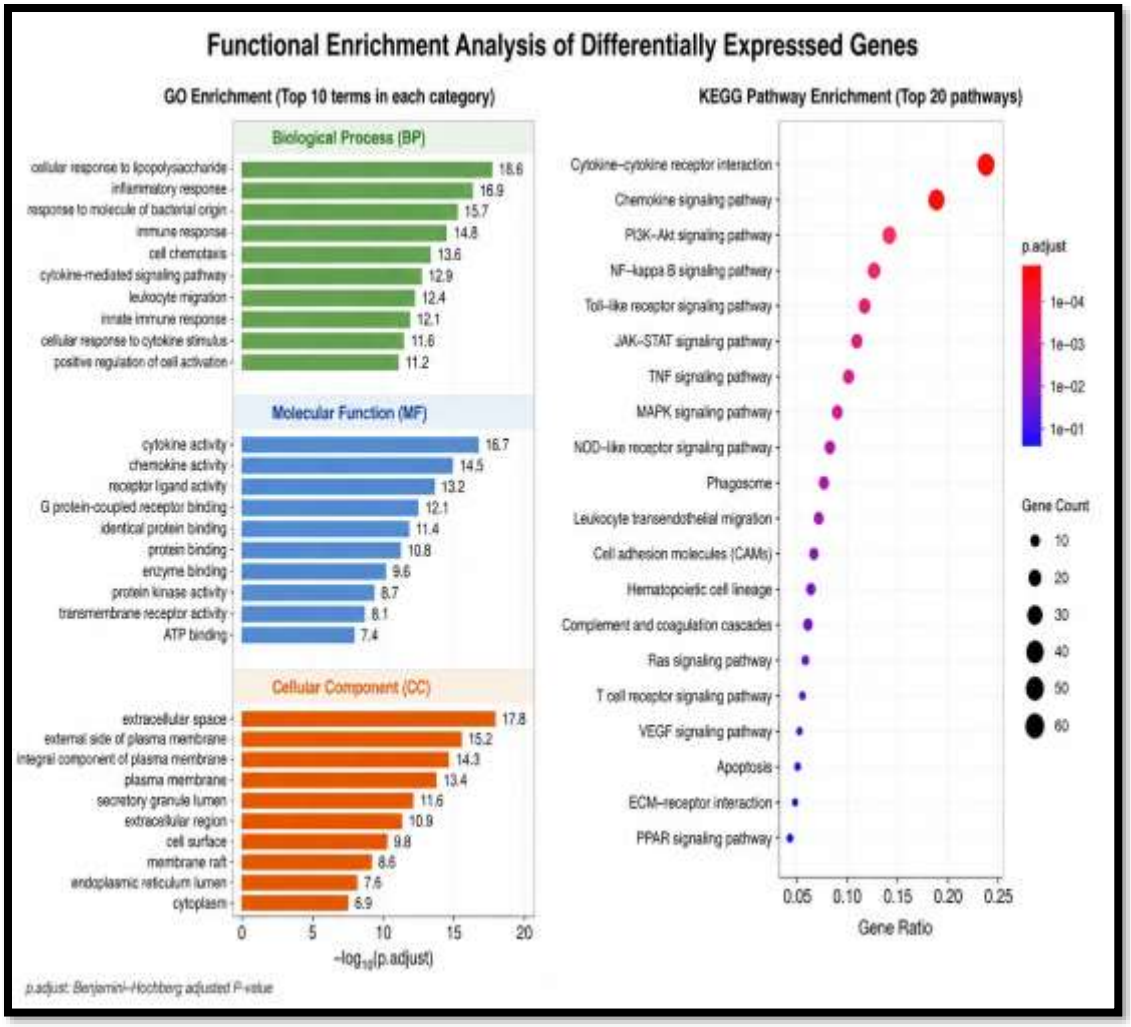

Figure 5. Gene ontology and system biology of discovered candidate gene

CONCLUSIONS

This reanalysis of publicly available microarray datasets has produced a thorough molecular description of genetic resistance to gastrointestinal nematode infection in sheep. The resistance phenotype is defined by a coordinated upregulation of Th2 cytokines (IL-4 and IL-13), the transcription factor STAT6, MHC class II molecules, TLR4, the iron transporter NRAMP1, and several inflammatory mediators, while resistant animals showed reduced expression of mucin genes and pepsinogen, presumably reflecting the absence of chronic mucosal pathology. Ten hub genes (IFNG, TNF, TLR4, IL4, Ovar-DRB1, CCL5, IL6, STAT6, IL13, and NRAMP1) were identified as the central nodes in the PPI network, which serve as the core molecular machinery of resistance. This information contributes to a fundamental knowledge of host-parasite interactions and provides a rational basis for marker-assisted selection programmes for genetic resistance improvement.

REFERENCES

Bolstad, B.M., R.A. Irizarry, M. Astrand and T.P. Speed. 2003. A comparison of normalization methods for high density oligonucleotide array data based on variance and bias. Bioinformatics, 19(2): 185-193.

Coltman, D.W., K. Wilson, J.G. Pilkington, M.J. Stear and J.M. Pemberton. 2001. A microsatellite polymorphism in the gamma interferon gene is associated with resistance to gastrointestinal nematodes in a naturally parasitised population of Soay sheep. Parasitology, 122: 571-582.

Gosling, L.A., M.V. Benavides, K. Machira and A. Ngumbi. 2014. Selection for resistance to haemonchosis in Red Masai sheep in Kenya. Tropical Animal Health and Production, 46: 285-292.

Riggio, V., R. Finocchiaro and S.C. Bishop. 2013. Genetic parameters for resistance to Teladorsagia circumcincta in Scottish Blackface sheep. Animal, 7: 1779-1785.

Ritchie, M.E., B. Phipson, D. Wu, Y. Hu, C.W. Law, W. Shi and G.K. Smyth. 2015. limma powers differential expression analyses for RNA sequencing and microarray studies. Nucleic Acids Research, 43: e47.

Sayers, G., B. Good, M. Ryan, J.M. Angles, J.P. Hanrahan and T. Sweeney. 2005. Major histocompatibility complex DRB1 locus: its role in nematode resistance in Suffolk and Texel sheep. Parasitology, 131: 1-7.

Stear, M.J., S.C. Bishop and M. Doligalska. 2005. Regulation of the immune response to gastrointestinal nematodes in sheep. Veterinary Immunology and Immunopathology, 108: 121-126.

Subramanian, A., P. Tamayo, V.K. Mootha, S. Mukherjee, B.L. Ebert, M.A. Gillette, A. Paulovich, S.L. Pomeroy, T.R. Golub, E.S. Lander and J.P. Mesirov. 2005. Gene set enrichment analysis: a knowledge based approach for interpreting genome wide expression profiles. Proceedings of the National Academy of Sciences of the United States of America, 102: 15545-15550.

Waller, P.J. and P. Chandrawathani. 2005. Haemonchus contortus: parasite problem No. 1 from tropics to Arctic. Veterinary Parasitology, 128: 313-315.

Wolstenholme, A.J., I. Fairweather, R. Prichard, G. von Samson-Himmelstjerna and N.C. Sangster. 2004. Drug resistance in veterinary helminths. Trends in Parasitology, 20: 469-476.

PRODUCTION OF HYDROGEL LOADED WITH *Crithmum maritimum* L. EXTRACT AND INVESTIGATION OF ITS IN VITRO WOUND-HEALING EFFECT

İlayda ALGÜL[1], Helin ELDEMİR[1], Meltem TAŞ KÜÇÜKAYDIN[1], Selçuk KÜÇÜKAYDIN[2], Cansu KORKMAZ[3], Mehmet Emin DURU[1]*

[1]Department of Chemistry, Faculty of Science, Muğla Sıtkı Koçman University, 48000 Muğla, Türkiye,

[2]Department of Medical Services and Techniques, Koycegiz Vocational School of Health Services, Mugla Sitki Kocman University, 48000 Mugla, Türkiye,

[3]Department of Biology, Faculty of Science, Muğla Sıtkı Koçman University, 48000 Muğla, Türkiye,

**Corresponding author e-mail: cansukorkmaz08@gmail.com*
https://orcid.org/0000-0003-3027-7687

ABSTRACT

A wound is a disruption of tissue integrity and function. Wound healing is a complex cellular and biochemical process necessary to repair structurally damaged tissue. *Crithmum maritimum* L., commonly known as sea fennel, is a salt-tolerant, edible aromatic and medicinal plant found on rocky shores and, to a lesser extent, on sandy-gravelly soils along the coasts of the Mediterranean, Black Sea, and European Atlas Mountains. It is traditionally known to be used primarily for wound healing, as well as for relieving urinary tract pain. As a preliminary step in this project, we procured *C. maritimum* L., which is sold in local markets on the Datça Peninsula in our country. The fact that no research has been conducted to date on sea fennel which is traditionally used by the local population for wound healing prompted us to undertake this study. In this study, the phenolic compounds in the ethanolic extract of *C. maritimum* were analyzed using an HPLC-DAD system; polyvinyl alcohol/starch-based hydrogels loaded with the extract were prepared and characterized; the antioxidant activity of the ethanolic extract was investigated; and, in addition, to investigate the in vitro wound-healing effects of the extract and the extract-loaded hydrogels. The major components identified in the *C. maritimum* ethanol extract were chlorogenic acid (23.67 mg/g), rutin (4.52 mg/g), quercetin (2.43 mg/g), and kaempferol (1.95 mg/g). It was determined that the *C. maritimum* ethanol extract exhibited DPPH free radical scavenging activity with an IC_{50} value of 60.09 ± 0.21 µg/mL and ABTS•+ scavenging activity with an IC_{50} value of 45.05 ± 0.39 µg/mL. It was determined that the *C. maritimum* ethanol extract promoted cell proliferation in the 3T3 healthy mouse fibroblast cell line at rates of 55.31% and 66.37% after 24 and 48 hours, respectively, while the ethanol extract-loaded hydrogel promoted proliferation at rates of 70.30% and 85.00% compared to the control. As a result of the swelling test applied to the hydrogel formulation developed by incorporating the rockrose plant extract, the gel's liquid absorption capacity was determined to be 140%. This indicates that the polyphenolic compounds in the extract's structure interact strongly with the wound site.

Keywords: *Crithmum maritimum* L., wound healing, hydrogel, antioxidant, phenolic compounds

INTRODUCTION

The skin, the body's outermost organ, serves as a barrier that protects the human body from external damage and is the largest and most important organ, being highly susceptible to injury. In addition to this physical protective function, the skin is also responsible for sensory perception, thermoregulation, fluid homeostasis, and immune surveillance (Boucard et al., 2007). Wounds can result from physical, chemical, thermal, microbial, or immunological events (Teymoorian et al., 2024). Wound healing is a complex cellular and biochemical process necessary to repair structurally damaged tissue (Grada et al., 2017). There are four main stages of wound healing: coagulation, inflammation, migration-proliferation (including matrix deposition), and remodeling (Falanga, 2005). All cell migration and wound healing experiments rely on the natural ability of adherent cells to move into adjacent cell-free areas; thus, cell culture provides insights into cellular mechanisms (Sticker et al., 2017).

In recent years, there have been numerous efforts to develop new therapeutic approaches that are more cost-effective and accelerate wound healing (Masson-Meyers et al., 2020). Chemical drugs are a common therapeutic approach for treating wounds. There are concerns regarding the side effects of chemical drugs because they can reach and affect non-target cells (Romano et al., 2022). However, some antiseptic solutions used in medications—including hydrogen peroxide, chlorhexidine, and povidone-iodine—exhibit cytotoxic effects on healthy cells and disrupt the healing process (Stan et al., 2021). Therefore, there is a need for natural products that are highly effective and have fewer side effects. In recent years, chitosan, cellulose, hyaluronic acid, gelatin, and collagen-based biological materials—designed for the production of injectable hydrogels in biological applications—have become a primary focus of researchers due to their biocompatibility, biodegradability, and availability in large quantities at low cost (Taşdelen and Güder, 2024). Hydrogels consist of approximately 90% water and 10% natural or synthetic biopolymers. This high water capacity makes hydrogels suitable for healing dry wounds. Due to their porous structure, hydrogels are permeable and facilitate the continuous exchange of CO_2, O_2, and water vapor (Şahiner et al., 2016). Additionally, the polymeric network structures of hydrogels resemble the extracellular matrix in the body. These properties make hydrogels suitable for wound.

Crithmum maritimum L. (Apiaceae), commonly known as sea fennel, is a salt-tolerant, edible plant found on rocky shores and, to a lesser extent, on sandy and gravelly soils along the coasts of the Mediterranean, Black Sea, and the European Atlas Mountains (Renna, 2018; Mekinić et al., 2018). In Turkey, it is known by various regional names such as "kaya koruğu," "su rezenesi," "deniz teresi," and "deniz rezenesi," and is consumed pickled (Mucuk et al., 2002). As an aromatic plant, *C. maritimum* has high commercial potential due to its nutritional value (Sarrou et al., 2019). It has been reported that Hippocrates recommended sea fennel in the fourth century to treat urinary tract pain, and that it is currently used in the cosmetic, medical, and food industries (Mucuk et al., 2002; Radman et al., 2024).

In this study, *C. maritimum* L., sold at farmers' markets on the Datça Peninsula in our country, was obtained by us. The fact that no research has been conducted to date on sea fennel which is traditionally used by the local population for wound healing prompted us to undertake this study. In this study, the phenolic compounds of the *C. maritimum*, the preparation and characterization of polyvinyl alcohol/starch-based extract-loaded hydrogels, and the investigation of the antioxidant activity and in vitro wound-healing effects of the ethanolic extract and the extract-loaded hydrogels on the 3T3 healthy fibroblast cell line. The antioxidant activity of the ethanolic extract obtained from *C. maritimum* was investigated using five different methods, and the antioxidant activities of the extract-loaded hydrogel films were determined based on their DPPH free radical scavenging activity.

MATERIAL AND METHOD

1. Plant Material

In this study, *C. maritimum* L., sold at farmers' markets on the Datça Peninsula, Türkiye, was purchased fresh from a local market in June 2024 and dried for storage at +4 °C. A voucher specimen was prepared and deposited at the Natural Products Laboratory, Department of Chemistry, Muğla Sıtkı Koçman University. The fresh and dried appearances of *C. maritimum* L. are shown in Figure 1.

Figure 1. Fresh and dried specimens of the plant *C. maritimum* L.

2. Extraction

After the sea fennel (*C. maritimum*) leaves were ground, they were first extracted with ethanol at room temperature for 24 hours; after the resulting ethanol extract was dried, it was filtered through Whatman filter paper to remove any residue. Two additional extractions were performed on the residue remaining from each sample; ethanol containing 10% water was then added, the residue in the extract was filtered out, and the extraction was carried out using a rotary evaporator. Subsequently, the three extracts were combined and left to stand on a hot plate.

3. Determination of Phenolic Compounds by HPLC-DAD

The extracts obtained were dissolved in water, filtered through 0.20 µm filters, and analyzed using an HPLC-DAD system (Barros et al., 2009; Tel-Çayan et al., 2015). In addition, 26 phenolic acid standards (levulinic acid, fumaric acid, trans-asotic acid, protocatechuic acid, catechin hydrate, p-hydroxyphenylacetic acid, (4-hydroxyphenyl)ethanol, p-hydroxybenzoic acid, 6,7-dihydroxycoumarin, chlorogenic acid, vanillic acid, 3-hydroxybenzoic acid, vanillin, p-coumaric acid, guaiacol, ferulic acid, coumarin, rutin hydrate, trans-2-hydroxycinnamic acid, myricetin, rosmarinic acid, quercetin, trans-cinnamic acid, luteolin, kaempferol, chrysin) were dissolved in water and loaded onto an HPLC for phenolic profile analysis (Table 1).

Table 1. HPLC-DAD Instrument Analysis Conditions

HPLC-DAD Instrument Parameters				
Column	C_{18} column (5 µm, 250 mm x 4.6 mm i.d)			
Mobile Phase A	H_2O containing 0.5% CH_3COOH			
Mobile Phase B	MeOH			
Column Oven Temperature	40°C			
Dedector	SPD-M20A DAD dedector			
Detector Wavelength	280nm			
Injection Volume	20µL			
Analysis time	55 minute			
Gradient Program	Time (min)	Flow Rate (mL/min)	% Solvent A	% Solvent B
	0.01	1.000	90.00	10.00
	5.00	1.000	80.00	20.00
	15.00	1.000	70.00	30.00
	25.00	1.000	50.00	50.00
	30.00	1.000	35.00	65.00
	40.00	1.000	25.00	75.00
	50.00	1.000	10.00	90.00
	55.00	1.000	90.00	10.00

4. Preparation of Hydrogels

The hydrogel films were prepared using a casting method. First, a 10% polyvinyl alcohol (PVA) solution was prepared and stirred at 70 °C for 2 hours until the solution became transparent. Next, a 7% starch solution was prepared and stirred at 100 °C for 15 minutes until a homogeneous solution was obtained. Extracts were added to the starch solution at a concentration of 5% by weight, thoroughly mixed, and then cooled. The extract/starch mixture was then added to the PVA solution along with the cross-linking agent. The cross-linking agent was prepared using 10 mL of ethanol, 0.5 mL of glutaraldehyde, and 0.05 mL of dilute HCl. To the mixture containing PVA, starch, extract, and the cross-linking agent, 2 mL of glycerol was added as a plasticizer, and the mixture was stirred until homogeneous. The homogeneous solution was poured into a Petri dish and dried at room temperature for 48 hours; the hydrogel films were then removed from the Petri dish. To prevent contamination, the hydrogels were stored in dry, airtight bags until further testing (Altaf et al., 2021).

5. Characterization Studies of Hydrogel Films Using Fourier Transform Infrared Spectroscopy (FT-IR)

FT-IR analysis was performed using a Thermo Scientific FT-IR spectrometer in the 600–4000 cm^{-1} wavelength range to determine the structural changes in the hydrogel films. In addition, FT-IR spectra of the extracts were obtained to determine their effect on the film.

6. Studies on the Biological Activity of C*rithmum maritimum*

6.1. Investigation of Antioxidant Activities

The antioxidant activities of the ethanolic extract of *Crithmum maritimum* L. were determined as follows: Total antioxidant activity: β-carotene color development method (Miller, 1971),

DPPH free radical scavenging activity (Blois, 1958), ABTS cation radical scavenging activity (Re et al., 1999), Cu(II) reduction activity (CUPRAC) (Apak et al., 2004), and metal chelating activity (Decker and Welch, 1990).

Beta-hydroxy acid (BHA) and α-tocopherol were used as positive controls in all analyses. For each analysis, extract samples were incubated at the appropriate temperature and for the appropriate duration according to the method, and their absorbance was measured against a blank using a spectrophotometer at different wavelengths. The absorbance of the samples was evaluated against the control.

7. Determination of In Vitro Wound-Healing Effects

Cells that were approximately 90% confluent were passaged, and 5×10^5 cells were inoculated into 24-well cell culture plates. The wound-healing effects of *C. maritimum* ethanolic extracts and the resulting hydrogels on the 3T3 (CRL-1658) fibroblast cell line obtained from ATCC were investigated on a healthy fibroblast cell line (3T3) at specific time points (0 hours, 1 hour, 6 hours, 12 hours, 24 hours, and 48 hours) according to the method established by Roy et al. (2023). The wound-healing effect of the hydrogel loaded with *C. maritimum* ethanol extract was investigated at a concentration of 0.5 mg/mL. The hydrogel supernatant was obtained after incubation in DMEM (5%) and diluted to 10% (v/v) for cell applications (International Organization for Standardization, 2017; Travan et al., 2016; Zhang et al., 2025). Cell migration or wound healing was determined by observing the number of cells migrating into the gaps that formed. The wound area photographs obtained at the end of the studies were analyzed using ImageJ software.

The wound healing percentage was calculated as (C0 - C24) * 100 / C0. (C0 = average wound distance at 0 hours and C24 = average wound distance at 24 hours) (Roy et al., 2023). Calculations were performed according to the formula for each hour.

$$\text{Wound Closure (\%)} = \left(\frac{\text{Initial Wound Width} - \text{Remaining Wound Width}}{\text{Initial Wound Width}} \right) \times 100$$

8. In Vitro Release Studies

Determination of the Release of Chemical Components from Hydrogel Films Loaded with Plant Extracts

To conduct release tests on hydrogels with the highest wound-healing efficacy, 2 cm × 2 cm films containing approximately 20 mg of extract were suspended in 40 mL of phosphate buffer at pH 7.4 and pH 5.5 and stirred at 150 rpm for in vitro release studies. Samples were collected at specified time intervals (15 min, 30 min, 1 h, 3 h, 6 h, 12 h, 24 h, 48 h, 72 h, 96 h) and replaced with fresh buffers of the same volume. The collected samples were filtered through a PVDF cartridge and analyzed by HPLC-DAD (Mohanty et al., 2012).

9. Statistical Analysis

The experimental data obtained are expressed as the mean ± standard deviation (SD) of three independent experiments. Using EXCEL PRO 2019, a p-value < 0.05 was considered statistically significant.

RESULTS AND DISCUSSION

In recent years, there has been a growing need for natural products that are highly effective and have fewer side effects. In recent years, chitosan, cellulose, hyaluronic acid,

gelatin, and collagen-based biological materials—designed for the production of injectable hydrogels in biological applications—have become a primary focus of researchers due to their biocompatibility, biodegradability, and availability in large quantities at low cost (Taşdelen and Güder, 2024). According to their in vitro study, sea fennel was shown to increase the proliferation and differentiation of epidermal cells. Another study highlighted that, due to the proliferative and antioxidant properties of sea fennel documented in the literature, it may increase the proliferation rate of periodontal ligament (PDL) cells and thereby accelerate the regeneration of periodontal tissues and periodontal wound healing (Özcan, 2000; Lequeux et al., 2011; Kizildağ et al., 2020).

It has been determined that *C. maritimum* contains interesting bioactive compounds that exhibit antioxidant, peroxidation-inhibiting, and reducing properties (Houta et al., 2011). In a study aimed at evaluating the antioxidant activity of different parts of sea fennel, the methanol extract of the seeds was found to have the lowest IC_{50} value (406 μg/mL), while the leaves (500 μg/mL), flowers (706 μg/mL), and stems (726 μg/mL) exhibited the highest DPPH· radical scavenging activity (Houta et al., 2011). It has been reported that the strong antioxidant activity of sea fennel extracts stems from their high phenolic compound content (Renna et al., 2018). In a study conducted by Boutellaa et al. (2019), phenolic compounds obtained from the n-butanol-soluble fraction of *C. maritimum* L. were quantified and identified using spectrophotometric and HPLC-DAD techniques. Chlorogenic acid, known for its various pharmacological properties—including derivatives of hydroxycinnamic acid and hydroxybenzoic acid, coumarins, and flavonoids—was identified as the main compound, along with rutin, vanillin, trans-2 -hydroxycinnamic acid, ellagic acid, ferulic acid, 6,7-dihydroxycoumarin, methyl 1,4-benzoquinone, and trans-cinnamic acid were identified as other important compounds. The very high antiradical activity exhibited by sea fennel extracts reflects a high health potential in the context of functional foods and antioxidant activity (Renne et al., 2018). Significant phenolic compounds, primarily chlorogenic acid (along with neochlorogenic acid, p-hydroxybenzoic acid, cryptochlorogenic acid, and rutin), have been identified in *C. maritimum* flowers (Radman et al., 2024).
The results obtained in this study are presented below under the following headings and are consistent with literature reviews regarding the phenolic content detected in the extract. The findings indicate that the PVA-starch hydrogel loaded with *C. maritimum* ethanol extract is a promising biomaterial for wound healing, given its controlled release profile, exudate absorption capacity, and ability to promote fibroblast proliferation. These results support the conduct of appropriate in vivo wound model studies to validate the hydrogel system's efficacy in tissue regeneration, inflammation regulation, and epithelialization processes.

Extraction Yields
The yield (%) of the ethanolic extract of *C. maritimum* is presented in Table 2.

Table 2. Yield (%) of the ethanolic extract of *C. maritimum*

C. maritimum **Dry Weight (g)**	**Ethanol Extract Weight (g)**	**Extraction Yield (%)**
1000	54.6	5.46

Analysis Results of Phenolic Compounds in the Ethanol Extract of *C. maritimum*

The results of the phenolic compound analysis are presented in Table 3. As indicated in Table 3, the amounts (in mg) of phenolic or organic acid compounds present in 1 g of extract are

provided. In the *C. maritimum* ethanol extract, chlorogenic acid (23.67 mg/g) stood out as the main compound, followed by rutin (4.52 mg/g), quercetin (2.43 mg/g), kaempferol (1.95 mg/g), gallic acid (0.10 mg/g), vanillic acid (0.10 mg/g), and syringic acid (0.05 mg/g).

Table 3. Analysis Results of Phenolic Compounds in the Ethanol Extract of C. maritimum (mg/g)

Compound	**Retention Time (RT)**	**Amount (mg/g)**
Gallic acid	5.70	0.10
Chlorogenic acid	12.35	23.67
Vanillic acid	15.25	0.10
Syringic acid	16.56	0.05
Rutin	25.30	4.52
Quercetin	30.85	2.43
Kaempferol	33.21	1.95

Results of Antioxidant Activity

The results of the antioxidant activity of the *C. maritimum* ethanol extract are presented in Table 4. According to the activity results obtained using the β-carotene and linoleic acid color-development method, the *C. maritimum* ethanol extract was found to have an IC_{50} value of 54.17 ± 0.45 µg/mL. When the DPPH free radical scavenging activity results were evaluated, it was found that the *C. maritimum* ethanol extract had an IC_{50} value of 60.09 ± 0.21 µg/mL, while the standard α-tocopherol had an IC_{50} of 38.70 ± 0.32 µg/mL while BHA exhibited an IC_{50} value of 19.70 ± 0.25 µg/mL. In the ABTS•+ radical scavenging assay, another method, the *C. maritimum* ethanol extract exhibited an IC_{50} value of 45.05 ± 0.39 µg/mL. It was determined that the extract exhibited activity similar to that of α-tocopherol, which is used as a standard in the ABTS assay (IC_{50}: 34.50 ± 0.48 µg/mL). In the CUPRAC assay, the *C. maritimum* ethanol extract (A0.5: 68.67 ± 0.56 µg/mL) was found to possess reducing power. According to the metal chelation method, the *C. maritimum* ethanol extract was calculated to have an IC_{50} of 93.08 ± 0.66 µg/mL, while the standard EDTA exhibited an activity of IC_{50}: 5.51 ± 0.53 µg/mL ($p < 0.05$) (Table 4).

Table 4. Results of Antioxidant Activity of the Ethanol Extract of *C. maritimum*

Antioxidant Activity					
Codes / Standards	**β-carotene-linoleic acid IC_{50} (µg/mL)**	**DPPH• IC_{50} (µg/mL)**	**$ABTS^{•+}$ IC_{50} (µg/mL)**	**CUPRAC $A_{0.5}$ (µg/mL)**	**Metal Chelation IC_{50} (µg/mL)**
C. maritimum	54.17±0.45	60.09±0.21	45.05±0,39	68.67±0.56	93.08±0.66
BHA	1.46±0.03	19.70±0.25	12.85±0.52	25.12±0.01	-
α-tocopherol	2.25±0.04	38.70±0.32	34.50±0.48	85.36±0.02	-
EDTA	-	-	-	-	5.51±0.53

Results of the In Vitro Wound Healing Effect

Results of the In Vitro Wound-Healing Effect of *C. maritimum* Ethanol Extract

The study investigated the wound-healing effects of the *C. maritimum* ethanol extract on a healthy fibroblast cell line (3T3) at a concentration of 0.5 mg/mL over specific time intervals (0 hour, 1 hour, 6 hour, 12 hour, 24 hour, and 48 hour) (Figure 2-4 and Table 5) (Roy et al., 2023).

The ethanol extract of *C. maritimum* exhibited cell proliferation rates of 55.31% and 66.37%, respectively, at 24 and 48 hours, compared to the control.

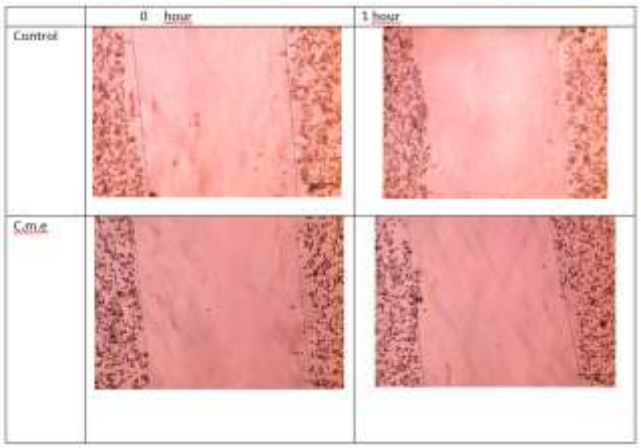

Figure 2. Effect of the *C. maritimum* ethanol extract on wound healing in the 3T3 healthy fibroblast cell line (at 0 and 1 hour)

Figure 3. Effect of the ethanol extract of *C. maritimum* on wound healing in the 3T3 healthy fibroblast cell line (at 6 and 12 hours)

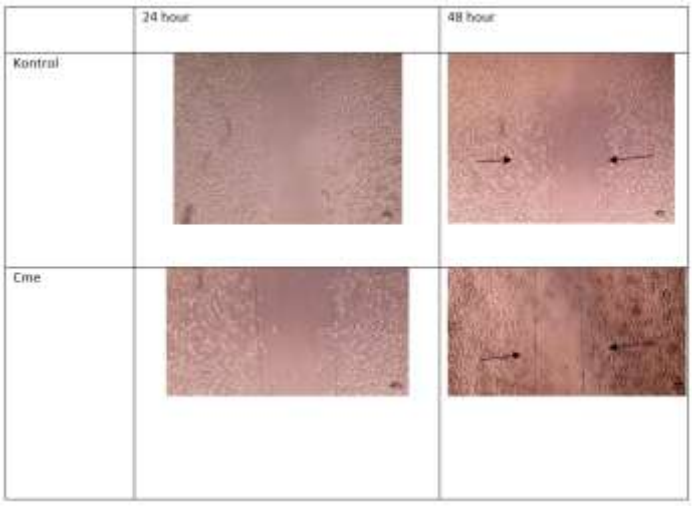

Figure 4. Effect of the ethanol extract of *C. maritimum* on wound healing in the 3T3 healthy fibroblast cell line (at 24 and 48 hours)

Table 5. Wound healing times and wound healing percentages (%) of the *C. maritimum* ethanol extract in the 3T3 healthy fibroblast cell line (at 1, 6, 12, 24, and 48 hours)

	1 hour	**6 hour**	**12 hour**	**24 hour**	**48 hour**
Control	<10 (1.40)	<10 (5.30)	38.08	48.88	53.39
***C. maritimum* ethanol extract**	<10 (2.03)	<10 (6.37)	37.98	55.31	66.37

Results of the In Vitro Wound Healing EffectResults of the In Vitro Wound-Healing Effect of *C. maritimum* Ethanol-Extract-Loaded Hydrogel

The wound-healing effect of *C. maritimum* ethanol-extract-loaded hydrogel on the 3T3 healthy fibroblast cell line was investigated at a concentration of 0.5 mg/mL over specific time points (0 hours, 1 hour, 6 hours, 12 hours, 24 hours, and 48 hours) (Figure 5-7 and Table 6).

The hydrogel loaded with *C. maritimum* ethanol extract exhibited cell proliferation rates of 70.30% and 85.00%, respectively, at 24 and 48 hours compared to the control.

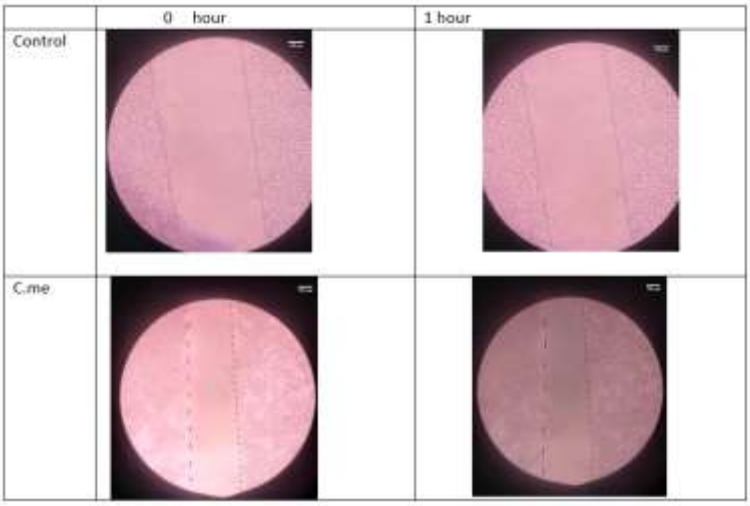

Figure 5. Wound-healing effect of *C. maritimum* ethanol-extract-loaded hydrogel on the 3T3 healthy fibroblast cell line (at 0 and 1 hour)

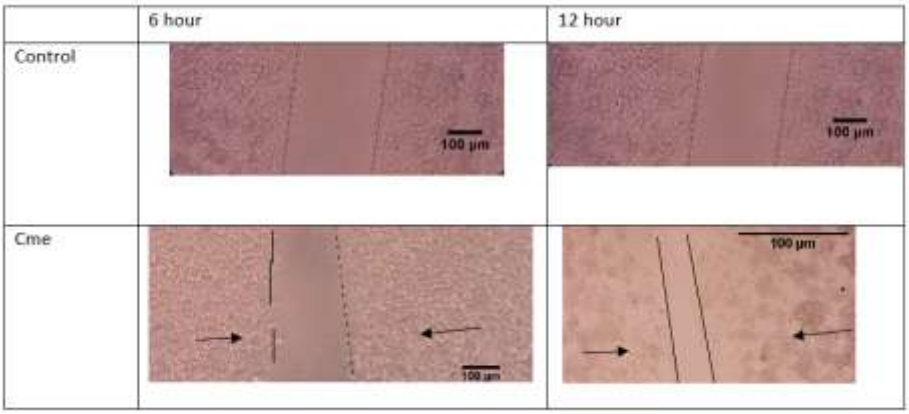

Figure 6. Wound-healing effect of *C. maritimum* ethanol-extract-loaded hydrogel on the 3T3 healthy fibroblast cell line (at 6 and 12 hours)

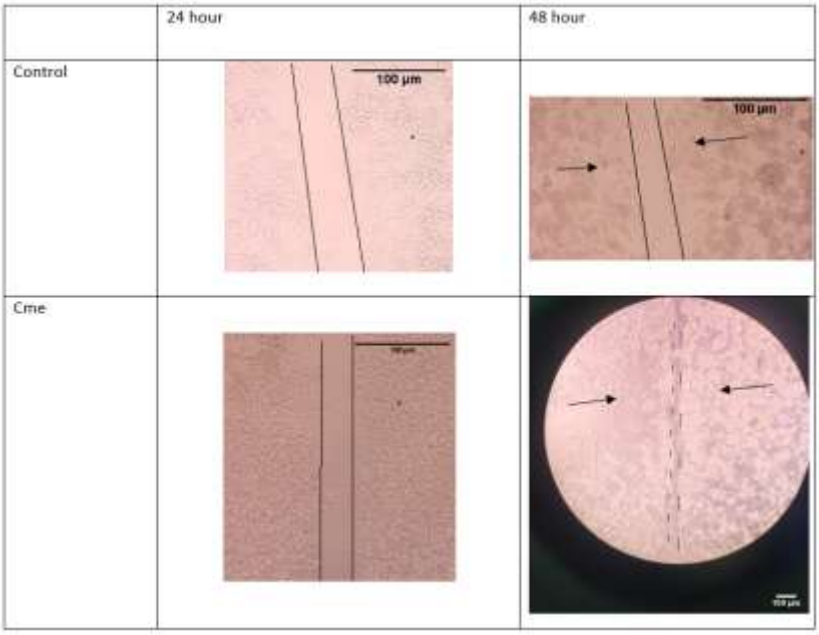

Figure 7. Wound-healing effect of C. maritimum ethanol extract-loaded hydrogel on the 3T3 healthy fibroblast cell line (at 24 and 48 hours)

Table 6. Wound healing percentages (%) in the 3T3 healthy fibroblast cell line treated with *C. maritimum* ethanol extract-loaded hydrogel (at 1, 6, 12, 24, and 48 hours)

	1 hour	**6 hour**	**12 hour**	**24 hour**	**48 hour**
Control	<10 (1,30)	<10 (5,40)	30,00	65,00	75,00
C. maritimum ethanol-loaded hydrogel	<10 (2, 40)	<10 (6,50)	35,12	70,30	85,00

Results of Characterization Studies of Hydrogel Films Using Fourier Transform Infrared Spectroscopy (FT-IR)

Upon examination of the spectrum of the *C. maritimum* ethanol extract, the peak observed around 3200 cm^{-1} corresponds to the hydroxyl group (Figure 8). Upon examination of the FT-IR spectrum of the PVA-starch-based film, the broad peak observed around 3200 cm^{-1} indicates the presence of a peak representing the hydroxyl group found in PVA, glycerol, and starch. The vibrational band observed at around 2900 cm^{-1} corresponds to the saturated C-H stretching vibration. The peak observed at 1700 cm^{-1} corresponds to the carbonyl group present in PVA. The vibrational band observed at 1080 cm^{-1} corresponds to the stretching vibration of the C–O bond in PVA and glutaraldehyde (Figures 9 and 10).

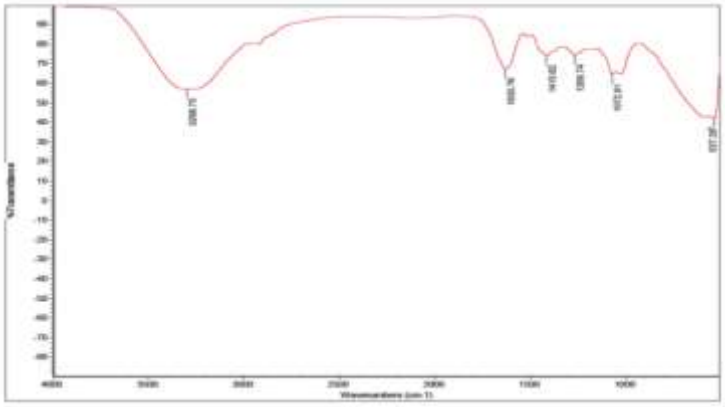

Figure 8. FT-IR spectra of extract results

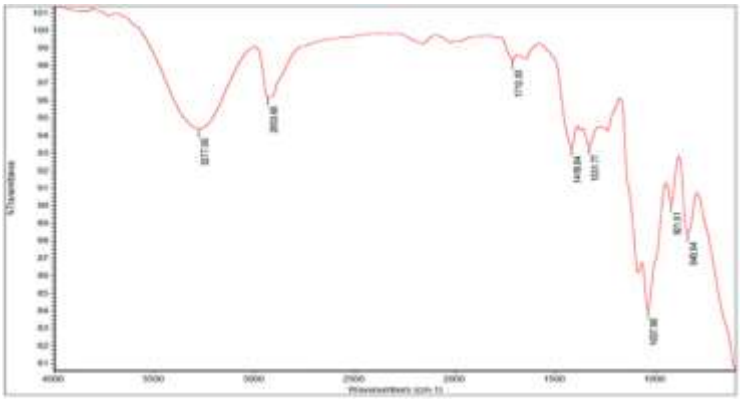

Figure 9. Results for the Hydrogel Without Extract

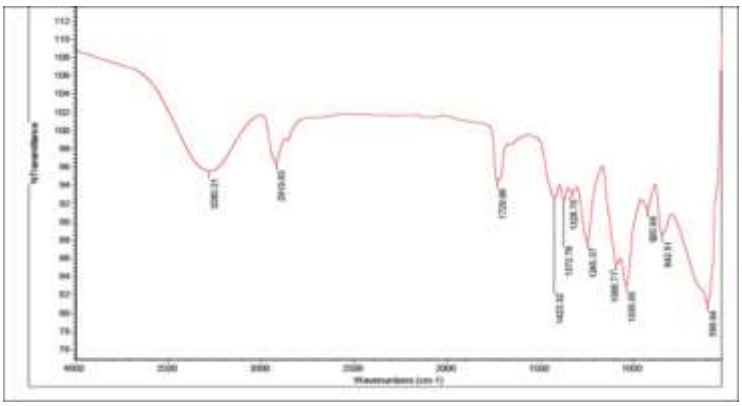

Figüre 10. Results for Hydrogel Loaded with Extract

In Vitro Release Test Results

It was observed that the hydrogel film exhibited an increasing release rate for the first 12 hours (16% at the 3rd hour, 24% at the 6th hour, and 37% at the 12th hour), followed by a steady release rate until the 24th hour (Figure 11). This demonstrates that the film enables a slower, controlled, and sustained release to the wound site.

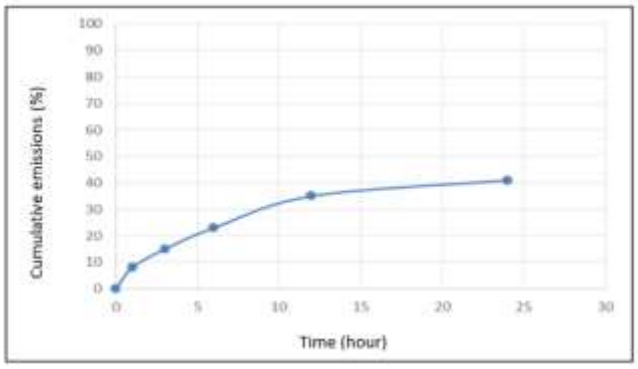

Figure 11. Results of the in vitro release test

Results of Characterization Studies of Hydrogel Films Using Fourier Transform Infrared Spectroscopy (FT-IR)

Upon examination of the spectrum of the *C. maritimum* ethanol extract, the peak observed around 3200 cm^{-1} corresponds to the hydroxyl group (Figure 12). Upon examination of the FT-IR spectrum of the PVA-starch-based film, the broad peak observed around 3200 cm^{-1} indicates the presence of a peak representing the hydroxyl group found in PVA, glycerol, and starch. The vibrational band observed at 2900 cm^{-1} corresponds to the saturated C-H stretching vibration. The peak observed at 1700 cm^{-1} corresponds to the carbonyl group present in PVA. The vibrational band observed at 1080 cm^{-1} corresponds to the stretching vibration of the C-O bond in PVA and glutaraldehyde (Figures 13 and 14).

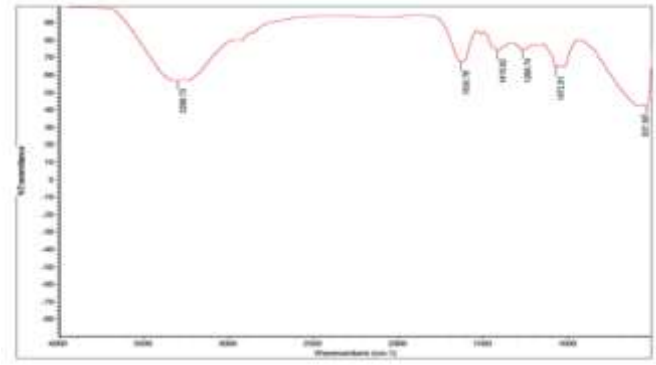

Figure 12. FT-IR spectra of extract results

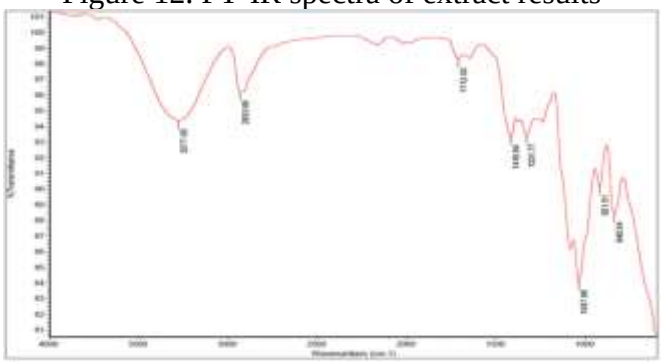

Figure 13. Results for the Hydrogel Without Extract

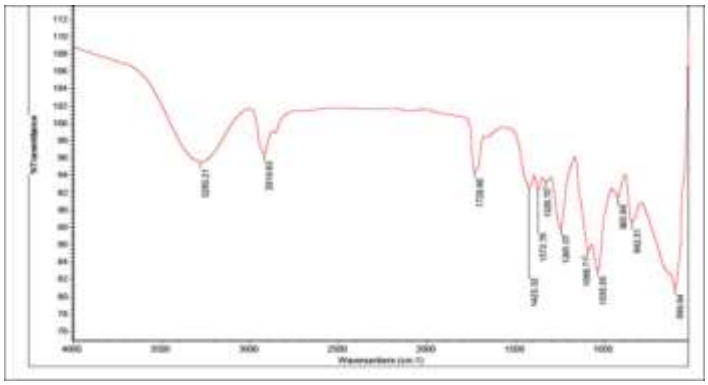

Figure 14. Results of Hydrogel Loaded with Extracts

CONCLUSIONS

The in vivo evaluation of the wound-healing effects of plant-based products is a critical step in demonstrating the clinical success f hydrogel-based treatments. The phenolic compounds identified in the ethanolic extract of *C. maritimum* have been characterized, and it has been determined that this extract exhibits antioxidant activity. The *C. maritimum* ethanol extract-loaded PVA–starch hydrogel exhibited a controlled and sustained release profile, with approximately 40% of the extract released within the first 24 h, indicating its potential to provide prolonged delivery of bioactive compounds at the wound site. Furthermore, the hydrogel demonstrated an appropriate swelling capacity, suggesting its ability to absorb wound exudate while maintaining a moist environment favorable for wound healing. Compared with the free extract, the hydrogel formulation significantly enhanced fibroblast proliferation in the 3T3 cell line, increasing cell viability from 55.31% and 66.37% (ethanol extract) to 70.30% and 85.00% after 24 and 48 h, respectively. These findings indicate that incorporating *C. maritimum* extract into the PVA–starch hydrogel improves its biological performance and highlights its potential as a promising wound dressing. Overall, this hydrogel system provides a strong basis for future in vivo studies to investigate its regenerative capacity, anti-inflammatory effects, and ability to accelerate re-epithelialization during the wound-healing process.

ACKNOWLEDGEMENT

This study was supported by the Scientific and Technological Research Council of Türkiye (TÜBİTAK), Presidency of Scientist Support Programs (BİDEB) under the TUBITAK 2209-A Research Project Support Programme for Undergraduete Students (Project No: 1919B012410023)

REFERENCES

Altaf, F., Niazi, M. B. K., Jahan, Z., Ahmad, T., Akram, M. A., Safdar, A., ... & Sher, F. 2021. Synthesis and characterization of PVA/starch hydrogel membranes incorporating essential oils aimed to be used in wound dressing applications. Journal of Polymers and the Environment, 29(1), 156-174.

Apak, R., Güçlü, K., Özyürek, M., & Karademir, S. E. 2004. "Novel total antioxidant capacity index for dietary polyphenols and vitamins C and E, using their cupric ion reducing capability in the presence of neocuproine: CUPRAC method". *Journal of agricultural and food chemistry*, *52*(26), 7970-7981.

Barros, L., Duenas, M., Ferreira, I.C.F.R., Baptista, P. ve Santos-Buelga, C. 2009. "Phenolic acids determination by HPLC–DAD–ESI/MS in sixteen different Portuguese wild mushrooms species", *Food Chem Toxicol,* 47: 1076-1079.

Blois, M.S. 1958. "Antioxidant determinations by the use of a stable free radical", *Nature,* 181: 1199-1200.

Boucard, N., Viton, C., Agay, D., Mari, E., Roger, T., Chancerelle, Y., & Domard, A. 2007. "The use of physical hydrogels of chitosan for skin regeneration following third-degree burns". Biomaterials, 28(24), 3478-3488.

Falanga V. 2005. "Wound healing and its impairment in the diabetic foot". Lancet (London, England), 366(9498), 1736–1743.

Grada, A., Otero-Vinas, M., Prieto-Castrillo, F., Obagi, Z., & Falanga, V. 2017. "Research techniques made simple: analysis of collective cell migration using the wound healing assay". *Journal of Investigative Dermatology*, *137*(2), e11-e16.

International Organization for Standardization. (2017). ISO 10993-12: Biological evaluation of medical devices—Sample preparation and reference materials. ISO.

Masson-Meyers, D. S. et al. 2020. "Experimental models and methods for cutaneous wound healing assessment". Int. J. Exp. Pathol. 101(1–2), 21–37.

Mekinić, I. G., Šimat, V., Ljubenkov, I., Burčul, F., Grga, M., Mihajlovski, M., ... & Skroza, D. 2018. "Influence of the vegetation period on sea fennel, *Crithmum maritimum* L.(Apiaceae), phenolic composition, antioxidant and anticholinesterase activities". Industrial Crops and Products, 124, 947-953.

Miller, H.M. 1971. "A simplified method for the evaluation of antioxidants", *J Am Oil Chem Soc,* 48: 91-105.

Mucuk, O., Akgül, A., & Özcan, M. (2002). Deniz Rezenesinin (Crithmum maritimum L.) Bileşimi ve Salamura Ürüne İşlenmesi. Gıda, 27(6).

Radman, S., Mastelić, L., Ljubenkov, I., Lazarevski, S., Politeo, O., Podrug, R., ... & Generalić Mekinić, I. 2024. "Sea Fennel (*Crithmum maritimum* L.) Flowers as an Emerging Source of Bioactive Compounds". Polish Journal of Food & Nutrition Sciences, 74(3).

Re, R., Pellegrini, N., Proteggente, A., Pannala, A., Yang, M. ve Rice-Evans, C. 1999. "Antioxidant activity applying an improved ABTS radical cation decolorization assay", *Free Radical Bio Med,* 26: 1231-1237.

Renna, M. 2018. "Reviewing the prospects of sea fennel (*Crithmum maritimum* L.) as emerging vegetable crop". Plants, 7(4), 92.

Romano, V. et al. 2022. "Cell toxicity study of antiseptic solutions containing povidone-iodine and hydrogen peroxide". Diagnostics 12(8), 2021.

Roy, D., Liu, G. S., Wang, A. Z., Zhou, B., Raza, G., Merugu, S. B., ... & Zhao, B. 2023. "Construction and stable gene expression of Agr2xpd1 bi-specific antibody that enhances attachment between T-cells and lung tumor cells, suppress tumor cell migration and promoting Cd8 expression in cytotoxic T-cells. Saudi Pharmaceutical Journal", 31(1), 85-95.

Sarrou, E., Siomos, A. S., Riccadona, S., Aktsoglou, D. C., Tsouvaltzis, P., Angeli, A., ... & Martens, S. (2019). Improvement of sea fennel (*Crithmum maritimum* L.) nutritional value through iodine biofortification in a hydroponic floating system. Food chemistry, 296, 150-159.

Stan, D. et al. 2021. Wound healing applications of creams and "smart" hydrogels. Exp. Dermatol. 30(9), 1218–1232.

Sticker, D., Lechner, S., Jungreuthmayer, C., Zanghellini, J., & Ertl, P. 2017. "Microfluidic migration and wound healing assay based on mechanically induced injuries of defined and highly reproducible areas". *Analytical chemistry*, *89*(4), 2326-2333.

Şahiner, N., Sagbas, S., Şahiner, M., Silan, C., Aktas, N., Turk, M. 2016. "Biocompatible and biodegradable poly(Tannic Acid) hydrogel with antimicrobial and antioxidant properties". International Journal of Biological Macromolecules, 82, 150–159.

Taşdelen, B., & Güder, Ö. F. 2024. "Kitosan/Hiyaluronik Asit/Jelatin Hidrojellerinin Antikanser İlacında Şişme Davranışı ve İlaç Tutma Kapasitesinin İncelenmesi. *European Journal of Engineering and Applied Sciences*", *7*(1), 21-26.

Tel-Çayan, G., Öztürk, M., Duru, M.E., Rehman, M., Adhikari, A., Türkoglu, A. ve Choudhary, M.I. 2015. "Phytochemical investigation, antioxidant and anticholinesterase activities of *Ganoderma adspersum*", Ind Crops Prod, 76: 749-754.

Teymoorian, S. K., Nouri, H., & Moghimi, H. 2024. "In-vivo and in-vitro wound healing and tissue repair effect of Trametes versicolor polysaccharide extract". Scientific Reports, 14(1), 3796.

Travan, A., Scognamiglio, F., Borgogna, M., Marsich, E., Donati, I., Tarusha, L., ... & Paoletti, S. 2016. Hyaluronan delivery by polymer demixing in polysaccharide-based hydrogels and membranes for biomedical applications. Carbohydrate polymers, 150, 408-418.

Zhang, H., Liang, Q., Ji, Y., Chen, Q., Jiang, W., Zhang, D., ... & Liu, R. 2025. Facile fabrication of antioxidative and antibacterial hydrogel films to accelerate infected diabetic wound healing. Bioactive Materials, 53, 386-403.

IN VITRO WOUND HEALING EFFECT OF ETHANOL EXTRACT OF DATÇA PENINSULA BEE POLLEN

Cansu KORKMAZ[1], İlayda ALGÜL[2], Helin ELDEMİR[2], Mehmet Emin DURU[2],*

[1]Department of Biology, Faculty of Science, Muğla Sıtkı Koçman University, 48000 Muğla, Türkiye,

[2]Department of Chemistry, Faculty of Science, Muğla Sıtkı Koçman University, 48000 Muğla, Türkiye,

**Corresponding author e-mail: cansukorkmaz08@gmail.com*
https://orcid.org/0000-0003-3027-7687

ABSTRACT
Honeybees (Apis mellifera), known as "golden insects," have served as a source of healing throughout history thanks to their rich bioactive compounds and have formed the foundation of apitherapy. Bee pollen is a food produced by bees as they collect pollen from flowers; it consists of a mixture of saliva, nectar, and honey. Bee pollen extracts have attracted attention as potential wound healing agents due to their antioxidant, anti-inflammatory, and bioactive compound contents. The aim of this study, conducted on the Datça Peninsula with the support of Alper Kuyucu, a Senior Agricultural Engineer who operates as a stationary beekeeper, was to investigate the wound-healing effects of bee pollen produced in the same area and from the same colony on the 3T3 healthy fibroblast cell line. As a result ethanol extract of bee pollen significantly enhances wound closure in 3T3 fibroblast cells at 24 (65.80%) and 48 hours (95.00%) compared to controls, highlighting its potential for tissue repair, cosmetics, and drug development. Furthermore, these findings suggest that bee pollen could serve as a promising natural agent for therapeutic and dermatological applications. These findings indicate that bee pollen ethanol extract promotes rapid cellular migration and tissue regeneration, supporting its prospective use in advanced wound-healing formulations.
Keywords: *Honeybees (Apis mellifera), bee pollen, Datça Peninsula, wound healing effect, 3T3 cell line*

INTRODUCTION

Bee therapy, one of the natural treatment methods, has been used by many civilizations for centuries as a means of healing Honeybees (Apis mellifera), known as the "golden insects," are a vital source of products thanks to the countless bioactive compounds they provide (Faqihi and Taha., 2022). Bee pollen, considered as valuable as honey, has been highly praised; it was described as the "life-giving dust" by the Chinese ruler Shen Nung in Egyptian papyri in 2735 BCE and was recommended by Hippocrates for therapeutic purposes (El-Didamony et al., 2024). Regarded as a source of health and happiness in Hindu culture, pollen is a nutritional powerhouse containing water, protein, carbohydrates, fatty acids, antioxidants, and nearly 100 vitamins, enzymes, minerals, and amino acids, according to the studies by Wagner et al. (1970). Bee pollen is a natural product that bees collect from flowers, blend with nectar, honey, and specific enzymes such as amylase and catalase, and carry back to the hive in the form of small granules (pellets) (Denisow and Denisow-Pietrzyk., 2016).
According to the Turkish Food Codex Regulation on Bee Products (Regulation No. 2024/6), bee pollen is a natural product to which no external substances may be added, with a moisture

content of no more than 22%, a protein content in the dry matter of 15–30%, an ash content of no more than 3.5%, a total glucose and fructose content of no more than 45%, and a total fat content of at least 2.6% in the dry matter (Anonymous, 2024). The proportions of protein, carbohydrates, fatty acids, vitamins, polyphenols, phytosterols, and carotenoid pigments it contains vary depending on ecological factors such as flora, geographic location, and season (Denisow and Denisow-Pietrzyk., 2016; El-Didamony et al., 2024). Consumed as food since ancient times, these pollen granules possess antioxidant, antimicrobial, anticancer, and immune-modulating properties (Yildiz et al., 2014).

This study, conducted on the Datça Peninsula—an area featuring a distribution of endemic plants—with the support of the Muğla Province Beekeepers' Association (MAYBİR) and stationary beekeeper and Senior Agricultural Engineer Alper Kuyucu, aimed to investigate the wound-healing effects of bee pollen (produced in the same area and from the same colony) on the 3T3 healthy fibroblast cell line over specific time periods (12 h, 24 h, and 48 h).

MATERIAL AND METHODS

1. Obtaining a Bee Pollen Sample

In this study, Alper KUYUCU, a member of MAYBİR and a professional agricultural engineer who produces bee products other than honey in the Marmaris–Datça region, collected 500 grams of bee pollen from 30 separate colonies—one out of every 10 colonies—for use in our research during the summer of 2024.

2. Extraction

Bee pollen were first extracted with ethanol at room temperature for 24 hours; after the resulting ethanol extract was dried, it was filtered through Whatman filter paper to remove any residue. Two additional extractions were performed on the residue remaining from each sample; ethanol containing 10% water was then added, the residue in the extract was filtered out, and the extraction was carried out using a rotary evaporator. Subsequently, the three extracts were combined and left to stand on a hot plate.

3. Determination of In Vitro Wound-Healing Effects

Cells that were approximately 90% confluent were passaged, and 5×10^5 cells were inoculated into 24-well cell culture plates. The wound-healing effects ethanol extract of Datça Peninsula bee pollen the resulting on the 3T3 (CRL-1658) fibroblast cell line obtained from ATCC were investigated according to the method established by Roy et al. (2023), on a healthy fibroblast cell line (3T3) at specific time points (0 hour, 12 hour, 24 hour, and 48 hour). The wound-healing effect of ethanol extract of Datça Peninsula bee pollen was investigated at a concentration of 0.5 mg/mL. Cell migration or wound healing was determined by observing the number of cells migrating into the gaps that formed. The wound area photographs obtained at the end of the studies were analyzed using ImageJ software.

The wound healing percentage was calculated as (C0 - C24) * 100 / C0. (C0 = average wound distance at 0 hours and C24 = average wound distance at 24 hours) (Roy et al., 2023). Calculations were performed according to the formula for each hour.

$$\text{Wound Closure (\%)} = \left(\frac{\text{Initial Wound Width} - \text{Remaining Wound Width}}{\text{Initial Wound Width}} \right) \times 100$$

4. Statistical Analysis

All experimental data are expressed as the mean ± standard deviation (SD) of three independent experiments, and analyses were performed using Excel Pro 2019.

RESULTS AND DISCUSSION

Results of the In Vitro Wound-Healing Effect of Ethanol Extract of Datça Peninsula Bee Pollen

Natural products hold great potential for preventive treatments. Many people prefer natural compounds found in plants, such as phytochemicals, as part of complementary and alternative therapies. However, because many bioactive natural compounds have not been extensively studied and have not been approved as drugs, they cannot be used directly in treatment (Ju et al., 2016). Natural products are part of complementary and alternative therapies. Bee products are used as an adjunct in the treatment of metabolic disorders such as diabetes, obesity, hyperlipidemia, and associated cardiovascular problems. Bee pollen extracts, which stand out as potential wound-healing agents thanks to their antioxidant and anti-inflammatory properties and rich bioactive components, are drawing particular attention. It has been reported that these extracts make significant contributions to wound repair by supporting tissue regeneration and regulating cellular responses involved in the healing process (Olczyk et al., 2016; Bedjih et al., 2025).

The wound healing results obtained using an ethanol extract at a concentration of 0.5 mg/mL of bee pollen from the Datça Peninsula on the 3T3 fibroblast cell line at specific time points (0 h, 12 h, 24 h, and 48 h) compared to the control are presented in Figures 1 and 2 and Table 1. Treatment with the ethanol extract of Datça Peninsula bee pollen resulted in wound closure rates of 25.90%, 65.80%, and 95.00% at 12, 24, and 48 hours, respectively, compared to 33.54%, 51.81%, and 90.00% in the control group. At 24 and 48 hours, the ethanol extract bee pollen exhibited higher wound closure rates (65.80% and 95.00%, respectively) compared to the control group (51.81% and 90.00%). The results demonstrate that the ethanol extract of bee pollen significantly enhances wound closure in 3T3 fibroblast cells, particularly at 24 and 48 hours compared to the control group. These results suggest that bee pollen could serve as a novel target in both cosmetics and drug development by contributing to fibroblast proliferation. According to the results of the Sidak's multiple comparisons test following the two-way repeated measures ANOVA (Two-way RM ANOVA), the wound closure rates between the Control and Pe (Bee pollen ethanol extract) groups showed statistically significant differences at 12 hours ($P = 0.034$) and 24 hours ($P = 0.0059$). In contrast, the difference between the groups at 48 hours was not statistically significant ($P = 0.8956$). (Figure 2). These findings indicate that the extract holds promising potential as a natural therapeutic agent for tissue repair and wound healing applications.

	Pe	Control
0 hour		
12 hour	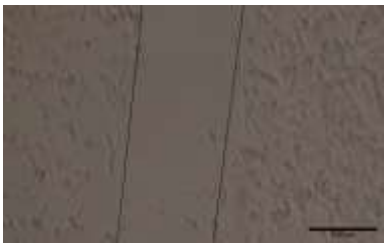	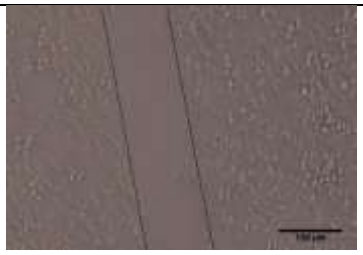
24 hour	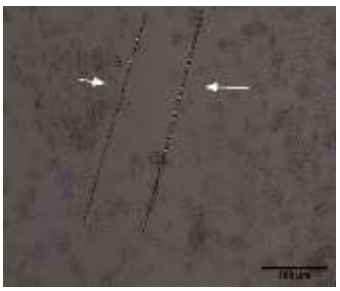	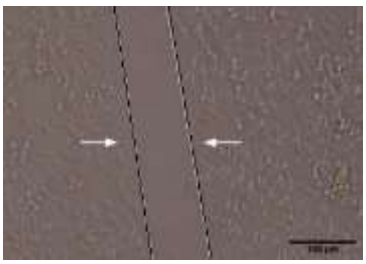
48 hour	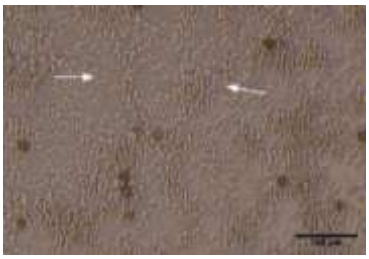	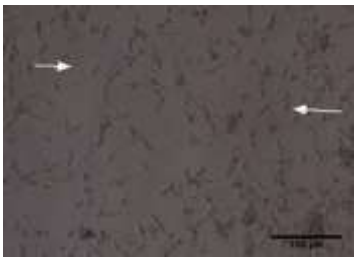

Figüre 1. Effect of the ethanol extract of Datça Peninsula bee pollen on wound healing in the 3T3 healthy fibroblast cell line (at 0h, 12h, 24h and 48 hour)

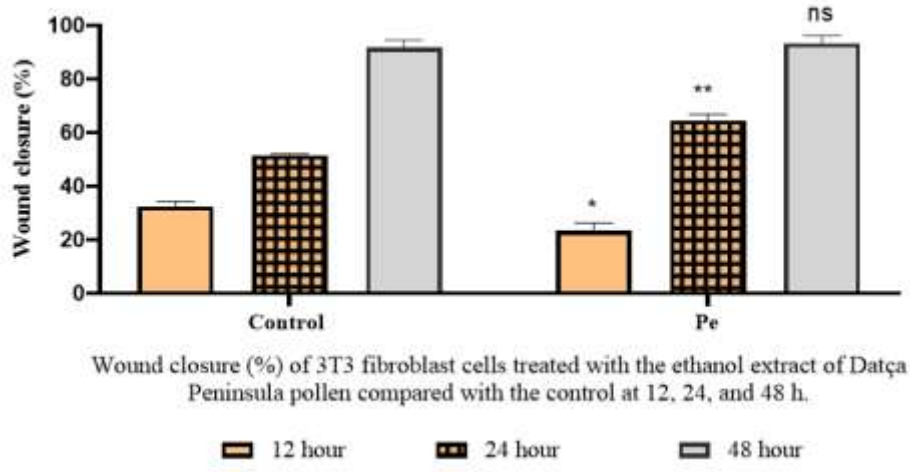

Figure 2. Wound closure (%) of 3T3 fibroblast cells treated with the ethanol extract of Datça Peninsula bee pollen compared with the control at 12, 24, and 48 h.

(Data are presented as mean ± SD. *P < 0.05, **P < 0.01, ns: not significant. Two-way RM ANOVA followed by Sidak's multiple comparisons test).

Table 1. Wound healing (%) of 3T3 fibroblast cells treated with the ethanol extract of Datça Peninsula bee pollen compared with the control at 12, 24, and 48 h.

	12 hour	**24 saat**	**48 saat**
Control	33.54	51.81	90
Ethanol extract of Datça Peninsula bee pollen	25.90	65.80	95

CONCLUSIONS

Natural products are part of complementary and alternative therapies. According to this study results at 24 and 48 hours, the ethanol extract bee pollen of Datça Peninsula exhibited higher wound closure rates (65.80% and 95.00%, respectively) compared to the control group (51.81% and 90.00%). In particular, the achievement of higher wound closure rates compared to the control group at later time points (24 h and 48 h) This suggests that this bee pollen extract could be a promising natural agent for tissue repair and wound healing, with potential for future complementary combination studies.

ACKNOWLEDGEMENT

Authors would like to thank the Muğla Provincial Beekeepers' Association (MAYBİR) and Alper Kuyucu, a senior agricultural engineer engaged in stationary beekeeping, for their valuable contributions.

REFERENCES

Anonymous (2024). Türk gıda kodeksi. Arı ürünleri tebliği (2024/6). Tarım ve Orman Bakanlığı. 25 Mayıs 2024 tarih ve 32527 sayılı Resmî Gazete, Ankara.

Bedjih, F., Ouchemoukh, S., Amessis-Ouchemoukh, N., Otmani, A., Zaidi, H., Kara, Y., ... & Kolaylı, S. (2025). Biochemical properties of different Algerian bee pollen samples. Mediterranean Journal of Nutrition and Metabolism, 18(1), 48-68.

Denisow, B., & Denisow-Pietrzyk, M. (2016). Biological and therapeutic properties of bee pollen: a review. Journal of the Science of Food and Agriculture, 96(13), 4303-4309.

El-Didamony, S. E., Gouda, H. I., Zidan, M. M., & Amer, R. I. (2024). Bee products: An overview of sources, biological activities and advanced approaches used in apitherapy application. Biotechnology Reports, 44, e00862.

Faqihi, R. A., & Taha, E. A. H. (2022). Apitherapy as an Alternative medicine: Article review. African Journal of Biological Sciences, 18(2), 43-57.

Ju, H. M., Yu, K. W., Cho, S. D., Cheong, S. H., & Kwon, K. H. (2016). "Anti-cancer effects of traditional Korean wild vegetables in complementary and alternative medicine", Complementary Therapies in Medicine, 24, 47-54.

Olczyk, P., Koprowski, R., Kaźmierczak, J., Mencner, L., Wojtyczka, R., Stojko, J., ... & Komosinska-Vassev, K. (2016). Bee pollen as a promising agent in the burn wounds treatment. Evidence-Based Complementary and Alternative Medicine, 2016(1), 8473937.

Wagner, H., Dobler, I., & Thiem, I. (1970). Effect of royal jelly on the peripheral blood and survival rate of mice after irradiation of the entire body with X-rays.

Yildiz, O. K. T. A. Y., Karahalil, F. A. T. M. A., Can, Z., Sahin, H., & Kolayli, S. E. V. G. (2014). Total monoamine oxidase (MAO) inhibition by chestnut honey, pollen and propolis. Journal of enzyme inhibition and medicinal chemistry, 29(5), 690-694.

ANALYSIS RESULTS OF PHENOLIC COMPONENTS and CHEMOMETRIC ANALYSIS IN GRAPES PRODUCED WITH DIFFERENT AGROECOLOGICAL PRACTICES

Cansu KORKMAZ[1], Fatih ÇAYAN[2], Oğuzhan SOLTEKİN[3], Mehmet Emin DURU[4]*

[1]Department of Biology, Faculty of Science, Muğla Sıtkı Koçman University, 48000 Muğla, Türkiye,

[2]Department of Chemistry and Chemical Processing Technologies, Muğla Vocational School, Muğla Sıtkı Koçman University, 48000 Muğla, Türkiye,

[3]Manisa Viticulture Research Institute, Turkish Ministry of Agriculture and Forestry, 45125 Manisa, Türkiye,

[4]Department of Chemistry, Faculty of Science, Muğla Sıtkı Koçman University, 48000 Muğla, Türkiye,

**Corresponding author e-mail: cansukorkmaz08@gmail.com*
https://orcid.org/0000-0003-3027-7687

ABSTRACT

The climate-induced rising temperatures and severe water stress create physiological pressure on grapevines, negatively suppressing the accumulation of phenolic compounds that are critical for health. This study investigated the effects of integrated agroecological strategies on the phenolic components and chemometric profiles of grapes to mitigate the adverse impacts of climate change on Mediterranean viticulture. In this study, the phenolic compound profile of grapes grown under different production conditions (alfalfa, biohydrogel, plant growth-promoting rhizobacteria) was determined using an HPLC-DAD system. In this context, the findings regarding grapes obtained from the experimental plots of the Ministry of Agriculture and Forestry's Manisa Viticulture Research Institute were investigated based on the control group of the study. It was determined that flavonoids such as kaempferol and apigenin were dominant across all treatments. This indicates that phenylpropanoid metabolism is active and that the plant's defense and adaptation mechanisms are robust. According to the findings obtained, it was determined that different production conditions (alfalfa, biohydrogel, and plant growth-promoting rhizobacteria) had a significant effect on the phenolic component profile and chemometric properties of grapes, substantially increasing secondary metabolite accumulation compared to the control group. Moreover, this is primarily because phenolic compounds are predominantly distributed within the skin and seeds of the grape.

Keywords: *Phenolic profile, Grape, Alfalfa, biohydrogel, growth-promoting rhizobacteria (PGP), HPLC (DAD), Chemometrıc analysis*

INTRODUCTION

Phenolic compounds constitute the most abundant group of compounds in grapes and wine after carbohydrates and fruit acids (Van de Wiel et al., 2001; Lopez-Velez et al., 2003). In the grape berry, phenolic compounds are generally located in the skin and seeds. While 60-70% of the

polyphenols extractable from grape tissues are found in the seeds, 28-35% are located in the berry skin. The amount extractable from the pulp is as low as 10% (Anonymous, 2003). Indeed, Mozetic et al. (2006) determined that the total amount of phenolic compounds in the berry skin of the white grape variety Rebula was 3.5 times higher than that in the pulp.

The quantity and characterization of flavan-3-ol monomers and procyanidins extracted from Vitis vinifera fruit depend on varying degrees of ripening and water content. As ripening progressed, the extraction yield of phenolic compounds per berry decreased, with flavan-3-ol monomers showing a more rapid decline. The mean degree of polymerization of procyanidins remained unchanged, while their thiolytic degradation decreased. As fruit maturity increased, the resistance of extracted procyanidins to acid-catalyzed thiolysis increased. Water content in the vine affected polyphenol amounts, indicating that the compositional effect was cultural (Kennedy et al., 2000).

In this study, to determine phenolic compounds profile of grapes grown under different production conditions (alfalfa, biohydrogel, growth-promoting rhizobacteria), grapes were extracted with methanol at room temperature. Firstly, For HPLC analysis, the obtained grapes extracts were dissolved in methanol and subjected to phenolic profile analysis using an HPLC-DAD system (Shimadzu 20 AT series high-performance liquid chromatograph, Shimadzu Corporation, Japan) with reference phenolic acid standards (Barros et al., 2009; Tel-Çayan et al., 2015). Secondly, in this study the effects of various agroecological practices (alfalfa cover cropping, biohydrogel application, and plant growth-promoting (PGP) bacteria) on the phenolic profile and chemometric analysis of grapes were evaluated under water-limited conditions. In this study, grapes obtained from the experimental plots of the Ministry of Agriculture and Forestry's Manisa Viticulture Research Institute are presented below under the relevant headings, based on the control group of the study.

MATERIAL AND METHODS

Determination of Phenolic Compounds by HPLC-DAD

In this study, to investigate the phenolic compounds of grapes approximately 100 g of each sample was dried in a lyophilizer. The resulting water extracts were stored in a cool and dark environment until analysis. For HPLC analysis, the obtained grapes extracts were dissolved in methanol, filtered through a 0,20µm PTFE filter, and subjected to phenolic profile analysis using an HPLC-DAD system (Shimadzu 20 AT series high-performance liquid chromatograph, Shimadzu Corporation, Japan) with reference phenolic acid standards (Barros et al., 2009; Tel-Çayan et al., 2015).

Qualitative and quantitative results were obtained through retention times using peak spiking (co-injection) with standards and peak area calculations. HPLC operating conditions, including column specifications, mobile phase, detector, injection volume, and analysis time, are presented in Table 1.

Table 1. HPLC Operating Conditions

HPLC-DAD Instrument Parameters				
Column	C18 column (5 µm, 250 mm x 4.6 mm i.d)			
Mobile Phase A	H_2O containing %0,5'lik CH_3COOH			
Mobile Phase B	MeOH			
Column Oven Temperature	40°C			
Detector	SPD-M20A DAD detector			
Detection Wavelength	280nm			
Injection Volume	20µL			
Analysis Time	55 minutes			
Gradient Program	Time (min)	Flow (mL/min)	% Solvent A	% Solvent B
	0.01	1.000	90.00	10.00
	5.00	1.000	80.00	20.00
	15.00	1.000	70.00	30.00
	25.00	1.000	50.00	50.00
	30.00	1.000	35.00	65.00
	40.00	1.000	25.00	75.00
	50.00	1.000	10.00	90.00
	55.00	1.000	90.00	10.00

RESULTS AND DISCUSSION

Analysis Results of Phenolic Components in Grapes Produced with Different Cultivation Techniques

The codes and yields of the extracts obtained from the extraction study conducted to investigate the phenolic components of the grape samples, which are the subjects of this study, are presented in Table 2.

Table 2. Codes and extraction yields (% w/w) of grapes grown under different cultivation techniques

Sample Name and Production Conditions	**Sample Code**	**Extraction Solvent**	**Fresh Weight of Material (g)**	**Net Weight of Extract (g)**	**Extract Yield (%)**
Aqueous extract of grape grown with alfalfa	YÜS	Water	100	16.39	16.39
Aqueous extract of grape grown without alfalfa	YYÜS	Water	100	14.73	14.73
Aqueous extract of grape grown with biohydrogel	BHÜS	Water	100	12.72	12.72
Aqueous extract of grape grown without biohydrogel	BHYÜS	Water	100	11.94	11.94
Aqueous extract of grape grown with PGP	PGPÜS	Water	100	11.06	11.06
Aqueous extract of grape grown without PGP	PGPYÜS	Water	100	10.79	10.79

In this study, to examine the changes in phenolic compounds of grape juices obtained from vines subjected to different cultivation techniques under drought stress, lyophilized grape juice samples were analyzed comparatively against control groups using an HPLC-DAD system. The results obtained from these analyses are presented in Table 3.

Table 3. Phenolic compound analysis results of grapes produced in study experimental plots via HPLC-DAD (mg/g extract)

No	Reference Compounds	YÜS	YYÜS	BHÜS	BHYÜS	PGPÜS	PGPYÜS
1	Oxalic acid	-	-	-	-	-	-
2	Fumaric acid	-	-	-	-	-	-
3	Gallic acid	-	-	-	-	-	-
4	Protocatechuic acid	-	-	-	-	-	-
5	Methyl-1,4-benzoquinone	-	-	-	-	-	-
6	Catechin hydrate	-	-	-	-	-	-
7	*p*-Hydroxy phenyllactic acid	-	-	-	-	-	-
8	4-Quinoline carboxaldehyde	-	-	-	-	-	-
9	Chlorogenic acid	-	-	-	-	-	-
10	4-Hydroxybenzoic acid	-	-	-	-	-	-
11	6,7-Dihydroxycoumarin	-	-	-	-	-	-
12	Caffeic acid	-	-	-	-	-	-
13	Cyanidin chloride	-	-	-	-	-	-
14	Syringic acid	-	-	-	-	-	-
15	Vanillin	-	-	-	-	-	-
16	*p*-Coumaric acid	-	-	-	-	-	-
17	Taxifolin	-	-	-	-	-	-
18	Guaiacol	-	-	-	-	-	-
19	Ferulic acid	-	-	-	-	-	-
20	*m*-Coumaric acid	-	-	-	-	-	-
21	Coumarin	-	-	-	-	-	-
22	Rutin	-	-	-	-	-	-
23	2-Hydroxycinnamic acid	0.17	0.30	0.30	0.30	-	-
24	Myricetin	-	-	-	-	-	-
25	Rosmarinic acid	-	-	-	-	-	-
26	3,4-Dimethoxycinnamic acid	-	-	-	-	-	-
27	Quercetin	-	-	-	-	-	-
28	Naringenin	-	-	0.45	-	-	-
29	trans-Cinnamic acid	-	-	-	-	-	-
30	Pinobanksin	-	-	-	-	0.46	0.49
31	Hesperetin	-	-	-	-	-	-
32	Kaempferol	3.17	3.10	3.29	3.20	1.62	1.58
33	Apigenin	0.89	0.82	0.88	0.85	1.24	1.15
34	Chrysin	-	-	-	-	-	-
35	Galangin	-	-	-	-	-	-
36	4-Hexylresorcinol	-	-	-	-	-	-
37	Artepillin C	-	-	-	-	-	-

An examination of Table 3 reveals that the diversity of phenolic compounds in grape juice is more limited compared to that in the leaves. This is attributed to the fact that phenolic compounds are predominantly localized in the grape skin and seeds (Kennedy et al., 2000; Mozetic et al., 2006). Flavonoids such as kaempferol and apigenin were identified as the dominant compounds across all treatments. This finding indicates that the phenylpropanoid

metabolism is highly active and that the plant's defense and adaptation mechanisms remain robust (Kuljarusnont et al., 2024; Ninkuu et al., 2025). The increase in 2-hydroxy cinnamic acid content in the clover treatment suggests that the early stages of the phenylpropanoid pathway are activated and that this treatment up-regulates the secondary metabolism (Sharma et al., 2019). Conversely, the decrease in certain phenolic compounds observed in the hydrogel and PGP treatments points to a metabolic reallocation within the plant under stress conditions (Wani et al., 2016; Commisso et al., 2016; Kuljarusnont et al., 2024; Ninkuu et al., 2025).

Phenolic Compound Amounts per Serving in Grape Juices Produced in Study Applications

Based on the phenolic compound analysis results determined by HPLC-DAD (Table 4) and the grape juice extraction yields (Table 5), the phenolic compound contents per portion (defined as 100 g of grape juice) were calculated. The per-serving amounts of phenolic compounds in grape juices obtained via different cultivation techniques are presented in Tables 5.4 and 5.5. Accordingly, the phenolic compound contents in 100 g of grape juice derived from grapes produced in the clover trial plot are detailed in Table 4

Table 4. Phenolic compound amounts per serving in grapes produced in clover and non-clover grapevine production plots (mg/100 g grape juice)

No	Reference Compounds	YÜS	YYÜS
1	2-Hydroxycinnamic acid	2.79	4.41
2	Kaempferol	51.95	45.66
3	Apigenin	13.77	12.08

As shown in Table 4, when comparing the per-serving phenolic compound amounts in grape juices produced with clover application, it is observed that vines in plots with clover cover crops are enriched in flavonoids, such as kaempferol and apigenin, compared to the control group, whereas the content of 2-hydroxycinnamic acid is decreased. The reduction in 2-hydroxycinnamic acid indicates that this compound is consumed in the flavonoid biosynthesis process, and the carbon flux in the phenylpropanoid metabolism is channeled toward the flavonoid pathway (Sharma et al., 2019).

When investigating the effect of cover crop applications with clover (*Medicago sativa* L.) on grape phenolic composition, it is evident that this treatment promotes flavonoid biosynthesis and increases the concentrations of kaempferol and apigenin compared to the control. It has been reported in the literature that cover crops used in vineyards increase total phenolic compounds and, in particular, the flavonoid fraction in grapes and wine, making flavonoids the dominant components over non-flavonoid phenolics (Xi et al., 2010). Similarly, cover crop treatments have been shown to significantly increase flavonol content (Peng et al., 2021; Luo et al., 2025). Conversely, the relative decrease in phenolic acids, such as hydroxycinnamic acids, can be explained by the redirection of carbon flux within the phenylpropanoid metabolism toward flavonoid biosynthesis (Dixon and Paiva, 1995; Vogt, 2010; Luo et al., 2025). Furthermore, it is suggested that intercropping with clover modulates the secondary metabolite distribution by reducing oxidative stress and balancing the metabolic state of the plant (Jeder et al., 2021). The results obtained in this project regarding the clover application are in strong agreement with those reported in the literature (Dixon and Paiva, 1995; Vogt, 2010; Xi et al., 2010; Liu et al., 2021; Peng et al., 2021; Patil et al., 2024).

Table 5. Amounts of phenolic compounds and organic acids per serving in grapes produced in vine production areas with and without hydrogel application (mg/100 g grape juice)

No	Reference Compounds	BHÜS	BHYÜS
1	2-Hydroxycinnamic acid	3.82	3.28
2	Naringenin	5.72	-
3	Kaempferol	41.85	38.21
4	Apigenin	11.19	10.15

It was determined that flavonoids, such as kaempferol and apigenin, increased significantly under the clover treatment, while this increase continued at a lower level under the hydrogel application; in contrast, flavonoids either showed a limited increase or remained stable under the PGP application (Tables 4–5). The literature reports that cover crops particularly promote flavonoid biosynthesis and cause flavonoids to become the dominant components in the phenolic profile of grapes (Xi et al., 2010; Peng et al., 2022). It is known that hydrogel applications create moderate stress conditions by partially alleviating water stress in the plant, which supports the production of secondary metabolites (Agaba et al., 2010; Farooq et al., 2009). Conversely, it has been reported that plant growth-promoting rhizobacteria (PGPR) stimulate growth by reducing stress levels in the plant, which may lead to a decrease or stabilization in the production of secondary metabolites (Egamberdieva et al., 2017; Vacheron et al., 2013). Indeed, the findings from the PGP application within the scope of our project, showing a limited increase in flavonoids, are consistent with this mechanism. On the other hand, it was determined that the amount of pinobanksin decreased in the PGP-treated plot compared to the control group (Table 6). It is noted that flavanone derivatives such as pinobanksin are among the plant defense metabolites and that a decline in these compounds may be observed when stress is reduced (Dixon and Paiva, 1995). Furthermore, while not detected in other treatments, the presence of naringenin was identified only in the hydrogel application. Naringenin is a key intermediate in flavonoid biosynthesis and can be detected under conditions where metabolic flux is balanced and intermediate accumulation occurs (Falcone Ferreyra et al., 2012). This indicates that the hydrogel application exerts a balancing effect on secondary metabolism.

Table 6. Per-serving amounts of phenolic compounds and organic acids in grapes produced in PGP-treated and non-PGP-treated grapevine production plots (mg/100 g grape juice)

No	Referance Compounds	PGPÜS	PGPYÜS
1	Pinobanksin	5.09	5.28
2	Kaempferol	17.92	17.05
3	Apigenin	13.71	12.41

Chemometric Analysis of Phenolic Compounds and Organic Acids in Grapevine Leaves Grown with Different Drought-Resistance Cultivation Techniques

The chemometric analyses performed based on the phenolic compound profiles of grapevine leaves are presented in Figure 1 and Figure 2. As can be observed in both figures, the effects of different cultivation techniques on secondary metabolism are clearly demonstrated.

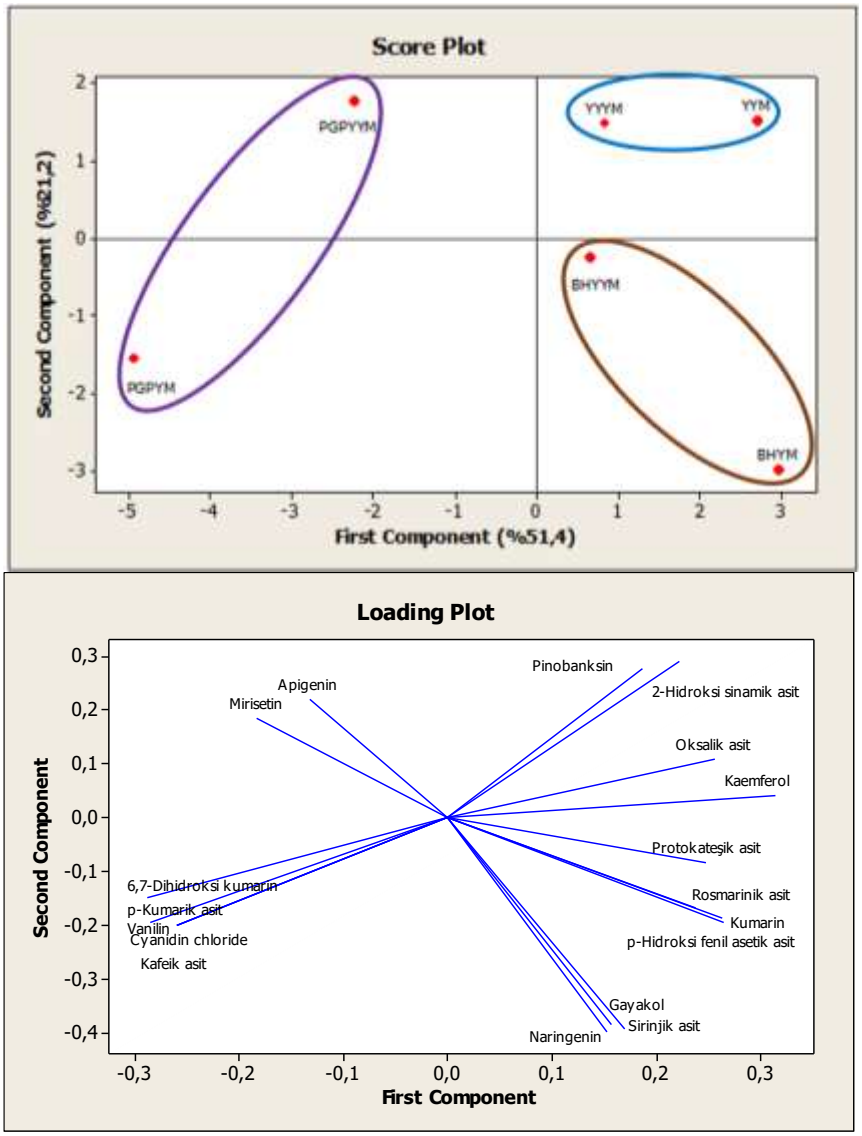

Figure 1. Principal Component Analysis (PCA) and Hierarchical Cluster Analysis (HCA) results based on phenolic compound and organic acid profiles of grapevine leaves grown with different cultivation techniques

The PCA results indicate that the samples are clearly differentiated based on their phenolic compound compositions. The principal components (PC1 and PC2) explain the majority of the total variance, revealing that the differences, particularly between flavonoids and phenolic acids, are the primary determinants in the distribution of the samples (Figure 1). The more compact clustering observed in some groups depending on the application suggests that these treatments exert a more stable and homogeneous effect on phenolic metabolism, whereas the wider dispersion of other groups indicates an enhancement in metabolic diversity. It has been extensively reported in the literature that PCA is an effective method for elucidating the variation in plant metabolites and the impacts of environmental/agronomic treatments (Jolliffe and Cadima, 2016).

Regarding the Hierarchical Cluster Analysis (HCA) results, the samples form significant groups based on their phenolic compound similarities (Figure 1). Notably, the clustering of replicates from the same application into similar groups demonstrates that the treatments have distinct and reproducible effects on the phenolic profile. The close proximity of certain applications within the clusters suggests that these techniques exert similar effects on the phenylpropanoid

metabolism. HCA is widely recognized as a reliable method for the classification of biochemical and metabolomic data (Caesar et al., 2018; Bu et al., 2019).

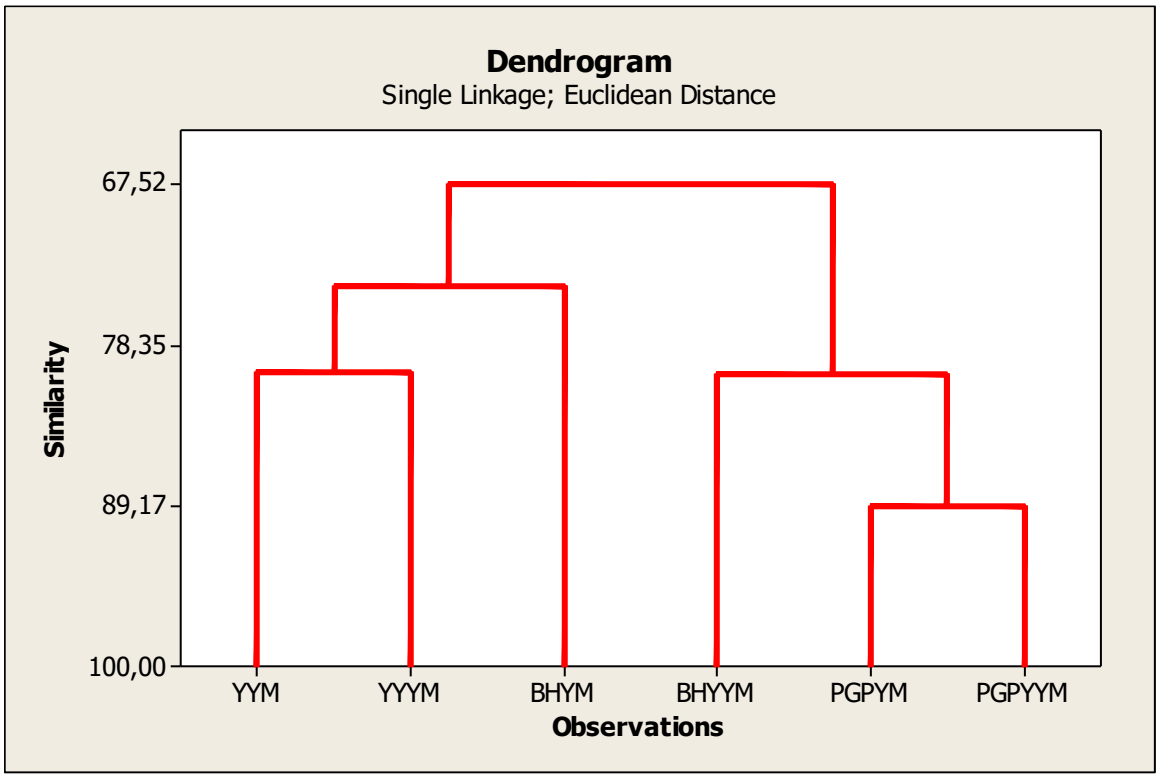

Figure 2. Dendrogram showing the hierarchical clustering of grapevine leaves grown with different cultivation techniques, based on phenolic compound and organic acid profiles.

In the dendrogram analysis presented in Figure 2 the similarity and distance relationships between samples are clearly visualized. While short branch lengths signify high similarity and low variation in terms of phenolic compound profiles, long branches indicate greater metabolic divergence. In this context, the clustering of certain applications at shorter distances suggests that these groups possess a more homogeneous and balanced phenolic composition, whereas the wider dispersion of others indicates an enhancement in metabolic diversity. Dendrogram analysis is widely utilized in the literature for interpreting metabolic profile differences and elucidating inter-sample relationships (Wishart, 2008).

Chemometric analyses based on the phenolic constituents of grapevine leaves cultivated with different techniques demonstrate that these techniques exert significant impacts on the secondary metabolism of the leaves. When PCA and HCA results are evaluated collectively, it is evident that these treatments play both a discriminative and a guiding role in the phenolic profile. It is particularly noteworthy that while some treatments increase homogeneity in phenolic components, others promote metabolic diversity. These results substantiate that the phenylpropanoid metabolism is a dynamic system sensitive to environmental and agronomic factors, and the findings are in strong alignment with those reported in the literature (Dixon and Paiva, 1995; Jolliffe and Cadima, 2016).

CONCLUSIONS

This study demonstrates that integrated agroecological practices significantly impact the secondary metabolism of grapevine leaves. Flavonoids such as kaempferol and apigenin were identified as the dominant compounds across all treatments, indicating that the phenylpropanoid metabolism remains highly active and that the plant's defense and adaptation mechanisms are robust. Furthermore, these outcomes are closely attributed to the fact that phenolic compounds are predominantly localized in the grape skin and seeds. Overall, chemometric analyses based on these phenolic constituents confirm that different cultivation techniques exert substantial effects on metabolic profiles, offering valuable strategies for sustainable and climate-resilient viticulture.

ACKNOWLEDGEMENT

The authors are grateful for the conditions that the Partnership for Research and Innovation in the Mediterranean Area (PRIMA), the Scientific and Technological Research Council of Turkiye (TUBITAK), and the European Union provided in the development of the VineProtect project (10.54499/PRIMA/0011/2021 and TUBITAK-122N043).

REFERENCES

Agaba, H., Orikiriza, L. J. B., Esegu, J. F. O., Obua, J., Kabasa, J. D., & Hüttermann, A. (2010). Effects of hydrogel amendment to different soils on plant available water and survival of trees under drought conditions. Clean–Soil, Air, Water, 38(4), 328-335.

Anonymous (2003). Polyphenolics, Inc. Technical Publication I. Http://Www.Polyphenolics.Com/Research/Research.Htm.

Barros, L., Falcão, S., Baptista, P., Freire, C., Vilas-Boas, M., & Ferreira, I. C. (2008). Antioxidant activity of Agaricus sp. Mushrooms by chemical, biochemical and electrochemical assays. Food Chemistry, 111(1), 61-66.

Bu, J., Liu, W., Pan, Z., & Ling, K. (2019). Comparative Study of Hydrochemical Classification Based on Different Hierarchical Cluster Analysis Methods. International Journal of Environmental Research and Public Health, 17(24), 9515.

Caesar LK, Kvalheim OM, Cech NB. (2018). Hierarchical cluster analysis of technical replicates to identify interferents in untargeted mass spectrometry metabolomics. Anal Chim Acta. 2018 Aug 27;1021:69-77.

Commisso M., Toffali K., Strazzer P., Stocchero M., Ceoldo S., Baldan B., et al. (2016). Impact of phenylpropanoid compounds on heat stress tolerance in carrot cell cultures. Front. Plant Sci. 7, 1439.

Dixon RA and Paiva NL. (1995). Stress-Induced Phenylpropanoid Metabolism. Plant Cell. 1995 Jul;7(7):1085-1097.

Egamberdieva, D., Wirth, S. J., Alqarawi, A. A., Abd_Allah, E. F., & Hashem, A. (2017). Phytohormones and Beneficial Microbes: Essential Components for Plants to Balance Growth and Stress Tolerance. Frontiers in Microbiology, 8, 1580.

Falcone Ferreyra, M. L., Rius, S. P., & Casati, P. (2012). Flavonoids: Biosynthesis, biological functions, and biotechnological applications. Frontiers in Plant Science, 3, 222.

Farooq, M., Wahid, A., Kobayashi, N., Fujita, D., & Basra, S. M. A. (2009). Plant drought stress: effects, mechanisms and management. Agronomy for Sustainable Development, 29(1), 185-212.

Jeder, S. Nouaırı, I., Melkı, F., Chebıl, S. ., Louatı, F., Mhadhbı, H., & Zrıbı, K. (2021). Effect of intercropping alfalfa on physiological and biochemical parameters of young grapevine plants

cultivated on agricultural and contaminated soils. Notulae Botanicae Horti Agrobotanici Cluj-Napoca, 49(1), 12017.
Jolliffe, I.T. and Cadima, J. (2016). Principal Component Analysis: A Review and Recent Developments. Philosophical Transactions of the Royal Society A: Mathematical, Physical and Engineering Sciences, 374, Article 20150202.
Kennedy, J., Matthews, M. ve Waterhouse, A.L. (2000). Changes in grape seed polyphenols during fruit ripening, Pyhtochemistry, 55, 77-85.
Kuljarusnont S, Iwakami S, Iwashina T, Tungmunnithum D. Flavonoids and Other Phenolic Compounds for Physiological Roles, Plant Species Delimitation, and Medical Benefits: A Promising View. Molecules. 2024 Nov 14;29(22):5351.
Lopez Velez, M., Martınez, F., Del Valle- Rıbes, C. (2003). The Study Of Phenolic Compounds As Natural Antioxidants İn Wine. Critical Reviews İn Food Science And Nutrition, 43 (3): 233-244.
Luo, X., Wu, J., Li, H., Wang, X., Wang, W., Li, H., Li, K., & Bai, S. (2025). Integrative Analysis of Transcriptomic and Metabolomic Profiles Identifies Distinct Dynamic Changes in Primary and Secondary Metabolites in Grape Berries Under Fruit-Specific Light Exposure. Horticulturae, 11(5), 481.
Mozetič, B., Simčič, M., & Trebše, P. (2006). Anthocyanins and hydroxycinnamic acids of Lambert Compact cherries (Prunus avium L.) after cold storage and 1-methylcyclopropene treatment. Food Chemistry, 97(2), 302-309.
Ninkuu, V., Liu, Z., Qin, A., Xie, Y., Song, X., & Sun, X. (2025). Impact of straw returning on soil ecology and crop yield: A review. Heliyon, 11(2), e41651.
Patil, H., Naik, R., & Paramasivam, S. K. (2024). Utilization of banana crop ligno-cellulosic waste for sustainable development of biomaterials and nanocomposites. International Journal of Biological Macromolecules, 282, 137065.
Peng, J., Ma, J., Wei, X., Zhang, C., Jia, N., Wang, X., ... & Wang, Z. (2021). Accumulation of beneficial bacteria in the rhizosphere of maize (Zea mays L.) grown in a saline soil in responding to a consortium of plant growth promoting rhizobacteria. Annals of Microbiology, 71(1), 40.
Sharma A, Shahzad B, Rehman A, Bhardwaj R, Landi M, Zheng B. (2019). Response of Phenylpropanoid Pathway and the Role of Polyphenols in Plants under Abiotic Stress. Molecules. 2019 Jul 4;24(13):2452.
Tel-Çayan, G., Öztürk, M., Duru, M.E., Rehman, M., Adhikari, A., Türkoglu, A. ve Choudhary, M.I. (2015) Phytochemical investigation, antioxidant and anticholinesterase activities of Ganoderma adspersum, Ind Crops Prod, 76: 749-754.
Vacheron, J., Desbrosses, G., Bouffaud, M. L., Touraine, B., Moënne-Loccoz, Y., Muller, D., Legendre, L., Wisniewski-Dyé, F., & Prigent-Combaret, C. (2013). Plant growth-promoting rhizobacteria and root system functioning. Frontiers in Plant Science, 4, 356.
Van De Wıel, A., Van Golde, P.H.M., Hart, H.C.H. (2001). Blessing Of The Grape. European Journal Of Internal Medicine, 12: 484-489.
Vogt T. (2010). Phenylpropanoid biosynthesis. Mol Plant. 2010 Jan;3(1):2-20.
Wani, S. H., Kumar, V., Shriram, V., & Sah, S. K. (2016). Phytohormones and their metabolic engineering for abiotic stress tolerance in crop plants. The Crop Journal, 4(3), 162-176.
Wishart, D. S. (2008). Metabolomics: Applications to food science and nutrition research. Trends in Food Science & Technology, 19(9), 482-493.
Xi, Z., ZHANG, Z., CHENG, Y., & LI, H. (2010). The Effect of Vineyard Cover Crop on Main Monomeric Phenols of Grape Berry and Wine in Vitis viniferal L. Cv. Cabernet Sauvignon. Agricultural Sciences in China, 9(3), 440-448.

KEFE CUMIN (*Laser trilobum* (L.) Borkh.) in TURKISH CUISINE

Sema AY[1], Sevgi ÇALIŞKAN[1]

[1] Niğde Ömer Halisdemir Üniversity, Faculty of Agricultural Sciences and Technologies, Department of Plant Production and Technologies Niğde-Türkiye

Corresponding author e-mail: sema_ay@mail.ohu.edu.tr

ABSTRACT

Kefe cumin (*Laser trilobum* (L.) Borkh.) is a perennial herbaceous species belonging to the *Apiaceae* (Umbelliferae) family and is commonly known as cumin. The species grows naturally in certain regions of Türkiye and is also referred to by various regional vernacular names, including Kefe cumin, mountain cumin, *sıra baharatı*, and *geyik sırası*. Chemical analyses have shown that the aerial parts and fruits of the plant contain high levels of d-limonene and perillaldehyde. Widely distributed throughout the flora of Türkiye, *Laser trilobum* has become integrated into the gastronomic and ethnobotanical traditions of the regions where it naturally occurs, resulting in its diverse range of uses. Kefe cumin has a long-standing history in traditional Anatolian medicine and continues to be widely used by local communities as a medicinal plant. Herbal tea prepared by boiling the seeds has been reported to be traditionally consumed for the management of diabetes, hypertension, and digestive system disorders. The ethnobotanical applications of the species play an important role in the traditional culinary culture of the Mediterranean and Southeastern Anatolia regions, where it is valued as an aromatic ingredient. From a gastronomic perspective, the spice obtained by drying and grinding the seeds into a powder is widely used as a flavoring agent in meat dishes and traditional beverages, particularly in the provinces of Mersin, Adana, and Hatay. In this context, the increasing popularity of the species in recent years, supported by both scientific evidence reported in the literature and the traditional practical knowledge of local communities, has renewed interest in its economic and medicinal importance. In conclusion, the conservation of the species' rich phytochemical composition and cultural value is of great importance for sustainable agriculture and local development strategies.

Keywords:
Laser trilobum, Turkish cuisine, ethnobotany, d-limonene, perillaldehyde.

INTRODUCTION

Medicinal and aromatic plants have always been key players of human history, shaping nutrition, health, and culture. Notably, members of the Apiaceae family hold a vital role in both gastronomy and traditional therapeutics, largely attributed to their essential oils, phenolic substances, and unique flavor profiles. In addition to species of high economic value such as cumin (*Cuminum cyminum* L.), fennel (*Foeniculum vulgare*), anise (*Pimpinella anisum*), and coriander (*Coriandrum sativum*), there exist locally utilized species that remain comparatively underexplored (Davis, 1972). Among these, *Laser trilobum* (L.) Borkh. (commonly referred to as 'kefe kimyonu' in Turkish) is a perennial herbaceous plant of the genus *Laser* within the Apiaceae family, occurring naturally in various regions of Türkiye (Tekgüler et al., 2025). Despite its distribution across temperate regions of Asia and Europe, encompassing Iran, the Caucasus, Türkiye, the Balkans, and Central Europe, *L. trilobum* has received comparatively

little attention relative to other members of the Apiaceae family (Baser et al., 1993; Vahdat et al., 2006). Local practices in Türkiye include consuming the shoots as vegetables and using its aromatic, cumin-flavored fruits as a spice sold in local markets (Chizzola, 2007; Parlatan et al., 2009).

Represented within Turkish flora, *L. trilobum* is naturally distributed in high-altitude areas (Demir & Kan, 2025) and is locally designated by several common names, including 'dağ kimyonu', 'kefe kimyonu', 'kamun', and 'sıra' (Baytop, 1994; Şenkardeş & Tuzlacı, 2014; Agar & Tosun, 2025). Traditionally, the fruits of *L. trilobum* are dried and used as a culinary spice, and in some areas, they are used in traditional healing practices. However, studies focusing on the gastronomic usage of the species is constrained, with existing information relying largely on ethnobotanical surveys. This highlights the need for a more detailed scientific evaluation of the plant's gastronomic potential.

Growing interest in natural flavors and functional foods has led to the re-evaluation of regional spices. Because consumers increasingly select natural flavor compounds instead of synthetic additives, species like *L. trilobum* hold growing significance for the food industry. In this framework, systematically investigating the species' botanical features, chemical composition, and traditional uses represents a critical priority.

2.Ecological Features and Natural Distribution

L. trilobum is a perennial species native to the temperate regions of Eurasia, with a distribution extending from Eastern and Central Europe across the Balkans and Crimea to the Caucasus, Türkiye, the Levant, and northern Iran. Türkiye constitutes one of the major centers of natural distribution and harbors substantial genetic diversity of this species within its native populations (WCVP, 2025). The species is typically found at elevations ranging from 700 to 2,000 m, where it inhabits sun-exposed slopes, forest clearings, rocky sites, and calcareous soils (Demir & Kan, 2025). Its perennial life cycle and extensive root system enable it to withstand prolonged periods of water limitation, suggesting a considerable capacity to persist under drought-prone conditions. Together, these ecological and physiological characteristics make *L. trilobum* a potentially valuable genetic resource for understanding plant adaptation to increasing drought and other environmental stresses associated with climate change.

The combination of its distinctive morphological traits and ecological adaptability underscores the importance of *L. trilobum* not only as a component of the natural flora but also as a species with considerable potential for gastronomy and the sustainable use of endemic plant resources.

3.History and Distribution of Kefe Cumin

L. trilobum (L.) Borkh. is one of the Apiaceae species native to Europe and Western Asia. The species was first described by Carl Linnaeus as *Laserpitium trilobum* and was later reclassified as *L. trilobum* by Borkhausen. This name is currently accepted as the valid taxonomic designation in international community (POWO, 2025). Its common name, "kefe kimyonu" ("Kefe cumin"), derives from the cumin-like aroma of its dried, ground fruits.

In terms of geographic distribution, *L. trilobum* has a naturally wide range. It occurs across the temperate zone of Asia (North Caucasus and Transcaucasia, the eastern Aegean islands, Iran, Lebanon, Syria, and Türkiye) as well as in various regions of Europe (in Eastern Europe: the Baltic states, Middle and South European Russia, Crimea, Ukraine, Austria, Czechoslovakia, Germany, Hungary, Albania, Bulgaria, Greece, Italy, Romania, and European Türkiye, along with the territories of the former Yugoslavia). It is distributed across a broad phytogeographic area extending from Southeastern and Central Europe through the Balkans, the Black Sea Basin,

the Caucasus, Anatolia, and into northern Iran (WCVP, 2025). This distribution pattern indicates that the species is capable of adapting to a wide range of climatic and topographic conditions.

Türkiye is recognized as one of the species' natural centers of distribution. Natural populations occur particularly in the Taurus Mountains, the Amanos Mountains, the Central Taurus range, and the higher elevations of the Mediterranean Region. In addition, the species has been reported to occur in certain high-altitude areas of Central Anatolia and in the mountainous regions of Southeastern Anatolia (Davis, 1972). This distribution indicates that *L. trilobum* possesses broad ecological tolerance, capable of adapting to both steppe and forest-steppe transition zones (Demir & Kan, 2025).

Research on *L. trilobum* has intensified considerably over the past three decades, with the existing literature focusing largely on its essential oil composition, antimicrobial activity, phytochemical profile, and ethnobotanical uses, while studies on its gastronomic applications remain scarce. Cultivation of Kefe cumin at a commercial scale has not yet become established in Türkiye, and plants are majorily wild-harvested from natural populations - a practice that raises concerns regarding the long-term sustainability of these populations.

4. Historical Use of Kefe Cumin as a Spice

Numerous species belonging to the Apiaceae family have been used as spices throughout history (Ngahang Kamte et al., 2018). *Laser trilobum* is also an aromatic species of this family, and its fruits are particularly used as a spice in local cuisines after being dried and ground. However, the literature provides no direct evidence indicating that the plant was widely used in the Ottoman palace cuisine or documented historical culinary sources. Therefore, from a scientific perspective, it is more appropriate to consider the historical use of Kefe cumin within the context of local culinary practices and ethnobotanical traditions.

Etnobotanical studies conducted in Türkiye have reported that the dried fruits are ground and consumed as a spice; in some regions, the fruits are also boiled and traditionally used for conditions such as digestive disorders, abdominal pain, and the common cold (Bulut et al., 2014; Güneş et al., 2017). In addition, extracts obtained from these plants have been reported to reduce the formation of biogenic amines and limit microbial contamination in cheese and meat products (Ehsani et al., 2016).

The primary reason for the use of Kefe cumin as a spice is its high essential oil content and characteristic citrus-like aroma. The essential oil of *Laser trilobum* fruits contains limonene at very high proportions, ranging from 26% to 91%. Owing to its high limonene content, the plant possesses a distinctive and intense odor and aroma profile (Ferahoğlu & Kırıcı, 2023). In particular, ground fruits provide a pronounced aroma even when used in small amounts, thereby enhancing the sensory characteristics of traditional recipes. Nowadays, the increasing consumer demand for natural flavoring agents is expected to bring Kefe cumin back into focus in the fields of gastronomy and functional food research.

5. Phytochemical Composition of Kefe Cumin

Aromatic plants belonging to the Apiaceae family are known to contain high levels of essential oils and secondary metabolites with biological activities (Spinozzi et al., 2021; Thivia et al., 2021). *Laser trilobum* is one of the species exhibiting these characteristics. The fruits constitute

the plant organ with the highest essential oil content (Agar & Tosun, 2025). In a GC-MS analysis conducted by Ferahoğlu and Kırıcı (2023) on fruits collected from the Mersin region, the essential oil content was determined to be 4.4%, with d-limonene and perillaldehyde accounting for approximately 95% of the oil. These two monoterpene compounds are considered to be largely responsible for the characteristic aroma and biological activity of Kefe cumin. Studies have shown that the composition of essential oil constituents varies considerably among different organs of the plant. While **perillaldehyde and limonene** are the major constituents in the fruits, **β-caryophyllene** and **α-pinene** have been identified as the predominant constituents in the leaves and stems and in the rhizomes, respectively (Agar & Tosun, 2025). This indicates that different organs of the plant may have distinct utilization potentials in terms of pharmacological applications and food technology.

Studies reported in the literature have demonstrated that the essential oils of *Laser trilobum* exhibit antimicrobial activity against certain Gram-positive and Gram-negative pathogenic bacteria (Nazzaro et al., 2013). In addition, its antioxidant capacity has been suggested to potentially slow oxidative deterioration, thereby indicating its potential as a natural food preservative (Akgül, 1992; Parlatan et al., 2005; Drobac et al., 2017). However, as a substantial proportion of the existing studies have been conducted at the laboratory scale, further comprehensive research is needed to evaluate its potential applications in food systems.

From a phytochemical perspective, *Laser trilobum* stands out as a noteworthy species in the development of functional foods, natural preservatives, and herbal products, not only due to its aromatic properties but also because of the bioactive monoterpenes and sesquiterpenes it contains (Drobac et al., 2017). The available data indicate that controlled cultivation practices may have positive effects on essential oil yield and composition, representing an important opportunity for enhancing the economic value of the species.

6. Use of Kefe Cumin in Turkish Cuisine

Türkiye is one of the countries where wild aromatic plants are widely incorporated into culinary culture, owing to its diverse climatic zones and rich flora. Many species belonging to the *Apiaceae* family are used not only for medicinal purposes but also as spices. Ethnobotanical studies have demonstrated that plants locally referred to as “cumin” in Türkiye are not limited to *Cuminum cyminum*; *Carum carvi, Grammosciadium daucoides,* and *Laser trilobum* are also regionally used for similar purposes (Tuncay and Yeşil, 2019).

6.1 Traditional Forms of Use

Although the number of scientific publications concerning the gastronomic use of *Laser trilobum* is limited, available studies have reported that, in Turkish traditional practices, young shoots are consumed as vegetables, while the aromatic fruits, which have a cumin-like flavor, are ground and used as a spice and sold in local markets (Baser et al., 1993; Chizzola, 2007; Parlatan et al., 2009). Ferahoğlu & Kırıcı (2023) reported that, in samples collected from the Mersin region, the fruits are locally known as “Kefe cumin” and that essential oil is obtained from the dried fruits. The same study indicated that the species is not cultivated in Türkiye and that its use relies largely on fruits collected from natural populations.

A comprehensive ethnobotanical study conducted in the Hatay region revealed that *Laser trilobum* is used as a spice in local dishes (Keskin & Alpınar, 2002), and that this practice represents one of the traditional uses that had not previously been documented in detail in the

literature. The study emphasizes that this plant constitutes a part of the local gastronomic heritage and highlights the importance of preserving traditional knowledge systems.

Use in Cheese and Dairy Products

Aromatic species belonging to the *Apiaceae* family have been used in cheese production in Anatolia for many years (Öztürk et al., 2000; Çakmakçı & Şensoy, 2015). Although standardized cheese production studies specifically involving *Laser trilobum* are limited, ethnobotanical records indicate that ground fruits are added in some regions to impart flavor to herb-infused cheese and dairy products similar to *çökelek*. The primary reason for this use is that volatile compounds such as limonene and perillaldehyde, which are present at high concentrations in the fruits, provide a characteristic citrus-like aroma.

Use in Meat and Meat Products

One of the strongest pieces of scientific evidence regarding the use of Kefe cumin in meat products comes from the study conducted by Akgül and Kıvanç (1989). The study demonstrated that the addition of *Laser trilobum* spice to *köfte*, a traditional product of Turkish cuisine, inhibited the growth of *Staphylococcus aureus*. This finding indicates that the plant has potential not only as a flavoring agent but also in food preservation due to its natural antimicrobial properties. These findings are consistent with current trends toward the use of natural preservatives and provide a scientific basis for considering Kefe cumin as a functional spice.

Use in Local Dishes

It is not possible to state with certainty that specific recipes incorporating Kefe cumin have been scientifically validated. Nevertheless, based on the traditional knowledge of local communities, the plant appears to be used as a flavoring agent in meat dishes and certain regional spice blends. An ethnobotanical study conducted in Hatay reported that *Laser trilobum* is used as a spice in local dishes and noted that the species is obtained through traditional wild harvesting and constitutes one of the aromatic plants used in the local cuisine (Güzel & Kayıkçı, 2023). However, the existing literature does not provide standardized recipes specifying the particular dishes in which the plant is used or the quantities employed. Instead, available information primarily concerns the use of the spice obtained from the dried fruits in Hatay cuisine and regional spice blends. This is significant in demonstrating the strong relationship between Anatolian culinary culture and biological diversity.

Evaluation from the Perspective of Gastronomy and Functional Foods

In recent years, the growing consumer preference for natural sources of flavoring agents and preservatives over synthetic additives has increased interest in wild aromatic plants. Considering the high essential oil content of *Laser trilobum*, its predominant limonene and perillaldehyde constituents, and its antioxidant and antimicrobial activities, the species has considerable potential for use as a functional spice.

However, studies in the field of gastronomy are largely based on ethnobotanical observations. Standardized recipes, sensory analyses, consumer acceptance studies, and food technology applications remain insufficiently developed. Therefore, future interdisciplinary research is expected to elucidate in greater detail the various uses of Kefe cumin in Turkish cuisine.

CONCLUSION

Laser trilobum (L.) Borkh. is one of the important aromatic plants occurring naturally in the flora of Türkiye and locally known as “Kefe cumin.” The available scientific evidence indicates that the dried fruits of the species are used as a spice, may exhibit natural antimicrobial activity in meat products, and are traditionally incorporated into local dishes in some regions. However, the number of scientific publications concerning its use in Turkish cuisine remains limited.

In light of the growing interest in natural aromatic plants, investigating the controlled cultivation, gastronomic applications, sensory properties, and potential applications of Kefe cumin in food technology is of considerable importance. Furthermore, documenting local gastronomic knowledge and developing sustainable utilization models will contribute both to the conservation of biological diversity and to the enrichment of Türkiye’s gastronomic heritage.

REFERENCES

Agar, O. T. & Tosun, B. (2025). Chemical Composition of Essential Oils from Cultivated Laser trilobum (L.) Borkh. in Different Plant Parts. Turkish Journal of Agriculture - Food Science and Technology, 13(s1): 2308-2316, https://doi.org/10.24925/turjaf.v13is1.2308-2316.7743

Akgül, A. (1992). The essential oil composition of Turkish *Laser trilobum* (L.) Borkh. fruits. Journal of Essential Oil Research, 4, 89–90.

Akgül, A., & Kıvanç, M. (1989). Effect of Laser trilobum spice on natural microflora of köfte, a Turkish ground meat product. National Center for Biotechnology Information. 1991;35(2):149-54. doi: 10.1002/food.19910350206.

Baser, K. H. C., T., Ö., & Kirimer, N. (1993). The Essential Oil of Laser trilobum Fruit of Turkish Origin. Journal of Essential Oil Research, 5(4), 365-369. https://doi.org/https://doi.org/10.1080/10412905.1993.9698244

Baytop, T.(1994). Türkçe Bitki Adları Sözlüğü. Türk Dil Kurumu Yayınları No:578, s.508.

Bulut, G., Tuzlacı, E., Doğan, A., & Şenkardeş, İ. (2014). An ethnopharmacological review on the Turkish *Apiaceae* species. Journal of Faculty Pharmacy of Istanbul University, 44(2): 163-179.

Chizzola, R. (2007). Composition of the essential oil from *Laser trilobum* grown in the wild in Vienna. Chemistry of Natural Compounds, 43(4), 484-486. https://doi.org/https://doi.org/10.1007/s10600-007-0171-5

Çakmakçı, Ö. & Şensoy, S. (2015). Otlu Peynirde Kullanılan Yabani Otlar ve Belirgin Özellikleri. GAP VII. Tarım Kongresi, Şanlıurfa, Türkiye, 28 Nisan - 01 Mayıs 2015, ss.411-416.

Davis, P. H. (Ed.). (1972). Flora of Turkey and the East Aegean Islands (Vol. 4). Edinburgh University Press.

Demir, S. & Kan, Y. (2025). Kimyon Olarak Bilinen Bitki Türleri ve Değerlendirmesi. Kırşehir Ahi Evran Üniversitesi Ziraat Fakültesi Dergisi, 5(2): 128-158.

Ehsani, A., Hashemi, M., Naghibi, S. S., Mohammadi, S. H., & Khalili Sadaghiani, S. (2016). Properties of *Bunium persicum* essential oil and its application in Iranian white cheese

against Listeria monocytogenes and Escherichia coli O157:H7. Journal of Food Safety, 36(4), 563–570. https://doi.org/10.1111/jfs.12277

Ferahoğlu, E., & Kırıcı, S. (2023). Mersin'de Yetişen Kefe Kimyonu (*Laser trilobum*) Meyvelerinden Elde Edilen Uçucu Yağın Kimyasal Bileşenleri. Biological Diversity and Conservation. 16 (1): 1-5.

Güneş, S., Savran, A., Paksoy, M. Y., Koşar, M., Çakılcıoğlu, U. (2017). Ethnopharmacological survey of medicinal plants in Karaisalı and its surrounding (AdanaTurkey). Journal of herbal medicine, 8: 68-75.

Güzel, Y., & Kayıkçı, S. (2023). Traditional Foraged Spice, Sauce, and Egg-Painting Plants of Hatay, Türkiye: Bringing the Traditional into Commerce. *ANADOLU Journal of Aegean Agricultural Research Institute*, *33*(2), 237-258.

Keskin, M. E., Alpınar, K. (2002). Kışlak (Yayladağı-Hatay) hakkında etnobotanik bir araştırma. Ot Sistematik Botanik Dergisi, 9(2), 91 - 100.

Nazzaro, F., Fratianni, F., De Martino, .L, Coppola, R. & De Feo, V. (2013). Effect of essential oils on pathogenic bacteria. Pharmaceuticals, 6, 1451-1474.

Ngahang Kamte, S. L., Ranjbarian, F., Cianfaglione, K., Sut, S., Dall'Acqua, S., Bruno, M., Afshar, F.H., Iannarelli, R., Benelli, G., Cappellacci, L., &. (2018). Identification of highly effective antitrypanosomal compounds in essential oils from the *Apiaceae* family. Ecotoxicol. Environ. Saf. 2018, 156, 154–165.

Öztürk, A., Öztürk, S. & Kartal, Ş. (2000). Van otlu peynirlerine katılan bitkilerin özellikleri ve kullanılışları. Ot Sistematik Botanik Dergisi, 7(2):167-179.

Parlatan, A. (2005). Kefe kimyonu (Laser trilobum L.) meyvesinin bazı kimyasal özelliklerinin ve ekstraktının antibakteriyal etkisinin belirlenmesi.

Parlatan, A., Sariçoban, C., & Özcan, M. M. (2009). Chemical composition and antimicrobial activity of the extracts of Kefe cumin (*Laser trilobum* L.) fruits from different regions. International Journal of Food Sciences and Nutrition, 60(7), 606-617. https://doi.org/https://doi.org/10.3109/09637480801993938

Plants of the World Online. Royal Botanic Gardens, Kew. *Laser trilobum* (L.) Borkh.

Spinozzi, E., Maggi, F., Bonacucina, G., Pavela, R., Boukouvala, M. C., Kavallieratos, N. G., Canale, A., Romano, D., Desneux, N., Wilke, A.B.B., Beier, J. C. & Benelli, G. (2021). Apiaceae essential oils and their constituents as insecticides against mosquioes-A revive. Industrial Crops & Products, 171 (2021) 113892.

Şenkardeş, İ., & Tuzlacı, E. (2014). Gündoğmuş (Antalya/Türkiye) yöresinden bazı etnobotanik bilgiler. Clinical and Experimental Health Sciences, 4(2), 63-75. doi: 10.5455/musbed.20140303070652.

Tekgüler, B., Koca, I., Pashazadeh, H., Ali Redha, A. & Karadeniz, B. (2025). Chemical Composition, Antioxidant Capacity, and Volatile Profile of *Laser trilobum* (Kefe Cumin) Seeds Grown in Turkey. Foods 2025 Conference, The 6th International Electronic Conference on Foods, 28-30 October 2025, Organised by MDPI, Online.

Thivia, P., Gamage, A., Piumali, D., Merah, O. & Madhujith, T. (2021). *Apiaceae* as an Important Source of Antioxidants and Their Applications. Cosmetics 2021, 8, 111. https://doi.org/10.3390/cosmetics8040111

Tuncay, H. O., & Yeşil, Y. (2019). Comparative fruit anatomy and morphology of four species known as cumin in Turkey. KSU J. Agric Nat 22(4): 547-556.

Vahdat, M., Eslami, B., Dabiri, H., Khalilzadeh, M., Tajbakhsh, M., & Larijani, K. (2006). Essential oil composition of *Laser trilobum* (L.) Borkh. Umbelliferae herbs growing wild in Iran. J. Sci. I. A. U. (JSIAU), 16(60), 20-23. https://www.sid.ir/FileServer/JE/95920066004

World Checklist and Bibliography of Vascular Plants (WCVP) (2025). *Cuminum cyminum* L., *Carum carvi* L., *Laser trilobum* Borkh. *Bunium persicum* (Boiss.) B.Fedtsch, *Bunium bulbocastanum* L., *Cuminum setifolium* (Boiss.) Rech. f. Kew Science. http://www.kew.org https://powo.science.kew.org

DISTRIBUTION OF SUGAR COMPONENTS AND CHEMOMETRIC ANALYSIS IN GRAPES PRODUCED WITH DIFFERENT AGROECOLOGICAL PRACTICES

Cansu KORKMAZ[1], Selçuk KÜÇÜKAYDIN[2], Fatih ÇAYAN[3], Esra ALBAZ[4], Mehmet Emin DURU[5]*

[1]Department of Biology, Faculty of Science, Muğla Sıtkı Koçman University, 48000 Muğla, Türkiye,
[2]Department of Medical Services and Techniques, Koycegiz Vocational School of Health Services, Mugla Sitki Kocman University, 48000 Mugla, Türkiye,
[3]Department of Chemistry and Chemical Processing Technologies, Muğla Vocational School, Muğla Sıtkı Koçman University, 48000 Muğla, Türkiye,
[4]Manisa Viticulture Research Institute, Turkish Ministry of Agriculture and Forestry, 45125 Manisa, Türkiye,
[5]Department of Chemistry, Faculty of Science, Muğla Sıtkı Koçman University, 48000 Muğla, Türkiye,

**Corresponding author e-mail: cansukorkmaz08@gmail.com*
https://orcid.org/0000-0003-3027-7687

ABSTRACT

Protecting and optimizing fruit quality parameters—specifically the sugar profile—under water deficit conditions induced by climate change in viticulture is of critical importance for both yield and processing quality. This study aimed to determine the distribution of sugar components in grapes produced using different agroecological practices and to examine the obtained data through chemometric analyses. In this study, the sugar profiles of grapes produced using various cultivation techniques aimed at growing grapevines with reduced water usage were determined using an HPLC system. Based on the results, the analysis of sugar components in grape juice revealed that fructose ranged from 7.15 to 8.17 g/100 g and glucose from 6.15 to 8.52 g/100 g, showing an increasing tendency compared to the control group across the treatment groups, with total sugar accumulation particularly enhanced in the alfalfa and biohydrogel treatments. The glucose/fructose ratio in the grapes produced across the treatment plots was determined to remain within the range of 0.81 to 1.08, indicating that carbon metabolism was maintained in a balanced manner and that the practices did not disrupt fruit ripening physiology. This comprehensive dataset clearly demonstrates that the applied system not only enhances drought tolerance but also provides a robust metabolic optimization supporting quality in terms of phenolic compounds, aromatic metabolites, and sugar composition. In additionally, Chemometric analyses (PCA and HCA) reveal that PGP application forms a distinct cluster and promotes a more homogeneous sugar composition, whereas alfalfa and biohydrogel treatments induce greater metabolic variation. According to the findings obtained, it was determined that different production conditions (alfalfa, biohydrogel, and plant growth-promoting rhizobacteria) had a significant effect on the sugar profile and chemometric properties of grapes, substantially increasing secondary metabolite accumulation compared to the control group.

Keywords: *Sugar profile, Grape, Alfalfa, biohydrogel, growth-promoting rhizobacteria (PGP), HPLC, Chemometrıc analysis*

INTRODUCTION

The most significant risk for viticulture is the future increase in sugar content of grapes due to rising temperatures (Lakatos and Mitre., 2023). Adverse environmental conditions can independently cause heat and water stress in grapevines, affecting internal parameters such as sugar and acid content, the development of phenolic compounds, and yield (Hewitt et al., 2023). According by Lakatos and Mitre (2023) have been reported, the effect of the aridity index on the past and future occurrence of maximum sugar content for six grape varieties was analyzed. Glucose and fructose are the dominant sugars in grapes, complemented by sucrose accumulation (Fontes et al., 2011). Sugar accumulation in grapes is directly proportional to their growth and development (Manning et al., 2001). In this respect, the content and composition of glucose, fructose, and sucrose play an important role in the formation of fruit quality (Liu et al., 2017; Zhong et al., 2023). Glucose and fructose constitute the vast majority (97.88%–99.86%) of the sugar composition of grapes. During the ripening process, the balance between these two sugars ranges from 0.74 to 1.05 (Li et al., 2020). In a study conducted by Eyduran et al. (2015) on table grape varieties in Turkey, fructose and glucose levels were found to range from 8.03 to 15.55 g/100 g and 9.51 to 16.47 g/100 g, respectively, with the highest accumulation observed in the white seedless grape variety "Sultaniye". Similarly, Liu et al. (2006) reported major glucose and fructose levels ranging from 45.86 to 122.89 mg/ mL^{-1} and 47.64 to 131.04 mg/mL^{-1} in grape berries over a two-year period.
In this study, to determine sugar profile of grapes grown under different production conditions (alfalfa, biohydrogel, growth-promoting rhizobacteria analysis using an HPLC system (Shimadzu 20 AT series high-performance liquid chromatograph, Shimadzu Corporation, Japan) Secondly, in this study the effects of various agroecological practices (alfalfa cover cropping, biohydrogel application, and plant growth-promoting (PGP) bacteria) on the sugar profile and chemometric analysis of grapes were evaluated under water-limited conditions. In this study, grapes obtained from the experimental plots of the Ministry of Agriculture and Forestry's Manisa Viticulture Research Institute are presented below under the relevant headings, based on the control group of the study.

MATERIAL AND METHODS

Determination of Sugar Components by HPLC

The grape samples produced within the scope of this study were pressed in a cotton cheesecloth to extract their juice, and the remaining pomace was washed with ultrapure water and pressed again; the resulting grape juice was then lyophilized. The grape juice extract thus obtained was stored in a dark and cool environment until sugar component analyses were performed. The amounts (%) of glucose, fructose, sucrose, and maltose in the grape samples were determined using an HPLC system. A Shodex NH2P-50 4E (5 µm, 250x4.6 mm) column and a Shimadzu RI 20 A model refractive index (RI) detector were used. The detector temperature was set to 30 °C, and the mobile phase used was 75% ACN (acetonitrile) + 25% ultrapure water. Standards and samples were injected into the instrument with a mobile phase flow rate of 1 mL/min and an injection volume of 10 µL. First, pure glucose, fructose, sucrose, and maltose standards were prepared with ultrapure water at concentrations of 0.125%, 0.25%, 0.50%, and 1%, filtered through a Millipore 0.45 µm membrane filter, and injected into the system to construct a 4-point calibration curve. The lyophilized grape juice extracts (2.5 g) were weighed into a volumetric flask (25 mL), and 15 mL of ultrapure water was added. After the mixture was completely dissolved by vortexing for 5 minutes, the volume was completed to 25 mL with ultrapure water using a Pasteur pipette and homogenized by vortexing. The samples were

transferred to vials and injected into the HPLC system under the specified conditions to determine their sugar profiles [AOAC 977.20 (2005)].

RESULTS AND DISCUSSION

Distribution Of Sugar Components in Grapes Produced With Different Cultivation Techniques Against Drought

The codes and yields of the extracts obtained from the extraction study conducted to investigate the sugar profile of the grape samples, which are the subjects of this study, are presented in Table 1.

Table 1. Codes and extraction yields (% w/w) of grapes grown under different cultivation techniques

Sample Name and Production Conditions	**Sample Code**	**Extraction Solvent**	**Fresh Weight of Material (g)**	**Net Weight of Extract (g)**	**Extract Yield (%)**
Aqueous extract of grape grown with alfalfa	YÜS	Water	100	16.39	16.39
Aqueous extract of grape grown without alfalfa	YYÜS	Water	100	14.73	14.73
Aqueous extract of grape grown with biohydrogel	BHÜS	Water	100	12.72	12.72
Aqueous extract of grape grown without biohydrogel	BHYÜS	Water	100	11.94	11.94
Aqueous extract of grape grown with PGP	PGPÜS	Water	100	11.06	11.06
Aqueous extract of grape grown without PGP	PGPYÜS	Water	100	10.79	10.79

Within the scope of the project, the sugar profiles of grapes produced using various cultivation techniques aimed at achieving grapevine cultivation with reduced water usage were determined using an HPLC system. The results obtained are presented in Table 2.

Table 2. Comparison of glucose, fructose, and sucrose contents in grapes grown under different agroecological applications (g/100 g grape juice)

Sample Code	Fructose	Glucose	Fructose + Glucose)	Glucose/Fructose	Sucrose
YÜS	7.92	6.75	14.67	0.85	2.01
YYÜS	2	7.59	6.15	13.74	0.81
BHÜS	3	7.85	7.72	15.57	0.98
BHYÜS	4	7.15	7.33	14.48	1.02
PGPÜS	5	8.17	8.19	16.36	1.00
PGPYÜS	6	7.88	8.52	16.40	1.08

The sugar profiles of grapes produced using various cultivation techniques within the scope of the project were determined using an HPLC system, and the results are presented in Table 2. Fructose and glucose are the dominant sugars in the grape juices, constituting the major part of the sugar composition. It has been reported that fructose and glucose accumulation is predominant in grape juice, complemented by sucrose, and that sugar accumulation in grapes is directly proportional to growth and development (Manning et al., 2001; Fontes et al., 2011). In this respect, the content and composition of glucose, fructose, and sucrose play a significant role in fruit quality formation (Liu et al., 2017; Zhong et al., 2023). Glucose and fructose account for approximately 97.88%–99.86% of the sugar composition in grapes. The balance between these two sugars varies between 0.74 and 1.05 during the ripening process (Li et al., 2020).

An examination of Table 2. reveals that the fructose content ranges from 7.15 to 8.17 g/100 g, while glucose ranges from 6.15 to 8.52 g/100 g. Alfalfa biohydrogel, and PGP applications were found to increase fructose levels in grape juice compared to the control groups. While glucose levels were higher in the alfalfa and biohydrogel-treated vines than in the control groups, glucose levels in the PGP-treated area were lower than in the control. Regarding the sum of fructose and glucose, alfalfa and biohydrogel treatments provided higher sugar accumulation than the control, whereas values in PGP-treated areas remained lower than the control. These findings are consistent with those reported in the literature (Liu et al., 2006; Eyduran et al., 2015; Zhong et al., 2023).

When evaluating the effects on sugar metabolism in PGP applications, it is known that these microorganisms optimize photosynthetic activity and carbon metabolism (Yang et al., 2009). The glucose/fructose ratios in this study, ranging from 0.81 to 1.08, confirm that hexose sugars accumulated in a balanced manner during the ripening process and that these values remain within physiological limits (Kliewer, 1967; Li et al., 2020). The fact that the different agronomic techniques applied did not create any negative impact on sugar metabolism, and that this ratio remained more balanced—particularly in PGP applications—is associated with the potential of plant growth-promoting microorganisms to optimize carbon distribution (Vacheron et al., 2013; Egamberdieva et al., 2017). Consequently, it is evaluated that PGP applications have a regulatory effect on carbon metabolism in grapes and contribute to the stabilization of sugar composition.

Chemometric Analysis of Sugar Components in Grapes Produced With Different Cultivation Techniques Against Drought

The results of the chemometric analysis conducted regarding the sugar components of grape juices produced with different cultivation techniques within the scope of the project are presented in Figures 1 and 2.

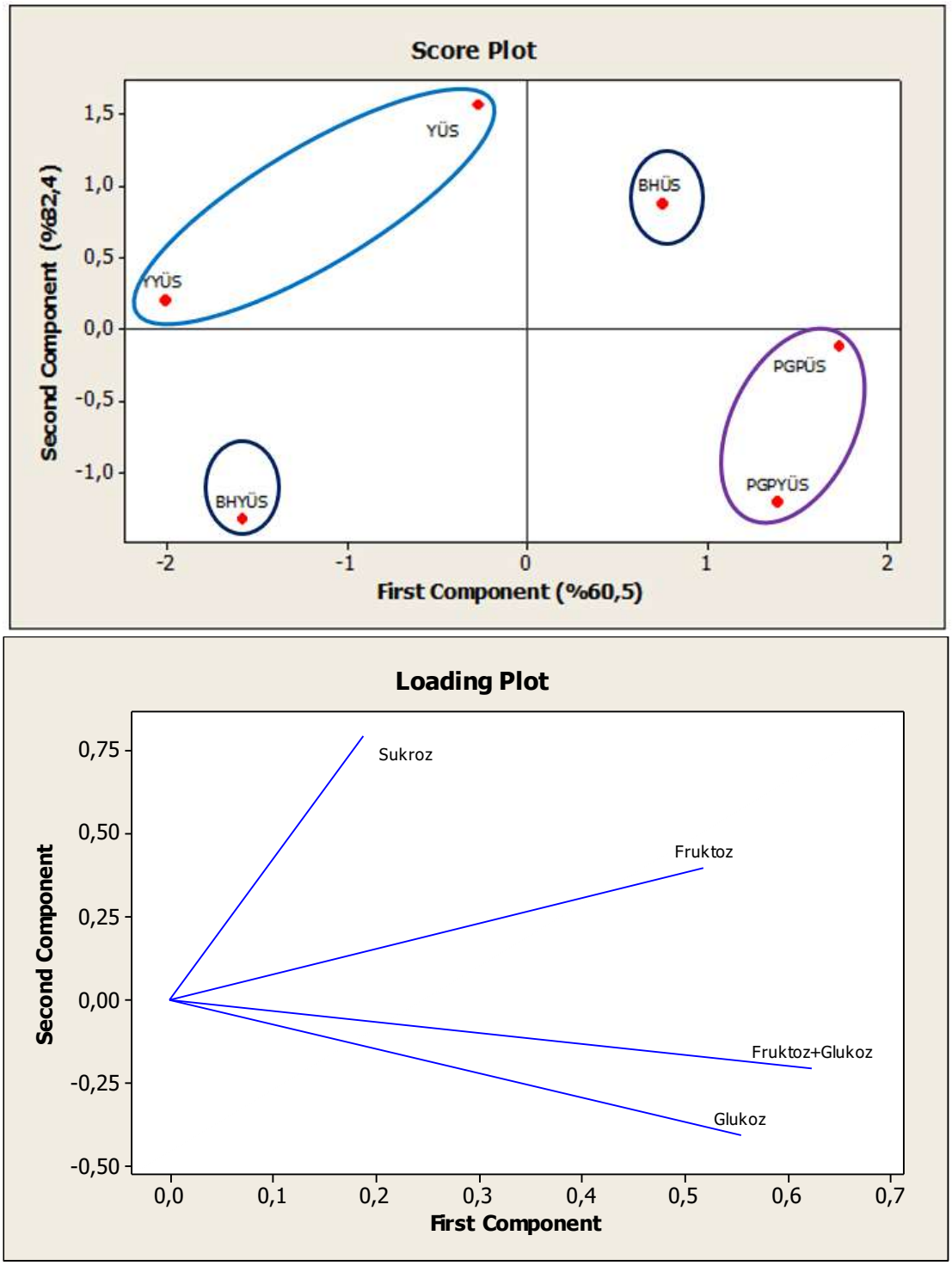

Figure 1**.** Results of the chemometric analysis (PCA and HCA) regarding the sugar components of grape juices produced with different cultivation techniques

The chemometric analyses based on sugar components (PCA and HCA) presented in Figures 1 and 2 clearly demonstrate the effects of the treatments on grape metabolism. The PCA results indicate that PGP application creates a more homogeneous and stable structure regarding sugar composition, whereas alfalfa and biohydrogel treatments exhibit higher variation. HCA and dendrogram analyses support these findings, confirming that the PGP treatment forms a distinct cluster and exerts a regulatory effect on carbon metabolism (Figures 1 and 2). These results are

consistent with the literature regarding the balancing role of plant growth-promoting (PGP) microorganisms in sugar metabolism (Vacheron et al., 2013; Egamberdieva et al., 2017).
When the analytical results for phenolic compounds and organic acids in grapevine leaves and grape juices, along with the sugar profiles of the grape juices, are evaluated as a whole, it is observed that the chemometric analyses (PCA, HCA, and dendrograms) support all findings and clearly reveal the metabolic impacts of the treatments. PCA analyses show that the treatments create distinct separations in terms of phenolic and sugar composition, while HCA and dendrogram analyses reveal that these differences manifest as statistically significant clusters. Specifically, it has been determined that PGP application leads to a more homogeneous metabolic profile, whereas alfalfa and biohydrogel treatments result in higher metabolic diversity. This clearly proves that the phenylpropanoid metabolism is a dynamic and tunable system, highly sensitive to environmental and agronomic factors

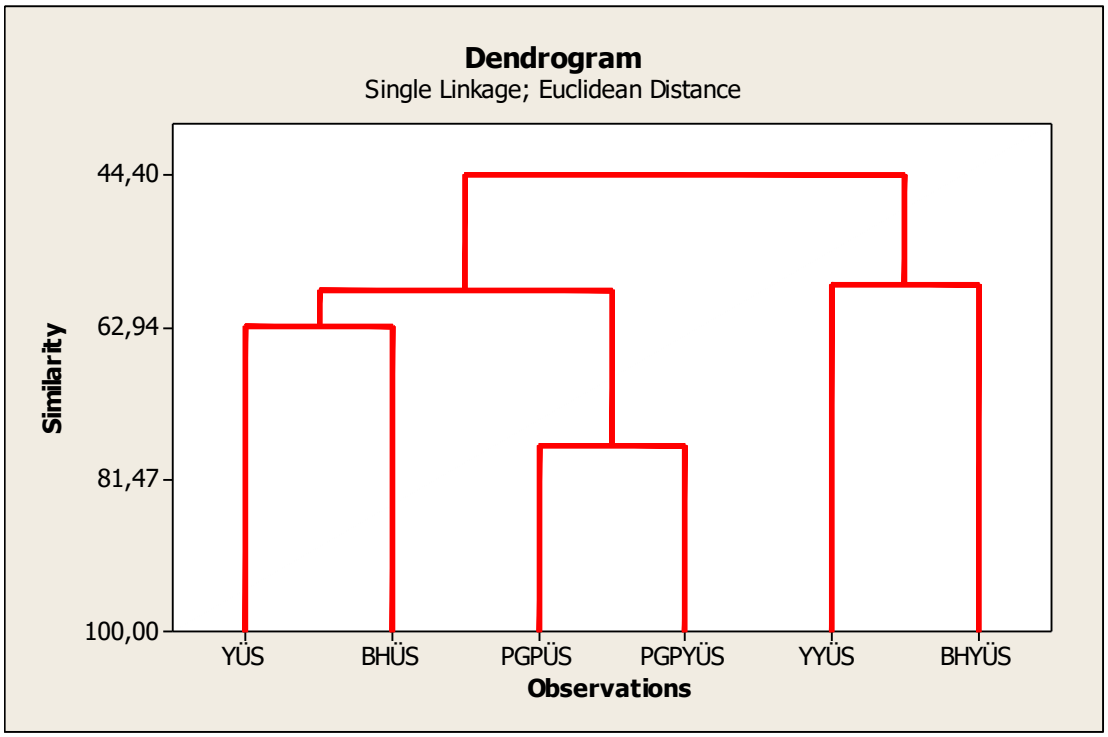

Figure 2. Dendrogram analysis regarding the sugar components of grape juices produced with different cultivation techniques.

CONCLUSIONS

In this study, the sugar profiles of grapes produced using various cultivation techniques aimed at growing grapevines with reduced water usage were determined using an HPLC system. Highlighting the critical importance of water conservation in viticulture, this study demonstrates that sustainable agronomic techniques can maintain or enhance key fruit quality parameters and sugar metabolism under water-limited conditions. Fructose and glucose were identified as the dominant sugars in the grape juice across all treatments, accounting for the vast majority of the total sugar composition. Alfalfa and biohydrogel treatments successfully enhanced overall sugar accumulation, whereas PGP applications exhibited a distinct regulatory effect, maintaining a balanced distribution between hexose sugars. The glucose-to-fructose ratios remained well within normal physiological limits (0.81–1.08), confirming that the tested

agroecological practices did not negatively impact sugar metabolism and effectively contributed to the stabilization of fruit quality and carbon allocation.

ACKNOWLEDGEMENT

The authors are grateful for the conditions that the Partnership for Research and Innovation in the Mediterranean Area (PRIMA), the Scientific and Technological Research Council of Turkiye (TUBITAK), and the European Union provided in the development of the VineProtect project (10.54499/PRIMA/0011/2021 and TUBITAK-122N043).

REFERENCES

AOAC (2005) Association of Official Analytical Chemist, Official Methods of Analysis. 18th Edition, AOAC International, Suite 500, 481 North Frederick Avenue, Gaithersburg, Maryland 20877-2417, USA.

Egamberdieva, D., Wirth, S. J., Alqarawi, A. A., Abd_Allah, E. F., & Hashem, A. (2017). Phytohormones and Beneficial Microbes: Essential Components for Plants to Balance Growth and Stress Tolerance. Frontiers in Microbiology, 8, 1580.

Eyduran, S. P., Akin, M., Ercisli, S., Eyduran, E., & Maghradze, D. (2015). Sugars, organic acids, and phenolic compounds of ancient grape cultivars (Vitis vinifera L.) from Igdir province of Eastern Turkey. Biological research, 48(1), 2.

Fontes, N., Gerós, H., & Delrot, S. (2011). Grape berry vacuole: A complex and highly dynamic organelle. Journal of Experimental Botany, 62(14), 4885-4900.

Hewitt S., Hernández-Montes E., Dhingra A., Keller M. (2023). Impact of heat stress, water stress, and their combined effects on the metabolism and transcriptome of grape berries. Sci. Rep. 2023;13:9907.

Kliewer, W. M. (1967). Annual cyclic changes in the concentration of free amino acids in grapevines. American Journal of Enology and Viticulture, 18(3), 126-137.

Lakatos, L., & Mitre, Z. (2023). Effect of drought on the future sugar content of wine grape varieties till 2100: Possible adaptation in the Hungarian Eger wine region. Biomolecules, 13(7), 1143.

Li J., Zhang C., Liu H., Liu J., Jiao Z. (2020). Profiles of sugar and organic acid of fruit juices: a comparative study and implication for authentication. J. Food Qual. 2020, 7236534. doi: 10.1155/2020/7236534.

Liu X. J., An X. H., Liu X., Hu D. G., Wang X. F., You C. X., et al. (2017). MdSnRK1.1 interacts with MdJAZ18 to regulate sucrose-induced anthocyanin and proanthocyanidin accumulation in apple. J. Exp. Bot. 68 (11), 2977–2990.

Liu, H. F., Wu, B. H., Fan, P. G., Li, S. H., & Li, L. S. (2006). Sugar and acid concentrations in 98 grape cultivars analyzed by principal component analysis. Journal of the Science of Food and Agriculture, 86(10), 1526-1536.

Manning K., Davies C., Bowen H. C., White P. J. (2001). Functional characterization of two ripening-related sucrose transporters from grape berries. Ann. Bot. 87 (1), 125–129.

Vacheron, J., Desbrosses, G., Bouffaud, M. L., Touraine, B., Moënne-Loccoz, Y., Muller, D., Legendre, L., Wisniewski-Dyé, F., & Prigent-Combaret, C. (2013). Plant growth-promoting rhizobacteria and root system functioning. Frontiers in Plant Science, 4, 356.

Yang J, Kloepper JW, Ryu CM. (2009), Rhizosphere bacteria help plants tolerate abiotic stress. Trends Plant Sci. 2009 Jan;14(1):1-4.

Zhong, H., Yadav, V., Wen, Z., Zhou, X., Wang, M., Han, S., ... & Wu, X. (2023). Comprehensive metabolomics-based analysis of sugar composition and content in berries of 18 grape varieties. Frontiers in Plant Science, 14, 1200071.

SECONDARY METABOLITE PROFILE AND CHEMOMETRIC ANALYSIS OF GRAPE LEAVES GROWN DIFFERENT AGROECOLOGICAL PRACTICES

Cansu KORKMAZ[1], Meltem TAŞ KÜÇÜKAYDIN[2], Selçuk KÜÇÜKAYDIN[3], Fatih ÇAYAN[4], Nurdan GÜNGÖR SAVAŞ[5], Mehmet Emin DURU[2]*

[1]Department of Biology, Faculty of Science, Muğla Sıtkı Koçman University, 48000 Muğla, Türkiye,
[2]Department of Chemistry, Faculty of Science, Muğla Sıtkı Koçman University, 48000 Muğla, Türkiye,
[3]Department of Medical Services and Techniques, Koycegiz Vocational School of Health Services, Mugla Sitki Kocman University, 48000 Mugla, Türkiye
[4]Department of Chemistry and Chemical Processing Technologies, Muğla Vocational School, Muğla Sıtkı Koçman University, 48000 Muğla, Türkiye,
[5]Manisa Viticulture Research Institute, Turkish Ministry of Agriculture and Forestry, 45125 Manisa, Türkiye

**Corresponding author e-mail: cansukorkmaz08@gmail.com*
https://orcid.org/0000-0003-3027-7687

ABSTRACT

The effects of climate change on agricultural production systems are becoming more evident with each passing day, particularly in the Mediterranean basin.Within the scope of this study, it was aimed to reduce water consumption in grapevine cultivation and to elucidate the metabolic responses of plants to drought stress, thereby contributing to the sustainable management of water resources under climate change conditions. Accordingly, alfalfa (cover crop), biohydrogel, and plant growth-promoting rhizobacteria (PGP) applications were implemented under conditions where water demand was reduced by 50%; the results obtained were compared with those from fully irrigated control plots. To determine the volatile secondary metabolite profiles of grapevine leaves grown under different production conditions (alfalfa, biohydrogel, growth-promoting rhizobacteria), essential oils were extracted via steam distillation from fresh leaves harvested before the fruit ripening stage. The component analysis of these oils was conducted using Gas Chromatography (GC) and Gas Chromatography-Mass Spectrometry (GC-MS) systems. Although aldehyde compounds were present in low quantities in the plots where alfalfa was applied, the relative abundances of terpenoids and compounds with aromatic ester and benzenoid structures were determined to have increased. In the analysis of secondary metabolites, it was found that terpenoids were present at high levels ranging from 29.46% to 43.55% in all treatments, and that aromatic ester/benzenoid compounds reached levels as high as 16.25% particularly in the alfalfa treatment. In contrast, the fact that aldehydes—known as stress biomarkers—were present only in the control and alfalfa-free systems at levels ranging from 0.42% to 0.99%, and were completely absent in the biohydrogel and PGP treatments, was interpreted as evidence that lipid peroxidation was suppressed and oxidative stress was effectively controlled. Moreover, it has been shown through experimental studies that hydrogel applications reduce water stress in plants and improve physiological performance.

Keywords: *Secondary metabolite, Alfalfa, biohydrogel, growth-promoting rhizobacteria (PGP), Gas Chromatography (GC), Gas Chromatography-Mass Spectrometry (GC-MS), Chemometrıc analysis*

INTRODUCTION

Viticulture is a production system that is highly sensitive to climatic conditions; environmental variables such as temperature, precipitation patterns, relative humidity, and wind directly affect grape yield and quality. For this reason, the grapevine is considered an indicator plant that reflects the effects of climate change early and distinctly (Bucur et al., 2019). In arid and semi-arid regions, low and irregular rainfall poses a significant threat to agricultural production due to water scarcity. Deficit irrigation techniques are of vital importance for efficiently managing these limited water resources, ensuring optimal soil moisture in the root zone, and increasing water use efficiency without compromising crop quality (Panigrahi et al., 2011; Pereira et al., 2011). However, since these methods involve high-cost systems that require specialized expertise, they generally offer advantages only in the cultivation of high-value crops (Uysal et al., 2024). Today, the Mediterranean basin continues to account for a significant portion of global grape production; in countries such as Spain, France, Italy, Portugal, Morocco, and Türkiye, viticulture not only generates economic value but also contributes to the preservation of the rural landscape, local culture, and agricultural biodiversity (OIV, 2023; Santillán et al., 2019).

Microorganisms living in the plant root zone directly influence many processes, such as nutrient cycling, root development, stress tolerance, water use efficiency, and disease resistance (Berendsen et al., 2012; Compant et al., 2019). It has been reported that bacterial groups such as Proteobacteria, Actinobacteria, and Firmicutes are particularly dominant in the *Vitis vinifera* L. rhizosphere and that these microorganisms perform critical functions related to plant development (Vega-Avila et al., 2015).

In this study, to determine the volatile secondary metabolite profiles of grapevine leaves grown under different production conditions (alfalfa, biohydrogel, growth-promoting rhizobacteria), essential oils were extracted via steam distillation from fresh leaves harvested before the fruit ripening stage. The component analysis of these oils was conducted using Gas Chromatography (GC) and Gas Chromatography-Mass Spectrometry (GC-MS) systems. Within the scope of this study, the effects of various agroecological practices (alfalfa cover cropping, biohydrogel application, and plant growth-promoting (PGP) bacteria) on the secondary metabolite profile and chemometric analysis of grapevines were evaluated under water-limited conditions. The analysis results for grapevine leaves obtained from the experimental plots of the Ministry of Agriculture and Forestry's Manisa Viticulture Research Institute are presented below under the relevant headings, based on the control group of the study.

MATERIAL AND METHODS

Chemical Analysis of Essential Oils Extracted From Grapevine Leaves

1. Extraction of Essential Oils

Grape leaves collected from the field were boiled fresh in water for approximately three hours using a Clevenger-type apparatus to extract the essential oil via hydrodistillation. Due to the low yield of essential oil, the oil was extracted from the Clevenger apparatus using hexane. The essential oil, now in a mixture with hexane, was then dried with anhydrous sodium sulfate and stored in a refrigerator at +4 °C until analysis.

2. Gas Chromatography (GC) Analysis

The essential oil components obtained from grape leaves via hydrodistillation were analyzed using a Shimadzu GC-17AAF gas chromatograph. The percentage compositions of the essential oil components were calculated using the GC Solution software based on the gas

chromatogram. In addition, the characterization of the components was supported by considering their retention times and calculating their Kovats index values. The GC analysis conditions are presented in Table 1.

Table 1. GC Analysis Conditions

Column	:	DB-1 capillary column (0.25 id x 30 m)
Dedector	:	FID
Carrier Gas	:	He
Makeup/Fuel Gases	:	High-purity (99.999%) dry air and hydrogen
Injection Temperature	:	250^{o}C
Column Temperature	:	The sample was held at 60°C for 5 minutes. It was then heated to 280°C at a rate of 4°C per minute and held at 280°C for 15 minutes.
Detector Temperature	:	280^{o}C
Split Ratio	:	1:50
Injection Volume	:	0.2µL

3. Gas Chromatography-Mass Spectrometry (GC-MS) Analysis

A Varian 2100 GC-MS instrument was used to characterize the volatile oil components of grape leaves. NIST 2014 library data, as well as the spectrophotometric atlases titled “Eight Peak Index of Mass Spectra,” “Monoterpenes,” and “Identification of Essential Oils by Ion Trap Mass Spectroscopy,” were used to identify the components. Retention times and Kovats index values were instrumental in determining the components. In addition, the analyses of the volatile oil components were confirmed by comparing them with literature data, retention times obtained by analyzing reference substances individually under the same chromatographic conditions, and by using reference substances as internal standards to account for potential interference. The GC-MS analysis conditions are presented in Table 2.

Table 2. GC-MS Analysis Conditions

Column	:	DB-1 capillary column (30 m x 0.25mm, 0.25µm)
Carrier Gas	:	He
Injection Temperature	:	280^{o}C
Column Temperature	:	The sample was held at 60°C for 5 minutes. It was then heated to 290°C at a rate of 4°C per minute and held at 290°C for 10 minutes.
Split Ratio	:	1:50
Ion Source Temperature	:	150 ^{o}C
Electron Energy	:	70 eV
Mass Range	:	28-450 m/z
Scan Range	:	0.01
Injection Volume	:	0.2µL

RESULTS AND DISCUSSION

Evaluation of The Secondary Metabolite Profile And Class Distribution Of Grapevine Leaves Grown Under Different Production Conditions

Within the scope of this study, it was aimed to reduce water consumption in grapevine cultivation and to elucidate the metabolic responses of plants to drought stress, thereby contributing to the sustainable management of water resources under climate change conditions. Accordingly, alfalfa (cover crop), biohydrogel, and plant growth-promoting rhizobacteria (PGP) applications were implemented under conditions where water demand was reduced by 50%; the results obtained were compared with those from fully irrigated control plots.

To determine the volatile secondary metabolite profiles of grapevine leaves grown under different production conditions, essential oils were extracted via steam distillation from fresh leaves harvested before the fruit ripening stage. The component analysis of these oils was conducted using Gas Chromatography (GC) and Gas Chromatography-Mass Spectrometry (GC-MS) systems. The codes and descriptions of the essential oil samples obtained from the grapevine leaves are presented in Table 3 while the qualitative and quantitative data of the identified volatile secondary metabolites and their distributions at the compound class level are presented in Table 4.

Table 3. Identification codes for essential oil samples obtained from grapevine leaves produced under different production conditions

Sample Description and Production Condition	Sample Code
Essential oil from grapevine leaves grown in the alfalfa-mulched field	YY
Essential oil from grapevine leaves grown in the field without alfalfa	YYY
Essential oil from grapevine leaves grown in the biohydrogel-treated field	BHY
Essential oil from grapevine leaves grown in the field without biohydrogel	BHYY
Essential oil from grapevine leaves grown in the PGP-treated field	PGPY
Essential oil from grapevine leaves grown in the field without PGP	PGPYY

Table 4. Secondary metabolite components and compound classes of grapevine leaves produced under different production conditions against drought stress

COMPOUND NAME	RI	YY (%)	YYY (%)	BHY (%)	BHYY (%)	PGPY (%)	PGPYY (%)
2,4-Hexadien-1-ol	859	2.98	0.57	-	-	-	-
cis-3-Hexen-1-ol	862	6.21	4.76	-	-	8.55	4.11
trans-2-Hexen-1-ol	865	0.92	1.04	-	-	1.59	0.41
1-Hexanol	889	2.17	1.39	-	-	-	-
Heptanal	877	0.07	-	-	-	-	-
(E,E)-2,4-Hexadienal	883	0.11	0.05	-	-	-	-
cis-2-Heptenal	923	0.09	0.02	-	-	-	-
Benzaldehyde	926	0.09	0.04	-	-	-	-
2,2,6-Trimethyl-6-vinyltetrahydro-2H-pyran	957	0.68	0.12	-	-	-	-
1-Octen-3-ol	961	0.05	-	-	-	-	-
6-Methyl-5-hepten-2-one	966	0.07	-	-	-	-	-
Camphene	968	0.83	0.26	-	-	-	-
(E,E)-2,4-Heptadienal	980	0.02	-	-	-	-	-
Isolimonene	985	0.99	0.16	-	-	-	-
cis-3-Hexen-1-yl acetate	990	5.65	4.30	-	-	6.36	4.76
Hexyl acetate	994	0.39	0.22	-	-	-	-
Isooctanol	1001	0.16	0.17	-	-	-	-
D-Limonene	1014	0.39	0.09	-	-	-	-
2,2,6-Trimethylcyclohexanone	1012	0.19	0.04	-	-	-	-
Phenylacetaldehyde	1018	0.48	0.22	-	-	-	-
cis-Ocimene	1026	0.12	-	-	-	-	-
α-Isophorone	1042	0.13	-	-	-	-	-
γ-Terpinene	1046	0.13	-	-	-	-	-
cis-Linalool oxide	1057	0.53	0.31	-	-	1.07	0.81
Terpineolene	1074	0.90	0.31	-	-	-	-
cis-2-Pentenyl butanoate	1081	0.02	0.06	-	-	-	-
Linalool	1083	7.21	5.98	-	-	14.11	13.88
Hotrienol	1085	0.88	1.59	-	-	1.79	1.80
n-Hexyl propionate	1088	0.07	-	-	-	-	-

α-Cyclocitral	1095	0.07	0.03	-	-	-	-
Myrcenol	1104	0.14	0.08	-	-	-	-
p-Mentha-1,3,8-triene	1118	0.03	-	-	-	-	-
p-Mentha-8-en-1-ol	1149	0.09	-	-	-	-	-
cis-3-Hexenyl butanoate	1157	0.67	2.49	-	-	0.59	0.03
Hexyl butanoate	1173	0.08	0.19	-	-	-	-
Terpinen-4-ol	1175	0.33	0.11	-	-	-	-
cis-3-Nonen-1-ol	1178	0.12	0.07	-	-	-	-
Isopinocarveol	1181	0.18	-	-	-	-	-
α-Terpineol	1184	0.48	0.16	-	-	-	0.03
trans-3-Hexenyl butanoate	1196	19.98	21.34	9.05	6.89	28.44	23.28
Isopulegol	1208	0.25	0.15	-	-	-	-
α-Ionene	1211	0.05	0.07	-	-	-	-
p-Menth-1-en-9-al	1213	0.29	0.10	-	-	-	-
β-Cyclocitral	1215	0.80	0.48	-	-	0.56	-
4-tert-Butylcyclohexanone	1218	-	0.09	-	-	1.16	1.42
β-Citral	1222	0.83	0.64	-	-	2.87	3.88
β-Citronellol	1225	0.59	0.37	-	-	-	-
cis-3-Hexenyl isovalerate	1227	6.52	7.28	3.99	4.15	6.49	8.95
Cyclohexyl methacrylate	1228	1.77	-	-	-	0.67	-
n-Hexyl isovalerate	1230	1.22	2.64	-	-	-	-
4,4-Dimethyl-5-nonenal	1238	0.05	0.04	-	-	-	-
Nerol	1239	1.72	2.88	3.80	4.36	7.97	10.64
cis-2-Decenal	1246	0.07	0.05	-	-	-	-
p-(2-Methylallyl)phenol	1250	0.12	0.04	-	-	-	-
α-Citral	1252	0.16	-	-	-	-	-
4-Hexenyl pentanoate	1271	0.15	0.33	-	-	-	-
1,4-Dihydrothujopsene	1293	1.48	2.75	-	-	5.19	7.01
3-Methylcyclohexyl 2-butenoate	1315	0.62	1.32	1.50	2.88	0.54	0.79
Benzyl butyrate	1327	-	0.07	-	-	-	-
1,1,6-Trimethyl-1,2-dihydronaphthalene	1329	0.82	0.43	-	-	-	0.61
α-Ionone	1331	2.27	3.91	-	-	2.26	3.32
1,1,2,3,3-Pentamethylindane	1335	0.05	0.01	-	-	-	-
cis-β-Hexenyl caproate	1360	3.94	5.62	10.30	11.42	4.35	5.60
4-Hexenyl hexanoate	1379	0.87	1.30	5.21	3.86	1.15	1.24
2-Hexenyl hexanoate	1383	0.21	0.30	-	-	-	-
β-Phenylethyl isobutyrate	1385	0.21	0.33	-	-	-	-
β-Caryophyllene	1403	0.10	0.01	-	-	-	-
4-(2,4,4-Trimethylcyclohexa-1,3-dienyl)but-3-en-2-one	1407	1.16	0.07	-	-	-	-
cis-3-Hexenyl trans-2-hexenoate	1409	0.22	0.40	-	-	-	-
β-Phenylethyl butyrate	1411	0.17	1.43	-	-	-	-
β-Ionone epoxide	1416	0.06	0.07	1.67	0.43	-	-
2,2,3,3-Tetramethyl-1-indanone	1414	0.11	-	-	-	-	-
Dihydro-pseudo-ionone	1421	0.41	0.13	1.00	0.77	-	-

4-(2,4,4-Trimethylcyclohexa-1,5-dienyl)but-3-en-2-one	1435	0.31	0.08	-	-	-	-
4-(2,6,6-Trimethylcyclohexa-1,5-dienyl)but-3-en-2-one	1447	0.51	0.17	-	-	-	-
β-Ionone	1452	1.65	2.20	3.48	2.93	0.34	0.08
(E,E)-α-Farnesene	1465	0.16	0.13	-	-	-	-
α-Farnesene	1482	0.61	0.78	3.64	2.86	0.24	0.18
Unidentified	-	0.20	-	-	-	-	-
γ-Himachalene	1498	0.05	-	-	-	-	-
trans-Nerolidol	1538	0.23	0.19	-	-	-	-
cis-3-Hexenyl benzoate	1542	0.49	1.03	16.25	12.80	0.78	1.59
n-Hexyl benzoate	1549	-	0.12	-	-	-	-
Allo-aromadendrene oxide	1570	0.04	-	-	-	-	-
Phenylethyl caproate	1601	0.00	0.13	-	-	-	-
cis-3-Hexenyl salicylate	1642	0.01	0.09	-	-	-	-
Unidentified	-	0.10	-	-	-	-	-
Unidentified	-	0.07	-	-	-	-	-
Hexahydrofarnesyl acetone	1842	0.07	1.12	2.07	2.91	-	-
Farnesyl acetone	1928	0.16	0.11	-	-	-	-
Isophytol	1944	0.52	0.13	-	-	-	-
Sinapinic acid	1967	0.05	0.09	-	-	-	-
n-Heptadecanol	1974	0.34	0.03	-	-	-	-
Phytol	2009	11.47	12.61	13.81	15.78	1.15	1.93
Heneicosane	2142	0.19	0.36	6.49	7.81	0.46	0.91
Pentacosane	2511	0.07	0.33	3.44	2.09	0.46	0.69
Docosa-1,3-dien-1-ol	2518	0.12	0.12	-	-	-	-
Tricosanol	2554	0.29	0.46	7.34	9.65	0.64	1.61
Heptacosane	2709	0.24	0.22	6.96	8.41	0.21	0.45
Total		100.00	100.00	100.00	100.00	100.00	100.00
Classification of Compounds	Proportion (%)						
Aldehydes		0.99	0.42	-	-	-	-
Alcohols		13.36	8.61	7.34	9.65	10.78	6.13
Terpenoids		38.43	39.49	29.46	30.05	37.56	43.55
Fatty acid derivatives		40.85	48.12	30.06	29.20	47.91	44.65
Aromatic esters and benzenoids		3.26	2.00	16.25	12.80	1.45	2.20
Ketones		2.24	0.45	-	-	1.16	1.42
Aliphatic hydrocarbons		0.50	0.90	16.90	18.30	1.14	2.06

The analysis results indicate that the volatile secondary metabolites found in grapevine leaves consist primarily of aldehydes, alcohols, terpenoids, aromatic compounds, and hydrocarbons. However, it has been determined that the relative abundances of these compound classes exhibit significant variations depending on the applied production conditions. Aldehyde compounds were detected at low levels only in the alfalfa-treated (YY) and non-alfalfa control (YYY) plots (0.99% and 0.42%, respectively), whereas these compounds were not detected in the biohydrogel and PGP applications. It was observed that terpenoids varied between 29.46% and 43.55% in all samples, while fatty acid derivatives were found to be among the dominant compound classes, ranging from 29.20% to 48.12%. When evaluated in terms of aromatic esters

and benzenoid compounds, it was determined that these compounds increased in the biohydrogel-treated field (BHY) and the alfalfa-cultivated field (YY) compared to the control group (16.25% and 3.26%, respectively), whereas they were found at lower levels (1.45%) in the PGP-treated field (Table 4).

Although aldehyde compounds were present in low quantities in the plots where alfalfa was applied, the relative abundances of terpenoids and compounds with aromatic ester and benzenoid structures were determined to have increased. In particular, the presence of β-ionone and its derivatives, hexahydrofarnesyl acetone and various aromatic esters at higher rates in these groups indicates that the secondary metabolism has shifted in a different direction. This situation points to a systemic metabolic reprogramming at a level that cannot be explained solely by the reduction of stress. The reduction of evaporation by cover crops like alfalfa by covering the soil surface, the stabilization of soil moisture, and the enhancement of microbial activity in the root zone are evaluated as fundamental reasons for the effect of this application on secondary metabolism. Various studies have shown that cover crops reduce evaporation and protect soil moisture by creating a physical barrier on the soil surface; furthermore, they improve soil structure, increase water-holding capacity, and significantly raise microbial activity (Haruna et al., 2020). Additionally, it is anticipated that alfalfa's increase in soil fertility through nitrogen fixation may have contributed to the activation of the phenylpropanoid and isoprenoid metabolic pathways.

As in the plots where alfalfa was applied, an increase in terpenoids and aromatic compounds was observed in the plots where PGP bacteria were applied. However, it is understood that this increase is more limited compared to the alfalfa application and that it occurs as a strengthening of the existing metabolic structure rather than a complete change in the metabolite profile. It is known that PGP bacteria interact with plant roots to increase the production of phytohormones such as indole-3-acetic acid (IAA), regulate ethylene levels through the ACC deaminase enzyme, and trigger systemic resistance (ISR) mechanisms in the plant. These mechanisms have been reported to improve water and nutrient uptake by increasing root development and to raise the plant's tolerance against abiotic stresses (Gupta and Pandey, 2019). These biochemical processes lead to the activation of enzymatic pathways responsible for secondary metabolite synthesis, particularly increasing terpenoid production. In their study, Velásquez et al. (2020) revealed that microbial inoculation causes an increase in terpenoid compounds. In our study, the fact that the quantities of terpenoids such as linalool, linalyl acetate, β-ionon ve α-farnesen in the grapevine leaves in the PGP-treated field have increased compared to the control group is in full compliance with the findings reported by Velásquez et al. (2020). The data obtained in this study are consistent with the aforementioned literature and reveal that PGP application strengthens the adaptive metabolic response in the plant.

In the secondary metabolites of grapevine leaves in the field where biohydrogel application was performed, no significant increase was observed in terms of terpenoids, while an increase was detected in aromatic esters and benzenoid compounds. This shows that biohydrogel contributes to the preservation of the existing metabolic balance by reducing the plant's water stress rather than directly activating secondary metabolite biosynthesis. In addition to these, it is known that biohydrogel improves plant water potential and prevents the formation of oxidative stress by increasing the water-holding capacity in the soil (Agbna and Zaidi, 2025). Therefore, biohydrogel can be evaluated as a buffer mechanism that prevents the occurrence of stress rather than increasing secondary metabolite diversity. Indeed, it is clearly stated in the literature that biohydrogels create a continuous and balanced water source in the root zone by increasing the water-holding capacity in the soil, thereby increasing the resistance of plants against drought stress and reducing stress-induced metabolic disturbances (Agbna and Zaidi, 2025). Moreover, it has been shown through experimental studies that hydrogel applications reduce water stress in plants and improve physiological performance (Kargar et al., 2017).

Chemometric Analysis of Secondary Metabolite Components in Grapevine Leaves Cultivated Under Different Production Conditions

The qualitative and quantitative results of volatile secondary metabolites in grapevine leaves cultivated under three different methods against drought stress were analyzed chemometrically. The results of the chemometric analysis, which considered all volatile secondary metabolite components, are presented in Figure 1 and Figure 2.

As illustrated in Figure 1, it is observed that the volatile secondary metabolites of grapevine leaves treated with PGP bacteria (PGPY) and those untreated (PGPYY, control group) clustered together. Similarly, grapevine leaves treated with biohydrogel (BHY) and those untreated (BHYY, control group) also clustered together; however, they occupied distinct regions due to differences in specific components. In contrast, the volatile secondary components of grapevine leaves from the alfalfa-treated (YY) and non-treated (YYY) fields were found to form distinct clusters in the Principal Component Analysis (PCA). Nevertheless, the hierarchical clustering dendrogram indicates that they cluster together (Figure 1 and Figure 2). According to the chemometric analysis results, the three different methods tested for drought stress in grapevine cultivation clustered in distinct regions regarding their volatile secondary metabolites, indicating that the cultivation technique directly contributes to the biosynthesis of secondary metabolites.

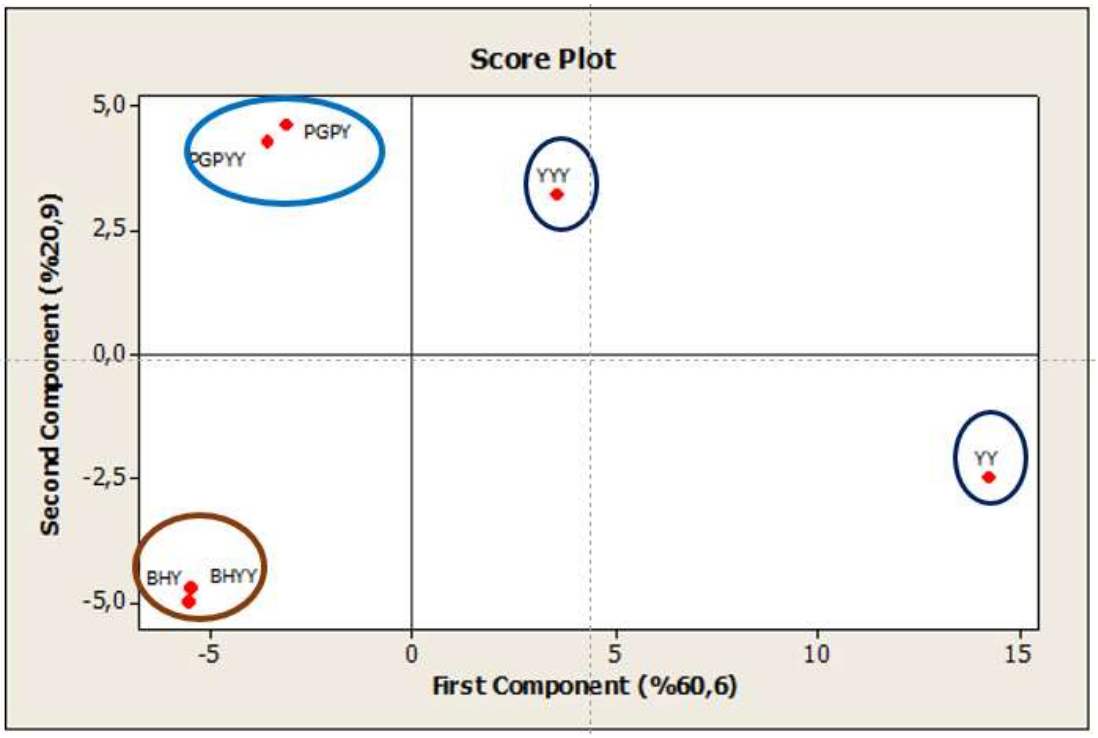

Figure 1. Principal Component Analysis (PCA) results of secondary metabolite components in grapevine leaves cultivated under different production conditions

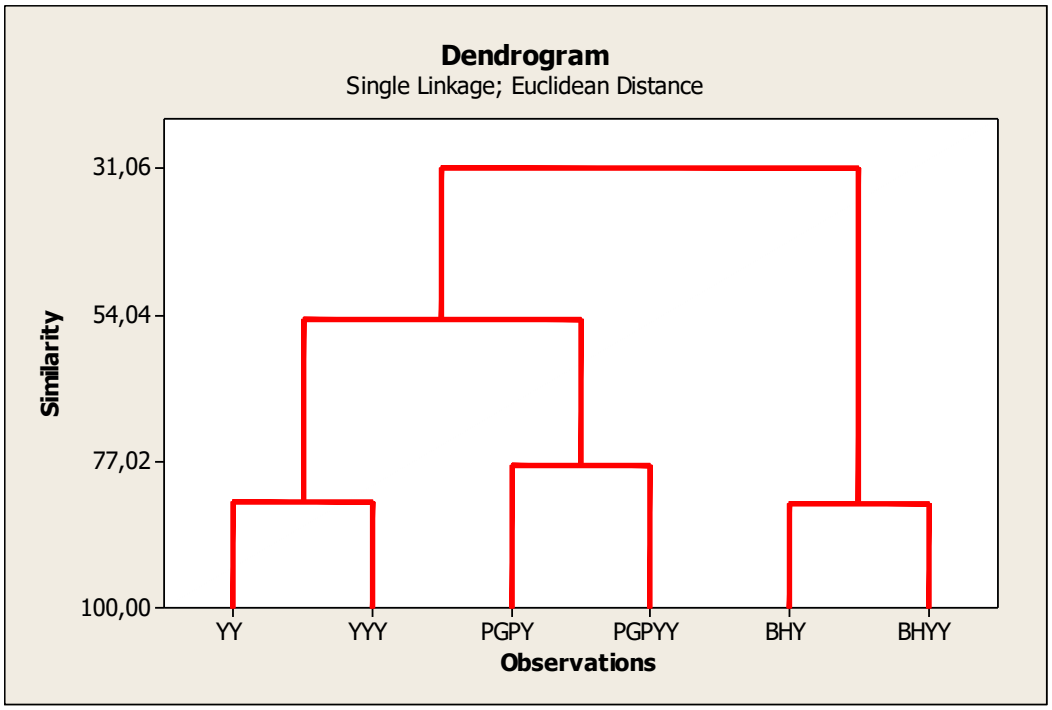

Figure 2. Dendrogram of volatile secondary metabolite components in grapevine leaves cultivated under different production conditions

Chemomitric analysis results concerning the volatile secondary metabolite components of the samples within the scope of the study are presented in Figures 3 and 4.

Based on the volatile secondary metabolite compound classes in the leaves of grapevines subjected to Biohydrogel application (BHY) versus those not subjected (BHYY, control group), Principal Component Analysis (PCA) reveals that the grapevines grown using these methods cluster separately from those grown using the other two techniques. Furthermore, while the volatile secondary metabolite compound classes in the leaves of vines subjected to PGB application (PGBY) and those not subjected (PGBYY, control group) cluster together in terms of PCA, the secondary metabolites of grapevine leaves grown in the field without alfalfa also fall within this same cluster (Figure 3). The fact that the volatile secondary metabolite compound classes in the leaves of grapevines grown in the alfalfa-planted field cluster differently from the other techniques and their respective control groups clearly demonstrates the effect of water-deficit management methods on the plant's secondary metabolite production. Hierarchical Cluster Analysis (HCA) revealed that the volatile metabolites cluster into two main groups based on compound classes: one group consists of leaves from grapevines treated with Biohydrogel, while the other comprises samples from PGB-treated and alfalfa-planted areas (Figure 4). Additionally, the dendrogram indicates that the secondary metabolites of grapevine leaves in the alfalfa-planted field cluster differently from both the control group and the PGB-treated field. Just as in the chemometric analyses performed on volatile secondary compounds, the results based on compound classes also indicate that the three distinct methods applied for water-deficit management elicit different responses in the plant, suggesting that the biosynthetic pathways involved may differ. The distinct clustering based on compound classes confirms the hypothesis that cultivation techniques directly contribute to secondary metabolite biosynthesis.

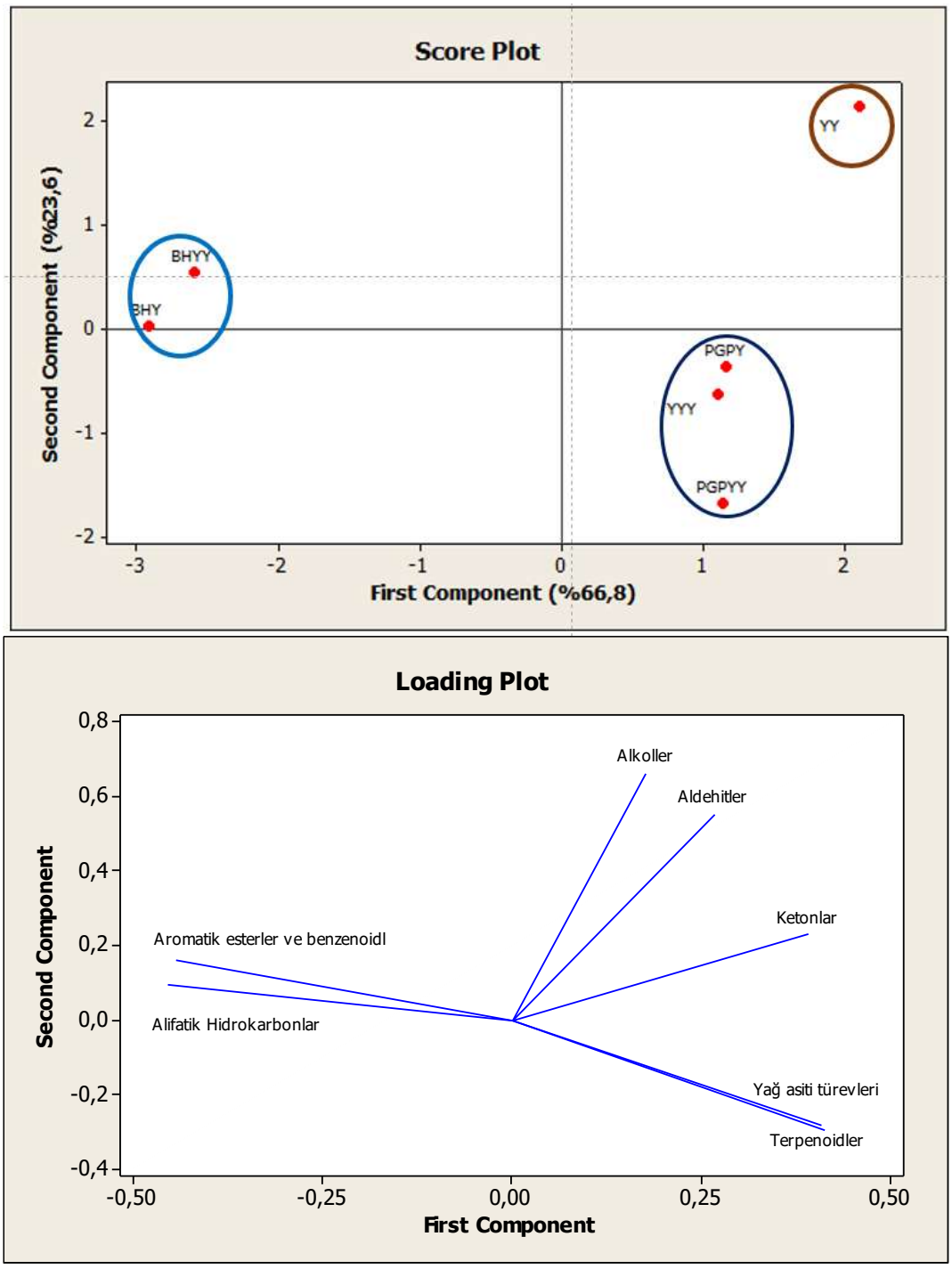

Figure 3. Results of Principal Component Analysis (PCA) and Hierarchical Cluster Analysis (HCA) regarding the volatile secondary metabolite compound classes of grapevine leaves produced under different cultivation conditions.

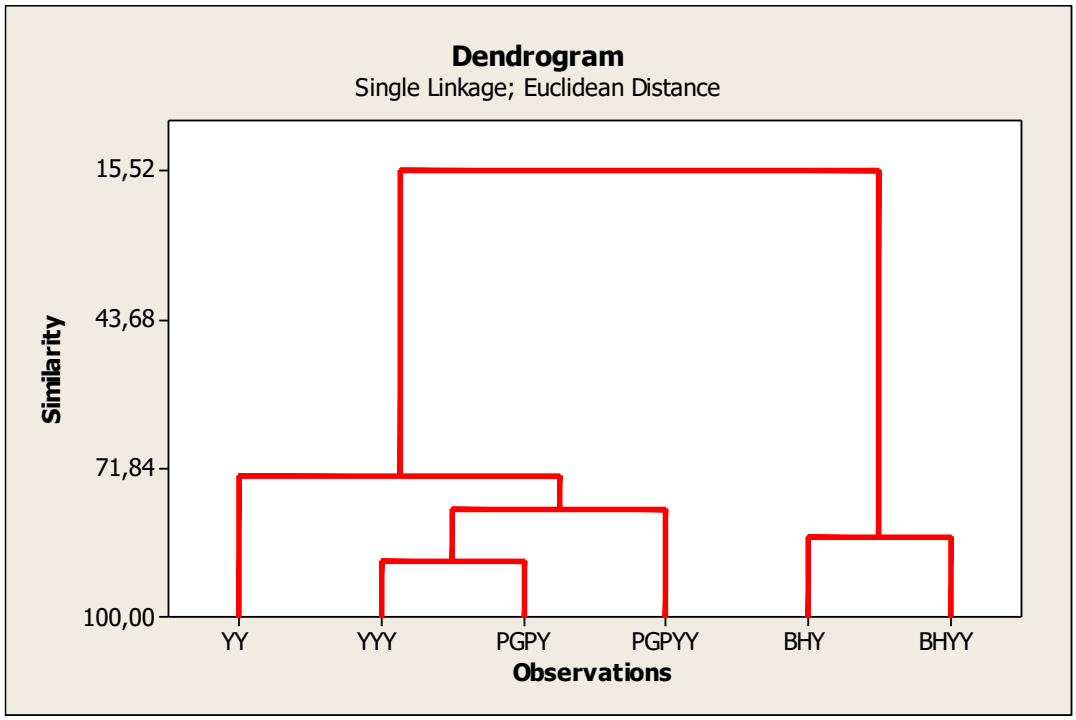

Figure 4. Dendrogram of volatile secondary metabolite compound classes of grapevine leaves produced under different cultivation conditions.

CONCLUSIONS

Based on the analysis of secondary metabolites, terpenoids predominated across all treatments, accounting for 29.46% to 43.55% of the total composition, while aromatic esters and benzenoids peaked at 16.25% specifically in the alfalfa treatment. Notably, aldehydes—widely recognized as biomarkers of oxidative stress—were detected solely in the control and alfalfa-free systems (0.42% to 0.99%) and were entirely absent in the biohydrogel and plant growth-promoting (PGP) treatments. This absence strongly indicates that these sustainable management practices effectively suppressed lipid peroxidation and successfully mitigated oxidative stress in the plants.

ACKNOWLEDGEMENT

The authors are grateful for the conditions that the Partnership for Research and Innovation in the Mediterranean Area (PRIMA), the Scientific and Technological Research Council of Turkiye (TUBITAK), and the European Union provided in the development of the VineProtect project (10.54499/PRIMA/0011/2021 and TUBITAK-122N043).

REFERENCES

Agbna, G.H.D. Zaidi, S.J. (2025) Hydrogel Performance in Boosting Plant Resilience toWater Stress-A Review, Gels, 11, 276.

Berendsen RL, Pieterse CM, Bakker PA. (2012). The rhizosphere microbiome and plant health. Trends Plant Sci. 2012 Aug;17(8):478-86. doi: 10.1016/j.tplants.2012.04.001. Epub 2012 May 5. PMID: 22564542.

Bucur, G. M., Cojocaru, G. A., & Antoce, A. O. (2019). The climate change influences and trends on the grapevine growing in Southern Romania: A long-term study. In BIO Web of Conferences (Vol. 15, p. 01008). EDP Sciences.

Compant, S., Samad, A., Faist, H., & Sessitsch, A. (2019). A review on the plant microbiome: Ecology, functions, and emerging trends in microbial application. *Journal of Advanced Research, 19*, 29–37.

Gupta S and Pandey S. (2019). ACC Deaminase Producing Bacteria With Multifarious Plant Growth Promoting Traits Alleviates Salinity Stress in French Bean (Phaseolus vulgaris) Plants. Front Microbiol. 2019 Jul 9;10:1506.

Haruna, S. I., Anderson, S. H., Udawatta, R. P., Gantzer, C. J., Phillips, N. C., Cui, S., & Gao, Y. (2020). Improving soil physical properties through the use of cover crops: A review. Agrosystems, Geosciences & Environment, 3(1), e20105.

Kargar, M. , Suresh, R. , Legrand, M. , Jutras, P. , Clark, O. and Prasher, S. (2017). Reduction in Water Stress for Tree Saplings Using Hydrogels in Soil. Journal of Geoscience and Environment Protection, 5, 27-39.

OIV, 2023. Descriptor list for grape vine varieties and Vitis species. Available at: https://www.oiv.int/what-we-do/data-discovery-report?oiv (Accessed: 11 November 2024).

Panigrahi, P., Sahu, N. N., & Pradhan, S. (2011). Evaluating partial root-zone irrigation and mulching in okra (*Abelmoschus esculentus* L.) under a sub-humid tropical climate. Journal of Agriculture and Rural Development in the Tropics and Subtropics (JARTS), 112(2), 169-175.

Pereira, L. S., Oweis, T., & Zairi, A. (2002). Irrigation management under water scarcity. Agricultural water management, 57(3), 175-206.

Santillán, D., Garrote, L., Iglesias, A., & Sotes, V. (2020). Climate change risks and adaptation: New indicators for Mediterranean viticulture. Mitigation and adaptation strategies for global change, 25(5), 881-899.

Uysal, Y., Doğaroğlu, Z. G., Makas, M. N., & Çaylali, Z. (2024). Boosting Water Retention in Agriculture: Vine Biochar-Doped Hydrogels' Swelling and Germination Effects. Global Challenges, 8(5), 2300254.

Vega-Avila, A. D., Gumiere, T., Andrade, P. A. M., Lima-Perim, J. E., Durrer, A., Baigori, M., ... & Andreote, F. D. (2015). Bacterial communities in the rhizosphere of Vitis vinifera L. cultivated under distinct agricultural practices in Argentina. Antonie Van Leeuwenhoek, 107(2), 575-588.

Velásquez, A., Vega-Celedón, P., Fiaschi, G., Agnolucci, M., Avio, L., Giovannetti, M., ... & Seeger, M. (2020). Responses of Vitis vinifera cv. Cabernet Sauvignon roots to the arbuscular mycorrhizal fungus Funneliformis mosseae and the plant growth-promoting rhizobacterium Ensifer meliloti include changes in volatile organic compounds. Mycorrhiza, 30(1), 161-170.

PHYTOCHEMICAL PROFILE OF ESSENTIAL OILS IN KEFE CUMIN (*Laser trilobum* (L.) Borkh.)

Sema AY[1], Sevgi ÇALIŞKAN[1], Caner YAVUZ[2]

[1] Niğde Ömer Halisdemir Üniversity, Faculty of Agricultural Sciences and Technologies, Department of Plant Production and Technologies Niğde-Türkiye
[2]Niğde Ömer Halisdemir Üniversity, Faculty of Agricultural Sciences and Technologies, Department of Agricultural Genetic Engineering Niğde-Türkiye
Corresponding author e-mail: sema_ay@mail.ohu.edu.tr

ABSTRACT

Kefe cumin (Laser trilobum (L.) Borkh.) is a perennial herbaceous species belonging to the Apiaceae (Umbelliferae) family. Although it is not cultivated in Türkiye, it is known to occur naturally in many regions of the country. The species is known by various regional vernacular names, including Kefe cumin, mountain cumin, sıra baharatı, and geyik sırası. As a species widely distributed throughout the flora of Türkiye, *Laser trilobum* occupies an important place in the gastronomic and ethnobotanical traditions of the regions where it naturally occurs. From a gastronomic perspective, the spice obtained by drying and grinding the fruits into a powder is widely used as a flavoring agent in meat dishes and traditional beverages, particularly in the provinces of Mersin, Adana, and Hatay. The fruits of Kefe cumin, a medicinal and aromatic plant, have been reported to be rich in mineral nutrients. The major constituents of the plant's essential oil are known to be d-limonene and perillaldehyde. These monoterpenoid compounds are responsible for the characteristic lemon-like aroma and distinctive woody odor profile of the fruits. The essential oil composition of fruit samples collected from different geographical regions has been reported to exhibit variation. Furthermore, significant differences have been reported in the proportions of essential oil constituents among different plant parts. The rich essential oil content of Kefe cumin demonstrates its considerable potential and indicates that the species is of significant economic and industrial value among medicinal and aromatic plants. In conclusion, given its rich phytochemical properties and diverse traditional uses, further scientific research is required to better understand and fully explore the potential of *Laser trilobum*.

Keywords: *Laser trilobum*, d-limonene, perillaldehyde, medicinal and aromatic plants.

INTRODUCTION

Medicinal and aromatic plants are plants that contain bioactive compounds in one, several, or all of their organs, such as leaves, stems, flowers, bulbs, tubers, and fruits (Mokhtarzadeh et al., 2023). Owing to the presence of alkaloids, terpenoids, and phenolic compounds, these plants are used in the pharmaceutical, perfumery, cosmetic, and food industries (Bayram et al., 2010). This wide range of applications has enabled medicinal and aromatic plants to occupy an important place in human history from the past to the present.

Among medicinal and aromatic plants, the Apiaceae family is a large family that includes important medicinal and aromatic plants such as cumin, coriander, anise, fennel, and dill. Plants belonging to the Apiaceae family, also known as the parsley family, are frequently preferred for their use as flavoring and aromatic agents, spices, and medicinal purposes.Members of the Apiaceae family, which have been known to be used in medicine since ancient times, have

attracted the attention of researchers because they are frequently preferred as raw materials in the pharmaceutical, cosmetic, and perfumery industries (Sayed-Ahmad et al., 2017).

One of the common characteristics of species belonging to this family is their richness in essential oil content. Owing to the essential oils they contain and their compositions, the utilization potential of these plants also becomes more diverse. One of these species, Laser trilobum (L.) Borkh., is among the species worthy of phytochemical evaluation due to its characteristic essential oil components and traditional uses (Demir & Kan, 2025; Ferahoğlu & Kırıcı, 2023).

Laser trilobum (L.) Borkh. (Kefe cumin) and Cuminum cyminum L. (cultivated cumin) both belong to the Apiaceae family; however, they are distinct species belonging to different genera (Laser and Cuminum). Therefore, although the designation "Kefe cumin" may botanically suggest that this plant is a species of cultivated cumin, its relationship with true cumin is limited to the family level. In addition to this botanical distinction, Kefe cumin differs from the commonly used cultivated cumin by its sharp and distinctive woody aroma. This distinction has led to promising views that, owing to its rich essential oil composition, Kefe cumin may serve as an alternative in the food industry (Demir & Kan, 2025) and may also represent a novel spice for use in gastronomy (Bayraktar, 2009).

The essential oil content and composition of plants have been reported to vary depending on geographical and genetic variation, physiological characteristics, and environmental conditions (Chizzola, 2010). The wide geographical distribution of Laser trilobum and its ability to grow under different ecological conditions indicate that its essential oil composition may also be influenced by these environmental differences (Ferahoğlu & Kırıcı, 2023; Bayraktar, 2009). Indeed, the literature has reported that the proportions of limonene and perillaldehyde, which are the major constituents of the essential oil, vary over a wide range in fruit samples collected from different countries and regions, particularly Türkiye, Serbia, Austria, and Iran. In addition, a limited number of studies have investigated plant organs other than the fruit (rhizome, leaf, and herba) and have observed that the essential oil composition of these organs differs qualitatively from that of the fruit (Ferahoğlu & Kırıcı, 2023; Drobac et al., 2017; Chizzola, 2007).

However, these findings are scattered throughout the literature, and no comprehensive review has been found that simultaneously evaluates the effects of variables such as geographical origin (country, region, and province), altitude, and plant organ on essential oil composition. The aim of this study is to review, in light of the available literature, the differences in the essential oil content of Laser trilobum samples collected from different regions, countries, and provinces, as well as the variations in essential oil composition among different plant organs.

General Information About Kefe Cumin

Laser trilobum is a naturally growing perennial herbaceous species belonging to the Apiaceae family that has not been sufficiently studied (Uçan Türkmen et al., 2024). The plant is also known by names such as Kefe cumin, mountain cumin, wild cumin, and sıra cumin (Tosun, 2021). It is referred to as “sıra baharatı” and “sıra kimyonu” in the Mersin region (Bayraktar, 2009), “kemun-kamun” in Kahramanmaraş (Üstüner, 2022), and “geyik sırası” in the Hatay region (Özmen, 2010).

Laser trilobum reaches a height of 50–120 cm, has trilobed glabrous leaves, and is characterized by white umbel-type flowers. Its fruits are elliptical in shape, measuring 5–10 mm in length and 2–4 mm in width (Ferahoğlu & Kırıcı, 2023). The plant flowers in spring, and its seeds are harvested in June and July. It is known to grow in forested areas, under trees such as pine and oak, in shrublands and semi-shaded habitats, and along the edges of vineyards (Parlatan et al., 2009). Kefe cumin has been reported to grow in calcareous soils (Chizzola, 2007), and its distribution ranges from approximately 500 to 1,800 m above sea level (Bayraktar, 2009).

Geographical Distribution of Kefe Cumin

Laser trilobum grows naturally in the Turkish provinces of Zonguldak, Gümüşhane, Samsun, Bolu, İstanbul, Edirne, Bursa, Balıkesir, İzmir, Muğla, Afyon, Konya, Ankara, Sivas, Kahramanmaraş, Erzincan, Eskişehir, Adana, Hatay, Isparta, and Mersin (Parlatan, 2005). Worldwide, it is naturally distributed in countries including Iran, Lebanon, Syria, Russia, Ukraine, Germany, Hungary, Albania, Bulgaria, Greece, Italy, and Romania (Demir & Kan, 2025). This broad geographical distribution indicates that the species can naturally occur under different ecological conditions.

Traditional Uses

The seeds of Kefe cumin (*Laser trilobum*) have a wide range of uses. The seeds of the plant are ground and used in dishes, particularly meat dishes, as an aromatic spice (Drobac et al., 2017; Chizzola, 2007; Parlatan et al., 2009). It has also been reported that the leaves of the plant are used as a vegetable (Chizzola, 2007). In addition, the plant is known to be used against ailments such as abdominal pain and cramps, hypertension, and diabetes. Furthermore, the prepared tea can be applied to the skin for the treatment of acne (Parlatan et al., 2009). In addition to its use in the treatment of diseases, it has been reported to be used for purposes of supporting the immune system (Demir & Kan, 2025).

Besides the widespread use of the plant fruits, the essential oil components obtained from the plant are also known to have a wide range of applications (Drobac et al., 2017; Ferahoğlu & Kırıcı, 2023; Parlatan, 2005). D-limonene, one of the important components of the essential oil of Kefe cumin, is a monoterpene that is also found in high proportions in citrus peels. D-limonene is used as a flavoring and aroma agent in the food industry, as a perfume component in the cosmetics sector, and as a natural solvent in the cleaning industry; it also has potential for the development of antimicrobial agents and biopesticides (Demir & Kan, 2025).

Perillaldehyde, another major component obtained from Kefe cumin fruits, also has a wide range of applications. Perillaldehyde is widely used as a flavoring additive in food products to impart a spice- and citrus-like flavor (Ferahoğlu & Kırıcı, 2023). In addition, various studies have demonstrated that it exhibits high efficacy against food spoilage, particularly that caused by fungi, and that it can therefore be considered as a natural food preservative (Tian et al., 2015). Furthermore, findings indicating that the compound has antidepressant (Ji et al., 2014), antitumor (Andrade et al., 2018), and anticancer (Zielińska et al., 2021) effects suggest that *L. trilobum* may be considered an important natural source of perillaldehyde for the pharmaceutical industry.

Essential Oil Content and Major Components

Essential oils contain a complex mixture of compounds with various functional groups, which contributes to different biological activities, such as antimicrobial and antioxidant activities (Abbaszadegan et al., 2016). The biological activities of essential oils produced by aromatic plants as secondary metabolites are directly related to the types of compounds they contain, the concentrations of these compounds, and the interactions among these compounds. In addition, the major components present in plants are among the principal groups of compounds that determine the biological and sensory properties of essential oils (Bakkali et al., 2008). Determining the essential oil composition of a plant is important not only for revealing its characteristic aroma profile but also for evaluating its potential biological activity and possible areas of application.

The determination of the chemical composition of *Laser trilobum* essential oil is of interest in terms of understanding the characteristic aroma profile and biological properties of the species. Determining the chemical composition and aroma profile of the plant's essential oil will contribute to identifying the potential areas of application of *Laser trilobum*. Several studies

addressing this subject are available in the literature. Some studies on the plant have obtained samples from different locations, helping to determine whether differences in location result in variations in the essential oil, whereas other studies have focused on determining the essential oil contents of different organs of plants obtained from the same location.

When essential oil analyses conducted on samples of different origins and plant organs in the literature are examined, variable results have also been obtained in fruits collected from different provinces of Türkiye. For example, Kefe cumin fruits obtained from the Mersin region were found to have an essential oil content of 4.4%, and the major components of the obtained essential oil were determined as perillaldehyde at 50% and d-limonene at 45% (Ferahoğlu & Kırıcı, 2023). In contrast, although the essential oil content was lower (2.7%) in fruits obtained from the Zonguldak region, the dominance of perillaldehyde continued here as well (68%), while d-limonene ranked second at 24% (Meriçli & Meriçli, 1986). The essential oil content of plant herba collected from the Artvin region was found to be 1.2%; the major components were determined as 73% perillaldehyde, 7.6% perill alcohol, and 7.6% E-caryophyllene, while limonene was detected at a low proportion of 2% (Bayraktar, 2009).

In a study comparing seeds obtained from different countries, the essential oil contents of samples originating from Germany, India, and Türkiye were found to be 4.4%, 4.8%, and 5.8%, respectively, and perillaldehyde and d-limonene were determined as the major components in all three origins (Parlatan et al., 2009). In samples collected from Iran, plant herba was used, and the essential oil content was reported as 2.2% as a result of the analysis. The major components of the essential oil were found to be α-pinene at 34% and β-caryophyllene at 17% (Vahdat et al., 2006). This result differed from the perillaldehyde and limonene dominance observed in previous studies and suggests that variation in chemical composition may also be influenced by factors such as climate, soil structure, and harvesting period, in addition to geographical origin.

In another study, samples collected from different locations in Austria were examined separately for leaf and fruit essential oils. The major components of the essential oil obtained from the leaves were found to be α-pinene at 12% and bornyl angelate at 67%, whereas the major components of the essential oil obtained from the fruits of the same plant were determined as perillaldehyde and limonene (Chizzola, 2007).

In another study, when the essential oils of plant fruits and rhizomes obtained from Serbia were examined, α-pinene was found at a proportion of 31% as the major component of the essential oil obtained from the rhizomes, whereas this component was found at 7% in the essential oil obtained from the fruits. The second major component of the essential oil obtained from the rhizomes was γ-terpinene at 9%, whereas this compound was not detected in the essential oil obtained from the fruits. The major component of the fruit essential oil was limonene at 51%, while this compound was present at 2% in the rhizomes. The second major component of the fruit essential oil was perillaldehyde at 26%, whereas this compound was not detected in the rhizomes. In addition, although carvone was present among the components of the fruit essential oil in a small amount, this compound was not detected in the rhizomes (Drobac et al., 2017).

A similar study was also observed in samples collected from the Lakes Region. While the essential oil content remained quite low at 0.14% in herba samples, the major components were found to be α-pinene (33.22%) and β-pinene (24.09%). In fruits, however, the essential oil content increased to 11.37%, and the major component was dl-limonene (53.67%) (Tosun, 2021). The aforementioned studies are presented comparatively in Table 1.

Table 1. Essential oil content and major components according to different origins and plant organs.

Origin/Region	**Plant Organ**	**Essential Oil Content**	**Major Components (%)**	**Reference**
Mersin (Türkiye)	Fruit	%4,4	Perillaldehyde 50%; d-Limonene 45%	Ferahoğlu ve Kırıcı, 2023
Zonguldak (Türkiye)	Fruit	%2,7	Perillaldehyde 68%; d-Limonene 24%	Meriçli ve Meriçli, 1986
Artvin (Türkiye)	Herba	%1,2	Perillaldehyde 73%; Perillyl alcohol 7.6%; E-Caryophyllene 7.6%; Limonene 2%	Bayraktar, 2009
Göller Yöresi (Türkiye)	Herba	%0,14±0,03	α-Pinene 33.22%; β-Pinene 24.09%; dl-Limonene 7.65%; β-Caryophyllene 12.53%	Tosun, 2021
Göller Yöresi (Türkiye)	Fruit	%11,37±0,15	α-Pinene 13.44%; dl-Limonene 53.67%; Perillaldehyde 29.34%	Tosun, 2021
Almanya	Seed	%4,4	Perillaldehyde and d-Limonene (Not specified)	Parlatan ve ark., 2009
Hindistan	Seed	%4,8	Perillaldehyde and d-Limonene (Not specified)	Parlatan ve ark., 2009
Türkiye	Seed	%5,8	Perillaldehyde and d-Limonene (Not specified)	Parlatan ve ark., 2009
İran	Herba	%2,2	α-Pinene 34%; β-Caryophyllene 17%	Vahdat ve ark., 2006
Avusturya	Leaf	%0,1-%0,2	α-Pinene 12%; Bornyl angelate 67%	Chizzola, 2007
Avusturya	Fruit	%4,0-%4,7	Perillaldehyde and limonene (Not specified)	Chizzola, 2007
Sırbistan	Rhizome	Oran belirtilmemiş	α-Pinene 31%; γ-Terpinene 9%	Drobac ve ark., 2017
Sırbistan	Fruit	%6,7	Limonene 51%; Perillaldehyde 26%; α-Pinene 7%; Carvone 0.5%	Drobac ve ark., 2017

CONCLUSION

The evaluation of the literature data reveals that the chemical composition of *Laser trilobum* essential oils can vary considerably depending on geographical origin and plant organ. In fruit samples, d-limonene and perillaldehyde generally predominate, whereas different compounds such as α-pinene, β-pinene, β-caryophyllene, bornyl angelate, and carvone have been found as

dominant or prominent components in some herba, leaf, and rhizome samples. In particular, the emergence of different essential oil profiles in different organs of the same plant demonstrates the importance of plant organ in determining essential oil composition. Indeed, the high proportion of bornyl angelate in the leaf essential oil of *L. trilobum* reveals a chemical profile different from the limonene and perillaldehyde that predominate in the fruits.
However, the fact that the existing studies were conducted under different geographical, ecological, and methodological conditions makes it difficult to attribute the observed differences to a single factor. For these reasons, although the studies demonstrate that the essential oil composition of *L. trilobum* varies according to geographical origin and plant organs, they also indicate the need for studies that help elucidate its relationship with cultivation conditions.

REFERENCES

Andrade, L. N., Severino, P., Amaral, R. G., Doria, G. A. A., da Silva, A., Alves, M., ... & de Sousa, D. P. (2018). Evaluation of cytotoxic and antitumor activity of perillaldehyde 1, 2-epoxide. *Journal of Medicinal Plants Research*, *12*(30), 590-600.

A. Abbaszadegan, A. Gholami, Y. Ghahramani, R. Ghareghan, M. Ghareghan, A. Kazemi, A. Iraji, Y. Ghasemi, Antimicrobial and cytotoxic activity of Cuminum cyminum as an intracanal medicament compared to chlorhexidine gel. Iran Endod. J., 11, 44-50 (2016). https://doi.org/10.7508/iej.2016.01.009

Bakkali, F., Averbeck, S., Averbeck, D., & Idaomar, M. (2008). Biological effects of essential oils–a review. *Food and chemical toxicology*, *46*(2), 446-475.

Bayraktar, Ş. (2009). *Asteraceae ve Umbelliferae familyasına ait bazı bitki türlerinin antimikrobiyal ve antioksidan aktivitelerinin araştırılması* (Doctoral dissertation, Yüksek Lisans Tezi, Fen Bilimleri Enstitüsü, Karadeniz Teknik Üniversitesi, Trabzon).

Bayram, E., Kırıcı, S., Tansı, S., Yılmaz, G., Kızıl, O. A. S., & Telci, İ. (2010). Tibbi ve aromatik bitkiler üretiminin arttirilmasi olanaklari. *TMMOB Ziraat Mühendisleri Odasi, Ziraat Mühendisligi VII. Teknik Kongresi*, *11*, 15.

Chizzola, R. (2007). Composition of the essential oil from Laser trilobum grown in the wild in Vienna. *Chemistry of Natural Compounds*, *43*(4), 484-486.

Chizzola, R. (2010). Essential oil composition of wild growing Apiaceae from Europe and the Mediterranean. *Natural Product Communications*, *5*(9), 1934578X1000500925.

Demir, S. & Kan, Y. (2025). Kimyon olarak bilinen Bitki Türleri ve değerlendirmesi. *Kırşehir Ahi Evran Üniversitesi Ziraat Fakültesi Dergisi*, 5(2), 128-158.

Drobac, M., Petrović, S., Milenković, M., Couladis, M., Kukić-Marković, J., & Niketić, M. (2017). Composition and antimicrobial properties of essential oils of laser trilobum rhizomes and fruits. *Natural product communications*, *12*(3), 1934578X1701200335.

Ferahoğlu, E., & Kırıcı, S. (2023). Chemical compositions of essential oil obtained from the fruits of Laser trilobum grown in Mersin. *Biodivers. Conserv*, *16*(1), 1-5.

Ji, W. W., Wang, S. Y., Ma, Z. Q., Li, R. P., Li, S. S., Xue, J. S., ... & Ma, S. P. (2014). Effects of perillaldehyde on alternations in serum cytokines and depressive-like behavior in

mice after lipopolysaccharide administration. *Pharmacology Biochemistry and Behavior, 116*, 1-8.

Meriçli, F., & Meriçli, A. H. (1986). Laser trilobum ve Cuminum cyminum meyvalarının uçucu yağları. *Marmara Pharmaceutical Journal, 2*(1), 85-95.

Mokhtarzadeh, S., Peker, A., Ertunç, E., Çakır, M. F., & Güngör, H. (2023). Tıbbi ve Aromatik Bitkileri Konusuna Genel Bir Bakış. *Düzce Üniversitesi Ziraat Fakültesi Dergisi, 1*(1), 1-7.

Özmen, M. (2010). Hatay-Erzin Başlamış Köyünden Derlenen Bitki Adları. *Erdem*, (58), 255-268.

Parlatan, A. (2005). Kefe kimyonu (Laser trilobum L.) meyvesinin bazı kimyasal özelliklerinin ve ekstraktının antibakteriyal etkisinin belirlenmesi.

Parlatan, A., Sariçoban, C., & Özcan, M. M. (2009). Chemical composition and antimicrobial activity of the extracts of Kefe cumin (Laser trilobum L.) fruits from different regions. *International Journal of Food Sciences and Nutrition*, *60*(7), 606-617.

Sayed-Ahmad, B., Talou, T., Saad, Z., Hijazi, A., & Merah, O. (2017). The Apiaceae: Ethnomedicinal family as source for industrial uses. *Industrial crops and products*, *109*, 661-671.

Tian, J., Zeng, X., Lü, A., Zhu, A., Peng, X., & Wang, Y. (2015). Perillaldehyde, a potential preservative agent in foods: Assessment of antifungal activity against microbial spoilage of cherry tomatoes. LWT-Food Science and Technology, 60(1), 63-70. doi: 10.1016/j.lwt.2014.08.014.

Tosun, B. (2021). Göller yöresi'nde yayılış gösteren apıaceae familyasına ait bazı bitki türlerinin ekonomik değerleri ile kültüre alma potansiyellerinin belirlenmesi. *Isparta University of Applied Sciences Graduate Education Institute. 243pp*.

Uçan Türkmen, F., Özkan, K., Koyuncu, G., & Erol, Ü. H. (2024). Laser trilobum L., Hypericum scabrum L., ve Teucrium polium L. bitkilerinin metanol ekstraktlarının antioksidan aktiviteleri, mikrobiyolojik özellikleri ve fenolik bileşen miktarlarının belirlenmesi. *Mustafa Kemal University Journal of Agricultural Sciences/Mustafa Kemal Üniversitesi Tarım Bilimleri Dergisi*, *29*(2).

Üstüner, T. (2022). Kahramanmaraş ilinde gıda olarak tüketilen bitki türlerinin ve kullanım amaçlarının belirlenmesi. *Turkish Journal of Weed Science*, *25*(1), 54-68.

VAHDAT, M., ESLAMI, B., Dabiri, H., KHALILZADEH, M., TAJBAKHSH, M., & LARIJANI, K. (2006). Essential oil composition of Laser trilobum (L.) Borkh. Umbelliferae herbs growing wild in Iran.

Zielińska-Błajet, M., Pietrusiak, P., & Feder-Kubis, J. (2021). Selected monocyclic monoterpenes and their derivatives as effective anticancer therapeutic agents. *International journal of molecular sciences*, *22*(9), 4763.

BIFUNCTIONAL $CoFe_2O_4$-ZnS:Mn CORE-SHELL NANOPARTICLES FOR NANOSCIENCE APPLICATIONS

Yeliz AKPINAR[1*]

[1] *Kırşehir Ahi Evran University, Art and Science Faculty, Department of Chemistry, Kırşehir, Türkiye*
Corresponding author e-mail: yeliz.akpinar@ahievran.edu.tr

ABSTRACT

In recent years, bifunctional nanomaterials with magnetic and optical properties have gained considerable attention in nanomedicine, especially for nanoscience applications. Materials show different properties at the nanoscale than at bulk size. In addition, as size decreases, nanoparticles develop richer surface properties. For example, a higher surface-to-volume ratio provides a larger surface area, increasing functional efficiency. Therefore, quantum dots (QDs) and magnetic nanoparticles are commonly used for their unique properties. Conventional quantum dots often contain highly toxic heavy metals, such as cadmium, which restricts their clinical translation. Manganese-doped zinc sulfide (ZnS:Mn) quantum dots have been developed to overcome this drawback and are a biocompatible, cadmium-free substitute with stable luminescence. In this study, we synthesized core-shell $CoFe_2O_4$-ZnS:Mn QD nanocomposites through co-precipitation and then successfully developed a dual-modal imaging platform. SEM morphology showed that the composite structure consisted of ZnS:Mn quantum dots inside the cobalt ferrite magnetic nanoparticles. Also, the Fluorescence spectra showed a strong and characteristic orange-pink emission around 630-700 nm, which corresponds to the 4T1→6A1 transition of Mn2+ ions. The coexistence of a strong magnetic response and bright luminescence indicates that these cadmium-free core-shell nanostructures are promising for targeted drug delivery and concurrent optical/magnetic resonance imaging.

Keywords: Nanoscience, Quantum Dots, Magnetic Nanoparticles

INTRODUCTION

Currently, nanotechnology is a hot topic in science. These researchs have led to the development of goods and methods that improve the efficiency of everyday life. The development of nanoscience is being driven by a number of issues, including the need for renewable energy sources, the identification and treatment of novel illnesses, and the growing need for food due to population expansion. The basic building elements of the scientific method of product development are nanostructures. Nano-sized materials are very helpful in biological research due to their special characteristics(Ahmad et al., 2025; Dowling, 2004; Hughes et al., 2025) .

Magnetic nanoparticles (MNPs) are a rapidly expanding class of metal nanoparticles (NPs) that have sparked a revolution in materials science due to their unique combination of advantageous properties, including high surface-to-volume ratio, superparamagnetism, size-dependent properties, and quantum confinement effects, with conventional bulk material characteristics(Chand & Vasquez-Guardado, 2025) . The weak plasmonic optical properties of magnetic nanoparticles limit their use in applications such as imaging. The absence of plasmonic properties, meaning they do not emit fluorescence when exposed to light at a specific wavelength, prevents their use as sensors. To overcome this limitation, composite structures were developed. Magnetic nanoparticles were combined with molecules or nanoparticles that have plasma or fluorescence emission properties, making them multifunctional(Corr et al.,

2008). The aim was to perform both magnetic applications such as MRI, hyperthermia, and magnetic targeting, and optical applications such as SERS detection and fluorescence detection, simultaneously(Mir et al., 2025; Sirgedaite et al., 2023; Wolfbeis, 2015).
Quantum dots (QDs) are semiconductor particles with optical and electronic (optoelectronic) characteristics that vary with size and composition. QDs are very tiny, usually ranging in size from 1.5 to 10.0 nm. QD nanotechnology has recently made significant inroads into a number of biological and electrical areas. Because of their special qualities—such as excellent photostability, size-dependent optical characteristics, high brightness and extinction coefficient, and significant Stokes shift—QDs have been shown to be effective. Due to their limited ability to display all of these characteristics, organic dyes or fluorophore molecules are unsuitable for many imaging and biosensing applications. Furthermore, because of their enormous surface area, ultrasmall QDs may provide additional benefits over another type nanomareials for creating multimodal/multifunctional probes(Bera et al., 2010; Maxwell et al., 2020) . Quantum dots based on cadmium are generally used due to their high emission properties. However, because cadmium-containing quantum dots are not stable under UV light, there is a possibility of cadmium ions leaching into the environment. Since cadmium has high toxicity, its use for biomedical purposes is problematic. Therefore, Cd-based quantum dots are coated with Zn-derived quantum dots. Alternatively, for biomedical applications, Zn and Mn-based or carbon-based quantum dots with lower toxicity are used (Hardman, 2006; Lin & Chen, 2023).
In the literature, nanocomposites containing multifunctional magnetic particles and quantum dots have been produced for this purpose. Some of these include: Wang et al. Fe_2O_3 Beads−CdSe/ZnS Quantum Dots nanocomposite(Wang et al., 2004); Xu et al. Fe_3O_4/SiO_2 and water-soluble CdSe−ZnS quantum dots (QDs) nanocopmpsite. (Xu et al., 2010); Tadesse et al. nitrogen doped carbon quantum dots/magnetite nanocomposites (Tadesse et al., 2018), and Bunkoed et al. graphene quantum dots and magnetite nanoparticles embedded in molecularly imprinted polymer (GQDs@Fe_3O_4/MIP) nanocomposites(Bunkoed et al., 2020).
In this study, Cobalt ferrite magnetic nanoparticles were modified with ZnS:Mn quantum dots. Quantum dots provided fluorimetric properties to magnetic nanoparticles

METHOD

1.) $CoFe_2O_4$ nanoparticles (MNPs) were created via co-precipitation. A 1:2 mole solution of $CoCl_2$ and $FeCl_3$ salts was prepared in a flask and mixed with a NaOH solution at 80°C for an hour. The resulting black particles were gathered using a magnet, and a solution of water was used for three magnetic washing processes. After that, it was dissolved in 50 mL deionized water (Roy et al., 2024)
2.) 1.0 ml $CoFe_2O_4$ nanoparticle (MNP) solutions were added to 10.0 ml 0.025 M Zn(NO3)2 and Mn(NO3)2 mixed solution.After 1 hour of mixing, 0.1 M Na2S solution was added to the previous solution. After 12 hours of mixing in a dark room, a gray-brownish precipitate was obtained and washed with dı water three times using a magnet.Finally, nanoparticles were dispersed in water. Supernatant was disposed of.
3.) To demonstrate the effect of nanocomposite ratios in optimization studies, the experiment was performed twice separately by adding 1.0 and 2.0 ml of magnetic particle solution to equal amounts of Zn and Mn ion mix solutions.

RESULTS AND DISCUSSION

The adherence of quantum dots to the magnetic nanoparticle surface was checked using a UV lamp. First, it was observed that the prepared ZnS:Mn QDs composites gave an orange color under UV light at a wavelength of 365 nm (Figure 1a). Then, the prepared nanocomposite was

visualized in daylight and under UV light at the same wavelength. The color, which was light gray-brown under daylight, appeared orange-pink under UV light (Figure 1b and 1c).

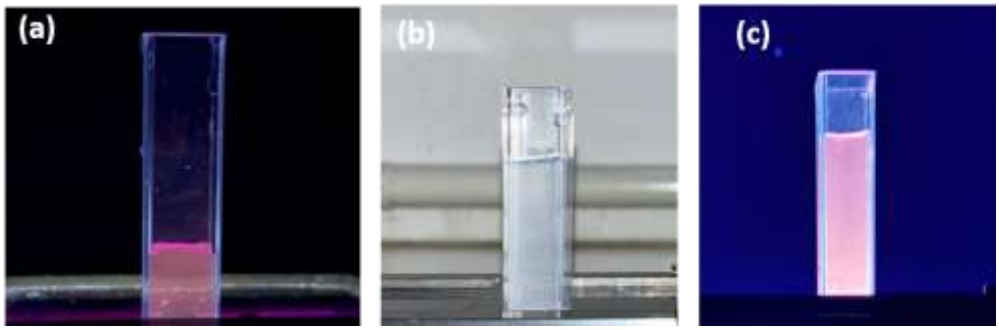

Figure 1. Image of a.) ZnS:Mn QDs under UV light, b.) Nanocomposite under solar light, c) nanocomposites under UV light.

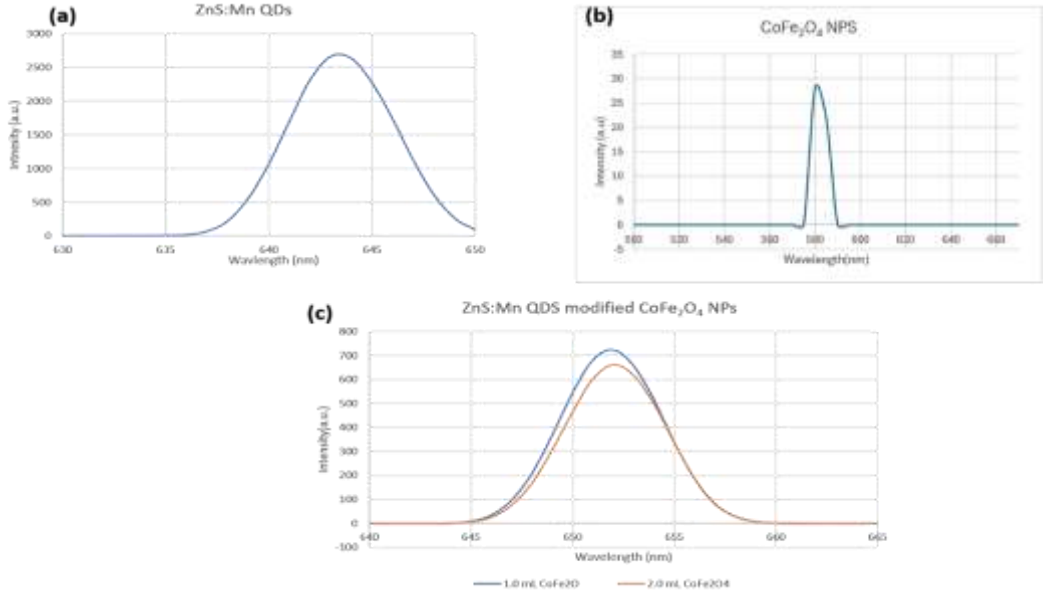

Figure 2. Emission spectrum of a.) ZnS:Mn quantum dots, b) $CoFe_2O_4$ NPs c.) ZnS:Mn quantum dots modified magnetic nanoparticles

Fluorescence Spectroscopy (FL) was used for emission measurements. For measurements, a quartz cell was used, and the device was adjusted to 320 nm excitation wavelength. ZnS:Mn quantum dots give emission at 642 nm(Figure 2a). These results are consistent with the literature (Patel et al., 2020). The fluorescence emission spectrum shown in Figure 2b corresponds to the prepared cobalt ferrite nanoparticles. It exhibits a peak at 580 nm that is either absent or negligibly weak. This wavelength does not coincide with the emission wavelength of ZnS:Mn quantum dots. ZnS:Mn quantum dots modified magnetic nanoparticles(nanocomposite) emitted at 652 nm. The wavelength shifted with agglomeration (Figure 2c). In addition, the emission intensity decreased significantly due to quenching caused by agglomeration of the magnetic nanoparticles. For optimization, we used 1.0 mL (blue line) and 2.0 mL (orange line) magnetic nanoparticles during synthesis, separately. Figure 2c indicated that there is no significant difference. As a result, the ratio of components is not effective for this method.

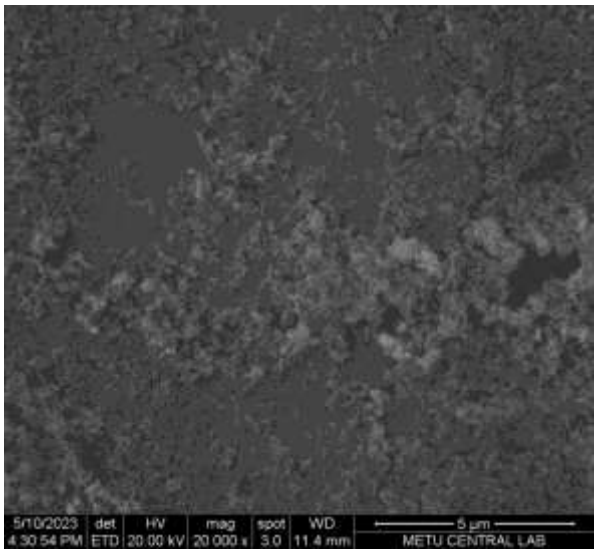

Figure 3. SEM images of ZnS:Mn quantum dots modified magnetic nanoparticles(Nanocomposites)

Figure 3 shows the SEM image of the prepared nanocomposite. In the image, the dark gray particles are magnetic nanoparticles, and the light gray particles are quantum dots attached to the magnetic particles.

CONCLUSIONS

This study aimed to produce a bifunctional nanomaterial by combining two different nanomaterials solely through adsorption, without the need for any interconnecting groups and an extra reaction step. The goal was to obtain a core-shell structure, but SEM images showed that the core-shell structure was not fully formed. Instead, a randomly distributed composite structure was formed. Fluorescence spectroscopy measurements and UV light beams showed that quantum dots in the structure adhered to the magnetic particle surface. In the future, other combination methods will be tried to produce more efficient emissions and a core-shell structure. Several techniques, including TEM, Zeta Potentiometer, VSM, and FTIR Spectroscopy, will improve characterization. The stability of the nanocomposite will also be tested. The produced particles will be used in imaging, biomedical applications,water splitting, and dye degradation as catalysts.

REFERENCES

Ahmad, K., Ahmad, R., Faizan, M., Farah, Ali, F., Yousaf, M. M., Ali, F., Niaz, W., Khan, T. U., Khan, S., Ali, S., Ahmed, I., & Hassan, H. (2025). A review of nanotechnology in food industry with implication for viable outlook and safety issues. *Hybrid Advances*, *10*, 100487. https://doi.org/10.1016/j.hybadv.2025.100487

Bera, D., Qian, L., Tseng, T.-K., & Holloway, P. H. (2010). Quantum Dots and Their Multimodal Applications: A Review. *Materials*, *3*(4), 2260–2345. https://doi.org/10.3390/ma3042260

Bunkoed, O., Raksawong, P., Chaowana, R., & Nurerk, P. (2020). A nanocomposite probe of graphene quantum dots and magnetite nanoparticles embedded in a selective polymer for the enrichment and detection of ceftazidime. *Talanta*, *218*, 121168. https://doi.org/10.1016/j.talanta.2020.121168

Chand, K., & Vasquez-Guardado, E. S. (2025). Magnetic Nanoparticles: Synthesis and Applications in Life Sciences. *ChemistryOpen*, *14*(12). https://doi.org/10.1002/open.202500214

Corr, S. A., Rakovich, Y. P., & Gun'ko, Y. K. (2008). Multifunctional Magnetic-fluorescent Nanocomposites for Biomedical Applications. *Nanoscale Research Letters*, *3*(3), 87. https://doi.org/10.1007/s11671-008-9122-8

Dowling, A. P. (2004). Development of nanotechnologies. *Materials Today*, *7*(12), 30–35. https://doi.org/10.1016/S1369-7021(04)00628-5

Hardman, R. (2006). A Toxicologic Review of Quantum Dots: Toxicity Depends on Physicochemical and Environmental Factors. *Environmental Health Perspectives*, *114*(2), 165–172. https://doi.org/10.1289/ehp.8284

Hughes, K. J., Ganesan, M., Tenchov, R., Iyer, K. A., Ralhan, K., Diaz, L. L., Bird, R. E., Ivanov, J., & Zhou, Q. A. (2025). Nanoscience in Action: Unveiling Emerging Trends in Materials and Applications. *ACS Omega*, *10*(8), 7530–7548. https://doi.org/10.1021/acsomega.4c10929

Lin, X., & Chen, T. (2023). A Review of in vivo Toxicity of Quantum Dots in Animal Models. *International Journal of Nanomedicine*, *Volume 18*, 8143–8168. https://doi.org/10.2147/IJN.S434842

Maxwell, T., Nogueira Campos, M. G., Smith, S., Doomra, M., Thwin, Z., & Santra, S. (2020). Quantum Dots. In *Nanoparticles for Biomedical Applications* (pp. 243–265). Elsevier. https://doi.org/10.1016/B978-0-12-816662-8.00015-1

Mir, A., Dashti, H., & Huyeh, M. R. (2025). Optical properties of magneto-plasmonic nanoparticles chain of Fe_3O_4@SiO_2@Ag and their sensing applications. *Scientific Reports*, *16*(1), 1506. https://doi.org/10.1038/s41598-025-31439-7

Patel, J., Jain, B., Singh, A. K., Susan, Md. A. B. H., & Jean-Paul, L. (2020). Mn-Doped ZnS Quantum dots–An Effective Nanoscale Sensor. *Microchemical Journal*, *155*, 104755. https://doi.org/10.1016/j.microc.2020.104755

Roy, P., Hoque, S. M., Akter, S., Liba, S. I., & Choudhury, S. (2024). Study on the chemical co-precipitation synthesized $CoFe_2O_4$ nanoparticle for magnetocaloric performance in the vicinity of superparamagnetic blocking temperature. *Heliyon*, *10*(14), e34413. https://doi.org/10.1016/j.heliyon.2024.e34413

Sirgedaite, G., Talaikis, M., Niaura, G., & Mikoliunaite, L. (2023). Magneto-plasmonic nanostructures for SERS: magnetite decorated by silver and gold nanoparticles. *New Journal of Chemistry*, *47*(1), 402–411. https://doi.org/10.1039/D2NJ04368H

Tadesse, A., RamaDevi, D., Hagos, M., Battu, G., & Basavaiah, K. (2018). Synthesis of nitrogen doped carbon quantum dots/magnetite nanocomposites for efficient removal of methyl blue dye pollutant from contaminated water. *RSC Advances*, *8*(16), 8528–8536. https://doi.org/10.1039/C8RA00158H

Wang, D., He, J., Rosenzweig, N., & Rosenzweig, Z. (2004). Superparamagnetic Fe_2O_3 Beads−CdSe/ZnS Quantum Dots Core−Shell Nanocomposite Particles for Cell Separation. *Nano Letters*, *4*(3), 409–413. https://doi.org/10.1021/nl035010n

Wolfbeis, O. S. (2015). An overview of nanoparticles commonly used in fluorescent bioimaging. *Chemical Society Reviews*, *44*(14), 4743–4768. https://doi.org/10.1039/C4CS00392F

Xu, Y., Karmakar, A., Wang, D., Mahmood, M. W., Watanabe, F., Zhang, Y., Fejleh, A., Fejleh, P., Li, Z., Kannarpady, G., Ali, S., Biris, A. R., & Biris, A. S. (2010). Multifunctional Fe_3O_4 Cored Magnetic-Quantum Dot Fluorescent Nanocomposites for RF Nanohyperthermia of Cancer Cells. *The Journal of Physical Chemistry C*, *114*(11), 5020–5026. https://doi.org/10.1021/jp9103036

MAPPING GROUND VEGETATION BIODIVERSITY OF FOREST ECOSYSTEMS THROUGH SPATIAL ANALYSIS

Doriana (Bode) XHULAJ[1], Enea MALAJ[2], Anjeza BEKOLLI[3]*

[1] Agricultural University of Tirana, Faculty of Environment and Agriculture, Department of Agronomic Sciences, Tirana, Albania
[2] Agricultural University of Tirana, Faculty of Forest Sciences, Forest Department, Tirana, Albania
[3] Agricultural University of Tirana, Faculty of Economy and Agribusiness, Department of Mathematics and Informatics, Tirana, Albania

Corresponding author email: dbode@ubt.edu.al

ABSTRACT

In this study, we assessed the diversity of the ground vegetation across 29 circular plots inside the Mediterranean forest of the National Park Divjake-Karavasta. Ground vegetation and associated shrub and tree species in the study area forest exhibit varying conservation significance when assessed against national Red List data. The majority of species are generally classified as Least Concern or are not explicitly listed due to their broad distribution and ecological resilience. Similarly, Mediterranean and maquis-associated taxa such as *Phillyrea angustifolia* L., *Erica arborea* L., *Rhamnus alaternus* L., *Paliurus spina-christi* Mill., and *Ruscus aculeatus* L. are considered stable, although they may be affected locally by fire regimes and land-use change. In contrast, certain species demonstrate higher conservation sensitivity at the national level. *Juniperus macrocarpa* remains associated with vulnerable coastal dune habitats and is considered Near Threatened in regional contexts, while *Pyrus pyraster* (L.) Burgsd. is characterized by fragmented populations and may also be regarded as Near Threatened locally. The descriptive analysis highlights that the 29 plots of the Divjaka Mediterranean forest are characterized by a vertically developed vegetation structure, but with significant horizontal heterogeneity, especially in the lower vegetation layers. These patterns highlight that, although most species fall under Least Concern globally, incorporating national-level conservation assessments is essential for accurately identifying ecologically sensitive vegetation clusters in spatial analyses such as SKATER, thereby improving biodiversity mapping and conservation planning in Albanian ecosystems.

Keywords: Biodiversity, Forest, Map, Structure, Spatial analyses

INTRODUCTION

Ground vegetation biodiversity in forest ecosystems is a critical yet often overlooked component that underpins overall ecological stability and function. This layer—comprising mosses, herbs, grasses, and low shrubs—supports complex food webs by providing habitat and nourishment for invertebrates, microorganisms, and small vertebrates, thereby sustaining higher trophic levels (Gilliam, 2007). It also plays a vital role in soil protection and nutrient cycling by reducing erosion, enhancing organic matter decomposition, and maintaining soil moisture, which are essential for long-term forest productivity (Whigham, 2004). Moreover, ground vegetation serves as a sensitive indicator of environmental change, reflecting the impacts of disturbances such as climate change, pollution, and land-use practices (De Frenne et

al., 2013). Its influence extends to forest regeneration processes, as it can either facilitate or inhibit tree seedling establishment, shaping species composition and forest succession over time (George & Bazzaz, 1999). Therefore, studying ground vegetation biodiversity is fundamental for effective forest conservation and sustainable ecosystem management.

Mapping ground vegetation diversity through Spatial "K"-luster Analysis by Tree Edge Removal (SKATER) is an effective approach for identifying spatial patterns and ecological heterogeneity within forest ecosystems (Assunção et al., 2006). SKATER is a spatial clustering technique that groups sampling units (such as vegetation plots) into homogeneous regions based on species composition while preserving geographic continuity, making it especially suitable for ecological studies (Assunção et al., 2006). By using measures of similarity or dissimilarity—often derived from species abundance or presence–absence data—the method constructs a minimum spanning tree and then iteratively removes edges to form clusters with internally similar biodiversity characteristics. This allows researchers to map distinct vegetation zones, detect gradients in species diversity, and better understand how environmental factors such as soil, elevation, or microclimate influence ground vegetation distribution. Applying SKATER to forest ground vegetation enhances the ability to visualize biodiversity patterns, supports more precise conservation planning, and improves decision-making in sustainable forest management by highlighting areas of high ecological value or vulnerability. This study aimed to identify and interpret the spatial structure of ground vegetation biodiversity in the Mediterranean forest of the National Park Divjakë-Karavasta, combining statistical and graphical methods to capture both ecological homogeneity and heterogeneity.

MATERIAL AND METHOD

Study area: Assessments have been carried out during May 2024, in the Mediterranean coniferous forests at the National Park of the Divjakë-Karavasta (Divjaka forest), defined as a forest with a variable mixture of at least two native coniferous species constituting ≥70 percent of the forest cover on sandy soils. A GIS procedure was used to randomly select plots in the forest area with at least 70 percent tree canopy cover. The center of the plot was located according to a systematic sampling design at the intersection of a 100×100-meter grid. About 29 circular plots with a radius of 11.28 meters (0.1 hectares) were designed.

Data monitoring: I. the monitoring of forest ground vegetation in the National Park of the Divjakë-Karavasta is carried out in accordance with the Manualin e planeve të mbareshtimit te pyjeve dhe kullotave (https://qeverisjavendore.gov.al/Manuali-i-planeve-te-mbareshtimit-te-pyjeve-dhe-kullotave-2019.pdf). In the pine forest habitat of Divjakë, we examined 29 plots as study areas and assessed 9 qualitative indicators, which provide us with descriptive information about the area under study. Specifically, for the 29 plots created, we assessed the following indicators: Land use category; Form of governance; Spatial distribution; Composition of the forest collection; Origin of the forest; Type of management; Main function; Vertical structure; Regeneration cuttings and Silvicultural mass.

1. The indicator Land use category contains the following defining criteria: Forests; Shrubs and/or herbaceous vegetation associations; Open areas with little or no vegetation; Pastures; Mines, construction areas and collection sites; Water areas and Burned areas.
2. The indicator Governance form contains the following classifications: Trunks; Coppice; Composite trunks; Composite coppice; Shrubs; Herbaceous vegetation areas; Pastures.
3. The indicator Main function of forests based on the Forest Management Manual (2019) should be determined for each test area. These functions are classified into: Productive; Protective; Social; Conservation.
4. The composition of the forest collection implies the participation of the main species of the test areas and is classified into: Simple and Mixed.

5. The spatial distribution indicator provides information on the distribution patterns of plant vegetation in the habitat plots under study by classifying them into: Not forested; Uniform; Scattered in clusters; Scattered in floors; Mosaic pattern; Irregular; Individuals.
6. The forest origin indicator. It is determined by referring to the dominant species of the areas under study. It is classified as natural or artificial. When the origin of the forest is (i) natural, then one of the specifications is selected in the field: with seed, Shoots; mixed; undetermined. If the forest has an origin of (ii) Planted-artificial, then the year of afforestation is noted.
7. The vertical structure of the forest is determined based on the crown levels of the stand, referring to the criteria: Simple (1 level); Two levels; Many levels.
8. Regenerative cutting. Field assessment of the presence of regeneration.
9. Silvicultural measures (what is recommended)
II. The structure of the ground vegetation cover is categorized in the field as follows: Medium-sized trees, shrubs and woody plants (3m<L.<5m); Tall shrubs (1.5m<L.<3m); Medium shrubs (0.5m<L.<1.50m); Low shrubs (0.05m<L.<0.5m); Shrubs near ground level (0.02m<L.<0.05m); Fern cover; Herbaceous cover. Code 0 = No presence in the test area; 1 = Rare species: close to zero cover; 2 = Scattered plants: CC ≤1%; 3 = Low plant number: CC 1-5%; 4 = Intermediate plant number: CC 5-10%; 5 = High plant number: CC 10-25%; 6 = CC 25-50%; 7 = CC 50-75%; 8 = CC >75%.

***Data analysis method*:** In this study, the SKATER (Spatial "K"-luster Analysis by Tree Edge Removal) analysis (Assuncao et al. 2006) is used to identify spatial patterns and homogeneous areas of vegetation structure in the test plots of the Divjaka Mediterranean forest. The spatial dependence test is applied through Moran's I coefficient to assess whether there is a spatial effect on the distribution of these variables, that is, whether geographically close surfaces present similarities in vegetation structure. After determining the spatial relationships, the SKATER method is applied, which is based on the construction of a neighborhood graph through the Minimum Spanning Tree (MST) algorithm (Anselin 1995; Huda et. al 2023). MST describes the minimal connections between test plots based on the similarity of vegetation structure, without creating cycles, and preserving the real spatial relationships between them.

RESULTS AND DISCUSSIONS

The monitoring of forest ground vegetation:

The data obtained in the field for 29 plots as study area plots in the Divjaka Mediterranean forest habitat were assessed for 9 indicators, providing us with descriptive information on the area under study. Specifically, for the indicator Land use category in the field assessment conducted for all 29 plots, we selected the criterion Forest for each plot in relation to this indicator. The type of forest management/form of governance helps us to understand how the forest is managed and used by the community. The indicator Form of governance results for all plots in the study are the same: coppice. This classification, referred to in the National Forest Inventory (IKP 2022), suggests a form of governance that bases renewal mainly on seed, and its management is done until the age when the trees reach considerable size.

Based on field observations and the current status of this forest ecosystem, our test areas provide a protective function, positively influencing the environment by mitigating climate change, preventing soil erosion, and supporting the circulation of materials. Of course, these areas also meet the criteria for social and conservation functions, as they serve as environments for recreation and tourism. At the same time, the Divjaka Mediterranean forest habitat, thanks to its high biodiversity, serves as an area of special scientific value.

For the spatial distribution indicator, the results suggest that six of the 29 plots (S1, S8, S9, S10, S11, S12) meet the criteria for the non-forested category, and four of the 29 plots in the study (S23, S24, S25, S26) fall into the Uniform distribution category (Figure 1). The data show

that 17 plots present a spatial distribution in stands, and only two plots (S16 and S18) present a spatial distribution with individuals. Knowing the composition of the forest stand is important because it shows not only which tree species make up the forest but also how it functions as an ecosystem. It helps in planning forest management, indicates the level of biodiversity, helps in protection from diseases and pests, affects natural regeneration, and allows the assessment of forest productivity. In this way, the composition of the forest stand is an indicator of the structure, health, and sustainability of the forest. In our case study, we estimated that among the 29 plots, only 5 (S1, S17, S19, S26) are characterized by a simple assemblage composition, while the other 24 plots are characterized by a mixed composition. This result shows that more than one species is present in most of our area, suggesting good biodiversity and, consequently, a greater variety of habitats for flora and fauna. In a forest ecosystem, the presence of a mixed species composition will help to cope with climate change better than areas represented by a small number of species or those with a single species.

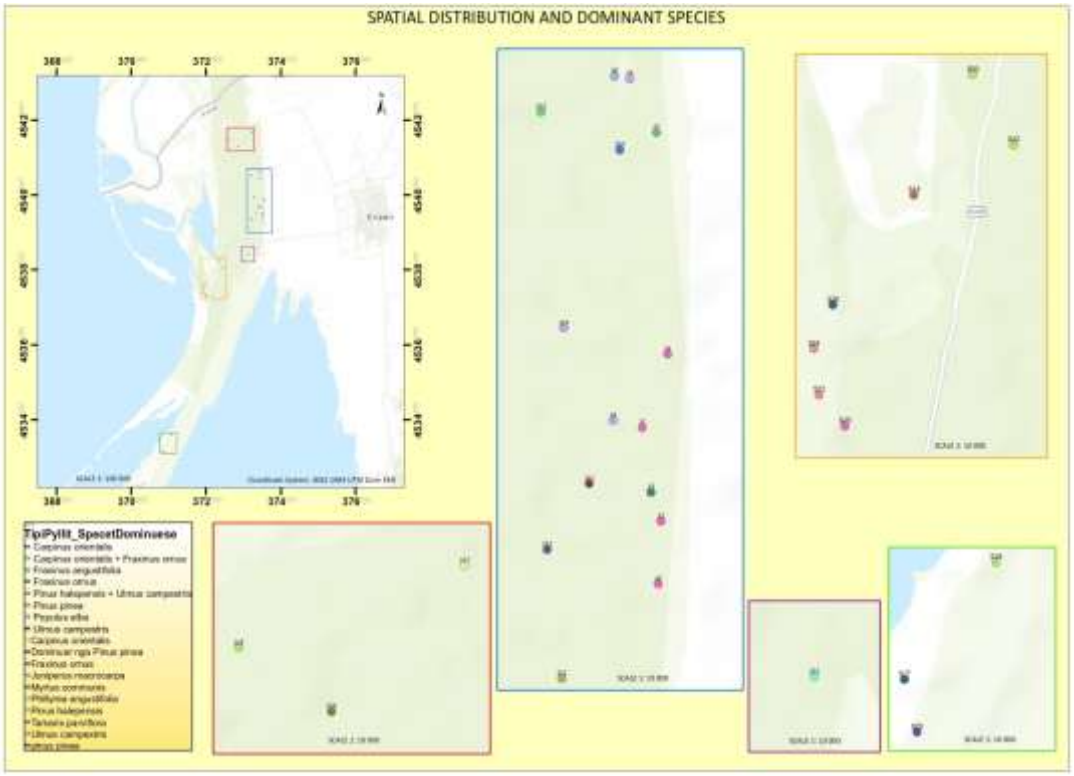

Figure 1. Spatial distribution of dominant forest tree species composition

To understand how this forest ecosystem was created, our field assessment of forest origin included two categories: (i) natural and (ii) planted-artificial. Based on the observations, four plots (S23, S24, S25, and S26) have a planted-artificial forest origin with seedlings. All other plots have a natural origin. Within this category, 22 plots have a seed-created origin; only one plot, S6, has a vegetative origin with shoots; and two other plots, S8 and S15, have a mixed forest formation origin (seed and shoots).

The vertical structure of the forest tells us about the division of the forest vegetation into layers according to height. Knowing it is important because it tells us about the ecological health of the forest under study, how light and moisture are distributed, whether natural regeneration is possible or not, etc. The data suggest the presence of a two-story vertical structure of the forest in 24 plots, i.e., we have two main layers of vegetation arranged vertically, one created by tall and mature trees which represent the main forest cover (canopy) and the lowest layer represented by small trees, shrubs and young plants which grow understory. Plots S2, S3, S6

and S7 are presented with a vertical structure with more than two stories, suggesting an even higher biological diversity in these areas, for better efficiency of sunlight use and for a healthy regeneration of vegetation. Only plot 1 is presented with a one-story structure.

If the management plan for this habitat included regeneration cuttings, in 29 plots from field observations we assessed their presence or absence. In none of our plots did we observe the presence of regeneration of this forest.

Silvicultural measures in a forest habitat are important as they suggest how this habitat is managed and improved to be as sustainable and healthy as possible. Regarding this indicator, we could choose to recommend between the options of: Forest Clearance; Thinning; Selective felling of individual trees; Selective felling in groups; Conversion; Afforestation. For all plots, we recommend clearing as a silvicultural measure in order for this forest to improve growth, regeneration, or overall health of the trees. This process would include the removal of unwanted vegetation, such as weeds, shrubs, or weak-growing trees that compete with young trees for light, water, and nutrients. Clearing would also help sunlight penetrate the forest floor, encourage natural regeneration of desired tree species, and reduce the risk of pests, disease, or fire. In this way, clearing would help create better conditions for a healthier and more productive forest.

Results of the SKATER spatial analysis based on the Structure of the terrestrial vegetation cover:

Descriptive analysis of vegetation cover structure was carried out for 29 test plots located in the Divjaka Mediterranean forest, based on seven categories representing different vertical levels of vegetation, from ground vegetation to woody plants with a height of 3–5 m. The assessment of cover was carried out through a semi-quantitative scale (0–8), which reflects the relative percentage of cover of each category in each test plot. The results show that the vegetation structure presents a good vertical development, with a significant presence of shrubs and medium-sized woody vegetation in most of the plots. The category of woody plants and shrubs with a height of 3–5 m shows medium to high values of cover in most of the plots, suggesting a successful consolidated stage of the forest. In this category, the main representative species of the 29 plots under study are: *Pinus pinea* L., *Ulmus campestris* L., *Pinus halepensis* Mill., *Cornus mas* L., *Fraxinus ornus* L., *Juniperus macrocarpa* S.et.Sm., *Carpinus orientalis* Mill., *Pyrus pyraster (L.)* Burgsd., *Paliurus spina-christi* Mill., *Carpinus betulus* L., *Crataegus monogyna* Jacq., *Myrtus communis* L., *Cercis siliquastrum* L., *Phillyrea latifolia* L., *Tamarix parviflora* DC., *Pistacia lentiscus* L., and *Pinus pinaster* Aiton.

Similarly, tall shrubs (1.5–3 m) and medium shrubs (0.5–1.5 m) present a relatively stable distribution, with values ranging from medium to high cover, indicating a significant density of the shrub understory. The main representative species observed in the field for the medium shrub category are: *Juniperus macrocarpa* S.et.Sm., *Carpinus orientalis* Mill., *Pyrus pyraster (L.)* Burgsd., *Phillyrea angustifolia* L., *Myrtus communis* L., *Phillyrea latifolia* L., *Erica arborea* L., *Rhamnus alaternus* L., *Tamarix parviflora* DC., *Pistacia lentiscus* L. and *Colutea arborescens* L.

In the test areas under consideration for the medium shrub category, in addition to the representatives of the above category, we find several other species, specifically: *Ruscus aculeatus* L., *Paliurus spina-christi* Mill., *Rubus ulmifolius* Schott., *Cornus sanguinea* L., *Rosa canina* L., and *Crataegus monogyna* Jacq.

Unlike the upper vegetation layers, the lower layers show a more pronounced variability between the test plots. Low vegetation (0.05–0.5 m) and shrubs near ground level (0.02–0.05 m) present variable values, reflecting local differences in microecological conditions, such as lighting, humidity, and natural or anthropogenic interventions. This heterogeneity in the lower vegetation layer suggests the presence of different microhabitats within the forest massif.

Fern cover is absent in all analyzed plots, indicating that this plant group does not constitute an important structural component in the study area. Meanwhile, herbaceous vegetation presents an uneven distribution, with some plots showing high cover values, while others have a very limited or absent presence. This indicates that the herbaceous component is significantly influenced by local terrain conditions and the overall canopy structure. The main species observed for this category are: *Juncus acutus* L., *Juncus maritimus* Lam., *Arthrocnemum macrostachyum* (Moric.) K.Koch, and *Phragmites australis* (Cav.) Trin. ex Steud.

Ground vegetation and associated shrub and tree species in the Mediterranean forest and coastal ecosystem of the Divjaka-Karavasta National Park exhibit varying conservation significance when assessed against national Red List data. The majority of species, including *Carpinus orientalis* Mill., *Phillyrea latifolia* L., *Myrtus communis* L., *Pistacia lentiscus* L., *Crataegus monogyna* Jacq., *Cornus sanguinea* L., *Rosa canina* L., *Rubus ulmifolius* Schott, *and Phragmites australis* (Cav.*)* Trin. ex Steud. are generally classified as Least Concern or are not explicitly listed due to their broad distribution and ecological resilience (Ministry of Tourism and Environment Albania, 2013; International Union for Conservation of Nature, 2024). Similarly, Mediterranean and maquis-associated taxa such as *Phillyrea angustifolia* L., *Erica arborea* L., *Rhamnus alaternus* L., *Paliurus spina-christi* Mill., *and Ruscus aculeatus* L. are considered stable, although they may be affected locally by fire regimes and land-use change (Barina et al., 2018; Euro+Med PlantBase, 2023). In contrast, certain species demonstrate higher conservation sensitivity at the national level. *Juniperus macrocarpa* S.et.Sm., remains associated with vulnerable coastal dune habitats and is considered Near Threatened in regional contexts (International Union for Conservation of Nature, 2024), while *Pyrus pyraster* is characterized by fragmented populations and may also be regarded as Near Threatened locally (Barina et al., 2018). Riparian and halophytic species such as *Tamarix parviflora* DC., *Juncus acutus* L., *Juncus maritimus* Lam., *and Arthrocnemum macrostachyum (*Moric.*)* K.Koch are typically not globally threatened but are ecologically sensitive due to their dependence on wetland and coastal habitats, which are under increasing anthropogenic pressure (Tzonev et al., 2019). Additionally, *Colutea arborescens* L. and *Ulmus minor* Mill. may show localized vulnerability due to habitat fragmentation and disease impacts (Allen et al., 2010; Barina et al., 2018). These patterns highlight that, although most species fall under Least Concern globally, incorporating national-level conservation assessments is essential for accurately identifying ecologically sensitive vegetation clusters in spatial analyses such as SKATER, thereby improving biodiversity mapping and conservation planning in Albanian ecosystems.

Moran's I test shows that only a subset of the vegetation structure variables exhibit statistically significant spatial dependence (Table 1). Herbaceous vegetation shows significant positive autocorrelation, suggesting that geographically close areas tend to have similar levels of herbaceous cover and form spatial clusters. In contrast, the woody/shrub layer with a height of 3–5 m shows negative autocorrelation, indicating local contrasts between neighboring areas and the presence of transitional zones in the vegetation structure. The other variables do not show statistical evidence for spatial autocorrelation, reflecting local or microhabitat variability without a clear spatial structure at the study scale. These results support the use of SKATER analysis, where variables with spatial structure and local contrasts are expected to contribute to the increase in SSD and to the separation of the Minimum Spanning Tree into ecologically homogeneous groups (Figure 2).

The construction of the Minimum Spanning Tree (MST) on the standardized vegetation structure variables revealed relationships with very different Sum of Squared Differences (SSD) values, reflecting different degrees of ecological heterogeneity between the test plots. The relationship S19–S25 presents the highest SSD value, which indicates a very pronounced change in vegetation structure and identifies the S19 plot as an ecologically separate unit from the rest of the study area. This plot does not present diversity, as the measurements performed

show that it is mainly represented only by individuals of the species *Tamarix parviflora* DC. (Malaj et al 2024).

Table 1. Spatial dependence test (Moran's I): Moran's I results for vegetation structure variables in 29 Divjaka Mediterranean forest test plots

Vegetation variable	Moran's I	p-value	z-score
Herbaceous vegetation	**0.212**	**0.028**	2.243
Woody plants & shrubs (3–5 m)	**−0.200**	**0.035**	−1.470
Medium shrubs (0.5–1.5 m)	−0.141	0.124	−1.086
Low shrubs (0.05–0.5 m)	0.067	0.167	0.924
Shrubs near ground level (0.02–0.05 m)	0.050	0.192	0.788
Tall shrubs (1.5–3 m)	−0.095	0.297	−0.578
Ferns	NaN	—	NaN

A second important contrast is observed in the relationship S22–S23, which separates a micro-zone composed of plots S23 and S24 from the rest of the forest massif. These two plots present low values of species diversity, which are similar to each other; S23 is represented by individuals of *Juniperus macrocarpa* S.et Sm.; *Pinus halepensis* Mill.; and *Tamarix parviflora* DC. Plot 24 differs from Plot 23 only by the presence of *Pinus pinaster* Ait., which replaces *Tamarix* sp.

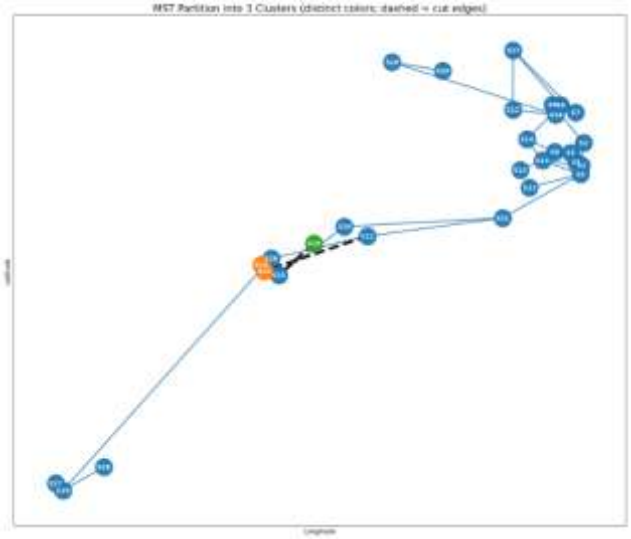

Figure 2. The Minimum Spanning Tree (MST) constructed on the Divjaka Mediterranean test plots, using as link weights the structural change of vegetation measured through Sum of Squared Differences (SSD) on standardized variables.

The graph illustrates the separation of the Minimum Spanning Tree (MST) into three spatial clusters by cutting the links with the highest SSD. The main cluster represents a relatively homogeneous vegetation structure, while the other two clusters identify a separate unit (S19) and a homogeneous micro-zone (S23–S24). The broken links indicate ecological boundaries and major transition zones between clusters. The full SSD values for all MST links result in three spatial clusters. The first cluster includes most of the areas and is characterized by a relatively homogeneous vegetation structure, representing the main ecological core of the Divjaka Pine. The second cluster consists only of area S19, which exhibits significantly different structural features and can be interpreted as a separate ecological zone or a unit with

specific local conditions. The third cluster includes areas S23 and S24, which form a homogeneous micro-zone, but distinct from the main cluster.

CONCLUSION

This study aimed to investigate the spatial organization of vegetation within the Divjaka Mediterranean Forest by integrating statistical and graphical approaches to characterize ecological homogeneity and heterogeneity. Moran's I analysis confirmed the presence of spatial autocorrelation and local spatial variation in several vegetation attributes, supporting the application of spatial clustering techniques. The Minimum Spanning Tree (MST) combined with the SKATER algorithm enabled the delineation of ecologically homogeneous clusters and the identification of distinct vegetation units that would be difficult to detect using conventional non-spatial methods. This integrated approach provides a robust framework for understanding vegetation spatial patterns and offers valuable support for forest management, ecological monitoring, and evidence-based conservation planning.

REFERENCES

Allen, E. A., et al. 2010. Dutch elm disease and its impact on elm populations. Forest Pathology.

Anselin, L. 1996. The Moran scatterplot as an ESDA tool to assess local instability in spatial association.

Assunção, R. M., M. C. Neves, G. Câmara, C. da Costa Freitas. 2006. Efficient regionalization techniques for socio-economic geographical units using minimum spanning trees. International Journal of Geographical Information Science. 20(7): 797–811.

Barina, Z., G. Somogyi, D. Pifkó, M. Rakaj. 2018. Checklist of vascular plants of Albania. Phytotaxa. 378(1): 1–339.

De Frenne, P., et al. 2013. Microclimate moderates plant responses to climate warming. Nature Climate Change.

Euro+Med PlantBase. 2023. Euro+Med PlantBase: the information resource for Euro-Mediterranean plant diversity.

George, L. O., F. A. Bazzaz. 1999. The fern understory as an ecological filter. Ecology.

Gilliam, F. S. 2007. The ecological significance of the herbaceous layer in temperate forest ecosystems. BioScience.

Huda, N. M., F. Fran, Y. Yundari, L. Fikadila, F. Safitri. 2023. Modified weight matrix using Prim's algorithm in Minimum Spanning Tree (MST) approach for GSTAR(1;1) model. BAREKENG: Journal of Mathematics and Its Applications. 17(1): 263–274.

International Union for Conservation of Nature (IUCN). 2024. The IUCN Red List of Threatened Species.

Legendre, P., L. Legendre. 2012. Numerical Ecology. 3rd English Edition. Elsevier. Amsterdam, The Netherlands. 990 pages.

Malaj, E., D. Bode. 2024. Assessing biodiversity in forest ecosystems using ecological indices: Case study of the Mediterranean Coniferous Forest at Divjakë-Karavasta National Park. International Journal of Ecosystems and Ecology Science. 14(4): 129–138. DOI: 10.31407/ijees14.417.

Ministry of Tourism and Environment. 2013. Red List of Albanian Flora and Fauna. Ministry of Tourism and Environment. Tirana, Albania.

Tzonev, R., et al. 2019. Vegetation diversity and habitat classification in the Balkans.

Whigham, D. F. 2004. Ecology of woodland herbs in temperate deciduous forests. Annual Review of Ecology, Evolution, and Systematics. 35: 583–621

HABITAT-BASED ANALYSIS OF SPECIES DIVERSITY IN DIVJAKË–KARAVASTA NATIONAL PARK

Doriana (Bode) XHULAJ[1], Enea MALAJ[2], Adelajda HALILI[3]*

[1]Agricultural University of Tirana, Faculty of Environment and Agriculture, Department of Agronomic Sciences, Tirana, Albania;
[2]Agricultural University of Tirana, Faculty of Forest Sciences, Forest Department, Tirana, Albania;
[3]Polytechnic University of Tirana, Faculty of Geology and Mining, Department of Mineral Resources Engineering, Tirana, Albania.

Corresponding author email: dbode@ubt.edu.al

ABSTRACT

The objective of this research was to assess the tree species diversity, structure, and composition within two different habitats of Divjakë-Karavasta National Park. Thirty-five circular sampling plots (0.1 ha each; radius 11.28 m) were established to characterize the tree communities within the study area. In total, 2,336 trees were inventoried. The Kulari (Argjinatura Shkumbin) forest contained 45 plant taxa distributed among 11 orders, 15 families, 19 genera, and 22 species, whereas the Gjeneruka forest comprised 31 taxa representing 8 orders, 10 families, 13 genera, and the same number of species (22). Analysis of the 15 sampling plots in the first forest habitat showed that the four most abundant tree species *Populus alba* L., *Ulmus campestris* L., *Cornus mas* L., and *Phillyrea latifolia* L. accounted for 57.41% of the total tree abundance. In the second forest habitat, based on data from 20 sampling plots, *Carpinus orientalis* Mill. was the dominant species, exhibiting the highest relative density (33%). It was followed by three members of the Fagaceae family: *Quercus cerris* L., *Quercus frainetto* Ten., and *Quercus robur* L. Differences in forest structure were examined through analyses of tree height and diameter-class distributions. Spatial variation in tree diversity was mapped in ArcGIS 10.5 using the Shannon, Simpson, and Species Richness indices. The results reveal distinct patterns of species diversity and stand structure between the two habitats, providing ecological evidence that can support biodiversity conservation, habitat management, and long-term monitoring within Divjakë–Karavasta National Park and other protected landscapes in Albania.

Keywords: Tree species, Habitat, Ecological diversity, Composition, Forest structure

INTRODUCTION

The Divjakë–Karavasta National Park region is home to the most significant and diverse ecosystem in Albania, offering great value in terms of biodiversity. It is recognized for its stunning natural scenery, wide variety of species, as well as its traditional economic practices and appeal as a tourist destination (Xhulaj et al. 2026). Evaluating the variety of tree species, their makeup, and the structure of forests in the habitats of the Divjakë–Karavasta National Park is important for understanding how the ecosystem functions and for effectively managing conservation efforts. These assessments offer valuable information about the ecological condition, ability to recover from disturbances, and the natural development processes of forest communities.

Comparative analysis of forest ecosystems is an essential approach for evaluating biodiversity, community composition, and ecological stability across different forest types. Ecological

indices are widely used to quantify species diversity, richness, evenness, dominance, and similarity, providing valuable information for biodiversity assessment and forest management. In recent years, these traditional ecological indices have increasingly been integrated with multivariate statistical techniques such as Pearson correlation and Principal Component Analysis (PCA) to better understand the relationships among ecological variables and the environmental factors driving forest ecosystem variation.

Lakićević and Srđević (2018) investigated the application of biodiversity indices in forest communities by comparing four forest ecosystems using the Shannon–Wiener, Simpson, Margalef, Berger–Parker, and Jaccard indices. The authors concluded that using multiple ecological indices provides a more comprehensive assessment of forest biodiversity than relying on a single measure (Lakićević & Srđević, 2018). Similarly, Stamin and Cosmulescu (2025) assessed vegetation diversity in three temperate forest ecosystems in southern Romania using a wider range of biodiversity indices. Statistical comparisons showed that larger forest ecosystems generally supported higher biodiversity, while variations in species distribution affected community evenness and dominance. The authors emphasized that combining several ecological indices provides a more accurate representation of forest ecosystem diversity and offers valuable information for conservation planning and sustainable forest management.

Although biodiversity indices quantify ecological diversity, they do not explain the relationships among ecological variables. Therefore, many recent studies (Sheng et al., 2024) have incorporated Pearson correlation analysis to evaluate associations between biodiversity indices and environmental factors. Likewise, Norbu et al. (2026) analyzed woody plant diversity in *Betula platyphylla* forests on the southeastern Tibetan Plateau using Pearson correlation to examine relationships among biodiversity indices, elevation, and soil characteristics.

To complement correlation analysis, researchers increasingly use Principal Component Analysis (PCA) to summarize complex ecological datasets and identify the principal environmental gradients influencing forest ecosystems. PCA reduces numerous correlated variables into a small number of independent principal components, facilitating interpretation of ecological variation among forest communities. Song et al. (2021) used PCA to investigate environmental factors affecting tree species abundance and richness in a subtropical forest. Pearson correlation analysis was also applied to evaluate relationships among environmental variables, demonstrating how PCA and correlation analysis complement one another in ecological research (Song et al., 2021). Similarly, Zhang et al. (2025) applied PCA in a forest health assessment study to reduce numerous forest health indicators into a smaller number of principal components before conducting classification analyses. Furthermore, Wang et al. (2025) integrated biodiversity indices, Pearson correlation, and PCA to investigate biomass accumulation and environmental adaptability in naturally regenerating subtropical forests. The combined analytical approach provided a comprehensive understanding of the ecological processes governing forest ecosystem development (Wang et al., 2025).

Ecological indices remain fundamental tools for comparative analysis of forest ecosystems by quantifying species richness, diversity, evenness, dominance, and community similarity. However, integrating these indices with Pearson correlation and PCA provides a more comprehensive understanding of forest ecosystem dynamics. Pearson correlation identifies significant relationships among biodiversity and environmental variables, whereas PCA reveals the principal ecological gradients responsible for variation among forest communities. Together, these methods offer a robust framework for comparing forest ecosystems, identifying biodiversity drivers, and supporting evidence-based conservation and sustainable forest management. The findings of our study will support managers in evaluating the conservation measures applied within these forest ecosystems in the protected area.

MATERIAL AND METHOD

Study area: The study took place in two distinct areas within Divjakë-Karavasta National Park: Habitat 1, referred to as the Kulari forest, which is part of the Argjinatura Shkumbin Economic Unit, and Habitat 2, known as the Gjeneruka forest. Divjakë-Karavasta National Park is a protected region located along the coastline of Albania. The park spans latitudes from 40° to 55° N and longitudes from 19° to 29° E.
Data collection: The ecological data were collected during the spring of 2024 to 2025 in two forest areas within the Divjakë-Karavasta National Park. Randomly selected plots were chosen based on a GIS method, focusing on regions with at least 70% tree coverage. Using a systematic approach, the center of each plot was placed at the intersection of a 100 by 100 meter grid. A total of thirty-five circular plots, each with a radius of 11.28 meters (equivalent to 0.1 hectares), were established.
Data analysis: A series of tree species composition indices, including the Shannon index (H') (Shannon, 1948), a unique measure of evenness (J') by index standardization Shannon (Elliot et. al., 1997), species richness (DMn), (Magurran, 2004) the Simpson index (D) (Simpson, 1949), the Berger-Parker index (d) (Berger & Parker, 1970), and the Clark-Evans (R) (Clark & Evans, 1954), were computed for this study in order to investigate the heterogeneity in the composition of the communities under study. The structural composition of trees was analyzed by comparing the tree height distribution and diameter classes. We used the geospatial tools in ArcGIS 10.5 to evaluate the diversity of tree species spatially by using ecological indices (e.g., Shannon, Simpson, Species Richness) and MVSP - Version 3.22 for other statistical analyses.

RESULTS AND DISCUSSIONS

Biodiversity indices provide complementary measures of community composition by assessing species diversity, richness, dominance, and spatial organization, offering a comprehensive assessment of ecological conditions (Magurran, 2004; Krebs, 1999). The biodiversity assessment of the 35 sampling plots revealed notable differences between Habitat 1 (Kulari forest) and Habitat 2 (Gjeneruka forest) in species diversity, richness, dominance, and spatial distribution. Descriptive statistics indicate that Habitat 1 generally exhibited greater biodiversity and a more stable community structure than Habitat 2.
Field observations across 15 plots in our Habitat 1 (Kulari forest) identified 45 plant taxa, comprising 11 orders, 19 genera, 15 families, 22 species, and 674 individuals. Among these, *Populus alba* L. accounted for 20.91% across 12 plots; *Ulmus campestris* L. and *Cornus mas* L. were present in all 11 plots, totaling 13.5%; and *Phillyrea latifolia* L. was present in 6 plots, totaling 9.5%. These three tree species were the most prevalent in the area. The mean stand density was 44.93 individuals ha^{-1}. In all 15 study plots, the number of tree species per unit area decreased as the tree trunk size increased. Based on the distribution of trunk sizes, the largest group of trees (79.67%) had a trunk diameter between 2 and 22 centimeters at breast height. The next largest group (13.2%) had diameters ranging from 26 to 46 centimeters, while the smallest group (4.89%) had diameters between 46 and 62 centimeters.
Field data from the 20 plots in Habitat 2 (Gjeneruka forest) of the Divjakë-Karavasta National Park indicate the presence of 10 families, consisting of 13 genera and a total of 22 species. The plots are predominantly characterized by the three principal families, Pinaceae, Corylaceae, and Fagaceae, accounting for 81.82% of the total, with 1360 individuals. In the plots taken in this habitat, the species presented an abundant status with a higher relative density at 33% for *Carpinus orientalis* Mill., followed by three species of the Fagaceae family (*Quercus cerris* L.; *Quercus frainetto* Ten. and *Quercus robur* L.). The average stand density was 75.54 trees per hectare, which suggests a forest that is moderately stocked, not too thin and not too dense. When

looking at the distribution of tree sizes across all 20 sampling plots, most of the trees—78.88% or 1311 trees—fell into the category of having a diameter at breast height (DBH) less than 10 cm. On the other hand, only a small percentage, 4.15% or 69 trees, had a DBH of 20 cm or more. The remaining trees, which made up 16.97% or 282 trees, had a DBH between 10 and 20 cm.

The Shannon diversity index considers both the variety of species and their relative abundance, making it one of the most widely utilized metrics for assessing community diversity. Because it indicates not just a rise in the number of species but also a more uniform distribution of individuals among those species, a higher value signifies greater diversity (Shannon & Weaver, 1949; Magurran, 2004). Habitat 1 had a higher maximum Shannon diversity (2.499) than Habitat 2 (2.245); the mean Shannon index was also higher in Habitat 1 (1.372) than in Habitat 2 (1.194), indicating that Habitat 1 generally supported a more diverse biological community. Although both habitats included plots with low diversity, Habitat 2 had a minimum value of zero, implying that at least one plot had no species diversity or was dominated by a single species (Table 1).

Table 1. Data analysis of the tree inventory of the two forest habitats inside Divjakë-Karavasta National Park

Diversity index/ 35 plots	Shannon H' value		Evenness J' value		Richness DMn value		Simpson D value		Berger-Parker d value		Clark-Evans R-value	
	Habitat 1	Habitat 2	Habitat 1	Habitat 2	Habitat 1	Habitat 2	Habitat 1	Habitat 2	Habitat 1	Habitat 2	Habitat 1	Habitat 2
	2.499	2.244	0.808	0.726	0.847	0.539	0.9	0.841	0.209	0.327	4.361	5.957
Average	1.372	1.194	0.793	0.672	0.941	0.681	0.686	0.591	0.46	0.55	4.886	6.63
Min	0.629	0	0.573	0	0.408	0.132	0.4	0.017	0.232	0.202	3.226	3.65
Max	2.096	2.051	0.952	0.933	1.434	1.376	0.9	0.869	0.777	1	6.303	9.774
Variance	0.169	0.313	0.012	0.055	0.11	0.093	0.015	0.059	0.019	0.052	1.098	3.516
Standard deviation	0.411	0.559	0.113	0.235	0.332	0.306	0.124	0.243	0.139	0.228	1.047	1.875
Coefficient of variation	29.98	46.87	14.29	34.95	35.27	44.91	18.14	41.24	30.4	41.54	21.44	28.28

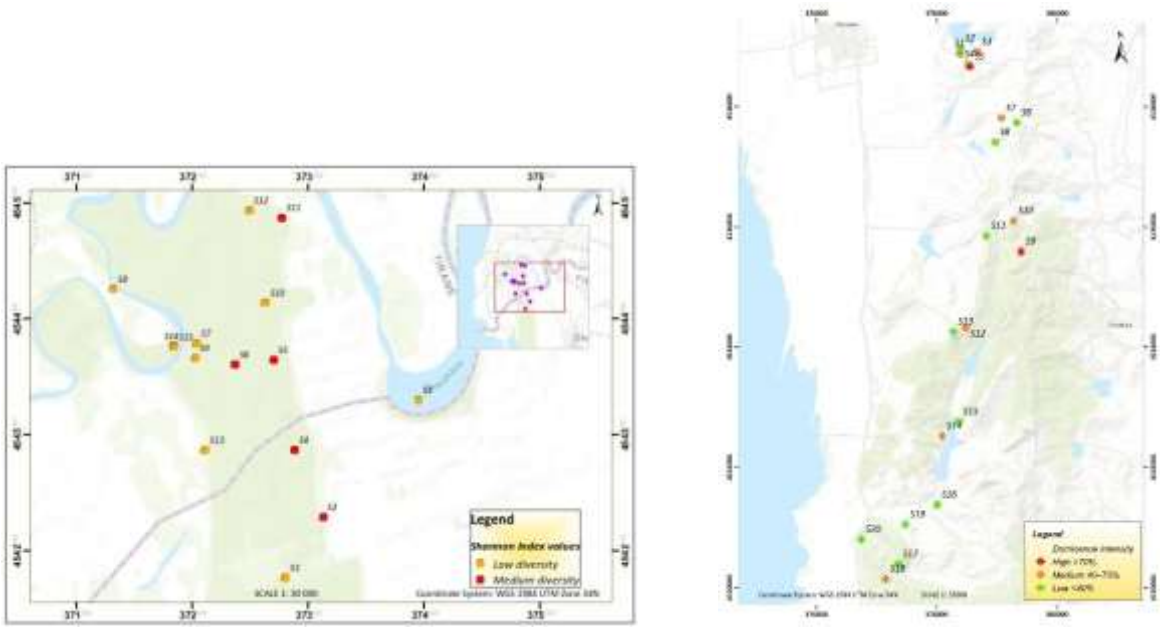

(b)

Figure 1. Mapping species diversity using Shannon Index values (a) Habitat 1(the Kulari forest) and (b) Habitat 2 (the Gjeneruka forest)

Shannon diversity showed much greater variability in Habitat 2, as evidenced by its higher variance (0.313) and standard deviation (0.560) compared with Habitat 1 (variance = 0.169; standard deviation = 0.411). Moreover, the coefficient of variation in Habitat 2 (46.88%) was greater than that in Habitat 1 (29.98%), indicating that species diversity was less consistent across plots in Habitat 2.

The Evenness Index (J') assesses how evenly individuals are distributed among species. Values close to one suggest a very equitable distribution of individuals, while lower values reflect dominance by only a few species (Pielou, 1966; Krebs, 1999).

Habitat 1 showed greater species evenness, with an average of 0.793 compared with 0.673 in Habitat 2. The maximum evenness values were similarly high in both habitats (0.952 and 0.934), indicating that some plots in each habitat had nearly equal species abundances. However, Habitat 2 again recorded a minimum value of zero, suggesting complete dominance by a single species in certain plots. Habitat 2 also exhibited greater variability (CV = 34.96%) than Habitat 1 (CV = 14.29%), indicating that the distribution of individuals among species was much less consistent.

These results indicate that species were more evenly distributed in Habitat 1, whereas Habitat 2 exhibited greater fluctuations in species dominance (Pielou, 1966; Magurran, 2004).

Species richness is the simplest measure of biodiversity and indicates the number of species in a community. Higher richness generally reflects greater habitat complexity and ecological suitability, although richness alone does not account for species abundances (Margalef, 1958; Magurran, 2004).

Habitat 1 recorded a higher average richness (0.941) than Habitat 2 (0.682). Although both habitats reached similar maximum richness values (1.434 and 1.376), Habitat 2 had a much lower minimum richness (0.132) than Habitat 1 (0.408). The coefficient of variation for richness was also higher in Habitat 2 (44.92%) than in Habitat 1 (35.27%), suggesting greater heterogeneity in species composition among plots. These findings indicate that Habitat 1 generally supported more species than Habitat 2, suggesting more favorable ecological conditions.

The Simpson Diversity Index (D) quantifies the probability that two individuals randomly selected from a community belong to different species. A higher value usually suggests higher diversity, as it means the community is not mainly composed of just one or a few species (Simpson, 1949; Krebs, 1999).

Habitat 1 exhibited a higher average Simpson index (0.686) than Habitat 2 (0.591), indicating greater species diversity. The maximum value was also higher in Habitat 1 (0.900) than in Habitat 2 (0.841). The lower minimum Simpson value in Habitat 2 (0.017) compared with Habitat 1 (0.400) suggests that some Habitat 2 plots were highly dominated by one or very few species. The greater variance, standard deviation, and coefficient of variation observed in Habitat 2 indicate less stable diversity across sampling plots. Overall, Simpson's index supports the conclusion that Habitat 1 possessed greater biodiversity and a more balanced community structure.

Berger–Parker Dominance Index (d) is used to measure the relative abundance of the most frequently occurring species within a community. A smaller value suggests less dominance by a single species and more variety among the species present, while a larger value shows that one species makes up a large share of the total population (Berger & Parker, 1970; Magurran, 2004).

Habitat 1 had a lower average dominance value (0.460) than Habitat 2 (0.551), indicating that no single species dominated most plots in Habitat 1. Conversely, Habitat 2's higher value suggests stronger dominance by one or a few species. Habitat 2 also reached the maximum possible value of 1.0, indicating complete dominance by a single species in at least one

sampling plot. Habitat 1 had a lower maximum dominance value of 0.777. Additionally, Habitat 2 exhibited greater variability (CV = 41.55%) than Habitat 1 (30.40%), indicating inconsistent patterns of species dominance across plots. These findings indicate that Habitat 2 had greater ecological dominance, which generally corresponds to lower community diversity.

The Clark–Evans index evaluates the spatial distribution of individuals within a population. Values greater than one indicate a regular (uniform) distribution, values close to one indicate a random distribution, and values below one indicate clustering (Clark & Evans, 1954). Both habitats showed R-values significantly higher than one, with averages of 4.886 in Habitat 1 and 6.630 in Habitat 2. This suggests that individuals were evenly distributed across both habitats rather than grouped together. Habitat 2 showed a higher average R-value, suggesting a stronger tendency toward uniform spacing of individuals. However, Habitat 2 also displayed greater variability (SD = 1.875; CV = 28.28%) than Habitat 1 (SD = 1.047; CV = 21.44%), indicating less consistency in spatial patterns among plots. The uniformly spaced distributions observed in both habitats may reflect competition among individuals or environmental factors promoting regular spacing (Clark & Evans, 1954; Krebs, 1999).

Results on the Pearson correlation matrix

Shannon diversity showed a very strong positive correlation with Simpson diversity (SDI) (r = 0.948), indicating that plots with higher Shannon diversity also tended to have higher Simpson diversity (Table 2). This is expected because both indices measure species diversity, though they differ in their sensitivity to rare and common species.

Shannon diversity was also strongly positively correlated with Margalef richness (DMn) (r = 0.782) and evenness (J′) (r = 0.758). These relationships indicate that increases in species richness and more equitable species distributions are associated with higher overall diversity. Conversely, Shannon diversity exhibited a very strong negative correlation with Berger–Parker dominance (r = −0.917), indicating that communities dominated by a single species tend to have substantially lower overall diversity. Only a weak positive correlation was observed between Shannon diversity and the Clark–Evans index (r = 0.344), suggesting that spatial distribution has only a limited association with species diversity.

Table 2. Pearson Correlation Matrix

Variables	H′	J′	DMn	SDI	d	R
H′ (Shannon)	1.000	0.758	0.782	0.948	-0.917	0.344
J′ (Evenness)	0.758	1.000	0.499	0.897	-0.877	-0.003
DMn (Margalef Richness)	0.782	0.499	1.000	0.712	-0.645	-0.133
SDI (Simpson Diversity)	0.948	0.897	0.712	1.000	-0.959	0.214
d (Berger–Parker)	-0.917	-0.877	-0.645	-0.959	1.000	-0.230
R (Clark–Evans)	0.344	-0.003	-0.133	0.214	-0.230	1.000

Evenness demonstrated a very strong positive correlation with Simpson diversity (r = 0.897), indicating that communities in which individuals are distributed more equally among species also exhibit greater diversity. The relationship between evenness and Margalef richness was moderate (r = 0.499), suggesting that the number of species alone does not necessarily determine how evenly individuals are distributed.

Evenness was strongly negatively correlated with Berger–Parker dominance (r = −0.877), confirming that dominance by a single species reduces the equitable distribution of individuals. The correlation between evenness and Clark–Evans R was essentially zero (r = −0.003), indicating no meaningful relationship between spatial pattern and species evenness.

Margalef Richness (DMn) exhibited a strong positive correlation with Simpson diversity (r = 0.712), indicating that plots containing more species generally possess higher overall diversity.

Richness showed a moderately strong negative correlation with Berger–Parker dominance (r = −0.645), suggesting that communities with greater numbers of species tend to be less dominated by a single species.

Simpson diversity exhibited the strongest negative correlation with Berger–Parker dominance (r = −0.959). This nearly perfect inverse relationship indicates that increases in species dominance are associated with substantial reductions in overall diversity. The weak positive relationship between Simpson diversity and Clark–Evans R (r = 0.214) suggests that spatial regularity has only a minor influence on species diversity.

Berger–Parker dominance showed a weak negative correlation with Clark–Evans R (r = −0.230). This indicates that communities with greater dominance by a single species are only slightly less likely to exhibit regular spatial distributions, and the association is relatively weak.

Results on PCA analysis

Principal Component Analysis (PCA) was conducted using six biodiversity indices (Shannon diversity, Pielou's evenness, Margalef richness, Simpson diversity, Berger–Parker dominance, and Clark–Evans R) measured across 35 sampling plots (Table 3). The first principal component (PC1) represents an overall biodiversity gradient, characterized by positive contributions from Shannon diversity, Simpson diversity, species richness, and evenness, and a strong negative contribution from Berger–Parker dominance. This indicates that plots with greater species diversity and more even communities are associated with lower species dominance. The second principal component (PC2) is associated primarily with the Clark–Evans R index, reflecting variation in the spatial arrangement of individuals that is largely independent of community diversity. Together, the PCA distinguish plots according to both community composition and spatial structure, providing an integrated assessment of biodiversity patterns among the sampling sites.

Table 3. Principal Component Analysis (PCA) based on data of the biodiversity indices

Principal Component	Eigenvalue	Variance Explained (%)	Cumulative (%)
PC1	4.382	**70.94**	70.94
PC2	1.149	**18.6**	89.55
PC3	0.551	8.92	98.47
PC4	0.062	1.01	99.47
PC5	0.017	0.27	99.75
PC6	0.016	0.25	100

Principal Component 1 (PC1) accounted for 70.94% of the total variance and represents a biodiversity gradient (Figure 4). Shannon diversity, Simpson diversity, Pielou's evenness, and Margalef richness all loaded positively on PC1, whereas Berger–Parker dominance loaded strongly in the opposite direction. This indicates that plots with higher diversity, greater species richness, and more even communities are associated with lower species dominance. Thus, PC1 distinguishes biologically diverse communities from communities dominated by one or a few species.

Principal Component 2 (PC2) explained an additional 18.60% of the total variance and was dominated by the Clark–Evans R index (loading = 0.918). This indicates that PC2 primarily represents spatial organization rather than species diversity. Because the biodiversity indices had relatively small loadings on PC2, spatial distribution appears to vary largely independently of diversity and dominance.

According to the Kaiser criterion (eigenvalues > 1), only PC1 and PC2 should be retained. Together they explain 89.55% of the total variance, indicating that the six biodiversity indices

can be summarized effectively by two ecological gradients: (1) community diversity versus dominance and (2) spatial distribution (Figure 3).

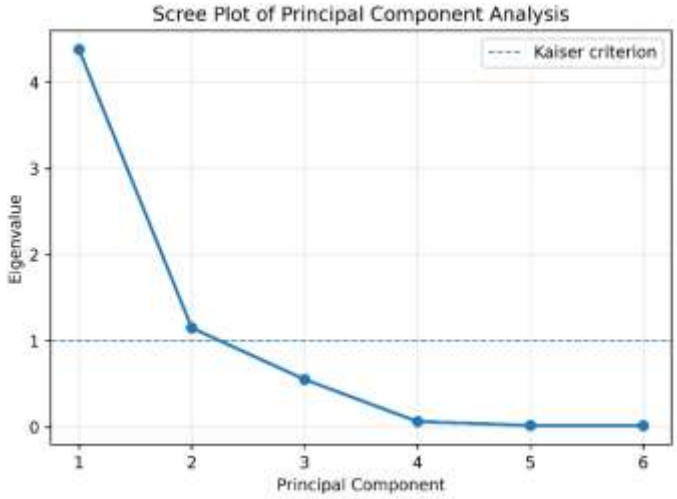

Figure 3. Scree plot showing the eigenvalues of the six principal components derived from the biodiversity indices

These PCA results agree with our Pearson correlation analysis. Shannon diversity, Simpson diversity, evenness, and richness are positively associated with one another, whereas Berger–Parker dominance is negatively associated with these indices. Clark–Evans R forms a largely independent dimension, reflecting spatial pattern rather than biodiversity. Habitat 1 (S1–S15) is expected to cluster toward the positive side of PC1 (Figure 4) because of generally higher diversity and lower dominance. Habitat 2 (S16–S35) is expected to show greater spread and include several plots associated with higher dominance (e.g., S16, S19, S25, S31).

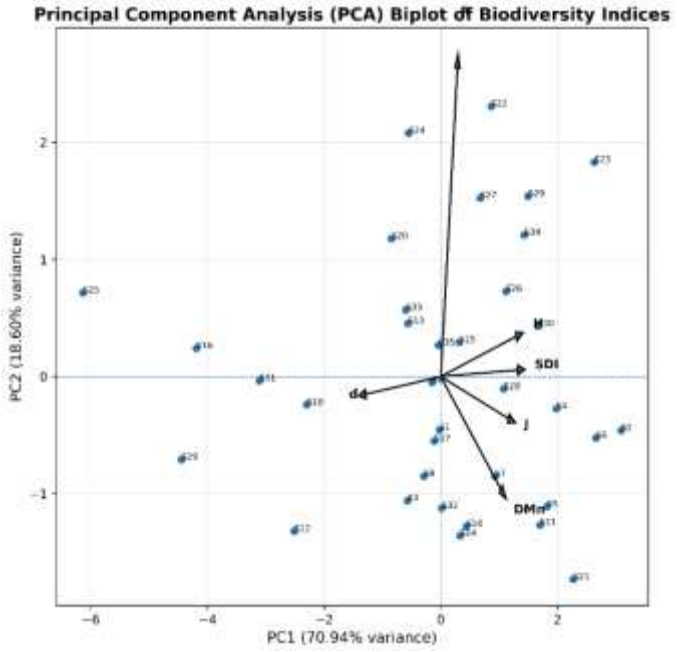

Figure 4. PCA biplot visualizes the relationships among six ecological indices within the two forest habitats inside Divjakë-Karavasta National Park

The first two principal components accounted for 89.55% of the total variation in the dataset, indicating that they captured the vast majority of the information contained in the six biodiversity indices. This high cumulative percentage demonstrates that the multidimensional variation among the sampling plots can be effectively summarized using only two principal components. Consequently, the remaining principal components contributed relatively little additional information, supporting the use of the first two components for interpreting the major ecological gradients and relationships among the biodiversity indices.

CONCLUSION

Analysis of species composition revealed clear differences in dominance patterns between the two forest habitats. In the first forest habitat, based on 15 sampling plots, the four most abundant tree species *Populus alba* L., *Ulmus campestris* L., *Cornus mas L.*, and *Phillyrea latifolia* L. collectively accounted for 57.41% of the total tree abundance. In contrast, the second forest habitat, represented by 20 sampling plots, was strongly dominated by *Carpinus orientalis* Mill., which exhibited the highest relative density (33%). This species was followed in abundance by three representatives of the Fagaceae family, *Quercus cerris* L., *Quercus frainetto* Ten., and *Quercus robur* L., indicating a distinct compositional structure compared with the first habitat.
The comparison between Habitat 1 and Habitat 2 of the Divjakë-Karavasta National Park revealed distinct differences in biodiversity and community structure. Overall, Habitat 1 exhibited higher diversity, species richness, and evenness, indicating a more balanced and heterogeneous biological community. In contrast, Habitat 2 showed greater variability among sampling plots and included several plots with higher Berger–Parker dominance values, suggesting that some communities were characterized by the dominance of one or a few species.
The Pearson correlation analysis demonstrated that Shannon diversity, Simpson diversity, species richness, and evenness were strongly and positively related in both habitats, whereas Berger–Parker dominance was negatively associated with these indices. This indicates that increases in species richness and evenness were consistently accompanied by higher biodiversity, while greater species dominance reduced overall community diversity. The Clark–Evans R index showed weak relationships with the diversity indices, suggesting that spatial distribution was largely independent of biodiversity patterns.
Principal Component Analysis supported these findings by showing that the first two principal components explained 89.55% of the total variation. The first principal component represented a gradient from communities with high diversity, richness, and evenness to those with high species dominance, while the second component reflected differences in spatial distribution. The PCA further indicated that Habitat 1 plots were generally associated with higher biodiversity values, whereas Habitat 2 exhibited a broader range of ecological conditions.
Overall, the results suggest that Habitat 1 provides more favorable conditions for maintaining diverse and evenly distributed biological communities, while Habitat 2 is more heterogeneous and contains areas where species dominance is more pronounced. These findings provide a valuable baseline for future biodiversity monitoring and can help guide habitat conservation and management strategies.

REFERENCES

Berger, W. H., F. L. Parker. 1970. Diversity of planktonic Foraminifera in deep-sea sediments. Science. 168(3937): 1345–1347.

Clark, P. J., F. C. Evans. 1954. Distance to nearest neighbor as a measure of spatial relationships in populations. Ecology. 35(4): 445–453.

Elliot, A. J., M. A. Church. 1997. A hierarchical model of approach and avoidance achievement motivation. Journal of Personality and Social Psychology. 72(1): 218–232.

Krebs, C. J. 1999. Ecological Methodology. 2nd Edition. Benjamin Cummings. 620 pages.

Lakićević, M., B. Srđević. 2018. Measuring biodiversity in forest communities: A role of biodiversity indices. Contemporary Agriculture. 67(1): 1–10.

Li, X., et al. 2025. Environmental filtering and dispersal limitation jointly shape the taxonomic, functional and phylogenetic diversity in a subtropical karst forest of China. Frontiers in Plant Science.

Magurran, A. E. 2004. Measuring Biological Diversity. Blackwell Publishing. Oxford, UK. 256 pages.

Margalef, R. 1958. Information theory in ecology. General Systems. 3: 36–71.

MVSP - A MultiVariate Statistical Package for Windows. Version 3.22. Kovach Computing Services. 2007. Available at: www.kovcomp.co.uk/mvsp/.

Norbu, T., et al. 2026. Woody plant diversity and community structure along elevational and soil gradients in *Betula platyphylla* forests, southeastern Tibetan Plateau. Ecology and Evolution.

Odum, E. P., G. W. Barrett. 2005. Fundamentals of Ecology. 5th Edition. Brooks/Cole. Belmont, California. 598 pages.

Pielou, E. C. 1966. The measurement of diversity in different types of biological collections. Journal of Theoretical Biology. 13: 131–144.

Shannon, C. E. 1948. A mathematical theory of communication. Bell System Technical Journal. 27: 379–423.

Sheng, Q., et al. 2024. Driving forces of herbaceous species diversity in natural broadleaf forests in Maoershan, Northeast China. Frontiers in Plant Science. 15.

Simpson, E. H. 1949. Measurement of diversity. Nature. 163: 688.

Song, X., et al. 2021. Disentangling environmental effects on the tree species abundance distribution and richness in a subtropical forest. Forests.

Stamin, F. D., S. Cosmulescu. 2025. Assessing the vegetation diversity of different forest ecosystems in southern Romania using biodiversity indices and similarity coefficients. Biology. 14(7): 869.

Wang, Y., et al. 2025. The synergistic effect of species diversity and functional diversity in subtropical naturally regenerating forests promotes environmental adaptability of biomass accumulation. Forest Ecosystems.

Xhulaj (Bode), D., E. Malaj, A. Halili. 2026. Biodiversity beneath the canopy: Understanding forest structure inside a protected area. Agriculture and Forestry. 72(2): 75–87. https://doi.org/10.17707/AgricultForest.72.2.05

Zhang, Y., et al. 2025. A data-driven approach to forest health assessment through multivariate analysis and machine learning techniques. Ecological Informatics.

CHANGES IN THE CONTENT OF LACTOSE AND FREE AMINO ACIDS DURING THE RIPENING OF SALTED CHEESE

Eva Ceka[1], Ida Kruti[2]

[1] Qiriazi University College, Professional Higher College in Food Technology, Tirana, 1001, Albania
eva.ceka@qiriazi.edu.al, https://orcid.org/0009-0009-4719-0941

[2] Qiriazi University College, Faculty of Education, Social Sciences and Sports, Tirana, 1001, Albania
ida.kruti@qiriazi.edu.al, https://orcid.org/0009-0009-7929-9722

Corresponding author e-mail: eva.ceka@qiriazi.edu.al

ABSTRACT

This study examined the changes in lactose content and free amino acid (FAA) levels during the ripening of cow's milk cheese treated with 20% brine (14–16 °C, 24 h). Two cheese variants were prepared from pasteurised cow's milk (3.8% fat): one coagulated with chymosin only (DLK) and one with chymosin supplemented with a microbial starter culture (DLK-S). Cheese samples were stored at 14–15 °C and analysed on days 12, 22 and 32 of ripening for moisture, pH, titratable acidity, sodium chloride, lactose and free amino acids. In the chymosin-only variant (DLK), the lactose content decreased gradually on days 12, 22 and 32. The FAA content remained low and essentially unchanged indicating that lactic acid bacteria originating from the milk alone exerted limited lactose-metabolising and proteolytic activity during the 32-day ripening period. By contrast, the starter-supplemented variant (DLK-S) showed a marked acceleration in both processes: lactose declined on day 12 and fell below the detection limit by day 32, while FAA levels increased steadily. A positive correlation between lactic acid production and lactose consumption was observed in both variants. These results confirm that the addition of a microbial starter culture to brine-salted cheese markedly enhances lactose catabolism and proteolysis during ripening. While the indigenous lactic acid bacteria in DLK maintained only a basal level of metabolic activity, the defined starter in DLK-S drove lactose to exhaustion by day 32 and produced FAA levels approximately five times higher than those in the chymosin-only cheese. The findings highlight the essential role of starter cultures in the development of flavour and aroma compounds in salted cheese during extended ripening.

Keywords: cheese ripening, salted cheese, brine treatment, lactose metabolism, free amino acids, proteolysis, starter culture, chymosin, cow's milk

INTRODUCTION

The application of salt to cheese curd is one of the most universal steps in cheese manufacture. Salt contributes directly to flavour, inhibits spoilage and pathogenic organisms, influences texture, and modulates the activity of ripening enzymes (Fox et al., 2004). This review examines how brine salting affects the metabolism of residual lactose and the proteolytic degradation of casein during cheese ripening, with particular attention to the interaction between salt concentration, starter culture activity and FAA accumulation.

The aim of this study was to investigate the changes in the content of lactose and free amino acids (FAA) during cheese ripening, with particular attention to the effects of two factors: (i)

the addition of a microbial starter culture (commercial yogurt) versus coagulation with chymosin alone omission of a salting treatment. Two cheese variants were produced from pasteurised cow's milk and monitored over their respective ripening periods for a suite of physicochemical indices, including moisture, pH, titratable acidity, sodium chloride, lactose and free amino acid content.

Salting methods and their effect on cheese composition

Brine salting involves immersing pressed cheese in a concentrated NaCl solution, typically 18–22% (w/v), at 10–16 °C for periods ranging from hours to days (Fox et al., 2004). Salt uptake is a diffusion-driven process: NaCl migrates inward while moisture migrates outward, creating a characteristic salt-in-moisture gradient that is highest at the surface and lowest at the centre (Kleter et al., 1984). This gradient has important implications for the spatial distribution of microbial activity and enzymatic ripening within the cheese.

In brine-salted cheeses, the time required for NaCl to reach inhibitory concentrations throughout the cheese is longer than in dry-salted varieties, which has consequences for controlling undesirable fermentations in the interior.

Effect of salt on LAB and lactose fermentation

Sodium chloride inhibits LAB primarily through the reduction of water activity (aw). As NaCl concentration increases, the aw decreases, creating osmotic stress that impairs bacterial growth, reduces sugar transport across the cell membrane, and inhibits glycolytic enzyme activity (Turner and Thomas, 1980). Sensitivity to NaCl varies among LAB species and strains.

At the salt-in-moisture levels typical of semi-hard cheeses (approximately 4–6% S/M), starter LAB growth is slowed but not arrested, and residual lactose is typically fermented to completion within the first weeks of ripening. At higher S/M levels, lactose fermentation may be significantly delayed, providing a potential substrate for late gas-producing organisms (McSweeney and Fox, 2004).

The anaerobic metabolism of lactate by Clostridium tyrobutyricum to butyrate and hydrogen gas known as late gas blowing is particularly associated with brine-salted cheeses in which NaCl has not yet penetrated to inhibitory concentrations (Kleter et al., 1984; Fox et al., 1990). Complete and timely fermentation of residual lactose by the starter culture is therefore an important quality parameter.

Proteolysis in salted cheese

The proteolytic agents in salted cheese are the same as in other cheese types: residual coagulant (chymosin), indigenous milk proteinases (plasmin), and LAB proteinases and peptidases (McSweeney, 2004; Upadhyay et al., 2004). However, their rates are modulated by NaCl.
Chymosin activity is relatively insensitive to NaCl at typical cheese concentrations, although high salt levels may alter the conformation of casein substrates (Fox and McSweeney, 1996b). Plasmin activity has been reported to be stimulated by moderate NaCl in some studies (Bastian and Brown, 1996). LAB peptidases are indirectly affected through salt's impact on cell viability and lysis kinetics, as these intracellular enzymes are released into the cheese matrix upon cell death (Kunji et al., 1996; Upadhyay et al., 2004).
The practical consequence is that salted cheeses exhibit slower FAA accumulation than unsalted equivalents. However, this slower rate allows for a more gradual and balanced development of

flavour compounds over extended ripening, which is characteristic of many valued aged varieties (McSweeney, 2004).

FAA and flavour development in salted cheese

FAA accumulation in salted cheese follows a characteristic pattern: an initial lag phase during which primary proteolysis generates large peptides, followed by a progressive increase as LAB peptidases hydrolyse these intermediates to individual amino acids (McSweeney, 2004). FAA levels may range from a few milligrams to several hundred milligrams per 100 g cheese, depending on the variety and ripening duration (McSweeney and Sousa, 2000).
These free amino acids serve as substrates for secondary catabolic reactions transamination, decarboxylation, deamination that produce volatile flavour compounds (Yvon and Rijnen, 2001; Curtin and McSweeney, 2004). In cheeses without a defined starter, FAA accumulation is typically much lower, reflecting the limited proteolytic capacity of indigenous NSLAB and the dominance of primary proteolysis by chymosin and plasmin, which generate large peptides but do not efficiently release individual amino acids (Christensen et al., 1999).

MATERIAL AND METHOD

Raw materials

Fresh cow's milk (10 litres) was obtained from a local dairy farm on the day of cheese manufacture. The milk had a fat content of 3.8% (w/w). The coagulant used was commercial bovine chymosin with a clotting strength of 1:10,000. A commercial plain yogurt was used as the source of microbial starter culture, providing a mixed population of lactic acid bacteria (principally Lactobacillus delbrueckii subsp. bulgaricus and Streptococcus thermophilus). All reagents for physicochemical analyses were of analytical grade.

Experimental design

The study employed a 2 × 2 factorial design with two factors: coagulation method (chymosin only vs. chymosin + starter culture) and salting treatment (salted vs. unsalted). This yielded four cheese variants, each designated by a sample code as follows:
- DLK – cheese coagulated with chymosin only, with salt treatment;
- DLK-S – cheese coagulated with chymosin + microbial starter culture, with salt treatment;

The salted variants (DLK and DLK-S) were analysed at three time points during ripening: days 12, 22 and 32.

Cheese manufacture

The 10 liters of milk were divided into two equal batches of 5 liters each. Each batch was used to produce salted variant as described below. The production protocol was identical for both batches up to the pressing step to produce feta cheese, after which the salting treatment was applied.

Salted variants (DLK and DLK-S)

The milk (5 litres, 3.8% fat) was pasteurised using a low-temperature, long-time (LTLT) protocol at 63–65 °C for 30 minutes, followed by rapid cooling to 1–2 °C. After tempering to

30 °C, the milk was divided into two portions. The first portion was coagulated by the addition of chymosin at a dose of 150 mg per 5 litres (strength 1:10,000) at 30 °C for 50–60 minutes to produce the DLK variant. The second portion received both chymosin (same dose) and 30 g of plain yogurt as a source of starter culture, and was coagulated under the same conditions (30 °C, 50–60 minutes) to produce the DLK-S variant.

Following coagulation, syneresis was allowed to proceed at 30 °C. The curd was then pressed under its own weight to facilitate whey expulsion. The pressed curd was immersed in a 20% (w/v) NaCl brine solution at 14–16 °C for 24 hours. After brining, the cheese samples were stored for ripening at 14–15 °C and sampled for analysis on days 12, 22 and 32.

Analytical methods

All physicochemical analyses were performed in duplicate on each cheese sample at the designated ripening time points. The following parameters were determined:

Moisture content

Moisture content was determined gravimetrically by drying a weighed sample in a thermostat oven at 105 °C until a constant weight was achieved (Ardö and Polychroniadou, Cheese Analysis Manual). The result was expressed as a percentage (%, w/w).

pH

The pH of each cheese sample was measured potentiometrically by inserting a calibrated glass electrode directly into the cheese mass at ambient temperature (Ardö and Polychroniadou, Cheese Analysis Manual).

Titratable acidity

Titratable acidity was determined by the potentiometric titration method (Ardö and Polychroniadou, Cheese Analysis Manual) and expressed as a percentage of lactic acid (%, w/w).

Sodium chloride (NaCl)

The NaCl content of the salted cheese samples (DLK and DLK-S) was determined by the Volhard method (Ardö and Polychroniadou, Cheese Analysis Manual) and expressed as a percentage (%, w/w). NaCl analysis was not performed on the unsalted variants (DLKP and DLK-SP), as no salt was added during their manufacture.

Lactose content

Lactose content was determined by the iodimetric method of Fine (1932), as described by James (1998, Analytical Chemistry of Food, Springer Science & Business). The result was expressed as mg lactose per 100 g cheese as shown in chart 1. Where the measured value fell below the sensitivity of the method, the result was reported as below the limit of detection (> LD).

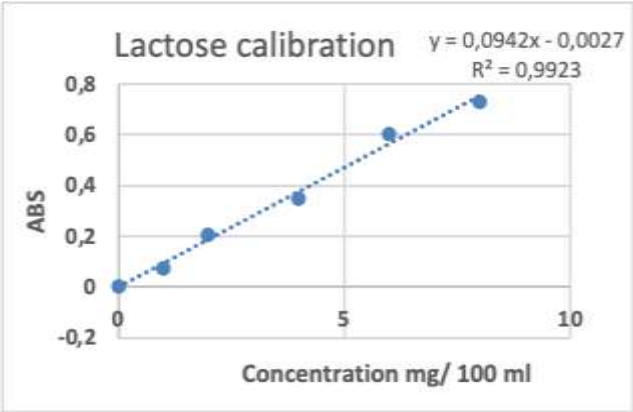

Chart 1. Lactose curbe calibration

Free amino acid (FAA) content

The content of free amino acids was determined spectrophotometrically using a ninhydrin-based colorimetric assay, with L-lysine as the calibration standard (Ardö and Polychroniadou, Cheese Analysis Manual). A calibration curve was constructed by plotting absorbance at 570 nm against known concentrations of L-lysine (µg/100 µl). The FAA content of each cheese sample was calculated from the calibration curve and expressed as mg FAA per 100 g cheese as shown on chart 2.

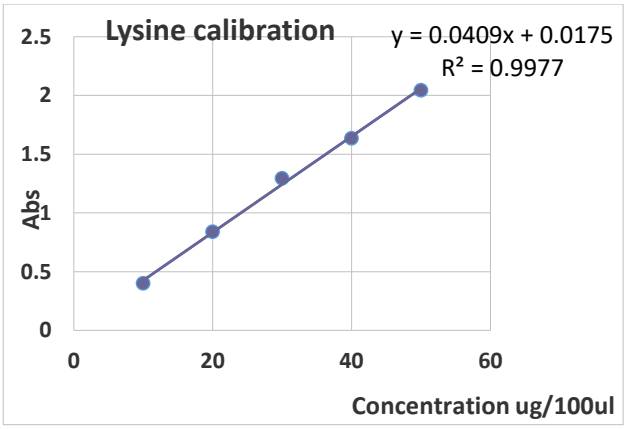

Chart 2. Lysine curbe calibration

RESULTS AND DISCUSSION

This section presents the results of the physicochemical analysis of two salted cheese variants: DLK (chymosin only) and DLK-S (chymosin + starter culture). Both were treated with 20% NaCl brine at 14–16 °C for 24 hours, then stored at 14–15 °C and analysed on days 12, 22 and 32 of ripening.

The chymosin-only salted variant (DLK), the lactose content decreased gradually on days 12, 22 and 32 of ripening, Fig 2. The FAA content remained low throughout. The pH declined slowly, while titratable acidity decreased. Moisture fell, and NaCl in brine stabilised at approximately 19–21%.

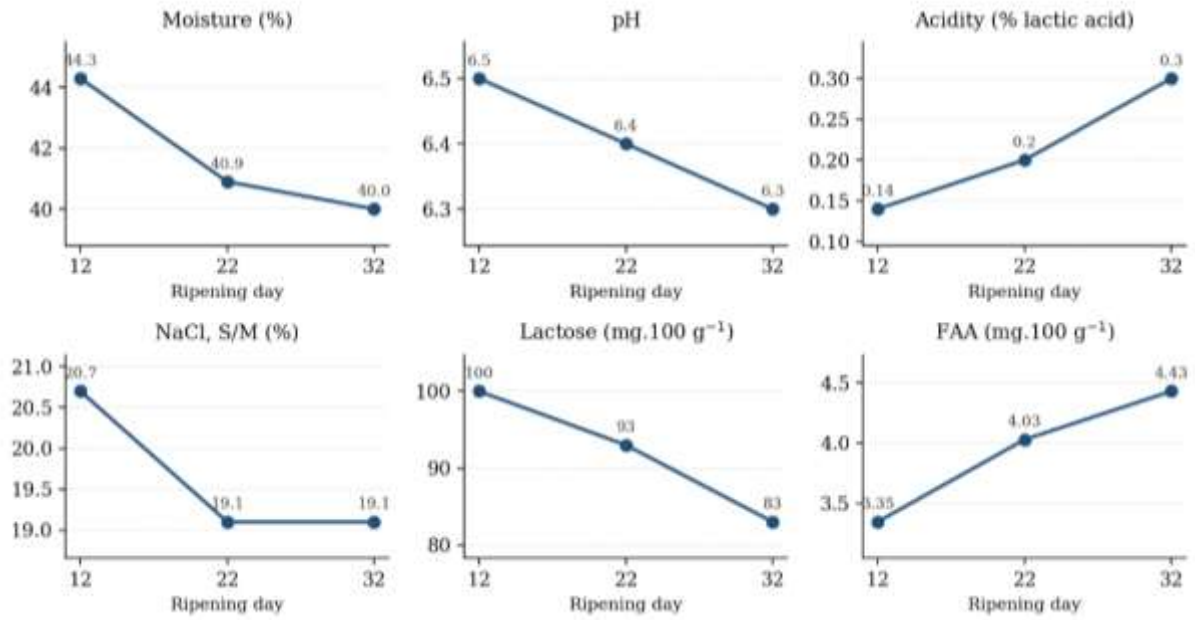

Fig 2. DLK cheese chymosin only, salted, changes during ripening from day 12 to day 32.

These results indicate that the indigenous lactic acid bacteria originating from the pasteurised milk exert limited metabolic activity throughout the 32-day ripening period in the presence of high salt concentrations and without a defined starter culture. The slow decline in lactose and the near-constant FAA levels suggest that the proteolytic activity observed is attributable primarily to the residual chymosin retained in the curd, which hydrolyses αs1-casein at the Phe_{23}–Phe_{24} bond as its primary site of action, and to a lesser extent to indigenous plasmin activity. The low FAA accumulation indicates that the peptidases necessary for the terminal stages of proteolysis are present in insufficient quantities without a starter-derived enzyme complement.

The starter-supplemented salted variant (DLK-S) exhibited a markedly different metabolic profile. Lactose was consumed rapidly and falling below the detection limit by day 32. The pH was substantially lower than in DLK at all time points, reflecting vigorous acid production by the starter LAB. Titratable acidity rose on day 12 to day 22 before stabilising on day 32, consistent with the near-exhaustion of lactose as a fermentable substrate Fig 3.

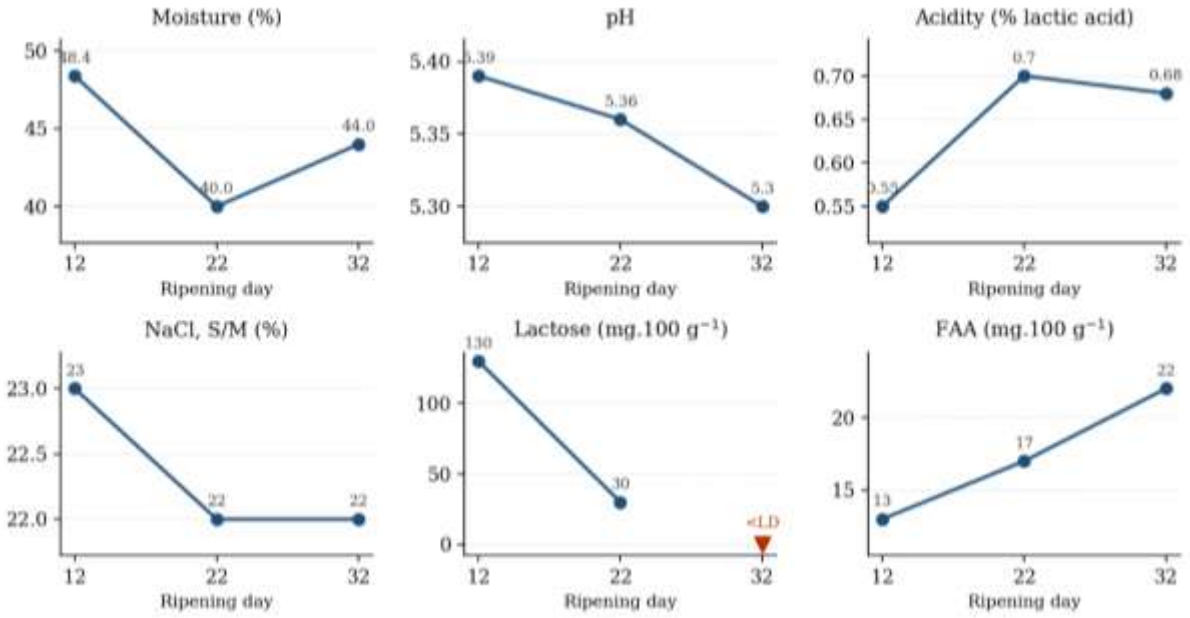

Fig 3. DLK-S cheese chymosin + starter, salted: changes during ripening from day 12 to day 32

The FAA content increased steadily approximately five times higher than in DLK at each corresponding time point. The continuous accumulation demonstrates that the proteolytic enzyme system of the starter LAB comprising cell envelope-associated proteinases and intracellular peptidases released upon cell lysis actively degrades the casein matrix throughout the ripening period.

A positive correlation was observed between lactic acid production and lactose consumption in both variants, confirming that lactose serves as the primary energy source for the LAB and that its fermentation to lactate drives the acidification of the cheese curd.

COMPARATIVE DISCUSSION

The comparison of DLK and DLK-S demonstrates that the addition of a microbial starter culture is the decisive factor in determining both the rate and extent of lactose metabolism and proteolysis in brine-salted cheese. While the indigenous microflora in DLK maintained only basal-level metabolic activity over 32 days, the defined starter in DLK-S drove lactose to exhaustion and produced FAA levels approximately five times higher.

The complete fermentation of residual lactose by day 32 in DLK-S is an important quality parameter, as unfermented lactose can serve as a carbon source for undesirable secondary microflora and contribute to defects during extended ripening. The elevated FAA levels represent a larger pool of substrates for secondary catabolic reactions that generate volatile flavour compounds.

LIMITATIONS

Several limitations should be considered. First, the earliest sampling point was day 12, so the initial phase of lactose fermentation (days 0–12) was not captured. Second, the NaCl values reported (19–23%) represent salt-in-moisture rather than salt-in-cheese; clarification is important as NaCl concentration strongly influences LAB activity. Third, the FAA assay reports total free amino acids using a single method calibrated with L-lysine, without resolving

individual amino acids. Fourth, no sensory evaluation was performed. Fifth, the experiment used a single production batch without biological replicates. Finally, the use of commercial yogurt as a starter precludes attribution of specific activities to defined bacterial strains.

CONCLUSIONS

Brine salting is a critical control point in cheese manufacture, simultaneously contributing to preservation, texture and flavour while modulating ripening biochemistry. Salt inhibits LAB growth and enzymatic activity in a concentration-dependent manner, slowing lactose fermentation and proteolysis. The use of a defined starter culture is essential for ensuring complete lactose fermentation and for providing the proteolytic enzyme complement necessary for sustained FAA release. The interplay between salt concentration, starter activity and ripening duration remains a key area for optimisation in consistent cheese quality production.

REFERENCES

Bastian, E.D. and Brown, R.J. (1996) Plasmin in milk and dairy products. International Dairy Journal, 6, pp. 435–457.

Christensen, J.E., Dudley, E.G., Pederson, J.A. and Steele, J.L. (1999) Peptidases and amino acid catabolism in lactic acid bacteria. Antonie van Leeuwenhoek, 76, pp. 217–246.

Collins, Y.F., McSweeney, P.L.H. and Wilkinson, M.G. (2003b) Lipolysis and free fatty acid catabolism in cheese: a review of current knowledge. International Dairy Journal, 13, pp. 841–866.

Curtin, A.C. and McSweeney, P.L.H. (2004) Catabolism of amino acids in cheese during ripening. In: Fox, P.F., McSweeney, P.L.H., Cogan, T.M. and Guinee, T.P. (eds.) Cheese: Chemistry, Physics and Microbiology, Vol. 1, 3rd edn. London: Elsevier, pp. 435–454.

Fox, P.F. and McSweeney, P.L.H. (1996b) Proteolysis in cheese during ripening. Food Reviews International, 12, pp. 457–509.

Fox, P.F., Lucey, J.A. and Cogan, T.M. (1990) Glycolysis and related reactions during cheese manufacture and ripening. CRC Critical Reviews in Food Science and Nutrition, 29, pp. 237–253.

Fox, P.F., McSweeney, P.L.H., Cogan, T.M. and Guinee, T.P. (eds.) (2004) Cheese: Chemistry, Physics and Microbiology, Vol. 1: General Aspects, 3rd edn. London: Elsevier.

Huffman, L.M. and Kristoffersen, T. (1984) Role of lactose in Cheddar cheese manufacture and ripening. New Zealand Journal of Dairy Science and Technology, 19, pp. 151–162.

Kleter, G., Lammers, W.L. and Vos, E.A. (1984) The influence of pH and concentration of lactic acid and NaCl on the growth of Clostridium tyrobutyricum in whey and cheese. Netherlands Milk and Dairy Journal, 38, pp. 31–41.

Kunji, E.R.S., Mierau, I., Hagting, A., Poolman, B. and Konings, W.N. (1996) The proteolytic system of lactic acid bacteria. Antonie van Leeuwenhoek, 70, pp. 187–221.

Law, J. and Haandrikman, A. (1997) Proteolytic enzymes of lactic acid bacteria. International Dairy Journal, 7, pp. 1–11.

McSweeney, P.L.H. (2004) Biochemistry of cheese ripening: introduction and overview. In: Fox, P.F., McSweeney, P.L.H., Cogan, T.M. and Guinee, T.P. (eds.) Cheese: Chemistry, Physics and Microbiology, Vol. 1, 3rd edn. London: Elsevier, pp. 347–360.

McSweeney, P.L.H. and Fox, P.F. (2004) Metabolism of residual lactose and of lactate and citrate. In: Fox, P.F., McSweeney, P.L.H., Cogan, T.M. and Guinee, T.P. (eds.) Cheese: Chemistry, Physics and Microbiology, Vol. 1, 3rd edn. London: Elsevier, pp. 361–372.

McSweeney, P.L.H. and Sousa, M.J. (2000) Biochemical pathways for the production of flavour compounds in cheese during ripening: a review. Le Lait, 80, pp. 293–324.

McSweeney, P.L.H., Olson, N.F., Fox, P.F., Healy, A. and Højrup, P. (1993) Proteolytic specificity of chymosin on bovine αs1-casein. Journal of Dairy Research, 60, pp. 401–412.

Parente, E. and Cogan, T.M. (2004) Starter cultures: general aspects. In: Fox, P.F., McSweeney, P.L.H., Cogan, T.M. and Guinee, T.P. (eds.) Cheese: Chemistry, Physics and Microbiology, Vol. 1, 3rd edn. London: Elsevier, pp. 123–148.

Smit, G., van Hylckama Vlieg, J.E.T., Smit, B.A., Ayad, E.H.E. and Engels, W.J.M. (2002) Fermentative formation of flavour compounds by lactic acid bacteria. Australian Journal of Dairy Technology, 57, pp. 61–68.

Turner, K.W. and Thomas, T.D. (1980) Lactose fermentation in Cheddar cheese and the effect of salt. New Zealand Journal of Dairy Science and Technology, 15, pp. 265–276.

Upadhyay, V.K., McSweeney, P.L.H., Magboul, A.A.A. and Fox, P.F. (2004) Proteolysis in cheese during ripening. In: Fox, P.F., McSweeney, P.L.H., Cogan, T.M. and Guinee, T.P. (eds.) Cheese: Chemistry, Physics and Microbiology, Vol. 1, 3rd edn. London: Elsevier, pp. 391–434.

Yvon, M. and Rijnen, L. (2001) Cheese flavour formation by amino acid catabolism. International Dairy Journal, 11, pp. 185–201.

CHANGES IN THE CONTENT OF LACTOSE AND FREE AMINO ACIDS DURING THE RIPENING OF UNSALTED CHEESE

Eva Ceka[1], *Ida Kruti*[2]

[1] *Qiriazi University College, Professional Higher College in Food Technology, Tirana, 1001, Albania*
eva.ceka@qiriazi.edu.al, https://orcid.org/0009-0009-4719-0941
[2] *Qiriazi University College, Faculty of Education, Social Sciences and Sports, Tirana, 1001, Albania*
ida.kruti@qiriazi.edu.al, https://orcid.org/0009-0009-7929-9722

Corresponding author e-mail: eva.ceka@qiriazi.edu.al

ABSTRACT

This study investigated the changes in lactose content and free amino acid (FAA) levels during the ripening of cow's milk cheese produced without salt treatment. Two cheese variants were prepared from pasteurised cow's milk (3.8% fat): one coagulated with chymosin only (DLKP) and one with chymosin supplemented with a microbial starter culture (DLK-SP). Cheese samples were stored at 14–15 °C and analysed on days 1, 3 (or 5) and 7 of ripening for moisture, pH, titratable acidity, lactose and free amino acids.
In the chymosin-only variant (DLKP), lactose decreased from 5 and 7, and FAA levels fell over the same period, reflecting limited proteolytic activity in the absence of a defined starter culture. The starter-supplemented variant (DLK-SP) exhibited an accelerated pattern: lactose declined on day 1 to day 3 and fell below the detection limit by day 7, while FAA levels were high, rising on days 1, 3 and 7. The pH of DLK-SP dropped accompanied by an increase in titratable acidity. The results demonstrate that in the absence of salt, the addition of a microbial starter culture stimulates both lactose catabolism and proteolysis from the earliest stages of ripening. The FAA content in the starter-supplemented unsalted cheese (DLK-SP) was higher than in any of the salted variants, indicating that the omission of salt with starter inoculation, creates conditions highly favourable for the enzymatic degradation of caseins and the release of flavour precursors. These findings suggest that unsalted cheese produced with a starter culture develops flavour and aroma compounds more rapidly than its salted counterparts.

Keywords: cheese ripening, unsalted cheese, lactose metabolism, free amino acids, proteolysis, starter culture, chymosin, cow's milk

INTRODUCTION

Cheese is among the most ancient and diverse fermented food products. While many commercial cheeses undergo a salting step, a number of traditional and artisanal varieties are produced with reduced salt or without salt entirely. The biochemical changes that occur during the ripening of unsalted cheese are of particular interest because the absence of sodium chloride removes a major regulatory factor that normally modulates microbial growth and enzymatic activity in the cheese matrix (Fox et al., 2004). This review examines the current understanding of the two principal biochemical events during the ripening of unsalted cheese: the catabolism

of residual lactose by lactic acid bacteria (LAB) and the proteolytic degradation of casein to peptides and free amino acids (FAA). These processes are the primary determinants of flavour and texture development (McSweeney, 2004). The aim of this study was to investigate the changes in the content of lactose and free amino acids (FAA) during cheese ripening, with particular attention to the effects of two factors: (i) the addition of a microbial starter culture (commercial yogurt) versus coagulation with chymosin alone without adding salt.

Residual lactose and its fermentation

During cheese manufacture, most of the lactose in milk is lost in the whey. Nevertheless, a small but significant amount remains in the curd at the end of production, quantified at approximately 0.8–1.0% for Cheddar-type cheeses (Huffman and Kristoffersen, 1984). The complete fermentation of this residual lactose during the early stages of ripening is essential for cheese quality, as unfermented lactose can serve as a carbon source for undesirable organisms such as Clostridium tyrobutyricum, which causes late gas blowing (Fox et al., 1990).

The rate and completeness of lactose fermentation depend primarily on the metabolic activity of the LAB population. In cheeses made with defined starters, organisms such as Lactococcus lactis ferment lactose rapidly to L-lactate via the homofermentative pathway (Parente and Cogan, 2004). Without a defined starter, indigenous non-starter lactic acid bacteria (NSLAB) ferment lactose more slowly and may produce both L- and D-lactate (Turner and Thomas, 1980).

In unsalted cheese, the absence of NaCl-induced osmotic stress allows LAB to grow more rapidly and ferment lactose more completely than in salted counterparts. Salt-in-moisture levels normally exert a significant inhibitory effect on LAB growth rates and metabolic activity (Turner and Thomas, 1980). When this inhibitory factor is removed, residual lactose may be exhausted within days rather than weeks.

Proteolysis: agents and mechanisms

Proteolysis is the most important primary biochemical event during the ripening of most rennet-coagulated cheeses (McSweeney, 2004). It contributes to flavour through the release of short peptides and free amino acids, influences texture through hydrolysis of the casein matrix, and provides substrates for secondary catabolic reactions (Upadhyay et al., 2004).

The residual coagulant most commonly chymosin is responsible for the initial hydrolysis of intact caseins into large and medium-sized peptides, with its primary cleavage sites well characterised (McSweeney et al., 1993). Plasmin, an indigenous serine proteinase associated with the casein micelle, also contributes to primary proteolysis (Bastian and Brown, 1996). The proteinases and peptidases of starter LAB and NSLAB are then responsible for degrading these peptides into short peptides and free amino acids (Kunji et al., 1996; Christensen et al., 1999).

The proteolytic system of Lactococcus comprises the cell envelope-associated proteinase lactocepin, which degrades caseins at the cell surface, and a diverse array of intracellular peptidases aminopeptidases, dipeptidases, tripeptidases and proline-specific peptidases released into the cheese matrix upon cell lysis (Law and Haandrikman, 1997; Upadhyay et al., 2004). These intracellular peptidases are essential for the terminal stages of proteolysis.

Free amino acids as flavour precursors

Free amino acids serve as substrates for secondary catabolic reactions transamination, decarboxylation, deamination and desulfurylation that generate many volatile compounds responsible for cheese aroma (Yvon and Rijnen, 2001; Curtin and McSweeney, 2004). The

catabolism of branched-chain amino acids yields aldehydes and alcohols; aromatic amino acid catabolism produces phenolic compounds; and sulfur-containing amino acid catabolism generates methanethiol and related volatiles that are important to cheese aroma even at very low concentrations (Smit et al., 2002; McSweeney and Sousa, 2000).

Implications for unsalted cheese ripening

In unsalted cheese, uninhibited LAB growth leads to faster lactose fermentation, more vigorous acid production, and more rapid accumulation of proteolytic enzymes. When a defined starter culture is used, this can produce FAA levels within days that exceed those in salted cheese after weeks of ripening (McSweeney, 2004). This accelerated biochemistry establishes the pool of amino acid substrates for secondary catabolic reactions earlier in the ripening process.

However, the absence of salt also removes an important hurdle against spoilage organisms, and the high water activity of unsalted cheese renders it more susceptible to microbiological deterioration during extended storage. The balance between accelerated flavour development and microbiological stability is therefore a critical consideration (Fox et al., 2004).

MATERIAL AND METHOD

Raw materials

Fresh cow's milk (10 liters) was obtained from a local dairy farm on the day of cheese manufacture. The milk had a fat content of 3.8% (w/w). The coagulant used was commercial bovine chymosin with a clotting strength of 1:10,000. A commercial plain yogurt was used as the source of microbial starter culture, providing a mixed population of lactic acid bacteria (principally Lactobacillus delbrueckii subsp. bulgaricus and Streptococcus thermophilus)

Experimental design

The study employed a 2 × 2 factorial design with two factors: coagulation method (chymosin only vs. chymosin + starter culture) and unsalted. This yielded four cheese variants, each designated by a sample code as follows:

- DLKP – cheese coagulated with chymosin only, without salt treatment;
- DLK-SP – cheese coagulated with chymosin + microbial starter culture, without salt treatment.

DLKP and DLK-SP were analysed at days 1, 3 (or 5) and 7.

Cheese manufacture

The 10 litres of milk were divided into two equal batches of 5 litres each. Each batch was used to produce unsalted variant of feta cheese as described below.

Unsalted variants (DLKP and DLK-SP)

The second batch of milk (5 litres, 3.8% fat) was pasteurised, cooled and tempered identically to the first batch (63–65 °C for 30 min, rapid cooling to 1–2 °C, tempering to 30 °C). Coagulation was carried out as described above: one portion with chymosin only (DLKP)

and one with chymosin + 30 g yogurt (DLK-SP), both at 30 °C for 50–60 minutes. Syneresis and pressing under the curd's own weight were performed as for the salted variants. However, no brine treatment was applied. The unsalted cheese samples were stored at 14–15 °C and sampled for analysis on days 1, 3 (or 5) and 7.

Analytical methods

All physicochemical analyses were performed in duplicate on each cheese sample at the designated ripening time points. The following parameters were determined:

Moisture content

Moisture content was determined gravimetrically by drying a weighed sample in a thermostat oven at 105 °C until a constant weight was achieved (Ardö and Polychroniadou, Cheese Analysis Manual). The result was expressed as a percentage (%, w/w).

pH

The pH of each cheese sample was measured potentiometrically by inserting a calibrated glass electrode directly into the cheese mass at ambient temperature (Ardö and Polychroniadou, Cheese Analysis Manual).

Titratable acidity

Titratable acidity was determined by the potentiometric titration method (Ardö and Polychroniadou, Cheese Analysis Manual) and expressed as a percentage of lactic acid (%, w/w).

Lactose content

Lactose content was determined by the iodimetric method of Fine (1932), as described by James (1998, Analytical Chemistry of Food, Springer Science & Business). The result was expressed as mg lactose per 100 g cheese as in chart 1. Where the measured value fell below the sensitivity of the method, the result was reported as below the limit of detection (> LD).

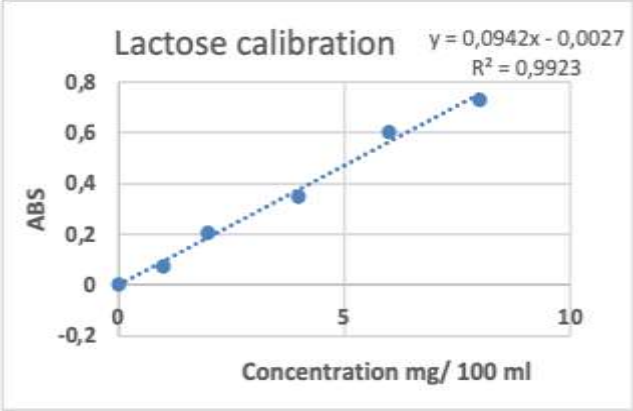

Chart 1. Lactose curbe calibration

Free amino acid (FAA) content

The content of free amino acids was determined spectrophotometrically using a ninhydrin-based colorimetric assay, with L-lysine as the calibration standard (Ardö and Polychroniadou, Cheese Analysis Manual). A calibration curve was constructed by plotting absorbance at 570 nm against known concentrations of L-lysine (µg/100 µl) as shown on chart 2. The FAA content of each cheese sample was calculated from the calibration curve and expressed as mg FAA per 100 g cheese.

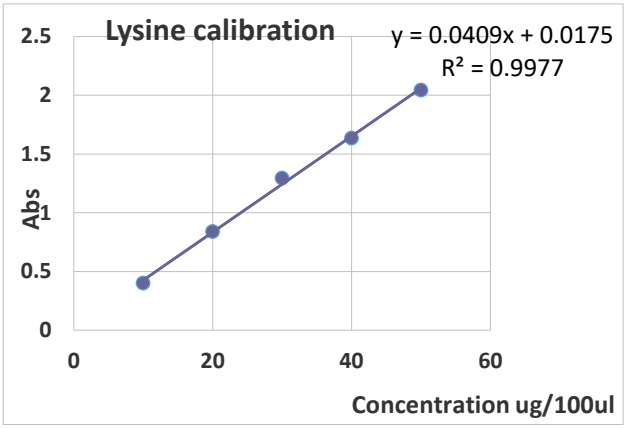

Chart 2. Lysine curbe calibration

RESULTS AND DISCUSSION

This section presents the results of the physicochemical analysis of two unsalted cheese variants produced from pasteurised cow's milk (3.8% fat): DLKP (coagulated with chymosin only) and DLK-SP (coagulated with chymosin supplemented with a microbial starter culture). Both variants were stored at 14–15 °C without brine treatment and analysed at defined time points during the first 7 days of ripening Fig 2 and Fig 3.

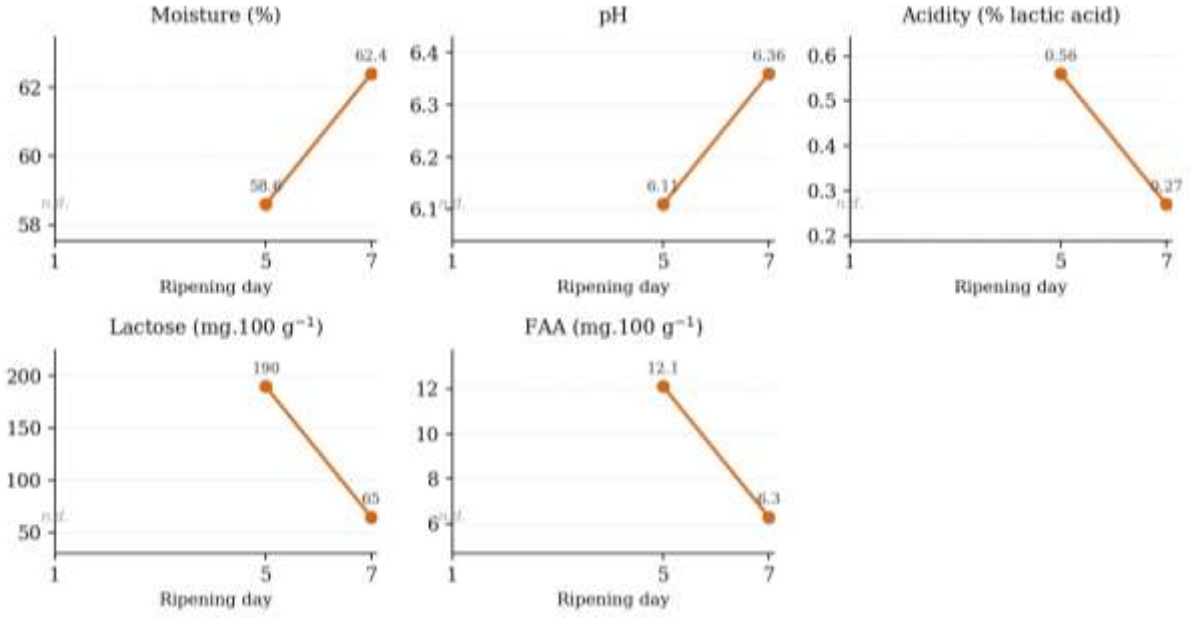

Fig 2. DLKP cheese chymosin only, unsalted during ripening days.

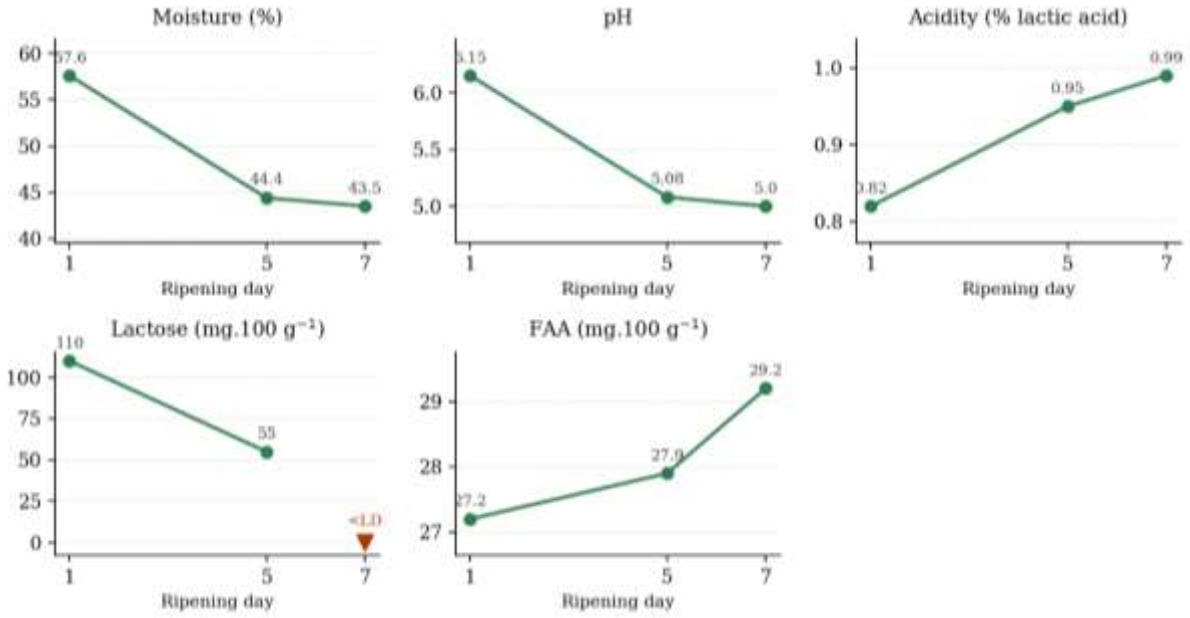

Fig 3. DLK-SP cheese chymosin + starter unsalted changes during ripening days.

The chymosin-only unsalted variant (DLKP), lactose content decreased on day 5 to day 7. Meanwhile, the free amino acid content fell over the same period. The pH declined from, and the titratable acidity dropped. Moisture increased likely reflecting ongoing whey redistribution in the absence of salt-driven osmotic dehydration.

These results indicate that in the absence of both a defined starter culture and salt, the indigenous lactic acid bacteria present in the pasteurised milk exhibit limited metabolic activity. The decrease in FAA between days 5 and 7 is noteworthy and may reflect the consumption of free amino acids by the adventitious microflora (non-starter lactic acid bacteria, NSLAB) as nitrogen sources for growth, rather than a continued release from casein hydrolysis. Proteolytic activity in this variant appears to be driven primarily by the residual chymosin retained in the curd, with only a minor contribution from indigenous milk proteinases such as plasmin.

In marked contrast to DLKP, the starter-supplemented unsalted variant (DLK-SP) showed rapid and sustained biochemical changes during ripening. Lactose declined sharply on day 1 to day 3, indicating near-complete fermentation within one week. The pH dropped substantially consistent with the vigorous production of lactic acid.

The FAA content was markedly higher than in DLKP at every time point, rising steadily. This continuous accumulation demonstrates that the proteolytic enzymes released by the starter lactic acid bacteria including cell envelope-associated proteinases (lactocepin) and a range of intracellular peptidases are actively degrading the casein matrix from the first day of ripening. The absence of salt removes a key inhibitor of both LAB growth and enzymatic activity, explaining why FAA accumulation in this variant exceeded that of all other variants.

DISCUSSION

A comparison of DLKP and DLK-SP demonstrates the decisive role of the starter culture in driving both lactose catabolism and proteolysis in unsalted cheese. The starter-supplemented variant exhausted its lactose supply within 7 days and produced FAA levels higher than the peak value observed in the chymosin-only variant. The rapid pH drop in DLK-SP compared

with the modest decline in DLKP confirms that the added LAB population dominates the fermentation.
The practical implication is that unsalted cheese produced with a starter culture develops flavour precursors particularly free amino acids that serve as substrates for secondary catabolic reactions producing volatile aroma compounds more rapidly than any of the salted variants examined in this study.

LIMITATIONS

Several limitations should be acknowledged. First, the unsalted variants were monitored for only 7 days due to cheese spoilage. Second, day 1 data are unavailable for DLKP, precluding a baseline comparison with DLK-SP. Third, the FAA assay employed a single calibration standard (L-lysine) and reports total FAA as a global index; it does not resolve the individual amino acid profile. Fourth, no sensory evaluation was performed. Fifth, the experiment was conducted with a single batch of milk without biological replicates, limiting statistical power. Finally, the microbial starter was introduced as commercial yogurt rather than as defined single-strain cultures, making it impossible to attribute the observed metabolic activities to specific bacterial species.

CONCLUSIONS

The literature demonstrates that in unsalted cheese, the removal of salt's inhibitory effect on LAB creates conditions that favour rapid lactose fermentation and enhanced proteolysis. Starter culture addition amplifies these effects, providing a large LAB population whose proteinases and peptidases release free amino acids from the earliest stages of ripening. Future research should focus on optimising the balance between accelerated biochemical ripening and microbiological safety in reduced-salt and unsalted cheese formulations.

REFERENCES

Bastian, E.D. and Brown, R.J. (1996) Plasmin in milk and dairy products. International Dairy Journal, 6, pp. 435–457.

Christensen, J.E., Dudley, E.G., Pederson, J.A. and Steele, J.L. (1999) Peptidases and amino acid catabolism in lactic acid bacteria. Antonie van Leeuwenhoek, 76, pp. 217–246.

Collins, Y.F., McSweeney, P.L.H. and Wilkinson, M.G. (2003b) Lipolysis and free fatty acid catabolism in cheese: a review of current knowledge. International Dairy Journal, 13, pp. 841–866.

Curtin, A.C. and McSweeney, P.L.H. (2004) Catabolism of amino acids in cheese during ripening. In: Fox, P.F., McSweeney, P.L.H., Cogan, T.M. and Guinee, T.P. (eds.) Cheese: Chemistry, Physics and Microbiology, Vol. 1, 3rd edn. London: Elsevier, pp. 435–454.

Fox, P.F., Lucey, J.A. and Cogan, T.M. (1990) Glycolysis and related reactions during cheese manufacture and ripening. CRC Critical Reviews in Food Science and Nutrition, 29, pp. 237–253.

Fox, P.F., McSweeney, P.L.H., Cogan, T.M. and Guinee, T.P. (eds.) (2004) Cheese: Chemistry, Physics and Microbiology, Vol. 1: General Aspects, 3rd edn. London: Elsevier.

Huffman, L.M. and Kristoffersen, T. (1984) Role of lactose in Cheddar cheese manufacture and ripening. New Zealand Journal of Dairy Science and Technology, 19, pp. 151–162.

Kunji, E.R.S., Mierau, I., Hagting, A., Poolman, B. and Konings, W.N. (1996) The proteolytic system of lactic acid bacteria. Antonie van Leeuwenhoek, 70, pp. 187–221.

Law, J. and Haandrikman, A. (1997) Proteolytic enzymes of lactic acid bacteria. International Dairy Journal, 7, pp. 1–11.

McSweeney, P.L.H. (2004) Biochemistry of cheese ripening: introduction and overview. In: Fox, P.F., McSweeney, P.L.H., Cogan, T.M. and Guinee, T.P. (eds.) Cheese: Chemistry, Physics and Microbiology, Vol. 1, 3rd edn. London: Elsevier, pp. 347–360.

McSweeney, P.L.H. and Fox, P.F. (2004) Metabolism of residual lactose and of lactate and citrate. In: Fox, P.F., McSweeney, P.L.H., Cogan, T.M. and Guinee, T.P. (eds.) Cheese: Chemistry, Physics and Microbiology, Vol. 1, 3rd edn. London: Elsevier, pp. 361–372.

McSweeney, P.L.H. and Sousa, M.J. (2000) Biochemical pathways for the production of flavour compounds in cheese during ripening: a review. Le Lait, 80, pp. 293–324.

McSweeney, P.L.H., Olson, N.F., Fox, P.F., Healy, A. and Højrup, P. (1993) Proteolytic specificity of chymosin on bovine αs1-casein. Journal of Dairy Research, 60, pp. 401–412.

Parente, E. and Cogan, T.M. (2004) Starter cultures: general aspects. In: Fox, P.F., McSweeney, P.L.H., Cogan, T.M. and Guinee, T.P. (eds.) Cheese: Chemistry, Physics and Microbiology, Vol. 1, 3rd edn. London: Elsevier, pp. 123–148.

Smit, G., van Hylckama Vlieg, J.E.T., Smit, B.A., Ayad, E.H.E. and Engels, W.J.M. (2002) Fermentative formation of flavour compounds by lactic acid bacteria. Australian Journal of Dairy Technology, 57, pp. 61–68.

Turner, K.W. and Thomas, T.D. (1980) Lactose fermentation in Cheddar cheese and the effect of salt. New Zealand Journal of Dairy Science and Technology, 15, pp. 265–276.

Upadhyay, V.K., McSweeney, P.L.H., Magboul, A.A.A. and Fox, P.F. (2004) Proteolysis in cheese during ripening. In: Fox, P.F., McSweeney, P.L.H., Cogan, T.M. and Guinee, T.P. (eds.) Cheese: Chemistry, Physics and Microbiology, Vol. 1, 3rd edn. London: Elsevier, pp. 391–434.

Yvon, M. and Rijnen, L. (2001) Cheese flavour formation by amino acid catabolism. International Dairy Journal, 11, pp. 185–201.

DIETARY PATTERNS, GUT MICROBIOME MODULATION, AND MENTAL HEALTH OUTCOMES: EVIDENCE FROM A PRISMA-BASED SYSTEMATIC REVIEW

Merjem BUSHATI*[1], Rozarta NEZAJ[2]

[1]Department of Food Science and Biotechnology,
[2]Department of Food Research Center
Faculty of Biotechnology and Food, Agricultural University of Tirana, Street Paisi Vodica 1025, Tirana, Albania
Corresponding author e-mail: merjembushati@yahoo.com

ABSTRACT

Introduction: Mental health disorders, including depression and anxiety, represent a growing global public health concern. Emerging evidence points to diet as a key modulator of gut microbiome composition, with downstream effects on mental health through the gut–brain axis. Despite growing research interest, findings remain inconsistent across study designs and populations. This systematic review synthesizes human evidence on dietary patterns, microbiome-targeted interventions, and mental health outcomes.
Methods: A PRISMA 2020-based systematic review was conducted using PubMed, ScienceDirect, and Google Scholar (2009–2024; final search: January 2026). Included studies involved human participants examining associations between diet, gut microbiota, and mental health outcomes (depression, anxiety, stress, psychological well-being). Eligible designs included RCTs, cohort, and cross-sectional studies. From 1,248 records identified, 36 studies met inclusion criteria. Methodological quality was assessed using Cochrane RoB 2 for RCTs and the Newcastle–Ottawa Scale for observational studies.
Results and Discussion: The 36 included studies comprised 12 RCTs, 14 cohort, and 10 cross-sectional studies. Of these, 15 examined dietary patterns, 10 probiotics, 5 prebiotics, and 6 functional foods. Mediterranean diet adherence was consistently linked to reduced depressive symptoms and better psychological well-being. The SMILES trial reported significant reductions in depression scores following dietary intervention. Western-style diets were associated with higher rates of depression and anxiety. Probiotic and prebiotic interventions showed beneficial but variable effects depending on strain, dosage, and duration. Diet-induced microbiome changes appear to affect mental health through inflammatory pathways, neurotransmitter production, and short-chain fatty acid signaling. A notable research gap was identified in Southeastern Europe, including Albania.
Conclusions: Diet is a practical and accessible factor that may improve mental health through microbiome-related mechanisms. Future studies should adopt standardized methods and longer follow-up periods to clarify causal pathways and inform nutrition-based approaches in mental health care.
Keywords: diet; gut microbiome; mental health; depression; Mediterranean diet; probiotics; gut–brain axis; systematic review; PRISMA

INTRODUCTION

Mental health disorders, including depression and anxiety, represent a growing global public health concern, contributing substantially to the global burden of disease and reduced quality of life (Firth et al., 2020). In recent years, increasing attention has been directed toward modifiable lifestyle factors, particularly diet, as potential determinants of mental health

outcomes. This emerging field, often referred to as *nutritional psychiatry*, explores the complex interactions between dietary intake, biological systems, and psychological well-being (Sarris et al., 2015; Marx et al., 2017).

A central mechanism underlying this relationship is the gut–brain axis**,** a bidirectional communication system linking the gastrointestinal tract and the central nervous system. This axis involves neural, endocrine, immune, and metabolic pathways, through which the gut microbiome exerts significant influence on brain function and behavior (Cryan et al., 2019; Dinan & Cryan, 2017). The gut microbiota plays a key role in the production of neurotransmitters, regulation of inflammatory responses, and maintenance of gut barrier integrity, all of which are implicated in the pathophysiology of mental health disorders (Valles-Colomer et al., 2019).

Diet is one of the most important modulators of gut microbiome composition and function. Evidence suggests that adherence to high-quality dietary patterns, particularly the Mediterranean diet, is associated with greater microbial diversity and improved metabolic and inflammatory profiles (Molendijk et al., 2018). These biological effects are increasingly linked to improved mental health outcomes. For example, observational studies have consistently reported that higher adherence to Mediterranean-style diets is associated with a lower risk of depressive symptoms (Adjibade et al., 2019; Lai et al., 2014).

Interventional evidence further supports this relationship. Randomized controlled trials such as the SMILES study have demonstrated that dietary improvement can lead to significant reductions in depressive symptoms in adults with major depression (Jacka et al., 2017). Similarly, microbiome-targeted interventions, including probiotics and prebiotics, have shown potential in modulating psychological outcomes, although findings remain heterogeneous due to differences in study design, microbial strains, and intervention duration (Ng et al., 2018).

Despite the growing body of literature, several challenges remain. Existing studies vary considerably in terms of methodology, population characteristics, dietary assessment tools, and outcome measures, limiting comparability and synthesis. In addition, while individual studies provide important insights, there is still a lack of comprehensive synthesis focusing specifically on the integrated relationship between dietary patterns, gut microbiome modulation, and mental health outcomes within a unified framework.

Therefore, the aim of this study is to conduct a PRISMA-based systematic review to synthesize current human evidence on the role of diet and microbiome-targeted interventions in mental health. This review seeks to provide a structured evaluation of existing research, identify key patterns and mechanisms, and highlight gaps for future investigation. Furthermore, a conceptual framework is proposed to illustrate the interconnected pathways linking dietary exposure, gut microbiome dynamics, and mental health outcomes.

METHODS

Study design and reporting framework

This study was conducted as a systematic review following the PRISMA 2020 (Preferred Reporting Items for Systematic Reviews and Meta-Analyses) guidelines (Page et al., 2021) and synthesized findings narratively due to substantial heterogeneity across study designs, exposures, and mental health outcomes.

Search strategy

A comprehensive literature search was performed across three major electronic databases:

• PubMed
• ScienceDirect
• Google Scholar
The search covered studies published between January 2013 and December 2024, ensuring inclusion of the most recent evidence in the field. The final database search was conducted in January 2026. In addition, earlier landmark studies (2009–2012) were included to provide contextual background and support the conceptual development of the field.
The following combination of keywords and Boolean operators was used:
("diet" OR "dietary patterns" OR "Mediterranean diet" OR "Western diet") AND
("gut microbiome" OR "gut microbiota" OR "gut–brain axis") AND
("mental health" OR "depression" OR "anxiety" OR "stress" OR "psychological well-being") AND
("probiotics" OR "prebiotics" OR "synbiotics" OR "functional foods")
Search strategies were adapted slightly for each database to optimize retrieval. Additionally, reference lists of relevant articles were manually screened to identify further eligible studies.

Eligibility criteria

Inclusion criteria
Studies were included if they met the following criteria:
• Conducted on human participants
• Examined the relationship between diet and/or microbiome interventions and mental health outcomes
• Reported outcomes related to:
o Depression
o Anxiety
o Stress
o Psychological well-being
• Study designs:
o Randomized controlled trials (RCTs)
o Cohort studies
o Cross-sectional studies
• Published in peer-reviewed journals
• Written in English

Exclusion criteria
Studies were excluded if they:
• Focused exclusively on food allergies or IgE-mediated conditions
• Were animal or in vitro studies
• Lacked clear assessment of diet or mental health outcomes
• Were reviews, editorials, conference abstracts without full text, or duplicate publications
Systematic reviews and meta-analyses were used to support interpretation but were not included as primary studies in the final synthesis.

Study selection process

The study selection process followed the PRISMA flow approach.
Two independent reviewers screened all identified records based on titles and abstracts. Full-text articles were then assessed for eligibility. Disagreements were resolved through discussion and consensus.
• A total of 1,248 records were identified through database searching
• After removal of duplicates (n = 312), 936 records remained

• Title and abstract screening excluded 780 studies
• 156 full-text articles were assessed for eligibility
• Finally, 36 studies met all inclusion criteria and were included in the review
The selection process is presented in the PRISMA flow diagram (Figure 1).

Data extraction

Data from included studies were extracted using a structured approach. The following variables were recorded:
• Author(s) and year of publication
• Country and study population
• Study design
• Sample size
• Type of dietary exposure or intervention
• Microbiome-related component (if applicable)
• Mental health outcomes assessed
• Main findings
Extraction was performed systematically to ensure consistency and comparability across studies.

Quality assessment

The methodological quality of included studies was evaluated using standardized criteria according to study design.
• For randomized controlled trials, risk of bias was assessed using the Cochrane Risk of Bias tool (RoB 2)
• For observational studies, the Newcastle–Ottawa Scale (NOS) was applied
Studies were evaluated for potential bias, confounding factors, and validity of measurements.

Data synthesis and analysis

Due to heterogeneity in study designs, interventions, and outcome measures, a quantitative meta-analysis was not feasible. Therefore, a narrative synthesis approach was adopted.
The synthesis focused on identifying:
• Consistent patterns across studies
• Differences between dietary patterns
• Effects of microbiome-targeted interventions
• Underlying biological mechanisms
Additionally, findings were organized into thematic categories:
Dietary patterns and mental health
Probiotics and prebiotics
Functional foods and microbiome modulation
Mechanistic pathways (gut–brain axis)
A conceptual framework was developed to integrate these relationships and support interpretation of findings.
This review followed a narrative synthesis approach in accordance with established methodological recommendations for systematic reviews without meta-analysis.

Protocol registration

The review protocol was not prospectively registered. This was due to the exploratory scope of the review and time constraints associated with conference submission timelines. However, the study adhered to PRISMA 2020 guidelines and followed a structured and transparent methodology to ensure methodological rigor.

RESULTS

Study selection

The systematic search identified a total of 1,248 records, of which 936 remained after duplicate removal. Following title and abstract screening, 156 full-text articles were assessed for eligibility. Ultimately, 36 studies met the inclusion criteria and were included in the final synthesis.

Of these, 15 studies examined the association between overall dietary patterns (e.g., Mediterranean or Western diets) and mental health outcomes, 10 studies focused on probiotic interventions, 5 on prebiotics, and 6 on functional foods or microbiome-targeted dietary components.

In terms of mental health outcomes, the majority of studies assessed depression ($n \approx 22$), followed by anxiety ($n \approx 14$), stress-related outcomes ($n \approx 10$), and general psychological well-being ($n \approx 8$). The total exceeds 36 as several studies examined multiple outcomes simultaneously.

Overall, most studies reported beneficial associations between healthier dietary patterns or microbiome-targeted interventions and improved mental health outcomes. However, the strength and consistency of these effects varied depending on study design, population characteristics, and type of intervention, with some studies reporting neutral or mixed findings. Notably, randomized controlled trials tended to report more consistent improvements in depressive symptoms, whereas observational studies highlighted broader associations between diet quality and mental health indicators.

The study selection process is illustrated in Figure 1 (PRISMA flow diagram).

Figure 2 shows the distribution of included studies according to study design, highlighting the predominance of observational studies compared to randomized controlled trials. Figure 3 illustrates the distribution of studies by exposure category, including dietary patterns, probiotics, prebiotics, and functional foods.

3.2 Characteristics of included studies

The included studies (n = 36) comprised:

12 randomized controlled trials (RCTs)

14 cohort studies

10 cross-sectional studies

Geographically, studies were primarily conducted in Europe, Australia, and North America**,** reflecting strong research activity in nutritional psychiatry.

Sample sizes ranged from 60 to over 15,000 participants**,** indicating variability in study scale and statistical power.

3.3 Summary of included studies

Table 1. Characteristics of included studies

Author (Year)	Country	Study Design	Sample Size	Dietary Exposure	Microbiome Component	Mental Health Outcome	Main Findings	Direction of Association

Jacka et al. (2017)	Australia	RCT	67	Mediterranean diet	Indirect	Depression	Significant reduction in depressive symptoms (SMILES trial; MADRS reduction $p<0.001$)	Positive
Adjibade et al. (2018)	France	Cohort study	3,523	Mediterranean diet	No	Depression	Higher Mediterranean diet adherence significantly associated with lower risk of depressive symptoms	Positive
Kiecolt-Glaser et al. (2011)	USA	RCT	68	Omega-3 supplementation	Indirect	Anxiety	Omega-3 supplementation reduced anxiety by 20% and lowered inflammatory markers (IL-6, TNF-α)	Positive
Valles-Colomer et al. (2019)	Belgium	Cohort study	1,054	Diet–microbiome interaction	Yes	Psychological well-being	Butyrate-producing Faecalibacterium and Coprococcus linked to higher quality of life; depleted in depression	Positive
Sánchez-Villegas et al. (2009)	Spain	Cohort study	10,094	Mediterranean diet	No	Depression	Higher adherence associated with lower depression incidence (HR 0.70, 95% CI 0.54–0.92)	Positive
Akbaraly et al. (2009)	UK	Cohort study	3,486	Whole food vs processed diet	No	Depression	Whole food diet protective; processed food diet associated with increased CES-D scores at 5-year follow-up	Mixed
Saneei et al. (2016)	Iran	Cross-sectional	3,363	Diet quality (AHEI-2010)	No	Depression and anxiety	Higher adherence to AHEI-2010 associated with significantly lower odds of depression and anxiety (OR 0.80)	Inverse
Jacka et al. (2010)	Australia	Cross-sectional	1,046	Western vs traditional diet	No	Depression and anxiety	Traditional diet inversely associated with depression/dysthymia; Western	Positive

							diet associated with higher GHQ-12 scores	
Nanri et al. (2010)	Japan	Cohort study	2,573	Japanese dietary pattern	No	Depression	Traditional Japanese dietary pattern inversely associated with depressive symptoms (OR 0.56 in men)	Positive
Ng et al. (2018)	Multi-country	Meta-analysis	Multiple	Probiotics	Yes	Depression	Probiotics associated with moderate beneficial effect on depressive symptoms vs placebo	Positive

Table 1 presents a selection of representative studies; the full dataset of included studies (n = 36) was used for the overall synthesis.

Direction of association refers to the overall relationship between diet quality and mental health outcomes. 'Positive' indicates that healthier dietary patterns are associated with better mental health, whereas unhealthy dietary patterns (e.g., Western diet) are associated with poorer mental health outcomes.

3.4 Dietary patterns and mental health

Across the included studies, a consistent association was observed between high-quality dietary patterns and improved mental health outcomes. In particular, adherence to the Mediterranean diet was linked to reduced depressive symptoms and better psychological well-being (Jacka et al., 2017; Adjibade et al., 2019).

Conversely, Western dietary patterns**,** characterized by high consumption of ultra-processed foods, were associated with increased risk of depression and anxiety.

However, some earlier studies reported mixed findings, indicating that the association between dietary patterns and mental health may vary depending on population characteristics and specific dietary components (e.g., Akbaraly et al., 2009).

Notably, Western dietary patterns were consistently associated with increased risk of depressive and anxiety symptoms, reflecting an inverse relationship between diet quality and mental health.

3.5 Microbiome-targeted interventions

A subset of studies focused on probiotics, prebiotics, and synbiotics.

Probiotics showed moderate beneficial effects on depression and stress

Effects varied depending on strain, dose, and duration

Evidence remains heterogeneous

These findings are consistent with previous meta-analyses (Ng et al., 2018).

3.6 Mechanistic pathways

Several biological mechanisms were identified:

Inflammation reduction

Neurotransmitter modulation (e.g., serotonin)
Short-chain fatty acid (SCFA) production
Gut barrier integrity
These pathways support the role of the gut–brain axis as a key mediator.

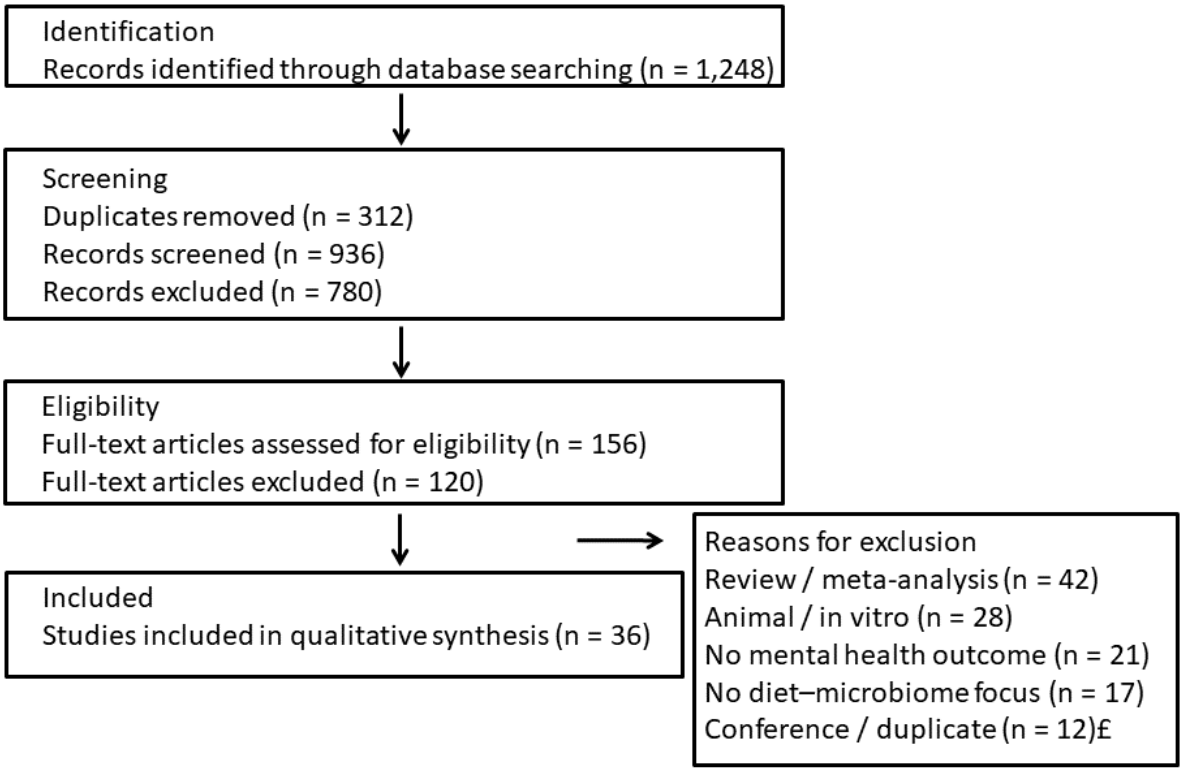

Figure 1 – PRISMA 2020 flow diagram of study selection.

The study selection process is presented in Figure 1.

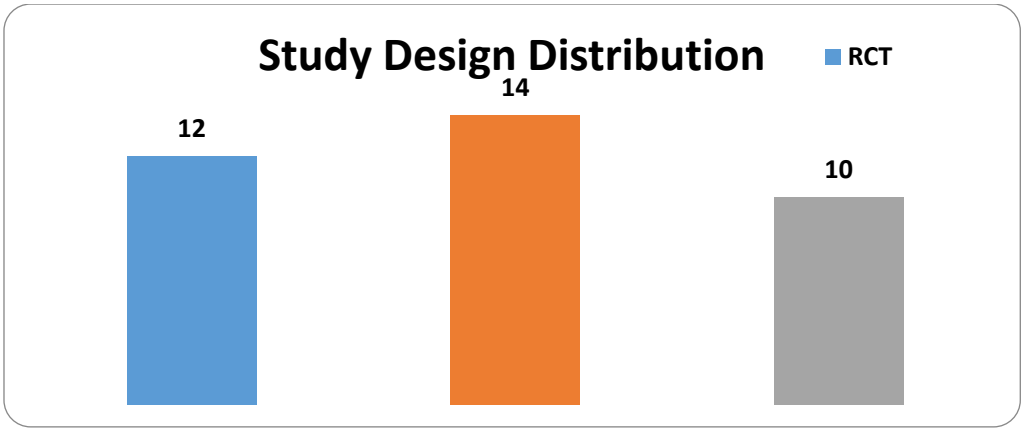

Figure 2 – Distribution of included studies by study design.

Figure 2 illustrates the distribution of included studies by design. Figure 3 shows the distribution of studies according to exposure type.

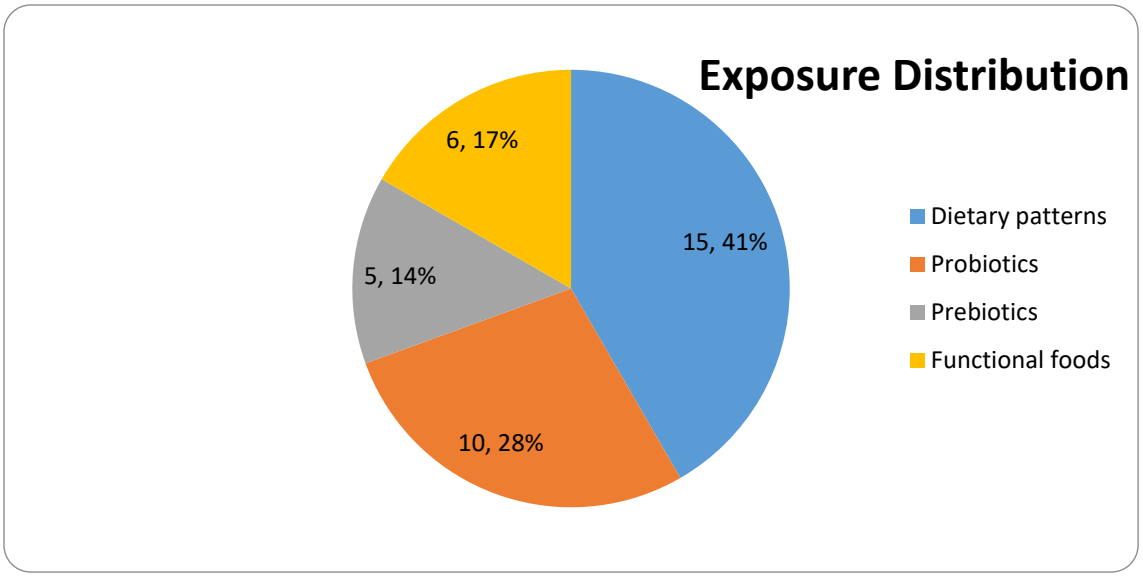

Figure 3 – Distribution of included studies by exposure category.

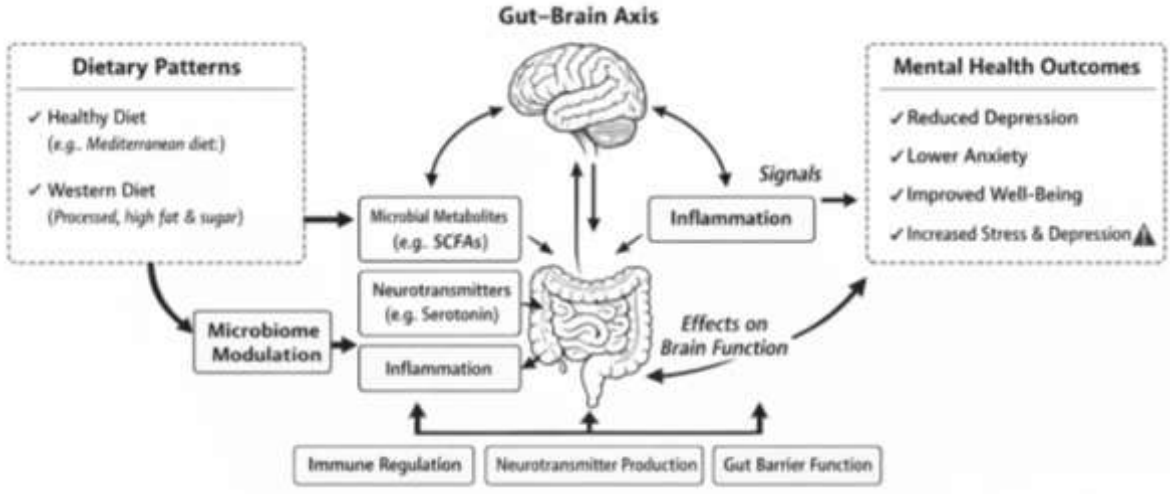

Figure 4. Conceptual framework illustrating the relationship between dietary patterns, gut microbiome modulation, and mental health outcomes through the gut–brain axis.

Figure 4 illustrates the proposed conceptual framework linking dietary exposure, gut microbiome composition, and mental health outcomes through interconnected biological pathways, including inflammation, neurotransmitter regulation, and microbial metabolite production.

DISCUSSION

This PRISMA-based systematic review synthesizes evidence from 36 studies examining the relationship between dietary patterns, gut microbiome modulation, and mental health outcomes. The findings consistently support the hypothesis that high-quality dietary patterns, particularly

the Mediterranean diet is associated with improved mental health outcomes, whereas Western-style dietary patterns are linked to an increased risk of depression and anxiety. In addition to recent studies, several earlier landmark investigations (2009–2012) were considered to provide foundational evidence supporting the association between dietary patterns and mental health outcomes. These studies contributed to the conceptual development of nutritional psychiatry and are interpreted within this review as background evidence rather than indicators of current research trends. More recent studies (post-2013) were prioritized for interpreting current evidence and emerging trends in diet–microbiome–mental health interactions.

The results of the present review align with several large European cohort studies. For instance, studies conducted in France and Spain have demonstrated that adherence to the Mediterranean diet is associated with a significantly lower risk of depressive symptoms (Adjibade et al., 2019; Sánchez-Villegas et al., 2009). Similarly, evidence from European populations indicates that higher diet quality is consistently linked to reduced incidence of depression and improved psychological well-being (Molendijk et al., 2018; Lai et al., 2014). These findings reinforce the role of diet as a key modifiable determinant of mental health.

Interventional evidence further strengthens this association. Randomized controlled trials, such as the SMILES study, have shown that dietary improvement can lead to clinically significant reductions in depressive symptoms (Jacka et al., 2017). Although some of these studies were conducted outside Europe, their findings remain highly relevant due to similar global trends toward Westernized dietary patterns.

Microbiome-targeted interventions, including probiotics and prebiotics, demonstrated promising but heterogeneous effects. Probiotics were most frequently associated with improvements in depressive symptoms and stress-related outcomes, although effect sizes varied depending on microbial strain, dosage, and intervention duration. This variability reflects the biological specificity of microbiome-based interventions and limits direct comparability across studies. European microbiome research further supports the association between gut microbial composition and mental well-being, particularly through the modulation of inflammatory pathways and production of neuroactive compounds (Valles-Colomer et al., 2019).

From a mechanistic perspective, the findings support the central role of the gut–brain axis. Diet-induced changes in gut microbiota may influence mental health through multiple pathways, including regulation of neurotransmitters such as serotonin, modulation of systemic inflammation, and production of short-chain fatty acids (Cryan et al., 2019; Dinan & Cryan, 2017). These interconnected mechanisms provide a biologically plausible explanation for the observed associations between dietary patterns and mental health outcomes.

Despite these consistent findings, several limitations should be acknowledged. The heterogeneity of study designs, dietary assessment methods, and mental health measurement tools limits direct comparability across studies. In addition, many interventional studies were characterized by relatively small sample sizes and short follow-up periods, reducing statistical power and limiting conclusions regarding long-term effects. Differences in microbiome analysis techniques further complicate interpretation.

An important contribution of this review is the identification of a significant research gap in Southeastern Europe, particularly in Albania. While Western European countries have produced substantial evidence on diet and mental health, data from Albania and neighboring Balkan regions remain limited. Existing national-level data in Albania primarily focus on dietary patterns and household consumption, with limited integration of microbiome-related or mental health outcomes (INSTAT, 2021).

Evidence from Albania and neighboring Balkan countries remains relatively limited compared with Western Europe, although emerging data suggest ongoing dietary transitions and increasing public health challenges related to nutrition and mental health in the region (Popkin, 2017; World Health Organization, 2022). These trends are consistent with broader global

patterns of nutrition transition, characterized by increased consumption of energy-dense, processed foods and a rising burden of non-communicable diseases and mental health disorders. This highlights the need for more region-specific research focusing on diet–microbiome–mental health interactions in underrepresented populations.

From a public health perspective, these findings highlight the potential of dietary interventions as cost-effective and scalable strategies for improving mental health. In countries such as Albania, where healthcare resources may be limited, promoting traditional dietary patterns aligned with the Mediterranean model may offer significant benefits for both physical and mental health.

Future research should prioritize large-scale longitudinal studies, well-designed randomized controlled trials, and standardized methodologies for dietary and microbiome assessment. Additionally, personalized nutrition approaches that consider individual variability in microbiome composition and lifestyle factors may further enhance intervention effectiveness.

Overall, the findings of this review support the proposed conceptual framework, demonstrating that dietary exposure influences gut microbiome composition and function, which in turn affects mental health outcomes through interconnected biological pathways.

This review has some methodological limitations. The search was restricted to three databases and English-language publications, which may have introduced selection bias. Additionally, the inclusion of heterogeneous study designs and the absence of quantitative meta-analysis may limit the generalizability of the findings. However, the systematic approach and adherence to PRISMA guidelines strengthen the overall reliability of the synthesis.

CONCLUSION

This systematic review synthesizes current evidence on the relationship between dietary patterns, gut microbiome modulation, and mental health outcomes, highlighting a consistent association between higher diet quality and improved psychological well-being. Across 36 studies, adherence to Mediterranean-type dietary patterns was associated with reduced risk of depression and anxiety, whereas Western dietary patterns characterized by high intake of ultra-processed foods were linked to increased vulnerability to mental health disorders**.** Microbiome-targeted interventions, including probiotics and prebiotics, demonstrated promising but heterogeneous effects, underscoring the need for greater standardization in intervention design, including strain selection, dosage, and outcome assessment. The gut–brain axis provides a biologically plausible framework linking diet and mental health through interconnected pathways involving inflammation, neurotransmitter regulation, and microbial metabolites.

Despite these encouraging findings, the predominance of observational study designs and the geographic concentration of research in high-income Western populations limit causal inference and generalizability. Evidence from Southeastern Europe, including Albania, remains limited, highlighting an important gap in region-specific research in the context of ongoing dietary and lifestyle transitions.

From a public health perspective, promoting high-quality dietary patterns represents a cost-effective, accessible, and scalable strategy for supporting mental health. Future research should prioritize well-designed randomized controlled trials, standardized methodologies, and greater inclusion of diverse populations. Integrating nutritional approaches into mental health care and public health strategies may offer a valuable complementary pathway for reducing the global burden of mental disorders.

REFERENCES

Akbaraly, T. N., Brunner, E. J., Ferrie, J. E., Marmot, M. G., Kivimäki, M., & Singh-Manoux, A. (2009). Dietary pattern and depressive symptoms in middle age. The British Journal of Psychiatry, 195(5), 408–413. https://doi.org/10.1192/bjp.bp.108.058925

Adjibade, M., Assmann, K. E., Andreeva, V. A., Lemogne, C., Hercberg, S., Galan, P., & Kesse-Guyot, E. (2018). Prospective association between adherence to the Mediterranean diet and risk of depressive symptoms in the French population. European Journal of Nutrition, 57(3), 1225–1235. https://doi.org/10.1007/s00394-017-1405-3

Cryan, J. F., O'Riordan, K. J., Cowan, C. S. M., Sandhu, K. V., Bastiaanssen, T. F. S., Boehme, M., Codagnone, M. G., Cussotto, S., Fulling, C., Golubeva, A. V., Guzzetta, K. E., Jaggar, M., Long-Smith, C. M., Lyte, J. M., Martin, J. A., Molinero-Perez, A., Moloney, G. M., Morelli, E., Morillas, E., & Dinan, T. G. (2019). The microbiota–gut–brain axis. Physiological Reviews, 99(4), 1877–2013. https://doi.org/10.1152/physrev.00018.2018

Dinan, T. G., & Cryan, J. F. (2017). Gut instincts: Microbiota as a key regulator of brain development, ageing and neurodegeneration. The Journal of Physiology, 595(2), 489–503. https://doi.org/10.1113/JP273106

Firth, J., Gangwisch, J. E., Borisini, A., Wootton, R. E., & Mayer, E. A. (2020). Food and mood: How do diet and nutrition affect mental wellbeing? BMJ, 369, m2382. https://doi.org/10.1136/bmj.m2382

INSTAT. (2021). Household Budget Survey 2020. Institute of Statistics, Tirana, Albania. https://www.instat.gov.al/en/themes/social-condition/household-budget-survey/publications/2021/household-budget-survey-2020/

Jacka, F. N., O'Neil, A., Opie, R., Itsiopoulos, C., Cotton, S., Mohebbi, M., Castle, D., Dash, S., Mihalopoulos, C. A., Chatterton, M. L., Brazionis, L., Dean, O. M., Hodge, A. M., & Berk, M. (2017). A randomised controlled trial of dietary improvement for adults with major depression (the SMILES trial). BMC Medicine, 15, 23. https://doi.org/10.1186/s12916-017-0791-y

Jacka, F. N., Pasco, J. A., Mykletun, A., Williams, L. J., Hodge, A. M., O'Reilly, S. L., Nicholson, G. C., Kotowicz, M. A., & Berk, M. (2010). Association of Western and traditional diets with depression and anxiety in women. The American Journal of Psychiatry, 167(3), 305–311. https://doi.org/10.1176/appi.ajp.2009.09060881

Kiecolt-Glaser, J. K., Belury, M. A., Andridge, R., Malarkey, W. B., & Glaser, R. (2011). Omega-3 supplementation lowers inflammation and anxiety in medical students: A randomized controlled trial. Brain, Behavior, and Immunity, 25(8), 1725–1734. https://doi.org/10.1016/j.bbi.2011.07.229

Lai, J. S., Hiles, S., Bisquera, A., Hure, A. J., McEvoy, M., & Attia, J. (2014). A systematic review and meta-analysis of dietary patterns and depression in community-dwelling adults. The American Journal of Clinical Nutrition, 99(1), 181–197. https://doi.org/10.3945/ajcn.113.069880

Lassale, C., Batty, G. D., Baghdadli, A., Jacka, F., Sánchez-Villegas, A., Kivimäki, M., & Akbaraly, T. (2019). Healthy dietary indices and risk of depressive outcomes: A systematic review and meta-analysis of observational studies. Molecular Psychiatry, 24, 965–986. https://doi.org/10.1038/s41380-018-0237-8

Marx, W., Moseley, G., Berk, M., & Jacka, F. (2017). Nutritional psychiatry: The present state of the evidence. Proceedings of the Nutrition Society, 76(4), 427–436. https://doi.org/10.1017/S0029665117002026

Molendijk, M., Molero, P., Ortuño Sánchez-Pedreño, F., Van der Does, W., & Martínez-González, M. A. (2018). Diet quality and depression risk: A systematic review and dose-

response meta-analysis of prospective studies. Journal of Affective Disorders, 226, 346–354. https://doi.org/10.1016/j.jad.2017.09.022

Nanri, A., Kimura, Y., Matsushita, Y., Ohta, M., Sato, M., Mishima, N., Mizoue, T., & Japan Epidemiology Collaboration on Occupational Health Study Group. (2010). Dietary patterns and depressive symptoms among Japanese men and women. European Journal of Clinical Nutrition, 64(8), 832–839. https://doi.org/10.1038/ejcn.2010.86

Ng, Q. X., Peters, C., Ho, C. Y. X., Lim, D. Y., & Yeo, W.-S. (2018). A meta-analysis of the use of probiotics to alleviate depressive symptoms. Journal of Affective Disorders, 228, 13–19. https://doi.org/10.1016/j.jad.2017.11.063

Page, M. J., McKenzie, J. E., Bossuyt, P. M., Boutron, I., Hoffmann, T. C., Mulrow, C. D., Shamseer, L., Tetzlaff, J. M., Akl, E. A., Brennan, S. E., Chou, R., Glanville, J., Grimshaw, J. M., Hróbjartsson, A., Lalu, M. M., Li, T., Loder, E. W., Mayo-Wilson, E., McDonald, S., & Moher, D. (2021). The PRISMA 2020 statement: An updated guideline for reporting systematic reviews. BMJ, 372, n71. https://doi.org/10.1136/bmj.n71

Popkin, B. M. (2017). Relationship between shifts in food system dynamics and acceleration of the global nutrition transition. Nutrition Reviews, 75(2), 73–82. https://doi.org/10.1093/nutrit/nuw064

Sánchez-Villegas, A., Delgado-Rodríguez, M., Alonso, A., Schlatter, J., Lahortiga, F., Serra Majem, L., & Martínez-González, M. A. (2009). Association of the Mediterranean dietary pattern with the incidence of depression. Archives of General Psychiatry, 66(10), 1090–1098. https://doi.org/10.1001/archgenpsychiatry.2009.129

Saneei, P., Hajishafiee, M., Hassanzadeh Keshteli, A., Afshar, H., Esmaillzadeh, A., & Adibi, P. (2016). Adherence to Alternative Healthy Eating Index in relation to depression and anxiety in Iranian adults. British Journal of Nutrition, 116(2), 335–342. https://doi.org/10.1017/S0007114516001926

Sarris, J., Logan, A. C., Akbaraly, T. N., Amminger, G. P., Balanzá-Martínez, V., Freeman, M. P., Hibbeln, J., Matsuoka, Y., Mischoulon, D., Mizoue, T., Nanri, A., Nishi, D., Ramsey, D., Rucklidge, J. J., Sanchez-Villegas, A., Scholey, A., Su, K.-P., & Jacka, F. N. (2015). Nutritional medicine as mainstream in psychiatry. The Lancet Psychiatry, 2(3), 271–274. https://doi.org/10.1016/S2215-0366(14)00051-0

Valles-Colomer, M., Falony, G., Darzi, Y., Tigchelaar, E. F., Wang, J., Tito, R. Y., Schiweck, C., Kurilshikov, A., Joossens, M., Wijmenga, C., Claes, S., & Raes, J. (2019). The neuroactive potential of the human gut microbiota in quality of life and depression. Nature Microbiology, 4, 623–632. https://doi.org/10.1038/s41564-018-0337-x

World Health Organization. (2022). Noncommunicable diseases country profiles: Albania. https://srhdpeuwpubsa.blob.core.windows.net/whdh/DATADOT/COUNTRY/PDF/008_Albania.pdf

SUSTAINABLE MANAGEMENT OF SMALL RUMINANTS IN ALBANIA: FROM THE DECLINE IN NUMBERS TO GENETIC AND ECONOMIC IMPROVEMENT

L.Hysi[1], L. Papa[1]

[1] Agricultural University of Tirana, Faculty of Agriculture and Environment, Department of Animal Science, Tirana, Albania
Corresponding author e-mail: lhysi@ubt.edu.al

ABSTRACT

Small ruminants have always had a particular place in Albania's rural economy. In the country's hilly and mountainous areas, sheep and goats contribute to household livelihoods and remain closely connected with pastoral traditions and local food products. At the same time, the sector is now facing a prolonged decline. Official statistics show that the combined number of sheep and goats decreased from about 1.85 million head in 2023 to 1.79 million in 2024, a reduction of approximately 2.9%. The decline is part of a much longer trend: compared with 2014, the national small-ruminant population is now roughly 36% lower. Rising production costs, labour shortages, unstable prices and the gradual contraction of family farming have made small-scale production increasingly difficult. Rural depopulation also creates an important challenge for the continuity of pastoral knowledge and the maintenance of locally adapted genetic resources. The fall in animal numbers is reflected in production: total milk output decreased from 900,569 to 876,688 tonnes between 2023 and 2024, while live-weight meat production also declined. This paper argues that genetic improvement should be treated as part of a wider recovery strategy rather than as a stand-alone technical intervention. Better animal identification and recording, selection based on performance, artificial insemination, genomic tools and conservation measures can improve productivity while protecting valuable local genetic resources. These measures, however, will only have a lasting effect if they are accompanied by better farm management, stronger producer cooperation, improved market access and more consistent public policies.

Keywords: Small ruminants; sustainable management; population dynamics; genetic improvement; technology transfer

INTRODUCTION

Sheep and goats occupy a distinctive place in Albania's agricultural landscape. Their importance is particularly visible in hilly and mountainous areas, where they provide milk and meat, make productive use of natural pastures and contribute to the income of a large number of rural households. Their role is also broader than production. Local breeds carry genetic characteristics developed under difficult environmental conditions, and livestock keeping is closely connected with pastoral knowledge, traditional products and the cultural identity of many rural communities.

The development of the sector over the last three decades has been uneven. Following the increase observed between 1991 and 1996, the number of small ruminants dropped sharply during the political and economic instability of 1997. The population recovered during the following years, declined again up to 2005 and then increased moderately until around 2016. Since then, however, the downward trend has become increasingly persistent. This recent decline is important because it is occurring at a time when many rural areas are already experiencing depopulation and a shortage of agricultural labour.

The problem therefore cannot be reduced to a simple fall in livestock numbers. When family flocks disappear, the sector loses production capacity, but it may also lose breeding animals, local knowledge and the practical experience needed to maintain indigenous breeds. The present paper reviews the recent development of Albania's small-ruminant sector, examines the main economic, structural, biological and institutional factors behind the decline, and considers how genetic improvement could be combined with better management and stronger value chains to support a more sustainable future.

MATERIALS AND METHODS

The study is based on a review and synthesis of official statistical and institutional information concerning the Albanian small-ruminant sector. Data on animal numbers, production and regional distribution for the period 2014–2024 were compiled from the Agricultural Reports and livestock publications of the National Institute of Statistics of Albania (INSTAT), including Livestock Statistics 2024, published in 2025, and Milk and Dairy Products 2024, published in 2025. Information on the conservation status of indigenous sheep and goat populations was taken from Government of Albania Decision (VKM) No. 1708 (2008), concerning in-situ conservation programmes.

The discussion of genetic improvement and conservation measures draws on FAO guidelines for the characterization and management of animal genetic resources (FAO, 2007; FAO, 2011; FAO, 2012; FAO, 2023), as well as information from the European Gene Bank Network for Animal Genetic Resources (EUGENA) and the IPARD III Rural Development Programme of Albania (European Commission, 2022). Time-series data were compared across years and animal categories in order to identify the direction and magnitude of changes. Production figures for meat, milk and cheese were also compared across the most recent years available. Regional data were considered in order to identify areas where small-ruminant production and local breed diversity remain particularly concentrated.

RESULTS AND DISCUSSION

The available statistics show a clear downward trend. The combined sheep and goat population fell from approximately 2.8 million head in 2014 to 1.792 million in 2024, corresponding to a reduction of about 36%. The decline became particularly pronounced after 2018. Between 2023 and 2024, the number of sheep decreased from 1.206 million to 1.177 million, while the number of goats fell from 640,000 to 615,000. Within these totals, milked sheep decreased from 1.006 million to 968,000 and milked goats from 512,000 to 501,000. These changes point to continuing pressure on family-based production systems and justify closer attention to the economic and genetic sustainability of the sector. (INSTAT, 2025) The recent population figures are summarized in Table 1 (INSTAT, 2025).

The decline in animal numbers is also visible in production. Live-weight meat production decreased from 135,483 tonnes in 2023 to 130,334 tonnes in 2024, a fall of 3.8%. Total national milk production fell by 2.7% between 2023 and 2024, from 900,569 to 876,688 tonnes. Cow's milk remains the largest component of national milk production, while goat's milk accounts for 7.7% and sheep's milk for 7.4%. Dairy processing also experienced a contraction: total cheese production decreased by 9.9% in 2024, with sheep-milk cheese declining by 5.9% and goat-milk cheese by 16.8%. These changes are relevant for small-ruminant farms because milk and traditional cheese products are among the main channels through which their production reaches the market. (INSTAT, 2025a; INSTAT, 2025b)

Table 1. Small-ruminant population dynamics in Albania, 2014–2024 (thousand head).

Category ('000 head)	**2014**	**2018**	**2021**	**2023**	**2024**
Small ruminants, total	2,800	2,781	2,256	1,846	1,792
Sheep, total	1,896	1,864	1,481	1,206	1,177
of which, ewes	1,419	1,366	1,116	1,006	968
Goats, total	904	917	775	640	615
of which, does	695	699	599	512	501

Source: INSTAT, historical Agricultural Reports; INSTAT (2025), Livestock Statistics 2024

Table 2. Sheep and goat meat production in Albania, selected years (thousand tonnes, live weight).

Category ('000 t)	**2014**	**2018**	**2021**	**2024**
Sheep meat	35.0	36.0	34.0	30.0
Goat meat	15.0	20.0	16.0	14.0

Source: INSTAT, historical Agricultural Reports; INSTAT (2025), Livestock Statistics 2024.

Table 3. Sheep and goat milk collection in Albania, 2020–2024 (thousand tonnes).

Category ('000 t)	**2020**	**2022**	**2023**	**2024**
Sheep milk	75.0	69.0	64.0	64.0
Goat milk	80.0	76.0	71.0	68.0

Source: INSTAT, historical Agricultural Reports; INSTAT (2025), Livestock Statistics 2024.

Production is not evenly distributed across the country. In 2024, Vlorë and Gjirokastër had the largest concentrations of sheep, accounting for 29.3% and 14.5% of the national total, respectively. This regional concentration is important when considering both the organization of production and the conservation of local genetic resources. (INSTAT, 2025)

Albania still has a valuable group of indigenous sheep and goat populations. Among sheep, Bardhoka, Ruda, Shkodranja, Lara e Polisit and the Recka (Komuna) population are recognized as local genetic resources. Goat populations include Caporja e Dragobisë, Dhija e Hasit, Dhija e Matit, Dhija e Velipojës, Dhija e Kallmetit, Caporja e Pogradecit, Dhija e Liqenasit and Dhija e Dukatit. Some of these populations, including Shkodranja and Lara e Polisit sheep and Caporja e Dragobisë and Dhija e Liqenasit goats, have been identified as endangered and are maintained through in-situ conservation programmes (Government of Albania, 2008).

The value of these animals is not necessarily expressed through maximum production under intensive conditions. Their strength is often their ability to remain productive under conditions in which high-yielding imported genotypes would require considerably more feed, management and veterinary support. This distinction is important when decisions about genetic improvement are made. A breed that produces less milk in a controlled system may nevertheless be the better choice for a mountain farm if it is better adapted to local pasture, climate and disease pressure.

Table 4. Comparative characteristics of local Albanian small-ruminant breeds and imported or crossbred genotypes.

Trait	**Local Albanian breeds**	**Imported / crossbred breeds**
Environmental adaptation	Very high; adapted to mountain terrain, drought and modest feed	Usually require more controlled feeding and management
Feed requirements	Low; efficient use of natural pasture	Higher; greater dependence on concentrated, high-quality feed
Milk yield per season	80–120 L (sheep); 150–300 L (goats)	200–300 L (sheep); 400–800 L (goats)
Milk fat content	High (6–8%); well suited to traditional cheese	Lower (3.5–5%); generally suited to fresh milk
Disease resistance	High natural tolerance to parasites and local climate	Often more sensitive; vaccination and hygiene require closer attention
Genetic conservation status	At risk; several populations are below 1,000 head	Widely available internationally

The reasons behind the present decline are interconnected. From an economic perspective, farms are exposed to rising production costs and fluctuations in farm-gate prices. Feed is one of the major production costs, while pasture resources are not always used efficiently because of degradation, management difficulties and uncertainty over land use. A large proportion of Albanian flocks are small and family-based, which can limit bargaining power and make it more difficult to establish stable links with collectors, processors and formal markets.

The structural weaknesses reinforce the economic ones. Farm fragmentation, limited cooperation among producers and the lack of reliable local collection and processing networks make it difficult to create consistent quantities and quality. The absence of a functioning and systematic animal identification and registration system is another major obstacle. Without reliable records, it is difficult to know which animals perform well, which breeding lines should be retained and where genetic improvement is actually taking place.

There are also biological and technical constraints. Breeding material is not always used within clearly defined selection programmes, performance recording remains limited, feeding is not always balanced according to physiological needs, and many farms continue to rely on management practices that restrict productivity. At the institutional level, support measures have not always been stable or clearly connected with productivity and quality, while cooperation among public authorities, universities and farmers remains insufficient. For these reasons, the current situation should be understood as a systemic problem rather than as a problem caused by animal genetics alone.

The consequences extend beyond the farm. Falling incomes can accelerate the disappearance of family farms, while lower domestic production increases reliance on imports. At the same time, Albania risks losing opportunities to develop higher-value products based on local milk, traditional cheese and other products associated with particular regions. Rural depopulation also means that pastoral knowledge is becoming harder to transmit from one generation to the next. In many mountain areas, the average age of farmers is already high, and the loss of active herders affects the way communal pastures are managed. Where grazing pressure becomes too high, pasture degradation can follow; where grazing is abandoned completely, other ecological changes may occur. In both cases, biodiversity and the ecological functions of pastoral landscapes may be affected.

Against this background, genetic improvement should be approached as a practical tool for strengthening the sector rather than as an isolated scientific exercise. The limited availability of

systematic performance records makes it difficult to compare the genetic and productive performance of Albanian flocks reliably with regional benchmarks. Nevertheless, the absence of consistent selection and recording remains an important constraint on genetic progress. A realistic improvement programme would begin with the establishment of a national breed registry compatible with FAO and EU approaches, followed by the identification and recording of superior animals within breed-specific nucleus farms. Selection should focus on traits that have direct value for farmers, including milk yield, growth, body weight and fertility.

More advanced technologies can then be introduced where the necessary infrastructure exists. Artificial insemination can accelerate the dissemination of desirable genetics, while genomic characterization based on SNP markers can help clarify relationships among local populations and identify genetic diversity that should be conserved. Gene banks for semen, somatic cells, ova and embryos can provide an additional safeguard for populations that are particularly vulnerable. These measures are especially relevant for breeds and populations such as Hasit, Dragobisë, Velipoja, Liqenas and Dukat goats and Shkodranja and Kolonjë sheep, where the loss of breeding animals could be difficult to reverse.

Experience from other European countries offers useful lessons, although their systems cannot simply be copied into Albania. Italy has linked genetic improvement with breed associations; France has developed extensive recording and selection systems that increasingly combine phenotypic and genomic information; Greece has connected local-breed conservation with geographical-origin branding. Kosovo and North Macedonia also provide examples of regional cooperation in genetic improvement. For Albania, the most appropriate model would likely be one that combines these lessons with the realities of small family farms and mountain production systems.

Genetic progress will have limited value if the economic environment of the farm does not improve at the same time. Farmers need simple records that allow them to understand what each animal actually costs and produces. Recording feed use and output, calculating the real cost per litre of milk or kilogram of meat, improving feeding according to physiological stage and making better use of local feed resources can all contribute to higher efficiency. Producer groups and cooperatives could also improve the position of farmers by enabling joint collection, processing and marketing. A nucleus-farm-and-satellite model may be particularly useful, allowing selected farms to produce breeding animals while neighbouring farms benefit from improved genetics.

A basic recording system would already represent a significant step forward. Individual animal identification, monthly milk recording and weighing of lambs and kids at birth and at approximately 45 and 90 days would generate information that is currently missing from many farms. Public support could be linked partly to the completion and quality of these records, creating an incentive for farmers to participate in the improvement system rather than treating subsidies simply as payment per head.

Policy support is equally important. A coherent national framework for small ruminants could bring together genetic improvement, pasture management and rural economic development. Subsidy schemes could increasingly reward performance, product quality, recording and conservation outcomes rather than animal numbers alone. Better veterinary and extension services in mountain areas, together with continued participation in programmes such as IPARD III, Horizon Europe and Interreg IPA Balkan–Med, could provide opportunities for investment, training and international cooperation.

CONCLUSIONS

The decline of Albania's small-ruminant sector is more than a reduction in livestock numbers. It reflects the combined effects of rising production costs, labour shortages, fragmented farms,

weak market organization, limited performance recording and inconsistent support systems. At the same time, the decline places pressure on a genetic heritage that has developed through generations of adaptation to Albania's diverse environments.

Reversing this trend will require more than introducing new technologies. Genetic improvement can provide an important foundation, but it needs to be connected with better farm management, reliable animal recording, stronger farmer cooperation, improved market access and policies that reward both productivity and conservation. The objective should not be to replace Albania's local breeds with imported genetics. Rather, improvement should increase the productivity of well-adapted animals while retaining the characteristics that make them valuable to mountain farming systems.

The future of the sector will ultimately depend on whether Albania can move from a model based largely on survival to one based on informed management and cooperation. Protecting local genetic resources, improving productivity and creating better economic opportunities are not separate goals. They are parts of the same transition, and together they can give small-ruminant farming a more sustainable and competitive future.

REFERENCES

European Commission. 2022. Commission Implementing Decision of 9.3.2022 adopting the IPA III Rural Development Programme (IPARD III) of the Republic of Albania for the years 2021–2027. Brussels.

EUGENA. n.d. European Gene Bank Network for Animal Genetic Resources. European Regional Focal Point for Animal Genetic Resources (ERFP). Available at: https://www.eugena-erfp.net.

FAO. 2007. Global Plan of Action for Animal Genetic Resources and the Interlaken Declaration. Rome.

FAO. 2011. Molecular Genetic Characterization of Animal Genetic Resources. FAO Animal Production and Health Guidelines No. 9. Rome.

FAO. 2012. Phenotypic Characterization of Animal Genetic Resources. FAO Animal Production and Health Guidelines No. 11. Rome.

Ajmone-Marsan, P., Boettcher, P.J., Colli, L., Ginja, C., Kantanen, J. & Lenstra, J.A. (eds.). 2023. Genomic characterization of animal genetic resources: Practical guide. FAO Animal Production and Health Guidelines No. 32. Rome, FAO. https://doi.org/10.4060/cc3079en.

Government of Albania. 2008. Decision (VKM) No. 1708, dated 29.12.2008, On the implementation of programmes for the in-situ conservation of autochthonous breeds of small ruminants.

INSTAT (National Institute of Statistics of Albania). 2025. Livestock Statistics 2024. Tirana.

INSTAT (National Institute of Statistics of Albania). 2025a. Livestock Statistics 2024. Tirana.

MOLECULAR CHARACTERIZATION OF ALBANIAN SHEEP AND GOAT BREEDS: A REVIEW OF GENETIC DIVERSITY AND POPULATION STRUCTURE

L.Hysi[1], L. Papa[1]

[1]Agricultural University of Tirana, Faculty of Agriculture and Environment, Department of Animal Science, Tirana, Albania.

Corresponding author: lhysi@ubt.edu.al

ABSTRACT

Albanian sheep and goat breeds represent an important component of the country's animal genetic resources and have been the subject of several molecular investigations over the last two decades. These studies have provided valuable information on the genetic diversity and population structure of indigenous breeds using different molecular marker systems. This review brings together the available evidence to provide an integrated overview of the current knowledge and to highlight its relevance for the conservation and sustainable management of Albanian small ruminant genetic resources. The published studies employed microsatellites (SSR), AFLP, mitochondrial DNA (mtDNA), and SNP markers to investigate the genetic diversity of sheep and goat breeds, although SNP-based studies remain comparatively limited compared to microsatellite-based research. Sheep breeds studied included Bardhoka, Ruda, Shkodrane, and Recka, together with several local goat populations. Although different approaches and sampling strategies were used, the studies reached similar conclusions: Albanian sheep and goat populations were consistently characterized by high genetic diversity, reflected in high allelic richness and heterozygosity. Most variation was observed within breeds, whereas differentiation among breeds was generally low to moderate, indicating preserved genetic variability. Population structure analyses also identified varying degrees of clustering and admixture, improving understanding of relationships among local breeds and their evolutionary history. These studies have established an important scientific foundation for the genetic characterization of Albanian sheep and goat breeds and have contributed significantly to the documentation of the country's animal genetic resources. Recent advances in genomic technologies provide new opportunities to complement the existing knowledge through genome-wide analyses, allowing a more detailed investigation of genetic diversity, population structure, inbreeding, admixture, and signatures of selection. The integration of these approaches with previous molecular studies will further support conservation programmes, sustainable breeding strategies, and the long-term preservation of Albania's indigenous sheep and goat breeds.

Keywords: Sheep, Goat, Breeds, Genetic diversity, Population structure, Molecular markers, Microsatellites.

INTRODUCTION

Sheep and goats are among the earliest domesticated livestock species and continue to play a fundamental role in global agriculture, food security, and rural livelihoods. According to the Food and Agriculture Organization (FAO), more than two billion sheep and goats are currently raised worldwide, providing meat, milk, fibre, hides, and other products while supporting the livelihoods of millions of smallholder farmers, particularly in marginal and mountainous regions (FAO, 2023). Beyond their economic value, indigenous sheep and goat breeds represent

an irreplaceable component of global animal genetic resources. Local breeds have evolved over centuries through a combination of natural selection and traditional breeding practices, resulting in populations that are well adapted to specific environmental conditions, disease challenges, and production systems (Groeneveld et al., 2010). Consequently, they constitute unique reservoirs of genetic variation that may prove essential for maintaining sustainable livestock production under future climatic and socio-economic scenarios (FAO, 2015).

The conservation of animal genetic resources has therefore become a global priority. The increasing replacement of indigenous breeds by highly specialized commercial populations has resulted in a continuous erosion of livestock biodiversity, raising concerns regarding the long-term sustainability of animal production systems (Taberlet et al., 2008). Molecular genetic tools have become indispensable for the characterization and conservation of livestock genetic resources. During the last three decades, DNA-based markers have progressively replaced traditional phenotypic and pedigree-based evaluations, allowing direct assessment of genetic diversity, population structure, phylogenetic relationships, and evolutionary history (Bruford et al., 2003). Microsatellite markers (SSR) represented the first generation of highly informative molecular markers widely adopted in livestock genetics because of their high polymorphism and codominant inheritance. Numerous international studies successfully applied microsatellites to estimate heterozygosity, allelic richness, genetic differentiation, and inbreeding in indigenous sheep and goat populations (Dalvit et al., 2008; Peter et al., 2007).

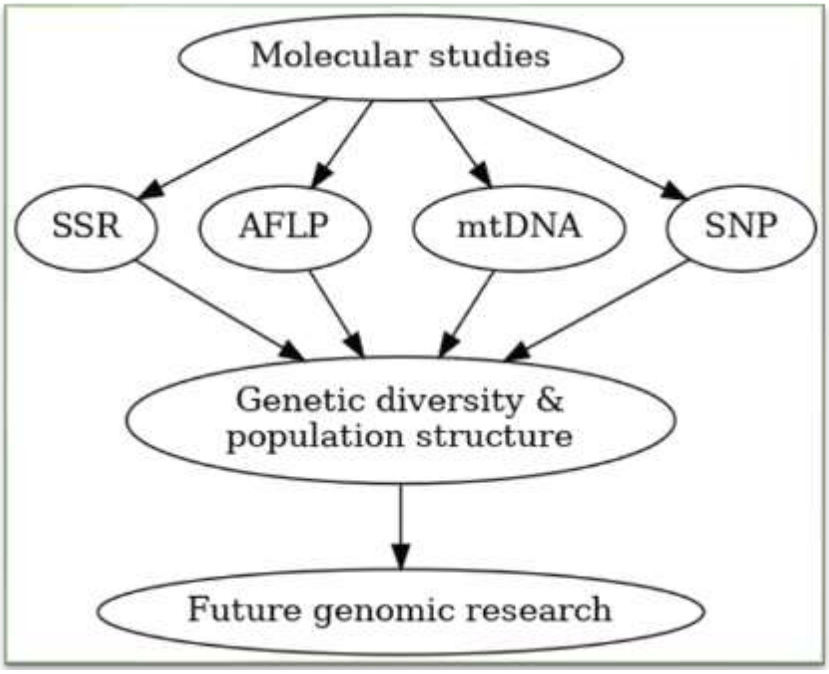

Figure 1. Molecular markers used for breed characterization

Subsequently, amplified fragment length polymorphism (AFLP) markers provided genome-wide information without requiring prior sequence knowledge and were extensively used for evaluating genetic relationships among livestock populations. More recently, the development of single nucleotide polymorphism (SNP) arrays and next-generation sequencing technologies has substantially improved the resolution of population genetic analyses. Genome-wide SNP datasets now enable the investigation of demographic history, genomic inbreeding, effective population size, signatures of selection, and adaptive genetic variation with unprecedented accuracy (Kijas et al., 2012; Colli et al., 2018). In parallel, mitochondrial DNA (mtDNA)

analyses have provided valuable insights into maternal lineages, domestication events, and phylogeographic relationships among livestock populations (Naderi et al., 2008).

Within Europe, numerous molecular studies have demonstrated that indigenous Mediterranean and Balkan sheep and goat breeds generally maintain high levels of genetic diversity despite relatively limited population sizes (Pariset et al., 2011; Ciani et al., 2020). These populations often exhibit weak to moderate genetic differentiation due to historical gene flow associated with transhumance, traditional grazing systems, and the long-term exchange of breeding animals among neighbouring regions. Such patterns have been reported in Italy, Greece, Spain, Serbia, Croatia, and Türkiye, highlighting the importance of extensive production systems in maintaining genetic diversity (Pariset et al., 2011; Colli et al., 2018).

Albania represents one of the biodiversity hotspots of the Balkan Peninsula and possesses several indigenous sheep and goat breeds that have adapted to diverse ecological conditions ranging from coastal Mediterranean areas to mountainous alpine environments. These breeds constitute valuable genetic resources because of their adaptation to low-input production systems, local diseases, and environmental constraints. During the past two decades, a series of molecular studies have investigated the genetic diversity and population structure of Albanian sheep and goat breeds using microsatellites, AFLP markers, SNPs, and mitochondrial DNA (Hoda et al., 2009; Hoda et al., 2011; Hykaj et al., 2013). Collectively, these studies have substantially improved the understanding of the genetic characteristics of Albanian livestock populations.

The objective of this review is to synthesize and evaluate the molecular genetic studies conducted on Albanian sheep and goat breeds, compare their principal findings with those reported for other Mediterranean and Balkan populations, and discuss their implications for the conservation and sustainable management of Albania's indigenous animal genetic resources.

MATERIAL AND METHOD

A comprehensive literature review was conducted to identify published molecular genetic studies on indigenous Albanian sheep and goat breeds. Relevant articles published between 2009 and 2023 were retrieved from Web of Science, Scopus, Google Scholar, PubMed and ScienceDirect using combinations of the keywords Albanian sheep, Albanian goat, genetic diversity, population structure, molecular markers, microsatellite (SSR), AFLP, SNP, and mtDNA.

For each selected publication, information on the year of publication, animal species, breeds investigated, sample size, molecular markers, analytical methods, and main findings was systematically extracted and summarized in comparative tables.

Given the heterogeneity of the reviewed studies regarding molecular markers, sample size, and analytical approaches, a qualitative comparative analysis was performed rather than a quantitative meta-analysis. The synthesis focused on genetic diversity, population structure, phylogenetic relationships, and conservation-related findings, while comparisons with similar studies from other Mediterranean and Balkan countries were included whenever appropriate.

RESULTS AND DISCUSSION

The molecular characterization of Albanian sheep and goat populations has mainly been carried out by researchers from the Agricultural University of Tirana, particularly Anila Hoda and collaborators. The available literature shows that work in this area was especially concentrated between 2009 and 2014. The sheep breeds most frequently studied were Bardhoka, Ruda, Shkodrane and Recka. Studies on goat genetic structure shows that the core work focused on six autochthonous Albanian goat breeds—Capore, Dukati, Hasi, Liqenasi, Mati and

Muzhake—while more recent work also examined Velipoja, Dragobia and Smokthina. Across the published studies, several marker systems were used, including microsatellites, AFLP markers, SNPs and mitochondrial DNA (mtDNA) D-loop sequences. These studies were designed to estimate genetic diversity, quantify breed differentiation, assess inbreeding, infer relationships among breeds and evaluate population structure and admixture.

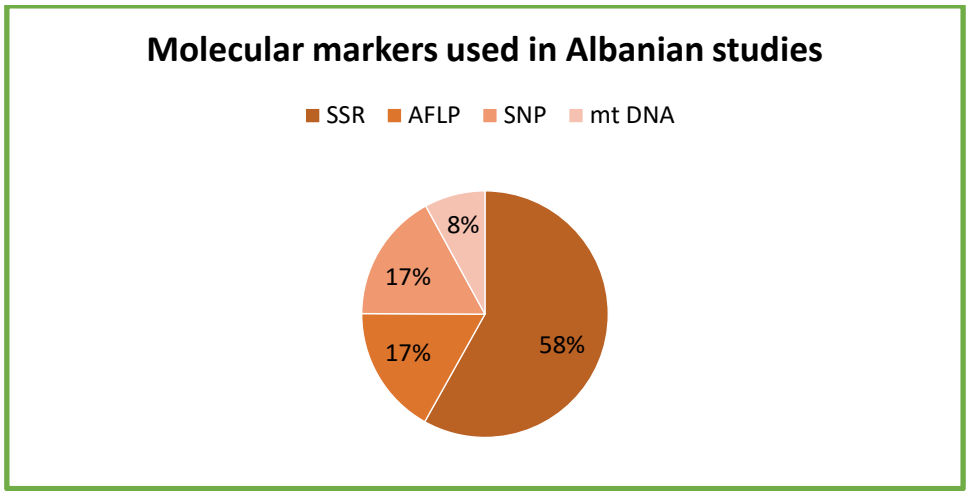

Figure 2. Molecular markers used in Albanian studies

The main molecular studies in sheep are presented in Table 1

Table 1. Sheep molecular studies

Year	Authors	Breeds	Sample size	Markers	Main findings
2009	Hoda A., Dobi P., Hykaj G.	Bardhoka, Ruda, Recka, Shkodrane	124	6 microsatellites	High diversity; FST=0.106; ~89% within-breed variation
2009	Hoda A. et al.	Bardhoka, Ruda, Shkodrane	93	31 microsatellites	K=2 clusters; strong admixture; weak separation
2010	Hykaj G., Hoda A.	Bardhoka, Ruda, Shkodrane	93	31 microsatellites	~98.9% variation within breeds; very low between
2011	Hoda A. et al.	Bardhoka, Ruda, Shkodrane	93	36 SNPs	Weak structure confirmed at genome level
2012	Hykaj G., Hoda A., Ajmone-Marsan P.	Bardhoka, Ruda, Shkodrane	93	AFLP markers	~96% within-individual variation; weak structure
2014	Hoda A. et al.	Recka	32	15 microsatellites	High heterozygosity; high allelic richness

The first molecular characterization conducted by Hoda. A., Dobi. P., Hykaj. G (2009) represented a milestone in the genetic evaluation of Albanian sheep populations. Using six microsatellite loci in four local breeds (Bardhoka, Ruda, Recka and Shkodrane), 124

individuals, the authors identified 98 alleles, corresponding to an average of 8.15 alleles per locus, demonstrating considerable allelic richness. Approximately 89% of the total genetic variation was distributed within breeds, while the genetic differentiation among breeds was relatively low (GST ≈ 0.106). Principal Component Analysis and Neighbor-Joining clustering further indicated that Bardhoka and Shkodrane were genetically more closely related than Recka, reflecting both geographical proximity and historical gene flow.

The second major study from 2009 focused specifically on population structure rather than only on diversity indices. It used 31 microsatellite markers to analyze Albanian sheep breeds, particularly the local breeds Bardhoka, Ruda and Shkodrane. The work was carried out in the framework of the ECONOGENE project, which aimed to support molecular characterization and conservation of local animal genetic resources. Similar findings were reported by Hykaj and Hoda (2010), who observed that 98.89% of molecular variation occurred within breeds, leaving only about 1.1% attributable to differences among breeds. Such values clearly indicate that historical migration, uncontrolled mating and the absence of strict breeding isolation have maintained substantial gene flow among Albanian sheep populations. The AFLP study performed by Hykaj et al. (2012) further confirmed this pattern. Although AFLP markers represent a different class of molecular markers, they also demonstrated that approximately 96% of the total molecular variation was distributed among individuals within breeds, whereas only a small fraction was explained by differences among breeds.

The transition from microsatellite markers to SNP technology represented another important step in the molecular characterization of Albanian sheep. Using 36 SNP markers, Hoda et al. (2011) again identified weak population structure and considerable admixture among Bardhoka, Ruda and Shkodrane breeds. Although SNPs are individually less polymorphic than microsatellites, their high reproducibility confirmed the conclusions obtained with previous marker systems and demonstrated the robustness of the observed population structure.

Breed-specific analysis of the Recka sheep (Hoda et al., 2014) further highlighted the rich genetic resources preserved within Albanian breeds. Analysis of 15 microsatellite loci identified 143 alleles, high observed heterozygosity (approximately 0.785), high polymorphic information content (PIC), and a very low inbreeding coefficient (FIS ≈ 0.013). These parameters indicate that Recka has retained substantial genetic variability and has experienced limited inbreeding despite its relatively restricted geographic distribution.

Taken together, the reviewed studies reveal a remarkably consistent pattern in Albanian sheep populations. Regardless of whether microsatellites, AFLP or SNPs were employed, the majority of genetic variation was consistently detected within breeds rather than among breeds. The estimated proportion of within-breed variation ranged from approximately 89% to 98.89%, while the corresponding among-breed component remained comparatively small.

Microsatellite analyses demonstrated high allelic diversity and substantial within-breed variation, AFLP analyses confirmed the predominance of within-population molecular variation, while SNP analyses independently supported weak genetic structuring. High within-breed diversity represents a valuable reservoir of genetic variation that may contribute to adaptation to local environmental conditions and traditional production systems. At the same time, the relatively low differentiation among breeds means that conservation strategies should consider both the preservation of individual breed identities and the maintenance of the broader genetic diversity present across Albanian sheep populations.

Table 2. Goat molecular studies

Year	Authors	Breeds	Sample size	Markers	Main analyses	Main findings
2011	Hoda A., Hykaj G., Dunner S., Obexer-Ruf G.	Capore, Dukati, Hasi, Liqenasi, Mati, Muzhake	183	30 microsatellites	Ho, He, FIS, FST	High diversity within-breed. Very low differentation among breeds.
2012	Hoda. A., Sena L., Hykaj G.	Capore, Dukati, Hasi, Liqenasi, Mati, Muzhake	185	AFLP	Nei's expected heterozygosity; Shannon index; FST;	High levels of within-breed genetic diversity
2012	Hykaj G., Hoda A., Bicoku Y., Papa L.	Muzhake	30	30 microsatellites	Allelic diversity, heterozygosity	High polymorphism
2012	Bozgo V., Hoda A., Bicoku Y., Bajramaj R.	Hasi, Bulçar, Çekin, Peza, and Velipoja	328	Visible markers (seven visible traits)	PCA, genetic distance	Phenotypic differentiation
2013	Hykaj G., Hoda A., Dobi P., Papa L., Bakiu R., Novaku M.	Capore, Dukati, Hasi, Liqenasi, Mati, Muzhake	185	26 SNPs	Genetic distance, genetic diversity	Most genetic variation occurs within individuals rather than between breeds
2014	Hoda A., Bicoku Y., Dobi P.	Capore, Dukati, Hasi, Liqenasi, Mati, Muzhake		77 mtDNA D-loop	Haplotype analysis	**High haplotype diversity** but **low nucleotide diversity**. Rich maternal gene pool.
2014	Hykaj G &Hoda A.	Capore, Dukati, Hasi, Liqenasi, Mati, Muzhake	185	Review article 31SSR, AFLP and 26 SNP markers	Genetic distance, genetic diversity	All microsatellite markers were highly polymorphic
2023	Hoda A, Hykaj G, Hysi L et al.	Velipoja, Dragobia, Smokthina	90	10 microsatellites	STRUCTURE, Ho, He	High diversity

The molecular studies conducted on Albanian indigenous goat breeds consistently demonstrate that these populations retain substantial levels of genetic diversity despite long-term adaptation to extensive production systems and the relatively small effective population sizes of several local breeds. Studies employing microsatellite markers (SSR), AFLP, SNPs and mitochondrial DNA (mtDNA) have produced remarkably consistent conclusions, indicating high within-breed genetic variability coupled with weak genetic differentiation among breeds (Hoda et al., 2011; Hoda et al., 2012; Hykaj et al., 2013; Hoda et al., 2014).

The first comprehensive molecular characterization of Albanian goat breeds was performed by Hoda et al. (2011) using 30 microsatellite loci in 183 unrelated animals representing six indigenous breeds (Capore, Dukati, Hasi, Liqenasi, Mati and Muzhake). The study identified a high degree of polymorphism across all loci, with expected heterozygosity ranging approximately from 0.71 to 0.76, while the mean number of alleles per locus exceeded ten. Genetic differentiation among breeds was very limited ($F_{ST} \approx 0.02$), indicating that approximately 98% of the total genetic variation was maintained within breeds.

The AFLP-based investigation by Hoda, Sena and Hykaj (2012) confirmed the microsatellite results using an independent marker system. AFLP analysis revealed a high level of polymorphism together with considerable within-population diversity. Shannon diversity indices and Nei's expected heterozygosity demonstrated that all six breeds possess abundant genetic variation, whereas Reynolds and Nei genetic distance estimates indicated only moderate differentiation among populations. Cluster analyses grouped genetically related breeds largely according to their geographical distribution, although substantial overlap among breeds remained evident.

Further evidence was provided by the SNP analysis conducted by Hykaj et al. (2013), in which 26 single nucleotide polymorphisms were used to evaluate genetic relationships among six Albanian goat breeds. Despite the lower polymorphism of individual SNP loci compared with microsatellites, the study confirmed weak to moderate population structure and relatively low assignment accuracy of individuals to their breed of origin.

Mitochondrial DNA analysis performed by Hoda et al. (2014) added an evolutionary perspective by investigating sequence variation within the mtDNA D-loop region. Several distinct haplotypes were identified among Albanian goat breeds, demonstrating considerable maternal lineage diversity. Phylogenetic analysis indicated that Albanian goats belong predominantly to the widespread European maternal lineage (haplogroup A), while the observed haplotype diversity suggests multiple historical maternal origins and long-term maintenance of maternal genetic variability.

The molecular characterization of the Muzhake breed using microsatellite markers demonstrated high heterozygosity and substantial allelic diversity, confirming that even geographically restricted populations have preserved considerable genetic variation. Similarly, analyses of three northern Albanian goat populations (Velipoja, Dragobia and Smokthina) revealed weak population subdivision despite clear phenotypic differences, emphasizing that morphological differentiation is not necessarily accompanied by marked genetic divergence (Hoda, Hykaj & Hysi et al., 2023).

Overall, the remarkable agreement among studies employing SSRs, AFLP, SNPs and mtDNA demonstrates that Albanian goat breeds represent valuable reservoirs of genetic diversity. The predominance of within-breed variation indicates that traditional extensive production systems have maintained genetic variability while limiting the development of strong genetic isolation among local breeds.

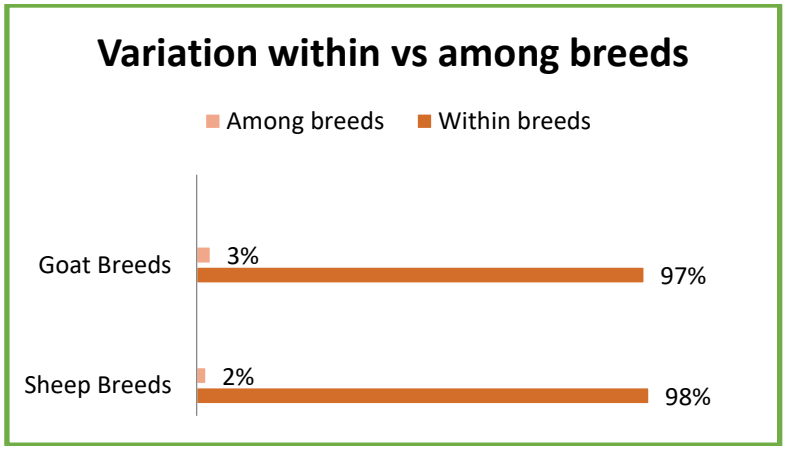

Figure 3. Variation within and among breeds

Comparison with international studies further demonstrates that Albanian sheep and goat breeds exhibit genetic diversity levels comparable to, or even exceeding, many indigenous European populations. Microsatellite analyses of Italian sheep breeds reported expected heterozygosity values between 0.65 and 0.75, while Greek and Balkan sheep populations generally showed values ranging from 0.68 to 0.77 (Dalvit et al., 2008; Ligda et al., 2009; Peter et al., 2007). Comparable patterns have also been described in several Balkan countries. Croatian Pramenka populations and Serbian indigenous breeds exhibit moderate to high allelic richness but weak genetic subdivision due to historical transhumance and gene flow among neighbouring populations (Šalamon et al., 2014). Likewise, Romanian Zackel-derived breeds show high within-population diversity and relatively low FST values (Kusza et al., 2015), closely resembling the genetic structure identified in Albanian sheep.

Similar estimates also have been reported for Mediterranean goat breeds, where expected heterozygosity usually ranges between 0.68 and 0.78 and FST values remain relatively low (Canon et al., 2006; Di Lorenzo et al., 2014). The Albanian studies therefore place local breeds among the genetically richest indigenous populations in southeastern Europe.

Similar values have also been described for Greek indigenous goats, where extensive traditional management has maintained high levels of within-population diversity (Ligda et al., 2009).Comparable patterns have been reported in Balkan countries. Serbian, Croatian and Romanian indigenous goat breeds generally exhibit expected heterozygosity values above 0.70, while FST values typically range between 0.02 and 0.06, indicating limited genetic differentiation among neighbouring populations (Ramljak et al., 2018; Kusza et al., 2015).

CONCLUSIONS

Both Albanian sheep and goat breeds constitute unique components of the European animal genetic heritage. Their high levels of genetic diversity, low inbreeding, considerable allelic richness and long-term adaptation to diverse ecological conditions underline the importance of implementing coordinated national conservation programmes while promoting the sustainable utilization of these valuable indigenous genetic resources.

REFERENCES

Bruford, M. W., Bradley, D. G., & Luikart, G. (2003). DNA markers reveal the complexity of livestock domestication and diversity. Nature Reviews Genetics, 4, 900–910.

Cañón, J., et al.(2006) "Geographical partitioning of goat diversity in Europe and the Middle East." Animal genetics 37.4 : 327-334.
Ciani, Elena, et al. "Genome-wide analysis of I talian sheep diversity reveals a strong geographic pattern and cryptic relationships between breeds." Animal Genetics 45.2 (2014): 256-266.
Ciani, E., Mastrangelo, S., Da Silva, A., Marroni, F., ..., Hoda, A., ..., & Lenstra, J. A. (2020). On the origin of European sheep as revealed by the diversity of the Balkan breeds and by optimizing population-genetic analysis tools. Genetics Selection Evolution, 52:25.
Colli, L., et al. (2018). Genome-wide SNP profiling of worldwide goat populations reveals strong partitioning of diversity and highlights post-domestication migration routes. Genetics Selection and Evolution, 50, 58..
Dalvit, C., et al. "Genetic diversity and variability in Alpine sheep breeds." Small Ruminant Research 80.1-3 (2008): 45-51.
Di Lorenzo, P., et al. (2014). Microsatellite analysis of Italian goat breeds. Small Ruminant Research.
FAO. (2015). The Second Report on the State of the World's Animal Genetic Resources for Food and Agriculture. Rome. .
FAO. (2023). FAOSTAT Statistical Database.
Groeneveld, L. F., et al. (2010). Genetic diversity in farm animals – a review. Animal Genetics, 41(Suppl. 1), 6–31.
Hoda A., Ajmone-Marsan P., Hykaj G. and Econogene consortium (2010). Genetic diversity in Albanian sheep breeds estimated by AFLP markers. Albanian Journal of Agricultural Sciences Vol 10(2), p 23-29
Hoda A., Dobi P., Hykaj G. and Econogene consortium (2009). Population structure in Albanian sheep breeds analyzed by microsatellite markers. Livestock Research for Rural Development 21 (11).
Hoda A., Sena L. and Hykaj G. (2012) Genetic diversity revealed by AFLP markers in Albanian goat breeds. Arch. Biol. Sci., Belgrade, 64 (2), 799-807. (IF = 0.356)
Hoda, A. , Hykaj, G. , Sena, L. and Delia (Veizaj), E. (2011). Population structure in three Albanian sheep breeds using 36 single nucleotide polymorphisms. Acta Agriculturae Scandinavica, Section A – Animal Science, 61: 1, 12 20 (IF 0.484).
Hoda, A., Biçoku, Y., & Dobi, P. (2014). Genetic diversity of Albanian goat breeds revealed by mtDNA sequence variation . Biotechnology & Biotechnological Equipment, 2014 Vol. 28, No. 1, 77–81, http://dx.doi.org/10.1080/13102818.2014.901672
Hoda, A., Hykaj G. , Dunner, S, Obexer-Ruff, G and Econogene Consortium (2011) Genetic diversity of Albanian goat breeds based on microsatellite markers. Arch. Zootec. 60 (230): 605-613
Hoda, A., Hykaj, G., Hysi, L., Bixheku, H. (2023): Genetic structure of three Albanian local goat breeds based on micosatellite markers. Agriculture and Forestry, 69 (2): 7-19. doi:10.17707/AgricultForest.69.2.01
Hoda, A., Vegara, M., & Bozgo, V. (2014).
Hoda, A.; Dobi, P., and G. Hyka. (2009). Population structure in Albanian sheep breeds analyzed by microsatellite markers. Livestock Research for Rural Development 21.
Hykaj G., Hoda A. (2014). Genetic diversity of albanian goat breeds estimated by molecular markers. Albanian J. Agric Sci., 13 (Special editidon): 249 252
Hykaj G., Hoda A., Biçoku Y. and Papa L. (2012). Genetic variability of Muzhake goat, estimated by microsatellite markers. Livestock Research for Rural Development. Volume 24, Article #126

Hykaj G., Hoda A., Dobi, P., Papa, L., Bakiu, R. and Novaku, M. (2013). Population structure and genetic distances betëeen six Albanian local goat breeds using 26 SNP markers. Livestock Research for Rural Development 25 (4) 2013

Kijas, J. W., et al. (2012). Genome-wide analysis of the world's sheep breeds reveals high levels of historic mixture and strong recent selection. PLoS Biology, 10(2), e1001258.

Kusza, Szilvia, et al. "Mitochondrial DNA variability in Gyimesi Racka and Turcana sheep breeds." Acta Biochimica Polonica 62.2 (2015): 273-280.Ligda, C., et al. (2009). Genetic diversity of Greek sheep and goat breeds. Small Ruminant Research.

Naderi, S., et al. (2008). The goat domestication process inferred from large-scale mitochondrial DNA analysis. Proceedings of the National Academy of Sciences, 105, 17659–17664.

Pariset, L., et al. (2011). Genetic diversity of sheep breeds from Albania, Greece, and Italy assessed by mitochondrial DNA and nuclear polymorphisms (SNPs). The Scientific World Journal, 2011, 186342, 1–19.

Peter, C., et al. (2007). Genetic diversity and subdivision of European sheep breeds. Journal of Animal Breeding and Genetics.

Ramljak, J., Bunevski, G., Bytyqi, H., Marković, B., Brka, M., Ivanković, A., ... & Medugorac, I. (2018). Conservation of a domestic metapopulation structured into related and partly admixed strains. Molecular ecology, 27(7), 1633-1650.

Taberlet, P., et al. (2008). Are cattle, sheep, and goats endangered species? Trends in Genetics, 24, 449–452.

Zeder, M. A. (2008). Domestication and early agriculture in the Mediterranean Basin. Proceedings of the National Academy of Sciences.

EVALUATION OF FLUORIDE AND CHLORIDE CONCENTRATIONS IN SULTANKÖY AND ALTINYAZI RESERVOIRS (TÜRKIYE): A COMPARATIVE AND DENTAL PUBLIC HEALTH APPROACH

Meltem Tekbaş Atay[1], Mediha Büyükgöze Dindar[1], Cem Tokatlı[2]*

[1]Trakya University, Faculty of Dentistry, Edirne / Türkiye
[2]Trakya University, İpsala Vocational School, Edirne / Türkiye

**Corresponding author: meltemtekbasatay@trakya.edu.tr*

ABSTRACT

In this comprehensive and detailed hydrochemical investigation, the seasonal water quality dynamics, spatial variations, and overall pollution profiles of the Sultanköy and Altınyazı Reservoirs, which hold immense strategic importance for extensive agricultural irrigation practices and regional freshwater reserves within the economically vital Meriç-Ergene Basin, were comparatively evaluated and monitored based on precise fluoride (F^-) and chloride (Cl^-) ion parameters. The extensive analytical results, laboratory data, and field observations revealed that despite both artificial aquatic systems being located within the exact same geographical area and climatic region, the fundamental hydrochemical characteristics and major anion compositions of these two crucial water bodies significantly differ on a critical basin scale. According to the quantitative findings of the monitoring program, Altınyazı Reservoir prominently stands out with its remarkably high chloride concentrations and elevated salinity indicators, whereas fluoride accumulation exhibits a much more dominant, persistent, and distinctive hydrochemical character throughout the Sultanköy Reservoir ecosystem. This sharp contrast in the dominant anion distribution and geochemical fingerprints of the reservoirs clearly points to highly differing anthropogenic pressures occurring along the specific drainage lines feeding the dams, the varying quality and volume of agricultural return waters draining from surrounding crop fields, or the distinct local lithological configurations and geological structures characterizing the respective drainage basins. Consequently, this comparative research study provides critical baseline data, scientific insights, and environmental indicators necessary for implementing sustainable water resource management strategies in the region, protecting aquatic ecosystems, and assessing the future long-term utilization potential and ecological safety of both reservoirs for irrigation and secondary purposes.

Keywords: Sultanköy Reservoir, Altınyazı Reservoir, Fluoride, Chloride, Dental health, Meriç-Ergene Basin

INTRODUCTION

In the 21st century, the degradation of freshwater ecosystems stands out as a paramount environmental crisis, severely jeopardizing aquatic biodiversity and public health (Helvacıoğlu et al., 2025; Din et al., 2023; Muhammad et al., 2025). As vital lentic components, artificial reservoirs perform indispensable functions in irrigation and municipal water supply. Nonetheless, intensifying anthropogenic stressors—primarily driven by agrochemical runoff and wastewater discharges—frequently induce severe water quality degradation in these critical water bodies (Çiçek et al., 2014; Köse et al., 2020; Ustaoğlu et al., 2022).

The Sultanköy and Altınyazı Dam Lakes represent two pivotal reservoirs in Edirne Province (Türkiye), serving as lifelines for regional drinking water supply and agricultural activities. Established by the General Directorate of State Hydraulic Works (DSİ) to sustain the socioeconomic and ecological equilibrium of the region, these reservoirs are increasingly subjected to anthropogenic threats (http://www2.dsi.gov.tr/). Persistent agricultural drainage and domestic waste loads introduce substantial amounts of contaminants into these lacustrine systems, threatening their long-term sustainability (Tokatlı et al., 2017; Tokatlı, 2019; 2020a; 2020b).

From a public health and dentistry perspective, monitoring specific hydrochemical parameters like fluoride is of utmost clinical significance. Fluoride is a crucial micronutrient fundamental for preventing dental caries, with municipal drinking water being its predominant intake vector (Andezhath et al., 1993; Güner et al., 2016; Tokatlı and Güner, 2018; Onur and Tokatlı, 2020; Tokatlı et al., 2022; 2023). However, its therapeutic window is remarkably narrow; chronic overexposure can precipitate debilitating conditions, most notably dental and skeletal fluorosis. Consequently, determining precise fluoride concentrations in regional water reserves remains a critical cross-disciplinary concern linking environmental science with preventive dentistry.

To address these pressing ecological and public health concerns, the present study was designed to execute a comparative hydrochemical assessment of the Sultanköy and Altınyazı Dam Lakes, with a primary focus on their fluoride (F) and chloride (Cl) profiles.

MATERIALS AND METHODS

Research Area and Sample Collection

Figure 1 illustrates the topographic configuration of the study area, including the spatial distribution of the selected monitoring stations across the Sultanköy and Altınyazı Dam Lakes. Within the scope of this study, surface water samples were systematically collected from the designated stations in the autumn season of 2024. The sampling strategy was specifically scheduled for a single campaign during autumn, as this transitional period marks the onset of significant seasonal precipitation. This hydrometeorological timing was strategically chosen to capture the critical phase where increased surface runoff and atmospheric depositions intensively flush the surrounding watershed, thereby significantly influencing the transport and concentration dynamics of fluoride and chloride ions within the reservoir ecosystems.

Fluoride and Chloride Analysis

Fluoride and chloride concentrations were quantified using spectrophotometric techniques, employing a Hach Lange DR 3900 spectrophotometer (https://tr.hach.com/) following APHA protocols (1998, 2017). For the determination of fluoride levels, the Hach Lange LCK 323 cuvette test kit was utilized. Concurrently, chloride concentrations were measured using the Hach Lange LCK 311 cuvette test kit. All analytical procedures were conducted in strict accordance with the manufacturer's protocols to ensure accuracy and reproducibility.

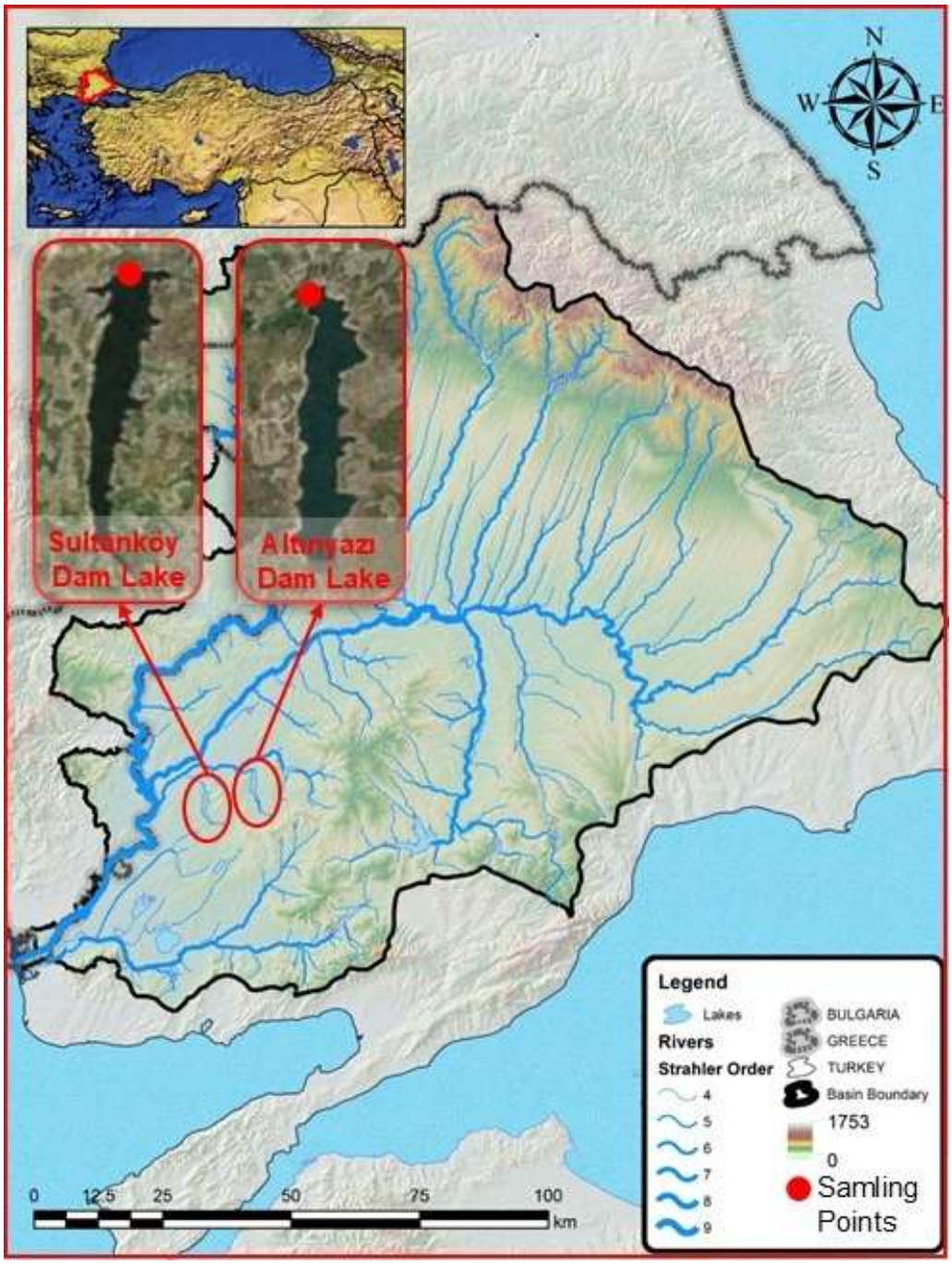

Figure 1. Meriç – Ergene Basin, investigated reservoirs and selected sampling stations

RESULTS AND DISCUSSION

The fluoride and chloride distributions in the Sultanköy and Altınyazı Dam Lakes are illustrated in Figure 2. The analytical results revealed distinct hydrochemical profiles for each reservoir. Chloride concentrations peaked in Altınyazı Dam Lake (158.00 ppm) compared to Sultanköy Dam Lake (89.00 ppm). Conversely, a completely opposite trend was observed for fluoride; Sultanköy Dam Lake exhibited significantly higher levels (0.418 ppm) than Altınyazı Dam

Lake (0.103 ppm), showing an approximately four-fold increase between these lentic ecosystems.

Fluoride is a vital trace element with double-edged clinical implications. While its deposition in dental tissues plays a fundamental role in preventing dental caries, excessive exposure can trigger substantial pathological risks depending on concentration and duration (Taghipour et al., 2016; Tokatlı et al., 2022; 2023). Because drinking water supplies serve as the primary exposure vector, maintaining optimal fluoride levels remains a critical cornerstone of dental public health and preventive dentistry. On the contrary, chronic ingestion above therapeutic thresholds can precipitate dental and skeletal fluorosis (Güner et al., 2016; Tokatlı and Güner, 2018; 2020; Jannat et al., 2022; Din et al., 2024).

In the present study, fluoride concentrations in both Sultanköy (0.418 ppm) and Altınyazı (0.103 ppm) reservoirs were well within the permissible drinking water limit of 1.5 ppm stipulated by TS266 (2005), EC (2007), and WHO (2011). Although both lakes pose no fluorosis risk, the significantly lower fluoride level in Altınyazı suggests that supplementary oral health strategies might be required if utilized for municipal supply to ensure adequate protection against caries. Turningly, the higher chloride levels in Altınyazı Dam Lake (158.00 ppm) point toward more intense agricultural runoff or evaporative concentration dynamics in its catchment area.

CONCLUSIONS

This study evaluated the comparative hydrochemistry of Sultanköy and Altınyazı Dam Lakes with a specific focus on fluoride and chloride dynamics. The results revealed a distinct environmental polarization between the two reservoirs; Altınyazı Dam Lake is characterized by higher chloride loads, likely driven by agricultural runoff, whereas Sultanköy Dam Lake exhibits a significantly more dominant fluoride character. From a clinical and dental public health perspective, the fluoride concentrations in both lentic ecosystems remain safely below the maximum permissible drinking water threshold of 1.5 ppm set by WHO, EC, and TS266, indicating no risk of dental or skeletal fluorosis for the local population. However, the remarkably low fluoride levels in Altınyazı Dam Lake highlight a potential insufficiency for optimal dental caries prevention if these waters are integrated into municipal supply grids. Ultimately, these baseline outputs underscore the necessity of cross-disciplinary monitoring strategies that bridge environmental watershed management with preventive dentistry to ensure the dual protection of ecosystem stability and regional oral health.

ACKNOWLEDGEMENTS

This study was supported by Trakya University Scientific Research Projects Unit under Project Code 2024/230. The author would like to thank Trakya University for the financial and institutional support provided throughout the research.

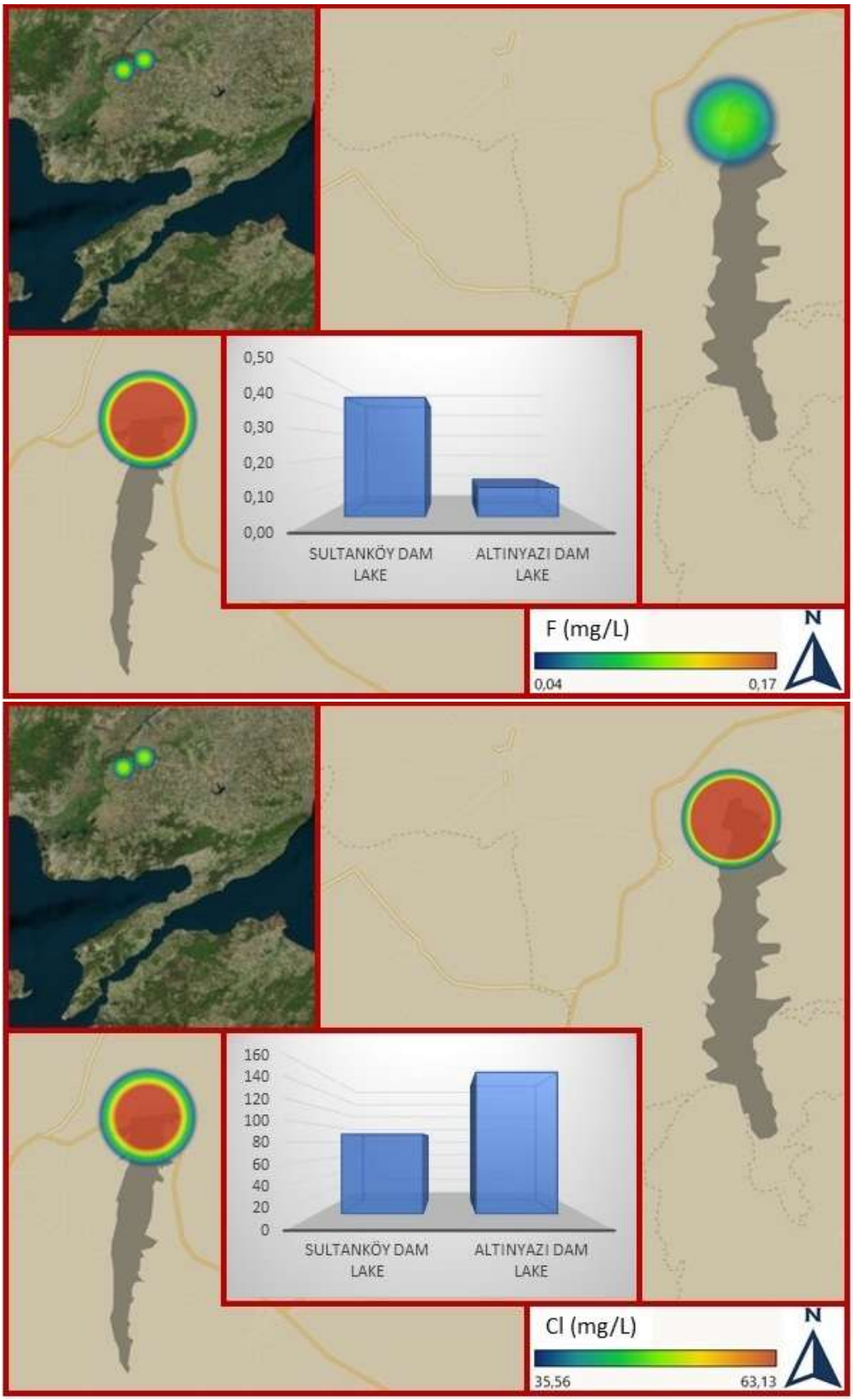

Figure 2. Fluoride and chloride levels in the investigated reservoirs

REFERENCES

Andezhath, S. K., Kumar, A., Bhatnagar, M., Bahudur, R., 1993. Prevalence of Endemic Fluorosis with Gastro-Intestinal Manifestations in People Living in Some North-Indian Villages. Fluoride, 26 (2): 97-104.

APHA, 1998. Standard Methods for the Examination of Water and Wastewater. American Public Health Association. Inc., Washington, DC.

APHA, 2017. American public health association (APHA). Stand. Methods Exam. Water Wastewater.

Çiçek, A., Köse, E., Emiroğlu, Ö., Tokatlı, C., Başkurt, S., Sülün, Ş., 2014. Boron and arsenic levels in water, sediment and tissues of Carassius gibelio (Bloch, 1782) in a dam lake. Polish Journal of Environmental Studies, 23 (5): 1843-1848.

Din, I. U., Wajid, A., Muhammad, S., Rehman, I., Tokatlı, C., 2024. Spatial Distribution and Potential Health Risk Assessment for Fluoride And nitrate Via Water Consumption in Pakistan. Journal Of Geochemical Exploration, 259: 107413.

EC (European Communities), 2007. European Communities (drinking water) (no. 2). Regulations 2007. S.I. No. 278 of 2007.

Güner, Ş., Uyar-Bozkurt, S., Haznedaroğlu, E., Menteş, A., 2016. Dental Fluorosis and Catalase Immunoreactivity of the Brain Tissues in Rats Exposed to High Fluoride Pre- and Postnatally. Biol Trace Elem Res., 174 (1): 150-157.

Helvacıoğlu, İ. A., Gülbaşı, A., Tokatlı, C., 2025. Evaluating the environmental sustainability awareness of paddy producers in the Meriç Plain (Northwest Türkiye): a comprehensive statistical approach. Acta Scientiarum Polonorum-Formatio Circumiectus, 24 (1): 3-13.

https://tr.hach.com/

Jannat, J. N., İslam, K. M. S., İslam, H. M. T., İslam, M. S., Khan, R., Bakar, S. M. A., Varol, M., Tokatlı, C., Chandra, P. S., İslam, A., İdris, A. M., Malafaia, G., Islam, A. R. T., 2022. Hydrochemical Assessment of Fluoride and Nitrate in Groundwater from East and West Coasts of Bangladesh and India. Journal of Cleaner Production, https://doi.org/10.1016/j.jclepro.2022.133675.

Köse, E., Emiroğlu, Ö., Çiçek, A., Aksu, S., Başkurt, S., Tokatlı, C., Şahin, M., Uğurluoğlu, A., 2020. Assessment of ecologic quality in terms of heavy metal concentrations in sediment and fish on Sakarya River and dam lakes, Turkey. Soil and Sediment Contamination: An International Journal, 29:3, 292-303.

Muhammad, S., Ahmed, T., Amin, S., Tokatlı, C., Ustaoğlu, F., 2025. Spatial distribution of hazard index via heavy metals consumption in water from the Himalayan lacustrine ecosystems. Physics and Chemistry of the Earth, 138: 103858.

Onur, Ş. G., Tokatlı, C., 2020. Comparison of Fluoride Contents in Terms of Teeth Health and Water Quality in Drinking Water at the Northern and Southern Regions of Meriç River Basin (Edirne/Turkey). International Journal of Agriculture, Environment and Food Sciences, 4 (2): 173-180.

Taghipour, N., Amini, H., Mosaferi, M., Yunesian, M., Pourakbar, M., Taghipour, H., 2016. National and Sub-National Drinking Water Fluoride Concentrations and Prevalence of Fluorosis and of Decayed, Missed and Filled Teeth in Iran from 1990 to 2015: A Systematic Review. Environmental Science and Pollution Research, 23 (6): 5077–5098.

Tokatlı, C., 2019. Use of the potential ecological risk index for sediment quality assessment: a case study of dam lakes in the Thrace part of the Marmara Region. Aquatic Sciences and Engineering, 34 (3): 90-95.

Tokatlı, C., 2020a. Pesticide accumulations in water and sediment of dam lakes located in Thrace part of Marmara Region (Turkey). Aquatic Research, 3 (3): 124-134.

Tokatlı, C., 2020b. Application of water quality index for drinking purposes in dam lakes: a case study of Thrace Region. Sigma Journal of Engineering and Natural Sciences, 38 (1): 393-402.
Tokatlı, C., Baştatlı, Y., Elipek, B., 2017. Water quality assessment of dam lakes located in Edirne Province (Turkey). Sigma Journal of Engineering and Natural Sciences, 35 (4): 743-750.
Tokatlı, C., Güner, Ş., 2018. Fluorine Accumulations in Drinking Water of Havsa District (Edirne, Turkey) and Assessment of Water Quality in Terms of Teeth Health. Sigma Journal of Engineering and Natural Sciences, 36 (3): 887-894.
Tokatlı, C., İslam, A. R. T., Güner, Ş. O., Ustaoğlu, F., İslam, S., Dindar, M. B., 2022. A Pioneering Study on Health Risk Assessment of Fluoride in Drinking Water in Thrace Region of Northwest Türkiye. Groundwater for Sustainable Development, https://doi.org/10.1016/j.gsd.2022.100836.
Tokatlı, C., Onur, Ş. G., Dindar, M. B., Malafaia, G., Islam, A. R. T., Muhammad, S., 2023. Spatial-Temporal Variability and Probabilistic Health Risk Assessment of Fluoride from Lentic Ecosystem, Türkiye. International Journal of Environmental Analytical Chemistry, https://doi.org/10.1080/03067319.2023.2198645.
TS 266, 2005. Sular-İnsani Tüketim Amaçlı Sular. Türk Standartları Enstitüsü, ICS 13.060.20.
Ustaoğlu, F., İslam, S., Tokatlı, C., 2022. Ecological and probabilistic human health hazard assessment of heavy metal in Sera Lake Nature Park sediments (Trabzon, Turkey). Arabian Journal of Geosciences, 15: 597.
WHO (World Health Organization), 2011. Guidelines for Drinking-water Quality. World Health Organization Library Cataloguing-in-Publication Data, NLM Classification: WA 675.

AGE-SPECIFIC PROBABILISTIC HEALTH RISKS OF FLUORIDE EXPOSURE VIA GROUNDWATER CONSUMPTION IN LOW AND HIGH ELEVATION AQUIFERS OF NORTHWEST TÜRKIYE

Mediha Büyükgöze Dindar[1], Meltem Tekbaş Atay[1], Cem Tokatlı[2]*

[1]Trakya University, Faculty of Dentistry, Edirne / Türkiye
[2]Trakya University, İpsala Vocational School, Edirne / Türkiye

**Corresponding author: medihabuyukgoze@trakya.edu.tr*

ABSTRACT

Chronic exposure to fluoride via drinking water consumption is a well-documented global public health concern due to its capacity to induce non-carcinogenic health complications, such as dental and skeletal fluorosis, depending on the dose and physiological susceptibility. This study presents a comparative and age-specific probabilistic health risk assessment of fluoride exposure for populations utilizing groundwater from two distinct topographic zones (high-elevation/slope and low-elevation/plain) in the İpsala district of Edirne province, Northwest Türkiye. To evaluate the toxicological and non-carcinogenic hazards across different human developmental stages, the Hazard Quotient (HQ) was mathematically modeled for four demographic cohorts: infants, children, teenagers, and adults. The probabilistic risk assessment demonstrated that fluoride-induced health hazards are significantly influenced by both the topographic origin of the water source and age-specific physiological characteristics. In the high-elevation slope zone, fluoride exposure poses a negligible non-carcinogenic risk for all studied groups, with HQ values remaining comfortably below the safe regulatory threshold (HQ < 1), ranging from 0.04680 for infants to 0.33150 for children. Conversely, a substantial increase in exposure hazards was characterized in the low-elevation plain zone. In this lower terrain, the calculated HQ for children escalated sharply to 0.80372, followed by teenagers (0.56733), adults (0.45459), and infants (0.11347). These findings reveal that while no cohort currently exceeds the absolute safety limit, the child population in the low-elevation plain zone approaches this critical benchmark closely. Consequently, children constitute the most vulnerable demographic segment to chronic fluoride exposure in this region. This study underscores the necessity of implementing age-specific public health monitoring and target-driven water management strategies, particularly within the low-lying plain sectors of the basin, to mitigate long-term fluoride health risks.

Keywords: Fluoride exposure, Probabilistic risk assessment, Hazard Quotient, Demographic cohorts, Children vulnerability, İpsala Basin

INTRODUCTION

Access to safe drinking water is a fundamental requirement for public health, particularly regarding geogenic contaminants like fluoride that possess a narrow margin of safety. While controlled fluoride intake prevents dental caries, chronic and excessive consumption triggers non-carcinogenic health complications such as dental or skeletal fluorosis (Andezhath et al., 1993; Taghipour et al., 2016; Din et al., 2024). Human health responses to fluoride ingestion are heavily dependent on age-specific physiological cohorts (infants, children, teenagers, and

adults) due to significant differences in daily water consumption rates and body weights. Among these groups, children are widely recognized as the most vulnerable demographic segment owing to their developing skeletal structures and higher fluid intake relative to body weight. Therefore, utilizing probabilistic health risk assessment tools, such as the Hazard Quotient (HQ), is essential to accurately model exposure scenarios for vulnerable populations rather than relying on oversimplified average values (Onur et al., 2019; Tokatlı et al., 2022; Rashid et al., 2024).

The Thrace Region of Northwest Türkiye heavily depends on groundwater aquifers for domestic supply. Although general water quality across the region has been widely documented, the specific impact of geomorphological features—namely topographic elevation differences—on age-specific fluoride exposure risks remains completely unaddressed (Tokatlı, 2019; 2020; Helvacıoğlu et al., 2025). Aquifers situated in high-elevation recharge slopes versus low-lying plain discharge zones exhibit distinct exposure profiles, making a critical knowledge gap for local public health management. To address this gap, this study aims to evaluate and compare the non-carcinogenic health hazards (HQ) of fluoride via groundwater consumption across four distinct demographic cohorts in the İpsala (Edirne) district, utilizing well waters operating at similar depths but at different topographic elevations. This research provides essential, data-driven clinical insights required for targeted public health interventions in the region.

MATERIALS AND METHODS

Research Area and Sample Collection

The investigation was conducted in the İpsala district of Edirne province, located within the hydrogeologically and structurally complex Ergene Basin in the Thrace region of Northwest Türkiye (Figure 1). To effectively characterize the influence of geomorphological and topographic variations on groundwater fluoride dynamics, representative groundwater samples were synchronized and collected during the summer season of 2026. The sampling strategy targeted two active production wells operating at identical depth intervals (about 100 m) but positioned within contrasting topographical configurations: a high-elevation (slope) setting and a low-elevation (plain) setting.

All field sampling procedures strictly adhered to international standard protocols for groundwater quality monitoring. Prior to capturing the samples, both production wells were continuously purged for approximately 15–20 minutes. This purging process was maintained until key in-situ physicochemical parameters reached complete stabilization, thereby guaranteeing the collection of undisturbed formation water. The collected hydrochemical samples were stored in pre-cleaned, high-density polyethylene bottles, immediately placed in insulated cooler boxes maintained at 4 ^{0}C to preserve chemical integrity, and rapidly transferred to the laboratory for subsequent analytical determination.

Fluoride Analysis

Fluoride concentrations were quantified spectrophotometrically using a high-performance Hach Lange DR 3900 laboratory spectrophotometer, strictly adhering to the standard methods established by the American Public Health Association (APHA, 1998, 2017). The analytical determination was executed utilizing precision-engineered Hach Lange LCK 323 cuvette test kits. To ensure the highest degree of analytical accuracy, reproducibility, and minimal instrumental drift, all preparation and measurement steps were conducted in rigorous compliance with the manufacturer's operational protocols.

Figure 1. Map of İpsala district

Health Risk Assessment

To address physiological and behavioral variations, the target population was stratified into four age cohorts: infants (<2 years), children (2–6 years), teenagers (6–16 years), and adults (>16 years). Daily fluoride exposure via drinking water ingestion for each demographic category was calculated using Equation 1. The non-carcinogenic health hazards were subsequently characterized using the Hazard Quotient (HQ) according to Equation 2 (Yousefi et al., 2018). An HQ threshold of less than 1.0 indicates a negligible toxicological risk, whereas values greater than 1.0 signify potential non-carcinogenic health concerns, indicating an increased probability of developing dental or skeletal fluorosis.

$$EDI = \frac{Cf \; x \; Cd}{Bw} \quad (1)$$

$$HQ = \frac{EDI}{RfD} \quad (2)$$

EDI: Estimation of fluoride consumption – daily (mg/kg/day)
C_f: Fluoride level in the investigated drinking water samples (mg/L)
C_d: Mean daily water intake (L/day) (the mean water consumption rates in infants, children, teenagers and adults were 0.08, 0.85, 2 and 2.5 L/day, respectively)
B_w: Body weight (kg) (body weights of investigated groups were considered 10, 15, 50 and 78 kg, respectively)
RfD: Reference dose (mg/kg/day) (it is 0.06 mg/kg/day for fluoride (EPA, 1992).

RESULTS AND DISCUSSION

The age-specific non-carcinogenic health risks triggered by chronic fluoride exposure via groundwater consumption were evaluated using the Hazard Quotient (HQ) modelling approach. The calculated probabilistic health risk indices for four distinct demographic cohorts (infants, children, teenagers, and adults) across contrasting topographic settings are comprehensively illustrated in Figure 2.

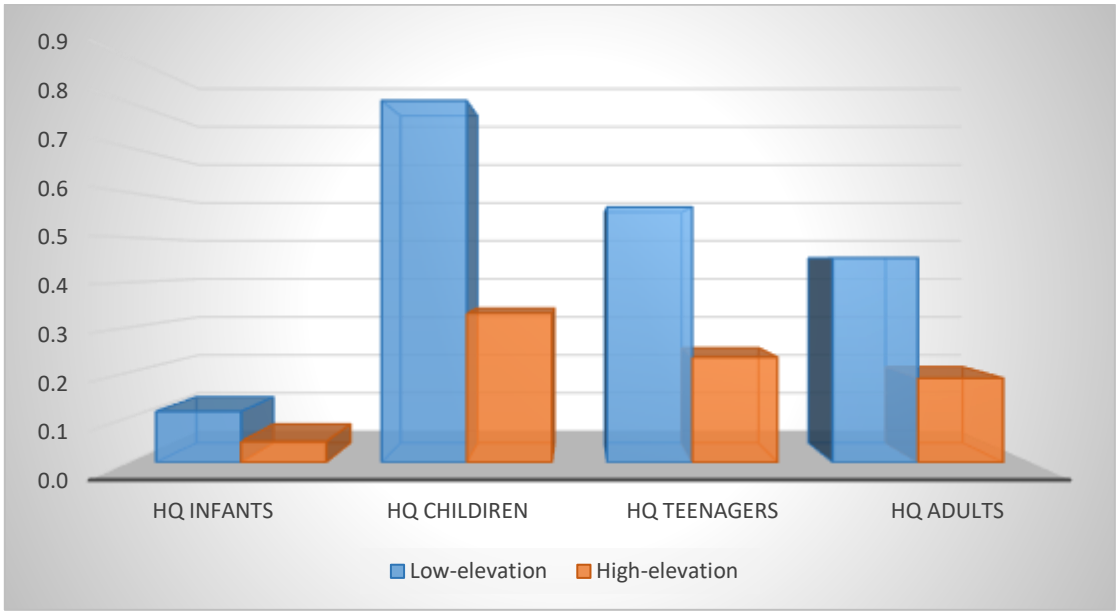

Figure 2. Probabilistic non-carcinogenic risk indices (HQ) of fluoride exposure

The outcomes of the probabilistic risk assessment revealed that non-carcinogenic health hazards fluctuate drastically depending on both the geomorphological location of the water source and the specific physiological traits of the exposed human cohorts (Taghipour et al., 2016; Tokatlı et al., 2022; Cao et al., 2023). For the high-elevation (slope) aquifer, the exposure modelling demonstrated completely negligible health risks. In this elevated recharge zone, the calculated HQ values for all demographic groups remained safely and comfortably below the critical regulatory threshold (HQ < 1). Specifically, the risk indices were modelled as 0.04680 for infants, 0.33150 for children, 0.23400 for teenagers, and 0.18750 for adults (Figure 2). These low values clearly indicate that chronic ingestion of groundwater from the slope sector poses no significant toxicological threat to the local population across any developmental stage.
Conversely, a dramatic and concerning elevation in exposure hazards was characterized in the low-elevation (plain) aquifer zone. In this low-lying discharge sector, the toxicological risks escalated sharply across all demographic segments. The calculated HQ values for the plain

aquifer followed a distinct order based on metabolic and consumption dynamics: children (0.80372) > teenagers (0.56733) > adults (0.45459) > infants (0.11347).
The most critical finding of this research is the pronounced vulnerability of the child cohort within the low-elevation plain zone. While no individual demographic group currently exceeds the absolute international safety threshold (HQ = 1), the child cohort's risk index reaches a critical threshold of 0.80372 (Figure 2). This high value indicates that children consuming water from the plain aquifer are approaching the non-carcinogenic safety boundary closely. This pronounced vulnerability observed in the younger population strongly corroborates broader global literature, which consistently demonstrates that children face substantially higher chronic exposure risks from drinking water consumption due to their significantly lower average body weights relative to their daily volumetric fluid ingestion rates (Gao et al., 2013; Tokatlı et al., 2023).

CONCLUSIONS

This study demonstrates a profound geomorphological control on age-specific probabilistic health risks from chronic fluoride exposure in the İpsala Basin. While the high-elevation slope aquifer poses completely negligible toxicological hazards for all demographic segments (HQ < 0.34), a substantial elevation in exposure vulnerability was characterized in the low-elevation plain zone. The Hazard Quotient (HQ) analysis revealed a strict age-dependent susceptibility order of children > teenagers > adults > infants. The most critical outcome is that children consuming groundwater from the low-elevation plain aquifer constitute the most vulnerable cohort, with their risk index reaching a critical threshold of 0.80372. Although no demographic group currently exceeds the absolute safety boundary (HQ = 1), the close proximity of the child cohort underscores a substantial risk for mild dental fluorosis under chronic long-term consumption. These findings indicate that regional water quality averages can obscure localized public health risks. Consequently, this study emphasizes the urgent need for target-oriented public health screening, pediatric dental monitoring, and age-specific protective water management strategies specifically tailored for the low-lying plain sectors of the region.

ACKNOWLEDGEMENTS

This study was supported by Trakya University Scientific Research Projects Unit under Project Code 2024/230. The author would like to thank Trakya University for the financial and institutional support provided throughout the research.

REFERENCES

Andezhath, S. K., Kumar, A., Bhatnagar, M., Bahudur, R., 1993. Prevalence of Endemic Fluorosis with Gastro-Intestinal Manifestations in People Living in Some North-Indian Villages. Fluoride, 26 (2): 97-104.
APHA, 1998. Standard Methods for the Examination of Water and Wastewater. American Public Health Association. Inc., Washington, DC.
APHA, 2017. American public health association (APHA). Stand. Methods Exam. Water Wastewater.
Cao, W., Zhang, Z., Guo, H., Fu, Y., Gao, C., Nan, T., Ren, Y., Li, Z., 2023. Spatial distribution and controlling mechanisms of high fluoride groundwater in the coastal plain of Bohai Rim, North China. Journal of Hydrology, 617: 128952.

Din, I. U., Wajid, A., Muhammad, S., Rehman, I., Tokatlı, C., 2024. Spatial Distribution and Potential Health Risk Assessment for Fluoride And nitrate Via Water Consumption in Pakistan. Journal Of Geochemical Exploration, 259: 107413.

EPA. 1992. Framework for Ecological Risk Assessment. Risk Assessment Forum. US Environmental Protection Agency, Washington, DC.

Gao, H. J., Jin, Y. Q., Wei, J. L. 2013. Health Risk Assessment of Fluoride in Drinking Water from Anhui Province in China. Environ. Monit. Assess., 185 (5), 3687–3695.

Helvacıoğlu, İ. A., Gülbaşı, A., Tokatlı, C., 2025. Evaluating the environmental sustainability awareness of paddy producers in the Meriç Plain (Northwest Türkiye): a comprehensive statistical approach. Acta Scientiarum Polonorum-Formatio Circumiectus, 24 (1): 3-13.

Onur, Ş. G., Sezgin, B. I., Tokatlı, C., Haznedaroğlu, E., Eda, A., İldeş, G. Ç., Kalaoğlu, E. E., Yazıcı, B., Menteş, A., 2019. Prevalence of dental fluorosis and dental caries in 3 districts of Edirne with different water fluoride levels. Journal of Yeditepe University Faculty of Dentistry, 15 (2): 219-223.

Rashid, A., Ayub, M., Gao, X., Khattak, S. A., Ali, L., Li, C., Ahmad, A., Khan, S., Rinklebe, J., Ahmad, P., 2024. Hydrogeochemical characteristics, stable isotopes, positive matrix factorization, source apportionment, and health risk of high fluoride groundwater in semiarid region. Journal of Hazardous Materials, 469: 134023.

Taghipour, N., Amini, H., Mosaferi, M., Yunesian, M., Pourakbar, M., Taghipour, H., 2016. National and Sub-National Drinking Water Fluoride Concentrations and Prevalence of Fluorosis and of Decayed, Missed and Filled Teeth in Iran from 1990 to 2015: A Systematic Review. Environmental Science and Pollution Research, 23 (6): 5077–5098.

Tokatlı, C., 2019. Use of the potential ecological risk index for sediment quality assessment: a case study of dam lakes in the Thrace part of the Marmara Region. Aquatic Sciences and Engineering, 34 (3): 90-95.

Tokatlı, C., 2020. Application of water quality index for drinking purposes in dam lakes: a case study of Thrace Region. Sigma Journal of Engineering and Natural Sciences, 38 (1): 393-402.

Tokatlı, C., Islam, A. R. T., Güner, Ş. O., Ustaoğlu, F., Islam, S., Dindar, M. B., 2022. A pioneering study on health risk assessment of fluoride in drinking water in Thrace region of northwest Türkiye. Groundwater for Sustainable Development, 19: 100836.

Tokatlı, C., Onur, Ş. G., Dindar, M. B., Malafaia, G., Islam, A. R. T., Muhammad, S., 2023. Spatial-temporal variability and probabilistic health risk assessment of fluoride from lentic ecosystem, Türkiye. International Journal of Environmental Analytical Chemistry, 104 (19): 8316–8335.

Yousefi, M., Ghoochani, M., Mahvi, A. H., 2018. Health Risk Assessment to Fluoride in Drinking Water of Rural Residents Living in the Poldasht City, Northwest of Iran, Ecotoxicol. Environ. Saf., 148: 426–430.

VARIATIONS IN FLUORIDE GEOCHEMISTRY OF GROUNDWATER IN THE İPSALA (EDIRNE) BASIN BASED ON TOPOGRAPHIC ELEVATION DIFFERENCES AND ITS EVALUATION FROM A DENTISTRY PERSPECTIVE

Meltem Tekbaş Atay[1], Mediha Büyükgöze Dindar[1], Cem Tokatlı[2]*

[1]Trakya University, Faculty of Dentistry, Edirne / Türkiye
[2]Trakya University, İpsala Vocational School, Edirne / Türkiye

**Corresponding author: meltemtekbasatay@trakya.edu.tr*

ABSTRACT

Groundwater geochemistry plays a pivotal role in public health, especially concerning elements with a narrow margin of safety such as fluoride. In this study, the fluoride dynamics of groundwater aquifers operated at similar depths (about 100 m) but located at different topographic elevations (high elevation/slope and low elevation/plain) in the İpsala district of Edirne province (Türkiye) were comprehensively investigated, and a clinical evaluation was conducted from the perspective of preventive dentistry. In addition to the primary fluoride parameter, physicochemical variables including pH and Electrical Conductivity (EC), which significantly govern fluoride hydrogeochemistry, mobilization, and dissolution kinetics, were systematically monitored in the sampled well waters. According to the analytical results, the groundwater fluoride concentration was measured as 0.351 ppm in the high-elevation (slope) well, whereas it reached 0.851 ppm in the low-elevation (plain) well. The concomitant sharp increase in EC levels (from 380 to 1919 µS/cm) and the alkaline shift in pH (from 7.42 to 7.53) from high to low elevations demonstrated that prolonged water-rock interactions, mineral dissolution, and alkaline anion exchange processes trigger significant geogenic fluoride enrichment in the low-lying plain aquifer. From a dental perspective, it was determined that groundwater from the high elevation contains insufficient fluoride for optimal dental caries prophylaxis (<0.5 ppm), potentially leaving the local consumer population susceptible to increased tooth decay. Conversely, groundwater from the low-elevation aquifer falls precisely within the optimal range (0.5 - 1.0 ppm) recommended for preventive dentistry, placing it at a critical hydrochemical threshold that requires close clinical monitoring for mild dental fluorosis risk, particularly in children, under scenarios of chronic long-term consumption.

Keywords: İpsala district, Groundwater hydrogeochemistry, Geogenic fluoride, Dental caries prophylaxis, Dental fluorosis

INTRODUCTION

Groundwater geochemistry plays a vital role in public health, particularly regarding trace elements like fluoride which exhibit a narrow safety margin for human health. While optimal fluoride levels (0.5 – 1.0 ppm) are essential for dental caries prophylaxis, sub-optimal exposure increases caries susceptibility, and chronic excessive consumption triggers dental fluorosis (Onur et al., 2019; Tokatlı et al., 2022). The mobilization of geogenic fluoride into aquifers is governed by water-rock interactions, alkaline anion exchange, and hydrodynamic gradients. Topographic elevation differences significantly dictate these processes by altering groundwater residence time and mineral dissolution rates from recharge (slope) to discharge (plain) zones (Rashid et al., 2024; Din et al., 2024).

Although the Thrace Region's water quality and environmental characteristics have been widely studied in recent years, the specific impact of geomorphological features and topographic elevation differences on fluoride hydrogeochemistry, along with its direct implications for preventive dentistry in the İpsala district, remain completely unaddressed (Tokatlı, 2019; 2020; Helvacıoğlu et al., 2025). This lack of spatial understanding presents a critical knowledge gap, as rural populations in this region heavily rely on shallow and deep aquifers for daily drinking water consumption.

Therefore, this study aims to systematically evaluate the variations in groundwater fluoride geochemistry between high-elevation (slope) and low-elevation (plain) aquifers within the İpsala (Edirne) Basin, specifically focusing on wells operating at identical depth intervals to eliminate confounding hydrogeological variables. By closely monitoring dissolved fluoride concentrations alongside critical in-situ parameters such as pH and Electrical Conductivity (EC), this research not only elucidates the exact geogenic release and alkaline anion exchange mechanisms driving fluoride enrichment in low-lying discharge zones but also provides essential, data-driven clinical insights into the dual dental health risks—namely dental caries susceptibility and dental fluorosis—for the local population.

MATERIALS AND METHODS

Research Area and Sample Collection

The study area is located in the İpsala district of Edirne province, situated within the structurally complex Ergene Basin in the Thrace region of Türkiye (Figure 1). To evaluate the impact of topographic elevation on groundwater fluoride dynamics, representative groundwater samples were collected in summer season of 2026 from two production wells operated at similar depths (about 100 m) but exhibiting distinct topographical settings: a high-elevation/slope aquifer and a low-elevation/plain aquifer. Sampling procedures were conducted in accordance with international standard methods. Before sample collection, the wells were purged for approximately 15 – 20 minutes until physicochemical parameters stabilized, ensuring the retrieval of representative formation water. Samples were collected in pre-cleaned polyethylene bottles, kept in cooler boxes at 4 ^{0}C, and immediately transferred to the laboratory for hydrogeochemical analysis.

Chemical Analysis

Physicochemical parameters, including hydrogen ion concentration (pH) and Electrical Conductivity (EC), were measured in situ at the wellhead immediately upon sample collection using a Hach HQ40D multiparameter digital meter equipped with robust, factory-calibrated IntelliCAL probes. To ensure analytical accuracy and minimize drift, the multiparameter device was cross-calibrated daily against standard buffer solutions and certified conductivity standards.

Following field measurements, dissolved fluoride concentrations were quantified spectrophotometrically under controlled laboratory conditions using a high-performance Hach DR3900 laboratory spectrophotometer, strictly following the globally recognized American Public Health Association protocols (APHA, 1998, 2017). For the precise determination of fluoride levels, the Hach LCK 323 cuvette test kit was employed. All spectrophotometric steps were performed in strict accordance with the manufacturer's operational instructions.

Figure 1. Map of İpsala district

RESULTS AND DISCUSSION

The hydrogeochemical parameters and fluoride concentrations of the groundwater wells vary significantly based on topographic elevation differences, as illustrated in Figure 2. The high-elevation (slope) well exhibited a pH of 7.42, an Electrical Conductivity (EC) of 380 µS/cm, and a lower fluoride concentration of 0.351 ppm. Conversely, in the low-elevation (plain) well, pH slightly increased to 7.53, while EC and fluoride levels escalated sharply to 1919 µS/cm and 0.851 ppm, respectively. The concomitant increase in EC and pH from the slope to the plain aquifer demonstrates a clear geogenic enrichment mechanism. In the low-lying plain area (discharge zone), prolonged water-rock interactions and alkaline anion exchange processes trigger the desorption of fluoride from sediment surfaces into the groundwater (Cao et al., 2023; Gao et al., 2023).

From a clinical preventive dentistry perspective, these results highlight distinct local public health implications. Groundwater from the high-elevation zone contains insufficient fluoride (0.351 ppm < 0.5 ppm) for optimal dental caries prophylaxis, leaving consumer populations at a higher risk for tooth decay. In contrast, the fluoride concentration in the low-elevation plain well (0.851 ppm) falls precisely within the optimal therapeutic window (0.5 – 1.0 ppm) recommended for preventing dental caries (EC, 2007; WHO, 2011; Tokatlı et al., 2024). However, because this value sits near the upper threshold of the optimal range, chronic consumption of this plain groundwater requires careful clinical monitoring, as it presents a potential threshold risk for mild dental fluorosis in children during critical periods of tooth development.

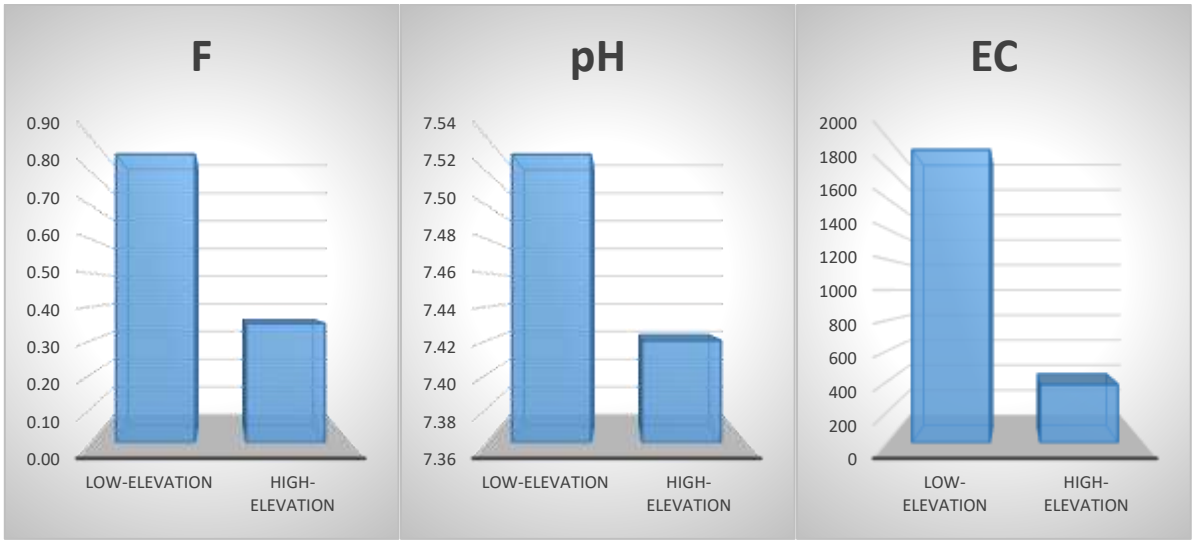

Figure 2. Fluoride (ppm), pH and EC (µS/cm) levels in the investigated wells

CONCLUSIONS

This study demonstrates that topographic elevation differences significantly influence groundwater fluoride geochemistry in the İpsala Basin, even at similar well depths. The transition from the high-elevation slope to the low-elevation plain triggers geogenic fluoride enrichment (from 0.351 to 0.851 ppm), driven by prolonged water-rock interactions and alkaline anion exchange as evidenced by elevated pH and EC levels.

From a dental health perspective, groundwater from the slope aquifer is sub-optimal and leaves the local population susceptible to dental caries. Conversely, the plain aquifer provides optimal levels for caries prophylaxis but requires clinical monitoring due to the threshold risk of mild dental fluorosis under chronic exposure. These findings underscore the critical need for integrating hydrogeochemical data with public health strategies in regional water management.

ACKNOWLEDGEMENTS

This study was supported by Trakya University Scientific Research Projects Unit under Project Code 2024/230. The author would like to thank Trakya University for the financial and institutional support provided throughout the research.

REFERENCES

APHA, 1998. Standard Methods for the Examination of Water and Wastewater. American Public Health Association. Inc., Washington, DC.

APHA, 2017. American public health association (APHA). Stand. Methods Exam. Water Wastewater.

Cao, W., Zhang, Z., Guo, H., Fu, Y., Gao, C., Nan, T., Ren, Y., Li, Z., 2023. Spatial distribution and controlling mechanisms of high fluoride groundwater in the coastal plain of Bohai Rim, North China. Journal of Hydrology, 617: 128952.

Din, I. U., Wajid, A., Muhammad, S., Rehman, I., Tokatlı, C., 2024. Spatial distribution and potential health risk assessment for fluoride and nitrate via water consumption in Pakistan. Journal of Geochemical Exploration, 259: 107413.

EC (European Communities), 2007. European Communities (drinking water) (no. 2). Regulations 2007. S.I. No. 278 of 2007.

Gao, X., Naseem, A., Luo, W., Rashid, A., Ma, S., Li, C., Zhang, X., 2024. Impact of microbial activity on fluoride release from sediments in areas with high fluoride groundwater: Mechanisms, sources and the lithology diversity. Science of The Total Environment, 955: 176940.

Helvacıoğlu, İ. A., Gülbaşı, A., Tokatlı, C., 2025. Evaluating the environmental sustainability awareness of paddy producers in the Meriç Plain (Northwest Türkiye): a comprehensive statistical approach. Acta Scientiarum Polonorum-Formatio Circumiectus, 24 (1): 3-13.

Onur, Ş. G., Sezgin, B. I., Tokatlı, C., Haznedaroğlu, E., Eda, A., İldeş, G. Ç., Kalaoğlu, E. E., Yazıcı, B., Menteş, A., 2019. Prevalence of dental fluorosis and dental caries in 3 districts of Edirne with different water fluoride levels. Journal of Yeditepe University Faculty of Dentistry, 15 (2): 219-223.

Rashid, A., Ayub, M., Gao, X., Khattak, S. A., Ali, L., Li, C., Ahmad, A., Khan, S., Rinklebe, J., Ahmad, P., 2024. Hydrogeochemical characteristics, stable isotopes, positive matrix factorization, source apportionment, and health risk of high fluoride groundwater in semiarid region. Journal of Hazardous Materials, 469: 134023.

Tokatlı, C., 2019. Use of the potential ecological risk index for sediment quality assessment: a case study of dam lakes in the Thrace part of the Marmara Region. Aquatic Sciences and Engineering, 34 (3): 90-95.

Tokatlı, C., 2020. Application of water quality index for drinking purposes in dam lakes: a case study of Thrace Region. Sigma Journal of Engineering and Natural Sciences, 38 (1): 393-402.

Tokatlı, C., Islam, A. R. T., Güner, Ş. O., Ustaoğlu, F., Islam, S., Dindar, M. B., 2022. A pioneering study on health risk assessment of fluoride in drinking water in Thrace region of northwest Türkiye. Groundwater for Sustainable Development, 19: 100836.

Tokatlı, C., Onur, Ş. G., Dindar, M. B., Malafaia, G., Islam, A. R. T., Muhammad, S., 2023. Spatial-temporal variability and probabilistic health risk assessment of fluoride from lentic ecosystem, Türkiye. International Journal of Environmental Analytical Chemistry, 104 (19): 8316–8335.

WHO (World Health Organization), 2011. Guidelines for Drinking-water Quality. World Health Organization Library Cataloguing-in-Publication Data, NLM Classification: WA 675.

ASSESSMENT OF ORGANIC POLLUTION AND BDI TREND IN THE ERZEN RIVER, ALBANIA (2014–2024)

Vjola Saliaga[1], Vjola Bakillari[1], Seit Shallari[1], Ferdi Brahushi[1], Fatbardh Sallaku[1], Ilir Kristo[1]

[1]Agricultural University of Tirana, Faculty of Agriculture and Ecology. Tirana, Albania

Corresponding Author email: violasaliaga@gmail.com

ABSTRACT

The rapid increase of economic activities including agriculture, industrial development, uncontrolled gravel abstraction and unregulated urban wastewater discharges and lack of adequate infrastructure and management, has significantly increased pressure on rivers quality in Albania, thereby contributing to enhanced pollution levels. Land use particularly nearby rivers for different industrial activities and agriculture represent one of major sources of many organic and inorganic pollutants in surface and groundwater. Meanwhile untreated municipal and industrial wastewater can significantly affect the ecological functioning of river ecosystems. This study aims to assess the long-term variation of organic pollution in the Erzeni River during 2014–2024 using the biodegradability index (BDI), calculated as the ratio of five-day biochemical oxygen demand to chemical oxygen demand (BOD_5/COD). Monitoring data covering the study period, reported in the annual environmental status reports published by the Albanian National Environmental Agency (NEA), together with the pressure analysis presented in the official Erzen River Basin Management Plan, were analyzed for two representative official monitoring sites. The results indicate persistent presence of organic pollution, particularly in areas affected by urban, industrial, and agricultural pressures. Individual BOD_5 concentrations range from 5 to 20 mg/L, with no clearly distinguishable seasonal pattern. BDI values showed relatively limited interannual variation and generally ranged between 0.5 and 0.6. The highest individual BDI (0.89) was observed in 2021 and the lowest (0.38) in October 2014. The predominance of BDI values above 0.5 indicates that a substantial proportion of the organic matter present in the river was readily biodegradable. However, the continued occurrence of measurable BOD_5 and COD concentrations throughout the studied period suggests persistent organic inputs. The EU WFD promotes the integrated management of water resources to support environmentally sustainable development and reduce pressures associated with excessive water abstraction and pollution. Albania has transposed such requirements in the national legislation and continuous to improve secondary legislation to better manage pollution control, environmental permitting, and water quality monitoring. Nevertheless, effective implementation of these requirements depends on robust monitoring systems, well-equipped laboratories, and clear data-sharing mechanisms. At present, these prerequisites are only partially established and operational. An integrated management approach is therefore required to (i) reduce organic and nutrient loads originating from urban wastewater discharges and agricultural activities, (ii) identify and control of heavy metal sources (urban/industrial sources), including the role of sediments in their accumulation and potential remobilization; and (iii) improve monitoring programmes through the systematic inclusion of WFD priority substances, thereby enabling a comprehensive and WFD-compliant water quality assessment of the Erzeni River.

Keywords: River pollution, BOD/COD ratio, freshwater quality assessment.

INTRODUCTION

EU Water Framework Directive representing the fundamental legal act in shaping the water management sector since 2000 across the European countries, foresees an analysis of anthropogenic impact, as a cyclical process, in the context of the river basin management planning (1). In Albania, this approach is embedded in the national legislation therefore chemical, and not only, pollution should be frequently measured and adequately controlled. This study aims to assess the long-term variation of organic pollution in the Erzen river using the biodegradability index (BDI), calculated as the ratio of BOD/COD, where both parameters represent routine analyses of the water quality and are significantly important in controlling the total content of pollution and the management of water environment (2).
The BDI must be smaller or equal to 1.0; the higher the value, the more serious the pollution of organic matter and the higher the level of biodegradability (3), (4); (5). Rivers are often considered a sink and source of many pollutants (6) and especially if there are discharges of industrial and/or urban wastewaters induced in the water system, they show high levels of BOD_5 and COD. High presence of organic matter in water leads to a decrease of dissolved oxygen due to consumption.

Official datasets for BOD_5 and COD concentrations during 2014–2024, as published by responsible authorities in regular reports, were analyzed in two NEA representative official monitoring sites. Albania has transposed EU WFD requirements in the main but its effective implementation however depends on robust monitoring systems, well-equipped laboratories and clear data-sharing/reporting mechanisms to ensure a better pollution control management, environmental permitting tools and adequate water quality monitoring. At present, these prerequisites are only partially established.

MATERIAL AND METHOD

Two NEA representative official monitoring sites were selected for this study (Ura Beshirit and Ura Sallmonaj) based on the analysis of pressures presented in the official river basin management plan including agriculture, various industrial activities and gravel mining upstream. Data series between 2014 – 2024, as officially reported by NEA through yearly environmental status reports (7) and the official river basin management plan for Erzen river basin (8) were analyzed and selected data have been plotted to identify BDI trend and potentially asses changes in pollution patters during these years.

Yearly individual mean data of the two selected monitoring sites were analyzed to observe any differences on BDI and be able to judge over the level of pollution. According to official reports, water samples have been taken on irregular seasonal basis over the years, between two to four times per year. All BOD > COD values were excluded to ensure credibility of the results and respective BDI ratio is not considered in the trend analysis.

RESULTS AND DISCUSSION

Individual BOD_5 values range from 5 to 20 mg/L, with no clearly distinguishable seasonal pattern. BDI values showed relatively limited interannual variation and generally ranged between 0.5 and 0.6. The highest individual BDI (0.89) was observed in 2021 and the lowest (0.38) in October 2014. The predominance of BDI values above 0.5 (Table 1) indicates that a substantial proportion of the organic matter present in the river was readily biodegradable.

Table 1 BDI Mean values for both official monitoring sites

Measurement	Year/Month	EbeM1-31 BDI	EsaM1-31 BDI
EM1	Apr-14	0.5	0.14
EM2	Jun-14	0.5	0.56
EM3	Aug-14	0.38	0.41
EM4	Mar-15	0.56	0.56
EM5	Sept-15	0.58	0.56
EM6	Nov-15	0.59	0.5
EM7	Feb-16	0.6	0.67
EM8	Apr-16	0.54	0.57
EM9	Aug-16	0.50	0.62
EM10	Oct-16	1	
EM11	May-17	1	1
EM12	Oct-17	0.64	0.63
EM13	Feb-18	1	1
EM14	Jul-18	1	1
EM15	Nov-18	0.62	0.58
EM16	Mar-19	0.03	0.57
EM17	May-19	0.07	0.63
EM18	Oct-19		0.56
EM19	Dec-19	0.40	
EM20	Feb-20	0.54	0.61
EM21	Apr-20	0.83	1
EM22	Oct-20	0.57	0.57
EM23	Mar-21	0.36	0.46
EM24	Oct-21	0.59	0.61
EM25	Mar-22	0.67	0.6
EM26	Sept-22	0.6	1
EM27	May-23	0.71	0.6
EM28	Sept-23	0.4	0.57
EM29	May-24	0.57	0.58
EM30	Oct-24	0.6	0.44
EM31	Dec-24	0.69	0.59

The BOD and COD fluctuates at both monitoring sites through the years and also on seasonal basis. (9) argues that this might be due to organic matter which comes from anthropogenic activities active in the study area (e,g plant extracts, solid wastes dumping, sewage discharges, and agricultural run-off. When BDI values range between 0.3 – 0.6 it confirms that the pollutants in waters belong to slow degradable category and >0.6 they are biodegradable (10). Results indicate persistent presence of organic pollution, particularly in areas affected by urban, industrial, and agricultural pressures and the continued occurrence of measurable BOD_5 and COD concentrations throughout the studied period suggests persistent organic inputs. BDI mean value, combining both monitoring sites increases through the years, particularly visible from 2014 to 2016 (Figure 1).

In a snapshot overview the trend is stable after 2022 showing lower values compared to an increased one before 2020. Nevertheless, the overall trend is near to 0.5 is mostly associated with consistent discharges of urban waters and agricultural activities in the areas nearby the river area.

Few cases were observed where the individual concentrations of BOD_5 and COD were excluded from the BDI analysis due to information inconsistency.

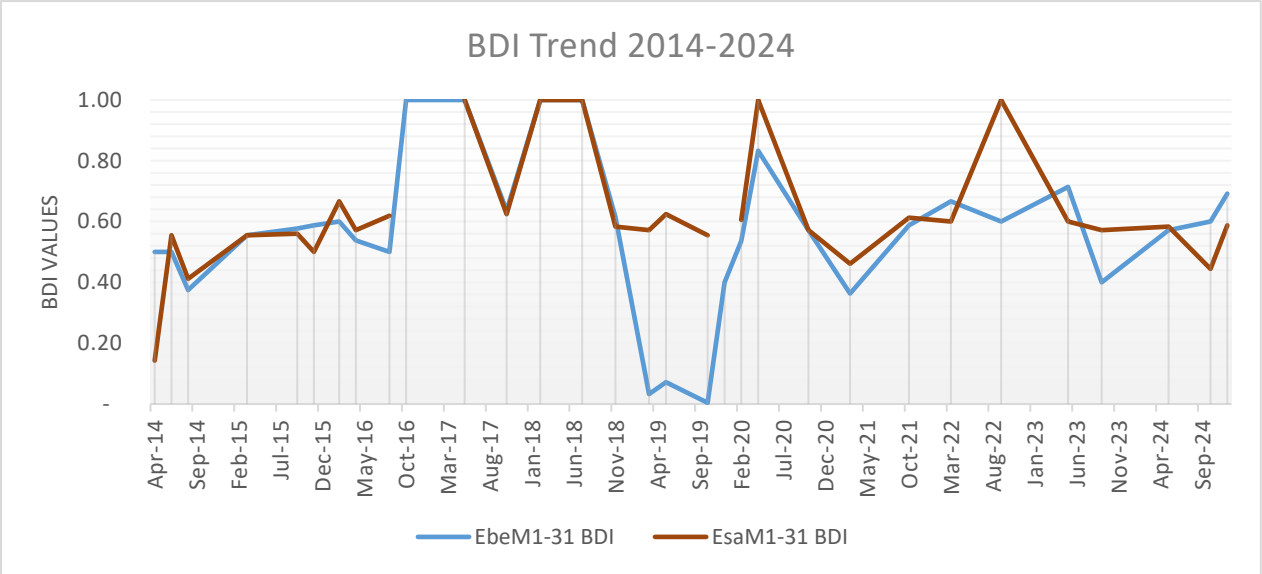

Figure 1 BDI trend concentration during 2014-2024

CONCLUSIONS

The predominance of BDI values above 0.5 indicates that a substantial proportion of the organic matter present in the river was readily biodegradable. Continued occurrence of measurable BOD_5 and COD concentrations throughout the studied period suggests persistent organic inputs. Higher BDI values in longer periods of time observed in the second monitoring site. An integrated management approach is therefore required to reduce organic and nutrient loads originating from urban wastewater discharges and agricultural activities, to identify and control of heavy metal sources (urban/industrial sources), including the role of sediments in their accumulation and potential remobilization, and to improve monitoring programmes through the systematic inclusion of WFD priority substances.

REFERENCES

[1]. EU. EU Water Framework Directive 2000/60/EC. 2000.

[2]. The testing of Chemical Oxygen Demand (COD) and Biological Oxygen Demand (BOD) of river water in Cipager Cirebon. Prambudy, H. Supriyatin, T. Setiawan , F. s.l. : IOP Publishing. Purpose LED Publishing. Conference sweries. , 2019.

[3]. Relationship, importance, and development of analytical techniques: COD, BOD, and, TOC in water—An overview through time. Aguilar-Torrejón J.A., Balderas-Hernández P., Roa-Morales G., Barrera-Díaz C.E., Rodríguez-Torres I., Torres-Blancas T.,. s.l. : SN Applied Sciences. A Springer Nature Journal , 2023, Vol. 5:118.

[4]. REVIEW ON BOD, COD AND BOD/COD RATIO: A TRIANGLE ZONE FOR TOXIC, BIODEGRADABLE AND STABLE LEVELS. Samudro, G. and Mangkoedihardjo, S. 4, s.l. : Research Gate, 2010, INTERNATIONAL JOURNAL Of ACADEMIC RESEARCH, Vol. 2.

[5]. Li, D. Sh. Liu. Water Quality Monitoring in Aquaculture. [book auth.] Daoling Li. Water Quality Monitoring and Management: Basis, Technology and Case Studies. s.l. : ELSEVIER. ISBN 978-0-12-811330-1, 2019, 12.

[6]. Dilution or enrichment: the effects of flood on pollutants in river waters. Zhou, M., et al. s.l. : Springer. Environmental Sciences Europe., 2022, SpringerOpen, Vol. 34:61.

[7]. AKM, Agjencia Kombetare e Mjedisit. Environmental Status Reports 2010-2020.

[8]. Ujore, Agjencia e Menaxhimit te Burimeve. Erzen River Basin Management Plan. AMBU. 2023. Official Plan.

[9]. Appraisal of seasonal variations in water quality of river Cauvery using multivariate analysis. Sharma, T R. Ravichandran, C. 1, s.l. : Informa UK Limited, trading as Taylor & Francis Group, 2021, Water Science ISSN: 2357-0008, Vol. 35, pp. 49-62.

[10]. Assessment of Organic Pollutant Index and Biodegradability Index in Determining River Pollution Load. Setyawan, A. Muhammad, F. Hermawan, F. s.l. : Purpose Led Publishing. IOP Conferences Series. , 2024, Earth and Environmental Science., Vol. 1414.

OPTIMIZING GOAT SPERM CRYOPRESERVATION: A TRADE-OFF BETWEEN KINEMATICS AND MEMBRANE INTEGRITY

Boubakeur Safsaf (1), Djemouai Boukhalfa (1), Karim Benhenia(2)

1 University of Batna 1 Hadj Lakhdar, ESPA Laboratory, Department of Veterinary Sciences, Institute of Veterinary and Agricultural Sciences, Batna, 05000, ALGERIA.
2 National Center for Biotechnology Research, BP E73-UV 03, Nouvelle Ville Ali Mendjli-, 25016, Constantine, ALGERIA

Corresponding author e-mail: boubaker.safsaf@univ-batna.dz

ABSTRACT

Cryopreservation of goat sperm is challenged by the vulnerability of the sperm plasma membrane to cold shock and oxidative stress-induced lipid peroxidation. Caprine spermatozoa possessing a high proportion of polyunsaturated fatty acids (PUFAs) and a low cholesterol-to-phospholipid ratio (0.30–0.35), which predisposes the membrane to cryoinjury, compound this vulnerability. Recent studies have reported on the use of cholesterol-loaded cyclodextrins (CLC) to stabilize the sperm plasma membrane and improve post-thaw semen quality. However, the role of seminal plasma (SP) during CLC-based cryopreservation remains debated. While SP supplies protective antioxidants and proteins, it also contains enzymes that degrade egg yolk-based extenders. This study evaluated the effect of pre-freeze washing (SP removal) on the functional characteristics of cryopreserved goat sperm. Overall, sperm quality was found to be comparable in washed and unwashed semen, with no significant differences in most kinematic parameters. However, unwashed sperm showed higher average path velocity (VAP), while washed sperm had significantly higher viability and straightness (STR). This suggests that, during caprine semen cryopreservation with CLC, membrane stability and kinematic performance exhibit a trade-off.

Keywords: Cryopreservation; caprine sperm; seminal plasma; sperm motility; membrane integrity

INTRODUCTION

Artificial insemination (AI) with frozen semen is a primary tool for achieving genetic progress in goat farming. In practice, however, its use is limited by inconsistent outcomes from semen freezing. These includes structural damage to sperm membrane & DNA which is catalyzed by lipid peroxidation (LPO) and by oxidative stress to which spermatozoa are exposed during freeze thaw cycle (Anand et al. 2016, Suwor et al. 2025). SP may also degrade milk extenders using enzymes and explained in detail below. The plasma membranes of goat spermatozoa has relatively high level of PUFA (polyunsaturated fatty acid) and low Cholesterol: PL (0.30-0.35)ratio, result in high membrane fluidity and hence are prone to cold shock (Anand et al. 2016, Aitken & West 1990, Darin- Bennett & White 1977, Simsek et al. 2025). These membranes aid in fertilisation normally but creates obstacles for semen during freezing process. The loss of cholesterol from the membranes during cryopreservation is another cause of cryoinjury on buck sperm (Amorim et al., 2009; Bailey et al., 2008).
The second is oxidative stress. If not neutralized by an effective antioxidant system, the oxidative stress results in lipid peroxidation (LPO), leading to loss of membrane fluidity and permeability, altering sperm metabolism (Sies, 1986; Bansal & Bilaspuri, 2011; Aitken et al.,

1989; Maxwell & Watson, 1996; Peris et al., 2007). Consequently a few methods were developed in relation to improve the cholesterol load in sperm via using cholesterol loaded cyclodextrin (CLC) method, which can be presented as addition of antioxidants and design of a new freeze medium (Konyali et al. 2013; Ashrafi et al. 2013; Kumar et al. 2025). The application of CLC was observed to reduce ROS and malondialdehyde formation, decrease of ATP depletion and preserve of the integrity of plasma membrane and acrosome in boar sperm following thawing (Zhang et al., 2024).

In spite of the membrane structure, the seminal plasma (SP) protection role in caprine semen cryopreservation is still controversial. Despite conferring protective components and enzymes to the sperm, SP enzymes can create adverse reactions with extender components. The buck seminal plasma has enzymes that can hydrolyze specific components of the classic extenders, like those found in milk or egg yolk. The main examples are EYCE (a phospholipase A2) and a BUSgp60 glycoprotein lipase, which are both capable of degrading egg yolk lipids into lyso-phospholipids and free fatty acids, both damaging for the sperm membrane and the acrosome (Pellicer-Rubio et al., 1997; Pellicer-Rubio & Combarnous, 1998; Esteve et al., 2025). Certain SP enzymes act on milk components similarly, complicating the use of milk-based extenders. For these reasons, despite evidence that SP helps maintain the viability and motility of cold-stored and frozen semen (Maxwell & Johnson, 1999; Azerêdo et al., 2001), standard practice in caprine semen cryopreservation calls for removing SP by centrifugation before freezing. However, it is not without its complications. Mechanical removal of SP by centrifugation may damage membrane integrity as well as impair sperm kinetics (Maxwell & Johnson, 1999; Azerêdo et al., 2001). Also, SP also contains protective elements like proteins and antioxidants that shield sperm cells from free radical mediated damage (Maxwell & Johnson, 1999; Azerêdo et al., 2001; Ohaneje et al., 2021) Thus, SP removal presents a dual-edged sword: it eliminates a source of enzymatic harm while also eliminating a source of protection. Given this duality, we examined how centrifugal removal of SP affects the quality of post-thaw goat semen. We hypothesized that centrifugation prior to freezing would shift the balance between two competing effects—the loss of toxic SP components and the mechanical stress/oxidative load introduced by centrifugation—and that this balance would be reflected in post-thaw sperm motility and membrane integrity.

MATERIAL AND METHOD

Animals and Semen Collection

Semen was collected from five Arbia breed bucks, selected based on semen volume, mass motility, individual motility, and sperm concentration. Two ejaculates were collected per buck, yielding a total of 10 ejaculates. The two ejaculates from each buck were pooled to obtain one sample per buck (n = 5). Each sample was divided into two aliquots and diluted to a concentration of 360×10^6 spermatozoa/mL.

Experimental Design

Table 1 summarizes the sperm processing for unwashed and washed groups. Both groups were incubated for 15 min at 22 °C in the presence of CLC.

Table 1. Sperm processing for unwashed and washed groups

Group	Treatment
Unwashed	Treated directly with 150 µL of Tris-based cryopreservation diluent containing cholesterol-loaded cyclodextrin (CLC).
Washed	Centrifuged twice at 500 × g for 15 min in 1 mL Tris-based cryoprotectant (CP) diluent, resuspended in an equal volume of Tris-based CP diluent after the second centrifugation, then treated with 150 µL of Tris-based cryopreservation diluent containing CLC.

Cryopreservation Protocol

Following CLC treatment, each sample was diluted threefold with an egg yolk-based freezing extender to obtain a final concentration of 120×10^6 spermatozoa/mL. The extended semen was loaded into 0.25 mL French straws, sealed, and equilibrated for 2 h at 4 °C. Straws were then frozen by holding them vertically 4 cm above liquid nitrogen vapor for 15 min before plunging into liquid nitrogen. For thawing, straws were immersed in a water bath at 37 °C for 40 s.

Post-Thaw Sperm Quality Assessment

Sperm Motility Analysis

Sperm motility was evaluated using a computer-assisted sperm analysis (CASA) system. Post-thaw semen suspensions were diluted 1:50 in Tris-based diluent and loaded onto a pre-warmed (37 °C) slide using a 10 µL pipette. The suspension was covered with an 18 × 18 mm coverslip and examined under a video-enhanced phase-contrast microscope (CROSS, 100× objective; Discovery Sensing, Inc., USA). Four fields per sample were captured, each containing ≥ 200 spermatozoa. Analysis settings: 25 frames/s, head area 20–90 µm², curvilinear velocity (VCL) > 10 µm/s (Tamayo-Canul et al., 2011). The following kinematic parameters were recorded (Table 2).

Table 2. Parameters studied and their description

Parameter	Description
TM	Total motility (%): percentage of spermatozoa with VCL > 10 µm/s
PM	Progressive motility (%): percentage of spermatozoa with VCL > 25 µm/s and straightness (STR) > 80%
VCL	Curvilinear velocity (µm/s)
VSL	Straight-line velocity (µm/s)
VAP	Average path velocity (µm/s)
LIN	Linearity (%)
ALH	Amplitude of lateral head displacement (µm)
BCF	Beat-cross frequency (Hz)
STR	Straightness (%)
WOB	Wobble (%)

Sperm Viability (Eosin-Nigrosin)

Sperm viability was evaluated using the eosin-nigrosin staining technique. A 10 µL semen suspension was mixed with 10 µL eosin-nigrosin solution, smeared on a slide, air-dried, and examined under a light microscope at 400× magnification. Two hundred spermatozoa were

counted per sample. Viable sperm excluded the dye (unstained), whereas non-viable sperm appeared red or pink (Björndahl et al., 2003; Vale et al., 2014).

Statistical Analysis

The calculation of means, standard error of the mean (SEM), and statistical analysis were performed using Statview 4.02 software (Abacus Concepts Inc., Berkeley, CA, USA). Values for each parameter are expressed as mean ± SEM. A two-way analysis of variance (ANOVA), followed by a Fisher post-hoc test, was used to determine the effect of washing the seminal plasma on the observed variation. Values were considered significant at $p<0.05$.

RESULTS AND DISCUSSION

Effect of Seminal Plasma Washing on Post-Thaw Sperm Parameters

The effects of seminal plasma washing on post-thaw caprine sperm quality parameters are summarized in Table 3.

Washing significantly improved viability (from 72.0% to 82.8%) and straightness (STR). Conversely, average path velocity (VAP) was significantly higher in unwashed samples (88.6 µm/s) compared to washed samples (76.3 µm/s). Total motility, progressive motility, and curvilinear velocity (VCL) were numerically higher in unwashed semen, though these differences did not reach statistical significance. VSL, LIN, ALH, BCF, and WOB were unaffected by treatment.

Table 3. Effects of seminal plasma washing on post-thaw caprine sperm parameters (mean ± SEM)

Parameter	Unwashed	Washed	P-value
Viability (%)	72.0 ± 0.9	82.8 ± 2.3	≤ 0.05
Total motility, TM (%)	92.4 ± 4.3	86.1 ± 0.2	0.20
Progressive motility, PM (%)	69.5 ± 3.1	57.2 ± 0.5	0.06
VCL (µm/s)	105.5 ± 3.2	91.5 ± 1.7	0.06
VSL (µm/s)	59.9 ± 3.0	57.0 ± 1.6	0.40
VAP (µm/s)	88.6 ± 2.2	76.3 ± 2.2	≤ 0.05
LIN (%)	56.9 ± 4.6	62.3 ± 0.6	0.30
ALH (µm)	2.2 ± 0.5	2.3 ± 0.05	0.80
BCF (Hz)	9.05 ± 1.0	9.8 ± 0.3	0.50
STR (%)	67.5 ± 5.0	74.6 ± 0.5	≤ 0.05
WOB (%)	84.1 ± 4.6	83.4 ± 0.8	0.80

Taken together, these data point to a trade-off rather than a clear advantage: washing protects membrane integrity and directional movement, whereas retaining SP preserves sperm velocity.

Discussion

Seminal plasma (SP) removal before freezing in an egg yolk–citrate extender with CLC had a complex effect on post-thaw buck sperm, consistent with the unusually lipid-rich, cryolabile structure of goat sperm membranes (Kumar et al., 2025). The post-wash rise in viability supports SP removal as conferring some membrane protection, while higher VAP and numerically greater total motility, progressive motility, and VCL in unwashed samples suggest SP also benefits motility. SP therefore plays both a protective and a damaging role: washing removes harmful enzymatic activity but also some motility-enhancing components.

This pattern sits within a genuinely mixed literature. Azerêdo et al. (2001) reported the opposite effect in frozen-thawed goat spermatozoa, where SP removal decreased motility and vigor rather than improving membrane integrity, whereas other work shows washing before 5 °C storage improves motility, acrosome integrity, and HOST response. The 10.8-point viability gain observed here thus fits an inconsistent evidence base, even though washing also removes metabolic components SP would otherwise supply (Kumar et al., 2025).

The likely mechanism is reduced SP-driven lipid damage. Pellicer-Rubio et al. (1997) and Pellicer-Rubio and Combarnous (1998) identified a bulbourethral lipase in buck SP that degrades sperm in milk-based extenders via free fatty acids and lysolecithins. An egg yolk–coagulating enzyme in goat semen (Roy, 1957) is, per Kumar et al. (2025), similarly detrimental in egg yolk media, hydrolyzing yolk lecithin into lysolecithin and priming the membrane for capacitation-like changes and acrosomal degeneration; washing likely reduces exposure to this agent. Watson (2000) similarly identified freeze-thaw as the most damaging stage of cryopreservation.

The contribution of SP to motility is different: it provides proteins, lipids, enzymes and antioxidants that buffer cold shock (Maxwell & Johnson, 1999), a stabilizing role also reported by Azerêdo et al. (2001). Here, unwashed samples reached VAP of 88.6 µm/s versus 76.3 µm/s for washed samples, with TM, PM, and VCL trending similarly — suggesting specific SP components support faster movement even as they compromise membrane integrity.

The extender system constrains these effects. CLC stabilizes membranes against cold and osmotic stress; Darin-Bennett and White (1977) showed ram and bull sperm carry a lower membrane cholesterol-to-phospholipid ratio than cold-tolerant species, and that introducing cholesterol raises resistance to chilling and osmotic shock while preserving viability and motility (Darin-Bennett & White, 1977; Salmon et al., 2016). Mocé et al. (2014) reported similar CLC benefits under fast and slow freezing, and Salmon et al. (2017) showed CLC improves resistance specifically to SP-mediated injury — explaining why VSL, LIN, ALH, BCF, and WOB were unaffected by washing, since mechanical (washing) and chemical (CLC) neutralization of SP damage may converge on the same outcome for these traits. CLC alone, however, is insufficient for optimal preservation, as confirmed by the present finding of differences in viability and STR between washed and unwashed samples. Under CLC, membranes maintained integrity and acceptable motility in both groups, but viability and STR were significantly higher in washed sperm ($p \leq 0.05$), possibly reflecting residual enzymatic damage in CLC-treated sperm, or, more likely, a selection effect in which washing removes dead and degenerate cells (Naing et al., 2011). Total motility, ALH, BCF, LIN, and WOB did not differ between groups, indicating no detrimental effect of SP once its damaging activity was partly blocked by CLC. Extensive washing can improve cryopreservation by removing deleterious enzymes and ROS-generating molecules (Naing et al., 2011), but the manipulation involved carries its own risk of physical damage to spermatozoa.

Work on Angora bucks offers a useful comparison: The benefit of centrifugation was found to be highly dependent on extender (Sarıözkan et al., 2010) where a Bioxcell extender outperformed standard Tris for post-thaw motility, membrane integrity, pregnancy rates and antioxidant activity. Washing is also laborious and carries the risk of sperm loss (Tuli & Holtz, 1994), so providing a strong extender together with cholesterol supplementation to reduce the need for washing has both operational and biological benefits.

Kozdrowski et al. (2007) provide a contrasting result: comparing plasma removal with 20% egg yolk against no removal with 1.5% egg yolk in French Alpine bucks, they found plasma removal improved VAP, VSL, STR, LIN, ALH, and motility — opposite to our VAP result. This likely reflects a confound, since egg yolk concentration (not plasma removal alone) differed between their groups, and egg yolk cholesterol is itself cold-protective; our design

held CLC and egg yolk constant, isolating SP's effect more cleanly and likely explaining our trade-off rather than a uniform improvement. Kozdrowski et al. (2007) also cite Leboeuf et al. (2000) on the bulbourethral-derived EYCE (a phospholipase A hydrolyzing egg-yolk lecithin to toxic lysolecithin) and Verstegen et al. (2002) on ALH, VAP, VSL, STR, and LIN as indices of fertilizing capacity. Still, results remain inconsistent: Tuli and Holtz (1994) found no benefit to plasma removal in Boer goats, and Ritar and Salamon (1991) attribute post-thaw variability to interacting effects of male, collection month, egg yolk concentration, and plasma removal — reinforcing that SP removal cannot be assessed independent of the extender system.

Santiago-Moreno et al. (2017) demonstrated that density gradient centrifugation was superior to washing methods in removing dead sperm with increased VSL, VAP, progression rates. This is yet another example of how it is the technique of removal not just that the dead sperm is removed that affects results. While it seemed as if dead cells and all our waste were disposed of, and that no physically trauma was done to our sample since the level of viablity did not decrease, it is obvious that some degree of functional compromise was performed, because of the increase in VAP (having successfully avoiding using to much force and too long centrifuge, following guidelines from Kumar et al. (2025).

VSL, LIN, ALH, BCF, and WOB were largely conserved across treatments, suggesting SP removal acts on survival and select velocity traits rather than the fundamental architecture of motility; within an egg yolk–citrate/CLC system, membrane stabilization preserves core motility patterns regardless of SP status. The primary effect of washing is thus a redistribution between viability and specific velocity traits, not a wholesale loss of motility.

Practically, washing is worthwhile when post-thaw survival and directional movement (STR) are the priority, as in controlled AI programs; where time and simplicity matter and CLC/egg yolk are already in the protocol, retaining SP is reasonable, since the viability cost is offset by higher velocity. The recommendation is thus conditional: washing improves viability and STR but is not strictly necessary when the extender system is already strongly cryoprotective.

To summarize, both our data and the literature support a bifunctional view of SP in goat semen cryopreservation: damaging membranes through lipase activity and enzyme–lipid interactions (Kumar et al., 2025) while also contributing to motility preservation. Washing improved viability and STR, while unwashed sperm retained higher VAP and a numerical edge in TM, PM, and VCL; under CLC-based cryopreservation, SP removal enhances membrane stability without being strictly essential for acceptable post-thaw quality.

CONCLUSIONS

Based on the study, washing seminal plasma before freezing improved post-thaw viability and straightness (STR) of goat sperm, whereas retaining seminal plasma preserved higher average path velocity (VAP) and a numerical advantage in total motility, progressive motility, and curvilinear velocity. These findings indicate a trade-off between membrane integrity and kinematic performance during CLC-based cryopreservation of caprine semen. While seminal plasma removal is not strictly essential when using cholesterol-loaded cyclodextrin and egg yolk-based extenders, it remains beneficial when the priority is post-thaw survival and directional movement for artificial insemination programs.

REFERENCES

Aitken, R. J., J. S. Clarkson, S. Fishel. 1989. Generation of reactive oxygen species, lipid peroxidation, and human sperm function. Biology of Reproduction, 41(1): 183-197.

Aitken, R. J., K. M. West. 1990. Analysis of the relationship between reactive oxygen species production and leukocyte infiltration in fractions of human semen separated on Percoll gradients. International Journal of Andrology, 13(6): 433-451.
Amorim, E. A. M., J. K. Graham, B. Spizziri, M. Meyers, C. A. A. Torres. 2009. Effect of cholesterol or cholesteryl conjugates on the cryosurvival of bull sperm. Cryobiology, 58(2): 210-214.
Anand, M., S. Yadav, J. Kumar, B. Yadav. 2016. Effect of different egg yolk concentration on chilled Barbari buck semen during short term storage. Journal of Animal Research, 6: 635-639.
Ashrafi, I., H. Kohram, F. F. Ardabili. 2013. Antioxidative effects of melatonin on kinetics, microscopic and oxidative parameters of cryopreserved bull spermatozoa. Animal Reproduction Science, 139(1-4): 25-30.
Azerêdo, G. A., C. R. Esper, K. T. Resende. 2001. Evaluation of plasma membrane integrity of frozen-thawed goat spermatozoa with or without seminal plasma. Small Ruminant Research, 41(3): 257-263.
Bailey, J. L., C. Lessard, J. Jacques, C. Bréque, I. Dobrinski, W. Zeng, H. L. Galantino-Homer. 2008. Cryopreservation of boar semen and its future importance to the industry. Theriogenology, 70(8): 1251-1259.
Bansal, A. K., G. S. Bilaspuri. 2011. Impacts of oxidative stress and antioxidants on semen functions. Veterinary Medicine International, 2011: Article ID 686137.
Björndahl, L., I. Söderlund, U. Kvist. 2003. Evaluation of the one-step eosin-nigrosin staining technique for human sperm vitality assessment. Human Reproduction, 18(4): 813-816.
Darin-Bennett, A., I. G. White. 1977. Influence of the cholesterol content of mammalian spermatozoa on susceptibility to cold-shock. Cryobiology, 14(4): 466-470.
Esteve, I. C., M. L. Mocé, E. A. Gómez, R. Martín-Montalbán, A. Martínez-Climent, E. Mocé. 2025. The detrimental impact of seminal plasma on the quality of cryopreserved sperm in goat bucks: Freezing–thawing as the most harmful step. Frontiers in Veterinary Science, 12: 1627878.
Konyali, C., C. Tomás, E. Blanch, E. A. Gómez, J. K. Graham, E. Mocé. 2013. Optimizing conditions for treating goat semen with cholesterol-loaded cyclodextrins prior to freezing to improve cryosurvival. Cryobiology, 67(2): 124-131.
Kozdrowski, R., A. Dubiel, W. Bielas, M. Dzięcioł. 2007. Two protocols of cryopreservation of goat semen with the use of computer-assisted semen analysis system. Acta Veterinaria Brno, 76(4): 601-604.
Kumar, A., K. K. Kanaka, H. Mehta, N. S. Thakur, G. Singh. 2025. A review of current challenges, influential factors, and advancements in goat semen cryopreservation. Archives of Current Research International, 25(3): 398-411.
Leboeuf, B., B. Restall, S. Salamon. 2000. Production and storage of goat semen for artificial insemination. Animal Reproduction Science, 62(1-3): 113-141.
Maxwell, W. M. C., L. A. Johnson. 1999. Physiology of spermatozoa at high dilution rates: The influence of seminal plasma. Theriogenology, 52(8): 1353-1362.
Maxwell, W. M. C., P. F. Watson. 1996. Recent progress in the preservation of ram semen. Animal Reproduction Science, 42(1-4): 55-65.
Mocé, E., C. Tomás, E. Blanch, J. K. Graham. 2014. Effect of cholesterol-loaded cyclodextrins on bull and goat sperm processed with fast or slow cryopreservation protocols. Animal, 8(5): 771-776.
Naing, S. W., H. Wahid, K. M. Azam, Y. Rosnina, A. B. Zuki, S. Kazhal, M. M. Bukar, et al. 2011. Effect of seminal plasma removal, washing solutions, and centrifugation regimes on Boer goat semen cryopreservation. Pertanika Journal of Tropical Agricultural Science, 34(2): 271-279.

Ohaneje, U. L., U. I. Osuagwuh, M. Alvarez-Rodríguez, I. Yáñez-Ortiz, A. Tabarez, M. J. Palomo. 2021. The re-addition of seminal plasma after thawing does not improve buck sperm quality parameters. Animals, 11(12): 3452.
Pellicer-Rubio, M. T., Y. Combarnous. 1998. Deterioration of goat spermatozoa in skimmed milk-based extenders as a result of oleic acid released by the bulbourethral lipase BUSgp60. Journal of Reproduction and Fertility, 112(1): 95-105.
Pellicer-Rubio, M. T., T. Magallon, Y. Combarnous. 1997. Deterioration of goat sperm viability in milk extenders is due to a bulbourethral 60-kilodalton glycoprotein with triglyceride lipase activity. Biology of Reproduction, 57(5): 1023-1031.
Peris, S. I., A. Morrier, M. Dufour, J. L. Bailey. 2007. Cryopreservation of ram semen facilitates sperm survival and in vitro fertilization. Theriogenology, 68(2): 289-298.
Ritar, A. J., S. Salamon. 1991. Effects of month of collection, method of processing, concentration of egg yolk and duration of frozen storage on viability of Angora goat spermatozoa. Small Ruminant Research, 42: 9-37.
Roy, A. 1957. Egg yolk-coagulating enzyme in the semen and Cowper's gland of the goat. Nature, 179(4554): 318-319.
Salmon, V. M., P. Leclerc, J. L. Bailey. 2016. Cholesterol-loaded cyclodextrin increases the cholesterol content of goat sperm to improve cold and osmotic resistance and maintain sperm function after cryopreservation. Biology of Reproduction, 94(4): 85.
Salmon, V. M., P. Leclerc, J. L. Bailey. 2017. Novel technical strategies to optimize cryopreservation of goat semen using cholesterol-loaded cyclodextrin. Cryobiology, 74: 19-24.
Santiago-Moreno, J., M. C. Esteso, C. Castaño, A. Toledano-Díaz, J. A. Delgadillo, A. López-Sebastián. 2017. Seminal plasma removal by density-gradient centrifugation is superior for goat sperm preservation compared with classical sperm washing. Animal Reproduction Science, 181: 141-150.
Sarıözkan, S., M. N. Bucak, P. B. Tuncer, U. Taşdemir, H. Kinet, P. A. Ulutaş. 2010. Effects of different extenders and centrifugation/washing on postthaw microscopic-oxidative stress parameters and fertilizing ability of Angora buck sperm. Theriogenology, 73(3): 316-323.
Sies, H. 1986. Biochemistry of oxidative stress. Angewandte Chemie International Edition in English, 25(12): 1058-1071.
Simsek, S., M. Hitit, M. Bodu, E. Memili. 2025. Sperm cell membranes of bulls and bucks associated with sperm fertility and freezability. Animals, 15(22): 3248.
Suwor, F., S. Kubota, S. Nawong, A. Thuangsanthia, M. Toyra, P. Paengkoum, S. Ponchunchoovong. 2025. Effects of cryoprotectant combinations on post-thawed sperm quality, biomolecular changes, DNA methylation, and pregnancy rates in Boer goat semen. Veterinary Sciences, 12(2): 178.
Tamayo-Canul, J., M. Alvarez, M. Mata-Campuzano, M. Alvarez-Rodríguez, P. de Paz, L. Anel, et al. 2011. Effect of storage method and extender osmolality on the quality of cryopreserved epididymal ram spermatozoa. Animal Reproduction Science, 129(3-4): 188-199.
Tuli, R. K., W. Holtz. 1994. Effect of glycerolization procedure and removal of seminal plasma on post-thaw survival and acrosome status from Boer goat spermatozoa. Theriogenology, 42(3): 547-555.
Verstegen, J., M. Iguer-Ouada, K. Onclin. 2002. Computer assisted semen analyzers in andrology research and veterinary practice. Theriogenology, 57(1): 149-179.
Watson, P. F. 2000. The causes of reduced fertility with cryopreserved semen. Animal Reproduction Science, 60-61: 481-492.
Zhang S., Zhang H., Liu K., Xu X., Qin Y., Xiao L., Zhou C., Wu J., Liu Y. and Bai J. (2024). Effect of cholesterol-loaded cyclodextrin treatment on boar sperm cryopreservation. Anim Biosci., 7;37(9):1558–1567. doi: 10.5713/ab.24.0030.

VALORIZATION OF AGRICULTURAL WASTE INTO ACTIVATED CARBON : CHARACTERIZATION AND PERFORMANCE FOR PHARMACEUTICAL POLLUTANT REMOVAL FROM WATER

*Belkharchouche Djanet * , Belkharchouche Drifa ***

***Laboratory of Energy Physics and Renewable Energies, University of Constantine 1, Algeria*

**Department of Process Engineering, University of Constantine 3, Algeria*

ABSTRACT

In this study, an activated carbon was prepared from **bean pods (Vicia faba)**, an abundant agricultural waste, by chemical activation. Two activating agents were compared : **phosphoric acid**, used at impregnation ratios of 100%, 150%, and 200%, and **sulfuric acid**, used at 200%. The results showed that the carbon activated with **200% phosphoric acid** exhibited the best performance, with an adsorption capacity of **107.5 mg/g**, compared to **90 mg/g** for the carbon activated with sulfuric acid, and only **2.98 mg/g** for the raw pods. The influence of several parameters on the adsorption process was also investigated, namely **pH, temperature, ionic strength, and initial pollutant concentration**. Adsorption equilibrium was reached within only **5 minutes** for concentrations below **150 mg/L**, reflecting rapid kinetics, satisfactorily described by the **pseudo-second-order kinetic model**. Fitting of the experimental data to the **Langmuir model** revealed monolayer adsorption. The thermodynamic study also allowed determination of the main parameters associated with the process, namely **Gibbs free energy, enthalpy, and entropy**. The properties of the resulting activated carbon, notably its **specific surface area and functional characteristics**, were investigated and confirmed by **BET, FTIR, and pHpzc** analyses. These results show that the valorization of bean pods into activated carbon constitutes a **sustainable, economical, and effective** approach for removing pharmaceutical residues present in water. This process fully falls within a **circular economy** approach, aimed at converting agricultural waste into high-value-added materials for the preservation and treatment of water resources.

Keywords: agricultural waste; activated carbon; adsorption; metoprolol; environment; remediation; circular economy.

INTRODUCTION

Pharmaceutical residues are increasingly detected in aquatic environments and represent an environmental concern due to their persistence and their potential effects on living organisms. Among these contaminants, metoprolol, a β-blocker widely used in the treatment of cardiovascular diseases, is frequently found in surface waters and wastewater treatment plant effluents, notably owing to its low biodegradability.

Among the various treatment techniques, adsorption onto activated carbon constitutes an effective method for removing organic micropollutants. However, the cost of conventional activated carbons encourages the development of alternative, economical, and sustainable materials, particularly from agricultural waste.

In this perspective, bean pods (Vicia faba) represent an interesting precursor for the production of activated carbons. Their valorization allows both the reduction of agricultural waste and the production of a high-value-added material. Chemical activation with H_3PO_4 (100, 150, and

200%) and H_2SO_4 (200%) was used to improve the textural and functional properties of the resulting materials.

Objective

Prepare and characterize activated carbons from bean pods, using H_3PO_4 and H_2SO_4 as activating agents, then evaluate their performance for the removal of pharmaceutical pollutants in aqueous media, using metoprolol as a model pollutant.

Experimental approach

Bean pods

↓

Chemical activation: H_3PO_4 / H_2SO_4

↓

Activated carbon

↓

Characterization: BET • FTIR • pHpzc

↓

Adsorption of metoprolol

↓

Water remediation

RESULTS

Textural characterization

Activation with H_3PO_4 strongly improves the textural properties of the bean pods. The BET specific surface area increases with the activation ratio and reaches its maximum value for BPPAC 200%.

Table 1. BET specific surface areas of the prepared activated carbons

Material	BPPAC 100%	BPPAC 150%	BPPAC 200%	BPSAC 200%
Cumulative pore volume V_{cum} (cm^3/g)	0.0731	0.0439	0.0417	0.0426
Total pore volume V_{tot} (cm^3/g)	18.835	34.435	43.248	40.331
Cumulative pore surface area S_{cum} (m^2/g)	16.674	9.791	7.545	9.791
S_{BET} (m^2/g)	1032.114	1040.744	1100.391	38.251
Average pore diameter ($4V_{tot}/S_{BET}$) (Å)	665.484	1323.499	1572.059	4.217

S(BET)
(m^2/g)

Material	
BPPAC 100%	1032.11
BPPAC 150%	1040.74
BPPAC 200%	1100.39
BPSAC 200%	38.25

BPPAC 200%: S(BET) = 1100.39 m^2/g

Adsorption performance

Chemical activation strongly improves the adsorption of metoprolol compared to the raw pods (2.98 mg/g). The best performance is obtained with carbons activated by H_3PO_4, particularly BPPAC 200%.

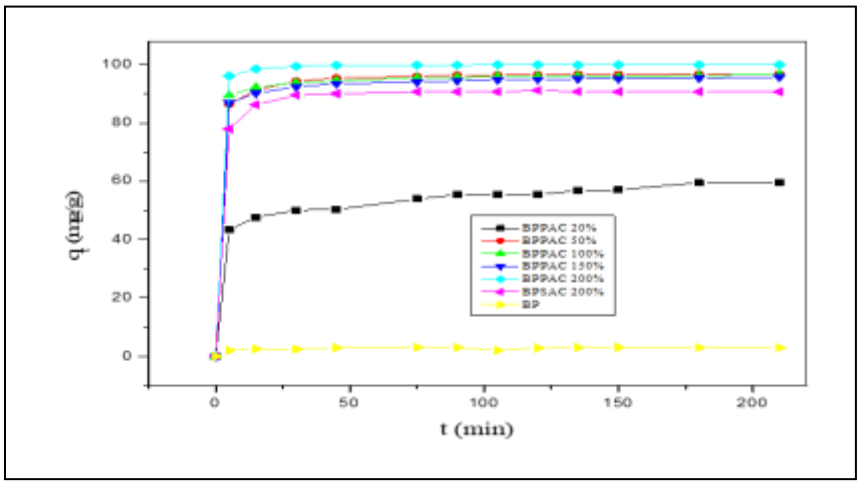

Figure 1. Effect of activation ratio on metoprolol adsorption.

Effect of pH

The adsorption capacity remains close to 78.38 mg/g in acidic media, then increases to a maximum of 94.55 mg/g at pH 10, before decreasing in more basic media.

pHpzc ≈ 4 | pKa ≈ 9.5 | q_e,max ≈ 94.55 mg/g at pH 10

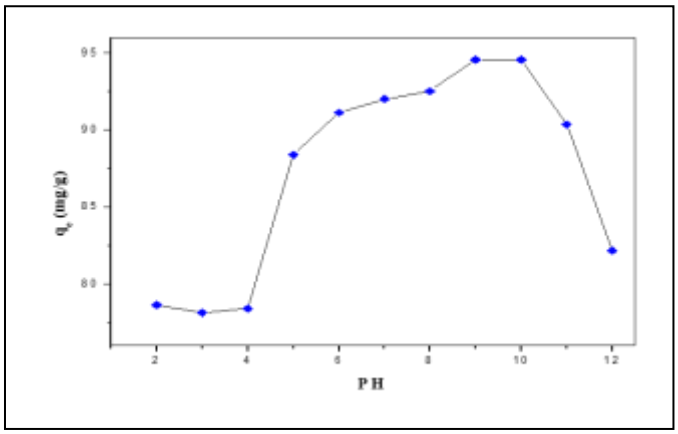

Figure 2. Effect of initial pH on metoprolol adsorption onto BPPAC.

Adsorption kinetics

Adsorption is rapid, with equilibrium reached within approximately 5 min for $C_0 < 150$ mg/L.
The pseudo-second-order (PSO) model describes the experimental data very well :
$R^2 = 0.9999–1.000$
The calculated adsorption capacities show excellent agreement with the experimental values.

Adsorption equilibrium
The equilibrium data show an excellent fit to the Langmuir 2 model.
20 °C: $R^2 = 0.998$
30 °C: $R^2 = 0.982$
50 °C: $R^2 = 0.995$
At 20 °C, the experimental capacity reaches $q_{e,exp} = 110.87$ mg/g.
These results are consistent with adsorption occurring mainly as a monolayer on the accessible sites of the activated carbon.

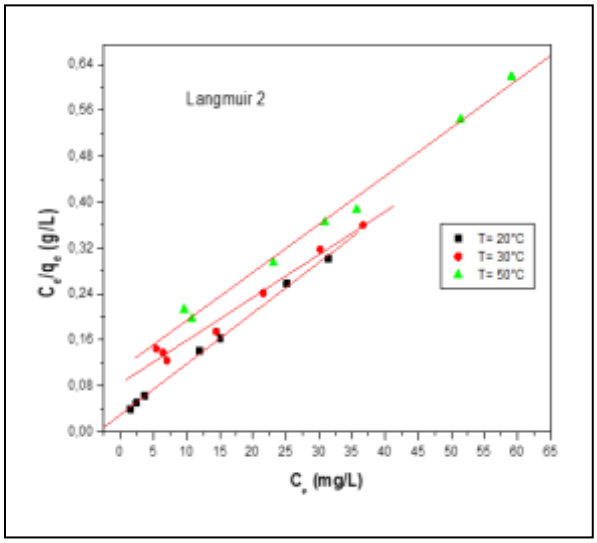

Figure 3. Linearization of the Langmuir 2 model for metoprolol adsorption onto BPPAC.

DISCUSSION

Surface properties
The high specific surface area of BPPAC 200% (1100.39 m^2/g) confirms the effectiveness of activation with H_3PO_4 in developing the textural properties of the material.
The FTIR analyses reveal changes in surface chemistry after activation, particularly in the oxygenated functional groups likely to contribute to interactions between the activated carbon and metoprolol.

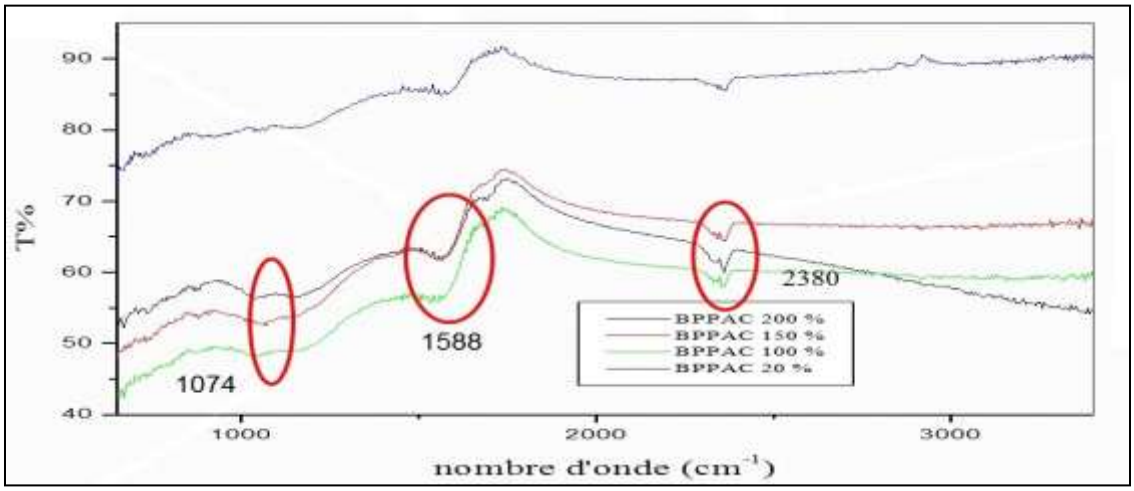

Figure 4. FTIR spectra of BPPAC carbons obtained at different H_3PO_4 activation ratios.

Adsorption mechanism
The relationship between the pHpzc of BPPAC ≈ 4 and the pKa of metoprolol ≈ 9.5 highlights the role of electrostatic interactions in the change of adsorption with pH.
The excellent fit to the pseudo-second-order model ($R^2 \approx 1$) describes the adsorption kinetics, while the Langmuir 2 model (R^2 up to 0.998) is consistent with adsorption occurring mainly as a monolayer.

Thermodynamics
The adsorption capacity decreases as the temperature increases :
20 °C → 110.87 mg/g
30 °C → 106.93 mg/g
50 °C → 95.44 mg/g
$\Delta G° < 0$ → thermodynamically favorable process
$\Delta H° < 0$ → exothermic process
$\Delta S° < 0$ → decreased disorder at the solid–solution interface
Overall interpretation
The performance of BPPAC results from the combined effect of its high specific surface area, its porous structure, its surface chemistry, and adsorbate–adsorbent interactions. These results confirm the value of activating bean pods with H_3PO_4 to produce an effective adsorbent for removing pharmaceutical pollutants in aqueous media.

CONCLUSION

BET specific surface area of BPPAC 200% = 1100.39 m^2/g
Maximum metoprolol removal = 98%
Fast equilibrium for $C_0 < 150$ mg/L ≈ 5 min
Pseudo-second-order model = $R^2 \approx 1$
Langmuir 2 model at 20 °C $R^2 = 0.998$
Maximum desorption = 60%

Activation of bean pods with H_3PO_4 at 200% yields the material with the best performance among the conditions studied. Metoprolol adsorption is rapid, well described by the pseudo-second-order model and consistent with adsorption occurring mainly as a monolayer according to the Langmuir model.

The process is thermodynamically favorable and exothermic ($\Delta G° < 0$; $\Delta H° < 0$). Desorption of up to 60% of the adsorbed metoprolol was achieved with a HNO_3 solution at 0.1 mol/L.
The valorization of bean pods into activated carbon constitutes a promising approach combining the removal of pharmaceutical pollutants, the valorization of agricultural waste, and the circular economy.

REFERENCES

V. Chander, B. Sharma, V. Negi, R.S. Aswal, P. Singh, R. Singh, and R. Dobhal, Pharmaceutical Compounds in Drinking Water, J Xenobiot, Jun 10., 6(1) (2016) 5774.
I. Villaescusa, N. Fiol, J. Poch, A. Bianchi, C. Bazzicalupi, Mechanism ofparacetamol removal by vegetable wastes: the contribution of p–pinteractions, hydrogen bonding and hydrophobic effect, Desalination. , 270(2011) 135–142.
J.R. Domínguez, T. González, P.E. Palo, M. Cuerda-Correa, Removal of common pharmaceuticals present in surface waters by Amberlite XAD-7 acrylic-ester resin: influence of pH and presence of other drugs, Desalination., 269 (2011)231–238.
A. de wilt, Y. He , N. Sutton, A. Langenhoff , H. Rijnaarts , Sorption and biodegradaion of six pharmaceutically active compounds under four different redox conditions , Chemosphere ., 193(2018) 811-819
R. Júlia, D. Andrade, M. F. Oliveira, M. G. C. da Silva, M.G. A. Vieira, Adsorption of Pharmaceuticals from Water and Wastewater Using Nonconventional Low-Cost Materials: J. Chem. Eng., 57 (2018) 9- 3103.

R.A. Figueroa, A.A. MacKay, Sorption of oxytetracycline to iron oxides and iron oxide-rich soils, Environ. Sci. Technol., 39 (2005) 6664–6671.
R.A. Figueroa, A. Leonard, A.A. MacKay, Modeling tetracycline antibiotic sorption to clays, Environ. Sci. Technol., 38 (2004) 476–483.
J.R.V. Pils, D.A. Laird, Sorption of tetracycline and chlortetracycline on K- and Ca-saturated soil clays, humic substances, and clay–humic complexes, Environ. Sci. Technol., 41 (2007) 1928–1933.
C. Gu, K.G. Karthikeyan, Interaction of tetracycline with aluminum and iron hydrous oxides, Environ. Sci. Technol., 39 (2005) 2660–2667.
T.X. Bui, H. Choi, Influence of ionic strength, anions, cations, and natural organic matter on the adsorption of pharmaceuticals to silica, Chemosphere., 80 (2010) 681–686.
J. Maszkowska , S. Stolte , J. Kumirska , P. Łukaszewicz, K. Mioduszewska, A. Puckowski , M. Caban , M. Wagil , P. Stepnowskia , A. Białk-Bielińska,Beta-blockers in the environment:Part II. Ecotoxicity study , Science of the total Environment. , 493 (2014) 1122-1126
R.S. Vardanyan, V.J. Hruby, In Synthesis of Essential Drugs., 2006
G. Stavroula , N. George, Z. K.A.Tzereme, M. P. M. K. Dimitrios, N. Bikiaris, Dimitra, A. Lambropoulou, Synthesis and characterization of modified carrageenan microparticles for the removal of pharmaceuticals from aqueous solutions , Colsurfb.,(2015)01.053.
D. Calamari, E. Zuccato, S. Castiglioni, R. Bagnati, R. Fanelli, Strategic survey of therapeutic drugs in the rivers Po and Lambro in Northern Italy, Environ. Sci. Technol., 37 (2003) 1241-1248.
J. Maszkowska, S. Stolte, J. Kumirska, P. Łukaszewicz, K. Mioduszewska, A. Puckowski, M. Caban, M. Wagil, P. Stepnowski, A. Białk-Bielińska, Beta-blockers in the environment: Part I. Mobility and hydrolysis study, Science of the Total Environment., 493 (2014) 1112-1121.

J. Maszkowska, S. Stolte, J. Kumirska, P. Łukaszewicz, K. Mioduszewska, A. Puckowski, M. Caban, M. Wagil, P. Stepnowski, A. Białk-Bielińska, Beta-blockers in the environment: Part II. Ecotoxicity study, Science of the Total Environment., 493 (2014) 1122-1126.

N. Gherbi, Z. Ziani, M. Khetib, D. Belkharchouche,A.H. Meniai, Experimental study and test of a new biosorbent prepared from bean peels to remove Rhodamine B from industrial wastewaters, Desalination and Water Treatment., (2021) 1–12.

M. Kwiatkowski,J. Sreńscek-Nazzal, B. Michalkiewicz,An analysis of the effect of the additional activation process on the formation of the porous structure and pore sizedistribution of the commercial activated carbon WG-12, Adsorption., (2017) 23:551–561.

M.A.Lillo, D. Cazorla-Amoros, A. Linares-Solano, Understanding chemical reactions between carbons and NaOH and KOH An insight into the chemical activation mechanism, Carbon., 41 (2003) 267–275.

MELATONIN AS A PROTECTANT AGAINST SALT AND DROUGHT STRESS: PRESERVATION OF ION BALANCE AND MEMBRANE INTEGRITY

Aygül Karaca[1]

[1]*Vocational School of Food, Agriculture and Livestock, Department of Crop and Animal Production, Bingöl University, Bingöl, Türkiye*

Corresponding author e-mail:akaraca@bingol.edu.tr

ABSTRACT

Global climate change poses a significant threat to agricultural production and food security, particularly by increasing the frequency and severity of abiotic stress factors such as salt and drought. These stress conditions lead to osmotic imbalance, ion toxicity (especially Na^+/K^+ imbalance), excessive reactive oxygen species (ROS) production, and disruption of cell membrane integrity in plants, resulting in growth and yield losses. Melatonin, a critical plant hormone, stands out in the fight against these negative effects due to its strong antioxidant properties and regulatory roles in stress response mechanisms. Melatonin improves essential physiological processes such as seed germination, photosynthesis, and carbon fixation, as well as enhancing stress tolerance by promoting the accumulation of osmolytes, sugars, and other endogenous hormones (auxins, gibberellic acid, and cytokinins). Furthermore, it enhances the activity of enzymatic and non-enzymatic antioxidant systems, enabling effective ROS clearance and regulating the expression of stress-responsive genes. Studies show that melatonin plays a significant role in maintaining Na^+/K^+ ion homeostasis, preserving cell membrane integrity, reducing lipid peroxidation, improving photosynthetic performance, and maintaining plant water balance under salt and drought stress. It also plays important roles in the regulation of stress-related genes and phytohormone signaling networks. These multifaceted effects of melatonin make it stand out as an environmentally friendly biostimulant in sustainable agricultural practices and a promising approach to enhancing stress tolerance against the negative impacts of climate change. A deeper understanding of melatonin's protective mechanisms on ion balance and membrane integrity will pave the way for innovative approaches to improving stress tolerance.

Keywords: melatonin, salt stress, drought stress, ion homeostasis, membrane integrity, antioxidant defense.

INTRODUCTION

Climate change is one of the most important factors threatening agricultural production and food security. Environmental stressors such as increasing temperatures, drought, floods, frost, and changing rainfall patterns directly and negatively affect the growth, development, and yield processes of plants. In particular, abiotic stress factors such as salinity, drought, extreme heat, and cold lead to significant changes in the physiological and molecular structures of plants. Recent studies allow us to understand more closely the adaptation mechanisms that plants develop against such stress conditions. Findings on how plants can survive in situations where multiple stressors occur simultaneously have reached remarkable dimensions (Li et al., 2009; Hu et al., 2023).

The two most common abiotic stress factors limiting agricultural production on a global scale are salinity and drought. According to the FAO's Global Report on Saline Soils published in 2024, approximately 1.38 billion hectares of land worldwide are affected by salinity, and

approximately one billion hectares are at risk of salinization. Climate change, dwindling water resources, and unsustainable land management indicate that these areas will expand even further in the coming years. Salt stress causes osmotic pressure and ion toxicity in plants, reducing the water uptake capacity of roots; this suppresses growth and development, leading to crop losses (Rozema and Flowers, 2008; Abobatta, 2020). Similarly, drought stress disrupts the water balance of plants by reducing the amount of water in the root zone, causing yield losses in many crops. In fact, yield losses caused by drought are higher compared to many other abiotic stress factors. Although the effect of drought varies depending on the plant species, developmental stage, and the duration and severity of the stress, it negatively affects growth and physiological activities at every stage of development (Valliyodan and Nguyen, 2006). In addition, drought disrupts the integrity of the cell membrane, negatively affecting ion transport and nutrient balance; it reduces the transpiration rate but does not limit nutrient uptake to the same extent (Farooq et al., 2012).

Plants develop numerous adaptation mechanisms at the morphological, physiological, biochemical, and molecular levels to minimize the negative effects of salinity and drought. Morphological changes such as reduced leaf area, slowed shoot growth, and increased root development, as well as physiological responses like stomatal closure, increased water use efficiency, and maintenance of cellular turgor, are just a few examples (Krasensky and Jonak, 2012). In addition, the accumulation of osmolytes such as proline, glycine betaine, and soluble sugars contributes to the maintenance of cellular osmotic balance, while the synthesis of stress-related proteins aids in the stabilization of biomolecules. However, salt and drought stress lead to disruption of cell membrane integrity, overproduction of reactive oxygen species (ROS), and particularly disruption of Na^+/K^+ ion homeostasis (Maryum et al., 2022). Loss of selective permeability of the cell membrane, disruption of ion balance, and ROS accumulation lead to decreased photosynthetic activity, slowed growth, and consequently, crop losses (Apel and Hirt, 2004; Chaves et al., 2009). Therefore, plants activate antioxidant defense systems to limit ROS accumulation and adapt to stress conditions by regulating phytohormone signaling networks (Rao et al., 2025).

Recent research highlights melatonin as a crucial signaling molecule in the regulation of these defense mechanisms. First identified as a neurohormone in animals, the discovery that melatonin is also synthesized in plants has increased interest in its role in regulating plant growth and development and abiotic stress tolerance (Arnao and Hernández-Ruiz, 2019; Ramasamy et al., 2023). In addition to its strong antioxidant properties, melatonin reduces ROS-induced oxidative damage by increasing the activity of antioxidant enzymes such as superoxide dismutase (SOD), catalase (CAT), and peroxidase (POD), promotes osmolyte accumulation, and regulates plant stress responses by interacting with phytohormones such as auxin, gibberellic acid, and cytokinin (Roychoudhury, 2023; Khan et al., 2024).

Among melatonin of protective effects against salt and drought stress, maintaining ion balance and membrane integrity is of critical importance. Studies show that melatonin applications contribute to ionic homeostasis by maintaining Na^+/K^+ ion balance, regulate membrane permeability by reducing lipid peroxidation occurring in the cell membrane, and thus protect cell integrity (Hassan et al., 2022; Zeng et al., 2022). Furthermore, melatonin has been reported to regulate the activity of various ion transporters, primarily Na^+/H^+ antiporters, strengthen the antioxidant defense system, and increase plant stress tolerance by modulating the expression of genes related to stress response (Wei et al., 2022). However, studies comprehensively addressing the physiological, biochemical, and molecular mechanisms of melatonin in maintaining ionic homeostasis and cell membrane integrity, particularly under salt and drought stress conditions, are limited. In this study, the role of melatonin in maintaining ionic balance and cell membrane integrity under salt and drought stress was evaluated in light of current

literature; These mechanisms have been shown to have potential contributions to increasing stress tolerance in plants and to sustainable agricultural practices.

MELATONIN BIOSYNTHESIS AND PHYSIOLOGICAL FUNCTIONS IN PLANTS

Melatonin, or N-acetyl-5-methoxytryptamine, is an important biomolecule with a very wide distribution in the biological world, found in almost all living organisms. First discovered in vertebrates, this molecule was considered for many years to be a neurohormone exclusive to animals (Lerner et al., 1958; Reiter, 1991). However, in 1995, two independent research groups revealed that melatonin is also found in plants, giving a completely different direction to studies in this field. These initial findings, especially on cereals, fruits, and vegetables, opened the door to research into the role of melatonin in plant physiology (Dubbels et al., 1995; Hattori et al., 1995). Today, it is known that melatonin is synthesized in very different organism groups such as bacteria, algae, higher plants, invertebrates, and vertebrates. This clearly demonstrates that melatonin is an evolutionarily well-established molecule with fundamental biological functions (Posmyk and Janas, 2009).

In all living organisms, the starting point for melatonin synthesis is tryptophan, an essential amino acid. Tryptophan is a precursor not only for melatonin but also for serotonin, found in all plants and animals, and indole-3-acetic acid (auxin), an important hormone in plants. Although melatonin can be produced from tryptophan via different biosynthetic pathways, the most widely accepted pathway is as follows: Tryptophan → Tryptamine → Serotonin → 5-methoxytryptamine → Melatonin. Numerous enzymes are involved in this conversion chain (Zhao et al., 2019). In the first step, the tryptophan decarboxylase (TDC) enzyme converts tryptophan to tryptamine. Next, the tryptamine 5-hydroxylase (T5H) enzyme comes into play and converts tryptamine into serotonin; the presence of this enzyme has been particularly proven in rice plants (Kang et al., 2007). In plants, the conversion from serotonin to 5-methoxytryptamine occurs via the acetylserotonin methyltransferase (ASMT/COMT) enzyme. This enzyme first converts serotonin to N-acetylserotonin (NAS). Finally, the 5-methoxytryptamine N-acetyltransferase/arylalkylamin N-acetyltransferase (SNAT/AANAT) enzyme completes the synthesis by converting this molecule into melatonin.

Melatonin is a signaling molecule that plays a key role in regulating daily (circadian) and seasonal rhythms in both plants and animals. In animals, melatonin synthesis increases during the dark and decreases during the light, and this cycle is considered a fundamental mechanism in the functioning of the biological clock (Reiter, 1991). A similar situation exists in plants; melatonin levels are regulated by photoperiod and circadian rhythm. However, this variation can differ depending on the plant species, developmental stage, and environmental conditions (Arnao and Hernández-Ruiz, 2015; 2020). The general trend is that melatonin synthesis peaks during the dark or just before sunrise. However, in some species, a second wave of synthesis can be observed during daylight hours due to oxidative stress triggered by high light intensity and temperature. This shows that melatonin not only regulates biological rhythms but is also active in sensing environmental signals and activating protective mechanisms against oxidative stress. With all these characteristics, melatonin is considered an important biostimulant that bridges the gap between photoperiodic responses and adaptation to environmental stress in plants.

In plants, melatonin is a versatile biomolecule that regulates growth and development. Its chemical structure and biosynthesis pathway are similar to indole-3-acetic acid (IAA) in the auxin group. Therefore, it can promote root formation, hypocotyl elongation, shoot development, and overall plant growth, exhibiting auxin-like effects, especially at low concentrations (Kanvar et al., 2018; Arnao and Hernández-Ruiz, 2020). However, the direction and intensity of these effects vary depending on the plant species, developmental stage, and the applied melatonin dose. Indeed, high concentrations of melatonin can even exhibit growth-

suppressive effects. Beyond this, melatonin supports plant development by playing a role in many physiological processes such as seed germination, photosynthesis, chlorophyll synthesis, regulation of root architecture, and delaying senescence.

One of melatonin's most notable properties is its function as a powerful antioxidant and stress regulator in plants (Yu et al., 2018). Melatonin, in addition to directly scavenging reactive oxygen species (ROS), limits oxidative damage by increasing the activity of antioxidant enzymes such as SOD, CAT, POD, and glutathione reductase (GR). This protects cell membrane integrity, reduces lipid peroxidation, and increases membrane stability. Furthermore, melatonin enhances plant tolerance to numerous abiotic stress conditions such as salinity, drought, low temperature, and heavy metal stress by promoting osmolyte accumulation, increasing photosynthetic efficiency, and regulating the expression of stress-related genes (Zhang et al., 2015; Zeng et al., 2022). With all these multiple effects, melatonin promotes plant growth. It stands out as a powerful regulatory molecule that stimulates and enhances stress tolerance.

MELATONIN-MEDIATED PROTECTION AGAINST SALT AND DROUGHT STRESS

Salinity and drought are the primary abiotic stress factors limiting growth and development in plants. These two stressors trigger a chain reaction of physiological disturbances in the plant, including osmotic pressure, ion toxicity, water imbalance, and excessive production of reactive oxygen species (ROS). In this process, the accumulation of Na^+ ions within the cell increases while K^+ uptake decreases; this imbalance leads to disruption of ion homeostasis, negatively affecting enzyme activity, metabolic processes, and photosynthesis performance. Simultaneously, excessive ROS production accelerates lipid peroxidation, impairs the selective permeability of the cell membrane, and leads to loss of membrane integrity. As a result of all these disruptions, electrolyte leakage from cells increases, water use efficiency decreases, and plant growth and yield are significantly reduced (Li et al., 2019; Yusuf et al., 2024).

Recent studies have shown that melatonin acts as a multifaceted regulator in mitigating these physiological and biochemical disruptions. Melatonin, as a powerful free radical scavenger, not only directly neutralizes ROS but also enhances plant defense capabilities by increasing the activity of antioxidant enzymes such as SOD, CAT, ascorbate peroxidase (APX), POD, and GR. It also contributes to maintaining cellular osmotic balance by promoting the accumulation of osmolytes and soluble sugars. Furthermore, it supports cell membrane stability by reducing lipid peroxidation and malondialdehyde (MDA) formation (Hassan et al., 2022; Pardo-Hernández et al., 2020).

One of melatonin's most notable effects is its regulatory role in maintaining ionic homeostasis. Studies have shown that melatonin application limits Na^+ accumulation and reduces K^+ loss by regulating the expression of Na^+/H^+ antiporters and high-affinity K^+ transporters, thus significantly contributing to the maintenance of intracellular Na^+/K^+ balance (Yan et al., 2020; 2021). Maintaining ion balance, preserving membrane integrity, and reducing oxidative damage allows for more efficient photosynthetic mechanisms. This slows down chlorophyll degradation, improves gas exchange, and increases water use efficiency. In addition, melatonin contributes to the regulation of genes related to stress responses and various phytohormone signaling networks, further strengthening the adaptation of plants to salt and drought conditions (Tahjib-Ul-Arif et al., 2025). With all these multifaceted protective effects, melatonin has great potential as an environmentally friendly and effective bio-stimulant in sustainable agricultural practices; It is considered one of the prominent biomolecules, especially in strategies aimed at maintaining ionic homeostasis and membrane integrity.

MOLECULAR MECHANISMS UNDERLYING MELATONIN-MEDIATED STRESS TOLERANCE

Melatonin not only functions as a powerful antioxidant in plants, but also plays a crucial role as a bioregulator, regulating numerous signaling pathways and enhancing tolerance to salinity and drought. Recent research reveals that the protective effect of melatonin is based on molecular processes such as the regulation of stress-related gene expression, coordination of signaling interactions between phytohormones, calcium (Ca^{2+})-mediated signal transduction, and control of nitric oxide (NO)-related redox mechanisms. All these mechanisms work together and interactively to maintain ion balance, preserve cell membrane integrity, and enable plants to adapt more successfully to stressful conditions (Gu et al., 2022; Ahmad et al., 2023; Pan et al., 2023).

One of melatonin's most critical roles is its ability to reshape the expression of stress-responsive genes. Under challenging conditions such as salt and drought, melatonin applications regulate the activity of stress-sensitive transcription factors and genes involved in defense mechanisms, enabling plants to more accurately interpret stress signals and develop appropriate defense strategies (Byeon and Back, 2014). In addition, melatonin controls ROS accumulation by increasing the expression of genes encoding enzymes related to the antioxidant defense system, minimizes oxidative damage, and contributes to the maintenance of cellular redox balance (Sheshadri et al., 2018; Gu et al., 2022). Particularly under salt stress, melatonin regulates genes associated with ion transport and homeostasis, limiting Na^+ accumulation in the cytoplasm, maintaining K^+ levels in balance, and thus reducing ion toxicity (Tahjib-Ul-Arif et al., 2025).

Another vital mechanism where melatonin exerts its influence is the coordination of complex signaling networks among phytohormones. Melatonin is no longer seen as a molecule acting alone; Melatonin is considered a regulator that shapes plant stress responses in interaction with abscisic acid (ABA), auxin (IAA), gibberellin acid (GA), cytokinins (CK), ethylene (ET), jasmonic acid (JA), and salicylic acid (SA) (Samanta and Roychoudhury, 2023). Particularly in conditions such as drought and salinity, melatonin's adjustments to ABA levels play a crucial role in controlling stomata, increasing water use efficiency, and maintaining osmotic balance. Melatonin also promotes root development via the auxin signaling pathway, supporting water and mineral uptake; it regulates cytokinin and gibberellin metabolism, ensuring continued growth. In addition, by interacting with JA and SA signaling pathways, it further strengthens antioxidant defenses and the activation of stress-related genes (Ahmad et al., 2023; Samanta and Roychoudhury, 2023).

Calcium (Ca^{2+}) is one of the key second messenger molecules involved in the transmission of stress signals in plants. Melatonin is known to regulate Ca^{2+}-mediated signal transduction, supporting the activation of stress response genes, the antioxidant defense system, and ionic homeostasis. This makes the adaptation mechanisms that plants develop against salt and drought stress more effective (Liu et al., 2020; Huang et al., 2022).

The effects of melatonin on stress tolerance are further enhanced by its interaction with NO. NO acts as an important signaling molecule in plants and, together with melatonin, plays a role in activating the antioxidant defense system, maintaining ROS balance, and regulating redox homeostasis. This interaction significantly contributes to mitigating oxidative damage, maintaining cell membrane integrity, and increasing plant tolerance to salt and drought (Pardo-Hernández et al., 2020; Ahmad et al., 2023; Kolupaev et al., 2024).

In summary, melatonin is a key player in plant defense against salinity and drought by activating multi-layered molecular mechanisms such as the regulation of stress response genes, coordination of phytohormone interactions, and management of Ca^{2+} and NO-mediated signaling pathways. This integrated signaling network provides a strong foundation for maintaining ionic homeostasis, preserving cell membrane integrity, and enhancing overall stress tolerance.

CONCLUSIONS

As the effects of global climate change become increasingly apparent, salinity and drought stand out as the most significant abiotic stressors threatening agricultural production and food security. These challenging conditions hinder plant growth and lead to yield losses through mechanisms such as osmotic imbalance, ion toxicity, oxidative damage, and disruption of cell membrane integrity. However, recent research reveals that melatonin acts as a versatile and powerful regulator in mitigating these negative effects. Melatonin significantly increases plant tolerance to salinity and drought by activating the antioxidant defense system, maintaining ion balance and cell membrane integrity, supporting photosynthetic activity, and regulating gene expression and phytohormone signaling networks. With all these properties, melatonin stands out as an environmentally friendly, effective, and promising bio-stimulant for sustainable agricultural practices. Further elucidation of the molecular mechanisms related to melatonin in different plant species and under varying stress conditions is of paramount importance. This will both increase the efficiency of melatonin in agricultural applications and make significant contributions to the development of new plant varieties with high stress tolerance.

REFERANSLAR

Abobatta, W. F. 2020. Plant responses and tolerance to combined salt and drought stress. In Salt and drought stress tolerance in plants: signaling networks and adaptive mechanisms (pp. 17-52). Cham: Springer International Publishing.

Ahmad, I., Song, X., Hussein Ibrahim, M. E., Jamal, Y., Younas, M. U., Zhu, G., ... & Adam Ali, A. Y. 2023. The role of melatonin in plant growth and metabolism, and its interplay with nitric oxide and auxin in plants under different types of abiotic stress. Frontiers in Plant Science, 14, 1108507.

Apel, K., & Hirt, H. 2004. Reactive oxygen species: Metabolism, oxidative stress, and signal transduction. Annual Review of Plant Biology, 55(1), 373-399.

Arnao, M. B., & Hernández-Ruiz, J. 2015. Functions of melatonin in plants: A review. Journal of Pineal Research, 59(2), 133-150.

Arnao, M. B., & Hernández-Ruiz, J. 2019. Melatonin: A new plant hormone and/or a plant master regulator? Trends in Plant Science, 24(1), 38-48.

Arnao, M. B., & Hernández-Ruiz, J. 2020. Is phytomelatonin a new plant hormone? Agronomy, 10(1), 95.

Byeon, Y., & Back, K. 2014. Melatonin synthesis in rice seedlings in vivo is enhanced at high temperatures and under dark conditions due to increased serotonin N-acetyltransferase and N-acetylserotonin methyltransferase activities. Journal of Pineal Research, 56(2), 189-195.

Chaves, M. M., Flexas, J., & Pinheiro, C. 2009. Photosynthesis under drought and salt stress: Regulation mechanisms from whole plant to cell. Annals of Botany, 103(4), 551-560.

Dubbels, R., Reiter, R. J., Klenke, E., Goebel, A., Schnakenberg, E., Ehlers, C., ... & Schloot, W. (1995). Melatonin in edible plants identified by radioimmunoassay and by high performance liquid chromatography-mass spectrometry. Journal of Pineal Research, 18(1), 28-31.

Farooq, M., Hussain, M., Wahid, A., & Siddique, K. H. M. 2012. Drought stress in plants: an overview. Plant responses to drought stress: From morphological to molecular features, 1-33.

Food and Agriculture Organization of the United Nations (FAO). 2024. Global status of salt-affected soils. FAO. https://doi.org/10.4060/cd3044en

Gu, Q., Xiao, Q., Chen, Z., & Han, Y. 2022. Crosstalk between melatonin and reactive oxygen species in plant abiotic stress responses: An update. International Journal of Molecular Sciences, 23(10), 5666.

Hassan, M. U., Mahmood, A., Awan, M. I., Maqbool, R., Aamer, M., Alhaithloul, H. A., ... & Qari, S. H. 2022. Melatonin-induced protection against plant abiotic stress: Mechanisms and prospects. Frontiers in Plant Science, 13, 902694.

Hattori, A., Migitaka, H., Iigo, M., Itoh, M., Yamamoto, K., Ohtani-Kaneko, R., ... & Reiter, R. J. 1995. Identification of melatonin in plants and its effects on plasma melatonin levels and binding to melatonin receptors in vertebrates. Biochemistry and Molecular Biology International, 35(3), 627-634.

Hu, J., Zhao, X., Gu, L., Liu, P., Zhao, B., Zhang, J., & Ren, B. 2023. The effects of high temperature, drought, and their combined stresses on the photosynthesis and senescence of summer maize. Agricultural Water Management, 289, 108525.

Huang, X., Tanveer, M., Min, Y., & Shabala, S. 2022. Melatonin as a regulator of plant ionic homeostasis: Implications for abiotic stress tolerance. Journal of Experimental Botany, 73(17), 5886-5902.

Kang, S., Kang, K., Lee, K., & Back, K. 2007. Characterization of tryptamine 5-hydroxylase and serotonin synthesis in rice plants. Plant Cell Reports, 26(11), 2009-2015.

Kanwar, M. K., Yu, J., & Zhou, J. 2018. Phytomelatonin: Recent advances and future prospects. Journal of Pineal Research, 65(4), e12526.

Khan, M., Hussain, A., Yun, B. W., & Mun, B. G. 2024. Melatonin: The multifaceted molecule in plant growth and defense. International Journal of Molecular Sciences, 25(12), 6799.

Kolupaev, Y. E., Yemets, A., Yastreb, T. O., & Blume, Y. 2024. Functional interaction of melatonin with gasotransmitters and ROS in plant adaptation to abiotic stresses. Frontiers in Plant Science, 15, 1505874.

Krasensky, J., & Jonak, C. 2012. Drought, salt, and temperature stress-induced metabolic rearrangements and regulatory networks. Journal of Experimental Botany, 63(4), 1593-1608.

Lerner, A. B., Case, J. D., Takahashi, Y., Lee, T. H., & Mori, W. 1958. Isolation of melatonin, the pineal factor that lightens melanocytes. Journal of the American Chemical Society, 80(10), 2587-2587.

Li, J., Liu, J., Zhu, T., Zhao, C., Li, L., & Chen, M. 2019. The role of melatonin in salt stress responses. International Journal of Molecular Sciences, 20(7), 1735.

Li, Y. P., Ye, W., Wang, M., & Yan, X. D. 2009. Climate change and drought: A risk assessment of crop-yield impacts. Climate Research, 39, 31-46.

Liu, J., Shabala, S., Zhang, J., Ma, G., Chen, D., Shabala, L., ... & Zhao, Q. 2020. Melatonin improves rice salinity stress tolerance by NADPH oxidase-dependent control of the plasma membrane K^+ transporters and K^+ homeostasis. Plant, Cell & Environment, 43(11), 2591-2605.

Maryum, Z., Luqman, T., Nadeem, S., Khan, S. M. U. D., Wang, B., Ditta, A., & Khan, M. K. R. 2022. An overview of salinity stress, mechanism of salinity tolerance and strategies for its management in cotton. Frontiers in Plant Science, 13, 907937.

Pan, Y., Xu, X., Li, L., Sun, Q., Wang, Q., Huang, H., ... & Zhang, J. 2023. Melatonin-mediated development and abiotic stress tolerance in plants. Frontiers in Plant Science, 14, 1100827.

Pardo-Hernández, M., López-Delacalle, M., & Rivero, R. M. 2020. ROS and NO regulation by melatonin under abiotic stress in plants. Antioxidants, 9(11), 1078.

Posmyk, M. M., & Janas, K. M. 2009. Melatonin in plants. Acta Physiologiae Plantarum, 31(1), 1-11.

Ramasamy, K., Karuppasami, K. M., Alagarswamy, S., Shanmugam, K. P., Rathinavelu, S., Vellingiri, G., ... & Kanagarajan, S. 2023. Role of melatonin in directing plant physiology. Agronomy, 13(9), 2405.

Rao, M. J., Duan, M., Zhou, C., Jiao, J., Cheng, P., Yang, L., ... & Zheng, B. 2025. Antioxidant defense system in plants: Reactive oxygen species production, signaling, and scavenging during abiotic stress-induced oxidative damage. Horticulturae, 11(5), 477.

Reiter, R. J. 1991. Pineal melatonin: Cell biology of its physiological interactions. Endocrine Reviews, 12(2), 151-181.
Roychoudhury, A. (Ed.). 2023. Advancement of melatonin research in plants: Multi-faceted role in regulating development and stress protection. CRC Press.
Rozema, J., & Flowers, T. 2008. Crops for a salinized world. Science, 322(5907), 1478-1480.
Samanta, S., & Roychoudhury, A. 2023. Crosstalk of melatonin with major phytohormones and growth regulators in mediating abiotic stress tolerance in plants. South African Journal of Botany, 163, 201-216.
Sheshadri, S., Nishanth, M., Yamine, V., & Simon, B. 2018. Effect of melatonin on the stability and expression of reference genes in Catharanthus roseus. Scientific Reports, 8(1), 1-11.
Tahjib-Ul-Arif, M., Zahan, I., Hossain, M. S., Imran, S., Hasanuzzaman, M., Dawood, M. F., ... & Brestic, M. 2025. Melatonin-mediated ionic homeostasis in plants: Mitigating nutrient deficiency and salinity stress. Discover Plants, 2(1), 143.
Valliyodan, B., & Nguyen, H. T. 2006. Understanding regulatory networks and engineering for enhanced drought tolerance in plants. Current Opinion in Plant Biology, 9(2), 189-195.
Wei, L., Zhao, H., Wang, B., Wu, X., Lan, R., Huang, X., ... & Zheng, Q. 2022. Exogenous melatonin improves the growth of rice seedlings by regulating redox balance and ion homeostasis under salt stress. Journal of Plant Growth Regulation, 41(6), 2108-2121.
Yan, F., Wei, H., Li, W., Liu, Z., Tang, S., Chen, L., ... & Li, G. 2020. Melatonin improves K^+ and Na^+ homeostasis in rice under salt stress by mediated nitric oxide. Ecotoxicology and Environmental Safety, 206, 111358.
Yan, F., Wei, H., Ding, Y., Li, W., Chen, L., Ding, C., ... & Li, G. 2021. Melatonin enhances Na^+/K^+ homeostasis in rice seedlings under salt stress through increasing the root H^+-pump activity and Na^+/K^+ transporters sensitivity to ROS/RNS. Environmental and Experimental Botany, 182, 104328.
Yu, Y., Lv, Y., Shi, Y., Li, T., Chen, Y., Zhao, D., & Zhao, Z. 2018. The role of phyto-melatonin and related metabolites in response to stress. Molecules, 23(8), 1887.
Yusuf, M., Saeed, T., Almenhali, H. A., Azzam, F., Hamzah, A. I. A. H., & Khan, T. A. 2024. Melatonin improved efficiency of 24-epibrassinolide to counter the collective stress of drought and salt through osmoprotectant and antioxidant system in pea plants. Scientia Horticulturae, 323, 112453.
Zeng, W., Mostafa, S., Lu, Z., & Jin, B. 2022. Melatonin-mediated abiotic stress tolerance in plants. Frontiers in Plant Science, 13, 847175.
Zhang, N., Sun, Q., Zhang, H., Cao, Y., Weeda, S., Ren, S., & Guo, Y. D. 2015. Roles of melatonin in abiotic stress resistance in plants. Journal of Experimental Botany, 66(3), 647-656.
Zhao, D., Yu, Y., Shen, Y., Liu, Q., Zhao, Z., Sharma, R., & Reiter, R. J. 2019. Melatonin synthesis and function: Evolutionary history in animals and plants. Frontiers in Endocrinology, 10, 249.

CRUSTACEAN COMMUNITY STRUCTURE AND SEASONAL DYNAMICS ALONG THE HIMARA COAST: A COMPARISON BETWEEN PORTO PALERMO AND QEPARO

Brunilda Veshaj[1], Denada Sota[1], Stela Ruci[2], Anisa Toska[2], Julinda Sinaj[1], Arlinda Kakaci[1], Sabrina Abazaj [1], Sajmir Beqiraj[2]*

[1]Department of Biology, Faculty of Technical and Natural Sciences, University "Ismail Qemali", Vlora, ALBANIA;
[2]Department of Biology, Faculty of Natural Sciences, University of Tirana, ALBANIA

**Corresponding author e-mail: brunilda.veshaj@univlora.edu.al*

ABSTRACT

Crustaceans are an important component of benthic communities and can provide valuable information on environmental conditions and ecological change in marine ecosystem. This study investigates the structure and seasonal dynamics of crustacean assemblages along the Himara coast, comparing the Porto Palermo protected area with the Qeparo coastal area. Sampling was conducted during four periods: autumn 2023, spring 2024, autumn 2024, and spring 2025. At each site and sampling period, three transects and three sampling areas were surveyed. A total of 58 crustacean taxa were recorded, and their abundance was quantified. In addition, the abundance and percentage cover of four balanid species (Cirripedia) were assessed to provide further information on the structure of the sessile crustacean community. Community composition and seasonal variation were analyzed using multivariate statistical approaches, including PERMANOVA, together with analyses of taxonomic richness and abundance. The study aims to determine whether crustacean assemblages differ significantly between Porto Palermo and Qeparo, whether community structure varies among seasons, and whether the magnitude and pattern of spatial differences change seasonally. The results will provide baseline information on the composition, abundance, and seasonal dynamics of crustacean assemblages and identify common and characteristic taxa in the two coastal areas. This information will contribute to the long-term ecological assessment of the Porto Palermo protected area and Qeparo coastal site.

Key words: benthic community, crustaceans, biodiversity, protected areas, seasonal variation, multivariate statistical analyses.

INTRODUCTION

Rocky coastal ecosystems are among the most heterogeneous marine habitats and support diverse benthic communities due to the structural complexity of the hard substrates (Gimenez et al. 2022). Crevices, cavities and associated algal communities provide suitable conditions for a wide range of organisms and contribute to the maintenance of high levels of coastal biodiversity. In the Mediterranean Sea, one of the areas with the highest marine biodiversity on a global scale, but also under constant anthropogenic pressure (Bianchi & Morri 2000; Coll et al. 2010), rocky coasts are particularly important habitats, where the composition and structure of the benthic community can vary significantly at relatively small spatial scales and across seasons (Marina et al. 2015; Sturaro et al. 2014; Sala et al. 2012).

Crustaceans constitute an important group of benthic marine communities. They include mobile taxa associated with rocky substrates and algal habitats, as well as sessile forms such as balanids (Cirripedia) (Hamdy et al. 2017).

For the crustacean community, seasonal changes can result in changes in species richness, abundance, and community composition (Scipione & Zupo 2010; Gambi et al. 1992; Rumbold et al. 2017). Recent studies have shown that the presence and dominance of crustaceans, both native and non-native, can vary significantly from month to month according to environmental context, highlighting that without repeated sampling, biodiversity changes unnoticed (Kazanavičiūtė et al. 2024).

The Ionian coast consists of extensive rocky habitats that support diverse marine benthic communities, where most studies have focused on macroinvertebrates, macroalgae and Posidonia oceanica meadows (Beqiraj et al., 2008; Beqiraj & Kashta, 2013; Beqiraj, 2014; Beqiraj & Ballesteros, 2018; Fraschetti et al., 2011; Kashta et al., 2005; Kashta et al., 2007; Kashta & Beqiraj, 2009; Kasemi et al., 2008; Kasemi et al., 2013; Pititto etal., 2009; Ruci et al., 2014; Ruci et al., 2023), but detailed studies on the spatial and seasonal dynamics of the crustacean community remain relatively limited (Vaso & Gjiknuri (1993).

A comparison of the two areas, Porto Palermo and Qeparo, across seasons may provide an opportunity to assess both spatial and temporal components of crustacean community structure (Sturaro et al. 2014; Di Franco et al. 2009).

The aim of this study is to identify the crustacean community structure and seasonal changes along the Himara coast, comparing the protected area of Porto Palermo (Beqiraj et al. 2008, Beqiraj & Kashta 2013, Beqiraj 2014), with the coastal area of Qeparo.

MATERIAL AND METHODS

Sample collection

Benthic crustaceans were collected from two sampling sites Qeparo (40°03'05"N19°48'45"E) and Porto Palermo Bay (40°03'41"N19°47'34"E) along the Himara coast, in shallow water, during four sampling periods: Autumn 2023, Spring 2024, Autumn 2024, and Spring 2025 (Fig. 1). At each site and sampling period, three transects were established, and within each transect three quadrats were randomly sampled (nine replicates per site per period), using conventional techniques for benthic samples from hard substrates, as described by Bianchi et al. (2003), Keklikoglou et al. (2018), Mikac et al. (2020), Salomidi (2003), and Zenetos et al. (2000). Each quadrat consisted of a standardized 50 × 50 cm frame, subdivided into 25 equal squares of 10 × 10 cm, to facilitate systematic counting of individuals. After collection, Samples were preserved using 4% formaldehyde solution and were taken to the laboratory for further analysis. Taxonomic identification of crustacean specimens followed standard identification guides for Mediterranean Crustacea including Ruffo (ed., 1982–1998, Parts 1–4), Riedl (1991), Argano et al. (1995), Zettler & Zettler (2017), and Trainito (2004). The nomenclature and systematic classification of all identified taxa were verified against the World Register of Marine Species (WoRMS).

Figure 1. Map of sampling sites: a) Porto Palermo; b) Qeparo

Statistical analyses

Statistical analysis assessed both univariate and multivariate characteristics of crustacean communities in Porto Palermo and Qeparo during the four sampling periods. Taxonomic richness and abundance were used to describe the main characteristics of the communities and to assess spatial and seasonal variability. Total abundance (N) was the number of individuals

recorded per replicate, summed across replicates for each zone and season. Taxonomic richness (S) was the number of crustacean taxa identified per replicate, zone, and season. We also calculated relative abundance for each taxon, following the approach used by (Kazanavičiūtė et al. 2024). This was the percentage of a taxon's abundance out of the total abundance in each zone-season combination. Relative abundance let us identify dominant and characteristic taxa, regardless of differences in sampling effort or total abundance between zones and seasons.

We assessed changes in crustacean community composition using multivariate analyses based on a Bray–Curtis similarity matrix (Bray & Curtis 1957) calculated from square-root transformed abundance data, following standard practice for community-level analyses (Clarke & Warwick 2001). We used non-metric multidimensional scaling (NMDS; Kruskal 1964; Clarke 1993) to show patterns of similarity between samples. We used PERMANOVA (Anderson 2001; McArdle & Anderson 2001) to test the effects of location and season, and their interaction, on community composition. The location × season interaction told us whether the difference between Porto Palermo and Qeparo stayed the same across seasons, or changed over time.

RESULTS AND DISCUSSION

There were 58 crustaceans identified from both localities for all periods. Out of this total number, 47 crustacean species were found in Porto Palermo while 40 crustacean species were found in Qeparo.

Richness and abundance both changed by site and season. Porto Palermo had more taxa than Qeparo in three of the four periods: 39 vs. 23 in autumn 2023, 31 vs. 25 in spring 2024, 28 vs. 25 in spring 2025. Only autumn 2024 was different Qeparo had slightly more taxa there (19 vs. 17) (Figure 2a).

Abundance told the opposite story. Qeparo had more individuals than Porto Palermo in both spring periods: 3955 vs. 1339 in 2024, 3848 vs. 1320 in 2025.

Porto Palermo remained higher only in autumn 2023 (2995 versus 1979). This shows something important: Porto Palermo has more species but fewer individuals; Qeparo has fewer species but with high peaks of abundance. Making them two areas with different dynamics (figure2b).

In Qeparo, one of the abundant taxa in all seasons was *Aphohyale crassipes*. The relative abundance of this taxon increased from autumn 2023 to autumn 2024. In addition, in spring 2024, *Heteroanais oerstedii* was one of the abundant taxa, whereas *Ptolyhyale eburnea* was valuable. In spring 2025, the most abundant taxon was *Autonoë angularis*. Moreover, *Protohyale schmidtii* had an obvious increase in this season (figure 3).

In Porto Palermo, *Aphohyale crassipes* was one of the dominating taxa in all seasons, particularly in autumn 2024. Another taxon that was abundant in autumn 2023 was *Pleonexes helleri*, whereas in spring 2024 and autumn 2024 *Elasmopus pocillimanus* had an obvious increase. Finally, in spring 2025, the abundant taxon was *Elasmopus pocillimanus* along with *Aphohyale crassipes* (figure 3).

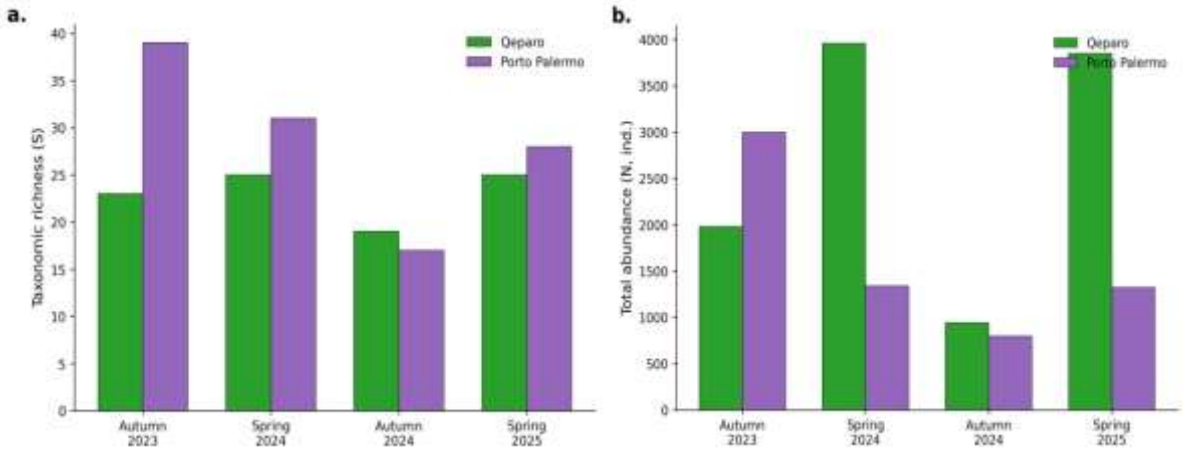

Figure 2: Taxonomic richness (a) and total abundance (b) of crustacean communities.

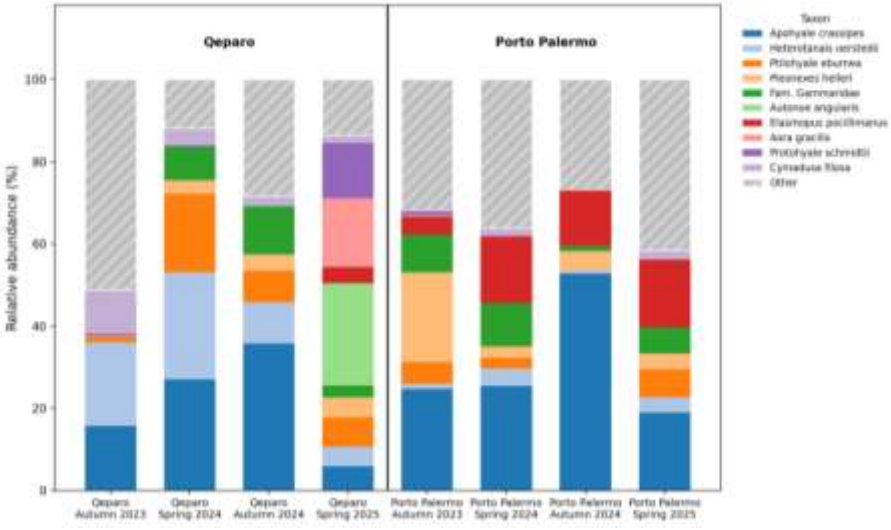

Figure 3: Seasonal abundance of dominant Crustacean taxa (Qeparo & Porto Palermo, 2023-2025)

Points corresponding to Qeparo and Porto Palermo communities (figure 4) partly intersect in the middle of the chart; therefore, the two communities share some similarities. However, the

distribution of the points belonging to Qeparo is broader than the distribution of points belonging to Porto Palermo.

Consequently, dispersion is the characteristic that differs the stability of the samples of the two communities. In particular, Qeparo is characterized by a higher diversity of the samples, while the samples from Porto Palermo are similar to each other.

Season is another characteristic that influences the location of the points. For instance, the points of spring 2025 (diamonds) for Qeparo community are isolated and positioned in the upper right corner. Moreover, the points of autumn 2024 (triangles) for the two communities are positioned below the other seasons' points. Thus, seasons influence the location of the sample almost as much as areas do.

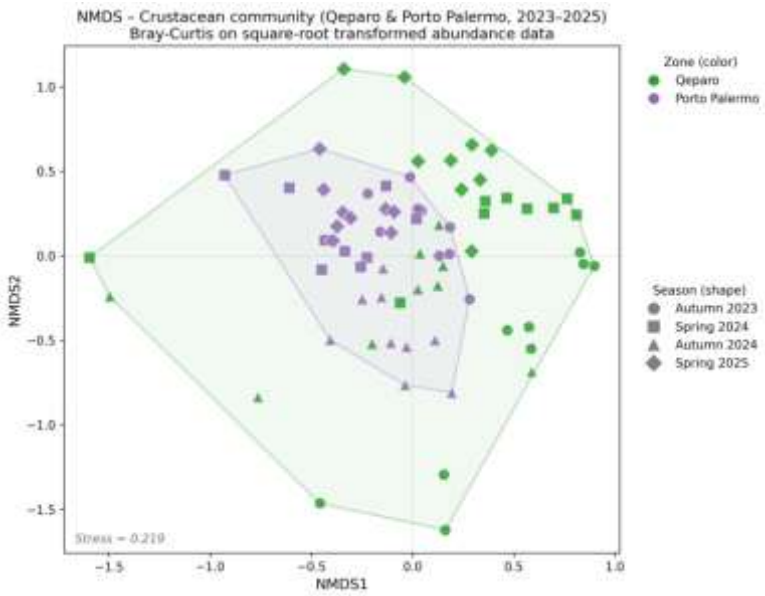

Figure 4: Comparison of the Crustacean community between the two sampling areas Qepare & Porto Palermo

The PERMANOVA analysis (Table 1) evidenced highly significant differences for both factors (zone and season) and their interaction. Assemblage structure different significantly between Qeparo and Porto Palermo (Pseudo-F = 11.11, P (perm) = 0.001), among the four sampling periods (Pseudo-F = 6.67, P(perm) = 0.001), and the zone × season interaction is also highly significant (Pseudo-F = 4.70, P(perm) = 0.001), indicating that spatial differences between the two sites are not consistent through time.

Such assemblage patterns were well represented by the nMDS plot (Figure 4), which showed partial separation between Qeparo and Porto Palermo samples, with greater dispersion of Qeparo replicates along both axes. This pattern is consistent with the higher temporal variability

in taxonomic composition and abundance recorded at Qeparo across the four sampling periods, as reported in Figure 2.

The residual variance (58.6%) remained comparatively high, a pattern commonly observed in crustacean assemblage data from hard-bottom habitats, and likely reflects fine-scale variability among replicates within each zone and season, in addition to the structuring effects of zone and season themselves.

Table 1. Results of (PERMANOVA) testing the effects of zone, season, and their interaction on crustacean assemblage structure, based on a Bray–Curtis resemblance matrix calculated from square-root transformed abundance data (999 permutations).

Source	Df	MS	Pseudo-F	P(perm)
Zone	1	1.7091	11.11	0.001
Season	3	1.0261	6.67	0.001
Zone × Season	3	0.7223	4.7	0.001
Res	64	0.1538		
Total	71			

CONCLUSIONS

A distinction was found between Porto Palermo and Qeparo. We documented 58 taxa of crustaceans in total. Porto Palermo had more taxa (47) than Qeparo (40) and shared 29 taxa.

The richness and abundance were inversely correlated. While Porto Palermo showed a higher number of species, Qeparo had more individuals. Qeparo had also higher peaks in abundance, which indicates different functioning of the sites instead of the latter being "richer".

The effect of the season was also observed. Zone × season interaction was significant, and thus the difference between Porto Palermo and Qeparo differed from season to season.

The dominant taxa are also telling their stories. *Apohyale crassipes* remained dominant in Porto Palermo throughout all four seasons. In Qeparo, the dominant taxon changed every season, first *Heterotanais oerstedii*, then *Ptilohyale eburnea*, then *Autonoe angularis* and *Protohyale schmidtii*. Thus, the Qeparo community shows a lower stability than the Porto Palermo community. In general, we can say this study gives an initial baseline on the crustacean community of this area of the Himara coast. This information will be useful for future monitoring of the protected Porto Palermo area in comparison to Qeparo as a reference area.

REFERENCES

Anderson, M.J. (2001). A new method for non-parametric multivariate analysis of variance. Austral Ecology, 26(1), 32–46.

Argano, R., Ferrara, F., Guglielmo, L., Riggio, S. & Ruffo, S. (1995). Crustacea Malacostraca II (Tanaidacea, Isopoda, Amphipoda, Euphausiacea). In: Minelli, A., Ruffo, S. & La Posta, S. (eds.), Checklist delle specie della fauna italiana, 30. Calderini, Bologna, pp. 1–52.

Beqiraj, S. (2014). Assessment and preparation of documents for the new proposed MPA Cape of Rodoni. Technical report, 61 pp.

Beqiraj, S., Ballesteros, E. (2018). Assessment of the state of marine biodiversity in the Albanian littoral. Albanian Conference on Biology and Environment (KShBM-ACBE), 28–30 September 2018, Prishtina.

Beqiraj, S., Kashta, L. (2013). Assessment and preparation of documents for the new proposed MPA Cape of Rodoni. Technical report.

Beqiraj, S., Kashta, L., Kuci, M., Kasemi, D., Mato, Xh., Gace, A. (2008). Benthic macrofauna of Posidonia oceanica meadows in the Albanian coast. Natura Montenegrina, 7(2), 55–69.

Bianchi, C.N., Morri, C., Chessa, L.A., Morganti, C., Pergent, G., Pergent-Martini, C., Sghaier, Y.R., Zenetos, A. (2003–2004). Hard bottoms. In: Mediterranean marine benthos: a manual of methods for its sampling and study. Biologia Marina Mediterranea, 11(suppl. 1), 185–215.

Bray, J.R., Curtis, J.T. (1957). An ordination of the upland forest communities of southern Wisconsin. Ecological Monographs, 27(4), 325–349.

Clarke, K.R. (1993). Non-parametric multivariate analyses of changes in community structure. Australian Journal of Ecology, 18(1), 117–143.

Clarke, K.R., Warwick, R.M. (2001). Change in marine communities: an approach to statistical analysis and interpretation, 2nd edition. PRIMER-E, Plymouth.

Coll, M., Piroddi, C., Steenbeek, J., Kaschner, K., Ben Rais Lasram, F., Aguzzi, J., Ballesteros, E., et al. (2010). The biodiversity of the Mediterranean Sea: estimates, patterns, and threats. PLoS ONE, 5(8), e11842.

Di Franco, A., Bussotti, S., Navone, A., Panzalis, P., Guidetti, P. (2009). Evaluating effects of total and partial restrictions to fishing on Mediterranean rocky-reef fish assemblages. Marine Ecology Progress Series, 387, 275–285.

Fraschetti, S., Beqiraj, S., Gačić, M., Mascle, J., Odorico, R. (2011). Scientific rationale for the proposed CIESM North Ionian Sea Marine Peace Park. CIESM Workshop Monographs, 87–96.

Gambi, M.C., Lorenti, M., Russo, G.F., Scipione, M.B., Zupo, V. (1992). Depth and seasonal distribution of some groups of the vagile fauna of the Posidonia oceanica leaf stratum: structural and trophic analyses. Marine Ecology, 13(1), 17–39.

Gimenez, G., Corriero, G., Beqiraj, S., Lazaj, L., Lazic, T., Longo, C., Mercurio, M., Nonnis Marzano, C., Zuccaro, M., Zuna, V., Pierri, C. (2022). Characterization of the Coralligenous Formations from the Marine Protected Area of Karaburun-Sazan, Albania. Journal of Marine Science and Engineering, 10(10), 1458.

Hamdy, R., Langeneck, J., Atta, M.M., Dorgham, M.M., El-Rashidy, H.H., Musco, L. (2017). Diversity and ecology of crustaceans from shallow rocky habitats along the Mediterranean coast of Egypt. Marine Biodiversity, 49, 221–233.

Kasemi, D., Beqiraj, S., Ruci, S. (2008). Macrozoobenthos of the rocky coasts of Vlora, Albania. Natura Montenegrina, 7(2), 133–143.

Kasemi, D., Ruci, S., Beqiraj, S. (2013). Data on macrozoobenthos of the Radhima coast, Vlora Bay, Albania. Natura Montenegrina, 12, 773–785.

Kashta, L., Beqiraj, S. (2009). Analysis of the proposed potential Marine Protected Areas. Protected Areas Gap Assessment and Marine Protected Areas Development in Albania (UNDP, GEF, MEFWA). Technical report, 81 pp.

Kashta, L., Beqiraj, S., Mato, Xh., Xhulaj, M., Gaçe, A., Mullaj, A. (2005). The inventory of habitats with Posidonia oceanica and littoral habitats in Albania. Technical Report. APAWA, Tirana. 86 pp.

Kashta, L., Xhulaj, M., Mato, Xh., Beqiraj, S., Gace, A. (2007). The state of Posidonia meadows along the Albanian coast: general evaluation. 3rd Mediterranean Symposium on Marine Vegetation, Marseilles, France, 121–125.

Kazanavičiūtė, E., Dickey, J.W.E., Soto, I., Haubrock, P.J., Kouba, A., Brennan, R.S., Steffen, G., Briski, E. (2024). Seasonal changes in biodiversity of native and non-native amphipod taxa under diverse environmental contexts. Marine Biology, 171, 156.

Keklikoglou, K. et al. (2018). [Reference requires verification from original source.]

Kruskal, J.B. (1964). Nonmetric multidimensional scaling: a numerical method. Psychometrika, 29(2), 115–129.

Marina, P., Rueda, J.L., Urra, J., Salas, C., Gofas, S., Moya, F., Garcia, T., Lopez-Gonzalez, N., Laiz-Carrion, R., Baro, J. (2015). Sublittoral soft bottom assemblages within a Marine Protected Area of the northern Alboran Sea. Journal of the Marine Biological Association of the United Kingdom, 95(8), 1–14.

McArdle, B.H., Anderson, M.J. (2001). Fitting multivariate models to community data: a comment on distance-based redundancy analysis. Ecology, 82, 290–297.

Pititto, F., Grenci, S., Dedej, Z., Gace, A., Kashta, L., Beqiraj, S., Acunto, S., Bulgheri, G., Cinelli, F., Sivini, N., Greco, R., Torchia, G. (2009). Cartography and protection of the Posidonia oceanica meadows along the Albanian coast. Biologia Marina Mediterranea, 16(1), 324–325.

Riedl, R. (1991). Fauna e Flora del Mediterraneo. Franco Muzzio Editore, Padova. 775 pp.

Ruci, S., Kasemi, D., Beqiraj, S. (2014). Data on macrozoobenthos in rocky areas of the Adriatic Sea of Albania. International Journal of Research in Applied, Natural and Social Sciences, 2, 63–70.

Ruci, S., Kasemi, D., Nasto, I., Toska, A., Beqiraj, S. (2023). Molluscs from Himara coast, Ionian Sea, Albania. V. International Agricultural, Biological & Life Science Conference, Edirne, Turkey, 18–20 September 2023, 1138–1146.

Ruffo, S. (ed.) (1982–1998). The Amphipoda of the Mediterranean (Parts 1–4). Mémoires de l'Institut Océanographique, Monaco, 13.

Rumbold, C., Obenat, S., Velazquez, S.N., Gancedo, B., Spivak, E. (2017). Seasonal variation of peracarid assemblages in natural and artificial marine environments of the Southwestern Atlantic Ocean. Marine Biodiversity, 48(4), 1743–1754.

Sala, E., Ballesteros, E., Dendrinos, P., Di Franco, A., Ferretti, F., Foley, D., Fraschetti, S., et al. (2012). The structure of Mediterranean rocky reef ecosystems across environmental and human gradients, and conservation implications. PLoS ONE, 7(2), e32742.

Scipione, M.B., Zupo, V. (2010). Crustacean amphipods from the seagrasses Zostera marina, Cymodocea nodosa and Posidonia oceanica in the Adriatic Sea (Italy): a first comparison. Zoologica Baetica, 21, 15–32.

Sturaro, N., Lepoint, G., Pérez-Perera, A., Vermeulen, S., Panzalis, P., Navone, A., Gobert, S. (2014). Seagrass amphipod assemblages in a Mediterranean marine protected area: a multiscale approach. Marine Ecology Progress Series, 506, 175–192.

Trainito, E. (2004). Atlante di Flora e Fauna del Mediterraneo. Il Castello srl, Milano, pp. 10–241.

Vaso, A., Gjiknuri, L. (1993). Decapod crustaceans of the Albanian coast. Crustaceana, 65(3), 390–407.

Zettler, M.L., Zettler, A. (2017). Marine and freshwater Amphipoda from the Baltic Sea and adjacent territories. Conch Books, Harxheim, Germany.

CHEMICAL PRETREATMENT OF ALGERIAN GOLD ORE: THE CASE OF AMESMESSA – HOGGAR-

Z. Chafi-Souici[a,b], M. Y. Baghdadi [a,b], N. Si Tayeb[a,b], K. Boughanem[b], W. Naitahmed[b], M. Louz[c], F. Tiour[d]*

[a] University of Bejaia, Faculty of Exact Sciences, Laboratory of Physical Chemistry of Materials and Catalysis (LPCMC), 06000 Bejaia, Algeria

[b] University of Bejaia, Faculty of Technology, Mining and Geology Department, 06000 Bejaia, Algeria

[c] University of Saad Dahlab, Faculty of Science and Technology, Department of Process Engineering, Blida, Algeria

[d] Laboratory of Materials Technology and Process Engineering, Department of Mining and Geology, Abderrahmane Mira University of Bejaia, Algeria

** Corresponding author e-mail: zahia.chafi@univ-bejaia.dz*

ABSTRACT

Refractory gold ores pose significant challenges to gold extraction and require effective pretreatment strategies to improve recovery. Their refractory behaviour mainly stems from complex mineralogical composition; gold particles may occur as fine disseminations or be associated with sulfide and gangue minerals, limiting their accessibility during conventional extraction processes such as direct cyanidation. As high-grade, readily treatable gold deposits become increasingly depleted, industrial interest has shifted toward refractory gold ores, which generally respond poorly to conventional extraction methods. Under standard cyanidation conditions, gold recovery from these ores is often limited, frequently remaining below 80%. This refractory behaviour may result from several factors, including cyanide-consuming elements. Copper, in particular, can strongly interfere with cyanidation at elevated concentrations because it forms stable cyanide complexes, increasing cyanide consumption and reducing cyanide available for gold dissolution. In this context, the present study aimed to evaluate the leaching behaviour of the investigated ore and determine suitable pretreatment and leaching conditions to improve gold extraction. For this purpose, cyanide leaching tests were conducted in conjunction with physicochemical and mineralogical characterisation of the ore. The results showed that cyanide consumption increased with increasing initial cyanide concentration, suggesting the presence of cyanide-reactive species, particularly copper- and iron-bearing minerals. These findings confirm the ore's refractory behaviour and emphasise the need for an optimised pretreatment strategy to reduce reagent consumption and enhance gold recovery. The NH_3–$Pb(NO_3)_2$ pretreatment increased gold recovery from 58% to 85% under 0.3 g/L NaCN conditions.

Keywords: Amesmessa ores, trace elements, gold recovery, DRX, pretreatment.

INTRODUCTION

Refractory gold ores represent an increasing challenge for the extractive metallurgy industry because their complex mineralogical composition often limits the effectiveness of conventional cyanidation. Gold may occur as fine inclusions or may be physically encapsulated within sulfide

and other gangue minerals, restricting contact between gold and the cyanide solution (La Brooy et al., 1994; Fernández et al., 2000). In addition, refractory ores may contain several mineralogical constituents and elements, including Fe, Cu, Zn, As, Sb, Pb, Hg, Se, Te, carbonaceous matter, and silicate phases, which can adversely affect cyanidation through cyanide consumption, oxygen consumption, passivation, preg-robbing, or other mechanisms (Larrabure & Rodríguez-Reyes, 2021). **Copper is particularly problematic** because readily cyanide-soluble copper minerals form stable copper–cyanide complexes, increasing cyanide consumption and potentially reducing gold extraction efficiency (Jiang et al., 2001; Bas et al., 2015).

During cyanide leaching, cyanide-soluble copper minerals may dissolve and form stable copper–cyanide complexes (Breuer et al., 2005; Medina & Anderson, 2020). These reactions consume free cyanide, decrease its availability for gold dissolution, and increase reagent consumption and operating costs (Oraby & Eksteen, 2014; Medina & Anderson, 2020). Dissolved copper–cyanide species may also complicate downstream gold recovery, cyanide recycling, and effluent detoxification (Adams et al., 2008). Consequently, the mineralogical form and concentration of cyanide-soluble copper are important parameters controlling the metallurgical performance of copper-bearing gold ores.

Several pretreatment strategies have therefore been investigated to minimise copper interference before gold cyanidation, including acid pre-leaching, oxidative treatment, roasting, bio-oxidation, and ammonia-based pretreatment (La Brooy et al., 1994; Bas et al., 2015). Alternative processing routes involving selective copper leaching and non-cyanide lixiviants such as glycine, thiosulfate, thiocyanate and chloride systems have also been proposed (Muir, 2011; Maganga et al., 2023). The effectiveness of these approaches depends strongly on copper mineralogy, gold association, and mineral liberation, making detailed mineralogical and chemical characterisation essential for selecting an appropriate treatment route (Maganga et al., 2023; Deschênes et al., 1997).

This issue is particularly relevant to gold resource development in southern Algeria, where several gold occurrences are distributed across the Hoggar region, including deposits in Tamanrasset, Ain Guezzam, and surrounding areas. Although these deposits represent important metallurgical potential, the mineralogical composition and processing behaviour of many occurrences remain insufficiently characterised, particularly their response to conventional cyanidation. The refractory behaviour of the Amesmessa ore is not primarily attributed to gold encapsulation, but to cyanide-consuming copper-bearing sulfide minerals, which reduce free cyanide availability and may promote gold surface passivation during cyanidation. A better understanding of these mineralogical constraints and their influence on reagent consumption and gold dissolution is therefore essential to evaluate the metallurgical potential of these resources and develop suitable processing strategies.

Although ammonia-assisted cyanidation has been previously investigated for copper–gold ores, most reported studies have focused on generic copper-rich ores or oxidised copper–gold systems. The novelty of this work lies in evaluating and optimising a combined ammonia–lead nitrate pretreatment strategy for the Algerian Amesmessa gold ore from the SARL Tinmerkadin Ech 82 deposit, located about 465 km southwest of Tamanrasset in southern Algeria. This study investigates the mineralogical and chemical characteristics of this refractory copper-bearing ore and examines how copper-bearing phases affect gold extraction, cyanide consumption, and subsequent gold adsorption onto activated carbon. Unlike previous studies, this work evaluates the ore's response at cyanide concentrations close to current plant operating conditions (300

ppm NaCN), establishing relationships between ore mineralogy, copper content, reagent consumption, and gold recovery. The results show that targeted chemical conditioning with ammonia–lead nitrate can overcome mineralogical constraints, particularly those associated with copper-bearing sulfides and cyanide-consuming species, providing a more efficient processing strategy for refractory copper–gold ores.

MATERIAL AND METHOD

A representative ore sample was collected from the SARL Tinmerkadin (Ech 82) gold ore deposit in the Amesmessa gold district, southern Algeria, approximately 465 km southwest of Tamanrasset. The sample was crushed to −4 mm using a jaw crusher, followed by a roll crusher, and then ground to obtain a particle size distribution of 80% passing 75 µm (d_{80} = 75 µm). The ground material was riffled into 300 g portions for the leaching experiments. Depending on the experimental series, 300 g of ore was contacted with 500 mL to 2 L of leaching solution in 1-L beakers or sealed rolling bottles and agitated at a constant speed for 24 h. The leaching solutions were prepared with deionised water and contained NaCN at concentrations ranging from 0.3 to 3 g/L, NH_3 from 0 to 1 M, and/or Pb $(NO_3)_2$ from 0 to 1000 g/t. The pH was maintained under alkaline conditions by periodically adding 1 M NaOH, with a range of 10.5–11.0 for direct cyanidation and 9.3–10.5 for pretreatment tests. Following leaching, the residues were filtered, dried, and digested with aqua regia under controlled heating conditions. Gold, silver, and copper concentrations were determined by atomic absorption spectrometry (AAS), while the mineralogical composition of the ore was characterised by X-ray diffraction (XRD), with phase identification performed using HighScore Plus software and the PAN-ICSD database. Gold recovery was calculated as the percentage of gold extracted relative to the ore's initial gold content:

$$Au\ recovery\ \% = \frac{Au\ extracted}{Initial\ Au\ content}\ x\ 100$$

3 RESULTS

Analytical characterisation (XRD+XRF)

X-ray diffraction (XRD) determined the sample's mineralogical composition. Phase analysis used HighScore Plus software and the PAN-ICSD database. The results (Figure 1) identified quartz as the dominant phase, consistent with the Amesmessa veins being composed almost entirely of quartz. Chalcopyrite, pyrite, sphalerite, and albite were also identified as secondary phases, confirming the presence of copper-bearing sulfide minerals in the ore. Chemical analysis of the ore sample (Table 1) using XRF for whole rock and AAS for minerals shows that the sample contains gold and copper in the leach solution, with a content of 14 g/t Au and 1% Cu. The ore sample consists predominantly of quartz (75% SiO_2) and, to a small extent, sulphide minerals (2.12% S in total).

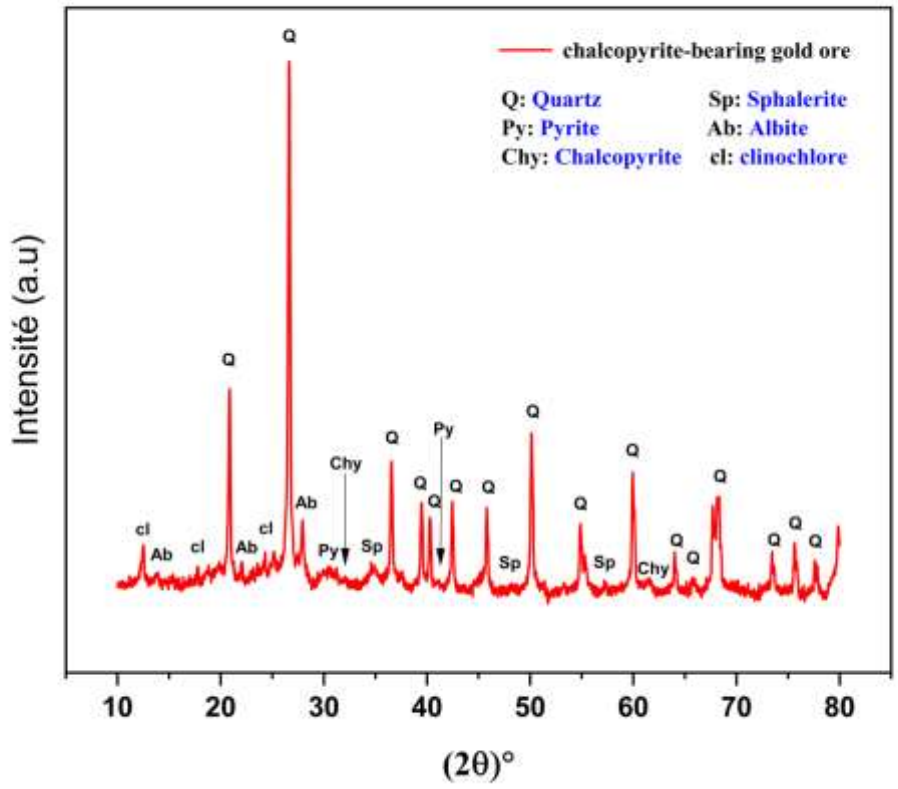

Figure 1. XRD pattern of the Amesmessa ore sample, showing quartz as the dominant phase with chalcopyrite, pyrite, and albite as secondary phases.

Table 1. Chemical and mineralogical compositions of ore and bulk concentrate samples.

w (SiO_2)/%	*w*(Fe_2O_3)/%	*w*(Al_2O_3)/%	*w*(CaO)/%	*w*(Ba)/%	*w*(S_{total})/%
75	5.30	1.04	0.77	0.02	2.12
w(Au)(g/t)	*w*(Ag)(g/t)	*w*(Cu)/ %	*w*(Pb)/ %	*w*(Zn)/%	*w*(Ni)/%
14	0.5	1	0.10	0.11	0.04

The presence of soluble minerals, particularly those containing Fe, S, and Cu, represents a major challenge in gold processing, as these species can significantly influence cyanide consumption, gold leaching kinetics, and the overall performance of downstream recovery operations (Sceresini, 2005; Muir, 2011; Dai et al., 2012). Among these impurities, copper is particularly detrimental because its high affinity for cyanide drives excessive reagent consumption by forming stable copper–cyanide complexes. Consequently, free cyanide available for gold dissolution decreases, reducing gold extraction efficiency when cyanide concentrations are insufficient (Bas et al., 2012). Muir (2011) reported that each 1% reactive copper in the ore may consume about 30 kg/t of NaCN, significantly increasing operating costs and negatively affecting the economic viability of cyanidation. For this reason**,** pretreatment is necessary to improve gold recovery in Amessmessa ores.

Effect of NaCN concentration on direct cyanidation of gold

Cyanide leaching (bottle-roll) tests were initially conducted to establish baseline conditions and determine optimal parameters for assessing gold recovery, following the industrial standard procedure commonly used to evaluate the cyanidation potential of gold ores. In each test, we agitated a prepared ore sample (300 g) in cyanide leaching solutions with NaCN concentrations ranging from 0.3 to 3 g/L. We continuously controlled the pH between 9.3 and 10.5 to ensure suitable cyanidation conditions. We estimated the composite sample's initial gold grade at 14 g/t. We performed six leaching tests under the experimental conditions summarised in Table 2, and present the results in Figure 2.

Table 2. Leaching experimental conditions

Test N°	1	2	3	4	5	6
NaCN (g/L)	0.3	0.5	1.0	1.5	3.0	0.5
NaOH (g/L)	0.5	0.7	0.9	1.2	1.8	0.7
Water volume (L)	1	1	1	1	1	2

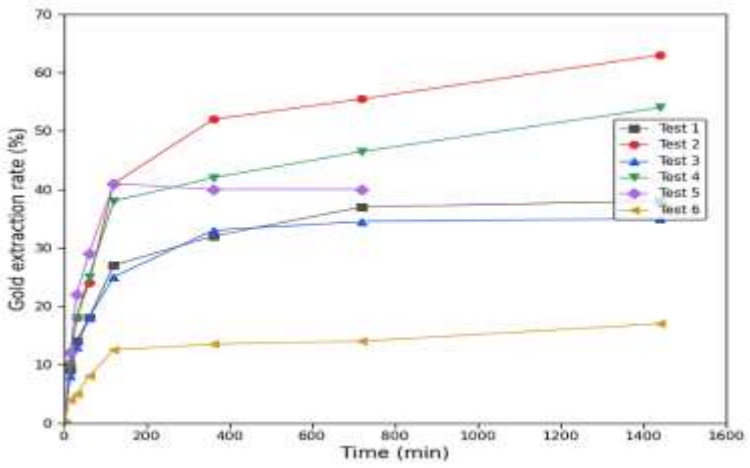

Figure 2. Effect of NaCN concentration on extraction of gold from ore

The results show a clear dependence of gold extraction kinetics on the operating conditions, particularly at prolonged agitation times. The generally low extraction rates across the six tests indicate cyanide-consuming species that limit gold dissolution. In this ore, XRD identified chalcopyrite as the main contributor to cyanide consumption and may explain the limited extraction efficiency. As shown in Figure 2, gold recovery was not proportional to NaCN concentration; the highest extraction rate was obtained at 0.5 g/L NaCN (Test 2), consistent with previous studies (Baghdadi et al., 2025). Increasing the cyanide concentration beyond this value did not improve gold recovery, indicating that additional cyanide was preferentially consumed by non-gold species rather than enhancing gold dissolution.

Ores pretreatment

To improve gold recovery, we investigated a pretreatment step to optimise the cyanidation process by reducing the impact of cyanide-consuming species. Preliminary characterisation of the ore revealed copper-bearing minerals, which can negatively affect gold leaching through excessive cyanide consumption and the formation of sulfide species that may promote gold surface passivation (Msumange et al., 2020). Therefore, two reagents were selected for conditioning prior to cyanidation: lead nitrate (50 g/t), which promotes the precipitation of free sulfide as insoluble lead sulfide (PbS) and limits gold surface passivation, and ammonia (0.5 and 1 mol/L), which reduces the detrimental effect of copper through selective complexation, thereby decreasing cyanide consumption. The underlying mechanisms involve complexation of copper ions and oxidation or removal of sulfide species to minimise passivating layers and enhance gold dissolution.

Pretreatment experiments used the same rolling-bottle setup as the direct cyanidation tests, with two conditioning times (1 h and 4 h) followed by cyanide leaching under alkaline conditions. The NaCN concentrations were maintained at 0.3 and 1 g/L, and the pH was continuously controlled at 9.3-10.5 to prevent the precipitation of copper at pH>10.5.

Effect of lead nitrate on the gold extraction rate

Lead nitrate aims to eliminate all species adsorbed on the gold surface, mainly S^{2-} sulfides.
The curve in Figure 3 illustrates the effect of adding lead nitrate on gold extraction kinetics.

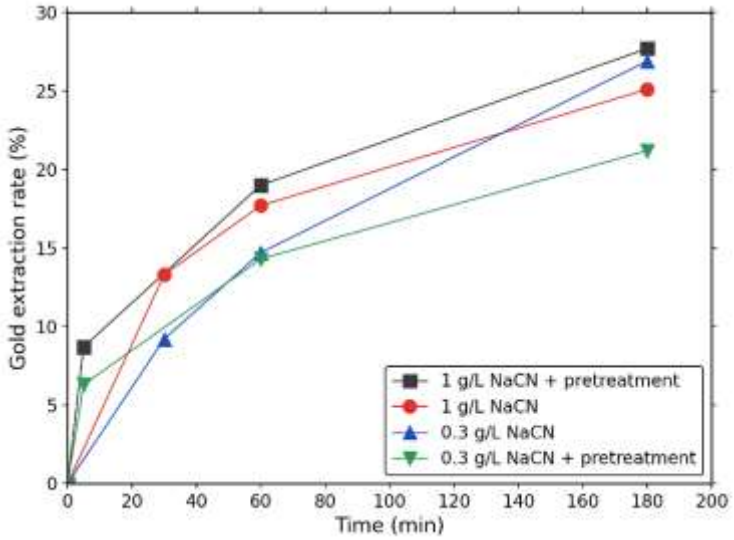

Figure 3**.** Effect of lead nitrate addition (50 g/t) on gold leaching kinetics

The curve shows the effect of adding lead nitrate (50 g/t) on extraction kinetics. Kinetics improved significantly at both cyanide concentrations (0.3 and 1 g/L). This result confirms the cyanide-consuming nature of the gold ore studied, where cyanide-consuming compounds adsorb onto the gold surface. The extraction rate is clearly proportional to cyanide concentration when using lead nitrate.
Extraction kinetics improved significantly at both cyanide concentrations tested (0.3 and 1 g/L) following lead nitrate pretreatment. This result is consistent with the ore's cyanide-overconsuming nature, in which compounds released during leaching adsorb onto the gold

surface, and confirms that the extraction rate is proportional to cyanide concentration when lead nitrate is used.

Ammonia effect

Compared with traditional cyanide leaching, the ammonia–cyanide system offers a more selective approach to gold recovery from copper–gold ores, with substantially lower cyanide consumption. (Muir et al., 1989). Figure 4 illustrates the time-dependent leaching profile for gold under increasing concentrations of NaCN and 0.5 mol/L NH_3.

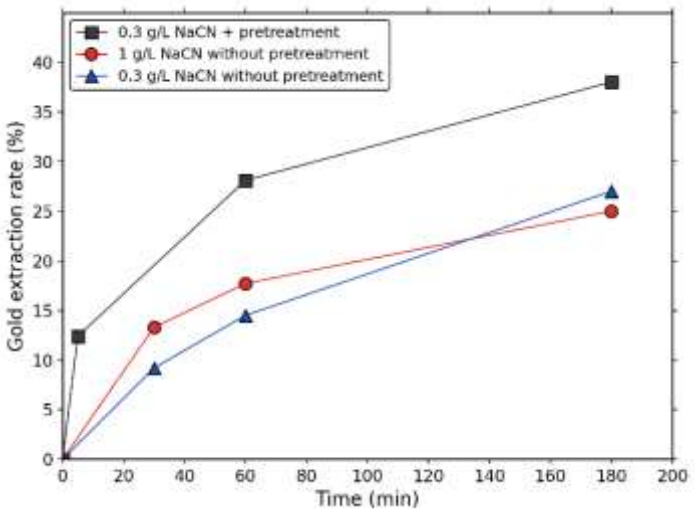

Figure 4. Effect of ammonia pretreatment (0.5 mol/L NH_3) on gold extraction kinetics,

The extraction kinetics demonstrate the significant impact of pretreatment on gold leaching performance. The pretreated sample using 0.3 g/L cyanide showed a rapid increase in gold recovery, reaching about 12% within the first few minutes, whereas both non-pretreated conditions showed nearly negligible extraction over the same period. This behaviour indicates that pretreatment effectively removes an initial kinetic barrier to gold dissolution, likely associated with surface passivation or cyanide-consuming species. The beneficial effect of pretreatment was maintained throughout leaching, with the pretreated sample achieving a final recovery of 38% after 180 minutes, compared with only 25–27% for the non-pretreated samples, an improvement of 10–13 percentage points despite the lower cyanide concentration. In contrast, the leaching profiles at 1 g/L and 0.3 g/L cyanide without pretreatment were nearly identical, with only a slight crossover at the end of the test, suggesting that increasing cyanide dosage alone does not significantly improve gold recovery. This limited improvement likely stems from preferential cyanide consumption by interfering minerals, such as copper-bearing phases and sulfides, rather than by gold dissolution. Overall, these results confirm that pretreatment plays a key role in overcoming mineralogical limitations, accelerating gold dissolution kinetics, and improving final recovery, while also enabling reduced cyanide consumption. Therefore, the pretreatment strategy is a promising approach for treating refractory copper–gold ores by improving leaching efficiency while reducing reagent requirements.

Effect of ammonia–lead nitrate mixture pretreatment on the extraction rate

To improve recovery rates, we ran a series of pretreatment tests, combining the two reagents (lead nitrate, NH_3) to investigate the mineral's behaviour and observe how the extraction rate evolves. For this, we ran five tests (without pretreatment; with 0.3 g/L NaCN; 0.5 mol/L NH_3; and 50 g/t Pb (NO_3) to evaluate the effect of pretreatment. Figure 5 illustrates the results.

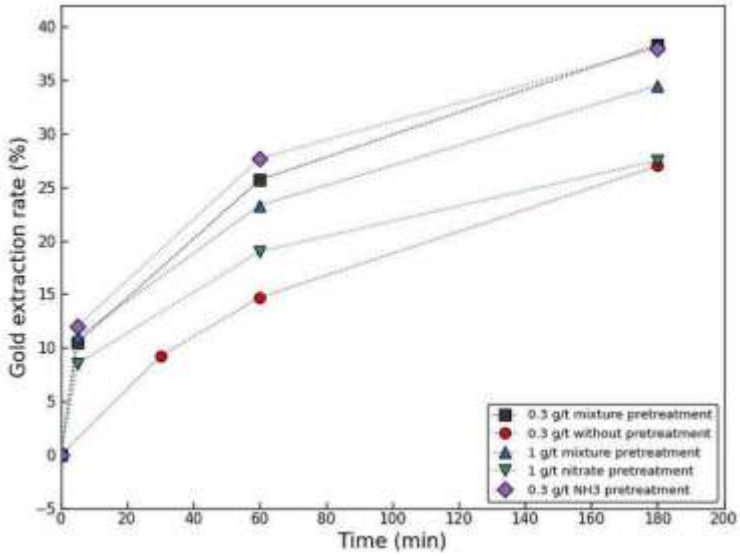

Figure 5. Effect of NH_3-Pb (NO_3) mixture on the gold extraction rate

Cyanidation with the NH_3–Pb $(NO_3)_2$ mixture yielded remarkable results at both 0.3 g/L (and 1 g/L cyanide. We recorded a clear improvement in kinetics and in recovery rate (10–12%). These results are more favourable than those obtained with lead nitrate alone. This result demonstrates the dual effect of the cyanogenic elements in our ore: one on the gold surface and the other in competition with cyanide complexation.

Both cases show high consumption, with ammonia alone (0.5 mol/L) and with the mixture, leading us to conclude that cyanide complexation is more favourable than passivation of the gold surface. In other words, the effect of cyanide consumption by copper has a greater impact than the passivation of the gold surface by sulfides.

To further optimise the mixture's effect, we repeated pretreatment using higher reagent doses and a longer conditioning time (4 h). Because the study aims to model the ore-treatment process on Amesmessa's current processing line, where the applied cyanide concentration is 0.3 g/L, 100 g/t $Pb(NO_3)_2$ and 1 mol/L NH_3.

Figure 6 demonstrates that ammonia pretreatment consistently provided higher gold extraction rates than lead nitrate alone, regardless of the reagent concentration applied. However, the combined ammonia–lead nitrate conditioning strategy exhibited the highest efficiency, confirming the synergistic effect of both reagents during the treatment of the copper-rich Amesmessa ore. Based on the calculated extraction yields, the optimised mixture pretreatment increased gold recovery from 58% without pretreatment to 85.9% under industrial processing conditions (0.3 g/L NaCN). Test 3, corresponding to the combined NH_3–$Pb(NO_3)_2$ pretreatment, achieved the highest recovery, showing that ammonia's simultaneous reduction of copper-related cyanide consumption and lead nitrate's mitigation of gold surface passivation

significantly improve cyanidation performance. These results confirm the effectiveness of the proposed pretreatment strategy in enhancing gold recovery from copper-bearing refractory ores under low-cyanide conditions.

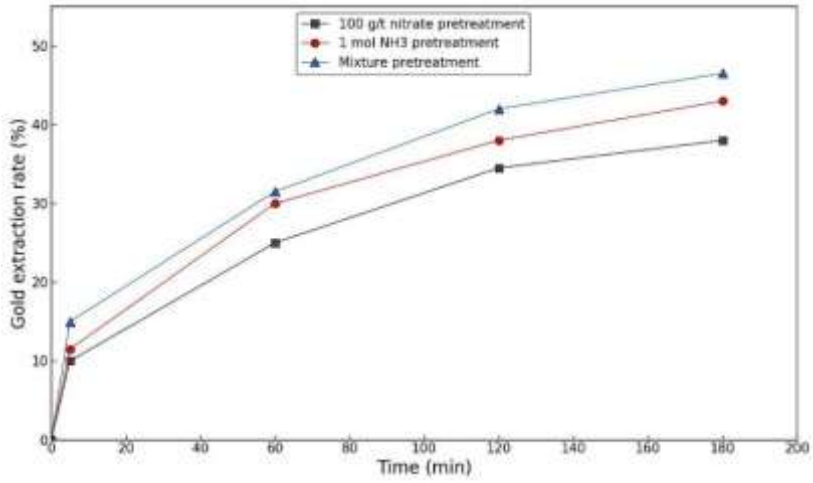

Figure 6. Effect of NH_3-Pb (NO_3) mixture on the gold extraction rate

CONCLUSION

Gold extraction from the Amesmessa ore is primarily based on cyanidation, a process whose efficiency depends on several critical factors, including ore mineralogical characteristics, cyanide concentration, and pH control under alkaline conditions. Experimental investigations were conducted at the Amesmessa mine laboratory using a representative sample collected from SARL Tinmerkadine (sample 820). These tests aimed to identify the optimal leaching parameters and pretreatment conditions required to enhance gold recovery. Based on the obtained results, the following conclusions can be drawn:
The X-ray diffraction spectrum of the ore reveals the presence of a predominant phase, quartz, in addition to other phases: chalcopyrite, pyrite, and albite.

Leaching kinetics improved after pretreatment with lead nitrate, confirming the cyanide-consumptive nature of the gold ore studied, in which cyanide-consuming compounds adsorb onto the gold surface.

Cyanidation using the NH_3–$Pb(NO_3)_2$ mixture yielded remarkable results in terms of increasing the extraction rate. This result demonstrates the dual effect of the cyanide-consumptive elements in our ore: one acting on the gold surface and the other competing with cyanide through complexation.

Industrial-scale optimisation remains necessary to further enhance gold recovery and ensure the practical applicability of the proposed leaching conditions. However, the results are promising. Pretreating with ammonia and lead nitrate (high doses, 4 hours) lifted recovery from 58% to 85%. This occurred under standard plant conditions (300 ppm NaCN). For copper-rich ore like this, it works.
The proposed pretreatment may reduce NaCN consumption, lower operating costs through improved gold recovery, and facilitate industrial application because the treatment conditions are close to those used at the Amesmessa processing plant. Further pilot-scale studies are required to confirm its economic and industrial feasibility.

REFERENCES

Adams, M., R. Lawrence, M. Bratty. 2008. Biogenic sulphide for cyanide recycle and copper recovery in gold–copper ore processing. *Minerals Engineering*, 21(6): 509–517.

Baghdadi, M. Y., Z. Chafi, M. Louz, T. Tahri, M. E. A. Benamar, S. Bellucci. 2025. Origin of the over consumption of cyanide during the leaching of the Amesmessa gold ore. *Naukovyi Visnyk Natsionalnoho Hirnychoho Universytetu*, (2): 26–32.

Bas, A. D., E. Koç, E. Y. Yazici, H. Deveci. 2015. Treatment of copper-rich gold ore by cyanide leaching, ammonia pretreatment and ammoniacal cyanide leaching. *Transactions of Nonferrous Metals Society of China*, 25(2): 597–607.

Breuer, P. L., X. Dai, M. I. Jeffrey. 2005. Leaching of gold and copper minerals in cyanide deficient copper solutions. *Hydrometallurgy*, 78(3–4): 156–165.

Deschênes, G., P. J. H. Prud'homme. 1997. Cyanidation of a copper-gold ore. *International Journal of Mineral Processing*, 50(3): 127–141.

Fernández, R. R., H. Y. Sohn, K. M. LeVier. 2000. Process for treating refractory gold ores by roasting under oxidizing conditions. *Mining, Metallurgy & Exploration*, 17: 1–6.

Jiang, T., Y. Z. Zhang, Y. B. Yang, Z. C. Huang. 2001. Influence of copper minerals on cyanide leaching of gold. *Journal of Central South University of Technology*, 8: 24–28.

La Brooy, S. R., H. G. Linge, G. S. Walker. 1994. Review of gold extraction from ores. *Minerals Engineering*, 7(10): 1213–1241.

Larrabure, G., J. C. F. Rodríguez-Reyes. 2021. A review on the negative impact of different elements during cyanidation of gold and silver from refractory ores and strategies to optimize the leaching process. *Minerals Engineering*, 173: 107194.

Maganga, S. P., A. Wikedzi, M. D. Budeba, S. V. Manyele. 2023. Overview of the Challenges and Opportunities in Processing Complex Gold-Copper Ores. *Mining, Metallurgy & Exploration*, 40: 2167–2185.

Medina, D., C. G. Anderson. 2020. A Review of the Cyanidation Treatment of Copper-Gold Ores and Concentrates. *Metals*, 10(7): 897.

Muir, D. M. 2011. A review of the selective leaching of gold from oxidised copper–gold ores with ammonia–cyanide and new insights for plant control and operation. *Minerals Engineering*, 24(6): 576–582.

Muir, D. M., S. R. La Brooy, C. Cao. 1989. Recovery of gold from copper-bearing ores. *Proceedings of the World Gold '89*, Littleton, Colorado, USA: SME, 363–374.

Oraby, E. A., J. J. Eksteen. 2014. The selective leaching of copper from a gold–copper concentrate in glycine solutions. *Hydrometallurgy*, 150: 14–19.

IDENTIFICATION OF *MACROSIPHUM ROSAE* IN ROSA SPP, SHRUBS, IN THE TIRANA AREA, ALBANIA

Florie REXHAJ [1], Dhurata SHEHU [1], Ajten Berxolli[1]*
Agricultural University of Tirana, Faculty of Agriculture and Environment, Plant Protection Department

Corresponding author e-mail:frexhaj@ubt.edu.al

ABSTRACT

Roses are considered one of the most sought-after plants worldwide. They have a high vitamin C content and are widely used for juices, jams, and syrups. In addition, they are also used as ornamental plants for decorating natural environments and indoor spaces such as homesand offices. Roses have also found favorable conditions for growth and cultivation in Albania. The city of Albania that carries the scent of roses is Permeti. Roses are susceptible to various pests and diseases that may affect their health and aesthetic appearance. Among the pests that attack roses especially at the beginning of spring, the most hazardous are aphids. The rose aphid, *Macrosiphum rosae*, is one of the most important pests of roses worldwide and causes economic damage. The aim of this study was to identify this pest in our country. The study was conducted during 2025, from early March to late October, in the Botanical Garden of the Agricultural University of Tirana. For aphid identification, field observations were carried out; specimens were prepared as fixed slide-mounted preparations and compared with taxonomic keys and standard descriptions. The species collected in the Botanical Garden corresponded to the description of *Macrosiphum rosae.* This study, confirmed the presence of this aphid in our country and it is role in causing significant damage to rose shrubs.

Keywords: Roses, *Macrosiphum rosae*, aphids ,identification, taxonomic key, microscope, pest.

INTRODUCTION

Rose is one of the most beautiful ornamental flowers in the world, and as suchit can be found in many houses and gardens in cities due to its especialcharacteristics such as stability, long period of floral initiation, different varieties,and, of course, its beauty. (Larson, R.A.,1992). Roses is an ornamental shrub up to two meters hight, with long thorns,with large, leafy, beautifull, clustered flowers, with a pleasant smel and in white, red, yellow,ect. It is also used for various perfumes and for decorations. (https://sq.wikipedia.org/wiki/Trandafili). Rose hasbeen most important crop in the floriculture industry. The genus Rosa includes 200 species and 18,000 cultivars. (Weiss,1997; Gudin,S, 2000). Those rose bushes can suffer from several problems such as diseases and pests. Roses are can to various types of pests and diseases that can affect their health and aesthetic appearance. (https://sq.jardineriaon.com.2025). Aphids or plant lice are serious pests of various crops including rose. (K.Zamir Rasib, et.al.,2021). Aphids feed on buds, shoots and leaves, colonies may persist throughout the year but are most numerous and troublesome in late spring and early summer. (Buczacki.S.T,et.al.,1998). Strong infestation by the aphid results in the deformation of stems, leaves and flowers. (Jaskiewiez, B.,1997). Roses can support several species of aphid in the spring and summer, the most common is usually Macrosiphum rosae (https://gd.eppo.int/taxon). Macrosiphum rosae, the

rose aphid, is a species of sap-sucking aphids in the subfamily Aphidinae. (Cichocka E., 2003), (Gudin, S., 2000). The rose aphid, Macrosiphum rosae, is one of the most important pests on roses in the world and it causes economic damage. (Mehrparvar M.,et.al.2016). This insect stops growth of leaf bud, flower buds and twigs by eating them and also prohibits flowering and causes weakness of flower buds. In severe infection, it causes deformated and mottledpetals which this reduces flowers beauty.(Mehrparvar et al. 2009). Aphids are observed in two colourful races: green and rosy-brown ones . It is a holocyclic, host alternating and olyphagous species (Cichocka E., 2003). In order to reduce the economic losses inflicted by roses aphids ,it is necessary to study different biological parameters of this pest species so that an effective management plan can be formulated (Yousuf I,et.al.,2020). Management is done with the development of thorough insect and disease scouting, record keeping, development of soundcultural and sanitation practices (David, J.S., 2001). Early detection is key. The sooner the presence of aphids is identified, the easier it will be to eradicate them and the less likely there will be serious damage to the plant.http://www.fjalori.shkenca.org/

MATERIALS AND METHODS

Time and place of study

The study was conducted during 2025 from the beginning of March to the end of October. The location for the study was chosen to be an area of the Tirana district within the Campus of the Agricultural University of Tirana. Many rose bushes of the genus Rosa spp are concentrated there. The purpose of this study was to identify *Macrosiphum rosae* in these rose bushes.
Tirana, being 30 km from the coast, has a hot subtropical-mediterranean climate with an average of 260-290 sunny days per year. Summer is hot and dry due to the dominance of subtropical high-pressure systems, while winter has moderate temperatures. Even in spring, temperatures have increased, favoring many diseases and pests.

Figure 1. Study area

Figure 2. Study area from (google earth)

Study method.

In this study, to identify the presence of *Macrosiphum rosa* (Linnaeus, 1758) in rose bushes in our country, the following was used:
• field observation
• slide-mounted specimens

• comparison with taxonomic keys and standard descriptions

To identify the pest in the laboratory, a weekly sampling method was used from March to the end of October. Each week, 5 rose bushes were selected and a branch of each rose bush was randomly cut as a sampling unit. Since most rose aphid colonies are located along a 10 - 15 cm length of the main part of the branches, these 15 cm of branches were selected and cut. These branches were placed in plastic bags where the sampling dates were marked on each sample, which were taken to the laboratory for examination with a magnifying glass and microscope.

Figure 3. Field observation for the identification of *M.rosa*

In addition to weekly sampling, the rose plants were carefully inspected, especially inside the branches and at the upper levels of the roots, collecting all aphids that were found with a small brush in a bottle of 70 % ethanol and then identified in the laboratory. Even during the hot summer months, June, July, August and September, checks were made three times a month to see if this aphid remained hidden in the rose plants or migrated to secondary plants. These samples, in addition to being analyzed with a magnifying glass and microscope, were also analyzed by preparing fixed preparations, which consists of a more in-depth analysis of the different parts of the fixed insect.

We based ourselves on the classical method according to (Hille Ris Lambers.1950 - 1970), for the preparation of fixed aphid preparations, the sequence of work used is as follows:

Preservation in 70-80 % alcohol

Maceration which serves to dissolve the soft fatty parts, as well as to bleach the sclerotized parts, where the insects become transparent and the individual parts are easily distinguished with a microscope. They were boiled in 10 % KOH for 30 min or they can be left for 24 hours in the environment until they become transparent.

Rinsing with distilled water.

They are placed in 50 ml of 70% alcohol and three drops of HCl, where they are left for 5 min for neutralization.

Fuchsin staining is performed (0.5 grams of fuchsin + 25 ml of 10 % HCl + 300ml of distilled water). The staining lasts 30 min.

The lice are placed in the center of the slide and 70 % alcohol is poured over them, leaving for 3 - 5 minutes.
Add one drop of Wintergreen 0.1% and leave for three minutes, remove the oil, dry the preparation and then add 3 drops of Canadian balsam, place the lamella and in this state the preparation is not moved for 6 days.

After the preparation of the fixed preparations, the specimens were analyzed with a steriomicroscope, and on the basis of the special characteristics of *Macrosiphum rosa*, its identification was possible. Identification of the pest was done by studying their morphological characters under microscope and comparing them with literature available on their morphology.

Figure 4. Stereomicroscope observation for the identification of *M.rosa*

RESULTS AND DISCUSSION.

The study was carried out on a 200 m^2 area planted with roses (*Rosa spp*.) within the Agricultural University of Tirana in the Botanical Garden. The identification of aphids was based on a combination of host plant, pest symptoms, morphological characters and comparison with taxonomic keys based on standard entomological literature of various authors. The host plant was rose bushes which is also the main host for these pests. From phytosanitary monitoring in the field with a magnifying hand lens, practical identification was achieved mainly through field observations and bioecological characteristics of the pest. Aphids were observed on young shoots in buds and on young leaves, dense colonies were observed, typical of rose aphids. The populations were mainly located in the young parts of the plant on young shoots and on the underside of the rose leaves where they fed on plant juices. The increase in the populations of these individuals during the spring in this area of Tirana was favored by moderate temperatures and high relative humidity. The damages were typical for the rose aphid (*Macrosiphum rosae*) such as: deformation of young shoots, wrinkling of leaves, slowing of development and secretion of honeydew which favors the development of black mold. Individuals of this species had an elongated body, which helps distinguish it from other types of plant aphids, green, pink or reddish in color, long antennae and thin legs. Another identifying feature was the relatively long black and cylindrical cornicles, as well as the elongated and light-colored tail typical of the rose aphid.

Figure 5. Monitoring symptoms on rose bushes

After field monitoring, the species were taken to the laboratory and their identification began, through the use of taxonomic keys and microscopic analysis of diagnostic parts.
The species collected in the botanical garden after examination, matched the description of *Macrosiphum rosae* through these features:

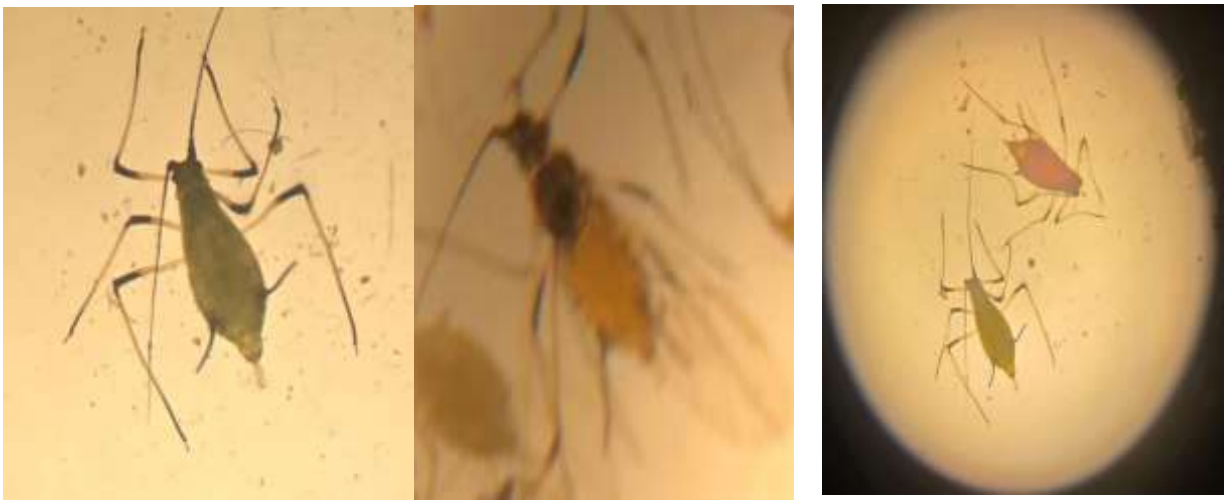

Figure 6. Identification of *Macrosiphum rosae* with a stereomicroscope

.

Wingless form (aptere)

Host plant is rose.
Body relatively large (2.2 - 3.6) elongated and thin, not short and oval.
Body color light green, pink or reddish brown.
Surface often shiny.
Antennae very long, 3.6 mm dark in color and with many rhinaria (sensory organs).
Siphonculi (cornicles) are long, straight, black, with a prominent reticulum at the tip.
The caudas i long, slender and light in color.

Legs long and thin and joints of legs dark in color

Even the winged form(alate) matched the description of the characters of *Macrosiphum rosae*:

Size 2.5 - 3.6 mm
Body shape more slender and elongated.
Thorax black, body color green
Head dark and sclerotized
Antennae long and with many sensors
Two pairs of transparent wings
Cornicles long, cylindrical black
The cuda is long and slender.
Long legs, thin tibia with black color.

DISCUSSION

The results of field observations and laboratory analyses confirmed the presence of the rose aphid *Macrosiphum rosae* (Linnaeus, 1758) in rose bushes cultivated in the territory of the Campus of the Agricultural University of Tirana. This species is considered one of the most widespread aphids of the family Aphididae that affects plants of the *Rosaceae* family and is widely reported in temperate and Mediterranean climate regions Blackman & Eastop (2000). During field monitoring, it was observed that these individuals formed dense colonies mainly on the vegetative tops and flower buds of the host plants. The infestation was accompanied by the presence of molasses on the leaf surface, as well as deformation and twisting of young plant tissues. Similar symptoms have been reported by David et al. (1975) and Heie. (1986-1995), who emphasize that the physiological damage caused by this species negatively affects the vegetative and aesthetic development of the rose.

The morphological characteristics of the observed individuals were consistent with the descriptions reported in the international literature. Body color ranged from light green to pink or reddish, while the alate and apterous forms presented obvious differences in the development of body structures, especially in pigmentation and wing development. According to Tomiuk & Wohmann (1990), this morphological variability is related to environmental factors and the biological stages of aphid development.

Morphological identification of *Macrosiphum rosae* was carried out through the analysis of external body characters observed with a stereomicroscope. The identification process was based on the use of taxonomic keys and on the comparison of the morphological structures of the alate and apterous forms. Morphometric characters were compared with the data presented by David et al. (1975), while diagnostic descriptions were based on the standard references of Blackman & Eastop (2000).

According to these authors, *M. rosae* is characterized by an elongated, spindle-shaped body, with a length ranging from 1.7 - 3.6 mm. The antennae and legs are relatively long, while the sphinuculi (cornicles) are cylindrical, black and well developed. The cauda appears elongated and with paler pigmentation compared to the rest of the body. These diagnostic characteristics were also found in the individuals analyzed during this study.

The agreement of the results obtained with the data of the international literature shows that the methodology used for the monitoring and identification of *M. rosae* was appropriate for the agroclimatic conditions of the Tirana area. Also, the results suggest that the climatic conditions of this area favor the development and reproduction of this species, especially during periods

of moderate temperatures and high relative humidity, factors which are considered important for the dynamics of aphid populations (Blackman & Eastop, 2000).

CONCLUSIONS

The presence of the rose aphid Macrosiphum rosae was confirmed in the agro-ecological conditions of our country.
Macrosiphum rosae represents an important pest for rose bushes and a potential vector of plant viruses.
Species identification was successsfully accomplished based on monitoring typical symptoms in the field of host plants.
The analysis of diagnostic morphological characters was carried out using taxonomic keys available in standard foreigen literature.
Wingless and winged forms were identified, indicating high adaptability and spread.
In addition to *M.rosae* ,other species of aphids were also identified on rose bushes, but the identification of other species was not the focus of our study.
It is essential to inspect rose bushes regularly, paying special attention to the transition periods between seasons.
Green aphids tend to hide on the underside of leaves, young shoots and flower buds.
It is advisable to inspect both sides of the leaves and not to forget the areas with softer growth, as they are often the first to settle there.
In the agroecological conditions of Albania the development of pest populations is favored by moderate spring temperatures and adequate relative humidity.
Continuous monitoring and implementation of integrated management strategies is recommended.

LITERATURA

Alford, David V. (2012). *Pests of Ornamental Trees, Shrubs and Flowers*. CRC Press. pp. 66–67. ISBN 978-1-84076-628-8.

Buczacki, S.T., & Harris, K.M. (1998). Pests, diseases and disorders of garden plants. 2 edn. London: HarperCollins.

Blackman, R. L, and Eastop, V. f. (2000,2026). Aphids onthe world's crops. An identification guide. Chiches-ter, UK: John Wiley & Sons.

Cichocka E., (2003.) Bionomia i parametry demograficzne populacji mszycy różano-szczeciowej (*Macrosiphum rosae* L.) [Biology and demografic parameters of *Macrosiphum rosae* L.]. Progress in Plant Protection/ Postępy w Ochronie Roslin 43 (2), 565-568 [in Polish].

David,S.K.(1975).A taxonomic review of *Macrosiphum* (Homoptera:Aphididae) in India.Oriental Insects 9(4).461-493.https://doi.org/10.1080/00305316.1970.10433978

David, J.S.,(2001). Aphids On trees and shrubs, Ohio StateUniversity Extension Fact Sheet, Department ofHorticulture and Crop Science Fyffe Court, Columbus Ohio.

Gudin, S.,(2000)Management Of Macrosiphum Rosae L. On Different Cultivars Of Rosa Indica L. By Using Different Botanical Extracts And Detergent Solution Rose: Genetics and breeding. Plant Breed.,17: 159–189.

Heie,O.E.(1986-1995).The Aphidoidea (Hemiptera) of Fennoscandia and Denmark. Scandinavian Science Press.

Hille Ris Lambers,D.(1950).Contributions to a monograph of the Aphididae of Europe

Insha YOUSUF, Abdul A.BUHROO.(March 3,2020). Acta agriculturae Slovenica,115/2,283-295 Seasonal incidence and bionomics of rose aphid, Macrosiphum rosae (Linnaeus,1758), (Hemiptera:Aphididae) in Kashmir, India. doi:10.14720/aas.2020.115.2.1173

Jaśkiewicz B., (1997) Species composition and dynamics of the aphid occurrence on selected decorative shrubs in the years 1973-1993]. Rozprawy Naukowe AR in Lublin 183, 1-93 [in Polish].https://gd.eppo.int/taxon/MACSRO/photos

K. ZAMIR RASIB* and M. RAZZAQ .(2021). Biological control of rose aphid (Macrosiphum rosae) using coccinellid beetle (Coccinella septempunctata) under field conditions in Gujranwala, Pakistan21-02-2021) Journal of Biological Control, 35(1): 44-47, 2021, DOI: 10.18311/jbc/2021/26307

Larson, R. A. (1992), Introduction to floriculture. Academic Press, Inc

Mohsen Mehrparvar Seyed Mozaffar Mansouri Bijan Hatami.(2016).Some bioecological aspects of the rose aphid,Macrosiphum rosae (Hemiptera:Aphididae) and its natural enemies September. Acta Universitatis Sapientiae Agriculture and Environment 8(1) DOI: 10.1515/ausae-2016-0007 .License .CC BY-NC-ND 4.0

Mehrparvar,M. M,mobli and B.hatami. (2008). Of rose aphid (Macrosiphum rosae L.) (Homoptera: Aphididae) on variouscultivars of rose and wild rose. Journal of agricultural and natural resources sciences and technologies twelveth year. 45: 711-718.

Quratulain , Muhammad Aslam , Muhammad Khalid Rafique , Mian Atiq Ahmad And Rashid Mahmood. (June 25,2015) Plant Protection Department, Govt. Of Punjab, Pakistan2pmas Arid Agriculture University, Rawalpindi, Pakistan3honeybee Research Institute, Narc, Islamabad,Pakistan.Pakistan Entomologist 2015, 37(1):15-20 https://www.researchgate.net/publication/282847988

Tomiuk, J,&Wohmann,K.(1990).Morphological variability and population structure in aphids.Entomologia Experimentalis et Applicata,54,123-130.

Wikipedia(30 nëntor 2024) “Shendeti.com.al” August 12, 2015. http://www.fjalori.shkenca.org/
https://sq.jardineriaon.com/ sëmundjet-e-shkurreve-të-trëndafilave.html

(https://sq.wikipedia.org/wiki/Trandafili).

https://gd.eppo.int/taxon).

POPULATION DYNAMICS OF THE POTATO TUBER MOTH (*PHTHORIMAEA OPERCULELLA*) IN THE DIVJAKË REGION, ALBANIA

Florie REXHAJ [1]Dhurata SHEHU [2],Ajten BERXOLLI[3]

Agricultural University of Tirana, Faculty of Agriculture and Environment, Plant Protection Department

Corresponding author e-mail:frexhaj@ubt.edu.al

ABSTRACT

Potato (*Solanum tuberosum* L.) is one of the most economically important agricultural crops in Albania. Among its major insect pests, the potato tuber moth, *Phthorimaea operculella* (Zeller, 1873), causes significant yield losses both in the field and during storage. The aim of this study was to evaluate the seasonal population dynamics of this pest under the agroecological conditions of the Divjakë region, one of the main potato-producing areas in Albania. The study was conducted from March to October 2025 in a 1-ha potato field planted with the Arizona cultivar. Population dynamics were monitored using two Delta Econex pheromone traps, and moth captures were recorded periodically throughout the growing season.The results showed that adult activity began in April, with low capture levels below the economic threshold. During the first potato production cycle (March – June), the pest population remained at low levels. The first generation was completed at the end of June in the epigeal part of the host plant. This infestation had no impact on the yield. A marked increase in moth captures was observed during July, August, and September, coinciding with temperatures ranging from 33 to 38°C and the development of successive generations. High temperatures and low humidity favored rapid reproduction, resulting in a significant increase in population density. A gradual decline in captures was recorded from late September through October, corresponding to decreasing temperatures and the end of the cropping cycle. The findings indicate that early potato production is exposed to a relatively low risk of infestation by *P. operculella*, whereas the second production cycle is considerably more vulnerable due to the accumulation of successive generations and favorable climatic conditions. Continuous monitoring using pheromone traps is an effective tool for predicting population fluctuations and supports.

Key words: Potato, (*Phthorimaea operculella),* monitoring, population, management.

INTRODUCTION

Potato (*S.tuberosum* L.) is the fourth major food crop around the world after rice (*Oryza sativa* L.), wheat (*Triticum* spp.L.), and maize (*Zea mays* L.). (Xu,J.et.al.,2019))&(Gao,Y.L.et.al.,2021). In Albania, potato production represents an important agricultural sector, with an annual output estimated at approximately 245,000–255,000 tons. (https://www.abaonline.al). However, potato production is challenged by many factors including pests and diseases, particularly *P. operculella.* (Graft, J.E.,1917). Phthorimaea operculella (Zeller, 1873), commonly known as the potato tuber moth, is a lepidopteran species belonging to the family Gelechiidae. (https://en.wikipedia.org/). The potato tuber moth, *Phthorimaea operculella* (Lepidoptera: Gelechiidae), is an oligophagous

pest that has been foundfeeding on more than 60 plants in different parts of the worldwith the majority of the hosts belonging to the Solanaceae family (Das,G.P et,al., 1994). It causes significant economic losses in potato production in subtropical and tropical areas.(Das,G.P,et.al.,1992). *P.operculella* is a pest of both field and storage conditions (Gilboa S.et.al.,1995). The damaging stage of the pest is the larva .(Lal, L, 1993).The larva attacks all vegetative parts of the potato, and most economic damage occurs to potato tubers both before harvest in the field and during storage. (R. S. Chandel et.al.,2019). Foliar damage by *P. operculella* to the potato plants does not usually cause significant yield losses. (Graft, J.E., 1917). Currently, pest management practices are effective in controlling *P.operculella.* https://www.sciencedirect.com **.**The use of synthetic pheromones that interfere with insect mating for pest control has been widely demonstrated in numerous Lepidoptera and other insect species. (Claudia Vasquez.,2009)**.** *Phthorimaea operculella* male moths are attracted to pheromones, which are concentrated chemicals of the female "scent" impregnated in a rubber septum in the center of a sticky liner insert within delta traps (Rondon, 2020). For its management, use of healthy seed, field sanitation, deep planting, and proper ridging contribute significantly. (R.S .Chandel ,et.al.,2019). Pesticide application is most widely used management strategy to control *P. operculella*. (Trivedi,T.P,et.al.,1992). As most of the economic damage occurs when *P. operculella* infests the tubers, so researchers should focus on management of this insect pest during tuber period. (Amone.S,et.al.,1998) & (Gao,Y.L.,2018).

MATERIAL AND METHODS

Time and place of study

The study was conducted from March to the end of October 2025 in the Divjaka region, one of the main potato-growing areas in Albania. The objective of the study was to analyze the seasonal population dynamics of the potato tuber moth (*Phthorimaea operculella*), identify periods of high infestation risk, and provide recommendations for the integrated management of this pest. The potato cultivar used in the study was Arizona.

Divjaka is located in the Western Lowland of Albania and is characterized by a typical Mediterranean climate, with mild, rainy winters and hot, dry summers. Average temperatures range from approximately 5–12°C in January to 30–35°C in July, providing favorable conditions for the development and population growth of *P. operculella* throughout the potato growing season.The soils in the Divjaka region are predominantly sandy and alluvial, providing highly favorable conditions for potato cultivation. In addition, the region's climatic conditions, characterized by high summer temperatures, adequate humidity, and the continuous cultivation of potato crops, create an optimal environment for the development and establishment of the potato tuber moth (*Phthorimaea operculella*). These environmental conditions favor the pest's survival, reproduction, and population growth throughout the entire growing season.

Figure 1. Stadi area in Divjaka

Study method

To monitor the population dynamics of the potato tuber moth (*Phthorimaea operculella*) in the Divjaka region, a pheromone-based monitoring system was employed. The experimental field covered an area of 1 ha, with a row spacing of 75 cm and a plant spacing of 30 cm.

Monitoring was carried out using triangular Econex Delta traps equipped with sticky inserts and species-specific sex pheromone lures. The traps were installed approximately 20 cm above the crop canopy, as adult moths typically fly close to the plants. Two traps per hectare were used: one placed in the center of the field and the other at the field margin, avoiding the direction of the prevailing wind to minimize interference with pheromone dispersion.

Under normal conditions, traps were inspected every seven days, whereas during periods of increased pest activity they were checked every 3–4 days. After each inspection, captured moths were counted, removed using forceps, and the data were recorded, leaving the sticky surface clean for the next assessment.

The pheromone lures were replaced every 4–6 weeks due to the high summer temperatures, which accelerated pheromone volatilization. Sticky inserts were replaced every 7–14 days, depending on the number of captured insects and the accumulation of dust. Frequent strong winds in the study area caused considerable dust deposition, reducing the adhesive efficiency of the trap surfaces.

To monitor the population dynamics of *Phthorimaea operculella*, regular weekly observations were conducted through visual inspections using a hand lens. Systematic monitoring enabled the assessment of the pest's population dynamics by first determining and recording its location within the crop, followed by continuous observations of population development throughout the growing season.

Figure 2. Monitoring plot

Figure 3 .Leaf damage

RESULTS AND DISCUSSION

Trap inspections began immediately after their installation in March. Initially, the traps were checked every morning until the first adult moths were captured. Thereafter, monitoring was carried out weekly through regular and systematic inspections. Captured moths were removed using forceps, and the number of individuals captured was recorded in a dedicated field notebook.

Table 1. Average weekly number of *Ph.operculella* adults captured for trap during the monitoring period.

Months	Average catch/trap/week
March	0
April	5
May	13
June	20
July	70
August	80 (peak)
September	60
October	29

As shown in table 1, the first adult flights of *Phthorimaea operculella* were recorded in April, with low trap catches during the first week. As temperatures increased, moth activity gradually intensified, reaching a monthly average of approximately 5 adults per trap per week. In May, moth activity remained below the economic threshold, with an average of 13 adults per trap per week.

During June, the average number of captured adults increased to 20 moths per trap per week. However, this population level did not pose a significant threat to potato production, as feeding damage was mainly confined to the above-ground (epigeal) parts of the plants, while the first potato crop had already completed its vegetative cycle.

In the following months, the number of captured adults increased markedly, corresponding to the rise in air temperature and the development of successive generations of the pest. Overlapping generations resulted in a continuous increase in the population, and the nature of the damage shifted predominantly to the potato tubers, where infestation levels became relatively high.

Graphic 1. Population Dynamics of *Phthorimaea operculella* in Divjakë (2025)

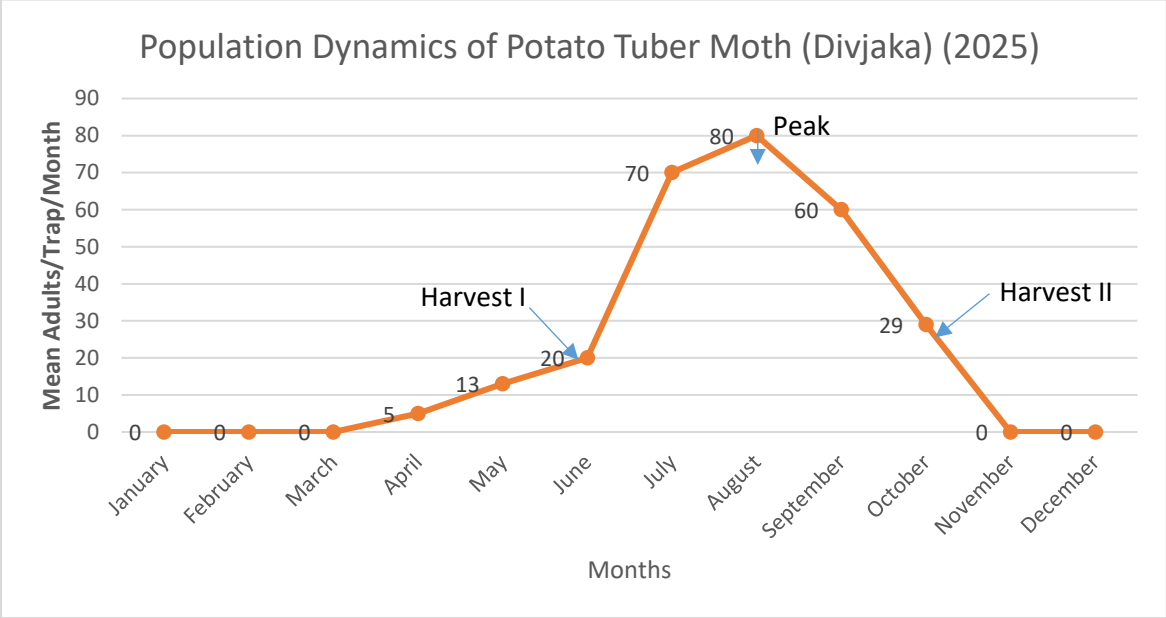

The data presented in graphic 1 also illustrate the seasonal population dynamics of *Phthorimaea operculella*. Adult moth activity began in April, with a monthly average of 5 adults per trap per week. During May, a gradual increase in moth activity was observed, reaching a monthly average of 13 adults per trap per week. This increase was favored by temperatures ranging from 24 to 28°**C** and the active vegetative growth of the potato crop.

The peak of the first generation was recorded in June, with a monthly average of 20 adults per trap per week. This generation completed its development primarily on the vegetative (epigeal) parts of the plant. Infestation of the above-ground plant tissues remained low and did not affect the yield of the first potato crop in the Divjaka region.

Figure 4. Harvest of the first potato crop in the Divjaka region, Albania (2025).

Successive generations of *Phthorimaea operculella* initially developed on potato tubers remaining in the field after harvest and on wild solanaceous host plants, particularly *Datura stramonium* L., before subsequently colonizing the second potato crop. The highest pest activity was recorded during July, August, and September, with average trap catches of 70, 80, and 60 adults per trap per week, respectively. The population peak occurred in August.

These population peaks coincided with high summer temperatures (33–38°C), which favored rapid population growth and the continuous development of successive generations. Under these climatic conditions, each generation was completed within approximately 22–24 days, resulting in a rapid increase in pest density.

In October, moth activity declined to an average of 29 adults per trap per week, mainly due to decreasing temperatures and the completion of the potato crop's growing season.

During the 2025 growing season, the second potato crop in the Divjaka region was severely affected by *P. operculella*. Prolonged high temperatures accelerated the development of successive generations, leading to intense tuber infestation and substantial yield losses.

The results obtained from monitoring with Econex Delta traps baited with species-specific sex pheromone lures demonstrated that this technique is an effective and reliable method for monitoring the seasonal population dynamics of *Phthorimaea operculella*. The information obtained can be used to identify periods of highest pest risk and to optimize the timing of integrated pest management (IPM) measures.

DISCUSSION

The results of this study demonstrated that the population dynamics of *Phthorimaea operculella* in the Divjaka region were primarily influenced by temperature and local agroecological conditions. The gradual increase in the number of male moths captured in Delta traps baited with sex pheromones from April to August is consistent with the findings of Rondon (2020) and Kroschel and Sporleder (2006), who reported that high temperatures accelerate pest development, shorten the life cycle, and promote the occurrence of multiple generations during the growing season.

Sex pheromone traps are widely recognized as a reliable tool for the early detection of adult moth activity and for determining the optimal timing of control measures within Integrated Pest Management (IPM) programs (Rondon, 2020; Sporleder et al., 2004). Similarly, Yan et al. (2023) reported that trap efficiency is influenced by trap height, trap type, and pheromone

dosage, with traps positioned at the crop canopy level capturing the highest numbers of male moths.

Our findings are also consistent with those of Aryal et al. (2020), who reported that *P. operculella* populations exhibit several seasonal peaks and that their development is strongly influenced by temperature and local agroecological conditions.

The completion of the first generation by the end of June indicates that the early potato crop in the Divjaka region is exposed to relatively low pest pressure. Harvesting of the first crop was completed in early June, before the potato tuber moth population reached the economic threshold. This observation is in agreement with the findings of Cota (2003), who concluded that the first potato crop is generally protected from economically significant damage by *P. operculella*, as infestations during this period are largely confined to the above-ground (epigeal) plant tissues and do not significantly affect tuber yield.

Overall, the results confirm that continuous monitoring using Delta traps baited with sex pheromones provides an effective method for tracking the seasonal population dynamics of *P. operculella*. Knowledge of these population trends is essential for identifying periods of greatest pest risk, optimizing the timing of control measures, and improving the effectiveness of Integrated Pest Management (IPM) strategies in potato production.

CONCLUSIONS

Monitoring *Phthorimaea operculella* populations using sex pheromone traps is essential for:

Early detection of the pest.

Determining the optimal timing for control measures.

Environmentally safe pest monitoring, as pheromone traps are highly species-specific and do not harm beneficial insects.

Evaluating the effectiveness of implemented pest management strategies.

Reducing unnecessary pesticide applications, thereby supporting sustainable Integrated Pest Management (IPM) programs.

The potato tuber moth (*Phthorimaea operculella*) completed several generations between June and the end of October under the climatic conditions of the Divjaka region. Early potato cultivars were exposed to relatively low pest pressure and were generally protected from economically significant damage.

In contrast, the second potato crop was highly vulnerable to infestation by *P. operculella*. Therefore, more intensive monitoring using sex pheromone traps is strongly recommended to ensure early detection and timely implementation of control measures.

The ability of *P. operculella* to produce multiple overlapping generations within a single growing season makes this pest particularly problematic in warm Mediterranean environments such as Divjaka.

Effective management of this key potato pest requires timely intervention before economic damage occurs through the implementation of an Integrated Pest Management (IPM) strategy that combines:

Agronomic (cultural) measures, including deeper planting of seed tubers, adequate soil covering (hilling), regular irrigation, removal of exposed tubers, and destruction of crop residues.
Physical and mechanical control methods.
Biological control measures.
Chemical control, applied only when pest populations exceed the economic threshold and in accordance with IPM principles.

LITERATURA

Arnone, S.; Musmeci, S.; Bacchetta, L.; Cordischi, N.; Pucci, E.; Cristofaro, M.; Sonnino, A. (1998) Research in *Solanum* spp. of sources of resistance to the potato tuber moth *Phthorimaea operculella* (Zeller). *Potato Res.* 1998, *41*, 39–49.

Aryal, S., et al. (2020). *Population dynamics of potato tuber moth (Phthorimaea operculella) under Nepalese agroecological conditions.*

Claudia Vasquez. (2009). Effect of Pheromone Trap Density on Mass Trapping of Male Potato Tuber Moth Phthorimaea operculella (Zeller) (Lepidoptera: Gelechiidae), and Level of Damage on Potato Tubers. Chilean Journal of Agricultural Research,

Cota, E.(2003,January). Bioecology and control of potato moth (*Phthorimaea operculella* , Zeller). Agricultural University of Tirana.

Das GP, Magallona ED, Raman KV, Adalla, CB (1992).Effects of different components of IPM in themanagement of the potato tuber moth in storage.Agric. Ecosyst. Environ. 4: 321-325

Das GP, Raman KV (1994). Alternate hosts of the potatotuber moth, Phthorimaea operculella (Zeller). CropProt. 13: 83-86.

Dekebol, A.;Aryal, S.;Jung, C. (2019).Suitability of tomato leaves for larval development of Potato tuber moth,*Phthorimaea operculella* (Zeller) (Lepidoptera: Gelechiidae). *Entomol. 49*, 258–264.

Gao, Y.L. Green control techniques for potato tuberworm (*Phthorimaea operculella*).(2021) *Sci. Agric*, *54*, 533–535.

Gao,Y.L. Potato tuberworm: A threat for China potatoes. *Entomol. Ornithol. Herpetol.* (2018), *7*, e132. https://en.wikipedia.org/wiki/Phthorimaea_operculella

Graft, J.E.(1917) The potato tubermoth. *Tech. Bull. USDA* 1917, *427*, 58.

Gilboa S, Podoler H (1995). Presence-absence sequentialsampling for potato tuberworm (Lepidoptera:Gelechiidae) on processing tomatoes: selection ofsample sites according to predictable seasonal trends.J. Econ. Entomol. 88: 1332-1336

Kroschel, J., & Sporleder, M. (2006). *Ecology and management of the potato tuber moth*.

Lal. L.; (1993) Potato tuber moth–bionomics and management. In: Chadha KL, Grewal JS (eds) Advances inHorticulture, Vol. 7- Potato. Malhotra Publishing House, New Delhi, pp 591–60201859-5

Rondon, S. I. (2020). *The Potato Tuberworm: A Literature Review of Its Biology, Ecology, and Control*. *American Journal of Potato Research*.

Rondon, S. I. (2020) Decoding *Phthorimaea operculella* (Lepidoptera: Gelechiidae) in the new age of change. J.Integr. Agr. 19, 316-324

R. S. Chandel 1 & Sumit Vashisth 2 & Saurbh Soni 1 &Rahul Kumar 1 & Vinod Kumar. (June2019). The Potato Tuber Moth, Phthorimaea operculella (Zeller), in India: Biology, Ecology, and Control . https://doi.org/10.1007/s11540-019-09426-z

Sporleder, M., Kroschel, J., et al. (2004). *Biology and ecology of the potato tuber moth under different environmental conditions.*
Trivedi, T. P. & Rajagopal, D. (1992). Distribution, biology, ecology and management of potato tuber moth, *Phthorimaea operculella* (Zeller) (Lepidoptera: Gelechiidae): A review. *Int. J. Pest Manage.* 38, 279–285
Yan, X., et al. (2023). *Effects of trap height, trap type and pheromone dose on monitoring efficiency of* Phthorimaea operculella.
Xu, J.; Zhu, J.H.; Yang, Y.L.; Tang, H.; Lv, H.P.; Fan, M.T.; Shi, Y.; Dong, D.F.; Wang, G.J.; Wang, W.X.;(2019). Status of major diseases and insect pests of potato and pesticide usage in China. *Sci. Agric*, *52*, 2800–2808. (In Chinese)
https://www.abaonline.al
https://en.wikipedia.org/).
https://www.sciencedirect.com

EVALUATION OF TOTAL PHENOLIC CONTENT, ANTIOXIDANT CAPACITY, AND ANTIMICROBIAL ACTIVITY OF *ELAEAGNUS ANGUSTIFOLIA* L.

Elanur KOÇ[1], Nagehan SALTAN[2], Gamze GÖGER[3]

[1] Anadolu University Department of Pharmaceutical Botany, Graduate School, Eskişehir, Türkiye
[2] Anadolu University Faculty of Pharmacy Department of Pharmaceutical Botany, Eskişehir, Türkiye
[3]Afyonkarahisar Health Sciences University, Faculty of Pharmacy, Department of Pharmacognosy, Afyonkarahisar, Türkiye

Corresponding author e-mail: elanurkoc97@gmail.com

ABSTRACT

Elaeagnus angustifolia L. (Elaeagnaceae), commonly known as Russian olive, is rich in bioactive compounds with potential health benefits. This study aimed to comprehensively evaluate the total phenolic content (TPC), antioxidant capacities, and antimicrobial activities of various extracts and decoctions obtained from the fruits and aerial parts of *E. angustifolia* collected from Eskişehir and Bursa provinces (Türkiye). TPC was determined via the Folin-Ciocalteu method and expressed as mg gallic acid equivalents per gram of extract (mg GAE/g). Antioxidant performance was evaluated using the DPPH radical scavenging assay (IC_{50}, mg/mL). Antimicrobial evaluation was conducted against *Escherichia coli* ATCC 8739, *Staphylococcus aureus* ATCC 6538, *Pseudomonas aeruginosa* ATCC 9027, *Candida parapsilosis* ATCC 22019, and *Candida albicans* ATCC 90028 using the broth microdilution method to determine Minimum Inhibitory Concentrations (MIC, µg/mL). Tetracycline and Amphotericin B were utilized as standard reference drugs.TPC values ranged widely from 16.8±0.02 to 67.8±0.06 mg GAE/g. The highest phenolic concentration was recorded in sample 5A (Eskişehir, aerial parts, 70% ethanol; 67.8 ±0.06 mg GAE/g), which concurrently exhibited the strongest DPPH radical scavenging activity with the lowest IC_{50} value (0.275±0.02 mg/mL). Conversely, sample 1E (Bursa, fruits, ethyl acetate) displayed the lowest TPC (16.8±0.02 mg GAE/g) and the weakest antioxidant capacity (IC_{50}: 2.101±0.05 mg/mL). The antimicrobial screening revealed variable efficacy across formulations. The highest antibacterial potency was observed in sample 1A against both *E. coli* and *S. aureus*, with a MIC value of 500 µg/mL. For antifungal action, sample 5B demonstrated the highest efficacy against *C. parapsilosis* with a MIC of 500 µg/mL. In contrast, *P. aeruginosa* exhibited strong resistance to almost all extracts (MIC >4000 µg/mL). The results demonstrate that *E. angustifolia* aerial parts and fruit formulations possess significant antioxidant and selective antimicrobial properties, which strongly correlate with their total phenolic levels. In particular, 70% ethanol extracts of aerial parts present promising profiles. These findings suggest that *E. angustifolia* could serve as a valuable natural source of bioactives for pharmaceutical and nutraceutical applications.

Keywords: *Elaeagnus angustifolia*, Antibacterial, Antifungal, DPPH, Total Phenolic Content

INTRODUCTION

Elaeagnus angustifolia L. can be identified by its distinctive small, elliptical pomes that are reddish-brown in color and measure about 1.5 to 2 cm long. Its leaves are long and elliptical,

featuring sharp tips and short stalks [Hamidpour et al., 2016; Saboonchian et al., 2014]. Because it shares a close visual resemblance with the common olive tree, people frequently call it wild olive, Russian olive, or oleaster, which is its most common English name. This deciduous species belongs to the Elaeagnaceae family and generally grows into a large shrub or a small tree between 2 and 7 meters tall, easily recognized by its silvery-green branches [Hamidpour et al., 2016; Hassanzadeh et al., 2018]. There are more than 90 species within the *Elaeagnus* genus, showing a broad geographical distribution across the semi-tropical regions of Asia, Europe, and North America. In several European countries, it is primarily favored as an urban ornamental plant; however, in Central and Eastern Anatolia, it is extensively cultivated for its edible fruits [Cansev et al., 2011]. Almost every part of the plant, including its roots, bark, blossoms, leaves, and fruits, exhibits notable medicinal qualities, paving the way for its versatile use in the food, pharmaceutical, and fragrance industries [Hassanzadeh et al., 2018]. In Russia, E. angustifolia has a long-standing reputation as a highly therapeutic plant and has been widely adopted in the folk medicine of various Asian and Trans-Caucasian regions due to its medicinal benefits [Abizov et al., 2008].

Herbal decoctions and infusions prepared from the leaves, flowers, bark, and fruits of local populations have been utilized for generations to manage a variety of health problems and physical conditions. For instance, drinking infusions made from its flowers or eating raw or cooked fruits is believed to help relieve coughs, colds, fevers, nausea, vomiting, jaundice, asthma, and diarrhea, while also being considered beneficial during tetanus management [Ahmadiani et al., 2000]. Ethnobotanical data from Iran indicate that traditional practitioners regularly recommend the fruits to ease pain in individuals suffering from joint inflammation, whereas they use the blossoms to treat tetanus. In the traditional medicine of Türkiye, a hot tea prepared from the flowering twigs of the plant is documented as a traditional remedy for treating diabetes in the Gönen district of Balıkesir province [Sarikaya et al., 2010]. Similarly, folk practices support using the fruit for its diuretic, tonic, antipyretic, and antidiarrheal actions, as well as for managing kidney complaints [Ayaz and Bertoft, 2001; Gurbuz et al., 2003]. Phytochemical analyses indicate that the *E. angustifolia* contains a rich diversity of secondary metabolites, such as flavonoids, polysaccharides, sitosterols, carotenoids, cardiac glycosides, terpenoids, coumarins, phenolcarboxylic acids, amino acids, saponins, vitamins, and tannins. In fact, these specific flavonoid components have drawn significant interest from food and medical scientists owing to their robust in vitro and in vivo antioxidant properties, along with their capacity to scavenge free radicals, interrupt radical chain pathways, and chelate metal ions (Liu and Yao, 2007). In addition to their role as antioxidants, the structural phenolics and terpenes found within these extracts are believed to be directly associated with the plant's antimicrobial modes of action, potentially breaking down microbial cell walls and interrupting internal pathways. The fruits are particularly high in proteins, sugars, vitamins (such as tocopherol, vitamin C, carotene), and major minerals including calcium, magnesium, potassium, sodium, and phosphorus, along with iron and manganese. They are also rich in substantial lipid and fatty acid fractions, including palmitic, palmitoleic, and linoleic acids, phospholipids, glycolipids [Hamidpour et al., 2016; Goncharova et al., 1995; Okmen and Turkcan, 2014; Sahan et al., 2015]. An earlier piece of research focused directly on analyzing the essential elements, polyphenolic levels, and total antioxidant potential of the fruits [Cansev et al., 2011]. Meanwhile, another study proposed that dried fruit flour could serve as a valuable functional ingredient in food formulations due to its dense nutritional properties [Sahan et al., 2013]. This high bioactive content in the different tissues of *E. angustifolia* explains its strong biological activities [Incilay, 2014]. Because of these qualities, current studies have explored incorporating the fruit into various food products to enhance their functional value [Sahan et al., 2013; Cakmakci et al., 2015].

The flowers and leaves are reported to concentrate large quantities of phenolic and flavonoid compounds [Saboonchian et al., 2014], while the fruits and seeds display strong antioxidant activity [Wang et al., 2012].

Modern pharmacological screenings continue to highlight the anti-inflammatory, antioxidant, antimicrobial, and anticancer potential of *E. angustifolia* [Hamidpour et al., 2016]. Furthermore, previous evaluations of *E. angustifolia* leaf extracts have highlighted their selective antibacterial efficacy against food pathogens, particularly demonstrating a maximum inhibition zone against *Yersinia enterocolitica*, while concurrently exhibiting prominent antioxidant activity through stable DPPH free-radical scavenging profiles [Okmen and Turkcan, 2014].

Therefore, the present study aimed to evaluate and compare the total phenolic contents, DPPH radical scavenging capacities, and antimicrobial profiles of 70% ethanol extracts, ethyl acetate extracts, and decoctions obtained from the fruits and aerial parts of *E. angustifolia*. To observe potential variations induced by geographic factors, plant materials were collected from Eskişehir and Bursa provinces (Türkiye). The antimicrobial potency was determined via Minimum Inhibitory Concentration (MIC) against a panel of pathogens, including *Escherichia coli*, *Staphylococcus aureus*, *Pseudomonas aeruginosa*, *Candida parapsilosis*, and *Candida albicans*. Ultimately, this research aims to contribute to the scientific understanding of the traditional uses of *E. angustifolia* and evaluate its potential as a natural source for future pharmaceutical and nutraceutical applications.

MATERIAL AND METHOD

Plant Material

In 2025, wild specimens of *Elaeagnus angustifolia* were gathered from the provinces of Bursa and Eskişehir. The botanical identification of the collected plants was performed using the diagnostic keys in Flora of Turkey and the East Aegean Islands (Davis, 1982) and supported by field photographs. The corresponding voucher specimens were authenticated and deposited at the Anadolu University Herbarium in Eskişehir, Türkiye under the voucher codes: ESSE 16286 and 16287).

To preserve the chemical integrity of thermolabile secondary metabolites, the freshly harvested aerial parts (comprising leaves and flowers) and fruits were first washed thoroughly under running tap water to remove physical debris, rinsed with distilled water, and subsequently left to dry at ambient room temperature in a well-ventilated, shaded area. Once completely dried, the plant materials were finely pulverized using a laboratory grinder before the extraction process. Solvent extraction was carried out using 70% ethanol and ethyl acetate, maintaining a material-to-solvent ratio of 10 g per 100 mL. This maceration process was repeated for three consecutive cycles, with each round lasting 8 hours. At the end of each cycle, the solution was filtered, and the remaining plant residue was remacerated with fresh solvent to optimize total yield. The collected filtrates were pooled and concentrated to dryness on a rotary evaporator at 37°C. Following the evaporation of the organic solvent, the remaining aqueous fraction of the ethanol extract was thoroughly dried using a freeze-dryer (lyophilizer). The crude dry extracts were maintained at +4°C for subsequent experimental steps. Additionally, aqueous decoctions of the fruit samples were prepared according to traditional methods. All crude dry extracts were tightly sealed and stored at +4 °C in dark glass vials until subsequent *in vitro* bioassays.

Figure 1. General view of *Elaeagnus angustifolia* during different vegetation periods: (a) flowering stage, (b) fruiting stage

Determination of Total Phenolic Content (TPC)

The total phenolic content (TPC) of the *E. angustifolia* extracts was evaluated colorimetrically utilizing the Folin-Ciocalteu reagent (FCR) protocol, with the final values expressed as milligrams of gallic acid equivalents per gram of dry weight (mg GAE/g DW) (Singleton et al., 1999). Briefly, a 0.20 mL aliquot of each extract was blended with 1560 µL of distilled water and 0.10 mL of the Folin-Ciocalteu reagent. Following a brief reaction interval spanning 1 to 8 minutes, the mixture was treated with 0.300 mL of a 20% sodium carbonate (Na_2CO_3) solution. The resulting reaction tubes were incubated at a controlled temperature of 25 °C for 2 hours. After incubation, the optical density (absorbance) was monitored at 760 nm employing a BioTek microplate spectrophotometer. Quantitative calculations were derived from a standard calibration curve constructed using a series of gallic acid concentrations ranging from 0.03 to 1 mg/mL. To guarantee experimental precision, a blank control was processed simultaneously, and all analyses were performed in triplicate; the results are presented as mean values ± standard deviation (SD).

DPPH Radical Scavenging Activity

The antioxidant potential of both the fruit and aerial part extracts of *E. angustifolia* was determined via the DPPH (2,2-diphenyl-1-picrylhydrazyl) radical scavenging method, adapting the methodology outlined by Agiel et al. (Agiel et al., 2024). A stock solution of DPPH was prepared at a concentration of 80 µg/mL. For the assay, 200 µL of each plant extract (dissolved in MeOH at an initial concentration of 5 mg/mL) was introduced into the first row of a 96-well microplate. The remaining wells were pre-filled with 100 µL of methanol (MeOH).

A series of two-fold serial dilutions was executed across the plate to achieve a final concentration gradient spanning from 5 mg/mL down to 0.039 mg/mL. The scavenging reaction was triggered by introducing 100 µL of the DPPH stock solution into each well, after which the plate was incubated in darkness for 30 minutes. In this experimental setup, gallic acid was

employed as the reference standard (positive control), a mixture of DPPH and MeOH functioned as the negative control, and pure MeOH was used as the blank.

Following incubation, the absorbance of the reaction mixtures was recorded at 517 nm at room temperature using a BioTek microplate spectrophotometer. The percentage of DPPH radical inhibition was calculated according to the standard formula reported in Reference 21. Half-maximal inhibitory concentration (IC_{50}) values were computed through non-linear regression analysis using SigmaPlot 13.0 software (SPSS Inc., Chicago, IL). All calculations are expressed as the mean values obtained from three independent experimental replicates.

DPPH Scavenged (%) = [(Abscontrol – Abssample)/Abscontrol] × 100

Antimicrobial Activities

The Gram-positive *Staphylococcus aureus* ATCC 6538 and Gram-negative *Escherichia coli* ATCC 8739, *Pseudomonas aeruginosa* ATCC 9027, and yeast *C. parapsilosis* ATCC 22019, and *C. albicans* ATCC 90028strains were used. The following antimicrobial agents used Tetracycline and Amphotericine B. Mueller-Hinton Agar (MHA), and Tryptic Soy Agar (TSA) were used to ensure the viability of the strains used in the study. The Mueller-Hinton Broth (MHB) and RPMI 1640 medium were used for the antimicrobial activity test. The initial concentration of the extracts was set at 8000 µg/mL. For the standards, the initial concentration was 128 µg/mL.

Antibacterial Activity (MIC, µg/ mL)

The microdilution technique (M-100-S16) for aerobic microorganisms published by the Clinical and Laboratory Standards Institute (CLSI) was used, with some modifications to the protocol (CLSI, 2006; Göger et al., 2018; Göger et al., 2023). To revive the standard culture strains to be used in antimicrobial susceptibility testing, they were inoculated into petri dishes containing Mueller Hinton Agar (MHA) and Tryptic Soy Agar (TSA) and incubated at 37°C for 24 hours. At the end of incubation, single colonies that had grown on the culture medium were transferred to tubes containing Mueller-Hinton Broth (MHB) and incubated at 37°C for 24 hours. After 18–24 hours of incubation, the cultures grown in the liquid medium were adjusted to a concentration of McFarland No. 0.5 (approximately 10^8 CFU/mL for bacteria) using a densitometer. For the experiment, microplate dishes with 96 “U”-type wells were used. After these steps, the microplate wells were sealed and incubated at 35–37°C for 16–20 hours. At the end of the incubation period, 15 µL of resazurin reagent was added to each well to determine the presence of growth. The plates were then incubated for an additional 1–2 hours at 37°C to allow for color development. At the end of incubation, the uncolored areas were identified as concentrations where no growth occurred, and the minimum inhibitory concentration (MIC) values were determined.

Anticandidal Activity (MIC, µg/ mL)

This procedure was performed using the microdilution technique (M27-A2) protocol for fungi published by the Clinical and Laboratory Standards Institute (CLSI, 2002). The standard *Candida* strains used in antifungal activity tests. To revive, the cultures were inoculated into petri dishes containing Sabouraud’s Dextrose Agar (SDA) and incubated at 37°C for 24 hours. At the end of incubation, single colonies that have grown on the medium were transferred to tubes containing 0.85% sodium chloride, vortexed thoroughly, and then adjusted to a turbidity of McFarland No. 0.5 (10^6 CFU/mL for yeast culture) using a turbidimeter. The culture was then diluted in RPMI medium to a concentration of 10^3 CFU/mL and used for the test. Serial two-fold dilutions were performed on the extracts, the plates are inoculated the microorganism and incubated at 35–37°C for 16–20 hours. At the end of the incubation period, a small amount of resazurin reagent was added to the plates to determine the presence of growth in the wells. At the end of incubation, areas that do not change color are identified as concentrations where no growth occurred.

RESULTS AND DISCUSSION

Total Phenolic Content (TPC) and Antioxidant Activity

The quantitative results for the total phenolic content (TPC) and DPPH radical scavenging capacities (IC_{50}) of the various E. angustifolia extracts (70% ethanol, ethyl acetate, and traditional decoctions) from Eskişehir and Bursa provinces are presented in Table 1. The evaluated samples demonstrated a wide variation in TPC, ranging from 16.8 ± 0.02 to 67.8 ± 0.06 mg GAE/g extract. The highest total phenolic concentration was observed in sample 5A (Eskişehir, aerial parts, 70% ethanol extract) with 67.8 ± 0.06 mg GAE/g extract, which concurrently exhibited the most potent DPPH radical scavenging activity with the lowest IC_{50} value of 0.275 ±0.02 mg/mL. This performance was followed by sample 1A (Bursa, aerial parts, 70% ethanol extract), which possessed a TPC of 50.8 ± 0.05 mg GAE/g extract and an IC_{50} of 0.361 ± 0.01 mg/mL. Sample 1B (Bursa, aerial parts, ethyl acetate extract) also showed a significant phenolic level (40.2 ± 0.05 mg GAE/g extract) and antioxidant capacity (IC_{50}: 0.430 ± 0.07 mg/mL). Conversely, lower phenolic contents and weaker antioxidant capacities were consistently found in the fruit extracts. The lowest phenolic concentration was recorded in sample 1E (Bursa, fruits, ethyl acetate extract) with 16.8 ± 0.02 mg GAE/g extract, exhibiting a high IC_{50} of 2.101 ± 0.05 mg/mL. This was followed by sample 5F (Eskişehir, fruits, ethyl acetate extract) with a TPC of 19.1 ± 0.03 mg GAE/g extract and an IC_{50} of 1.983 ±0.03 mg/mL. Generally, the aerial parts of *E. angustifolia* demonstrated a higher concentration of phenolic compounds and antioxidant performance compared to their corresponding fruit parts, regardless of the geographical origin.

Table 1. Data on TPC and DPPH$^{\bullet}$ Assay of *Elaeagnus angustifolia* extracts

Extracts	**Origin/Plant part**	**Solvent**	**TPC (mg GAE/g ext.)**	**DPPH (IC_{50} mg/mL)**
1A	Bursa, aerial parts	70% EtOH	50.8±0.05	0.361±0.01
1B	Bursa, aerial parts	Ethyl Acetate	40.2±0.05	0.430±0.07
1D	Bursa, fruits	70% EtOH	35.3±0.07	0.481±0.05
1E	Bursa, fruits	Ethyl Acetate	16.8±0.02	2.101±0.05
1F	Bursa, fruits	Decoction	26.9±0.04	1.562±0.06
5A	Eskişehir aerial parts	70% EtOH	67.8±0.06	0.275±0.02
5B	Eskişehir aerial parts	Ethyl Acetate	34.1±0.02	0.501±0.01
5D	Eskişehir, fruits	70% EtOH	32.9±0.02	0.513±0.05
5F	Eskişehir, fruits	Ethyl Acetate	19.1±0.03	1.983±0.03
5E	Eskişehir, fruits	Decoction	33.7±0.01	0.708±0.06
GA				0.002±0.0003

Values are expressed as mean ± SD (n = 3). TPC: Total Phenolic Content
mg GAE/g ext.: Total phenols expressed as gallic acid equal milligrams of gallic acid per gram (dry weight) of extract, GA: gallic acid

These results are consistent with prior findings in the literature. Saboonchian et al. (2014) observed that the flowers and leaves of *E. angustifolia* contain elevated levels of phenolic and flavonoid compounds compared to other parts. While Berktaş and Çam (2020) suggested that the bioactive content of the fruits might surpass that of the leaves in certain specific cultivars, our empirical data clearly demonstrate that the aerial parts of both the Bursa and Eskişehir populations possess a far superior phenolic and antioxidant profile.

Furthermore, our findings validate that the DPPH radical scavenging activity of *E. angustifolia* is correlated with its phenolic profile, which is in agreement with Faramarz et al. (2015). Comparing the extraction solvents, polar 70% ethanol proved to be the most efficient system for recovering potent radical-scavenging phenolics. This observation is supported by Si et al. (2011), who documented that polar fractions of *E. angustifolia* exhibit significant DPPH scavenging capacities, and Amini et al. (2019), who verified that polar leaf extracts possess excellent radical scavenging attributes due to their concentrated polar phenolic fractions.

Antimicrobial Activity

The minimum inhibitory concentrations (MIC, µg/mL) of the *E. angustifolia* extracts against five pathogenic strains are compiled in Table 2. The extracts demonstrated that the antimicrobial efficacy profile depends on the plant part and extraction solvent.

Table 2. *In Vitro* Antimicrobial Efficacy (MIC, µg/mL) of *E. angustifolia* Extracts

Extracts	*Escherichia coli*	*S. aureus*	*P. aeruginosa*	*C. parapsilosis*	*C. albicans*
1A	500	500	>4000	2000	4000
1B	1000	>4000	>4000	1000	4000
1D	>4000	>4000	>4000	4000	8000
1E	>4000	>4000	>4000	2000	8000
1F	>4000	>4000	>4000	8000	8000
5A	4000	>4000	>4000	2000	4000
5B	1000	>4000	4000	500	2000
5D	>4000	>4000	>4000	4000	8000
5F	4000	>4000	>4000	1000	2000
5E	>4000	>4000	>4000	1000	8000
TET	0.125	0.125	4	-	-
AMP	-	-	-	4>	128

TET: Tetracycline, AMP: Amphotericin B. Values are represented as MIC (µg/mL).

Among the tested extracts, the polar 70% ethanol extract of Bursa aerial parts (1A) displayed the most prominent antibacterial potency, inhibiting the growth of both the Gram-negative *E. coli* and the Gram-positive *S. aureus* at a low MIC of 500 µg/mL. Moderate antibacterial activities against *E. coli* were also observed for the ethyl acetate extracts of aerial parts from both Bursa (1B) and Eskişehir (5B), with a MIC of 1000 µg/mL. Conversely, the opportunistic pathogen *P. aeruginosa* displayed resistance against almost all tested formulations, with MIC values exceeding 4000µg/mL (with the sole exception of sample 5B, which yielded a MIC of 4000µg/mL). The fruit extracts, regardless of the solvent used, showed low antibacterial potential, with MIC values typically exceeding 4000µg/mL against all tested bacterial strains.

These findings strongly align with İncilay (2014), who observed that polar leaf and flower extracts of Turkish *E. angustifolia* possess strong antimicrobial action against Gram-positive bacteria, particularly *S. aureus*, whereas fruit extracts remain virtually inactive. Our results confirm that the fruit formulations (1D, 1E, 1F, 5D, 5F, 5E) are substantially less effective against bacterial pathogens, exhibiting MIC values ≥4000µg/mL. The general resistance of *P. aeruginosa* to our extracts is a widely recognized phenomenon among Gram-negative bacteria,

primarily arising from their highly selective outer membrane barrier. This resistance profile is supported by Okmen and Türkcan (2014), who reported that certain Gram-negative bacteria and yeast species display marked insensitivity to leaf extracts of *E. angustifolia*.

In the antifungal evaluation, the pathogenic yeast *C. parapsilosis* was found to be significantly more susceptible to the *E. angustifolia* extracts than *C. albicans*. The most notable anticandidal activity was achieved by sample 5B (Eskişehir, aerial parts, ethyl acetate extract) against *C. parapsilosis* with a MIC of 500µg/mL. This was followed by the ethyl acetate extracts of Bursa aerial parts (1B) and Eskişehir fruits (5F), which both inhibited *C. parapsilosis* at a MIC of 1000µg/mL. Interestingly, the aqueous decoction (INF) of Eskişehir fruits (5E) also exhibited promising antifungal activity against *C. parapsilosis* with a MIC of 1000µg/mL, which was superior to its organic solvent counterparts. The marked susceptibility of *Candida* species towards ethyl acetate formulations (such as 5B and 1B) suggests that relatively less polar solvents are efficient at extracting specific lipophilic constituents, such as terpenoids, lipophilic flavonoids, or fatty acids, which may possess targeted cell-membrane disrupting antifungal properties. This hypothesis regarding selective solvent extraction is supported by Khan et al. (2016), who demonstrated that less polar extracts (such as ethyl acetate and n-hexane) of *E. angustifolia* anatomical parts display specialized and powerful antifungal profiles compared to their highly polar counterparts.

It is well-established that the chemical composition and biological activities of medicinal plants vary significantly due to geographic, climatic, and edaphic conditions. In the present study, minor yet noteworthy variations were observed between the samples collected from Eskişehir and Bursa provinces. Specifically, while the Eskişehir population yielded the highest TPC and strongest antioxidant capacity (5A), the Bursa population demonstrated the most potent antibacterial profile against *E. coli* and *S. aureus* (1A). These differences emphasize the distinct role of regional microclimates, altitude, and soil chemistry in modulating the biosynthetically active pathways of *E. angustifolia*.

From an ethnobotanical perspective, these empirical results strongly validate the historical and traditional uses of this species. In the traditional folk medicine of Türkiye, Iran, and Pakistan, preparations (such as decoctions and infusions) of *E. angustifolia* are widely utilized to alleviate throat infections, fever, joint pain, and inflammatory conditions (Ali & Qaiser, 2009; Sarıkaya et al., 2010). The prominent antioxidant capacities and selective antimicrobial properties demonstrated by the aerial parts and fruit formulations in this study provide a robust, evidence-based scientific foundation for their traditional therapeutic claims.

CONCLUSIONS

In conclusion, this study provides a detailed and comparative pharmacological evaluation of wild *E. angustifolia* populations harvested from Eskişehir and Bursa provinces. The integrated findings confirm that the aerial parts, particularly when extracted with 70% ethanol, represent a valuable natural reservoir of phenolic antioxidants and selective antimicrobial agents. Additionally, the selective anticandidal potency of the ethyl acetate and traditional decoction formulations highlights the therapeutic promise of these extracts. These findings contribute valuable scientific data to the botanical and pharmaceutical literature, strongly supporting the potential application of *E. angustifolia* as a natural bioactive source for future pharmaceutical and nutraceutical developments.

ACKNOWLEDGEMENT

This work was supported by the Anadolu University Scientific Research Projects Coordination Unit under grant number TYL-2025-2878.

REFERENCES

Abizov, E. A., O. N. Tolkachev, S. D. Mal'Tsev, E. V. Abizova. 2008. Composition of biologically active substances isolated from the fruits of Russian olive (*Elaeagnus angustifolia*) introduced in the European part of Russia. Pharmaceutical Chemistry Journal. 42: 23-25.

Agiel, N., Y. B. Köse, Z. Gulcan, N. Saltan, M. Kürkçüoğlu, G. İşcan. 2024. Antioxidant and antimicrobial activity of the endemic *Mentha longifolia* subsp. *cyprica* growing in Cyprus. Phytochemistry Letters. 60: 243-248.

Ahmadiani, A., Hosseiny, J., Semnanian, S., Javan, M., Saeedi, F., Kamalinejad, M., Saremi, S. 2000. Antinociceptive and anti-inflammatory effects of *Elaeagnus angustifolia* fruit extract. Journal of Ethnopharmacology. 72: 287–292.

Ali, H., M. Qaiser. 2009. The ethnobotany of Chitral valley, Pakistan with particular reference to medicinal plants. Pakistan Journal of Botany. 41(4): 2009-2041.

Amini, M. H., A. Ahmady, A. M. Zhakfar, M. N. Sediqi, M. N., G. Babak. 2019. Preliminary phytochemical profile, in vitro antioxidant and sun protective activities of *Alhagi pseudalhagi* and *Elaeagnus angustifolia* L. Journal of Pharmaceutical Research International. 31(4): 1-13.

Ayaz, F. A., E. Bertoft. 2001. Sugar and phenolic acid composition of stored commercial oleaster fruits. Journal of Food Composition and Analysis. 14(5): 505-511.

Berktaş, S., M. Çam. 2020. Antioxidant and antidiabetic properties of oleaster (*Elaeagnus angustifolia* L.) fruits and leaves. Akademik Gıda. 18(3): 270-278.

Cansev, A., Y. Sahan, G. Celik, S. Taskesen, H. Ozbey. 2011. Chemical properties and antioxidant capacity of *Elaeagnus angustifolia* L. fruits. Asian Journal of Chemistry. 23: 2661-2665.

Clinical and Laboratory Standards Institute. 2002. Reference method for broth dilution antifungal susceptibility testing of yeasts: approved standard—second edition (M27-A2). Wayne, PA: CLSI.

Clinical and Laboratory Standards Institute. 2006. Methods for dilution antimicrobial susceptibility tests for bacteria that grow aerobically: approved standard—seventh edition (M7-A7). Wayne, PA: CLSI.

Çakmakçı, S., E. F. Topdaş, P. Kalin, H. Han, P. Şekerci, L. Köse, İ. Gülçin. 2015. Antioxidant capacity and functionality of oleaster (*Elaeagnus angustifolia* L.) flour and crust in a new kind of fruity ice cream. International Journal of Food Science and Technology. 50: 472-481.

Davis, P. H. 1982. Flora of Turkey and the East Aegean Islands. Edinburgh: Edinburgh University Press.

Faramarz, S., G. Dehghan, A. Jahanban-Esfahlan. 2015. Antioxidants in different parts of oleaster as a function of genotype. BioImpacts: BI. 5(2): 79-85.

Goncharova, N. P., V. N. Plugar', Y. V. Rashkes, A. S. Isamukhamedov, A. I. Glushenkova. 1995. Oxygenated fatty acids of the seeds of *Elaeagnus angustifolia*. Chemistry of Natural Compounds. 30(6): 661-665.

Göger, G., B. Demirci, S. Ilgın, F. Demirci. 2018. Antimicrobial and toxicity profiles evaluation of the Chamomile (*Matricaria recutita* L.) essential oil combination with standard antimicrobial agents. Industrial Crops and Products. 120: 279-285.

Göger, G., D. Yüksel, F. Göger, Y. B. Köse, F. Demirci. 2023. Antimicrobial evaluation of *Tripleurospermum callosum* (Boiss. & Heldr.) E. Hossain extracts using in vitro and in vivo *Caenorhabditis elegans* model against urinary system pathogens. International Journal of Environmental Health Research. 34:1466-1478.

Gürbüz, I., O. Üstün, E. Yesilada, E. Sezik, O. Kutsal. 2003. Anti-ulcerogenic activity of some plants used as folk remedy in Turkey. Journal of Ethnopharmacology. 88(1): 93-97.

Hamidpour, R., S. Hamidpour, M. Hamidpour, M. Shahlari, M. Sohraby, N. Shahlari, R. Hamidpour. 2016. Russian olive (*Elaeagnus angustifolia* L.): From a variety of traditional

medicinal applications to its novel roles as active antioxidant, anti-inflammatory, anti-mutagenic and analgesic agent. Journal of Traditional and Complementary Medicine. 7(1): 24-29.
Hassanzadeh, Z., H. Hassanpour. 2018. Evaluation of physicochemical characteristics and antioxidant properties of *Elaeagnus angustifolia* L. Scientia Horticulturae. 238: 83-90.
Incilay, G. 2014. Volatile composition, antimicrobial and antioxidant properties of different parts from *Elaeagnus angustifolia* L. Journal of Essential Oil Bearing Plants. 17(6): 1187-1202.
Khan, S. U., A. U. Khan, A. U. H. A. Shah, S. M. Shah, S. Hussain, M. Ayaz, S. Ayaz. 2016. Heavy metals content, phytochemical composition, antimicrobial and insecticidal evaluation of *Elaeagnus angustifolia*. Toxicology and Industrial Health. 32(1): 154-161.
Liu, Q., H. Y. Yao. 2007. Antioxidant activities of barley seeds extracts. Food Chemistry. 102: 732-737.
Okmen, G., O. Turkcan. 2014. A study on antimicrobial, antioxidant and antimutagenic activities of *Elaeagnus angustifolia* L. leaves. African Journal of Traditional, Complementary and Alternative Medicines. 11: 116-120.
Saboonchian, F., R. Jamei, S. S. Hosseini. 2014. Phenolic and flavonoid content of *Elaeagnus angustifolia* L. (leaf and flower). Avicenna Journal of Phytomedicine. 4: 231-238.
Sahan, Y., D. Gocmen, A. Cansev, G. Celik, E. Aydin, A. N. Dundar, D. Dulger, H. B. Kaplan, A. Kilci, S. Gucer. 2015. Chemical and techno-functional properties of flours from peeled and unpeeled oleaster (*Elaeagnus angustifolia* L.). Journal of Applied Botany and Food Quality. 88: 34-41.
Sarikaya, S., H. Öner, U. Ş. Harput. 2010. Türkiye florasında diyabet tedavisinde kullanılan tıbbi bitkiler. Ankara Üniversitesi Eczacılık Fakültesi Dergisi. 39: 317-342.
Si, C. L., P. P. Qin, Y. Y. Lu, L. Wu, H. H. Wang, L. F. Hui, Y. H. Ni. 2011. GC-MS analysis of chemical composition and free radical scavenging activity of *Elaeagnus angustifolia* Bark. Advanced Materials Research. 183: 854-858.
Singleton, V. L., R. Orthofer, R. M. Lamuela-Raventós. 1999. Analysis of total phenols and other oxidation substrates and antioxidants by means of Folin-Ciocalteu reagent. In: Oxidants and antioxidants part A. Amsterdam: Elsevier. 152-178.
Wang, Y., T. Guo, J. Li, S. Zhou, P. Zhao. 2012. Four flavonoid glycosides from the pulps of *Elaeagnus angustifolia* and their antioxidant activities. In: Proceedings of the 2012 2nd International Conference on Computer and Information Applications (ICCIA 2012). Atlantis Press, Paris, France.

EPILOBIUM PARVIFLORUM: BENEFITS FOR PROSTATE HEALTH VERSUS IATROGENIC RISKS A CLINICAL CASE AND IN SILICO PREDICTION

Beghriche Imene[1], Kadri Rayen[2] , A.H Fendri[3]

1. Professor assistant in pharmacology, University Constantine 3, Medicine faculty.
2. PhD, Applied Chemistry. Permanent Researcher Class B : In silico & Computational chemistry at CRSP Constantine
3. Professor at Didouche Mourad Hospital, central laboratory. University Constantine 3, Medicine faculty Constantine

Corresponding Autor: ***imene.beghriche@univ-constantine3.dz***

ABSTRACT

Background: *Epilobium parviflorum* is a perennial plant that grows in wetlands in Europe, Asia, and North Africa; traditionally used for urinary and prostate disorders, but its side effects and safety in patients receiving anticoagulant therapy remains poorly documented.
Case presentation: We report the case of a 69-year-old man treated with acenocoumarol for dilated cardiomyopathy who presented with an excessive international normalized ratio (INR) of 5.6 after daily consumption of *Epilobium parviflorum* herbal tea. The patient also had also elevated creatinine levels.
The patient's anticoagulant therapy was modified, and pharmacological and therapeutic monitoring was initiated, his kidney function was closely checked until it stabilized.
Methods: A follow-up of clinical and biological parameters was performed, and in silico analyses were carried out on the major phytoconstituents of *E. parviflorum* to explore possible mechanisms of interaction.
Results: Serum creatinine showed a gradual decrease after withdrawal of the infusion. In silico predictions suggested potential inhibition of CYP2C9 and CYP3A4 by myricetin and quercetin, which may explain the observed increase in anticoagulant effect.
Conclusion: This case highlights the risk of clinically significant herb-drug interactions and emphasizes the importance of systematically asking patients about herbal medicine use during anticoagulant treatment.

Keywords: *Epilobium parviflorum*; acenocoumarol; herb-drug interaction; in silico; CYP2C9; CYP3A4; case report

INTRODUCTION

Epilobium parviflorum, commonly known as small-flowered willowherb, is a medicinal plant traditionally used to manage conditions such as fever, rheumatic pain, headaches, and mucosal or skin infections. Recently, its popularity has grown significantly for treating benign prostatic hyperplasia (BPH) and other urinary disorders, despite limited scientific evidence regarding its efficacy and safety profile [1-3].

Fig. 1: Epilobium parviflorum

The aerial parts of *Epilobium* species are particularly rich in secondary metabolites (Fig. 2) [1]. These bioactive constituents are believed to drive the plant's anti-inflammatory, and antioxidant properties [4,5].

Fig. 2: Main secondary metabolites of the small-flowered willowherb

However, this complex chemical makeup also raises concerns about potential, yet poorly investigated, drug-plant interactions [6].

As the self-medication use of *E. parviflorum* for BPH rises, patients frequently combine it with conventional pharmacotherapy without realizing the associated risks. In particular, its high flavonoid and tannin content can alter the enzymatic and metabolic activity of various drugs, potentially modulating their therapeutic efficacy or inducing toxicity [6-8].

In this context, *E. parviflorum* is of particular interest in North Africa; notably, we successfully collected specimens in eastern Algeria (Constantine). Here, we report the long-term monitoring of a patient under acenocoumarol therapy who developed severe, excessive anticoagulation following the regular consumption of *E. parviflorum* herbal tea. To elucidate the underlying biological mechanisms, *in silico* ADMET and toxicity predictions were conducted on its major phytoconstituents.

MATERIAL AND METHODS

Data collection

this study reports the long-term monitoring of a patient receiving acenocoumarol who experienced excessive anticoagulation after consuming *Epilobium parviflorum* herbal tea.

Clinical information was collected during routine medical care, including INR measurements, therapeutic modifications and serum creatinine values obtained during and after discontinuation of herbal tea consumption.

1.2. In silico analysis

Three major phytochemicals reported in *E. parviflorum* (myricetin, quercetin and oenothein B) were selected based on phytochemical studies. Their chemical structures obtained from PubChem and inserted in SMILES format. The pharmacokinetic and toxicity profiles were evaluated using ADMETlab 3.0, a platform that predicts how a molecule is Absorbed, Distributed, Metabolized, Excreted, and how Toxic it might be, and ProTox 3.0, a tool specifically designed to predict organ toxicity.

Case description

The aerial parts of Epilobium spp are rich in secondary metabolites, mainly polyphenols such as flavonoids, phenolic acids and tannins, as well as lipophilic compounds such as steroids [1]. the small-flowered species are rich in flavonoids, mainly myricetin and quercetin, and in tannins, mainly oenothein B, giving them anti-inflammatory, analgesic, antioxidant, antibacterial and antiproliferative properties [4,6,7,8].

The complex constituents of Epilobium *spp* makes it dangerous in combination with medication.

The growing interest in certain species of fireweed for its potential efficacy in treating benign prostatic hyperplasia has led to an increase in its consumption, often without consideration of its potential risks [8].

To illustrate this risk, let's take the example of our patient, a 69-year-old man who presented for the first time to the hospital Didouche Mourad, Constantine, Algeria, for a haemostasis test. The result showed a low PT and an INR of 5.6.

The patient's history revealed that he was diabetic, in addition to having dilated cardiomyopathy for which he had been treated with acenocoumarol 4 mg, a vitamin K antagonist (VKA) for over a year at a dose of 3/4 tablet (Cp) - 1/2 Cp in alternation.

The last INR value recorded one month previously was within the therapeutic range **[2-3].**

As the patient's treatment remained unchanged, the questioning focused on his diet, which showed that he had no notion of the need for a diet adapted to his anticoagulant treatment. In addition, he had been taking a cup of fireweed-tea every evening for more than a week.

The high tannin and flavonoid content of E. parviflorum may explain the increase in INR and the risk of haemorrhage. In fact, tannins' ability to complex proteins gives them an inhibitory effect on multiple enzyme systems [9]. Flavonoids, such as myricetin and quercetin, also have an antiplatelet aggregation effect [10] in addition to an inhibitory effect on cytochrome P450 (CYP450) isoenzymes 2C9 and 3A4, which significantly increases the activity of anticoagulants [11-15].

A therapeutic education session was then required, and led to the following recommendations:

- Skip the day's anticoagulant intake and check the INR the next day,
- Explanation of the effects of acenocoumarol, the need for regular monitoring and the many interactions with drugs, food and plants,
- And finally, the need to stop taking herbal tea, which increased the effect of the VKA.

The patient was cooperative and receptive to the information, but he wanted to continue taking the herbal tea because since he started taking it, his prostate problems had disappeared, specifically his polyuria, incontinence, urinary retention and pelvic pain, which gave him a better quality of sleep.

We then advised limiting the daily amounts consumed and instituting withdrawal periods with close monitoring of INRs in order to manage the interaction and find the appropriate dosage.

The patient resumed his treatment at 1/2 Cp the following day, as he was unable to perform an INR.
Subsequent INR tests were carried out on D5 and D9 after resumption, and the results were between 2 and 3.
Our patient finally stopped taking herbal tea after a month and a half, which led us to increase the dosage (3/4 tablet).
During the period of continuous Epilobium consumption, serum creatinine remained moderately elevated (17 and 18.21 mg/L). After stopping of the herbal tea, creatinine level progressively decreased to 16.17 mg/L one month later and subsequently to 15.56 and 14.24 mg/L during follow-up (Table.1).

Table 1: Evolution of the patient's creatinine levels

Time	**Creatinine (mg/L)**	**Creatinine (µmol/L)**
During herbal tea	17	150.3
During herbal tea	18.21	161
1 month after discontinuation	16.17	143
Follow-up	15.56	137.5
Follow-up	14.24	125.88

The pharmacokinetic and toxicity profiles of the major bioactive compounds isolated from *Epilobium parviflorum* were evaluated using two complementary *in silico* platforms: ADMETlab 3.0 and ProTox 3.0 [16 - 17].
ADMETlab 3.0 was used to predict the absorption, distribution, metabolism, excretion, and toxicity (ADMET) properties of the selected phytoconstituents. A particular focus was placed on the potential of inhibition of CYP450 enzymes, with a particular emphasis on its capacity to inhibit CYP2C9 and CYP3A4. These isoforms play a critical role in the hepatic metabolism of a wide range of drugs, including oral anticoagulants such as acenocoumarol. The analysis revealed that myricetin and quercetin exhibited severe predicted inhibition against both CYP2C9 and CYP3A4, whereas oenothein B showed no predicted inhibition of CYP2C9 and only weak interaction with CYP3A4.
ProTox 3.0 was subsequently employed to evaluate organ-specific toxicity endpoints, with a particular emphasis on nephrotoxicity. The ProTox 3.0 predictions indicated a low ADMET risk for both myricetin and oenothein B, while quercetin triggered a ProTox Alert, suggesting a higher potential for adverse renal effects.
The results of the in-silico network pharmacology predictions are summarized in Table 2.

Table 2: ADMET prediction [16 - 17].

Compound	**CYP2C9/ Score**	**CYP3A4/ Score**	**Nephrotoxicity**
Myricetin	Inhibitor (0.995)	Inhibitor (0.999)	low ADMET risk
Quercetin	Inhibitor	inhibitor	ProTox alert
Oenothein B	no inhibition predicted	weak	low ADMET risk

DISCUSSION

This case highlights the significant, yet often overlooked, risks associated with the concurrent use of herbal remedies and conventional medications. Specifically, it demonstrates the potential for *Epilobium parviflorum* to interact negatively with acenocoumarol.

The high tannin and flavonoid content, of *E. parviflorum* appears to be the primary culprit in the observed increase in the patient's INR. They can inhibit enzyme systems, which are crucial for the metabolism of acenocoumarol. This leads to an enhanced anticoagulant effect, significantly increasing the risk of hemorrhage.

Interestingly, a gradual decrease in serum creatinine was observed after discontinuation of the herbal tea. Although this temporal association does not establish causality, it raises the hypothesis that prolonged exposure to Epilobium, direct or indirect (for example through dehydration, drug interaction, or underlying disease modulation), deserves further investigation.

The case emphasizes the importance of thorough patient history taking, particularly regarding the use of herbal remedies. Therapeutic education played a crucial role in this case, especially as the patients often fail to report the use of herbal remedies, which can lead to undetected drug interactions and adverse effects. This highlights the need for clinicians to proactively inquire about the use of herbal products.

CONCLUSION:

This case study demonstrates that the concomitant use of Epilobium parviflorum and acenocoumarol may expose patients to clinically significant drug-herb interactions. Long-term monitoring also revealed changes in renal function that coincided with the consumption of herbal tea, although a causal relationship cannot be confirmed.

In silico findings suggest that myricetin and quercetin from *E. parviflorum* may interfere with the specific cytochrome P450 pathways required for acenocoumarol metabolism, raising a significant concern for pharmacokinetic herb–drug interactions. In contrast, oenothein B appeared to present a more favorable safety profile with minimal CYP450 inhibition and low predicted nephrotoxicity.

It is the responsibility of physicians and pharmacists to regularly monitor their patients. They should systematically investigate the use of herbal medicines in patients undergoing anticoagulation therapy and report any adverse effects to the relevant pharmacovigilance center.

REFERENCES

1. Joseph E. Pizzorno, ND. Michael T. Murray, ND. Textbook of Natural. 5th Edition. (2020) 581-583

2. Revue prescrire, Se soigner avec des plantes n'est pas forcément sans risque. Septembre 2023.

3. Beghriche I, Belhachem A, Hamidene I, Fendri AH. Origanum vulgare and hemorrhagic risk, about a case. Annales de cardiologie et d'angeiologie 74 (2025) 101856.

4. Sebastian Granica, Jakub P. Piwowarski, Monika E. C zerwińska, Anna K. Kiss. Phytochemistry, pharmacology and traditional uses of different Epilobium species (Onagraceae):Areview.

5. Tomáš Bajer, David Šilha, Karel Ventura, Petra Bajerová. Composition and antimicrobial activity of the essential oil, distilled aromatic water and herbal infusion from Epilobium parviflorum Schreb. Industrial Crops and Products, Volume 100, June 2017, Pages 95-105

6. Radosław Kujawski* *et al*. Effect of Willow herb (Epilobium angustifolium L.) extract on gene expression of selected P450 cytochromes in rat liver – preliminary study. Herba Polonica Vol. 55 No 4 2009 ISSN: 0018-0599

7. Barbara Hevesi Tóth∗, Balázs Blazics, Ágnes Kéry. Polyphenol composition and antioxidant capacity of Epilobium species. Journal of Pharmaceutical and Biomedical Analysis 49 (2009) 26–31.
8. Olta Allkanjari, Annabella Vitalone. What do we know about phytotherapy of benign prostatic hyperplasia? Life Sciences Volume 126, 1 April 2015, Pages 42-56
9. Tanin — Le dictionnaire [Internet]. [Cited: 27 Février 2025]. Available at : https://dictionnaire.acadpharm.org/w/Tanin
10. Jing Wang , Yingying Hu , Qingqing Li , Ya-nan Liu, Jingjing Lin , Ren-ai Xu. Effects of myricetin and quercetin on ticagrelor metabolism and the underlying mechanism. Chemico-Biological Interactions. Volume 392, 1 April 2024, 110924
11. N. He, T. Edeki The inhibitory effects of herbal components on CYP2C9 and CYP3A4 catalytic activities in human liver microsomes Am J Ther, 11 (2004), pp. 206-212
12. Sudhir N. Umathe, Pankaj V. Dixit, Vijendra kumar, Kuldeep U. Bansod, Manish M. Wanjari Quercetin pretreatment increases the bioavailability of pioglitazone in rats: Involvement of CYP3A inhibition. biochemical pharmacology 75 (2008)1670–1676
13. M.M. Cotreau, L.L. von Moltke, M.C. Beinfeld, D.J. Greenblatt Methodologies to study the induction of rat hepatic and intestinal cytochrome P450 3A at the mRNA, protein, and catalytic activity level J Pharmacol Toxicol Methods, 43 (2000), pp. 41-54)
14. D. Lou, S.S. Bao, Y.H. Li, Q.M. Lin, S.F. Yang, J.Y. He Inhibitory mechanisms of myricetin on human and rat liver cytochrome P450 enzymes Eur. J. Drug Metab. Pharm., 44 (5) (2019), pp. 611-618
15. Zhize Ye , Hailun Xia , Jinyu Hu , Ya-nan Liu , Anzhou Wang , Jian-ping Cai , Guo-xin Hu, Ren-ai Xu. CYP3A4 and CYP2C19 genetic polymorphisms and myricetin interaction on tofacitinib metabolism Author links open overlay panel.
16. ADMETlab 3.0; [cited: 10 Decembre 2025], available at: https://admetlab3.scbdd.com/
17. ProTox-3.0 - Prediction of TOXicity of chemicals [cited: 10 Decembre 2025]

Abbreviations:
BPH: Benign prostatic hyperplasia
Cp: tablet
CYP450 :cytochrome P450 enzymes
D: Day
INR: International Normalized Ratio
PT: prothrombin time
Spp: species
VKA : vitamin K antagonist

Patient consent: Written informed consent was obtained.

Conflict of interest: None declared.

Funding: No external funding.

AMMONIUM ADSORPTION CAPACITY IN SOME SELECTED SOILS IN THE ISHËM RIVER BASIN, ALBANIA

Xhuljo Sema[1], Fatos Huqi[1], Vjola Bakillari[1], Eugen Skura[1], Fatbardh Sallaku[1], Seit Shallari[1] and Ilir Kristo[1]*

Department of Environment and Natural Resources, Faculty of Agriculture and Environment, Agricultural University of Tirana, Tirana, Albania

**Corresponding author e-mail: xhsema@ubt.edu.al*

ABSTRACT

Ammonium (NH_4^+) adsorption is an important soil process that regulates nitrogen retention, fertilizer use efficiency and NH_4^+ availability for plant uptake. By retaining NH_4^+ within the soil matrix, this process reduces nitrogen losses through leaching and nitrification, thereby enhancing nutrient conservation. However, excessive NH_4^+ adsorbed may temporarily reduce ammonium availability to plants, potentially limiting short-term nitrogen uptake. Therefore, quantifying the NH_4^+ adsorption capacity of soils is essential for optimizing nitrogen management in agricultural systems. In this study, NH_4^+ adsorption capacity of selected soils from the Ishëm River Basin was evaluated using batch adsorption experiments with 0.01 M $CaCl_2$ as the background electrolyte. Air-dried soil samples were equilibrated with NH_4Cl solutions containing 0, 5, 10, 20, 50 and 100 mg NH_4^+ L^{-1} at a soil-to-solution ratio of 1:10 for 24 h. The equilibrium NH_4^+ concentration was determined spectrophotometrically using the indophenol blue method and NH_4^+ adsorbed was calculated as the difference between the initial and equilibrium NH_4^+ concentrations. Results showed that NH_4^+ adsorption increased progressively with increasing initial ammonium concentration in all soils. Compared with the sandy soil (5.2% clay), soils with higher clay contents exhibited substantially greater NH_4^+ adsorption. The soil containing 62.5% clay reached a maximum adsorption of 394.86 mg kg^{-1}, corresponding to 39–76% of the applied NH_4^+, whereas the sandy soil reached only 150 mg kg^{-1} (9–30% of applied NH_4^+). The highest NH_4^+ adsorption was observed in the soil with an intermediate clay content (31.6%), reaching 506 mg kg^{-1} (47.47–65.1% of applied NH_4^+), likely due to the combined effects of clay minerals and its relatively high organic matter content (4.66%), which enhanced ammonium retention. Overall, the results highlight the important role of clay content in regulating NH_4^+ adsorption, with organic matter likely acting as a complementary factor that enhances ammonium retention.

Keywords: Ammonium adsorption; Batch adsorption experiments; Clay content; Organic matter; Ishëm River Basin

INTRODUCTION

To maximize crop yields, agricultural soils are extensively supplemented with nitrogen (N), which serves as a critical macronutrient for plant development and vegetative growth (Diaz & Rosenberg, 2008). Crop growth relies heavily on the uptake of nitrogen in its two primary inorganic states: nitrate (NO_3^-) and ammonium (NH_4^+) (Marschner, 1995). However, despite the fact that modern agricultural practices depend predominantly on mineral fertilizers to supply these forms, the actual utilization efficiency of these inputs remains very low (Yadav, 2024). Approximately half of the nitrogen applied to agricultural systems escapes plant uptake and may be lost into the environment via leaching, surface runoff, denitrification and volatilization (Anas et al., 2020).

The soil behavior of ammonium (NH_4^+) is notably unique compared to other inorganic nitrogen species. This ion is subject to multiple competing pathways: it can be fixed within clay mineral interlayers, adsorbed onto soil cation exchange sites, incorporated into microbial biomass or oxidized through the nitrification process (Havlin et al., 2014). Due to its positive charge, ammonium exhibits a robust affinity for soil particles, distinguishing its behavior from that of the highly mobile nitrate ion. Beyond its adsorption onto cation exchange complexes, NH_4^+ can undergo fixation within the structural interlayer lattices of particular clay minerals, where it remains temporarily inaccessible for plant uptake (Nieder et al., 2011). Primarily occurring in 2:1 type clay minerals such as illite and vermiculite, ammonium fixation is driven by specific interlayer zones that selectively bind NH_4^+ (Mortland, 1966).

The ammonium fixation capacity of a soil fluctuates in response to a complex pattern of physicochemical attributes. Factors such as wetting and drying dynamics, cation exchange capacity (CEC), temperature, pH, organic matter content, ammonium concentration and particle size distribution collectively modulate the magnitude of this fixation (Nommik & Vahtras, 1982; Clemente & Bernal, 2006).
Ammonium fixation has a dual effect on nitrogen dynamics in soil. It can protect NH_4^+ from rapid nitrification, thereby mitigating subsequent losses from denitrification and leaching (Scherer, 1993; Steffens & Sparks, 1999; Juang et al., 2001). On the other hand, can reduce the availability of fertilizer-derived NH_4^+ for crop uptake (Scherer et al., 2014).
The objective of this study was to evaluate the ammonium adsorption capacity of selected soil samples through laboratory adsorption experiments using calcium chloride ($CaCl_2$) as the background electrolyte and different initial ammonium concentrations. The study further aimed to assess the relationship between ammonium adsorption and selected soil physicochemical properties, providing insights into the mechanisms controlling nitrogen retention in soil.

MATERIALS AND METHODS

Soil sampling and analysis

The soil samples used in this study were collected from the Ishëm River Basin, located in central-western Albania. Sampling was carried out at a depth of 0–30 cm across the basin. The collected soil samples were transported to the laboratory and pretreated according to ISO 11464:2006. The samples were air-dried at room temperature, disaggregated and sieved through a 2 mm mesh to remove coarse fragments and visible roots.

The prepared soil samples were analyzed for selected physicochemical properties, including soil pH, measured in a 1:5 soil-to-water suspension according to ISO 10390:2021; electrical conductivity (EC), measured in a 1:5 soil-to-water extract according to ISO 11265:2025; soil organic matter, determined by the potassium dichromate oxidation method; total nitrogen (TN), determined using the Kjeldahl method according to ISO 11261:1995; total phosphorus (P-tot), determined using the molybdenum blue method according to ISO 6878:2004 and soil texture, determined by the hydrometer method according to ISO 11277:2020.

Determination of ammonium adsorption capacity

The ammonium adsorption capacity of the soil samples was determined using a batch equilibrium adsorption procedure adapted from previously published procedures for ammonium adsorption in soils (Ranjbar & Jalali, 2013; Sieczka & Koda, 2016).

For each treatment, 2.00 g of air-dried soil (<2mm) were weighed and transferred into 50 mL polypropylene centrifuge tubes. A 0.01 M calcium chloride ($CaCl_2$) solution was used as the background electrolyte to maintain constant ionic strength throughout the experiment. Ammonium solutions containing 0, 5, 10, 20, 50 and 100 mg NH_4-N L^{-1} were prepared from a 1000 mg NH_4-N L^{-1} stock solution using analytical-grade ammonium chloride (NH_4Cl) dissolved in 0.01 M $CaCl_2$. 20 mL of each working solution were added to the soil samples, resulting in a soil-solution ratio of 1:10 (w/v). Each treatment was prepared in duplicate.

To inhibit microbial nitrification during the equilibration period, three drops of chloroform ($CHCl_3$) were added to each centrifuge tube. The tubes were sealed and placed on an orbital shaker at 150 rpm for 24 h at room temperature (25 ± 1 °C) to allow adsorption equilibrium to be reached. Following equilibration, the suspensions were centrifuged at 3500 rpm for 15 min and the supernatants were filtered through 0.45 μm syringe membrane filters. The equilibrium ammonium concentration (C_e) was determined colorimetrically using the indophenol blue method at 655 nm with a UV–Vis spectrophotometer.

The amount of ammonium adsorbed by the soil (q, mg kg^{-1}) was calculated by mass balance as:

$$q = (C_0 - C_e) \times V/m$$

Where C_0 is the initial ammonium concentration (mg L^{-1}), C_e is the equilibrium ammonium concentration (mg L^{-1}), V is the volume of the solution (L), and m is the dry mass of the soil (kg).

The obtained adsorption data were used to evaluate the ammonium adsorption capacity of the investigated soils and to examine its relationship with the measured soil physicochemical properties.

RESULTS AND DISCUSSION

Physical Chemical properties of the selected soils

The physicochemical characteristics of the three soil samples are presented in Table 1. The soils showed considerable differences in clay, organic matter and total nitrogen content, while pH values ranged from 6.81 to 7.70, indicating slightly acidic to neutral conditions. Electrical conductivity (EC) was low in all samples (26.20–110.95 μS cm^{-1}), indicating the absence of salinity problems.

Table 1: Physical chemical properties of selected soils

Code	pH	EC	LO	W	P –Tot	TN	Clay	Silt	Sand
		μS cm^{-1}	%	%	mg kg^{-1}			%	
N1	7.59	110.95	4.66	5.41	247.10	2953.05	31.62	23.72	44.66
N2	7.70	83.20	1.90	8.66	182.81	2010.04	62.48	27.16	10.36
N3	6.81	26.20	0.94	3.19	246.41	1020.33	5.16	20.64	74.20

The greatest differences were observed in soil texture. Sample N2 had the highest clay content (62.48%), N1 presented an intermediate content (31.62%), while N3 was dominated by the sandy fraction (74.20%) and had only 5.16% clay. Since clay particles provide negatively charged exchange surfaces capable of retaining ammonium ions, the observed differences in

soil texture are expected to influence ammonium adsorption capacity. In contrast, the high sand content in N3 suggests a lower potential for ammonium retention due to its lower specific surface area and limited number of exchange sites (Nieder et al., 2011).
Organic matter content was highest in N1 (4.66%) and lowest in N3 (0.94%), while total nitrogen followed the same trend. This pattern reflects the well-known relationship between soil organic matter and nitrogen reserves, as organic matter constitutes the main nitrogen reservoir in most soils (Ladha et al., 2011; Ren et al., 2014).
These differences in texture, organic matter and nitrogen content indicate that the three soils present different physicochemical conditions, which are expected to affect their ability to adsorb NH_4^+.

Ammonium Adsorption Capacity

The experimental results showed that the amount of NH_4^+ adsorbed by the soils increased with increasing ammonium application rates (Table 2). However, the adsorption response of the three soils varied depending on their physicochemical characteristics. At all application levels, soils N1 and N2 exhibited considerably higher adsorption capacities compared to soil N3. At the highest NH_4^+ application rate (1000 mg kg^{-1}), soil N1 presented the highest amount of adsorbed NH_4^+ (506.33 mg kg^{-1}), followed by N2 (394.86 mg kg^{-1}), while N3 exhibited the lowest value (88.95 mg kg^{-1}).

The low adsorption capacity of soil N3 can be related to its predominantly sandy texture and very low clay content (5.16%), which limit the number of active exchange sites for NH_4^+ retention. In contrast, the higher clay content in N1 and N2 provided more favorable conditions for ammonium adsorption.
These findings are consistent with those reported by Nieder et al. (2011) who highlighted the important role of soil texture in ammonium fixation. Their study showed that coarse-textured soils generally retain much lower amounts of adsorbed NH_4^+ (10–90 mg kg^{-1}) than fine-textured soils (90–460 mg kg^{-1}). This difference is mainly attributed to the lower clay content and the smaller number of adsorption sites available in coarse soils, which limits their capacity to retain ammonium.

Table 2: Ammonium adsorption capacity and adsorption efficiency of the studied soils at different NH_4^+ application rates

Applied NH_4^+ (mg kg^{-1})	N1		N2		N3	
	Adsorbed NH_4^+ (mg kg^{-1})	Adsorption (%)	Adsorbed NH_4^+ (mg kg^{-1})	Adsorption (%)	Adsorbed NH_4^+ (mg kg^{-1})	Adsorption (%)
50	32.55	65.09	38.01	76.01	12.66	25.32
100	53.92	53.92	58.16	58.16	28.19	28.19
200	112.08	56.04	107.00	53.50	58.04	29.02
500	237.34	47.47	236.93	47.39	150.77	30.15
1000	506.33	50.63	394.86	39.49	88.95	8.89

When the results were expressed as percentage of NH_4^+ adsorbed, a slightly different behavior was observed between the soils. Soil N2 showed the highest adsorption efficiency at the lower application rates (76.01% at 50 mg kg^{-1} and 58.16% at 100 mg kg^{-1}), reflecting the influence of its high clay content (62.48%). However, with increasing NH_4^+ application rate, the relative adsorption efficiency decreased, while soil N1 maintained a higher adsorption percentage at the highest applied concentration (50.63% at 1000 mg kg^{-1}).

Although soil N2 had the highest clay content, the highest absolute adsorption capacity at the highest application rate was recorded in soil N1. This result suggests that in addition to the clay fraction, the higher organic matter content in N1 (4.66%) may have contributed to the increased capacity of the soil to retain NH_4^+, especially under conditions of high ammonium loading.

Overall, the results indicate that NH_4^+ adsorption is controlled by the interaction between soil texture and organic matter content. As documented by Nommik & Vahtras (1982), clay content appears to be one of the main factors determining adsorption capacity, while organic matter plays a complementary role in maintaining this capacity as ammonium concentrations increase.

Relationship between applied NH_4^+ and adsorbed NH_4^+

To better describe the relationship between the amount of NH_4^+ applied and adsorbed, the experimental data were fitted with a power regression model (Figure 1, Table 3). The model showed a very good relationship for soils N1 (R^2 = 0.9966) and N2 (R^2 = 0.9971), while a lower R^2 value (0.8241) was recorded for soil N3, indicating a greater variability in the adsorption process.

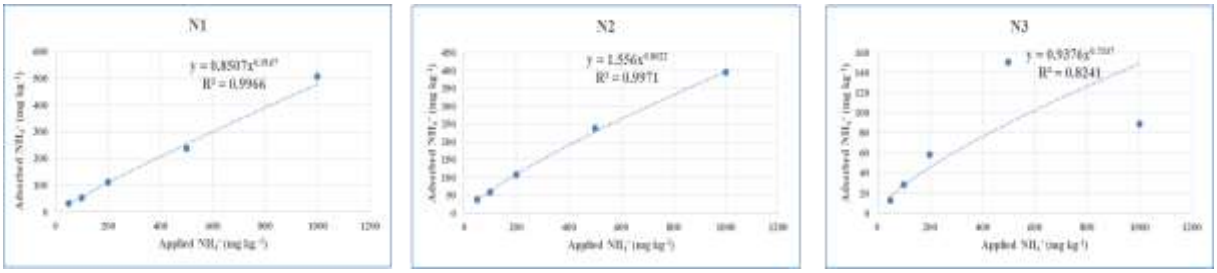

Figure 1: Relationship between applied NH_4^+ and adsorbed NH_4^+ described by a power regression model.

The value of the regression exponent (b) gradually decreased from N1 (0.9167) to N2 (0.8022) and N3 (0.7337), which indicates that with increasing NH_4^+ application rate, the increase in the adsorbed amount becomes less proportional.

Table 3: Power regression equations describing the relationship between applied and adsorbed NH_4^+ in the studied soils

Soil	Power regression equation	R^2 Value
N1	$y = 0.8507x^{0.9167}$	0.9966
N2	$y = 1.5560x^{0.8022}$	0.9971
N3	$y = 0.9376x^{0.7337}$	0.8241

The exponent of soil N1, which is closer to the value of 1, indicates that adsorption increased almost proportionally over the entire range of tested concentrations. In contrast, the lower value of the exponent for soil N3 indicates that the adsorption efficiency decreased more rapidly with increasing NH_4^+ application rate. These results are consistent with the differences in soil texture and organic matter content, discussed above.

CONCLUSIONS

The preliminary results obtained so far suggest that the adsorption capacity of NH_4^+ varied among the studied soils and was influenced by their physicochemical properties, particularly soil texture and organic matter content. In all soils, the amount of adsorbed NH_4^+ increased with increasing application rates, although clear differences in adsorption capacity were observed.

Soil N1 exhibited the highest adsorption capacity, while soil N3 showed the lowest. The lower adsorption capacity of N3 may be related to its low clay content and dominance of the sandy fraction. Although soil N2 had the highest clay content, the higher adsorption capacity observed in N1 suggests that, in addition to clay content, its higher organic matter content may have contributed to its greater ability to retain NH_4^+, especially at higher application rates.

The power regression model provided a good description of the relationship between applied and adsorbed NH_4^+, especially for soils N1 and N2, suggesting that this approach may be useful for describing NH_4^+ adsorption behavior in these soils. Overall, the findings indicate that NH_4^+ retention in soils is likely controlled by the combined influence of several physicochemical properties, with clay content and organic matter appearing to play important roles.

These findings represent the results obtained to date from the three soils investigated in this study. Further analyses are ongoing and the assessment will be extended to additional soil samples collected from different areas of the Ishëm River Basin to provide a more comprehensive understanding of NH_4^+ adsorption capacity and its relationship with soil physicochemical properties across the basin.

Acknowledgments

This research was carried out within the framework of the AMORE AL project. The project is funded by Austrian Partnership Programme in Higher Education and Research for Development (APPEAR) and supported by BOKU University, TU Wien and Karlsruhe Institute of Technology. The authors would like to express their sincere gratitude to all project partners and associated institutions for their valuable support, data provision and technical contributions.

REFERENCES

Anas, M., Liao, F., Verma, K. K., Sarwar, M. A., Mahmood, A., Chen, Z.-L., Li, Q., Zeng, X.-P., Liu, Y., & Li, Y.-R. (2020). Fate of nitrogen in agriculture and environment: Agronomic, eco-physiological and molecular approaches to improve nitrogen use efficiency. *Biological Research, 53*(1), Article 47. https://doi.org/10.1186/s40659-020-00312-4

Clemente, R., & Bernal, M. P. (2006). Fractionation of heavy metals and distribution of organic carbon in two contaminated soils amended with humic acids. *Chemosphere*, *64*(8), 1264–1273. https://doi.org/10.1016/j.chemosphere.2005.12.058

Diaz, R. J., & Rosenberg, R. (2008). Spreading dead zones and consequences for marine ecosystems. *Science, 321*(5891), 926–929. https://doi.org/10.1126/science.1156401

Havlin, J. L., Tisdale, S. L., Nelson, W. L., & Beaton, J. D. (2014). *Soil fertility and fertilizers: An introduction to nutrient management* (8th ed.). Pearson.

Juang, T. C., Wang, M. K., Chen, H. J., & Tan, C. C. (2001). Ammonium fixation by surface soils and clays. ***Soil Science, 166*(5), 345–352.** https://doi.org/10.1097/00010694-200105000-00005

Ladha, J. K., Reddy, C. K., Padre, A. T., & van Kessel, C. (2011). Role of nitrogen fertilization in sustaining organic matter in cultivated soils. *Journal of Environmental Quality*, 40(6), 1756–1766. https://doi.org/10.2134/jeq2011.0064

Marschner, H. (1995). *Mineral nutrition of higher plants* (2nd ed.). Academic Press.

Mortland, M. M. (1966). Ammonia interactions with soil minerals. In M. H. McVickar, W. P. Martin, I. E. Miles, & H. H. Tucker (Eds.), *Agricultural anhydrous ammonia: Technology and*

use (pp. 188–197). American Society of Agronomy. https://doi.org/10.2134/1966.nh3agricultural.c10

Nieder, R., Benbi, D. K., & Scherer, H. W. (2011). Fixation and defixation of ammonium in soils: A review. *Biology and Fertility of Soils, 47*(1), 1–14. https://doi.org/10.1007/s00374-010-0506-4

Nommik, H., & Vahtras, K. (1982). Retention and fixation of ammonium and ammonia in soils. In F. J. Stevenson (Ed.), *Nitrogen in agricultural soils* (Agronomy Monograph No. 22, pp. 123–171). American Society of Agronomy. https://doi.org/10.2134/agronmonogr22.c4

Ranjbar, F., & Jalali, M. (2013). *Measuring and modeling ammonium adsorption by calcareous soils*. **Environmental Monitoring and Assessment, 185**, 3191–3200. https://doi.org/10.1007/s10661-012-2782-y

Ren, T., Wang, J., Chen, Q., Zhang, F., & Lu, S. (2014). The effects of manure and nitrogen fertilizer applications on soil organic carbon and nitrogen in a high-input cropping system. *PLOS ONE*, 9(5), e97732. https://doi.org/10.1371/journal.pone.0097732

Scherer, H. W. (1993). Dynamics and availability of the non-exchangeable NH_4-N: A review. *European Journal of Agronomy, 2*(3), 149–160. https://doi.org/10.1016/S1161-0301(14)80124-X

Scherer, H. W., Feils, E., & Beuters, P. (2014). Ammonium fixation and release by clay minerals as influenced by potassium. *Plant, Soil and Environment, 60*(7), 325–331. https://doi.org/10.17221/202/2014-PSE

Sieczka, A., & Koda, E. (2016). *Kinetic and Equilibrium Studies of Sorption of Ammonium in the Soil–Water Environment in Agricultural Areas of Central Poland*. **Applied Sciences, 6(10), 269**. https://doi.org/10.3390/app6100269

Steffens, D., & Sparks, D. L. (1999). Effect of residence time on the kinetics of nonexchangeable ammonium release from illite and vermiculite. *Journal of Plant Nutrition and Soil Science, 162*(6), 599–605. https://doi.org/10.1002/(SICI)1522-2624(199912)162:6%3C599::AID-JPLN599%3E3.0.CO;2-Y

Yadav, M. (2024). Nitrogen uptake in wheat: A comprehensive study. *International Journal of Research in Agronomy, 7*(4), 101–103. https://doi.org/10.33545/2618060X.2024.v7.i4b.535

EVALUATION OF AMINO ACID DIGESTIBILITY AND PROTEIN QUALITY OF BLACK SOLDIER FLY LARVAE (Hermetia illucens) MEAL IN BROILER CHICKENS

Ruhollah Kianfar[1], Ghaith Raed Khalaf[1]

[1] University of Tabriz, Faculty of Agriculture, Department of Animal Sciences, Tabriz, Iran
Corresponding author e-mail: rkianfar@tabrizu.ac.ir

ABSTRACT

The search for sustainable protein alternatives has intensified due to increasing global population and environmental concerns associated with conventional protein sources. This study evaluated the standardized ileal digestibility (SID) of amino acids and protein quality of black soldier fly larvae (BSFL) (*Hermetia illucens*) meal compared to soybean meal in broiler chickens. A total of 70 male Ross 308 broiler chickens at 34 days of age were used in a completely randomized design with 7 treatments and 5 replicates. Experimental diets included purified diets containing BSFL meal or soybean meal as the sole protein source, a basal corn-soybean meal diet, mixture diets (50:50), and a nitrogen-free diet for measuring endogenous losses. All diets contained 0.5% chromic oxide. Birds were fed experimental diets from 34 to 38 days, and ileal digesta was collected at day 38. Chemical composition analysis showed BSFL meal contained 36.21% crude protein, significantly lower than soybean meal (43.45%). However, the SID of protein in BSFL meal (89.86%) was significantly higher than soybean meal (81.75%). Methionine digestibility in BSFL meal (91.93%) was substantially higher than soybean meal (75.17%), while lysine digestibility was 92.25% versus 88.52%, respectively. However, valine digestibility in BSFL meal (75.85%) was significantly lower than soybean meal (94.79%), and cystine digestibility (82.86%) was also lower than soybean meal (101.53%). The DIAAS value for BSFL meal (72.6%) was significantly higher than soybean meal (59.6%). Methionine + cystine was identified as the first-limiting amino acid for both sources. In conclusion, despite its lower protein concentration, BSFL meal exhibits high protein quality and digestibility, particularly for lysine and methionine, making it a viable alternative protein source. However, the lower digestibility of valine and cystine requires attention in diet formulation, and a synergistic combination with soybean meal is recommended for optimal results.

Keywords: Black soldier fly larvae, *Hermetia illucens*, Amino acid digestibility, Protein quality, DIAAS, Broiler chickens

INTRODUCTION

The global demand for animal protein is projected to increase by 70% by 2050, placing unprecedented pressure on feed protein sources (FAO, 2012). Soybean meal, the predominant plant protein source, faces sustainability challenges including deforestation, high water consumption, and reliance on genetically modified crops. Fish meal production is constrained by declining wild fish stocks (Tacon & Metian, 2008). Therefore, identifying sustainable, cost-effective alternatives has become essential for global food security.

Edible insects have emerged as promising alternatives due to their efficient feed conversion, ability to be reared on organic wastes, and favorable nutritional profiles (Van Huis et al., 2013;

Makkar et al., 2014). Among various species, black soldier fly (*Hermetia illucens*) has gained significant attention as a candidate for mass production. BSFL meal contains 35-45% protein and 15-35% fat, with a relatively balanced amino acid profile (Elwert et al., 2010; Schiavone et al., 2017). The insect is capable of converting a wide range of organic wastes into high-quality biomass, making it an environmentally sustainable protein source (Surendra et al., 2016; Abd El-Hack et al., 2020).

The presence of chitin in insect exoskeletons presents unique challenges for digestibility assessment. Chitin, a nitrogen-containing polysaccharide, may affect protein and amino acid digestibility, making accurate measurement essential for proper feed formulation (Finke, 2013; Jonas-Levi & Martinez, 2017). Modern poultry nutrition relies on standardized ileal digestibility (SID) values rather than total amino acid concentrations to formulate balanced diets (Ravindran & Bryden, 1999). This approach enables more precise matching of bird requirements and reduces nitrogen excretion (Wayne et al., 2010).

Recent studies have evaluated the amino acid digestibility of BSFL meal with varying results. Mahmoud and Ravindran (2025) reported SID coefficients of 0.83 for lysine, 0.89 for methionine, and 0.82 for threonine in black soldier fly prepupae meal. Alafif et al. (2025) reported SID ranges of 86.77-89.17% for BSFL amino acids, depending on rearing substrate. Bovera et al. (2015) demonstrated that BSFL meal could effectively replace soybean meal in broiler diets without negative effects on growth performance. Dabbou et al. (2018) and Lee et al. (2018) confirmed positive effects of BSFL meal on intestinal morphology and immune responses.

However, comprehensive studies comparing BSFL meal with soybean meal using the DIAAS methodology in the local context are limited. Therefore, this study was conducted to determine the standardized ileal amino acid digestibility and protein quality of BSFL meal compared to soybean meal in broiler chickens using the DIAAS methodology.

MATERIAL AND METHOD

Birds and Management

A total of 70 male Ross 308 broiler chickens at 34 days of age were obtained from a commercial flock and randomly assigned to 7 experimental treatments with 5 replicates (2 birds per replicate). Birds were housed in metabolic cages (30 × 40 cm) equipped with separate feeders and waterers in an environmentally controlled room with temperature maintained at 24±1°C and a lighting program of 23 hours light and 1 hour dark. All birds received commercial diets based on Ross 308 recommendations until 33 days of age and were fed experimental diets from 34 to 38 days.

Experimental Diets and Treatments

The experiment was conducted as a completely randomized design (CRD) with 7 treatments and 5 replicates. Experimental diets were formulated as semi-purified diets based on corn starch and glucose (as carbohydrate sources) and soybean oil (as fat source), with vitamins and minerals added according to Ross 308 requirements for the finisher period. All diets contained 0.5% chromic oxide (Cr_2O_3) as an indigestible marker and were formulated without free amino acids.

The experimental treatments included:

Basal diet (BD): Corn-soybean meal based diet

Nitrogen-free diet (NFD): For measuring basal endogenous amino acid losses

Purified BSFL diet: NFD + BSFL meal as the sole protein source

Purified soybean meal diet: NFD + soybean meal as the sole protein source

Mixture diet (50:50): BD + BSFL diet (1:1 ratio)

All feed ingredients were analyzed for chemical composition before diet formulation.

Sample Collection and Chemical Analysis

Birds were fed experimental diets from day 34 to 38 (4 days). At the end of day 38, all birds were slaughtered by cervical dislocation. The terminal ileum (from Meckel's diverticulum to 4 cm anterior to the ileo-cecal junction) was immediately dissected, and ileal digesta were gently flushed with distilled water, pooled per replicate, and stored at -20°C until analysis.

Proximate analysis: Dry matter, ash, crude protein, crude fat, and crude fiber were determined according to AOAC (2005) standard methods. Crude protein was determined by the Kjeldahl method (N × 6.25).

Chromic oxide measurement: Chromium concentration in diets and ileal digesta was measured by spectrophotometry according to Fenton and Fenton (1979).

Amino acid analysis: Amino acid concentrations were determined using ion-exchange chromatography (amino acid analyzer) following acid hydrolysis with 6N HCl at 110°C for 24 hours. For sulfur-containing amino acids (methionine and cystine), performic acid oxidation was performed prior to hydrolysis.

Calculations

Amino acid digestibility, digestible amino acid content, and DIAAS were calculated using standard formulas as described in Paper 1.

Statistical Analysis

Data were analyzed using the GLM procedure of SAS (version 9.4) in a completely randomized design. Treatment means were compared using Duncan's multiple range test at $P < 0.05$ significance level.

RESULTS AND DISCUSSION

Chemical Composition

The chemical composition of BSFL meal and soybean meal is presented in Table 1. BSFL meal contained 36.21% crude protein, significantly lower than soybean meal (43.45%). The total amino acid content in BSFL meal (34.42%) was slightly lower than soybean meal (36.18%).

Table 1. Chemical composition of black soldier fly larvae meal and soybean meal (% dry matter)

Parameter	BSFL Meal	Soybean Meal	SEM
Crude Protein	36.21c	43.45b	0.35
Crude Fat	31.50a	1.40b	0.44
Crude Fiber	14.90a	6.20b	0.33
Ash	11.40a	7.20b	0.29
Essential Amino Acids			
Lysine	2.28c	2.83b	0.04
Methionine	0.76b	0.68c	0.01
Arginine	1.61c	2.58b	0.03
Threonine	1.14c	1.77b	0.02
Valine	3.61b	1.76c	0.05
Leucine	2.26c	2.78b	0.05
Isoleucine	1.76b	1.62c	0.02
Phenylalanine	1.50c	1.82b	0.02
Histidine	1.03b	0.96c	0.01
Non-Essential Amino Acids			
Glutamic acid	3.96c	6.39b	0.10
Glycine	2.65b	1.62c	0.05
Alanine	2.16b	1.61c	0.04
Serine	2.14b	1.87c	0.03

a,b,c Values within rows with different superscripts differ significantly ($P < 0.05$)

The crude protein content of BSFL meal (36.21%) is within the range reported by other researchers (Elwert et al., 2010; Nyangena et al., 2020). The relatively lower protein concentration compared to soybean meal is primarily due to higher fat (31.50%) and ash (11.40%) content in BSFL meal. However, it is noteworthy that the total amino acid content (34.42%) is very close to crude protein (36.21%), indicating that the majority of nitrogen in BSFL meal is in the form of amino acids, with minimal non-protein nitrogen contribution from chitin. This finding is consistent with Finke (2013) who reported high protein recovery in BSFL meal.

When normalized per unit of protein (Table 2), BSFL meal had comparable lysine (6.32%) to soybean meal (6.57%) but significantly higher valine (10.03%), methionine (2.10%), and isoleucine (4.90%). The high valine proportion in BSFL protein is remarkable and indicates that BSFL meal is exceptionally rich in branched-chain amino acids, which are important for muscle protein synthesis.

Table 2. Amino acid composition of BSFL meal and soybean meal (% of protein)

Amino Acid	BSFL Meal	Soybean Meal	SEM
Lysine	6.32a	6.57a	0.10
Methionine	2.10a	1.59b	0.03
Arginine	4.48c	6.01a	0.09
Threonine	3.16c	4.12a	0.05
Valine	10.03a	4.08c	0.08
Leucine	6.29b	6.47b	0.10
Isoleucine	4.90a	3.77c	0.04
Phenylalanine	4.16a	4.22a	0.06
Histidine	2.86a	2.24c	0.02
Total Amino Acids	95.63a	84.16b	0.74

a,b,c Values within rows with different superscripts differ significantly (P < 0.05)

Apparent and Standardized Ileal Digestibility

Table 3 presents the apparent (AID) and standardized (SID) ileal digestibility values for BSFL meal and soybean meal. BSFL meal exhibited significantly higher SID for protein (89.86%) compared to soybean meal (81.75%). This superiority was also observed for most essential amino acids, with notable exceptions for valine and cystine.

Table 3. Apparent and standardized ileal digestibility of protein and amino acids in BSFL meal and soybean meal (%)

Parameter	AID		SID	
	BSFL	Soybean	BSFL	Soybean
Protein	88.55b	80.56c	89.86a	81.75b
Essential Amino Acids				
Lysine	90.29a	87.45b	92.25a	88.52b
Methionine	90.75b	73.88c	91.93b	75.17c
Arginine	94.42b	91.69c	95.97b	92.26c
Threonine	86.77c	90.45b	88.04c	91.30b
Valine	73.72c	90.82b	75.85c	94.79a
Leucine	87.72b	83.96c	89.18b	85.68c
Isoleucine	87.23b	88.57b	88.17b	89.59b
Phenylalanine	88.50a	83.57b	91.74a	87.26b
Histidine	94.18b	91.82c	95.51b	92.03c
Non-Essential Amino Acids				
Cystine	70.42c	92.94b	82.86b	101.53a
Glycine	90.30b	81.29c	91.24b	82.80c
Alanine	89.31b	90.76b	90.82b	92.91b

a,b,c Values within rows (AID or SID) with different superscripts differ significantly ($P < 0.05$)

The high digestibility of BSFL meal protein (89.86% SID) confirms its excellent amino acid availability despite the presence of chitin. This finding is consistent with Schiavone et al. (2017) who reported high nutrient digestibility for partially defatted BSFL meal, and with Alafif et al. (2025) who reported SID ranges of 86.77-89.17% for BSFL amino acids.

The most remarkable finding was the substantially higher methionine digestibility in BSFL meal (91.93% SID) compared to soybean meal (75.17% SID). This represents a significant competitive advantage, as methionine is the first limiting amino acid in poultry diets (Lemme

et al., 2004). The high lysine digestibility in BSFL meal (92.25% SID) also exceeds soybean meal (88.52% SID), indicating excellent lysine availability. Mahmoud and Ravindran (2025) reported SID coefficients of 0.89 for methionine and 0.83 for lysine in BSFL prepupae meal, which are slightly lower than our values (0.92 and 0.92, respectively). This difference may be due to differences in insect strain, rearing substrate, processing method, or life stage (larvae vs. prepupae).

However, two important limitations were identified. First, valine digestibility in BSFL meal (75.85% SID) was significantly lower than soybean meal (94.79% SID). This finding is consistent with Matin et al. (2021) who reported variable and sometimes low valine digestibility in insect meals (as low as 60%). The low valine digestibility may be partly due to binding of this amino acid to the chitin matrix or specific resistant protein structures. Rumpold and Schlüter (2013) suggested that chitin can bind to proteins and render them indigestible. Second, cystine digestibility in BSFL meal (82.86% SID) was lower than soybean meal (101.53% SID), likely due to stable disulfide bonds in insect proteins that are resistant to proteolytic enzymes.

Digestible Amino Acid Content

Table 4 presents the digestible amino acid content of BSFL meal and soybean meal. The standardized digestible protein content in BSFL meal (32.53 g/100g) was slightly lower than soybean meal (35.51 g/100g) due to the lower total protein concentration.

Table 4. Standardized digestible amino acid content of BSFL meal and soybean meal (g/100g)

Amino Acid	BSFL Meal	Soybean Meal
Digestible Protein	32.53c	35.51b
Lysine	2.10c	2.50b
Methionine	0.70b	0.51c
Arginine	1.55c	2.38b
Threonine	1.00c	1.62b
Valine	2.74b	1.66c
Leucine	2.02c	2.38b
Isoleucine	1.56b	1.45c
Phenylalanine	1.37c	1.58b
Histidine	0.99b	0.89c
Total Digestible Amino Acids	31.02c	32.90b

a,b,c Values within rows with different superscripts differ significantly ($P < 0.05$)

Despite the lower total digestible amino acid content, BSFL meal provides significant amounts of methionine (0.70 g/100g), which is 37% higher than soybean meal (0.51 g/100g). This is a valuable characteristic for poultry diets where methionine is often supplemented synthetically. However, the lower protein concentration of BSFL meal means that higher inclusion levels may be needed to achieve target protein levels.

Protein Quality Assessment (DIAAS)

Table 5 presents the DIAAS values for BSFL meal and soybean meal calculated based on Ross 308 starter requirements. BSFL meal had a significantly higher DIAAS value (72.6%) compared to soybean meal (59.6%). Methionine + cystine was identified as the first-limiting amino acid for both sources.

Table 5. DIAAS values for BSFL meal and soybean meal based on Ross 308 starter requirements

Amino Acid	Requirement (mg/g protein)	BSFL Meal	Soybean Meal
Methionine	24.09	89.3%	59.6%
Methionine + Cystine	43.64	72.6%	72.9%
Lysine	57.27	112.7%	122.9%
Threonine	38.18	80.5%	119.4%
Valine	43.64	193.0%	107.1%
Leucine	63.18	141.6%	106.1%
Isoleucine	38.18	125.6%	106.9%
Arginine	59.55	79.5%	112.5%
DIAAS Score		**72.6%**	**59.6%**

The DIAAS score of 72.6% for BSFL meal indicates that it is a "moderate" quality protein source (<75%), but still superior to soybean meal (59.6%). The limiting amino acid is the sulfur amino acid group (methionine + cystine), consistent with findings for other insect meals (Matin et al., 2021). However, the severity of this limitation is less pronounced than in soybean meal, where methionine alone is the limiting factor with a score of only 59.6%.

The high valine and leucine scores in BSFL meal (193.0% and 141.6%, respectively) are noteworthy, indicating that BSFL meal is exceptionally rich in branched-chain amino acids. This is consistent with the high valine concentration (10.03% of protein) observed in BSFL meal. These amino acids play key roles in muscle protein synthesis and energy metabolism (Wu et al., 2013).

Comparison of Methodologies

A comparison of the two methodology approaches (purified diet vs. complete diet) revealed interesting patterns. The complete diet method yielded significantly higher SID estimates for

some amino acids like valine (increased from 79.35% to 91.85%) and isoleucine (increased from 90.54% to 98.91%), indicating synergistic effects within the complete diet matrix. This suggests that in practical diets, the digestibility of certain amino acids in BSFL meal may be higher than estimated from purified diets alone.

CONCLUSIONS

Based on the comprehensive evaluation of black soldier fly larvae meal in this study, the following conclusions can be drawn:

Moderate protein concentration: BSFL meal contains 36.21% crude protein, lower than soybean meal (43.45%), but with most nitrogen (95.63%) in the form of amino acids.

Excellent digestibility: Despite the presence of chitin, BSFL meal shows high standardized ileal digestibility of protein (89.86%) and most amino acids, significantly higher than soybean meal (81.75%).

Superior methionine digestibility: Methionine digestibility in BSFL meal (91.93%) is substantially higher than soybean meal (75.17%), providing 37% more digestible methionine per unit weight.

Important limitations: Valine digestibility (75.85%) and cystine digestibility (82.86%) are significantly lower than soybean meal (94.79% and 101.53%, respectively), requiring attention in diet formulation.

Good protein quality: The DIAAS value of BSFL meal (72.6%) is significantly higher than soybean meal (59.6%), indicating superior inherent protein quality. The first-limiting amino acid is methionine + cystine for both sources.

Practical implications: BSFL meal can serve as a viable alternative protein source in poultry diets. However, its lower protein concentration means higher inclusion levels may be required to meet target protein levels. The optimal strategy involves synergistic combination with soybean meal, where BSFL meal provides high-quality methionine and soybean meal compensates for lysine and arginine.

Research needs: Future research should focus on optimizing rearing substrates and processing methods to improve valine and cystine digestibility, exploring the potential of enzymatic hydrolysis to enhance overall protein quality, and conducting long-term feeding trials to confirm the practical benefits of BSFL meal in commercial poultry production.

REFERENCES

Abd El-Hack, M. E., et al. (2020). Black soldier fly (Hermetia illucens) meal as a promising feed ingredient for poultry: A comprehensive review. *Agriculture*, 10(8), 339.

Alafif, M. A., et al. (2025). Effect of rearing substrate on amino acid digestibility and metabolizable energy of black soldier fly larvae meal in broilers. *Poultry Science*, 104(2), 103456.

AOAC. (2005). Official Methods of Analysis (18th ed.). Association of Official Analytical Chemists International.

Bovera, F., et al. (2015). Use of Tenebrio molitor larvae meal as protein source in broiler diet: Effect on growth performance and nutrient digestibility. *Journal of Animal Science*, 93(12), 5718-5725.

Dabbou, S., et al. (2018). Black soldier fly larvae meal in broiler diets: Effects on growth performance and gut morphology. *Animal*, 12(9), 1845-1853.

Elwert, C., et al. (2010). Nutrient composition of black soldier fly (Hermetia illucens) larvae. *Proceedings of the Society of Nutrition Physiology*, 19, 151.

FAO. (2012). Edible insects: Future prospects for food and feed security. Food and Agriculture Organization of the United Nations.
FAO. (2013). Dietary protein quality evaluation in human nutrition. Food and Agriculture Organization of the United Nations.
Fenton, T. W., & Fenton, M. (1979). An improved procedure for the determination of chromic oxide in feed and feces. *Canadian Journal of Animal Science*, 59(3), 631-634.
Finke, M. D. (2013). Complete nutrient content of four species of feeder insects. *Zoo Biology*, 32(1), 27-36.
Jonas-Levi, A., & Martinez, J. I. (2017). The overestimation of protein content in insects due to chitin. *Journal of Insects as Food and Feed*, 3(4), 247-252.
Lee, S., et al. (2018). Immunomodulatory effects of black soldier fly larvae meal in broilers. *Poultry Science*, 97(7), 2378-2385.
Lemme, A., Ravindran, V., & Bryden, W. L. (2004). Methionine as the first limiting amino acid in poultry diets. *World's Poultry Science Journal*, 60(2), 207-224.
Mahmoud, M., & Ravindran, V. (2025). Standardized ileal amino acid digestibility of black soldier fly prepupae meal in broilers. *Poultry Science*, 104(3), 104567.
Makkar, H. P., Tran, G., Heuzé, V., & Ankers, P. (2014). State-of-the-art on use of insects as animal feed. *Animal Feed Science and Technology*, 197, 1-33.
Matin, N., Utterback, P., & Parsons, C. M. (2021). Standardized ileal amino acid digestibility of insect meals in cecectomized roosters. *Poultry Science*, 100(7), 101189.
Nyangena, D. N., et al. (2020). Nutritional composition of black soldier fly larvae reared on different substrates. *Journal of Insects as Food and Feed*, 6(4), 361-370.
Ravindran, V., & Bryden, W. L. (1999). Amino acid digestibility in poultry: A review. *Australian Journal of Agricultural Research*, 50(5), 787-802.
Rumpold, B. A., & Schlüter, O. K. (2013). Nutritional composition and safety aspects of edible insects. *Molecular Nutrition & Food Research*, 57(5), 802-823.
Schiavone, A., et al. (2017). Nutritional value of partially defatted black soldier fly larvae meal for broiler chickens. *Journal of Animal Science and Biotechnology*, 8(1), 1-9.
Surendra, K. C., Olivier, R., Tomberlin, J. K., Jha, R., & Khanal, S. K. (2016). Bioconversion of organic wastes into biodiesel and animal feed via black soldier fly. *Renewable Energy*, 98, 197-202.
Tacon, A. G., & Metian, M. (2008). Global overview on the use of fish meal and fish oil in industrially compounded aquafeeds. *Aquaculture*, 285(1-4), 146-158.
Van Huis, A. (2013). Potential of insects as food and feed in assuring food security. *Annual Review of Entomology*, 58, 563-583.
Van Huis, A., Van Itterbeeck, J., Klunder, H., Mertens, E., Halloran, A., Muir, G., & Vantomme, P. (2013). Edible insects: Future prospects for food and feed security. FAO Forestry Paper 171.
Wayne, A., Ravindran, V., & Bryden, W. L. (2010). Endogenous amino acid losses in poultry. *World's Poultry Science Journal*, 66(3), 451-460.
Wu, G., et al. (2013). Nonessential amino acids in poultry nutrition. *Amino Acids*, 45(3), 421-434.

CURRENT APPROACHES TO THE VALORIZATION OF FERMENTED FOOD BY-PRODUCTS FOR FUNCTIONAL PRODUCT DEVELOPMENT

Ebru Isitmezoglu[1], Muge Uyarcan[2]

[1] Fersan Fermentation R&D Center, İzmir, Türkiye
[2] Manisa Celal Bayar University, Faculty of Engineering and Natural Sciences, Department of Food Engineering, Yunusemre/Manisa, Türkiye
Corresponding author e-mail: ebru.isitmezoglu@fersan.com.tr

ABSTRACT

Rapid population growth, uncontrolled industrial expansion, and changing consumption patterns have led to a significant increase in food industry waste, making it one of the most critical challenges threatening environmental and economic sustainability globally. This ecological crisis has necessitated minimizing food processing waste and reintegrating it into the economy through value-added applications, thereby highlighting the concepts of the circular bioeconomy, biorefineries, and green technology approaches. Solid and liquid by-products generated during the industrial production of fermented products, particularly wine, beer, dairy, soy, vinegar, and kombucha, exhibit remarkable functional and therapeutic potential owing to their high-value biological constituents, including proteins, free amino acids, polyphenolic antioxidants, and prebiotic oligosaccharides. To recover these bioactive compounds from cellular matrices while preserving their natural structural integrity, next-generation green technologies, such as ultrasound-assisted extraction, microwave-assisted extraction, supercritical fluid systems, and solid-state fermentation, have been widely employed. These recovered, or microbially resynthesized functional compounds can be utilized in a wide range of applications within the food, materials, biomedical, and healthcare sectors as antimicrobial preservatives capable of suppressing pathogenic microorganisms and cellular signaling mechanisms, nanotechnologically encapsulated nutraceuticals, active and intelligent packaging films, and biodegradable polymers (PLA/PHA) serving as sustainable alternatives to petrochemical-based materials. Fermented food by-products have also been successfully incorporated into functional foods, with brewer's spent grain being used in bread, pasta, and snack formulations and cheese whey being utilized in functional and sports beverages. These innovative valorization strategies not only drastically reduce the organic load associated with Chemical Oxygen Demand (COD) and Biological Oxygen Demand (BOD), thereby mitigating environmental impacts, but also provide promising solutions for producing functional products that support human health at the molecular level. Accordingly, this article reviews the most recent advances in the utilization of fermented food by-products as a source of bioactive compounds, the green technologies employed for their recovery, and their potential applications in functional product development.

Keywords: Fermented food by-product, Functional products, Fermentation, Sustainability, Valorization.

INTRODUCTION

Rapid population growth, uncontrolled industrial expansion, and changing consumption patterns have led to a significant increase in solid waste and by-products within the food industry, making sustainable waste management a critical global issue. The inadequacy of

current waste management policies results in a large portion of this organic biomass being released into nature as an environmental burden or incurring high disposal costs (Chetrariu and Dabija, 2020; Verma et al., 2021). However, modern biorefinery systems and circular bioeconomy approaches enable food processing wastes to be evaluated beyond the traditional concept of waste, transforming these resources into valuable raw materials that can be utilized in the production of high-value-added functional components, bioactive molecules, and sustainable biomaterials (Camargo et al., 2022; Faria et al., 2023). In this context, preventing biomass waste and converting wastes into functional products both serve sustainable development goals and offer innovative solutions to the food and pharmaceutical industries (Naibaho et al., 2025; Topi et al., 2025).

With a deep-rooted history and wide application in the food industry, the fermentation sector generates high amounts of organic by-products in direct proportion to the magnitude of its production volume (Swetha et al., 2023; Woraprayote et al., 2023). Pomace, peels, sediments, and wastewaters generated during the production of products such as wine, beer, fermented milk, fermented fruits and vegetables, vinegar, and kombucha constitute a significant source of valuable components such as secondary metabolites, proteins, dietary fiber, and fermentable sugars (Lac et al., 2024; Aradwad et al., 2025). Traditionally considered to have low added value and used primarily as animal feed or fertilizer, these byproducts are now emerging as valuable sources to produce nutraceuticals and bioactive peptides, which promote human health and reduce the risk of various diseases (Lopes et al., 2025).

Within the fermented food industry, the valorization of by-products originating specifically from wine and beer production into high-added-value components has become one of the research fields receiving intense interest in recent years. Grape pomace, peels, seeds, and sediments generated during industrial wine production contain high proportions of phenolic compounds with antioxidant and cardioprotective properties, such as anthocyanins, catechins, and proanthocyanidins (Suescun-Ospina et al., 2023; Constantin et al., 2024; Cánovas et al., 2025). Similarly, spent yeasts and malt rootlets generated during beer production are by-products rich in bioactive peptides, beta-glucans, and flavor-enhancing nucleotides that hold potential for use in functional food formulations (Halahlah et al., 2025; Couto et al., 2026; Soto-Maldonado et al., 2026). On the other hand, cheese whey, a major by-product of cheese manufacturing, not only serves as a valuable source for the recovery of bioactive proteins but can also be utilized as a carbon source in the microbial production of biodegradable bioplastics such as polyhydroxyalkanoates (Mota et al., 2026).

With rising consumer demands in recent years, studies focusing on the conversion of by-products generated during the production of fermented products, such as kombucha and vinegar, into high-added-value components have also gained importance (Maske et al., 2026). Cellulosic biofilm and acidic liquid by-products derived from kombucha production are utilized in the development of innovative functional products across a wide range of areas, from food packaging applications to the production of biomedical products (Vianna et al., 2025; Hartono et al., 2026). Similarly, by-products such as okara formed as a result of soy fermentation hold significant potential in the development of value-added food products thanks to their compositions rich in various bioactive phytochemicals and prebiotic dietary fibers (Zhou et al., 2019).

Ensuring the efficient recovery of bioactive compounds found in fermented food by-products while preserving their properties largely depends on the efficiency of the applied extraction and purification technologies. In this context, recent studies show that environmentally friendly and high-efficiency processes such as green synthesis approaches, ultrasound- and microwave-assisted extraction, supercritical fluid technologies, and solid-state fermentation are coming to the forefront as alternatives to conventional chemical methods that require high temperatures or the use of toxic solvents (Eche et al., 2025; Mia et al., 2025; Garzón et al., 2026).

Furthermore, utilizing nanotechnological carrier systems to enhance the bioavailability and stability of the recovered compounds stands out among current approaches in this field (Zhu et al., 2024; Mirzakulova et al., 2025). Among other applications, as a key component of holistic biorefinery approaches, the conversion of fermented food by-products into functional food ingredients, bioenergy sources and innovative agricultural products, such as feed additives aimed at reducing methane emissions, is also receiving notable attention (Selmi et al., 2025; Mato et al., 2026).

In this review, current recovery strategies, technological advancements, and application areas aimed at converting fermented food by-products into high-added-value products are discussed. Furthermore, the potential of these by-products for use in the development of functional products has been evaluated in terms of sustainable waste management and the circular bioeconomy, and future perspectives have been evaluated.

FERMENTED FOOD BY-PRODUCTS

Within the fermentation sector, one of the largest-volume subsectors of the global food industry ecosystem, millions of tons of organic waste and by-products are generated annually depending on the scale of production capacity. In sustainable waste management and circular economy approaches, these residues are evaluated differently than unprocessed traditional agricultural waste. The primary reason for this is that these by-products undergo controlled microbial bioprocesses, during which they are biochemically modified by the metabolic activities of microorganisms, acquiring a more stable and complex matrix structure (Chetrariu and Dabija, 2020; Eche et al., 2025). Based on the operational outputs of production processes, fermented food by-products are classified into two main groups: solid fractions, such as pomace, spent grain, sediments, and microbial biomass, and liquid phases, such as cheese whey, acidic waters, and post-fermentation liquids. These by-products are rich in high-quality proteins, free amino acids, soluble and insoluble dietary fibers, and microbial secondary metabolites making them an important raw material source for the recovery of high-added-value components in advanced biorefinery processes (Zhou et al., 2019; Mia et al., 2025).

When the distribution of fermented food by-products is examined according to industrial sources, the alcoholic and non-alcoholic fermented beverage sectors stand out in terms of volume. Brewer's spent grain and brewer's yeast, which are the primary by-products of brewing processes, rank among important biomass sources for the recovery of high-added-value components due to their compositions rich in lignocellulosic fibers and highly digestible microbial proteins (Naibaho et al., 2025; Couto et al., 2026; Soto-Maldonado et al., 2026). In the wine industry, grape pomace (including skins, seeds, and stalk residues) generated during the maceration and primary fermentation stages, alongside wine lees settled at the tank bottoms, are extensively discussed in the literature as fermented by-products rich in plant secondary metabolites, particularly phenolic compounds (Suescun-Ospina et al., 2023; Lopes et al., 2025; Topi et al., 2025). Regarding animal-derived fermented food by-products, the dairy industry constitutes a significant source. Particularly, cheese whey and acidic process waters generated from cheese and strained yogurt production possess significant potential for bioconversion and recovery processes thanks to their high-quality serum proteins (alpha-lactalbumin, beta-lactoglobulin) and lactose contents (Mirzakulova et al., 2025; Selmi et al., 2025; Mota et al., 2026). In plant-based fermentation processes, okara, a by-product of soybean processing; vinegar production by-products; and microbial biofilms formed during kombucha production stand out for their prebiotic oligosaccharide content, organic acid profiles, and high bacterial cellulose content, respectively. These unique compositional characteristics enable the utilization of these by-products as valuable raw material sources in functional product design (Zhou et al., 2019; Maske et al., 2024; Vianna et al., 2025; Hartono et al., 2026).

RECOVERY STRATEGIES FOR FERMENTED FOOD BY-PRODUCTS

The utilization of bioactive and functional components present in the composition of fermented food by-products in the formulations of value-added products depends on the effective separation of these components from complex cellular and polymeric structures without disrupting their integrity. In conventional extraction methods, the prolonged use of high temperatures and toxic organic solvents

causes the denaturation of temperature-sensitive phenolic compounds, the cleavage of peptide bonds, and a decrease in overall process efficiency. To overcome these disadvantages caused by conventional methods, focus has shifted toward innovative green technologies such as ultrasound- and microwave-assisted extraction systems and supercritical fluid technologies that aim to increase process efficiency while reducing environmental impacts. These advanced approaches shorten the processing time by facilitating the release of target bioactive components from the matrix into the solvent, while simultaneously minimizing energy consumption and waste generation derived from toxic chemical solvents (Swetha et al., 2023; Naibaho et al., 2025).

When the mechanisms of action of the innovative green extraction technologies are examined, it is stated that ultrasound-assisted extraction accelerates the mass transfer of bioactive compounds by mechanically disrupting cellular structures through cavitation waves generated in the liquid medium. In the literature, it is reported that this method has been successfully applied in the high-yield recovery of polyphenolic compounds with antioxidant properties from winemaking by-products (Constantin et al., 2024). Microwave-assisted extraction, based on the principle of electromagnetic heating, rapidly heats the water molecules within the target matrix, increasing intracellular pressure and causing the cell wall to rupture from the inside out. It is noted that this specific method significantly shortens the extraction time in obtaining functional compounds from lignocellulosic fermented by-products with complex structures, such as brewer's spent grain (Aradwad et al., 2025). On the other hand, supercritical fluid extraction offers a highly selective process without leaving toxic solvent residues or causing thermal degradation, primarily using carbon dioxide in a state above its critical temperature and pressure values. It is anticipated that this advanced technology is also considered one of the most promising green strategies for isolating high-purity and value-added nutraceutical components from fermented food industry by-products (Naibaho et al., 2025).

In addition to physical and chemical extraction methods, the direct application of biotechnological processes to fermented by-products is considered to play a significant role in recovery procedures. In this context, solid-state fermentation stands out as one of the primary approaches employed in the re-fermentation of solid fermented by-products with low water activity using specific mold or bacterial strains. During the solid-state fermentation process, it is reported that microorganisms secrete extracellular enzymes that hydrolyze cellulose, hemicellulose, and lignin complexes within the by-product matrix; thereby converting conjugated phenolic compounds bound to the plant cell wall into their free forms, significantly increasing the biological activity and antioxidant capacity of the material (Verma et al., 2021; Garzón et al., 2026). Since these functional hydrolysates and liquid extracts obtained through microbial or enzymatic processes exhibit structures sensitive to environmental factors, they are stabilized using micro/nanoencapsulation and nanotechnological carrier matrices to prevent potential oxidative or thermal degradation that may occur during the storage and end-use stages. It is stated that thanks to these applied protective systems, bioactive compounds can be successfully converted into final raw material forms suitable for industrial use (Mirzakulova et al., 2025; Mota et al., 2026).

APPLICATION OF FERMENTED FOOD BY-PRODUCTS

Today, complex organic by-products generated by high-volume production processes in the fermented food industry are being utilized in various industrial application within the framework of the circular bioeconomy, owing to their rich bioactive components (Chetrariu and Dabija, 2020; Eche et al., 2025). Broadly, these by-products have a wide utilization potential in areas such as the development of biodegradable packaging films, production of functional foods with enhanced nutritional value, renewable energy-focused biofuel production, active packaging technologies, recovery of antimicrobial components against foodborne pathogens and spoilage microorganisms, and biofilm control. Among these application areas, functional product development approaches hold a significant place; by utilizing the by-products in pasta, muffins, snacks, anthocyanin-rich kombucha-like beverages, and cheese whey-based sports drinks, the protein, dietary fiber, antioxidant, and mineral contents of the products can be enriched (Cánovas et al., 2025; Couto et al., 2026; Eche et al., 2025; Mirzakulova et al., 2025). On the other hand, by-products such as brewer's spent grain, which is rich in lignocellulosic fiber, and brewer's spent yeast, which is a microbial protein source, are

evaluated as valuable industrial raw materials not only in food formulations but also in biofuel production in line with sustainable clean energy goals (Couto et al., 2026). The utilization of fermented food by-products in materials technology also constitutes an important research area. High-added-value components obtained from these by-products through recovery and bioconversion strategies are also considered significant raw material sources in the development of bio-based and biodegradable packaging materials as alternatives to petroleum-based synthetic plastics. In this context, polylactic acid and polyhydroxyalkanoate-based biopolymers, which are obtained through the bioconversion of carbon sources recovered from by-products, can be used as matrices in the production of packaging materials with lower environmental impacts (Swetha et al., 2023; Selmi et al., 2025). In active packaging applications, antimicrobial peptides and polyphenol-rich antioxidant fractions recovered from fermented food by-products can be integrated into different packaging matrices to impart functional properties. By ensuring the controlled release of bioactive compounds onto the food contact surface, these systems contribute to the limitation of microbial growth and lipid oxidation, thereby offering significant potential for preserving food quality and extending shelf life (Vianna et al., 2025; Mota et al., 2026).

In addition to packaging applications, antimicrobial components recovered from fermented food by-products can also be utilized directly in foods as natural preservatives. In particular, the recovery of antimicrobial metabolites such as bacteriocins, organic acids, and hydrogen peroxide produced by lactic acid bacteria during fermentation from liquid by-products offers significant potential in terms of natural preservation strategies aimed at controlling the growth of foodborne pathogens (Woraprayote et al., 2023). The antimicrobial effects of these metabolites can emerge not only through direct mechanisms, such as the disruption of cell membrane integrity, but also through the suppression of the quorum sensing system, which regulates intercellular communication among bacteria, by certain components. The suppression of the quorum sensing mechanism can affect the expression of genes associated with virulence and biofilm formation, thereby limiting the ability of pathogens to adhere to surfaces and form protective biofilms (Zhu et al., 2024). Consequently, it is considered that contamination risks that may arise in food matrices can be successfully brought under control by means of these biological components without the need for chemical and synthetic preservatives.

FERMENTED FOOD BY-PRODUCTS IN FUNCTIONAL PRODUCT DEVELOPMENT

Fermented food by-products constitute a significant source for functional product development due to their content of nutritional and bioactive components such as proteins, dietary fiber, phenolic compounds, vitamins, and minerals (Aradwad et al., 2025; Mia et al., 2025). The incorporation of industrial by-products such as brewer's spent grain, grape pomace, and cheese whey into various food formulations improves the nutritional value of the products and imparts or enhances functional attributes such as antioxidant properties (Cánovas et al., 2025; Eche et al., 2025; Mirzakulova et al., 2025; Couto et al., 2026). While this approach allows for the development of novel products with enhanced nutritional and functional properties, it also contributes to the conversion of by-products generated in the food industry into value-added components (Mia et al., 2025). Table 1 presents recent studies on the utilization of these by-products in different product categories, including baked goods, snacks, and fermented beverages.

Table 1. Recent studies evaluating the utilization of fermented food by-products in functional product development

Functional Food Product	**Fermented Food By-product**	**Application Purpose**	**Results**	**References**
Anthocyanin-rich, kombucha-like fermented functional beverage	Wine lees and grape pomace	To evaluate the applicability of winemaking by-products (grape pomace and wine lees) as raw materials in the development of kombucha-like functional beverages.	The addition of wine lees contributed to increasing the antioxidant capacity by elevating the anthocyanin content of the functional beverage. Furthermore, it ensured the preservation of the microbial and physicochemical stability of the product during a 21-day storage period.	Cánovas et al. (2025)
Functional baked goods (muffins)	Brewer's spent grain (BSG)	To investigate the effects of different drying methods on the chemical composition, physicochemical properties, and bioactive compounds of BSG, and to evaluate the quality and consumer acceptance of BSG-fortified muffins.	The incorporation of 15% BSG flour yielded a 22.59% increase in total dietary fiber and a 13% increase in protein without affecting consumer acceptance.	Shih et al. (2020)
Functional baked goods (pasta)	Brewer's spent grain (BSG)	To evaluate the properties of bioprocessed BSG as an ingredient for pasta formulation and to verify its nutritional and antioxidant properties.	The 15% utilization of bioprocessed BSG increased protein digestibility (from approximately 76.22% to 88.52%) and lowered the predicted glycemic index.	Schettino et al. (2021)
Functional baked goods (bread)	Brewer's spent grain	To evaluate the effects of partially replacing wheat flour with brewers' spent grain on dough properties, bread quality, and nutritional value.	It has been reported that adding spent brewer's grain to bread formulations at a 10% rate contributes to improving nutritional properties by reducing the product's energy value from 225 kcal to 204–216 kcal, while increasing the	Czubaszek et al. (2022)

			dietary fiber content per 100 g of product from approximately 5 g to 10 g and the protein content from 13.4 g to 15 g.	
Functional and prebiotic beverages	Whey	To develop a functional beverage using whey protein isolate, inulin, and fruit juice concentrates, and to evaluate the bioactive properties of the obtained product.	Within the scope of evaluating whey, a liquid fermented food by-product, in the production of functional beverages, formulations containing 5% whey protein isolate, 4% inulin, and 10% fruit juice concentrate (apple, raspberry, or cranberry) were developed. It was reported that following digestion, the ACE (angiotensin-converting enzyme) inhibitory activity of these formulations reached 78.63%, and the DPPH radical scavenging activity reached 74.83%. Furthermore, they demonstrated antimicrobial activity by forming inhibition zones of up to 29.46 mm against pathogenic microorganisms.	Kotsaki et al. (2025)

As evident from the table, each waste material has a unique application area and imparts distinct value to the product. While cheese whey provides an ideal base for sports beverages owing to its liquid form and composition, brewer's spent grain is a highly effective source of fiber in solid form baked goods such as bread and pasta (Eche et al., 2025; Mirzakulova et al., 2025). Beverages derived from grape pomace, on the other hand, are developed for consumers who prefer antioxidant-rich products (Cánovas et al., 2025). At this point, the major challenge facing manufacturers is preserving the sensory quality of foods, as the conventional taste, texture, and aroma of the foods to which by-products are added may undergo changes (Eche et al., 2025; Couto et al., 2026). Determining the correct inclusion ratios and developing appropriate formulations are critical steps in consumer acceptance of these novel products (Eche et al., 2025).

SUSTAINABILITY AND FUTURE PERSPECTIVES OF FERMENTED FOOD BY-PRODUCT MANAGEMENT

The valorization of fermented food by-products in integrated biorefinery systems is of great importance in terms of the efficient utilization of industrial resources and the mitigation of the environmental impacts of food production. In particular, the discharge of cheese whey, acidic process waters, and other liquid by-products which possess a high organic load alongside high

chemical and biochemical oxygen demand into receiving environments without adequate treatment can lead to significant environmental problems in aquatic ecosystems, such as eutrophication, a reduction in dissolved oxygen levels, and the disruption of ecological balance (Selmi et al., 2025; Topi et al., 2025). In contrast, the recovery of these by-products via advanced biotechnological processes and their conversion into functional components, biopolymers, or biofuels not only alleviates the environmental and economic burden stemming from waste management but also contributes to the generation of value-added products and the attainment of circular economy objectives. Furthermore, studies based on life cycle assessments demonstrate that converting fermented food by-products into value-added products can, under appropriate process conditions, contribute to reducing greenhouse gas emissions and the overall environmental impacts of food production systems (Chetrariu and Dabija, 2020; Eche et al., 2025).

In the future, more effective utilization of metabolic engineering and artificial intelligence-supported bioprocess technologies is anticipated in the valorization of fermented food by-products. Microorganisms developed through genetic modification and targeted adaptation techniques could enable the high-yield conversion of complex carbon sources found in by-products into targeted functional components. Accordingly, the development of next-generation industrial strains aimed at the valorization of different by-products stands out as a prominent research area (Mia et al., 2025; Selmi et al., 2025). Furthermore, the development of smart encapsulation systems for the protection and controlled release of bioactive components is among the approaches that may gain significance in the future. Moreover, the utilization of biomaterials such as kombucha bacterial cellulose produced during the fermentation process carries substantial potential for the development of innovative products in the packaging and biomedical fields (Vianna et al., 2025; Hartono et al., 2026). Nevertheless, to transfer these approaches from laboratory and pilot scales to industrial production, provided that technical limitations related to scaling up are overcome, the economic viability of the processes is demonstrated, and standards concerning biosafety and regulatory frameworks are established, it can be stated that the biotechnological recovery of fermented food wastes will significantly contribute to global sustainability goals.

CONCLUSIONS

Fermented food by-products are not merely environmental concerns that requires disposal; they are considered high-potential raw material sources for the food industry due to their rich bioactive compounds. Approaches such as advanced green extraction techniques, solid-state fermentation, and enzymatic hydrolysis enable the recovery and bioconversion of valuable components from complex fermented matrices, allowing these by-products to be utilized as value-added resources in food, packaging, biofuel, and biotechnological applications. While contributing to the reintegration of fermented food by-products into the production cycle and the more efficient use of resources, this multifaceted valorization approach supports waste reduction, and the establishment of a sustainable value chain based on a zero-waste approach within the food supply chain. Consequently, it is anticipated that industrial upscaling efforts supported by process optimization, current legal regulations, and academia-industry collaborations will promote the widespread conversion of fermented food by-products into value-added products, thereby making significant contributions to the achievement of circular bioeconomy goals.

REFERENCES

Aradwad, P., Raut, S., Abdelfattah, A., Rauh, C., & Sturm, B. 2025. Brewer's spent grain: Unveiling innovative applications in the food and packaging industry. Comprehensive Reviews in Food Science and Food Safety, 24(3), e70150.

Camargo, D. A., Pereira, M. S., dos Santos, A. G., & Fleuri, L. F. 2022. Isolated and fermented orange and grape wastes: Bromatological characterization and phytase, lipase and protease source. Innovative Food Science & Emerging Technologies, 77, 102978.

Cánovas, B. M., Pérez-Novas, I., García-Viguera, C., Domínguez-Perles, R., & Medina, S. 2025. Assessment of Winery By-Products as Ingredients as a Base of "3S"(Safe, Salubrious, and Sustainable) Fermented Beverages Rich in Bioactive Anthocyanins. Foods, 14(14), 2514.

Chetrariu, A., & Dabija, A. 2020. Brewer's spent grains: Possibilities of valorization, a review. Applied Sciences, 10(16), 5619.

Constantin, O. E., Stoica, F., Rațu, R. N., Stănciuc, N., Bahrim, G. E., & Râpeanu, G. 2024. Bioactive components, applications, extractions, and health benefits of winery by-products from a circular bioeconomy perspective: A review. Antioxidants, 13(1), 100.

Couto, G. H., Bortolini, D. G., Hernandes, E. E., Hashimoto, E. H., Boettcher, D. L., Rodrigues, S. Á., ... & Pagnoncelli, M. G. B. 2026. Upcycling of Beer Processing Residues: Insights for Microbreweries Sustainability. ACS omega, 11(4), 4918-4939.

Czubaszek, A., Wojciechowicz-Budzisz, A., Spychaj, R., & Kawa-Rygielska, J. 2022. Effect of added brewer's spent grain on the baking value of flour and the quality of wheat bread. Molecules, 27(5), 1624.

Eche, V., Emenike, C. U., & Rupasinghe, H. V. 2025. Nutritional value of brewer's spent grain and consumer acceptance of its value-added food products. Foods, 14(16), 2900.

Faria, D. J., Carvalho, A. P. A. D., & Conte-Junior, C. A. 2023. Valorization of fermented food wastes and byproducts: Bioactive and valuable compounds, bioproduct synthesis, and applications. Fermentation, 9(10), 920.

Garzón, A. G., Pavón, Y., Aquino, M. E., & Drago, S. R. 2026. Valorization of brewing by-products: obtaining flavor-enhancing and antioxidant compounds from spent yeast. Sustainable Food Technology.

Halahlah, A., Abdessamie, K., Peltonen, S., & Thao, H. M. 2025. A review of innovative approaches to valorizing brewing by-products for food applications and consumer perceptions. Sustainable Food Technology.

Kotsaki, P., Aspri, M., & Papademas, P. 2025. Novel whey fermented beverage enriched with a mixture of juice concentrates: Evaluation of antimicrobial, antioxidant, and angiotensin I converting enzyme inhibitory (ACE) activities before and after simulated gastrointestinal digestion. Microorganisms, 13(7), 1490.

Lopes, J. D. C., Madureira, J., Margaça, F. M., & Cabo Verde, S. 2025. Grape pomace: A review of its bioactive phenolic compounds, health benefits, and applications. Molecules, 30(2), 362.

Maske, B. L., Ruiz, I., Vale, A. D. S., Sampaio, V. D. M., El Kadri, N. K., Soccol, C. R., & Pereira, G. V. 2024. Predicting the Microbiome and Metabolome Dynamics of Natural Apple Fermentation Towards the Development of Enhanced Functional Vinegar. Fermentation, 10(11), 552.

Mia, M. S., Ahmed, M. M., & Zzaman, W. 2025. Valorization of food waste into functional ingredients supports a sustainable strategy for the food industry. Discover Food, 5(1), 275.

Mirzakulova, A., Sarsembaeva, T., Suleimenova, Z., Kowalski, Ł., Gajdzik, B., Wolniak, R., & Bembenek, M. 2025. Whey: Composition, Processing, Application, and Prospects in Functional and Nutritional Beverages—A Review. Foods, 14(18), 3245.

Mota, J., Moura-Alves, M., Teixeira, A. F., Nóbrega, R., Lameirão, D., & Gonçalves, C. 2026. From Cheese Whey to Functional Ingredients: Upcycling Whey Proteins for Cardiovascular and Immunomodulatory Health—Evidence Mapping and Perspectives from Portugal. Foods, 15(5), 908.

Naibaho, J., Korzeniowska, M., Phimolsiripol, Y., & Gavahian, M. 2025. Value-added compounds from brewers' spent grain to develop bioactive-enriched food ingredients: Recent advances in sustainable extraction and considerations for industrial application. Food Bioscience, 107351.

Lac, D. H., Le Tan, N. T., & Nguyen, D. Q. 2024. Valorization of Fermentation Waste: Eco-Friendly Synthesis of Antimicrobial Bacterial Cellulose-Silver Nanocomposites Using Post-Fermentation Solution as a Reducing Agent. Chemical Engineering Transactions, 113, 277-282.

Schettino, R., Verni, M., Acin-Albiac, M., Vincentini, O., Krona, A., Knaapila, A., ... & Coda, R. 2021. Bioprocessed brewers' spent grain improves nutritional and antioxidant properties of pasta. Antioxidants, 10(5), 742.

Selmi, H., Presutto, E., Spano, G., Capozzi, V., & Fragasso, M. 2025. Valorising Whey: From Environmental Burden to Bio-Based Production of Value-Added Compounds and Food Ingredients. Foods, 14(21), 3646.

Shih, Y. T., Wang, W., Hasenbeck, A., Stone, D., & Zhao, Y. 2020. Investigation of physicochemical, nutritional, and sensory qualities of muffins incorporated with dried brewer's spent grain flours as a source of dietary fiber and protein. Journal of Food Science, 85(11), 3943-3953.

Soto-Maldonado, C., Espinosa, A., Bucarey, J. L., & Fuentes, L. 2026. Functional Benefits of Brewer's Spent Grain and the Challenge of Developing Food Ingredients for Human Health. Antioxidants, 15(2), 247.

Suescun–Ospina, S. T., Ávila–Stagno, J., Vera-Aguilera, N., Astudillo-Neira, R., Trujillo-Mayol, I., & Alarcón-Enos, J. 2023. Effects of drying method on bioactive compounds contents, rumen fermentation parameters and in vitro methane output of waste dried País grape (Vitis vinifera L.) marc. Food Bioscience, 51, 102154.

Swetha, T. A., Ananthi, V., Bora, A., Sengottuvelan, N., Ponnuchamy, K., Muthusamy, G., & Arun, A. 2023. A review on biodegradable polylactic acid (PLA) production from fermentative food waste-Its applications and degradation. International Journal of Biological Macromolecules, 234, 123703.

Topi, D., Arapi, D., & Seiti, B. 2025. Vine Pruning Residues and Wine Fermentation By-Products: A Non-Exploited Source of Sustainable Agriculture, Albania Case. Resources, 14(2), 29.

Verma, N., Kumar, V., & Bansal, M. C. 2021. Valorization of waste biomass in fermentative production of cellulases: a review. Waste and Biomass Valorization, 12(2), 613-640.

Vianna, N. D. M., Albagli, G., Pereira, A. D. S., & Amaral, P. F. 2025. From Tea Fermentation to New Technologies: Multisectoral Applications of Kombucha SCOBY Through the Lens of Methodi Ordinatio. Fermentation, 11(10), 589.

Woraprayote, W., Janyaphisan, T., Adunphatcharaphon, S., Sonhom, N., Showpanish, K., Rumjuankiat, K., ... & Petchkongkaew, A. 2023. Bacteriocinogenic lactic acid bacteria from Thai fermented foods: potential food applications. Food Bioscience, 52, 102385.

Zhou, R., Ren, Z., Ye, J., Fan, Y., Liu, X., Yang, J., ... & Li, J. 2019. Fermented soybean dregs by neurospora crassa: a traditional prebiotic food. Applied Biochemistry and Biotechnology, 189(2), 608-625.

Zhu, L., Li, J., Yang, J., Li, X., Lin, D., & Wang, M. 2024. Fermentation broth from fruit and vegetable waste works: Reducing the risk of human bacterial pathogens in soil by inhibiting quorum sensing. Environment International, 188, 108753.

COMBINED TOXICITY OF MICROPLASTICS AND CHEMICAL POLLUTANTS IN AQUATIC ORGANİSMS

Duygu Özhan TURHAN

Department of Biology, Faculty of Arts and Science, Inonu University, Malatya 44280, Turkey

duygu.turhan@inonu.edu.tr

ABSTRACT

Microplastics are widespread contaminants in aquatic ecosystems and have received increasing attention in recent years due to their potential environmental impacts. In aquatic environments, microplastics do not occur in isolation but coexist with heavy metals, pesticides, pharmaceuticals, and various organic contaminants. Their large surface area and physicochemical properties facilitate the adsorption of different chemicals onto their surfaces, raising concerns about their potential role in modifying the transport, bioavailability, and toxicity of coexisting pollutants.

This review aims to evaluate the toxicological effects of combined exposure to microplastics and chemical pollutants in aquatic organisms. Available evidence indicates that interactions between microplastics and heavy metals, pesticides, pharmaceuticals, and other organic contaminants may vary depending on polymer type, particle size, surface characteristics, aging processes, and the physicochemical conditions of the surrounding environment. Combined exposures have been associated with oxidative stress, alterations in antioxidant defense systems, neurotoxic and genotoxic responses, as well as adverse effects on growth, development, reproduction, and behavior. However, the influence of microplastics on the toxicity of coexisting chemicals is not uniform. Depending on the properties of the contaminant, microplastic characteristics, exposure duration, and concentration, combined exposure may result in synergistic, antagonistic, or additive effects.

Overall, interactions between microplastics and chemical pollutants represent an important factor that may modify the biological effects of contaminants in aquatic ecosystems. Considering combined effects alongside the toxicity of individual pollutants in environmental risk assessment may provide a more realistic understanding of exposure scenarios occurring in natural aquatic environments.
Keywords: microplastics, combined toxicity, aquatic organisms, environmental pollutants, ecotoxicology

INTRODUCTION

1. Definition and Environmental Formation of Microplastics

Plastic products are widely used in applications ranging from daily life to industry due to advantageous properties such as light weight, durability, versatility, and low production cost. However, the rapid increase in plastic use and the long-term persistence of the resulting plastic waste in the environment have made plastic pollution an important global environmental problem. Plastic materials entering the environment can fragment over time into smaller plastic particles under the influence of physical, chemical, and biological processes. Microplastics

(MPs) are generally defined as synthetic polymer particles with an upper size limit of 5 mm, although there is no definitive consensus regarding the lower size limit. Furthermore, the continued fragmentation of microplastics under environmental conditions may lead to the formation of nanoscale plastic particles (Li et al., 2018).

2. Environmental Transport and Distribution of Microplastics

Certain characteristics of microplastics, such as their light weight, diverse morphologies, and extremely long lifespans, contribute substantially to their transport between environmental compartments. These properties also make microplastics one of the most widespread pollutants worldwide. Nearly all plastics and plastic-derived materials are produced on land and enter different environments through various pathways. In most scenarios, land acts as the initial receiving compartment for microplastics, which subsequently enter the environment through direct littering, improper waste management, accidental losses during disposal, and industrial spills (Horton & Dixon, 2018).

3. Physicochemical Properties of Microplastics and Their Role as Chemical Carriers

An important chemical characteristic common to microplastics is their capacity to adsorb and accumulate environmental pollutants, including heavy metals and organic contaminants. Moreover, microplastics contain various chemical additives, such as plasticizers and flame retardants, suggesting that they may act as both a “carrier” and a “source” of other chemicals. Microplastics are generally resistant to chemical reactions; however, exposure to UV radiation can induce photochemical degradation and lead to higher fragmentation rates. In addition, the hydrophobic properties of microplastics can determine their interactions within aquatic habitats and organisms. Consequently, microplastics exhibit distinctive environmental pollutant characteristics that influence their distribution, uptake, and toxicity in aquatic species (Hasan et al., 2024).

4. Biological Effects of Microplastics on Aquatic Organisms

The adverse effects of microplastics on fish reproduction have also become a growing concern. For example, microplastics may have serious consequences for the endocrine systems of fish. Plasticizers and various bisphenol analogues and phthalates, which are important endocrine disruptors, may leach from microplastics into the environment. These chemicals may mimic or induce hormonal imbalances, potentially leading to reduced fertility rates, alterations in offspring growth, or even changes in sex ratios (Hasan et al., 2024).

Huang et al. (2024) exposed juvenile *Carassius auratus* to different concentrations of polystyrene microplastics (PS-MPs; 200, 800, and 3200 µg/L) for 32 days and evaluated their effects on growth, tissue damage, and gene expression. PS-MPs were reported to accumulate particularly in the gastrointestinal tract and gills, and exposure resulted in varying degrees of histopathological damage in the intestine, gills, brain, and liver. In addition, the severity of tissue damage increased with increasing PS-MP concentration, and changes were detected in the expression of the genes examined in the liver, intestine, and gills (Huang et al., 2024).

5. Interactions of Microplastics with Organic Pollutants and Heavy Metals

According to previous studies, microplastics can act as carriers capable of adsorbing and enriching heavy metals as well as organic pollutants such as polycyclic aromatic hydrocarbons

(PAHs), polychlorinated biphenyls (PCBs), pharmaceuticals, and personal care products (PPCPs) from water or soil. Microplastics are highly mobile. After adsorbing organic pollutants, they may transport these contaminants to new environments and cause adverse effects (Zhang et al., 2023).

Microplastics can adsorb and accumulate various organic pollutants, including persistent organic pollutants such as polycyclic aromatic hydrocarbons (PAHs) and polychlorinated biphenyls (PCBs), as well as different heavy metals. The adsorption of heavy metals onto microplastic surfaces is influenced by several factors, including the physicochemical properties of the particles, surface modifications, aging, and environmental conditions (Ateia et al., 2022).

6. Interactions of Microplastics with Antimicrobials and Microorganisms

Various studies have investigated the adsorption and desorption behavior of antibiotics, particularly macrolides and quinolones, on different types of MPs, mainly polystyrene, polyethylene, and polylactic acid. To date, most studies have focused on the adsorption properties of pristine MPs, whereas desorption behavior has been investigated to a more limited extent. However, a large proportion of MPs present in the environment are aged. Once antibiotics are adsorbed by MPs, they can be transported along with the movement of MPs. Therefore, determining whether adsorbed antibiotics can desorb from microplastic surfaces is important for assessing the risks that these pollutants may pose in new environments (Zhang et al., 2023).

The co-occurrence of MPs and antimicrobials in the environment raises concerns regarding their combined ecological effects. Antimicrobials, which have substantially improved human and animal health and agricultural productivity, now frequently contaminate the environment through sources such as agricultural runoff and industrial discharges. For example, hydrophobic polymers such as polyethylene or polystyrene readily adsorb nonpolar antimicrobials, whereas charged or functionalized surfaces can bind ionizable antibiotics such as sulfonamides or tetracyclines. Their environmental presence not only poses ecological risks but also contributes to the proliferation of resistance genes (Tang, 2025).

7. Combined Toxicity of Pollutant Mixtures

Interactions between microplastics and coexisting pollutants may result in synergistic, antagonistic, or additive effects. When MPs carry other pollutants such as DBP, their large surface area may enable them to accumulate greater amounts of contaminants through an adsorptive carrier effect, thereby increasing toxicity. Conversely, MPs may reduce the bioavailability of pollutants through adsorption and enrichment, thereby decreasing their bioaccumulation. In addition, whether the interaction is synergistic or antagonistic may depend on MP concentration. Aggregation, disaggregation, and the corresponding exposure levels vary among different MP concentrations, which can result in inconsistent toxicity responses (Liang et al., 2025).

Turhan et al. (2026) evaluated the individual and combined effects of polyethylene microplastics (PE-MPs) and deltamethrin (DEL) during the early life stages of *Xenopus laevis*. PE-MPs alone did not cause marked mortality or malformations in embryos but induced changes in biochemical responses. Under combined exposure to DEL and PE-MPs, additive, antagonistic, and synergistic interactions were reported depending on the biomarker and developmental stage. In embryos, additive effects were observed for GST and CaE, antagonistic

effects for AChE, while the CAT response showed antagonistic or synergistic characteristics depending on the DEL concentration (Turhan et al., 2026).

The toxic effects of mixtures of MPs and hazardous chemicals may differ from the inherent toxicity of the individual substances depending on factors such as mixture concentration and ratio and interactions among the components. During the embryonic development of the amphibian *Rhinella arenarum*, non-toxic concentrations of copper and nonylphenol produced toxic effects depending on the mixture ratio (Aronzon et al., 2020). In *Daphnia magna* exposed to a mixture of silver ions and two different metal oxide nanoparticles, a synergistic effect greater than the toxic effects of the individual substances was confirmed (Park et al., 2019).

Liang et al. (2025) evaluated the combined toxicity of polypropylene microplastic fibers (MPFs) and dibutyl phthalate (DBP) in *Chlorella vulgaris*. Combined exposure was reported to cause more pronounced effects on photosynthesis, oxidative stress, and metabolism than individual exposures. In addition, the direction of combined toxicity changed depending on MPF concentration, with synergistic interactions at high MPF concentrations and antagonistic interactions at low MPF concentrations.

Wang et al. (2022) investigated the individual and combined toxic effects of polyvinyl chloride microplastics (PVC-MPs) and di(2-ethylhexyl) phthalate (DEHP) on *Danio rerio* embryos and larvae. The study used 0.1 ppm PVC-MPs and 71 µg/L DEHP, representing an environmentally relevant concentration. Individual exposure to PVC-MPs and DEHP inhibited embryo hatching, whereas this effect was reduced under combined exposure. Individual exposures also caused toxic effects on oxidative stress and cardiac development, while these effects were alleviated during combined exposure. The researchers reported an antagonistic interaction between PVC-MPs and DEHP and suggested that adsorption of DEHP by PVC-MPs, thereby reducing its bioavailability and bioaccumulation, may contribute to this antagonistic effect.

Zhang et al. (2022) showed that aged microplastics increased the accumulation of roxithromycin in *Carassius auratus* tissues in a microplastic size-dependent manner. Both aged microplastics and roxithromycin significantly increased superoxide dismutase (SOD) and catalase (CAT) activities in the liver and intestine while suppressing acetylcholinesterase (AChE) activity in the brain. In addition, smaller aged microplastics intensified roxithromycin-induced damage in the liver, gills, and brain, whereas larger microplastics caused more severe intestinal damage.

Similarly, in a 28-day study evaluating the combined effects of oxytetracycline and polystyrene microplastics on juvenile yellow catfish (*Pelteobagrus fulvidraco*), neither oxytetracycline nor 100 µg/L microplastics alone significantly affected growth, antioxidant and digestive enzyme activities, or intestinal microbial diversity. In contrast, combined exposure to oxytetracycline and 100 µg/L polystyrene microplastics increased SOD and CAT activities, caused mild intestinal damage, and increased the abundance of Proteobacteria (Tang, 2025).

CONCLUSION

The available evidence indicates that interactions between microplastics and chemical pollutants may significantly modify their toxic effects in aquatic organisms. Depending on microplastic characteristics, pollutant properties, concentration, and exposure conditions, combined exposure may result in synergistic, additive, or antagonistic effects. These interactions can influence oxidative stress, neurotoxicity, growth, development, and other

biological responses. Therefore, evaluating microplastics and chemical pollutants separately may not adequately reflect exposure scenarios in natural aquatic environments. Further studies using environmentally relevant concentrations and different microplastic–pollutant combinations are needed to better understand these complex interactions and to improve ecological risk assessment.

REFERENCES

Aronzon, C. M., Peluso, J., & Coll, C. P. (2020). Mixture toxicity of copper and nonylphenol on the embryo-larval development of *Rhinella arenarum*. Environmental Science and Pollution Research, 27, 13985–13994. https://doi.org/10.1007/s11356-020-07857-7

Ateia, M., Ersan, G., Alalm, M. G., Boffito, D. C., & Karanfil, T. (2022). Emerging investigator series: Microplastic sources, fate, toxicity, detection, and interactions with micropollutants in aquatic ecosystems—A review of reviews. Environmental Science: Processes & Impacts, 24(2), 172–195. https://doi.org/10.1039/D1EM00443C

Hasan, A. K. M. M., Hamed, M., Hasan, J., Martyniuk, C. J., Niyogi, S., & Chivers, D. P. (2024). A review of the neurobehavioural, physiological, and reproductive toxicity of microplastics in fishes. Ecotoxicology and Environmental Safety, 282, 116712.

Horton, A. A., & Dixon, S. J. (2018). Microplastics: An introduction to environmental transport processes. WIREs Water, 5, e1268. https://doi.org/10.1002/wat2.1268

Huang, Y., Li, W., Dong, K., Li, X., Li, W., & Wang, D. (2024). Effect of polystyrene microplastic exposure on individual, tissue, and gene expression in juvenile crucian carp (*Carassius auratus*). Fishes, 9, 385.

Li, J., Liu, H., & Chen, P. (2018). Microplastics in freshwater systems: A review on occurrence, environmental effects, and methods for microplastics detection. Water Research, 137, 362–374.

Liang, L., Liang, Y., Su, M., Wang, Z., Zhou, Z., Zhou, X., & Jiang, Z. (2025). Combined toxicity of microplastic fibers and dibutyl phthalate on algae: Synergistic or antagonistic? Aquatic Toxicology, 281, 107290.

Park, C. B., Jung, J. W., Baek, M., Sung, B., Park, J. W., Seol, Y., Yeom, D. H., Park, J. W., & Kim, Y. J. (2019). Mixture toxicity of metal oxide nanoparticles and silver ions on *Daphnia magna*. Journal of Nanoparticle Research, 21, 166. https://doi.org/10.1007/s11051-019-4606-2

Tang, K. H. D. (2025). Combined toxicity of microplastics and antimicrobials on animals: A review. Antibiotics, 14(9), 896.

Turhan, D. O., Benli, C. A., Yurekli, M., & Güngördü, A. (2026). The single and combined effects of deltamethrin and polyethylene microplastics on the development and biochemical responses of *Xenopus laevis* in early life stages. Ecotoxicology, 35, 37.

Wang, H., Wang, Y., Wang, Q., Lv, M., Zhao, X., Ji, Y., Han, X., Wang, X., & Chen, L. (2022). The combined toxic effects of polyvinyl chloride microplastics and di(2-ethylhexyl) phthalate on the juvenile zebrafish (*Danio rerio*). Journal of Hazardous Materials, 440, 129711.

Zhang, P., Lu, G., Sun, Y., Zhang, J., Liu, J., & Yan, Z. (2022). Aged microplastics change the toxicological mechanism of roxithromycin on *Carassius auratus*: Size-dependent interaction and potential long-term effects. Environment International, 169, 107540.

Zhang, X., Liu, L., Chen, X., Li, J., Chen, J., & Wang, H. (2023). The fate and risk of microplastic and antibiotic sulfamethoxazole coexisting in the environment. Environmental Geochemistry and Health, 45(6), 2905–2915. https://doi.org/10.1007/s10653-022-01385-8

EFFECTS OF SEEDLING AGE AND GROWING SEASON ON TOTAL SOLUBLE CARBOHYDRATE CONTENT IN *Ginkgo biloba* L. SEEDLINGS

Fahrettin ATAR[1], Ali BAYRAKTAR[1]

[1] Karadeniz Technical University, Faculty of Forestry, Department of Forest Engineering, Trabzon, Türkiye
Corresponding author e-mail: alibayraktar@ktu.edu.tr

ABSTRACT

Carbohydrates play a fundamental role in plant growth and development by serving as the primary source of metabolic energy and by contributing to physiological adaptation under changing environmental conditions. The present study aimed to determine the variation in total soluble carbohydrate content of *Ginkgo biloba* L. seedlings with respect to seedling age and sampling time during the growing season. Two-, three-, and four-year-old seedlings were used as plant material. Leaf samples were collected from 20 seedlings in each age class (60 seedlings in total) at the beginning and at the end of the growing season. Total soluble carbohydrate content was determined using the phenol–sulfuric acid method described by Dubois et al. (1956), and the results were expressed as mg g^{-1} dry weight. Within each sampling period, differences among seedling ages were evaluated by one-way analysis of variance (ANOVA), followed by Duncan's multiple range test to identify homogeneous groups. In addition, changes in carbohydrate content between the beginning and the end of the growing season were compared for each seedling age using the independent samples *t*-test. At the beginning of the growing season, total soluble carbohydrate content increased with seedling age, with mean values of 90.77, 93.94, and 98.24 mg g^{-1} in two-, three-, and four-year-old seedlings, respectively. The differences among age classes were statistically significant ($p < 0.05$), and Duncan's test identified the four-year-old seedlings as the group with the highest carbohydrate content. In contrast, this pattern was reversed at the end of the growing season, when the highest carbohydrate content was recorded in two-year-old seedlings (133.77 mg g^{-1}), whereas the lowest value was observed in four-year-old seedlings (116.35 mg g^{-1}). Differences among age classes at the end of the growing season were highly significant ($p < 0.01$). Furthermore, Wilcoxon signed-rank test revealed significant differences in total soluble carbohydrate content between the beginning and the end of the growing season for each seedling age. The findings demonstrate that total soluble carbohydrate content in *Ginkgo biloba* seedlings is influenced not only by seedling age but also by the stage of the growing season. The reversal in carbohydrate distribution among age classes from the beginning to the end of the growing season suggests age-dependent differences in carbohydrate accumulation, utilization, and reserve allocation during seasonal growth. These results provide new insights into the physiological dynamics of carbohydrate metabolism in *Ginkgo biloba* seedlings and contribute to a better understanding of age-related physiological processes that may support future nursery management and silvicultural practices.

Keywords: Maidenhair tree; carbohydrate metabolism; seedling age; seasonal dynamics; physiological development

INTRODUCTION

Climate change is associated with numerous environmental challenges, including rising temperatures, alterations in precipitation regimes, drought, declining water resources, floods, and increases in the frequency and intensity of heat waves (Turan, 2018). Among these impacts, drought is one of the major environmental factors directly affecting plant growth and development. Due to its geographical location and climatic characteristics, Türkiye is among the countries facing considerable risks of drought and desertification (Tüfekçioğlu and Tüfekçioğlu, 2018). Indeed, according to the desertification risk map developed for Türkiye, 12.7% of the country's land area is classified as being at low risk, 53.2% at moderate risk, and 25.5% at high risk of desertification (TÜBİTAK, 2015).

Throughout their growth and development, plants exhibit a range of physiological, biochemical, and molecular responses to changing environmental conditions. The magnitude and nature of these responses may vary depending on genotype and species, the intensity and duration of environmental stress, plant age, and developmental stage (Bray, 1997). Therefore, when evaluating the physiological characteristics of plants, it is important to consider not only environmental conditions but also plant age and developmental stage.

Carbohydrates are fundamental organic compounds produced through photosynthesis and play essential roles in providing energy for plant growth and development, storing carbon, and facilitating its transport among different plant organs. In addition, soluble carbohydrates are important physiological components involved in plant adaptation to changing environmental conditions. Changes in environmental conditions can substantially affect the synthesis, utilization, and allocation of carbohydrates, particularly starch and sucrose (Wang and Stutte, 1992; Keller and Ludlow, 1993; Dien et al., 2019). Under stress conditions such as water limitation, changes in the balance between photosynthetic carbon gain and carbon consumption may increase plant dependence on non-structural carbohydrate reserves (Guehl et al., 1993).

Soluble sugars are considered not only important sources of metabolic energy but also key compounds involved in plant adaptation to environmental conditions. An accumulation of soluble carbohydrates under stress conditions has been reported in several plant species (Munns and Weir, 1981; Thomas, 1990; Guehl et al., 1993). Such increases may be associated with reduced sugar consumption resulting from decreased growth, starch hydrolysis, and changes in carbohydrate translocation among plant organs. Therefore, determining soluble carbohydrate concentrations in different plant organs and their variation throughout plant development is important for evaluating plant physiological status and responses to changing environmental conditions (Gill et al., 2001).

Ginkgo biloba L. is a unique gymnosperm and the only extant species of the family Ginkgoaceae (Shareena and Kumar, 2022). With an evolutionary history extending approximately 270 million years to the Permian period, *G. biloba* is commonly referred to as a "living fossil," as its fundamental morphological characteristics have remained relatively unchanged over a remarkably long geological period (Zhou and Zheng, 2003). Native to China, *G. biloba* is now widely cultivated throughout temperate regions and is particularly valued in urban forestry and landscape applications (Del Tredici, 1991).

Ginkgo biloba is a deciduous tree that can reach 20–35 m in height and has high ornamental value owing to its characteristic fan-shaped leaves, which turn bright yellow in autumn. Its tolerance to urban pollution, resistance to pests and diseases, adaptability to a wide range of environmental conditions, and remarkable longevity further enhance its value for use in urban environments (Stanković, 2016). The species is also of considerable pharmacological importance because of the various biologically active compounds present in its leaves and seeds and has consequently been the subject of extensive research on its ecological, physiological, and pharmacological properties (van Beek, 2002; Mahadevan and Park, 2008).

Because carbohydrate metabolism is closely associated with plant growth, development, and adaptation to environmental conditions, carbohydrate concentrations may vary depending on plant age and phenological stage. Particularly in perennial woody plants, seasonal changes in the balance among carbohydrate production, utilization, translocation, and storage may be reflected in leaf soluble carbohydrate concentrations. Therefore, determining changes in carbohydrate content among seedlings of different ages during the same growing season is important for elucidating age-related physiological differences.

The present study aimed to determine the variation in total soluble carbohydrate content of *Ginkgo biloba* seedlings in relation to seedling age and growing season. For this purpose, total soluble carbohydrate contents in the leaves of two-, three-, and four-year-old seedlings were determined at the beginning and end of the growing season, allowing comparisons both among seedling age classes and between sampling periods within each age class. The findings are expected to contribute to a better understanding of age- and season-related physiological changes in *G. biloba* seedlings and to provide useful information for future nursery management and landscape applications.

MATERIAL AND METHOD

The study was conducted using two-, three-, and four-year-old *Ginkgo biloba* L. seedlings grown under open-field conditions at the Research and Application Greenhouse of the Faculty of Forestry, Karadeniz Technical University (Figure 1). A total of 60 seedlings were included in the study, with 20 seedlings representing each age group. To evaluate age- and season-related changes in leaf total soluble carbohydrate content, leaf samples were collected at two different stages of the growing season: at the beginning of the growing season (May 2025) and at the end of the growing season (October 2025). Leaf samples obtained from the respective age groups during both sampling periods were subsequently used for the determination of total soluble carbohydrate content. According to the long-term climatic records for Trabzon Province covering the period from 1927 to 2023, where the Research and Application Greenhouse of the Faculty of Forestry is located, the mean annual temperature is 14.8 °C and the mean annual total precipitation is 828.9 mm.

Total soluble carbohydrate (TSC) content was quantified using the phenol–sulfuric acid assay based on the method of Dubois et al. (1956). Following collection, leaf samples were placed in paper bags and oven-dried at 65 °C for 48 h. The dried samples were subsequently ground to a fine powder, and 0.1 g of each sample was accurately weighed for analysis. Soluble carbohydrates were extracted from the powdered leaf material with 80% ethanol for 24 h. After extraction, the samples were centrifuged at 5000 rpm for 10 min, and the resulting supernatant was used for carbohydrate determination. For colorimetric analysis, a 50 µL aliquot of the supernatant was transferred into a glass tube and mixed with 1 mL of 5% phenol solution using a vortex mixer. Subsequently, 5 mL of sulfuric acid was added, and the mixture was thoroughly vortexed again. The reaction mixtures were allowed to stand at room temperature for 1 h to complete color development and cooling. Absorbance was then measured at 490 nm using 3-mL cuvettes. Total soluble carbohydrate concentrations were calculated from a standard calibration curve and expressed on a dry-weight basis as mg/g DW.

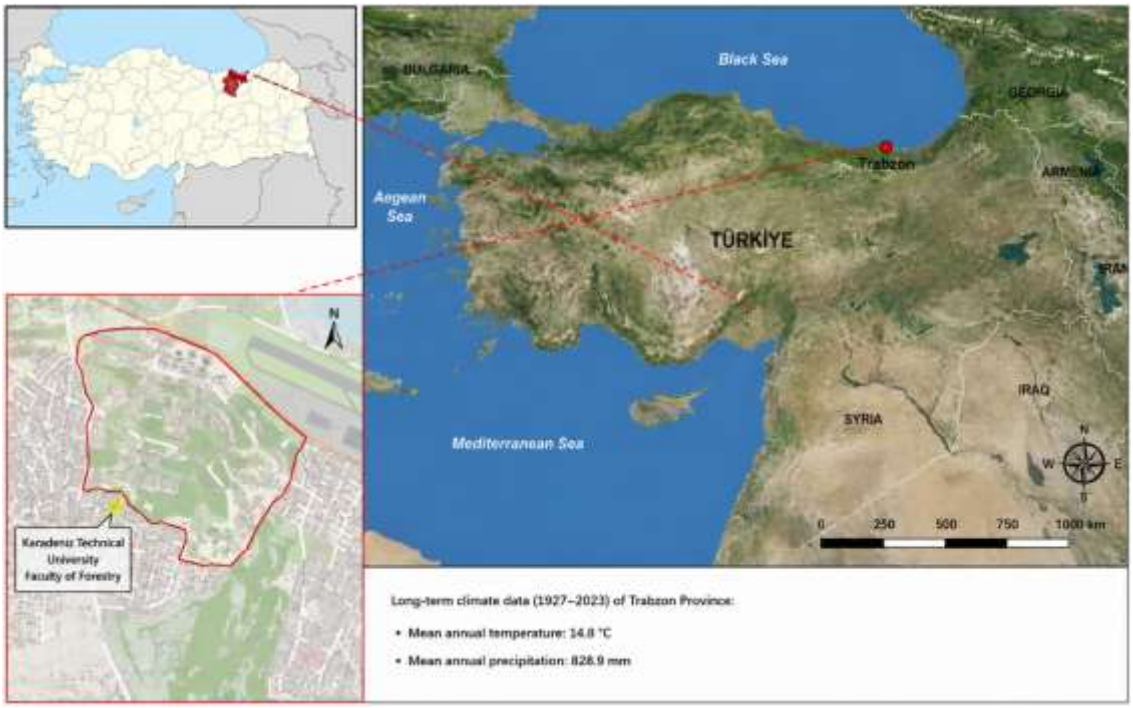

Figure 1. Geographical location of the study area

Statistical analyses were performed using IBM SPSS Statistics 23.0. Differences in total soluble carbohydrate content among two-, three-, and four-year-old *Ginkgo biloba* seedlings were analyzed separately for each sampling period using one-way analysis of variance (ANOVA). When significant differences were detected, Duncan's multiple range test was applied to identify homogeneous groups among seedling ages. In addition, total soluble carbohydrate contents measured at the beginning and at the end of the growing season were compared separately for each seedling age using the Wilcoxon signed-rank test. Statistical significance was evaluated at the $p < 0.05$ level.

RESULTS

Descriptive statistics for total soluble carbohydrate (TSC) content of two-, three-, and four-year-old *Ginkgo biloba* seedlings, together with the results of the Wilcoxon signed-rank test comparing May and October measurements, are presented in Table 1.

Table 1. TSC values of *Ginkgo biloba* seedlings of different ages

Seedling Age	Min. (mg/g)		Max. (mg/g)		Mean ± SE (mg/g)		Wilcoxon test Sig.
	May	Oct	May	Oct	May	Oct	
2-year-old	81.18	127.65	102.06	143.24	90.77 ± 2.45	133.77 ± 2.02	0.005
3-year-old	86.47	114.12	105.59	129.12	93.94 ± 2.13	120.53 ± 1.69	0.005
4-year-old	95.00	105.88	100.59	129.41	98.24 ± 0.65	116.35 ± 3.03	0.005

$p<0.01$: There is a statistically significant difference at the 99% confidence level

Total soluble carbohydrate content varied considerably according to seedling age and sampling period (Table 1). In May, the mean TSC content was highest in four-year-old seedlings (98.24 ± 0.65 mg/g), followed by three-year-old (93.94 ± 2.13 mg/g) and two-year-old seedlings (90.77 ± 2.45 mg/g). In October, however, this pattern was reversed, with the highest mean TSC content recorded in two-year-old seedlings (133.77 ± 2.02 mg/g), followed by three-year-old (120.53 ± 1.69 mg/g) and four-year-old seedlings (116.35 ± 3.03 mg/g). The TSC values ranged from 81.18 to 102.06 mg/g in two-year-old, 86.47 to 105.59 mg/g in three-year-old, and 95.00 to 100.59 mg/g in four-year-old seedlings in May. In October, the corresponding ranges increased to 127.65–143.24, 114.12–129.12, and 105.88–129.41 mg/g, respectively. Wilcoxon signed-rank test results showed that TSC content increased significantly from May to October in all three seedling age groups (p<0.01).
The results of one-way ANOVA examining differences in total soluble carbohydrate (TSC) content among seedling age groups in May and October are presented in Table 2.

Table 2. Results of variance analysis regarding TSC content of seedlings of different ages

		Sum of Squares	df	Mean Square	F	P
May	Between Groups	281.088	2	140.544	3.840	0.034
	Within Groups	988.133	27	36.598		
	Total	1269.221	29			
Oct	Between Groups	1653.391	2	826.696	15.410	0.000
	Within Groups	1448.445	27	53.646		
	Total	3101.836	29			

p<0.01: There is a statistically significant difference at the 99% confidence level
p<0.05: There is a statistically significant difference at the 95% confidence level

One-way ANOVA revealed significant differences in TSC content among the three seedling age groups in both sampling periods (Table 2). In May, the effect of seedling age on TSC content was statistically significant ($F = 3.840$, $p < 0.05$). A considerably stronger age-related difference was observed in October, when the ANOVA indicated a highly significant effect of seedling age on TSC content ($F = 15.410$, $p < 0.01$). These results demonstrate that TSC content differed among two-, three-, and four-year-old seedlings during both sampling periods, with the differences among age groups becoming more pronounced at the end of the growing season.

The results of Duncan's multiple range test showing differences in total soluble carbohydrate (TSC) content among seedling age groups in May and October are presented in Figure 2. In May, four-year-old seedlings had the highest mean TSC content (98.24 ± 0.65 mg/g) and were classified in group a, whereas two-year-old seedlings had the lowest mean value (90.77 ± 2.45 mg/g) and were classified in group b, indicating a significant difference between these two age groups. Three-year-old seedlings (93.94 ± 2.13 mg/g) were placed in the intermediate ab group and therefore did not differ significantly from either two- or four-year-old seedlings. In October, the trend changed markedly. Two-year-old seedlings exhibited the highest TSC content (133.77 ± 2.02 mg/g) and formed group a, while three-year-old (120.53 ± 1.69 mg/g) and four-year-old seedlings (116.35 ± 3.03 mg/g) were both classified in group b. Thus, in October, two-year-old seedlings had significantly higher TSC content than the other two age groups, whereas no significant difference was detected between three- and four-year-old seedlings.

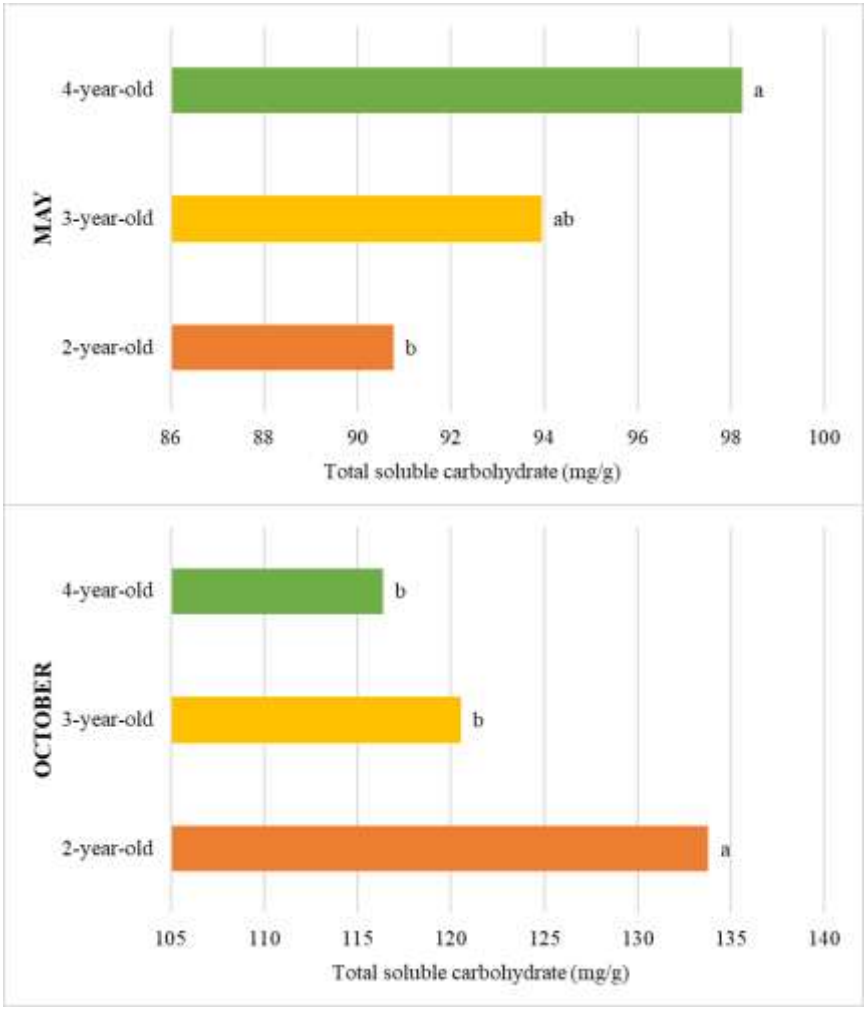

Figure 2. Duncan test results for May and October measurements of seedlings of different ages based on TSC content

DISCUSSION AND CONCLUSION

The present study demonstrated that total soluble carbohydrate (TSC) content in *Ginkgo biloba* leaves was influenced by both seedling age and sampling period. TSC content increased significantly from May to October in all three age groups; however, the magnitude of this increase differed among seedling ages. Moreover, the ranking of age groups changed considerably during the growing season. While four-year-old seedlings exhibited the highest TSC content in May, two-year-old seedlings had the highest value in October. These findings indicate that seasonal changes in carbohydrate metabolism in *G. biloba* seedlings are closely associated with developmental stage and that seedlings of different ages may differ in the balance between carbohydrate production, utilization, and allocation.

Seasonal variation in carbohydrate concentration is a characteristic feature of perennial woody plants because non-structural carbohydrates represent a dynamic balance between carbon acquisition through photosynthesis and carbon demand for growth, respiration, storage, and other metabolic processes. Soluble sugars also perform functions beyond carbon storage, including transport, energy metabolism and osmoregulation (Hartmann and Trumbore, 2016). A broad synthesis of seasonal NSC dynamics showed that soluble sugars, starch, and total NSC vary substantially during the year and that carbohydrate concentrations may increase as plants

approach the dormant period, particularly in temperate environments (Martínez-Vilalta et al., 2016). Therefore, the higher TSC concentrations observed in October in the present study may reflect changes in the source–sink balance toward the end of the growing season, when demand for active vegetative growth declines and a greater proportion of assimilated carbon may remain in soluble or reserve forms.

Evidence from *G. biloba* also supports pronounced seasonal regulation of carbohydrate metabolism. Guo et al. (2024), investigating seasonal development of current- and second-year xylem in *G. biloba*, reported marked seasonal changes in non-structural carbohydrate concentrations together with substantial changes in genes and metabolites involved in carbohydrate metabolism. They also found a positive association between ABA concentration and non-structural carbohydrate content, indicating that seasonal carbohydrate dynamics in *Ginkgo* are closely integrated with developmental and hormonal regulation. Similarly, Li et al. (2020) demonstrated pronounced physiological and transcriptomic changes in *G. biloba* leaves during the transition from green leaves to autumn senescence, including reductions in photosynthetic activity and substantial alterations in ABA- and jasmonic-acid-related pathways. These findings support the view that the increase in TSC observed from May to October in the present study occurred within a broader seasonal reorganization of carbon metabolism rather than simply representing continuous carbohydrate accumulation throughout the growing period.

Nevertheless, seasonal changes in individual soluble sugars do not necessarily follow the same direction as changes in total soluble carbohydrate content. Horbowicz et al. (2022) identified sucrose, glucose, and fructose as major soluble sugars in *G. biloba* leaves and reported substantial changes in their concentrations during natural leaf senescence. In particular, glucose and fructose declined as leaves progressed toward natural senescence, while sucrose metabolism also changed markedly. This apparent difference from the present results should be interpreted cautiously because the two studies evaluated different carbohydrate fractions and different phenological intervals. Horbowicz et al. (2022) quantified individual sugars during the relatively narrow transition from September to natural senescence in October, whereas the present study compared total soluble carbohydrates between May and October using the phenol–sulfuric acid assay. Thus, differences in sampling stage, analytical approach, and the carbohydrate fractions measured may explain the contrasting responses. Importantly, the October samples in the present study represent the end of the growing season and should not necessarily be considered equivalent to fully senescent leaves.

Another important finding was the reversal of the age-related differences between the two sampling periods. In May, TSC content increased with seedling age, and four-year-old seedlings had significantly higher TSC content than two-year-old seedlings. In October, however, two-year-old seedlings accumulated significantly more TSC than both three- and four-year-old seedlings. The seasonal increase was therefore proportionally strongest in the youngest seedlings and progressively smaller with increasing seedling age. Such differences may be associated with ontogenetic changes in source–sink relationships and carbohydrate allocation. Seedling age can influence photosynthetic carbon acquisition, growth demand, storage capacity, and the distribution of NSC among leaves, stems, and roots. For example, Han et al. (2025) demonstrated clear age-dependent differences in organ-specific NSC allocation and carbon coordination between one- and three-year-old *Pinus yunnanensis* seedlings, showing that developmental stage can substantially modify carbohydrate allocation strategies. Although that study involved another tree species and shade treatments, it provides physiological support for the age-dependent differences observed here.

Recent evidence obtained directly from *G. biloba* seedlings further emphasizes the importance of carbohydrate partitioning among plant organs. Tang et al. (2026) reported that defoliation of two-year-old *G. biloba* seedlings increased soluble sugar and starch concentrations in the

remaining leaves while decreasing carbohydrate reserves in stems and roots. Their results demonstrate that changes in leaf carbohydrate concentration can occur simultaneously with an opposite response in other organs and therefore reflect active redistribution of carbon within the plant. Accordingly, the higher October TSC concentration of two-year-old seedlings in the present study should not necessarily be interpreted as a greater whole-plant carbohydrate reserve. It may instead reflect age-specific differences in the retention, utilization, or translocation of carbohydrates in leaves. Measurements of soluble sugars and starch in stems and roots, together with leaf measurements, would be required to determine whether the age-related differences observed here represent differences in whole-plant carbon storage or primarily in organ-specific allocation.

Overall, the results indicate that both seedling age and seasonal development are important determinants of leaf TSC content in *G. biloba*. The significant increase from May to October in all age classes demonstrates a strong seasonal component, whereas the reversal in the ranking of age groups indicates that this seasonal response is age dependent. The relatively high TSC concentration of four-year-old seedlings at the beginning of the growing season and the pronounced late-season increase in two-year-old seedlings suggest differences in carbohydrate utilization and allocation among developmental stages. However, because the present study quantified total soluble carbohydrates only in leaves at two sampling dates, the underlying mechanisms cannot be attributed specifically to changes in photosynthesis, carbohydrate translocation, starch–sugar conversion, or environmental acclimation. Future studies incorporating repeated sampling throughout the growing season and simultaneous measurements of individual soluble sugars, starch, photosynthetic traits, and carbohydrate concentrations in leaves, stems, and roots would provide a more comprehensive understanding of age-dependent carbon dynamics in *G. biloba*. Nevertheless, the present findings demonstrate that seedling age should be considered when evaluating the physiological status and seasonal carbohydrate dynamics of *G. biloba* seedlings and provide a useful basis for future nursery and ecophysiological studies.

REFERENCES

Bray, E. 1997. Plant Responses to Water Deficit. *Trends in Plant Science*, 2: 48-54.

Del Tredici, P. 1991. Ginkgos and People - A Thousand Years of Interaction. *Arnoldia*, 51(2): 2-15.

Dien, D. C., T. Mochizuki, T. Yamakawa. 2019. Effect of Various Drought Stresses and Subsequent Recovery on Proline, Total Soluble Sugar and Starch Metabolisms in Rice (*Oryza sativa* L.) Varieties. *Plant Production Science*, 22(4): 530-545.

Gill, P. K., A. D. Sharma, P. Singh, S. S. Bhullar. 2001. Effect of Various Abiotic Stresses on the Growth, Soluble Sugars and Water Relations of Sorghum Seedlings Grown in Light and Darkness. *Bulgarian Journal of Plant Physiology*, 27: 72-84.

Guehl, J. M., A. Clement, P. Kaushal, G. Aussenac. 1993. Planting Stress, Water Status and Non-Structural Carbohydrate Concentrations in Corsican Pine Seedlings. *Tree Physiology*, 12(2): 173-183.

Guo, F., W. Yu, F. Fu, H. Hou, J. Zhang, J. Guo, P. Wu, Y. A. El-Kassaby, G. Wang. 2024. Physiological, Transcriptome and Metabolome Analyses Provide Molecular Insights to Seasonal Development in *Ginkgo biloba* Xylem. *Industrial Crops and Products*, 208: 117930.

Han, J., Y. Liu, W. Zhang, G. Duan, J. Chen, W. Zhu, J. Wu. 2025. The Age-Dependent Response of Carbon Coordination in the Organs of *Pinus yunnanensis* Seedlings under Shade Stress. *Plants*, 14(17): 2679.

Hartmann, H., S. Trumbore. 2016. Understanding the Roles of Nonstructural Carbohydrates in Forest Trees – From What We Can Measure to What We Want to Know. *New Phytologist*, 211(2): 386-403.

Horbowicz, M., J. Szablińska-Piernik, J. Góraj-Koniarska, K. Miyamoto, J. Ueda, M. Saniewski. 2022. Changes in Polar Metabolites Content during Natural and Methyl-Jasmonate-Promoted Senescence of *Ginkgo biloba* Leaves. *International Journal of Molecular Sciences*, 23(1): 266.

Keller, F., M. M. Ludlow. 1993. Carbohydrate Metabolism in Drought-Stressed Leaves of Pigeonpea (*Cajanus cajan*). *Journal of Experimental Botany*, 44(8): 1351-1359.

Li, W., L. Wang, Z. He, Z. Lu, J. Cui, N. Xu, B. Jin, L. Wang. 2020. Physiological and Transcriptomic Changes during Autumn Coloration and Senescence in *Ginkgo biloba* Leaves. *Horticultural Plant Journal*, 6(6): 396-408.

Mahadevan, S., Y. Park. 2008. Multifaceted Therapeutic Benefits of *Ginkgo biloba* L.: Chemistry, Efficacy, Safety, and Uses. *Journal of Food Science*, 73(1): R14-R19.

Martínez-Vilalta, J., A. Sala, D. Asensio, L. Galiano, G. Hoch, S. Palacio, F. I. Piper, F. Lloret. 2016. Dynamics of Non-Structural Carbohydrates in Terrestrial Plants: A Global Synthesis. *Ecological Monographs*, 86(4): 495-516.

Munns, R., R. Weir. 1981. Contribution of Sugars to Osmotic Adjustment in Elongating and Expanded Zones of Wheat Leaves during Moderate Water Deficits at 2 Light Levels. *Australian Journal of Plant Physiology*, 8(1): 93-105.

Shareena, G., D. Kumar. 2022. Traversing through Half a Century Research Timeline on *Ginkgo biloba*, in Transforming a Botanical Rarity into an Active Functional Food Ingredient. *Biomedicine and Pharmacotherapy*, 153: 113299.

Stanković, M. S. 2016. Biology and Ecology of *Ginkgo biloba* L. (Ginkgoaceae). In: Emmett Fisher (Ed.), *Ginkgo biloba: Biology, Uses and Health Benefits*. Nova Science Publishers, New York. 1-27.

Tang, W., S. Yu, W. Tang, T. Gao, Y. Liu, P. Yu, G. Wang, J. Guo. 2026. Dynamic Responses to Defoliation Timing and Intensity in *Ginkgo biloba* Seedlings: Integrated Physiological and Biochemical Perspectives. *Plant Growth Regulation*, 106: Article 42.

Thomas, H. 1990. Osmotic Adjustment in *Lolium perenne*: Its Heritability and the Nature of Solute Accumulation. *Annals of Botany*, 66(5): 521-530.

TÜBİTAK. 2015. *Desertification Report of Turkey*. Ankara, Türkiye.

Turan, E. S. 2018. Türkiye'nin İklim Değişikliğine Bağlı Kuraklık Durumu. *Doğal Afetler ve Çevre Dergisi*, 4(1): 63-69.

Tüfekçioğlu, A., M. Tüfekçioğlu. 2018. Kuraklık ve Orman Ekosistem Dinamikleri Etkileşimi. *Türkiye Ormancılık Dergisi*, 19(1): 103-108.

van Beek, T. A. 2002. Chemical Analysis of *Ginkgo biloba* Leaves and Extracts. *Journal of Chromatography A*, 967(1): 21-55.

Wang, Z., G. W. Stutte. 1992. The Role of Carbohydrates in Active Osmotic Adjustment in Apple under Water Stress. *Journal of the American Society for Horticultural Science*, 117(5): 816-823.

Zhou, Z., S. Zheng. 2003. The Missing Link in Ginkgo Evolution. *Nature*, 423(6942): 821-822.

ENVİRONMENTAL SURVEİLLANCE OF ESBL PRODUCİNG *ESCHERİCHİA COLİ* AND ANTİBİOTİC RESİSTANCE İN THE SHKUMBİNİ RİVER ECOSYSTEM, ALBANİA

Florian Plaku[1,2,], Ilir Kusi[1],*

Agricultural University of Tirana, Tirana, Albania

PhD Candidate at Veterinary Sciences, Agricultural University of Tirana, 1025 Tirana, Albania

fplaku@ubt.edu.al, ikusi@ubt.edu.al,

** Corresponding author e-mail: fplaku@ubt.edu.al*

ABSTRACT

Recent studies have demonstrated that ESBL-producing *E. coli* are globally common in aquatic environments such as lakes and rivers, detecting viable ESBL producers in a high proportion of water samples. The main objective of this study was to investigate the occurrence, diversity, and phenotypic and molecular characteristics of ESBL-producing *E. coli* in the aquatic environment, in the Shkumbini River Ecosystem. Antimicrobial susceptibility analysis of the ESBL producing E. coli revealed that 100 % of isolates were resistant to at least one antimicrobial agent in three or more antimicrobial categories thus characterized as multidrug resistant (MDR). Molecular characterization of ESBL producing isolates revealed the prevalence and diversity of the β-lactamase resistance genes among them. The most prevalent ESBL Genotype was blaCTX-M-1 (33.33%, 5/15). Overall, the findings of our study are worrisome, emphasizing the importance of rivers as potential reservoirs of antibiotic resistance genes (ARGs), imposing serious threats to public health as well as the necessity of a more detailed analysis of genomic features of ESBL *E. coli* isolates to better understand the pathogenic potential and the epidemic characteristics of them in the aquatic ecosystem. Considering the continuous interaction between aquatic ecosystems, human activities, and animal production systems, the detection of ESBL-producing E. coli in the Shkumbini River emphasizes the urgent need for coordinated One Health-based surveillance programs to identify transmission pathways and develop effective strategies for controlling the environmental dissemination of antimicrobial resistance.

Key words: ESBL-producing *E.Coli*, surface water, antibiotic resistance genes

INTRODUCTION

Our study encompassed a range of sampling locations, including areas impacted by human sewage and wastewater contaminated with animal waste from wet markets or slaughterhouses. We collected 8 samples from both upstream and downstream sites. The downstream samples provided valuable information on the presence and concentrations of ESBL-*E. coli*, primarily due to inputs from the surrounding community, including sewage discharges and waste. Furthermore, we conducted comprehensive analysis on the total E. coli present in the collected samples. Using these total *E. coli* counts, we calculated the proportion of colonies that were ESBL producers among the overall *E. coli* population (WHO). Furthermore, we undertook extensive analyses to thoroughly explore their antibiotic resistance profiles, while concurrently investigating the presence of ESBL genes.

MATERIALS AND METHODS

The proposed methodology introduces a realistic approach to the selection of sampling locations based on field survey and the use of geospatial techniques to account for the impact of human activities (Vikas, 2015). The water from the Shkumbin river has been and is used for different purposes like bathing, washing of clothes, and also for agriculture.

During the study we implemented a standardizes sampling protocol in which the minimum depth of 30 cm below the water surface was consistently maintained, with no samples exceeding 50 cm. Sampling was conducted at predetermined locations, predominantly on bridges. Each sample, consisting of 1 liter, was promptly transferred to a thermos and stored for up to 8 hours for preservation. To ensure proper preservation, we decided to store the samples in refrigerator as immediate analysis was not conducted at that time (Claiborne), (ISO, 2006-08). The concentration of ESBL-*E.Coli* in water exhibit considerable variation doe to the variability of fecal contamination levels different type of waste and the availability of no-contaminated water source as rainfall and upland spring. Because of this we have in front of us a major challenge in accurately prediction water contamination levels in other sampling periods. Therefore, to ensure the presence of countable numbers of colonies, multiple 10-fold dilutions of each sample were analyzed. Another approach was utilized simultaneously due to its advantage of allowing us to isolate pure strains of a single species or segregate strains from a mixed population, selectively reducing or removing unknown organisms. This reduction is achieved thought a repeated process of suspending an initial solution into fixed volumes of liquid diluent (ISO 6.-1. , 2017). After confirming the presence of gas in the tubes, we proceed with indole test as means to differentiate between E. Coli and Enterobacter aerogenes (ISENBERG, 1958) (MacWilliams, 2009). Simultaneously in order to obtain accurate result, a volume of 100 ml from the sample was filtered through a membrane with pore size of 0.45 mm (ISO 8. , 2018). To determine the presence of ESBL activity, the membrane was incubated on TBX (Tryptone Bile X-glucuronide) agar plate supplemented with 4μg/ml CTX (Cefotaxime). By adhering to established protocol and employing rigorous purification techniques, we successfully isolated a total of 16 colonies of ESBL *E. coli* (ISO 7. , 2023) (WHO).

After isolating the Esbl colonies, we continued with phenotypic confirmation methods to confirm their presence. These methods are based on the principle that clavulanic acid can inhibit ESBL enzymes, resulting in a synergistic effect when combined with CTX and Ceftazidime. We conducted the tests using antibiotic disks: Cefoxitin (FOX), Cefotaxime (CTX), Ceftazidime (CAZ), Aztreonam (ATM) and Amoxycillin/Clavulanic Acid (AMC). The incubation was performed at a temperature of 37°C for a period of 16-18 hours (EUCAST, July 2017) (WHO).

To extract genomic DNA from individual bacterial colonia simple method was applied. Carefully selecting 1 to 5 individual colonies (depending from their size) from the agar plate,

to ensure an ample quantity of DNA. Those colonies have been collected by using a sterile inoculating loop and then resuspended in 100 µl sterile deionized H2O. This suspension was placed at 97 ◦C and "cooked" for 5–10 minutes using a water bath, after that solution was shake for 5 minutes at a rate of approximately 2000-6000 oscillations per minute. To separate the supernatant containing DNA we centrifuge the cell lysate at 15,000 × g, 5–15 minutes. Usually, a small volume ranging from 1-5 µl is added to a PCR reagent mix (Edward R. B. Moore, January 2004) (Omar B. Ahmed, 2017).

For every DNA extracted a various PCR multiplex were employed for molecular characterization including: Mcr-1, Mcr-2, Mcr-3, Mcr-4, Mcr-5 (Rebelo Ana Rita, Euro Surveill. 2018); ShV, OXA 1, TEM; OXA, NMD, KPC (Bogaerts P, 2013) (Dallenne C, 2010); CTX-M 8/ 25; IMP, VIM; CTX-M 1, CTX-M 2, CTX-M 9 (M.C. El bouamri, 2015,) (Bogaerts P, 2013).

RESULTS

The table, displays the findings of six samples that tested positive for ESBL in E. coli. These E. coli organisms were found in 100 ml water samples that were collected. Out of the six samples that showed growth, 15 distinct colonies were selected based on suspicion of ESBL. After conducting synergy tests, we were able to isolate 15 distinct E. coli colonies that tested positive for ESBL.

Antibiograms were performed for each of the isolated strains to determine their antibiotic resistance profiles. The obtained results have shown higher resistance of strains towards Streptomycin was 93.33%, Ampicillin 93.33%, 73.33% Gentamycin, 40% Tetracycline and Trimethoprim, 33.33% Ciprofloxacin,26.67% Chloramphenico,13.33% Meropenem and no resistance at all from Imipenem.

Molecular characterization of ESBL producing isolates revealed the prevalence and diversity of the β-lactamase resistance genes among them. The most prevalent ESBL Genotype was blaCTX-M-1 (33.33%, 5/15).

DISCUSSION

Based on the performed analyses, it is evident that ESBL genes are in circulation in Elbasan region. In relation to antibiotics, the antibiogram indicates the development of resistance against commonly utilized antibiotics in Albania. Following his trend is anticipated to yield more significant repercussions in the future, imposing serious threats to public health as well as the necessity of a more detailed analysis of genomic features of ESBL *E. coli* isolates to better understand the pathogenic potential and the epidemic characteristics of them.

ACKNOWLEDGMENTS

I would like to acknowledge and extend my gratitude to prof. Ilir Kusi, Charalampos Kotzamanidis, Erinda Lika, for their invaluable guidance, mentorship and constructive feedback throughout the course of this research.

REFERENCES

Bogaerts P, R. d. (2013). Validation of carbapenemase and extended-spectrum β-lactamase multiplex endpoint PCR assays according to ISO 15189. *J Antimicrob Chemother*, 1576-1582.

Claiborne, K. E. (OCTOBER 1949). Effect of Age and Storage Temperature on Bacteriological Water Samples. *American Water Works Association*, 948-952.

Dallenne C, D. C. (2010). Development of a set of multiplex PCR assays for the detection of genes encoding important beta-lactamases in Enterobacteriaceae. *J Antimicrob Chemother*, 490-495.

Edward R. B. Moore, A. A. (January 2004). *Molecular Microbial Ecology Manual Second EditionChapter: 1.6.1.* Kluwer Academic Publishers.

EUCAST. (July 2017). *guidelines for detection of resistance mechanisms and specific resistances of clinical and/or epidemiological importance.*

ISENBERG, H. D. (1958). Indole reactions in bacteria. *Journal of bacteriology*, 682–690.

ISO, 1. (2006-08). *Water quality — Sampling for microbiological analysis.*

ISO, 6.-1. (2017). *Microbiology of the food chain — Preparation of test samples, initial suspension and decimal dilutions for microbiological examination — Part 1: General rules for the preparation of the initial suspension and decimal dilutions.*

ISO, 7. (2023). *Water quality — Requirements for the performance testing of membrane filters used for direct enumeration of microorganisms by culture methods.*

ISO, 8. (2018). *Water quality — General requirements and guidance for microbiological examinations by culture.*

M.C. El bouamri, L. A. (2015,). Molecular characterization of extended spectrum β-lactamase-producing Escherichia coli in a university hospital in Morocco, North Africa. *African Journal of Urology*, 161-166.

MacWilliams, M. P. (2009). *Indole Test Protocol.* American Society for Microbiology.

Omar B. Ahmed, A. S. (2017). Quality improvement of the DNA extracted by boiling method in. *International Journal of Bioassays*, 5347-5349.

Rebelo Ana Rita, B. V.-G. (Euro Surveill. 2018). Multiplex PCR for detection of plasmid-mediated colistin resistance determinants,mcr-1, mcr-2, mcr-3, mcr-4 and mcr-5 for surveillance purposes. *European Centre for Disease Control and Prevention (ECDC)*.

Vikas, V. (2015). “Design of Sampling Locations for River Water Quality Monitoring Considering Seasonal Variation of Point and Diffuse Pollution Loads.” Environmental Monitoring and Assessment 187.6 (2015): n. pag. Web. *Springer* , 187:376.

WHO. (n.d.). *integrated global surveillance on ESBL-producing E. coli using a “One Health” approach:*.

EVALUATION OF THE ANNUAL PLAN AND SUBJECT CONTENT OF THE CLIMATE, ENVIRONMENT AND INNOVATIVE SOLUTIONS COURSE BY SCIENCE EDUCATION STUDENTS

Nurcan Özkan[1]

[1] *Trakya University, Education Faculty, Mathematics and Sciences Education Department, Edirne, Turkey*
Corresponding author e-mail: nurcanozkan@hotmail.com

ABSTRACT

The rapid changes in science and technology, the evolving needs of individuals and society, and the innovations and advancements in learning and teaching theories and approaches have directly impacted the roles expected of individuals. This transformation defines an individual who produces knowledge, uses it functionally in life, solves problems, thinks critically, is entrepreneurial, determined, possesses communication skills, can empathize, and contributes to society and culture, etc. For these reasons, the Climate, Environment, and Innovative Solutions Curriculum aims to contribute to students becoming individuals who can find solutions to the problems in our environment. The curriculum, within the framework of virtue, values, and actions, aims to guide students from actions to values, from values to virtuous individuals, and from virtuous individuals to the ultimate goal of becoming peaceful individuals in a livable environment. The Climate, Environment, and Innovative Solutions course curriculum addresses climate change, the interaction of environmental systems with humans, and environmental problems. The program also includes topics such as environmental problems, the fundamentals of innovative solutions, and efforts to develop innovative solutions. Given that the environment and environmental problems occupy a significant place in our lives today, and because children need to be educated and develop attitudes on these issues from a young age, this research aims to evaluate the Climate, Environment, and Innovative Solutions Course Curriculum and Annual Plan implemented in Turkey, as perceived by university students. For this purpose, a qualitative research method was used in the study. As a data collection method, 22 final-year science education students who went to schools for internships were asked to evaluate the curriculum on A4 paper, and then the data were interpreted. When students' statements are evaluated, it is seen that the program is effective in some areas and unsuccessful in others.

Keywords: Climate, Environment and Innovative Solutions, Curriculum, Annual plan, Science education students

INTRODUCTION

Human activities in the human environment cause air, water, soil, noise, and light pollution on the one hand, and on the other hand, they play a significant role in global climate change by increasing global warming. Furthermore, the issue of sharing water and energy resources has transformed from an environmental challenge into an international economic and political problem. Reversing this worsening trend as soon as possible has become one of humanity's most important tasks. At this point, it is not enough to simply protect the natural environment; solutions to the problems must also be found, and a safe, clean, and sustainable understanding of the natural environment must be developed. Action plans at local, national,

and global levels that mitigate the impact of environmental challenges and protect and improve the environment need to be implemented worldwide. To leave a more livable world for future generations, the current lifestyle, which is based on "more production" and "more consumption," must first transform into a sustainable lifestyle free from waste. An important point to emphasize is that the use and management of natural resources should be approached in a way that ensures their sustainability and passes them on to future generations, rather than in a destructive and damaging manner (Ministry of National Education, 2026).

Climate change is predicted to increasingly threaten the future security and well-being of humanity (Türkeş, 2022). This threat is making its effects felt more and more each day, without any distinction between underdeveloped and developing countries. Despite the Intergovernmental Panel on Climate Change (IPCC) reports demonstrating that climate change is caused by human activities, it is still not considered a serious problem by countries (Aydın and Demirbaş, 2020). Climate change has affected human life throughout history. However, after the industrial revolution in the 19th century, humans also began to influence the climate through their activities, and the impact of humans on climate change began to increase (Şen, 2022; Karaaslan and Çetin, 2025).

With the increase in environmental problems, people's perspectives on nature have changed. The previously dominant romantic viewpoint has gradually given way to an attitude that investigates and questions environmental problems (Kılıç, 2013; Dere and Çinikaya; 2023). When examining the development of environmental education in the 20th century, it is necessary to mention some important steps. Firstly, the books "The Silent Spring" and "Our Synthetic Environment," published in 1962, created significant awareness of the global impact of chemical products (Ünder, 1996). In 1971, an international study entitled "Study of Man's Impact on Climate" was published with the support of the Swedish Academy of Sciences (Hulme, 2016; Dere and Çinikaya; 2023).

Six years after Turkey signed the Paris Agreement in 2015, it was ratified by the Grand National Assembly of Turkey (TBMM) on October 6, 2021, and published in the Official Gazette (Official Gazette, October 7, 2021). Following the ratification of the agreement, the name of the Ministry of Environment and Urbanization was changed to "Ministry of Environment, Urbanization and Climate Change" in order to draw attention to the issue of climate change (Official Gazette, October 29, 2021). Article 12 of the Paris Agreement emphasizes that signatory countries should provide climate change education and cooperate to raise public awareness of climate change (Official Gazette, October 7, 2021).

As is known, with environmental problems reaching a global dimension, environmental education has been on the agenda of many international meetings since the 1970s. In Turkey, environmental responsibility is addressed within the framework of cooperation between the state and citizens, as stipulated in Article 56 of the 1982 Constitution. In 1999, a protocol was signed between the Ministry of Environment and Forestry and the Ministry of National Education aiming to include environmental issues in various levels of education (preschool, primary, secondary, and apprenticeship training) and to organize in-service training courses on environmental education for students and teachers nationwide. Essentially, in Turkey, until the Paris Agreement was signed in 2015, environmental issues were covered in subjects such as life skills, science, social studies, geography, and biology. The Climate, Environment and Innovative Solutions course is a brand new course introduced as an elective in high schools as part of the Ministry of National Education's (MEB) curriculum update. This course is not a direct replacement for a specific old course; rather, it is a new, focused curriculum added to the elective course pool by expanding its scope.

One of the tools that prepares individuals to both combat climate change and adapt to its effects is education (Açıkalın, Sarı and Erçetin, 2024). Education has a positive impact on our thoughts, behaviors, and communication with present and future generations in the fight against

climate change (Mochizuki and Bryan, 2015; Karaaslan and Çetin, 2025). One of the most important aspects of combating and adapting to climate change is effective environmental education. Effective environmental education will make individuals and society better prepared for the consequences of climate change. Climate change education, which is particularly linked to environmental education, stands out in this preparation (Karaaslan and Çetin, 2025).

Understanding the causes and consequences of climate change and discussing appropriate responses aims to increase individuals' attitudes and motivation to make informed decisions and take responsible actions (Anderson, 2010). Climate change education should aim to prepare children for a rapidly changing, uncertain, and risky future (Stevenson et al., 2017).

With the 21st century, environmental education, with its multidisciplinary structure, occupies a unique position within both formal (preschool, primary, secondary, high school, and undergraduate) and non-formal education. Within this scope, the Climate, Environment and Innovative Solutions Curriculum aims to enable students to recognize, develop interest and curiosity about nature and their immediate environment, to have a positive attitude, to understand the relationship between humans and the environment, to view a livable environment as a legacy for future generations within the framework of sustainability, to have knowledge about the causes and consequences of climate change in the world and in Turkey and to take responsibility in this context, to have knowledge about environmentally friendly technologies, to become familiar with environmentally related professions, and to adopt the principles of environmental ethics. In this context, the Climate, Environment and Innovative Solutions course plays an important role in raising individuals who can generate knowledge, solve problems, evaluate events with a critical perspective, possess advanced communication skills, have high empathy, and contribute to social and cultural development (Ministry of National Education, 2022; Gülersoy and Gülersoy, 2023).

The Climate, Environment, and Innovative Solutions course will enable students to perceive the variable and dynamic environment from a holistic perspective. While the concept of "environment" considers the natural and human environment as a whole, the concept of "environmental" refers to events and phenomena related to the environment. This course focuses primarily on the various environmental problems arising from the interaction of natural and human systems, and how to address these problems. For students to understand and evaluate these focused problems and ways to cope with them, and to develop their own solutions, they first need to have a holistic perspective. Students can gain a holistic perspective when they see examples of human impacts on an environmental system, the resulting environmental problems, and proposed solutions to ensure the sustainability of environmental systems, all presented together.

The aim of this research is to compare the 2026 Environment, Climate and Innovative Solutions Curriculum and its topics, published by the Ministry of National Education (MEB), from various perspectives as viewed through the lens of student approaches.

MATERIAL AND METHOD

The study was structured according to a qualitative research approach. In this context, the data used in the research were obtained from materials in which students' opinions were collected in writing. The study was conducted using data collected from 22 final-year students taking the Environmental Education course in the Science Education Department of the Faculty of Education at Trakya University during the Fall semester of the 2025-2026 academic year. The students consisted of 2 male and 20 female individuals. They were asked to express their impressions and experiences from their internships and program reviews on A4 paper. These data were then coded sequentially from 1 to 22. Below, some students' statements are presented and evaluated in the findings section.

RESULTS AND DISCUSSION

The Climate, Environment, and Innovative Solutions course consists of 6 units. The number of learning outcomes and durations for each unit are presented in Table 1. Based on this content, some of the data obtained from 22 students in this section are presented below.
The student in the S1 group expressed their thoughts about the course as follows: “This course aims to create environmental awareness and a sense of sustainable living among students. The inclusion of fundamental topics such as the concept of the environment, ecosystems, the use of natural resources, environmental problems, and climate change in the annual plan demonstrates that environmental education is addressed from a holistic perspective. Presenting the topics sequentially also helps children establish cause-and-effect relationships. Addressing the issue of climate change by linking it to human activities and environmental problems enables students to connect this process to their daily lives. Addressing environmental issues from both local and global perspectives helps children develop a sense of responsibility towards the environment.”

Table 1. Units, number of learning outcomes, and class hours for the Climate, Environment, and Innovative Solutions course (Ministry of National Education. 2026).

UNIT	Number of Learning Outcomes	Lesson Hours	Percentage%
1 CLIMATE CHANGE	1	8	11
2. ENVIRONMENT AND HUMANITY	4	10	14
3. ENVIRONMENTAL PROBLEMS	5	22	30
4. FUNDAMENTALS OF INNOVATIVE SOLUTIONS TO ENVIRONMENTAL PROBLEMS	4	10	14
5. DEVELOPING INNOVATIVE SOLUTIONS TO ENVIRONMENTAL PROBLEMS	4	18	25
SCHOOL-BASED PLANNING *	-	4	6
TOTAL	18	72	100

Student code S3 provides positive feedback regarding the course's contribution to developing students' environmental awareness. “The fact that the annual plan does not limit itself to addressing environmental issues solely at the institutional knowledge level, but focuses on current environmental crises such as climate change and sustainability, is considered a positive approach. Connecting the topics to the disciplines of biology, chemistry, and geography helps students perceive the ecosystem as a holistic structure rather than in separate parts. Addressing concepts such as carbon footprint, in particular, allows students to question their own environmental impact and develop a green career mindset. It is believed that this content-rich plan will significantly improve ecological literacy levels if theoretical knowledge is supported by students analyzing the problems they encounter in their living environment.”

The student code S4 indicates that the course is student-centered. "It has a holistic structure that addresses environmental and climate issues from a local to a global perspective. The content begins with the human-nature relationship and continues with topics such as cyclical nature, environmental problems, global climate change, the effects of climate change in Turkey, and sustainable development. The content aims to develop environmental awareness, a sense of responsibility, and an understanding of sustainable living among students. In addition to theoretical knowledge, the program prioritizes connecting it to daily life, project-based work, and raising awareness. Overall, the annual plan has a current, functional, and student-centered

content aimed at raising individuals who are sensitive, conscious, and active in addressing the environmental and climate issues of our time."

The student in course S6 finds the course insufficient in terms of content depth, application, and critical thinking, and expresses their thoughts as follows. "The annual curriculum in secondary education provides an important framework for developing environmental awareness and understanding of climate change.

The plan covers current issues such as climate change, the environment and people, environmental problems, and the foundations of innovative solutions to environmental problems. However, I believe the content is largely superficial, and fundamental scientific concepts such as greenhouse gases, the matter cycle, and the climate crisis are not explored in depth.

The limited number of weekly lesson hours leads to a large number of learning outcomes being achieved in a short period of time, and especially to project-based and application-based studies not being carried out effectively. Although projects and awareness-raising activities have been mentioned, the explanations for their implementation and evaluation are not clear enough. I also think that the repetition of teaching methods and techniques in a similar way for weeks on end causes the plan to remain monotonous in practice. I observe that the course content focuses primarily on developing individual awareness, and that the economic, social, and political dimensions of environmental problems are not sufficiently explored.

In conclusion, while the plan is functional in terms of raising basic awareness, I can say that it has areas that need improvement in terms of content depth, practicality, clarity of measurement and evaluation, and critical thinking skills."

Student S7 states that the subjects are covered superficially due to the low number of weekly class hours. "The annual plan for the climate, environment, and innovative solutions course implemented in secondary education provides an important framework for raising environmental awareness and understanding of climate change.

The plan covers current issues such as human-nature relations, environmental problems, global climate change, and sustainable development. However, it appears that the content is largely superficial, and fundamental scientific concepts such as greenhouse gases, the matter cycle, and the climate crisis are not explored in depth.

The limited number of weekly lesson hours leads to a large number of learning outcomes being delivered in a short period of time, and especially to project-based and application-based studies not being carried out effectively. Although projects and awareness-raising activities have been mentioned, the explanations regarding the implementation and evaluation of these activities are not sufficiently clear. Furthermore, the repetition of teaching methods and techniques in a similar manner throughout the weeks leads to the plan remaining monotonous in practice.

The course content appears to focus primarily on developing individual awareness, while the economic, social, and political dimensions of environmental problems are not adequately explored. In conclusion, while the plan is functional in terms of raising basic awareness, it has areas that need improvement in terms of content depth, practicality, clarity of measurement and evaluation, and critical thinking skills."

The student with code S8 expresses the positive and negative aspects of the course. "The annual plan for the Environmental Education and Climate Change course generally demonstrates a holistic, systematic, and student-centered approach.

The plan follows a flow that begins with "Climate Change" and ends with "School-based planning. This enables students to understand environmental and climate issues from simple to complex, and from local to global. Including current concepts such as ecological footprint, climate crisis, zero waste, recycling, and upcycling makes it easier for students to connect them to their daily lives.

In addition to direct instruction, active student participation is encouraged through methods and techniques such as field trips, observation, drama, project design, station activities, and brainstorming. The use of tools and resources such as textbooks, whiteboards, interactive whiteboards, slides, the internet, photographs, videos, and documentaries is planned. While the use of the internet and video is mentioned, the use of technological tools such as climate modeling, CO_2 monitoring applications, and digital mapping could be further encouraged. The plan could diversify methods such as more experimental and field studies, and digital simulations.

The emphasis placed on values such as justice, responsibility, respect, and patriotism in each learning outcome demonstrates that the course aims not only at imparting knowledge but also at developing attitudes and behaviors.

The plan incorporates Türkiye's specific impacts of climate change, mitigation efforts, and projects such as zero waste, enabling students to engage with the realities of the country. The inclusion of green professions and future employment fields demonstrates the course's aim to contribute to students' future plans. Different literacy areas are covered, such as environmental, water, agricultural, food, and financial literacy.

Students' awareness of global citizenship could also be strengthened by placing more emphasis on issues such as climate justice, global cooperation, and sustainable living practices. Overall, this plan stands out as a balanced and feasible plan aimed at developing environmental literacy in students. The suitability of the topics and learning outcomes for the age group, and their integration with values education, are the plan's strongest points."

The student code S10 indicates that the course helps students develop into environmentally conscious, responsible, and aware individuals. "Upon reviewing its content, I see that it is a contemporary course that aims not only to impart environmental knowledge to students, but also to cultivate students as environmentally conscious, responsible, and aware individuals. Activities such as project design, poster and brochure creation, and informing the local community encourage active student participation and ensure that learned information is applied to daily life. It's also very good that the achievements encompass local, national, and global dimensions. However, the program also has some limitations. The high number of learning objectives and the dense content in some units can lead to superficial learning, especially in classroom applications. Trying to fit such broad topics as global climate change, disasters, environmental pollution, and sustainability into a limited number of class hours can make time management difficult for teachers. Another issue is the potential for environmental problems and the climate crisis to instill intense anxiety and feelings of hopelessness in students. Furthermore, making field studies and observation activities focused on local environmental issues mandatory will enhance the retention of learning. The program can be strengthened with solution-oriented activities and more hands-on fieldwork."

Students coded S11 express current issues and solution-oriented thinking skills more effectively. "The spiral, holistic structure aimed at transforming environmental awareness from knowledge to behavior is reflected in the subject matter. The plan begins with climate change and progresses through topics such as the environment and people, environmental problems, the foundations of innovative solutions to environmental problems, developing innovative solutions to environmental problems, and school-based planning. The content is related to students' daily lives and includes concepts such as ecological footprint and greenhouse gases. The aim is to develop students' problem-solving skills, responsibility, and social awareness through sustainable development.

In general, the plan aims to cultivate individuals who are sensitive to environmental issues, by not only providing knowledge but also developing attitudes, values, and behaviors. In this respect, the course content contributes to students' ability to evaluate local and global

environmental problems in terms of cause-and-effect relationships and to acquire solution-oriented thinking skills."

The student with code S12 focused on the contribution of the course to responsibility and awareness. "When the 'Climate, Environment and Innovative Solutions' course curriculum is examined, it can be seen that the content is designed in a holistic structure that not only identifies environmental problems but also aims to equip students with multifaceted and vital competencies such as environmental, water, agricultural, and food literacy. In particular, integrating current and strategic issues such as the "zero waste" project and recycling into the curriculum encourages students to acquire practical skills in waste management, such as designing projects and developing products, rather than simply possessing theoretical knowledge. Furthermore, linking the causes and consequences of global climate change to its effects specific to Turkey, and exemplifying sustainable living models such as ecological villages in tranquil cities, demonstrates that the course aims to instill in students a global vision as well as a sense of local responsibility."

The student in question, code S14, argues that the course aims to make students responsible and environmentally conscious. "The purpose of the annual plan is to ensure lasting environmental awareness. It is holistic and continuousIt is student-centered. Looking at the first unit, climate change, it discusses greenhouse gases and global warming. I can say that this gives the topic a global dimension for the students. The second unit is Environment and Human. This unit discusses human-environment interaction and the harmony of the natural balance. The environmental problems unit aims to enable students to interpret human activities that cause environmental problems; to analyze the environmental impacts of air pollution, water scarcity and pollution, and soil degradation; and to interpret the environmental impacts of biodiversity loss. The importance of the student's sense of responsibility is emphasized. Production and consumption habits are discussed. Examples from daily life are given to enable the student to integrate the topic into their daily life. The unit "Fundamentals of Innovative Solutions to Environmental Problems" aims to enable students to analyze the importance of environmental rights and participation in solving environmental problems, to reason about environmental problems within the context of struggle strategies, to critique economic and social projects within the scope of the responsibilities imposed by international environmental agreements, and to interpret innovative projects in terms of their causes and consequences for environmental sustainability. The aim of the "Innovative Solutions to Environmental Problems" unit is for students to be able to empathize with stakeholders affected by the environmental problems they observe, to evaluate the research problem they have defined regarding developing innovative solutions to environmental problems, to develop innovative ideas for solving the defined problem, and to design a model for the innovative idea they have developed. Finally, this annual plan aims to foster a sense of responsibility and environmental awareness in students. The annual plan aims to help us develop a holistic perspective."

Student S16 expressed very positive opinions regarding the course. "Upon examining the annual plan for the 'Climate, Environment, and Innovative Solutions' course taught in secondary education, it is evident that the topics are addressed in a meaningful and pedagogically coherent manner. The plan's approach, starting with climate change and concluding with the concept of school-based planning, allows students to grasp environmental and climate issues from simple to complex, and from local to global levels. This structure contributes to understanding environmental problems in terms of cause-and-effect relationships.

Including current and frequently encountered concepts such as ecological footprint, climate crisis, zero waste, recycling, and upcycling in the annual plan makes it easier for students to relate the course content to their daily lives. In addition, addressing topics such as sustainable energy use, transportation, production and consumption habits, natural resource management, population growth, and migration helps students understand the multifaceted

nature of environmental problems. Furthermore, including different literacy areas such as environmental, water, agricultural, food, and financial literacy in the plan is an important element in supporting students' development as informed individuals.

The course delivery avoids relying solely on lectures; instead, it incorporates methods and techniques such as field trips, drama, role-playing, project development, station work, discussions, and case studies, encouraging active student participation and learning through doing. The use of tools such as textbooks, interactive whiteboards, visual and auditory materials, the internet, videos, and documentaries also aims to increase the retention of learning.

One of the striking aspects of the plan is that each learning outcome is linked to values such as justice, responsibility, respect, patriotism, and accountability. This demonstrates that the course aims not only to impart knowledge but also to develop environmentally conscious attitudes and behaviors.

In conclusion, the annual plan for the "Climate, Environment and Innovative Solutions Course" offers comprehensive and holistic content that addresses knowledge, skills, and values dimensions together, aiming to develop an awareness of sustainable living among students."
Student S20 states that the course is not only about transferring information but also about aiming for behavioral change. "Upon reviewing the annual plan, it is evident that the course has a holistic approach that addresses cognitive, affective, and behavioral goals together. The course content aims not only to teach students environmental concepts, but also to develop awareness and a sense of responsibility towards environmental problems.

The inclusion of current and globally significant topics such as climate change, global warming, greenhouse gases, carbon footprint, and sustainability in the introductory unit of the plan directly links the course to contemporary environmental issues. In this context, students become aware of the economic, social, and political consequences of climate change.

Furthermore, the inclusion of fundamental environmental concepts such as environment, ecosystem, biodiversity, and human-nature relations provides students with the necessary foundation to understand the global environmental problems discussed in later units.

The inclusion of individual and societal responsibilities towards environmental problems, environmental awareness, and environmental ethics in the annual plan demonstrates that the course is structured not only to impart knowledge but also to aim for behavioral change."

The student with code S21 argues that, with the necessary adjustments and enrichments, the course will be effective in raising environmentally conscious and responsible individuals. "The course generally has current and functional content aimed at instilling environmental awareness and climate change consciousness. The units' progression towards the relationship between the environment and people, and towards developing innovative solutions to environmental problems, shows that the topics are arranged from simple to complex. Including topics related to daily life such as ecological footprint consumption habits, water and energy conservation, helps students understand environmental problems in a concrete way. Furthermore, the program's strengths include supporting student active participation through project presentations and awareness-raising activities. The "Climate Change and Turkey" unit also allows students to become aware of its effects on our country. However, the high subject density in some units may create practical difficulties in terms of class hours.

The limited depth of the discussion of scientific concepts and the insufficient inclusion of concrete examples for measurement and evaluation are areas where the program needs improvement. While the impacts of disasters and climate change are significant, practical studies could be increased. Consequently, with necessary adjustments and enhancements, this course has the potential to play an effective role in fostering environmentally conscious and responsible individuals. or example, I used the book used in this course as a resource for preparing a lecture presentation. The topic was global climate change. The information is very vague, and it creates difficulties because the information given to the student is not fully related

to science. Topics related to science, such as the greenhouse effect and the carbon cycle, can be elaborated on in more detail."

The S22 program emphasized student development on a unit basis. "According to the annual plan I reviewed, the course comprises 6 units, 18 learning outcomes, and 72 lesson hours. The topics start with fundamental concepts and progress to more complex and global issues. This approach is good. It puts the student at the center. The topics raise the student's awareness. This is an important point. The first unit, "Climate Form," has quite detailed content. The topic addresses a current issue, including its causes and effects. However, it could have been supported with more examples from daily life. Students could have been asked to prepare materials such as drawings and posters. The second unit is "Environment and Human." This unit emphasizes establishing interaction between the student and their environment and fostering awareness of their surroundings. Out-of-school learning is included here, which is good but insufficient. More flexibility is needed in this area, adapting to city and school conditions. Depending on the school's circumstances, some lessons could be taught in the schoolyard, allowing for flexibility. In the second unit of "Circular Nature," the students were encouraged to become aware of the natural events happening around them. In the unit covering water and matter cycles, technological materials can be used to support the topics, contributing to more understandable and lasting learning. The environmental problems unit (Unit 3) specifically addresses environmental pollution. He/she presented this both locally and globally. That's good. However, he asked for an explanation and calculation of a concept like ecological footprint with examples. It would have been better if he/she had first specified what it is. The students may not have seen or heard of this concept before. It ensures greater sustainability. The unit on the foundations of innovative solutions to environmental problems addresses the importance of environmental rights and participation in solving environmental problems, reasoning about environmental issues, the ability to critique economic and social projects within the framework of responsibilities imposed by international environmental agreements, and the interpretation of innovative projects in terms of their causes and consequences for environmental sustainability. This unit aims to develop analytical, reasoning, and critical thinking skills. Connections are made to real life situations. In these respects, the topics are good. It aims to raise students as more conscious and sensitive citizens. I believe that this course should include more extracurricular learning activities (trips to national parks, etc.) to foster greater sensitivity and awareness by being in close contact with the environment."

DISCUSSION AND CONCLUSIONS

"The curriculum of the 'Climate, Environment and Innovative Solutions' course aims to contribute to the goal of enabling students to become individuals who can develop solutions to environmental problems." The curriculum aims for students to progress from actions to values, from values to virtuous individuals, and from virtuous individuals to the ultimate goal of being a "Peaceful Individual in a Livable Environment" within the framework of the Virtue-Value-Action Framework (Ministry of National Education, 2026).

The Climate, Environment, and Innovative Solutions Curriculum addresses climate change, the interaction of environmental systems with humans, and environmental problems. The curriculum also includes topics such as environmental problems, the fundamentals of innovative solutions, and the development of innovative solutions (Ministry of National Education, 2026).

The effectiveness of curriculum programs depends on the learning outcomes being at least at the understanding level of the cognitive process steps (Anderson and Krathwohl, 2001). This statement should not be interpreted as meaning that the learning outcomes included in the curriculum are more at the understanding level than at the cognitive process level. As the analysis results show, the Climate, Environment, and Innovative Solutions Curriculum focuses

more on learning outcomes at the comprehension level, while the number of learning outcomes at the higher-level cognitive process stages—analysis and creation, as well as application and evaluation—is insufficient. Compared to other curricula (Gökler, 2012; Büyükalan and Baysal, 2019; İlhan and Gülersoy, 2019a; İlhan and Gülersoy, 2019b; İlhan and Gülersoy, 2019c; Özdemir, 2020; Öztürk et al., 2020; Akhan, 2021; Alkın Şahin et al., 2022; Koca, 2022), the positive aspect is the existence of learning outcomes at the level of creation. Indeed, Mayer (2002) states that effective teaching is achieved through gains related to the application, analysis, evaluation, and creation steps of the cognitive process dimension (Gülersoy and Gülersoy, 2023).

The inadequacy of learning outcomes at the application and evaluation levels highlights a negative aspect of the program. In summary, it suggests that the course will not be sufficiently effective in achieving meaningful learning in terms of knowledge accumulation and cognitive process dimensions (Gülersoy and Gülersoy, 2023).

Education on disasters caused by climate change will become even more important in the future. In this regard, it has been observed that the learning outcomes and concepts related to disasters are included. Educating children about disasters is crucial for increasing societal resilience (Mızrak, 2018). Within the framework of this program, activities where students learn by doing and experiencing are needed to increase resilience against disasters. Education given only theoretically remains in underlined sentences in books, erased blackboards, and notebooks where notes are taken (Dere and Çinikaya; 2023).

Finally, it is deemed appropriate that the program is insufficient in terms of out-of-school learning environments and that the achievements related to out-of-school learning environments should be increased. However, research conducted in various fields within the literature highlights the cognitive, affective, and psychomotor contributions of out-of-school learning environments (Uludağ, 2017; Kuo et al., 2019; Altınbay and Gümüş, 2020; Bolu, 2021; Dere and Çifçi, 2022; Yıldız, 2022). Utilizing these pedagogical contributions can more effectively support the aims of environmental education (Dere and Çinikaya; 2023).

REFERENCES

Açıkalın, Ş, N., E. Sarı, Ş. Ş. Erçetin. 2024. Role of Education in Awareness on Climate Change. Current Perspectives in Social Sciences, 28(1): 56-63. https://doi.org/10.53487/atasobed.1454546

Akhan, O. 2021. Examining the Learning Outcomes in the 12th-Grade Republic of Turkey Revolution History and Kemalism Curriculum Based on the Revised Bloom's Taxonomy. ZfWT, 13(2): 109-124.

Alkın Şahin, S., N. Tunca Güçlü, C. D. Atan. 2022. Ortaokul Fen Bilimleri Dersi Öğretim Programı (2018) Kazanımlarının Mühendislik ve Tasarım Becerileri Açısından İncelenmesi. Uluslararası Batı Karadeniz Sosyal ve Beşerî Bilimler Dergisi, 6(1): 1-25.

Altınbay, R., N. Gümüş. 2020. Sosyal Bilgiler Öğretmenlerinin Sanal Tur Uygulamalarıyla İlgili Görüşleri. Journal of Innovative Research in Teacher Education, 1(1): 60-71. https://doi.org/10.29329/jirte.2020.321.5

Anderson, L., D. E. Krathwohl. 2001. A Taxonomy for Learning, Eaching and Assessing: A Revision of Bloom's Taxonomy of Educational Objectives. New York: Addison Wesley Longman Inc.

Anderson, A. 2010, September 16. Combating Climate Change Through Quality Education. Washington, DC: Brookings Global Economy and Development.

Aydın, R., M. Demirbaş. 2020. 21. Yüzyılın En Büyük Tehdidi: Küresel İklim Değişikliği. Ecological Life Sciences, 15(4): 163-179.
https://www.doi.org/10.12739/NWSA.2020.15.4.5A0143

Bolu, A. 2021. Okul Dışı Öğrenme Ortamlarının Fen Eğitimine Katkısına Yönelik Yönetici ve Öğretmen Görüşleri. Yayımlanmamış Yüksek Lisans Tezi, Pamukkale Üniversitesi.
Büyükalan Filiz, S., S. B. Baysal. 2019. Sosyal Bilgiler Dersi Öğretim Programı Kazanımlarının Revize Edilmiş Bloom Taksonomisine Göre Analizi. İnönü Üniversitesi Eğitim Fakültesi Dergisi, C/S. 20(1): 234-253.
Dere, F., T. Çifçi. 2022. Okul Öncesi Öğretmenlerinin Okul Dışı Öğrenme Ortamlarının Pedagojik Katkılarına İlişkin Görüşleri. Cumhuriyet International Journal of Education, 11(4): 681-695. https://doi.org/10.30703/cije.1116818
Dere, İ., C. Çinikaya. 2023. 2015 Çevre Eğitimi ve 2022 Çevre Eğitimi ve İklim Değişikliği Programlarının Çeşitli Boyutlar Açısından Karşılaştırılması. International Journal of Geography and Geography Education (IGGE), C/S. 49: 80-96.
Gökler, Z. S. 2012. İlköğretim İngilizce Dersi Hedefleri Kazanımları SBS Soruları ve Yazılı Sınav Sorularının Yeni Bloom Taksonomisine Göre Değerlendirilmesi. Yayınlanmamış Yüksek Lisans Tezi, Eskişehir Osmangazi Üniversitesi, Eğitim Bilimleri Enstitüsü, Eskişehir.
Gülersoy, A. E., Ö. Gülersoy. 2023. Çevre Eğitimi ve İklim Değişikliği Dersi (6, 7 veya 8. Sınıflar) Öğretim Programı Kazanımlarının Yenilenmiş Bloom Taksonomisi Bilişsel Alan Basamaklarına Göre Değerlendirilmesi. Jass Studies-The Journal of Academic Social Science Studies, 16(97): 1-16.
Hulme, M. 2016. İklim Değişikliği Konusunda Neden Anlaşamıyoruz? M. Özenç (Çev.). Alfa Yayıncılık.
İlhan, A., A. E. Gülersoy. 2019a. 10. Sınıf Coğrafya Dersi Öğretim Programı Kazanımlarının Yenilenmiş Bloom Taksonomisine Göre Değerlendirilmesi. lnternational Journal of Geography and Geography Education (IGGE), C/S. 39: 10-28.
İlhan, A., A. E. Gülersoy. 2019b. 9. Sınıf Coğrafya Dersi Öğretim Programı Kazanımlarının Yenilenmiş Bloom Taksonomisine (Bilişsel Alan) Göre Değerlendirilmesi. II. Uluslararası Coğrafya Eğitimi Kongresi (UCEK-2019), 8-10 Kasım, Eskişehir. 15
İlhan, A., A. E. Gülersoy. 2019c. 12. Sınıf Coğrafya Dersi Öğretim Programı Kazanımlarının Yenilenmiş Bloom Taksonomisine Göre Değerlendirilmesi. II. Uluslararası Coğrafya Eğitimi Kongresi (UCEK-2019), 8-10 Kasım, Eskişehir.
Karaaslan, H., T. Çetin. 2025. Çevre Eğitimi ve İklim Değişikliği Dersi (6, 7 veya 8. Sınıflar) Öğretim Programının Disiplinlerarası Öğretim Açısından Değerlendirilmesi. SDU International Journal of Educational Studies, 12(1): 67-80. Doi: 10.33710/sduijes.1662378
Kılıç, S. 2013. Çevre Etiği. Orion Kitabevi.
Koca, H. K. 2022. Ortaöğretim Din Kültürü ve Ahlak Bilgisi Öğretim Programı'nda Bulunan Bilişsel Kazanımların Yenilenmiş Bloom Taksonomisi'ne Göre İncelenmesi. Marife, C/S. 22 (1): 293-313.
Ministry of National Education. 2022. Çevre Eğitimi ve İklim Değişikliği Dersi Öğretim Programı (Ortaokul 6, 7 veya 8. Sınıflar), Ankara: Millî Eğitim Bakanlığı.
Ministry of National Education. 2026. İklim, Çevre ve Yenilikçi Çözümler Yıllık Plan 2025-2026. https://cografyahocasi.com/yillik-planlar/iklim-cevre-ve-yenilikci-cozumler-yillik plan.html?__cf_chl_f_tk=1hyjRSfMjV2mzwkCfppgF9z03dJyll6eVUcIkDHSG2c-1782939001-1.0.1.1
VAOfbe4djqjJgYx617.q2.vwsWyAwoBadOvq0JWTo_k#google_vignette
Kuo, M., M. Barnes, C. Jordan. 2019. Do Experiences with Nature Promote Learning? Converging evidence of a cause-and-effect relationship. Frontiers in Psychology, 10: 1-9. https://doi.org/10.3389/fpsyg.2019.00305
Mayer, R. E. 2002. Rote Versus Meaningful Learning. Theory Into Practice, C/S. 41(4): 226-232.
Mızrak, S. 2018. Eğitim, Afet Eğitimi ve Afete Dirençli Toplum. MSKU Eğitim Fakültesi Dergisi, 5(1): 56-67. https://doi.org/10.21666/ muefd.321970

Mochizuki, Y., A. Bryan. 2015. Climate Change Education in the Context of Education for Sustainable Development: Rationale and Principles. Journal of Education for Sustainable Development, 9(1): 4-26. https://doi.org/10.1177/0973408215569109

Official Gazette. October 7. 2021. Paris anlaşmasının onaylanmasının uygun bulunduğuna dair kanun. 20 Mayıs 2023 tarihinde https://www. resmigazete.gov.tr/eskiler/2021/10/20211007-7.pdf adresinden edinilmiştir.

Official Gazette. October 29. 2021. Bazı cumhurbaşkanlığı kararnamelerinde değişiklik yapılması hakkında cumhurbaşkanlığı kararnamesi. 20 Mayıs 2023 tarihinde https://www.resmigazete.gov.tr/eskiler/2021/10/20211029-35.pdf adresinden edinilmiştir.

Özdemir, Y. 2020. 2018 Lise Fizik, Kimya ve Biyoloji Öğretim Programlarının Yeni Bloom Taksonomisine Göre Karşılaştırmalı Analizi. Yayınlanmamış Yüksek Lisans Tezi, Marmara Üniversitesi, Eğitim Bilimleri Enstitüsü, İstanbul.

Öztürk, G., A. Karamete, G. Çetin. 2020. An Analysis of Learning Outcomes in Information Technologies and Software Curriculum based on Revised Bloom's Taxonomy. Cukurova University Faculty of Education Journal, C/S. 49(2): 1061-1097.

Stevenson, R. B., J. Nicholls, H. Whitehouse. 2017. What is Climate Change Education? Curriculum Perspectives, 37: 67-71. https://doi.org/10.1007/s41297-017-0015-9

Şen, Z. 2022. İklim Değişikliği ve Türkiye. Çevre, Şehir ve İklim Dergisi, 1(1): 1-19.

Türkeş, M. 2022. İklim Diplomasisi ve İklim Değişikliğinin Ekonomi Politiği. Bilim ve Ütopya, 332: 31-45.

Uludağ, G. 2017. Okul Dışı Öğrenme Ortamlarının Fen Eğitiminde Kullanılmasının Okul Öncesi Dönemdeki Çocukların Bilimsel Süreç Becerilerine Etkisi. Yayımlanmamış Doktora Tezi. Hacettepe Üniversitesi.

Ünder, H. 1996. Çevre Felsefesi. Doruk Yayımcılık.

Yıldız, E. 2022. Okul Öncesi Öğretmenlerinin Okul Dışı Öğrenme Ortamlarını Kullanma Durumlarının Değerlendirilmesi. Bayburt Eğitim Fakültesi Dergisi, 17(33): 94-127. https://doi.org/10.35675/befdergi.826566

Andrade, A., A. Vigliocco, S. Alemano, A. Llanes G. Abdala. 2013. Comparative Morpho-Biochemical Responses of Sunflower Lines Sensitive and Tolerant to Water Stress. American Journal of Plant Sciences, 4(12C): 156-167.

Ahmed S, Ahmad R, Ashraf MY, Ashraf M, Waraich EA. 2009. Sunflower (*Helianthus annuus* L.) response to drought stress at germination and seedling growth stages. *Pak. J. Bot*. 41(2): 647-654.

Arslan, B., Kaya, Y. 2019. Hybrid Sunflower Seed Production and Certification. Seed Science and Seed Technologies Book. 4 Volumes, 839-374. BISAB. Ankara, Turkey. 2154 pages.

Arslan, Ö., A. S. Balkan Nalçaiyi, Ş. Çulha Erdal, V. Pekcan, Y. Kaya, N. Çiçek, Y. Ekmekçi. 2020. Analysis of drought response of sunflower inbred lines by chlorophyll a fluorescence induction kinetics. Photosynthetica. 58 (SI): 163-172.

Ciçek, N., V. Pekcan, Ö. Arslan, Ş. Çulha Erdal, A. S. Balkan Nalçaiyi, A. N. Çil, V Şahin, Y. Kaya, Y. Ekmekçi. 2019. Assessing drought tolerance in field-grown sunflower hybrids by chlorophyll fluorescence kinetics. Brazilian Journal of Botany. 7(25): 1-12.

Ghaffari, M., M. Toorchi, M. Valizadeh, M. R. Shakiba. 2012. Morpho - Physiological Screening of Sunflower Inbred Lines under Drought Stress Condition. Turkish Journal of Field Crops.17(2):185-190.

Jocic, S., D. Miladinovic, Kaya Y. 2015. Breeding and Genetics of Sunflower. N. Dunford, E. M. Force (Ed) Sunflower: Chemistry, Production, Processing, and Utilization. 710 pages. AOCS (American Oil Chemistry Society. 1-26.

GENOMIC PREDICTION OF HEAD DIAMETER IN SUNFLOWER: COMPARING GWAS-DERIVED AND GENOME-WIDE FEATURE SETS ACROSS MACHINE LEARNING MODELS

[KEMAL AKKANAT]¹[EVREN OSMA]²

¹ [Computer Engineering Department, Engineering Faculty, Trakya University, Edirne, Türkiye]

2 [Natural Gas and Installation Technology, Vocational School, Beykent University, İstanbul, Türkiye]

Corresponding author e-mail: [evrenosma@beykent.edu.tr]

ABSTRACT

Head diameter is a key yield component in sunflower, yet most genomic studies of the trait stop at association mapping and rarely move toward predictive modeling. This gap matters because breeders care less about which SNP sits where and more about whether a genotype's future performance can be forecast before it ever reaches the field. Here we compared genomic prediction accuracy for head diameter across three feature representations, a compact GWAS-derived SNP set, a principal component set summarizing genome-wide variation, and a correlation-based LD-pruned set, using data from 274 sunflower accessions genotyped at 226,779 SNPs. Five models spanning linear and nonlinear families, Ridge, Lasso, Random Forest, XGBoost, and a multilayer perceptron, were evaluated under five-fold cross-validation. The best combination paired XGBoost with the GWAS-SNP feature set, reaching a mean R^2 of 0.632, consistently outperforming both larger genome-wide feature sets. A marker count analysis further showed that predictive accuracy plateaus once the number of markers approaches the size of the significant GWAS pool, around 112 SNPs; beyond that point, additional markers add little. These results indicate that a compact, association-informed marker panel can rival or exceed genome-wide predictors, offering a genotyping strategy that is both cheaper and more interpretable for sunflower breeding programs.

Keywords: Sunflower, Genomic prediction, GWAS, Machine learning, Head diameter, Marker economy

1. INTRODUCTION

Sunflower occupies a peculiar position among the world's oilseed crops: it supplies a substantial share of global vegetable oil while tolerating drought and marginal soils better than many of its competitors, standing out as a crop capable of stable yield across a wide range of environmental conditions (Badouin et al., 2017). That resilience is tied to a genome that took unusually long to characterize: the species carries roughly 3.6 gigabases of highly repetitive sequence, a technical obstacle that delayed the arrival of a usable reference genome for years (Badouin et al., 2017). When the assembly was finally resolved, it revealed clues about oil metabolism, flowering time, and the broader evolution of the Asterid lineage, opening the door to genome-scale association studies in a crop that had previously relied on far coarser tools (Badouin et al., 2017).

Among the traits breeders track in sunflower, head diameter holds a curious dual status: it is not merely one of several component traits determining seed yield, but also one of the easiest to measure in the field. Because it is comparatively easy to measure under field conditions, it has become a favorite target across breeding programs regardless of season or location (Delen

et al., 2022). Prior GWAS-based work on this trait reported substantial heritable variation: a panel of 342 accessions evaluated across the 2019, 2020, and 2022 growing seasons was combined into a single multi-year BLUP, yielding a broad-sense heritability estimate of 0.88 (Delen et al., 2022). That association study, conducted across 226,779 SNPs using both the mixed linear model and farmCPU, identified 106 and 8 significant markers respectively, of which 53 and 21 were located near annotated genes (Delen et al., 2022). A later version of the same work, extended to disc diameter, appeared in Plant Direct (Delen et al., 2024).

Genome-wide association studies (GWAS) test large numbers of single-nucleotide polymorphisms (SNPs)—individual DNA sequence variants—for statistical association with a trait of interest, and the statistical machinery behind such studies has become fairly standardized. Mixed linear models are widely used to control spurious associations driven by population structure (Yu et al., 2006), while farmCPU, introduced a decade later, offers a computationally leaner alternative that iterates between fixed and random effect components (Liu et al., 2016). Principal components are commonly used as covariates to correct for population stratification (Price et al., 2006), and PLINK remains a standard tool for filtering, pruning, and formatting genotype data for association analysis (Purcell et al., 2007).

What this literature does not yet do for sunflower is push past association mapping into prediction — and that next step matters. Significant SNPs become genuinely useful to a breeder once they can forecast the performance of untested individuals, and that forecasting task is where machine learning enters the picture; breeding programs benefit more from markers that improve prediction than from markers that are significant only in a statistical sense. Whether such methods actually improve on classical genomic prediction, and whether a compact GWAS-informed marker set can substitute for a full genome-wide panel, are questions that recent work in several other crops has begun to answer. The next section reviews that evidence before turning to the specific hypotheses tested here.

2. RELATED WORK

Whether machine learning genuinely outperforms classical genomic best linear unbiased prediction (GBLUP) remains an open question across crop species, with the answer depending on the trait, the population, and dataset size. In maize, GBLUP outperformed deep learning methods in eight of nine tested scenarios once a genotype-by-environment interaction term was included, yet the ranking reversed almost entirely once that term was dropped (Barreto et al., 2024). Sugarcane presents a starker case: because the crop is a highly non-additive, clonally propagated polyploid, an extended GBLUP model outpaced most machine learning approaches, with only a carefully tuned random forest coming close (Chen et al., 2023). In wheat, by contrast, deep learning methods surpassed GBLUP for two of five traits while performing comparably on the remaining three (Montesinos-López, A. et al., 2024). No single method wins consistently, which is precisely why feature engineering, rather than model choice alone, deserves closer scrutiny.

A more directly relevant question is whether a small set of markers, chosen for statistical significance in a prior GWAS, can match or beat predictions built from an entire genome-wide marker panel; evidence from several crops suggests it can. In oats, a study of 195 cultivars found that GWAS-derived marker subsets predicted plant height more accurately than the full genome-wide panel, with the best accuracy for that trait reached using only 100 GWAS-derived markers (Peng et al., 2025). A related pattern was reported in Russian sturgeon aquaculture, where GWAS-based SNP prioritization outperformed alternative selection strategies at densities of 10,000 markers and above, improving prediction accuracy by as much as 3.4 percent relative to whole-genome sequencing (Song, H. et al., 2025). In wheat, a framework called GRE, combining GWAS with random forest feature selection, produced marker subsets

that significantly outpredicted randomly chosen SNPs of the same size (Song, M. et al., 2025). Three unrelated crops, three converging conclusions: GWAS-informed feature selection can improve prediction without requiring the full marker panel.

Machine learning has also been folded directly into the GWAS pipeline itself, rather than applied only downstream of it. In soybean, support vector machines and random forests compared against classical MLM and farmCPU surfaced a richer set of marker-trait relationships tied to yield components than the classical methods alone (Yoosefzadeh-Najafabadi et al., 2021). The same research group later predicted multi-year yield component traits using an ensemble of a multilayer perceptron, a radial basis function network, and random forest, partially overcoming the limitations any single model showed on its own (Yoosefzadeh-Najafabadi et al., 2022). Wheat has recently seen a similarly direct comparison. Traditional GWAS tools were pitted against several machine learning approaches, including XGBoost and random forest, and the machine learning side proved particularly valuable for traits where epistatic effects appear to dominate (Milek et al., 2026).

Sample size remains an important limitation in these comparisons, particularly for deep learning methods: a recent review of multimodal deep learning approaches for genomic prediction noted that instability under small datasets is an expected outcome rather than an anomaly, since generalization capacity suffers when architectural complexity is not balanced against sample size (Montesinos-López, O. A. et al., 2024). This limitation is directly relevant here, as the present study works with a few hundred accessions rather than several thousand.

Taken together, this body of work supports two working expectations. Nonlinear ensemble methods often, though not always, edge out linear baselines, and compact GWAS-informed marker sets often rival or beat much larger genome-wide feature representations. Neither expectation has been tested in sunflower for head diameter, which is the gap this study addresses. We test three hypotheses. First, a small GWAS-selected SNP set should yield prediction accuracy comparable to, or better than, features derived from the entire genome. Second, nonlinear machine learning models, particularly Random Forest and XGBoost, should outperform the linear Ridge and Lasso baselines. Third, prediction accuracy should plateau once the number of markers used exceeds the informative core of the GWAS signal, a pattern with direct implications for how many markers a breeding program actually needs to genotype.

Table 1 situates the present study alongside these related comparisons of GWAS-informed and genome-wide prediction strategies across crop species.

Table 1. Summary of related GWAS-informed genomic prediction studies compared with the present study.

Study	Crop / system	Feature sets compared	Key finding
Barreto et al., 2024	Maize	GBLUP vs. deep learning (multi-environment, with/without G×E)	GBLUP outperformed deep learning in 8 of 9 scenarios when G×E was modeled; ranking reversed once the G×E term was dropped
Chen et al., 2023	Sugarcane	Extended GBLUP vs. machine learning	GBLUP outperformed most ML methods; only a carefully tuned random forest came close
Montesinos-López, A. et al., 2024	Wheat	Deep learning vs. GBLUP (5 traits)	Deep learning surpassed GBLUP for 2 of 5 traits and performed comparably on the remaining 3
Peng et al., 2025	Oats	100 GWAS-derived SNPs vs. full genome-wide panel (195 cultivars)	GWAS-derived subset predicted plant height more accurately than the full panel
Song, H. et al., 2025	Russian sturgeon	GWAS-prioritized SNPs (≥10,000 markers) vs. alternative selection strategies	Improved prediction accuracy by up to 3.4% relative to whole-genome sequencing
Song, M. et al., 2025	Wheat	GWAS + random forest (GRE)-selected subset vs. random SNPs of equal size	Selected subset significantly outperformed random SNPs of the same size
This study	**Sunflower**	**112 GWAS-SNP set vs. 100-component PCA vs. LD-pruned set (274 accessions, 226,779 SNPs)**	**GWAS-SNP set outperformed both genome-wide sets across all five models; XGBoost reached R^2 = 0.632, and accuracy plateaued near 112 markers**

3. MATERIALS AND METHODS

3.1 Plant materials, phenotyping, and genotyping data

Phenotypic data were drawn from a panel of 342 sunflower accessions evaluated for head diameter across the 2019, 2020, and 2022 growing seasons, following the design established by Delen and colleagues (Delen et al., 2022). Best linear unbiased predictions (BLUPs) combining the three seasons served as the trait values used throughout this study. After filtering for complete genotype and phenotype records, 274 accessions remained available for modeling.

Genotyping by sequencing yielded 226,779 SNPs across the panel, consistent with the marker density reported in the source study (Delen et al., 2022). Markers with a minor allele frequency at or below 0.05 were excluded prior to downstream analysis.

3.2 GWAS SNP selection and feature set construction

The GWAS-informed feature set was built from the union of significant SNPs identified by the two association mapping approaches applied in the source study, the mixed linear model (Yu et al., 2006) and farmCPU (Liu et al., 2016). Combining the significant hits from both methods

yielded a pool of 112 SNPs, which formed the basis of the GWAS-SNP feature set used in every subsequent model. Three feature representations were built and compared side by side.

The GWAS-SNP feature set used the 112 markers described above directly as model inputs. This set was intentionally compact and biologically anchored, since every marker had already cleared a significance threshold in prior association testing.

The PCA feature set summarized genome-wide variation using principal components derived from the full genome-wide marker panel. Components were retained up to the point where they cumulatively explained 65 percent of total genetic variance (Price et al., 2006), resulting in 100 components used as predictors. This set captures broad genome-wide structure but is less directly interpretable than individual markers, since a single component blends thousands of markers at once.

The LD-pruned feature set removed redundant, highly correlated markers from the genome-wide panel using a correlation-based pruning procedure, loosely following the spirit of standard LD-pruning workflows (Purcell et al., 2007). This step used pairwise correlation thresholding rather than PLINK's canonical linkage disequilibrium algorithm, a simplification that speeds computation without fully replicating the population-genetic rigor of a PLINK-based pipeline.

3.3 Models

Five models were trained on each of the three feature sets, spanning both linear and nonlinear families. Ridge (Hoerl and Kennard, 1970) and Lasso (Tibshirani, 1996) were implemented as standard regularized linear regressions. Random Forest (Breiman, 2001) and XGBoost (Chen and Guestrin, 2016) were configured as ensemble tree methods with typical hyperparameter ranges for tabular genomic data. A multilayer perceptron was included to represent a deep learning baseline, given its established but variable track record in genomic prediction settings with modest sample sizes (Montesinos-López, O. A. et al., 2024).

3.4 Evaluation, robustness checks, and software

Model performance was assessed under five-fold cross-validation, with R^2, root mean squared error, mean absolute error, and Pearson correlation reported for each model and feature set combination (Table 2 and Table 3).

To probe how prediction accuracy scales with marker density, subsets of K = 10, 25, 50, 100, 150, and 250 markers were tested for Random Forest, Ridge, and XGBoost, tracing an accuracy curve intended to reveal whether, and where, performance saturates (Table 4).

Because the phenotype data combines BLUP values across 2019, 2020, and 2022 without separate year-level records, a genuine leave-one-year-out external test was not possible. Two complementary robustness checks were used instead. The first repeated five-fold cross-validation across ten independent fold splits. The second ran thirty repetitions of a random train-test holdout at a 20 percent test proportion (Table 5). Analyses were implemented in Python using scikit-learn for the linear and Random Forest models, XGBoost for the boosted tree model, and PyTorch for the multilayer perceptron.

4. RESULTS

4.1 Phenotypic distribution

Head diameter values across the 342 phenotyped accessions followed a broadly unimodal distribution with a mean of 14.73 cm, a median of 15.07 cm, a standard deviation of 3.05 cm, and a mild negative skew (-0.38), consistent with a polygenic quantitative trait shaped by many

loci of small effect. Figure 1 marks the mean with a dashed line and the median with a dotted line, and shows values ranging from a minimum of 6.79 cm to a maximum of 22.76 cm. The 274 accessions used for model training and evaluation are the subset of this panel with complete paired genotype and phenotype records.

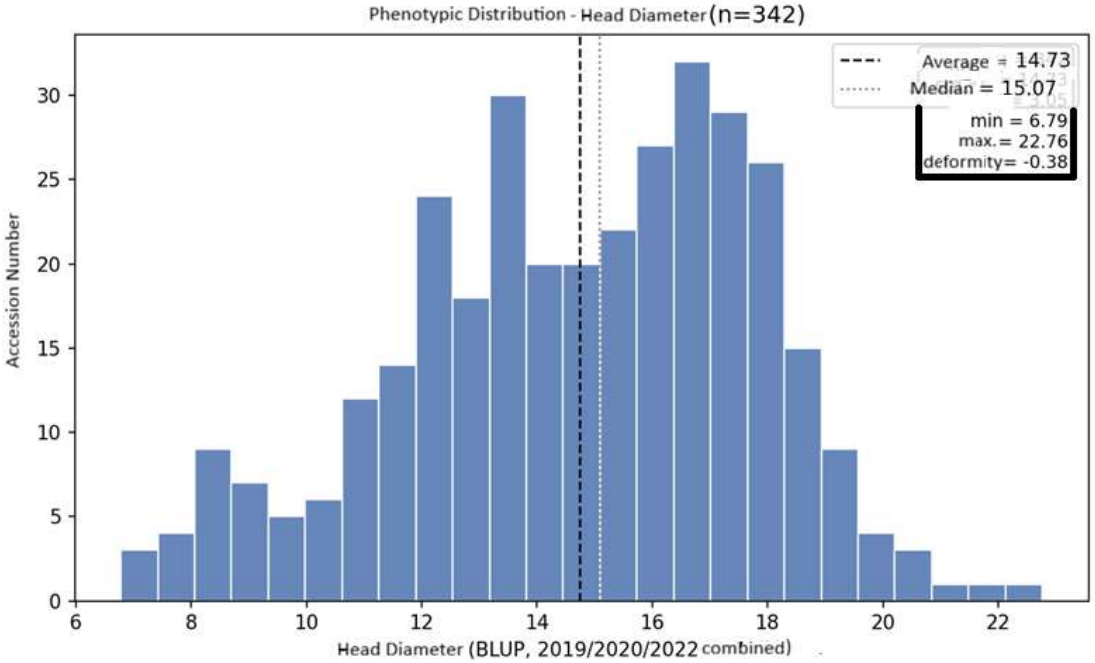

Figure 1. Distribution of head diameter BLUP values (2019/2020/2022 combined) across 342 sunflower accessions. Dashed line: mean (14.73 cm); dotted line: median (15.07 cm).

4.2 Model by feature set performance

Table 2 summarizes mean R^2 across five-fold cross-validation for every model and feature set combination.

Table 2. Mean R^2 by model and feature set (five-fold cross-validation).

Feature set	Lasso	MLP	Random Forest	Ridge	XGBoost
GWAS-SNP	0.611	0.302	0.593	0.500	0.632
LD-pruned	0.452	-1.104	0.519	0.504	0.566
PCA	0.163	-0.282	0.414	0.066	0.434

The best combination overall paired XGBoost with the GWAS-SNP feature set, reaching a mean R^2 of 0.632. Every model, without exception, performed best on the GWAS-SNP set and worst on the PCA set, a pattern that held regardless of whether the underlying algorithm was linear or tree based. Lasso on the GWAS-SNP set came remarkably close to XGBoost, at 0.611, suggesting that once the feature set itself is well chosen, even a comparatively simple linear model can perform competitively. The multilayer perceptron struggled across the board and turned sharply negative on the LD-pruned set, at -1.104, a clear sign of overfitting given the small sample size relative to the dimensionality of that feature set.

Table 3 breaks the GWAS-SNP result down further, reporting root mean squared error, mean absolute error, and Pearson correlation alongside R^2 for every model. XGBoost led on every metric simultaneously, not just R^2, with the lowest RMSE (1.880 cm) and MAE (1.518 cm) and the highest Pearson correlation (0.806) of any model on any feature set.

Table 3. Cross-validated performance metrics (mean ± SD), GWAS-SNP feature set.

Model	R^2	RMSE (cm)	MAE (cm)	Pearson r
Lasso	0.611 ± 0.061	1.944 ± 0.127	1.561 ± 0.154	0.794 ± 0.040
MLP	0.302 ± 0.300	2.565 ± 0.499	1.783 ± 0.210	0.652 ± 0.133
Random Forest	0.593 ± 0.095	1.986 ± 0.251	1.554 ± 0.162	0.782 ± 0.053
Ridge	0.500 ± 0.131	2.191 ± 0.255	1.683 ± 0.192	0.733 ± 0.073
XGBoost	0.632 ± 0.105	1.880 ± 0.265	1.518 ± 0.188	0.806 ± 0.058

Figure 2 places these same feature-set comparisons side by side as a bar chart, making it easier to see at a glance which model and feature-set combination is best suited to predicting head diameter. Error bars show one standard deviation of R^2 across the five folds, giving a visual sense of how consistent each combination was across different data partitions.

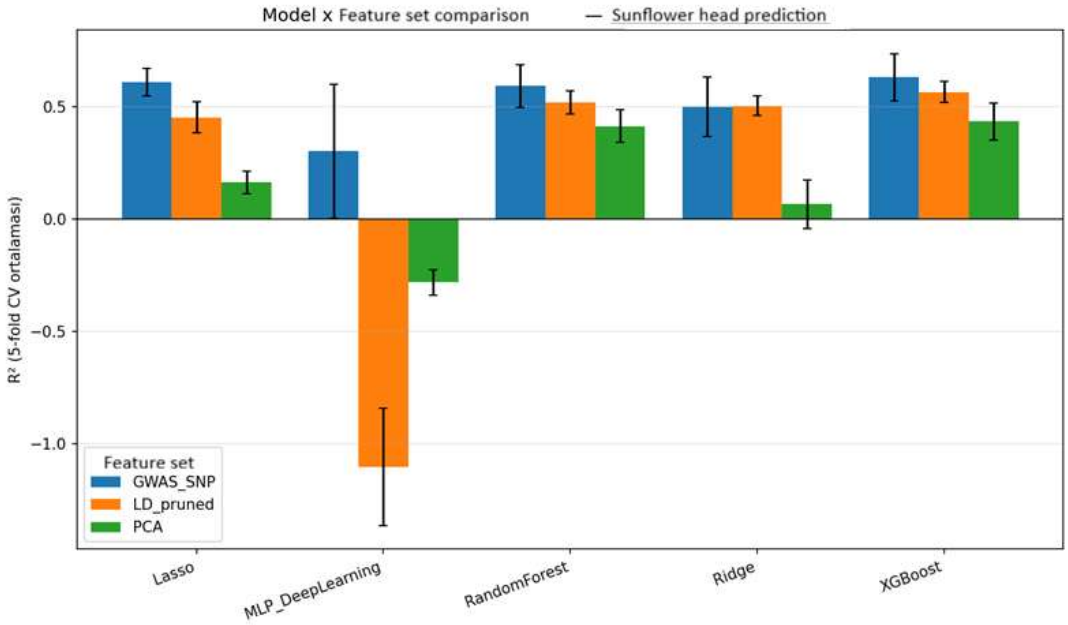

Figure 2. Mean cross-validated R^2 for each of the five models, grouped by feature set (GWAS-SNP, LD-pruned, PCA). Error bars show one standard deviation across folds.

4.3 Marker count and prediction accuracy

The marker count curve reinforced the pattern already visible in Table 2. Table 4 reports the full marker-density sweep, K = 10 to 250, for Random Forest, Ridge, and XGBoost.

Table 4. Mean R^2 as a function of marker count (K), five-fold cross-validation.

K	Random Forest	Ridge	XGBoost
10	0.502	0.452	0.522
25	0.510	0.442	0.524
50	0.513	0.441	0.543
100	0.509	0.458	0.556
150	0.595	0.500	0.659
250	0.595	0.500	0.659

Because the GWAS-SNP pool contains only about 112 markers in total, values of K beyond that point, namely K = 150 and K = 250, necessarily reuse the entire pool once it is exhausted, and the accuracy curve flattens as a result, identically for every model in Table 4. This flattening is not an artifact of the experimental design; it is itself evidence for marker economy, showing that no additional significant GWAS-SNPs remained available beyond the initial 112 to meaningfully push accuracy any higher. XGBoost benefited most from additional markers up to the plateau, climbing from 0.522 at K = 10 to 0.659 at K = 150, while Ridge gained comparatively little (0.452 to 0.500) over the same range.

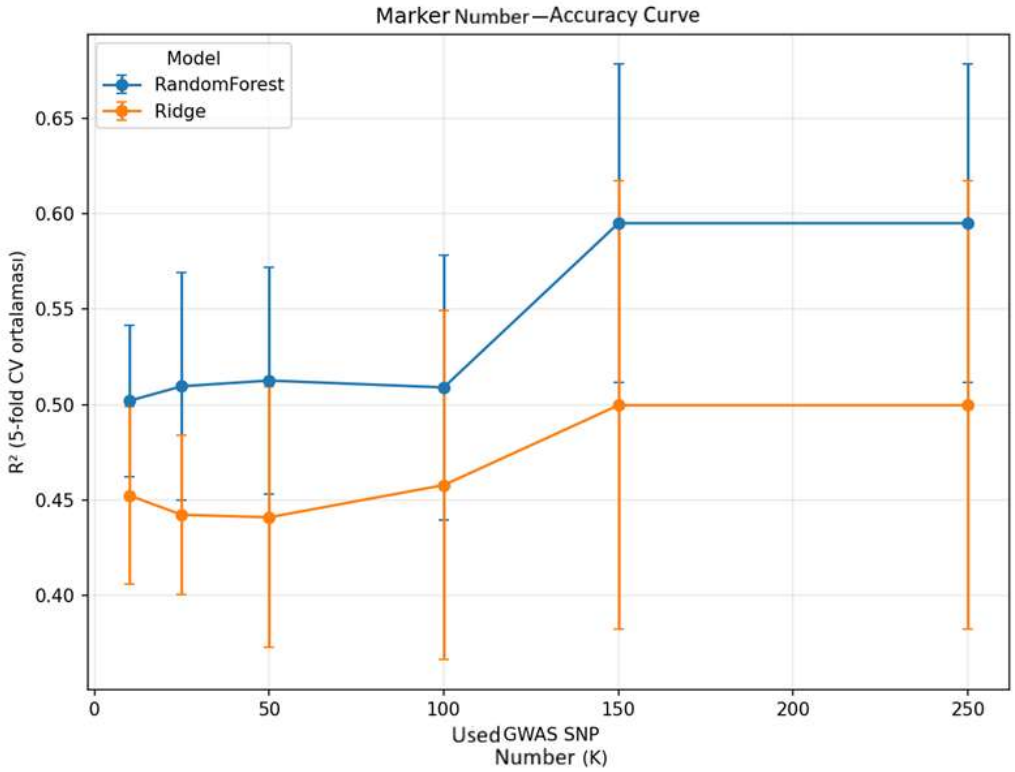

Figure 3. Marker count versus prediction accuracy, K = 10 to 250, for Random Forest and Ridge. The curve plateaus beyond the size of the significant GWAS-SNP pool (~112 markers).

4.4 Feature importance, SHAP analysis, and robustness checks

For the best performing combination, XGBoost trained on the GWAS-SNP set, gain-based feature importance identified which SNPs the model relied on most heavily (Table 6, Figure 4), while SHAP values described the direction and magnitude of each SNP's contribution to

predicted head diameter (Table 7, Figure 5). Together, these two views offer a biological explanation for why the GWAS-SNP set outperformed the larger feature sets. A small number of large-effect loci appear to dominate the signal, a pattern consistent with the concentrated genetic architecture reported by the original GWAS study for this trait (Delen et al., 2022).

Table 6. Top 15 SNPs by XGBoost gain-based feature importance, GWAS-SNP set.

Rank	SNP	Gain importance
1	NC_035442.2-15637958	0.506
2	NC_035442.2-14716876	0.169
3	NC_035442.2-12398885	0.073
4	NC_035442.2-14792234	0.042
5	NC_035442.2-15671785	0.028
6	NC_035442.2-10938079	0.026
7	NC_035442.2-14716897	0.014
8	NC_035442.2-17411583	0.013
9	NC_035442.2-17411417	0.011
10	NC_035448.2-31775666	0.008
11	NC_035442.2-94651944	0.008
12	NC_035445.2-52020671	0.007
13	NC_035442.2-14923270	0.006
14	NC_035445.2-100405520	0.006
15	NC_035448.2-31754150	0.005

Figure 4 renders the Table 6 ranking as a bar chart, making the relative size of each SNP's contribution easier to compare visually. Because gain-based importance only reflects how often and how effectively a marker is used to split the tree, it identifies which loci the model relies on most heavily without indicating whether higher genotype dosage raises or lowers predicted head diameter, a direction that is recovered separately below.

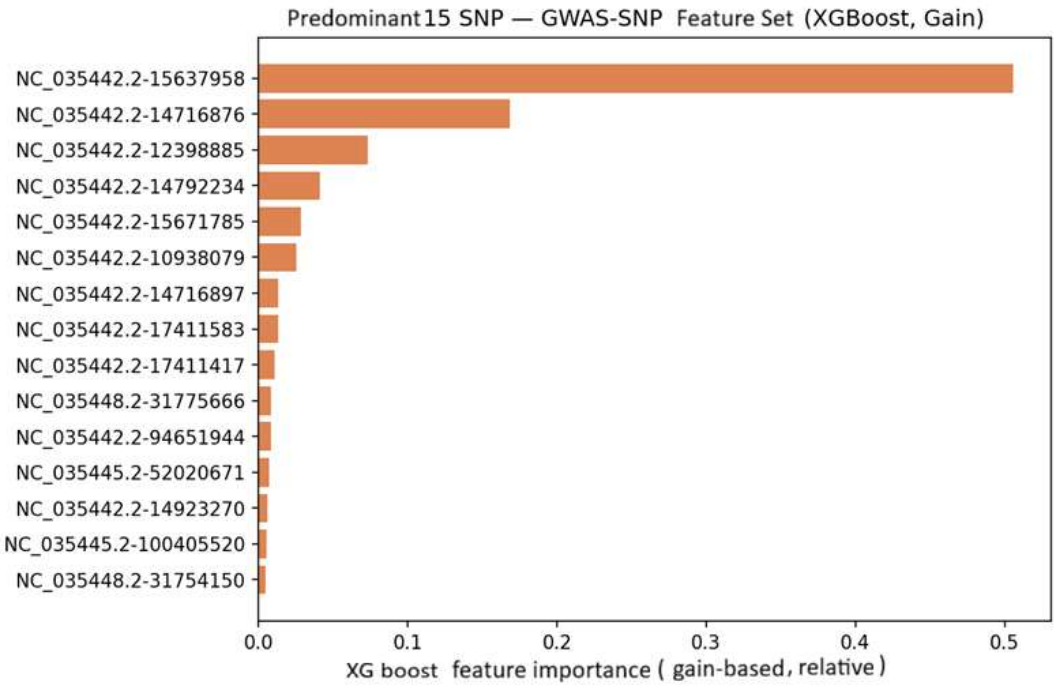

Figure 4. XGBoost gain-based feature importance, top 15 SNPs (GWAS-SNP set).

To recover that missing directional information, Table 7 reports SHAP (SHapley Additive exPlanations) values for the same set of top-ranked GWAS-SNP markers. Alongside the mean absolute SHAP value, which measures the overall magnitude of each SNP's contribution, the table also lists the mean signed SHAP value, indicating whether a marker's typical effect on predicted head diameter is positive or negative.

Table 7. Top 15 SNPs by mean absolute SHAP value, GWAS-SNP set (XGBoost).

Rank	SNP	Mean |SHAP|	Mean signed SHAP
1	NC_035445.2-100405520	0.658	0.001
2	NC_035435.2-160345299	0.600	-0.021
3	NC_035445.2-52020671	0.484	-0.002
4	NC_035437.2-67450339	0.405	0.001
5	NC_035436.2-20355884	0.349	0.000
6	NC_035442.2-14794596	0.327	0.011
7	NC_035442.2-10938079	0.300	-0.035
8	NC_035442.2-15637958	0.210	-0.008
9	NC_035448.2-31775666	0.202	-0.025
10	NC_035442.2-14716897	0.190	-0.030
11	NC_035448.2-31753915	0.171	0.028
12	NC_035442.2-94651944	0.140	0.014
13	NC_035442.2-17411417	0.131	-0.011
14	NC_035442.2-14716876	0.097	-0.008
15	NC_035442.2-15271146	0.084	0.009

Figure 5 visualizes these results as a SHAP beeswarm plot, with each point representing one accession. Point color encodes genotype dosage from low to high, and horizontal position encodes the SHAP value, capturing both the direction and magnitude of that SNP's contribution to the predicted trait. Unlike the gain-based ranking in Table 6 and Figure 4, this view makes it possible to see whether increasing dosage at a given SNP tends to raise or lower predicted head diameter, offering a more concrete basis for biological interpretation.

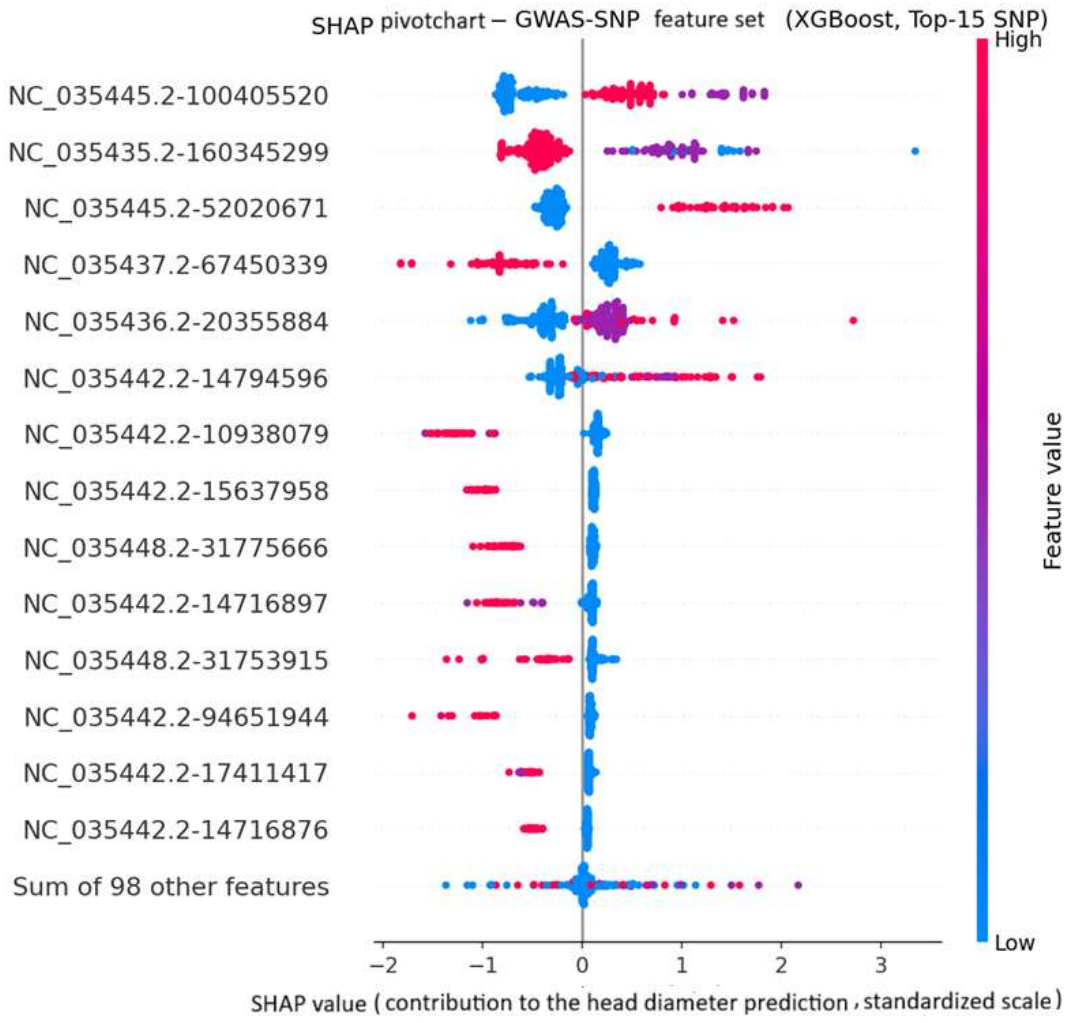

Figure 5. SHAP summary plot for the top 15 SNPs, GWAS-SNP feature set (XGBoost).

Two complementary robustness checks were run for the GWAS-SNP feature set: ten independent repeats of five-fold cross-validation, and thirty repetitions of a random train/test holdout at a 20 percent test proportion. Table 5 summarizes the resulting mean R^2 for each model alongside the original single-split figures from Table 2.

Table 5. Mean R^2 under three validation schemes, GWAS-SNP feature set.

Model	Single 5-fold CV	Repeated CV (10×5-fold)	External holdout (30×)
Lasso	0.611	0.595	0.571
Random Forest	0.593	0.591	0.588
Ridge	0.500	0.482	0.493
XGBoost	0.632	0.631	0.619

Figure 6 shows the full distribution of R^2 values behind the repeated-CV column in Table 5, rather than just its mean. Because ten independent reshuffles of the five-fold split were run for each model, fifty R^2 values are plotted per model, giving a fuller picture of how much the estimated accuracy depends on the specific way the data happen to be partitioned.

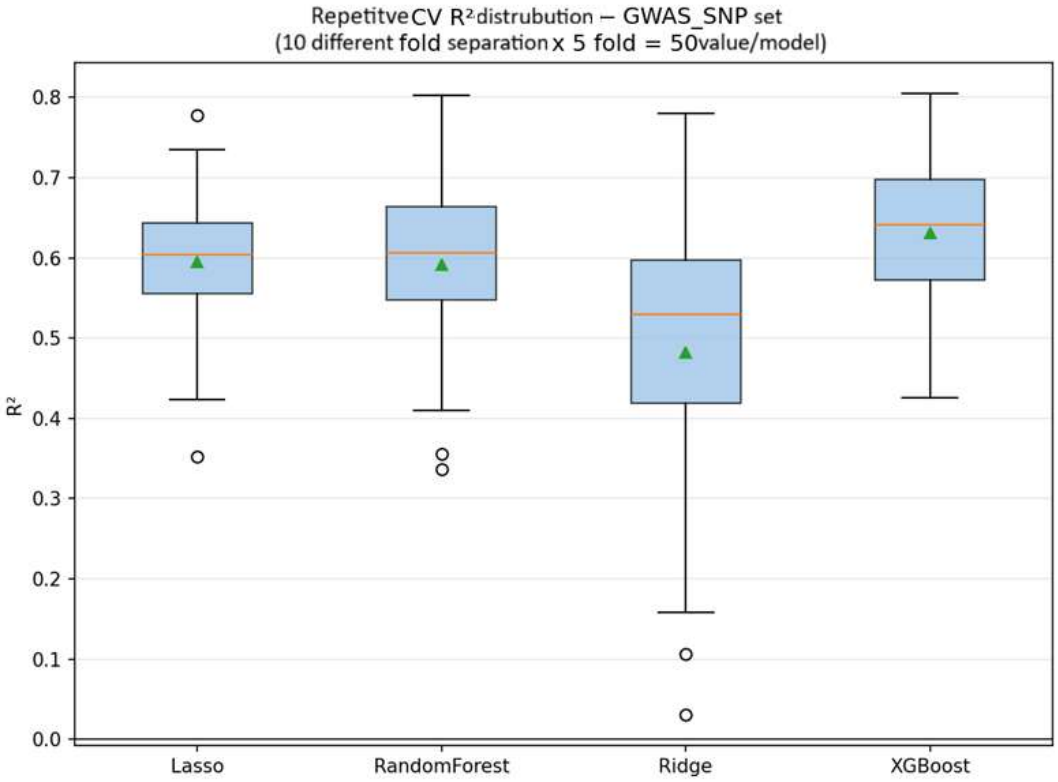

Figure 6. Distribution of R^2 across repeated 5-fold CV runs, GWAS-SNP feature set.

Within each boxplot in Figure 6, the green triangle marks the mean and the orange line marks the median R^2 across the fifty repeats. Figure 7 then steps back and compares all three validation schemes from Table 5 directly. A genuine leave-one-year-out external test could not be performed here, because the phenotype data combine BLUP values from the 2019, 2020, and 2022 seasons into a single record per accession rather than keeping separate year-level measurements; the repeated cross-validation and random holdout schemes shown below therefore serve as complementary robustness checks, confirming that the single-split results reported earlier in Table 2 are not simply an artifact of one particular, arbitrary partition of the data.

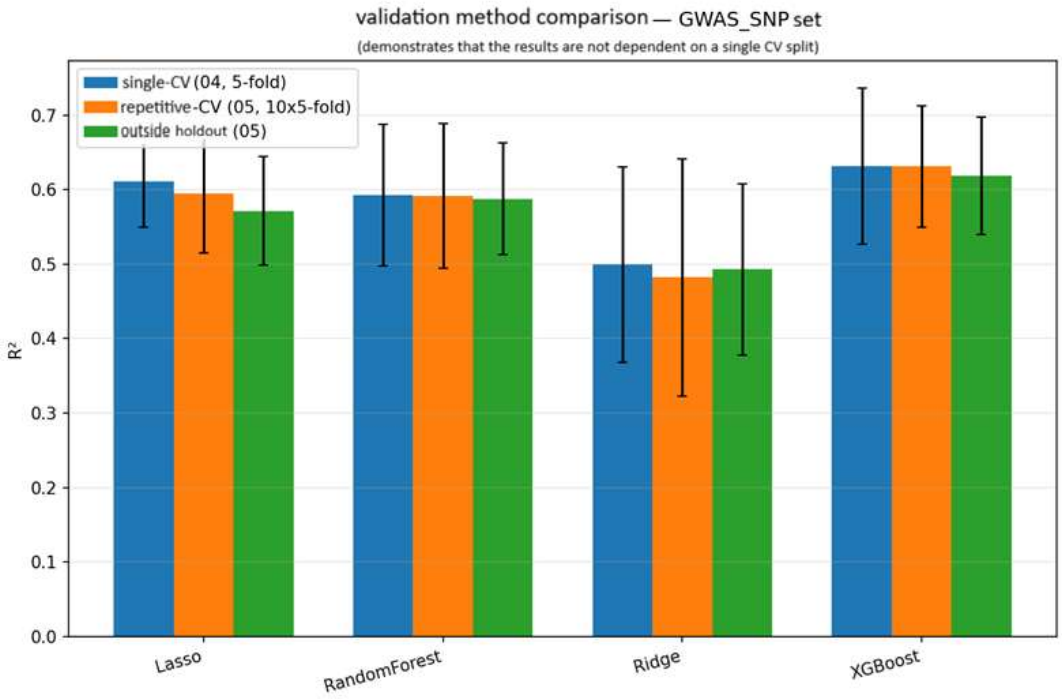

Figure 7. Mean R^2 across the three validation schemes in Table 5.

5. DISCUSSION

The central finding of this study is unambiguous: across every model tested, the GWAS-SNP feature set won, and it did not win by a narrow margin. XGBoost paired with GWAS-SNP markers reached a mean R^2 of 0.632 (Table 2, Table 3), outperforming the same algorithm trained on 100 principal components by nearly 0.2 in absolute terms. This supports H1 directly: a modest, biologically curated set of 112 markers carried more predictive signal than either a 100-dimensional summary of genome-wide variation or a correlation-pruned marker panel drawn from the same 226,779-SNP pool. The likely explanation lies in signal concentration. If head diameter is influenced by a relatively small number of loci with sizable individual effects, as the SHAP results in Table 7 and Figure 5 and the underlying association mapping both suggest (Delen et al., 2022), then feature sets built around those specific loci will naturally carry more usable information per predictor than diffuse, genome-wide summaries built to capture variance rather than trait-relevant signal.

The comparison between model families offers a more qualified answer to H2. XGBoost did edge out every other model on the GWAS-SNP set, and Random Forest also outperformed both linear baselines on two of the three feature sets. Yet the margin between XGBoost and Lasso on the GWAS-SNP set was small, just two hundredths of R^2. This narrow gap suggests that once the feature set itself has been well chosen, the choice of algorithm matters less than the literature sometimes implies. It echoes the maize and wheat findings summarized earlier, where the relative advantage of machine learning over linear or classical genomic prediction shifted depending on trait, dataset size, and whether interaction effects were modeled explicitly (Montesinos-López, A. et al., 2024; Barreto et al., 2024). Here, on a dataset of 274 accessions, nonlinear methods offered a real but not overwhelming advantage, and simpler linear models remained surprisingly competitive as long as they were fed the right inputs.

H3 was also supported, and the marker count curve in Table 4 and Figure 3 is arguably the most breeding-relevant result in this study. Accuracy climbed steadily as markers were added up to roughly the size of the significant GWAS pool, then flattened. Because K = 150 and K = 250

exceed the available pool of 112 significant SNPs, those higher values necessarily recycle the same markers, and the resulting plateau is a direct demonstration that additional genome-wide markers beyond the GWAS-informed core add little further predictive value. This mirrors what has already been observed in oats, where the best prediction accuracy for plant height was reached using just 100 GWAS-derived markers (Peng et al., 2025), and in sturgeon breeding, where GWAS-based SNP prioritization delivered the largest gains at moderate marker densities before returns diminished (Song, H. et al., 2025).

The practical implication for breeding programs is straightforward: achieving high prediction accuracy with a small, biologically meaningful marker panel lowers genotyping cost directly, a benefit that matters most for small and mid-sized programs operating under tight budgets. The oat study made this point explicitly, noting that a GWAS-informed marker strategy could both optimize prediction rates and reduce the number of markers a small-scale breeding program needs to genotype (Peng et al., 2025). The same logic applies with even more force in sturgeon aquaculture, where long generation intervals make genotyping cost a particularly critical constraint, and where GWAS-based SNP selection has already been proposed as a practical breeding strategy for exactly that reason (Song, H. et al., 2025). Sunflower breeding programs, especially those without access to dense genome-wide panels, stand to benefit from an analogous approach.

Several limitations temper these conclusions. It is worth remembering that association is not the same thing as proof. A SNP tied statistically to head diameter is not automatically the gene responsible for it, and confirming that link at the molecular level remains a separate task left to future research. The sample size, 274 accessions, is modest for genomic prediction work, and it likely explains the volatility seen in the multilayer perceptron results, consistent with reviews noting that deep learning models tend to destabilize on small datasets when architectural complexity outpaces available data (Montesinos-López, O. A. et al., 2024). The LD-pruned feature set relied on a simplified correlation-based method rather than a full PLINK pipeline, a shortcut that may have understated the true performance achievable from a properly pruned genome-wide panel (Purcell et al., 2007). The phenotype itself was a single multi-year BLUP rather than separate yearly measurements, which ruled out a genuine external validation across growing seasons and limited robustness testing to the resampling-based approaches reported in Table 5 instead.

Future work should address each of these gaps directly. A full PLINK-based LD-pruning pipeline would offer a fairer comparison against the GWAS-SNP set. An external test year, collected independently of the training panel, would provide the kind of validation that resampling alone cannot fully replace. Finally, deeper SHAP-based interrogation of the top-ranked SNPs in Table 7, paired with functional annotation, could help confirm or refute candidate gene hypotheses near the loci this study flagged as most influential.

6. CONCLUSION

This study shows that a compact, GWAS-derived panel of 112 SNPs predicts sunflower head diameter more accurately than either a 100-component genome-wide PCA representation or a correlation-pruned marker set drawn from the same 226,779-SNP pool, with XGBoost on the GWAS-SNP set reaching a mean R^2 of 0.632. Prediction accuracy plateaued once marker counts approached the size of the significant GWAS pool, reinforcing the case for marker economy. Together, these results suggest that breeding programs working with sunflower head diameter do not need dense genome-wide panels to forecast performance accurately: a small, interpretable, biologically grounded marker set can do the job just as well, and often better, while costing considerably less to genotype.

REFERENCES

Badouin, H., J. Gouzy, C. J. Grassa, F. Murat, et al. 2017. The sunflower genome provides insights into oil metabolism, flowering and Asterid evolution. *Nature*. 546(7656): 148-152.

Barreto, C. A. V., K. O. G. Dias, I. C. de Sousa, C. F. Azevedo, A. C. C. Nascimento, L. J. M. Guimarães, C. T. Guimarães, M. M. Pastina, M. Nascimento. 2024. Genomic prediction in multi-environment trials in maize using statistical and machine learning methods. *Scientific Reports*. 14: 1062.

Breiman, L. 2001. Random forests. *Machine Learning*. 45(1): 5-32.

Chen, T., C. Guestrin. 2016. XGBoost: A scalable tree boosting system. *Proceedings of the 22nd ACM SIGKDD International Conference on Knowledge Discovery and Data Mining*. 785-794.

Chen, Y., et al. 2023. Genomic prediction with machine learning in sugarcane, a complex highly polyploid clonally propagated crop with substantial non-additive variation for key traits. *The Plant Genome*. 16(4).

Delen, Y., R. V. Mural, G. Xu, S. Palali Delen, J. C. Schnable, J. Yang, I. Dweikat. 2022. Dissecting the genetic architecture of sunflower head diameter using genome-wide association study. *bioRxiv*.

Delen, Y., R. V. Mural, S. Palali-Delen, G. Xu, J. C. Schnable, I. Dweikat, J. Yang. 2024. Dissecting the genetic architecture of sunflower disc diameter using genome-wide association study. *Plant Direct*. 8(10).

Hoerl, A. E., R. W. Kennard. 1970. Ridge regression: Biased estimation for nonorthogonal problems. *Technometrics*. 12(1): 55-67.

Liu, X., M. Huang, B. Fan, E. S. Buckler, Z. Zhang. 2016. Iterative usage of fixed and random effect models for powerful and efficient genome-wide association studies. *PLoS Genetics*. 12(2): e1005767.

Milek, J. J., S. Michel, A. Buchelt, A. Holzinger, E. M. Molin. 2026. Applying traditional and machine learning-based GWAS approaches for marker-trait identification in wheat. *Frontiers in Plant Science*. 16: 1734247.

Montesinos-López, A., L. Crespo-Herrera, S. Dreisigacker, et al. 2024. Deep learning methods improve genomic prediction of wheat breeding. *Frontiers in Plant Science*. 15: 1324090.

Montesinos-López, O. A., M. Chavira-Flores, Kismiantini, L. Crespo-Herrera, C. Saint Piere, H. Li, R. Fritsche-Neto, K. Al-Nowibet, A. Montesinos-López, J. Crossa. 2024. A review of multimodal deep learning methods for genomic-enabled prediction in plant breeding. *Genetics*. 228(4): iyae161.

Peng, J., X. Lei, T. Liu, Y. Xiong, J. Wu, Y. Xiong, M. You, J. Zhao, J. Zhang, X. Ma. 2025. Integration of machine learning and genome-wide association study to explore the genomic prediction accuracy of agronomic trait in oats (Avena sativa L.). *The Plant Genome*. 18(1).

Price, A. L., N. J. Patterson, R. M. Plenge, M. E. Weinblatt, N. A. Shadick, D. Reich. 2006. Principal components analysis corrects for stratification in genome-wide association studies. *Nature Genetics*. 38(8): 904-909.

Purcell, S., B. Neale, K. Todd-Brown, et al. 2007. PLINK: a tool set for whole-genome association and population-based linkage analyses. *American Journal of Human Genetics*. 81(3): 559-575.

Song, H., W. Wang, T. Dong, X. Yan, C. Geng, S. Bai, H. Hu. 2025. Prioritized SNP selection from whole-genome sequencing improves genomic prediction accuracy in sturgeons using linear and machine learning models. *International Journal of Molecular Sciences*. 26(14): 7007.

Song, M., S. Zhang, S. Qiu, R. Qin, C. Zhao, Y. Wu, H. Sun, G. Liu, F. Cui. 2025. GRE: A framework for significant SNP identification associated with wheat yield leveraging GWAS-random forest joint feature selection and explainable machine learning genomic selection algorithm. *Genes*. 16(10): 1125.

Tibshirani, R. 1996. Regression shrinkage and selection via the lasso. *Journal of the Royal Statistical Society: Series B*. 58(1): 267-288.

Yoosefzadeh-Najafabadi, M., D. Tulpan, M. Eskandari. 2021. Application of machine learning and genetic optimization algorithms for modeling and optimizing soybean yield using its component traits. *PLOS ONE*. 16(4): e0250665.

Yoosefzadeh-Najafabadi, M., S. Torabi, D. Torkamaneh, D. Tulpan, I. Rajcan, M. Eskandari. 2022. Machine-learning-based genome-wide association studies for uncovering QTL underlying soybean yield and its components. *International Journal of Molecular Sciences*. 23(10): 5538.

Yu, J., G. Pressoir, W. H. Briggs, et al. 2006. A unified mixed-model method for association mapping that accounts for multiple levels of relatedness. *Nature Genetics*. 38(2): 203-208.

ELUCIDATING OXYGEN-CENTERED INTERACTIONS IN EUGENOL ADSORPTION ON ZN-DOPED *BIPHENYL NANOPARTICLES*

FATMA KANDEMIRLI[1], SERAP SENTURK DALGIC[2], SEYFETTIN DALGIC[2]

[1]Biomedical Engineering Department, Faculty of Engineering & Architecture, Kastamonu University, Kastamonu, Turkiye
[2]Department of Physics, Faculty of Science, Trakya University, 22030 Edirne, Turkiye

ABSTRACT

The interaction of bioactive molecules with functionalized aromatic nanostructures is of significant interest for applications in drug delivery and nanoscale sensing. In this study, the adsorption behavior of eugenol on Zn-doped biphenyl nanoparticles was investigated using density functional theory (DFT) calculations. Fully optimized geometries and energy analyses were performed to determine the preferred binding configurations and to elucidate the nature of the interaction mechanisms. The results reveal that the adsorption process is predominantly governed by interactions involving the oxygen-containing functional groups of eugenol, particularly the hydroxyl (-OH) moiety, which exhibits strong affinity toward the Zn active sites. This interaction is characterized by partial coordination between the oxygen atom and the Zn center, accompanied by charge transfer from the eugenol molecule to the nanoparticle surface. The calculated interaction energies indicate the formation of stable complexes, suggesting a favorable adsorption process. Such metal–oxygen interactions in doped nanostructures have been widely reported as key contributors to enhanced binding affinity and stability (Bader, 1990; Grimme, 2008). Furthermore, electronic structure analysis demonstrates significant redistribution of electron density and modification of frontier molecular orbitals upon adsorption, indicating potential changes in the electronic properties of the system. These findings are consistent with previous studies highlighting the role of heteroatom doping in tuning adsorption characteristics and enhancing molecular interactions in aromatic nanomaterials (Novoselov et al., 2004). Overall, this study provides detailed molecular-level insight into eugenol adsorption on Zn-doped biphenyl nanoparticles and supports their potential application as effective carriers for bioactive compounds.

Key words: Zn-doped biphenylene nanotube; eugenol; DFT; M06-2X; adsorption; QTAIM; RDG/NCI; density of states; nonlinear optical response; molecular sensing

INTRODUCTION

Eugenol (4-allyl-2-methoxyphenol) is a phenylpropanoid found at high abundance in clove essential oil. Its phenolic hydroxyl, methoxy substituent, allyl chain, and aromatic π system create chemically nonequivalent regions for coordination, hydrogen bonding, electrostatic attraction, and dispersion. These structural features underpin eugenol's reported antioxidant, antimicrobial, anti-inflammatory, analgesic, and antibiofilm activities (Pramod et al., 2010; Ulanowska and Olas, 2021; Ribeiro et al., 2024). They also make eugenol a useful molecular probe for asking how a bioactive aromatic compound engages a metal-modified carbon surface. Recent DFT studies of isolated and solvated eugenol and of eugenol adsorption on doped nanocages further illustrate how strongly the predicted response depends on molecular environment and substrate composition (Genç et al., 2025; de Paul Zoua et al., 2024). A molecular-level description of the present interaction is relevant to adsorption-based

recognition and to the preliminary design of carrier or sensing materials, while practical use additionally requires selectivity, release, toxicity, and transport studies.

Carbon nanostructures offer extended polarizable frameworks whose local electronic properties can be modified by curvature, finite size, edge termination, defects, and substitutional doping. Introducing a metal atom into a carbon network can redistribute charge and create a localized site that is more chemically responsive than the undoped framework. Prior calculations and reviews have shown that heteroatom or transition-metal modification can alter adsorption energies and frontier states of nanotube models (Durgun et al., 2004; Stoyanov et al., 2009; Zhang et al., 2014; Boshir Ahmed et al., 2023). In the present work, the calculated substrate is a finite Zn-substituted biphenylene nanotube fragment, denoted ZnBPNT. All mechanistic and electronic interpretations below refer specifically to this finite-cluster model.

Eugenol can approach ZnBPNT through at least three chemically plausible motifs. The methoxy oxygen may donate lone-pair density toward Zn; the phenolic oxygen may form a related oxygen-centered contact while retaining its O-H bond; or the aromatic face may engage the Zn-containing region through a spatially broader π-mediated interaction. These alternatives need not show the same ranking for every descriptor. A short contact can reflect localized coordination, whereas a larger fragment charge transfer or a smaller frontier-orbital separation can arise from delocalized coupling. Likewise, the most negative interaction energy need not yield the most favorable adsorption energy if the fragments pay different deformation penalties. The study therefore compares structural, energetic, electronic, topological, and response descriptors rather than using any single quantity as a proxy for binding.

The M06-2X meta-hybrid functional was selected because its high fraction of exact exchange and empirical parametrization generally provide useful performance for main-group thermochemistry and many noncovalent interactions (Zhao and Truhlar, 2008). Aromatic adsorption nevertheless remains challenging: dispersion, basis-set superposition, finite-cluster boundaries, and metal-site electronic structure can each influence small relative energies. High-level studies of aromatics on carbon nanotubes indicate that π–π and CH···π contributions can be substantial (Kar et al., 2008; Grimme, 2008; Pan and Xing, 2008), while experiments on phenolic adsorption emphasize the roles of aromaticity and substituent pattern (Lin and Xing, 2008). Consequently, numerical rankings separated by only a few tenths of a kilocalorie per mole should be regarded as effectively degenerate at the present level rather than as definitive selectivity.

Electronic descriptors were included to determine whether adsorption perturbs the finite ZnBPNT model. HOMO and LUMO energies, orbital distributions, fragment-resolved density of states, and charge redistribution can reveal coupling, but they do not directly supply a periodic band gap or electrical conductance. In the same way, static dipole moment, polarizability, and first hyperpolarizability describe molecular response tensors rather than macroscopic device performance. These distinctions are important because computational sensor studies sometimes equate a HOMO-LUMO shift with a measured resistance change without calculating transport. Here, the electronic analyses are used as screening-level evidence of perturbation, consistent with the broader literature on doped-carbon sensing models (Gowri Sankar and Udhayakumar, 2013; Wang and Yeow, 2009; Lu et al., 2015; Zhang et al., 2017; Zeng et al., 2018; Mubarok et al., 2022).

Real-space analyses provide a complementary view. The quantum theory of atoms in molecules (QTAIM) characterizes electron-density topology at critical points, whereas the reduced-density-gradient/noncovalent-interaction (RDG/NCI) approach maps attractive, weakly dispersive, and repulsive regions using $\mathrm{sign}(\lambda_2)\rho$ (Bader, 1990; Espinosa et al., 2002; Johnson et al., 2010). Molecular electrostatic-potential surfaces identify electron-rich oxygen and π regions that can face the Zn site (Suresh and Anila, 2023). Combined with adsorption, interaction, and deformation energies, these tools help distinguish localized Zn···O contacts

from the extended aromatic interaction. Multiwfn provides a consistent wavefunction-analysis platform for these descriptors (Lu and Chen, 2012).
This chapter therefore addresses three questions: which of the methoxy-directed, hydroxyl-directed, and phenyl-directed configurations are energetically competitive; how an implicit aqueous environment changes their structure and thermodynamics; and which electronic or topological signatures accompany adsorption. The analysis also separates supported conclusions from screening hypotheses. In particular, it treats desorption-time estimates as model-dependent, avoids converting finite-cluster orbital gaps into conductivity claims, and identifies the computational checks still needed before the material can be described as a selective carrier or sensor.

COMPUTATIONAL METHODS

Molecular Models and Adsorption Configurations

The isolated eugenol molecule, a finite Zn-substituted biphenylene nanotube fragment, and three eugenol/ZnBPNT complexes were optimized. Complex 1 (C1) places the methoxy oxygen O1 toward Zn; Complex 2 (C2) places the phenolic oxygen O2 toward Zn; and Complex 3 (C3) brings the center of the eugenol phenyl ring toward the Zn-containing region. Gas-phase and water-labelled continuum calculations were considered for each configuration. The three starting orientations probe distinct local minima rather than an exhaustive adsorption landscape, so the resulting ranking applies to the sampled motifs.
The optimized structures were treated as vibrational minima on the basis of positive listed lowest-frequency values. Because the units and detailed frequency treatment for those values were not retained in the computational metadata, they were not used quantitatively. The model is finite; consequently, its orbital energies and broadened density-of-states curves are molecular-cluster descriptors. They should not be interpreted as the band structure of an infinite biphenylene nanotube. Reproducible use of the finite model requires reporting its stoichiometry, edge termination, exact Zn substitution site, total charge, and spin multiplicity together with the optimized coordinates.

Electronic-Structure Protocol and Solvation

Density-functional calculations were carried out at the M06-2X/6-31G(d) level for the isolated fragments and the complexes. Geometry optimization and harmonic vibrational analysis were performed at the same stated level. An implicit aqueous treatment was applied to the same adsorption motifs. The electronic-structure software/revision, total charge and spin multiplicity, numerical thresholds, continuum variant, cavity definition, radii, and non-electrostatic solvent terms were not retained in the available computational metadata. The aqueous results are therefore comparative model estimates rather than protocol-independent hydration thermodynamics, and all tabulated structures are compared only on a like-for-like basis.
A 6-31G(d) description is computationally economical for a cluster of this size, but it is modest for quantitative metal-organic adsorption. Pople-type 6-31G basis functions are available for Zn (Rassolov et al., 1998), yet the present basis lacks diffuse functions and is not a high-accuracy choice for virtual orbitals, response properties, or weak binding. M06-2X was developed and benchmarked primarily for main-group thermochemistry and noncovalent interactions; its use at a Zn coordination site therefore needs an independent method check. No counterpoise-corrected adsorption energies were available. The absolute binding magnitudes may contain basis-set superposition error, and small C1-C3 differences should not be overinterpreted. A defensible validation hierarchy would include def2-TZVP or def2-TZVPD quality single points, a Zn-appropriate effective-core-potential/basis alternative, counterpoise

calculations, and a second functional. These checks are recommendations for future validation and are not represented as calculations already performed.
Several settings could not be verified: software revision, model formula and edge passivation, Zn-site indexing, total charge and multiplicity, integration grid, convergence thresholds, frequency scaling, and the exact continuum-solvation keyword. These unavailable settings limit exact reproduction and cross-method comparison. Only quantities with reproducible definitions are reported. A complete data record should include the missing metadata, optimized coordinates, and representative input files.

Energy, Charge, and Desorption Descriptors

Adsorption energy was defined as Eads = Ecomplex - Eeugenol(opt) - EZnBPNT(opt), so negative values indicate stabilization relative to the separately optimized fragments. Interaction energy was evaluated with each fragment frozen in its geometry within the complex: Eint = Ecomplex - Eeugenol(in complex) - EZnBPNT(in complex). The deformation penalty is Edef = Eads - Eint and is positive when fragment distortion costs energy. The tabulated identity Eads = Eint + Edef is satisfied within rounding for all six structures. Zero-point-corrected values and thermal free energies supplied by the harmonic calculations were used for the comparison. Because the frequency treatment and concentration convention are undocumented, the association free energies are method- and standard-state-sensitive. No additional 1 atm-to-1 M correction was applied.
Fragment charge transfer was taken from the reported population analysis as the electron transfer from eugenol to ZnBPNT. Because the population scheme was not retained in the computational metadata, these values are used to compare trends only. A screening desorption time was calculated from $\tau = \nu_0^{-1} \exp(|E_{ads,ZPE}|/RT)$, with T = 298.15 K and $\nu_0 = 10^{12}$ s^{-1}; this equation reproduces the tabulated values exactly. It assumes that the desorption barrier equals the magnitude of the ZPE-corrected adsorption energy and therefore is not a calculated kinetic barrier. In solution it omits diffusion, explicit solvent exchange, and competitive hydration.

Wavefunction, DOS, and Nonlinear-Optical Analyses

HOMO and LUMO energies and isosurfaces were examined for isolated eugenol, ZnBPNT, and C1-C3. Broadened TDOS, PDOS, and OPDOS curves were generated with Multiwfn 3.8. The spectra contain fragment-resolved contributions, but the complete atom-to-fragment mapping, broadening function, normalization, and energy reference were unavailable. The curves are therefore used only to assess aggregate state redistribution; specific adsorbate-framework-Zn assignments are not made. Positive and negative OPDOS features were interpreted conventionally as bonding and antibonding contributions at the corresponding orbital energies. Because a finite cluster has discrete levels, the curves visualize state mixing; the vertical reference is not a periodic-material Fermi level.
Electrostatic-potential, QTAIM, and RDG/NCI analyses were evaluated from the optimized wavefunctions. QTAIM interpretation used ρ, the $\nabla^2\rho$, and the total energy density H at an identified interaction critical point. Only gas-phase C1 and C2 critical-point values whose identity and numerical scale were internally consistent were retained. The aqueous C1 entry was excluded because its density, Laplacian, ELF, and sign(λ_2)ρ corresponded to a covalent intramolecular critical point and lay outside the displayed NCI range, indicating a mismatched critical-point assignment.
The molecular dipole magnitude, mean polarizability, polarizability anisotropy, and total first hyperpolarizability were obtained from the calculated response tensors. Polarizabilities are reported in 10^{-24} esu and β in 10^{-30} esu. Additional ΔQ and Q_off columns were excluded because their values are not electron-transfer charges and no reproducible definition was

available. Static molecular β values are treated as comparative response descriptors, not as bulk second-order susceptibility or an experimentally demonstrated optical switching signal.

RESULTS AND DISCUSSION

Geometry, Vibrational Minima, and Charge Redistribution

The optimized structures are summarized in Fig. 1 and the principal contacts in Table 1. In the gas phase, C1 and C2 form nearly equal Zn···O separations of 2.116 and 2.118 Å, respectively. C3 has a longer 2.699 Å Zn-to-phenyl-center distance, as expected for a spatially distributed aromatic contact. Water changes the contacts only modestly: C1 lengthens by 0.026 Å, C2 shortens by 0.002 Å, and C3 shortens by 0.048 Å. Geometry therefore establishes that both oxygen sites can approach Zn locally, but it cannot by itself rank methoxy versus hydroxyl adsorption.

The listed lowest-frequency values are positive and range from 4.05 to 15.33, but their units and frequency treatment were not retained. If they are wavenumbers in cm^{-1}, they correspond to very soft motions for which rigid-rotor/harmonic-oscillator entropies are especially sensitive. Free energies should therefore be compared more cautiously than electronic or ZPE-corrected energies. In addition, the presence of a reported local minimum does not prove global stability: alternative rotations, edge contacts, and adsorption sites were not sampled systematically.

Net charge transfer from eugenol to ZnBPNT is 0.1383, 0.1137, and 0.1447 e for gas-phase C1-C3. The corresponding water values rise to 0.1474, 0.1215, and 0.1620 e. C3 therefore gives the largest fragment charge displacement despite its longer geometric contact. This is chemically plausible for a delocalized phenyl interaction, but the trend should not be equated with a stronger localized bond. C2 gives the smallest transfer in both media, showing that the phenolic oxygen can form a short contact without producing the largest whole-fragment electron redistribution.

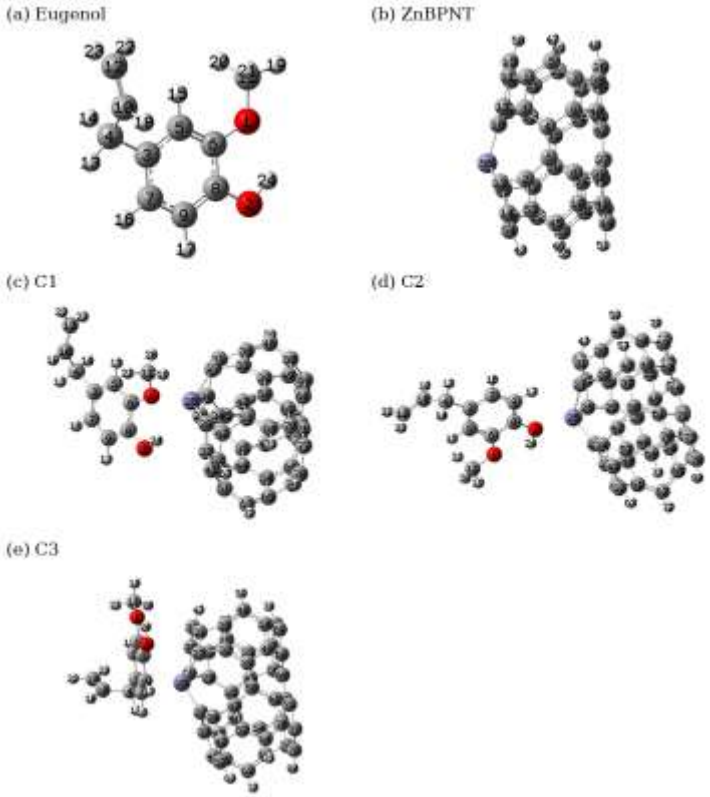

Fig. 1: Optimized gas-phase structures: (a) eugenol, (b) ZnBPNT, (c) methoxy-directed C1, (d) hydroxyl-directed C2, and (e) phenyl-directed C3. Atom numbers follow the optimized models.

Table 1: Principal contacts, reported fragment charge transfer to ZnBPNT, and screening desorption-time estimates at 298.15 K. O1 is methoxy oxygen and O2 is phenolic oxygen.

Motif	Medium	Contact (Å)	q to ZnBPNT (e)	τ (s)
C1, O1···Zn	Gas	2.116	0.1383	5.41×10^{2}
C2, O2···Zn	Gas	2.118	0.1137	2.84×10^{-2}
C3, ring···Zn	Gas	2.699	0.1447	3.73×10^{2}
C1, O1···Zn	Water	2.142	0.1474	4.46×10^{-4}
C2, O2···Zn	Water	2.116	0.1215	1.59×10^{-8}
C3, ring···Zn	Water	2.651	0.1620	1.76×10^{-4}

The screening desorption times span many orders of magnitude because of the exponential energy dependence. Gas-phase estimates are 5.41×10^{2} s for C1, 2.84×10^{-2} s for C2, and 3.73×10^{2} s for C3; water-labelled estimates are far shorter. These numbers help compare the six calculations under one assumed prefactor, but they are not recovery times measured or obtained from transition states. In particular, using a continuum adsorption energy as a solution-phase desorption barrier ignores solvent reorganization and mass transport. They are therefore retained only as transparent screening descriptors.

Adsorption, Interaction, Deformation, and Free Energies

The energy decomposition in Table 2 changes the initial structural picture. Gas-phase ZPE-corrected adsorption energies are -20.10, -14.26, and -19.88 kcal mol^{-1} for C1-C3. C1 is nominally lowest, but its 0.22 kcal mol^{-1} separation from C3 is far below the expected uncertainty of the functional/basis model. The scientifically defensible interpretation is that the methoxy-directed and phenyl-directed minima are effectively co-preferred at this level, whereas hydroxyl-directed C2 is clearly less favorable by about 5.6-5.8 kcal mol^{-1}.

Table 2: Zero-point-corrected energy components and thermal association free energies (kcal mol^{-1}). Negative Eads and Eint denote stabilization; Edef is the positive deformation penalty.

Motif	Medium	Eads,ZPE	Eint,ZPE	Edef,ZPE	ΔGads
C1	Gas	-20.10	-22.90	2.80	-9.03
C2	Gas	-14.26	-21.56	7.30	-2.97
C3	Gas	-19.88	-22.88	3.00	-7.35
C1	Water	-11.80	-13.29	1.49	0.04
C2	Water	-5.73	-12.25	6.51	5.15
C3	Water	-11.25	-12.21	0.96	1.73

C1 and C3 also have essentially identical gas-phase interaction energies (-22.90 and -22.88 kcal mol^{-1}). Their adsorption difference arises from deformation costs of 2.80 and 3.00 kcal mol^{-1}. C2 still has a favorable interaction energy of -21.56 kcal mol^{-1}, but a 7.30 kcal mol^{-1} deformation penalty substantially weakens its net adsorption. This distinction resolves an apparent contradiction: similar 2.12 Å Zn···O distances in C1 and C2 do not imply similar

adsorption because the hydroxyl-directed geometry requires much greater reorganization of the fragments.

Thermal corrections preserve the gas-phase ranking. Association free energies are -9.03 kcal mol^{-1} for C1, -2.97 for C2, and -7.35 for C3. The less negative values relative to Eads,ZPE reflect the entropic cost of bringing two molecular fragments together. C1 remains nominally most favorable, followed by C3. Given low-frequency modes and the missing standard-state correction, however, the exact free-energy spacing should not be viewed as high-accuracy thermodynamics.

The implicit aqueous treatment weakens all ZPE-corrected adsorption energies to -11.80, -5.73, and -11.25 kcal mol^{-1}. C1 and C3 remain close, whereas C2 remains distinctly weaker. Interaction energies similarly decrease in magnitude to -13.29, -12.25, and -12.21 kcal mol^{-1}. The C3 deformation penalty falls to only 0.96 kcal mol^{-1}, indicating that its extended aromatic geometry accommodates the interaction with little distortion. C2 retains a large 6.51 kcal mol^{-1} penalty, again explaining why a short Zn···O2 distance is not sufficient for strong net adsorption.

Aqueous association free energies are 0.04, 5.15, and 1.73 kcal mol^{-1} for C1-C3. On the uncorrected continuum/RRHO convention reported here, C1 is approximately thermoneutral and C2/C3 are positive after thermal and entropic terms. Their signs must not be treated as protocol-independent, however. For a bimolecular association, changing from a 1 atm ideal-gas convention to 1 M at 298.15 K would shift ΔG by about -1.89 kcal mol^{-1}, enough to change the signs of C1 and C3 but not C2. Low-frequency entropy treatment can also move values on this scale. The robust conclusion is therefore that the aqueous estimates are substantially less favorable than the gas-phase values and are sensitive to standard state and RRHO treatment, not that spontaneous solution binding has been definitively excluded. Explicit hydration and conformational sampling would be needed to predict binding in solution.

Overall, the energetic results support two mechanistic regimes. C1 uses localized methoxy-O···Zn interaction and low deformation; C3 uses a broader aromatic contact with nearly identical intrinsic interaction and larger fragment charge transfer. C2 forms a geometrically short phenolic-O···Zn contact but pays a much larger deformation cost. Oxygen-centered attraction is qualitatively important, but the numerical results do not establish phenolic-OH adsorption as the strongest configuration. The nominal optimum is C1, and C1/C3 are effectively degenerate within method uncertainty.

Frontier Orbitals and Electrostatic Response

The gas-phase ZnBPNT HOMO is -5.032 eV; the corresponding LUMO is -2.584 eV and the molecular gap is 2.447 eV. Isolated eugenol has a much larger 8.041 eV gap. After adsorption, gas-phase gaps are 2.517, 2.629, and 2.472 eV for C1-C3. All three are slightly larger, not smaller, than that of bare ZnBPNT. C3 has the smallest gap among the complexes but increases the bare-cluster value by 0.0245 eV. C2 produces the largest increase, 0.1819 eV.

The same pattern holds in the aqueous calculations. The ZnBPNT gap is 2.595 eV, compared with 2.615, 2.757, and 2.612 eV for C1-C3. Thus adsorption changes the gap by about 0.02 eV for C1 and C3 and 0.16 eV for C2. These shifts demonstrate configuration-dependent orbital perturbation but do not support the earlier claim of adsorption-induced gap narrowing. Nor can they be translated directly into conductivity: the model is a finite molecule, Kohn-Sham eigenvalue differences are not quasiparticle gaps, and no electrode coupling or transport calculation was performed.

The orbital isosurfaces in Fig. 2 nevertheless show that adsorption redistributes frontier density across the coupled structure. The HOMO and LUMO remain largely associated with the extended ZnBPNT framework, while the eugenol orientation changes the local amplitude and

degree of mixing. The larger C3 fragment charge transfer is consistent with electronic communication through the aromatic system even though its gap shift is small. C2's larger gap change coexists with its weaker adsorption, reinforcing that electronic perturbation and thermodynamic stability are distinct observables.

Table 3: Frontier molecular-orbital energies and HOMO-LUMO separations for isolated species and the three adsorption motifs.

System	Medium	HOMO (eV)	LUMO (eV)	Gap (eV)
Eugenol	Gas	-6.841	1.201	8.041
Eugenol	Water	-7.044	1.009	8.053
ZnBPNT	Gas	-5.032	-2.584	2.447
ZnBPNT	Water	-5.044	-2.449	2.595
C1	Gas	-4.877	-2.360	2.517
C1	Water	-5.056	-2.441	2.615
C2	Gas	-4.847	-2.218	2.629
C2	Water	-5.137	-2.380	2.757
C3	Gas	-4.797	-2.326	2.472
C3	Water	-5.022	-2.410	2.612

Electrostatic-potential surfaces locate negative potential around both eugenol oxygen atoms and a delocalized potential over the aromatic ring. The electron-rich methoxy oxygen faces the Zn region in C1, and the phenolic oxygen does so in C2. C3 instead aligns its π surface with the Zn-containing zone. These maps rationalize the three starting orientations but cannot quantify binding by themselves because the displayed colors depend on a chosen electron-density isosurface and potential scale. Their value is mechanistic: they identify complementary regions consistent with the optimized contacts and charge redistribution.

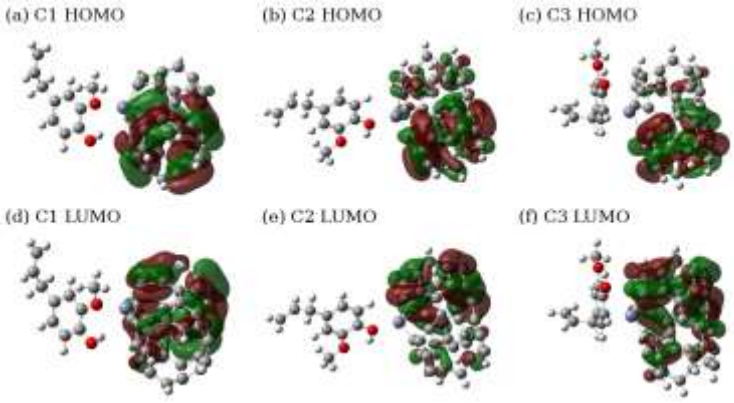

Fig. 2: Gas-phase HOMO and LUMO isosurfaces of C1-C3. Because the numerical isovalue was not retained, comparisons are qualitative.

Nonlinear-Optical Response Descriptors

The response properties in Table 4 are reported with corrected units. Gas-phase ZnBPNT has a dipole moment of 1.034 D, mean polarizability of 76.27×10^{-24} esu, anisotropy of 34.66×10^{-24} esu, and first hyperpolarizability of 79.94×10^{-30} esu. Eugenol is much less polarizable because of its smaller electron cloud. Complex polarizabilities cluster near 91-93 $\times 10^{-24}$ esu, close to

the additive scale expected from the two fragments. Adsorption therefore changes the spatial distribution of response more clearly than it produces a large superadditive polarizability.

Table 4: Static molecular response descriptors: dipole moment μ, mean polarizability α and anisotropy Δα (10^{-24} esu), and first hyperpolarizability β (10^{-30} esu).

System	Medium	μ (D)	α	Δα	β
Eugenol	Gas	1.022	15.95	10.54	3.05
Eugenol	Water	1.311	20.61	13.83	1.97
ZnBPNT	Gas	1.034	76.27	34.66	79.94
ZnBPNT	Water	2.146	139.21	56.56	289.05
C1	Gas	1.818	92.89	29.18	58.29
C1	Water	2.931	160.50	51.78	265.23
C2	Gas	2.397	90.78	28.25	43.63
C2	Water	2.833	149.23	53.87	184.55
C3	Gas	2.400	92.79	31.95	66.95
C3	Water	3.990	161.37	57.79	260.54

Among gas-phase complexes, dipole moments are 1.818, 2.397, and 2.400 D for C1-C3. Their β values are 58.29, 43.63, and 66.95 × 10^{-30} esu. C3 has the largest β of the three complexes, but it remains below the isolated ZnBPNT value. Thus a larger permanent dipole or fragment charge transfer does not guarantee a larger first hyperpolarizability. The tensor response depends on the directions and energy denominators of field-induced charge redistribution, not simply on static charge separation (Junqueira et al., 2016; Song and Wang, 2021; Tsapi et al., 2023).

The aqueous calculations produce much larger values: β is 265.23, 184.55, and 260.54 × 10^{-30} esu for C1-C3, and the isolated aqueous ZnBPNT value is 289.05 × 10^{-30} esu. Relative to ZnBPNT in the same environment, adsorption lowers β by about 8.2%, 36.2%, and 9.9% for C1-C3; the corresponding gas-phase decreases are about 27.1%, 45.4%, and 16.2%. Thus the large water-labelled numbers reflect solvent polarization, not an adsorption-induced enhancement over the bare substrate. Complex 3 also has the largest dipole moment (3.990 D), mean polarizability (161.37 × 10^{-24} esu), and anisotropy (57.79 × 10^{-24} esu). These static continuum values remain qualitative because diffuse functions are absent and the response is basis sensitive. Frequency dependence, orientation, aggregation, symmetry, and bulk susceptibility remain untested.

QTAIM and RDG/NCI Evidence

The internally consistent gas-phase QTAIM values are summarized in Table 5. At the selected C1 and C2 Zn···O critical points, ρ is 0.0562 and 0.0534 a.u., the Laplacian is positive (0.2595 and 0.2587 a.u.), and H is modestly negative (-0.0128 and -0.0105 a.u.). A positive Laplacian indicates local density depletion typical of a closed-shell interaction, while negative H indicates a stabilizing potential-energy contribution and some shared character. For a metal-oxygen contact, the combined pattern is better described as coordination-like or intermediate than as either a purely covalent bond or a weak van der Waals contact.

Table 5: Internally consistent gas-phase QTAIM descriptors at the selected Zn···O critical points. Aqueous values are excluded pending critical-point reassignment.

Descriptor (a.u.)	C1 gas	C2 gas
ρ at CP	0.056178	0.053387
$\nabla^2\rho$	0.259524	0.258729
G(r)	0.077697	0.075178
V(r)	-0.090513	-0.085674
H(r)	-0.012816	-0.010496
ELF	0.084840	0.077107

C1 has slightly larger ρ and a more negative H than C2, consistent with its lower deformation-corrected adsorption energy and larger fragment charge transfer. The differences are modest, so QTAIM supports rather than independently proves the energetic ranking. The aqueous C1 critical-point row was excluded because its ρ of 0.30004 a.u., negative Laplacian, ELF of 0.931, and sign(λ_2)ρ of -0.30004 are characteristic of a covalent bond critical point and are incompatible with the plotted NCI range and the 2.142 Å Zn···O contact. Interpreting that row as an intermolecular critical point would be scientifically unsafe.

The gas-phase RDG scatter plots in Fig. 3 show low-gradient features on the negative side of sign(λ_2)ρ for all three motifs, consistent with attractive interaction regions. They also contain near-zero features associated with dispersion and positive regions associated with steric crowding. Because only two-dimensional scatter plots are available, individual features cannot be assigned spatially to a particular Zn···O or aromatic contact; that assignment would require consistently scaled three-dimensional NCI isosurfaces. The plots therefore demonstrate the coexistence of interaction regimes but do not provide an adsorption energy or a unique bond classification (Johnson et al., 2010).

Taken together, geometry, energy decomposition, and real-space topology give a coherent picture. C1 forms a localized methoxy-O···Zn contact with favorable interaction and limited distortion. C2 forms a similar-distance phenolic-O···Zn contact, but the required geometry is costly. C3 gains comparable intrinsic stabilization from a more distributed aromatic contact. This multimodal interpretation is stronger than using an isolated critical-point value or the color of an NCI surface to rank configurations.

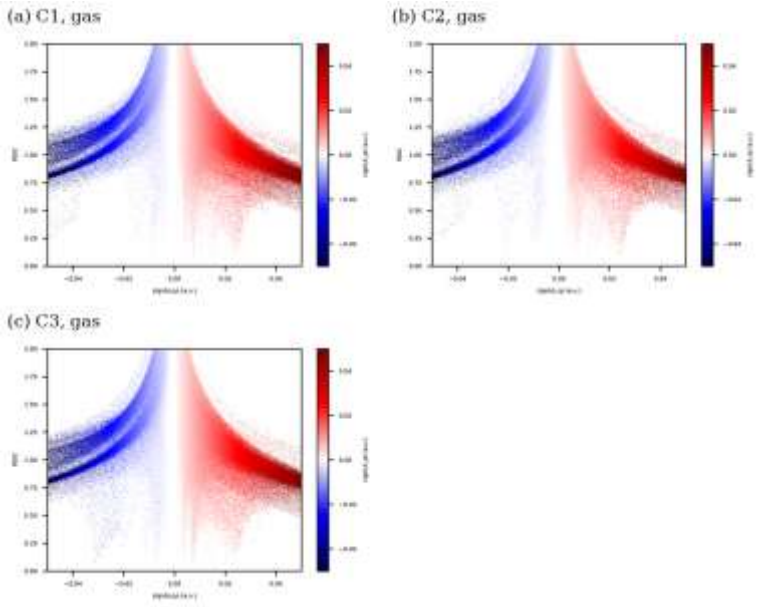

Fig. 3: Gas-phase RDG versus sign(λ_2)ρ plots for C1-C3. Blue/negative regions denote attractive interactions, near-zero regions weak dispersion, and red/positive regions steric repulsion.

TDOS, PDOS, OPDOS, and Implications for Sensing

The broadened TDOS/PDOS/OPDOS curves in Figs. 4-6 are qualitatively similar across the six complex-medium cases because the carbon framework supplies most molecular states. Multiple projected contributions overlap in occupied regions, indicating aggregate state mixing rather than an electronically isolated eugenol molecule. Because the complete atom-to-fragment mapping was unavailable, the curves are not used to assign a specific adsorbate-framework-Zn hybridization pathway. Their peak positions and heights also depend on the projection, broadening, and normalization and cannot rank adsorption energies quantitatively.

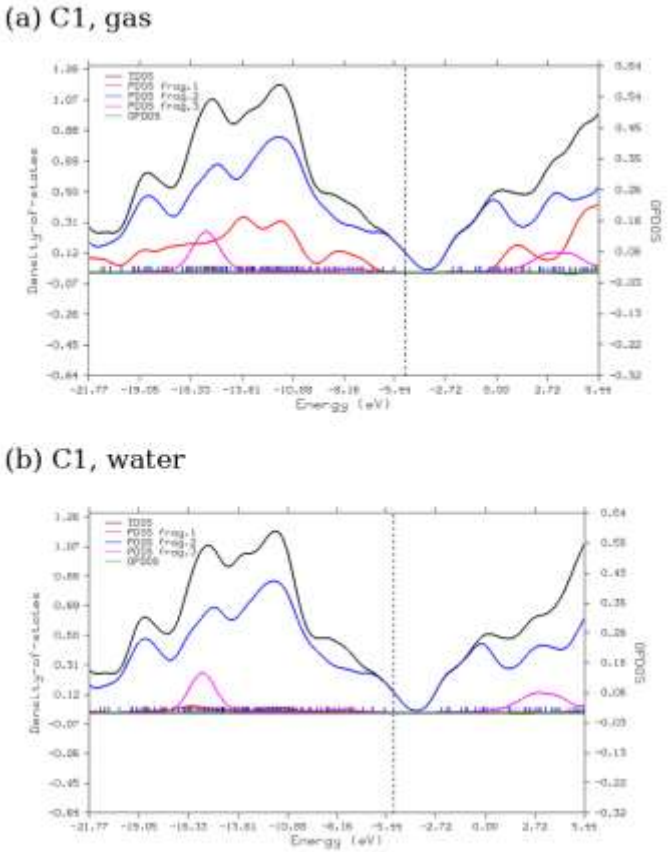

Fig. 4: TDOS, fragment-resolved PDOS, and OPDOS curves for C1 in (a) gas and (b) the water-labelled continuum calculation. Curves are broadened finite-cluster molecular-state distributions.

(a) C2, gas

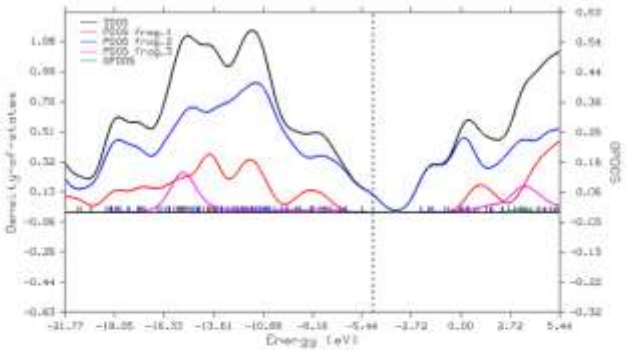

(b) C2, water

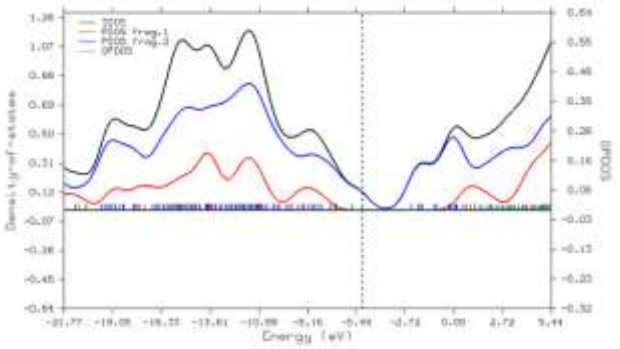

Fig. 5: TDOS, fragment-resolved PDOS, and OPDOS curves for C2 in (a) gas and (b) the water-labelled continuum calculation. Curves are broadened finite-cluster molecular-state distributions.

(a) C3, gas

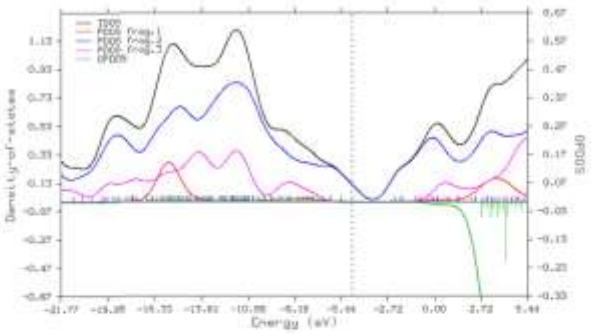

(b) C3, water

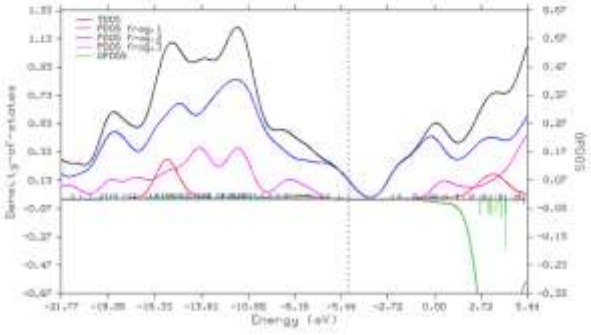

Fig. 6: TDOS, fragment-resolved PDOS, and OPDOS curves for C3 in (a) gas and (b) the water-labelled continuum calculation. Curves are broadened finite-cluster molecular-state distributions.

C3 also shows negative OPDOS features in the unoccupied region above roughly +2 eV relative to the plot reference. Negative OPDOS there denotes antibonding combinations among the selected fragments. Because these states are unoccupied in the ground state, their presence does not contradict the favorable C3 adsorption energy. It instead reflects the expected formation of bonding and antibonding combinations when molecular subsystems mix (Rangger et al., 2010). Ground-state stabilization must be assessed from occupied-state contributions and total energies.

Adsorption clearly perturbs several descriptors: fragment charges change by 0.11-0.16 e, dipoles and response tensors are configuration dependent, and frontier-state distributions mix. The gap shifts relative to bare ZnBPNT are nevertheless small for C1 and C3, and no current-voltage, transmission, selectivity, or competitive-adsorption calculation was performed. It is therefore appropriate to describe ZnBPNT as electronically responsive in this molecular model, not as a validated eugenol sensor. Experimental or transport-level confirmation would require a defined device geometry, electrode coupling, realistic coverage, competing analytes, humidity, and signal-to-noise assessment.

The carrier interpretation is similarly provisional. Favorable gas-phase adsorption and moderate interaction in an implicit medium suggest that Zn substitution can create recognition motifs, but the positive modeled aqueous association free energies show that spontaneous solution binding is not established. Drug-delivery use would additionally require loading capacity, desorption under physiological conditions, colloidal stability, toxicity, and biocompatibility. The

calculations identify hypotheses and relative interaction motifs; they do not replace these biological and materials tests.

Scope, Uncertainty, and Validation Priorities

Several limitations control the precision of the conclusions. The sampled adsorption landscape contains only three starting orientations; the finite model may exhibit edge effects; the basis is modest and uncorrected for BSSE; and the implicit-solvent protocol is incompletely specified. Low-frequency harmonic modes affect entropy, while a single optimized structure omits configurational averaging. Population charges and orbital energies are method dependent. These limitations do not erase robust trends such as the large C2 deformation penalty, but they prevent a 0.22 kcal mol^{-1} C1-C3 difference from being treated as chemical selectivity.

The next computational stage should verify model composition and charge/multiplicity, document the solvation keyword and standard state, perform counterpoise and larger-basis single points, rescan orientations, and use quasi-harmonic or ensemble free energies. Explicit water molecules around the oxygen and Zn sites would test competitive hydration. A complete QTAIM analysis must track the same atom pair and critical point across environments. Periodic or sufficiently extended models, followed by transport or work-function calculations, are needed before invoking conductivity-based sensing. These checks would convert the present descriptor study into a reproducible quantitative assessment.

CONCLUSION

A consistent reanalysis of the three optimized motifs shows that eugenol can engage the Zn-substituted biphenylene nanostructure through localized oxygen contacts or a distributed aromatic interaction. C1 (methoxy O1⋯Zn) and C3 (phenyl-directed) have virtually identical gas-phase intrinsic interaction energies and ZPE-corrected adsorption energies; their 0.22 kcal mol^{-1} difference is not significant at the present level. C2 (phenolic O2⋯Zn) forms an equally short contact but is weakened by a much larger deformation penalty. The aqueous continuum reduces binding magnitudes and yields standard-state- and RRHO-sensitive association free energies near zero or above on the reported convention.

Adsorption redistributes fragment charge and frontier density, but it increases rather than narrows the finite-cluster HOMO-LUMO gap. Corrected NLO units show strong solvent polarization without demonstrating a bulk optical response. Gas-phase QTAIM descriptors support coordination-like Zn⋯O contacts, while RDG and projected-state analyses reveal additional delocalized interactions. An anomalous aqueous critical-point assignment and undefined response columns were excluded rather than overinterpreted.

The defensible outcome is therefore a molecular-level screening result: Zn substitution creates multiple interaction motifs and measurable descriptor changes, with methoxy-directed and phenyl-directed structures co-competitive. Claims of selective sensing, aqueous capture, drug delivery, or device performance require larger-basis/BSSE validation, explicit-solvent sampling, verified topology, competing analytes, transport calculations, and experiment. This bounded interpretation preserves the useful mechanistic information while aligning the conclusions with the actual evidence.

REFERENCES

1. Bader, R. F. W. (1990). Atoms in molecules: A quantum theory. *Oxford University Press*. doi:10.1093/oso/9780198551683.001.0001

2. Boshir Ahmed, M., Alom, J., Hasan, M. S., Asaduzzaman, M., Rahman, M. S., Hossen, R., Abu Hasan Johir, M., Alam, M. T., Zhou, J. L., Zhu, Y., and Zargar, M. (2023). General

doping chemistry of carbon materials. *ChemNanoMat*, 9(4), e202200482. doi:10.1002/cnma.202200482
3. de Paul Zoua, V., Bine, F. K., Pagoré, I. F., Fouegue, A. D. T., and Ntieche, R. A. (2024). A DFT study of eugenol adsorption onto pure and Si-doped $Al_{12}N_{12}$ and $B_{12}N_{12}$ fullerene-like nanocages. *Computational and Theoretical Chemistry*, 1240, 114807. doi:10.1016/j.comptc.2024.114807
4. Durgun, E., Dag, S., Ciraci, S., and Gülseren, O. (2004). Energetics and electronic structures of individual atoms adsorbed on carbon nanotubes. *The Journal of Physical Chemistry B*, 108(2), 575-582. doi:10.1021/jp0358578
5. Espinosa, E., Alkorta, I., Elguero, J., and Molins, E. (2002). From weak to strong interactions: A comprehensive analysis of the topological and energetic properties of the electron density distribution involving X-H···F-Y systems. *The Journal of Chemical Physics*, 117(12), 5529-5542. doi:10.1063/1.1501133
6. Genç, F., Mohammed, W. N. R., and Kandemirli, F. (2025). Computational study of the structural, electronic, and thermodynamic properties of eugenol in the gas phase and solvated environments. *Cumhuriyet Science Journal*, 46(4), 741-752. doi:10.17776/csj.1732415
7. Gowri Sankar, P. A., and Udhayakumar, K. (2013). Electronic properties of boron- and silicon-doped (10,0) zigzag single-walled carbon nanotubes upon gas molecular adsorption: A DFT comparative study. *Journal of Nanomaterials*, 2013, 293936. doi:10.1155/2013/293936
8. Grimme, S. (2008). Do special noncovalent π–π stacking interactions really exist? *Angewandte Chemie International Edition*, 47(18), 3430-3434. doi:10.1002/anie.200705157
9. Johnson, E. R., Keinan, S., Mori-Sánchez, P., Contreras-García, J., Cohen, A. J., and Yang, W. (2010). Revealing noncovalent interactions. *Journal of the American Chemical Society*, 132(18), 6498-6506. doi:10.1021/ja100936w
10. Junqueira, G. M. A., Mendonça, J. P. A., Lima, A. H., Quirino, W. G., and Sato, F. (2016). Enhancement of nonlinear optical properties of graphene oxide-based structures: Push-pull models. *RSC Advances*, 6(97), 94437-94450. doi:10.1039/C6RA18314J
11. Kar, T., Bettinger, H. F., Scheiner, S., and Roy, A. K. (2008). Noncovalent π–π stacking and CH···π interactions of aromatics on the surface of single-wall carbon nanotubes: An MP2 study. *The Journal of Physical Chemistry C*, 112(50), 20070-20075. doi:10.1021/jp807809u
12. Lin, D., and Xing, B. (2008). Adsorption of phenolic compounds by carbon nanotubes: Role of aromaticity and substitution of hydroxyl groups. *Environmental Science & Technology*, 42(19), 7254-7259. doi:10.1021/es801297u
13. Lu, J., Zhang, X., Wu, X., Dai, Z., and Zhang, J. (2015). A Ni-doped carbon nanotube sensor for detecting oil-dissolved gases in transformers. *Sensors*, 15(6), 13522-13532. doi:10.3390/s150613522
14. Lu, T., and Chen, F. (2012). Multiwfn: A multifunctional wavefunction analyzer. *Journal of Computational Chemistry*, 33(5), 580-592. doi:10.1002/jcc.22885
15. Mubarok, F. A., Sari, H. C., Firdaus, M., Pratiwi, W. E., Ivansyah, A. L., and Muttaqien, F. (2022). Density functional theory investigation on the interaction of F_2 with (4,0) SWCNT and X-doped (4,0) SWCNT for gas-sensor applications. *Diamond and Related Materials*, 130, 109463. doi:10.1016/j.diamond.2022.109463
16. Novoselov, K. S., Geim, A. K., Morozov, S. V., Jiang, D., Zhang, Y., Dubonos, S. V., Grigorieva, I. V., and Firsov, A. A. (2004). Electric field effect in atomically thin carbon films. *Science*, 306(5696), 666-669. doi:10.1126/science.1102896
17. Pan, B., and Xing, B. (2008). Adsorption mechanisms of organic chemicals on carbon nanotubes. *Environmental Science & Technology*, 42(24), 9005-9013. doi:10.1021/es801777n
18. Pramod, K., Ansari, S. H., and Ali, J. (2010). Eugenol: A natural compound with versatile pharmacological actions. *Natural Product Communications*, 5(12), 1999-2006. doi:10.1177/1934578X1000501236

19. Rangger, G. M., Romaner, L., Hofmann, O. T., Heimel, G., Ramsey, M. G., and Zojer, E. (2010). Analysis of bonding between conjugated organic molecules and noble metal surfaces using orbital overlap populations. *Journal of Chemical Theory and Computation*, 6(11), 3481-3489. doi:10.1021/ct100449c
20. Rassolov, V. A., Pople, J. A., Ratner, M. A., and Windus, T. L. (1998). 6-31G* basis set for atoms K through Zn. *The Journal of Chemical Physics*, 109(4), 1223-1229. doi:10.1063/1.476673
21. Ribeiro, T. A. N., dos Santos, G. A., dos Santos, C. T., Soares, D. C. F., Saraiva, M. F., Leal, D. H. S., and Sachs, D. (2024). Eugenol as a promising antibiofilm and anti-quorum-sensing agent: A systematic review. *Microbial Pathogenesis*, 196, 106937. doi:10.1016/j.micpath.2024.106937
22. Song, Y.-D., and Wang, Q.-T. (2021). Investigations of electronic and nonlinear optical properties of superalkali-adsorbed biphenylene-based sheets by first-principles calculations. *Optik*, 242, 166830. doi:10.1016/j.ijleo.2021.166830
23. Stoyanov, S. R., Titov, A. V., and Král, P. (2009). Transition-metal- and nitrogen-doped carbon nanostructures. *Coordination Chemistry Reviews*, 253(23-24), 2852-2871. doi:10.1016/j.ccr.2009.03.011
24. Suresh, C. H., and Anila, S. (2023). Molecular electrostatic potential topology analysis of noncovalent interactions. *Accounts of Chemical Research*, 56(13), 1884-1895. doi:10.1021/acs.accounts.3c00193
25. Tsapi, C. T., Tasheh, S. N., Nkungli, N. K., Fouegue, A. D. T., Alongamo, C. I. L., and Ghogomu, J. N. (2023). Exohedral adsorption of N-(4-methoxybenzylidene) isonicotinohydrazone onto $X_{12}N_{12}$ nanocages and the effect on its NLO properties. *Journal of Chemistry*, 2023, 5287422. doi:10.1155/2023/5287422
26. Ulanowska, M., and Olas, B. (2021). Biological properties and prospects for the application of eugenol—A review. *International Journal of Molecular Sciences*, 22(7), 3671. doi:10.3390/ijms22073671
27. Wang, Y., and Yeow, J. T. W. (2009). A review of carbon-nanotube-based gas sensors. *Journal of Sensors*, 2009, 493904. doi:10.1155/2009/493904
28. Zeng, Y., Lin, S., Gu, D., and Li, X. (2018). Two-dimensional nanomaterials for gas-sensing applications: The role of theoretical calculations. *Nanomaterials*, 8(10), 851. doi:10.3390/nano8100851
29. Zhang, X., Cui, H., Gui, Y., and Tang, J. (2017). Mechanism and application of carbon nanotube sensors in SF_6 decomposition-product detection: A review. *Nanoscale Research Letters*, 12, 177. doi:10.1186/s11671-017-1945-8
30. Zhang, Y., Zhang, J., and Su, D. S. (2014). Substitutional doping of carbon nanotubes with heteroatoms and their chemical applications. *ChemSusChem*, 7(5), 1240-1250. doi:10.1002/cssc.201301166
31. Zhao, Y., and Truhlar, D. G. (2008). The M06 suite of density functionals for main-group thermochemistry, thermochemical kinetics, noncovalent interactions, excited states, and transition elements. *Theoretical Chemistry Accounts*, 120(1-3), 215-241. doi:10.1007/s00214-007-0310-x

IN VIVO AND *IN SILICO* INVESTIGATION OF THE GASTROPROTECTIVE ACTIVITY OF ALEPPO PINE (*PINUS HALEPENSIS* MILL.) EXTRACT

BRIKA Aya[1], ZEGHAD Nadia[2], NOUI Amira[3]

[1] Department of Biochemistry and Cellular and Molecular Biology, Faculty of Natural and Life Sciences. Constantine 1 University, Constantine, Algeria,
[2] Department of Plant Biology. Constantine 1 University, Constantine, Algeria.
[3] Biotechnology Research Center (C.R.B.T), Constantine, Algeria.
Corresponding author e-mail: aya.brika@doc.umc.edu.dz

ABSTRACT

The present study aimed to evaluate the gastroprotective activity of hydromethanolic bark extract of Pinus halepensis (PHE) using both in vivo and in silico approaches. Gastric ulcers were induced in albino Wistar rats using an HCl/Ethanol model. PHE was administered at 250, 500, and 1000 mg/kg, with omeprazole (20 mg/kg) as the reference drug. Molecular docking of twelve LC-MS/MS-identified compounds was conducted against the gastric proton pump (H^+/K^+-ATPase). 3D structures of the ligands were sourced from PubChem, and the crystallographic structure of the gastric proton pump was obtained from the Protein Data Bank (PDB ID: 5YLU). Docking simulations were conducted using FlexX software. A clear dose-dependent effect was observed, with inhibition rates reaching 33.91 ± 1.02%, 51.08 ± 4.73%, and 62.04 ± 2.73% for the 250, 500, and 1000 mg/kg doses, respectively. The UI decreased from 70.37 ± 4.2 in the control group to 46.46 ± 0.72 (250 mg/kg), 34.55 ± 3.33 (500 mg/kg), and 26.73 ± 1.92 (1000 mg/kg). At the highest dose (1000 mg/kg). Macroscopic examination of the gastric mucosa demonstrated that pretreatment with PHE at the highest dose (1000 mg/kg) resulted in near-complete restoration of mucosal integrity compared to the untreated control group. Docking simulations of identified compounds against H^+/K^+-ATPase highlighted quercetin (−26.74 KJ/mol) and catechin (−25.95 KJ/mol) as the most promising candidates, both surpassing omeprazole (−18.49 KJ/mol) in binding affinity. Molecular interaction analysis revealed that the best compounds established multiple stabilizing contacts within the active site of H^+/K^+-ATPase. These findings suggest that *Pinus halepensis* bark extract possesses potent gastroprotective properties, likely mediated by the antisecretory activity of its flavonoid constituents, highlighting PHE as a promising candidate for future anti-ulcer therapeutic development.

Keywords: *Pinus halepensis*, gastroprotective effect, ulcer index, molecular docking, gastric proton pump.

INTRODUCTION

Gastric ulcers remain a major global health concern, resulting from an imbalance between aggressive factors and gastric mucosal defenses. Although conventional treatments are available, their side effects and increasing drug resistance highlight the need for safer alternatives (Chitapanarux et al., 2023). Medicinal plants are promising sources of bioactive compounds with antioxidant, anti-inflammatory, and gastroprotective properties (Aman et al., 2025). *Pinus halepensis* is traditionally recognized for its biological activities related to oxidative stress and tissue protection, suggesting potential gastroprotective effects. Therefore, this study aimed to evaluate the gastroprotective activity of *P. halepensis* extract and investigate its possible mechanisms using complementary *in vivo* and *in silico* approaches.

MATERIAL AND METHOD

Plant material

The plant material was collected in June 2023 from Djbel El Ouahch forest, Constantine, eastern Algeria, identified, and dried under appropriate conditions prior to extraction.

Extraction

The hydroalcoholic extract of *Pinus halepensis* (PHE) was obtained by maceration using a methanol/water mixture (70/30, *v/v*) (Boudebbaz et al., 2025).

In vivo anti-ulcer activity

Healthy *Wistar* rats were fasted for 48 h, and acute gastric ulcers were induced using HCl/ethanol (80/20) (Zeghad et al., 2026). Animals received *Pinus halepensis* extract (0.25–1.00 g/kg) or omeprazole (0.02 g/kg). Gastric lesions were assessed using ImageJ, and the ulcer index and gastroprotection were calculated (Kim et al., 2020).

In silico molecular docking against the gastric proton pump

Molecular docking was performed to evaluate the interactions of LC-MS/MS-identified *Pinus halepensis* phytoconstituents with gastric H^+/K^+-ATPase (PDB ID: 5YLU). Ligand structures were obtained from PubChem, and omeprazole was used as the reference compound. Docking simulations were performed using LeadIT v2.1.8, and binding affinities were expressed as ΔG (kJ/mol) (Hioual et al., 2014).

RESULTS AND DISCUSSION

In Vivo Anti-Ulcer Activity

The results of the anti-ulcer activity summarized in Table 1, demonstrate a clear dose-dependent gastroprotective effect of PHE across the three tested doses (0.25, 0.50, and 1.00 g/kg body weight), and surpassing the reference drug at both 0.50 g/kg and 1.00 g/kg. The gastric mucosal protective effect of PHE may be primarily attributed to its phenolic compounds, which are known for their significant anti-ulcerogenic activity and ability to protect the gastric mucosa (Boudebbaz et al., 2025; Bakry et al., 2023).

Table 1. Effects of *Pinus halepensis* bark extract on ulcer index, ulcer inhibition in HCl/ethanol-induced gastric ulcerated rats.

Animal's group	Ulcer index	Inhibition (%)
Normal group	-	-
Control group	70.37 ± 4.2 ^{d}	0.00 ^{a}
Standard (Omeprazol 0.02 g/kg)	43.35 ± 2.16 ^{c}	38.57 ± 3.18 ^{b}
PHE 0.25 g/kg	46.46 ± 0.72 ^{a}	33.91 ± 1.02 ^{a}
PHE 0.50 g/kg	34.55 ± 3.33 ^{a}	51.08 ± 4.73 ^{a}
PHE 1.00 g/kg	26.73 ± 1.92 ^{a}	62.04 ± 2.73 ^{a}

PHE: *Pinus halepensis* extract. Values are expressed as Mean ± SD (n=6). Analysis of variance (ANOVA one-factor and Tukey Tests) revealed statistical difference ($P<0.05$). Different superscripts (a, b, c...) for values in the same columns are statistically different.

In silico molecular docking against the gastric proton pump

Molecular docking was performed to investigate the interaction of Catechin, Quercetin, Naringenin, and Luteolin with gastric H^+/K^+-ATPase (PDB ID: 5YLU), using omeprazole as the reference inhibitor. Binding affinities are presented in Table 2.

Table 2. Scoring functions of the phytoconstituents from *P. halepensis* docked to the gastric proton pump

Compounds	**Gastric Proton Pump (5YLU)**
	Scoring Function (KJ/mol)
Omeprazol	-18.4919
Catechin	-25.9543
Quercetin	-26.7423
Naringenin	-22.8859
Luteolin	-23.1306

Quercetin (−26.7423 KJ/mol) showed the strongest binding affinity, followed by Catechin (−25.9543 KJ/mol), with both displaying more favorable scores than Omeprazole (−18.4919 KJ/mol). Luteolin and Naringenin (−23.1306 KJ/mol and −22.8859 KJ/mol, respectively) also showed favorable interactions with H^+/K^+-ATPase. These affinities may be related to their hydroxyl groups and aromatic rings, which promote hydrogen-bonding and hydrophobic interactions (Shahidi & Dissanayaka, 2023; Lešnik et al., 2025). Overall, the findings support the potential contribution of these polyphenols to gastroprotection through proton pump inhibition.

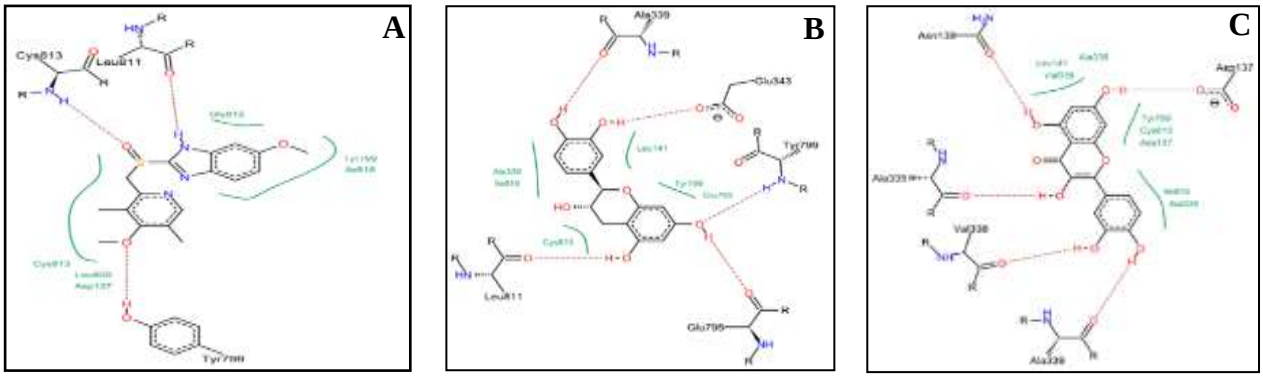

Figure 1. Binding interactions of omeprazole (A), catechin (B), and quercetin (C) within the gastric H^+/K^+-ATPase active site. Hydrogen bonds are represented by purple dashed lines, and hydrophobic interactions are highlighted in green.

CONCLUSIONS

Pinus halepensis shows promising gastroprotective potential due to its bioactive compounds with antisecretory properties. Combining *in vivo* experiments and *in silico* analyses suggests that this plant may help protect the gastric mucosa and act on key molecular targets involved in ulcer formation. These findings support further studies to validate its use as a natural anti-ulcer agent.

REFERENCES

Aman, A., Kumari, J., & Rajbhar, R. (2025). A review on herbal potential for treatment of peptic ulcer. *International Journal of Pharmaceutical Research and Applications.* 10(4), 560–569. https://doi.org/10.35629/4494-1004560569

Bakry, S., Naser, A., Negoumy, S., Kassem, M., Abdel-Sattar, E., & Meselhy, M. (2023). Phenolic acids-rich fraction from Ficus drupacea leaves for the prevention and treatment of ethanol-induced gastric mucosal injury in rats. Inflammopharmacology, 31(3), 1423 - 1436. https://doi.org/10.1007/s10787-023-01158-4.

Beiranvand, M., Bahramikia, S., & Dezfoulian, O. (2021). Evaluation of antioxidant and anti-ulcerogenic effects of Eremurus persicus (Jaub & Spach) Boiss leaf hydroalcoholic extract on ethanol-induced gastric ulcer in rats. *Inflammopharmacology*, 29(5), 1503 - 1518. https://doi.org/10.1007/s10787-021-00868-x

Boudebbaz, K., Brouk, M., Laalem, R., & Zabaiou, N. (2025). Gastroprotective properties of flavonoid-rich extract of Pulicaria odora against ethanol-induced gastric ulcer in mice. *Heliyon*, 11(1), e41625. https://doi.org/10.1016/j.heliyon.2025.e41625

Chitapanarux, T., Kongkarnka, S., Wannasai, K., & Sripan, P. (2023). Prevalence and factors associated with atrophic gastritis and intestinal metaplasia: A multivariate, hospital-based, statistical analysis. *Cancer Epidemiology*, 82, 102309. https://doi.org/10.1016/j.canep.2022.102309

De Araújo, E., Guerra, G., Andrade, A., Fernandes, J., Da Silva, V., De Aragão Tavares, E., De Araújo, A., De Araújo Júnior, R., & Zucolotto, S. (2021). Gastric ulcer healing property of *Bryophyllum pinnatum* leaf extract in chronic model in vivo and gastroprotective activity of its major flavonoid. *Frontiers in Pharmacology*, 12. https://doi.org/10.3389/fphar.2021.744192.

Hioual, K., Chikhi, A., Bensegueni, A., Merzoug, A., Boucherit, H., Mokrani, E. H., Teniou, S., & Merabti, B. (2014). Successful challenge: A key step in infectious diseases treatment using computer-aided drug design. *International Journal of Biological Sciences and Applications*, 1(1), 11–14.

Kim, Y. S., Lee, J. H., Song, J., & Kim, H. (2020). Gastroprotective effects of Inulae flos on HCl/ethanol-induced gastric ulcers in rats. *Molecules*, 25(23). https://doi.org/10.3390/molecules25235623

Lešnik, S., Jukič, M., & Bren, U. (2025). Unveiling polyphenol-protein interactions: A comprehensive computational analysis. *Journal of Cheminformatics*, 17(1), 50. https://doi.org/10.1186/s13321-025-00997-3

Oueslati, S., Beji, R., Kalai, F., Soufiani, M., Zorrig, W., Aissam, S., Msaada, K., & Modafar, E. (2023). Antioxidant potentialities and gastroprotective effect of *Reichardia picroides* extracts on Ethanol/HCl induced gastric ulcer rats. *International Journal of Environmental Health Research*, 34, 1088 - 1099. https://doi.org/10.1080/09603123.2023.2198760.

Shahidi, F., & Dissanayaka, C. (2023). Phenolic-protein interactions: insight from in-silico analyses – A review. *Food Production, Processing and Nutrition*, 5(1), 2. https://doi.org/10.1186/s43014-022-00121-0.

Zeghad, N., Hefny Gad, M., Madi, A., Ahmed, E., Sihem, H., & Belkhiri, A. (2026). Gastroprotective effect of an Algerian hydroalcoholic *Punica granatum L*. peel extract against ethanol/HCl-induced gastric mucosal injury in Wistar rats. *Current Issues in Pharmacy and Medical Sciences*, 38(4), 270–275. https://doi.org/10.12923/cipms-2025-0043.

ANALYSIS OF SPECIES DIVERSITY AND DISTRIBUTION PATTERNS OF THE APIACEAE FAMILY IN THE NAKHCHIVAN AUTONOMOUS REPUBLIC

Novruzi Nurlana[1]

[1]Nakhchivan Teachers İnstitution
Nakhchivan AR, Azerbaijan
E-mail: nnurlana91@mail.ru

ABSTRACT

The present study provides a comprehensive analysis of the species diversity, distribution patterns, ecological characteristics, and phytochemical potential of the Apiaceae family in the Nakhchivan Autonomous Republic. The family is represented by 57 genera and 107 species, making it one of the most species-rich plant groups within the regional flora and an important component of local biodiversity. Particular attention is given to rare and endangered taxa, especially *Prangos acaulis* (DC.) Bornm., which is included in the Red Book of Azerbaijan and plays a significant role in the conservation of regional plant diversity. The study integrates floristic, ecological, and recent pharmacological data to evaluate the biological and applied significance of this species. *P. acaulis* is characterized as a drought-tolerant xerophytic plant distributed mainly in mountainous and semi-arid environments, where it contributes to ecosystem stability, vegetation dynamics, and adaptation to arid climatic conditions. Phytochemical investigations reveal a diverse composition of bioactive compounds, including essential oils, flavonoids, coumarins, and terpenoids, with notable variation across different plant organs. These variations are closely related to environmental conditions and ecological factors. Recent studies (2023–2026) demonstrate that *P. acaulis* exhibits significant antibacterial, antifungal, antioxidant, anti-inflammatory, cytotoxic, and immunomodulatory activities, highlighting its potential for therapeutic applications. Furthermore, the application of plant extracts in nanotechnology has shown enhanced bioactivity, improved bioavailability, and increased therapeutic efficiency, indicating promising prospects for pharmaceutical development and innovative drug design. Despite these advances, several research gaps remain, particularly regarding *in vivo* effects, toxicological evaluation, and dose–response relationships, which require further detailed investigation. Overall, the findings emphasize the ecological importance and pharmacological potential of *P. acaulis*, as well as the urgent need for its conservation, rational utilization, and sustainable management within the region.

Keywords: Apiaceae; *Prangos acaulis*; biodiversity; Nakhchivan Autonomous Republic; phytochemistry; pharmacological activity; essential oils; antioxidant activity; conservation; nanotechnology

INTRODUCTION

Plants belonging to the Apiaceae (Umbelliferae) family are predominantly perennial, biennial, or annual herbaceous species, comprising approximately 300–450 genera and 3,700–4,000 species. The family is morphologically characterized by its distinctive umbel-type inflorescence, which represents one of its primary diagnostic features. Members of this family are typically aromatic and contain essential oils as well as various biologically active compounds. Owing to these properties, they are widely utilized both as food and in pharmacological applications. Notable representatives include vegetable species such

as *Daucus carota* and *Apium graveolens*, as well as spice and essential oil-bearing plants such as *Anethum graveolens*, *Coriandrum sativum*, *Cuminum cyminum*, and *Foeniculum vulgare*. Medicinal species within this family exhibit spasmolytic, antiseptic, and digestive-enhancing properties.

The family is geographically distributed across almost all continents. However, it exhibits its greatest species diversity in temperate climatic zones, particularly in the Mediterranean region, the Caucasus, and Central Asia, as well as in mountainous and semi-desert areas. In contrast, it is relatively less represented in tropical regions. Within the flora of the Nakhchivan Autonomous Republic, the Apiaceae family is among the most species-rich families, represented by 57 genera and 107 species.

Among the members of the Apiaceae family occurring in Azerbaijan, particularly within the flora of the Nakhchivan Autonomous Republic, several rare and endangered species included in the Red Book of the Republic of Azerbaijan can be identified. These include *Prangos acaulis* (DC.) Bornm., *Eryngium wanaturii* Woronow, *Ferula persica* Willd., *Ferula szowitsiana* DC., *Grammosciadium platycarpum* (Boiss. & Hausskn.) Schischk., *Stenotaenia macrocarpa* Freyn & Sint. ex Freyn, and *Zeravschania pauciradiata* (Tamamsch.) M. Pimen. These species possess significant scientific and ecological importance in terms of the conservation of regional biodiversity.

Prangos acaulis (DC.) Bornm. — a representative of the genus *Prangos* L. (Apiaceae), commonly known as stemless prangos, belongs to a genus comprising approximately 25 species distributed across the Mediterranean region, Asia Minor, Iran, Afghanistan, Central Asia, and Eastern India. Of these, six species occur in the Caucasus, five in Azerbaijan, and four species are recorded within the territory of the Nakhchivan Autonomous Republic. The conservation status of the species is classified as Lower Risk (LR) [Conservation Dependent (CD)]. In Azerbaijan, *P. acaulis* is distributed exclusively within the Nakhchivan Autonomous Republic. It occurs mainly in the lower and middle mountain belts, particularly in areas such as Ardic Mountain, Garagush Mountain, Daridagh, Agridagh, and Kotamdagh. The species grows on stony-gravelly, calcareous-clayey, and grassy slopes. Despite its relatively wide distribution within the region, its natural populations are steadily declining due to intensive harvesting by local populations as a food plant. The species reproduces by seeds.

Biological characteristics: *Prangos acaulis* (DC.) Bornm. is a perennial herb densely covered with curly hairs. The stem is surrounded at the base by remnants of old leaves, cylindrical in shape, and branched in the middle part into broad, shield-like structures, reaching a height of 15–40 cm. Basal leaves are long-petiolate with short, leathery sheaths; the leaf blade is generally triangular-ovate in outline and three- to four-times pinnately divided. Stem leaves are significantly smaller than basal leaves, sessile on the sheath, with upper leaves being simply pinnate and divided into numerous linear elongated segments (1–3 cm long). The inflorescence is an umbel with (4) 5–6 rays; umbellets and involucels contain 9–10 flowers, with central flowers often sterile. Involucral bracts are linear or lanceolate-linear and pubescent. Fruits are elongated, 12–18 mm long, with membranous, undulate wings and serrated margins. The species flowers in April–May and produces fruits in May–June. It is a xerophytic species with both nutritional and medicinal value. The species belongs to the Atropatenean floristic geographical element. The decline in population size and number is primarily associated with limiting ecological and zoogenic factors. In addition, intensive collection during spring represents a major constraint on natural regeneration. However, as the species is included in the Red Book of the Nakhchivan Autonomous Republic, conservation measures have been developed to ensure its protection and sustainable use. Given that its populations are relatively threatened, the habitats of this species within the Zangezur National Park and the Arpachay State Nature Reserve should be placed under strict monitoring.

Prangos acaulis, one of the rare representatives of the Apiaceae family, has recently attracted considerable attention due to its phytochemical and pharmacological properties. Contemporary studies indicate that this species contains a rich spectrum of bioactive compounds, including essential oils, flavonoids, coumarins, and terpenoids. Variations in chemical composition have been observed among different plant organs (leaves, flowers, and stems). In particular, α-pinene (~39%) predominates in the leaves, whereas limonene and other terpene compounds are more abundant in the flowers. These findings suggest that the species is sensitive to ecological factors, with its chemical profile varying depending on environmental conditions.

Recent studies (2023–2026) have demonstrated that *Prangos acaulis* possesses significant pharmacological potential. Extracts of the plant have been reported to exhibit antibacterial and antifungal activities, with pronounced efficacy against *Streptococcus mutans*, including the inhibition of biofilm formation. Moreover, the high content of phenolic compounds indicates strong antioxidant and anti-inflammatory properties, which are essential for cellular protection and the prevention of various diseases. Experimental investigations have revealed that plant extracts exert cytotoxic effects against HT-29 and MCF-7 cell lines, with these effects being further enhanced when formulated as chitosan-based nanoformulations. In addition, immunomodulatory properties of the species have been reported, suggesting its involvement in cytokine regulation and immune response modulation.

One of the emerging directions in contemporary research is the application of plant extracts in nanotechnology. This approach enhances the efficacy of bioactive compounds and enables the achievement of higher therapeutic effects at lower doses, which is considered promising for the future development of pharmaceutical formulations.

From an ecological perspective, *Prangos acaulis* is primarily distributed in mountainous and semi-arid regions and is characterized as a drought-tolerant species. Variations in the composition of its essential oils depending on climatic and soil conditions indicate its sensitivity to environmental factors. This feature makes the species a valuable indicator for studying climate–vegetation relationships.

Nevertheless, several gaps remain in the existing body of research. In particular, the effects of the species under *in vivo* conditions have not been sufficiently investigated, its toxicological profile has not been fully characterized, and dose–response relationships remain unclear. Furthermore, more detailed studies on its flavonoid composition and microelement content are required.

MATERIALS AND METHODS

The study was based on field investigations, herbarium analyses, and a comprehensive review of relevant scientific literature. Field surveys were conducted across different ecological zones of the Nakhchivan Autonomous Republic, including mountainous and semi-arid regions, to identify species distribution and habitat characteristics. Plant specimens were collected, identified, and classified according to standard taxonomic methods. Morphological and ecological characteristics of *Prangos acaulis* were examined in situ, and its distribution areas were recorded. In addition, data on phytochemical composition and pharmacological properties were obtained from recent scientific publications (2023–2026), focusing on essential oils, bioactive compounds, and biological activities such as antimicrobial, antioxidant, and cytotoxic effects.

RESULTS AND DISCUSSION

The results indicate that the Apiaceae family is widely represented in the Nakhchivan Autonomous Republic, with significant species diversity concentrated in mountainous and

semi-arid zones. Among the identified species, *Prangos acaulis* occupies a distinct ecological niche and demonstrates high adaptability to xerophytic conditions.

Morphological analysis shows that the species is a perennial herb with characteristic umbel inflorescences and well-developed reproductive structures. Its distribution is mainly associated with stony and calcareous soils in lower and middle mountain belts.

Phytochemical studies confirm that *P. acaulis* contains a rich composition of essential oils, flavonoids, coumarins, and terpenoids. The variation in chemical composition among plant organs indicates its sensitivity to environmental conditions. Pharmacological investigations reveal significant antibacterial, antifungal, antioxidant, anti-inflammatory, cytotoxic, and immunomodulatory activities.

Recent advances in nanotechnology have further enhanced the therapeutic potential of plant extracts, demonstrating improved efficacy at lower concentrations. However, insufficient *in vivo* studies and limited toxicological data remain key limitations in the current research.

CONCLUSION

The Apiaceae family plays a significant role in the flora of the Nakhchivan Autonomous Republic, contributing to regional biodiversity and ecological stability. *Prangos acaulis*, as a rare and endangered species, possesses considerable ecological and pharmacological importance. The study highlights its rich phytochemical composition and diverse biological activities, indicating strong potential for future pharmaceutical applications. At the same time, the species is under threat due to environmental pressures and overharvesting, necessitating effective conservation measures. Further research is required to investigate its *in vivo* effects, toxicological properties, and dose–response relationships. The integration of modern approaches, including nanotechnology, may provide new opportunities for the sustainable use and application of this species.

REFERENCES

İbadullayeva, S.C. (2005). *Azərbaycan florasının Kərəvüzkimiləri (Apiaceae Lindl.)*. Bakı, 373 s.

Nurlanə Novruzi. Qaraquş dağının florası və bitkiliyi. 377 s. Bakı. 2025.

Nurlanə Novruzi. Dərələyəz silsiləsinin nadir bitkiləri. 304 s. Məktəb nəşriyyatı. 2024.

Safarova, F., Ismayilova, V., & Nasirova, A. (2023). *Apiaceae Lindl. in Flora of Nakhchivan Autonomous Republic: Poisonous species of the celery family*. Biodiversity & Environment Journal, 1(1), 1–6.

Sərkərov, S.V., Qasımova, G.Q., & Heydərov, İ.G. (2017). *Azərbaycan florasında Apiaceae fəsiləsinin faydalı növlərinin öyrənilməsi*. AMEA Botanika İnstitutunun əsərləri, 37, 38, 44.

Talıbov, T.H., İbrahimov Ə.Ş., İbrahimov Ə.M. Naxçıvan Muxtar Respublikası florasının taksonomik spektri (Ali sporlu, çılpaqtoxumlu və örtülütoxumlu bitkilər)./ İkinci nəşr, Naxçıvan: Əcəmi, -2021, -426 s.

Askerov, A.M. (2006). *Azərbaycan florası*. Bakı.

Constance, L. (1971). *History of the classification of Umbelliferae*. Academic Press.

Grossheim, A.A. (1967). *Flora Kavkaza*. Moskva–Leninqrad.

Mozaffari, A.S., Kamkar, A., & Archana, G. (2013). *Ethnobotany and medicinal uses of plants*. Journal of Medicinal Plants Research.

Plunkett, G.M., Soltis, D.E., & Soltis, P.S. *Evolutionary patterns in Apiaceae*. Systematic Botany.

Stevens, P.F. (2001–). *Angiosperm Phylogeny Website – Apiaceae*.

MORPHOLOGICAL AND ANATOMICAL INVESTIGATIONS ON *PHLOMIS PUNGENS* WILLD. FROM ESKİŞEHİR

İlayda ERTÜRK[1], Nagehan SALTAN[2]

[1] Anadolu University, Department of Pharmaceutical Botany, Graduate School, Eskisehir, Türkiye
[2] Anadolu University, Department of Pharmaceutical Botany, Eskişehir, Turkey
Corresponding author e-mail: ilaydaerturk1@gmail.com

ABSTRACT

The genus *Phlomis* L. (Lamiaceae), colloquially known in Anatolia as "ballık otu," "çalba," "şalba," or "calba," has widespread traditional uses ranging from herbal teas to wound-healing, analgesic, and tonic applications. In this study, *Phlomis pungens* Willd. (Syn: *P. herba-venti L. subsp. pungens* (Willd.) Maire ex De Filipps), naturally distributed around Eskişehir, was evaluated from a botanical perspective. The morphological and anatomical features of the species were characterized using light microscopy to establish diagnostic criteria for accurate taxonomic identification. Morphological measurements revealed that *P. pungens* is a perennial herb reaching 55 cm in height and 0.3–0.5 cm in stem diameter, with a quadrangular stem covered by dense stellate-tomentose hairs. Cauline leaves are simple to occasionally lobed, arranged in a decussate pattern, measuring 2.5–14.7 × 0.3–4.8 cm. The inflorescence comprises up to 40 verticillasters, with each cluster bearing 3 to 11 zygomorphic, bilabiate flowers supported by linear-subulate bracts. The 5-toothed actinomorphic calyx measures 8–11 × 3–5 mm, and the pink-to-purple corolla lobes measure 8–11 × 4–9 mm with four epipetalous stamens. Anatomical analyses demonstrated angular collenchyma in stem corners, a dorsiventral leaf mesophyll, sinuous anticlinal epidermal cell walls, and diacytic stomata on both leaf surfaces accompanied by characteristic multicellular stellate and dendroid non-glandular trichomes. Providing robust morphological and anatomical data for this traditionally utilized species is of significant importance. These findings will not only facilitate accurate taxonomic identification and ensure safe therapeutic use but will also serve as a foundational reference for future pharmacological and phytochemical research.

Keywords: *Phlomis pungens*, anatomy, morphology, diagnostic characters.

INTRODUCTION

Due to its geographical location, climatic diversity, and soil structure, Türkiye ranks among the richest countries globally in terms of floristic diversity, situated at the intersection of three phytogeographies: European-Siberian, Mediterranean, and Iran-Turanian (Tekin, 2025).
Within this diverse flora Lamiaceae is the third largest family in Türkiye, represented by 574 species of annual or perennial herbs and shrubs distributed across the Mediterranean Region and Northern Hemisphere. Members of this family possess substantial economic, pharmacological, and industrial importance owing to their characteristic essential oils, aromatic constituents, and therapeutic properties (Üren, 2015; Adawe, 2021). Members of Lamiaceae are globally widespread, occurring in all continents except polar regions, with significant concentration in temperate zones such as Southwest Asia and South America (Tahravi, 2021). Taxonomically, the family is distinguished by quadrangular stems, opposite or decussate exstipulate leaves, and zygomorphic, bilabiate flowers bearing four epipetalous stamens and a bicarpellary, four-lobed superior ovary with a gynobasic style yielding four nutlets (Üren, 2015; Adawe, 2021). The presence of specialized glandular trichomes secreting essential oils and

phenolic compounds imparts substantial economic, pharmacological, and cosmetic value to the family, underpinning its extensive application in perfumery, food, flavoring, and traditional phytotherapy (Tahravi, 2021; Korkmaz, 2022).

Within Lamiaceae, the genus *Phlomis* L. occupies an important taxonomic and ethnomedicinal position. According to the Flora of Turkey, this genus is represented by a total of 44 species and 9 varieties, 10 of which are hybrids. In the List of Vascular Plants of Turkey, the genus Phlomis is recorded as 46 species and 11 varieties, 13 of which are hybrid species (Tekin, 2025). Morphologically, *Phlomis* taxa are perennial herbs or subshrubs characterized by a softly villous, stellate, or dendroid indumentum, simple leaves with entire to crenate-dentate margins, and axillary verticillasters subtended by distinct bracts (Üren, 2015; Adawe, 2021). Their adaptation to arid, rocky, and calcareous habitats reflects high ecological tolerance and xerophytic specialization (Tekin, 2025). Etymologically, the generic name *Phlomis* is derived from the Ancient Greek word “phlox” (meaning "flame," referring to the historical use of its woolly leaves as lamp wicks), while the specific epithet “pungens” translates to "piercing" or "puncturing," denoting its sharp calyx teeth (Ceylan, 2026).

Known colloquially in Anatolia as "ballık otu," "çalba," "şalba," or "calba," *Phlomis* taxa have extensive ethnobotanical applications, commonly utilized as herbal teas and traditional remedies for their wound-healing, analgesic, anti-inflammatory, and tonic effects.

Herbal infusions prepared from their flowering aerial parts are used to relieve gastrointestinal disorders and support liver, kidney, and cardiovascular health. In addition, they are folkly used to treat diabetes, stomach ulcers, hemorrhoids, inflammation, and wounds. (Arıca and Fırat, 2026).

Phlomis pungens Willd. (*Synonyms: Phlomis herba-venti* var. *pungens* (Willd.) Schmalh., *Phlomitis pungens* (Willd.) Rchb. ex T.Nees, *P. herba-venti* L. subsp. *pungens* (Willd.) Maire ex De Filipps) is an important representative of this genus, distributed naturally across Central Anatolia, including the Eskişehir province.

Despite the widespread therapeutic usage of *Phlomis* species, interspecific morphological similarities and regional phenotypic variations frequently lead to taxonomic confusion and adulteration in commercial herbal raw materials. Micro-anatomical characters such as trichome morphology, stoma architecture, and vascular bundle organization serve as indispensable diagnostic markers for resolving taxonomic ambiguities and ensuring botanical quality control. Therefore, the present study was conducted to determine the detailed macromorphological and light microscopic anatomical characteristics of *Phlomis pungens* specimens collected from natural habitats around Eskişehir. By providing comprehensive structural and diagnostic criteria, this work aims to facilitate accurate species delimitation, ensure safe therapeutic utilization, and establish a reliable botanical baseline for subsequent phytochemical, pharmacological, and systematic evaluations.

MATERIAL AND METHOD

Plant specimens of *Phlomis pungens* were collected from natural populations in Central Anatolia: [B3] Eskişehir: Beylikova, 39°50'00" N, 31°11'37" E, 870 m, 21 June 2025. Voucher specimens were identified according to Davis’s *Flora of Turkey and the East Aegean Islands* and deposited in the Herbarium of the Faculty of Pharmacy, Anadolu University (ESSE 16734). Morphological examinations were performed on 20 randomly selected individuals from the collected herbarium and fresh materials. Vegetative and floral characters were measured using millimetric paper. The measured parameters were tabulated and compared with taxonomic descriptions in *Flora of Turkey* and related literature. Macromorphological details of vegetative and reproductive organs (stems, leaves, bracts, and flowers) were photographed using an Olympus SZX12 stereomicroscope equipped with the Kameram® digital imaging software.

For anatomical evaluations, plant tissues (stems and leaves) fixed in 70% ethanol were used. Transverse sections of the mid-stem, leaf midrib, and lamina, as well as superficial sections of the adaxial and abaxial leaf epidermises, were obtained manually using the free-hand sectioning technique with commercial razor blades. The anatomical sections were examined using an Olympus BX51 light microscope equipped with an Olympus EP50 digital camera system. All anatomical layers, vascular organizations, stomatal types, and trichome indumentum were documented and scaled (µm).

RESULTS AND DISCUSSION

Morphological Characters

Phlomis pungens Willd. has a quadrangular stem covered with a stellate-tomentose indumentum, measuring 14–55 cm in height and 0.3–0.5 cm in diameter. The species typically produces 5 to 40 verticillasters, each containing more than 20 flowers. The leaf apex is acute, and the margins are crenate to serrate. The leaf base is cuneate or attenuate, tapering towards the petiole. The lamina exhibits pinnate-reticulate venation and is densely covered with stellate hairs. The leaves are 2.5–14.7 cm in length and 0.3–4.8 cm in width, while the corolla is 0.8–1.1 cm long and 0.4–0.9 cm wide. The corolla is purple-lilac, zygomorphic, bilabiate, and covered with stellate hairs. The calyx measures 0.8–1.1 cm in length and 0.3–0.5 cm in width. The leaves are generally simple, sometimes lobed, and arranged in a decussate pattern. The flowers are zygomorphic and bilabiate. The calyx is usually 5-toothed and actinomorphic, comprising three short and two long teeth, with distinct venation extending from the base to the teeth. The stamens are four in number, inserted into the corolla tube. The anthers are dithecal, consisting of two thecae housing the pollen sacs. The bracts are linear-subulate in shape, measuring 0.7–1.4 cm in length, and are covered with stellate or dendroid hairs forming a tomentose-villous indumentum (Figure 1).

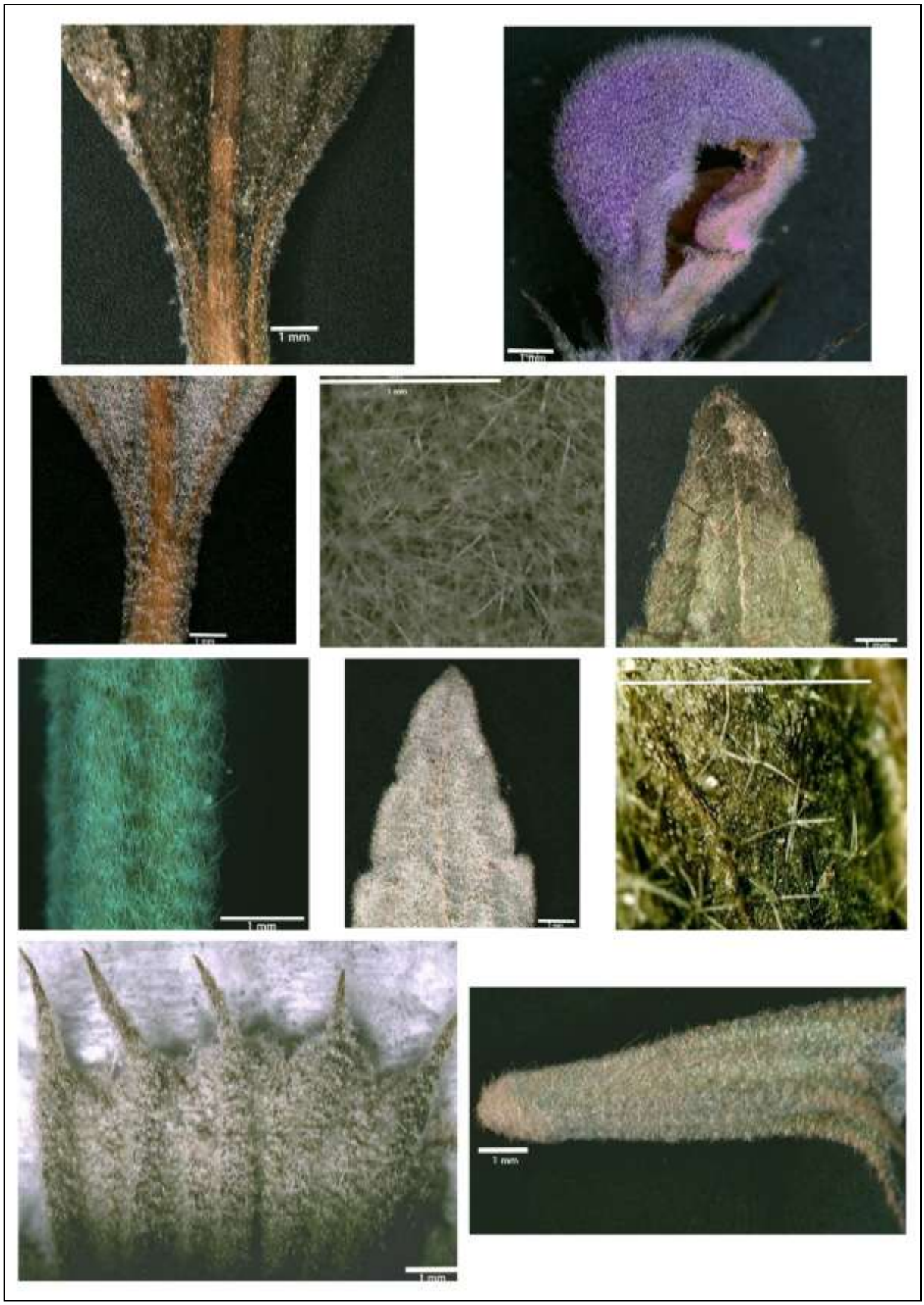

Figure 1. Stereomicroscope images of the morphological characters of *Phlomis pungens*.

Table 1. Macromorphological measurements of *Phlomis pungens* specimens collected from Eskişehir

Morphological Characters	**Measured Range (Min–Max)**	**Flora of Turkey (Davis, 1982)**	**Sarıkaya A. G., Fakir H. (2016)**
Vegetative Characters			
Plant height (cm)	14.0–55.0	70	-
Stem diameter (cm)	0.3–0.5		-
Internodal distance (cm)	2.5–11.0	-	-
Number of leaves per plant	32–166	-	-
Leaf length (cm)	2.5–14.7	5-13	2.2-11.5
Leaf width (cm)	0.3–4.8	1-6	0.4-4.2
Petiole length (cm)	0.2–7.2	10	0.2-7.7
Inflorescence & Floral Characters			
Number of verticillasters per plant	5–40	2-15	-
Distance between verticillasters (cm)	1.8–7.6	-	-
Number of flowers per verticillaster	3–11	-	-
Number of bracts per verticillaster	10–28	-	-
Bract length (cm)	0.7–1.4	1.1-1.7	-
Calyx length (cm)	0.8–1.1	0.8-1.5	-
Calyx width (cm)	0.3–0.5	-	-
Corolla length (cm)	0.8–1.1	1.5-2.5	-
Corolla width (cm)	0.4–0.9	-	-
Stamen length (cm)	0.8–1.5		

Anatomical Characters

Stem Anatomy

The stem is typically quadrangular, a characteristic feature of the family. It is surrounded by a single-layered epidermis with a cutinized outer wall that serves as a protective layer. Multicellular stellate or dendroid non-glandular and glandular trichomes emerge from the epidermis. Beneath the epidermis lies the collenchyma tissue, which is distinctly thickened at the corners. The cortical parenchyma is situated between the collenchyma and the vascular cylinder. Immediately beneath the cortical parenchyma lies the central cylinder (stele). The vascular tissues are arranged sequentially inward as sclerenchyma, phloem, vascular cambium, and xylem. The innermost part of the stem is occupied by the pith region (Figure 2).

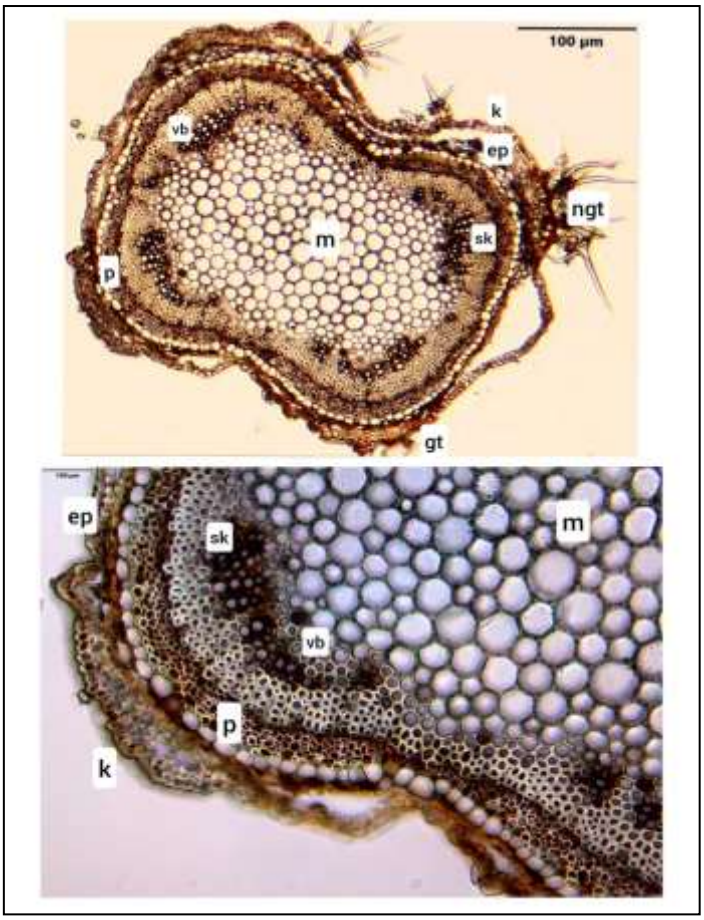

Figure 2. Light micrographs of *P. pungens* stem cross-sections. (ep: epidermis, k: collenchyma, p: parenchyma, sk: sclerenchyma, vb: vascular bundle, m: pith, ngt: non-glandular trichome, gt: glandular trichome; Scale bars = 100 µm).

Leaf Cross-Section

The midrib is surrounded by a single-layered epidermis on both the adaxial (upper) and abaxial (lower) surfaces. Multicellular stellate and dendroid non-glandular trichomes emerge from the epidermis. Immediately beneath the epidermis lies the collenchyma tissue, characterized by its thickened cell walls. The vascular bundle is located in the innermost central region. Within the vascular bundle, the phloem is oriented toward the abaxial (lower) surface, whereas the xylem faces the adaxial (upper) surface. In the transition zone from the midrib to the lamina, the mesophyll layer becomes distinct. In this region, the palisade parenchyma is composed of cylindrical, longitudinally elongated cells (Figure 3).

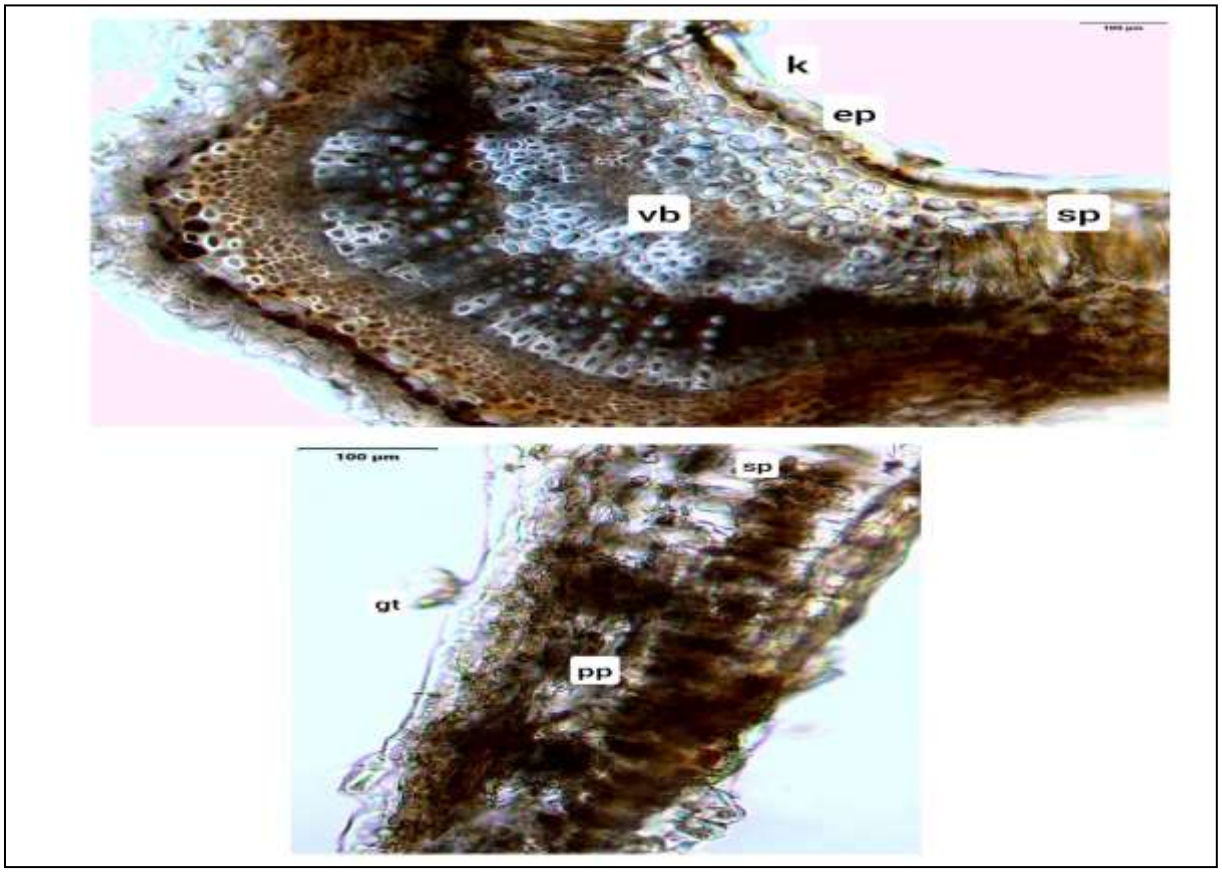

Figure 3. Light micrographs of *P. pungens* leaf cross-sections. (ep: epidermis, k: collenchyma, vb: vascular bundle, pp: palisade parenchyma, sp: spongy parenchyma, gt: glandular trichome; Scale bars = 100 µm).

Leaf Adaxial Surface Section

The anticlinal walls of the epidermal cells are sinuous. The stomata are of the diacytic type, each enclosed by two guard cells. Additionally, multicellular stellate non-glandular trichomes are present, characterized by pointed apices, thickened cell walls, and bases embedded within the epidermis (Figure 4).

Figure 4.

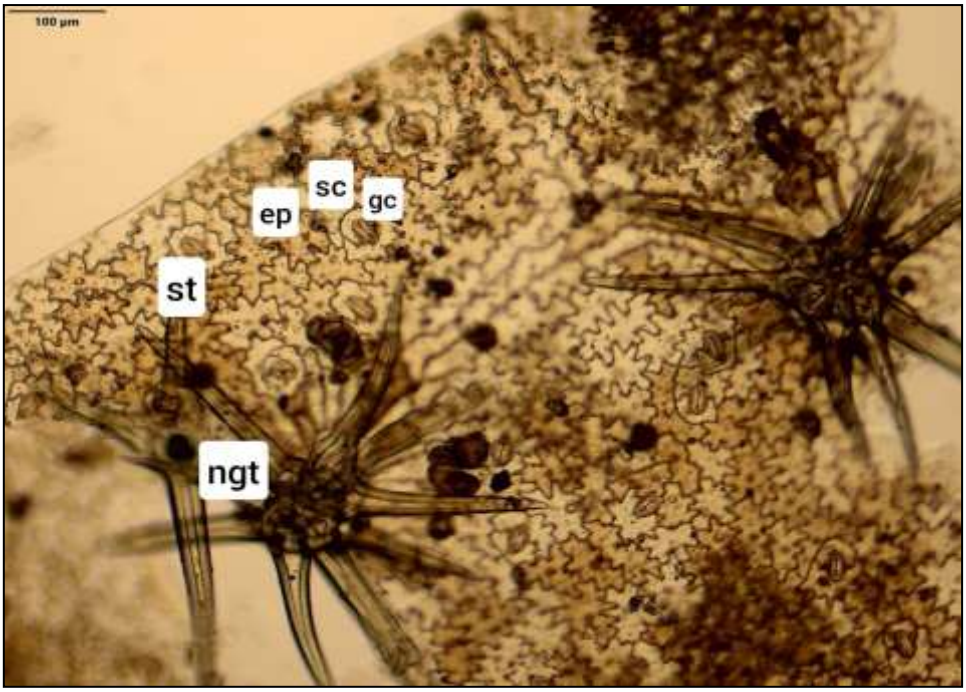

Micrograph of leaf adaxial surface. (ep: epidermal cell, st: stoma, sc: subsidiary cell, gc: guard cell, ngt: non-glandular trichome; Scale bar = 100 µm).

Leaf Abaxial Surface Section

The anticlinal walls of the epidermal cells are sinuous, and diacytic stomata are present. The abaxial surface exhibits a denser indumentum compared to the adaxial surface. The non-glandular trichomes are stellate or dendroid in structure, with their basal portion emerging from the epidermis and extending into long, pointed arms (Figure 5).

Figure 5.

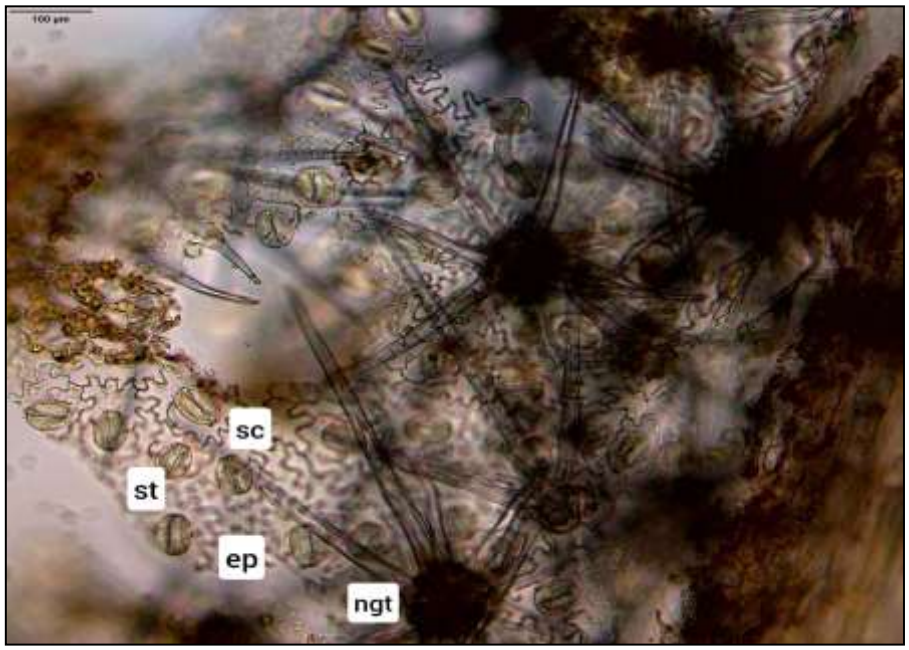

Micrograph of leaf abaxial surface showing denser indumentum. (ep: epidermal cell, st: stoma, sc: subsidiary cell, ngt: non-glandular trichome; Scale bar = 100 µm).

Trichomes

The multicellular stellate and dendroid non-glandular trichomes are characterized by long, pointed arms (Figure 6).

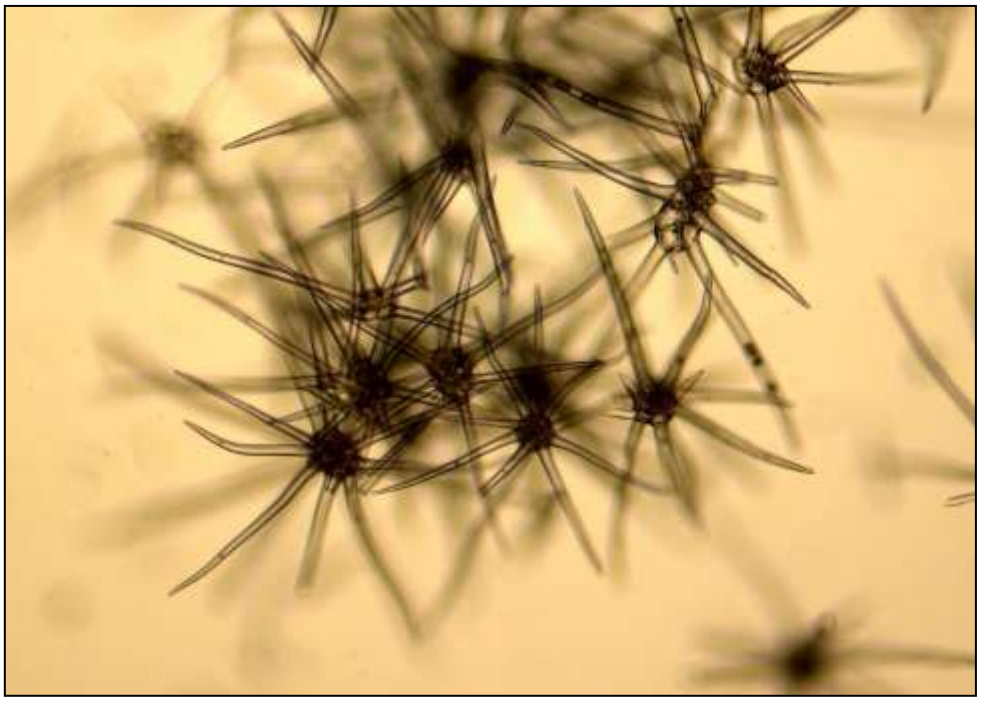

Figure 6. Multicellular stellate and dendroid non-glandular trichomes of *Phlomis pungens*

The morphological and anatomical results obtained in this study are broadly consistent with the available literature, with minor variations reflecting local population dynamics (Table 1). Specifically, Sarıkaya and Fakir (2016) reported leaf length as 2.2–11.5 cm, leaf width as 0.4–4.2 cm, and petiole length as 0.2–7.7 cm, whereas in the present study, these parameters were measured as 2.5–14.7 cm, 0.3–4.8 cm, and 0.2–7.2 cm, respectively. Similarly, while Davis (1982) documented a maximum plant height of up to 70 cm, the individuals examined herein reached a maximum height of 55 cm. In addition, Davis (1982) reported bract length as 1.1–1.7 cm and calyx length as 0.8–1.5 cm, while our measurements indicated ranges of 0.7–1.4 cm and 0.8–1.1 cm, respectively.

From an ecological and functional perspective, Tekin (2025) reported that *Phlomis* taxa typically inhabit arid and rocky terrains, conferring substantial environmental tolerance and adaptability. The specimens evaluated in this study were collected from the semi-arid steppe habitats of Eskişehir, where detailed micro-anatomical analyses revealed well-developed xeromorphic adaptations most notably a dense indumentum of thick-walled stellate/dendroid trichomes and angular collenchyma. These anatomical findings strongly corroborate the ecological observations of Tekin (2025), demonstrating the structural specialization of *P. pungens* to arid environments.

CONCLUSIONS

Phlomis is a taxon belonging to the Lamiaceae family, represented by 46 species in Türkiye. In this study, *P. pungens*, naturally distributed around Eskişehir, was evaluated from a botanical perspective. The species is characterized by quadrangular stems with dense stellate indumentum, decussate leaves (2.5–14.7 × 0.3–4.8 cm), and 5–40 verticillasters containing

bilabiate flowers with epipetalous stamens. Anatomically, the presence of angular collenchyma, dorsiventral mesophyll, sinuous epidermal anticlinal walls, and diacytic stomata on both leaf surfaces represents definitive diagnostic markers.

Based on the comparative literature review, *P. pungens* populations in and around Eskişehir possess a denser indumentum composed of thicker-walled stellate trichomes compared to populations growing in other regions. This dense indumentum serves as a critical ecophysiological adaptation to xerophytic conditions by reducing boundary layer wind velocity, minimizing transpiration, lowering UV radiation absorption, and providing physical defense against herbivorous insects.

Providing these comprehensive morpho-anatomical standards will ensure accurate taxonomic delimitation, support quality control for safe therapeutic use, and provide a solid baseline for future phytochemical research.

ACKNOWLEDGEMENT

This work was supported by the Anadolu University Scientific Research Projects Coordination Unit under grant number TYL-2026-3370.

REFERENCES

Adawe AM, 2021. Eskişehir Civarında Yetişen Bazı Lamiaceae Türlerinin Kimyasal ve Biyolojik Profillerinin Belirlenmesi. Doktora Tezi, Anadolu Üniversitesi, Lisansüstü Eğitim Enstitüsü, Eskişehir, Türkiye.

Arıca E, Fırat M, 2026. Unveiling The Phytochemical Landscape of *Phlomis pungens Willd:* LC-MS/MS Insights Into Antioxidant and Multi-Enzyme Inhibitory Potential. Records of Natural Products. 20(4):e26023755.

Ceylan Ş, 2026. *Phlomis herba-venti* subsp. *pungens* (Willd.) Maıre Ex Defilipps Bitkisinin Enzim İnhibisyonu ve Antioksidan Etkisinin Değerlendirilmesi ve Fitokimyasal Analizi. Yüksek Lisans Tezi, Gazi Üniversitesi, Sağlık Bilimleri Enstitüsü, Ankara, Türkiye.

Davis PH, 1982. Flora of Turkey and East Aegean Islands 7, Edinburg University Press, Edinburgh.

Korkmaz FJW, 2022. *Phlomis pungens* var. *hirta* Bitkisinin Sitotoksik ve Antigenotoksik Etkilerinin Bazı In Vitro Testlerle Araştırılması. Yüksek Lisans Tezi, Balıkesir Üniversitesi, Fen Bilimleri Enstitüsü, Balıkesir, Türkiye.

Sarıkaya AG, Fakir H, 2016. The Morphological And Distribution Areas Characteristics Of Native *Phlomis* L. (Lamiaceae) Taxa In The Lakes District, Turkey. Turkish Journal of Forestry. 17(2): 85-93.

Üren MC, 2015. Bazı *Phlomis* Türleri Üzerine Fitokimyasal Araştırma. Doktora Tezi, Süleyman Demirel Üniversitesi, Fen Bilimleri Enstitüsü, Isparta, Türkiye.

Tahravi L, 2021. Bazı Lamiaceae Familyası Bitkilerinin Osteoartrite Karşı Etkilerinin Matriks Metalloproteinaz-3 (Mmp-3) İnhibitör Etki Tayini ile Tespiti. Yüksek Lisans Tezi, Hacettepe Üniversitesi, Sağlık Bilimleri Enstitüsü, Ankara, Türkiye.

Tekin F, 2025. *Phlomis armeniaca* Willd. Bitki Ekstresinin Fitokimyasal Analizi ve İn-Vitro Preadipoz Hücre Hatları Üzerinde Antidiyabetik Potansiyelinin Araştırılması. Doktora Tezi, Ankara Yıldırım Beyazıt Üniversitesi, Halk Sağlığı Enstitüsü, Ankara, Türkiye.

ASSESSMENT OF SELECTED MACRO- AND MICRONUTRIENT CONCENTRATIONS IN SOILS AND WHEAT IN THE NARLI PLAIN

Ömer Faruk DEMİR[1]

[1]*Kahramanmaraş Sütçü İmam University, Faculty of Agriculture, Department of Soil Science and Plant Nutrition, Kahramanmaraş, Türkiye*

Corresponding author e-mail: demirfaruk@ksu.edu.tr

ABSTRACT

Evaluating soil nutrient availability together with plant nutrient concentrations provides a comprehensive understanding of crop nutritional status. Accordingly, this study aimed to assess the macro- and micronutrient status of wheat grown in the Narlı Plain of Kahramanmaraş, Türkiye. Soil samples were collected from a depth of 0–30 cm, and flag leaf samples were collected immediately before heading from 11 wheat-growing fields. Soil samples were analyzed for pH, calcium carbonate ($CaCO_3$) and organic matter contents, available phosphorus (Olsen-P), exchangeable potassium (K), calcium (Ca), and magnesium (Mg), and DTPA-extractable iron (Fe), zinc (Zn), copper (Cu), and manganese (Mn). Plant samples were analyzed for P, K, Ca, Mg, Fe, Zn, Cu, and Mn concentrations. The soils were slightly to moderately alkaline, with organic matter contents ranging from 2.13% to 4.50% and $CaCO_3$ contents ranging from 19.84% to 41.09%. Soil Olsen-P concentrations varied between 7.98 and 35.38 mg kg^{-1}, while the mean DTPA-extractable Fe, Zn, Cu, and Mn concentrations were 11.73, 1.05, 1.50, and 9.65 mg kg^{-1}, respectively. The mean exchangeable K, Ca, and Mg concentrations were 339.55, 3461, and 1145 mg kg^{-1}, respectively. The mean P, K, Ca, and Mg concentrations in wheat flag leaves were 0.28%, 2.60%, 0.80%, and 0.18%, respectively, whereas the mean Fe, Zn, Cu, and Mn concentrations were 97.93, 21.84, 6.75, and 40.41 mg kg^{-1}, respectively. The results showed that wheat grown in the Narlı Plain was generally adequately supplied with the macro- and micronutrients examined. However, the variation in soil and plant nutrient concentrations among the sampled fields suggests that wheat nutrient status may be influenced by differences in soil nutrient reserves, fertilizer management, and other soil properties. These findings highlight the importance of evaluating soil and plant analyses together when developing field-specific nutrient management strategies for wheat production in the region.

Keywords: Calcareous soil, flag leaf, mineral nutrition, wheat.

INTRODUCTION

Determining the mineral nutritional status of wheat grown in calcareous soils represents an important diagnostic challenge because soil nutrient reserves do not necessarily correspond to the availability of these nutrients to plants. High soil pH and $CaCO_3$ content may restrict nutrient uptake by roots by altering nutrient speciation in the soil solution, adsorption–desorption equilibria, and precipitation reactions. Therefore, the presence of an adequate reserve of a particular nutrient in the soil does not necessarily indicate that the nutrient can be taken up by plants in sufficient amounts (Hinsinger, 2001; Marschner, 2012; Xue et al., 2016). Recent studies conducted in calcareous soils have also demonstrated that these conditions may affect nutrient uptake and fertilizer-use efficiency in wheat (Martínez-Ríos et al., 2024; Zaheri Abdehvand et al., 2024; Demirkaya & Gülser, 2025).

In calcareous and alkaline soils, P may form sparingly soluble compounds with Ca or become immobilized through retention on $CaCO_3$ surfaces. Similarly, high pH and the presence of carbonate and bicarbonate ions may reduce the solubility and root availability of Fe, Zn, Mn, and Cu. Zinc availability, in particular, is strongly influenced by interactions among soil pH, carbonate content, P status, organic matter, and clay minerals (Chen et al., 2019; Martínez-Ríos et al., 2024). Consequently, wheat grown in calcareous soils may exhibit marginal or latent nutrient deficiencies even in the absence of visible deficiency symptoms. However, the relationship between soil $CaCO_3$ content and plant nutritional status is not straightforward. Nutrient availability in the root zone is governed by the combined effects of soil pH and $CaCO_3$ content, as well as texture, organic matter, cation exchange capacity, soil moisture, and rhizosphere processes. Plant nutrient uptake may also vary depending on genotype, root-system characteristics, growth stage, fertilization history, and interactions among nutrients (White & Brown, 2010; Marschner, 2012). Therefore, $CaCO_3$ content alone may not provide an adequate basis for assessing plant nutritional status in calcareous soils.

Soil analyses provide information on the potential availability of nutrients and the nutrient-supplying capacity of the soil, whereas plant tissue analyses reflect the integrated outcome of soil–root processes as expressed in plant nutrient uptake. However, because elemental concentrations in plant tissues vary with the sampled organ and growth stage, the results should be interpreted using appropriate sampling times and established sufficiency ranges (Jones et al., 1991; Reuter & Robinson, 1997; Lemaire et al., 2019). Flag leaves collected immediately before heading constitute suitable diagnostic material for assessing the nutrient status of wheat. Accordingly, the combined use of soil and plant analyses enables a more comprehensive assessment of nutrient deficiencies and limitations to nutrient uptake.

The Narlı Plain, located south of Kahramanmaraş, is an important agricultural production area characterized by soils developed from alluvial and colluvial parent materials. Variations in topographic position and soil-forming conditions have resulted in considerable heterogeneity in the physical and chemical properties of the plain's soils (Yakupoğlu et al., 2012; Yakupoğlu & Demirci, 2013). Previous studies conducted in the region have shown that this variability is also reflected in soil pH, $CaCO_3$ content, and nutrient concentrations (Saltalı et al., 2018). Total and active $CaCO_3$ contents have also been reported to be associated with the availability of certain metallic micronutrients in the soils of the plain (Kadifeci et al., 2024). Nevertheless, field-based information on the extent to which soil nutrient levels are reflected in the nutritional status of wheat remains limited. Accordingly, this study aimed to determine selected physical and chemical properties of calcareous agricultural soils under wheat cultivation in the Narlı Plain and to evaluate the macro- and micronutrient status of wheat through combined soil and flag-leaf analyses. The relationships between soil $CaCO_3$ content and P, K, Ca, Mg, Fe, Zn, Cu, and Mn concentrations in wheat flag leaves were also investigated.

MATERIAL AND METHOD

Study area

The study was conducted in wheat-growing areas of the Narlı Plain, located within the administrative boundaries of Pazarcık district, Kahramanmaraş Province, southern Türkiye. Situated approximately 30 km southeast of Kahramanmaraş city center, the plain covers an area of approximately 26,500 ha and lies within a transitional zone between Mediterranean and continental climatic conditions (Saltalı et al., 2018).

The soils of the Narlı Plain have developed predominantly from alluvial and colluvial parent materials transported from the surrounding uplands and deposited across the plain. Variations in depositional environments and topographic positions have resulted in pronounced spatial variability in the physical and chemical properties of these soils (Yakupoğlu et al., 2012;

Yakupoğlu & Demirci, 2013). The soils of the region have generally been characterized as neutral to slightly alkaline and as having varying $CaCO_3$ contents. Moreover, their total and active $CaCO_3$ contents may influence the availability of metallic micronutrients (Kadifeci et al., 2024).

The study area comprised fields under wheat cultivation within the Narlı Plain. Eleven wheat-growing fields were selected to represent the spatial variability in soil properties and plant nutritional status across the plain. The geographical coordinates of the soil and flag-leaf sampling points were recorded during fieldwork. The location of the study area within Türkiye and Kahramanmaraş Province, together with the distribution of the sampling points across the Narlı Plain, is presented in Figure 1.

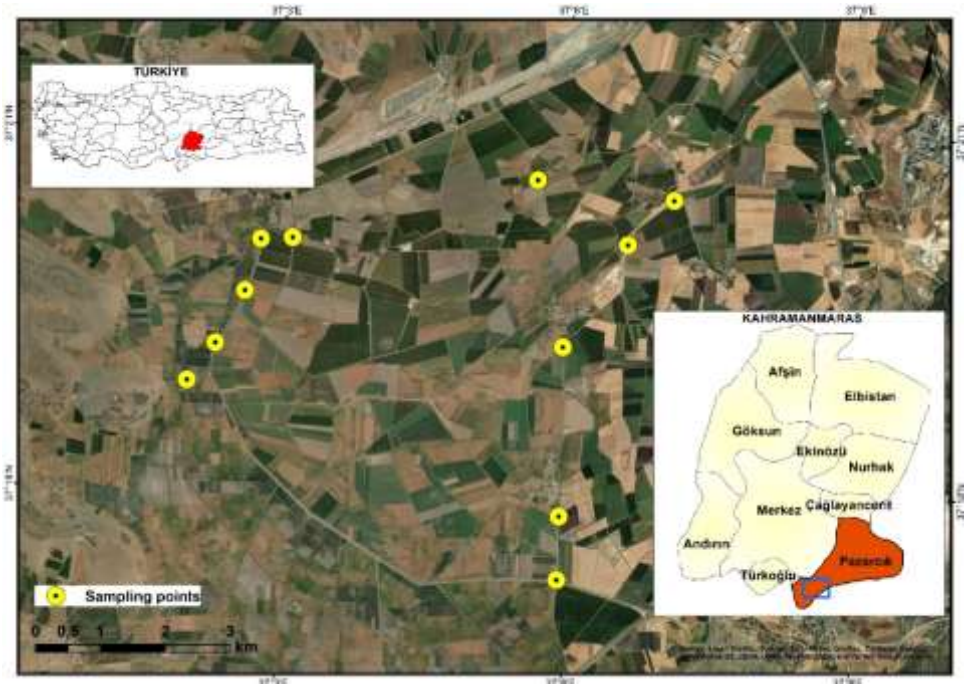

Figure 1. Location of the study area and distribution of soil and wheat flag-leaf sampling points in Narlı Plain

Soil and Plant Sampling and Preparation for Analysis

Soil samples were collected from a depth of 0–30 cm at 11 wheat-growing fields selected across the Narlı Plain, and the coordinates of the sampling points were recorded using a Global Positioning System (GPS). Composite soil samples representing each sampling point were transported to the laboratory, air-dried under ambient conditions, and passed through a 2-mm sieve. The prepared samples were labelled and stored in sealed plastic containers under cool and dry conditions until analysis (Richards, 1954).

Plant samples were collected simultaneously from the same fields where the soil samples were obtained. To assess the nutritional status of wheat, 25–30 representative flag leaves were collected from each field immediately before heading (Jones et al., 1991). The leaf samples were washed with distilled water to remove surface dust and other residues and subsequently oven-dried at 65 °C for 48 h. The dried plant material was ground and homogenized, transferred to labelled polyethylene bags, and stored under refrigerated conditions until chemical analysis (Jones & Case, 1990).

Soil and Plant Analyses

Soil pH and electrical conductivity (EC) were determined in saturated soil paste according to the methods described by Peech (1965) and Richards (1954), respectively. Total calcium carbonate ($CaCO_3$) content was measured using a Scheibler calcimeter (Loeppert & Suarez, 1996), whereas soil organic matter was determined using the Walkley–Black wet oxidation method (Nelson & Sommers, 1996). Available P was determined using the Olsen method based on extraction with 0.5 M $NaHCO_3$ at pH 8.5 (Olsen et al., 1954). Exchangeable K, Ca, and Mg were extracted with 1 N ammonium acetate (NH_4OAc) at pH 7.0 (Thomas, 1982). Plant-available Fe, Zn, Cu, and Mn were determined using the DTPA extraction method (Lindsay & Norvell, 1978). The concentrations of K, Ca, Mg, Fe, Zn, Cu, and Mn in the soil extracts were measured using an Agilent 240AA atomic absorption spectrophotometer (AAS).

A 0.50-g portion of each ground plant sample was wet-digested on a hot plate using a mixture of 5 mL HNO_3 and 4 mL $HClO_4$ until a clear solution was obtained (Jones & Case, 1990). Following digestion, the solutions were filtered and brought to a known volume with deionized water. Phosphorus concentration in the plant samples was determined spectrophotometrically using the vanadomolybdophosphoric yellow colour method. Potassium, Ca, Mg, Fe, Zn, Cu, and Mn concentrations were measured using an Agilent 240AA atomic absorption spectrophotometer.

Statistical Analyses

Minimum, maximum, and mean values for the soil and plant variables were calculated using Microsoft Office Excel. Relationships between soil $CaCO_3$ content and P, K, Ca, Mg, Fe, Zn, Cu, and Mn concentrations in wheat flag leaves were examined using two-tailed Pearson correlation analysis in IBM SPSS Statistics 23.0 (IBM Corp., Armonk, NY, USA). Statistical significance was accepted at $p < 0.05$, and graphical presentations of the results were prepared using Microsoft Office Excel.

RESULTS AND DISCUSSION

Characteristic Properties of the Study-Area Soils

Soil pH values ranged from 7.43 to 7.79, with a mean of 7.56. Electrical conductivity values varied between 303 and 501 μS cm^{-1}, averaging 349 μS cm^{-1}. Soil $CaCO_3$ contents ranged from 19.84% to 41.09%, with a mean of 27.95%, whereas organic matter contents varied between 2.13% and 4.50%, with a mean of 2.85%. Based on these results, the soils were generally characterized as slightly alkaline and non-saline, with high to very high $CaCO_3$ contents and moderate organic matter levels.

Table 1. Descriptive statistics of selected physicochemical properties of the study area soils

	pH	**EC**	**Lime**	**OM**
		(μS/cm)		%
Min	7,43	303	19,84	2,13
Max	7,79	501	41,09	4,50
Mean	7,56	349	27,95	2,85

Macronutrient Status of the Study-Area Soils

Evaluation of the macronutrient contents of soil samples collected from the Narlı Plain revealed different sufficiency levels among the nutrients examined. According to Cottenie (1980), available P concentrations of 8–25 mg kg^{-1} are classified as sufficient, whereas concentrations of 25–80 mg kg^{-1} are considered high (Figure 2). Based on these thresholds, the mean available P concentration (22.5 mg kg^{-1}) was within the sufficient range; 54.5% of the samples were classified as sufficient and 45.5% as high. However, because the minimum concentration was close to the lower limit of the sufficiency range, the mean value should be interpreted together with the variability among sampling sites.

The mean exchangeable K concentration (340 mg kg^{-1}) exceeded the ≥161 mg kg^{-1} threshold above which Kaiser and Piotrowski (2024) did not recommend K fertilization for wheat under Minnesota conditions. While 63.6% of the samples reached or exceeded this threshold, 36.4% had K concentrations within the range of 95–160 mg kg^{-1}. Therefore, the high mean K concentration should not be interpreted as indicating a uniform K status across all sampling sites. Because this threshold was developed for a different region, it should be used as a comparative benchmark rather than directly applied to fertilizer recommendations for the Narlı Plain.

Regarding exchangeable Ca, 45.5% of the samples were classified as sufficient (1150–3500 mg kg^{-1}), whereas 54.5% were classified as high (3500–10,000 mg kg^{-1}). The mean Ca concentration (3461 mg kg^{-1}) was close to the upper limit of the sufficient range. Accordingly, the results did not indicate Ca deficiency in the investigated soils under the classification system used. For exchangeable Mg, 72.7% of the samples were classified as high (480–1500 mg kg^{-1}) and 27.3% as very high (>1500 mg kg^{-1}). The mean Mg concentration (1145 mg kg^{-1}) was within the high range, and all samples exceeded the sufficiency range, indicating that the soils generally had high exchangeable Mg concentrations (Cottenie, 1980).

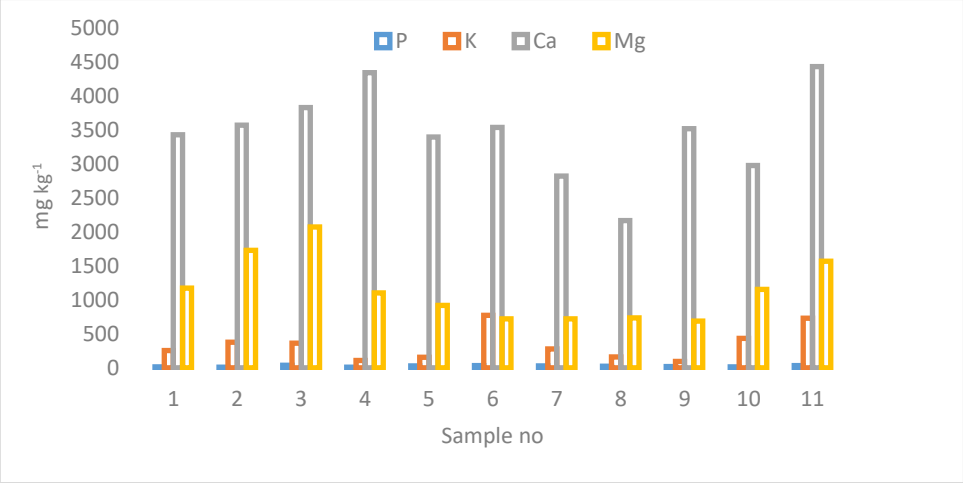

Figure 2. Distribution of available P and exchangeable cations

Micronutrient Status of the Study-Area Soils

The DTPA-extractable micronutrient concentrations of the soil samples collected from the Narlı Plain varied among the sampling sites (Figure 3). Iron (Fe) concentrations ranged from 8.88 to 23.52 mg kg^{-1}, with a mean of 11.73 mg kg^{-1}. Zinc (Zn) concentrations varied between 0.54 and 2.90 mg kg^{-1}, averaging 1.05 mg kg^{-1}. Copper (Cu) concentrations ranged from 1.08 to 2.20 mg kg^{-1}, with a mean of 1.50 mg kg^{-1}, whereas manganese (Mn) concentrations varied between 3.36 and 28.80 mg kg^{-1}, averaging 9.65 mg kg^{-1}. The mean concentrations of the micronutrients followed the order Fe > Mn > Cu > Zn.

Soil micronutrient status was evaluated using the critical levels reported for maize by Lindsay and Norvell (1978) as comparative benchmarks. In all samples, Fe, Cu, and Mn concentrations exceeded their respective critical levels of 4.5, 0.2, and 1.0 mg kg^{-1}. Thus, according to these thresholds, no indication of Fe, Cu, or Mn deficiency was identified in the investigated soils. However, the critical values reported for Mn and Cu were proposed tentatively and should therefore be interpreted with caution.

Based on the critical Zn level of 0.8 mg kg^{-1}, 45.5% of the samples were classified as deficient and 54.5% as sufficient. Although the mean Zn concentration (1.05 mg kg^{-1}) exceeded the critical threshold, the occurrence of concentrations below this value in 45.5% of the samples demonstrates that soil Zn status should not be evaluated solely on the basis of the mean. Zinc was the only micronutrient for which values below the critical level were detected, indicating a potential Zn deficiency at some sampling sites that warrants further investigation. Nevertheless, because the thresholds used were originally established for maize, definitive conclusions regarding wheat nutritional status should be supported by plant tissue analyses and crop-specific sufficiency criteria.

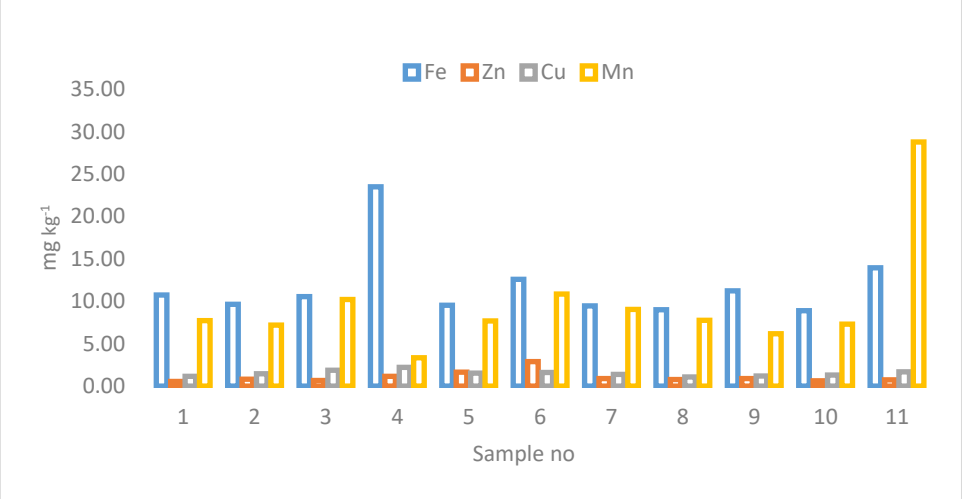

Figure 3. Distribution of DTPA-extractable Fe, Zn, Cu and Mn concentrations

Flag-Leaf Macronutrient Concentrations in Wheat

Macronutrient concentrations in wheat flag leaves varied among the sampling sites. Phosphorus concentrations ranged from 0.21% to 0.38%, with a mean of 0.28%. Potassium concentrations varied between 2.13% and 3.33%, averaging 2.60%. Calcium concentrations exhibited a relatively wide variation, ranging from 0.40% to 1.61%, with a mean of 0.80%. Magnesium concentrations ranged from 0.14% to 0.24%, with a mean of 0.18% (Figure 4). Among the macronutrients examined, K had the highest mean concentration, whereas Mg had the lowest.

The plant analysis results indicated that wheat grown in the study area generally had an adequate macronutrient status. When compared with the critical concentrations and sufficiency ranges reported for wheat, P and K concentrations were considered sufficient at all sampling sites (Jones et al., 1991; Reuter & Robinson, 1997; Plank & Donohue, 2000). In particular, the mean P (0.28%) and K (2.60%) concentrations exceeded the reported critical levels for wheat, indicating no apparent nutritional deficiency in these elements.

The variation in Ca concentrations from 0.40% to 1.61% indicated considerable differences among the sampling sites in Ca uptake or accumulation within plant tissues. Nevertheless, all measured Ca concentrations exceeded the critical level reported for wheat. Magnesium concentrations varied within a narrower range and averaged 0.18%. Because even the lowest

Mg concentration (0.14%) was above the critical level, no evident Mg deficiency was identified in the wheat plants (Jones et al., 1991; Reuter & Robinson, 1997; Plank & Donohue, 2000).

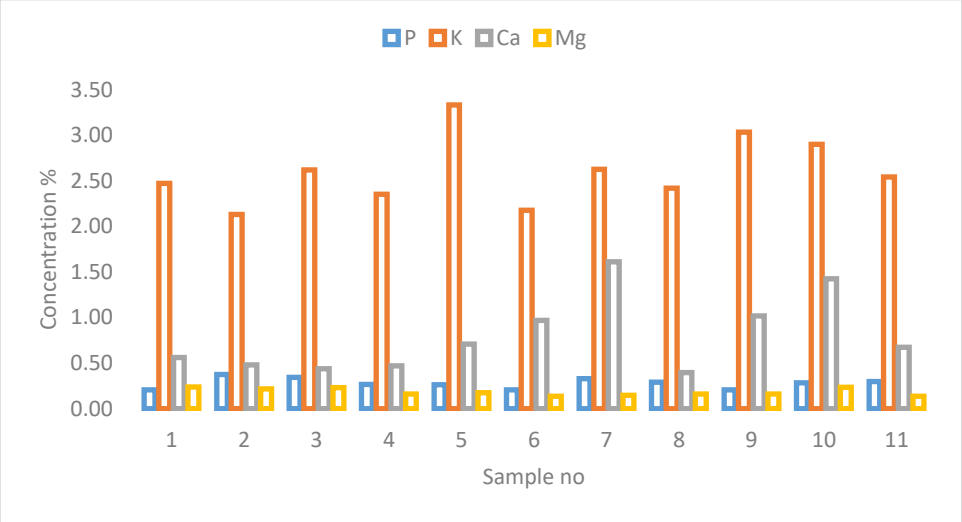

Figure 4. Foliar concentrations of macronutrients in wheat

Micronutrient Status of Wheat Flag Leaves

Micronutrient concentrations in wheat flag leaves varied among the sampling sites. Iron concentrations ranged from 69.00 to 156.75 mg kg^{-1}, with a mean of 97.93 mg kg^{-1}. Zinc concentrations varied between 17.50 and 30.00 mg kg^{-1}, averaging 21.84 mg kg^{-1}. Copper concentrations ranged from 4.50 to 8.75 mg kg^{-1}, with a mean of 6.75 mg kg^{-1}, whereas Mn concentrations varied between 16.00 and 54.25 mg kg^{-1}, averaging 40.41 mg kg^{-1} (Figure 5).

Based on the critical concentrations and sufficiency ranges reported for wheat, Fe, Zn, and Mn concentrations were generally considered adequate (Jones et al., 1991; Reuter & Robinson, 1997; Plank & Donohue, 2000). Iron concentrations of at least 69.00 mg kg^{-1} at all sampling sites indicated no evident Fe deficiency. Similarly, the observed Zn concentrations indicated that the wheat plants generally had an adequate Zn nutritional status.

Although the mean Cu concentration was within the sufficient range, the lowest value of 4.50 mg kg^{-1}, recorded at sampling site 2, was close to the critical level of approximately 5 mg kg^{-1} reported for wheat. Therefore, Cu nutrition was generally adequate, although a marginal Cu status may have occurred at this sampling site (Jones et al., 1991; Reuter & Robinson, 1997). Manganese concentrations indicated adequate nutrition at most sampling sites; however, the minimum concentration recorded at sampling site 11 was close to the lower limit of the sufficiency range.

Overall, wheat grown in the study area was adequately supplied with Fe, Zn, Cu, and Mn, although Cu and Mn concentrations approached the lower sufficiency limits at some sampling sites. Because tissue micronutrient concentrations may be influenced by soil pH, $CaCO_3$ and organic matter contents, nutrient availability, and interactions among elements, the combined interpretation of soil and plant analyses provides a more reliable assessment of wheat nutritional status (Reuter & Robinson, 1997).

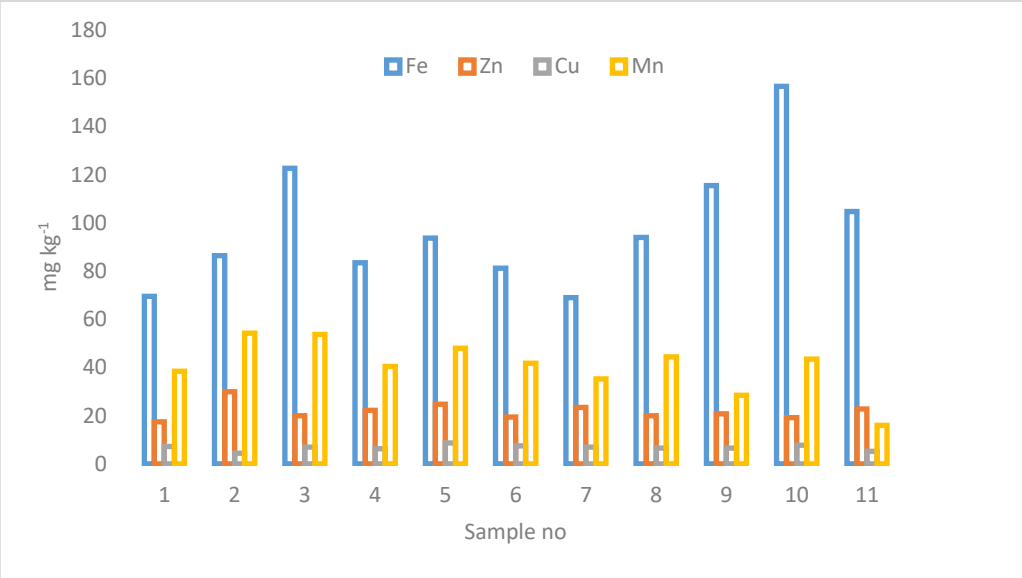

Figure 5. Foliar micronutrient concentrations in wheat

Relationships between soil lime and plant nutrients

No statistically significant correlations were detected between soil $CaCO_3$ content and P, K, Ca, Mg, Fe, Zn, Cu, or Mn concentrations in wheat flag leaves ($p > 0.05$; Table 2). Correlation coefficients ranged from −0.268 to 0.228, indicating no apparent linear relationship between soil $CaCO_3$ content and the macro- or micronutrient concentrations of wheat across the sampled fields. These findings suggest that variation in wheat nutritional status cannot be explained solely by soil $CaCO_3$ content and may also be influenced by soil nutrient reserves, fertilization practices, other soil properties, and plant-related factors. Nevertheless, because of the limited sample size (n = 11), the results should be interpreted within the context of the study area and sampling conditions (Table 2).

Table 2 Pearson correlation coefficients between soil lime and nutrient concentrations in wheat flag leaves

Plant nutrient	Pearson's r	p value	Significance
P	0,033	0,923	ns
K	−0,137	0,688	ns
Ca	−0,268	0,425	ns
Mg	0,228	0,500	ns
Fe	−0,028	0,934	ns
Zn	0,005	0,987	ns
Cu	−0,227	0,503	ns
Mn	0,001	0,998	ns

Note: Pearson correlation coefficients were calculated using 11 paired soil and flag-leaf samples (n = 11). ns: not significant ($p > 0.05$; two-tailed).

CONCLUSION

Wheat grown in the calcareous agricultural soils of the Narlı Plain was generally adequately supplied with P, K, Ca, Mg, Fe, Zn, Cu, and Mn. Available P and exchangeable K, Ca, and Mg concentrations in the soils were predominantly sufficient or high, while no clear deficiency of Fe, Cu, or Mn was identified. However, Zn concentrations were below the critical threshold in

45.5% of the soil samples, indicating a potential risk of Zn deficiency in some production fields. Plant analysis revealed no evident nutrient deficiencies, although Cu and Mn concentrations approached the lower limits of the sufficiency ranges at certain sampling sites. The absence of significant relationships between soil $CaCO_3$ content and nutrient concentrations in wheat flag leaves ($p > 0.05$) indicated that variation in plant nutritional status could not be explained solely by soil $CaCO_3$ content. Consequently, the combined interpretation of soil and plant analyses is recommended for a reliable assessment of wheat nutritional status in the Narlı Plain, with particular attention to the regular monitoring of Zn, Cu, and Mn.

REFERENCES

Chen, X.-X., Zhang, W., Wang, Q., Liu, Y.-M., Liu, D.-Y., & Zou, C.-Q. (2019). Zinc nutrition of wheat in response to application of phosphorus to a calcareous soil and an acid soil. Plant and Soil, 434(1–2), 139–150. https://doi.org/10.1007/s11104-018-3820-5

Cottenie, A. (1980). Soil and plant testing as a basis of fertilizer recommendations (FAO Soils Bulletin No. 38/2). Food and Agriculture Organization of the United Nations. https://openknowledge.fao.org/handle/20.500.14283/d8502e

Demirkaya, S., & Gülser, C. (2025). Biochar innovations for sustainable agriculture: Acidification and zinc enrichment strategies to improve calcareous soil fertility and wheat yield. Soil and Water Research, 20(2), 105–118. https://doi.org/10.17221/77/2024-SWR

Hinsinger, P. (2001). Bioavailability of soil inorganic P in the rhizosphere as affected by root-induced chemical changes: A review. Plant and Soil, 237(2), 173–195. https://doi.org/10.1023/A:1013351617532

Jones, J. B. Jr., and V. W. Case 1990. Sampling, Handling, and analyzing plant tissue samples, chapter 15. In R.L. Westerman (ed) Soil Testing and Plant Analysis, Third Edition, SSSA, Madison, Wisconsin, USA, pp. 390-420. https://doi.org/10.2136/sssabookser3.3ed.c15

Jones, J. B., Jr., Wolf, B., & Mills, H. A. (1991). Plant analysis handbook: A practical sampling, preparation, analysis, and interpretation guide. Micro-Macro Publishing. https://openlibrary.org/books/OL12110790M/Plant_Analysis_Handbook

Kadifeci, H., Dikici, H., & Demir, Ö. F. (2024). Effect of active lime on the availability of metal micronutrients. Turkish Journal of Agricultural and Natural Sciences, 11(2), 347–356. https://doi.org/10.30910/turkjans.1407307

Kaiser, D. E., & Piotrowski, K. (2024). Fertilizing wheat in Minnesota. University of Minnesota Extension. https://extension.umn.edu/agriculture/crop-production/nutrient-management-for-minnesota-crops/fertilizing-wheat-in-minnesota

Lemaire, G., Sinclair, T., Sadras, V., & Bélanger, G. (2019). Allometric approach to crop nutrition and implications for crop diagnosis and phenotyping: A review. Agronomy for Sustainable Development, 39, Article 27. https://doi.org/10.1007/s13593-019-0570-6

Lindsay, W. L., & Norvell, W. A. (1978). Development of a DTPA soil test for zinc, iron, manganese, and copper. Soil Science Society of America Journal, 42(3), 421–428. https://doi.org/10.2136/sssaj1978.03615995004200030009x

Loeppert, R. H., & Suarez, D. L. (1996). Carbonate and gypsum. In D. L. Sparks (Ed.), Methods of Soil Analysis: Part 3—Chemical Methods (pp. 437–474). Soil Science Society of America and American Society of Agronomy, Madison, WI, USA. https://doi.org/10.2136/sssabookser5.3.c15

Marschner, P. (Ed.). (2012). Marschner's mineral nutrition of higher plants (3rd ed.). Academic Press. https://doi.org/10.1016/C2009-0-63043-9

Martínez-Ríos, O., Bravo-Vinaja, Á., San-Martín-Hernández, C., Hidalgo-Moreno, C. I., Sánchez-de-Jesús, M. A., Llampallas-Díaz, J. D., Santillan-Balderas, D. R., & García-Preciado,

J. C. (2024). Zinc deficiency in calcareous soils: A bibliometric analysis from 1989 to 2024. Agriculture, 14(12), Article 2285. https://doi.org/10.3390/agriculture14122285
Nelson, D. W., & Sommers, L. E. (1996). Total carbon, organic carbon, and organic matter. In D. L. Sparks (Ed.), Methods of soil analysis: Part 3. Chemical methods (pp. 961–1010). Soil Science Society of America. https://doi.org/10.2136/sssabookser5.3.c34
Olsen, S. R., Cole, C. V., Watanabe, F. S., & Dean, L. A. (1954). Estimation of available phosphorus in soils by extraction with sodium bicarbonate (USDA Circular No. 939). U.S. Department of Agriculture. https://archive.org/details/estimationofavai939olse
Peech, M. (1965). Hydrogen-ion activity. In C. A. Black (Ed.), Methods of soil analysis: Part 2. Chemical and microbiological properties (pp. 914–926). American Society of Agronomy. https://doi.org/10.2134/agronmonogr9.2.c9
Plank, C. O., & Donohue, S. J. (2000). Small grain—Barley, oats, rye, wheat. In C. R. Campbell (Ed.), Reference sufficiency ranges for plant analysis in the Southern Region of the United States (pp. 29–31). Southern Cooperative Series Bulletin No. 394. https://paperzz.com/doc/8950152/reference-sufficiency-ranges-for-plant-analysis-in-the-so
Reuter, D. J., & Robinson, J. B. (Eds.). (1997). Plant analysis: An interpretation manual (2nd ed.). CSIRO Publishing. https://www.publishing.csiro.au/book/437
Richards, L.A. (1954). Diagnosis and Improvement of Saline and Alkali Soils. Agriculture Handbook, No:60, U.S. Department of Agriculture. U.S. Government Printing Office, Washington D.C., 166.
Saltalı, K., Gündoğan, R., Demir, Ö. F., Kara, Z., Yakupoğlu, T., Dikici, H., & Yılmaz, K. (2018). Narlı Ovası topraklarının ağır metal kapsamı üzerine çimento fabrikası baca tozlarının etkileri. Toprak Su Dergisi, 7(1), 11–20. https://doi.org/10.21657/topraksu.410113
Thomas, G. W. (1982). Exchangeable cations. In A. L. Page, R. H. Miller, & D. R. Keeney (Eds.), Methods of soil analysis: Part 2. Chemical and microbiological properties (2nd ed., pp. 159–165). American Society of Agronomy and Soil Science Society of America. https://doi.org/10.2134/agronmonogr9.2.2ed.c9
White, P. J., & Brown, P. H. (2010). Plant nutrition for sustainable development and global health. Annals of Botany, 105(7), 1073–1080. https://doi.org/10.1093/aob/mcq085
Xue, Y., Xia, H., Christie, P., Zhang, Z., Li, L., & Tang, C. (2016). Crop acquisition of phosphorus, iron and zinc from soil in cereal/legume intercropping systems: A critical review. Annals of Botany, 117(3), 363–377. https://doi.org/10.1093/aob/mcv182
Yakupoğlu, T., & Demirci, D. (2013). Kahramanmaraş-Narli Ovasi Topraklarinin Erozyona Duyarliliklari İle Bazi Toprak Özellikleri Arasindaki İlişkiler. Anadolu Tarım Bilimleri Dergisi, 28(1), 33-38. https://izlik.org/JA62SJ38AJ
Yakupoğlu, T., Saltalı, K., & Karagöktaş, M. (2012). Narlı Ovası'nda toprak aşınabilirliğinin pedotransfer yaklaşımı ile tahminlenmesi. KSÜ Doğa Bilimleri Dergisi, 15(2), 59–67. https://izlik.org/JA98BP96FZ
Zaheri Abdehvand, Z., Karimi, D., Rangzan, K., & Mousavi, S. R. (2024). Assessment of soil fertility and nutrient management strategies in calcareous soils of Khuzestan Province: A case study using the Nutrient Index Value method. Environmental Monitoring and Assessment, 196(6), Article 503. https://doi.org/10.1007/s10661-024-12665-4

EFFECTS OF MYCORRHIZA-BASED MICROBIAL FERTILIZERS ON BASIL (*Ocimum basilicum* L.) AGRICULTURAL CHARACTERISTICS UNDER DEFICIT IRRIGATION CONDITIONS

Alaattin BOZKUŞ[1], Onur Ali KORUCU[1], Mehmet GÜMÜŞ[1], Halil Han KOCAÖMEROĞLU[1], Elif Azra AKIN[1], İsmail Emrah TAVALI[1], Hüseyin OK[2]*

[1] Department of Soil Science and Plant Nutrition, Faculty of Agriculture, Akdeniz University, 07059 Antalya, Türkiye

[2] Department of Plant Production and Technologies, Faculty of Agricultural Sciences and Technologies, Cyprus International University, 99258 Nicosia, Türkiye

** Correspondence: etavali@akdeniz.edu.tr*

ABSTRACT

The application of microbial fertilizers on plants has gained increasing importance as a sustainable strategy to enhance crop stress tolerance and plant productivity under challenging deficit irrigation conditions. This study aimed to evaluate the effects of various mycorrhiza-based microbial fertilizer formulations on the growth performance of broad-leaved basil (*Ocimum basilicum* L.) grown in a sandy-loam calcareous soil. The study focused on how these microbial amendments influence plant resilience across four deficit irrigation levels: full irrigation (SS100) and three deficit irrigation regimes (SS80, SS60, and SS40). The results indicated that deficit irrigation conditions severely restricted vegetative growth parameters in unfertilized control groups. However, microbial fertilization significantly alleviated the adverse effects of drought stress. Basil plants treated with mycorrhizal formulations, particularly dual or combined microbial treatments, exhibited notable improvements in plant growth dynamics. Key parameters including plant height, root collar diameter, and total leaf number were positively affected by the microbial amendments even under high water deficit. Additionally, plants treated with microbial fertilizers recorded significantly higher chlorophyll levels (SPAD values), demonstrating sustained photosynthetic efficiency under stress. At harvest, a substantial increase in fresh biomass accumulation was observed in mycorrhiza-treated plots compared to the control group, highlighting the role of these symbiotic microorganisms in optimizing root surface area and nutrient uptake. Overall, mycorrhiza-based applications emerged as highly effective inputs for mitigating drought-induced limitations in basil cultivation.

Keywords: Mycorrhiza, Biostimulants, Drought tolerance, Sustainable agriculture

INTRODUCTION

The rapidly increasing global population, dwindling freshwater resources, and irregular rainfall patterns triggered by global climate change are among the most significant ecological problems threatening agricultural production. In particular, in semi-arid climate zones such as the Mediterranean Basin (e.g., the southern coasts of Türkiye), plants frequently face water scarcity (drought) stress throughout their growing seasons (IPCC, 2021). Drought stress leads to a decrease in cell turgor pressure, stomatal closure, accumulation of reactive oxygen species (ROS) causing oxidative damage, and consequently a significant reduction in photosynthesis,

nutrient uptake, and ultimately biomass and economic yield in plants (Augé, 2001; Dimkpa et al., 2009).

Basil (*Ocimum basilicum* L.), belonging to the Lamiaceae family, is a high-value annual plant with wide applications in the food, pharmaceutical, and cosmetic industries, classified as a medicinal and aromatic plant. Basil plants have significant economic importance due to their volatile oils, phenolic compounds, and antioxidants. However, the plant is highly sensitive to soil moisture deficiency during its vegetative growth period (Daza-Torres et al., 2017). In basil plants grown under water scarcity, the leaf area index decreases, fresh herb yield decreases, and the market value of the plant diminishes. Therefore, developing alternative, environmentally friendly agronomic strategies that will ensure the sustainability of basil production and increase abiotic stress tolerance under deficit irrigation conditions is critically important.

Intensive chemical fertilization, used in traditional agriculture to increase yields, leads to salinity accumulation in the soil, groundwater pollution, and disruption of the soil microbiota. In recent years, the use of microbial fertilizers (biostimulants) such as Arbuscular Mycorrhizal Fungi (AMF) and Plant Growth Promoting Rhizobacteria (PGPR) as alternatives to these chemical inputs has attracted great interest in terms of agricultural sustainability (Calvo et al., 2014; Backer et al., 2018). AMF forms extraradical hyphae networks by establishing a symbiotic relationship with plant roots; these hyphae take up and transport low-mobility nutrients such as water and phosphorus from soil pores that the plant's normal root system cannot reach (Ruiz-Lozano et al., 2012). At the same time, mycorrhiza and beneficial rhizobacteria improve root architecture by promoting indole acetic acid (IAA) synthesis in the plant and provide osmotic protection against water stress by increasing antioxidant enzyme activities (Bharti et al., 2016).

The main objective of this study is to comparatively determine the effects of different mycorrhiza-derived microbial fertilizer formulations on parameters reflecting the agricultural characteristics of Large-Leaf Basil (*Ocimum basilicum* L.) grown under restricted irrigation conditions. The primary reason for focusing on basil in this study is the lack of comprehensive literature on the specific morpho-physiological responses of combined microbial fertilizer applications at different water stress levels, despite the high economic value of the species. The study is based on the hypothesis that microbial symbiosis can compensate for yield losses under restricted irrigation by increasing water use efficiency.

MATERIAL AND METHODS

Research Area and Soil Characteristics

This study was conducted in the autumn of 2025 in the Research and Application Greenhouse of the Faculty of Agriculture, Akdeniz University (36° 53' 33" N, 30° 38' 52" altitude 50m). According to meteorological data collected throughout the experiment, the average daily temperature of the area was 16.0 °C, the average daily sunshine duration was 6-7 hours, the average daily open surface evaporation was 2.5 mm to 3.0 mm/day, the average daily rainfall was 4.6 mm, the average daily wind speed was 2.9 m/s, and the average relative humidity was 64%. The greenhouse floor was covered with black plastic mulch, and the greenhouse had top and side ventilation systems.

The experiment was carried out under controlled conditions with natural sunlight, under a homogeneous temperature and relative humidity regime throughout the growing period. The growing medium used in the experiment was obtained soil from a depth of 0-30 cm from the Aksu Application Area of Akdeniz University. This soil is classified as "Typic Xerofluvent" based on its physical and chemical properties, formed on alluvial parent material called the "Tehnelli Series" (Sarı et al., 2009).

Analysis of the potting soil revealed a slightly alkaline pH (pH 7.9), low electrical conductivity (salinity), high lime content, cation exchange capacity (CEC) ranging from 18.9-19.3 meq/100g, and a sandy-loam texture (Table 1). Overall, the soil has a low organic matter content (1.6%), a high bulk density (1.40 g/cm³), and a low water-holding capacity (available water 8.96%) due to its composition. These physical characteristics indicate that the soil is prone to rapid water loss and provides an ideal testing environment for drought stress trials.

Table 1. Soil physical and chemical properties

Parameter	Content
pH	7.9
EC (dS/m)	0.38
Total N (%)	0.09
Available P (mg/kg)	8.4
CEC (me/100g)	18.9
Exchangeable Na (me/100g)	0.1
Exchangeable K (me/100g)	0.3
Exchangeable Ca (me/100g)	18.5
Exchangeable Mg (me/100g)	2.4
Lime (%)	30.5
Organic matter (%)	1.6
Sand (%)	44.3
Loam (%)	39.1
Clay (%)	16.6

Plant Material and Applications

In the experiment, commercially standardized large-leaf basil (*Ocimum basilicum* L. cv. Vilmorin) seedlings were used as plant material. The experiment was established using a Randomized Complete Block Design in a factorial arrangement, with 5 different fertilizer applications x 4 different irrigation levels x 3 replications, totaling 60 pots (one plant per pot). The pots were placed in a north-south direction, taking care to avoid placing the same applications side by side to minimize the shading effect (edge effect). Details regarding mycorrhiza-based microbial fertilization and other fertilization treatments in the experiment are given in Table 2.

Table 2. Fertilizer materials and their contents applied to potting soil in the experiment

Application	Content
MG+A	Application of the microbial preparation called Krishiza (contains arbuscular mycorrhizal fungus and microorganism spores)
MG+B	Application of the microbial fertilizer called Indigo (contains arbuscular mycorrhizal fungus and microorganism spores)
MG+A+B	Combined (dual) application of Krishiza and Indigo preparations
OG+	Application of standard chemical fertilizer (does not contain microbial inoculant)
OG-MG-	Negative control group without mycorrhiza or chemical fertilizer application

Irrigation Regime

Irrigation was applied to all trial subjects when 40% of the available water capacity of the soil was consumed based on the water requirements of the basil plant (Allen et al., 1998; Daza-Torres et al., 2017). Irrigation procedures were determined by the gravimetric (weighing) method based on the field capacity and wilting point data of the pots, and 4 different irrigation levels were created (Table 3).

Table 3. Water restriction rates applied to basil plants in the experiment

Irrigation level	Content
SS100	Full Irrigation (No Stress) where 100% of the plant's water needs are met
SS80	Slightly Restricted Irrigation (80% of the water lost is replenished)
SS60	Moderately Restricted Irrigation (60% of the water lost is replenished)
SS40	Severely Restricted Irrigation (40% of the water lost is replenished) (Heavy water stress)

The water levels in the pots were checked at regular intervals using a precision balance, and the amount of moisture lost was measured, with water added to the pots according to their group size. In addition, a standard liquid chemical fertilization (fertigation) program was applied to all pots in equal volumes throughout the experiment to meet the plants' basic nutrient needs.

Experimental Procedure and Measurements

Following the preparation of soil, filling it into pots (September 24), and bringing it to field capacity, seedlings were planted on October 10 after being treated with microbial preparations using the root dipping (inoculation) method. During the growing season, hoeing, disease/pest (entomological) controls, and specific treatments (October 23-30) were carried out. Phenological readings were taken at 5 different measurement times (Time points 1-5; e.g., October 20, November 14, November 25, etc.) during the vegetation period.

Plant height (cm): Measured from the soil surface to the apical bud using a ruler. Root collar diameter (mm): Measured just above the soil surface with a digital caliper. Plant crown width (cm): Determined by measuring the distance between the two widest points of the plant. Number of leaves (pieces/plant): Determined by counting the number of fully opened non-chlorotic functional leaves. Chlorophyll content (SPAD): Measured from fully developed leaves at the mid/upper nodes of the plant using a SPAD-502 (Konica Minolta) portable chlorophyll meter. Fresh weight (g/plant): Above-ground biomass of plants was determined by weighing with a precision balance (0.01 g) at the last harvest on December 12th.

Statistical Analyses

The obtained data were statistically evaluated using the SPSS (Version 23.0) software package. The main effects and interactions of the Application (AAP), Irrigation Level (IL), and Measurement Time (MT) factors on growth parameters were tested at a 5% significance level ($P<0.05$) using a three-way factorial analysis of variance (ANOVA) with Type III sums of squares. Statistically significant differences were separated using the Least Significant Difference (LSD) test.

RESULTS

The effects of different microbial fertilizer applications (MFA), limited irrigation levels (LI), and measurement time (MT) on plant growth parameters were investigated. It was determined that the applications (MFA) had a highly significant effect ($P<0.001$) on root collar diameter, leaf number, chlorophyll content, and fresh weight, and a significant effect ($P<0.01$) on plant height and crown width. In addition to the main factors, the Application × Irrigation Level (MFAxLI) interaction was found to be statistically significant only in root collar diameter ($P<0.05$) (Table 4).

Table 4. Effects of microbial fertilization at different measurement times and different irrigation levels on plant growth parameters

	Plant Growth Parameters					
	Root collar diameter (mm)	**Plant height (cm)**	**Plant Crown Width (cm)**	**Number of leaves (pieces)**	**Chlorophyll Content (SPAD)**	**Plant weight (g)**
microbial fertilizer applications (MFA)						
MG+A	5.48 a[1]	38.43 a	26.38 a	58.93 a	41.72 a	102.50 a
MG+B	5.04 b	38.43 a	25.38 ab	53.20 ab	40.97 a	85.83 a
MG+A+B	5.55 a	39.33 a	24.60 ab	58.65 a	41.50 a	91.25 a
OG+	5.04 b	35.51 b	23.25 bc	50.33 b	41.51 a	81.66 a
OG-MG-	4.72 c	35.11 b	22.21 c	42.28 c	38.28 b	49.16 b
limited irrigation levels (LI)						
SS100	5. 36 a	38.38 a	24.21	53.28	39.37 b	83.33
SS80	5.17 ab	36.62 ab	24.50	54.46	39.89 b	82.33
SS60	5.16 ab	38.72 a	24.50	52.00	41.91 a	79.00
SS40	4.97 b	35.73 b	24.24	50.97	42.02 a	83.66
measurement time (MT)						
1.	3.25 e	12.01 e	11.68 e	8.23 d	33.70 d	-
2.	4.00 d	23.33 d	18.10 d	13.60 d	38.77 c	-
3.	5.47 c	42.65 c	23.48 c	50.71 c	41.56 b	-
4.	6.02 b	50.68 b	29.85 b	78.71 b	48.23 a	-
5.	7.08 a	58.15 a	38.71 a	112.13 a	41.72 b	-
ANOVA						
MFA	10.751***[2]	4.772**[3]	4.868**	11.132***	10.157***	7.900***
LI	2.773*[4]	3.310*	NS [5]	NS	11.558***	NS
MT	215.473***	481.759***	192.924***	455.584***	137.655***	-
MFA×LI	2.020*	NS	NS	NS	NS	NS
MFA×MT	NS	NS	NS	2.830***	2.710**	-
LI×MT	NS	NS	NS	NS	NS	-
MFA×LI×MT	NS	NS	NS	NS	NS	-

[1] Means within columns followed by different letters are significantly different according to LSD test at $p < 0.05$.. [2] Significant at $p < 0.001$ level. [3] **; Significant at $p < 0.01$ level. [4] *; Significant at $p < 0.05$ level. [5] NS: not significant.

Root Collar Diameter and Plant Height

Root collar diameter (RCD) in plants is a critical parameter reflecting the capacity of vascular bundles for water and nutrient transport. According to the research findings, the highest RCD values were obtained from the MG+A+B (5.55 mm) and MG+A (5.48 mm) plots containing mycorrhiza and microbial treatment, and these treatments were statistically in the same "a" group (Table 4). The lowest root collar diameter was observed in the OG-MG-control group (4.72 mm, "c" group) without any fertilizer/microbial application. When examined according to irrigation levels; full irrigation (SS100) provided the highest diameter development with 5.36 mm, while severe water stress (SS40) reduced this value to 4.97 mm (P<0.05).

Similarly, plant height values were significantly affected by the MFA. MG+A+B (39.33 cm), MG+A (38.43 cm), and MG+B (38.43 cm) applications statistically significantly increased plant height compared to the OG+ (35.51 cm) and OG-MG- control groups (35.11 cm) without microbial inoculant. Regarding the irrigation regimes, a fluctuating trend was observed where the highest vegetative height was noted under moderate water restriction (SS60 with 38.72 cm) and full irrigation (SS100 with 38.38 cm), whereas severe water stress (SS40) suppressed the average plant height to 35.73 cm (Table 4).

Plant Crown Width and Number of Leaves

Plant crown width and leaf number are directly related to the plant's net assimilation area (photosynthetic surface). Analysis data show that mycorrhizal applications increase crown width. MG+A application (26.38 cm) ranked first in group "a", while the OG-MG-control group

(22.21 cm) remained in group "c". Although the effect of irrigation level on crown width was not statistically significant (NS), the highest numerical values were measured at SS60 (24.50 cm) and SS80 (24.50 cm) levels (Table 4).
In terms of total leaf number, the MG+A (58.93 leaves/plant) and MG+A+B (58.65 leaves/plant) combinations increased leaf formation by approximately 40% compared to the control group (42.28 leaves/plant) (P<0.001). As expected, the measurement time factor showed a linear increase correlated with plant phenology; the average leaf number, which was 8.23 in the 1st measurement, reached 112.13 leaves/plant in the 5th measurement before harvest. The MFA×MT interaction on leaf number was also found to be significant (P<0.001) (Table 4); this demonstrates that microbial fertilizers stimulate leaf organogenesis much faster in later growth stages compared to the control group.

Chlorophyll Content (SPAD Values)
SPAD values, which represent chlorophyll concentration, showed quite interesting responses to microbial fertilization and water restriction factors. While the average SPAD value in control plants (OG-MG-) was 38.28, MG+A (41.72) and MG+A+B (41.50) applications statistically increased chlorophyll levels (P<0.001) and were placed in group "a" (Table 4).
A much more striking finding emerged in the differences between irrigation levels (SS). While the average SPAD value was 39.37 under full irrigation (SS100) conditions without water stress, this value increased to 42.02 at the SS40 level with severe water restriction and to 41.91 at the SS60 level (P<0.001). Specifically, this physiological response indicates that the severity of water restriction increased the amount of chlorophyll per unit area in the leaves.

Plant Weight (Biomass)

Harvest fresh weight (biomass), the most fundamental indicator of agricultural success in basil cultivation, was the parameter that most clearly reflected the effect of microbial fertilizers (P<0.001). At the end of the experiment, the average fresh weight of the MG+A application, which contains mycorrhiza and beneficial bacteria alone, was measured as 102.50 g. This was followed by the MG+A+B combined application with 91.25 g. In contrast, the average fresh weight in the OG-MG- control group, which received only inorganic base fertilization and no microbial support, was only 49.16 g. This explicitly indicates that the mycorrhizal formulation (MG+A) increased the plant fresh biomass by 108% (more than double) compared to the control group in the overall average. Interestingly, the statistical analysis revealed that the deficit irrigation levels did not exert a significant main effect (NS) on the total fresh weight, implying that the robust root infrastructure promoted by microbial inoculation effectively buffered potential biomass losses across different water availability levels (Table 4).

DISCUSSION

The findings clearly demonstrate the supportive effects of beneficial microorganisms (AMFs) applied to the soil on plant morphology and biomass. The calcareous, low-organic-matter, and sandy-loam soil used in the experiment has low water-holding capacity, making the plants susceptible to water stress. The findings support the idea that microbial fertilizers activate tolerance mechanisms despite these challenging soil characteristics and irrigation limitations.
In the study, mycorrhizal (MG+A) and combined microbial fertilizer (MG+A+B) applications significantly increased the height, root collar diameter, and leaf number of basil plants compared to the control group. Mycorrhizal fungi establish a symbiotic relationship by settling in the root cortex cells of the plant. Through their hyphal networks (extraradical mycelium), they transfer water and nutrients with slow diffusion (especially phosphorus, zinc, and copper)

from micro-pores inaccessible to the roots to the plant (Dimkpa et al., 2009; Calvo et al., 2014). This observed promotion in plant height and root collar diameter can be explained by improved plant nutrition and consequently increased meristematic cell division. Similar studies on basil plants (Copetta et al., 2006) also confirm that AMF inoculation optimizes vegetative parameters. The fact that combined application (MG+A+B) yields result as successful as single applications is a result of the synergistic interaction between these combined applications; because such applications can promote the germination of mycorrhizal spores and the root infection rate (Barea et al., 1992).

One of the most striking results of the study is that increased water restriction (SS60 and SS40) statistically increases the amount of chlorophyll (SPAD value) in basil plants compared to the SS100 level. Water stress generally causes the degradation of photosynthetic pigments (chlorosis). This phenomenon is primarily driven by the 'concentration effect' under drought stress. To minimize transpirational water loss, plants restrict leaf cell expansion. Consequently, the reduction in total leaf area combined with increased leaf thickness elevates the relative chlorophyll density per unit surface area, directly reflected in higher SPAD indices (Rouphael et al., 2012). The higher SPAD values (41.72) in plants treated with microbial fertilizer compared to the control group (38.28) are related to the fact that beneficial microorganisms facilitate the uptake of essential elements for chlorophyll biosynthesis, such as nitrogen (N) and magnesium (Mg), thus ensuring that the photosynthetic apparatus remains more robust against stress.

The fresh weight findings, the most important outcome of the experiment, proved that microbial fertilizers are an indispensable tool for maintaining plant production under water stress. The fact that the biomass amount in the control plots was almost half that of the plants treated with microbial inoculant shows how much water stress conditions suppress the metabolism of uninoculated plants. Mycorrhizal plants (especially the MG+A formulation) can maintain cellular turgor even at low soil moisture levels and continue carbon assimilation (biomass formation) by increasing the expression of "aquaporin" genes, which regulate water flow into the plant body through the roots, and by optimizing stomatal conductivity (Ruiz-Lozano et al., 2012).

CONCLUSION

The results of this study, conducted on basil (*Ocimum basilicum* L.) grown under limited irrigation conditions (drought stress) in calcareous soils with low organic matter and poor water retention capacity typical of the Mediterranean Basin, can be summarized as follows: Mycorrhiza-based microbial fertilizer applications (especially MG+A and MG+A+B combinations) statistically increased plant height, root collar diameter, and crown width ($P<0.001$) compared to the control group grown under conventional cultivation, resulting in a stronger and more structurally resistant plant architecture. The number of leaves, an indicator of the vegetative capacity of the plants, was approximately 40% higher in pots inoculated with microbial fertilizers compared to the control group. Severe water restriction (SS40) caused a concentration effect by concentrating chlorophyll content per unit leaf area. Microbial fertilizers supported photosynthetic capacity by maintaining chlorophyll integrity at a higher level against this physiological pressure of stress. Regarding agricultural yield, the most critical finding was that Mycorrhiza (MG+A) application increased the fresh biomass of basil by 108% compared to control crops in limited irrigation scenarios. In conclusion, against the backdrop of global climate change scenarios where drought increasingly limits agricultural productivity, transitioning from intensive chemical inputs to integrated mycorrhizal formulations stands out as a high-efficiency, agronomically viable, and ecologically sustainable strategy to secure crop yields. Further studies could investigate how this microbial symbiosis regulates water stress

genes at the molecular (transcriptomic) level and its effects on the essential oil profile, which determines the economic importance of basil, under field conditions.

ACKNOWLEDGEMENTS

In this study, the phase of conducting pot experiments under modern greenhouse conditions was supported by Dean's Office of the Faculty of Agriculture at Akdeniz University.

REFERENCES

Allen, R. G., Pereira, L. S., Raes, D., & Smith, M. (1998). Crop evapotranspiration: Guidelines for computing crop water requirements (FAO Irrigation and Drainage Paper 56). Rome, Italy: FAO.

Augé, R. M. (2001). Water relations, drought and vesicular-arbuscular mycorrhizal symbiosis. Mycorrhiza, 11(1), 3-42. https://doi.org/10.1007/s005720100097

Backer, R., Rokem, J. S., Ilangumaran, G., Lamont, J., Praslickova, D., Ricci, E., Subramanian, S., & Smith, D. L. (2018). Plant growth-promoting rhizobacteria: Context, mechanisms of action, and roadmap to commercialization of biostimulants for sustainable agriculture. Frontiers in Plant Science, 9, 1473. https://doi.org/10.3389/fpls.2018.01473

Barea, J. M., Azcon, R., & Azcon-Aguilar, C. (1992). Vesicular-arbuscular mycorrhizal fungi in nitrogen-fixing systems. In Methods in Microbiology (Vol. 24, pp. 391-416). Academic Press.

Bharti, N., Pandey, S. S., Barnawal, D., Patel, V. K., & Kalra, A. (2016). Plant growth promoting rhizobacteria Dietzia natronolimnaea modulates the expression of stress responsive genes providing protection of wheat from salinity stress. Scientific Reports, 6, 34768.

Calvo, P., Nelson, L., & Kloepper, J. W. (2014). Agricultural uses of plant biostimulants. Plant and Soil, 383(1-2), 3-41.

Copetta, A., Lingua, G., & Berta, G. (2006). Effects of three AM fungi on growth, distribution of glandular hairs, and essential oil production in Ocimum basilicum L. var. Genovese. Mycorrhiza, 16(7), 485-494.

Daza-Torres, M. C., Arias-Prado, P. C., Reyes-Trujillo, A., & Urrutia-Cobo, N. (2017). Basil (*Ocimum basilicum* L.) water needs calculated from the crop coefficient. Ingeniería e Investigación, 37(3), 8-16.

Dimkpa, C. O., Weinand, T., & Asch, F. (2009). Plant–rhizobacteria interactions alleviate abiotic stress conditions. Plant, Cell & Environment, 32(12), 1682-1694.

IPCC. (2021). Climate Change 2021: The Physical Science Basis. Contribution of Working Group I to the Sixth Assessment Report of the Intergovernmental Panel on Climate Change. Cambridge University Press.

Rouphael, Y., Cardarelli, M., Schwarz, D., Franken, P., & Colla, G. (2012). Effects of drought on nutrient uptake and assimilation in vegetable crops. In Plant Responses to Drought Stress (pp. 171-195). Springer, Berlin, Heidelberg.

Ruiz-Lozano, J. M., Porcel, R., Azcón, C., & Aroca, R. (2012). Regulation by arbuscular mycorrhizae of the integrated physiological response to salinity in plants: New challenges in physiological and molecular studies. Journal of Experimental Botany, 63(11), 4033-4048.

Sarı, M., Özcan, H., Bahtiyar, M., & Çelik, N. (2009). Akdeniz Üniversitesi Aksu Çiftliği Topraklarının Temel Fiziksel ve Kimyasal Özellikleri. Akdeniz Üniversitesi Ziraat Fakültesi Dergisi, 22(1), 1-10.

THE IMPORTANCE OF BEHAVIORAL INDICATORS FOR ANIMAL WELFARE AND HERD MANAGEMENT IN DAIRY CATTLE

Mustafa KİBAR[1,], Ramazan ERKMEN[2]*

[1] Siirt University, Faculty of Agriculture, Department of Animal Science, Siirt, Türkiye
[2] Lidersan Dairy Farm, Feed and Ration Management Department, Gaziantep, Türkiye

** Corresponding author e-mail: mustafakibar@siirt.edu.tr*

ABSTRACT

Cattle behaviors are among the important biological indicators used in evaluating the physiological state, health level, adaptation to environmental conditions, and welfare of animals. Regular monitoring of behaviors such as feeding, rumination, resting, movement, social interaction, estrus, water consumption, and defecation contribute to the early diagnosis of diseases, the evaluation of management practices, and the improvement of production performance. In this review, first, the basic approaches used in the evaluation of cattle behaviors and the relationship between behavior and animal welfare are discussed; then, behavioral indicators such as body condition, feed intake, heat stress, estrus behaviors, rumen fill, housing hygiene, resting behavior, bunk and stall design, foot health, fecal consistency, and water consumption are evaluated in line with the current literature. In addition, the contributions of behavioral indicators to animal health, welfare, his decision-making processes in herd management, and the applicability of these indicators in field conditions are also addressed. Furthermore, the importance of behavioral observations in monitoring herd management, animal health, and welfare is emphasized. Literature findings show that the use of behavior-based evaluations together with appropriate feeding and housing practices can provide significant contributions to improving animal welfare, identifying diseases at an early stage, and increasing production performance. Additionally, regular and systematic monitoring of behaviors can contribute to making more accurate and timely decisions in herd management. In conclusion, systematic monitoring and evaluation of cattle behaviors are considered a fundamental management tool for sustainable production, effective herd management, and the development of animal welfare in modern dairy cattle enterprises.

Keywords: Cattle behavior, Animal welfare, Ethology, Behavioral indicators, Dairy farming, Herd management

INTRODUCTION

Animal behavior and behavioral indicators are among the primary criteria used in the assessment of animal welfare. Scientific evaluation of animal welfare requires jointly considering the preservation of animals' health and biological functions, their negative and positive emotional states, and their ability to express species-typical natural behaviors (Fraser, 2009). Evaluating cattle behaviors in relation to environmental conditions and rearing practices highlights the importance of behavior in livestock research (Sahu et al., 2020). Cattle have a wide behavioral repertoire, and much of their time is spent on feeding, rumination, and resting behaviors (Kilgour, 2012). Behavioral indicators, particularly behaviors such as vocalization, can provide useful information for assessing animals' physiological and psychological states (Watts and Stookey, 2000). In addition, behavior-based observation and assessment approaches enable systematic on-farm monitoring of animal welfare (Grandin, 2015). In recent years, with

the development of precision livestock farming technologies, feeding, rumination, activity, and other behavioral indicators in dairy cattle can be continuously monitored with sensor-based monitoring systems. These technologies allow objective assessment of behavioral and welfare indicators and are used as an important approach in monitoring animal welfare (Stygar et al., 2021).

Cattle behaviors encompass a broad behavioral repertoire including feeding, rumination, resting, movement, responses to environmental stressors, estrus signs, housing use, foot health, water consumption, and social interactions. Joint evaluation of these behaviors contributes not only to the assessment of individual animal health but also to a holistic evaluation of herd welfare and farm management. In this review, the main approaches used in the evaluation of cattle behaviors and the importance of behavioral indicators for animal health, welfare, and herd management are discussed in line with the current literature; the role of behavior-based assessment in modern dairy cattle enterprises is presented.

Assessment of cattle behaviors and animal welfare

Cattle display a characteristic behavioral repertoire composed of feeding, rumination, resting, locomotion, and social behaviors, and the assessment of these behaviors is important for defining normal behavioral patterns (Kilgour, 2012). Vocal behaviors are also among the key behavioral indicators that provide information about animals' biological processes and welfare status (Watts and Stookey, 2000). Today, behavioral and welfare indicators in dairy cattle can be monitored and assessed objectively using sensor technologies, and these technologies are used as important tools in welfare assessment (Stygar et al., 2021).

Tinbergen (1963) framed behavioral research around four fundamental questions: the mechanism of behavior expression, development (ontogeny), adaptive function, and evolutionary history. Font (2023) emphasizes that evaluating these four questions together continues to be a fundamental approach for understanding animal behavior.

Animal-based indicators such as body condition, cleanliness, lying behavior, lameness, and social behaviors are used in the assessment of cattle welfare (Welfare Quality®, 2009). Body condition score is regarded as an important indicator related to production, health, and welfare in dairy cattle (Roche et al., 2009). In addition, behavioral observations alongside other animal-based measures are primary approaches used for practical welfare assessment (Grandin, 2015). Evaluations of the effects of different housing systems on cattle behavior, as well as assessments of good nutrition and appropriate housing conditions, are also considered when examining cattle welfare (Özçelik Metin and Asan, 2016; Şahin and Uğurlu, 2016).

Stress is one of the key factors affecting the behavior of dairy cattle. Stressors such as pain, disease, heat stress, social stress, and housing-related comfort problems can cause changes in feeding behavior, social interactions, and other behavioral responses (Jurkovich et al., 2024). Therefore, monitoring stress-related behavioral changes constitutes an important component of the animal welfare approach, which is based on the joint assessment of health, affective state, and the ability to express natural behaviors (von Keyserlingk et al., 2009; Grandin, 2015).

Behavioral indicators and their use in herd management

Body condition scoring is an important indicator used to assess energy reserves in dairy cattle and is closely related to health, productivity, and welfare (Roche et al., 2009). Low condition scores are associated with negative energy balance and health problems, while high condition scores are linked to metabolic disorders and periparturient issues (Roche et al., 2009). When interpreting condition scores, the animal's physiological stage and nutritional status are evaluated together (NASEM, 2021).

Feed access and feed bunk space are major environmental factors affecting feeding behavior in dairy cattle. Grouping strategy, social dominance, bunk space, and feed accessibility can influence feeding behavior and feed intake; excessive crowding can reduce feeding activity and alter resting and rumination behaviors (Grant and Albright, 2001). Ensuring adequate feed access is also among the key elements considered in welfare assessments of dairy cattle (Göncü et al., 2016).

Increased stocking density at the bunk affects feeding and social behaviors in dairy cows. As bunk density increases, feeding time decreases while aggressive behaviors and the frequency of displacement from the feed bunk increase. Cows with lower social rank are particularly more frequently displaced under high-density conditions. Based on these findings, researchers recommend avoiding excessive bunk crowding and using feed barriers that provide physical separation to reduce competition (Huzzey et al., 2006).

Rumen fill score, one of the behavioral and physiological indicators used to assess nutritional status, is based on visual inspection of the left paralumbar fossa. This scoring system was developed to monitor the relationship between nutritional status and fertility in dairy cattle (Zaaijer and Noordhuizen, 2003).

Rumination behavior is an important behavioral indicator closely related to rumen functions and the operation of the digestive system (Allen, 1997; Beauchemin, 2018). During rumination, re-chewing of feed particles and increased saliva secretion contribute to the maintenance of the rumen environment (Allen, 1997; Beauchemin, 2018). This behavior largely occurs during resting and is closely associated with lying behavior (Schirmann et al., 2012). Rumination time is used as a useful indicator in the assessment of health and metabolic status and can now be monitored via sensor technologies (Soriani et al., 2013; Beauchemin, 2018). Physically effective fiber plays an important role in maintaining rumination behavior (Allen, 1997; Beauchemin, 2018). Diets adequate in physically effective fiber stimulate chewing and rumination behavior, increase saliva secretion, and help maintain rumen pH (Allen, 1997). The physical characteristics of fiber and particle size are important ration attributes that affect rumination behavior (Beauchemin, 2018).

Fecal consistency is a trait that can vary according to changes in dietary composition in dairy cattle and can be assessed by visual scoring. Differences in dietary fiber and protein levels and variations in feedstuffs can affect fecal dry matter, neutral detergent fiber (NDF), acid detergent fiber (ADF), starch, and pH characteristics, in addition to fecal consistency. However, it has been reported that fecal consistency cannot be accurately predicted using only diet components and animal performance parameters, and that the relationship between fecal consistency and feeding is influenced by many factors (Ireland-Perry and Stallings, 1993).

Water intake and drinking behavior in lactating dairy cows are related to dry matter intake, milk yield, the dry matter content of the rations, and environmental conditions. A significant portion of water intake occurs during feeding and after milking (Cardot et al., 2008). Additionally, drinker cleanliness and the condition of technical equipment on dairy farms are among the measures considered in the assessment of animal welfare (Ceco and Önk, 2024).

Increased locomotor activity is observed in cows during estrus. Mounting other animals and allowing themselves to be mounted, restlessness, increased walking activity, and vocalization are the main behavioral signs observed during estrus. In modern dairy operations, the intensity of estrus signs may be reduced and become difficult to detect visually due to factors such as high milk yield and housing and flooring conditions (Roelofs et al., 2010). Sensor technologies such as pedometers, accelerometers, activity sensors, and image analysis systems are used to objectively and continuously monitor behavioral changes (Stygar et al., 2021).

Foot health is an important factor affecting behavior in dairy cattle. Animals that develop lameness show changes in behavior and lying behavior, and their welfare is adversely affected (Cook and Nordlund, 2009; İzci et al., 2021). Barn design, flooring characteristics, and resting

areas are among the important environmental factors in the development of lameness (Cook and Nordlund, 2009). Therefore, regular hoof care and provision of appropriate flooring and resting conditions are considered fundamental practices to prevent lameness (Cook and Nordlund, 2009; İzci et al., 2021). Regular assessment of the proper functioning of milking machine components—vacuum system, pulsation system, and other technical parts—is important for maintaining milking performance and udder health (Mein et al., 2004).

Effects of environmental factors on behavior and welfare

Heat stress is an important environmental factor that adversely affects behavior and welfare in dairy cattle. During heat stress, behavioral and physiological changes such as increased respiration rate, panting, longer standing times, and decreased feed intake are observed. Prolonged heat stress can have negative effects on milk yield, reproductive performance, and animal welfare. Therefore, improving environmental conditions and providing appropriate cooling practices during hot periods are among the primary approaches to reducing heat stress (Polsky and von Keyserlingk, 2017; Lees et al., 2019; Erzurum and Uysal Erzurum, 2020).

Resting behavior is an important behavioral indicator used in the assessment of animal welfare in dairy cattle. The characteristics of resting areas, stall design, and comfort directly affect animals' lying and standing behaviors. Appropriate resting conditions are associated with longer lying times, while inadequate resting conditions can increase standing time (Cook et al., 2004). Inappropriate stall designs and inadequate resting conditions can hinder the ability to enter the lying area, reduce resting duration, and increase standing time (Cook and Nordlund, 2009). Sufficient lying time is important for the welfare of dairy cattle, and prolonged standing is associated with an increased risk of lameness (Tucker et al., 2021). Frequent position changes, reluctance to enter the lying area, and abnormal lying postures are also important behavioral indicators used to evaluate the comfort of resting areas (Cook and Nordlund, 2009; Tucker et al., 2021; Haley et al., 2001).

Barn design and equipment placement are important environmental factors that influence dairy cattle behavior. The placement of the neck rail can affect stall use, and insufficient stall length, width, and forward lunge space can restrict lying-down and rising movements, negatively impacting resting behavior (Tucker et al., 2005; Cook and Nordlund, 2009; Tucker et al., 2021). Designing stalls to fit animals' body dimensions is important to support appropriate resting behavior.

Keeping bedding clean and dry and effectively removing manure are among the fundamental management practices recommended for the control of environmental mastitis (Hogan and Smith, 2012).

Literature review

The reviewed literature shows that behavioral indicators such as feeding, rumination, resting, locomotion, estrus, water intake, and social behaviors are important measures for assessing animal health, welfare, and herd management in dairy cattle. Additionally, animal-based indicators like body condition score, rumen fill score, fecal evaluation, and lameness, when used alongside behavioral assessments, contribute to a more comprehensive welfare evaluation. Sensor-based precision livestock technologies enable continuous and objective monitoring of behavioral changes, offering significant advantages for early detection of health problems, improvement of reproductive management, and enhancement of decision-support processes in herd management. The literature commonly emphasizes that appropriate feeding, barn design, and environmental management practices positively influence behavioral patterns and thereby support the sustainability of animal welfare and production performance.

CONCLUSIONS

Cattle behaviors are reliable biological indicators for assessing animals' physiological state, health status, adaptation to environmental conditions, and welfare. Joint evaluation of feeding, rumination, resting, movement, reproductive behaviors, social interactions, water intake, and other behavioral parameters enables comprehensive assessment not only of individual animal health but also of herd-level welfare and the effectiveness of farm management.

Because changes in behavioral indicators often appear before clinical signs, these observations gain importance for early detection of diseases, identification of metabolic disorders, detection of environmental stressors, and development of appropriate management strategies. Therefore, evaluating behavioral observations together with feeding management, housing conditions, foot health, reproductive management, and other routine herd-management practices contribute both to the protection of animal welfare and to the sustainable improvement of production performance.

Recent advances in precision livestock technologies have made it possible to assess behaviors objectively, continuously, and in real time via sensors, image analysis systems, and automated monitoring technologies. Using these technologies alongside traditional behavioral observations facilitates early detection of health problems, supports decision-making processes in herd management, and enables more effective monitoring of animal welfare.

In conclusion, behavior-based assessments stand out as an indispensable management tool for sustainable production, effective herd management, and the improvement of animal welfare in modern dairy cattle enterprises. In the future, integration of behavioral observations with precision livestock technologies and automated monitoring systems will play an important role in developing sustainable animal production by enabling earlier, more accurate, and more holistic assessments of animal health and welfare.

Declaration of artificial intelligence use

During the preparation of this review, artificial intelligence-supported tools were utilized for the purposes of grammatical editing, improving the academic expression structure, and ensuring content organization. However, all scientific content, data, and citations in the text are based on sources provided by the author. The artificial intelligence tool was not used for generating new information, adding data, or creating scientific inferences; it was used solely as a supportive tool in the process of reorganizing existing texts and ensuring their compliance with academic writing standards.

REFERENCES

Allen, M. S. (1997). Relationship between fermentation acid production in the rumen and the requirement for physically effective fiber. Journal of Dairy Science, 80(7), 1447–1462. https://doi.org/10.3168/jds.S0022-0302(97)76074-0

Beauchemin, K. A. (2018). Invited review: Current perspectives on eating and rumination activity in dairy cows. Journal of Dairy Science, 101(6), 4762–4784. https://doi.org/10.3168/jds.2017-13706

Cardot, V., Le Roux, Y., and Jurjanz, S. (2008). Drinking behavior of lactating dairy cows and prediction of their water intake. Journal of Dairy Science, 91(6), 2257–2264. https://doi.org/10.3168/jds.2007-0711

Ceco, A., and Önk, K. (2024). Kars ili süt sığırcılığı işletmelerinde hayvan refahının barınak ve yetiştirme şartları açısından değerlendirilmesi. Veterinary Sciences and Practices. https://doi.org/10.17094/vetsci.1528284

Cook, N. B., and Nordlund, K. V. (2004). *Behavioral needs of the transition cow and considerations for special needs facility design*. Veterinary Clinics of North America: Food Animal Practice, 20(3), 495–520. https://doi.org/10.1016/j.cvfa.2004.06.011

Cook, N. B., and Nordlund, K. V. (2009). The influence of the environment on dairy cow behavior, claw health and herd lameness dynamics. Veterinary Journal, 179(3), 360–369. https://doi.org/10.1016/j.tvjl.2007.09.016

Cook, N. B., Bennett, T. B., and Nordlund, K. V. (2004). Effect of free stall surface on daily activity patterns in dairy cows. Journal of Dairy Science, 87(9), 2912–2922. https://doi.org/10.3168/jds.S0022-0302(04)73422-5

Erzurum, O., and Uysal Erzurum, A. B. (2020). Sıcaklık stresinin süt sığırlarının refahı üzerine etkileri. Hayvansal Üretim, 61(1), 49–54. https://doi.org/10.29185/hayuretim.546607

Font, E. (2023). 50 years of the Nobel Prize to Lorenz, Tinbergen, and von Frisch: Integrating behavioral function into an ethology for the 21st century. Frontiers in Ethology, 2, Article 1270913. https://doi.org/10.3389/fetho.2023.1270913

Fraser, D. (2009). *Assessing animal welfare: Different philosophies, different scientific approaches*. Zoo Biology, 28(6), 507–518. https://doi.org/10.1002/zoo.20253

Göncü, S., Koluman, N., Serbester, U., and Görgülü, M. (2016). Süt sığırcılığında refah istekleri ve kritik kontrol noktaları. Çukurova Tarım ve Gıda Bilimleri Dergisi, 31(1), 9–20. https://izlik.org/JA38JH56ED

Grandin, T. (2015). Improving Animal Welfare: A Practical Approach (2nd ed.). CABI.

Grant, R. J., and Albright, J. L. (2001). Effect of animal grouping on feeding behavior and intake of dairy cattle. Journal of Dairy Science, 84(E. Suppl.), E156–E163. https://doi.org/10.3168/jds.S0022-0302(01)70210-X

Haley, D. B., Rushen, J., and de Passillé, A. M. (2001). Assessing cow comfort: Effects of two floor types and two tie stall designs on the behaviour of lactating dairy cows. Applied Animal Behaviour Science, 71(2), 105–117. https://doi.org/10.1016/S0168-1591(00)00175-1

Hogan, J. S., and Smith, K. L. (2012). Managing environmental mastitis. Veterinary Clinics of North America: Food Animal Practice, 28(2), 217–224. https://doi.org/10.1016/j.cvfa.2012.03.009

Huzzey, J. M., DeVries, T. J., Valois, P., and von Keyserlingk, M. A. G. (2006). Stocking density and feed barrier design affect the feeding and social behavior of dairy cattle. Journal of Dairy Science, 89(1), 126–133. https://doi.org/10.3168/jds.S0022-0302(06)72075-6

Ireland-Perry, R. L., and Stallings, C. C. (1993). *Fecal consistency as related to dietary composition in lactating Holstein cows*. Journal of Dairy Science, 76(4), 1074–1082. https://doi.org/10.3168/JDS.S0022-0302(93)77436-6

İzci, C., Çuhadar Erdal, F., and Yıldız, M. (2021). Süt sığırlarında topallık: Hayvan refahı ve davranışına etkisi üzerine bir değerlendirme. Ziraat Fakültesi Dergisi, 58(4), 629–639. https://doi.org/10.20289/zfdergi.870888

Jurkovich, V., Hejel, P., and Kovács, L. (2024). A Review of the Effects of Stress on Dairy Cattle Behaviour. Animals, 14(14), 2038. https://doi.org/10.3390/ani14142038

Kilgour, R. J. (2012). In pursuit of "normal": A review of the behaviour of cattle at pasture. Applied Animal Behaviour Science, 138(1–2), 1–11. https://doi.org/10.1016/j.applanim.2011.12.002

Lees, A. M., Sejian, V., Wallage, A. L., Steel, C. C., Mader, T. L., Lees, J. C., and Gaughan, J. B. (2019). The impact of heat load on cattle. Animals, 9(6), 322. https://doi.org/10.3390/ani9060322

Mein, G. A., Reinemann, D. J., Ohnstad, I., and Rasmussen, M. D. (2004). Milking machine testing and evaluation. In A. V. Hillerton (Ed.), Milk Machine Testing and Mastitis Prevention. British Mastitis Conference Proceedings.

NASEM. (2021). National Academies of Sciences, Engineering, and Medicine. *Nutrient Requirements of Dairy Cattle: Eighth Revised Edition*. National Academies Press. https://doi.org/10.17226/25806

Özçelik Metin, M., and Asan, H. (2016). Sütçü sığırlarda refah kalitesinin değerlendirilmesi I: İyi beslenme ve iyi barınak. Mehmet Akif Ersoy Üniversitesi Veteriner Fakültesi Dergisi, 1(2), 91–98. https://doi.org/10.24880/maeuvfd.287353

Polsky, L., and von Keyserlingk, M. A. G. (2017). Invited review: Effects of heat stress on dairy cattle welfare. Journal of Dairy Science, 100(11), 8645–8657. https://doi.org/10.3168/jds.2017-12651

Roche, J. R., Friggens, N. C., Kay, J. K., Fisher, M. W., Stafford, K. J., and Berry, D. P. (2009). Body condition score and its association with dairy cow productivity, health, and welfare. Journal of Dairy Science, 92(12), 5769–5801. https://doi.org/10.3168/jds.2009-2431

Roelofs, J. B., van Eerdenburg, F. J. C. M., Soede, N. M., and Kemp, B. (2010). Various behavioral signs of estrous and their relationship with time of ovulation in dairy cattle: A review. Theriogenology, 74(3), 327–344. https://doi.org/10.1016/j.theriogenology.2010.01.014

Sahu, B. K., Parganiha, A., and Pati, A. K. (2020). Behavior and foraging ecology of cattle: A review. Journal of Veterinary Behavior, 40, 50–74. https://doi.org/10.1016/j.jveb.2020.08.004

Schirmann, K., Chapinal, N., Weary, D. M., Heuwieser, W., and von Keyserlingk, M. A. G. (2012). Rumination and its relationship to feeding and lying behavior in Holstein dairy cows. Journal of Dairy Science, 95(6), 3212–3217. https://doi.org/10.3168/jds.2011-4741

Soriani, N., Trevisi, E., and Calamari, L. (2013). Relationships between rumination time, metabolic conditions, and health status in dairy cows during the transition period. Journal of Animal Science, 91(6), 2891–2901. https://doi.org/10.2527/jas.2012-5741

Stygar, A. H., Gómez, Y., Berteselli, G. V., Dalla Costa, E., Canali, E., Niemi, J. K., Llonch, P., and Pastell, M. (2021). A systematic review on commercially available and validated sensor technologies for welfare assessment of dairy cattle. Frontiers in Veterinary Science, 8, 634338. https://doi.org/10.3389/fvets.2021.634338

Şahin, E., and Uğurlu, N. (2016). Farklı barınak sistemlerinde süt sığırı davranışları. Bahri Dağdaş Hayvancılık Araştırma Dergisi, 5(1), 25–32. https://izlik.org/JA82RL67TE

Tinbergen, N. (1963). On aims and methods of ethology. Zeitschrift für Tierpsychologie, 20(4), 410–433. https://doi.org/10.1111/j.1439-0310.1963.tb01161.x

Tucker, C. B., Jensen, M. B., de Passillé, A. M., Hänninen, L., and Rushen, J. (2021). *Invited review: Lying time and the welfare of dairy cows*. Journal of Dairy Science, 104(1), 20–46. https://doi.org/10.3168/jds.2019-18074

Tucker, C. B., Weary, D. M., and Fraser, D. (2005). Influence of neck-rail placement on free-stall preference, use, and cleanliness of dairy cattle. Journal of Dairy Science, 88(8), 2730–2737. https://doi.org/10.3168/jds.S0022-0302(05)72984-4

Von Keyserlingk, M. A. G., Rushen, J., de Passillé, A. M., and Weary, D. M. (2009). Invited review: The welfare of dairy cattle—Key concepts and the role of science. *Journal of dairy science*, *92*(9), 4101-4111. https://doi.org/10.3168/jds.2009-2326

Watts, J. M., and Stookey, J. M. (2000). Vocal behaviour in cattle: The animal's commentary on its biological processes and welfare. Applied Animal Behaviour Science, 67(1–2), 15–33. https://doi.org/10.1016/S0168-1591(99)00108-2

Welfare Quality®. (2009). Welfare Quality® Assessment Protocol for Cattle. Welfare Quality® Consortium, Lelystad, Netherlands.

Zaaijer, D., and Noordhuizen, J. P. T. M. (2003). A novel scoring system for monitoring the relationship between nutrition and fertility in dairy cows: The rumen fill score. Cattle Practice, 11, 205–211.

AN EVALUATION ON SUSTAINABLE WATER MANAGEMENT IN DAIRY CATTLE ENTERPRISES FROM GLOBAL WATER SECURITY

Mustafa KİBAR[1,], Ramazan ERKMEN[2]*

[1] Siirt University, Faculty of Agriculture, Department of Animal Science, Siirt, Türkiye
[2] Lidersan Dairy Farm, Feed and Ration Management Department, Gaziantep, Türkiye

** Corresponding author e-mail: mustafakibar@siirt.edu.tr*

ABSTRACT

Water is one of the indispensable natural resources for the continuity of life, the protection of ecosystems, and the sustainability of agricultural production. However, population growth, climate change, water pollution, and increasing water demand are progressively increasing the pressure on water resources on a global scale. The agricultural sector is one of the areas where freshwater resources are most intensively used. Within the agricultural sector, intensive water use is carried out in dairy cattle enterprises. In these enterprises, water stands out as one of the fundamental inputs of production due to the drinking water requirements of animals, feed production, milking systems, and the cleaning of equipment and housing. In this review, the current status of global water resources and water security, the causes of water pollution, and current approaches toward the protection of water resources are evaluated; subsequently, sustainable water management practices in dairy cattle enterprises and current studies regarding water resources and water management in dairy cattle enterprises in Türkiye are discussed in detail. Literature findings show that regular monitoring of water use in enterprises, reduction of water losses, evaluation of alternative water resources, dissemination of practices for water reuse, and the adoption of appropriate management strategies can increase water use efficiency. Furthermore, ensuring continuous access for animals to an adequate amount and appropriate quality of drinking water is of great importance as a fundamental necessity for protecting animal health, welfare, and production performance. In conclusion, the dissemination of sustainable water management in dairy cattle enterprises will provide significant long-term contributions to the protection of water resources, the support of environmental sustainability, and the development of sustainable milk production.

Keywords: Water security, Water pollution, Sustainable water management, Dairy farming, Water resources, Water use efficiency

INTRODUCTION

Water is one of the indispensable natural resources for the continuation of human life, the maintenance of ecosystem continuity, and the conduct of economic activities (Kato and Kansha, 2024). Although approximately 71% of the Earth's surface is covered by water, the amount of usable freshwater resources is quite limited. About 96.5% of total water resources consist of saline water in the oceans, while only approximately 2.5% qualify as freshwater. A large portion of freshwater is stored in glaciers, permanent snow cover, and groundwater; consequently, the share of directly usable surface freshwater resources for human daily life, agricultural production, and ecosystem sustainability is very small. Despite their extremely limited volume, rivers are of central importance for meeting people's daily water needs, sustaining agricultural production, and ensuring ecosystem continuity. This situation indicates that usable freshwater resources are quantitatively constrained and that effective management and sustainable use of

water resources have become a strategic priority at the global level (U.S. Geological Survey, 2019).

With the rapid growth of the global population, the need for safe drinking water, sanitation, and hygiene services has also increased. Globally, between 2000 and 2024 approximately 2.2 billion people gained access to safely managed drinking water, and 2.8 billion people gained access to safely managed sanitation services. Nevertheless, continued inequalities between regions in access to safe water, sanitation, and basic hygiene services demonstrate that the global water crisis is not only an environmental issue but also a significant social problem (WHO, 2025). In Türkiye, the per capita renewable freshwater amount of approximately 642 m^3/person/year and the annual freshwater withdrawal reaching 54.7% of renewable water resources highlight the current pressure on water resources and necessitate the development of strategies for effective water management (FAO, 2025). Pressure on water resources is expected to increase further in the future. With the intensification of the global water cycle due to climate change, it is estimated that by 2050 the population at risk of flooding will reach approximately 1.6 billion, and the population experiencing water scarcity for at least part of the year will reach 4.8–5.7 billion people. Therefore, developing holistic approaches for the sustainable management of water resources and using existing water resources more efficiently are among the global priority targets (UNESCO, 2018).

On the other hand, pollutants originating from industrial, urban, and agricultural activities adversely affect water quality, creating important problems for both environmental sustainability and human health. The agricultural sector is one of the most intensive users of freshwater resources, and in dairy cattle enterprises water management is considered a fundamental component of sustainable production due to animals' drinking water requirements, milking systems, cleaning operations, and feed production (Kato and Kansha, 2024; Lin et al., 2022; Akhtar et al., 2021; FAO, 2025; Monteiro et al., 2023). Accordingly, evaluating approaches to increase water use efficiency in dairy cattle enterprises is important for the protection of water resources and the support of sustainable animal production. In this review, first the current status of global water resources and water security is addressed, followed by water pollution and current approaches to the protection of water resources; subsequently, sustainable water management in dairy cattle enterprises and studies on water resources and water management in dairy cattle enterprises in Türkiye are evaluated.

The current status of global water resources and water security

Although approximately 71% of the Earth's surface is covered by water, the vast majority of that water (about 96.5%) is saline water in the oceans. Only roughly 2.5% of total water resources qualify as freshwater, of which approximately 68.7% is stored in glaciers and permanent snow cover and about 30% in groundwater. Only about 1.2% of freshwater exists as surface water such as lakes and rivers; within these, lakes account for roughly 20.9% while rivers make up only about 0.49% of surface freshwater. Despite their extremely limited volume, rivers are of central importance for meeting people's daily water needs, sustaining agricultural production, and ensuring ecosystem continuity. This situation reveals that usable freshwater resources are quantitatively very limited and unevenly distributed across the globe, and that effective management, sustainable use, and protection of water resources are strategic priorities at the global level (U.S. Geological Survey, 2019).

Global population rose from 6.2 billion to 8.2 billion between 2000 and 2024, during which significant but uneven progress was made in access to water, sanitation, and hygiene services. In this period, approximately 2.2 billion people gained access to safely managed drinking water and 2.8 billion to safely managed sanitation services. However, while the population lacking

access to drinking water has generally declined, this number has increased in low-income countries and in some urban areas. Similarly, improvements in access to safely managed sanitation occurred faster in rural areas while remaining limited in urban areas, and deficiencies persist in low-income countries. Moreover, the number of people without basic hygiene services rose from 427 million to 502 million in low-income countries, indicating that the gains are not evenly distributed across regions and income groups and that the global water crisis is deepening particularly among disadvantaged populations (WHO, 2025).

Türkiye's long-term average total renewable freshwater resources are reported as 53.6 km^3/year, and per capita renewable freshwater is approximately 642 m^3/person/year. Annual total freshwater withdrawal in Türkiye is about 58.5 km^3, of which 73.9% is used for agricultural irrigation, 15.2% for municipal (domestic) services, and 10.9% for industry. The fact that annual freshwater withdrawal reaches 54.7% of renewable freshwater resources indicates significant pressure on Türkiye's water resources and underscores that effective management and efficient use of water resources are strategic necessities (FAO, 2025).

Pressure on global water resources is expected to increase further in the future. Currently more than 2 billion people lack access to safely managed drinking water, and more than twice that number lack safely managed sanitation services. With rapidly growing global population, water demand is expected to increase by about one-third by 2050; accelerating consumption, environmental degradation, and the multifaceted impacts of climate change necessitate new approaches for managing limited freshwater resources. Climate change is intensifying the global water cycle, increasing the risks of floods and droughts. It is estimated that the population at risk of flooding, currently 1.2 billion, will reach 1.6 billion by 2050 (about 20% of the world population), and that the population affected by land degradation and drought already reaches 1.8 billion. Meanwhile, about 3.6 billion people currently live in areas with potential water scarcity for at least one month of the year; this number is projected to rise to 4.8–5.7 billion by 2050. These figures make the development of holistic approaches for sustainable management of water resources and more efficient use of existing water resources global priorities (UNESCO, 2018).

Water pollution and protection of water resources

Large volumes of wastewater are generated by industrial activities, and these wastewaters can contain high pollutant loads and toxic components, thereby causing serious problems for environmental sustainability and public health. Because the quantity of wastewater produced, pollutant concentration, and types of pollutants vary significantly by sector, these characteristics must be accurately identified and assessed in order to determine appropriate treatment technologies. Therefore, effective management of wastewater and the application of suitable treatment methods are considered fundamental components of the sustainable use of water resources (Kato and Kansha, 2024).

A literature review using keywords such as water pollution, water quality, health, and cancer evaluated 85 studies. The findings indicate that more than 80% of wastewater generated by human activities is discharged into rivers and oceans without any treatment, a situation that not only causes environmental pollution but also creates conditions for the emergence of more than 50 diseases. Degradation of water quality is responsible for a significant portion of global disease burden and child mortality, and it plays an important role in the spread of enteric infections such as diarrheal diseases. The impacts of water pollution on human health are evident but can vary depending on factors such as region, age, and gender. Researchers emphasize that interventions and strengthened management practices are needed to improve water quality and reduce adverse health effects (Lin et al., 2022).

Pressure on water quality does not originate solely from anthropogenic activities; global warming, land-use changes, and natural geological processes also threaten the sustainability of water resources. In addition to pollutants from industrial waste, urban settlements, and agricultural activities (pesticide and fertilizer applications), natural processes complicate the behavior of heavy metals and inorganic substances in water systems. Therefore, interdisciplinary research, the development of flexible regulations, and strengthened international cooperation are reported to be necessary to sustainably protect water quality (Akhtar et al., 2021).

Practices for protecting water resources are not limited to large-scale environmental policies; they also include measures that can be implemented at the individual level. Even very small leaks from taps can cause significant water losses over the long term. For example, if a single tap leaks at a rate of just one drop per minute, it results in approximately 0.4 L per day and about 146 L per year (U.S. Geological Survey [USGS], 2018). According to Turkish Statistical Institute (TSI) data, Türkiye's population in 2025 is 86,092,168 and the average household size is 3.08 persons, which corresponds to approximately 28 million households. In this case, a single tap leaking one drop per minute in each household would cause an annual national water loss of about 4.08 billion liters (approximately 4.08 million m^3). Similarly, in Istanbul, with about 5.1 million households, this amount would reach approximately 747 million liters per year (about 747 thousand m^3). This example demonstrates that water losses that seem negligible at the individual level can become substantial waste at the national scale, and that simple measures such as repairing tap leaks can make an important contribution to the sustainable management of water resources (TSI, 2025; 2026).

There are various practical measures that can be implemented at the individual level to increase water savings and protect existing water resources. Key practices to reduce domestic water consumption include running washing machines and dishwashers only when fully loaded, keeping taps closed when not in use, and shortening shower durations. In addition, promptly repairing all leaks in plumbing systems and preferring water-saving devices that limit flow in toilet cisterns and showerheads contribute to efficient water use. These practices should be considered not only in domestic settings but also in livestock enterprises with high water consumption, particularly dairy cattle farms.

Sustainable water management in dairy cattle enterprises

In dairy cattle enterprises, water is a fundamental input used not only to meet animals' drinking water requirements but also across many stages of production such as milking systems, equipment and housing cleaning, and feed production. Therefore, the sustainable use of water resources is considered an important necessity for ensuring production continuity under increasing water scarcity conditions and for improving water use efficiency in livestock. Recent studies indicate that technological applications, appropriate farm management, and approaches for water reuse are key strategies for increasing water use efficiency in dairy cattle enterprises (Monteiro et al., 2023; Higham et al., 2017).

Regular monitoring of water use on dairy farms is considered one of the most important practices for improving water use efficiency. Research shows substantial differences among farms in water use for the milking unit, animals' drinking water consumption, and leaks in water distribution systems. Regular measurement and monitoring of water use help farms estimate their water needs more accurately, identify differences in usage, and manage existing water resources more effectively (Higham et al., 2017). In addition, proper feeding of animals, adequate ventilation of housing, and regular maintenance and repair of water, wastewater, and

irrigation systems are fundamental farm management practices that contribute to reducing the water footprint (Monteiro et al., 2023).

Evaluating alternative water sources to reduce dependency on freshwater is an important component of sustainable water management. On-farm rainwater harvesting and the reuse of suitably treated wastewater for irrigation and manure removal systems are among the practices that can improve water use efficiency (Willers et al., 1999). Reusing water recovered from heat-exchanger systems used to cool milk after milking and applying technological equipment in irrigation systems are also recommended measures to reduce water consumption (Monteiro et al., 2023).

Sustainable water management includes not only reducing the volume of water used but also ensuring continuous access for animals to an adequate quantity and quality of drinking water. Considering environmental factors that affect animals' water consumption, maintaining uninterrupted access to water resources, and adopting appropriate water management practices are of great importance for preserving animal welfare, health status, and production performance (Bak Jensen and Vestergaard, 2021; Singh et al., 2022).

Water resources in Türkiye and water management in dairy cattle enterprises

Türkiye is among the countries experiencing significant pressure on water resources in terms of renewable freshwater per capita. According to FAO data, Türkiye's long-term average total renewable freshwater resources are 53.6 km^3/year, and the renewable freshwater amount per capita is reported as approximately 642 m^3/person/year. The annual total freshwater withdrawal in Türkiye is approximately 58.5 km^3, of which 73.9% is used in agricultural irrigation, 15.2% in municipal (domestic) services, and 10.9% in the industrial sector. Additionally, the fact that the annual total freshwater withdrawal reaches 54.7% of renewable freshwater resources indicates a considerable level of pressure on Türkiye's water resources and reveals that effective management and efficient use of water resources are a strategic necessity (FAO, 2025).

Studies on water use, water quality, and water management in dairy cattle enterprises in Türkiye have been increasing in recent years. Yaylak and Yavuz (2016) reported that ensuring continuous access to an adequate quantity and appropriate quality of drinking water for dairy cattle is one of the fundamental requirements for animal health, welfare, and production performance. The same study stated that placing water troughs in sufficient numbers and suitable locations, cleaning them regularly, and planning water distribution systems according to farm capacity are among the basic practices that should be considered on farms.

Koçbeker and Bahtiyarca (2017) reported that insufficient quantity or low-quality drinking water in dairy cattle can negatively affect feed intake and milk yield; therefore, for sustainable dairy farming, in addition to providing the quantity and quality of water that animals need, proper planning of water management is also of great importance.

Recent studies carried out in Türkiye show that a significant portion of water use in milk production originates from feed production, animals' drinking water consumption, and water used in barns and milking units. In a study conducted at Ankara University Haymana Research and Practice Farm, the water footprint of milk production was calculated; by evaluating the shares of feed production, animals' drinking water consumption, and water used in barns and milking units in total water consumption, the total water consumption per 1 liter of milk production was determined as 1112.3 L (Çolak et al., 2025).

Additionally, in a study conducted in dairy cattle enterprises in the Kütahya province, it was determined that a significant portion of the farms were located close to water resources and that inappropriate manure storage practices posed an environmental risk for water resources. The study emphasized that farms should be planned taking into account appropriate infrastructure and management practices to prevent water and environmental pollution (Peypazar and Kılıç, 2021).

CONCLUSIONS

The increasing pressure on water resources on a global scale has made the sustainable management of water one of the priority issues for agricultural production systems. Factors such as limited freshwater resources, population growth, climate change, and water pollution make the more effective and efficient use of water mandatory. In this context, developing holistic approaches for the protection of water resources and increasing water use efficiency play an important role in achieving sustainable development goals.

In dairy cattle enterprises, water is one of the fundamental inputs used in many stages of production, such as feed production, milking systems, and the cleaning of equipment and barns, in addition to meeting the drinking water requirements of the animals. Therefore, the regular monitoring of water use in enterprises, reduction of water losses, evaluation of alternative water sources, dissemination of practices for water reuse, and the adoption of appropriate enterprise management strategies provide significant contributions to increasing water use efficiency. Furthermore, ensuring continuous access for animals to drinking water in sufficient quantity and appropriate quality is one of the fundamental components of not only water management but also the protection of animal health, welfare, and production performance.

Considering the existing pressure on water resources in Türkiye, the dissemination of practices for sustainable water management in dairy cattle enterprises is of great importance. Regular monitoring of water use at the enterprise level, the use of water-saving technologies, the development of appropriate infrastructure practices, and the adoption of management strategies that will reduce environmental risks will contribute to both the protection of water resources and sustainable milk production.

In conclusion, sustainable water management in dairy cattle enterprises should be considered a fundamental necessity in terms of protecting water resources, supporting environmental sustainability, improving animal welfare, and ensuring the long-term sustainability of production systems. The up-to-date information presented in this review provides a comprehensive evaluation that can contribute to practices for the more effective management of water use in dairy cattle enterprises and to future research.

Declaration on the use of artificial intelligence

During the preparation process of this review, AI-powered tools were utilized for the purposes of grammatical editing of the texts, improving the academic expression structure, and ensuring content organization. However, all scientific content, data, and citations in the text are based on the sources provided by the author. The artificial intelligence tool was not used for the purpose of generating new information, adding data, or creating scientific inferences; it was used only as a supportive tool in the process of reorganizing existing texts and making them compliant with academic writing standards.

REFERENCES

Akhtar, N., Syakir Ishak, M. I., Bhawani, S. A., and Umar, K. (2021). Various natural and anthropogenic factors responsible for water quality degradation: A review. Water, 13(19), 2660. https://doi.org/10.3390/w13192660

Bak Jensen, M., and Vestergaard, M. (2021). Freedom from thirst-do dairy cows and calves have sufficient access to drinking water?. https://doi.org/10.3168/jds.2021-20487

Çolak, M. S., Polat, H. E., Yıldırım, A. C., and Alptekin, N. D. (2025). The Water Footprint of Raw Milk Production on A Dairy Farm. *Ziraat Fakültesi Dergisi*, *20*(2), 89-100. https://doi.org/10.54975/isubuzfd.1819179

FAO. (2025). Food and Agriculture Organization of the United Nations. AQUASTAT core database. https://data.apps.fao.org/aquastat/

Higham, C. D., Horne, D., Singh, R., Kuhn-Sherlock, B., and Scarsbrook, M. R. (2017). Temporal and spatial water use on irrigated and nonirrigated pasture-based dairy farms. *Journal of dairy science*, *100*(8), 6772-6784. https://doi.org/10.3168/jds.2016-12200

Kato, S., and Kansha, Y. (2024). Comprehensive review of industrial wastewater treatment techniques. Environmental Science and Pollution Research, 31(39), 51064-51097. https://doi.org/10.1007/s11356-024-34584-0

Koçbeker, V. D., and Bahtiyarca, Y. (2017). The Effect of The Amount and Quality of Potable Water on Dairy Cattle. *The Turkish Journal Of Occupational / Environmental Medicine and Safety*, *2*(1(3), 420-435. https://izlik.org/JA57PC86AT

Lin, L., Yang, H., and Xu, X. (2022). Effects of water pollution on human health and disease heterogeneity: a review. Frontiers in environmental science, 10, 880246. https://doi.org/10.3389/fenvs.2022.880246

Monteiro, A., Santos, S., and Pereira, J. L. (2023). Efficient water use in dairy cattle production: A Review. *The Open Agriculture Journal*, *17*(1). https://doi.org/10.2174/0118743315270668231127190323

Peypazar, Z. B., and Kılıç, İ. (2021). Süt Sığırı İşletmelerinin Çevre Kirliliği Potansiyellerinin Değerlendirilmesi: Kütahya İli Örneği. *Uludağ Üniversitesi Mühendislik Fakültesi Dergisi*, *26*(1), 15-28. https://doi.org/10.17482/uumfd.811129

Singh, A. K., Bhakat, C., and Singh, P. (2022). A review on water intake in dairy cattle: associated factors, management practices, and corresponding effects. *Tropical Animal Health and Production*, *54*(2), 154. https://doi.org/10.1007/s11250-022-03154-2

TSI. (2025). Turkish Statistical Institute. Adrese Dayalı Nüfus Kayıt Sistemi Sonuçları, 2025. Adrese Dayalı Nüfus Kayıt Sistemi Sonuçları - 2025 - Veri Portalı - TÜİK

TSI. (2026). Turkish Statistical Institute. İstatistiklerle Aile, 2025. İstatistiklerle Aile - 2025 - Veri Portalı - TÜİK

U.S. Geological Survey. (2018). Drip calculator: How much water does a leaking faucet waste? https://www.usgs.gov/tools/drip-calculator-how-much-water-does-a-leaking-faucet-waste

U.S. Geological Survey. (2019, October 25). The distribution of water on, in, and above the Earth. https://www.usgs.gov/media/images/distribution-water-and-above-earth

UNESCO. (2018). United Nations Educational, Scientific and Cultural Organization. The United Nations World Water Development Report 2018: Nature-based solutions for water. https://unesdoc.unesco.org/ark:/48223/pf0000261424

WHO. (2025). World Health Organization, and United Nations Children's Fund. Progress on household drinking water, sanitation and hygiene 2000–2024: Special focus on inequalities. https://www.who.int/publications/i/item/9789240115149

Willers, H. C., Karamanlis, X. N., and Schulte, D. D. (1999). Potential of closed water systems on dairy farms. Water Science and Technology, 39(5), 113-119. https://doi.org/10.1016/S0273-1223(99)00092-X

Yaylak, E., and Yavuz, M. (2016). Sığırlarda İçme Suyu Kalitesi ve Suluk Yönetimi. Journal of Animal Production, 57(2), 57-67. https://izlik.org/JA32TF68XC

INFLUENCE OF BASAL WOUNDING AND AUXIN APPLICATIONS ON ROOTING PERFORMANCE OF HARDWOOD CUTTINGS OF *Podocarpus macrophyllus* var. *macrophyllus*

Ali BAYRAKTAR[1]

[1] *Karadeniz Technical University, Faculty of Forestry, Department of Forest Engineering, Trabzon, Türkiye*
Corresponding author e-mail: alibayraktar@ktu.edu.tr

ABSTRACT

Vegetative propagation through stem cuttings is widely used for the large-scale production of ornamental plants because it enables the preservation of desirable parental characteristics and the multiplication of selected cultivars and varieties. *Podocarpus macrophyllus* (Thunb.) Sweet var. *macrophyllus* is an ornamental evergreen conifer native to East Asia and widely cultivated in parks, gardens, and urban landscapes because of its attractive foliage, adaptability to pruning, and aesthetic value. Therefore, enhancing the rooting success of hardwood cuttings is important for the efficient vegetative propagation of the variety. This study aimed to evaluate the effects of basal wounding and different auxin applications on the rooting performance of hardwood cuttings collected from a male stock plant of *P. macrophyllus* var. *macrophyllus*.

The experiment included eight treatments consisting of a control, basal wounding, and applications of indole-3-butyric acid (IBA) and α-naphthalene acetic acid (NAA) at concentrations of 6000, 8000, and 10000 ppm. At the end of the rooting period, rooting percentage, callus percentage, root length, and root number were determined. The data were subjected to one-way analysis of variance (ANOVA). Although no statistically significant differences were detected among the treatments ($p > 0.05$), clear differences in rooting responses were observed. The highest mean rooting percentage (53.3%) was achieved with the IBA 6000 ppm treatment, compared with only 16.7% in the control treatment, whereas the highest mean callus percentage (30.0%) was obtained in the basal wounding, IBA 8000 ppm, and NAA 6000 ppm treatments. The greatest mean root length (6.4 cm) was recorded following NAA 10000 ppm application. Likewise, the highest mean root number (10.6 roots per cutting) was obtained with NAA 6000 ppm, followed closely by NAA 8000 ppm (10.5 roots per cutting). In contrast, the control treatment generally produced lower rooting performance than auxin-treated cuttings.

Overall, IBA applications were more effective in improving rooting percentage, whereas NAA treatments promoted root system quality by increasing both root length and root number. These findings suggest that auxin application may improve the rooting potential of *P. macrophyllus* var. *macrophyllus* hardwood cuttings, thereby supporting the large-scale production of high-quality nursery stock for ornamental landscape use.

Keywords: Ornamental plant, clonal propagation, stem cuttings, adventitious rooting

INTRODUCTION

The genus *Podocarpus* L'Hér. ex Pers., belonging to the family Podocarpaceae, comprises approximately 98–115 species and is recognized as the largest genus within the family and the second-largest genus of extant conifers after *Pinus* L. (Debreczy and Rácz, 2011; Farjon, 2017; POWO, 2026). *Podocarpus macrophyllus* (Thunb.) Sweet is an evergreen tree of considerable

ornamental value, particularly appreciated for its use in landscape design and bonsai cultivation, while also offering important economic, medicinal, and ecological benefits (Abdillahi et al., 2010; Chen et al., 2023; Deng et al., 2023; Liang et al., 2025). Its economic value is further reflected in the use of its wood as timber (Abdillahi et al., 2010). Moreover, bioactive compounds such as terpenoids, flavonoids, and steroids reported in *P. macrophyllus* highlight its medicinal potential through their antitumor, antioxidant, and anti-inflammatory activities (Kim et al., 2021; Deng et al., 2023; Mohamed et al., 2023). In addition to these benefits, *P. macrophyllus* can contribute to improving urban air quality through its capacity to retain atmospheric particulate matter (Chen et al., 2023). *P. macrophyllus* var. *macrophyllus*, which is naturally distributed in Taiwan, southeastern China, and Japan, is particularly valued for ornamental use due to its attractive form and evergreen foliage (Cheng et al., 2007). Given these characteristics, the development of efficient propagation methods for *P. macrophyllus* var. *macrophyllus* is essential for the production of high-quality and uniform planting material.

Plant propagation is an essential component of the horticultural sector (Loconsole et al., 2024). Vegetative propagation is widely used in ornamental plant production, particularly for the multiplication of selected genotypes while preserving their desirable characteristics (Ürgenç, 1982, 1992; Hartmann et al., 2002; Oinam et al., 2011). Among vegetative propagation techniques, stem cutting is a simple, rapid, and cost-effective method that enables the production of large numbers of genetically uniform plants (Kaviani and Negahdar, 2017; Druege et al., 2019; Ross et al., 2021). Adventitious roots, which develop from non-root tissues in response to stimuli such as stress and wounding (Gogna et al., 2022), are crucial for successful propagation by stem cuttings (Assis et al., 2004; Oinam et al., 2011).

Adventitious root formation is particularly important in the cutting propagation of economically valuable ornamental plants used in landscaping (Geiss et al., 2009). The process is complex and governed by the interaction of various endogenous and exogenous factors. Endogenous factors include genotype, physiological age and condition of the stock plant, cutting type and position, carbohydrate and mineral nutrient status, and endogenous hormonal balance, whereas exogenous factors include the application of plant growth regulators, light, temperature, water availability, wounding, and rooting conditions (da Costa et al., 2013; Druege et al., 2019; Yıldırım et al., 2020; Kumar et al., 2022; Bayraktar, 2025). Among these factors, auxins play a key role in adventitious root formation and are widely used to promote rooting in stem cuttings (Druege et al., 2019; Kumar et al., 2022). Indole-3-butyric acid and α-naphthaleneacetic acid are among the exogenously applied auxins commonly used to stimulate adventitious rooting (Loconsole et al., 2024). In addition, wounding is an effective practice in cutting propagation that can promote adventitious root formation (Hartmann et al., 2002; Zhou, 2005).

Despite considerable advances in propagation by cuttings, low rooting efficiency remains a major constraint in ornamental plant nursery production, resulting in substantial economic losses (Loconsole et al., 2024). In *P. macrophyllus*, vegetative propagation by cuttings may also present difficulties, with rooting success being influenced by several factors, including cutting type, basal wounding, and the application of auxins (Menegusso et al., 2021). Therefore, this study aimed to evaluate the effects of basal wounding and different concentrations (6000, 8000, and 10000 ppm) of indole-3-butyric acid and α-naphthaleneacetic acid on the rooting performance of hardwood cuttings collected from a male plant of *P. macrophyllus* var. *macrophyllus*. Rooting and callus percentages, root length, and root number were assessed to compare treatment effectiveness and identify the most suitable treatment for the vegetative propagation of this variety.

MATERIAL AND METHOD

Hardwood cuttings of *Podocarpus macrophyllus* (Thunb.) Sweet var. *macrophyllus* were collected from a healthy and vigorous male stock plant growing on the Kanuni Campus of Karadeniz Technical University (KTU), Trabzon, Türkiye, at the end of October, when the current-season shoots were fully mature and completely lignified. Hardwood cuttings measuring 12–14 cm in length were prepared from these shoots. The basal cut of each cutting was made immediately below a node using a sharp and sterilized knife. The leaves on the lower portion of each cutting were removed, while a few healthy leaves were retained at the apical portion. Approximately half of the lamina of each retained leaf was removed to reduce transpirational water loss while maintaining photosynthetic activity.

The experiment included eight treatments comprising untreated cuttings (control, C), basal wounding (W), and indole-3-butyric acid (IBA) and α-naphthaleneacetic acid (NAA) applied at concentrations of 6000, 8000, and 10000 ppm. Hereafter, the treatments are referred to as IBA 6000 ppm, IBA 8000 ppm, IBA 10000 ppm, NAA 6000 ppm, NAA 8000 ppm, and NAA 10000 ppm, respectively.

In the basal wounding treatment, two diagonal cuts, each approximately 5 mm in length, were made across the basal end of each cutting to form an X-shaped wound. IBA and NAA were applied at 6000, 8000, and 10000 ppm as follows: the basal ends of the cuttings were dipped directly into the respective hormone powder, and excess powder was gently removed before inserting the cuttings into the rooting medium. Control cuttings received no auxin treatment and were not subjected to basal wounding.

Following treatment application, the cuttings were inserted into a heated rooting bed containing perlite as the rooting substrate, with approximately half of each cutting embedded in the medium. The perlite layer was maintained at a depth of 20 cm. The experiment was arranged in a completely randomized design with three replications, each consisting of 10 cuttings, resulting in 30 cuttings per treatment. A total of eight treatments were evaluated, comprising 240 cuttings in the entire experiment. Rooting was carried out under controlled environmental conditions with an air temperature of 20 ± 2°C, a bottom-heated rooting bed temperature of 25 ± 2°C, and a relative humidity of 75 ± 5%.

At the end of the rooting period, all cuttings were carefully removed from the rooting medium, and adhering perlite particles were gently removed from the roots prior to evaluation. Rooting percentage, callus percentage, root length, and root number were determined for each treatment. A cutting was considered rooted if it had developed at least one adventitious root measuring 1 cm or longer. Rooting percentage was calculated by dividing the number of rooted cuttings by the total number of cuttings and multiplying the result by 100. Callus percentage was calculated as the proportion of cuttings that formed callus tissue at the cutting base. The length of the longest primary root was determined by measuring the distance from the base of the cutting to the tip of the longest primary root using a ruler and expressed in centimetres. Root number was determined by counting all adventitious roots formed on each rooted cutting.

Statistical analyses were performed using IBM SPSS Statistics 27. The effects of the treatments on rooting percentage, callus percentage, root length, and root number were evaluated using one-way analysis of variance (ANOVA), with statistical significance accepted at $p < 0.05$. Means and standard deviations were calculated for all measured variables. Frequency distributions were generated for rooting and callus percentages, whereas minimum and maximum values were determined for root length and root number. The results were presented graphically to facilitate comparisons among treatments.

RESULTS

Following a rooting period of 149 days, all cuttings were removed from the rooting bed and evaluated for rooting percentage, callus formation, root length, and root number. The frequency distributions of rooting and callus percentage among treatments are presented in Figure 1.

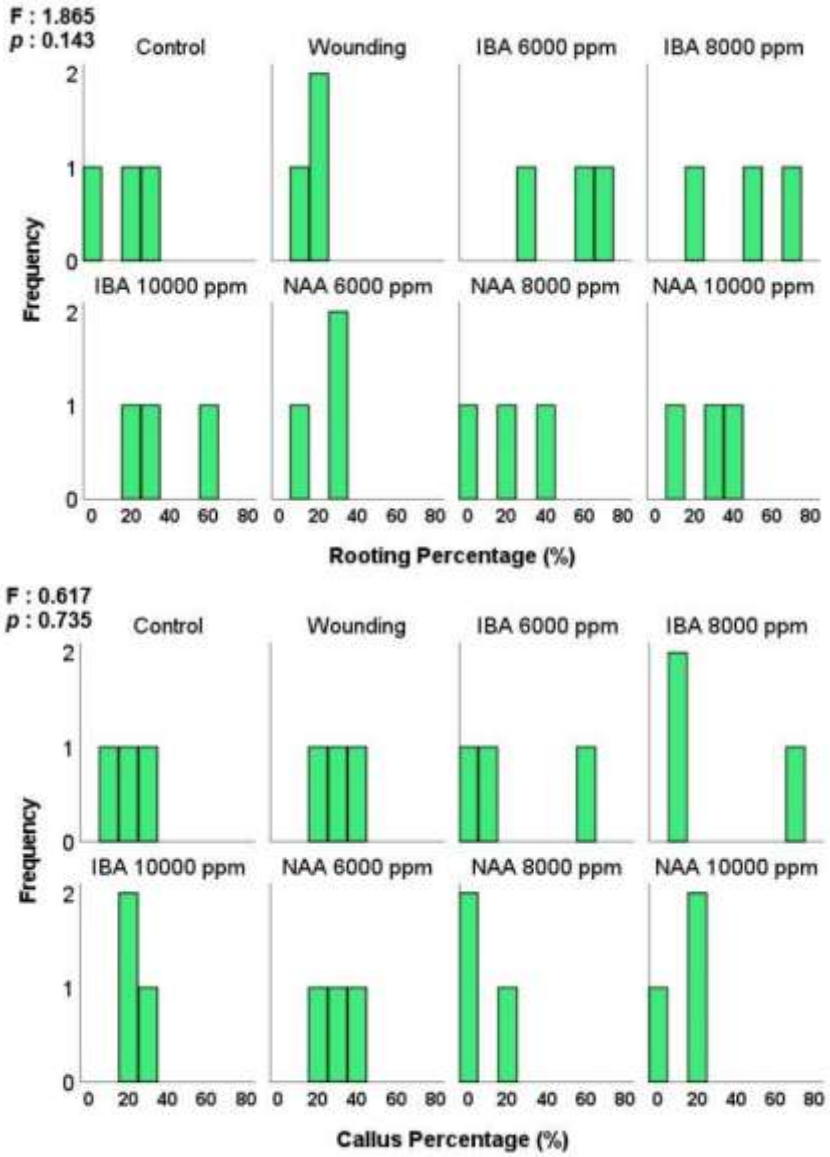

Figure 1. Frequency distributions of rooting and callus percentages by treatment, with one-way ANOVA results

As shown in Figure 1, one-way ANOVA revealed no statistically significant differences ($p > 0.05$) among treatments for either rooting percentage or callus percentage. Nevertheless, the frequency distributions of rooting and callus percentages varied among treatments, and considerable variation was also observed among replicates within each treatment. The rooting and callus percentages recorded for each replicate within each treatment ranged from 0% to 70%. A notable finding was that the highest rooting percentages recorded in the individual replicates (70%) occurred exclusively in the IBA 6000 and IBA 8000 ppm treatments, followed by the IBA 10000 ppm treatment with a maximum of 60%, whereas the remaining treatments did not exceed 40%. In addition, the highest callus formation percentage recorded among the

individual replicates (70%) was observed in the IBA 8000 ppm treatment, whereas none of the remaining treatments reached this value. Figure 2 presents the minimum and maximum values of root length and root number, together with the corresponding one-way ANOVA results.

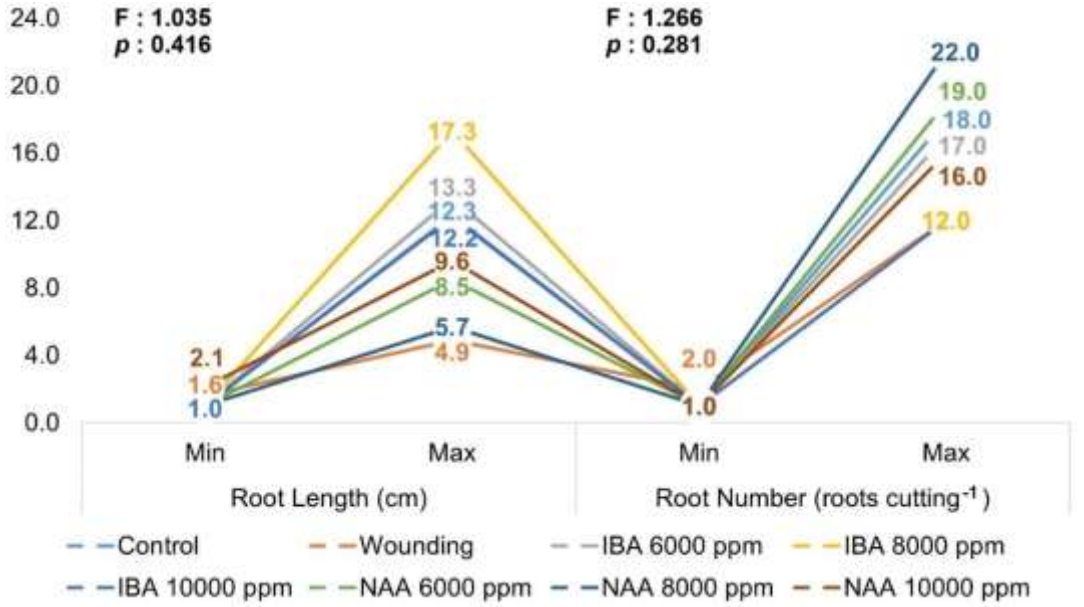

Figure 2. Minimum and maximum root length and root number values by treatment, with one-way ANOVA results

One-way ANOVA detected no statistically significant differences among treatments for either root length or root number ($p > 0.05$). However, differences in the minimum and maximum values were evident among treatments. Minimum root length was 1.0 cm in six treatments, whereas the wounding and NAA 10000 ppm treatments exhibited slightly higher minimum values of 1.6 and 2.1 cm, respectively. Maximum root length values ranged from 4.9 to 17.3 cm across treatments, with the highest value recorded in the IBA 8000 ppm treatment and a maximum of 12.3 cm observed in the control. Across treatments, root number ranged from 1 to 22 roots per cutting. The highest value was associated with the NAA 8000 ppm treatment (22 roots per cutting), whereas a maximum of 18 roots per cutting was observed in the control treatment. The mean rooting percentage, callus percentage, and their corresponding standard deviations for each treatment are presented in Figure 3.

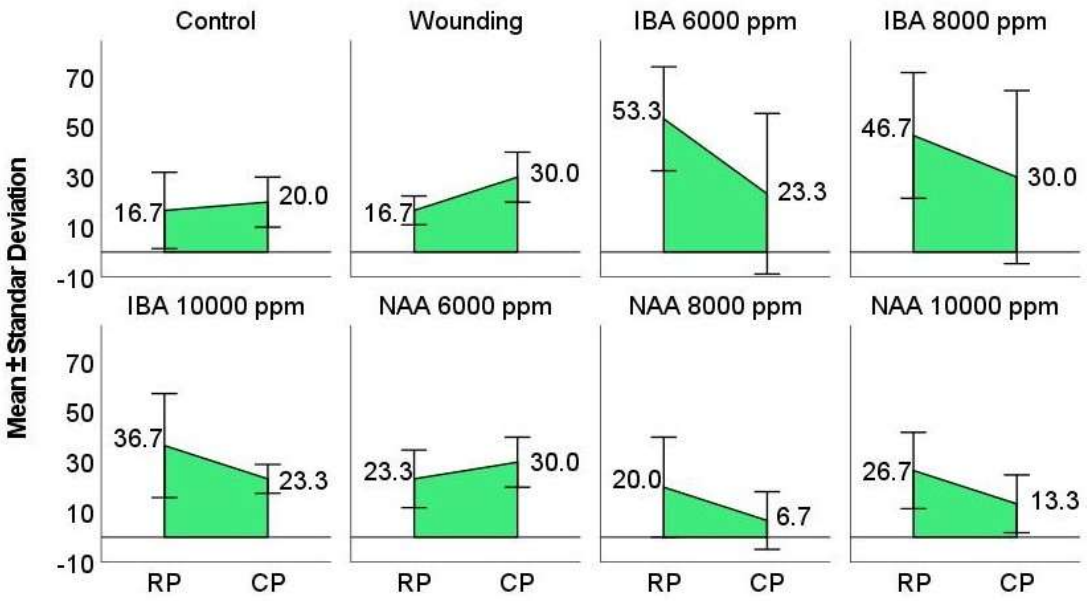

Figure 3. Mean rooting and callus percentages with standard deviations for each treatment

Figure 3 shows that the mean rooting percentage was greatest in the IBA 6000 ppm treatment (53.3%), followed by IBA 8000 ppm (46.7%) and IBA 10000 ppm (36.7%). Mean rooting percentages in the control, wounding, and NAA treatments ranged from 16.7% to 26.7%. In contrast, mean callus percentages showed a different pattern, with the highest values (30.0%) recorded in the wounding, IBA 8000 ppm, and NAA 6000 ppm treatments. Mean callus percentage was 23.3% in the IBA 6000 ppm and IBA 10000 ppm treatments, 20.0% in the control, 13.3% in the NAA 10000 ppm treatment, and 6.7% in the NAA 8000 ppm treatment. Figure 4 summarizes the mean root length and root number, together with standard deviations, for each treatment.

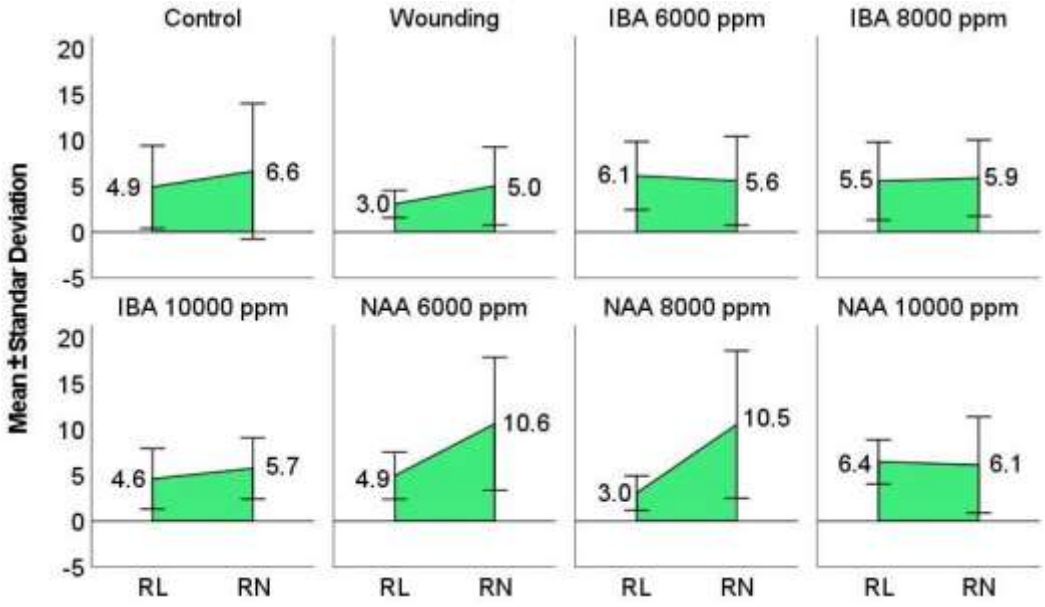

Figure 4. Mean root length and root number with standard deviations for each treatment

The mean root length values ranged from 3.0 to 6.4 cm among treatments. The greatest mean root length was obtained in the NAA 10000 ppm treatment (6.4 cm), closely followed by the

IBA 6000 ppm treatment (6.1 cm). In contrast, the lowest mean root length (3.0 cm) was observed in the wounding and NAA 8000 ppm treatments, while the control treatment had a mean root length of 4.9 cm. Unlike root length, mean root number reached its highest values in the NAA 6000 ppm (10.6 roots per cutting) and NAA 8000 ppm (10.5 roots per cutting) treatments. The control treatment exhibited a mean of 6.6 roots per cutting, while the remaining treatments produced mean root numbers ranging from 5.0 to 6.1 roots per cutting. A representative photograph of *P. macrophyllus* var. *macrophyllus* hardwood cuttings showing rooting, callus formation, and loss of viability is presented (Figure 5).

Figure 5. Rooting, callus formation, and loss of viability in *P. macrophyllus* var. *macrophyllus* hardwood cuttings

DISCUSSION AND CONCLUSION

The present study demonstrated that basal wounding and exogenous auxin applications produced different rooting responses in hardwood cuttings of *Podocarpus macrophyllus* var. *macrophyllus* collected from a male stock plant, although the differences among treatments were not statistically significant. Nevertheless, the observed trends indicated that auxin type and concentration may differentially influence individual components of the rooting process. In particular, IBA treatments were associated with higher rooting percentages, with the highest mean rooting percentage (53.3%) obtained in the IBA 6000 ppm treatment, compared with 16.7% in the untreated control. Callus formation showed a different response pattern, with the highest mean callus percentage (30.0%) recorded in the wounding, IBA 8000 ppm, and NAA 6000 ppm treatments. Regarding root system development, NAA treatments were more prominent in promoting root system development, as reflected by the greatest mean root length (6.4 cm) in the NAA 10000 ppm treatment and the highest mean root numbers in the NAA 6000 ppm (10.6 roots per cutting) and NAA 8000 ppm (10.5 roots per cutting) treatments. These findings suggest that, under the experimental conditions of the present study, IBA was more effective in increasing rooting percentage and overall rooting success, whereas NAA tended to promote root growth and root system development.

Similar trends have been reported in previous studies on *P. macrophyllus*. Güney et al. (2024), who investigated the effects of different rooting bed temperatures and auxin applications on hardwood cuttings of *P. macrophyllus* var. *maki*, found no statistically significant differences

in rooting percentage, callus percentage, root length, or root number, despite numerical variation among treatments. The highest mean rooting percentage (63.33%) was obtained with IAA 5000 ppm at a rooting bed temperature of 25 ± 2°C and with IAA 3000 ppm at 20 ± 2°C. These treatments were followed by NAA 5000 ppm at 25 ± 2°C and IBA 3000 ppm at 20 ± 2°C, both of which resulted in a mean rooting percentage of 56.67%. Regarding callus formation, the highest mean callus percentage at a rooting bed temperature of 25 ± 2°C was obtained with IBA 3000 ppm (25.0%). At 20 ± 2°C, the highest mean value (20.0%) was recorded in the control, IBA 3000 ppm, and IBA 5000 ppm treatments. In terms of root development, the greatest mean root length (11.25 cm) was recorded with IBA 5000 ppm at 25 ± 2°C, whereas the highest mean root number (7.24 roots per cutting) was obtained with IBA 3000 ppm at 20 ± 2°C. These findings are broadly consistent with the present study, particularly in terms of the absence of statistically significant differences among treatments and the numerical variation in rooting responses associated with auxin applications. However, Güney et al. (2024) used hardwood cuttings of var. *maki* collected in March and applied IBA, IAA, and NAA at concentrations of 3000 and 5000 ppm, whereas the present study used hardwood cuttings of var. *macrophyllus* collected at the end of October and evaluated IBA and NAA at 6000, 8000, and 10000 ppm. Furthermore, the rooting period was 217 days in their study compared with 149 days in the present study. Differences in variety, cutting collection time, auxin type and concentration, and rooting period may therefore have contributed to the variation in rooting responses observed between the two studies. Menegusso et al. (2021) evaluated the effects of IBA concentration and application method (0, 500, 1000, and 1500 mg L^{-1}; hydroalcoholic solution and talc), as well as cutting type and basal lesion type (basal and apical cuttings; wedge, bevel, and horizontal lesions), on the rooting of *P. macrophyllus* in two separate experiments. In the first experiment, the application of IBA as a hydroalcoholic solution resulted in a maximum rooting percentage of 78.29% at 550 mg L^{-1}, while root number and root length were not significantly affected by IBA concentration or application method. In the second experiment, basal cuttings showed high rooting percentages ranging from 84.44 to 91.11% across the three lesion types, with no significant differences among them, whereas in apical cuttings the bevel treatment resulted in a significantly lower rooting percentage (51.11%) than the wedge (82.22%) and horizontal (77.78%) treatments. These findings are partially consistent with the present study, in which the highest rooting percentage was also obtained with IBA, although at a substantially higher concentration (6000 ppm), whereas basal wounding alone did not result in a comparable improvement in rooting.

Studies on other *Podocarpus* species further indicate that rooting responses may vary considerably depending on auxin concentration and plant material. In *P. neriifolius,* Hossain et al. (2019) obtained the highest rooting percentage (61.3%) and root number (9.8 roots per cutting) with 0.8% IBA, whereas the greatest root length (6.0 cm) was recorded with a lower IBA concentration of 0.4%. In *P. falcatus*, Negash and van Staden (2003) showed that stock plant age markedly affected the rooting performance of cuttings treated with IBA. Cuttings from younger stock plants (3 months and 2 years old) achieved rooting percentages of up to 80% and responded positively to 20–80 µg IBA, whereas higher concentrations inhibited rooting. In contrast, cuttings from older stock plants (4 and 8 years old) showed lower rooting percentages but produced more roots. These findings, together with the results of the present study, suggest that the auxin concentration associated with a high rooting percentage does not necessarily result in greater root length or root number, and that the rooting response to auxin may also depend on characteristics of the stock plant. Rooting substrate has also been shown to influence several components of rooting performance in *Podocarpus*. Gerding et al. (1996) reported that the rooting percentage of *P. nubigena* cuttings varied considerably among rooting substrates, ranging from 20 to 87%, with the highest rooting percentage obtained in a 2:1 mixture of composted bark and pumice. Root length also varied among substrates from 2.8 to

4.5 cm, with the longest roots recorded in the same 2:1 mixture. Root number ranged from 7.2 to 17.6 roots per cutting, with the highest value obtained in a 1:2 mixture of composted bark and pumice. In addition, callus formation was more prevalent in substrates associated with lower rooting percentages. These findings highlight the importance of the physical and chemical properties of rooting substrates in determining rooting performance. Taken together, previous studies on different *Podocarpus* species indicate that rooting performance may be influenced by several factors, including auxin concentration, stock plant age, and rooting substrate. The variation among these studies further suggests that these factors may differentially affect individual rooting parameters, including rooting and callus percentages, root length, and root number. This pattern is also consistent with the present study, in which different auxin treatments showed distinct numerical trends among the evaluated rooting parameters despite the absence of statistically significant differences among treatments. In addition, positive effects of exogenous auxin applications and basal wounding on adventitious rooting have been reported in numerous studies across different plant species (Al-Salem and Karam, 2001; Blythe, 2012; Yıldırım et al., 2020).

In conclusion, the present study provides useful insights into the rooting performance of hardwood cuttings obtained from male *P. macrophyllus* var. *macrophyllus*. The results indicate that auxin applications can contribute to rooting and root system development, with IBA showing potential for improving rooting success and NAA for promoting root growth and root system development. Basal wounding alone did not provide a clear advantage under the experimental conditions. Overall, the findings may contribute to the development of effective cutting propagation practices for this ornamental variety. Further studies should evaluate different auxin concentrations and rooting conditions, as well as the combined application of wounding and auxins. In addition, studies including both male and female individuals would be valuable for determining whether sex influences rooting performance and for further improving propagation protocols for *P. macrophyllus* var. *macrophyllus*.

REFERENCES

Abdillahi, H. S., G. I. Stafford, J. F. Finnie, J. van Staden. 2010. Ethnobotany, phytochemistry and pharmacology of *Podocarpus* sensu latissimo (sl). *South African Journal of Botany*, 76(1): 1-24.

Al-Salem, M. M., N. S. Karam. 2001. Auxin, wounding, and propagation medium affect rooting response of stem cuttings of *Arbutus andrachne*. *HortScience*, 36(5), 976-978.

Assis, T. F., A. G. Fett-Neto, A. C. Alfenas. 2004. Current techniques and prospects for the clonal propagation of hardwoods with emphasis on eucalyptus. In: Walter, C., M. Carson. (Eds.) Plantation Forest Biotechnology for the 21st Century. Research Signpost, Thiruvananthapuram, India, 1109-1119.

Bayraktar, A. 2025. Çelikle bitki üretiminde köklenme başarısını etkileyen faktörler arasında yaralamanın yeri. In: Özrenk, K., A. Bolat. (Eds.) Ziraat ve Orman Ürünleri Alanında Uluslararası Derleme, Araştırma ve Çalışmalar. Serüven Yayınevi, Ankara, Türkiye, 307-329.

Blythe, E. K. 2012. Hardwood cutting propagation of Confederate rose using auxin and wounding treatments. *Horttechnology*, 22(4), 476-478.

Chen, Y., Y. Xu, X. Liang, W. Yan, R. Zhang, Y. Yan, S. Qin. 2023. Foliar particulate matter retention and toxic trace element accumulation of six roadside plant species in a subtropical city. *Scientific Reports*, 13(1): 12831.

Cheng, K. T., F. L. Hsu, S. H. Chen, P. K. Hsieh, H. S. Huang, C. K. Lee, M. H. Lee. 2007. New constituent from *Podocarpus macrophyllus* var. *macrophyllus* shows anti-tyrosinase effect and regulates tyrosinase-related proteins and mRNA in human epidermal melanocytes. *Chemical and Pharmaceutical Bulletin*, 55(5): 757-761.

da Costa, C. T., M. R. de Almeida, C. M. Ruedell, J. Schwambach, F. S. Maraschin, A. G. Fett-Neto. 2013. When stress and development go hand in hand: Main hormonal controls of adventitious rooting in cuttings. *Frontiers in Plant Science*, 4: 133.

Debreczy, Z., Z. Rácz. 2011. *Conifers around the World*. 2 vols. DendroPress, Budapest.

Deng, Z., F. Sheng, S. Y. Yang, Y. Liu, L. Zou, L. L. Zhang. 2023. A comprehensive review on the medicinal usage of *Podocarpus* species: Phytochemistry and pharmacology. *Journal of Ethnopharmacology*, 310: 116401.

Druege, U., A. Hilo, J. M. Pérez-Pérez, Y. Klopotek, M. Acosta, F. Shahinnia, …, M. R. Hajirezaei. 2019. Molecular and physiological control of adventitious rooting in cuttings: Phytohormone action meets resource allocation. *Annals of Botany*, 123(6): 929-949.

Farjon, A. 2017. A handbook of the World's conifers. 2nd ed. Brill, Leiden.

Geiss, G., L. Gutierrez, C. Bellini. 2009. A*dventitious root formation: New insights and perspectives*. Wiley-Blackwell, Hoboken, NJ, USA.

Gerding, V., M. E. Hermosilla, R. Grez. 1996. Substrata of composted bark for vegetative propagation of *Podocarpus nubigena* Lindl. and *Eucryphia cordifolia* Cav. stalk stem cutting. *Revista Bosque*, 17(2): 57-64.

Gogna, M., R. Kumar, L. D. Tiwari, A. Tailor, A. Kumari, S. Mehta. 2022. Chapter 15 - Strigolactones: A new player in regulating adventitious root formation. In: Husen, A. (Ed.) Plant Biology, Sustainability and Climate Change, Environmental, Physiological and Chemical Controls of Adventitious Rooting in Cuttings. Academic Press, 343-366.

Güney, D., A. Bayraktar, İ. Turna. 2024. *Podocarpus macrophyllus* var. *maki* Siebold & Zucc. çeliklerinin köklendirilmesinde farklı ortam sıcaklıkları ile fitohormon uygulamalarının etkileri. In: Bolat, İ., Ü. Ayata, G. Ulay. (Eds.) Orman Mühendisliği Alanında Araştırmalar ve Değerlendirmeler-Aralık 2024. Gece Kitaplığı, Ankara, Türkiye, 51-64.

Hartmann, T. H., D. E. Kester, F. T. Davies, R. L. Geneve. 2002. *Plant propagation: Principles and practices*. 7th ed. Prentice Hall, Upper Saddle River, NJ.

Hossain, M. A., M. A. Islam, M. A. K. Azad, M. M. Rahman, W. Shumi, N. A. A. Shukor. 2019. Propagation of an endangered gymnosperm tree species (*Podocarpus neriifolius* D. Don.) by stem cuttings in non-mist propagator. *Pertanika Journal of Tropical Agricultural Science*, 42(1): 237-250.

Kaviani, B., N. Negahdar. 2017. Propagation, micropropagation and cryopreservation of *Buxus hyrcana* Pojark., an endangered ornamental shrub. *South African Journal of Botany*, 111: 326-335.

Kim, C., D. Le, M. Lee. 2021. Diterpenoids isolated from *Podocarpus macrophyllus* inhibited the inflammatory mediators in LPS-induced HT-29 and RAW 264.7 cells. *Molecules*, 26(14): 4326.

Kumar, A., A. Choudhary, H. Kaur, K. Sangeetha, S. Mehta, A. Husen. 2022. Physiological and environmental control of adventitious root formation in cuttings: An overview. *Environmental, Physiological and Chemical Controls of Adventitious Rooting in Cuttings*, 1-24.

Liang, X., D. Zhong, C. Zhang, Y. Pan, C. Zhang, H. Guo, …, Y. Feng. 2025. Effects of different cultivation substrates on the growth of *Podocarpus macrophyllus* and the rhizosphere soil microbial community structure. *Agronomy*, 15(5): 1055.

Loconsole, D., E. Scaltrito, A. E. Sdao, G. Cristiano, B. de Lucia. 2024. Application of commercial seaweed extract-based biostimulants to enhance adventitious root formation in ornamental cutting propagation protocols: A review. *Frontiers in Horticulture*, 3: 1371090.

Menegusso, F. J., F. Villa, D. F. D. Silva, L. S. D. Silva, G. Ritter, T. Eberling. 2021. Vegetative propagation of an ornamental conifer: Some techniques in podocarpo cutting. *Ciência Rural*, 51(9): e20180896.

Mohamed, N. Z., L. Shaaban, S. Safan, A. S. El-Sayed. 2023. Phytochemical and metabolic profiling of the different *Podocarpus* species in Egypt: Potential antimicrobial and antiproliferative activities. *Heliyon*, 9(9): e20034.

Negash, L., J. van Staden. 2003. Vegetative propagation of the threatened East African yellowwood (*Podocarpus falcatus*). *South African Journal of Botany*, 69(2): 170-175.

Oinam, G., E. Yeung, L. Kurepin, T. Haslam, A. Lopez-Villalobos. 2011. Adventitious root formation in ornamental plants: I. General overview and recent successes. *Propagation of Ornamental Plants*, 11: 78-90.

POWO. 2026. Plants of the World Online. Facilitated by the Royal Botanic Gardens, Kew. http://www.plantsoftheworldonline.org/ (accessed 17 August 2026).

Ross, S. G., M. Souza-Pérez, N. Ávila, F. Pietro, A. M. González. 2021. Stem cutting anatomy and biochemical responses associated with competence for adventitious root differentiation in *Acca sellowiana* (Myrtaceae). *Trees*, 35: 1221-1232.

Ürgenç, S. 1982. *Orman ağaçları ıslahı*. İstanbul Üniversitesi Orman Fakültesi Yayınları, Yayın No. 293, İstanbul, 414 s.

Ürgenç, S. 1992. *Ağaç ve süs bitkileri fidanlık ve yetiştirme tekniği*. İstanbul Üniversitesi Orman Fakültesi Yayınları, Üniversite Yayın No. 3676, Fakülte Yayın No. 418, İstanbul.

Yıldırım, N., A. Bayraktar, F. Atar, D. Güney, M. Öztürk, İ. Turna. 2020. Effects of different genders and hormones on stem cuttings of *Salix anatolica*. *Journal of Sustainable Forestry*, 39: 300-308.

Zhou, L. 2005. *Salt tolerance, propagation and provenance evaluation of Taxodium as a landscape and coastal wetland tree*. Master's thesis. Department of Horticulture, Stephen F. Austin State University, Nacogdoches, TX.

AI-ASSISTED HIGH-THROUGHPUT PHENTYPING IN *ARABIDOPSIS THALIANA*: CURRENT APPROACHES

NURAN EKICI

Trakya University, Faculty of Education, Department of Science Education, Edirne, Turkey

ABSTRACT

Arabidopsis thaliana is one of the most widely used model organisms in research on plant genetics, molecular biology, developmental biology, and plant biotechnology due to its short life cycle, small genome, ease of transformation, and extensive mutant collections. In recent years, alongside advancements in imaging technologies, high-throughput phenotyping (HTP) systems have enabled the rapid, accurate, and reproducible assessment of the morphological, physiological, and developmental traits of plants. However, analyzing the large volumes of image and phenotype data obtained from these systems is a time-consuming and labor-intensive process using traditional methods. For this reason, artificial intelligence-based approaches—particularly machine learning, deep learning, and computer vision techniques—have become a significant area of research in plant phenotyping studies. The aim of this study is to evaluate artificial intelligence-assisted high-throughput phenotyping approaches in *Arabidopsis thaliana* and to outline current developments in this field by examining scientific studies published in the Web of Science, Scopus, and PubMed databases between 2020 and 2026. In this context, prominent image analysis methods, deep learning-based approaches, and high-throughput phenotyping platforms in the literature have been examined. Within the scope of the studies reviewed, artificial intelligence applications for leaf and root phenotyping, monitoring plant growth, image analysis, and determining abiotic stress responses were evaluated, and the current software and platforms developed for these purposes were summarized. Furthermore, the contributions of AI-driven phenotyping approaches to elucidating genotype-phenotype relationships, more accurately assessing plant development, and efficiently analyzing large-scale phenotypic data have been discussed. In conclusion, it is considered that AI-powered high-throughput phenotyping approaches accelerate data analysis processes in *Arabidopsis thaliana* research, enhance the accuracy of phenotypic assessments, and possess broad application potential ranging from fundamental plant biology to sustainable agriculture and plant biotechnology. With the advancement of artificial intelligence algorithms and the widespread adoption of high-throughput phenotyping systems, it is anticipated that these technologies will be utilized more effectively in plant research in the future and will make significant contributions to the development of new research areas.

Keywords: *Arabidopsis thaliana*, artificial intelligence, high-throughput phenotyping, deep learning, plant phenotyping

INTRODUCTION

Model organisms are experimental systems that contribute to elucidating the fundamental mechanisms underlying biological processes and enable the findings obtained to be applied to other living organisms. They are widely used in basic and applied research due to their short life cycles, well-characterized genetics, ease of cultivation, and rich genetic resources. In plant

sciences, model organisms play a significant role in understanding plant development, gene functions, environmental stress responses, and molecular regulatory mechanisms (Meinke et al., 1998; Koornneef and Meinke, 2010; Provart et al., 2016).
Among these model organisms, *Arabidopsis thaliana* is considered the most important model species in plant biology due to its small genome (approximately 135 Mb), short life cycle, high seed yield, ease of transformation, and extensive mutant collections. Being the first plant to have its full genome sequenced has led to its widespread use in genetic and molecular studies and paved the way for numerous research projects in the fields of developmental biology, physiology, genetics, genomics, and plant biotechnology. Furthermore, the ability to examine in detail the physiological and molecular responses to various environmental conditions has made this species an indispensable model for phenotyping studies as well (Arabidopsis Genome Initiative, 2000; Koornneef and Meinke, 2010; Provart et al., 2016).

Plant phenotyping is one of the fundamental research fields that enables the quantitative and qualitative assessment of the morphological, physiological, biochemical, and developmental characteristics of plants. Since traditional phenotyping methods rely largely on manual observations and measurements, they are time-consuming and labor-intensive and may be subject to observer-dependent variations. In contrast, high-throughput phenotyping (HTP) systems developed in recent years enable the analysis of large numbers of plants with high accuracy in a short time by utilizing imaging technologies, sensor systems, and automated data collection platforms. These developments have made it possible to obtain phenotypic data more rapidly, reliably, and reproducibly, particularly in large-scale experiments (Fahlgren et al., 2015; Yang et al., 2020).
With the widespread adoption of high-throughput phenotyping systems, the volume of image and phenotype data obtained has increased significantly. The inadequacy of traditional methods in analyzing large datasets has accelerated the integration of artificial intelligence-based approaches into plant phenotyping studies (Pieruschka and Schurr, 2019). Machine learning, deep learning, and computer vision techniques yield successful results in the automated determination of numerous phenotypic traits, such as leaf area, plant growth, root architecture, flowering time, and signs of environmental stress. Thus, data analysis processes are accelerated, human-induced errors are reduced, and a contribution is made to the more accurate assessment of genotype-phenotype relationships (Fahlgren et al., 2015; Yang et al., 2020).
The recent increase in the number of studies conducted in the field of AI-driven high-throughput phenotyping has made it necessary to systematically evaluate the body of knowledge in this area. This study examines artificial intelligence-assisted high-throughput phenotyping approaches in *Arabidopsis thaliana*, based on scientific studies published in the Web of Science, Scopus, and PubMed databases between 2020 and 2026. In this context, the importance of *Arabidopsis thaliana* as a model organism, the development of high-throughput phenotyping systems, and current applications regarding leaf and root phenotyping—utilizing artificial intelligence-based analysis methods, plant growth monitoring, and the assessment of abiotic stress responses—have been examined. Furthermore, the contributions of AI-driven phenotyping approaches to plant biology research have been evaluated, and potential areas for future research have been discussed.

The Importance of *Arabidopsis thaliana* as a Model Organism

Arabidopsis thaliana is an annual herbaceous plant belonging to the Brassicaceae (mustard) family and is the most widely used model organism in the fields of plant biology, molecular genetics, developmental biology, and plant biotechnology. Today, it is preferred as an experimental system in much of the fundamental research conducted in plant sciences and serves as the initial application site for newly developed methods. Model organisms are living things that are studied extensively to understand biological processes and that allow the knowledge gained to be applied to other species. The primary reasons for the adoption of *A. thaliana* as a model organism are its short life cycle, its small and well-defined genome, the ease with which it can be cultivated under laboratory conditions, and the availability of a robust research infrastructure for genetic studies (*Arabidopsis* Genome Initiative, 2000) (Fig. 1).

One of the most important advantages of *A. thaliana* is its short life cycle, allowing it to go from seed to seed in approximately 6–8 weeks. This feature enables researchers to examine numerous generations within a single year. For instance, in a study investigating the effect of a gene on plant development, different generations can be compared within a few months rather than waiting several years. This enables experiments to be completed in less time and reduces research costs (Koornneef and Meinke, 2010).

The genome size of *A. thaliana* is approximately 135 Mb (megabases), and it contains approximately 27,000 genes. It marked a significant milestone in molecular biology research as the first plant species to have its genome fully sequenced. A small genome facilitates gene identification, mutation analysis, gene expression studies, and bioinformatics analyses. The availability of organized and reliable genomic data provides a significant advantage, particularly in AI-driven bioinformatics studies (Hou et al., 2022).

A. thaliana is one of the plants that can be transformed quite easily via *Agrobacterium tumefaciens* (Bélanger et al., 2024) In the floral dip technique - the most widely used method- foreign genes can be transferred to the plant by dipping the flowers into a bacterial suspension. This method is quite fast and economical compared to many other plant species. For this reason, the determination of gene functions, gene silencing studies, and CRISPR/Cas-based gene editing research are frequently conducted on *A. thaliana* (Zlobin et al., 2020).

Fig. 1: Rosette structure in *Arabidopsis thaliana*. (Small RNA Pathways in Plants, PLoS Biology) (2004); Wikimedia Commons,
CC BY 2.5.

Extensive mutant collections for *A. thaliana* have been established worldwide (Alonso et al., 2003). Researchers can easily obtain mutants lacking a specific gene, lines exhibiting gene overexpression, and T-DNA insertion mutants. This situation enables the same biological phenomenon to be investigated by different research groups using standard materials. *A.*

thaliana is a small plant and can be grown in a very small space. Hundreds or even thousands of plants can be grown simultaneously in a growth room or climate chamber. This feature offers a significant advantage, particularly for high-throughput phenotyping (HTP) studies. The ability to raise many individuals under the same environmental conditions increases the reliability of the obtained phenotypic data (Fahlgren et al., 2015).

High-throughput phenotyping systems developed in recent years are predominantly tested on *A. thaliana.* The primary reasons for this are the ability to analyze numerous plants in a single image due to their small rosette structure, the suitability of the leaves for easy segmentation, the ability to visualize root development in transparent media, and the capacity to acquire large amounts of image data in a short time. With the aid of these features, machine learning, deep learning, and computer vision algorithms are trained and validated on *A. thaliana* images (**Maraveas, 2024)**.

A. thaliana is not merely a model used to understand its own biology. Image analysis algorithms, artificial intelligence models, and phenotyping platforms developed using this plant can subsequently be adapted to economically important crops such as wheat, rice, maize, tomatoes, soybeans, and canola **(Maraveas, 2024; Kaya, 2025)**. Therefore, *A. thaliana* serves as a "testing platform" for the development and validation of new technologies **(Maraveas, 2024)**.

Phenotyping

Phenotyping is the process of systematically evaluating the observable and measurable traits of an organism that emerge from the interaction between its genetic makeup (genotype) and environmental conditions **(Fahlgren et al., 2015; Yang et al., 2020).** Plant phenotyping involves determining the observable or qualitative characteristics related to growth, development, morphology, physiology, and responses to stress **(Maraveas, 2024)**. The concept of phenotype does not refer solely to the plant's external appearance. Leaf number, leaf area, plant height, root length, flowering time, biomass, photosynthesis rate, water use, chlorophyll content, and responses to stress conditions such as drought or salinity are also part of the phenotype **(Yang et al., 2020; Maraveas, 2024)**. In short, phenotyping is the process of measuring how a plant grows, develops, and responds to environmental conditions. For many years in plant biology, most of the research has focused on the identification of genes. However, the presence of a gene alone is not sufficient; what matters is demonstrating how that gene affects the plant's appearance, development, or physiology. Therefore, phenotyping is one of the most important research steps for understanding the relationship between genotype and phenotype **(Fahlgren et al., 2015)**. For example, two *Arabidopsis* plants can be genetically different. This difference may manifest in leaf size, root development, drought tolerance, and flowering time. Phenotyping studies enable the objective measurement of these differences **(Maraveas, 2024)**.

Traits Examined in Plant Phenotyping

Phenotyping studies may involve the assessment of different characteristics, depending on the aim of the research **(Yang et al., 2020; Maraveas, 2024)**. These may include the plant's morphological, physiological, and developmental characteristics, as well as the stress responses it exhibits under various stress conditions **(Yang et al., 2020)**. Morphological characteristics are measurements related to the plant's external appearance. Examples include plant height, leaf area, number and shape, rosette diameter, leaf angle, root length, number of lateral roots, and the number of flowers, fruits, or siliques. These characteristics can be easily measured through image analysis. Physiological characteristics are measurements related to the plant's life

processes. Examples of these include photosynthesis rate, stomatal conductance, chlorophyll content, leaf temperature, water use, respiration, and transpiration. These characteristics are generally determined using sensors and specialized imaging systems **(Maraveas, 2024; Kaya, 2025)**.

Developmental characteristics refer to the development of the plant over time. Examples include germination time, leaf formation rate, growth rate, flowering time, and senescence. **(Yang et al., 2020).** These traits can be evaluated through time-series analysis using images captured at specific intervals. Phenotyping is also used to determine how plants respond to environmental conditions. Examples include drought, salt stress, heat stress, cold stress, heavy metal stress, nutrient deficiencies, and interactions with diseases and pests. Such studies are of great importance, particularly in terms of plant breeding **(Maraveas, 2024; Kaya, 2025)**.

Phenotyping Process

In the past, phenotyping was largely performed manually. The researchers were measuring plant height with a ruler, counting the leaves one by one, determining root lengths, and tabulating the results. Although these methods were reliable, they were time-consuming, labor-intensive, and subject to observer-dependent variations **(Fahlgren et al., 2015; Yang et al., 2020)**. With the advancement of technology, camera systems, image analysis, and artificial intelligence-driven methods have come into use, making it possible to analyze large numbers of plants rapidly and under standardized conditions **(Maraveas, 2024; Kaya, 2025)**.

The Relationship Between Phenotyping and Artificial Intelligence

In modern phenotyping studies, data obtained from imaging systems reach very large volumes. It is not possible to manually evaluate images of thousands of plants taken at different times. For this reason, artificial intelligence-based methods are used. Machine learning and deep learning algorithms can automatically recognize leaves, analyze root systems, monitor plant growth, classify signs of disease and stress, and measure phenotypic traits with high accuracy. Thus, the phenotyping process becomes faster, objective, and reproducible **(Fahlgren et al., 2015; Maraveas, 2024)**.

Arabidopsis thaliana is one of the most suitable model plants for phenotyping research due to its small size and short life cycle **(Fahlgren et al., 2015; Yang et al., 2020)**. In phenotyping studies conducted on this species, parameters such as rosette size, leaf number, leaf area, root architecture, flowering time, and stress responses are frequently evaluated. In recent years, these features can be analyzed automatically by AI-powered phenotyping systems on thousands of plants in a short period of time **(Maraveas, 2024; Kaya, 2025)**.

The Emergence of Artificial Intelligence in Plant Phenotyping

Plant phenotyping is a fundamental research field aimed at measuring the morphological, physiological, and developmental characteristics of plants **(Yang et al., 2020; Maraveas, 2024)**. For many years, these measurements were performed manually by researchers, with traits such as plant height, leaf number, root length, and biomass being evaluated individually **(Fahlgren et al., 2015)**. However, because of rapid advancements in molecular biology, genomics, and imaging technologies, the number of plants examined in studies and the volume of data generated have increased significantly. This situation has rendered traditional phenotyping methods inadequate and prompted researchers to develop faster, more reliable, and automated analysis methods. This need is precisely the reason for incorporating artificial intelligence technologies into plant phenotyping **(Maraveas, 2024; Kaya, 2025)**.

Modern phenotyping systems can generate thousands of images daily using high-resolution cameras, hyperspectral imaging systems, thermal cameras, and various sensors **(Maraveas, 2024)**. For instance, consider an *Arabidopsis thaliana* experiment where 500 plants are photographed each day; if the experiment lasts 30 days, the number of images requiring evaluation by the researcher reaches 15,000. Manually analyzing such large datasets is a process that is both time-consuming and prone to error **(Fahlgren et al., 2015; Maraveas, 2024)**. Artificial intelligence algorithms, however, analyze these images rapidly, offering significant convenience to the researcher **(Maraveas, 2024; Kaya, 2025)**.

In traditional phenotyping studies, researchers measure plant height with a ruler, count leaves individually, determine root lengths, and record the results in data tables **(Fahlgren et al., 2015; Yang et al., 2020)**. While these procedures are feasible for a small number of plants, they result in a significant loss of time in studies involving hundreds or thousands of individuals. AI-powered image analysis systems can automatically perform these same tasks in a much shorter time **(Ubbens et al., 2025; Kaya, 2025)**.

Differences in assessment among researchers may arise during manual measurements. For instance, determining leaf boundaries, counting small leaves, and measuring root length can vary from person to person. This situation may reduce the reproducibility of the results. Since artificial intelligence algorithms evaluate the same image using the same criteria, they enable the acquisition of more standardized and objective measurements **(Maraveas, 2024; Ubbens et al., 2025)**.

Phenotyping is not limited to measurements taken at a single point in time; in many studies, it requires monitoring over a period of days or weeks during the initial stages **(Fahlgren et al., 2015; Yang et al., 2020)**. For instance, it is important to regularly record traits such as new leaf formation, rosette growth, root development, and the timing of expansion **(Yang et al., 2020)**. AI-powered systems can automatically track the developmental process by comparing images captured at various time points **(Ubbens et al., 2025)**.

Manually assessing certain phenotypic traits is quite difficult. For instance, the reliable analysis of characteristics such as leaf shape variation, venation patterns, root architecture, stomatal density, trichome (leaf hair) count, leaf color, and stress symptoms has become possible through image processing and artificial intelligence techniques. Therefore, artificial intelligence is employed not only to accelerate measurements but also to analyze complex traits that are challenging to evaluate with the human eye (Watt et al., 2020).

Thousands of different genotypes are evaluated in plant breeding studies. Researchers aim to identify individuals possessing traits such as drought tolerance, high yield, or disease resistance. Artificial intelligence-powered phenotyping systems facilitate the identification of candidate individuals with desired traits by analyzing large numbers of plants in a short time. This both shortens the research duration and enhances the effectiveness of plant breeding programs **(Fahlgren et al., 2015; Yang et al., 2020; Maraveas, 2024; Kaya, 2025)**.

The aim of using artificial intelligence in plant phenotyping is not to replace the researcher. The researcher plans the experiment, grows the plants, defines the biological question, and interprets the obtained results. Artificial intelligence, on the other hand, serves as a powerful tool that supports the researcher's decision-making process by rapidly and accurately analyzing large datasets derived from images **(Yang et al., 2020; Singh et al., 2021; Maraveas, 2024).**

The primary reason for using artificial intelligence in plant phenotyping is the need to analyze the vast amounts of data generated by modern imaging systems rapidly, accurately, and in a standardized manner **(Fahlgren et al., 2015; Yang et al., 2020)**. AI-based image analysis methods enable the automated assessment of plants' morphological, physiological, and developmental traits, thereby reducing human error and significantly accelerating research processes. These advancements make significant contributions to numerous fields, ranging

from fundamental plant biology to plant breeding and sustainable agriculture (Singh et al., 2021; Maraveas, 2024).

AI-Assisted Phenotyping Methods

AI-powered phenotyping is the process of automatically analyzing image and sensor data obtained from plants using computer algorithms (Table 1). Through this approach, plant organs such as leaves, roots, stems, flowers, and fruits can be evaluated rapidly, accurately, and reproducibly (Singh et al., 2021).

Computer Vision

Computer vision is a field of artificial intelligence that enables computers to recognize objects by analyzing images obtained from cameras or sensors. Its key capabilities include analyzing digital images, attempting to recognize plants in a manner like the human eye, distinguishing between plant parts such as leaves, roots, stems, and flowers, determining the locations of objects within an image, and analyzing multiple plants in a single image. Applications in plant phenotyping include leaf identification, leaf count calculation, leaf area measurement, rosette diameter determination, root system imaging, flower and fruit counting, identification of disease symptoms, and early detection of drought symptoms **(Fahlgren et al., 2015; Yang et al., 2020; Singh et al., 2021; Maraveas, 2024)**. Its significance in *Arabidopsis thaliana* research lies in the ability to easily recognize the rosette structure, automatically segment the leaves, analyze multiple plants within a single image, and serve as the foundation for high-throughput phenotyping systems **(Tsaftaris et al., 2016; Yang et al., 2020; Maraveas, 2024)**. In short, computer vision enables the computer to "see" the plant.

Image Analysis

Image analysis is the process of extracting biologically meaningful information from images of plants. It converts images into numerical data and enables measurements to be taken. It reduces the need for human intervention, can analyze large datasets, and performs the same measurement in a standardized way across every image **(Fahlgren et al., 2015; Tsaftaris et al., 2016; Yang et al., 2020)**. Morphological traits measurable via image analysis includes leaf area, number, and shape; rosette size; plant height; root length; and the number of lateral roots, flowers, and siliques **(Yang et al., 2020; Singh et al., 2021)**. Leaf color, chlorophyll content, leaf temperature, water status, and signs of drought are physiological traits that can be measured through image analysis **(Yang et al., 2020; Maraveas, 2024)**. Developmental characteristics—such as growth rate, time of leaf formation, time of flowering, and the senescence process—can also be measured using image analysis. In *A. thaliana* studies, image analysis has been used to monitor leaf growth, evaluate root development, compare mutants, determine stress conditions, and investigate genotype-phenotype relationships **(Tsaftaris et al., 2016; Yang et al., 2020; Maraveas, 2024)**. In short, image analysis enables the computer to take measurements from the plant.

Deep Learning

Deep learning is an artificial intelligence method capable of automatically recognizing objects by learning from many images. Deep learning works with large datasets. It does not require the user to write the rules one by one. It can learn from the images on its own. It can also make

accurate predictions on new images. It can recognize complex patterns **(LeCun et al., 2015; Tsaftaris et al., 2016; Singh et al., 2021; Maraveas, 2024)**. Its tasks in plant phenotyping include the automatic identification of leaves, individual leaf segmentation, root system analysis, recognition of disease symptoms, classification of drought stress, monitoring of plant growth, and the identification of small structures such as stomata and trichomes (Singh et al., 2021; Maraveas, 2024).

The deep learning models used are CNN (Convolutional Neural Network), Mask R-CNN, U-Net, and AutoML **(LeCun et al., 2015; Singh et al., 2021; Maraveas, 2024)**. CNN (Convolutional Neural Network) can recognize leaves and roots and detect symptoms of disease if a disease has occurred in the plant **(Krizhevsky et al., 2012; Singh et al., 2021)**. Mask R-CNN, on the other hand, identifies each leaf of the plant as a separate object. It can calculate the leaf area. It can serve to separate the siliques and the flowers (Ronneberger et al., 2015; Tsaftaris et al., 2016). The task of U-Net is to perform leaf and root segmentation. It also analyzes cell and tissue images **(Ronneberger et al., 2015; Tsaftaris et al., 2016)**. AutoML, on the other hand, automatically selects the most suitable artificial intelligence model to be used in phenotyping. In this way, the need for the user's programming knowledge is reduced **(Maraveas, 2024)**. Deep learning has been employed in *A. thaliana* for leaf and root phenotyping, rosette analysis, growth monitoring, stress analysis, and the evaluation of genotype-phenotype relationships **(Yang et al., 2020; Singh et al., 2021; Maraveas, 2024)**. In summary, deep learning enables the computer to learn how to recognize and analyze plants.

Table 1: Relationships between artificial intelligence concepts used in plant phenotyping

Concept	Primary Duty
Computer vision	Identifies the plant and its organs in the image.
Image analysis	It takes measurements from recognized structures and obtains numerical data.
Deep learning	It enables the computer to learn these processes and execute them automatically and with high accuracy.

Artificial Intelligence-Assisted Phenotyping Applications in *Arabidopsis thaliana*

AI-powered phenotyping systems enable the rapid, accurate, and automated assessment of various organs of *Arabidopsis thaliana* and its responses to environmental stresses. Analyses of leaves, roots, and abiotic stress responses have been among the most intensively studied application areas in recent years **(Yang et al., 2020; Singh et al., 2021; Maraveas, 2024)**.

Leaf Analysis

Leaf analysis is the examination of the morphological and physiological characteristics of leaves for the purpose of evaluating the plant's growth, development, and responses to environmental conditions **(Fahlgren et al., 2015; Yang et al., 2020)**. Leaf number, leaf area, leaf length and width, leaf shape, rosette diameter, leaf angle, leaf growth rate, leaf color, signs of chlorosis and necrosis, and leaf senescence are traits that can be measured using artificial intelligence **(Tsaftaris et al., 2016; Yang et al., 2020; Singh et al., 2021; Maraveas, 2024)**. Leaf analysis is important because it enables the visualization of plant growth rates, aids in identifying genetic differences, facilitates the comparison of mutant plants, reveals early signs

of environmental stress, and allows for the monitoring of plant development over time **(Fahlgren et al., 2015; Yang et al., 2020; Maraveas, 2024)**.

The number of leaves is used to assess the plant's development rate and growth status. Leaf area provides information about the plant's growth and photosynthetic capacity. Leaf shape helps determine genetic differences and environmental influences. Rosette diameter is an important metric indicating the overall growth performance of *A. thaliana*. The leaf growth rate reveals the plant's developmental dynamics through time-series imagery **(Fahlgren et al., 2015; Yang et al., 2020)**. Leaf color can provide information about chlorophyll content, nutritional status, and signs of stress. In the analysis of stomata, stomatal density, stomatal size, and the degree of opening are automatically determined. Information regarding gas exchange and water loss can also be obtained. Trichome (leaf hair) analysis involves evaluating trichome count, density, and distribution through image analysis. Trichome number and distribution can be used to evaluate plant development and responses to certain environmental stresses **(Tsaftaris et al., 2016; Yang et al., 2020)**. In leaf vein network analysis, vein structure and vein density are examined. By examining the vascular structure and density, water and nutrient transport as well as developmental differences can be evaluated **(Yang et al., 2020; Maraveas, 2024)**.

Deep learning algorithms separate leaves from the background (segmentation), identify each leaf as a distinct object, automatically calculate leaf area, determine growth rates by comparing daily images, and track the same plant over time **(Ronneberger et al., 2015; He et al., 2017; Tsaftaris et al., 2016; Singh et al., 2021)**. Many systems developed in the literature automatically analyze rosette development, leaf size, leaf number, and the growth curve **(Fahlgren et al., 2015; Yang et al., 2020; Maraveas, 2024)**. For example, the APTES system can identify individual leaves and automatically perform detailed morphological measurements using an enhanced Cascade Mask R-CNN model (Zhai et al., 2025).

Root Analysis

Root analysis refers to phenotyping practices aimed at evaluating a plant's below-ground development and root architecture **(Fahlgren et al., 2015; Yang et al., 2020)**. Primary root length, lateral root number, lateral root length, root density, root growth rate, root branching pattern, root angle, and total root length are traits that can be measured using artificial intelligence **(Tsaftaris et al., 2016; Yang et al., 2020; Singh et al., 2021; Maraveas, 2024)**. Root analysis is an important process, as it indicates the plant's water uptake capacity, provides information on nutrient uptake, and enables the assessment of drought tolerance. It also reveals differences between genotypes. It also helps in understanding the plant's adaptation to environmental conditions. Computer vision and deep learning methods separate roots from the background, identify primary and lateral roots, track root growth day by day, and quantitatively analyze root architecture **(Ronneberger et al., 2015; Tsaftaris et al., 2016; Singh et al., 2021)**. In *A. thaliana* studies, AI-based platforms such as ChronoRoot can monitor root development as time series, calculate root growth rates, and automatically assess changes in root architecture. These systems are widely used, particularly in studies on drought and nutrient deficiency **(Gaggion et al., 2021)**.

Abiotic Stress Analysis

Abiotic stress analysis is the assessment of the responses of plants to environmental factors such as drought, salinity, heat, cold, and nutrient deficiency **(Yang et al., 2020)**. Stresses in

plants—such as drought stress, salt stress, high-temperature stress, low-temperature stress, nutrient deficiencies, and oxidative stress—can be detected using artificial intelligence **(Singh et al., 2021; Maraveas, 2024)**. Symptoms such as changes in leaf color, wilting, leaf curling, leaf temperature, reduced growth rate, changes in the rosette area, slowed root development, and alterations in light reflectance properties can be analyzed by artificial intelligence **(Fahlgren et al., 2015)**. Plants under stress exhibit small changes that are difficult to detect with the naked eye. Artificial intelligence can identify these changes at an early stage, classify different stress levels, predict the severity of stress, and help the researcher make faster decisions (Yang et al., 2020; Maraveas, 2024).

Arabidopsis is one of the most frequently used model plants in stress studies, such as those concerning drought and salinity. AI-powered systems can distinguish stressed plants from healthy ones, identify signs of drought by analyzing leaf images, and classify stress levels using hyperspectral or RGB imagery **(Singh et al., 2021; Maraveas, 2024)**. These studies contribute to the development of plant varieties resistant to stress conditions for future agricultural production **(Yang et al., 2020; Maraveas, 2024)**. Artificial intelligence-enabled phenotyping applications in *A. thaliana* enable the automated analysis of leaves, roots, and environmental stress **(Fahlgren et al., 2015; Yang et al., 2020; Maraveas, 2024)**. With the help of computer vision and deep learning algorithms, plant growth, development, and responses to environmental changes can be evaluated with high accuracy, thereby enabling a more comprehensive examination of genotype-phenotype relationships **(Tsaftaris et al., 2016; Singh et al., 2021; Maraveas, 2024)**.

Current Software

Numerous software programs have been developed to enable the rapid and accurate analysis of images obtained in high-throughput phenotyping studies. These software programs automatically evaluate the morphological and physiological characteristics of plants using computer vision, image analysis, and deep learning methods. Some of the most frequently used software programs in *Arabidopsis thaliana* studies are APTES, ChronoRoot, and PlantCV **(Fahlgren et al., 2015;** Zhai et al., 2025**; Gaggion et al., 2021) (Table 2)**.

Table 2: Comparison of Software for Phenotyping

Software	Primary Aim	Key Feature
APTES	Leaf phenotyping	Individual recognition and segmentation of leaves
ChronoRoot	Root phenotyping	Monitoring root development over time
PlantCV	General phenotyping	An open-source platform capable of analyzing different types of images.

APTES

(*Arabidopsis* Phenotyping Platform Based on Deep Learning)

The purpose of using APTES is to automatically identify *Arabidopsis* rosette leaves and analyze their phenotypic traits **(**Zhai et al., 2025**) (Fig. 2)**. Its key feature is that it is based on deep

learning. It uses the Mask R-CNN algorithm. It can identify individual leaves. It performs leaf segmentation. Calculates leaf area. Determines the number of leaves. Measures rosette size.

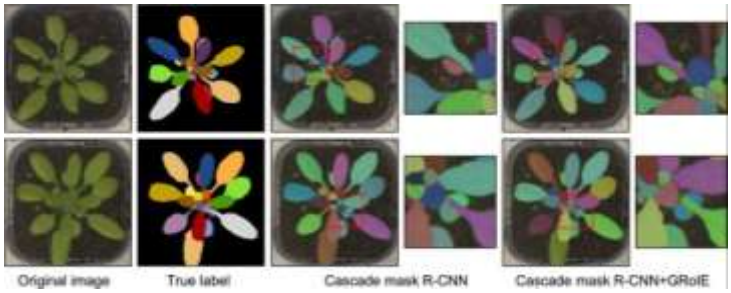

Fig. 2: Leaf instance segmentation results and phenotypic trait extraction in *A. thaliana* (Zhai et al., 2025), CC BY 4.0.

It can analyze different developmental stages. Its advantages are that it reduces the need for manual measurement, ensures high accuracy, can analyze many images in a short time, and is suitable for time-series studies. It yields successful results with *Arabidopsis* images. Areas of application include leaf phenotyping, mutant analysis, growth monitoring, and the investigation of genotype-phenotype relationships **(Yang et al., 2020;** Zhai et al., 2025**)**.

ChronoRoot

It is possible to automatically monitor the development of the Arabidopsis root system over time using ChronoRoot **(Gaggion et al., 2021) (Fig. 3)**. ChronoRoot is based on deep learning. It performs root segmentation. It identifies the primary root. Identifies lateral roots. Tracks daily root development. Analyzes root architecture. Generates time-series data. Its advantages include analyzing root development without the need for manual measurement, revealing dynamic growth changes, and processing large datasets. It can examine the root architecture in detail. It is used in root phenotyping, drought studies, nutrient element research, monitoring root development, and plant physiology research **(Gaggion et al., 2021; Yang et al., 2020)**.

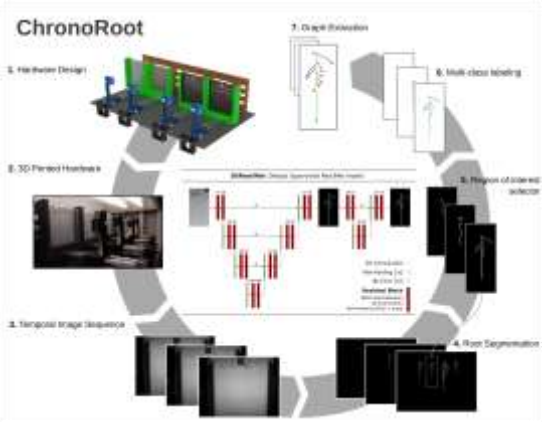

Fig. 3: Components of the ChronoRoot system and the root phenotyping process (Gaggion et al., 2021), CC BY 4.0.

PlantCV

The purpose of PlantCV is to process plant images and analyze phenotypic traits using open-source tools **(Gehan et al., 2017) (Fig. 4)**. It is open source. It is Python-based. It has a modular structure. It can analyze RGB images. It can work with hyperspectral images. It can evaluate thermal images. It can analyze fluorescence images. Customizable by the user. The characteristics it can analyze include leaf area, leaf count, plant height, plant width, color analysis, signs of chlorosis, signs of necrosis, biomass estimation, and plant segmentation (Singh et al., 2021). Its primary advantage is that it is free. It has a large user community. It can be used with various plant species. It can analyze large datasets. It is constantly being updated. Its areas of application include *Arabidopsis* research, plant breeding, agricultural phenotyping, stress physiology, and image analysis studies **(Gehan et al., 2017; Yang et al., 2020)**.

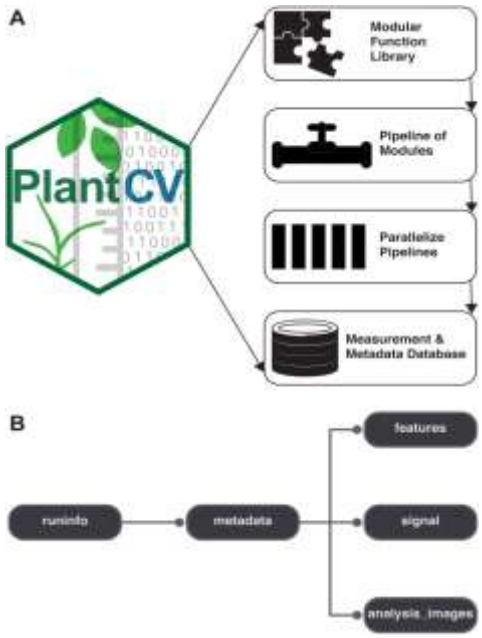

Fig. 4: PlantCV's image analysis components. (Gehan et al., 2017),

CC BY 4.0.

CONCLUSION AND FUTURE PERSPECTIVE

Conclusion

Arabidopsis thaliana is one of the most widely used model organisms in plant biology, thanks to its short life cycle, small and well-characterized genome, ease of genetic transformation, and extensive mutant collections. Due to these characteristics, it is also used as an important research model in the development and validation of AI-powered, high-throughput phenotyping systems. High-throughput phenotyping technologies enable the rapid and reliable analysis of large amounts of data obtained from imaging systems and sensors. However, the increase in the volume of this data has rendered traditional manual assessment methods inadequate, making the use of computer vision, image analysis, and deep learning-based artificial intelligence approaches essential. Thanks to software developed in recent years such as APTES, ChronoRoot, and PlantCV leaf development, root architecture, plant growth, and abiotic stress responses can be analyzed with high accuracy. These technologies not only accelerate the data

analysis process but also contribute to conducting research that is more objective, reproducible, and highly accurate.

AI-powered phenotyping approaches:

- Enable the analysis of large volumes of image data in a short time.
- Reduce time loss associated with manual measurements.
- Minimize human-induced measurement variations.
- Allow for the monitoring of plant growth over time.
- Enable the automated assessment of leaves, roots, and other morphological structures.
- Contribute to the early detection of abiotic stress symptoms.
- Support a more detailed examination of genotype-phenotype relationships.
- Facilitate the identification of candidate genotypes in plant breeding programs.

Future Perspective

Rapid advancements in artificial intelligence technologies are significantly shaping the future of plant phenotyping research. In the coming years, phenotyping processes are expected to become increasingly automated using more advanced algorithms, more powerful imaging systems, and computers with higher processing capacities.

In particular,

- the combined use of multiple imaging techniques (RGB, hyperspectral, thermal, and 3D imaging),
- the integration of multiple data sources with artificial intelligence,
- the joint analysis of genomic, transcriptomic, and phenomics data,
- the development of open-source software,
- the widespread adoption of cloud-based analysis platforms, and
- the development of real-time phenotyping systems

will make significant contributions to the future advancement of this field.

Adapting methods developed on *Arabidopsis thaliana* following appropriate validation studies to economically important crops such as wheat, rice, maize, and tomatoes offer significant opportunities for sustainable agriculture, plant breeding, and food security.

AI-powered high-throughput phenotyping is regarded not merely as a technological innovation in plant research, but as a significant approach that transforms research processes. Methods developed using *Arabidopsis thaliana* enable a more detailed understanding of plant **development and the more effective analysis of phenotypic data. It is anticipated that, with the future advancement of AI algorithms and the widespread adoption of high-throughput phenotyping systems, these technologies will be utilized more effectively**

across a broad spectrum of applications ranging from basic plant biology to plant biotechnology and sustainable agriculture.

REFERENCES

Alonso, J.M. *et al.* (2003). Genome-Wide Insertional Mutagenesis of *Arabidopsis thaliana*.*Science* 301,653-657. https://doi.org/10.1126/science.1086391

The Arabidopsis Genome Initiative. (2000). *Analysis of the genome sequence of the flowering plant Arabidopsis thaliana*. *Nature*, 408, 796–815. https://doi.org/10.1038/35048692

Bélanger, J.G., Copley, T.R., Hoyos-Villegas, V. et al. (2024). A comprehensive review of in planta stable transformation strategies. *Plant Methods* 20, 79. https://doi.org/10.1186/s13007-024-01200-8

Fahlgren, N., Gehan, M. A., & Baxter, I. (2015). Lights, camera, action: high-throughput plant phenotyping is ready for a close-up. *Current opinion in plant biology*, *24*, 93-99. https://doi.org/10.1016/j.pbi.2015.02.006

Gaggion, N., Ariel, F., Daric, V., Lambert, É., Legendre, S., Roulé, T., Camoirano, A., Milone, D. H., Crespi, M., Blein, T., & Ferrante, E. (2021). *ChronoRoot: High-throughput phenotyping by deep segmentation networks reveals novel temporal parameters of plant root system architecture*. *GigaScience, 10*(7), giab052. https://doi.org/10.1093/gigascience/giab052

Gehan, M. A., Fahlgren, N., Abbasi, A., Berry, J. C., Callen, S. T., Chavez, L., Doust, A. N., Feldman, M. J., Gilbert, K. B., Hodge, J. G., Hoyer, J. S., Lin, A., Liu, S., Lizárraga, C., Lorence, A., Miller, M., Platon, E., Tessman, M., & Sax, T. (2017). *PlantCV v2: Image analysis software for high-throughput plant phenotyping*. *PeerJ*, *5*, e4088. https://doi.org/10.7717/peerj.4088

He, K., Gkioxari, G., Dollár, P., & Girshick, R. (2017). *Mask R-CNN*. Proceedings of the IEEE International Conference on Computer Vision (ICCV), 2961–2969.

Hou, X., Wang, D., Cheng, Z., Wang, Y., & Jiao, Y. (2022). A near-complete assembly of an *Arabidopsis thaliana* genome. *Molecular plant*, *15*(8), 1247-1250. https://doi.org/10.1016/j.molp.2022.05.014

Kaya, C. (2025). Optimizing crop production with plant phenomics through high-throughput phenotyping and AI in controlled environments. *Food and Energy Security*, *14*(1), e70050. https://doi.org/10.1002/fes3.70050

Koornneef, M., & Meinke, D. (2010). The development of *Arabidopsis* as a model plant. *The Plant Journal*, *61*(6), 909–921. https://doi.org/10.1111/j.1365-313X.2009.04086.x

Krizhevsky, A., Sutskever, I., & Hinton, G. E. (2012). *ImageNet classification with deep convolutional neural networks. Advances in Neural Information Processing Systems*, 25, 1097–1105.

LeCun, Y., Bengio, Y. & Hinton, G. (2015). Deep learning. *Nature* **521**, 436–444. https://doi.org/10.1038/nature14539

Maraveas, C. (2024). Image analysis artificial intelligence technologies for plant phenotyping: Current state of the art. *AgriEngineering*, *6*(3), 3375–3407. https://doi.org/10.3390/agriengineering6030193

Meinke, D. W., Cherry, J. M., Dean, C., Rounsley, S. D., & Koornneef, M. (1998). *Arabidopsis thaliana*: a model plant for genome analysis. *Science*, *282*(5389), 662-682. https://doi.org/10.1126/science.282.5389.662

Pieruschka, R., & Schurr, U. (2019). *Plant phenotyping: Past, present, and future*. ***Plant Phenomics*, 2019,** 7507131. https://doi.org/10.34133/2019/7507131

Provart, N. J., Alonso, J., Assmann, S. M., Bergmann, D., Brady, S. M., Brkljacic, J., ... McCourt, P. (2016). 50 years of *Arabidopsis* research: Highlights and future directions. *New Phytologist*, *209*(3), 921–944. https://doi.org/10.1111/nph.13687

Singh, A., Jones, S., Ganapathysubramanian, B., Sarkar, S., Mueller, D., Sandhu, K., & Nagasubramanian, K. (2021). Challenges and opportunities in machine-augmented plant stress phenotyping. *Trends in plant science*, *26*(1), 53-69. https://doi.org/10.1016/j.tplants.2020.07.010

Ronneberger, O., Fischer, P., & Brox, T. (2015). *U-Net: Convolutional Networks for Biomedical Image Segmentation.* In *Medical Image Computing and Computer-Assisted Intervention (MICCAI)* (pp. 234–241).

Tsaftaris, S. A., Minervini, M., & Scharr, H. (2016). *Machine learning for plant phenotyping needs image processing*. ***Trends in Plant Science,*** **21**(12), 989–991. https://doi.org/10.1016/j.tplants.2016.10.002

Ubbens, J., Stavness, I., Pound, M. P., & Guo, W. (2025). Deep learning in plant phenotyping: the first ten years. *Plant Phenomics*, 100062. https://doi.org/10.1016/j.plaphe.2025.100062

Watt, M., et al. (2020). Phenotyping: New Windows into the Plant for Breeders. *Annual Review of Plant Biology*, 71, 689–712. https://doi.org/10.1146/annurev-arplant-042916-041124

Zhai, R., Tang, N., Liu, Z., Tao, S., Huang, Y., Jiang, X., Du, A., Wang, J., Luo, T., Liu, J., Garzon-Martínez, G. A., Corke, F. M. K., Doonan, J. H., & Yang, W. (2025). *APTES: A high-throughput deep learning–based Arabidopsis phenotypic trait estimation system for individual leaves and siliques*. *aBIOTECH*, *6*(4), 744–762. https://doi.org/10.1007/s42994-025-00239-y

Zlobin, N. E., Lebedeva, M. V., & Taranov, V. V. (2020). CRISPR/Cas9 genome editing through *in planta* transformation. *Critical Reviews in Biotechnology*, *40*(2), 153–168. https://doi.org/10.1080/07388551.2019.1709795

MORPHOMETRIC VARIATION AND GROWTH PATTERNS OF INTERTIDAL LIMPETS (*PATELLA* SPP.) ALONG THE SOUTHERN COAST OF ALBANIA

Ina NASTO[1], Engjëllushe PASHAJ[1], Kristiana LUSHNJARI[1]*

[1] Department of Biology, Faculty of Technical and Natural Sciences,

University "Ismail Qemali" Vlore, Albania

**Corresponding Author: ina.nasto@univlora.edu.al*

ABSTRACT

Morphometric variation in intertidal limpets of the genus *Patella* (Mollusca: Gastropoda) has been found to vary in relation to environmental, ecological and habitat-related factors, and thus represents an important study subject. The objective of the present study has thus been to investigate morphometric variation and growth in different species of *Patella* occurring in intertidal rocky areas along the southern coast of Albania. A total of 397 specimens from the genus *Patella* were analyzed. These specimens were from the archive of the Laboratory of the Department of Biology, Faculty of Technical and Natural Sciences, University "Ismail Qemali" Vlore, Albania. The material was collected from 7 coastal areas along the southern coast of Albania: Triport, Karaburun Peninsula, Akuarium, Llaman, Porto Palermo, Qeparo and Sarandë (Ksamil). A total of 4 species of genus *Patella* were identified, including: *Patella caerulea*, *P. rustica*, *P. ulyssiponensis* and *Cymbula safiana (Patella nigra)*. *Cymbula safiana (Patella nigra*) was considered separately for morphological characterization rather than for comparison with the rest of species of genus *Patella*. In order to assess the morphological differences between the species and between the populations from different locations, as well as to establish the morphometric correlations and the growth patterns, were carried out analyses of correlation and regression among the studied variables. Results. Large amount of morphological variation was recorded among the four species of the genus *Patella* and among the seven studied locations. Shell morphometry, expressed by means of several morphometric ratios, and by means of correlations between all the measured parameters, allowed an accurate assessment of the studied species' growth, of their ecological adaptation, and of their population structure.This study contributes to knowledge on biodiversity of marine species in coastal waters of Albania. It provides data on morphological variations of intertidal species of limpets and their ecological adaptations to environment of rocky shores. Data obtained can be used in assessments of biodiversity and in ecological monitoring, as well as for conservation of species of rocky shores.

Keywords: *Patella*, morphometric variation, shell morphology, growth patterns, gastropods, rocky shore ecosystems, southern Albanian coast.

INTRODUCTION

The genus *Patella* (Patellidae) comprises 37 species of marine Gastropods distributed in four genera: *Patella*, *Cymbula*, Helcion, and Scutellastra (Ridgway, 1998; Espinosa et al., 2010; Belmokhtar et al., 2022). These species of marine gastropods inhabit rocky intertidal areas, known as the mediolittoral zone of the benthic environment of the Mediterranean Sea (Bellan-Santini, 1985; Urra et al., 2017; Caballero et al., 2009). The different species of the family PateLLidae show a wide variety of characters, which allow their identification, including their preference for certain levels of exposure to waves (Buttivant, 2019). Some species like *Cymbula xandros* (Philippi, 1844) are epiphytic and live on algae, while others like *Patella rustica*

(Linnaeus, 1758) live on the rocky bottom and among the epibenthic algae of the shallow subtidal of the littoral zone (Riedl, 1991). In the Mediterranean area, five species of the genus *Patella* are present: *Patella caerulea* (Linnaeus, 1758); *Patella rustica* (Linnaeus, 1758) = *Patella lusitanica* (Gmelin, 1791); *Patella ulyssiponensis* (Gmelin, 1791); *Patella ferruginea* (Gmelin, 1791), listed as Vulnerable by Espinosa et al. (2007); and *Patella depressa* (Jickeli, 1885), so far only recorded in the Alboran Sea (Gofas et al., 2011); Cascales-Soler et al. (2023).

All abiotic and biotic factors influence the variation of morphological characters in *Patella* species, which determine their growth, shell morphology, distribution, mortality and reproduction. The presence of radula and eroding activity of each species determines their preference for different types of substrate and their ability to remove irregularities of substrate to maintain their body wet (Guelorget and Perthuisot, 1983). Wave exposure, slope and tidal levels determine distribution of species within rocky shores. Most species show high tolerance to thermal and desiccation stresses although some species are more sensitive than others (Williams & Morritt, 1995; Harley, 2008; Miller et al., 2009; Fraser et al., 2010; Christofoletti et al., 2011; Prusina et al., 2014; Bouzaza & Mezali, 2018; da Silva Freitas, 2021; Belmokhtar et al., 2022).

In this study were analyzed three species of *Patella (P. caerulea, P. rustica and P. ulyssiponensis)* and also the species *Cymbula safiana (Patella nigra)* in order to study their distribution, biodiversity and their morphological variability.

MATERIAL AND METHOD

For the purpose of this study 397 specimens were taken from the archived material of the Laboratory of the Department of Biology, University “Ismail Qemali” Vlora, which had originated from seven localities of the southern coast of Albania, namely: Triport, Karaburun Peninsula (specimens of this locality had been collected from two habitats, i.e. upper and lower shores), Akuarium, Llaman, Porto Palermo, Qeparo and Sarandë (Ksamil). The preserved specimens, after having been cleaned from any organic material, were rinsed with water and left to dry at room temperature. In the following, only specimens with intact and well preserved shells have been considered for the purpose of this study, whereas specimens with damaged shells have been excluded from the material under consideration.

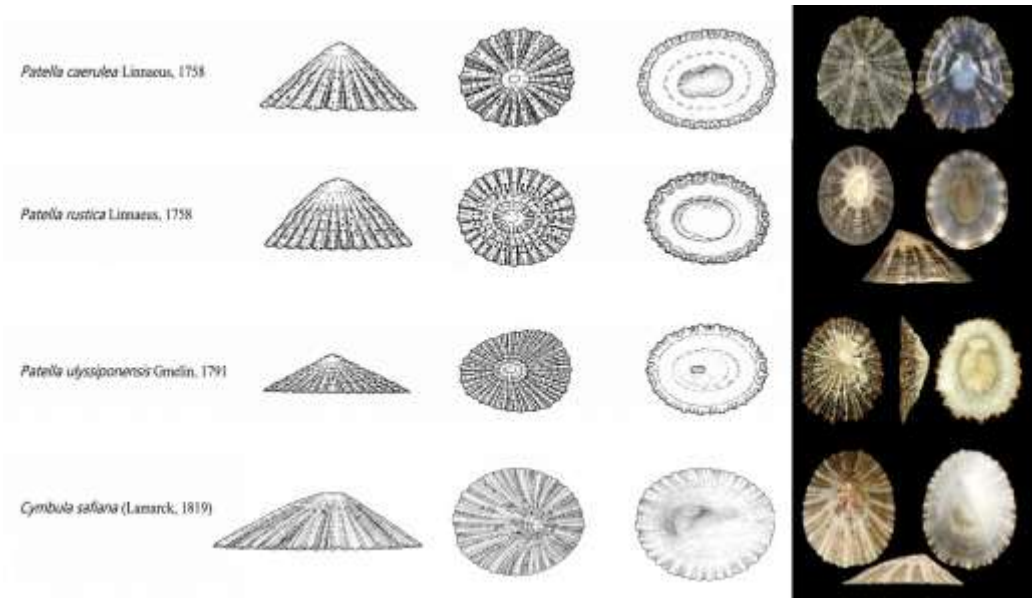

Figure. 1. Shell morphology of *Patella caerulea*, *P. rustica*, *P. ulyssiponensis*, and *Cymbula safiana*, showing lateral (left), dorsal (central), and internal (right) views (Adapted from Cabral., (2007).

For species identification the morphology of the shell, the shell height, the apex position and the number of radial ribs as well as the external and internal shell coloration were analyzed. For morphometric analysis of the studied *Patella* species four shell parameters were measured on 397 specimens using a digital caliper with an accuracy of 0.1 mm: the shell length (SL), the shell width (SW), the shell width at the apex (SWA) and the shell height (SH). Three morphometric ratios were calculated for each specimen. The first ratio is the basal ellipticity which was calculated by dividing the shell width (SW) by the shell length (SL). The second ratio is the basal eccentricity that was calculated by dividing the shell width at the apex (SWA) by the shell width (SW) and the third ratio is the conicity that was calculated by dividing the shell height (SH) by the shell length (SL). The morphometric data were presented as mean values± SD.

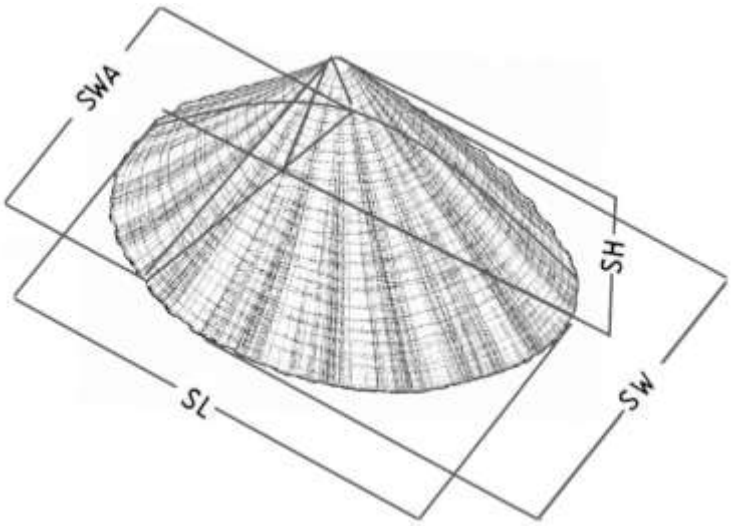

Figure. 2. Shell morphometric variables were measured: shell length (SL), shell width (SW), shell width at apex (SWA) (Adapted from Cabral., (2007)

Significant differences among the groups were tested using a one-way ANOVA test. Normality test, including a Kolmogorov–Smirnov test and a Shapiro–Wilk test, was used to assess normality of the data before the ANOVA test. Differences among means were assessed using post-hoc comparisons, when required. To investigate correlations between the morphometric variables, Pearson's correlation coefficient was used. The principal components analysis (PCA) was used to determine the principal components of the shell morphology variation of the four *Patella* species. Linear discriminant analysis (LDA) was performed to determine how well the variables separated the four species, and the degree of variation between the species.

RESULTS AND DISCUSSION

Species composition and spatial distribution

Four species of limpets, including three species of the genus *Patella* (*P. caerulea*, *P. rustica*, *P. ulyssiponensis*) and *Cymbula safiana* (*C. safiana*), were found at seven localities along the southern coast of Albania (Fig. 3).

Figure. 3. Spatial distribution and relative composition of Patella caerulea, P. rustica, P. ulyssiponensis, and Cymbula safiana across the seven sampling areas: 1. Triport, 2. Karaburun, 3. Akuarium, 4. Llaman, 5. Porto Palermo, 6. Qeparo, and 7. Ksamil (Sarandë region). Pie charts indicate the relative contribution of each species at each sampling site.

Species distribution varies greatly between individual sites. In Karaburun for example, *P. caerulea* comprises the biggest portion of the entire sampled fauna. Although *P. rustica* is

distributed in most of the sampled sites, its relative contribution to the whole of species present varies greatly. In contrast, *P. ulyssiponensis* has a limited distribution across sites and is found in greatest numbers in Karaburun, Llaman and Porto Palermo. The distribution of *C. safiana* is by far the most restricted and is found in greatest numbers in the two aforementioned sites, Llaman and Qeparo. Hence, it can be concluded that the distribution of species of limpets varies greatly between individual sites and is greatly affected by the environmental conditions of the local habitats. These sites vary greatly in terms of substrate, exposure to waves, hydrodynamic conditions and availability of food. *P. caerulea* seems to have the greatest ecological flexibility and therefore the greatest distribution amongst sites. The two former species have a more restricted distribution and therefore seem to have a greater affinity to specific habitats.

Descriptive statistics of shell morphometric parameters

Table 1 lists the mean (± SD) of four shell morphometric characteristics for four species of limpets from around the Southern Coast of Albania. *P. rustica* had the greatest mean SL of the four species of limpets recorded from around the Southern Coast of Albania (mean = 22.21 ± 4.05 mm; N = 131; Table 1). *P. caerulea* had the greatest mean SW of the four species of limpets recorded from around the Southern Coast of Albania (mean = 17.75 ± 5.12 mm; N = 67; Table 1). The greatest mean SWA of the four species of limpets recorded from around the Southern Coast of Albania was also found in *P. caerulea* (mean = 16.12 ± 4.96 mm; N = 64; Table 1). *Cymbula safiana* had the lowest mean value for SW of the four species of limpets recorded from around the Southern Coast of Albania (mean = 12.73 ± 3.65 mm; N = 15; Table 1). The same species also had the lowest mean value for SWA of the four species of limpets recorded from around the Southern Coast of Albania (mean = 11.59 ± 3.37 mm; N = 13; Table 1). Shell height showed the greatest amount of interspecific variation (Table 1). In this characteristic, the greatest mean value for the four species of limpets recorded from around the Southern Coast of Albania was found in *P. rustica* (mean = 6.95 ± 1.90 mm; N = 98; Table 1). The smallest mean value for shell height was found in *Cymbula safiana* (mean = 4.33 ± 1.29 mm; N = 25; Table 1). Furthermore, in terms of interspecific variation, *Cymbula safiana* had the lowest mean value for all four of the morphometric variables recorded in this study (Table 1). This species of limpet thus appears to have the smallest shells of all four species recorded from around the Southern Coast of Albania.

Table 1. Mean shell morphometric measurements (± SD, mm) of *Patella caerulea, P. rustica, P. ulyssiponensis, and Cymbula safiana* across the study area. SL, shell length; SW, shell width; SWA, shell width at apex; SH, shell height.

Morphometric parameters	***P.caerulea***	***P.rustica***	***P.ulyssiponensis***	***Cymbula safiana***
SL, shell length **(mm)**	21.62±5.82	22.21±4.05	19.18±4.58	16.54 ±4.67
SW, shell width **(mm)**	17.75±5.12	17.50±4.71	14.73±3.76	12.73±3.65
SWA shell width at apex **(mm)**	16.12±4.96	16.09±3.02	13.67±3.71	11.59 ±3.37
SH, shell height **(mm)**	4.95±1.62	6.95±1.90	4.87±1.21	4.33± 1.29

Morphometric analysis of *Patella caerulea*

A total number of 236 specimens of *P. caerulea* were included in the morphometric analysis. Mean and range values for four of the shell morphometric parameters were as follows: Shell Length (SL) 11.0-37.6 mm, mean 21.43 ± 5.56 mm; Shell Width (SW) 8.2-31.5 mm, mean 17.50 ± 4.89 mm; Shell Width at Apex (SWA) 7.1-29.2 mm, mean 15.90 ± 4.74 mm; and Shell

Height (SH) 2.4-9.9 mm, mean 4.87 ± 1.55 mm. In addition to these, four shape parameters were calculated, namely, Basal Ellipticity (BE) 0.804-0.859, mean 0.814 ± 0.055; Basal Eccentricity (BEC) 0.562-0.906, mean 0.908 ± 0.088; Conicity (C) 0.160-0.292, mean 0.226 ± 0.034; and Basal Circular Symmetry (BCS) 0.947-0.974, mean 0.962 ± 0.006. While great amounts of variation occurred in the four shell size parameters, much less variation was found for the four shape ratios. These results suggest a great amount of variation for *P. caerulea* from the seven sampling stations of the southern coast of Albania.

Descriptive Statistics

A summary of the morphometric variables for *P. caerulea* included in the analysis of *P. caerulea* from the southern coast of Albania are listed in Table 2. The mean value and standard deviation for the SL, SW, SWA and SH for 236 *P. caerulea* are 21.43 ± 5.56 mm, 17.50 ± 4.89 mm, 15.90 ± 4.74 mm, 4.87 ± 1.55 mm, respectively. For the shape ratios basal ellipticity, basal eccentricity and conicity the mean values and standard deviations for the 236 *P. caerulea* are 0.814 ± 0.055, 0.908 ± 0.088 and 0.226 ± 0.034 respectively. The SL ranged from 11.0 mm to 37.6 mm with the greatest amount of variation occurring between the longest and shortest individual shells (37.6 mm and 11.0 mm, respectively). The SW, SWA and SH ranged from 8.2 mm to 31.5 mm, 7.1 mm to 29.2 mm and 2.4 mm to 9.9 mm respectively with the greatest amount of variation between the largest and smallest individual shells being for the SW (31.5 mm and 8.2 mm, respectively). The shape ratios all showed relatively narrow ranges of variation with the greatest amount of variation for basal eccentricity (0.908 ± 0.088) and the smallest amount of variation for conicity (0.226 ± 0.034).

Table 2. Descriptive statistics of morphometric traits of *Patella caerulea* (N = 236).

Descriptive Statistics					
Patella caerulea	N	Minimum	Maximum	Mean	Std. Deviation
SL, shell length (mm)	236	11.0000	37.6000	21.431780	5.5640532
SW, shell width (mm)	236	8.2000	31.5000	17.495339	4.8900876
SWA shell width at apex (mm)	236	7.1000	29.2000	15.899576	4.7357985
SH, shell height (mm)	236	2.4000	9.9000	4.868644	1.5547155
Basal ellipticity (SW/SL)	236	.6193	.9574	.814228	.0552952
Basal eccentricity (SWA/SW)	236	.6270	1.8687	.908253	.0882797
Conicity (SH/SL)	236	.1270	.3216	.226188	.0344255
Valid N (listwise)	236				

One-Way ANOVA

The one-way ANOVA testing for the differences among the seven stations revealed significant differences for all the measured variables, except for basal eccentricity. Thus, shell length (SL; $F_{6,229} = 6.654$, $p < 0.001$), shell width (SW; $F_{6,229} = 7.711$, $p < 0.001$), shell width at apex (SWA; $F_{6,2}229 = 8.053$, $p < 0.001$), and shell height (SH; $F_{6,2}{}^{29} = 2.886$, $p = 0.010$) all exhibited significant variation among the stations. Additionally, the two shape ratios, i.e., basal ellipticity (SW/SL; $F_{6,229} = 4.005$, $p = 0.001$) and conicity (SH/SL; $F_{6,2}{}^{29} = 13.032$, $p < 0.001$), also showed considerable variation among the sampling stations. However, the basal eccentricity (SWA/SW; $F_{6,2}{}^{29} = 0.687$, $p = 0.661$) did not exhibit any significant variation among the stations. The results of the Tukey HSD post-hoc tests for the highest F-values, which were for Ksamil (Station 7), revealed that the largest limpets occurred in this station. In comparison, the

Karaburun (Station 2) limpets generally were smaller than those found in the remaining six stations. A similar trend was found for the Akuarium (Station 3), Llaman (Station 4), and Porto Palermo (Station 5) stations, with the largest limpets occurring in these stations as well. In terms of the differences between Karaburun and Llaman, for the three variables SL, SW, and SWA, the largest differences occurred between these two stations. For the remaining two variables, i.e., SH and basal ellipticity, the differences between the respective pairs of stations were generally not as large, with the largest differences found between the Qeparo (Station 6) and Akuarium (Station 3) stations. The largest conicity values were found in the Triport (Station 1) and Porto Palermo (Station 5) stations, and the remaining largest conicity values were found in the Ksamil (Station 7) and Qeparo (Station 6) stations.

Table 3. One-way ANOVA results for morphometric parameters of *Patella caerulea* among the seven sampling stations along the southern Albanian coast.

Table 3. One-way ANOVA results for morphometric parameters of *Patella caerulea* among the seven sampling stations along the southern Albanian coast.

One-Way ANOVA

Patella caerulea		Sum of Squares	df	Mean Square	F	Sig.
SL, shell length (mm)	Between Groups	1080.124	6	180.021	6.654	.000
	Within Groups	6195.168	229	27.053		
	Total	7275.292	235			
SW, shell width (mm)	Between Groups	944.565	6	157.427	7.711	.000
	Within Groups	4674.980	229	20.415		
	Total	5619.545	235			
SWA shell width at apex (mm)	Between Groups	918.280	6	153.047	8.053	.000
	Within Groups	4352.250	229	19.005		
	Total	5270.530	235			
SH, shell height (mm)	Between Groups	39.927	6	6.655	2.886	.010
	Within Groups	528.101	229	2.306		
	Total	568.028	235			
Basal ellipticity (SW/SL)	Between Groups	.068	6	.011	4.005	.001
	Within Groups	.650	229	.003		
	Total	.719	235			
Basal eccentricity (SWA/SW)	Between Groups	.032	6	.005	.687	.661
	Within Groups	1.799	229	.008		
	Total	1.831	235			
Conicity (SH/SL)	Between Groups	.071	6	.012	13.032	.000
	Within Groups	.208	229	.001		
	Total	.279	235			

Canonical Discriminant Analysis (CDA)

In this analysis, we examined the amount of explained variance of seven functions using Wilks' Lambda test for each of them. The overall model included all seven functions ($p < 0.001$; $\lambda = 0.412$; $\chi2 = 202.449$; $df = 42$). Therefore, combined, the seven functions greatly differentiate between limpets collected from the seven study sites (Fig. 4).

Also the second canonical function explained significant part of between-station variation after the first function had been removed (Wilks' Λ=.795, $\chi2(30)$=52.316, p=.007). None of the following functions (3 to 6) were, however, significant (Wilks' Λ-values from .887 to .980; $\chi2$-

values from 27.415 to 5.259; and p-values from .124 to .385) and thus they did not add any information that would improve station discrimination. Therefore, the first two functions are considered to be sufficient for an interpretation of data.

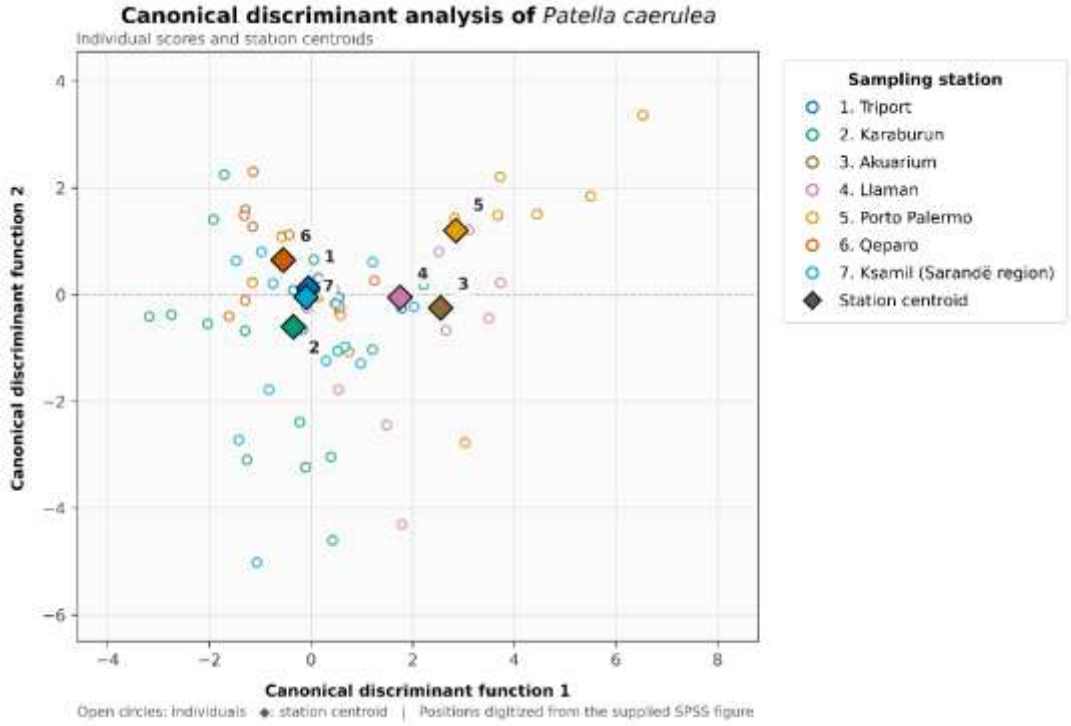

Canonical Discriminant Analysis (CDA)

Figure 4. Canonical discriminant analysis results for morphometric parameters of *Patella caerulea* among the seven sampling stations along the southern Albanian coast.

The canonical plot shows that instead of complete differentiation between the stations, there is partial differentiation. The greatest differentiation is shown by the Porto Palermo samples on the first canonical function, whereas the Akuarium and Llaman samples are displaced in a positive direction of Function 1. The Qeparo samples show some differentiation on Function 2, whereas the Triport, Karaburun and Ksamil samples are largely concentrated in the center of the canonical space and thus show a great deal of overlap between them. This overlap between several of the stations suggests that in addition to significant geographical variation, there are also some morphological features that are shared by different populations of the species.

In terms of equality of covariance matrices, a very significant Box's M test provided evidence against the equality of the covariance matrices for the seven groups of limpets. It must, however, be noted that Box's M test is not necessarily a reliable criterion when sample sizes are relatively small and/or when there are singular covariance matrices. In terms of these latter criteria, it was found that there were several singular covariance matrices for this study (see Table 5). Therefore, results from the classification into the seven groups, obtained using a Discriminant Function Analysis (DFA) of the same set of morphological measurements, must be treated with a considerable amount of reserve, and conclusions based on these results are best made with extreme caution.

Morphometric comparison among species

Variation between species in shell length, width, at apex and height of the four Patellidae species (*Patella caerulea*, *P. rustica*, *P. ulyssiponensis* and *Cymbula safiana*) was tested for

using a one-way ANOVA. All the studied species differed for all of the studied variables (Table 4). The highest amount of variation between species for the studied shell characteristics, was for conicity of the shell. It is concluded, that the morphometric variables, used in the present study, can effectively be used for species discrimination in the genus *Patella* and Cymbula. This is in accordance with findings of a number of previous morphological studies on species within the Patellidae family (e.g. for *P.* vulgata, *P.* aprica, *P.* mesatrii, and *P.* granulata, see: Reid 1965; Mikkelsen & Bieler 2007; Reid 2007; Wesselingh 2007; Nordsieck 1979).

Table 4. One-way ANOVA results for morphometric and shell-shape variables among the *Patella* species and *Cymbula safiana*.

In addition to interspecific variation in the absolute values of the four morphometric variables, also significant interspecific variation was found in the several aspects of the shell shape (i.e. in the shape indices). In fact, the results of the One-way ANOVA showed significant differences among the species for the variables shell width at apex (SWA; $F_{(}3,406_{)} = 12.448$, $p < 0.001$), and for the variables expressing the degree of elliptical and eccentric basal outline (i.e. basal ellipticity SW/SL; $F_{(}3,406_{)} = 14.783$, $p < 0.001$; and basal eccentricity SWA/SW; $F_{(}3,406_{)} = 1.894$, $p = 0.130$, respectively). Only the last variable showed non-significant differences among species. So, the three *Patella* species and *Cymbula safiana*, in addition to significantly different absolute values of the four studied variables (i.e. SL, SW, SWA, and SH), also significantly differ in several aspects of the shell shape, with highest interspecific variation found for the variables expressing the shell conicity (i.e. SH/SL; $F_{(}3,406_{)} = 106.148$, $p < 0.001$). In particular, the highest F-value (i.e. 106.148) was found for the variable conicity, which, as already mentioned, expresses the shell profile and therefore it is the variable that better represents the differences in the aspect of the shell shape found among the species.

Table 4. One-way ANOVA results for morphometric and shell-shape variables among the Patella species and Cymbula safiana.

One-Way ANOVA

		Sum of Squares	df	Mean Square	F	Sig.
SL, shell length (mm)	Between Groups	899.547	3	299.849	11.040	.000
	Within Groups	11026.837	406	27.160		
	Total	11926.384	409			
SW, shell width (mm)	Between Groups	875.762	3	291.921	14.558	.000
	Within Groups	8141.174	406	20.052		
	Total	9016.936	409			
SWA shell width at	Between Groups	716.984	3	238.995	12.448	.000
apex (mm)	Within Groups	7795.006	406	19.200		
	Total	8511.990	409			
SH, shell height	Between Groups	296.129	3	98.710	41.730	.000
(mm)	Within Groups	960.371	406	2.365		
	Total	1256.501	409			
Basal ellipticity	Between Groups	.132	3	.044	14.783	.000
(SW/SL)	Within Groups	1.211	406	.003		
	Total	1.343	409			
Basal eccentricity	Between Groups	.034	3	.011	1.894	.130
(SWA/SW)	Within Groups	2.412	406	.006		
	Total	2.446	409			
Conicity (SH/SL)	Between Groups	.477	3	.159	106.148	.000
	Within Groups	.609	406	.001		
	Total	1.086	409			

Canonical Discriminant Analysis (CDA) between species

The results from the Canonical Discriminant Analysis between the species revealed significant multivariate differentiation among the four species. The test for the three canonical functions revealed that they collectively defined between species differences (Wilks' $\lambda = 0.412$, $\chi^2 = 357.469$, df = 21, $P < 0.001$). The analysis of the remaining two canonical functions, after removal of the first, also revealed significant between species differences (Wilks' $\lambda = 0.824$, $\chi^2 = 78.180$, df = 12, $P < 0.001$). However, test for the third canonical function, alone, revealed that it did not significantly between species differences (Wilks' $\lambda = 0.987$, $\chi^2 = 5.259$, df = 5, $P = 0.385$). Thus, most of the significant between species differences were contained within the first two canonical functions (Figs 4 and 5). The results of the Canonical Discriminant Analysis support previous morphological studies (e.g., Williamson, 1981), that used a range of morphological characters to identify between species differences in Mediterranean Patellidae.

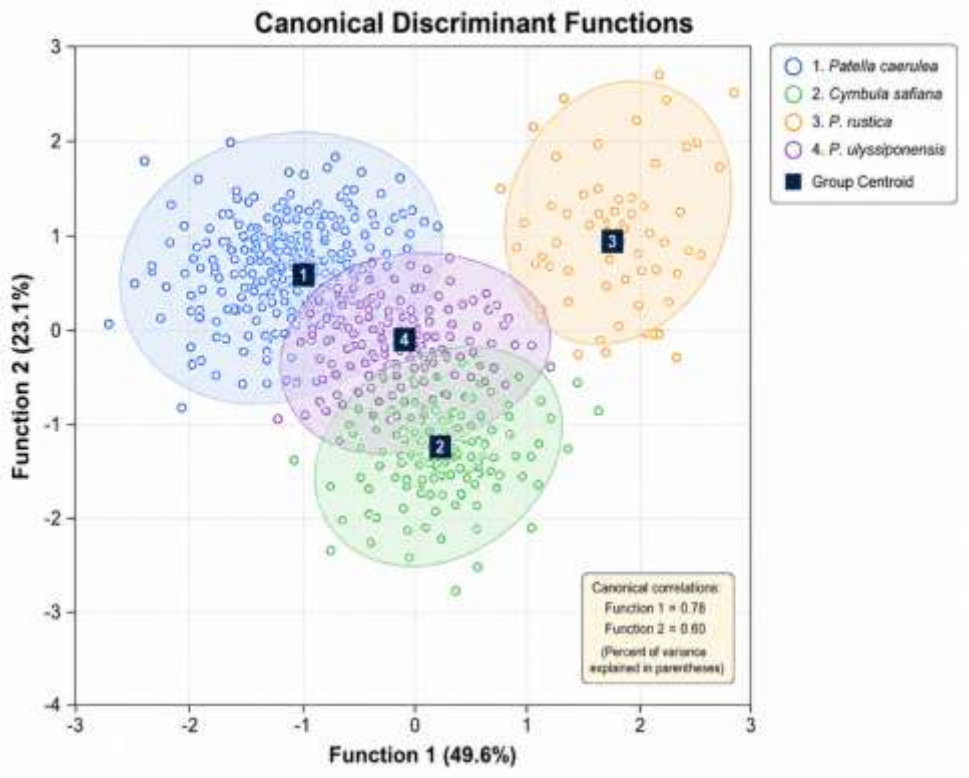

Figure 4. Canonical discriminant analysis results for morphometric parameters among the Patella *caerulea, P. rustica, P. ulyssiponensis*, and *Cymbula safiana* species in seven sampling stations along the southern Albanian coast.

Fig. 4 presents the Canonical Discriminant Analysis (CDA) results, obtained by using the morphometric parameters of the four Patellidae species as variables in the analysis, and the seven sampling localities as cases. The three canonical functions, together, are able to significantly and fully discriminate among the four species of limpets. Thus, Functions 1, 2, and 3, altogether, account for 94.149% of the variability in the original data matrix. In addition, it is worth noticing that, the discrimination among species, provided by the canonical functions, is highly significant. Thus, Function 1, independently of the others, is able to significantly and fully discriminate among the four species of limpets. Similarly, the remaining Functions, 2 and 3, together, are also able to provide significant and additional discriminatory information among the species of limpets.

CONCLUSIONS

The spatial distribution of four species of Patellidae limpets (*Patella caerulea*, *P. rustica*, *P. ulyssiponensis*, *Cymbula safiana*) was investigated at seven intertidal stations along the southern coast of Albania. The four species showed a heterogeneous distribution among the investigated localities. The most widely distributed species was *P. caerulea*, whereas *P. ulyssiponensis* and, especially, *C. safiana* were represented by only a few individuals at a small number of localities. Our findings are in agreement with previous studies that reported the distribution of and the morphology of limpets to be affected by several habitat-related factors including the type of substrate on which they live, the degree of exposure to hydrodynamical forces, thermal conditions and desiccation stress.

Geographical Variation of Shell Morphology in Individuals of *P. caerulea*: *P. caerulea* studied at seven locations of southern Albanian coast showed significant differences in most of the studied morphometric characteristics (Table 5, Figure 3). The three proportional characteristics of shape i.e., basal ellipticity, conicity and basal eccentricity showed the highest variability.

Conicity showed the greatest variability among the three characteristics, with the highest values recorded at Ksamil. In contrast, the eccentricity of the base of the shell was found to be rather stable among all the studied characteristics (Table 5). The highest variation was recorded for conicity, followed by other characteristics. Overall, results of present study support the previous findings (Cabral, 2007; Bouzaza & Mezali, 2018; Vafidis et al., 2020; Belmokhtar et al., 2022) regarding the high degree of phenotypic variability in morphology of the shells of the intertidal limpets, which is a function of their environmental plasticity.

It is worth noting that, as shown in the previous section, the morphological differentiation of *P. caerulea* populations from different sampling stations is partial. As in fact already highlighted by previous research on intertidal limpets, this type of geographical differentiation is in fact typical of species that display high phenotypic plasticity. Therefore, even if the analyzed populations show some differences in their morphological characteristics, they also display a considerable number of similarities. This fact therefore does not seem to be contradicting with the previously reported information, but rather it appears to be a confirmation of it. However, it is worth to reiterate that the analysis of the discriminant functions and of the groups' classification has to be considered with some caution, as already highlighted in the previous section.

Patella rustica differed from the other three species for the highest values of the shell height (SH) and conicity (SH/SL) while for the lowest values for the width of the base at the apex (SWA). In contrast, basal eccentricity (SWA/SW) did not differ significantly among the four species ($F_{3,30(}$= 1.894; p = 0.130). These results suggest that, in the examined species, the highest values of conicity are associated with the highest values of shell height. The examined species, therefore, are characterized by high values of conicity that, in addition to the dimensions of the shell, are considered useful for the interspecific discrimination of Mediterranean species of the genus *Patella* (Cabral, 2007; Bouzaza & Mezali, 2018; Belmokhtar et al., 2022).

Canonical discriminant function analysis showed that significant multivariate discrimination between the four species existed, and that all three of the canonical functions, in total, explained significant amounts of between species variance. Thus, while it is true that some amount of between species variance remains unexplained by these functions (most of which would, in any case, probably be noise rather than real information), shell morphology in the four species of limpets nevertheless provides useful, discriminatory information among the species. But, of course, that information must be considered within the framework of the overall morphological characteristics of the species. That is, as stated above, in absolute terms, none of the between species variance was explained by any of the functions (i.e. all of the functions explained zero amount of variance between species), in relative terms, however, the first two of the three functions collectively explained a highly significant amount of between species variance.

In conclusion, this study documents significant amounts of both spatial and interspecific morphological variation within the recently introduced *Patella caerulea* as well as three native *Patella* species (*P. rustica*, *P. ulyssiponensis* and *Cymbula safiana*) along the southern Albanian coast. Shell morphometry provided effective means for interspecific classification; however, considerable amounts of interspecific as well as intraspecific variation precluded complete, taxon-specific grouping. Future studies employing larger, more balanced sample sizes of individual species in conjunction with a variety of environmental, ecological and molecular-based variables will be necessary to accurately assess to what extent of variability is due to phenotypic plasticity, as opposed to genetically fixed characters, and the specific environmental variables which govern these patterns. In the interim, this study serves as a fundamental, quantitative morphometric framework for these four Mediterranean species in this specific region.

REFERENCES

Begon, M., Harper, J. L., & Townsend, C. R. (1996). Ecology: Individuals, populations and communities (2nd ed.). Blackwell Scientific Publications.

Bellan-Santini, D. (1985). The Mediterranean benthos: Reflections and problems raised by a classification of the benthic assemblages. In M. Moraitou-Apostolopoulou & V. Kiortsis (Eds.), Mediterranean marine ecosystems (pp. 19–48). Springer US.

Belmokhtar, F., Belmokhtar, R., Kerfouf, A., & Hamed, M. B. B. (2022). Morphometric analysis of three Mediterranean limpets *Patella* caerulea Linnaeus, 1758, P. rustica Linnaeus, 1758 and the endangered P. ferruginea Gmelin, 1791 (Gastropoda Patellidae) from the Algerian West Coast. Biodiversity Journal, 13(3), 483–494.

Bouzaza, Z., & Mezali, K. (2018). Discriminant-based study of the shell morphometric relationships of *Patella* caerulea (Gastropoda: Prosobranchia) of the western Mediterranean Sea. Turkish Journal of Zoology, 42(5), 513–522.

Buttivant, H. (2019). Rock pool: Extraordinary encounters between the tides. Duckworth Books.

Caballero, R., Fernandez-Gonzalez, F., Badia, R. P., Molle, G., Roggero, P. P., Bagella, S., ... Ispikoudis, I. (2009). Grazing systems and biodiversity in Mediterranean areas: Spain, Italy and Greece. Pastos, 39(1), 9–154.

Cabral, J. (2007). Shape and growth in European Atlantic *Patella* limpets (Gastropoda, Mollusca): Ecological implications for survival. Web Ecology, 7, 11–21.

Cascales-Soler, A., Ramos-Esplá, A. A., & Forcada, A. (2023). Reviewing the knowledge on the genus *Patella* in the Mediterranean Sea: Testing the effect of protection on the mean abundance and size of *Patella* ferruginea. Frontiers in Marine Science, 10, 1158470.

Christofoletti, R. A., Takahashi, C. K., Oliveira, D. N., & Flores, A. A. V. (2011). Abundance of sedentary consumers and sessile organisms along the wave exposure gradient of subtropical rocky shores of the south-west Atlantic. Journal of the Marine Biological Association of the United Kingdom, 91, 961–967.

Corte-Real, H. B. S. M., Hawkins, S. J., & Thorpe, J. P. (1996). Population differentiation and taxonomic status of the exploited limpet *Patella* candei in the Macaronesian islands (Azores, Madeira, Canaries). Marine Biology, 125, 141–152.

Cossignani, T. (1992). Atlante delle conchiglie del Medio Adriatico. L'Informatore Piceno.

Cossignani, T., & Ardovini, R. (2011). Malacologia mediterranea: Atlante delle conchiglie del Mediterraneo: 7500 foto a colori. L'Informatore Piceno.

da Silva Freitas, D. C. A. (2021). Effects of climate change on limpets (*Patella* spp.): Biology and distribution [Master's thesis, Universidade do Porto].

Fraser, C. M. L., Coleman, R. A., & Klein, J. C. (2010). Up or down? Limpet orientation on steeply sloped substrata. Aquatic Biology, 11, 91–98. https://doi.org/10.3354/ab00294

Gofas, S., Salas, C., & Moreno, D. (2011). Moluscos marinos de Andalucía (Vol. 1). Universidad de Málaga, Servicio de Publicaciones e Intercambio Científico.

Guelorget, O., & Perthuisot, J.-P. (1983). Le domaine paralique: Expressions géologiques, biologiques et économiques du confinement (16th ed.). Presse de l'École Normale Supérieure.

Harley, C. D. G. (2008). Tidal dynamics, topographic orientation, and temperature-mediated mass mortalities on rocky shores. Marine Ecology Progress Series, 371, 37–46. https://doi.org/10.3354/meps07711

Miller, L. P., Harley, C. D. G., & Denny, M. W. (2009). The role of temperature and desiccation stress in limiting the local-scale distribution of the owl limpet, Lottia gigantea. Functional Ecology, 23, 756–767. https://doi.org/10.1111/j.1365-2435.2009.01567.x

Nobles, C. (1993). Taxonomy, morphology and population genetics of Mediterranean *Patella* [Doctoral dissertation, University of Liverpool].

Prusina, I., Sarà, G., De Pirro, M., Dong, Y. W., Han, G. D., Glamuzina, B., & Williams, G. A. (2014). Variations in physiological responses to thermal stress in congeneric limpets in the Mediterranean Sea. Journal of Experimental Marine Biology and Ecology, 456, 34–40.

Riedl, R. (1991). Fauna e flora del Mediterraneo: Dalle alghe ai mammiferi; una guida sistematica alle specie che vivono nel mar Mediterraneo.

Tlig-Zouari, S., Rabaoui, L., Fguiri, H., Diawara, M., & Ben Hassine, O. K. (2011). Morphometric characterization of the limpet *Patella* ferruginea along the Tunisian coasts. Cahiers de Biologie Marine, 52, 269–278. https://doi.org/10.21411/CBM.A.C1C76657

Urra, J., Gofas, S., Rueda, J. L., Marina, P., Mateo-Ramírez, Á., Antit, M., & Salas, C. (2017). Biodiversity and biogeographical patterns of molluscan assemblages in vegetated and unvegetated habitats in the northern Alboran Sea (W Mediterranean Sea). Marine Biodiversity, 47(1), 187–201.

Vafidis, D., Drosou, I., Dimitriou, K., & Klaoudatos, D. (2020). Population characteristics of the limpet *Patella* caerulea (Linnaeus, 1758) in Eastern Mediterranean (Central Greece). Water, 12, 1186.

Williams, G. A., & Morritt, D. (1995). Habitat partitioning and thermal tolerance in a tropical limpet, Cellana grata. Marine Ecology Progress Series, 124, 89–103. https://doi.org/10.3354/meps124089.

ADVANCES IN SEED COATING TECHNOLOGIES FOR VEGETABLE CROPS

Nusret Özbay [1] and Aygül Karaca[2]*

[1]Department of Horticulture, Faculty of Agriculture, Bingöl University, Bingöl, Türkiye;

[2]Vocational School of Food, Agriculture and Livestock, Department of Crop and Animal Production, Bingöl University, Bingöl, Türkiye, akaraca@bingol.edu.tr

**Corresponding author's e-mail: nozbay@bingol.edu.tr*

ABSTRACT

Vegetable crop production relies on rapid, uniform, and vigorous seed germination to ensure successful crop establishment and high productivity. However, vegetable seeds often exhibit poor emergence, low vigor, irregular germination, and increased susceptibility to biotic and abiotic stresses, limiting stand establishment and yield potential. Seed coating technology has emerged as an effective pre-sowing seed enhancement strategy that improves seed performance by delivering protective and bioactive compounds directly to the seed surface. In addition to facilitating seed handling and precision sowing, modern coating systems function as carriers for fungicides, insecticides, micronutrients, plant growth regulators, biostimulants, beneficial microorganisms, and nanomaterials, thereby promoting germination, seedling vigor, and stress resilience. Recent advances in biodegradable polymers, bio-based coating materials, and controlled-release formulations have further strengthened the role of seed coatings in sustainable vegetable production. This review summarizes recent developments in seed coating technologies, with particular emphasis on the principal coating approaches, including film coating, encrusting, pelleting, and priming-plus-coating, and their applications in economically important vegetable crops such as tomato, pepper, brassicas, onion, carrot, and lettuce. The effects of coating materials and functional additives on germination, seedling establishment, stress tolerance, disease suppression, and crop productivity are critically discussed. Finally, current challenges, emerging innovations, and future research directions for the development of environmentally friendly and high-performance seed coating systems are highlighted to support sustainable and climate-resilient vegetable production.

Keywords: seed coating, vegetable seeds, film coating, pelleting, biostimulants, sustainable agriculture, seed enhancement.

1. INTRODUCTION

Vegetable species hold a significant place in agricultural production due to their high economic value and important role in human nutrition. For efficient and high-quality vegetable production, rapid and homogeneous germination of seeds, regular emergence, and strong seedling development are of great importance. In instance, plant density and production performance in later developmental phases are effectively determined by uniform plant emergence in the early stages of production. However, exact seed dispersion and mechanical sowing can be challenging due to the small, light, and irregularly shaped seeds found in many vegetable species. Unwanted plant density and erratic plant emergence might result from improper seed distribution after sowing. Furthermore, environmental conditions such as drought, salinity, low or high temperatures, and soil-borne pathogens can negatively affect

germination and early seedling development, limiting plant emergence (Javed et al., 2022; Biswal et al., 2026).

Technologies that improve the physical properties of seeds, facilitate the sowing process, and simultaneously support germination and early plant development play a significant role in mitigating these problems. Seed coating is one such technology. Applying various materials to a seed's surface or surrounding area without changing its genetic makeup is the basis of seed coating. Seeds can be coated to alter their size, shape, weight, and surface characteristics, which facilitates their transportation, processing, and use with precision planting equipment. In particular, coating small and irregularly shaped seeds makes them more uniformly shaped and enables more accurate planting. In order to facilitate planting and enhance seed and plant performance, one of the primary goals of contemporary seed coating technology is to apply the active ingredients to the seed surface in the appropriate amounts and as uniformly as possible (Afzal et al., 2020).

From an application that only modifies the physical characteristics of seeds, seed coating technology has developed into a multipurpose system that provides the seed with a variety of active ingredients. Nutrients, pesticides, fungicides, plant growth regulators, biostimulants, and beneficial microorganisms can all be transported using coating materials. The direct delivery of active ingredients to the seed and growing root zone during germination is made possible by the presence of these substances surrounding the seed. In order to guaranty that the applied material is both present on the seed surface and functional during germination and early development, the coating system serves as a carrier (Afzal et al., 2020; Biswal et al., 2026).

Seed coating serves more purposes than just making planting easier. Appropriate coating systems can help improve seed performance against environmental stresses, support seed germination and seedling development, and allow more focused application of specific plant protection products. Specifically, direct delivery of active ingredients around the seed can minimize needless applications and enable concentration of application to the intended area. Seeds can be physiologically supported during germination and the early stages of seedling development, in addition to being physically improved, by adding biostimulants, nutrients, and microbial components to seed coating systems. Because of these characteristics, seed coating is a useful technology for more sustainable production systems and precision agriculture (Afzal et al., 2020; Javed et al., 2022).

In recent years, there has been a significant diversification in the materials and techniques utilized in seed coating technologies. Among the techniques frequently applied to vegetables and other horticultural plants are film coating, encrustation, and pelleting. Furthermore, coating systems utilizing seaweed extracts, polymers, naturally derived materials, microbial inoculants, and other biologically active materials are being developed. Microencapsulation, controlled release, and nanoscale coating are examples of more sophisticated technologies that present new opportunities for safeguarding active ingredients surrounding the seed and releasing them under appropriate circumstances. One strategy that can offer substitutes for conventional coating systems is the use of biodegradable polymers and biologically derived active substances in sustainable horticultural production (Gong et al., 2025; Biswal et al., 2026).

The characteristics of the coating material, the thickness of the coating, the kind and concentration of the active ingredient, the physical and physiological characteristics of the seed, and environmental factors can all affect how effective seed coating technologies are. By restricting the seed's access to water and oxygen, an excessively thick or inappropriate coating layer can postpone germination. In contrast, a suitable coating system developed taking into account seed characteristics and growing conditions can improve seed sowing performance while supporting germination, emergence, and early seedling development. Therefore, the

coating material and application method should be evaluated according to the characteristics of each vegetable species (Afzal et al., 2020; Javed et al., 2022).

The main objectives of seed coating are:
• To facilitate seed processing and sowing;
• To deliver active substances directly to the spermosphere;
• To improve germination and seedling establishment;
• To reduce pesticide use through targeted application of active substances;
• To support precision agriculture and sustainable crop production.

These advancements in seed coating technologies have the potential to combine seed protection and early development support with precision planting in the same application, especially in vegetable varieties with small and irregularly shaped seeds. Today, research focuses not only on improving the physical properties of seeds but also on developing new and sustainable coating systems for the efficient delivery of nutrients, biostimulants, and biological agents, supporting germination and seedling development, and using resources more efficiently (Afzal et al., 2020; Biswal et al., 2026).

2. MAJOR SEED COATING TECHNOLOGIES

Seed coating technologies are evaluated under different methods depending on the amount of material applied, the properties of the coating layer, and the physical changes it creates on the seed. The main approaches commonly used in vegetable seeds are film coating, encrustation, and pelleting, and the combined application of seed priming and coating stands out as an important approach to improving seed performance. These methods offer different advantages in terms of improving the sowingability and homogeneous emergence of seeds, efficient transport of active components, and supporting germination and early seedling development (Biswal et al., 2026).

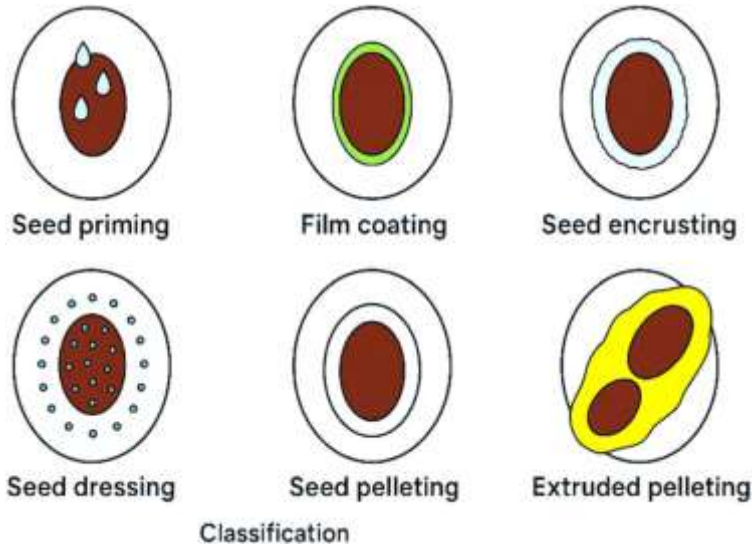

Fig. 2 Classification of seed coating technologies (Biswal et al., 2026).

2.1 FILM COATING

Film coating is a technology based on applying a thin and homogeneous layer of coating material to the seed surface, usually in an amount not exceeding 5% of the seed weight (Pedrini et al., 2017). Coating materials mostly consist of polymers, pigments, plasticizers, and colorants; polymer-based binders ensure the dissolution or **homogeneous distribution of**

active components within the coating (Taylor and Harman, 1990; Qiu et al., 2005). Rotary coating systems are the most commonly used equipment in commercial applications, while fluidized bed systems are used more limitedly. One of the important advantages of film coating is that it allows the application of different active components to the seed without significantly altering its size and shape. Therefore, it can be used in the delivery of plant growth regulators, nutrients, biostimulants, and plant protection products. For example, it has been reported that applying a film coating containing 0.0075% uniconazole to Brassica napus L. seeds can reduce the negative effects of flood stress and increase antioxidant enzyme activities (Willenborg et al., 2004). However, it has been noted that the application did not have a significant effect on germination. Similarly, it has been reported that germination performance improved in canola seeds coated with a polymer film under low temperature and humidity stress conditions (Pedrini et al., 2018). These findings suggest that film coating can be used in delivering active ingredients to the seed and supporting early plant development under stress conditions.

2.2 PELLETING

Pelletizing is the application of a thick coating layer in the form of aggregates or pellets around the seed. This method is particularly preferred for processing small or irregularly shaped seeds (Taylor et al., 2001; Pedrini et al., 2020). Pelletizing is a technique that provides a greater weight increase by applying liquids and inert materials (such as diatomaceous earth, talc, and bentonite) to the seed surface; therefore, it is considered a continuation of the mini-pelletizing process (Afzal et al., 2020). This process can also be performed using a rotary drum or rotary pan. However, pelletizing generally transforms the seed morphology into a larger, spherical shape that is difficult to distinguish from the original seed shape (Halmer, 2000). Pelletizing contributes to the improvement of planting with mechanical planting equipment by increasing the weight percentage by 500-5000%. It facilitates planting for garden plants with small seeds or irregular seed shapes, including lettuce and tomatoes (Kangsopa et al., 2018; Javed et al., 2022). Newly pelleted seeds should be dried before packaging and storage.

2.3 ENCRUSTING

Encrustation is a seed coating method that involves applying liquid and solid particulate materials to the seed, completely coating it while preserving its original shape (Taylor, 2020). Encrusted seeds can also be called mini pellets or, in some cases, coated seeds. The main equipment used in obtaining encrusted seeds is a rotary coater and a coating pan. Due to the high amount of water used during encrustation, the coated seeds must be dried to their original moisture content before packaging and storage. The increase in seed weight after encrustation can vary between 8% and 500% (Afzal et al., 2020).

Encrusted seeds have been reported to improve seedling emergence. Encrusted fescue seeds before storage showed significantly higher germination rates compared to seeds encrusted after storage or those without any treatment (Olivera et al., 2017). However, the thickness of the coating layer or the amount of coating on the seed can affect the germination rate, and encrusted seeds are reported to germinate in a longer time compared to film-coated seeds (Gorim and Asch, 2012). The amount of binder used during encrustation can also alter the mechanical properties of the coating, such as integrity, compressive strength, and dispersal time after wetting (Qiu et al., 2020).

2.4 PRIMING COMBINED WITH COATING

The strategy of combining the physiological preparation of the seed for germination with the protective and transport qualities of the coating is known as "combined seed priming and coating." Before going through the coating process, seeds are dried to the proper moisture content after carefully absorbing water to start metabolic processes during priming. This application can promote more uniform seedling emergence and hasten the germination process of seeds. The combined application of priming and coating has the potential to enhance the performance of seeds and seedlings in the early developmental stage, particularly in challenging environmental conditions like low temperatures, drought, and salinity (Pedrini et al., 2017; Afzal et al., 2020).

In addition to enhancing the seed's physical characteristics, the coating procedure that comes after priming enables the introduction of active ingredients into the seed environment, including nutrients, biostimulants, plant growth regulators, and biological agents. Therefore, the protection and regulated transport of active substances offered by coating support the physiological benefits of priming. According to reports, this method has a lot of potential, especially when it comes to strong seedling development, quick and uniform emergence, and improved seed performance under stressful circumstances (Pedrini et al., 2017; Afzal et al., 2020; Qiu et al., 2020). Priming, however, may have an impact on the seeds' storage qualities. Since the storage life of primed seeds may be reduced, ensuring appropriate drying and controlled storage conditions after application is crucial. Therefore, in systems where priming and coating are used together, priming conditions, drying level, coating material properties, and storage conditions should be evaluated as a whole (Gorim and Asch, 2017; Pedrini et al., 2017).

3. MATERIALS USED IN SEED COATING

Seed coating materials determine the physical properties of the coating as well as ensuring the efficient and homogeneous transport of active ingredients to the seed surface. The materials used generally include polymers and binders, fillers and active ingredients, as well as biostimulants, nutrients, plant protection products, and beneficial microorganisms. The selection of the coating material should be made considering the properties of the component to be applied, the target dose, the coating method, and the physical properties of the seed. A suitable combination of materials and equipment is important to ensure homogeneous adhesion of the coating to the seed surface while preventing mechanical damage to the seeds (Zhang et al., 2022; Biswal et al., 2026).

3.1 POLYMERS AND BINDERS

Polymers and binders contribute to the formation of a homogeneous coating layer and the maintenance of coating stability by ensuring the adhesion of coating materials to the seed surface. They also support the retention of coating components on the seed surface, the regulation of water uptake, and the transport of active substances to the seed. Binders include biologically derived substances like starch, cellulose derivatives, alginate, chitosan, proteins, and natural gums, as well as synthetic polymers like polyvinyl alcohol (PVA) and polyacrylates. Biodegradable polymers are becoming more and more popular, especially when it comes to lowering environmental effects and creating sustainable farming methods (Ryu et al., 2006; Kimmelshue et al., 2019; Sohail et al., 2022; Biswal et al., 2026).

3.2 FILLERS

Fillers are frequently used inert bulking materials that allow seeds to be physically altered, especially during the encrustation and pelleting processes (Zhang et al., 2022). They can be made from a single substance or by combining several different substances. Fillers influence seed size, shape, and planting accuracy by adding to the volume and structural characteristics of the seed coating. Additionally, they may aid in the regulated release of active components (Afzal et al., 2020).

3.3 ACTIVE INGREDIENTS

The functional elements of seed coating systems that have a direct impact on seed and seedling performance are called active ingredients. These components are primarily used to protect seeds from biotic stressors or to enhance plant performance during germination, seedling emergence, early development, and stress situations. Plant protection products, plant nutrients, biostimulants, plant growth regulators, and beneficial microorganisms are the primary active ingredients found in seed coatings (Afzal et al., 2020).

Insecticides, nematicides, fungicides, and other protective agents are used to shield seeds from pests and diseases, particularly during germination and seedling emergence. However, choosing the right dose and formulation is crucial because high doses of some protective agents can have a detrimental effect on germination and seedling development (Rocha et al., 2019). Nutrients, on the other hand, can support early nutrient utilization by ensuring the delivery of microelements such as nitrogen (N), phosphorus (P), potassium (K), boron (B), copper (Cu), manganese (Mn), molybdenum (Mo), and zinc (Zn) to the seed environment. It has been reported that these applications can have positive effects on germination, plant development, and yield (Sohail et al., 2022).

Biostimulants and plant growth regulators are also increasingly used in seed coating systems. The application of plant growth regulators such as salicylic acid, gibberellic acid, and abscisic acid, as well as various biostimulants, via coating can contribute to supporting germination and early seedling development and increasing stress tolerance. In particular, direct delivery of the active ingredient to the seed environment during the early development stage is a significant advantage that can increase the effectiveness of the application (Amirkhani et al.; 2016; Afzal et al., 2020; Chen et al., 2024).

Beneficial microorganisms also constitute an important group of active ingredients. Microorganisms such as plant growth promoting bacteria (PGPB/PGPR), Trichoderma species and arbuscular mycorrhizal fungi can be applied to the seed surface via seed coating. These microorganisms can support root colonization, nutrient uptake and plant development; It can also increase plant resilience under some biotic and abiotic stress conditions (Maity et al., 2018; Rocha et al., 2019). In particular, direct application of biological agents to the seed strengthens the biological function of the coating technology by ensuring the presence of active microorganisms in the seed and root zone in the early period.

As a result, the type of active ingredient, its dose, distribution within the coating and release characteristics are the main factors that determine the success of the seed coating application. Homogeneous delivery of active ingredients to the seed in a suitable coating matrix; It can support germination, seedling development and stress tolerance while reducing unnecessary input use. Therefore, the choice of active ingredient should be evaluated not only based on the targeted biological effect, but also on the seed type, coating method and growing conditions (Afzal et al., 2020; Sohail et al., 2022).

4. APPLICATIONS OF SEED COATING IN VEGETABLE CROPS

4.1 IMPROVED SOWING QUALITY

To achieve uniform plant emergence and suitable plant density in vegetable cultivation, even and controlled seed distribution during sowing is essential. Individual dosing and placement at suitable intervals in precision sowing machines can be difficult when dealing with small and irregularly shaped seeds, especially those of lettuce, carrots, onions, and celery. By improving the uniformity of the seeds' size and shape, seed coating applications can help achieve more accurate seed separation and placement during mechanical sowing (Taylor et al., 1990; Pedrini et al., 2017). Research using a variety of seed coating applications has shown how these benefits affect different kinds of vegetables. For vegetable varieties with tiny, irregularly shaped seeds, pelletizing stands out as a crucial application in enhancing precision sowing performance. Pelleting lettuce (Lactuca sativa L.) seeds enhances their physical characteristics, making it simpler to separate and place them at the right intervals in precision seeding machines. This helps direct seeding systems better control plant density (Hill, 1999; Halmer, 2008). Similarly, due to the small, light, and irregular structure of carrot (*Daucus carota* L.) seeds, pelleting allows these seeds to acquire physical and mechanical properties more suitable for mechanical seeding. Hacıyusufoğlu and Akbaş (2019) reported that pelleting changed the size, shape, and weight characteristics of carrot seeds, and that this change is important for seeding. A similar advantage is seen in onion (*Allium cepa* L.) seeds. Karayel et al. (2020) compared the performance of naked and pelleted onion seeds in a vacuum precision seeding machine and revealed that a more suitable seed distribution was obtained in pelleted seeds. Also, Yogeesha et al. (2017) reported that pelleting onion seeds facilitated seed handling and created a more uniform seed structure. In contrast, film coating can be a more suitable option in situations where a significant change in seed size is undesirable. For example, in economically valuable vegetable species such as tomatoes (*Solanum lycopersicum* L.), film coating allows the application of coating materials without significantly altering the initial size of the seed and contributes to maintaining the existing seed calibration in precision planting systems (Halmer, 2008). These studies show that the seed size and shape of the vegetable species and the planting system used should be evaluated together when choosing the coating method. While film coating enables the application of coating materials without appreciably changing the seed size, pelleting allows the seeds to acquire more uniform physical characteristics, particularly in small and irregularly shaped seeds. Therefore, depending on the features of the vegetable species and the specifications of the precision planting systems, various coating techniques may offer varying benefits.

4.2 CROP PROTECTION

During the early stages of germination and seedling development, seeds are extremely vulnerable to diseases, especially those brought on by soil-borne pathogens. Particularly in vegetable cultivation, pathogens like Pythium, Rhizoctonia, and Fusarium can adversely affect germination and seedling emergence, resulting in large losses. Fungicides and other protective active ingredients can be directly applied to the seed environment using seed coating technologies, providing targeted protection during the plant's most vulnerable early developmental stage (Taylor and Harman, 1990; Halmer, 2008). Compared to large-field applications, concentrating active ingredients around the seed environment allows for direct application to the target area and the use of fewer protective agents. Numerous studies have shown how this method can be applied to vegetable species. Fungicide-containing coatings are applied to tomato (Solanum lycopersicum L.) seeds, especially to suppress Fusarium,

Rhizoctonia, and Pythium species that cause dumping-off diseases. During germination, protective elements on the seed surface can create a protective environment that lowers the likelihood that young root and stem tissues will come into contact with pathogens (Taylor and Harman, 1990). Similarly, soil-borne diseases that affect Brassica group vegetables (cabbage, broccoli, cauliflower, and kale) in their early stages of development are managed through seed treatments. According to Taylor et al. (1998), using fungicides in conjunction with seed guaranties that the active ingredients are delivered straight to the seed area and that targeted application can minimize needless pesticide use. Coating applications are also used in onion (*Allium cepa* L.) seeds to prevent potential fungal diseases, particularly during germination and seedling development. Fungicides applied to seeds by encrustation and film coating guaranty the presence of protective elements surrounding the seed and their efficacy during the early stages of development (Halmer, 2008). As a result, it can help prevent diseases that might arise during the seed and early seedling stages.

A novel strategy for managing disease is the application of biological agents in seed coatings, in addition to chemical fungicides. In particular, species of Bacillus, Pseudomonas, and Trichoderma can prevent the spread of disease in a number of ways, including by competing with pathogens, generating antagonistic compounds, and boosting the plant's defense mechanisms (Nigro et al., 2014). Beneficial microorganisms can be present in the seed and root zone from the start of germination by coating the seed surface with these microorganisms. Biological seed applications have substantial potential for lowering chemical inputs and creating more sustainable disease management systems, according to Pedrini et al. (2020). In conclusion, coating vegetable seeds with chemical and biological protective components can help suppress soil-borne pathogens, particularly during germination and seedling emergence. However, the type and dosage of the active ingredient used, along with the target pathogen, vegetable species, and coating formulation, may all affect how well the application works.

4.3 ENHANCED GERMINATION AND STAND ESTABLISHMENT

Applications of seed coatings can enhance the sowing qualities of seeds as well as promote early seedling development and faster, more uniform germination. Particularly in challenging environmental circumstances, germination and seedling emergence can be supported by the appropriate microenvironment produced by the coating materials surrounding the seed and the active ingredients in the formulation (Halmer, 2008; Pedrini et al., 2017). Research on vegetable species also demonstrates that this effect can change based on the species and application technique. For instance, it has been noted that under low temperature and humidity stress conditions, canola seeds coated with polymer film perform better during germination (Taylor et al., 1998). Similarly, it has been found that applying encrustation to onion seeds can boost the germination rate, vigor index, root length, and shoot length; additionally, applying a coating that contains thiram specifically promotes the development of seedlings. These findings demonstrate that seed coating technologies can effectively promote germination and guaranty stronger seedling formation when utilized with suitable formulations.

4.4 NUTRIENT AND BIOSTIMULANT DELIVERY

Through the direct application of nutrients and biostimulants to the seed environment made possible by seed coating technologies, these elements can be used more effectively during germination and the early stages of seedling development. Specifically, the incorporation of microelements and components that promote plant growth into coating formulations guaranties that nutrients are situated near the seed and young root zone, which enhances the efficiency of nutrient utilization (Pedrini et al., 2017). Additionally, by allowing the controlled release of

nutrients to the seed environment, new generation formulations like hydrogel coatings based on alginate can support nutrient supply during early development (Skrzypczak et al., 2021). Similarly, it has been reported that seed coatings can support root development, seedling growth, and nutrient uptake in vegetable production by transporting microorganisms, microelements, and biologically active components. As a result, seed coating is regarded as a carrier system that transports nutrients and biostimulants to the intended area rather than just an application that physically modifies the seed surface.

4.5 BIOLOGICAL SEED COATINGS

In order to ensure that beneficial microorganisms are present around the seed during germination and the early stages of seedling development, biological seed coatings are a sustainable application method. When incorporated into seed coating formulations, microorganisms like Bacillus, Pseudomonas, and Trichoderma, in particular, can support colonization in the root zone and suppress soil-borne pathogens (Nigro et al., 2014; Pedrini et al., 2017). In vegetable cultivation, these types of biological coatings are reported to be used not only for disease suppression but also for supporting root development and plant growth. However, the ability of the coating material to maintain the viability of the microorganisms and ensure their proper adhesion to the seed is a crucial factor for the success of the application. Therefore, biological seed coatings are being considered as an alternative or complementary approach to chemical seed treatments in more sustainable vegetable production systems.

4.6 IDENTIFICATION AND TRACEABILITY

In addition to their physical and biological functions, seed coatings can also be used to identify and trace seeds. Coating materials can be given different colors and visual features, especially in order to easily distinguish different varieties, seed lots and application types. Colored coatings can facilitate rapid identification of seeds during processing and storage stages, while also reducing the risk of mixing or misuse of different applications (Halmer, 2008; Pedrini et al., 2020). In addition, associating the coating color or appearance with a specific seed lot or application can contribute to supporting quality control in production and distribution processes. For this reason, seed coating technologies are considered not only as an application that improves planting and seed performance, but also as a practical tool to support the identification, quality control and traceability of seeds throughout the production chain.

5. EMERGING SEED COATING TECHNOLOGIES

More controlled, targeted, and effective delivery of active ingredients to the seed is the focus of recent developments in seed coating technologies, which go beyond conventional coating applications. Specifically, next-generation coating systems with nutrients, nanomaterials, and beneficial microorganisms present substantial chances to improve seed performance, increase stress tolerance, and improve resource utilization efficiency (Afzal et al., 2020). As a result of these advancements, seed coating is becoming a multifunctional delivery and seed enhancement technology rather than just a physical coating application.

5.1. MICROBIAL SEED COATINGS

The use of microorganisms that promote plant growth, particularly growth-promoting bacteria (PGPB), rhizobacteria, and beneficial fungi, in seed coatings holds significant potential for supporting nutrient uptake and plant growth, and suppressing soil-borne diseases and pathogens (Ma, 2019; Rocha et al., 2019). Applying beneficial microorganisms via seed coating allows for their direct delivery to the seed zone, enabling the use of lower inoculum amounts and

offering an effective inoculation method (Scott, 1990; Taylor and Harman, 1990; Cho et al., 2000). The use of suitable carrier materials contributes to the adhesion of microorganisms to the seed surface and their protection against external environmental conditions, thus supporting their viability within the coating (Deaker et al., 2004; Tufail et al., 2018; Głodowska et al., 2017). Indeed, while it has been reported that biotic stress is reduced and emergence and early plant development are supported in seeds coated with microorganisms that promote plant growth (Głodowska et al., 2017), pelleting sesame seeds with the E681 strain has been found to reduce the incidence of seedling damping-off disease (Ryu et al., 2006). With these characteristics, microbial seed coatings are considered a new generation approach that supports seed performance and early plant development, contributes to biological disease management, and has potential for sustainable production systems.

5.2. NANO-SEED COATINGS

An emerging strategy that makes it possible to precisely and carefully deliver nutrients, growth regulators, and other biologically active substances to seeds is the integration of nanotechnology into seed coating systems. By facilitating the adhesion of coating components to the seed surface and the controlled release of active substances, the high surface area and distinctive physicochemical characteristics of nanoscale materials can enhance germination and seedling development (Singh et al., 2024). In particular, the use of ZnO, Si, and other nanomaterials can have beneficial effects on root development, water and nutrient uptake, and the encapsulation of nutrients and biostimulants within nanocarriers supports the metabolic activity of the seed (Okan, 2020; Al Jabri et al., 2022; Singh et al., 2024). Additionally, by holding water inside the coating and releasing it to the seed gradually, nano-coatings can help maintain the water status of seeds during drought conditions. For instance, controlled water release has been reported to be possible with graphene oxide and hydrogel-based nanomaterials (Silva et al., 2025). Furthermore, according to Singh et al. (2024), nano-coating systems may enhance seed performance and seedling resilience in the face of abiotic stressors like heat, salinity, and drought. These characteristics set nano-seed coatings apart as a cutting-edge seed coating technology that seeks to enhance germination, early seedling development, and stress tolerance by facilitating the precise and regulated delivery of active ingredients.

5.3. NUTRIENT-ENHANCED COATINGS

The availability of sufficient nutrients during the early stages of plant development is crucial for healthy germination and seedling growth. Coating seeds with appropriate amounts of macro and especially microelements allows nutrients to be directly deposited around the seed, reducing nutrient losses and increasing nutrient use efficiency (Scott, 1989; Farooq et al., 2012). The use of microelements such as Zn, B, Fe, Mn, Cu, Mg, and Mo in seed coatings has shown positive results on germination, emergence, plant development, and yield in various plant species (Afzal et al., 2020). However, since direct contact of high amounts of macroelement coatings with the seed can cause phytotoxicity and negatively affect germination and seedling development, it is recommended to create a protective starting or boundary layer between the nutrient-containing layer and the seed (Scott, 1989). Reducing nutrient losses through seed coating can also contribute to lower production costs compared to traditional soil applications (Farooq et al., 2012). Furthermore, it has been reported that maize seeds coated with slow-release N-P-K exhibit improved emergence and yield characteristics compared to conventional fertilizer application (Dong et al., 2016). Therefore, nutrient-enriched coatings are considered an effective seed coating approach that supports early plant development and has the potential to reduce nutrient losses and fertilization costs.

6. CHALLENGES

Although seed coating technologies offer significant advantages, the success of the application depends on the proper optimization of the coating formulation and coating thickness. Inappropriate coating properties or excessive coating thickness can negatively affect germination and seedling development by limiting the seed's water and oxygen uptake (Javed et al., 2022). Furthermore, the use of polymers, nutrients, pesticides, and biological agents within the same coating system makes maintaining compatibility and biological efficacy between these components a crucial technical requirement (Afzal et al., 2020). In systems where priming and coating are applied together, the potential decrease in seed storage performance necessitates ensuring appropriate storage conditions after application. In addition, dust-off generated during coating or during planting and transport poses a significant problem in terms of the dispersal of active ingredients into the environment; therefore, the coating must adhere strongly to the seed surface and be resistant to abrasion (Langlet et al., 2024). The persistence of non-biodegradable synthetic polymers in the environment and the formation of microplastics are becoming increasingly important for the sustainability of seed coating technologies (Sohail et al., 2022; Langlet et al., 2024). Therefore, future research should focus on achieving a suitable balance between coating efficacy and germination, storability, compatibility of active ingredients, and environmental safety.

7. FUTURE PERSPECTIVES

In the future, environmentally friendly, precise, and product- and environmental condition-specific coating systems are expected to come to the forefront in the development of seed coating technologies. Increasing the use of biodegradable and biologically derived polymers constitutes an important research area in terms of reducing the environmental impact of synthetic coating materials (Sohail et al., 2022; Langlet et al., 2024). In addition, the more effective incorporation of microbial inoculants and plant biostimulants into coating systems offers new opportunities for improving the resistance of seeds to biotic and abiotic stresses (Afzal et al., 2020). The development of smart coatings that can release active substances in a controlled manner in response to environmental signals such as humidity, temperature, or pathogen presence can contribute to the widespread adoption of precise and needs-based applications in the future. Additionally, faster determination of appropriate coating compositions for various vegetable types and production conditions can be made possible through the use of artificial intelligence and data-driven approaches in coating formulation design. Developing coating formulations tailored to crop and environmental conditions holds great promise for enhancing seed performance and the resilience of production systems in production areas facing stresses like drought, salinity, and high temperatures. Additionally, tracking seed variety, applied coating, and batch information throughout the production chain can be facilitated by the development of digital systems that allow the traceability of coated seeds.

CONCLUSION

By combining developments in materials science, biotechnology, and precision agriculture, seed coating technologies have developed into a sophisticated platform for seed development. In addition to improving mechanical planting performance, targeted germination, seedling emergence, plant protection, and nutrient delivery, modern coating systems also allow for a decrease in chemical inputs. The sustainability and resource efficiency of vegetable production systems are anticipated to be further improved by emerging technologies like biodegradable polymers, microbial inoculants, nanotechnology, environmentally responsive smart coatings, and AI-powered formulation designs. In order to meet the increasing demand for high-quality,

long-lasting, and ecologically friendly vegetable production, coating formulations must be continuously developed and optimized for various vegetable types and production conditions.

REFERENCES

Afzal, I., Javed, T., Amirkhani, M., & Taylor, A. G. 2020. Modern Seed Technology: Seed Coating Delivery Systems for Enhancing Seed and Crop Performance. Agriculture, 10(11), 526. https://doi.org/10.3390/agriculture10110526

Al Jabri, H., Saleem, M. H., Rizwan, M., Hussain, I., Usman, K., & Alsafran, M. 2022. Zinc oxide nanoparticles and their biosynthesis: overview. Life, 12(4), 594.

Amirkhani, M., Netravali, A. N., Huang, W., & Taylor, A. G. 2016. Investigation of soy protein–based biostimulant seed coating for broccoli seedling and plant growth enhancement. HortScience, 51(9), 1121-1126.

Biswal, B. C., Mishra, S., Jaiswal, K., Mohanty, S., & Dash, D. (2026). Seed coating innovations for sustainable horticulture enhancing germination, crop resilience and resource efficiency. Discover Sustainability, 7(1), 426. https://doi.org/10.1007/s43621-026-02826-5

Chen, B., Fu, J., Zheng, Y., Liu, G., Fu, L., & Li, Y. 2024. Biostimulants in agriculture: innovations in seed treatment and coating technologies. Seed Science and Technology, 52(3), 227-249.

Cho, S., Seo, H., Oh, Y., Lee, E., Choi, I., Jang, Y., Song, Y., & Min, T. 2000. Selection of coating materials and binders for pelleting onion (Allium cepa L.) seed. Journal of the Korean Society for Horticultural Science, 41, 593–597.

Deaker, R., Roughley, R. J., & Kennedy, I. R. 2004. Legume seed inoculation technology—A review. Soil Biology and Biochemistry, 36(8), 1275–1288.

Dong, Y. J., He, M. R., Wang, Z. L., Chen, W. F., Hou, J., Qiu, X. K., & Zhang, J. W. 2016. Effects of new coated release fertilizer on the growth of maize. Journal of soil science and plant nutrition, 16(3), 637-649.

Farooq, M., Wahid, A., & Siddique, K. H. 2012. Micronutrient application through seed treatments: a review. Journal of soil science and plant nutrition, 12(1), 125-142.

Javed, T., Afzal, I., Shabbir, R., Ikram, K., Zaheer, M. S., Faheem, M., ... & Iqbal, J. 2022. Seed coating technology: An innovative and sustainable approach for improving seed quality and crop performance. Journal of the Saudi Society of Agricultural Sciences, 21(8), 536-545. https://doi.org/10.1016/j.jssas.2022.03.003

Gong, M., Zheng, M., Li, X., Li, Y., Qiao, Z., Ren, Y., & Lv, G. 2025. A microbial microencapsulation design of seed coating technology to boost wheat seed performance in saline soil. Chemical and Biological Technologies in Agriculture, 12(1), 97.

Gorim, L., & Asch, F. 2012. Effects of composition and share of seed coatings on the mobilization efficiency of cereal seeds during germination. Journal of agronomy and crop science, 198(2), 81-91.

Gorim, L., & Asch, F. 2017. Seed coating increases seed moisture uptake and restricts embryonic oxygen availability in germinating cereal seeds. Biology, 6(2), 31.

Głodowska, M., Schwinghamer, T., Husk, B., & Smith, D. 2017. Biochar based inoculants improve soybean growth and nodulation. Agricultural Sciences, 8, 1048–1064.

Hacıyusufoğlu, A. F., & Akbaş, T. 2019. Some physico-mechanical properties of carrot (Daucus carota L.), cherry belle (Rhaphanus sativus L.) and nigella (Nigella sativa L.) seeds coated with pellets. Akademik Ziraat Dergisi, 8(1), 21-26.

Halmer, P. 2008. Seed technology and seed enhancement. Acta Horticulturae, 771, 17–26.

Halmer, P. 2000. Commercial seed treatment technology. In M. Black & J. D. Bewley (Eds.), Seed technology and its biological basis (pp. 257–286). Sheffield Academic Press.

Hill, H. J. 1999. Recent developments in seed technology. Journal of New seeds, 1(1), 105-112.

Kangsopa, J., Hynes, R.K., Siri, B. 2018. Lettuce seeds pelleting: A new bilayer matrix for lettuce (Lactuca sativa) seeds. Seed Science and Technology, 46(3): 521-531.
Karayel, D., Hacıyusufoğlu, A. F., Çanakcı, M., & Topakcı, M. 2020. Performance of a large seed vacuum planter for bare and pelleted onion seeds. Mediterranean Agricultural Sciences, 33(2), 253-258.
Kimmelshue, C., Goggi, A. S., & Cademartiri, R. 2019. The use of biological seed coatings based on bacteriophages and polymers against Clavibacter michiganensis subsp. nebraskensis in maize seeds. Scientific reports, 9(1), 17950.
Langlet, R., Valentin, R., Morard, M., & Raynaud, C. D. 2024. Transitioning to Microplastic-Free Seed Coatings: Challenges and Solutions. Polymers, 16(14), 1969.
Ma, Y. 2019. Seed coating with beneficial microorganisms for precision agriculture. Biotechnology advances, 37(7), 107423.
Maity, A., Vijay, D., Gupta, C. K., Singh, S. K., Wasnik, V. K., & Ghosh, P. K. 2018. Polymer film coating mediated delivery of pesticide enhances germination, vigour and shelf life of cowpea seeds under biotic stress and natural ageing. Range Management and Agroforestry, (2), 215-223.
Nigro, M., Vinale, F., Lorito, M., Marra, R., Woo, S. L., & Lanzuise, S. 2014. Trichoderma-based products and their widespread use in agriculture. The Open Mycology Journal, 8(1), 71-126.
Okan, N. O. 2020. TiO2 nanopartiküllerin Nohut (Cicer arietinum L.) Bitkisininin In Vitro çimlenmesi, büyümesi Ve Rejenerasyonuna Etkileri (Master's thesis, Necmettin Erbakan University (Turkey)).
Olivera, M. E., Ferrari, L., Araoz, S., & Postulka, E. B. 2017. Improvements on physiological seed quality of Festuca arundinacea schreb by encrusting technology: Products and storage effects. Science, 10, 33-37.
Pedrini, S., Merritt, D. J., Stevens, J., & Dixon, K. 2017. Seed coating: science or marketing spin?. Trends in plant science, 22(2), 106-116.
Pedrini, S., Bhalsing, K., Cross, A. T., & Dixon, K. W. 2018. Protocol Development Tool (PDT) for seed encrusting and pelleting. Seed Science and Technology, 46(2), 393-405.
Pedrini, S., Balestrazzi, A., Madsen, M. D., Bhalsing, K., Hardegree, S. P., Dixon, K. W., & Kildisheva, O. A. 2020. Seed enhancement: getting seeds restoration-ready. Restoration Ecology, 28, S266-S275.
Qiu, J., Wang, R., Yan, J., & Hu, J. 2005. Seed film coating with uniconazole improves rape seedling growth in relation to physiological changes under waterlogging stress. Plant Growth Regulation, 47(1), 75-81.
Qiu, Y., Amirkhani, M., Mayton, H., Chen, Z., & Taylor, A. G. 2020. Biostimulant seed coating treatments to improve cover crop germination and seedling growth. Agronomy, 10(2), 154.
Rocha, I., Ma, Y., Souza-Alonso, P., Vosátka, M., Freitas, H., & Oliveira, R. S. 2019. Seed coating: a tool for delivering beneficial microbes to agricultural crops. Frontiers in plant science, 10, 1357.
Ryu, C. M., Kim, J., Choi, O., Kim, S. H., & Park, C. S. 2006. Improvement of biological control capacity of Paenibacillus polymyxa E681 by seed pelleting on sesame. Biological Control, 39(3), 282-289.
Singh, S., Pathak, S., Singh, J., Kamboj, M., & Singh, V. 2024. Nano-seed coating technologies for enhancing vegetable seed performance and stress tolerance. Journal of Agriculture and Ecology Research International, 25(6), 278-295.
Silva, F. G. D., Souza, E. S., Fonseca, J. D. D. S., Melo, S. D., Barros, J. E. K., & Barros, B. S. 2025. Effect of sugarcane bagasse-derived graphene oxide on bean seed germination. Materials Research, 28(Suppl 1), e20250060.

Sohail, M., Pirzada, T., Opperman, C. H., & Khan, S. A. 2022. Recent advances in seed coating technologies: transitioning toward sustainable agriculture. Green Chemistry, 24(16), 6052-6085.

Scott, J. M. 1989. Seed coatings and treatments and their effects on plant establishment. Advances in agronomy, 42, 43-83.

Skrzypczak, D., Jarzembowski, Ł., Izydorczyk, G., Mikula, K., Hoppe, V., Mielko, K. A., ... & Witek-Krowiak, A. 2021. Hydrogel alginate seed coating as an innovative method for delivering nutrients at the early stages of plant growth. Polymers, 13(23), 4233.

Taylor, A. G., & Harman, G. E. 1990. Concepts and technologies of selected seed treatments. Annual Review of Phytopathology, 28, 321–339.

Taylor, A. G., Allen, P. S., Bennett, M. A., Bradford, K. J., Burris, J. S., & Misra, M. K. (1998). Seed enhancements. Seed science research, 8(2), 245-256.

Taylor, A.G., Eckenrode, C.J., Straub, R.W., 2001. Seed coating technologies and treatments for onion: challenges and progress. HortScience, 36(2): 199- 205.

Taylor, A. G. 2020. Seed storage, germination, quality, and enhancements. In The physiology of vegetable crops (pp. 1-30). Wallingford UK: CABI.

Tufail, M. S., Krebs, G. L., Ahmad, J., & Southwell, A. 2018. The effect of Rhizobium seed inoculation on yields and quality of forage and seed of berseem clover (Trifolium alexandrinum L.) and its impact on soil fertility and smallholder farmer's income. Journal of Animal and Plant Sciences, 28, 1493–1500.

Willenborg, C. J., Gulden, R. H., Johnson, E. N., & Shirtliffe, S. J. 2004. Germination characteristics of polymer-coated canola (Brassica napus L.) seeds subjected to moisture stress at different temperatures. Agronomy journal, 96(3), 786-791.

Yogeesha, H. S., Panneerselvam, P., Bhanuprakash, K., & Hebbar, S. S. (2017). Standardization of protocol for seed pelleting in onion (Allium cepa) to improve seed handling.

Zhang, K., Khan, Z., Yu, Q., Qu, Z., Liu, J., Luo, T., ... & Luo, L. (2022). Biochar coating is a sustainable and economical approach to promote seed coating technology, seed germination, plant performance, and soil health. Plants, 11(21), 2864.

DAIRY WASTEWATER AS A SUBSTITUTE OF FAT IN GLUTEN FREE COOKIES FORMULATION: A CHALLENGE FOR AGROFOOD SUSTAINABILTY SECTOR

Nawal Benkrizi[1], Farouk Benabdi[2], Lahouari Dahloum[3], Sarah Hireche[1]

[1] Higher School of Agronomy, Agronomy Department, Mostaganem, Algeria

[2] Abdelhamid Ben Badis University, English Department, Laboratory of Languages, literature and Civilization/African History, Algeria

[3] Abdelhamid Ben Badis University, Agronomy Department, Laboratory of Agrobiotechnology, Genetic Resources, and Modelling, Mostaganem, Algeria

Corresponding author e-mail: n.benkrizi@esa-mosta.dz

ABSTRACT

Sustainable development has seen significant growth in recent years in agriculture, particularly in the food industry sector. As a part of this initiative, the food industry has focused on the valorization and recycling of industrial waste from food production in order to reduce costs and protect the environment. The most common example is the use of dairy effluents, such as dairy wastewater. Our study focused on the use of dairy wastewater, specifically first rinse water (excluding CIP system water), in the formulation of gluten-free and low-fat cookies. In this type of formulation, the purpose of dairy wastewater was to replace fat. First, a sample of this dairy wastewater, obtained from processed cheese production, was sampled and its quality was tested. The quality control included standard physicochemical, nutritional, and microbiological analyses. The physicochemical analysis involved measuring pH, Dornic acidity, density, conductivity, and freezing point; the nutritional analysis consisted of dry matter content, ash content, butyric acid content, protein content, and lactose content; the microbiological analysis encompassed the enumeration of *E. coli*, *Enterococci*, and *sulfite-reducing Clostridium*. Second, the cookies made with dairy wastewater were prepared using two gluten-free flours: oat and quinoa. After baking the cookies, a sensory evaluation by a panel of 30 tasters was conducted. The questionnaire of the sensory test determined the evaluation of the parameters of appearance, shape, taste, persistence, mouthfeel, smell and texture. Therefore, a total of 30 samples of dairy wastewater were analyzed. These samples were found to be relatively acidic, with a pH of approximately 6 and an acidity assessed at 53.33°D. The fat content was high, compared to the protein content, estimated at approximately 8.5% and 1.7% respectively. The tasters unanimously approved of the use of dairy wastewater in the preparation of the reduced-fat, gluten-free cookies.

Keywords: Sustainable development, Dairy wastewater, Valorization, Recycling dairy effluent Cookies.

INTRODUCTION

Sustainability is a global concept, driven by several factors, including environmental pollution. The concept of sustainability emerged in the agricultural sector to support farmers and entrepreneurs by offering potential solutions to their problems. Today, sustainable development also aims to address the challenges faced by manufacturers in the agri-food sector. The most common example of this is the dairy sector, known for its high daily production and significant organic waste output [1,2].

Dairy effluents vary depending on the type of production [3], ranging from whey to rinsing, washing, and disinfection water [4]. These effluents are rich in nutrients (proteins, fats, sugars, etc.) [5] as well as bacteria [6] that contaminate soils and groundwater. This dairy wastewater contamination has thus become a global problem [2], sparking the need for treatment and/or recycling. Nevertheless, most of the solutions have been limited to treating this dairy wastewater for the production of biomass, biopolymers, biofertilizers, and primarily energy [4]. Nowadays, research is moving towards new food solutions, which are increasingly focused on the reuse of nutrients from dairy wastewater in the formulation of other food products**,** such as the production of confectionery based on lactose from dairy wastewater [4].
Following this approach, this study aims to reuse the dairy wastewater from rinsing processed cheese in the production of gluten-free cookies. This dairy wastewater, a by-product of fermented food, will likely bring lightness and tenderness to the finished product. Furthermore, the dairy wastewater is incorporated through basic heat treatment and simple filtration, without resorting to complex processes such as extraction and concentration, thus minimizing production costs.

MATERIEL AND METHODS

This research was conducted from February 2025 to June 2025, where 30 samples of dairy wastewater were collected in sterile vials and subjected to analytical characterization tests (Figure 1). The dairy wastewater studied came from the first rinse of the pipes and tanks of the processed cheese production line and was free of any chemicals indicated by the clean-in-place process to ensure its safety for reuse in food. The dairy wastewater was filtered twice and treated at a high temperature (140°C for 2–3 seconds).

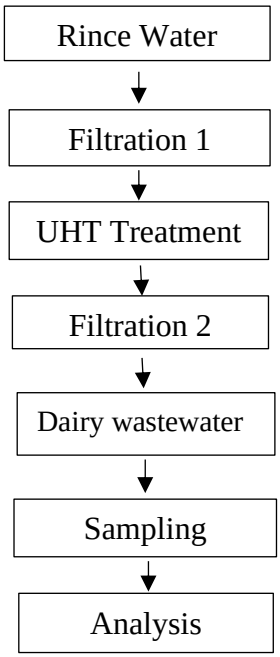

Figure 1: Dairy wastewater diagram process methodology

These samples first underwent microbiological analysis to ensure the safety of this water type. The parameters analyzed included the detection of fecal contaminants related to dairy, such as *E. coli* (ISO 9308-1:2014), *Enterococci* (ISO 7899-2:2000), and *sulfite-reducing Clostridium* (ISO 15213:2023). However, physicochemical and nutritional parameters, including density, conductivity, freezing point, ash content, protein content, and lactose content were measured directly using an Ultrasonic Portable Milkanalyser (Milkotronic Ltd-Bulgaria). Therefore, pH was measured using a pH meter; acidity was determined via an acid-base titration with sodium hydroxide (N/9) and phenolphthalein as a color indicator. The total dry extract was determined with a desiccator at 120°C until evaporation of water and the butyric content was quantified by the conventional Van Gulik Method (ISO 3433: 2008).

Following the quality control of the dairy wastewater samples, they were incorporated into quinoa and oat-based cookies. It is important to note that in this study, the dairy wastewater replaced the usual fat, which is butter. The cookie recipe included, in the following order of ingredients: dairy wastewater, sugar, salt, egg, flour, baking powder, chocolate chips, and dried fruit (Figure 2). The dough was then refrigerated for approximately one hour to make it pliable. The cookie dough was baked at approximately 180°C for 15 minutes, then cooled and packaged in boxes. Finally, the prepared cookies were analyzed by a panel of 30 untrained tasters; the coded samples were placed on plates with a glass of water. The tasting sheet allowed for the evaluation of appearance, shape, taste, persistence, mouthfeel, smell, crunchiness, sandy texture, tenderness, softness, moisture and friability on a hedonic scale of 1 to 9.

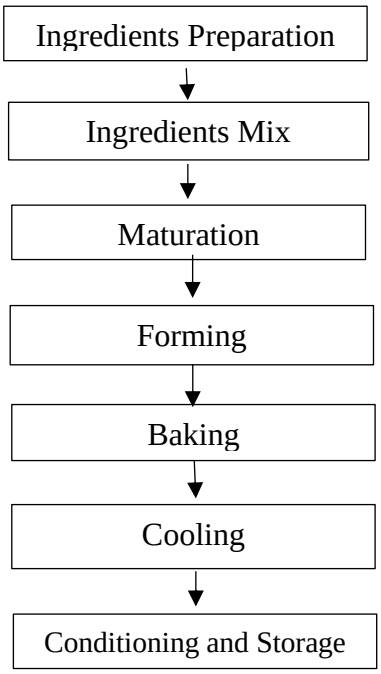

Figure 2: Diagram of cookies process

RESULTS AND DISCUSSION

After the recovery of dairy wastewater from cheese production, it appeared as a solid state. Its texture was similar to that of creamy butter or a spread (Figure 3). Microbiological analyses revealed that the dairy wastewater was free of fecal contamination.

Figure 3: Dairy wastewater aspect

Regarding the physicochemical parameters, the results showed interesting and exploitable properties (Table 1). The pH was relatively more acidic than milk (6.09 vs. 6.4) and more alkaline than cheese (5.8). Our results were similar to those of [7], where the pH of the dairy wastewater was measured at 6.07. As for acidity, it is relatively high, measured at 53.33°D, compared to that of milk, which is normalized to 18°D. However, it was observed that the acidity of the dairy wastewater varied depending on the processed cheese production and the amount of water used for rinsing (recipe and residues), ranging between 50°D and 60°D. Our results confirm the hypothesis put forward by [8] that the properties of the dairy wastewater depend on both the type of product and the process. The conductivity value fluctuated at 4.89 mS cm−1, corresponding to the quantity of electrolytes (minerals). This value was almost identical to that of [7], which was 4.75 mS cm−1.

Table 1: Physicochemical characterization of dairy wastewater

Parameters	**pH**	**Acidity**	**Density**	**Conductivity**	**Frozen Point**
Dairy wastewater	6.09±0.25	53.33±5.77	14.72±1.87	4.89±0.81	-0.326±0.03

Similarly, in terms of nutritional properties, dairy wastewater exhibited a relatively rich nutrient composition (Table 2). Its total dry extract (TDE) proved quite interesting, approaching that of milk. Dairy wastewater showed a high mineral content (which explains the conductivity results) and a high fat content of 1.046% and 8.5%, respectively. However, dairy wastewater was low in protein and lactose content with 1.74% and 2.62%, respectively.

Table 2: Nutritional characterization of dairy wastewater

Parameters	**TDE**	**Ash**	**BAC**	**PC**	**Lac**
Dairy wastewater	13.35±8.87	1.046±0.71	8.5±0.5	1.74±0.29	2.62±0.43

TDE: Total dry extract; BAC: Butyric acid content; PC: Protein content; Lac: Lactose

After baking, the cookies were cooled and arranged on plates (Figure 4). These cookies were presented to an untrained panel of 30 consumers, who were given tasting notes. The results of the sensory analysis are shown in Figure 5.

Figure 4: Oat and quinoa cookies presentation

The scores were satisfactory, ranging from 6 to 7.5 for most attributes, including appearance, shape, taste, persistence, mouthfeel, smell, tenderness, softness, moisture, and friability. Only the crunchiness and sandy texture received scores below 4. This perception confirmed that the dairy wastewater, which is rich in fat, contributed to the cookies' tenderness and soft texture rather than the crunchy or sandy effect. These results are close to the original cookie recipe, as crunchiness is more associated to the puff pastry and the sandy texture to the shortbread biscuit.

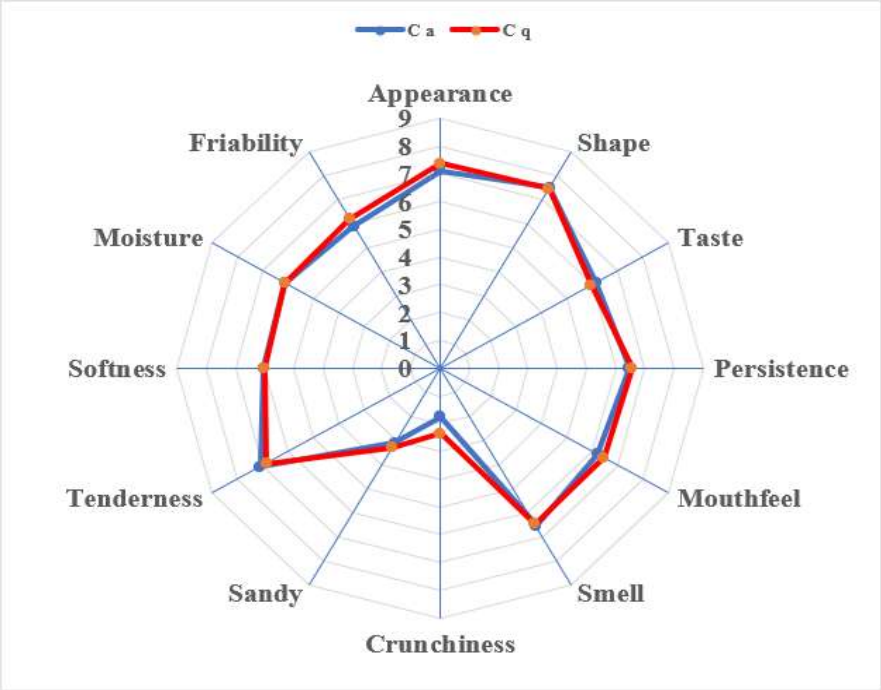

Figure 5: Sensory perception of the panelists
Ca: Oat cookies; Cq: Quinoa cookies

Regarding the use of gluten-free flours, it was observed that the shape, texture, aroma, and soft, moist feel were nearly identical for both cookies. However, the appearance, mouthfeel, and

crumbly texture (friability) were more appreciated in the quinoa flour cookies. Conversely, the oat flour cookies received higher marks for taste parameters, specifically sweetness and tenderness. Ultimately, the quinoa flour cookies were rated higher than the oat flour cookies.

CONCLUSION

This study demonstrated that dairy effluents, such as dairy wastewater, can be recycled into food products other than dairy. Dairy wastewater proved to be a good alternative for reducing production costs and preserving the environment. Dairy wastewater is a by-product composed of nutrients that can be used to enrich the production of other food products such as cookies. Dairy wastewater helped guarantee the quality of gluten-free cookies, while ensuring their sensory acceptability.

REFERENCES

[1] Albuquerque ML, Rodrigues-Silva A, Ribeiro AR, Chávez CM, de Cássia Santana G, da S. Martins A, Amorim CC, Starling MCVM. Ecotoxicity assessment of dairy wastewater: environmental risks and regulatory needs. Ecotoxicology (2026) 35:102 https://doi.org/10.1007/s10646-026-03088-7
[2] Patel MB, Solanki A, Patel k, Pal S. Study the efficiency of moving bed bio-film reactor (MBBR) for dairy wastewater treatment. International journal of novel research and development (2026) 11:6.
[3] Janczukowicz W, Debowski M, Pesta J, Zieliński M. Composition of wastewater originated from the particular sections of dairy production. Polish journal of natural sciences (2006) 20(1):307-324.
[4] Chalannavar RK, Gunagi VU, Hosamani PA, Divakar MS, Malabadi RB. Dairy waste by-products: An updated Review. International Journal of Biological and Pharmaceutical Sciences Archive (2026) 11(01):034-040 https://doi.org/10.53771/ijbpsa.2026.11.1.0013
[5] Shi W, Healy MG, Ashekuzzaman SM, Daly K, Leahy JJ, Fenton O. Dairy processing sludge and co-products: A review of present and future re-use pathways in agriculture. J. Clean. Prod. (2021) 314:128035.
[6] Garcha S, Verma N, Brar SK. Isolation, characterization and identification of microorganisms from unorganized dairy sector wastewater and sludge samples and evaluation of their biodegradability. Water Resour. Ind. (2016) 16:19-28.
[7] Lenartowicz M, Jurík L, Aydın E, Válek A, Kaletová T. Nutrient Removal and Recovery from Dairy Wastewater via Co-Cultivation of Scenedesmus obliquus and Lemna minor. Water (2026) 18:1859 https://doi.org/10.3390/w18151859
[8] Cvetković BR, Memišin N, Nježić Z, Pezo L, Juodeikiene G, Vitas J and Ilić N. Addressing wastewater challenges in the dairy industry: a focused case study. Journal of Dairy Research (2025) 92:135-145 https://doi.org/10.1017/ S0022029925101131

FARMING PRACTICES EFFECT ON THE QUALITY OF THE MONTBELIARDE BREED MILK FROM THE WILAYA OF MOSTAGANEM

Nawal Benkrizi[1], Farouk Benabdi [2], Lahouari Dahloum[3], Hanane Belharret [1]

[1] Higher School of Agronomy, Agronomy Department, Mostaganem, Algeria

[2] Abdelhamid Ben Badis University, English Department, Laboratory of Languages, literature and civilization/African History, Algeria

[3] Abdelhamid Ben Badis University, Agronomy Department, Laboratory of Agrobiotechnology, Genetic Resources, and Modelling, Mostaganem, Algeria

Corresponding author e-mail: n.benkrizi@esa-mosta.dz

ABSTRACT

As demonstrated by several studies, livestock farming practices are synonymous with yield and quality for farmers. They influence the quality of animal products as well as the zootechnical parameters of the animals themselves. However, dairy cattle are not exempted from this equation; where farming practices play a limiting role in mastering the quality of milk and dairy products. For this purpose, a study was conducted in this context on three farms in the wilaya of Mostaganem; it is a Mediterranean region located in the northwest of Algeria. These farms were characterized by raising only one breed of imported cows, belonging to the French breed 'the Montbéliarde'. Therefore, the experimental approach was structured around two axes; the first axis included a prospecting (survey) and the second axis an analytical part. First, the survey was carried out using a questionnaire that primarily gathered information on farming practices. Second, the sampling process consisted of six 250ml samples collected from each farm. They were collected in sterile vials after the morning mixed milking from several Montbéliarde cows. Then, the samples underwent physicochemical analysis and lactic acid bacteria enumeration to link the effects of farming practices to milk quality. The physicochemical analysis performed, by using a lactoscan, allowed for the determination of pH, density, conductivity, ash, protein content, fat content, and lactose content. The enumeration of lactic acid bacteria was carried out on MRS medium incubated at 30°C for 24 hours. A total of 18 milk samples were analyzed and showed a minimal fat content and a moderate protein content estimated at approximately 3%. The lactic acid bacteria count was approximately 260 x 10^6 UFC.

Keywords: Farming practices, Quality, Dairy cattle, Montbéliarde, Questionnaire.

INTRODUCTION

The Montbéliarde is the most common dairy breed in France after the Holstein [1]. However, the Montbéliarde is also considered as a dual-purpose breed, producing both milk and meat [2]. It is generally considered as a robust [3] and highly productive breed. In northern Cameroon, production reaches approximately 9.1 kg per day per cow [4]. This breed is also known for its high-quality of hard cheeses, such as Gruyère and Emmental [5][6].

Nevertheless, milk production depends on both internal breed-related factors and external factors [7]. The most studied limiting factors are external factors that are not genetically linked to the animal. Breeding practices have been the subject of several studies and have shown a significant effect on milk production. Therefore, this study aims to investigate the effect of

breeding practices implemented in the wilaya of Mostaganem on the quality of the imported Montbéliarde breed.

MATERIAL AND METHODES

This research was conducted in May 2023 in the wilaya of Mostaganem, a coastal city bordering the Mediterranean Sea to the north. It is characterized by a humid climate, mild temperatures, and average rainfall of approximately 90 mm.

This research focused on three farms raising Montbéliarde cows; the Montbéliarde is a mountain dairy breed imported from France. The aim of this study was to investigate the impact of farming practices implemented in the Mostaganem province on the milk quality of Montbéliarde cows. The farms ranged in size from 4,500 hectares to 8,600 hectares, a factor that directly influences cow behavior and milk production. A questionnaire was distributed to the farmers to gather as much information as possible about their farming practices. This questionnaire consisted of two parts: the first concerned the farmers' personal information, and the second covered the farming practices employed.

Subsequently, milk sampling was carried out in the morning, with six 250 ml samples collected from each farm. This sampling included mixed milk to randomize the samples and exclude internal factors affecting the cows (age and stage of lactation). These samples were collected in sterile containers to prevent and avoid contamination. The samples underwent physicochemical analysis using an Ultrasonic Portable Milkanalyser (Milkotronic Ltd-Bulgaria) to measure pH, density, conductivity, protein content, butyric acid content, lactose content, dry matter content degreased, and ash content (Figure 1).

Figure 1: Milkotronic Ltd-Bulgaria

Lactic acid bacteria counts were performed on MRS medium at 30°C for 24 hours. Decimal dilutions up to 10^{-9}, depending on the bacterial load, were prepared (Figure 2). Then each 1 ml dilution was inoculated using the pour-plate technique on MRS medium (Figure 2).

Figure 2: Enumeration of lactic acid bacteria

RESULTS AND DISCUSSION

The questionnaire results showed a similarity between farm 2 and farm 3 (Table 1). Only the breeder from farm 1 refused to disclose information about their farm; this explains the absence of results for farm 1. The results are identical for both farms (farm 2 and 3) regarding the farmer's level of education (primary), the breeding method (natural), the housing method (free-range), the water trough and its distribution method (collective/restricted), and the quantity of forage distributed per herd per day (4 kg).
Regarding the other parameters, milk production was found to be higher on farm 2 than on farm 3 (10L vs. 9L). It was also noted that the diet was richer at farm 2 than at farm 3, with diversified meals including forage, concentrate, hay, straw, and pasture. Conversely, farm 3 relied more heavily on concentrate (9 kg per herd per day) than on green forage, as clearly indicated by the pasture area, which was estimated at 3 hectares for farm 3 compared to 4 hectares for farm 2.

Table 1: Characteristics of Montbéliarde farms in Mostaganem

Parameters	**Farm 2**	**Farm 3**
Breeder institution	Primary	Primary
Milk production	10L	9L
Grazing area	4 Hectares	3 Hectares
Feeding	Forage, concentrate, pasture, hay and straw	Forage, concentrate and pasture
Forage ration/herd/day	4Kg	4Kg
Concentrate	Seeds and oilseed cakes	Not mentioned
Concentrate ratio/herd/day	4Kg	9Kg
Hay	Grasses and legumes	Not mentioned
Straw	Maize, sorghum and barley	Not mentioned
Unlimited water	No	No
Watering trough	Collective	Collective
Milking	Automatic and manual	Manual
Stalling	Free	Free
Reproduction	Naturel	Naturel

As for the physicochemical results shown in Table 2, they appeared to be within normal limits, with a pH between 6.4 and 6.8 and a density of 28 to 34 or 35. However, the pH of the milk

from farm 1 was high (7), suggesting that the cows were probably at the end of lactation or had an early infection.

Table 2: Physicochemical parameters of Montbéliarde milk from the 3 studied farms

Parameters **Farms**	**pH**	**D**	**C**
Farme1	7±0.15	33.2±0.11	5.02±0.07
Farm 2	6.57±0.0068	33.04±0.16	5.18±0.036
Farm 3	6.56±0.0087	33.13±0.16	5.1±0.017

D: Density; C: Conductivity

The results of the nutritional quality assessment of Montbéliarde milk are presented in Table 3. The fat content was higher in the milk from cows on farms 2 and 3, and rather low in the milk from cows on farm 1 (2.46% vs. 1.83%). According to the questionnaire results, on farms 2 and 3, the breeders fed their cows with concentrate, hence the higher fat content (2.44% on farm 2 and 2.48% on farm 3). The 1.83% fat content for the milk from farm 1 suggests that the cows were either not fed concentrate or received at least 4 kg/herd/day. Regarding protein content, the levels were higher in the milk from farms 2 and 3 than from farm 1 (3.04% vs. 3.03% vs. 2.95%, respectively). Our results are lower than those of [8], where the milk from Montbéliarde cows contained 3.58% fat and 3.18% protein. Their cows' diet was based primarily on corn and wheat bran. Similarly, for [9], the fat content of Montbéliarde milk was estimated at 3.8% and the protein at 3.3%, which is higher than our results. Their cows' diet was based on grazing in the summer and corn silage or haylage in the winter. The SNF was assessed at 8.68%, which represented a smaller quantity compared to our results estimated on average at 9.79%.
It is clear that feed and feed ratio influenced the composition of Montbéliarde milk. Lactose content was fairly similar for all the milk samples, around 4.4%, as lactose levels are generally stable in milk. Ash content was also stable and similar for all the milk samples.

Table 3: Nutritional parameters of Montbéliarde milk from the 3 studied farms

Parameters **Farms**	**F**	**P**	**L**	**SNF**	**Ash**
Farm 1	1.83±0.02	2.95±0.003	4.34±0.04	9.62±0.03	0.61±0.0001
Farm 2	2.44±0.03	3.04±0.008	4.53±0.005	9.89±0.03	0.65±0.0001
Farm 3	2.48±0.001	3.03±0.0001	4.53±0.002	9.86±0.042	0.63±0.0157

F: Fat; P: Protein; L: Lactose; SNF: Solid Non-Fat

The results obtained from the lactic acid bacteria count (Table 4) showed an increased count for the milk from farms 2 and 3 (222 x 10^6 CFU and 228 x 10^6 CFU, respectively). In contrast, the milk from farm 1 showed a lower count (144 x 10^6 CFU). Lactic acid bacteria represent the original flora of the milk; that is, they are naturally present and do not represent a source of contamination. Therefore, by comparing the quality parameter results with the lactic acid bacteria count, it can be observed that the lactic acid bacteria count was higher in the milk with a higher nutrient content, namely the milk from farms 2 and 3. By contrast, the count was lower in the milk from farm 1, where the nutrient content is lower. This suggests that the lactic acid bacteria load increased with the amount of nutrients in the milk., which is likely linked to the quantity and type of feed ingested by the Montbéliarde cow.

Table 4: Lactic Acid Flora

Parametres **Farmes**	**LAB**
Farm 1	144.10^6
Farm 2	222.10^6
Farm 3	228.10^6

LAB: Lactic Acid Bacteria

CONCLUSION

This study suggests that the Montbéliarde cow breed adapts easily to different climates. Originally from a rather cold climate, it has successfully adapted to warm temperate and humid climates, where its milk production is estimated at 9 liters to 10 liters per day. However, this production is linked to the farming practices employed. A well-balanced diet with a good ratio of feed and protein ensures good milk quality; a high quantity of concentrate increases the fat content. On the contrary, a high quantity of forage increases the protein content.
Farming practices also influence the load of lactic acid bacteria. An increase in nutrients leads to an increase in the quantity of lactic acid bacteria in the milk. It is important to know that lactic acid bacteria are a good indicator of milk quality, especially for milk intended for processing, specifically milk that will undergo fermentation. This process allows for the natural production of raw fermented products such as Lben (fermented milk), Raib (fermented milk), and more refined fermented products with enhanced flavors, such as yogurt and cheeses. This represents a good alternative for artisanal and/or traditional industries that prefer to rely on natural, practical, and inexpensive processes.

REFERENCES

[1] Balandraud N, Mosnier C, Delaby L, Dubief F. Holstein ou Montbéliarde : des différences phénotypiques aux conséquences économiques à l'échelle de l'exploitation. INRA Prod. Anim (2018) 31(4) : 337-352 https://doi.org/10.20870/productions-animales.2018.31.4.2394
[2] France Conseil Élevage. Résultats de contrôle laitier espèces bovine – France 2017. Institut de l'élevage (2018).
[3] Pires JAA, De La Torre A, Barreto-Mendes L, Cassar-Malek, Ortigues-Marty, Blanc F. Production and metabolic responses of Montbéliarde and Holstein cows during the periparturient period and a sequential feed-restriction challenge. J. Dairy Sci. (2025) 108(2) :1495-1508.
[4] Ngom RV, Akoussa AM, Ema PJN, Njapdounke PK, Yakouba B, Souley HEH, Koumai PH, Zangue HA. Performance, biosecurity practices and antimicrobial usage in Montbéliarde dairy farms in Northern Cameroon. Springer Nature Journal. Nature portfolio (2026) 16:21367 | https://doi.org/10.1038/s41598-026-50197-8
[5] Allouche L, Madani T, Mechmeche M, Bouchemal A. Reproductive performance of Montbeliard cows reared under subtropical environment: effects of heat stress and acclimatization duration. Livestock Research for Rural Development (2018) 30(7): 128.
[6] Sadek RR, Abou-Bakr S, Nigm AA, Ibrahim AEAM, Badr MM, Awad MAA. Evaluation of milk yield and reproductive performance of pure Holstein and its F1 crossbreds with Montbeliarde in Egypt. World's Veterinary Journal (2021) 11(3):489-497 https://dx.doi.org/10.54203/scil.2021.wvj63

[7] Bujko J, Candrák J, Strapák P, Hrnčár C, Bogucki M, Kasarda R. Evaluation of milk components and somatic cell count in Montbéliarde dairy cows. Contemporary Agriculture (2025) 74(3-4):149-153 https://doi.org/10.2478/contagri-2025-0018
[8] Larbaoui D, Meribai A, Kouidri A, Khodja AMN, Nouani A, Mouloud M. Influence of Dairy Cows Race and Diet on Milk Composition in Algeria. Life Sci J (2013) 10(4):3017-3025 http://www.lifesciencesite.com
[9] Sobczuk-Szul M, Pogorzelska-Przybyłek P, Momot M, Nogalski Z. Content of Selected Macroelements and Zinc in Relation to Stage of Lactation of Montbéliarde and Polish Holstein-Friesian Cows. Appl. Sci. (2025) 15:144 https://doi.org/ 10.3390/app15010144

TAXONOMIC REVISION OF THE FAMILY LILIACEAE IN THE FLORA OF ALBANIA

Saliaj O[1]., Gjeta E.[1], Mullaj A.[2]

[1]Research Center of Flora and Fauna, Faculty of Natural Sciences, University of Tirana, Albania

[2]Center for Scientific Research, Projects and Innovation, University College of Business, Tirana, Albania

ABSTRACT

The family Liliaceae has historically represented one of the most broadly circumscribed groups within monocotyledonous plants in the Albanian flora. In *Flora e Shqipërisë* (*Flora of Albania*, Vol. 4), the family was treated in a traditional taxonomic sense and included 25 genera characterized by considerable morphological diversity. However, advances in molecular phylogenetics and the development of modern classification systems during recent decades have substantially redefined the circumscription of Liliaceae, resulting in the transfer of numerous genera to several distinct families. The present study provides a critical taxonomic revision of Liliaceae in Albania through a comparative analysis between the traditional treatment presented in *Flora of Albania* and contemporary international taxonomic databases, including *Euro+Med PlantBase* and the *Plants of the World Online* (POWO) database of the Royal Botanic Gardens, Kew. Additional information was obtained from the *Distribution Atlas of Vascular Plants in Albania*, the *Checklist of Albanian Flora*, and other relevant botanical and taxonomic literature. The results demonstrate that, of the 25 genera traditionally included within Liliaceae, only five genera are currently accepted as members of the family: *Erythronium*, *Fritillaria*, *Gagea*, *Lilium*, and *Tulipa*. Most of the remaining genera have been reassigned to families such as Asparagaceae, Amaryllidaceae, Asphodelaceae, Colchicaceae, Melanthiaceae, Smilacaceae, and Nartheciaceae. The revised Albanian Liliaceae flora includes taxa of considerable floristic, phytogeographical, and conservation importance, including endemic and subendemic species such as *Tulipa albanica*, *Tulipa kosovarica*, *Fritillaria ionica*, and *Lilium chalcedonicum*. This study highlights the importance of integrating modern phylogenetic concepts into national floristic treatments and contributes to the taxonomic standardization and updated interpretation of the Albanian vascular flora.

Keywords: Albania; Balkan flora; floristic revision; Liliaceae; nomenclature; plant taxonomy

INTRODUCTION

The flora of Albania has been the subject of extensive botanical research over many decades. *Flora e Shqipërisë* (*Flora of Albania)* represents the most comprehensive and important contribution to the study of the country's vascular plants. It documents 3,235 species and 689 subspecies, grouped into 165 families and 300 genera. The work was published in four volumes (I, 1988; II, 1992; III, 1996; IV, 2000) by the Institute of Biological Research of the Academy of Sciences of Albania. The compilation of this flora was primarily based on material preserved in the National Herbarium, comprising more than 150,000 specimens, and also incorporated numerous contributions from Albanian and international botanists who conducted field expeditions throughout the country.

Liliaceae family is of considerable botanical and ecological importance, comprising many species with wide distribution in temperate regions of the Northern Hemisphere. Globally, it includes taxa of significant horticultural, medicinal, and ornamental value, while in the Balkan Peninsula it is represented by several native species adapted to diverse habitats ranging from lowland ecosystems to alpine zones. In the context of Balkan flora, *Liliaceae* contributes to regional plant diversity and serves as an important group for biogeographical and evolutionary studies, particularly due to its complex taxonomic history and recent revisions based on molecular data (Euro+Med PlantBase; Plants of the World Online).

The family *Liliaceae*, as treated in *Flora e Shqipërisë* (Vol. 4), included 25 genera. However, according to updated taxonomic revisions based on modern phylogenetic systems and international databases such as the Euro+Med PlantBase and Plants of the World Online, the circumscription of this family has been significantly reduced. These revisions reflect major advances in plant systematics, resulting in a redefinition of generic boundaries and the reassignment of many taxa formerly included in *Liliaceae* to other families.

This study aims to reassess the Liliaceae taxa reported in Albania based on *Flora e Shqipërisë* and update their nomenclature in accordance with international databases.

MATERIALS AND METHODS

The study was based on a critical revision of the family Liliaceae in Albania through the comparison of traditional floristic sources with contemporary taxonomic databases and recent literature. Initially, volume 4 of *Flora e Shqipërisë* (*Flora of Albania*; Vangjeli et al., 2000) was systematically examined in order to compile the taxa traditionally included within Liliaceae in the Albanian flora.

Subsequently, the recorded taxa were revised and updated according to current taxonomic concepts using major international plant databases, including Euro+Med PlantBase and the Plants of the World Online (POWO) database of the Royal Botanic Gardens, Kew. Nomenclatural updates and taxonomic standardization were primarily based on Euro+Med PlantBase. Additional information was obtained from the *Distribution Atlas of Vascular Plants in Albania* (Barina, 2017), the *Checklist of Albanian Flora* (Barina et al., 2018), and other relevant published studies.

All collected data were critically evaluated and organized in order to identify taxonomic and nomenclatural changes and to provide an updated overview of the family Liliaceae in Albania according to contemporary classification systems.

RESULTS AND DISCUSSIONS

Following a critical revision of the family *Liliaceae* in *Flora e Shqipërisë* (Flora of Albania, Vol. 4; Vangjeli et al., 2000), it was found that the family was originally represented by 25 genera. However, according to updated taxonomic treatments based on Euro+Med PlantBase and the Plants of the World Online (POWO) database, only five genera are currently retained within *Liliaceae*: *Tulipa* L., *Lilium* Tourn. ex L., *Gagea* Salisb., *Fritillaria* Tourn. ex L., and *Erythronium* L.

The remaining genera have been redistributed into several families, most notably *Asparagaceae*, reflecting significant advances in phylogenetic understanding and modern taxonomic restructuring of monocotyledons. The full list of taxa and their updated classification is presented in Table 1.

Tab 1: Updated classification of *Liliaceae* genera in Albania

Genus	Family in *Flora e Shqipërisë*	Updated Family
Allium L.	Liliaceae Juss.	Amaryllidaceae J. St.-Hil.
Aloe L.	Liliaceae Juss.	Asphodelaceae Juss.
Anthericum L.	Liliaceae Juss.	Asparagaceae Juss.
Asparagus L.	Liliaceae Juss.	Asparagaceae Juss.
Asphodeline Rchb.	Liliaceae Juss.	Asphodelaceae Juss.
Asphodelus L.	Liliaceae Juss.	Asphodelaceae Juss.
Bellevalia Lapeyr.	Liliaceae Juss.	Asparagaceae Juss.
Colchicum L.	Liliaceae Juss.	Colchicaceae DC.
Convallaria L.	Liliaceae Juss.	Asparagaceae Juss.
Hyacinthus L.	Liliaceae Juss.	Asparagaceae Juss.
Muscari Mill.	Liliaceae Juss.	Asparagaceae Juss.
Narthecium Huds.	Liliaceae Juss.	Nartheciaceae Bjurzon
Ornithogalum L.	Liliaceae Juss.	Asparagaceae Juss.
Paris L.	Liliaceae Juss.	Melanthiaceae Batsch
Polygonatum Mill.	Liliaceae Juss.	Asparagaceae Juss.
Ruscus L.	Liliaceae Juss.	Asparagaceae Juss.
Scilla L.	Liliaceae Juss.	Asparagaceae Juss.
Smilax L.	Liliaceae Juss.	Smilacaceae Vent.
Urginea Steinh.	Liliaceae Juss.	Asparagaceae Juss.
Veratrum L.	Liliaceae Juss.	Melanthiaceae Batsch

For the five genera currently retained within *Liliaceae family (Tulipa* L., *Lilium* Tourn. ex L., *Gagea* Salisb., *Fritillaria* Tourn. ex L., and *Erythronium* L.), a reassessment was conducted based on updated taxonomic databases and other references described in the methodology. The corresponding data are presented in Table 2.

Tab 2: Representation of updated Liliaceae taxa in the National Herbarium of Albania

Genus	Taxon	Status in Albania
Erythronium L.	*Erythronium dens-canis* L.	Native
Fritillaria L.	*Fritillaria gussichiae* (Degen & Dörfl.) Rix	Native
	Fritillaria ionica Halácsy	Subendemic (Albania and Greece)
	Fritillaria ionica Halácsy subsp. *ionica*	Subendemic (Albania and Greece)
	Fritillaria ionica subsp. *thessala* (Boiss.) Kamari	Native
	Fritillaria macedonica Bornm.	Native
	Fritillaria messanensis Raf.	Native
	Fritillaria messanensis Raf. subsp. *messanensis*	Presence doubtful
	Fritillaria messanensis subsp. *gracilis* (Ebel) Rix	Native
	Fritillaria messanensis subsp. *neglecta* (Parl.) Nyman	Native
	Fritillaria montana W. D. J. Koch	Native
	Fritillaria pontica Wahlenb.	Native
Gagea Salisb.	*Gagea amblyopetala* Boiss. & Heldr	Native
	Gagea bohemica (Zauschn.) Schult. & Schult.f.	Native
	Gagea fragifera (Vill.) Ehr. Bayer & G. López	Native
	Gagea lutea (L.) Ker Gawl.	Native
	Gagea minima (L.) Ker Gawl.	Native
	Gagea pratensis (Pers.) Dumort.	Native
	Gagea pusilla (F. W. Schmidt) Sweet	Native
	Gagea villosa (M.Bieb.) Sweet	Native
Lilium L.	*Lilium albanicum* Griseb.	Native
	Lilium candidum L.	Native
	Lilium chalcedonicum L.	Subendemic (Albania and Greece)
	Lilium martagon L.	Native
	Lilium carniolicum Bernh. W. D. J. Koch	Native
	Lilium lancifolium Thunb.	Cultivated
Tulipa L.	*Tulipa albanica* Kit Tan & Shuka	Endemic
	Tulipa gesneriana L.	Cultivated
	Tulipa kosovarica Kit Tan, Shuka & Krasniqi	Subendemic (Albania and Kosovo)
	Tulipa sylvestris L.	Native
	Tulipa sylvestris subsp. *australis* (Link) Pamp.	Native

Table 2 summarizes the currently accepted genera and taxa of the family Liliaceae occurring in Albania, according to contemporary taxonomic concepts. The table also provides information on the phytogeographical status of each taxon in Albania, including native, endemic, subendemic, cultivated, and doubtful taxa.

Among the represented genera, *Fritillaria* is the richest in taxa, comprising several species and subspecies distributed across different ecological and mountainous regions of the country. The genus is of particular phytogeographical importance due to the presence of Balkan subendemics such as *Fritillaria ionica* Halácsy, restricted to Albania and Greece. The occurrence of multiple infraspecific taxa within *Fritillaria messanensis* Raf. further reflects the taxonomic complexity of the genus in the Balkan Peninsula. One taxon, *Fritillaria messanensis* Raf. subsp. *messanensis*, is considered doubtful in Albania, indicating the need for additional field investigations and herbarium revision to confirm its distribution.

The genus *Gagea* is represented by several native taxa, most of which are characteristic elements of open grasslands, rocky habitats, and montane ecosystems. Although none of the Albanian representatives are endemic, the genus contributes significantly to the spring geophyte flora of the country and demonstrates considerable ecological diversity.

The genus *Lilium* includes taxa of high ornamental and conservation value. Particularly noteworthy is *Lilium albanicum* Griseb., an important Balkan species associated with mountainous habitats. *Lilium chalcedonicum* L. is treated as a subendemic species shared between Albania and Greece, emphasizing the floristic connections between southwestern Balkan territories. The presence of cultivated taxa such as *Lilium lancifolium* Thunb. indicates the inclusion of non-native ornamental elements occasionally recorded in floristic sources.

The genus *Tulipa* is especially significant from a biogeographical and conservation perspective. *Tulipa albanica* Kit Tan & Shuka represents one of the most important endemic taxa of the Albanian flora and highlights Albania as a center of plant diversity in the Balkan Peninsula. In addition, *Tulipa kosovarica* Kit Tan, Shuka & Krasniqi is considered subendemic to Albania and Kosovo, further emphasizing the regional importance of the western Balkans for the diversification of the genus. Native representatives such as *Tulipa sylvestris* L. and its subspecies *australis* remain characteristic components of natural and semi-natural habitats, whereas *Tulipa gesneriana* L. is mainly cultivated.

Overall, the updated circumscription of Liliaceae in Albania reflects a substantial reduction in the number of included genera compared to the traditional treatment in *Flora e Shqipërisë*. The remaining taxa largely consist of bulbous geophytes with high floristic, phytogeographical, ornamental, and conservation significance. The presence of endemic and subendemic taxa further underlines the importance of Albania within the Balkan floristic region and highlights the need for continued taxonomic, chorological, and conservation-oriented studies on the family.

REFERENCES

Barina, Z., Somogyi, G., Pifko, D. & Rakaj, M. (2018). Checklist of vascular plants of Albania. – Phytotaxa 378: 1-339. https://doi.org/10.11646/phytotaxa.378.1.1.

Barina, Z. (2017). Distribution atlas of vascular plants in Albania – Budapest: Hungarian Natural History Museum, ISBN 978-963-9877-29-0

Vangjeli, J., Ruçi, B., Mullaj, A., Qosja, Xh., & Paparisto, K. (2000). *Flora e Shqipërisë* [Flora of Albania], Vol. 4. Tirana: Academy of Sciences of the Republic of Albania, Biological Research Center.

Euro+Med PlantBase (https://europlusmed.org/)

Plants of the World Online (POWO) database (Royal Botanic Gardens, Kew; https://powo.science.kew.org)

VEGETABLE POWDERS AS NATURAL COLORANTS İN BREAD: EFFECTS ON COLOR, PHYSİCAL, TEXTURAL, MOİSTURE, AND SENSORY PROPERTİES

Öznur EYMİR[1], Tekmile CANKURTARAN KÖMÜRCÜ[2]

Necmettin Erbakan University Meram Vocational School Food Processing Department Flour and Flour Products Technology Program, Konya, Türkiye
[2]Necmettin Erbakan University, Engineering Faculty, Food Engineering Department, Konya, Türkiye
Corresponding author e-mail: tekmilecankurtaran@gmail.com

ABSTRACT

The replacement of synthetic food colorants with natural alternatives has become an important strategy for developing clean-label bakery products. This study investigated the effects of pumpkin, red cabbage, spinach, red beet, and red bell pepper powders on the color, physical, textural, moisture, and sensory properties of wheat bread. Bread samples were prepared by replacing wheat flour with 4% vegetable powder using the straight dough method. Instrumental color measurements (L*, a*, b*, SI, and hue) were performed on both crust and crumb. Loaf weight, loaf volume, specific volume, moisture content, and texture profile parameters (hardness, adhesiveness, springiness, cohesiveness, chewiness, and resilience) were determined. Sensory evaluation was conducted using a 7-point hedonic scale to assess appearance, taste, odor, crumb structure, and overall acceptability. Vegetable powder incorporation significantly affected bread quality characteristics ($P < 0.05$). Spinach bread exhibited the lowest lightness, loaf volume, and specific volume, together with the highest hardness and chewiness, indicating the formation of a compact crumb structure. In contrast, red beet and red bell pepper breads maintained loaf volume and specific volume comparable to the control while producing attractive natural coloration. Moisture content varied significantly among formulations, ranging from approximately 36.4% to 39.2%, with spinach bread showing the highest moisture level and red beet bread the lowest. Sensory evaluation revealed that pumpkin and red bell pepper breads received sensory scores comparable to the control for most attributes, whereas red cabbage bread showed significantly lower consumer acceptance, particularly for taste and odor. Overall, the results demonstrate that vegetable powders can successfully replace synthetic colorants in bread production while generating distinctive natural colors. Among the evaluated vegetables, red bell pepper and pumpkin showed the greatest potential for developing clean-label colored breads by maintaining desirable technological quality together with high consumer acceptability.

Keywords: bread, vegetable powders, natural colorants, clean-label, sensory evaluation, texture profile analysis.

INTRODUCTION

Bread is one of the oldest and most widely consumed cereal-based foods worldwide, providing a substantial proportion of daily dietary energy and nutrients in many populations. Owing to its affordability, convenience, and consumer acceptance, bread has become an ideal vehicle for nutritional enrichment and functional ingredient incorporation (Cauvain, 2015; Gómez & Martinez, 2018). In recent years, increasing consumer awareness of the relationship between diet and health has encouraged the bakery industry to develop products with enhanced

nutritional quality while maintaining desirable technological and sensory properties (Dziki et al., 2021; Mir et al., 2017).

Visual appearance is among the first quality attributes influencing consumers' purchasing decisions, and color is considered one of the most critical factors affecting product acceptability. Consumers frequently associate bright and natural colors with freshness, quality, and nutritional value. Consequently, there has been growing interest in replacing synthetic food colorants with naturally derived pigments obtained from plant materials. This trend is strongly associated with the increasing demand for clean-label foods, where consumers prefer products formulated with recognizable, minimally processed, and naturally sourced ingredients (Asioli et al., 2017; Sigurdson et al., 2017).

Vegetables are excellent sources of natural pigments as well as bioactive compounds including phenolic compounds, carotenoids, betalains, chlorophylls, vitamins, minerals, and dietary fiber. Besides imparting attractive colors, these compounds may contribute antioxidant activity and improve the nutritional profile of bakery products (Sharma et al., 2022; Ktenioudaki & Gallagher, 2012). Pumpkin is particularly rich in carotenoids, especially β-carotene, which produces desirable yellow-orange coloration while serving as an important precursor of vitamin A (Murkovic et al., 2002). Red cabbage contains anthocyanins responsible for its characteristic purple coloration together with remarkable antioxidant capacity (Wu & Prior, 2005). Spinach provides chlorophyll pigments, lutein, minerals, and folates that contribute both nutritional value and green coloration (Ferruzzi & Blakeslee, 2007). Red beet is recognized as one of the richest dietary sources of betalains, pigments exhibiting high coloring capacity and antioxidant activity (Clifford et al., 2015). Likewise, red bell pepper contains considerable amounts of carotenoids such as capsanthin and capsorubin, which contribute vivid red coloration and antioxidant potential (Howard et al., 2000).

The incorporation of vegetable powders into bread formulations may significantly influence dough rheology and bread quality because these ingredients contain considerable amounts of dietary fiber and non-gluten components. Fiber competes with gluten proteins for water, interrupts gluten network formation, and alters gas retention during fermentation, thereby affecting loaf volume, crumb structure, and texture (Rosell et al., 2009; Gómez et al., 2011). Depending on the type and concentration of vegetable powder, changes in hardness, cohesiveness, springiness, chewiness, moisture retention, and crumb porosity have been reported in numerous studies (Ktenioudaki & Gallagher, 2012; Dziki et al., 2021).

Several researchers have investigated vegetable-enriched breads produced with pumpkin, beetroot, spinach, carrot, tomato, broccoli, or other vegetable powders. These studies generally reported improvements in antioxidant capacity, dietary fiber, mineral composition, and consumer perception of naturalness. However, technological responses varied considerably depending on the vegetable source because pigment composition, particle size, fiber characteristics, and water absorption capacity differ substantially among vegetables (Bhol & Bosco, 2014; Sharma et al., 2022). Therefore, comparative studies evaluating different vegetable powders under identical processing conditions remain limited and are necessary to identify suitable natural colorants capable of providing both desirable appearance and acceptable technological performance.

In the present study, wheat breads enriched with pumpkin, red cabbage, spinach, red beet, and red bell pepper powders were comparatively evaluated. Instrumental color measurements were performed to determine the effects of different vegetable pigments on bread color. In addition, loaf weight, loaf volume, specific volume, and texture profile parameters, including hardness, adhesiveness, springiness, cohesiveness, chewiness, and resilience, were determined to evaluate technological quality. The results provide valuable insights into the application of vegetable powders as natural coloring agents for developing clean-label bread products with improved visual appeal while maintaining satisfactory physical quality.

MATERIAL AND METHODS

Materials

Commercial refined wheat flour, compressed baker's yeast, salt, and tap water were used for bread production. Pumpkin (*Cucurbita moschata*), red cabbage (*Brassica oleracea* var. *capitata* f. rubra), spinach (*Spinacia oleracea*), red beet (*Beta vulgaris*), and red bell pepper (*Capsicum annuum* L.) powders were incorporated into the bread formulations as natural coloring agents. All ingredients were obtained from local suppliers and stored under appropriate conditions until use.

Bread preparation

Bread samples were prepared according to the straight dough method with slight modifications. The control formulation consisted of wheat flour, compressed yeast (3.0 g/100 g flour), salt (1.5 g/100 g flour), and water. Wheat flour was partially replaced with each vegetable powder at the predetermined substitution level 4%.

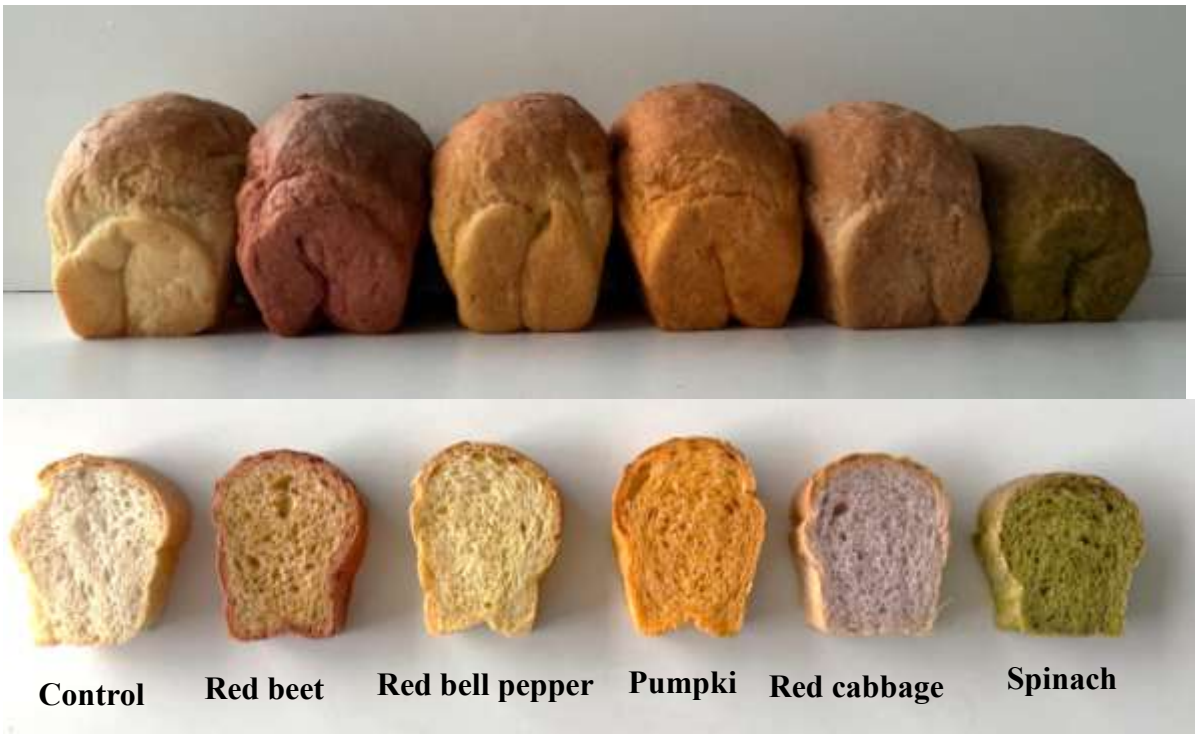

Figure 1. Representative external and crumb appearances of the control and vegetable-powder-enriched breads.

The ingredients were mixed using a laboratory mixer (Hobart N50, Offenburg, Germany) until optimum dough development. Doughs were fermented in a fermentation cabinet (Fimak FMD 16, Konya, Türkiye) at 30°C and 75–80% relative humidity for two successive 30-min bulk fermentation periods, with folding after each fermentation step. Subsequently, the doughs were moulded and subjected to a final proofing at 30°C for 60 min. Baking was carried out in a deck oven (Fimak Rokon Classic FRN10 G, Konya, Türkiye) preheated to 230 ± 5°C. After baking, loaves were cooled at room temperature for 60 min prior to physical analyses. Crust color, loaf weight, loaf volume, and specific volume were determined after cooling. Crumb color and texture profile analyses were performed after 24 h of storage (**Figure 1**).

Color measurement

The color characteristics of bread crust and crumb were determined using the procedure described in Section 2.2 (ham madde renk analiziyle aynı yöntem). Crumb color was measured on bread slices with a thickness of 2.5 cm, while crust color was measured directly on the loaf

surface. Five measurements were taken from different locations of each loaf, and the mean values were reported. Color parameters including L* (lightness), a* (redness/greenness), and b* (yellowness/blueness) were recorded.

Loaf weight, loaf volume, and specific volume

Bread loaves were weighed after cooling for 60 min following baking. Loaf volume was determined using the rapeseed displacement method according to Elgün et al. (2001). Specific volume was calculated as the ratio of loaf volume to loaf weight and expressed as cm^3/g.

$$\textit{Specific volume } (cm^3/g) = \textit{loaf volume } (cm^3) / \textit{loaf weight } (g)$$

Texture profile analysis (TPA)

Texture profile analysis was carried out using a TA.XT Plus Texture Analyzer (Stable Micro Systems Ltd., Surrey, UK) equipped with a 30-kg load cell and a 36-mm cylindrical probe. Bread slices (2.5 cm thickness) were analyzed after 24 h of storage at room temperature. The test conditions were set as follows: pre-test speed of 1 mm/s, test speed of 5 mm/s, post-test speed of 5 mm/s, and compression distance of 5 mm. The parameters determined included hardness, adhesiveness, springiness, cohesiveness, chewiness, and resilience.

Moisture content

Crumb moisture content was determined 24 h after baking by the oven-drying method. Homogenized crumb samples were dried at 105 °C to constant mass, and moisture content was expressed as percentage wet basis (AACC, 2000).

Sensory evaluation

Sensory evaluation was conducted with 20 untrained panelists from Necmettin Erbakan University who regularly consumed bakery products. Coded bread samples were presented in randomized order under ambient conditions. Taste, odor, appearance, crumb structure, and overall acceptability were evaluated using a 7-point hedonic scale (1 = dislike extremely; 7 = like extremely). Drinking water was provided for palate cleansing between samples (Meilgaard et al., 2016).

Statistical analysis

All analytical measurements were carried out in triplicate, and results were expressed as mean ± standard deviation. Data were analyzed using JMP statistical software, version 10.0 (SAS Institute Inc., Cary, NC, USA). One-way analysis of variance (ANOVA) was performed, and means were compared using Tukey's HSD test at $p < 0.05$.

RESULTS AND DISCUSSION

Crust color characteristics

The color parameters of breads enriched with different vegetable powders are presented in **Figure 2**. Incorporation of vegetable powders significantly affected the color characteristics of the bread samples ($P < 0.05$), confirming that the natural pigments present in the vegetables were retained to varying extents after the baking process. The extent of color modification depended on the pigment composition of each vegetable powder, resulting in distinct changes in lightness, redness, yellowness, color saturation, and hue angle. The L* value, representing lightness, decreased significantly in all vegetable-enriched breads compared with the control sample ($P < 0.05$). The control bread exhibited the highest L* value, indicating the lightest crumb, whereas spinach bread showed the lowest L* value, producing the darkest crumb among all formulations. Red beet bread also displayed relatively low lightness, while pumpkin, red cabbage, and red bell pepper breads exhibited intermediate L* values. The reduction in lightness can be attributed to the intrinsic color intensity of the vegetable powders, which replaced part of the wheat flour and consequently darkened the crumb. Similar decreases in L* values have been reported in breads fortified with spinach, beetroot, carrot, and other vegetable powders, where the presence of natural pigments reduced crumb brightness after baking

(Ktenioudaki & Gallagher, 2012; Sharma et al., 2022). In addition, thermal reactions occurring during baking, including Maillard reactions and caramelization, may further contribute to crumb darkening, particularly in formulations containing vegetables rich in reducing sugars.

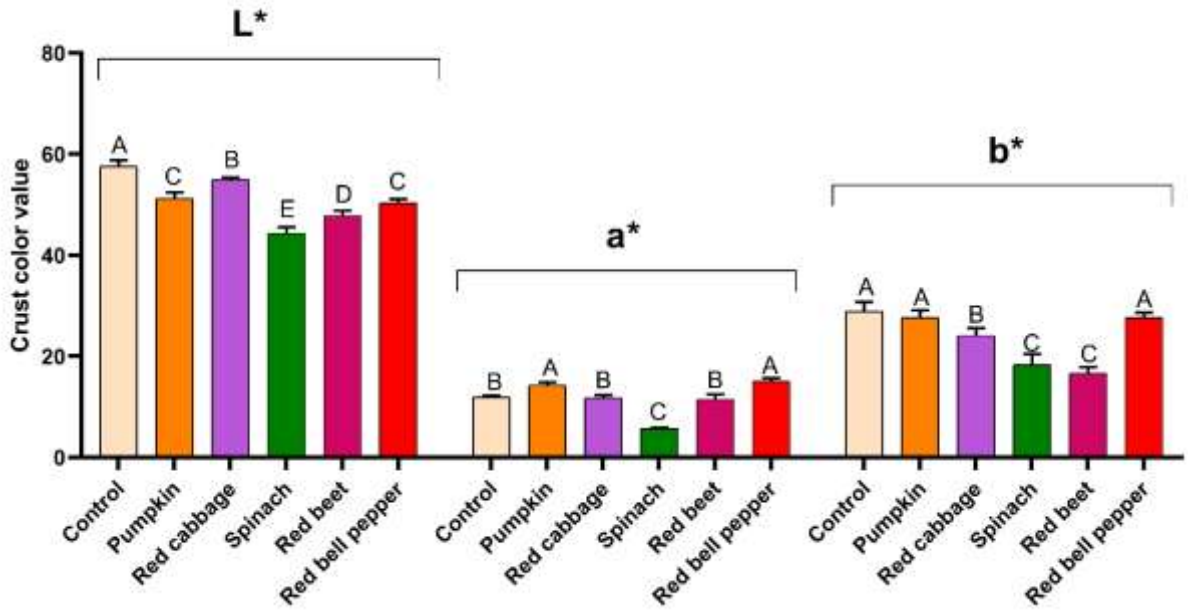

Figure 2. Crust L*, a*, and b* values of breads containing different vegetable powders. Different letters indicate significant differences ($p < 0.05$).

Significant differences were also observed in the a* values among bread samples. Red bell pepper and pumpkin breads exhibited the highest positive a* values, indicating enhanced redness, whereas spinach bread showed the lowest a* value because of the predominance of chlorophyll pigments that shifted the color toward the green region. Red cabbage and red beet breads produced intermediate redness values despite containing anthocyanins and betalains, respectively. The relatively moderate a* value observed in beet bread may be associated with the partial thermal degradation of betalains during baking, whereas anthocyanins in red cabbage are known to be sensitive to pH and temperature changes, which may also reduce color intensity. Previous studies have demonstrated that chlorophylls are susceptible to thermal degradation, while anthocyanins and betalains may undergo structural changes under baking conditions, resulting in reduced color stability compared with carotenoid pigments (Sigurdson et al., 2017; Clifford et al., 2015).

The b* values were likewise significantly influenced by vegetable powder incorporation. The highest b* values were observed in the control, pumpkin, and red bell pepper breads, whereas spinach and red beet breads exhibited the lowest values ($P < 0.05$). These findings are consistent with the pigment composition of the vegetables. Pumpkin and red bell pepper are rich in carotenoids, particularly β-carotene, capsanthin, and capsorubin, which impart yellow-orange coloration and therefore increase positive b* values. In contrast, chlorophyll-rich spinach and betalain-rich beetroot shifted the color away from the yellow axis, resulting in lower b* values. Similar trends have been reported in vegetable-fortified bakery products, where carotenoid-rich ingredients increased yellowness while green leafy vegetables reduced b* values because of chlorophyll dominance (Howard et al., 2000; Murkovic et al., 2002).

Color saturation, expressed as the saturation index, differed significantly among formulations **(Figure 3**). The control, pumpkin, and red bell pepper breads exhibited the highest chroma values, indicating brighter and more vivid colors. Conversely, spinach and red beet breads

presented significantly lower chroma values, suggesting less saturated and comparatively duller crumb colors. Chroma reflects the purity and intensity of color; therefore, higher values indicate a more vivid appearance that may enhance consumer perception of freshness and attractiveness. The reduced chroma observed in spinach bread may result from partial degradation of chlorophyll pigments during baking, whereas pigment interactions within the bread matrix could also contribute to lower saturation.

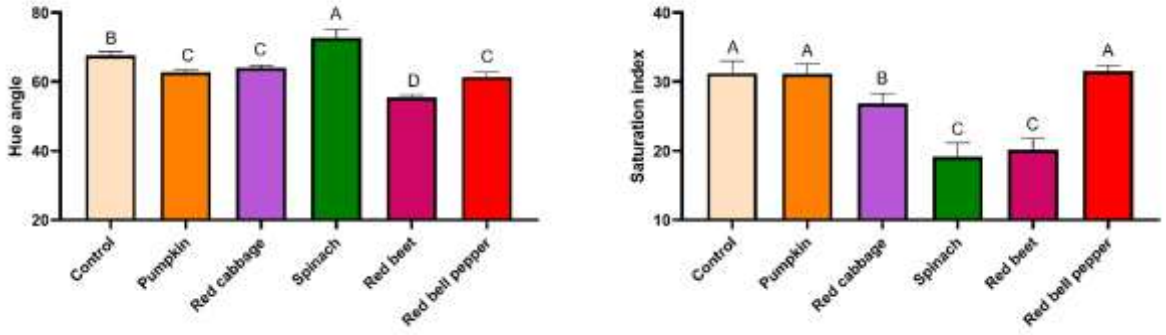

Figure 3. Crust hue angle and saturation index of breads containing different vegetable powders. Different letters indicate significant differences ($p < 0.05$).

The hue angle further differentiated the color characteristics of the bread samples. Spinach bread exhibited the highest hue angle, reflecting the dominance of green pigments, whereas red beet bread showed the lowest hue angle because of the strong contribution of red-purple betalains. Pumpkin, red cabbage, and red bell pepper breads displayed intermediate hue values, indicating balanced yellow, orange, and red color characteristics. Variations in hue angle demonstrate that each vegetable powder generated a distinct visual appearance, emphasizing the importance of pigment composition in determining the final bread color.

Crumb color characteristics

The instrumental color characteristics of bread crumbs prepared with different vegetable powders are presented in Figure 2. Similar to crust color, vegetable powder incorporation significantly affected all color parameters of the bread crumb ($P < 0.05$). However, the differences observed in crumb color more accurately reflect the contribution of the vegetable pigments because the crumb is less affected by Maillard browning and caramelization than the crust.

The L* values of bread crumbs decreased significantly following the incorporation of vegetable powders ($P < 0.05$). The control bread exhibited the highest lightness, whereas spinach bread showed the lowest L* value, indicating the darkest crumb among all formulations. Pumpkin bread remained relatively light, while red cabbage and red bell pepper produced intermediate L* values. The reduction in crumb lightness is mainly associated with the intrinsic color intensity of the incorporated vegetable powders, which diluted the white color of refined wheat flour. Spinach powder produced the greatest decrease in L* because of its high chlorophyll concentration, whereas the relatively high lightness of pumpkin bread can be attributed to the naturally lighter yellow pigments of carotenoids. Similar reductions in crumb lightness have been reported for breads enriched with spinach, beetroot, carrot, and other vegetable ingredients, where the replacement of wheat flour with pigmented plant materials resulted in darker crumb structures (Ktenioudaki & Gallagher, 2012; Dziki et al., 2021).

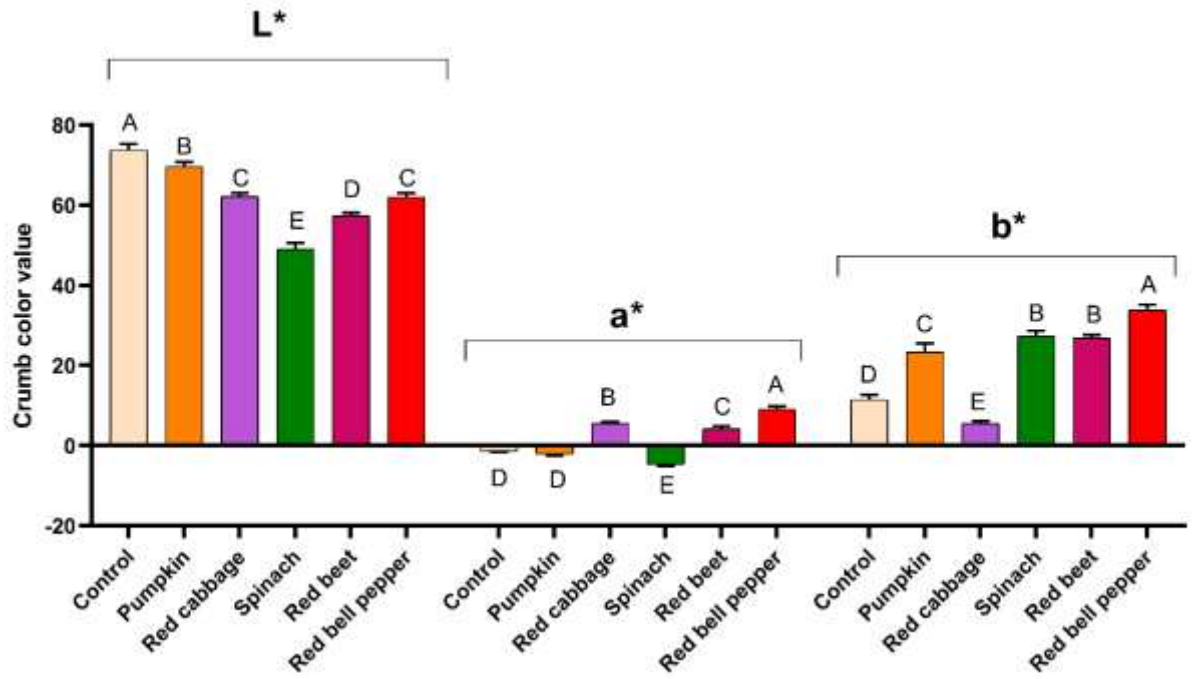

Figure 4. Crumb L*, a*, and b* values of breads containing different vegetable powders. Different letters indicate significant differences ($p < 0.05$).

Marked differences were also observed in the a* values. Pumpkin and control breads exhibited slightly negative a* values, indicating a tendency toward green rather than red. In contrast, red cabbage, red beet, and especially red bell pepper significantly increased positive a* values ($P < 0.05$), demonstrating enhanced redness of the crumb. Red bell pepper bread exhibited the highest a* value, reflecting the high concentration of carotenoid pigments, particularly capsanthin and capsorubin. Red cabbage and red beet also increased redness owing to anthocyanins and betalains, respectively. Conversely, spinach bread showed negative a* values because chlorophyll pigments shifted the color toward the green axis. These findings clearly demonstrate that the botanical origin of the vegetable powder largely determines the chromatic properties of bread crumb. Previous studies have similarly reported that chlorophyll-rich vegetables decrease a* values, whereas carotenoid-, anthocyanin-, and betalain-containing ingredients enhance redness in cereal products (Sigurdson et al., 2017; Clifford et al., 2015).

The b* values were significantly affected by vegetable type. Red bell pepper bread exhibited the highest b* value, followed by spinach and red beet breads, whereas the control bread showed comparatively lower yellowness. The lowest b* value was observed in red cabbage bread. The high yellowness of red bell pepper bread is attributed to its abundant carotenoid composition, while pumpkin also produced a noticeable increase in b* because of β-carotene. Although spinach contains green chlorophyll pigments, the presence of lutein and other yellow carotenoids likely contributed to its relatively high b* value. In contrast, anthocyanin-rich red cabbage shifted the overall color toward the purple region, thereby reducing yellowness. Similar behavior has been reported in previous studies evaluating the influence of vegetable pigments on bakery products (Howard et al., 2000; Murkovic et al., 2002).

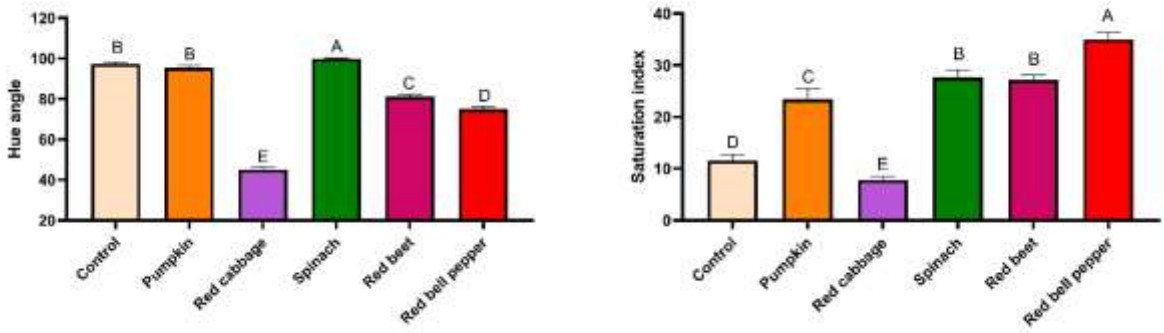

Figure 5. Crumb hue angle and saturation index of breads containing different vegetable powders. Different letters indicate significant differences ($p < 0.05$).

The saturation index demonstrated considerable variation among bread samples (**Figure 5**). Red bell pepper bread exhibited the highest chroma value, indicating the most vivid and saturated crumb color, whereas the control and red cabbage breads showed significantly lower chroma values ($P < 0.05$). Pumpkin, spinach, and red beet breads displayed intermediate saturation levels. Chroma represents color intensity, and higher values indicate stronger visual impact. The pronounced chroma of red bell pepper bread suggests that carotenoid pigments remained relatively stable during baking, whereas the lower saturation observed in red cabbage bread may be explained by the thermal sensitivity of anthocyanins, which are susceptible to degradation under baking conditions.

Significant differences were likewise observed for the hue angle, confirming that each vegetable powder generated a distinct color tone in the crumb. Spinach bread exhibited the highest hue angle, reflecting the predominance of green pigments. In contrast, red cabbage bread showed the lowest hue angle because of the strong contribution of anthocyanins, producing a purple-reddish crumb. Red beet and red bell pepper breads also exhibited reduced hue angles compared with the control, indicating a shift toward red coloration, whereas pumpkin bread maintained hue values close to those of the control due to its yellow-orange carotenoid profile.

Physical properties

Vegetable powder type significantly influenced loaf weight, loaf volume, and specific volume (**Figure 6**). Loaf weight was highest in spinach bread, while red cabbage bread was intermediate; the control, pumpkin, red beet, and red bell pepper breads formed a lower statistical group. Because dough pieces were prepared on an equal flour basis but water was added to obtain optimum dough development, the higher baked weight of spinach bread is consistent with greater water retention rather than greater dry-matter input.

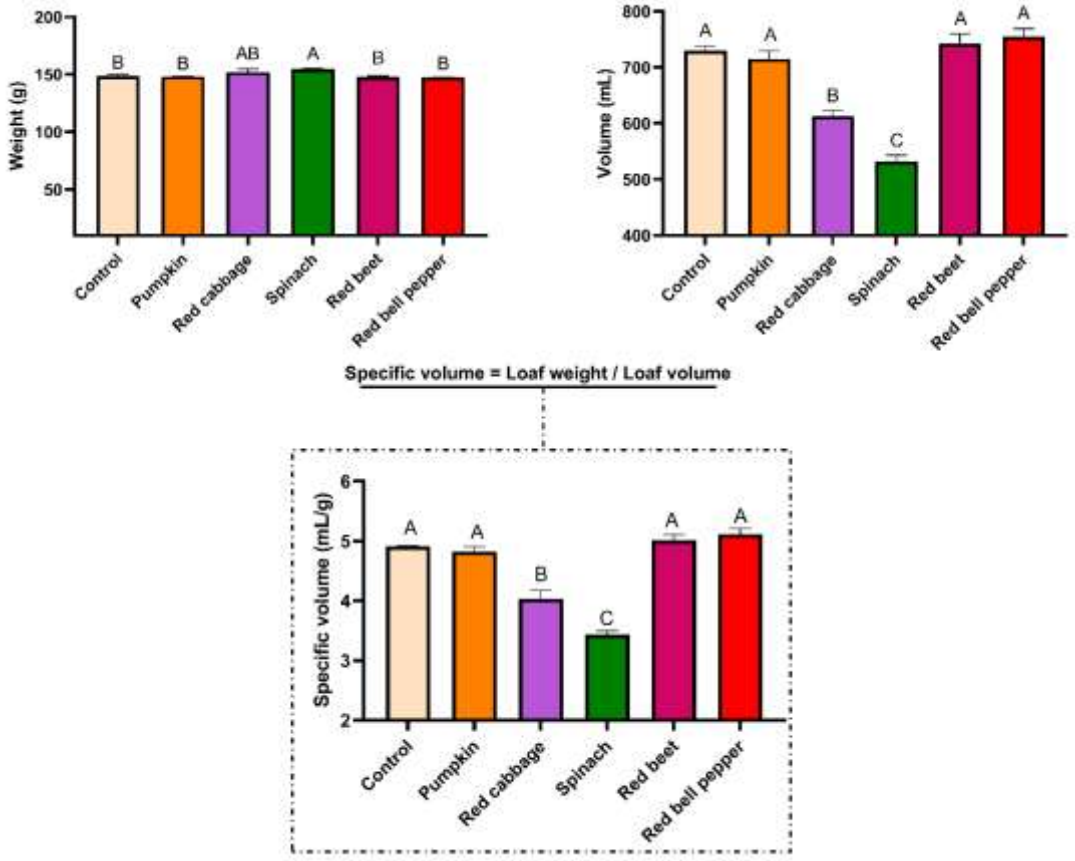

Figure 6. Loaf weight, loaf volume, and specific volume of breads containing different vegetable powders. Different letters indicate significant differences ($p < 0.05$).

The control, pumpkin, red beet, and red bell pepper breads had comparable loaf volumes and specific volumes. Red cabbage caused a moderate decrease, whereas spinach produced the lowest values for both parameters. These results indicate that the effect was not an inevitable consequence of adding 4% vegetable powder, but depended on powder composition. Fiber and non-gluten particles can dilute or disrupt the gluten network and modify water distribution, thereby reducing gas retention and loaf expansion (Ktenioudaki and Gallagher, 2012). Reduced volume after pumpkin enrichment has been reported at higher substitution levels (Różyło et al., 2014; Aljahani, 2022), while spinach powder has also been shown to alter the physicochemical properties of bread (Junejo et al., 2021). In the present study, the limited changes observed for pumpkin, red beet, and red bell pepper show that these powders were technologically compatible with the formulation at 4%.

Moisture content

Crumb moisture content differed significantly among the formulations ($p < 0.05$) and ranged from approximately 36.4 to 39.2% (Figure 7). Spinach bread had the highest moisture content, followed by red cabbage, whereas the control had an intermediate value. Pumpkin and red bell pepper were statistically similar to the control, while red beet bread had the lowest moisture content. The high moisture of spinach bread corresponded with its greater loaf weight and may reflect the water-binding capacity of its fiber-rich solids. Conversely, the lower moisture of red beet bread indicates that pigment source alone does not predict water retention. Ingredient-specific fiber structure, soluble solids, and interactions with the starch–gluten matrix are likely involved. Because formulation water was adjusted to optimum dough development, the

moisture differences should be interpreted as the combined result of water requirement and retention during baking.

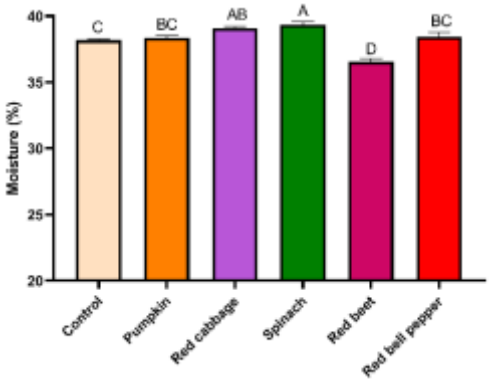

Figure 7. Moisture content of breads containing different vegetable powders. Different letters indicate significant differences ($p < 0.05$).

Texture profile properties

The texture profile parameters of the breads are presented in Table 1. Spinach bread had the highest hardness (2197.95 g) and chewiness (1097.29 g), consistent with its lower loaf volume and specific volume. A smaller, denser loaf generally contains less expanded gas-cell structure and therefore requires greater force during compression. Red cabbage bread also showed increased hardness (1574.12 g), although its chewiness did not differ from the control because its cohesiveness was significantly lower. By contrast, red bell pepper bread exhibited the lowest hardness (979.48 g), while pumpkin and red beet breads remained statistically comparable with the control.

Adhesiveness was markedly more negative in red cabbage bread, whereas the remaining samples did not differ significantly. Springiness was unaffected by vegetable powder type, indicating that the crumb recovered similarly after compression. Cohesiveness and resilience were lowest in red cabbage bread; spinach retained values comparable with the control despite its greater firmness. Thus, hardness alone did not describe the entire crumb response. The combination of high hardness and high chewiness in spinach bread points to a compact but internally cohesive matrix, whereas the red cabbage crumb was firm yet structurally less cohesive. Similar ingredient-dependent changes in loaf structure and texture have been observed in breads enriched with pumpkin, spinach, and beetroot ingredients (Różyło et al., 2014; Junejo et al., 2021; Cui et al., 2022).

Table 1. Texture profile parameters of breads containing different vegetable powders.

	Hardness (g)	Adhesiveness	Springiness	Cohesiveness	Chewiness (g)	Resilience
Control	1054.20±124.98bc	-6.77±11.12a	0.92±0.02a	0.53±0.04a	526.09±93.70b	0.16±0.02a
Pumpkin	1140.43±128.34bc	-6.79±5.51a	0.95±0.01a	0.47±0.02ab	510.32±79.64b	0.14±0.01ab
Red cabbage	1574.12±113.91b	-36.72±4.19b	0.91±0.05a	0.41±0.03b	565.85±49.37b	0.10±0.02b
Spinach	2197.95±377.89a	-2.51±2.17a	0.95±0.02a	0.52±0.05a	1097.29±25.28a	0.17±0.03a
Red beet	1154.41±131.83bc	-5.51±19.48a	0.90±0.07a	0.47±0.02ab	489.26±39.23b	0.14±0.01ab
Red bell pepper	979.48±112.32c	-1.47±1.00a	0.96±0.02a	0.48±0.03ab	444.37±26.95b	0.14±0.01ab

Values are mean ± standard deviation. Different lowercase letters within the same column indicate significant differences ($p < 0.05$).

Sensory properties

Sensory scores differed according to vegetable source (Figure 8). Control and red bell pepper breads received the highest taste scores, while pumpkin remained statistically close to the

control. Spinach and red beet received intermediate scores, and red cabbage was least preferred for taste. A similar pattern was observed for odor: control and red bell pepper breads had the highest ratings, pumpkin and spinach were comparable or only slightly lower, whereas red cabbage obtained the lowest score. The lower acceptance of red cabbage may be related to its characteristic sulfurous notes and the unfamiliar flavor–color combination in bread.

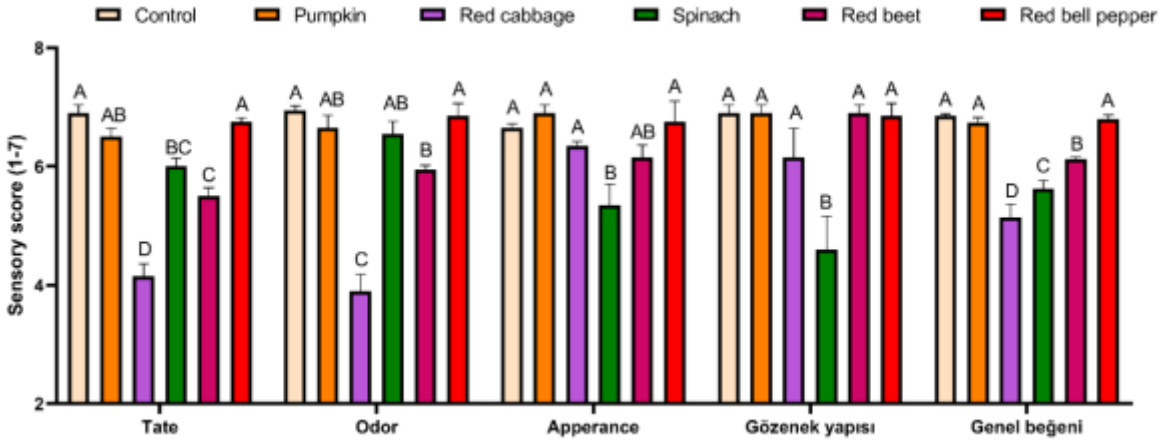

Figure 8. Sensory scores of breads containing different vegetable powders. Different letters within each attribute indicate significant differences ($p < 0.05$).

Appearance scores were high for the control, pumpkin, red bell pepper, and red beet breads. Red cabbage remained acceptable but was lower than the leading formulations, while spinach received the lowest appearance score. For crumb structure, the control, pumpkin, red beet, and red bell pepper breads formed the highest statistical group. Spinach received the lowest crumb-structure score, in agreement with its low specific volume and high instrumental hardness. Overall acceptability was highest for red bell pepper and was statistically comparable with the control and pumpkin breads. Red beet received a moderately high score, whereas spinach and especially red cabbage were less preferred. These findings demonstrate that a strong natural color does not by itself ensure acceptance; flavor compatibility and crumb structure are also decisive. The favorable performance of pumpkin agrees with reports that modest pumpkin incorporation can retain acceptable bread quality (Różyło et al., 2014; Aljahani, 2022), while the lower rating of spinach is consistent with the sensory limitations reported as spinach enrichment increases (Junejo et al., 2021).

CONCLUSION

Pumpkin, red cabbage, spinach, red beet, and red bell pepper powders produced clearly distinguishable natural colors in wheat bread at a 4% flour-replacement level. Their technological effects, however, were strongly dependent on vegetable type. Spinach caused the greatest structural change, as evidenced by higher moisture and loaf weight, lower loaf volume and specific volume, and increased hardness and chewiness. Red cabbage also reduced loaf expansion and cohesiveness and received the lowest taste, odor, and overall-acceptability ratings. In contrast, pumpkin and red bell pepper breads maintained physical and textural properties close to the control and achieved high sensory acceptance. Red beet produced attractive coloration and acceptable texture and sensory quality, although it had the lowest crumb moisture. Overall, red bell pepper and pumpkin powders were the most promising natural colorants under the tested conditions. The results apply specifically to the 4% incorporation level; future work should evaluate concentration-dependent responses, pigment

retention, antioxidant capacity, storage stability, and formulation-specific water absorption before industrial application.

REFERENCES

AACC. (2000). Approved Methods of the American Association of Cereal Chemists (10th ed.). American Association of Cereal Chemists, St. Paul, MN, USA.

Aljahani, A. H. (2022). Wheat-yellow pumpkin composite flour: Physico-functional, rheological, antioxidant potential and quality properties of pan and flat bread. Saudi Journal of Biological Sciences, 29(5), 3432–3439. https://doi.org/10.1016/j.sjbs.2022.02.040

Asioli, D., Aschemann-Witzel, J., Caputo, V., Vecchio, R., Annunziata, A., Næs, T., and Varela, P. (2017). Making sense of the "clean label" trends: A review of consumer food choice behavior and discussion of industry implications. Food Research International, 99, 58–71. https://doi.org/10.1016/j.foodres.2017.07.022

Cauvain, S. P. (2015). Technology of Breadmaking (3rd ed.). Springer, Cham. https://doi.org/10.1007/978-3-319-14687-4

Cui, R., Fei, Y., and Zhu, F. (2022). Physicochemical, structural and nutritional properties of steamed bread fortified with red beetroot powder and their changes during breadmaking process. Food Chemistry, 383, 132547. https://doi.org/10.1016/j.foodchem.2022.132547

Elgün, A., Ertugay, Z., Certel, M., and Kotancılar, H. G. (2001). Tahıl ve Ürünlerinde Analitik Kalite Kontrolü ve Laboratuvar Uygulama Kılavuzu (4th ed.). Atatürk University Faculty of Agriculture Publications, Erzurum, Türkiye.

Junejo, S. A., Rashid, A., Yang, L., Xu, Y., Kraithong, S., and Zhou, Y. (2021). Effects of spinach powder on the physicochemical and antioxidant properties of durum wheat bread. LWT, 150, 112058. https://doi.org/10.1016/j.lwt.2021.112058

Ktenioudaki, A., and Gallagher, E. (2012). Recent advances in the development of high-fibre baked products. Trends in Food Science & Technology, 28(1), 4–14. https://doi.org/10.1016/j.tifs.2012.06.004

Meilgaard, M. C., Civille, G. V., and Carr, B. T. (2016). Sensory Evaluation Techniques (5th ed.). CRC Press, Boca Raton, FL.

Różyło, R., Gawlik-Dziki, U., Dziki, D., Jakubczyk, A., Karaś, M., and Różyło, K. (2014). Wheat bread with pumpkin (Cucurbita maxima L.) pulp as a functional food product. Food Technology and Biotechnology, 52(4), 430–438. https://doi.org/10.17113/ftb.52.04.14.3587

Sigurdson, G. T., Tang, P., and Giusti, M. M. (2017). Natural colorants: Food colorants from natural sources. Annual Review of Food Science and Technology

DEVELOPMENT OF GLUTEN-FREE CHICKPEA CHIPS ENRICHED WITH COLD-PRESSED BLACK CUMIN SEED CAKE

Öznur EYMİR[1], Tekmile CANKURTARAN KÖMÜRCÜ[2]

Necmettin Erbakan University Meram Vocational School Food Processing Department Flour and Flour Products Technology Program, Konya, Türkiye

[2]Necmettin Erbakan University, Engineering Faculty, Food Engineering Department, Konya, Türkiye

Corresponding author e-mail: tekmilecankurtaran@gmail.com

ABSTRACT

The valorization of agro-industrial by-products offers a sustainable approach to reducing food-processing waste and developing value-added food products. Black cumin (*Nigella sativa* L.) seed cake, remaining after cold-pressed oil extraction, contains appreciable amounts of dietary fiber, protein, residual oil, and bioactive compounds and may therefore be utilized in gluten-free food formulations. This study investigated the effects of replacing chickpea flour with black cumin seed cake powder at levels of 1, 2, 3, 4, and 5% (w/w) on the quality characteristics of gluten-free chickpea chips. Instrumental color (L*, a*, b*, saturation index, and hue angle), physical properties (diameter, thickness, and spread ratio), textural characteristics (hardness and fracturability), and sensory acceptability were evaluated. Black cumin seed cake incorporation significantly affected the color and hardness of the chips ($p < 0.05$). Increasing the seed cake level progressively reduced L*, a*, b*, and saturation index values, resulting in darker and less saturated products. Chip diameter increased slightly, whereas thickness and spread ratio were not significantly affected. Hardness decreased progressively with increasing seed cake incorporation, while instrumental fracturability remained unchanged. Sensory evaluation showed that all formulations received scores above 5 on a 7-point hedonic scale. However, the samples containing 4 and 5% seed cake had significantly lower overall acceptability scores than the control, whereas formulations containing up to 3% maintained comparable overall acceptability. These findings indicate that cold-pressed black cumin seed cake can be incorporated into gluten-free chickpea chips, with 3% representing the highest tested level that maintained sensory acceptance comparable to the control. Its use provides a potential strategy for valorizing an oil-processing by-product in gluten-free snack formulations.

Keywords: black cumin seed cake, gluten-free chips, chickpea flour, by-product utilization, texture, color.

INTRODUCTION

The demand for gluten-free foods has increased in recent years due to the growing awareness of celiac disease, non-celiac gluten sensitivity, and consumer interest in alternative cereal and legume-based products. However, many commercially available gluten-free products are formulated mainly with refined starches and generally contain lower amounts of protein, dietary fiber, minerals, and bioactive compounds than their gluten-containing counterparts. Therefore, the development of nutritionally improved gluten-free products using naturally gluten-free and nutrient-dense raw materials remains an important area of food research.

Chickpea (*Cicer arietinum* L.) flour is a promising ingredient for gluten-free food formulations because of its favorable nutritional and technological properties. It is an important source of protein, complex carbohydrates, dietary fiber, vitamins, minerals, and unsaturated fatty acids. Compared with starch-based gluten-free ingredients, chickpea flour can improve the protein and fiber contents of gluten-free bakery and snack products. Its water-binding and structure-forming properties also support its use in products such as bread, biscuits, crackers, and chips (Melini et al., 2017; Vinod et al., 2023). Previous studies have demonstrated that chickpea flour can be successfully used as the principal ingredient in gluten-free crackers and can provide acceptable physical, textural, and sensory characteristics (Tomić et al., 2022).

In parallel with the development of nutrient-rich foods, the valorization of agro-industrial by-products has become increasingly important for reducing food-processing waste and promoting sustainable production. Cold-pressed oil production generates considerable quantities of seed cake, which is often used as animal feed or discarded despite containing valuable nutrients and bioactive constituents. Incorporating these by-products into food formulations can reduce waste while creating value-added functional ingredients.

Black cumin (*Nigella sativa* L.) is an oilseed traditionally used as a spice and valued for its characteristic aroma and bioactive components. After cold-press oil extraction, the remaining black cumin seed cake retains substantial amounts of protein, dietary fiber, residual oil, minerals, phenolic compounds, and other bioactive constituents (Zaky et al., 2021; Krawęcka et al., 2022). Black cumin seed cake has consequently attracted attention as a potential functional ingredient for the enrichment of bakery products, pasta, gluten-free foods, muffins, and fermented beverages. Its incorporation may increase the protein, dietary fiber, mineral, and antioxidant contents of food products while supporting the sustainable utilization of an oil-processing by-product (Krawęcka et al., 2022; Yabacı Karaoğlan, 2025). Despite its nutritional and sustainability advantages, the use of black cumin seed cake may also modify product quality. Its naturally dark color can decrease product lightness, while its fiber, protein, and residual lipid fractions can affect water absorption, dough structure, expansion, hardness, and fracture behavior. Moreover, the characteristic aroma and slightly bitter or intense flavor of black cumin may restrict its use at high incorporation levels (Yabacı Karaoğlan, 2025). Therefore, determining an appropriate incorporation level is important for balancing functional enrichment with technological quality and sensory acceptance. Oilseed press cakes have previously been evaluated in chickpea-based gluten-free products. Tomić et al. (2022), for example, demonstrated that pumpkin seed press cake could be successfully combined with chickpea flour to produce gluten-free crackers with improved nutritional and functional characteristics. Similarly, black cumin seed cake has been incorporated into pasta and bakery formulations, where it significantly affected product composition and technological properties (Krawęcka et al., 2022). Nevertheless, information concerning the use of cold-pressed black cumin seed cake in gluten-free chickpea chips, particularly its effects on color, physical dimensions, texture, and sensory acceptance, remains limited.

Therefore, the objective of the present study was to develop gluten-free chickpea chips enriched with cold-pressed black cumin seed cake powder at incorporation levels of 1, 2, 3, 4, and 5%. The effects of replacing chickpea flour with black cumin seed cake powder on the instrumental color, physical properties, textural characteristics, and sensory acceptability of the chips were investigated. The study also aimed to identify an appropriate incorporation level that would enable the valorization of black cumin seed cake without adversely affecting the technological and sensory quality of the final product.

MATERIAL AND METHODS

Materials

Chickpea flour, salt, garlic powder, red pepper powder, and cumin were obtained from a local retail market in Konya, Türkiye. Black cumin (*Nigella sativa* L.) seed cake, which remained after cold-press oil extraction, was obtained from (Superex Supercritical, Konya, Türkiye). Before use, the seed cake was ground using a laboratory mill and passed through a 300 µm sieve to obtain a uniform powder. All ingredients were stored under dry conditions at room temperature until use.

Experimental Design

Six gluten-free chickpea chip formulations were prepared: a control without black cumin seed cake powder and five formulations containing 1, 2, 3, 4, and 5% (w/w) seed cake powder. Black cumin seed cake powder was incorporated by replacing the corresponding amount of chickpea flour. The quantities of salt, garlic powder, red pepper powder, and cumin were kept constant in all formulations.

Production of Gluten-Free Chickpea Chips

Gluten-free chickpea chips were produced using a modified version of the method described by Aslan et al. (2023). Chickpea flour, black cumin seed cake powder, salt, garlic powder, red pepper powder, and cumin were mixed using a planetary mixer (Hobart N50; Hobart Canada Inc., Ontario, Canada). Water was gradually added during mixing until a homogeneous, firm, and workable dough was obtained. Because the water absorption capacity of the formulations varied depending on the seed cake level, the amount of water was adjusted according to the consistency of each dough.

The resulting dough was wrapped in cling film and rested in the dark at room temperature for 30 min to ensure adequate hydration. After hydration, the dough was divided into portions weighing 2.5 g. Each dough portion was compressed and baked between two Teflon-coated plates preheated to 300 °C for 2.5 min. The chips were subsequently cooled to room temperature (25 ± 2 °C), sealed in polyethylene bags, and stored at room temperature until analysis.

Color analysis

The surface color of the chickpea chip samples was measured using a Minolta CR-400 colorimeter (Minolta Camera Co., Ltd., Osaka, Japan). The results were expressed according to the CIELAB color system as L* (lightness; 0 = black and 100 = white), a* (redness-greenness), and b* (yellowness-blueness) (Francis, 1998).

The saturation index (SI), representing color intensity, was calculated using Equation (1):

$$SI = \sqrt{a^{*2} + b^{*2}}$$

The hue angle (h°) was calculated from the a* and b* values using Equation (2), with quadrant correction where necessary:

$$h^{\circ} = \tan^{-1}\left(\frac{b^{*}}{a^{*}}\right)$$

For samples with a* < 0 and b* > 0, 180° was added to the calculated value.

Determination of Physical Properties

The diameter and thickness of the chip samples were measured using a digital caliper with a precision of 0.01 mm (Mitutoyo, Japan). Measurements were performed at five different positions for each sample, and the mean values were reported in millimeters.
The spread ratio was calculated as the ratio of chip diameter to chip thickness according to Equation (3) (AACC, 2000):

$$Spread\ ratio = \left(\frac{Diameter\ (mm)}{Thickness\ (mm)}\right)$$

Instrumental Texture Analysis

The textural properties of the chickpea chips were determined 2 h after baking using a TA-XT2i Texture Analyzer (Stable Micro Systems, Surrey, UK) equipped with a three-point bending rig (HDP/3PB). The instrument was operated under the following conditions: 30 kg load cell, 1.0 mm/s pre-test speed, 3.0 mm/s test speed, 10.0 mm/s post-test speed, 5 mm test distance, and 50 g trigger force.
Hardness was defined as the maximum force required to break the sample and was expressed in grams. Fracturability was determined from the distance at which the first major break occurred on the force-distance curve and was expressed in millimeters. Measurements were performed on five individual chips from each formulation.

Sensory Evaluation

Sensory evaluation was conducted with 20 untrained panelists from Necmettin Erbakan University (Konya, Türkiye) who regularly consumed snack and bakery products. The samples were coded with randomly assigned three-digit numbers and presented to the panelists in randomized order under ambient conditions. Color appearance, odor, taste, crispness, and overall acceptability were evaluated using a 7-point hedonic scale (1 = dislike extremely and 7 = like extremely). Drinking water was provided for palate cleansing between samples.

Statistical analysis

All analyses were carried out in duplicate. The data were analyzed using JMP statistical software, version 10.0 (SAS Institute Inc., Cary, NC, USA). One-way analysis of variance (ANOVA) was used to determine the effect of black cumin seed cake incorporation level on the measured quality characteristics. When the effect was statistically significant, mean values were compared using Tukey's honestly significant difference (HSD) test. Differences were considered statistically significant at $p < 0.05$. The results were expressed as mean ± standard deviation.

RESULTS AND DISCUSSION

Color Properties of Gluten-Free Chickpea Chips

The color properties of the gluten-free chickpea chips enriched with black cumin seed cake powder are presented in **Figure 1.** Color is an important quality attribute of snack products because it directly influences product appearance and initial consumer perception. The incorporation of black cumin seed cake powder significantly affected all measured color parameters of the chips ($p < 0.05$).

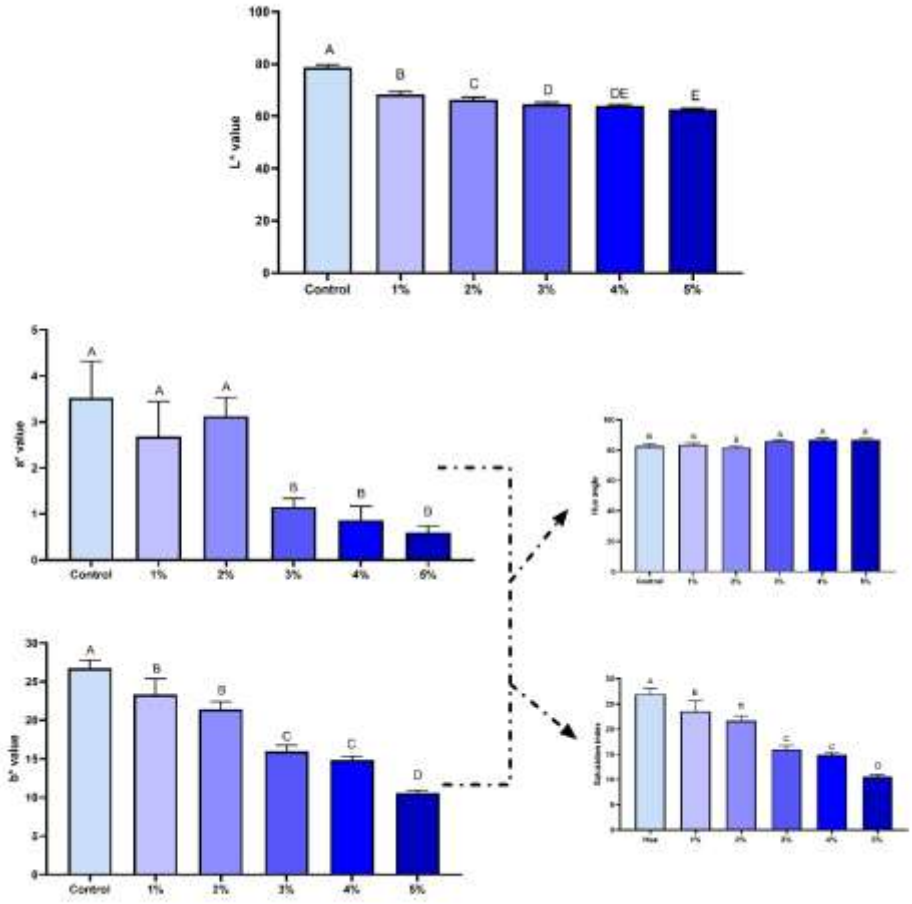

Figure 1. Effect of black cumin seed cake powder incorporation on the L*, a*, b*, hue angle, and saturation index values of gluten-free chickpea chips. Bars represent mean ± standard deviation. Different uppercase letters above the bars indicate significant differences among formulations according to Tukey's HSD test ($p < 0.05$).

The control chips exhibited the highest L* value, approximately 78, indicating a comparatively light-colored product. Increasing the black cumin seed cake level from 1 to 5% caused a progressive and significant reduction in L*, with the value decreasing to approximately 62 in the formulation containing 5% seed cake. The control and all enriched formulations were assigned to different statistical groups, except for the partial similarity observed between the 4 and 5% formulations. These findings demonstrated that even a relatively low level of black cumin seed cake produced a noticeable darkening of the chickpea chips. The reduction in lightness was primarily associated with the intrinsically dark color of black cumin seed cake. The high baking temperature may also have contributed to color development through non-enzymatic browning reactions. Różyło et al. (2021) similarly found that the addition of black cumin pressing waste progressively reduced the L* value of gluten-free starch bread, confirming the strong influence of this dark-colored by-product on product appearance. A comparable effect has also been reported in chickpea-based gluten-free crackers enriched with pumpkin seed press cake, in which the type and level of press-cake flour markedly affected instrumental color (Tomić et al., 2022). These findings support the view that the color response observed in the present chips resulted from both the replacement of light-colored chickpea flour and the thermal behavior of seed-cake components during baking.

The a* values of the chips also decreased with increasing seed cake incorporation. The control, 1%, and 2% formulations exhibited comparatively higher a* values and were statistically similar to one another ($p > 0.05$). However, the a* value decreased sharply when the seed cake level reached 3%, and the formulations containing 3–5% seed cake formed a separate statistical group. This decrease indicated a reduction in the red component of the chip surface color. A similar concentration-dependent trend was observed for b*. The control chips had the highest b* value, approximately 26–27, whereas the 5% seed cake formulation had the lowest value, approximately 10–11. Incorporation of only 1% seed cake significantly reduced b*, while further reductions occurred as the substitution level increased. The decreased b* values indicated that the characteristic yellow color of chickpea flour became less dominant as the proportion of the dark-colored seed cake increased.

The saturation index (SI) progressively decreased from approximately 27 in the control to approximately 10–11 in the 5% formulation. This result indicated a gradual reduction in color intensity or chromaticity. The decrease in SI was consistent with the simultaneous reductions in a* and b*. In contrast, the hue angle increased slightly at seed cake levels of 3% and above. The control, 1%, and 2% formulations were statistically similar, while the samples containing 3–5% seed cake formed a second statistical group with higher hue-angle values. Therefore, black cumin seed cake not only darkened the chips but also shifted their overall surface color toward a less saturated and more neutral appearance. Overall, replacing the relatively light-colored chickpea flour with black cumin seed cake produced darker and less saturated chips. This behavior agrees with the darkening reported for black cumin pressing-waste-enriched starch bread (Różyło et al., 2021), while the study of Tomić et al. (2022) demonstrates that press-cake enrichment can produce ingredient-specific color changes in chickpea-based gluten-free crackers. The effect of this visual change on product preference was therefore considered together with the sensory color-appearance scores in the present study.

Physical Properties of Gluten-Free Chickpea Chips

The diameter, thickness, and spread ratio values of the gluten-free chickpea chips are presented in **Figure 2.** Black cumin seed cake incorporation had a limited effect on the physical dimensions of the products. The diameter of the control chips was approximately 40.8 mm. The diameter remained statistically unchanged at the 1% incorporation level, whereas a slight increase was observed with further increases in black cumin seed cake. The formulations containing 3, 4, and 5% seed cake exhibited the highest diameter values, approximately 42–43 mm, and were statistically similar to one another. The 2% formulation showed an intermediate value and did not differ significantly from either the lower- or higher-incorporation groups. The slight increase in diameter may have resulted from changes in dough consistency and deformation during compression. Yüksel et al. (2025) showed that cold-pressed black cumin seed meal altered dough rheological behavior, particularly extensograph energy and extensibility, although farinograph water absorption did not differ significantly from the control. Tomić et al. (2022) likewise demonstrated that replacing chickpea flour with seed press-cake flour modified the physicochemical behavior of gluten-free cracker formulations. Because all dough portions in the present study had the same mass and were compressed under the same conditions, formulation-related differences in dough deformability may have contributed to lateral expansion. However, water was added according to dough workability rather than at a fixed level; consequently, the contributions of ingredient composition and formulation-specific water addition cannot be separated. In contrast to diameter, chip thickness was not significantly affected by black cumin seed cake incorporation ($p > 0.05$). The thickness values were approximately 1.6–1.9 mm, and all formulations were included in the same statistical group. Although the 5% formulation showed a numerically lower mean thickness than the other samples, the relatively high variability prevented this difference from reaching statistical significance.

The spread ratio showed a numerical increase from approximately 21.5 in the control to 26 in the formulation containing 5% black cumin seed cake. However, no statistically significant differences were observed among the formulations ($p > 0.05$). The numerical increase in spread ratio at the highest incorporation level resulted from the combination of a slightly greater diameter and a lower mean thickness. Nevertheless, the statistical results demonstrated that replacing up to 5% of chickpea flour with black cumin seed cake did not adversely affect the overall shape or dimensional stability of the chips. These findings are technologically important because major changes in diameter, thickness, or spread ratio could result in nonuniform baking, undesirable appearance, and inconsistencies in packaging. The absence of substantial changes in these parameters indicated that black cumin seed cake powder could be incorporated at levels of up to 5% without requiring major modification of the shaping and baking process.

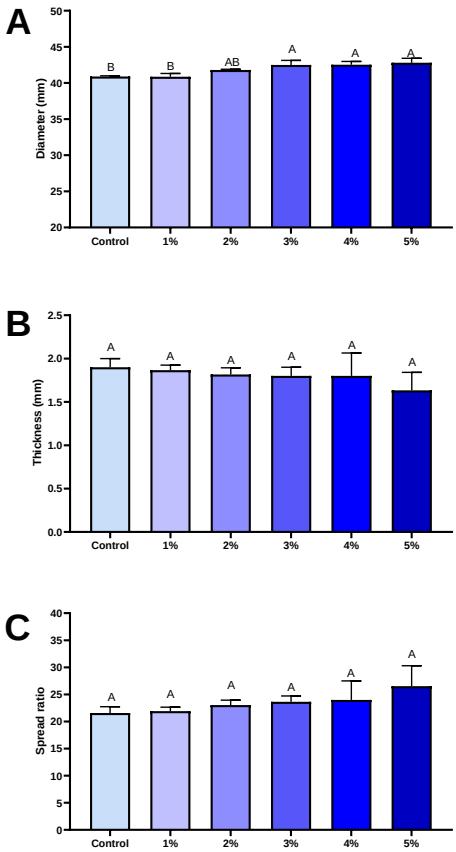

Figure 2. Effect of black cumin seed cake powder incorporation on the diameter, thickness, and spread ratio of gluten-free chickpea chips. Bars represent mean ± standard deviation. Different uppercase letters above the bars indicate significant differences among formulations according to Tukey's HSD test ($p < 0.05$).

Textural Properties of Gluten-Free Chickpea Chips

The hardness and fracturability values of the gluten-free chickpea chips are shown in Figure 3. Black cumin seed cake incorporation caused a progressive reduction in hardness. The control chips exhibited the highest value, approximately 2,400 g, whereas the 5% formulation displayed the lowest value, approximately 950 g. The control was significantly harder than the samples containing 3-5% seed cake, while the 1 and 2% formulations showed intermediate values. A

hardness-reducing effect of black cumin pressing waste was also observed by Różyło et al. (2021) in gluten-free starch bread. In chickpea-based gluten-free crackers, Tomić et al. (2022) further showed that the origin and level of seed press-cake flour can substantially modify product texture. In the present formulation, dilution of the chickpea starch matrix together with the fiber, protein, and residual lipid fractions of the seed cake may have contributed to the reduction in breaking force. Nevertheless, because dough rheology and microstructure were not measured, the mechanism responsible for this change cannot be conclusively established.

The direction and magnitude of textural changes caused by press-cake ingredients depend on the food matrix, substitution level, water content, and processing conditions. Krawęcka et al. (2022) reported that black cumin cake affected the processing and texture of pasta, whereas Różyło et al. (2021) observed reductions in hardness, springiness, and chewiness in gluten-free starch bread. Tomić et al. (2022) also documented formulation-dependent textural responses in chickpea-based crackers containing pumpkin seed press cake. Despite the marked reduction in hardness in the present study, fracturability remained statistically unchanged ($p > 0.05$), with values within a narrow range of approximately 33-34 mm. Thus, black cumin seed cake reduced the maximum breaking force without significantly changing the instrumental fracture distance. Sensory crispness nevertheless declined at the higher incorporation levels, indicating that instrumental fracture distance alone did not fully represent perceived crispness.

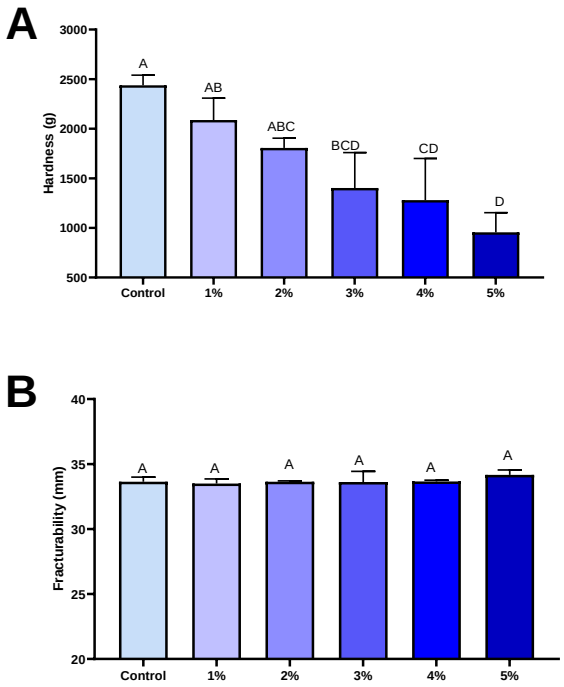

Figure 3. Effect of black cumin seed cake powder incorporation on the hardness (A) and fracturability (B) of gluten-free chickpea chips. Bars represent mean ± standard deviation. Different uppercase letters above the bars indicate significant differences among formulations according to Tukey's HSD test ($p < 0.05$).

Sensory Properties of Gluten-Free Chickpea Chips

The sensory scores of gluten-free chickpea chips enriched with black cumin seed cake powder are presented in Figure 4. All formulations received mean scores above 5 on the 7-point hedonic scale for color appearance, odor, taste, crispness, and overall acceptability. Thus,

although increasing the seed cake level caused reductions in some sensory scores, none of the formulations was evaluated negatively by the panelists.

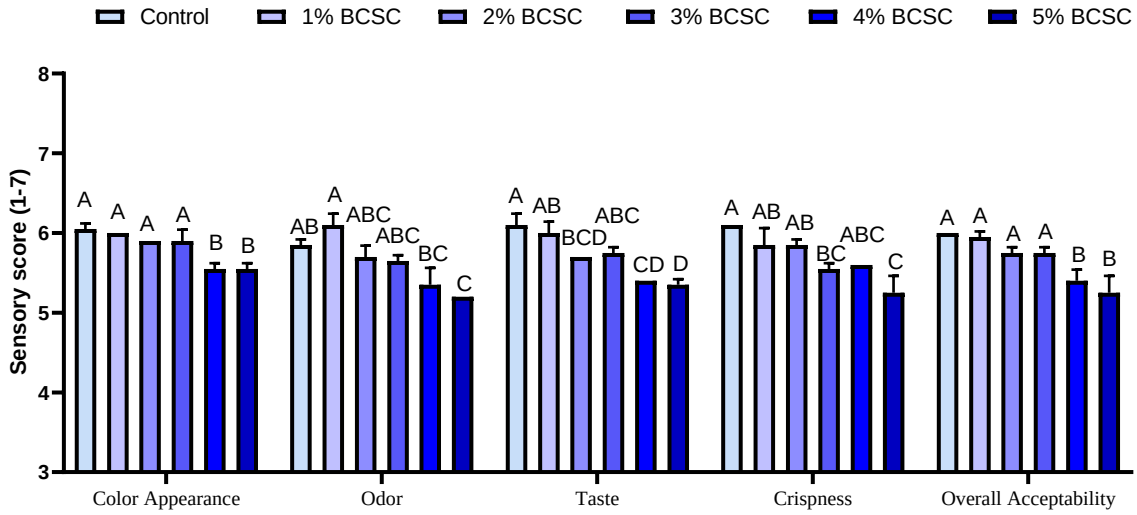

Figure 4. Sensory scores of gluten-free chickpea chips containing different levels of black cumin seed cake (BCSC) powder. Samples were evaluated for color appearance, odor, taste, crispness, and overall acceptability using a 7-point hedonic scale. Bars represent mean ± standard deviation. Different uppercase letters within each sensory attribute indicate significant differences among formulations according to Tukey's HSD test ($p < 0.05$).

The color appearance scores generally decreased with increasing black cumin seed cake incorporation. The control and the formulations containing 1, 2, and 3% seed cake received similar scores of approximately 5.8–6.1 and did not differ significantly from one another ($p > 0.05$). By contrast, the 4 and 5% formulations received significantly lower scores of approximately 5.5. This decrease was consistent with the instrumental color results, which showed progressive reductions in L*, a*, b*, and saturation index values. Therefore, the darker and less saturated appearance produced at higher seed cake concentrations was also perceived by the panelists. Nevertheless, the scores of the 4 and 5% formulations remained above the midpoint of the hedonic scale, indicating that their darker appearance was still reasonably acceptable.

Odor scores showed a similar concentration-dependent tendency. The formulation containing 1% black cumin seed cake received the highest odor score, slightly exceeding that of the control. This finding suggests that a low concentration of the seed cake contributed a characteristic aroma that was favorably perceived. However, odor scores gradually decreased as the incorporation level increased, and the 5% formulation received the lowest score. Black cumin contains characteristic volatile compounds, particularly those associated with its essential-oil fraction, which can provide a desirable aroma at low concentrations but may become dominant at higher levels. The statistical grouping showed substantial overlap among the control and intermediate formulations, whereas the difference was most evident between the 1 and 5% samples.

Black cumin seed cake incorporation also significantly affected taste scores ($p < 0.05$). The control and 1% formulations received the highest scores, approximately 6.0–6.1, while the 2 and 3% formulations showed moderately lower values. Taste scores declined further in the 4 and 5% formulations, which formed the lowest statistical groups. The reduction observed at higher substitution levels may be associated with the intense characteristic taste of black cumin

and the increased contribution of phenolic and other flavor-active compounds remaining in the seed cake after cold pressing. Previous research has similarly demonstrated that increasing black cumin concentration can reduce the sensory scores of enriched bakery products, despite improving their nutritional and functional properties (Awulachew et al., 2025). Therefore, the amount incorporated into a snack formulation should be carefully controlled to balance functional enrichment with taste acceptance.

Crispness scores decreased progressively as the black cumin seed cake level increased. The control received the highest score, approximately 6.1, whereas the 5% formulation received the lowest score, approximately 5.2. The control and lower seed cake levels showed overlapping statistical groups, while the highest incorporation level differed significantly from the control. This sensory trend partly agreed with the instrumental texture results. Instrumental hardness decreased markedly with increasing seed cake incorporation, indicating that the enriched chips required less force to break. Although fracturability remained statistically unchanged, panelists perceived some reduction in crispness at the higher substitution levels. This difference is reasonable because instrumental fracture measurements quantify specific mechanical properties, whereas sensory crispness is a complex perception involving sound, brittleness, hardness, and the breakdown behavior of the product during mastication.

Overall acceptability was highest for the control and the formulation containing 1% black cumin seed cake, with scores close to 6.0. The 2 and 3% formulations received slightly lower scores but remained statistically similar to the control. A significant reduction was observed at the 4 and 5% incorporation levels, which received scores of approximately 5.4 and 5.2, respectively. The decline in overall acceptability at these levels was consistent with the lower color appearance, taste, odor, and crispness scores. Despite these reductions, all samples had overall acceptability scores above 5, demonstrating that chickpea chips containing up to 5% black cumin seed cake remained sensorially acceptable. However, the 1–3% formulations provided a better balance between seed cake incorporation and consumer acceptance. In particular, the 3% formulation may be considered the highest suitable enrichment level without a significant loss of overall acceptability compared with the control. By contrast, although the 4 and 5% formulations contained greater quantities of the value-added ingredient, their darker color, more pronounced flavor, and lower perceived crispness reduced panelists' preference.

Overall, the sensory findings showed that black cumin seed cake could be successfully incorporated into gluten-free chickpea chips at low-to-moderate levels. Considering the sensory results together with the instrumental measurements, an incorporation level of up to 3% appears most appropriate for maintaining consumer acceptance while enabling the valorization of this cold-pressed oil by-product.

CONCLUSION

This study demonstrated that cold-pressed black cumin seed cake can be successfully utilized as a value-added ingredient in the production of gluten-free chickpea chips. Its incorporation at levels of 1–5% significantly affected the color, texture, and sensory properties of the chips, while causing only limited changes in their physical dimensions. Increasing the black cumin seed cake level resulted in darker and less saturated products, as indicated by the reductions in L*, a*, b*, and saturation index values. The diameter increased slightly, whereas thickness and spread ratio remained statistically unchanged. Hardness progressively decreased with increasing seed cake incorporation, while fracturability was not significantly affected. These results indicated that the enriched chips became easier to bite without losing their characteristic brittle structure.

Although all formulations received sensory scores above 5 on the 7-point hedonic scale, the samples containing 4 and 5% black cumin seed cake had significantly lower overall acceptability scores. In contrast, incorporation levels of up to 3% maintained overall

acceptability comparable to that of the control. Therefore, 3% black cumin seed cake can be recommended as the most suitable maximum incorporation level for achieving functional enrichment without adversely affecting the sensory quality of gluten-free chickpea chips.

Overall, the use of black cumin seed cake in chickpea-based chips offers a promising strategy for the valorization of a cold-pressed oil-processing by-product and the development of more sustainable gluten-free snack products. Further studies should investigate the nutritional composition, bioactive compounds, antioxidant activity, storage stability, and consumer acceptance of the developed chips.

REFERENCES

AACC (2000) Approved methods of analysis, 10th edn. American Association of Cereal Chemists, St. Paul

Aslan, M., Olcay, N., Ertas, N., & Demir, M. K. (2023). Effect of purple carrot powder substitution on some physical, chemical and sensory properties of chips samples.

Awulachew, M. T. (2025). Effect of partial replacement of wheat with fava bean and black cumin flours on nutritional properties and sensory attributes of bread. *Engineering Proceedings*, *87*(1), 8.

Francis, F. J. (1998). Colour analysis. Food analysis, 2, 599-612.

Krawęcka, A., Sobota, A., Sykut-Domańska, E., Physic, A., and Zarzycki, P. (2022). Effect of black cumin cake addition on the chemical composition, glycemic index, antioxidant activity, and cooking quality of durum wheat pasta. Molecules, 27(19), 6342. https://doi.org/10.3390/molecules27196342

Melini, V., Melini, F., Luziatelli, F., and Ruzzi, M. (2017). Legumes as functional ingredients in gluten-free bakery and pasta products. Annual Review of Food Science and Technology, 8, 81–100. https://doi.org/10.1146/annurev-food-030216-030045

Różyło, R., Piekut, J., Wójcik, M., Kozłowicz, K., Smolewska, M., Krajewska, M., Szmigielski, M., and Bourekoua, H. (2021). Black cumin pressing waste material as a functional additive for starch bread. Materials, 14(16), 4560. https://doi.org/10.3390/ma14164560

Tomić, J., Škrobot, D., Popović, L., Dapčević-Hadnađev, T., Čakarević, J., Maravić, N., and Hadnađev, M. (2022). Gluten-free crackers based on chickpea and pumpkin seed press cake flour: Nutritional, functional and sensory properties. Food Technology and Biotechnology, 60(4), 488–498. https://doi.org/10.17113/ftb.60.04.22.7685

Vinod, B. R., Pati, S., and Prabhasankar, P. (2023). Chickpea as a promising ingredient substitute in gluten-free bread making: An overview of technological and nutritional benefits. International Journal of Gastronomy and Food Science, 34, 100815.

Yabacı Karaoğlan, S. (2025). Cold-pressed black cumin (Nigella sativa L.) cake as a functional ingredient in sustainable food systems. International Journal of Agriculture, Environment and Food Sciences, 9(Special), 349–357. https://doi.org/10.31015/2025.si.34

Yüksel, Y., Kiralan, M., and Ramadan, M. F. (2025). Effect of cold-pressed Nigella sativa seed meal on dough quality and nutritional value of bread. Food Science and Technology International, 31(4), 338–347. https://doi.org/10.1177/10820132231207904

Zaky, A. A., Shim, J. H., & Abd El-Aty, A. M. (2021). A review on extraction, characterization, and applications of bioactive peptides from pressed black cumin seed cake. Frontiers in Nutrition, 8, 743909.

SYSTEM OF BULGARIAN PLANT GENETIC RESOURCES DOCUMENTATION – DESIGN, STRUCTURE AND STATUS

Nikolaya VELCHEVA[1], Simona CHEPERIGOVA[1]

[1] Institute of Plant Genetic Resources "Konstantin Malkov", Sadovo, Plovdiv district, Agricultural Academy, Bulgaria
Corresponding author e-mail: nikolaya_velcheva@abv.bg

ABSTRACT

Plant genetic resources (PGR) constitute a fundamental component of agricultural biodiversity and include genetic material of actual or potential value for food and agriculture. Their effective conservation and sustainable utilization require not only appropriate storage conditions but also a reliable, standardized and continuously updated documentation system. The Bulgarian system for plant genetic resources documentation was developed as an integrated information framework supporting the conservation, management, characterization, evaluation, exchange and utilization of germplasm maintained in the National Genebank at the Institute of Plant Genetic Resources "Konstantin Malkov" – Sadovo. The documentation system integrates passport information, taxonomic and geographical data, collecting and acquisition information, biological status, storage conditions, regeneration, evaluation and characterization data, as well as information related to the distribution and use of accessions. Its structure follows the FAO/Bioversity Multi-Crop Passport Descriptors and the requirements of the European Search Catalogue for Plant Genetic Resources (EURISCO), thereby providing compatibility and interoperability with European and international information networks. The system incorporates functional modules for accession registration, passport data management, expedition documentation, accession searching, storage and regeneration management, and controlled data access. An important feature of the system is the distinction between a public interface for researchers and other users and a protected management environment for authorized genebank specialists. Open access to passport information, including mobile access, increases the visibility and usability of Bulgarian plant genetic resources. The system also supports the National Inventory of plant genetic resources and the transfer of validated and harmonized data to EURISCO. The documentation framework provides traceability of accessions from acquisition and registration through storage, regeneration, characterization and distribution. Its implementation contributes to the modernization and digitalization of genebank management and strengthens the role of the Bulgarian National Genebank as a national and international information centre for plant genetic resources.

Keywords: Accession, GeneBankSystem, Descriptors, Expedition, Introduction, Crop breeding.

INTRODUCTION

Plant genetic resources for food and agriculture represent an essential component of agricultural biodiversity and provide the genetic basis for crop improvement, adaptation and sustainable food production. The diversity of crops, traditional varieties, landraces, breeding materials and crop wild relatives provides genetic variation that may be valuable for adaptation to changing environmental conditions, emerging pests and diseases, and new production systems. The

conservation of this diversity is therefore directly associated with long-term food security and the resilience of agricultural systems (Salgotra & Chauhan, 2023).

Modern agriculture relies increasingly on a relatively limited number of high-performing cultivars. This tendency may contribute to genetic erosion and the loss of traditional varieties and locally adapted populations. Landraces and traditional populations may contain valuable characteristics associated with adaptation to local environmental conditions, disease resistance, quality traits and specific consumer preferences. Consequently, their conservation in genebanks, combined where possible with in situ and on-farm conservation, is an important component of sustainable management of agricultural biodiversity (Raggi et al., 2021).

Ex situ conservation in genebanks provides an effective mechanism for the long-term preservation of plant genetic resources. However, the biological material alone is insufficient to ensure its effective future use. The scientific and practical value of an accession depends strongly on the availability, accuracy and completeness of information associated with it. Documentation has to allow the identity, origin, biological status, storage history, reproduction, characterization and utilization of each accession to be traced throughout its conservation cycle. The documentation of plant genetic resources is therefore an integral part of genebank management (FAO, 2013; ECPGR, 2021).

The Bulgarian National Genebank, located at the Institute of Plant Genetic Resources "Konstantin Malkov" – Sadovo, maintains collections comprising local populations, traditional varieties, modern cultivars, breeding lines, genetic stocks and crop wild relatives. The collections are managed through a specialized documentation system that integrates information generated during accession acquisition, registration, conservation, regeneration, characterization, evaluation and distribution. The system was developed through long-term interdisciplinary cooperation between researchers from IPGR-Sadovo and computer scientists (Stoyanova-Doycheva et al., 2020; Malinov et al., 2025).

The development of a standardized documentation framework in Bulgaria is also closely related to European and international initiatives for harmonization and exchange of plant gene pool information (Goritschnig et al., 2024). The Bulgarian National Genebank participates in the European Search Catalogue for Plant Genetic Resources (EURISCO) and coordinates the maintenance of the Bulgarian National Inventory. The system applies the FAO/Bioversity Multi-Crop Passport Descriptors, which provide a common structure for passport information and facilitate data exchange between national and international information systems.

The importance of interoperable documentation systems has increased with the development of digital infrastructures for plant genetic resources. Standardized information enables data aggregation, validation, searching and dissemination, while open access increases the potential for researchers, breeders and other stakeholders to identify and use conserved germplasm. Digitalization is therefore not simply a technical transformation of records into databases, but a means of improving the quality, accessibility, interoperability and long-term value of plant genetic resources information (Mendel et al., 2017; Cicova et al., 2026).

The objective of this study was to describe the design, structure and current status of the Bulgarian plant genetic resources documentation system, with particular emphasis on the information architecture of the GeneBankSystem at IPGR-Sadovo, the implementation of standardized descriptors, the documentation of enrichment of collections, data management and the integration of national information with EURISCO.

MATERIAL AND METHOD

Source of information

The study was based on the methodological framework for plant genetic resources enrichment and documentation developed for the Bulgarian National Genebank at IPGR-Sadovo. The documentation procedures, database structure, passport descriptors, expedition records, GeneBankSystem modules and principles of data exchange were analyzed.

The methodological framework follows international standards, particularly the FAO/Bioversity Multi-Crop Passport Descriptors (FAO/Bioversity, 2017), the FAO Genebank Standards for Plant Genetic Resources for Food and Agriculture (FAO, 2013), and the documentation and quality-management principles promoted by European program (ECPGR).

Structure of accession documentation

The basic documentation unit is the accession. Each accession receives a unique identification – catalogue number (COLLNUMB) at registration, which remains associated with the genetic resource throughout its storage, evaluation, regeneration and utilization.

The national accession number (ACCENUMB) is generated according to the established registration system and is not reused for another genetic resource.

The passport database is structured according to the FAO/Bioversity MCPD and EURISCO standards. The main groups of descriptors include:

taxonomic identification;
accession identification;
origin and acquisition;
collecting information;
geographical coordinates;
elevation;
biological status;
breeding and ancestral information;
collecting/acquisition source;
donor information;
storage conditions;
access and exchange status;
additional identifiers and remarks.

Four core fields – NICODE (National Inventory code), INSTCODE (Institute code), ACCENUMB and GENUS, provide the essential identification structure of an accession within the EURISCO framework. Their combination is intended to ensure uniqueness of the record and reduce duplication.

The system also supports the use of persistent unique identifiers PUID (Digital Object Identifier from FAO), which provide the possibility of unambiguous identification of a genetic resource at the global level.

Documentation of collecting expeditions

Expeditions constitute an important mechanism for enriching the Bulgarian genebank collections, particularly through the collection of local varieties, landraces, farmer populations and crop wild relatives. During collecting missions, seed or vegetative material is collected together with information concerning geographic location, environmental conditions, local names, cultivation practices and traditional uses.

The documentation system includes a dedicated expedition module. It records the participants, financing organization, project, geographic and ecological characteristics of the area, and the collected accessions. Search filters facilitate retrieval of expedition records according to different criteria.

A standardized questionnaire has also been developed for interviews with farmers maintaining local varieties. The questionnaire includes expedition identification, collection date, collector, geographic location, environmental characteristics, information about the farmer, taxonomic information and local accession name, as well as information about farm size, reasons for growing the accession, production destination, seed sources and traditional uses.

GenaBankSystem (https://genbank.uni-plovdiv.net/) architecture

The Bulgarian genebank documentation system is a web-based platform designed for integrated management of information associated with the conservation, study and distribution of plant genetic resources. It consists of two interconnected functional environments.

The public component provides external users with access to accession information and searching by passport data. The protected component is available to authorized users through authentication and is intended for documentation specialists and collection curators responsible for managing accessions in the active and base collections.

The system integrates several functional modules, including:

registration of new accessions;
passport-data management;
accession searching;
expedition documentation;
storage and regeneration information;
characterization and evaluation data;
accession distribution;
data administration and updating.

This modular structure allows information associated with an accession to be maintained as a continuous record rather than as isolated datasets.

Data quality, updating and protection

Data quality is maintained through continuous updating, validation and correction. Curators are responsible for maintaining reliable information for the collections under their responsibility, while documentation specialists are responsible for the quality of passport information introduced during accession registration.

When information for a particular descriptor is unavailable and cannot be established from other sources, the field remains unfilled rather than being populated with unsupported information. Data entered into the system must remain compatible with the European exchange format to facilitate automated transfer to international information networks.

The system also provides data protection and continuity through electronic registration and archival copies maintained on primary and backup servers.

RESULTS AND DISCUSSION

Integrated documentation framework

The analysis demonstrates that the Bulgarian documentation system has evolved from a MS Access database register Phyto 2000 into an integrated digital framework for the management of plant genetic resources. GeneBankSystem connects accession identity with information generated at different stages of the conservation process.

The documentation starts with accession acquisition and registration and continues through storage, regeneration, evaluation, characterization and distribution. Consequently, the accession record represents not only a passport description but also a dynamic information resource reflecting the history and status of the genetic material.

The main categories of operational data include evaluation and characterization results, germination information, regeneration and multiplication records, storage type and distribution to users. Regular updating of these records supports the reliability and traceability of the

collections. This approach corresponds to the principle that documentation should support the complete management cycle of a genebank accession rather than only its initial registration.

Standardization of passport data

One of the main strengths of the Bulgarian system is its alignment with the FAO/Bioversity Multi-Crop Passport Descriptors and EURISCO. Standardization makes it possible to describe accessions using a common taxonomy and data structure.

The database contains descriptors for taxonomic identity such as GENUS, SPECIES, SPAUTHOR, SUBTAXA and CROPNAME. Origin and collecting descriptors include COLLNUMB, COLLCODE (Collecting institute code), ORIGCTY (Country of origin), COLLSITE (Location of collecting site), COLLDATE (Collecting date) and COLLSRC (Collecting/acquisition source). Geographic information is represented through latitude, longitude and elevation.

The biological status descriptor SAMPSTAT (Biological status) allows accessions to be differentiated as wild material, traditional cultivars/landraces, breeding and research material, genetic stocks, and advanced or improved cultivars. This provides an important basis for distinguishing different categories of genetic resources within the national collection.

The system also documents storage categories, including seed collections, medium- and long-term storage, field collections, *in vitro* collections.

Such standardization is particularly important when national data are incorporated into international catalogues. EURISCO uses standardized passport descriptors to enable data exchange and facilitate access to information on European genebank collections.

Unique identification and traceability

Traceability is a central principle of the Bulgarian documentation system. Each accession receives a unique national accession number, while additional identifiers may link it to collecting institutions, donor institutions, previous catalogue numbers or other databases. The ACCENUMB identifier is assigned at registration and cannot subsequently be reused for another accession. The system therefore preserves the identity of an accession even if the original biological material is lost. This approach provides continuity between physical germplasm and its digital representation. It also supports the identification of duplicates, the management of regeneration activities and the interpretation of research data associated with individual accessions. The use of additional identifiers, donor accession numbers and persistent identifiers creates opportunities for linking national records with other institutional and international information resources.

Documentation of plant genetic resources

A specific strength of the Bulgarian system is its capacity to document local plant genetic resources collected directly from traditional agricultural systems. Local varieties and landraces are frequently maintained by small-scale farmers and gardeners outside formal breeding programmes. Their documentation therefore requires information that goes beyond conventional passport descriptors. The expedition questionnaire developed within the methodological framework records not only the identity and geographical origin of the accession but also farmer-related information, cultivation practices, reasons for maintaining the material, production destinations, seed sources and traditional uses. This additional information increases the cultural, historical and practical value of the accession record. It can also support future research on the relationship between genetic resources, traditional knowledge, agricultural practices and local food systems. The inclusion of collecting-site information and geographic coordinates also creates opportunities for analysis. Geographic descriptors can be used to identify areas of concentration of particular genetic resources, support future collecting missions and contribute to analyses of adaptation and diversity.

In essence, the introduction activity of international free germplasm exchange, which is carried out by the genebank in Sadovo using SMTA (FAO, 2006), serves the crop improvement

programs of the breeding institutes in Bulgaria. Accessions are introduced upon special requests with diverse geographical origins for study in the conditions of the country and for use as donors of valuable traits as ecological plasticity, resistance to a given pathogen, high productivity, etc. The main partners of the National Genebank in the exchange are: GRIN (USA), ICARDA, NordGen, IPK (Germany), INRA (France), John Innes Center (Great Britain).
The genebank conserves seeds of Bulgarian advanced varieties and breeding lines, the result of crop improvement programs, for long-term storage, which are registered in the GeneBankSystem with data on pedigree, breeding institution and access level.
Integration of the National Inventory with EURISCO
The Bulgarian National Genebank is presented in EURISCO and performs a coordinating role in relation to the Bulgarian National Inventory. The National Inventory integrates passport information from collections maintained by different Bulgarian scientific institutions. The National Focal Point is responsible for collecting, validating, harmonizing and periodically submitting information to EURISCO Intranet. Thus, the documentation system functions not only as an institutional database but also as a national information infrastructure connecting different plant genetic resources collections. The national-to-European data transfer is represented on the Figure 1.

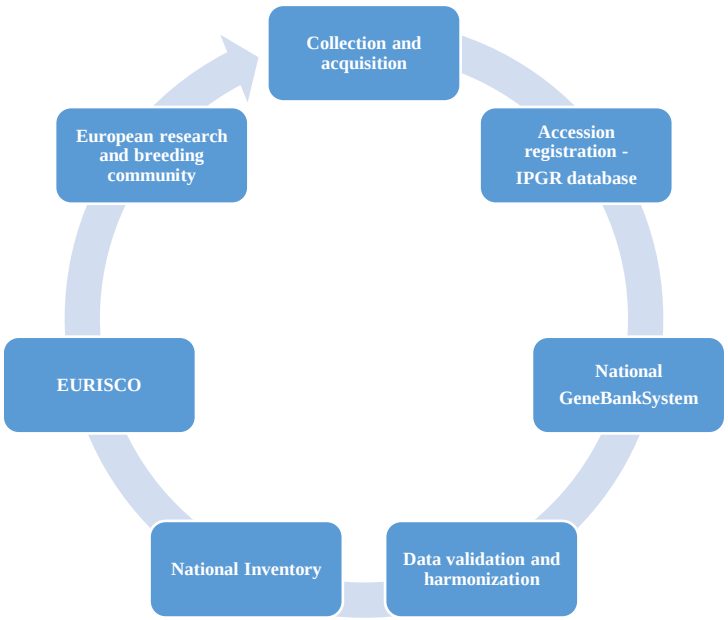

Figure 1. Integration of the Bulgarian National Inventory with European plant genetic resources community system

Such interoperability increases the international visibility of Bulgarian plant genetic resources and facilitates their identification for scientific research, breeding and conservation activities. According to Mendel et al. (2026), improved data management and documentation contribute to the visibility and usability of genebank collections. The integration with EURISCO further strengthens this role by providing a standardized European environment for accessing passport information.

Open access and user-oriented information services
The transition from an internal database to a web-based information environment represents an important development in the Bulgarian GeneBankSystem. The public interface provides

external users with access to accession information, while the protected component enables professional management of the collections.
Open access is available in both Bulgarian and English, and a mobile application has been developed to facilitate access by external users.
This approach is consistent with the broader development of digital infrastructures for genebank and responds to the increasing demand for accessible and interoperable information. Open access does not replace the physical conservation of germplasm; rather, it increases the visibility of conserved material and enables potential users to identify resources before requesting biological material.
The availability of standardized passport information is particularly important for breeders and researchers because it allows them to search collections according to crop, taxonomic identity, geographical origin, biological status and other characteristics.
Data security and quality management
The implementation of data backup and controlled access is another important element of the system. Information is maintained in electronic registers and backed up on primary and secondary servers, reducing the risk of data loss and supporting continuity of genebank operations. Data quality is further supported by defined responsibilities among documentation and conservation specialists and collection curators. Information may be corrected or supplemented when new evidence becomes available. This is particularly important for historical accessions, for which passport information may initially be incomplete. The system therefore follows a dynamic model of documentation in which accession records are considered continuously improvable rather than static records created only at the time of acquisition.
Current status and development potential
The current documentation framework provides an integrated digital environment for managing accession information in the Bulgarian National Genebank. Its main achievements include standardized passport documentation, unique accession identification, expedition documentation, integration of storage and regeneration information, evaluation and characterization records, public access and interoperability with EURISCO.
According to ECPGR (2023) and Velcheva et al. (2026) the system provides a foundation for further digital development. The GeneBankSystem explicitly defines the documentation framework as a dynamic structure that is expanded and updated with innovative techniques by IS-PGR-SADOVO public financed project. Future development is focus on increasing the interoperability of phenotypic datasets, improving geospatial functionality, strengthening links between passport and characterization data, expanding and implementing additional mechanisms for data validation and quality control. An important future direction is also the integration of more detailed characterization and evaluation datasets. While passport data provide the identity and origin of accessions, characterization and evaluation data provide the information needed to assess their actual value for breeding, research and sustainable agriculture.

CONCLUSIONS

The Bulgarian GeneBankSystem represents an integrated digital framework for the management of information associated with the national germplasm collections maintained at the National Genebank of IPGR-Sadovo.
The system combines accession registration, standardized passport documentation, collecting and expedition information, geographical data, biological status, storage and regeneration records, characterization and evaluation information, and distribution data. The use of FAO/Bioversity Multi-Crop Passport Descriptors and alignment with EURISCO provide an internationally compatible structure for data exchange and interoperability.

A major achievement is the introduction of a unique and traceable accession identification system that maintains the connection between the physical genetic resource and its digital record throughout the accession conservation process. The expedition module enables the documentation of local varieties and landraces together with information on their traditional cultivation and utilization.

The integration of the Bulgarian documentation system with the National Inventory and EURISCO increases the visibility of Bulgarian plant genetic resources and facilitates their discovery and potential use by researchers, breeders and other stakeholders. The public web interface and mobile access further support the open-access principle.

The system provides mechanisms for data quality control, updating, backup and controlled access, which are essential for the long-term reliability of genebank documentation.

Overall, the Bulgarian GeneBankSystem demonstrates that digital documentation is an essential component of modern germplasm management. By connecting physical conservation with standardized, interoperable and accessible information, the system strengthens the capacity of the Bulgarian National Genebank to conserve, document, study and promote the sustainable use of plant genetic resources. Its modular and dynamic structure provides a basis for further integration of new data types, innovative technologies and European and international information infrastructures.

ACKNOWLEDGEMENTS

The research work was carried out under the project IS-PGR-SADOVO “Intelligent system for managing Bulgarian plant gene pool, conserved in the genebank of IPGR-Sadovo” with the financial support of the Ministry of Education and Science, Contract number KP-06-H86/9/09.12.2024 of Bulgarian National Science Fund.

REFERENCES

Cicova, I., Mendel, Ľ., Zetochova, E., Varga, M., & Hauptvogel, R. 2026. Evaluation and Documentation of Plant Genetic Resources in the Genebank of the Slovak Republic. Journal of Mountain Agriculture on the Balkans, Vol. 29, Issue 1, 775–812.

ECPGR. 2021. Plant Genetic Resources Strategy for Europe. Rome, Italy.

ECPGR. 2023. Operational Guide for the Bulgarian Genebank. Institute of Plant Genetic Resources “Konstantin Malkov”, Sadovo.

FAO. 2006. Standard Material Transfer Agreement. Rome, Italy.

FAO. 2013. Genebank Standards for Plant Genetic Resources for Food and Agriculture. Rome, Italy. ISBN 978-92-5-108262-1.

FAO/Bioversity. 2017. Multi-Crop Passport Descriptors. Rome, Italy.

Goritschnig, S., Weise, S., Guzzon, F., Maggioni, L., van Hintum, T., Steffensen, L. L., et al. 2024. Strengthening European research cooperation on plant genetic resources conservation and use. Genetic Resources, S2, 119–134.

Malinov, P., Madanska, S., Doychev, E., Kostadinova-Tsankova, L., Stoyanov, I., & Wassilew, K. 2025. Cross-Platform Integration of Ontologies and Information Extraction for Plant Genetic Resources for the Bulgarian National GeneBank. Proc. of 2025 International Conference Automatics and Informatics (ICAI), 305-309.

Mendel, Ľ., Cicova, I., Zetochova, E., Hauptvogel, R., Varga, M., & Velcheva, N. 2026. Development, Modernization, and Standardization of IS GRISS (Genetic Resources Information System of Slovakia). Journal of Mountain Agriculture on the Balkans, Vol. 29, Issue 1, 748–774.

Mendel, Ľ., Hauptvogel, P., & Čičová, I. 2019. Plant genetic resources information system of Slovakia as the primary source of the information. Agrobiodiversity for Improving of Nutrition, Health and Quality of Life, 3, 178–185.
Raggi, L., Caproni, L., & Negri, V. 2021. Landrace added value and accessibility in Europe: what a collection of case studies tells us. Biodiversity and Conservation, 30, 1031–1048.
Salgotra, R. K., & Chauhan, B. S. 2023. Genetic diversity, conservation, and utilization of plant genetic resources. Genes, 14(1), 174.
Stoyanova-Doycheva, A., Doychev, E., Stoyanov, S., & Toskova, A. 2020. An Intelligent Gene Bank Management System. Proc. of 2020 International Conference Automatics and Informatics (ICAI), 1-5.
Velcheva, N., Cheperigova, S., Stoyanova-Doycheva, A., Madanska, S., & Malinov, P. 2026. Methodological Guide for the Enrichment and Documentation of Plant Genetic Resources. Paisii Hilendarski University Press, Plovdiv. ISBN (print): 978-619-281-168-6, ISBN (online) 978-619-281-175-4, 58 p.

PLATFORM FOR ACCESS TO SEEDS AND SCIENTIFIC KNOWLEDGE – RESULTS FROM THE IS-PGR-SADOVO PROJECT

Nikolaya VELCHEVA[1], Valko NESHEV[1]

[1] Institute of Plant Genetic Resources "Konstantin Malkov", Sadovo, Plovdiv district, Agricultural Academy, Bulgaria
Corresponding author e-mail: nikolaya_velcheva@abv.bg

ABSTRACT

The GeneBankSystem was developed to enhance transparency, collaboration, and innovation in plant genetic resources management. Coordinated by the Institute of plant genetic resources – Sadovo, the initiative aims to provide open and structured access to seed collections and research data. The platform integrates passport data, phenotypic and agronomic evaluations, and documentation of conserved germplasm, ensuring long-term preservation and accessibility. The creation of a database for phenotypic evaluation of seeds from different plant species is of a key importance for the management, scientific value, and sustainability of the genebank. The MARViN VisionLine measuring equipment is a high-tech analysis system that uses computer vision to precisely measure color, shape, size, and other visual parameters of seeds. It detects color anomalies and creates color-calibrated images for documentation. The results are characterized by high accuracy, precision, flexibility, and the ability to integrate into other information systems. A collection of common bean (*Phaseolus vulgaris L.*) with diverse geographical origin was analysed. The new data complement the passport, evaluation, and characterization records of the accessions. By promoting open science principles, the digital platform supports plant breeders, researchers, farmers, and policymakers in developing resilient and sustainable crop varieties. A key result is the digitization and systematization of national plant genetic resources collections, aligned with international standards for biodiversity conservation. The platform also strengthens knowledge transfer between science and practice, fostering innovation in agriculture under changing climate conditions. Overall, the GeneBankSystem contributes to the conservation of agrobiodiversity while advancing open access to scientific knowledge at national and international levels.

Keywords: Common bean, Genebank collection, Phenotyping, Conservation, Digitalization.

INTRODUCTION

Plant genetic resources for food and agriculture constitute an essential foundation for crop improvement, food security, adaptation to climate change, and sustainable agricultural development. Genebanks play a central role in conserving this diversity *ex situ* and in ensuring that valuable genetic material remains available for research, breeding, education, and future generations. However, the increasing size and complexity of genebank collections require advanced information systems capable not only of storing passport information but also of integrating characterization, evaluation, spatial, experimental, and monitoring data (Weise et al., 2020).

The National Genebank at the Institute of Plant Genetic Resources (IPGR) – Sadovo maintains *ex situ* plant gene pool of Bulgaria. The scale of the collection creates significant requirements for efficient registration, monitoring, documentation, storage, evaluation, and retrieval of information (Desheva et al., 2026). The IS-PGR-SADOVO project, entitled "Intelligent system

for managing Bulgarian plant gene pool, conserved in the genebank of IPGR-Sadovo", was designed to address these requirements through the development of intelligent components for the existing GeneBankSystem (Velcheva et al., 2025b).

A major objective of the project is to improve the management of processes associated with the conservation, research, and access to plant genetic resources. The system is being developed to support both specialized genebank personnel and external users, including researchers and other stakeholders with different levels of expertise. An important component is the development of a public information portal with intelligent access based on semantic models, allowing more complete and efficient access to information about conserved germplasm (Stoyanov et al., 2025).

The project combines several complementary technological approaches: an information system for genebank management, semantic modelling through GeneBankOntology, intelligent assistance for control germination testing, sensor-based monitoring of storage conditions, and integration of data generated by external seed-analysis equipment. These components create a digital environment in which biological material, scientific information, experimental results, and spatial data can be connected (Malinov et al., 2025).

Particular attention was given to phenotypic and biometric characterization. The establishment of a relational database for phenotypic evaluation is important for increasing the scientific value and long-term usability of genebank collections (Neshev & Velcheva, 2025). The acquisition of MARViN VisionLine and MARViN SmartLine systems enabled automated digital analysis of seed morphology and quality characteristics, generating standardized images and structured datasets that can subsequently be incorporated into the GeneBankSystem.

A new approach to the digital management of *ex situ* plant genetic resources has been developed at the Institute of Plant Genetic Resources "Konstantin Malkov" – Sadovo, Agricultural Academy. Particular emphasis is placed on the digitalization of characterization and evaluation data, which complement conventional passport information and increase the scientific value and usability of genebank collections. The establishment of a relational database for phenotypic evaluation of different plant species provides an important basis for systematic management, long-term preservation, scientific analysis, and future integration of genebank data into international information platforms. Such an approach facilitates information exchange among genebanks and provides wider access to genetic resources and associated scientific knowledge (Velcheva et al., 2025a).

The present paper summarizes the main results achieved during the first stage of the IS-PGR-SADOVO project, with particular emphasis on digital access to plant genetic resources, semantic information management, phenotyping, and the integration of scientific data into the genebank conservation system.

The aim of the study analyze the implementation of digital technologies for precise phenotypic analysis of seeds in the genebank as a tool for sustainable conservation, characterization, and evaluation of plant genetic resources.

MATERIAL AND METHOD

GeneBankSystem and digital documentation

The research activities were carried out using the information infrastructure of the National Genebank at IPGR-Sadovo and the GeneBankSystem. The system was developed to support the registration, storage, regeneration, monitoring, characterization, and evaluation of plant genetic resources.

During the first stage of the IS-PGR-SADOVO project, the existing system was analysed and expanded with additional functionalities for reproduction management and geremination testing. According to the data check 31.08.2026, 53,970 accessions are registered in the

GeneBankSystem by passport data. A significant amount of work was devoted to integrating reproduction records that had previously not been completely available in the old documentation Phyto 2000 database.

Scripts were developed for importing reproduction data, followed by manual verification and clarification of temporary reproduction numbers and their corresponding accessions. At the reported stage, more than 50,000 reproduction records existed, of which approximately 9,500 had been entered into the database together with associated geremination control-tests information. This data integration provides a basis for more reliable management of the collection.

Intelligent management of geremination control-tests

The GeneBankSystem was expanded with functionalities supporting the management of geremination control-tests. These include transferring seeds between storage collections, filtering accessions and reproduction records according to selected characteristics, exporting data in Excel format, and generating QR codes for individual storage records.

The QR-code functionality provides direct access to information concerning a specific reproduction and its geremination control-tests. A laboratory dashboard was designed to support the monitoring of recently processed reproductions and those requiring subsequent geremination control-tests (Figure 1).

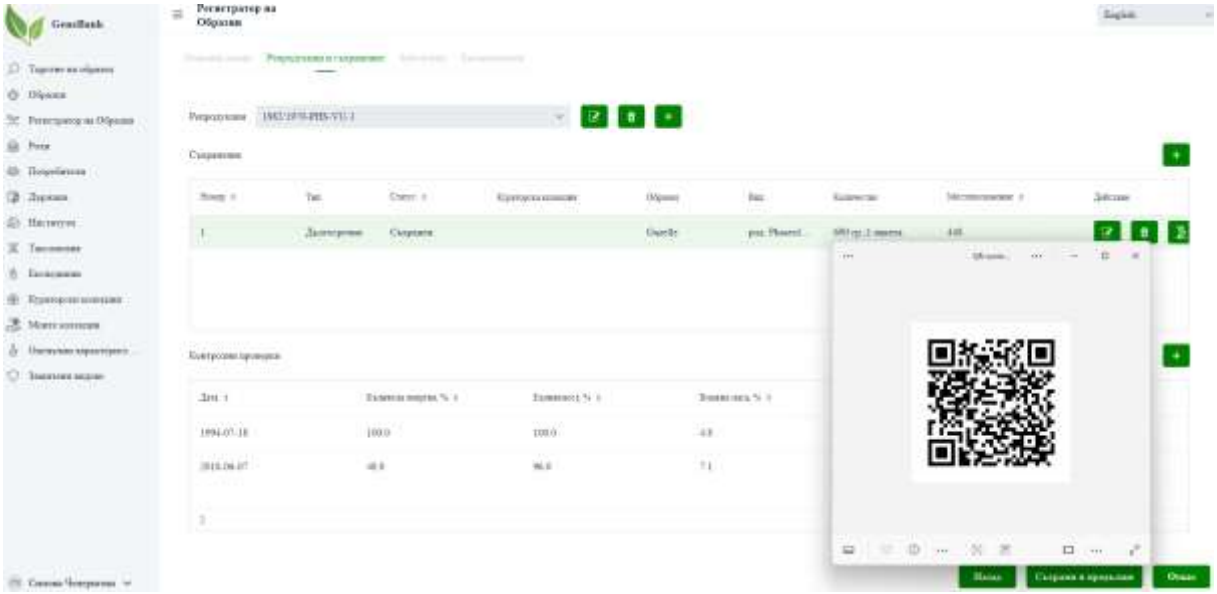

Figure 1. Generating a QR code for a seed reproduction of a common bean accession

Semantic modelling and external access

The GeneBankOntology was developed as a semantic representation of knowledge concerning plant genetic resources conserved in the National Genebank. Passport information was structured in accordance with EURISCO requirements and the FAO/Bioversity Multi-Crop Passport Descriptors (2017). The ontological model links accession identifiers with taxonomic information, collection sites, geographic coordinates, altitude, and other passport descriptors. Evaluation characteristics are also associated with individual accessions.

EURISCO uses standardized passport descriptors and also provides access to phenotypic information, supporting data discovery and exchange among genebanks and users. This approach follows the international documents towards interoperable documentation of plant genetic resources for food and agriculture (Maggioni et al., 2014; FAO, 2021) and the Operational Guide for the Bulgarian Genebank (ECPGR, 2023).

Monitoring of seed-storage conditions

A sensor network was designed and implemented to monitor temperature and relative humidity in the seed-storage facilities. The network covers the active collection and designated laboratory areas. The sensors provide continuous measurements and transmit data to server infrastructure. The system supports real-time visualization, threshold-based notifications, and storage of historical measurements. Central information displays were installed, while measurements are also logged on servers for subsequent analysis (Figure 2).

Figure 2. Screenshot of temperature and humidity data from the genebank storage facilities

Continuous monitoring of storage conditions provides an additional protection for the biological material and complements the digital documentation system.

Digital phenotyping and seed analysis

The digitalization of characterization and evaluation data is one of the components of the project. To support this activity, two high-tech seed-analysis systems, MARViN VisionLine and MARViN SmartLine (Figure 3), were acquired (MARViTECH, 2026).

Figure 3. Measuring system for digital seed analysis - MARViN SmartLine and MARViN VisionLine

The systems use computer vision, cameras, and dedicated software to measure seed colour, shape, size, and other visual parameters. They can detect colour anomalies and generate colour-calibrated images suitable for documentation and scientific analysis. Their main advantages include high accuracy, precision, flexibility, and the potential for integration with other information systems.

MARViN VisionLine generates images and structured analytical data, including seed length, width, area, perimeter, shape, colour characteristics, weight, percentage of damaged seeds, automatically determined quality class, and information on the date of analysis. The resulting data can be exported in CSV, XLS, XLSX, and other tabular formats.

MARViN SmartLine provides automated counting, measurement, and classification of seeds based on digital image processing. The system generates seed images, analytical reports, and statistical information, including number of seeds, size, shape, area, colour characteristics, damaged seed percentage, and quality indicators.

The data generated by the two systems are intended for integration into the GeneBankSystem, where they can be linked to accession identifiers and other passport, characterization, and evaluation information. This creates a basis for the development of a database for phenotypic and biometric information.

Experimental evaluation of the common bean collection

A collection of 80 common bean (*Phaseolus vulgaris* L.) accessions with diverse geographical origins was studied within the framework of a PhD thesis study conducted at the Department of Plant Genetic Resources of IPGR-Sadovo. During 2024-2026, the accessions were evaluated through field observations and biometric measurements using international descriptors. Biological, morphological, and quality-related characteristics were assessed in two replications. In 2025, the seed material of the investigated collection was additionally analysed using the MARViN VisionLine system. This allowed conventional field-based characterization to be complemented by digital seed phenotyping and standardized image-based measurements. This approach enabled the integration of biological, morphological, visual, and spatial information into a unified digital documentation environment.

RESULTS AND DISCUSSION

Development of an integrated digital platform

The first stage of the IS-PGR-SADOVO project resulted in significant expansion of the GeneBankSystem towards an integrated digital platform for the management and utilization of plant genetic resources. The system now incorporates functionalities for passport data, reproduction management, germination control-tests, data filtering, Excel export and QR-code identification. These functions improve the traceability of conserved material and reduce the dependence on manual searching and fragmented documentation.

The integration of reproduction information was particularly important because a large number of reproduction records were not initially linked to the corresponding accessions in the database. Their gradual integration creates a more complete digital representation of the physical collection.

The platform therefore moves beyond the role of a conventional accession database. It increasingly functions as an integrated knowledge environment in which biological material is connected with scientific, technical, and environmental information.

Digitalization of characterization and evaluation information

One of the important results of the project is the establishment of a technological basis for digitalizing characterization and evaluation information from *ex situ* collections. The creation of a database for phenotypic information provides a structured environment in which measurements generated from different experiments and plant species can be stored, linked to

accession identifiers, analysed, and subsequently shared. This is particularly important because phenotypic information may retain scientific value long after the completion of the original experiment.

The international development of EURISCO demonstrates the importance of this approach. EURISCO currently contains extensive phenotypic information in addition to passport data, and recent developments have focused on improving the standardization and FAIRness of phenotypic datasets.

The approach implemented at IPGR-Sadovo therefore corresponds to the broader development of genebank information systems from simple passport-data repositories towards integrated platforms supporting characterization, evaluation, visualization, and utilization of germplasm.

Digital phenotyping using MARViN systems

The introduction of MARViN VisionLine and SmartLine significantly increased the capacity of IPGR-Sadovo for standardized digital analysis of seed material. The systems generate both images and quantitative data, allowing seed characteristics to be documented in a reproducible digital format. This is particularly valuable for morphological traits such as seed length, width, area, perimeter, shape, colour, and damaged seed percentage.

The generated digital images provide a permanent visual record of the analysed accessions. In combination with structured measurements, they can be used for comparative analyses, statistical evaluation, and subsequent identification of accessions with desirable characteristics. The integration of these data into the GeneBankSystem will further increase their value by linking individual measurements to accession identity, passport information, evaluation data, and geographic origin.

Characterization and valorization of the common bean collection

The common bean collection provided a practical case study for the application of the new digital approach (Figure 4). The combination of field observations and computer-vision-based seed analysis enabled the creation of a more comprehensive accession profile. Instead of representing an accession only by its passport data, the digital record can include its geographical origin, phenological characteristics, biometric measurements, seed morphology, colour characteristics, digital images, and other quality-related parameters.

Figure 4. Result of common bean seed analysis with MARViN VisionLine

The analysis of the data from the Marvin seed analyzer was carried out on the average values

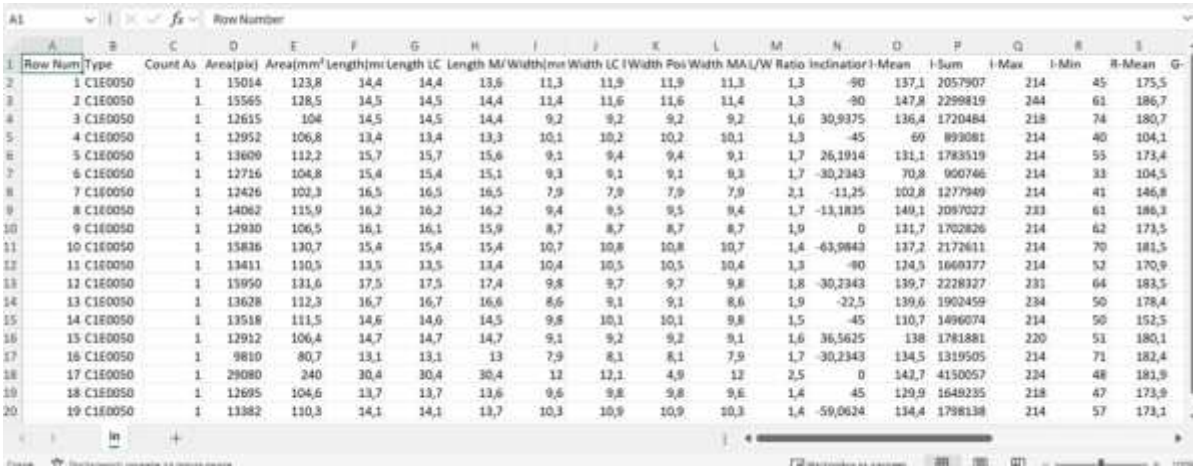

Row Num	Type	Count As	Area(pix)	Area(mm²	Length(mi	Length LC	Length Mi	Width(mi	Width LC	Width Pos	Width MA	L/W Ratio	Inclination	I-Mean	I-Sum	I-Max	I-Min	R-Mean	G-
1	C1E0050	1	15014	123,8	14,4	14,4	13,6	11,3	11,9	11,9	11,3	1,3	-90	137,1	2057907	214	45	175,5	
2	C1E0050	1	15565	128,5	14,5	14,5	14,4	11,4	11,6	11,6	11,4	1,3	-90	147,8	2299819	244	61	186,7	
3	C1E0050	1	12615	104	14,5	14,5	14,4	9,2	9,2	9,2	9,2	1,6	30,9375	136,4	1720484	218	74	180,7	
4	C1E0050	1	12952	106,8	13,4	13,4	13,3	10,1	10,2	10,2	10,1	1,3	-45	69	893081	214	40	104,1	
5	C1E0050	1	13609	112,2	15,7	15,7	15,6	9,1	9,4	9,4	9,1	1,7	26,1914	131,1	1783519	214	55	173,4	
6	C1E0050	1	12716	104,8	15,4	15,4	15,1	9,3	9,1	9,1	9,3	1,7	-30,2343	70,8	900746	214	33	104,5	
7	C1E0050	1	12426	102,3	16,5	16,5	16,5	7,9	7,9	7,9	7,9	2,1	-11,25	102,8	1277949	214	41	146,8	
8	C1E0050	1	14062	115,9	16,2	16,2	16,2	9,4	9,5	9,5	9,4	1,7	-13,1835	149,1	2097022	233	61	186,3	
9	C1E0050	1	12930	106,5	16,1	16,1	15,9	8,7	8,7	8,7	8,7	1,9	0	131,7	1702826	214	62	173,5	
10	C1E0050	1	15836	130,7	15,4	15,4	15,4	10,7	10,8	10,8	10,7	1,4	-63,9843	137,2	2172611	214	70	181,5	
11	C1E0050	1	13411	110,5	13,5	13,5	13,4	10,4	10,5	10,5	10,4	1,3	-90	124,5	1669377	214	52	170,9	
12	C1E0050	1	15950	131,6	17,5	17,5	17,4	9,8	9,7	9,7	9,8	1,8	-30,2343	139,7	2228327	231	64	183,5	
13	C1E0050	1	13628	112,3	16,7	16,7	16,6	8,6	9,1	9,1	8,6	1,9	-22,5	139,6	1902459	234	50	178,4	
14	C1E0050	1	13518	111,5	14,6	14,6	14,5	9,8	10,1	10,1	9,8	1,5	-45	110,7	1496074	214	50	152,5	
15	C1E0050	1	12912	106,4	14,7	14,7	14,7	9,1	9,2	9,2	9,1	1,6	36,5625	138	1781881	220	51	180,1	
16	C1E0050	1	9810	80,7	13,1	13,1	13	7,9	8,1	8,1	7,9	1,7	-30,2343	134,5	1319505	214	71	182,4	
17	C1E0050	1	29080	240	30,4	30,4	30,4	12	12,1	4,9	12	2,5	0	142,7	4150057	224	48	181,9	
18	C1E0050	1	12695	104,6	13,7	13,7	13,6	9,6	9,8	9,8	9,6	1,4	45	129,9	1649235	218	47	173,9	
19	C1E0050	1	13382	110,3	14,1	14,1	13,7	10,3	10,9	10,9	10,3	1,4	-59,0624	134,4	1798138	214	57	173,1	

of the traits, including: morphological parameters (length, width, area, perimeter) and intensity of the color indicators.

The analysis grouped the accessions into 5 groups, with the traits that influence their grouping being the perimeter of the seeds (perimeter mm) and the color of the seeds. The largest group unites all accessions with white seed color (40 accessions), the data are compared with the qualitative visual assessment of the trait – seed color according to the evaluation descriptors list. The other accessions are distributed in groups with a predominant brown color in several shades and black with small seeds. The collection is dominated by accession with kidney-shaped seeds (comparison was made with a qualitative assessment of the trait – seed shape).

Figure 5. Digital imagines of common bean seeds – output from the MARViN VisionLine

Accessions demonstrated promising agronomic characteristics and potential value for plant breeding programmes. These observations highlight the importance of curator collections maintained in genebanks as sources of potentially valuable variation for crop improvement.
The results demonstrate that the role of a genebank extends beyond long-term conservation. Conserved accessions can represent a reservoir of traits that may be used in breeding programmes aimed at improving productivity, quality, adaptation, and resilience under changing environmental conditions.

Local common bean populations as valuable genetic resources

The local common bean populations collected through expeditions represent an important component of Bulgarian agricultural biodiversity. Their value is associated not only with their genetic diversity but also with their adaptation to specific local environmental conditions and traditional agricultural practices.
The digital documentation of these populations makes it possible to preserve information that might otherwise be lost, including the location of origin, altitude, geographic coordinates, morphological characteristics, and visual features of the seed.
The spatial visualization developed within the project provides an accessible way of exploring the geographic distribution of local accessions. The combination of maps, passport information, morphological data, and seed images creates a more complete picture of the conserved genetic diversity.
This integrated approach may support future studies of relationships between geographical origin, environmental conditions, and phenotypic variation. It can also facilitate the identification of accessions for further evaluation and breeding.

Open access and knowledge transfer

A central principle of the developed platform is to increase access to information associated with conserved genetic resources. The digitalization of *ex situ* collections makes it possible to provide structured information to a wider range of users and to improve the connection between conservation and utilization.
Local common bean populations should not only be collected and conserved but also characterized, documented, and made visible to the scientific and agricultural community. Their potential value can only be fully realized when researchers and breeders are able to identify relevant accessions and obtain sufficient information to assess their suitability for further use.

The GeneBankSystem provides a technological basis for this process by connecting passport information with phenotypic, biometric, visual, geographic, and evaluation data. The development of filter search further improves the accessibility and interpretability of the information.

Open access to information should be understood in the context of applicable rules governing access to genetic resources and associated benefit-sharing requirements. International systems such as EURISCO demonstrate the importance of making standardized information discoverable and reusable while respecting the rights and conditions associated with the underlying genetic material.

The proposed approach supports knowledge transfer between genebanks, research institutions, breeding programmes, farmers, and other stakeholders in the agri-food chain. It can therefore contribute to a transition from passive conservation towards active conservation and sustainable utilization of plant genetic resources (Westengen et al., 2018).

Contribution to breeding and climate-resilient agriculture

The combination of digital phenotyping and genebank documentation provides opportunities for identifying genetic resources with characteristics potentially useful for crop improvement. The common bean case study demonstrates how traditional local material can be evaluated using modern technologies and transformed into structured digital information. The value of these datasets is not limited to current research. Properly documented phenotypic data can be reused for future analyses, comparative studies, modelling, and breeding applications. This is particularly important under global climate change, when genetic diversity adapted to different environmental conditions may become increasingly valuable.

Digital documentation also reduces the risk that valuable knowledge associated with conserved accessions will be lost. By linking the seed material with its characterization history, images, measurements, and geographic origin, the system preserves both the biological resource and the knowledge generated about it.

CONCLUSIONS

The IS-PGR-SADOVO project has established an important technological basis for improving access to seeds and scientific knowledge associated with Bulgarian plant genetic resources conserved at the National Genebank of IPGR-Sadovo.

The main achievement is the development of an integrated digital environment that connects accession documentation, reproduction and germination testing information, semantic knowledge, phenotypic data, digital seed images, geographic information, and environmental monitoring.

The establishment of a database for characterization and evaluation data is a particularly important step towards the digitalization of *ex situ* collections. It creates opportunities for systematic storage, analysis, exchange, and future reuse of phenotypic information and provides a foundation for integration with national and international information platforms.

The acquisition and application of MARViN VisionLine and MARViN SmartLine introduced computer-vision-based digital phenotyping into the characterization of the genebank collections. The systems provide standardized measurements and digital images of seed morphology and quality characteristics and create opportunities for linking these data with accession passport information.

The evaluation of 80 *Phaseolus vulgaris* L. accessions of diverse geographical origin demonstrated the practical value of combining field observations, biometric measurements, international descriptors, and digital seed analysis. Promising accessions with potentially valuable agronomic characteristics were identified, emphasizing the importance of curator collections as sources of material for future crop breeding programmes.

The development of GeneBankOntology and semantic search provides a further step towards intelligent and user-oriented access to genebank knowledge. By connecting taxonomic, passport, evaluation, and visual information, the system can make complex scientific information more accessible to different categories of users.
The project demonstrates that digitalization of *ex situ* collections should not be considered merely as a technical conversion of records into electronic format. It represents a strategic approach to increasing the visibility, scientific value, accessibility, and sustainable utilization of plant genetic resources.
The integration of seed material, scientific data, digital images, phenotypic information, and geographic origin creates a foundation for stronger cooperation between genebanks, researchers, crop breeders, farmers, and other stakeholders. The GeneBankSystem contributes not only to the conservation of Bulgarian agrobiodiversity but also to the transfer of scientific knowledge and the development of resilient and sustainable agriculture under changing climatic conditions.

ACKNOWLEDGEMENTS

The research work was carried out under the project IS-PGR-SADOVO “Intelligent system for managing Bulgarian plant gene pool, conserved in the genebank of IPGR-Sadovo” with the financial support of the Ministry of Education and Science, Contract number KP-06-H86/9/09.12.2024 of Bulgarian National Science Fund.

REFERENCES

Desheva, G., Velcheva, N., Neshev, V., Uzundzhalieva, K., & Masheva, V. 2026. The seed storability of crops under medium-term storage condition in the genebank of Bulgaria. Bulgarian Journal of Crop Science, 63(3), 84-89.
ECPGR. 2023. Operational Guide for the Bulgarian Genebank. European Cooperative Programme for Plant Genetic Resources.
FAO. 2021. Global information systems and documentation of plant genetic resources for food and agriculture. Commission on Genetic Resources for Food and Agriculture. Food and Agriculture Organization of the United Nations.
FAO/Bioversity. 2017. Multi-Crop Passport Descriptors (MCPD). Rome, Italy.
Maggioni, L., van Hintum, T. J. L., & Lipman, E. 2014. Tailoring the documentation of plant genetic resources in Europe to the needs of the user: Workshop of the ECPGR Documentation and Information Working Group, 20-22 May 2014, Prague, Czech Republic.
Malinov, P., Doychev, E., Madanska, S., & Stoyanova-Doycheva, A. 2025. Intelligent warning component for control checks in the GeneBank system, Proceedings of the International Scientific Conference, “Informatics, mathematics, education and their applications“ - IMEA’2025, Pamporovo, Bulgaria.
MARViTECH. 2026. MARViN VisionLine and MARViN SmartLine: Digital seed analysis systems. Technical documentation.
Neshev, V. & Velcheva, N. 2025. Survey and Grouping of *Phaseolus vulgaris* Accessions by Passport, Characterization and Evaluation Descriptors. Journal of Mountain Agriculture on the Balkans, Vol. 28(3), 185-202.
Stoyanov, S., Belichev, B., Tabakova-Komsalova, V., Stoyanov, I., & Kostadinova-Tsankova, L. 2025. Monitoring in the National Gene Bank, Proceedings of the International Scientific Conference, “Informatics, mathematics, education and their applications“ - IMEA’2025, 25 – 27 November 2025, Pamporovo.

Velcheva, N., Desheva G., Uzundzhalieva K., Stoyanova-Doycheva A., Doukovska L. & Neshev V. 2025a. Innovative techniques for monitoring and efficient management of the Bulgarian genebank. Scientific Papers. Series B, Horticulture. Vol. LXIX, Issue 1, 544-550.
Velcheva, N., Stoyanova-Doycheva, A., & Doukovska, L. 2025b. Intelligent System for Managing Bulgarian Plant Gene Pool as a Target Object of IS-PGR-SADOVO Project. Journal of Mountain Agriculture on the Balkans, Vol. 28(5), 1076-1090.
Weise, S., Lohwasser, U., & Oppermann, M. (2020). Document or lose it on the importance of information management for genetic resources conservation in genebanks. Plants, 9(8), 1050.
Westengen, O. T., Skarbø, K., Mulesa, T. H., & Berg, T. 2018. Access to genes: Linkages between genebanks and farmers' seed systems. Food Security, (1), 9-25.

CURRENT STATUS AND PROBLEMS OF SHEEP FARMERS: THE CASE OF REŞADİYE DİSTRİCT, TOKAT PROVİNCE

Rüveyda YÜZBAŞIOĞLU

Tokat Gaziosmanpaşa University, Faculty of Agriculture, Department of Agricultural Economics, Tokat, Türkiye

Corresponding author e-mail: ruveyda.kiziloglu@gop.edu.tr.

ABSTRACT

Sheep farming plays an important role in the sustainability of rural economies and livestock production; however, the sector is increasingly affected by rising production costs as well as structural, technical, and institutional challenges. This study aims to examine the socioeconomic characteristics of sheep farming enterprises in Reşadiye district of Tokat Province, determine their production costs, and classify the major problems encountered by sheep farmers using factor analysis. The primary data were collected through face-to-face surveys with 117 sheep farming enterprises selected using stratified sampling. Descriptive statistics and exploratory factor analysis were employed to analyze the data. The average age of the farmers was 44.35 years, while their average experience in sheep farming was 19 years. In addition, 84.62% of the farmers were engaged in both crop and livestock production. The average total production cost was calculated as TRY 69,180.47 per enterprise. Variable costs accounted for 92.08% of total production costs, while fixed costs represented 7.92%. Among variable costs, concentrate and roughage feed costs constituted the largest cost component, with a combined share of 60.94%, followed by veterinary and animal health costs at 15.32%. The share of total feed costs in variable costs increased with farm size. The problems encountered by sheep farmers were grouped into four factors: structural, policy-related, and environmental problems; institutional support and production conditions; technical infrastructure and farm continuity; and production risks and resource constraints. These four factors explained 55.104% of the total variance. The findings indicate that the sustainability of sheep farming enterprises requires an integrated approach addressing not only production costs but also structural, institutional, technical, and production-related challenges. Accordingly, more efficient use of feed and pasture resources, strengthened support and agricultural extension services, measures to alleviate animal health and shepherd availability problems, and regional policies supporting the intergenerational continuity of sheep farming enterprises are recommended.

Keywords: Sheep farming, Production costs, Factor analysis, Farmers' problems

INTRODUCTION

Sheep farming is an important agricultural activity that enables the utilization of poor-quality pastures, fallow land, crop residues, and areas unsuitable for crop production by converting these resources into animal products such as meat, milk, wool, hair, and hides. In particular, sheep farming occupies an important place in the agricultural sector due to its role in the efficient utilization of natural resources, its contribution to rural income and employment, and its importance for the sustainability of livestock production. In addition to utilizing marginal and agriculturally disadvantaged areas, extensive sheep farming also plays an important role in

the provision of ecosystem services, the maintenance of rural populations, and the prevention of land abandonment (Bertolozzi-Caredio et al., 2021).

Rising production costs and inadequate producer prices in sheep and goat farming are among the main factors adversely affecting the economic sustainability of farms. Vouraki et al. (2020) reported that increasing production costs and inadequate farm-gate prices exert significant financial pressure on farms in the European small ruminant sector. This situation highlights the importance of jointly evaluating production costs and the economic challenges faced by sheep farms.

Sheep farming holds an important position in the global livestock sector. According to FAO (2023), there are approximately 1.2 billion sheep worldwide. Türkiye is also among the leading countries in the world in terms of its sheep population. According to 2024 data from the Turkish Statistical Institute (TURKSTAT), the sheep population in Türkiye increased by 4.8% compared with the previous year, reaching 44.081 million head (TURKSTAT, 2024). Sheep farming in Türkiye is generally characterized by the predominance of indigenous breeds and a feeding system largely based on pasture and grazing. In addition, the generally small scale of farms, difficulties in accessing production inputs, inadequacies in product marketing and utilization, and the limited share received by producers from product prices are among the major challenges facing the sector.

The distribution of the sheep population in Türkiye varies across regions and provinces. Tokat Province is one of the provinces where sheep farming is widely practiced due to its natural resources, rural structure, and livestock production activities. According to TURKSTAT (2024), Tokat Province has a total sheep population of 373,951 head, while Reşadiye District, which constitutes the study area, has a sheep population of 33,096 head. This situation underscores the importance of examining the existing structure and economic characteristics of sheep farming in Reşadiye District, as well as the problems faced by sheep farmers.

The economic sustainability of sheep farming is closely related not only to the income generated from production but also to the costs incurred during the production process. Bertolozzi-Caredio et al. (2021) stated that low profitability in sheep farming is associated with low selling prices and rising production costs, particularly increasing feed costs. Feed, labor, veterinary and animal health services, housing, energy, and other production inputs can significantly affect the cost structure and economic sustainability of sheep farms. Studies conducted in Türkiye have also demonstrated that factors such as feed, labor, pasture availability, access to shepherds, and marketing are important for the economic and structural sustainability of sheep farms (Çiçek et al., 2022; Gürer and Ulutaş, 2021; Mohamud and Çevrimli, 2023). Benoit et al. (2020) demonstrated that the economic performance of different sheep farming systems may be affected by technical and market-related risks and that farms develop different adaptation mechanisms in response to these risks.

However, the factors affecting the sustainability of sheep farming are not limited to production costs. Economic, structural, technical, and institutional challenges, including input prices, inadequate pasture and water resources, animal diseases, difficulties in finding shepherds, marketing opportunities, agricultural support policies, access to technical knowledge and extension services, and farm succession to future generations, may affect the continuity of production. Therefore, in addition to identifying the problems faced by sheep farmers, classifying these problems into their underlying dimensions is important for developing appropriate solutions and policies that address producers' needs.

The aim of this study is to determine the socioeconomic characteristics of sheep farms in Reşadiye District of Tokat Province, estimate production costs according to farm-size groups, and classify the main problems faced by sheep farmers using factor analysis. The findings are expected to contribute to the assessment of the economic and structural conditions of sheep

farming in the region and to the development of solutions aimed at enhancing the sustainability of sheep farms.

MATERIAL AND METHOD

Study Area and Data Collection

The primary material of the study consisted of primary data collected through face-to-face surveys from sheep farms in Reşadiye District of Tokat Province. Sheep farming is carried out in a total of 52 villages within the study area. The sheep population was taken into consideration in selecting the villages to be included in the study, and villages where sheep farming was concentrated were included in the research area. Accordingly, the survey was conducted in 10 villages, representing approximately 20% of the villages where sheep farming is practiced in the district.

At the farm level, data were collected on the socioeconomic characteristics of sheep farmers, farm structure, sheep production activities, production costs, and the problems faced by sheep farmers.

Sampling Method

Among the 52 villages where sheep farming is practiced in the study area, 10 villages were purposively selected based on the concentration of the sheep population. Sheep farms operating in the selected villages constituted the study population.

Prior to determining the sample size, the coefficient of variation was calculated based on the number of sheep owned by the farms constituting the population. The coefficient of variation is a measure used to determine whether the units within a population or sample exhibit a homogeneous or heterogeneous structure (Güneş & Arıkan, 1985; Şimşek, 2019). The calculated coefficient of variation was above 75%, indicating that the population had a heterogeneous structure. Therefore, the stratified sampling method was used to determine the sample size.

The farms were divided into three strata according to the number of sheep owned. The first stratum consisted of farms with 5–50 sheep, the second stratum of farms with 51–150 sheep, and the third stratum of farms with 151 sheep or more. The sample size was calculated at a 90% confidence level with a 1% deviation from the mean, and the number of farms to be surveyed was determined as 117. The proportional allocation method was used to distribute the sample among the strata (Çiçek & Erkan, 1996; Semerci, 2021). Accordingly, 33 farms from Stratum I, 39 farms from Stratum II, and 45 farms from Stratum III were included in the sample.

The following equation for the stratified sampling method was used to determine the sample size:

$$n = \frac{N.\sum N_h\,(S_h)^2}{N^2D^2 + \sum N_h\,(S_h)^2}$$

Where; n represents the sample size, N represents the total number of farms in the population, N_h represents the number of farms in the *h*th stratum, S_h represents the standard deviation of the *h*th stratum, and D represents the value associated with the allowable margin of error.

As a result of the sampling calculation, the number of farms to be surveyed within the scope of the study was determined as 117. The proportional allocation method was used to distribute the determined sample size among the strata (Çiçek & Erkan, 1996; Semerci, 2021). Accordingly, 33 farms from Stratum I, 39 farms from Stratum II, and 45 farms from Stratum III were included in the sample.

Table 1. Distribution of farms in the population by strata and number of farms selected for the sample

Stratum	Farm Size (head)	Mean (head)	Number of Farms (N_h)	Standard Deviation	Number of Farms in the Sample
I	5-50	27	72	14.23	33
ll	51-150	98	86	26.49	39
lll	151+	318	99	189.80	45
TOPLAM		163	257	173.05	117

The distribution of the 117 farms among the villages was based on the sheep population of the 10 villages included in the study. These villages had a total sheep population of 27,089 head, and the number of surveys to be conducted in each village was determined proportionally according to each village's share of the total sheep population. The following equation was used to calculate the sample size for each village:

$$n_i = \frac{N_i}{\sum_{i=1}^{10} N_i} * 117$$

Where:
n_i: number of surveys to be conducted in the *i*th village
N_i: sheep population of the *i*th village
$\sum_{i=1}^{10} N_i$: total sheep population of the 10 villages included in the study (27,089 head)
117: total sample size
The calculated values were rounded to the nearest whole number to determine the distribution of the sample size across the villages.

Table 2. Sheep population of the villages included in the study and proportional distribution of the sampled farms

Village	Sheep Population (head)	Share of Total (%)	Number of Sampled Farms
Çamlıkaya	4.392	16.21	19
Bereketli	3.722	13.74	16
Baydarlı	3.568	13.17	15
Cimitekke	3.292	12.15	14
Bereketli-Çakraz	2.525	9.32	11
Kuyucak	2.488	9.18	11
Bozçalı	2.256	8.33	10
Çınarcık	1.635	6.04	7
Nebişeyh	1.615	5.96	7
Cimitekke-Keteniği	1.596	5.89	7
Total	27.089	100.00	117

Data Analysis
Descriptive statistics were used to evaluate the data obtained from the study. Variables related to the socioeconomic characteristics of sheep farmers and farm structure were evaluated using frequencies, percentages, and mean values. Production costs associated with sheep farming

were calculated by considering variable and fixed costs, and the shares of individual cost items in total production costs were determined.

Exploratory factor analysis was applied to classify the main problems faced by sheep farmers into a smaller number of meaningful dimensions. Factor analysis is a multivariate statistical method that enables a large number of interrelated variables to be grouped into a smaller number of meaningful factors (Aksoy & Özdemir, 2026; Küley Ağır et al., 2025).

Production costs associated with sheep farming were calculated by considering variable and fixed costs. Variable costs included animal material, concentrate and roughage feed, veterinary and animal health expenses, labor, water, electricity and heating, livestock insurance, guard dog, shearing, and marketing expenses. General administrative expenses were calculated as 3% of total variable costs excluding general administrative expenses. Fixed costs included depreciation of sheep housing capital, maintenance and repair expenses for sheep housing, and depreciation of machinery capital. The shares of individual cost items in variable and fixed costs, as well as the proportions of variable and fixed costs in total production costs, were also calculated.

The suitability of the dataset for factor analysis was assessed using the Kaiser-Meyer-Olkin (KMO) measure of sampling adequacy and Bartlett's Test of Sphericity. A KMO value of 0.50 or above was considered acceptable, while a statistically significant Bartlett's Test of Sphericity was regarded as an indication that the correlation structure among the variables was suitable for factor analysis (Aksoy & Özdemir, 2026; Küley Ağır et al., 2025). Cronbach's Alpha coefficient was used to assess the internal consistency of the scale.

The analysis yielded a KMO value of 0.514 and a Cronbach's Alpha coefficient of 0.807, while Bartlett's Test of Sphericity was statistically significant ($p < 0.001$). Factors with eigenvalues greater than 1 were retained, and the Varimax rotation method was applied to improve factor interpretability (Küley Ağır et al., 2025). Variables with factor loadings of 0.40 or higher were considered in the interpretation of the factors. As a result of the analysis, four factors were identified, explaining 55.10% of the total variance.

RESULTS AND DISCUSSION

Socioeconomic Characteristics of Sheep Farmers

The overall mean age of the sheep farmers included in the study was 44.35 years. By farm-size group, the mean age was 43.43 years in Group I, 45.91 years in Group II, and 43.41 years in Group III. The similarity of the mean ages indicates that there was no marked difference in age among the farm-size groups. These results indicate that sheep farming in Reşadiye District is predominantly carried out by middle-aged farmers.

The professional experience of the farmers in sheep farming averaged 19.00 years. The mean professional experience was 13.42 years in Group I, 21.61 years in Group II, and 19.13 years in Group III, indicating that farmers in Group II had the highest average level of professional experience. Overall, the fact that the farmers had been engaged in sheep farming for a relatively long period indicates that they had accumulated considerable knowledge and experience in the sector.

The findings regarding the age of the farmers are similar to those reported in previous studies on sheep farmers in Türkiye. Çiçek et al. (2022) reported a mean age of 45.9 years for sheep farmers across Türkiye, while Gürer and Ulutaş (2021) reported a mean age of 45.15 years for farmers in Niğde and Aksaray provinces. Similarly, Köseman et al. (2022) found that 63.1% of sheep farmers in Malatya Province were in the 31–50 age group. When evaluated together with these studies, the mean age of 44.35 years determined in Reşadiye is largely consistent with the findings in the literature and suggests that sheep farming is predominantly carried out by middle-aged farmers in different regions.

In terms of professional experience, the mean of 19 years determined in Reşadiye was lower than the averages of 27.5 years reported by Çiçek et al. (2022) for Türkiye as a whole and 23.65 years reported by Gürer and Ulutaş (2021). In contrast, Tweldebirhan et al. (2025) reported an average farming experience of approximately 20 years among farmers in Ethiopia, which is close to the result obtained in Reşadiye. These results indicate that although sheep farmers in Reşadiye have less professional experience than those examined in some studies conducted in Türkiye, they nevertheless have considerable production experience in sheep farming.

Table 3. Some characteristics of sheep farmers regarding age and professional experience

Characteristics	Group I	Group II	Group III	Overall
Age (years)	43.43	45.91	43.41	44.35
Professional experience (years)	13.42	21.61	19.13	19.00

The educational status of the sheep farmers was examined, and middle school graduates had the highest share in the overall distribution at 29.06%, followed by primary school graduates at 26.50% and high school graduates at 22.22%. The proportions of associate degree and bachelor's degree graduates were 11.97% and 7.69%, respectively, while 2.56% of the farmers were illiterate. When farmers with a middle school education or higher were considered together, their share in the total was 70.94%. This finding indicates that the educational status of the sheep farmers included in the study was not concentrated solely at the basic education level.

When evaluated by farm-size group, middle school graduates ranked first in Group I with 30.30%, followed by associate degree graduates with 24.24% and high school graduates with 21.21%. In Group II, primary school graduates had the highest share at 33.33%, while the proportion of middle school graduates was 20.51%. In Group III, middle school graduates ranked first with 35.56%, while primary school and high school graduates each accounted for 28.89%. Although the distributions differed descriptively among the groups, no statistical significance test was conducted to examine the relationship between education level and farm size; therefore, these differences should be interpreted at the descriptive level.

The educational structure identified in Reşadiye differs from that reported in some sheep farming studies conducted in different regions of Türkiye. Çiçek et al. (2022) found that 51.3% of sheep farmers across Türkiye were primary school graduates, 18.7% were middle school graduates, and 13.3% were high school graduates, while university graduates accounted for only 6.0%. In the same study, the proportions of primary school, middle school, and high school graduates in the Black Sea Region were reported as 40.0%, 26.7%, and 20.0%, respectively. Similarly, Mohamud and Çevrimli (2023) reported that 51.6% of farmers in Selçuklu District of Konya Province were primary school graduates, 21.0% were middle school graduates, and 16.1% were high school graduates. In a study conducted in Malatya by Köseman et al. (2022), 70.2% of the farmers were primary school graduates, while middle school–high school graduates and college–university graduates accounted for 25.3% and 4.5%, respectively.

Compared with these studies, the educational status of sheep farmers in Reşadiye was not concentrated at the primary school level and was more evenly distributed across middle school, high school, and higher education levels. In particular, the combined share of associate and bachelor's degree graduates was 19.66%. The relatively high level of education may provide farms with a potential advantage in accessing and evaluating information on new production techniques, animal health practices, support programs, and farm management.

Indeed, Gürer and Ulutaş (2021) found that an increase in farmers' education level had a positive and statistically significant effect on the likelihood of continuing sheep farming, with an odds ratio of 1.513 for the education variable. This result indicates that education level is

one of the socioeconomic characteristics that should be considered in relation to the sustainability of sheep farms.

Table 4. Distribution of sheep farmers by educational status

Educational status	Group I		Group II		Group III		Overall	
	F	%	F	%	F	%	F	%
Illiterate	1	3.03	2	5.13	0	0.00	3	2.56
Primary school	5	15.15	13	33.33	13	28.89	31	26.50
Middle school	10	30.30	8	20.51	16	35.56	34	29.06
High school	7	21.21	6	15.38	13	28.89	26	22.22
Associate degree	8	24.24	5	12.82	1	2.22	14	11.97
Bachelor's degree	2	6.06	5	12.82	2	4.44	9	7.69
Total	33	100.00	39	100.00	45	100.00	117	100.00

When the income sources of the sheep farmers were examined, the combination of crop and livestock production was found to be the most common production structure, accounting for 84.62%. The proportion of farmers engaged exclusively in livestock production was 15.38%, while 3.42% considered livestock production as a supplementary source of income. In addition, 46.15% of the farmers received retirement income, and 55.56% had household members earning non-agricultural income. These findings indicate that sheep farming in Reşadiye is largely carried out in combination with other agricultural activities and that the income structure of farm households is not based solely on livestock production.

Similar issues concerning income diversification have also been addressed in sheep farming studies conducted in different regions. Gürer and Ulutaş (2021) reported that the proportions of sheep farms with non-agricultural income in Niğde and Aksaray were 3% and 26%, respectively. In Reşadiye, however, 55.56% of the farmers had household members earning non-agricultural income, indicating that income sources outside agricultural activities also played an important role in the households included in the study. Nevertheless, caution should be exercised when directly comparing these proportions because the studies differ in how non-agricultural income was defined.

Köseman et al. (2022) reported that 73.2% of sheep farmers in Malatya were not engaged in any other commercial activity apart from sheep farming. In Reşadiye, however, 84.62% of the farmers carried out crop and livestock production together, while retirement income and non-agricultural income earned by household members were also common. This indicates that sheep farming is an agricultural activity sustained alongside different sources of household income. This structure suggests that income sources should be considered together when evaluating the role of sheep farming within the household economy in Reşadiye.

Table 5. Some characteristics of sheep farmers regarding production and income structure

Income and production characteristic	F	%
Crop and livestock production	99	84.62
Livestock production only	18	15.38
Livestock production as a supplementary source of income	4	3.42
Retirement income	54	46.15
Household members with non-agricultural income	65	55.56

Note: The first two categories indicate the structure of production activities and are mutually exclusive. Since the remaining variables allow multiple responses, the sum of all percentages in the table exceeds 100%.

Production Costs in Sheep Farming Enterprises

When production costs in sheep farming enterprises were examined according to farm-size groups, total cost per farm was determined as TRY 13,619.66 in Group I, TRY 34,125.36 in Group II, and TRY 104,411.87 in Group III, while the overall average total cost was calculated as TRY 69,180.47. Total production costs increased markedly from Group I to Group III. This indicates that as farm size increases, the amount of inputs used in production and the associated total costs also increase.

An examination of the structure of variable costs showed that feed expenses constituted the most important cost item across all farms. The average concentrate feed cost per farm was TRY 28,316.00, accounting for 44.45% of variable costs, while roughage cost amounted to TRY 10,508.00 and accounted for 16.49%. When concentrate and roughage were considered together, total feed costs reached TRY 38,824.00 and represented 60.94% of variable costs. Feed costs were followed by veterinary and animal health expenses at 15.32% and labor costs at 6.24%. These findings indicate that production costs in the sheep farms examined were largely concentrated around feed expenses.

By farm-size group, the share of feed costs in variable costs increased with farm size. When concentrate and roughage costs were considered together, the share of total feed costs was calculated as 37.37% in Group I, 57.00% in Group II, and 64.60% in Group III. In contrast, the share of veterinary and animal health expenses declined from 25.58% in Group I to 15.42% in Group II and 12.97% in Group III. The share of labor costs was 6.60%, 6.83%, and 6.33% in Groups I, II, and III, respectively, showing a relatively similar distribution across farm sizes. These results indicate that feed costs become increasingly dominant within the variable cost structure, particularly in larger farms.

An examination of fixed costs showed that depreciation of sheep housing capital was the most important fixed cost item in all farm-size groups. Its share in fixed costs was 80.66% in Group I, 75.26% in Group II, and 65.38% in Group III, while the overall share was 69.69%. In contrast, the share of sheep housing maintenance and repair costs increased from 18.62% to 25.61% with increasing farm size, while the share of machinery capital depreciation increased from 0.71% to 9.01%. This distribution indicates that the internal structure of fixed costs also changes as farm size increases.

When the cost structure identified in Reşadiye is evaluated together with the findings of sheep farming studies conducted in different regions of Türkiye, similarities are observed particularly regarding the importance of feed costs. Çiçek et al. (2022) reported that feed costs accounted for 47.55% of total costs and labor costs for 30.12% in sheep farms across Türkiye. Similarly, Mohamud and Çevrimli (2023) determined that feed costs accounted for 46.1% of total production costs in sheep farms in Selçuklu District of Konya Province. In Reşadiye, feed costs also ranked first, accounting for 60.94% of variable costs, supporting the importance of feed expenses in the economic structure of sheep farms. However, caution should be exercised when directly comparing these ratios because the classification of cost items and the cost totals used to calculate percentages may differ among studies.

The international literature also emphasizes the importance of feed costs for the economic performance of sheep farms. Bertolozzi-Caredio et al. (2021) reported that feed expenses constituted a substantial proportion of total costs in extensive sheep farms in the Aragón region of Spain and that feed costs were a key determinant of the economic sustainability of farms. Theodoridis et al. (2022) demonstrated that increasing on-farm feed production is important for reducing dependence on purchased feed and controlling production costs. Similarly, Papadopoulou et al. (2021) emphasized the importance of utilizing pasture resources for the economic sustainability of small ruminant farms.

Overall, feed expenses constitute the main cost component in the cost structure of sheep farms in Reşadiye, and their relative share in variable costs increases as farm size increases. This

result indicates that, particularly for larger farms, improving on-farm feed production, increasing the availability of high-quality roughage resources, and ensuring the efficient use of existing pasture resources are important for controlling production costs.

Table 6. Distribution of production costs in sheep farming enterprises

Cost items	Group I (TRY)	%	Group II (TRY)	%	Group III (TRY)	%	Overall (TRY)	%
Animal material cost	1,753.57	16.53	1,795.80	6.06	1,817.00	1.86	1,803.00	2.83
Concentrate feed	3,428.57	32.32	12,919.35	43.61	45,763.00	46.87	28,316.00	44.45
Roughage	535.71	5.05	3,967.74	13.39	17,314.00	17.73	10,508.00	16.49
Veterinary and animal health	2,714.28	25.58	4,567.73	15.42	12,661.00	12.97	9,757.00	15.32
Labor costs	700.00	6.60	2,022.58	6.83	6,181.00	6.33	3,973.00	6.24
Water	46.42	0.44	237.09	0.80	408.00	0.42	289.00	0.45
Electricity and heating	267.85	2.52	427.41	1.44	766.00	0.78	621.00	0.97
Livestock insurance	0.00	0.00	361.29	1.22	2,811.00	2.88	1,874.00	2.94
Guard dog expenses	353.57	3.33	1,151.61	3.89	3,758.00	3.85	2,522.00	3.96
Shearing costs	471.42	4.44	1,016.12	3.43	2,520.00	2.58	1,706.00	2.68
Marketing costs	28.57	0.27	295.16	1.00	790.00	0.81	480.00	0.75
General administrative expenses (3%)	309.00	2.91	862.86	2.91	2,843.67	2.91	1,855.47	2.91
Total variable costs	10,608.96	100.00	29,624.74	100.00	97,632.67	100.00	63,704.47	100.00
Depreciation of sheep housing capital	2,428.57	80.66	3,387.09	75.26	4,432.20	65.38	3,816.00	69.69
Sheep housing maintenance and repair costs	560.71	18.62	936.12	20.80	1,736.00	25.61	1,291.00	23.58
Depreciation of machinery capital	21.42	0.71	177.41	3.94	611.00	9.01	369.00	6.73
Total fixed costs	3,010.70	100.00	4,500.62	100.00	6,779.20	100.00	5,476.00	100.00
Grand total costs	13,619.66	–	34,125.36	–	104,411.87	–	69,180.47	–

Note: General administrative expenses were calculated as 3% of total variable costs excluding general administrative expenses. Percentage values represent the shares of variable cost items in total variable costs and the shares of fixed cost items in total fixed costs.

When the total production costs of sheep farms were evaluated in terms of variable and fixed costs, variable costs accounted for a higher share of total costs in all farm-size groups. In Group I, variable costs constituted 77.89% of total costs, while fixed costs accounted for 22.11%. In Group II, the share of variable costs increased to 86.81%, whereas the share of fixed costs was 13.19%. In Group III, the share of variable costs reached the highest level at 93.51%, while the share of fixed costs declined to 6.49%. Across all farms, variable costs accounted for 92.08% of total production costs, whereas fixed costs represented 7.92%.

Across the farm-size groups, the share of variable costs in total production costs increased from Group I to Group III, whereas the relative share of fixed costs decreased. The absolute value of fixed costs increased from TRY 3,010.70 in Group I to TRY 4,500.62 in Group II and TRY 6,779.20 in Group III. Nevertheless, the decline in the share of fixed costs in total production costs from 22.11% to 6.49% indicates that, as farm size increased, the increase in variable costs

was greater than the increase in fixed costs. Indeed, variable costs increased from TRY 10,608.96 in Group I to TRY 97,632.67 in Group III.

This structure becomes clearer when evaluated together with the cost composition presented in Table 6. As farm size increased, the relative importance of feed costs within variable costs also increased. The combined share of concentrate and roughage costs was 37.37% in Group I, increasing to 57.00% in Group II and 64.60% in Group III. Therefore, as farm size increased, total production costs not only increased in absolute terms, but the cost structure also became increasingly concentrated in variable costs, particularly feed expenses.

The variable and fixed cost structure identified in Reşadiye is generally consistent with findings reported in the literature. Mohamud and Çevrimli (2023) found that variable costs accounted for 95% of total production costs and fixed costs for 5% in sheep farms in Selçuklu District of Konya Province. In Reşadiye, variable costs accounted for 92.08% of total production costs, while fixed costs represented 7.92%, indicating that production costs in sheep farms consist predominantly of variable costs. However, because the classification of cost items and, in particular, the way components such as labor are included in cost calculations may differ among studies, the cost calculation methods used should be considered when comparing these ratios.

Table 7. Distribution of variable and fixed costs by farm-size groups

Cost structure	Group I	Group II	Group III	Overall
Variable costs (TRY)	10,608.96	29,624.74	97,632.67	63,704.47
Share of variable costs (%)	77.89	86.81	93.51	92.08
Fixed costs (TRY)	3,010.70	4,500.62	6,779.20	5,476.00
Share of fixed costs (%)	22.11	13.19	6.49	7.92
Total costs (TRY)	13,619.66	34,125.36	104,411.87	69,180.47
Total (%)	100.00	100.00	100.00	100.00

Note: Percentage values represent the shares of variable and fixed costs in total production costs.

Classification of the Main Problems in Sheep Farming Using Factor Analysis

Exploratory factor analysis was applied to classify the main problems faced by sheep farmers into a smaller number of meaningful dimensions. The Kaiser-Meyer-Olkin (KMO) measure of sampling adequacy and Bartlett's Test of Sphericity were used to assess the suitability of the dataset for factor analysis. The KMO value was calculated as 0.514, indicating that sampling adequacy was at the minimum acceptable level for factor analysis. Bartlett's Test of Sphericity was statistically significant ($\chi^2 = 957.597$; $df = 153$; $p < 0.001$). This result indicates that the correlation matrix was not an identity matrix and that sufficient relationships existed among the variables to allow factor analysis to be applied. The Cronbach's Alpha coefficient, calculated to assess the internal consistency of the scale, was 0.807, indicating a good level of internal consistency among the variables used.

As a result of the factor analysis, the problems faced by sheep farmers were grouped under four main factors, which together explained 55.10% of the total variance. This result indicates that the problems encountered by sheep farmers cannot be grouped under a single dimension and that different problem areas need to be considered together. The contents and naming of the factors are evaluated in detail in the following tables.

Similar methods have been used in studies analyzing the multidimensional structure of small ruminant farms. Siasiou et al. (2021) examined 551 sheep and goat farms in Greece using multivariate analysis methods and identified five factors through principal component analysis, explaining 61.22% of the total variance. The KMO value in their study was calculated as 0.571, and Bartlett's Test of Sphericity was statistically significant ($p < 0.001$). Although the KMO

value of 0.514 and the total explained variance of 55.10% obtained in the Reşadiye study were lower than those reported by Siasiou et al. (2021), both studies demonstrate that a large number of variables can be classified under a smaller number of factors. These findings support the use of factor analysis as a method for classifying multidimensional characteristics and problem areas related to small ruminant farms.

Table 8. Tests of suitability for factor analysis

Test / Statistic	Value
Kaiser-Meyer-Olkin (KMO)	0.514
Bartlett's Approx. Chi-Square	957.597
Degrees of freedom (df)	153
Significance (p)	<0.001
Cronbach's Alpha	0.807

As a result of the factor analysis, four factors with eigenvalues greater than 1 were obtained, explaining 55.104% of the total variance. After Varimax rotation, the eigenvalue of the first factor was 3.003, explaining 16.686% of the total variance. The eigenvalue of the second factor was 2.955, accounting for 16.415% of the variance; the eigenvalue of the third factor was 2.217, accounting for 12.319%; and the eigenvalue of the fourth factor was 1.743, accounting for 9.685% of the variance.

After rotation, the contributions of the first and second factors to the total variance were quite similar. Together, these two factors explained 33.101% of the total variance. With the addition of the third factor, the cumulative explained variance increased to 45.420%, and with the inclusion of the fourth factor, it reached 55.104%. This distribution indicates that no single factor dominated the explanation of the problems faced by sheep farmers and that the total variance was distributed across different dimensions of the problems.

Table 9. Variance explained by the factors

Factor	Eigenvalue after rotation	Explained variance (%)	Cumulative variance (%)
1	3.003	16.686	16.686
2	2.955	16.415	33.101
3	2.217	12.319	45.420
4	1.743	9.685	55.104

An examination of the rotated factor loadings showed that the first factor consisted of constantly changing policies (0.813), problems related to guard dogs (0.718), problems arising from sheep housing (0.663), difficulties in obtaining grants (0.663), and wild animal attacks (0.518). Since variables related to policy, farm structure, and environmental conditions were grouped together under this factor, this dimension was named "Structural, Policy, and Environmental Problems." The highest loading within the factor was associated with constantly changing policies (0.813), indicating that problems related to policy implementation were the most prominent component of this dimension.

In the second factor, insufficient support (0.807) and the limited number of informational seminars (0.788) had the highest factor loadings. These variables were followed by water shortages (0.595), marketing problems (0.585), and difficulties in finding shepherds (0.549). Since institutional support and information services were grouped together with basic conditions essential for sustaining production, this dimension was named "Institutional Support

and Production Conditions." This structure indicates that farmers' problems are not limited to financial support but also include information and extension services, marketing, water availability, and labor supply.

The third factor consisted of problems in forage production (0.803), lack of modern technical facilities (0.642), and the lack of a successor to take over the farm (0.504). Since problems related to the technical structure of production and the transfer of the farm to future generations were grouped under the same factor, this dimension was named "Technical Infrastructure and Farm Continuity." This factor indicates that, in addition to existing technical conditions, the ability of sheep farms to continue operating in the future constitutes an important area of concern for their sustainability.

In the fourth factor, animal diseases had the highest factor loading at 0.881. Insufficient education (0.519), inadequate or unavailable pasture (0.506), and high feed prices (0.444) were also included in this factor. Since animal health risks were grouped together with production resources such as farmers' knowledge level, pasture availability, and feed costs, this dimension was named "Production Risks and Resource Constraints." The particularly high factor loading of animal diseases indicates that health-related risks were the most prominent component of this dimension.

Overall, the factor analysis results indicate that the problems faced by sheep farmers in Reşadiye District are not solely economic in nature; rather, they are grouped into four main dimensions encompassing structural and policy conditions, environmental risks, institutional support, production conditions, technical infrastructure, farm continuity, and constraints related to production resources.

Findings in the literature also support the multidimensional nature of the problems encountered in sheep farming. Nyam et al. (2022) classified the problems faced by small-scale sheep farmers in South Africa into four main components using principal component analysis and identified marketing, diseases and parasites, high feed costs, inadequate capital, professional knowledge, housing, labor, water, and pasture conditions as important problem areas. These results indicate that the problems identified in Reşadiye may also emerge in different production systems in economic, technical, structural, and production-resource dimensions.

The findings regarding farm continuity are also consistent with the literature. Siasiou et al. (2021) evaluated variables related to the current status and future of farms under a separate factor and demonstrated that farm succession and the tendency to continue production are important for the future of farms. Bertolozzi-Caredio et al. (2021) identified rural depopulation, labor shortages, and weak generational renewal among the factors threatening the continuity of extensive sheep farming. These findings support the inclusion of the lack of a successor to take over the farm within the farm continuity dimension identified in Reşadiye.

Similar results have also been reported regarding institutional support and production conditions. Gürer and Ulutaş (2021) found that an increase in the share of small ruminant support payments in the value of production positively affected farmers' likelihood of continuing sheep farming. The same study also reported that difficulties in finding shepherds negatively affected the decision to continue production. These results support the inclusion of insufficient support and difficulties in finding shepherds within the same problem dimension in Reşadiye.

In terms of production risks and resource constraints, Mohamud and Çevrimli (2023) identified inadequate pasture, animal diseases, increasing costs, marketing, and difficulties in finding shepherds among the major problems faced by sheep farms. Çiçek et al. (2022) also reported that pasture availability and productivity, family labor, shepherd availability, product prices, and marketing opportunities are important for the structure and sustainability of sheep farms. These findings support the production risks and resource constraints dimension identified in Reşadiye.

Overall, the factor analysis results show that the problems faced by sheep farmers in Reşadiye emerge across different structural, institutional, technical, and production-related dimensions. Therefore, measures aimed at ensuring the sustainability of sheep farming should not focus solely on production costs; they should also consider support and extension services, technical infrastructure, pasture and feed resources, animal health, labor supply, and the intergenerational continuity of farms together.

Table 10. Classification of the main problems faced by sheep farmers according to factors

Factor / Dimension	Variable	Factor loading
Factor 1: Structural, policy, and environmental problems	Constantly changing policies	0.813
	Problems related to guard dogs	0.718
	Problems arising from sheep housing	0.663
	Difficulties in obtaining grants	0.663
	Wild animal attacks	0.518
Factor 2: Institutional support and production conditions	Insufficient support	0.807
	Limited number of informational seminars	0.788
	Water shortages	0.595
	Marketing problems	0.585
	Difficulties in finding shepherds	0.549
Factor 3: Technical infrastructure and farm continuity	Problems in forage production	0.803
	Lack of modern technical facilities	0.642
	Lack of a successor to take over the farm	0.504
Factor 4: Production risks and resource constraints	Animal diseases	0.881
	Insufficient education	0.519
	Inadequate or unavailable pasture	0.506
	High feed prices	0.444

CONCLUSIONS AND RECOMMENDATIONS

This study examined the socioeconomic characteristics and production costs of sheep farms in Reşadiye District of Tokat Province and classified the main problems faced by sheep farmers using factor analysis. The results showed that the mean age of the farmers was 44.35 years and their average professional experience in sheep farming was 19 years. The fact that 84.62% of the farmers were engaged in both crop and livestock production indicates that sheep farming in the study area is carried out in an integrated manner with other agricultural activities. In addition, the prevalence of retirement income and non-agricultural income sources within the household indicates a diversified income structure among farm households.

In terms of production costs, the overall average total cost per farm was calculated as TRY 69,180.47. When concentrate and roughage costs were considered together, total feed costs accounted for 60.94% of variable costs, making feed the most important component of the cost structure. Feed costs were followed by veterinary and animal health expenses at 15.32% and labor costs at 6.24%. Variable costs accounted for 92.08% of total production costs, while fixed costs accounted for 7.92%. Across farm-size groups, the share of variable costs in total costs increased from 77.89% to 93.51%, whereas the share of fixed costs decreased from 22.11% to 6.49%. Furthermore, total feed costs accounted for 37.37% of variable costs in Group I, 57.00% in Group II, and 64.60% in Group III, indicating that the relative importance of feed costs increased with farm size. These findings demonstrate that production costs in sheep farms consist predominantly of variable costs and that the cost structure differs across farm-size groups.

The factor analysis grouped the problems faced by sheep farmers into four main dimensions: "Structural, Policy, and Environmental Problems," "Institutional Support and Production Conditions," "Technical Infrastructure and Farm Continuity," and "Production Risks and Resource Constraints." Together, these factors explained 55.104% of the total variance. Constantly changing policies, insufficient support, problems in forage production, and animal diseases had the highest factor loadings within their respective factors. These results demonstrate that the problems encountered in sheep farming are not limited to economic and cost-related issues but have a multidimensional structure encompassing structural, policy, institutional, technical, and production-related risks.

Based on the findings of the study, priority should be given to measures aimed at reducing feed costs, which constitute a major component of the cost structure of sheep farms. Improving farms' capacity to produce high-quality roughage, encouraging forage crop production, and protecting and efficiently utilizing existing pasture resources may contribute to reducing dependence on purchased feed and the associated cost burden. In particular, the increasing relative importance of feed costs as farm size increases highlights the importance of measures related to feed production and procurement for larger farms.

Based on the factor analysis results, it is recommended that access to support and grant programs be facilitated, predictability in agricultural support policies be improved, and training, information, extension, and advisory services for sheep farmers be strengthened. In addition, marketing opportunities should be improved and the effectiveness of producer organizations should be enhanced. Measures that take regional conditions into account should also be developed to address problems that directly affect the production process, including shepherd availability, water and housing conditions, animal diseases, inadequate pasture, and wild animal attacks.

The inclusion of the lack of a successor to take over the farm within the "Technical Infrastructure and Farm Continuity" dimension indicates that intergenerational continuity should also be considered in relation to the long-term sustainability of sheep farming. Therefore, developing measures that encourage young people to remain in or enter sheep farming is important for facilitating the transfer of farms to future generations.

In conclusion, the sustainability of sheep farming in Reşadiye District is shaped by several interrelated factors, including production costs, feed and pasture resources, institutional support, technical infrastructure, animal health, labor availability, marketing opportunities, and the intergenerational continuity of farms. Therefore, policies aimed at ensuring the continuity of sheep farming in the region should be developed through a comprehensive approach that takes regional conditions into account.

REFERENCES

Aksoy, A., Özdemir, F. N. 2026. Besi sığırcılığı işletmelerinde karşılaşılan riskler ve sürdürülebilirlik yaklaşımları (Erzurum ili örneği). Tekirdağ Ziraat Fakültesi Dergisi, 23(3): 975–989. https://doi.org/10.33462/jotaf.1762375

Benoit, M., Joly, F., Blanc, F., Dumont, B., Sabatier, R., Mosnier, C. 2020. Assessment of the buffering and adaptive mechanisms underlying the economic resilience of sheep-meat farms. Agronomy for Sustainable Development, 40: 34. https://doi.org/10.1007/s13593-020-00638-z

Bertolozzi-Caredio, D., Bardají, I., Coopmans, I., Soriano, B., Garrido, A. 2021. Key steps and dynamics of family farm succession in marginal extensive livestock farming. Journal of Rural Studies, 83: 131–141.

Çiçek, A., Erkan, O. 1996. Tarım ekonomisinde araştırma ve örnekleme yöntemleri. GOP Üniversitesi Ziraat Fakültesi Yayınları.

Çiçek, A., Ayyıldız, M., Erdal, G., Erdal, H. 2022. Türkiye'de koyun yetiştiriciliğinin önemi ve ekonomik analizi. MAS Journal of Applied Sciences, 7(Özel Sayı): 1303–1322. https://doi.org/10.5281/zenodo.7529826

FAO. 2023. FAOSTAT: Crops and livestock products. Food and Agriculture Organization of the United Nations.

Güneş, T., Arıkan, R. 1985. Tarım ekonomisi istatistiği. Ankara Üniversitesi Ziraat Fakültesi Yayınları, Yayın No. 924.

Gürer, B., Ulutaş, Z. 2021. TR71 Bölgesinde işletmelerin koyun yetiştiriciliği faaliyetine devam etme olasılığını etkileyen faktörlerin analizi. Anadolu Tarım Bilimleri Dergisi, 36: 63–72. https://doi.org/10.7161/omuanajas.773460

Köseman, A., Kul, S., Şeker, İ. 2022. Malatya ilindeki koyunculuk işletmelerinin yapısal özellikleri ve yetiştiricilerin sosyo-ekonomik durumu. Fırat Üniversitesi Sağlık Bilimleri Veteriner Dergisi, 36(1): 1–9.

Küley Ağır, B., Ekinci, M. S., Çelik, Ş. 2025. Türkiye'de yem bitkileri üretimi ve hayvan varlığı arasındaki ilişki: Faktör analizi yaklaşımı. Adnan Menderes Üniversitesi Ziraat Fakültesi Dergisi, 22(1): 137–144. https://doi.org/10.25308/aduziraat.1673063

Mohamud, A. H., Çevrimli, M. B. 2023. Technical and economic analysis of sheep breeding enterprises in Selcuklu District of Konya Province. Kocatepe Veterinary Journal, 16(3): 342–356. https://doi.org/10.30607/kvj.1278117

Nyam, Y. S., Bahta, Y. T., Oduniyi, O. S., Matthews, N. 2022. Smallholder sheep farmers' perception of production constraints and competitiveness strategies in South Africa. Scientific African, 16: e01192. https://doi.org/10.1016/j.sciaf.2022.e01192

Papadopoulou, A., Ragkos, A., Theodoridis, A., Skordos, D., Parissi, Z., Abraham, E. 2021. Evaluation of the contribution of pastures on the economic sustainability of small ruminant farms in a typical Greek area. Agronomy, 11(1): 63. https://doi.org/10.3390/agronomy11010063

Semerci, A. 2021. Tarım işletmelerinde tarımsal kredi kullanım durumunun analizi. Türk Tarım ve Doğa Bilimleri Dergisi, 8(2): 396–410.

Siasiou, A., Karelakis, C., Galanopoulos, K., Mitsopoulos, I., Lagka, V. 2021. Typology of management of transhumant sheep and goat farms in Greece: Proposals for the system continuity. European Journal of Agriculture and Food Sciences, 3(1): 84–89. https://doi.org/10.24018/ejfood.2021.3.1.228

Şimşek, G. 2019. Kırşehir ilinde küçükbaş hayvan yetiştiriciliği yapan işletmelerin teknik ve ekonomik yapılarının belirlenmesi. Yüksek lisans tezi, Ahi Evran Üniversitesi, Fen Bilimleri Enstitüsü.

Theodoridis, A., Vouraki, S., Morin, E., Koutouzidou, G., Arsenos, G. 2022. Efficiency analysis and identification of best practices and innovations in dairy sheep farming. Sustainability, 14(21): 13949. https://doi.org/10.3390/su142113949

TÜİK. 2024. Hayvansal üretim istatistikleri, 2024. Türkiye İstatistik Kurumu.

Tweldebirhan, M. D., Kesse, S., Woldesemayat, A. A., Edea, Z., Armar, A. J., Nigussie, H., Dadi, H., Haile, A. 2025. Farming typology and socio-economic analysis in sub-alpine ecosystem, Simien Mountain National Park, Ethiopia. East African Journal of Veterinary and Animal Sciences, 9(2): 55–68.

Vouraki, S., Skourtis, I., Psichos, K., Jones, W., Davis, C., Johnson, M., Riaguas Rupérez, L., Theodoridis, A., Arsenos, G. 2020. A decision support system for economically sustainable sheep and goat farming. Animals, 10(12): 2421. https://doi.org/10.3390/ani10122421

A REVIEW OF THE MECHANICAL BEHAVIOR OF AUXETIC TPMS-BASED FUNCTIONALLY GRADED STRUCTURES

TOLGA SOLAR[1], CANER SOLAR[2], PINAR AYDAN DEMIRHAN[3]

[1]Arel University, Engineering Faculty, Turkey
[2,3]Trakya University, Engineering Faculty, Turkey

ABSTRACT

Functionally graded materials (FGMs) enable spatial tailoring of mechanical properties by gradually varying material composition or structural characteristics, thereby reducing abrupt transitions commonly encountered in conventional composite systems. In recent years, triply periodic minimal surface (TPMS) architectures and auxetic structures with negative Poisson's ratio have attracted increasing attention because of their potential for lightweight design, deformation control, energy absorption, and impact resistance. TPMS architectures such as Gyroid, Primitive, Diamond, and I-WP provide smooth and continuous geometries, while auxetic behavior offers distinctive transverse deformation mechanisms. Their combination with functional grading provides a promising framework for tailoring the static, vibration, buckling, and dynamic responses of advanced lightweight structures. This review critically and comparatively examines recent developments in auxetic TPMS-based and functionally graded structures, with emphasis on geometrical design strategies, additive manufacturing, experimental characterization, mechanical behavior, and engineering applications. Particular attention is given to the relationships among topology, auxetic mechanism, grading strategy, manufacturing fidelity, and structural response. Current research limitations and future directions toward manufacturable, experimentally validated, and application-oriented auxetic TPMS systems are also discussed.

Key words: Auxetic structures, triply periodic minimal surfaces (TPMS), functionally graded materials (FGMs), sandwich structures, mechanical behavior.

INTRODUCTION

Mechanical metamaterials derive their macroscopic properties primarily from engineered architecture rather than solely from constituent materials. Among them, auxetic structures are particularly attractive because their negative Poisson's ratio can provide favorable deformation characteristics together with enhanced energy absorption, indentation resistance, and impact performance. These properties have motivated their investigation in protective systems, biomedical devices, automotive components, and lightweight engineering structures (Daynes, 2025; Novak et al., 2026). In parallel, functionally graded porous sandwich structures have been investigated as lightweight structural systems in which spatial variations in material properties and porosity can be used to tailor stiffness and static response (Solar and Demirhan, 2025).
Triply periodic minimal surface (TPMS) architectures have emerged as promising alternatives to conventional strut-based lattices because of their smooth and continuous geometries, high connectivity, and favorable mechanical efficiency. Primitive, Gyroid, Diamond, and I-WP are among the most frequently investigated TPMS topologies, although their responses vary considerably with topology, relative density, material properties, and loading conditions (Chen and Wang, 2026; Engel et al., 2026). The integration of TPMS architectures into functionally

graded porous sandwich structures has also been investigated for improving and tailoring their static structural response (Solar et al., 2025).

An important development has been the deliberate modification of TPMS architectures to generate auxetic behavior. Since conventional TPMS geometries are not universally auxetic, several geometrical strategies have been proposed, including buckling-induced deformation, coordinate transformation, unit-cell rotation, dual-period mapping, and shape-function optimization. Zheng et al. (2021) introduced a buckling-induced TPMS-derived auxetic metamaterial, while Wang et al. (2023) transformed a Gyroid architecture into a continuous auxetic tubular configuration. Liu et al. (2023) and Kim et al. (2024) subsequently demonstrated controllable auxeticity and deformation-dependent stiffness using modified Primitive-based architectures.

More recent research has shifted from simply achieving a negative Poisson's ratio toward simultaneously controlling auxeticity, stiffness, isotropy, deformation stability, and energy absorption. Daynes (2025) demonstrated TPMS-based configurations with positive, zero, and negative Poisson's ratios while addressing elastic isotropy, whereas Novak et al. (2026) showed that functional grading can stabilize auxetic deformation by suppressing localization and out-of-plane instability. Accordingly, this review examines the relationships among TPMS topology, auxetic mechanisms, functional grading, additive manufacturing, and mechanical response, with particular emphasis on compression, energy absorption, vibration, buckling, engineering applications, current challenges, and future research needs.

Table 1. Classification of the reviewed studies according to the integration strategy of auxeticity, TPMS and functional grading

Study	Main architecture	Design approach	Main contribution
Zheng et al. (2021)	Modified TPMS	Buckling-induced auxeticity	Introduced a mathematically defined 3D auxetic TPMS-derived structure
Wang et al. (2023)	Gyroid tubular TPMS	Coordinate transformation	Developed seamless auxetic tubular TPMS structures
Liu et al. (2023)	Primitive TPMS	Dual-period deformation	Enabled controllable NPR through geometric parameters
Kim et al. (2024)	Rotated Primitive TPMS	Unit-cell rotation	Achieved auxeticity with deformation-dependent stiffness
Daynes (2025)	Primitive TPMS	Shape-function mapping	Combined tunable Poisson's ratio with elastic isotropy
Novak et al. (2026)	Graded re-entrant AUXTPMS	Porosity grading	Improved deformation stability and sustained auxetic response

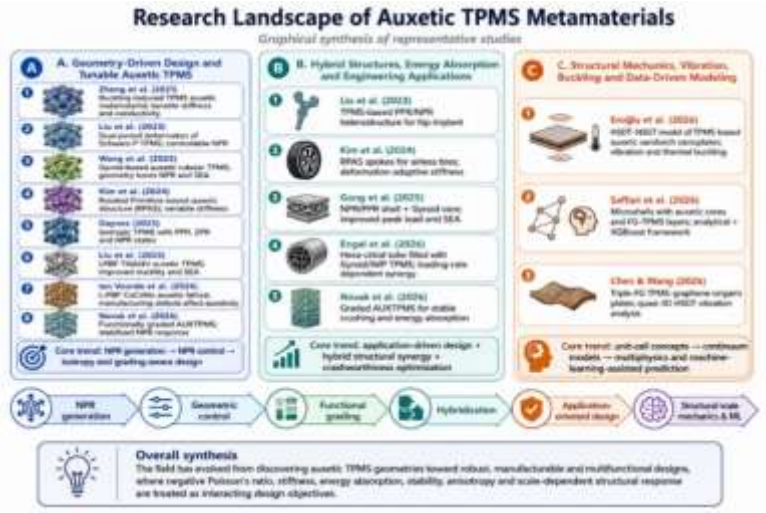

Fig. 1: Research landscape of auxetic TPMS metamaterials.

Design Strategies and Functional Grading of Auxetic TPMS Structures

Auxetic behavior in TPMS-based structures is generally achieved through deliberate geometric modification rather than being an inherent characteristic of conventional TPMS topologies. Recent design strategies therefore focus on activating rotational, bending, and buckling mechanisms while simultaneously controlling stiffness, anisotropy, deformation stability, and manufacturability (Kim et al., 2024; Novak et al., 2026). The evolution of these approaches is illustrated in Fig. 2.

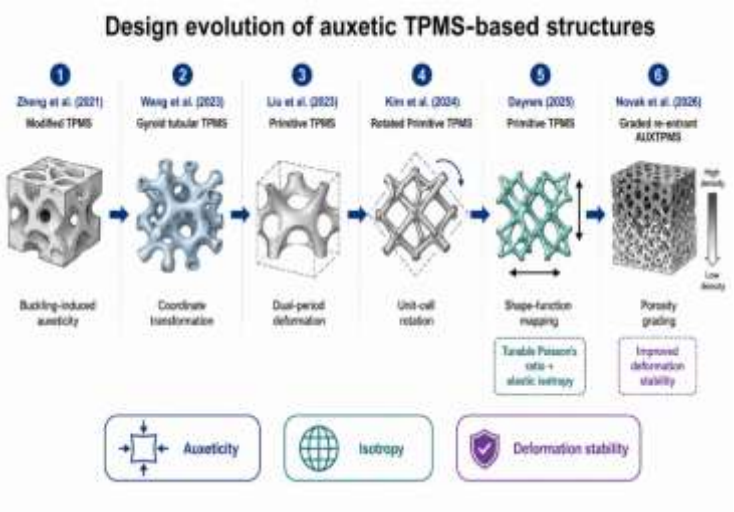

Fig. 2: Design evolution of auxetic TPMS-based structures. Original schematic synthesized from Zheng et al. (2021), Wang et al. (2023), Liu et al. (2023), Kim et al. (2024), Daynes (2025), and Novak et al. (2026).

Geometrical strategies for inducing auxetic behavior

Several geometrical approaches have been proposed to generate negative Poisson's ratio behavior in TPMS-derived structures. A modified TPMS architecture based on buckling-

induced deformation was among the early three-dimensional approaches, demonstrating that structural instability could be intentionally used to produce an auxetic response (Zheng et al., 2021). A different strategy transformed a Gyroid-type TPMS from Cartesian to cylindrical coordinates, producing a continuous tubular auxetic architecture suitable for additive manufacturing (Wang et al., 2023).

Primitive TPMS has subsequently become an important basis for controllable auxetic design. Dual-period deformation functions and Bézier-based transformations were applied to the P-surface to obtain tunable three-dimensional negative Poisson's ratio behavior (Liu et al., 2023). Unit-cell rotation was also used to generate oblique connections and deformation-dependent stiffness in rotated Primitive structures, providing a direct route toward application-oriented designs such as airless tires (Kim et al., 2024).

More recently, shape-function mapping and level-set optimization have enabled simultaneous control of Poisson's ratio and elastic isotropy. At a relative density of 20%, Poisson's ratios ranging approximately from +0.29 to −0.38 were demonstrated, including positive, zero, and auxetic configurations (Daynes, 2025). These developments indicate a transition from simply generating auxeticity toward programming several mechanical properties within the same TPMS-based architecture.

Functional grading of auxetic TPMS architectures

Functional grading introduces an additional design variable by allowing porosity, relative density, wall thickness, or other geometrical parameters to vary spatially. Unlike conventional FGMs, where grading is commonly associated with changes in material composition, TPMS-based structures can also achieve spatial property variation through geometry alone.

Current evidence shows that grading does not necessarily increase all mechanical properties simultaneously. Thickness-graded auxetic TPMS lattices exhibited altered deformation characteristics but did not consistently outperform homogeneous configurations in peak mechanical performance (ten Voorde et al., 2026). In contrast, porosity grading in re-entrant AUXTPMS structures promoted sequential crushing, reduced deformation localization, and suppressed out-of-plane instability, thereby maintaining the auxetic response over a wider strain range (Novak et al., 2026).

These findings suggest that one of the principal benefits of functional grading is deformation control rather than universal strength enhancement. Grading can therefore be used to regulate where deformation initiates, how collapse propagates, and how long the auxetic mechanism remains active.

Emerging multi-parameter and hybrid grading concepts

Recent studies have extended functional grading beyond a single geometrical parameter. A Triple-FG TPMS–graphene-origami system was proposed in which TPMS architecture, origami folding degree, and reinforcement content were graded independently, enabling multi-parameter control of dynamic response (Chen and Wang, 2026).

Hybrid concepts have also combined different architected mechanisms within separate structural components. For example, butterfly-shaped auxetic cores have been integrated with FG-TPMS face layers and graphene platelet reinforcement, demonstrating a multi-level design approach in which auxetic and TPMS functions are combined without necessarily being incorporated into the same unit cell (Saffari et al., 2026).

Overall, current design strategies are evolving from isolated auxetic unit cells toward graded, hybrid, and multi-parameter architected systems in which geometry, material distribution, and deformation mechanisms are tailored simultaneously.

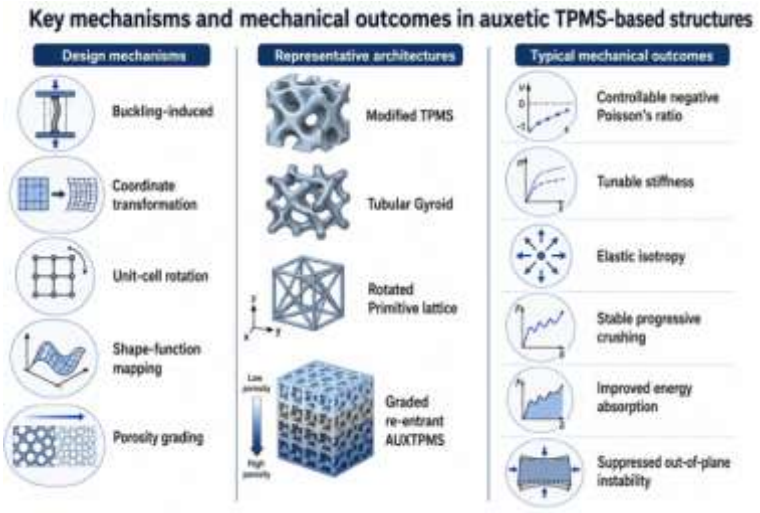

Fig. 3: Principal design mechanisms, representative architectures and typical mechanical outcomes of auxetic TPMS-based structures. Original schematic synthesized from the reviewed literature.

Mechanical Behavior of Auxetic TPMS-Based Structures

The mechanical response of auxetic TPMS-based structures is governed by the combined effects of topology, relative density, grading strategy, deformation mechanism, parent material, and loading condition. Most experimental studies focus on compression and energy absorption, whereas recent analytical investigations have extended the field toward vibration, buckling, and multifunctional structural behavior.

Compression behavior and energy absorption

Compression remains the most extensively investigated loading condition because it directly reveals auxetic deformation, collapse mechanisms, and energy-absorption capability. Recent studies indicate that achieving a stronger negative Poisson's ratio does not necessarily lead to simultaneous improvements in stiffness, strength, and energy absorption.

Homogeneous CoCrMo auxetic TPMS lattices fabricated by L-PBF exhibited apparent Poisson's ratios as low as approximately −0.1443, energy absorption up to 37.93 J/cm³, and compressive strength up to 231.44 MPa. However, the thickness-graded configuration did not consistently outperform the homogeneous structures in peak mechanical properties (ten Voorde et al., 2026).

High auxetic deformation has also been demonstrated in Ti6Al4V TPMS-based tubular metamaterials. An optimized configuration achieved an effective auxetic strain of 17.173% and a specific energy absorption (SEA) of 16.6 J/g, illustrating the possibility of combining pronounced auxeticity with high energy absorption while retaining an inherent trade-off with structural strength (Liu et al., 2025).

Functional grading can provide additional benefits by controlling the collapse sequence rather than simply increasing peak strength. Porosity-graded re-entrant AUXTPMS structures maintained negative Poisson's ratio behavior over a wider strain range and suppressed out-of-plane instability. Metallic specimens exhibited SEA values of 2.63 J/g for aluminium and 5.05 J/g for stainless steel (Novak et al., 2026).

Hybridization provides another route for improving compressive performance. The integration of a Gyroid core into NPR cylindrical shells increased both peak load and SEA by approximately 47% in selected configurations (Gong et al., 2025). However, such improvements can be loading-rate dependent. TPMS-filled hexa-chiral tubes showed increases of up to 104% in mass-specific energy absorption under quasi-static loading, whereas comparable benefits were not maintained under dynamic loading because of changes in the deformation behavior of the base material (Engel et al., 2026).

Overall, these findings demonstrate that auxeticity alone does not determine compressive performance. Topology, grading, hybrid interaction, material behavior, and loading rate must be considered simultaneously.

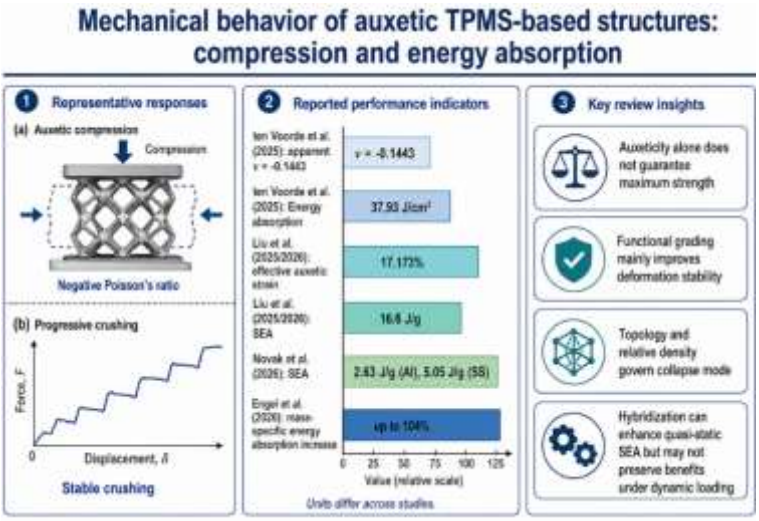

Fig. 4: Summary of representative compression responses, reported performance indicators and main review insights for auxetic TPMS-based structures. Original review figure synthesized from the reviewed literature.

Vibration and dynamic response

Compared with compression, vibration studies remain relatively limited. Nevertheless, recent investigations demonstrate that TPMS topology and functional grading can also be used to tailor the dynamic behavior of lightweight auxetic structures.

In Triple-FG TPMS–graphene-origami plates, natural frequencies were strongly affected by TPMS topology, grading pattern, and reinforcement distribution. Among the investigated configurations, P-type TPMS produced the highest natural frequencies, while increasing porosity generally reduced the fundamental frequency. The combined FGV-X/FGP-O grading configuration provided the highest response among the examined pattern combinations (Chen and Wang, 2026).

Machine-learning-assisted approaches have also been introduced for rapid prediction of vibration characteristics. For cylindrical microshells incorporating butterfly-shaped auxetic cores and FG-TPMS face layers, XGBoost models achieved coefficients of determination ranging from 98.84% to 99.91%, demonstrating the potential of data-driven methods for efficient performance prediction (Saffari et al., 2026).

These studies indicate a transition from geometry-based vibration analysis toward multi-parameter structural models combining functional grading, reinforcement distribution, foundation effects, and data-driven prediction.

Buckling and structural stability

Structural stability is becoming increasingly important as auxetic TPMS concepts are extended from cellular compression specimens to sandwich plates and other load-bearing systems. Functional grading has been shown to suppress out-of-plane instability and promote more stable progressive deformation in re-entrant AUXTPMS architectures (Novak et al., 2026).

At smaller structural scales, coupled vibration and buckling behavior has been investigated for sandwich nanoplates containing TPMS-based auxetic cores. Porosity, TPMS topology, nonlocal effects, strain-gradient effects, temperature, and external electric and magnetic fields were shown to modify both natural frequency and stability. Increasing porosity and nonlocal effects generally reduced effective stiffness, whereas strain-gradient effects increased structural rigidity (Eroğlu et al., 2026).

These results demonstrate that stability in auxetic TPMS structures is governed not only by geometry, but also by scale-dependent effects, environmental conditions, and multiphysics interactions. Buckling can therefore be considered both a failure mechanism and a controllable design parameter.

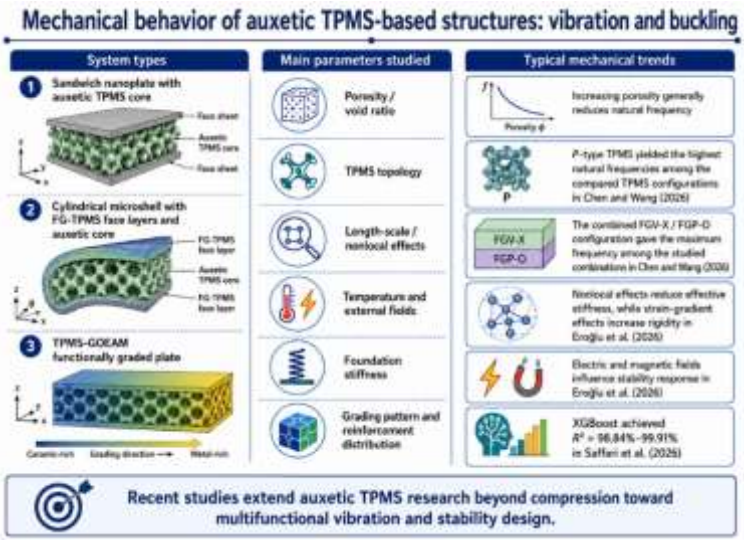

Fig. 5: Summary of system types, governing parameters and main mechanical trends reported in vibration and buckling studies of auxetic TPMS-based structures. Original review figure synthesized from the reviewed literature.

Comparative discussion

Overall, three trends emerge from the reviewed mechanical studies. First, auxetic TPMS architectures can provide favorable energy absorption and progressive deformation, although stronger auxeticity does not automatically correspond to higher strength or stiffness. Second, functional grading appears particularly useful for controlling deformation localization and structural stability. Third, recent analytical studies are extending auxetic TPMS research beyond compression toward vibration, buckling, multiphysics coupling, and data-driven structural design.

Table 2. Summary of the main mechanical findings in the reviewed studies

Study	Mechanical focus	Main reported result	Review interpretation
ten Voorde et al. (2026)	Compression / auxeticity / energy absorption	Apparent \(\nu \approx -0.1443\); energy absorption = 37.93 J/cm³; compressive strength up to 231.44 MPa	Strong performance, but grading does not automatically improve all peak properties.
Liu et al. (2025)	Compression / auxetic strain / SEA	Effective auxetic strain = 17.173%; SEA = 16.6 J/g	Strong auxeticity can coexist with good energy absorption, but trade-offs remain.
Novak et al. (2026)	Graded compression / stability / SEA	SEA = 2.63 J/g (Al), 5.05 J/g (SS); grading stabilizes collapse and prolongs NPR behavior	Functional grading is most valuable as a stability-control mechanism.
Gong et al. (2025)	Hybrid compression / peak load / SEA	Gyroid core improved compressive performance, with increases around 47% in some NPR-shell cases	Shell–core interaction can significantly improve compressive behavior.
Engel et al. (2026)	Quasi-static and dynamic crushing	Mass-specific energy absorption increase up to 104% under quasi-static loading	Hybridization can be beneficial, but the advantage may diminish under dynamic loading.
Chen and Wang (2026)	Free vibration / graded auxetic plate	P-type TPMS produced the highest frequencies; increasing porosity reduced frequency; FGV-X/FGP-O gave the highest response	TPMS topology and grading pattern strongly govern dynamic behavior.
Saffari et al. (2026)	Free vibration / ML-assisted prediction	XGBoost R^2 = 98.84–99.91%	Data-driven prediction is becoming relevant in architected TPMS systems.
Eroğlu et al. (2026)	Vibration / buckling / stability	Porosity reduces frequency; nonlocal effects soften the structure; strain-gradient effects increase rigidity; external fields affect stability	Buckling and vibration depend on topology, scale effects and coupled physical fields.

Additive Manufacturing and Experimental Characterization

Additive manufacturing (AM) is a key enabling technology for auxetic TPMS-based structures because their continuous curvature, internal cavities, and spatially varying geometries are difficult to realize using conventional manufacturing methods. The reviewed studies employ different AM routes depending on the parent material, structural scale, and intended mechanical response. Metallic structures are predominantly fabricated using laser powder bed fusion (LPBF), whereas polymeric and elastomeric architectures have been produced using material extrusion, selective laser sintering (SLS), direct ink writing (DIW), and digital light processing (DLP) (Wang et al., 2023; Daynes, 2025; Novak et al., 2026; Engel et al., 2026).

Additive manufacturing routes

Metal-based AM has enabled the fabrication of complex TPMS-derived auxetic structures with relatively high load-carrying capacity. Gyroid-derived tubular architectures were successfully produced using LPBF, demonstrating the feasibility of manufacturing continuous auxetic geometries without assembling separate cellular components (Wang et al., 2023). CoCrMo auxetic TPMS lattices were also fabricated by L-PBF, although process resolution imposed limitations on the smallest manufacturable features (ten Voorde et al., 2026). Similarly, Ti6Al4V structures produced by LPBF showed measurable differences between numerical and experimental stiffness because of manufacturing imperfections such as unmelted particles and lack-of-fusion defects (Liu et al., 2025).

Polymer-based AM provides greater flexibility for investigating large and recoverable auxetic deformation. TPU-95A structures with positive, zero, and negative Poisson's ratios were manufactured by material extrusion and tested under compression (Daynes, 2025). Rubber-based rotated Primitive structures were produced using a customized DIW process combined with photocuring and thermal vulcanization, demonstrating the manufacturability of flexible auxetic TPMS concepts for airless-tire applications (Kim et al., 2024).

Other AM routes have also been successfully applied. Graded AUXTPMS structures were fabricated from PA2200 using SLS, while selected configurations were additionally produced from stainless steel and aluminium alloys for material comparison (Novak et al., 2026). DLP was used to manufacture photopolymer hexa-chiral/TPMS hybrid structures for quasi-static and dynamic testing (Engel et al., 2026), whereas FFF with PLA enabled experimental investigation of concave cylindrical shells, Gyroid cores, and their hybrid configurations (Gong et al., 2025). Post-processing can also introduce additional functionality; electroless nickel coating substantially increased the stiffness and conductivity of a flexible TPMS-derived auxetic metamaterial while retaining its auxetic mechanism (Zheng et al., 2021).

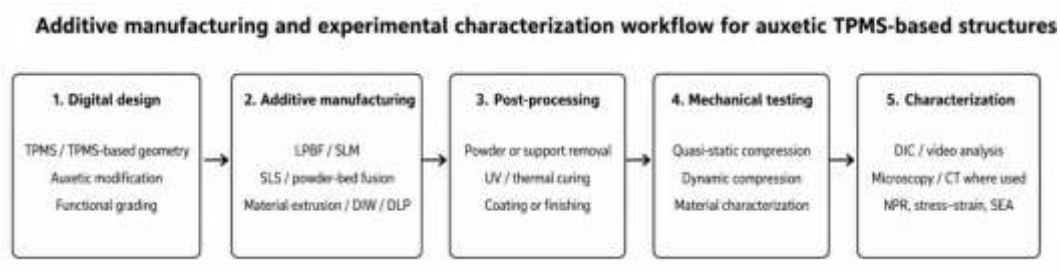

Fig. 6: Additive manufacturing and experimental characterization workflow

Experimental characterization

Quasi-static compression is the dominant experimental method in the reviewed literature because it simultaneously provides information on stress–strain response, collapse mechanisms, energy absorption, and negative Poisson's ratio behavior. However, the measurement techniques vary substantially among studies.

Digital image correlation (DIC) and related optical techniques are particularly valuable because auxetic deformation cannot always be adequately characterized using global force–displacement measurements alone. Three-dimensional deformation fields measured during compression showed generally good agreement with numerical predictions and enabled direct evaluation of negative Poisson's ratio behavior (Liu et al., 2023). Video image analysis combined with DIC was similarly used to compare uniform and graded AUXTPMS structures and to quantify longitudinal and transverse deformation during progressive collapse (Novak et al., 2026).

Experimental characterization has also been used to evaluate anisotropy. TPMS-based PPR, ZPR, and NPR specimens were tested in three loading orientations, allowing predicted elastic isotropy and Poisson's ratio behavior to be assessed experimentally (Daynes, 2025).

Dynamic testing remains comparatively limited. Quasi-static and dynamic compression tests on TPMS-filled hexa-chiral structures showed that mechanical benefits observed under slow loading may diminish at higher loading rates (Engel et al., 2026). This highlights the need to extend experimental validation toward impact, fatigue, vibration, and buckling conditions.

Table 3. Additive manufacturing and experimental characterization in representative reviewed studies

Study	Material	Manufacturing route	Experimental characterization	Main manufacturing/experimental insight
Zheng et al. (2021)	Flexible printed material + Ni coating	3D printing + electroless plating	Compression, mechanical and conductivity measurements	Ni coating substantially increased stiffness and conductivity while retaining auxetic behavior.
Wang et al. (2023)	Metallic system	LPBF	Compression + numerical validation	AM enabled seamless Gyroid-derived auxetic tubular structures.
Liu et al. (2023)	Flexible resin	3D printing	Compression + DIC	DIC confirmed 3D NPR deformation and generally good numerical–experimental agreement.
Kim et al. (2024)	Rubber-based ink	DIW + UV-assisted curing + vulcanization	Compression / tire deformation	Demonstrated manufacturability of flexible TPMS-based auxetic tire structures.
Daynes (2025)	TPU-95A	Material extrusion	Multi-direction compression, LVDT, transverse measurements	Enabled experimental validation of tunable Poisson's ratio and elastic isotropy.
Liu et al. (2025)	Ti6Al4V	LPBF	Compression + FEA comparison	Manufacturing defects produced measurable deviations from ideal numerical predictions.
Gong et al. (2025)	PLA	FFF	Tensile material tests + quasi-static compression	Provided direct comparison of shell, Gyroid core and hybrid deformation/failure modes.
ten Voorde et al. (2026)	CoCrMo	L-PBF	Compression + microscopy	Process resolution constrained minimum feature size; experiments confirmed strong NPR and energy absorption.
Novak et al. (2026)	PA2200; selected SS316L and AlSi10Mg	SLS / powder-bed fusion	ISO compression + VIA + DIC	Grading stabilized the auxetic deformation; different parent materials changed SEA.
Engel et al. (2026)	Photopolymer resin	DLP	Quasi-static + dynamic compression	Demonstrated that quasi-static benefits of hybridization are loading-rate dependent.

Review synthesis

The reviewed studies demonstrate that additive manufacturing is not merely a fabrication step but an integral part of the process–structure–property relationship in auxetic TPMS systems. Polymer-based AM facilitates large and recoverable deformation, whereas metallic LPBF offers higher strength but introduces greater sensitivity to geometric resolution and process defects. Full-field optical techniques such as DIC are increasingly important for characterizing local auxetic deformation, while experimental research remains strongly concentrated on quasi-

static compression. Broader validation under dynamic, fatigue, vibration, and buckling conditions therefore remains necessary.

Fig. 7: Typical workflow for the design, additive manufacturing, post-processing and experimental characterization of auxetic TPMS-based structures. Original review schematic synthesized from the reviewed literature.

Engineering Applications of Auxetic TPMS-Based Structures

Auxetic TPMS-based structures are increasingly being considered for engineering applications requiring lightweight design, deformation control, energy absorption, and structural adaptability. The reviewed literature mainly identifies four application areas: biomedical implants, automotive and crashworthiness components, aerospace and protective systems, and vibration-control or multifunctional structures.

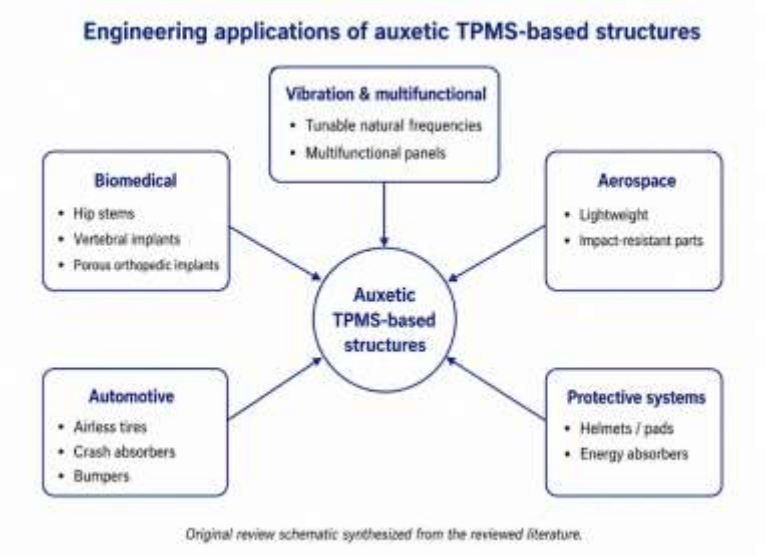

Fig. 8: Representative engineering application areas of auxetic TPMS-based structures. Original review schematic synthesized from the reviewed literature.

Biomedical applications

Controlled porosity, tunable stiffness, and negative Poisson's ratio behavior make auxetic TPMS architectures attractive for load-bearing biomedical applications. A TPMS-based heterostructure combining positive- and negative-Poisson's-ratio regions was proposed for hip stems to improve mechanical interaction at the bone–implant interface. The opposing transverse deformation of the two regions increased the contact area between the implant and surrounding bone during loading (Liu et al., 2023).
Ti6Al4V auxetic TPMS structures have also been proposed as candidates for artificial vertebral body implants because of their high ductility, tunable auxetic response, and energy-absorption capability (Liu et al., 2025). These studies indicate that biomedical applications require a balance among auxeticity, stiffness matching, porosity, strength, and long-term durability.

Automotive and crashworthiness applications

Automotive applications primarily exploit the energy absorption and deformation-dependent stiffness of auxetic TPMS structures. Rotated Primitive-based architectures were incorporated into airless tire spokes, where increasing stiffness with deformation improved shock absorption and limited excessive local deformation compared with conventional spoke concepts (Kim et al., 2024).
Gyroid-derived auxetic tubular architectures have also been proposed for crash absorbers, bumpers, and other protective tubular components because of their continuous geometry and controllable deformation (Wang et al., 2023). Hybrid NPR-shell/Gyroid-core structures further demonstrated improved peak load and energy absorption through interaction between the outer shell and internal TPMS core (Gong et al., 2025).

Aerospace and protective systems

The high specific properties and energy-dissipation capability of auxetic TPMS structures also make them promising for aerospace and protective applications. Ti6Al4V TPMS-based auxetic metamaterials have been suggested for lightweight aerospace components requiring enhanced deformation capacity and energy absorption (Liu et al., 2025). Gyroid-derived tubular structures have similarly been associated with impact-resistant aerospace and protective components (Wang et al., 2023).
Hybrid NPR-shell/Gyroid-core architectures have been proposed for aerospace buffer structures, anti-collision systems, and personal protective equipment (Gong et al., 2025). However, most available experimental evidence remains based on quasi-static compression, and validation under impact, repeated loading, and fatigue conditions is still limited.

Vibration control and multifunctional applications

Recent studies extend the application scope beyond compression and crashworthiness. Multi-parameter grading of TPMS–auxetic composite plates enables natural frequencies to be tailored through changes in topology, porosity, and reinforcement distribution, indicating potential for lightweight vibration-control and multifunctional structural panels (Chen and Wang, 2026).
These developments suggest that auxetic TPMS architectures may progressively evolve from passive energy-absorbing systems toward multifunctional structures integrating load carrying, vibration control, sensing, and adaptive mechanical response.

Table 4. Representative engineering applications of auxetic TPMS-based structures

Application area	Representative study	Architecture	Functional advantage	Application potential
Hip implant	Liu et al. (2023)	P-TPMS NPR + G-TPMS PPR heterostructure	Improved bone–implant contact and tunable stiffness	Hip stems and porous orthopedic implants
Vertebral implant	Liu et al. (2025)	Ti6Al4V auxetic TPMS tubular structure	High ductility, NPR and energy absorption	Artificial vertebral body implants
Airless tire	Kim et al. (2024)	Rotated Primitive TPMS	Variable stiffness and shock absorption	Non-pneumatic tire spokes
Crashworthiness	Wang et al. (2023)	Gyroid-derived auxetic tube	Lightweight energy absorption and controllable deformation	Vehicle crash absorbers and tubular protectors
Protective structures	Gong et al. (2025)	NPR shell + Gyroid core	Improved peak load and SEA	Aerospace buffers, anti-collision and personal protection
Vibration control	Chen and Wang (2026)	Triple-FG TPMS–auxetic plate	Tunable natural frequencies	Lightweight vibration-controlled panels

Review synthesis

The reviewed applications show a transition from material-level auxetic demonstrations toward application-oriented structural design. Biomedical applications emphasize interface mechanics and stiffness compatibility, automotive and protective systems focus on energy absorption and progressive collapse, while recent analytical studies extend the concept toward vibration and multifunctional behavior. Consequently, practical design should target a balanced combination of auxeticity, stiffness, strength, stability, energy absorption, and manufacturability rather than maximizing the negative Poisson's ratio alone.

Current Challenges and Future Research Directions

Despite the rapid development of auxetic TPMS-based structures, several challenges continue to limit their transition from conceptual designs to reliable engineering systems. The main limitations identified in the reviewed literature concern direct integration of functional grading with auxetic TPMS architectures, inconsistent performance metrics, limited experimental validation, manufacturing fidelity, multifunctional optimization, and application-level verification.

Limited direct integration of functional grading and auxetic TPMS

A major research gap is the limited number of studies in which auxeticity, TPMS architecture, and functional grading are directly integrated within the same structure. Most available studies focus either on modified auxetic TPMS architectures or on hybrid systems in which auxetic and TPMS mechanisms are located in separate structural components. Direct grading of an already

auxetic TPMS architecture remains comparatively uncommon (ten Voorde et al., 2026; Novak et al., 2026).
Future studies should therefore investigate spatial variation of relative density, wall thickness, unit-cell geometry, and auxetic parameters within directly graded AUXTPMS architectures. Such designs could provide greater control over both local deformation and global structural response.

Lack of standardized comparison criteria

Direct comparison among published studies remains difficult because different materials, relative densities, unit-cell dimensions, loading conditions, and performance indicators are employed. Some studies characterize auxeticity through apparent Poisson's ratio, whereas others report effective auxetic strain, stiffness, peak load, SEA, or stability-related parameters. More consistent reporting of relative density, Poisson's ratio, mechanical properties, loading conditions, deformation range, and energy-absorption metrics would improve comparison between different architectures and facilitate the development of more general design guidelines.

Limited experimental validation

Experimental research remains strongly concentrated on quasi-static compression. Although this loading condition is appropriate for characterizing auxetic deformation and progressive collapse, many proposed applications are subjected to dynamic, cyclic, or stability-related loading conditions.
Differences between quasi-static and dynamic responses have already demonstrated that performance improvements observed at low loading rates may not necessarily remain under dynamic conditions (Engel et al., 2026). Furthermore, several advanced vibration and stability models remain primarily numerical or analytical and require broader experimental verification (Chen and Wang, 2026; Eroğlu et al., 2026).
Future experimental studies should therefore place greater emphasis on dynamic loading, impact, fatigue, vibration, buckling, post-buckling, and long-term cyclic behavior.

Manufacturing fidelity and as-built geometry

Additive manufacturing introduces deviations between ideal numerical geometries and fabricated structures. Thin walls, small connections, and graded features are particularly sensitive to manufacturing resolution, surface irregularities, and process-induced defects. Such imperfections may substantially alter stiffness and deformation behavior relative to idealized numerical predictions (Liu et al., 2025).
Process-resolution limitations have also been identified as an important constraint in metallic auxetic TPMS structures (ten Voorde et al., 2026). Consequently, future numerical models should increasingly incorporate measured as-built geometry and experimentally characterized defects rather than relying exclusively on ideal CAD models.

Limited multifunctional and multi-objective optimization

Recent studies have expanded auxetic TPMS research toward vibration, buckling, energy absorption, and multifunctional systems. However, most optimization strategies still focus on one or a limited number of performance indicators.

Practical structures generally require simultaneous consideration of auxeticity, stiffness, strength, stability, energy absorption, mass, and manufacturability. Future research should therefore employ multi-objective optimization strategies capable of identifying suitable compromises between competing mechanical requirements.

Application-level validation

Although promising concepts have been proposed for biomedical implants, airless tires, protective structures, and aerospace components, many remain at the proof-of-concept stage. Application-specific requirements are considerably more demanding than demonstrating negative Poisson's ratio behavior under laboratory compression.
Biomedical structures, for example, require consideration of fatigue, stiffness compatibility, biocompatibility, and long-term implant–bone interaction. Automotive and protective systems require impact-rate sensitivity, repeated loading resistance, and reliable energy absorption under realistic service conditions.
Future research should therefore progress from generic mechanical characterization toward service-condition-based and application-specific validation.

Table 5. Summary of the main research gaps, current limitations, their significance, and corresponding future research needs in auxetic TPMS-based structures.

Research gap	Current limitation	Why it matters	Future need
Direct FG auxetic TPMS studies are limited	Few studies combine auxeticity, TPMS and grading in the same architecture	Limits understanding of true structure–grading coupling	More direct graded auxetic TPMS designs
Lack of standardized metrics	Different studies report different parameters and test conditions	Difficult to compare performance across the literature	More consistent reporting of density, NPR, SEA, stiffness and loading conditions
Experimental validation is narrow	Most tests are quasi-static compression only	Real applications require broader validation	Dynamic, fatigue, vibration and buckling experiments
Manufacturing fidelity issues	As-built defects alter the designed behavior	Numerical results may overestimate actual performance	Stronger integration of AM process–geometry–property analysis
Multifunctional optimization is limited	Most studies optimize one response at a time	Practical structures require balanced performance	Multi-objective design frameworks
Application-level validation is incomplete	Many studies remain proof-of-concept	Engineering transfer remains limited	Service-condition-based validation

Section synthesis

The reviewed challenges show that the field is now moving from demonstrating auxetic TPMS concepts toward establishing reliable, manufacturable and application-ready structural systems. The main research need is no longer simply to create a TPMS-based structure with a negative

Poisson's ratio, but to understand how topology, grading, manufacturing quality and loading environment interact to determine actual performance.
In this sense, the most important future direction is the development of integrated design approaches that connect: geometry + grading + manufacturing + experimental validation + application requirement within a unified framework.

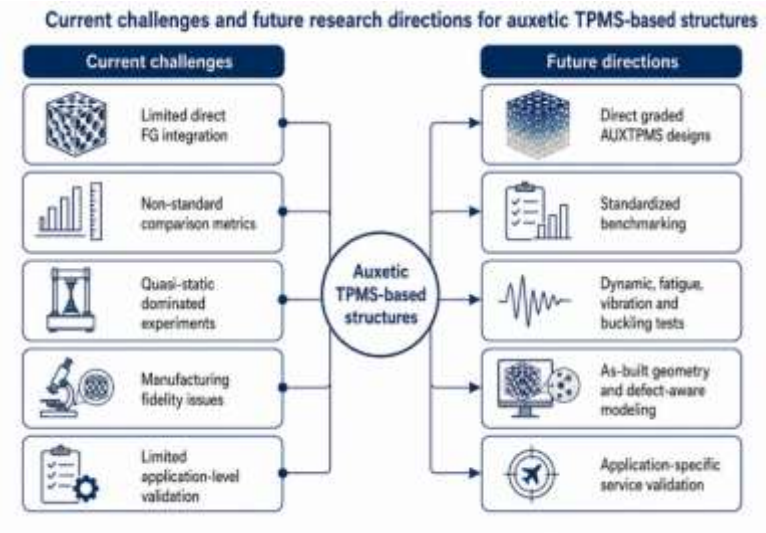

Fig. 9: Current challenges and future research directions for auxetic TPMS-based structures.

CONCLUSION

This review examined recent developments in auxetic TPMS-based and functionally graded structures with particular emphasis on geometrical design, functional grading, mechanical behavior, additive manufacturing, and engineering applications. The reviewed literature demonstrates that conventional TPMS architectures are not universally auxetic, and negative Poisson's ratio behavior generally requires deliberate geometrical modification through mechanisms such as rotation, buckling, coordinate transformation, or shape-function-based design.
Functional grading provides an additional means of tailoring structural response; however, its contribution should not be interpreted solely in terms of increased stiffness or strength. The available studies indicate that grading can be particularly effective in controlling deformation localization, progressive collapse, and the stability of the auxetic response. Mechanical performance therefore depends on the combined effects of topology, relative density, material properties, grading strategy, loading condition, and manufacturing quality.
Additive manufacturing has enabled increasingly complex metallic, polymeric, and elastomeric auxetic TPMS structures, but deviations between ideal and as-built geometries remain an important challenge. Experimental research is still dominated by quasi-static compression, whereas dynamic loading, fatigue, vibration, buckling, and long-term service behavior require substantially greater attention.
Overall, auxetic TPMS-based structures are evolving from geometry-driven metamaterial concepts toward graded, programmable, and multifunctional architected systems. Future progress will depend on the integrated optimization of auxeticity, stiffness, strength, stability, energy absorption, and manufacturability, together with experimentally validated designs under realistic service conditions. In particular, the limited number of studies directly combining functional grading with auxetic TPMS architectures represents a significant opportunity for future research.

REFERENCES

Chen, C., & Wang, T. (2026). Dynamic response of triple-functionally graded porous–auxetic nanocomposites: Coupling TPMS architectures with graphene origami metamaterials. *Thin-Walled Structures, 225*, 114851. https://doi.org/10.1016/j.tws.2026.114851

Daynes, S. (2025). Elastically isotropic auxetic and zero-Poisson's ratio TPMS-based metamaterials. *Virtual and Physical Prototyping, 20*(1), e2449569. https://doi.org/10.1080/17452759.2024.2449569

Engel, A., Movahedi, N., Novak, N., & Jung, A. (2026). Combining strut-based and sheet-based lattices: Quasi-static and dynamic performance of auxetic hexa-chiral tubes filled with TPMS structures for enhanced energy absorption. *Composites Part A: Applied Science and Manufacturing, 211*, 110179. https://doi.org/10.1016/j.compositesa.2026.110179

Eroğlu, M., Koç, M. A., & Esen, İ. (2026). Coupled magneto-electro-thermal buckling and vibration analysis of TPMS-based auxetic core sandwich nanoplates within the framework of HSDT and NSGT. *Journal of Thermal Stresses*. Advance online publication. https://doi.org/10.1080/01495739.2026.2631649

Gong, J., Ma, Z., Wei, Y., Song, G., & Hao, W. (2025). Compressive response of concave negative Poisson's ratio cylindrical shell/TPMS core composite structures. *Materials & Design, 259*, 114827. https://doi.org/10.1016/j.matdes.2025.114827

Kim, D.-Y., Kim, H.-S., Kamath, S. S., Hou, X., Choi, J.-W., & Park, S.-H. (2024). TPMS-based auxetic structure for high-performance airless tires with variable stiffness depending on deformation. *Scientific Reports, 14*(1), 11419. https://doi.org/10.1038/s41598-024-62101-3

Liu, B., Feng, J., Lin, Z., He, Y., & Fu, J. (2023). Controllable three-dimension auxetic structure design strategies based on triply periodic minimal surfaces and the application in hip implant. *Virtual and Physical Prototyping, 18*(1), e2170890. https://doi.org/10.1080/17452759.2023.2170890

Liu, F., Zhang, X., Chen, J., Liang, H., Luo, T., & Xu, J. (2025). Additive manufactured 3D auxetic metamaterial designed by minimal surfaces with enhanced ductility. *Journal of Alloys and Compounds, 1036*, 181679. https://doi.org/10.1016/j.jallcom.2025.181679

Novak, N., Al-Ketan, O., Grebo, A., Krstulović-Opara, L., Borovinšek, M., Ren, Z., & Vesenjak, M. (2026). Image-modulated implicit-field design of graded re-entrant triply periodical minimal surface with stabilised auxetic response. *physica status solidi (b), 263*, e70249. https://doi.org/10.1002/pssb.70249

Saffari, P. R., Senjuntichai, T., Askarinejad, S., Shalchy, F., & Saffari, P. R. (2026). Vibration analysis of cylindrical microshells with auxetic cores and triply periodic minimal surface layers using a hybrid analytical-machine learning framework. *Curved and Layered Structures, 13*(1), 20250044. https://doi.org/10.1515/cls-2025-0044

Solar, C., Demirhan, P. A., & Taşkın, V. (2025). Investigation of static behavior of functionally graded porous sandwich beams with TPMS core. *Proceedings of the Estonian Academy of Sciences, 74*(2), 109–114. https://doi.org/10.3176/proc.2025.2.04

Solar, T., & Demirhan, P. A. (2025). Static analysis of functionally graded porous sandwich beams. In *Proceedings of the VII. International Agricultural, Biological & Life Science Conference* (pp. 107–120). Istanbul, Türkiye.

ten Voorde, M. J. A., Moutablaleh, H., & Mehrpouya, M. (2026). Compressive and energy absorption properties of CoCrMo 3D auxetic lattice structures fabricated by L-PBF. *Thin-Walled Structures, 221*, 114316. https://doi.org/10.1016/j.tws.2025.114316

Wang, W., Jin, Y., Mu, Y., Zhang, M., & Du, J. (2023). A novel tubular structure with negative Poisson's ratio based on gyroid-type triply periodic minimal surfaces. *Virtual and Physical Prototyping, 18*(1), e2203701. https://doi.org/10.1080/17452759.2023.2203701

Zheng, X., Guo, X., & Watanabe, I. (2021). A mathematically defined 3D auxetic metamaterial with tunable mechanical and conduction properties. *Materials & Design, 198*, 109313. https://doi.org/10.1016/j.matdes.2020.109313

DEVELOPMENT OF AN ENVİRONMENTALLY SAFE DEFOLİATİON TECHNOLOGY BASED ON PH-SENSİTİVE DEFOLİANTS

Yusupov Xurshidjon Esojon o'g'li, Ergashev Dilmurod Adiljanovich, Ismoilov Muminjon Yusupovich

International Institute of Food Technology and Engineering, Al-Fergani Street, 204, Fergana City, Fergana Region, 150105, Uzbekistan.
Professor of the Fergana State University, 19 Murabbiylar Street, Fergana City, 150100, Uzbekistan.
E-Mail Address: xurshidjonyusupov50@gmail.com

ABSTRACT

The application of defoliants in modern agriculture plays an important role in facilitating mechanized harvesting, reducing labor costs, and increasing production efficiency. However, conventional defoliants often exhibit high chemical activity and may persist in soil and water environments for extended periods, resulting in environmental contamination and adverse effects on non-target organisms. Therefore, the development of environmentally safe defoliation technologies has become a significant challenge in sustainable agriculture and green chemistry.This study aims to develop an environmentally safe defoliation technology based on pH-sensitive defoliants and to investigate the possibility of controlling defoliant activity according to environmental pH conditions. The proposed concept is based on the assumption that pH-sensitive systems can selectively activate defoliants in the naturally acidic microenvironment of plant leaf surfaces while maintaining low activity in soil and aquatic environments. Such selective activation may reduce the chemical burden on the environment and improve the ecological safety of defoliation practices. The research was conducted using a modeling approach to evaluate the pH-dependent behavior of a pH-sensitive system. Three model environments representing acidic (pH ≈ 5), neutral (pH ≈ 7), and alkaline (pH ≈ 8) conditions were prepared. The activity of the model system was assessed through indicator-based observations under different pH conditions. The results demonstrated that the highest activity was observed in the acidic environment, while significantly lower activity was recorded under neutral and alkaline conditions. These findings indicate a strong dependence of system activity on environmental pH. The obtained results confirm the feasibility of utilizing pH-sensitive systems for controlled defoliant activation. The proposed approach may contribute to reducing environmental pollution, protecting soil and water resources, and preserving beneficial microorganisms. Furthermore, it provides a scientific basis for the development of next-generation environmentally friendly defoliants and sustainable agricultural technologies. The study highlights the potential of pH-responsive systems as an effective strategy for improving the environmental safety and efficiency of defoliation processes.

Keywords: defoliants, pH-responsive defoliants, environmental safety, environment, controlled activity, sustainable agriculture

.

INTRODUCTION

The use of defoliants in modern agriculture plays a significant role in facilitating mechanized harvesting, simplifying the picking process, and reducing labor costs. However, many conventional defoliants exhibit high biological activity and may persist in soil and aquatic environments for extended periods, thereby exerting adverse effects on environmental components. Consequently, ecological problems such as reduced soil fertility, inhibition of beneficial microbial activity, and contamination of water resources may arise.

In recent years, the growing demand for environmentally safe agricultural technologies based on the principles of green chemistry has become increasingly evident. In this context, controlling the activity of defoliants not by increasing their concentration but by adapting their performance to environmental conditions represents an important scientific challenge. In particular, utilizing the naturally acidic microenvironment of plant leaf surfaces to activate defoliants only at the required site and time may significantly enhance environmental safety.

This study is aimed at developing an environmentally safe defoliation technology based on pH-sensitive defoliants. The proposed approach is expected to reduce the chemical load associated with defoliation processes, contribute to environmental protection, and support the development of sustainable agricultural practices [1].

Research Objective. The objective of this study is to develop an environmentally safe defoliation technology based on pH-sensitive defoliants and to provide a scientific rationale for controlling the activity of defoliants as a function of environmental pH conditions [2,3].

Research Tasks:

1. To analyze the pH-dependent activity mechanisms of defoliants based on available scientific literature.
2. To develop an environmentally controlled model of defoliants using pH-responsive carrier systems such as coatings, gels, or adsorbents.
3. To model and compare the activity of defoliants under different pH conditions.
4. To establish criteria for evaluating the environmental safety of pH-sensitive defoliants.
5. To substantiate the practical applicability of the proposed technology [4].

Scientific Novelty:

1. A concept for controlling defoliant activity based on environmental pH rather than chemical concentration is proposed.
2. A model for transforming conventional defoliants into environmentally controlled systems through the use of pH-sensitive carrier materials has been developed.
3. A mechanism has been substantiated whereby defoliants remain active in the naturally acidic microenvironment of leaf surfaces while becoming passive in soil and aquatic environments.
4. A novel conceptual approach for ensuring environmentally safe defoliation processes has been developed [5].

RESEARCH OBJECT AND METHODOLOGY

The object of this study is the defoliation process and the defoliants used therein. The subject of the research is the activity of defoliants modified with pH-sensitive carrier systems and the mechanisms ensuring their environmental safety [6,7].
The following research methods were employed during the implementation of the project [8]:
- Analysis and synthesis of scientific literature;
- Modeling method (development of the operating mechanism of pH-sensitive defoliants);
- Comparative analysis (comparison of defoliant activity under different pH conditions);
- Observation method;
- Analysis and interpretation of results using graphical and tabular representations.

Practical Part:
The research was carried out through modeling the pH-dependent activity of defoliants. Rather than synthesizing an actual defoliant, a model system representing the operating mechanism of pH-sensitive defoliants was employed [9].
Stage 1. Preparation of pH Environments.
Three model environments with different pH values were prepared for the experiments:
- pH ≈ 5 (model of the acidic microenvironment of leaf surfaces);
- pH ≈ 7 (neutral environment model);
- pH ≈ 8 (model approximating soil conditions).

Stage 2. Modeling of the pH-Sensitive System.
A pH-responsive indicator-based model system was selected. This system was used as a simulation tool to mimic the pH-dependent activity of defoliants.
Stage 3. Evaluation of Activity.
An equal amount of the model system was introduced into each pH environment. Changes in color and the manifestation of activity indicators were subsequently observed. The appearance of color was considered an indicator of the active state of the defoliant, whereas the absence or disappearance of color was interpreted as a passive state.
Stage 4. Recording and Analysis of Results.
The experimental observations were recorded in tabular form. The activity levels were compared according to pH values, and the obtained results were presented graphically to illustrate the relationship between environmental pH and defoliant activity.

RESULTS

During the study, the activity of the pH-sensitive model system was observed in environments with different pH values. The results showed that the model system exhibited high activity in an acidic environment (pH ≈ 5), while its activity decreased significantly in a neutral environment (pH ≈ 7). In an alkaline environment (pH ≈ 8), the activity was minimal.

Table 1. Activity of the Defoliant Model Depending on pH Value

pH Value	**Environment Description**	**Observed Condition**	**Activity Level (%)**
5	Leaf surface model (acidic)	Strong color change	90%
7	Neutral environment model	Weak color intensity	30 %
8	Soil environment model (alkaline)	Almost no color change	15%

Figure 1. Presents the graphical relationship between pH value and the activity of the defoliant model.

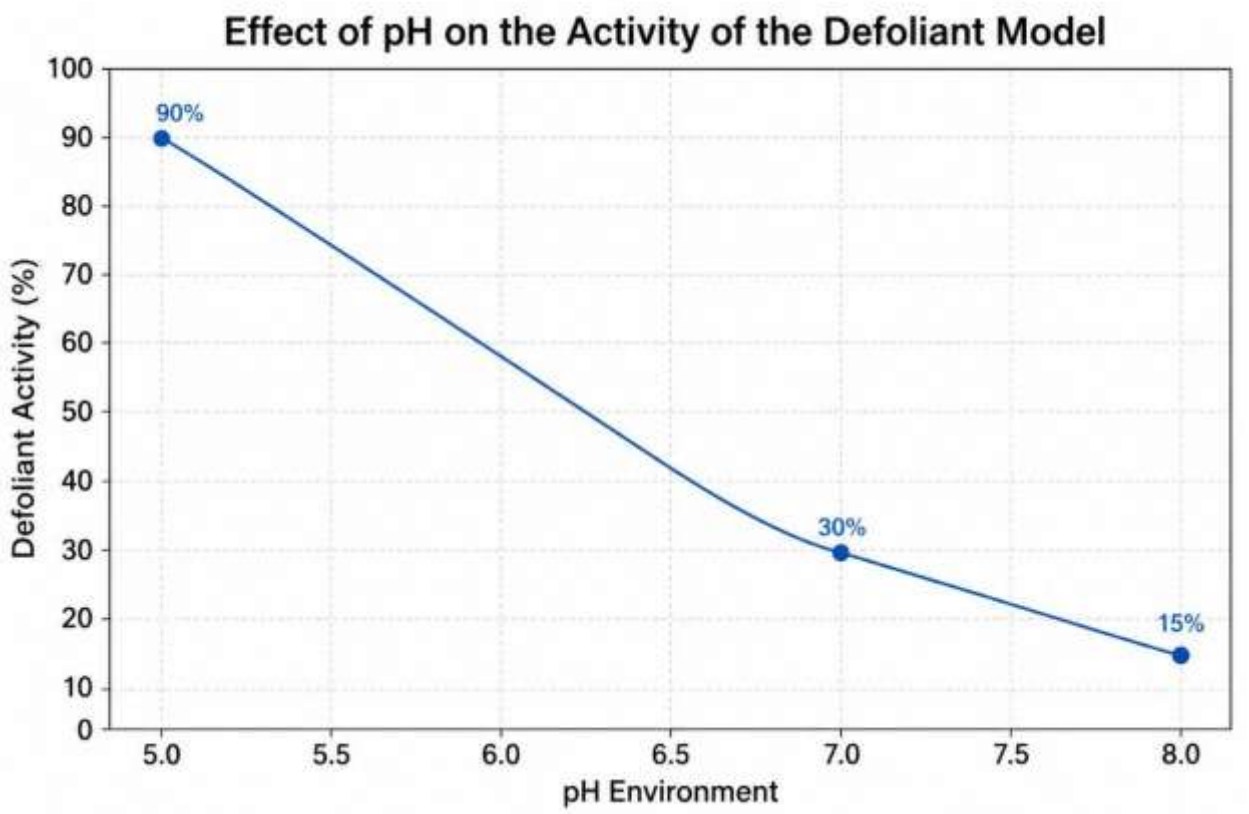

The obtained results indicate that the activity level of pH-sensitive systems is directly dependent on the pH value of the surrounding environment. This finding confirms that defoliants can remain active in the acidic microenvironment of leaf surfaces while becoming passive in soil and aquatic environments.

Expected Results:

- The dependence of defoliant activity on environmental pH will be scientifically substantiated using pH-sensitive systems.
- The mechanism by which defoliants remain active in the acidic microenvironment of leaf surfaces and passive in soil and water environments will be modeled.
- The potential of pH-sensitive defoliants to ensure an environmentally safe defoliation process will be demonstrated.
- The reduction of the chemical load released into the environment during the defoliation process will be scientifically justified.

Practical Significance of the Research*:* The results of this study provide an opportunity to organize the defoliation process in agriculture in an environmentally safe manner. The technology developed on the basis of pH-sensitive defoliants can contribute to reducing soil and water contamination, preserving the activity of beneficial microorganisms, and promoting sustainable agricultural development. Furthermore, the findings of this research may be applied in the future improvement of defoliant production technologies.
Research Limitations: No experiments were conducted using actual defoliants in this study. The experiments were performed using an indicator-based model system representing the pH-dependent activity of defoliants. Therefore, the obtained results are conceptual and modeling-based in nature.

CONCLUSION

The development of an environmentally safe defoliation technology based on pH-sensitive defoliants can reduce the negative environmental impact of the defoliation process. The concept of controlling defoliant activity according to environmental pH conditions enables the defoliation process to become more environmentally safe and controllable. The obtained results confirm the scientific validity of the proposed approach.

REFERENCES

1. Taiz, L., Zeiger, E., Møller, I. M., & Murphy, A. (2015). Plant Physiology and Development. Sunderland, MA: Sinauer Associates.
2. Grossmann, K. (2010). Auxin herbicides: Current status of mechanism and mode of action. Pest Management Science, 66, 113–120.
3. Yang, S. F., & Hoffman, N. E. (1984). Ethylene biosynthesis and its regulation in higher plants. Annual Review of Plant Physiology, 35, 155–189.
4. Sterling, T. M., & Hall, J. C. (1997). Mechanism of action of natural auxins and synthetic auxin herbicides. Pest Management Science, 50, 231–243.
5. Anastas, P. T., & Warner, J. C. (2000). Green Chemistry: Theory and Practice. Oxford: Oxford University Press.
6. Kah, M., & Brown, C. D. (2007). Adsorption of pesticides on soil and sediment. Chemosphere, 67, 204–213.
7. Khot, L. R., Sankaran, S., Maja, J. M., Ehsani, R., & Schuster, E. W. (2012). Applications of nanomaterials in agricultural production and crop protection. Crop Protection, 35, 64–70.
8. Gupta, P., Vermani, K., & Garg, S. (2002). Hydrogels: From controlled release to pH-responsive drug delivery. Drug Discovery Today, 7, 569–579.
9. Qiu, Y., & Park, K. (2001). Environment-sensitive hydrogels for drug delivery. Advanced Drug Delivery Reviews, 53(3), 321–339. https://doi.org/10.1016/S0169-409X(01)00203-4
10. Sinha, V. R., & Kumria, R. (2001). Polysaccharides in colon-specific drug delivery. International Journal of Pharmaceutics, 224, 19–38.

BIOSAFETY CONSIDERATIONS AND TECHNICAL ADVANCES IN THE PREPARATION OF SARS-COV-2 SPIKE PSEUDOVIRUSES

Zehra Köseoğlu[1], Nazife Gencer[2], Seval Cing Yıldırım[1], İbrahim Halil Yıldırım[3]

[1] Department of Biology, Division of Biotechnology, Faculty of Arts and Sciences, İnönü University, Malatya, Türkiye
[2] Department of Medical Microbiology, Division of Basic Medical Sciences, Faculty of Medicine, Kırşehir Ahi Evran University, Kırşehir, Türkiye
[3] Department of Medical Biology, Division of Basic Medical Sciences, Faculty of Medicine, Kırşehir Ahi Evran University, Kırşehir, Türkiye

ABSTRACT

The COVID-19 pandemic created an urgent need for experimental platforms that could support the safe and efficient study of SARS-CoV-2 entry, neutralization, and antiviral inhibition under more accessible laboratory conditions. In this context, spike-pseudotyped viral systems emerged as powerful alternatives to assays based on authentic SARS-CoV-2 because they reproduce the viral entry step while lacking full replication competence. This feature enabled their broad use in biosafety level 2 (BSL-2) laboratories and expanded research capacity beyond highly specialized high-containment facilities. Over time, SARS-CoV-2 pseudovirus systems evolved from emergency-response tools into versatile experimental platforms for neutralization assays, entry inhibitor screening, variant comparison, vaccine evaluation, and mechanistic studies of spike biology. Their increasing value has been driven by two major developments: first, biosafety-oriented improvements in vector architecture and packaging design, including multi-plasmid strategies, self-inactivating transfer systems, and refined lentiviral backbones; and second, technical advances that improve production efficiency, assay sensitivity, and biological relevance, such as optimized spike constructs, reporter-based readouts, host-cell engineering, and variant-adapted assay conditions. Recent studies have further demonstrated that these systems are scalable, applicable in resource-limited laboratory settings, and useful not only for neutralization analysis but also for investigating spike biogenesis and intracellular processing. Comparisons among HIV-1-, MLV-, and VSV-based backbones have also shown that platform choice can directly influence yield, workflow, and experimental interpretation. In addition to the broader literature, thesis-based laboratory implementation and chapter-based conceptual work from our group support the practical and methodological relevance of these platforms in SARS-CoV-2-related experimental design. Overall, the available evidence indicates that SARS-CoV-2 spike pseudovirus technology has become a mature, flexible, and indispensable framework for viral entry research, translational virology, and early-stage antiviral discovery.

Keywords: SARS-CoV-2, pseudovirus, spike protein, biosafety, lentiviral vector, VSV, neutralization assay

INTRODUCTION

The emergence of SARS-CoV-2 created an immediate need for systems capable of rapidly evaluating viral entry, antibody-mediated neutralization, and potential antiviral candidates. However, work with authentic SARS-CoV-2 requires high-containment infrastructure, most commonly BSL-3 laboratories, which limited access for many research groups during the pandemic and beyond (Millet et al., 2019; Chen & Zhang, 2021). In response to this challenge,

pseudovirus systems became one of the most widely adopted surrogate models because they preserve the viral entry properties of the authentic virus while eliminating full replication capacity, thereby substantially reducing experimental risk (Li et al., 2018; Nie et al., 2020).

Among all SARS-CoV-2 structural proteins, the spike glycoprotein occupies a central position because it mediates receptor recognition and membrane fusion through interaction with angiotensin-converting enzyme 2 (ACE2) and host proteases such as TMPRSS2 and furin (Walls et al., 2020; Wang et al., 2020; Hoffmann et al., 2020). For that reason, most SARS-CoV-2 pseudovirus platforms are designed around spike-pseudotyped particles built on alternative viral backbones, allowing researchers to model the entry process in a tractable and safer way (Crawford et al., 2020; Johnson et al., 2020).

Initially, these systems were used mainly as substitutes for live-virus assays. Yet the field developed rapidly, and pseudovirus platforms soon became essential tools for variant comparison, neutralizing antibody assessment, vaccine evaluation, and screening of entry inhibitors (Nie et al., 2020; Schmidt et al., 2020; Xiang et al., 2022). More recent studies further demonstrated that these assays can be deployed in laboratories with limited infrastructure, making them relevant not only for advanced research centers but also for broader diagnostic and drug-screening applications (Manu et al., 2024). Manu et al. (2024) strengthened this practical dimension by showing that a lentiviral assay based on p8.91, the luciferase reporter plasmid pCSFLW, and spike-expression constructs could be used in ACE2-expressing HEK293 cells for both compound screening and plasma neutralization analysis. In addition to the broader literature, a thesis from our group on pseudovirus production for SARS-CoV-2 neutralization antibody testing and a complementary book chapter on lentiviral vector design further support the methodological relevance of these platforms (Köseoğlu, 2023; Köseoğlu & Cing Yıldırım, 2023).

Biosafety framework of SARS-CoV-2 pseudovirus systems

The major biosafety advantage of pseudovirus systems lies in their replication-defective architecture. These particles are generally engineered for single-round infection, meaning they can enter susceptible cells and express a reporter signal but cannot complete a productive replication cycle or generate infectious progeny. This design markedly reduces biological risk compared with authentic SARS-CoV-2 and explains why such systems can be used under BSL-2 conditions in many settings (Millet et al., 2019; Nie et al., 2020; Chen & Zhang, 2021).

Nevertheless, the biosafety of pseudoviruses does not depend solely on the absence of replication. It is also determined by the organization of the vector system itself. In lentiviral platforms, for example, safety has progressively improved through the separation of viral functions into multiple plasmids, removal of unnecessary accessory elements, and use of self-inactivating transfer constructs (Dull et al., 1998; Maetzig et al., 2011; Tareen et al., 2013). These design principles reduce the theoretical possibility of recombination and increase control over the production system. Consequently, modern third-generation lentiviral systems are widely regarded as safer than earlier vector generations for laboratory applications involving pseudotyping (Dull et al., 1998; Chen & Zhang, 2021). This perspective is also consistent with our chapter-based work, which emphasizes third-generation lentiviral systems, SIN vectors, and chimeric 5′LTR designs as key biosafety layers in pseudovirus production (Köseoğlu & Cing Yıldırım, 2023).

Another important issue is the choice of viral backbone. SARS-CoV-2 spike pseudoviruses are most commonly generated using HIV-1-based lentiviral particles, murine leukemia virus (MLV)-based retroviral particles, or vesicular stomatitis virus (VSV)-based systems (Li et al., 2018; Chen & Zhang, 2021; Trischitta et al., 2024). Each system has advantages and limitations. Lentiviral systems are highly versatile and widely used in neutralization assays. MLV-based systems are also useful for entry studies, whereas VSV-based systems often provide strong

signal intensity and high infectious yield. This diversity indicates that biosafety is best understood not as a simple yes-or-no category, but as a combination of vector design, laboratory workflow, and experimental purpose. Trischitta et al. (2024) additionally noted that HIV-1- and MLV-based systems are generally easier and less time-consuming than VSV-based workflows, whereas VSV systems often provide higher particle yields; they also emphasized that VSV and MLV platforms may be considered safer than HIV systems in some methodological contexts.

Operational biosafety remains essential even when replication-defective systems are used. Appropriate institutional approval, personnel training, controlled workflow, physical containment practices, personal protective equipment, and validated decontamination measures are still required. Dahiya et al. (2023), for instance, explicitly noted that their pseudovirus work was conducted under institutional biosafety approval. This point is particularly important in a scientific meeting context because the use of a lower-risk surrogate does not eliminate the need for rigorous biosafety governance.

Technical advances in pseudovirus preparation

One of the main reasons pseudovirus systems remain highly relevant is the steady refinement of their technical design. Early studies largely aimed to generate functional particles for proof-of-concept assays, whereas more recent work has focused on reproducibility, yield optimization, host-cell susceptibility, variant-adapted calibration, and assay scalability.

A critical determinant of assay performance is the biological readiness of the target cell. Since spike-mediated entry depends on ACE2 binding and proteolytic activation, cells that express ACE2 together with TMPRSS2 or furin often provide improved sensitivity and more robust readouts (Hoffmann et al., 2020). Condor Capcha et al. (2021) demonstrated that viral entry signals could be enhanced when ACE2 was co-expressed with one or more activating proteases, emphasizing that pseudovirus assay quality depends not only on the particles produced but also on the receptor–protease context of the recipient cells. This work also illustrated how assay design can be streamlined into a relatively rapid workflow suitable for entry and neutralization studies.

Reporter selection constitutes another major technical variable. Fluorescent reporters such as GFP are valuable for visual confirmation, imaging, and qualitative assessment of infection, whereas luciferase-based systems generally provide greater sensitivity and wider dynamic range for quantitative neutralization and inhibitor screening (Crawford et al., 2020; Nie et al., 2020). Consequently, the choice of reporter should not be treated as a trivial technical detail; rather, it should reflect the intended analytical purpose of the study, whether that is visualization, quantification, or high-throughput screening.

Production efficiency has also emerged as a key focus of recent studies. Johnson et al. (2020) emphasized that spike-pseudotyping efficiency can vary markedly depending on construct design and packaging conditions. Extending this line of work, Fujioka et al. (2022) showed that conventional transient-expression VSV pseudotyping may produce a large proportion of particles lacking spike on their surface. According to their findings, excessive spike expression in producer cells may interfere with parental VSV infection and thereby reduce the yield of properly pseudotyped virions. To overcome this limitation, they developed a strategy using stable spike-expressing cell lines, which substantially improved the generation of spike-bearing VSV pseudoviruses with higher infectious yield. This contribution is particularly important because it shows that technical optimization is not limited to transfection efficiency, but also involves controlling spike expression biology in producer cells.

Another major advance is the growing recognition that optimization cannot be generalized across all SARS-CoV-2 variants. Sun et al. (2022) developed an HIV-1-based luciferase pseudovirus neutralization assay that included Alpha, Beta, Gamma, Kappa, and Omicron variants and found that the optimal spike-plasmid-to-backbone ratio and collection time

differed among variants. Notably, Omicron/BA.1 required a distinct optimal condition compared with earlier variants, demonstrating that pseudovirus systems must be recalibrated as spike evolution changes entry behavior and assay performance. This finding is highly relevant to current research because it underscores that pseudovirus platforms are dynamic systems that need continuous updating in response to viral evolution.

The expansion of pseudovirus technology into laboratories with limited infrastructure is another noteworthy development. Manu et al. (2024) established a lentiviral pseudovirus assay for both compound screening and neutralization analysis and emphasized that the system was scalable, practical, and suitable for medium- to high-throughput applications without requiring higher-level containment facilities. Their study is valuable not only methodologically but also strategically, because it demonstrates that pseudovirus-based assays can democratize access to SARS-CoV-2 functional studies across research settings with unequal resources. Their study also provides concrete methodological detail by using ACE2-HEK293 target cells and luciferase readout to quantify infection, and by defining a working titer threshold for assay use (Manu et al., 2024).

Our chapter-based review also describes transfer, envelope, and packaging plasmids as the core functional modules of lentiviral pseudovirus production and highlights HEK293T-based workflows as widely used experimental platforms (Köseoğlu & Cing Yıldırım, 2023). In parallel, the thesis work from our group supports the practical feasibility of producing pseudoviruses for SARS-CoV-2 neutralization-related applications within a modular lentiviral framework (Köseoğlu, 2023).

Applications in neutralization assays and variant assessment

SARS-CoV-2 spike pseudoviruses have become central tools for evaluating neutralizing antibodies, candidate vaccines, therapeutic monoclonal antibodies, and entry inhibitors (Crawford et al., 2020; Nie et al., 2020; Schmidt et al., 2020). Because these systems directly model spike-dependent entry, they are especially useful for studying how changes in spike structure alter neutralization susceptibility.

This role became even more important with the emergence of variants of concern. Sun et al. (2022) showed that Omicron/BA.1 exhibited marked resistance to some monoclonal antibodies and substantial immune evasion against convalescent plasma, whereas other antibodies retained activity with reduced potency. These findings highlight the importance of pseudovirus systems in rapidly identifying neutralization escape phenotypes before such data can be extensively generated with authentic virus. Similarly, other pseudovirus-based analyses have shown that neutralizing responses may differ substantially among variants, reinforcing the need for continuous variant-aware assay interpretation (Xiang et al., 2022; Trischitta et al., 2024).

In addition to antibody studies, pseudovirus systems have become valuable in early-stage compound screening. Because they can be used safely, rapidly, and at scale, they serve as effective prescreening platforms before authentic-virus confirmation. Manu et al. (2024) directly demonstrated this utility by identifying compounds that altered pseudovirus infectivity and by validating neutralizing activity in convalescent plasma. Thus, pseudovirus assays now occupy an important translational position between basic virology and applied antiviral discovery.

From entry assays to mechanistic studies of spike biology

A particularly important conceptual development in the field is the use of pseudovirus systems not only as entry readouts but also as tools to investigate spike biogenesis, processing, and intracellular trafficking. Dahiya et al. (2023) contributed to this direction by using lentivirus-based SARS-CoV-2 spike pseudoviruses in HEK293T cells expressing virus-specific intrabodies targeting the polybasic cleavage site of spike. Their approach allowed the

simultaneous evaluation of pseudovirus output and the intracellular fate of spike protein, showing that pseudovirus platforms can also serve as mechanistic systems for understanding how spike is processed and assembled.

This shift expands the scientific role of pseudovirus technology. The field is no longer limited to asking whether spike-bearing particles can enter cells or whether antibodies can block them. It is increasingly equipped to explore how spike is synthesized, trafficked, cleaved, stabilized, and incorporated into particles. Such studies suggest that future optimization may involve not only changing plasmid ratios or reporter types but also deliberately engineering intracellular spike handling in producer cells.

Limitations and future perspectives

Despite their strengths, pseudovirus systems have inherent limitations. Most importantly, they primarily model the entry phase of infection and therefore cannot fully reproduce the complete replication cycle, accessory protein functions, host responses, or pathogenic complexity of authentic SARS-CoV-2 (Chen & Zhang, 2021; Xiang et al., 2022). For this reason, pseudovirus data should ideally be interpreted alongside authentic-virus studies when possible.

In addition, the chosen viral backbone may influence particle morphology, spike density, and entry behavior. HIV-1-, MLV-, and VSV-based systems are highly useful, but none can be regarded as a perfect structural surrogate for native SARS-CoV-2 (Li et al., 2018; Trischitta et al., 2024). Assay outputs can also vary according to target cell line, reporter system, packaging design, spike construct, harvest timing, and titration strategy. These sources of variability create ongoing standardization challenges across laboratories. In this regard, Trischitta et al. (2024) emphasized that yield, safety, and operational complexity differ among HIV-1, MLV, and VSV backbones, reinforcing the idea that platform choice directly influences assay interpretation and standardization.

Looking ahead, three needs stand out. First, stronger inter-laboratory standardization is required in terms of producer cells, target cells, plasmid architecture, and readout methods. Second, continuing viral evolution demands variant-specific optimization rather than static protocol transferability. Third, the field is likely to move further toward biologically informed engineering strategies, including stable producer cell lines, regulated spike expression, and intracellular modulation of spike processing. Together, these directions suggest that pseudovirus technology is maturing from an emergency substitute into a robust, flexible, and enduring platform for viral entry research and antiviral development.

CONCLUSION

SARS-CoV-2 spike pseudovirus systems have developed into mature and highly adaptable platforms that combine biosafety, analytical flexibility, and practical scalability. Their value lies not only in enabling lower-risk studies of viral entry, but also in their continual methodological refinement through improved vector design, host-cell engineering, reporter selection, and variant-responsive optimization. Recent studies further show that these systems can support scalable neutralization and compound-screening workflows, can be adapted to resource-limited laboratories, and can even be repurposed for mechanistic studies of spike biogenesis and intracellular regulation. Taken together, the literature, our thesis-based work, and our chapter-based synthesis indicate that pseudovirus technology is no longer simply a provisional response to the COVID-19 crisis. Rather, it has become a durable experimental framework for studying viral entry, neutralization escape, and early-stage antiviral discovery.

REFERENCES

Chen, M., & Zhang, X.-E. (2021). Construction and applications of SARS-CoV-2 pseudoviruses: A mini review. *International Journal of Biological Sciences, 17*(6), 1574–1580. https://doi.org/10.7150/ijbs.59184

Condor Capcha, J. M., Lambert, G., Dykxhoorn, D. M., Salerno, A. G., Hare, J. M., Whitt, M. A., Pahwa, S., Jayaweera, D. T., & Shehadeh, L. A. (2021). Generation of SARS-CoV-2 spike pseudotyped virus for viral entry and neutralization assays: A 1-week protocol. *Frontiers in Cardiovascular Medicine, 7*, 618651. https://doi.org/10.3389/fcvm.2020.618651

Crawford, K. H. D., Eguia, R., Dingens, A. S., Loes, A. N., Malone, K. D., Wolf, C. R., Chu, H. Y., Tortorici, M. A., Veesler, D., Murphy, M., Pettie, D., King, N. P., Balazs, A. B., & Bloom, J. D. (2020). Protocol and reagents for pseudotyping lentiviral particles with SARS-CoV-2 spike protein for neutralization assays. *Viruses, 12*(5), 513. https://doi.org/10.3390/v12050513

Dahiya, S., Singh, S., & Sehrawat, S. (2023). Protocol for investigating the biogenesis of SARS-CoV-2 S pseudoviruses in HEK293T cells transduced to express the virus-specific intrabodies. *STAR Protocols, 4*(1), 101977. https://doi.org/10.1016/j.xpro.2022.101977

Dull, T., Zufferey, R., Kelly, M., Mandel, R. J., Nguyen, M., Trono, D., & Naldini, L. (1998). A third-generation lentivirus vector with a conditional packaging system. *Journal of Virology, 72*(11), 8463–8471. https://doi.org/10.1128/JVI.72.11.8463-8471.1998

Fujioka, Y., Kashiwagi, S., Yoshida, A., Satoh, A. O., Fujioka, M., Amano, M., Yamauchi, Y., & Ohba, Y. (2022). A method for the generation of pseudovirus particles bearing SARS coronavirus spike protein in high yields. *Cell Structure and Function, 47*(1), 43–53. https://doi.org/10.1247/csf.21047

Hoffmann, M., Kleine-Weber, H., Schroeder, S., Krüger, N., Herrler, T., Erichsen, S., Schiergens, T. S., Herrler, G., Wu, N.-H., Nitsche, A., Müller, M. A., Drosten, C., & Pöhlmann, S. (2020). SARS-CoV-2 cell entry depends on ACE2 and TMPRSS2 and is blocked by a clinically proven protease inhibitor. *Cell, 181*(2), 271–280.e8. https://doi.org/10.1016/j.cell.2020.02.052

Johnson, M. C., Lyddon, T. D., Suarez, R., Salcedo, B., LePique, M., Graham, M., Ricana, C., Robinson, C., & Ritter, D. G. (2020). Optimized pseudotyping conditions for the SARS-CoV-2 spike glycoprotein. *Journal of Virology, 94*(21), e01062-20. https://doi.org/10.1128/JVI.01062-20

Köseoğlu, Z. (2023). *SARS-CoV-2 nötralizasyon antikor testlerinde kullanılmak üzere pseudovirüslerin üretimi* [Master's thesis]. İnönü University.

Köseoğlu, Z., & Cing Yıldırım, S. (2023). Pseudovirüs üretimine yönelik olarak lentiviral vektörlerin tasarlanması ve geliştirilmesi. In M. Ç. Sayıl & R. Öztürk (Eds.), *Doğa bilimleri ve matematikte ileri ve çağdaş çalışmalar* (pp. 115–129). Duvar Yayınları.

Li, Q., Liu, Q., Huang, W., Li, X., & Wang, Y. (2018). Current status on the development of pseudoviruses for enveloped viruses. *Reviews in Medical Virology, 28*(1), e1963. https://doi.org/10.1002/rmv.1963

Maetzig, T., Galla, M., Baum, C., & Schambach, A. (2011). Gammaretroviral vectors: Biology, technology, and application. *Viruses, 3*(6), 677–713. https://doi.org/10.3390/v3060677

Manu, A. A., Owusu, I. A., Oyawoye, F. O., Languon, S., Barikisu, I. A., Tawiah-Eshun, S., Quaye, O., Donkor, K. J., Paemka, L., Amegatcher, G. A., Denyoh, P. M. D., Oduro-Mensah, D., Awandare, G. A., & Quashie, P. K. (2024). Development and utility of a SARS-CoV-2 pseudovirus assay for compound screening and antibody neutralization assays. *Heliyon, 10*, e31392. https://doi.org/10.1016/j.heliyon.2024.e31392

Millet, J. K., Tang, T., Nathan, L., Jaimes, J. A., Hsu, H.-L., Daniel, S., & Whittaker, G. R. (2019). Production of pseudotyped particles to study highly pathogenic coronaviruses in a

biosafety level 2 setting. *Journal of Visualized Experiments, 145*, e59010. https://doi.org/10.3791/59010

Nie, J., Li, Q., Wu, J., Zhao, C., Hao, H., Liu, H., Zhang, L., Nie, L., Qin, H., Wang, M., Lu, Q., Li, X., Sun, Q., Liu, J., Fan, C., Huang, W., & Wang, Y. (2020). Establishment and validation of a pseudovirus neutralization assay for SARS-CoV-2. *Emerging Microbes & Infections, 9*(1), 680–686. https://doi.org/10.1080/22221751.2020.1743767

Schmidt, F., Weisblum, Y., Muecksch, F., Hoffmann, H.-H., Michailidis, E., Lorenzi, J. C. C., Mendoza, P., Rutkowska, M., Bednarski, E., Gaebler, C., Agudelo, M., Cho, A., Wang, Z., Gazumyan, A., Cipolla, M., Caskey, M., Robbiani, D. F., Nussenzweig, M. C., Rice, C. M., & Hatziioannou, T. (2020). Measuring SARS-CoV-2 neutralizing antibody activity using pseudotyped and chimeric viruses. *Journal of Experimental Medicine, 217*(11), e20201181. https://doi.org/10.1084/jem.20201181

Sun, H., Xu, J., Zhang, G., Han, J., Hao, M., Chen, Z., Fang, T., Chi, X., & Yu, C. (2022). Developing pseudovirus-based neutralization assay against Omicron-included SARS-CoV-2 variants. *Viruses, 14*(6), 1332. https://doi.org/10.3390/v14061332

Tareen, S. U., Nicolai, C. J., Campbell, D. J., Nagarajan, L., & Kingsman, S. M. (2013). A Rev-independent gag/pol eliminates detectable psi-gag recombination in lentiviral vectors. *BioResearch Open Access, 2*(6), 421–430. https://doi.org/10.1089/biores.2013.0024

Trischitta, P., Tamburello, M. P., Venuti, A., & Pennisi, R. (2024). Pseudovirus-based systems for screening natural antiviral agents: A comprehensive review. *International Journal of Molecular Sciences, 25*(10), 5188. https://doi.org/10.3390/ijms25105188

Walls, A. C., Park, Y.-J., Tortorici, M. A., Wall, A., McGuire, A. T., & Veesler, D. (2020). Structure, function, and antigenicity of the SARS-CoV-2 spike glycoprotein. *Cell, 181*(2), 281–292.e6. https://doi.org/10.1016/j.cell.2020.02.058

Wang, Q., Zhang, Y., Wu, L., Niu, S., Song, C., Zhang, Z., Lu, G., Qiao, C., Hu, Y., Yuen, K.-Y., Wang, Q., Zhou, H., Yan, J., & Qi, J. (2020). Structural and functional basis of SARS-CoV-2 entry by using human ACE2. *Cell, 181*(4), 894–904.e9. https://doi.org/10.1016/j.cell.2020.03.045

Xiang, Q., Li, L., Wu, J., Tian, M., & Fu, Y. (2022). Application of pseudovirus system in the development of vaccines, antiviral drugs, and neutralizing antibodies. *Microbiological Research, 258*, 126993. https://doi.org/10.1016/j.micres.2022.126993

FROM FEAR TO AWARENESS: THE DUALITY OF SKIN MICROBIOME REALITY AND MEDIA REPRESENTATION THROUGH CASE STUDY ANALYSIS

Blerina VRENOZI[1], Daniela MYRTAJ[2]

[1]Research Center of Flora and Fauna, Faculty of Natural Sciences, University of Tirana, Petro Nini Luarasi 80, 1010, Tirana, Albania
[2]Department of Biology, Faculty of Natural Sciences, University of Tirana, Boulevard "Zog I", 1001, Tirana, Albania

Corresponding author e-mail: blerina.vrenozi@fshn.edu.al

ABSTRACT

Human skin is a complex ecosystem that is home to millions of microorganisms known as the skin microbiome. These microorganisms play a vital role in regulating the immune system and protecting against pathogens. However, the media represents a significant discrepancy between scientific reality and how the skin is portrayed. Digital and traditional platforms consistently promote biologically unrealistic, sterile beauty standards that misrepresent normal microbial variation and trigger severe social stigmatization. Using a qualitative, multi-case study methodology, this paper examines the discrepancy between biological facts and media-driven aesthetic myths. We examined three distinct narratives: a ten-year autoethnographic experience of *Acne vulgaris*; the systemic aesthetic bullying of participant Stelina Kurila on Big Brother VIP Albania 5; and the digital activism of skin-positivity advocate Maia. Our findings reveal that media channels systematically moralize and misidentify biological dysbiosis as a failure of personal hygiene. They utilize a divisive normalization mechanism that marginalizes affected individuals. In contrast, skin-positivity movements successfully challenge these unscientific standards of perfection. This study concludes that aligning cultural narratives with genomic reality by shifting public communication from media-induced fear to evidence-based scientific awareness is a critical psychosocial and public health intervention, necessary for the mental well-being and social integration of individuals living with visible dermatological conditions.

Keywords: Skin microbiome, *Acne vulgaris,* Mass media, Aesthetic bullying, Stigmatization

INTRODUCTION

The human skin, the body's largest and most exposed organ, covers an average surface area of approximately 1.8 m² and accounts for about 15% of an adult's body weight (Belkaid and Segre, 2014; McKenna et al., 2024; McGrath, 2025). Contemporary microbiology no longer classifies the skin as merely a physical barrier. Instead, the skin is conceptualized as a dynamic, complex ecosystem and meta-organism comprising the macroscopic host and vast communities of symbiotic bacteria, fungi, and viruses (Belkaid and Segre, 2014; Byrd et al., 2018). Advances in molecular biology have shifted the scientific view of the skin from a passive covering to an active "immunological organ" (Grice and Segre, 2011; McGrath, 2025). The cutaneous microbiome is a "guardian of health" that regulates innate and adaptive immune responses, defends against invading pathogens, and supports critical physiological processes such as wound healing (Sanford and Gallo, 2013; Belkaid and Segre, 2014; Byrd et al., 2018). The healthy skin microbiome is taxonomically dominated by four primary bacterial phyla: Actinobacteria, Firmicutes, Proteobacteria, and Bacteroidetes (Grice et al., 2009). Beneficial species, such as *Staphylococcus epidermidis*, act as primary defenders by producing

antimicrobial peptides and other molecules that inhibit pathogen colonization and modulate host immunity (Sanford and Gallo, 2013; Belkaid and Segre, 2014; Nakatsuji et al., 2018). Conversely, *Cutibacterium acnes* is a lipophilic commensal, naturally dominates sebaceous units but is often unfairly associated with pathology. In reality, *C. acnes* usually contributes to inflammation only when the microbial balance is disrupted, a state of dysbiosis (Fitz-Gibbon et al., 2013; Sanford and Gallo, 2013; Byrd et al., 2018).

However, the intersection of skin health and social perception is heavily influenced by the media, where physical appearance plays a significant role in shaping self-esteem and social integration, particularly among adolescents and young adults (Dalgard et al., 2015; Cohen et al., 2017; Yousaf et al., 2020). Dermatological conditions are more than just a cosmetic nuisance. They often cause significant psychological distress, including anxiety, depression, low self-esteem, and social isolation, similar to the distress experienced with chronic, disabling illnesses, such as arthritis or diabetes (Barankin and DeKoven, 2002; Dalgard et al., 2015; Germain et al., 2021; Christensen and Jafferany, 2023). Visible skin disorders often expose patients to stigmatization, teasing, and aesthetic cyberbullying (Luck-Sikorski et al., 2022; Chernyshov et al., 2024; Alfahaad et al., 2025). However, the media often oversimplifies this biological complexity. Digital platforms such as Instagram and TikTok promote heavily edited, filtered, and idealized images of perfect skin, establishing an unrealistic and sterile beauty standard by systematically removing natural pores and texture (Magin et al., 2011; Fardouly et al., 2015). This media construct consequently fosters a culture of fear regarding the skin's ecosystem, leading to an unnecessary obsession with aggressive disinfection and the overuse of cosmetic products (Basch et al., 2015). Recent studies on the skin-brain axis have revealed a possible link between certain bacterial species, including *Cutibacterium*, and positive psychological well-being, suggesting that a balanced microbiome is associated with reduced stress and improved mood (Luck-Sikorski et al., 2022; Tyson-Carr et al., 2025).

This article examines the significant contrast between the biological reality of the skin microbiome and media-driven aesthetic myths, analyzing how personal and digital media affect public perception. Through content analysis, we identify trends in dermatological representations, distinguishing media channels that foster pathophobia and misinformation (Vrenozi and Lugaj, 2025) from those that promote evidence-based health communication (Kite et al., 2023). This communication gap reflects broader public health dynamics in Albania, where inadequate scientific literacy fosters societal anxiety toward other medically significant taxa, allowing sensationalized fear to overshadow clinical reality (Vrenozi, 2025). Transitioning public discourse toward genomic realism, biological naturalism, and body diversity requires replacing media-induced panic with scientific awareness.

MATERIAL AND METHOD

This research uses a qualitative and analytical approach that combines media content analysis with case studies to examine the relationship between dermatological health and media narratives. The primary methodology involves systematically monitoring prominent Albanian media outlets, including Top Channel, TikTok, Instagram, JOQ Albania, Anabel Magazine, and Iliria News. These outlets were selected based on their significant public reach and influence on social discourse. Three case studies are analyzed to illustrate the tangible, real-world impact of these media narratives on psychological well-being and social integration.

1. A personal autoethnographic story: It involves the decade-long experience of one patient with *Acne vulgaris* from 2014 to 2024 (D. Myrtaj, personal communication). The story explores the tension between individual clinical reality and the “sterile” beauty standards promoted by the media.

2. Media representation of a reality show participant: This case study examined the public discourse surrounding Stelina Kurila during her time on the reality TV show Big Brother VIP Albania 5 in 2026. The case study examined public and digital responses, demonstrating how traditional and social media platforms can trigger intense public scrutiny and aesthetic judgment based on skin appearance. This case was chosen because of its high visibility, which sparked a national debate on skin appearance and health. Several media outlets documented the scandal, their editorial positions on natural beauty, and celebrities' reactions. A few examples are included here, such as Anabel Magazine (January 6, 2026) and Iliria News (January 5, 2026), as well as digital platforms such as Top Channel, JOQ Albania, TikTok, and Instagram.
3. Digital activism of a skin-positivity creator: This case study, taken from Maia's story in Changing Faces (March 7, 2023), examines the effect of digital activism in promoting skin positivity and challenging societal norms regarding beauty standards. It highlights narratives that challenge unrealistic beauty ideals and celebrate natural beauty.
By combining these three case studies, the manuscript aims to bridge the gap between contemporary biological science and the media's perception of the skin microbiome.

RESULTS AND DISCUSSIONS

Case Study 1. Autoethnographic Narrative of Acne vulgaris: Transitioning from media-induced fear to scientific awareness in acne management

The autoethnographic narrative highlights a profound discrepancy between the skin's biological reality and its hyper-sanitized media depiction (Magin et al., 2011), presenting a ten-year story of living with *Acne vulgaris* (D. Myrtaj, personal communication) (Figure 1). Although often dismissed as a minor cosmetic nuisance, the resulting psychological morbidity, including severe anxiety and depression, is clinically comparable in quality-of-life impairment to chronic, disabling conditions such as type 2 diabetes, heart disease, and severe arthritis (Barankin and DeKoven, 2002; Dalgard et al., 2015; Christensen and Jafferany, 2023). Throughout this decade, the patient was constantly exposed to unrealistic, sterile aesthetic standards on digital platforms like Instagram and TikTok, which filter out natural pores and texture to establish an unscientific baseline of perfection (Magin et al., 2011; Fardouly et al., 2015; tirananews, January 6, 2026).

Figure 1. The face images of the autoethnographic clinical progress: **A**- Started treatment 01.02.2024; **B**- After treatment 07.07.2026 ©danielamyrtaj

Because the human face represents the primary locus of the "social and relational self," the inability to meet this standard precipitated profound self-stigma and social anxiety (Barankin and DeKoven, 2002; Magin et al., 2011; Germain et al., 2021), compounded by "aesthetic bullying" from a public that moralizes cutaneous pathology as a failure of hygiene (Luck-

Sikorski et al., 2022; Chernyshov et al., 2024; Alfahaad et al., 2025). To achieve this ideal, the patient initially adopted aggressive, media-promoted "bacterial destruction" protocols (Basch et al., 2015). However, rather than providing relief, these sterilization methods damaged the outermost layer of the epidermis, stripping the vital extracellular lipid matrix and elevating the skin's naturally acidic pH, which ultimately exacerbated her acne severity (Grice and Segre, 2011; Sanford and Gallo, 2013; McGrath, 2025).

The decisive turning point in both the patient's clinical management and psychological well-being was reached through scientific literacy, reframing the skin not as an unhygienic surface to sterilize, but as a living meta-organism (Belkaid and Segre, 2014; Byrd et al., 2018). According to the hologenome theory, the human host and resident cutaneous microbiota coexist in a symbiotic relationship in which commensals actively calibrate local immunological networks (Belkaid and Segre, 2014; Byrd et al., 2018; Nakatsuji and Gallo, 2019). The patient successfully destigmatized her condition and transformed a decade of fear into a managed reality by transitioning her internal narrative from a moralizing language of "uncleanliness" and "failure" to biological homeostasis (Magin et al., 2011; Alfahaad et al., 2025). This shift repositioned *Cutibacterium acnes* as a vital lipophilic commensal that contributes to inflammation only in a state of dysbiosis (Fitz-Gibbon et al., 2013; Sanford and Gallo, 2013; Byrd et al., 2018), and highlighted *Staphylococcus epidermidis* as an essential "guardian of health" that secretes antimicrobial peptides to defend the host and regulate immune responses (Sanford and Gallo, 2013; Belkaid and Segre, 2014; Nakatsuji and Gallo, 2019). This alignment of cultural perception with genomic reality significantly reduced her psychological burden, enabling her to abandon makeup as a "mask" and accept natural skin variation (Tyson-Carr et al., 2025).

The culture of mass media's perfection filters out the reality of the human meta-organism (Magin et al., 2011; Fardouly et al., 2015), leaving the public shocked by natural appearance and detached from its genomic reality (Belkaid and Segre, 2014; Byrd et al., 2018). The true scandal is not the presence of *C. acnes*, but our collective failure to recognize its evolutionary role as a protective symbiont (Fitz-Gibbon et al., 2013; Sanford and Gallo, 2013). Replacing media myths with scientific education is critical for cutaneous immune homeostasis and psychological well-being (Tyson-Carr et al., 2025). In the Albanian context, addressing these public misconceptions requires a systematic shift in communication strategies. Regional surveys reveal significant public knowledge gaps and low preparedness regarding local biological exposures (Vrenozi, 2025). This educational shift is essential to destigmatize visible skin conditions and promote a broader biological naturalism (Changing Faces, March 7, 2023; Alfahaad et al., 2025).

Case Study 2. Public Perception of Cutaneous Health on Reality Television: "Aesthetic Bullying" and Hygiene Stigmatization

The 2026 season of Big Brother VIP Albania 5 provided a contemporary example of "aesthetic bullying" under constant 24/7 public surveillance (Anabel Magazine, January 6, 2026; Top Channel, 2026). One notable incident occurred when participant Stelina Kurila appeared on camera without makeup (Joker Albania, 2026; Iliria News, January 5, 2026) (Figure 2/A). Screenshots of her bare face quickly circulated across TikTok, Instagram, and Albanian portals like JOQ, Anabel, and Iliria News, triggering highly judgmental, offensive, and mocking commentary (Figure 2/A, B) (Anabel Magazine, January 6, 2026; Iliria News, January 5, 2026; Joker Albania, 2026; JOQ Albania, 2026; tirananews, January 6, 2026). This negative reaction to her visible *Acne vulgaris* highlights how the high visibility of facial lesions, particularly in central regions like the forehead and nose, attracts disproportionate public scrutiny, leading to

severe external stigmatization, anxiety, and negative social impressions (Barankin and DeKoven, 2002; Germain et al., 2021; McKenna et al., 2024; Alfahaad et al., 2025).

Figure 2. The face images: S. Kurrila: **A**- BBV appearance 05.01.2026 ©ilirianews.al; **B**-treatment 02.03.2026 ©ledaaesthetic; Maia's: **C** and **D**- Social media vs Reality 07.03.2023 ©changingfaces.org.uk

Anabel Magazine (January 6, 2026) pointed out the profound irony that, although the show is categorized as reality, viewers were shocked by it. This backlash demonstrates the public's shifting perception of healthy skin, replacing it with the computer-enhanced standard of perfection seen on Instagram. This shift has driven a divisive normalization mechanism that categorizes natural biological variations as other or abnormal (Magin et al., 2011; Alfahaad et al., 2025; Anabel Magazine, January 6, 2026). Social media commentators have relied on erroneous stereotypes that moralize skin conditions, characterizing Kurila's acne as a scandal, filth, or a personal failure of hygiene and self-care (Alfahaad et al., 2025; Anabel Magazine, January 6, 2026; Iliria News, January 5, 2026; JOQ Albania, 2026). These judgments ignore that acne is a complex biological process involving microbial dysbiosis, hormonal shifts, and inflammatory dynamics, rather than a lack of cleanliness. Individuals with acne often invest significant resources in high-quality skincare products and dermatological treatments (Magin et al., 2011; Alfahaad et al., 2025; Anabel Magazine, January 6, 2026; Ruci, March 2, 2026). The media's focus on Stelina's aesthetic deviation aligns with mass media's consistent promotion of the ideal of perfect skin, such as hyper-idealized celebrity accounts on Instagram (Cohen et al., 2017) (Table 1).

Table 1. Comparative analysis of media representation, public perception, and biological reality of skin microorganisms

Feature	Presentation in Media	Public Perception	Scientific Evidence	Gaps in Albanian Media	References
Cutaneous Microbiota	Portrayed as pathogens requiring complete eradication for hygiene	Pathophobia; associating natural bacterial presence with filth and infection	Symbiotic ecosystem essential for physical barrier homeostasis and immunity	Binary framing; omission of ecological complexity and host-microbe mutualism	(Grice and Segre, 2011; Belkaid and Segre, 2014; Byrd et al., 2018; JOQ Albania, 2026; Top Channel, 2026)

Feature	Presentation in Media	Public Perception	Scientific Evidence	Gaps in Albanian Media	References
Acne vulgaris	Portrayed as a superficial blemish or failure of personal hygiene	Triggers profound self-stigma, shame, and social isolation	Driven by genetic barriers, hormonal shifts, and follicular dysbiosis	Prioritizes commercial product marketing over microbiological explanations	Barankin and DeKoven, 2002; Fitz-Gibbon et al., 2013; Sanford and Gallo, 2013; Alfahaad et al., 2025; Anabel Magazine, January 6, 2026; JOQ Albania, 2026; Top Channel, 2026
Aesthetic Standards (Perfect skin)	Digitally filtered, edited, and hyper-idealized images across media platforms	Induces unrealistic beauty expectations, self-stigma, and appearance dissatisfaction	The healthy epidermis has natural texture, variations, and vital symbiotic microbes	Prioritizes artificial cosmetic perfection over biological and genomic realism	Barankin and DeKoven, 2002; Magin et al., 2011; Fardouly et al., 2015; Byrd et al., 2018; Alfahaad et al., 2025; Joker Albania, January 5, 2026; tirananews, January 6, 2026
Cutaneous Interventions	Cosmetic products marketed as universal, over-the-counter therapeutic cures	Uncritical product trust, delaying medical care in favor of self-medication	Requires professional clinical diagnosis and personalized, evidence-based therapy	Prioritizes commercial product marketing over clinical and scientific facts	Basch et al., 2015; Yousaf et al., 2020; Alfahaad et al., 2025; Ruci, March 2, 2026; Top Channel, 2026
Social Media "Skin Care"	Unregulated, simplified cosmetic advice promoted by non-medical influencers	High susceptibility to health misinformation and hazardous, unverified skin practices	Most digital advice lacks clinical grounding, empirical evidence, or safety verification	Omission of scientific screening, peer verification, or medical oversight	Basch et al., 2015; Yousaf et al., 2020; Iliria News, January 5, 2026; Joker Albania, January 5, 2026; tirananews, January 6, 2026
Educational Media Role	Infrequent, isolated health campaigns or authentic patient narratives	Fosters public empathy, health literacy, and destigmatization	Strategic health communication reduces public stigma and builds support	Omission of systematic health campaigns; untapped educational capacity	Luck-Sikorski et al., 2022; Kite et al., 2023; Alfahaad et al., 2025; Vrenozi and Lugaj, 2025; Top Channel, 2026

In response, Albanian public figures, including O. Marashi, A. Musta, F. Haxhialiu, and L. Brati, criticized this hypocrisy. They noted that a public that demands naturalness is repulsed by its biological reality (Anabel Magazine, January 6, 2026). The resulting cyberbullying created a toxic social environment, inflicting severe psychological distress, including anxiety, social withdrawal, and diminished self-esteem, that can be as disabling as the clinical condition itself (Dalgard et al., 2015; Germain et al., 2021; Luck-Sikorski et al., 2022; Chernyshov et al., 2024; Alfahaad et al., 2025). To remediate this social "inflammation", mass media platforms must transition from spaces of aesthetic judgment and public panic to public health advocates that promote scientific awareness, eliminate misinformation, and destigmatize natural cutaneous variations (Basch et al., 2015; Kite et al., 2023; Vrenozi and Lugaj, 2025).

Case Study 3. Digital Activism and the Skin-Positivity Movement: The psychosocial transition from stigmatization to communication through acne positivity

Maia's longitudinal experience as a digital activist and content creator illustrates that having a visible facial dermatological condition during adolescence increases the risk of severe social discrimination and bullying (Barankin and DeKoven, 2002; Luck-Sikorski et al., 2022; Changing Faces, March 7, 2023). Her personal history of schoolyard harassment and derogatory online comments led to severe social anxiety and low self-worth. This aligns with clinical evidence showing that the psychological distress caused by visible facial lesions is comparable in severity to that caused by disabling systemic diseases (Barankin and DeKoven, 2002; Changing Faces, March 7, 2023; Alfahaad et al., 2025). Initially, she used heavy makeup as a defensive mask to conceal her skin and manage daily social interactions, a widely documented coping mechanism used to mitigate stigma (Barankin and DeKoven, 2002; Changing Faces, March 7, 2023).

Eventually, Maia repurposed her digital platforms to join the acne positivity movement, posting unedited, natural images of her face (Figure 2/C, D) to challenge the beauty industry's standard practice of using digital enhancement to project a flawless, "sterile" aesthetic (Magin et al., 2011; Cohen et al., 2017; Changing Faces, March 7, 2023). This shift highlights how a new model of health communication can treat digital networks as therapeutic environments and sources of social support (Basch et al., 2015; Yousaf et al., 2020; Kite et al., 2023). By reframing natural skin variation as a component of a living meta-organism rather than an aesthetic failure, such movements provide the empathy and inclusivity needed to remediate social dysbiosis and improve patients' quality of life (Belkaid and Segre, 2014; Byrd et al., 2018; Changing Faces, March 7, 2023; Alfahaad et al., 2025). If our social perception, or "social skin", is integral to health, then mass media must complement public health by eliminating misinformation and promoting a new aesthetic of genomic realism that aligns cultural narratives with biological reality (Barankin and DeKoven, 2002; Magin et al., 2011; Fitz-Gibbon et al., 2013; Basch et al., 2015; Kite et al., 2023; Tyson-Carr et al., 2025; Vrenozi and Lugaj, 2025). Aligning cultural narratives with genomic realities is essential to alleviating the psychological burden imposed by unscientific standards of cutaneous perfection (Magin et al., 2011; Fardouly et al., 2015; Tyson-Carr et al., 2025).

CONCLUSIONS

This study's analysis reveals a profound, systemic discrepancy between contemporary scientific understanding of the skin and its depiction in the media. While biological research conceptualises the skin as a dynamic 'meta-organism' and an active immunological organ, media platforms consistently project a reductive, 'sterile' version of the human body. This

computer-enhanced ideal, which systematically removes pores, texture, and natural variations, forces individuals to view healthy biological processes as 'aesthetic failures' or evidence of personal neglect. The case studies of Stelina Kurila and Maia, along with the personal autoethnographic story, highlight the severe psychosocial consequences of this media construct. Visible dermatological conditions are not merely cosmetic concerns; they can lead to psychological distress, including anxiety, depression, and social withdrawal, at levels comparable to those experienced with chronic disabling illnesses.

Transitioning public discourse from 'aesthetic bullying' towards inclusivity requires a fundamental shift in literacy. Ultimately, replacing media-driven myths with scientific facts about the skin microbiome is essential for destigmatisation. Understanding the role of biological homeostasis and the protective function of commensal microorganisms can help society move away from a 'culture of fear' and towards a more inclusive understanding of body diversity. Promoting scientific awareness is not just a clinical necessity but also a vital step in safeguarding the mental health and social integration of individuals living with visible skin conditions.

REFERENCES

Alfahaad, H., Alsaiari, S., Alfarwan, W., Farhan, A., Alahmari, S. 2025. Public behaviours toward patients with dermatological diseases: a comprehensive review of public perception determinants. Advances in Dermatology and Allergology/Postępy Dermatologii i Alergologii, 42(6), 521–526. https://doi.org/https://doi.org/10.5114/ada.2025.154833

Anabel Magazine. 2026, January 6. *Pa bërë asgjë, Stelina i acaroi shumë, po* shumë njerëzit. https://www.anabelmagazine.com/pa-bere-asgje-stelina-i-acaroi-shume-po-shume-njerezit-i85735/

Barankin, B., DeKoven, J. 2002. Psychosocial effects of common skin diseases. Canadian Family Physician, 48(4), 712-716. https://pubmed.ncbi.nlm.nih.gov/12046366/

Basch, C. H., Basch, C. E., Hillyer, G. C., Reeves, R. 2015. YouTube Videos Related to Skin Cancer: A Missed Opportunity for Cancer Prevention and Control. Journal of Medical Internet Research Cancer, 1, e1. https://doi.org/doi:10.2196/cancer.4204

Belkaid, Y., Segre, J. A. 2014. Dialogue between skin microbiota and immunity. Science, 346(6212), 954-959. https://doi.org/https://doi.org/10.1126/science.1260144

Byrd, A. L., Belkaid, Y., Segre, J. A. 2018. The human skin microbiome. Nature Reviews Microbiology, 16(3), 143-155. https://doi.org/https://doi.org/10.1038/nrmicro.2017.157

Changing Faces. 2023, March 7. Maia's story: It's ok to have acne. UK’s leading charity for everyone with a scar, mark or condition on their face or body. https://www.changingfaces.org.uk/story/maias-story-its-ok-to-have-acne/

Chernyshov, P., Tomas-Aragones, L., Manolache, L., Pustisek, N., Darlenski, R., Marron, S., Koumaki, D., Pochynok, T., Szepietowski, J., Wala-Zielinska, K., Wójcik, E., Szepietowska, M., Lisicki, B., Tsidylo, I. G., Chernyshov, A. V., Poot, F., Magin, P. 2024. Bullying in persons with skin diseases. Journal of the European Academy of Dermatology and Venereology, 38(4), 752-760. https://doi.org/https://doi.org/10.1111/jdv.19683

Christensen, R. E., Jafferany, M. 2023. Psychiatric and psychological aspects of skin diseases. Clinical Dermatology, 41(1), 75-81. https://doi: 10.1016/j.clindermatol.2023.03.006.

Cohen, R., Newton-John, T., Slater, A. 2017. The relationship between Facebook and Instagram appearance-focused activities and body image concerns in young women. Body Image, 23, 183-187. https://doi.org/10.1016/j.bodyim.2017.10.002

Dalgard, F. J., Gieler, U., Tomas-Aragones, L., Lien, L., Poot, F., Jemec, G. B., Misery, L., Szabo, C., Linder, D., Sampogna, F., Evers, A. W. M., Halvorsen, J. A., Balieva, F., Szepietowski, J., Romanov, D., Marron, S. E., Altunay, I. K., Finlay, A. Y., Salek, S. S., Jörg, K. 2015. The psychological burden of skin diseases: a cross-sectional multicenter study among dermatological outpatients in 13 European countries. Journal of Investigative Dermatology, 135(4), 984-991. https://doi.org/DOI: 10.1038/jid.2014.530

Fardouly, J., Diedrichs, P. C., Vartanian, L. R., Halliwell, E. 2015. Social comparisons on social media: The impact of Facebook on young women's body image concerns and mood. Body Image, 13, 38-45. https://doi.org/https://doi.org/10.1016/j.bodyim.2014.12.002

Fitz-Gibbon, S., Tomida, S., Chiu, B.-H., Nguyen, L., Du, C., Liu, M., Elashoff, D., Erfe, M. C., Loncaric, A., Kim, J., Modlin, R. L. M., Jeff F., Sodergren, E., Craft, N., Weinstock, G. M., Li, H. 2013. *Propionibacterium acnes* strain populations in the human skin microbiome associated with acne. Journal of Investigative Dermatology, 133(9), 2152-2160. https://doi.org/https://doi.org/10.1038/jid.2013.21

Germain, N., Augustin, M., François, C., Legau, K., Bogoeva, N., Desroches, M., Toumi, M., Sommer, R. 2021. Stigma in visible skin diseases–a literature review and development of a conceptual model. Journal of the European Academy of Dermatology and Venereology, 35(7), 1493-1504. https://doi.org/DOI: 10.1111/jdv.17110

Grice, E. A., Kong, H. H., Conlan, S., Deming, C. B., Davis, J., Young, A. C., NISC Comparative Sequencing Program, Bouffard, G. G., Blakesley, R. W., Murray, P. R., Green, E. D., Turner, M. L., Segre, J. A. 2009. Topographical and temporal diversity of the human skin microbiome. Science, 324(5931), 1190-1192. https://doi.org/doi: 10.1126/science.1171700

Grice, E. A., Segre, J. A. 2011. The skin microbiome. Nature Reviews Microbiology, 9(4), 244-253. https://doi.org/https://doi.org/10.1038/nrmicro2537

Iliria News. 2026, January 5. Stelina e "Big Brother" frikëson ndjekësit, shfaqet pa 'make up' në ambientet e shtëpisë. https://ilirianews.al/stelina-e-big-brother-frikeson-ndjekesit-shfaqet-pa-make-up-ne-ambientet-e-shtepise/

Joker Albania. 2026, January 5. Photo post. TikTok. https://www.tiktok.com/@jokeralbania.al/photo/7591882363383287042

JOQ Albania. 2026. Online news and social media platform. https://joq-albania.com/

Kite, J., Chan, L., MacKay, K., Corbett, L., Reyes-Marcelino, G., Nguyen, B., Bellew, W., Freeman, B. 2023. A model of social media effects in public health communication campaigns: systematic review. Journal of Medical Internet Research, 25, e46345. https://doi.org/doi:10.2196/46345

Luck-Sikorski, C., Roßmann, P., Topp, J., Augustin, M., Sommer, R., Weinberger, N. 2022. Assessment of stigma related to visible skin diseases: a systematic review and evaluation of patient-reported outcome measures. Journal of the European Academy of Dermatology and Venereology, 36(4), 499-525. https://doi.org/https://doi.org/10.1111/jdv.17833

Ruci, A. 2026, March 2. Video post [@ledaaesthetic]. Instagram. https://www.instagram.com/reel/DVY8FOcjX3m/

Magin, P., Adams, J., Heading, G., Pond, D. 2011. 'Perfect skin', the media and patients with skin disease: a qualitative study of patients with acne, psoriasis and atopic eczema. Australian Journal of Primary Health, 17(2), 181-185. https://doi.org/https://doi.org/10.1071/PY10047

McGrath, J. A. 2025. Structure and function of skin, hair, and nails. Medicine, 53(7), 417-422. https://doi.org/10.1016/j.mpmed.2025.04.013

McKenna, M., Allman, M., Hargest, R. 2024. Surgical anatomy of the skin. Surgery (Oxford), 42(11), 781-787. https://doi.org/10.1016/j.mpsur.2024.08.008

Nakatsuji, T., Chen, T. H., Butcher, A. M., Trzoss, L. L., Nam, S.-J., Shirakawa, K. T., Zhou, W., Oh, J., Otto, M., Fenical, W., Gallo, R. L. 2018. A commensal strain of *Staphylococcus epidermidis* protects against skin neoplasia. Science Advances, 4(2), eaao4502. https://doi.org/https://doi.org/10.1126/sciadv.aao4502

Nakatsuji, T., Gallo, R. L. 2019. The role of the skin microbiome in atopic dermatitis. Annals of Allergy, Asthma and Immunology, 122(3), 263-269. https://doi:10.1016/j.anai.2018.12.003

Sanford, J. A., Gallo, R. L. 2013. Functions of the skin microbiota in health and disease. Seminars in Immunology, 25(5), 370-377. https://doi.org/https://doi.org/10.1016/j.smim.2013.09.005

tirananews. 2026, January 6. Photo post [@tirananews.al]. Instagram. https://www.instagram.com/p/DTKsBTFiOhM/

Top Channel. 2026. Big Brother VIP Albania. https://bigbrothervip.top-channel.tv/

Tyson-Carr, J., Leng, J., Scott, M., Adams, S., Hoptroff, M., Murphy, B., Fallon, N., Paterson, S., Thomas, A., Giesbrecht, T., Roberts, C. 2025. Body site-specific associations between human skin microbiome composition and psychological wellbeing. British Journal of Dermatology, 193(Supplement_2), ii6-ii14. https://doi.org/https://doi.org/10.1093/bjd/ljaf17

Vrenozi, B. 2025. Envenomation by the Mediterranean black widow spider Latrodectus tredecimguttatus (Araneae: Theridiidae) in Albania: hospital case studies and local knowledge. Arachnology, 20(2), 287-297. https://doi.org/10.13156/arac.2025.20.2.287

Vrenozi, B., Lugaj, A. 2025. Medically significant spiders (Arachnida: Araneae) and hymenopterans (Insecta: Hymenoptera) of Albania: A comprehensive review of ecology and venom toxicity. Polish Journal of Entomology, 94, 13-35. https://doi.org/https://doi.org/10.5604/01.3001.0054.9620

Yousaf, A., Hagen, R., Delaney, E., Davis, S., Zinn, Z. 2020. The influence of social media on acne treatment: a cross-sectional survey. Pediatric Dermatology, 37(2), 301-304. https://doi.org/https://doi.org/10.1111/pde.14091

ASSESSMENT OF URBAN AIR QUALITY IN ELBASAN (ALBANIA) BASED ON AIR MONITORING DATA

Raimonda Totoni (LILO)[1], Vanela Gjeci[2]

[1]Polytechnic University of Tirana, Faculty of Mathematical Engineering and Physical Engineering, Department of Chemical Chemistry, Albania

[2] National Environmental Agency, Albania

Corresponding author e-mail: rtotoni@gmail.com

ABSTRACT

Urban air pollution is a growing environmental and public health challenge in Albania, driven by rapid urbanization and inadequate infrastructure. Elbasan, a major city with a strong industrial legacy, is particularly vulnerable. This study aims to evaluate urban air quality in Elbasan city using 2023 monitoring data, generated through measurements conducted by the National Environmental Agency (NEA) for key pollutants, including PM_{10}, NO_2, CO, O_3, SO_2, and C_6H_6. The analysis of the monitoring data shows that for some of the main pollutants (NO_2 and PM_{10}), the concentrations measured during 2023 exceeded or were very close to the limit values established by international air quality standards. The annual average NO_2 concentration (32.94µg/m³) remains below the EU limit of 40 µg/m³ but is approximately 3.5 times higher than the 2021 WHO guideline of 10 µg/m³. Regarding PM_{10}, the annual average concentration (47.85 µg/m³) slightly exceeds the EU limit (40 µg/m³) but is more than three times higher than the WHO guideline value (15 µg/m³). Additionally, daily PM_{10} concentrations frequently surpass both EU and WHO daily limits, indicating exceedances of both short-term and long-term air quality standards. Seasonal analysis shows that air quality is poorest during winter, when pollutants such as PM_{10}, NO_2, CO, and C_6H_6 reach their highest concentrations and most frequent exceedances. This pattern is driven by both winter meteorological conditions and increased human activities. These results also demonstrate that, especially during the colder months, residents of Elbasan are exposed to air pollution levels that may harm health, with children, older adults, and people with pre-existing health conditions being the most vulnerable.
Keywords: Urban air quality; Air pollution; Air quality monitoring; Elbasan

INTRODUCTION

Currently, air pollution is acknowledged as one of the foremost environmental hazards to global human health. In particular, the World Health Organization reported that exposure to air pollution is the cause of more than seven million premature deaths annually and it is associated with several health problems such as asthma, chronic bronchitis, lung cancer, and cardiovascular diseases (WHO, 2021). In addition to the negative impacts on human health, air pollution also has a significant impact on the environment, leading to loss of biodiversity, ecosystem deterioration and degradation of soil and water quality (EEA, 2022).

The major sources of urban air pollution are vehicular traffic, domestic heating, industry and inappropriate waste disposal. The relative importance of these sources varies depending on the pollutant and the local context (EEA, 2022). In addition, meteorological parameters such as wind speed, wind direction, temperature and atmospheric stability play an important role in the

dispersion, accumulation and concentration of air pollutants and thus have an impact on the urban air quality (EEA, 2022)

The National Environment Report (NEA, 2023) points out that air pollution in major Albanian cities has become a serious environmental and public health problem, driven by rapid urbanization, increasing traffic density and lack of sustainable infrastructure. In this context, accurate determination and ongoing monitoring of the air quality are key to the assessment of pollution levels, identification of pollution sources, and to support data-driven environmental policies to protect the public health and promote sustainable urban growth.

Elbasan is one of the major cities in Albania. In the last decades, it has experienced many urban and socioeconomic changes, which have resulted in increasing environmental problems, especially in terms of air quality and its impacts on public health. The city is situated in the central part of Albania, in the valley of the Shkumbin River at an average altitude of about 110m above sea level. It has a Mediterranean climate with moderate winters, hot summers, and seasonal rainfall patterns.

Since the 1990s, rapid urban growth and domestic migration have fueled the spread of residential zones, often haphazardly and at the expense of farmland. This demographic growth has added to the strain on metropolitan infrastructure and services, leading to more traffic, higher energy consumption and more generated waste. These and the continuous growth of the city has made air pollution one of the major environmental problems in the city.

Prior to the 1990s, Elbasan was a major industrial center in Albania and was known as one of the most polluted regions in the country. While industrial activity has declined, pollution of air, water and soil remains a serious environmental problem with pollutants often exceeding national and international standards.

Today, Elbasan is one of the most polluted cities in Albania regarding its air quality. Unregulated industrial discharges, absence of regular environmental monitoring, poor compliance with environmental regulations and limited emission reduction efforts have been blamed for the decreasing air quality, especially around industrial facilities. Surveillance of data shows high levels of particulate matter, nitrogen dioxide , and carbon monoxide (AKM 2026). Pollution levels are typically highest during the colder months, when residential heating with wood and fossil fuels increases emissions, while unfavorable meteorological conditions reduce atmospheric dispersion and promote the accumulation of pollutants.

The objective of this study is to give a detailed assessment of the existing air quality in Elbasan, based on the monitoring data of 2023 obtained from the measurements carried out by the National Environmental Agency (NEA) for significant pollutants such as PM_{10}, NO_2, CO, O_3, SO_2 and C_6H_6. It aims also to identify the main air pollutants, their temporal variations, and the main factors contributing to air pollution. The findings are expected to improve the understanding of the city's air quality status and provide important information for developing effective environmental governance and pollution control strategies.

MATERIAL AND METHOD

The data on air pollutants monitoring used in this study were collected from National Agency of Environment (NEA), the institution responsible for environmental monitoring in Albania. The measurements were performed in the city of Elbasan in the period January-December 2023.

The automated instrument monitored continuously, logging the concentration of each contaminant each hour. The monitoring station is classified as an urban station and the sampling area is mainly residential.

The analysis is concentrated on six airborne pollutants: PM_{10}, NO_2, CO, SO_2, O_3, and C_6H_6. The data set includes continuous hourly measurements, from which monthly and annual averages were derived. This information provides a general overview of the seasonal variation of air quality and enables comparison with national standards, as well as international standards and guidelines set by the European Union and the World Health Organization (WHO). The monthly and annual averages obtained were used to analyze the air quality in Elbasan, to identify seasonal pollution patterns and to assess the influence of factors such as the weather conditions, traffic volume and economic activities. The collected monitoring data was processed and analyzed by Microsoft Excel 2016 for mathematical and statistic calculations.

A limitation of the study is the lack of data on the monitoring of $PM_{2.5}$ in 2023, considering that it is one of the most harmful air. In addition, technical problems with the monitoring equipment resulted in incomplete data sets for some pollutants, limiting the accuracy of assessing seasonal trends.

RESULTS AND DISCUSSION

Table 1 presents the average monthly and annual concentrations of sulfur dioxide (SO_2), ozone (O_3), carbon monoxide (CO), nitrogen dioxide (NO_2), particulate matter (PM_{10}), and benzene (C_6H_6) measured in the city of Elbasan during 2023.

Table 1. Average monthly and annual concentrations of the main air pollutants in the city of Elbasan during 2023

Parameter	**SO_2 µg/m³**	**O_3 µg/m³**	**CO mg/m³**	**NO_2 µg/m³**	**PM_{10} µg/m³**	**C_6H_6 µg/m³**
January	1.93	25.66	6.13	23.22	-	2.85
February	1.11	35.5	6.99	28.09	-	1.53
March	0.65	-	-	48.19	-	1.13
April	1.31	-	-	-	-	-
May	2.94	17.48	1.71	42.75	39.9	2.04
June	8.46	51.62	1.1	25.82	38.48	0.87
July	8.74	76.29	0.54	27.04	48.34	0.79
August	2.73	70.12	0.51	28.78	61.41	2.67
September	3.47	64.37	0.39	32.6	45.61	2.7
October	5.04	45.96	0.69	29.47	42.29	1.84
November	1.97	32.75	0.45	34.32	40.84	3.36
December	2.42	23.1	0.61	42.05	65.92	4.82
Annual average	3.40	44.29	1.91	32.94	47.85	2.24

Based on these data, graphical analyses, interpretation, and discussion are presented for each monitored air quality parameter.

Sulfur dioxide

Sulfur dioxide (SO_2) is a major air pollutant primarily emitted from industrial processes and the combustion of sulfur-containing fossil fuels. High SO_2 concentrations can irritate respiratory system, aggravate asthma and cause acid rain and environmental acidification (WHO, 2021). Figure 1 presents the monthly and annual means of SO_2 concentrations measured in Elbasan during 2023.

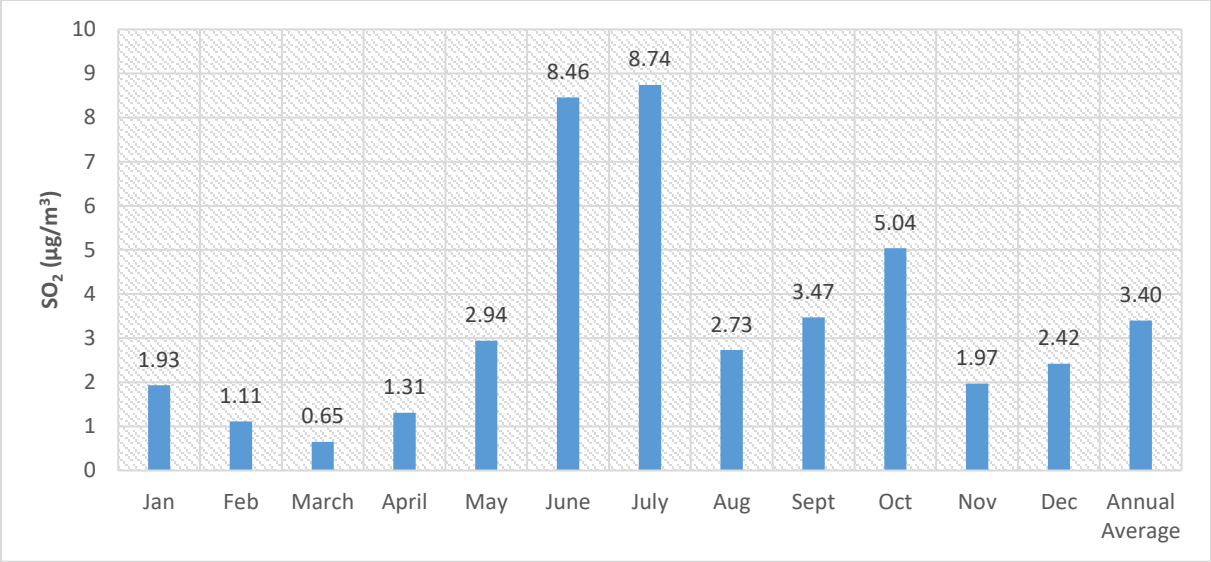

Figure 1. SO_2 concentration ($\mu g/m^3$) in the urban air of Elbasan during 2023

The annual average concentration of SO_2 as shown in Figure 1 was 3.4 $\mu g/m^3$. Since the air quality standards for SO_2 are based on hourly and 24-hour concentrations, the monitoring data were compared with the corresponding guideline values. The average concentrations over 24 h ranged from 0.25 to 13.03 $\mu g/m^3$, being below the limits of the European Union (125 $\mu g/m^3$) and WHO (40 $\mu g/m^3$), indicating that SO_2 pollution did not pose a significant air quality problem during the study period.

Maximum concentrations of SO_2 were found in June and July, and minimum in February and March. This seasonal pattern is different from that of some international studies where SO_2 levels are usually higher in winter and reach their lowest levels during summer (Lin et al., 2012; Wang et al., 2018). The relatively higher summer concentrations in Elbasan can be explained with the local meteorological conditions such as dry weather and low wind speeds that limits the dispersion of pollutants.

Ozone

Tropospheric ozone (O_3) is a secondary air pollutant formed by photochemical reactions of nitrogen oxides (NOx) and volatile organic compounds (VOCs) in the presence of sunlight. High concentrations of ozone can have a negative impact on the health of the respiratory system, especially for children, elderly people and those who already suffer from respiratory diseases

(WHO, 2021). Monthly and annual mean concentrations of O_3 measured in the city of Elbasan for 2023 are shown in figure 2.

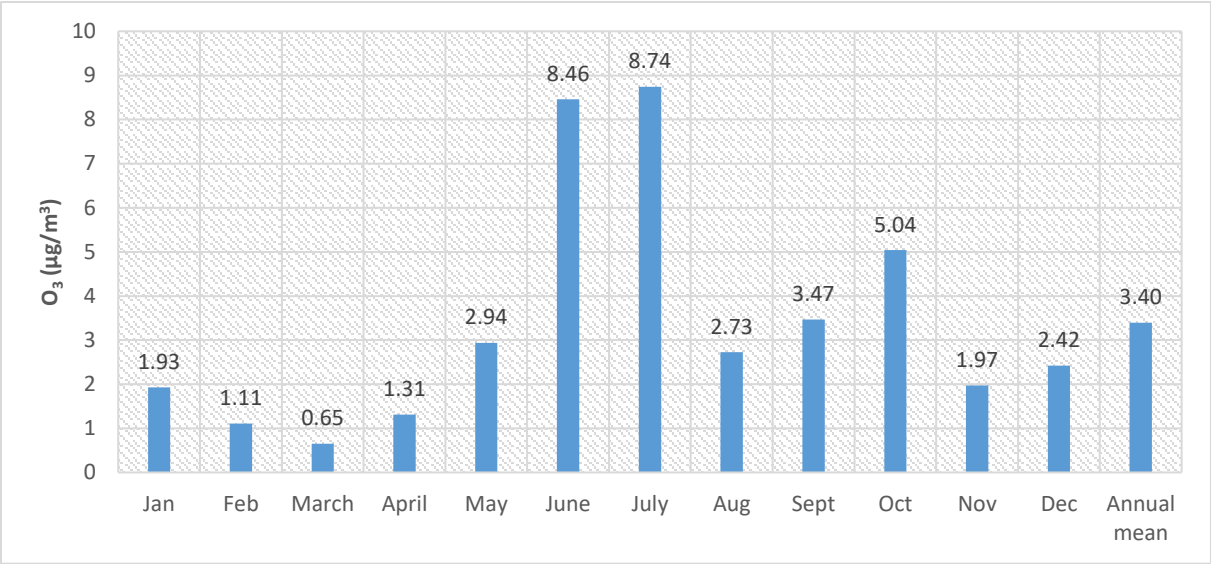

Figure 2. O_3 concentration (µg/m^3) in the urban air of Elbasan during 2023

The average annual concentration of O_3 was 44.29 µg/m^3. The ozone concentrations resulted to be higher in the warm season (June–September) than in the cold season (October–February). This trend is consistent with the typical seasonal pattern driven by stronger solar radiation and higher temperatures that enhance photochemical ozone formation. Hourly data analysis also indicated that ozone peaks around mid-day when solar radiation is the highest, consistent with the diurnal pattern of photochemical ozone formation (U.S. EPA, 2020) .

According to the European Union Air Quality Directive the maximum daily 8-hour average ozone (O_3) concentration should not exceed 120 µg/m³, whereas the WHO Air Quality Guidelines (2021) recommend a maximum daily 8-hour average of 100 µg/m³ and a peak-season average of 60 µg/m³. The analysis of the monitoring data of 2023 shows that the hourly O_3 concentrations in Elbasan exceeded the WHO peak-season guideline of 60 µg/m^3 in 21.4 % of the measurements, mainly in June-September, while 3.8 % of the measurements exceeded the 100 µg/m^3 guideline. However, the EU and Albanian limit value of 120 µg/m^3 was not exceeded. These results indicate that ozone pollution in summer may present a potential risk to public health and vegetation even when the current EU and national standards are met.

Nitrogen dioxide

Nitrogen dioxide (NO_2) is a major air pollutant produced mainly by the high-temperature combustion of fossil fuels from road traffic, industrial activities, and power generation. Exposure to elevated NO_2 levels is associated with adverse respiratory effects and contributes to the formation of ground-level ozone and secondary particulate matter, with negative impacts on both human health and ecosystems (WHO, 2021; EEA, 2024). Figure 3 presents the average monthly and annual NO_2 concentrations measured in the city of Elbasan during 2023.

As shown in this figure, the annual mean NO_2 concentration in Elbasan during 2023 was 32.94 µg/m³. This value is below the EU and Albanian annual limit of 40 µg/m³, but more than three times higher than the WHO Air Quality Guideline of 10 µg/m³, indicating a potential health concern may arise from exposure to this pollutant (WHO, 2021; Directive 2008/50/EC).

The highest monthly concentrations were recorded in March, May, and December, when average levels exceeded 40 µg/m³. Daily concentrations during these months were also frequently above the WHO recommended daily guideline.

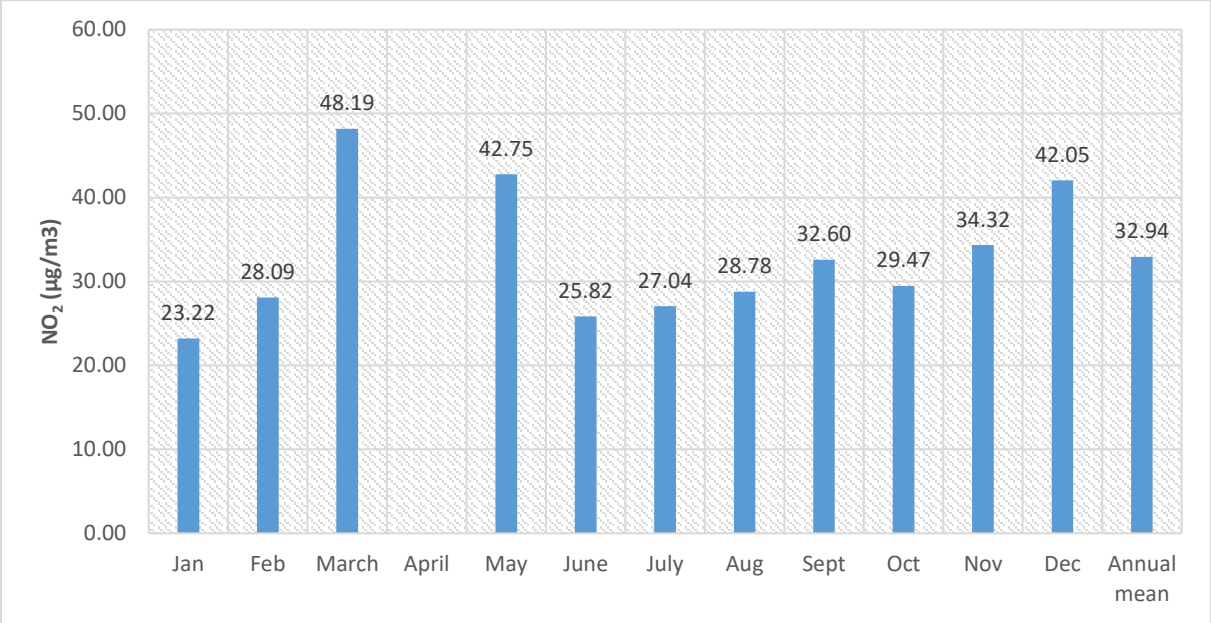

Figure 3. NO_2 concentration (µg/m^3) in the urban air of Elbasan during 2023

The observed seasonal variation generally follows the typical pattern reported in the literature, with higher NO_2 concentrations during the colder months due to increased fossil fuel combustion for residential heating (Guion et al., 2025), higher vehicle emissions, reduced atmospheric dispersion, and lower solar radiation (U.S. EPA, 2016). On a daily scale, NO_2 concentrations peaked during the morning and evening, corresponding to periods of increased traffic intensity, while daytime concentrations tend to decrease as atmospheric mixing and dilution increase (U.S. EPA, 2016;Voiculescu et al., 2020).

Carbon monoxide

Carbon monoxide (CO) is a toxic air pollutant produced mainly from the incomplete combustion of fossil fuels. Its main sources are emissions from vehicles, industry, residential heating with wood or coal and biomass burning, including forest fires. CO is especially harmful to human health as it binds with hemoglobin and decreases the blood's capacity to transport oxygen to organs and tissues, which may result in cardiovascular and respiratory effects at high exposure levels (WHO, 2021).

Figure 4 presents monthly and annual average concentrations of CO measured in the city of Elbasan during the year 2023. According to the monitoring data, the average annual concentration of CO in Elbasan in 2023 was 1.91 mg/m^3. The highest concentrations were observed in January and February, in accordance with the typical seasonal pattern of elevated CO concentrations during the colder months due to the increased combustion of fossil fuels for heating and poorer atmospheric dispersion (U.S. EPA, 1979; Gratsea et al., 2017). The highest daily CO concentrations were observed in the morning and evening, corresponding to hours of increased traffic and lower atmospheric mixing, while lower levels were observed during the midday hours.

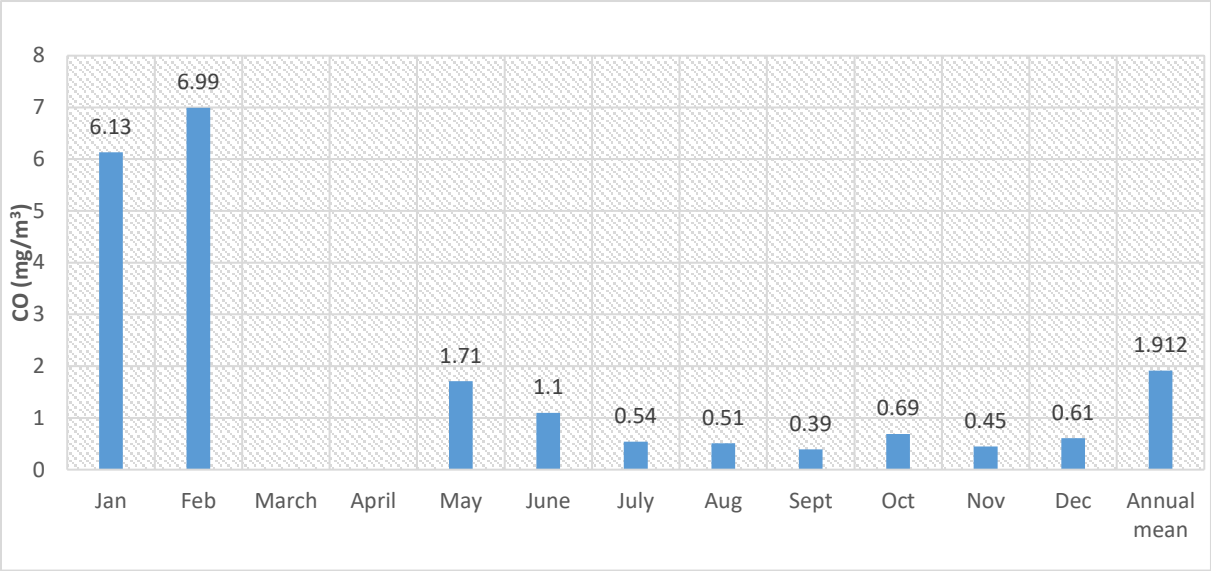

Figure 4. CO concentration (mg/m^3) in the urban air of Elbasan during 2023

When considering compliance with air quality standards note that the EU Air Quality Directive and national standards of Albania establish the maximum daily 8-hour average CO concentration at 10 mg/m^3. Monitoring data indicate that in 2023 the CO concentrations in Elbasan did not exceed this limit. However, according to the WHO Air Quality Guidelines (2021), the recommended 24-hour average should not exceed 4 mg/m³. The daily CO concentrations measured during the months January and February, consistently exceeded this guideline, suggesting that CO pollution may pose a potential health risk during the winter season despite compliance with current EU and national standards.

Particulate matter PM_{10}

Particulate matter with aerodynamic diameter ≤ 10 μm and ≤ 2.5 μm (PM_{10} and $PM_{2.5}$) are among the most important air pollutants of concern for human health. These particles are small enough to penetrate deep into the respiratory system. The high health hazard of $PM_{2.5}$ are related with their ability to cross the lung barrier and enter the bloodstream, contributing to cardiovascular and respiratory diseases, stroke and lung cancer (Abriha-Molnáret al., 2020). Short and long term exposure to particulate matter has been associated with increased morbidity and mortality (WHO, 2021; WHO, 2024).

The NEA's air quality monitoring data for Elbasan in 2023 are incomplete: $PM_{2.5}$ data are entirely unavailable, while PM_{10} data cover only May–December. The data gap impedes a reliable evaluation of the extent of these health-relevant pollutants and thus air pollution in the city.

The average concentration calculated from the available PM_{10} measurements is 47.85 μg/m^3, which is above the EU annual limit value of 40 μg/m^3 and more than three times the WHO guideline value of 15 μg/m^3. However, since the available measurements cover only May–December, this value should be interpreted as an average for the available monitoring period rather than as a fully representative calendar-year average.

The figure 5 presents monthly average for PM_{10} concentrations and calculated annual mean in Elbasan for 2023. The highest concentrations were observed in August and December, when the monthly averages greatly exceeded the applicable annual standard. During these months mean daily concentrations also exceeded the corresponding daily limit or guideline values, which are 50 μg/m^3 under the EU standard and 45 μg/m^3 under the WHO recommendation.

These results indicate that Elbasan was subject to PM_{10} pollution above the air quality standards for both short and long terms during the monitoring period.

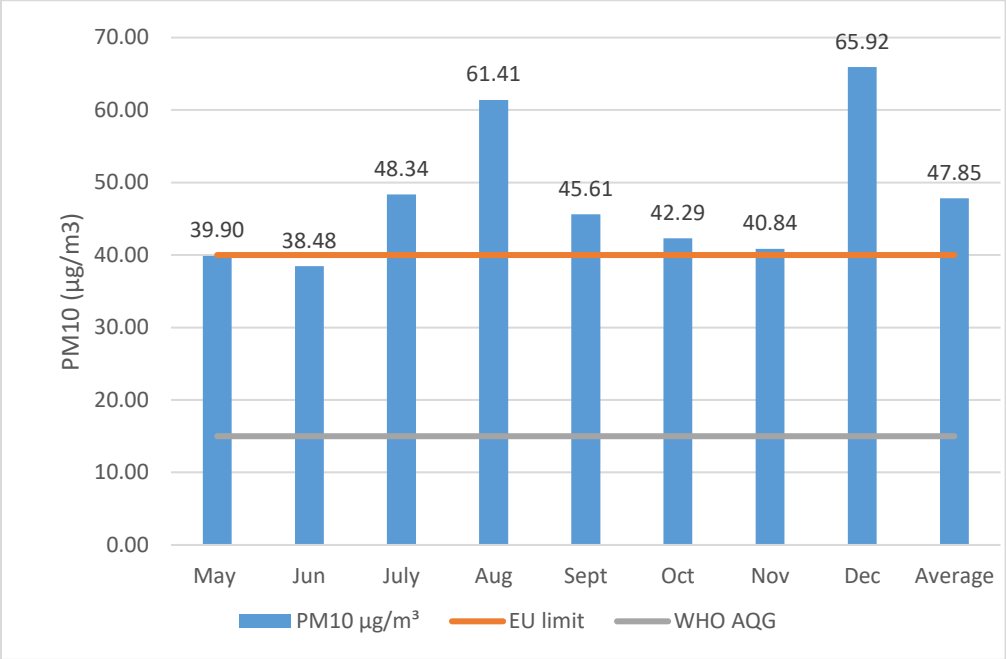

Figure 5. PM10 concentration (µg/m^3) in the urban air of Elbasan during 2023

Benzene C_6H_6

Benzene (C_6H_6) is a dangerous air pollutant that is emitted primarily from fuel combustion, vehicle exhaust, fuel evaporation, and industrial processes. Inhalation is the main way of exposure. Short-term exposure to high benzene levels can cause headache, dizziness, tiredness and irritation of the eyes and respiratory system, whereas long-term exposure may damage the bone marrow, decrease the white blood cells and is associated with an increased risk of leukaemia. International Agency for Research on Cancer (IARC) has classified benzene as carcinogenic to humans – Group 1 (IARC, 2018). It is also caracterized as a known human carcinogen by the US EPA (WHO, 2019; US EPA, 2003).

Figure 6 shows the monthly and annual mean concentrations of C_6H_6 in the city of Elbasan in 2023. As can be seen from the figure, the average annual concentration of benzene has resulted in 2.24 µg/m^3, with the highest concentrations being recorded in January, November and December. This trend matches usual seasonal variations in benzene concentrations which are generally higher in winter due to increased fuel combustion for heating, less atmospheric dispersion due to stable conditions and inversions, and less efficient photochemical breakdown (Baudic et al., 2025; Zhang et al., 2014).

The average annual concentration of benzene was below the EU limit of 5 µg/m^3 However, concentrations increased substantially during the colder months, approaching the EU limit value in December. From a public health perspective, these levels remain relevant because benzene is a known human carcinogen, and the WHO states that no safe level of exposure to airborne benzene can be recommended. The risk assessments of WHO show that even low levels of benzene are associated with an increased lifetime risk of leukemia (WHO, 2019; WHO, 2024).

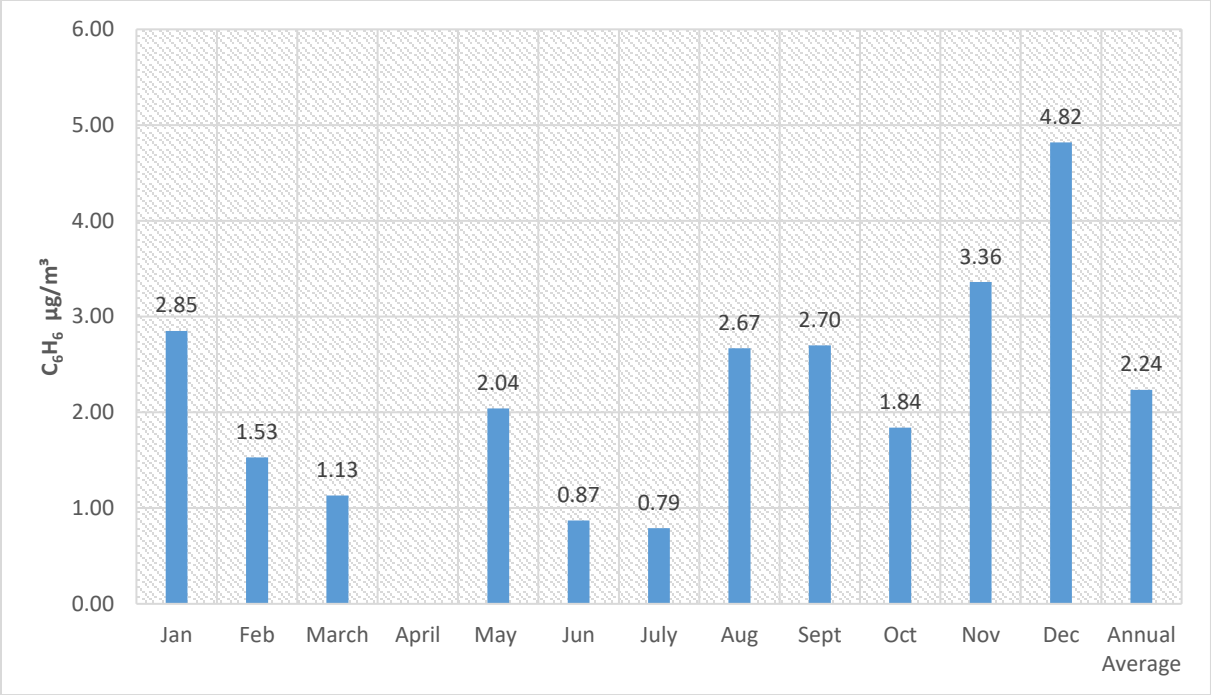

Figure 6. C_6H_6 concentration (µg/m^3) in the urban air of Elbasan during 2023

CONCLUSIONS

The analysis of the data obtained from the air quality monitoring in the city of Elbasan during the year 2023 is a useful basis for the evaluation of the urban air pollution of the city. The results indicate that air quality remains a concern, with several key pollutants exceeding or approaching national and EU limit values. Some pollutants that meet EU standards are still above WHO health-based guideline levels.

The seasonal analysis reveals that the air quality is generally worse in winter, with higher concentrations of PM10, NO_2, CO, and C_6H_6. This trend of pollution is mostly caused by increased burning of fuels for heating, lower temperatures and poor atmospheric dispersion due to temperature inversions.

Air pollution in Elbasan is influenced by multiple sources, particularly road traffic, industrial activities, residential heating, and the use of low-quality fuels. Open waste burning and agricultural activities may also contribute to pollutant levels. Effective control of these sources, together with strengthened air quality monitoring, would contribute to improving urban air quality and reducing potential adverse impacts on public health.

REFERENCES

Agjencia Kombëtare e Mjedisit (AKM). (2026). *Raporti vjetor për cilësinë e mjedisit 2025*

Alemayehu, Y.A., Asfaw, S.L. & Terfie, T.A. (2020). Exposure to urban particulate matter and its association with human health risks. *Environ Sci Pollut Res* **27**, 27491–27506 (2020).

https://doi.org/10.1007/s11356-020-09132-1Baudic, A., et al. (2025). Measurement report: Exploring the variations in ambient BTEX in urban Europe and their environmental health implications. *Atmospheric Chemistry and Physics, 25*, 625–648. https://doi.org/10.5194/acp-25-625-2025European

Environment Agency (EEA). (2022). *Air quality in Europe 2022: Sources and emissions of air pollutants in Europe.* EEA Report No 05/2022. Copenhagen: European Environment Agency.

European Environment Agency (EEA). (2022). *Dispersal of air pollutants.* Air and Health – Local authorities, health and environment.

European Environment Agency. (2024). Air quality in Europe – 2024 report. European Environment Agency.

European Parliament and Council. (2008). Directive 2008/50/EC of 21 May 2008 on ambient air quality and cleaner air for Europe. Official Journal of the European Union, L152, 1–44.

Gratsea, M., Liakakou, E., Stavroulas, I., et al. (2017). The combined effect of reduced fossil fuel consumption and increasing biomass combustion on Athens' air quality, as inferred from long term CO measurements. *Atmospheric Chemistry and Physics, 17*, 14041–14054. https://doi.org/10.5194/acp-17-14041-2017

Guion, A., Couvidat, F., Guevara, M., & Colette, A. (2025). Country- and species-dependent parameters for the heating degree day method to distribute NOx and PM emissions from residential heating in the EU 27: Application to air quality modelling and multi-year emission projections. *Atmospheric Chemistry and Physics, 25*, 2807–2827. https://doi.org/10.5194/acp-25-2807-2025

International Agency for Research on Cancer (IARC).(2018). Benzene. IARC Monographs on the Evaluation of Carcinogenic Risks to Humans, Volume 120. IARC Monographs – Benzene

Lin, W., Xu, X., Ma, Z., Zhao, H., Liu, X., & Wang, Y. (2012). Characteristics and recent trends of sulfur dioxide at urban, rural, and background sites in North China: Effectiveness of control measures. *Journal of Environmental Sciences, 24*(1), 34–49. https://doi.org/10.1016/S1001-0742(11)60727-4

U.S. Environmental Protection Agency. (1979). *Air quality criteria for carbon monoxide*. U.S. Environmental Protection Agency

U.S. Environmental Protection Agency. (2016). Integrated science assessment for oxides of nitrogen—Health criteria (Final report, January 2016) (EPA/600/R-15/068). U.S. Environmental Protection Agency.

U.S. Environmental Protection Agency. (2020). *Integrated science assessment for ozone and related photochemical oxidants: Seasonal patterns*. U.S. Environmental Protection Agency.

US Environmental Protection Agency. (2003). Benzene (CASRN 71-43-2), IRIS. US EPA – Benzene IRIS Assessment

Voiculescu, M., Constantin, D.-E., Condurache-Bota, S., Călmuc, V., Roșu, A., & Dragomir Bălănică, C. M. (2020). Role of meteorological parameters in the diurnal and seasonal variation of NO_2 in a Romanian urban environment. *International Journal of Environmental Research and Public Health, 17*(17), 6228. https://doi.org/10.3390/ijerph17176228

Wang, L., Wang, Y., Sun, Y., Sun, J., & Zhang, X. (2018). Analysis of SO_2 pollution changes of Beijing-Tianjin-Hebei region over China based on OMI observations from 2006 to 2017. *Advances in Meteorology, 2018,* Article 8746068. https://doi.org/10.1155/2018/8746068

World Health Organization (2024). Health consequences of air pollution on populations.

World Health Organization. (2019). Exposure to benzene: A major public health concern. WHO – Exposure to benzene

World Health Organization. (2021). WHO global air quality guidelines: Particulate matter ($PM_{2.5}$ and PM_{10}), ozone, nitrogen dioxide, sulfur dioxide and carbon monoxide. World Health Organization. https://apps.who.int/iris/handle/10665/345329

Zhang, Y., et al. (2014). Spatial/temporal variations and source apportionment of VOCs monitored at community scale in an urban area. *PLOS ONE*, *9*(4), e95734. https://doi.org/10.1371/journal.pone.0095734

MICROSPORIDIAL AND NEMATODE INFECTIONS IN THE PREDATORY BEETLE Calosoma sycophanta L. (COLEOPTERA: CARABIDAE) -REARING LABORATORIES IN TÜRKİYE

Tuğba Sağlam Güvendik[1,2], Mustafa Yaman[3]

[1]Department of Wildlife Ecology and Management, Faculty of Forestry, Isparta University of Applied Sciences, Isparta 32260, Türkiye
[2]Department of Biomedical Engineering, Faculty of Technology, Isparta University of Applied Sciences, Isparta 32260, Türkiye
[3]Department of Biology, Faculty of Arts and Science, Bolu Abant İzzet Baysal University, 14030, Bolu, Türkiye

Corresponding author e-mail: tugbasaglam32@hotmail.com

ABSTRACT

Calosoma sycophanta (Linnaeus, 1758), commonly known as the forest caterpillar hunter (FCH), is a large ground beetle that has long been recognized as an effective predatory species in the biological control of lepidopteran pests. In Türkiye, *C. sycophanta* is mass-reared in insect production facilities for the biological control of the pine processionary moth, *Thaumetopoea* spp. (Denis & Schiffermüller). However, despite being mass-produced through considerable effort and expense, *C. sycophanta* alone is insufficient to effectively suppress high-density infestations of the pine processionary moth. In addition, pathogenic viruses, bacteria, fungi, protists, and nematodes may cause chronic infections in predatory insects reared in laboratories for biological control. The use of healthy insects can significantly enhance the efficacy and overall success of biological control programs. This study investigated the current distribution of microsporidial and nematode infections in insect rearing laboratories used for biological control programs across Türkiye. From seven rearing laboratories in Türkiye (Antalya, Balıkesir, Bursa, Isparta, İzmir/Bergama, Manisa and Sakarya/Geyve) 447 dead adult specimens of *C. sycophanta* were procured. To find infected individuals, the beetles were dissected in Ringer's solution and examined under a light microscope at magnifications of 400–1000×. The study revealed that microsporidian infection was detected exclusively in samples obtained from the mass-rearing laboratory in Antalya province, whereas nematode infection was detected only in samples collected from the laboratory in Bursa province. The results showed that microsporidian infection was detected in samples collected from Antalya and Sakarya/Geyve, whereas nematode infection was detected exclusively in samples collected from Bursa. The prevalence of microsporidian infection was 19.0% in samples from Antalya, while it was 9.5% in samples from Sakarya/Geyve. In samples collected from Bursa, nematode infection was detected at a prevalence of 10.2%. In conclusion, to maximize the effectiveness of *C. sycophanta* as a biological control agent and to ensure the success of mass-rearing programs, adult beetles should be routinely screened for potential pathogens before mass rearing begins, and only pathogen-free populations should be selected for production.

Keywords: *Calosoma sycophanta, Microsporidia, Nemotode, Rearing Laboratories, Türkiye*

INTRODUCTION

Calosoma sycophanta (Linnaeus, 1758), commonly known as the forest caterpillar hunter, is a large ground beetle that has long been recognized as an effective predator in the biological

control of Lepidopteran pests. It feeds on a wide range of Lepidopteran species, including Dasychira pudibunda, Euproctis chrysorrhoea, Hyphantria cunea, Lymantria dispar, Lymantria monacha, Thaumetopoea spp. and Tortrix viridana thereby playing an important role in the natural suppression of pest populations (Çanakçıoğlu, 1993; Oğurlu, 2000; Kanat and Mol 2008; Yaman et al., 2019a). In Turkey, C. sycophanta, which plays an important role particularly in the natural suppression of pine processionary moth (T. pityocampa) populations, is mass-reared in insectaries for use in biological control programs (Tosun, 1977; Oğurlu, 2000; Kanat, 2002). However, these rearing programs require considerable effort and substantial costs (Kanat and Özbolat 2006; Yaman et al., 2019a). C. sycophanta, by feeding on both larval and pupal stages of T. pityocampa, is considered an effective biological control agent for regulating pine processionary moth population density during outbreak periods (Kanat and Mol 2008). The use of healthy individuals in biological control programs enhances the efficacy of biological control (Yaman et al., 2010a; Bjørnson and Oi 2014). Pathogenic viruses, bacteria, fungi, protists, and nematodes can cause chronic infections in predatory insects reared in laboratories for biological control. Therefore, the use of healthy insects in biological control programs can significantly enhance their efficacy and overall success (Yaman et al., 2016; Yaman et al., 2019a). It is well known that high mortality rates are observed during the mass rearing of C. sycophanta and after the released individuals are introduced into their natural environment. A substantial proportion of these mortalities is believed to be associated with diseases, as supported by previous studies on diseases affecting similar predatory insects (Yaman and Radek 2007; Yaman et al., 2010a; 2010b). Therefore, the mass rearing of C. sycophanta should aim to produce healthy individuals capable of surviving in the natural environment and reproducing successful1ly. To improve production efficiency, disease-causing agents in C. sycophanta should be identified during mass rearing, and rearing laboratories should be routinely screened for these pathogens. This study investigated the current distribution of microsporidian and nematode infections in C. sycophanta populations from insect rearing laboratories used for biological control programs across Türkiye.

MATERIAL AND METHOD

Insect Samples

From seven rearing laboratories in Türkiye (Antalya, Balıkesir, Bursa, Isparta, İzmir/Bergama, Manisa and Sakarya/Geyve) 447 dead adult specimens of *C. sycophanta* were procured.

Microscopic Examination

Firstly, the samples were taken for macroscopic examination. C. sycophanta adult samples were dissected in Ringer's solution and then prepared wet smears including host fat body, malpighian tubules, gut epithelium, and hemolymph were examined for the presence of the entomopathogen infection under a light microscope at a magnification of 400–1000X. When infection was found, the slides were air-dried and fixed with methanol, then stained with freshly prepared 5% solution of Giemsa stain. They were then washed in running tap water, air-dried, and examined under a microscope (Yaman et al., 2019b;Yaman and Sağlam Güvendik 2024).

RESULTS AND DISCUSSION

In this study, Microsporidian infection was detected in samples obtained from the mass-rearing laboratories in Antalya and Sakarya/Geyve, whereas Nematode infection was detected exclusively in samples collected from the laboratory in Bursa province (Table 1).

Table 1. Prevalence of Microsporidian and Nematode infections in *Calosoma sycophanta* populations

Location	Number of examined	Number of Microsporidia	Microsporidian infection (%)	Number of Nematode	Nematode infection (%)	Total (%)
Antalya	43	8	19	-	-	19
Balıkesir	103	-	-	-	-	-
Bursa	49	-	-	5	10.2	10.2
Isparta	10	-	-	-	-	-
İzmir/Bergama	84	-	-	-	-	-
Manisa	74	-	-	-	-	-
Sakarya/Geyve	84	8	9.5	-	-	9.5
Total	447	16	3.6	5	1.1	4. 7

The presence of a microsporidian pathogen in C. sycophanta adults reared in insectaries in Türkiye was first reported by Yaman et al. (2016). A microsporidian pathogen was detected in *C. sycophanta* adults from Demirci (Manisa), Selçuk (İzmir), Burhaniye (Balıkesir), and Antalya, and the infection site in the host was identified as the hemolymph (blood cells) (Yaman et al., 2016). In the present study, a microsporidian pathogen was detected in C. sycophanta adults from Antalya and Sakarya/Geyve, and, consistent with the findings of Yaman et al. (2016), the infection was observed predominantly in the hemolymph (blood cells) of the host. The prevalence of microsporidian infection was 19.0% in samples obtained from Antalya, whereas the prevalence was 9.5% in samples obtained from Sakarya/Geyve (Table 1). In a study investigating the distribution of a microsporidian pathogen in C. sycophanta populations obtained from rearing laboratories in Türkiye, the prevalence of microsporidiosis was found to vary among C. sycophanta populations from different regions of Türkiye across different years, with a particularly increasing trend in the occurrence of microsporidian infection in Antalya over the years (Yaman et al., 2019a). In the present study, microsporidian infection was still detected in C. sycophanta populations in Antalya in 2026. In contrast, no previous record of microsporidian infection had been reported from Sakarya/Geyve. In the present study, microsporidian infection was detected for the first time in the C. sycophanta rearing laboratory in Sakarya/Geyve.

Microsporidia cause chronic diseases in predatory insects reared in laboratories for biological control, thereby reducing their foraging ability and fecundity (Yaman et al., 2010b; Bjørnson and Oi 2014). Additionally, microsporidia have been shown to prolong larval and pupal development and reduce the fecundity and survival rates of adult predatory insects (Bjørnson and Keddie 1999; Joudrey and Bjørnson 2007; Bjørnson and Oi 2014).

In the samples examined, the pathogen's spore is the most characteristic stage. Light microscopy examinations of live and dead samples revealed the presence of pathogen spores in the intestine and body cavity (Figure 1). The presence of infection spores was confirmed using the Giemsa staining technique (Figure 2). Giemsa-stained spores were measured. Giemsa-stained spores measured $3.18 \pm 0.59 \times 1.63 \pm 0.26$ µm.

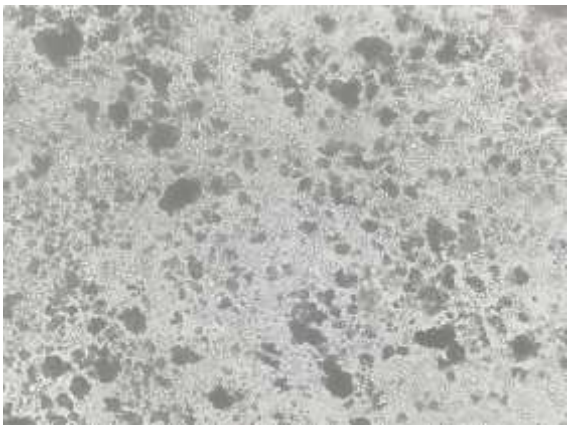

Figure 1. Light microscopy micrographs of microsporidian infection in Calosoma sycophanta

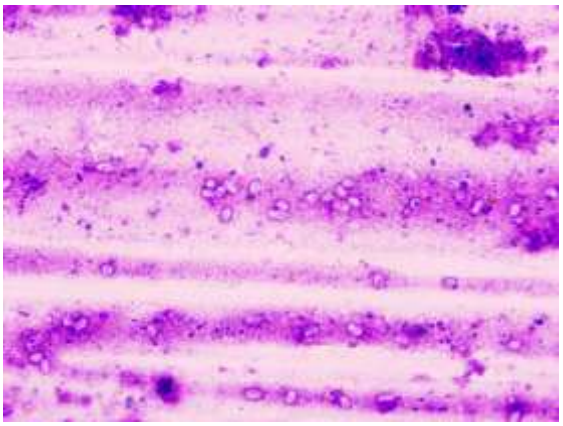

Figure 2. Light microscopy micrographs of Giemsa-stained microsporidian spores in *Calosoma sycophanta*

The infective juvenile stages of nematodes that cause diseases in insects enter their insect hosts through the mouth, anus, or directly through the cuticle. They penetrate the intestinal wall and enter the hemocoel, usually causing the host insect to die within 24–72 hours. Therefore, nematode infection in C. sycophanta is also undesirable. A literature review revealed that nematodes were detected in C. sycophanta individuals in Türkiye as part of a project conducted by Yaman (2007). In the present study, nematode infection was detected at a relatively high prevalence of 10.2% in samples obtained from Bursa (Table 1, Figure 3).

Figure 3. Light microscopy micrographs of nematode in Calosoma sycophanta

CONCLUSIONS

In conclusion, to maximize the effectiveness of *C. sycophanta* as a biological control agent and ensure the success of mass-rearing programs, it is of great importance that adult beetles be routinely screened for potential pathogens before rearing begins and that only pathogen-free populations be used for production. Given that individuals may be exposed to stress in mass-rearing laboratories because the environmental conditions encountered in nature cannot be fully replicated, and that stress may increase susceptibility to infections, pathogens should be regularly monitored and kept under control throughout the rearing process.

ACKNOWLEDGMENT

This study was supported by Scientific and Technological Research Council of Türkiye (TUBITAK) under the Grant Number 125N695. The authors thank to TUBITAK for their supports.

REFERENCES

Bjørnson, S., Keddie, A. 1999. Effects of Microsporidium phytoseiuli (Microsporidia) on the performance of the predatory mite, *Phytoseiulus persimilis* (Acari: Phytoseiidae). Biological Control 15: 153-161.

Bjørnson S., Oi D. 2014. Microsporidia biological control agents and pathogens of beneficial insects. In: Weiss, L.M., Becnel, J.J. (editors). Microsporidia: Pathogens of Opportunity. Chichester, UK: Wiley, pp. 635-686.

Çanakçıoğlu, H. 1993. Orman Entomolojisi (Özel Bölüm). İstanbul Üniversitesi Orman Fakültesi Yayınları, Yayın No:3523, Orman Fakültesi Yayın No:412, x+458 s. (Genişletilmiş 2. Baskı).

Joudrey, P., Bjørnson, S. 2007. Effects of an unidentified microsporidium on the convergent lady beetle, *Hippodamia convergens* Guerin-Meneville (Coleoptera: Coccinellidae), used for biological control. Journal of Invertebrate Pathology, 94: 140-143.

Kanat M. 2002. Çam Keseböceği (*Thaumetopoea pityocampa* Schiff.)'ne karşı Biyolojik Mücadelede *Calosoma sycophanta* L.'nın Kullanımı. Ülkemiz Ormanlarında Çam Keseböceği Sorunu ve Çözüm Önerileri Sempozyumu (Ed. M. Kanat), Kahramanmaraş, Turkey, p. 93-101.

Kanat, M., Özpolat, M. 2006. Mass production and release of *Calosoma sycophanta* L. (Coleoptera: Carabidae) used against the pine processionary moth, *Thaumetopoea pityocampa* (Schiff.) (Lepidoptera. Thaumetopoediae) in biological control. Turkish Journal of Zoology ,30: 181-185.

Kanat, M., Mol, T. 2008. The effect of *Calosoma sycophanta* L.(Coleoptera: Carabidae) feeding on the pine processionary moth, *Thaumetopoea pityocampa* (Denis & Schiffermüller)(Lepidoptera: Thaumetopoeidae), in the laboratory. Turkish Journal of Zoology, *32*(4): 367-372.

Oğurlu İ. 2000. Biyolojik Mücadele. Süleyman Demirel Üniversitesi Yayın No: 8, Orman Fakültesi Yayın No:1.

Tosun I. 1977. Akdeniz Bölgesi İğne Yapraklı Ormanlarında Zarar Yapan Böcekler ve Önemli Türlerin Parazit ve Yırtıcıları Üzerinde Araştırmalar. Orman Bakanlığı, OGM Sıra No: 612, Seri No:24, Ankara.

Yaman M. 2007. Avcı Böcek *Calosoma sycophanta* (L.) (Coleoptera: Carabidae)'nın Üretimini ve Yararlılığını Etkileyen Hastalık Etmenlerinin Belirlenmesi. TOVAG-TÜBİTAK 1001 Projesi, Proje No:114O722.

Yaman, M. ve Radek, R., 2007. "Infection of the predator beetle Rhizophagus grandis Gyll. (Coleoptera, Rhizophagidae) with the insect pathogenic alga Helicosporidium sp. (Chlorophyta: Trebouxiophyceae)", Biological Control.

Yaman, M., Radek, R., Weiser, J. ve Toguebaye, B., 2010a. "Unikaryon phyllotretae sp. n. (Protista, Microspora), a new microsporidian pathogen of Phyllotreta undulata", Folia Parasitologica.

Yaman, M., Radek, R., Weiser, J., Aydın, Ç. 2010b. A microsporidian pathogen of the predatory beetle *Rhizophagus grandis* (Coleoptera: Rhizophagidae). Folia Parasitologica, 57: 233-236.

Yaman, M., Eroğlu, M., Radek, R. 2016. Occurrence of a microsporidium in the predatory beetle *Calosoma sycophanta* L.(Coleoptera: Carabidae). Turkish Journal of Agriculture and Forestry, *40*(3): 420-424.

Yaman, M., Uzuner, S., Emirzeoğlu Güner B.G., Ayar, Ö., Ertürk, Ö., Eroğlu, M. 2019a. Distribution of microsporidial infection in the predator beetle, *Calosoma sycophanta* (Coleoptera: Carabidae)-rearing laboratories in Turkey. Turkish Journal of Agriculture and Forestry, *43*(6): 586-592.

Yaman, M., Algı, G., Radek, R. 2019b. Morphological, ultrastructural and molecular identification of a new microsporidian pathogen isolated from *Crepidodera aurata* (Coleoptera, Chrysomelidae). Turkish Journal of Zoology, 43: 407–415.

Yaman, M., Sağlam Güvendik T. 2024. The first record and occurrence of microsporidian pathogen, *Chytridiopsis* cf. *typographi* (Microspora) in *Pityokteines curvidens* (Coleoptera, Curculionidae) populations in Türkiye. Turkish Journal of Forestry, 25(4): 380-382.

A PRELIMINARY SURVEY OF NEMATODES AND GREGARINE IN Ips sexdentatus (BOERNER) (COLEOPTERA: CURCULIONIDAE, SCOLYTINAE) POPULATIONS FROM THE WESTERN MEDITERRANEAN REGION (ANTALYA, BURDUR AND ISPARTA), TÜRKİYE

Tuğba Sağlam Güvendik[1,2], Mustafa Yaman[3]

[1]Department of Wildlife Ecology and Management, Faculty of Forestry, Isparta University of Applied Sciences, Isparta 32260, Türkiye

[2]Department of Biomedical Engineering, Faculty of Technology, Isparta University of Applied Sciences, Isparta 32260, Türkiye

[3]Department of Biology, Faculty of Arts and Science, Bolu Abant İzzet Baysal University, 14030, Bolu, Türkiye

Corresponding author e-mail: tugbasaglam32@hotmail.com

ABSTRACT

Ips sexdentatus Boerner (Coleoptera: Curculionidae: Scolytinae) is one of the most destructive bark beetle species, responsible for substantial economic damage in coniferous forests of the Western Mediterranean Region, Türkiye. Pheromone trapping, together with mechanical and chemical control strategies, has long been employed for the management of this pest. However, increasing concerns regarding environmental sustainability have intensified interest in biological control agents and their associated natural enemies. In contrast, entomopathogenic organisms, as natural enemies of insects, possess several advantages over chemical insecticides. Entomopathogenic organisms play an important role as biological control agents against insect pests because of their widespread distribution and high prevalence of infection in insect populations. This preliminary study aimed to determine the presence of nematodes and gregarines in *I. sexdentatus* specimens collected from the Western Mediterranean Region (Antalya, Burdur and Isparta), Türkiye. A total of 120 adult *I. sexdentatus* specimens, including 85 live and 35 dead individuals, were examined in this study. Each beetle was dissected in a physiological solution (0.8% NaCl) and examined microscopically at magnifications of 400×-1000×. The study revealed that the gregarine pathogen was detected only in live *I. sexdentatus* specimens from Burdur province. Nematodes were abundantly detected in the hemolymph of both live and dead *I. sexdentatus* specimens from Isparta, Antalya and Burdur provinces. The detected gregarine pathogen co-occurred with nematodes. The highest nematode infection rates in the examined samples were found in Burdur (34.3%), Isparta (30%), and Antalya (20%). The average infection rate was 31%. The gregarine infection rate was found only in Burdur, at 1.4%. The detected natural enemies may play an important role in the biological control of *I. sexdentatus*, as they have the potential to affect its survival and reproductive capacity. Therefore, this preliminary study provides important baseline data for future studies on the natural enemies of *I. sexdentatus* in the Western Mediterranean Region of Türkiye.

Keywords: *Ips sexdentatus, Gregarine, Nematode, Western Mediterranean Region, Türkiye*

INTRODUCTION

Ips sexdentatus Boerner (Coleoptera: Curculionidae: Scolytinae) is one of the most important and destructive bark beetle species causing severe economic damage and losses in coniferous forests of the Western Mediterranean Region of Türkiye (Sarıkaya et al., 2012). It is a quarantine pest included in the EPPO A2 List and is recognized as one of the most important bark beetle species causing damage to forest ecosystems in Türkiye (EPPO, 2016; Erdoğan, 2024). *I. sexdentatus* was first recorded in Türkiye in 1928 by Bernhard in the spruce forests of Trabzon province. It was subsequently recorded in different regions of Türkiye, where pheromone traps have been widely used as the primary method for its control (Defne, 1954; Chararas, 1966; Beşceli ve Ekici, 1969; Tosun, 1975; Serez, 1984; Sekendiz, 1991; Yüksel, 1996, Cebeci, 2003; Eyüboğlu, 2011; Akkuzu ve Güzel, 2015; Özcan, 2017; Şahin, 2019; Erdoğan, 2024). Adult *I. sexdentatus* are highly efficient fliers, enabling them to actively search for and locate suitable host trees. In the Antalya, Burdur, and Isparta regions, its population may occasionally reach higher levels, and depending on climatic conditions, it can cause outbreaks (Sarıkaya et al., 2012). Although pheromone trapping, mechanical control, and chemical control methods have long been employed for the management of *I. sexdentatus*, these conventional control strategies have often provided limited effectiveness, highlighting the need for alternative and more sustainable approaches to its management. In Türkiye, several chemical insecticides, including cypermetrin and fenitrothion, have also been used to control this pest. However, due to the adverse effects of chemical insecticides on the environment and beneficial insects, as well as their unintended effects on natural predators and parasitoids, chemical control is no longer widely preferred for the management of this pest (Yüksel, 1998; Sevim et al., 2012). Nowadays, growing concerns about environmental sustainability have significantly increased interest in biological control agents and their associated natural enemies. Entomopathogenic organisms, which are natural enemies of insects, offer several advantages over chemical insecticides. Entomopathogenic organisms play an important role as biological control agents against insect pests due to their widespread distribution and high infection prevalence in insect populations (Yaman, 2007; Sevim et al., 2012). In this context, this preliminary study aimed to determine the presence of nematodes and gregarines in *Ips sexdentatus* specimens collected from the Western Mediterranean Region of Türkiye, particularly from Antalya, Burdur, and Isparta provinces.

MATERIAL AND METHOD

Insect Samples

A total of 120 adult *Ips sexdentatus* specimens were collected from the provinces of Antalya, Burdur and Isparta in Türkiye. The sampled individuals consisted of 85 live and 35 dead beetles.

Microscopic Examination

Firstly, the samples were subjected to macroscopic examination. Adult *Ips sexdentatus* specimens were dissected in physiological saline (0.8% NaCl), and wet smears prepared from the fat body, Malpighian tubules, gut epithelium, and hemolymph were examined for the presence of entomopathogenic infections under a light microscope at 400–1000× magnification (Sağlam et al., 2021).

RESULTS AND DISCUSSION

Both live and dead *Ips sexdentatus* specimens were examined in this study. The results revealed the occurrence of gregarine pathogens and nematode infections in the examined *I. sexdentatus*

specimens. The gregarine pathogen was detected only in live specimens collected from Burdur Province (Figure 1). Nematodes, however, were detected in high abundance in the hemolymph of both live and dead *I. sexdentatus* specimens collected from Isparta, Antalya, and Burdur provinces (Figure 2). Additionally, the gregarine pathogen detected in Burdur Province was co-detected with nematodes.

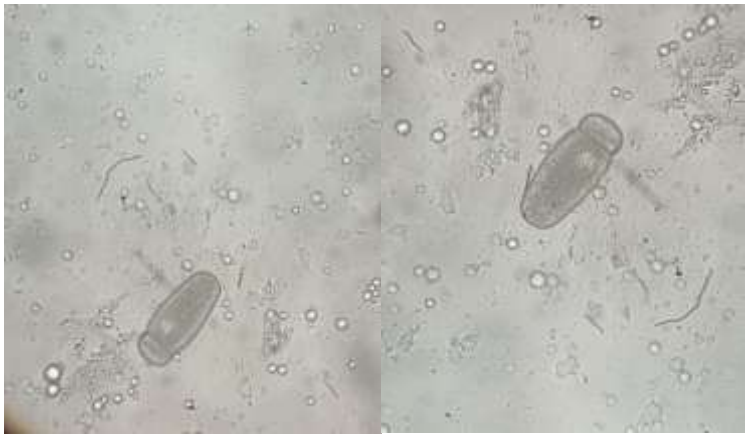

Figure 1. Light microscopy micrographs of gregarine in *Ips sexdentatus*

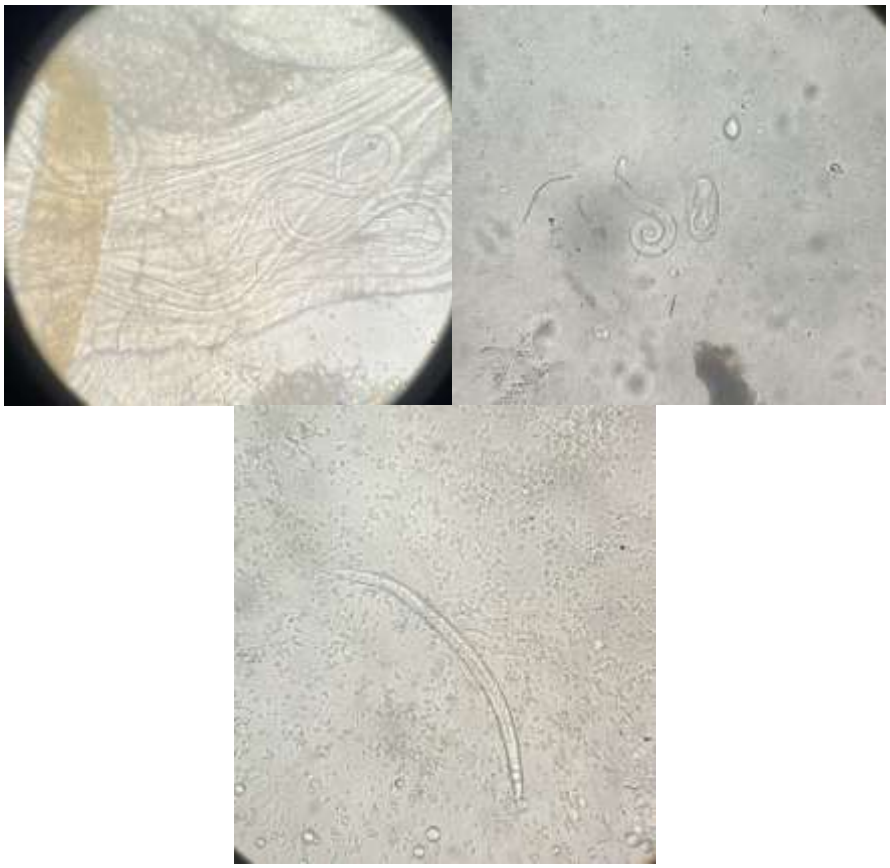

Figure 2. Light microscopy micrographs of nematode in *Ips sexdentatus*

The gregarine pathogen of *I. sexdentatus* was first reported in Türkiye by Yaman (2007). Additionally, the study reported the occasional co-occurrence of a gregarine and a nematode

parasite within the same host. In the present study, the gregarine pathogen detected in Burdur Province was also detected in association with nematodes.

Eugregarines that parasitize the midgut epithelial cells cause the most pronounced pathological changes during the intracellular and intercellular developmental stages of their trophozoites (Lipa, 1967; Yaman, 2007). Tanada ve Kaya (1993). It has been reported that midgut damage caused by gregarine infection can be readily repaired through the proliferation and differentiation of cells within the regenerative crypts, and that the pathological effects of gregarines are generally limited. However, the effects of nematode parasites on *I. sexdentatus* have been previously investigated (Lieutier, 1980, 1982, 1984). These two natural enemies may simultaneously reduce the host's lifespan and reproductive potential (Yaman, 2007). In the present study, nematodes were detected in both live and dead *I. sexdentatus* specimens collected from Isparta, Antalya, and Burdur provinces, while both nematode and gregarine parasites were simultaneously detected in specimens collected from Burdur Province.

The infection rates of gregarines detected in *I. sexdentatus* were reported as 27.4% in Bulgaria (Takov et al., 2007), 16.7–45.5% in Austria (Wegensteiner et al., 2005), and 6% in Türkiye (Yaman, 2007). In the present study, the gregarine infection rate was detected exclusively in Burdur province, at 1.4% (Table 1).

Table 1. Gregarine and Nematode Infections in *Ips sexdentatus* Populations in the Western Mediterranean Region

	Alive sample	**Nematode**	**Gregarine**	**Total (%) (alive)**	**Dead sample**	**Nematode**	**Total (%) (dead)**	**Total (%)**
Antalya	15	3	-	20	5	1	20	20
Burdur	50	18	1	36 Nematode 2 Gregarine	20	6	30	34.3 Nematode 1.4 Gregarine
Isparta	20	7	-	35	10	2	20	30
Toplam	85	28	1	33 Nematode 1.2 Gregarine	35	9	26	31 Nematode 0.8 Gregarine

In the present study, nematode parasites were detected in the hemolymph of both live and dead *I. sexdentatus* specimens. The nematode infection rates were 34.3% in Burdur, 30% in Isparta, and 20% in Antalya. The mean infection rate was 31% (Table 1). Rühm (1956) recorded three nematode species, *Contortylenchus acuminata*, *Parasitaphelenchus acuminati* and *Parasitorhabditis acuminata* in the hemolymph of *Ips acuminatus.* However, nematodes associated with species of the genus *Ips* have been reported to belong to the orders Diplogasterida, Rhabditida, and Tylenchida (Grucmanova and Holusa 2013; Yaman et al., 2016). In future stages of the study, the nematodes detected will be identified to the genus or species level.

CONCLUSIONS

The detected natural enemies may play an important role in the biological control of *Ips sexdentatus*, as they have the potential to affect its survival and reproductive capacity. Therefore, this preliminary study provides important baseline data for future studies on the natural enemies of *I. sexdentatus* in the Western Mediterranean Region of Türkiye.

REFERENCES

Akkuzu, E., Guzel, H. 2015. Edge effects of black pine forests on *Ips sexdentatus* (Boern.) abundance. Šumarski List, 9 (10): 447-453.

Beşceli, O., Ekici, M. 1969. Doğu Ladini (*Picea orientalis* L.) Mıntıkasında *Ips sexdentatus'* un Biyolojisi ve Mücadelesi. Ormancılık Araştırma Enstitüsü Yayınları Teknik Bülten Serisi No: 32, Ankara 35 pp.

Cebeci, H. 2003. The Entomological Problems on Plantations in İstanbul Province at Istanbul Forest Regional Directory. Institute of Graduate Studies in Science and Engineering, Istanbul University, (Unpublished) PhD. Thesis in, Istanbul, 207 pp (in Turkish with abstract in English).

Chararas, C. 1966. *Ips sexdentatus* and other bark beetle species on Picea orientalis. Journal of Forestry Research Institute, 12 (1): 3-37.

Defne, M. 1954. *Ips sexdentatus* Boerner kabuk böceğinin Çoruh ormanlarındaki durumu ve tevlit ettiği zararlar. İstanbul Üniversitesi Orman Fakültesi Dergisi, 4 (2): 80-91.

EPPO, 2016. *Ips sexdentatus* (IPSXSE). (Web page: https://gd.eppo.int/taxon/IPSXSE/categorization) (Date accessed: January 2026).

Erdoğan, C. 2024. Investigation of possible use of pheromone trap for adult population development and control of Ips sexdentatus (Börner, 1776)(Coleoptera: Scolytidae) damaging black pine in Başkent University Bağlıca Campus afforestation area. Turkish Journal of Entomology, *48*(1): 3-14.

Eyüboğlu, B. 2011. Research on The Biology, Damage and Struggle of Ips sexdentatus In Torul, Gumushane. Artvin Coruh University, (Unpublished), M. Sc. Thesis, Artvin, 61 pp (in Turkish with abstract in English).

Grucmanova S., J. Holusa 2013. Nematodes associated with bark beetles, with focus on the genus Ips (Coleoptera: Scolytinae) in Central Europe. Acta Zoologica Bulgarica, 65: 547-556.

Lieutier, F. 1980. Le parasitisme d'*Ips sexdentatus* (Boern) (Coleoptera: Scolytidae) par les ne´matodes du genre Parasitaphelenchus Fuchs. Relations avec le parasitisme par Contortylenchus diplogaster (v. Lins.). Rev. Ne´matol. 3: 271-281.

Lieutier, F. 1982. Effect of the endoparasitic nematodes on the oviposition of the bark beetle *Ips sexdentatus* Boerner (Insecta: Coleoptera). Acta Oecologica. Oecologia Applicata, 3: 191-204.

Lieutier, F. 1984. Observations sur le parasitisme d'Ips sexdentatus (Insecta: Scolytidae) par le Parasitorhabditis ipsophila (Nematoda:Rhabditidae). Annales de Parasitologie Humaine et Comparée, 59: 507- 520.

Lipa, J.J. 1967. Studies on gregarines (Gregarinomorpha) of arthropods in Poland. Acta Protozoologica. V: 97-179.

Özcan, G.E. 2017. The impacts of Ips sexdentatus on the moisture content of Anatolian black pine trees. Journal of Forestry Faculty, 17 (1): 99-106.

Rühm W. 1956. Die Nematoden der Ipiden. – Parasitologische Schriftenreihe, 6: 435. P.

Sağlam, T., Yaman, M., Ertürk, Ö. 2021. Distribution and occurrence of *Vairimorpha plodiae* (Opisthokonta: Microspora) in the indian meal moth, *Plodia interpunctella* (Lepidoptera: Pyralidae) populations: an extensive field study. Acta Protozoologica, *60*, 31-36.

Sarikaya, O., Avci, M., Yildirim, S. 2012. Flight activity and biology of *Ips sexdentatus* Boerner in Black pine (Pinus nigra Arnold) forests of Isparta, Turkey. In *International Scientific*

Conference, Forests in the future–Sustainable use, risks and challenges, Institute of Forestry, Belgrade, Republic of Serbia (pp. 597-604).
Sekendiz, O.A. 1991. *Abies nordmanniana* (Stev.) Spach.'nın Doğu Karadeniz Bölümü Ormanlarındaki Zararlı Böcekleri ile Koruma ve Savaş Yöntemleri. Orman Genel Müdürlüğü Yayınları, Yayın No: 678, Sıra No: 73, 200 pp.
Serez, M. 1984. *Ips sexdentatus* savaşında *Ips typographus*'un feromon dispenseri "İpslure" nin kullanılması. K.T.Ü. Orman Fakültesi Dergisi, 7 (1):35-43.
Sevim, A., Gökçe, C., Erbaş, Z., Özkan, F. 2012. Bacteria from *Ips sexdentatus* (Coleoptera: Curculionidae) and their biocontrol potential. *Journal of basic microbiology*, *52*(6): 695-704.
Şahin, M. 2019. Effect of Type, Color and Hanging Height of *Ips sexdentatus* Pheromone Traps on Capture Rates. Graduate School of Natural and Applied Sciences, Kastamonu University, (Unpublished) M.Sc. Thesis, Kastamonu, 56 pp (in Turkish with abstract in English).
Takov D, Doyche D, Wegensteiner R, Pilarska D. 2007. Study of Bark Beetle (Coleoptera, Scolytidae) Pathogens from Coniferous stands in Bulgaria. Acta Zoologica Bulgarica, 59: 87-96.
Tanada, Y., Kaya, H.K. 1993. Protozoan infection: Apicomplexa, Microspora. In: Insect Pathology, Academic Press, San Diego, pp 414-458.
Tosun, I. 1975. Akdeniz Bölgesi iğne yapraklı ormanlarında zarar yapan böcekler ve önemli türlerin parazit ve yırtıcıları üzerine araştırmalar. İ.Ü. Orman Fakültesi Dergisi, 26 (2): 218-254.
Wegensteiner R, Pernek M, Weiser J. 2005. Occurrence of *Gregarina typographi* (Sporozoa, Gregarinidae) and of *Metschnikowia typographi* (Ascomycota, Metschnikowiaceae) in Ips sexdentatus (Col., Scolytidae) from Austria. In: *Proceedings of the 10th European Meeting: Invertebrate pathogens in biological control:* Present and Future at Locorotondo, pp. 23-9.
Yaman, M. 2007. *Gregarina typographi* Fuchs, a gregarine pathogen of the six-toothed pine bark beetle, *Ips sexdentatus* (Boerner)(Coleoptera: Curculionidae, Scolytinae) in Turkey. Turkish Journal of Zoology, *31*(4): 359-363.
Yaman, M., Algi, G., Unal, S., Guner, B.G. 2016. Survey of pathogens and parasites of the engraver beetle *Ips acuminatus* (Gyllenhal, 1827)(Coleoptera: Curculionidae: Scolytinae) in Turkey. Acta zoologica bulgarica, *68*(1), 127-130.
Yüksel, B. 1996. Investigations on the Damaging Insects Species and of Some Predators and Parasites Species at the Oriental Spruce in Turkey. Graduate School of Natural and Applied Science, Karadeniz Technical University, (Unpublished) PhD. Thesis, Trabzon, Türkiye, 240 pp (in Turkish with abstract in English).
Yüksel, B. 1996. Investigation on biologies of *Ips sexdentatus* and its control. İstanbul University Publication, İstanbul.
Yüksel, B. 1998. Türkiye'de doğu ladini (*Picea orientalis* (L.) ormanlarında zarar yapan böcek türleri ile bunların yırtıcı ve parazitleri-II (Yırtıcı ve Parazitler). Orman Bakanlığı Doğu Karadeniz Ormancılık Araştırma Enstitüsü, Teknik Bülten, 6 (1): 85.

DISTRIBUTION AND RAW MATERIAL RESERVES OF FERULA VARIA (SCHRENK) TRAUTV. AND FERULA FOETIDA (BUNGE) REGEL IN THE FLORA OF UZBEKISTAN

Ilkhom Mukumov[1], Murtazo Hasanov[1], Nodira Nurullayeva[1], Feruza Dzhumaniyozova[2]*

[1]Department of Botany, Samarkand State University, Samarkand, 140163,Uzbekistan
[2]Department of Biology, Zarmed University, Samarkand,140105, Uzbekistan

1 Corresponding author: ilhommuqumov65@gmail.com

ABSTRACK

The genus Ferula L. is distributed primarily in arid desert and mountainous regions. There are 48 species of this genus in Uzbekistan. Ferula species are medicinal, essential oil, fodder and honey plants. Many species of Ferula contain a large amount of resin and are used in soap making, dye production, as well as in the textile and paper industries. The article analyzes the distribution and reserves of some species of the genus based on the methodology of M.G. Pimenov, K.A. Pupikina and others. *F. varia* is distributed in mountainous and foothill areas, and *F. foetida* - in desert areas. The reserve of *F.varia* is 41,21±2,49 tons on an area of 1512 hectares, and the reserve of *F.foetida* is 6564,74±233,88 tons on an area of 14037 hectares.

Key words: ferula, fodder, food, honey, medicinal plants, field studies, herbarium materials, chemical composition.

INTRODUCTION

The genus *Ferula* L. belongs to the tribe Peucedaneae Dumort., subfamily Apioideae Drude, family Apiaceae Lindl. (Umbelliferae). At present, approximately 180–210 species of the genus Ferula are known. These are perennial herbaceous geophytic plants. The genus is distributed almost exclusively within the central regions of Eurasia, with the greatest species diversity concentrated in Central Asia and the adjacent territories of Iran and Afghanistan. In Central Asia, 106 species have been recorded, of which 48 species occur in Uzbekistan. Most species of Ferula inhabit arid climatic zones, particularly desert and mountainous regions [2,9,10,15].
The flora of Uzbekistan is highly diverse; however, in recent years, climate change and anthropogenic impacts have significantly influenced plant diversity and vegetation cover [2,5,11]. The majority of Ferula species, according to their seasonal developmental rhythm, belong to the group of ephemeroids - perennial plants characterized by a short annual period of growth and development and a prolonged dormancy period occurring during unfavorable seasons. The underground organ of Ferula species is represented by a thickened storage root. The genus includes both giant species, such as *F. gigantea* (2–2.5 m in height), and dwarf species, such as *F. nuda* (25–30 cm).
The name *Ferula* L., originally proposed by Tournefort (1700), was later adopted by Carl Linnaeus (1753), under which the genus entered scientific botanical nomenclature. During the eighteenth century, botanical knowledge of this genus accumulated gradually, as botanists described new species, sometimes not from natural habitats but from specimens cultivated in botanical gardens [3,10].
A significant contribution to the study of the genus Ferula L. was made by such researchers as E.Regel, B.A.Fedtschenko, B.M. Kozo-Polyansky, M.P.Petrov, L.A.Utkin, I.A.Zakharyants,

I.T. Vasilchenko, E.P. Korovin, R.V.Kamelin, M.S. Baitenov, M.G. Pimenov, Kh.A.Nishanbaeva, S.Melibaev, as well as scientists from Iran, Afghanistan, Turkey, and China [3].

Species of the genus *Ferula* L. are considered promising essential oil-bearing, forage, food, melliferous, and medicinal plants. They represent an exceptionally rich source of biologically active compounds, including essential oils, coumarins, sesquiterpene lactones, esters, and other natural substances. Since ancient times, plants of this genus have attracted the attention of researchers from various scientific fields, including botany, chemistry, and pharmacology [4,12,17].

For nearly a thousand years, species of the genus *Ferula* have played an important role in folk and traditional medicine, particularly owing to their oleo-gum-resins such as asafoetida, sagapenum, galbanum, and others [1].

Many Ferula species containing considerable amounts of resin may be utilized in the soap-making, paint and varnish, textile, and paper industries. The fruits of Ferula species contain proteins and other nutritive substances and are used as nutrient-rich poultry feed, as well as in the treatment of haemonchosis in animals.

Species of *Ferula* may also be applied in other sectors of the national economy. Numerous species are regarded as valuable forage plants, especially in desert and semi-desert ecosystems, while some are also used as hay-producing plants. Important forage species include *F. foetida*, *F. varia*, *F. kuhistanica*, *F. karatavica*, *F. tenuisecta* and others.

Among the representatives of the genus *Ferula* L. occurring in Uzbekistan, particular attention is given to the mountain species *F. tenuisecta*, *F. kuhistanica*, *F. tadshikorum*, as well as the desert species *F. foetida* and *F. varia* (Fig.1-2). The latter species are also recognized as valuable forage plants and are used in the establishment of artificial agrophytocenoses aimed at enriching the fodder resources for livestock breeding in the South-Western Kyzylkum region.

It should be emphasized that numerous species of *Ferula* L. are widely used in agriculture as forage plants. They are readily consumed by cattle and sheep, with both the aerial parts and fruits serving as feed resources. The inclusion of fruits of *F. foetida* in cattle diets has been reported to increase milk productivity.

Plants of the genus *Ferula* L. occupy an important position in the formation of the vegetation cover of Uzbekistan. Species such as *F. kuhistanica*, *F. foetida*, *F. tenuisecta*, and others are regarded as important edificators with significant landscape-forming value [7,8,9].

Fig. 1. General appearance of *F. varia*

Fig.2. General view of *F. foetida*

RESEARCH OBJECTIVES

The aim of the present study was to investigate the biological and ecological characteristics, as well as the growth and developmental patterns, of different *Ferula* species under various ecological conditions of their habitats. The study also focused on the development of scientific and practical foundations for the adaptive utilization of agroecological resources, including the optimization of floristic composition, assessment of biological diversity, and evaluation of the resource potential of natural vegetation.

MATERIALS AND METHODS

The following methods were employed during the research. Species identification and taxonomic verification were carried out using the multi-volume publication “Key to the Plants of Central Asia” (Vol. I–X, 1963–2016). The assessment of productivity and reserves of aboveground biomass was conducted according to the methods proposed by M.E. Pimenova et al. (1970), M.E. Pimenova (1971), M.G. Pimenov et al. (1976), and K.A. Pupykina et al. (2019) [10,16,17,18,19].The nomenclature of the studied species follows the publications “Key to the Plants of Central Asia” (1963–2016) and the database Plants of the World Online [5].

RESULTS AND DISCUSSION

As a result of field investigations conducted during 2020–2024 within the territory of Uzbekistan, extensive research surveys were carried out and herbarium specimens were collected. The collected material was subsequently processed and analyzed together with relevant literature sources. Among the representatives of the genus *Ferula* L. occurring in Uzbekistan, approximately 39 species are resin-containing, 39 are essential oil-bearing, 4 are starch-producing, 22 are melliferous, 13 are forage plants, 10 are edible, and 22 possess medicinal properties.

To determine the reserves of plant raw materials, experimental plots measuring 10 × 10 m were established. In the Navoi region, nine populations of *F. varia* located at elevations of 250–600 m above sea level were investigated, covering a total area of 1,512 ha (Fig. 3). It was determined that the average biological reserve within the investigated territories in 2024 (Table 1) amounted to an exploitable reserve of 41.21 ± 2.49 tons.

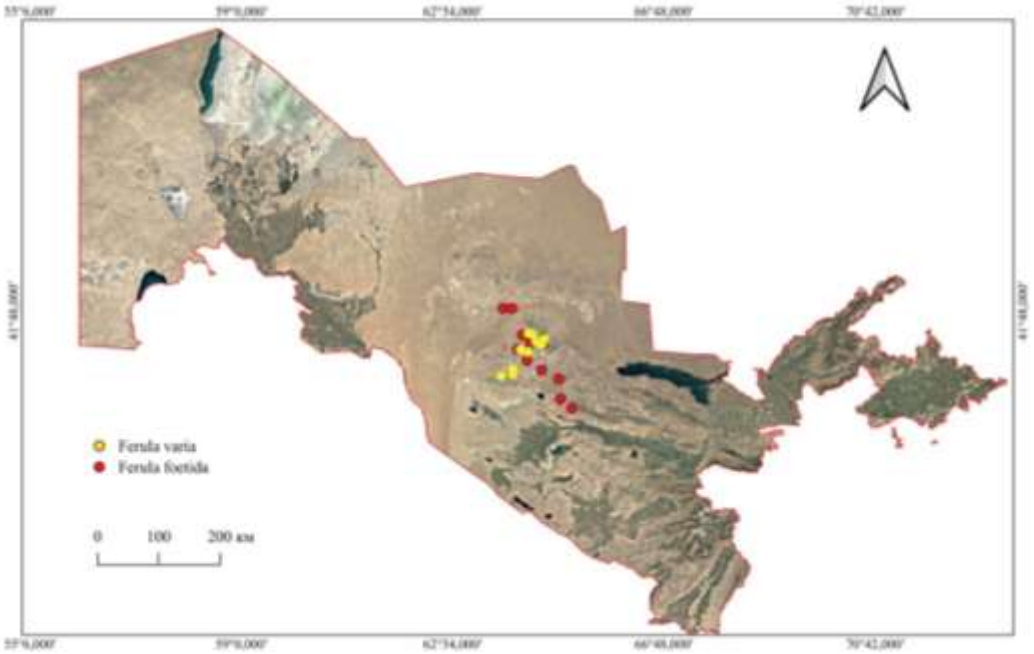

Fig. 3. Map of the studied species *F. varia* and *F. foetida.*

Table 1.

Area of Thickets and Reserves of Aboveground Biomass of *F. varia* (Air-Dry Weight), 2024

№	Key area	Category	Area of thickets, ha	Exploitable reserve of raw material, t
1.	Kuljuktau	2	175	1,91±0,12
2.	Zarafshan – Dovgistau (15 km)	1	912	28,51±1,98
3.	Navoi-Zarafshan (175 km)	2	102	1,87±0,09
4.	Navoi-Zarafshan (176 km)	1	27	0,29±0,01
5.	Navoi-Zarafshan (177 km)	1	196	6,12±0,24
6.	Navoi-Zarafshan(178 km)	2	72	0,89±0,03
7.	Navoi-Zarafshan (185 km)	2	11	0,62±0,01
8.	Navoi-Zarafshan (187 km)	2	8	0,91±0,05
9.	Navoi-Zarafshan (193 km)	2	9	0,09±0,004
	Total:		**1512**	**41,21±2,49**

Fourteen surveyed habitats of *F. foetida* located at elevations of 140–500 m above sea level covered a total area of 14,037 ha. It was determined that the average biological reserve within the investigated territories in 2024 amounted to an exploitable raw material reserve of 6564.74 ± 233.88 tons (Table 2).

Table 2.

Area of Thickets and Reserves of Aboveground Biomass of *F. foetida* (Air-Dry Weight), **2024**

№	Key area	Category	Area of thickets, ha	Exploitable reserve of raw material, t
1.	Ayakagit-ma District	2	793	311,41±10,77
2.	Shingeldy Village District	1	1118	694,94±19,11
3..	Bolokarak Village District	1	391	160,11±6,12
4.	Dovgistav Mine District	2	147	52,48±1,43
5.	Amantav Mine District	2	884	352,72±11,88
6.	Vicinity of the Kuljuktau Mountains (Zhamanzhar-say)	2	1326	587,55±21,35
7.	Vicinity of the Kuljuktau Mountains	1	512	159,13±7,86
8.	Along the Zarafshan–Tamdy road	2	3625	2321,81±71,43
9.	Along the Zhonkeldy–Shofirkon road	2	1403	559,80±22,15
10.	Along the Navoi–Zarafshan road (62 km)	1	1280	405,89±19,89
11.	Along the Navoi–Zarafshan road (92–94 km)	1	460	199,96±8,19
12.	Along the Navoi–Zarafshan road (195 km)	1	95	33,12±1,17
13.	Along the Navoi–Zarafshan road (207–221 km)	1	1820	630,63±29,52
14.	Along the Navoi–Uchkuduk road (262–263 km)	1	183	95,19±3,01
	Total:		**14037**	**6564,74±233,88**

CONCLUSIONS

Considering the above-mentioned data and based on the analysis of the obtained research results, the current status of the resources of *F. varia* and *F. foetida* in Uzbekistan has been determined. At present, the average area of resource significance in the Navoi region amounts to 15,549 ha. The analysis of long-term scientific data demonstrates that the exploitable raw material reserves of *F. varia* and *F. foetida* in Uzbekistan are undergoing a significant decline.

REFERENCES

Ahmadi, K. S., Hadjiakhoondi, A., Delnavazi, M. R., Tofighi, Z., Ajani, Y., and Kiashi, F. (2020). Chemical composition and biological activity of Ferula aucheri essential oil. Res. J. Pharmacogn. 7 (2), 21–31. doi:10.22127/RJP. 2020.210354.1537

Ilkhom Mukumov, Zebunisso Nomozova, Murtazo Hasanov, Nodira Nurullayeva, Zebokhon Rasulova Genus *Ferula* L. In The Flora Of The Hissar Ridge. E3S Web of Conferences 650, 02002 (2025) ICENIS https://doi.org/10.1051/e3sconf/202565002002

F. Djumaniyozova, A. Nurniyozov, I. Mukumov. Features of the distribution of species of the genus Ferula L. on the territory of the Turan lowland. E3S Web of Conferences 510, 03008 (2024). https://doi.org/10.1051/e3sconf/202451003008.

Jing Yi Zhao, Xin Yong Guo, Zhi Jia Tian. Transcriptome and metabolome analysis of the regulatory network of bioactive compounds synthesis in different growth stages of two medicinal edible Ferula. Scientia Horticulturae 338 (2024) 113770. https://doi.org/10.1016/j.scienta.2024.113770

Plants of the World Online [electronic resource] URL. www. powo.science.kew.org

Poonam Mahendra, Shradha Bisht. Ferula asa foetida: Traditional uses and pharmacological activity. Pharmacognosy Reviews. July-December (2012) Vol 6. Issue 12.

Ravi Kumar, Niketa Yadav Dinesh Kumar, Amit Rana, Sanatsujat Singh, Ramesh Chauhan, Ashok Kumar, Satbeer Singh. Ferula assa-foetida L., an important Central and South Asian traditional spice and medicinal herb: A comprehensive review. Journal of Applied Research on Medicinal and Aromatic Plants 41 (2024) 100548. https://doi.org/10.1016/j.jarmap.2024.100548

Shailja Choudhary, Bhawna Walia, Gitika Chaudhary. Ferula asafetida (Hing): A Review Based Upon its Ayurvedic and Pharmacological Properties. Int. J. Pharm. Sci. Rev. Res., 68(2), Article No. 06, Pages: 31-39. DOI link: (2021) http://dx.doi.org/10.47583/ijpsrr.2021.v68i02.006

Ubaid Yaqoob, Irshad Ahmad Nawchoo. Distribution and Taxonomy of Ferula L.: A Review. Research & Reviews: Journal of Botany. 15-23 © STM Journals 2016. All Rights Reserved. ISSN: 2278-2222(online) Volume 5, Issue 3. (2016)

Z.Jumayeva, N.Nurullayeva, A.Nozimova, X.Tursunboev, G.Dosjanova. Dynamics and characteristics of allergenic plant pollen in the Republic of Uzbekistan. E3S Web of Conferences 498, 02015 (2024) https://doi.org/10.1051/e3sconf/202449802015.

Zahra Aghaali, Jun-Li Yang, Mohammad Reza Naghavi, MeisamZargar. Removing limitations surrounding terpenoid biosynthesis by biotechnological techniques in Ferula sp.: A review. Current Plant Biology 41 (2025) 100455.https://doi.org/10.1016/j.cpb.2025.100455

Vinogradova V.M. Genus Ferula L. (Apiaceae) in Central Asia. News of the System of Higher Plants. Leningrad, 1990. 27, pp. 113-120. In Russian.

Korovin E.P. Umbelliferae. In: Flora of Uzbekistan. Tashkent, 1959. Vol. 4, pp. 257-470. In Russian.

Melibaev S. Biology and Resources of *Ferula tenuisecta* Korov. and *F. kuhistanica* Korov. as Sources of Estrogenic Preparations. Abstract of Cand. Dissertation. Tashkent, 1985. 21 p. In Russian.

Key to the Plants of Central Asia. Critical summary of flora. In volumes I-XI. Tashkent: Fan, 1968 – 2016. In Russian.

Pimenov M.G., Demidova L.S., Pimenova M.E., Sdobnina L.I. Raw material reserves of the Siberian swollen carp in the south-eastern Transbaikalia // Rast. resources. 1976. T.12, issue. 3, pp. 329-339. In Russian.

Pimenov M.G., Klyuykov E.V. Umbelliferae of Kyrgyzstan. Moscow, ed. KMK Moscow, 2002. 286 p. In Russian.

Pimenov M.G., Ostraumova T.A. Umbelliferae of Russia. Moscow, 2012. p.8. In Russian.

Pupykina K.A., Khasanova S.R., Kudashkina N.V., Galiakhmetova E.Kh., Shakirova P.P. Resource science and standardization of medicinal plant materials. Ufa: Russia; 2019. 117 p. In Russian.

ASSESSMENT OF ORGANIC POLLUTION AND BDI TREND IN THE ERZEN RIVER, ALBANIA (2014–2024)

Vjola Saliaga[1], Vjola Bakillari[1], Seit Shallari[1], Ferdi Brahushi[1], Fatbardh Sallaku[1], Ilir Kristo[1]

[1]Agricultural University of Tirana, Faculty of Agriculture and Ecology. Tirana, Albania

Corresponding Author email: violasaliaga@gmail.com

ABSTRACT

The rapid increase of economic activities including agriculture, industrial development, uncontrolled gravel abstraction and unregulated urban wastewater discharges and lack of adequate infrastructure and management, has significantly increased pressure on rivers quality in Albania, thereby contributing to enhanced pollution levels. Land use particularly nearby rivers for different industrial activities and agriculture represent one of major sources of many organic and inorganic pollutants in surface and groundwater. Meanwhile untreated municipal and industrial wastewater can significantly affect the ecological functioning of river ecosystems. This study aims to assess the long-term variation of organic pollution in the Erzeni River during 2014–2024 using the biodegradability index (BDI), calculated as the ratio of five-day biochemical oxygen demand to chemical oxygen demand (BOD_5/COD). Monitoring data covering the study period, reported in the annual environmental status reports published by the Albanian National Environmental Agency (NEA), together with the pressure analysis presented in the official Erzen River Basin Management Plan, were analyzed for two representative official monitoring sites. The results indicate persistent presence of organic pollution, particularly in areas affected by urban, industrial, and agricultural pressures. Individual BOD_5 concentrations range from 5 to 20 mg/L, with no clearly distinguishable seasonal pattern. BDI values showed relatively limited interannual variation and generally ranged between 0.5 and 0.6. The highest individual BDI (0.89) was observed in 2021 and the lowest (0.38) in October 2014. The predominance of BDI values above 0.5 indicates that a substantial proportion of the organic matter present in the river was readily biodegradable. However, the continued occurrence of measurable BOD_5 and COD concentrations throughout the studied period suggests persistent organic inputs. The EU WFD promotes the integrated management of water resources to support environmentally sustainable development and reduce pressures associated with excessive water abstraction and pollution. Albania has transposed such requirements in the national legislation and continuous to improve secondary legislation to better manage pollution control, environmental permitting, and water quality monitoring. Nevertheless, effective implementation of these requirements depends on robust monitoring systems, well-equipped laboratories, and clear data-sharing mechanisms. At present, these prerequisites are only partially established and operational. An integrated management approach is therefore required to (i) reduce organic and nutrient loads originating from urban wastewater discharges and agricultural activities, (ii) identify and control of heavy metal sources (urban/industrial sources), including the role of sediments in their accumulation and potential remobilization; and (iii) improve monitoring programmes through the systematic inclusion of WFD priority substances, thereby enabling a comprehensive and WFD-compliant water quality assessment of the Erzeni River.

Keywords: River pollution, BOD/COD ratio, freshwater quality assessment.

INTRODUCTION

EU Water Framework Directive representing the fundamental legal act in shaping the water management sector since 2000 across the European countries, foresees an analysis of anthropogenic impact, as a cyclical process, in the context of the river basin management planning (1). In Albania, this approach is embedded in the national legislation therefore chemical, and not only, pollution should be frequently measured and adequately controlled. This study aims to assess the long-term variation of organic pollution in the Erzen river using the biodegradability index (BDI), calculated as the ratio of BOD/COD, where both parameters represent routine analyses of the water quality and are significantly important in controlling the total content of pollution and the management of water environment (2).
The BDI must be smaller or equal to 1.0; the higher the value, the more serious the pollution of organic matter and the higher the level of biodegradability (3), (4); (5). Rivers are often considered a sink and source of many pollutants (6) and especially if there are discharges of industrial and/or urban wastewaters induced in the water system, they show high levels of BOD_5 and COD. High presence of organic matter in water leads to a decrease of dissolved oxygen due to consumption.

Official datasets for BOD_5 and COD concentrations during 2014–2024, as published by responsible authorities in regular reports, were analyzed in two NEA representative official monitoring sites. Albania has transposed EU WFD requirements in the main but its effective implementation however depends on robust monitoring systems, well-equipped laboratories and clear data-sharing/reporting mechanisms to ensure a better pollution control management, environmental permitting tools and adequate water quality monitoring. At present, these prerequisites are only partially established.

MATERIAL AND METHOD

Two NEA representative official monitoring sites were selected for this study (Ura Beshirit and Ura Sallmonaj) based on the analysis of pressures presented in the official river basin management plan including agriculture, various industrial activities and gravel mining upstream. Data series between 2014 – 2024, as officially reported by NEA through yearly environmental status reports (7) and the official river basin management plan for Erzen river basin (8) were analyzed and selected data have been plotted to identify BDI trend and potentially asses changes in pollution patters during these years.

Yearly individual mean data of the two selected monitoring sites were analyzed to observe any differences on BDI and be able to judge over the level of pollution. According to official reports, water samples have been taken on irregular seasonal basis over the years, between two to four times per year. All BOD > COD values were excluded to ensure credibility of the results and respective BDI ratio is not considered in the trend analysis.

RESULTS AND DISCUSSION

Individual BOD_5 values range from 5 to 20 mg/L, with no clearly distinguishable seasonal pattern. BDI values showed relatively limited interannual variation and generally ranged between 0.5 and 0.6. The highest individual BDI (0.89) was observed in 2021 and the lowest (0.38) in October 2014. The predominance of BDI values above 0.5 (Table 1) indicates that a substantial proportion of the organic matter present in the river was readily biodegradable.

Table 1 BDI Mean values for both official monitoring sites

Measurement	Year/Month	EbeM1-31 BDI	EsaM1-31 BDI
EM1	Apr-14	0.5	0.14
EM2	Jun-14	0.5	0.56
EM3	Aug-14	0.38	0.41
EM4	Mar-15	0.56	0.56
EM5	Sept-15	0.58	0.56
EM6	Nov-15	0.59	0.5
EM7	Feb-16	0.6	0.67
EM8	Apr-16	0.54	0.57
EM9	Aug-16	0.50	0.62
EM10	Oct-16	1	
EM11	May-17	1	1
EM12	Oct-17	0.64	0.63
EM13	Feb-18	1	1
EM14	Jul-18	1	1
EM15	Nov-18	0.62	0.58
EM16	Mar-19	0.03	0.57
EM17	May-19	0.07	0.63
EM18	Oct-19		0.56
EM19	Dec-19	0.40	
EM20	Feb-20	0.54	0.61
EM21	Apr-20	0.83	1
EM22	Oct-20	0.57	0.57
EM23	Mar-21	0.36	0.46
EM24	Oct-21	0.59	0.61
EM25	Mar-22	0.67	0.6
EM26	Sept-22	0.6	1
EM27	May-23	0.71	0.6
EM28	Sept-23	0.4	0.57
EM29	May-24	0.57	0.58
EM30	Oct-24	0.6	0.44
EM31	Dec-24	0.69	0.59

The BOD and COD fluctuates at both monitoring sites through the years and also on seasonal basis. (9) argues that this might be due to organic matter which comes from anthropogenic activities active in the study area (e,g plant extracts, solid wastes dumping, sewage discharges, and agricultural run-off. When BDI values range between 0.3 – 0.6 it confirms that the pollutants in waters belong to slow degradable category and >0.6 they are biodegradable (10). Results indicate persistent presence of organic pollution, particularly in areas affected by urban, industrial, and agricultural pressures and the continued occurrence of measurable BOD_5 and COD concentrations throughout the studied period suggests persistent organic inputs. BDI mean value, combining both monitoring sites increases through the years, particularly visible from 2014 to 2016 (
Figure 1).
In a snapshot overview the trend is stable after 2022 showing lower values compared to an increased one before 2020. Nevertheless, the overall trend is near to 0.5 is mostly associated with consistent discharges of urban waters and agricultural activities in the areas nearby the river area.

Few cases were observed where the individual concentrations of BOD_5 and COD were excluded from the BDI analysis due to information inconsistency.

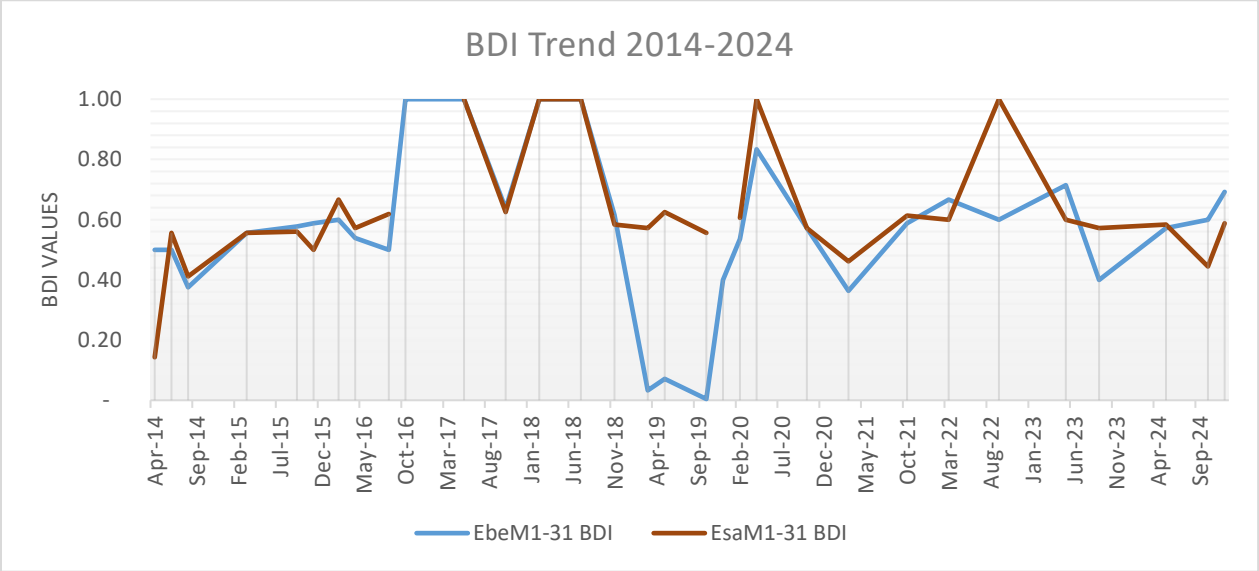

Figure 1 BDI trend concentration during 2014-2024

CONCLUSIONS

The predominance of BDI values above 0.5 indicates that a substantial proportion of the organic matter present in the river was readily biodegradable. Continued occurrence of measurable BOD_5 and COD concentrations throughout the studied period suggests persistent organic inputs. Higher BDI values in longer periods of time observed in the second monitoring site. An integrated management approach is therefore required to reduce organic and nutrient loads originating from urban wastewater discharges and agricultural activities, to identify and control of heavy metal sources (urban/industrial sources), including the role of sediments in their accumulation and potential remobilization, and to improve monitoring programmes through the systematic inclusion of WFD priority substances.

REFERENCES

1]. EU. EU Water Framework Directive 2000/60/EC. 2000.
[2]. The testing of Chemical Oxygen Demand (COD) and Biological Oxygen Demand (BOD) of river water in Cipager Cirebon. Prambudy, H. Supriyatin, T. Setiawan , F. s.l. : IOP Publishing. Purpose LED Publishing. Conference sweries. , 2019.
[3]. Relationship, importance, and development of analytical techniques: COD, BOD, and, TOC in water—An overview through time. Aguilar Torrejón J.A., Balderas Hernández P., Roa Morales G., Barrera Díaz C.E., Rodríguez Torres I., Torres Blancas T.,. s.l. : SN Applied Sciences. A Springer Nature Journal , 2023, Vol. 5:118.
[4]. REVIEW ON BOD, COD AND BOD/COD RATIO: A TRIANGLE ZONE FOR TOXIC, BIODEGRADABLE AND STABLE LEVELS. Samudro, G. and Mangkoedihardjo, S. 4, s.l. : Research Gate, 2010, INTERNATIONAL JOURNAL Of ACADEMIC RESEARCH, Vol. 2.
[5]. Li, D. Sh. Liu. Water Quality Monitoring in Aquaculture. [book auth.] Daoling Li. Water Quality Monitoring and Management: Basis, Technology and Case Studies. s.l. : ELSEVIER. ISBN 978-0-12-811330-1, 2019, 12.
[6]. Dilution or enrichment: the effects of flood on pollutants in river waters. Zhou, M., et al. s.l. : Springer. Environmental Sciences Europe., 2022, SpringerOpen, Vol. 34:61.
[7]. AKM, Agjencia Kombetare e Mjedisit. Environmental Status Reports 2010-2020.
[8]. Ujore, Agjencia e Menaxhimit te Burimeve. Erzen River Basin Management Plan. AMBU. 2023. Official Plan.
[9]. Appraisal of seasonal variations in water quality of river Cauvery using multivariate analysis. Sharma, T R. Ravichandran, C. 1, s.l. : Informa UK Limited, trading as Taylor & Francis Group, 2021, Water Science ISSN: 2357-0008, Vol. 35, pp. 49-62.
[10]. Assessment of Organic Pollutant Index and Biodegradability Index in Determining River Pollution Load. Setyawan, A. Muhammad, F. Hermawan, F. s.l. : Purpose Led Publishing. IOP Conferences Series. , 2024, Earth and Environmental Science., Vol. 1414.

EFFECT OF PLANTING DENSITY AND NUMBER OF STEMS ON THE YIELD OF THE HAZELNUT CULTIVAR 'ATA-BABA' IN AZERBAIJAN

Ayhan AHMADOV[1], Huseyn IDRISOV[1]

[1] Azerbaijan State Agricultural University, Agronomy Faculty, Horticulture Department, Ganja, Azerbaijan

Corresponding author e-mail: ayhan.ehmedov@gmail.com

ABSTRACT

This study was conducted to determine the effects of planting density and stem number on yield and pomological characteristics of the local hazelnut (*Corylus avellana* L.) cultivar 'Ata-baba' under the ecological conditions of Azerbaijan during 2023-2025. The experiment was established at the Zagatala Experimental Station using two planting schemes (6×7 m and 7×3 m) and different stem number treatments (7, 15, and 20 stems for 6×7 m; 4, 8, and 12 stems for 7×3 m). Growth parameters, leaf area, stem thickening, fruit weight, kernel ratio, kernel weight, nut number per husk, and yield per shrub and per hectare were evaluated. The results showed that leaf area generally decreased with increasing stem number among the regulated treatments, and was lowest of all in the untreated control. Stem thickening was generally highest in south-facing stems among the managed treatments, though this pattern did not hold in the untreated control. In the 7×3 m scheme, the highest yield per shrub was obtained from the 12-stem treatment (5.389 kg), whereas in the 6×7 m scheme the 15-stem treatment produced the highest yield (9.981 kg); yield in the untreated control remained lower than in any managed treatment in both schemes (3.485 kg and 5.861 kg, respectively, in 2024). Kernel ratio was highest at moderate stem densities, while fruit weight was highest at low-to-moderate densities depending on planting scheme; both were substantially higher in all managed treatments than in the untreated control, whose kernel ratio remained around 37-38% regardless of scheme or year. Yield per hectare increased with higher planting density despite slight reductions in individual nut traits. However, yield in 2025 was lower than in 2024, likely due to climatic factors and increased damage from the brown marmorated stink bug. Overall, the findings indicate that optimal stem number depends on planting density, and moderate stem densities (12 stems in 7×3 m and 15 stems in 6×7 m) provide the best balance between vegetative growth, yield, and nut quality for the 'Ata-baba' cultivar in Azerbaijan.

Keywords: *Corylus avellana* L., 'Ata-baba', planting density, stem number, hazelnut yield, Azerbaijan, Brown Marmorated Stink Bug.

INTRODUCTION

European hazelnut (*Corylus avellana* L.), a species belonging to the *Betulaceae* family, is a perennial shrub that has been cultivated in Azerbaijan since ancient times. Azerbaijan is among the leading hazelnut-producing countries in the world, with the main production concentrated in the northern regions of the country. Most of the hazelnut production in the country is carried out by small-scale farms, where the plants are cultivated in a multi-stem shrub form similar to the "ocak" system in Turkiye (Islam, 2018; Ahmadov, 2025). Smallholder farmers account for 60-70% of the country's total annual hazelnut output, and Zagatala together with the surrounding northwestern districts supplies the majority of national production (FAO, 2023).

Naturally reaching heights of 3-10 meters and capable of producing numerous suckers (Mehlenbacher, 1991), the European hazelnut in Azerbaijan has traditionally been propagated by separating root suckers from the parent plant. Due to its prolific sucker production, it is typically cultivated with a varying number of stems per plant. Because suckering aptitude varies among cultivars and continues throughout the growing season, regular removal of unwanted suckers is considered essential for keeping stem number and canopy density under control in multi-stemmed hazelnut orchards (Pacchiarelli et al., 2022).

In other countries, different training systems and corresponding planting schemes are applied for hazelnut cultivation (Beyhan, 2007). High planting density increases competition among plants for resources such as light, water, and nutrients, which may reduce yield and nut quality. However, with proper management, it is possible to maintain high yield and nut quality even at higher planting densities (Portarena et al., 2024).

Traditionally, hazelnut is grown in a multi-stem bush form in Turkiye, Italy, and Spain. When mechanical harvesting is intended, trees are trained on a single trunk. Some newly established young orchards in Oregon State, certain European countries, and other hazelnut-producing nations are being cultivated using the Vase training system (Baldwin, 2015). This shift away from the traditional multi-stemmed shrub form is largely driven by the goal of improving light penetration into the canopy and enabling mechanized orchard operations, even though multi-stemmed systems remain widespread in the Mediterranean basin and allow gradual plant renewal through sucker selection (Pacchiarelli et al., 2026).

Although numerous studies have been conducted on hazelnut planting density and training systems (Bignami et al., 2004; Beyhan, 2007; Ellena et al., 2012; Sokol, 2017; Balta et al., 2024; Portarena et al., 2024; Pacchiarelli et al., 2025), there appears to be a lack of sufficient research in this area within our country.

The main objective of the study is to investigate the yields of the Ata-baba hazelnut cultivar, which is the main cultivar grown in Azerbaijan, under different planting schemes and with different stem numbers during the 2023-2025 period, and to determine the most suitable number of stems for each planting scheme. During the research, additional vegetative and fruit parameters were also measured.

MATERIAL AND METHOD

The research was conducted during 2023-2025 in a hazelnut orchard located at the Zagatala Experimental Station of the Research Institute of Horticulture and Tea Growing. As the experimental material, plants of the local hazelnut cultivar *Ata-baba* were used under two different planting schemes (6×7 m and 7×3 m). For each planting scheme, different stem number treatments were determined. For the 6×7 m planting scheme, stem number treatments of 7, 15, and 20 stems were applied, while for the 7×3 m planting scheme, 4, 8, and 12 stems were selected. In addition, one untreated control variant for each scheme was included in the study. The control variant consisted of shrubs within the same planting scheme in which the number of stems had not been regulated and no systematic agrotechnical management practices had been applied. For each stem number treatment, 4 shrubs were chosen (8 shrubs in total with two replications).

In November 2023, the selected plants were pruned according to the predetermined stem numbers. During pruning, excess stems, including suckers, were removed, and only the specified number of stems was retained. Suckers were pruned twice a year, in November and July.

To determine annual stem thickening, stem circumference measurements were taken at the beginning and end of the vegetation period. Circumference was measured at 1 m above ground level for four stems located in four different directions using a flexible measuring tape (cm), and the measurement points were marked with oil-based paint (Figure 1). The same point was re-measured at the end of the vegetation period (after leaf fall and before pruning). Annual lateral thickening (ΔC) was calculated as follows:

$$\Delta C = C_2 - C_1 \quad (1)$$

Where: C_1 is the circumference measured at the beginning of the vegetation period (cm);

C_2 is the circumference measured at the end of the vegetation period (cm).

Leaf area was calculated using the leaf area estimation formula proposed by Cristofori et al. (2007):

$$LA = 2.59 + 0.74LW \quad (2)$$

Where: LA is leaf area (cm^2);

L is leaf length;

W is leaf width.

The first harvest was carried out on 4 September 2024 and on 5 September 2025. Fruits were collected manually from the ground by shaking the stems and were separated into husked and dehusked nuts, placed into separate bags according to stem number and planting scheme. On the same day, nuts were dehusked and weighed using an electronic balance with a sensitivity of 0.001 kg, and yields were recorded for each treatment. Harvesting was repeated five times at four-day intervals.

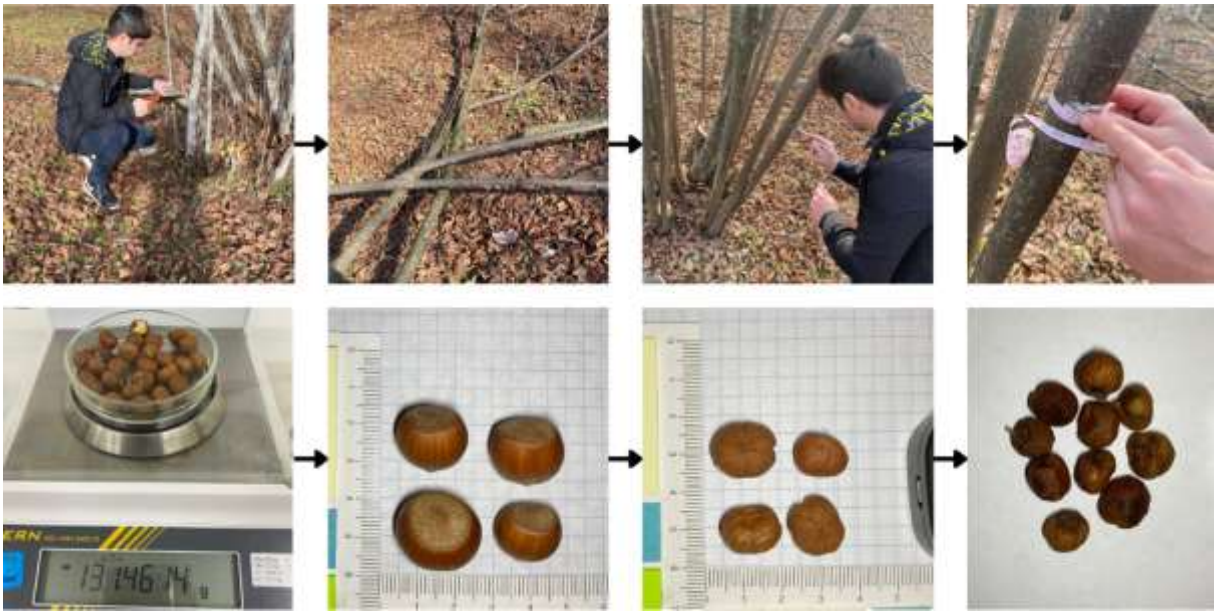

Figure 1. Sequential steps of the experimental workflow for field data collection and morphological characterization of *Corylus avellana* L. cv. Ata-baba

After the final harvest and weighing, yield per individual shrub was determined, and mean yield was calculated for each treatment.

In both years, the number of nuts per husk, nut and kernel weight, kernel percentage, and the percentages of empty and rotten nuts were determined, allowing the calculation of the percentage of healthy nuts. In recent years, the intensity of the brown marmorated stink bug has increased in the country, resulting in higher levels of damaged and rotten nuts.

Nut and kernel weights were determined by weighing 100 nuts using a balance with 0.01 g sensitivity. Kernel yield was calculated as the ratio of kernel weight to nut weight.

Data were analyzed separately for each planting scheme using one-way Analysis of Variance (ANOVA), with stem number (including the untreated control) as the factor. Where ANOVA indicated significant differences ($p<0.05$), Duncan's Multiple Range Test was performed to separate the means and identify the most productive stem densities. The analyses were conducted using SPSS Statistics (IBM Corp., Version 26.0, Armonk, NY, USA).

RESULTS AND DISCUSSION

Leaf area varied depending on the number of stems and the planting scheme, and in general it was higher at lower stem numbers. In the 7×3 planting scheme, the highest leaf area was recorded in the treatment with 4 stems (121.5 cm²). This was followed by the 12-stem (86.8 cm²) and 8-stem (85.2 cm²) treatments, which were close to each other. In the 6×7 planting scheme, the highest leaf area was observed in the 7-stem treatment (108.4 cm²), followed by the 15-stem treatment (92.6 cm²) and the 20-stem treatment (84.5 cm²). The untreated control recorded the lowest leaf area of all variants in both planting schemes, at 75±6.27 cm² in the 7×3 m scheme and 80.6±9.13 cm² in the 6×7 m scheme. This pattern is consistent with findings that denser hazelnut canopies intercept less photosynthetically active radiation at the lower and inner canopy levels, which limits leaf expansion and reduces fruit number and weight compared with more open canopy structures (Gutiérrez-Gamboa et al., 2025).

Table 1. Average Leaf Area (cm^2) of Hazelnut Cultivar ‘Ata-baba’ Under 7×3 m and 6×7 m Planting Schemes with Different Stem Numbers

Average leaf area (cm²) under the 7×3 planting scheme			
4 stems	**8 stems**	**12 stems**	**Control**
121.5±12.06	85.2±5.30	86.8±6.88	75±6.27
Average leaf area (cm²) under the 6×7 planting scheme			
7 stems	**15 stems**	**20 stems**	**Control**
108.4±8.32	92.6±5.08	84.5±4.71	80.6±9.13

Differences were observed in stem thickening depending on stem orientation. In all treatments of the 6×7 planting scheme, except for the 20-stem treatment and control, the greatest thickening was observed in south-facing stems, while the least thickening generally occurred in north-facing stems. The second highest thickening was recorded in east-facing stems, followed by west-facing stems. In the 7×3 planting scheme, the greatest stem thickening was observed in the south-facing stems of the 4-stem treatment (2.98 cm), whereas among the stem-number treatments the lowest thickening was recorded in the north-facing stems of the same treatment (1.04 cm); the untreated control showed even less thickening overall, with the smallest change recorded in the east-facing stems (0.03 cm). In the 6×7 planting scheme, the highest thickening was observed in the south-facing stems of the 15-stem treatment (3.14 cm), while among the stem-number treatments the lowest thickening was recorded in the east-facing stems of the 7-stem treatment (0.72 cm), the control again showed minimal thickening in all directions, with the smallest change recorded in the east-facing stems (0.03 cm).

Table 2. Annual Circumferential Stem Thickening (cm) across Different Cardinal Directions Under the 7×3 m and 6×7 m Planting Schemes

Circumferential stem thickening under the 7×3 planting scheme												
North-facing				**South-facing**			**East-facing**			**West-facing**		
Stem number	**2024 (cm)**	**2025 (cm)**	**Change (cm)**	**2024 (cm)**	**2025 (cm)**	**Change (cm)**	**2024 (cm)**	**2025 (cm)**	**Change (cm)**	**2024 (cm)**	**2025 (cm)**	**Change (cm)**
4	22.39	23.42	1.04	21.85	24.84	2.98	23.64	26.47	2.83	19.75	21.04	1.29
8	24.87	26.12	1.26	18.90	21.63	2.73	19.56	22.01	2.45	21.23	22.77	1.54
12	18.24	19.78	1.54	17.77	20.57	2.79	20.1	22.26	2.17	16.58	18.78	2.2
Control	17.59	17.68	0.09	16.18	16.34	0.16	19.16	19.19	0.03	14.14	14.58	0.44
Circumferential stem thickening under the 6×7 planting scheme												
North-facing				**South-facing**			**East-facing**			**West-facing**		
Stem number	**2024 (cm)**	**2025 (cm)**	**Change (cm)**	**2024 (cm)**	**2025 (cm)**	**Change (cm)**	**2024 (cm)**	**2025 (cm)**	**Change (cm)**	**2024 (cm)**	**2025 (cm)**	**Change (cm)**
7	22.61	23.61	1.00	20.98	22.70	1.73	19.19	19.91	0.72	17.58	18.87	1.29
15	18.97	20.94	1.98	19.19	22.33	3.14	14.79	17.77	2.98	19.94	22.33	2.39
20	18.49	21.13	2.64	17.58	20.13	2.54	13.66	16.55	2.89	13.91	16.61	2.70
Control	12.88	13.26	0.38	18.22	18.31	0.09	16.18	16.21	0.03	17.44	17.5	0.06

Compared to 2024, fruit weight was higher in all treatments in 2025. Under the 7×3 planting scheme, the highest mean fruit weight was recorded in the 4-stem treatment (1.84 g), whereas under the 6×7 planting scheme it was observed in the 15-stem treatment (2.15 g). The lowest fruit weight in the 7×3 scheme was found in the 12-stem treatment in 2024 (1.64 g); in 2025, however, the untreated control recorded the lowest fruit weight of all variants (1.68 g), just below the 12-stem treatment (1.71 g). Under the 6×7 planting scheme, the lowest fruit weight in both years was consistently found in the 20-stem treatment (1.86-1.91 g), remaining lower than the control (1.97-2.01 g).

An increase in kernel percentage was also observed in the second year compared with the first year. The highest kernel percentage was recorded in the 12-stem treatment under the 7×3 planting scheme (54.88%) and in the 15-stem treatment under the 6×7 planting scheme (56.86%). Among the stem-number treatments, the lowest kernel percentage was observed in the 8-stem treatment under the 7×3 planting scheme (46.97-52.94% across years) and in the 20-stem treatment under the 6×7 planting scheme (49.05-49.16% across years). The untreated control, however, recorded by far the lowest kernel percentage overall: only 38.03-38.08% in the 7×3 scheme and 37.06-38.04% in the 6×7 scheme, roughly 9-19 percentage points below every managed treatment.

Table 3. Yield Performance and Pomological Characteristics of Cultivar ‘Ata-baba’ Under Different Planting Schemes and Stem Densities (2024-2025)

Fruit weight, kernel ratio, and kernel weight under the 7×3 planting scheme								
	2024				**2025**			
№	**4 stems**	**8 stems**	**12 stems**	**Control**	**4 stems**	**8 stems**	**12 stems**	**Control**
Fruit weight (g)	1.79±0.12^{a}	1.67±0.14^{b}	1.64±0.13^{b}	1.67±0.14^{b}	1.84±0.11^{a}	1.81±0.14^{a}	1.71±0.11^{b}	1.68±0.09^{b}
Kernel ratio (%)	50.4±2.04^{a}	46.97±1.04^{b}	50.62±1.53^{a}	38.08±1.59^{c}	53.76±1.36^{a}	52.94±0.97^{a}	54.88±1.35^{a}	38.03±1.4^{b}
Kernel weight (g)	0.913±0.06^{a}	0.790±0.07^{c}	0.837±0.05^{b}	0.641±0.05^{d}	0.999±0.07^{a}	0.963±0.07^{ab}	0.948±0.09^{b}	0.645±0.06^{c}
Shell thickness	1.06±0.12^{a}	1.07±0.15^{a}	0.93±0.1^{b}	1.07±0.09^{a}	1.07±0.19^{b}	1.13±0.18^{ab}	1.01±0.16^{c}	1.18±0.13^{a}
Nut number per husk	2.2±0.64^{a}	2.2±0.7^{a}	2.02±0.77^{ab}	1.78±0.79^{b}	2.16±0.82^{a}	1.92±0.67^{ab}	1.88±0.75^{ab}	1.66±0.75^{b}
Average yield (kg)	3.537±0.49^{c}	4.663±0.58^{b}	5.389±0.54^{a}	3.485±0.93^{c}	3.342±0.51^{b}	4.090±0.69^{a}	4.572±0.67^{a}	3.275±0.87^{b}
Yield per hectare (kg)	1684±232	2220±276	2565±259	1659±444	1591±240	1947±330	2176±318	1559±412
Fruit weight, kernel ratio, and kernel weight under the 6×7 planting scheme								
	2024				**2025**			
№	**7 stems**	**15 stems**	**20 stems**	**Control**	**7 stems**	**15 stems**	**20 stems**	**Control**
Fruit weight (g)	2.07±0.16^{a}	2.09±0.13^{a}	1.86±0.14^{c}	1.97±0.15^{b}	2.12±0.14^{a}	2.15±0.15^{a}	1.91±0.12^{c}	2.01±0.14^{b}
Kernel ratio (%)	49.05±0.74^{b}	53.41±1.63^{a}	49.05±1.26^{b}	37.06±0.23^{c}	52.14±2.61^{b}	56.86±0.97^{a}	49.16±0.82^{c}	38.04±1.08^{d}
Kernel weight (g)	0.997±0.09^{b}	1.097±0.08^{a}	0.927±0.07^{c}	0.738±0.06^{d}	1.042±0.06^{b}	1.242±0.1^{a}	0.956±0.05^{c}	0.761±0.05^{d}
Shell thickness	1.08±0.1^{a}	0.94±0.15^{b}	1.08±0.11^{a}	1.08±0.14^{a}	1.1±0.18^{a}	1.01±0.15^{b}	1.11±0.15^{a}	1.13±0.19^{a}
Nut number per husk	2.16±0.79^{ab}	1.98±0.8^{b}	2.38±0.78^{a}	1.94±0.87^{b}	2.14±0.67^{a}	1.92±0.75^{ab}	2.2±0.78^{a}	1.8±0.78^{b}
Average yield (kg)	6.571±0.59^{b}	9.981±2.03^{a}	9.71±0.96^{a}	5.861±1.37^{b}	6.025±1.33^{b}	9.07±0.80^{a}	8.275±1.61^{a}	5.021±1.34^{b}
Yield per hectare (kg)	1564±140	2375±482	2311±229	1395±326	1434±316	2159±189	1969±383	1195±320

Under the 7×3 planting scheme, the highest kernel weight was recorded in the 4-stem treatment (0.999 g), while the lowest among the stem-number treatments was in the 12-stem treatment (0.948 g). The untreated control recorded the lowest kernel weight overall (0.641-0.645 g). Under the 6×7 planting scheme, the highest kernel weight was observed in the 15-stem treatment (1.242 g), and the lowest among the treatments in the 20-stem treatment (0.956 g), with the control again recording the lowest value overall (0.738-0.761 g).

The number of stems per plant did not demonstrate a consistent or significant linear correlation with the number of nuts per husk across the experimental periods. In the 7×3 planting scheme, a marginal downward trend was observed as stem density increased (e.g., from 2.2 to 2.02 in 2024). However, this pattern was not replicated in the 6×7 scheme, which exhibited a non-linear relationship where the mid-range density (15 stems) produced the fewest nuts per husk (1.98 in 2024 and 1.92 in 2025) before increasing again at 20 stems.

In a related study, Bak and Karadeniz (2021) investigated different stem numbers across two hazelnut cultivars and reported that fruit and kernel weights typically decrease as the number of stems increases. While our findings in the 7×3 planting scheme align with this observation, the 6×7 scheme showed a distinct deviation from this trend. Furthermore, while Bak and Karadeniz (2021) noted that the number of nuts per husk increases with higher stem counts, our results indicated a more stable or non-linear response, suggesting that planting density and layout may influence these parameters differently.

Differences were observed in yield indicators among planting schemes and stem numbers. Overall, yield values in 2025 were lower compared to 2024. This is thought to be related both to climatic conditions and to the increasing spread of the Brown Marmorated Stink Bug, which has become a serious problem in Azerbaijan in recent years. Year-to-year climatic variability, particularly temperature fluctuations during the growing season, has similarly been identified as a significant driver of interannual hazelnut yield variation in other production regions (An et al., 2020; Ahmadov, 2024).

Under the 7×3 planting scheme, the highest yield was recorded in the 12-stem variant (5.389 kg), followed by the 8-stem (4.663 kg) and 4-stem (3.537 kg) variants; yield in the untreated control was lower still (3.485 kg). In the 6×7 planting scheme, the highest yield was observed in the 15-stem variant (9.981 kg), followed by the 20-stem (9.71 kg) and 7-stem (6.571 kg) variants, with the untreated control again yielding the least (5.861 kg).

According to the 7×3 planting scheme, yield per hectare for the 4-stem variant in 2024 and 2025 was 1684±232 kg and 1591±240 kg, respectively; for the 8-stem variant, 2220±276 kg and 1947±330 kg; for the 12-stem variant, 2565±259 kg and 2176±318 kg; and for the control 1659±444 kg and 1559±412 kg respectively. In the 6×7 planting scheme, yield per hectare was 1564±140 kg and 1434±316 kg for the 7-stem variant, 2375±482 kg and 2159±189 kg for the 15-stem variant, 2311±229 kg and 1969±383 kg for the 20-stem variant and 1395±326 kg and 1195±320 kg for the control in 2024 and 2025, respectively.

Portarena et al. (2024) report that although yield efficiency is highest under medium-density planting, the highest yield per hectare is observed under high-density planting. Bignami et al. (2004) also state that high plant density is associated with higher productivity. Erdoğdu (2025) notes that productivity in the early years is higher in denser plantings, while in later years it is possible to maintain yield stability through different horticultural management methods. Balta et al. (2024) also report a positive correlation between plant density and yield per hectare.

It should be noted that yield was expressed as fresh weight, since it was measured immediately after harvest.

Özpınar and Yıldırım (2025) note that the damage rate of the brown marmorated stink bug is closely related to its population density. They report that the damage rate ranged between 31% and 53% during 2023-2024 in Türkiye. This pest is now recognized as a major global threat to

tree fruit and nut crops, and rising temperatures associated with climate change are expected to further favor its spread and the number of generations it completes per year (Pajač Beus et al., 2024). In hazelnut orchards specifically, direct feeding on developing kernels by the brown marmorated stink bug has been shown to cause substantial economic losses, underlining the need for integrated monitoring and management programs as the pest becomes established in new production regions such as Azerbaijan (Walton et al., 2022).

Table 4. Percentage of Normal and Abnormal Fruits of Ata-baba Cultivar (2024-2025)

Variant	**Normal (%)**	**Semi-damaged (%)**	**Empty (%)**	**Rotten (%)**	**Twin (%)**
2024					
Ata-baba (6×7)	88.52	4.09	3.51	3.22	0.64
Ata-baba (7×3)	83.07	2.88	11.18	2.56	0.32
2025					
Ata-baba (6×7)	79.64	7.58	4.39	7.58	0.80
Ata-baba (7×3)	78.62	4.61	13.28	3.22	0.27

CONCLUSIONS

Planting density and stem number significantly affected vegetative growth, yield, and nut characteristics of the 'Ata-baba' hazelnut cultivar under Azerbaijani conditions. Among the regulated treatments, leaf area decreased as stem number increased, and leaf area was lowest of all in the untreated control. Stem thickening was generally greatest in south-facing stems among the managed treatments, although this pattern did not hold in the untreated control, where north-facing stems thickened most in the 6×7 m scheme. Under the 7×3 m planting scheme, the highest yield was obtained with 12 stems per shrub, whereas in the 6×7 m scheme, 15 stems provided the best yield performance; yield in the untreated control remained lower than in any managed treatment in both schemes. Extremely high stem numbers did not proportionally increase yield and negatively affected certain fruit traits, while, regardless of stem number, all regulated treatments markedly improved kernel ratio and kernel weight compared with the unmanaged control. Yield per hectare increased with planting density; however, production in 2025 declined compared to 2024, likely due to climatic stress and increased damage from the brown marmorated stink bug. Moderate stem densities (12 stems at 7×3 m and 15 stems at 6×7 m) are recommended for optimizing yield and nut quality of the 'Ata-baba' cultivar in Azerbaijan, and the results confirm that actively managing stem number (even at non-optimal levels) is preferable to leaving shrubs unpruned.

REFERENCES

Ahmadov, A. 2024. The impact of climate change on hazelnut cultivation. Turkish Journal of Food and Agriculture Sciences, 6(2): 106-115.
Ahmadov, A. 2025. Hazelnut culture in Azerbaijan. Bahçe, 54(2): 129-138.
An, N., M. T. Turp, M. Türkeş, M. L. Kurnaz. 2020. Mid-term impact of climate change on hazelnut yield. Agriculture, 10(5): 159.
Bak, T., T. Karadeniz. 2021. Effects of branch number on quality traits and yield properties of European hazelnut (Corylus avellana L.). Agriculture, 11(5): 437.
Baldwin, B. J. 2015. The growth and productivity of hazelnut cultivars (Corylus avellana L.) in Australia. PhD Thesis, University of Western Sydney, Australia.

Balta, F., M. Yılmaz, O. Karakaya, K. Çalışkan, T. Yarılgaç, S. Z. Bostan, S. Uzun. 2024. Effect of Plant Density on Nut Traits, Nut Yield, Cluster Distribution and Chemical Components in Çakıldak (Corylus avellana L.) Hazelnut Cultivar. Applied Fruit Science, 66(6): 2295-2305.
Beyhan, N. 2007. Effects of planting density on yield and quality characteristics of hazelnut (cv. Palaz) in a hedgerow training system. Canadian Journal of Plant Science, 87(3): 595-597.
Bignami, C., G. Bertazza, S. Bizzarri, A. Bruziches, C. Cammilli, V. Cristofori. 2004. Effect of high density and dynamic tree spacing on yield and quality of the hazelnut cultivar 'Tonda Gentile Romana'. Acta Horticulturae, 686: 263-270.
Cristofori, V., Y. Rouphael, E. Mendoza-de Gyves, C. Bignami. 2007. A simple model for estimating leaf area of hazelnut from linear measurements. Scientia Horticulturae, 113(2): 221-225.
Ellena, M., P. Sandoval, A. González, J. Jequier, M. Contreras, C. San Martín. 2012. Advantages of high density planting of hazelnut orchards in South Chile: preliminary data. Acta Horticulturae, 1052: 235-240.
Erdoğdu, A. 2025. Farklı Dikim Mesafelerinin Yomralı Fındık Çeşidinde Bitki Gelişimi ve Verime Başlama Üzerine Etkileri. Yüksek Lisans Tezi, Ordu Üniversitesi, Fen Bilimleri Enstitüsü, Ordu, Türkiye.
FAO. 2023. Hazelnut sector in Azerbaijan: Options for green energy interventions along the value chain. Environment and Natural Resources Management Working Paper No. 98. FAO, Baku, Azerbaijan. https://doi.org/10.4060/cc8599en
Gutiérrez-Gamboa, G., M. Araya-Alman, M. Zúñiga-Sánchez, M. González, M. J. Lisperguer Fernández, S. Romero-Bravo. 2025. The impacts of light interception on yield and kernel parameters in hazelnut production. Horticulturae, 11(2): 156.
İslam, A. 2018. Hazelnut culture in Turkey. Akademik Ziraat Dergisi, 7(2): 259-266.
Mehlenbacher, S. A. 1991. Hazelnuts (Corylus). Genetic Resources of Temperate Fruit and Nut Crops, 290: 791-838.
Özpınar, A., S. Yıldırım. 2025. Çatalpınar (Ordu) İlçesinde Fındık Zararlısı Halyomorpha halys (Stål)'ın Bazı Biyolojik Özelliklerinin Belirlenmesi. ÇOMÜ Ziraat Fakültesi Dergisi, 13(2): 363-371.
Pacchiarelli, A., C. Silvestri, V. Cristofori. 2022. Advances in sucker control for sustainable European hazelnut (Corylus avellana L.) cultivation. Plants, 11(24): 3416.
Pacchiarelli, A., C. Silvestri, M. Muganu, V. Cristofori. 2025. Influence of the Plant Training System on Yield and Nut Traits of European Hazelnut (Corylus avellana L.) Cultivar Nocchione. Agronomy, 15(2): 345.
Pacchiarelli, A., R. Cristofori, C. Silvestri, V. Cristofori. 2026. European hazelnut: Plant training, planting layouts and pruning innovations. Agronomy, 16(5): 511.
Pajač Beus, M., D. Lemić, S. Skendžić, D. Čirjak, I. Pajač Živković. 2024. The brown marmorated stink bug (Hemiptera: Pentatomidae)—A major challenge for global plant production. Agriculture, 14(8): 1322.
Portarena, S., S. Proietti, S. Moscatello, C. Zadra, N. Cinosi, C. Traini, D. Farinelli. 2024. Effect of Tree Density on Yield and Fruit Quality of the Grafted Hazelnut Cultivar 'Tonda Francescana®'. Foods, 13(20): 3307.
Sokol, M. 2017. Cultivation of hazelnut tree trained with double vertical spindle shape. Acta Horticulturae, 1226: 251-254.
Walton, V. M., D. T. Dalton, B. Miller, E. T. Harris, E. Mirandola, G. Tait, S. Mermer. 2022. Economic impact and management of brown marmorated stink bug, Halyomorpha halys (Stål) (Hemiptera: Pentatomidae), in Oregon hazelnut orchards. Acta Horticulturae, 1379: 425-432.

RESISTANCE TO COPPER IN ESCHERICHIA COLI ISOLATES FROM ARUGULA

Fatma Özdemir[1], *Seza Arslan*[1], *Sueda Kabucu*[1]

[1] *Bolu Abant Izzet Baysal University, Faculty of Arts and Sciences, Department of Biology, 14030 Gölköy / Bolu, Türkiye*

Corresponding author e-mail: sudi.kabucu@gmail.com

ABSTRACT

Vegetables, including arugula, are essential components of a balanced diet due to their low caloric content and high nutritional value, contributing significantly to human health. Arugula, as cruciferous vegetable, is a rich source of fiber, vitamins A, C, K, B9, and various minerals, and possess antioxidant properties like neutralizing free radicals. Heavy metals are chemical elements that have toxic effects in living organisms. Environmental factors such as soil, water, and air pollution all contribute to heavy metal contamination in foods, particularly vegetables. Consumption of vegetables contaminated with heavy metals and foodborne pathogens, including *Escherichia coli*, could cause a significant concern to public health due to their tendency to bioaccumulation in the body and their toxic effects. The purpose of this study was to examine the resistance to heavy metal copper in the *E. coli* isolates from arugula using the broth microdilution method to determine the minimum inhibitory concentration (MIC) and the PCR method to amplify the *pcoR* gene, which encodes copper resistance. *E. coli* isolates from arugula and reference strains, including *E. coli* ATCC 8739 and *Enterobacter cloacae* NCIMB 13597, were tested for copper resistance. All tested arugula *E. coli* isolates had an MIC of 1600 µg/mL. The presence of the *pcoR* gene encoding copper resistance was detected in none of the arugula *E. coli* isolates. *E. coli* ATCC 8739 and *E. cloacae* NCIMB 13597 contained the *pcoR* gene and had MICs of 1600 µg/mL. In conclusion, in this study, *E. coli* isolates from arugula plants were evaluated for resistance to copper, a heavy metal that poses a risk to human health.

Keywords: copper resistance, *pcoR* gene, *Escherichia coli*, minimum inhibitory concentration, arugula

INTRODUCTION

Leafy green vegetables play an important role in a healthy lifestyle thanks to their fiber, vitamin, and antioxidant content. Arugula, a member of the Brassicaceae family, is a vegetable favored for its slightly bitter, tangy flavor in various applications, such as salads, smoothies, and sauces. The consumption of arugula is steadily increasing due to the vitamins, polyphenols, and other health-beneficial compounds it contains. In addition, its bioactive compounds have been associated with beneficial effects on gastrointestinal and cardiovascular health, as well as anticancer activity (Inestroza-Lizardo et al., 2016; Najmi et al., 2023; Santos et al., 2024).

Heavy metals are one of the most concerning environmental pollutants because of their toxicity, persistence in the environment, and facility to bioaccumulate along the food chain (Liao et al., 2023; Heydari et al., 2025). Primary sources of heavy metals are such as weathering rocks, volcanic activity, marine aerosols (Halem et al., 2024). Moreover, heavy metals can be detected in the environment as a result of fossil fuel combustion, agrochemical fertilizer use, sewage sludge supplementing, and industrial deposition processes (Halem et al., 2024).

Vegetables that are grown in soils contaminated with heavy metals can accumulate these heavy metals in their tissues' health (Santos et al., 2024). The accumulation of heavy metals in plants has numerous adverse effects, such as stunted growth and a reduced capacity for photosynthesis (Ojo et al., 2023). Through this process, heavy metals can enter the food chain, and consumption of these plants adversely affects human health, such as blindness, immunosuppressive functions and neurological damage (Ojo et al., 2023; Santos et al., 2024; Heydari et al., 2025).

Exposure of soil microorganisms to heavy metals leads to a reduction in microbial diversity and enzymatic activities (Ojo et al., 2023; Heydari et al., 2025). Bacteria have developed mechanisms to tolerate the toxic effects caused by heavy metals. Examples of these resistance mechanisms include enzymatic detoxification, intracellular and extracellular sequestration, efflux pumps, and active transport (Ojo et al., 2023).

Heavy metals are naturally occurring elements with atomic numbers above 20 and densities more than 5 g/cm³. Many heavy metals are essential for various biological processes (Mihdir et al., 2016; Gillieatt and Coleman, 2024). Essential metals include Zn, Cu, Mn, Fe, Co, Mo, and Ni. However, excessive concentrations of these metals can exert toxic effects on living organisms (Gillieatt and Coleman, 2024).

Although copper is an essential metal, the accumulation of excessive amounts within the cell is toxic to bacteria. Consequently, bacteria have developed copper resistance mechanisms. These resistance mechanisms are generally mediated by genes located on bacterial plasmids. In *E. coli*, the structural genes *pcoA, pcoB, pcoC*, and *pcoD* function in copper resistance, while the *pcoR* gene acts as a DNA-binding regulatory protein involved in the regulation of copper resistance genes (Chihomvu et al., 2015). Excessive copper intake, depending on the period of exposure, can cause major immediate or chronic adverse consequences such as cardiovascular diseases, neurological diseases, gastrointestinal issues and renal dysfunction (Najmi et al., 2023).

Escherichia coli is a rod-shaped, Gram-negative bacterium that belongs to the *Enterobacteriaceae* family. (Bhunia, 2008). It is generally motile and facultatively anaerobic and commonly occurs in the intestinal tract of humans and other warm-blooded animals (WHO, 2018; CDC, 2024). Although most *E. coli* strains are harmless and part of the normal intestinal microbiota, certain pathogenic strains such as Shiga toxin-producing *E. col*i (STEC), Enterohemorrhagic *E. coli* (EHEC) and Enteropathogenic *E. coli* (EPEC) can cause foodborne diseases ranging from mild diarrhea to severe bloody diarrhea (FDA, 2020; CDC, 2024).

Among the pathogenic *E. coli* strains, STEC is of particular concern because it can progress to hemolytic uremic syndrome (HUS) (WHO, 2018; CDC, 2024). Although most STEC infections are self-limiting, HUS can develop particularly in young children and older adults and may result in acute kidney failure.

Fresh vegetables can become contaminated with *E. coli* through direct contact with animals or through contact with faecally contaminated soil, irrigation water and during harvesting (FDA, 2020).

Heavy metal resistance is considerable because heavy metals are persistent in the environment, cannot be degraded and can cause long-term selective pressure among the bacterial populations. This selective pressure can be the cause of dissemination of metal resistance. In addition, heavy metal resistance may be associated with antibiotic resistance through co-selection, as resistance determinants against metals and antibiotics can be located on the same mobile genetic elements, such as plasmids and transposons (Heydari et al., 2025). Therefore, exposure to heavy metals can contribute to the dissemination of antimicrobial resistance among the bacterial populations. The widespread occurrence of heavy metals in agricultural environments makes investigating

heavy metal resistance in foodborne bacteria such as *E. coli* is important for a food safety concern (Mihdir et al., 2016; Gillieatt and Coleman, 2024).
The aim of this study is to investigate the resistance of *E. coli* isolates from arugula to copper, a heavy metal that is harmful to human health. The resistance of isolates to metal was evaluated using the broth microdilution method, and the presence of the *pcoR* gene, which is responsible for copper resistance, was determined using PCR.

MATERIALS AND METHODS

Bacterial isolates

Nine *Ecoli* isolates that were isolated from arugula by Özdemir (2024) and as reference, *E. coli* ATCC 8739 and *E. cloacae* NCIMB 13597 are used as a positive control in this experiment. Nine *E. coli* isolates and reference strains stored in stock culture at -20 °C in Tryptic Soy Broth with 20% glycerol. These isolates were activated from stock cultures using Tryptic Soy Broth for 24 hours at 37°C. After that, the culture streaked on to Eosin Methylene Blue (EMB) agar (Merck, Germany) for obtaining pure colonies exhibiting a suspicious metallic green sheen characteristic of *E. coli*. For further analyses, the selected colonies exhibiting metallic green sheen were subcultured on to EMB agar (Merck, Germany).

Minimum inhibitory concentration of heavy metal copper

The minimum inhibitory concentration assay (MIC) was used to assess copper resistance in nine *E. coli* isolates. The MIC was defined as the lowest concentration of copper that completely inhibited visible bacterial growth. Growth inhibition was determined by measuring the absorbance at 600 nm using a Thermo Electron Corporation microplate reader. All experiments were done in triplicate, with *E. coli* ATCC 8739 and *E. cloacae* NCIMB 13597 serving as control strains.
The MIC of copper was determined by the broth microdilution method using sterile U-bottom 96 well microtiter plates according to the Clinical and Laboratory Standards Institute standards (CLSI, 2012). Previously cultured *E. coli* isolates cultured on Eosin Methylene Blue (EMB) agar were collected using a sterile cotton loop and suspended in Mueller Hinton Broth (MHB). The bacterial suspension was adjusted to 0.5 McFarland, which corresponds to roughly 1×10^8 colony forming units (CFU) per mL. The suspension diluted 1:150 ratio in MHB. Copper solutions prepared by two-fold serial dilution in MHB. Final copper concentrations ranged from 3200 to 6.25 µg/mL. For each test, sterility and growth controls are included and the microtiter plates were incubated (37 °C/ 24 hours).

Minimum bactericidal concentration of heavy metal copper

The Clinical and Laboratory Standards Institute (2012) defined the minimum bactericidal concentration (MBC) as the lowest concentration capable of killing 99.9% of the bacterial population. MBC values were calculated using the findings of the minimal inhibitory concentration (MIC) test. Briefly, 10 µL of sample from the first eight wells were spot-inoculated onto Mueller Hinton Agar and incubated at 37 °C for 24 hours.

DNA extraction and identification of the *E. coli* isolates

E. coli isolates were inoculated into 5 mL of sterile Tryptic Soy Broth (TSB) and incubated overnight at 37 °C. After that, 950 µL of each culture was transferred to sterile microcentrifuge

tubes and centrifuged. Bacterial genomic DNA then isolated utilizing the cetyltrimethylammonium bromide (CTAB) method (Ausubel et al., 1991). For further PCR analysis, the extracted DNA was suspended in TE buffer and stored at −20 °C.
For species-level identification of *E. coli*, the *uspA* gene, which is encode the *E. coli* specific universal stress protein A, was amplified by PCR as previously described by Chen and Griffiths (1998). The PCR reaction was expected to yield an 884-bp amplicon. PCR amplification were performed in a T100 thermocycler (Bio-Rad). The reaction mixture had a final volume of 50 µL and contained 31.7 µL of PCR-grade water, 5 µL of 10X buffer, 4 mM $MgCl_2$, 0.2 mM dNTP mix (Amplicon), 0.4 µM of each primer, 4 µL of template DNA and 1.5 U of Taq polymerase (Thermo Scientific). The PCR cycling conditions were as follows: an initial denaturation at 94 °C/ 5 min; 30 cycles of denaturation at 94 °C/ 2 min, annealing at 60 °C/ 1 min, and extension at 72 °C/ 1 min; followed by a final extension at 72 °C/ 10 min. The products of PCR were separated on a 1% agarose gel and analyzed by agarose gel electrophoresis using a Bio-Rad system. *E. coli* ATCC 8739 was used as a positive control.

PCR amplification of the *pcoR* gene

The *pcoR* gene, which is related with copper resistance, was detected by PCR amplification. The *pcoR* gene encodes a transcriptional regulatory protein involved in the copper resistance. The primer for the *pcoR* gene were the forward primer, 5' CAGGTCGTTACCTGCAGCAG 3', and the reverse primer, 5' CTCTGATCTCCAGGACATATC 3' (Trajanovska et al., 1997). The expected PCR product size is 636 bp. The amplification performed in a total volume of 50 µL. Each 50 µL PCR reaction mixture contained 30.7 µL of PCR-grade water (AppliChem), 5 µL of 10× buffer (Thermo Scientific), 4 µL of $MgCl_2$ (Thermo Scientific), 1 µL of dNTP mix (Amplicon), 2 µL of each primer pair, 0.3 µL of Taq DNA polymerase (Thermo Scientific), and 5 µL of template DNA. The PCR amplification was carried out in a Bio- Rad T100 thermal cycler with an initial denaturation step at 94 °C for 8 minutes, followed by 35 cycles comprising denaturation at 94 °C / 1 minute, annealing at 64 °C / 1 minute, and extension at 72 °C / 90 seconds, with a final extension at 72 °C/ 8 minutes. All PCR products separated on %1 agarose gel by electrophoresis. The products stained with ethidium bromide and visualized (DNR Minilumi). A 100 bp ladder (Vivantis) used to determine the size of the amplified DNA fragments. *E. coli* ATCC 8739 and *E. cloacae* NCIMB 13597 were used as a positive control in the experiment.

RESULTS AND DISCUSSION

In this study, a total of nine *E. coli* isolates from arugula and two positive reference strains, *E. coli* ATCC 8739 and *E. cloacae* NCIMB 13597, were evaluated for heavy metal copper resistance by using both phenotypic and genotypic methods. Figure 1 presents the results of the phenotypic characteristics of copper resistance *E. coli* isolates from arugula and two positive controls based on MIC and MBC values obtained by the broth microdilution method. The MBC/MIC ratio is given in Figure 2. The heavy metal copper showed bactericidal activity against all *E. coli* isolates from arugula. Figure 3 shows a representative image of the minimal bactericidal concentration of heavy metal copper against *E. coli* isolates. The copper resistance is associated with the *pcoR* gene and is performed by PCR amplification. The *pcoR* gene was not detected in any of the nine *E. coli* isolates except for the reference strains. The representative PCR products of the *pcoR* gene in the *E. coli* isolates from arugula are shown in Figure 4.

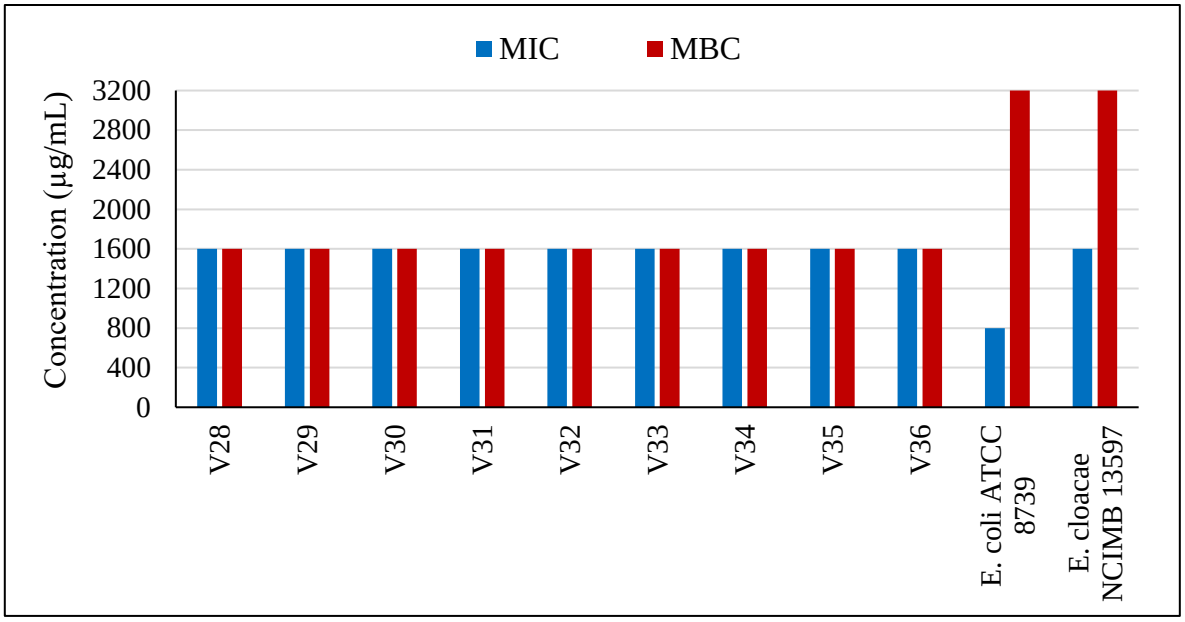

Figure 1. Minimum inhibitory concentration (MIC) and minimum bactericidal concentration (MBC) of heavy metal copper against the *E. coli* isolates from arugula and two positive control strains.

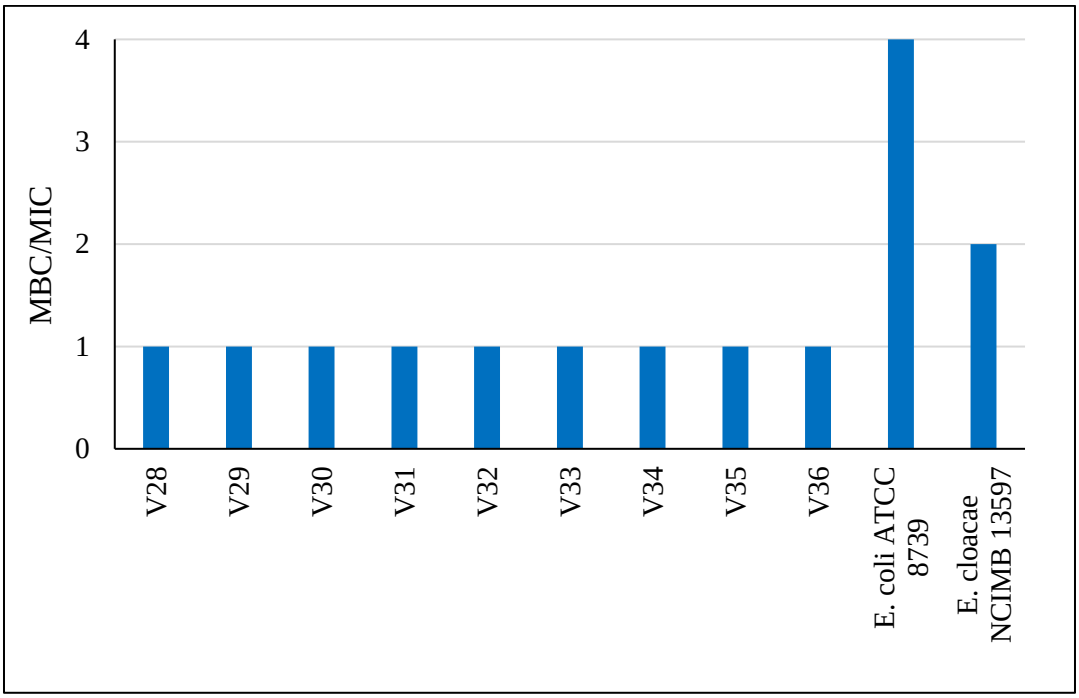

Figure 2. Ratio of minimum bactericidal concentration (MBC) to minimum inhibitory concentration (MIC) for heavy metal copper in the *E. coli* isolates from arugula and two positive controls. MBC/MIC ratio ≤ 4 means bactericidal activity and > 4 bacteriostatic activity.

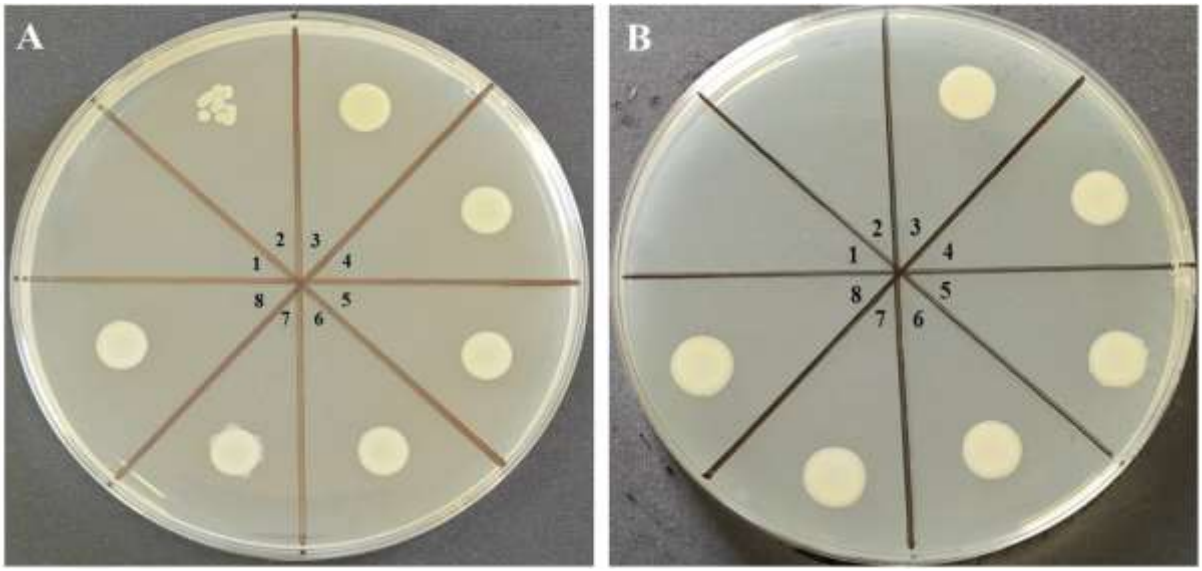

Figure 3. The representative image for the minimum bactericidal concentration (MBC) of the heavy metal copper against *E. cloacae* NCIMB 13597 (A) and V30 arugula *E. coli* isolate (B). The concentrations shown by the numbers 1-8 are 3200, 1600, 800, 400, 200, 100, 50, and 25 µg/mL.

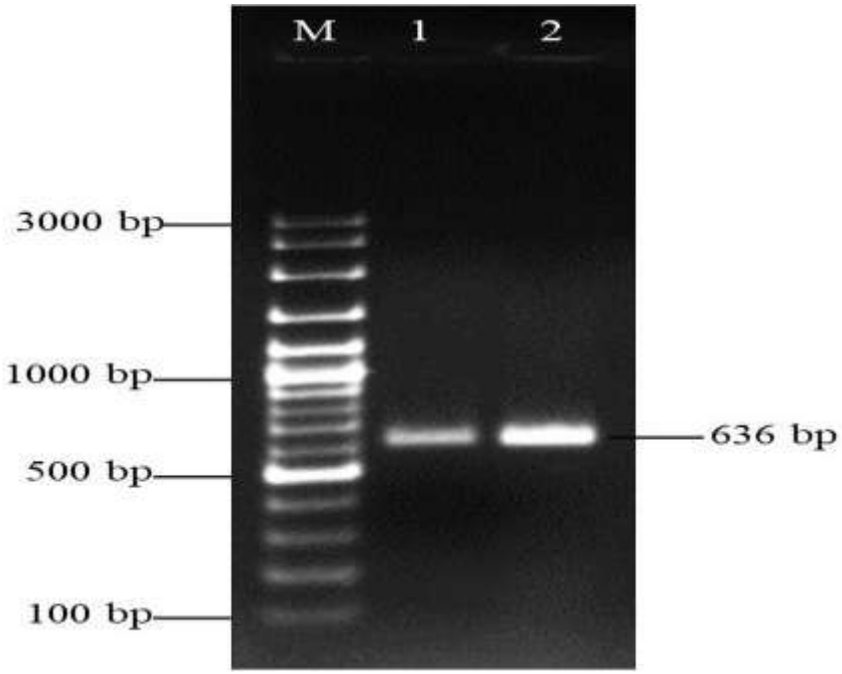

Figure 4. Agarose gel electrophoresis displaying polymerase chain reaction amplification of the *pcoR* gene (636 bp). Lane M: DNA ladder (100 bp). Lanes 1-2: *E. coli* ATCC 8739 and *E. cloacae* NCIMB 13597 positive reference strains for the *pcoR* gene.

In the current study, all tested *E. coli* isolates from arugula exhibited a MIC of 1600 µg/mL for the heavy metal, copper. Moreover, the *pcoR* gene associated with copper resistance was not detected among the *E. coli* isolates. Furthermore, the copper MIC values of *E. coli* ATCC 8739 and *E. cloacae* NCIMB 13597 were 800 and 1600 µg/mL, respectively. However, these reference strains, *E. coli* ATCC 8739 and *E. cloacae* NCIMB 13597, had the *pcoR* gene. These conflicts may suggest that copper tolerance may be mediated by other resistance mechanisms than the *pcoR* gene.

Dahanayake et al. (2016) reported that 37% of *Aeromonas* spp. isolates were resistant to copper. Najmi et al. (2023) investigated nine different heavy metals in leafy vegetables and reported that arugula has the highest heavy metal concentration among the other vegetables. The copper concentration in arugula ranged from 5.36 to 9.18 mg/kg dry weight. Nguyen et al. (2025) investigated the *pcoR* gene in *E. coli* and *S.* Typhimurium isolates, which are obtained from goat feces, and reported a prevalence of 9.36%. Islam et al. (2025) detected the *pcoR* gene among the *E. coli* isolates and reported a Cu^{2+} MIC of 2000 µg/mL.

In this study, the isolates showed a Cu^{2+} MIC of 1600 µg/mL and didn't show the *pcoR* gene. These results may suggest that the response of *E. coli* to heavy metal copper may not be dependent on the *pcoR* gene. Other copper efflux mechanisms may contribute to copper tolerance. Similar to our findings, Sendolo et al. (2022) didn't detect heavy metal resistance traits in clinical isolates; on the other hand, environmental isolates showed resistance-associated traits to silver and arsenic. The absence of copper-associated determinants in the study, as well as the absence of the *pcoR* gene, may imply that heavy metal resistance disruption varies depending on the bacterial source and environment.

CONCLUSIONS

This study evaluated the heavy metal copper resistance of *E. coli* isolates obtained from arugula. The MIC values of copper against all tested isolates were 1600 µg/ mL. The *pcoR* gene, which is linked to copper resistance, was not found in any of the examined *E. coli* isolates. In conclusion, studies regarding resistance to the heavy metal copper in *E. coli* isolates obtained from arugula, a popular vegetable, are important because heavy metal resistance poses potential threats to human health and food safety.

REFERENCES

Ausubel, F. M., Kingston, R. E., Brent, R., Moore, D. D., Seidman, J. G., Smith, J. A., et al. (1991). *Current protocols in molecular biology*. Greene Publishing Associates and Wiley Interscience.

Bhunia, A. K. (2008). *Foodborne microbial pathogens: Mechanisms and pathogenesis*. New York: Springer.

CDC (Centers for Disease Control and Prevention). (2024). *E. coli infection (Escherichia coli)*. https://www.cdc.gov/ecoli/php/technical-info/index

Chen, J., and Griffiths, M. W. (1998). PCR differentiation of *Escherichia coli* from other Gram-negative bacteria using primers derived from the nucleotide sequences flanking the gene

encoding the universal stress protein. *Letters in Applied Microbiology, 27*, 369–371. https://doi.org/10.1046/j.1472-765X.1998.00445.x

Chihomvu, P., Stegmann, P., and Pillay, M. (2015). Characterization and structure prediction of partial length protein sequences of *pcoA, pcoR* and *chrB* genes from heavy metal resistant bacteria from the Klip River, South Africa. *International Journal of Molecular Sciences*, *16*(4), 7352-7374. https://doi.org/10.3390/ijms16047352

CLSI (Clinical and Laboratory Standards Institute). (2012). Methods for dilution antimicrobial susceptibility tests for bacteria that grow aerobically-Ninth Edition, Approved standard, M7-A9. Wayne, PA, USA.

Dahanayake, P. S., Hossain, S., Wickramanayake, M. V. K. S., and Heo, G. J. (2019). Antibiotic and heavy metal resistance genes in *Aeromonas* spp. isolated from marketed Manila Clam (Ruditapes philippinarum) in Korea. *Journal of applied microbiology*, *127*(3), 941-952. https://doi.org/10.1111/jam.14355

FDA (Food and Drug Administration) (2020). *E. coli* and foodborne illness: Information for the public, FDA actions, and recommendations. https://www.fda.gov/news-events/public-health-focus/e-coli-and-foodborne-illness

Gillieatt, B. F., and Coleman, N. V. (2024). Unravelling the mechanisms of antibiotic and heavy metal resistance co-selection in environmental bacteria. *FEMS Microbiology Reviews*, *48*(4), fuae017. https://doi.org/10.1093/femsre/fuae017

Halem, A. A., El-Beltagi, H. S., Al-Dossary, O., Alsubaie, B., Henawy, A. R., Rezk, A. A., Almutairi, H. H., Mohamed, A. A., Elarabi, N. I., and Abdelhadi, A. A. (2024). Omics technology draws a comprehensive heavy metal resistance strategy in bacteria. *World Journal of Microbiology and Biotechnology*, *40*(6), 193. https://doi.org/10.1007/s11274-024-04005-y

Heydari, A., Kim, N. D., Biggs, P. J., Horswell, J., Gielen, G. J., Siggins, A., Bromhead, C., Meza-Alvarado, J.C., and Palmer, B. R. (2025). Antibiotic and heavy metal resistance in bacteria from contaminated agricultural soil: Insights from a New Zealand airstrip. *Antibiotics*, *14*(2), 192. https://doi.org/10.3390/antibiotics14020192

Inestroza-Lizardo, C., Silveira, A. C., and Escalona, V. H. (2016). Metabolic activity, microbial growth and sensory quality of arugula leaves (Eruca vesicaria Mill.) stored under non-conventional modified atmosphere packaging. *Scientia Horticulturae*, *209*, 79-85. http://dx.doi.org/10.1016/j.scienta.2016.06.007

Islam, M. R., Hossain, M. M., Mishu, M. A., and Ghosh, A. (2025). Co-exposure to heavy metals and antibiotics enhances resistance and transcriptional adaptation in enteric pathogens from poultry. *Total Environment Microbiology*, 100039. https://doi.org/10.1016/j.temicr.2025.100039

Liao, J., Xu, Y., Zhang, Z., Zeng, L., Qiao, Y., Guo, Z., Chen, J., Jia, B., Shang, C., and Chen, S. (2023). Effect of Cu addition on sedimentary bacterial community structure and heavy metal resistance gene abundance in mangrove wetlands. *Frontiers in Marine Science*, *10*, 1157905. https://doi.org/10.3389/fmars.2023.1157905

Mihdir, A., Assaeedi, A. S., Abulreesh, H. H., and Osman, G. E. (2016). Detection of heavy metal resistance genes in an environmental *Pseudomonas aeruginosa* isolate. *British Microbiology Research Journal*, *17*(1), 1-9. DOI: 10.9734/BMRJ/2016/28655

Najmi, A., Albratty, M., Al-Rajab, A. J., Alhazmi, H. A., Javed, S. A., Ahsan, W., Rehman, Z. ur, Hassani, R., and Alqahtani, S. S. (2023). Heavy metal contamination in leafy vegetables grown in Jazan region of Saudi Arabia: assessment of possible human health hazards. *International Journal of Environmental Research and Public Health*, *20*(4), 2984. https://doi.org/10.3390/ijerph20042984

Nguyen, T. K., Truong, T. T., Nguyen, T. T., Tran, D. D., Dang, T. T. C., and Tran, B. C. (2025). Antibiotic resistance and pathogenicity of Shiga-toxin-producing *Escherichia coli* (STEC) and non-STEC isolated from goats in the Mekong Delta, Vietnam. *Journal of Advanced Veterinary and Animal Research*, *12*(2), 420. http://doi.org/10.5455/javar.2025.l908

Ojo, G. J., Onile, O. S., Momoh, A. O., Oyeyemi, B. F., Omoboyede, V., Fadahunsi, A. I., and Onile, T. (2023). Physiochemical analyses and molecular characterization of heavy metal-resistant bacteria from Ilesha gold mining sites in Nigeria. *Journal of Genetic Engineering and Biotechnology*, *21*(1), 172. https://doi.org/10.1186/s43141-023-00607-5

Özdemir F. (2024). Multilocus sequence typing, phylogenetic grouping, serotyping, extended-spectrum beta-lactamases and antimicrobial resistance of *Escherichia coli* in vegetables. *Journal of Biological Research-Thessaloniki*, 31:10.

Santos, J. L. O., Bueno, G. M. G. B., de Moraes Flores, É. L., Ogava, L. E., de Souza Dias, F., and Leite, O. D. (2024). Support vector machine in the elementomic evaluation of arugula (Eruca Sativa) and lettuce (Lactuca sativa) grown in soils from a decommissioned mining area. *Journal of Food Composition and Analysis*, *135*, 106702. https://doi.org/10.1016/j.jfca.2024.106702

Sendolo, D., Baysah, G., and Ezeamagu, C. O. (2022). Detection of heavy metal-resistance gene in bacteria isolated from clinical and environmental sources using polymerase chain reaction (PCR). *Pan-African Journal of Health and Environmental Science*, *1*(2), 83-92. https://doi.org/10.56893/ajhes.2022-v1i2.239

Trajanovska, S., Britz, M. L., and Bhave, M. (1997). Detection of heavy metal ion resistance genes in Gram-positive and Gram-negative bacteria isolated from a lead-contaminated site. *Biodegradation*, *8*(2), 113-124. https://doi.org/10.1023/A:1008212614677

WHO (World Health Organization). (2018, February 7). *E. coli*. https://www.who.int/news-room/fact-sheets/detail/e-coli

MODELING PROBABILISTIC HEALTH RISKS OF FLUORIDE EXPOSURE FROM LENTIC ECOSYSTEMS IN THRACE REGION OF TÜRKIYE

Mediha Büyükgöze Dindar[1], Meltem Tekbaş Atay[1], Cem Tokatlı[2]*

[1]Trakya University, Faculty of Dentistry, Edirne / Türkiye
[2]Trakya University, İpsala Vocational School, Edirne / Türkiye

**Corresponding author: medihabuyukgoze@trakya.edu.tr*

ABSTRACT

In this comprehensive and detailed toxicological investigation, we aimed to model the non-carcinogenic health hazards and potential physiological effects of fluoride exposure from the Sultanköy and Altınyazı Dam Lakes (Northwest Türkiye) for local consumers using an advanced probabilistic risk assessment approach. Based on the long-term hydrochemical datasets of these reservoirs, a multi-pathway probabilistic human health risk assessment was performed to systematically address inherent uncertainties in various environmental exposure parameters. The Hazard Quotient (HQ) values via the drinking water ingestion pathway were simulated across four distinct age cohorts: infants, children, teenagers, and adults, to capture age-dependent susceptibility. The probabilistic risk characterization revealed that the simulated HQ values for fluoride did not exceed the critical toxicological threshold of 1.0 in either reservoir, demonstrating that these surface waters pose no immediate adverse systemic health hazards or chronic fluorosis risks for the regional population. Across all evaluated demographic categories, the highest risk orientation was consistently observed in children, followed by teenagers, adults, and infants, respectively. In a comparative framework, the estimated risk indices for Sultanköy Dam Lake were systematically higher across all age groups than those calculated for Altınyazı Dam Lake due to varying baseline anion levels. From a preventive dentistry and public health perspective, while both aquatic ecosystems are completely safe from a dental or skeletal fluorosis standpoint, the prominently lower exposure profiles in Altınyazı Dam Lake suggest a potential deficit in meeting the daily optimal fluoride requirements necessary for dental caries mitigation, emphasizing the need for targeted nutritional and dental planning in the region.

Keywords: Probabilistic risk assessment, Fluoride exposure, Hazard Quotient, Preventive dentistry, Public health

INTRODUCTION

Fluoride is a double-edged trace element that exerts a foundational control on human oral health. While its integration into dental tissues mitigates dental caries, drinking water remains the primary exposure vector globally (Andezhath et al., 1993; Güner et al., 2016; Tokatlı and Güner, 2018; Onur and Tokatlı, 2020). Dietary habits, pharmaceuticals, and geogenic or industrial processes also contribute to the cumulative fluoride load (Tokatlı et al., 2022; 2023). However, due to its narrow therapeutic index, sustained ingestion above optimal thresholds shifts its profile from cariostatic to toxic, posing risks of endemic dental and skeletal fluorosis. To address these concerns, health risk assessments have become vital in public health management to delineate the toxicological boundaries of environmental contaminants (Taghipour et al., 2016; Jannat et al., 2022; Din et al., 2024). Recently, integrating probabilistic

modeling into these frameworks has advanced water resource management. Unlike deterministic estimations, probabilistic risk assessment accounts for natural variations and uncertainties in physiological factors, body weights, and water ingestion rates, enabling the precise identification of vulnerable demographic cohorts for targeted preventive dentistry interventions.

In Northwest Türkiye, the Sultanköy and Altınyazı Dam Lakes represent two pivotal reservoirs in Edirne Province, serving as lifelines for regional drinking water supply and agricultural activities. Established by the General Directorate of State Hydraulic Works (DSİ), these ecosystems are increasingly subjected to anthropogenic threats, where agricultural drainage and domestic wastes introduce substantial contaminant loads (http://www2.dsi.gov.tr/; Tokatlı et al., 2017; Tokatlı, 2019; 2020a; 2020b). Unlike dynamic lotic systems, these stagnant dam lakes are highly susceptible to the long-term accumulation of chemical constituents driven by intense evaporation and diffuse catchment runoff, directly affecting public health safety.

Given these ecological characteristics, this study was designed to bridge environmental hydrochemistry with preventive medical modeling. The explicit objectives were (1) to evaluate the spatial non-carcinogenic health hazards of fluoride exposure from these critical lentic ecosystems and (2) to systematically quantify these potential risks across distinct age cohorts using a comprehensive probabilistic risk assessment approach.

MATERIALS AND METHODS

Research Area and Sample Collection

The topographic configuration of the study area and the spatial distribution of the monitoring stations across the Sultanköy and Altınyazı Dam Lakes are illustrated in Figure 1. Surface water sampling was systematically executed during a single field campaign in the autumn season of 2024. This specific transitional period was strategically selected to coincide with the onset of significant seasonal precipitation. The primary hydrometeorological objective of this timing was to capture the critical phase where intensified surface runoff and atmospheric deposition flush the catchment area, heavily influencing the transport dynamics and concentration variations of fluoride and chloride ions within these lentic ecosystems.

Fluoride Analysis

Fluoride concentrations were quantified using spectrophotometric techniques, employing a Hach Lange DR 3900 spectrophotometer (https://tr.hach.com/) following APHA protocols (1998, 2017). For the determination of fluoride levels, the Hach Lange LCK 323 cuvette test kit was utilized. All analytical procedures were conducted in strict accordance with the manufacturer's protocols to ensure accuracy and reproducibility.

Health Risk Assessment

To address physiological and behavioral variations, the target population was stratified into four age cohorts: infants (<2 years), children (2–6 years), teenagers (6–16 years), and adults (>16 years). Daily fluoride exposure via drinking water ingestion for each demographic category was calculated using Equation 1. The non-carcinogenic health hazards were subsequently characterized using the Hazard Quotient (HQ) according to Equation 2 (Yousefi et al., 2018). An HQ threshold of less than 1.0 indicates a negligible toxicological risk, whereas values greater than 1.0 signify potential non-carcinogenic health concerns, indicating an increased probability of developing dental or skeletal fluorosis.

$$EDI = \frac{Cf\ x\ Cd}{Bw} \quad (1)$$

$$HQ = \frac{EDI}{RfD} \quad (2)$$

EDI: Estimation of fluoride consumption – daily (mg/kg/day)
C_f: Fluoride level in the investigated drinking water samples (mg/L)
C_d: Mean daily water intake (L/day) (the mean water consumption rates in infants, children, teenagers and adults were 0.08, 0.85, 2 and 2.5 L/day, respectively)
B_w: Body weight (kg) (body weights of investigated groups were considered 10, 15, 50 and 78 kg, respectively)
RfD: Reference dose (mg/kg/day) (it is 0.06 mg/kg/day for fluoride (EPA, 1992).

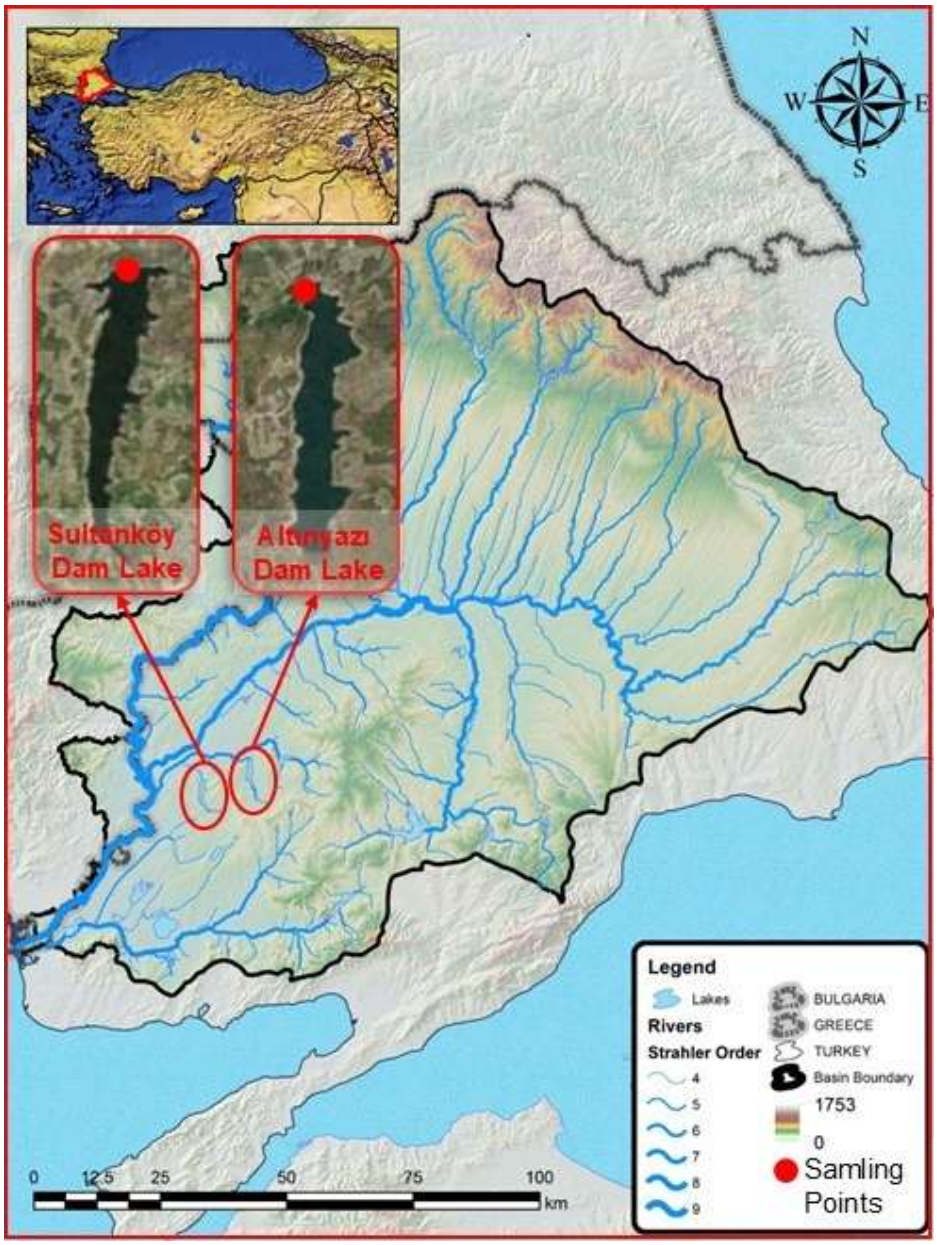

Figure 1. Meriç – Ergene Basin, investigated reservoirs and selected sampling station

RESULTS AND DISCUSSION

The simulated non-carcinogenic risk indices for the studied reservoirs are illustrated in Figure 2. The probabilistic risk characterization for the four distinct age cohorts revealed that all

calculated Hazard Quotient (HQ) values were systematically below the critical safety threshold of 1.0, indicating a negligible risk of severe fluorosis among the local population. Specifically, Sultanköy Dam Lake displayed systematically higher risk indices across all cohorts (Infants: 0.05573, Children: 0.39478, Teenagers: 0.27867, Adults: 0.22329) than Altınyazı Dam Lake (Infants: 0.01373, Children: 0.09728, Teenagers: 0.06867, Adults: 0.05502). The modeled outputs showed distinct demographic variations where children consistently exhibited the highest HQ values in both systems (0.39478 for Sultanköy and 0.09728 for Altınyazı), followed by teenagers, adults, and infants, respectively.

These health hazards and exposure risks are closely linked to demographic variables and population-specific consumption characteristics (Taghipour et al., 2016; Tokatlı et al., 2022). The trend of children experiencing the highest susceptibility aligns with global literature highlighting that younger populations face higher chronic risks from drinking water due to their lower body weights relative to daily ingestion rates (Gao et al., 2013; Tokatlı et al., 2023).

From a preventive dentistry perspective, while these low indices guarantee absolute safety against fluorosis, they also introduce a critical oral health concern. The remarkably low exposure profiles, particularly in Altınyazı Dam Lake, suggest that fluoride exposure risks fall drastically below the daily optimal levels necessary for dental caries mitigation. These findings emphasize that probabilistic exposure modeling is an essential tool to balance toxicological safety and oral health protection in regional water supplies.

CONCLUSIONS

In this study, the non-carcinogenic health hazards of fluoride exposure from Sultanköy and Altınyazı Dam Lakes were modeled using a probabilistic approach across four age groups. All simulated Hazard Quotient (HQ) values remained well below the critical threshold of 1.0, indicating a negligible risk of dental or skeletal fluorosis for local consumers. Children were identified as the most vulnerable cohort in both systems, followed by teenagers, adults, and infants, while Sultanköy Dam Lake systematically displayed higher risk indices than Altınyazı Dam Lake. From a public health perspective, these low exposure profiles—especially in Altınyazı Dam Lake—suggest a potential deficit in meeting the optimal daily fluoride ingestion required for dental caries mitigation.

ACKNOWLEDGEMENTS

This study was supported by Trakya University Scientific Research Projects Unit under Project Code 2024/230. The author would like to thank Trakya University for the financial and institutional support provided throughout the research.

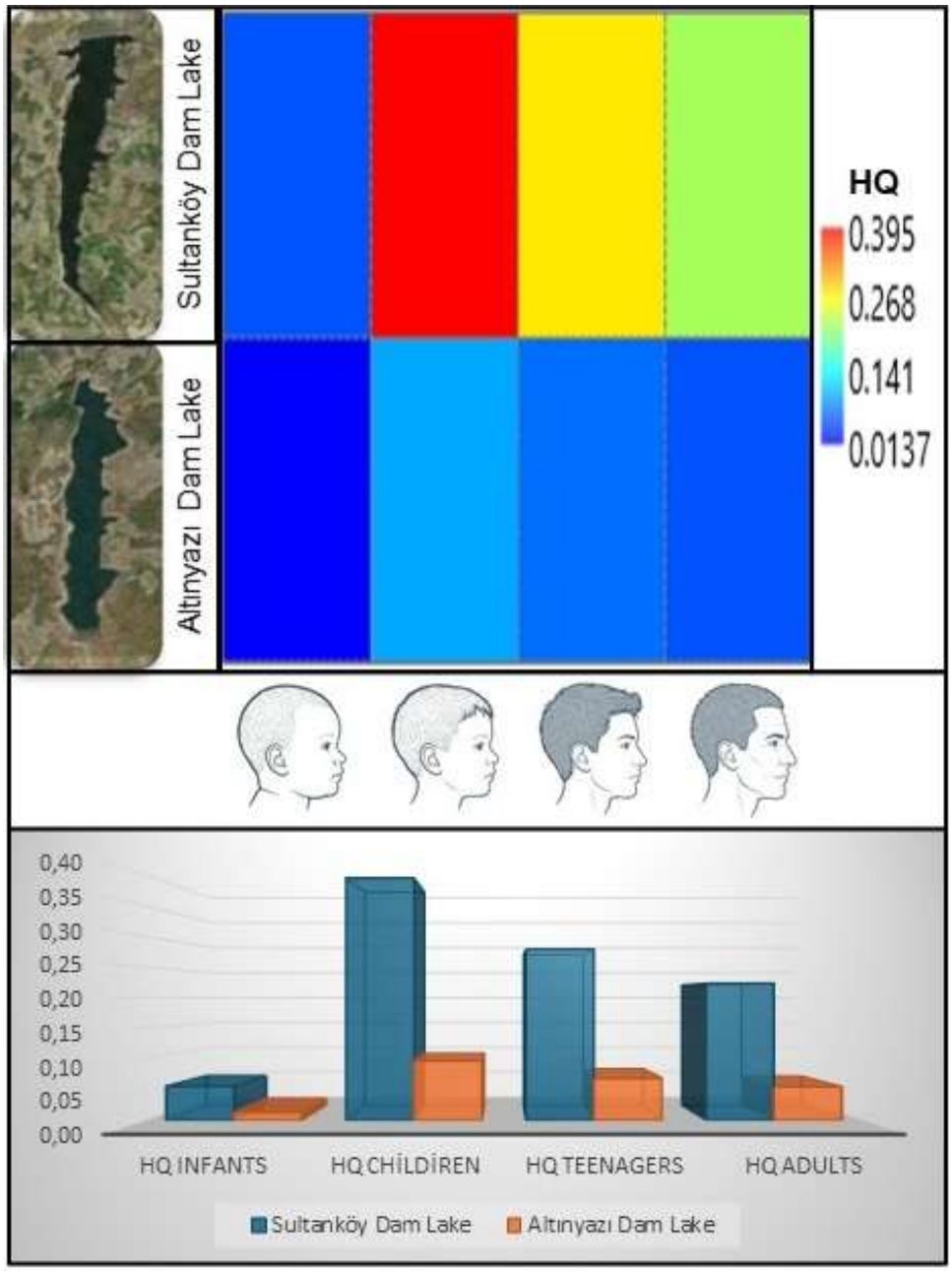

Figure 2. Probabilistic non-carcinogenic risk indices (HQ) of fluoride exposure

REFERENCES

Andezhath, S. K., Kumar, A., Bhatnagar, M., Bahudur, R., 1993. Prevalence of Endemic Fluorosis with Gastro-Intestinal Manifestations in People Living in Some North-Indian Villages. Fluoride, 26 (2): 97-104.

APHA, 1998. Standard Methods for the Examination of Water and Wastewater. American Public Health Association. Inc., Washington, DC.

APHA, 2017. American public health association (APHA). Stand. Methods Exam. Water Wastewater.

Din, I. U., Wajid, A., Muhammad, S., Rehman, I., Tokatlı, C., 2024. Spatial Distribution and Potential Health Risk Assessment for Fluoride And nitrate Via Water Consumption in Pakistan. Journal Of Geochemical Exploration, 259: 107413.

EPA. 1992. Framework for Ecological Risk Assessment. Risk Assessment Forum. US Environmental Protection Agency, Washington, DC.
Gao, H. J., Jin, Y. Q., Wei, J. L. 2013. Health Risk Assessment of Fluoride in Drinking Water from Anhui Province in China. Environ. Monit. Assess., 185 (5), 3687–3695.
Güner, Ş., Uyar-Bozkurt, S., Haznedaroğlu, E., Menteş, A., 2016. Dental Fluorosis and Catalase Immunoreactivity of the Brain Tissues in Rats Exposed to High Fluoride Pre- and Postnatally. Biol Trace Elem Res., 174 (1): 150-157.
http://www2.dsi.gov.tr/
Jannat, J. N., İslam, K. M. S., İslam, H. M. T., İslam, M. S., Khan, R., Bakar, S. M. A., Varol, M., Tokatlı, C., Chandra, P. S., İslam, A., İdris, A. M., Malafaia, G., Islam, A. R. T., 2022. Hydrochemical Assessment of Fluoride and Nitrate in Groundwater from East and West Coasts of Bangladesh and India. Journal of Cleaner Production, https://doi.org/10.1016/j.jclepro.2022.133675.
Onur, Ş. G., Tokatlı, C., 2020. Comparison of Fluoride Contents in Terms of Teeth Health and Water Quality in Drinking Water at the Northern and Southern Regions of Meriç River Basin (Edirne/Turkey). International Journal of Agriculture, Environment and Food Sciences, 4 (2): 173-180.
Taghipour, N., Amini, H., Mosaferi, M., Yunesian, M., Pourakbar, M., Taghipour, H., 2016. National and Sub-National Drinking Water Fluoride Concentrations and Prevalence of Fluorosis and of Decayed, Missed and Filled Teeth in Iran from 1990 to 2015: A Systematic Review. Environmental Science and Pollution Research, 23 (6): 5077–5098.
Tokatlı, C., 2019. Use of the potential ecological risk index for sediment quality assessment: a case study of dam lakes in the Thrace part of the Marmara Region. Aquatic Sciences and Engineering, 34 (3): 90-95.
Tokatlı, C., 2020a. Pesticide accumulations in water and sediment of dam lakes located in Thrace part of Marmara Region (Turkey). Aquatic Research, 3 (3): 124-134.
Tokatlı, C., 2020b. Application of water quality index for drinking purposes in dam lakes: a case study of Thrace Region. Sigma Journal of Engineering and Natural Sciences, 38 (1): 393-402.
Tokatlı, C., Baştatlı, Y., Elipek, B., 2017. Water quality assessment of dam lakes located in Edirne Province (Turkey). Sigma Journal of Engineering and Natural Sciences, 35 (4): 743-750.
Tokatlı, C., Güner, Ş., 2018. Fluorine Accumulations in Drinking Water of Havsa District (Edirne, Turkey) and Assessment of Water Quality in Terms of Teeth Health. Sigma Journal of Engineering and Natural Sciences, 36 (3): 887-894.
Tokatlı, C., İslam, A. R. T., Güner, Ş. O., Ustaoğlu, F., İslam, S., Dindar, M. B., 2022. A Pioneering Study on Health Risk Assessment of Fluoride in Drinking Water in Thrace Region of Northwest Türkiye. Groundwater for Sustainable Development, https://doi.org/10.1016/j.gsd.2022.100836.
Tokatlı, C., Onur, Ş. G., Dindar, M. B., Malafaia, G., Islam, A. R. T., Muhammad, S., 2023. Spatial-Temporal Variability and Probabilistic Health Risk Assessment of Fluoride from Lentic Ecosystem, Türkiye. International Journal of Environmental Analytical Chemistry, https://doi.org/10.1080/03067319.2023.2198645.
Yousefi, M., Ghoochani, M., Mahvi, A. H., 2018. Health Risk Assessment to Fluoride in Drinking Water of Rural Residents Living in the Poldasht City, Northwest of Iran, Ecotoxicol. Environ. Saf., 148: 426–430.

EVALUATION OF FLUORIDE AND CHLORIDE CONCENTRATIONS IN SULTANKÖY AND ALTINYAZI RESERVOIRS (TÜRKIYE): A COMPARATIVE AND DENTAL PUBLIC HEALTH APPROACH

Meltem Tekbaş Atay[1], Mediha Büyükgöze Dindar[1], Cem Tokatlı[2]*

[1]Trakya University, Faculty of Dentistry, Edirne / Türkiye
[2]Trakya University, İpsala Vocational School, Edirne / Türkiye

**Corresponding author: meltemtekbasatay@trakya.edu.tr*

ABSTRACT

In this comprehensive and detailed hydrochemical investigation, the seasonal water quality dynamics, spatial variations, and overall pollution profiles of the Sultanköy and Altınyazı Reservoirs, which hold immense strategic importance for extensive agricultural irrigation practices and regional freshwater reserves within the economically vital Meriç-Ergene Basin, were comparatively evaluated and monitored based on precise fluoride (F^-) and chloride (Cl^-) ion parameters. The extensive analytical results, laboratory data, and field observations revealed that despite both artificial aquatic systems being located within the exact same geographical area and climatic region, the fundamental hydrochemical characteristics and major anion compositions of these two crucial water bodies significantly differ on a critical basin scale. According to the quantitative findings of the monitoring program, Altınyazı Reservoir prominently stands out with its remarkably high chloride concentrations and elevated salinity indicators, whereas fluoride accumulation exhibits a much more dominant, persistent, and distinctive hydrochemical character throughout the Sultanköy Reservoir ecosystem. This sharp contrast in the dominant anion distribution and geochemical fingerprints of the reservoirs clearly points to highly differing anthropogenic pressures occurring along the specific drainage lines feeding the dams, the varying quality and volume of agricultural return waters draining from surrounding crop fields, or the distinct local lithological configurations and geological structures characterizing the respective drainage basins. Consequently, this comparative research study provides critical baseline data, scientific insights, and environmental indicators necessary for implementing sustainable water resource management strategies in the region, protecting aquatic ecosystems, and assessing the future long-term utilization potential and ecological safety of both reservoirs for irrigation and secondary purposes.

Keywords: Sultanköy Reservoir, Altınyazı Reservoir, Fluoride, Chloride, Dental health, Meriç-Ergene Basin

INTRODUCTION

In the 21st century, the degradation of freshwater ecosystems stands out as a paramount environmental crisis, severely jeopardizing aquatic biodiversity and public health (Helvacıoğlu et al., 2025; Din et al., 2023; Muhammad et al., 2025). As vital lentic components, artificial reservoirs perform indispensable functions in irrigation and municipal water supply. Nonetheless, intensifying anthropogenic stressors—primarily driven by agrochemical runoff and wastewater discharges—frequently induce severe water quality degradation in these critical water bodies (Çiçek et al., 2014; Köse et al., 2020; Ustaoğlu et al., 2022).

The Sultanköy and Altınyazı Dam Lakes represent two pivotal reservoirs in Edirne Province (Türkiye), serving as lifelines for regional drinking water supply and agricultural activities. Established by the General Directorate of State Hydraulic Works (DSİ) to sustain the socioeconomic and ecological equilibrium of the region, these reservoirs are increasingly subjected to anthropogenic threats (http://www2.dsi.gov.tr/). Persistent agricultural drainage and domestic waste loads introduce substantial amounts of contaminants into these lacustrine systems, threatening their long-term sustainability (Tokatlı et al., 2017; Tokatlı, 2019; 2020a; 2020b).

From a public health and dentistry perspective, monitoring specific hydrochemical parameters like fluoride is of utmost clinical significance. Fluoride is a crucial micronutrient fundamental for preventing dental caries, with municipal drinking water being its predominant intake vector (Andezhath et al., 1993; Güner et al., 2016; Tokatlı and Güner, 2018; Onur and Tokatlı, 2020; Tokatlı et al., 2022; 2023). However, its therapeutic window is remarkably narrow; chronic overexposure can precipitate debilitating conditions, most notably dental and skeletal fluorosis. Consequently, determining precise fluoride concentrations in regional water reserves remains a critical cross-disciplinary concern linking environmental science with preventive dentistry.

To address these pressing ecological and public health concerns, the present study was designed to execute a comparative hydrochemical assessment of the Sultanköy and Altınyazı Dam Lakes, with a primary focus on their fluoride (F) and chloride (Cl) profiles.

MATERIALS AND METHODS

Research Area and Sample Collection

Figure 1 illustrates the topographic configuration of the study area, including the spatial distribution of the selected monitoring stations across the Sultanköy and Altınyazı Dam Lakes. Within the scope of this study, surface water samples were systematically collected from the designated stations in the autumn season of 2024. The sampling strategy was specifically scheduled for a single campaign during autumn, as this transitional period marks the onset of significant seasonal precipitation. This hydrometeorological timing was strategically chosen to capture the critical phase where increased surface runoff and atmospheric depositions intensively flush the surrounding watershed, thereby significantly influencing the transport and concentration dynamics of fluoride and chloride ions within the reservoir ecosystems.

Fluoride and Chloride Analysis

Fluoride and chloride concentrations were quantified using spectrophotometric techniques, employing a Hach Lange DR 3900 spectrophotometer (https://tr.hach.com/) following APHA protocols (1998, 2017). For the determination of fluoride levels, the Hach Lange LCK 323 cuvette test kit was utilized. Concurrently, chloride concentrations were measured using the Hach Lange LCK 311 cuvette test kit. All analytical procedures were conducted in strict accordance with the manufacturer's protocols to ensure accuracy and reproducibility.

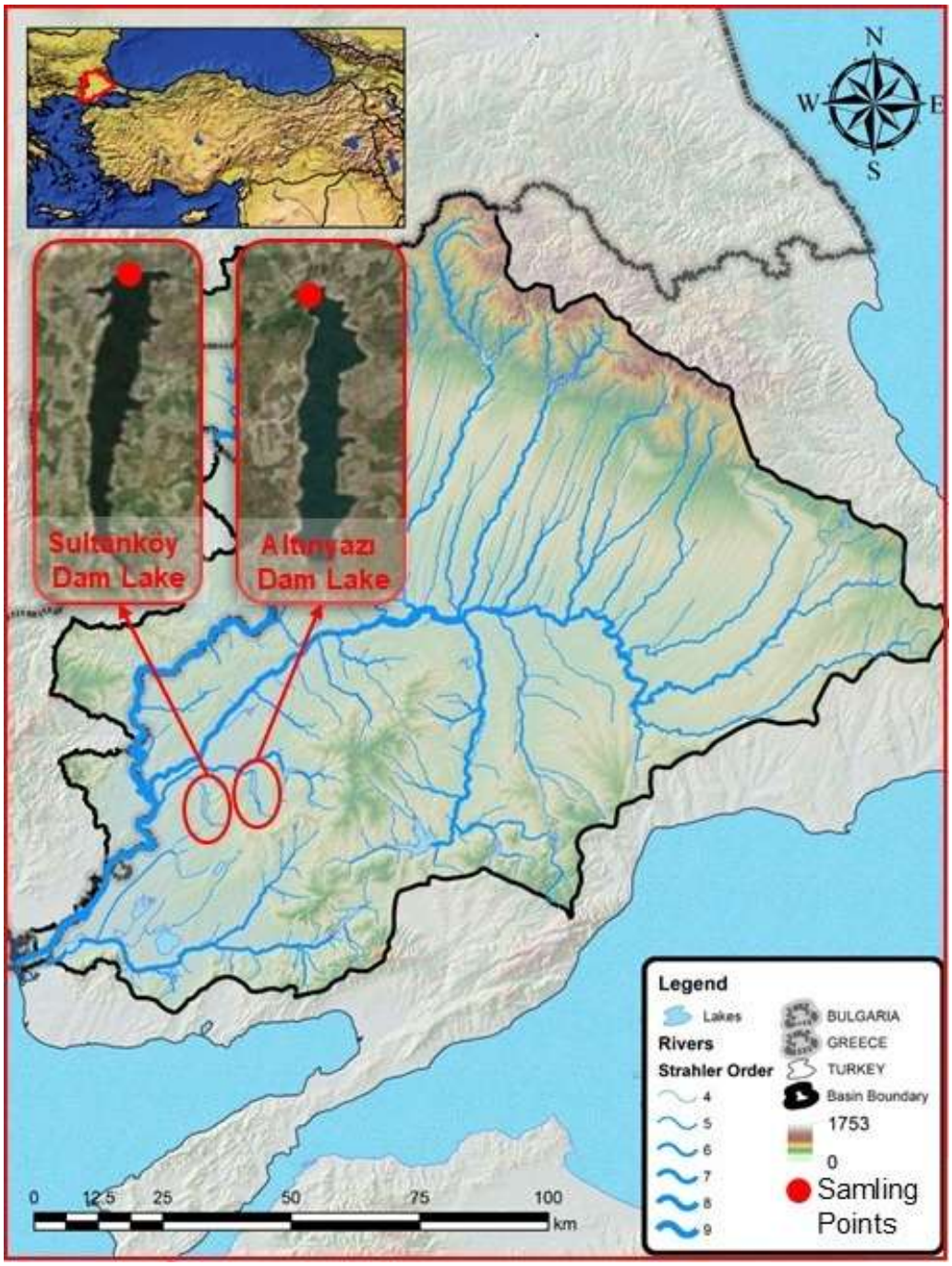

Figure 1. Meriç – Ergene Basin, investigated reservoirs and selected sampling stations

RESULTS AND DISCUSSION

The fluoride and chloride distributions in the Sultanköy and Altınyazı Dam Lakes are illustrated in Figure 2. The analytical results revealed distinct hydrochemical profiles for each reservoir. Chloride concentrations peaked in Altınyazı Dam Lake (158.00 ppm) compared to Sultanköy Dam Lake (89.00 ppm). Conversely, a completely opposite trend was observed for fluoride; Sultanköy Dam Lake exhibited significantly higher levels (0.418 ppm) than Altınyazı Dam Lake (0.103 ppm), showing an approximately four-fold increase between these lentic ecosystems.

Fluoride is a vital trace element with double-edged clinical implications. While its deposition in dental tissues plays a fundamental role in preventing dental caries, excessive exposure can trigger substantial pathological risks depending on concentration and duration (Taghipour et al., 2016; Tokatlı et al., 2022; 2023). Because drinking water supplies serve as the primary exposure vector, maintaining optimal fluoride levels remains a critical cornerstone of dental public health and preventive dentistry. On the contrary, chronic ingestion above therapeutic thresholds can precipitate dental and skeletal fluorosis (Güner et al., 2016; Tokatlı and Güner, 2018; 2020; Jannat et al., 2022; Din et al., 2024).

In the present study, fluoride concentrations in both Sultanköy (0.418 ppm) and Altınyazı (0.103 ppm) reservoirs were well within the permissible drinking water limit of 1.5 ppm stipulated by TS266 (2005), EC (2007), and WHO (2011). Although both lakes pose no fluorosis risk, the significantly lower fluoride level in Altınyazı suggests that supplementary oral health strategies might be required if utilized for municipal supply to ensure adequate protection against caries. Turningly, the higher chloride levels in Altınyazı Dam Lake (158.00 ppm) point toward more intense agricultural runoff or evaporative concentration dynamics in its catchment area.

CONCLUSIONS

This study evaluated the comparative hydrochemistry of Sultanköy and Altınyazı Dam Lakes with a specific focus on fluoride and chloride dynamics. The results revealed a distinct environmental polarization between the two reservoirs; Altınyazı Dam Lake is characterized by higher chloride loads, likely driven by agricultural runoff, whereas Sultanköy Dam Lake exhibits a significantly more dominant fluoride character. From a clinical and dental public health perspective, the fluoride concentrations in both lentic ecosystems remain safely below the maximum permissible drinking water threshold of 1.5 ppm set by WHO, EC, and TS266, indicating no risk of dental or skeletal fluorosis for the local population. However, the remarkably low fluoride levels in Altınyazı Dam Lake highlight a potential insufficiency for optimal dental caries prevention if these waters are integrated into municipal supply grids. Ultimately, these baseline outputs underscore the necessity of cross-disciplinary monitoring strategies that bridge environmental watershed management with preventive dentistry to ensure the dual protection of ecosystem stability and regional oral health.

ACKNOWLEDGEMENTS

This study was supported by Trakya University Scientific Research Projects Unit under Project Code 2024/230. The author would like to thank Trakya University for the financial and institutional support provided throughout the research.

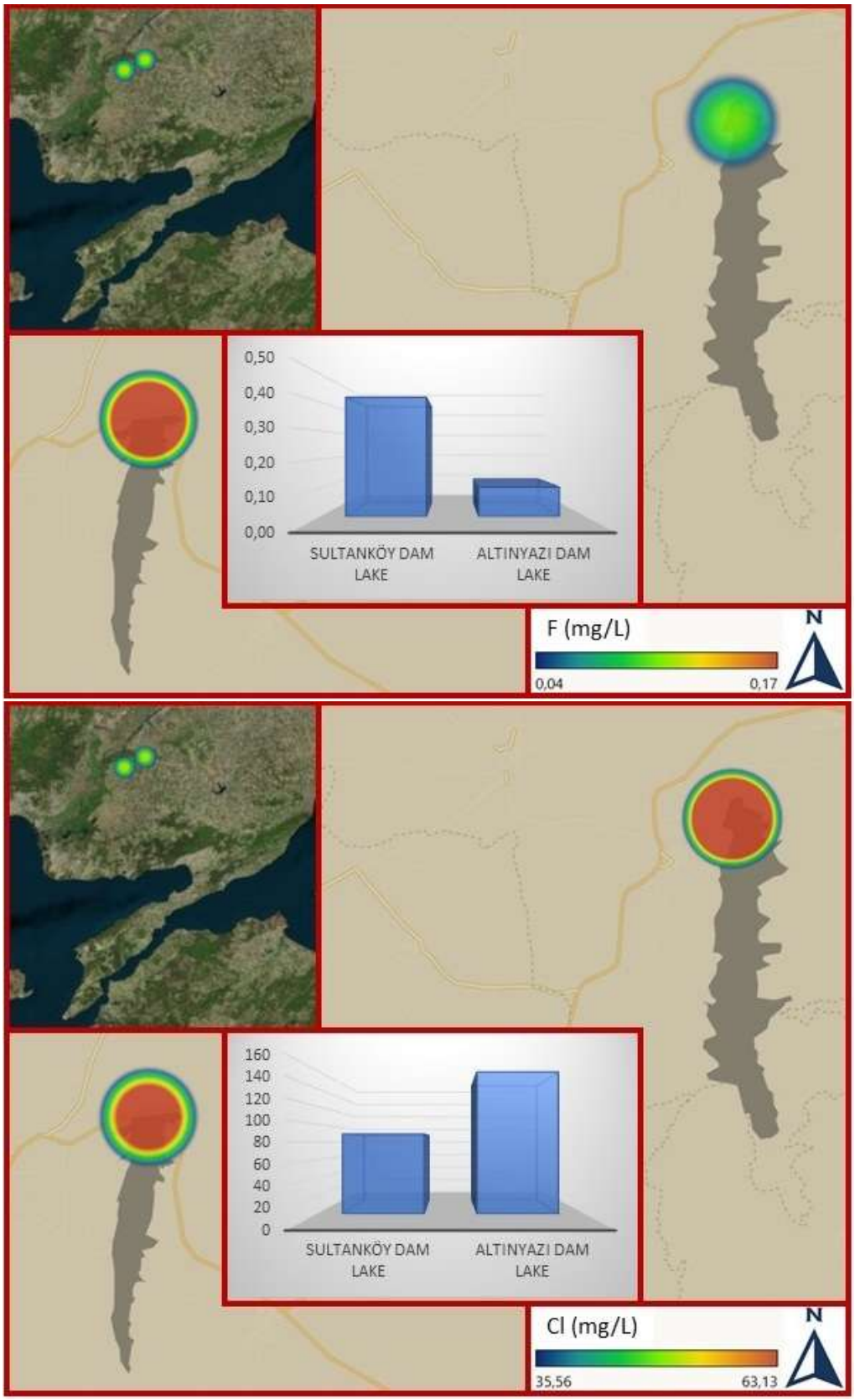

Figure 2. Fluoride and chloride levels in the investigated reservoirs

REFERENCES

Andezhath, S. K., Kumar, A., Bhatnagar, M., Bahudur, R., 1993. Prevalence of Endemic Fluorosis with Gastro-Intestinal Manifestations in People Living in Some North-Indian Villages. Fluoride, 26 (2): 97-104.

APHA, 1998. Standard Methods for the Examination of Water and Wastewater. American Public Health Association. Inc., Washington, DC.

APHA, 2017. American public health association (APHA). Stand. Methods Exam. Water Wastewater.

Çiçek, A., Köse, E., Emiroğlu, Ö., Tokatlı, C., Başkurt, S., Sülün, Ş., 2014. Boron and arsenic levels in water, sediment and tissues of Carassius gibelio (Bloch, 1782) in a dam lake. Polish Journal of Environmental Studies, 23 (5): 1843-1848.

Din, I. U., Wajid, A., Muhammad, S., Rehman, I., Tokatlı, C., 2024. Spatial Distribution and Potential Health Risk Assessment for Fluoride And nitrate Via Water Consumption in Pakistan. Journal Of Geochemical Exploration, 259: 107413.

EC (European Communities), 2007. European Communities (drinking water) (no. 2). Regulations 2007. S.I. No. 278 of 2007.

Güner, Ş., Uyar-Bozkurt, S., Haznedaroğlu, E., Menteş, A., 2016. Dental Fluorosis and Catalase Immunoreactivity of the Brain Tissues in Rats Exposed to High Fluoride Pre- and Postnatally. Biol Trace Elem Res., 174 (1): 150-157.

Helvacıoğlu, İ. A., Gülbaşı, A., Tokatlı, C., 2025. Evaluating the environmental sustainability awareness of paddy producers in the Meriç Plain (Northwest Türkiye): a comprehensive statistical approach. Acta Scientiarum Polonorum-Formatio Circumiectus, 24 (1): 3-13.

https://tr.hach.com/

Jannat, J. N., İslam, K. M. S., İslam, H. M. T., İslam, M. S., Khan, R., Bakar, S. M. A., Varol, M., Tokatlı, C., Chandra, P. S., İslam, A., İdris, A. M., Malafaia, G., Islam, A. R. T., 2022. Hydrochemical Assessment of Fluoride and Nitrate in Groundwater from East and West Coasts of Bangladesh and India. Journal of Cleaner Production, https://doi.org/10.1016/j.jclepro.2022.133675.

Köse, E., Emiroğlu, Ö., Çiçek, A., Aksu, S., Başkurt, S., Tokatlı, C., Şahin, M., Uğurluoğlu, A., 2020. Assessment of ecologic quality in terms of heavy metal concentrations in sediment and fish on Sakarya River and dam lakes, Turkey. Soil and Sediment Contamination: An International Journal, 29:3, 292-303.

Muhammad, S., Ahmed, T., Amin, S., Tokatlı, C., Ustaoğlu, F., 2025. Spatial distribution of hazard index via heavy metals consumption in water from the Himalayan lacustrine ecosystems. Physics and Chemistry of the Earth, 138: 103858.

Onur, Ş. G., Tokatlı, C., 2020. Comparison of Fluoride Contents in Terms of Teeth Health and Water Quality in Drinking Water at the Northern and Southern Regions of Meriç River Basin (Edirne/Turkey). International Journal of Agriculture, Environment and Food Sciences, 4 (2): 173-180.

Taghipour, N., Amini, H., Mosaferi, M., Yunesian, M., Pourakbar, M., Taghipour, H., 2016. National and Sub-National Drinking Water Fluoride Concentrations and Prevalence of Fluorosis and of Decayed, Missed and Filled Teeth in Iran from 1990 to 2015: A Systematic Review. Environmental Science and Pollution Research, 23 (6): 5077–5098.

Tokatlı, C., 2019. Use of the potential ecological risk index for sediment quality assessment: a case study of dam lakes in the Thrace part of the Marmara Region. Aquatic Sciences and Engineering, 34 (3): 90-95.

Tokatlı, C., 2020a. Pesticide accumulations in water and sediment of dam lakes located in Thrace part of Marmara Region (Turkey). Aquatic Research, 3 (3): 124-134.

Tokatlı, C., 2020b. Application of water quality index for drinking purposes in dam lakes: a case study of Thrace Region. Sigma Journal of Engineering and Natural Sciences, 38 (1): 393-402.
Tokatlı, C., Baştatlı, Y., Elipek, B., 2017. Water quality assessment of dam lakes located in Edirne Province (Turkey). Sigma Journal of Engineering and Natural Sciences, 35 (4): 743-750.
Tokatlı, C., Güner, Ş., 2018. Fluorine Accumulations in Drinking Water of Havsa District (Edirne, Turkey) and Assessment of Water Quality in Terms of Teeth Health. Sigma Journal of Engineering and Natural Sciences, 36 (3): 887-894.
Tokatlı, C., İslam, A. R. T., Güner, Ş. O., Ustaoğlu, F., İslam, S., Dindar, M. B., 2022. A Pioneering Study on Health Risk Assessment of Fluoride in Drinking Water in Thrace Region of Northwest Türkiye. Groundwater for Sustainable Development, https://doi.org/10.1016/j.gsd.2022.100836.
Tokatlı, C., Onur, Ş. G., Dindar, M. B., Malafaia, G., Islam, A. R. T., Muhammad, S., 2023. Spatial-Temporal Variability and Probabilistic Health Risk Assessment of Fluoride from Lentic Ecosystem, Türkiye. International Journal of Environmental Analytical Chemistry, https://doi.org/10.1080/03067319.2023.2198645.
TS 266, 2005. Sular-İnsani Tüketim Amaçlı Sular. Türk Standartları Enstitüsü, ICS 13.060.20.
Ustaoğlu, F., İslam, S., Tokatlı, C., 2022. Ecological and probabilistic human health hazard assessment of heavy metal in Sera Lake Nature Park sediments (Trabzon, Turkey). Arabian Journal of Geosciences, 15: 597.
WHO (World Health Organization), 2011. Guidelines for Drinking-water Quality. World Health Organization Library Cataloguing-in-Publication Data, NLM Classification: WA 675.

IMPACTS OF THE 2023 TÜRKİYE EARTHQUAKES ON THE AGRICULTURE SECTOR OF HATAY PROVINCE

A. Aytekin POLAT[1]

[1]*Hatay Mustafa Kemal University, Agriculture Faculty, Department of Horticulture, Antakya, Hatay/Turkey*

Corresponding author e mail: aapolat@mku.edu.tr

ABSTRACT

On 6 February 2023, two major earthquakes (Mw 7.7 and Mw 7.6) struck Kahramanmaraş, Türkiye, followed by a third earthquake (Mw 6.4) in Hatay on 20 February 2023. These earthquakes were among the most devastating disasters in the history of the Republic of Türkiye, affecting approximately 14 million people across 11 provinces. The affected region accounts for nearly 16% of the country's agricultural production, with Hatay being one of the provinces that experienced the greatest destruction. This study assessed the impacts of the February 2023 earthquakes on the agricultural and food sector in Hatay using a mixed-methods approach combining official statistical data, field observations, damage assessment reports, and semi-structured interviews with farmers. The earthquakes caused approximately 24,000 fatalities in Hatay and resulted in the destruction or severe damage of 80,323 buildings. Agricultural lands, irrigation systems, livestock facilities, storage infrastructure, and other production assets sustained extensive damage. According to official records, 2,861 cattle, 13,625 small ruminants, 5,529 barns and livestock shelters, and 9,381 beehives were lost or damaged, while the poultry sector was affected in 39 commercial enterprises. In addition, disruptions in the supply of essential agricultural inputs, including seeds, fertilizers, feed, and irrigation water, significantly constrained agricultural production. Labor shortages caused by large-scale migration and damage to rural infrastructure further delayed agricultural recovery. The findings indicate that the February 2023 earthquakes caused multidimensional disruptions extending well beyond direct physical damage, affecting agricultural production, supply chains, labor availability, and rural livelihoods. Strengthening disaster preparedness, rehabilitating agricultural infrastructure, and integrating resilience-based policies into long-term agricultural recovery strategies are essential for improving the sustainability and resilience of agroecosystems in earthquake-prone regions.

Keywords: agricultural production, disaster recovery, earthquake impacts, Hatay, Türkiye

INTRODUCTİON

Natural disasters threaten human life and the sustainability of many sectors, particularly agriculture. Among these disasters, earthquakes are especially significant because of their frequent occurrence and their widespread impacts (Agızan et al., 2023). In addition to causing delays and interruptions in agricultural activities, earthquakes damage production resources, irrigation infrastructure, and agricultural land through landslides, faulting, and ground fissures. They also trigger migration, reduce agricultural labor availability, and disrupt production systems, ultimately decreasing both the quantity and quality of agricultural products and contributing to higher food prices (Polat, 2025).

Due to its geographical location, Türkiye is highly prone to earthquakes. Between 1900 and 2023, the country experienced 269 damaging or fatal earthquakes, including 20 events with a magnitude of Mw ≥7.0. Among these, the 2023 Kahramanmaraş earthquakes, together with the 1939 Erzincan and 1999 Gölcük earthquakes, rank as the most destructive in terms of casualties and economic losses (PSB, 2023).

On February 6, 2023, two major earthquakes of Mw 7.7 and Mw 7.6 struck Pazarcık and Elbistan (Kahramanmaraş), followed by a Mw 6.4 earthquake in Yayladağı (Hatay) on February 20. These events represent one of the largest natural disasters in the history of the Republic of Türkiye and one of the most devastating earthquake sequences worldwide. The earthquakes affected approximately 120,000 km² and 14 million people across 11 provinces, causing 53,537 fatalities and 107,204 injuries (PSB, 2024). More than half a million buildings sustained damage, including residential, commercial, public, educational, healthcare, and historical structures, resulting in severe disruption to communication, energy, and transportation infrastructure (PSB, 2024).

The affected region encompasses approximately 4.03 million hectares of fertile agricultural land and accounts for nearly 16% of Türkiye's agricultural production, 15.3% of its agricultural gross domestic product, and 18.7% of its agricultural and forestry exports (PSB, 2023). These provinces produce 16.2% of the country's field crops, 26% of its fruit, and 15.2% of its vegetables, while also containing 13% of the national cattle population and 17.8% of the small ruminant population (TurkStat, 2023a). Hatay, the province most severely affected by the earthquakes, contributes 1.3% of Türkiye's gross domestic product and 1.6% of its agricultural gross domestic product (PSB, 2024). The province is one of the country's leading agricultural production and export centers, accounting for 15.6% of Türkiye's fresh fruit and vegetable exports in 2023. Its agricultural exports reached USD 818 million, with lemons, oranges, and mandarins representing the principal export commodities (Anonymous, 2023a).

Because agriculture constitutes the dominant economic activity in much of the disaster region, the earthquakes had profound consequences for agricultural production and food security. Extensive damage occurred to irrigation systems, livestock shelters, food processing facilities, grain silos, storage infrastructure, fisheries, and agricultural supply chains. Large-scale migration further reduced agricultural labor availability and disrupted production activities. According to the Food and Agriculture Organization (FAO), more than 20% of Türkiye's agricultural production was affected, and the initial economic loss in the agricultural sector was estimated at TL 24.2 billion (USD 1.3 billion) (FAO, 2023a, b).

This study evaluates the strategic importance of Hatay within Türkiye's agricultural sector, assesses the impacts of the 2023 earthquakes on agricultural production and infrastructure, identifies the major challenges faced by the sector, and proposes recommendations to strengthen agricultural resilience, safeguard food security, and improve the sustainability of agricultural supply chains following major natural disasters.

MATERİALS AND METHODS

The study was conducted in Hatay province, one of the regions most severely affected by the devastating earthquakes of February 6 and 20, 2023, and a region of significant importance to Türkiye’s agricultural production. Hatay, located in the Mediterranean Region of Türkiye (Figure 1), lies between 35°52′–37°04′ N latitude and 35°40′–36°35′ E longitude, at an average elevation of approximately 80 m, and is one of the oldest settlements in the country. A typical Mediterranean climate prevails in the area, with average annual temperatures ranging between 15.1°C and 20.0°C. The combination of favorable climatic conditions, soil characteristics, and topography allows for the cultivation of a wide variety of agricultural products. The province also plays a significant role in both domestic and international agricultural markets.

Figure 1. Location of Hatay Province, in Turkey.

Hatay is one of the provinces most affected by the disaster. Located at the southern tip of Turkey, Hatay is among the oldest settlements in the country. Antakya, the province's central city, has historically been a significant trade center due to its strategic location and multicultural structure. The history of Antakya dates back to 40,000 years ago. Throughout its history, Antakya has remained important and was the third-largest city of the Roman Empire. Historical records and digital photogrammetry indicate that Hatay has experienced 30 recorded earthquakes, seven of which completely destroyed the city, showing that it has been rebuilt multiple times (Beyen et al., 2003; Yüksel, 2023; Çimen, 2023; Candan, 2023). With the 2023 earthquakes, Hatay has now been destroyed for the eighth time.

This study was conducted using both quantitative and qualitative research techniques. Quantitative data were obtained from official reports and secondary sources in the literature and analyzed through document and report review methods. In this context, statistical data for Hatay province were collected from the databases and reports of the Turkish Statistical Institute, the Presidency of the Republic of Türkiye Strategy and Budget Directorate, the Hatay Provincial Directorate of Agriculture and Forestry, the Food and Agriculture Organization, and the Union of Chambers of Turkish Engineers and Architects.

Qualitative data were obtained through field observations and on-site investigations, as well as through individual and group interviews conducted with farmers to assess the impacts of the earthquakes on agricultural activities.

In the first stage of the study, the pre-earthquake structure of Hatay's agricultural sector was analyzed. All data were processed and analyzed using Microsoft Excel and presented in tabular form to facilitate interpretation. In the subsequent stage, the impacts of the earthquakes on the province's agricultural structure, including the extent of damage and destruction, were evaluated using tables and photographic evidence. Based on the findings, recommendations were developed to support the sustainability of agricultural production in the earthquake-affected region and to enhance the effectiveness of support mechanisms for the agricultural sector.

RESULTS AND DİSCUSSİON

General Information About the Province

General data on Hatay Province, including population, population density, and agricultural land availability, are summarized in Table 1. As shown, 275,578 hectares-50% of the province's total land area of 552,400 hectares-consist of agricultural land.

Table 1. General Information on Hatay Province (Anonymous,2023b; 2024)

Population (people)	1.686.043
Total Land Area of the Province (ha)	552.400
Altitude (m)	85
Population Density (per km²)	287
Coastline Length on the Mediterranean (km)	183
Number of Districts	15
Total Agricultural Land (ha)	275.578
Pasture Land (ha)	17.253
Fallow Land (da)	50.891
Forest Area (ha)	219.604

Physical and Geographical Features of Hatay Province

Located in southern Turkey along the eastern shores of the Gulf of Iskenderun, Hatay is bordered by the Mediterranean Sea to the west, Syria to the south and east, Adana to the northwest, Osmaniye to the north, and Gaziantep to the northeast. The province consists of 15 districts (Figure 2). Excluding lakes, Hatay covers an area of 5,524 km². Mountains make up 46.1% of the province's terrain, plains 33.5%, and plateaus 20.4% (Anonymous, 2023b).

Figure 2. Map of Hatay Province (Anonymous,2024)

Population and Settlement

Hatay and its surrounding region, where traces of human activity date back to the 3rd millennium BCE, is one of the earliest settled areas in Anatolia. It has drawn attention due to its dense settlement and demographic characteristics during various historical periods. Reliable population data for Hatay is available from 1940 onward. In that year, the province had a population of 246,138. According to the Address-Based Population Registration System (ADNKS), Hatay's population in 2022 (before the earthquake) was 1,686,043, including 847,128 men and 838,915 women (Anonymous, 2023b).

Structure of the Province's Agricultural Sector Before the Earthquake*Hatay's Place in Türkiye's Agricultural Production*: *Field Crop, Vegetable and Fruit Production*

Owing to its favorable climate, fertile soils, diverse agroecological conditions, and long growing season, Hatay is one of Türkiye's leading agricultural production provinces. Approximately 275,578 ha of agricultural land support intensive production of field crops, vegetables, fruits, and livestock, making the province one of the country's most important agricultural centers.

Hatay ranks first nationally in the production of sweet potato, chard, parsley, and dill, supplying approximately 76%, 72%, 65%, and 64% of Türkiye's total production, respectively. The province is also one of the country's leading citrus-producing regions, ranking second in mandarin production and third in the production of oranges, lemons, grapefruit, and total citrus fruits, contributing approximately 21% of national citrus production. In addition, olive cultivation represents a major component of the provincial economy, with approximately 14.2 million trees producing 178,933 tons of olives annually, equivalent to about 11% of Türkiye's total production and ranking the province third nationally.

Hatay also ranks among the leading producers of several other high-value crops, including carrot, loquat, grapefruit, seed cotton, banana, onion, apricot, garlic, cultivated mushroom, and persimmon. This highly diversified production structure highlights the province's strategic importance for Türkiye's agricultural economy.

Overall, Hatay makes substantial contributions to the national production of fruits, vegetables, citrus, olives, and cotton. Consequently, disruptions to agricultural production in the province have implications that extend beyond the regional level, affecting national agricultural output, food supply chains, agricultural exports, and food security.

Livestock Production and Fisheries

In addition to crop production, Hatay has a well-developed livestock sector comprising cattle, sheep and goat farming, poultry production, beekeeping, and aquaculture. These activities constitute an important component of the provincial agricultural economy and provide substantial income and employment for rural communities.

Prior to the February 2023 earthquakes, Hatay had 141,444 cattle, 558,609 small ruminants, 1,026,159 poultry, and 111,959 beehives, demonstrating the significant contribution of livestock production to the province's agricultural economy. The steadily increasing number of beehives also reflects the growing importance of beekeeping in the region.

Hatay also has an important fisheries and aquaculture sector supported by four fishing harbors. Although the province accounts for approximately 1.6% of Türkiye's total marine aquaculture production, its aquaculture production capacity had increased steadily before the earthquake, reflecting continued investment and the growing importance of this sector within the provincial economy.

Overall, the combined strength of the crop, livestock, and fisheries sectors highlights Hatay's strategic importance within Türkiye's agricultural system. Consequently, the extensive damage caused by the February 2023 earthquakes affected not only regional agricultural production but also national food supply chains, agricultural exports, and food security.

Agro-Based Industry

Hatay has a well-developed agro-based industry, with food manufacturing representing the largest industrial sector and accounting for 26.02% of all industrial enterprises. Until the 1970s, industrial development was closely linked to agriculture, particularly cotton production in the Amik Plain, which stimulated the establishment of numerous ginning and pressing factories as well as food, cottonseed oil, and olive oil processing facilities.

Today, agro-industrial activities remain concentrated on the processing, packaging, and marketing of major agricultural commodities, including wheat, cotton, citrus fruits, olives, onions, parsley, and tomatoes. Most of these enterprises are located in Antakya, İskenderun, Samandağ, and Dörtyol (UCTEA, 2024)

Damage to Agricultural Production after the Earthquakes

Overall Earthquake Damage in Hatay Province

According to the Ministry's Damage Assessment Report dated January 22, 2024, a total of 250,086 residential buildings in Hatay were classified as urgently demolished, destroyed, severely damaged, or moderately damaged. In addition, 44,060 commercial buildings and 2,581 barns and haylofts sustained similar levels of damage (PSB, 2024). Overall, approximately 56%

of the province's building stock was damaged or destroyed, while in central Antakya the damage rate reached 85–90%.

The earthquakes claimed 24,147 lives and caused widespread destruction of housing, public buildings, commercial facilities, and critical infrastructure, including water supply, sewage, transportation, and airport facilities. Damage to the Port of İskenderun also temporarily disrupted maritime transportation. The disaster triggered large-scale migration from Hatay, with estimates ranging from 563,751 to 775,000 displaced people (Erkılıç, 2024; FAO, 2023a). The collapse of residential areas, workplaces, and public services severely affected the province's social and economic structure and created significant challenges for post-disaster recovery.

Damage to Agricultural Production Infrastructure

The earthquakes of February 6 and 20, 2023 caused extensive damage to agricultural production infrastructure and rural settlements throughout Hatay Province, with Antakya, Defne, Samandağ, Kırıkhan, and Arsuz among the most severely affected districts. Damage extended to cultivated land, irrigation systems, agricultural machinery, grain silos, storage facilities, greenhouses, livestock units, food-processing plants, cotton gins, olive oil facilities, aquaculture enterprises, cold storage units, and agricultural input suppliers.

Impact on Crop Production

Agricultural infrastructure and greenhouse equipment across Hatay suffered significant damage, adversely affecting greenhouse cultivation. Seeds, fertilizers, pesticides, plant protection products, and stored produce were also damaged.

Due to heavy damage to tractors and other agricultural machinery, combined with a shortage of inputs, equipment, and labor, and difficulties in accessing agricultural land, land preparation for the spring season-which should have started in February-was either not conducted or delayed in many areas. This led to a decline in crop yield and quality.

In crop production areas, substantial losses occurred in fertilizers, seeds, plant protection products, and irrigation equipment. While seed loss remained limited in Belen and Hassa districts, fertilizer loss ranged between 25% and 50% in Altınözü, Antakya, Defne, and Erzin. In Arsuz, approximately 50% of irrigation pumps were damaged, and in Kırıkhan, many grain silos were affected (FAO, 2023a).

Vegetable growers experienced yield losses due to difficulties in accessing fungicides and plant nutrition products. In Samandağ, 50–75% of irrigation equipment, greenhouses, food processing units, and agricultural warehouses were severely damaged. In Kırıkhan, Samandağ, and Altınözü, major losses in agricultural mechanization were reported. Furthermore, the use of greenhouses as temporary shelters by displaced urban residents or rural dwellers unable to return to their homes significantly reduced greenhouse production.

In some regions, ruptures along fault lines and ground slippages caused fruit trees to be uprooted and orchards to suffer major deformations. For example, a new valley 300 meters long, 50 meters wide, and 40 meters deep formed in an olive grove in the Tepehan neighborhood of Altınözü district (Figure 3).

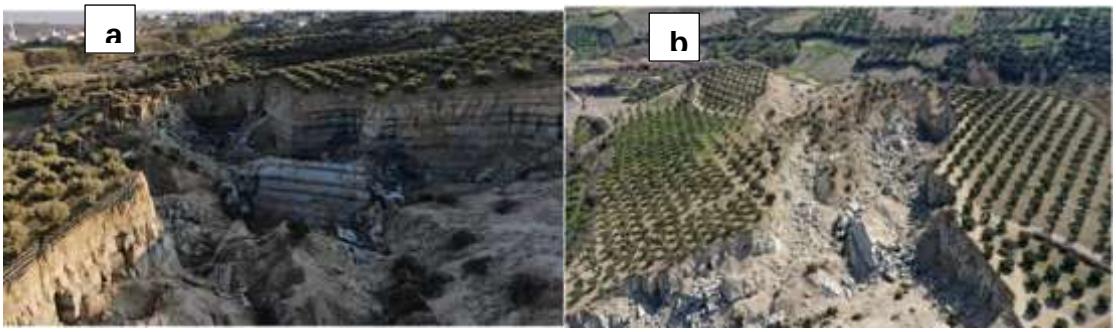

Figure 3. A split olive grove caused by the earthquake (DNA, 2023)

Impact on Livestock Production

The earthquakes caused extensive damage to the livestock sector in Hatay Province. A total of 2,861 cattle and 13,625 small ruminants were lost, while 305 corrals, 5,224 barns, and 9,381 beehives were damaged (Figure 4). The greatest losses were recorded in Antakya, Kırıkhan, Hassa, Kumlu, and Samandağ, highlighting the severe impact on districts where livestock production is a major agricultural activity.

Figure 4. Collapsed barns and corrals after the earthquake

The poultry sector was also significantly affected, with damage reported in 39 poultry enterprises, including four layer farms and one broiler operation. In several broiler farms, the collapse of feed silos and transportation disruptions caused mass bird mortality, resulting in substantial production losses (Akdemir et al., 2023).

The dairy sector experienced considerable disruption. Approximately 500 milking machines were damaged in Samandağ, while milk processing facilities in Defne and Samandağ sustained severe damage. Power outages interrupted milking operations, leading to animal health problems, reduced milk production, and increased veterinary costs. In addition, damage to feed mills, processing plants, storage facilities, transportation infrastructure, and the cold chain disrupted feed supply and milk marketing, causing significant economic losses for livestock producers.

Impact on the Fisheries Sector

The fisheries sector also suffered extensive damage. Fishing ports in İskenderun, Samandağ, Arsuz, and Dörtyol experienced severe damage to operational facilities and cold-chain infrastructure. Approximately 60% of fishing boats were damaged or destroyed; in Samandağ alone, 30 of 100 boats were completely destroyed and another 30 were partially damaged. The Food and Agriculture Organization estimated the total economic loss at approximately USD 4.5 million (FAO, 2023a, c). In addition, the İskenderun Fishing Port, which served as both a

landing site and a shelter for approximately 250 fishing vessels, sustained extensive structural damage (Figure 5).

Figure 5. Fishing port in İskenderun, Hatay

As the İskenderun Fishing Port remained out of service until repairs were completed, fishing vessels were temporarily relocated to Madenli Fishing Port, located 22 km away. According to the Ministry of Transport and Infrastructure, the total damage to fishing ports was estimated at TL 489.7 million. Hatay's ornamental fish sector was also severely affected: one production facility was completely destroyed, another ceased operations following the death of its owner, and two additional farms experienced extensive fish losses due to earthquake-induced failures of earthen ponds.

Impact on Agricultural Tools and Equipmen

The earthquakes caused extensive damage to agricultural machinery and equipment across Hatay Province. A total of 410 tractors and 6,914 agricultural tools and equipment were damaged (Figure 6). Tractor losses were highest in Kırıkhan (150), followed by Antakya (122) and Hassa (69), whereas damage to agricultural machinery and equipment was most severe in Antakya (4,125 units), followed by Kırıkhan (1,749) and Kumlu (536). These losses substantially reduced agricultural mechanization capacity, thereby hindering agricultural production and post-earthquake recovery efforts.

Figure 6. Tractors and machinery buried under rubble

Impact on Agro-Industry

The earthquakes caused extensive damage to Hatay's agro-industrial sector. In districts such as Antakya, Kırıkhan, and Samandağ, widespread building collapses and severe damage to food-processing facilities brought agro-industrial activities to a standstill. Damage to transportation, energy, water supply, sewage, and communication infrastructure further disrupted agricultural production, processing, and marketing.

Following the disaster, 2,798 sales and mass-consumption enterprises and 485 manufacturing enterprises ceased operations. Business closures were concentrated in Antakya (1,760 sales enterprises and 313 manufacturing enterprises), followed by Kırıkhan and Samandağ. In addition, 485 agricultural production and processing facilities became non-operational, including 335 bakeries, 29 fruit packing and processing facilities, 20 milk processing plants, and smaller numbers of slaughterhouses, egg-packing, spice-processing, and edible oil filling facilities. These losses severely disrupted the agricultural value chain by reducing the region's capacity to process, distribute, and market agricultural products.

Of the 121 facilities established under the Ministry of Agriculture and Forestry's Rural Development Program, 55 sustained earthquake damage, with total losses estimated at approximately TL 150.5 million (Table 14).

Table 14. Damage to Rural Development Enterprises by Sector

Sector	**Number of Enterprises**	**Estimated Loss (TL)**
Cotton (Ginning Factory)	13	50.000.000
Greenhouse	7	5.500.000
Cold Storage Facility	2	15.000.000
Livestock (Dairy Production)	2	20.000.000
Winery	1	1.000.000
Flour Factory	4	5.000.000
Animal Feed Factory	2	24.000.000
Olive Oil Factory	24	30.000.000
Total	**55**	**150.500.000**

Impact on Migration, Agricultural Labor, and Land Use

The earthquakes triggered large-scale migration, resulting in severe labor shortages in the agricultural sector. According to AFAD, approximately 564,000 people migrated from Hatay, while the Food and Agriculture Organization estimated the number at 775,000 (FAO, 2023a). This population displacement significantly disrupted planting and harvesting activities, threatening the sustainability of agricultural production.

According to the Farmer Registration System, the number of registered farmers in Hatay declined from 21,712 in 2022 to 20,044 in 2023. In addition, 7,913 decares of pastureland were rezoned for post-disaster housing and 424 decares for industrial development (Anonymous, 2023b). The establishment of container settlements and temporary shelters on agricultural land further reduced the area available for cultivation and negatively affected rural livelihoods.

Impact on the Physical Structure of Agricultural Lands

The earthquakes caused significant changes to the physical structure of agricultural lands. Soil uplift, fault-induced ground deformation, and topographic changes were observed across the affected areas, resulting in inconsistencies between land parcel records and geographic information system (GIS) data. Surface ruptures and ground displacement disrupted land consolidation projects and cadastral systems, while in some locations, large fault-induced valleys split fruit orchards into two (Figure 7).

Figure 7. Valley formed in an olive grove due to earthquake-induced landslide (DNA, 2023).

Impact on Logistics and Foreign Trade

The earthquakes caused severe liquefaction and lateral spreading in Antakya, Samandağ, and İskenderun, resulting in extensive damage to airports, highways, and railways and seriously disrupting transportation throughout Hatay. Blocked roads further restricted access to the affected areas during the emergency response period.

According to FAO field assessments, liquefaction along the İskenderun coast caused parts of the port to subside by approximately 1.5 m below sea level, severely damaging port infrastructure and forcing the temporary suspension of operations (FAO, 2023a). Numerous export-ready containers were destroyed, and fires at the port (Figure 8) caused the spoilage of food and agricultural products, resulting in substantial economic losses. Because the Port of İskenderun is a strategic logistics hub for Hatay, the Çukurova Region, and Eastern and Southeastern Anatolia, the disruption of its operations adversely affected regional agro-industrial activities and foreign trade (Özsalman and Yıldırım, 2024; Ketboga, 2024).

Figure 8. Burned container depot in İskenderun Port (a); post-earthquake condition of the depot (b) (UCTEA, 2023).

Liquefaction in the Amik Plain also damaged the Antakya–Cilvegözü highway, Hatay Airport runway (Figure 9), and railway infrastructure, leading to the suspension of civilian air transport and further restricting freight movement.

Previous studies have shown that earthquake-related damage to transportation infrastructure significantly disrupted both exports and imports (Özsalman and Yıldırım, 2024; Bardakçı and Demirtaş, 2023; Can et al., 2024). Hatay was among the three provinces experiencing the greatest export losses, and together these provinces accounted for 7.5 percentage points of the overall 11.1% decline in exports recorded across the earthquake-affected region.

Figure 9. Damaged runway (a) and airport connection roads (b) at Hatay Airport (UCTEA, 2023; Gokceoglu, 2023)

Impact on Production and Foreign Trade

The earthquakes caused widespread damage to production infrastructure in Hatay, temporarily bringing commercial activities to a standstill. Physical destruction of production facilities, workforce losses due to fatalities and migration, and disruptions to transportation and supply chains significantly reduced production capacity and export performance. In particular, damage to the road network (Figure 10) severely hindered logistics operations, resulting in production delays, order cancellations, and substantial losses in foreign trade (Yucel, 2023).

Figure 10. Earthquake damage to highways between Hatay-Kırıkhan (a) and Kırıkhan-Reyhanlı (b)

Debris Management and Its Impact on Ecosystems

The post-earthquake debris removal process was often conducted without adequate environmental safeguards, resulting in substantial impacts on natural ecosystems and agricultural landscapes. Unregulated disposal of rubble threatened biodiversity-rich areas in Hatay (Figure 11a), while debris dumping near residential areas and agricultural land (Figures 11b and 11c), including fruit and vegetable production areas, created environmental and public health concerns and disrupted agricultural activities.

Olive groves, mandarin orchards, and other agricultural lands were buried beneath debris, causing considerable economic losses and hindering agricultural recovery. In addition, the transport and disposal of construction waste contributed to the contamination of surface and groundwater (Figures 11b and 11c), posing potential risks to soil quality, agricultural production, and the food chain. The Asi River and the Mileyha Wetland, where the river flows into the Mediterranean Sea, were heavily affected by construction waste, while dust and

particulate matter generated during debris removal (Figure 11d) further threatened environmental quality and human health (UCTEA, 2024).

Figure 11. Rubble dump areas: (a) Composition of waste in dump sites; (b-c) Rubble sites in İskenderun Sarımazı and Pirinçlik—located near settlements, agricultural land, and groundwater recharge zones; (d) Dust cloud formed after dumping (UCTEA, 2023).

CONCLUSION

This study provides a comprehensive assessment of the impacts of the February 6 and 20, 2023 earthquakes on the agricultural production system of Hatay Province, the region most severely affected by the disaster. The earthquakes caused extensive damage to agricultural infrastructure, including farmland, irrigation systems, greenhouses, storage facilities, livestock production units, and agro-industrial enterprises. Beyond physical destruction, they significantly disrupted agricultural production, supply chains, rural livelihoods, and the province's capacity to sustain food production.

The findings indicate that losses in crop, livestock, fisheries, and agro-industrial sectors, together with damage to transportation and logistics infrastructure and large-scale migration, considerably weakened the regional agricultural economy and reduced agricultural productivity. Based on these findings, the following recommendations are proposed:

a) Reconstruct agricultural infrastructure through district-based prioritization, with emphasis on irrigation systems, greenhouses, livestock shelters, agricultural machinery, and rural enterprises.

b) Mitigate labor shortages by supporting the return of displaced farmers and agricultural workers through housing, financial assistance, and social support programs.

c) Update GIS databases and the Farmer Registration System to address land record inconsistencies caused by earthquake-induced land deformation.

d) Strengthen the resilience of logistics infrastructure, including ports, transportation networks, cold-chain facilities, processing plants, and agricultural supply systems.

e) Promote disaster-resilient agriculture through risk reduction strategies, early warning systems, resilient agricultural insurance schemes, continuous monitoring of fault-affected areas,

and sustainable land management practices. Urgent recovery priorities include restoring access to agricultural inputs, irrigation water, credit, and markets to enable producers to resume agricultural activities.

In conclusion, the agricultural losses experienced in Hatay represent not only a regional challenge but also a national concern for food security and agricultural sustainability. Long-term recovery will require an integrated, data-driven, and locally adapted reconstruction strategy that simultaneously supports agricultural production, rural livelihoods, and the resilience of the agricultural sector.

REFERENCES

Ağızan, K.; Bayramoğlu, Z.; Amri, H.I.B.F. 2023. Discussion of the Effects of Earthquake Disaster on Agricultural Production and Marketing (In Turkish, with English abstract). In M. Direk (Ed.), Proceedings of the 2nd International Conference on Sustainable Ecological Agriculture, pp: 217-229.

Akdemir, S.; Sahli, Z.; Kougnigan, E.; Tuna, K.E.; Ortulu, M.; Akinci, S.; Narci, G.; Ismailla, I.S. 2023. Socio-economic impact of the earthquakes of February 2023 on agricultural production of Türkiye. Scientific Papers. Series "Management, Economic Engineering in Agriculture and Rural Development, 23(2), 21-28.

Anonymous. Hatay Governorship, 2023a. Available online: http://www.hatay.gov.tr/hatayda-tarim (Accessed on 05 June 2025).

Anonymous. Hatay Directorate of Provincial Agriculture and Forestry, 2023b. Available online: https://hatay.tarimorman.gov.tr/Menu/55/Tarimsal-Veriler(Accessed on 05 June 2025).

Anonymous. Hatay Agricultural Investment Guide. Ministry of Agriculture and Forestry, General Directorate of Agricultural Reform, Agricultural Investor Advisory Office, 2024. Available online: https://www.tarimorman.gov.tr/TRGM/TARYAT/Belgeler/Tarımsal yatırım rehberi/ Hatay Tarımsal yatırım rehberi.pdf (Accessed on 05 June 2025).

Bardakçı, H.; Demirtaş, F. 2023.The Impact of Natural Disasters on International Trade: Evaluation of The Results of the Earthquakes in Turkey in 2023(In Turkish, with English abstract). Avrasya Dosyası Dergisi, 14(1), 183-204.

Beyen, K.; Erdik, M.; Mazmanoğlu, C.; Ekmekçioğlu, Z. 2003. Seismic Activity of Antakya from Past to Present and an Evaluation of Necessary Measures in Light of an International Conference (In Turkish). Türkiye Mühendislik Haberleri, 423, (2003/1), 51-53.

Can, B.A.; Gerdan, S.; Aslan, R. 2024. The Effects of 6 February 2023 Earthquakes on the Production and Marketing Process of Firms in the Agriculture and Food Sector: The Case of Malatya Province, Türkiye. Sustainability, 16, 9479. https:// doi.org/ 10.3390/su16219479

Candan, M. Destroyed seven times, reborn from its ashes seven times: Hatay (In Turkish), 2023. Available online: https://www.gazeteduvar.com.tr/7-kere-yikildi-7-kere-kullerinden-yeniden-dogdu-hatay-haber-1646757(Accessed on 05 June 2025).

Çimen, M. 2023 *Earthquakes in Hatay in a Historical Perspective* (In Turkish). Available online: https://bbnhaber.com.tr/yazarlar/ mustafa-cimen/tarihi-surec-icerisinde-hatay-depremleri -4197(Accessed on 05 June 2025).

Demirören News Agency(DNA). 2023. The olive grove was split in two in the earthquake; a 50-meter-wide valley was formed. Available online: https://www.dha.com.tr/yerel-haberler/hatay/altinozu/ zeytinlik-depremde-ikiye-bolundu-50-metre-geni-2204469 (Accessed on 05 June 2025).

Erkılıç, O. 2024. Hatay in the First Year After the Earthquake: Half of the Total Death Toll is from Hatay (Turkish). Available online: https://www.voaturkce.com/a/depremin-birinci-yilinda-hatay/7470105.html (Accessed on 05 June 2025).

Food and Agriculture Organization. 2023a. Türkiye: Agricultural sector needs assessment for earthquake-impacted provinces. Available online: https://doi.org/10.4060/cc6884en (Accessed on 05 June 2025).
Food and Agriculture Organization. 2023b. Türkiye earthquakes: initial assessment indicates losses of more than 20 percent in food production. Available online: https://www.preventionweb.net/news/turkiye-earthquakes-initial-assessment-indicates-losses-more-20-percent-food-production (Accessed on 05 June 2025).
Food and Agriculture Organization. 2023c. Türkiye initial assessment on possible impacts of earthquake in 11 provinces. Available online: https://www.fao.org/3/cc4779en/cc4779en.pdf (Accessed on 05 June 2025).
Gokceoglu, C. 2023. 6 February 2023 Kahramanmaraş – Türkiye Earthquakes: A General Overview. The International Archives of the Photogrammetry, Remote Sensing and Spatial Information Sciences, Volume XLVIII-M-1-2023 39th International Symposium on Remote Sensing of Environment (ISRSE-39) "From Human Needs to SDGs", 24–28 April 2023, Antalya, Türkiye, p.417-424.
Ketboga, M. 2024. The effects of the two major earthquakes on 6 February 2023 on the activities of foreign trade firms operating in Malatya Province and suggestions for solutions to the problems encountered. Igdır University Journal of Social Sciences, 35, 493–505.
Özsalman, E.; Yıldırım, U.T. 2024. The effects of the 6 February 2023 Kahramanmaras earthquakes on foreign trade: The case of 11 provinces. Journal of Academic Approaches, 15, 598–617.
Polat, A.A. 2025. The Effects of February 2023 Earthquakes Centered in Kahramanmaraş and Hatay, Türkiye on The Region's Agricultural Sector. Scientific Papers. Series "Management, Economic Engineering in Agriculture and Rural Development, 25 (4), 703-715.
Presidency of Strategy and Budget. Presidency of the Republic of Türkiye. 2023. 2023-Kahramanmaras-and-Hatay-Earthquakes-Report. Ankara, Turkiye, 2023. 140p. Available online: https://www.sbb.gov.tr/wp-content/uploads/2023/03/2023 Kahramanmaras-and-Hatay Earthquakes - Report.pdf (Accessed on 05 June 2025).
Presidency of Strategy and Budget. Presidency of the Republic of Türkiye. 2024. Kahramanmaras and Hatay Earthquakes Reconstruction and Development Report. Ankara, 2024. 133p. Available online: https://www.sbb.gov.tr/wp-content/uploads/2024/02/Kahramanmaras-ve-Hatay-Depremleri-Yeniden-Imar-ve-Gelisme-Raporu-1.pdf(Accessed on 05 June 2025).
The Union of Chambers of Turkish Engineers and Architects (UCTEA). 2023. Kahramanmaraş Earthquake Report. Available online: https://www.tmmob.org.tr/sites/default/files/ tmmob_deprem_raporu_son_4agustos-part-2-2.pdf (Accessed on 05 June 2025).
The Union of Chambers of Turkish Engineers and Architects (UCTEA). 2024. Second-Year Evaluation Report by TMMOB on the February 6, 2023 Kahramanmaraş Earthquakes (In Turkish). Available online: https://www.tmmob.org.tr/ sites/default/files/ ikinciyil_degerlendirme.pdf (Accessed on 05 June 2025).
Turkish Statistical Institute. Statistics on Crop Production, 2023a. Available online: ttps://data.tuik.gov.tr/ Kategori/GetKategori?p= Tarim-111(Accessed on 05 June 2025).
Turkish Statistical Institute. Statistics on Livestock Production, 2023b. Available online: https://biruni.tuik.gov.tr/hayvancilikapp/hayvancilik. zul (Accessed on 05 June 2025).
Yücel, A. 2023. Earthquakes in Turkey have disrupted supply chains. Available online: https://www.ekonomim.com/ekonomi/turkiyedeki-depremler-tedarik-zincirlerine-darbe-vurdu-haberi-684389 (Accessed on 05 June 2025).
Yüksel, Ş. 2023. Antakya's Earthquake Story (In Turkish, with English abstract). Modular Journal, 6(2),102-106.

INFLUENCE OF QUINCE ROOTSTOCKS ON VEGETATIVE GROWTH, INFLORESCENCE TRAITS, FLOWERING, AND FRUIT SET OF LOQUAT IN HIGH-DENSITY ORCHARDS

Atila Aytekin POLAT[1]

[1]*Hatay Mustafa Kemal University, Faculty of Agriculture, Department of Horticulture, Antakya, 31034 Hatay, Türkiye,*

Corresponding author e-mail: aapolat@mku.edu.tr

ABSTRACT

High production costs remain a major constraint for loquat cultivation. The expansion of loquat orchards in Turkey depends on cost reduction, increased productivity, and the supply of early and profitable products. High-density orchards using dwarf or semi-dwarf early cultivars offer a potential solution. The aim of the study is to investigate the vegetative growth and phenological characteristics of the loquat cultivar grafted on some quince rootstocks. In the experiment, 'Hafif Çukurgöbek (HÇG)' loquat cultivar grafted on three Quince rootstocks (BA 29, Quince A = MA, Quince C = MC) was used. The experiment was laid out in a completely randomized design with 5 replications and 6 plants were used in each replicate. In the study, vegetative growth parameters such as annual shoot length, trunk diameter of stock and scion and also structure canopy, phenological observations such as *inflorescence characteristics* (number of peduncles per cluster, number of flower buds per cluster, and number of flowers per cluster), and fruit set ratios (percent blossom ratios, % initial fruit set, and % final fruit set) of the cultivar/rootstock combinations were determined. Quince-C rootstock gave higher values in terms of annual shoot length, scion and rootstock diameter compared to Quince-A and BA-29 rootstocks. The differences between the rootstocks in terms of vegetative parameters were found to be statistically significant at 5% level. According to the three-year average, the flowering rate was found the highest in BA-29 rootstock, the lowest in MA rootstock. MA rootstock yielded the lowest value in the ratio of fruit harvested, while MC and BA-29 gave close values to each other. The data shows that BA-29 and MC give better results than the MA rootstock.

Keywords: loquat, quince rootstocks, vegetative growth, flowering, fruit set

INTRODUCTION

Loquat (*Eriobotrya japonica* Lindl.) is an evergreen fruit species belonging to the family Rosaceae within the order Rosales. It is mainly cultivated under subtropical climatic conditions, generally between latitudes 20° and 35° in both hemispheres. Loquat trees can tolerate winter temperatures down to –10 °C; however, flowers and developing fruits are susceptible to damage at approximately –3 °C (Polat, 2019).

Due to its early ripening period—coinciding with a season when most other fruit species are not yet harvested—loquat commands high market demand and premium prices. For this reason, it represents an economically valuable fruit crop for both producers and consumers (Polat and Kaşka, 1991; Polat, 1996; Özçağıran et al., 2011). Nevertheless, loquat trees typically reach heights of 5–10 m and develop large, spreading canopies, which increase production costs and complicate cultural practices. Controlling tree vigor is therefore essential, and the use of dwarfing rootstocks is among the most effective approaches. Dwarfing rootstocks enable high-

density planting systems that facilitate pruning, spraying, thinning, and especially harvesting, thereby reducing labor requirements while improving yield, fruit quality, and marketable production.

Considerable research has been conducted to identify suitable dwarfing rootstocks for many fruit species. In particular, clonal quince rootstocks—also evaluated in the present study—have been widely and successfully used in pear production, where they provide significant vigor control and improved orchard management. However, studies investigating their potential use in loquat cultivation remain limited. Previous research on loquat rootstocks has primarily focused on graft compatibility with wild *Eriobotrya* species (Zhang et al., 2007, 2010, 2011), graft success on loquat seedlings and quince rootstocks (Polat and Kaşka, 1992a, 1992b; Pio et al., 2010; Polat, 2018a, 2019, 2020, 2021b, 2021c), effects on vegetative growth (Polat and Kaşka, 1992a, 1992b; Polat, 1995; Baratta et al., 2001; Pio et al., 2007), and tolerance to salinity in irrigation water or soils (Garcia-Legaz et al., 2005; Lopez et al., 2007; Manuel et al., 2008). Despite these efforts, the identification of effective dwarfing rootstocks for loquat—comparable to those used in apple and pear—remains a critical research need for the development of high-density orchards.

One of the major constraints limiting the expansion of loquat cultivation is the large canopy size of trees grafted onto seedling rootstocks, which increases the cost of cultural operations, particularly pruning and fruit thinning. Reducing production costs, improving productivity, and achieving earlier yields are therefore essential objectives. Previous high-density planting studies have reported promising results, including reduced tree size (e.g., average heights around 1.87 m) and substantially lower labor requirements. These findings indicate that high-density loquat production with dwarf trees can provide earlier cropping, higher yield per unit area, and improved economic returns.

Several studies have suggested that quince can be used as a rootstock for loquat (Morton, 1987; Lin et al., 1999; Pio et al., 2007; Hummer and Janick, 2010; Badenes et al., 2013; Polat, 2018b). Earlier reports (Polat and Kaşka, 1992a, 1992b; Polat, 1995) indicated that quince rootstocks induced approximately 20–25% dwarfing compared with loquat seedlings, and BA-29 in particular was recommended for evaluation in high-density loquat orchards (Polat et al., 2003, 2004). Likewise, Pio et al. (2007) emphasized quince as a promising rootstock due to its capacity to reduce tree size and facilitate orchard operations.

Although some literature indicates that quince rootstocks have a dwarfing effect on loquats, studies that evaluate the effects of these rootstocks on fruit yield, quality, and vegetative growth are scarce. There is also a lack of comparative studies detailing how different quince rootstocks affect these characteristics. Therefore, in a study initiated in 2016 and still ongoing, the effects of clonal quince, hawthorn, and loquat seedling rootstocks on vegetative growth, flowering phenology, fruit set, fruit quality, and yield in loquats are being investigated. Preliminary data have been obtained regarding the effects of quince rootstocks on the vegetative development, phenological traits, yield, and fruit quality parameters of loquat cultivars grafted onto them, but it has been stated that these results are not yet conclusive and that the studies must be continued (Akkuş and Polat, 2021, 2022). This paper, which is part of the ongoing research, presents a comparative analysis of the effects of Quince-A, Quince-C and BA 29 rootstocks on vegetative growth of the HÇG loquat cultivar.

MATERIAL AND METHODS

Material

This study was conducted in Hatay, Turkey (36°12′E, 36°52′N; 80 m a.s.l.) over three consecutive years: 2018, 2019, and 2020. The experimental site is characterized by a typical Mediterranean climate, with an average annual temperature of 18.3°C and an annual precipitation of 1168 mm, most of which occurs during the winter and spring seasons. The soil

at the site is alkaline (pH 7.76), contains low levels of lime (2.4%), moderate salinity (EC: 446 µS/cm), and has a sandy-loam texture (57.37% sand, 25.32% loam, and 12% clay).
One-year-old 'Hafif Çukurgöbek' loquat trees, budded onto BA-29, Quince-A, and Quince-C quince rootstocks, were planted in January 2017 at a spacing of 1.0 × 0.5 m (equivalent to 2000 trees per decare) (Figure 1). Drip irrigation and standard horticultural practices were applied throughout the study period. Trees were trained using the open-center system.

Rootstocks and Varieties
The rootstocks BA-29, Quince-C, and Quince-A used in the experiment were originally selected at the East Malling Research Station, United Kingdom.
'Hafif Çukurgöbek' is an early-maturing loquat cultivar selected in Turkey (Demir, 1987). It produces medium-sized, orange-colored fruits that are very tasty and sweet. The cultivar is self-fertile and resistant to black spot disease caused by *Spilocaea eriobotryae*.

Method
The experiment was designed as a completely randomized design (CRD) with five replications. Each replication consisted of six plants.

Inflorescence Characteristics, Flowering, and Fruit Set Rate
For each rootstock, ten trees were selected, and four shoots per tree were used for the following measurements: number of peduncles per cluster, number of flower buds per cluster, and number of flowers per cluster. In accordance with the methodology described by Polat (2007, 2015) and Akkuş and Polat (2022), these observations were conducted at approximately 3-day intervals starting when the clusters first became visible on the shoots.
The flowering rate (%), initial fruit set (%), and small and final fruit set ratios (%) were calculated according to the methods proposed by Westwood (1995) and Polat (2007, 2015). To determine fruit set rate, four branches were selected randomly (one in each cardinal direction) and were tagged. Approximately 250-300 flower buds were counted at the pre-blossom phase on each of the selected branches. Thus, ca. 1000-1200 flower buds were selected on each tree. The flowers of each tagged branch were counted, and blossom rate was calculated as the proportion of the flower to bud number. At the end of blossoming, the number of initial fruits was counted, and initial fruit set percentage was calculated dividing this value by the flower number. Final fruit set percentage was determined by calculating the proportion of the number of harvested fruits to the number of flowers.

Vegetative Growth Measurements
Tree vegetative growth was assessed at mid of May every years measuring the following parameters:
Annual shoot length (cm): The length of four shoots per tree (one for each cardinal direction) was measured with a 5-meter measuring tape.
Trunk diameter (mm): Trunk diameters of both the scion and rootstock (5 cm above and below the graft union) were measured with a digital caliper (Mitutoyo, Kawasaki, Japan) with 0.01 mm sensitivity.
Crown height (cm): The vertical distance between the first branching point of the scion (or tree trunk) and the trees apex was measured with a 5-meter measuring tape.
Tree height (cm): The vertical distance between the bud union and the tree apex was measured with a 5-meter measuring tape.

Data Analysis and Statistics

The data were analyzed using analysis of variance (ANOVA) based on a completely randomized design. Mean comparisons were performed using Tukey's HSD multiple comparison test at the 0.01 significance level (Steel and Torrie, 1980). Percentage values were subjected to angular (arcsine) transformation to improve normality prior to ANOVA.

RESULTS AND DISCUSSION

Inflorescence Characteristics, Flowering, and Fruit Set Rate

Inflorescence Traits

The results presented in Table 1 show that the rootstock had significant effects on the number of peduncles per cluster, flowering rate, and final fruit set. Trees on Quince-C produced significantly higher number of peduncles per cluster than BA-29 (Table 1).

Table 1. The effects of rootstocks on the inflorescences properties, blossoming and fruit set rates of 'Hafif Çukurgöbek' loquat cultivar (2018–2020).

Rootstocks	No. of peduncle per cluster	No. of flower buds per cluster	No. of flowers per cluster	Flowering Rate (%)	Initial fruit set (%)	Small fruit(%)	Final fruit(%)
Quince-A	15.8 ab	142.7	118. 5	82.9 b	12.0	6.9	2.5 b
Quince-C	16.5 a	148.8	137.5	91.9 a	10.6	6.0	4.6 a
BA-29	14.7 b	139.4	128.2	93.1 a	10.8	6.2	4.8 a
Significance	**	NS	NS	**	NS	NS	**

(x) Means within each column followed by different letters are significantly different according to Tukey's HSD test at $p < 0.01$. (y) NS: Not significant.

In the literature, the number of studies evaluating comprehensively inflorescence characteristics, flowering behavior, and fruit set rates for trees grafted onto the rootstocks used in our research is fairly limited. Akkuş and Polat (2022) and Polat and Sezer (2022) reported that, in trees grafted onto the Quince-A rootstock, the number of peduncles per cluster ranged between 12.8 and 17.7, the number of flower buds per cluster ranged between 172.2 and 128.0, and the number of open flowers ranged between 150.3 and 102.5. In the same studies, these parameters were reported to be, respectively, 10.5–19.5, 133.2–156.5, and 124.8–143.8 for trees on Quince-C rootstock, and 10.83–16.69, 131.80–143.17, and 119.41–132.64 for trees on BA-29 rootstock. In an earlier study, the numbers of peduncles, flower buds, and open flowers were reported to be, respectively, 9.0, 123.3, and 115.3 in trees grafted onto hawthorn rootstock, and 10.3, 156.9, and 139.6 in trees grafted onto loquat seedling rootstock (Polat, 2023). These values are substantially similar to those obtained in the present study.

Flowering Rate (%)

Rootstock effect on flowering rate was highly significant ($p < 0.01$) with trees on Quince-C (91.9%) and BA-29 (93.1%) exhibiting higher flowering rates than those on Quince-A (82.9%)(Table 1). This suggests that Quince-A restricted vegetative growth and partially reduced flowering potential. Polat and Sezer (2022) reported flowering rates of 91.6%, 93.5%, and 90.7% for trees grafted onto Quince-A, Quince-C, and BA-29 rootstocks, respectively, while Akkuş and Polat (2022) found, for trees grafted onto same rootstocks, values of 80.1%, 91.9%, and 92.7%, respectively. In another study, the flowering rate was 93.5% in plants grafted onto hawthorn rootstock and 89.0% in those grafted onto loquat seedling rootstock (Polat, 2023). The findings obtained in our study are consistent with these reported values.

Initial Fruit Set (%)

Although differences among rootstocks were not statistically significant ($p > 0.05$), trees on Quince-A displayed slightly higher initial fruit set than BA-29 and Quince-C (Table 1). Previous studies have reported that the initial fruit set rate ranged between 8.4% and 13.8% in trees on Quince-A rootstock, between 9.8% and 11.0% in trees on Quince-C, and between 10.5% and 10.9% in trees on BA-29 (Akkuş and Polat, 2022; Polat and Sezer, 2022). In another study, this parameter was found to be 11.2% in trees grafted onto hawthorn rootstock, and 10.0% in those grafted onto loquat seedling rootstock (Polat, 2023). The findings obtained in our study are consistent with these previous reports.

Percent of Small Fruit (%)

Although differences between rootstocks in *percent of small fruit* were not statistically significant, trees on Quince-A tended to have higher percent of small fruit, suggesting possible limitations in resources allocation to fruit (Table 1). Akkuş and Polat (2022) and Polat and Sezer (2022) reported small fruit ratios ranging between 4.5% and 8.0% for trees on Quince-A, between 5.3% and 6.3% for trees on Quince-C, and between 6.1% and 6.2% for trees on BA-29 rootstocks. Polat (2023) found that the small fruit ratio was 7.9% and 5.6% in trees on hawthorn rootstock and loquat seedling rootstock, respectively.

Final Fruit Set (%)

The final fruit set rate was significantly affected by the rootstock ($p < 0.01$). Trees on BA-29 (4.8%) and Quince-C (4.6%) exhibited higher fruit retention compared to those on Quince-A (2.5%), suggesting that trees on Quince-A, despite a relatively high flowering rate, were more prone to fruit drop. Previous studies (Akkuş and Polat, 2022; Polat and Sezer, 2022) reported that the final fruit set (fruit harvested) rates were 2.2–3.0%, 3.7–5.2%, and 4.7–4.9% for trees on Quince-A, Quince-C, and BA-29 rootstocks, respectively. Polat (2023) found that the final fruit set rates was 6.3% in plants grafted onto hawthorn rootstock, and 4.2% in those grafted onto loquat seedling rootstock. Overall, Quince-C and BA-29 rootstocks induced the highest overall performance in terms of flowering and fruit set, confirming that these rootstocks are more suitable for the 'Hafif Çukurgöbek' loquat cultivar. These findings are consistent with previous studies by Polat et al. (2004), Durgaç et al. (2006), Polat (2018), Akkuş and Polat (2022), and Polat and Sezer (2022), who reported significant effects of quince rootstocks on loquat flowering intensity and fruit set

Vegetative growth

Regarding annual shoot length and trunk diameters of both scion and rootstock, plants grafted onto the Quince-C rootstock exhibited more vigorous growth and significantly higher values compared to those on Quince-A and BA-29 rootstocks (Figures 2–4).

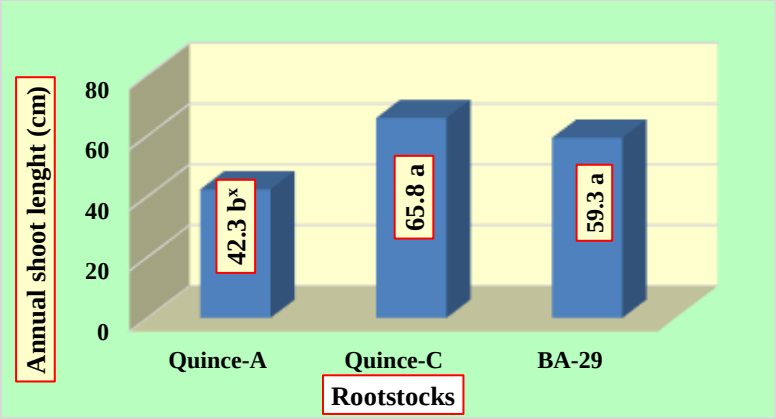

Figure 2. Average annual shoot length of 'Hafif Çukurgöbek' loquat grafted onto quince rootstocks during 2018–2020.

(x) Means followed by different lowercase letters indicate significant differences according to Tukey's test at $p < 0.05$.

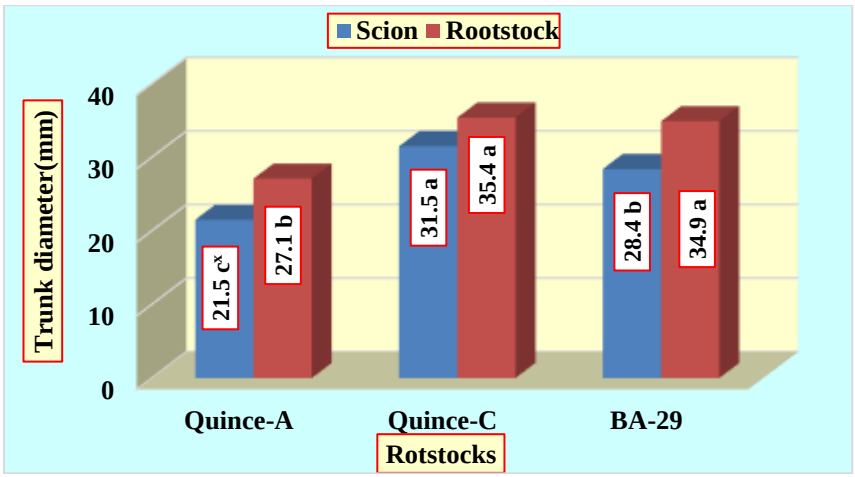

Figure 3. Average scion and rootstock trunk diameters of 'Hafif Çukurgöbek' loquat grafted onto quince rootstocks during 2018–2020.
(x) Means followed by different lowercase letters within the same parameter indicate significant differences according to Tukey's test at $p < 0.05$.

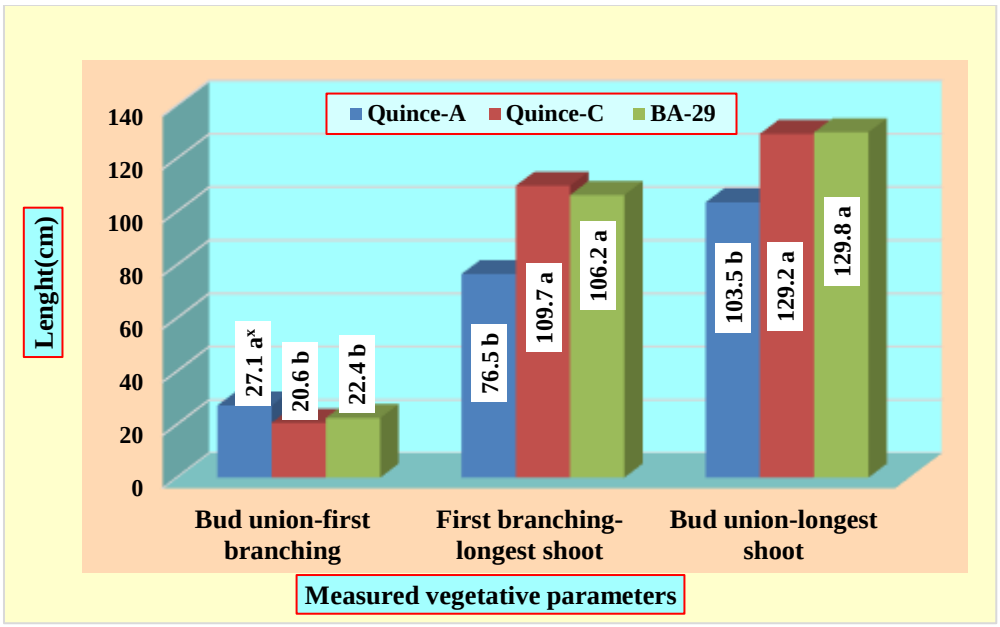

Figure 4. Some vegetative growth parameters of 'Hafif Çukurgöbek' loquat grafted onto quince rootstocks (2018–2020 average).
(x) Means followed by different lowercase letters within the same parameter indicate significant differences according to Tukey's test at $p < 0.05$.

The Quince-A rootstock showed lower values than the other two rootstocks for all parameters except for the distance between the budding point and the first branching on the trunk. In this particular measurement, Quince-A recorded the greatest distance, followed by BA-29, while Quince-C exhibited the shortest. Differences among rootstocks in terms of vegetative growth parameters were statistically significant at the 5% level.
Tree growth was initially rapid; however, crop load and pruning management appeared to regulate tree height and canopy volume. Currently, most trees have nearly occupied their allotted planting space, with average heights ranging from 1.51 to 1.85 m and trunk diameters

between 27.01 mm and 38.54 mm. These results are consistent with those reported by Hueso et al. (2007) in their study on the 'Magdal' cultivar grafted onto Quince-C rootstock.
In previous studies, Polat and Kaşka (1992a) reported an average shoot growth of 23.4 cm for plants grafted onto the Quince-A rootstock. Polat (1995) measured scion diameters in loquat seedlings ('Akko-XIII' and 'Armut Şekilli' cultivars) grafted onto Quince-A rootstocks as 18.24 mm, 30.15 mm, and 36.39 mm, and seedling heights as 74.3 cm, 120.2 cm, and 124.4 cm during the period between 1993 and 1995, respectively. The values obtained in the present study are consistent with those reported by Polat and Kaşka (1992a) and Polat (1995).

CONCLUSION

Reducing vegetative growth is very important in loquat cultivation due to its very high tree size. The most effective method for this is the use of dwarfing rootstocks such as quince (Cydonia oblonga). In this study, the effect of Quince-A, Quince-C and BA 29 quince clone rootstocks on phenological properties, flowering and fruit set rates of the HCG variety was studied in detail. Our preliminary findings indicate that dwarfing quince rootstocks are suitable for intensive loquat plantings. Among the rootstocks tested, BA-29 and Quince-C outperformed Quince-A. However, it is of great benefit to continue the further work to make a definitive judgment about the possibilities of using BA-29, and Quince-C rootstocks as new dwarfing rootstocks. Therefore, researches need to be continued, especially to determine all the characteristics regarding yield and fruit quality.

REFERENCES

Akkuş, S. and Polat, A.A. 2021. Investigation of vegetative growth, yield and fruit quality characteristics of 'Hafif Çukurgöbek' loquat cultivar grafted on different quince rootstocks. *Harran Tarım ve Gıda Bilimleri Dergisi*, 25(3), pp. 279-286. dio: 10.29050/harranziraat.910900

Akkuş, S., Polat, A.A. 2022. Effect of some quince rootstocks on inflorescence properties, flowering and fruit set in loquat (*Eriobotrya japonica* Lindl.). *KSU. Journal of Agriculture and Nature*, 25 (2), pp. 253-257. doi:10.18016/ksutarimdoga.vi.910339

Badenes, M.L., Janick, J., Lin, S., Zhang, Z., Liang, G.L., and Wang W. 2013. Breeding Loquat. *Plant Breeding Reviews,* 37, pp. 259-296.

Baratta, B., Campisi, G. and Raimondo, A. 2001. Vegetative and productive behaviour of Japanese loquat in various graft combinations. *Rivista di Frutticoltura e di Ortofloricoltura, 63,* pp. 61-64.

Demir, S. 1987. *Yenidünya Yetiştiriciliği.* T.C. Tarım Orman ve Köyişleri Bakanlığı Antalya Narenciye Araştırma Enstitüsü Müdürlüğü. Genel Yayın, 12, 31p.

Durgaç, C., Polat, A.A. and Kamiloğlu, O. 2006. Determining performances of some loquat (*Eriobotrya japonica*) cultivars under mediterranean coastal conditions in Hatay, Turkey. *New Zealand Journal of Crop and Horticultural Science*, 34, pp. 225- 230. doi: 10.1080/01140671.2006.9514411

García-Legaz, M.F., Gomez, E.L., Beneyto, J.M., Torrecillas, A. and Sánchez- Blanco, M.J. 2005. Effects of salinity and rootstock on growth, water relations, nutrition and gas exchange of loquat. *Journal of Horticultural Science & Biotechnology, 80,* pp. 199-203. doi: 10.1016/j.jplph.2007.07.022.

Hueso, J.J., Cañete, M.L. and Cuevas, J. 2007. High density loquat orchards: Plant selection and management. *Acta Horticulturae*, 750, pp. 349-353. doi: 10.17660/ActaHortic.2007.750.55

Hummer, K.E. and Janick J. 2009. Rosaceae: Taxonomy, Economic Importance, Genomics. in Kevin, M.F. and Susan, E.G (eds) *Genetics and Genomics of Rosaceae*, Springer

Science+Business Media, LLC, 233 Spring Street, New York, NY 10013, USA, pp.1-18.Doi: 10.1007/978-0-387-77491-6
Lin, S., Sharpe, R.H. and Janick, J. 1999. Loquat: Botany and Horticulture. in Jules, J. (ed.). *Horticultural Reviews*, 23, Wiley, New York, pp. 234-276. Doi: 10.1002/9780470650752.ch5
Lopez-Gomez, E., San Juan, M.A., Diaz-Vivancos, P., Mataix Beneyto, J., Garcia-Legaz, M.F. and Hernandez, J.A. 2007. Effect of rootstocks grafting and boron on the antioxidant systems and salinity tolerance of loquat plants (*Eriobotrya japonica* Lindl.). *Environmental and Experimental Botany*, 160, pp. 151-158. doi: 10.1016/j.envexpbot.2006.10.007
Manuel, F.G., Elvira, L., Jorge, M.B., Alejandra, N. and Jesus Sanchez-Blanco, M. 2008. Physiological behaviour of loquat and anger rootstocks in relation to salinity and calcium addition. *Journal of Plant Physiology* 165, pp.1041-1060.
Morton, J.F. 1987. Loquat. in Morton, J.F.(ed), *Fruits of Warm Climates*, Creative Resource Systems, Winterville, FL, pp 103-108.
Özçağıran, R., Ünal, A., Özeker, E. and İsfendiyaroğlu, M. 2011. *Ilıman İklim Meyve Türleri*: *Yumuşak Çekirdekli Meyveler* Cilt-II, Ege Üniversitesi Yayınları**,** Ziraat Fakültesi Yayınları, No: 556. İzmir, Turkey.
Pio, R., Dall'Orto, F.A.C., Barbosa, W., Chagas, E.A., Ojima, M. and Feldberg, N.P. 2007. Yield performance of loquat trees grafted on quince cultivar Portugal. *Pesquisa Agropecuária Brasileira*, 42(12), pp. 1715-1719. doi: 10.1590/S0100-204X2007001200007
Pio, R., Chagas, E.A., Barbosa, W., Signorini, G. and Feldberg, N.P. 2010. Intergeneric grafting of loquat cultivars using 'Japonese' quince tree as rootstock. *Ciência e Agrotecnologia,* 34(6), pp. 1452-1457. doi: 10.1590/S1413-70542010000600014
Polat, A.A. and Kaska, N. 1991. Investigation on the determination of most suitable buddings time and method for the loquat (*Eriobotrya japonica* Lindl.) under Adana ecological conditions. *Turkish Journal of Agriculture and Forestry* 15, pp. 975-986.
Polat, A.A. and Kaska, N. 1992a. An investigation on the usage of Quince-A as a rootstock for loquat. *Turkish Journal of Agriculture and Forestry* 16, pp. 745-755.
Polat, A.A. and Kaska, N. 1992b. Determination of budding success in loquats budded on Quince- C rootstock. *Bahçe* 21, pp. 9-11.
Polat, A.A. 1995. The effects of Quince-A rootstock on vegetative growth of loquat plants. *Derim* 12, pp. 84-88.
Polat, A.A. 1996. Akdeniz bölgemiz için önemli meyve türü: yenidünya (*Eriobotrya japonica* Lindl.). *MKÜ. Ziraat Fakültesi Dergisi***,** 1(1), pp. 39-46.
Polat, A.A. 2018a. The budding success in loquat (*Eriobotrya japonica* Lindl.) on different quince rootstock. *The 9th International Scientific Agriculture Symposium "AGROSYM 2018"*, Jahorina, Bosnia and Herzegovina. 4-7 October 2018,
Polat, A.A. 2018b. *Loquat Production in Turkey*: *Present State and Future*. LAP Lambert Academic Publishing, 69 p.
Polat, A.A. 2019. Bazı ayva anaçlarına yapılan yenidünya aşılarında aşı başarısı. *Avrasya 5. Uluslararası Uygulamalı Bilimler Kongresi*, Adana, Türkiye, s: 18-23.
Polat, A.A. 2020. Alıç anaçlarına yapılan yenidünya aşılarında aşı başarısının saptanması. *Manas Journal of Agriculture Veterinary and Life Sciences*, 10(1), pp. 1-5.
Polat, A.A. 2021b. Investigation on the usage of hawthorn (*Crataegus* spp) as rootstock for loquat (*Eriobotrya japonica* Lindl.). *Harran Tarım ve Gıda Bilimleri Dergisi,* 25(1), pp. 86-91. doi: 10.29050/harranziraat.774496
Polat, A.A. 2021c. Isıtmasız sera koşullarında yapılan yenidünya aşılarında aşı başarısının belirlenmesi. *Kahramanmaraş Sütçü İmam Üniversitesi, Tarım ve Doğa Dergisi* 24(1), pp.76-82. doi: 10.18016/ksutarimdoga.vi.741591
Polat, A.A., Durgaç, C., Kamiloğlu, Ö. and Çalışkan, O. 2003. Sık dikim ve örtüaltı yetiştirme tekniklerinin yenidünyalarda erkencilik verim ve kaliteye etkilerinin belirlenmesi. TÜBİTAK

Tarım, Orman ve Gıda Teknolojileri Araştırma Grubu, ARP – 2336, Antakya, Hatay, Türkiye, pp:68.

Polat; A.A., Durgaç, C. and Çalışkan, O. 2004. Effects of different planting space on the vegetative growth, yield and fruit quality of loquat. *Acta Horticulturae*, 632, pp.189-195. doi: 10.17660/ActaHortic.2004.632.23

Steel, R. and Torrie, J.H. 1980. *Principles and procedures of statistics*. 2nd ed. New York, McGraw-Hill.

Zhang, H.L., Lin, S.Q., Hu, Y.L., Li, J.G., Yang, X.H. and He, X.L. 2007. Photesynthetic characteristics of young 'Zaozhong No.62 loquat trees grafted on different rootstocks. *Acta Horticulturae*, 750, pp. 381-387. doi: 10.17660/ActaHortic.2007.750.61

Zhang, H.L., Zhang, K., Lin, S.Q.and Li, J.G. 2010. Screening wild eriobotrya species as rootstocks for loquat. *Journal of Horticultural Science & Biotechnology*, 85(5), pp. 399-404. doi: 10.1080/14620316.2010.11512687

ANATOMICAL EVALUATION OF EARLY-STAGE GRAFT COMPATIBILITY OF COTONEASTER NUMMULARIA WITH APPLE, PEAR, QUINCE, AND HAWTHORN

Remzi UĞUR[1], Ömer ATAGÜL[2]*

[1] Gaziantep University, Nurdagi Vocational High School, Department of Park and Garden Plants, Gaziantep, Türkiye
[2] Eastern Mediterranean Transitional Zone Agricultural Research Institute Directorate, Kahramanmaraş, Türkiye

**Corresponding author: remzibey@hotmail.com*

ABSTRACT

The conservation of natural plant genetic resources and the evaluation of wild woody species adapted to environmental stress conditions as alternative rootstocks are important objectives in rootstock breeding. In this study, the early-stage graft compatibility of *Cotoneaster nummularia*, a species naturally distributed in Anatolia, with the apple cultivar Golden Delicious, pear cultivar Deveci, quince cultivar Eşme, and hawthorn cultivar Polat Efe was evaluated anatomically. Healthy and vigorously growing *C. nummularia* genotypes were selected as rootstocks, and dormant budding was performed in September 2025. Approximately 11 months after grafting, three samples were collected from the graft union of each combination. Longitudinal sections were evaluated for the graft union line, cambial and vascular continuity, necrotic tissues, and parenchymatous tissue formation. Visual differences in starch distribution were also assessed using a 1% iodine–potassium iodide (IKI) solution. Golden Delicious/*C. nummularia* showed vascular discontinuity, necrotic areas, irregular xylem orientation, and extensive parenchymatous tissue formation, indicating early-stage anatomical incompatibility. In Eşme/*C. nummularia*, anatomical union formation occurred, but scion growth ceased; this combination was therefore considered incompatible. Deveci/*C. nummularia* largely established cambial and vascular continuity, although the graft union trace remained visible in the wood tissue. Polat Efe/*C. nummularia* most closely resembled the self-grafted *C. nummularia*/*C. nummularia* control, particularly in regular cambial–vascular continuity and the near disappearance of the graft union line. These findings indicate high early-stage anatomical compatibility between *C. nummularia* and Polat Efe hawthorn. Long-term trials with additional hawthorn genotypes are required before *C. nummularia* can be recommended as a rootstock.

Keywords: *Cotoneaster nummularia*, rootstock breeding, graft compatibility, graft union, vascular continuity.

INTRODUCTION

Anatolia is one of the world's important regions in terms of plant genetic resources and biodiversity due to its diverse climatic zones and habitats (Kaya & Raynal, 2001; Ambarlı et al., 2016; Duman et al., 2024). Türkiye is reported to harbor approximately 12,000 plant taxa, of which nearly 32% are endemic (Duman et al., 2024). The ecological heterogeneity of Anatolia supports the coexistence of wild and cultivated plant forms and provides suitable habitats for numerous woody species of the Rosaceae family (Ercisli, 2004; Basbag et al.,

2017). Long-term environmental selection can generate considerable genetic variation within natural populations, making them valuable sources of material for rootstock breeding (Ercisli, 2004). Genetic diversity related to geographic origin has been reported in *Prunus microcarpa* populations (Nas et al., 2011). In addition, naturally occurring *Prunus cerasifera* × *P. microcarpa* hybrids have been evaluated as potential rootstock materials (Uğur et al., 2021a). Therefore, the identification, conservation, and characterization of natural genetic resources are important for the development of new cultivars and rootstocks adapted to diverse environmental conditions (Ambarlı et al., 2016; Duman et al., 2024). Anatolia is home to wild genetic resources of several economically important Rosaceae genera, including Malus, Pyrus, Cydonia, Crataegus, Sorbus, Amygdalus, and Prunus (Ercisli, 2004). The potential use of wild Prunus species, including *Prunus domestica*, *P. cerasifera*, *P. divaricata*, *P. spinosa*, *P. microcarpa*, *P. scoparia*, *P. amygdalus*, and *P. arabica*, in rootstock breeding has also been investigated (Uğur, 2022; Uğur et al., 2023).

Rootstocks can influence scion vigor, precocity, yield, and fruit quality, as well as plant responses to different soil conditions, diseases, and abiotic stresses (Uğur et al., 2023; Ling et al., 2025). Wild species that naturally persist under adverse conditions such as drought, high temperature, salinity, high soil pH, and calcareous or nutrient-poor soils represent potentially valuable materials for rootstock breeding. Studies evaluating *Prunus scoparia* as a rootstock for almond under drought conditions (Abbasi et al., 2019) and reporting the effects of *P. microcarpa* on growth, yield, and nutrient uptake in apricot (Uğur, 2022; Uğur et al., 2021b) provide examples of the potential use of wild species in rootstock improvement.

This approach also supports the investigation of other wild members of the Rosaceae family as potential rootstock materials. One such species is *Cotoneaster nummularia* Fisch. & C.A.Mey. *C. nummularia* is a perennial wild species naturally occurring in Anatolia and has been reported to inhabit a wide range of environments, including dry slopes, limestone-derived soils, and eroded areas (Zengin et al., 2014; Basbag et al., 2017; Ravanbakhsh et al., 2018). This ecological distribution provides a rationale for experimentally investigating the species as a potential rootstock.

A substantial proportion of the research conducted on *C. nummularia* has focused on its ecological, phytosociological, and phytochemical characteristics. Zengin et al. (2014) reported the presence of various phenolic compounds in leaf and fruit extracts of naturally occurring *C. nummularia* from Anatolia. Although these findings do not directly demonstrate its suitability as a rootstock, they indicate that the species represents a biologically characterized wild genetic resource within the Rosaceae family. In contrast, experimental information regarding the potential use of *C. nummularia* as a rootstock for pome fruit species is currently lacking. Previous studies evaluating wild woody species as rootstocks (Nas et al., 2011; Abbasi et al., 2019; Uğur et al., 2021a; Uğur et al., 2021b; Uğur, 2022; Uğur et al., 2023; Ling et al., 2025) provide a scientific framework for investigating *C. nummularia* for this purpose.

Based on this knowledge gap, the present study aimed to evaluate the early-stage anatomical graft compatibility of naturally occurring *Cotoneaster nummularia* with Golden Delicious apple, Deveci pear, Eşme quince, and Polat Efe hawthorn. The study was conducted during 2025–2026 at the experimental grounds of Gaziantep University, Islahiye Vocational School, and in the laboratories of the Eastern Mediterranean Transitional Zone Agricultural Research Institute.

MATERİALS AND METHODS

Plant Material

The rootstock material consisted of naturally occurring *C. nummularia* genotypes growing on the campus of Gaziantep University, Islahiye Vocational School, located within the Eastern Mediterranean Transitional Zone. Commercially grown cultivars, namely Golden Delicious apple, Deveci pear, Eşme quince, and Polat Efe hawthorn, were used as scion material.

Methods

Survey and preparation of plants for grafting: A survey conducted in May 2025 identified six *C. nummularia* genotypes as potential rootstock candidates. Healthy individuals showing no visible disease symptoms and vigorous growth were selected. The selected genotypes were maintained under regular irrigation and cultural practices until September 2025. Eight branches suitable for grafting, each approximately 4–5 mm in diameter, were retained on each genotype.

Grafting and plant maintenance: In September 2025, dormant budding was performed on the selected *C. nummularia* rootstock candidates. Four rootstock–scion combinations were established: Golden Delicious apple/*C. nummularia*, Deveci pear/*C. nummularia*, Eşme quince/*C. nummularia*, and Polat Efe hawthorn/*C. nummularia*. A self-grafted *C. nummularia*/*C. nummularia* combination served as the anatomical control.

Irrigation and routine plant maintenance were continued after grafting. In March 2026, the grafted branches were cut back above the graft union to promote bud sprouting. Root suckers and vigorous watershoots were removed throughout the growing period, and routine irrigation and maintenance practices were continued from March to August 2026.

Collection of graft samples and anatomical examination: Approximately 11 months after grafting, three samples were collected from the graft union of each rootstock–scion combination and fixed in FAA solution (Sass, 1964). A total of 100 mL of FAA solution was prepared using 50 mL of 96% ethanol, 5 mL of glacial acetic acid, 10 mL of 37% formaldehyde, and 35 mL of distilled water. The samples were kept in the fixative for at least three days and were then transferred to 70% ethanol (Baş, 1998).

For macroscopic anatomical evaluation, longitudinal sections were prepared through the graft union, and the cut surfaces were smoothed using No. 0 waterproof sandpaper. A 1% iodine–potassium iodide (IKI) solution was applied to assess visual differences in starch distribution within the tissues. IKI staining intensity in the rootstock and scion tissues, the appearance of the graft union line, the structure of the bark and wood tissues, and the presence of necrotic tissue were evaluated together (Ünal, 1984; Ünal & Özçağıran, 1986; Watanabe & Nakazotomi, 1990; Tekintaş, 1991; Polat & Kaşka, 1992; Tekintaş & Dolgun, 1996; Kankaya et al., 1999).

Anatomical examinations were carried out in the laboratories of the Eastern Mediterranean Transitional Zone Agricultural Research Institute. Because the observations were qualitative and descriptive, no inferential statistical analysis was performed; the combinations were compared on the basis of the anatomical criteria described above.

RESULTS

Anatomical and IKI observations for all graft combinations are summarized in Table 1 and illustrated in Figures 1–5.

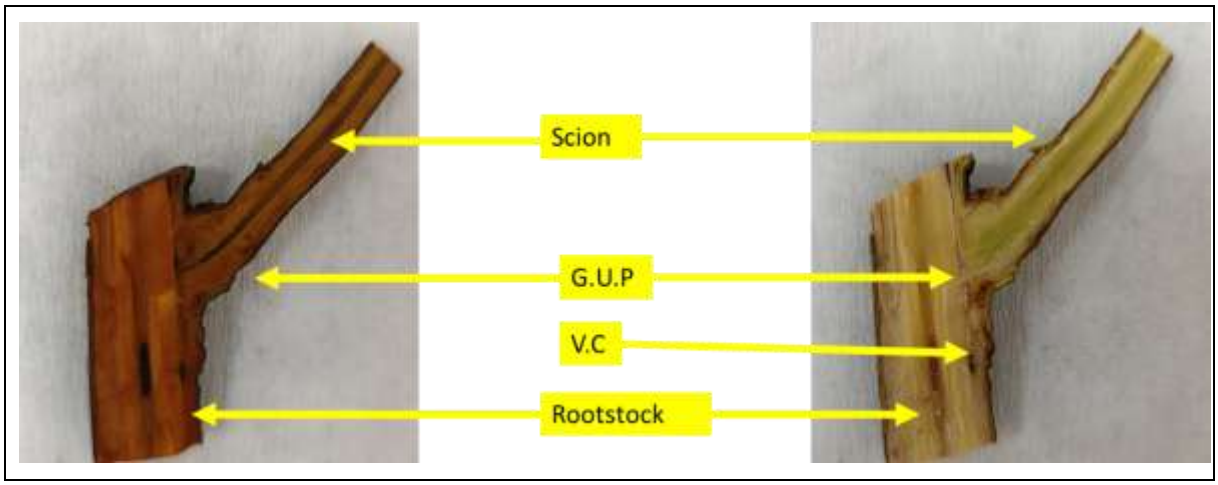

Figure 1. Anatomical images of the Golden Delicious apple/*C. nummularia* graft combination
G.U.P.: graft union point; V.C.: vascular cambium

The Golden Delicious apple/*C. nummularia* graft union showed vascular discontinuity, bark thickening, necrosis, and changes in xylem orientation. Following IKI staining, the rootstock and scion tissues exhibited different staining intensities, with pronounced darkening along the graft union line. In the woody tissue beneath the bark, the union line was deep and clearly defined, while xylem continuity was weak. Limited vascular differentiation and the predominance of parenchymatous tissue indicated that complete anatomical integration had not yet been achieved during the early stage of graft union development.

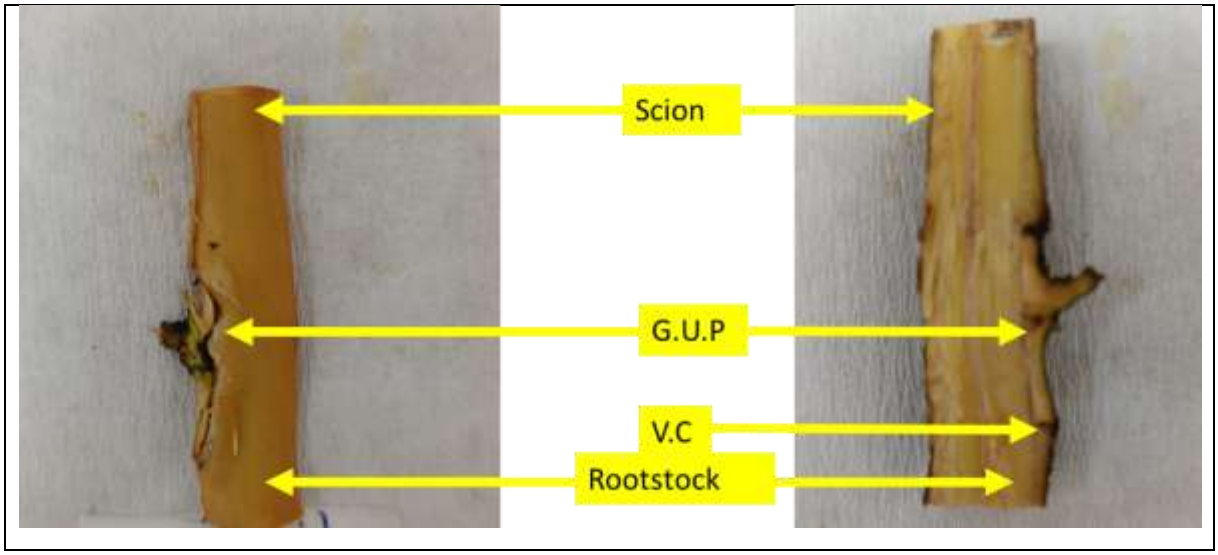

Figure 2. Anatomical images of the Eşme quince/*C. nummularia* graft combination

In the Eşme quince/*C. nummularia* combination, anatomical formation of the graft union was observed, but scion growth did not continue. This finding suggests that the initial formation of union tissue alone may not be sufficient for functional and long-term rootstock–scion compatibility. Because the method used did not directly measure nutrient or assimilate transport, no inference was made regarding the physiological mechanism underlying the growth failure. Based on the cessation of scion growth, the combination was considered incompatible at the early stage.

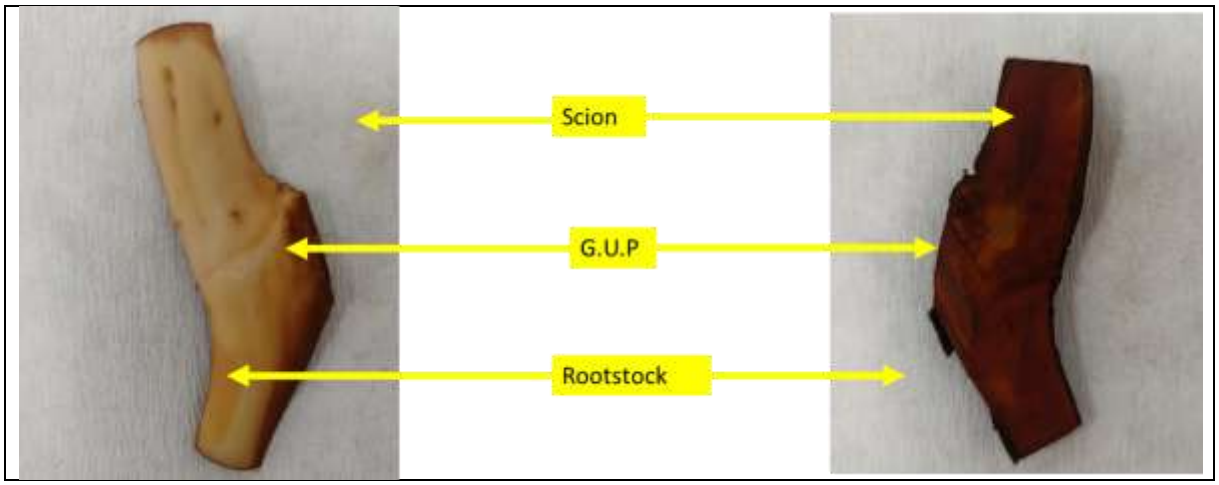

Figure 3. Anatomical images of the Deveci pear/*C. nummularia* graft combination

In the Deveci pear/*C. nummularia* combination, no obvious vascular discontinuity was observed at the graft union, and cambial continuity was largely maintained. Despite the change in orientation along the graft axis, the rootstock and scion tissues showed similar staining intensity after IKI treatment. This stained pattern suggested limited starch accumulation at the graft union; however, IKI staining does not provide a direct measure of assimilate or phloem transport. After removal of the bark, the graft union remained visible in the wood tissue as a shallow depression, indicating that the anatomical trace of the union had not completely disappeared.

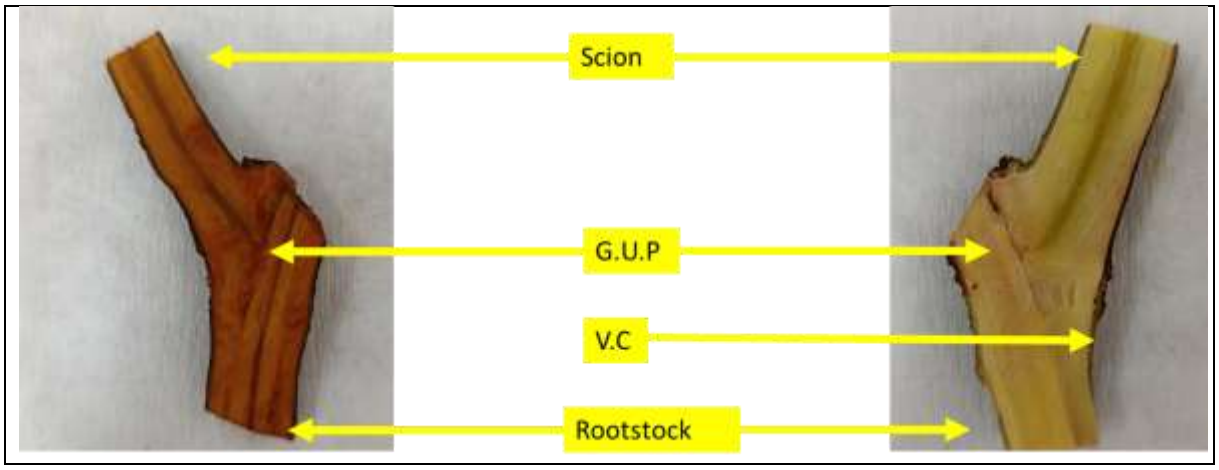

Figure 4. Anatomical images of the Polat Efe hawthorn/*C. nummularia* graft combination

In the Polat Efe hawthorn/*C. nummularia* combination, no obvious discontinuity was observed in the vascular tissues, and cambial continuity was well established at the graft union. Only a slight change in tissue orientation was observed along the graft axis. The rootstock and scion tissues showed similar staining intensity after IKI treatment, suggesting no marked local starch accumulation at the graft union. After removal of the bark, no distinct graft scar or depression was observed in the wood tissue, and the union line appeared smooth and continuous. These findings indicate a high degree of anatomical compatibility during the early stages of graft union development.

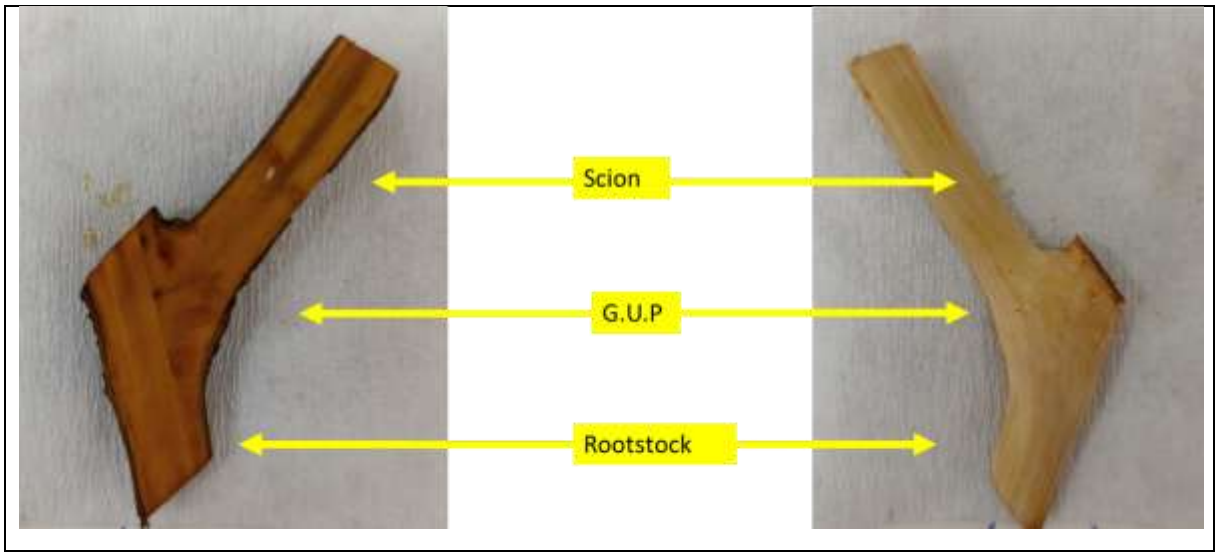

Figure 5. Anatomical images of the self-grafted *C. nummularia*/*C. nummularia* control combination

The *C. nummularia*/*C. nummularia* homograft combination was used as the control. No obvious discontinuity was observed in the vascular tissues at the graft union, and cambial continuity was well established. Following IKI treatment, the rootstock and scion tissues exhibited similar staining intensity, suggesting no marked local starch accumulation. After removal of the bark, no depressed union line was evident in the wood tissue, and the surface appeared smooth. The close anatomical similarity between the Polat Efe hawthorn/*C. nummularia* combination and the control supports the high degree of early-stage graft compatibility observed in this combination.

DİSCUSSİON AND CONCLUSION

Successful graft compatibility should not be inferred solely from continued shoot growth. Stable union formation also requires callus development, differentiation of a new cambial layer, and re-establishment of functional vascular connections. Disrupted cambial development, insufficient vascular differentiation, and persistent undifferentiated parenchymatous or callus tissue at the graft union are recognized anatomical indicators of incompatibility (Uğur et al., 2023).

Although genetic relatedness may increase the probability of graft compatibility, compatibility is combination-specific and cannot be predicted solely from taxonomic proximity. In addition, some forms of localized or delayed incompatibility may not become evident during the first years after grafting (Ling et al., 2025). Therefore, the approximately 11-month observation period in this study represents only early-stage graft union development.

The Golden Delicious apple/*C. nummularia* combination showed vascular discontinuity, bark thickening, necrotic areas, altered xylem orientation, and abundant parenchymatous tissue at the graft union. These abnormalities indicate incomplete anatomical integration and are consistent with features reported for incompatible graft combinations (Uğur et al., 2023; Ling et al., 2025). IKI staining also differed between rootstock and scion tissues, with darkening along the graft union; however, because IKI staining does not directly quantify assimilate transport, this observation should be interpreted only as a qualitative indication of local starch distribution. Although Zengin et al. (2014) reported phenolic compounds in *C. nummularia*,

their study did not examine graft unions, so the abnormalities observed here cannot be attributed directly to phenolic metabolism.

The Eşme quince/*C. nummularia* combination displayed a different form of graft failure. Anatomical union tissue developed, but scion growth did not continue. Thus, initial tissue union alone was insufficient to demonstrate functional compatibility. Because nutrient and assimilate transport were not measured directly, the physiological cause of the growth failure could not be determined. This finding also illustrates why early anatomical continuity and subsequent scion performance should be evaluated together (Uğur et al., 2023; Ling et al., 2025).

In the Deveci pear/*C. nummularia* combination, cambial continuity was largely maintained and no obvious vascular discontinuity was detected, supporting early-stage anatomical compatibility. Rootstock and scion tissues showed similar IKI staining intensity, while the graft union remained visible as a shallow trace in the wood. Consequently, the combination should be regarded as promising at the early stage but still requires long-term evaluation for growth, mechanical stability, and delayed incompatibility (Uğur et al., 2023; Ling et al., 2025).

Among the heterograft combinations, Polat Efe hawthorn/*C. nummularia* showed the closest anatomical resemblance to the homograft control. Cambial continuity was well established, no obvious vascular discontinuity was observed, and no distinct graft scar or indentation remained on the wood surface. Similar IKI staining intensity in rootstock and scion tissues further supported a high degree of early-stage anatomical compatibility. This result, however, applies only to the Polat Efe genotype tested and should not be generalized to all hawthorn cultivars or genotypes (Nas et al., 2011; Abbasi et al., 2019; Uğur et al., 2021a).

The self-grafted *C. nummularia*/*C. nummularia* control showed the most uniform anatomical integration, with regular cambial continuity, no evident vascular discontinuity, similar IKI staining on both sides of the union, and no depressed graft line in the wood. Its close resemblance to the Polat Efe/*C. nummularia* combination strengthens the evidence for high early-stage compatibility in that heterograft.

Taken together, the combinations should not be forced into a single linear compatibility ranking because the Golden Delicious and Eşme combinations failed in different ways. Golden Delicious/*C. nummularia* showed clear anatomical incompatibility, whereas Eşme/*C. nummularia* formed union tissue but failed to sustain scion growth. Deveci/*C. nummularia* showed substantial anatomical continuity but retained a visible graft trace, while Polat Efe/*C. nummularia* most closely approached the homograft control. Both anatomical union characteristics and continued scion growth should therefore be considered when interpreting compatibility.

From a rootstock-breeding perspective, the close anatomical similarity between Polat Efe/*C. nummularia* and the control justifies further investigation of *C. nummularia* as a potential hawthorn rootstock. More broadly, evaluating wild woody genetic resources may help identify stress-adapted material for sustainable rootstock breeding in Türkiye (Ercisli, 2004; Ambarlı et al., 2016; Duman et al., 2024). Nevertheless, the present findings are preliminary and do not establish species-level compatibility.

The principal limitations of this study were the approximately 11-month observation period, the descriptive sample design, the qualitative interpretation of IKI staining, and the absence of direct quantitative measurements of xylem and phloem function. Accordingly, the findings should be interpreted as early anatomical indicators rather than definitive evidence of long-term physiological compatibility.

Future studies should evaluate xylem and phloem continuity separately using histological methods and quantify traits such as callus thickness and vascular element number. Phenolic compounds should be analyzed in rootstock, graft-union, and scion tissues, and IKI-based observations should be validated by quantitative carbohydrate analyses. Long-term trials should also include a wider range of hawthorn genotypes and assess environmental adaptation, vegetative growth, yield, and fruit quality (Zengin et al., 2014; Uğur et al., 2023).

Table 1. Anatomical and IKI observations of the graft union in different rootstock–scion combinations

Combination	**Cambial/vascular continuity**	**Graft union line**	**Necrosis / excessive parenchyma**	**IKI appearance**	**Anatomical assessment**
C. nummularia / *C. nummularia*	Very good	Indistinct/smooth	Absent	Similar staining intensity	Control (reference anatomical appearance)
Polat Efe hawthorn / *C. nummularia*	Very good	Almost completely disappeared	Not evident	Similar staining intensity	High early-stage anatomical compatibility
Deveci pear / *C. nummularia*	Established	Visible graft union line; not completely disappeared	Not evident	Similar staining intensity	Compatible at the early stage; anatomical trace remains
Eşme quince / *C. nummularia*	Anatomical union observed; vascular function not confirmed	Details not specified	Not specified	Not specified	Union formed; scion growth did not continue (incompatible)
Golden Delicious apple / *C. nummularia*	Discontinuous/poor	Deep and distinct	Evident	Heterogeneous; darkening at the graft union	Clear early-stage anatomical incompatibility

REFERENCES

Abbasi, F., Khadivi, A., Taghizadeh, M., & ValizadehKaji, B. (2019). Micropropagation of Prunus scoparia, a suitable rootstock for almond under drought conditions. *International Journal of Fruit Science, 19(2)*, 221–230. https://doi.org/10.1080/15538362.2018.1539695

Ambarlı, D., Zeydanlı, U. S., Balkız, Ö., Aslan, S., Karaçetin, E., Sözen, M., Ilgaz, Ç., Gürsoy Ergen, A., Lise, Y., Demirbaş Çağlayan, S., Welch, H. J., Welch, G., Turak, A. S., Bilgin, C. C., Özkil, A., & Vural, M. (2016). An overview of biodiversity and conservation status of steppes of the Anatolian Biogeographical Region. *Biodiversity and Conservation, 25*, 2491–2519. https://doi.org/10.1007/s10531-016-1172-0

Baş, M. (1998). *Farklı Prunus klon ve çöğür anaçlarının bazı kayısı çeşitleriyle uyuşma düzeyi, bitki besin maddeleri alımı ve büyümeye etkileri üzerinde araştırmalar* [Doctoral dissertation, Çukurova University].

Basbag, M., Cacan, E., Sayar, M. S., & Karan, H. (2017). Some shrub and tree taxa in the grassland-pasture and natural vegetation of Turkey. *Middle East Journal of Science, 3(2)*, 115–128. https://doi.org/10.23884/mejs.2017.3.2.06

Duman, H., Doğan, M., Atlı, Ö., & Celep, F. (2024). Ex situ and in situ conservation approaches in species-rich Anatolian steppe ecosystem: A case study from Ankara, Türkiye. *Ecologies, 5*, 664–678. https://doi.org/10.3390/ecologies5040039

Ercisli, S. (2004). A short review of the fruit germplasm resources of Turkey. *Genetic Resources and Crop Evolution, 51(4)*, 419–435. https://doi.org/10.1023/B:GRES.0000023458.60138.79

Kankaya, A., Özyiğit, S., Tekintaş, F. E., & Seferoğlu, G. H. (1999). Bazı erik ve kayısı çeşitlerinin Pixy anacı ile uyuşmalarının belirlenmesi. In *Türkiye III. Ulusal Bahçe Bitkileri Kongresi* (pp. 295–299).

Kaya, Z., & Raynal, D. J. (2001). Biodiversity and conservation of Turkish forests. *Biological Conservation, 97*, 131–141. https://doi.org/10.1016/S0006-3207(00)00069-0

Ling, J., Yu, W., Yang, L., Zhang, J., Jiang, F., Zhang, M., Wang, Y., & Sun, H. (2025). Rootstock breeding of stone fruits under modern cultivation regime: Current status and perspectives. *Plants, 14(9)*, 1320. https://doi.org/10.3390/plants14091320

Nas, M. N., Bolek, Y., & Bardak, A. (2011). Genetic diversity and phylogenetic relationships of Prunus microcarpa C.A. Mey. subsp. tortusa analyzed by simple sequence repeats (SSRs). *Scientia Horticulturae, 127*, 220–227. https://doi.org/10.1016/j.scienta.2010.09.018

Polat, A. A., & Kaşka, N. (1992). Quince-A anacının bazı yenidünya çeşitleriyle uyuşma durumu ve aşı kaynaşmasının meydana gelişi üzerinde araştırmalar. *Doğa Türk Tarım ve Ormancılık Dergisi, 16(4)*, 773–788.

Ravanbakhsh, H., Hamzeh'ee, B., & Moshki, A. (2018). Ecology and phytosociology of Cotoneaster shrublands in Central Alborz of Iran. *Dendrobiology, 79*, 47–60. https://doi.org/10.12657/denbio.079.005

Sass, J. E. (1964). *Botanical microtechnique*. Iowa State University Press.

Tekintaş, F. E. (1991). Farklı anaçlar üzerine aşılanan turunçgil tür ve çeşitlerinde aşı kaynaşmalarının anatomik ve histolojik olarak incelenmesi üzerinde bir araştırma. *Yüzüncü Yıl Üniversitesi Ziraat Fakültesi Dergisi, 1(2)*, 68–81.

Tekintaş, F. E., & Dolgun, O. (1996). Badem çöğürlerine aşılı bazı şeftali ve nektarin çeşitlerinin uyuşma durumlarının incelenmesi üzerine bir araştırma. *Yüzüncü Yıl Üniversitesi Ziraat Fakültesi Dergisi, 6(1)*, 51–54.

Uğur, R. (2022). Prunus microcarpa: A potential rootstock for apricots. *Turkish Journal of Agriculture and Forestry, 46(1),* 49–58. https://doi.org/10.3906/tar-2107-14

Uğur, R., Gündeşli, M. A., & Palaz, E. B. (2021a). PCPM (Prunus cerasifera × Prunus microcarpa) hybrid rootstock candidate: Identification and production possibilities with hardwood cutting. *International Journal of Agriculture, Environment and Food Sciences, 5(3),* 360–364. https://doi.org/10.31015/jaefs.2021.3.14

Uğur, R., Paydaş, S., & Sarıdaş, M. A. (2023). Rootstock breeding and rootstock-scion interaction in Prunus species. *Journal of Erciyes Agriculture and Animal Science, 6(2),* 7–10. https://doi.org/10.55257/ethabd.1283481

Uğur, R., Yılmaz, C. H., Polat, M., Altun, Ö., & Özatar, H. O. (2021b). Investigation of leaf nutrient content of some apricot varieties grafted on Prunus microcarpa rootstock. In *Proceedings of the III Balkan Agricultural Congress (AGRIBALKAN 2021)*.

Ünal, A. (1984). Ayva anaçlarının bazı armut çeşitleriyle uyuşma durumları üzerinde araştırmalar. *Ege Üniversitesi Ziraat Fakültesi Dergisi, 21(3),* 141–155.

Ünal, A., & Özçağıran, R. (1986). Göz aşısında aşı kaynaşmasının meydana gelişi üzerinde bir araştırma. *Doğa Türk Tarım ve Ormancılık Dergisi, 10(3),* 399–407.

Watanabe, S., & Nakazotomi, N. (1990). Formation of the graft union in apple T-budding. *Bulletin of Yamagata University, Agricultural Science, 11(1),* 149–153.

Zengin, G., Uysal, A., Güneş, E., & Aktümsek, A. (2014). Survey of phytochemical composition and biological effects of three extracts from a wild plant (Cotoneaster nummularia Fisch. et Mey.): A potential source for functional food ingredients and drug formulations. *PLOS ONE, 9(11),* e113527. https://doi.org/10.1371/journal.pone.0113527

FUNCTIONAL HERBAL TEA BLENDS: PHENOLIC PROFILES, ANTIOXIDANT ACTIVITIES, AND IN VITRO DIGESTIBILITY ASSESSMENT BY SOTAX DISSOLUTION TEST

Turgay Çetinkaya[1], Fatih Bildik[2], Serap Sağlam[3], Gökçe Gürün[1]*

[1] Division of Aquatic Biotechnology, Department of Aquatic Biotechnology and Genomics, Faculty of Aquatic Sciences, Istanbul University, 34134 Istanbul, Türkiye

[2] Department of Food Engineering, Faculty of Chemistry and Metallurgy, Istanbul Technical University, 34469, Istanbul, Türkiye

[3] Botany Division, Department of Biology, Faculty of Science, Istanbul University, 34134, Istanbul, Türkiye

[*]Corresponding author: turgaycetinkaya@istanbul.edu.tr

ABSTRACT

Interest in herbal teas is steadily increasing due to their potential health benefits. In this study, fennel (*Foeniculum vulgare*), lemon balm (*Melissa officinalis* L.), hibiscus (*Hibiscus sabdariffa* L.), green tea (*Camellia sinensis* L.), freeze-dried Ottoman strawberries, and lavender (*Lavandula angustifolia*) were used to develop three functional herbal tea prototypes, and their antioxidant activities, FTIR spectral characteristics, and in vitro dissolution behaviours were evaluated. Three prototypes were prepared based on their targeted effects on the digestive system. Prototype 1 (P1), formulated with fennel (30%), lemon balm (24%), hibiscus (16%), green tea (14%), freeze-dried strawberry (12%), and lavender (4%), was designed to promote balanced digestion. Prototype 2 (P2) contained fennel (26%), lemon balm (20%), hibiscus (24%), green tea (12%), freeze-dried strawberry (14%), and lavender (4%) and was formulated to stimulate bowel activity. Prototype 3 (P3) was formulated with fennel (34%), lemon balm (30%), hibiscus (10%), green tea (10%), freeze-dried strawberry (12%), and lavender (4%), emphasising digestive comfort through increased proportions of fennel and lemon balm and reduced proportions of hibiscus and green tea. Fourier Transform Infrared Spectroscopy (FTIR) spectra revealed characteristic absorption bands associated with the diverse phytochemical and structural components of the plant mixtures. Antioxidant activity was evaluated using ABTS and DPPH radical-scavenging assays. P3 exhibited the strongest antioxidant performance among the three formulations, showing the highest ABTS radical-scavenging activity and the lowest IC_{50} value (9.65 and 9.71). The DPPH IC_{50} values were measured as 10.26, 9.73, and 9.71; and ABTS IC_{50} values were 10.26, 10.75 and 9.65, for P1, P2, and P3, respectively. The Trolox-equivalent antioxidant capacity determined by the ABTS assay exceeded 90 μmol TE g^{-1} in all tested formulations. The SOTAX dissolution test demonstrated rapid and extensive in vitro release under simulated gastrointestinal pH conditions (pH 1.2, 4.5, and 6.8), with cumulative dissolution values approaching 99-100% after 30 min. Consequently, P3, in which the proportions of fennel and lemon balm were increased while those of hibiscus and green tea were reduced, emerged as the most promising formulation based on its antioxidant performance and dissolution behaviour. These findings suggest that combining plant-based ingredients in appropriate ratios may influence the functional characteristics of herbal tea blends. The results provide a basis for further studies involving simulated gastrointestinal digestion, bioaccessibility, and bioavailability of the bioactive compounds.

Keywords: Functional herbal tea,

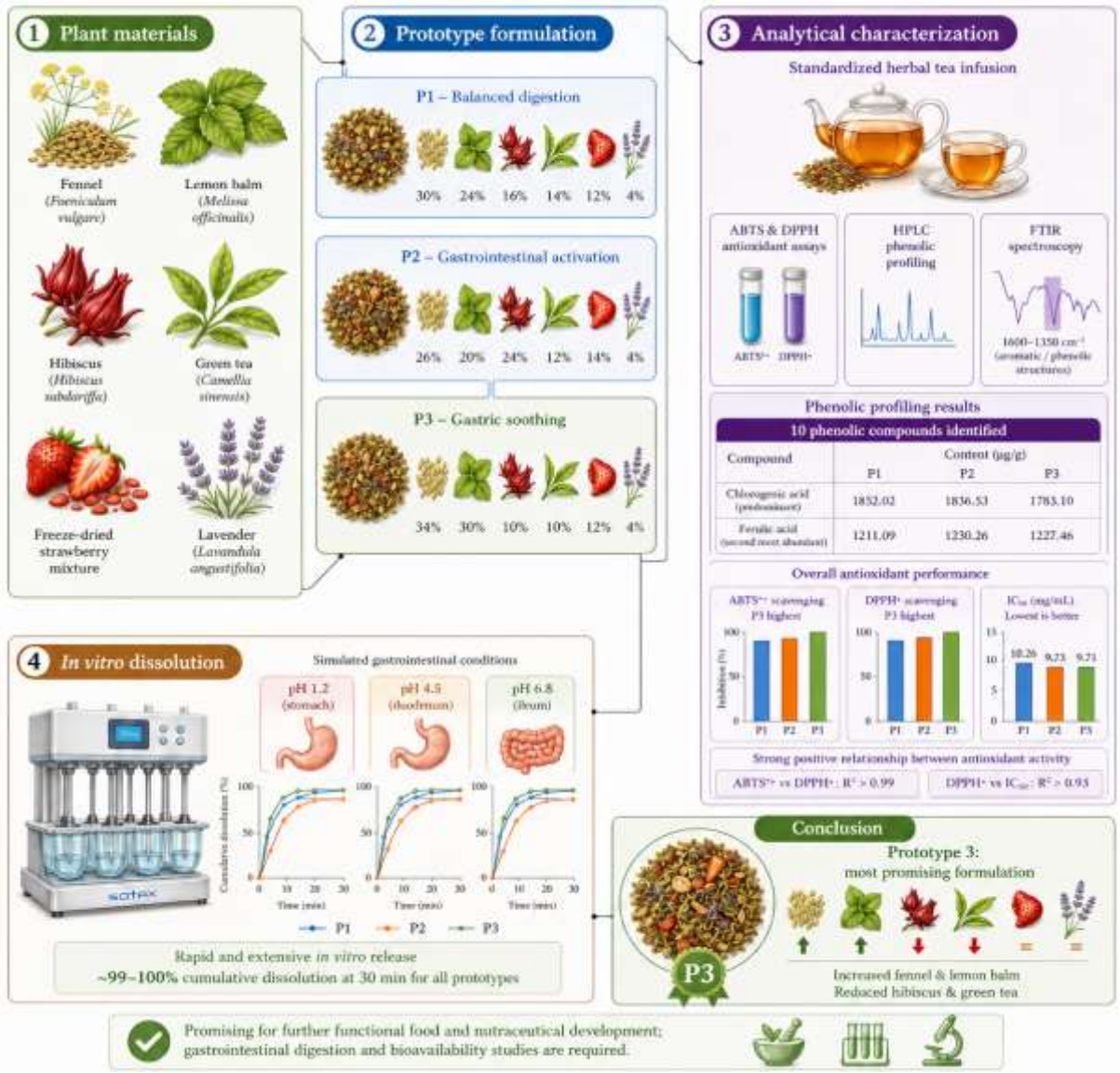

Graphical abstract. Development and multi-level characterization of functional herbal tea prototypes and determination of antioxidant performance and *in vitro* dissolution behavior (Created with https://illustrae.co).

INTRODUCTION

Oxidative stress, characterized by an imbalance between the production of reactive oxygen species (ROS) and the antioxidant defense system, is implicated in the pathogenesis of numerous chronic diseases, including gastrointestinal disorders (Halliwell, 2012). ROS are highly reactive molecular species containing at least one unpaired electron, which enables them to readily interact with cellular components and initiate chain reactions that may impair normal cellular functions and contribute to tissue damage (Phaniendra et al., 2015; Pooja et al., 2025). Consequently, the identification of effective dietary sources of antioxidants has received increasing attention in the context of disease prevention and health promotion.

Growing consumer interest in natural and functional products has increased the demand for plant-derived foods and beverages with antioxidant properties. Plant materials contain diverse secondary metabolites, particularly polyphenols, flavonoids, phenolic acids, and other

phytochemicals, which can contribute to their antioxidant potential (Yeh and Yen, 2006; Holst and Williamson, 2008; Martins et al., 2016; Intrasook et al., 2024). Herbal teas and infusions are therefore of particular interest as convenient sources of bioactive compounds. Depending on the plant species and the solubility of its constituents, infusions can be prepared from various plant parts, including leaves, flowers, fruits, seeds, roots, and bark. The extraction of bioactive compounds is strongly influenced by preparation conditions, particularly temperature and infusion time. Campanella et al. (2003) reported that a 5-min hot-water infusion provided optimal extraction of antioxidant compounds from both conventional and green tea; prolonged infusion and subsequent cooling may promote precipitation or micelle formation, potentially reducing the measurable antioxidant capacity and polyphenol content of the extract. The biological activity of plant-derived antioxidants is determined not only by their individual concentrations but also by their interactions within complex plant matrices. When different plant materials are combined, their bioactive constituents may exhibit additive, synergistic, or antagonistic interactions, resulting in antioxidant activity that cannot necessarily be predicted from the activity of the individual components. Thus, changing the relative proportions of the same plant materials may substantially modify the overall antioxidant capacity of the resulting infusion. Such interactions are particularly relevant for multifunctional herbal tea formulations, in which plants with complementary phytochemical profiles may be combined to target different physiological functions (Seeram, 2008).

The potential health effects of herbal teas are also influenced by the bioaccessibility and bioavailability of their phytochemicals. Although many plant-derived compounds demonstrate substantial antioxidant activity *in vitro*, their biological effects following ingestion depend on digestion, metabolism, absorption, and individual physiological factors (Heim et al., 2002; Espín et al., 2007; Holst and Williamson, 2008). Some compounds may be absorbed in their original form, whereas others undergo extensive metabolic transformation before exerting biological activity. Therefore, antioxidant capacity should be interpreted within the broader context of the composition and potential bioavailability of the phytochemicals present in the formulation.

Several plant materials are particularly relevant to the development of antioxidant-rich herbal tea formulations. *Melissa officinalis* L. (lemon balm) contains rosmarinic acid and flavonoids and has been associated with antioxidant and antispasmodic properties (Barros et al., 2013; Ülgen et al., 2023). *Foeniculum vulgare* (fennel) contains characteristic volatile constituents such as anethole and fenchone and is traditionally used for digestive and carminative purposes (Rahimi and Ardekani, 2013). *Hibiscus sabdariffa* L. (roselle) is rich in anthocyanins and protocatechuic acid and exhibits substantial radical-scavenging activity (Da-Costa-Rocha et al., 2014). *Camellia sinensis* L. (green tea) is a major dietary source of catechins, particularly epigallocatechin gallate, which contributes substantially to its antioxidant activity (Khan and Mukhtar, 2007). Strawberry (*Fragaria* spp.) is also a significant source of phenolic compounds and vitamin C, and freeze-drying can help preserve these compounds and the fruit's sensory characteristics (Giampieri et al., 2012). *Lavandula angustifolia* (lavender), traditionally used in herbal preparations and beverages, contains phenolic and volatile constituents that may contribute to its antioxidant and sensory properties (Cavanagh and Wilkinson, 2002; Batiha et al., 2023).

Despite the well-documented antioxidant potential of individual plant materials, the effects of combinations of multiple botanical products at different proportions remain insufficiently characterized. In particular, information on how formulation ratios influence the radical-scavenging capacity of multifunctional herbal tea blends is limited. Understanding these effects may facilitate the development of functional tea formulations with optimised antioxidant properties. Therefore, the present study aimed to develop and evaluate functional herbal tea

prototypes formulated from six plant matrices: *Foeniculum vulgare*, *Melissa officinalis* L., *Hibiscus sabdariffa* L., *Camellia sinensis* L., a freeze-dried strawberry preparation, and *Lavandula angustifolia*, combined at different proportions to target specific gastrointestinal functions. The prototypes were designed to represent three functional concepts: balanced digestion, intestinal activation, and gastric soothing. Their antioxidant capacities were evaluated using the ABTS and DPPH radical-scavenging assays, while FTIR analysis was performed for molecular characacterization and an *in vitro* dissolution test was conducted using a SOTAX dissolution system. The study further aimed to compare the effects of formulation ratios on antioxidant activity and dissolution behaviour and to identify the blend composition providing the highest antioxidant activity.

MATERIALS AND METHODS

2.1. Plant Materials and Prototype Formulations

Five plant materials were purchased from the Spice Bazaar (Mısır Çarşısı), Istanbul, Türkiye, and used to prepare three different functional herbal tea prototypes: fennel (*Foeniculum vulgare*), lemon balm (*Melissa officinalis* L.), hibiscus (*Hibiscus sabdariffa* L.), green tea (*Camellia sinensis* L.), and lavender (*Lavandula angustifolia*). Black strawberry, hairy strawberry, and Ottoman strawberry collected from Zonguldak and freeze-dried for 48 hours. The plant materials were blended at different proportions to develop three prototypes according to their targeted effects on the digestive system as demonstrated in Figure 1. Prototype 1 (P1) (balanced digestion) was formulated with fennel (30%), lemon balm (24%), hibiscus (16%), green tea (14%), freeze-dried strawberry 12%), and lavender (4%). Prototype 2 (P2) (intestinal activation/motility) contained fennel (26%), lemon balm (20%), hibiscus (24%), green tea (12%), freeze-dried strawberry (14%), and lavender (4%). Prototype 3 (P3) (gastric soothing) was formulated with fennel (34%), lemon balm (30%), freeze-dried strawberry (12%), hibiscus (10%), green tea (10%), and lavender (4%).

The prototypes were designed according to their targeted effects on the digestive system and developed with the inspiration of studies by Cho et al. (2026) and Teterovska et al. (2025). P1 was intended to support balanced digestion and reduce gas and bloating, P2 to support intestinall activity and motility, and P3 to provide a soothing effect on the stomach.

Figure 1. Visual appearance of the developed herbal tea prototypes (P1, P2, and P3, respectively).

2.2. Determination of Antioxidant Activity

The DPPH free-radical scavenging activity of the herbal tea mixture samples was determined based on the method described by Wang et al. (2012). Briefly, 0.1 mL of each sample solution was mixed with 3.9 mL of methanolic 64 µM DPPH solution. Following incubation in the dark, the absorbance was measured spectrophotometrically at 517 nm. The remaining DPPH concentration and overall antiradical capacity were quantified using a Trolox standard calibration curve prepared over a concentration range of 0-200 µg/mL. The IC_{50} value, defined as the sample concentration required to scavenge 50% of the initial DPPH radicals, was calculated accordingly. The percentage of DPPH inhibition was calculated using the Equation 1:

$$DPPH\ \ Scavenging\ Activity = 1 - \frac{Asample}{Acontrol} x100 \quad (1)$$

In the control assay, methanol was used instead of the sample solution.

2.3. Identification and Quantification of Phenolic Compounds

Phenolic compounds in the herbal tea infusions were identified and quantified using a Shimadzu HPLC system (Shimadzu, Japan) equipped with binary gradient pumps, an autosampler, and a diode array detector. Prior to analysis, samples were filtered through a 45 µm membrane filter and transferred into HPLC vials. Chromatographic separation was performed on a reversed-phase C18 column using acetonitrile (solvent A) and 0.75% (v/v) aqueous formic acid (solvent B) as the mobile phase. The flow rate was 1.0 mL min^{-1} and the injection volume was 10 µL. Detection at 220 nm was used for lutein, apigenin, hesperidin, and hydroxycinnamic acid; 306 nm for quercetin and quercetin-3-galactoside; and 330 nm for caftaric acid, ferulic acid, and chlorogenic acid. Phenolic compounds were identified by comparison of their retention times and UV-Vis spectral characteristics with analytical reference standards. Quantification was performed using external calibration curves over a concentration range of 10-50 µg mL^{-1}, with high linearity (R^2 = 1.000). The concentrations were calculated from the corresponding calibration curves and expressed as µg g^{-1} of sample.

2.4. FTIR Spectroscopy

Spectroscopic characterization of the herbal tea mixture samples was performed using FTIR spectrometer (Thermo Scientific, Nicolet iS5, Waltham, USA). High-resolution spectra were acquired over the wavenumber range of 500-4000 cm^{-1} by 37 scans at a spectral resolution of 4 cm^{-1}. Spectral processing and baseline evaluation was performed using OMNIC 9.0 software.

2.5. *In Vitro* Dissolution Test

The *in vitro* dissolution behavior of the herbal tea mixture samples was evaluated using a Sotax AT-MD dissolution system (Sotax AG, Switzerland) in accordance with the United States Pharmacopeia (USP 42-NF 37). The dissolution test was performed at a paddle rotation speed of 100 rpm and a temperature of 36.5°C. Three dissolution media were used: HCI solution at pH 1.2, acetate buffer at pH 4.5, and phosphate buffer at pH 6.8. For each condition, 100 mL of dissolution medium was prepared.

For the dissolution analysis, 5 mL of each sample was transferred into a 100 mL volumetric flask and diluted to volume with the dissolution medium, followed by thorough mixing. After 30 min, 5 mL of the sample solution was withdrawn and placed in an ultrasonic bath for 1 min and then allowed to cool. Subsequently, 1 mL of the sample solution was transferred into a separate 10 mL volumetric flask, diluted to volume with dissolution medium, and thoroughly mixed. A sodium chloride saline solution (10 mg) was used to prepare the blank solution. The pH values of the dissolution media were measured using a pH meter. The absorbance of the samples was measured against the blank solution using a UV-Vis spectrophotometer over the wavelength range of 200-400 nm, with a wavelength accuracy of ±0.1 nm, in accordance with USP 42-NF 37.

3. RESULTS AND DISCUSSION

3.1. Antioxidant Activity of the Herbal Tea Prototypes

The ABTS radical-scavenging profiles of P1, P2, and P3 are presented in Figures 2. P1 exhibited a relatively regular increase in radical-scavenging activity with increasing sample concentration (Figure 2A), indicating a consistent antioxidant response across the tested concentration range. P2 showed a similar concentration-dependent response, although its antioxidant performance remained relatively close to that of P1 (Figure 2B). Among the three formulations, P3 exhibited the most pronounced ABTS radical-scavenging response, with the highest antioxidant performance across the tested concentrations (Figure 2C). The overall Trolox-equivalent antioxidant capacity of all prototypes exceeded 90 μmol TE g^{-1}, indicating a substantial antioxidant potential of the developed herbal tea blends. IC_{50} values for P1, P2, and P3 samples were 10.26, 10.75 and 9.65, respectively. The superior performance of P3 is particularly noteworthy because its formulation contained lower proportions of green tea and hibiscus than P1 and P2, while the proportions of fennel and lemon balm were increased. Green tea and hibiscus are generally recognized as important sources of catechins and anthocyanins, respectively. Therefore, the higher antioxidant response of P3 suggests that the activity of a multi-component herbal blend cannot be predicted solely from the proportion of a single plant with high individual antioxidant capacity.

Instead, the observed response may reflect interactions among phenolic compounds originating from different botanical sources. Such interactions may be additive, synergistic, or antagonistic depending on the composition and relative proportions of the components. In P3, the increased contribution of *M. officinalis* and *F. vulgare* may have contributed to the enhanced antioxidant response through their phenolic constituents, including rosmarinic acid and flavonoids in lemon balm and phenolic compounds in fennel. However, the present results do not establish a specific molecular mechanism of synergy and should therefore be interpreted as evidence of a formulation-dependent antioxidant effect rather than direct proof of synergism.

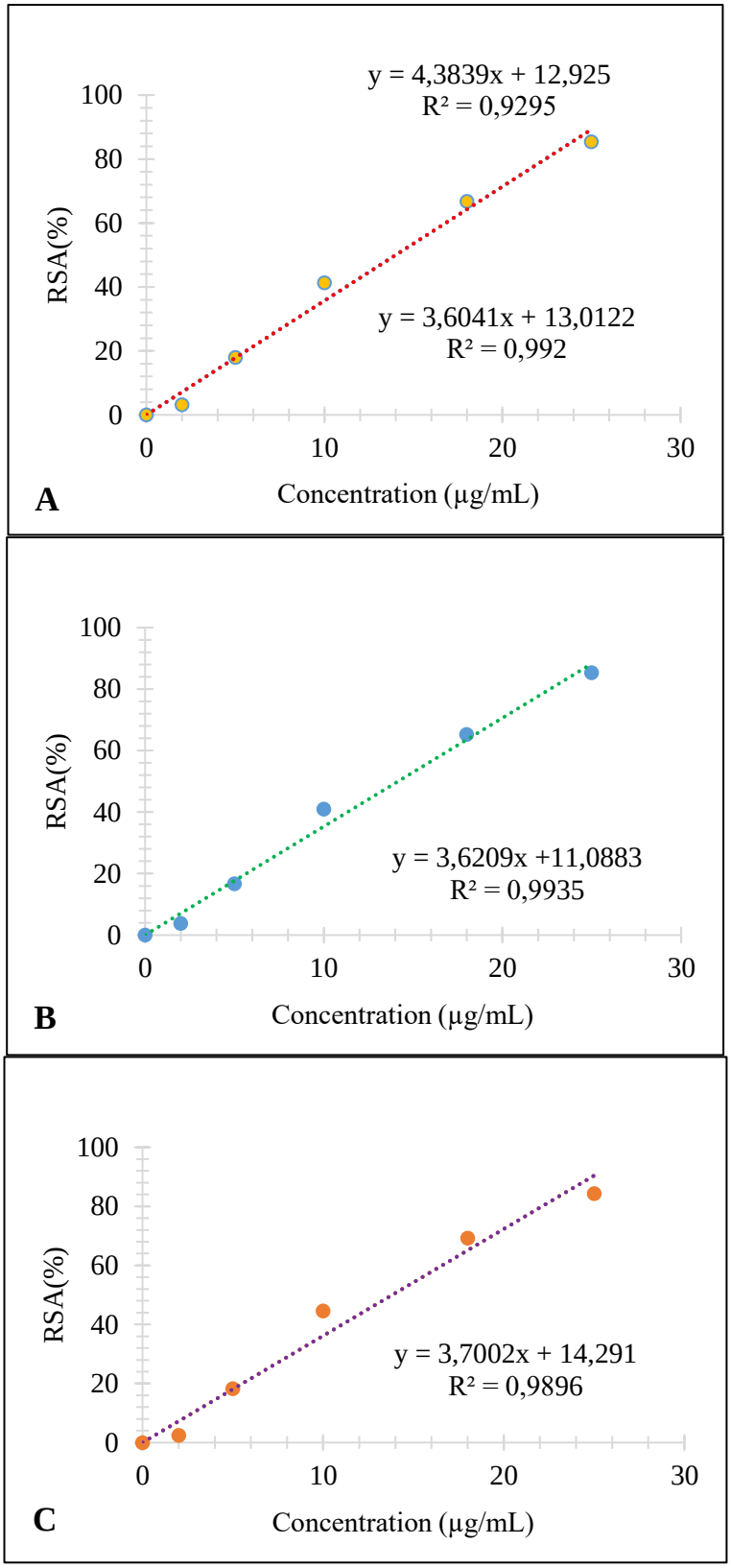

Figure 2. ABTS radical-scavenging activity curve of P1 (A), P2 (B), P3 (C) samples.

The DPPH assay provided complementary information on the radical-scavenging efficiency of the prototypes. Consistent with the ABTS results, P3 exhibited the strongest DPPH radical-scavenging performance among the formulations. The IC_{50} values were measured as 10.26,

9.73, and 9.71 for P1, P2, and P3, respectively. Because a lower IC_{50} value indicates a greater radical-scavenging efficiency, P3 showed the highest efficiency, followed closely by P2 and P1.

Although the differences in IC_{50} values were relatively small, the consistent ranking of P3 as the most effective formulation in both ABTS and DPPH assays strengthens the evidence that its specific botanical composition provided a more favorable antioxidant profile. The similarity between P1 and P2 further suggests that moderate changes in the proportions of individual ingredients did not substantially alter their overall radical-scavenging efficiency. The IC_{50} profiles of the three prototypes are presented in Figures 3.

The antioxidant capacity of the developed formulations was also consistent with previous observations for commercial herbal teas. Apak et al. (2006) reported substantial antioxidant capacities among commercially available tea products, including green tea. The antioxidant responses observed in the present study therefore support the potential of appropriately formulated herbal tea blends as sources of dietary antioxidants. The superior antioxidant performance of P3 is particularly noteworthy because the formulation contained lower proportions of green tea and hibiscus, despite the well-established antioxidant potential of these materials. Green tea is rich in catechins, including epigallocatechin gallate, whereas *H. sabdariffa* is characterized by anthocyanins and other phenolic compounds with radical-scavenging activity (Da-Costa-Rocha et al., 2014; Khan and Mukhtar, 2007). The higher antioxidant response of P3 therefore suggests that the antioxidant activity of a botanical mixture cannot be predicted solely from the concentration of the plant material generally recognized as having the strongest individual antioxidant activity.

Instead, interactions among phytochemicals originating from different plant materials may contribute to the overall response. Such interactions can be synergistic, additive, or antagonistic, depending on the composition and relative proportions of the components (Seeram, 2008). In P3, the increased contribution of *M. officinalis* and *F. vulgare* may have contributed to the observed antioxidant response. *M. officinalis* contains rosmarinic acid and flavonoid derivatives, whereas *F. vulgare* contains phenolic compounds and characteristic volatile constituents such as anethole and fenchone (Barros et al., 2013; Rahimi and Ardekani, 2013). Their combined contribution may have enhanced the radical-scavenging capacity of the formulation. However, the present data do not allow a specific molecular mechanism of synergy to be established, and further component-specific interaction studies would be required to confirm this interpretation.

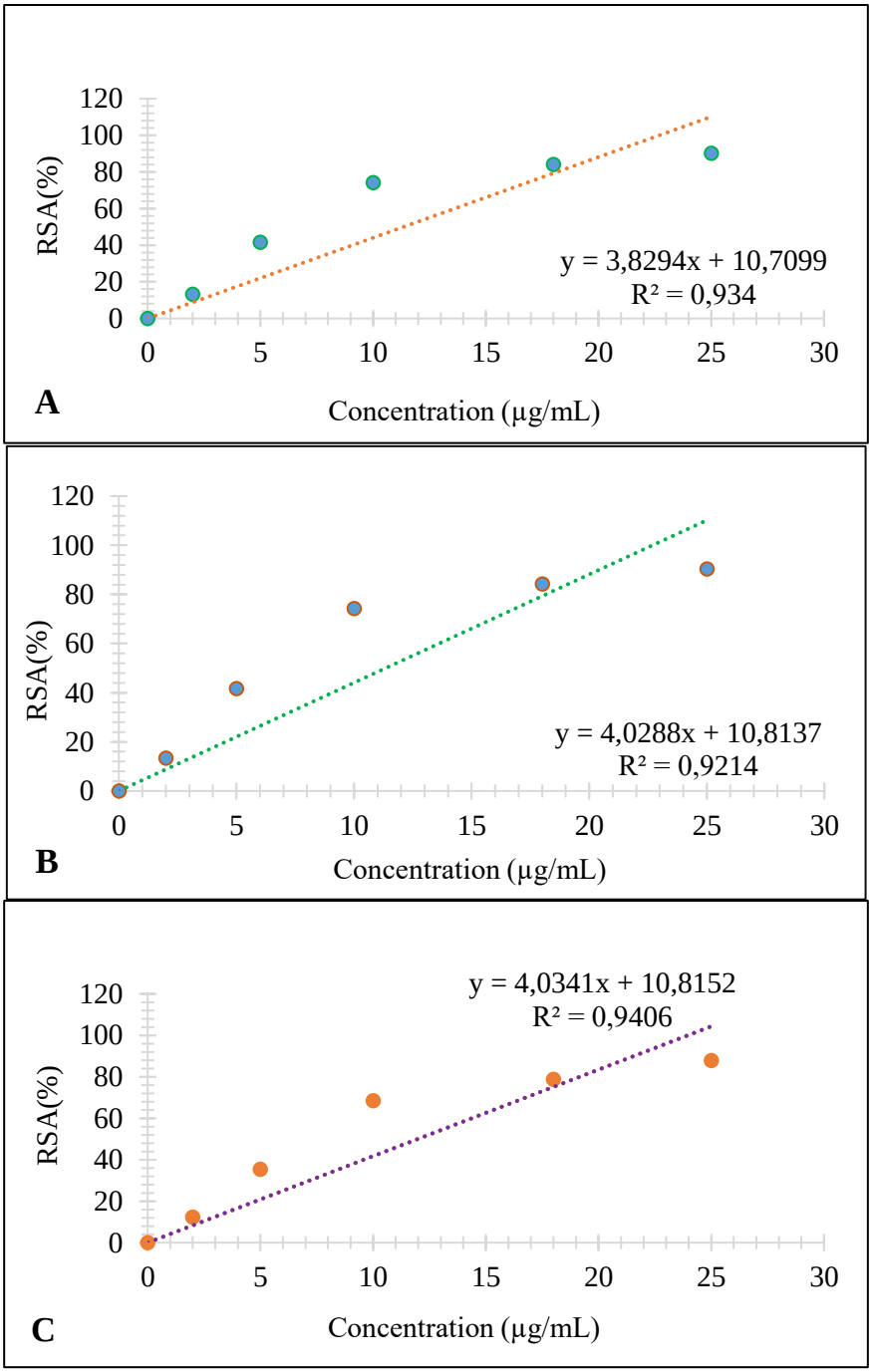

Figure 3. DPPH radical-scavenging activity curve of P1 (A), P2 (B), P3 (C) samples.

Although the prototypes differed in the relative proportions of the six botanical ingredients, all formulations exhibited substantial antioxidant activity. The IC_{50} differences among the prototypes indicate that the antioxidant potential of the blends was influenced not only by the presence of individual antioxidant-rich plants but also by their relative proportions.

3.2. Identification and Quantification of Phenolic Compounds

HPLC-DAD analysis was performed to characterise and quantify the individual phenolic compounds present in the three herbal tea prototypes. The phenolic compounds were identified and quantified by comparing their chromatographic characteristics with those of phenolic

reference standards. The HPLC-DAD chromatogram of the phenolic reference standard used for compound identification and quantification is presented in Figure 4.

HPLC-DAD analysis identified ten phenolic compounds in the three herbal tea prototypes (P1, P2, and P3), comprising six phenolic acids, three flavonols, and one flavone (**Table 2**). Chlorogenic acid was the most abundant phenolic compound detected in all three prototypes, followed by ferulic acid and hydroxycinnamic acid. Among the remaining phenolic acids, caffeic, vanillic, and syringic acids were detected at comparatively lower concentrations. Within the flavonoid group, quercetin was the predominant flavonol, followed by kaempferol and myricetin, while apigenin was the only flavone detected. Overall, the phenolic profiles of the three prototypes were dominated by phenolic acids, particularly chlorogenic acid and ferulic acid, whereas flavonols and flavones were present at substantially lower levels.

Among the other phenolic acids, vanillic acid ranged from 825.40 to 835.30 µg/g, caffeic acid from 889.45 to 892.50 µg/g, syringic acid from 664.81 to 712.45 µg/g, and hydroxycinnamic acid from 1038.65 to 1042.11 µg/g across the three prototypes. The concentrations of the detected flavonols ranged from 188.35 to 215.80 µg/g for quercetin, 75.30 to 91.25 µg/g for kaempferol, and 28.60 to 45.70 µg/g for myricetin. Apigenin, the detected flavone, ranged from 99.80 to 125.80 µg/g among the prototypes.

P1 contained 1852.02 ± 0.01 µg/g chlorogenic acid, 825.40 ± 0.15 µg/g vanillic acid, and 892.30 ± 0.12 µg/g caffeic acid. The highest concentration of chlorogenic acid was observed in P1, whereas the lowest concentration was detected in P3. Hydroxycinnamic acid showed only minor variation among the prototypes, with the highest concentration observed in P3 and the lowest in P2. In contrast, the individual phenolic compounds showed different distribution patterns among the prototypes, indicating that the relative proportions of the botanical ingredients influenced the phenolic composition of the resulting herbal tea formulations.

Table 1. Phenolic contents of the functional herbal tea prototypes (mean ± SD).

	Compounds (µg/g)	**P1**	**P2**	**P3**
Phenolic acids	Chlorogenic acid	1852.02 ±0.01	1836.53 ±0.24	1783.1±0.42
	Hydroxycinnamic acid	1042.9±0.18	1038.65±0.20	1042.11±0.05
	Vanilic acid	825.4 ±0.15	830.74 ±0.42	835.3 ±0.8
	Caffeic acid	892.30 ±0.12	889.45 ±0.32	892.5±0.14
	Syringic acid	664.81 ±0.05	675.45 ±0.28	712.45 ±0.25
	Ferulic acid	1211.09±0.32	1230.26±0.25	1227.46±0.48
Flavonols	Quercetin	188.35±0.09	195.3±0.11	215.8±0.28
	Kaempferol	88.15 ±0.02	91.25 ±0.05	75.3 ±0.05
	Myricetin	28.60 ±0.01	45.7 ±0.02	39.9 ±0.02
Flavons	Apigenin	99.8±0.08	125.8±0.13	115.5±0.19

The predominance of chlorogenic and ferulic acids across the prototypes may have contributed to their antioxidant properties, given the recognized radical-scavenging capacity of phenolic acids. However, the differences in antioxidant activity among the prototypes cannot be attributed to a single phenolic compound. Rather, the overall antioxidant response may reflect

the combined contribution and interactions of multiple phenolic constituents, including phenolic acids, flavonols, and flavones. This observation is consistent with the antioxidant results obtained from the ABTS and DPPH assays and further supports the importance of optimizing the relative proportions of individual botanical materials in multifunctional herbal tea formulations.

3.4. FTIR Characterization

FTIR spectroscopy was used to characterize the major functional groups present in the herbal tea formulations. The spectra showed characteristic absorption bands associated with aliphatic, phenolic, aromatic, carbonyl, and carbohydrate-containing constituents of the plant matrices (Figure 4).

Absorption bands observed at approximately 3012 and 2908 cm^{-1}, together with bands around 2801 and 2783 cm^{-1}, were associated with C–H stretching vibrations of aliphatic CH_2 and CH_3 groups. The broad region between approximately 3100 and 2750 cm^{-1} may also include C–H stretching vibrations associated with phenolic and other aromatic constituents. The spectral region between 1900 and 1100 cm^{-1} corresponded predominantly to the fingerprint region of the plant matrices and included stretching and bending vibrations associated with C=C, C–O–H, and C–O–C groups. Absorption bands in the 1600–1350 cm^{-1} region were consistent with aromatic and phenolic structures, including C–O-related vibrations associated with phenolic acids. A band occurring approximately between 1700 and 1655 cm^{-1} may be associated with carbonyl (C=O) stretching, including esterified components such as pectic substances. Additional bands around 1480 and 1410 cm^{-1} may be related to C–H deformation and other vibrations of aromatic and aliphatic constituents. The region between approximately 1410 and 750 cm^{-1} showed several characteristic bands attributable to organic acids, polysaccharides, and other plant-derived components.

The fingerprint region between approximately 1300 and 850 cm^{-1} contained bands potentially associated with C–O and C–C stretching vibrations of flavonoids, glycosides, anthocyanins, and polysaccharides. Bands in the 800–710 cm^{-1} region may additionally be related to C–O stretching and O–C–H bending vibrations. Overall, the FTIR spectra confirmed the presence of diverse oxygenated and aromatic functional groups consistent with the complex phytochemical composition of the herbal tea mixtures.

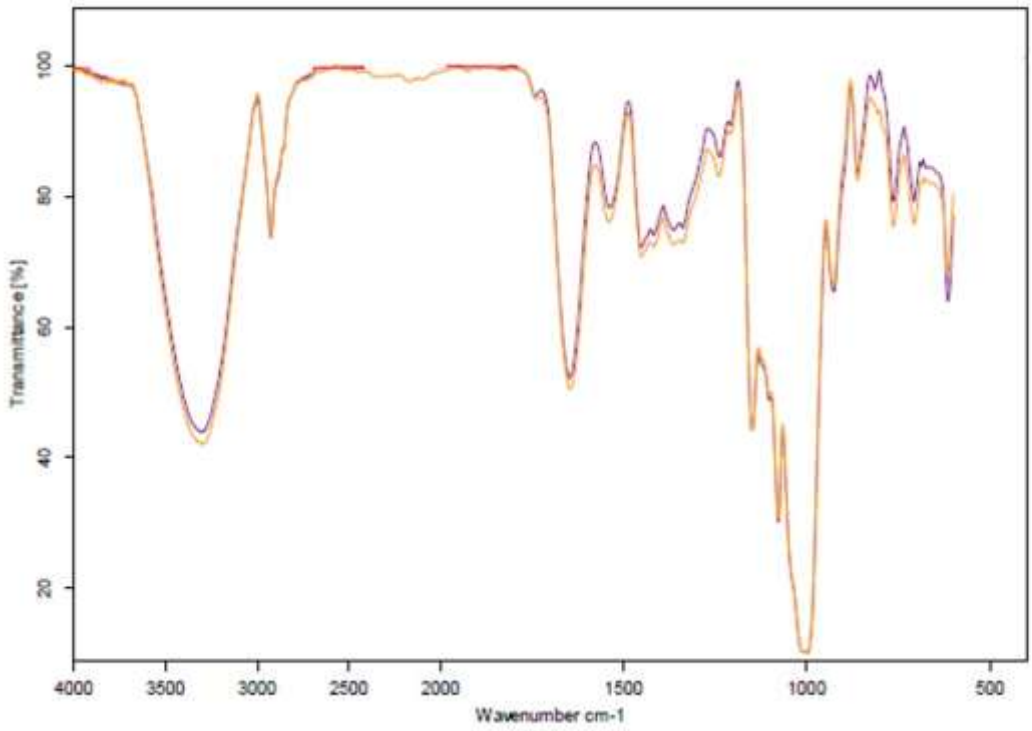

Figure 4. FTIR spectra of the herbal tea formulations.

3.5. *In Vitro* Dissolution Test

The *in vitro* dissolution behavior of the pilot herbal tea mixtures was evaluated under different gastrointestinal pH conditions. The formulations demonstrated rapid release, with cumulative dissolution generally exceeding 80% by 20 min and approaching a plateau within approximately 15 min.

At pH 1.2, the control formulation showed cumulative dissolution values of 68.0 ± 2.4%, 79.8 ± 3.1%, 89.0 ± 2.9%, and 98.8 ± 2.0% at 5, 10, 15, and 30 min, respectively. The corresponding 30-min values for batches 1-3 were 99.9 ± 1.2%, 100.0 ± 0.5%, and 100.0 ± 1.0%, respectively. At pH 4.5, the control reached 90.5 ± 2.0% dissolution at 15 min and 99.5 ± 2.0% at 30 min. The corresponding 30-min dissolution values for batches 1-3 were 99.7 ± 1.2%, 99.4 ± 1.9%, and 99.9 ± 1.3%, respectively. A similar pattern was observed at pH 6.8. The control reached 90.2 ± 3.0% at 15 min and 98.8 ± 2.0% at 30 min, whereas the three batches reached approximately 99-100% dissolution at 30 min. These results indicate that the tested formulations exhibited rapid and extensive dissolution across the simulated gastrointestinal pH conditions.

Table 2. Mean cumulative dissolution (%) ± RSD (%) of the herbal tea mixture batches at different gastrointestinal pH conditions.

Dissolution Medium	Sample	Mean Cumulative Dissolution (%) ± RSD (%)			
		5 min	10 min	15 min	30 min
Hydrochloric acid (pH 1.2)					
	Control	68.0±2.4	79.8±3.1	89.0±2.9	98.8±2.0
	P1	70.1±1.2	82.5±1.8	92.9±2.0	99.9±1.2
	P2	72.0±0.5	85.1±1.6	95.5±0.4	100.0±0.5
	P3	72.6±2.0	85.5±2.2	94.0±1.6	100.0±1.0
Acetate buffer (pH 4.5)					
	Control	67.0±3.0	78.0±2.5	90.5±2.0	99.5±2.0
	P1	70.5±1.8	79.5±1.1	92.0±1.5	99.7±1.2
	P2	71.5±1.5	80.5±2.2	93.9±1.1	99.4±1.9
	P3	73.0±2.7	82.0±2.3	92.5±2.5	99.9±1.3
Phosphate buffer (pH 6.8)					
	Control	68.0±2.5	77.5±2.0	90.2±3.0	98.8±2.0
	P1	71.5±2.0	80.0±2.6	95.0±1.2	99.0±1.10
	P2	69.5±1.4	85.2±1.4	93.2±1.2	100.0±0.2
	P3	70.0±1.5	83.8±1.0	95.8±0.6	99.9±0.4

The relatively low RSD values observed at the different sampling times indicate good repeatability of the dissolution profiles. The convergence of dissolution values toward approximately 99-100% at 30 min further suggests that the major soluble constituents of the formulations were efficiently released under the tested conditions. However, dissolution should be interpreted as an indicator of ***in vitro*** **release**, rather than direct evidence of bioavailability. Although rapid dissolution may facilitate subsequent absorption, actual bioavailability depends on additional processes, including gastrointestinal stability, enzymatic transformation, intestinal permeability, metabolism, and systemic disposition. Therefore, the high dissolution observed in the present study demonstrates favorable in vitro release characteristics but does not by itself establish *in vivo* bioavailability.

CONCLUSION

This study demonstrated that the formulation ratio of six botanical materials significantly influenced the phenolic composition and antioxidant properties of the developed herbal tea prototypes. Among the formulations, P3 showed the most promising overall antioxidant performance, characterized by a comparatively higher phenolic contribution and lower IC_{50} value, together with strong ABTS and DPPH radical-scavenging activity (R^2 = 0.990-0.994 for ABTS and R^2 = 0.929-0.941 for DPPH). The high correlations observed between TPC and antioxidant activity further highlighted the contribution of phenolic compounds to the antioxidant capacity of the formulations. HPLC analysis identified chlorogenic and ferulic acids as the predominant phenolic constituents, while FTIR analysis confirmed the presence of characteristic functional groups associated with the complex phytochemical composition of the plant mixtures. In addition, the formulations exhibited rapid and extensive *in vitro* dissolution,

reaching approximately 99-100% cumulative release at 30 min under the tested gastrointestinal pH conditions. Overall, these findings indicate that optimizing the relative proportions of botanical ingredients can enhance antioxidant performance without simply increasing the amount of individual plant materials, supporting P3 as a promising candidate for further functional dried capsule tea or nutraceutical development. Nevertheless, simulated gastrointestinal digestion and Caco-2 cell models should be employed in future studies to evaluate the stability, bioaccessibility, and intestinal uptake of the bioactive compounds. Comprehensive sensory and consumer acceptance studies, besides pilot- and industrial-scale validation, are also recommended to assess the practical applicability and commercialization potential of the optimized formulation for further studies.

Data Avaılabılıty

The data that support the findings of this study are available on request from the corresponding author.

Author Contrıbutıons

T.C. (Methodology, Supervision, Project administration, Writing-original draft; Writing-review & editing), F.B. (Data curation, Methodology, Resources, Validation, Writing-original draft), S.S. (Methodology, Conceptualisation, Validation, Writing-original draft), G.G (Methodology, Visualization, Writing-review & editing; Writing-original draft).

Fundıng

This research received no external funding.

Conflıct Of Interest

The authors declare no conflicts of interest.

REFERENCES

Apak, R., Güçlü, K., Özyürek, M., Esin Karademir, S., Erçağ, E. (2006). The cupric ion reducing antioxidant capacity and polyphenolic content of some herbal teas. *International journal of food sciences and nutrition*, *57*(5-6), 292-304. https://doi.org/10.1080/09637480600798132

Barros, L., Dueñas, M., Dias, M. I., Sousa, M. J., Santos-Buelga, C., Ferreira, I. C. (2013). Phenolic profiles of cultivated, in vitro cultured and commercial samples of Melissa officinalis L. infusions. *Food chemistry*, *136*(1), 1-8. https://doi.org/10.1016/j.foodchem.2012.07.107

Batiha, G. E. S., Teibo, J. O., Wasef, L., Shaheen, H. M., Akomolafe, A. P., Teibo, T. K. A., Papadakis, M. (2023). A review of the bioactive components and pharmacological properties of Lavandula species. *Naunyn-schmiedeberg's Archives of Pharmacology*, *396*(5), 877-900. https://doi.org/10.1007/s00210-023-02392-x

Campanella, L., Bonanni, A., Tomassetti, M. (2003). Determination of the antioxidant capacity of samples of different types of tea, or of beverages based on tea or other herbal products, using a superoxide dismutase biosensor. *Journal of pharmaceutical and biomedical analysis*, *32*(4-5), 725-736. https://doi.org/10.1016/S0731-7085(03)00180-8

Cavanagh, H. M. A., Wilkinson, J. M. (2002). Biological activities of lavender essential oil. *Phytotherapy research*, *16*(4), 301-308. https://doi.org/10.1002/ptr.1103

Chen, D., Milacic, V., Chen, M. S., Wan, S. B., Lam, W. H., Huo, C., Dou, Q. P. (2008). Tea polyphenols, their biological effects and potential molecular targets. *Histology and histopathology*, *23*(4), 487. https://doi.org/10.14670/hh-23.487

Cho, M. S., Lee, I. S., Kim, J., Park, J. W., Kim, J., & Ko, S. J. (2026). Multi-herb formulations modulating gut microbiota: A systematic review and data-driven analysis. *Journal of Ethnopharmacology*, 122082.

Da-Costa-Rocha, I., Bonnlaender, B., Sievers, H., Pischel, I., Heinrich, M. (2014). Hibiscus sabdariffa L.–A phytochemical and pharmacological review. *Food chemistry*, *165*, 424-443. https://doi.org/10.1016/j.foodchem.2014.04.002

Espín, J. C., García-Conesa, M. T., Tomás-Barberán, F. A. (2007). Nutraceuticals: facts and fiction. *Phytochemistry*, *68*(22-24), 2986-3008. https://doi.org/10.1016/j.phytochem.2007.09.014

Halliwell, B. (2012). Free radicals and antioxidants: updating a personal view. *Nutrition reviews*, *70*(5), 257-265. https://doi.org/10.1111/j.1753-4887.2012.00476.x

Heim, K. E., Tagliaferro, A. R., Bobilya, D. J. (2002). Flavonoid antioxidants: chemistry, metabolism and structure-activity relationships. *The Journal of nutritional biochemistry*, *13*(10), 572-584. https://doi.org/10.1016/S0955-2863(02)00208-5

Holst, B., Williamson, G. (2008). Nutrients and phytochemicals: from bioavailability to bioefficacy beyond antioxidants. *Current opinion in biotechnology*, *19*(2), 73-82. https://doi.org/10.1016/j.copbio.2008.03.003

Intrasook, J., Tsusaka, T. W., Anal, A. K. (2024). Trends and current food safety regulations and policies for functional foods and beverages containing botanicals. *Journal of food and drug analysis*, *32*(2), 112. https://doi.org/10.38212/2224-6614.3499

Kapravelou, G., Martínez, R., Andrade, A. M., López Chaves, C., López-Jurado, M., Aranda, P., Porres, J. M. (2015). Improvement of the antioxidant and hypolipidaemic effects of cowpea flours (Vigna unguiculata) by fermentation: Results of in vitro and in vivo experiments. *Journal of the Science of Food and Agriculture*, *95*(6), 1207-1216. https://doi.org/10.1002/jsfa.6809

Khan, N., Mukhtar, H. (2007). Tea polyphenols for health promotion. *Life sciences*, *81*(7), 519-533. https://doi.org/10.1016/j.lfs.2007.06.011

Martins, N., Barros, L., Ferreira, I. C. (2016). In vivo antioxidant activity of phenolic compounds: Facts and gaps. *Trends in Food Science & Technology*, *48*, 1-12. https://doi.org/10.1016/j.tifs.2015.11.008

Oktay, M., Gülçin, İ., Küfrevioğlu, Ö. İ. (2003). Determination of in vitro antioxidant activity of fennel (Foeniculum vulgare) seed extracts. *LWT-Food Science and Technology*, *36*(2), 263-271. https://doi.org/10.1016/S0023-6438(02)00226-8

Phaniendra, A., Jestadi, D. B., Periyasamy, L. (2015). Free radicals: properties, sources, targets, and their implication in various diseases. *Indian journal of clinical biochemistry*, *30*(1), 11-26. https://doi.org/10.1007/s12291-014-0446-0

Pooja, G., Shweta, S., Patel, P. (2025). Oxidative stress and free radicals in disease pathogenesis: A review. *Discover Medicine*, *2*(1), 104. https://doi.org/10.1007/s44337-025-00303-y

Rahimi, R., Ardekani, M. R. S. (2013). Medicinal properties of Foeniculum vulgare Mill. in traditional Iranian medicine and modern phytotherapy. *Chinese journal of integrative medicine*, *19*(1), 73-79. https://doi.org/10.1007/s11655-013-1327-0

Seeram, N. P. (2008). Berry fruits: compositional elements, biochemical activities, and the impact of their intake on human health, performance, and disease. *Journal of agricultural and food chemistry*, *56*(3), 627-629. https://doi.org/10.1021/jf071988k

Singleton, V. L., Orthofer, R., Lamuela-Raventós, R. M. (1999). Analysis of total phenols and other oxidation substrates and antioxidants by means of folin-ciocalteu reagent. In *Methods in enzymology* (Vol. 299, pp. 152-178). Academic press. https://doi.org/10.1016/S0076-6879(99)99017-1

Teterovska, R., Skotele, R. E., Maurina, B., & Sile, I. (2025). Medicinal plants in food supplements for gastrointestinal disorders: critical assessment of health claims on gastric acid regulation. *Nutrients*, *17*(23), 3674.

Ulgen, C., Yıldırım, A., Turker, A. (2023). Melissa officinalis: Antibacterial and antioxidant potential, phenolic profile and enzyme activities. *Kahramanmaraş Sütçü İmam Üniversitesi Tarım ve Doğa Dergisi*, *26*(5), 1075-1085. https://doi.org/10.18016/ksutarimdoga.vi.1170784

Ulgen, C., Yıldırım, A., Turker, A. (2023). Melissa officinalis: Antibacterial and antioxidant potential, phenolic profile and enzyme activities. *Kahramanmaraş Sütçü İmam Üniversitesi Tarım ve Doğa Dergisi*, *26*(5), 1075-1085. https://doi.org/10.18016/ksutarimdoga.vi.1170784

Wang, P., Aronson, W. J., Huang, M., Zhang, Y., Lee, R. P., Heber, D., Henning, S. M. (2010). Green tea polyphenols and metabolites in prostatectomy tissue: implications for cancer prevention. *Cancer Prevention Research*, *3*(8), 985-993. https://doi.org/10.1158/1940-6207.CAPR-09-0210

Wang, T., Jónsdóttir, R., Liu, H., Gu, L., Kristinsson, H. G., Raghavan, S., Ólafsdóttir, G. (2012). Antioxidant capacities of phlorotannins extracted from the brown algae Fucus vesiculosus. *Journal of agricultural and food chemistry*, *60*(23), 5874-5883. https://doi.org/10.1021/jf3003653

Yeh, C. T., Yen, G. C. (2006). Modulation of hepatic phase II phenol sulfotransferase and antioxidant status by phenolic acids in rats. *The Journal of nutritional biochemistry*, *17*(8), 561-569. https://doi.org/10.1016/j.jnutbio.2005.10.008

EFFECTS OF MYCORRHIZA-BASED MICROBIAL FERTILIZERS ON BASIL (Ocimum basilicum L.) AGRICULTURAL CHARACTERISTICS UNDER DEFICIT IRRIGATION CONDITIONS

Alaattin BOZKUŞ[1], Onur Ali KORUCU[1], Mehmet GÜMÜŞ[1], Halil Han KOCAÖMEROĞLU[1], Elif Azra AKIN[1], İsmail Emrah TAVALI[1], Hüseyin OK[2]*

[1] Department of Soil Science and Plant Nutrition, Faculty of Agriculture, Akdeniz University, 07059 Antalya, Türkiye

[2] Department of Plant Production and Technologies, Faculty of Agricultural Sciences and Technologies, Cyprus International University, 99258 Nicosia, Türkiye

** Correspondence: etavali@akdeniz.edu.tr*

ABSTRACT

The application of microbial fertilizers on plants has gained increasing importance as a sustainable strategy to enhance crop stress tolerance and plant productivity under challenging deficit irrigation conditions. This study aimed to evaluate the effects of various mycorrhiza-based microbial fertilizer formulations on the growth performance of broad-leaved basil (*Ocimum basilicum* L.) grown in a sandy-loam calcareous soil. The study focused on how these microbial amendments influence plant resilience across four deficit irrigation levels: full irrigation (SS100) and three deficit irrigation regimes (SS80, SS60, and SS40). The results indicated that deficit irrigation conditions severely restricted vegetative growth parameters in unfertilized control groups. However, microbial fertilization significantly alleviated the adverse effects of drought stress. Basil plants treated with mycorrhizal formulations, particularly dual or combined microbial treatments, exhibited notable improvements in plant growth dynamics. Key parameters including plant height, root collar diameter, and total leaf number were positively affected by the microbial amendments even under high water deficit. Additionally, plants treated with microbial fertilizers recorded significantly higher chlorophyll levels (SPAD values), demonstrating sustained photosynthetic efficiency under stress. At harvest, a substantial increase in fresh biomass accumulation was observed in mycorrhiza-treated plots compared to the control group, highlighting the role of these symbiotic microorganisms in optimizing root surface area and nutrient uptake. Overall, mycorrhiza-based applications emerged as highly effective inputs for mitigating drought-induced limitations in basil cultivation.

Keywords: Mycorrhiza, Biostimulants, Drought tolerance, Sustainable agriculture

INTRODUCTION

The rapidly increasing global population, dwindling freshwater resources, and irregular rainfall patterns triggered by global climate change are among the most significant ecological problems threatening agricultural production. In particular, in semi-arid climate zones such as the Mediterranean Basin (e.g., the southern coasts of Türkiye), plants frequently face water scarcity

(drought) stress throughout their growing seasons (IPCC, 2021). Drought stress leads to a decrease in cell turgor pressure, stomatal closure, accumulation of reactive oxygen species (ROS) causing oxidative damage, and consequently a significant reduction in photosynthesis, nutrient uptake, and ultimately biomass and economic yield in plants (Augé, 2001; Dimkpa et al., 2009).

Basil (*Ocimum basilicum* L.), belonging to the Lamiaceae family, is a high-value annual plant with wide applications in the food, pharmaceutical, and cosmetic industries, classified as a medicinal and aromatic plant. Basil plants have significant economic importance due to their volatile oils, phenolic compounds, and antioxidants. However, the plant is highly sensitive to soil moisture deficiency during its vegetative growth period (Daza-Torres et al., 2017). In basil plants grown under water scarcity, the leaf area index decreases, fresh herb yield decreases, and the market value of the plant diminishes. Therefore, developing alternative, environmentally friendly agronomic strategies that will ensure the sustainability of basil production and increase abiotic stress tolerance under deficit irrigation conditions is critically important.

Intensive chemical fertilization, used in traditional agriculture to increase yields, leads to salinity accumulation in the soil, groundwater pollution, and disruption of the soil microbiota. In recent years, the use of microbial fertilizers (biostimulants) such as Arbuscular Mycorrhizal Fungi (AMF) and Plant Growth Promoting Rhizobacteria (PGPR) as alternatives to these chemical inputs has attracted great interest in terms of agricultural sustainability (Calvo et al., 2014; Backer et al., 2018). AMF forms extraradical hyphae networks by establishing a symbiotic relationship with plant roots; these hyphae take up and transport low-mobility nutrients such as water and phosphorus from soil pores that the plant's normal root system cannot reach (Ruiz-Lozano et al., 2012). At the same time, mycorrhiza and beneficial rhizobacteria improve root architecture by promoting indole acetic acid (IAA) synthesis in the plant and provide osmotic protection against water stress by increasing antioxidant enzyme activities (Bharti et al., 2016).

The main objective of this study is to comparatively determine the effects of different mycorrhiza-derived microbial fertilizer formulations on parameters reflecting the agricultural characteristics of Large-Leaf Basil (*Ocimum basilicum* L.) grown under restricted irrigation conditions. The primary reason for focusing on basil in this study is the lack of comprehensive literature on the specific morpho-physiological responses of combined microbial fertilizer applications at different water stress levels, despite the high economic value of the species. The study is based on the hypothesis that microbial symbiosis can compensate for yield losses under restricted irrigation by increasing water use efficiency.

MATERIAL AND METHODS

Research Area and Soil Characteristics

This study was conducted in the autumn of 2025 in the Research and Application Greenhouse of the Faculty of Agriculture, Akdeniz University (36° 53' 33" N, 30° 38' 52" altitude 50m). According to meteorological data collected throughout the experiment, the average daily temperature of the area was 16.0 °C, the average daily sunshine duration was 6-7 hours, the average daily open surface evaporation was 2.5 mm to 3.0 mm/day, the average daily rainfall

was 4.6 mm, the average daily wind speed was 2.9 m/s, and the average relative humidity was 64%. The greenhouse floor was covered with black plastic mulch, and the greenhouse had top and side ventilation systems.

The experiment was carried out under controlled conditions with natural sunlight, under a homogeneous temperature and relative humidity regime throughout the growing period. The growing medium used in the experiment was obtained soil from a depth of 0-30 cm from the Aksu Application Area of Akdeniz University. This soil is classified as "Typic Xerofluvent" based on its physical and chemical properties, formed on alluvial parent material called the "Tehnelli Series" (Sarı et al., 2009).

Analysis of the potting soil revealed a slightly alkaline pH (pH 7.9), low electrical conductivity (salinity), high lime content, cation exchange capacity (CEC) ranging from 18.9-19.3 meq/100g, and a sandy-loam texture (Table 1). Overall, the soil has a low organic matter content (1.6%), a high bulk density (1.40 g/cm³), and a low water-holding capacity (available water 8.96%) due to its composition. These physical characteristics indicate that the soil is prone to rapid water loss and provides an ideal testing environment for drought stress trials.

Table 1. Soil physical and chemical properties

Parameter	Content
pH	7.9
EC (dS/m)	0.38
Total N (%)	0.09
Available P (mg/kg)	8.4
CEC (me/100g)	18.9
Exchangeable Na (me/100g)	0.1
Exchangeable K (me/100g)	0.3
Exchangeable Ca (me/100g)	18.5
Exchangeable Mg (me/100g)	2.4
Lime (%)	30.5
Organic matter (%)	1.6
Sand (%)	44.3
Loam (%)	39.1
Clay (%)	16.6

Plant Material and Applications

In the experiment, commercially standardized large-leaf basil (*Ocimum basilicum* L. cv. Vilmorin) seedlings were used as plant material. The experiment was established using a Randomized Complete Block Design in a factorial arrangement, with 5 different fertilizer applications x 4 different irrigation levels x 3 replications, totaling 60 pots (one plant per pot). The pots were placed in a north-south direction, taking care to avoid placing the same applications side by side to minimize the shading effect (edge effect). Details regarding mycorrhiza-based microbial fertilization and other fertilization treatments in the experiment are given in Table 2.

Table 2. Fertilizer materials and their contents applied to potting soil in the experiment

Application	Content
MG+A	Application of the microbial preparation called Krishiza (contains arbuscular mycorrhizal fungus and microorganism spores)
MG+B	Application of the microbial fertilizer called Indigo (contains arbuscular mycorrhizal fungus and microorganism spores)
MG+A+B	Combined (dual) application of Krishiza and Indigo preparations
OG+	Application of standard chemical fertilizer (does not contain microbial inoculant)
OG-MG-	Negative control group without mycorrhiza or chemical fertilizer application

Irrigation Regime

Irrigation was applied to all trial subjects when 40% of the available water capacity of the soil was consumed based on the water requirements of the basil plant (Allen et al., 1998; Daza-Torres et al., 2017). Irrigation procedures were determined by the gravimetric (weighing) method based on the field capacity and wilting point data of the pots, and 4 different irrigation levels were created (Table 3).

Table 3. Water restriction rates applied to basil plants in the experiment

Irrigation level	Content
SS100	Full Irrigation (No Stress) where 100% of the plant's water needs are met
SS80	Slightly Restricted Irrigation (80% of the water lost is replenished)
SS60	Moderately Restricted Irrigation (60% of the water lost is replenished)
SS40	Severely Restricted Irrigation (40% of the water lost is replenished) (Heavy water stress)

The water levels in the pots were checked at regular intervals using a precision balance, and the amount of moisture lost was measured, with water added to the pots according to their group size. In addition, a standard liquid chemical fertilization (fertigation) program was applied to all pots in equal volumes throughout the experiment to meet the plants' basic nutrient needs.

Experimental Procedure and Measurements

Following the preparation of soil, filling it into pots (September 24), and bringing it to field capacity, seedlings were planted on October 10 after being treated with microbial preparations using the root dipping (inoculation) method. During the growing season, hoeing, disease/pest (entomological) controls, and specific treatments (October 23-30) were carried out. Phenological readings were taken at 5 different measurement times (Time points 1-5; e.g., October 20, November 14, November 25, etc.) during the vegetation period.

Plant height (cm): Measured from the soil surface to the apical bud using a ruler. Root collar diameter (mm): Measured just above the soil surface with a digital caliper. Plant crown width (cm): Determined by measuring the distance between the two widest points of the plant. Number of leaves (pieces/plant): Determined by counting the number of fully opened non-chlorotic functional leaves. Chlorophyll content (SPAD): Measured from fully developed leaves at the mid/upper nodes of the plant using a SPAD-502 (Konica Minolta) portable chlorophyll meter. Fresh weight (g/plant): Above-ground biomass of plants was determined by weighing with a precision balance (0.01 g) at the last harvest on December 12th.

Statistical Analyses

The obtained data were statistically evaluated using the SPSS (Version 23.0) software package. The main effects and interactions of the Application (AAP), Irrigation Level (IL), and Measurement Time (MT) factors on growth parameters were tested at a 5% significance level (P<0.05) using a three-way factorial analysis of variance (ANOVA) with Type III sums of squares. Statistically significant differences were separated using the Least Significant Difference (LSD) test.

RESULTS

The effects of different microbial fertilizer applications (MFA), limited irrigation levels (LI), and measurement time (MT) on plant growth parameters were investigated. It was determined that the applications (MFA) had a highly significant effect (P<0.001) on root collar diameter, leaf number, chlorophyll content, and fresh weight, and a significant effect (P<0.01) on plant height and crown width. In addition to the main factors, the Application × Irrigation Level (MFAxLI) interaction was found to be statistically significant only in root collar diameter (P<0.05) (Table 4).

Table 4. Effects of microbial fertilization at different measurement times and different irrigation levels on plant growth parameters

	Plant Growth Parameters					
	Root collar diameter (mm)	**Plant height (cm)**	**Plant Crown Width (cm)**	**Number of leaves (pieces)**	**Chlorophyll Content (SPAD)**	**Plant weight (g)**
microbial fertilizer applications (MFA)						
MG+A	5.48 a[1]	38.43 a	26.38 a	58.93 a	41.72 a	102.50 a
MG+B	5.04 b	38.43 a	25.38 ab	53.20 ab	40.97 a	85.83 a
MG+A+B	5.55 a	39.33 a	24.60 ab	58.65 a	41.50 a	91.25 a
OG+	5.04 b	35.51 b	23.25 bc	50.33 b	41.51 a	81.66 a
OG-MG-	4.72 c	35.11 b	22.21 c	42.28 c	38.28 b	49.16 b
limited irrigation levels (LI)						
SS100	5. 36 a	38.38 a	24.21	53.28	39.37 b	83.33
SS80	5.17 ab	36.62 ab	24.50	54.46	39.89 b	82.33
SS60	5.16 ab	38.72 a	24.50	52.00	41.91 a	79.00
SS40	4.97 b	35.73 b	24.24	50.97	42.02 a	83.66
measurement time (MT)						
1.	3.25 e	12.01 e	11.68 e	8.23 d	33.70 d	-
2.	4.00 d	23.33 d	18.10 d	13.60 d	38.77 c	-
3.	5.47 c	42.65 c	23.48 c	50.71 c	41.56 b	-
4.	6.02 b	50.68 b	29.85 b	78.71 b	48.23 a	-
5.	7.08 a	58.15 a	38.71 a	112.13 a	41.72 b	-
ANOVA						
MFA	10.751***[2]	4.772**[3]	4.868**	11.132***	10.157***	7.900***
LI	2.773*[4]	3.310*	NS [5]	NS	11.558***	NS
MT	215.473***	481.759***	192.924***	455.584***	137.655***	-
MFA×LI	2.020*	NS	NS	NS	NS	NS
MFA×MT	NS	NS	NS	2.830***	2.710**	-
LI×MT	NS	NS	NS	NS	NS	-
MFA×LI×MT	NS	NS	NS	NS	NS	-

[1] Means within columns followed by different letters are significantly different according to LSD test at $p < 0.05$.. [2] Significant at $p < 0.001$ level. [3] **; Significant at $p < 0.01$ level. [4] *; Significant at $p < 0.05$ level. [5] NS: not significant.

Root Collar Diameter and Plant Height

Root collar diameter (RCD) in plants is a critical parameter reflecting the capacity of vascular bundles for water and nutrient transport. According to the research findings, the highest RCD values were obtained from the MG+A+B (5.55 mm) and MG+A (5.48 mm) plots containing mycorrhiza and microbial treatment, and these treatments were statistically in the same "a" group (Table 4). The lowest root collar diameter was observed in the OG-MG-control group (4.72 mm, "c" group) without any fertilizer/microbial application. When examined according to irrigation levels; full irrigation (SS100) provided the highest diameter development with 5.36 mm, while severe water stress (SS40) reduced this value to 4.97 mm ($P<0.05$).

Similarly, plant height values were significantly affected by the MFA. MG+A+B (39.33 cm), MG+A (38.43 cm), and MG+B (38.43 cm) applications statistically significantly increased plant height compared to the OG+ (35.51 cm) and OG-MG- control groups (35.11 cm) without microbial inoculant. Regarding the irrigation regimes, a fluctuating trend was observed where the highest vegetative height was noted under moderate water restriction (SS60 with 38.72 cm) and full irrigation (SS100 with 38.38 cm), whereas severe water stress (SS40) suppressed the average plant height to 35.73 cm (Table 4).

Plant Crown Width and Number of Leaves

Plant crown width and leaf number are directly related to the plant's net assimilation area (photosynthetic surface). Analysis data show that mycorrhizal applications increase crown width. MG+A application (26.38 cm) ranked first in group "a", while the OG-MG-control group (22.21 cm) remained in group "c". Although the effect of irrigation level on crown width was not statistically significant (NS), the highest numerical values were measured at SS60 (24.50 cm) and SS80 (24.50 cm) levels (Table 4).

In terms of total leaf number, the MG+A (58.93 leaves/plant) and MG+A+B (58.65 leaves/plant) combinations increased leaf formation by approximately 40% compared to the control group (42.28 leaves/plant) ($P<0.001$). As expected, the measurement time factor showed a linear increase correlated with plant phenology; the average leaf number, which was 8.23 in the 1st measurement, reached 112.13 leaves/plant in the 5th measurement before harvest. The MFA×MT interaction on leaf number was also found to be significant ($P<0.001$) (Table 4); this demonstrates that microbial fertilizers stimulate leaf organogenesis much faster in later growth stages compared to the control group.

Chlorophyll Content (SPAD Values)

SPAD values, which represent chlorophyll concentration, showed quite interesting responses to microbial fertilization and water restriction factors. While the average SPAD value in control plants (OG-MG-) was 38.28, MG+A (41.72) and MG+A+B (41.50) applications statistically increased chlorophyll levels ($P<0.001$) and were placed in group "a" (Table 4).

A much more striking finding emerged in the differences between irrigation levels (SS). While the average SPAD value was 39.37 under full irrigation (SS100) conditions without water stress, this value increased to 42.02 at the SS40 level with severe water restriction and to 41.91 at the SS60 level ($P<0.001$). Specifically, this physiological response indicates that the severity of water restriction increased the amount of chlorophyll per unit area in the leaves.

Plant Weight (Biomass)

Harvest fresh weight (biomass), the most fundamental indicator of agricultural success in basil cultivation, was the parameter that most clearly reflected the effect of microbial fertilizers ($P<0.001$). At the end of the experiment, the average fresh weight of the MG+A application, which contains mycorrhiza and beneficial bacteria alone, was measured as 102.50 g. This was followed by the MG+A+B combined application with 91.25 g. In contrast, the average fresh weight in the OG-MG- control group, which received only inorganic base fertilization and no microbial support, was only 49.16 g. This explicitly indicates that the mycorrhizal formulation (MG+A) increased the plant fresh biomass by 108% (more than double) compared to the control group in the overall average. Interestingly, the statistical analysis revealed that the deficit irrigation levels did not exert a significant main effect (NS) on the total fresh weight, implying that the robust root infrastructure promoted by microbial inoculation effectively buffered potential biomass losses across different water availability levels (Table 4).

DISCUSSION

The findings clearly demonstrate the supportive effects of beneficial microorganisms (AMFs) applied to the soil on plant morphology and biomass. The calcareous, low-organic-matter, and sandy-loam soil used in the experiment has low water-holding capacity, making the plants susceptible to water stress. The findings support the idea that microbial fertilizers activate tolerance mechanisms despite these challenging soil characteristics and irrigation limitations.

In the study, mycorrhizal (MG+A) and combined microbial fertilizer (MG+A+B) applications significantly increased the height, root collar diameter, and leaf number of basil plants compared to the control group. Mycorrhizal fungi establish a symbiotic relationship by settling in the root cortex cells of the plant. Through their hyphal networks (extraradical mycelium), they transfer water and nutrients with slow diffusion (especially phosphorus, zinc, and copper) from micro-pores inaccessible to the roots to the plant (Dimkpa et al., 2009; Calvo et al., 2014). This observed promotion in plant height and root collar diameter can be explained by improved plant nutrition and consequently increased meristematic cell division. Similar studies on basil plants (Copetta et al., 2006) also confirm that AMF inoculation optimizes vegetative parameters. The fact that combined application (MG+A+B) yields result as successful as single applications is a result of the synergistic interaction between these combined applications; because such applications can promote the germination of mycorrhizal spores and the root infection rate (Barea et al., 1992).

One of the most striking results of the study is that increased water restriction (SS60 and SS40) statistically increases the amount of chlorophyll (SPAD value) in basil plants compared to the SS100 level. Water stress generally causes the degradation of photosynthetic pigments (chlorosis). This phenomenon is primarily driven by the 'concentration effect' under drought stress. To minimize transpirational water loss, plants restrict leaf cell expansion. Consequently, the reduction in total leaf area combined with increased leaf thickness elevates the relative chlorophyll density per unit surface area, directly reflected in higher SPAD indices (Rouphael et al., 2012). The higher SPAD values (41.72) in plants treated with microbial fertilizer compared to the control group (38.28) are related to the fact that beneficial microorganisms facilitate the uptake of essential elements for chlorophyll biosynthesis, such as nitrogen (N) and

magnesium (Mg), thus ensuring that the photosynthetic apparatus remains more robust against stress.

The fresh weight findings, the most important outcome of the experiment, proved that microbial fertilizers are an indispensable tool for maintaining plant production under water stress. The fact that the biomass amount in the control plots was almost half that of the plants treated with microbial inoculant shows how much water stress conditions suppress the metabolism of uninoculated plants. Mycorrhizal plants (especially the MG+A formulation) can maintain cellular turgor even at low soil moisture levels and continue carbon assimilation (biomass formation) by increasing the expression of "aquaporin" genes, which regulate water flow into the plant body through the roots, and by optimizing stomatal conductivity (Ruiz-Lozano et al., 2012).

CONCLUSION

The results of this study, conducted on basil (*Ocimum basilicum* L.) grown under limited irrigation conditions (drought stress) in calcareous soils with low organic matter and poor water retention capacity typical of the Mediterranean Basin, can be summarized as follows: Mycorrhiza-based microbial fertilizer applications (especially MG+A and MG+A+B combinations) statistically increased plant height, root collar diameter, and crown width ($P<0.001$) compared to the control group grown under conventional cultivation, resulting in a stronger and more structurally resistant plant architecture. The number of leaves, an indicator of the vegetative capacity of the plants, was approximately 40% higher in pots inoculated with microbial fertilizers compared to the control group. Severe water restriction (SS40) caused a concentration effect by concentrating chlorophyll content per unit leaf area. Microbial fertilizers supported photosynthetic capacity by maintaining chlorophyll integrity at a higher level against this physiological pressure of stress. Regarding agricultural yield, the most critical finding was that Mycorrhiza (MG+A) application increased the fresh biomass of basil by 108% compared to control crops in limited irrigation scenarios. In conclusion, against the backdrop of global climate change scenarios where drought increasingly limits agricultural productivity, transitioning from intensive chemical inputs to integrated mycorrhizal formulations stands out as a high-efficiency, agronomically viable, and ecologically sustainable strategy to secure crop yields. Further studies could investigate how this microbial symbiosis regulates water stress genes at the molecular (transcriptomic) level and its effects on the essential oil profile, which determines the economic importance of basil, under field conditions.

ACKNOWLEDGEMENTS

In this study, the phase of conducting pot experiments under modern greenhouse conditions was supported by Dean’s Office of the Faculty of Agriculture at Akdeniz University.

REFERENCES

Allen, R. G., Pereira, L. S., Raes, D., & Smith, M. (1998). Crop evapotranspiration: Guidelines for computing crop water requirements (FAO Irrigation and Drainage Paper 56). Rome, Italy: FAO.

Augé, R. M. (2001). Water relations, drought and vesicular-arbuscular mycorrhizal symbiosis. Mycorrhiza, 11(1), 3-42. https://doi.org/10.1007/s005720100097

Backer, R., Rokem, J. S., Ilangumaran, G., Lamont, J., Praslickova, D., Ricci, E., Subramanian, S., & Smith, D. L. (2018). Plant growth-promoting rhizobacteria: Context, mechanisms of action, and roadmap to commercialization of biostimulants for sustainable agriculture. Frontiers in Plant Science, 9, 1473. https://doi.org/10.3389/fpls.2018.01473

Barea, J. M., Azcon, R., & Azcon-Aguilar, C. (1992). Vesicular-arbuscular mycorrhizal fungi in nitrogen-fixing systems. In Methods in Microbiology (Vol. 24, pp. 391-416). Academic Press.

Bharti, N., Pandey, S. S., Barnawal, D., Patel, V. K., & Kalra, A. (2016). Plant growth promoting rhizobacteria Dietzia natronolimnaea modulates the expression of stress responsive genes providing protection of wheat from salinity stress. Scientific Reports, 6, 34768.

Calvo, P., Nelson, L., & Kloepper, J. W. (2014). Agricultural uses of plant biostimulants. Plant and Soil, 383(1-2), 3-41.

Copetta, A., Lingua, G., & Berta, G. (2006). Effects of three AM fungi on growth, distribution of glandular hairs, and essential oil production in Ocimum basilicum L. var. Genovese. Mycorrhiza, 16(7), 485-494.

Daza-Torres, M. C., Arias-Prado, P. C., Reyes-Trujillo, A., & Urrutia-Cobo, N. (2017). Basil (*Ocimum basilicum* L.) water needs calculated from the crop coefficient. Ingeniería e Investigación, 37(3), 8-16.

Dimkpa, C. O., Weinand, T., & Asch, F. (2009). Plant–rhizobacteria interactions alleviate abiotic stress conditions. Plant, Cell & Environment, 32(12), 1682-1694.

IPCC. (2021). Climate Change 2021: The Physical Science Basis. Contribution of Working Group I to the Sixth Assessment Report of the Intergovernmental Panel on Climate Change. Cambridge University Press.

Rouphael, Y., Cardarelli, M., Schwarz, D., Franken, P., & Colla, G. (2012). Effects of drought on nutrient uptake and assimilation in vegetable crops. In Plant Responses to Drought Stress (pp. 171-195). Springer, Berlin, Heidelberg.

Ruiz-Lozano, J. M., Porcel, R., Azcón, C., & Aroca, R. (2012). Regulation by arbuscular mycorrhizae of the integrated physiological response to salinity in plants: New challenges in physiological and molecular studies. Journal of Experimental Botany, 63(11), 4033-4048.

Sarı, M., Özcan, H., Bahtiyar, M., & Çelik, N. (2009). Akdeniz Üniversitesi Aksu Çiftliği Topraklarının Temel Fiziksel ve Kimyasal Özellikleri. Akdeniz Üniversitesi Ziraat Fakültesi Dergisi, 22(1), 1-10.

INVESTIGATION OF QUANTITATIVE AND QUALITATIVE CHARACTERISTICS OF PROPOLIS PRODUCED BY TWO HONEY BEE BREEDS IN TWO TYPES OF HIVES

Maghsoud Besharati

Département of Animal Science, Ahar Faculty of Agriculture and Natural Resources, University of Tabriz, Tabriz, Iran

Corresponding author e-mail: mbesharati@tabrizu.ac.ir

ABSTRACT

Propolis, often referred to as "bee glue," is a resinous substance collected by honey bees from plant buds, exudates, and bark, and mixed with beeswax and salivary enzymes. It plays a vital role in hive hygiene and structural integrity, and has gained global recognition for its diverse biological properties, including antioxidant, antimicrobial, anti-inflammatory, and anticancer activities. As worldwide demand for natural health products continues to rise, propolis has emerged as a commercially valuable hive product. However, its chemical composition and yield are highly variable and influenced by several factors, including bee genetics, local flora, environmental conditions, and hive design. This variability poses significant challenges for standardisation and quality control, and highlights the need for region-specific studies. The present study was undertaken to evaluate the effects of two key factors, hive floor type (open vs. closed bottom) and honey bee breed (native Iranian vs. Carnica), on the quantitative production and qualitative characteristics of propolis in the geographical region of Bostanabad, Iran. A total of 32 colonies were standardised and evenly assigned to four experimental groups: (1) closed-bottom hives with native bees, (2) open-bottom hives with native bees, (3) closed-bottom hives with Carnica bees, and (4) open-bottom hives with Carnica bees. Propolis was collected using plastic traps with 3-mm mesh grids over a two-month period under uniform management conditions. Harvested samples were weighed, and their physicochemical properties, including moisture, ash content, pH, total phenolic content, total flavonoid content, antioxidant activity (DPPH radical-scavenging assay), soluble and insoluble solid fractions, and mineral element profiles, were analysed using standard laboratory methods. The results revealed significant differences in propolis yield among the treatments. The highest production (61.25 g per colony) was recorded in closed-bottom hives housing native Iranian bees, whereas the lowest yield (47.87 g) was obtained from open-bottom hives with Carnica bees ($p < 0.05$). This suggests that both genetic predisposition and hive microclimate influence resin-collecting behaviour. Interestingly, total phenolic content, flavonoid content, DPPH scavenging activity, ash percentage, and moisture content did not differ significantly across treatments ($p > 0.05$), indicating that these quality attributes were relatively stable under the study conditions. In contrast, the proportion of soluble solids was highest in native-bee colonies kept in closed-bottom hives, which may reflect subtle differences in resin origin or processing. The pH of propolis from native bees was consistently lower than that from Carnica bees, pointing to

breed-related chemical variation. Mineral analysis showed that closed-bottom hives with native bees yielded propolis with higher concentrations of calcium, phosphorus, copper, magnesium, manganese, and chromium compared to other groups ($p < 0.05$). These minerals are nutritionally and biologically relevant, contributing to propolis's overall bioactivity. Taken together, these findings demonstrate that both hive type and bee breed significantly affect the quantity and certain quality parameters of propolis. The superior performance of native Iranian bees in closed-bottom hives may reflect better adaptation to local environmental conditions and resource availability. From a practical perspective, this study provides valuable evidence for local beekeepers and producers seeking to optimise propolis yield and quality. It also underscores the importance of region-specific management strategies and the need for further research on seasonal variation, harvesting methods, and the chemical characterisation of active compounds. Ultimately, this work contributes to the broader goal of developing sustainable, high-value propolis production systems that support both apicultural livelihoods and the growing natural health product industry.

Keywords: Propolis; honey bee breed; hive type; antioxidant activity; phenolic compounds; mineral elements; propolis yield; Apis mellifera; Carnica bee; native Iranian bee; beekeeping management

1. INTRODUCTION

Propolis is a resinous hive product collected by honey bees from plant buds, exudates, bark, and other plant-derived sources and subsequently modified with beeswax and bee secretions. Within the colony, it serves as an important component of the social defense system by contributing to hive sealing, structural maintenance, and the inhibition of microbial growth. Beyond its biological role in the colony, propolis has attracted considerable scientific and commercial interest because of its diverse biological activities, including antioxidant, antimicrobial, anti-inflammatory, and other health-promoting properties (Bankova et al., 2000; Fokt et al., 2010; Anjum et al., 2019). Consequently, propolis is increasingly considered a valuable secondary hive product with potential applications in pharmaceutical, food, nutraceutical, and cosmetic industries.

The chemical composition and biological properties of propolis are highly variable. Unlike honey and royal jelly, whose major constituents are largely derived from the bees themselves, propolis is strongly dependent on the botanical resources available to foraging colonies. Plant species, geographical location, climate, season, and availability of resinous materials can therefore result in substantial differences in the chemical profile of propolis. More than hundreds of chemical constituents have been identified in propolis, with polyphenols, flavonoids, phenolic acids, terpenoids, and other plant-derived compounds contributing to its biological activity (Bankova et al., 2006; Kasote et al., 2022). This considerable chemical diversity is one of the major challenges in establishing consistent quality criteria for propolis and limits the direct comparison of samples originating from different geographical regions.

In addition to environmental and botanical factors, characteristics of the honey bee colony may influence both the quantity and composition of collected propolis. Honey bee genotypes and

races differ in their propolis-hoarding behavior and in their ability or tendency to collect plant resins. Evidence from different honey bee populations indicates that genetic and morphometric characteristics can be associated with differences in propolis-collecting capability (Koo & Park, 1997; Kekeçoğlu et al., 2020). Such differences may be particularly important when comparing locally adapted honey bee populations with introduced or selected genotypes under the same environmental conditions. The behavioral response of bees to resin availability and their ability to identify and transport suitable resinous materials may consequently affect the amount and characteristics of propolis accumulated within a colony.

Hive design is another potentially important management factor affecting propolis collection. The physical structure of the hive can modify the microenvironment of the colony and may influence the number and location of gaps or surfaces that bees attempt to seal with propolis. Experimental evidence has shown that modifications of hive interiors can alter propolis-hoarding behavior, while differences among hive designs have also been associated with variation in propolis production and quality (Hodges et al., 2019; Kiziltas & Erkan, 2020). Thus, optimizing hive design may provide a relatively simple management strategy for increasing the recovery of propolis as a commercial hive product. However, the response to a particular hive design may depend on the genetic characteristics of the colonies and the environmental conditions under which they are maintained.

Despite the increasing interest in propolis as a high-value apicultural product, information concerning the interaction between honey bee genotype and hive design under the environmental conditions of Iran remains limited. In particular, comparative information on propolis production by native Iranian honey bees and Carnica bees maintained in different hive-bottom configurations is scarce. Because native bees may be better adapted to local environmental conditions and available plant resources, their propolis-collecting behavior may differ from that of introduced or selected bee genotypes. At the same time, the use of closed- or open-bottom hives may modify colony conditions and consequently influence resin collection. Therefore, the present study was conducted to evaluate the effects of honey bee genotype and hive bottom type on the production and selected physicochemical and functional characteristics of propolis under the environmental conditions of Bostanabad, northwestern Iran. Native Iranian and Carnica honey bee colonies were maintained in wooden hives with either closed or open bottoms under standardized management conditions. The study was designed to determine whether these two practical factors could influence propolis yield and selected quality attributes and thereby provide useful information for improving propolis production in local beekeeping systems.

2. MATERIALS AND METHODS

2.1. Experimental design and propolis collection

The experiment was conducted using 32 honey bee colonies representing two honey bee genotypes: native Iranian honey bees (*Apis mellifera*) and Carnica bees (F1 hybrid). Colonies were randomly assigned to four experimental treatments according to honey bee genotype and hive bottom type: native bees in closed-bottom hives, native bees in open-bottom hives, Carnica bees in closed-bottom hives, and Carnica bees in open-bottom hives. Each treatment included

eight colonies. Before the beginning of the experiment, colonies were standardized to six frames of adult bees and five brood frames and maintained under similar management conditions.

Propolis was collected using plastic propolis traps equipped with 3-mm grids. The traps were installed in the experimental colonies and left in place for two months. At the end of the collection period, the propolis from each colony was removed, weighed, and recorded as propolis yield (g colony^{-1}). Samples intended for laboratory analyses were transferred to the laboratory, stored at −19 °C, and subsequently processed for physicochemical and biochemical analyses.

2.2. Propolis extraction

For analyses of phenolic compounds, flavonoids, and antioxidant activity, raw propolis samples were powdered and extracted with 80% ethanol. Briefly, 100 g of powdered raw propolis was mixed with 200 mL of 80% ethanol and shaken for 48 h at room temperature. The extract was filtered to remove residual wax and insoluble materials, kept at −10 °C for 24 h, and subsequently concentrated using a rotary evaporator at 45 °C. The concentrated extracts were stored in dark glass containers until analysis.

2.3. Physicochemical and antioxidant analyses

Selected physicochemical characteristics of the raw propolis samples were determined, including moisture, ash, pH, and soluble and insoluble solid fractions. Soluble and insoluble solids were determined by extracting 1 g of powdered propolis with 250 mL of 80% ethanol, followed by stirring, filtration, and weighing of the insoluble fraction. The soluble fraction was calculated from the difference between the initial sample weight and the insoluble fraction. Propolis pH was determined using a pH meter after preparation of the sample solution, with calibration performed using standard buffer solutions. Ash content was determined by drying the sample followed by incineration at 550 °C until a constant ash residue was obtained.

Total flavonoid content was determined using the aluminum chloride colorimetric method, with quercetin used as the reference standard. Absorbance was measured at 415 nm and results were expressed as quercetin equivalents. Total phenolic content was determined using the Folin–Ciocalteu colorimetric method, with gallic acid used as the reference standard, and expressed as mg gallic acid equivalents per gram of sample.

Antioxidant activity was evaluated using the DPPH radical-scavenging assay. Propolis extract was reacted with a methanolic DPPH solution and incubated for 30 min in the dark at room temperature. Absorbance was measured at 517 nm using a spectrophotometer. Radical-scavenging activity was calculated as the percentage inhibition of DPPH radicals relative to the control.

2.4. Mineral analysis

The mineral composition of propolis samples was determined to characterize differences in selected mineral elements among the experimental treatments. The concentrations of calcium, phosphorus, magnesium, iron, copper, manganese, zinc, sodium, potassium, and chromium were evaluated and expressed on a concentration basis. Selected additional elements, including nickel, lead, and aluminum, were also determined as part of the mineral profile.

2.5. Statistical analysis

Data were analyzed using the General Linear Model (GLM) procedure of SAS. The experimental treatments were considered as the statistical factor, and treatment means were

compared using Duncan's multiple range test. Differences were considered statistically significant at $P < 0.05$. The statistical model was:

$$Y_{ij} = \mu + T_j + e_{ij}$$

where $Y_{ij}$is the observed value, $\mu$is the overall mean, $T_j$is the effect of treatment, and $e_{ij}$is the experimental error.

3. RESULTS AND DISCUSSION

3.1. Propolis yield

Propolis yield differed significantly among the four experimental treatments ($P = 0.037$). Native Iranian honey bee colonies maintained in closed-bottom hives produced the greatest amount of propolis (61.25 g colony^{-1}), whereas the lowest yield was obtained from Carnica colonies maintained in open-bottom hives (47.87 g colony^{-1}). Native bees in open-bottom hives and Carnica bees in closed-bottom hives showed intermediate values of 56.62 and 53.62 g colony^{-1}, respectively (Table 1).

The greater propolis production observed in native colonies, particularly under the closed-bottom hive condition, suggests that both colony genotype and hive environment may influence resin-hoarding behavior. The relatively higher production by native bees may partly reflect adaptation to the local environment and the plant resources available in the study area. Previous studies have similarly reported differences in propolis-collecting ability among honey bee races and ecotypes, indicating that genetic characteristics can contribute to variation in resin collection (Koo and Park, 1997; Kekeçoğlu et al., 2020). Differences among hive designs have also been reported, supporting the possibility that hive structure can modify the conditions that stimulate bees to deposit and accumulate propolis (Kiziltas and Erkan, 2020).

The magnitude of the observed differences should nevertheless be interpreted within the specific environmental and management conditions of the present study. Propolis production is influenced by several factors, including botanical resources, geographical location, season, colony characteristics, and collection method. Therefore, the superior performance of native bees in the present experiment should not be generalized to all regions or seasons. Rather, it provides evidence that the choice of bee genotype and hive configuration can be relevant considerations when propolis production is an important objective of beekeeping.

3.2. Physicochemical characteristics of propolis

Moisture and ash contents were not significantly affected by the experimental treatments ($P > 0.05$). Moisture ranged from 1.25 to 1.85%, while ash content ranged from approximately 1.05 to 1.89%. These values indicate relatively low moisture and ash contents across all treatments and suggest that the basic physicochemical characteristics of the collected raw propolis were relatively consistent under the conditions of the experiment.

The pH values ranged from 5.46 to 5.73. Although the statistical analysis did not indicate a significant treatment effect ($P = 0.2279$), propolis obtained from native bee colonies showed numerically lower pH values than propolis collected from Carnica colonies. This numerical difference may indicate some variation in the chemical characteristics of propolis associated with bee genotype; however, the absence of statistical significance means that this observation should be considered cautiously. Previous research has indicated that propolis pH can vary

according to geographical origin, botanical sources, and other factors affecting its chemical composition.

A significant difference was observed in the soluble fraction of propolis ($P = 0.0089$). The highest soluble-solid content was recorded in propolis from native bees maintained in closed-bottom hives (24.23%), whereas the lowest value occurred in native bees maintained in open-bottom hives (22.87%). The corresponding insoluble fractions showed the reverse pattern. Total solids remained high and relatively consistent among treatments, ranging from approximately 98.15 to 98.74%.

The variation in soluble and insoluble fractions may reflect differences in the type and relative proportions of plant-derived resins collected by the colonies. Propolis composition is strongly dependent on botanical and geographical origin, while bee genotype and hive conditions may influence resin-collection preferences and the material ultimately deposited in the hive. Similar variability in the physicochemical composition of propolis from different bee populations and hive conditions has been reported previously. Thus, the higher soluble fraction observed in the native-bee/closed-bottom treatment may represent a potentially useful quality-related characteristic, although chemical profiling of individual compounds would be required to establish its biological significance.

3.3. Phenolic compounds and antioxidant activity

In contrast to propolis yield and soluble solids, the principal antioxidant-related characteristics evaluated in this study were relatively stable among treatments. Total flavonoid content ranged from 0.93 to 1.28 mg quercetin equivalents g^{-1}, total phenolic content ranged from approximately 326 to 345 mg gallic acid equivalents g^{-1}, and DPPH radical-scavenging activity ranged from approximately 85.6 to 89.4%. None of these parameters differed significantly among the experimental treatments ($P > 0.05$).

The absence of significant differences in these parameters despite the clear difference in propolis yield is noteworthy. It suggests that, under the environmental conditions and collection period of this experiment, the factors affecting the quantity of propolis collected did not produce a corresponding change in its overall phenolic and antioxidant characteristics. The phenolic content of propolis is generally strongly associated with botanical origin, and substantial differences among geographical regions have been reported. Therefore, the relatively similar phenolic and antioxidant profiles observed among the four treatments may indicate that colonies had access to a broadly similar pool of resin-producing plants during the experimental period.

The results also emphasize an important distinction between propolis quantity and quality. Increasing the amount of propolis collected does not necessarily imply an increase in total phenolic concentration or antioxidant activity. For practical propolis production, both yield and chemical characteristics should therefore be considered when evaluating the effect of beekeeping management practices.

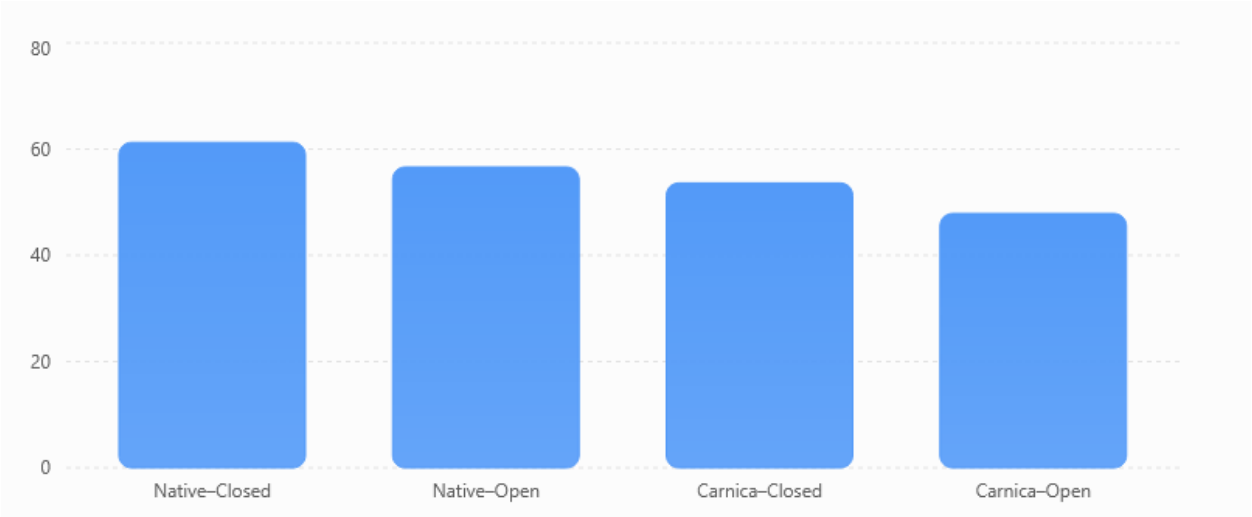

Figure 1. Propolis yield of native Iranian and Carnica honey bee colonies maintained in closed- and open-bottom hives. Values represent treatment means; the treatment effect was significant ($P = 0.037$).

3.4. Mineral composition

Mineral analysis demonstrated clearer treatment-related differences than those observed for phenolic and antioxidant characteristics. Propolis obtained from native bee colonies maintained in closed-bottom hives generally contained higher concentrations of several measured mineral elements than samples from the other treatments. In particular, calcium, phosphorus, copper, magnesium, manganese, iron, zinc, sodium, potassium, and chromium showed higher numerical concentrations in this treatment, with several of these differences reaching statistical significance.

The differences in mineral composition may be related to the botanical sources of the resins collected by the bees, as mineral profiles can vary among propolis samples according to geographical and environmental conditions. Trace and major elements have previously been investigated as potential indicators of the origin and characteristics of propolis. The greater concentrations observed in propolis from native colonies in closed-bottom hives therefore suggest that this treatment may have influenced either the source of collected resin or the relative incorporation of mineral-containing materials into the final propolis.

However, the mineral findings should not be interpreted as evidence that higher mineral concentrations necessarily indicate superior biological quality. Some elements may contribute to the nutritional or functional profile of propolis, whereas potentially toxic elements such as lead require separate consideration in quality-control studies. The present results primarily demonstrate that mineral composition was more responsive to the experimental treatments than the broad antioxidant indicators measured in this study.

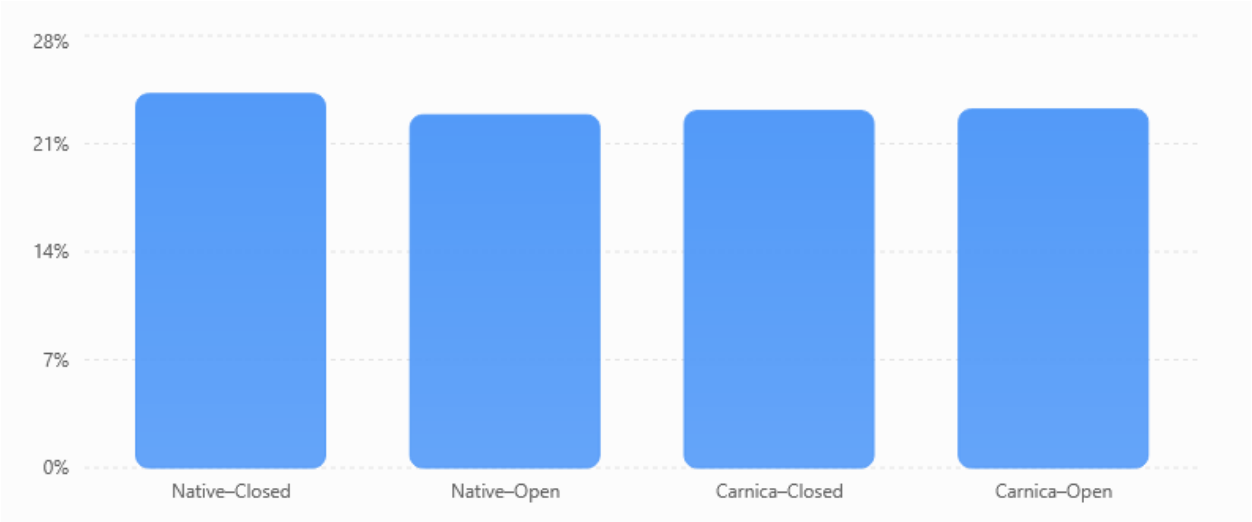

Figure 2. Soluble-solid fraction of propolis collected from native Iranian and Carnica honey bee colonies maintained in closed- and open-bottom hives. Treatment differences were significant ($P = 0.0089$).

CONCLUSION

The present study demonstrated that honey bee genotype and hive bottom design can influence propolis production under the environmental conditions of northwestern Iran. Native Iranian honey bee colonies maintained in closed-bottom hives produced the highest amount of propolis, whereas Carnica colonies in open-bottom hives showed the lowest production. In contrast, moisture, ash content, total phenolic content, total flavonoid content, and DPPH radical-scavenging activity were relatively stable among the experimental treatments. A significant difference was observed in the soluble fraction of propolis, while the mineral profile also showed treatment-related variation, particularly in propolis obtained from native colonies maintained in closed-bottom hives. These findings indicate that increasing propolis yield does not necessarily result in proportional changes in its broad phenolic or antioxidant characteristics. From a practical perspective, the use of native Iranian bees in closed-bottom hives appears promising for improving propolis yield under the conditions evaluated in this study. Nevertheless, these findings should be interpreted within the specific geographical and seasonal context of the experiment. Further studies covering different seasons, locations, botanical resources, and longer collection periods are warranted to determine the consistency of these effects and to identify the specific chemical compounds responsible for differences in propolis quality.

Anjum, S. I., Ullah, A., Khan, K. A., Attaullah, M., Khan, H., Ali, H., Bashir, M. A., Tahir, M., Ansari, M. J., Ghramh, H. A., Adgaba, N., & Dash, C. K. (2019). Composition and functional properties of propolis (bee glue): A review. *Saudi Journal of Biological Sciences, 26*(7), 1695–1703. https://doi.org/10.1016/j.sjbs.2018.08.013

Bankova, V. (2005). Recent trends and important developments in propolis research. *Evidence-Based Complementary and Alternative Medicine, 2*, 29–32. https://doi.org/10.1093/ecam/neh059

Bankova, V., Popova, M., & Trusheva, B. (2006). Plant sources of propolis: An update from a chemist's point of view. *Natural Product Communications, 1*(11), 1071–1078. https://doi.org/10.1177/1934578X0600101118

Bankova, V., de Castro, S. L., & Marcucci, M. C. (2000). Propolis: Recent advances in chemistry and plant origin. *Apidologie, 31*(1), 3–15. https://doi.org/10.1051/apido:2000102

Christov, R., Trusheva, B., Popova, M., Bankova, V., & Bertrand, M. (2006). Chemical composition of propolis from Canada, its antiradical activity and plant origin. *Natural Product Research, 20*(6), 531–536. https://doi.org/10.1080/14786410500056918

Kekeçoğlu, M., Eroğlu, N., Kambur, M., & Uçak, M. (2020). The relationships between propolis collecting capability and morphometric features of some honey bee races and ecotypes in Anatolia. *Journal of Agricultural Sciences, 26*(1), 71–77. https://doi.org/10.15832/ankutbd.447319

Kekeçoğlu, M., Keskin, M., Birinci, C., Birinci, E., & Kolaylı, S. (2021). Effects of honey bee race and season on propolis composition. *Journal of Agricultural Sciences, 27*(3), 292–297. https://doi.org/10.15832/ankutbd.619996

Kiziltas, H., & Erkan, C. (2020). The effects of different beehives on propolis production and quality. *Food Science and Technology, 41*, 222–228. https://doi.org/10.1590/fst.20120

Koo, M. H., & Park, Y. K. (1997). Investigation of flavonoid aglycones in propolis collected by two different varieties of bees in the same region. *Bioscience, Biotechnology, and Biochemistry, 61*(2), 367–369. https://doi.org/10.1271/bbb.61.367

Velikova, M., Bankova, V., Sorkun, K., Houcine, S., Tsvetkova, I., & Kujumgiev, A. (2000). Propolis from the Mediterranean region: Chemical composition and antimicrobial activity. *Zeitschrift für Naturforschung C, 55*(9–10), 790–793. https://doi.org/10.1515/znc-2000-9-1019

INFLUENCE OF THE MALE EFFECT ON ESTRUS RESPONSE IN CARPATHIAN GOATS RAISED IN TWO CONTRASTING CLIMATIC AREAS OF ROMANIA

Laura MARINICĂ [1,3,4], Andreea Hortanse ANGHEL [1,2,3], Dorina NADOLU [1,2], Daniela JITARIU [3], Constantin PASCAL [4]

[1]National Association of Goat Breeders of Romania, 248, I.C. Bratianu Boulevard, Constanța, Romania
[2]Institute of Research and Developement for Sheep and Goat Breeding Palas-Constanța, 248, I.C. Bratianu Boulevard, Constanța, Romania
[3]Faculty of Natural Sciences and Animal Sciences, Ovidius University of Constanta, Constanța, Romania
[4]Faculty of Food and Animal Sciences, Iași University of Life Sciences, No.8, Mihail Sadoveanu Alley, Iasi, România

Corresponding author e-mail: ahanghel@yahoo.com

ABSTRACT

The male effect is considered one of the most efficient natural methods for stimulating ovarian activity and synchronizing estrus in goats, representing a practical alternative to hormonal protocols in extensive and semi-extensive production systems. The present study was conducted to evaluate the influence of the male effect on estrus response in Carpathian goats raised under two contrasting climatic conditions in Romania. A total of 100 clinically healthy adult females were equally distributed between a dry and a humid climatic area and assigned to control and experimental groups. In the experimental groups, females were completely isolated from bucks for 60 days before the breeding season, after which one buck was introduced for every 25 females. Estrus was monitored daily for 15 days following buck introduction and both the proportion of females exhibiting estrus and the interval between buck introduction and estrus onset were recorded. The application of the male effect significantly improved reproductive performance in both climatic areas. In the dry area, the proportion of females exhibiting estrus increased from 68% in the control group to 92% in the experimental group, while in the humid area it increased from 72% to 96%. In addition, a considerably higher proportion of females expressed estrus within the first five days after buck introduction, demonstrating a more synchronized reproductive response. Although reproductive performance was slightly higher in the humid area, the male effect proved highly effective under both environmental conditions, indicating that climatic factors may influence the intensity, but not the efficiency, of the reproductive response. The results demonstrate that the male effect is a simple, low-cost and hormone-free reproductive management strategy capable of improving estrus synchronization in Carpathian goats and can be successfully applied under different climatic conditions to increase the efficiency of breeding management.

Keywords: goats, estrus, male, effect, reproductive

INTRODUCTION

Reproductive performance is an important component of goat production because it influences herd replacement, the organization of mating and kidding and the continuity of milk and meat production. Goats are generally classified as seasonally polyestrous animals, although the onset and duration of reproductive activity vary according to breed, latitude, photoperiod,

physiological status, nutrition and production system (Luo et al., 2019; Souza-Fabjan et al., 2021; Šavorić et al., 2024). At temperate latitudes, the annual variation in day length is the main environmental factor controlling reproductive seasonality, while climatic conditions and forage availability may further modify the reproductive response.

The seasonal pattern of reproduction can limit the organization of breeding programmes and the planned distribution of kidding throughout the year. Hormonal protocols based on progestogens, prostaglandins and gonadotropins are commonly used to induce or synchronize estrus. Although these treatments can provide a controlled reproductive response, their application requires additional animal handling and increases production costs. Repeated hormonal treatments may also reduce estrus response and reproductive performance through endocrine and immune changes (Sun et al., 2024). For these reasons, increasing attention has been directed towards non-hormonal methods that can be more easily integrated into extensive and semi-extensive production systems.

The male effect is a natural reproductive management method based on the introduction of bucks after a period of separation from females. Contact with a sexually active male can stimulate luteinizing hormone secretion, follicular development, ovulation and estrous behaviour in females with reduced or absent ovarian activity (Chemineau, 1987; Delgadillo et al., 2009). The response is initiated mainly by olfactory signals but is reinforced by visual, auditory and behavioural stimuli. Consequently, complete separation before buck introduction is generally recommended to increase the response of females when contact is re-established.

The effectiveness of the male effect depends on several factors associated with both females and males. In females, live weight, body condition, previous reproductive activity and nutritional status can influence the proportion of animals that ovulate or exhibit estrus after buck introduction (Gallego-Calvo et al., 2015, 2018). In males, sexual activity, age, feeding level, photoperiodic treatment and the intensity of behavioural interactions with females may modify the reproductive response. Delgadillo et al. (2020) found that undernutrition reduced body weight, testicular size and odour intensity in bucks and increased the interval between buck introduction and the onset of estrous behaviour in females. Subsequent research showed that nutritional supplementation improved the sexual response of bucks managed under semi-extensive conditions and increased their ability to stimulate reproductive activity in females (Delgadillo et al., 2021).

The sexual activity of males may also affect the proportion of females that show estrus and ovulation. Photoperiod-treated bucks can improve estrus expression and reproductive performance, particularly in breeds characterized by pronounced reproductive seasonality (Zarazaga et al., 2021). However, high testosterone concentrations at the time of buck introduction do not appear to be an essential condition for inducing ovarian activity, suggesting that the response results from the combined action of several behavioural and physiological signals (Zarazaga et al., 2022).

The male-to-female ratio is another factor that may affect the degree of contact between animals and the intensity of stimulation. Ratios ranging from one buck per five females to one buck per 20 females have produced stronger reproductive responses than lower male availability, such as one buck per 30 females (Zarazaga et al., 2018). Nevertheless, climatic and management conditions may modify these responses. Alves et al. (2014) obtained high estrus rates in Anglo-Nubian goats during both dry and rainy periods, although some reproductive indicators were more favourable during the rainy season. These differences may be associated with changes in feed availability, nutritional status and environmental stress.

Climatic conditions can influence reproduction directly through temperature and humidity and indirectly through their effects on pasture growth and feed quality. Although goats are considered well adapted to a wide range of environments, prolonged exposure to high temperatures can alter endocrine function, feed intake and reproductive performance (Danso et

al., 2024). In extensive and semi-extensive systems, dry conditions may also reduce the availability and nutritional value of forage, whereas more favourable rainfall can support a more stable supply of feed. The reproductive response to the male effect should therefore be evaluated in relation to the environmental and management conditions in which the animals are raised.

The Carpathian goat is widely raised in Romania, particularly in traditional production systems; however, information regarding its estrous response following the controlled introduction of bucks remains limited. Moreover, few studies have compared the effectiveness of the same male-effect protocol in Carpathian goats maintained under contrasting climatic conditions.

Therefore, the present study aimed to evaluate the influence of the male effect on estrus response in Carpathian goats raised in a dry and a humid climatic area of Romania. The proportion of females that showed estrus during the first 15 days and the distribution of estrus onset after buck introduction were compared to determine whether climatic conditions were associated with differences in the intensity and synchronization of the reproductive response.

MATERIALS AND METHODS

The study was conducted between August and September 2025 on two goat farms located in regions of Romania with contrasting climatic conditions. The first farm was situated in a dry region of south-eastern Romania, characterized by higher mean annual temperatures, reduced annual precipitation and frequent periods of water deficit during the growing season. The second farm was located in a more humid northern region, characterized by moderate temperatures, higher precipitation and conditions favorable for vegetation growth and pasture availability.

The climatic characterization of the two regions was based on mean annual temperature, mean temperature during the breeding season, annual precipitation, relative humidity and the mean annual number of rainy days. In the dry region, the mean annual temperature was 12.5°C, the mean temperature during the breeding season was 18.6°C, annual precipitation was 420 mm, relative humidity was 63% and the mean annual number of rainy days was 85. In the humid region, the corresponding values were 9.8°C, 15.2°C, 720 mm, 76% and 125 days, respectively. Climatic data were obtained from the Romanian National Meteorological Administration (ANM, https://www.meteoromania.ro/clima/).

A total of 100 clinically healthy adult Carpathian females were included in the study, with 50 females selected from each farm. Within each climatic region, the animals were divided into a control group and an experimental group, each consisting of 25 females. Therefore, the control group included 50 females, with 25 animals from each region, while the experimental group consisted of another 50 females distributed in the same manner. All animals were maintained under the usual feeding and management conditions of the farms throughout the study.

The females in the control groups were managed according to the usual reproductive practices of each farm. They were not subjected to a prior period of separation from males and therefore did not undergo the protocol based on male presence. Reproductive activity proceeded under the routine conditions of the farms and these groups served as the basis for comparison when evaluating the influence of male presence on estrus expression.

The females in the experimental groups were completely isolated from males for 60 days before the beginning of the breeding period. During this interval, all direct and indirect contact between females and males was prevented, including visual, olfactory and auditory contact. At the end of the isolation period, one breeding male was introduced into each experimental group of 25 females, corresponding to a male-to-female ratio of 1:25. The day of male introduction was designated as Day 0 and the males remained with the females throughout the 15 day observation period. Monitoring of the control and experimental groups began on the same date in each climatic region.

Estrous behavior was monitored daily for 15 consecutive days. Females were considered to be in estrus when they showed behavioral signs of sexual receptivity and accepted mounting by the male. The number of females that showed estrus was recorded individually for each group. Estrus response was calculated as the number of females that showed estrus divided by the total number of females in the respective group and multiplied by 100.

To assess the distribution and degree of synchronization of the reproductive response, the interval between the beginning of the observation period and the first detection of estrus was recorded for each female. According to the time of estrus onset, the females were classified into three intervals: 1-5 days, 6-10 days and 11-15 days.

The numbers and proportions of females that showed estrus were calculated for each group and climatic region. Differences between the control and experimental groups were assessed using Pearson's chi-square test. The same test was applied to compare the proportions of females that showed estrus within the three observation intervals. Statistical significance was established at $P < 0.05$ and the results were expressed as numbers of females and percentages.

RESULTS AND DISCUSSION

The proportion of females that showed estrus within the first 15 days after male introduction was used to evaluate the reproductive response in the two climatic regions (Table 1).

Table 1. Estrus response of Carpathian females according to climatic region and group

Climatic Area	**Group**	**n**	**Females in estrus**	**%**	**P-value**
Dry Area	Control	25	17	68,00	P=0,034
	Experimental	25	23	92,00	
Humid Area	Control	25	18	72,00	P=0,022
	Experimental	25	24	96,00	

The presence of the male stimulated estrus expression in Carpathian females in both regions. In the dry region, the proportion of females that showed estrus increased from 68.00% in the control group to 92.00% in the experimental group, representing an increase of 24.00 percentage points. In the humid region, the corresponding proportion increased from 72.00% to 96.00%, resulting in the same increase of 24.00 percentage points.

Statistical analysis revealed significant differences between the control and experimental groups in both the dry region ($P = 0.034$) and the humid region ($P = 0.022$), confirming the influence of male presence on estrus expression.

The reproductive response was numerically slightly higher in the humid region, where 96.00% of the experimental females showed estrus, compared with 92.00% in the dry region. Nevertheless, the increase relative to the control group was identical in both regions. Therefore, male presence produced a clear reproductive response under both climatic conditions (Figure 1).

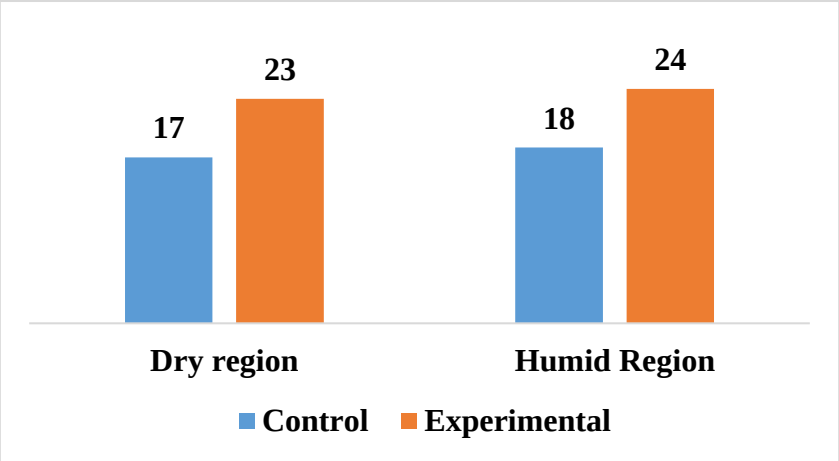

Figure 1. Distribution of estrus expression during the first 15 days following male introduction

In addition to the proportion of females that showed estrus, the time interval between male introduction and estrus onset was analyzed to assess the degree of synchronization of reproductive activity.

Estrus expression was concentrated mainly within the first five days after male introduction. In the dry region, the proportion of females that showed estrus during the 1-5 day interval increased from 20.00% in the control group to 56.00% in the experimental group. In the humid region, the corresponding values increased from 28.00% to 68.00%.

The proportions of females that showed estrus during the 6-10 day and 11-15 day intervals were lower in the experimental groups than in the control groups. This distribution indicates that male introduction promoted an earlier and more synchronized reproductive response. Highly significant differences were recorded for the 1-5 day interval in both the dry region ($P = 0.009$) and the humid region ($P = 0.004$). Differences between groups during the 6-10 day and 11-15 day intervals were not statistically significant ($P > 0.05$) (Table 2).

Table 2. Distribution of females that showed estrus according to the time interval following male introduction

Climatic Region	**Group**	**n**	**1-5 days**	**%**	**6-10 days**	**%**	**11-15 days**	**%**
Dry Area	Control	25	5	20,00	7	28,00	5	20,00
	Experimental	25	14	56,00	6	24,00	3	12,00
P-value			**0,009**		**0,754**		**0,439**	
Humid Area	Control	25	7	28,00	6	24,00	5	20,00
	Experimental	25	17	68,00	5	20,00	2	8,00
P-value			**0,004**		**0,733**		**0,218**	

Note: n - number of females.

The introduction of males after a 60 day separation period increased both the proportion of females that showed estrus and the concentration of estrus onset within the first five days. These findings are consistent with the neuroendocrine mechanism described by Chemineau (1987) and subsequently detailed by Delgadillo et al. (2009). According to this mechanism, olfactory, visual, auditory and behavioral stimuli emitted by the male activate the hypothalamic-pituitary-ovarian axis, promoting luteinizing hormone secretion, follicular development and ovulation.

The earlier concentration of estrus expression observed in the experimental groups is also supported by Augusto et al. (2020). In prepubertal Saanen goats, exposure to a sexually active male resulted in estrous behavior occurring two weeks earlier than in females maintained without male stimulation. These authors recorded estrus in 70.00% of the stimulated animals, compared with 44.00% in the control group. Although the breed, age and experimental design differed from those of the present study, both studies indicate that sociosexual stimulation can increase the proportion of responsive females and promote an earlier estrous response.

The slightly higher numerical response recorded in the humid region may be associated with differences in environmental and nutritional conditions. A more consistent availability of feed resources in regions with higher rainfall may contribute to maintaining a favorable body condition and metabolic status. By contrast, water deficit and variations in the availability and quality of vegetation in dry regions may reduce the energy and protein intake required for normal reproductive activity. However, because each climatic region was represented by one farm, the observed differences cannot be attributed exclusively to climatic conditions.

These findings are supported by Danso et al. (2024), who reported that although goats have a strong capacity to adapt to high temperatures, prolonged exposure to heat stress may cause endocrine and metabolic changes that negatively affect reproductive performance. High temperatures and reduced feed availability can influence reproductive activity in both females and males.

The results are also comparable to those reported by Alves et al. (2014), who evaluated the male effect in Anglo-Nubian goats during dry and rainy seasons. Their findings demonstrated that this method can be applied successfully under different climatic conditions, although some reproductive indicators were more favorable during the rainy season. Similarly, the present study recorded a slightly earlier and more concentrated estrus response in the humid region.

The high estrus response observed in the present study is also consistent with the findings of Viana Neto et al. (2015), who reported that 94.50% of dairy goats showed estrus following biostimulation through the male effect during rainy and dry seasons. This value was intermediate between the 92.00% recorded in the dry region and the 96.00% recorded in the humid region in the present study. Despite differences in breed and management conditions, the similarity between these values demonstrates that controlled male introduction can produce a high estrus response under contrasting environmental conditions.

From a practical perspective, male presence represents an effective method for reproductive management on goat farms in Romania, where many herds are raised under extensive or semi-extensive systems and the use of hormonal treatments may be limited by their cost. The method can contribute to a more efficient organization of the breeding season and facilitate the grouping of kidding events without the use of hormonal protocols. Its effectiveness may be supported by ensuring appropriate nutritional conditions and adapting reproductive management to the environmental characteristics of each region.

CONCLUSIONS

The male effect was effective in stimulating and synchronizing reproductive activity in Carpathian goats in both climatic regions. Following male introduction after a 60 day separation period, the proportion of females that showed estrus within the first 15 days increased from 68.00% to 92.00% in the dry region and from 72.00% to 96.00% in the humid region.

The protocol also promoted an earlier onset of estrus. During the first five days following male introduction, the proportion of females that showed estrus increased from 20.00% to 56.00% in the dry region and from 28.00% to 68.00% in the humid region, indicating more effective synchronization of reproductive activity in the experimental groups.

Although the reproductive response was numerically slightly higher in the humid region, male presence produced a clear and statistically significant response under both climatic conditions. Therefore, this method can be applied in regions with different climatic characteristics, provided that appropriate nutritional and management conditions are ensured.

From a practical perspective, the male effect represents a simple, low-cost and hormone-free method for reproductive management in Carpathian goat herds. Its application may contribute to a more efficient organization of the breeding season and facilitate the grouping of kidding events in extensive and semi-extensive production systems.

REFERENCES

Alves, C.G.T., Almeida-Irmao, J.M., Moura, M.T., Silva, J.C.F., Deus, P.R., Neves, J.P., Bartolomeu, C.C., Lima, P.F., Oliveira, M.A.L. 2014. Influence of male-to-female ratio and climatic conditions on the reproductive performance of Anglo-Nubian goats. Boletim de Indústria Animal, 71(3): 284-290.

Augusto, L., Rodrigues, A.D., Merighe, G.K.F., Oliveira, S.A., Bomfim, G.F., Negrão, J.A. 2020. Influence of male on estrus behavior, estradiol and progesterone release and puberty onset on prepubertal Saanen goats. Semina: Ciencias Agrárias, 41(4): 1247-1258.

Chemineau, P. 1987. Possibilities for using bucks to stimulate ovarian and oestrous cycles in anovulatory goats - A review. Livestock Production Science, 17: 135-147.

Danso, F., Iddrisu, L., Lungu, S.E., Zhou, G., Ju, X. 2024. Effects of heat stress on goat production and mitigating strategies: A review. Animals, 14(12): 1793.

Delgadillo, J.A., Gelez, H., Ungerfeld, R., Hawken, P.A.R., Martin, G.B. 2009. The male effect in sheep and goats: revisiting the dogmas. Behavioural Brain Research, 200(2): 304-314.

Delgadillo, J.A., Lemiere, A., Flores, J.A., Bedos, M., Hernandez, H., Vielma, J., Guerrero-Cervantes, M., Zarazaga, L.A., Keller, M., Chemineau, P. 2020. Undernutrition reduces the body weight and testicular size of bucks exposed to long days but not their ability to stimulate reproduction of seasonally anestrous goats. Animal, 14(12): 2562-2569.

Delgadillo, J.A., Sifuentes, P.I., Flores, M.J., Espinoza-Flores, L.A., Andrade-Esparza, J.D., Hernandez, H., Keller, M., Chemineau, P. 2021. Nutritional supplementation improves the sexual response of bucks exposed to long days in semi-extensive management and their ability to stimulate reproduction in goats. Animal, 15(2): 100114.

Gallego-Calvo, L., Gatica, M.C., Guzman, J.L., Zarazaga, L.A. 2015. Reproductive performance response to the male effect in goats is improved when doe live weight/body condition score is increasing. Animal Reproduction Science, 156: 51-57.

Gallego-Calvo, L., Gatica, M.C., Guzman, J.L., Zarazaga, L.A. 2018. Reproductive responses to sexually active buck of does treated with melatonin when body weight/body condition is increasing or decreasing. Animal Reproduction Science, 190: 75-84.

Luo, J., W. Wang, S. Sun. 2019. Research advances in reproduction for dairy goats. Asian-Australas Journal of Animal Sciences, 32(8): 1284-1295.

Souza-Fabjan, J.M.G., Correia, L.F.L., Batista, R.I.T.P., Locatelli, Y., Freitas, V.J.F., Mermillod, P. 2021. Reproductive Seasonality Affects In Vitro Embryo Production Outcomes in Adult Goats. Animals, 11, 873.

Sun, S., Lv, M., Niu, H., Luo, J. 2024. Influence of repeated estrus synchronization treatment on hormone secretion, growth, and development of dairy goats. Frontiers in Veterinary Science, 10.

Savoric, J., V. Stevanovic, S. Vince, I. Matic, J. Grizelj, M. Lojkic, N. Macesic, M. Samardzija, T. Karadjole, B. Spoljaric. 2024. Reproductive success in goats: A review of selected impacting factors. Veterinarska Stanica, 55(5): 585-593.

Viana Neto, A.M., Flores Salles, M.G., Salles Rodrigues, I.C., Figueiredo Freitas, V.J., Noronha Moura, A.A.A., De Araujo, A.A. 2015. Insemination of dairy goats with estrus induced by the male effect during rainy and dry seasons in Northeastern Brazil. Journal of Advances in Agriculture, 4(1): 350-355.

Zarazaga, L.A., Gatica, M.C., Gallego-Calvo, L., Guzman, J.L. 2018. When using photostimulated bucks to induce the male effect in female goats living at Mediterranean latitudes, a male:female ratio of 1:20 is optimum. Journal of Applied Animal Research, 46(1): 883-887.

Zarazaga, L.A., Gatica, M.C., Delgado-Pertinez, M., Hernandez, H., Guzman, J.L., Delgadillo, J.A. 2021. Photoperiod-treatment in Mediterranean bucks can improve the reproductive performance of the male effect depending on the extent of their seasonality. Animals, 11(2): 400.

Zarazaga, L.A., Gatica, M.C., De La Rosa, I., Delgado-Pertíñez, M., Guzmán, J.L. 2022. The high testosterone concentrations of the bucks used in the male effect is not a prerequisite for obtaining high ovarian activity in goats from Mediterranean latitudes. Animals, 12(8): 954.

https://www.meteoromania.ro/clima/.

VALORIZATION OF PLANT-BASED BY-PRODUCTS FOR ALTERNATIVE PROTEIN PRODUCTION IN SUSTAINABLE FOOD SYSTEMS: CURRENT APPROACHES AND FOOD APPLICATIONS

Sude Cansın GÜNGÖR[1], Müge UYARCAN[1]

[1]Manisa Celal Bayar University, Faculty of Engineering and Natural Sciences, Food Engineering Department, Manisa, Türkiye

Corresponding author e-mail: gungorsudecansin@gmail.com

ABSTRACT

The accelerating expansion of the world population, changing dietary habits, and the continuous increase in protein consumption necessitate a re-evaluation of traditional animal and plant-based protein production systems in terms of environmental, economic, and sustainability. In particular, the high greenhouse gas emissions, intensive land and water use, and adverse effects on biodiversity associated with animal-based protein production have positioned the development of sustainable alternative protein sources as one of the leading research priorities on a global scale. In this regard, the utilization of plant-based by-products generated in the food industry for alternative protein production has emerged as a significant strategy in terms of both the circular bioeconomy and the zero-waste approach. By-products such as fruit and vegetable processing residues, brewer's spent grain, spent coffee grounds, oilseed meals, cereal bran, and legume hulls are among the potential raw materials that can be converted into high-value-added protein sources, owing to their rich content of protein, dietary fiber, polyphenols, and other bioactive compounds. However, lignocellulosic components such as cellulose, hemicellulose, pectin, and lignin present in the plant cell wall limit the recovery of protein; consequently, conventional extraction methods exhibit significant disadvantages, including low yield, prolonged processing time, and high chemical consumption. To overcome these limitations, green technologies such as ultrasound-, enzyme-, and microwave-assisted extraction, supercritical fluid extraction, deep eutectic solvents, pulsed electric field, high hydrostatic pressure, and membrane filtration have emerged as alternative approaches. In addition, the production of microbial proteins—particularly single-cell protein—from lignocellulosic biomass through fermentation bioprocesses, as well as algae- and insect-based bioconversion systems, stand out as innovative approaches that enable the conversion of low-value biomass into protein sources with high added value. These technologies not only enhance protein yield, purity, and functional properties but also significantly reduce energy consumption, organic solvent use, and environmental impact. Owing to their superior techno-functional properties such as emulsification, foaming, water- and oil-binding capacity, and gelation the recovered proteins are utilized in numerous food applications, including plant-based meat analogues, dairy alternatives, functional beverages, and enriched bakery products. Nevertheless, variability in raw material composition, the industrial scalability of extraction processes, food safety, regulatory frameworks, and consumer acceptance remain among the key challenges in this field. This review examines current extraction and bioconversion approaches for the utilization of plant-based by-products in alternative protein production, along with the functional food applications of these proteins and their potential contributions to sustainable food systems.

Keywords: Alternative proteins, Plant-based by-products, Green extraction, Sustainable food systems.

INTRODUCTION

The global agri-food system faces the dual challenge of meeting the nutritional needs of a rapidly growing population while reducing the environmental burden of food production. The global population is projected to reach 8.6 billion by 2030, 9.7–9.8 billion by 2050, and approximately 11.2 billion by 2100. Meeting these demands is expected to require a substantial increase in food production, while land, water, and energy resources are becoming increasingly scarce (Choręziak et al., 2025; Dhiman et al., 2026; Leite et al., 2026).

The anticipated increase in food demand is particularly critical for protein supply. Protein requirements are influenced by factors such as age, health status, and physical activity; an average adult is estimated to require approximately 1–1.6 g of protein per kilogram of body weight per day. Meat has traditionally been a major protein source because of its complete amino acid composition and cultural acceptance. However, the projected doubling of meat demand by 2050, driven by population growth, urbanization, and changing dietary preferences, would intensify pressure on land, water, and energy resources. Animal agriculture is estimated to generate approximately 7.1 gigatonnes of carbon dioxide (CO_2) annually and to account for about 14.5% of total greenhouse gas emissions (Singh & Krishania, 2026). Livestock production is also associated with deforestation, habitat conversion, biodiversity loss, soil degradation, water pollution, overgrazing, and desertification. In addition, the misuse and overuse of antibiotics in intensive animal production have been linked to the rise of antibiotic resistance (Malila et al., 2024). Consequently, the development of alternative protein sources has become a strategic priority. Balancing animal-derived proteins with plant proteins and other alternatives could contribute to more sustainable food systems, support biodiversity, and improve the distribution of high-quality proteins across populations (Choręziak et al., 2025).

Alternative proteins can be obtained from plants, fungi, insects, algae, and cultured meat. They generally contain lower levels of saturated fatty acids and may provide bioactive compounds, making them relevant to the prevention of lifestyle-related health conditions (Sarathy et al., 2025). Compared with animal-based production, plant-based foods require less land and water and generate lower CO_2 emissions. They may also help reduce fluctuations in the availability and price of protein-rich foods caused by extreme weather events, pandemics, conflicts, and inflation (Ahmad et al., 2025; Hadidi et al., 2024).

Beyond conventional plant sources, agri-food by-products represent an abundant and underutilized reservoir of proteins, amino acids, lipids, fatty acids, sugars, dietary fibers, pigments, minerals, vitamins, peptides, and other bioactive compounds. Relevant materials include husks, straw, stover, peels, pomace, seeds, spent grains, shells, bran, organs, whey, factory vegetable-oil residues, and other agricultural by-products. These streams are increasingly investigated for the recovery of food ingredients, food enzymes, food additives, and bioactive compounds, including compounds with antimicrobial activity (Leite et al., 2026; Ospina-Maldonado et al., 2024). Recovered components have been incorporated into functional beverages, nutrient-enriched snacks, and food supplements (Ververis et al., 2026). Particularly, protein-rich plant-based co-products offer significant potential as value-added ingredients in food applications due to their balanced amino acid compositions, low contaminant levels, and superior technological functionalities, such as emulsifying, gelling, and foaming properties. Their recovery, however, is complicated by the lignocellulosic or oleaginous matrices in which the proteins are embedded (Gaber et al., 2025). Protein extraction is therefore a critical step in

determining the yield, purity, nutritional quality, and techno-functional performance of plant protein ingredients and hydrolysates. Conventional approaches, including solvent-based extraction and alkaline extraction, remain widely used because they are operationally simple and relatively inexpensive. Nevertheless, these methods may require large quantities of water or chemicals, consume substantial energy, exhibit limited selectivity, and promote protein denaturation or degradation, thereby reducing nutritional and functional quality (Bekiroglu et al., 2025; Sabaghi & Seyedalmoosavi, 2025; Gaber et al., 2025). These limitations of traditional methods have increased the need for more environmentally friendly and resource-efficient approaches promoting the development of green extraction technologies. Green extraction technologies, including ultrasound-, enzyme-, and microwave-assisted extraction, supercritical fluid extraction, deep eutectic solvents, pulsed electric field, high hydrostatic pressure, and membrane filtration, offer promising strategies for improving protein recovery while reducing the environmental impact associated with conventional extraction processes (Khalid et al., 2025; Sabaghi & Seyedalmoosavi, 2025; Gaber et al., 2025). In addition, the production of microbial proteins, particularly single-cell protein, from lignocellulosic biomass through fermentation bioprocesses, as well as algae- and insect-based bioconversion systems, represents an innovative approach for converting low-value biomass into high-value protein sources (Leite et al., 2026; Rajput et al., 2026). These approaches can improve protein yield, purity, and functional properties while contributing to reduced energy consumption, chemical use, and environmental impact (Dhiman et al., 2026). The selection and optimization of these extraction and bioconversion approaches should balance process efficiency, cost, and protein purity according to the requirements of different industrial applications (Sabaghi & Seyedalmoosavi, 2025).

The value of extracted proteins in food manufacture is commonly assessed through techno-functional properties, including solubility or dispersibility, water- and oil-holding capacity, emulsifying and foaming behavior, and gelation. However, they are highly dependent on the extraction method, protein aggregation state, and composition of the surrounding food matrix, particularly in plant-derived proteins (Naibaho, 2027). Physical structure-modifying treatments, including high-pressure processing (HPP), ultrasound, pulsed electric fields (PEF), cold atmospheric plasma, and extrusion, can further improve the functionality of protein-rich by-products. These treatments may reduce antinutritional factors, promote protein unfolding, and enhance solubility by modifying protein structure and fiber composition. Such changes can facilitate the incorporation of valorized by-products into new food applications (Chen & Ozturk, 2026).

Technological advancements in the recovery and processing of proteins are also contributing to the development of the alternative protein sector. These advancements not only contribute to improving the sensory and nutritional attributes of alternative protein products, including taste, texture, and nutritional quality, but also accelerate research and development activities and market growth through investments made by major food and technology companies in the sector. Accordingly, the integration of alternative proteins into existing food systems is not limited solely to the replacement of animal-derived proteins; rather, it is increasingly regarded as part of a broader transition toward more sustainable, resilient, and ethical protein production models. In this context, agri-food residues, processing by-products, and industrial wastewater represent protein-rich yet underutilized resources with considerable potential for protein recovery (Dhiman et al., 2026). In particular, plant-based proteins play an important role in modern food systems owing to their potential to enhance protein accessibility, support environmental sustainability, and contribute to the prevention of chronic diseases. The applications of these proteins encompass a broad range of products, from meat analogues and dairy alternatives to protein supplements and functional beverages (Mia et al., 2026).

This review comprehensively examines the potential of agricultural and industrial by-products for alternative protein production, innovative green extraction methods for protein recovery, and the applications of the recovered proteins in various food products.

Plant-Based By-Products As Sustainable Protein Sources

Food loss and waste represent major sustainability challenges for global food systems. Approximately one-third of the food produced worldwide, corresponding to nearly 1.3 billion tonnes annually, is lost or wasted and contributes an estimated 8–10% of global greenhouse-gas emissions (Boudalia et al., 2026). In this context, the valorization of plant-based by-products generated during food processing is considered a viable strategy that can contribute to the more efficient utilization of existing agricultural resources and the diversification of alternative protein sources.

Over the past two decades, plant proteins have attracted sustained interest as nutritious and sustainable sources of essential amino acids. While serving as an alternative to animal-derived proteins, which are costly or inadequately available in developing nations, they are increasingly being incorporated into daily diets in developed countries, particularly in vegan food products (Akhtar et al., 2022). In addition to their availability, cost-effectiveness, and versatile functional properties within food systems, the utilization of plant-based proteins has increased in parallel with growing consumer interest in more affordable and environmentally sustainable diets and the widespread adoption of veganism and vegetarianism in Western societies (Munialo et al., 2022; Coronel-León et al., 2026). The growing interest in plant-based proteins has also highlighted the importance of valorizing plant-based by-products, generated at various stages of the food supply chain such as harvesting, processing, and refining, as protein sources. These by-products include oilseed meals derived from soybean, sunflower, and canola processing; fruit and vegetable residues originating from juice production, such as apple pomace, citrus peel, and grape pomace; cereal milling by-products like wheat and rice bran; and hulls obtained from legume processing (Shawky et al., 2025). In addition to proteins, these by-products contain dietary fiber, carbohydrates, minerals, vitamins, phenolics, flavonoids, carotenoids, and other bioactive compounds (Danciu et al., 2026; Khalid et al., 2025).

The protein content of plant-based by-products varies depending on the source and the nature of the by-product. On a dry-matter basis, fruit and vegetable pomaces generally contain 8–15% protein, whereas peels contain approximately 2–10% and pulps 1–5%. With approximately 10-25% protein and 15-65% lipid contents, seeds are considered among the more protein-dense fractions. These nutritional attributes render fruit seeds, pomaces, and kernels valuable resources for valorization (Danciu et al., 2026; Khalid et al., 2025).

The significance of valorizing plant-based by-products becomes increasingly apparent when considering their production volumes. Fruit- and vegetable-processing residues account for approximately 16% of total food by-products and contribute about 6% of global greenhouse-gas emissions. Brewer's spent grain (BSG) represents approximately 85% of the brewing industry's solid by-products, with global production exceeding 39 million tonnes annually. Similarly, several million tons of spent coffee grounds are generated annually, and this material constitutes a significant waste stream originating from coffee production (Danciu et al., 2026).

Cereal processing by-products constitute a significant group among plant-based protein sources. Global cereal production exceeds 2.8 billion tons annually (FAO, 2023), and milling and dehulling processes generate various fractions such as pericarp, aleurone layer, embryo, and bran. Despite their nutritional value, these fractions, which contain fibers, bioactive peptides, lipids, phenolic compounds, phytosterols, and other health-promoting components in

addition to proteins, are frequently utilized as animal feed or discarded (Aït-Kaddour et al., 2024).

Brewers' spent grain, a prominent example of cereal processing by-products, contains approximately 60% carbohydrates (including roughly 50% dietary fiber), 30% protein, and 10% lipids, in addition to minerals and bioactive polyphenols. Its protein fraction is dominated by water-insoluble hordeins and glutelins. Moreover, its content of ferulic acid, *p*-coumaric acid, caffeic acid, arabinoxylan, and β-glucan is reported to contribute to its antioxidant, anti-inflammatory, hepatoprotective, and prebiotic potential (Danciu et al., 2026). With global beer production approaching 180 million tonnes per year, BSG production is estimated to correspond to approximately 20% of this volume and to represent approximately 85% of the brewing industry's solid by-products (Aït-Kaddour et al., 2024; Saberian et al., 2024).

Spent coffee grounds (SCG) are also among the plant-based by-products that can be valorized for their protein and other valuable components. The disposal of SCG, generated in massive quantities, poses a significant challenge from an environmental management perspective. On a dry basis, SCG generally contain 6–16% protein, 10–18% lipids, and 60–70% total dietary fiber, mainly in the form of cellulose, hemicellulose, and lignin. They also contain chlorogenic acid, caffeine, melanoidins, diterpenes such as kahweol and cafestol, galactomannan, arabinogalactan, and other phenolic compounds (Choe, 2025; Danciu et al., 2026).

Oilseed meals and cakes constitute another notable group of plant-based by-products, distinguished by their protein content. Approximately 39% of oilseed meals and press cakes are generated during food production and processing, with substantial quantities arising from the processing of soybeans, sunflower, rapeseed, pumpkin seeds, hemp seeds, and other oil-bearing crops (Chen & Ozturk, 2026). Although traditionally utilized as low-value animal feed or discarded, the protein content of oilseed meals can reach up to 50% on a dry matter basis, thereby presenting significant potential for utilization in human nutrition (Kanimozhi et al., 2026). Furthermore, oilseed by-products also contain lipids and other valuable bioactive compounds (Aït-Kaddour et al., 2024).

Overall, plant-based agro-industrial by-products hold considerable potential for the diversification of alternative protein sources, owing to their high production volumes, protein content, and other nutritional and bioactive components (Nirmal et al., 2025). The valorization of these resources, traditionally utilized as animal feed or discarded, can contribute to the diversification of the protein supply without requiring additional agricultural inputs, thereby supporting circular and resource-efficient food systems (Naibaho, 2027).

Emerging Extraction, Processing And Bioconversion Technologies For Alternative Proteins

The primary objective of any extraction procedure is to maximize recovery of the target compound while minimizing adverse changes to its properties and limiting the co-extraction of undesired constituents (Chandran et al., 2024). Protein extraction is particularly challenging because plant proteins are often tightly entrapped within cell walls and intracellular cotyledon matrices, and interactions with the extraction solvent can modify their structural characteristics. Efficient extraction therefore requires technologies that can disrupt plant-cell integrity and facilitate protein release (Chandran et al., 2023).

In protein recovery, solvent extraction and alkaline extraction-isoelectric precipitation are among the widely used conventional methods due to their reliance on simple, reliable, and well-defined protocols. Solvent extraction commonly employs organic solvents such as hexane,

ethanol, acetone, and methanol to recover proteins and other constituents from finely ground plant materials. After the protein-rich liquid fraction is separated from the solid residue, the proteins are precipitated and the solvent is evaporated or recovered for reuse (Kaur et al., 2025).

Isoelectric precipitation following alkaline extraction is another widely utilized conventional method in the industrial production of plant-based protein isolates and concentrates. This method exploits the pH-dependent solubility properties of proteins. In the initial stage, the pH is typically elevated to a range of 8-10 through the addition of sodium hydroxide to induce protein solubilization, during which fiber-rich fractions are separated. Subsequently, the pH is lowered to approximately 4.0-4.5 via acid addition. Under these isoelectric conditions, where protein solubility reaches a minimum, the proteins are recovered through precipitation (Nartea et al., 2023).

Conventional methods have long been used to produce plant-protein concentrates and isolates because of their operational simplicity, established protocols, and relatively low initial set-up costs. Nevertheless, their reliance on intensive chemical and thermal treatments creates important technological and environmental constraints. These methods may involve high energy consumption, environmental contamination, hazardous solvent residues, and reduced extraction quality or protein recovery (Ahmad et al., 2025). Incomplete protein recovery and heat- or pH-induced denaturation may additionally impair protein solubility, emulsifying capacity, and textural properties. Therefore, these limitations restrict the use of recovered proteins in food formulations in which such functionalities are essential and underscore the need for extraction approaches that combine high recovery efficiency with reduced environmental impacts and improved protein quality (Shawky et al., 2025).

In this context, various advanced extraction technologies have been developed and optimized for protein recovery over the past decade. Methods employing ultrasound-assisted extraction (UAE), enzyme-assisted extraction, microwave-assisted extraction (MAE), supercritical fluid extraction, and deep eutectic solvents present considerable potential for enhancing protein yield, purity, and functional properties while mitigating resource requirements and environmental burdens (Issa et al., 2025).

Ultrasound-assisted extraction, also known as sonoprocessing, is a promising non-thermal technology for protein recovery and modification. Compared with conventional methods, sonication can reduce processing time, energy consumption, and chemical use, potentially lowering the carbon footprint of protein processing. UAE uses mechanical sound waves at frequencies above the range of human hearing, generally above 20 kHz. In food processing, high-power ultrasound commonly operates at frequencies between 20 and 100 kHz (Ahmad et al., 2025). The effectiveness of UAE is primarily attributed to acoustic cavitation. Alternating compression and rarefaction cycles generate microbubbles in the liquid extraction medium. These bubbles grow and collapse violently within microseconds, producing localized high pressures and temperatures, intense hydrodynamic shear forces, and high-velocity liquid microjets (Ahmad et al., 2025; Chen & Ozturk, 2026). The implosion of these bubbles generates localized extreme conditions of temperatures up to 5000 K and pressures of 50 MPa, alongside high-velocity liquid microjets (approximately 400 km/h) and intense shear forces (Sharma et al., 2026). This cell-disruption mechanism is particularly relevant to agro-industrial residues, in which cellulose, hemicellulose, pectin, and lignin form rigid lignocellulosic barriers that restrict protein release into the liquid phase. Unlike conventional extraction, which may produce limited structural disruption, ultrasound can damage cell-wall architecture and facilitate protein liberation from the matrix (Gumus & Yildiz, 2024). UAE generally requires shorter treatment times and lower temperatures than conventional methods, which may help preserve the

structure of sensitive proteins. It is also considered environmentally favorable because it can reduce the need for strong chemicals and excessive energy inputs (Kaur et al., 2025).

Enzyme-assisted extraction uses biocatalysts to accelerate biological reactions and has increasingly been applied to reduce the need for harsh chemicals, shorten extraction times, and improve extraction efficiency. In plant-protein extraction, enzymes degrade the complex cell-wall structure composed of hemicellulose, cellulose, and lignin, thereby facilitating the release of intracellular proteins. Commercial preparations used for this purpose include Pectinex Ultra SP-L, Pectinex UF, Viscozyme L, pectinase, and cellulase, which provide hemicellulase, cellulase, and pectinase activities. Proteases such as Alcalase and Protex can additionally facilitate the passage of smaller protein fragments through the disrupted cell wall by hydrolyzing proteins into smaller molecules (Akyüz et al., 2024). The efficiency of enzyme-assisted extraction depends on enzyme type and concentration, the enzyme-to-substrate ratio, temperature, and extraction time. Protein yield and purity are also associated with the extent of cell-wall disruption. Optimal pH conditions are therefore required to prevent enzyme inactivation and protein denaturation. Typical extraction conditions involve alkaline pH values of 8–10 and temperatures of 45–60 °C (Huang et al., 2024).

Microwave-assisted extraction is a rapid, energy-efficient, and environmentally favorable technology for recovering proteins and other value-added constituents from agro-industrial by-products (Aït-Kaddour et al., 2024; Ligarda-Samanez et al., 2025). It uses non-ionizing electromagnetic waves in the frequency range of 300 MHz to 300 GHz. Frequencies of 2.45 GHz are commonly used in domestic systems, whereas 915 MHz or 2.45 GHz are typically applied at industrial scale (Sharma et al., 2026). Unlike conduction- or convection-based heating, MAE produces rapid and volumetric heating throughout the material (Hadidi et al., 2024). During microwave treatment, polar molecules in the plant matrix interact directly with electromagnetic radiation through dipole rotation and ionic conduction, generating dielectric heating (Maqsood et al., 2025). Free water molecules within biological cells are particularly important microwave-absorbing regions. Their rapid heating and vaporization increase intracellular pressure and generate abrupt temperature and pressure gradients, causing intracellular water to expand and cell-wall and membrane structures to rupture (Bagasettihalli Kariyappa et al., 2025; Hadidi et al., 2024; Shawky et al., 2025). The resulting cellular disruption promotes deeper solvent penetration, increases the solubilization rate of target proteins and bioactive compounds, and accelerates their release into the extraction medium through improved mass transfer (Bagasettihalli Kariyappa et al., 2025; Shawky et al., 2025). In addition to its rapid heating profile, MAE can reduce solvent requirements and extraction time while improving extraction efficiency compared with conventional processes. Its ability to operate synergistically with other techniques, including UAE and enzyme-assisted extraction, also supports its integration into biorefinery frameworks designed to recover high-value constituents from plant-based agro-industrial residues (Maqsood et al., 2025).

Supercritical-fluid extraction is another green alternative to conventional extraction. It uses non-toxic solvent systems, operates at low temperatures and over short extraction times, enhances diffusion, and reduces energy consumption. Its performance depends on the optimization of pressure, temperature, extraction time, and CO_2 flow rate, as well as on matrix characteristics such as moisture content, particle size, porosity, and shape. These parameters influence extraction selectivity and yield. The resulting extracts may contain high-value compounds with relevant biological activities, purity, and stability, supporting their potential use as functional-food ingredients (Calleja-Gómez et al., 2024).

Eutectic-mixture frameworks offer non-toxic and highly selective alternatives for biomolecule separation. Their mild thermal operating conditions can support structural stability during dissolution, while their solvent systems can dissolve complex protein matrices while preserving native three-dimensional conformation. Customizable polarity ranges, localized pH zones, and fluid-dynamic properties facilitate intact mass transfer into the liquid phase (Mohammad, 2026). The efficacy of deep-eutectic-solvent extraction depends largely on the selection of the hydrogen-bond acceptor and donor. These components collectively determine key solvent properties, including polarity, viscosity, hydrogen-bonding capacity, and pH. The polarity of the deep eutectic solvent must also correspond to the target compound. Hydrophilic deep eutectic solvents are generally more suitable for extracting phenolic compounds and polar proteins. In addition, the extensive hydrogen-bond network in these solvents can disrupt hydrogen bonds within the plant cell-wall matrix and facilitate the separation of intracellular proteins (Khalid et al., 2025).

In addition to green extraction technologies, bioconversion of low-value agricultural and food-processing residues provides an alternative route for protein production within a circular bioeconomy framework. In particular, microbial proteins, especially single-cell protein, can be produced from lignocellulosic residues and food waste through submerged or solid-state fermentation using bacteria, yeasts, fungi, and microalgae. These microorganisms can convert low-cost waste streams into protein-rich biomass, with single-cell protein generally containing high levels of protein and requiring relatively low land and water inputs, thereby supporting waste valorization and resource efficiency (Rajput et al., 2026; Sekoai et al., 2024). Similarly, algae-based systems have attracted attention as alternative protein platforms, with microalgae such as *Spirulina* and *Chlorella* reported as protein-rich biomass sources for food and feed applications (Navarré et al., 2025; Sekoai et al., 2024). Insect-based bioconversion, particularly using black soldier fly larvae (*Hermetia illucens*), also enables the conversion of organic waste streams into protein- and lipid-rich biomass, further contributing to circular waste-to-protein systems (Dhiman et al., 2026). These bioconversion approaches therefore provide complementary strategies for converting underutilized biomass and organic waste streams into value-added protein sources (Bai et al., 2026; Dhiman et al., 2026).

Physical Modification And Structuring Of Proteins Derived From Plant-Based By-Products

The incorporation of proteins recovered from agro-industrial by-products into food systems as functional ingredients depends on the controlled manipulation of their molecular conformation (Ligarda-Samanez et al., 2025; Rasool et al., 2026). Physical processing techniques employed for this purpose can be categorized into two groups: non-thermal physical treatments and structuring techniques that impart specific structural and textural properties to the proteins. While high-pressure processing and pulsed electric fields are among the non-thermal physical treatments; extrusion, electrospinning, and three-dimensional (3D) printing are the primary techniques utilized for protein structuring. These physical and mechanical processes, which do not require chemical or enzymatic inputs, can facilitate the enhancement of techno-functional properties by inducing controlled modifications in the protein structure (Ahmad et al., 2025; Farsani et al., 2026).

The effects of physical treatments on protein structure are highly dependent on processing conditions. Non-thermal processes, in particular, can alter weak non-covalent interactions such as hydrogen bonds and hydrophobic interactions, thereby inducing protein unfolding and the exposure of hydrophobic amino acid residues and free sulfhydryl groups. Consequently, these structural modifications can yield enhancements in solubility, interfacial emulsion stability, and

foaming capacity (Ahmad et al., 2025; Ligarda-Samanez et al., 2025). However, these effects vary depending on the processing conditions; while insufficient treatment leads to limited structural modifications, over-processing can result in irreversible denaturation, aggregation, or the loss of bioactivity. Furthermore, although these technologies generally facilitate the preservation of nutritional composition under mild conditions, the energy requirements—particularly those of high-pressure processing—must be taken into consideration during process design (Bekiroglu et al., 2025).

Among these techniques, high-pressure processing, also known as high hydrostatic pressure processing, is a non-thermal technology based on the application of pressures up to 800 MPa to food systems for a duration of several minutes. The uniform transmission of pressure throughout the medium ensures that the treatment effect is largely independent of product composition, size, and shape, thereby preserving the macroscopic integrity of the product. The impact of HPP on proteins is driven by the disruption of hydrophobic, electrostatic, and hydrogen bond interactions; a phenomenon that can subsequently influence molecular rearrangement, gelation, and aggregation (Chen & Ozturk, 2026). At appropriate pressure levels, the destabilization of the secondary, tertiary, and quaternary structures of proteins can result in partial or complete unfolding, the dissociation of subunits, a decrease in α-helical content, and an increase in β-sheet and random coil conformations. The exposure of hydrophobic residues, sulfhydryl groups, and charged side chains consequently alters the surface properties and interaction potential of the proteins (Mia et al., 2026). The manifestation of these structural modifications in functional properties depends on pressure intensity, holding time, temperature, pH, ionic strength, protein structure, and the composition of the food matrix. While moderate pressure levels can enhance solubility, emulsification, or gelation, excessive pressure can diminish techno-functional performance due to aggregation, denaturation, and phase separation (Ahmad et al., 2025).

The pulsed electric field process is based on inducing a transmembrane potential difference and electroporation through the application of short, high-voltage pulses of 20–80 kV cm^{-1} for durations of 1–100 μs to plant, microbial, and fungal cells. The resulting transient or permanent nanopores increase membrane permeability, thereby facilitating the release of intracellular water, ions, metabolites, and proteins, while the microchannels that enhance solvent-solute mobility accelerate mass transfer and improve substrate accessibility for microbial metabolism (Sharma et al., 2026). PEF can also alter protein conformation by promoting protein unfolding, charge redistribution, and the exposure of hydrophobic regions via electric field-induced molecular polarization (Teng et al., 2025). These modifications can enhance solubility, water-holding capacity, emulsification, and foaming properties; meanwhile, the inactivation of lipoxygenase, trypsin inhibitor activity, and allergenic structures can contribute to the improvement of flavor and nutritional value. However, an increase in processing intensity can alter the volatile compound profile and promote the formation of oxidative volatile compounds (Anbarasan et al., 2023).

In addition to the physical modification of proteins, structuring techniques are employed to generate desired structural properties in food applications. Among these, extrusion is a continuous thermal process widely utilized in the processing of plant-based proteins due to its short processing time, high efficiency, cost-effectiveness, and technological maturity. Through the combined effects of temperature, pressure, and shear forces, the material is mixed, homogenized, extruded, expanded, and transformed into organized fibrous protein structures (Xiao et al., 2023). Although low-moisture extrusion is generally performed at a moisture content of approximately 30%, moisture levels ranging from 10% to 35% have also been reported; this method yields dry, porous textured vegetable proteins suitable for use in

rehydrated products such as nuggets and burgers. High-moisture extrusion (HME), on the other hand, is typically applied at 50-70% moisture, though moisture levels in the range of 40-80% can also be utilized. While this process facilitates the formation of fibrous structures resembling muscle tissue, it can enhance chewiness and mouthfeel; furthermore, it can promote protein gelation, recombination, and fat emulsification (Zhang et al., 2021; Bisht et al., 2025; Imran et al., 2026). The capability of HME to provide low energy input, zero waste discharge, high production efficiency, and a desirable product texture—owing to its prevention of product expansion and reduction of viscous energy dissipation—supports its utilization in the development of plant-based meat alternatives (Zhang et al., 2021).

In addition to extrusion, electrospinning and 3D printing are also utilized in the structuring of plant-based proteins. Electrospinning involves the dissolution and denaturation of plant proteins in alkaline reagents, followed by their coagulation through a spinneret to generate a fibrous material composed of organized proteins. In 3D printing, on the other hand, the molten protein is extruded through a nozzle and deposited in layers to form a fibrous structure (Xiao et al., 2023; Zahari et al., 2022).

Applications In Sustainable Food Systems

In the valorization of plant-based proteins recovered from agro-industrial by-products as food ingredients, it is crucial that they exhibit functional properties that are equivalent to, superior to, or distinct from existing protein alternatives (Ismail et al., 2020). The properties of proteins, such as solubility, emulsification, gelation, binding, and water and oil holding capacities, directly influence their potential applications across various food systems (Ciugureanu et al., 2025). In this context, plant proteins can be utilized in diverse product categories, including meat and dairy alternatives, protein-rich beverages, bakery products, pasta, and snacks (Du & Yang, 2024).

Plant-based meat alternatives constitute one of the prominent application areas for alternative proteins. In contrast to the complex architecture of animal meat, which consists of muscle, fat, and connective tissues, plant proteins predominantly exist in globular conformations. This structural discrepancy complicates the mimicking of the fibrous structure, texture, aroma, and mouthfeel of animal meat. Consequently, structuring techniques are employed to transform plant proteins into meat-like structures (Kaplan et al., 2025; Samad et al., 2024). The stability of the resulting structures, along with their physicochemical and sensory properties during cooking, is crucial for consumer acceptance. Modified proteins with enhanced thermal stability can mitigate undesired denaturation during thermal processing, while high solubility coupled with strong binding, water-holding, and oil-holding capacities can contribute to the structural integrity of the product (Keerthi et al., 2025). Coconut, butter, sunflower, canola, and sesame oils can enhance juiciness and tenderness; however, excessive fat content can exert a lubricating effect, thereby interfering with the protein denaturation that is crucial for the development of a meat-like texture (Samad et al., 2024). Consequently, protein functionality, lipid composition, and structuring technology must be evaluated in conjunction in the formulation of plant-based meat alternatives (Boukid, 2021). Current studies evaluating proteins derived from plant-processing by-products in meat-analogue formulations and the structural features of the resulting products are summarized in Table 1.

Table 1. Current studies evaluating proteins derived from plant-processing by-products in meat-analogue formulations

By-Product Protein Source	**Application**	**Findings**	**References**
Okara flour (29.35% protein), a soybean-processing by-product	Incorporation at 0–40% into high-moisture meat analogues (HMMA) formulated with soy protein isolate, wheat gluten, and corn starch	Increasing okara reduced protein density but increased dietary fiber from 0 to 7.59 g/100 g at 40% incorporation. Fibrous anisotropy was maintained up to 20% okara, whereas higher levels reduced firmness, cohesiveness, and elasticity and disrupted protein alignment and gel functionality.	Aussanasuwannakul et al., 2025
Biji (okara/soybean curd residue), a protein-containing soybean-processing by-product	Used at 5, 10, 15, and 20 g in plant-based patties	Biji addition improved water-holding capacity, crude protein content, and textural properties while reducing cooking loss and dimensional shrinkage. The 20 g formulation exhibited the highest WHC and protein content and the lowest cooking loss, with reduced levels of undesirable volatile compounds.	Nam et al., 2024
Brewer's spent grain, a protein- and fiber-rich brewery by-product	Incorporation into soy protein isolate-based high-moisture meat analogues	BSG improved texturization, reduced hardness, and increased in vitro protein digestibility (74.58–76.15%). Incorporation levels up to 23.4% were suitable for texturization, whereas higher levels impaired fibrous structure formation.	da Silva et al., 2024
Pineapple edible pomace (6.52 ± 0.34% protein) and peel pomace (4.61 ± 0.15% protein)	Partial replacement of soy protein isolate during extrusion for meat analogue production	Pineapple pomace enhanced expansion ratio, water absorption index (optimized at 150.39%), and degree of texturization, promoting a meat-like fibrous structure.	Lu et al., 2025

Jackfruit by-products	Jackfruit by-products at different levels (18%, 38%, 58%, and 78%)	A formulation containing 58% jackfruit by-products and 20% wheat gluten achieved the highest sensory acceptance and provided higher protein (20.67 ± 3.96 g) and dietary fiber contents than the commercial meat analogue (14.26 ± 1.38 g protein).	(Hamid et al., 2020)

Dairy alternatives and protein-rich beverages constitute another prominent application area for plant-based proteins. These products serve as viable alternatives, particularly for consumers with lactose intolerance or milk protein allergies (Alehosseini et al., 2025). While cow's milk contains approximately 3.3 g of protein per 100 mL, the protein content of plant-based beverages varies significantly depending on the source used. Soy beverages contain about 4.0–4.8 g of protein per 100 mL; conversely, this value ranges from 0.3 to 0.7 g in rice beverages and is generally below 1 g in almond, oat, and coconut beverages (Yadav et al., 2026).

In the development of plant-based beverages, sensory and physicochemical properties are as critical as protein content. The emergence of beany, bitter, or off-flavors in these products, alongside a high starch content that negatively affects textural quality, can limit consumer acceptance. Furthermore, volatile compounds such as hexanal, hexanol, and pentanal, which can be generated as a result of lipid oxidation, can also contribute to off-flavors (Pointke et al., 2022). Acidification, fermentation, ultrasonication, and membrane filtration can be employed to improve protein functionality and sensory quality, whereas the blending of different proteins can contribute to the enhancement of amino acid profiles and beverage characteristics. These products can be targeted towards vegetarians, individuals with lactose intolerance or milk allergies, athletes, infants, and health-conscious consumers (Sabaghi & Seyedalmoosavi, 2025).

Among dairy products, plant-based cheese alternatives represent a more challenging application area because the technological functionality of dairy cheese is largely associated with the casein matrix. In these products, milk fat and/or proteins are partially or completely replaced by plant-based fats, oils, and proteins. The functional properties of the products largely depend on their fat, protein, dry matter, and calcium content. The inability of plant proteins to fully replicate the technological functionality of casein, coupled with their higher molecular weight compared to milk proteins, leads to functional differences. Therefore, achieving the characteristic texture, elasticity, and melting behavior of dairy cheese in plant-based alternatives poses a significant technological challenge, while modified starch can be utilized to mimic some of these properties (Kowalczewski et al., 2025).

In addition to meat and dairy alternatives, plant-based proteins can also be utilized in the formulations of bakery products, pasta, and snacks. Bread, cakes, pastries, and other bakery products rank among the staple foods widely consumed across different societies. Cereal-based snacks, on the other hand, enjoy a widespread consumption pattern as convenient and ready-to-eat products (Boukid et al., 2024). However, these products are associated with several challenges in the contemporary context. The first concerns the elevated sugar and fat content typically found in bakery products, which has been linked to weight gain and the onset of non-communicable diseases, including diabetes, cardiovascular disease, and obesity. The second challenge relates to product deterioration, which encompasses chemical, physical, and

microbiological alterations occurring in baked goods over time. Given that plant proteins are rich in bioactive compounds—such as antioxidant dietary fibers and phenolic compounds—their incorporation into the formulation of bakery and pasta products may be expected to contribute to the mitigation of these issues (Ahanchi et al., 2024). Furthermore, plant-based proteins can contribute to the quality enhancement of these products owing to their relatively high protein content and functional properties such as emulsification and gelation. On the other hand, mitigating off-flavors, enhancing processing efficiency, and raising consumer awareness are crucial for the broader utilization of plant-based proteins in snack products (Sabaghi & Seyedalmoosavi, 2025). The findings of current studies on the use of proteins derived from plant-processing by-products in the formulation of milk substitutes, bakery products, and extruded snacks are summarized in Table 2.

Table 2. Current studies evaluating proteins derived from plant-processing by-products in milk substitutes, bakery products, and extruded snacks

By-Product Protein Source	**Application**	**Findings**	**References**
Protein isolated from potato juice	Potato protein isolate was incorporated into plant-based cheese analogues as a protein source and functional ingredient	The optimized formulation (5% potato protein, 12% fat, 25% modified potato starch) showed increased hardness and viscosity and desirable melting properties, supporting its use as a lower-fat dairy cheese alternative in hot foods	Kowalczewski et al., 2025
Brewer's spent grain protein (BSGP)	Combined with lentil protein isolate to develop plant-based milk alternatives	Lentil–BSGP blending increased the proxy in vitro Digestible Indispensable Amino Acid Score (PIVDIAAS) from 0.48 and 0.50 for lentil protein and BSGP alone to 0.83, while improving sedimentation and creaming stability and emulsion whiteness.	Boeck et al., 2024
Pumpkin, sunflower, and walnut oilseed cakes	Development of vegan yoghurt-like fermented beverages through lactic fermentation	Oilseed cake-based beverages contained 3.7–4.6% protein and up to 1.9% fiber, with lower syneresis (14–18%) and enhanced polyphenol and antioxidant contents. Pumpkin- and walnut-based formulations showed the best sensory acceptance, and all products remained microbiologically safe for 14 days	Radu et al., 2025

By-Product Protein Source	Application	Findings	References
Defatted hemp cake	Utilization of defatted hemp cake (DHC; 34.50% protein), an oil-processing by-product, at 5–10% in corn grits for extruded snack production	Increasing DHC addition reduced expansion ratio and fracturability while increasing bulk density and hardness. The optimized formulation contained 5% DHC, 15% moisture, and 150 °C extrusion temperature, demonstrating the potential of DHC as a protein-rich by-product for extruded snack production	Jozinović et al., 2017
Brewer's spent grain, sugar beet pulp, and apple pomace	Incorporation of brewer's spent grain (11.08% protein at 15% addition), sugar beet pulp (SBP; 8.08% protein at 15% addition), and apple pomace (AP; 7.07% protein at 15% addition) at 5–15% into corn grits for directly expanded extruded snacks	BSG and SBP increased protein content, with a more pronounced effect for BSG, while AP reduced protein content. All by-products increased soluble and insoluble dietary fiber, with SBP providing the greatest improvement in fiber content. The addition of 5–15% by-products enhanced the nutritional value of corn snacks, with 10–15% incorporation enabling a "high in fiber" claim	Jozinovi´c et al., 2021
Spent coffee grounds	Incorporated into shortbread biscuits at concentrations ranging from 0% to 10%.	Increasing SCG addition proportionally increased protein content (5.54–7.08%) and enhanced dietary fiber and antioxidant properties. The 10% SCG formulation showed the highest protein content, favorable aroma, reduced hardness, and good storage stability	Koay et al., 2023
Sunflower seed cake	Protein enrichment of gluten-free bread using sunflower seed cake, an oil-processing by-product (up to 15%).	Sunflower cake increased protein content from 7.44 to 9.69% (d.b.) and enhanced fiber and polyphenol contents. The 15% formulation exhibited the most favorable sensory acceptance and desirable textural properties, supporting its use as a protein-rich by-product for gluten-free bread.	Blicharz-Kania et al., 2023

By-Product Protein Source	Application	Findings	References
Brewer's spent grain flour	Utilization of brewer's spent grain flour (BSGF; 15.5 ± 0.14 g protein/100 g) at 40–60% as a protein-rich by-product in chocolate cakes	BSGF increased protein, dietary fiber, zinc, and antioxidant capacity, with 60% substitution providing the highest nutritional enrichment. The 40% formulation achieved the best consumer acceptance, supporting BSGF as a functional protein-rich ingredient for bakery products	Paiva et al., 2025
Brewer's spent grain	Protein enrichment of bread using brewer's spent grain (16.6 ± 1.6% protein) at 15–30% flour substitution	Protein content increased from 7.5% to 8.1% and 11.3%, while dietary fiber increased from 7.4% to 16.4% and 24.4% with 15% and 30% BSG, respectively. The 15% BSG formulation reduced shelf life from 14 to 12 days, whereas 30% BSG reduced it to 6 days at 20 °C	Papadimitriou et al., 2026

CONCLUSIONS AND FUTURE DIRECTIONS

Driven by population growth, climate change, and resource constraints, the growing interest in sustainable, healthy, and ethical food options underscores the significance of plant-based and alternative protein sources. In this context, the valorization of agro-industrial by-products—such as oilseed meals, cereal brans, and fruit and vegetable pomaces—into high-value protein sources offers substantial potential for mitigating the environmental impacts of conventional protein production and supporting the circular bioeconomy. Advanced green technologies, including ultrasound-, enzyme-, and microwave-assisted extraction, supercritical fluid extraction, and deep eutectic solvents, enable the recovery of functional proteins and bioactive compounds while reducing chemical waste and environmental footprints. Nevertheless, the utilization of the resulting proteins, particularly in meat and dairy alternatives, entails various challenges in terms of achieving the targeted structural, sensory, and nutritional properties. Therefore, alongside protein recovery, their functional and structural characteristics in food applications must also be considered. Future studies must focus on multi-objective optimization strategies that comprehensively evaluate the relationships among extraction and processing conditions, structural transformations of proteins, sensory properties, and nutritional functionality. Furthermore, the holistic consideration of criteria such as sensory quality, nutritional value, environmental impact, safety, and economic accessibility is crucial for the effective utilization of proteins derived from agro-industrial by-products in food systems.

REFERENCES

Ahanchi, M., Sugianto, E. C., Chau, A., Khoddami, A. 2024. Quality Properties of Bakery Products and Pasta Containing Spent Coffee Grounds (SCGs): A Review. *Foods*. 13: 3576.

Ahmad, T., Esposito, F., Rauf, M. A., Inam-ur-Raheem, M., Cirillo, T., Aadil, R. M. 2025. A Review on Recent Processing and Bioprocessing Developments in Alternative Proteins: Sources, Modification Methods, Economic Feasibility, and Future Challenges. *Food and Bioprocess Technology*. 19: 54.

Aït-Kaddour, A., Hassoun, A., Tarchi, I., Loudiyi, M., Boukria, O., Cahyana, Y., Ozogul, F., Khwaldia, K. 2024. Transforming plant-based waste and by-products into valuable products using various "Food Industry 4.0" enabling technologies: A literature review. *Science of the Total Environment*. 955: 176872.

Akhtar, S., Ismail, T., Layla, A., Hussain, M., Qamar, M. 2022. An overview of plant-based protein rich products. In: *Plant Protein Foods*. 27-60.

Akyüz, A., Tekin, İ., Aksoy, Z., Ersus, S. 2024. Plant protein resources, novel extraction and precipitation methods: A review. *Journal of Food Process Engineering*. 47(10): e14758.

Alehosseini, E., McSweeney, P. L. H., Miao, S. 2025. Recent updates on plant protein-based dairy cheese alternatives: Outlook and challenges. *Critical Reviews in Food Science and Nutrition*. 65(30): 6846-6860.

Aussanasuwannakul, A., Pantoa, T., Pengpinit, W. 2025. Structure–Function Relationships in High-Moisture Meat Analogues: Effects of Soybean Residue (Okara) on Plant Protein–Starch Gels. *Gels*. 11: 805.

Bagasettihalli Kariyappa, P., Sethi, S., Arora, B. 2025. Extraction and characterization of plant-based proteins from agro-processing by-products—A review. *Food Biomacromolecules*. 2(3): 403-417.

Bai, X., Gong, Y., Wei, W., Wang, W., Zhuang, M., Yang, Y. 2026. Global production potential and environmental benefits of alternative proteins from biowaste. *Resources, Conservation and Recycling*. 228: 108818.

Bekiroglu, H., Acar, Z. D., Sagdic, O. 2025. Sustainable plant-based protein hydrolysates: Utilization of waste proteins modified by enzymatic hydrolysis in techno-functional applications. *International Journal of Biological Macromolecules*. 148823.

Bisht, A., Murugan, G., Hussain, M., Abdi, G. 2025. Current advancements in alternative protein sources: Plant-based, cultured meat, and insect proteins for a sustainable future. *Food Bioscience*. 107708.

Blicharz-Kania, A., Pecyna, A., Zdybel, B., Andrejko, D., Marczuk, A. 2023. Sunflower seed cake as a source of nutrients in gluten-free bread. *Scientific Reports*. 13(1): 10864.

Boudalia, S., Symeon, G. K., Dotas, V., Gueboudji, Z., Kouadri, I., Sehili, B., B., Terfa, M. T., Smeti, S., Gueroui, Y., Bousbia, A. 2026. The valorization of agrifood byproducts and waste to advance the sustainable development goals: Current state and new perspectives. *Sustainability*. 18(5): 2165.

Boukid, F. 2021. Plant-based meat analogues: From niche to mainstream. *European food research and technology*, *247*(2), 297-308.

Boukid, F., Mefleh, M., Mameri, H., Rosell, C. M. 2024. Plant protein innovations in snacks and bakery: Synergy of market trends and scientific advances. *Food Bioscience*. 62: 105580.

Calleja-Gomez, M., Roig, P., Pateiro, M., Dominguez-Valencia, R., Lorenzo, J. M., Fernandez-Lopez, J., J., Viuda-Martos, M., Pérez-Álvarez, J., Martínez-Zamora, L., Nieto, G., Peñalver, R., Carrillo, C. 2024. Health-promoting benefits of plant-based by-product extracts obtained by innovative technologies. *Current Opinion in Food Science*. 57: 101161.

Chandran, A. S., Kashyap, P., Thakur, M. 2024. Effect of extraction methods on functional properties of plant proteins: A review. *eFood*. 5(3): e151.

Chandran, A. S., Suri, S., Choudhary, P. 2023. Sustainable plant protein: an up-to-date overview of sources, extraction techniques and utilization. *Sustainable Food Technology*. 1(4): 466-483.

Chen, J., & Ozturk, O. K. 2026. Valorization of plant-based protein-rich byproducts through physical processing techniques: A review. *International Journal of Biological Macromolecules*, 150308.

Chen, L., Lin, X., Xia, Y. 2026. Plant-based meat alternatives: Advancements in ingredients, processing, consumer perception, and future directions. *Journal of Future Foods*.

Choe, U. 2025. Valorization of spent coffee grounds and their applications in food science. *Current Research in Food Science*. 10: 101010.

Choręziak, A., Rosiejka, D., Michałowska, J., Bogdański, P. 2025. Nutritional quality, safety and environmental benefits of alternative protein sources—An overview. *Nutrients*. 17(7): 1148.

Ciugureanu, I., Bulgaru, V., Gurev, A., Ghendov-Moşanu, A. 2025. Plant-based proteins: sources, extraction methods and functional perspectives for the sustainable food industry. *Journal of Engineering Science*. (4): 80-103.

da Silva, A. M. M., Lima, M. A., Koksel, F., Sato, A. C. K. 2024. Incorporation of brewer's spent grain into plant-based meat analogues: benefits to physical and nutritional quality. *International Journal of Food Science and Technology*. 59(6): 3870-3882.

Danciu, C. A., Mag, A. G., Stanciu, C., Vidu, L., Stanciu, M. 2026. Valorization of plant-based food by-products through green extraction of bioactive compounds for functional food. *Molecules*. 31(4): 646.

Dhiman, S., Mukherjee, G., Kumar, A., Krishan, B. 2026. Alternative proteins from waste streams: a circular economy roadmap for sustainable food systems. *Sustainable Food Technology*. 4(3): 2266-2294.

Du, X., Yang, J. (Eds.). 2024. *Flavor-associated applications in health and wellness food products*. Springer. 3-19.

FAO, 2023. FAO Cereal Supply and Demand Brief | Food and Agriculture Organization of the United Nations.

Farsani, M. S., Forooghi, E., Rastegar, H. 2026. Plant-Based Hydrocolloids as Functional and Sustainable Alternatives to Gelatin in Food Systems: Sources, Properties, Applications, and Critical Challenges. *Food Hydrocolloids for Health*. 100293.

Gaber, J., Tayane, S., Bejjaoui, B., M'Hamdi, N. 2025. Sustainable protein extraction from co-products using an integrated bio-inspired process. In: *E3S Web of Conferences*. 680: 00055.

Hadidi, M., Aghababaei, F., Gonzalez-Serrano, D. J., Goksen, G., Trif, M., McClements, D. J., Moreno, A. 2024. Plant-based proteins from agro-industrial waste and by-products: Towards a more circular economy. *International Journal of Biological Macromolecules*. 261: 129576.

Hamid, M. A., Tsia, F. L. C., Okit, A. A. B., Xin, C. W., Cien, H. H., Harn, L. S., Patrick, P. N., Samirin, S., Azizi, W. A. A. W., Irfanian, A., Yee, C. F. 2020. The application of Jackfruit by-product on the development of healthy meat analogue. In: *IOP Conference Series: Earth and Environmental Science*. 575(1): 012001.

Huang, J., Zhang, M., Mujumdar, A. S., Semenov, G., Luo, Z. 2024. Technological advances in protein extraction, structure improvement and assembly, digestibility and bioavailability of plant-based foods. *Critical Reviews in Food Science and Nutrition*. 64(31): 11556-11574.

Imran, M., Huang, B., Adil, M., Aleem, K., Waseem, M., Manzoor, M. F., Javed, M. R., Saleem, M., Shrestha, N. K., Karabulut, G., Goksen, G. 2026. Harnessing novel proteins for advancing plant-based meat analogs. *Journal of Food Composition and Analysis*. 108778.

Ismail, B. P., Senaratne-Lenagala, L., Stube, A., Brackenridge, A. 2020. Protein demand: Review of plant and animal proteins used in alternative protein product development and production. *Animal Frontiers*. 10(4): 53-63.

Issa, R., Issa, S., Rajapakse, H. 2025. Next-generation extraction technologies for plant proteins: Enhancing yield, functionality, and sustainability. *Journal of Biological Methods*. 13(1): e99010084.

Jozinović, A., Ačkar, Đ., Jokić, S., Babić, J., Balentić, J. P., Banožić, M., Šubarić, D. 2017. Optimisation of Extrusion Variables for the Production of Corn Snack Products Enriched with Defatted Hemp Cake. *Czech Journal of Food Sciences*. 35(6): 507.

Jozinović, A., Šubarić, D., Ačkar, Đ., Babić, J., Orkić, V., Guberac, S., Miličević, B. 2021. Food industry by-products as raw materials in the production of value-added corn snack products. *Foods*. 10(5): 946.

Kanimozhi, N. V., Nagalakshmi, S., Sukumar, M. 2026. Microbial fermentation strategies for enhancing sensory and nutritional quality of plant-based protein foods. *Food Wellness*. 100046.

Kaur, S. P., Sagar, N. A., Rani, N. 2025. Alternative proteins: Innovations in sources, processing, and consumption. *Frontiers in Sustainable Food Systems*. 9: 1641712.

Keerthi, R., Praveena, U., Pillai, P. K., Ragavan, K. V., Anandharamakrishnan, C. 2025. Role of chemically-modified proteins for the formulation of plant-based animal-product alternatives. *Food Hydrocolloids*. 168: 111545.

Khalid, L., Jabeen, I., Ahmad, T., Inam-ur-Raheem, M., Shahid, A., Cirillo, T., Esposito, F. 2025. Valorization of fruit and vegetable by-products for protein extraction and their functional applications in food and non-food sectors. *Food and Bioproducts Processing*.

Koay, H. Y., Azman, A. T., Zin, Z. M., Portman, K. L., Hasmadi, M., Rusli, N. D., Hasmadi, M., Aidat, O., Zainol, M. K. 2023. Assessing the impact of spent coffee ground (SCG) concentrations on shortbread: A study of physicochemical attributes and sensory acceptance. *Future Foods*. 8: 100245.

Kowalczewski, P. Ł., Smarzyński, K., Biegalski, J., Muzolf-Panek, M., Cais-Sokolińska, D., Ruszkowska, M., Lewandowicz, J., Miedzianka, J., Wróbel, M. M., Kačániová, M.,

Baranowska, H. M. 2025. Insight into the potato protein-based vegan cheese: A comprehensive study on physicochemical, mechanical and molecular properties. *Food Science and Technology International*. 32(4): 385-399.

Leite, A., Vasconcelos, L., Teixeira, A., Rodrigues, S. S. 2026. Valorization of By-Products for Functional Ingredients in Meat and Meat Replacers: A Circular Bioeconomy Approach. *Foods*. 15(9): 1567.

Ligarda-Samanez, C. A., Huamán-Carrión, M. L., Calsina-Ponce, W. C., Cruz, G. D. L., Calderón Huamaní, D. F., Cabel-Moscoso, D. J., Garcia-Espinoza, A. J., Sucari-León, R., Aroquipa-Durán, Y., Muñoz-Saenz, J. C., Muñoz-Melgarejo, M., Jilaja-Carita, E. E. 2025. Technological innovations and circular economy in the valorization of agri-food by-products: advances, challenges and perspectives. *Foods*. 14(11): 1950.

Lu, V. L., Gavahian, M., Lin, J. 2025. Textural properties of plant-based meat analogue extrudates enriched with pineapple processing by-product powder. *International Journal of Food Science and Technology*. 60(1): vvae080.

Malila, Y., Owolabi, I. O., Chotanaphuti, T., Sakdibhornssup, N., Elliott, C. T., Visessanguan, W., Karoonuthaisiri, N., Petchkongkaew, A. 2024. Current challenges of alternative proteins as future foods. *npj Science of Food*. 8(1): 53.

Maqsood, S., Khalid, W., Kumar, P., Benmebarek, I. E., Rasool, I. F. U., Trif, M., Moreno, A., Esatbeyoglu, T. 2025. Valorization of plant-based agro-industrial waste and by-products for the production of polysaccharides: Towards a more circular economy. *Applied Food Research*. 5(1): 100954.

Mia, M. S., Rahman, O., Nabi, M. H. B., Ahmed, M. M., Rayhan, M. A., Mithun, M. H., Niaz, M. I., Zzaman, W. 2026. High-Pressure Modifications of Plant-Based Proteins: Enhancing Quality and Techno-Functionality for Food Applications. *Future Foods*. 101086.

Mohammad, R. 2026. Deep eutectic solvents in plant-based protein extraction: Limitations and applications. *European Food Science and Engineering*. 7(1): 33–41.

Munialo, C. D., Stewart, D., Campbell, L., Euston, S. R. 2022. Extraction, characterisation and functional applications of sustainable alternative protein sources for future foods: A review. *Future Foods*. 6: 100152.

Naibaho, J. 2027. Techno-functional properties of proteins from agro-industrial side streams: Relevance for food processing and structure–function considerations. *Food Hydrocolloids*. 113092.

Nam, J. K., Lee, J. Y., Jang, H. W. 2024. Quality characteristics and volatile compounds of plant-based patties supplemented with biji powder. *Food Chemistry: X*. 23: 101576.

Nartea, A., Kuhalskaya, A., Fanesi, B., Orhotohwo, O. L., Susek, K., Rocchetti, L., Di Vittori, V., Bitocchi, E., Pacetti, D., Papa, R. 2023. Legume byproducts as ingredients for food applications: Preparation, nutrition, bioactivity, and techno-functional properties. *Comprehensive Reviews in Food Science and Food Safety*. 22(3): 1953-1985.

Navarré, A., Musto, L., Nazareth, T. 2025. Beyond meat substitution: A multifaceted review of plant-based and alternative proteins, from environmental impact to analytical technologies. *Foods*. 14(13): 2312.

Nirmal, N., Anyimadu, C. F., Khanashyam, A. C., Bekhit, A. E. D. A., Dhar, B. K. 2025. Alternative protein sources: addressing global food security and environmental sustainability. *Sustainable Development*. 33(3): 3958-3969.

Ospina-Maldonado, S., Martin-Gómez, H., Cardoso-Ugarte, G. A. 2024. From waste to wellness: a review on the harness of food industry by-products for sustainable functional food production. *International Journal of Food Science and Technology*. 59(11): 8680-8692.

Paiva, C. F., Almeida, T. D. S. F. D., Arelhano, G. E., Alvarado, A. V. R., Menezes, M. B. D., Argandoña, E. J. S., Gomes, I. L. D. A., Moya, A. M. T. M., Filho, P. S. L., Santos, E. F. D. 2025. Potential of brewer's spent grain as a nutritional ingredient in bakery products. *Plant Foods for Human Nutrition*. 80(1): 12.

Papadimitriou, A. B., Betsa, D., Pavlopoulos, C., Papadopoulou, K., Dermesonlouoglou, E., Giannakourou, M. C., Lyberatos, G. 2026. Valorization of brewer's spent grain via its incorporation into bakery products. *Waste and Biomass Valorization*. 1-16.

Pointke, M., Albrecht, E. H., Geburt, K., Gerken, M., Traulsen, I., Pawelzik, E. 2022. A comparative analysis of plant-based milk alternatives part 1: composition, sensory, and nutritional value. *Sustainability*. 14(13): 7996.

Radu, O., Capcanari, T., Boiștean, A., Covaliov, E. 2025. Biotechnological valorisation of oilseed cakes in the formulation of vegan yoghurt-like fermented beverages. *Beverages*. 11(6): 164.

Rajput, S. D., Pandey, N., Keshavkant, S. 2026. Bioconversion of agricultural waste into bacterial single-cell protein: recent advances and modelling approaches. *Systems Microbiology and Biomanufacturing*. 6(2): 47.

Rasool, I. F. U., Koraqi, H., Adil, M. Z., Aziz, A., Sehar, H., Kumar, P., Ghazala, A., Moreno, A., Khalid, W., Esatbeyoglu, T. 2026. Extraction of Plant Protein Using the Green Procedures: Functional Development Toward Sustainable Development Goals (SDGs). *Applied Food Research*. 102131.

Sabaghi, M., Seyedalmoosavi, M. M. 2025. Applications of sustainable proteins in food and feed, and perspectives on health and circular bioeconomy. *International Journal of Biological Macromolecules*. 309: 143193.

Saberian, H., Yazdi, A. P. G., Nejatian, M., Bazsefidpar, N., Mohammadian, A. H., Rahmati, M., Assadpour, E., Jafari, S. M. 2024. Brewers' spent grain as a functional ingredient in bakery, pasta, and cereal-based products. *Future Foods*. 10: 100479.

Sarathy, S. P., Ravikumar, H., Nanjan, P., Alagesan, N., Chua, B. L. 2025. Plant-based protein: A multi-nutritional sustainable alternative to animal foods and their structure, functions, and relationship: A review. *International Journal of Biological Macromolecules*. 321: 146465.

Sekoai, P. T., Roets-Dlamini, Y., O'Brien, F., Ramchuran, S., Chunilall, V. 2024. Valorization of food waste into single-cell protein: an innovative technological strategy for sustainable protein production. *Microorganisms*. 12(1): 166.

Sharma, V., Hamill, R. M., Cabral, E. M., Burgess, C. M., Barry-Ryan, C. 2026. Conventional and emerging pre-treatments for plant protein fermentation: prospects for next-generation plant-based meat analogues. *Food Research International*. 120007.

Shawky, E., Zhu, W., Tian, J. 2025. A review of innovative extraction technologies for protein recovery from plant-based by-products: A step toward zero-waste processing. *International Journal of Biological Macromolecules*. 315: 144301.

Singh, S., Krishania, M. 2026. A review on advancing sustainable vegan meat alternatives through scalable production of plant-based smart proteins. *Trends in Food Science & Technology*. 105497.

Ververis, E., Favata, A., Koffas, N., Zakidou, P. 2026. Agri-food by-product valorisation and safety in sustainable food systems: Hidden hazards, risk–benefit trade-offs, challenges and opportunities. *Food Chemistry Advances*. 101299.

Xiao, X., Zou, P. R., Hu, F., Zhu, W., Wei, Z. J. 2023. Updates on plant-based protein products as an alternative to animal protein: Technology, properties, and their health benefits. *Molecules*. 28(10): 4016.

Yadav, A. K., Ronya, N., Rathaur, A., Rai, D. C., Trivedi, H., Patel, V. 2026. Plant-based milk alternatives: processing, nutritional profile, bioactive compounds and health implications. *Food Nutrition*. 100061.

Zahari, I., Östbring, K., Purhagen, J. K., Rayner, M. 2022. Plant-based meat analogues from alternative protein: A systematic literature review. *Foods*. 11(18): 2870.

Zhang, T., Dou, W., Zhang, X., Zhao, Y., Zhang, Y., Jiang, L., Sui, X. 2021. The development history and recent updates on soy protein-based meat alternatives. *Trends in Food Science & Technology*. 109: 702-710.

FOODBORNE MYCOTOXINS AND THE HUMAN MICROBIOME: A HACCP-BASED RISK ASSESSMENT APPROACH

Natalija Atanasova-Pancevska[1*], Aleksandra Markovska[2], Daniela Todevska[3]

[1]Ss. Cyril and Methodius University in Skopje, Faculty of Natural Sciences and Mathematics – Skopje, Institute of Biology, Department of Microbiology and Microbial Biotechnology, Skopje, North Macedonia
[*]corresponding author: natalijaap@gmail.com, natalija@pmf.ukim.mk

[2] Quality Consulting, North Macedonia

[3] Faculty of Agriculture, Goce Delcev University, Stip, North Macedonia

ABSTRACT

Mycotoxins, toxic secondary metabolites produced by fungi such as *Aspergillus*, *Fusarium*, and *Penicillium*, represent one of the most significant chemical hazards in food systems. They contaminate cereals, nuts, fruits, and processed products, posing risks not only through acute toxicity but also via chronic exposure that can disrupt the human gut microbiome. The microbiome, a complex ecosystem of bacteria, fungi, and archaea, plays a central role in digestion, immune regulation, and metabolic homeostasis. Evidence suggests that mycotoxins such as aflatoxins, ochratoxin A, fumonisins, and deoxynivalenol can alter microbial diversity, reduce beneficial taxa, and promote dysbiosis, thereby increasing susceptibility to gastrointestinal disorders, metabolic dysfunction, and immune imbalance. This review synthesizes current knowledge on the ecological interactions between foodborne mycotoxins and the human microbiome, emphasizing the need for integrated risk assessment. The Hazard Analysis and Critical Control Points (HACCP) framework provides a systematic approach to identifying and controlling hazards at critical points in food production and processing. Applying HACCP principles to mycotoxin contamination involves monitoring agricultural practices, storage conditions, and processing steps where fungal growth and toxin production are most likely. By incorporating **microbiome-focused biomarkers**, such as microbial diversity indices, short-chain fatty acid levels, NF-κB activation, and metabolomic signatures, into HACCP risk assessment, food safety management can evolve beyond traditional toxicological thresholds to include microbial resilience and host health outcomes. Case studies highlight how HACCP interventions, including improved grain storage, rapid detection methods, and biocontrol strategies, reduce mycotoxin exposure. Ultimately, aligning HACCP with microbiome research offers a proactive strategy to mitigate the long-term health consequences of mycotoxin contamination. This interdisciplinary approach underscores the importance of integrating food safety, microbiology, and public health perspectives to safeguard consumer wellbeing and ensure sustainable food systems.

Keywords: Foodborne mycotoxins, Human gut microbiome, Microbiome dysbiosis, HACCP framework, Critical control points, Risk assessment, Food safety management

INTRODUCTION

Mycotoxins are toxic secondary metabolites produced by fungi such as *Aspergillus*, *Fusarium*, and *Penicillium*. They contaminate staple foods including cereals, nuts, coffee, dried fruits, and spices, and represent one of the most significant chemical hazards in food safety (Khan, 2024).

Chronic exposure to mycotoxins has long been associated with hepatotoxicity, nephrotoxicity, immunosuppression, and carcinogenesis (Mafe & Büsselberg, 2026). More recently, attention has shifted to their impact on the **human gut microbiome**, a complex ecosystem essential for digestion, immune regulation, and metabolic homeostasis.

Evidence indicates that mycotoxins disrupt microbial diversity, reduce beneficial taxa, and promote dysbiosis. For example, deoxynivalenol (DON) impairs short-chain fatty acid production and increases intestinal inflammation (Mafe & Büsselberg, 2026), while aflatoxin B_1 alters microbial composition and epithelial barrier integrity (Khan, 2024). These bidirectional interactions are critical: gut microbes can metabolize and detoxify certain mycotoxins, but they can also bioactivate others, amplifying toxicity (Mafe & Büsselberg, 2026).

The **Hazard Analysis and Critical Control Points (HACCP)** framework provides a systematic approach to identifying and controlling hazards at critical points in food production. Applying HACCP principles to mycotoxin contamination involves monitoring agricultural practices, storage conditions, and processing steps where fungal growth and toxin production are most likely (Khan, 2024). Integrating microbiome endpoints into HACCP risk assessment could enhance food safety management by considering not only toxicological thresholds but also microbial resilience and host health outcome

TYPES OF FOODBORNE MYCOTOXINS

Aflatoxins

Produced mainly by *Aspergillus flavus* and *A. parasiticus*, aflatoxins are potent hepatotoxins and carcinogens. Aflatoxin B_1 is the most toxic, linked to liver cancer and immune suppression (Mafe & Büsselberg, 2024). Studies show that aflatoxins disrupt gut microbial balance, reducing beneficial *Lactobacillus* and *Bifidobacterium* populations, while increasing opportunistic pathogens (Mafe & Büsselberg, 2026).

Ochratoxin A (OTA)

Generated by *Aspergillus* and *Penicillium* species, OTA contaminates cereals, coffee, and dried fruits. It is nephrotoxic and immunotoxic, and recent findings suggest it alters gut microbial composition, impairing epithelial barrier function and promoting dysbiosis (Khan, 2024). OTA exposure has been linked to reduced microbial diversity and increased inflammatory signaling pathways such as NF-κB (Mafe & Büsselberg, 2026).

Fumonisins

Produced by *Fusarium verticillioides*, fumonisins contaminate maize and maize-based products. Fumonisin B_1 interferes with sphingolipid metabolism and has been associated with esophageal cancer (Mafe & Büsselberg, 2024). In the gut, fumonisins disrupt microbial communities and impair short-chain fatty acid production, contributing to intestinal inflammation (Mafe & Büsselberg, 2026).

Deoxynivalenol (DON)

Also known as vomitoxin, DON is produced by *Fusarium graminearum* and contaminates wheat, barley, and maize. DON induces gastrointestinal distress and immune dysregulation. It reduces microbial richness, impairs SCFA production, and increases pro-inflammatory cytokines, thereby exacerbating dysbiosis (Khan, 2024; Mafe & Büsselberg, 2026).

Zearalenone (ZEN)

Produced by *Fusarium* species, ZEN is an estrogenic mycotoxin found in maize and wheat. It disrupts hormonal balance and reproductive health. In the gut, ZEN alters microbial

composition and may promote the growth of taxa capable of metabolizing estrogen-like compounds, further complicating host–microbe interactions (Mafe & Büsselberg, 2026)

MICROBIOME IMPACTS OF FOODBORNE MYCOTOXINS

The gut microbiome refers to the diverse community of microorganisms living in the digestive tract, primarily in the intestines. These microorganisms play essential roles in digestion, nutrient absorption, and the synthesis of certain vitamins and hormones. The balance and composition of the gut microbiome can significantly impact overall health, including metabolic function, mental health, and immune response.

Each individual has a unique gut microbiome influenced by various factors, including genetics, diet, lifestyle, and environmental exposures. Maintaining a balanced and diverse gut microbiome is crucial for supporting various bodily functions and promoting overall well-being.

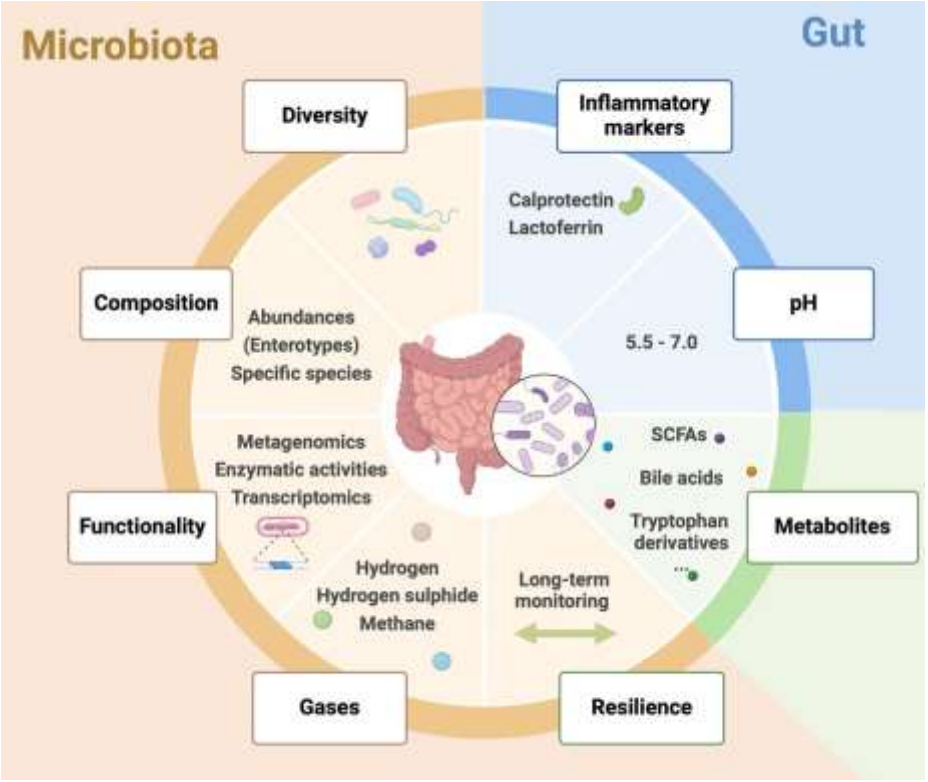

Figure 1. Potential markers of a healthy gut microbiota. A healthy gut microbiota is characterised by a diverse and balanced community of microorganisms that perform vital functions for the host. Several key markers have been proposed to assess these, including microbial diversity, composition (abundances, enterotypes, specific species), functionality (metagenomics, enzymatic activities, transcriptomics) and resilience (through long-term monitoring). Production of important metabolites like SCFAs, bile acids and tryptophan derivatives, as well as gases (hydrogen, hydrogen sulfide, methane), are potential indicators. Additionally, gut health indicators such as pH levels and the presence of inflammation markers (like calprotectin, lactoferrin) can be used for assessing overall gut health. SCFAs, short-chain fatty acids (from Van Hul et al., 2024).

Exposure to foodborne mycotoxins can disrupt this balance, leading to microbiome dysbiosis and downstream health consequences

Alterations in Microbial Diversity

Aflatoxins, particularly aflatoxin B_1, reduce beneficial taxa such as *Lactobacillus* and *Bifidobacterium* while promoting opportunistic pathogens (Chałaśkiewicz et al., 2025). This imbalance increases intestinal permeability and weakens epithelial barrier integrity (Mafe & Büsselberg, 2026).

Metabolic Effects

Deoxynivalenol (DON) is one of the most studied mycotoxins. It reduces the production of short-chain fatty acids (SCFAs), which are crucial for gut health and immune modulation. DON exposure also elevates pro-inflammatory cytokines, contributing to chronic intestinal inflammation (Li et al., 2019). Fumonisins, especially fumonisin B_1, disrupt sphingolipid metabolism and alter microbial composition, reducing *Clostridiaceae* and *Campylobacteraceae* while increasing *Ruminococcaceae* and *Faecalibacterium* (Yunus Zeebone et al., 2023; Zhang et al., 2021).

Immune Dysregulation

Ochratoxin A (OTA) is nephrotoxic and immunosuppressive, but also directly affects the microbiome. OTA activates NF-κB signaling, leading to chronic inflammation and reduced microbial diversity (Więckowska et al., 2025; Izco et al., 2021). Dysbiosis caused by OTA increases susceptibility to infections and metabolic disorders.

Bidirectional Interactions

The relationship between mycotoxins and the microbiome is **bidirectional**. Gut microbes can metabolize and detoxify certain mycotoxins, but they may also bioactivate others, amplifying toxicity (Mafe & Büsselberg, 2026). This dual role highlights the need for integrated risk assessment approaches that consider microbial resilience alongside toxicological thresholds.

HACCP CONTROL POINTS FOR MYCOTOXIN MANAGEMENT

The **Hazard Analysis and Critical Control Points (HACCP)** framework provides a systematic approach to identifying, evaluating, and controlling hazards in food production. When applied to mycotoxins, HACCP emphasizes prevention at critical stages rather than relying solely on end-product testing. Integrating microbiome considerations into HACCP adds a novel dimension, ensuring that food safety strategies also protect gut microbial health.

1. ***Primary Production (Agriculture)***

Critical Control Point (CCP): Crop cultivation and harvesting

Mycotoxins such as aflatoxins and fumonisins originate in the field, particularly under warm and humid conditions (Khan, 2024).

Preventive measures: crop rotation, resistant varieties, biocontrol agents (e.g., *Aspergillus flavus* biocompetitive strains).

Microbiome relevance: reducing contamination at source minimizes downstream exposure that disrupts gut microbial diversity

2. ***Post-Harvest Handling and Storage***

Critical Control Point (CCP): Grain drying and storage

Improper drying and high moisture favor fungal growth and OTA production (Izco et al., 2021).

Preventive measures: rapid drying to <13% moisture, controlled humidity, aeration systems.

Microbiome relevance: OTA exposure is linked to NF-κB activation and dysbiosis (Więckowska et al., 2025).

3. ***Processing and Manufacturing***

Critical Control Point (CCP): Milling, sorting, and detoxification steps

DON and ZEN often persist through processing; sorting and cleaning reduce contamination (Li et al., 2019).

Emerging technologies: enzymatic detoxification, microbial biotransformation.

Microbiome relevance: microbial detoxification strategies may preserve gut microbial resilience.

4. *Distribution and Retail*

Critical Control Point (CCP): Packaging and transport

Contamination can occur during storage and distribution if conditions favor fungal growth.

Preventive measures: HACCP monitoring of supply chains, traceability systems.

Microbiome relevance: minimizing chronic low-dose exposure reduces risk of long-term dysbiosis.

5. ***Consumption and Public Health Monitoring***

Critical Control Point (CCP): Consumer awareness and biomarker surveillance

Incorporating microbiome-sensitive biomarkers into HACCP risk assessment could provide early warning of subclinical effects (Mafe & Büsselberg, 2026).

Public health programs should integrate dietary monitoring with microbiome analysis to assess cumulative impacts.

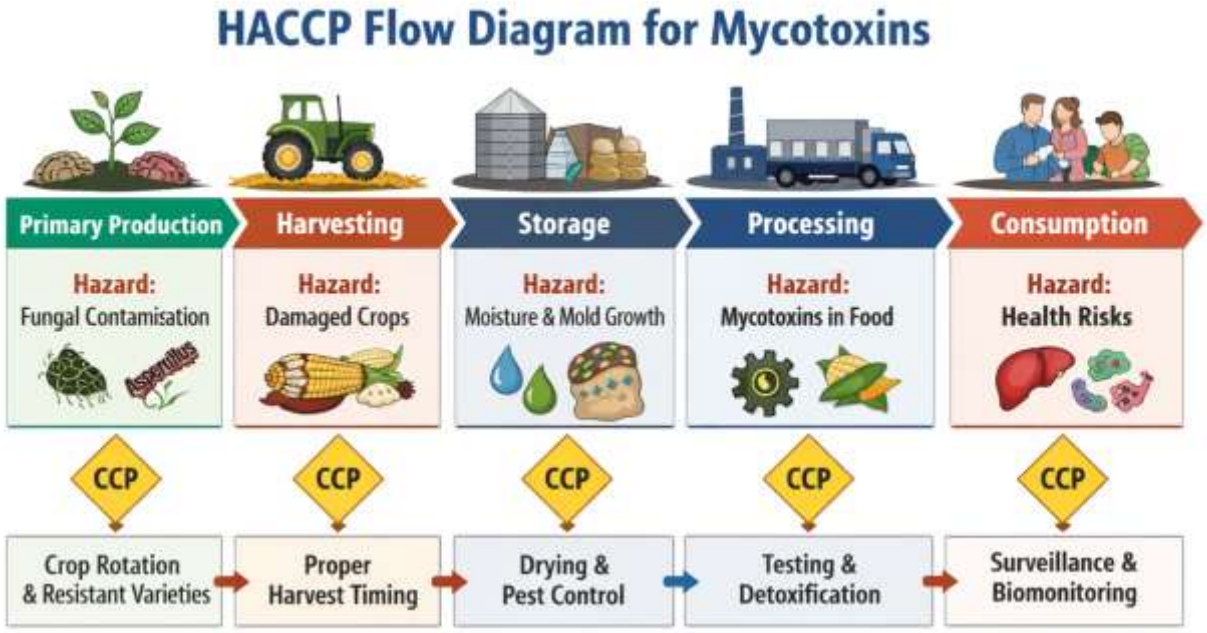

Figure 2. HACCP flow diagram for mycotoxin control in food systems

MICROBIOME BIOMARKERS IN FOOD SAFETY

In recent years, food safety science has begun to recognize that the **human gut microbiome** is not only a passive target of dietary contaminants but also an active participant in shaping health outcomes. This realization has led to the proposal of **microbiome biomarkers** as complementary tools within HACCP-based risk assessment frameworks. Unlike traditional monitoring, which focuses on detecting chemical residues such as aflatoxins or fumonisins in food products, microbiome biomarkers provide a **biological readout** of how these toxins affect host physiology even at low, chronic exposure levels.

One of the most widely studied indicators is **microbial diversity**. Healthy gut ecosystems are characterized by high richness and evenness, measured through indices such as Shannon and Simpson. Exposure to aflatoxin B_1 has been shown to reduce microbial diversity, weakening the resilience of the gut ecosystem and increasing susceptibility to opportunistic pathogens (Chałaśkiewicz et al., 2025). This decline in diversity can therefore serve as an early warning biomarker of toxin-induced dysbiosis.

Another critical set of biomarkers involves **short-chain fatty acids (SCFAs)**, including acetate, propionate, and butyrate. These metabolites are produced by gut microbes during fiber fermentation and play essential roles in maintaining intestinal barrier integrity and modulating immune responses. Studies demonstrate that deoxynivalenol (DON) and fumonisins significantly reduce SCFA production, leading to impaired gut function and chronic inflammation (Li et al., 2019; Yunus Zeebone et al., 2023). Monitoring SCFA levels in fecal or blood samples thus provides a functional biomarker of microbiome health under toxin stress.

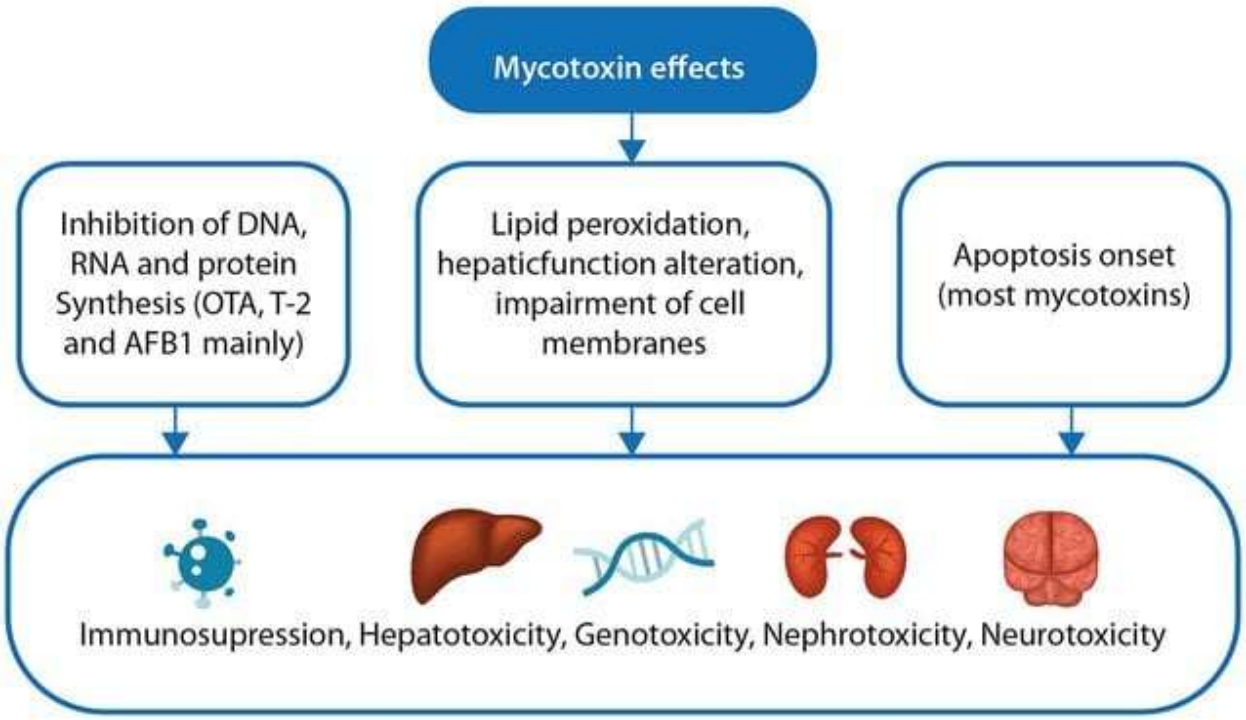

Figure 3. Major mechanisms of mycotoxin toxicity and their effects. Different mechanisms of mycotoxins can affect different organs and tissues in birds such as inhibition of protein synthesis, lipid peroxidation, hepatic function impairment, apoptosis modulation, among others. DNA, deoxyribonucleic acid; RNA, ribonucleic acid; OTA, ochratoxin; AFB1, aflatoxin B1 (from Gómez-Osorio et al., 2024).

The immune system offers another layer of biomarker evidence. Mycotoxins such as ochratoxin A (OTA) activate **NF-κB signaling**, resulting in elevated levels of pro-inflammatory cytokines like IL-6 and TNF-α. These cytokines are measurable in serum and reflect immune dysregulation linked to microbiome imbalance (Więckowska et al., 2025; Izco et al., 2021). Their inclusion in HACCP monitoring would allow food safety systems to capture not only chemical hazards but also their biological consequences.

Beyond immune markers, **metabolomic signatures** provide a systems-level perspective. Alterations in bile acids, sphingolipids, and estrogen-like metabolites have been associated with fumonisin and zearalenone exposure (Zhang et al., 2021). These shifts reveal how toxins disrupt host–microbe metabolic interactions, offering highly specific biomarkers for risk assessment.

Finally, **probiotic resilience markers** highlight the protective role of beneficial microbes. The survival and activity of taxa such as *Lactobacillus* and *Bifidobacterium* under toxin stress can serve as indicators of microbiome robustness. Probiotic supplementation has been shown to mitigate DON and OTA effects, suggesting that resilience markers could guide preventive interventions within HACCP frameworks (Mafe & Büsselberg, 2026).

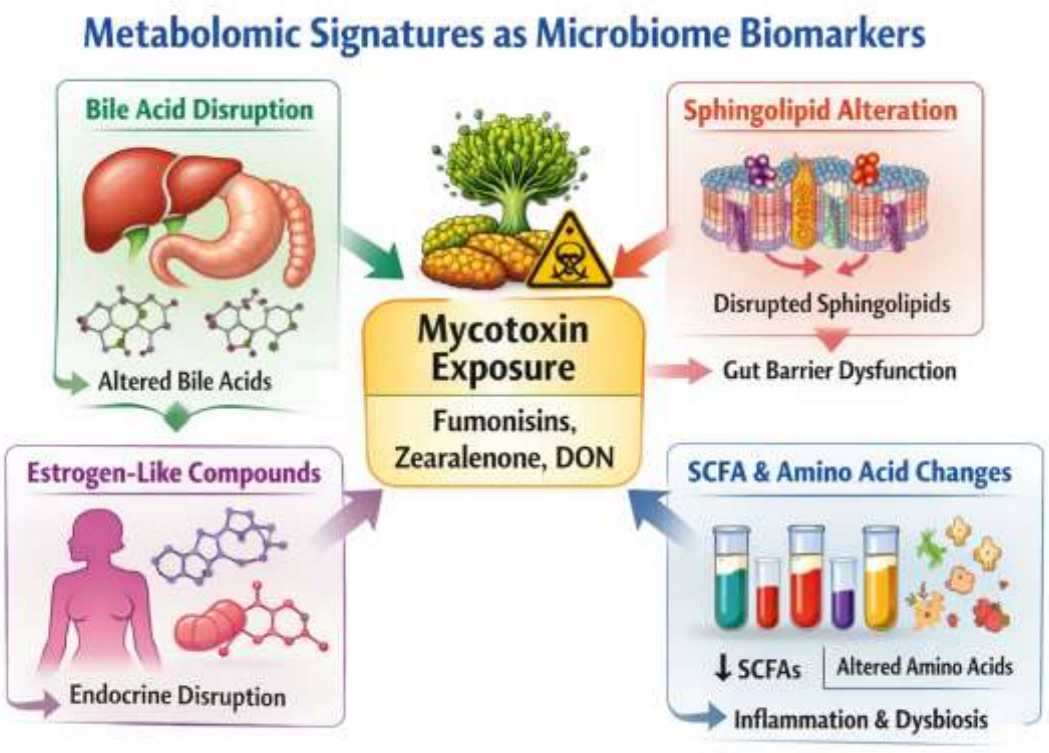

Figure 4. Metabolomic signatures as microbiome biomarkers in food safety. Mycotoxin exposure alters bile acid metabolism, sphingolipid integrity, estrogen-like compounds, and SCFA/amino acid profiles, providing measurable indicators of toxin impact on gut health.

CONCLUSION

The interplay between **foodborne mycotoxins** and the **gut microbiome** represents a critical frontier in modern food safety research. Mycotoxins such as aflatoxins, ochratoxin A, deoxynivalenol, fumonisins, and zearalenone exert not only direct toxicological effects but also profound influences on microbial composition, metabolism, and immune regulation. These interactions reshape the intestinal ecosystem, leading to dysbiosis, inflammation, and metabolic imbalance.

Integrating microbiome-based indicators into the HACCP framework transforms food safety from a purely chemical surveillance system into a **biological risk-assessment model**. By monitoring microbial diversity, SCFA production, cytokine activation, and metabolomic signatures, HACCP can detect early biological responses to contamination long before clinical symptoms appear. This approach aligns with the principles of preventive toxicology and precision nutrition, emphasizing resilience and health maintenance rather than reactive control.

REFERENCES

Chałaśkiewicz, A., Kowalska, M., Nowak, J., & Wiśniewski, P. (2025). Aflatoxin B1 exposure and gut microbiome dysbiosis: Implications for intestinal barrier function. *Toxins, 17*(2), 145. https://doi.org/10.3390/toxins17020145

Gómez-Osorio, L.-M., Vasiljevic, M., Raj, J., Chaparro-Gutierréz, J. J., & López-Osorio, S. (2024). Mycotoxins and coccidiosis in poultry – co-occurrence, interaction, and effects. *Frontiers in Veterinary Science, 11*, 1387856. https://doi.org/10.3389/fvets.2024.1387856

Izco, M., Vettorazzi, A., de Toro, M., Sanz, M., & López de Cerain, A. (2021). Oral sub-chronic ochratoxin A exposure induces gut microbiota alterations in mice. *Toxins, 13*(2), 106. https://doi.org/10.3390/toxins13020106

Khan, R. (2024). Mycotoxins in food: Occurrence, health implications, and control strategies – A comprehensive review. *Toxicon, 248*, 108038. https://doi.org/10.1016/j.toxicon.2024.108038

Li, J., Liu, H., & Chen, J. P. (2019). Metagenomic analysis of gut microbiota alteration in a mouse model exposed to deoxynivalenol. *Toxicology and Applied Pharmacology, 372*, 47–56. https://doi.org/10.1016/j.taap.2019.03.018

Mafe, A. N., & Büsselberg, D. (2024). Mycotoxins in food: Cancer risks and strategies for control. *Foods, 13*(21), 3502. https://doi.org/10.3390/foods13213502

Mafe, A. N., & Büsselberg, D. (2026). Microbiome–mycotoxin interactions and probiotic strategies: Implications for gut health and cancer. *Frontiers in Nutrition, 13*, 1783295. https://doi.org/10.3389/fnut.2026.1783295

Van Hul, M., Cani, P. D., Petifils, C., De Vos, W. M., Tilg, H., & El-Omar, E. M. (2024). What defines a healthy gut microbiome? *Gut, 73*(11), 1893–1908. https://doi.org/10.1136/gutjnl-2024-333378

Więckowska, M., Szelenberger, R., Poplawski, T., Zielińska, E., & Kowalczyk, A. (2025). Gut as a target of ochratoxin A: Toxicological insights and the role of microbiota. *International Journal of Molecular Sciences, 26*(19), 9438. https://doi.org/10.3390/ijms26199438

Yunus Zeebone, Y., Bóta, B., Halas, V., Tóth, Á., & Fébel, H. (2023). Gut faecal microbial and health marker response to dietary fumonisins in weaned pigs. *Toxins, 15*(5), 328. https://doi.org/10.3390/toxins15050328

Zhang, F., Chen, Z., Jiang, L., Wang, Y., & Liu, H. (2021). Response of fecal bacterial flora to fumonisin B1 exposure in BALB/c mice. *Toxins, 13*(9), 612. https://doi.org/10.3390/toxins13090612

CHEMICAL STATUS ASSESSMENT OF THE URBAN LANA RIVER, ALBANIA, UNDER THE EU WATER FRAMEWORK DIRECTIVE

Vjola Bakillari[1], Vjola Saliaga[1], Fatos Huqi[1], Xhuljo Sema[1], Irena Duka[1], Ferdi Brahushi[1], Ilir Kristo[1], Fatbardh Sallaku[1] and Seit Shallari[1]*

Department of Environment and Natural Resources, Faculty of Agriculture and Environment, Agricultural University of Tirana, Tirana, Albania

**Corresponding author e-mail: vbakillari@ubt.edu.al*

ABSTRACT

Maintaining or achieving Good chemical status of surface waters is a fundamental objective of the European Union Water Framework Directive (WFD) (2000/60/EC). Urban rivers are particularly vulnerable to multiple anthropogenic pressures, including untreated wastewater discharges, stormwater runoff, and diffuse urban pollution, which collectively contribute to the deterioration of water quality. In Albania, comprehensive assessments of spatial variations in the chemical status of urban rivers remain limited, constraining the identification of pollution pressures and the prioritization of effective management measures required to support WFD implementation. This study investigates how urban influence is reflected in the chemical status of the Lana River, an urbanized tributary of the Ishëm River Basin. Monitoring was conducted from April 2024 to February 2026 at Lana 1, upstream, representing the key entry point of urban influence, and Lana 2, representing the site where urban pressures are accumulated. Lana 1 was monitored quarterly and Lana 2 monthly to capture pollution intensity and temporal variability. The investigated parameters included pH, electrical conductivity (EC), biochemical oxygen demand (BOD_5), chemical oxygen demand (COD), and the priority substances cadmium (Cd), nickel (Ni), and lead (Pb). Metals were determined by atomic absorption spectroscopy (AAS) and assessed against the corresponding Annual Average Environmental Quality Standards (AA-EQS). The results revealed a clear spatial deterioration in water quality along the urban reach of the river. Mean pH remained relatively stable, changing only from 7.73 at Lana 1 to 7.69 at Lana 2, whereas mean EC increased from 579 to 833 µS/cm. Median BOD_5 and COD values increased from 22.42 to 80.0 mg/L and from 61.80 to 160 mg/L, indicating increased dissolved loads and intensified organic pollution consistent with the cumulative influence of urban pressures. Mean concentrations also increased downstream, from 0.56 to 0.71 µg/L for Cd, 18.86 to 25.49 µg/L for Pb, and 12.38 to 14.26 µg/L for Ni. Cd, Pb, and Ni exhibited frequent exceedances of their corresponding AA-EQS, with the most pronounced downstream increases observed for Cd and Pb. Overall, the integration of physicochemical indicators with priority-substance compliance revealed downstream water-quality deterioration along the urban reach of the Lana River and shows that for the investigated priority substances, for a period of two years of consistent quality monitoring, the river water failed to achieve good chemical status. The upstream-downstream monitoring approach, as applied in this case study, provides an evidence basis for prioritizing wastewater pollution control and strengthening pollutant source-oriented monitoring in compliance with WFD requirements for river management.

Keywords: Chemical status assessments, Priority substances, Wastewater pressure

INTRODUCTION

Urban rivers are among the aquatic systems most strongly affected by anthropogenic pressures because they receive pollutant inputs from densely populated and highly modified catchments. Untreated or insufficiently treated wastewater, stormwater runoff, industrial discharges and diffuse urban sources can alter physicochemical conditions and introduce organic matter, nutrients and potentially toxic substances into receiving waters. These pressures commonly

generate longitudinal changes in water quality, often characterized by increasing pollutant concentrations downstream of urban areas (Glińska-Lewczuk et al., 2016; Szklarek et al., 2021; Wiesner-Sękala and Kończak, 2023). Electrical conductivity (EC), biochemical oxygen demand (BOD_5) and chemical oxygen demand (COD) provide complementary evidence of changes in dissolved and organic loads, although they do not independently determine chemical status under the Water Framework Directive.

Among urban contaminants, cadmium (Cd), lead (Pb) and nickel (Ni) are of particular environmental concern because of their persistence, toxicity and potential effects on aquatic ecosystems. Their occurrence in rivers may be associated with municipal and industrial effluents, urban runoff, atmospheric deposition, contaminated sediments and natural catchment characteristics. Recent investigations of a small urban river in Poland demonstrated spatial and seasonal variability in Cd, Pb, Ni, and other metals and highlighted the relevance of stormwater drainage and urban catchment characteristics for their distribution (Śniady et al., 2026). European-scale monitoring has also shown that temporal trends in Cd and Pb concentrations differ considerably among catchments in response to changes in pollutant emissions and catchment-specific characteristics (Eklöf et al., 2024). Investigations of surface waters affected by municipal and industrial discharges have also reported exceedances of Environmental Quality Standards for priority metals, confirming that these substances remain relevant constraints on the achievement of good chemical status (Wiesner-Sękala and Kończak, 2023).

Under the European Union Water Framework Directive (WFD), good chemical status requires compliance with Environmental Quality Standards (EQS) for priority substances (European Parliament and Council, 2000). Directive 2008/105/EC and its amendment, Directive 2013/39/EU, establish Annual Average Environmental Quality Standards (AA-EQS) for assessing long-term exposure to priority pollutants in surface waters (European Parliament and Council, 2008, 2013). Physicochemical parameters provide supporting information on general water-quality conditions, whereas WFD chemical-status classification is determined by compliance with the applicable EQS for priority substances.

However, evidence concerning upstream-downstream changes and the chemical status of urban rivers in Albania remains limited. Previous investigations have identified substantial anthropogenic pressures and water-quality deterioration within the Ishëm River Basin, but detailed assessments of individual urban tributaries remain scarce (Keci et al., 2021). This information gap restricts the identification of pollution gradients and the prioritization of wastewater-control and source-oriented monitoring measures. Upstream-downstream monitoring provides a practical means of directly comparing water-quality conditions along a defined river reach, particularly when observations from two stations are paired in time (Chen et al., 2021).

This study assessed how urban influence was reflected in water quality and chemical status along the Lana River, an urbanised tributary of the Ishëm River Basin. It aimed to identify downstream changes in pH, EC, BOD_5 and COD, quantify spatial and temporal variations in Cd, Pb and Ni, and assess whether their concentrations complied with the corresponding AA-EQS. The upstream-downstream monitoring design was applied to compare water-quality conditions at the upstream entry to the main urban reach with those observed after the accumulation of urban pressures.

MATERIALS AND METHODS

Study area and monitoring design

The Lana River is an urban tributary of the Ishëm River Basin that flows through Tirana, the largest and most densely populated city in Albania. The river receives cumulative pressures associated with urban development, including wastewater discharges, stormwater runoff, and diffuse inputs from the surrounding catchment. An upstream-downstream monitoring design was therefore applied to evaluate changes in water quality along its urban reach.

Two monitoring stations were selected (Figure 1). Lana 1 was located at the upstream entry to the main urban reach and represented conditions before the accumulation of the principal urban pressures. Lana 2 was located downstream of the urban area and was selected to represent the cumulative influence of wastewater and other urban pollutant inputs. The two stations were used to assess downstream changes in physicochemical conditions and priority-metal concentrations.

Monitoring was conducted from April 2024 to February 2026, covering 17 sampling campaigns. Lana 1 was sampled quarterly, providing eight observations during the study period, whereas Lana 2 was sampled monthly to capture greater temporal variability in downstream water quality. Eight sampling dates common to both stations were used for paired upstream-downstream statistical comparisons.

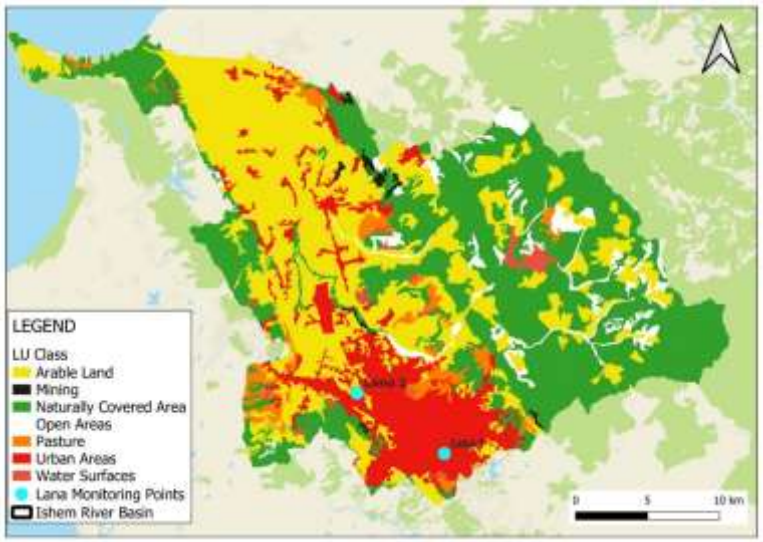

Figure 1. Location of the Lana River monitoring stations within the Ishëm River Basin.

Water sampling and analytical methods

Water samples were collected at both monitoring stations and transported to the laboratory of the Agricultural University of Tirana. Their preservation and subsequent analysis followed established laboratory procedures within the EN ISO/IEC 17025 accreditation framework. All investigated parameters were determined under laboratory conditions.

The physicochemical parameters included pH, electrical conductivity (EC), biochemical oxygen demand (BOD_5), and chemical oxygen demand (COD). Electrical conductivity was

expressed in µS/cm, while BOD_5 and COD were expressed in mg/L. These parameters were selected to characterize general water-quality conditions and changes in dissolved and organic loads along the investigated river reach.

The investigated priority metals were cadmium (Cd), nickel (Ni) and lead (Pb). Their total concentrations were determined by atomic absorption spectroscopy using a NOVAA 800D instrument and expressed in µg/L. Laboratory quality-control procedures were applied during sample preparation and instrumental analysis in accordance with the accredited analytical methods.

Environmental Quality Standard assessment

Measured Cd, Pb, and Ni concentrations were evaluated against the Annual Average Environmental Quality Standards established for inland surface waters under Directive 2008/105/EC, as amended by Directive 2013/39/EU. The applicable AA-EQS values were 1.2 µg/L for Pb and 4.0 µg/L for Ni. For Cd, the applicable AA-EQS ranges from 0.08 to 0.25 µg/L, depending on the water-hardness class.

Individual monitoring results were compared with the corresponding AA-EQS to identify the occurrence and frequency of concentrations above these reference values. Overall compliance was evaluated by comparing the mean concentration of each investigated metal with its corresponding AA-EQS. In accordance with the WFD "one-out, all-out" principle, non-compliance with the applicable AA-EQS for any of the investigated priority substances was interpreted as failure to achieve good chemical status with respect to the substances included in this study.

Statistical analysis

Descriptive statistics, including mean, median, minimum, maximum, and standard deviation, were calculated to characterize the distribution and temporal variability of each parameter at the two monitoring stations. Because the stations were sampled at different frequencies, all available observations were used for the station-specific descriptive analysis.

Upstream-downstream statistical comparisons were restricted to the eight dates on which both stations were sampled. The Wilcoxon signed-rank test was applied to the paired observations because of the small sample size and without assuming a normal distribution of the data. This non-parametric approach is suitable for evaluating paired water-quality observations collected using an upstream-downstream monitoring design and has been applied in comparable river assessments (Chen et al., 2021). Statistical significance was established at $p < 0.05$.

RESULTS AND DISCUSSION

Descriptive statistical analysis was used to characterize the distribution and temporal variability of the investigated physicochemical parameters and priority-metal concentrations. The results showed clear differences between the upstream and downstream monitoring stations.

Physicochemical water-quality characteristics

The physicochemical results showed clear differences between the upstream and downstream monitoring stations (Table 1). Mean pH remained relatively stable, changing only from 7.73 at

Lana 1 to 7.69 at Lana 2. In contrast, EC increased substantially along the investigated urban reach. Mean EC increased from 579.64 µS/cm at Lana 1 to 833.19 µS/cm at Lana 2, indicating a greater dissolved ionic load downstream.

More pronounced changes were observed for the organic-pollution indicators. Median BOD_5 increased from 22.42 mg/L at Lana 1 to 80.00 mg/L at Lana 2, while median COD increased from 61.80 to 160.00 mg/L. Mean BOD_5 and COD were also substantially higher at Lana 2. The increases observed in BOD_5, COD, and EC provide complementary evidence of higher dissolved loads and intensified organic pollution after the river passes through the main urban area.

The wide concentration ranges and high standard deviations of BOD_5 and COD indicate substantial temporal variability and the influence of individual high-concentration events. Although elevated values were already recorded at Lana 1, their higher downstream values indicate further deterioration associated with the accumulation of urban pressures. Similar patterns have been reported in urban rivers affected by municipal wastewater, stormwater runoff, and diffuse urban inputs (Glińska-Lewczuk et al., 2016; Szklarek et al., 2021).

Table 1. Descriptive statistics of physicochemical parameters at the Lana River monitoring stations

Parameter	Station	Range	Mean	Median	SD
pH	Lana 1	7.20–8.20	7.73	7.78	0.33
	Lana 2	7.34–7.92	7.69	7.74	0.15
EC (µS/cm)	Lana 1	535–686	579.64	572.5	48.53
	Lana 2	628–1307	833.19	812.4	141.29
BOD_5 (mg/L)	Lana 1	0.61–206	49.69	22.42	67.54
	Lana 2	2.74–310	106.7	80	82.81
COD (mg/L)	Lana 1	0.50–469	115.88	61.8	152.7
	Lana 2	5.34–706	230.38	160	191.31

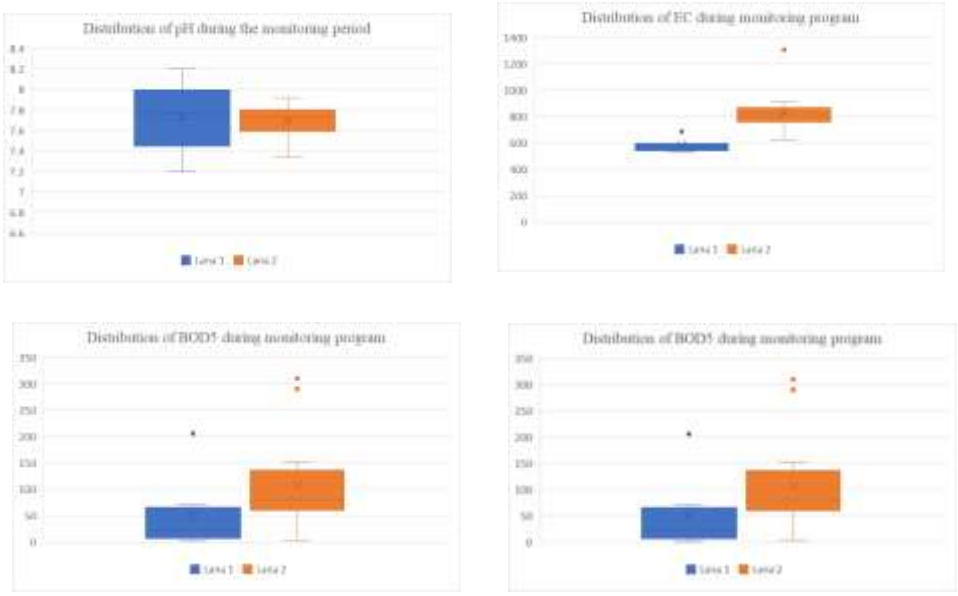

Figure 2. Distribution of pH, EC, BOD_5 and COD values during the monitoring period

Priority-metal concentrations and AA-EQS compliance

Cd, Pb, and Ni were detected at both stations and showed higher mean concentrations at Lana 2 (Table 2). Mean Cd increased from 0.56 to 0.71 µg/L, while the wider range and higher standard deviation at Lana 2 indicate greater temporal variability downstream. This pattern may reflect intermittent pollutant inputs or changes in hydrological conditions during individual monitoring campaigns.

Pb showed the largest absolute downstream increase, with its mean concentration rising from 18.86 µg/L at Lana 1 to 25.49 µg/L at Lana 2. The relatively high mean and median concentrations at both stations indicate persistent Pb contamination rather than an effect caused exclusively by isolated concentration peaks. Mean Ni increased from 12.38 to 14.26 µg/L and exhibited substantial temporal variability at both stations.

The downstream increases in Cd, Pb and Ni are consistent with cumulative pollutant inputs along the urban reach. Potential sources include municipal and industrial effluents, road and stormwater runoff, atmospheric deposition, and the mobilization of contaminated suspended material or sediments. Ni may also be influenced by natural catchment characteristics and therefore cannot be attributed exclusively to urban pollution. Comparable variability in Cd, Ni, Pb and other metals has been reported in the Bogdanka River, a small urban river affected by stormwater drainage and urban catchment pressures (Śniady et al., 2026).

Table 2. Descriptive statistics of Cd, Pb, and Ni concentrations at the Lana River monitoring stations (µg/L)

Parameter	Station	Range	Mean	Median	SD
Cd (µg/L)	Lana 1	0.354–0.837	0.56	0.55	0.16
	Lana 2	0.130–2.171	0.71	0.72	0.43
Pb (µg/L)	Lana 1	11.95–28.48	18.86	19.86	5.62
	Lana 2	10.66–37.90	25.5	24.9	7.36
Ni (µg/L)	Lana 1	0.05–23.60	12.38	14.36	8.91
	Lana 2	0.06–29.94	14.27	14.39	8.35

Comparison with the applicable AA-EQS revealed frequent concentrations above the corresponding reference values at the downstream station. At Lana 2, Pb exceeded the AA-EQS of 1.2 µg/L in all observations. Cd exceeded the upper hardness-dependent AA-EQS of 0.25 µg/L in 16 of 17 observations (94.1%), while Ni exceeded its AA-EQS of 4.0 µg/L in 15 of 17 observations (88.2%). Mean concentrations of all three metals were also above their corresponding AA-EQS values, indicating non-compliance during the monitoring period. Overall, Pb represented the most persistent concern, while Cd and Ni showed frequent concentrations above their corresponding reference values.

Although metal contamination was already evident at Lana 1, the higher mean concentrations at Lana 2 indicate additional deterioration along the urban reach. Studies on surface waters affected by municipal and industrial discharges have similarly reported elevated metal concentrations and failure to comply with the applicable Environmental Quality Standards (Wiesner-Sękala and Kończak, 2023).

Under the WFD "one-out, all-out" principle, the observed non-compliance indicates that the investigated river reach failed to achieve good chemical status with respect to Cd, Pb, and Ni. These findings identify priority-metal contamination as a persistent pressure and underline the importance of strengthening urban pollution-control measures along the Lana River.

Upstream-downstream statistical comparison

The upstream-downstream differences were evaluated using eight monitoring dates common to both stations. EC, BOD_5, COD, Cd, Pb, and Ni were consistently higher at Lana 2 during the paired monitoring campaigns. The Wilcoxon signed-rank test confirmed statistically significant downstream increases for all six parameters ($p=0.0078$; Table 3). In contrast, pH did not differ significantly between the stations ($p=0.25$).

These findings confirm that downstream deterioration was reflected in dissolved loads, organic-pollution indicators, and priority-metal concentrations, whereas pH remained comparatively stable. The findings are consistent with the value of paired upstream-downstream monitoring for identifying changes along a defined river reach while reducing the influence of temporal variation between observations (Chen et al., 2021).

The results should nevertheless be interpreted within the limitations of the monitoring design. The stations were sampled at different frequencies, and individual wastewater and stormwater outlets were not monitored. Consequently, the study identifies a clear upstream-downstream pollution gradient but does not quantify the contribution of specific emission sources. Additional source-oriented and rainfall-event monitoring supported by river-discharge data would improve the identification of the processes controlling pollutant variability.

Table 3. Wilcoxon signed-rank test results for paired observations at Lana 1 and Lana 2.

Parameter	Number of pairs	Test statistic (W)	p-value	Statistical result
pH	8	8.5	0.25	Not significant
EC	8	0	0.0078	Significant increase
BOD_5	8	0	0.0078	Significant increase
COD	8	0	0.0078	Significant increase
Cd	8	0	0.0078	Significant increase
Pb	8	0	0.0078	Significant increase
Ni	8	0	0.0078	Significant increase

CONCLUSIONS

The integrated assessment of physicochemical parameters and priority-metal concentrations revealed clear downstream deterioration along the urban reach of the Lana River. While pH remained relatively stable, EC, BOD_5, and COD increased significantly at Lana 2, indicating higher dissolved loads and intensified organic pollution. Cd, Pb, and Ni concentrations also increased downstream, with the most pronounced changes observed for Pb and Cd.

Frequent AA-EQS exceedances, particularly at the downstream station, demonstrate persistent priority-metal contamination. Under the WFD “one-out, all-out” principle, the observed non-compliance indicates that the investigated river reach failed to achieve good chemical status with respect to the three priority substances included in this study.

The two-year upstream-downstream dataset provides new evidence of the cumulative influence of urban pressures on an under-investigated Albanian river. Although individual pollution sources were not investigated separately, the monitoring results clearly demonstrated downstream deterioration in water quality. These findings support the prioritization of wastewater-pollution control and more source-oriented monitoring, particularly at specific discharge points and during rainfall-related events, to strengthen WFD-based management of the Lana River.

Acknowledgments

This study was supported by the APPEAR project No. 320 AMoRE-Al, "Assessment of Pollutant Emissions to Support River Basin Management in Albania under the EU Water Framework Directive", funded by the Austrian Development Agency (ADA).

REFERENCES

1. Chen, Y., Wang, Y., Chia, B., Wang, D. (2021). Upstream-downstream water quality comparison of restored channelized streams. *Ecological Engineering*, 170, 106367. DOI:10.1016/j.ecoleng.2021.106367

2. EklÖf, K., von Brömssen, C., Huser, B., Äkerblom, S., Augustaitis, A., Braaten, H.F.V., de Wit, H.A., Dirnböck, T., Elustondo, D., Grandin, U., Holubová, A., Kleemola, S., Krám, P., Lundin, L., Löfgren, S., Markensten, H., Moldan, F., Pihl Karlsson, G., Rönnback, P., Valinia, S. and Vuorenmaa, J. (2024). Trebds in mercury, lead and cadmium concentrations in 27 European streams and rivers: 2000-2020. Environmental pollution, 360, 124761. https://doi.org/10.1016/j.envpol.2024.124761

3. European Parliament and Council (2000). Directive 2000/60/EC establishing a framework for Community action in the field of water policy (Water Framework Directive). *Official Journal of the European Communities*, L 327, 22.12.2000, pp. 1–73. http://data.europa.eu/eli/dir/2000/60/2026-05-10

4. European Parliament and Council (2008). Directive 2008/105/EC on environmental quality standards in the field of water policy. *Official Journal of the European Union*, L 348, 24.12.2008, pp. 84-97. http://data.europa.eu/eli/dir/2008/105/oj

5. European Parliament and Council (2013). Directive 2013/39/EU amending Directives 2000/60/EC and 2008/105/EC as regards priority substances in the field of water policy. *Official Journal of the European Union*, L 226, 24.08.2013, pp. 1-17. http://data.europa.eu/eli/dir/2013/39/oj

6. Glińska-Lewczuk, K., Golaś, I., Koc, J., Gotkowska-Plachta, A., Harnisz, M. and Rochwerger, A. (2016). The impact of urban areas on the water quality gradient along a lowland river. Environmental Monitoring and Assessment, 188, 624. DOI:10.1007/s10661-016-5638-z

7. Keci, E., Matalla, O., and Gjeci, V. (2021) Water quality status in the Ishmi River, Albania over the period 2014-2019 and prospective towards the achievements of EU WFD objectives in its basin. Proceedings of the 5th International Scientific Conference EMAN 2021-Economics and Management: How to Cope with Disrupted Times, pp. 435-446 DOI: https://doi.org/10.31410/EMAN.2021.435

8. Śniady, I., Stryniak, I., Szponar, J. and Siepak, M. (2026). Heavy metals pollution and toxicity assessment in a small urban river: Analysis of the Bogdanka River catchment (Poznań, Poland). Geographia Polonica, 99(1), 121-142. doi: https://doi.org/10.7163/GPol.0320

9. Szlarek, S., Kiedrzyńska, E., Kiedrzyński, M., Mankiewicz-Boczek, J., Mitsch, WJ. and Zalewski, M. (2021). Comparing ecotoxicological and physicochemical indicators of municipal wastewater effluent and river water quality in a Baltic Sea catchment in Poland. Ecological Indicators, 126, 107611. https://doi.org/10.1016/J.ECOLIND.2021.107611

10. Wiesner-Sękala, M. and Kończak, B. (2023). Assessment of the impact of industrial and municipal discharges on the surface water body status (Poland). Sustainability, 15(2), 997. https://doi.org/10.3390/su15020997

COMBINED TOXICITY OF MICROPLASTICS AND CHEMICAL POLLUTANTS IN AQUATIC ORGANISMS

Duygu Özhan TURHAN

Department of Biology, Faculty of Arts and Science, Inonu University, Malatya, Turkey

duygu.turhan@inonu.edu.tr

ABSTRACT

Microplastics are widespread contaminants in aquatic ecosystems and have received increasing attention in recent years due to their potential environmental impacts. In aquatic environments, microplastics do not occur in isolation but coexist with heavy metals, pesticides, pharmaceuticals, and various organic contaminants. Their large surface area and physicochemical properties facilitate the adsorption of different chemicals onto their surfaces, raising concerns about their potential role in modifying the transport, bioavailability, and toxicity of coexisting pollutants. This review aims to evaluate the toxicological effects of combined exposure to microplastics and chemical pollutants in aquatic organisms. Available evidence indicates that interactions between microplastics and heavy metals, pesticides, pharmaceuticals, and other organic contaminants may vary depending on polymer type, particle size, surface characteristics, aging processes, and the physicochemical conditions of the surrounding environment. Combined exposures have been associated with oxidative stress, alterations in antioxidant defense systems, neurotoxic and genotoxic responses, as well as adverse effects on growth, development, reproduction, and behavior. However, the influence of microplastics on the toxicity of coexisting chemicals is not uniform. Depending on the properties of the contaminant, microplastic characteristics, exposure duration, and concentration, combined exposure may result in synergistic, antagonistic, or additive effects. Overall, interactions between microplastics and chemical pollutants represent an important factor that may modify the biological effects of contaminants in aquatic ecosystems. Considering combined effects alongside the toxicity of individual pollutants in environmental risk assessment may provide a more realistic understanding of exposure scenarios occurring in natural aquatic environments.

Keywords: microplastics, combined toxicity, aquatic organisms, environmental pollutants, ecotoxicology

INTRODUCTION

1. Definition and Environmental Formation of Microplastics

Plastic products are widely used in applications ranging from daily life to industry due to advantageous properties such as light weight, durability, versatility, and low production cost. However, the rapid increase in plastic use and the long-term persistence of the resulting plastic waste in the environment have made plastic pollution an important global environmental problem. Plastic materials entering the environment can fragment over time into smaller plastic particles under the influence of physical, chemical, and biological processes. Microplastics (MPs) are generally defined as synthetic polymer particles with an upper size limit of 5 mm,

although there is no definitive consensus regarding the lower size limit. Furthermore, the continued fragmentation of microplastics under environmental conditions may lead to the formation of nanoscale plastic particles (Li et al., 2018).

2. Environmental Transport and Distribution of Microplastics

Certain characteristics of microplastics, such as their light weight, diverse morphologies, and extremely long lifespans, contribute substantially to their transport between environmental compartments. These properties also make microplastics one of the most widespread pollutants worldwide. Nearly all plastics and plastic-derived materials are produced on land and enter different environments through various pathways. In most scenarios, land acts as the initial receiving compartment for microplastics, which subsequently enter the environment through direct littering, improper waste management, accidental losses during disposal, and industrial spills (Horton & Dixon, 2018).

3. Physicochemical Properties of Microplastics and Their Role as Chemical Carriers

An important chemical characteristic common to microplastics is their capacity to adsorb and accumulate environmental pollutants, including heavy metals and organic contaminants. Moreover, microplastics contain various chemical additives, such as plasticizers and flame retardants, suggesting that they may act as both a “carrier” and a “source” of other chemicals. Microplastics are generally resistant to chemical reactions; however, exposure to UV radiation can induce photochemical degradation and lead to higher fragmentation rates. In addition, the hydrophobic properties of microplastics can determine their interactions within aquatic habitats and organisms. Consequently, microplastics exhibit distinctive environmental pollutant characteristics that influence their distribution, uptake, and toxicity in aquatic species (Hasan et al., 2024).

4. Biological Effects of Microplastics on Aquatic Organisms

The adverse effects of microplastics on fish reproduction have also become a growing concern. For example, microplastics may have serious consequences for the endocrine systems of fish. Plasticizers and various bisphenol analogues and phthalates, which are important endocrine disruptors, may leach from microplastics into the environment. These chemicals may mimic or induce hormonal imbalances, potentially leading to reduced fertility rates, alterations in offspring growth, or even changes in sex ratios (Hasan et al., 2024).

Huang et al. (2024) exposed juvenile *Carassius auratus* to different concentrations of polystyrene microplastics (PS-MPs; 200, 800, and 3200 µg/L) for 32 days and evaluated their effects on growth, tissue damage, and gene expression. PS-MPs were reported to accumulate particularly in the gastrointestinal tract and gills, and exposure resulted in varying degrees of histopathological damage in the intestine, gills, brain, and liver. In addition, the severity of tissue damage increased with increasing PS-MP concentration, and changes were detected in the expression of the genes examined in the liver, intestine, and gills (Huang et al., 2024).

5. Interactions of Microplastics with Organic Pollutants and Heavy Metals

According to previous studies, microplastics can act as carriers capable of adsorbing and enriching heavy metals as well as organic pollutants such as polycyclic aromatic hydrocarbons (PAHs), polychlorinated biphenyls (PCBs), pharmaceuticals, and personal care products

(PPCPs) from water or soil. Microplastics are highly mobile. After adsorbing organic pollutants, they may transport these contaminants to new environments and cause adverse effects (Zhang et al., 2023).

Microplastics can adsorb and accumulate various organic pollutants, including persistent organic pollutants such as polycyclic aromatic hydrocarbons (PAHs) and polychlorinated biphenyls (PCBs), as well as different heavy metals. The adsorption of heavy metals onto microplastic surfaces is influenced by several factors, including the physicochemical properties of the particles, surface modifications, aging, and environmental conditions (Ateia et al., 2022).

6. Interactions of Microplastics with Antimicrobials and Microorganisms

Various studies have investigated the adsorption and desorption behavior of antibiotics, particularly macrolides and quinolones, on different types of MPs, mainly polystyrene, polyethylene, and polylactic acid. To date, most studies have focused on the adsorption properties of pristine MPs, whereas desorption behavior has been investigated to a more limited extent. However, a large proportion of MPs present in the environment are aged. Once antibiotics are adsorbed by MPs, they can be transported along with the movement of MPs. Therefore, determining whether adsorbed antibiotics can desorb from microplastic surfaces is important for assessing the risks that these pollutants may pose in new environments (Zhang et al., 2023).

The co-occurrence of MPs and antimicrobials in the environment raises concerns regarding their combined ecological effects. Antimicrobials, which have substantially improved human and animal health and agricultural productivity, now frequently contaminate the environment through sources such as agricultural runoff and industrial discharges. For example, hydrophobic polymers such as polyethylene or polystyrene readily adsorb nonpolar antimicrobials, whereas charged or functionalized surfaces can bind ionizable antibiotics such as sulfonamides or tetracyclines. Their environmental presence not only poses ecological risks but also contributes to the proliferation of resistance genes (Tang, 2025).

7. Combined Toxicity of Pollutant Mixtures

Interactions between microplastics and coexisting pollutants may result in synergistic, antagonistic, or additive effects. When MPs carry other pollutants such as DBP, their large surface area may enable them to accumulate greater amounts of contaminants through an adsorptive carrier effect, thereby increasing toxicity. Conversely, MPs may reduce the bioavailability of pollutants through adsorption and enrichment, thereby decreasing their bioaccumulation. In addition, whether the interaction is synergistic or antagonistic may depend on MP concentration. Aggregation, disaggregation, and the corresponding exposure levels vary among different MP concentrations, which can result in inconsistent toxicity responses (Liang et al., 2025).

Turhan et al. (2026) evaluated the individual and combined effects of polyethylene microplastics (PE-MPs) and deltamethrin (DEL) during the early life stages of *Xenopus laevis*. PE-MPs alone did not cause marked mortality or malformations in embryos but induced changes in biochemical responses. Under combined exposure to DEL and PE-MPs, additive, antagonistic, and synergistic interactions were reported depending on the biomarker and developmental stage. In embryos, additive effects were observed for GST and CaE, antagonistic

effects for AChE, while the CAT response showed antagonistic or synergistic characteristics depending on the DEL concentration (Turhan et al., 2026).

The toxic effects of mixtures of MPs and hazardous chemicals may differ from the inherent toxicity of the individual substances depending on factors such as mixture concentration and ratio and interactions among the components. During the embryonic development of the amphibian *Rhinella arenarum*, non-toxic concentrations of copper and nonylphenol produced toxic effects depending on the mixture ratio (Aronzon et al., 2020). In *Daphnia magna* exposed to a mixture of silver ions and two different metal oxide nanoparticles, a synergistic effect greater than the toxic effects of the individual substances was confirmed (Park et al., 2019).

Liang et al. (2025) evaluated the combined toxicity of polypropylene microplastic fibers (MPFs) and dibutyl phthalate (DBP) in *Chlorella vulgaris*. Combined exposure was reported to cause more pronounced effects on photosynthesis, oxidative stress, and metabolism than individual exposures. In addition, the direction of combined toxicity changed depending on MPF concentration, with synergistic interactions at high MPF concentrations and antagonistic interactions at low MPF concentrations.

Wang et al. (2022) investigated the individual and combined toxic effects of polyvinyl chloride microplastics (PVC-MPs) and di(2-ethylhexyl) phthalate (DEHP) on *Danio rerio* embryos and larvae. The study used 0.1 ppm PVC-MPs and 71 µg/L DEHP, representing an environmentally relevant concentration. Individual exposure to PVC-MPs and DEHP inhibited embryo hatching, whereas this effect was reduced under combined exposure. Individual exposures also caused toxic effects on oxidative stress and cardiac development, while these effects were alleviated during combined exposure. The researchers reported an antagonistic interaction between PVC-MPs and DEHP and suggested that adsorption of DEHP by PVC-MPs, thereby reducing its bioavailability and bioaccumulation, may contribute to this antagonistic effect.

Zhang et al. (2022) showed that aged microplastics increased the accumulation of roxithromycin in *Carassius auratus* tissues in a microplastic size-dependent manner. Both aged microplastics and roxithromycin significantly increased superoxide dismutase (SOD) and catalase (CAT) activities in the liver and intestine while suppressing acetylcholinesterase (AChE) activity in the brain. In addition, smaller aged microplastics intensified roxithromycin-induced damage in the liver, gills, and brain, whereas larger microplastics caused more severe intestinal damage.

Similarly, in a 28-day study evaluating the combined effects of oxytetracycline and polystyrene microplastics on juvenile yellow catfish (*Pelteobagrus fulvidraco*), neither oxytetracycline nor 100 µg/L microplastics alone significantly affected growth, antioxidant and digestive enzyme activities, or intestinal microbial diversity. In contrast, combined exposure to oxytetracycline and 100 µg/L polystyrene microplastics increased SOD and CAT activities, caused mild intestinal damage, and increased the abundance of Proteobacteria (Tang, 2025).

CONCLUSION

The available evidence indicates that interactions between microplastics and chemical pollutants may significantly modify their toxic effects in aquatic organisms. Depending on microplastic characteristics, pollutant properties, concentration, and exposure conditions, combined exposure may result in synergistic, additive, or antagonistic effects. These interactions can influence oxidative stress, neurotoxicity, growth, development, and other

biological responses. Therefore, evaluating microplastics and chemical pollutants separately may not adequately reflect exposure scenarios in natural aquatic environments. Further studies using environmentally relevant concentrations and different microplastic–pollutant combinations are needed to better understand these complex interactions and to improve ecological risk assessment.

REFERENCES

Aronzon, C. M., Peluso, J., & Coll, C. P. (2020). Mixture toxicity of copper and nonylphenol on the embryo-larval development of *Rhinella arenarum*. Environmental Science and Pollution Research, 27, 13985–13994. https://doi.org/10.1007/s11356-020-07857-7

Ateia, M., Ersan, G., Alalm, M. G., Boffito, D. C., & Karanfil, T. (2022). Emerging investigator series: Microplastic sources, fate, toxicity, detection, and interactions with micropollutants in aquatic ecosystems—A review of reviews. Environmental Science: Processes & Impacts, 24(2), 172–195. https://doi.org/10.1039/D1EM00443C

Hasan, A. K. M. M., Hamed, M., Hasan, J., Martyniuk, C. J., Niyogi, S., & Chivers, D. P. (2024). A review of the neurobehavioural, physiological, and reproductive toxicity of microplastics in fishes. Ecotoxicology and Environmental Safety, 282, 116712.

Horton, A. A., & Dixon, S. J. (2018). Microplastics: An introduction to environmental transport processes. WIREs Water, 5, e1268. https://doi.org/10.1002/wat2.1268

Huang, Y., Li, W., Dong, K., Li, X., Li, W., & Wang, D. (2024). Effect of polystyrene microplastic exposure on individual, tissue, and gene expression in juvenile crucian carp (*Carassius auratus*). Fishes, 9, 385.

Li, J., Liu, H., & Chen, P. (2018). Microplastics in freshwater systems: A review on occurrence, environmental effects, and methods for microplastics detection. Water Research, 137, 362–374.

Liang, L., Liang, Y., Su, M., Wang, Z., Zhou, Z., Zhou, X., & Jiang, Z. (2025). Combined toxicity of microplastic fibers and dibutyl phthalate on algae: Synergistic or antagonistic? Aquatic Toxicology, 281, 107290.

Park, C. B., Jung, J. W., Baek, M., Sung, B., Park, J. W., Seol, Y., Yeom, D. H., Park, J. W., & Kim, Y. J. (2019). Mixture toxicity of metal oxide nanoparticles and silver ions on *Daphnia magna*. Journal of Nanoparticle Research, 21, 166. https://doi.org/10.1007/s11051-019-4606-2

Tang, K. H. D. (2025). Combined toxicity of microplastics and antimicrobials on animals: A review. Antibiotics, 14(9), 896.

Turhan, D. O., Benli, C. A., Yurekli, M., & Güngördü, A. (2026). The single and combined effects of deltamethrin and polyethylene microplastics on the development and biochemical responses of *Xenopus laevis* in early life stages. Ecotoxicology, 35, 37.

Wang, H., Wang, Y., Wang, Q., Lv, M., Zhao, X., Ji, Y., Han, X., Wang, X., & Chen, L. (2022). The combined toxic effects of polyvinyl chloride microplastics and di(2-ethylhexyl) phthalate on the juvenile zebrafish (*Danio rerio*). Journal of Hazardous Materials, 440, 129711.

Zhang, P., Lu, G., Sun, Y., Zhang, J., Liu, J., & Yan, Z. (2022). Aged microplastics change the toxicological mechanism of roxithromycin on *Carassius auratus*: Size-dependent interaction and potential long-term effects. Environment International, 169, 107540.

Zhang, X., Liu, L., Chen, X., Li, J., Chen, J., & Wang, H. (2023). The fate and risk of microplastic and antibiotic sulfamethoxazole coexisting in the environment. Environmental Geochemistry and Health, 45(6), 2905–2915. https://doi.org/10.1007/s10653-022-01385-8

EVALUATION OF MODULAR LIQUID FERTILIZERS CONTAINING SNP, SA-NA, NA-NAA, CPPU AND GA3 IN TERMS OF ROOT DEVELOPMENT, STRESS MANAGEMENT AND FRUIT DEVELOPMENT

Gökhan Yaşar[1], Burcu Köse[1], Ahmet Akbulut[1], Hatice Deniz Öncel[1]*

[1]İGSAŞ R&D Center, Kütahya, Türkiye
**Corresponding Author: Gökhan Yaşar, İGSAŞ R&D Center, Kütahya, Türkiye. E-mail: gokhan.yasar@igsas.com.tr*

ABSTRACT

This study evaluates modular plant activation strategies containing sodium nitrophenolate (SNP), sodium salicylate (SA-Na), the sodium salt of naphthaleneacetic acid (Na-NAA), forchlorfenuron (CPPU) and gibberellic acid (GA3), with respect to their potential contributions to rooting, stress management and fruit development. These compounds are associated, respectively, with photosynthetic activation and rapid physiological response, stress signalling and systemic resistance, adventitious rooting, cytokinin-like cell division and fruit enlargement, and gibberellin-related developmental regulation, including germination, shoot elongation and flowering. Integrating such compounds into fertilizer-related liquid formulations may create considerable product value; however, this compound group also represents the most regulation-sensitive family addressed in this line of work, given concerns related to dosage, phenological timing, residue levels and phytotoxicity. Rather than proposing a single combined formulation, this study outlines three separate modules: a stress management module, a rooting module, and a fruit enlargement and quality module. For peer-reviewed publication, each module should be supported by an independent dose-response trial and a corresponding safety evaluation.

Keywords: *plant growth regulator; sodium nitrophenolate; sodium salicylate; NAA; CPPU; GA3*

1. INTRODUCTİON

Plant growth regulators and physiological activators are compounds that, even at low doses, can direct plant developmental processes. Unlike conventional fertilizers, they do not act primarily by supplying nutrients; instead, they can influence photosynthesis, hormonal balance, root formation, flowering, fruit set and stress defence. For this reason, the boundary between a fertilizer formulation and a growth-regulator approach must be considered carefully from both a scientific and a regulatory standpoint.

In-house evaluation notes have assessed SNP, SA-Na, Na-NAA, CPPU and GA3 for distinct intended uses. SNP has been associated with rapid onset of action and support for photosynthesis; SA-Na with systemic resistance and stress management; Na-NAA with root development; CPPU with fruit enlargement; and GA3 with objectives such as germination, cluster elongation and fruit length.

The scientific value of this study lies not in combining these compounds into a single recipe, but in organising them into target-specific modules. In this way, distinct physiological objectives — rooting, stress management and fruit development — can be measured independently, and the resulting formulation claims become more scientifically defensible.

2. MATERİALS AND METHODS

2.1 Materials

The modular compound groups considered in this study are defined as follows: an SNP-based photosynthesis and growth activation group; an SA-Na-based stress and systemic resistance support group; an Na-NAA-based rooting group; a CPPU-based fruit-enlargement group; and a GA3-based germination, elongation and flowering group.

2.2 METHODS

For the stress management module, a control, a micronutrient/amino-acid base product, an SA-Na-containing product, and an SA-Na + SNP combination are compared.

For the rooting module, seedling or cutting trials are used to measure rooting percentage, root number, root length and root dry weight.

For the fruit-enlargement module, CPPU and GA3 applications are tested at separate doses according to phenological stage; fruit size, firmness, dry matter, soluble solids content, acidity and possible residue risks are monitored.

Rather than disclosing a complete recipe for each module, the active-ingredient class, application window, dose range and safety criteria should be reported in the publication text. Compliance with residue limits and relevant regulations must be explicitly addressed for ethical and regulatory reasons.

2.3 Statistical Analysis

Regression analysis is used for dose-response relationships, analysis of variance (ANOVA) for treatment group comparisons, and appropriate ordinal-data methods for phytotoxicity scores. Multivariate principal component analysis (PCA) may additionally be applied to fruit quality datasets.

3. RESULTS

The target physiological effects of SNP, SA-Na, Na-NAA, CPPU and GA3 have been clearly defined; however, field efficacy or dose-response results are not yet available in the current documentation. These compounds carry high potential for product development, but confirmatory field data remain to be generated.

The literature indicates that NAA/auxin applications can support adventitious root formation; that CPPU applications can be effective on fruit size and quality parameters; that GA3 applications have been studied in citrus and other fruit species in relation to flowering and fruit set; and that salicylic acid and nitrophenolate compounds may contribute to mechanisms associated with stress tolerance and photosynthesis.

Table 1. Proposed publication framework for the modular activation groups.

Module	Compound Class	Main Target	Measurable Output
Stress management	SA-Na + SNP	Antioxidant defence and photosynthesis	SPAD, Fv/Fm, electrolyte leakage
Rooting	Na-NAA + amino acid/phosphorus support	Adventitious root formation	Rooting %, root number, root length
Fruit enlargement	CPPU + Ca/B support	Cell division and fruit growth	Fruit weight, diameter, firmness
Flowering/elongation	GA3 module	Shoot, flower and fruit development	Cluster length, fruit set, quality

4. DİSCUSSİON

This compound group carries high publication value, yet it is simultaneously the most sensitive topic addressed in this line of work. Compounds such as CPPU, GA3 and NAA-type substances may fall under plant-growth-regulator or pesticide/registration regimes in many countries. For this reason, in the academic text, the product group should be defined not as a "fertilizer" claim, but as a "controlled physiological activation module," and regulatory compliance should be noted separately.

Compounds such as SNP and SA-Na can be positioned more compatibly with stress-management products. The Na-NAA rooting module and the CPPU/GA3 fruit-development module should be tested separately from one another. Combining a large number of growth-regulating compounds within a single formulation complicates scientific interpretation; a modular approach improves both publication quality and product safety.

5. CONCLUSION

If properly modularised, the SNP, SA-Na, Na-NAA, CPPU and GA3 compound group has the potential to yield at least one comprehensive full-length article, together with two additional application-focused technical articles, produced within an in-house research and development framework. At the current stage, the literature basis is strong; however, definitive efficacy claims should not be made until field and dose-response data are completed

Declarations

Ethics Approval: This study is a laboratory-scale fertilizer and plant activation formulation development study and does not involve human or animal experimentation. If a field trial is conducted on living plant material, internal institutional permits and relevant local regulatory records should be obtained prior to submission.

Author Contributions:

Burcu Köse: Project management.

Ahmet Akbulut: Experimental design, data collection and initial draft.

Gökhan Yaşar: Methodology, manuscript review.

Hatice Deniz Öncel: Literature review and analysis.

Funding: This study was carried out within the scope of an in-house research and development project.

Conflict of Interest: The authors declare that this product development study is an in-house R&D activity, and that the academic interpretations presented are limited to the current experimental results and the relevant literature.

Acknowledgements: The authors thank the R&D and Antalya plant teams for their contribution to the laboratory and field planning processes.

REFERENCES

Garmendia, A., Beltrán, R., Zornoza, C., García-Breijo, F. J., Reig, J., & Merle, H. (2019). Gibberellic acid in Citrus spp. flowering and fruiting: A systematic review. PLoS ONE, 14(9), e0223147. https://doi.org/10.1371/journal.pone.0223147

Ghimire, B. K., Kim, S. H., Yu, C. Y., & Chung, I. M. (2022). Biochemical and physiological changes during early adventitious root formation in Chrysanthemum indicum Linné cuttings. Plants, 11(11), 1440. https://doi.org/10.3390/plants11111440

Khan, M. I. R., Fatma, M., Per, T. S., Anjum, N. A., & Khan, N. A. (2015). Salicylic acid-induced abiotic stress tolerance and underlying mechanisms in plants. Frontiers in Plant Science, 6, 462. https://doi.org/10.3389/fpls.2015.00462

Liu, Z., et al. (2025). Compound sodium nitrophenolate improves photosynthesis and forage quality in Hemarthria compressa. Agronomy, 15(11), 2526. https://doi.org/10.3390/agronomy15112526

Lyu, B., et al. (2024). Sequential application of 1-naphthalenacetic acid and putrescine promotes the developmental growth of adventitious roots in chrysanthemum cuttings. The Horticulture Journal, 93(4), 395-405.

Przybysz, A., Gawrońska, H., & Gajc-Wolska, J. (2014). Biological mode of action of a nitrophenolates-based biostimulant: Case study. Frontiers in Plant Science, 5, 713. https://doi.org/10.3389/fpls.2014.00713

Xie, X., et al. (2024). Effect of forchlorfenuron (CPPU) on fruits quality and residue analysis in kiwifruits. Journal of Food Composition and Analysis, 132, 106296.

Yang, H., Fang, R., Luo, L., Yang, W., Huang, Q., Yang, C., Hui, W., Gong, W., & Wang, J. (2023). Uncovering the mechanisms of salicylic acid-mediated abiotic stress tolerance in horticultural crops. Frontiers in Plant Science, 14, 1226041. https://doi.org/10.3389/fpls.2023.1226041

POTENTIAL OF A MICRONUTRIENT, AMINO ACID AND PLANT SIGNALING COMPOUND-BASED LIQUID FERTILIZER FOR FROST AND POST-STRESS NUTRITION

Gökhan Yaşar[1]*, Burcu Köse[1], Ahmet Akbulut[1], Hatice Deniz Öncel[1]

[1]İGSAŞ R&D Center, Kütahya, Türkiye

*Corresponding Author: Gökhan Yaşar, İGSAŞ R&D Center, Kütahya, Türkiye. E-mail: gokhan.yasar@igsas.com.tr

ABSTRACT

This manuscript evaluates a liquid fertilizer concept containing micronutrients, amino acids and plant signaling compounds, developed for frost and post-stress nutrition. The formulation combines Zn, Mn, Fe, Cu, B and Mo, an amino acid fraction, ammonium nitrogen, and low-dose nitrophenolate/salicylate-based activators. Laboratory-scale preparation indicated that the formulation could be positioned for orchard recovery after frost, protection of chlorophyll-related functions, reduction of micronutrient-limitation risk, and mitigation of stress-induced physiological decline. The literature supports the relevance of foliar nutritional strategies for frost tolerance, the stress-regulatory role of salicylic acid, and the photosynthesis-promoting effects of nitrophenolate-based biostimulants. The manuscript frames the product as a field-trial-ready formulation concept rather than a final efficacy claim.

Keywords: *liquid fertilizer; frost stress; micronutrients; amino acids; sodium nitrophenolate; sodium salicylate*

1. INTRODUCTİON

With climate change, late spring frosts, temperature fluctuations, drought and salinity have become major risks limiting yield and quality, particularly in fruit growing and protected cultivation. Low-temperature injury in plants is associated with disruption of membrane integrity, increased reactive oxygen species, suppression of photosynthesis, and disturbance of mineral nutrient balance. For this reason, pre- and post-frost nutrition strategies should be regarded not merely as a fertilization practice but as a physiological recovery management approach.

Micronutrients play a critical role in enzyme activity, chlorophyll synthesis, oxidative stress management and reproductive development. Zinc is involved in protein synthesis and auxin metabolism; manganese in photosystem II and enzymatic reactions; iron in chlorophyll and electron transport; copper in redox enzymes; boron in cell wall integrity, flowering and fruit set; and molybdenum in nitrogen metabolism. Balanced micronutrient application can support the plant's recovery capacity, particularly during stress periods.

Protein hydrolysates and free amino acids form an important group within plant biostimulants. Beyond serving as a nitrogen source, these compounds are considered signaling molecules or precursor metabolites that may influence osmotic regulation, nutrient uptake, root development and stress response. The addition of low-dose salicylate- and nitrophenolate-based activators to this structure aims to give the product a physiologically supportive function in addition to its nutritional role.

2. MATERİALS AND METHODS

2.1 Materials

The liquid fertilizer family addressed in this study combines micronutrients, an amino acid fraction and plant signaling compounds. For reasons of commercial confidentiality, exact recipe proportions are not disclosed in the manuscript; components are described in functional groups. The laboratory equipment used included a mixing vessel, a precision balance and measuring vessels.

2.2 Methods

In laboratory preparation, micronutrient salts were added to the mixing vessel in a controlled sequence; after homogenization was achieved, the amino acid fraction and the low-dose physiological activator components were added. The visual homogeneity, sedimentation tendency, application suitability and product positioning of the mixture were evaluated.

For field validation, a three-stage protocol is proposed: a pre-frost protective application, a post-frost recovery application, and a control/comparison application. The main parameters to be measured are leaf chlorophyll index, electrolyte leakage, visual frost-damage score, shoot vitality, fruit set, leaf micronutrient analysis, and final yield/quality parameters.

2.3 Statistical Analysis

Once field data are available, analysis of variance should be performed using a factorial design incorporating treatment, dose and time factors; means should be compared using Tukey's or Duncan's test; non-parametric tests should be used where necessary for ordinal measures such as the frost-damage score.

3. RESULTS

In the laboratory mixture, micronutrients, amino acids and activator components were successfully combined within a single product family. Internal evaluation notes indicated a favourable assessment of the product's potential use in frost-related and post-stress nutrition in orchards. This finding is not sufficient on its own to support a commercial efficacy claim, but it provides a technical feasibility signal for initiating field trials.

The literature review supports three scientific rationales for this approach. First, foliar mineral applications may have measurable effects on low-temperature tolerance. Second, salicylate signaling is associated with antioxidant defence and stress-related gene expression. Third, nitrophenolate-based compounds have been linked to photosynthetic pigments and carbon assimilation. Designing these three mechanisms together with micronutrient- and amino-acid-based nutrition distinguishes this liquid fertilizer approach from conventional micronutrient fertilizers.

Table 1. Scientific rationale and proposed validation parameters for the formulation.

Component Group	Expected Function	Proposed Validation Parameter
Micronutrients	Enzyme activity, chlorophyll and nutrient balance	Leaf Zn, Mn, Fe, Cu, B, Mo analysis
Amino acid fraction	Post-stress nitrogen and metabolic support	Free amino acids, total N, growth measurements
Salicylate-based component	Antioxidant defence and stress signaling	MDA, SOD/CAT/POD, electrolyte leakage
Nitrophenolate-based component	Photosynthesis and growth activation	SPAD, Fv/Fm, biomass, shoot development

4. DİSCUSSİON

The formulation addressed in this study can be interpreted as a hybrid approach combining mineral nutrition with a biostimulant strategy. Because membrane stability, osmotic adjustment and antioxidant defence come to the forefront under frost stress, products based solely on macronutrient application may not be sufficient under all conditions. For this reason, using micronutrients together with amino acid and signaling components may provide broader physiological targets for post-stress recovery.

At the same time, salicylate, nitrophenolate and similar activator compounds are sensitive components with respect to dose, phenological timing and product regulation. In the manuscript, these components should be addressed under the assumption of controlled, low-dose and regulation-compliant use. For peer-reviewed publication, the product's effect must be demonstrated through comparison of a control, micronutrients alone, amino acids alone, and the combined formulation.

5. CONCLUSİON

This study shows that a liquid fertilizer combining micronutrients, amino acids and plant signaling compounds can be developed into a publishable manuscript addressing frost and post-stress nutrition. The current laboratory data are sufficient to support the skeleton of a full research article, but field data are required for any efficacy claim. The strongest publication framework would be a frost/stress trial comparing the combined formulation against micronutrient-only and control treatments.

Declarations

Ethics Approval: This study is a laboratory-scale fertilizer and plant nutrition formulation development study and does not involve human or animal experimentation. If a field trial is conducted on living plant material, internal institutional permits and relevant local regulatory records should be obtained prior to submission.

Author Contributions:

Burcu Köse: Project management.

Ahmet Akbulut: Experimental design, data collection and initial draft.

Gökhan Yaşar: Methodology, manuscript review, literature and analysis.

Hatice Deniz Öncel: Literature review and analysis.

Funding: This study was carried out within the scope of an in-house research and development project.

Conflict of Interest: The authors declare that this product development study is an in-house R&D activity, and that the academic interpretations presented are limited to the current experimental results and the relevant literature.

Acknowledgements: The authors thank the R&D and Antalya plant teams for their contribution to the laboratory and field planning processes.

REFERENCES

Ahmed, N., Zhang, B., Deng, L., et al. (2024). Micronutrients and their effects on horticultural crop quality, productivity and sustainability. Scientia Horticulturae, 323, 112512. https://doi.org/10.1016/j.scienta.2023.112512

Colla, G., Hoagland, L., Ruzzi, M., Cardarelli, M., Bonini, P., Canaguier, R., & Rouphael, Y. (2017). Biostimulant action of protein hydrolysates: Unraveling their effects on plant physiology and microbiome. Frontiers in Plant Science, 8, 2202. https://doi.org/10.3389/fpls.2017.02202

Donderalp, V., & Dursun, A. (2022). Improvement of frost tolerance in tomato by foliar application of potassium sulphate. Scientia Horticulturae, 295, 110868. https://doi.org/10.1016/j.scienta.2021.110868

Khan, M. I. R., Fatma, M., Per, T. S., Anjum, N. A., & Khan, N. A. (2015). Salicylic acid-induced abiotic stress tolerance and underlying mechanisms in plants. Frontiers in Plant Science, 6, 462. https://doi.org/10.3389/fpls.2015.00462

Liu, Z., et al. (2025). Compound sodium nitrophenolate improves photosynthesis and forage quality in Hemarthria compressa. Agronomy, 15(11), 2526. https://doi.org/10.3390/agronomy15112526

Yang, H., Fang, R., Luo, L., Yang, W., Huang, Q., Yang, C., Hui, W., Gong, W., & Wang, J. (2023). Uncovering the mechanisms of salicylic acid-mediated abiotic stress tolerance in horticultural crops. Frontiers in Plant Science, 14, 1226041. https://doi.org/10.3389/fpls.2023.1226041

DEVELOPMENT OF SLOW-RELEASE UAN-28, UAN-32, UAN-33 AND UAN-34 LIQUID NITROGEN FERTILIZERS: NITROGEN USE EFFICIENCY AND LOW-TEMPERATURE STABILITY

Gökhan Yaşar, Ahmet Akbulut, Deniz Öncel, Burcu Köse & Halit Duran

İGSAŞ Research and Development Unit, Türkiye

ABSTRACT

Urea ammonium nitrate (UAN) solutions are widely used liquid nitrogen fertilizers because they combine urea, ammonium and nitrate nitrogen in a homogeneous fluid phase and permit accurate metering in soil and fertigation systems. Their technical performance, however, is governed by two independent but interacting issues: nitrogen transformation after application and phase stability during storage. The urea fraction may hydrolyze rapidly and contribute to ammonia volatilization under unfavorable surface-application conditions, whereas concentrated UAN solutions can crystallize when temperature falls below their salt-out temperature. This study develops an integrated formulation and validation framework for UAN-28, UAN-32, UAN-33 and UAN-34 products designed to delay urea-N transformation while maintaining acceptable low-temperature stability. The formulation strategy is based on nitrogen mass balance, controlled urea/ammonium nitrate ratio, optional ammonium thiosulfate (ATS) addition, and evaluation of stabilizing or urease-inhibiting auxiliaries. A 5% ATS-supported design matrix calculated with 35% N ammonium nitrate, 46.6% N urea and 12% N ATS produced theoretical total N values of 32.25, 33.28 and 34.62% for the UAN-32, UAN-33 and UAN-34 candidates, respectively. The calculations show that increasing N grade is achieved mainly by reducing water from 15.77 to 9.87%, which simultaneously narrows the solution-stability window. Literature data indicate that conventional UAN-28 has a substantially lower salt-out temperature than UAN-32, while urease inhibitors such as NBPT and, under some conditions, ATS can reduce or delay ammonia loss from surface-applied UAN. Accordingly, the paper proposes a validation sequence based on ISO 23381 salt-out testing, total-N analysis, density, pH, visual clarity, cold-storage and re-dissolution observations, soil incubation, ammonia-volatilization measurements, and plant uptake/yield tests. The framework distinguishes a stabilized or enhanced-efficiency UAN from a true controlled-release fertilizer: a slow-release claim should only be made after release or transformation kinetics are experimentally demonstrated. The resulting approach provides a technically defensible basis for pilot-scale optimization of concentrated UAN products combining nitrogen-use-efficiency objectives with improved storage reliability.

Keywords: UAN, liquid nitrogen fertilizer, enhanced-efficiency fertilizer, slow release, urease inhibition, ammonium thiosulfate, nitrogen use efficiency, salt-out temperature, crystallization

INTRODUCTION

Nitrogen (N) is one of the principal nutrients controlling crop yield and quality, yet fertilizer-N efficiency is determined not only by the amount applied but also by the chemical form of N, the rate of transformation in soil, placement, moisture, temperature, pH, residue cover and the timing of crop demand. Urea-containing fertilizers are particularly sensitive to post-application hydrolysis. Urease catalyzes the conversion of urea to ammoniacal forms; during this process, transient alkalization around the fertilizer zone can increase the proportion of gaseous ammonia

and therefore the risk of N loss. This mechanism is especially relevant when urea-containing fertilizers are left on the soil surface without sufficient rainfall, irrigation or mechanical incorporation (Cantarella et al., 2018; Liu et al., 2019).

Urea ammonium nitrate solution is a useful platform for N management because it contains three agronomically relevant N pools in a single liquid product. Approximately one-half of the N in conventional UAN is commonly associated with urea, while the ammonium nitrate fraction supplies both ammonium and nitrate. The nitrate fraction is immediately mobile and plant available, ammonium can be retained temporarily by soil exchange sites before nitrification, and urea undergoes hydrolysis before entering the ammonium pool. This multi-form distribution provides flexibility for injection, banding and precise liquid application, but also means that the product cannot be evaluated as a single chemical species.

The agronomic objective of a delayed-N UAN formulation is to extend the period during which a portion of the urea-derived N remains available for crop uptake and to reduce avoidable losses. In liquid UAN, this goal is more appropriately approached through stabilization of N transformation than through a physical coating, because the product is already an aqueous solution. Urease inhibitors can temporarily slow urea hydrolysis; nitrification inhibitors can affect the subsequent conversion of ammonium to nitrate. Their performance depends strongly on soil and environmental conditions. Cantarella et al. (2018) reported that NBPT is one of the most established urease inhibitors and can substantially reduce ammonia losses from urea-based fertilizers. UAN-specific studies have also shown reductions in volatilization with NBPT-containing treatments, although the magnitude of the benefit is affected by application method and environment (Grant et al., 1996; Goos, 2013; Liu et al., 2019).

Ammonium thiosulfate (ATS) is technologically interesting because it adds both N and sulfur and can also interact with urea hydrolysis. Sullivan and Havlin (1992) demonstrated that thiosulfate oxidation products, particularly tetrathionate, can contribute to urease inhibition in soil. In a greenhouse study with surface-applied UAN, Goos (2013) reported lower ammonia losses for several additive systems, including ATS, compared with unamended UAN. However, other field observations have shown a weaker ATS response than NBPT under particular soil and climatic conditions (Grant et al., 1996). ATS should therefore be treated as a multifunctional formulation component whose agronomic effect requires direct validation rather than as a universal urease-inhibitor substitute.

A second and independent challenge is the physical stability of concentrated UAN during storage and transportation. UAN is a concentrated salt solution, and its dissolved-solids capacity decreases as temperature falls. Below the salt-out temperature, urea and/or nitrate-containing crystals may precipitate, producing sediment, concentration gradients, blocked transfer systems and non-uniform product application. Commercial guidance places the salt-out temperature of UAN-28 near -18 °C and conventional UAN-32 near approximately -2 to 0 °C, depending on composition and product specification. These data illustrate the fundamental trade-off: higher nutrient concentration reduces the quantity of water transported per unit N, but also decreases the margin against low-temperature crystallization.

For liquid fertilizers, ISO 23381:2020 specifically addresses determination of the salt-out (crystallization) temperature. This is more directly relevant to UAN product development than general freezing-point methods developed for other aqueous systems. An R&D program for high-analysis UAN should therefore separate the concepts of freezing, supercooling, first-crystal appearance, salt-out temperature and re-dissolution behavior. A formulation that remains visually clear for a short period at a target temperature may still crystallize during prolonged storage, while a product that forms crystals may remain commercially manageable if the crystals readily re-dissolve under defined recirculation and warming conditions.

The objective of the present study is to convert these agronomic and physicochemical requirements into a unified development framework for UAN-28, UAN-32, UAN-33 and UAN-

34. The specific aims are: (i) to establish a mass-balance approach for target N grades; (ii) to evaluate an ATS-supported composition matrix for UAN-32/33/34; (iii) to identify the consequences of decreasing water content on low-temperature stability; (iv) to define the analytical and agronomic tests required before a slow-release or enhanced-efficiency claim is made; and (v) to provide a pilot-scale decision structure suitable for subsequent laboratory and field validation.

MATERIAL AND METHOD

Materials and formulation components

The formulation framework uses urea, ammonium nitrate (AN) and process water as the principal UAN components. For calculation purposes, the theoretical N content of urea was taken as 46.6% and that of the AN raw material as 35.0%. ATS, when used, was treated as a 12% N sulfur-containing liquid component. Ammonium sulfate (AS) may be considered in exploratory low-temperature or sulfur-enrichment studies, but it was not included in the principal UAN-32/33/34 design matrix evaluated here. The actual certificate-of-analysis values of all raw materials should replace theoretical values before pilot production.

The slow-release concept was operationally defined as delayed N transformation rather than as a presumed release claim. Candidate auxiliaries can include urease inhibitors, nitrification inhibitors, or chemically compatible N-containing stabilizer systems. Because the present source dataset does not specify final commercial doses for these auxiliaries, no unverified dose is assigned in this manuscript. Each additive must instead be tested at its supplier-recommended active-ingredient range and evaluated for compatibility, storage stability, pH, phytotoxicity and agronomic response.

Table 1. Principal formulation components and their technical roles.

Component	Primary function	Development relevance
Urea	Amide-N source	Main N fraction targeted for delayed hydrolysis and improved N-use efficiency.
Ammonium nitrate	Ammonium- and nitrate-N source	Provides rapid-availability N forms and contributes strongly to ionic strength and salt-out behavior.
Process water	Solvent phase	Controls concentration, density, viscosity, heat balance and crystallization margin.
ATS	N + S liquid component	Provides sulfur and may influence urease activity; its effect on crystallization must be measured in the complete formulation.
AS (optional)	N + S solid component	Potential sulfur and ionic-composition modifier; requires separate solubility and salt-out evaluation.
Urease inhibitor / stabilizer	Delays urea hydrolysis	Candidate enhanced-efficiency component; must be validated by soil incubation and ammonia-loss tests.
Nitrification inhibitor (optional)	Delays NH4+ oxidation	Potential complementary strategy; should not be assumed to reduce ammonia volatilization.

Formulation design and nitrogen mass balance

The first design step was selection of the target nominal N grade. UAN-28 was used as the low-temperature reference class because its larger water fraction provides a wider solubility margin. UAN-32 represents the common high-analysis commercial grade, whereas UAN-33 and UAN-34 were treated as progressively more concentrated development targets. The total N content was calculated from the mass fraction and N assay of each N-bearing component according to Eq. (1):

$$Ntotal\ (\%) = 0.466 \cdot murea + 0.350 \cdot mAN + 0.120 \cdot mATS + fAS\text{-}N \cdot mAS$$

where m is the mass percentage of each component in the finished product and fAS-N is the measured N fraction of ammonium sulfate when AS is included. For AN, one-half of the AN-derived N was assigned to nitrate-N and one-half to ammoniacal-N for theoretical N-form distribution. ATS-derived N was assigned to ammoniacal-N. Final grade designation must be based on laboratory analysis rather than calculation alone.

Table 2. Starting composition matrix and theoretical total nitrogen. Values are wt.% of finished product.

Specification	NH4NO3	Urea	ATS	H2O	Theoretical total N
UAN-28 reference*	40.00	30.00	0.00	30.00	27.98
UAN-32 + ATS	45.43	33.80	5.00	15.77	32.25
UAN-33 + ATS	46.73	35.03	5.00	13.24	33.28
UAN-34 + ATS	48.66	36.47	5.00	9.87	34.62

**UAN-28 is shown as a conventional reference composition for comparison; the UAN-32/33/34 + ATS values are the source formulation matrix evaluated in this study.*

Table 3. Theoretical distribution of nitrogen forms in the starting matrix (percentage points of product mass).

Specification	Urea-N	Ammoniacal-N	Nitrate-N	Total N
UAN-28 reference	13.98	7.00	7.00	27.98
UAN-32 + ATS	15.75	8.55	7.95	32.25
UAN-33 + ATS	16.32	8.78	8.18	33.28
UAN-34 + ATS	17.00	9.12	8.52	34.62

Laboratory preparation sequence

Laboratory preparation is proposed as a controlled dissolution procedure. Process water is charged first and agitation is started. The solution is then brought to approximately 35-55 °C, avoiding unnecessary overheating. Urea is introduced gradually until a homogeneous solution is obtained, followed by controlled AN addition while temperature, visual clarity and pH are monitored. ATS and other compatible liquid auxiliaries are added only after the main UAN phase is fully dissolved. The batch is then adjusted to its target mass, mixed to homogeneity and filtered when required before analytical sampling.

For pilot work, the procedure should be managed under the facility's process-safety rules for ammonium-nitrate-containing systems. Raw-material contamination, incompatible metals, unintended organic contamination, local overheating and uncontrolled evaporation can alter both safety and product composition. The purpose of the 35-55 °C range is to support dissolution, not to define a fixed industrial set point; the minimum temperature that provides complete dissolution and reproducible product quality should be preferred.

Low-temperature stability and crystallization testing

Salt-out temperature should be determined according to ISO 23381:2020, which is specifically intended for liquid fertilizers. For development screening, this measurement should be supplemented with fixed-temperature storage at selected temperatures relevant to the intended market. The original development plan proposes observations at 0, -5 and -10 °C. For each condition, the recorded endpoints should include time to first visible crystal, crystal abundance, sedimentation, phase separation, viscosity change, and the temperature/time required for complete re-dissolution after warming and recirculation.

The terms "freezing point" and "salt-out temperature" should not be used interchangeably in reporting. UAN can precipitate dissolved fertilizer salts before the bulk aqueous phase behaves as a fully frozen system. Accordingly, the primary product-development endpoint is salt-out/crystallization behavior. ASTM D1177 can provide a general conceptual reference for laboratory freezing-point observation in aqueous systems, but ISO 23381 is the more appropriate cited method for liquid fertilizer crystallization.

Nitrogen-transformation and agronomic validation

The enhanced-efficiency claim requires an untreated UAN control and at least one candidate stabilized formulation. Soil incubation should quantify the persistence of urea-N and the accumulation of ammoniacal and nitrate N over time. A parallel volatilization system should quantify cumulative ammonia loss. Closed or semi-closed chambers with acid traps may be used provided the method is validated and identical conditions are applied to all treatments. Measurements should be conducted under controlled soil moisture, temperature and pH conditions that are relevant to the intended use environment.

Pot or field trials should then compare plant N uptake, above-ground biomass, chlorophyll or canopy indicators when appropriate, final yield, and N-use-efficiency indices. Application method must be treated as a major factor because surface-applied UAN has a different volatilization risk than injected or incorporated UAN. A treatment that reduces ammonia loss under surface application may show little yield benefit when the same product is immediately incorporated into soil, as demonstrated in UAN field research (Liu et al., 2019).

Quality-control parameters and data evaluation

For replicated laboratory or agronomic trials, treatment means should be evaluated using an appropriate experimental design and inferential statistics. A randomized complete block design is suitable for many pot and field experiments, while completely randomized designs may be adequate for homogeneous laboratory incubations. Replication number, model structure, significance threshold and post-hoc comparison method must be reported with the actual dataset; they are not fixed in the present formulation-design dataset.

Table 4. Minimum analytical and performance validation plan for candidate UAN products.

Parameter	Purpose	Recommended evaluation
Total N (%)	Confirm grade and mass balance	Validated total-N method (e.g., Kjeldahl/Dumas or an equivalent fertilizer method).
Density at 20 °C	Batch consistency and logistics	Calibrated density measurement at controlled temperature.
pH	Chemical stability and application compatibility	Direct pH measurement with calibrated electrode.
Clarity / sediment	Single-phase quality	Visual assessment before and after cold storage; filtration record where applicable.
Salt-out temperature	Primary cold-stability endpoint	ISO 23381:2020.
Cold-storage stability	Longer-term practical risk	Fixed-temperature holds at 0, -5 and -10 °C or market-specific conditions.
Re-dissolution behavior	Recoverability after crystallization	Record warming temperature, time and mixing requirement.
Urea hydrolysis	Evidence of delayed transformation	Controlled soil incubation versus untreated UAN.
NH3 volatilization	Evidence of N-loss reduction	Validated chamber/trap method versus untreated UAN.
Plant N uptake / yield	Agronomic confirmation	Pot or replicated field trial with suitable statistical analysis.

RESULTS AND DISCUSSION

Calculated formulation performance and nitrogen balance

The ATS-supported starting matrix produced theoretical total-N values of 32.25, 33.28 and 34.62% for the UAN-32, UAN-33 and UAN-34 candidates, respectively (Table 2). The UAN-32 and UAN-33 candidates are therefore close to their nominal grade designations on a theoretical basis. The UAN-34 candidate, however, calculates to 34.62% N with the assumed raw-material assays. This is an important formulation-development result: the candidate should either be rebalanced toward the desired nominal specification or intentionally treated as a higher-analysis experimental grade after laboratory confirmation. The value should not be silently rounded to 34.0% N.

The N-form calculations also show that approximately one-half of the total N remains in the urea pool across the matrix, while the remainder is divided between ammoniacal and nitrate N. In the UAN-32 + ATS candidate, the calculated urea-N, ammoniacal-N and nitrate-N values are 15.75, 8.55 and 7.95 percentage points, respectively. ATS contributes 0.60 percentage point N while increasing the ammoniacal fraction. This distribution retains the functional logic of

UAN: an immediately available nitrate fraction, an ammonium fraction and a larger urea fraction that is the principal target for delayed hydrolysis.
The most consequential compositional trend is the reduction in water. From UAN-32 + ATS to UAN-34 + ATS, the water fraction decreases from 15.77 to 9.87%. This raises nutrient density but also increases dissolved-solids loading and decreases the thermodynamic margin against crystallization. Therefore, a high nominal N value cannot be treated as an independent optimization objective; the grade, cold stability, density, viscosity, pumpability and re-dissolution behavior must be optimized as a coupled system.

Low-temperature stability: implications of concentration and multicomponent formulation

Commercial reference data illustrate the expected concentration effect. UAN-28 is commonly reported with a salt-out temperature near -18 °C, whereas UAN-32 is typically near -2 to 0 °C, with the exact value depending on composition and product specification. The broader low-temperature margin of UAN-28 is therefore a useful reference when screening additives or process changes. In contrast, UAN-33 and UAN-34 cannot be assigned a reliable salt-out temperature from grade number alone; their values must be measured because small changes in water, AN/urea ratio and additional salts can substantially alter crystallization behavior.
The 5% ATS matrix is particularly important in this respect. ATS adds a third major dissolved salt system and contributes useful sulfur, but the UAN-32 + ATS formulation contains only 15.77% water, considerably less than a conventional UAN-32 reference composition. Consequently, any favorable multicomponent/eutectic effect of ATS must be large enough to offset the reduced water fraction if a lower crystallization temperature is to be achieved. The formulation therefore should not be described as cold-stable merely because ATS is present. Its actual salt-out temperature and storage behavior are experimental questions.

Table 5. Low-temperature interpretation framework for the UAN development series.

Grade / candidate	Reference or design information	Development interpretation
UAN-28	Literature salt-out approximately -18 °C	Useful low-temperature reference; larger water fraction gives broader stability margin.
Conventional UAN-32	Literature salt-out approximately -2 to 0 °C	Commercial benchmark for concentrated UAN.
UAN-32 + 5% ATS	15.77% water; 32.25% theoretical N	Must be measured: added salt complexity may help or hurt crystallization depending on full composition.
UAN-33 + 5% ATS	13.24% water; 33.28% theoretical N	Narrower expected stability window; prolonged cold-storage testing required.
UAN-34 + 5% ATS	9.87% water; 34.62% theoretical N	Highest crystallization-risk candidate in the present matrix; grade balance and salt-out behavior are critical.

Historical liquid-fertilizer work shows that modifying the ionic composition can lower crystallization temperature in some UAN-containing systems. Sulfur-containing UAN formulations based on ammonium sulfate have been reported with lower crystallization

temperatures when the overall composition and water content were appropriately balanced, and urea-formaldehyde-containing solutions have also been described as depressing salt-out temperature in certain high-N liquid blends. Such examples support the feasibility of formulation engineering, but they cannot be transferred directly to the present system without testing because the phase behavior is composition specific.

Delayed urea transformation and ammonia-loss control

The agronomic part of the concept is supported by a substantial body of work on urease inhibition. NBPT delays urea hydrolysis and thereby reduces the rapid local increase in ammoniacal N and pH that promotes ammonia volatilization. A broad review by Cantarella et al. (2018) reported a strong average reduction in ammonia loss from NBPT-treated urea, although the response varied with crop and environment. The mechanism is especially relevant to UAN because a major fraction of its N is urea-N.

UAN-specific evidence confirms that formulation additives can alter ammonia loss. Goos (2013) compared several additives in greenhouse studies and reported average 14-day ammonia-loss reductions relative to untreated UAN of 40% with ATS, 40% with calcium thiosulfate, 51% with an NBPT-containing product and 65% with NBPT plus calcium thiosulfate. However, the literature is not uniform. Grant et al. (1996) found NBPT effective with UAN under zero-till conditions while ATS had little influence in their particular field microplots. These contrasting results emphasize that ATS efficacy depends on soil and environmental conditions and that formulation screening must be followed by site-relevant validation.

The chemistry proposed for ATS is also different from direct NBPT inhibition. Sullivan and Havlin (1992) showed that thiosulfate itself did not directly inhibit purified urease to the same extent as oxidation products formed in soil and identified tetrathionate as an important inhibitory species. This helps explain why ATS performance can vary with soil moisture, temperature, pH and oxidation conditions. In practical product development, ATS should therefore be evaluated simultaneously as a sulfur nutrient, an ionic formulation component and a potentially variable contributor to delayed urea hydrolysis.

Slow-release versus stabilized UAN: claim definition

A key scientific issue is terminology. A liquid UAN containing a urease inhibitor does not automatically become a classical controlled-release fertilizer in the same sense as a coated granule or a slowly soluble N compound. The more defensible initial classification is an enhanced-efficiency or stabilized UAN with delayed N transformation. The term “slow-release characteristic” can be used as a development objective, but a final slow-release claim requires time-resolved evidence showing that the relevant N fraction is transformed or becomes plant available more slowly than the untreated control.

This distinction improves the quality of the research design. If the only demonstrated result is reduced ammonia volatilization, the supported claim is N-loss mitigation. If soil incubation additionally demonstrates slower urea disappearance or delayed mineral-N conversion, the supported claim expands to delayed transformation. If plant and release-kinetic data show prolonged N availability without yield or phytotoxicity penalties, a stronger slow-release or controlled-availability claim may then be justified. The manuscript therefore treats claim strength as an evidence hierarchy rather than as an assumption built into the formulation name.

Table 6. Evidence required for progressively stronger product claims.

Claim level	Minimum evidence	Interpretation
Physically stable UAN	N grade, pH, density, clarity, salt-out/cold-storage data	Supports product handling and storage specification only.
Stabilized / enhanced-efficiency UAN	Above + lower NH3 loss and/or altered N-transformation kinetics vs. untreated UAN	Supports reduced-loss or delayed-transformation positioning.
Slow-release characteristic	Above + time-resolved release/transformation and plant-availability evidence	Supports a measured slower availability profile under defined conditions.
Agronomically superior product	Above + replicated plant uptake, yield and NUE response	Supports crop-performance claims for the tested use conditions.

Integrated product-development decision path

The results of the calculation and literature assessment support a sequential rather than one-step development strategy. First, each candidate must meet its N-grade target after real raw-material assays are inserted into the mass balance. Second, the candidate must remain chemically and physically compatible at ambient temperature. Third, salt-out temperature and extended cold-storage behavior must be determined. Only formulations that pass these physical screens should proceed to detailed N-transformation and agronomic testing. This order prevents resources being spent on biologically promising additives that produce an unstable commercial liquid.

UAN-28 is well suited to early compatibility and inhibitor screening because its higher water content reduces the risk that a negative result is caused only by inadequate solubility. UAN-32 should then serve as the principal commercial benchmark. UAN-33 and UAN-34 should be treated as advanced high-analysis variants and should not advance unless their cold stability, re-dissolution behavior and analytical N values remain acceptable. Within this sequence, ATS-containing and non-ATS controls are required to separate sulfur-nutrition effects from urease-inhibition and phase-stability effects.

The final product decision should be based on a multi-criteria matrix rather than on a single freezing or N-value result. A technically successful candidate should combine: target total N; reproducible N-form distribution; acceptable pH and density; low sediment formation; sufficiently low salt-out temperature for the intended logistics chain; complete and practical re-dissolution after cold exposure; reduced ammonia loss or delayed urea transformation versus untreated UAN; and no adverse effect on crop performance or application equipment.

CONCLUSIONS

This study converts an initial UAN formulation concept into a full technical framework for developing UAN-28, UAN-32, UAN-33 and UAN-34 liquid nitrogen fertilizers with delayed N transformation and improved low-temperature reliability. The calculated ATS-supported matrix gives 32.25, 33.28 and 34.62% total N for the UAN-32, UAN-33 and UAN-34 candidates, respectively. The UAN-34 candidate therefore requires particular attention to grade adjustment and analytical confirmation rather than simple nominal labeling.

The formulation calculations identify water content as the central physical trade-off. Increasing the target N grade from UAN-32 to the high-analysis UAN-34 candidate reduces water from 15.77 to 9.87%, which is expected to narrow the crystallization-stability window. ATS may provide agronomic sulfur value and may influence urea hydrolysis, but its net effect on cold stability cannot be inferred from composition alone. Salt-out temperature must be measured on the finished formulation, preferably using ISO 23381:2020, and complemented by prolonged cold-storage and re-dissolution tests.

From an agronomic perspective, the literature supports the use of urease-inhibition strategies to reduce ammonia loss from urea-containing fertilizers, including UAN, but treatment response is sensitive to soil, climate and application method. The most scientifically defensible development pathway is therefore to describe early candidates as stabilized or enhanced-efficiency UAN and reserve a slow-release claim for formulations that demonstrate delayed transformation/release kinetics and sustained plant availability in comparative experiments.

For subsequent pilot and field development, the highest-priority measurements are real total N, density, pH, salt-out temperature, 0/-5/-10 °C storage behavior, re-dissolution, urea-hydrolysis kinetics, cumulative ammonia volatilization, plant N uptake and yield. Integrating these endpoints provides a robust decision basis for selecting a commercially viable UAN formulation that improves nitrogen-use efficiency without sacrificing storage and handling performance.

REFERENCES

ASTM International. 2026. ASTM D1177-22(2026), Standard Test Method for Freezing Point of Aqueous Engine Coolants. ASTM International, West Conshohocken, PA, USA. doi:10.1520/D1177-22R26.

Cantarella, H., Otto, R., Soares, J. R., Silva, A. G. B. 2018. Agronomic efficiency of NBPT as a urease inhibitor: A review. Journal of Advanced Research, 13: 19-27. doi:10.1016/j.jare.2018.05.008.

Goos, R. J. 2013. Effects of fertilizer additives on ammonia loss after surface application of urea-ammonium nitrate fertilizer. Communications in Soil Science and Plant Analysis, 44(12): 1909-1917. doi:10.1080/00103624.2013.783061.

Grant, C. A., Brown, K. R., Bailey, L. D., Jia, S. 1996. Volatile losses of NH3 from surface-applied urea and urea ammonium nitrate with and without the urease inhibitors NBPT or ammonium thiosulphate. Canadian Journal of Soil Science, 76(3): 417-419. doi:10.4141/cjss96-050.

International Organization for Standardization. 2020. ISO 23381:2020, Determination of salt out (crystallization) temperature of liquid fertilizers. ISO, Geneva, Switzerland.

Jones, C. A., Koenig, R. T., Ellsworth, J. W., Brown, B. D., Jackson, G. D. 2013. Management of urea fertilizer to minimize volatilization. Montana State University Extension, Bozeman, MT, USA.

Liu, S., Wang, X., Yin, X., Savoy, H. J., McClure, A., Essington, M. E. 2019. Ammonia volatilization loss and corn nitrogen nutrition and productivity with efficiency enhanced UAN and urea under no-tillage. Scientific Reports, 9: 6610. doi:10.1038/s41598-019-42912-5.

Matczuk, D., Skiba, U., Matyjaszczyk, E. 2021. Effectiveness of the use of urease inhibitors in agriculture: A review. International Agrophysics, 35: 197-208.

Sullivan, D. M., Havlin, J. L. 1992. Thiosulfate inhibition of urea hydrolysis in soils: Tetrathionate as a urease inhibitor. Soil Science Society of America Journal, 56(3): 957-960. doi:10.2136/sssaj1992.03615995005600030045x.

UNIDO and International Fertilizer Development Center. 1998. Fertilizer Manual. Kluwer Academic Publishers, Dordrecht, The Netherlands.

University of Tennessee Extension. 2018. Enhanced-efficiency nitrogen fertilizer as a tool to control nitrogen losses and improve nitrogen use efficiency. University of Tennessee Institute of Agriculture, Knoxville, TN, USA.
Yara North America, Inc. UAN-32 Urea Ammonium Nitrate Solution 32-0-0: Technical Bulletin. Typical analysis and salting-out temperature data.
US Patent 4,239,522. 1980. Fertilizer solutions containing sulfur and having low crystallization temperature.
US Patent Application US20090133457A1. 2009. High nitrogen liquid fertilizer.

DEVELOPMENT OF NOVEL FERTILIZER SYSTEMS FROM DOLOMITE BY NITRIC ACID AND MAGNESIUM-BASED PROCESSING ROUTES

Gökhan Yaşar, Ahmet Akbulut, Deniz Öncel, Burcu Köse & Halit Duran

İGSAŞ Research and Development Unit, Türkiye

ABSTRACT

Dolomite [CaMg(CO3)2] is an abundant carbonate mineral that can serve not only as a liming material but also as a local feedstock for soluble calcium- and magnesium-containing fertilizers. This paper develops a process-oriented framework for converting dolomite into value-added fertilizer intermediates through two complementary routes: direct nitric-acid digestion of raw dolomite to obtain mixed calcium-magnesium nitrate liquor, and a calcination-assisted route designed to facilitate selective magnesium hydroxide recovery and subsequent magnesium oxide production. The source process concept combines particle-size control, optional calcination, nitric-acid dissolution, pH-controlled precipitation, filtration, recycle of nitrate-containing mother liquor, and final liquid or suspension formulation. Stoichiometric calculations for pure dolomite show that 100 kg of CaMg(CO3)2 requires 136.69 kg pure HNO3 and can theoretically generate 88.98 kg anhydrous Ca(NO3)2 and 80.43 kg anhydrous Mg(NO3)2 while releasing 47.73 kg CO2. Complete calcination would yield approximately 30.41 kg CaO and 21.86 kg MgO equivalents per 100 kg pure dolomite. These calculations are design values and must be corrected for ore purity, acid excess, free water, hydration state and process losses. Recent literature demonstrates that uncalcined dolomite can be digested with nitric acid and subsequently neutralized with ammonia to produce liquid N-Ca-Mg fertilizers, while earlier patent literature shows that nitrate-containing slaking media can improve magnesium hydroxide filterability in dolomite-based separation processes. On this basis, the paper proposes an experimental matrix covering raw versus calcined dolomite, particle size, acid stoichiometry, reaction temperature, pH, residence time, precipitation reagent, cake washing and mother-liquor recycle. Recommended validation includes XRD, XRF/ICP-OES, TGA/DSC, SEM-EDS, total N, Ca, Mg, heavy metals, density, pH, crystallization behavior, filtration rate and agronomic tests. The resulting framework provides a technically defensible basis for laboratory and pilot-scale development of nitrate-based liquid fertilizers, magnesium hydroxide suspensions and MgO precursors from dolomite without presenting unverified target values as experimental results.

Keywords: Dolomite, nitric acid, calcium nitrate, magnesium nitrate, magnesium hydroxide, liquid fertilizer, filtration, calcination, process development

INTRODUCTION

Calcium (Ca) and magnesium (Mg) are essential plant nutrients with distinct physiological roles. Magnesium is the central atom of chlorophyll and participates in enzyme activation, energy transfer and carbon assimilation, whereas calcium contributes to cell-wall structure, membrane stability, root development and the quality of many horticultural crops. The agronomic value of Ca and Mg therefore depends not only on total nutrient content but also on mineral solubility, delivery route and the chemical environment in which the nutrients are applied.

Dolomite is a double carbonate commonly represented as CaMg(CO3)2. Pure dolomite contains, on a theoretical oxide-equivalent basis, approximately 30.41% CaO and 21.86%

MgO, with the remainder corresponding largely to CO2 released during complete thermal decomposition (Olszak-Humienik & Jablonski, 2015). Natural ores deviate from this ideal composition because calcite, silica, iron-bearing phases, aluminosilicates and trace elements may be present. These impurities are important for fertilizer development because acid digestion can transfer both nutrients and undesirable elements into solution.

Natural dolomite can be applied directly as a liming or soil-conditioning material, but the carbonate lattice dissolves comparatively slowly under many soil conditions. Chemical conversion offers a route to transform the mineral into more soluble nitrate salts or into Mg(OH)2/MgO products with controlled particle properties. Acid-leaching studies have already demonstrated that dolomite can be converted to magnesium salts, while Turkish work by Yildirim and Akarsu (2010) showed that high-purity MgO can be produced through a leach-precipitation-pyrohydrolysis route. Sulfuric-acid processing has likewise been used to produce magnesium sulfate heptahydrate, with particle size, acid ratio, temperature and filtration identified as critical variables (Rashad & Baioumy, 2005).

Nitric acid is particularly attractive in a fertilizer-oriented flowsheet because nitrate introduced during mineral dissolution remains a plant nutrient rather than a non-fertilizer counter-ion. Recent research demonstrated the production of liquid nitrogen-calcium-magnesium fertilizers by digesting finely ground, uncalcined dolomite with nitric acid, neutralizing the acidic liquor with ammonia and adding nitrogenous components (Didžiulytė & Šlinkšienė, 2025). Historical patent literature also describes the simultaneous production of magnesia and calcium nitrate from dolomite and highlights a persistent industrial challenge: Mg(OH)2 precipitates may be difficult to filter unless slurry conditioning, particle size and the ionic composition of the mother liquor are controlled (DE830943C; DE1912865A1; US2912306A).

The present work therefore treats dolomite conversion as a fertilizer-process design problem rather than as a single reaction. The objective is to define a laboratory-to-pilot framework for (i) direct production of Ca/Mg nitrate fertilizer liquor, (ii) selective recovery of magnesium hydroxide as a suspension or MgO precursor, and (iii) integration of the calcium- and nitrogen-rich mother liquor into fertilizer products. The study expands the initial project draft with stoichiometric mass balances, a route-comparison matrix, analytical requirements, a filtration strategy, process risks and a structured experimental validation plan. Because the project is still at the process-development stage, calculated and literature-supported values are clearly distinguished from future experimental results.

MATERIAL AND METHOD

Materials and raw-material characterization

The primary raw material is dolomite ore. Before reaction testing, each ore lot should be homogenized, dried to constant mass where appropriate, crushed and milled to defined size fractions. The minimum characterization set should include XRF or wet-chemical major-element analysis, loss on ignition (LOI), XRD phase identification and ICP-OES or equivalent analysis for Ca, Mg, Fe, Al, Mn and regulated trace elements. TGA/DSC is recommended to identify the actual decomposition profile of the selected ore because calcination behavior depends on impurity content, particle size, CO2 partial pressure and heating history.

Process reagents include nitric acid, deionized water, ammonia solution and/or sodium hydroxide for pH control and Mg(OH)2 precipitation. Calcium nitrate solution or nitrate-rich wash water is included as a potential slaking/conditioning medium for the calcined route. Antifoam may be used during carbonate digestion because rapid CO2 evolution can cause severe foaming. Flocculant should be screened only after baseline filtration behavior has been established so that any improvement can be attributed to a defined mechanism.

Table 1. Main materials and their intended process functions.

Material	Primary role	Critical quality / control point
Dolomite ore	Ca and Mg source	CaO/MgO equivalent, mineralogy, LOI, Fe/Al/Si, heavy metals, particle size
Nitric acid	Carbonate/oxide dissolution and nitrate source	Assay, density, acid feed rate, stoichiometric excess
Ammonia solution	Neutralization and Mg(OH)2 precipitation option	NH3 assay, pH endpoint, residual ammonium
Sodium hydroxide	Alternative Mg(OH)2 precipitant	NaOH assay, Na introduction into product liquor
Calcium nitrate liquor / wash water	Slaking or slurry-conditioning medium	Ca(NO3)2 concentration, recycle impurity build-up
Deionized water	Dissolution, washing and formulation	Conductivity and water balance
Antifoam / flocculant	Optional process aids	Compatibility, dose-response and fertilizer acceptability

Particle-size preparation

The source process draft proposes comparison of controlled particle-size fractions and cites a sub-0.84 mm target for some calcined-dolomite filtration concepts. The experimental plan should therefore include at least three fractions rather than treating a single grind as optimal. A practical screening set is <0.25 mm, 0.25-0.50 mm and 0.50-0.84 mm. Finer material should increase reactive surface area during acid digestion, but excessive fines can increase slurry viscosity and produce compact, poorly permeable filter cakes. Particle size must consequently be optimized jointly with reaction conversion and filtration rate.

Route A: direct nitric-acid digestion of raw dolomite

For the direct fertilizer route, raw dolomite is charged to a temperature-controlled, agitated reactor and nitric acid is added gradually to control foaming and heat release. The main idealized reaction is:

$$CaMg(CO3)2 + 4HNO3 \rightarrow Ca(NO3)2 + Mg(NO3)2 + 2CO2\uparrow + 2H2O \quad (1)$$

The reaction should be operated as an acid-digestion experiment with measured rather than assumed endpoints. Variables include acid concentration, acid/dolomite stoichiometric ratio, temperature, particle size and residence time. The initial source draft proposed 50-75 °C as a reaction window. A recent fertilizer study provides a useful lower-temperature reference: uncalcined dolomite (<0.25 mm) was decomposed with 45% HNO3 for approximately 50 min with the maximum temperature kept below 50 °C, followed by filtration and ammonia neutralization (Didžiulytė & Šlinkšienė, 2025). Accordingly, the present paper treats 35-75 °C as a screening space rather than declaring one temperature as optimum before testing.

Route B: calcination-assisted conversion and magnesium separation

The calcination-assisted route is intended to increase reactivity and create an oxide-rich intermediate. Complete idealized decomposition is represented by:

$$CaMg(CO3)2 \rightarrow CaO + MgO + 2CO2\uparrow \quad (2)$$

The original process draft proposed 1150-1450 °C as a screening range. This high-temperature range should not be adopted uncritically as the default operating condition. Thermal literature shows that dolomite decomposition is strongly dependent on atmosphere and mineralogy and that oxide formation occurs at substantially lower temperatures in many systems; temperatures that are unnecessarily high may increase energy demand and sintering. Therefore, the recommended laboratory design is to determine the ore-specific TGA/DSC decomposition profile first and then compare a lower calcination window (for example 800-1050 °C) with a limited high-temperature condition from the original project concept. The key output is not furnace temperature itself, but conversion, residual carbonate, oxide reactivity, specific surface behavior and downstream filtration performance.

Calcined solids can be slaked or conditioned in water, calcium nitrate solution or recycled nitrate-containing wash liquor. Historical dolomite patents report that nitrate-containing slaking media can alter the physical form of hydrated solids and improve Mg(OH)2 filterability. This concept will be treated as an experimental hypothesis rather than as an assumed benefit.

Nitric-acid conversion of calcined dolomite

The idealized reaction of the calcined CaO-MgO mixture with nitric acid is:

$$CaO + MgO + 4HNO3 \rightarrow Ca(NO3)2 + Mg(NO3)2 + 2H2O \quad (3)$$

Compared with raw-carbonate digestion, the calcined route eliminates reaction CO2 during the acid step but shifts CO2 release to the furnace and adds a substantial energy requirement. This trade-off should be quantified experimentally through acid consumption, conversion, residence time, filtration behavior and product concentration.

Selective magnesium hydroxide precipitation

Magnesium can be recovered from nitrate liquor by increasing pH. With sodium hydroxide, the simplified precipitation reaction is:

$$Mg(NO3)2 + 2NaOH \rightarrow Mg(OH)2\downarrow + 2NaNO3 \quad (4)$$

NaOH provides straightforward pH control but transfers sodium nitrate to the liquid phase. For a fertilizer plant this may be undesirable depending on the final product specification and sodium limits. Ammonia therefore deserves parallel evaluation because it introduces nitrogen rather than sodium. A simplified representation is:

$$Mg(NO3)2 + 2NH3 + 2H2O \rightarrow Mg(OH)2\downarrow + 2NH4NO3 \quad (5)$$

The ammonia route can create an ammonium-nitrate-rich mother liquor with direct fertilizer value, but precipitation chemistry is affected by ammonium concentration, ionic strength and pH. The process must therefore be optimized experimentally. The source draft proposed pH 8.5-10.5; this range is retained as a screening interval, with pH titration curves and dissolved Mg/Ca analyses used to determine the actual selectivity window.

Theoretical mass balance

Stoichiometric calculations were performed for ideal CaMg(CO3)2 using molar masses of 184.399 g mol−1 for dolomite and 63.012 g mol−1 for HNO3. These values provide a transparent basis for acid planning and theoretical yields, but do not account for ore impurities, incomplete conversion, hydrates, entrained mother liquor or process losses.

Table 2. Theoretical material balance for 100 kg of pure dolomite.

Item	Theoretical value	Interpretation
Pure HNO3 requirement	136.69 kg	4 mol HNO3 per mol dolomite
56% HNO3 solution equivalent	244.08 kg	Stoichiometric solution mass; operating excess not included
65% HNO3 solution equivalent	210.29 kg	Stoichiometric solution mass; operating excess not included
Ca(NO3)2, anhydrous equivalent	88.98 kg	Theoretical calcium-nitrate salt basis
Mg(NO3)2, anhydrous equivalent	80.43 kg	Theoretical magnesium-nitrate salt basis
CO2 released in raw-acid route	47.73 kg	Gas load from carbonate decomposition
CaO after complete calcination	30.41 kg	Oxide-equivalent fraction of pure dolomite
MgO after complete calcination	21.86 kg	Oxide-equivalent fraction of pure dolomite
Total calcined oxides	52.27 kg	Ideal residual solid after complete CO2 removal
Mg(OH)2 theoretical precipitate	31.63 kg	If all Mg is selectively recovered as Mg(OH)2
Pure NaOH for full Mg precipitation	43.38 kg	Stoichiometric value for Eq. 4
Pure NH3 for full Mg precipitation	18.47 kg	Stoichiometric value for Eq. 5

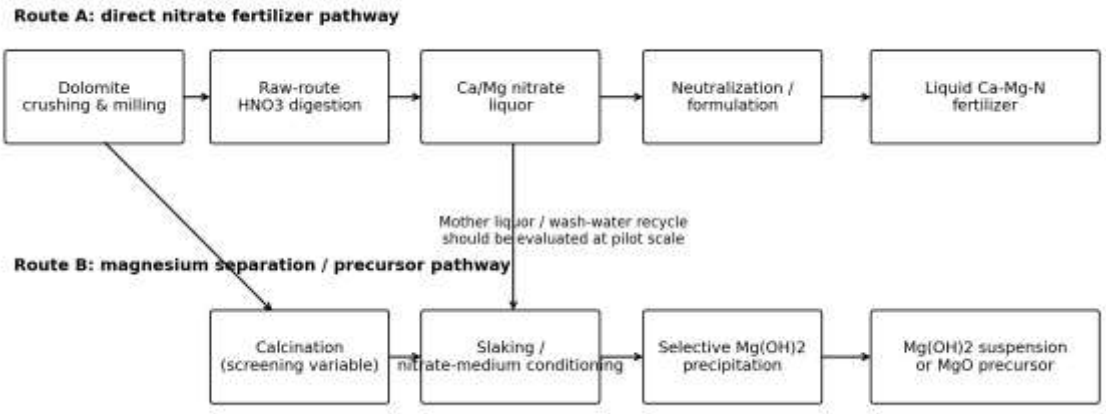

Figure 1. Proposed integrated process routes for dolomite-derived fertilizer products. Route A prioritizes direct nitrate-fertilizer liquor; Route B adds calcination/slaking and selective magnesium recovery.

Experimental design and process variables

The project should be executed as a staged design rather than a full-factorial experiment from the first batch. Stage 1 establishes raw-material variability and direct-acid baseline behavior. Stage 2 compares raw and calcined routes. Stage 3 focuses on Mg(OH)2 selectivity and filtration. Stage 4 integrates the best conditions into fertilizer formulations and agronomic validation. Each quantitative laboratory condition should be performed with sufficient replication for statistical evaluation after the screening stage.

Table 3. Proposed laboratory screening matrix.

Factor	Suggested screening levels	Primary responses
Dolomite condition	Raw; calcined at ore-specific lower window; selected high-temperature condition	Conversion, acid demand, Ca/Mg recovery
Particle size	<0.25; 0.25-0.50; 0.50-0.84 mm	Dissolution time, slurry rheology, filtration
HNO3 concentration	45%; 56%; 65% or plant-available grades	Reaction control, final concentration, safety
Acid stoichiometry	100%; 110%; 120-140% of calculated demand	Residual solids, free acidity, impurity dissolution
Reaction temperature	35; 50; 65; 75 °C screening	Conversion, foaming, residence time
Residence time	15; 30; 50/60; 90 min	Approach to dissolution plateau
Precipitation reagent	NaOH; NH3 solution	Mg recovery, Ca carryover, mother-liquor value
Precipitation pH	8.5; 9.0; 9.5; 10.0; 10.5	Mg(OH)2 yield/selectivity and filterability
Slaking medium	Water; Ca(NO3)2 solution; recycled wash liquor	Particle morphology and filter rate
Cake washing	0; 1; 2 wash stages	Nitrate removal, CaO impurity, yield loss

Analytical methods and performance criteria

ICP-OES should be used to quantify dissolved Ca, Mg and trace metals in reaction liquors and wash streams. XRF is suitable for rapid major-oxide analysis of raw and calcined solids, while XRD should be used to identify dolomite, calcite, CaO, MgO, Mg(OH)2 and other crystalline phases. TGA/DSC provides the thermal decomposition profile and supports selection of a calcination window. SEM-EDS is recommended for comparing raw mineral morphology, calcined porous structures and precipitated Mg(OH)2 agglomerates.

For fertilizer products, total nitrogen, nitrate-N and ammoniacal-N should be measured with validated fertilizer methods appropriate to the formulation. Density, pH, conductivity, viscosity, insoluble matter and crystallization/low-temperature stability should be characterized for liquid products. For Mg(OH)2 and MgO products, MgO equivalent, CaO contamination, moisture,

LOI and particle-size distribution are important quality attributes. Heavy-metal screening is essential because nitric acid can solubilize trace elements originally present in the ore.

Table 4. Recommended analytical package for process validation.

Sample / product	Analyses	Purpose
Raw dolomite	XRF, XRD, ICP-OES, LOI, TGA/DSC, particle size	Feedstock composition and variability
Calcined dolomite	XRD, XRF, LOI, TGA check, particle size	Carbonate conversion and oxide formation
Acid digestion liquor	ICP-OES (Ca/Mg/impurities), free acidity, pH, density	Dissolution efficiency and impurity transfer
Mg(OH)2 cake	MgO eq., CaO impurity, moisture, XRD, SEM-EDS	Selectivity, morphology and product quality
Mother liquor	Ca, Mg, nitrate-N, ammoniacal-N, Na where relevant	Recycle and fertilizer integration
Liquid fertilizer	Total N, CaO/MgO eq., pH, density, viscosity, insolubles, crystallization	Commercial-formulation quality
Agronomic samples	Plant biomass/yield, tissue Ca/Mg/N, soil available Ca/Mg	Nutrient-use performance

RESULTS AND DISCUSSION

Stoichiometric potential of dolomite as a fertilizer feedstock

The theoretical balance in Table 2 illustrates why dolomite is attractive for integrated fertilizer processing. One hundred kilograms of pure mineral contains the equivalent of 30.41 kg CaO and 21.86 kg MgO, and complete reaction with nitric acid converts these alkaline-earth components into nitrate salts while introducing fertilizer N from the acid. On an anhydrous salt basis, the ideal mixed Ca(NO3)2-Mg(NO3)2 product contains approximately 17.93% N, 17.95% CaO equivalent and 12.90% MgO equivalent. Actual liquid products will contain water, excess acid or neutralization products, so their nutrient analysis will be lower and must be determined experimentally.

The same balance also identifies the dominant process load in the raw-dolomite route: CO2 evolution. The theoretical release is 47.73 kg CO2 per 100 kg pure dolomite. At laboratory scale this primarily affects foaming and reactor headspace; at pilot and industrial scale it becomes a gas-handling, ventilation and capacity issue. Controlled acid addition, adequate freeboard and antifoam screening are therefore process-design requirements rather than optional operational details.

Direct digestion versus calcination-assisted processing

The two routes serve different product objectives. Direct nitric-acid digestion avoids the thermal-energy penalty of calcination and is well suited to liquid Ca-Mg-N fertilizer development. The 2025 Sustainability study is particularly relevant because it demonstrated a direct sequence of dolomite → nitric acid → ammonia water → urea → ammonium nitrate and reported stable liquid fertilizer formulations after further nitrogen enrichment. By contrast, the calcination-assisted route becomes more attractive when selective Mg(OH)2 or MgO is the

priority, because conversion to reactive oxides and controlled slaking can create a solid-liquid separation pathway not available in a simple mixed nitrate solution.

Table 5. Technical comparison of the two principal process routes.

Criterion	Route A: raw dolomite + HNO3	Route B: calcination-assisted
Primary target	Liquid Ca-Mg nitrate fertilizer liquor	Mg(OH)2 / MgO plus nitrate-rich co-product
Energy demand	Lower; no calcination furnace	Higher; furnace and gas handling required
Gas evolution	CO2 during acid digestion	CO2 mainly during calcination
Reaction rate	Controlled by mineral dissolution and particle size	Potentially faster oxide-acid reaction after calcination
Solid-liquid separation	Mainly insoluble-gangue filtration	Critical Mg(OH)2 precipitation and cake filtration
Main risk	Foaming, excess acidity, impurity dissolution	Sintering, energy use, filterability, Ca carryover
Fertilizer integration	Directly favorable	Requires mother-liquor/product integration
Best initial use	Fast laboratory proof of concept	Second-stage route for higher-value Mg products

Calcination temperature should be treated as an optimization variable

A key improvement over the initial process draft is the treatment of calcination temperature as a measured optimization variable rather than a fixed 1150-1450 °C requirement. Olszak-Humienik and Jablonski (2015) showed that the thermal decomposition of natural dolomite is strongly condition-dependent and confirmed complete conversion to CaO and MgO under suitable thermal conditions. Didžiulytė and Šlinkšienė (2025) explicitly avoided a 1050 °C calcination step in their fertilizer route because of its energy demand. These observations do not invalidate high-temperature testing; they indicate that very high temperatures should be justified by downstream benefits such as reactivity, phase purity or filtration. Excessive firing may promote sintering and reduce the reactive surface of the oxide product. TGA/DSC-guided furnace trials are therefore a more defensible development strategy.

Acid stoichiometry, concentration and impurity control

The ideal reaction requires four moles of HNO3 per mole of dolomite. Real ores require an operational allowance because non-dolomite carbonate phases and acid-consuming impurities may be present, while incomplete mixing or passivation can prevent stoichiometric acid from reaching full conversion. The recent direct-fertilizer study used an acid charge stated as 140% of the stoichiometric amount for its specific dolomite. This supports testing controlled acid excess, but it should not be copied as a universal recipe. Excess acid can increase Ca/Mg recovery yet also dissolve more Fe, Al and trace metals, increase neutralization demand and lower the nutrient concentration of the finished fertilizer if large amounts of neutralizing solution are then required. The optimum is therefore the minimum acid excess that provides reproducible nutrient recovery and an acceptable impurity profile.

Magnesium hydroxide precipitation and filtration as the decisive separation step

Mg(OH)2 precipitation is chemically simple but industrially demanding because fine precipitates can form gelatinous or low-permeability cakes. Historical patent DE830943C emphasized the practical importance of generating a more filterable precipitate and described slaking burned dolomite in calcium-nitrate-containing solution before reaction with nitrate liquor. The related US2912306A patent reported a lime-poor magnesia product and improved filtration when nitrate-conditioned slaking was used. DE1912865A1 similarly described the conversion of MgO-containing dolime solids to Mg(OH)2 in chloride-containing mother liquor. Although these documents are old, they highlight a modern process-development principle: precipitation yield alone is not sufficient; particle morphology, cake permeability, wash demand and mother-liquor recovery determine the economic feasibility of the separation.

For the present project, pH should therefore be increased stepwise while measuring dissolved Mg and Ca, rather than simply targeting the upper end of the 8.5-10.5 screening range. Filterability should be quantified as filtrate volume per unit area per unit time, cake moisture and wash-water demand. SEM-EDS and particle-size analysis can then be used to connect operating conditions with precipitate morphology. The best precipitation condition is the one that balances Mg recovery, low Ca contamination and practical filtration.

Product-development opportunities

Table 6. Dolomite-derived product families and proposed development logic.

Product family	Principal chemistry	Development objective	Key validation
Liquid Ca-Mg-N fertilizer	Ca(NO3)2 + Mg(NO3)2, optionally NH4NO3/urea	High-solubility Ca/Mg with nitrogen	N/Ca/Mg analysis, pH, density, crystallization, crop compatibility
Mg-rich liquid fertilizer	Mg(NO3)2-rich separated liquor	Rapid Mg supply via fertigation/foliar routes	Mg concentration, Ca selectivity, phytotoxicity
Mg(OH)2 suspension	Mg(OH)2 dispersed phase	Suspension fertilizer / soil-pH functionality	Particle size, sedimentation, redispersibility, Mg availability
MgO precursor	Dried/calcined Mg(OH)2	Higher-purity Mg product for agricultural or industrial use	MgO assay, CaO impurity, LOI, surface/reactivity
Calcium nitrate co-product	Ca(NO3)2-rich mother liquor	Fertilizer integration and Ca value recovery	Ca/N ratio, Mg carryover, crystallization behavior
Organomineral product	Dolomite-derived solids/liquors + organic matrix	Slower nutrient release / soil-conditioning concept	Nutrient release, stability, agronomic trial

For the first laboratory milestone, the direct liquid Ca-Mg-N route is the lowest-complexity product because it avoids selective separation. A second milestone should focus on Mg(OH)2

recovery only after the nitrate liquor and impurity profile are characterized. Product diversification should follow measured process behavior rather than forcing all product families through one flowsheet.

Process safety, environmental control and scale-up

Nitric-acid digestion requires corrosion-resistant equipment, controlled reagent addition, temperature monitoring and effective ventilation. The carbonate reaction itself primarily generates CO2, but nitric acid handling and contact with reducing contaminants or inappropriate materials can create additional hazards. Industrial design should therefore include closed or semi-closed reaction equipment, scrubber capacity where required, materials-of-construction review and procedures that prevent contamination of nitrate-rich liquors with incompatible organic or combustible materials.

Calcination shifts a large portion of the environmental burden from the wet reaction to the furnace. Energy use and direct process CO2 must be included in route comparison. Mother-liquor and wash-water recycle can reduce wastewater and recover nitrate value, but repeated recycle can also concentrate Na, Cl, Fe, Al or other impurities. A purge strategy should be defined from measured impurity accumulation rather than assumed closed-loop operation.

Pilot-scale decision criteria

Table 7. Recommended stage-gate criteria before pilot scale.

Stage	Decision question	Minimum evidence before progression
1. Feedstock	Is the dolomite sufficiently consistent?	Representative XRF/XRD/ICP data from multiple lots; impurity and heavy-metal profile
2. Direct digestion	Can Ca and Mg be recovered reproducibly?	Mass balance, residual solids, acid consumption, reaction time and foam control
3. Product liquor	Is a stable fertilizer-grade liquid feasible?	N/Ca/Mg analysis, pH, density, viscosity, crystallization and storage observations
4. Mg separation	Can Mg(OH)2 be recovered selectively and filtered?	Mg recovery, Ca impurity, cake rate/moisture, washing requirement
5. Recycle	Can mother liquor/wash water be reused safely?	Ion accumulation profile, product quality after repeated recycle cycles
6. Agronomy	Does chemical availability translate to crop response?	Replicated greenhouse or field response versus commercial/reference fertilizers
7. Economics	Does the selected route justify scale-up?	Reagent, energy, water, filtration, drying and waste-management balance

Limitations of the present study

The present manuscript is a process-development paper based on the project draft, stoichiometric calculations and published literature/patent evidence. The target conditions listed in Tables 3-7 are experimental design ranges, not measured optima. No experimental recovery percentage, filtration rate, impurity level or agronomic response is claimed for the İGSAŞ dolomite project until the corresponding laboratory data are generated. This distinction is essential for scientific publication and will allow future measured results to replace the design targets without rewriting the conceptual framework.

CONCLUSIONS

Dolomite can be treated as a strategic Ca-Mg feedstock for fertilizer-process development rather than only as a low-solubility liming mineral. The most direct route is nitric-acid digestion of finely ground raw dolomite, producing a mixed Ca/Mg nitrate liquor that can be neutralized and formulated as a liquid fertilizer. This pathway minimizes thermal energy demand and is supported by recent experimental literature on liquid N-Ca-Mg fertilizer production.

A calcination-assisted route is justified when the project objective expands to selective Mg(OH)2 recovery or MgO production. However, calcination temperature should be selected from ore-specific TGA/DSC and downstream performance rather than fixed at the highest temperature. The separation challenge is not merely chemical precipitation: Mg recovery, Ca contamination, particle morphology, cake permeability, washing and mother-liquor recycle must be optimized together.

The theoretical balance establishes a transparent baseline: per 100 kg pure dolomite, the stoichiometric requirement is 136.69 kg pure HNO3, with theoretical formation of 88.98 kg Ca(NO3)2 and 80.43 kg Mg(NO3)2 and release of 47.73 kg CO2. These values must be corrected with actual ore assay, acid excess and process losses before scale-up.

The recommended development sequence is therefore: feedstock characterization → direct nitric-acid digestion baseline → calcination comparison where needed → selective precipitation/filtration study → fertilizer formulation and low-temperature stability → mother-liquor recycle assessment → greenhouse/field validation → techno-economic evaluation. This staged approach can generate the measured process data required for a final peer-reviewed article and can also identify potentially protectable process know-how for the PYP 75-3120-026 “Dolomitten Farklı Gübre Üretim Projesi”.

ACKNOWLEDGEMENTS

This manuscript was prepared within the scope of the planned PYP 75-3120-026 “Dolomitten Farklı Gübre Üretim Projesi”. The authors acknowledge the planned contributions of the İGSAŞ R&D team and collaborating analytical laboratories. Experimental data and institution-specific funding information should be updated before journal or congress submission.

REFERENCES

Abdel-Aal, E. A. (1995). Possibility of utilizing Egyptian dolomite ores for production of magnesium oxide by acid leaching. Fizykochemiczne Problemy Mineralurgii, 29, 55-65.

Didžiulytė, E., & Šlinkšienė, R. (2025). Use of amino acids and organic waste extracts to improve the quality of liquid nitrogen-calcium-magnesium fertilizers. Sustainability, 17(15), 7081. https://doi.org/10.3390/su17157081

German Patent DE830943C. (1952). Production of magnesia and calcium nitrate from dolomite.

German Patent DE1912865A1. (1970). Magnesium hydroxide production from dolomite and salt solution.

Olszak-Humienik, M., & Jablonski, M. (2015). Thermal behavior of natural dolomite. Journal of Thermal Analysis and Calorimetry, 119, 2239-2248. https://doi.org/10.1007/s10973-014-4301-6

Rashad, M. M., & Baioumy, H. M. (2005). Chemical processing of dolomite associated with the phosphorites for production of magnesium sulfate heptahydrate. The European Journal of Mineral Processing and Environmental Protection, 5(2), 174-183.

US Patent 2,912,306. (1959). Method of producing magnesia and calcium nitrate from dolomite.
Yildirim, M., & Akarsu, H. (2010). Preparation of magnesium oxide (MgO) from dolomite by leach-precipitation-pyrohydrolysis process. Physicochemical Problems of Mineral Processing, 44(1), 257-272.

DEVELOPMENT AND PERFORMANCE EVALUATİON OF WATER-RETENTİVE HYDROGEL FORMULATİONS TO IMPROVE WATER USE EFFİCİENCY İN AGRİCULTURE

Halit Duran[1],, Deniz Öncel[1], Ahmet Akbulut[1], Gökhan Yaşar[1], Burcu Köse[1]

İGSAŞ, R&D Center, Kütahya, Türkiye.

**Corresponding Author: Halit Duran, İGSAŞ R&D Center, Kütahya, Türkiye. Phone: +90 5066476419; E-mail: halit.duran@igsas.com.tr*

ABSTRACT

Water scarcity driven by climate change, population growth, and irregular rainfall patterns has made efficient water use in agriculture a critical issue for sustainable food production. Agricultural activities account for a large share of global freshwater consumption, and a significant portion of irrigation water is lost through evaporation, surface runoff, and deep percolation. Consequently, the need for technologies that can increase soil water retention capacity and improve irrigation efficiency is growing steadily. In recent years, hydrogel-based superabsorbent polymers have emerged as promising materials due to their ability to absorb large amounts of water and release it in a controlled manner to the plant root zone when needed. In this study, a water-retentive hydrogel formulation with properties comparable to commercial agricultural hydrogels was developed, and its potential agricultural performance was evaluated. The formulation was prepared using superabsorbent polymeric structures, organic stabilizers, and cross-linking agents. Laboratory- and pot-scale trials were planned to determine the water absorption capacity, swelling behavior, soil moisture retention performance, and effects on plant growth of the developed hydrogel recipe. Different hydrogel doses will be applied to the soil under controlled irrigation conditions, and the results will be compared with control groups. The developed hydrogel formulations are expected to reduce soil moisture loss, extend irrigation intervals, and support plant growth by providing a more stable moisture environment in the root zone. The system developed is also expected to contribute to sustainable agricultural practices by improving irrigation efficiency in arid and semi-arid regions. This study is expected to provide a basis for controlled-release fertilizer systems, biodegradable hydrogel technologies, and climate-resilient agricultural practices.

Keywords: Hydrogel, Water retention capacity, Sustainable agriculture, Superabsorbent polymer, Irrigation efficiency, Soil moisture

INTRODUCTION

Due to global climate change and increasing water consumption, the water resources available for agricultural production are steadily decreasing. The agricultural sector accounts for approximately 70% of total freshwater use worldwide, and significant water losses occur in current irrigation systems. In agricultural activities carried out particularly in arid and semi-arid regions, the inefficient use of water leads to yield losses and increased economic damage.

Superabsorbent polymers (SAPs), which enable water to be retained in the soil for longer periods, have become one of the key research areas in sustainable agricultural practices in recent years. These polymers can absorb hundreds of times their own weight in water and release the

stored water back to the plant root zone in a controlled manner. Guilherme et al. (2015) reported that hydrogel applications reduce water stress and positively affect plant growth. Montesano et al. (2015) reported that controlled water release provides a reduction in irrigation frequency and an improvement in plant growth. In addition, Ekebafe et al. (2011) stated that superabsorbent polymers improve the soil-water relationship under arid conditions.

However, the high cost of existing commercial hydrogel products, the low biodegradability shown by some products, and their variable performance under different soil conditions make it necessary to develop new formulations. For this reason, developing more economical, environmentally friendly, and high-performance water-retentive hydrogel systems is of great importance.

The main objective of this study is to develop a new hydrogel formulation that can be used in agricultural applications and to evaluate the effects of the developed formulation on water retention capacity and plant growth.

MATERIAL AND METHOD

In this study, superabsorbent polymer, organic additives, cross-linking agents, and stabilizer components are used in the preparation of the hydrogel formulation. A polyacrylate-based superabsorbent material is preferred as the main polymeric structure. Cellulose derivatives are utilized to increase the mechanical strength of the formulation.

The agricultural soil to be used in the trials will be homogenized, sieved, and used under standard moisture conditions. Fast-growing test plants have also been selected for the pot trials.

In preparing the hydrogel formulation, superabsorbent polymer, organic additive, and cross-linking agent will be mixed at determined ratios. The mixture will be homogenized under controlled temperature and left to cure for a specific period. The resulting hydrogel structure will be dried and converted into granular form.

The following parameters will be examined to evaluate the performance of the prepared formulations:

Water absorption capacity

Swelling ratio

Water release time

Stability in soil

Resistance to repeated wetting-drying cycles

Controlled pot trials will be conducted to determine hydrogel performance. The trial groups are planned to be formed as follows:

Control group: soil without hydrogel

Trial group 1: soil containing 0.2% hydrogel

Trial group 2: soil containing 0.5% hydrogel

Trial group 3: soil containing 1.0% hydrogel

The following measurements will be taken at specific intervals:

Soil moisture percentage

Irrigation frequency

Plant height

Number of leaves

Fresh and dry biomass amount

RESULTS AND DISCUSSION

It is anticipated that the developed hydrogel formulations will retain water in the soil for longer periods compared to the control group. In particular, formulations with high absorption capacity are expected to extend irrigation intervals and reduce water losses.

In the hydrogel-treated groups, plant height, leaf development, and biomass amount are predicted to be higher than in the control group.

The results to be obtained are anticipated to demonstrate that superabsorbent hydrogel applications can provide significant advantages in agricultural water management. In line with studies in the literature, the developed formulation is expected to increase soil moisture retention capacity.

The positive effects of hydrogel applications on plant growth are particularly important in terms of reducing water stress. It is thought that the reduction in irrigation frequency could both decrease water consumption and reduce production costs.

Formulations containing organic additives are considered to offer advantages in terms of environmental sustainability and could be integrated with controlled-release fertilizer systems.

CONCLUSIONS

Within the scope of this study, the water-retentive hydrogel formulation developed is considered to be a significant material that can improve agricultural irrigation efficiency. It is thought that the developed formulation could reduce irrigation frequency and support plant growth by retaining soil moisture for longer periods.

In future studies, it is recommended that greenhouse and open-field trials be conducted to evaluate performance under different climate and soil conditions. In addition, new formulation development studies using biodegradable raw materials could be carried out.

REFERENCES

Ekebafe, L. O., Ogbeifun, D. E., & Okieimen, F. E. (2011). Polymer applications in agriculture. Biokemistri, 23(2), 81–89.

Guilherme, M. R., Aouada, F. A., Fajardo, A. R., Martins, A. F., Paulino, A. T., Davi, M. F. T., Rubira, A. F., & Muniz, E. C. (2015). Superabsorbent hydrogels based on polysaccharides for application in agriculture as soil conditioner and nutrient carrier: A review. European Polymer Journal, 72, 365–385. https://doi.org/10.1016/j.eurpolymj.2015.04.017

Montesano, F. F., Parente, A., Santamaria, P., Sannino, A., & Serio, F. (2015). Biodegradable superabsorbent hydrogel increases water retention properties of growing media and plant growth. Agriculture and Agricultural Science Procedia, 4, 451–458. https://doi.org/10.1016/j.aaspro.2015.03.051

EVALUATION OF THE EFFECTIVENESS OF PLANT-BASED BUILDING MATERIALS IN TERMS OF RESOURCE AND ENERGY EFFICIENCY

Emine İLHAN[1], Esma MIHLAYANLAR[2]

[1] Trakya University, Institute of Science, Architecture Department, Edirne, Turkey

[2] Trakya University, Architecture Department, Edirne, Turkey

Corresponding author e-mail: emineiilhan41@gmail.com

ABSTRACT

Maintaining a clean and healthy environment is directly linked to the preservation of ecosystems and biodiversity. In this context, the use of eco-friendly materials is gaining increasing importance in the construction sector. Energy efficiency, resource utilization, and material selection are among the fundamental assessment criteria in widely used green building certification systems. Energy efficiency improves as the level of naturalness of construction materials increases and the extent of their processing decreases. Research indicates that prioritizing the use of plant-based materials in building design and construction is essential for minimizing energy consumption. Plant-based construction materials—particularly those derived from renewable sources and possessing low embodied energy—represent a significant alternative to traditional materials; consequently, the use of bio-based and biocomposite materials is rising within the industry as part of a sustainability-oriented approach. Plant-based materials stand out due to their natural, eco-friendly, and sustainable characteristics; they hold significant global potential in the construction materials sector thanks to their renewability, ability to reduce carbon footprints, contribution to occupant health, and excellent insulation performance. For these reasons, plant-based construction materials are viewed as a crucial step toward achieving sustainability goals in the construction industry. Researching, developing, and promoting the use of these materials is of great importance for sustainable building design. This study aims to evaluate the effectiveness of plant-based construction materials in terms of resource and energy efficiency. Within this scope, the study examines the role of plant-based construction materials in sustainable building production and their relationship with the life cycle assessment approach. The potential contribution these materials can make to the sustainable construction sector is being examined by analyzing their role within national and international regulations, green building certification systems (BREEAM, LEED, CASBEE, GBTool, etc.), and life cycle assessment tools.

Keywords: Plant-based building materials, Life cycle assessment, Green building certificate systems, Energy use, Embodied energy.

INTRODUCTION

Driven by population growth, industrialization, and urbanization, the construction sector is characterized by high energy and raw material consumption and significant environmental impact. Regarding the sectoral distribution of energy consumption in Türkiye as of 2024, the largest shares belong to the industrial (32.2%) and transportation (28.5%) sectors. These are followed by the residential sector (23.8%) and the agriculture and livestock sector (10.8%) (ghg-turkiye.com, 2024). Assessing the environmental performance of buildings requires considering not only energy requirements during the operational phase but also the entire life

cycle of building materials, spanning from pre-production to disposal. Furthermore, chemicals, volatile organic compounds (VOCs), and formaldehyde—utilized or generated during raw material sourcing, production, and transportation—can pose risks to indoor air quality and human health (Zorlu, 2019). Consequently, it is crucial to consider environmental criteria such as low embodied energy, the use of renewable raw material sources, recyclability, and low water consumption when evaluating materials. In particular, the European Union's targets to reduce carbon emissions by 55% by 2030 and achieve climate neutrality by 2050 are driving efforts toward more efficient resource and energy use within the construction sector (eu.immib.org, 2023). The environmental issues and consumption patterns associated with the construction sector necessitate the consideration of sustainable materials that enhance energy and resource efficiency while minimizing environmental impact. Plant-based building materials offer an alternative to conventional materials due to their derivation from renewable sources, low embodied energy potential, carbon sequestration capabilities, and thermal and acoustic insulation performance. An examination of international examples reveals that various raw materials—such as wood, bamboo, hemp, straw bales, cork, mycelium, flax fiber, and rice husks—are utilized in diverse building types, ranging from residences and educational facilities to cultural centers and high-rise structures. These global applications demonstrate the technical, environmental, and economic viability of plant-based building materials, thereby serving as a guide for future initiatives in Türkiye. Figure 1 illustrates the geographical distribution of selected buildings worldwide that utilize plant-based building materials. The examples examined show that a variety of plant-based materials are employed across diverse building typologies, including educational facilities, cultural centers, residences, pavilions, and high-rise structures.

Figure 1. Examples of buildings worldwide that utilize plant-based construction materials.

Information regarding the examples shown on the map is presented in Table 1. These examples demonstrate the applicability of plant-based building materials across various climatic conditions and building types.

Table 1. Selected examples of buildings worldwide utilizing plant-based construction materials and their characteristics.

BUILDING NAME	YEAR	LOCATION	BUILDING TYPE	PLANT MATERIAL USED	APPLICATION AREA
Brock Commons Tallwood House (archdaily.com, 2017).	2017	Canada	Student Dormitory	CLT Panel Glulam	Structural Material
Hy-Fi Pavilion (MoMA PS1) (architizer.com, 2026)	2014	USA	Pavilion	Mycelium Brick	Structural Material
BaleHaus (University of Bath) (bath.ac.uk, 2026).	2010	England	Project Building	Straw bale panels	Structural and Protective Material
HemPod (University of Bath) (bath.ac.uk, 2010)	2010	England	Project Building	Hempcrete	Structural and Protective Material
Cork House (archdaily.com,2026a) .	2019	England	Housing	Mushroom Block	Structural Material
Growing Pavilion (thegrowingpavilion.com, 2026).	2019	Holland	Pavilion	Mycelium, Hemp Fiber, and Reed Fiber Biocomposite Panel	Detail Material
Hybrid Flax Pavilion (icd.uni-stuttgart.de, 2026).	2024	Germany	Pavilion	Flax Fiber Reinforced Biocomposite	Structural Material
GAIA (ricehouse.it, 2026).	2018	Italy	Project Building	Rice Husk and Rice Straw Biocomposite	Protective Material
Mjøstårne (moelven-com, 2026).	2019	Norway	Skyscraper	Glued Laminated Timber (Glulam) Cross-Laminated Timber (CLT)	Structural Material
Sara Kulturhus (whitearkitekter.com, 2026).	2021	Sweden	Cultural Center and Hotel	Glued Laminated Timber (Glulam) Cross-Laminated	Structural Material

				Timber (CLT)	
Asakusa Culture Tourist Information Center (archdaily.com, 2026b).	2012	Japan	Cultural Center	Glued Laminated Timber (glulam)	Structural Material
Bamboo Pavilion (archdaily.com, 2026c).	2018	Chinese	Pavilion	Bamboo	Structural Material
Green School Bali (archdaily.com, 2026d).	2007	Indonesia	Education Campus	Bamboo	Structural and Detail Material

Figure 2 illustrates the geographical distribution of traditional practices involving the use of plant-based building materials in Türkiye. Depending on local conditions, wood is observed to be widely used in various regions, particularly in Safranbolu Houses and the Eastern Black Sea Region. While straw is utilized as an additive in adobe construction in the Central Anatolia Region, reed is traditionally used for roofing and shading structures along the Mediterranean coast. These examples demonstrate that plant-based building materials are employed in Türkiye, particularly within the context of traditional building culture.

Figure 2. Examples of traditional buildings in Türkiye that utilize plant-based construction materials.

MATERIAL AND METHOD

This study investigates the role of plant-based building materials in sustainable building production and their relationship with the life cycle assessment (LCA) approach; it also examines the criteria for their use and evaluation within green building rating systems, as well as the approaches employed within the LCA framework. Based on the data obtained, the study analyzes the potential of plant-based building materials to reduce resource and energy consumption, prevent waste, and contribute to sustainable building production**.**

The study seeks to answer the following research questions:
What is the potential of plant-based building materials to reduce resource, energy, and waste consumption in architecture?

What is the role of plant-based building materials within green building rating systems?

CLASSIFICATION OF BUILDING MATERIALS AND RELEVANT REGULATIONS

"Construction material" refers to the various elements—defined by their specific properties—that constitute the physical environment and structural components essential for human life (Eriç, 2002). While material properties are generally examined under two main categories—intrinsic and extrinsic properties (Bayraktar, 2010)—materials are classified based on various criteria such as intended use, production method, origin, form, and physical and chemical characteristics (Şimşek, 2003). In addition to traditional materials like stone, wood, and brick, technological advancements have led to the use of a wide range of construction materials, including steel, concrete, plastics, composites, biomaterials, and smart materials. Plant-based construction materials are those in which at least one of the primary components is derived from renewable biological sources, plant biomass, or agricultural waste (Le et al., 2023). Plant fibers, starches, oils, and various agricultural wastes can be utilized in their production. Lignocellulosic sources—such as sugarcane, bamboo, jute, kenaf, rice stalks and husks, wheat, corn, hemp, straw, and flax—are among the primary raw materials that can be utilized in the production of construction materials (Youngquist et al., 1994). The quantities of global fiber sources are presented in Table 2.

Table 2. Quantity of global fiber sources (arastirma.tarimorman.gov., 2024; Yazıcı, 2024)

Fiber sources in the world	Quantity (tons)
Barley	143,3 million
Jute (2022)	3.503,448
Coconut (2022)	1.939,429
Flax (2022)	875,995
Hemp (2021)	274,883
Kenaf (2022)	224,926
Sisal (2022)	213,305
Sunflower	52,048
Cotton	51,8
Ramie (2022)	7,625

The diversity and widespread nature of agricultural production in Turkey facilitate the generation of various plant-based wastes and allow them to be utilized as raw material sources for the production of building materials. Table 3 shows the status of agricultural wastes in Turkey—specifically those suitable for use as fibers. Such materials, derived from renewable resources, can be classified as green building materials because, under appropriate production and usage conditions, they contribute to reducing environmental burdens and enhancing the comfort of building occupants.

Table 3. Production quantities of fiber sources in Türkiye (arastirma.tarimorman.gov., 2024; tuik.gov., 2025)

Turkey's fiber sources	Annual (Million Metric Tons)
Wheat	17,9
Corn	8,5
Barley	6
Cotton	2.2
Sunflower	1,8
Rice	1,19
Oats	0.3
Rye	0.2

The use of renewable resources and the repurposing of agricultural waste in the construction sector allow plant-based materials to be addressed within the framework of resource efficiency and the circular economy. The fibers used in the production of these materials can be classified as natural or man-made, depending on their method of extraction. Natural fibers offer significant advantages in construction materials due to their low cost, low specific gravity, ease of processing, low energy requirements, and favorable thermal and acoustic properties. However, they also possess characteristics that must be taken into account, such as low resistance to moisture and fire, property fluctuations due to weather conditions, and susceptibility to biological degradation.

LEGAL REGULATIONS ON BUILDING MATERIALS

In Turkey, the construction materials sector encompasses various product groups such as concrete, cement, steel, wood, glass, ceramics, and insulation materials. Technical standards and conformity requirements form the basis for the production and use of construction materials, with these standards established by the relevant national authorities (Bringas, 2004). Amidst growing environmental concerns, the resource and energy efficiency of construction materials, as well as their environmental impacts, are gaining increasing importance within the scope of regulations and standards. The Construction Products Regulation mandates that construction products meet seven basic requirements: mechanical resistance and stability; safety in case of fire; hygiene, health, and the environment; safety and accessibility in use; protection against noise; energy economy and heat retention; and the sustainable use of natural resources (Construction Products Regulation, 2013). While the Energy Efficiency Law and the Regulation on Energy Performance in Buildings establish criteria for reducing energy consumption and improving energy performance in buildings, the Environmental Impact Assessment (EIA) Regulation aims to evaluate the potential environmental impacts of projects. Furthermore, the Waste Management Regulation sets out principles for waste reduction, reuse, recovery, and disposal without harming the environment. Regulations concerning air, water, and soil pollution also support the control of environmental impacts that may arise from the production processes of construction materials. When these regulations are considered collectively, it becomes evident that the selection of construction materials requires taking into account not only technical performance but also energy consumption, resource utilization, emissions, waste generation, and environmental impacts throughout the material's life cycle. Various approaches—such as TSE and ISO standards, Environmental Product Declarations

(EPD), eco-labeling, green building certification systems, and Life Cycle Assessment (LCA)—are utilized to evaluate the environmental impacts of construction materials. These systems enable the determination and comparison of energy and resource consumption, emissions, waste generation, and environmental impacts from the production stage through to the end of the material's service life. LCA, in particular, serves as a crucial tool for sustainable material selection by facilitating a systematic evaluation of environmental impacts arising throughout the material's life cycle. In this context, the aforementioned standards, evaluation methods, and certification systems provide a fundamental framework for assessing plant-based construction materials in terms of resource and energy efficiency.

LIFE CYCLE ASSESSMENT-LCA and BUILDING CERTIFICATION SYSTEMS

As environmental impacts have increasingly intensified worldwide, awareness regarding environmental consciousness and sustainability has also grown. In this context, it is crucial to address the principles and strategies underpinning sustainable architecture in a manner that ensures their compatibility and mutual reinforcement. Life Cycle Assessment (LCA)—one such approach—serves as a systematic method enabling the combined evaluation of qualitative and quantitative data to determine the environmental impacts of structures and building materials. LCA is a method used to assess the environmental performance of a product or material. While the traditional "cradle-to-grave" approach in life cycle assessments covers the processes spanning from raw material sourcing to the end of a product's service life, the "cradle-to-cradle" approach prioritizes the reuse and recovery of materials rather than treating them as waste after use. Developed by McDonough and Braungart, this approach offers a sustainable design philosophy that supports the circular use of resources, renewable energy, and environmental health (McDonough & Braungart, 2016). Within this approach, evaluating the energy requirements associated with the production and use of building materials is just as important as the efficient use of resources throughout their life cycle. Embodied energy refers to the total energy consumed by a building material throughout its life cycle—spanning raw material sourcing, production, transportation, construction, use, maintenance, reuse, recycling, and disposal (Cabeza et al., 2014). As a key criterion for assessing the environmental performance of building materials, embodied energy plays a significant role in sustainable material selection by helping to reduce energy consumption and carbon emissions. Plant-based materials represent a significant alternative in sustainable building design, as they are derived from renewable sources and—in the case of certain types—possess the potential for carbon storage alongside low production energy requirements.

There are numerous certification systems used by various countries around the world to assess the environmental impact of buildings. Brief information regarding the most widely used certification systems is presented in Table 4.

Table 4. Green building systems used in different countries

Certificate	Country	Publication Year	Number of Certified Buildings	Reference Year
LEED	ABD	1998	107.319 (usgbc.org, 2025b)	2025
BREAM	England	1990	More than 1.045,000 (breeam.com, 2025a)	2025
GREEN STAR	Australia	2003	More than 5.500 (gbca.org.au, 2025)	2025
DGNB	Germany	2009	12.900 (dgnb.de, 2"024)	2024
CASBEE	Japan	2001	More than 5.105 (ibecs.or.jp, 2026)	2026
SBTOOL	Canada	1998		
BEAM PLUS	Hong Kong	1996	2165 (beamsociety.org, 2025)	2025
B.E.S.T.	Türkiye	2013	23 (dilekasan.com, 2022)	2022
YeS –TR	Türkiye	2021	Resmi veri bulunmamaktadır	2021
IGBC	India	2001	More than 18.620 (igbc.in, 2026)	2026

To outline the assessment approaches of certification systems regarding construction materials, material categories, their sub-categories, and assessments concerning plant-based materials were examined separately and compared in Table 5.

Table 5. Comparison of Material Categories in Green Building Certification Systems

Certification System	Material Category	Score/Weight of the Material Category	Subcategories of the Material Category and Evaluation of Plant-Based Materials	
LEED (usgbc.org, 2025a)	Materials and Resources	18 Point	Zero Waste Operations Planning	Precondition
			Quantify and Evaluate Embodied Carbon	Precondition
			Reuse of Buildings and Materials	3
			Reducing Embodied Carbon	6

			Low-Emission Materials	2
			Building Product Selection and Procurement	5
			Building Product Selection and Procurement	2
BREEAM (BRE, 2025)	Material	14 Point +4 example	Building life cycle assessment	7+ 3 example
			Environmental product declarations	1
			Responsibility regarding resource use in construction materials	4+1 example
			Durability and flexibility	1
			Material efficiency	1
GREEN STAR (gbca.org, 2022)	Material	14 Point	Life cycle impacts	7
			Environmental product declarations	3
			Sustainable products	3
			Construction and demolition waste	1
DGNB (DGNB, 2024)	Ecology	%40	Climate protection and energy	100+15 bonus
			Risks to the local environment	100+22,5 bonus
			Responsible use of resources	100+27,5 bonus
			Drinking water demand and wastewater generation	100+27,5 bonus
			Land use	100
			On-site biodiversity	100
CASBEE (ibecs.or.jp, 2025).	L2; Resources and materials	---	Resources and Materials	
			Continued use of the existing structural framework	
			Use of recycled materials as structural materials	
			Use of recycled materials as non-structural materials	

			Sustainable forestry for wood	
			Efforts to increase the reusability of components and materials	
SBTOOL (enicbcmed.eu, 2023)	Energy and Resource Consumption	---	Degree of reuse of suitable existing structures	
			Material intensity	
			Local materials	
			Design for deconstruction	
			Renewable materials	
			Recycled materials	
			Design for adaptability	
BEAM PLUS (BEAM, 2025)	Materials and waste (MW)	14 Point + 22 bonus	Minimal waste sorting facilities	Precondition
			Building reuse	2 bonus+1 bonus
			Modular and standardized design	1+1 bonus
			Prefabrication	1+3 bonus
			Durable and flexible design	1+2 bonus
			Sustainable forest products	1+1 bonus
			Recycled materials	1+2 bonus
			Ozone-depleting substances	2
			Regional materials	1+2 bonus
			Use of green products	2+4 bonus
			Life cycle assessment	1+1 bonus
			Adaptability and deconstruction	1+1 bonus
			Advanced waste sorting facilities	2+2 bonus
B.E.S.T (cedbik.org, 2025)	Material and Resource Use	14 Point	Use of eco-friendly materials	3
			Utilization of existing building elements	3
			Reuse of materials	3

			Use of local materials	3
			Durable materials	2
YeS-TR (tuca.gov, 2024)	Construction Material and Life Cycle Assessment (LCA)	100 Point	Building Material Life Cycle Assessment (LCA) and Environmental Product Declaration (EPD)	25
			Health Product Declaration (HPD)	21
			Radiation Emission	5
			Responsible Sourcing	8
			Local Sourcing	6
			Use of Reused, Refurbished, or Recycled Materials	26
			Use of Durable Materials	9
IGBC (IGBC, 2016)	Building materials and resources	16 Point	Sustainable architecture and design	5
			Site selection and planning	14
			Water conservation	19
			Energy efficiency	30
			Building materials and resources	16
			Indoor environmental quality	9
			Innovation and development	7

In green building certification systems, materials are evaluated based on general criteria such as "sustainable building materials," "use of environmentally friendly materials," and "low-emission materials." However, the unique characteristics of plant-based materials—such as renewability, low embodied energy, carbon storage, biodegradability, and resource efficiency—are not directly addressed. Therefore, it is important to develop specific and distinguishing criteria within certification systems to make the environmental advantages of plant-based building materials more visible.

CONCLUSIONS

The creation of the built environment and the production of building materials result in the consumption of natural resources and energy. The study demonstrates that sustainable building production does not depend solely on material selection; rather, proper design, appropriate construction techniques, and conscious usage must be addressed holistically.

To promote the widespread use of plant-based materials, it is crucial to utilize rapidly renewable plants—cultivable with low energy and water consumption—and agricultural waste in the production of building materials. Sustainability criteria such as carbon footprint, recyclability, life-cycle performance, and reusability need to be more extensively integrated into standards and assessment systems. Furthermore, the adoption of material and digital product passports will strengthen resource efficiency and the circular economy approach by enabling the monitoring of material composition, service life, environmental impacts, and potential for reuse.

Future research should conduct a detailed analysis of the life cycle of plant-based building materials—spanning production, usage, and disposal—in terms of energy consumption, carbon footprint, and resource utilization. It is important to compare the environmental and technical performance of various materials—such as hemp, straw, bamboo, flax, and fungi—against traditional building materials, and to evaluate properties like mechanical strength, fire resistance, moisture behavior, and thermal performance under varying climatic conditions. Furthermore, the application of BIM, energy simulations, and digital modeling methods can help predict how these materials perform in different types of structures. Additionally, research is needed on aspects such as cost, production capacity, supply chains, and the use of local resources when scaling up from laboratory studies to industrial production. Beyond the economic and sectoral barriers affecting the widespread adoption of these materials, it is also crucial to examine the levels of awareness and acceptance among designers, practitioners, and end-users. Finally, increasing interdisciplinary research will contribute to a more comprehensive understanding of the environmental, technical, and economic potential of plant-based building materials.

Note: “This study was supported by the Trakya University Scientific Research Projects (TÜBAP) Coordination Office under project number FYL-2026-4632.”

REFERENCES

arastirma.tarimorman.gov. (2024). 2024—Temmuz Tarım Ürünleri Piyasa Raporu. Accessed from the address https://arastirma.tarimorman.gov.tr/tepge/Menu/27/Tarim-Urunleri-Piyasalari on November 5,2025.

archdaily.com (2026a). Accessed from the address https://www.archdaily.com/938586/cork-house-matthew-barnett-howland-plus-dido-milne-plus-oliver-wilton on July 17,2026.

archdaily.com (2026b). Accessed from the address https://www.archdaily.com/251370/asakusa-culture-and-tourism-center-kengo-kuma-associates on July 15,2026.

archdaily.com (2026c). Accessed from the address https://www.archdaily.com/905690/bamboo-pavilion-zuo-studio on July 15,2026.

archdaily.com (2026d). Accessed from the address https://www.archdaily.com/81585/the-green-school-pt-bambu on July 15,2026.

archdaily.com (2017). Accessed from the address https://www.archdaily.com/879625/inside-vancouvers-brock-commons-the-worlds-tallest-timber-structured-building on July 25,2026.

architizer.com (2026). Accessed from the address https://architizer.com/projects/hy-fi/ on July 23, 2026
bath.ac.uk (2010). Accessed from the address https://www.bath.ac.uk/announcements/low-carbon-hemp-house-put-to-the-test/ on July 13, 2026.
bath.ac.uk (2026). Accessed from the address https://www.bath.ac.uk/case-studies/bath-researchers-develop-houses-with-zero-carbon-footprint/ on July 13,2026.
Bayraktar, F. T. (2010). Türkiye' de Yapı Malzemesi Yaşam Döngüsü Değerlendirmesi İçin Bir Sistem Önerisi (Publication No:310403) [Master's Thesis, Istanbul Technical University, Institute of Science]. YÖK Ulusal Tez Merkezi.
BEAM. (2025). *BEAM Plus New Buildings Version 2.0*. BEAM Society Limited
beamsociety.org. (2025). Accessed from the address https://www.beamsociety.org.hk/en/ on September 9, 2025.
BRE. (2025). BREEAM International New Construction Version 7. BRE Global.
breeam.com. (2025a). Explore BREEAM. Accessed from the address https://tools.breeam.com/projects/explore/map.jsp?sectionid=0&projectType=&rating=&certNo=&buildingName=&client=&developer=&certBody=&assessor=&addressPostcode=&countryId=7&partid=10023&Submit=Search on August 31, 2025
Bringas, J. E. (2004). Handbook of Comparative World Steel Standards (3. bs). ASTM International100 Barr Harbor Drive, PO Box C700, West Conshohocken, PA 19428-2959. https://doi.org/10.1520/DS67C-EB
Cabeza, L. F., Rincón, L., Vilariño, V., Pérez, G., & Castell, A. (2014). Life Cycle Assessment (LCA) and Life Cycle Energy Analysis (LCEA) of Buildings and the Building Sector: A Review. Renewable and Sustainable Energy Reviews, 29, 394-416.
cedbik.org. (2025). Binalarda Ekolojik ve Sürdürülebilir Tasarım B.E.S.T Konut ve Ticari Sertifikası. Accessed from the address https://www.cedbik.org/best on September 9, 2025.
DGNB. (2024). DGNB System – Kriterienkatalog Kleine Wohngebäude Sanierung / Neubau Versıon 2024.
dgnb.de. (2024). DGNB in Figures. Accessed from the address https://www.dgnb.de/en/dgnb/about-dgnb/dgnb-in-figures?utm_source on January 29,2026.
dilekasan.com. (2022). Türkiye Yeşil Bina Sertifikaları. Accessed from the address https://www.dilekasan.com/turkiye-yesil-bina-sertifikalari/?utm_source on January 29,2026.
enicbcmed.eu (2023), Accessed from the address https://www.enicbcmed.eu/sites/default/files/2024-04/SBTool_Manual_Booklet.pdf on April 5,2025.
eu.immib.org. (2023). Avrupa Yeşil Mutabakatı. Accessed from the address https://eu.immib.org.tr/avrupa-yesil-mutabakati/ on August 22,2025.
Eriç, M. (2002). Yapı Fiziği ve Malzemesi. Literatür Yayınları.
gbca.org. (2022). Rating system. Accessed from the address https://new.gbca.org.au/green-star/rating-system/ on August 31,2025.
gbca.org.au. (2025). Green Star Project Directory. Accessed from the address https://www.gbca.org.au/project-directory.asp?utm_source on September 1,2025.
ghg-turkiye.com (2024). *Enerji İzleme Platformu*. Accessed from the address https://ghg-turkiye.com/enerji-platformu on June7,2026.
IGBC. (2016). IGBC Green New Buildings Rating System (Version 3.0). Indian Green Building Council.
ibecs.or.jp. (2025). İbecs.or.jp. Accessed from the address https://www.ibecs.or.jp/CASBEE/english/ on September 9,2025.
ibecs.or.jp. (2026). CASBEE建築評価認証物件一覧. CASBEE建築評価認証物件一覧. Accessed from the address

https://www.ibecs.or.jp/CASBEE/certified_buld/CASBEE_certified_buld_list.htm on September7,2025.
icd.uni-stuttgart.de (2026). Accessed from the address https://www.icd.uni-stuttgart.de/projects/hybrid-flax-pavilion/ on July 21,2026.
igbc.in. (2026). Confederation of Indian Industry. Accessed from the address https://igbc.in/about-us on September 9,2025
Le, D. L., Salomone, R., & Nguyen, Q. T. (2023). Circular Bio-Based Building Materials: A Literature Review of Case Studies and Sustainability Assessment Methods. Building and Environment, 244(1). https://doi.org/10.1016/j.buildenv.2023.110774
McDonough, W., & Braungart, M. (2016). Cradle to Cradle Certıfied Product Standard Versıon 3.1. y Cradle to Cradle Products Innovation Institute.
moelven-com.(2026). Accessed from the address https://www-moelven-com.translate.goog/mjostarnet/?_x_tr_sl=en&_x_tr_tl=tr&_x_tr_hl=tr&_x_tr_pto=tc on July 24,2026.
ricehouse.it (2026). Accessed from the address https://www.ricehouse.it/en/storie/gaia/ on July 23,2026.
Şimşek, O. (2003). Yapı Malzemesi 1. BETA yayınları.
thegrowingpavilion.com (2026). Accessed from the address https://thegrowingpavilion.com/about/ on July 19,2026.
tuik.gov. (2025). Bitkisel Üretim 2.Tahmini, 2025. Accessed from the address https://data.tuik.gov.tr/Bulten/Index?p=Bitkisel-Uretim-2.Tahmini-2025-53938 on November 5, 2025.
usgbc.org. (2025a). LEED v5. Accessed from the address https://www.usgbc.org/leed/v5 on September 19,2025.
usgbc.org. (2025b). LEED Project Directory. Accessed from the address https://www.usgbc.org/projects on August 24,2025.
whitearkitekter.com (2026). Accessed from the address https://whitearkitekter.com/project/sara-cultural-centre/ on July 25,2026.
Yapı Malzemeleri Yönetmeliği. (2013)
Yazıcı, L. (2024). Lif Bitkileri: Dünya ve Ülkemizde Mevcut Durumun Değerlendirilmesi. İçinde Tarım Bilimleri Alanında Multidisipliner Güncel Çalışmalar IV (ss. 105-130). İKSAD yayınevi.
Youngquist, J. A., English, B. E., Scharmer, R. C., Chow, P., & Shook, S. R. (1994). Literature review on use of nonwood plant fibers for building materials and panels (FPL-GTR-80; s. FPL-GTR-80). U.S. Department of Agriculture, Forest Service, Forest Products Laboratory. https://doi.org/10.2737/FPL-GTR-80
Zorlu, K. (2019). Yapı Malzemelerinin İç Mekan Hava Kalitesine Etkisi Üzerine Bir Araştırma (Publication No:620433) [Master's Thesis, Gebze Technical University, Institute of Science]. YÖK Ulusal Tez Merkezi.

YSTEM OF BULGARIAN PLANT GENETIC RESOURCES DOCUMENTATION – DESIGN, STRUCTURE AND STATUS

Nikolaya VELCHEVA[1], Simona CHEPERIGOVA[1]

[1] Institute of Plant Genetic Resources "Konstantin Malkov", Sadovo, Plovdiv district, Agricultural Academy, Bulgaria

Corresponding author e-mail: nikolaya_velcheva@abv.bg

ABSTRACT

Plant genetic resources (PGR) constitute a fundamental component of agricultural biodiversity and include genetic material of actual or potential value for food and agriculture. Their effective conservation and sustainable utilization require not only appropriate storage conditions but also a reliable, standardized and continuously updated documentation system. The Bulgarian system for plant genetic resources documentation was developed as an integrated information framework supporting the conservation, management, characterization, evaluation, exchange and utilization of germplasm maintained in the National Genebank at the Institute of Plant Genetic Resources "Konstantin Malkov" – Sadovo. The documentation system integrates passport information, taxonomic and geographical data, collecting and acquisition information, biological status, storage conditions, regeneration, evaluation and characterization data, as well as information related to the distribution and use of accessions. Its structure follows the FAO/Bioversity Multi-Crop Passport Descriptors and the requirements of the European Search Catalogue for Plant Genetic Resources (EURISCO), thereby providing compatibility and interoperability with European and international information networks. The system incorporates functional modules for accession registration, passport data management, expedition documentation, accession searching, storage and regeneration management, and controlled data access. An important feature of the system is the distinction between a public interface for researchers and other users and a protected management environment for authorized genebank specialists. Open access to passport information, including mobile access, increases the visibility and usability of Bulgarian plant genetic resources. The system also supports the National Inventory of plant genetic resources and the transfer of validated and harmonized data to EURISCO. The documentation framework provides traceability of accessions from acquisition and registration through storage, regeneration, characterization and distribution. Its implementation contributes to the modernization and digitalization of genebank management and strengthens the role of the Bulgarian National Genebank as a national and international information centre for plant genetic resources.

Keywords: Accession, GeneBankSystem, Descriptors, Expedition, Introduction, Crop breeding.

INTRODUCTION

Plant genetic resources for food and agriculture represent an essential component of agricultural biodiversity and provide the genetic basis for crop improvement, adaptation and sustainable food production. The diversity of crops, traditional varieties, landraces, breeding materials and crop wild relatives provides genetic variation that may be valuable for adaptation to changing environmental conditions, emerging pests and diseases, and new production systems. The

conservation of this diversity is therefore directly associated with long-term food security and the resilience of agricultural systems (Salgotra & Chauhan, 2023).

Modern agriculture relies increasingly on a relatively limited number of high-performing cultivars. This tendency may contribute to genetic erosion and the loss of traditional varieties and locally adapted populations. Landraces and traditional populations may contain valuable characteristics associated with adaptation to local environmental conditions, disease resistance, quality traits and specific consumer preferences. Consequently, their conservation in genebanks, combined where possible with in situ and on-farm conservation, is an important component of sustainable management of agricultural biodiversity (Raggi et al., 2021).

Ex situ conservation in genebanks provides an effective mechanism for the long-term preservation of plant genetic resources. However, the biological material alone is insufficient to ensure its effective future use. The scientific and practical value of an accession depends strongly on the availability, accuracy and completeness of information associated with it. Documentation has to allow the identity, origin, biological status, storage history, reproduction, characterization and utilization of each accession to be traced throughout its conservation cycle. The documentation of plant genetic resources is therefore an integral part of genebank management (FAO, 2013; ECPGR, 2021).

The Bulgarian National Genebank, located at the Institute of Plant Genetic Resources "Konstantin Malkov" – Sadovo, maintains collections comprising local populations, traditional varieties, modern cultivars, breeding lines, genetic stocks and crop wild relatives. The collections are managed through a specialized documentation system that integrates information generated during accession acquisition, registration, conservation, regeneration, characterization, evaluation and distribution. The system was developed through long-term interdisciplinary cooperation between researchers from IPGR-Sadovo and computer scientists (Stoyanova-Doycheva et al., 2020; Malinov et al., 2025).

The development of a standardized documentation framework in Bulgaria is also closely related to European and international initiatives for harmonization and exchange of plant gene pool information (Goritschnig et al., 2024). The Bulgarian National Genebank participates in the European Search Catalogue for Plant Genetic Resources (EURISCO) and coordinates the maintenance of the Bulgarian National Inventory. The system applies the FAO/Bioversity Multi-Crop Passport Descriptors, which provide a common structure for passport information and facilitate data exchange between national and international information systems.

The importance of interoperable documentation systems has increased with the development of digital infrastructures for plant genetic resources. Standardized information enables data aggregation, validation, searching and dissemination, while open access increases the potential for researchers, breeders and other stakeholders to identify and use conserved germplasm. Digitalization is therefore not simply a technical transformation of records into databases, but a means of improving the quality, accessibility, interoperability and long-term value of plant genetic resources information (Mendel et al., 2017; Cicova et al., 2026).

The objective of this study was to describe the design, structure and current status of the Bulgarian plant genetic resources documentation system, with particular emphasis on the information architecture of the GeneBankSystem at IPGR-Sadovo, the implementation of standardized descriptors, the documentation of enrichment of collections, data management and the integration of national information with EURISCO.

MATERIAL AND METHOD

Source of information

The study was based on the methodological framework for plant genetic resources enrichment and documentation developed for the Bulgarian National Genebank at IPGR-Sadovo. The

documentation procedures, database structure, passport descriptors, expedition records, GeneBankSystem modules and principles of data exchange were analyzed.
The methodological framework follows international standards, particularly the FAO/Bioversity Multi-Crop Passport Descriptors (FAO/Bioversity, 2017), the FAO Genebank Standards for Plant Genetic Resources for Food and Agriculture (FAO, 2013), and the documentation and quality-management principles promoted by European program (ECPGR).
Structure of accession documentation
The basic documentation unit is the accession. Each accession receives a unique identification – catalogue number (COLLNUMB) at registration, which remains associated with the genetic resource throughout its storage, evaluation, regeneration and utilization.
The national accession number (ACCENUMB) is generated according to the established registration system and is not reused for another genetic resource.
The passport database is structured according to the FAO/Bioversity MCPD and EURISCO standards. The main groups of descriptors include:
taxonomic identification;

accession identification;

origin and acquisition;

collecting information;

geographical coordinates;

elevation;

biological status;

breeding and ancestral information;

collecting/acquisition source;

donor information;

storage conditions;

access and exchange status;

additional identifiers and remarks.

Four core fields – NICODE (National Inventory code), INSTCODE (Institute code), ACCENUMB and GENUS, provide the essential identification structure of an accession within the EURISCO framework. Their combination is intended to ensure uniqueness of the record and reduce duplication.
The system also supports the use of persistent unique identifiers PUID (Digital Object Identifier from FAO), which provide the possibility of unambiguous identification of a genetic resource at the global level.
Documentation of collecting expeditions
Expeditions constitute an important mechanism for enriching the Bulgarian genebank collections, particularly through the collection of local varieties, landraces, farmer populations and crop wild relatives. During collecting missions, seed or vegetative material is collected

together with information concerning geographic location, environmental conditions, local names, cultivation practices and traditional uses.
The documentation system includes a dedicated expedition module. It records the participants, financing organization, project, geographic and ecological characteristics of the area, and the collected accessions. Search filters facilitate retrieval of expedition records according to different criteria.
A standardized questionnaire has also been developed for interviews with farmers maintaining local varieties. The questionnaire includes expedition identification, collection date, collector, geographic location, environmental characteristics, information about the farmer, taxonomic information and local accession name, as well as information about farm size, reasons for growing the accession, production destination, seed sources and traditional uses.
GenaBankSystem (https://genbank.uni-plovdiv.net/) architecture
The Bulgarian genebank documentation system is a web-based platform designed for integrated management of information associated with the conservation, study and distribution of plant genetic resources. It consists of two interconnected functional environments.
The public component provides external users with access to accession information and searching by passport data. The protected component is available to authorized users through authentication and is intended for documentation specialists and collection curators responsible for managing accessions in the active and base collections.
The system integrates several functional modules, including:
registration of new accessions;

passport-data management;

accession searching;

expedition documentation;

storage and regeneration information;

characterization and evaluation data;

accession distribution;

data administration and updating.

This modular structure allows information associated with an accession to be maintained as a continuous record rather than as isolated datasets.
Data quality, updating and protection
Data quality is maintained through continuous updating, validation and correction. Curators are responsible for maintaining reliable information for the collections under their responsibility, while documentation specialists are responsible for the quality of passport information introduced during accession registration.
When information for a particular descriptor is unavailable and cannot be established from other sources, the field remains unfilled rather than being populated with unsupported information. Data entered into the system must remain compatible with the European exchange format to facilitate automated transfer to international information networks.
The system also provides data protection and continuity through electronic registration and archival copies maintained on primary and backup servers.

RESULTS AND DISCUSSION

Integrated documentation framework

The analysis demonstrates that the Bulgarian documentation system has evolved from a MS Access database register Phyto 2000 into an integrated digital framework for the management of plant genetic resources. GeneBankSystem connects accession identity with information generated at different stages of the conservation process.

The documentation starts with accession acquisition and registration and continues through storage, regeneration, evaluation, characterization and distribution. Consequently, the accession record represents not only a passport description but also a dynamic information resource reflecting the history and status of the genetic material.

The main categories of operational data include evaluation and characterization results, germination information, regeneration and multiplication records, storage type and distribution to users. Regular updating of these records supports the reliability and traceability of the collections. This approach corresponds to the principle that documentation should support the complete management cycle of a genebank accession rather than only its initial registration.

Standardization of passport data

One of the main strengths of the Bulgarian system is its alignment with the FAO/Bioversity Multi-Crop Passport Descriptors and EURISCO. Standardization makes it possible to describe accessions using a common taxonomy and data structure.

The database contains descriptors for taxonomic identity such as GENUS, SPECIES, SPAUTHOR, SUBTAXA and CROPNAME. Origin and collecting descriptors include COLLNUMB, COLLCODE (Collecting institute code), ORIGCTY (Country of origin), COLLSITE (Location of collecting site), COLLDATE (Collecting date) and COLLSRC (Collecting/acquisition source). Geographic information is represented through latitude, longitude and elevation.

The biological status descriptor SAMPSTAT (Biological status) allows accessions to be differentiated as wild material, traditional cultivars/landraces, breeding and research material, genetic stocks, and advanced or improved cultivars. This provides an important basis for distinguishing different categories of genetic resources within the national collection.

The system also documents storage categories, including seed collections, medium- and long-term storage, field collections, *in vitro* collections.

Such standardization is particularly important when national data are incorporated into international catalogues. EURISCO uses standardized passport descriptors to enable data exchange and facilitate access to information on European genebank collections.

Unique identification and traceability

Traceability is a central principle of the Bulgarian documentation system. Each accession receives a unique national accession number, while additional identifiers may link it to collecting institutions, donor institutions, previous catalogue numbers or other databases. The ACCENUMB identifier is assigned at registration and cannot subsequently be reused for another accession. The system therefore preserves the identity of an accession even if the original biological material is lost. This approach provides continuity between physical germplasm and its digital representation. It also supports the identification of duplicates, the management of regeneration activities and the interpretation of research data associated with individual accessions. The use of additional identifiers, donor accession numbers and persistent identifiers creates opportunities for linking national records with other institutional and international information resources.

Documentation of plant genetic resources

A specific strength of the Bulgarian system is its capacity to document local plant genetic resources collected directly from traditional agricultural systems. Local varieties and landraces are frequently maintained by small-scale farmers and gardeners outside formal breeding programmes. Their documentation therefore requires information that goes beyond

conventional passport descriptors. The expedition questionnaire developed within the methodological framework records not only the identity and geographical origin of the accession but also farmer-related information, cultivation practices, reasons for maintaining the material, production destinations, seed sources and traditional uses. This additional information increases the cultural, historical and practical value of the accession record. It can also support future research on the relationship between genetic resources, traditional knowledge, agricultural practices and local food systems. The inclusion of collecting-site information and geographic coordinates also creates opportunities for analysis. Geographic descriptors can be used to identify areas of concentration of particular genetic resources, support future collecting missions and contribute to analyses of adaptation and diversity.

In essence, the introduction activity of international free germplasm exchange, which is carried out by the genebank in Sadovo using SMTA (FAO, 2006), serves the crop improvement programs of the breeding institutes in Bulgaria. Accessions are introduced upon special requests with diverse geographical origins for study in the conditions of the country and for use as donors of valuable traits as ecological plasticity, resistance to a given pathogen, high productivity, etc. The main partners of the National Genebank in the exchange are: GRIN (USA), ICARDA, NordGen, IPK (Germany), INRA (France), John Innes Center (Great Britain).

The genebank conserves seeds of Bulgarian advanced varieties and breeding lines, the result of crop improvement programs, for long-term storage, which are registered in the GeneBankSystem with data on pedigree, breeding institution and access level.

Integration of the National Inventory with EURISCO

The Bulgarian National Genebank is presented in EURISCO and performs a coordinating role in relation to the Bulgarian National Inventory. The National Inventory integrates passport information from collections maintained by different Bulgarian scientific institutions. The National Focal Point is responsible for collecting, validating, harmonizing and periodically submitting information to EURISCO Intranet. Thus, the documentation system functions not only as an institutional database but also as a national information infrastructure connecting different plant genetic resources collections. The national-to-European data transfer is represented on the Figure 1.

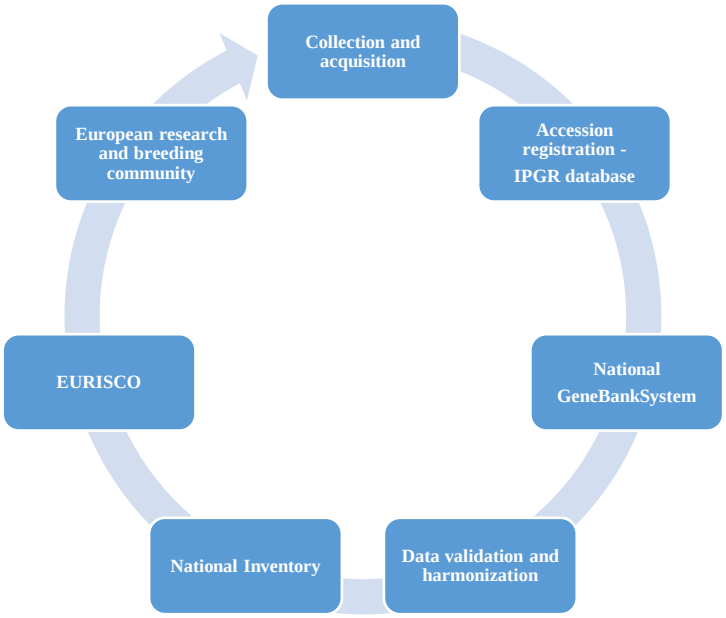

Figure 1. Integration of the Bulgarian National Inventory with European plant genetic resources community system

Such interoperability increases the international visibility of Bulgarian plant genetic resources and facilitates their identification for scientific research, breeding and conservation activities. According to Mendel et al. (2026), improved data management and documentation contribute to the visibility and usability of genebank collections. The integration with EURISCO further strengthens this role by providing a standardized European environment for accessing passport information.

Open access and user-oriented information services

The transition from an internal database to a web-based information environment represents an important development in the Bulgarian GeneBankSystem. The public interface provides external users with access to accession information, while the protected component enables professional management of the collections.

Open access is available in both Bulgarian and English, and a mobile application has been developed to facilitate access by external users.

This approach is consistent with the broader development of digital infrastructures for genebank and responds to the increasing demand for accessible and interoperable information. Open access does not replace the physical conservation of germplasm; rather, it increases the visibility of conserved material and enables potential users to identify resources before requesting biological material.

The availability of standardized passport information is particularly important for breeders and researchers because it allows them to search collections according to crop, taxonomic identity, geographical origin, biological status and other characteristics.

Data security and quality management

The implementation of data backup and controlled access is another important element of the system. Information is maintained in electronic registers and backed up on primary and secondary servers, reducing the risk of data loss and supporting continuity of genebank operations. Data quality is further supported by defined responsibilities among documentation and conservation specialists and collection curators. Information may be corrected or supplemented when new evidence becomes available. This is particularly important for historical accessions, for which passport information may initially be incomplete. The system therefore follows a dynamic model of documentation in which accession records are considered continuously improvable rather than static records created only at the time of acquisition.

Current status and development potential

The current documentation framework provides an integrated digital environment for managing accession information in the Bulgarian National Genebank. Its main achievements include standardized passport documentation, unique accession identification, expedition documentation, integration of storage and regeneration information, evaluation and characterization records, public access and interoperability with EURISCO.

According to ECPGR (2023) and Velcheva et al. (2026) the system provides a foundation for further digital development. The GeneBankSystem explicitly defines the documentation framework as a dynamic structure that is expanded and updated with innovative techniques by IS-PGR-SADOVO public financed project. Future development is focus on increasing the interoperability of phenotypic datasets, improving geospatial functionality, strengthening links between passport and characterization data, expanding and implementing additional mechanisms for data validation and quality control. An important future direction is also the integration of more detailed characterization and evaluation datasets. While passport data provide the identity and origin of accessions, characterization and evaluation data provide the information needed to assess their actual value for breeding, research and sustainable agriculture.

CONCLUSIONS

The Bulgarian GeneBankSystem represents an integrated digital framework for the management of information associated with the national germplasm collections maintained at the National Genebank of IPGR-Sadovo.

The system combines accession registration, standardized passport documentation, collecting and expedition information, geographical data, biological status, storage and regeneration records, characterization and evaluation information, and distribution data. The use of FAO/Bioversity Multi-Crop Passport Descriptors and alignment with EURISCO provide an internationally compatible structure for data exchange and interoperability.

A major achievement is the introduction of a unique and traceable accession identification system that maintains the connection between the physical genetic resource and its digital record throughout the accession conservation process. The expedition module enables the documentation of local varieties and landraces together with information on their traditional cultivation and utilization.

The integration of the Bulgarian documentation system with the National Inventory and EURISCO increases the visibility of Bulgarian plant genetic resources and facilitates their discovery and potential use by researchers, breeders and other stakeholders. The public web interface and mobile access further support the open-access principle.

The system provides mechanisms for data quality control, updating, backup and controlled access, which are essential for the long-term reliability of genebank documentation.

Overall, the Bulgarian GeneBankSystem demonstrates that digital documentation is an essential component of modern germplasm management. By connecting physical conservation with standardized, interoperable and accessible information, the system strengthens the capacity of the Bulgarian National Genebank to conserve, document, study and promote the sustainable use of plant genetic resources. Its modular and dynamic structure provides a basis for further integration of new data types, innovative technologies and European and international information infrastructures.

ACKNOWLEDGEMENTS

The research work was carried out under the project IS-PGR-SADOVO “Intelligent system for managing Bulgarian plant gene pool, conserved in the genebank of IPGR-Sadovo” with the financial support of the Ministry of Education and Science, Contract number KP-06-H86/9/09.12.2024 of Bulgarian National Science Fund.

REFERENCES

Cicova, I., Mendel, Ľ., Zetochova, E., Varga, M., & Hauptvogel, R. 2026. Evaluation and Documentation of Plant Genetic Resources in the Genebank of the Slovak Republic. Journal of Mountain Agriculture on the Balkans, Vol. 29, Issue 1, 775–812.

ECPGR. 2021. Plant Genetic Resources Strategy for Europe. Rome, Italy.

ECPGR. 2023. Operational Guide for the Bulgarian Genebank. Institute of Plant Genetic Resources “Konstantin Malkov”, Sadovo.

FAO. 2006. Standard Material Transfer Agreement. Rome, Italy.

FAO. 2013. Genebank Standards for Plant Genetic Resources for Food and Agriculture. Rome, Italy. ISBN 978-92-5-108262-1.

FAO/Bioversity. 2017. Multi-Crop Passport Descriptors. Rome, Italy.

Goritschnig, S., Weise, S., Guzzon, F., Maggioni, L., van Hintum, T., Steffensen, L. L., et al. 2024. Strengthening European research cooperation on plant genetic resources conservation and use. Genetic Resources, S2, 119–134.

Malinov, P., Madanska, S., Doychev, E., Kostadinova-Tsankova, L., Stoyanov, I., & Wassilew, K. 2025. Cross-Platform Integration of Ontologies and Information Extraction for Plant Genetic

Resources for the Bulgarian National GeneBank. Proc. of 2025 International Conference Automatics and Informatics (ICAI), 305-309.
Mendel, Ľ., Cicova, I., Zetochova, E., Hauptvogel, R., Varga, M., & Velcheva, N. 2026. Development, Modernization, and Standardization of IS GRISS (Genetic Resources Information System of Slovakia). Journal of Mountain Agriculture on the Balkans, Vol. 29, Issue 1, 748–774.
Mendel, Ľ., Hauptvogel, P., & Čičová, I. 2019. Plant genetic resources information system of Slovakia as the primary source of the information. Agrobiodiversity for Improving of Nutrition, Health and Quality of Life, 3, 178–185.
Raggi, L., Caproni, L., & Negri, V. 2021. Landrace added value and accessibility in Europe: what a collection of case studies tells us. Biodiversity and Conservation, 30, 1031–1048.
Salgotra, R. K., & Chauhan, B. S. 2023. Genetic diversity, conservation, and utilization of plant genetic resources. Genes, 14(1), 174.
Stoyanova-Doycheva, A., Doychev, E., Stoyanov, S., & Toskova, A. 2020. An Intelligent Gene Bank Management System. Proc. of 2020 International Conference Automatics and Informatics (ICAI), 1-5.
Velcheva, N., Cheperigova, S., Stoyanova-Doycheva, A., Madanska, S., & Malinov, P. 2026. Methodological Guide for the Enrichment and Documentation of Plant Genetic Resources. Paisii Hilendarski University Press, Plovdiv. ISBN (print): 978-619-281-168-6, ISBN (online) 978-619-281-175-4, 58 p.

EFFECT OF FERTILIZATION REGIME AND UMBEL ORDERS ON HETEROBLASTY OF CARROT SEEDS

Alexander Trayanov[1], Nikolay Panayotov[2], Valentin Panchev[2], Kostadin Trayanov[3]

[1]Maritsa Vegetable Crops Research Institute, 32 „Brezovsko shosse" Str., 4003 Plovdiv, Agricultural Academy - Sofia, Bulgaria
[2]Agricultural University - Plovdiv, 12 „Mendeleev" Blvd., 4000 Plovdiv, Bulgaria
[3]Geosemselect LTD, Bulgaria

Corresponding author e-mail: alexander_traqnov@abv.bg

ABSTRACT

The long flowering period in carrots, starting with the flowers from the central umbel and continuing with those from the umbels on the branches of the I, II and III order, leads to the formation and maturation of seeds at different stages of the mother plant. This determines the different quality of the seeds, as well as the presence of heteroblasty in the resulting seed production. The main objective of the present study is to investigate the influence of the nutrient regime and the order of the umbels on the quality of the seeds in carrots. Three levels of NPK were studied, as follows: N – 0, 50, 70, 90 kg.ha^{-1}, P – 0, 90, 140, 190 kg.ha^{-1} and K – 0, 100, 150, 200 kg.ha^{-1}, applied once and twice. The share of individual umbels in the formation of the total seed yield, the linear dimensions of the seed – length, width and thickness, mass of 1000 seeds, the quality of the seeds by determining the germination energy, germination, mean germination time and uniformity of germination, as well as the morphological features of the seedlings – length of the embryo root and hypocotyl, and fresh and dry mass of the seedlings were determined. The different nutrient regime affects the quality of the seeds and the morphological parameters of the seedlings in carrots, helping to reduce the quality difference. This is most clearly observed when fertilizing with $N_{90}P_{90}K_{200}$, as well as with $N_{90}P_{190}K_{100}$ (once application) and $N_{90}P_{90}K_{200}$ (twice application), where the differences in germination energy and germination between seeds from individual orders are the smallest.

Key words: *Daucus carota* L., heteroblasty, germination, seed, vigour, yield

INTRODUCTION

Flowering in carrots begins with the flowers from the central umbel and continuing sequentially with the umbels on the first, second, and third order branches. This period is characterized by a long duration, with seeds forming and ripening at different stages of the mother plant's development and under different climatic conditions. This leads to the formation of seeds with different quality (Panayotov, 2005). A number of authors Manimurugan et al., (2017), Thakur et al. (2015), Panayatov (2010), Pereira et al. (2008) point out the importance of umbel order on carrot seed quality. Sutradhar et al. (2017) claim that seeds from the central umbel are with the highest quality, followed by those obtained from umbels I, II and III orders. A similar opinion is expressed by Kumar et al. (2017), who found a decrease in seed viability with increasing umbels order. All of this clearly shows the presence of heteroblasty in carrot seeds. There are various approaches that help reduce differences in seed quality. One of them is optimizing the nutritional regime when growing carrot seed plants. According to Noor et al. (2019) and Kano et al. (2012), seed vigour increased after application of higher levels of

phosphorus and potassium. In attempts to optimize the nutritional regime in carrot seed production, Iqbal et al. (2023) indicated that fertilization with $N_{150}P_{125}K_{65}$ kg.ha^{-1} resulted in an increase in seed yield and quality, as well as a decrease in their heteroblasty. In their studies, Ilyas et al. (2013) and Panayotov (2015) express the opinion that phosphorus plays an important role in better insemination of plants and obtaining seeds of equal quality. A similar conclusion ware reached by Lefarmo et al. (2019).

For successful carrot seed production is essential importance the control of carrot fly (Psila rosae Fabr.). This pest is widespread in Europe, North America and New Zealand (Collier & Finch, 1996; Ramert & Ekbom, 1996; Sivasubramaniam, 1996). In the 1950s, chemical control with the pest was carried out using organochlorine compounds (Wright & Coaker, 1968). In modern plant protection practice, insecticides from the group of synthetic pyrethroids are widely used to control of carrot fly.

The main objective of the present study was to determine the differences in carrot seed quality depending on the fertilization regime and umbel order.

MATERIAL AND METHOD

The experiments were carried out during the period 2017-2019 in the Experimental Field and Laboratory of the Department of "Horticulture" at the Agricultural University - Plovdiv, Bulgaria with carrots, variety Tushon. Seed production was carried out using the technology adopted in Bulgaria by preliminary production of stecklings (Murtazov et al., 1984). The stecklings were produced by sowing at the end of June and harvesting in mid-November, after which they were placed for storage during the winter period in a pit. Soil preparation was carried out by deep autumn plowing and furrow profiling in the spring. The stecklings were planted in mid-March according to a scheme of 80x30 cm. Each variant was presented in four replicates with a experimental plot size of 7 m^2 and a explored area of 6 m^2 (Barov, 1982).

Two fertilization regimes were studied: 1. Once fertilization, by applying the entire amount of phosphorus and potassium fertilizers in the fall before deep plowing and nitrogen during planting; 2. Double fertilization - half of the phosphorus and potassium fertilizers were applied before autumn deep plowing, the other half in the spring before planting, and nitrogen fertilizer - half before planting, and the other part during the growing season at the beginning of flowering. The following variants with different fertilization levels in kg.ha^{-1} and application term were studied:: once fertilization: 1.$N_0P_0K_0$ – control; 2.$N_{70}P_{140}K_{150}$ (recomended); 3.$N_{50}P_{90}K_{100}$; 4.$N_{50}P_{90}K_{200}$; 5.$N_{50}P_{190}K_{100}$; 6.$N_{50}P_{190}K_{200}$; 7.$N_{90}P_{90}K_{100}$; 8.$N_{90}P_{90}K_{200}$; 9.$N_{90}P_{190}K_{100}$; 10.$N_{90}P_{190}K_{200}$ and twice fertilization: 11.$N_{50}P_{90}K_{100}$; 12.$N_{50}P_{90}K_{200}$; 13.$N_{50}P_{190}K_{100}$; 14.$N_{50}P_{190}K_{200}$; 15.$N_{90}P_{90}K_{100}$; 16.$N_{90}P_{90}K_{200}$; 17.$N_{90}P_{190}K_{100}$; 18.$N_{90}P_{190}K_{200}$. The different fertilizer rates are determined based on the recommended fertilization for carrot seed production in Bulgaria $N_{70}P_{140}K_{150}$ (Madzharova, 1968; Kolev et al. 1977).

The following fertilizers were used: ammonium nitrate (N 34%), triple superphosphate (P2O5 46%) and potassium sulfate (K2O 50%). During the vegetation of the seed plants, all necessary cultural practices were carried out for their normal development. The seed production was harvested when 60-70% of the seeds were fully mature, and the rest were waxy ripe. The seed stalks were placed for 10 days for post-harvest ripening of the seeds. The seeds from the umbels of the individual orders – central (king), I, II and III, were cleaned separately, after which their linear dimensions – length, width and thickness – were determined (Panayotov, 2015), the mass of 1000 seeds was determined according to the requirements of ISTA (2013). The percentage contribution of individual umbels to the total seed yield was calculated. The germination energy and germination of the seeds from the central umbel and umbels I, II and III order were determined according to the requirements of ISTA (2013). The mean germination time was calculated using the formula proposed by Battle and Whittington (Wellington, 1972). The

uniformity of germination was determined using the Strona method described in detail in Panayotov (2015). The vigor index was calculated using the "Initial vegetative productivity of seeds" method (Panayotov, 2013). The length of the embryo root and hypocotyl was determined on the day of germination determination, by measuring 10 seedlings in four replicates. The fresh mass of one seedling was assessed by measurement of each developed seedling from the three replicates on scale accurate to the third digit and divided into the number of these seedlings. The dry mass of the seedling was determined using a drying oven according to the method described by Black et al. (2008).

During the period of steckling production and the cultivation of seed plants yellow sticky traps were placed to detect the presence of the carrot fly (*Psila rosae* Fabr.).

If an infestation is detected, various insecticides from the synthetic pyrethroid group will be used for control.

Due to the similarity in trends over the three years of the experiment, the results shown are the average three-year data.

The data from the study were subjected to analysis of variance (Fowel and Cohen, 1992), and the least significant differences between the individual variants were calculated using the Fisher test at $p = 0.05$, according to the ANOVA method.

RESULTS AND DISCUSSION

The formation of high and quality seed yields in carrots depends of many factors with ecological and agrotechnological character. For the normal development of seed plants, correct plant protection is essential, especially against pests. During the vegetation period, when field experiments were carried out, no pests with an economic threshold of harmfulness were observed. Carrot seed plants are characterized by a specific morphology, which determines the different participation of individual umbels in the formation of the yield. On average for all tested variants, the share of first-order umbels is 50.61%, followed by second-order umbels with 30.57% (Figure 1). This is due to the larger number of umbels that develop along the branches from first and second order. The umbels from the last III order and the umbels from the central stems are characterized by the least participation. A similar opinion is expressed by Panayotov (2010) and Mengistu and Yamoah (2010), who point out that despite the largest size of the central umbel, as well as the largest weight of the seeds formed in it, the first-order umbels have a major share in the yield, which is related to their greater number.

The participation of the central umbel in productivity is highest after once and twice fertilization with the $N_{50}P_{90}K_{200}$ combination - 16.24 and 15.67%, respectively. The share of first-order umbels increases more significantly after the application of $N_{90}P_{90}K_{100}$ (once) and $N_{90}P_{190}K_{100}$ (twice). A once application of $N_{50}P_{190}K_{200}$, as well as a twice application of $N_{90}P_{90}K_{200}$ and $N_{50}P_{90}K_{200}$ leads to a more significant increase in the percentage share of umbels from second and third order in the total seed yield.

The mass of 1000 seeds is an important indicator that is closely related and depends on the size and density of the seeds. Its importance is also determined by the fact that it directly participates in determining the seeding rate (Mihov et al., 2014).

In carrots, the mass of 1000 seeds decreases smoothly with increasing umbel order. For unfertilized plants, i.e. when developing without additional impact, compared to that of the central umbel, it decreases by 3.38% for the first order and significantly more for the second and third, respectively 19.30 and 27.82% (Figure 2).

In the central umbel, this indicator has the highest value for the option fertilized once with $N_{50}P_{90}K_{100}$ – 1.276 g, followed by $N_{50}P_{90}K_{200}$ and $N_{90}P_{90}K_{200}$ again applied once – 1.269 and 1.178 g, respectively. When applying mineral fertilizers twice, an increase was recorded for the combinations $N_{90}P_{90}K_{200}$ – 1.206 g and $N_{50}P_{90}K_{200}$ – 1.110 g.

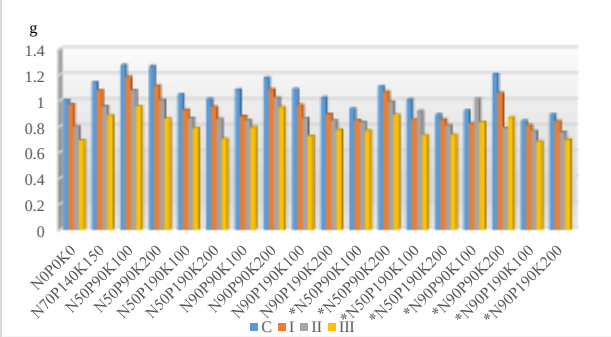

* twice fertilization; C – central umbel; I, II, III – orders;

Figure 1. Share of umbels in the formation of seed yield denending on the fertizition regime and umbel order, (%)

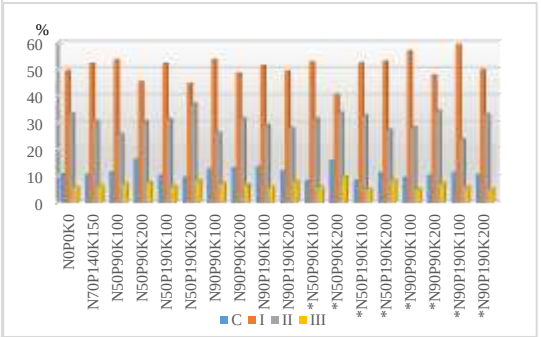

* twice fertilization; C – central umbel; I, II, III – orders;

Figure 2. Mass of 1000 seeds depending on the fertilization regime and umbel order, (g)

Seeds from the first-order umbels are characterized by a maximum absolute mass after once application of $N_{50}P_{90}K_{100}$ – 1.184 g, which represents an increase of 0.103 g compared to the fertilized control and 0.249 g compared to the zero control. Fertilization with $N_{50}P_{90}K_{200}$ and $N_{90}P_{90}K_{200}$ leads to produce seeds with the highest mass at the other time of application of mineral fertilizers – 1.071 g and 1.060 g, respectively. A similar pattern was observed for the seeds of the last two orders – II and III.

The applied fertilization levels reduce the existing heteroblasty in carrot seeds. This applies especially to seeds of the III and II order compared to the central umbel and the I order. This decrease is stronger observed in most variants with twice fertilization and compared to the unfertilized dcontrol it is more than doble compared to all previous orders. The reduction in heteroblasty between seeds from the central umbel and from the first order is weaker.

The linear dimensions of seeds have important practical significance for seed cleaning, sorting and mechanized sowing (Panayotov, 2015; Black et al., 2008). The seeds from the central umbel are characterized by the highest values of the three linear dimensions, followed by those from the first-order umbel (Table 1).

A more significant decrease in length, width and thickness is found in seeds from umbels of the II and especially III order. Panayotov (2010) also reaches a similar conclusion. Fertilizing the carrot seed plants with $N_{50}P_{90}K_{200}$ and $N_{90}P_{90}K_{200}$ at both terms leads to an increase in the linear dimensions of the seeds in individual umbels. A stronger decrease in heteroblasty of the seeds, however, is observed after the application of $N_{50}P_{190}K_{100}$ (once) and $N_{50}P_{190}K_{100}$ and $N_{50}P_{190}K_{200}$ (twice).

To determine the quality of seeds, the most important thing is to establish the basic vital indicators - germination energy and germination. The highest germination energy for all orders was recorded for the variant with single fertilization $N_{90}P_{90}K_{200}$, with the exception of the first order where it was with a twice fertilization. For the central umbel it reaches 83.44% and decreases by 4.12% for seeds of the first order, by 8.78% for those of the second order and by 13.0% for those of the third order (Figure 3). A similar trend was observed for germination (Figure 4).

From this it can be assumed that seeds that were formed at an earlier stage of the development of the mother plants ripen better, accumulate more nutrients and are characterized by higher quality. A similar opinion is expressed by Sutradhar et al. (2017).

Depending on the applied nutritional regime, the heteroblasty in germination energy and seed germination decreases, and this is observed more clearly in seeds from the first-order umbels compared to those from the central umbel, especially well expressed after once fertilization with $N_{90}P_{90}K_{200}$ and $N_{90}P_{190}K_{100}$, as well as twice with $N_{90}P_{90}K_{100}$ and $N_{90}P_{90}K_{200}$.

Mean germination time is an important indicator that better determines the vital status of seeds (Panayotov, 2015).

Table 1. Linear dimensions of carrot seeds depending on the fertilization regime and umbel order (mm)

Variants	C			I			II			III		
	L	W	T	L	W	T	L	W	T	L	W	T
Once fertilization												
$N_0P_0K_0$	2.73	1.08	0.49	2.59	1.03	0.46	2.35	0.96	0.44	2.33	0.94	0.35
$N_{70}P_{140}K_{150}$	2.77	1.18	0.52	2.74	1.19	0.52	2.55	1.09	0.51	2.31	0.92	0.45
$N_{50}P_{90}K_{100}$	2.80	1.16	0.53	2.66	1.09	0.48	2.55	1.02	0.50	2.39	0.93	0.44
$N_{50}P_{90}K_{200}$	3.00	1.12	0.52	2.77	1.19	0.55	2.53	1.08	0.49	2.33	1.02	0.48
$N_{50}P_{190}K_{100}$	2.79	1.18	0.50	2.73	1.16	0.49	2.42	1.06	0.45	2.29	1.02	0.42
$N_{50}P_{190}K_{200}$	2.74	1.08	0.53	2.56	1.00	0.53	2.57	0.97	0.48	2.40	0.88	0.49
$N_{90}P_{90}K_{100}$	2.83	1.09	0.46	2.68	1.08	0.48	2.53	0.96	0.44	2.40	0.89	0.42
$N_{90}P_{90}K_{200}$	2.85	1.15	0.51	2.70	1.10	0.49	2.59	1.01	0.44	2.31	0.96	0.40
$N_{90}P_{190}K_{100}$	2.71	1.09	0.50	2.60	1.03	0.46	2.36	1.01	0.45	2.24	0.96	0.42
$N_{90}P_{190}K_{200}$	2.70	1.14	0.51	2.59	1.03	0.47	2.61	1.02	0.46	2.29	0.93	0.39
Twice fertilization												
$N_{50}P_{90}K_{100}$	2.63	1.11	0.50	2.62	1.11	0.52	2.44	1.04	0.45	2.23	0.97	0.43
$N_{50}P_{90}K_{200}$	2.78	1.14	0.51	2.80	1.07	0.47	2.47	0.98	0.44	2.34	0.99	0.43
$N_{50}P_{190}K_{100}$	2.62	1.06	0.52	2.58	1.00	0.47	2.43	0.95	0.42	2.30	0.89	0.38
$N_{50}P_{190}K_{200}$	2.64	1.08	0.56	2.58	1.07	0.51	2.41	1.04	0.46	2.23	0.94	0.41
$N_{90}P_{90}K_{100}$	2.72	1.13	0.52	2.51	1.01	0.50	2.44	1.00	0.41	2.22	0.92	0.42
$N_{90}P_{90}K_{200}$	2.74	1.16	0.50	2.64	1.04	0.48	2.55	1.05	0.45	2.30	1.01	0.41
$N_{90}P_{190}K_{100}$	2.75	1.12	0.49	2.47	1.04	0.49	2.42	1.01	0.45	2.27	0.92	0.40
$N_{90}P_{190}K_{200}$	2.90	1.16	0.56	2.68	1.10	0.50	2.45	1.03	0.45	2.11	0.79	0.34
LSD p=0.05%	**0.29**	**0.12**	**0.05**	**0.21**	**0.12**	**0.08**	**0.20**	**0.09**	**0.06**	**0.22**	**0.13**	**0.09**

L – length; W – width; T – thickness; C – central umbel; I, II, III – order;

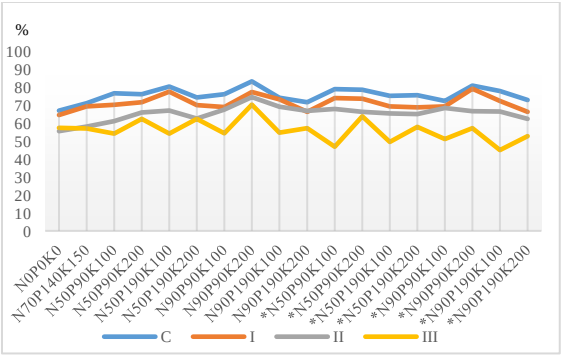

* twice fertilization; C – central umbel; I, II, III – orders;

Figure 3. Germination energy of carrot seeds depending on the fertilization regime and umbel order, (%)

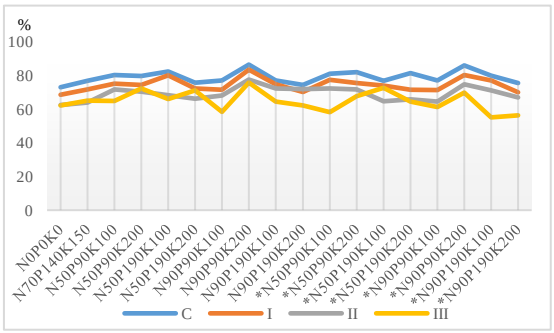

* twice fertilization; C – central umbel; I, II, III – orders;

Figure 4. Germination of carrot seeds depending on the fertilization regime and umbel order, (%)

The number of days required for germination of seeds from the central umbel and the first-order umbels is about 4 (Table 2). Regardless of the small differences, it can be noted that the seeds from the central umbel germinate faster, with the shortest period was recorded for the combination $N_{90}P_{190}K_{200}$, applied twice (3.32 days). For seeds from first-order umbels, mean germination time decreases significantly after twice fertilization with $N_{90}P_{90}K_{100}$ (3.79 days). Seeds from the second-order umbels and especially from the third-order umbels germinate much more slowly. The most days for this – 6.05 and 6.31, were required, respectively, for once fertilization with $N_{50}P_{90}K_{100}$ for the second umbel and for a twice fertilization with $N_{90}P_{90}K_{100}$ for the third order seeds, which is approximately 3 days more than the values for the central umbel.

Table 2. Sowing qualities of carrot seeds depending on the fertilization regime and umbel order

Variants	Mean germination time (days)				Uniformity of germination (%)			
	C	I	II	III	C	I	II	III
Once fertilization								
$N_0P_0K_0$	3.52	4.23	4.31	5.42	13.84	11.90	8.76	7.82
$N_{70}P_{140}K_{150}$	3.65	3.84	5.42	5.79	15.70	13.10	10.26	11.00
$N_{50}P_{90}K_{100}$	3.68	4.49	6.05	6.10	11.91	11.92	11.14	10.15
$N_{50}P_{90}K_{200}$	3.46	3.98	4.43	5.99	15.17	13.74	11.43	8.16
$N_{50}P_{190}K_{100}$	3.95	3.88	4.90	5.81	10.64	12.71	11.98	8.38
$N_{50}P_{190}K_{200}$	3.97	3.92	4.90	5.63	12.48	13.16	9.68	9.53
$N_{90}P_{90}K_{100}$	3.77	5.13	5.86	6.03	15.16	11.90	9.23	8.25
$N_{90}P_{90}K_{200}$	3.58	4.08	4.60	5.30	14.04	16.07	13.24	12.32
$N_{90}P_{190}K_{100}$	3.72	4.17	4.87	6.13	12.68	10.99	11.40	9.42
$N_{90}P_{190}K_{200}$	3.98	4.36	4.87	4.95	13.21	9.99	9.47	10.84
Twice fertilization								
$N_{50}P_{90}K_{100}$	3.71	4.07	5.11	6.01	12.75	12.15	11.62	7.49
$N_{50}P_{90}K_{200}$	3.69	4.37	4.83	5.62	13.31	11.42	9.50	9.92
$N_{50}P_{190}K_{100}$	3.75	4.28	4.77	6.13	14.07	12.37	12.93	9.30
$N_{50}P_{190}K_{200}$	3.75	3.89	4.73	5.15	11.78	13.78	9.44	9.36
$N_{90}P_{90}K_{100}$	3.52	3.79	4.78	6.31	12.07	12.73	9.82	7.19
$N_{90}P_{90}K_{200}$	3.64	4.07	5.16	5.75	12.11	15.50	11.53	10.31
$N_{90}P_{190}K_{100}$	3.72	4.17	5.01	5.29	13.01	12.80	9.35	8.99
$N_{90}P_{190}K_{200}$	3.32	4.11	5.01	6.21	15.06	10.10	10.71	6.65
LSD p=0.05%	**0.55**	**0.79**	**0.92**	**1.27**	**4.11**	**3.54**	**1.92**	**2.41**

C – central umbel; I, II, III – orders;

It can be pointed out that the seeds of the last, third order, which are characterized by the lowest quality, germinate almost twice slowly compared to the seeds from the central stems and the umbels of the first-order branches.

The heteroblasty between the seeds from the central umbel and the first umbels is higher only for the variant $N_{90}P_{90}K_{100}$, applied once, while for $N_{50}P_{190}K_{200}$ in the same regime and for $N_{50}P_{190}K_{200}$ when applied twice, it is almost absent.

The differences in mean germination time between seeds of the first and second order are also insignificant, increasing slightly with a twice application of the higher fertilizer rates, and compared to the central umbel, the differences reach almost one day, but are lower compared to the control.

The strongest heteroblasty was recorded for the seeds from the third order, compared to those from the central stems, with the difference for the fertilized and unfertilized controls being approximately two days, while with the optimization of the nutritional regime it decreases, especially for $N_{90}P_{190}K_{200}$ and $N_{50}P_{190}K_{200}$ (once) and $N_{50}P_{190}K_{200}$ and $N_{90}P_{190}K_{100}$ (twice).
According to Copeland and McDonald (2001), uniformity of seed germination is essential for better crop establishment.
Most uniformity germinate the seeds from central umbel, follow from umbels with higher order – I, II and III. A higher percentage of uniformity germinated seeds from the central umbel was found in the fertilized control – 15.70%. Close to this result are the variants fertilized with $N_{50}P_{90}K_{200}$ (15.17%) and $N_{90}P_{90}K_{100}$ (15.16%) applied once, as well as with twice fertilization with maximum amounts of the three fertilizers $N_{90}P_{190}K_{200}$ (15.06%).
Germination efficiency decreases with increasing umbel order, reaching it's minimum in seeds of the last third order. However, optimizing the nutritional regime improves seed quality, which is particularly evident when applying $N_{90}P_{90}K_{200}$ at both fertilization terms.
The heteroblasty between the seeds from the central umbel and those from the first-order umbels decreased more significantly after twice fertilization with $N_{90}P_{90}K_{100}$, as well as with the combination $N_{50}P_{90}K_{100}$, regardless of the method of application. Higher heteroblasty was reported between seeds of the second and third order, compared to those from the central umbel, with a decrease observed after fertilization with $N_{90}P_{90}K_{200}$.
The morphological characteristics of the seedlings are essential for determining the viability of the seeds. Different fertilizer rates, as well as the method of fertilization, affect the length of the different parts of carrot seedlings.
The maximum length of the embryo root in the seeds from the central umbel was recorded after twice fertilization with $N_{90}P_{190}K_{100}$ – 2.54 cm (Figure 5). At the first application period of mineral fertilizers, it reaches a greater length in the variants $N_{50}P_{90}K_{100}$ and $N_{50}P_{90}K_{200}$ – 2.39 cm, followed by $N_{90}P_{90}K_{200}$ – 2.31 cm.
A more significant growth of the embryo root for the seedlings from first-order umbels was observed after twice fertilization with $N_{90}P_{90}K_{100}$ – 2.77 cm, in contrast to the zero control, where only 1.77 cm was recorded. Good results are also found for the variants $N_{90}P_{190}K_{100}$ (twice) and $N_{50}P_{190}K_{100}$ (once), 2.48 cm and 2.51 cm, respectively.
A relatively shorter embryo root, in most of the tested fertilization methods, develops the seeds of the second and especially the third order. In the first case, once fertilization has the strongest effect at levels $N_{90}P_{190}K_{100}$, $N_{90}P_{90}K_{200}$ and $N_{50}P_{90}K_{100}$, and when applying fertilizer rates twice, the maximum length is recorded for the variant $N_{50}P_{190}K_{100}$. Once fertilization with $N_{90}P_{90}K_{100}$ and twice fertilization with $N_{50}P_{90}K_{200}$ causes the development of seedlings with the longest embryo root in the seeds of the last third order. The difference in seed quality from different umbels decreases more significantly after once application of $N_{50}P_{90}K_{200}$ and twice application of $N_{50}P_{190}K_{100}$.
Different levels of N, P and K, as well as their frequency of application, have weak effect on hypocotyl length in carrot seedlings. A more significant increase in the values of the monitored indicator for the seeds of all orders was recorded after a once fertilization with $N_{90}P_{90}K_{200}$, as well as after $N_{90}P_{190}K_{200}$ for the twice method of the applying mineral fertilizers (Figure 6).
This indicator is less affected by heteroblasty. Nevertheless, optimizing the nutrient regime leads to it's reduction, and this is more significantly observed in the variants fertilized once with $N_{90}P_{90}K_{100}$ and with $N_{90}P_{90}K_{200}$, and twice with $N_{50}P_{190}K_{200}$.

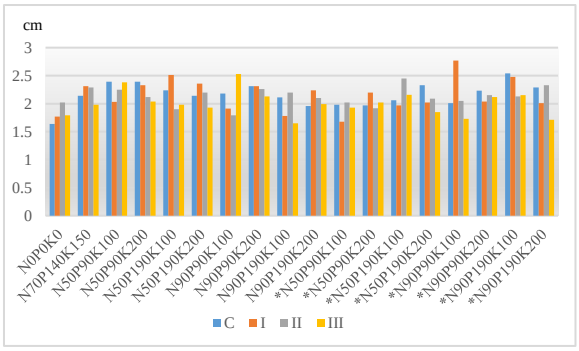

* twice fertilization; C – central umbel; I, II, III – orders;

Figure 5. Length of the embryo root of carrot seedlings depending on the fertilization regime and umbel order, (cm)

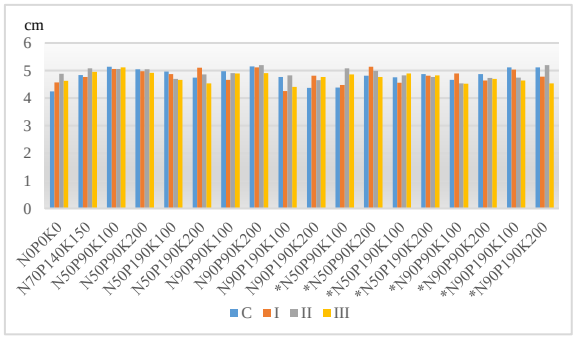

* twice fertilization; C – central umbel; I, II, III – orders;

Figure 6. Length of the hypocotyl of carrot seedlings depending on the fertilization regime and umbel order, (cm)

Seedling fresh mass is a main parameter in many tests to determine seed vigour (Copeland and McDonalds, 2001; Black et al, 2008; Panayotov, 2015). This determines it's importance for a more complete characterization of the vital status of vegetable seeds.

The fresh mass of the seedlings from the seeds from the central umbel increased significantly in the variant fertilized twice with $N_{90}P_{90}K_{200}$ (13.25 mg) (Table 3). This represents an increase of 27.89% compared to the unfertilized control and 12.67% compared to the fertilized control. At the first term of application of mineral fertilizers increase increase in mass was observed at $N_{50}P_{90}K_{100}$ – 12.85 mg.

The mass of one seedling in the seeds of I order umbels is highest after application of $N_{50}P_{90}K_{100}$ (once) – 12.30 mg, as opposed to the zero and fertilized controls, where it is 10.50 mg and 11.57 mg, respectively.

For seeds from secondary umbels, the weight of the pods for most of the tested combinations is around 10 mg. A more significant increase was found with the fertilizer rate $N_{90}P_{90}K_{200}$ (once application) – 11.37 mg, which is represent with 0.93 mg and 1.37 mg more than the recommended rate and when growing plants without fertilization.

The values obtained for the seeds from the last, third order, are in range from 7.87 mg for $N_{90}P_{90}K_{100}$ (twice) to 10.30 mg for $N_{50}P_{90}K_{100}$ and $N_{90}P_{90}K_{200}$, again applied twice.

Good results have also been reported for $N_{50}P_{90}K_{200}$ regardless of the method of application. A more significant reduction in differences between seeds from individual orders is found for $N_{50}P_{90}K_{200}$ at both application terms, as well as for $N_{90}P_{190}K_{100}$ (once).

Determining the parameters of the absolute dry mass of the seedlings makes it possible to gain an idea of the physiological status of the seeds. The presence of higher values also determines the suitability subsequently from these seeds to be formed a better plants.

The seedlings from the central umbel developed a higher absolute mass after twice fertilizations with maximum amounts of the three fertilizers – 4.55%. A good result is also reported for the combination $N_{50}P_{90}K_{100}$ – 4.33%. At the first application period, the highest percentage was reported for the fertilizer rate $N_{50}P_{190}K_{100}$ (4.21).

The absolute dry mass for the seedlings from the first-order umbels for most of the variants is about 4%. A weak decrease was found in once application of $N_{50}P_{190}K_{100}$.

A more significant increase in the values of the monitored indicator in the second-order canopies was found for the variant fertilized twice with $N_{90}P_{90}K_{100}$ (3.66%), which represents an increase of 0.78% compared to the zero control and 0.44% compared to the fertilizer rate used to the moment in carrot seed production.

For the umbels of the last III order, the data obtained are in range from 2.66% for $N_{50}P_{190}K_{200}$ to 4.22% for $N_{50}P_{90}K_{200}$ and $N_{90}P_{190}K_{200}$ applied twice.

In this indicator, the heteroblasty between seeds from umbels with different orders is less affected by the applied nutritional regime. Regardless of this, it can be noted that a decrease is observed after fertilization with $N_{90}P_{190}K_{100}$ (once) and $N_{90}P_{90}K_{100}$ (twice).

Table 3. Morphological characteristics of carrot seedlings depending on the fertilization regime and umbel order

Variants	Fresh mass of one seedling (mg)				Absolute dry mass of seedlings (%)			
	C	I	II	III	C	I	II	III
Once fertilization								
$N_0P_0K_0$	10.36	10.50	10.00	10.22	3.99	3.29	2.88	3.22
$N_{70}P_{140}K_{150}$	11.76	11.57	10.44	8.45	3.33	3.33	3.22	3.44
$N_{50}P_{90}K_{100}$	12.85	12.30	10.38	9.27	3.88	3.72	3.55	3.66
$N_{50}P_{90}K_{200}$	11.56	12.01	10.34	10.28	3.63	3.33	2.99	3.77
$N_{50}P_{190}K_{100}$	10.09	10.79	9.83	8.97	4.21	2.88	3.21	3.55
$N_{50}P_{190}K_{200}$	8.49	10.74	9.67	8.88	3.73	3.44	2.55	3.32
$N_{90}P_{90}K_{100}$	11.07	9.55	9.70	9.68	3.86	3.77	2.99	3.33
$N_{90}P_{90}K_{200}$	11.17	10.20	11.37	9.64	3.66	3.21	2.66	3.11
$N_{90}P_{190}K_{100}$	9.08	10.20	9.45	10.00	3.88	3.11	3.11	2.99
$N_{90}P_{190}K_{200}$	9.43	10.88	10.14	9.66	3.77	2.99	3.33	2.99
Twice fertilization								
$N_{50}P_{90}K_{100}$	9.03	10.18	10.07	10.30	4.33	4.22	3.21	3.88
$N_{50}P_{90}K_{200}$	11.04	10.72	10.51	10.23	3.99	3.88	3.33	4.22
$N_{50}P_{190}K_{100}$	10.56	9.22	10.28	8.76	3.55	3.66	2.99	2.88
$N_{50}P_{190}K_{200}$	11.51	10.59	8.56	9.33	3.66	3.66	3.10	2.66
$N_{90}P_{90}K_{100}$	9.71	11.33	9.63	7.87	3.88	3.66	3.66	3.33
$N_{90}P_{90}K_{200}$	13.25	9.50	9.88	10.30	3.88	3.88	3.55	3.77
$N_{90}P_{190}K_{100}$	11.68	10.98	10.36	9.75	3.88	3.88	3.22	3.66
$N_{90}P_{190}K_{200}$	12.58	9.84	9.76	8.85	4.55	3.77	3.33	4.22
LSD p=0.05%	**3.03**	**2.38**	**2.47**	**3.28**	**0.96**	**0.81**	**0.90**	**0.80**

C – central umbel; I, II, III – orders;

CONCLUSIONS

The seed yield of carrots is formed primarily from the seeds from the first-order and second-order umbels. Once fertilization with $N_{90}P_{90}K_{100}$ and double fertilization with $N_{90}P_{190}K_{100}$ lead to an increase in the percentage participation of these umbels in the formation of the total seed yield.

As a result of the applied fertilization levels and regimes, heteroblasty between seeds from umbels with different order were reduced in most indicators. This is most significantly observed when fertilizing with $N_{90}P_{90}K_{200}$, as well as with $N_{90}P_{190}K_{100}$ (once) and $N_{90}P_{90}K_{200}$ (twice), where the differences in germination energy and germination between seeds from individual orders are the smallest.

The highest absolute mass and linear dimensions were found for seeds from the central umbel and they decreasing with increasing umbel order. A more significant increase in their values

and a decrease in the heteroblasty was reported after fertilization with $N_{50}P_{90}K_{100}$, $N_{50}P_{90}K_{200}$ and $N_{90}P_{90}K_{200}$.

The length of the embryo root in seeds of all orders increased after twice fertilization with $N_{90}P_{90}K_{100}$ and $N_{90}P_{190}K_{100}$, while that of the hypocotyl increased more significantly as a result of a once fertilization with $N_{90}P_{90}K_{200}$, as well as with $N_{90}P_{190}K_{200}$ for the twice method of applying of the mineral fertilizers.

The fresh mass of one seedling increases after fertilization with $N_{50}P_{90}K_{100}$ and $N_{90}P_{90}K_{200}$, regardless of the method of application. The seedling developed higher absolute dry mass as a result of twice fertilizations with $N_{90}P_{190}K_{200}$ and $N_{50}P_{90}K_{200}$, as well as and once fertilization with $N_{50}P_{190}K_{100}$. These two indicators are weakly influenced by umbel order.

REFERENCES

Barov, V. 1982. Analyses and schemes of field experiments. National Agriculture and Industrial Complex, Sofia: 668. (Bg)

Black, M., J. Bewley, P. Halmer. 2008. The encyclopedia of seed science, technology and uses. Cromwell Press, Trowbridge, UK: 828.

Copeland, L.O., M. B. Mc Donald. 2001. Longevity and deterioration. In: Copeland, L.O. (ed.). Principles of seed science and technology, Chapman & Hall Ltd., London: 181-220.

Collier, R. H., S. Finch. 1996. Field and laboratory studies on the effects of temperature on the development of the carrot fly (*Psila rosae* F.). Annals of Applied Biology, 128(1):1-11.

Fowel, J., L. Cohen. 1992. Practicle statistics for field biology, Publishing house John Wiley & Sons, New York: 272.

Iqbal, M, F., R. A. Majeed, S. Najeebullah, S. B. Baran, M. Touseef, M. S. Saeed, F. Hussain, M. A. Mahesar. 2023. Determination of several NPK levels on the growth and seed yield of carrot (*Daucus carota* L.), Annals of Agriculture and Environment, 1(1): 17-20.

Ilyas, M., G. Ayub, N. Ahmad, O. Ullah, S. Hassan, R. Ullah. 2013. Effect of different stickling size and phosphorous levels on seed production in carrot (*Daucus carota* L.), Middle East Journal of Scientific Research, 17(3): 280-286.

ISTA. 2013. International Rules for Seed Testing, International Seed Testing Association, Bassersdorf, CH-Switzerland.

Kolev, N., A. Michov, St. Buchvarov. 1977. Vegetable seed production. Zemizdat, Sofia: 403. (Bg)

Kano, C., A. Cardoso, R. Villas Bôas. 2012. Phosphorus rates on yield and quality of lettuce seeds. Horticultura Brasileira, 30: 695-698.

Kumar, A., B. Aferoza, S. Mushtaq, A. Nabi, S. Mufti. 2017. Standartization of spacing and steckling size for quality seed production of carrot (*Daucus carota* L.) under Kashmir valley conditions. Annals of Biology, 33(1): 117-119.

Lefarmo, T., W. Mohammed, K. Woldetsadik. 2019. Effect of blended NPS fertilizer, root type and root treatment on yield and yield component of carrot (Daucus carota L.) seed at Haramaya, Eastern Ethiopia. J. Hortic. Sci. For., 1: 203.

Madzharova, D. 1968. Root vegetable crops. Publishing by Academy of Agricultural Science, Sofia: 184. (Bg)

Mihov, Kr., N. Panayotov, S. Filipov, T. Babrikov, K. Kostadinov, D. Haitova. 2014. Manual for exercises in vegetable production with seed production. Publishing house of the Agricultural University-Plovdiv: 168. (Bg)

Murtazov, T., Il. Minkov, Ghr. Petrov. 1984. Vegetable production with selection and seed production of vegetable crops. Christo G. Danov, Plovdiv: 379. (Bg)

Manimurugan, C., V.K. Pandita, B.S. Tomar, N. Gupta, P.M. Singh. 2017. Effect of plant density and foliar nutrient application on seed yield and quality in Asiatic carrot (*Daucus carota* L.). Indian Journal of Agricultural Sciences, 87(3): 419-424.

Mengistu, T., Ch. Yamoah. 2010. Effect of sowing date and planting density on seed production of carrot (*Daucus carota* var. *sativa*) in Ethiopia. African Journal of Plant Science, 4(8): 270-279.

Noor, A., K. Ziaf, M. Amjad, R. Ahmad. 2019. Potash application enhances the yield and seed attributes of carrot by improving the quality of tertiary umbel seeds. Pak. J. Agri. Sci., 56(1): 83-94.

Panayotov, N. 2015. Seed science and factors of seed production of the vegetable crops. Publishing house of the Agricultural University-Plovdiv: 290. (Bg)

Panayotov, N. 2013. Initial vegetative production of the seeds – method for determination of vigor. Journal of Crop science, Academy of Agricultural Science, 50: 52-57. (Bg)

Panayotov, N. 2005. Technological managenment and factors influencing seed quality of vegetable crops, In: Dris Ramdane (ed.). Vegetables: Growing Environment and Mineral Nutrition, WFL Publisher, Helsinki, Finland: 138-165.

Panayotov, N. 2010. Heterogeneity of carrot seeds depending on their position on the mother plant. Folia Horticulturae, 22(1): 25-30.

Pereira, R.S., W.M. Nascimento, J. V. Vieira. 2008. Carrot seed germination and vigor in response to temperature and umbel orders, Scientific Agriculture, 65: 145-150.

Ramert, B., B. Ekbom. 1996. Intercropping as a management strategy against carrot rust fly (diptera: Psilidae): A test of enemies and resource concentration hypotheses. Environmental Entomology, 25(5): 1092-1100.

Sivasubramaniam, W. 1996. The role of monitoring, reduced-rate insecticides and insecticide placement in the control of carrot rust fly (*Psila rosae* F.) in Canterbury, New Zealand. (Ph.D., Lincoln University).

Sutradhar, H., V.K. Pandita, B.S. Tomar, R.N. Yadav. 2017. Studies on contribution of umbel order on seed yield and quality under different planting ratio and plant spacing in carrot hybrid, Pusa Vasuda. Vegetable Science, 44(2): 91-94.

Thakur, A.K., A. Vikram, H.S. Kanwar, R.K. Bhardwaj. 2015. Effect of storage and umbel orders on seed quality of European carrot cultivar Solan Rachna under cold desert conditions of Himachal Pradesh. International Journal of Bio-resource and Stress Management, 6(1): 63-67.

Welington, P. S. 1972. Handbook for seedling evaluation, Proceeding of the International Seed Testing Association, 35: 175.

Wright, D. W., T. H. Coaker. 1968. Development of dieldrin resistance in carrot fly in England, Plant Pathology, 17: 178-181.

DEVELOPMENT AND PERFORMANCE EVALUATİON OF NPK-BASED SLOW-RELEASE FERTİLİZER FORMULATİONS

Halit DURAN[1], Gökhan YAŞAR[1], Ahmet AKBULUT[1], Deniz ÖNCEL[1], Burcu KÖSE[1]

İGSAŞ Ar-Ge Merkezi, Kocaeli, Türkiye.
**Corresponding Author: Halit Duran, İGSAŞ Ar-Ge Merkezi, Kocaeli, Türkiye.*

E-mail: halit.duran@igsas.com.tr

ABSTRACT

Rising fertilizer consumption coupled with declining nutrient use efficiency has emerged as a major challenge for sustainable agriculture. Conventional NPK fertilizers suffer from substantial nutrient losses following soil application due to mechanisms such as leaching, volatilization, and fixation. Nitrogen loss via ammonia volatilization and nitrate leaching, in particular, leads to both economic inefficiency and environmental hazards. Consequently, interest in slow-release fertilizer technologies capable of releasing nutrients in a controlled manner aligned with crop demand has grown significantly. In this study, a slow-release NPK fertilizer formulation was developed using polymer coating systems and stabilizing additives to regulate nutrient release dynamics and enhance fertilizer use efficiency. The formulation aims to attenuate rapid dissolution in soil and ensure sustained nutrient availability within the root zone. Laboratory and soil incubation experiments were designed to evaluate nutrient release kinetics, granule crushing strength, water stability, and controlled-release performance. Furthermore, various coating ratios and formulation combinations will be investigated to identify the optimal release profile. Pot trials were planned to examine the effects of the developed fertilizer on plant growth parameters, nutrient uptake, and crop-water relations. The developed slow-release NPK formulation is expected to minimize nutrient losses, boost fertilizer efficacy, and contribute to sustainable agricultural production while mitigating environmental pollution risks associated with over-fertilization. This study serves as a foundational reference for biodegradable coating technologies, controlled-release nutrient delivery systems, and next-generation smart fertilizer applications.

Keywords: Slow-release fertilizer, NPK fertilizer, Controlled nutrient release, Sustainable agriculture, Polymer coating, Fertilizer efficiency

INTRODUCTION

With the rapid increase in world population, achieving high yields in agricultural production has become imperative. This has led to increased use of chemical fertilizers; however, the low use-efficiency of conventional fertilizers has brought about significant environmental and economic problems. A substantial portion of applied fertilizers is lost from the soil or dispersed into the environment before being taken up by plants.

Ammonia volatilization and nitrate leaching, in particular, significantly reduce the use-efficiency of nitrogenous fertilizers. In phosphorus fertilizers, the amount of phosphorus available for plant uptake remains limited due to the problem of soil fixation. For this reason, the development of slow-release fertilizer systems capable of releasing nutrients in a controlled manner has become an important area of research for sustainable agriculture.

The literature indicates that polymer-coated fertilizers reduce nutrient losses and have a positive effect on plant growth. Shaviv (2001) reported that controlled-release fertilizers increase plant nutrition efficiency. Trenkel (2010) stated that slow-release fertilizer technologies offer significant advantages in reducing environmental losses. Similarly, Azeem et al. (2014) noted that polymer-coated fertilizers improve fertilizer use-efficiency by enhancing controlled-release performance.
However, the high cost of existing commercial products, the environmental sustainability disadvantages of some coating materials, and their variable performance under different soil conditions necessitate the development of new formulations.
The aim of this study is to develop a slow-release NPK fertilizer formulation using polymer coating technologies and to evaluate the effects of the developed system on controlled nutrient release and plant growth.

MATERIAL AND METHOD

Commercial fertilizer raw materials will be used as sources of nitrogen, phosphorus, and potassium in the study. The formulation was designed using biopolymer- and synthetic polymer-based coating agents in order to impart controlled-release properties. In addition, binding additives and stabilizers were used to increase granule strength.

The soil samples to be used in the trials are planned to be standardized and maintained under controlled moisture conditions. Fast-growing test plants were preferred for the pot trials.

NPK fertilizer granules will be prepared in specified ratios and coated using a controlled coating system. During the coating process, the polymer solution will be sprayed onto the granule surface, followed by a drying step at a specific temperature.

The following analyses are planned in order to determine the performance of the prepared formulations:

- Nutrient element release profile
- Granule strength
- Moisture absorption
- Coating homogeneity

Nutrient release behavior will be examined through soil incubation tests. Soil samples will be taken at different time intervals to analyze the release amounts of nitrogen, phosphorus, and potassium.

The following groups were established for the pot trials:

- Control group: Conventional NPK fertilizer
- Treatment group 1: Slow-release fertilizer with 0.5% coating ratio
- Treatment group 2: Slow-release fertilizer with 1% coating ratio
- Treatment group 3: Slow-release fertilizer with 2% coating ratio

The following parameters are planned to be measured throughout plant development:

- Plant height
- Leaf number

- Chlorophyll content
- Fresh and dry biomass
- Soil nutrient content

RESULTS AND DISCUSSION

The developed slow-release NPK formulations are expected to provide more controlled nutrient release compared to conventional fertilizers. In particular, granules with a higher coating ratio are thought to extend the nutrient release duration.

In the soil incubation tests, nitrogen losses are expected to be lower than those of the control group. Phosphorus is also expected to remain in a plant-available form in the soil for a longer period.

In the pot trials, plant growth parameters are expected to be higher in the groups treated with slow-release fertilizer. The increase in plant height, leaf development, and biomass is thought to result from the continuity of nutrient supply.

The results to be obtained indicate that NPK formulations providing controlled release could improve fertilizer use-efficiency. It is considered that slow-release systems could minimize environmental impacts, particularly by reducing nitrogen losses.

Consistent with studies reported in the literature, it has been determined that polymer coating systems control the rate of nutrient release and have a positive effect on plant growth.

The use of biodegradable coating materials may provide a significant advantage in terms of environmental sustainability. In addition, the use of the developed systems together with hydrogel and inhibitor technologies may offer important opportunities for next-generation smart fertilizer systems.

CONCLUSIONS

Within the scope of this study, it was evaluated that the slow-release NPK fertilizer formulation developed could improve fertilizer use-efficiency by providing controlled nutrient release. It is thought that the developed system, by reducing nutrient losses, could provide both economic and environmental advantages.

In future studies, it is recommended that open-field trials be conducted to evaluate performance under different climate and soil conditions. In addition, the development of new, environmentally friendly formulations using biodegradable polymer coating systems can be targeted.

REFERENCES

Azeem, B., KuShaari, K., Man, Z. B., Basit, A., & Thanh, T. H. (2014). Review on materials & methods to produce controlled release coated urea fertilizer. Journal of Controlled Release, 181, 11–21. https://doi.org/10.1016/j.jconrel.2014.02.020

Shaviv, A. (2001). Advances in controlled-release fertilizers. Advances in Agronomy, 71, 1–49. https://doi.org/10.1016/S0065-2113(01)71011-5

Trenkel, M. E. (2010). Slow- and controlled-release and stabilized fertilizers: An option for enhancing nutrient use efficiency in agriculture. International Fertilizer Industry Association.

Wu, L., Liu, M., & Liang, R. (2008). Preparation and properties of a double-coated slow-release NPK compound fertilizer with superabsorbent and water-retention. Bioresource Technology, 99(3), 547–554. https://doi.org/10.1016/j.biortech.2006.12.027

PERFORMANCE OF THE COMBINED TILLAGE MACHINE IN CLAY SOILS

Tuğba KARAKÖSE[1], Ali TEKGÜLER[2]

*[1]Ondokuz Mayis University, Faculty of Agriculture, Department of Agricultural Machinery and Technologies Engineering, Atakum, Samsun, TÜRKİYE. *Corresponding Author: tugba.karakose@omu.edu.tr*

[2]Ondokuz Mayıs University, Samsun Vocational School, Department of Agricultural Machinery, İlkadım, Samsun, TÜRKİYE.

atekgul@omu.edu.tr

ABSTRACT

Conventional tillage methods in clay and moisty soils lead to adverse effects such as soil compaction, plow pan formation, and excessive clodding. This complicates seedbed preparation and reduces field sprout emergence rates. In heavy clay soils with high moisture content and poor drainage, ridge sowing should be applied to protect the seeds from groundwater. A new prototype machine consisting of a lister and a rotary tiller has been designed for use in areas with these soil and climate characteristics. The ridges created by this machine were processed with the rotary tiller to prepare them for sowing. In the research, the performance of the prototype machine at an average soil moisture content of 25%, the minimum observable moisture level, was compared against conventional methods using physical and mechanical parameters such as bulk density, porosity, penetration resistance, and aggregate size distribution. As a result, no statistically significant difference was found between the plow + prototype tillage and the prototype tillage treatments. It was proven that the prototype machine can be used effectively on its own under clayey and humid conditions. By forming ridges in a single pass to protect seeds from groundwater—replacing the conventional 4-pass tillage system, this machine provides a significant advantage in terms of time, labor, and fuel consumption.

Keywords: Conventional tillage Ridge tillage, Poor drainage, Clay Soil

INTRODUCTION

Agricultural soils are frequently degraded as a consequence of intensive and improper management practices. Mitigating this degradation requires the adoption of appropriate tillage methods, enhancing soil organic matter content, preserving microbial populations, and transitioning toward sustainable agricultural systems. The incorrect application of conventional tillage practices often results in significant drawbacks, including soil compaction, plough pan formation, excessive soil pulverization, and rapid moisture loss (Alvarez et al.1995, Pierce,1983, Eckert, 1987).

In regions experiencing excessive soil moisture during the sowing period, seed germination is seriously affected. While tillage can facilitate drainage and reduce moisture levels in the root zone (Ketcheson, 1980) , ridge sowing offers an effective mechanical solution by elevating the seedbed. Ridges protect seeds from waterlogging and prevent decay (Fulton et al.1996), and

previous studies have demonstrated that ridge sowing can achieve yields comparable to conventional tillage (CT) in poorly drained soils (Erbach, 1982, Stone and Heslop, 1987).

Achieving optimal friability (mellowness) in heavy-textured clay soils is highly challenging when moisture levels are elevated. Heavy clay soils possess a high capacity for water and nutrient retention; however, internal water movement is slow, and soil aeration rates are low. Consequently, these soils must be tilled within a narrow, optimum moisture range. As moisture content increases, clay soil transitions into a plastic consistency, eventually becoming slurry-like and adhering strongly to tillage tools. Conversely, when these soils dry after improper tillage, large, hard clods are formed due to their dense aggregate structure. Breaking down these clods consumes excessive energy, making the preparation of an ideal seedbed extremely difficult (Canbolat et al., 2013).

Soil physical properties, climatic conditions, and topography are primary determinants of crop yield. Declining yields coupled with rising input costs threaten the economic viability of small-scale agricultural enterprises. A primary indicator of yield reduction in heavy clay soils is a low field sprout emergence rate, primarily driven by dense soil structures and rising groundwater levels following heavy rainfall. Even when sowing is mechanically feasible in wet soils, seeds are prone to rotting. Furthermore, seeds trapped beneath large clods suffer from poor seed-to-soil contact and fail to germinate, while emerging sprouts often lack the mechanical strength to penetrate the crusted surface. In poorly managed heavy clay soils, seedling emergence rates can drop by up to 40%, frequently necessitating costly and labor-intensive replanting. This results in wasted fuel energy, labor inefficiency, delays in the cropping calendar, and excessive seed consumption.

While conventional listers (Bernacki et al. 1972, Merfield et al.2020) and modified rotary cultivators (Mandal, 2013, Salokhe and Ramalingam, 2001,Destain and Houmy,1990) have been utilized for years, their operational designs have seen limited development for extreme conditions. When high soil moisture is combined with a heavy clay texture, soil adheres to the blades and clogs the spaces between rotary tines, rendering standard equipment inoperable. Currently, there is a critical lack of machinery capable of operating efficiently under high-moisture clay soil conditions.

The objective of this study was to evaluate the operational performance of a prototype soil-tilling machine developed for heavy-textured agricultural soils prone to high moisture levels from drainage problems under the lowest soil moisture conditions recorded in the field. Accordingly, performance was evaluated based on some physical and mechanical soil parameters during field trials conducted at an average soil moisture content of 25%.

MATERIALS AND METHODS

The field trials were conducted in a heavy-textured clay soil comprising 50.47% clay, 21.08% silt, and 28.45% sand. During the experiments, the average soil moisture content at the prototype machine's working depth of 100 mm was 25%. The technical specifications of the tractor used during the field trials are summarized in Table 1. In addition to the newly designed prototype machine, a conventional mouldboard plough and a tandem disc harrow were used for comparison.

Table 1. Technical specifications of the tractor utilized in field trials.

Power generation, kW (2270 min^{-1})	64.5 (88 BG)
Torque, (Nm) / Engine cycle (min^{-1})	335/1360
Max lifting force of the lifting arms mounted on the rear points, (kN)	33
Total weight (Kg)	3500
Front axle (Kg)	1190
Rear Axle (Kg)	2310

The prototype machine is an integrated implementation consisting of a specialized lister (ridger) and a rotary cultivator (Fig. 1). To overcome high soil hardness while minimizing energy consumption, the rotary cultivator was designed to process only the active sowing rows rather than the entire soil surface.

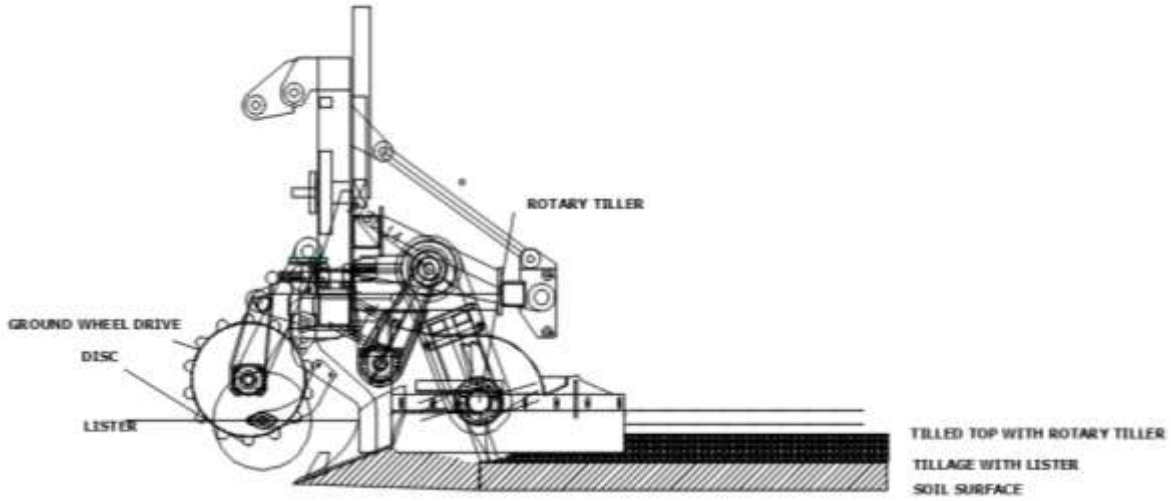

Figure 1. prototype machine

Preliminary field trials were conducted to determine the optimal ridge geometry capable of maintaining structural integrity without degrading until seedling emergence under heavy clay conditions (Fig. 2). The finalized ridge profile was configured with a 700 mm row spacing, a 350-400 mm ridge-top width, a 150-200 mm ridge height, and 45° side slope angles. Tillage along the ridges was executed by the rotary cultivator at an operational depth of 100 mm.

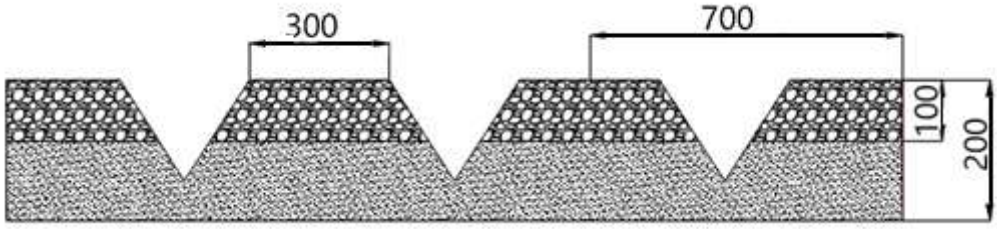

Figure 2. The ridge shape

The experimental layout was arranged in a Randomized Complete Block Design consisting of 24 plots, each measuring 10 x 5 m, arranged across eight rows. Three distinct tillage treatments were evaluated; Conventional Tillage (CT): Mouldboard ploughing followed by disc harrowing (3 passes). Combined Tillage (Plough + Prototype): Mouldboard ploughing followed by direct seedbed preparation using the prototype machine. Direct Prototype Tillage (Prototype machine): Single-pass direct seedbed preparation using only the prototype machine.

To determine bulk density (BD) and total soil porosity (SP), undisturbed core samples were collected after tillage from two depths (0-100 mm and 100-200 mm) in three replicates per plot. BD and moisture content were determined gravimetrically according to standard methods (Blake and Hartge,1986), and total porosity was calculated from BD and particle density (Dursun, 2015).

Soil penetration resistance (PR) was measured using an Eijkelkamp hand-pushed electronic cone penetrometer (Kukal and Aggarwal, 2003). Soil particle size distribution following tillage was determined using a vibrating sieve set according to standard testing procedures (Keçecioğlu, 1967). The six initial size fractions (<1, 1-2, 2-4, 4-6.3, 6.3-8, and >10mm) were categorized into three primary agronomic clod size classes: 1 mm, 1<x<10 mm (ideal seedbed aggregate size), and >10 mm.

Statistical analyses were performed using SPSS v21 Base software. Analysis of variance (ANOVA) was conducted to evaluate the effects of the tillage treatments on soil physical properties. When significant differences were detected, treatment means were compared using the Least Significant Difference (LSD) test at a significance level of $P < 0.05$.

RESULTS AND DISCUSSION

Due to high regional precipitation, the experimental soil does not dry sufficiently during the spring sowing season. Prior to tillage operations, soil moisture was 25.69% and 32.81%, the baseline BD values at depths of 0-100 and 100-200 mm were 1.22g cm^{-3} and 1.26 g cm^{-3}, respectively, while baseline SP values were 53.96% and 52.45%.

Table 3.1. Soil BD and SP values across different tillage treatments and depths.

Treatment	BD (g cm^{-3}) (100 mm)	SP (%) (100 mm)	BD (g cm^{-3}) (200 mm)	SP (%) (200 mm)
CT	1.22b	53.64b	1.23	53.41
Direct Prototype Tillage	1.10a	58.49a	1.28	51.48
Combined Tillage (Plough + Prototype)	1.10a	58.13a	1.24	52.99

Means within a column followed by different superscript letters are significantly different ($P < 0.05$)

Following tillage, significant differences in both BD and SP were observed among treatments at the 0-100 mm depth ($P < 0.05$), whereas no statistically significant differences were detected at the 100-200 mm depth (Table 3.1). At the surface layer (0-100 mm), the lowest BD (1.10 g cm^{-3}) and highest porosity (58.49% and 58.13%) were achieved by the Direct Prototype Tillage and Combined Tillage treatments, significantly outperforming CT (1.22g cm^{-3} BD and 53.64% porosity).

BD values exceeding 1.60 g cm^{-3} are known to severely restrict root proliferation in general agricultural soils (Raper et al., 1999). However, in heavy clay soils (e.g., 45% clay content), root development can be hindered at thresholds as low as 1.39 g cm^{-3} (Pierce et al., 1983; Fulton et al., 1996). In the present study, all post-tillage BD values remained well below these critical thresholds, indicating that none of the tillage systems created physical barriers to plant growth. As BD decreased, SP increased predictably. Similar inverse relationships in clay soils have been reported by Kasap (2023), although the prototype machine achieved superior surface porosity compared to standard rotary treatments.

Soil penetration resistance values did not differ significantly among the tillage treatments across any of the measured depths ($P > 0.05$). The maximum penetration resistance recorded before and after tillage did not exceed 0.61MPa. The lowest penetration resistance was observed in plots processed with the Combined Tillage system (Plough + Prototype). Hakansson and Lipiec (2000) established that mechanical impedance exceeding 3.0 MPa completely halts root elongation. The values recorded in our trials are substantially lower than this critical limit, confirming optimal soil looseness. These findings align with Bulut (2015), who recorded a minimum penetration resistance of 0.78 MPa (0-150 mm) in heavy soils, and are consistent with the mechanization results of Karaağaç (2007). The particle size distribution following seedbed preparation is a crucial indicator of tillage efficiency, particularly in plastic clay soils. The percentage of aggregates larger than 10 mm and within the ideal 1-10 mm range showed statistically significant differences among treatments ($P < 0.05$), while the fine fraction (<1 mm) showed no significant difference (Table 3.2).

Table 3.2. Post-tillage soil particle size distribution (%) across treatments.

Treatment	10<x	1<x<10	x<1
CT	83.88a	15.76b	1.20
Direct Prototype Tillage	60.01b	38.23a	1.74
Combined Tillage (Plough + Prototype)	55.78b	42.45a	1.76

Means within a column followed by different superscript letters are significantly different ($P < 0.05$)

CT resulted in an excessively coarse seedbed, with 83.88% of soil clods exceeding 10 mm and only 15.76% falling within the agronomically desirable 1-10 mm range. In contrast, Direct Prototype Tillage and Combined Tillage significantly reduced the proportion of large clods (>10 mm) to 60.01% and 55.78%, respectively, while more than doubling the fraction of ideal seedbed aggregates (1-10 mm to 38.23% and 42.45%).

This aggregate size distribution achieved by the prototype machine closely approaches the optimal soil fragmentation criteria required for rapid crop emergence in heavy soils (Dursun,

2015). Furthermore, the proportion of dust-like fine particles (<1 mm) remained below 2.00% across all treatments, indicating that the prototype machine successfully fragmented heavy clay without causing structural over-pulverization or increasing erosion risks. The proportion of seedbed-ready aggregates (<10 mm) obtained with the prototype was higher than the 13.55% (conventional) and 15.30% (rotary tillage) reported by Pınar (1992), and superior to the fragmentation ratios observed by Kasap (2023) in similar soil textures. Moreover, these findings reinforce Karaköse et al. (2026), who demonstrated that specialized ridge-rotary systems maintain superior clod fragmentation efficacy at moisture levels ranging from 25% to 37% compared to CT implements.

CONCLUSION

Field evaluations of the newly developed prototype machine, engineered specifically for poorly drained and heavy clay soils, demonstrated superior agronomic and mechanical performance compared to Conventional multi-pass tillage. At a challenging soil moisture content of 25%, the prototype successfully formed structurally stable ridges that maintained their geometry following rainfall, effectively elevating the seedbed and protecting seeds from groundwater saturation.

The prototype machine produced significantly better soil fragmentation and lower surface BD than conventional tillage. Importantly, statistical analyses revealed no significant difference in seedbed quality between the two-stage Combined Tillage (ploughing followed by the prototype) and the single-pass Direct Prototype Tillage. This confirms that the prototype machine can be operated independently as a primary and secondary tillage implementation in heavy clay soils. By consolidating a Conventional four-stage seedbed preparation process into a single pass, the prototype implement offers a sustainable agricultural solution that prevents deep soil compaction, reduces equipment wear, and maximizes both fuel and labor efficiency.

REFERENCES

Alvarez R., Santanatoglia, O.J., & Garcia, R.. 1995. Soil respiration and carbon inputs from crops in a wheat–soyabean rotation under different tillage systems. *Soil Use Manage.* 1995.*11*, p. 45–50. https://doi.org/10.1111/j.1475-2743.1995.tb00495.x.

Bernacki, H., Haman, J., Kanafojski, C. Z., & Wiszniewicz, E.1972. Agricultural machines, theory and construction. *US Dept. Of commerce, National technical İnformation Service*. 1972.Virginia.

Blake, G. R., and Hartge, K. H. Bulk density.1986. *Methods of soil analysis: Part 1 Physical and mineralogical methods*, p.363-375. https://doi.org/10.2136/sssabookser5.1.2ed.c13.

Bulut, O. N. 2015. *Buğday tarımında farklı toprak işleme yöntemlerinin toprak özellikleri, tarla filiz çıkışı ve verim üzerine etkileri* (Master's thesis). Gaziosmanpaşa Üniversitesi, Ziraat Fakültesi, Biyosistem Mühendisliği Anabilim Dalı, Tokat, Türkiye.

Canbolat, M., Barik, K., ve Özgül, M. 2013. Erzurum yöresinde farklı ana materyaller üzerinde oluşmuş üç toprak profilinin kıvam limitleri ve şişmebüzülme karakteristikleri. Atatürk Üniversitesi Ziraat Fakültesi Dergisi, 30(2).

Destain, M. F., & Houmy, K.1987. Effects of design and kinematic parameters of rotary cultivators on soil structure. Soil and Tillage Research, 1990. 17(3-4), 291-301. https://doi.org/10.1016/0167. (90)90042-C.

Dursun, İ.. *Toprak İşleme Alet ve Makinaları*. Ankara üniversitesi. 2015.Yayın no:1614. Ankara (Turkish).

Eckert, D. J. Evaluation of ridge planting systems on a poorly drained lake plain soil. *Journal of soil and water conservation*, 1987.42(3), p.208-211. https://doi.org/10.1080/00224561.1987.12456076.

Erbach, D. C. 1982. Tillage for continuous corn and corn-soybean rotation. *Transactions of the ASAE*, 1982.*25*(4), p.906-0911. https://doi: 10.13031/2013.33638.

Fulton, J.P., Wells, L.G., Shearer, S.A. & Barnhisel, R.I., 1996. Spatial Variation of Soil Physical Properties: A Precussor to Precision Tillage. *ASAE Paper No.961002.International Meeting*, 1996.*Phoenix*, Arizona.

Håkansson, I. & Lipiec, J. 1987. A review of the usefulness of relative bulk density values in studies of soil structure and compaction. *Soil and Tillage Research*, 2000. 53(2), p. 71-85. https://doi.org/10.1016/S0167, (99)00095-1.

Karaağaç, H. A., & Barut, Z. B. 2007. İkinci ürün silajlık mısır tarımında farklı toprak işleme ve ekim sistemlerinin teknik ve ekonomik yönden karşılaştırılması. *Tarım Makinaları Bilimi Dergisi*, *3*(1), 33-40.

Karaköse, T., Tekgüler, A., & Beyhan, M. A. 2026. Development of a Ridge Sowing Machine for Clay Soil Conditions and Determination of Its Field Performance. *Applied Sciences*, *16*(11), 5525.

Kasap, A. 2023. *Comparison of different tillage methods in chickpea (Cicer arietinum L.) cultivation* (Doctoral dissertation). Department of Agricultural Machinery and Technologies Engineering, Graduate School of Natural and Applied Sciences, Ankara University, Ankara, Türkiye.

Keçecioğlu, G.1967. Toprak Kanalında Çeşitli Toprak işleme Aletleri Üzerinde Bir Araştırma. *Ege Üniversitesi Ziraat Fakültesi Yayınları*. p.93 (Turkish).

Ketcheson, J. W. 1980. Effect of Tillage on Fertilizer Requirements for Corn on a Silt Loam Soil. *Agronomy Journal*.72(3), p.540-542. https://doi.org/10.2134/agronj1980.00021962007200030031x.

Kukal, S. S., and Aggarwal, G. C. 2003. Puddling depth and intensity effects in rice–wheat system on a sandy loam soil: I. Development of subsurface compaction.*Soil and Tillage Research. 72*(1), 1-8. https://doi.org/10.1016/S0167-1987(03)00093-X.

Mandal, S. K., Bhattacharya, B., & Mukherjee, S. 2013. Optimization of design parameters for rotary tiller's blade. power. 4(5).

Merfield, C. N., Bennett, J. R., Berry, N. A., Bluon, A., O'Connell, D. M., & Hodge, S. 2020. The potential of mini-ridging for controlling intrarow weeds: estimating minimum lethal burial depth. Weed Research. 60(5), 353-362. https://doi.org/10.1111/wre.12441.

Pınar, Y., Uzun, Z., Onuk, V., Bat, N.K., ve Tekgüler, A. 1992. "Tohum yatağı hazırlama yöntemlerinin toprağın bazı fiziksel özelliklerine etkileri." *14.Tarımsal mekanizasyon kongresi bildiri kitabı.* Samsun.

Pierce, F.J., Larson, W.E., Dowdy, R.H. & Graham, W.A.P. 1983. Productivity of Soils: Assessing Long-Term Changes Due to Erosion. *Journal Soil and Water Cons*., 38., p.39-44. https://doi.Org/10.1080/00224561.1983.12436244.

Raper, R. L., Reeves, D. W., Burt, E. C., & Torbert, H. A. 1994. Conservation tillage and traffic effects on soil condition. *Transactions of the ASAE*. 37, p. 763-768. https://doi: 10.13031/2013.28138.

Salokhe, V. M., & Ramalingam, N. 2001. Effects of direction of rotation of a rotary tiller on properties of Bangkok clay soil. Soil and Tillage research, 2001. 63(1-2), 65-74. https://doi.org/10.1016/S0167-1987(01)00235-5

Stone, J. A. & Heslop, L. C. 1987. Blade cultivator, ridge, and moldboard plow tillage comparison on a poorly drained soil. *Transactions of the ASAE*. 30, p.61-0064. https://doi: 10.13031/2013.30402.

PHENOTYPIC AND GENOTYPIC RESISTANCE TO HEAVY METAL ZINC IN ESCHERICHIA COLI

Seza Arslan[1], Fatma Özdemir[1], Sueda Kabucu[1]

[1] Bolu Abant Izzet Baysal University, Faculty of Arts and Sciences, Department of Biology, 14030 Gölköy / Bolu, Türkiye

Corresponding author e-mail: sudi.kabucu@gmail.com

ABSTRACT

Many pathogens, including *Escherichia coli* causing serious infections, pose a significant risk to human health worldwide. *E. coli* is a commensal bacterium that is widely found in the human gastrointestinal tract. Some strains of *E. coli* can cause gastrointestinal and extraintestinal infections in humans due to the acquisition of pathogenetic factors through mobile genetic elements, such as plasmids, bacteriophages, pathogenicity islands, and transposons. Heavy metals are pollutants that cause serious harm to the environment and human health due to their toxicity, persistence in the environment, and bioaccumulative properties. Heavy metals contribute to antimicrobial resistance in bacteria through co-selection and cross-resistance. Although some metals, such as zinc, are crucial for microbes, they can be toxic at high concentrations or impose selective pressure on bacteria. The aim of this study was to investigate the resistance to heavy metal zinc in multidrug-resistant (MDR) *Escherichia coli* isolates using phenotypic analysis by the broth microdilution method and genotypic analysis by the PCR-based amplification of the *zntA* gene associated with zinc resistance. All MDR *E. coli* isolates had minimum inhibitory concentration (MIC) and minimum bactericidal concentration (MBC) values higher than 3200 µg/mL. Out of the zinc-resistant MDR isolates, 85.7% were positive for the *zntA* gene, encoding resistance to zinc. However, 14.3% of the MDR isolates with an MIC of >3200 µg/mL did not carry the *zntA* gene. The results of this study demonstrate the presence of zinc resistance both phenotypically and genotypically. The zinc-resistant MDR *E. coli* isolates from food in this study might constitute potential risks to human health.

Keywords: zinc resistance, *zntA* gene, *Escherichia coli*, minimum inhibitory concentration

INTRODUCTION

Escherichia coli is a Gram negative, short rod, aerobic, generally motile organism. Most of the strains are not pathogenic and exist in the intestinal tract of warm blooded animals (Bhunia, 2008). The pathogenic strains cause disease inside the intestinal tract and in the extraintestinal sites like hemolytic uremic syndrome, urinary tract infection, septicemia, and meningitis (Dworkin et al., 2006; Bhunia, 2008).

Pathogenic *E. coli* strains are categorized into different pathotypes according to their virulence characteristics and pathogenic mechanisms. In addition, pathogenic *E. coli* strains are serologically classified based on their capsular(K), somatic (O), and flagellar (H) antigens. The most important pathotypes clinically as they cause a serious threat to human health and are responsible for a large proportion of diarrhoeal diseases (Bhunia, 2008). Pathogenic strains of *E. coli* colonise the intestinal epithelium and damage host cells through various virulence factors. These bacteria may affect the function of ion transport systems, cause excessive fluid loss, inhibit protein synthesis, alter the host cell cytoskeleton, and eventually induce cell death. Collectively, these pathogenic mechanisms lead to the development of a wide range of gastrointestinal infections (Meng et al., 2007; Bhunia, 2008).

Heavy metals are poisonous, persistent and bioaccumulative in nature. They are metallic and non-metallic materials. Certain heavy metals such as zinc, copper and nickel are essential for basic biological activities but can be hazardous when they cross permissible limits. Chromium, unlike other metals such as cadmium and lead, is very toxic to living things even in small quantities (Chen et al., 2018; Peshkov et al., 2025). Zinc occurs naturally and as a result of human activities in the environment. It can be naturally released into the environment by rock weathering, volcanic eruptions, air dust, and forest fires. On the other hand, anthropogenic sources of emission include industrial waste, burning of fossil fuels, and a number of industrial processes (Hussain et al., 2022; Peshkov et al., 2025). It is widespread in soil, water, atmosphere, plants, and living organisms (Hussain et al., 2022).

Humans can inhale heavy metals via contaminated air, ingest them via contaminated water and food, and absorb them via skin contact (Afolabi et al., 2023). Zinc is a transition trace metal and is an essential cofactor and key player in cell growth and development processes in most living organisms (Adekanmbi et al., 2020; Schuindt et al., 2026). Many fundamental biological processes, including transcription to translation and cell division to metabolism, depend on zinc (Schuindt et al., 2026). Its chemical properties allow for stable interactions with most proteins, supporting enzyme and protein functionality (Berg and Shi, 1996; Adekanmbi et al., 2020).

High amounts of zinc are potentially hazardous to humans, microbes and other living species. A high level of zinc release in the environment results in the disruption of microbial communities and the selection of zinc tolerant microorganisms (Hussain et al., 2022). Heavy metals exposure and their bioaccumulation may cause adverse health effects, such as weight loss, decreased immunity, cancer, hepatotoxicity, cardiovascular diseases and reproductive disorders (Halema et al., 2024; Peshkov et al., 2025). A high zinc concentration disrupts metal homeostasis, enters cells through non-specific transport systems, and inhibits enzyme activity and disrupts normal cell functions. For these reasons, intracellular zinc concentration must be controlled by zinc homeostasis systems such as the ZntA-mediated efflux system (Nies, 1999).

Bacteria have evolved methods to defend themselves from heavy metal exposure. Heavy metal resistance genes may be found on bacterial chromosomes, transposons, or plasmids. Their presence promotes horizontal gene transfer and the spread of heavy metal and antibiotic resistance genes (Halema et al., 2024). Bacteria have specific uptake and efflux systems to maintain zinc homeostasis (Hussain et al., 2022). The ZnuABC transporter system ensures proper zinc intake by increasing zinc uptake from exogenous sources. Alternatively, bacteria activate a detoxifying mechanism to prevent the build up of high zinc concentrations as intracellular zinc levels rise. The P-type ATPase zntA exports excess zinc from the cytoplasm. The CzcCBA efflux system, a resistant nodulation division transporter, regulates zinc export across the cell membrane (Nies, 1999; Hussain et al., 2022). These coordinated uptake and efflux systems maintain intracellular zinc levels, allowing bacteria to adapt under heavy metal stress conditions and resist zinc toxicity (Hussain et al., 2022).

Multidrug resistance refers to a bacterium exhibiting resistance to at least one antibiotic from more than three different classes of antimicrobials. Exposure to this bacterium risks human and animal health by complicating infection treatments. Furthermore, antibiotic resistance has emerged as a serious public health concern, as antibiotic use facilitates the spread of antibiotic resistance genes throughout the food chain. Furthermore, heavy metal-induced selective pressure in environmental reservoirs contributes to the spread and persistence of antibiotic resistance genes (Vats et al., 2022; Nguyen et al., 2025).

Water and soil are contaminated with heavy metals from both natural and anthropogenic sources (Gillieatt and Coleman, 2024). These hazardous metals may enter the human body as a result of heavy metal contamination in foods, particularly vegetables. The presence of heavy metal contaminants in the environment poses growing threats to food safety and human health. Moreover, heavy metals can cause and prolong antimicrobial resistance in food-borne bacteria

(Mihdir et al., 2016; Vats et al., 2022). Therefore, the aim of this study is to investigate heavy metal zinc resistance among the multidrug-resistant (MDR) *E. coli* isolates from vegetables. The broth microdilution method was performed phenotypically to determine the minimum inhibitory concentration (MIC) for zinc. The *zntA* gene responsible for zinc resistance was detected genotypically by using PCR.

MATERIALS AND METHODS

Bacterial isolates

The reference strains *Escherichia coli* ATCC 35218, *E. coli* K-12, and seven multidrug-resistant (MDR) *E. coli* isolates previously isolated and identified from vegetables (Özdemir, 2024) were used in this study. All isolates stored in sterile Eppendorf tubes at -20 °C in Brain Heart Infusion broth (Merck) containing 20% glycerol in the stock bacterial culture collection were revived. The MDR *E. coli* isolates were activated from stock cultures using Brain Heart Infusion broth (37°C / 24 h). Then, the culture was streaked on Eosin Methylene Blue (EMB) (Merck, Germany) to obtain individual colonies showing characteristics of a metallic green sheen. These colonies were subcultured onto Brain Heart Infusion agar (Merck, Germany) and used for further study.

Phenotypic characterization

Determination of minimum inhibitory concentration of heavy metal zinc

The minimum inhibitory concentration (MIC) of heavy metal zinc quantitatively on a U-bottom sterile 96-well microtiter plate (LP Italiana) was determined by the broth microdilution method according to CLSI recommendations (CLSI, 2012). Heavy metal zinc ($ZnCl_2$) was obtained from Sigma-Aldrich. All multidrug-resistant (MDR) *E. coli* isolates were streaked on Eosin Methylene Blue (EMB) agar (Merck). The petri plates were incubated at 37°C for 24 h. Later, several colonies with a green metallic sheen from the EMB agar were selected and suspended on Mueller Hinton Broth (MHB). The bacterial suspension turbidity was adjusted to a 0.5 McFarland (around 10^8 colony forming units (CFU) / mL). Adjusted suspension was diluted at 1:150 ratio in MHB and inoculated to each well of a microtiter plate. Two-fold dilutions of the zinc metal were prepared in MHB on wells of the microtiter plates. Heavy metal zinc was tested at concentrations ranging from 3200 to 6.25 µg/ mL. Each test consisted of a sterility control well (only MHB) and a growth control well (MHB with bacterial culture but no zinc). The microtiter plates were incubated for 24 h at 37°C. After incubation, the MIC was defined as the lowest visible concentration of the heavy metal zinc that completely inhibited bacterial growth. The absorbance was determined at 600 nm using a Thermo Electron Corporation microplate reader. The tests were conducted in triplicates. In this study, the references *E. coli* K-12 and *E. coli* ATCC 35218 were utilized controls.

Detection of minimum bactericidal concentration of heavy metal zinc

After incubation (37°C/ 24 h), the minimum bactericidal concentration (MBC) is the lowest concentration of an agent that inhibits 99.9% of bacterial growth (CLSI, 2012). The MBC was determined, after reading, In order to detect viable cells, 10 µL of the first eight dilutions, ranging from 3200 to 25 µg/mL, were seeded as a spot inoculation onto MHB and incubated at 37°C for 24 h.

Genotypic characterization

Genomic DNA extraction

A single colony of the multidrug-resistant (MDR) *E. coli* was suspended in the 5 mL Brain Heart Infusion (BHI) broth and incubated for 24 h at 37°C. Later, 1.5 mL of culture suspension was transferred into a sterile microcentrifuge tube. After centrifugation, DNA of the MDR *E. coli* isolates was isolated using the cetyl trimethyl ammonium bromide (CTAB) method (Ausubel et al., 1991). The DNA was stored in TE buffer (10 mM Tris, 1mM EDTA) and kept at -20°C for further PCR analysis.

PCR identification of the *E. coli* isolates

For species-level identification, *uspA* gene (*E. coli* specific universal stress protein A) was amplified by PCR, as previously described (Chen and Griffiths, 1998). All PCR reactions were performed in a T100 thermocycler (Bio-Rad). A 50 µL The reaction mixture included 1.5 U Taq polymerase (Thermo Scientific), 5 µl 10X buffer, 4 mM $MgCl_2$, 0.2 mM dNTP mix (Amplicon), 0.4 µM primers, 4 µL template, and 31.7 µL PCR water. The cycles were 94°C/ 5 min for the first cycle; 94°C/ 2 min, 60°C/ 1 min, and 72°C/ 1 min for the next 30 cycles; and 72°C/ 10 min for the final cycle. The PCR products were determined on a 1% agarose gel and analyzed by agarose gel electrophoresis (Bio-Rad). *E. coli* ATCC 35218 strain was employed as a positive control.

PCR identification of the *zntA* gene

The *zntA* gene was detected using PCR, which encodes a zinc export protein that is responsible for heavy metal resistance, particularly zinc. The primers for the *zntA* gene were the forward primer, 5'-ATC GTC CGC TCG CTG TAT CTC T-3', and the reverse primer, 5'-CCG CCT TTT CCC CTC ACC CTA ACC-3' (Rensing et al., 1997). The predicted size was 2374 bp. The PCR amplification was performed in 50 µL as a final volume; 30.7 µL PCR water (AppliChem), 5 µL 10X buffer, 4 µL $MgCl_2$, 1 µL dNTP mix (Amplicon), 2 µL forward and reverse primer, 0.3 µL Taq DNA polymerase (Thermo Scientific), and 5 µL DNA template. PCR amplification was carried out in a Bio-Rad T100 thermal cycler under the following conditions: an initial denaturation at 94 °C for 8 min, followed by 35 cycles of denaturation at 94 °C for 1 min, primer annealing at 64 °C for 1 min, extension at 72 °C for 90 sec, and a final extension at 72 °C for 8 min. The amplified PCR products were separated by electrophoresis on a 1% agarose gel, stained with ethidium bromide and visualized (DNR Minilumi). A 100-bp DNA ladder (Vivantis) for DNA fragment size determination on gel electrophoresis was used. In all experiments, the reference strains, including *E. coli* K-12 and *E. coli* ATCC 35218, were used as positive controls.

RESULTS AND DISCUSSION

Nowadays, excessive and inappropriate use of antimicrobial drugs and heavy metals in aquaculture and animal farming may accelerate the spread of antimicrobial resistance through co-selection (Seiler et al., 2012). In this investigation, multidrug-resistant (MDR) *E. coli* isolates from vegetables were evaluated for resistance to heavy metal zinc ($ZnCl_2$) using both phenotypic and genotypic methods.

Table 1 displays the results of phenotypic and genotypic characterization for zinc resistance by the broth microdilution method and for the presence of Zn (II)-translocating P-type ATPase, encoded by the *zntA* gene, responsible for zinc resistance.

All MDR *E. coli* isolates from vegetable samples and tested reference strains, including *E. coli* K-12 and *E. coli* ATCC 35218, showed a minimum inhibitory concentration (MIC) for zinc greater than 3200 µg/ mL (Table 1). Furthermore, the minimum bactericidal concentrations (MBCs) for zinc were found to be higher than 3200 µg/mL for all MDR *E. coli* isolates and tested reference control strains, such as *E. coli* K-12 and *E. coli* ATCC 35218 (Table 1). Figure 1 illustrates a representative MBC image of *E. coli* K-12 and an MDR *E. coli* isolate from spinach (V11).

Table 1. Resistance to heavy metal zinc among the multidrug-resistant *E. coli* isolates

No	Isolate	Source	MIC (µg/mL)	MBC (µg/mL)	*zntA* gene
1	V10	Spinach	> 3200	> 3200	+
2	V11	Spinach	> 3200	> 3200	+
3	V13	Spinach	> 3200	> 3200	-
4	V17	Lettuce	> 3200	> 3200	+
5	V25	Lettuce	> 3200	> 3200	+
6	V26	Lettuce	> 3200	> 3200	+
7	V27	Lettuce	> 3200	> 3200	+
E. coli K-12			> 3200	> 3200	+
E. coli ATCC 35218			> 3200	> 3200	+

MIC, Minimum inhibitory concentration; MBC, Minimum bactericidal concentration.

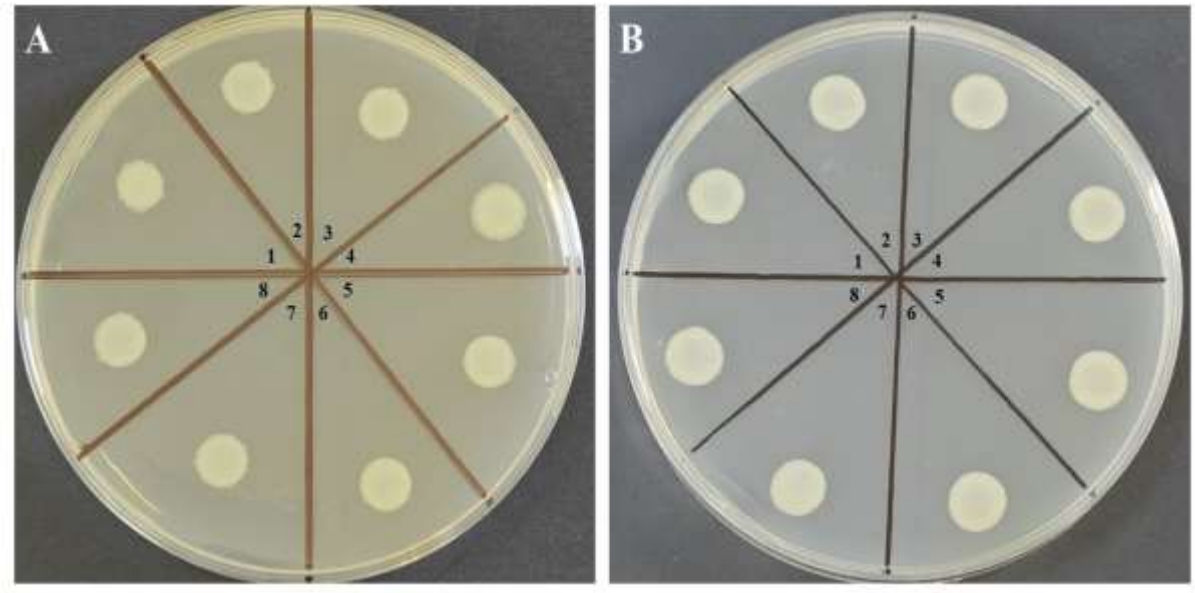

Figure 1. The agar plates represent the minimum bactericidal concentration (MBC) of heavy metal zinc against *E. coli* K-12 (A) and a spinach MDR *E. coli* isolate (B). The concentrations shown by the numerals 1-8 are 3200, 1600, 800, 400, 200, 100, 50, and 25 mg/mL.

The presence of the *zntA* gene associated with zinc resistance was performed by PCR amplification. Only six (85.7%) of the seven MDR *E. coli* isolates had the *zntA* gene identified by PCR (Table 1). The representative PCR products of the *zntA* gene in the MDR *E. coli* isolates from vegetables are shown in Figure 2.

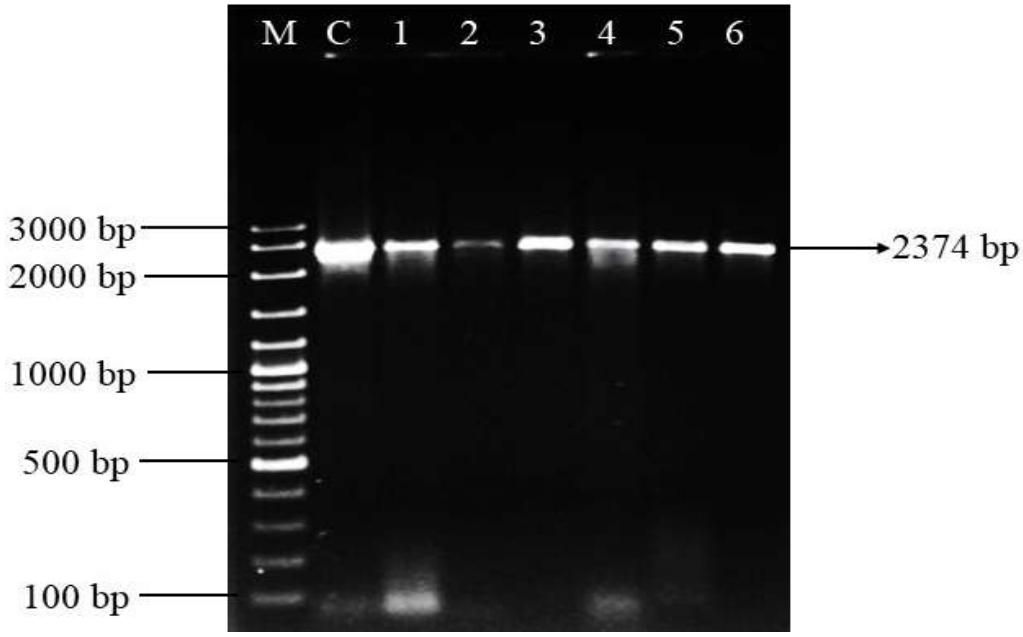

Figure 2. Agarose gel electrophoresis of the PCR amplification of the *zntA* gene (2374 bp) in six MDR *E. coli* isolates from vegetables, except the spinach *E. coli* isolate. M: 100 bp marker (Vivantis), C: positive *E. coli* K-12 strain, Lanes 1-7: MDR *E. coli* isolates in this study.

In this study, a high level (85.7%) of zinc resistance was observed among the seven multidrug resistant (MDR) *E. coli* isolates, suggesting a potential association between zinc and multidrug resistance. Similar observations were reported by Cufaoğlu et al. (2022), who reported that 89% of the *E. coli* isolates were resistant to at least three antibiotics. Among the eight heavy metals, zinc resistance was detected in 62%, with minimum inhibitory concentration (MIC) values reaching 3200 µg/mL. Additionally, PCR amplification of the Cufaoğlu et al. (2022) 20 isolates with high zinc MIC values revealed that 85% carried the *zntA* gene. In our study, PCR amplification indicated that the six MDR *E. coli* isolates (85.7%) carried the *zntA* gene (Figure 2). Yang et al. (2018) found that 77% of *E. coli* isolates contained the zntA gene, with MIC values ranging from 400 to 1600 µg/mL. Vidhyaparkavi et al. (2017) demonstrated that *zntA* expression increased in response to zinc exposure, confirming its importance in bacterial zinc tolerance. On the other hand, the mere presence of the *zntA* gene does not explain zinc resistance. For example, Adekanmbi et al. (2020) showed that some isolates of *E. coli* do not have the *zntA* gene, suggesting that maybe other mechanisms and systems contribute to zinc tolerance.

CONCLUSIONS

The present research revealed that the phenotypic and genotypic resistance characteristics of multidrug-resistant (MDR) *E. coli* isolates from vegetables to the heavy metal zinc. All MDR isolates were zinc resistant, and all except one carried the *zntA* gene, which is associated with zinc resistance. As a result, the existence and dissemination of heavy metal resistance in MDR *E. coli* isolates from vegetables might pose risks to human health and food safety.

REFERENCES

Adekanmbi, A. O., Adeleke, O. J., Aremu, O. O., and Olaposi, A. V. (2020). Molecular characterization, antibiogram and distribution of *zntA* gene in zinc-resistant *Escherichia coli* population recovered from anthropogenically-influenced surface water sources in Nigeria. *Meta Gene, 26*, 100789. https://doi.org/10.1016/j.mgene.2020.100789

Afolabi, O. O., Wali, E., Asomaku, S. O., Ogbuehi, N. C., Bosco-Abiahu, L. C., Orji, M. C., and Emelu, V. O. (2023). Ecotoxicological and health risk assessment of toxic metals and metalloids burdened soil due to anthropogenic influence. *Environmental Chemistry and Ecotoxicology, 5*, 29-38. http://dx.doi.org/10.1016/j.enceco.2022.12.002

Ausubel, F. M., Kingston, R. E., Brent, R., Moore, D. D., Seidman, J. G., Smith, J. A., et al. (1991). *Current protocols in molecular biology*. Greene Publishing Associates and Wiley Interscience.

Becerra-Castro, C., Machado, R. A., Vaz-Moreira, I., and Manaia, C. M. (2015). Assessment of copper and zinc salts as selectors of antibiotic resistance in Gram-negative bacteria. *Science of the Total Environment, 530*, 367-372. https://doi.org/10.1016/j.scitotenv.2015.05.102

Berg, J. M., and Shi, Y. (1996). The galvanization of biology: a growing appreciation for the roles of zinc. *Science*, *271*(5252), 1081-1085. DOI: 10.1126/science.271.5252.1081

Bhunia, A. K. (2008). *Foodborne microbial pathogens: Mechanisms and pathogenesis*. New York: Springer.

Chen, L., Zhou, S., Shi, Y., Wang, C., Li, B., Li, Y., and Wu, S. (2018). Heavy metals in food crops, soil, and water in the Lihe River Watershed of the Taihu Region and their potential health risks when ingested. *Science of The Total Environment*, *615*, 141-149. https://doi.org/10.1016/j.scitotenv.2017.09.230

Cufaoglu, G., Cengiz, G., Onaran Acar, B., Yesilkaya, B., Ayaz, N. D., Levent, G., and Goncuoglu, M. (2022). Antibiotic, heavy metal, and disinfectant resistance in chicken, cattle, and sheep origin *E. coli* and whole-genome sequencing analysis of a multidrug-resistant *E. coli* O100: H25 strain. *Journal of Food Safety, 42*(5), e12995. https://doi.org/10.1111/jfs.12995

Dworkin, M. (Ed.). (2006). *The prokaryotes: A handbook on the biology of bacteria* (3rd ed., Vol. 6: Proteobacteria: Gamma subclass). Springer. https://doi.org/10.1007/0-387-30746-X

Gillieatt, B. F., and Coleman, N. V. (2024). Unravelling the mechanisms of antibiotic and heavy metal resistance co-selection in environmental bacteria. *FEMS Microbiology Reviews*, *48*(4), fuae017. DOI: 10.1093/femsre/fuae017

Halem, A. A., El-Beltagi, H. S., Al-Dossary, O., Alsubaie, B., Henawy, A. R., Rezk, A. A., Almutairi, H. H., Mohamed, A. A., Elarabi, N. I., and Abdelhadi, A. A. (2024). Omics technology draws a comprehensive heavy metal resistance strategy in bacteria. *World Journal of Microbiology and Biotechnology*, *40*(6), 193. https://doi.org/10.1007/s11274-024-04005-y

Hussain, S., Khan, M., Sheikh, T. M. M., Mumtaz, M. Z., Chohan, T. A., Shamim, S., and Liu, Y. (2022). *Zinc essentiality, toxicity, and its bacterial bioremediation: a comprehensive insight. Frontiers in Microbiology 13: 900740*. https://doi.org/10.3389/fmicb.2022.900740

Meng, J., Doyle, M. P., Zhao, T., Zhao, S. (2007). Enterohemorrhagic *Escherichia coli*. In Doyle M.C, Beushat L.R (Eds.) *Food Microbiology* (pp. 249-269). ASM Press.

Mihdir, A., Assaeedi, A. S., Abulreesh, H. H., and Osman, G. E. (2016). Detection of heavy metal resistance genes in an environmental *Pseudomonas aeruginosa* isolate. *British Microbiology Research Journal*, *17*(1), 1-9. DOI: 10.9734/BMRJ/2016/28655

Nies, D. H. (1999). Microbial heavy-metal resistance. *Applied Microbiology and Biotechnology*, *51*(6), 730-750. org/ 10. 1007/ s10534- 026- 00828-4.

Peshkov, S. A., Nikiyan, H. N., Sizentsov, A. N., and Davydova, O. K. (2025). Sorption of Heavy Metals (Pb, Cd, Co, and Zn) by Bacteria of the Genus *Bacillus*: An Investigation of the Ability and Consequences of Bioaccumulation. *International Journal of Microbiology*, 1, 4067880. https://doi.org/10.1155/ijm/4067880

Rensing, C., Mitra, B., Rosen, B.P. (1997). The *zntA* gene of *Escherichia coli* encodes a Zn (II)-translocating P-type ATPase. Proceedings of the National Academy of Sciences of the United States of America (PNAS). 94: 14326-14331.

Schuindt, C. P., Batista, B. B., Cesetti, L., Lima Neto, S. P., Soldati, T., and da Silva Neto, J. F. (2026). The genes *zntA* and *zntR* encoding a P-type ATPase and its activator confer zinc and cadmium resistance in *Chromobacterium violaceum*. *BioMetals*, 1-19. https://doi. org/10.1007/s10534-026-00828-4

Seiler, C., Berendonk, T. U. 2012. Heavy metal driven co-selection of antibiotic resistance in soil and water bodies impacted by agriculture and aquaculture. *Frontiers in Microbiology*, 3: 399.

Vats, P., Kaur, U.J., Rishi, P. (2022). Heavy metal-induced selection and proliferation of antibiotic resistance: A review. *Journal of Applied Microbiology*. 132: 4058-4076.

Vidhyaparkavi, A., Osborne, J., and Babu, S. (2017). Analysis of *znt A* gene in environmental *Escherichia coli* and additional implications on its role in zinc translocation. *3 Biotech*, *7*(1), 9. DOI 10.1007/s13205-017-0613-0

Yang, S., Deng, W., Liu, S., Yu, X., Mustafa, G. R., Chen, S., He, L., Ao, X., Yang, Y., Zhou, K., Li, B., Han, X., Xue, X., and Zou, L. (2020). Presence of heavy metal resistance genes in *Escherichia coli* and *Salmonella* isolates and analysis of resistance gene structure in *E. coli* E308. *Journal of Global Antimicrobial Resistance*, *21*, 420-426. https://doi.org/10.1016/j.jgar.2020.01.009

ASSESSMENT OF SELECTED MACRO- AND MICRO NUTRIENT CONCENTRATIONS IN SOILS AND WHEAT IN THE NARLI PLAIN

Ömer Faruk DEMİR

Kahramanmaraş Sütçü İmam University, Faculty of Agriculture, Department of Soil Science and Plant Nutrition, Kahramanmaraş, Türkiye

Corresponding author e-mail: demirfaruk@ksu.edu.tr

ABSTRACT

Evaluating soil nutrient availability together with plant nutrient concentrations provides a comprehensive understanding of crop nutritional status. Accordingly, this study aimed to assess the macro- and micronutrient status of wheat grown in the Narlı Plain of Kahramanmaraş, Türkiye. Soil samples were collected from a depth of 0–30 cm, and flag leaf samples were collected immediately before heading from 11 wheat-growing fields. Soil samples were analyzed for pH, calcium carbonate ($CaCO_3$) and organic matter contents, available phosphorus (Olsen-P), exchangeable potassium (K), calcium (Ca), and magnesium (Mg), and DTPA-extractable iron (Fe), zinc (Zn), copper (Cu), and manganese (Mn). Plant samples were analyzed for P, K, Ca, Mg, Fe, Zn, Cu, and Mn concentrations. The soils were slightly to moderately alkaline, with organic matter contents ranging from 2.13% to 4.50% and $CaCO_3$ contents ranging from 19.84% to 41.09%. Soil Olsen-P concentrations varied between 7.98 and 35.38 mg kg^{-1}, while the mean DTPA-extractable Fe, Zn, Cu, and Mn concentrations were 11.73, 1.05, 1.50, and 9.65 mg kg^{-1}, respectively. The mean exchangeable K, Ca, and Mg concentrations were 339.55, 3461, and 1145 mg kg^{-1}, respectively. The mean P, K, Ca, and Mg concentrations in wheat flag leaves were 0.28%, 2.60%, 0.80%, and 0.18%, respectively, whereas the mean Fe, Zn, Cu, and Mn concentrations were 97.93, 21.84, 6.75, and 40.41 mg kg^{-1}, respectively. The results showed that wheat grown in the Narlı Plain was generally adequately supplied with the macro- and micronutrients examined. However, the variation in soil and plant nutrient concentrations among the sampled fields suggests that wheat nutrient status may be influenced by differences in soil nutrient reserves, fertilizer management, and other soil properties. These findings highlight the importance of evaluating soil and plant analyses together when developing field-specific nutrient management strategies for wheat production in the region.

Keywords: Calcareous soil, flag leaf, mineral nutrition, wheat.

INTRODUCTION

Determining the mineral nutritional status of wheat grown in calcareous soils represents an important diagnostic challenge because soil nutrient reserves do not necessarily correspond to the availability of these nutrients to plants. High soil pH and $CaCO_3$ content may restrict nutrient uptake by roots by altering nutrient speciation in the soil solution, adsorption–desorption equilibria, and precipitation reactions. Therefore, the presence of an adequate reserve of a particular nutrient in the soil does not necessarily indicate that the nutrient can be taken up by plants in sufficient amounts (Hinsinger, 2001; Marschner, 2012; Xue et al., 2016). Recent studies conducted in calcareous soils have also demonstrated that these conditions may affect

nutrient uptake and fertilizer-use efficiency in wheat (Martínez-Ríos et al., 2024; Zaheri Abdehvand et al., 2024; Demirkaya & Gülser, 2025).

In calcareous and alkaline soils, P may form sparingly soluble compounds with Ca or become immobilized through retention on $CaCO_3$ surfaces. Similarly, high pH and the presence of carbonate and bicarbonate ions may reduce the solubility and root availability of Fe, Zn, Mn, and Cu. Zinc availability, in particular, is strongly influenced by interactions among soil pH, carbonate content, P status, organic matter, and clay minerals (Chen et al., 2019; Martínez-Ríos et al., 2024). Consequently, wheat grown in calcareous soils may exhibit marginal or latent nutrient deficiencies even in the absence of visible deficiency symptoms. However, the relationship between soil $CaCO_3$ content and plant nutritional status is not straightforward. Nutrient availability in the root zone is governed by the combined effects of soil pH and $CaCO_3$ content, as well as texture, organic matter, cation exchange capacity, soil moisture, and rhizosphere processes. Plant nutrient uptake may also vary depending on genotype, root-system characteristics, growth stage, fertilization history, and interactions among nutrients (White & Brown, 2010; Marschner, 2012). Therefore, $CaCO_3$ content alone may not provide an adequate basis for assessing plant nutritional status in calcareous soils.

Soil analyses provide information on the potential availability of nutrients and the nutrient-supplying capacity of the soil, whereas plant tissue analyses reflect the integrated outcome of soil–root processes as expressed in plant nutrient uptake. However, because elemental concentrations in plant tissues vary with the sampled organ and growth stage, the results should be interpreted using appropriate sampling times and established sufficiency ranges (Jones et al., 1991; Reuter & Robinson, 1997; Lemaire et al., 2019). Flag leaves collected immediately before heading constitute suitable diagnostic material for assessing the nutrient status of wheat. Accordingly, the combined use of soil and plant analyses enables a more comprehensive assessment of nutrient deficiencies and limitations to nutrient uptake.

The Narlı Plain, located south of Kahramanmaraş, is an important agricultural production area characterized by soils developed from alluvial and colluvial parent materials. Variations in topographic position and soil-forming conditions have resulted in considerable heterogeneity in the physical and chemical properties of the plain's soils (Yakupoğlu et al., 2012; Yakupoğlu & Demirci, 2013). Previous studies conducted in the region have shown that this variability is also reflected in soil pH, $CaCO_3$ content, and nutrient concentrations (Saltalı et al., 2018). Total and active $CaCO_3$ contents have also been reported to be associated with the availability of certain metallic micronutrients in the soils of the plain (Kadifeci et al., 2024). Nevertheless, field-based information on the extent to which soil nutrient levels are reflected in the nutritional status of wheat remains limited. Accordingly, this study aimed to determine selected physical and chemical properties of calcareous agricultural soils under wheat cultivation in the Narlı Plain and to evaluate the macro- and micronutrient status of wheat through combined soil and flag-leaf analyses. The relationships between soil $CaCO_3$ content and P, K, Ca, Mg, Fe, Zn, Cu, and Mn concentrations in wheat flag leaves were also investigated.

MATERIAL AND METHOD

Study area

The study was conducted in wheat-growing areas of the Narlı Plain, located within the administrative boundaries of Pazarcık district, Kahramanmaraş Province, southern Türkiye. Situated approximately 30 km southeast of Kahramanmaraş city center, the plain covers an area of approximately 26,500 ha and lies within a transitional zone between Mediterranean and continental climatic conditions (Saltalı et al., 2018).

The soils of the Narlı Plain have developed predominantly from alluvial and colluvial parent materials transported from the surrounding uplands and deposited across the plain. Variations in depositional environments and topographic positions have resulted in pronounced spatial variability in the physical and chemical properties of these soils (Yakupoğlu et al., 2012; Yakupoğlu & Demirci, 2013). The soils of the region have generally been characterized as neutral to slightly alkaline and as having varying $CaCO_3$ contents. Moreover, their total and active $CaCO_3$ contents may influence the availability of metallic micronutrients (Kadifeci et al., 2024).

The study area comprised fields under wheat cultivation within the Narlı Plain. Eleven wheat-growing fields were selected to represent the spatial variability in soil properties and plant nutritional status across the plain. The geographical coordinates of the soil and flag-leaf sampling points were recorded during fieldwork. The location of the study area within Türkiye and Kahramanmaraş Province, together with the distribution of the sampling points across the Narlı Plain, is presented in Figure 1.

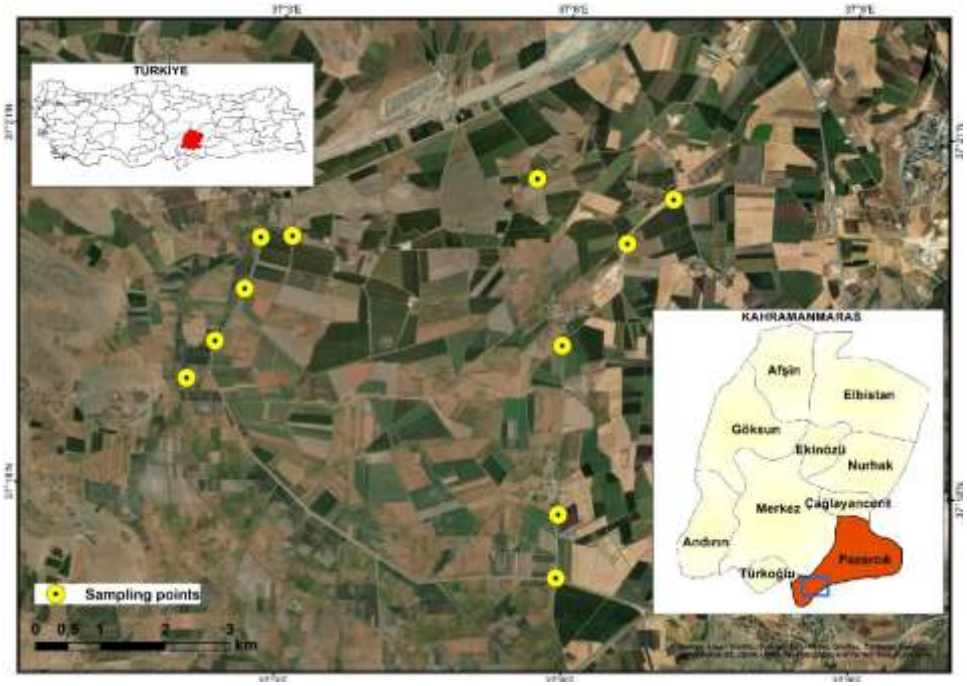

Figure 1. Location of the study area and distribution of soil and wheat flag-leaf sampling points in Narlı Plain

Soil and Plant Sampling and Preparation for Analysis

Soil samples were collected from a depth of 0–30 cm at 11 wheat-growing fields selected across the Narlı Plain, and the coordinates of the sampling points were recorded using a Global Positioning System (GPS). Composite soil samples representing each sampling point were transported to the laboratory, air-dried under ambient conditions, and passed through a 2-mm sieve. The prepared samples were labelled and stored in sealed plastic containers under cool and dry conditions until analysis (Richards, 1954).

Plant samples were collected simultaneously from the same fields where the soil samples were obtained. To assess the nutritional status of wheat, 25–30 representative flag leaves were collected from each field immediately before heading (Jones et al., 1991). The leaf samples were washed with distilled water to remove surface dust and other residues and subsequently oven-dried at 65 °C for 48 h. The dried plant material was ground and homogenized, transferred

to labelled polyethylene bags, and stored under refrigerated conditions until chemical analysis (Jones & Case, 1990).

Soil and Plant Analyses

Soil pH and electrical conductivity (EC) were determined in saturated soil paste according to the methods described by Peech (1965) and Richards (1954), respectively. Total calcium carbonate ($CaCO_3$) content was measured using a Scheibler calcimeter (Loeppert & Suarez, 1996), whereas soil organic matter was determined using the Walkley–Black wet oxidation method (Nelson & Sommers, 1996). Available P was determined using the Olsen method based on extraction with 0.5 M $NaHCO_3$ at pH 8.5 (Olsen et al., 1954). Exchangeable K, Ca, and Mg were extracted with 1 N ammonium acetate (NH_4OAc) at pH 7.0 (Thomas, 1982). Plant-available Fe, Zn, Cu, and Mn were determined using the DTPA extraction method (Lindsay & Norvell, 1978). The concentrations of K, Ca, Mg, Fe, Zn, Cu, and Mn in the soil extracts were measured using an Agilent 240AA atomic absorption spectrophotometer (AAS). A 0.50-g portion of each ground plant sample was wet-digested on a hot plate using a mixture of 5 mL HNO_3 and 4 mL $HClO_4$ until a clear solution was obtained (Jones & Case, 1990). Following digestion, the solutions were filtered and brought to a known volume with deionized water. Phosphorus concentration in the plant samples was determined spectrophotometrically using the vanadomolybdophosphoric yellow colour method. Potassium, Ca, Mg, Fe, Zn, Cu, and Mn concentrations were measured using an Agilent 240AA atomic absorption spectrophotometer.

Statisitical analyses

Minimum, maximum, mean, and standard deviation values for the soil and plant variables were calculated using Microsoft Office Excel. Relationships between soil $CaCO_3$ content and P, K, Ca, Mg, Fe, Zn, Cu, and Mn concentrations in wheat flag leaves were examined using two-tailed Pearson correlation analysis in IBM SPSS Statistics 23.0 (IBM Corp., Armonk, NY, USA). Statistical significance was accepted at $p < 0.05$, and graphical presentations of the results were prepared using Microsoft Office Excel.

RESULTS AND DISCUSSION

Characteristic Properties of the Study-Area Soils

Soil pH values ranged from 7.43 to 7.79, with a mean of 7.56. Electrical conductivity values varied between 303 and 501 µS cm^{-1}, averaging 349 µS cm^{-1}. Soil $CaCO_3$ contents ranged from 19.84% to 41.09%, with a mean of 27.95%, whereas organic matter contents varied between 2.13% and 4.50%, with a mean of 2.85%. Based on these results, the soils were generally characterized as slightly alkaline and non-saline, with high to very high $CaCO_3$ contents and moderate organic matter levels.

Table 1. Descriptive statistics of selected physicochemical properties of the study area soils

	pH	**EC**	**Lime**	**OM**
		(µS/cm)		%
Min	7,43	303	19,84	2,13
Mak	7,79	501	41,09	4,50
Ort	7,56	349	27,95	2,85

Macronutrient Status of the Study-Area Soils

Evaluation of the macronutrient contents of soil samples collected from the Narlı Plain revealed different sufficiency levels among the nutrients examined. According to Cottenie (1980), available P concentrations of 8–25 mg kg^{-1} are classified as sufficient, whereas concentrations of 25–80 mg kg^{-1} are considered high. Based on these thresholds, the mean available P concentration (22.5 mg kg^{-1}) was within the sufficient range; 54.5% of the samples were classified as sufficient and 45.5% as high. However, because the minimum concentration was close to the lower limit of the sufficiency range, the mean value should be interpreted together with the variability among sampling sites.

The mean exchangeable K concentration (340 mg kg^{-1}) exceeded the ≥161 mg kg^{-1} threshold above which Kaiser and Piotrowski (2024) did not recommend K fertilization for wheat under Minnesota conditions. While 63.6% of the samples reached or exceeded this threshold, 36.4% had K concentrations within the range of 95–160 mg kg^{-1}. Therefore, the high mean K concentration should not be interpreted as indicating a uniform K status across all sampling sites. Because this threshold was developed for a different region, it should be used as a comparative benchmark rather than directly applied to fertilizer recommendations for the Narlı Plain.

Regarding exchangeable Ca, 45.5% of the samples were classified as sufficient (1150–3500 mg kg^{-1}), whereas 54.5% were classified as high (3500–10,000 mg kg^{-1}). The mean Ca concentration (3461 mg kg^{-1}) was close to the upper limit of the sufficient range. Accordingly, the results did not indicate Ca deficiency in the investigated soils under the classification system used. For exchangeable Mg, 72.7% of the samples were classified as high (480–1500 mg kg^{-1}) and 27.3% as very high (>1500 mg kg^{-1}). The mean Mg concentration (1145 mg kg^{-1}) was within the high range, and all samples exceeded the sufficiency range, indicating that the soils generally had high exchangeable Mg concentrations (Cottenie, 1980).

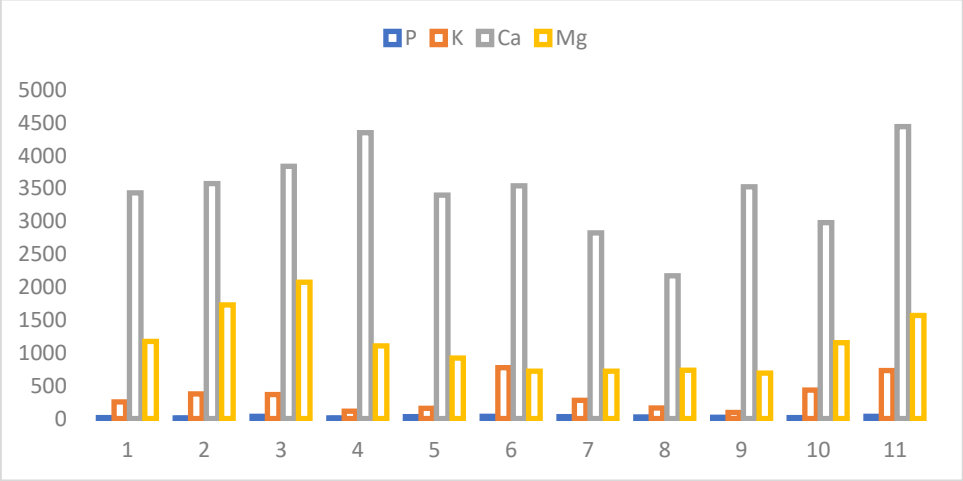

Figure 2. Distribution of available P and exchangeable cations

Micronutrient Status of the Study-Area Soils

The DTPA-extractable micronutrient concentrations of the soil samples collected from the Narlı Plain varied among the sampling sites (Figure 2). Iron (Fe) concentrations ranged from 8.88 to 23.52 mg kg^{-1}, with a mean of 11.73 mg kg^{-1}. Zinc (Zn) concentrations varied between 0.54 and 2.90 mg kg^{-1}, averaging 1.05 mg kg^{-1}. Copper (Cu) concentrations ranged from 1.08 to 2.20 mg kg^{-1}, with a mean of 1.50 mg kg^{-1}, whereas manganese (Mn) concentrations varied

between 3.36 and 28.80 mg kg^{-1}, averaging 9.65 mg kg^{-1}. The mean concentrations of the micronutrients followed the order Fe > Mn > Cu > Zn.

Soil micronutrient status was evaluated using the critical levels reported for maize by Lindsay and Norvell (1978) as comparative benchmarks. In all samples, Fe, Cu, and Mn concentrations exceeded their respective critical levels of 4.5, 0.2, and 1.0 mg kg^{-1}. Thus, according to these thresholds, no indication of Fe, Cu, or Mn deficiency was identified in the investigated soils. However, the critical values reported for Mn and Cu were proposed tentatively and should therefore be interpreted with caution.

Based on the critical Zn level of 0.8 mg kg^{-1}, 45.5% of the samples were classified as deficient and 54.5% as sufficient. Although the mean Zn concentration (1.05 mg kg^{-1}) exceeded the critical threshold, the occurrence of concentrations below this value in 45.5% of the samples demonstrates that soil Zn status should not be evaluated solely on the basis of the mean. Zinc was the only micronutrient for which values below the critical level were detected, indicating a potential Zn deficiency at some sampling sites that warrants further investigation. Nevertheless, because the thresholds used were originally established for maize, definitive conclusions regarding wheat nutritional status should be supported by plant tissue analyses and crop-specific sufficiency criteria.

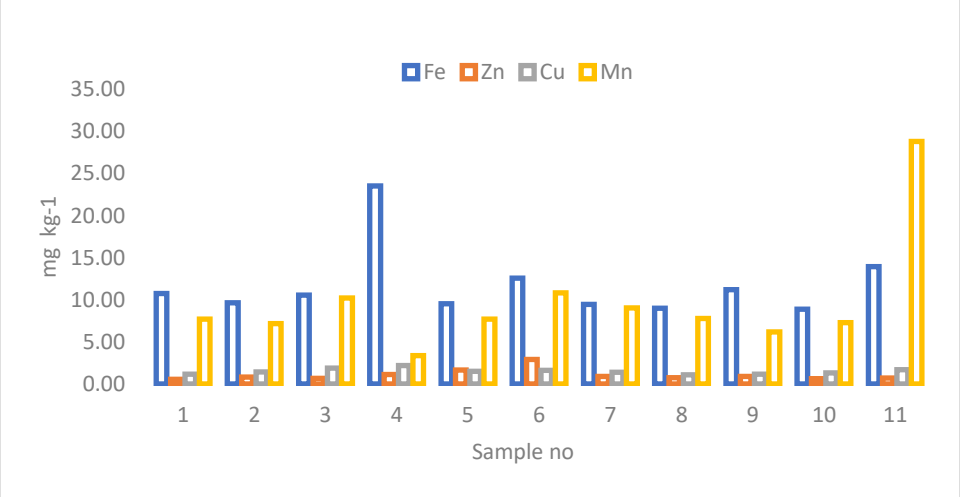

Figure 3. Distribution of DTPA-extractable Fe, Zn, Cu, Mn and Ni concentrations

Flag-Leaf Macronutrient Concentrations in Wheat

Macronutrient concentrations in wheat flag leaves varied among the sampling sites. Phosphorus concentrations ranged from 0.21% to 0.38%, with a mean of 0.28%. Potassium concentrations varied between 2.13% and 3.33%, averaging 2.60%. Calcium concentrations exhibited a relatively wide variation, ranging from 0.40% to 1.61%, with a mean of 0.80%. Magnesium concentrations ranged from 0.14% to 0.24%, with a mean of 0.18% (Figure 5). Among the macronutrients examined, K had the highest mean concentration, whereas Mg had the lowest.

The plant analysis results indicated that wheat grown in the study area generally had an adequate macronutrient status. When compared with the critical concentrations and sufficiency ranges reported for wheat, P and K concentrations were considered sufficient at all sampling sites (Jones et al., 1991; Reuter & Robinson, 1997; Plank & Donohue, 2000). In particular, the mean P (0.28%) and K (2.60%) concentrations exceeded the reported critical levels for wheat, indicating no apparent nutritional deficiency in these elements.

The variation in Ca concentrations from 0.40% to 1.61% indicated considerable differences among the sampling sites in Ca uptake or accumulation within plant tissues. Nevertheless, all measured Ca concentrations exceeded the critical level reported for wheat. Magnesium concentrations varied within a narrower range and averaged 0.18%. Because even the lowest Mg concentration (0.14%) was above the critical level, no evident Mg deficiency was identified in the wheat plants (Jones et al., 1991; Reuter & Robinson, 1997; Plank & Donohue, 2000).

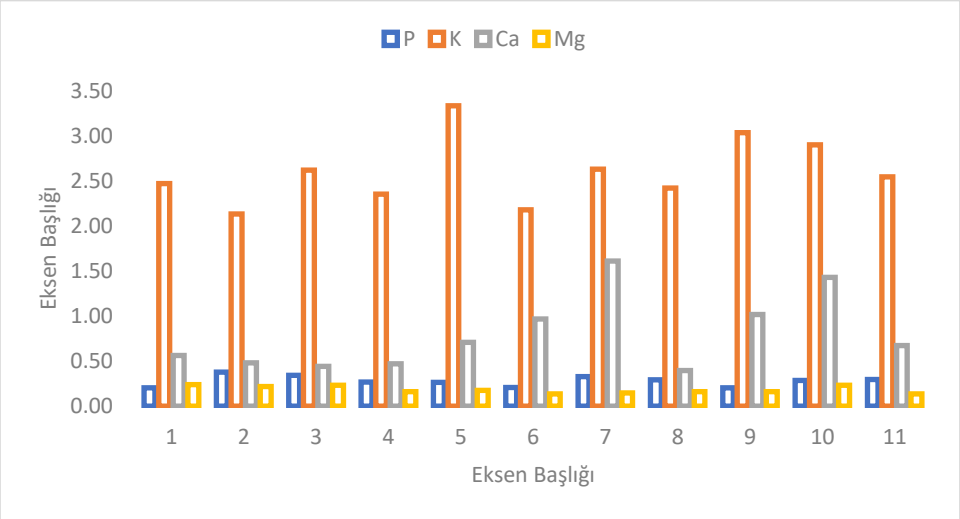

Figure 4. Foliar concentrations of macronutrients in wheat

Micronutrient Status of Wheat Flag Leaves

Micronutrient concentrations in wheat flag leaves varied among the sampling sites. Iron concentrations ranged from 69.00 to 156.75 mg kg^{-1}, with a mean of 97.93 mg kg^{-1}. Zinc concentrations varied between 17.50 and 30.00 mg kg^{-1}, averaging 21.84 mg kg^{-1}. Copper concentrations ranged from 4.50 to 8.75 mg kg^{-1}, with a mean of 6.75 mg kg^{-1}, whereas Mn concentrations varied between 16.00 and 54.25 mg kg^{-1}, averaging 40.41 mg kg^{-1} (Figure 6).

Based on the critical concentrations and sufficiency ranges reported for wheat, Fe, Zn, and Mn concentrations were generally considered adequate (Jones et al., 1991; Reuter & Robinson, 1997; Plank & Donohue, 2000). Iron concentrations of at least 69.00 mg kg^{-1} at all sampling sites indicated no evident Fe deficiency. Similarly, the observed Zn concentrations indicated that the wheat plants generally had an adequate Zn nutritional status.

Although the mean Cu concentration was within the sufficient range, the lowest value of 4.50 mg kg^{-1}, recorded at sampling site 2, was close to the critical level of approximately 5 mg kg^{-1} reported for wheat. Therefore, Cu nutrition was generally adequate, although a marginal Cu status may have occurred at this sampling site (Jones et al., 1991; Reuter & Robinson, 1997). Manganese concentrations indicated adequate nutrition at most sampling sites; however, the minimum concentration recorded at sampling site 11 was close to the lower limit of the sufficiency range.

Overall, wheat grown in the study area was adequately supplied with Fe, Zn, Cu, and Mn, although Cu and Mn concentrations approached the lower sufficiency limits at some sampling sites. Because tissue micronutrient concentrations may be influenced by soil pH, $CaCO_3$ and organic matter contents, nutrient availability, and interactions among elements, the combined

interpretation of soil and plant analyses provides a more reliable assessment of wheat nutritional status (Reuter & Robinson, 1997).

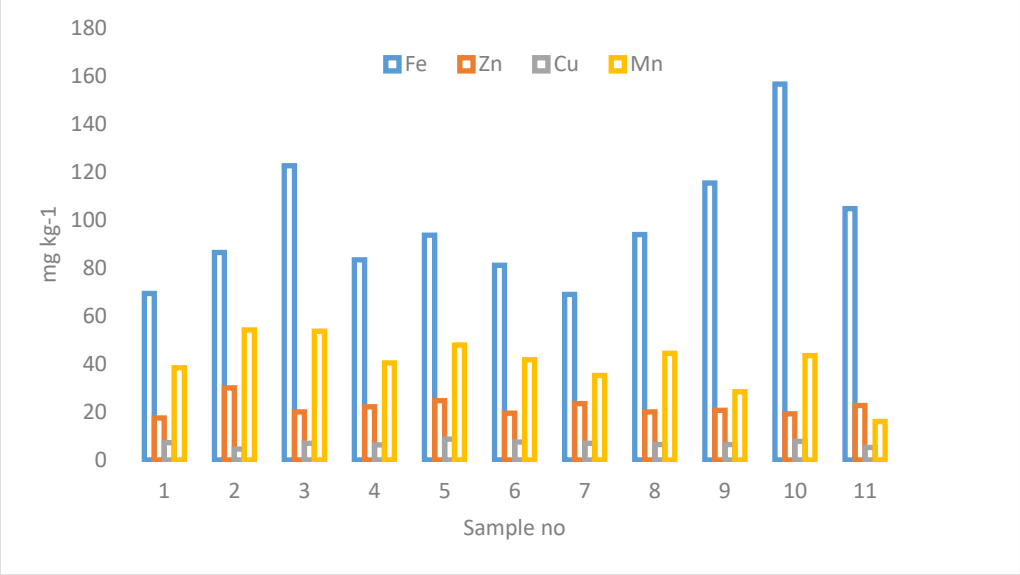

Figure 5. Foliar micronutrient concentrations in wheat

Relationships between soil lime and plant nutrients

No statistically significant correlations were detected between soil $CaCO_3$ content and P, K, Ca, Mg, Fe, Zn, Cu, or Mn concentrations in wheat flag leaves ($p > 0.05$; Table 2). Correlation coefficients ranged from −0.268 to 0.228, indicating no apparent linear relationship between soil $CaCO_3$ content and the macro- or micronutrient concentrations of wheat across the sampled fields. These findings suggest that variation in wheat nutritional status cannot be explained solely by soil $CaCO_3$ content and may also be influenced by soil nutrient reserves, fertilization practices, other soil properties, and plant-related factors. Nevertheless, because of the limited sample size ($n = 11$), the results should be interpreted within the context of the study area and sampling conditions (Table 2).

Table 2 Pearson correlation coefficients between soil lime and nutrient concentrations in wheat flag leaves

Plant nutrient	Pearson's r	p value	Significance
P	0,033	0,923	ns
K	−0,137	0,688	ns
Ca	−0,268	0,425	ns
Mg	0,228	0,500	ns
Fe	−0,028	0,934	ns
Zn	0,005	0,987	ns
Cu	−0,227	0,503	ns
Mn	0,001	0,998	ns

Note: Pearson correlation coefficients were calculated using 11 paired soil and flag-leaf samples ($n = 11$). ns: not significant ($p > 0.05$; two-tailed).

CONCLUSION

Wheat grown in the calcareous agricultural soils of the Narlı Plain was generally adequately supplied with P, K, Ca, Mg, Fe, Zn, Cu, and Mn. Available P and exchangeable K, Ca, and Mg concentrations in the soils were predominantly sufficient or high, while no clear deficiency of Fe, Cu, or Mn was identified. However, Zn concentrations were below the critical threshold in 45.5% of the soil samples, indicating a potential risk of Zn deficiency in some production fields. Plant analysis revealed no evident nutrient deficiencies, although Cu and Mn concentrations approached the lower limits of the sufficiency ranges at certain sampling sites. The absence of significant relationships between soil $CaCO_3$ content and nutrient concentrations in wheat flag leaves ($p > 0.05$) indicated that variation in plant nutritional status could not be explained solely by soil $CaCO_3$ content. Consequently, the combined interpretation of soil and plant analyses is recommended for a reliable assessment of wheat nutritional status in the Narlı Plain, with particular attention to the regular monitoring of Zn, Cu, and Mn.

REFERENCES

Peech, M. (1965). Hydrogen-ion activity. In C. A. Black (Ed.), Methods of soil analysis: Part 2. Chemical and microbiological properties (pp. 914–926). American Society of Agronomy. https://doi.org/10.2134/agronmonogr9.2.c9

Chen, X.-X., Zhang, W., Wang, Q., Liu, Y.-M., Liu, D.-Y., & Zou, C.-Q. (2019). Zinc nutrition of wheat in response to application of phosphorus to a calcareous soil and an acid soil. Plant and Soil, 434(1–2), 139–150. https://doi.org/10.1007/s11104-018-3820-5

Cottenie, A. (1980). Soil and plant testing as a basis of fertilizer recommendations (FAO Soils Bulletin No. 38/2). Food and Agriculture Organization of the United Nations. https://openknowledge.fao.org/handle/20.500.14283/d8502e

Demirkaya, S., & Gülser, C. (2025). Biochar innovations for sustainable agriculture: Acidification and zinc enrichment strategies to improve calcareous soil fertility and wheat yield. Soil and Water Research, 20(2), 105–118. https://doi.org/10.17221/77/2024-SWR

Thomas, G. W. (1982). Exchangeable cations. In A. L. Page, R. H. Miller, & D. R. Keeney (Eds.), Methods of soil analysis: Part 2. Chemical and microbiological properties (2nd ed., pp. 159–165). American Society of Agronomy and Soil Science Society of America. https://doi.org/10.2134/agronmonogr9.2.2ed.c9

Hinsinger, P. (2001). Bioavailability of soil inorganic P in the rhizosphere as affected by root-induced chemical changes: A review. Plant and Soil, 237(2), 173–195. https://doi.org/10.1023/A:1013351617532

Jones, J. B. Jr., and V. W. Case 1990. Sampling, Handling, and analyzing plant tissue samples, chapter 15. In R.L. Westerman (ed) Soil Testing and Plant Analysis, Third Edition, SSSA, Madison, Wisconsin, USA, pp. 390-420. https://doi.org/10.2136/sssabookser3.3ed.c15

Jones, J. B., Jr., Wolf, B., & Mills, H. A. (1991). Plant analysis handbook: A practical sampling, preparation, analysis, and interpretation guide. Micro-Macro Publishing. https://openlibrary.org/books/OL12110790M/Plant_Analysis_Handbook

Kadifeci, H., Dikici, H., & Demir, Ö. F. (2024). Effect of active lime on the availability of metal micronutrients. Turkish Journal of Agricultural and Natural Sciences, 11(2), 347–356. https://doi.org/10.30910/turkjans.1407307

Kaiser, D. E., & Piotrowski, K. (2024). Fertilizing wheat in Minnesota. University of Minnesota Extension. https://extension.umn.edu/agriculture/crop-production/nutrient-management-for-minnesota-crops/fertilizing-wheat-in-minnesota

Lemaire, G., Sinclair, T., Sadras, V., & Bélanger, G. (2019). Allometric approach to crop nutrition and implications for crop diagnosis and phenotyping: A review. Agronomy for Sustainable Development, 39, Article 27. https://doi.org/10.1007/s13593-019-0570-6

Lindsay, W. L., & Norvell, W. A. (1978). Development of a DTPA soil test for zinc, iron, manganese, and copper. Soil Science Society of America Journal, 42(3), 421–428. https://doi.org/10.2136/sssaj1978.03615995004200030009x

Marschner, P. (Ed.). (2012). Marschner's mineral nutrition of higher plants (3rd ed.). Academic Press. https://doi.org/10.1016/C2009-0-63043-9

Martínez-Ríos, O., Bravo-Vinaja, Á., San-Martín-Hernández, C., Hidalgo-Moreno, C. I., Sánchez-de-Jesús, M. A., Llampallas-Díaz, J. D., Santillan-Balderas, D. R., & García-Preciado, J. C. (2024). Zinc deficiency in calcareous soils: A bibliometric analysis from 1989 to 2024. Agriculture, 14(12), Article 2285. https://doi.org/10.3390/agriculture14122285

Nelson, D. W., & Sommers, L. E. (1996). Total carbon, organic carbon, and organic matter. In D. L. Sparks (Ed.), Methods of soil analysis: Part 3. Chemical methods (pp. 961–1010). Soil Science Society of America. https://doi.org/10.2136/sssabookser5.3.c34

Olsen, S. R., Cole, C. V., Watanabe, F. S., & Dean, L. A. (1954). Estimation of available phosphorus in soils by extraction with sodium bicarbonate (USDA Circular No. 939). U.S. Department of Agriculture. https://archive.org/details/estimationofavai939olse

Plank, C. O., & Donohue, S. J. (2000). Small grain—Barley, oats, rye, wheat. In C. R. Campbell (Ed.), Reference sufficiency ranges for plant analysis in the Southern Region of the United States (pp. 29–31). Southern Cooperative Series Bulletin No. 394. https://paperzz.com/doc/8950152/reference-sufficiency-ranges-for-plant-analysis-in-the-so

Reuter, D. J., & Robinson, J. B. (Eds.). (1997). Plant analysis: An interpretation manual (2nd ed.). CSIRO Publishing. https://www.publishing.csiro.au/book/437

Richards, L.A. (1954). Diagnosis and Improvement of Saline and Alkali Soils. Agriculture Handbook, No:60, U.S. Department of Agriculture. U.S. Government Printing Office, Washington D.C., 166.

Saltalı, K., Gündoğan, R., Demir, Ö. F., Kara, Z., Yakupoğlu, T., Dikici, H., & Yılmaz, K. (2018). Narlı Ovası topraklarının ağır metal kapsamı üzerine çimento fabrikası baca tozlarının etkileri. Toprak Su Dergisi, 7(1), 11–20. https://doi.org/10.21657/topraksu.410113

White, P. J., & Brown, P. H. (2010). Plant nutrition for sustainable development and global health. Annals of Botany, 105(7), 1073–1080. https://doi.org/10.1093/aob/mcq085

Xue, Y., Xia, H., Christie, P., Zhang, Z., Li, L., & Tang, C. (2016). Crop acquisition of phosphorus, iron and zinc from soil in cereal/legume intercropping systems: A critical review. Annals of Botany, 117(3), 363–377. https://doi.org/10.1093/aob/mcv182

Yakupoğlu, T., & Demirci, D. (2013). Kahramanmaraş-Narli Ovasi Topraklarinin Erozyona Duyarliliklari İle Bazi Toprak Özellikleri Arasindaki İlişkiler. Anadolu Tarım Bilimleri Dergisi, 28(1), 33-38. https://izlik.org/JA62SJ38AJ

Yakupoğlu, T., Saltalı, K., & Karagöktaş, M. (2012). Narlı Ovası'nda toprak aşınabilirliğinin pedotransfer yaklaşımı ile tahminlenmesi. KSÜ Doğa Bilimleri Dergisi, 15(2), 59–67. https://izlik.org/JA98BP96FZ

Zaheri Abdehvand, Z., Karimi, D., Rangzan, K., & Mousavi, S. R. (2024). Assessment of soil fertility and nutrient management strategies in calcareous soils of Khuzestan Province: A case study using the Nutrient Index Value method. Environmental Monitoring and Assessment, 196(6), Article 503. https://doi.org/10.1007/s10661-024-12665-4

COMPARATIVE EVALUATION OF DROUGHT TOLERANCE IN DIVERSE TRITICUM SPECIES USING THERMAL RETENTION, MEMBRANE DAMAGE, AND STRESS INDICES

Oğuzhan Önal[1], İmren Kutlu[1], Koç Mehmet Tuğrul[2]

[1]Eskişehir Osmangazi University, Faculty of Agriculture, Department of Field Crops, Eskişehir, Türkiye

[2]Eskişehir Osmangazi University, Faculty of Agriculture, Department of Soil Science and Plant Nutrition, Türkiye

Corresponding author e-mail: oguzhanonal44@gmail.com

ABSTRACT

The identification of drought-tolerant wheat germplasm is essential for developing climate-resilient cultivars. This study evaluated drought tolerance in 96 genotypes representing eight *Triticum* groups, including durum landraces, durum breeding lines, Polish wheat, Khorasan wheat, bread wheat landraces, Indian dwarf wheat, and tetraploid and hexaploid check cultivars. Drought responses were assessed using unmanned aerial vehicle (UAV)-derived thermal retention, membrane damage, and complementary drought stress indices. Thermal images acquired at the tillering and heading stages were processed using Pix4D, and the resulting thermal index values were used to calculate thermal retention (TE retention), while membrane damage was determined using the electrolyte leakage method. Grain yield under irrigated and water-deficit conditions was used to calculate the Relative Efficiency Index (REI), Stress Non-Stress Production Index (SNPI), Modified Stress Tolerance Index 1 (K1STI), and Modified Stress Tolerance Index 2 (K2STI). Principal component analysis (PCA) was performed separately for tetraploid and hexaploid materials to investigate relationships among physiological traits and drought indices. Substantial variation was observed among and within wheat groups for all evaluated traits. Membrane damage and TE Retention showed considerable genotypic variation, while drought indices revealed contrasting response patterns among genotypes. Durum breeding lines exhibited relatively higher SNPI values and broader variation than the other tetraploid groups, while bread wheat landraces showed substantial variability for the modified stress tolerance indices. PCA discriminated genotypes according to membrane damage, TE retention, and drought index profiles, identifying several durum breeding lines and Khorasan wheat genotypes with favorable drought-response characteristics. The integration of UAV-derived thermal traits, membrane damage, and complementary drought indices effectively characterized drought responses across genetically diverse wheat materials and provides a practical approach for identifying promising germplasm for wheat improvement programs.

Keywords: drought tolerance, UAV thermal imaging, membrane stability, stress indices, *Triticum* spp.

INTRODUCTION

Drought is one of the most severe abiotic stresses limiting wheat (*Triticum* spp.) production worldwide and is expected to intensify under changing climatic conditions. As one of the world's principal staple crops, wheat supplies nearly 20% of the calories and protein consumed by the global population, making the development of drought-resilient cultivars essential for sustaining future food security (Ashfaq et al., 2022). Water deficit adversely affects plant growth, photosynthesis, assimilate partitioning, and grain filling, ultimately reducing grain yield. However, the magnitude of yield loss largely depends on drought severity, duration, and the developmental stage at which stress occurs, making drought tolerance one of the most complex traits targeted in wheat breeding (Ashfaq et al., 2022; Ghanem & Al-Farouk, 2024).

The genus *Triticum* encompasses a broad range of cultivated species differing in ploidy level, evolutionary origin, genetic constitution, and adaptation to diverse agroecological environments. Ancient wheats and traditional landraces have recently attracted renewed interest because they represent valuable reservoirs of genetic diversity that may contain adaptive alleles lost during modern breeding (Lopes et al., 2015). Comparative evaluation of genetically diverse wheat groups therefore provides an opportunity to identify novel sources of drought tolerance and broaden the genetic basis of future breeding programs. Nevertheless, information describing the comparative physiological responses of diverse *Triticum* groups under water-deficit conditions remains limited, particularly when evaluated using integrated phenotyping approaches.

Conventional drought screening has primarily relied on grain yield measured under irrigated and stress conditions. Although yield remains the ultimate breeding target, it is strongly influenced by environmental variation and genotype × environment interactions, frequently limiting its effectiveness as the sole selection criterion (Ahmad et al., 2022). Consequently, physiological traits and complementary drought tolerance indices have become increasingly important for improving selection efficiency. Among physiological traits, membrane damage estimated by electrolyte leakage has been widely accepted as a reliable indicator of cellular injury caused by drought stress. Water deficit promotes oxidative stress, leading to lipid peroxidation, disruption of membrane integrity, and increased electrolyte leakage; therefore, genotypes exhibiting lower membrane damage generally possess greater tolerance to drought (Shahid et al., 2022).

Recent advances in high-throughput phenotyping have substantially improved the evaluation of drought responses in breeding populations. In particular, unmanned aerial vehicle (UAV)-based thermal imaging enables rapid, non-destructive, and repeated assessment of crop performance under field conditions. Thermal information derived from UAV platforms has been successfully associated with canopy temperature, plant water status, transpiration, biomass production, and grain yield, allowing the early identification of drought-responsive genotypes while greatly increasing phenotyping efficiency compared with conventional field measurements (Ashfaq et al., 2022; Awais et al., 2023; Das et al., 2022; Mali et al., 2025). The integration of UAV-assisted thermal phenotyping with physiological measurements therefore provides a powerful approach for characterizing drought adaptation in genetically diverse germplasm.

To complement physiological measurements, numerous drought tolerance indices have been proposed to simultaneously evaluate genotype performance under stress and non-stress environments (Jalili et al., 2026). Classical indices, including Mean Productivity (MP), Geometric Mean Productivity (GMP), Harmonic Mean (HM), and Stress Tolerance Index (STI), have been widely used for drought evaluation, whereas recently developed indices such

as Relative Efficiency Index (REI), Stress Non-Stress Production Index (SNPI), and Modified Stress Tolerance Indices (K1STI and K2STI) provide improved discrimination of genotypes exhibiting both high productivity and stable performance across contrasting environments (Jalili et al., 2026). Furthermore, multivariate statistical techniques, particularly principal component analysis (PCA), facilitate the simultaneous interpretation of physiological traits and drought indices, enabling more reliable identification of drought-tolerant germplasm than the use of individual parameters alone (Al-Ashkar, 2024; Jalili et al., 2026).

Although UAV-derived thermal traits, membrane damage, and drought tolerance indices have individually been used to characterize drought responses in wheat, studies integrating these complementary approaches across genetically diverse *Triticum* groups remain scarce. Therefore, the present study aimed to comparatively evaluate drought tolerance in 96 genotypes representing eight wheat groups using UAV-derived thermal responses, membrane damage, and complementary drought indices (REI, SNPI, K1STI, and K2STI). In addition, principal component analysis was performed separately for tetraploid and hexaploid materials to investigate the relationships among physiological traits, drought indices, and genotypic responses under contrasting water regimes.

MATERIAL AND METHOD

Plant Materials and Experimental Design

A total of 96 wheat genotypes representing diverse *Triticum* species were used as plant material in this study. The germplasm consisted of 90 accessions obtained from the United States Department of Agriculture (USDA) National Plant Germplasm System (NPGS), including 45 tetraploid genotypes (11 *T. durum* landraces, 14 *T. durum* breeding lines, 5 *T. polonicum*, and 15 *T. turanicum*) and 45 hexaploid genotypes (34 *T. aestivum* landraces and 11 *T. sphaerococcum*). Detailed information on the evaluated genotypes is presented in Table 1.

Table 1. Information about the genotypes used in the study.

Ploidy	Species	Genotype Code	Plant ID	Plant Name	Collected from/Pedigree
Tetraploid	*T. durum_landrace*	D3	PI 73376	2529/Kara Kilchik	Azerbaijan
		D4	PI 73318	2650/Kara glianikh	Azerbaijan
		D28	PI 172562	Akbasak-24	Türkiye
		D33	PI 341350	Beyaz Kunduru	Elazığ
		D35	PI 167669	Kara	Ankara
		D45	PI 166706	Kunduru-5	Ankara
		D66	PI 173475	Menceki-4	Elazığ
		D82	PI166243	Sahman-6	Konya
		D90	PI 341345	Sari-5	Eskişehir
		D96	PI 341353	Sari Kilcik	Ankara
		D115	PI 585192	Uveyik-12	Çorum
	T. durum_lines	OR2	PI 655356	OR971849	Westbred 881/5/D.130-16/4/Uveyik 162/ 61.130//HC6654/3/Akbasak/Oviachic 65
		OR3	PI 655360	OR9801900	Westbred 881/5/D.130-16/4/Uveyik 162/ 61.130//HC6654/3/Akbasak/Oviachic 65
		OR4	PI 655361	OR9801915	Quilafen/5/Uveyik 162/61.130//HC6654/ 3/Akbasak/Oviachic 65/4/Westbred 881
		OR12	PI 655370	OR2000007	Uveyik 162/61.130//HC6654/3/Akbasak/ Oviachic 65/4/Vic
		OR13	PI 655371	OR2000008	Uveyik 162/61.130//HC6654/3/Akbasak/ Oviachic 65/4/Vic
		OR19	PI 655416	OR2010496	Uveyik 162/61.130//HC6654/3/Akbasak/ Oviachic 65/4/Renville/5/H7092-12
		OR21	PI 655421	OR2010506	Uveyik 162/61.130//HC6654/3/Akbasak/ Oviachic 65/4/Renville/5/H7092-12
		OR25	PI 655426	OR2010518	Uveyik 162/61.130//HC6654/3/Akbasak/ Oviachic 65/4/Renville/5/H7092-12

		OR26	PI 655427	OR2010519	Uveyik 162/61.130//HC6654/3/Akbasak/ Oviachic 65/4/Renville/5/H7092-12
		OR27	PI 655428	OR2010520	Uveyik 162/61.130//HC6654/3/Akbasak/ Oviachic 65/4/Renville/5/H7092-12
		OR29	PI 655435	OR2010543	Westbred 881/Parus/4/Uveyik 162/61.130// HC6654/3/Akbasak/Oviachic 65
		OR30	PI 655450	OR2000008	Uveyik 162/61.130//HC6654/3/Akbasak/ Oviachic 65/4/Vic
		OR32	PI 655471	OR2000005	Uveyik 162/61.130//HC6654/3/Akbasak/ Oviachic 65/4/Vic
		OR38	PI 655482	OR2010525	Vic/Brindur/4/Uveyik 162/61.130// HC6654/3/Akbasak/Oviachic 65
	T. polonicum	P1	CItr 14139	CI 14139	Unknown
		P2	CItr 14140	CI 14140	Unknown
		P3	PI 306548	2939	Romania
		P4	PI 306549	2941	Romania
		P5	PI 167622	Mika	Balıkesir, Turkey
	T. turanicum	T8	PI 211668	1473	Ankara
		T13	PI115815	15992-15	Türkiye
		T14	PI 254213	15992-13	Türkiye
		T16	PI 113392	1N1	Khorasan, Iran
		T17	PI 254203	263-a-10	Iran
		T34	PI 113393	2N4	Iraq
		T35	PI 537992	73/3	Adıyaman,
		T37	PI 184543	Arrancada F3	Aveiro, Portugal
		T38	PI 67343	Australian Pouland	Victoria, Australia
		T42	CItr 14095	CI 14095	Unknown
		T44	PI127106	Dandan-i-Shutur	Fāryāb, Afghanistan
		T57	PI 210386	Heath	Iran
		T60	PI 481582	IQ 97	Iraq
		T87	PI 192658	Meknes	Morocco
		T95	PI 166959	Turnadili	Çankırı
	T. durum_checks	KZLTN	Registered Cultivar	Kızıltan	Türkiye
		EMNBY	Registered Cultivar	Eminbey	Türkiye
		KMBT	Registered Cultivar	Kümbet	Türkiye
Hexaploid	*T. aestivum_landrace*	A2	PI 211669	1482	Ankara
		A4	PI 211656	1152-1	Ankara
		A6	PI 559622	84TK613-001.0	Erzurum
		A7	PI 559623	84TK617-001.0	Erzurum
		A10	PI 173494	Asure	Malatya
		A20	PI 24485	Kara Bugdai	Toshkent, Uzbekistan
		A26	PI 166873	Kirik-5	Ağrı
		A29	PI 178018	Kirik-8	Ağrı
		A53	PI 263152	Kirik-32	Kars
		A73	PI 166868	Köse-3	Bingöl
		A80	PI 166826	Köse-10	Erzincan
		A95	PI341619	Kunduru-4	Kahramanmaraş
		A110	PI 166884	Menceki-11	Tunceli
		A111	PI 166891	Menceki-12	Tunceli
		A116	PI 166707	Sarı Başak-3	Eskişehir
		A119	PI178041	Sünter-1	Afyonkarahisar
		A126	PI 166602	Sünter-8	Bilecik
		A138	PI 341321	Sünter-20	Eskişehir
		A149	PI166303	Sünter-31	Yozgat
		A159	PI 470316	79TK035-189 (Tir)	Bitlis
		A162	PI 166790	Tir-5	Van
		A178	PI 560692	TU85-088-01-3	Ağrı
		A181	PI 560695	TU85-088-01-6	Ağrı

T.sphaerococcum	A186	PI 560589	TU85-012-06	Bitlis
	A189	PI 560654	TU85-053-03	Bitlis
	A192	PI 560657	TU85-056-05-1	Bitlis
	A194	PI 560659	TU85-056-05-3	Bitlis
	A199	PI 560677	TU85-072-03	Bitlis
	A204	PI 560819	TU86-22-01-1	Siirt
	A205	PI 560820	TU86-22-01-2	Siirt
	A213	PI 560618	TU85-033-02-2	Van
	A215	PI 560620	TU85-033-03-2	Van
	A223	PI 560859	TU86-46-01-1	Van
	A226	PI 560862	TU86-46-01-4	Van
	S2	PI 278650	971	United Kingdom
	S3	PI 190982	2531	Portugal
	S4	PI115818	23824	Punjab, India
	S8	PI 277142	Acarp	India
	S19	PI 272581	I-1-3573	Pest, Hungary
	S20	PI 277164	Randhawai	Punjab, Pakistan
	S23	PI 282452	TRI 3008	India
	S25	PI 40942	Linaza	Punjab, Pakistan
	S26	PI 40943	Wernerianum	Punjab, Pakistan
	S27	PI 40944	Humboldti	Punjab, Pakistan
	S28	PI 323439	Unknown-1	Wien, Austria
T. aestivum_checks	MFTBY	Registered Cultivar	Müfitbey	Türkiye
	REİS	Registered Cultivar	Reis	Türkiye
	ESPE	Registered Cultivar	Esperia	Türkiye

Six commercially grown wheat cultivars were included as check varieties. The tetraploid checks comprised the durum wheat cultivars Kızıltan, Eminbey, and Kümbet, whereas the hexaploid checks consisted of the bread wheat cultivars Müfitbey, Reis, and Esperia.

The experimental soil had a clay texture, with a salt content of 0.06%, lime content of 8.24%, organic matter content of 2.65%, and a pH of 7.73. The amounts of plant-available P_2O_5 and K_2O in the soil were 10.31 and 271.93 kg da^{-1}, respectively. Climatic conditions during the 2023–2024 growing season differed from the long-term averages (1991–2022). The mean temperature during the growing period was 11.2°C, compared with the long-term average of 8.9°C, while total precipitation was 249.2 mm, approximately 15% lower than the long-term average of 294.5 mm. The difference was particularly pronounced during the later stages of crop development. Precipitation in April, June, and July was only 11.8, 5.6, and 4.4 mm, respectively, compared with the corresponding long-term averages of 44.1, 24.2, and 15.0 mm. In addition, June and July were warmer than the long-term averages, with mean temperatures of 22.9 and 23.7°C, respectively. These conditions indicate that the crop experienced relatively warm and dry conditions, particularly during the later part of the growing season.

Field experiments were established on 26 October 2023 under two contrasting water regimes, irrigated (IR) and rainfed (RF), using an augmented experimental design. Each genotype was sown with a plot drill at a seeding density of 500 plants m^{-2} in four-row plots, each 4 m in length with 25 cm row spacing. Phosphorus fertilizer was applied at sowing at a rate of 8 kg P_2O_5 da^{-1}, whereas nitrogen fertilizer was applied according to soil analysis recommendations to provide a total of 14 kg N da^{-1}, split between sowing and the stem elongation stage.

Physiological evaluations were performed using leaf samples collected at the tillering (Zadoks 30) and heading (Zadoks 58) growth stages under both irrigated and rainfed conditions. The experimental plots were harvested on 19 July 2024 using a plot combine harvester, and grain yield was determined for each genotype under both water regimes.

UAV-Based Thermal Imaging and Thermal Retention Analysis

High-throughput thermal phenotyping was performed using a DJI Mavic 2 Enterprise Advanced unmanned aerial vehicle (UAV) equipped with an integrated thermal infrared (TIR) camera. The thermal sensor had a resolution of 640 × 512 pixels and operated within the 8–14 μm spectral range. Thermal image acquisition was conducted at the tillering (Zadoks 30) and heading (Zadoks 58) growth stages under both irrigated (IR) and rainfed (RF) conditions. To minimize the influence of environmental variation on thermal measurements, all UAV flights were conducted under clear-sky conditions between 10:00 and 12:00 h, with wind speeds below 12 m s^{-1}. Images were acquired at an altitude of 15 m above ground level (AGL), with approximately 80% forward overlap and 70% side overlap, ensuring sufficient image overlap for orthomosaic generation.

Thermal images, from which orthomosaic maps were created using Pix4Dmapper software (Pix4D SA, Lausanne, Switzerland), were processed using the zonal statistics tool in ArcGIS to obtain average thermal index values derived from the image at the plot level under irrigated and rain-fed conditions. The image-derived thermal index reflects relative variation in canopy thermal conditions but does not represent absolute canopy temperature. To characterize the relative thermal response of each genotype to water deficit, the thermal index obtained under rainfed conditions was normalized to the corresponding value under irrigated conditions. This stress-to-irrigated ratio was termed thermal retention (TE retention) in the present study and was calculated separately for the tillering and heading stages as follows:

TE Retention = Thermal Index (RF) / Thermal Index (IR)

where Thermal Index (RF) and Thermal Index (IR) represent the plot-level image-derived thermal index values obtained under rainfed and irrigated conditions, respectively. A TE Retention value of 1.0 indicates no relative change in the thermal index between the two water regimes, whereas values above or below 1.0 indicate proportionally higher or lower thermal index values under rainfed conditions, respectively.

Membrane Damage Determination

Membrane damage was determined using the electrolyte leakage method described by Sairam et al. (1997) with slight modifications. At both the tillering (Zadoks 30) and heading (Zadoks 58) growth stages, three leaf discs (2 cm in diameter) were collected from irrigated (control) and rainfed (drought-stressed) plants. The discs were rinsed thoroughly with distilled water, gently blotted dry, and transferred into test tubes containing 20 mL of distilled water. Samples were incubated on a rotary shaker at 250 rpm for 4 h at room temperature, after which the initial electrical conductivity (EC_1) was measured using a conductivity meter.

Subsequently, the samples were autoclaved at 121°C for 15 min to completely disrupt the cell membranes and release the remaining electrolytes. After cooling to room temperature, the final electrical conductivity (EC_2) was recorded. Electrolyte leakage (EL) was calculated according to the following equation (Sairam et al., 1997):

$EL\ (\%) = (EC_1 / EC_2) \times 100$

Membrane damage (%) was subsequently calculated using the electrolyte leakage values of drought-stressed and irrigated plants according to the following equation:

Membrane damage (%) = [(ELstress−ELcontrol) / (100 − ELcontrol)] × 100

where ELstress and ELcontrol represent the electrolyte leakage percentages measured under rainfed and irrigated conditions, respectively.

Drought Tolerance Indices

Grain yield obtained under irrigated (Yp) and rainfed (Ys) conditions was used to calculate four complementary drought tolerance indices. The relative efficiency index (REI) was calculated as: REI = $(Ys_i / \bar{Y}s) \times (Yp_i / \bar{Y}p)$ according to Hossain et al. (1990).

The modified stress tolerance index 1 (K1STI) and modified stress tolerance index 2 (K2STI) were calculated according to Farshadfar and Sutka (2002) using the following equations: K1STI = $(Yp^2 / \bar{Y}p^2) \times STI$ and K2STI = $(Ys^2 / \bar{Y}s^2) \times STI$

The stress non-stress production index (SNPI) was calculated according to Moosavi et al. (2008) as: SNPI = [(Yp + Ys) / (Yp − Ys)]^(1/3) × (Yp × Ys × Ys)^(1/3)

where Yp and Ys represent grain yield under irrigated and rainfed conditions, respectively, while $\bar{Y}p$ and $\bar{Y}s$ denote the corresponding mean yields of all genotypes under irrigated and rainfed conditions. These indices were selected because they simultaneously evaluate genotype productivity under favorable and water-deficit environments and provide complementary information on drought tolerance and yield stability.

Statistical Analysis

Descriptive statistics were calculated for all physiological traits and drought tolerance indices to summarize the variation among wheat groups. The distributions of membrane damage, TE retention, REI, SNPI, K1STI, and K2STI were visualized using boxplots.

To investigate the relationships among physiological traits and drought tolerance indices and to identify the major sources of variation, principal component analysis (PCA) was performed separately for tetraploid and hexaploid wheat materials. The analysis included membrane damage at tillering (MDTL) and heading (MDHD), TE retention at tillering (TERTL) and heading (TERHD), and the four drought tolerance indices (REI, SNPI, K1STI, and K2STI). Prior to PCA, all variables were standardized to zero mean and unit variance to eliminate differences in measurement scales.

PCA biplots were generated to visualize the distribution of genotypes and the relationships among the evaluated variables. Descriptive statistics, boxplots, principal component analysis, and graphical visualizations were performed using R software (version 4.5.2; R Core Team, Vienna, Austria) with the ggplot2, ggrepel, factoextra, and dplyr packages.

RESULTS AND DISCUSSION

Thermal Retention Responses under Drought Conditions

The TE retention parameter showed substantial variation among wheat groups at both the tillering (TL) and heading (HD) stages (Figure 1), indicating marked genotypic differences in the relative thermal response between rainfed and irrigated conditions. As observed for

membrane damage, within-group variation was generally pronounced, highlighting considerable genetic diversity in thermal responses to water deficit.

At the tillering stage (Figure 1A), the tetraploid checks (DWC) exhibited TE retention values relatively close to 1.0, with a comparatively narrow distribution across the three check cultivars. Likewise, the hexaploid checks (BWC) displayed a relatively narrow distribution. In contrast, Polish wheat (P) and durum lines (OR) showed much broader distributions, reflecting greater genotypic variability. Among individual genotypes, A159 exhibited a high TE retention value (1.52) within the bread wheat landrace group, whereas D115 showed the lowest value (0.56) among the durum landraces. Considerable variation was also observed within Indian dwarf wheat, where TE Retention ranged from 0.46 (S26) to 1.24 (S23).

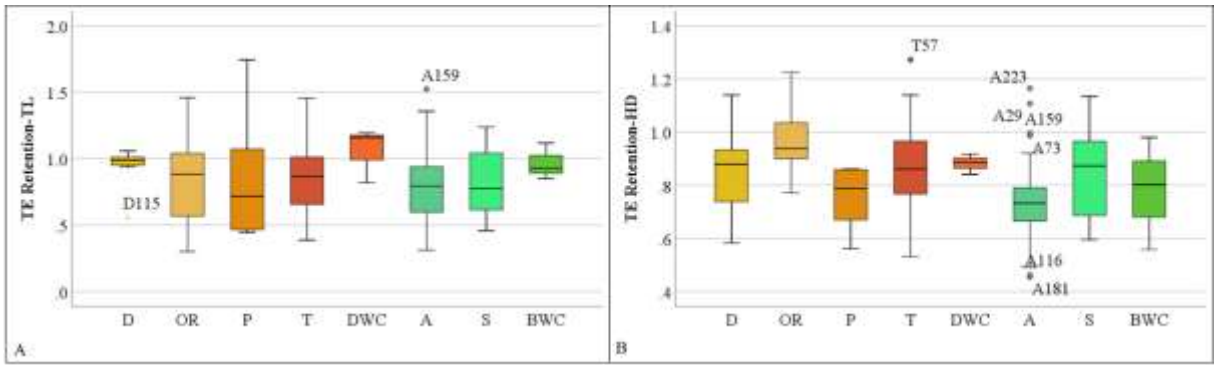

Figure 1. Thermal retention in the examined wheat genotypes under drought stress.

At the heading stage (Figure 1B), group differences became less pronounced, with most median values ranging approximately between 0.75 and 0.95. Nevertheless, several individual genotypes deviated markedly from their respective group distributions. Genotype T57 exhibited the highest TE retention value (1.27), while A223 (1.16), A29 (1.11), and A159 (1.00) showed relatively high values within the bread wheat landrace group. Conversely, A181 and A116 exhibited the lowest values (0.46), corresponding to substantially lower thermal index values under rainfed than under irrigated conditions.

The relatively narrow distributions observed for the tetraploid and hexaploid check cultivars indicate less genotypic variation in their relative thermal responses, whereas the broader distributions detected within several landrace and genetically diverse groups demonstrate substantial within-group variability. In particular, bread wheat landraces, durum lines, and Indian dwarf wheat contained genotypes with markedly contrasting TE retention values, providing useful variation for evaluating thermal responses to water deficit.

UAV-based thermal imaging has increasingly been used for high-throughput assessment of crop responses to water deficit because thermal characteristics can provide information related to plant water status and physiological responses to drought (Qin et al., 2022; Mali et al., 2025; Sharma et al., 2025; Cudjoe et al., 2026). As TE retention represents the ratio of the thermal index under rainfed to irrigated conditions (RF/IR), values close to 1.0 indicate a relatively small change between water regimes. Several genotypes remained close to unity, including D90 and D82 at tillering and A159, OR4, S3, and A73 at heading. However, pronounced stage-dependent responses were also observed. For example, P2 decreased from 1.74 at tillering to 0.79 at heading, OR32 from 1.46 to 0.91, whereas T37 increased from 0.43 to 1.14. These shifts indicate that genotypic thermal responses to water deficit were strongly influenced by developmental stage.

Thermal traits have been widely used to characterize wheat responses to water deficit because canopy thermal behavior is associated with plant water status, stomatal regulation, and transpirational cooling (Blum et al., 1989; Bhandari et al., 2021; Qin et al., 2022). In the present study, TE retention was used as a relative thermal-response parameter rather than as an independent measure of drought tolerance. Therefore, genotypes with values close to unity were considered to exhibit greater thermal stability between water regimes, while their overall drought performance was evaluated together with membrane damage and yield-based stress indices.

Membrane Damage Responses of Wheat Groups under Drought Stress

Membrane damage varied considerably among the evaluated wheat groups at both the tillering (TL) and heading (HD) growth stages (Figure 2), indicating substantial genetic variation in cellular responses to drought stress. However, variation within groups was generally greater than that among groups, demonstrating the broad diversity of drought adaptation mechanisms present within the evaluated Triticum germplasm.

At the tillering stage (Figure 2A), Indian dwarf wheat (S) exhibited the highest mean membrane damage (8.08%), followed by the hexaploid checks (BWC) (5.91%), bread wheat landraces (A) (5.05%), and tetraploid checks (DWC) (4.23%). In contrast, Khorasan wheat (T) (2.28%) and durum lines (OR) (2.31%) showed the lowest average membrane damage. The Indian dwarf wheat group also exhibited the greatest variability (SD = 7.49; CV = 92.66%), with membrane damage ranging from only 0.68% (S25) to 23.57% (S26). Similarly, bread wheat landraces displayed a broad range of responses, varying from 0.14% (A111) to 14.70% (A162), reflecting the large physiological diversity within this germplasm. In comparison, durum lines showed a narrower distribution despite a similar mean value, with OR32 (0.28%), OR25 (0.37%), and OR38 (0.47%) exhibiting the lowest membrane damage, whereas OR27 (6.12%) represented the most susceptible genotype within this group.

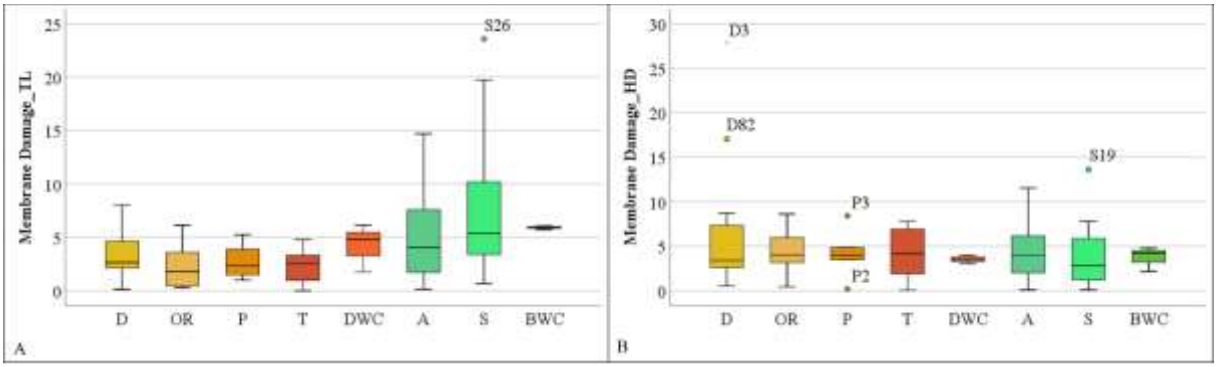

Figure 2. Membrane damage in the examined wheat genotypes under drought stress.

At the heading stage (Figure 2B), membrane damage became more uniform among wheat groups, with group means ranging from 3.54% (tetraploid checks) to 7.03% (durum landraces). However, several individual genotypes showed exceptionally high injury. Genotype D3 exhibited the greatest membrane damage (27.86%), followed by D82 (17.04%), resulting in the highest coefficient of variation for the durum landrace group (CV = 117.83%). Likewise, S19 (13.62%) represented a highly susceptible Indian dwarf wheat genotype, whereas P2 (0.20%), D45 (0.53%), S27 (0.09%), and T44 (0.31%) maintained remarkably low membrane damage, suggesting superior preservation of membrane integrity under drought conditions.

Maintenance of membrane integrity is considered one of the earliest physiological mechanisms associated with drought tolerance because drought-induced oxidative stress increases

membrane permeability and electrolyte leakage (Bajji et al., 2002). Consequently, genotypes exhibiting lower membrane damage are generally considered more capable of maintaining cellular function under water-deficit conditions. The broad within-group variation observed in the present study agrees with previous reports demonstrating that membrane damage is an effective physiological criterion for discriminating drought tolerance among wheat genotypes (Öztürk et al., 2016; Ghanem & Al-Farouk, 2024). Moreover, the large variability observed particularly within bread wheat landraces and Indian dwarf wheat suggests that these germplasm groups constitute valuable reservoirs of allelic diversity for future drought-tolerance breeding.

Drought Tolerance Indices

Considerable variation was observed among wheat groups and individual genotypes for all four drought tolerance indices (Figure 3), indicating marked differences in drought adaptation and yield stability under contrasting moisture conditions. Although the distribution patterns differed among indices, substantial within-group variation was consistently observed, reflecting the wide genetic diversity present in the evaluated *Triticum* germplasm.

The relative efficiency index (REI) showed relatively similar median values among most wheat groups, whereas the check cultivars displayed narrower distributions than the landrace groups (Figure 3A). The highest REI values were recorded for genotypes D115 (4.08), P1 (3.03), S20 (2.82) and A194 (2.64), indicating superior yield performance under rainfed conditions relative to irrigated conditions. In contrast, several genotypes, including D3 (0.04), A205 (0.11) and OR12 (0.23), exhibited considerably lower REI values, suggesting greater sensitivity to water deficit. The relatively broad distributions observed within bread wheat landraces and Indian dwarf wheat indicate substantial genetic diversity for drought adaptation within these groups. Group means for REI were relatively similar, ranging from 0.98 in the tetraploid checks to 1.23 in durum landraces, but within-group variability was much greater in the genetically diverse germplasm. Durum landraces and Polish wheat showed particularly high variation for REI, with CV values of 97.50 and 95.65%, respectively, whereas tetraploid checks were much more uniform (CV = 4.81%). Several individual accessions clearly exceeded their respective group distributions, emphasizing that genotype-level selection may be more informative than comparisons based only on group means. Because REI combines yield performance relative to the population means under both stress and non-stress conditions, the high values of these genotypes indicate comparatively favorable performance across the two environments rather than drought response based solely on yield under stress.

Greater differentiation among groups was evident for SNPI (Figure 3B). Mean SNPI was highest in the tetraploid checks (10.62), Khorasan wheat (9.87), and durum breeding lines (9.47), whereas Indian dwarf wheat had a markedly lower mean of 1.43. However, the high mean of the tetraploid checks was accompanied by relatively low variability (CV = 26.9%), while durum breeding lines displayed much greater variation (CV = 88.0%), largely reflecting the exceptionally high SNPI of OR32 (36.04). Other prominent genotypes included A10 (18.49), T13 (18.28), A4 (16.35), P1 (15.33), and OR21 (14.77). This pattern is particularly relevant because SNPI was specifically proposed to identify genotypes combining high and relatively stable yield under both irrigated and non-irrigated conditions. Moosavi et al. (2008), working with bread and durum wheat, reported positive relationships of SNPI with yield under both conditions and with several productivity-based indices and recommended it for identifying genotypes with desirable performance across stress and non-stress environments. The exceptionally high SNPI of OR32 therefore distinguishes this genotype from the broader durum

breeding-line population, although its overall drought response should be evaluated together with the other indices rather than on SNPI alone.

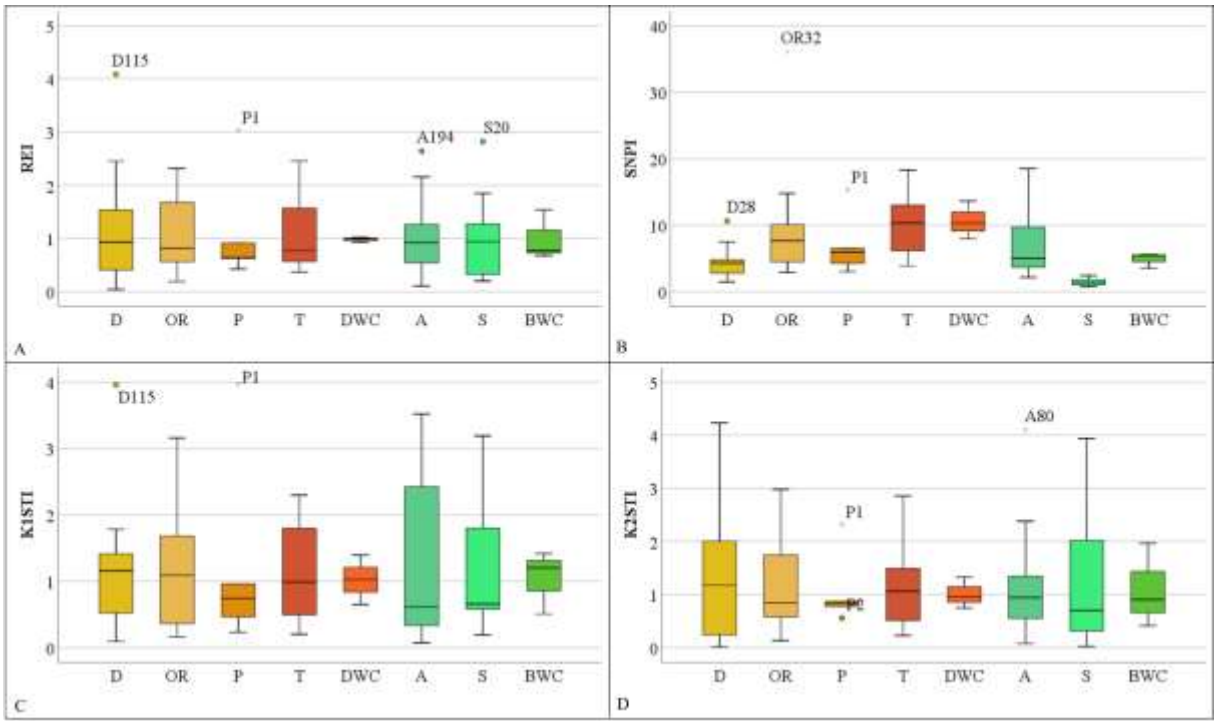

Figure 3. Drought tolerance indices in the examined wheat genotypes under drought stress.

The modified stress tolerance indices also revealed pronounced genotypic variation (Figures 3C and 3D). For K1STI, group means ranged from 1.02 in tetraploid checks to 1.28 in bread wheat landraces, but the magnitude of within-group variation was much greater than the differences among means. Polish wheat had the highest CV for K1STI (120.19%), followed by bread wheat landraces (93.59%) and durum landraces (89.11%). P1 (3.97), D115 (3.96), A194 (3.52), A7 (3.43), and S20 (3.19) occupied the upper end of the K1STI distribution. K2STI showed a similarly broad response, with D115 (4.23), A80 (4.10), S2 (3.94), S3 (3.61), D96 (3.39), and OR30 (2.98) among the highest-ranking genotypes. Particularly large variation for K2STI occurred in durum landraces and Indian dwarf wheat, both of which had CV values above 100%, whereas tetraploid checks were considerably more homogeneous (CV = 28.81%). Farshadfar and Sutka (2002) developed the modified stress tolerance index by applying correction coefficients to STI to improve discrimination among genotypes differing in performance under stress and non-stress environments. Their results also emphasized that genotype classification based on a single drought criterion can be contradictory and that modified indices can provide additional discrimination among contrasting response types.

Yield-based drought indices have long been recognized as effective tools for identifying superior genotypes because they simultaneously consider productivity under stress and non-stress conditions rather than evaluating yield in a single environment (Fernandez, 1992; Moosavi et al., 2008). Similarly, the modified stress tolerance indices proposed by Farshadfar and Sutka (2002) provide improved discrimination among genotypes differing in drought adaptation. The contrasting rankings obtained from REI, SNPI, K1STI, and K2STI are therefore biologically and statistically informative rather than inconsistent. Drought indices differ in the relative weight they assign to yield potential, yield under stress, and stability between environments. Fernandez (1992) emphasized that an effective selection criterion should

preferentially identify genotypes with high performance under both stress and non-stress conditions, while also demonstrating that different indices can favor different response groups. This explains why some genotypes were outstanding for a particular index but not consistently superior for all four indices. For example, OR32 was exceptional for SNPI (36.04) but showed more moderate REI (1.64) and K2STI (0.85), whereas D115 combined the highest REI (4.08) with very high K1STI (3.96) and K2STI (4.23). P1 similarly combined high REI (3.03), SNPI (15.33), and the highest K1STI (3.97). A194 also performed consistently well for REI (2.64) and K1STI (3.52), while T44 combined relatively high REI (2.46) and K2STI (2.86). Thus, D115 and P1 in particular exhibited favorable performance across several complementary yield-based criteria rather than superiority based on a single index.

Overall, the high coefficients of variation within several landrace and breeding groups demonstrate that drought-response diversity was often greater within taxonomic groups than suggested by their group means. This is particularly important for breeding because selection at the individual-genotype level can reveal useful accessions that would be obscured by group-level comparisons. Moosavi et al. (2008) emphasized the advantage of combining several indices and multivariate analysis rather than relying on a single drought criterion. This multi-index approach is also consistent with the recent declaration of Jalili et al. (2026), which incorporates REI, K1STI, K2STI, and SNPI among a broader set of complementary stress tolerance indices for comprehensive genotype evaluation in plant breeding. Khan (2025) also demonstrated that different drought indices provide complementary information and that the combined use of correlation analysis and PCA improves discrimination of genotypes with favorable yield performance across contrasting environments. Similarly, some wheat studies have emphasized that drought adaptation is better characterized through the integration of yield-based indices with physiological and agronomic responses rather than reliance on a single criterion (Ghanem and Al-Farouk, 2024). Accordingly, the consistent performance of D115 and P1 across several yield-based indices, together with the distinctive profiles of OR32, A194, T44, and other high-ranking genotypes, identifies a focused set of candidates for further evaluation. Their classification as drought-tolerant material, however, requires integration of these yield-based responses with membrane damage and Thermal Retention, which was subsequently achieved through PCA.

Principal Component Analysis

Principal component analysis (PCA) was performed separately for the tetraploid and hexaploid wheat materials to investigate the relationships among thermal retention, membrane damage, and drought tolerance indices and to visualize the distribution of genotypes according to their drought responses (Figure 4). The first two principal components explained 56.2% of the total variation in tetraploid wheat (PC1 = 37.5%, PC2 = 18.7%) and 50.1% in hexaploid wheat (PC1 = 31.0%, PC2 = 19.1%), revealing distinct multivariate response patterns within the two ploidy groups.

In the tetraploid materials (Figure 4A), REI and K1STI showed similar vector orientations, indicating that these indices represented relatively similar patterns of genotype differentiation. K2STI was also positioned in the upper-left region of the biplot, whereas SNPI was oriented toward the lower-left quadrant. The contrasting orientation of SNPI and membrane damage at tillering (MDTL) suggested that these variables represented different dimensions of the drought response. This differentiation among yield-based indices is consistent with Farshadfar et al. (2012), who showed through PCA that SNPI, K1STI, and K2STI differed in their relationships with grain yield under rainfed and irrigated conditions.

The thermal variables also showed stage-dependent patterns. TERTL and TERHD were oriented toward different regions of the biplot, indicating that the relative thermal response to water deficit differed between tillering and heading. Similarly, MDTL and MDHD showed contrasting orientations, suggesting that drought-induced membrane injury was also dependent on developmental stage. The separation of the thermal and membrane-damage vectors from several yield-based indices indicates that these physiological measurements contributed information that was not fully represented by yield-derived drought indices alone.

The distribution of tetraploid genotypes further illustrated this multivariate diversity. D115, T44, and D96 were separated from much of the population, reflecting distinctive combinations of drought-response traits, while OR32, T38, T17, and D3 also occupied relatively extreme positions in the ordination space. The tetraploid check cultivars KZLTN, EMNBY, and KMBT were located comparatively closer to the central region than several of the more widely dispersed landrace and breeding accessions. Notably, D115 was differentiated in the same multivariate analysis in which it had already exhibited the highest REI and high K1STI and K2STI values, strengthening its identification as a promising tetraploid candidate when multiple drought-response criteria are considered together.

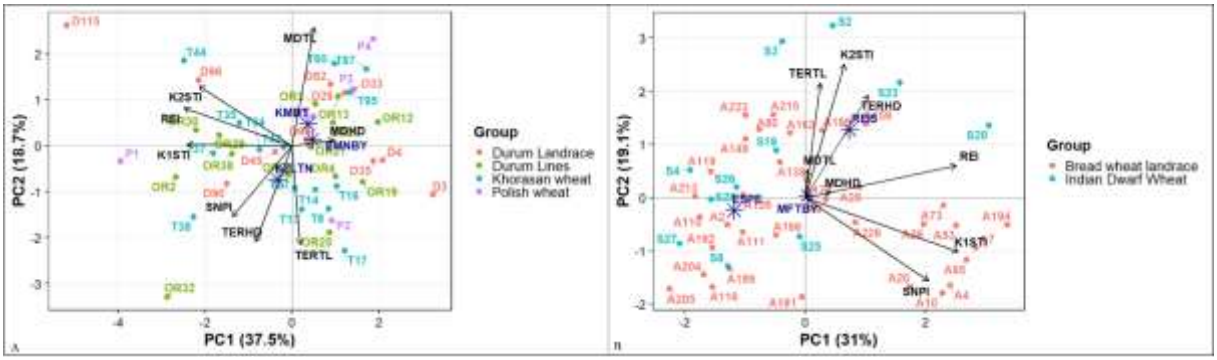

Figure 4. PCA biplot illustrating the multivariate relationships between wheat genotypes and drought stress indicators

For the hexaploid wheat materials (Figure 4B), REI, K1STI, and SNPI were projected predominantly toward the positive side of PC1, showing broadly similar orientations and contributing strongly to genotype differentiation along this axis. K2STI was more strongly oriented toward positive PC2, while the thermal retention variables were also represented primarily along the second component. Membrane damage variables showed shorter vectors than several drought tolerance indices, suggesting a comparatively smaller contribution to genotype differentiation represented by the first two components. Thus, as observed in the tetraploid material, the first two PCs represented different components of drought response rather than a single uniform tolerance axis.

Bread wheat landraces displayed broad dispersion across the biplot, demonstrating substantial within-group diversity. Several landraces, including A194, A95, A7, and A4, were positioned in the region associated with yield-based drought indices, whereas A205, A181, A116, and A204 occupied contrasting regions of the ordination space. Among Indian dwarf wheat genotypes, S2, S3, and S23 were positioned more closely to K2STI and the positive-PC2 region containing the thermal-response vectors, whereas S25, S27, and S8 showed contrasting multivariate positions. Among the bread wheat checks, MFTBY was located relatively close to the central region, whereas REIS and ESPE occupied different positions, indicating that the check cultivars did not exhibit a completely homogeneous multivariate response.

The joint use of REI, SNPI, K1STI, and K2STI is particularly relevant because these indices provide complementary rather than interchangeable information on genotype performance under contrasting water regimes. Jalili et al. (2026) classified REI as a stress-tolerance index, K1STI and K2STI as modified indices intended for environment-specific selection, and SNPI as a composite index useful when selection based on a single criterion is insufficient. The authors further demonstrated that a genotype ranking highly for an individual modified index may perform poorly according to other stress-related criteria, emphasizing that genotype selection should not rely on a single index. This interpretation agrees with the contrasting rankings observed in the present study, where D115 and P1 performed favorably across several indices, whereas OR32 was distinguished predominantly by its exceptionally high SNPI. Moosavi et al. (2008) and Farshadfar et al. (2012) similarly emphasized the value of combining complementary drought indices for genotype discrimination rather than relying on a single selection criterion.

Importantly, yield-based drought indices describe the agronomic outcome of stress but do not fully capture the physiological heterogeneity underlying that performance. The inclusion of thermal retention and membrane damage therefore added independent physiological dimensions to the yield-based assessment, allowing genotypes with similar agronomic performance to be distinguished according to differences in their canopy-level and cellular responses. This is particularly relevant for drought screening because comparable yield responses may result from different physiological strategies, which cannot be resolved through yield-derived indices alone. The use of thermal imaging together with conventional physiological traits has similarly improved the characterization of genotypic variation under water deficit in wheat (Ashfaq et al., 2022; Qin et al., 2022). Thus, the separation of thermal, membrane-damage, and yield-based variables observed in the present biplots supports their complementary value for multidimensional drought characterization.

The developmental-stage dependence observed for thermal retention in the present study is also physiologically relevant. Qin et al. (2022) reported that UAV-derived canopy thermal responses were associated with physiological traits related to plant water status and photosynthetic functioning under water deficit, while the strength of thermal discrimination varied with developmental stage and stress intensity. Thus, the contrasting orientations of TERTL and TERHD in the present PCA should not be regarded as inconsistent responses but rather as evidence that canopy thermal behavior under drought is dynamic across crop development. Repeated thermal phenotyping may therefore provide information that would be lost by measurements restricted to a single growth stage.

From a breeding perspective, thermal phenotyping is particularly attractive because drought-induced changes in stomatal regulation and transpiration can alter canopy thermal behavior before their consequences are fully expressed in final grain yield. UAV-based thermal imaging additionally provides rapid, non-destructive, and spatially extensive phenotyping of large numbers of breeding materials, offering potential as an intermediate physiological indicator of drought response (Qin et al., 2022; Das et al., 2022). However, thermal responses should not be considered stand-alone measures of drought tolerance because they are affected by developmental stage, stress intensity, and the physiological mechanisms regulating canopy cooling. Their interpretation together with membrane damage and final yield-based indices therefore provides a stronger basis for genotype evaluation than any of these components alone.

Overall, PCA demonstrated that thermal retention, membrane damage, and drought tolerance indices provided complementary information for differentiating drought responses among wheat genotypes. Their integration is biologically relevant because they represent different

levels of drought response: canopy-level thermal regulation, cellular membrane injury, and agronomic performance under contrasting water regimes. The broad dispersion observed particularly among landrace and breeding materials highlights substantial physiological and agronomic diversity within these germplasm groups. Accordingly, the combined approach allowed genotypes to be evaluated not merely for favorable yield-based index values, but for the extent to which these agronomic responses were accompanied by distinct thermal and membrane-level responses. Such multidimensional screening may provide a more robust basis for identifying promising drought-adapted germplasm for subsequent validation and use in wheat improvement programs.

An additional noteworthy finding of the present analysis was that the previously selected tolerant and sensitive genotypes could also be differentiated, to a considerable extent, using the independent set of variables evaluated here. The original tolerant (T) and sensitive (S) classification had been established from a broader set of traits using a PCA-based selection index, whereas the present analysis was based specifically on membrane damage, Thermal Retention, and complementary yield-based drought indices. Despite these methodological differences, most of the previously selected T/S pairs retained a broadly contrasting response pattern across the variables evaluated here, although the degree of separation varied among wheat groups (data not shown). This agreement suggests that the original classification captured drought-response differences that were also detectable through physiological and yield-based indicators not used in exactly the same combination during the initial selection.

The relevance of the multivariate discrimination obtained in the present study is further supported by the subsequent-season evaluation of 16 selected genotypes from the same germplasm. Based on the broader drought-response assessment conducted during the same screening season, contrasting tolerant and sensitive genotypes were selected from each wheat group and evaluated in the following growing season using UAV-derived canopy temperature, DREB expression, and a broader set of yield-based drought indices (Önal et al., 2026). Several of the original selections showed consistent responses across seasons. In particular, D115, which exhibited the highest REI and high K1STI and K2STI values in the present study, subsequently showed one of the most stable drought-response profiles, with the lowest TOL and among the lowest SDI and highest YSI and RSI values. MFTBY also maintained favorable performance across productivity and stability criteria, whereas previously selected sensitive genotypes such as T57 and A223 showed comparatively high drought sensitivity in the subsequent season. However, some genotypes showed less consistent classifications across years, emphasizing the influence of seasonal conditions and the importance of combining multiple physiological and agronomic criteria rather than assigning drought tolerance from a single season or index (Önal et al., 2026).

CONCLUSIONS

The present study demonstrated substantial variation in drought responses among diverse *Triticum* germplasm based on thermal retention, membrane damage, and complementary drought tolerance indices. The combined evaluation of physiological and yield-based responses revealed considerable within-group variation, particularly among landrace and breeding materials, emphasizing the importance of genotype-level evaluation rather than reliance on group means alone. D115 and P1 were particularly notable for their favorable performance across several yield-based drought indices, while other genotypes, including OR32, A194, and T44, exhibited distinctive response profiles that warrant further evaluation. PCA revealed that the evaluated traits represented distinct but complementary dimensions of drought response, enabling clearer differentiation among genotypes with contrasting physiological and agronomic

profiles. Notably, the present set of traits also broadly supported the tolerant and sensitive classifications previously established using a broader set of traits and a PCA-based selection index. Overall, the integration of UAV-derived thermal phenotyping, membrane damage, and complementary drought tolerance indices provides a practical multidimensional approach for high-throughput drought screening and the identification of promising germplasm for wheat improvement programs.

ACKNOWLEDGEMENTS

We are grateful for the financial support provided by the Eskişehir Osmangazi University Scientific Research Projects Coordination Unit (Project No. FOA-2024-3007). This manuscript is derived from a portion of the data generated during the ongoing PhD research of the first author.

REFERENCES

Ahmad, A., Z. Aslam, T. Javed, S. Hussain, A. Raza, R. Shabbir, F. Mora-Poblete, T. Saeed, F. Zulfiqar, M. M. Ali, M. Nawaz, M. Rafiq, H. S. Osman, M. Albaqami, M. A. A. Ahmed, M. Tauseef. 2022. Screening of heat (*Triticum aestivum* L.) genotypes for drought tolerance through agronomic and physiological response. Agronomy. 12(2): 287.

Al-Ashkar, I. 2024. Multivariate analysis techniques and tolerance indices for detecting bread wheat genotypes of drought tolerance. Diversity. 16(8): 489.

Ashfaq, W., G. Brodie, S. Fuentes, D. Gupta. 2022. Infrared thermal imaging and morpho-physiological indices used for wheat genotypes screening under drought and heat stress. Plants. 11(23): 3269.

Awais, M., W. Li, M. J. M. Cheema, Q. U. Zaman, A. Shaheen, B. Aslam, W. Zhu, M. Ajmal, M. Faheem, S. Hussain, A. A. Nadeem, M. M. Afzal, C. Liu. 2023. UAV-based remote sensing in plant stress imagine using high-resolution thermal sensor for digital agriculture practices: A meta-review. International Journal of Environmental Science and Technology. 20(1): 1135-1152.

Bajji, M., J. M. Kinet, S. Lutts. 2002. The use of the electrolyte leakage method for assessing cell membrane stability as a water stress tolerance test in durum wheat. Plant Growth Regulation. 36(1): 61-70.

Bhandari, M., Q. Xue, S. Liu, B. A. Stewart, J. C. Rudd, P. Pokhrel, B. Blaser, K. Jessup, J. Baker. 2021. Thermal imaging to evaluate wheat genotypes under dryland conditions. Agrosystems, Geosciences & Environment. 4(2): e20152.

Blum, A., L. Shpiler, G. Golan, J. Mayer. 1989. Yield stability and canopy temperature of wheat genotypes under drought-stress. Field Crops Research. 22(4): 289-296.

Cudjoe, D. K., Y. Sun, S. Li, W. Guo. 2026. Spatial and temporal scales in plant phenotyping for crop water stress assessment: A review. The Plant Phenome Journal. 9(1): e70073.

Das, S., J. Christopher, M. R. Choudhury, A. Apan, S. Chapman, N. W. Menzies, Y. P. Dang. 2022. Evaluation of drought tolerance of wheat genotypes in rain-fed sodic soil environments using high-resolution UAV remote sensing techniques. Biosystems Engineering. 217: 68-82.

Farshadfar, E., Z. Moradi, P. Elyasi, B. Jamshidi, R. Chaghakabodi. 2012. Effective selection criteria for screening drought tolerant landraces of bread wheat (*Triticum aestivum* L.). Annals of Biological Research. 3(5): 2507-2516.

Farshadfar, E., J. Sutka. 2002. Screening drought tolerance criteria in maize. Acta Agronomica Hungarica. 50(4): 411-416.

Fernandez, G. C. J. 1992. Effective selection criteria for assessing plant stress tolerance. In: Adaptation of Food Crops to Temperature and Water Stress. AVRDC, Shanhua, Taiwan. 257-270.

Ghanem, H. E., M. O. Al-Farouk. 2024. Wheat drought tolerance: Morpho-physiological criteria, stress indexes, and yield responses in newly sand soils. Journal of Plant Growth Regulation. 43(7): 2234-2250.
Hossain, A. B. S., R. G. Sears, T. S. Cox, G. M. Paulsen. 1990. Desiccation tolerance and its relationship to assimilate partitioning in winter wheat. Crop Science. 30(3): 622-627.
Jalili, A., H. Sabouri, Z. Shoaei. 2026. A comprehensive web-based platform for calculation of abiotic stress tolerance indices in plant breeding. Scientific Reports. 16(1): 7995.
Khan, A. A. 2025. Drought tolerance indices: Genetic parameter estimation and application in discriminating tolerant wheat genotypes. Genetika. 57(3): 377-397.
Lopes, M. S., I. El-Basyoni, P. S. Baenziger, S. Singh, C. Royo, K. Ozbek, H. Aktas, E. Ozer, F. Ozdemir, A. Manickavelu, T. Ban, P. Vikram. 2015. Exploiting genetic diversity from landraces in wheat breeding for adaptation to climate change. Journal of Experimental Botany. 66(12): 3477-3486.
Mali, S. S., M. Scobie, J. Baillie, C. Plant, S. Shammi, A. Das. 2025. Integrating UAV-based multispectral and thermal infrared imageries with machine learning for predicting water stress in winter wheat. Precision Agriculture. 26(3): 44.
Moosavi, S. S., B. Yazdi Samadi, M. R. Naghavi, A. A. Zali, H. Dashti, A. Pourshahbazi. 2008. Introduction of new indices to identify relative drought tolerance and resistance in wheat genotypes. Desert. 12(2): 165-178.
Önal, O., İ. Kutlu, K. M. Tuğrul. 2026. Integrating UAV-based thermal imaging, DREB expression, and mathematical indices to evaluate drought tolerance in diverse *Triticum* species. International Journal of Agriculture, Forestry and Life Sciences. 10(2): 76-87.
Öztürk, A., B. Taşkesenligil, K. Haliloğlu, M. Aydin, Ö. Çağlar. 2016. Evaluation of bread wheat genotypes for early drought resistance via germination under osmotic stress, cell membrane damage, and paraquat tolerance. Turkish Journal of Agriculture and Forestry. 40(2): 146-159.
Qin, W., J. Wang, L. Ma, F. Wang, N. Hu, X. Yang, Y. Xiao, Y. Zhang, Z. Sun, Z. Wang, K. Yu. 2022. UAV-based multi-temporal thermal imaging to evaluate wheat drought resistance in different deficit irrigation regimes. Remote Sensing. 14(21): 5608.
Sairam, R. K., P. S. Deshmukh, D. S. Shukla. 1997. Tolerance of drought and temperature stress in relation to increased antioxidant enzyme activity in wheat. Journal of Agronomy and Crop Science. 178(3): 171-178.
Shahid, S., Q. Ali, S. Ali, F. A. Al-Misned, S. Maqbool. 2022. Water deficit stress tolerance potential of newly developed wheat genotypes for better yield based on agronomic traits and stress tolerance indices: Physio-biochemical responses, lipid peroxidation and antioxidative defense mechanism. Plants. 11(3): 466.
Sharma, H., H. Sidhu, A. Bhowmik. 2025. Remote sensing using unmanned aerial vehicles for water stress detection: A review focusing on specialty crops. Drones. 9(4): 241.

ASSESSMENT OF SELECTED MACRO- AND MICRONUTRIENT CONCENTRATIONS IN SOILS AND WHEAT IN THE NARLI PLAIN

Ömer Faruk DEMİR
Kahramanmaraş Sütçü İmam University, Faculty of Agriculture, Department of Soil Science and Plant Nutrition, Kahramanmaraş, Türkiye

Corresponding author e-mail: demirfaruk@ksu.edu.tr

ABSTRACT

Evaluating soil nutrient availability together with plant nutrient concentrations provides a comprehensive understanding of crop nutritional status. Accordingly, this study aimed to assess the macro- and micronutrient status of wheat grown in the Narlı Plain of Kahramanmaraş, Türkiye. Soil samples were collected from a depth of 0–30 cm, and flag leaf samples were collected immediately before heading from 11 wheat-growing fields. Soil samples were analyzed for pH, calcium carbonate ($CaCO_3$) and organic matter contents, available phosphorus (Olsen-P), exchangeable potassium (K), calcium (Ca), and magnesium (Mg), and DTPA-extractable iron (Fe), zinc (Zn), copper (Cu), and manganese (Mn). Plant samples were analyzed for P, K, Ca, Mg, Fe, Zn, Cu, and Mn concentrations. The soils were slightly to moderately alkaline, with organic matter contents ranging from 2.13% to 4.50% and $CaCO_3$ contents ranging from 19.84% to 41.09%. Soil Olsen-P concentrations varied between 7.98 and 35.38 mg kg^{-1}, while the mean DTPA-extractable Fe, Zn, Cu, and Mn concentrations were 11.73, 1.05, 1.50, and 9.65 mg kg^{-1}, respectively. The mean exchangeable K, Ca, and Mg concentrations were 339.55, 3461, and 1145 mg kg^{-1}, respectively. The mean P, K, Ca, and Mg concentrations in wheat flag leaves were 0.28%, 2.60%, 0.80%, and 0.18%, respectively, whereas the mean Fe, Zn, Cu, and Mn concentrations were 97.93, 21.84, 6.75, and 40.41 mg kg^{-1}, respectively. The results showed that wheat grown in the Narlı Plain was generally adequately supplied with the macro- and micronutrients examined. However, the variation in soil and plant nutrient concentrations among the sampled fields suggests that wheat nutrient status may be influenced by differences in soil nutrient reserves, fertilizer management, and other soil properties. These findings highlight the importance of evaluating soil and plant analyses together when developing field-specific nutrient management strategies for wheat production in the region.

Keywords: Calcareous soil, flag leaf, mineral nutrition, wheat.

INTRODUCTION

Determining the mineral nutritional status of wheat grown in calcareous soils represents an important diagnostic challenge because soil nutrient reserves do not necessarily correspond to the availability of these nutrients to plants. High soil pH and $CaCO_3$ content may restrict nutrient uptake by roots by altering nutrient speciation in the soil solution, adsorption–desorption equilibria, and precipitation reactions. Therefore, the presence of an adequate reserve of a particular nutrient in the soil does not necessarily indicate that the nutrient can be taken up by plants in sufficient amounts (Hinsinger, 2001; Marschner, 2012; Xue et al., 2016). Recent studies conducted in calcareous soils have also demonstrated that these conditions may affect nutrient uptake and fertilizer-use efficiency in wheat (Martínez-Ríos et al., 2024; Zaheri Abdehvand et al., 2024; Demirkaya & Gülser, 2025).

In calcareous and alkaline soils, P may form sparingly soluble compounds with Ca or become immobilized through retention on $CaCO_3$ surfaces. Similarly, high pH and the presence of carbonate and bicarbonate ions may reduce the solubility and root availability of Fe, Zn, Mn, and Cu. Zinc availability, in particular, is strongly influenced by interactions among soil pH, carbonate content, P status, organic matter, and clay minerals (Chen et al., 2019; Martínez-Ríos et al., 2024). Consequently, wheat grown in calcareous soils may exhibit marginal or latent nutrient deficiencies even in the absence of visible deficiency symptoms. However, the relationship between soil $CaCO_3$ content and plant nutritional status is not straightforward. Nutrient availability in the root zone is governed by the combined effects of soil pH and $CaCO_3$ content, as well as texture, organic matter, cation exchange capacity, soil moisture, and rhizosphere processes. Plant nutrient uptake may also vary depending on genotype, root-system characteristics, growth stage, fertilization history, and interactions among nutrients (White & Brown, 2010; Marschner, 2012). Therefore, $CaCO_3$ content alone may not provide an adequate basis for assessing plant nutritional status in calcareous soils.

Soil analyses provide information on the potential availability of nutrients and the nutrient-supplying capacity of the soil, whereas plant tissue analyses reflect the integrated outcome of soil–root processes as expressed in plant nutrient uptake. However, because elemental concentrations in plant tissues vary with the sampled organ and growth stage, the results should be interpreted using appropriate sampling times and established sufficiency ranges (Jones et al., 1991; Reuter & Robinson, 1997; Lemaire et al., 2019). Flag leaves collected immediately before heading constitute suitable diagnostic material for assessing the nutrient status of wheat. Accordingly, the combined use of soil and plant analyses enables a more comprehensive assessment of nutrient deficiencies and limitations to nutrient uptake.

The Narlı Plain, located south of Kahramanmaraş, is an important agricultural production area characterized by soils developed from alluvial and colluvial parent materials. Variations in topographic position and soil-forming conditions have resulted in considerable heterogeneity in the physical and chemical properties of the plain's soils (Yakupoğlu et al., 2012; Yakupoğlu & Demirci, 2013). Previous studies conducted in the region have shown that this variability is also reflected in soil pH, $CaCO_3$ content, and nutrient concentrations (Saltalı et al., 2018). Total and active $CaCO_3$ contents have also been reported to be associated with the availability of certain metallic micronutrients in the soils of the plain (Kadifeci et al., 2024). Nevertheless, field-based information on the extent to which soil nutrient levels are reflected in the nutritional status of wheat remains limited. Accordingly, this study aimed to determine selected physical and chemical properties of calcareous agricultural soils under wheat cultivation in the Narlı Plain and to evaluate the macro- and micronutrient status of wheat through combined soil and flag-leaf analyses. The relationships between soil $CaCO_3$ content and P, K, Ca, Mg, Fe, Zn, Cu, and Mn concentrations in wheat flag leaves were also investigated.

MATERIAL AND METHOD

Study area

The study was conducted in wheat-growing areas of the Narlı Plain, located within the administrative boundaries of Pazarcık district, Kahramanmaraş Province, southern Türkiye. Situated approximately 30 km southeast of Kahramanmaraş city center, the plain covers an area of approximately 26,500 ha and lies within a transitional zone between Mediterranean and continental climatic conditions (Saltalı et al., 2018).

The soils of the Narlı Plain have developed predominantly from alluvial and colluvial parent materials transported from the surrounding uplands and deposited across the plain. Variations in depositional environments and topographic positions have resulted in pronounced spatial

variability in the physical and chemical properties of these soils (Yakupoğlu et al., 2012; Yakupoğlu & Demirci, 2013). The soils of the region have generally been characterized as neutral to slightly alkaline and as having varying $CaCO_3$ contents. Moreover, their total and active $CaCO_3$ contents may influence the availability of metallic micronutrients (Kadifeci et al., 2024).

The study area comprised fields under wheat cultivation within the Narlı Plain. Eleven wheat-growing fields were selected to represent the spatial variability in soil properties and plant nutritional status across the plain. The geographical coordinates of the soil and flag-leaf sampling points were recorded during fieldwork. The location of the study area within Türkiye and Kahramanmaraş Province, together with the distribution of the sampling points across the Narlı Plain, is presented in Figure 1.

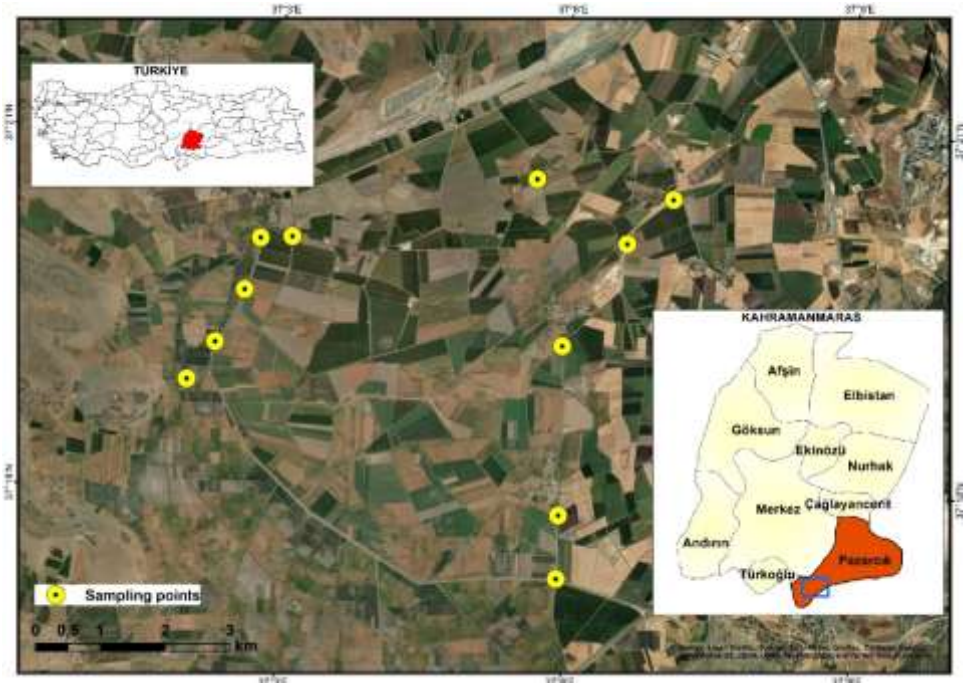

Figure 1. Location of the study area and distribution of soil and wheat flag-leaf sampling points in Narlı Plain

Soil and Plant Sampling and Preparation for Analysis

Soil samples were collected from a depth of 0–30 cm at 11 wheat-growing fields selected across the Narlı Plain, and the coordinates of the sampling points were recorded using a Global Positioning System (GPS). Composite soil samples representing each sampling point were transported to the laboratory, air-dried under ambient conditions, and passed through a 2-mm sieve. The prepared samples were labelled and stored in sealed plastic containers under cool and dry conditions until analysis (Richards, 1954).

Plant samples were collected simultaneously from the same fields where the soil samples were obtained. To assess the nutritional status of wheat, 25–30 representative flag leaves were collected from each field immediately before heading (Jones et al., 1991). The leaf samples were washed with distilled water to remove surface dust and other residues and subsequently oven-dried at 65 °C for 48 h. The dried plant material was ground and homogenized, transferred to labelled polyethylene bags, and stored under refrigerated conditions until chemical analysis (Jones & Case, 1990).

Soil and Plant Analyses

Soil pH and electrical conductivity (EC) were determined in saturated soil paste according to the methods described by Peech (1965) and Richards (1954), respectively. Total calcium carbonate ($CaCO_3$) content was measured using a Scheibler calcimeter (Loeppert & Suarez, 1996), whereas soil organic matter was determined using the Walkley–Black wet oxidation method (Nelson & Sommers, 1996). Available P was determined using the Olsen method based on extraction with 0.5 M $NaHCO_3$ at pH 8.5 (Olsen et al., 1954). Exchangeable K, Ca, and Mg were extracted with 1 N ammonium acetate (NH_4OAc) at pH 7.0 (Thomas, 1982). Plant-available Fe, Zn, Cu, and Mn were determined using the DTPA extraction method (Lindsay & Norvell, 1978). The concentrations of K, Ca, Mg, Fe, Zn, Cu, and Mn in the soil extracts were measured using an Agilent 240AA atomic absorption spectrophotometer (AAS).

A 0.50-g portion of each ground plant sample was wet-digested on a hot plate using a mixture of 5 mL HNO_3 and 4 mL $HClO_4$ until a clear solution was obtained (Jones & Case, 1990). Following digestion, the solutions were filtered and brought to a known volume with deionized water. Phosphorus concentration in the plant samples was determined spectrophotometrically using the vanadomolybdophosphoric yellow colour method. Potassium, Ca, Mg, Fe, Zn, Cu, and Mn concentrations were measured using an Agilent 240AA atomic absorption spectrophotometer.

Statistical Analyses

Minimum, maximum, and mean values for the soil and plant variables were calculated using Microsoft Office Excel. Relationships between soil $CaCO_3$ content and P, K, Ca, Mg, Fe, Zn, Cu, and Mn concentrations in wheat flag leaves were examined using two-tailed Pearson correlation analysis in IBM SPSS Statistics 23.0 (IBM Corp., Armonk, NY, USA). Statistical significance was accepted at $p < 0.05$, and graphical presentations of the results were prepared using Microsoft Office Excel.

RESULTS AND DISCUSSION

Characteristic Properties of the Study-Area Soils

Soil pH values ranged from 7.43 to 7.79, with a mean of 7.56. Electrical conductivity values varied between 303 and 501 µS cm^{-1}, averaging 349 µS cm^{-1}. Soil $CaCO_3$ contents ranged from 19.84% to 41.09%, with a mean of 27.95%, whereas organic matter contents varied between 2.13% and 4.50%, with a mean of 2.85%. Based on these results, the soils were generally characterized as slightly alkaline and non-saline, with high to very high $CaCO_3$ contents and moderate organic matter levels.

Table 1. Descriptive statistics of selected physicochemical properties of the study area soils

	pH	**EC**	**Lime**	**OM**
		(µS/cm)		%
Min	7,43	303	19,84	2,13
Max	7,79	501	41,09	4,50
Mean	7,56	349	27,95	2,85

Macronutrient Status of the Study-Area Soils

Evaluation of the macronutrient contents of soil samples collected from the Narlı Plain revealed different sufficiency levels among the nutrients examined. According to Cottenie (1980), available P concentrations of 8–25 mg kg^{-1} are classified as sufficient, whereas concentrations of 25–80 mg kg^{-1} are considered high (Figure 2). Based on these thresholds, the mean available P concentration (22.5 mg kg^{-1}) was within the sufficient range; 54.5% of the samples were classified as sufficient and 45.5% as high. However, because the minimum concentration was close to the lower limit of the sufficiency range, the mean value should be interpreted together with the variability among sampling sites.

The mean exchangeable K concentration (340 mg kg^{-1}) exceeded the ≥161 mg kg^{-1} threshold above which Kaiser and Piotrowski (2024) did not recommend K fertilization for wheat under Minnesota conditions. While 63.6% of the samples reached or exceeded this threshold, 36.4% had K concentrations within the range of 95–160 mg kg^{-1}. Therefore, the high mean K concentration should not be interpreted as indicating a uniform K status across all sampling sites. Because this threshold was developed for a different region, it should be used as a comparative benchmark rather than directly applied to fertilizer recommendations for the Narlı Plain.

Regarding exchangeable Ca, 45.5% of the samples were classified as sufficient (1150–3500 mg kg^{-1}), whereas 54.5% were classified as high (3500–10,000 mg kg^{-1}). The mean Ca concentration (3461 mg kg^{-1}) was close to the upper limit of the sufficient range. Accordingly, the results did not indicate Ca deficiency in the investigated soils under the classification system used. For exchangeable Mg, 72.7% of the samples were classified as high (480–1500 mg kg^{-1}) and 27.3% as very high (>1500 mg kg^{-1}). The mean Mg concentration (1145 mg kg^{-1}) was within the high range, and all samples exceeded the sufficiency range, indicating that the soils generally had high exchangeable Mg concentrations (Cottenie, 1980).

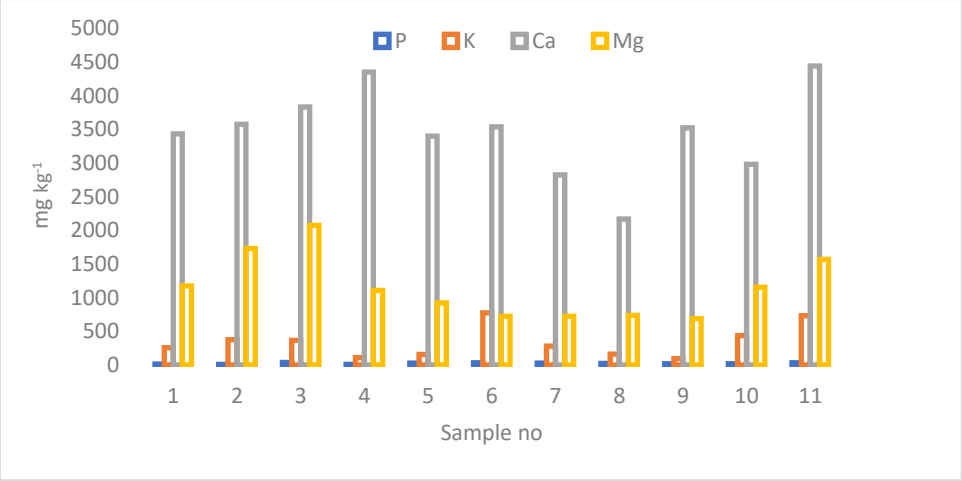

Figure 2. Distribution of available P and exchangeable cations

Micronutrient Status of the Study-Area Soils

The DTPA-extractable micronutrient concentrations of the soil samples collected from the Narlı Plain varied among the sampling sites (Figure 3). Iron (Fe) concentrations ranged from 8.88 to 23.52 mg kg^{-1}, with a mean of 11.73 mg kg^{-1}. Zinc (Zn) concentrations varied between 0.54 and 2.90 mg kg^{-1}, averaging 1.05 mg kg^{-1}. Copper (Cu) concentrations ranged from 1.08 to 2.20 mg kg^{-1}, with a mean of 1.50 mg kg^{-1}, whereas manganese (Mn) concentrations varied

between 3.36 and 28.80 mg kg^{-1}, averaging 9.65 mg kg^{-1}. The mean concentrations of the micronutrients followed the order Fe > Mn > Cu > Zn.

Soil micronutrient status was evaluated using the critical levels reported for maize by Lindsay and Norvell (1978) as comparative benchmarks. In all samples, Fe, Cu, and Mn concentrations exceeded their respective critical levels of 4.5, 0.2, and 1.0 mg kg^{-1}. Thus, according to these thresholds, no indication of Fe, Cu, or Mn deficiency was identified in the investigated soils. However, the critical values reported for Mn and Cu were proposed tentatively and should therefore be interpreted with caution.

Based on the critical Zn level of 0.8 mg kg^{-1}, 45.5% of the samples were classified as deficient and 54.5% as sufficient. Although the mean Zn concentration (1.05 mg kg^{-1}) exceeded the critical threshold, the occurrence of concentrations below this value in 45.5% of the samples demonstrates that soil Zn status should not be evaluated solely on the basis of the mean. Zinc was the only micronutrient for which values below the critical level were detected, indicating a potential Zn deficiency at some sampling sites that warrants further investigation. Nevertheless, because the thresholds used were originally established for maize, definitive conclusions regarding wheat nutritional status should be supported by plant tissue analyses and crop-specific sufficiency criteria.

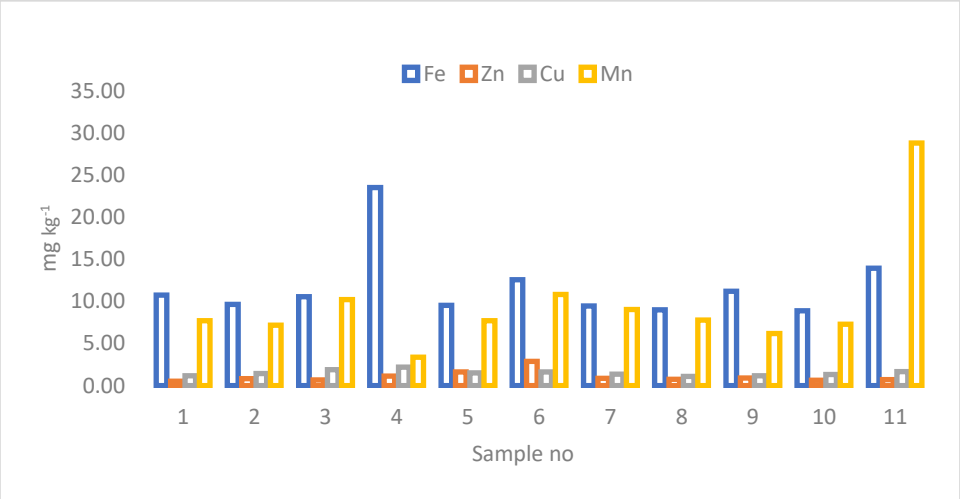

Figure 3. Distribution of DTPA-extractable Fe, Zn, Cu and Mn concentrations

Flag-Leaf Macronutrient Concentrations in Wheat

Macronutrient concentrations in wheat flag leaves varied among the sampling sites. Phosphorus concentrations ranged from 0.21% to 0.38%, with a mean of 0.28%. Potassium concentrations varied between 2.13% and 3.33%, averaging 2.60%. Calcium concentrations exhibited a relatively wide variation, ranging from 0.40% to 1.61%, with a mean of 0.80%. Magnesium concentrations ranged from 0.14% to 0.24%, with a mean of 0.18% (Figure 4). Among the macronutrients examined, K had the highest mean concentration, whereas Mg had the lowest.

The plant analysis results indicated that wheat grown in the study area generally had an adequate macronutrient status. When compared with the critical concentrations and sufficiency ranges reported for wheat, P and K concentrations were considered sufficient at all sampling sites (Jones et al., 1991; Reuter & Robinson, 1997; Plank & Donohue, 2000). In particular, the mean P (0.28%) and K (2.60%) concentrations exceeded the reported critical levels for wheat, indicating no apparent nutritional deficiency in these elements.

The variation in Ca concentrations from 0.40% to 1.61% indicated considerable differences among the sampling sites in Ca uptake or accumulation within plant tissues. Nevertheless, all measured Ca concentrations exceeded the critical level reported for wheat. Magnesium concentrations varied within a narrower range and averaged 0.18%. Because even the lowest Mg concentration (0.14%) was above the critical level, no evident Mg deficiency was identified in the wheat plants (Jones et al., 1991; Reuter & Robinson, 1997; Plank & Donohue, 2000).

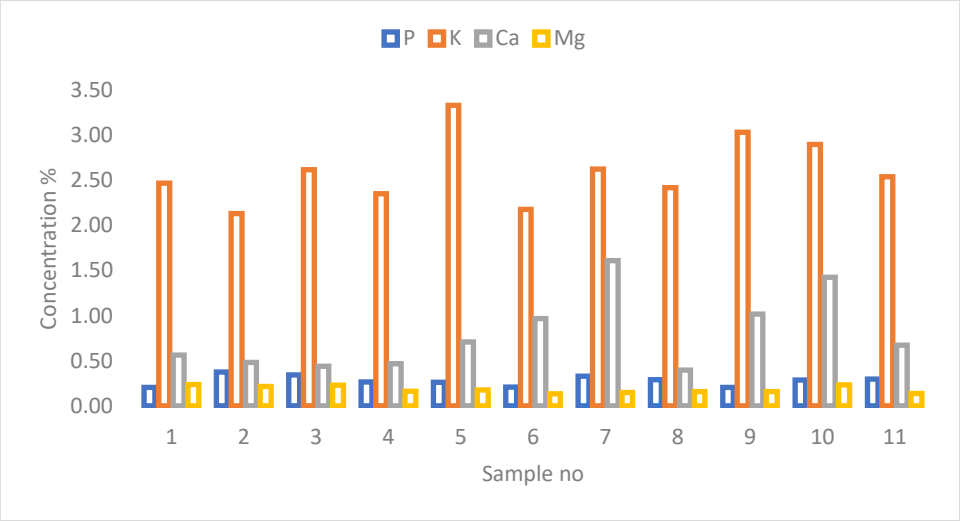

Figure 4. Foliar concentrations of macronutrients in wheat

Micronutrient Status of Wheat Flag Leaves

Micronutrient concentrations in wheat flag leaves varied among the sampling sites. Iron concentrations ranged from 69.00 to 156.75 mg kg^{-1}, with a mean of 97.93 mg kg^{-1}. Zinc concentrations varied between 17.50 and 30.00 mg kg^{-1}, averaging 21.84 mg kg^{-1}. Copper concentrations ranged from 4.50 to 8.75 mg kg^{-1}, with a mean of 6.75 mg kg^{-1}, whereas Mn concentrations varied between 16.00 and 54.25 mg kg^{-1}, averaging 40.41 mg kg^{-1} (Figure 5).

Based on the critical concentrations and sufficiency ranges reported for wheat, Fe, Zn, and Mn concentrations were generally considered adequate (Jones et al., 1991; Reuter & Robinson, 1997; Plank & Donohue, 2000). Iron concentrations of at least 69.00 mg kg^{-1} at all sampling sites indicated no evident Fe deficiency. Similarly, the observed Zn concentrations indicated that the wheat plants generally had an adequate Zn nutritional status.

Although the mean Cu concentration was within the sufficient range, the lowest value of 4.50 mg kg^{-1}, recorded at sampling site 2, was close to the critical level of approximately 5 mg kg^{-1} reported for wheat. Therefore, Cu nutrition was generally adequate, although a marginal Cu status may have occurred at this sampling site (Jones et al., 1991; Reuter & Robinson, 1997). Manganese concentrations indicated adequate nutrition at most sampling sites; however, the minimum concentration recorded at sampling site 11 was close to the lower limit of the sufficiency range.

Overall, wheat grown in the study area was adequately supplied with Fe, Zn, Cu, and Mn, although Cu and Mn concentrations approached the lower sufficiency limits at some sampling sites. Because tissue micronutrient concentrations may be influenced by soil pH, $CaCO_3$ and organic matter contents, nutrient availability, and interactions among elements, the combined interpretation of soil and plant analyses provides a more reliable assessment of wheat nutritional status (Reuter & Robinson, 1997).

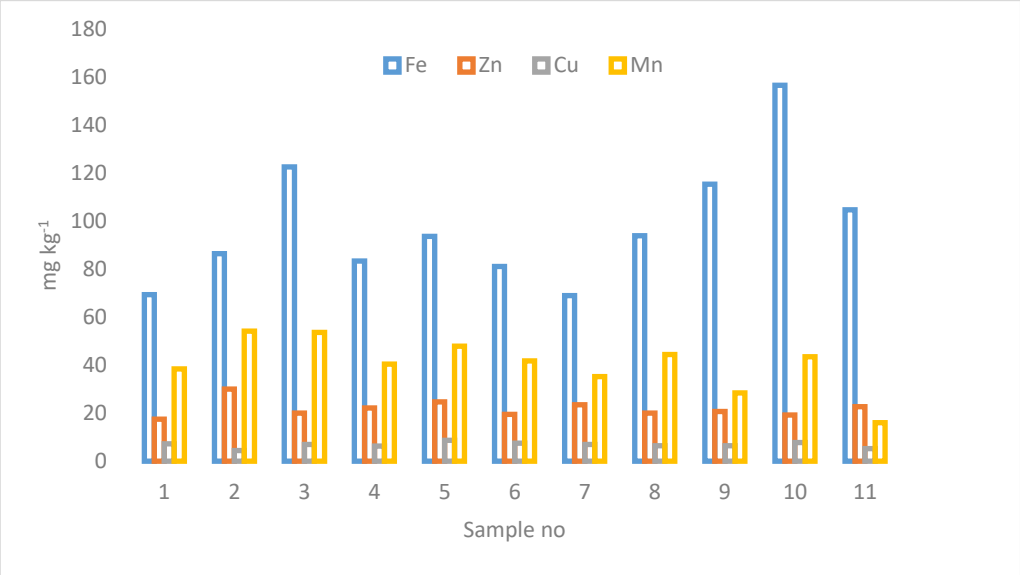

Figure 5. Foliar micronutrient concentrations in wheat

Relationships between soil lime and plant nutrients

No statistically significant correlations were detected between soil $CaCO_3$ content and P, K, Ca, Mg, Fe, Zn, Cu, or Mn concentrations in wheat flag leaves ($p > 0.05$; Table 2). Correlation coefficients ranged from −0.268 to 0.228, indicating no apparent linear relationship between soil $CaCO_3$ content and the macro- or micronutrient concentrations of wheat across the sampled fields. These findings suggest that variation in wheat nutritional status cannot be explained solely by soil $CaCO_3$ content and may also be influenced by soil nutrient reserves, fertilization practices, other soil properties, and plant-related factors. Nevertheless, because of the limited sample size ($n = 11$), the results should be interpreted within the context of the study area and sampling conditions (Table 2).

Table 2 Pearson correlation coefficients between soil lime and nutrient concentrations in wheat flag leaves

Plant nutrient	Pearson's r	p value	Significance
P	0,033	0,923	ns
K	−0,137	0,688	ns
Ca	−0,268	0,425	ns
Mg	0,228	0,500	ns
Fe	−0,028	0,934	ns
Zn	0,005	0,987	ns
Cu	−0,227	0,503	ns
Mn	0,001	0,998	ns

Note: Pearson correlation coefficients were calculated using 11 paired soil and flag-leaf samples ($n = 11$). ns: not significant ($p > 0.05$; two-tailed).

CONCLUSION

Wheat grown in the calcareous agricultural soils of the Narlı Plain was generally adequately supplied with P, K, Ca, Mg, Fe, Zn, Cu, and Mn. Available P and exchangeable K, Ca, and Mg concentrations in the soils were predominantly sufficient or high, while no clear deficiency of Fe, Cu, or Mn was identified. However, Zn concentrations were below the critical threshold in 45.5% of the soil samples, indicating a potential risk of Zn deficiency in some production fields. Plant analysis revealed no evident nutrient deficiencies, although Cu and Mn concentrations approached the lower limits of the sufficiency ranges at certain sampling sites. The absence of significant relationships between soil $CaCO_3$ content and nutrient concentrations in wheat flag leaves ($p > 0.05$) indicated that variation in plant nutritional status could not be explained solely by soil $CaCO_3$ content. Consequently, the combined interpretation of soil and plant analyses is recommended for a reliable assessment of wheat nutritional status in the Narlı Plain, with particular attention to the regular monitoring of Zn, Cu, and Mn.

REFERENCES

Chen, X.-X., Zhang, W., Wang, Q., Liu, Y.-M., Liu, D.-Y., & Zou, C.-Q. (2019). Zinc nutrition of wheat in response to application of phosphorus to a calcareous soil and an acid soil. Plant and Soil, 434(1–2), 139–150. https://doi.org/10.1007/s11104-018-3820-5

Cottenie, A. (1980). Soil and plant testing as a basis of fertilizer recommendations (FAO Soils Bulletin No. 38/2). Food and Agriculture Organization of the United Nations. https://openknowledge.fao.org/handle/20.500.14283/d8502e

Demirkaya, S., & Gülser, C. (2025). Biochar innovations for sustainable agriculture: Acidification and zinc enrichment strategies to improve calcareous soil fertility and wheat yield. Soil and Water Research, 20(2), 105–118. https://doi.org/10.17221/77/2024-SWR

Hinsinger, P. (2001). Bioavailability of soil inorganic P in the rhizosphere as affected by root-induced chemical changes: A review. Plant and Soil, 237(2), 173–195. https://doi.org/10.1023/A:1013351617532

Jones, J. B. Jr., and V. W. Case 1990. Sampling, Handling, and analyzing plant tissue samples, chapter 15. In R.L. Westerman (ed) Soil Testing and Plant Analysis, Third Edition, SSSA, Madison, Wisconsin, USA, pp. 390-420. https://doi.org/10.2136/sssabookser3.3ed.c15

Jones, J. B., Jr., Wolf, B., & Mills, H. A. (1991). Plant analysis handbook: A practical sampling, preparation, analysis, and interpretation guide. Micro-Macro Publishing. https://openlibrary.org/books/OL12110790M/Plant_Analysis_Handbook

Kadifeci, H., Dikici, H., & Demir, Ö. F. (2024). Effect of active lime on the availability of metal micronutrients. Turkish Journal of Agricultural and Natural Sciences, 11(2), 347–356. https://doi.org/10.30910/turkjans.1407307

Kaiser, D. E., & Piotrowski, K. (2024). Fertilizing wheat in Minnesota. University of Minnesota Extension. https://extension.umn.edu/agriculture/crop-production/nutrient-management-for-minnesota-crops/fertilizing-wheat-in-minnesota

Lemaire, G., Sinclair, T., Sadras, V., & Bélanger, G. (2019). Allometric approach to crop nutrition and implications for crop diagnosis and phenotyping: A review. Agronomy for Sustainable Development, 39, Article 27. https://doi.org/10.1007/s13593-019-0570-6

Lindsay, W. L., & Norvell, W. A. (1978). Development of a DTPA soil test for zinc, iron, manganese, and copper. Soil Science Society of America Journal, 42(3), 421–428. https://doi.org/10.2136/sssaj1978.03615995004200030009x

Loeppert, R. H., & Suarez, D. L. (1996). Carbonate and gypsum. In D. L. Sparks (Ed.), Methods of Soil Analysis: Part 3—Chemical Methods (pp. 437–474). Soil Science Society of America

and American Society of Agronomy, Madison, WI, USA. https://doi.org/10.2136/sssabookser5.3.c15

Marschner, P. (Ed.). (2012). Marschner's mineral nutrition of higher plants (3rd ed.). Academic Press. https://doi.org/10.1016/C2009-0-63043-9

Martínez-Ríos, O., Bravo-Vinaja, Á., San-Martín-Hernández, C., Hidalgo-Moreno, C. I., Sánchez-de-Jesús, M. A., Llampallas-Díaz, J. D., Santillan-Balderas, D. R., & García-Preciado, J. C. (2024). Zinc deficiency in calcareous soils: A bibliometric analysis from 1989 to 2024. Agriculture, 14(12), Article 2285. https://doi.org/10.3390/agriculture14122285

Nelson, D. W., & Sommers, L. E. (1996). Total carbon, organic carbon, and organic matter. In D. L. Sparks (Ed.), Methods of soil analysis: Part 3. Chemical methods (pp. 961–1010). Soil Science Society of America. https://doi.org/10.2136/sssabookser5.3.c34

Olsen, S. R., Cole, C. V., Watanabe, F. S., & Dean, L. A. (1954). Estimation of available phosphorus in soils by extraction with sodium bicarbonate (USDA Circular No. 939). U.S. Department of Agriculture. https://archive.org/details/estimationofavai939olse

Peech, M. (1965). Hydrogen-ion activity. In C. A. Black (Ed.), Methods of soil analysis: Part 2. Chemical and microbiological properties (pp. 914–926). American Society of Agronomy. https://doi.org/10.2134/agronmonogr9.2.c9

Plank, C. O., & Donohue, S. J. (2000). Small grain—Barley, oats, rye, wheat. In C. R. Campbell (Ed.), Reference sufficiency ranges for plant analysis in the Southern Region of the United States (pp. 29–31). Southern Cooperative Series Bulletin No. 394. https://paperzz.com/doc/8950152/reference-sufficiency-ranges-for-plant-analysis-in-the-so

Reuter, D. J., & Robinson, J. B. (Eds.). (1997). Plant analysis: An interpretation manual (2nd ed.). CSIRO Publishing. https://www.publishing.csiro.au/book/437

Richards, L.A. (1954). Diagnosis and Improvement of Saline and Alkali Soils. Agriculture Handbook, No:60, U.S. Department of Agriculture. U.S. Government Printing Office, Washington D.C., 166.

Saltalı, K., Gündoğan, R., Demir, Ö. F., Kara, Z., Yakupoğlu, T., Dikici, H., & Yılmaz, K. (2018). Narlı Ovası topraklarının ağır metal kapsamı üzerine çimento fabrikası baca tozlarının etkileri. Toprak Su Dergisi, 7(1), 11–20. https://doi.org/10.21657/topraksu.410113

Thomas, G. W. (1982). Exchangeable cations. In A. L. Page, R. H. Miller, & D. R. Keeney (Eds.), Methods of soil analysis: Part 2. Chemical and microbiological properties (2nd ed., pp. 159–165). American Society of Agronomy and Soil Science Society of America. https://doi.org/10.2134/agronmonogr9.2.2ed.c9

White, P. J., & Brown, P. H. (2010). Plant nutrition for sustainable development and global health. Annals of Botany, 105(7), 1073–1080. https://doi.org/10.1093/aob/mcq085

Xue, Y., Xia, H., Christie, P., Zhang, Z., Li, L., & Tang, C. (2016). Crop acquisition of phosphorus, iron and zinc from soil in cereal/legume intercropping systems: A critical review. Annals of Botany, 117(3), 363–377. https://doi.org/10.1093/aob/mcv182

Yakupoğlu, T., & Demirci, D. (2013). Kahramanmaraş-Narli Ovasi Topraklarinin Erozyona Duyarliliklari İle Bazi Toprak Özellikleri Arasindaki İlişkiler. Anadolu Tarım Bilimleri Dergisi, 28(1), 33-38. https://izlik.org/JA62SJ38AJ

Yakupoğlu, T., Saltalı, K., & Karagöktaş, M. (2012). Narlı Ovası'nda toprak aşınabilirliğinin pedotransfer yaklaşımı ile tahminlenmesi. KSÜ Doğa Bilimleri Dergisi, 15(2), 59–67. https://izlik.org/JA98BP96FZ

Zaheri Abdehvand, Z., Karimi, D., Rangzan, K., & Mousavi, S. R. (2024). Assessment of soil fertility and nutrient management strategies in calcareous soils of Khuzestan Province: A case study using the Nutrient Index Value method. Environmental Monitoring and Assessment, 196(6), Article 503. https://doi.org/10.1007/s10661-024-12665-4

WINE QUALITY AND SAFETY: THE ROLE OF SULFITES, SULFATES AND PHOSPHATES IN MICROBIOLOGICAL STABILITY

Sulltanë Ajçe[1], Adrian Maho[2]

[1]Department of Agrifood, Faculty of Agriculture, Fan. S. Noli University, Korce, Albania
[2]Department of Agronomy, Faculty of Agriculture, Fan. S. Noli University, Korce, Albania
Corresponding author e-mail: sajce@unkorce.edu.al (Orcid ID: 0009-0009-5737-4461)

ABSTRACT

Sulphites, Sulphates and phosphates play a significant role in microbiological stability, quality and safety of wines. This study aims to evaluate the impact of Sulphur dioxide (SO_2), sulphates SO_4^{2-} and Phosphate (PO_4^{3-}compounds on control of microbial growth and on key physicochemical properties of wine. Sulphites are widely used as preservatives due tu their antimicrobial and antioxidant activity, effectively inhibiting the growth of undersirable microorganisms such as wild yeasts, lactic acid bacteria and acetic acid bacteria. In contrast, phosphates contribute indirectly by supporting yeast metabolism during fermentation and stabilizing the chemical environment of the wine. Wine samples were analyzed for free and total SO_2, phosphate content, pH, acidity and microbial load using standard analytical and microbiological methods. The results demonstrate that appropriate level of sulphites significantly reduce microbial contamination and prevent spoilage, thereby enhancing shelf life and sensory quality. However, excessive sulphite concentrations may pose health concerns and negatively affect organoleptic properties. Phosphates were found to influence fermentation efficiency and microbial balance, although their direct antimicrobial effect is limited. In conclusion, the combined management of sulphites and phosphates is essential for maintaining wine stability, ensuring microbiological safety, and achieving high-quality products. Optimizing their concentrations in accordance with regulatory limits is crucial for balancing technological benefits and consumer health protection.

Keywords: *SO_4^{2-}, SO_2, PO_4^{3-}, Acetobacter spp., microbial load, assurance quality, food safety*

INTRODUCTION

Wine is a product produced by the fermentation of grape juice. It is produced from grapes of the species Vitis vinifera and a large number of varieties and cultivars.(Troja, R. 2005) The concentration of mineral salts in wine is regulated according to international standards and European Union legislation, to guarantee food safety and the quality of wines.(Troja, R. 2005) Wine contains the following elements and mineral salts:Sulfates SO_4^{2-}, phosphates PO_4^{3-}, potassium K^+, calcium Ca^{2+}, magnesium Mg^{2+} and in low concentrations sodium Na^+. (Bourgeois, C. M., & Larpent, J. P. 1989). Mineral salts in wine are inorganic compounds that come from grapes, soil, agricultural water (from irrigation) and technological practices during the winemaking process. They play an important role in biochemical reactions during fermentation, in the chemical quality, microbiological (stability of microorganisms) and organo-sensory characteristics of wine (body, taste). The origin of mineral salts in wine is from the vineyard soils, during the grape ripening phase, the use of mineral fertilizers (sulfates, phosphates) in the vineyards, agricultural water for irrigation and chemical and biological additives during the fermentation and stabilization process of must for wine. The balance of mineral salts directly affects the resistance to microbiological diseases (spoiling) of wine. Sulphates in wine have a significant impact on the taste, chemical stability and microbial

activity (yeast, lactic and acetic bacteria) of grape must and wine. At high concentrations they can inhibit and limit microbial activity. Their presence is related to natural and technological factors during wine production. Grapes absorb sulfates from the root (soil), especially in soils with high sulfur content. Sulfur is an important element for plants. Experimental measurements show that during the grape ripening period, a greater amount of sulfates accumulates and these pass into the final product (wine). Water used for irrigation increases the amount of sulfates. The use of phytosanitary components used to protect grapes from fungal diseases contributes to an increase in the concentration of sulfates (Formisano, M. 1990). Technological use of SO_2 during the sulfitation process. SO_2 is used as a preservative and antioxidant in wine. The oxidation of SO_2 converts them into sulfates, increasing their total concentration. [1] Phosphates in wine are natural compounds and additives that serve as an important source of phosphorus. Their levels range from 70 mg/L to 500 mg/L in white wines, and from 150 mg/L to 1000 mg/L in red wines. Their sources fall into three main categories: Soil and Grapes (Natural Source): Phosphorus is an essential nutrient for grapevines, which is naturally absorbed from the soil. (Jay, J. M. 1985). Most of the phosphate in wine originates from the grapes themselves and the crushing process. Fertilized Soil: To optimize soil chemistry and provide optimal nutrient levels to the vines, viticulturists use phosphate-based mineral fertilizers. Diammonium Phosphate (Added Additive): During the fermentation process, winemakers often add Diammonium Phosphate (DAP) as a nutritional supplement. This additive helps yeast (the fungi that carry out the fermentation) process sugar and produce alcohol more quickly. (Prifti, D. 2007)

MATERIAL AND METHOD

Physico-chemical analyses (Bindashi, H., & Frashëri, M. 1984)
Preparation of wine samples for physico-chemical analyses:(Frashëri, M., & Prifti, D. 1997)
Removal of carbon dioxide with an ultrasonic device
Method Reference ISO (International Organization for Standardization), ISO 6632
Preparation of wine sample for analysis.
Before determining the physico-chemical analyses, the wine must be decarbonated. For this, 300-400 ml of wine are poured into a large glass, heated, preferably to 20-250C, and placed in an ultrasonic device until the gas is removed (it is removed quickly). If the wine contains suspended matter, then after removing the carbon dioxide it is filtered through a dry filter paper. To determine reducing sugars, sulfates and phosphates in wine, the wines are decolorized with activated carbon or centrifugation, filtered and diluted before the chemical analysis of the determination.
Determination of free sulfuric acid
Method Reference ISO 6632
Ripper Method (Iodometry)
For red wines: In a 250 ml glass beaker, 10 ml of red wine, 1 ml of 1% starch solution, 1 ml of sulfuric acid (1:3) are added and titrated with a 0.01N iodine solution. The color change is determined by comparing it with a 250 ml glass beaker containing 10 ml of red wine, 1 ml of 1% starch solution, 1 ml of sulfuric acid (1:3), but without added iodine. The comparison is made with a white, well-lit surface. The number of ml of iodine solution consumed is indicated by N. The same determination is made on the desulphite sample by boiling with air cooling, during 45 min or by oxidation with two drops of 10 volumes of hydrogen peroxide (3%), the number of milliliters of iodine consumed is marked with N_1. For common analyses N_1=0.2 ml. The content in free sulfuric acid in mg per liter is calculated using the following formula. (AOAC. 2005)

For white wines: For white wine the determination is simpler. Take 50 ml of wine with a pipette and pour it into a 200-300 ml Erlenmeyer flask, add 2 ml of starch solution and 1-2 ml of sulfuric acid solution (1:3) and immediately titrate with
0.02 N iodine solution, stirring continuously until with a single drop the liquid takes on a stable blue color for 10 seconds. In another Erlenmeyer flask, 50 ml of wine, 1 ml of starch, 1 ml of sulfuric acid and 0.5 ml of hydrogen peroxide are added to oxidize SO_2, stirring occasionally, and after 5 minutes, titration is performed as above.
Determination of total sulfuric acid
In common practice, an approximate and simplified process is used: In a 250-300 ml conical flask, 10 ml of 0.1 N sodium hydroxide solution and 25 ml of red or white wine are added, immersing the tip of the pipette in the alkaline solution. Stir and leave to stand for 5 minutes in the cold. Then, 5 ml of sulfuric acid solution (1:3), 1 ml of 1% starch solution are added and titrated with iodine solution at 4 g per liter. The total sulfuric acid content in mg/l is calculated using the following formula: Where: N-number of ml of iodine solution with 4 grams per liter consumed. Note: Due to the rapid oxidation sulfuric acid, the first analysis that is made to the wine after opening the bottles is free and total sulfuric gas.

Figure 2. Iris Spectrophotometer Apparatus (*AOAC. 2005)*

Determination of Sulfates in Wine
Wavelength 420 nm
The wine sample must be filtered and decolorized (with activated carbon) or with lead acetate. Decolorization with Chemical Reagents (Lead Acetate). A precipitate is formed with the compound (protein and phenols). We added a little lead acetate to the sample until a precipitate form, then filtered. Activated carbon is the safest, simplest and most widely used method in wine analysis, only the filtration is carried out completely so that no particles remain. (Tini, V., & Ciudici, P. 2000)
We take 50-100 ml of wine, where we add 0.5-1 g of activated carbon. We mix it for 5-10 minutes. We let it stand for a while (or shake it lightly with a magnet). We filter it with filter paper (or membrane). The filtrate should be clear and without strong color. Phosphates (Wavelength) 700-880 nm according to the Spectrophotometric method (Iris Spectrophotometer). Standard norms for sulfates and phosphates in wine according to oenological practices and the International Organisation of Vine and Wine and the legislation of the European Union
Sulfates SO_4^{2-} in wine. Reference method ISO 9280. Spectrophotometric method at wavelength $\lambda = 420$ nm. Typical value: 200-600 mg/L → normal in most wines. It can reach up to 800 mg/L in some cases depending on the processing. 1000 mg /L It is considered high and can affect the taste (bitter/salty taste) and stability. Sulfates are actually related to the use of SO_2 and technological processing. Interpretation of sulfates should be done together with the parameters pH, SO2, mineralization.

Determination of Phosphates PO_4^{3-} in wines

Decolorization and filtration of red wine samples for sample preparation. Then we diluted the samples 2:10 to eliminate interferences during the determination of phosphates with the Spectrophotometer at wavelength λ = 880 nm

Reference method ISO 6878. Spectrophotometric method: Acceptable values 100-400 mg/L (as PO_4^{3-}) or 30-120 mg/L as P. High values: 500 mg/L may indicate contamination, high use of additives or special raw materials. Phosphates are important for: yeast nutrition during fermentation and biological stability.

Parameter Normal Value High Value

Sulphates 200-600 mg/L > 1000 mg/L

Phosphates 100-400 mg/L > 500 mg/L

A value of 600 mg/L phosphates in wines is above the norm and indicates the high use of phosphate fertilizers in vineyards, nutritional supplements for yeasts during fermentation or contamination from water, equipment, and higher concentration from the raw material. High phosphate values in wines affect chemical stability by causing turbidity and precipitation during the technological process and in the final product. This then requires stabilization, filtration and treatment of wines.

Microbiological Analysis of Wines of "ÇEÇI" Winery [7]

Determination and Identification of Acetic Bacteria (Acetobacter spp.) and Lactic Acid Bacteria in the Field Bromthymol Blue Agar.

Determination of mycorrhizal microflora on PDA (chloramphenicol) medium. Reference method ISO/CD 21527

Bromthymol blue agar medium is a selective medium for the identification of acetic and lactic acid bacteria. After incubation at 370C, the color changes from yellow to blue-green when acetic acid bacteria grow. (Shabani, L. 2003)

BROMTIMOL BLUE AGAR MEDIUM

Agar 1.5 g / 100 ml, Peptone 1 g / 100 ml, Yeast extract 0.5 g / 100 ml, NaCl 0.5 g / 100 ml, Bromtimol blue 2 mg / 100 ml

PDA MEDIUM (Potato Dextrose Agar) (For fungal load) (Gilliland, S. E. 1985) medium with a high polysaccharide content that favors the development of yeasts and molds, is a medium that favors the development of molds and yeasts and can be supplemented with other ingredients, e.g., acids and antibiotics to inhibit the development of bacterial loads. It is recommended for evaluating mold and yeast loads in food products as well as other foods and cosmetic products. It is sometimes used to grow fungal cultures in clinical trials. It is prepared with an infusion of dehydrated potatoes (200 ml of infusion containing 4 g of potato extract; 20 g of dextrose and 15 g of starch per 1 liter of medium. The pH of the medium is 5.6 +/- 0.2 at 25°C. Then, the count is made after 24 hours and after 48 hours for bacteria and after 7 days for yeasts and molds. Colonies with Bromthymol blue agar plates are counted after 48 hours, while those with Sabourand agar and PDA after 72 hours because molds develop more slowly (Frashëri, M., & Prifti, D. 1997). The counting of colonies is done by turning the plate upside down and placing it on a dark background (dark paper plate). The colonies appear in the form of dots of various sizes and shapes. The colonies that are counted are considered to be descendants of the cells of microorganisms; therefore, according to the number of colonies grown, the amount of microorganisms present can be determined in the air at the time of sowing (cultivation). Bromthymol blue agar media were used for acetic and lactic bacteria, Sabourand agar and PDA media for molds and yeasts. Two replicates for each sample and three decimal dilutions were used (Jay, J. M. 1985).

RESULTS AND DISCUSSION

Determination of sufates SO_4^{2-} and phosphates PO_4^{3-} in analyzed samples of bottled wines, with Spectrophotometer, after deggasing and decolorization.

Table. ***Content of sulphates SO_4^{2-} and phosphates PO_4^{3-} in analyzed samples of bottled wines***

Samples	**SO_4^{2-} (sulphates) mg/L**	**PO_4^{3-} (phosphates) mg/L**
"KABËRNET"Wine	92	600
"MERLOT"Wine	56	600
"TOKAI"Wine	170	168

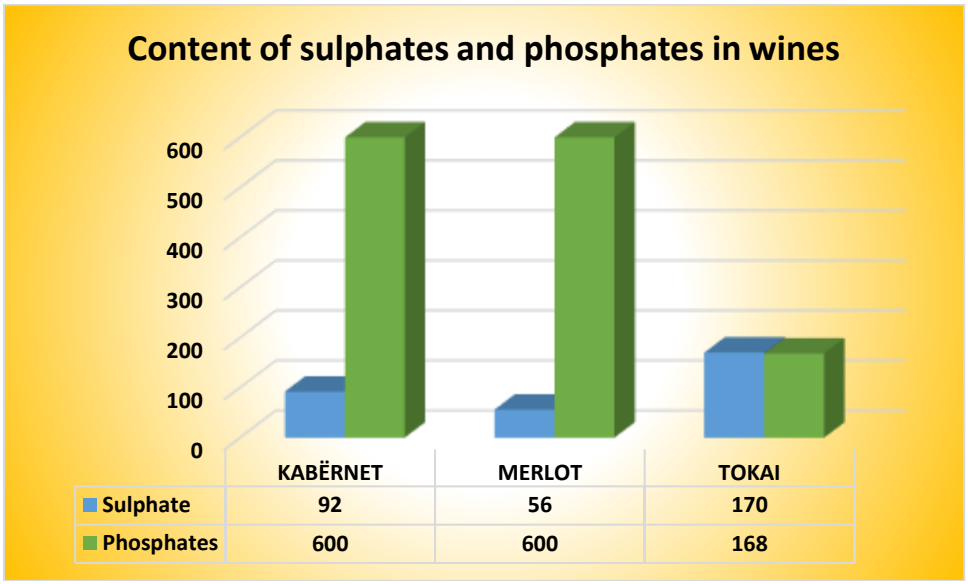

Graph 1. ***Content of sulphates (SO_4^{2-}) and phosphates (PO_4^{3-}) in analyzed samples of bottled wines***

Content of total, free and bound SO_2 in the wines analyzed

Table 1. Determination of total, free and bound SO_2 content in the analyzed wines

Samples	Total SO_2 (mg/L)	Free SO_2 (mg/L)	**Bound SO_2 = Total SO_2- free SO_2 (mg/L)**
"KABËRNET"wine	128	26,24	101,76
"MERLOT"wine	167,8	12,8	155
"TOKAI" wine	198	7,87	190,13

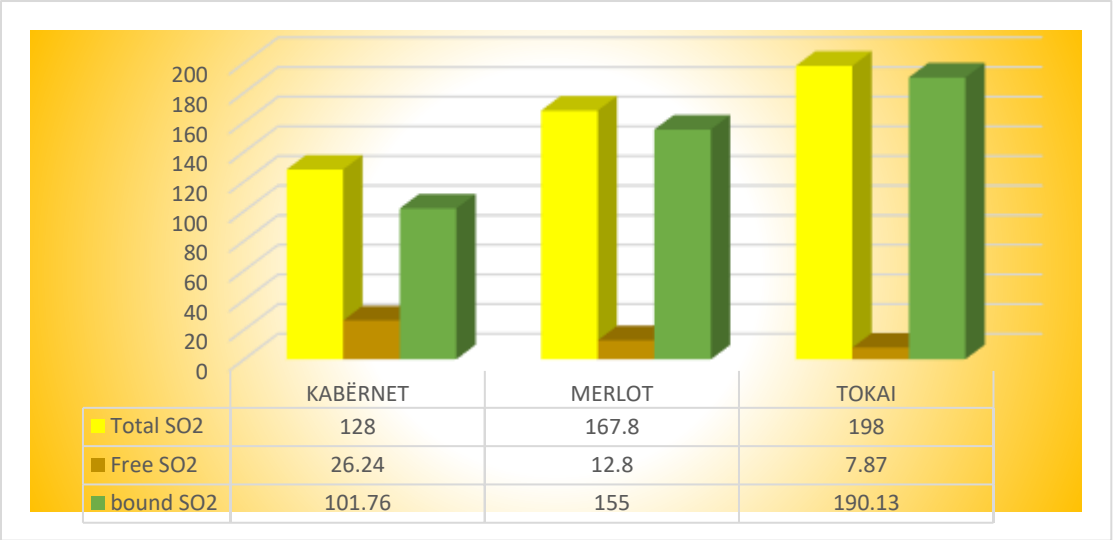

Graph 2. ***Content of mg/L*** **total, free and bound** ***SO₂*** **in the wines analyzed**

From the graphic presentation it is clear that:
Total SO_2 ranges from 128 mg/L in Cabernet wine to 198 mg/L in Tokai wine. According to the standard, it should not be more than 220 mg/l. This results in the total sulfur gas being within the parameters required to protect the wine from oxidation and bacterial diseases.
Free SO_2 It ranges from 7.87 mg/L in Tokai wine to 26.24 in Cabernet wine. According to the Standard, it should not be > 30 mg/L.

MICROBIOLOGICAL ANALYSIS

Table 2. Microbiological control of wines from the "Çeçi" Winery, Gurishtë, Albania

Samples	**Dilution**	**The Parallels**	**Terrenet ushqyese**						
			PDA(Potato dextroze agar)		**Sabourand (Chloramphenicol)**			**Bromthymol Blue Agar (*Acetobacter aceti* *Lactic Acid Bacteria)***	
			Incubation time		Incubation time			Incubation time	
			48 hours	**72 hours**	**24 hours**	**48 hours**	**7 days**	**48 hours**	**72 hours**
KABËRNET	10^{-1}	I II Average		20 16 18			- - -	24 20 22	30 20 25
	10^{-2}	I II Aver.		18 16 17			- - -	15 13 14	20 20 20
	10^{-3}	I II Aver.		- - -			- - -	12 10 11	15 11 13
MERLOT	10^{-1}	I II Aver.		15 15 15			6 4 5	22 14 18	26 20 23
	10^{-2}	I II Aver.		20 18 19			5 - 2.5	18 16 17	22 20 21
	10^{-3}	I II Aver.		26 - 13			- - -	12 8 10	16 14 15
TOKAI	10^{-1}	I II Aver.		12 17 14.5			10 10 10	14 14 14	18 16 17
	10^{-2}	I II Aver.		2 - 1			8 1 4.5	12 12 12	16 16 16
	10^{-3}	I II Aver.		1 5 3			6 - 3	10 10 10	14 14 14

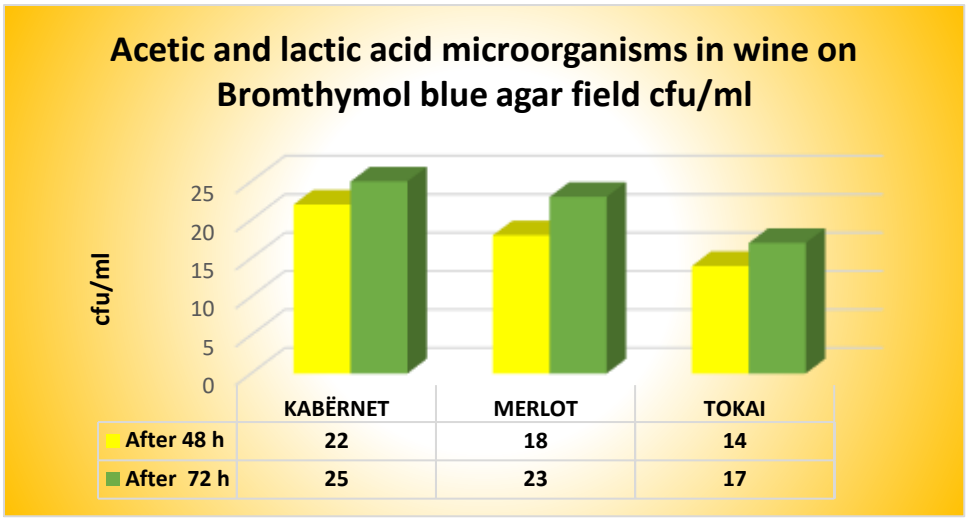

Graph 3. Amount of microorganisms grown on Bromthymol blue agar medium, after 48 hours and 72 hours of incubation, at temperature 37^0C

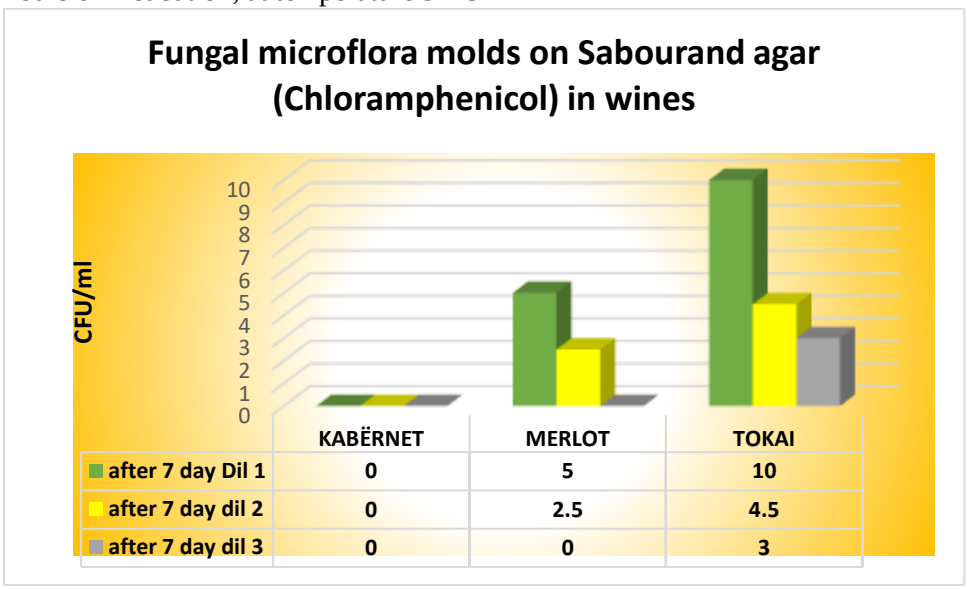

Graph 4. Fungal microflora (molds) on Sabourand Agar (Chloramphenicol) medium in wines, after 7 days of incubation, at temperature 25 ^{0}C

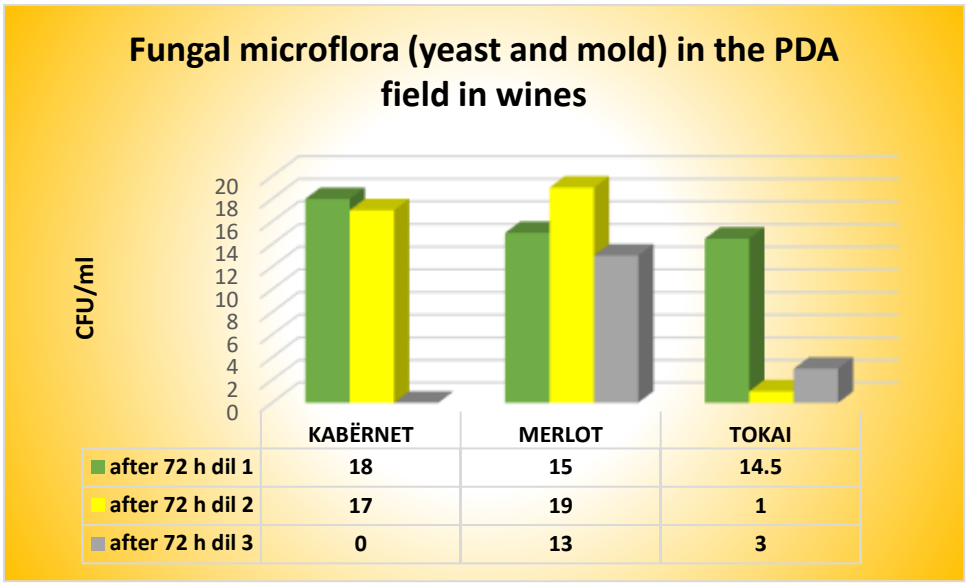

Graph 5. ***Fungal microflora (yeast and mold) on PDA (potato dextrose agar) medium in wines, after 72 hours of incubation, at room temperature 25 ^{0}C***

CONCLUSIONS

At the end of this study to determine the physical and chemical analyses of all types of "Winery Wines, Çeçi", we can draw some conclusions and recommendations.
Cabernet: The total extract is excellent (38.49 g/L) which promises a full-bodied wine. Monitoring only for the stability of phosphates so that it does not create a bottom after 6 months in the bottle.
Merlot: It has balanced parameters (pH 3.38, good total acidity, low volatile acidity 0.38 g/L). It is a stable wine.
Tokai: Requires care. It should be sold/consumed quickly on the market and stored in a cold chain. High Phosphate Management (Cabernet and Merlot Wines)
Problem discovered: The value of 600 mg/L of phosphates in both red wines is above the normal oenological limit (100–400 mg/L). This may come from excessive use of yeast nutrients (DAP - Diammonium Phosphate) during fermentation or from treatments in the vineyard.
Risk: High phosphates in the final product cause phosphate turbidity after bottling.
Recommendation: Adjustment of yeast nutrients: Reduce the dose of DAP during alcoholic fermentation in subsequent years and prefer organic nutrients (based on yeast autolysate), which do not increase inorganic phosphate residues. Reduce the use of chemical fertilizers containing phosphorus in the vineyard.
Microbiological Analysis. Gram-stained preparations for colonies grown on Bromthymol blue agar were short Gram-positive bacilli, while on PDA medium, colonies of beige, yellow and orange yeasts grew. The orange colonies, when identified under the microscope, resulted in elliptical clusters of *Rhodotorula spp*. On Sabourand medium, black molds grew, which after being identified under the microscope at x40, x100 magnification were of the genus *Aspergillus spp.* In the three analyzed wines, the mold load was within the limit values.
The number of colonies on the media used for the analyzed wines was within the allowed norms (<200cfu/ml) (State standards. 1982)
From the experiments performed, all three analyzed samples resulted qualitative from a physico-chemical and microbiological point of view.

REFERENCES

AOAC. 2005. Official Methods of Analysis of AOAC International. 18th ed. AOAC International, Gaithersburg, Maryland, USA: 6-269.
Bindashi, H., & Frashëri, M. 1984. *Food product analyses*: 110-126.
Bourgeois, C. M., & Larpent, J. P. 1989. *Microbiologie Alimentaire. Vol. II: Les Fermentations Alimentaires*: 6-69.
Formisano, M. 1990. *Microbiologia Industriale*: 3-126.
Gilliland, S. E. 1985. *Bacterial Starter Cultures for Foods*:56-59.
Jay, J. M. 1985. *Modern Food Microbiology*: 52-68.
Frashëri, M., & Prifti, D. 1997. *Technical microbiology practicum*:112-125.
Prifti, D. 2007. *Food Microbiology*: 92-123.
Shabani, L. 2003. *Microbiology of Fermented Food*: 96-113.
State Standards. 1982. *States standards for food products*: 3-16.
Troja, R. 2005. *Food Chemistry and Technology*: 65-96
Tini, V., & Ciudici, P. 2000. *Microbiologia degli Alimenti Fermentati*: 66-78
Zambonelli, C. 1998. *Microbiologia e Biotecnologia del Vino*: 11-330.
Zigori, V., & Kongoli, R. 2004. *Science and Technique*: 22-357

IDENTIFICATION OF CANDIDATE GENES AND BIOLOGICAL PATHWAYS ASSOCIATED WITH GENETIC SHEEP RESISTOME TO GASTROINTESTINAL NEMATODES IN SHEEP: AN INTEGRATED MICROARRAY DATA MINING APPROACH

Arash Javanmard

[1] *Department of Animal Science, Faculty of Agriculture, University of Tabriz, Tabriz, Iran*

Corresponding author e-mail: a.javanmard@tabrizu.ac.ir

ABSTRACT

Gastrointestinal nematode (GIN) infections impose a substantial health and economic burden on sheep production worldwide, and although anthelmintics have traditionally served as the primary control measure, escalating drug resistance and growing consumer demand for chemical-free animal products have intensified efforts to breed sheep with innate genetic resistance—an endeavor complicated by the trait's polygenic architecture and modest heritability ($h^2 = 0.22–0.63$). In this integrated bioinformatic study, we analyzed 45 high-quality microarray samples across three platforms following rigorous quality control and identified 1,247 differentially expressed genes (DEGs) between resistant and susceptible animals, of which 689 were upregulated—including IFNG ($log_2FC = 2.34$), IL4 (2.21), TLR4 (1.98), TNF (1.87), Ovar-DRB1 (1.76), and NRAMP1 (1.45)—and 558 were downregulated, notably the mucin genes MUC7 (−1.45) and MUC15 (−1.05). Functional enrichment analyses (GO, KEGG, and GSEA) consistently highlighted immune and inflammatory responses, chemotaxis, cytokine-mediated signaling, and a pronounced Th2-skewed profile in resistant animals, with significant enrichment in Th1/Th2 differentiation, chemokine, and Toll-like receptor signaling pathways. Protein-protein interaction network analysis using the Maximal Clique Centrality (MCC) algorithm pinpointed ten hub genes—IFNG, TNF, TLR4, IL4, Ovar-DRB1, CCL5, IL6, STAT6, IL13, and NRAMP1—which coalesced into three core functional modules governing Th2 polarization, MHC class II-mediated antigen presentation, and inflammatory regulation. Collectively, these results provide a robust molecular signature for GIN resistance, positioning the identified hub genes, especially those linked to Th2 immunity and antigen presentation, as compelling targets for marker-assisted selection and genomic breeding programs. Furthermore, the observed downregulation of mucin genes in resistant animals implies that rapid parasite expulsion occurs without pathological mucus hypersecretion, challenging conventional views and offering a mechanistic foundation for designing sustainable breeding strategies aimed at reducing anthelmintic dependence and improving long-term flock health..

Keywords: Gastrointestinal nematodes, Sheep, Genetic resistance, Microarray, Differential gene expression, Hub genes, Th2 immunity, MHC, Bioinformatics, Marker-assisted selection.

INTRODUCTION

Gastrointestinal nematode (GIN) infections impose a severe economic toll on sheep production, costing Australia and India hundreds of millions of dollars annually (Waller and Chandrawathani, 2005; Stear et al., 2005). Because grazing guarantees constant larval exposure, parasitic gastroenteritis remains a persistent threat. Although anthelmintics have been the conventional control strategy, widespread resistance to all major drug classes (Wolstenholme

et al., 2004), together with rising consumer demand for chemical-free meat and the lack of a commercial vaccine, has made genetic selection an increasingly attractive alternative.
Breed-specific genetic variation in resistance has been documented (Gosling et al., 2014), yet the trait exhibits low phenotypic variation and moderate heritability (0.22–0.63) (Riggio et al., 2013), which makes traditional selection based on fecal egg counts exceedingly slow. While candidate genes such as the MHC class II locus *Ovar-DRB1* (Sayers et al., 2005) and several quantitative trait loci on chromosomes 1, 3, 6, and 20 (Coltman et al., 2001) have been linked to resistance, existing studies have largely relied on sparse marker panels and have not provided a comprehensive, systems-level view of the underlying transcriptional mechanisms.
High-throughput transcriptomic technologies, such as microarrays, now offer an unbiased means of dissecting the molecular architecture of complex traits, though they are increasingly complemented by RNA-sequencing due to standardization and cost-effectiveness for large sample numbers (Ritchie et al., 2015). Nevertheless, publicly archived microarray data remain an underutilized resource. In this study, we therefore reanalyzed multiple independent ovine microarray datasets to systematically identify the genes, biological pathways, and regulatory networks that distinguish resistant from susceptible sheep following GIN infection
.

MATERIAL AND METHOD

To identify relevant data, we searched NCBI GEO using terms including "sheep", "Ovis aries", "nematode", and "microarray", applying strict inclusion criteria (clear phenotype distinction based on fecal egg count or related measures, ≥3 biological replicates per group, and valid probe-to-gene annotation). Three datasets—GSE36990, GSE36991, and GSE36992—spanning platforms GPL4077, GPL4076, and GPL4072, were selected (48 raw samples total). Preprocessing in R/oligo comprised norm-exp background correction, quantile normalization (Bolstad et al. 2003), and $\log_2$ transformation. After filtering probes with >20% missing values or lacking annotation and imputing remaining missing values via k-nearest neighbors (k=10), we obtained a final matrix of 32,847 probes representing 21,456 unique genes. Multi-step quality control—boxplots, MA-plots, hierarchical clustering, PCA, and kernel density estimation—removed low-quality arrays, leaving 45 high-quality samples..

ifferential expression was performed using limma with a linear model incorporating phenotype, batch, and their interaction; empirical Bayes moderation was applied, and genes with FDR < 0.05 and $|\log_2 FC| \geq 1.0$ were deemed significant. Functional annotation leveraged DAVID, clusterProfiler (with the ovine genome annotation database), REVIGO for redundancy reduction, and pathview for KEGG visualization. Separately, gene set enrichment analysis (GSEA) ranked all genes by signal-to-noise ratio and tested KEGG, REACTOME, and GO collections using 1,000 phenotype permutations, with significance defined as |NES| > 1.5 and FDR < 0.25 (Subramanian et al., 2005).

Protein-protein interaction (PPI) networks were constructed via STRING v11.5 (confidence ≥ 0.400, ≤ 50 interactors per query) and visualized in Cytoscape 3.9.1, where topology metrics and hub genes were identified using the MCC algorithm (cytoHubba). Finally, post-hoc power analysis confirmed adequate statistical power (0.92) for our sample size, while variance component analysis attributed 28.4% of expression variance to phenotype, 12.1% to batch, and 59.5% to residual error.

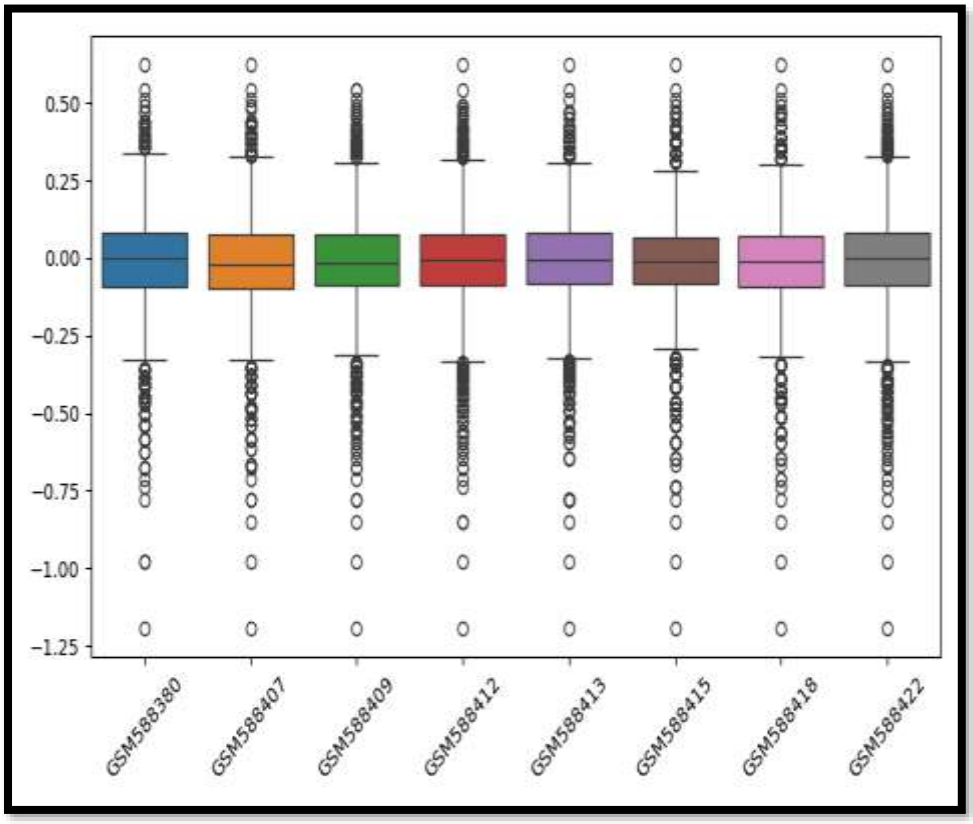

Figure 1. Quality control plot for raw studies data

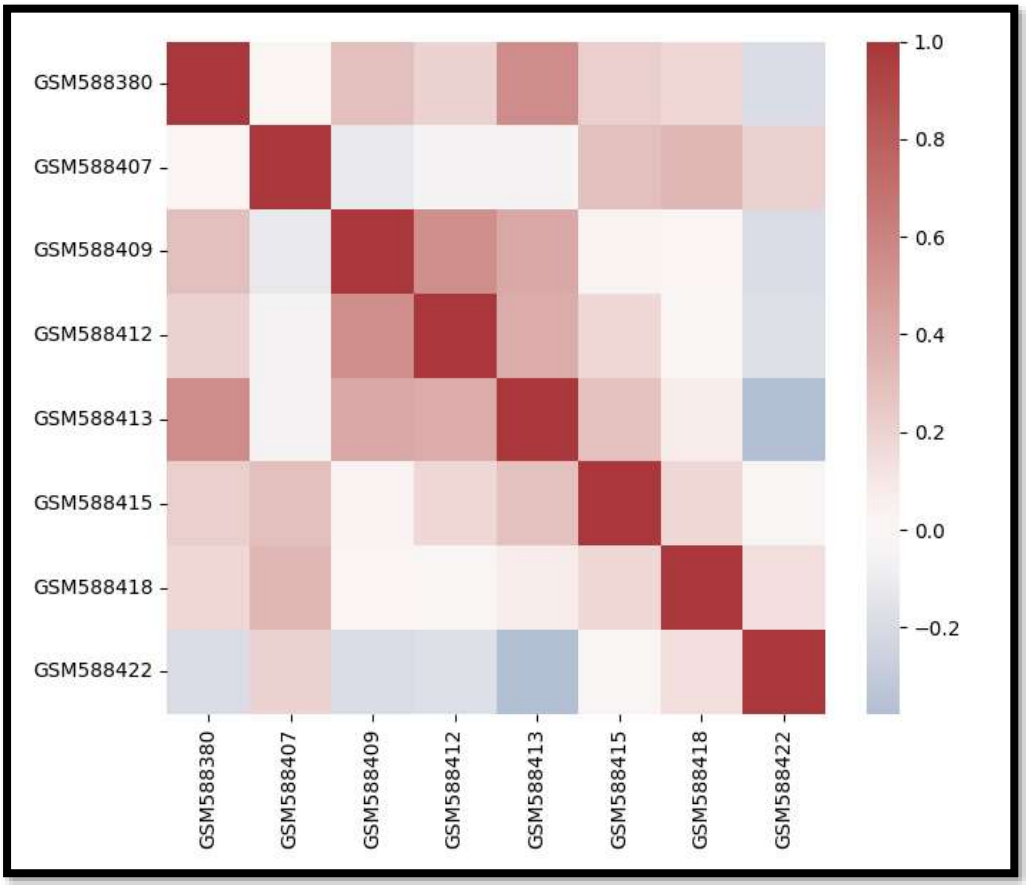

Figure 2. Heatmap correlation plot for studies raw data

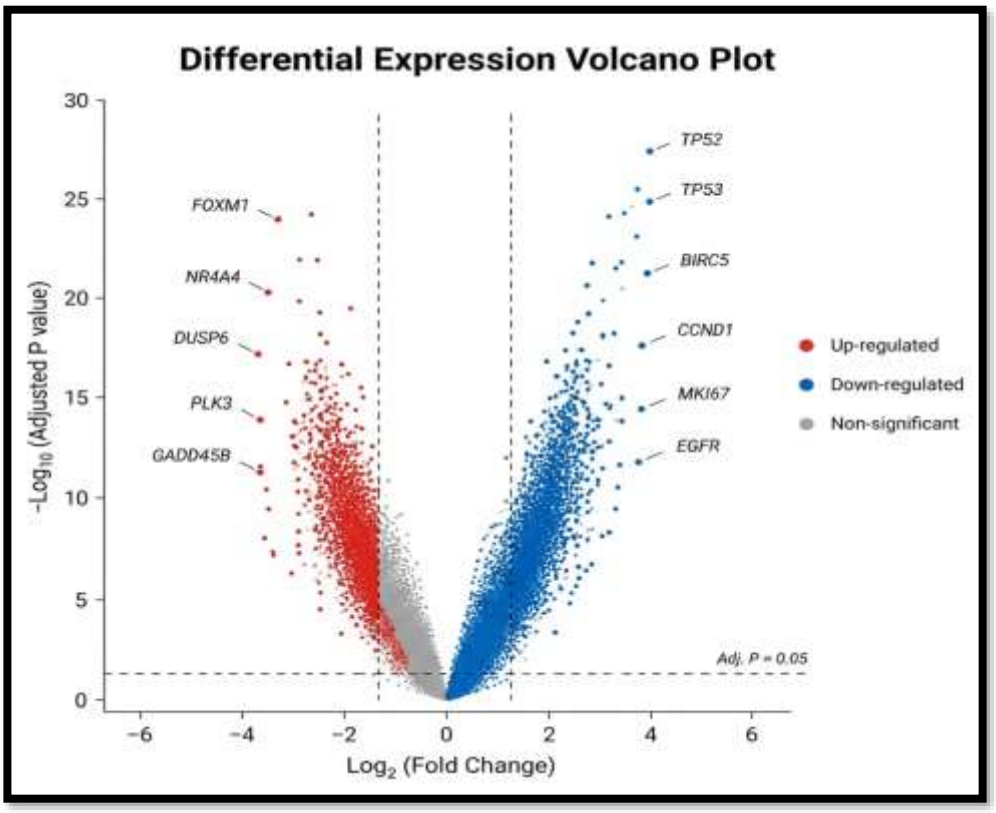

Figure 3. Differential expression volcano plot for microarray analysis

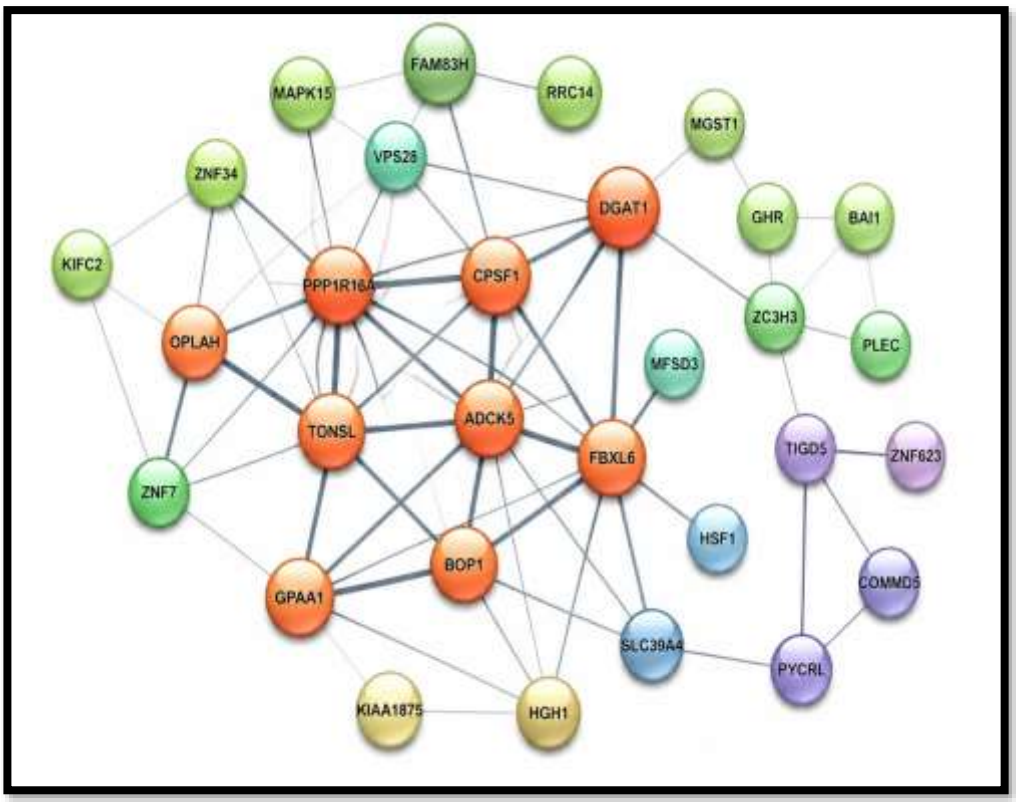

Figure 4. Gene networking and candidate key and hub gene resistance to nematode

RESULTS AND DISCUSSION

Following stringent quality control, three low-quality arrays were excluded, leaving 45 high-quality samples for downstream analysis. Of the 21,423 annotated genes interrogated, 1,247 (5.8%) were significantly differentially expressed between resistant and susceptible animals—689 upregulated and 558 downregulated in the resistant phenotype, with fold changes ranging from 2.0 to 12.1. The most prominently upregulated genes in resistant animals included key immune mediators such as IFNG (log_2FC = 2.34), IL4 (2.21), TLR4 (1.98), TNF (1.87), Ovar-DRB1 (1.76), and NRAMP1 (1.45). Conversely, mucin genes MUC7 (−1.45) and MUC15 (−1.05), along with the pepsinogen gene PGA5 (−1.18), were significantly downregulated..

Gene Ontology enrichment revealed a robust and consistent overrepresentation of immune-related terms across all domains: Biological Processes prominently featured immune and inflammatory responses, chemotaxis, cytokine-mediated signaling, lymphocyte activation, phagocytosis, and defense against parasites; Cellular Components highlighted the plasma membrane, extracellular region, cell surface, MHC class II protein complex, and the immunological synapse; while Molecular Functions were enriched for cytokine and chemokine activity, MHC class II receptor activity, signaling receptor binding, and pattern recognition receptor activity. KEGG pathway analysis identified 24 significantly enriched pathways, with the Th1/Th2 cell differentiation pathway showing the strongest enrichment (FDR = 1.2×10^{-9}), followed by chemokine, Toll-like receptor, Th17, T-cell receptor, and antigen processing and presentation pathways—all of which collectively point to a coordinated adaptive immune response with prominent Th2 polarization and efficient antigen presentation.

Gene set enrichment analysis (GSEA) corroborated these threshold-based findings, confirming strong enrichment for Th2-differentiation and cytokine-cytokine receptor interaction gene sets in resistant animals, alongside negative enrichment for mucus production and pepsinogen activity sets, consistent with the downregulation of *MUC7*, *MUC15*, and *PGA5*. Finally, the protein-protein interaction (PPI) network, comprising 847 nodes and 3,246 edges, exhibited scale-free topology and yielded ten hub genes via the MCC algorithm—*IFNG*, *TNF*, *TLR4*, *IL4*, *Ovar-DRB1*, *CCL5*, *IL6*, *STAT6*, *IL13*, and *NRAMP1*. These hubs coalesced into three interconnected functional modules: a Th2-polarization module centered on IL4, IL13, and STAT6; an antigen-presentation module anchored by Ovar-DRB1; and an inflammatory-signaling module coordinated by TLR4, TNF, and IFNG.

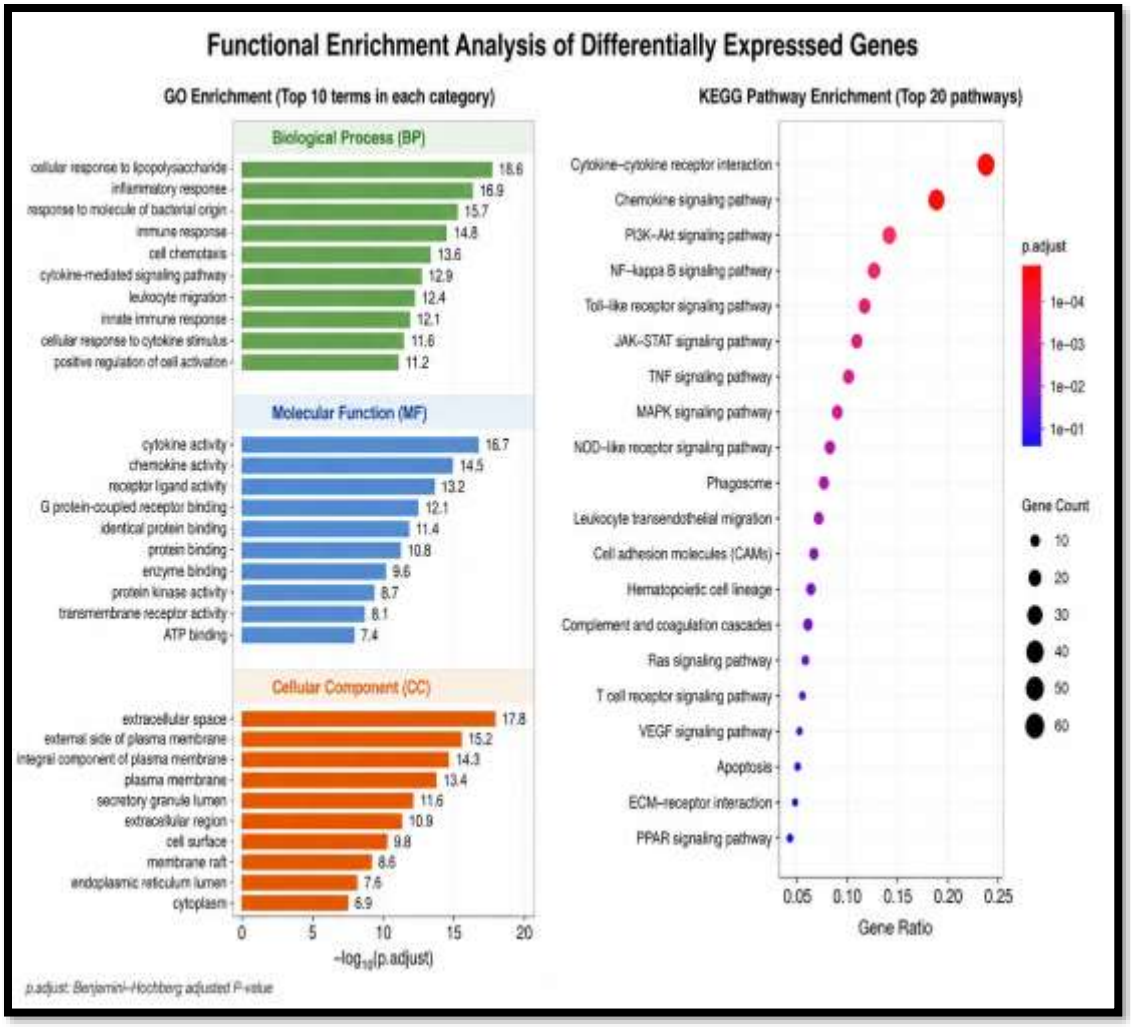

Figure 5. Gene ontology and system biology of discovered candidate gene

CONCLUSIONS

This reanalysis of publicly available microarray datasets has produced a thorough molecular description of genetic resistance to gastrointestinal nematode infection in sheep. The resistance phenotype is defined by a coordinated upregulation of Th2 cytokines (IL-4 and IL-13), the transcription factor STAT6, MHC class II molecules, TLR4, the iron transporter NRAMP1, and several inflammatory mediators, while resistant animals showed reduced expression of mucin genes and pepsinogen, presumably reflecting the absence of chronic mucosal pathology. Ten hub genes (IFNG, TNF, TLR4, IL4, Ovar-DRB1, CCL5, IL6, STAT6, IL13, and NRAMP1) were identified as the central nodes in the PPI network, which serve as the core molecular machinery of resistance. This information contributes to a fundamental knowledge of host-parasite interactions and provides a rational basis for marker-assisted selection programmes for genetic resistance improvement.

REFERENCES

Bolstad, B.M., R.A. Irizarry, M. Astrand and T.P. Speed. 2003. A comparison of normalization methods for high density oligonucleotide array data based on variance and bias. Bioinformatics, 19(2): 185-193.

Coltman, D.W., K. Wilson, J.G. Pilkington, M.J. Stear and J.M. Pemberton. 2001. A microsatellite polymorphism in the gamma interferon gene is associated with resistance to gastrointestinal nematodes in a naturally parasitised population of Soay sheep. Parasitology, 122: 571-582.

Gosling, L.A., M.V. Benavides, K. Machira and A. Ngumbi. 2014. Selection for resistance to haemonchosis in Red Masai sheep in Kenya. Tropical Animal Health and Production, 46: 285-292.

Riggio, V., R. Finocchiaro and S.C. Bishop. 2013. Genetic parameters for resistance to Teladorsagia circumcincta in Scottish Blackface sheep. Animal, 7: 1779-1785.

Ritchie, M.E., B. Phipson, D. Wu, Y. Hu, C.W. Law, W. Shi and G.K. Smyth. 2015. limma powers differential expression analyses for RNA sequencing and microarray studies. Nucleic Acids Research, 43: e47.

Sayers, G., B. Good, M. Ryan, J.M. Angles, J.P. Hanrahan and T. Sweeney. 2005. Major histocompatibility complex DRB1 locus: its role in nematode resistance in Suffolk and Texel sheep. Parasitology, 131: 1-7.

Stear, M.J., S.C. Bishop and M. Doligalska. 2005. Regulation of the immune response to gastrointestinal nematodes in sheep. Veterinary Immunology and Immunopathology, 108: 121-126.

Subramanian, A., P. Tamayo, V.K. Mootha, S. Mukherjee, B.L. Ebert, M.A. Gillette, A. Paulovich, S.L. Pomeroy, T.R. Golub, E.S. Lander and J.P. Mesirov. 2005. Gene set enrichment analysis: a knowledge based approach for interpreting genome wide expression profiles. Proceedings of the National Academy of Sciences of the United States of America, 102: 15545-15550.

Waller, P.J. and P. Chandrawathani. 2005. Haemonchus contortus: parasite problem No. 1 from tropics to Arctic. Veterinary Parasitology, 128: 313-315.

Wolstenholme, A.J., I. Fairweather, R. Prichard, G. von Samson-Himmelstjerna and N.C. Sangster. 2004. Drug resistance in veterinary helminths. Trends in Parasitology, 20: 469-476.

IN VIVO AND IN SILICO INVESTIGATION OF THE GASTROPROTECTIVE ACTIVITY OF ALEPPO PINE (PINUS HALEPENSIS MILL.) EXTRACT

BRIKA Aya[1], ZEGHAD Nadia[2], NOUI Amira[3]

[1] Department of Biochemistry and Cellular and Molecular Biology, Faculty of Natural and Life Sciences. Constantine 1 University, Constantine, Algeria,
[2] Department of Plant Biology. Constantine 1 University, Constantine, Algeria.
[3] Biotechnology Research Center (C.R.B.T), Constantine, Algeria.
Corresponding author e-mail: aya.brika@doc.umc.edu.dz

ABSTRACT

The present study aimed to evaluate the gastroprotective activity of hydromethanolic bark extract of Pinus halepensis (PHE) using both in vivo and in silico approaches. Gastric ulcers were induced in albino Wistar rats using an HCl/Ethanol model. PHE was administered at 250, 500, and 1000 mg/kg, with omeprazole (20 mg/kg) as the reference drug. Molecular docking of twelve LC-MS/MS-identified compounds was conducted against the gastric proton pump (H^+/K^+-ATPase). 3D structures of the ligands were sourced from PubChem, and the crystallographic structure of the gastric proton pump was obtained from the Protein Data Bank (PDB ID: 5YLU). Docking simulations were conducted using FlexX software. A clear dose-dependent effect was observed, with inhibition rates reaching 33.91 ± 1.02%, 51.08 ± 4.73%, and 62.04 ± 2.73% for the 250, 500, and 1000 mg/kg doses, respectively. The UI decreased from 70.37 ± 4.2 in the control group to 46.46 ± 0.72 (250 mg/kg), 34.55 ± 3.33 (500 mg/kg), and 26.73 ± 1.92 (1000 mg/kg). At the highest dose (1000 mg/kg). Macroscopic examination of the gastric mucosa demonstrated that pretreatment with PHE at the highest dose (1000 mg/kg) resulted in near-complete restoration of mucosal integrity compared to the untreated control group. Docking simulations of identified compounds against H^+/K^+-ATPase highlighted quercetin (−26.74 KJ/mol) and catechin (−25.95 KJ/mol) as the most promising candidates, both surpassing omeprazole (−18.49 KJ/mol) in binding affinity. Molecular interaction analysis revealed that the best compounds established multiple stabilizing contacts within the active site of H^+/K^+-ATPase. These findings suggest that *Pinus halepensis* bark extract possesses potent gastroprotective properties, likely mediated by the antisecretory activity of its flavonoid constituents, highlighting PHE as a promising candidate for future anti-ulcer therapeutic development.

Keywords: *Pinus halepensis*, gastroprotective effect, ulcer index, molecular docking, gastric proton pump.

INTRODUCTION

Gastric ulcers remain a major global health concern, resulting from an imbalance between aggressive factors and gastric mucosal defenses. Although conventional treatments are available, their side effects and increasing drug resistance highlight the need for safer alternatives (Chitapanarux et al., 2023). Medicinal plants are promising sources of bioactive compounds with antioxidant, anti-inflammatory, and gastroprotective properties (Aman et al., 2025). *Pinus halepensis* is traditionally recognized for its biological activities related to oxidative stress and tissue protection, suggesting potential gastroprotective effects. Therefore, this study aimed to evaluate the gastroprotective activity of *P. halepensis* extract and investigate its possible mechanisms using complementary *in vivo* and *in silico* approaches.

MATERIAL AND METHOD

Plant material

The plant material was collected in June 2023 from Djbel El Ouahch forest, Constantine, eastern Algeria, identified, and dried under appropriate conditions prior to extraction.

Extraction

The hydroalcoholic extract of *Pinus halepensis* (PHE) was obtained by maceration using a methanol/water mixture (70/30, *v/v*) (Boudebbaz et al., 2025).

In vivo anti-ulcer activity

Healthy *Wistar* rats were fasted for 48 h, and acute gastric ulcers were induced using HCl/ethanol (80/20) (Zeghad et al., 2026). Animals received *Pinus halepensis* extract (0.25–1.00 g/kg) or omeprazole (0.02 g/kg). Gastric lesions were assessed using ImageJ, and the ulcer index and gastroprotection were calculated (Kim et al., 2020).

In silico molecular docking against the gastric proton pump

Molecular docking was performed to evaluate the interactions of LC-MS/MS-identified *Pinus halepensis* phytoconstituents with gastric H^+/K^+-ATPase (PDB ID: 5YLU). Ligand structures were obtained from PubChem, and omeprazole was used as the reference compound. Docking simulations were performed using LeadIT v2.1.8, and binding affinities were expressed as ΔG (kJ/mol) (Hioual et al., 2014).

RESULTS AND DISCUSSION

In Vivo Anti-Ulcer Activity

The results of the anti-ulcer activity summarized in Table 1, demonstrate a clear dose-dependent gastroprotective effect of PHE across the three tested doses (0.25, 0.50, and 1.00 g/kg body weight), and surpassing the reference drug at both 0.50 g/kg and 1.00 g/kg. The gastric mucosal protective effect of PHE may be primarily attributed to its phenolic compounds, which are known for their significant anti-ulcerogenic activity and ability to protect the gastric mucosa (Boudebbaz et al., 2025; Bakry et al., 2023).

Table 1. Effects of *Pinus halepensis* bark extract on ulcer index, ulcer inhibition in HCl/ethanol-induced gastric ulcerated rats.

Animal's group	Ulcer index	Inhibition (%)
Normal group	-	-
Control group	70.37 ± 4.2 ^{d}	0.00 ^{a}
Standard (Omeprazol 0.02 g/kg)	43.35 ± 2.16 ^{c}	38.57 ± 3.18 ^{b}
PHE 0.25 g/kg	46.46 ± 0.72 ^{a}	33.91 ± 1.02 ^{a}
PHE 0.50 g/kg	34.55 ± 3.33 ^{a}	51.08 ± 4.73 ^{a}
PHE 1.00 g/kg	26.73 ± 1.92 ^{a}	62.04 ± 2.73 ^{a}

PHE: *Pinus halepensis* extract. Values are expressed as Mean ± SD (n=6). Analysis of variance (ANOVA one-factor and Tukey Tests) revealed statistical difference ($P<0.05$). Different superscripts (a, b, c...) for values in the same columns are statistically different.

In silico molecular docking against the gastric proton pump

Molecular docking was performed to investigate the interaction of Catechin, Quercetin, Naringenin, and Luteolin with gastric H^+/K^+-ATPase (PDB ID: 5YLU), using omeprazole as the reference inhibitor. Binding affinities are presented in Table 2.

Table 2. Scoring functions of the phytoconstituents from *P. halepensis* docked to the gastric proton pump

Compounds	**Gastric Proton Pump (5YLU)**
	Scoring Function (KJ/mol)
Omeprazol	-18.4919
Catechin	-25.9543
Quercetin	-26.7423
Naringenin	-22.8859
Luteolin	-23.1306

Quercetin (−26.7423 KJ/mol) showed the strongest binding affinity, followed by Catechin (−25.9543 KJ/mol), with both displaying more favorable scores than Omeprazole (−18.4919 KJ/mol). Luteolin and Naringenin (−23.1306 KJ/mol and −22.8859 KJ/mol, respectively) also showed favorable interactions with H^+/K^+-ATPase. These affinities may be related to their hydroxyl groups and aromatic rings, which promote hydrogen-bonding and hydrophobic interactions (Shahidi & Dissanayaka, 2023; Lešnik et al., 2025). Overall, the findings support the potential contribution of these polyphenols to gastroprotection through proton pump inhibition.

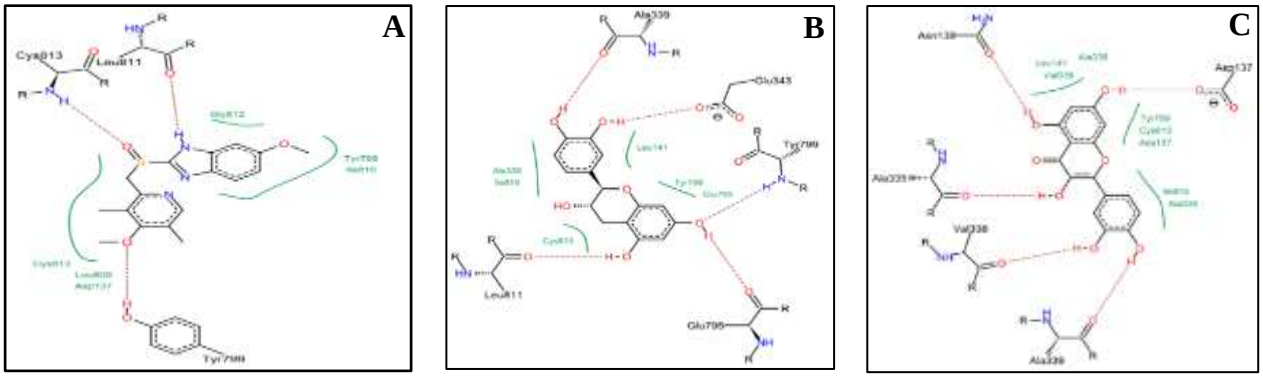

Figure 1. Binding interactions of omeprazole (A), catechin (B), and quercetin (C) within the gastric H^+/K^+-ATPase active site. Hydrogen bonds are represented by purple dashed lines, and hydrophobic interactions are highlighted in green.

CONCLUSIONS

Pinus halepensis shows promising gastroprotective potential due to its bioactive compounds with antisecretory properties. Combining *in vivo* experiments and *in silico* analyses suggests that this plant may help protect the gastric mucosa and act on key molecular targets involved in ulcer formation. These findings support further studies to validate its use as a natural anti-ulcer agent.

REFERENCES

Aman, A., Kumari, J., & Rajbhar, R. (2025). A review on herbal potential for treatment of peptic ulcer. *International Journal of Pharmaceutical Research and Applications.* 10(4), 560–569. https://doi.org/10.35629/4494-1004560569

Bakry, S., Naser, A., Negoumy, S., Kassem, M., Abdel-Sattar, E., & Meselhy, M. (2023). Phenolic acids-rich fraction from Ficus drupacea leaves for the prevention and treatment of ethanol-induced gastric mucosal injury in rats. Inflammopharmacology, 31(3), 1423 - 1436. https://doi.org/10.1007/s10787-023-01158-4.

Beiranvand, M., Bahramikia, S., & Dezfoulian, O. (2021). Evaluation of antioxidant and anti-ulcerogenic effects of Eremurus persicus (Jaub & Spach) Boiss leaf hydroalcoholic extract on ethanol-induced gastric ulcer in rats. *Inflammopharmacology*, 29(5), 1503 - 1518. https://doi.org/10.1007/s10787-021-00868-x

Boudebbaz, K., Brouk, M., Laalem, R., & Zabaiou, N. (2025). Gastroprotective properties of flavonoid-rich extract of Pulicaria odora against ethanol-induced gastric ulcer in mice. *Heliyon*, 11(1), e41625. https://doi.org/10.1016/j.heliyon.2025.e41625

Chitapanarux, T., Kongkarnka, S., Wannasai, K., & Sripan, P. (2023). Prevalence and factors associated with atrophic gastritis and intestinal metaplasia: A multivariate, hospital-based, statistical analysis. *Cancer Epidemiology*, 82, 102309. https://doi.org/10.1016/j.canep.2022.102309

De Araújo, E., Guerra, G., Andrade, A., Fernandes, J., Da Silva, V., De Aragão Tavares, E., De Araújo, A., De Araújo Júnior, R., & Zucolotto, S. (2021). Gastric ulcer healing property of *Bryophyllum pinnatum* leaf extract in chronic model in vivo and gastroprotective activity of its major flavonoid. *Frontiers in Pharmacology*, 12. https://doi.org/10.3389/fphar.2021.744192.

Hioual, K., Chikhi, A., Bensegueni, A., Merzoug, A., Boucherit, H., Mokrani, E. H., Teniou, S., & Merabti, B. (2014). Successful challenge: A key step in infectious diseases treatment using computer-aided drug design. *International Journal of Biological Sciences and Applications*, 1(1), 11–14.

Kim, Y. S., Lee, J. H., Song, J., & Kim, H. (2020). Gastroprotective effects of Inulae flos on HCl/ethanol-induced gastric ulcers in rats. *Molecules*, 25(23). https://doi.org/10.3390/molecules25235623

Lešnik, S., Jukič, M., & Bren, U. (2025). Unveiling polyphenol-protein interactions: A comprehensive computational analysis. *Journal of Cheminformatics*, 17(1), 50. https://doi.org/10.1186/s13321-025-00997-3

Oueslati, S., Beji, R., Kalai, F., Soufiani, M., Zorrig, W., Aissam, S., Msaada, K., & Modafar, E. (2023). Antioxidant potentialities and gastroprotective effect of *Reichardia picroides* extracts on Ethanol/HCl induced gastric ulcer rats. *International Journal of Environmental Health Research*, 34, 1088 - 1099. https://doi.org/10.1080/09603123.2023.2198760.

Shahidi, F., & Dissanayaka, C. (2023). Phenolic-protein interactions: insight from in-silico analyses – A review. *Food Production, Processing and Nutrition*, 5(1), 2. https://doi.org/10.1186/s43014-022-00121-0.

Zeghad, N., Hefny Gad, M., Madi, A., Ahmed, E., Sihem, H., & Belkhiri, A. (2026). Gastroprotective effect of an Algerian hydroalcoholic *Punica granatum L*. peel extract against ethanol/HCl-induced gastric mucosal injury in Wistar rats. *Current Issues in Pharmacy and Medical Sciences*, 38(4), 270–275. https://doi.org/10.12923/cipms-2025-0043.

COMPARATIVE EFFECTS OF EDTA AND DTPA ON THE STABILITY OF ASCORBIC ACID DURING CAPILLARY ELECTROPHORETIC DETERMINATION IN LEMON JUICE

Ahmet Dursun[1]

[1] *Hatay Mustafa Kemal University, Agriculture Faculty, Food Engineering Department, Hatay, Turkey*

Corresponding author e-mail: adursun@mku.edu.tr

ABSTRACT

The oxidation of ascorbic acid especially in presence of metal catalysts can occur during sample preparation, resulting in an inaccurate measurement of its capillary electrophoretic determination. This study was performed in order to compare the effect of ethylenediaminetetraacetic acid (EDTA) and diethylenetriaminepentaacetic acid (DTPA) on the stability of ascorbic acid in lemon juice. Lemon juice was prepared freshly and then mixed (1:1 v/v) with EDTA or DTPA at concentrations of 0 (untreated), 0.5, 1.0 and 2.0 mM and measured either immediately or after 6 h waiting at room temperature. The external calibration curve ranged from 1.56125 to 100 µg/mL and had a higher linearity (R^2=0.99985), with limits of detection and quantification of 1.57 and 4.77 µg/mL, respectively. The recovery of this method was 95% which revealed a satisfactory analytical accuracy. The concentration of chelator had a significant effect on the initial ascorbic acid concentration measurement ($P < 0.001$). However, after waiting for 6 h, both the type ($P < 0.01$) and concentration ($P < 0.001$) of chelator significantly influenced ascorbic acid stability. The highest ascorbic acid concentration was found in samples treated with DTPA in comparison with EDTA-treated ones. These results showed that oxidation begins during sample preparation and suggested that adding approximately 1.0 mM of DTPA is an effective strategy to improve the reliability of capillary electrophoretic determination of ascorbic acid in food matrices.

Keywords: Oxidation, Ascorbic acid, Lemon juice, Metal-chelate complexes

INTRODUCTION

Ascorbic acid (Vitamin C) is one of the most important water-soluble antioxidants which is naturally present in fruits and vegetables and plays an important role in human nutrition due to its participation in collagen synthesis, iron absorption, immunity function, and oxidative stress protection (Yin et al., 2022). Additionally, ascorbic acid is commonly used in the food industry for retarding lipid oxidation, protecting color and flavor of foods, and improve product stability (Gérard et al., 2019). For this reason, the accurate determination of ascorbic acid is essential for quality control, nutritional labeling, and evaluation of food processing and storage conditions.

Different analytical techniques have been applied for the determination of ascorbic acid including titration, spectrophotometry, high-performance liquid chromatography (HPLC), and capillary electrophoresis (CE) (Suntornsuk et al., 2002; Uckoo et al., 2011). Among those, CE has received much attention due to its high separation efficiency, rapid analysis, low quantity of reagent, and minimal sample preparation (Maria Rizelio et al., 2012). Furthermore, CE could

be considered an eco-friendly analytical technique due to low solvents consumption (Topaloğlu & Dursun, 2026).

However, despite its advantages, the analysis of ascorbic acid by using CE has been found to be difficult due to the fact that it is very susceptible to oxidation during sample preparation and analysis. The oxidation of ascorbic acid into dehydroascorbic acid is greatly accelerated by oxygen, light, high temperatures, alkaline conditions, and especially by metal ions like Fe^{2+} and Cu^{2+} (Zinellu et al., 2006). This oxidation process not only reduces the amount of ascorbic acid but may also adversely affect electrophoretic performance through the alteration of peak area, migration time, peak symmetry, and theoretical plate number, thereby compromising analytical precision and accuracy.

In order to prevent oxidation catalyzed by metal ions, chelators are commonly added during the sample preparation stage. In particular, ethylenediaminetetraacetic acid (EDTA) has been widely used to maintain the stability of ascorbic acid through complexation with trace metal ions, and some studies have shown the positive impact of EDTA on maintaining ascorbic acid stability in fruit juices and biological samples (Cancalon, 2001; Zinellu et al., 2006). On the other hand, diethylenetriaminepentaacetic acid (DTPA), a chelator with a higher affinity for many transition metal ions compared to EDTA (Karak et al., 2016), has been successfully applied as a stabilizing agent in biological samples to minimize the oxidation of ascorbic acid. As reported by Collie et al. (2021), perchloric acid/DTPA-based stabilization effectively decreased the oxidation of ascorbic acid during sample storage; however, substantial oxidation occurred during sample preparation, which highlighted the importance of sample preparation stage in determining the ascorbic acid content. Despite the extensive use of EDTA in several CE analysis of ascorbic acid, there is no systematic study has been conducted on the effect of EDTA and DTPA in capillary electrophoretic determination of ascorbic acid in lemon juice.

Lemon juice constitutes an appropriate model matrix for the investigation of the stabilizing effect of chelator because it naturally contains relatively high concentrations of ascorbic acid, as well as trace metal ions that can oxidize this compound (Davey et al., 2000). Moreover, the evaluation of stabilization strategies particularly relevant for routine laboratory analysis, as sample handling and waiting at room temperature could increase the oxidative degradation.

Therefore, the aim of the present study was the investigation of the effect of EDTA and DTPA at various concentrations on the stability of ascorbic acid in the process of CE analysis of lemon juice. In order to simulate possible delays associated with sample processing in routine experiments, samples (with and without pretreatment) were kept at room temperature for up to 6 h prior to analysis. The impact of chelator was assessed according to the change in the content of ascorbic acid. The results of the present study can be used to improve the reliability and reproducibility of CE analysis of ascorbic acid in fruit juices.

MATERIAL AND METHOD

L-ascorbic acid, ethylenediaminetetraacetic acid (EDTA), diethylenetriaminepentaacetic acid (DTPA), boric acid and sodium hydroxide were purchased from Merck. Ultra-pure water was used throughout the study for the preparation of all solutions. Standard stock solution of L-ascorbic acid was freshly prepared on the day of analysis.

The fresh lemons were purchased from a local market (Hatay, Türkiye). Prior to analysis, the fruits were washed with tap water, and then by distilled water and dried. The peels were manually removed, and then the edible part was homogenized by using a laboratory homogenizer (HGB2WTG4, Waring Commercial, USA). Lemon juice was obtained by

filtering the homogenate through coarse filter paper and immediately used for subsequent analyses. The physicochemical characteristics of freshly prepared lemon juice were determined. The pH was measured at room temperature using a calibrated digital pH meter (HI2211, Hanna Instruments, Woonsocket, USA). The total soluble solids were determined using a digital refractometer (DR201-95, A. Krüss Optronic GmbH, Hamburg, Germany) and expressed as ^{o}Briks. The titratable acidity was determined by titration with standardized 0.1 N NaOH solution and expressed as g of citric acid per 100 mL of lemon juice. All the measurements were performed in triplicates.

In order to assess the impact of metal chelation on stability of ascorbic acid, freshly prepared lemon juice was divided into two experimental groups corresponding EDTA and DTPA. Each experimental group was further subdivided into 4 concentrations (0 (control), 0.5, 1.0, and 2.0 mM) of chelators. The concentrations of chelators were selected considering previous studies that used about 1 mM of EDTA to stabilize ascorbic acid (Spínola et al., 2012). Moreover, both low and high concentrations were used to determine the effect of concentration-dependent metal chelation and to identify the minimal concentration that stabilizes ascorbic acid adequately. Lemon juice was mixed with each chelator in equal volumes (1:1 v/v). In one group, the samples were analyzed immediately after preparation to represent the initial measured concentration (0 h). The other group of samples was kept for 6 h at room temperature to evaluate the effects of EDTA and DTPA on oxidation of ascorbic acid. Ascorbic acid concentration was calculated from the external standard technique.

Capillary electrophoresis-diode array detection (CE-DAD) method was used for ascorbic acid determination (7100, Agilent Technologies, Palo Alto, USA). The separations were carried out in an uncoated fused-silica capillary (50 µm i.d., 64.5 cm total length, G1600-61232, Agilent) using 30 mM borate buffer (pH 9.0) as background electrolyte. The detection wavelength was set at 270 nm. The samples and standards were injected to the capillary by hydrodynamically at 50 mbar 5 s (Cancalon, 2001). Prior to analysis, the CE system was conditioned according to the manufacturer's instructions.

Ascorbic acid measured from initial (0 h) and after waiting for 6 h samples were analyzed separately using a two-way ANOVA with chelator (EDTA and DTPA) and concentration (0, 0.5, 1, and 2 mM) as fixed factor in a completely randomized design. Duncan's multiple range test was applied for post-hoc comparison of means determined as significant at $P < 0.05$. Statistical analysis was performed using SPSS statistical software (Version 26, IBM, USA).

RESULTS AND DISCUSSION

The pH, total soluble solids (TSS), and titratable acidity determined in lemon juice were 2.65, 5.85 (^{o}Briks) and 4.55 g citric acid/100 mL, respectively. The measured pH is in accordance with the higher acidic nature of lemon juice and agrees well with the previous findings reported by Uçan et al. (2014). However, the authors reported higher TSS and titratable acidity compared to those obtained in the present study. These differences could be attributed to the type of lemon used, fruit maturity, cultivation and management conditions (Sun et al., 2019; Di Vaio et al., 2023).

The main analytical characteristics of the CE method were summarized in Table 1. A seven-point calibration curve was constructured within the concentration range of 1.56125-100 µg/mL. The calibration curve exhibited good linearity between the analyte concentration and peak area with a coefficient of determination (R^2=0.99985). The obtained linearity was higher than that of Dresler & Maksymiec (2013) who reported a R^2 of 0.988 for ascorbic acid using CE in plants. The response factor was determined as 2.35, which indicates a stable analytical response of the CE method within the calibration range. The low variation in response factor

(CV <5%) confirmed repeatability of the CE method. The limit of detection (LOD) and quantification (LOQ) were 1.57 µg/mL and 4.77 µg/mL, respectively. These values indicated that the CE method provides good sensitivity, necessary to detect natural concentrations of ascorbic acid in lemon juice. The LOD obtained from the present study were comparable to those reported for CE methods used borate electrolytes and UV detection (Dresler & Maksymiec, 2013). A higher LOD (10 mg/mL) of ascorbic acid had been previously reported for beverages analyzed by CE (Liu et al., 2014). Method accuracy was evaluated by recovery experiments (Table 1). The representative electropherograms of the native and ascorbic acid-spiked samples of lemon juice were shown in Fig 1. The mean recovery of 95% demonstrated a satisfactory analytical accuracy and negligible matrix interference. The confidence interval of 95% (81.2-109%) confirmed the reliability of the analytical method as well (Table 1). According to internationally analytical validation guidelines (ICH, 1996), recovery values of 80-110% are generally considered acceptable for food analysis. Similarly, Liao et al. (2001) obtained the recovery rates of 95-105% for ascorbic acid in fruit juices, including lemon.

Table 1. Analytical calibration characteristics and validation parameters of the applied capillary electrophoresis method for the determination of ascorbic acid in lemon juice.

Calibration characteristics	
Concentration range (µg/mL)	1.56125-100
Equation (y=ax±b)	y=2.07*x*+1.69
Determination coefficient (R^2)	0.99985
Limit of detection (LOD, µg/mL)	1.57
Limit of quantification (LOQ, µg/mL)	4.77
Response factor	2.35
CV of Response factor (%)	4.65
Method accuracy	
Real concentration (µg/mL)	50.0
Non-spiked sample (µg/mL)	32.2±1.52
Spiked sample (µg/mL)	79.8±4.04
Recovery (%)	95.2±5.44
CI 95% (lower-upper)	81.2-109

CV: Coefficient of variation. CI: Confidence interval. The data were expressed as mean±standard error (n=3).

The influence of EDTA and DTPA at different concentrations on the stability of ascorbic acid in lemon juice was presented in Table 2. The concentration dependents effects of both chelators were illustrated in Fig 2. The ascorbic acid concentration after the preparation of samples ranged between 334 and 445 µg/mL, depending on the concentration of chelators. The ascorbic acid concentration in the present study was consistent with the findings reported by (Uçan et al., 2014), who showed a significant reduction in ascorbic acid level from 420 µg/mL to 345 µg/mL during the processing. Similarly, it has been reported that the ascorbic acid concentrations in lemon juice decreased steadily during ripening from 31.4 to 23.7 mg/100 g (Di Matteo et al., 2021). The chelator concentration had a significant effect on the ascorbic acid content initially measured ($P < 0.001$). The samples with 1.0 and 2.0 mM chelator concentration showed higher concentrations of ascorbic acid in comparison to other treatments, regardless of the type of chelator used (Table 2, Fig 2).

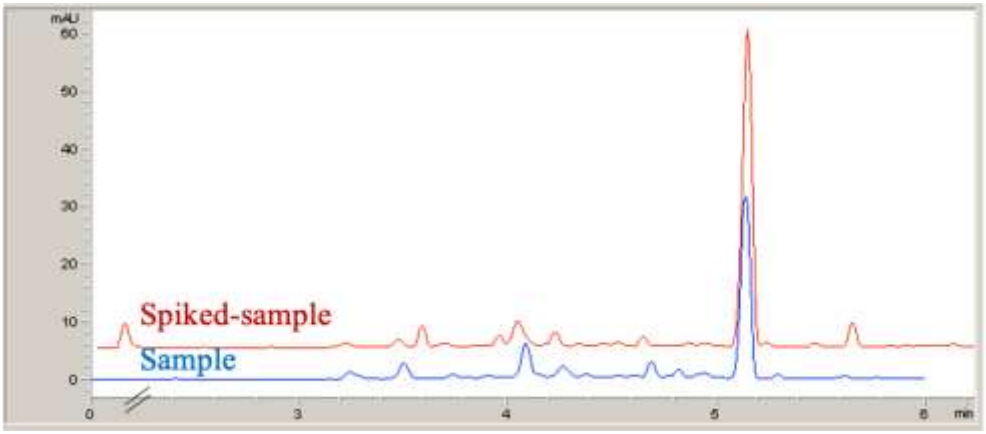

Figure 1. Capillary electropherograms of native and ascorbic acid-spiked lemon juice samples.

Table 2. Effects of DTPA and EDTA concentration on the measured ascorbic acid concentration in lemon juice analyzed immediately and after 6 h waiting at room temperature.

Chelator	Concentration (mM)	Ascorbic acid (µg/mL)	
		Initial	After 6 h
DTPA	0 (Control)	336±17.6	244±2.19
	0.5	334±9.39	327±8.88
	1.0	410±15.5	333±10.3
	2.0	445±25.0	353±6.00
EDTA	0 (Control)	336±25.2	239±10.1
	0.5	386±18.4	308±13.1
	1.0	409±13.9	309±4.10
	2.0	406±12.3	306±11.0
Chelator (A)			
DTPA		381±16.3	315±12.9
EDTA		384±11.8	291±9.96
P value		*0.831*	*0.002*
Concentration (B)			
0 mM (Control)		336^{b}±13.8	242^{b}±4.76
0.5 mM		360^{b}±14.7	318^{a}±8.26
1.0 mM		410^{a}±9.30	321^{a}±7.43
2.0 mM		425^{a}±15.2	330^{a}±11.9
P value		*<0.001*	*<0.001*
Interaction (A x B)		*0.135*	0.172

The data were expressed mean±standard error (n=3). $^{a-b}$Different lowercase letters within the same column indicate significant differences among chelator concentration ($P < 0.05$).

The initial ascorbic acid concentration obtained in the samples treated with chelators indicate that oxidative degradation of ascorbic acid begins immediately after tissue disruption and juice extraction before analysis. Mechanical homogenization leads to damage to cellular compartments, resulting in the interaction of ascorbic acid with endogenous metal ions and oxidative enzymes in the presence of oxygen (Spínola et al., 2012). That means oxidation of ascorbic acid may even in the stage of sample handling before the beginning of instrumental analysis when metal-catalyzed reactions are not appropriately controlled. Moreover, it has been

reported that significant loss of ascorbic acid happens immediately after the extraction of juice and in the next stages of processing (Davey et al., 2000; Uçan et al., 2014). Although the low pH (2.6) of lemon juice may be considered to keep ascorbic acid stable, acidic matrix alone is not enough to inhibit oxidation process. Previous studies have shown that metal ions like Fe^{3+} and Cu^{+2} still have the ability to oxidize of ascorbic acid even in acidic matrix by metal mediated electron transfer reaction (Bradshaw et al., 2011; Pullar et al., 2018).

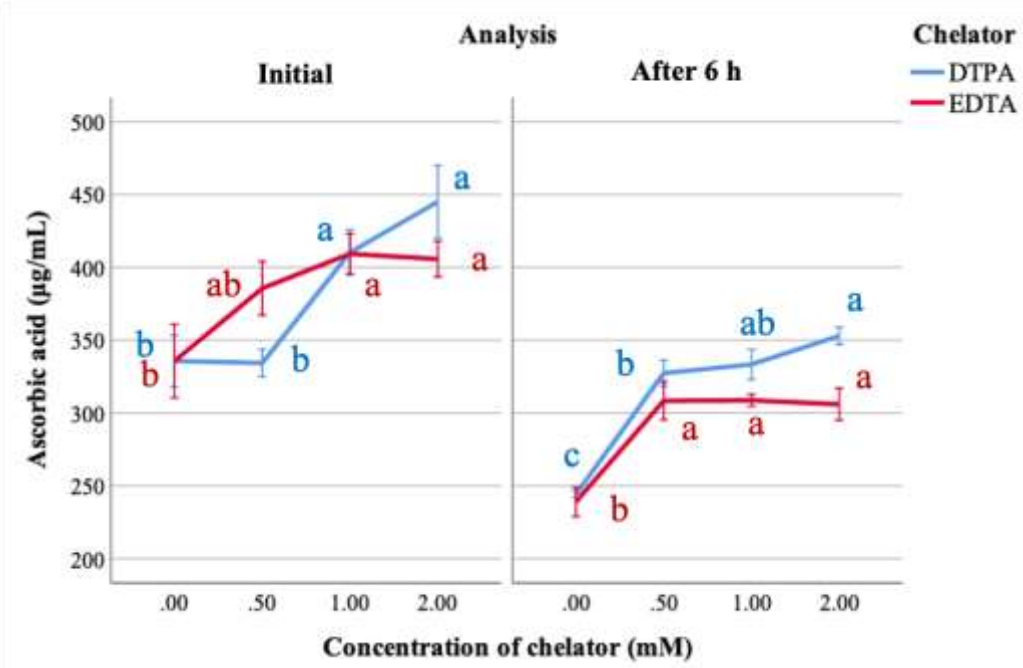

Figure 2. Effects of DTPA and EDTA concentrations on the measured ascorbic acid concentration (µg/mL) in lemon juice analyzed initial and after 6 h at room temperature. Error bar represents standard error (n=3). [a-c]Different lowercase letters indicate significant differences among chelator concentration within each chelator treatment ($P < 0.05$).

Upon waiting for 6 h after preparation of the samples, the concentration of ascorbic acid was decreased in all samples (Table 2, Fig 2). However, the addition of chelator minimized the amount of oxidation compared to the untreated control. Significant effects of both chelator concentration ($P < 0.001$) and chelator type ($P < 0.01$) were noted upon waiting for 6 h after preparation of the samples. In general, samples treated with DTPA had more amounts of ascorbic acid concentration (315 µg/mL) than those treated with EDTA (291 µg/mL). It should be stated that DTPA provided more effective protection against oxidation during prolonged sample handling. Pullar et al. (2018) demonstrated that ascorbic acid oxidation occurred rapidly in the process of sample preparation and processing, and the catalysts of this process was the transition metal ions. Addition of DTPA inhibited metal-catalyzed oxidation of the substance, while EDTA act less effectively because complexes between EDTA and metal ions retained redox activity at physiological pH. These results were shown in consistence well with those of the present study. Calculated losses also show the protective effects of both chelators. Without any chelator, about 28% of initial ascorbic acid were lost during 6 h period. On the contrary, losses from samples treated EDTA were about 24%, while losses from DTPA treated samples were about 17% (Fig 3). This higher efficiency of DTPA is expected because of the stronger complex formation ability of DTPA for metal ions compared with EDTA. Namely, DTPA molecule has an additional amino-carboxylate group, which provides it with larger stability

constants with Fe^{3+} and some other metal ions. Indeed, comparative studies have demonstrated that DTPA forms more stable complexes with iron than EDTA (Zhou et al., 2010).

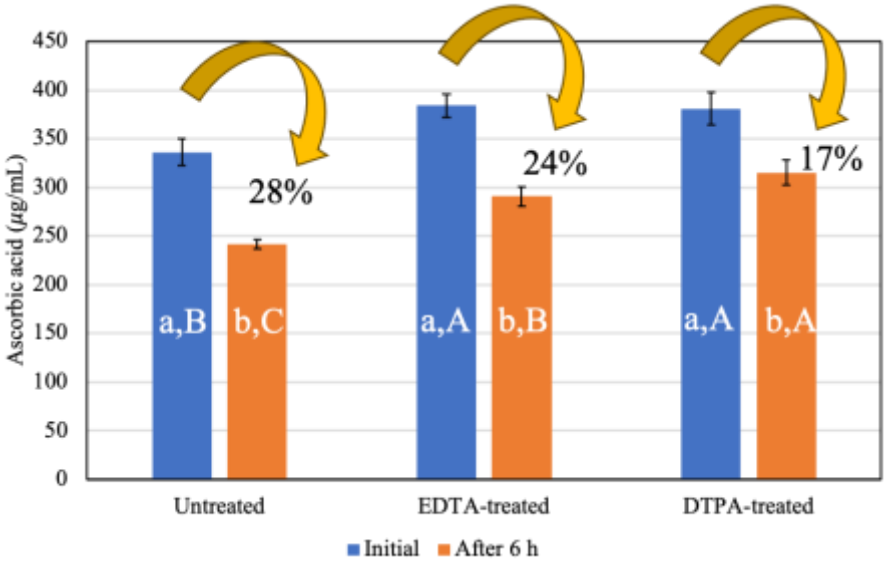

Figure 3. Changes in ascorbic acid concentration in untreated, EDTA- and DTPA-treated lemon juice after 6 h of waiting at room temperature. Arrows indicate the percentage loss of ascorbic acid. Error bar represents standard error (n=3). [a,b]Different lowercase letters indicate significant differences among analysis time within each treatment ($P < 0.05$). [A-C]Different uppercase letters indicate significant differences among treatments at the same analysis time ($P < 0.05$).

The concentration dependent effects observed in the present study further confirm that practicality of 1.0 mM as an adequate concentration for routine CE determination of ascorbic acid. While the samples which were treated with 2.0 mM chelator had numerically higher amounts of ascorbic acid than samples which were treated with 1.0 mM chelator, the difference did not statistically significant (Fig 2). In this case, it should be suggested that the majority of catalytically active metal ions can probably already be efficiently complexed at approximately 1.0 mM concentration under the experimental conditions of lemon juice analysis. Hence, increase in the chelator concentration to a value above 1.0 mM cannot appear to provide any analytical advantages but will result in more reagent usage. Moreover, previous studies have noted the susceptibility of ascorbic acid to its oxidation in the course of sample preparation. Collie et al. (2021) showed that the stabilization with perchloric acid/DTPA successfully prevented the oxidation of plasma ascorbate during frozen storage; however, considerable oxidation could take place during sample processing. Similarly, the present findings confirm this statement to a food matrix by noting the crucial influence of sample preparation rather than storage alone constitutes on the ascorbic acid quantification. Therefore, the incorporation of an appropriate chelating agent immediately after extraction appears to be essential for minimizing metal-catalyzed oxidation.

CONCLUSIONS

From an analytical perspective, based on the results obtained from the present study, the addition of about 1.0 mM EDTA or DTPA seem to be sufficient to improve the immediate determination of ascorbic acid through CE. However, when analysis is not performed directly and waiting for a while at room temperature becomes necessary, DTPA would be more

appropriate due to the higher capability of protecting native ascorbic acid. These results offer a practical guidance for routine capillary electrophoretic determination of vitamin C in citrus matrices and potentially any other food which is sensitive to metal-mediated oxidation. Moreover, the present investigation was limited to only one matrix, as well as a short time interval (6 h) under room temperature conditions. Further research should investigate the efficacy of EDTA and DTPA in different matrices with varying metal content along with different time periods and temperatures.

REFERENCES

Aguilar-Hernández, M. G., Núñez-Gómez, D., Forner-Giner, M. Á., Hernández, F., Pastor-Pérez, J. J., & Legua, P. (2020). Quality Parameters of Spanish Lemons with Commercial Interest. Foods, 10(1), 62. https://doi.org/10.3390/foods10010062

Bradshaw, M. P., Barril, C., Clark, A. C., Prenzler, P. D., & Scollary, G. R. (2011). Ascorbic Acid: A Review of its Chemistry and Reactivity in Relation to a Wine Environment. Critical Reviews in Food Science and Nutrition, 51(6), 479–498. https://doi.org/10.1080/10408391003690559

Cancalon, P. F. (2001). Routine analysis of ascorbic acid in citrus juice using capillary electrophoresis. Journal of AOAC International, 84(3), 987–991.

Collie, J. T., Hudson, E. P., Deane, A. M., Bellomo, R., & Greaves, R. F. (2021). A Stabilizing Agent, PCA/DTPA, Improves Plasma Storage Life for the Chromsystems Vitamin C Assay up to Six Months. Annals of Laboratory Medicine, 41(4), 414–418. https://doi.org/10.3343/alm.2021.41.4.414

Davey, M. W., Montagu, M. V., Inze, D., Sanmartin, M., Kanellis, A., Smirnoff, N., Benzie, I. J., Strain, J. J., Favell, D., & Fletcher, J. (2000). Plant L-ascorbic acid: Chemistry, function, metabolism, bioavailability and effects of processing. Journal of the Science of Food and Agriculture, 80(7), 825–860. https://doi.org/10.1002/(SICI)1097-0010(20000515)80:7%3C825::AID-JSFA598%3E3.0.CO;2-6

Di Matteo, A., Di Rauso Simeone, G., Cirillo, A., Rao, M. A., & Di Vaio, C. (2021). Morphological characteristics, ascorbic acid and antioxidant activity during fruit ripening of four lemon (Citrus limon (L.) Burm. F.) cultivars. Scientia Horticulturae, 276, 109741. https://doi.org/10.1016/j.scienta.2020.109741

Di Vaio, C., Cirillo, A., Catalano, C., & La Malfa, S. (2023). A Decade-Long Quantitative–Qualitative Characterization of 18 Lemon Cultivars. Horticulturae, 9(11), 1186. https://doi.org/10.3390/horticulturae9111186

Dresler, S., & Maksymiec, W. (2013). Capillary zone electrophoresis for determination of reduced and oxidised ascorbate and glutathione in roots and leaf segments of Zea mays plants exposed to Cd and Cu. Acta Scientiarum Polonorum Hortorum Cultus, 12(6), 143–155.

Gérard, V., Ay, E., Graff, B., Morlet-Savary, F., Galopin, C., Mutilangi, W., & Lalevée, J. (2019). Ascorbic Acid Derivatives as Potential Substitutes for Ascorbic Acid To Reduce Color Degradation of Drinks Containing Ascorbic Acid and Anthocyanins from Natural Extracts. Journal of Agricultural and Food Chemistry, 67(43), 12061–12071. https://doi.org/10.1021/acs.jafc.9b05049

ICH (1996). ICH Harmonised Tripartite Guideline: Validation of Analytical Procedures: Methodology (Q2B) (CPMP/ICH/281/95). The European Agency for the Evaluation of Medicinal Products.

Karak, T., Paul, R. K., Das, D. K., & Boruah, R. K. (2016). Complexation of DTPA and EDTA with Cd2+: Stability constants and thermodynamic parameters at the soil-water interface. Environmental Monitoring and Assessment, 188(12), 670. https://doi.org/10.1007/s10661-016-5685-5

Liao, T., Jiang, C.-M., Wu, M.-C., Hwang, J.-Y., & Chang, H.-M. (2001). Quantification ofL-ascorbic acid and total ascorbic acid in fruits and spinach by capillary zone electrophoresis. Electrophoresis, 22(8), 1484–1488. https://doi.org/10.1002/1522-2683(200105)22:8%3C1484::AID-ELPS1484%3E3.0.CO;2-9

Liu, F.-J., Ding, G.-S., & Tang, A.-N. (2014). Simultaneous separation and determination of five organic acids in beverages and fruits by capillary electrophoresis using diamino moiety functionalized silica nanoparticles as pseudostationary phase. Food Chemistry, 145, 109–114. https://doi.org/10.1016/j.foodchem.2013.08.035

Maria Rizelio, V., Gonzaga, L. V., Borges, G. D. S. C., França Maltez, H., Costa, A. C. O., & Fett, R. (2012). Fast determination of cations in honey by capillary electrophoresis: A possible method for geographic origin discrimination. Talanta, 99, 450–456. https://doi.org/10.1016/j.talanta.2012.06.009

Pullar, J., Bayer, S., & Carr, A. (2018). Appropriate Handling, Processing and Analysis of Blood Samples Is Essential to Avoid Oxidation of Vitamin C to Dehydroascorbic Acid. Antioxidants, 7(2), 29. https://doi.org/10.3390/antiox7020029

Spínola, V., Mendes, B., Câmara, J. S., & Castilho, P. C. (2012). An improved and fast UHPLC-PDA methodology for determination of L-ascorbic and dehydroascorbic acids in fruits and vegetables. Evaluation of degradation rate during storage. Analytical and Bioanalytical Chemistry, 403(4), 1049–1058. https://doi.org/10.1007/s00216-011-5668-x

Sun, Y., Singh, Z., Tokala, V. Y., & Heather, B. (2019). Harvest maturity stage and cold storage period influence lemon fruit quality. Scientia Horticulturae, 249, 322–328. https://doi.org/10.1016/j.scienta.2019.01.056

Suntornsuk, L., Gritsanapun, W., Nilkamhank, S., & Paochom, A. (2002). Quantitation of vitamin C content in herbal juice using direct titration. Journal of Pharmaceutical and Biomedical Analysis, 28(5), 849–855. https://doi.org/10.1016/S0731-7085(01)00661-6

Topaloğlu, F., & Dursun, A. (2026). Chloride-based salt determination in meat bouillon and bone broth: A comparative evaluation of Mohr titration and capillary electrophoresis. Journal of Food Measurement and Characterization. https://doi.org/10.1007/s11694-026-04655-6

Uçan, F, Ağçam, E, & Akyıldız, A. (2014). Doğal Bulanık Limon Suyu Üretimi Üzerinde Bir Araştırma. Gıda, 39(1), 25–32.

Uckoo, R. M., Jayaprakasha, G. K., Nelson, S. D., & Patil, B. S. (2011). Rapid simultaneous determination of amines and organic acids in citrus using high-performance liquid chromatography. Talanta, 83(3), 948–954. https://doi.org/10.1016/j.talanta.2010.10.063

Yin, X., Chen, K., Cheng, H., Chen, X., Feng, S., Song, Y., & Liang, L. (2022). Chemical Stability of Ascorbic Acid Integrated into Commercial Products: A Review on Bioactivity and Delivery Technology. Antioxidants, 11(1), 153. https://doi.org/10.3390/antiox11010153

Zhou, S., Zhang, B., Sturm, E., Teagarden, D. L., Schöneich, C., Kolhe, P., Lewis, L. M., Muralidhara, B. K., & Singh, S. K. (2010). Comparative Evaluation of Disodium Edetate and Diethylenetriaminepentaacetic Acid as Iron Chelators to Prevent Metal -Catalyzed Destabilization of a Therapeutic Monoclonal Antibody. Journal of Pharmaceutical Sciences, 99(10), 4239–4250. https://doi.org/10.1002/jps.22141

Zinellu, A., Sotgia, S., Deiana, L., & Carru, C. (2006). Pre-analytical factors affecting ascorbic and uric acid quantification in human plasma. Journal of Biochemical and Biophysical Methods, 67(2–3), 95–105. https://doi.org/10.1016/j.jbbm.2006.01.006

APPLICATION OF ORGANIC FERTILIZERS FOR SUSTAINABLE AGRICULTURE

*Zhanar Yessenbayeva 1**

[1]Satbayev University; Almaty, The Republic of Kazakhstan;

Corresponding author e-mail: zh.yessenbayeva@satbayev.university

ABSTRACT

The increasing demand for environmentally sustainable agricultural practices has accelerated the development and application of organic fertilizers as alternatives to conventional mineral fertilizers. Organic fertilizers not only supply essential nutrients for plant growth but also improve soil structure, enhance microbial activity, increase organic matter content, and contribute to long-term soil fertility. This review summarizes recent advances in the application of organic fertilizers, with particular emphasis on vermicompost and innovative biocapsulated fertilizer technologies. The paper discusses the classification of organic fertilizers, their agronomic and environmental benefits, and their role in improving nutrient use efficiency while reducing nutrient losses and environmental pollution. Particular attention is given to biodegradable vermicompost-based biocapsulated fertilizers, which enable the controlled release of nutrients and support sustainable nutrient management. A conceptual model of a vermicompost-based biocapsulated fertilizer is presented to illustrate its potential as an environmentally friendly solution for enhancing soil fertility and crop productivity. The findings indicate that integrating organic fertilizers with controlled-release technologies represents a promising strategy for achieving sustainable agriculture and supporting the transition toward circular bioeconomy principles.

Keywords: organic fertilizers, sustainable agriculture, vermicompost, soil fertility, nutrient cycling, organic waste

INTRODUCTION

Agricultural intensification has substantially increased global food production over recent decades. However, the excessive use of mineral fertilizers has resulted in numerous environmental problems, including soil degradation, nutrient imbalance, water pollution, greenhouse gas emissions, and loss of soil biodiversity. Consequently, sustainable agricultural practices have become increasingly important for ensuring long-term food security while protecting natural ecosystems. Organic fertilizers represent one of the most promising approaches to sustainable crop production. Produced from plant residues, animal manure, compost, vermicompost, and other organic wastes, these materials recycle nutrients back into agricultural soils and contribute to the circular economy. Unlike synthetic fertilizers, organic fertilizers improve both the physical and biological properties of soil while gradually releasing essential nutrients. Among various organic fertilizers, vermicompost has attracted particular attention because of its high nutrient content, beneficial microorganisms, humic substances, and plant growth regulators. Numerous studies have demonstrated that vermicompost enhances seed germination, root development, nutrient uptake, and crop yield.

The aim of this review is to summarize recent advances in the application of organic fertilizers for sustainable agriculture, with particular emphasis on vermicompost and its contribution to improving soil fertility and crop productivity.

Types of Organic Fertilizers

Organic fertilizers originate from naturally occurring biological materials and vary considerably in their chemical composition and agronomic performance. Figure 1 illustrates the major types of organic fertilizers commonly used in agriculture, including farmyard manure, compost, vermicompost, green manure, poultry manure, and bio-organic fertilizers enriched with beneficial microorganisms.

Figure 4. Composition of the substrates used for vermicomposting (cattle manure, organic food waste, CaO_2, paper waste, and fallen leaves), %.

Chemical characterization of the samples was carried out to determine the content of organic matter (humus), total nitrogen (N), total phosphorus (P), and total potassium (K) in the vermicompost. The results of the chemical analysis are summarized in Table 2.

Table 2. Chemical composition of vermicompost samples.

Sample	Humus, %	Total nitrogen (N), mg kg^{-1}	Available phosphorus (P_2O_5), mg kg^{-1}	Available potassium (K_2O), mg kg^{-1}
1	34.7	66.75 ± 0.05	322 ± 0.01	1865 ± 0.8
2	33.0	236.75 ± 0.01	462 ± 0.06	1415 ± 0.5
3	41.5	393.25 ± 0.03	442 ± 0.03	2045 ± 0.9
4	23.1	1145.75 ± 0.60	407 ± 0.02	2760 ± 0.7
5	10.9	16.375 ± 0.03	422 ± 0.05	4375 ± 0.8
6	11.8	133.0 ± 0.02	417 ± 0.09	3170 ± 0.6
7	1.9	4.6 ± 0.04	32 ± 0.02	620 ± 0.07

Based on the results of the chemical analysis presented above, the vermicompost samples can be ranked according to decreasing humus content as follows: III > I > II > IV > VI > V. The difference in humus content between samples I and II was insignificant, indicating similar levels of organic matter. The highest humus content was observed in Sample III. Fallen leaves are rich in organic matter, and under favorable conditions red Californian earthworms (*Eisenia fetida*) are capable of converting up to 30% of this material into vermicompost during a single composting cycle. In contrast, the control sample exhibited considerably lower concentrations of humus and essential biogenic nutrients. These findings indicate that the activity of red Californian earthworms, together with their associated beneficial microorganisms, effectively accelerates the decomposition of organic residues and enhances the accumulation of humus as well as plant-essential nutrients in the resulting vermicompost.

CONCLUSIONS

This study demonstrated the effectiveness of vermicomposting as a sustainable biotechnology for the recycling of organic waste into high-quality organic fertilizer. Seven different substrate formulations were evaluated to investigate the influence of substrate composition on the physicochemical properties of the resulting vermicompost. The vermicomposting process, carried out over a period of 90 days using Eisenia fetida, resulted in the efficient decomposition and stabilization of organic matter under controlled environmental conditions.

The chemical analyses revealed considerable differences among the experimental treatments. Vermicompost produced from substrates containing cattle manure and plant-derived organic materials exhibited higher humus content and improved concentrations of essential nutrients, including nitrogen, phosphorus, and potassium. Spectroscopic analysis of humic and fulvic acids further indicated an increased degree of humification and structural complexity in the vermicompost compared with the initial substrate, confirming the formation of stable humic substances during the vermicomposting process. The obtained results demonstrate that substrate composition plays a crucial role in determining vermicompost quality and nutrient availability. The synergistic interaction between Eisenia fetida and associated microorganisms accelerated the transformation of organic residues into a biologically active and nutrient-rich fertilizer.

Overall, the findings confirm that vermicomposting is an environmentally friendly and economically viable approach for organic waste management. The produced vermicompost has considerable potential for improving soil fertility, enhancing nutrient cycling, and supporting sustainable agricultural production while simultaneously reducing the environmental burden associated with organic waste disposal. Future studies should focus on evaluating the long-term agronomic performance of vermicompost under field conditions and optimizing substrate formulations to maximize fertilizer quality and crop productivity.

Funding

This research was funded by the Young Scientist Project (2025-2027), grant No. AP25794509, titled «Development of biocapsulated fertilizers based on organic waste and their implementation in agriculture», supported by the Committee of Science of the Ministry of Science and Higher Education of the Republic of Kazakhstan.

REFERENCES

Brady, N.C.; Weil, R.R. *The Nature and Properties of Soils*, 15th ed.; Pearson: New York, 2017.

Principles and Applications of Soil Microbiology; Pearson Education, 2007.

Palm, C.A.; Myers, R.J.K.; Nandwa, S.M. Combined use of organic and inorganic nutrient sources for soil fertility maintenance. In: *Replenishing Soil Fertility in Africa*; SSSA Special Publication 51, 1997.

Bernal, M.P.; Alburquerque, J.A.; Moral, R. Composting of animal manures and chemical criteria for compost maturity assessment. *Bioresource Technology*. 2009, 100, 5444–5453.

Hargreaves, J.C.; Adl, M.S.; Warman, P.R. A review of the use of composted municipal solid waste in agriculture. *Agriculture, Ecosystems & Environment*. 2008, 123, 1–14.

Epstein, E. *The Science of Composting*. CRC Press, 1997.

Domínguez, J.; Edwards, C.A. Vermicomposting organic wastes: A review. In: *Soil Zoology for Sustainable Development in the 21st Century*; 2011.

Arancon, N.Q.; Edwards, C.A. *Vermiculture Technology: Earthworms, Organic Wastes, and Environmental Management*. CRC Press, 2011.

Lim, S.L.; Wu, T.Y.; Lim, P.N.; Shak, K.P.Y. The use of vermicompost in sustainable agriculture: Impact on plant growth and soil fertility. *Pedosphere*. 2015, 25, 831–846.

Atiyeh, R.M.; Arancon, N.Q.; Edwards, C.A.; Metzger, J.D. The influence of earthworm-processed pig manure on plant growth. *Bioresource Technology*. 2002, 84, 7–14.

Snapp, S.S.; Swinton, S.M.; Labarta, R. et al. Evaluating cover crops for benefits, costs and performance. *Agronomy Journal*. 2005, 97, 322–332.

Sarrantonio, M.; Gallandt, E. The role of cover crops in North American cropping systems. *Journal of Crop Production*. 2003, 8, 53–74.

Sharpley, A.N.; McDowell, R.W.; Kleinman, P.J.A. Phosphorus loss from land to water. *Plant and Soil*. 2001, 237, 287–307.
Eghball, B.; Power, J.F. Phosphorus- and nitrogen-based manure and compost applications. *Soil Science Society of America Journal*. 1999, 63, 895–901.
Vessey, J.K. Plant growth promoting rhizobacteria as biofertilizers. *Plant and Soil*. 2003, 255, 571–586.
Adesemoye, A.O.; Kloepper, J.W. Plant–microbes interactions in enhanced fertilizer-use efficiency. *Applied Microbiology and Biotechnology*. 2009, 85, 1–12.
Bashan, Y.; de-Bashan, L.E. How the plant growth-promoting bacterium *Azospirillum* promotes plant growth. *Advances in Agronomy*. 2010, 108, 77–136.
Bhattacharyya, P.N.; Jha, D.K. Plant growth-promoting rhizobacteria (PGPR): Emergence in agriculture. *World Journal of Microbiology and Biotechnology*. 2012, 28, 1327–1350.
Orlov, D.S. *Humus Acids of Soils and the General Theory of Humification*. Moscow State University Press, Moscow, Russia, 1990.
International Humic Substances Society (IHSS). Isolation of Soil Humic and Fulvic Acids. Available at: https://humic-substances.org/methods/

INFLUENCE OF REMOVING THE OUTER SCALES OF THE CORM ON THE DEVELOPMENT AND PRODUCTIVITY OF GLADIOLI

Valentin Panchev

Agricultural University - Plovdiv, 12, Mendeleev Blvd.

e-mail: valentin_panchev@abv.bg

ABSTRACT

Gladiolus are one of the main flower crops used both for cut flowers. They are growing through corms. This also determined the scope of the study. The main goal of this article is to study the influence of removing the outer scales of the corm on the growth performance of different varieties of gladioli. The experiments were conducted with three varieties of gladiolus: Amsterdam, Oasis and Fado. The corms scales were removed immediately before planting. Whole unpeeled corms, planted at the same time and scheme, were used as controls. Planting was carried out during the period 25. 03. -5.04. 2023-2025 according to the 15 x 15 cm scheme. The phenological development of plants was observed - beginning and mass emergence, formation of the first leaves, appearance of the flower stalks, beginning and end of flowering. In the full flowering phase, biometric studies were carried out – flower stalk height, number of leaves, leaf length, fresh and dry weight of leaves, leaf area, number of flowers, length and diameter of the average flower. It was found that plants from peeled corms developed more dormant buds. These plants formed more leaves, with a larger area and weight. No changes in the height of the flower stalks were observed. Phenological development was close between the two methods of cultivation. Peeling of the corms in most plants caused the formation of a larger number of flower stalks, which led to a larger total number of flowers. The Fado variety emerged with the highest decorative value.

Key words: corm, gladiolus, vegetative mass, flower, phenology

INTRODUCTION

Flower production is a leading direction in industrial floriculture, with the genus Gladiolus (Gladiolus, family Iridaceae) ranking second among the main cut flower crops worldwide (Farhat T., 2004; Raj et al., 2009; Azim et al., 2019). The crop is widespread and is grown both in the field and in greenhouse conditions (Bai et al., 2009). Its high market value is determined by its valuable decorative qualities – spectacular inflorescences with rich color diversity, erect stems and great durability (Bose et al., 2003; Manning and Peter, 2008; Memon et al., 2013; Azim, 2019).

Most modern varieties (Gladiolus x grandiflora) are complex polyhybrids obtained through interspecific hybridization (Barnard, 1972; Huxley et al., 1992). In genetic terms, combinatorial selection (Denisa et al., 2012; Hort et al., 2012) and other methods, such as the application of RAPD markers (Pragya et al., 2010), are basic research tools for assessing genetic relationships and creating new adaptive genotypes.

In Bulgaria, the majority of planting material is of Dutch origin, but successful selection programs have also been carried out in our country, leading to the creation of highly competitive local varieties, such as the variety "Iva" (Ivanova et al., 2019).

In a biotechnological aspect, propagation is complemented by in vitro methods with stem explants under the influence of growth regulators (Meira et al., 1990).

However, the expression of genetic potential depends strongly on environmental factors and the applied agrotechnics. The light regime in the "4–6 leaf" phase is particularly critical, where the deficiency slows down morphogenesis (Shillo and Halevy, 1996). Studies in our country show that later planting dates accelerate development (Kaninski et al., 2012), with mid-April being the most favorable time for planting (Ivanova et al., 2016).

The application of gibberellic acid GA_3 also has a positive effect (Suman et al., 2012). Since different varieties react specifically, continuous variety testing and quality pre-sowing preparation of the planting material are mandatory. For example, the varieties Snow-Princes/Snow White and American Beauty are much earlier flowering than the Magic variety (Kamble et al., 2004).

A major factor in production is the low natural propagation coefficient, and obtaining high-quality new corms takes several growing seasons (Bose et al., 2003; Takatsu et al., 2005; Ramzan et al., 2010). To overcome this factor and improve germination, controlled temperature storage (Carpenter et al., 1991) and pre-sowing chemical treatment with potassium nitrate KNO_3 (Ramzan et al., 2010; Mushtaq et al., 2012; Memon et al., 2013) are used.

Along with chemical and physical methods (Aladjadjiyan, 2007), mechanical effects on the structure of the planting material also play an important role. The outer dry scales of the corm perform a protective function during storage, but after planting they can act as a physical and chemical barrier (through the inhibitors contained in them), limiting the access of moisture and oxygen to the dormant bud, which delays germination. The effects of removing these scales on the biometric indicators of the aboveground biomass and underground reproductive organs are not well studied and require detailed experimental clarification. In this regard, the main objective of the present study is to study the influence of removing the outer scales of the corm on the rate of germination and subsequent development, as well as to investigate a number of phenological characteristics of different gladiolus varieties grown in Bulgarian conditions.

MATERIAL AND METHODS

The research activity was carried out during the period 2023 – 2025. in the Experimental Field and the Scientific Laboratory at the Department of Horticulture of the Agricultural University – Plovdiv, Bulgaria. The object of the study is three modern gladiolus varieties Gladiolus x grandiflora, namely the variety "*Fado*", the variety "*Oasis*" and the variety "*Amsterdam*".

The main preparation of the area began in the fall with pre-plowing application of mineral fertilizers in doses of 15 kg.da^{-1} phosphorus, in the form of triple superphosphate and 20 kg.da^{-1} potassium, in the form of potassium sulfate. This was followed by deep plowing and the formation of evenly raised beds. Fine pre-sowing cultivation of the surface layer was carried out in the spring. Twenty days before planting, pre-sowing nitrogen fertilization with ammonium nitrate in a dose of 24 kg.da^{-1} active substance nitrogen was applied.

The experiment was set up using a randomized method in three replications, with each experimental plot including 100 plants. Planting was carried out according to a 15 x 15 cm scheme in the period 5 - 10 April.

Two variants of planting material preparation were studied. The first variant was the experimental one, for which peeled corms were used. In them, the outer covering scales of the corms were removed mechanically immediately before planting in the soil. The second variant is the control one with unpeeled corms. In it, whole, structurally intact unpeeled corms were used, planted on the same day, under the same scheme and depth.

During the vegetation period, all standard and approved agrotechnical practices for the country (watering, weeding, plant protection) necessary for the normal growth and development of the plants were applied, according to the guidelines of the Institute of Ornamental and Medicinal Plants (Bistrichanov et al., 2008).

The indicators related to the phenological and vegetative development, as well as the decorative and productive qualities of the plants, were recorded during and after the vegetation. The measurements were made according to the methodology of Dimova et al. (2012), when exactly 10% of the plants in the respective plot enter the given phase. The measurements were carried out on 10 plants from each repetition, selected randomly. The obtained experimental data were subjected to mathematical and statistical processing by one-factor analysis of variance One-way ANOVA by the Fisher method, described by Fowel and Cohen (1992). The significance of the differences between the mean values was tested by the criterion for the least significant difference (LSD) at a critical significance level of p = 5.0%. Due to unidirectionality and high similarity in the trends in individual years, the final results presented in the study represent average values from the three-year experimental period.

RESULTS AND DISCUSSION

Immediately before planting, a biometric characterization of the corms was carried out, including measuring their diameter, height and weight. Table 1 shows the initial biometric indicators of the planting material. It is clear from it that the variety "*Amsterdam*" is characterized by the highest average values for all three measured indicators: corm height, diameter and weight, respectively 2.80cm, 4.10cm and 28.60g for the unpeeled controls and height 2.5cm, diameter 3.9cm and weight 27.73g for the peeled ones, and the variety "*Fado*" has the lowest values - for the unpeeled ones: height 2.2cm, diameter 2.8cm and weight 16.91g, and for the peeled ones height 1.9cm, diameter 2.7cm and weight 16.16g. After mechanical removal of the outer scales, a natural decrease in the parameters was observed in all three varieties.

Table 1. Morphological characteristics of a gladiolus corm.

Variety		**Unpeeled**			**Peeled**		
		Height (cm)	Diameter (cm)	Weight (g)	Height (cm)	Diameter (cm)	Weight (g)
1	*Fado*	2,6	3,6	26,14	2,4	3,5	25,84
2	*Oasis*	2,2	2,8	16,91	1,9	2,7	16,16
3	*Amsterdam*	2,8	4,1	28,60	2,5	3,9	27,73
LSD p=5.0%		0,28	0,48	2,02	0,33	0,33	1,06

The effect of peeling corms on the dynamics of germination and subsequent phenophases is presented in Table 2. One of the most significant results in the present study is the establishment of an accelerated germination rate in the variants with removed outer scales. In peeled corms, all phenophases occur on average 2-3 days earlier compared to the control. The earliest germinates the variety "*Fado*", followed by the varieties "*Oasis*" and "*Amsterdam*" respectively 25, 27 and 32 days for the control and 21, 25 and 28 days for peeled corms. This effect is due to the elimination of the mechanical barrier of the dry scales and the facilitation of the entry of moisture and oxygen to the corm. The trend is similar for the appearance of the first, third leaf and flowering stem.

Table 2. Phenological observation of different gladiolus varieties (days after sprouting).

Variety		*Fado*	*Oasis*	*Amsterdam*	LSD p=5.0%
Unpeeled	Sprouting*	25	27	32	2,0
	Appearance of First leaf	11	16	9	2,0
	Appearance of Third leaf	22	29	19	2,0
	Appearance of flower stalk	43	48	53	2,75
Peeled	Sprouting*	21	25	28	2,0
	Appearance of First leaf	9	14	7	2,0
	Appearance of Third leaf	21	26	18	2,0
	Appearance of flower stalk	41	46	50	2,0

*Days after planting

The accelerated vegetative start in the peeled variants also reflects directly on the generative development. The flowering start phase in the peeled bulbs is earlier, as can be seen from Table 3. The earliest of the peeled bulbs to start flowering is the '*Fado*' variety at 89 days after germination, followed by the '*Oasis*' variety - 94 days and the '*Amsterdam*' variety - 102 days, while in the unpeeled ones this happens at 91, 95 and 104 days respectively. Since all three tested varieties show a specific varietal reaction, the flowering duration is almost identical in both variants with a difference of only one day. The '*Fado*' variety has the shortest flowering, with the peeled ones lasting 61 days and the unpeeled ones - 62. The '*Oasis*' variety has a flowering duration of 63 and 64 days, respectively for unpeeled and peeled corms. Plants from peeled bulbs of the *Amsterdam* variety bloom the longest - 67 days. In the unpeeled variety, the variety retains its superiority with a flowering duration of 66 days. As a result of the faster start of flowering and the varietal specificity, the end of flowering phase also occurs earlier.

Table 3. Phenological observation of different gladiolus varieties (days after sprouting).

Variety		**Unpeeled**			**Peeled**		
		Begging of flowering	End of flowering	Flowering duration	Begging of flowering	End of flowering	Flowering duration
1	*Fado*	91	153	62	89	150	61
2	*Oasis*	95	158	63	94	158	64
3	*Amsterdam*	104	170	66	102	169	67
LSD p=5.0%		2,0	2,75	3,33	3,16	2,00	4,21

Removing the scales reduces the delay in the initial development of the plants, while at the same time increasing the number of developed dormant buds, and this is evident from Table 4. In all studied varieties, a tendency towards the formation of a larger number of flowering stalks is observed, with the control having average values of 1.2 for the "*Fado*" variety, 1.6 for the "*Oasis*" variety and 2.4 for the "*Amsterdam*" variety, while in the peeled varieties the values for the varieties are 3.4, 3.6 and 3.9, respectively. In terms of height, diameter and mass of the flower stalk, the reported data show a negligible difference between the control and experimental variants, but we can still summarize that the values for these indicators for the flowering stems that emerged from unpeeled corms are higher than those of the unpeeled ones,

with the exception of the "*Oasis*" variety with a stem height of 105.4 cm in the peeled ones and 104.6 in the control.

Table 4. Morphological characteristics of the flower stalk.

Variety		*Fado*	*Oasis*	*Amsterdam*	LSD p=5.0%
Unpeeled	Number of developed flower stalks	1,2	1,6	2,4	0,8
	Heigh of a flower stalk (cm)	97,1	104,6	127,7	1,9
	Diameter of a flower stalk (cm)	2,4	2,2	2,6	0,2
	Weight of a flower stalk (g)	37,8	40,6	46,3	1,74
Peeled	Number of developed flower stalks	3,4	3,6	3,9	1,42
	Heigh of a flower stalk (cm)	96,5	105,4	127,3	2,65
	Diameter of a flower stalk (cm)	2,3	2,1	2,5	0,2
	Weight of a flower stalk (g)	37,4	40,1	45,9	1,59

The data in Table 5 indicate that the removal of the scales has a strong stimulating effect on the number of leaves. In peeled bulbs, a greater number of leaves per plant is recorded compared to unpeeled ones, approximately three times more. In plants from the experimental variant of the "*Fado*" variety, their number is 24.8, unlike the control - only 8.3 pcs. In the "*Oasis*" variety, the readings are similar, and in the "*Amsterdam*" variety, the values are the highest - 11.3 pcs for the control and 33.6 pcs for the tested variant. A direct relationship is noted with the number of flower stalks formed. At the expense of the number of leaves, all other studied indicators, namely leaf area, length, width, fresh and dry mass, show smaller values in the variant with peeled corms, but the differences are insignificant.

Table 5. Morphological characteristics of the leaves.

Variety		*Fado*	*Oasis*	*Amsterdam*	LSD p=5.0%
Unpeeled	Number of leaves	8,3	9,0	11,3	1,44
	Weight of a leaf (g)	13,4	9,1	11,6	1,41
	Leaf area (cm^2)	210,1	112,6	157,3	1,9
	Leaf dry mass (g)	2,6	1,3	1,9	0,49
	Length of a leaf (cm)	76,5	60,2	68,5	9,15
	Width of a leaf (cm)	3,5	2,6	3,2	1,04
Peeled	Number of leaves	24,8	27,2	33,6	7,08
	Weight of a leaf (g)	13,2	7,7	9,8	0,86
	Leaf area (cm^2)	208,3	108,8	149,2	1,95
	Leaf dry mass (g)	2,4	1,1	1,5	0,54
	Length of a leaf (cm)	75,1	60,6	67,6	9,26
	Width of a leaf (cm)	3,4	2,3	2,9	1,12

The number of developed flowers in the spike inflorescence has been shown to decrease in plants grown from peeled bulbs. As can be seen in Table 6, in the control they are 12.3 pcs, 11.1 pcs and 16.2 pcs respectively for the varieties "*Fado*", "*Oasis*" and "*Amsterdam*", and in the experimental variant they are 11.8 pcs, 10.4 pcs and 14.6 pcs respectively. The length, diameter and mass of the single flower are affected in the same way. In the "*Fado*" variety, the length of the flower is 9.5 cm in the control variant and only 9.1 cm for the experimental variant. Similar data were recorded for the "*Oasis*" variety - the length is 10.2 cm in the control and only 9.8 cm in the experimental variant. The largest difference was recorded for the "*Amsterdam*" variety, where the data are 9.6 cm and 8.8 cm respectively. The data are similar for the other indicators.

Table 6. Morphological characteristics of the flowers.

Variety		*Fado*	*Oasis*	*Amsterdam*	LSD p=5.0%
Unpeeled	Number of flowers	12,3	11,1	16,2	0,82
	Length of a flower (cm)	9,5	10,2	9,6	0,86
	Diameter of a flower (cm)	10,1	11,4	10,7	0,85
	Weight of a flower (g)	7,4	6,1	6,8	0,86
Peeled	Number of flowers	11,8	10,4	14,6	0,79
	Length of a flower (cm)	9,1	9,8	8,8	0,63
	Diameter of a flower (cm)	9,7	11,1	9,9	1,52
	Weight of a flower (g)	7,1	5,7	6,2	1,03

CONCLUSIONS

Based on the three-year study conducted on the influence of pre-sowing removal of the covering scales in the gladiolus varieties "*Fado*", "*Oasis*" and "*Amsterdam*", the following important conclusions can be made:

1. Mechanical peeling of corms immediately before planting eliminates the protective barrier of dry scales, thus shortening the germination time and accelerating the entry into the various phenophases.

2. Removal of the scales stimulates the development of more dormant buds, which leads to a powerful increase in the total number of flowering stalks and in direct correlation with the increased number of leaves.

3. As a result of removing the outer scales of the corm, the total productivity increases at the expense of the single flower. Redistributed energy leads to a higher total number of flowers per plant, but is reflected in a slight, statistically insignificant decrease in the dimensions (length, diameter and mass) of the single leaves and flowers.

4. The three studied varieties respond specifically to the applied manipulation. The variety "*Amsterdam*" retains the highest absolute values in terms of total vegetative and generative biomass, while the variety "*Fado*" emerges as the earliest flowering variety with the highest decorative value.

REFERENCES

Aladjadjiyan, A. (2007) - Research the connections between vitality and physical properties at carrots (Daucus carota L.), Nantes variety, treated with ultrasound and laser rays. Scientific works of Bulgarian Union of the Scienties, III, 128-133.

Azim, M. H. (2019). Progeny test of crosses among different cultivars of gladiolus. Journal of plant production, agronomy, breeding and horticulture, 41(4), 29-44

Bai, J., J.L. Carrion-I-Silvestre, 2009. Structural changes, common stochastic trends, and unit roots in panel data. The Review of Economic Studies, 76(2), 471-501.

Barnard, T.T. (1972). On hybrids and hybridization. In: Lewis, G.J., Obermeyer, A.A. & Barnard, T.T. Gladiolus, a revision of the South African species. Journal of South Africa Botany, 10, 304–310.

Bistrichanov, S., Ivanova, I., Kaninski, A. (2008). Technology for cut flower production in gladiolus in the open, approved by the Expert Council of the Academy of Agricultural Science. Protocol №14/10.04.2008 (Bg).

Bose, T.K., Yadav, L.P. & Pal, P. 2003. Gladiolus. In: Commercial Flowers. Department of Horticulture, Bidhan Chandra Krishi. Naya Prokash,1-33.

Carpenter, W.J., Wilfret, G.J., Cornell, J.A. (1991). Temperature and relative humidity govern

Denisa, H. O. R. A., Cantor, M., Erzsebet, B. U. T. A., Andriescu, I. (2012). Researches regarding intraspecific hybridization of Gladiolus L. species in order to obtain novel ornamental varieties. Bulletin of University of Agricultural Sciences and Veterinary Medicine Cluj-Napoca. Horticulture, 69(1).

Dimova, D., E. Marinkov, 2012. Experimental design and biometry, Publish house of Agricultural University-Plovdiv, 65-79 (Bg).

Farhat, T. (2004). Plant characteristic and vase life of gladiolus flowers as influenced by the preharvest and npk application and postharvest chemical treatment. M.Sc. (hons). thesis, Pmas-Aaur, 1-22.

Fowel J., L. Cohen. (1992). Practical statistics for field biology. John Wiley & Sons, New York. 227 pages. Germination and storage of gladiolus seed. Hortscience, 26(8), 1054-1057.

Horţ, D., Cantor, M., Buta, E. & Andriescu, I. (2012). Researches regarding intraspecific hybridization of Gladiolus L. Species in order to obtain novel ornamental varieties. Bulletin of the University of Agricultural Sciences and Veterinary Medicine Cluj-Napoca. Horticulture, 69(1), 172-177.

Huxley, A., Griffiths, M. & Levy, M. (1992). Gladiolus. In: eds. Griffiths, M. & Huxley, A.J The new royal horticultural society dictionary of gardening, New York: Stockton Press, 2, 25-45.

Ivanova, I., Kaninski, A., & Galeva, A. 2019. Iva - a new Bulgarian variety of gladiolus. Bulgarian Journal of Crop Science, 56(5).

Ivanova, Iv., Ivanova, V., Dimitrov, D. (2016). Influence of planting data on growth and cut flowers of gladiolus. Dcoratyviuju ir sodo augalu sortimento, technologiju ir aplinkos optimizimizavis Mokso darbai, vol. 7(12), 142-145.

Kamble, B. S., Reddy, B. S., Patil, R. L. T., Kulkarni, B. S. (2004). Performance of gladiolus (Gladiolus hybridus Hort.) cultivars for flowering and flower quality. Journal of Ornamental Horticulture, volume 7, Issue 3 and 4, 51-56.

Kaninski, A., Ivanova, I., Galeva, A., 2012. Ekaterina – New Bulgarian variety, Plant science. XLIX, No 3, 64-67.

Manning, J & Peter, G. (2008). The Iris Family. Natural History & Classification. Portland, Oregon, USA. Timber Press, 138–142.

Meira, Z., Halevy A. H., Shilo, R., 1990, Organs and Plantlets Regeneration of Gladiolus through Tissue Culture., Annals of Botany Company, Volume 34, Issue 3, 671–676.

Memon, S. A., Baloch, A. R., Baloch, M. A., Keerio, M. I. (2013). Pre-soaking treatment and foliar application of KNO3 on growth and flower production of gladiolus (Gladiolus hortulanus). Journal of Agricultural Technology, Vol. 9(5): 1347-1366

Mushtaq, S., Ishfaq, A. H., Syed, Z, Ul, H., Muhammad, A., Muhammad, A. S., Rizwan R., Misbah, R., Muhammad, A., Muhammad, S. I. (2012). Evaluation of seed priming on germination of Gladiolus alatus. African journal of biotechnology, 11(52), 11520-11523.

Pragya, K., Bhat,V., Misra, R. L., Ranjan, J. K., 2010. Analysis of diversity and relationships among Gladiolus cultivars using morphological and RADP markers. Indian Journal of Agricultural Science, 80(9), 766-72.

Raj, S. K., Srivastava, A., Chandra, G. & Singh, B. P. (2009). Characterization of cucumber mosaic virus isolate infecting Gladiolus cultivars and comparative evaluation of serological and molecular methods for sensitive diagnosis. Current science, 83(9), 1132-1137.

Ramzan, A., Hafiz, I. A., Ahmad, T. & N. Abbasi, A. (2010). Effect of priming with potassium nitrate and dehusking on seed germination of gladiolus (Gladiolus alatus) Pakistan Journal of Botany, 42(1): 247-258.

Shillo, R. A., Halevy, H., 1996, The effect of various environmental factors on flowering of gladiolus. I. Light intensity. Scientia Horticulturae,Volume 4, Issue 2, Pages 131-137.

Takatsu. Y., Suzuki, K., Yamada, T., Inoue, E., Gonai, T., Nogi, M., Kasumi, M. (2005). Interspecific hybridization of wild gladiolus species using a dendrogram based rapid analysis. Proceeding of IX International Symposium on Flower Bulbs, ISHS. Eds.: Okubo, H., Miller, W.B. & Chastagner, G.A., Acta Horticulturae, 673, 475-480.

RESEARCH ON THE SPECIFICITY OF BIOCHEMICAL PATHWAYS IN ARCHAEA

Bihter Sude ARCA[1], Emirhan TULUMTAŞ[1], Cihat ÇELİK[2,], Ender BÜYÜKGÜZEL[3], Kemal BÜYÜKGÜZEL[1]*

[1] Zonguldak Bülent Ecevit University, Department of Biology, Science Faculty, Zonguldak TR-67100, Türkiye
[2] Zonguldak Bülent Ecevit University, Çaycuma Food and Agriculture Vocational School, Department of Chemistry and Chemical Processing Technologies, Zonguldak TR-67900, Türkiye
[3] Zonguldak Bülent Ecevit University, Department of Molecular Biology and Genetics, Science Faculty, Zonguldak TR-67100, Türkiye
Corresponding author e-mail: cihatcelik1@gmail.com

ABSTRACT

For many years, archaea were categorized alongside bacteria due to their structural similarities. However, the work of Carl R. Woese in the 1970s revealed their distinct molecular structures, establishing these organisms as one of the three domains of life (Bacteria, Archaea, and Eukaryota). While metabolic pathways are generally well-conserved in other domains, archaea have been found to possess variant pathways containing various novel enzymes with a different control mechanism. This difference, in particular, involves specific biochemical mechanisms involving deviations from central carbohydrate metabolism, classical glycolysis, and pentose phosphate pathways. Central carbohydrate metabolism is fundamental to energy production and biosynthetic activities in living organisms. Currently, research on glycolytic enzymes from various phylogenetic lineages has revealed a structure composed of canonical and novel enzymes in archaeal variants of the Embden-Meyerhof-Parnas (EMP) and Entner-Doudoroff (ED) pathways. These differences are known to be pronounced in species resistant to extreme conditions such as high temperatures, high salinity, extreme pH, and high pressure. Archaeal metabolic systems include kinases that utilize ADP instead of ATP, ferredoxin-dependent oxidoreductases, and phosphorylation-independent energy conversion mechanisms. These characteristics have demonstrated that archaeal enzymes hold significant potential for biotechnological applications. Furthermore, due to their high resilience, archaea are used as fundamental model organisms in astrobiology research. From a broad perspective, this study addresses the discovery process of archaea, their resistance mechanisms to extreme conditions, fundamental biochemical differences in central carbohydrate metabolism derived from molecular and genetic data, as well as the structure, function, enzymatic constituents, and regulation of archaeal glycolytic pathways. Additionally, current biotechnological application fields and their potential roles in space research are evaluated.

Keywords: Archaea, Carbohydrate metabolism, Embden-Meyerhof-Parnas pathway, Entner-Doudoroff pathway, ADP-dependent kinases.

INTRODUCTION

Until the last quarter of the 20th century, the phylogenetic and evolutionary classification of life was fundamentally understood within the framework of the prokaryote-eukaryote

dichotomy. Due to their similar microscopic morphological characteristics and cellular dimensions, archaea were classified alongside prokaryotes/bacteria for many years. However, in the late 1970s, small subunit ribosomal RNA (16S/18S rRNA) sequence analyses conducted by Carl R. Woese and George E. Fox revealed that these organisms are distinct from both bacteria and eukaryotes at the molecular level. Today, building upon this evolutionary discovery, Woese et al. redefined the cellular organization of life, definitively demonstrating that living organisms consist of three primary domains at the cellular level: Bacteria, Archaea, and Eukaryota (Woese and Fox, 1977; Woese et al., 1990). While fundamental metabolic pathways and cellular processes are known to be highly conserved phylogenetically in bacteria and eukaryotes, archaea stand out due to the unique metabolic strategies they have developed throughout evolutionary history. In archaea, variant metabolic pathways containing numerous novel enzymes with distinct catalytic regulatory mechanisms have been identified. These unique differences become particularly pronounced in central carbohydrate metabolism, which is critically important for basic cellular energy production. Archaea possess specific biochemical mechanisms involving alternative intermediates and distinct enzymatic catalysts that show marked deviations from classical glycolysis and pentose phosphate pathways. Advancing technologies and recent research focusing on the glycolytic enzymes of phylogenetic lineages have unveiled a complex network composed of both canonical and non-canonical enzymes within the archaeal variants of the classical Embden-Meyerhof-Parnas (EMP) and Entner-Doudoroff (ED) pathways. It has become clear that these metabolic innovations are especially prominent in extremophilic species adapted to harsh environmental conditions that push the boundaries of life, such as extreme temperature (hyperthermophilia), high salinity (extreme halophilia), extreme pH values (extreme acidophilia/alkaliphilia), and high hydrostatic pressure (piezophilia). From a biochemical perspective, archaeal metabolic systems diverge significantly from conventional phosphorylation processes. For instance, specific kinases that utilize ADP instead of ATP in glycolytic steps, the use of ferredoxin-dependent oxidoreductases as reducing equivalents instead of NAD(P)+, and energy conversion mechanisms that bypass phosphorylation steps constitute key characteristic features of this group. These adaptations in archaea indicate a high potential for biotechnological, industrial, and pharmaceutical applications, owing to the resilience of archaeal enzymes under harsh industrial conditions. Furthermore, the robust resistance mechanisms exhibited by archaea in the Earth's most challenging ecosystems have made them essential model organisms in astrobiological research aimed at searching for life in extraterrestrial environments.

Although archaea were initially confused with bacteria due to their morphologically anucleate and organelle-lacking structures, they exhibit a profile close to eukaryotes in terms of genetic information processing mechanisms, while completely diverging from both groups in their unique membrane lipid chemistry (Woese et al., 1990; Siebers and Schönheit, 2005). While bacterial and eukaryotic membranes contain straight-chain fatty acids linked to a glycerol-3-phosphate (G3P) backbone via ester bonds, archaeal membranes feature isoprenoid (diphytanyl or phytanyl) chains attached to a glycerol-1-phosphate (G1P) backbone via ether linkages. These ether bonds and isoprenoid rings enable the cell membranes of hyperthermophilic archaea to maintain structural integrity and prevent proton leakage even under extreme temperature and extreme pH conditions (Koga and Morii, 2007). Furthermore, peptidoglycan (murein), the key structural component of the bacterial cell wall, is absent in archaea; instead, structures such as pseudomurein, S-layers (proteinaceous surface layers), or heteropolysaccharides are present.

From a metabolic perspective, archaea possess an exceptionally broad spectrum of life strategies, including chemosynthesis, fermentation, autotrophy, and heterotrophy. They constitute the dominant life forms in the most challenging ecosystems of the biosphere (Sato

and Atomi, 2011). However, molecular ecology and metagenomic studies have proven that archaea are not restricted to extreme environments; they are also widespread in ocean surface waters, temperate soils, and even within the human microbiota (DeLong, 1992).
It was previously assumed that central carbohydrate metabolism, which is responsible for cellular energy production and the synthesis of structural building blocks in other domains of life, was strictly conserved throughout evolutionary history. However, biochemical and genomic investigations in archaea have demonstrated that these canonical pathways harbor numerous unusual modifications and entirely novel enzyme families (Verhees et al., 2003; Bräsen et al., 2014).

Molecular And Bıochemıcal Features Unıque To Archaea

To understand archaeal metabolism, it is essential to first comprehend the primary phylogenetic groups constituting this domain and their molecular adaptations. Currently, based on phylogenomic analyses and genomic data, archaea are classified within Euryarchaeota, the TACK supergroup (Thaumarchaeota, Aigarchaeota, Crenarchaeota, Korarchaeota), the Asgard supergroup (such as Lokiarchaeota) branching from TACK, and the cellularly/genomically reduced DPANN supergroup.
The majority of biochemical and metabolic studies have focused on the two initially discovered primary phyla, Euryarchaeota and Crenarchaeota. Euryarchaeota represents a metabolically highly heterogeneous group that encompasses extreme halophiles, methanogens, and certain hyperthermophiles. Species within this group frequently utilize modified mEMP and modified mED pathways for glucose catabolism, distinct from classical routes, and possess enzymatic mechanisms such as ADP-dependent glucokinase/phosphofructokinase or non-phosphorylating GAPDH. Crenarchaeota, on the other hand, predominantly consists of hyperthermophilic and acidophilic species; these organisms possess energy and carbon metabolisms adapted to harsh thermophilic conditions, such as sulfur oxidation/reduction or branched ED pathways. On the other hand, the discovery of novel phyla, particularly those included within the TACK and Asgard supergroups, has demonstrated that archaeal metabolism is not solely restricted to adaptation to extreme conditions. Eukaryotic Signature Proteins (ESPs), which form the foundation of eukaryotic cellular complexity, membrane remodeling, and vesicular mechanisms, have been identified within the genomes of these archaea. This finding proves that the ancestral molecular systems governing intracellular trafficking and organellar dynamics originally emerged in archaea (Spang et al., 2015).
From the perspective of biochemical adaptations, hydrophobic core packing, salt bridges, disulfide bonds, and oligomeric complexations, which confer protein stability in archaea exposed to extreme temperatures and pressures, are particularly noteworthy. To prevent intracellular metabolites from undergoing thermal degradation at elevated temperatures, such as the isomerization and degradation of triose-phosphates or 1,3-bisphosphoglycerate, archaea have evolved alternative pathway adaptations that bypass canonical glycolytic steps or incorporate high-affinity, stable enzymes (Verhees et al., 2003).

CENTRAL CARBOHYDRATE METABOLISM AND GLYCOLYTIC DEVIATIONS

The classical glycolytic pathway (EMP) serves as the fundamental catabolic route conserved across all bacterial and eukaryotic systems, generating a net yield of 2 moles of ATP and 2 moles of NADH during the conversion of 1 mole of glucose into 2 moles of pyruvate. In the canonical EMP pathway, hexoses are phosphorylated by hexokinase (HK) or glucokinase (GLK), converted to fructose-6-phosphate (F6P) by phosphoglucose isomerase (PGI), and subsequently transformed into fructose-1,6-bisphosphate (F1,6BP) through phosphofructokinase (PFK). F1,6BP is then cleaved into dihydroxyacetone phosphate (DHAP)

and glyceraldehyde-3-phosphate (GAP) by fructose-1,6-bisphosphate aldolase (FBPA) (Nelson and Cox, 2000). In archaea, however, this process follows biocatalytic steps that diverge markedly from classical paradigms (Verhees et al., 2003; Bräsen et al., 2014).

Modified Embden-Meyerhof-Parnas (EMP) Pathway

Glucose catabolism proceeds through a modified EMP pathway in model organisms, particularly the anaerobic hyperthermophilic euryarchaeota *Pyrococcus furiosus* and *Thermococcus kodakarensis*, alongside the microaerophilic crenarchaeote *Thermoproteus tenax* (Selig et al., 1997; Siebers and Schönheit, 2005; Verhees et al., 2003). The principal points of divergence in this modified pathway comprise the following steps:

Glucose Phosphorylation: ADP-Dependent Glucokinases and ROK Hexokinases

While classical glycolysis consumes ATP to phosphorylate glucose, most hyperthermophilic archaea utilize ADP-dependent glucokinase (ADP-GLK) as the phosphate donor instead of ATP. First identified in *Pyrococcus furiosus*, the ADP-GLK enzyme converts glucose into glucose-6-phosphate (G6P) while releasing AMP (Kengen et al., 1995).

ADP-GLK enzymes belong to the ribokinase superfamily. Crystal structure analyses revealed that these enzymes share no sequence or fold homology with ATP-dependent hexokinases (Ito et al., 2001). This preference for ADP allows glycolytic flux to continue uninterrupted even under severe stress conditions where the intracellular ATP/ADP ratio declines. Conversely, glucose phosphorylation remains ATP-dependent in crenarchaeal species such as *Aeropyrum pernix* and *Thermoproteus tenax*, though the reaction is catalyzed by broad-substrate-specificity hexokinases belonging to the ROK family (Hansen et al., 2002).

Isomerization and Phosphofructokinase Deviations (ADP-PFK, PP_i-PFK)

Beyond the classical bacterial and eukaryotic PGI enzymes, two novel isomerase classes involved in the conversion of G6P to F6P have been identified in archaea: bifunctional PGI/PMI (which also exhibits phosphomannose isomerase activity) and cupin-type PGI (cPGI), a metalloenzyme structure (Hansen et al., 2002; Hansen et al., 2005). The active center of cPGI enzymes contains Fe^{2+} or Ni^{2+} ions and displays no sequence similarity to classical PGIs.

The key regulatory step of glycolysis, the conversion of F6P to F1,6BP, proceeds irreversibly via ATP-dependent phosphofructokinase (PFK-A) in canonical systems. In archaea, two principal unconventional alternatives exist:

ADP-Dependent Phosphofructokinase (ADP-PFK): In Pyrococcus and Thermococcus species, F6P phosphorylation is likewise driven by ADP (F6P + ADP → F1,6BP + AMP) (Tuininga et al., 1999). The identification of ADP-PFK and ADP-GLK enzymes confirmed that the preparatory phase of glycolysis in hyperthermophilic Euryarchaeota relies entirely on ADP.

Pyrophosphate-Dependent Phosphofructokinase (PP_i-PFK): In *Thermoproteus tenax*, F6P is phosphorylated using inorganic pyrophosphate (PP_i). This reaction is reversible, functioning bidirectionally in both glycolysis and gluconeogenesis depending on the cellular energy charge (Siebers et al., 1998).

Glyceraldehyde-3-Phosphate Oxidation: Non-Phosphorylating GAPDH (GAPN) and GAPOR

The most radical biochemical deviation within the archaeal EMP pathway occurs during the oxidation of triose phosphates (GAP). In classical glycolysis, GAP is oxidized to 1,3-bisphosphoglycerate (1,3BPG) by GAPDH with the incorporation of inorganic phosphate (P_i), followed by substrate-level phosphorylation (SLP) catalyzed by PGK to generate ATP. In most hyperthermophilic archaea, the 1,3BPG intermediate exhibits extreme thermal instability, possessing a half-life of merely a few seconds at elevated temperatures. Consequently, archaea

have evolved two distinct enzymatic mechanisms that completely bypass the formation of 1,3BPG (Bräsen et al., 2014):

-Non-Phosphorylating Glyceraldehyde-3-Phosphate Dehydrogenase (GAPN): Converts GAP directly and irreversibly into 3-phosphoglycerate (3PG). The reaction consumes no P_i and yields no ATP synthesis, instead reducing $NADP^+$ or NAD^+ to form NAD(P)H (Reher et al., 2007).

-GAP:Ferredoxin Oxidoreductase (GAPOR): Present in anaerobic hyperthermophiles such as *Pyrococcus furiosus*, this enzyme contains iron-sulfur (Fe-S) clusters and a tungsten-pterin center, coupling GAP oxidation directly to the reduction of ferredoxin (Fd) (Mukund and Adams, 1995). The operation of GAPN or GAPOR eliminates the 2 moles of ATP typically generated by the classical GAPDH/PGK enzymatic pair. This substitution reduces the net ATP yield of the modified EMP pathway to zero or negative values (Selig et al., 1997).

Modified Entner-Doudoroff (ED) Pathway Variants

In bacteria such as *Pseudomonas* species, the classical ED pathway relies on the oxidation of glucose to gluconate, its subsequent phosphorylation to form 2-keto-3-deoxy-6-phosphogluconate (KDPG), and the cleavage of KDPG into pyruvate and GAP via KDPG aldolase. In archaea, however, the ED pathway diverges into two principal modified variants (Ahmed et al., 2005; Siebers and Schönheit, 2005):

Semi-phosphorylated ED Pathway

Operating in organisms such as *Halobacterium salinarum*, *Haloferax volcanii*, and *Thermoplasma acidophilum*, this route begins with the oxidation of glucose to gluconate by glucose dehydrogenase (GDH), followed by dehydration to 2-keto-3-deoxygluconate (KDG) via gluconate dehydratase (GAD). At this stage, KDG undergoes phosphorylation by ATP-dependent KDG kinase (KDGK) to yield KDPG, which is subsequently cleaved into 1 mole of pyruvate and 1 mole of GAP by KDPG aldolase (KDPGA). The resulting GAP is then processed down to pyruvate through modified EMP pathway enzymes (Reher et al., 2007).

Non-phosphorylated ED Pathway

Identified in extreme thermoacidophilic crenarchaeotes such as *Sulfolobus solfataricus* and *Sulfolobus acidocaldarius*, this pathway involves no phosphorylated intermediates. Following the formation of KDG, KDG aldolase (KDGA) directly cleaves non-phosphorylated KDG into pyruvate and non-phosphorylated glyceraldehyde (GA). GA is subsequently oxidized to glycerate by glyceraldehyde dehydrogenase (DH), phosphorylated to 2-phosphoglycerate (2PG) by glycerate kinase, and ultimately converted to pyruvate via enolase and pyruvate kinase steps (Lamble et al., 2003). The net ATP yield of this non-phosphorylated pathway is zero.

Pentose Metabolism and Pentose Phosphate Pathway Deviations

The classical pentose phosphate pathway (PPP) represents the primary metabolic network supplying ribose-5-phosphate (R5P) for nucleotide synthesis and NADPH for biosynthetic reducing power. In most archaea, however, the oxidative phase of the classical PPP, involving glucose-6-phosphate dehydrogenase and 6-phosphogluconate dehydrogenase, is entirely absent (Bräsen et al., 2014). Instead, archaea rely on reversed non-oxidative PPP steps or unique alternative pathways, such as hexulose-6-phosphate synthase (HPS) and 3-hexulose-6-phosphate isomerase (PHI) replacing transaldolase, to synthesize pentoses (Soderberg, 2005). For pentose catabolism, they employ specialized dehydratase and dehydrogenase cascades operating through dicarboxylic acid intermediates, which diverge completely from bacterial systems.

Bıotechnologıcal Applıcatıons And Astrobıologıcal Potentıal Of Archaea

Enzymes exhibiting high stability obtained from archaea (extremozymes) offer significant operational advantages in industrial biotechnology (Özkan and Başbülbül, 2021). Archaeal amylases, glucoamylases, and pullulanases involved in carbohydrate metabolism retain their catalytic activity even under elevated temperatures (>90°C), extreme pH levels, and in the presence of organic solvents. For instance, amylolytic enzymes derived from Pyrococcus species eliminate cooling costs during industrial starch processing by simultaneously reducing viscosity and hydrolyzing starch into glucose at high temperatures (Vieille and Zeikus, 2001). Similarly, ADP-dependent glucokinases (ADP-GLK) exhibit prolonged shelf life and exceptional stability as enzymatic components in commercial biosensor kits used for blood glucose quantification and analytical measurement of clinical ATP/ADP ratios (Sakuraba et al., 2002). Furthermore, promiscuous archaeal isomerases and aldolases providing broad substrate specificity facilitate high selectivity and yield in the industrial-scale biosynthesis of high-value rare sugars from aldoses.

Astrobiology is an interdisciplinary field investigating the origin, evolution, and distribution limits of life in the universe. The remarkable resilience of archaea toward hostile environmental conditions, alongside their non-canonical metabolic pathways, renders them primary model organisms in extreme environment simulations (Rothschild and Mancinelli, 2001; DasSarma et al., 2020).

CONCLUSIONS

Research on central carbohydrate metabolism in archaea demonstrates that metabolic flexibility and evolutionary adaptability across life are far broader than previously recognized. The archaeal variants of classical EMP and ED pathways feature highly unique biocatalysts, including ADP-dependent kinases, cupin-type isomerases, GAPN, and GAPOR. These modifications enable the bypass of thermally unstable intermediates under extreme environmental conditions while optimizing cellular energy balance. As genome editing technologies become more broadly implemented in archaeal systems, future investigations will elucidate the functions of currently uncharacterized archaeal enzymes.

REFERENCES

Ahmed, H., Ettema, T. J., Tjaden, B., Geerling, A. C., Van Der Oost, J., Siebers, B. (2005). The semi-phosphorylative Entner–Doudoroff pathway in hyperthermophilic archaea: a re-evaluation. Biochemical Journal, 390(2): 529-540.

Bräsen, C., Esser, D., Rauch, B., Siebers, B. (2014). Carbohydrate metabolism in Archaea: current insights into unusual enzymes and pathways and their regulation. Microbiology and Molecular Biology Reviews, 78(1): 89-175.

DasSarma, S., DasSarma, P., Laye, V. J., Schwieterman, E. W. (2020). Extremophilic models for astrobiology: haloarchaeal survival strategies and pigments for remote sensing. Extremophiles, 24(1): 31-41.

DeLong, E. F. (1992). Archaea in coastal marine environments. Proceedings of the National Academy of Sciences, 89(12): 5685-5689.

Hansen, T., Reichstein, B., Schmid, R., Schönheit, P. (2002). The first archaeal ATP-dependent glucokinase, from the hyperthermophilic crenarchaeon Aeropyrum pernix, represents a monomeric, extremely thermophilic ROK glucokinase with broad hexose specificity. Journal of Bacteriology, 184(21): 5955-5965.

Hansen, T., Schlichting, B., Felgendreher, M., Schönheit, P. (2005). Cupin-type phosphoglucose isomerases (Cupin-PGIs) constitute a novel metal-dependent PGI family representing a convergent line of PGI evolution. Journal of Bacteriology, 187(5): 1621-1631.

Ito, S., Fushinobu, S., Yoshioka, I., Koga, S., Matsuzawa, H., Wakagi, T. (2001). Structural basis for the ADP-specificity of a novel glucokinase from a hyperthermophilic archaeon. Structure, 9(3): 205-214.

Kengen, S. W., Tuininga, J. E., de Bok, F. A., Stams, A. J., de Vos, W. M. (1995). Purification and Characterization of a Novel ADP-dependent Glucokinase from the Hyperthermophilic Archaeon *Pyrococcus furiosus*. Journal of Biological Chemistry, 270(51): 30453-30457.

Koga, Y., Morii, H. (2007). Biosynthesis of ether-type polar lipids in archaea and evolutionary considerations. Microbiology and Molecular Biology Reviews, 71(1): 97-120.

Lamble, H. J., Heyer, N. I., Bull, S. D., Hough, D. W., Danson, M. J. (2003). Metabolic pathway promiscuity in the archaeon *Sulfolobus solfataricus* revealed by studies on glucose dehydrogenase and 2-keto-3-deoxygluconate aldolase. Journal of Biological Chemistry: 278(36), 34066-34072.

Mukund, S., Adams, M. W. (1995). Glyceraldehyde-3-phosphate ferredoxin oxidoreductase, a novel tungsten-containing enzyme with a potential glycolytic role in the hyperthermophilic archaeon *Pyrococcus furiosus*. Journal of Biological Chemistry: 270(15), 8389-8392.

Nelson, D. L., Cox, M. M. (2000). Lehninger principles of biochemistry (Vol. 631, pp. 842-843). New York: Worth publishers.

Özkan, G., Başbülbül, G. (2021). Diversity of thermophilic archaea and their biotechnological uses. Biological Diversity and Conservation, 14(1): 155-166.

Reher, M., Gebhard, S., Schönheit, P. (2007). Glyceraldehyde-3-phosphate ferredoxin oxidoreductase (GAPOR) and nonphosphorylating glyceraldehyde-3-phosphate dehydrogenase (GAPN), key enzymes of the respective modified Embden–Meyerhof pathways in the hyperthermophilic crenarchaeota *Pyrobaculum aerophilum* and *Aeropyrum pernix*. FEMS Microbiology Letters, 273(2): 196-205.

Rothschild, L. J., Mancinelli, R. L. (2001). Life in extreme environments. Nature, 409(6823): 1092-1101.

Sakuraba, H., Yoshioka, I., Koga, S., Takahashi, M., Kitahama, Y., Satomura, T., Kawakami, R., Ohshima, T. (2002). ADP-dependent Glucokinase/Phosphofructokinase, a Novel Bifunctional Enzyme from the Hyperthermophilic Archaeon *Methanococcus jannaschii*. Journal of Biological Chemistry, 277(15): 12495-12498.

Sato, T., Atomi, H. (2011). Novel metabolic pathways in Archaea. Current Opinion in Microbiology, 14(3): 307-314.

Selig, M., Xavier, K. B., Santos, H., Schönheit, P. (1997). Comparative analysis of Embden-Meyerhof and Entner-Doudoroff glycolytic pathways in hyperthermophilic archaea and the bacterium *Thermotoga*. Archives of Microbiology, 167(4): 217-232.

Siebers, B., Klenk, H. P., Hensel, R. (1998). PPi-dependent phosphofructokinase from *Thermoproteus tenax*, an archaeal descendant of an ancient line in phosphofructokinase evolution. Journal of Bacteriology, 180(8): 2137-2143.

Siebers, B., Schönheit, P. (2005). Unusual pathways and enzymes of central carbohydrate metabolism in Archaea. Current Opinion in Microbiology, 8(6): 695-705.

Soderberg, T. I. M. (2005). Biosynthesis of ribose-5-phosphate and erythrose-4-phosphate in archaea: a phylogenetic analysis of archaeal genomes. Archaea, 1(5): 347-352.

Spang, A., Saw, J. H., Jørgensen, S. L., Zaremba-Niedzwiedzka, K., Martijn, J., Lind, A. E., ... Ettema, T. J. (2015). Complex archaea that bridge the gap between prokaryotes and eukaryotes. Nature, 521(7551): 173-179.

Tuininga, J. E., Verhees, C. H., van der Oost, J., Kengen, S. W., Stams, A. J., de Vos, W. M. (1999). Molecular and biochemical characterization of the ADP-dependent phosphofructokinase from the hyperthermophilic archaeon *Pyrococcus furiosus*. Journal of Biological Chemistry, 274(30): 21023-21028.

Verhees, C. H., Kengen, S. W., Tuininga, J. E., Schut, G. J., Adams, M. W., De Vos, W. M., Oost, J. V. D. (2003). The unique features of glycolytic pathways in Archaea. Biochemical Journal, 375(2): 231-246.
Vieille, C., Zeikus, G. J. (2001). Hyperthermophilic enzymes: sources, uses, and molecular mechanisms for thermostability. Microbiology and Molecular Biology Reviews, 65(1): 1-43.
Woese, C. R., Fox, G. E. (1977). Phylogenetic structure of the prokaryotic domain: the primary kingdoms. Proceedings of the National Academy of Sciences, 74(11): 5088-5090.
Woese, C. R., Kandler, O., Wheelis, M. L. (1990). Towards a natural system of organisms: proposal for the domains Archaea, Bacteria, and Eucarya. Proceedings of the National Academy of Sciences, 87(12): 4576-4579.

BIFUNCTIONAL CoFe2O4-ZnS:Mn CORE-SHELL NANOPARTICLES FOR NANOSCIENCE APPLICATIONS

Yeliz AKPINAR[1*]

[1] *Kırşehir Ahi Evran University, Art and Science Faculty, Department of Chemistry, Kırşehir, Türkiye*
Corresponding author e-mail: yeliz.akpinar@ahievran.edu.tr

ABSTRACT

In recent years, bifunctional nanomaterials with magnetic and optical properties have gained considerable attention in nanomedicine, especially for nanoscience applications. Materials show different properties at the nanoscale than at bulk size. In addition, as size decreases, nanoparticles develop richer surface properties. For example, a higher surface-to-volume ratio provides a larger surface area, increasing functional efficiency. Therefore, quantum dots (QDs) and magnetic nanoparticles are commonly used for their unique properties. Conventional quantum dots often contain highly toxic heavy metals, such as cadmium, which restricts their clinical translation. Manganese-doped zinc sulfide (ZnS:Mn) quantum dots have been developed to overcome this drawback and are a biocompatible, cadmium-free substitute with stable luminescence. In this study, we synthesized core-shell $CoFe_2O_4$-ZnS:Mn QD nanocomposites through co-precipitation and then successfully developed a dual-modal imaging platform. SEM morphology showed that the composite structure consisted of ZnS:Mn quantum dots inside the cobalt ferrite magnetic nanoparticles. Also, the Fluorescence spectra showed a strong and characteristic orange-pink emission around 630-700 nm, which corresponds to the 4T1→6A1 transition of Mn2+ ions. The coexistence of a strong magnetic response and bright luminescence indicates that these cadmium-free core-shell nanostructures are promising for targeted drug delivery and concurrent optical/magnetic resonance imaging.

Keywords: Nanoscience, Quantum Dots, Magnetic Nanoparticles

INTRODUCTION

Currently, nanotechnology is a hot topic in science. These researchs have led to the development of goods and methods that improve the efficiency of everyday life. The development of nanoscience is being driven by a number of issues, including the need for renewable energy sources, the identification and treatment of novel illnesses, and the growing need for food due to population expansion. The basic building elements of the scientific method of product development are nanostructures. Nano-sized materials are very helpful in biological research due to their special characteristics(Ahmad et al., 2025; Dowling, 2004; Hughes et al., 2025) .

Magnetic nanoparticles (MNPs) are a rapidly expanding class of metal nanoparticles (NPs) that have sparked a revolution in materials science due to their unique combination of advantageous properties, including high surface-to-volume ratio, superparamagnetism, size-dependent properties, and quantum confinement effects, with conventional bulk material characteristics(Chand & Vasquez-Guardado, 2025) . The weak plasmonic optical properties of magnetic nanoparticles limit their use in applications such as imaging. The absence of plasmonic properties, meaning they do not emit fluorescence when exposed to light at a specific wavelength, prevents their use as sensors. To overcome this limitation, composite structures

were developed. Magnetic nanoparticles were combined with molecules or nanoparticles that have plasma or fluorescence emission properties, making them multifunctional(Corr et al., 2008). The aim was to perform both magnetic applications such as MRI, hyperthermia, and magnetic targeting, and optical applications such as SERS detection and fluorescence detection, simultaneously(Mir et al., 2025; Sirgedaite et al., 2023; Wolfbeis, 2015).

Quantum dots (QDs) are semiconductor particles with optical and electronic (optoelectronic) characteristics that vary with size and composition. QDs are very tiny, usually ranging in size from 1.5 to 10.0 nm. QD nanotechnology has recently made significant inroads into a number of biological and electrical areas. Because of their special qualities—such as excellent photostability, size-dependent optical characteristics, high brightness and extinction coefficient, and significant Stokes shift—QDs have been shown to be effective. Due to their limited ability to display all of these characteristics, organic dyes or fluorophore molecules are unsuitable for many imaging and biosensing applications. Furthermore, because of their enormous surface area, ultrasmall QDs may provide additional benefits over another type nanomareials for creating multimodal/multifunctional probes(Bera et al., 2010; Maxwell et al., 2020) . Quantum dots based on cadmium are generally used due to their high emission properties. However, because cadmium-containing quantum dots are not stable under UV light, there is a possibility of cadmium ions leaching into the environment. Since cadmium has high toxicity, its use for biomedical purposes is problematic. Therefore, Cd-based quantum dots are coated with Zn-derived quantum dots. Alternatively, for biomedical applications, Zn and Mn-based or carbon-based quantum dots with lower toxicity are used (Hardman, 2006; Lin & Chen, 2023).

In the literature, nanocomposites containing multifunctional magnetic particles and quantum dots have been produced for this purpose. Some of these include: Wang et al. Fe_2O_3 Beads−CdSe/ZnS Quantum Dots nanocomposite(Wang et al., 2004); Xu et al. Fe_3O_4/SiO_2 and water-soluble CdSe−ZnS quantum dots (QDs) nanocopmpsite. (Xu et al., 2010); Tadesse et al. nitrogen doped carbon quantum dots/magnetite nanocomposites (Tadesse et al., 2018), and Bunkoed et al. graphene quantum dots and magnetite nanoparticles embedded in molecularly imprinted polymer (GQDs@Fe_3O_4/MIP) nanocomposites(Bunkoed et al., 2020).

In this study, Cobalt ferrite magnetic nanoparticles were modified with ZnS:Mn quantum dots. Quantum dots provided fluorimetric properties to magnetic nanoparticles

METHOD

1.) $CoFe_2O_4$ nanoparticles (MNPs) were created via co-precipitation. A 1:2 mole solution of $CoCl_2$ and $FeCl_3$ salts was prepared in a flask and mixed with a NaOH solution at 80°C for an hour. The resulting black particles were gathered using a magnet, and a solution of water was used for three magnetic washing processes. After that, it was dissolved in 50 mL deionized water (Roy et al., 2024)

2.) 1.0 ml $CoFe_2O_4$ nanoparticle (MNP) solutions were added to 10.0 ml 0.025 M Zn(NO3)2 and Mn(NO3)2 mixed solution.After 1 hour of mixing, 0.1 M Na2S solution was added to the previous solution. After 12 hours of mixing in a dark room, a gray-brownish precipitate was obtained and washed with dı water three times using a magnet.Finally, nanoparticles were dispersed in water. Supernatant was disposed of.

3.) To demonstrate the effect of nanocomposite ratios in optimization studies, the experiment was performed twice separately by adding 1.0 and 2.0 ml of magnetic particle solution to equal amounts of Zn and Mn ion mix solutions.

RESULTS AND DISCUSSION

The adherence of quantum dots to the magnetic nanoparticle surface was checked using a UV lamp. First, it was observed that the prepared ZnS:Mn QDs composites gave an orange color under UV light at a wavelength of 365 nm (Figure 1a). Then, the prepared nanocomposite was visualized in daylight and under UV light at the same wavelength. The color, which was light gray-brown under daylight, appeared orange-pink under UV light (Figure 1b and 1c).

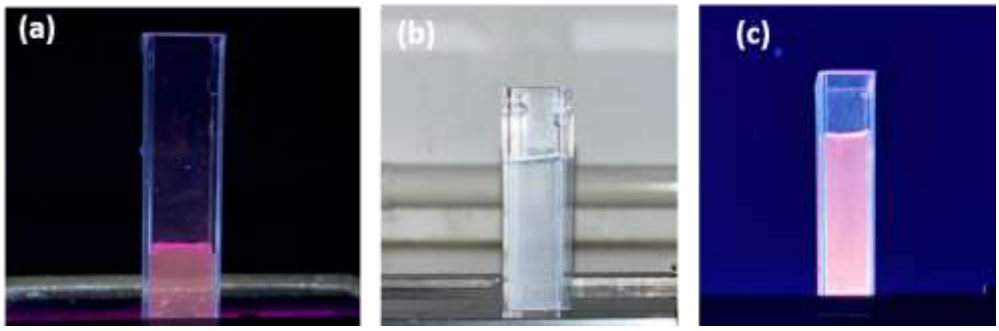

Figure 1. Image of a.) ZnS:Mn QDs under UV light, b.) Nanocomposite under solar light, c) nanocomposites under UV light.

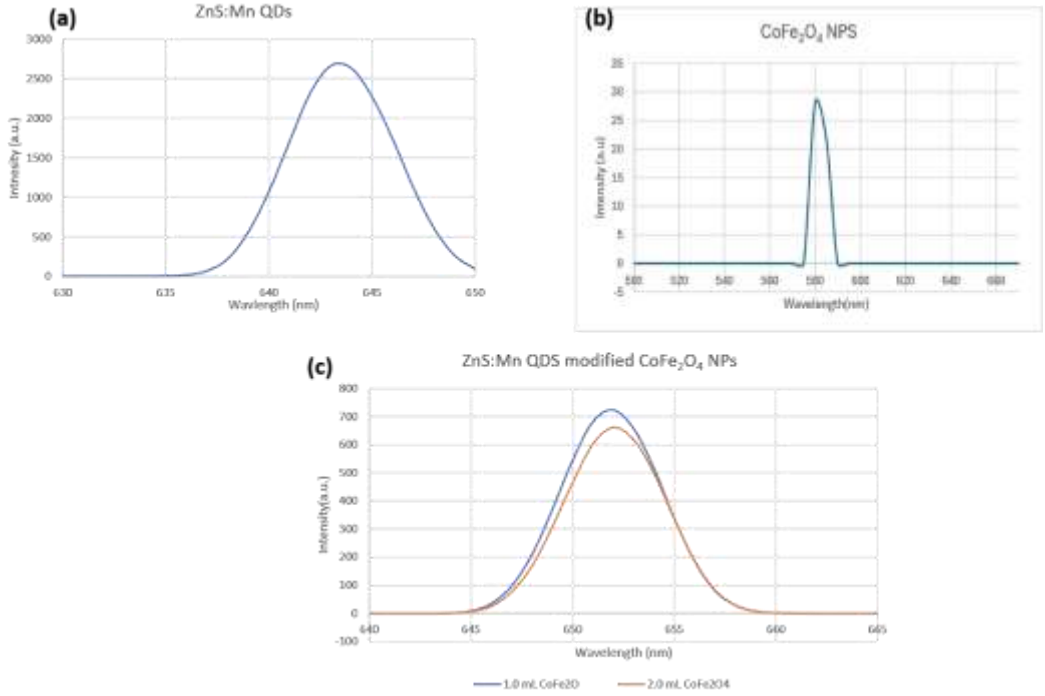

Figure 2. Emission spectrum of a.) ZnS:Mn quantum dots, b) $CoFe_2O_4$ NPs c.) ZnS:Mn quantum dots modified magnetic nanoparticles

Fluorescence Spectroscopy (FL) was used for emission measurements. For measurements, a quartz cell was used, and the device was adjusted to 320 nm excitation wavelength. ZnS:Mn quantum dots give emission at 642 nm(Figure 2a). These results are consistent with the literature (Patel et al., 2020). The fluorescence emission spectrum shown in Figure 2b corresponds to the prepared cobalt ferrite nanoparticles. It exhibits a peak at 580 nm that is either absent or negligibly weak. This wavelength does not coincide with the emission

wavelength of ZnS:Mn quantum dots. ZnS:Mn quantum dots modified magnetic nanoparticles(nanocomposite) emitted at 652 nm. The wavelength shifted with agglomeration (Figure 2c). In addition, the emission intensity decreased significantly due to quenching caused by agglomeration of the magnetic nanoparticles. For optimization, we used 1.0 mL (blue line) and 2.0 mL (orange line) magnetic nanoparticles during synthesis, separately. Figure 2c indicated that there is no significant difference. As a result, the ratio of components is not effective for this method.

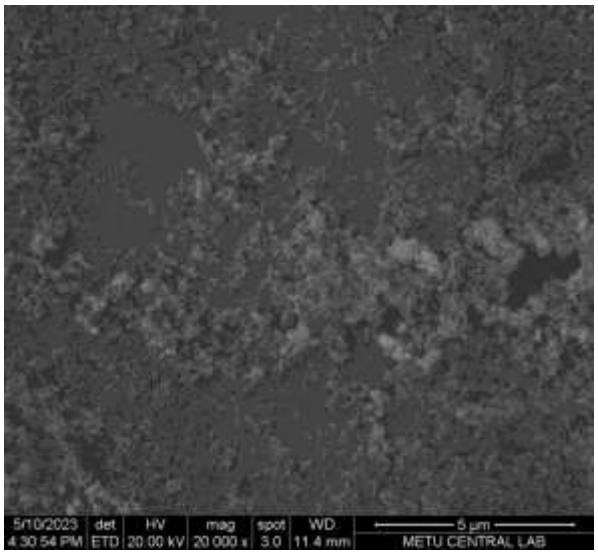

Figure 3. SEM images of ZnS:Mn quantum dots modified magnetic nanoparticles(Nanocomposites)

Figure 3 shows the SEM image of the prepared nanocomposite. In the image, the dark gray particles are magnetic nanoparticles, and the light gray particles are quantum dots attached to the magnetic particles.

CONCLUSIONS

This study aimed to produce a bifunctional nanomaterial by combining two different nanomaterials solely through adsorption, without the need for any interconnecting groups and an extra reaction step. The goal was to obtain a core-shell structure, but SEM images showed that the core-shell structure was not fully formed. Instead, a randomly distributed composite structure was formed. Fluorescence spectroscopy measurements and UV light beams showed that quantum dots in the structure adhered to the magnetic particle surface. In the future, other combination methods will be tried to produce more efficient emissions and a core-shell structure. Several techniques, including TEM, Zeta Potentiometer, VSM, and FTIR Spectroscopy, will improve characterization. The stability of the nanocomposite will also be tested. The produced particles will be used in imaging, biomedical applications,water splitting, and dye degradation as catalysts.

REFERENCES

Ahmad, K., Ahmad, R., Faizan, M., Farah, Ali, F., Yousaf, M. M., Ali, F., Niaz, W., Khan, T. U., Khan, S., Ali, S., Ahmed, I., & Hassan, H. (2025). A review of nanotechnology in food

industry with implication for viable outlook and safety issues. *Hybrid Advances, 10,* 100487. https://doi.org/10.1016/j.hybadv.2025.100487

Bera, D., Qian, L., Tseng, T.-K., & Holloway, P. H. (2010). Quantum Dots and Their Multimodal Applications: A Review. *Materials*, *3*(4), 2260–2345. https://doi.org/10.3390/ma3042260

Bunkoed, O., Raksawong, P., Chaowana, R., & Nurerk, P. (2020). A nanocomposite probe of graphene quantum dots and magnetite nanoparticles embedded in a selective polymer for the enrichment and detection of ceftazidime. *Talanta*, *218*, 121168. https://doi.org/10.1016/j.talanta.2020.121168

Chand, K., & Vasquez-Guardado, E. S. (2025). Magnetic Nanoparticles: Synthesis and Applications in Life Sciences. *ChemistryOpen*, *14*(12). https://doi.org/10.1002/open.202500214

Corr, S. A., Rakovich, Y. P., & Gun'ko, Y. K. (2008). Multifunctional Magnetic-fluorescent Nanocomposites for Biomedical Applications. *Nanoscale Research Letters*, *3*(3), 87. https://doi.org/10.1007/s11671-008-9122-8

Dowling, A. P. (2004). Development of nanotechnologies. *Materials Today*, *7*(12), 30–35. https://doi.org/10.1016/S1369-7021(04)00628-5

Hardman, R. (2006). A Toxicologic Review of Quantum Dots: Toxicity Depends on Physicochemical and Environmental Factors. *Environmental Health Perspectives*, *114*(2), 165–172. https://doi.org/10.1289/ehp.8284

Hughes, K. J., Ganesan, M., Tenchov, R., Iyer, K. A., Ralhan, K., Diaz, L. L., Bird, R. E., Ivanov, J., & Zhou, Q. A. (2025). Nanoscience in Action: Unveiling Emerging Trends in Materials and Applications. *ACS Omega*, *10*(8), 7530–7548. https://doi.org/10.1021/acsomega.4c10929

Lin, X., & Chen, T. (2023). A Review of in vivo Toxicity of Quantum Dots in Animal Models. *International Journal of Nanomedicine*, *Volume 18*, 8143–8168. https://doi.org/10.2147/IJN.S434842

Maxwell, T., Nogueira Campos, M. G., Smith, S., Doomra, M., Thwin, Z., & Santra, S. (2020). Quantum Dots. In *Nanoparticles for Biomedical Applications* (pp. 243–265). Elsevier. https://doi.org/10.1016/B978-0-12-816662-8.00015-1

Mir, A., Dashti, H., & Huyeh, M. R. (2025). Optical properties of magneto-plasmonic nanoparticles chain of Fe_3O_4@SiO_2@Ag and their sensing applications. *Scientific Reports*, *16*(1), 1506. https://doi.org/10.1038/s41598-025-31439-7

Patel, J., Jain, B., Singh, A. K., Susan, Md. A. B. H., & Jean-Paul, L. (2020). Mn-Doped ZnS Quantum dots–An Effective Nanoscale Sensor. *Microchemical Journal*, *155*, 104755. https://doi.org/10.1016/j.microc.2020.104755

Roy, P., Hoque, S. M., Akter, S., Liba, S. I., & Choudhury, S. (2024). Study on the chemical co-precipitation synthesized $CoFe_2O_4$ nanoparticle for magnetocaloric performance in the vicinity of superparamagnetic blocking temperature. *Heliyon*, *10*(14), e34413. https://doi.org/10.1016/j.heliyon.2024.e34413

Sirgedaite, G., Talaikis, M., Niaura, G., & Mikoliunaite, L. (2023). Magneto-plasmonic nanostructures for SERS: magnetite decorated by silver and gold nanoparticles. *New Journal of Chemistry*, *47*(1), 402–411. https://doi.org/10.1039/D2NJ04368H

Tadesse, A., RamaDevi, D., Hagos, M., Battu, G., & Basavaiah, K. (2018). Synthesis of nitrogen doped carbon quantum dots/magnetite nanocomposites for efficient removal of methyl blue dye pollutant from contaminated water. *RSC Advances*, *8*(16), 8528–8536. https://doi.org/10.1039/C8RA00158H

Wang, D., He, J., Rosenzweig, N., & Rosenzweig, Z. (2004). Superparamagnetic Fe_2O_3 Beads−CdSe/ZnS Quantum Dots Core−Shell Nanocomposite Particles for Cell Separation. *Nano Letters*, *4*(3), 409–413. https://doi.org/10.1021/nl035010n

Wolfbeis, O. S. (2015). An overview of nanoparticles commonly used in fluorescent bioimaging. *Chemical Society Reviews*, *44*(14), 4743–4768. https://doi.org/10.1039/C4CS00392F

Xu, Y., Karmakar, A., Wang, D., Mahmood, M. W., Watanabe, F., Zhang, Y., Fejleh, A., Fejleh, P., Li, Z., Kannarpady, G., Ali, S., Biris, A. R., & Biris, A. S. (2010). Multifunctional Fe_3O_4 Cored Magnetic-Quantum Dot Fluorescent Nanocomposites for RF Nanohyperthermia of Cancer Cells. *The Journal of Physical Chemistry C*, *114*(11), 5020–5026. https://doi.org/10.1021/jp9103036

BIOMECHANICAL FORCES GENERATED BY ORTHODONTIC APPLIANCES IN THE TREATMENT OF DENTAL AND SKELETAL MALOCCLUSIONS: A NARRATIVE REVIEW

Mirana BORIÇI[1], Çeljana TOTI[2], Rozarta NEZAJ[2]

[1]Department of Dentistry, Faculty of Medical Sciences, Albanian University, Tirana
[2]Faculty of Dental Medicine, University of Medicine, Tirana

Corresponding author e-mail: rozartanezaj@gmail.com

ABSTRACT

Background: Orthodontic treatment relies on controlled mechanical forces to modify tooth position and correct dental and skeletal malocclusions. Their clinical effects depend on force magnitude, direction, duration, point of application, force–moment relationships, anchorage, and biological tissue response. **Aim:** This narrative review examines the biomechanical forces generated by commonly used orthodontic appliances and their relationship with biological response and the management of dental and skeletal malocclusions. **Material and Method:** Peer-reviewed literature addressing orthodontic biomechanics, force–moment relationships, biological mechanisms of tooth movement, anchorage, and appliance-generated force systems was narratively reviewed. Evidence concerning fixed appliances, elastics and springs, temporary skeletal anchorage devices (TADs), and clear aligners was considered and synthesized according to biomechanical principles and clinical applications. **Results and Discussion:** Orthodontic force systems determine the pattern of tooth movement through interactions among force, moment, and the center of resistance. Mechanical loading induces biological responses involving the periodontal ligament and alveolar bone, including cellular activity, inflammatory signaling, bone resorption, and bone formation. Fixed appliances provide versatile three-dimensional control, while elastics and springs introduce additional force vectors. TADs enhance skeletal anchorage, whereas clear aligners generate forces and moments through appliance deformation and tooth–aligner interaction. Available evidence remains heterogeneous regarding optimal force magnitude and the predictability of newer appliance systems. **Conclusions:** Effective orthodontic treatment requires integration of malocclusion characteristics, desired tooth movement, force–moment relationships, anchorage requirements, appliance selection, and biological response. A biomechanically informed approach may facilitate controlled treatment, while further clinical research is needed to establish the predictability of emerging technologies.

Keywords: Orthodontic biomechanics; Orthodontic forces; Orthodontic appliances; Malocclusion; Orthodontic tooth movement; Anchorage; Clear aligners.

INTRODUCTION

Orthodontic treatment relies on the controlled application of mechanical forces to modify tooth position and correct dental and skeletal malocclusions. The clinical effect of an orthodontic force is determined by its magnitude, direction, point of application, and duration, together with the moment generated around the tooth and the characteristics of the supporting tissues (Hocevar, 1981; Proffit et al., 2018).

Orthodontic biomechanics provides the mechanical basis for predicting and controlling tooth movement. A force applied to a tooth may produce translation, rotation, or a combination of these movements, depending on the relationship between its line of action and the center of resistance (Hocevar, 1981). Consequently, orthodontic tooth movement should not be considered simply as a response to force magnitude; rather, it reflects the complete force–moment system acting on the tooth and its supporting structures.

The biological response is equally important. Mechanical loading of the periodontal ligament produces cellular, vascular, inflammatory, and molecular responses that contribute to periodontal ligament adaptation and alveolar bone remodeling (Asiry, 2018; Li et al., 2018; Li et al., 2021). Tooth movement therefore represents a dynamic interaction between mechanical stimulation and biological tissue response.

Different orthodontic appliances are capable of generating different force systems. Fixed appliances allow interaction between brackets and archwires, while elastics, springs, temporary skeletal anchorage devices (TADs), and clear aligners provide additional or alternative mechanisms for force delivery (Proffit et al., 2018; Dalessandri et al., 2014; Park et al., 2021; Iliadi et al., 2019). The selection and activation of these systems should be related to the desired tooth movement and anchorage requirements.

The treatment of malocclusion further illustrates the importance of biomechanical planning. Sagittal, vertical, transverse, and space-related discrepancies may require different force vectors and anchorage strategies. Consequently, patients within the same broad malocclusion category may have substantially different biomechanical requirements.

The aim of this narrative review is to examine the biomechanical forces generated by commonly used orthodontic appliances and their relationship with biological tissue response and the clinical treatment of dental and skeletal malocclusions. The review specifically addresses fundamental force–moment relationships, biological mechanisms associated with orthodontic tooth movement, appliance-generated force systems, anchorage considerations, and the clinical implications of these principles for individualized orthodontic treatment planning.

MATERIALS AND METHODS

This work was conducted as a narrative review of peer-reviewed scientific literature addressing orthodontic biomechanics and the biological response to orthodontic forces.

The literature was considered according to four interconnected areas: fundamental biomechanical principles, biological mechanisms of orthodontic tooth movement, force systems generated by orthodontic appliances, and clinical application in the treatment of malocclusion.

Relevant literature concerning force magnitude and direction, force–moment relationships, periodontal and alveolar responses, fixed orthodontic appliances, elastics, springs, skeletal anchorage, and clear aligner systems was considered. Particular emphasis was placed on established biomechanical literature, systematic reviews, and clinically relevant studies addressing the mechanical and biological mechanisms of orthodontic tooth movement (Hocevar, 1981; Theodorou et al., 2019; Dalessandri et al., 2014; Iliadi et al., 2019).

The evidence was synthesized narratively rather than quantitatively. Findings were interpreted in relation to the intended type of tooth movement, anchorage requirements, appliance characteristics, and biological response. No meta-analysis or pooled effect calculation was undertaken because the purpose of this review was to provide an integrated clinical overview rather than a quantitative estimate of treatment effects.

As a narrative review, the present work does not claim to represent an exhaustive systematic review of all available literature. Instead, it provides a focused synthesis of established biomechanical and biological concepts and contemporary evidence relevant to orthodontic force application and the treatment of malocclusion.

RESULTS AND DISCUSSION

Fundamental Biomechanical Principles

Orthodontic biomechanics describes the mechanical principles governing the application of forces to teeth and their supporting structures. Its clinical purpose is to establish a predictable relationship between an applied force system and the resulting tooth movement (Hocevar, 1981; Proffit et al., 2018).

A force applied to a tooth can produce translational and/or rotational effects depending on its magnitude, direction, and line of action. When the line of action does not pass through the center of resistance, a moment is generated. The combined control of force and moment is therefore fundamental to determining the resulting pattern of tooth movement (Hocevar, 1981).

The center of resistance represents a theoretical point within the tooth-supporting system at which application of a force can produce translational movement. Its position is influenced by the morphology of the tooth and the characteristics of its periodontal support. The center of rotation, in contrast, is determined by the applied force–moment system and changes according to the relationship between force and moment (Hocevar, 1981).

The moment-to-force (M/F) relationship is an important determinant of orthodontic tooth movement. Changes in this ratio alter the center of rotation and consequently influence whether movement is predominantly tipping, translation, or root movement (Hocevar, 1981; Proffit et al., 2018). This relationship is particularly relevant during space closure, torque expression, intrusion, extrusion, and movements requiring accurate root positioning.

Force Magnitude and Duration

The biological and mechanical effects of orthodontic force are influenced by both force magnitude and duration. Current evidence does not support a single universally optimal force magnitude for every type of orthodontic movement (Theodorou et al., 2019).

A systematic review concluded that forces between 50 and 100 cN may be appropriate for bodily orthodontic tooth movement, patient comfort, and potentially fewer side effects. However, the authors emphasized substantial methodological heterogeneity and weak-to-moderate evidence, indicating that these findings should not be interpreted as a universal force prescription (Theodorou et al., 2019).

Accordingly, force selection should be related to the intended movement, appliance characteristics, anchorage requirements, and biological response rather than to an isolated numerical value.

Anchorage

Anchorage refers to resistance to unwanted movement of teeth or other anatomical structures during orthodontic treatment. Because orthodontic force systems generate reciprocal reactions, control of these reactive forces is essential for achieving the intended treatment objective (Proffit et al., 2018).

Conventional anchorage relies primarily on teeth and their supporting structures. TADs provide an additional source of skeletal anchorage and have expanded the range of force systems available when conventional anchorage is insufficient (Dalessandri et al., 2014; Park et al., 2021).

Clinical success of TADs is influenced by patient-, device-, and management-related factors. Their use therefore remains dependent on appropriate biomechanical and clinical planning.

Biological Response to Orthodontic Forces

Orthodontic tooth movement results from a coordinated biological response to mechanical loading of the periodontal ligament and surrounding alveolar tissues. Application of an orthodontic force changes the mechanical environment of the periodontal ligament and initiates cellular, vascular, inflammatory, and molecular responses involved in tissue remodeling (Asiry, 2018; Li et al., 2018; Li et al., 2021).

Mechanical loading produces areas of compression and tension and modifies cellular activity, extracellular matrix organization, and local tissue signaling (Li et al., 2018; Li et al., 2021).

Orthodontic tooth movement depends on coordinated remodeling of the periodontal ligament and alveolar bone. Mechanical loading can initiate inflammatory and cellular responses that participate in bone resorption and formation (Asiry, 2018; Li et al., 2018; Li et al., 2021).

Osteoclast-mediated bone resorption contributes to tooth displacement in areas subjected to appropriate mechanical and biological stimuli, while osteoblast activity contributes to bone formation and adaptation (Li et al., 2018; Li et al., 2021).

The RANK/RANKL/OPG system has an important role in regulating osteoclast differentiation and activity during orthodontic tooth movement (Yamaguchi, 2009). Inflammatory and signaling mediators also participate in the tissue response to orthodontic loading (Asiry, 2018; Li et al., 2021).

The relationship between orthodontic force and biological response cannot be reduced to a simple linear relationship between force magnitude and rate of tooth movement. The response depends on the type of movement, force characteristics, tissue condition, and individual biological variability (Li et al., 2021; Theodorou et al., 2019).

Root resorption is one clinically relevant adverse outcome associated with orthodontic tooth movement, although its occurrence is multifactorial and cannot be attributed to force magnitude alone (Weltman et al., 2010).

Biomechanical Forces Generated by Orthodontic Appliances

Fixed Orthodontic Appliances

Fixed appliances provide a versatile system for controlling tooth movement through interactions between brackets, archwires, and auxiliary components. The resulting force and moment systems are influenced by archwire dimensions and material properties, bracket geometry, activation, and tooth position (Proffit et al., 2018).

During alignment, flexible archwires can generate forces for correction of displaced and rotated teeth. As treatment progresses, stiffer archwires and auxiliary mechanics may be used to improve three-dimensional control and facilitate torque expression and root positioning.

Elastics and Springs

Elastics and springs provide additional force vectors that can be incorporated into orthodontic mechanics. Interarch elastics may generate sagittal and vertical components, and their effects depend on attachment sites and direction of application. Because these systems generate reciprocal forces, appropriate anchorage control is essential (Proffit et al., 2018).

Elastomeric materials may undergo force degradation during clinical use. A systematic review demonstrated that orthodontic elastomeric power chains undergo force decay over time, which may influence their mechanical performance (Halimi et al., 2012).

Springs may be incorporated into fixed appliance systems for space opening, space closure, distalization, or other controlled movements. Their mechanical characteristics depend on material properties, activation, geometry, and deactivation behavior.

Temporary Anchorage Devices

TADs have expanded the biomechanical possibilities of orthodontic treatment by providing skeletal anchorage when conventional dental anchorage may be insufficient. Their use can facilitate movements such as intrusion, distalization, mesialization, and retraction while reducing reliance on reciprocal dental movement (Dalessandri et al., 2014; Park et al., 2021).

The biomechanical advantage of TADs depends on their position, stability, direction of force application, and relationship to the desired tooth movement. Clinical success is also influenced by patient-, device-, and treatment-related factors.

Skeletal anchorage therefore does not eliminate the need for biomechanical planning; instead, it provides an additional anchorage point from which force and moment systems can be designed.

Clear Aligner Systems

Clear aligners generate orthodontic forces through elastic deformation of the appliance and its interaction with individual teeth. The resulting forces and moments depend on aligner

geometry, material properties, tooth morphology, planned movement, and auxiliary features such as attachments.

A systematic review and meta-analysis evaluated the forces and moments generated by aligner-type appliances for different orthodontic tooth movements. The evidence was based on in-vitro laboratory studies, and the authors emphasized that the findings should be interpreted within the specific experimental conditions. Tipping and rotation were among the most frequently examined movements (Iliadi et al., 2019).

Recent evidence has also investigated the combined use of clear aligners and temporary skeletal anchorage devices for selected complex tooth movements, including intrusion, extrusion, and distalization. However, the evidence remains relatively limited. A 2025 systematic review identified 14 records for qualitative analysis and emphasized the need for further research to optimize clinical outcomes (Marinelli et al., 2025).

Application of Biomechanical Principles to Malocclusion

The clinical application of orthodontic biomechanics becomes particularly relevant when mechanical principles are translated into treatment strategies for specific malocclusion patterns. Conventional classifications provide a useful description of sagittal, vertical, and transverse discrepancies, but they do not independently determine the mechanical strategy required for correction.

Sagittal Malocclusions

Class II and Class III malocclusions represent common sagittal discrepancies, but their biomechanical management varies according to the relative contribution of dental and skeletal components.

In Class II treatment, interarch elastics can generate combinations of sagittal and vertical force components and may contribute to correction through reciprocal dental effects. Their use therefore requires appropriate anchorage control and consideration of the resultant force vector (Proffit et al., 2018).

Class III correction similarly depends on the underlying diagnosis. Dental Class III relationships may be addressed through controlled dentoalveolar compensation, whereas skeletal Class III discrepancies may require orthopedic or surgical approaches depending on growth status and severity.

Vertical Malocclusions

Vertical malocclusions require careful control of intrusive and extrusive force systems. Deep-bite correction may involve incisor intrusion, posterior extrusion, or a combination of movements depending on facial pattern, incisor position, and periodontal conditions.

Intrusion is particularly sensitive to the location and direction of the applied force. Skeletal anchorage has expanded the possibility of applying intrusive forces with reduced dependence on conventional dental anchorage (Dalessandri et al., 2014; Park et al., 2021).

Open-bite correction presents a different biomechanical challenge. Depending on the underlying etiology, treatment may involve anterior extrusion, posterior intrusion, dentoalveolar compensation, growth modification, or orthognathic intervention.

Transverse Malocclusions

Transverse discrepancies may involve dental, dentoalveolar, or skeletal components. This distinction is important because dental expansion primarily modifies tooth inclination and dentoalveolar relationships, whereas skeletal expansion aims to modify the transverse skeletal relationship.

The biomechanical response to expansion is influenced by age, skeletal maturity, appliance design, activation protocol, and periodontal anatomy. The choice of expansion mechanism should therefore consider the source and magnitude of the discrepancy.

Crowding and Space Management

Crowding may be managed through combinations of arch development, interproximal enamel reduction, distalization, space redistribution, or extraction, depending on severity and distribution.

Following extraction, space closure requires careful control of anchorage and incisor movement. The force–moment relationship influences the pattern of anterior tooth movement and the distribution of anchorage demands (Hocevar, 1981; Proffit et al., 2018).

For non-extraction treatment, expansion and distalization can provide additional space in selected patients, but periodontal and anatomical limits of dental movement must be respected.

Complex and Combined Malocclusions

Many patients present with combinations of sagittal, vertical, transverse, and dental discrepancies. In these cases, individual force systems may interact and produce secondary effects that influence other components of treatment.

For example, sagittal mechanics may generate vertical effects, while transverse expansion may modify dental inclination and periodontal loading. Similarly, space closure may influence incisor torque and anchorage requirements.

Complex treatment therefore requires consideration of combined mechanical effects rather than evaluation of each movement independently.

Individualized Biomechanical Treatment Planning

Traditional malocclusion classifications remain clinically useful, but classification alone does not define the complete biomechanical requirements of treatment. Patients within the same malocclusion category may differ in skeletal pattern, dental compensation, periodontal support, facial morphology, anchorage requirements, and treatment objectives.

Biomechanical diagnosis can therefore complement conventional classification by identifying the specific movements required and the mechanical conditions necessary to achieve them.

The first step in biomechanical treatment planning is identification of the discrepancy requiring correction. The mechanical objective should then be defined in terms of the desired movement, such as bodily movement, controlled tipping, root movement, intrusion, extrusion, rotation, distalization, or mesialization.

Different orthodontic appliances generate different combinations of forces and moments. Fixed appliances provide extensive control through bracket–archwire interactions, whereas elastics, springs, skeletal anchorage, and clear aligners provide additional or alternative mechanisms for force delivery (Proffit et al., 2018; Dalessandri et al., 2014; Park et al., 2021; Iliadi et al., 2019).

Anchorage control is central to individualized treatment planning because orthodontic force systems generate reciprocal reactions. Conventional dental anchorage may be sufficient in some cases, whereas skeletal anchorage may be advantageous when greater anchorage control is required (Dalessandri et al., 2014; Park et al., 2021).

Biomechanical planning must also account for the biological response of periodontal and alveolar tissues. Individual variability in periodontal support, root morphology, alveolar anatomy, and tissue response may influence the clinical expression of an otherwise similar mechanical system (Asiry, 2018; Li et al., 2018; Li et al., 2021).

Digital and Computational Biomechanics

Digital technologies have increasingly influenced orthodontic diagnosis and treatment planning. Three-dimensional imaging, digital models, virtual setups, and computational approaches can facilitate visualization of dental and skeletal relationships and may assist in planning complex movements.

Finite element analysis can provide information concerning stress and strain distributions associated with different force systems and has been increasingly used to investigate orthodontic tooth movement and appliance–periodontium interactions. However, computational predictions should be interpreted cautiously because model assumptions, material properties, boundary conditions, and biological simplifications can influence the results (Cattaneo and Cornelis, 2021).

Recent systematic evidence concerning finite element analysis of clear aligners has also highlighted substantial methodological heterogeneity and limited standardization in the assessment of aligner biomechanics (Cao et al., 2025).

A digitally planned tooth position should therefore not be considered equivalent to a guaranteed biological outcome. Clinical results remain dependent on the actual force system, appliance fit and activation, patient compliance when relevant, tissue remodeling, and treatment execution.

Limitations and Future Perspectives

The literature addressing orthodontic biomechanics encompasses experimental studies, clinical investigations, systematic reviews, and computational models with substantial variation in study design, appliance characteristics, force systems, outcome measures, and patient populations. This heterogeneity limits direct comparison between studies and prevents formulation of universally applicable biomechanical prescriptions.

The biological response to orthodontic force is also variable. Although established biomechanical principles provide a theoretical basis for predicting tooth movement, differences in periodontal anatomy, alveolar bone morphology, root characteristics, tissue response, and treatment conditions may influence clinical outcomes (Asiry, 2018; Li et al., 2018; Li et al., 2021).

Evidence concerning newer technologies, particularly clear aligners, skeletal anchorage-assisted mechanics, and computational modeling, continues to evolve. Evidence regarding their long-term clinical advantages and ability to consistently improve treatment predictability remains heterogeneous (Iliadi et al., 2019; Marinelli et al., 2025; Cao et al., 2025). Future research should integrate biomechanical measurements with clinical and biological outcomes. Standardized reporting of force magnitude, direction, duration, anchorage conditions, appliance characteristics, and treatment outcomes would improve comparability between studies.

Three-dimensional imaging, digital models, intraoral scanning, and computational biomechanical analysis may provide additional opportunities for patient-specific treatment planning. However, future studies should determine whether computational predictions correspond sufficiently to actual clinical tooth movement (Cattaneo and Cornelis, 2021; Cao et al., 2025). Technological sophistication should not replace established clinical diagnosis and biomechanical principles. The principal future challenge is to determine when and for whom a particular biomechanical strategy provides a clinically meaningful therapeutic advantage.

CONCLUSIONS

Orthodontic treatment is fundamentally based on the interaction between mechanical force systems and the biological response of dentoalveolar tissues. Correction of malocclusion therefore requires more than appliance selection or application of a predetermined force. It requires understanding the relationship between malocclusion characteristics, desired tooth movement, force–moment relationships, anchorage requirements, and tissue response.

Fixed appliances, elastics, springs, temporary skeletal anchorage devices, and clear aligner systems can generate different biomechanical environments and consequently provide different possibilities for controlling orthodontic tooth movement (Proffit et al., 2018; Dalessandri et al., 2014; Park et al., 2021; Iliadi et al., 2019). Their clinical application should be determined by the treatment objective and mechanical requirements of the individual case.

An integrated approach linking malocclusion diagnosis, desired tooth movement, force–moment requirements, anchorage control, appliance characteristics, and biological considerations provides a rational framework for individualized orthodontic treatment planning.

Digital and computational technologies may further support biomechanical planning, but their predictions should be interpreted within the limitations of current evidence and validated against clinical outcomes. Overall, orthodontic biomechanics provides a mechanistic bridge between diagnosis and treatment and may contribute to more controlled tooth movement, rational appliance selection, and treatment strategies adapted to individual anatomical and biological conditions.

REFERENCES

Asiry MA. 2018. Biological aspects of orthodontic tooth movement: a review of literature. *Saudi Journal of Biological Sciences*. 25(6):1027-1032. doi:10.1016/j.sjbs.2018.03.008.
Cao H, Hua X, Yang L, Aoki K, Shang S, Lin D. 2025. A systematic review of biomechanics of clear aligners by finite element analysis. *BMC Oral Health*. 25:1026. doi:10.1186/s12903-025-06295-6.
Cattaneo PM, Cornelis MA. 2021. Orthodontic tooth movement studied by finite element analysis: an update. What can we learn from these simulations? *Current Osteoporosis Reports*. 19(2):175-181. doi:10.1007/s11914-021-00664-0.
Dalessandri D, Salgarello S, Dalessandri M, Lazzaroni E, Piancino M, Paganelli C, Maiorana C, Santoro F. 2014. Determinants for success rates of temporary anchorage devices in orthodontics: a meta-analysis (n > 50). *European Journal of Orthodontics*. 36(3):303-313. doi:10.1093/ejo/cjt049.
Halimi A, Benyahia H, Doukkali A, Azeroual MF, Zaoui F. 2012. A systematic review of force decay in orthodontic elastomeric power chains. *International Orthodontics*. 10(3):223-240. doi:10.1016/j.ortho.2012.06.013.
Hocevar RA. 1981. Understanding, planning, and managing tooth movement: orthodontic force system theory. *American Journal of Orthodontics*. 80(5):457-477. doi:10.1016/0002-9416(81)90243-8.
Iliadi A, Koletsi D, Eliades T. 2019. Forces and moments generated by aligner-type appliances for orthodontic tooth movement: a systematic review and meta-analysis. *Orthodontics & Craniofacial Research*. 22(4):248-258. doi:10.1111/ocr.12333.
Li Y, Jacox LA, Little SH, Ko CC. 2018. Orthodontic tooth movement: the biology and clinical implications. *Kaohsiung Journal of Medical Sciences*. 34(4):207-214. doi:10.1016/j.kjms.2018.01.007.
Li Y, Zhan Q, Bao M, Yi J, Li Y. 2021. Biomechanical and biological responses of periodontium in orthodontic tooth movement: up-date in a new decade. *International Journal of Oral Science*. 13(1):20. doi:10.1038/s41368-021-00125-5.
Marinelli G, Inchingolo AM, Inchingolo AD, Ferrante L, Avantario P, Campanelli M, Palermo A, Inchingolo F, Dipalma G. 2025. Temporary anchorage devices in clear aligner therapy: a systematic review. *Bioengineering*. 12(5):531. doi:10.3390/bioengineering12050531.
Park KH, Choi JY, Kim KA, Kim SJ, Chung KR, Kim SH. 2021. Critical issues concerning biocreative strategy in contemporary temporary skeletal anchorage device orthodontics: a narrative review. *Orthodontics & Craniofacial Research*. 24(Suppl. 1):39-47. doi:10.1111/ocr.12444.
Proffit WR, Fields HW, Larson BE, Sarver DM. 2018. *Contemporary Orthodontics*. 6th ed. St Louis: Elsevier.
Theodorou CI, Kuijpers-Jagtman AM, Bronkhorst EM, Wagener FADTG. 2019. Optimal force magnitude for bodily orthodontic tooth movement with fixed appliances: a systematic review. *American Journal of Orthodontics and Dentofacial Orthopedics*. 156(5):582-592. doi:10.1016/j.ajodo.2019.05.011.
Weltman B, Vig KWL, Fields HW, Shanker S, Kaizar EE. 2010. Root resorption associated with orthodontic tooth movement: a systematic review. *American Journal of Orthodontics and Dentofacial Orthopedics*. 137(4):462-476. doi:10.1016/j.ajodo.2009.06.021.
Yamaguchi M. 2009. RANK/RANKL/OPG during orthodontic tooth movement. *Orthodontics & Craniofacial Research*. 12(2):113-119. doi:10.1111/j.1601-6343.2009.01444.x.

DESIGN AND IMPLEMENTATION OF AN OFF-GRID SOLAR-POWERED DRIP IRRIGATION SYSTEM WITH A SOIL MOISTURE CONTROLLER FOR DAYTIME IRRIGATION OF OLIVE GROVES IN CANAKKALE

Görkem Şen

Trakya University, Ipsala Vocational School, Electronics and Automation Department, Edirne, Türkiye

gorkemsen@trakya.edu.tr

ABSTRACT

The olive tree is a typical Mediterranean climate plant characterized by dry and hot summers and capable of surviving with minimal water. However, if olive trees are irrigated, they exhibit increased bud formation and flowering, higher fruit production, larger fruit size, greater yield per tree, and a higher amount of olive oil. In recent years, renewable energy resources have been preferred in irrigation applications in order to both reduce fossil fuel-based energy consumption and irrigation costs. The use of solar energy as a renewable energy resource for agricultural irrigation has been steadily increasing. In this study, an off-grid solar-powered, soil moisture-controlled daytime drip irrigation system is implemented in an olive grove located in Ezine, Çanakkale. The mentioned irrigation system essentially includes a 12 Volt submersible pump, two photovoltaic panels (12 Volt, 340 Watt) and a control unit. The control unit determines the conditions under which the submersible pump operates and basically consists of a circuit breaker, a solar charge controller, a battery, a digital timer, and a soil moisture controller. The function of the battery in the control unit is to continuously provide energy needs of control circuits. Thus, control settings can remain constant at all times. In addition, since the battery is not used to power the submersible pump, a low-cost system can be designed using a low-capacity battery. Thanks to a digital timer, the solar drip irrigation system can operate at scheduled intervals during the daytime on a weekly basis. With the help of the soil moisture controller, efficient drip irrigation can be carried out based on the predetermined set value of soil moisture. In this design, the soil moisture controller continuously measures soil moisture with a sensor. If the level of soil moisture is below the set value and the time is between 9:00 and 18:00, the control unit allows irrigation. On the other hand, if the soil moisture level is above the set value or the time is outside the specified time range, irrigation is prevented. Owing to the drip irrigation system mentioned, water needs of olive trees are met during the daytime by controlling soil moisture. In this way, economical irrigation is achieved while agricultural productivity is enhanced. By preventing unnecessary irrigation, efficient use of water is possible. Additionally, this study can be used in any area where a sustainable irrigation system is required.

Keywords: Off-grid solar system, Renewable energy, Solar-powered irrigation, Sustainable production, Soil moisture-controlled system, Photovoltaic system

INTRODUCTION

In traditional irrigation systems, pumps powered either by electricity or fossil fuels are used. Electric pumps generally obtain the energy they need either from the power grid or from generators that run on fossil fuels. In any case, the required energy relies on fossil fuels. As is well known, fossil fuels are not unlimited and their reserves are steadily decreasing. Moreover,

the use of these fuels not only causes greenhouse gas (GHG) emissions but also releases pollutants such as benzene, carbon monoxide, sulfur oxides, and ammonia. Therefore, the transition to renewable energy resources (RES) in agricultural irrigation, where energy is essential, has become increasingly important (Mirahmad et al., 2026).

Nowadays, when people think of RESs, solar and wind energy are usually the first that come to mind. Solar energy is one of the most important RESs, as it is clean, free, and easily accessible, making it a key contributor to electricity generation worldwide. However, a country's geographical location directly determines how much it can benefit from solar energy. Türkiye has rich solar energy potential because it is located in a sunny region of the Earth, between the 36th - 42nd northern parallels and the 26th - 45th east meridians, which provides an advantage over most other countries (Kotcioğlu, 2011). Solar energy potential atlas of Türkiye is given in Figure 1. Solar energy potential is directly proportional to the duration of sunlight in specific regions, and Türkiye demonstrates considerable capacity for power generation from solar energy, as evidenced in Figure 1 (Kabalci et al., 2016).

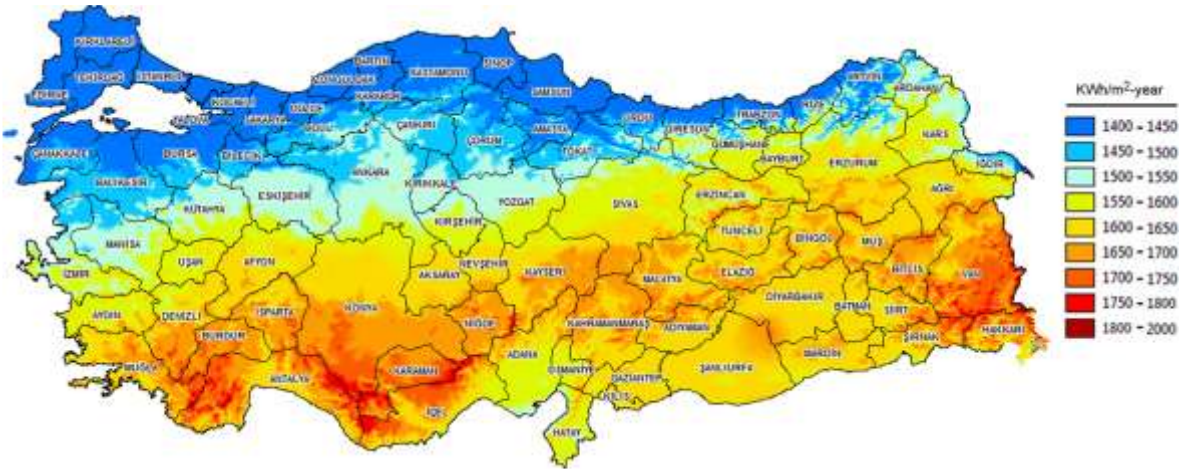

Figure 1. Solar energy potential atlas of Türkiye (Kabalci et al., 2016)

Solar-powered systems are consistently finding various application areas (Şen, 2024). One of them is a solar-powered agricultural irrigation (Şen, 2023). These systems reduce operational costs while supporting environmental sustainability. They can be used in regions with limited access to electricity, improve water efficiency, and lower GHG emissions. In addition, they ease labor and boost production. Being reliable, scalable, and integrable with a battery unit, they provide a sustainable solution for agricultural irrigation (Hossain et al., 2024).

With the integration of sensors suitable for agricultural irrigation systems, the concept of smart irrigation systems has emerged. For example, soil moisture sensors provide real-time measurements. Farmers can evaluate the relevant soil moisture data to accurately assess the water needs of trees or crops. Soil moisture data are used to determine at what intervals and how much water should be supplied to trees or crops. When irrigation is carried out based on soil moisture data, the soil moisture level is maintained at an optimum level, allowing trees or crops to access necessary nutrients and reducing the risk of water stress (Wanyama et al.,2023). Drip irrigation is a micro-irrigation technology that delivers controlled amounts of water and nutrients directly to the root zone of trees or crops through networks of pipes and drippers. Replacing inefficient irrigation methods with drip irrigation has been shown to reduce water losses during irrigation by 20% to 76% and to increase crop water productivity by 15%. Farmers who adopt drip irrigation can achieve water savings while simultaneously improving crop yields (Grant et al., 2022).

Olive trees are among the most resilient traditional dryland fruit species under water stress conditions. Although olive trees are generally drought-tolerant, not all phenological stages exhibit the same level of resistance, and the combination of the duration and severity of water stress is critical. Flowering, fruit set, and oil accumulation phases are the most sensitive stages to water stress conditions (Molina-Moral et al., 2022).

In this study, the off-grid solar-powered, soil moisture-controlled daytime drip irrigation system is implemented in an olive grove located in Ezine, Çanakkale, Türkiye. The proposed irrigation system essentially includes a 12 Volt direct current (DC) submersible pump, two photovoltaic (PV) panels and a control unit. The control unit basically consists of a circuit breaker, a solar charge controller, a battery, a digital timer, and a soil moisture controller. The battery in the control unit serves to continuously supply power to control circuits, ensuring that the settings remain stable at all times. Since it does not drive the DC submersible pump, a low-capacity battery can be used, making the system more cost-effective. With the soil moisture controller, drip irrigation can be efficiently managed according to the preset soil moisture level. Thanks to the digital timer, the solar drip irrigation system can operate at scheduled intervals during the daytime on a weekly basis. Owing to the installed drip irrigation system, water needs of olive trees are met during the daytime by controlling soil moisture.

MATERIAL AND METHOD

Study Area

Çanakkale is located in the Marmara Region of Türkiye and holds a strategic position, connecting the continents of Asia and Europe. Çanakkale has 12 districts and the study is carried out in Ezine district of Çanakkale. The location of Ezine in Türkiye is shown in Figure 2.

Figure 2. The location of Ezine in Türkiye

Ezine is situated in the transitional zone between the Marmara and the Aegean regions. Known for its natural beauty and fertile plains, Ezine enjoys an advantageous location in terms of both sea and land transportation. Consequently, climatic characteristics of both regions are also reflected in Ezine. Winters are generally mild and rainy, with precipitation predominantly occurring as rainfall. Meteorological records indicate that November, December, March, and April are the months with the highest precipitation. In contrast, summers are hot and dry. July

and August are the warmest months, with average temperatures ranging between 25°C and 35°C, and precipitation is typically scarce during this period. Therefore, agricultural irrigation constitutes a significant necessity, particularly in the summer season. Furthermore, due to its settlement being surrounded by hills, Ezine exhibits relatively high average humidity levels (Şen, 2023).

The olive tree is a species that is sensitive to climate conditions. Ezine is one of the regions in Çanakkale where olive cultivation is carried out intensively. The mentioned irrigation study is applied on almost three-acre of olive grove in Ezine shown in Figure 3.

Figure 3. The olive grove in Ezine

Design and Realization of the Proposed System

In this study, the off-grid solar-powered system is implemented in an approximately three-acre olive grove in Ezine, Çanakkale, Türkiye which performs drip irrigation only during the daytime by taking soil moisture levels into account. The overall schematic of the proposed irrigation system is shown in Figure 4, and its photograph is presented in Figure 5, respectively.

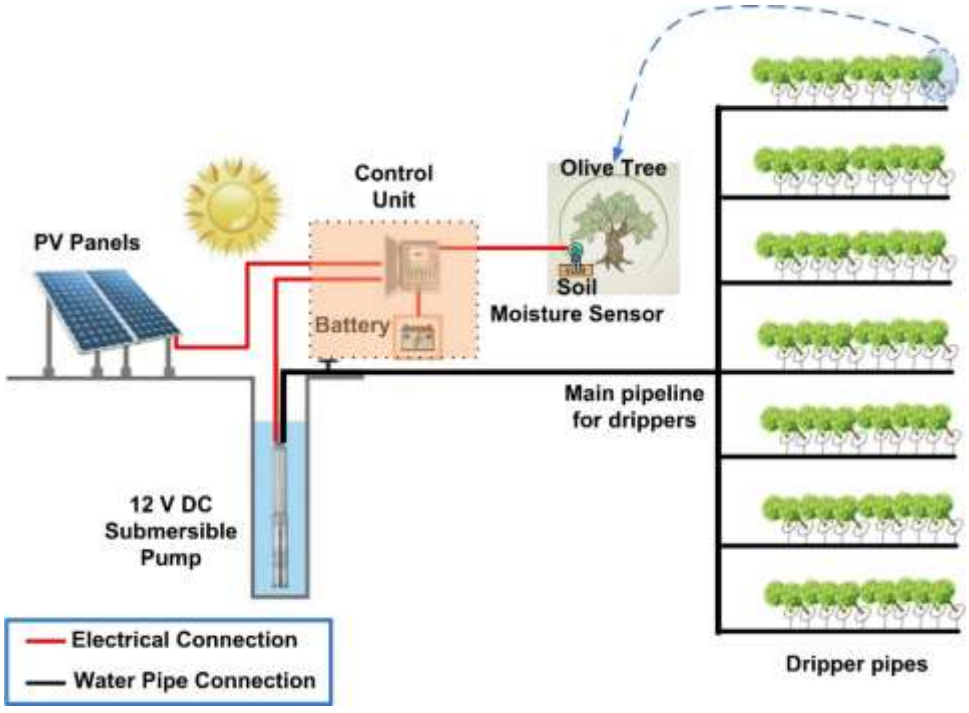

Figure 4. The overall scheme of the proposed irrigation system

Figure 5. Photograph of the proposed irrigation system

As illustrated in Figures 4 and 5, the electrical structure of the proposed irrigation system comprises three main parts, namely PV panels, the DC submersible pump, and the control unit. In the proposed irrigation system, there are two PV panels. Values of each PV panels are 12 Volt and 170 Watt. 12 Volt, 340 Watt DC source is obtained by connecting these PV panels in parallel. Characteristics of PV panel are shown in Table 1.

Table 1. Characteristics of PV panels

Name	Rating
Panel Maximum Power	205 W
Peak Voltage	21.45V
Peak Current	9.6 A
Open Circuit Voltage	25.92 V
Short Circuit Current	9.9 A

There is an artesian well with a depth of thirty-three meters in the mentioned olive grove. The water level is about six meters below the ground. 12 Volt DC submersible pump is located at

thirteen meters below the ground. Characteristics of 12 Volt DC submersible pump are shown in Table 2.

Table 2. Characteristics of DC submersible pump

Name	Rating
Voltage	12 V
Power Consumption	130 W
Speed	2850 r/min
Maximum Flow Rate (Qmax)	2 m^3/h
Maximum Head (Hmax)	35 m

The last main part of the proposed irrigation system is the control unit which consists of the circuit breaker, the solar charge controller, the battery, the digital timer, and the soil moisture controller. Photograph of the control unit of the proposed irrigation system is shown in Figure 6.

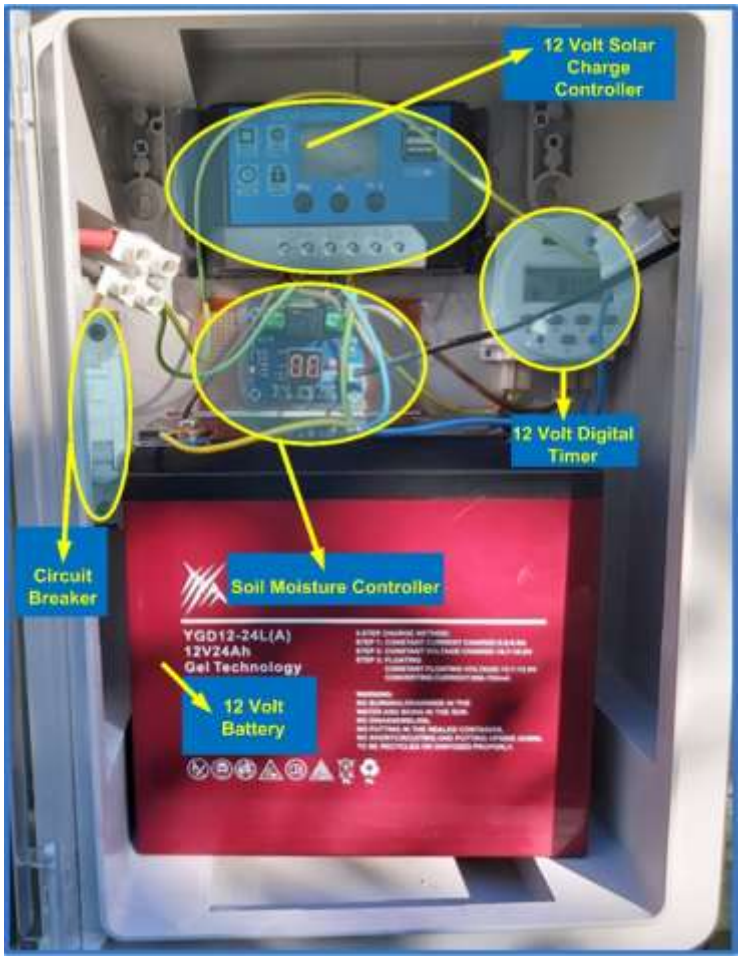

Figure 6. Control unit of the proposed system

The circuit breaker not only protects the system against electrical faults but also acts as an on-off controller for PV panels.
The solar charge controller serves to regulate energy transfer from PV panels to the battery, protecting the battery from overcharging. The solar charge controller's some characteristics are shown in Table 3.

Table 3. Some characteristics of solar charge controller

Name	Rating
Rated Charge Current	10 A
Operating Voltage	12/24Volt auto sensing/auto switching
Control Method	Pulse width modulation (PWM) pulse-duration modulation charge mode
Working Temperature	-35ºC to +60ºC

Another important component of the control unit is the battery. The system employs a 12-Volt, 24-Ah gel battery. A higher-capacity battery group is not selected, as the chosen battery is intended to continuously supply power only to control circuits.
The soil moisture controller is powered directly by the battery voltage, that is, 12 Volts. Through the probe connected to the soil moisture controller, the level of soil moisture in the root zone of the selected olive tree is measured. Using the adjustment buttons on soil moisture controller, the soil moisture value that will serve as a reference for drip irrigation can be set. Based on this set value, the relay in the soil moisture controller switches on and off to control the current flow of the DC submersible pump.
The digital timer like the soil moisture controller, is powered directly by the battery voltage. It can be programmed multiple times to allow current to flow at desired times throughout the week. In addition, if required, the current flow of the DC submersible pump can also be manually enabled or disabled.
The general electrical connection of the proposed irrigation system, introduced with its photograph in Figure 5, is illustrated in Figure 7.

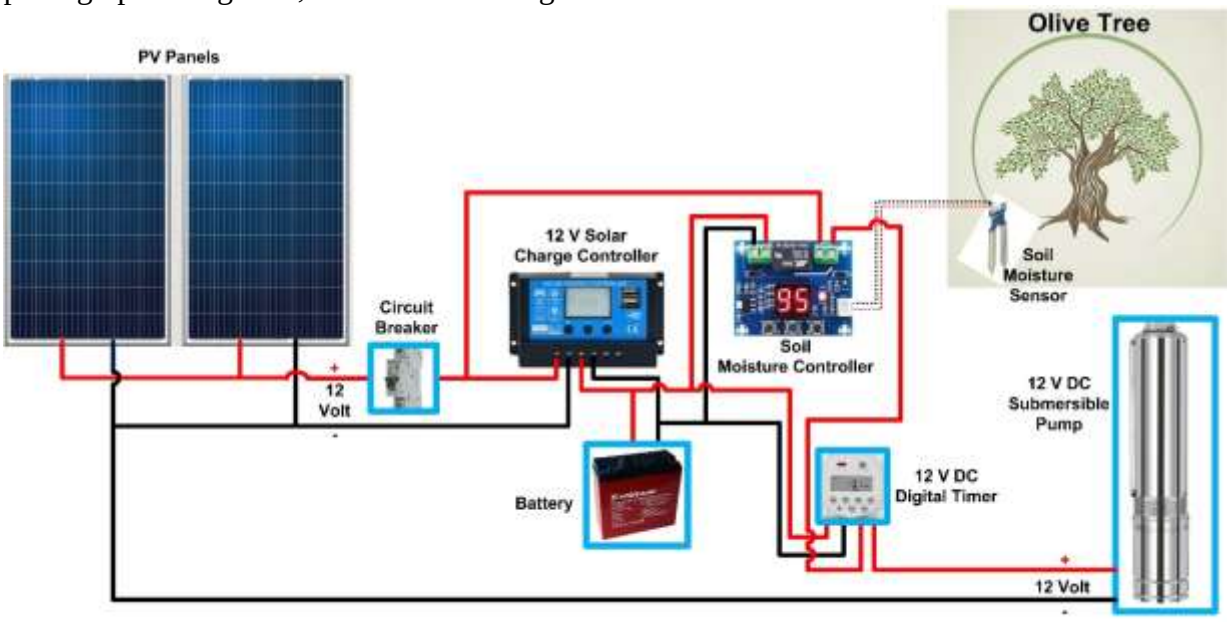

Figure 7. General electrical connection scheme of the proposed system

Operation of the Proposed System

The operating steps of the proposed daytime irrigation system are as follows:
PV panels are connected to the solar charge controller via the circuit breaker. The circuit breaker in the system has two main functions. Its first function is to electrically disconnect PV panels

when needed. Its second function is to protect the entire system by cutting off the current flow in case of electrical faults.

The battery is charged through the solar charge controller during periods when sunlight is available. The solar charge controller's settings need to be adjusted according to the battery's specifications.

The battery continuously supplies energy needs of the soil moisture controller and the digital timer. In this way, settings of these two parts within the control unit remain unchanged.

The battery does not supply power to the DC submersible pump. Therefore, its capacity has been selected solely to continuously supply power to the control unit.

The soil moisture controller continuously measures the level of the soil moisture of the selected olive tree. If the measured soil moisture level is below the set moisture value, the relay inside the soil moisture controller allows the current flow from PV panels to the relevant terminal of the digital timer. However, if the measured value is above the set moisture value, it prevents the current flow from PV panels to the relevant terminal of digital timer.

The digital timer is set to allow the current flow from the soil moisture controller to the DC submersible pump between 09:00 and 18:00 every day of the week. During these specified time intervals, if the soil moisture controller permits the current flow, PV panels energize the DC submersible pump and drip irrigation begins. In contrast, when the soil moisture controller and the digital timer do not simultaneously allow the current flow, PV panels can not energize the DC submersible pump. Consequently, drip irrigation can not be performed.

As a result, it has been determined that olive trees in the mentioned olive grove are successfully irrigated using the drip irrigation method every day of the week between 09:00 and 18:00, taking into account soil moisture level.

CONCLUSIONS

This study provides an example of the development of sustainable irrigation practices in olive groves. In this study, the off-grid solar-powered, soil moisture-controlled daytime drip irrigation system is designed and installed for olive grove irrigation in Ezine district of Çanakkale province. The soil moisture-controlled irrigation is targeted only during daytime. Thus, since the low-capacity battery is used that only supplies continuous power to control circuits, the system is established with lower installation costs compared to alternatives with high-capacity battery units. Additionally, as irrigation is carried out based on soil moisture, water needs of olive trees are met at the most appropriate time, while unnecessary irrigation is prevented. Moreover, this study presents a model that can be applied not only to olive groves but also to different plant species and various climatic conditions. Therefore, implementing these solar-powered irrigation systems will contribute to the development of our farmers as well as the economic and agricultural growth of our country.

REFERENCES

Grant F., Sheline C., Sokol J., Amrose S., Brownell E., Nangia V., Winter V A. G. 2022. Creating A Solar-Powered Drip Irrigation Optimal Performance Model (SDrOP) to Lower The Cost of Drip Irrigation Systems for Smallholder Farmers. Applied Energy. 323: 119563.

Hossain S., Hassan M., Shayem A. 2024. Design and Analysis of Solar Irrigation Systems for Sustainable Rice Cultivation in Bangladesh. 6th International Conference on Electrical Engineering and Information & Communication Technology (ICEEICT). 02-04 May 2024. Dhaka, Bangladesh.

Kabalci Y., Kabalci E., Canbaz R., Calpbinici A. 2016. Design and Implementation of a Solar Plant and Irrigation System with Remote Monitoring and Remote Control Infrastructures. Solar Energy. 139: 506–517.

Kotcioğlu I. 2011. Clean and Sustainable Energy Policies in Turkey. Renewable and Sustainable Energy Reviews. 15(9): 5111-5119.

Mirahmad M. R., Rizi A. P., Jafari M. 2026. Comparative Life Cycle Assessment of Solar, Grid, and Diesel Energy Sources for Pressurized Irrigation: A Case Study from Iran. Energy Conversion and Management: X. 30: 101754.

Molina-Moral J.C., Moriana-Elvira A., Pérez-Latorre F.J. 2022. The Sustainability of Irrigation Strategies in Traditional Olive Orchards. Agronomy. 12(1): 64.

Şen G. 2023. Economic Analysis of 340 W Solar Based Drip Irrigation System and Comparison with Its Gasoline-Based Equivalent in Türkiye. V. Balkan Agricultural Congress (AGRIBALKAN 2023). 20-23 September 2023. Edirne, Türkiye.

Şen G. 2024. Design and Application of An Automatic Pet Feeder with Two-Way Splitter Suitable for Grid-Connected or Solar-Powered Use. VI. International Agricultural, Biological & Life Science Conference (AGBIOL 2024). 18-20 September 2024. Edirne, Türkiye.

Wanyama J., Soddo P., Nakawuka P., Tumutegyereize P., Bwambale E., Oluk I., Mutumba W., Komakech A J. 2023. Development of A Solar Powered Smart Irrigation Control System Kit. Smart Agricultural Technology. 5: 100273.

DESIGN AND APPLICATION OF AN OFF-GRID SOLAR-BASED, SOIL MOISTURE-CONTROLLED DRIP IRRIGATION SYSTEM FOR OLIVE GROVES IN TURKIYE

Görkem Şen

Trakya University, Ipsala Vocational School, Electronics and Automation Department, Edirne, Türkiye

gorkemsen@trakya.edu.tr

ABSTRACT

Olive trees are grown mostly in countries bordering the Mediterranean basin, such as Türkiye, Spain, Italy, Greece, Tunisia, Portugal, Syria, Libya, Morocco and Algeria. Although the olive tree is a species resistant to drought conditions, it is one of the agricultural products that will be most affected by global climate change. Therefore, water resources should be managed carefully, and appropriate irrigation strategies should be implemented. The use of solar energy in agricultural irrigation is increasing day by day, as this energy is both an environmentally friendly approach and an economical solution in the long term. In this study, the installation of an off-grid solar-based, soil moisture-controlled 24-hour drip irrigation system is performed in an olive grove located in Ezine, Çanakkale. The drip irrigation system contains two photovoltaic (PV) panels (12 Volt, 340 Watt), a battery group (12 Volt), a 12 Volt submersible pump and a control unit. The control unit defines the operating conditions of the submersible pump and consists of a circuit breaker, a solar charge controller, a digital timer and a soil moisture controller. The solar charge controller allows PV panels to charge the battery group. The battery group provides the energy needs of both the control circuits and the submersible pump, enabling drip irrigation. To ensure 24/7 drip irrigation capability, the battery group must have sufficient power capacity. The designed system can be operated at various times throughout the day and night, owing to the digital timer. Thanks to the soil moisture controller, effective drip irrigation can be carried out by taking into account the predefined soil moisture threshold. In this application, the soil moisture controller constantly measures soil moisture using a sensor. If the soil moisture level falls below the specified threshold and the time is within the set time period, the control unit allows the battery group to power the submersible pump. If the soil moisture level exceeds the specified threshold or the time is outside the set time period, the control unit does not allow the battery group to power the submersible pump. With this solar-based irrigation system, olive trees' water needs are continuously met by considering soil moisture. Thus, an efficient, eco-friendly, cost-effective, and sustainable drip irrigation is realized and agricultural efficiency is increased. Additionally, this study can be used in any agricultural estate and the mentioned solar-based irrigation system will constantly support the development of the agricultural sector.

Keywords: Off-grid photovoltaic system, Solar based drip irrigation, Renewable energy, Sustainable production, Soil moisture-controlled system

INTRODUCTION

Water is a highly critical resource for agricultural production and accounts for about 70% of total freshwater use worldwide (Sidik et al., 2025). Agricultural irrigation systems are designed

to mitigate adverse effects of insufficient rainfall and to promote the growth of crops or trees. In the developing world, crop yields in irrigated areas are consistently higher than those in rain-fed areas (Bhavsar et al., 2023).

While various agricultural irrigation methods exist, nowadays systems that both use water efficiently and provide crops or trees with the exact amount of irrigation they need have come to the forefront due to global climate change. Drip irrigation is a method that ensures significant water savings. Water is supplied drop by drop directly to the root zone of crops or trees. With its effective use, evaporation and surface runoff of water can be controlled (Ahmed and Fernando, 2017). Since it can be installed both above and below ground, it enables sufficient and efficient agricultural irrigation. However, the potential clogging of drippers can negatively affect irrigation efficiency (Junjie et al., 2012). Due to continuous reliance on inefficient traditional irrigation methods, significant water losses have occurred and pressure on water resources has increased, particularly in arid and semi-arid regions (Sidik et al., 2025). Therefore, the use of drip irrigation systems is important.

Agricultural irrigation conducted only through drip irrigation cannot be considered a fully water-efficient system on its own. Utilizing sensor technology in agricultural irrigation and establishing an appropriate automation system supports sustainable agricultural production (Bhavsar et al., 2023). In particular, integrating soil moisture sensors into irrigation systems enhances efficiency in irrigation management. Through the soil moisture sensor, the soil moisture level of the relevant crop or tree can be measured in real time. Based on the data obtained instantly, it can be used to irrigate them according to their needs (Sidik et al., 2025).

If agricultural irrigation is to be carried out with appropriate automation, the choice of the electricity source to be used becomes important. In agricultural irrigation, the power grid or fossil fuel-based generators are generally used. However, in rural areas, access to fossil fuels or the power grid is not always easy. Therefore, off-grid electricity sources are needed (Grant et al., 2022). The integration of renewable energy resources (RES) into agricultural irrigation systems supports the sustainability of agriculture.

It is possible to use solar energy, one of the RESs, to meet the electrical power demand of agricultural irrigation systems. Solar energy stands out as one of the most important RESs thanks to its almost zero operating costs, long service life, and inexhaustible energy supply (Şen, 2023). The use of solar energy reduces dependence on environmentally harmful fossil fuels (Sidik et al., 2025). Türkiye's geographical location provides a significant advantage for generating electrical power from solar energy (Şen, 2024). Figure 1 shows Türkiye's solar energy potential map.

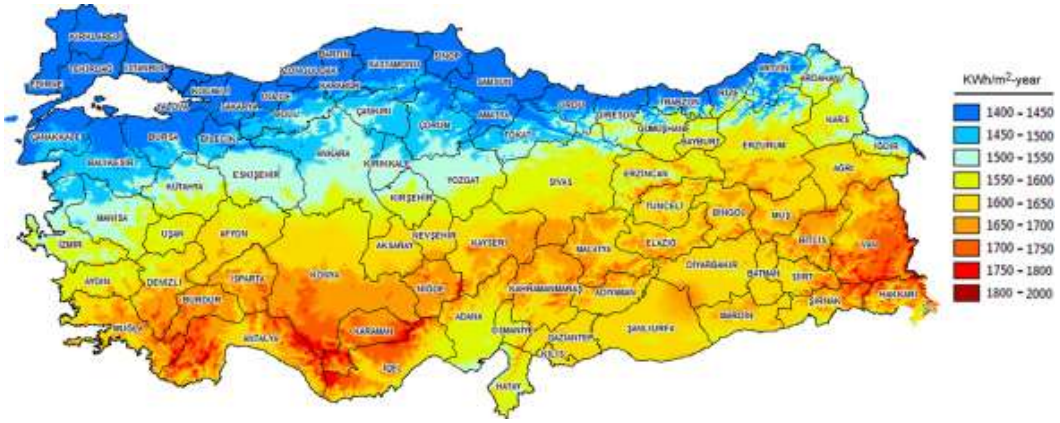

Figure 1. Türkiye's solar energy potential map (Kabalci et al., 2016)

Olive trees are a characteristic species of the Mediterranean basin, representing around 96% of the trees in the region. Olive trees are drought-resistant and have adapted well to arid and semi-arid areas with low water availability. Olive trees are traditionally cultivated using the dry farming method; nevertheless, the yield improvements provided by supplementary irrigation have led to growing interest in water use in olive cultivation. In olive trees, fruit development occurs in three main stages: flowering, pit hardening, and post-pit hardening. These stages differ in their tolerance to water stress. Flowering and post-pit hardening are water-sensitive stages. In contrast, pit hardening is recognized as a drought-tolerant stage. Therefore, additional irrigation during the water-sensitive stages of the plant cycle improves vegetative growth. It increases olive production, which also results in a greater amount of olive oil. The main reason for this increase is that the fruits are larger and there is a higher yield of fruit per tree (Yorulmaz et al., 2019).

In this study, the installation of an off-grid solar-based, soil moisture-controlled 24-hour drip irrigation system is performed in an olive grove located in Ezine, Çanakkale, Türkiye. The installed system contains two photovoltaic (PV) panels (12 Volt, 340 Watt), a battery group (12 Volt), a 12 Volt direct current (DC) submersible pump and a control unit. The control unit defines the operating conditions of the submersible pump and consists of a circuit breaker, a solar charge controller, a digital timer and a soil moisture controller. The battery group supplies energy to both the control circuits and the DC submersible pump, enabling drip irrigation. Thanks to the digital timer, the mentioned system can be operated at different times during the day and night. Irrigation is carried out effectively by considering the soil moisture threshold determined by the soil moisture controller. With this proposed irrigation system, olive trees' water needs are continuously met by controlling soil moisture.

DESIGN AND IMPLEMENTATION OF THE PROPOSED SYSTEM

Study Area

Çanakkale is located in the Marmara Region of Türkiye. Like Istanbul, it connects the continents of Asia and Europe. The city has many districts, one of which is Ezine. Ezine lies in the southwest of Çanakkale, along the coast of the Aegean Sea. Ezine's location within Türkiye is shown in Figure 2.

Figure 2. Ezine's location within Türkiye

Çanakkale is one of the leading areas in Türkiye in terms of olive cultivation. Ezine, in particular, is an important center for olive and olive oil production. The proposed solar-based agricultural irrigation system is established on approximately three acres of olive grove in Ezine, as shown in Figure 3.

Figure 3. The olive grove in Ezine in which the study is undertaken

General Structure of the System

In this study, a system capable of performing drip irrigation at any time of the day by taking soil moisture into account is implemented in an approximately 3-acre olive grove located in Ezine, Çanakkale, Türkiye. The structural schematic of the implemented irrigation system is shown in Figure 4, and image of the system is presented in Figure 5, respectively.

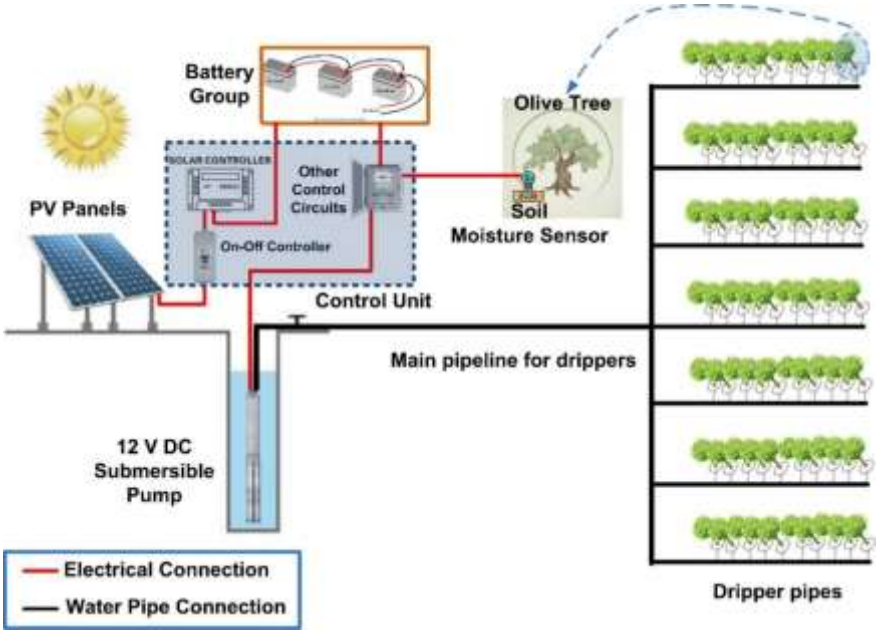

Figure 4. Structural schematic of the proposed solar-based irrigation system

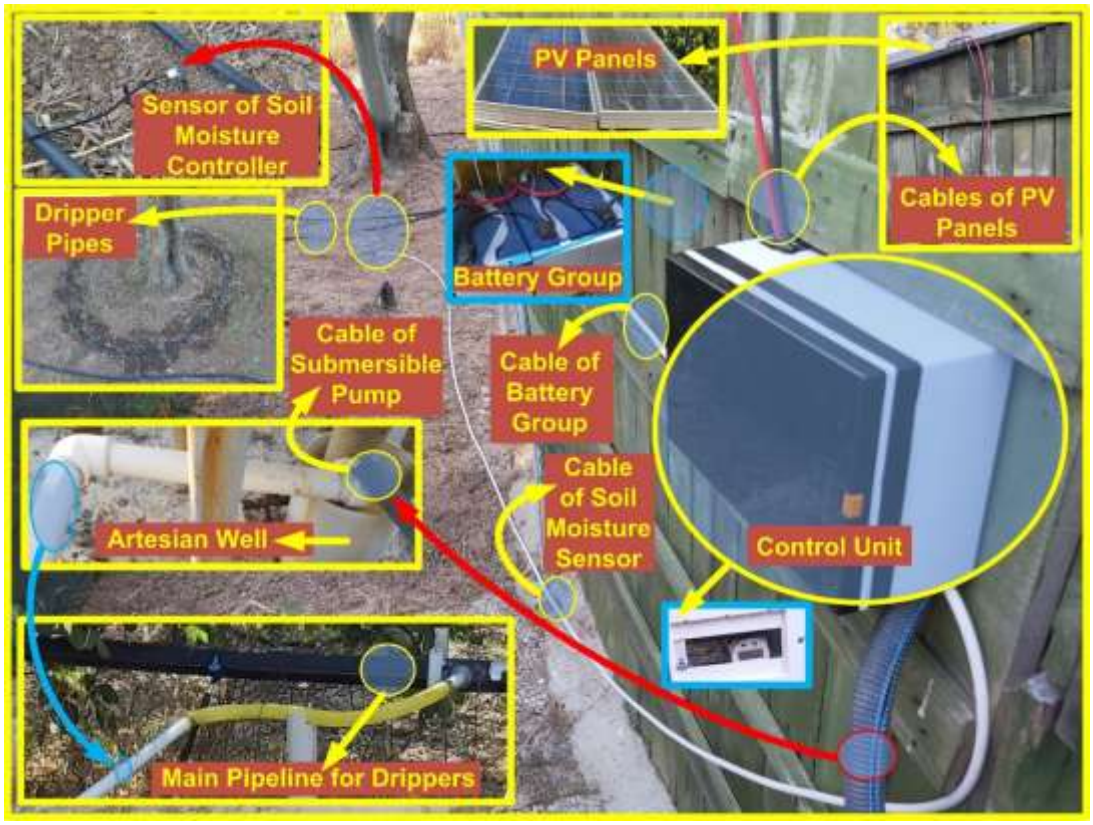

Figure 5. Image of the proposed solar-based irrigation system

As showed in Figures 4 and 5, the electrical configuration of the presented solar-based irrigation system comprises four main parts, namely PV panels, the battery group, the control unit and the DC submersible pump.
In the presented drip irrigation system, there are two PV panels and values of each PV panels are 12 Volt and 170 Watt. Also, these PV panels are connected in parallel to obtain 12 Volt, 340 Watt DC source. PV panels' technical parameters are shown in Table 1.

Table 1. Technical parameters of PV panels

Name	Rating
Panel Maximum Power	205 W
Peak Voltage	21.45V
Peak Current	9.6 A
Open Circuit Voltage	25.92 V
Short Circuit Current	9.9 A

The battery group consists of three 12 Volt, 100Ah gel batteries connected in parallel. The capacity of the battery group has been kept high because, in addition to supplying power to circuits in the control unit, it is also intended to supply energy requirements of the DC submersible pump.
Another important part of the presented solar-based irrigation system is the control unit which consists of the circuit breaker, the solar charge controller, the soil moisture controller and the

digital timer. Photograph of the control unit within the proposed solar-based irrigation system is shown in Figure 6.

Figure 6. Control unit within the proposed solar based irrigation system

Within the system, the circuit breaker fulfills two primary roles. Firstly, it protects the entire system in case of a possible electrical fault. Secondly, it acts as an on-off controller that disconnects or connects PV panels to the system whenever required.
The solar charge controller manages the energy transfer from PV panels to the battery group. It keeps the battery group safe from overcharging. Some parameters of the solar battery charge controller are shown in Table 2.

Table 2. Some parameters of solar charge controller

Name	Rating
Rated Charge Current	10 A
Operating Voltage	12/24Volt auto sensing/auto switching
Control Method	Pulse width modulation (PWM) pulse-duration modulation charge mode
Working Temperature	-35ºC to +60ºC

The digital timer and the soil moisture control circuit are powered by the voltage of battery group. Both of these elements of the control unit contain relays that perform switching in the main circuit. The terminals of these relays are connected in series and are electrically positioned between the battery group and the DC submersible pump. Thus, via these relays, the battery group either energizes the DC submersible pump or it doesn't. The digital timer can be

programmed multiple times during desired intervals of the week. Thus, the relay of the digital timer allows current flow during the specified time periods. The soil moisture control circuit, through its sensor, measures the soil moisture level in the root zone of the relevant olive tree. Using the buttons on the circuit, the soil moisture threshold for drip irrigation can be set. Based on this set soil moisture threshold, the relay inside the soil moisture controller allows current flow. As a result, for the battery group to energize the DC submersible pump and enable drip irrigation, both these relays mentioned must allow current flow.
The last main part of the presented solar-based irrigation system is DC submersible pump. There is an artesian well with a depth of thirty-three meters in the olive grove where the study is carried out. The water level is about six meters below the ground and DC submersible pump is located at thirteen meters below the ground. DC submersible pump's technical parameters are shown in Table 3.

Table 3. Technical parameters of DC submersible pump

Name	Rating
Voltage	12 V
Power Consumption	130 W
Speed	2850 r/min
Maximum Flow Rate (Qmax)	2 m^3/h
Maximum Head (Hmax)	35 m

The overall electrical connection scheme of presented solar-based irrigation system, introduced with its image in Figure 5, is shown in Figure 7.

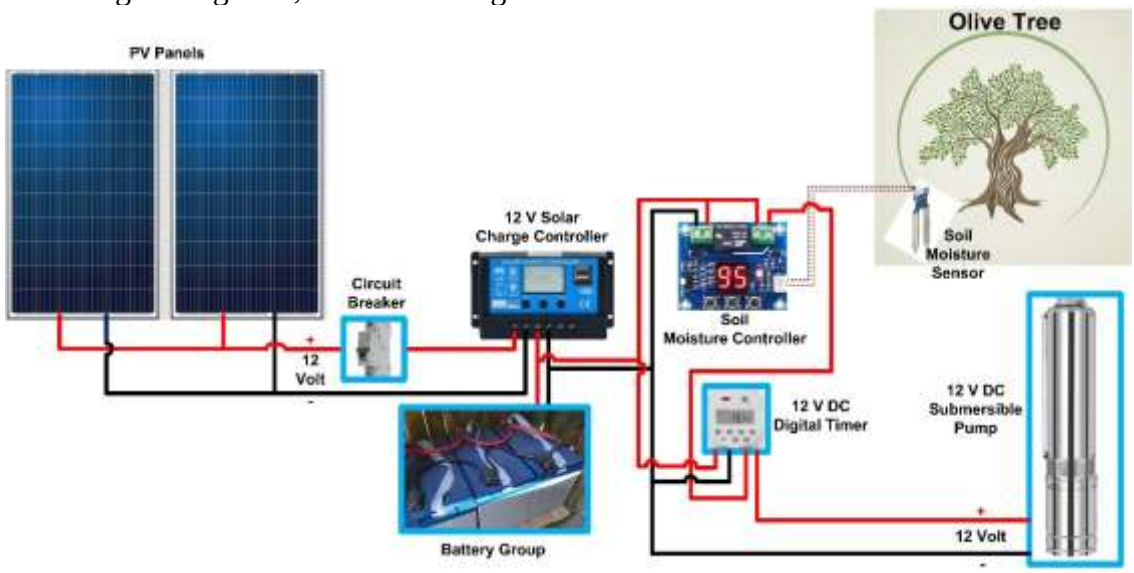

Figure 7. Overall electrical connection scheme of the presented solar-based irrigation system

Operation of the System

The operating steps of the proposed daily irrigation system are as follows:
The circuit breaker is electrically located between PV panels and the solar charge controller. This component protects the system by cutting off the circuit current in case of a possible electrical fault and also allows PV panels to be easily disconnected from the system electrically whenever needed.

The battery group is charged throughout the day via the solar charge controller. The solar charge controller is adjusted according to specifications of batteries that make up the battery group.

The battery group meets energy needs of both control circuits (the soil moisture controller and the digital timer) and the DC submersible pump. Since control circuits remain continuously powered, preset values for control are not erased. In addition, the battery group has been selected with a high energy capacity to meet the energy demand of the DC submersible pump.

The soil moisture controller continuously measures the soil moisture value of the selected olive tree. If the measured soil moisture level is below the specified threshold, the relay inside the controller allows the current from the battery group to flow to the relevant terminal of the digital timer. However, if the measured soil moisture level is above the specified threshold, the current flow from the battery group to the relevant terminal of the digital timer is not permitted.

The digital timer can be programmed to allow the current flow from the relay of soil moisture controller to the DC submersible pump at any time of the day, regardless of whether it is daytime or nighttime. During the programmed time intervals, if the soil moisture controller permits the current flow, the battery group energizes the DC submersible pump and drip irrigation begins. Otherwise, if both the soil moisture controller and the digital timer do not simultaneously allow the current flow, the battery group cannot energize the DC submersible pump. Consequently, drip irrigation cannot be performed.

As a result, it has been determined that olive trees in the mentioned olive grove are successfully irrigated using the solar-based drip irrigation method, taking into account the soil moisture level at any time of the day.

CONCLUSIONS

As impacts of global climate change on agricultural production continue to increase, priority is being given to the efficient management of water resources and the use of RESs. In this study, the off-grid solar-based, soil moisture-controlled 24-hour drip irrigation system is designed and installed for olive grove irrigation in Ezine district of Çanakkale province. The proposed system includes the battery group with high energy capacity and the digital timer. The use of these elements makes it possible to carry out agricultural irrigation around the clock. In addition, thanks to the soil moisture sensor integrated into the system, olive trees are irrigated only when needed. This approach not only prevents unnecessary use of water but also helps ensure optimal irrigation of olive trees. As a result, this application offers a holistic solution that brings together the principles of sustainability, efficiency, and environmental responsibility in agricultural production. This approach can help reduce the negative impacts of climate change and support food security. This practice, tested in the olive grove, can be adapted to agricultural areas of different scales or used for the irrigation of other crops. The proposed study is considered to contribute to the development of sustainable agriculture.

REFERENCES

Ahmed D. I., Fernando X. 2017. Solar-powered Drip-Irrigation for Rural Bangladesh. 2017 IEEE Canada International Humanitarian Technology Conference (IHTC), 21-22 July 2017. Toronto, Canada.

Bhavsar D., Limbasia B., Mori Y., Aglodiya M. I., Shah M. 2023. A Comprehensive And Systematic Study In Smart Drip And Sprinkler Irrigation Systems. Smart Agricultural Technology. 5: 100303.

Grant F., Sheline C., Sokol J., Amrose S., Brownell E., Nangia V., Winter V A. G. 2022. Creating A Solar-Powered Drip Irrigation Optimal Performance Model (SDrOP) to Lower The Cost of Drip Irrigation Systems for Smallholder Farmers. Applied Energy. 323: 119563.

Junjie F., Xiuqiao H., Guoliang Z., Zhong D., Guanghui D., Yang L. 2012. Research and Application on the Movable Subsurface Drip Irrigation System. World Automation Congress 2012 (WAC 2012). 24-28 June 2012. Puerto Vallarta, Mexico.

Kabalci Y., Kabalci E., Canbaz R., Calpbinici A. 2016. Design and Implementation of a Solar Plant and Irrigation System with Remote Monitoring and Remote Control Infrastructures. Solar Energy. 139: 506–517.

Şen G. 2023. Design And Implementation of An Off-Grid Solar Based Semi-Automatic Drip Irrigation System for Olive Groves In Canakkale. V. Balkan Agricultural Congress (AGRIBALKAN 2023). 20-23 September 2023. Edirne, Türkiye.

Şen G. 2024. Design And Implementation of A Solar-Based Automatic Pet Feeder And Water Dispenser. VI. International Agricultural, Biological & Life Science Conference (AGBIOL 2024). 18-20 September 2024. Edirne, Türkiye.

Sidik A. R., Tawakal A., Sumirat G. S., Narputro P. 2025. Smart Irrigation Based on Soil Moisture Sensors with Photovoltaic Energy for Efficient Agricultural Water Management: A Systematic Literature Review. Engineering Proceedings. 107(1):17.

Yorulmaz A., Erinç H., Tatlı A., Tekin A. 2019. The Effect of Irrigation On Olive And Olive Oil Characteristics. Gıda / The Journal of Food. 44(6), 1081-1091.

EXTRACTION AND STRUCTURAL CHARACTERIZATION OF HUMIC ACIDS DERIVED FROM NITRIC ACID-ASSISTED COW MANURE COMPOST

R. Ghallab[1], A. Kemmouche[2,3], B. Kebabi[4], H. Boughrara[4], I, Khettabi[2]

[1]Ecole Nationale Polytechnique de Constantine (ENPC), Malek Ibn Nabi
[2] Ecole Nationale Supérieure de Biotechnologie (ENSB), Taoufik Khaznadar
[3]Laboratoire de Conception et Application de Molécules Bioactives
[4] Université Constantine 1

ABSTRACT

Humic substances are widely employed in agriculture due to their capacity to enhance crop yields and improve soil quality. Among these, humic acid often exhibits superior efficacy. This study aims to isolate and characterize humic substances, particularly humic acid, for subsequent agricultural applications. The raw material was cow manure compost pretreated with nitric acid, containing 36.68% C and 6.47% N. Characterization was performed using X-ray diffraction (XRD), Fourier-transform infrared spectroscopy (FTIR) and UV–visible (UV–Vis) spectroscopy. XRD patterns revealed ordered, graphite-like aromatic domains within the extracted humic acid, while UV–Vis and FTIR analyses confirmed the clear distinction between humic acid and fulvic acid and highlighted the higher aromaticity and structural complexity of humic acid compared with the more oxygen-rich, reactive fulvic acid. These features indicate that nitric-acid–assisted cow manure compost is a promising source of functional humic fractions for soil conditioning and sustainable agricultural use.

INTRODUCTION

The rapid growth and clustering of urban, agro-industrial and livestock activities in limited areas has greatly increased the generation and accumulation of organic wastes, which often become sources of soil, air and water pollution. To manage these wastes safely and efficiently, their recycling through agricultural use has received considerable attention, whether as organic fertilizers, soil amendments, or substrates for soilless cultivation systems (Sánchez-Monedero et al., 1996).Humic substances (HS) represent the highly transformed fraction of non-living natural organic matter, formed from complex organic compounds whose structures vary widely in complexity. They are often referred to as the “black gold of agriculture” because of their agronomic value (Cristina et al., 2020). Beyond their fertilizing effect, humic substances play a key role in the transport, immobilization and degradation of organic and mineral contaminants

such as pesticides, polycyclic aromatic hydrocarbons and heavy metals in soils and aquatic environments, a role that arises from their particular chemical and structural features (Koriko et al., 2013).

Humic substances are made of long carbon chains that resist microbial breakdown and are mainly composed of carbon, oxygen, hydrogen, nitrogen and sulphur. They contain many types of organic structures, such as polypeptides, polysaccharides, esters, ethers, phenols, lipids, quinones, aromatic rings, and various aliphatic compounds.

They are usually divided into three fractions based on solubility: humic acid, fulvic acid and humin. Humic acid consists of both aromatic and aliphatic acids, fulvic acid is smaller, more oxidized and soluble over a wide pH range, while humin is the heaviest fraction and remains insoluble in both acidic and alkaline solutions.

Their functional groups dissociate and give humic substances an overall negative charge, which allows them to strongly bind positively charged ions and molecules. Thanks to this chemical behaviour, they can improve soil fertility and water retention, stimulate root development and nutrient uptake, influence plant physiology and yield, and help remediate polluted soils and wastewater (Mosa et al., 2020).

In this context, the objective of the present study is to isolate and characterize humic substances in order to enable their subsequent use in agricultural systems.

MATERIALS AND METHODS

1.1. The preparation of the raw material

The raw material used in this study is caw manure chemically treated by nitric acid, as detailed by (Ghallab et al., 2024):

A fixed quantity of collected manure is weighed both before and after drying to calculate its moisture content. After this, the dried manure is ground in a ball mill to create a uniform texture. Particles under 250 micrometers are separated via sieving and stored in dry bags for future use.

Next, 3 grams of this dried, ground manure are combined with 15 mL of nitric acid (at the specified concentration of 0.5 M) to form a paste. The paste's pH is then adjusted to neutral using a potassium hydroxide solution. The final product is dried and stored for later application.

1.2. Separation of Humic Acid

The Humic Substances (HA: Humic Acid and FA: Fulvic Acid) were separated from manure compost according to (Gomes Junior et al., 2019) as follows:

The extraction was conducted using a solution of 0.1 mol L-1 NaOH (1:10, v: v) under a nitrogen (N_2) atmosphere. The mixture was stirred for 4 hours and then centrifuged at 3000 g for 20 minutes. The supernatant was acidified to pH 1.5 using 6 mol L^{-1} HCl and allowed to sit overnight at 4°C. After centrifugation, the supernatant (FA) was stored. The Has were solubilized and precipitated two more times, then treated for 16 hours with a solution of HCl: HNO3 diluted at 1:20 (v: v). The solution was added gradually under stirring until complete dissolution, noting the required volume. The HAs solution was then titrated to pH 7.0 using a solution of 0.1 mol L-1 KOH. Finally, then dried by lyophilization and stored.

1.3. Characterisation of Humic Acid

The crystalline structure and mineral composition of HA were evaluated via X-ray diffraction (XRD) on a Bruker D8 ADVANCE diffractometer. Measurements occurred at 25°C, scanning the 2θ range of 10–90° at 0.015° steps per second.

Ultraviolet (UV) and Fourier transform infrared (FTIR) spectroscopy were used to characterise humic acids. UV absorbance values were measured using a Jenway UV-visible spectrophotometer with plastic cuvettes (1cm x 1cm) at 25 ˚C. A Shimadzu IRAffinity-1S Fourier transform infrared spectrophotometer was used. Samples were analysed over the mid-infrared range from 400 to 4000 cm^{-1}.

RESULTS AND DISCUSSION

1.4. Characterization of Humic Acid by XDR

The XRD pattern in Fig. 1 shows a highly crystalline HA structure, with sharp peaks at 2θ = 24°, 28°, and 58°. These distinct peaks confirm ordered molecular arrangements in HA, despite its macromolecular nature and variable composition.

Key features include the prominent G band at ~2θ = 24°, linked to graphite-like aromatic groups (Sudiono et al., 2017), consistent with the (002) graphite peak seen in prior HA studies (Balmori et al., 2012). A secondary peak at ~28° and a broader, weaker one at 58° indicate HS-specific structures. Additional sharp, unidentified peaks suggest organic impurities or residual crystalline phases from extraction.

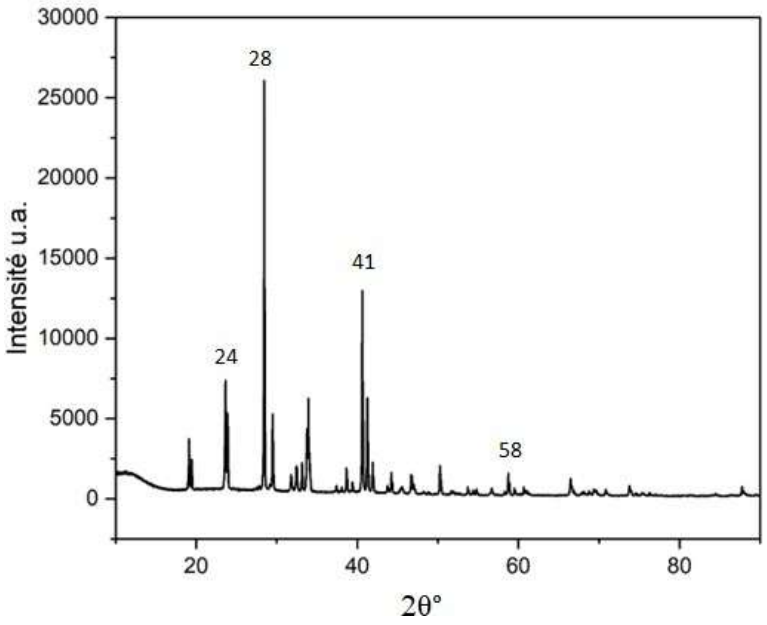

Figure 1. XRD Pattern of HA

1.5. Analysis of separated HS by Ultraviolet-Visible Spectroscopy

The E4/E6 ratio, based on absorbance at 472 and 665 nm, is a widely accepted parameter commonly used to characterize humic substances (HS), including humic acids (HA) and fulvic acids (FA). According to the literature, a ratio below 5 indicates the presence of HAs, which are known for their long carbon chains, high molecular weight, and aromatic structures. A ratio above 5 suggests the presence of FA, which are more oxygenated and carry more carboxylic groups. They are also generally lower in molecular weight and more chemically reactive (Koriko., 2010).

Table 1. Welt ratio Results

Abs	E_4 (465nm)	E_6 (665nm)	E_4/E_6
HA	0.087	0.02	4.35
FA	0.074	0.01	7.4

The data in (table 1) reflect these trends: the HA sample has an E_4/E_6 ratio of 4.35, confirming its identity as HA; the FA sample has a ratio of 7.4, indicating its identity as FA. These results align with previous studies' findings, including those by Aylaj et al. (2023). This validates the usefulness of the Welt ratio in distinguishing HS types based on their chemical characteristics and behaviour in soil systems.

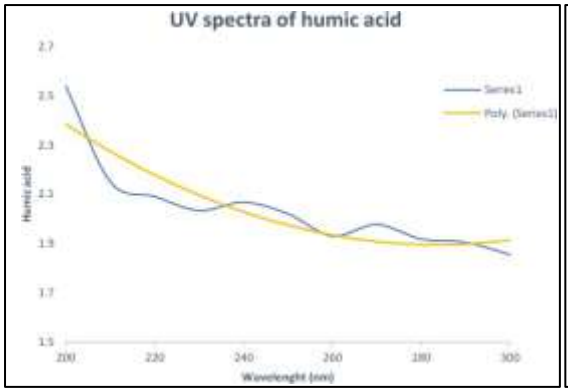

Figure 2a. spectra of HA from 200 to 300nm

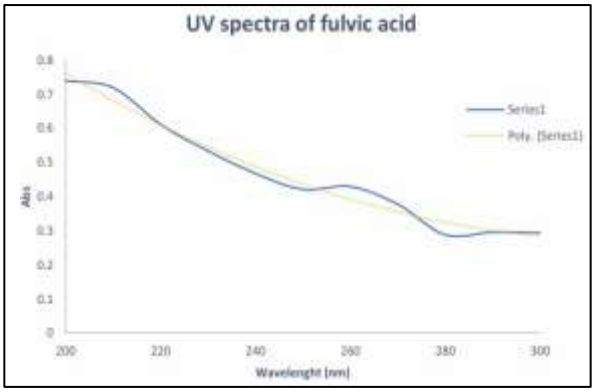

Figure 2b. UV spectra of FA from 200 to 300nm

The UV-Vis spectra of humic acid (HA) and fulvic acid (FA), recorded between 200 and 300 nm (Figures 2.a and 2.b), showed a steady drop in absorbance as the wavelength increased, which is a typical trait of humic substances. As noted by Uyguner et al (2007), these spectra tend to be broad and lack sharp peaks, with intensity gradually fading at higher wavelengths. Subtle shoulder bumps between 240 and 290 nm hint at the presence of aromatic or unsaturated structures like C=C, C=O, or N=N groups (Purmalis & Klavins, 2013). Interestingly, HA consistently absorbed more strongly than FA, particularly at shorter wavelengths, which points to its greater molecular complexity and larger size.

1.6. HA and FA Analysis using Fourier Transform Infrared Spectroscopy

The FTIR spectrum of humic acid (Figure 3.a) displays key peaks that reflect its complex molecular structure. A broad band between 3700–3400 cm^{-1} indicates O–H stretching, typical of hydroxyl groups in alcohols, phenols, and carboxylic acids. The peak near 2920 cm^{-1} corresponds to C–H stretching in aliphatic or methoxy groups, suggesting the presence of alkyl chains. A sharp peak at 1635 cm^{-1} is mainly associated with C=O stretching from carbonyl compounds and possibly C=C bonds in aromatic structures. A weaker band at 1380 cm^{-1} points to CH_3 bending vibrations, while peaks in the fingerprint region—such as those around 993, 800, and 472 cm^{-1}—are linked to aromatic C–H out-of-plane bending and possibly sulfur-containing groups (Koriko., 2010).

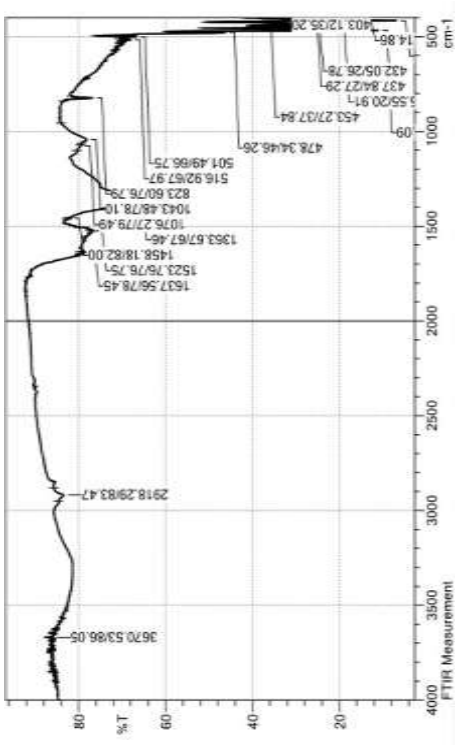

Figure 3.a. FTIR spectrum of HA

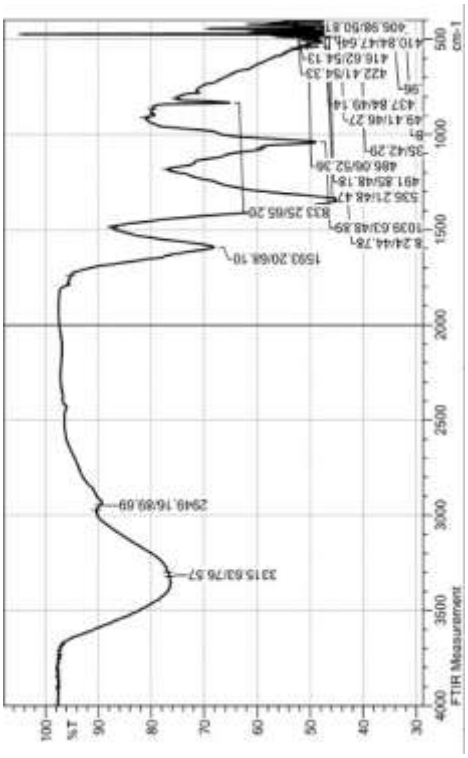

Figure 3.b. FTIR spectrum of FA

The FTIR spectrum of fulvic acid (Figure 3.b) shows several notable differences compared to that of humic acid. A broad peak around 3315 cm^{-1} indicates O–H stretching, pointing to the presence of hydroxyl groups, carboxylic acids, and phenols—similar to HA but slightly shifted. The band at 2949 cm^{-1} corresponds to C–H stretching vibrations from aliphatic chains or methoxy groups, suggesting FA also contains alkyl structures. A distinct peak at 1593 cm^{-1} is linked to C=C or C=O stretching in aromatic or conjugated systems, which appears more prominent in FA, indicating a greater presence of such structures. Additional peaks between 1170 and 1030 cm^{-1} are associated with C–O–C bonds, typical of esters or carbohydrates. Finally, signals below 600 cm^{-1} suggest the presence of aromatic or possibly sulfur-containing groups.

Both HA and FA share some functional groups, but FA is more reactive and contains more oxygen-based functional groups, such as phenols and carboxyls. Meanwhile, HA shows a more complex molecular structure, with more diverse functional groups, including sulphur-containing components and a higher degree of aromaticity. These differences in structure and functionality make each substance unique in its chemical behaviour and potential applications (Niu et al., 2019).

CONCLUSION

The study successfully isolated humic substances, particularly humic acid, from nitric-acid–treated cow manure compost and provided a detailed structural characterization using XRD, UV–Vis and FTIR spectroscopy. XRD analysis revealed that the extracted humic acid retains ordered, graphite-like aromatic domains together with additional crystalline features, indicating a structured but chemically heterogeneous macromolecule.

UV–Vis measurements, including the E4/E6 ratio and spectral shape, confirmed the clear differentiation between humic acid and fulvic acid, in line with their expected molecular size, degree of condensation and oxygenation, and supported their correct assignment as distinct humic fractions. FTIR spectra further highlighted both shared and distinct functional groups in HA and FA, showing that fulvic acid is richer in oxygen-containing, more reactive moieties, whereas humic acid displays greater aromaticity and a broader diversity of functional groups, including possible sulphur-containing structures.

Taken together, these results demonstrate that cow manure compost, after nitric-acid pretreatment, is a suitable and valuable source of structurally well-defined humic fractions with complementary properties, making them promising candidates for use as soil conditioners and functional inputs in sustainable agriculture. The distinct structural features and reactivities of HA and FA identified in this work can guide their targeted application in improving soil quality, nutrient dynamics and remediation of contaminated environments

REFERENCES

- Aylaj, M., Sisouane, M., Tahiri, S., Mouchrif, Y., & El Krati, M. (2023). Effects of humic acid extracted from organic waste composts on Turnip culture (Brassica rapa subsp. rapa) in a sandy soil. Journal of Ecological Engineering, 24(7).
- Balmori, D. M., Domínguez, C. Y. A., Carreras, C. R., Rebatos, S. M., Farías, L. B. P., Izquierdo, F. G., ... & García, A. C. (2019). Foliar application of humic liquid extract from vermicompost improves garlic (Allium sativum L.) production and fruit quality. *International Journal of Recycling of Organic Waste in Agriculture*, *8* (Suppl 1), 103-112.
- Cristina, G., Camelin, E., Ottone, C., Garofalo, S. F., Jorquera, L., Castro, M., ... & Tommasi, T. (2020). Recovery of humic acids from anaerobic sewage sludge: Extraction, characterization and encapsulation in alginate beads. *International Journal of Biological Macromolecules*, *164*, 277-285.

COMPARISON OF VOLATILE AROMA PROFILES OF NATURALLY GROWING DAFFODIL (Narcissus tazetta L.) FLOWERS FROM ADANA AND MERSIN PROVINCES

Yakup POLAT[1], Hatice DEMİRCİOĞLU[2], Şevket ALP[3], Nesibe Ebru KAFKAS[4]*

[1,2,4]Çukurova University, Faculty of Agriculture, Department of Horticulture, Adana, Türkiye

[3]Van Yüzüncü Yıl University, Faculty of Architecture and Design, Department of Landscape Architecture, Van, Türkiye

**Corresponding author: yakupyyu@gmail.com*

ABSTRACT

Daffodil (*Narcissus tazetta* L.) is an important geophyte for cut-flower production, landscape design, potted-plant use, and the perfumery and cosmetics industries because of its natural distribution across the Mediterranean Basin, showy flower clusters, and characteristic fragrance. The presence of native and naturalized Narcissus taxa in Türkiye makes this plant group important not only as ornamental material but also as a genetic resource with a long-standing place in collective cultural memory through its distinctive scent. This study aimed to characterize the volatile aroma profiles of naturally occurring N. tazetta flowers from Adana and Mersin provinces and to compare regional differences. Volatile organic compounds in the flower samples were analyzed using headspace solid-phase microextraction coupled with gas chromatography–mass spectrometry (HS-SPME/GC-MS), classified by chemical group, and evaluated according to their relative percentages in the total volatile fraction. The results revealed clear chemical differentiation between the Adana and Mersin populations. Ketones were dominant in the Adana samples (56.26%), whereas the Mersin samples exhibited a more balanced profile comprising ketones (37.90%), alcohols (33.47%), and terpenes (15.56%). The Adana population was characterized by a high proportion of 1-(2-methylphenyl)ethanone, while the Mersin population contained higher levels of linalool (21.15%) and (E)-β-ocimene (9.65%). These findings indicate that natural N. tazetta populations warrant further evaluation for aromatic genotype selection, ornamental breeding, perfumery and cosmetic applications, and conservation of genetic resources.

Keywords: Aroma profile, Daffodil, HS-SPME/GC-MS, Natural population, *Narcissus tazetta* L, Volatile organic compounds.

1. INTRODUCTION

Narcissus L. is a bulbous geophyte genus in the family Amaryllidaceae, with a broad distribution extending from the Mediterranean Basin to southern Europe, North Africa, and parts of Asia. Although the Iberian Peninsula is regarded as a major center of diversity for the genus, *Narcissus tazetta* L. is among the species notable for its extensive range, from the

Mediterranean coasts to China and Japan (Fernandes, 1968; Davis, 1984; Blanchard, 1990; Mathew, 2002; Kington, 1989; Rivera et al., 2003). The occurrence of native and naturalized Narcissus taxa in the flora of Türkiye makes the country an important reservoir of genetic resources for the genus (Alp et al., 2015).

N. tazetta is considered one of the most widespread naturally occurring daffodil species in Türkiye. Alp et al. (2015) reported that the species occurs naturally along the Black Sea, Aegean, Marmara, and Mediterranean coastal belts as well as in Southeastern Anatolia, and that two subspecies and double-flowered forms are found in Anatolia. More recently, Zeybekoğlu et al. (2025) investigated *N. serotinus* s.l. populations from southwestern Türkiye using a cytogenomic approach and demonstrated pronounced cytogenetic diversity associated with polyploidy and hybridization in this taxonomically complex group, emphasizing the importance of Türkiye as a region for speciation and hybridization within Narcissus.

Historically, daffodils have been cultivated in Anatolia and throughout the Mediterranean cultural landscape for the pleasant fragrance of their flowers, becoming part of urban culture and traditional garden heritage. Different forms were reportedly cultivated in southern Anatolia during the Roman period and in İstanbul during the Ottoman era, and some forms were subsequently introduced to Europe through İstanbul (Baytop and Mathew, 1984; Zarifikhosroshahi et al., 2021). Today, daffodils are used as garden perennials, cut flowers, potted plants, and outdoor ornamentals; their fragrant flowers also have value for the perfumery and cosmetics industries (Hanks, 2002; Zarifikhosroshahi et al., 2021).

Floral scent is a complex trait produced by varying proportions and combinations of volatile organic compounds. These compounds may function as ecological signals in plant–pollinator interactions while also having economic value in the perfumery, cosmetics, aromatherapy, and ornamental-plant sectors (Jurgens et al., 2000; Kim et al., 2000). Headspace solid-phase microextraction (HS-SPME), particularly when coupled with GC-MS, is widely used for floral scent analysis because it allows volatile compounds to be sampled with minimal disturbance of the natural scent profile (Barták et al., 2003; Chen et al., 2013). However, the quantitative composition of floral volatiles may be influenced by geographic environment, ecological conditions, harvest time, and flowering stage (Edris et al., 2008).

In a previous study on aroma compounds of *N. tazetta* ecotypes originating from Türkiye, volatile constituents of flowers collected from İzmir, Siirt, and Şırnak/Cizre were identified by HS-SPME/GC-MS, with β-ocimene and benzyl acetate reported among the principal aroma compounds (Zarifikhosroshahi et al., 2021). That study demonstrated that natural ecotypes from different regions of Türkiye may differ in aroma composition. Nevertheless, the comparative aroma profiles of natural populations from Adana and Mersin, both located within the Mediterranean coastal belt, merit separate investigation.

The aim of this study was therefore to determine the volatile organic compound profiles of naturally occurring *N. tazetta* flowers from Adana and Mersin provinces using HS-SPME/GC-MS, compare differences in chemical groups and dominant compounds between the two regions, and evaluate the findings in relation to aromatic genotype selection, ornamental plant breeding, perfumery and cosmetics applications, and conservation of natural populations.

2. MATERIALS AND METHODS

2.1. Plant material and sampling

The plant material consisted of *N. tazetta* flowers collected from naturally occurring populations in Adana and Mersin provinces. Samples were obtained during the natural flowering period from healthy, fully opened flowers. The two locations were selected because both provinces are situated within the Mediterranean coastal zone, fall within the natural distribution range of *N. tazetta*, and contain local populations traditionally recognized for their pronounced fragrance. After collection, flowers were transported to the laboratory under conditions designed to minimize the loss of volatile compounds, and analyses were conducted without delay.

2.2. HS-SPME/GC-MS analysis

Volatile organic compounds in the flower samples were determined by headspace solid-phase microextraction coupled with gas chromatography–mass spectrometry (HS-SPME/GC-MS). HS-SPME is a rapid, solvent-free sample-preparation technique in which volatile compounds released from floral material into the headspace are adsorbed onto a coated fiber. Compared with thermal extraction methods such as hydrodistillation, this approach is preferred in floral-scent studies because it can provide a closer representation of the flower's natural volatile profile (Barták et al., 2003; Chen et al., 2013; Zarifikhosroshahi et al., 2021).

During analysis, volatile compounds released from the flower samples were adsorbed onto an SPME fiber and subsequently thermally desorbed into the GC-MS system for separation and identification. Compound identification was based on retention time, retention index, and mass-spectral library matches. Identified compounds were classified into the major chemical groups of aldehydes, alcohols, esters, acids, ketones, and terpenes.

2.3. Data evaluation

Each compound detected in the Adana and Mersin samples was evaluated according to its relative percentage of the total volatile compounds. First, the overall distributions of the major chemical groups were compared, after which the principal compounds within each group were examined. The findings were interpreted in terms of regional differences in aroma profile, potential chemotypic differentiation, and aromatic genotype selection. Because the study was descriptive and comparative in nature, the results were evaluated on the basis of relative volatile-compound percentages.

3. RESULTS

3.1. Regional distribution of volatile-compound groups

The volatile-compound composition of naturally occurring N. tazetta flowers differed between the Adana and Mersin populations. Ketones were the dominant chemical group in the Adana population, accounting for 56.26% of the total profile. In the Mersin population, ketones accounted for 37.90%, whereas alcohols (33.47%) and terpenes (15.56%) occurred at substantially higher proportions than in Adana (Table 1).

Table 1. Distribution of volatile-compound groups in naturally occurring N. tazetta flowers from Adana and Mersin (%)

Chemical group	Adana (%)	Mersin (%)	Regional pattern
Aldehydes	–	0.40	Detected only at a low level in Mersin
Alcohols	25.51	33.47	Higher in Mersin
Esters	11.32	12.17	Similar in the two regions
Acids	0.46	0.50	Very low and similar in both regions
Ketones	56.26	37.90	Markedly higher in Adana
Terpenes	6.45	15.56	Markedly higher in Mersin

3.2. Dominant aroma compounds

Among the compounds identified, 1-(2-methylphenyl)ethanone was the most abundant ketone in both regions. It represented 56.26% of the total volatile compounds in Adana and 37.71% in Mersin. Linalool was markedly more abundant in Mersin (21.15%) than in Adana (11.33%). Similarly, (E)-β-ocimene accounted for 9.65% in Mersin but only 2.77% in Adana. Benzyl acetate was detected at comparable levels in Adana (3.08%) and Mersin (2.76%) (Table 2).

Table 2. Major volatile compounds detected in naturally occurring N. tazetta flowers from Adana and Mersin (%)

Chemical group	Compound	Adana (%)	Mersin (%)	Interpretation
Ketone	1-(2-Methylphenyl)ethanone	56.26	37.71	Dominant compound defining the Adana profile
Alcohol	Linalool	11.33	21.15	Key compound contributing to the floral character of Mersin
Ester	Benzyl acetate	3.08	2.76	Comparable levels in both regions
Ester	Hydrocinnamyl acetate	5.08	5.44	High and similar in both regions
Terpene	(E)-β-Ocimene	2.77	9.65	Markedly higher in Mersin
Terpene	3,7-Dimethyl-1,3,6-octatriene	1.47	3.33	Higher in Mersin
Alcohol	1,8-Cineole	1.44	4.06	Higher in Mersin
Alcohol	Benzenepropanol	3.62	5.11	Higher in Mersin

3.3. Detailed results by compound group

Among aldehydes, hexanal was detected only in the Mersin samples, at 0.40%. Although present at a low level, hexanal may contribute green and fresh odor notes. No aldehyde was detected in the Adana samples at a reportable proportion of the total profile.

Alcohols constituted an important compound group in both regions; however, their total proportion was higher in Mersin (33.47%) than in Adana (25.51%). This difference was mainly attributable to higher levels of linalool, 1,8-cineole, and benzenepropanol in the Mersin samples. The particularly high linalool content in Mersin (21.15%) suggests that this population may be distinguished by a stronger floral scent character.

The total ester fractions were similar in Adana (11.32%) and Mersin (12.17%). Benzyl acetate and hydrocinnamyl acetate were among the major esters in both populations. Previous studies have identified benzyl acetate as one of the characteristic aroma compounds of N. tazetta and other Narcissus taxa; its occurrence in both the Adana and Mersin populations is therefore

consistent with the literature (Mookherjee et al., 1989; Chen et al., 2013; Zarifikhosroshahi et al., 2021). Ketones were the principal aroma-compound group in the Adana population. Their total proportion was 56.26% in Adana compared with 37.90% in Mersin. The high value observed in Adana was largely attributable to 1-(2-methylphenyl)ethanone, indicating that the Adana population has a distinctive ketone-dominated chemical profile.

The Mersin population was clearly distinguished by its terpene fraction. Total terpenes accounted for 15.56% in Mersin compared with 6.45% in Adana. This difference was primarily associated with the high proportion of (E)-β-ocimene in Mersin (9.65%). β-Ocimene has previously been reported as an important aroma compound in daffodils (Melliou et al., 2007; Chen et al., 2013; Ruíz-Ramón et al., 2014; Zarifikhosroshahi et al., 2021).

3.4. Detailed list of compounds

Table 3. Volatile compounds identified in Adana and Mersin samples and their relative abundances (%)

Chemical group	Compound	Adana (%)	Mersin (%)
Aldehydes	Hexanal	–	0.40
Alcohols	2-Ethyl-1-hexanol	0.12	–
Alcohols	Benzyl alcohol	0.63	–
Alcohols	1,8-Cineole	1.44	4.06
Alcohols	Linalool	11.33	21.15
Alcohols	Benzeneethanol	0.72	0.35
Alcohols	α-Terpineol	2.97	–
Alcohols	Benzenepropanol	3.62	5.11
Alcohols	Geraniol	0.11	–
Alcohols	O-Methoxybenzyl alcohol	0.19	0.18
Alcohols	2-Methoxy-benzeneethanol	3.11	1.77
Alcohols	3-Phenyl-2-propen-1-ol	–	0.20
Alcohols	2-Methoxy-benzenepropanol	1.27	0.65
Esters	(E)-3-Hexen-1-ol acetate	–	0.38
Esters	Acetic acid, hexyl ester	–	0.25
Esters	Benzyl acetate	3.08	2.76
Esters	Acetic acid, nonyl ester	–	0.21
Esters	Acetic acid, 2-phenylethyl ester	2.22	1.80
Esters	Hydrocinnamyl acetate	5.08	5.44
Esters	(Z)-3-Phenyl-2-propenoic acid, methyl ester	0.24	–
Esters	(E)-Cinnamyl acetate	–	0.22
Esters	Benzoic acid methyl ester	0.15	–
Esters	Isoeugenyl acetate	0.14	–
Esters	Benzyl benzoate	0.65	0.87
Acids	Acetic acid	0.46	0.50
Ketones	1-(2-Methylphenyl)ethanone	56.26	37.71
Ketones	4-(4-Methoxyphenyl)-2-butanone	–	0.19
Terpenes	Limonene	–	0.23
Terpenes	(E)-β-Ocimene	2.77	9.65
Terpenes	3,7-Dimethyl-1,3,6-octatriene	1.47	3.33
Terpenes	1,3,8-Para-menthatriene	0.29	0.31
Terpenes	2,6-Dimethyl-2,4,6-octatriene	–	0.87
Terpenes	1,3-Methoxy-benzene	0.10	–
Terpenes	1-Methoxy-4-(1-propenyl)-benzene	1.82	1.17

-: not detected

4. DISCUSSION

This study compared the volatile aroma profiles of naturally occurring N. tazetta flowers from Adana and Mersin provinces. The results showed that the two populations differed in both the

overall distribution of volatile-compound groups and the identity of their dominant compounds. These findings support the initial expectation that natural populations may exhibit regional differentiation in aroma profile. The dominance of ketones and the high proportion of 1-(2-methylphenyl)ethanone in the Adana population indicate a ketone-dominated chemical character, whereas the higher proportions of alcohols and terpenes in Mersin—particularly linalool and (E)-β-ocimene—suggest that these compounds play a greater role in defining the Mersin aroma profile.

The most striking finding was that ketones accounted for more than half of the total volatile profile in the Adana samples. In contrast, the lower ketone proportion and higher alcohol and terpene fractions in Mersin demonstrate that pronounced regional chemical differentiation may occur within the same species. This supports the view that natural populations should be evaluated not only on the basis of morphological and phenological traits but also according to their volatile-compound profiles when selecting aromatic genotypes.

4.1. Odor characteristics of the identified chemical groups

The sensory meaning of an aroma profile becomes more informative when the relative abundance of chemical groups is considered together with odor descriptors reported in the literature for the compounds that constitute those groups. Acetophenone-derived ketones, including 1-(2-methylphenyl)ethanone, which dominated the Adana profile, are generally associated with sweet, balsamic, almond-like, and heavy floral notes. The ketone-rich Adana profile may therefore be expected to produce an intense, sweet, full-bodied scent impression largely shaped by a single dominant compound.

In the Mersin population, linalool is associated with fresh, sweet, and floral notes; 1,8-cineole with cool, camphoraceous and eucalyptus-like notes; and (E)-β-ocimene with warm, herbaceous, and airy-floral notes. Hexanal, detected only in Mersin, may add a fresh-cut green-grass character that enhances perceived freshness. Benzyl acetate, which occurred at similar proportions in both populations, is a characteristic floral constituent of daffodil and jasmine scents and may therefore provide a shared floral identity. Taken together, the Mersin profile points toward a fresher, floral-terpenic, relatively complex, lighter, and more airy scent impression.

4.2. Potential effects of fragrance on human perception in landscape and cut-flower use

In landscape settings, fragrance is generally perceived outdoors at some distance from the plant, with volatile compounds dispersed by air movement. A Mersin-type profile dominated by highly volatile compounds with relatively low odor thresholds, such as linalool and (E)-β-ocimene, may have greater potential to create a fresh, pleasant, and relaxing scent impression around walkways, seating areas, and recreational spaces. Such fresh-floral emissions may contribute to a positive and invigorating user experience in outdoor environments. By contrast, the ketone-rich, intensely sweet Adana profile may be perceived less as a broadly dispersed fresh scent and more as a pronounced, full-bodied fragrance at close range, potentially making it more suitable for specialized settings where strong scent perception in close proximity is desired.

In cut-flower and indoor use, fragrance is perceived within a confined space and typically at close range. Under these conditions, the intense and persistent character of the ketone-

dominated Adana profile could readily fill an indoor environment; however, dominance by a single heavy-sweet note could, over time, be perceived as overpowering by some users. In contrast, the fresher, more balanced, floral-terpenic Mersin profile may provide a lighter and more refined scent impression that remains pleasant over a longer period indoors. The two populations may therefore offer different perceptual advantages depending on the distance and spatial context in which the fragrance is experienced.

4.3. Comparison with previous studies and methodological–sensory limitations

In the earlier study of Turkish ecotypes, β-ocimene and benzyl acetate were reported as major aroma constituents in samples from İzmir, Siirt, and Şırnak/Cizre, while both the number and relative abundance of compounds varied among locations (Zarifikhosroshahi et al., 2021). In the present study, the main differentiation between the Adana and Mersin samples was associated less with a β-ocimene–benzyl acetate axis and more with variation in ketones, linalool, and terpenes. Such differences may be related to ecological conditions at the collection sites, genetic structure of the populations, flowering stage, harvest time, and analytical conditions. Edris et al. (2008) likewise reported that the quantitative composition of floral aroma can vary with geographic environment and harvest time.

An important limitation is that odor perception cannot be explained solely by the percentage composition of volatile compounds. Odor thresholds differ substantially among compounds, and constituents such as linalool and (E)-β-ocimene may contribute disproportionately to perceived scent even when present at relatively low concentrations. In addition, synergistic and masking interactions among compounds may make the overall odor impression differ from the simple sum of individual components. Because the present study did not include a sensory panel or gas chromatography–olfactometry (GC-O), the interpretations of odor character and potential human perception presented above should be regarded as predictions based on odor descriptors reported in the literature and should be validated through sensory testing. Furthermore, HS-SPME/GC-MS results can be influenced by technical factors such as fiber type, extraction time, temperature, sample quantity, and the phenological stage of the flowers.

4.4. Conservation and genetic resource value

The findings demonstrate that natural daffodil populations in Türkiye should be regarded not only as components of floristic diversity or sources of ornamental plant material but also as valuable genetic resources in terms of aroma profile. Alp et al. (2015) reported that natural Narcissus populations in Türkiye occur particularly along the Taurus Mountains within the Mediterranean climatic zone and that native and naturalized populations are exposed to pressures such as urbanization, removal of gardens, and uncontrolled collection from the wild. In this context, the distinct aroma profiles observed in the Adana and Mersin populations, together with their potential suitability for different uses, provide an additional scientific rationale for conserving and domesticating local populations. Populations that are differentiated by volatile-compound profile may be maintained in ex situ collections, developed as controlled propagation material, and incorporated into ornamental breeding programs.

5. CONCLUSIONS

In this study, the volatile aroma profiles of naturally occurring N. tazetta flowers from Adana and Mersin provinces were characterized using HS-SPME/GC-MS and the two populations

were compared. The results showed that the populations exhibited distinct chemical profiles in terms of both volatile-compound groups and dominant constituents.

Ketones were the dominant chemical group in the Adana population (56.26%), with 1-(2-methylphenyl)ethanone alone accounting for 56.26% of the profile. In the Mersin population, ketones represented 37.90%, alcohols 33.47%, and terpenes 15.56%; linalool (21.15%) and (E)-β-ocimene (9.65%) were particularly prominent.

This chemical differentiation also points to two contrasting tendencies in scent character. The ketone-rich Adana profile may be associated with a sweet, full-bodied, and intense fragrance, whereas the Mersin profile, rich in linalool, 1,8-cineole, and (E)-β-ocimene, suggests a fresher, floral-terpenic, and more airy character. On this basis, Mersin-type populations with fresher and more diffusible fragrance profiles may be especially suitable for landscape settings around walking and resting areas, while Adana-type populations with stronger and more persistent fragrance may be more appropriate for cut-flower and specialized uses where scent is intended to be perceived at close range. These interpretations, however, are predictions based on odor descriptors reported for the identified compounds and should be validated through sensory analysis.

The study is limited to samples from two locations and did not include sensory evaluation. Accordingly, the findings represent the volatile-compound profiles of the sampled Adana and Mersin populations under the specific sampling conditions used here, and direct conclusions regarding fragrance preference or perceived scent intensity should not be drawn solely from chemical percentages. Broader generalization will require comparative analyses across multiple years, flowering stages, and a larger number of natural populations.

Based on the present findings, future studies should conduct multi-location aroma screening of natural N. tazetta populations; complement chemical analyses with gas chromatography–olfactometry (GC-O) and sensory panel tests to account for odor thresholds and synergistic effects; incorporate genotypes with contrasting fragrance and use profiles into ex situ collections; and develop domestication programs based on controlled propagation.

REFERENCES

Alp, Ş., Zeybekoğlu, E., Salman, A. and Özzambak, M.E. 2015. Ülkemizin doğal ve doğallaşmış nergis türleri ve karşılaştığı sorunlar. Selçuk Tarım Bilimleri Dergisi, 3(2): 304–308.

Barták, P., Bednář, P., Čáp, L., Ondráková, L. and Stránský, Z. 2003. SPME - A valuable tool for investigation of flower scent. Journal of Separation Science, 26(8): 715–721.

Baytop, T. and Mathew, B. 1984. The Bulbous Plants of Turkey. B.T. Batsford Ltd., London.

Blanchard, J.W. 1990. Narcissus: A Guide to Wild Daffodils. Alpine Garden Society, Woking.

Chen, H.C., Chi, H.S. and Lin, L.Y. 2013. Headspace solid-phase microextraction analysis of volatile components in Narcissus tazetta var. chinensis Roem. Molecules, 18(11): 13723–13734.

Davis, P.H. 1984. Flora of Turkey and the East Aegean Islands. Vol. 8. Edinburgh University Press, Edinburgh.

Edris, A.E., Chizzola, R. and Franz, C. 2008. Isolation and characterization of the volatile aroma compounds from the concrete headspace and the absolute of Jasminum sambac flowers grown in Egypt. European Food Research and Technology, 226(3): 621.
Fernandes, A. 1968. Keys to the identification of native and naturalized taxa of the genus Narcissus L. Daffodil and Tulip Year Book, 37–66.
Hanks, G.R. 2002. Narcissus and Daffodil: The Genus Narcissus. Taylor & Francis, London.
Jurgens, A., Webber, A.C. and Gottsberger, G. 2000. Floral scent compounds of Amazonian Annonaceae species pollinated by small beetles and thrips. Phytochemistry, 55(6): 551–558.
Kim, H.J., Kim, K., Kim, N.S. and Lee, D.S. 2000. Determination of floral fragrances of Rosa hybrida using solid-phase trapping-solvent extraction and gas chromatography-mass spectrometry. Journal of Chromatography A, 902(2): 389–404.
Kington, S. 1989. The International Daffodil Checklist. Royal Horticultural Society, London.
Mathew, B. 2002. Classification of the genus Narcissus. In: Hanks, G.R. (Ed.), Narcissus and Daffodil: The Genus Narcissus. Taylor & Francis, London.
Melliou, E., Kalpoutzakis, E., Tsitsa, E. and Magiatis, P. 2007. Composition of the essential oils of Narcissus tazetta and Narcissus serotinus from Greece. Journal of Essential Oil-Bearing Plants, 10(2): 101–103.
Mookherjee, B.D., Trenkle, R.W. and Wilson, R.A. 1989. Live vs. dead. Part II. A comparative analysis of the headspace volatiles of some important fragrance and flavor raw materials. Journal of Essential Oil Research, 1(2): 85–90.
Rivera, D., De Castro, C.O., Ruiz, S.R. and Ariza, F.A. 2003. The origin of cultivation and wild ancestors of daffodils (Narcissus subgenus Ajax) from an analysis of early illustrations. Scientia Horticulturae, 98(4): 307–330.
Ruíz-Ramón, F.F., Águila, D.J., Egea-Cortines, M. and Weiss, J. 2014. Optimization of fragrance extraction: daytime and flower age affect scent emission in simple and double narcissi. Industrial Crops and Products, 52: 671–678.
Zarifikhosroshahi, M., Alp, Ş. and Kafkas, N.E. 2021. Characterization of aroma compounds of Daffodil (Narcissus tazetta L.) ecotypes from Turkey. International Journal of Agriculture, Forestry and Life Sciences, 5(1): 101–105.
Zeybekoğlu, E., Koçyiğit, M., Alp, Ş., Tuna, M. and Özzambak, M.E. 2025. Cytogenomic differentiation of Narcissus serotinus s.l. in southwestern Turkey: Insights into polyploidy and hybridization. Sylwan, 169(10): 76–95.

DETERMINATION OF POMOLOGICAL AND CHEMICAL CHARACTERISTICS OF GILABURU (Viburnum Opulus L.) FRUITS GROWN IN TUŞBA DISTRICT, VAN PROVINCE

Yakup POLAT[1], Şevket ALP[2], Muzaffer BAYRAM[2], Ferit ÇELİK[3], Nesibe Ebru KAFKAS[4]

[1,4]Department of Horticulture, Faculty of Agriculture, Çukurova University, Adana, Türkiye
[2]Department of Landscape Architecture, Faculty of Architecture and Design, Van Yüzüncü Yıl University, Van, Türkiye
[3]Department of Horticulture, Faculty of Agriculture, Van Yüzüncü Yıl University, Van, Türkiye

Corresponding author email: yakupyyu@gmail.com

ABSTRACT

Gilaburu (*Viburnum opulus* L.) is a multipurpose shrub species in the family Adoxaceae that can be used as a fruit crop, ornamental plant, medicinal plant, and source of functional food ingredients. This study was conducted to determine selected pomological and chemical characteristics of gilaburu fruits grown in Tuşba district of Van Province and to evaluate the quality potential of the species under high-altitude, semi-arid conditions. Mean fruit weight, fruit length, fruit width, and cluster weight were 0.57 g, 9.30 mm, 10.19 mm, and 34.96 g, respectively. The fruit flesh ratio was 87.04%, and mean seed weight was 0.07 g. Color measurements yielded L*, a*, b*, Chroma, and Hue values of 27.32, 35.20, 26.68, 44.24, and 36.86°, respectively. Chemical analyses showed total soluble solids (TSS) of 13.3%, titratable acidity of 2.00%, and pH of 3.51. The findings indicate that gilaburu fruits grown under Van/Tuşba conditions, with their high flesh ratio, pronounced red coloration, suitable TSS content, and acidic character, have potential for use in juice, vinegar, fermented beverages, jam, marmalade, and as functional food ingredients. Owing to its showy flowers, red fruit clusters, and autumn foliage coloration, gilaburu also stands out as a multipurpose shrub that can provide both aesthetic and productive functions in edible landscape designs.

Keywords: Edible landscapes, Functional food, Gilaburu, Pomological characteristics, Semi-arid area, *Viburnum opulus* L.

1. INTRODUCTİON

Interest in functional foods, local genetic resources, alternative fruit species capable of adapting to climate change, and multifunctional landscape plants has increased steadily in recent years. Population growth, food-security concerns, urbanization pressure, and the effects of climate change on agricultural production have created a need to consider not only conventional high-yielding crops but also wild or semi-domesticated species with high nutritional and ecological value. In this context, edible fruit-bearing shrubs offer considerable potential for both food production and landscape design.

Gilaburu (*Viburnum opulus* L.) is a deciduous, perennial species in the family Adoxaceae that typically grows as a shrub. Internationally, the species is known by common names such as European cranberrybush, guelder rose, snowball tree, and cramp bark, whereas in Türkiye it is known by regional names including gilaburu, gilaboru, gilebor, and giligili (Kajszczak et al., 2020; Karabulut and Kaynarca, 2024). Its natural distribution extends across Europe, North Africa, northern Asia, Russia, and parts of Türkiye. In Türkiye, it is traditionally recognized

particularly in Kayseri and several other regions, where the fruits are processed into local products.

Gilaburu fruits are bright red, sour, and astringent, and are characterized by high acidity. Although these sensory properties limit direct fresh consumption, the fruits can be processed into products such as juice, fermented beverages, vinegar, jam, marmalade, pickles, tea, and dietary supplements (Güney and Gündeşli, 2022; Karabulut and Kaynarca, 2024). Previous studies have shown that gilaburu fruits are rich in phenolic compounds, organic acids, flavonoids, anthocyanins, vitamins, minerals, and various other bioactive constituents (Kajszczak et al., 2020; Ömeroğlu Gülada et al., 2025). Accordingly, the species is regarded as a valuable raw material for the functional food industry because of its antioxidant, antimicrobial, anti-inflammatory, and other biological activities.

Gilaburu is noteworthy not only for food and medicinal uses but also from a landscape architecture perspective. Its shrub form, showy white flowers, bright red fruit clusters, and autumn foliage coloration give the plant high visual value. The edible landscape approach is a sustainable landscape concept in which fruit, vegetables, medicinal and aromatic plants, and edible ornamentals are integrated according to aesthetic design principles, thereby combining productive and visual functions (Concklin et al., 2025; Zheng and Chou, 2023). In this context, gilaburu stands out as a multifunctional shrub capable of providing both aesthetic value and edible products.

Ecologically, *V. opulus* is most commonly associated with moist habitats, streambanks, forest clearings, and soils rich in organic matter. Nevertheless, selection studies conducted in the Kayseri region reported that gilaburu genotypes occur at elevations of 1,290–1,645 m, indicating that the species can also be considered for high-altitude environments (Gündoğar, 2013). Van Province, by contrast, differs markedly from typical gilaburu habitats because of its high elevation, continental climate, cold winters, dry summers, and semi-arid ecological conditions. Determining the quality characteristics of gilaburu fruits grown in Tuşba district, Van Province, is therefore important for evaluating the species' performance outside its typical natural habitat and its potential for adaptation.

The aim of this study was to determine selected pomological and chemical characteristics of gilaburu fruits grown in Tuşba district, Van Province, and, based on the findings, to assess the species' potential for adaptation, functional-food use, and edible-landscape applications under high-altitude, semi-arid conditions.

2. MATERİALS AND METHODS

2.1. Plant Material

The study material consisted of mature fruit samples collected from gilaburu (*Viburnum opulus* L.) plants grown in Tuşba district of Van Province. Tuşba is located in the Eastern Anatolia Region and is characterized by high elevation, a continental climate, cold winters, dry summers, and semi-arid ecological conditions. In this respect, the study area differs from the moist natural habitats with which *V. opulus* is generally associated. Fruit samples were collected at full maturity, when the fruits had developed their characteristic red color (Figure 1.). Healthy, undamaged fruit clusters representative of the plants were selected for sampling. The collected material was transported to the laboratory under appropriate conditions, and analyses were conducted shortly thereafter.

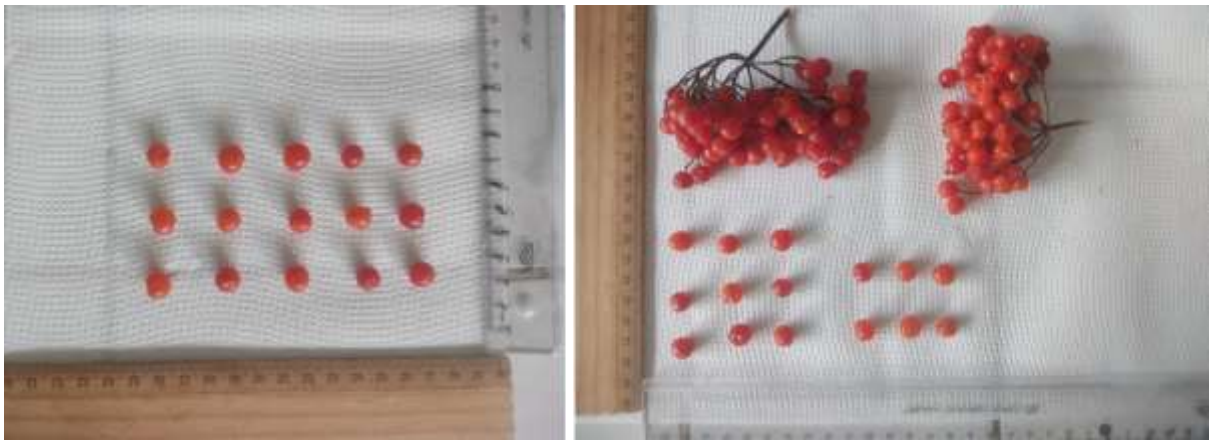

Figure 1. Fruits used as material.

2.2. Pomological Analyses

Pomological analyses included fruit weight, fruit length, fruit width, skin thickness, cluster weight, fruit flesh ratio, and seed characteristics. Fruit weight was measured in grams (g) using a precision balance (Polat et al., 2024). Fruit length and width were measured in millimeters (mm) with a digital caliper. Cluster weight was determined by weighing intact fruit clusters, and skin thickness was measured with a digital caliper.

Seed weight was determined by separating the seeds from the fruits and weighing them on a precision balance. Fruit flesh ratio was calculated as a percentage (%) by subtracting seed weight from fruit weight and dividing the resulting value by fruit weight. These parameters were used to assess the suitability of the fruit for fresh-market and processed products.

2.3. Color Analyses

Fruit skin color was measured on five fruits randomly selected from each of three replicates to represent the genotype, using a Minolta CR-400 colorimeter (Minolta Co., Tokyo, Japan). Measurements were expressed in the CIELAB color space as L*, a*, and b* values. L* indicates lightness on a scale from black (0) to white (100), while a* and b* define chromatic coordinates in the color plane perpendicular to L*. Positive a* values indicate red and negative a* values green; positive b* values indicate yellow and negative b* values blue. Before measurement, the instrument was calibrated using a standard white calibration plate. Chroma (C*), which describes color saturation or vividness, and Hue angle (h°), which describes the dominant color component, were calculated from the measured a* and b* values (Polat et al., 2024).

$C^* = (a^{*2} + b^{*2})^{1/2}$, $h^\circ = \tan^{-1}(b^*/a^*)$

2.4. Chemical Analyses

Pieces were taken from randomly selected fruits and pressed to obtain juice. The juice was filtered and pooled to produce a homogeneous juice sample.

Total soluble solids (TSS): TSS content was determined as °Brix using a digital refractometer (Atago, Japan). A portion of fruit juice was placed on the refractometer prism, and the reading was recorded as percentage TSS (Uzun et al., 2015).

Titratable acidity: A 1 mL aliquot of fruit juice was titrated with 0.1 N NaOH to pH 8.1, and titratable acidity was expressed as a percentage of malic acid (Cemeroğlu, 2007).

pH determination: A 10 mL fruit juice sample was transferred to a suitable container, and the electrode of a digital pH meter was immersed in the sample. The value was recorded after the reading had stabilized.

2.5. Data Analysis

The data obtained in the study were evaluated using descriptive statistical methods. For each trait, the mean, minimum, maximum, standard deviation (SD), and coefficient of variation (CV, %) were calculated. The findings were interpreted in terms of fruit quality, suitability for processed products, functional-food potential, and the feasibility of growing gilaburu under high-altitude, semi-arid conditions.

3. RESULTS

The pomological, color, and chemical characteristics of gilaburu (*Viburnum opulus* L.) fruits grown in Tuşba district, Van Province, are presented in Table 1.

Table 1. Pomological, color, and chemical characteristics of gilaburu fruits grown in Tuşba district, Van Province.

Characteristic	Mean	Min.	Max.	SD	CV (%)
Fruit weight (g)	0.565	0.520	0.610	0.031	5.48
Fruit length (mm)	9.298	8.900	9.700	0.273	2.94
Fruit width (mm)	10.185	9.800	10.600	0.259	2.54
Skin thickness (mm)	0.430	0.380	0.480	0.032	7.44
Cluster weight (g)	34.955	29.820	40.910	5.020	14.36
Fruit flesh ratio (%)	87.035	84.800	89.200	1.820	2.09
Seed weight (g)	0.073	0.060	0.090	0.010	13.70
Seed length (mm)	7.763	7.400	8.100	0.228	2.94
Seed width (mm)	8.693	8.300	9.100	0.254	2.92
Seed thickness (mm)	1.823	1.780	1.860	0.022	1.22
L* (Lightness)	27.315	25.100	29.800	1.520	5.57
a* (Redness)	35.203	32.700	37.500	1.620	4.60
b* (Yellowness)	26.678	20.900	32.100	5.348	20.05
Chroma (Saturation)	44.243	41.200	47.100	1.945	4.40
Hue angle (°)	36.863	34.200	39.100	1.610	4.37
TSS (%)	13.300	13.200	13.400	-	-
Titratable acidity (%)	2.003	1.980	2.040	0.026	1.31
pH	3.513	3.500	3.520	-	-

SD: Standard deviation; CV: Coefficient of variation; TSS: Total soluble solids

For pomological characteristics, mean fruit weight was 0.565 g, with values ranging from 0.520 to 0.610 g. Mean fruit length and width were 9.298 mm and 10.185 mm, respectively. These results indicate that the fruits were slightly wider than they were long, giving them a nearly round morphology. Mean skin thickness was 0.430 mm, ranging from 0.380 to 0.480 mm. Mean

cluster weight was 34.955 g, with a range of 29.820–40.910 g. Among the pomological traits, cluster weight had the highest coefficient of variation (14.36%), indicating greater sample-to-sample variability than the other parameters.

The mean fruit flesh ratio was 87.035%. Its low coefficient of variation (2.09%) indicates that this trait was highly consistent among samples. Mean seed weight was 0.073 g, while mean seed length, width, and thickness were 7.763, 8.693, and 1.823 mm, respectively. The very low coefficient of variation for seed thickness (1.22%) indicates that this was one of the most stable traits among the samples.

For fruit skin color, the mean L* value was 27.315, indicating a relatively dark appearance. The positive and high a* value (mean 35.203) reflects pronounced red coloration. The mean b* value was 26.678. Mean Chroma was 44.243, indicating high color saturation, while the mean Hue angle was 36.863°. Taken together, these color parameters show that gilaburu fruits grown under Tuşba conditions had a vivid, saturated, and visually attractive red color. Among the color traits, b* showed the greatest variation (20.05%).

For chemical characteristics, mean titratable acidity was 2.003%, with values ranging from 1.980 to 2.040%. The low coefficient of variation for acidity (1.31%) indicates that the fruits were highly homogeneous in this respect. Mean TSS was 13.300%, and mean pH was 3.513. A TSS value of approximately 13% together with a pH of around 3.5 indicates that the fruits had a distinctly acidic character.

4. DİSCUSSİON

The findings of this study show that gilaburu (V. opulus) can produce fruit under the conditions of Tuşba district, Van Province, and that these fruits possess quality attributes suitable for processing. Given that the species is most commonly associated with moist habitats and soils rich in organic matter, the results obtained in a high-altitude, semi-arid environment are noteworthy in terms of the ecological adaptability of gilaburu. They suggest that the species may be considered not only in its traditional growing regions but also in other ecological settings where suitable microclimatic and management conditions can be provided.

Overall, the pomological characteristics of fruits grown under Tuşba conditions were consistent with the typical morphology of gilaburu fruit. Their nearly round shape, occurrence in clusters, and high fruit flesh ratio (87.04%) support the species' potential for processed products. Selection studies conducted in the Kayseri region have shown that gilaburu genotypes can be evaluated at high elevations and may differ substantially in fruit quality characteristics (Gündoğar, 2013). The present findings likewise indicate that ecological conditions, genotype, and growing environment may play important roles in determining fruit characteristics.

A high fruit flesh ratio is an important characteristic that enhances the suitability of gilaburu for processed products such as juice, purée, vinegar, fermented beverages, jam, and marmalade. The relatively low seed proportion compared with the flesh may also be considered advantageous in terms of processing yield. In this context, the Tuşba samples showed a profile more suited to processed-product development than to direct fresh consumption. The astringent and sour taste of gilaburu fruit can limit fresh consumption; however, these same characteristics may contribute desirable flavor and acidity balance in fermented or heat-processed products.

Color parameters provide important indications of both visual quality and landscape value. The high Chroma value (44.24) and pronounced a* value (35.20) indicate a vivid, saturated red fruit color, a feature of value for both consumer perception and potential use as a natural color source in the food industry. Numerous studies have reported that gilaburu is rich in phenolic compounds, anthocyanins, and other bioactive constituents (Kajszczak et al., 2020; Karabulut and Kaynarca, 2024; Ömeroğlu Gülada et al., 2025). The high red color intensity observed here

may therefore be regarded not only as an indicator of visual quality but also as a preliminary finding warranting more detailed investigation of pigment content and functional compounds.

The chemical characteristics show that gilaburu fruits grown in Tuşba had a distinctly acidic character and a soluble-solids content suitable for processed products. A pH of 3.51 and titratable acidity of 2.00% may offer technological advantages in products such as juice, vinegar, fermented beverages, and jam. Arslan et al. (2018) reported a TSS content of 11.3% and a pH of 3.20 for wild-growing gilaburu fruits from Ardahan and its surroundings. The higher pH observed in the present study suggests that the chemical characteristics of gilaburu fruits may vary with growing region. Such differences may result from genotype, ecological conditions, growing environment, and harvest time. Nevertheless, the functional-food potential of gilaburu cannot be comprehensively characterized on the basis of TSS, pH, and titratable acidity alone. Future studies should therefore determine phenolic content, anthocyanin content, organic-acid profiles, antioxidant capacity, mineral composition, and sensory properties to provide a more complete assessment of the nutritional and functional value of gilaburu fruits.

This study also provides a useful basis for evaluating the suitability of gilaburu for edible landscape design. The edible landscape approach integrates food production with aesthetic and ecological functions within the same design; plants are expected not only to yield edible products but also to contribute visual quality, support pollinators, and create seasonal landscape effects (Concklin et al., 2025; Zheng and Chou, 2023). With its shrub form, showy white flowers, bright red fruit clusters, autumn foliage coloration, and edible fruits, gilaburu is particularly well suited to this approach and stands out as a multifunctional shrub that can serve both productive and aesthetic purposes in high-altitude, semi-arid regions.

The study was based on a limited number of samples, and the results should therefore be regarded as a preliminary assessment of gilaburu fruits grown under Tuşba conditions. Studies covering multiple years, different locations, and larger sample groups will be needed to evaluate the regional adaptability of the species more reliably. In addition, separate assessment of irrigation, soil properties, management conditions, genotypic variation, and microclimatic effects will be important for explaining the performance of gilaburu in semi-arid, high-altitude environments.

5. CONCLUSİON

This study showed that gilaburu (Viburnum opulus L.) fruits grown in Tuşba district, Van Province, possess quality characteristics that may be valuable under high-altitude, semi-arid conditions. The results demonstrate that the species can produce fruit under these ecological conditions, that the fruits have characteristics suitable for processed products, and that the plant has noteworthy potential for edible landscape design.

With a high fruit flesh ratio (87.04%), pronounced red coloration (Chroma: 44.24), acidic character (titratable acidity: 2.00%; pH: 3.51), and total soluble solids content of 13.3%, gilaburu fruits have potential for use in juice, vinegar, fermented beverages, jam, marmalade, and as functional food ingredients. Although their astringent and sour taste may restrict fresh consumption, these same attributes can become advantages in processed products by contributing characteristic flavor, color, and acidity balance.

The results suggest that Viburnum opulus may be considered as an alternative fruit species for Tuşba and other high-altitude, semi-arid areas with similar conditions. Because of its showy flowers, red fruit clusters, autumn foliage coloration, and edible fruits, the species may also be used as a multipurpose shrub in edible landscape applications, where it can combine aesthetic and productive functions.

This study provides preliminary evidence regarding the cultivation potential of gilaburu outside its typical natural habitat. To establish regional adaptation more reliably, future studies should include multiple years and locations, larger sample sizes, and advanced biochemical analyses, including antioxidant capacity, total phenolic content, anthocyanin content, organic-acid profiles, mineral composition, and sensory evaluation.

REFERENCES

Arslan, M., Erbil, N., & Murathan, Z. tuğba. (2018). Ardahan ve Çevresinde Yabani Olarak Yetişen Gilaburu Meyve Ekstraktının Antimikrobiyal, Antioksidan ve Antimutajenik Aktivitelerinin Araştırılması. Gümüşhane Üniversitesi Fen Bilimleri Dergisi, 8(1), 18-25. https://doi.org/10.17714/gumusfenbil.294719

Cemeroğlu. B.. 2007. Gıda Analizleri. (s.168-171) Gıda Teknolojisi Derneği Yayınları. No:34. Ankara. Türkiye

Concklin, M., Wallace, V., Siegel-Miles, A. 2025. Sustainable Edible Landscapes. UConn Extension, College of Agriculture, Health and Natural Resources, University of Connecticut.

Gündoğar, R. 2013. Kayseri Yöresinde Yetişen Gilebor (*Viburnum opulus* L.) Genotiplerinin Belirlenmesi. Doktora Tezi, Ordu Üniversitesi Fen Bilimleri Enstitüsü, Bahçe Bitkileri Anabilim Dalı, Ordu, 61 s.

Güney, M., Gündeşli, M.A. 2022. The necessities of cranberry bush (*Viburnum opulus*) evaluation for horticultural cultivation. MAS Journal of Applied Sciences, 7(4): 1033–1041. DOI: 10.5281/zenodo.7379762.

Kajszczak, D., Zakłos-Szyda, M., Podsędek, A. 2020. *Viburnum opulus* L.—A review of phytochemistry and biological effects. Nutrients, 12(11): 3398. DOI: 10.3390/nu12113398.

Karabulut, Ş.Y., Kaynarca, G.B. 2024. Gilaburu (*Viburnum opulus* L.) meyvesi: Önemi, bileşimi ve gıda endüstrisinde kullanım potansiyeli. Niğde Ömer Halisdemir Üniversitesi Mühendislik Bilimleri Dergisi, 13(3): 1047–1055. DOI: 10.28948/ngumuh.1315024.

Ömeroğlu Gülada, B., Złotek, U., Gawlik, U., Kowalczyk, D., Taşkın, D., Taşkın, T., Jakubczyk, A., Güneş, F.E. 2025. Impact of *Viburnum opulus* L. fruit extracts on the physicochemical, sensory, and bioactive properties of wheat waffles. Molecules, 30: 4677. DOI: 10.3390/molecules30244677.

Taşkın, O., Aşık, B.B., İzli, N. 2019. Gilaburu bitkisinin (*Viburnum opulus* L.) meyve, sap ve yaprağının mineral içeriği. KSÜ Tarım ve Doğa Dergisi, 22(2): 178–182. DOI: 10.18016/ksutarimdoga.vi.484362.

Uzun. S.. Balta. M. F.. Kaya. T. ve Karakaya. O.. 2015. Çamaş (ordu) yöresinde yetişen yerel elma genotiplerinin fenolojik ve pomolojik özellikleri. Akademik Ziraat Dergisi. 2 (1). 28-33.

Polat, Y., Çelik, F., & Küçüker, E. (2024). Şanlıurfa Yöresinde Selekte Edilen Nar (Punica granatum L.) Genetik Kaynaklarının Agromorfolojik ve Fiziko-Kimyasal Özellikleri. Turkish Journal of Agricultural and Natural Sciences, 11(1), 226-238.

Zheng, Z.W., Chou, R.J. 2023. The impact and future of edible landscapes on sustainable urban development: A systematic review of the literature. Urban Forestry & Urban Greening, 84: 127930. DOI: 10.1016/j.ufug.2023.127930.

IDENTIFICATION OF BIOFILM-ASSOCIATED MICROORGANISMS IN ALBANIAN DAIRY PROCESSING ENVIRONMENTS USING SELECTIVE CULTURE MEDIA AND MALDI-TOF MASS SPECTROMETRY

Arbnora Durmishaj[1,2], Rozeta Hasalliu[1]

1 Department of Food Science and Biotechnology Agricultural University of Tirana, Albania

2 Department of Engineering and Food Technology, University "Isa Boletini"-Mitrovicë, Kosovo

Corresponding author e-mail: arbnora.durmishaj@gmail.com

ABSTRACT

Biofilms formed on food-contact surfaces in dairy processing environments represent a major challenge to food safety due to their ability to harbor persistent microorganisms that can withstand routine cleaning and disinfection procedures. The present study aimed to identify the cultivable microbiota associated with biofilm-positive environmental samples collected from dairy processing facilities by integrating conventional microbiological cultivation with matrix-assisted laser desorption/ionization time-of-flight mass spectrometry (MALDI-TOF MS). Environmental swab samples previously confirmed as biofilm-positive were cultured on Bengal Rose Chloramphenicol Agar, de Man, Rogosa and Sharpe (MRS) Agar, Baird-Parker Agar supplemented with Egg Yolk Tellurite, Coliform Chromogenic Agar, and Tryptic Soy Agar. Colonies displaying distinct morphological characteristics were purified and identified by MALDI-TOF MS. A total of **47 representative isolates** were successfully identified, corresponding to **14 bacterial species** belonging to **eight genera**. The identified microbiota was dominated by members of the genera ***Staphylococcus, Enterococcus, and Escherichia, while Citrobacter, Corynebacterium, Klebsiella, Enterobacter, and Rothia*** were recovered less frequently. The predominant species included *Staphylococcus aureus*, *Escherichia coli*, *Enterococcus faecalis*, *Enterococcus hirae*, *Staphylococcus saprophyticus*, *Citrobacter freundii*, *Corynebacterium falsenii*, and *Klebsiella oxytoca*. Additional isolates comprised *Staphylococcus lugdunensis*, *Staphylococcus warneri*, *Staphylococcus haemolyticus*, *Staphylococcus carnosus*, *Enterobacter cloacae*, and *Rothia kristinae*. The recovery of hygiene indicator bacteria together with opportunistic pathogens demonstrates the high microbial diversity associated with dairy biofilms and emphasizes their potential role as reservoirs of persistent contamination. The combined approach enabled comprehensive characterization of microorganisms colonizing biofilm-positive surfaces, demonstrating the coexistence of diverse bacterial and fungal populations within dairy processing environments. Selective culture media facilitated the targeted isolation of specific microbial groups, while MALDI-TOF MS provided rapid, accurate, and reproducible identification, significantly reducing the time required for microbial characterization compared with conventional biochemical methods. The findings contribute to a better understanding of microbial persistence in food-processing environments and provide valuable information for improving environmental monitoring programs, optimizing sanitation protocols, and developing effective biofilm control strategies to enhance dairy product safety and quality.

Keywords: Biofilms; Dairy processing environment; MALDI-TOF MS; Selective culture media; Microbial identification; Food safety.

INTRODUCTION

Biofilms formed on food-contact surfaces in dairy processing environments represent a major challenge to food safety due to their ability to harbor persistent microorganisms that can withstand routine cleaning and disinfection procedures. Product contamination by pathogenic and spoilage bacteria has been linked to the presence of biofilms [2]. Microorganisms on wet surfaces have the ability to aggregate, grow into microcolonies, and produce biofilm. Biofilms are matrix protected microbial communities, often attached to a surface. It is the key feature that distinguishes a biofilm from attached bacteria and facilitates increased resistance to disinfecting agents, UV-radiation and desiccation [1].

This study aimed to identify the cultivable microbiota associated with biofilm-positive environmental samples collected from Albanian dairy processing facilities by integrating conventional microbiological cultivation with matrix-assisted laser desorption-ionization time-of-flight mass spectrometry (MALDI-TOF MS).

MATERIAL AND METHOD

Environmental swab samples previously confirmed as biofilm-positive were collected from dairy processing environments. The samples were cultured on a range of selective and non-selective culture media to facilitate the recovery of different microbial groups, including **Bengal Rose Chloramphenicol Agar (BRCA), de Man, Rogosa and Sharpe (MRS) Agar, Baird-Parker Agar supplemented with Egg Yolk Tellurite, Coliform Chromogenic Agar,** and **Tryptic Soy Agar (TSA).** Following incubation, colonies exhibiting distinct morphological characteristics were selected and subjected to purification on **TSA** to obtain isolated cultures suitable for subsequent identification. The purified isolates were identified using matrix-assisted laser desorption/ionization time-of-flight mass spectrometry (MALDI-TOF MS). The resulting identification data were subsequently analyzed using descriptive statistics to summarize the distribution of the recovered isolates according to bacterial species and genus (figure 1).

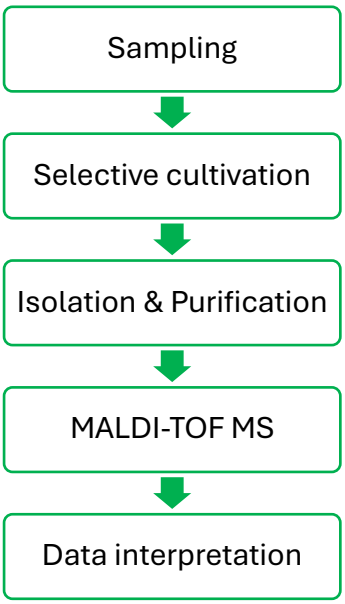

Figure 1. Study workflow

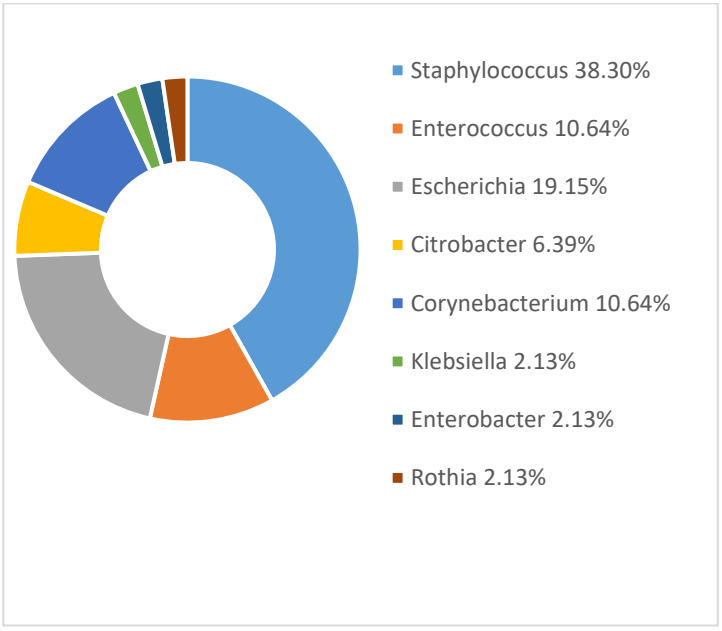

Figure 2. Distribution of 47 isolates across 8 genera

RESULTS AND DISCUSSION

The microbiological characterization of biofilm-positive surfaces revealed a diverse bacterial community comprising 47 isolates, 14 species belonging to eight genera (figure 2). The microbial profile was predominantly represented by *Staphylococcus*, *Enterococcus*, and *Escherichia*, genera frequently associated with food-processing environments and capable of persisting on environmental surfaces. Their recovery from biofilm-positive sites indicates that these microorganisms may contribute to the establishment and maintenance of microbial communities on surfaces within dairy-processing facilities.

The detection of potentially pathogenic or opportunistic microorganisms, including *Staphylococcus aureus*, *Escherichia coli*, and *Enterococcus* spp., is of particular relevance from a food-safety perspective. Their presence on environmental surfaces may represent a potential source of cross-contamination, particularly when such sites are located in areas with direct or indirect contact with equipment or food products. The association of these microorganisms with biofilm-positive surfaces is also important because biofilm-associated cells can be more difficult to remove through routine cleaning and disinfection procedures, potentially contributing to their persistence within the processing environment.

In addition to the predominant genera, the recovery of *Citrobacter*, *Corynebacterium*, *Klebsiella*, *Enterobacter*, and *Rothia* demonstrates the heterogeneous nature of the microbiota associated with biofilm-positive surfaces. The presence of multiple bacterial genera suggests that dairy-processing biofilms should be considered complex microbial communities rather than populations dominated by a single organism. Such diversity may reflect differences in surface characteristics, environmental conditions, nutrient availability, moisture, and cleaning practices across sampling locations.

MALDI-TOF MS provided species-level identification of the recovered isolates and allowed the characterization of the microbial diversity associated with the biofilm-positive samples. The technique offered a rapid and reproducible approach for identification and was particularly useful for distinguishing closely related bacterial isolates within the recovered microbiota. Its application therefore represents a valuable tool for environmental microbiological monitoring and for obtaining a more detailed characterization of microorganisms associated with biofilm formation.

CONCLUSIONS

Biofilm-positive environments in Albanian dairies harbor a diverse microbiota comprised of 47 isolates, 14 species and 8 genera.
The predominance of *Staphylococcus*, *Enterococcus* and *Escherichia* underscores their key role in biofilm persistence.
Selective culture media combined with MALDI-TOF MS provides a powerful approach for comprehensive microbial characterization
These findings support the improvement of environmental monitoring, sanitation protocols and biofilm control strategies to enhance dairy product safety and quality.

REFERENCES

[1] Bridier A, Sanchez-Vizuete P, Guilbaud M, Piard JC, Naïtali M, Briandet R. 2015. Biofilm-associated persistence of food-borne pathogens. Food Microbiology, 45(PB):167–178.

[2] Chmielewski RAN, Frank JFF. 2003. Biofilm formation and control in food processing facilities. Comprehensive Reviews in Food Science And Food Safety, 2(1):22–32.
[3] Maes S, Huu SN, Heyndrickx M, Weyenberg S Van, Steenackers H, Verplaetse A, Vackier T, Sampers I, Raes K, De Reu K. 2017. Evaluation of two surface sampling methods for microbiological and chemical analyses to assess the presence of biofilms in food companies. Journal of Food Protection, 80(12):2022–2028.
[4] Masuko, T., Minami, A., Iwasaki, N., Majima, T., Nishimura, S., Lee, Y.C. 2005. Carbohydrate analysis by a phenol-sulfuric acid method in microplate format. Anal. Biochem., 339, pp. 69-72, 10.1016/j.ab.2004.12.001.
[5] Quijada NM, Mann E, Wagner M, Rodríguez-Lázaro D, Hernández M, Schmitz-Esser S. 2018. Autochthonous facility-specific microbiota dominates washed-rind Austrian hard cheese surfaces and its production environment. International Journal of Food Microbiology, 267(August 2017):54–61.
[6] Wagner EM, Pracser N, Thalguter S, Fischel K, Rammer N, Pospíšilová L, Alispahic M, Wagner M, Rychli K. 2020. Identification of biofilm hotspots in a meat processing environment: Detection of spoilage bacteria in multi-species biofilms. International Journal of Food Microbiology, 328:108668.
[7] Weber M, Liedtke J, Plattes S, Lipski A. 2019. Bacterial community composition of biofilms in milking machines of two dairy farms assessed by a combination of culture dependent and -independent methods. PLoS ONE, 14(9):1–21.

INTEGRATED CULTURE, PCR AND MALDI-TOF WORKFLOW FOR IMPROVED DETECTION OF LISTERIA SPP. IN ALBANIAN DAIRY PROCESSING ENVIRONMENTS

Arbnora Durmishaj[1], Rozeta Hasalliu[1], Kathrin Rychli[2], Anila Kopali[1]

1 Department of Food Science and Biotechnology Agricultural University of Tirana, Albania

2 Centre for Food Science and Veterinary Public Health, University of Veterinary Medicine Vienna, Vienna, Austria

Corresponding author e-mail: arbnora.durmishaj@gmail.com

ABSTRACT

Listeria monocytogenes remains a major concern in dairy processing due to its persistence on environmental surfaces and its potential to contaminate ready-to-eat products. This study evaluated an integrated workflow combining selective culture, conventional PCR and MALDI-TOF MS for the confirmation of *Listeria* isolates recovered from Albanian dairy processing environments. A total of 100 environmental swab samples were collected from three Albanian dairy processing plants. Following a two-step enrichment and selective cultivation protocol, presumptive colonies were confirmed by conventional PCR targeting the 16S rRNA and hly genes and subsequently identified by MALDI-TOF MS. Among the 100 environmental samples, **13 samples produced presumptive** *Listeria* **colonies** after selective cultivation. PCR analysis confirmed the presence of **nine** *Listeria* **spp. isolates and one** *Listeria monocytogenes* **isolate**, while the remaining presumptive colonies were PCR-negative. MALDI-TOF analysis demonstrated that *Listeria innocua* was the predominant environmental species (90%), whereas *L. monocytogenes* represented only 10% of confirmed isolates. Positive isolates originated from both food-contact and non-food-contact surfaces, indicating multiple potential contamination niches within dairy facilities. The findings demonstrate that integrating selective culture with molecular and proteomic confirmation significantly improves the reliability of environmental *Listeria* surveillance. The combined workflow provides an effective approach for identifying contamination hotspots, supporting targeted sanitation strategies, improving routine microbiological monitoring, and strengthening food safety management systems in dairy processing plants

Keywords: *Listeria monocytogenes*; *Listeria innocua*; dairy industry; environmental monitoring; PCR; MALDI-TOF MS.

INTRODUCTION

Microbial life abounds on surfaces in both natural and industrial environments, one of which is the food industry. A solid substrate, water and some nutrients are sufficient to allow the construction of a microbial fortress, a so-called biofilm. [1]

The foodborne pathogen *Listeria monocytogenes*, responsible for listeriosis a rare but severe infection disease, can survive in the food processing environment for month or even years. So-

called persistent *L. monocytogenes* strains greatly increase the risk of (re)contamination of food products, and are therefore a great challenge for food safety. [2]

Listeria monocytogenes is able to form biofilms on various surfaces and this ability is thought to contribute to persistence in the environment and on contact surfaces in the food industry. Extracellular DNA (eDNA) is a component of the biofilm matrix of many bacterial species and was shown to play a role in biofilm establishment of *L. monocytogenes*. [4]

In dairy-processing environments, the organism may be introduced through raw materials, water, animals, personnel or equipment and may persist in wet and difficult-to-clean niches such as drains, floors, pipes, hoses, joints and equipment surfaces.

Detection of presumptive *Listeria* colonies by selective culture is useful for recovery of viable microorganisms but does not by itself provide reliable species-level identification. Molecular methods can provide additional confirmation, while MALDI-TOF MS can support rapid species-level identification of cultured isolates. An integrated workflow therefore combines complementary information from culture, molecular detection and proteomic identification

MATERIAL AND METHOD

Sampling strategy

Environmental samples were collected from three Albanian dairy companies. Sampling covered six processing zones: reception, pasteurization, production, packaging, storage and cooling room. Sampling sites were selected with a focus on critical locations associated with product spoilage and potential cross-contamination. Samples were collected following routine cleaning and disinfection procedures.

Enrichment and selective cultivation

Samples were processed using a two-step enrichment and selective cultivation workflow. The first enrichment was performed in Half Fraser Broth, followed by plating on RapidLMono and PALCAM selective media. After evaluation of the first plating step, a second enrichment was performed in Full Fraser Broth, followed by a second plating step on RapidLMono and PALCAM. Colonies with morphology compatible with *Listeria* were considered presumptive isolates and were selected for further confirmation.

Conventional PCR and gel electrophoresis

Presumptive isolates were subjected to conventional PCR targeting 16S rRNA and hly. The 16S rRNA target was used for confirmation of the *Listeria* genus, while hly was included as a virulence-associated target relevant to *L. monocytogenes*. PCR products were evaluated by gel electrophoresis. Isolates producing the expected molecular confirmation pattern were retained for downstream identification.

MALDI-TOF MS identification

PCR-confirmed isolates were subjected to MALDI-TOF MS for species-level identification. The resulting protein spectral profiles were compared with the available reference database, allowing assignment of isolates to *Listeria* species.

Table 1: From sampling to species identification results

Analytical stage	n	%
Environmental samples	100	100%
Presumptive *Listeria* samples	13	13%
PCR-confirmed isolates	10	10%
L. innocua among confirmed isolates	9	90%
L. monocytogenes among confirmed isolates	1	10%

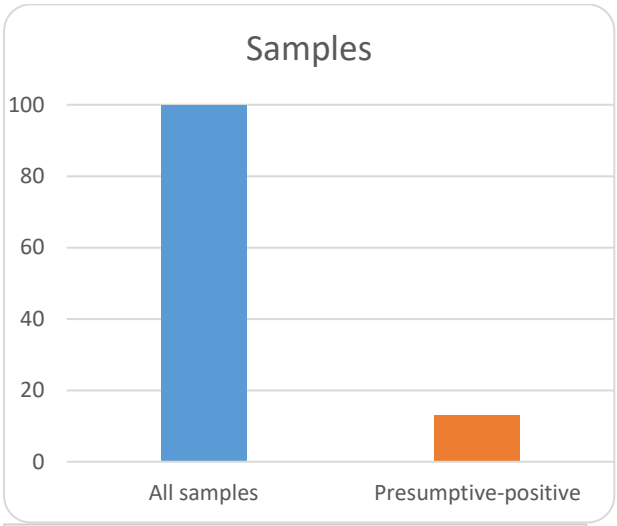

Figure 1. Presumptive isolates

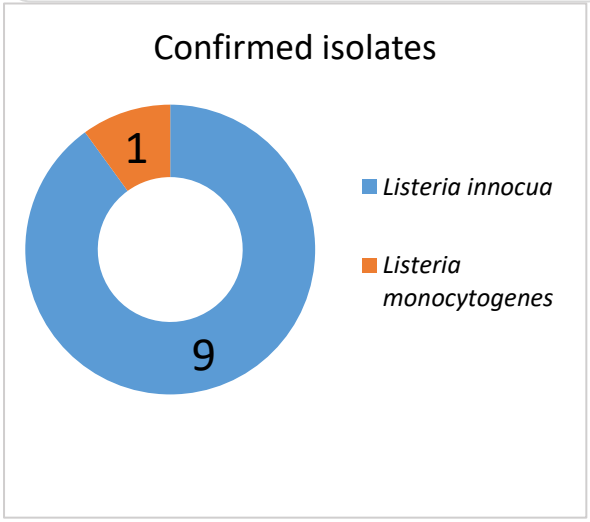

Figure 2. MALDI-TOF results

RESULTS AND DISCUSSION

A total of 100 environmental swabs were investigated. Presumptive *Listeria* colonies were recovered from 13 samples, corresponding to a presumptive-positive rate of 13% (figure 1). Of the 13 presumptive colonies, 10 were confirmed by PCR, corresponding to a confirmation rate of 76.9% among presumptive colonies. The confirmed set comprised nine other *Listeria spp*. isolates and one *Listeria monocytogenes* isolate according to the study workflow and subsequent species-level identification.

MALDI-TOF MS identified nine of the 10 confirmed isolates as *Listeria innocua* and one as *Listeria monocytogenes* (figure 2). Therefore, *L. innocua* accounted for 90% of confirmed isolates and *L. monocytogenes* for 10%. *L. innocua* was the predominant *Listeria* species recovered from the investigated dairy-processing environments.

Positive isolates originated from different environmental surface types, including both food-contact and non-food-contact surfaces. Food-contact sites represent a potential direct route to product contamination, whereas non-food-contact sites may function as environmental reservoirs or transfer points. The distribution of positive sites indicates that environmental monitoring should not be restricted to direct food-contact surfaces.

The present study demonstrates the value of an integrated analytical strategy for environmental surveillance of *Listeria* in dairy-processing facilities. The three analytical stages used in this study provide complementary information. Selective culture supports recovery of viable presumptive isolates; PCR provides molecular confirmation; and MALDI-TOF MS enables rapid species-level identification of cultured isolates. The combination can therefore increase confidence in environmental surveillance compared with reliance on a single analytical method.

CONCLUSIONS

A total of 100 environmental samples were investigated across three Albanian dairy plants. Thirteen samples (13%) yielded presumptive *Listeria* colonies. Ten isolates were confirmed by PCR. *L. innocua* predominated (90%) among confirmed isolates while *L. monocytogenes* represented 10%. Positive isolates were recovered from both food-contact and non-food-contact surfaces The combination of selective culture, PCR and MALDI-TOF MS provides a practical integrated strategy for environmental *Listeria* surveillance.

REFERENCES

[1] Bridier A, Sanchez-Vizuete P, Guilbaud M, Piard JC, Naïtali M, Briandet R. 2015. Biofilm-associated persistence of food-borne pathogens. Food Microbiology, 45(PB):167–178.

[2] Rychli, K., Grunert, T., Ciolacu, L., Zaiser, A., Razzazi-Fazeli, E., Schmitz-Esser, S., Ehling-Schulz, M., Wagner, M. 2016 **Exoproteome analysis reveals higher abundance of proteins linked to alkaline stress in persistent** *Listeria monocytogenes* **strains.** Int. J. Food Microbiol., 218 (2016), pp. 17-26, 10.1016/j.ijfoodmicro.2015.11.002

[3] Wagner EM, Pracser N, Thalguter S, Fischel K, Rammer N, Pospíšilová L, Alispahic M, Wagner M, Rychli K. 2020. Identification of biofilm hotspots in a meat processing environment: Detection of spoilage bacteria in multi-species biofilms. International Journal of Food Microbiology, 328:108668.

[4] Zetzmann, M., Okshevsky, M., Endres, J., Sedlag, A., Caccia, N., Auchter, M., Waidmann, M.S., Desvay, M., Meyer, R.L., Reidel, C.U. 2015. **DNase-sensitive and -resistant modes of biofilm formation by** *Listeria monocytogenes* Front.Microbiol., 6 pp. 1-11, 10.3389/fmicb.2015.01428

DOPING EFFECT ON BIPHENYLENE NANOTUBES: A DFT STUDY

Serap Senturk Dalgic[1], Dilek Kuzalic Burucu[2], Seyfettin Dalgic[1], Fatma Kandemirli[3]*

[1] Department of Physics, Faculty of Science, Trakya University, Edirne, Turkey
[2] Electrical and Electronic Engineering Department, Faculty of Engineering and Architecture, Istanbul Beykent University, Istanbul, Turkey
[3] Biomedical Engineering Department, Faculty of Engineering and Architecture, Kastamonu University, Kastamonu, Turkey
Corresponding author e-mail: dserap@yahoo.com

ABSTRACT

Biphenylene nanotubes (BPNTs) have recently emerged as promising one-dimensional carbon nanostructures owing to their unique non-hexagonal topology. BPNTs are carbon allotropes composed of alternating four-, six-, and eight-membered carbon rings. BPNTs offer a clear alternative to Carbon Nanotubes (CNTs) because their high surface reactivity is well suited to sensor applications. This study aims to comprehensively evaluate the potential of pristine BPNTs and Al-, Si-atom-doped BPNTs (Al-BPNTs) and (Si-BPNTs) for nanosensor applications by examining their structural, electronic, and quantum-chemical properties using Density Functional Theory (DFT) calculations. As reported, pristine BPNTs are semi-metallic, irrespective of their chirality. Changes in the electronic band gap (E_g), the density of states (DOS) of pristine BPNT, and the charge density difference (CDD) due to Al-, Si- atom doping have been observed in both gas and water phases. The results reveal that the BPNT exhibits intrinsic metallic behaviour with a high density of states at the Fermi level, making it a highly sensitive platform for nanosensor applications. Doping effects are dominant. A widening of the band gap is observed with Si- atom doping. The Fermi energy level and HOMO-LUMO energies change slightly, and the sensor signal remains detectable. These findings demonstrate that atomic doping provides a practical strategy for tuning the electronic properties of BPNTs for future nanosensor designs.

Keywords: Metal -Doped Biphenylene Nanotubes (BPNTs), Sensors, DFT

INTRODUCTION

The biphenylene network contains four-, six- and eight-membered carbon rings. Hudspeth et al. (2010) examined its sheet and one-dimensional derivatives, including nanotubes; Fan et al. (2021) subsequently synthesized the two-dimensional network. Atomic doping changes its electronic and catalytic behaviour (Ren et al., 2022). Esfandiarpour et al. (2022) investigated CO_2 adsorption on pristine, Al- and Si-doped BPNTs, providing a gas-phase reference for the isolated supports.

Related nanotube studies connect optimized geometries and charge distributions with frontier orbitals in BMSF-BENZ, tretinoin and Aldara systems (Al-Sawaff et al., 2021; Genç et al., 2025; Dalgic et al., 2025). Here, pristine, Al- and Si-doped BPNTs are compared in gas and implicit water using the same hydrogen-terminated cluster. The analysis covers geometry, cohesive energy, electrostatic potential, frontier orbitals and charge redistribution, together with the effect of hydrogen polarization functions.

MATERIAL AND METHOD

The neutral clusters contain 56 atoms: $C_{48}H_8$ or $C_{47}H_8M$ (M = Al, Si), with eight terminal hydrogens and a dopant fraction of 2.083%. Pristine and Si-BPNT are restricted singlets; Al-BPNT has 303 electrons and is an unrestricted doublet. For Al, $\langle S^2 \rangle$ is 0.9232–0.9333 before annihilation and 0.7692–0.7706 afterward (pure doublet: 0.75). The alpha-HOMO of Al-BPNT is singly occupied.

DFT calculations (Hohenberg and Kohn, 1964; Kohn and Sham, 1965) used Gaussian 09, Revision E.01 for clusters and A.02 for some isolated atoms. M06-2X (Zhao and Truhlar, 2008) was used with gas/6-31G(d) (G-d), gas/6-31G(d,p) (G-dp) and water/6-31G(d) (W-d). The (d,p) basis adds hydrogen polarization (Hariharan and Pople, 1973). Water used the integral equation formalism polarizable continuum model (IEFPCM) with ε = 78.3553 (Tomasi et al., 2005; Scalmani and Frisch, 2010).

Geometry optimization and harmonic frequency analysis used default integration settings for clusters and UltraFine for isolated atoms in water. Final optimizations met all four convergence criteria. Some subsequent frequency jobs exceeded the maximum-displacement threshold while satisfying both force criteria.

The signed cohesive energy per atom was calculated from cluster and neutral isolated-atom SCF energies at the corresponding basis set and environment:

$$E_{coh} = \frac{E_{cluster} - \Sigma_A n_A E_A(atom)}{N}, \; N = 56 \quad (1)$$

N = 56 includes hydrogens. More negative E_{coh} indicates stronger binding relative to triplet C and Si, and doublet Al and H references. Energies used 1 hartree = 27.211386245988 eV. The gas-to-water change was $E_{water}(R_{water}) - E_{gas}(R_{gas})$ at 6-31G(d). This energy difference includes continuum polarization and geometry relaxation.

The gap between the highest occupied molecular orbital (HOMO) and the lowest unoccupied molecular orbital (LUMO) was evaluated separately for each spin channel s:

$$E_{g,s} = \varepsilon_{LUMO,s} - \varepsilon_{HOMO,s} \quad (2)$$

Chemical potential (μ), hardness (η) and electrophilicity (ω) were estimated from frontier orbitals (Parr and Pearson, 1983; Parr et al., 1999):

$$\mu = \frac{\varepsilon_{HOMO} + \varepsilon_{LUMO}}{2}; \; \eta = \frac{E_g}{2}; \; \omega = \frac{\mu^2}{2\eta} \quad (3)$$

The Fermi-energy estimate was $E_{F,s} = \mu_s$, and the work-function estimate was $\Phi_s \approx -E_{F,s}$ with $E_{vac} = 0$. For Al, these are spin-channel estimates. Changes in E_g and Φ were calculated relative to pristine BPNT under the same condition:

$$\Delta X\,(\%) = 100 \times \frac{X_{doped} - X_{pristine}}{X_{pristine}} \quad (4)$$

Gas (G-d) and water (W-d) density of states (DOS) spectra span −10 to +3 eV. For Al, $0.5(DOS_\alpha + DOS_\beta)$ is shown with the alpha gap. Natural population analysis (NPA) used total density, including both Al spin populations (Reed et al., 1985). GaussView (Dennington et al., 2009) displayed structures, orbitals and molecular electrostatic potentials (MEP), mapped from −0.025 to +0.025 a.u.

Charge density difference (CDD) maps used Multiwfn (Lu and Chen, 2012; Lu, 2024) and VESTA (Momma and Izumi, 2011):

$$\Delta\rho_{def}(r) = \rho_{BPNT}(r) - \sum_A \rho_{A,ref}(r - R_A) \quad (5)$$

Positive and negative deformation densities denote accumulation and depletion relative to free atoms. The ±0.004 e/bohr³ maps were compared with NPA charges; neutral C and H reference densities were gas-phase quintet and doublet states, respectively.

RESULTS AND DISCUSSION

Optimized geometries and cohesive energies

All nine structures retain the BPNT framework and have 162 positive harmonic frequencies; the lowest frequencies range from 110.040 to 127.432 cm^{-1}. Figure 1 compares the optimized gas and water structures. The Si-C distances are shorter than Al-C distances under every condition (Table 1). Water slightly lengthens the Al-C contacts, whereas the Si-C distances change in both directions.

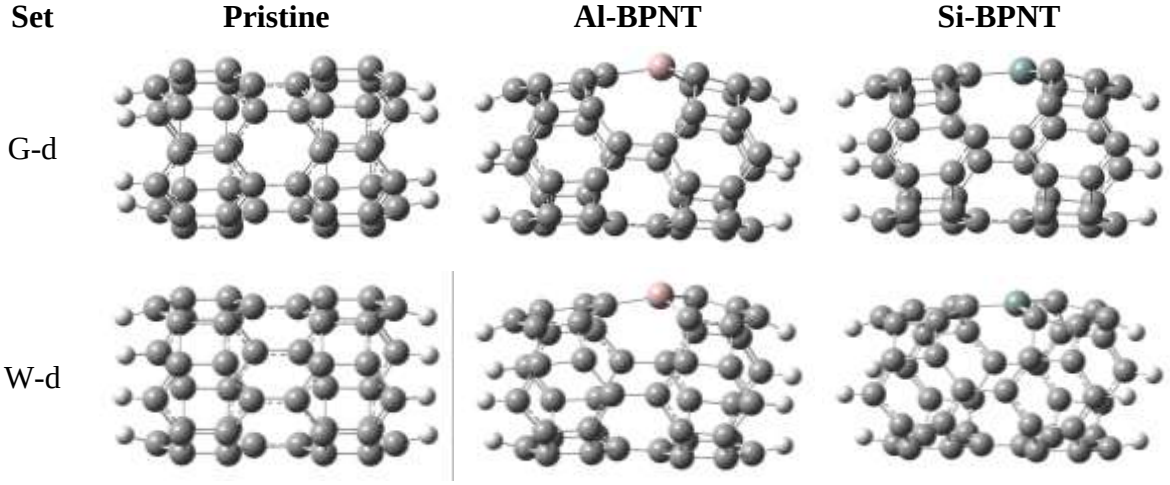

Figure 1. Optimized structures in gas (G-d, top) and water (W-d, bottom). Carbon is grey, hydrogen white, Al pink and Si teal.

Table 1. Local geometry, dopant NPA charge, lowest harmonic frequency and cohesive energy.

Set	Model	M–C range (Å)	q_M (e)	ν_{min} (cm^{-1})	E_{coh} (eV $atom^{-1}$)
G-d	Pristine	—	—	127.432	−6.110
G-d	Al	1.857–1.881	+1.756	115.367	−6.005
G-d	Si	1.735–1.773	+1.747	112.797	−6.027
G-dp	Pristine	—	—	121.337	−6.115
G-dp	Al	1.857–1.881	+1.756	115.517	−6.010
G-dp	Si	1.735–1.773	+1.747	112.878	−6.032
W-d	Pristine	—	—	122.394	−6.097
W-d	Al	1.861–1.884	+1.781	116.372	−5.991
W-d	Si	1.739–1.769	+1.794	110.040	−6.013

M–C spans the three nearest carbon atoms. Cohesive energies include all 56 atoms.

Cohesive energies become less negative in the order pristine, Si-BPNT and Al-BPNT. Pristine BPNT thus has the strongest binding relative to the selected atomic references. The gas-to-water cluster energy changes are −6.873, −7.524 and −7.212 kcal mol^{-1} for pristine, Al- and Si-BPNT, respectively.

Molecular electrostatic potential

The MEP maps show an approximately symmetric distribution for pristine BPNT and local changes near the dopants (Figure 2). The two gas-phase basis sets give similar patterns. Water changes the contrast over the central framework, particularly for Si-BPNT.

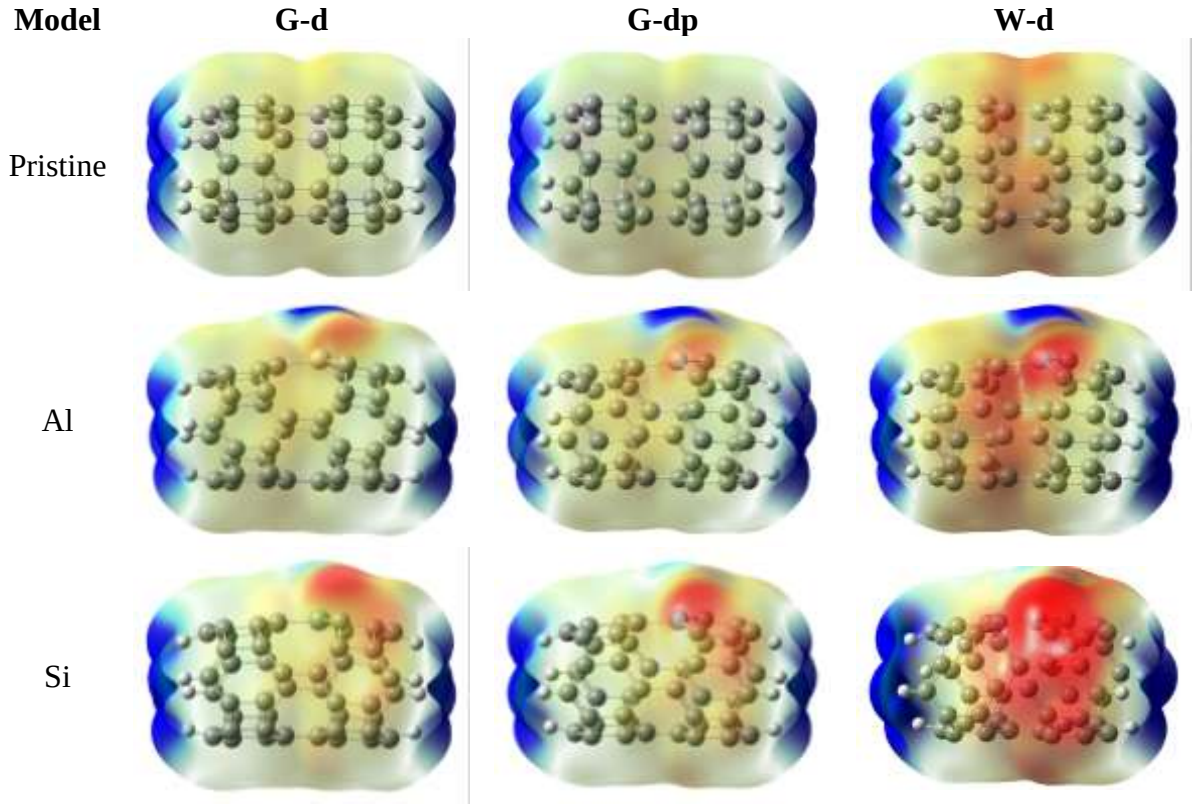

Figure 2. MEP maps in gas and water; potential range −0.025 to +0.025 a.u.

Frontier orbitals and density of states

The G-d frontier gaps are 2.522 eV for pristine BPNT, 2.654 eV for Al α and 2.497 eV for Si-BPNT (Table 2). Al raises both alpha frontier levels, especially the LUMO, widening the gap. Si lowers both levels and stabilizes the LUMO more strongly, narrowing the gas-phase gap. The Al beta gap is larger than the alpha gap.

Table 2. Frontier orbital energies and molecular gaps (eV).

Set	Model	Spin	HOMO	LUMO	Gap
G-d	Pristine	α = β	−5.285	−2.763	2.522
G-d	Al	α	−5.208	−2.554	2.654
G-d	Al	β	−5.232	−2.492	2.740
G-d	Si	α = β	−5.346	−2.849	2.497
G-dp	Pristine	α = β	−5.281	−2.761	2.520
G-dp	Al	α	−5.206	−2.553	2.653
G-dp	Al	β	−5.230	−2.490	2.741
G-dp	Si	α = β	−5.344	−2.848	2.496
W-d	Pristine	α = β	−5.290	−2.755	2.535
W-d	Al	α	−5.218	−2.538	2.680
W-d	Al	β	−5.234	−2.478	2.757
W-d	Si	α = β	−5.382	−2.807	2.575

Adding hydrogen polarization functions changes the gaps by no more than about 0.002 eV. In water, both dopants increase the gap relative to pristine BPNT. The gas-to-water gap increases are approximately 0.013, 0.026 and 0.077 eV for pristine, Al α and Si-BPNT, respectively. The largest change occurs for Si. Figure 3 compares the nearby occupied and virtual levels. These are molecular gaps of finite clusters, rather than periodic band gaps.

Water lowers the Si-BPNT HOMO by 0.035 eV and raises its LUMO by 0.042 eV, giving the 0.077 eV increase in their separation. The two shifts act in opposite directions, so their midpoint changes much less than the gap. The gas-to-water changes in the Fermi-energy estimate are 0.0008, 0.0025, 0.0058 and 0.0033 eV for pristine BPNT, Al alpha, Al beta and Si-BPNT, respectively.

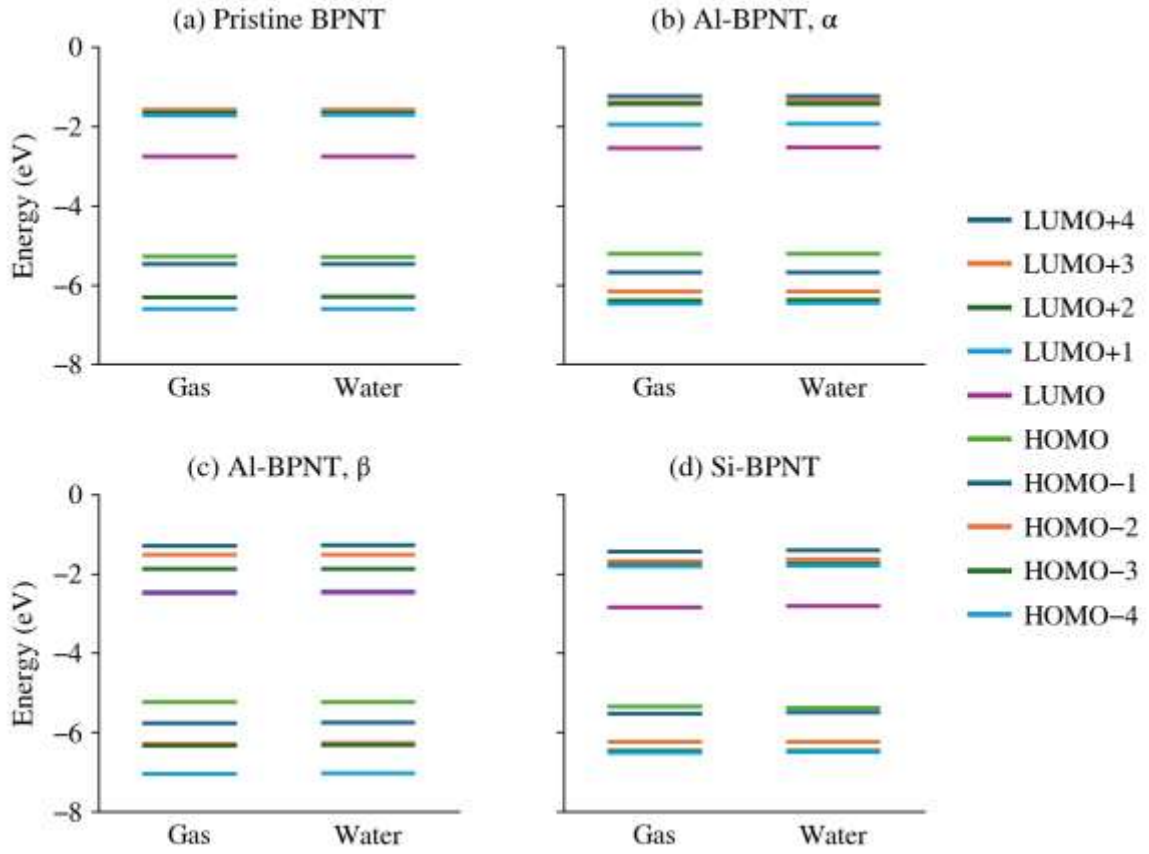

Figure 3. Orbital energies in gas (G-d) and water (W-d) at 6-31G(d). Colours identify levels from HOMO−4 to LUMO+4; Al alpha and beta channels are shown separately.

Figure 4 compares the gas and water DOS spectra. The principal peak patterns and the separation of occupied and virtual levels are retained in water, while the frontier gap increases for each model. Al retains distinct alpha and beta contributions. These spectra describe discrete levels of hydrogen-terminated clusters. The metallic tubes reported by Hudspeth et al. (2010) concern extended structures; the present finite-cluster gaps do not establish metallic transport.

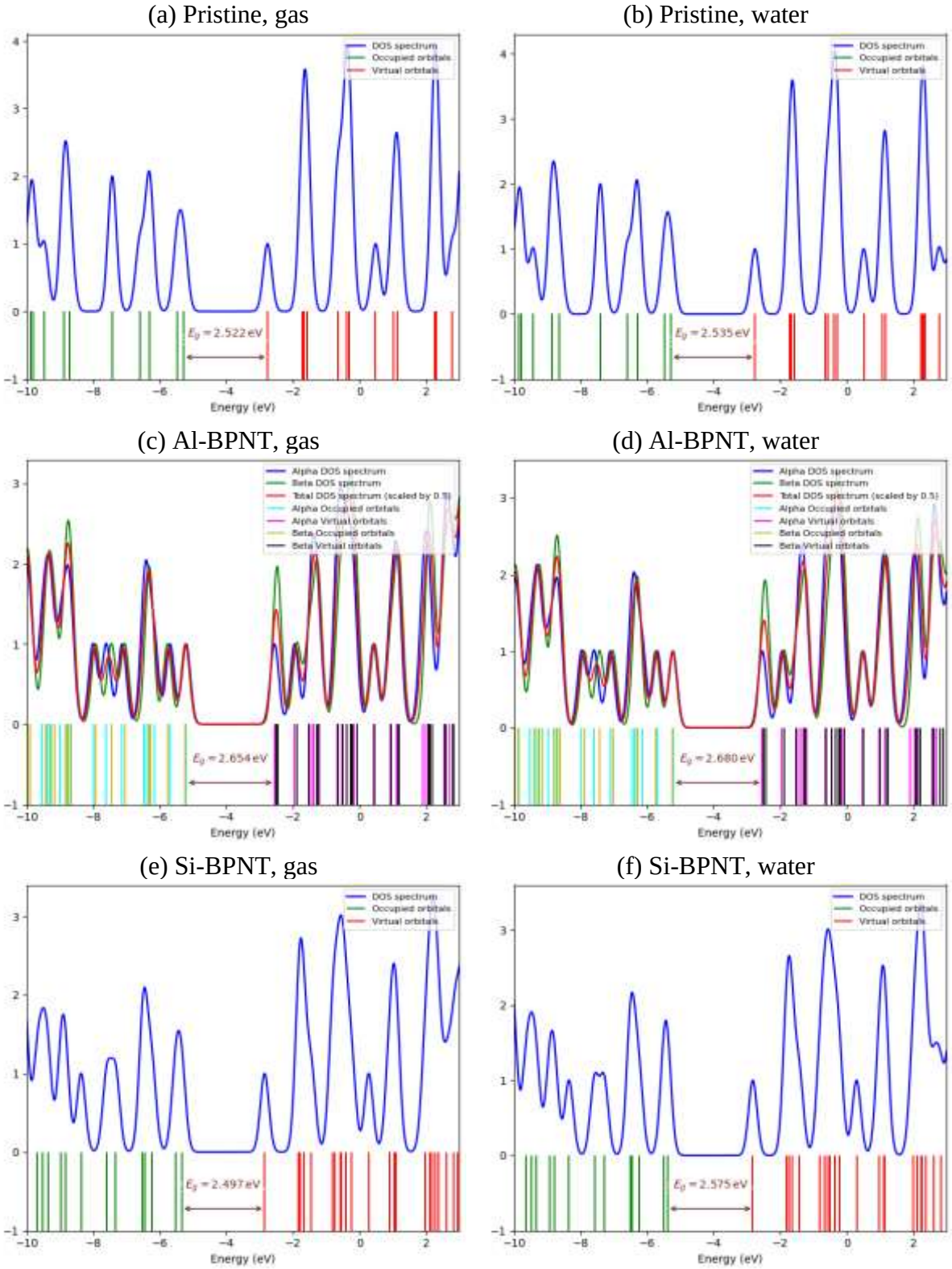

Figure 4. DOS spectra at M06-2X/6-31G(d): gas (left) and water (right). Sticks mark occupied and virtual levels. For Al, the red curve is $0.5(DOS_\alpha + DOS_\beta)$; gap labels refer to alpha orbitals.

In the orbital surfaces (Figure 5), the pristine HOMO extends relatively evenly over the framework, whereas Al-BPNT has a more asymmetric distribution. The Al alpha-HOMO is the singly occupied orbital; its spatial pattern therefore describes the open-shell channel.

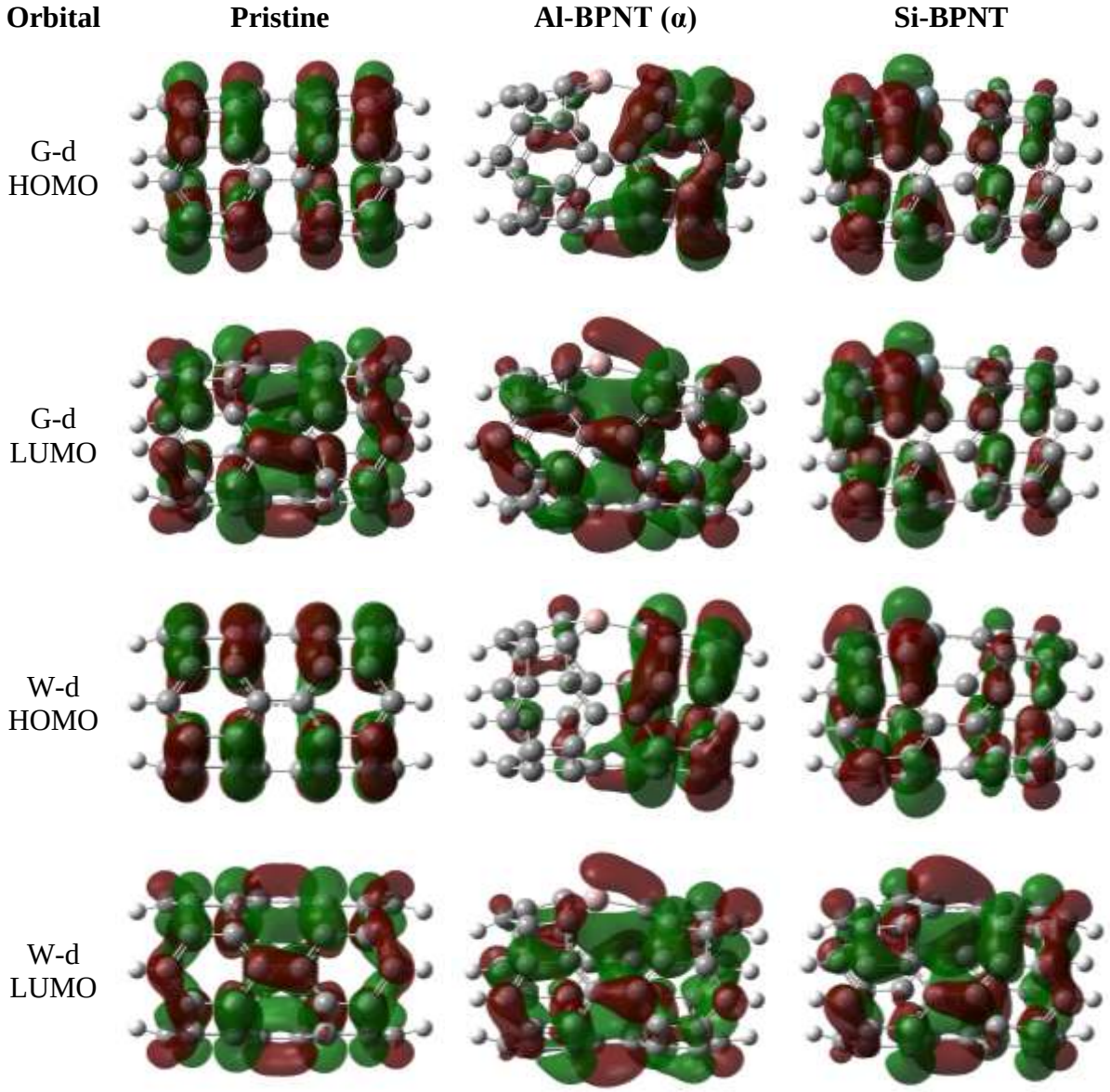

Figure 5. HOMO and LUMO surfaces in gas (G-d) and water (W-d). Alpha orbitals are shown for Al in both phases. Red and green denote opposite orbital phases.

Quantum molecular descriptors

Si-BPNT has the most negative chemical potential, the largest work-function estimate and the highest electrophilicity under all three conditions (Table 3). Al has the greatest hardness in both spin channels. At G-d, the work-function estimate decreases by 3.549% for Al α and increases by 1.840% for Si. The Si gap change switches from negative in gas to positive in water, whereas its work-function change remains positive.

Table 3. Orbital-based descriptors (eV) and changes relative to pristine BPNT (%).

Set	Model	$E_F = \mu$	η	ω	Φ	ΔE_g (%)	$\Delta\Phi$ (%)
G-d	Pristine	−4.024	1.261	6.419	4.024	—	—
G-d	Al α	−3.881	1.327	5.675	3.881	5.237	−3.549
G-d	Al β	−3.862	1.370	5.442	3.862	8.654	−4.023
G-d	Si	−4.098	1.249	6.723	4.098	−0.976	1.840
G-dp	Pristine	−4.021	1.260	6.416	4.021	—	—
G-dp	Al α	−3.879	1.327	5.672	3.879	5.277	−3.521
G-dp	Al β	−3.860	1.370	5.436	3.860	8.750	−4.005
G-dp	Si	−4.096	1.248	6.721	4.096	−0.946	1.865
W-d	Pristine	−4.023	1.267	6.385	4.023	—	—
W-d	Al α	−3.878	1.340	5.613	3.878	5.726	−3.591
W-d	Al β	−3.856	1.378	5.394	3.856	8.751	−4.147
W-d	Si	−4.094	1.287	6.512	4.094	1.569	1.779

$\Phi \approx -E_F$ with $E_{vac} = 0$. Al α and β are separate spin-channel estimates; $\Delta X = 100(X_{doped} - X_{pristine})/X_{pristine}$.

These quantities provide an electronic reference for comparing the isolated supports in sensing applications. A detectable signal depends on the support–analyte response and cannot be inferred from the isolated-support descriptors alone.

Charge redistribution

The deformation-density surfaces show a repeated pattern along pristine BPNT in gas and water (Figure 6). Al produces pronounced changes near the protruding doped region, whereas Si retains a more regular outline. These patterns accompany the local bond-length differences. The Al and Si NPA charges rise from +1.756 and +1.747 e in gas to +1.781 and +1.794 e in water, respectively. The increases are +0.025 e for Al and +0.047 e for Si, consistent with the stronger solvent-induced change in the Si frontier gap. The surface maps locate redistribution relative to free atoms; NPA provides the corresponding atom-centred population comparison.

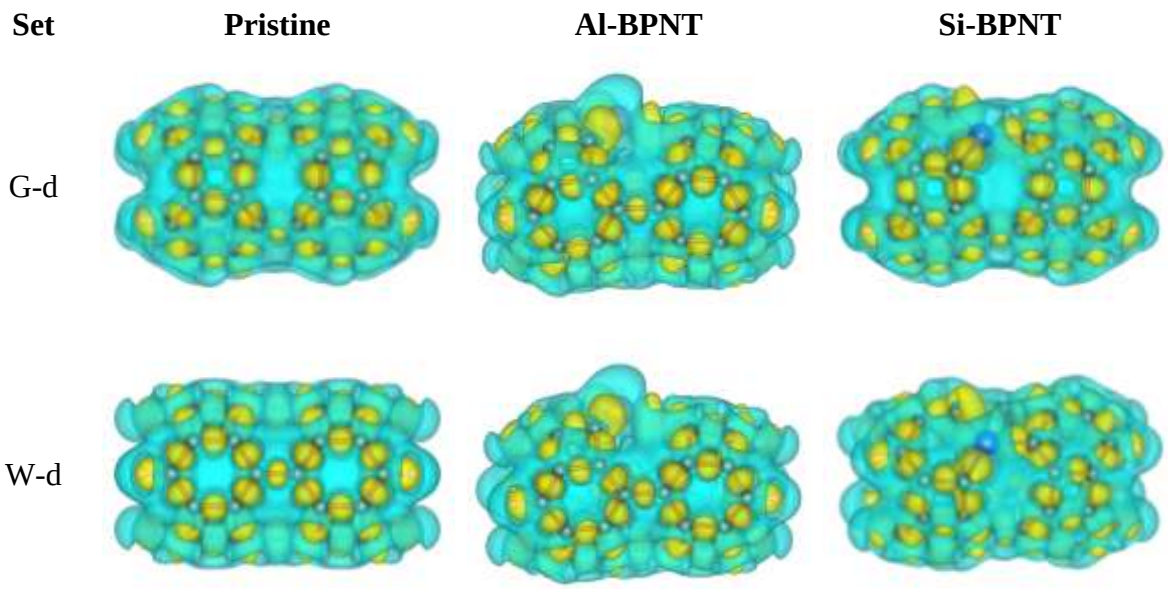

Figure 6. Deformation densities in gas (G-d, top) and water (W-d, bottom) at ±0.004 e/bohr³. Yellow and cyan denote accumulation and depletion relative to the free-atom reference in equation (5).

Comparison with published BPNT results

Table 4 compares the isolated supports with Esfandiarpour et al. (2022) at gas-phase M06-2X/6-31G(d,p). The earlier model contains 120 framework sites and eight hydrogens, compared with 48 sites and eight hydrogens here; the dopant fractions are 0.833% and 2.083%, respectively. Both studies give the gap order Al > pristine > Si. Al raises the gap by about 0.133 eV here and 0.19 eV in the earlier work, while Si lowers it by about 0.024 and 0.06 eV.

Table 4. Isolated BPNT comparison at M06-2X/6-31G(d,p): this work and Esfandiarpour et al. (2022).

Quantity	Pristine		Al		Si	
	This work	2022	This work	2022	This work	2022
HOMO (eV)	−5.281	−5.32	−5.206	−5.15	−5.344	−5.31
LUMO (eV)	−2.761	−3.11	−2.553	−2.75	−2.848	−3.16
Gap (eV)	2.520	2.21	2.653	2.40	2.496	2.15
E_{coh} (eV atom^{-1})	−6.115	−8.10	−6.010	−8.06	−6.032	−8.04
Mean M–C (Å)	—	—	1.873	1.86	1.757	1.75
q_M (e)	—	—	+1.756	+1.70	+1.747	+1.71

Current Al frontier values are alpha-channel values; the published pair is not spin-labelled. Mean M–C uses the three nearest carbon atoms. Published values are from Tables 3–4 and sections 3.2–3.3; atomic-reference states for the published cohesive energies are unspecified.

The mean Al-C and Si-C distances agree closely with the reported 1.86 and 1.75 Å, and both studies give dopant charges near +1.7 e. Pristine BPNT has the most negative cohesive energy in both studies, but the Al/Si order differs. Absolute cohesive energies depend on cluster composition and isolated-atom reference states, which limits direct numerical comparison.

The present pristine, Al and Si gaps exceed the 2022 values by approximately 0.31, 0.25 and 0.35 eV, respectively. The agreement is therefore strongest for the direction of the doping effect, local bond lengths and dopant charges.

CONCLUSIONS

Al and Si doping modify the local geometry and electronic structure of finite BPNTs. Si-C contacts are shorter than Al-C contacts, and cohesive energies are most negative for pristine BPNT, followed by Si-BPNT. Al widens the frontier gap in both media. Si narrows the gas-phase gap but widens it relative to pristine BPNT in water. Si also yields the largest work-function estimate and the larger solvent-induced gap and dopant-charge changes. The MEP, orbital and deformation-density maps locate the electronic redistribution around the dopants. The small Fermi-energy shifts and distinct gap responses characterise doping and solvent effects on the isolated supports.

REFERENCES

Al-Sawaff, Z. H., Dalgic, Senturk S., Kandemirli, F. 2021. Theoretical study of the adsorption of BMSF-BENZ drug for osteoporosis disease treatment on Al-doped carbon nanotubes (Al-CNT) as a drug delivery vehicle. European Journal of Chemistry, 12(3), 314–322. https://doi.org/10.5155/eurjchem.12.3.314-322.2143

Dalgic, Senturk S., Burucu, D. K., Dalgic, S., Kandemirli, F. 2025. A comparative DFT study on the interaction of Aldara drug molecule with SiC and Si-carbon nanotubes. Journal of Applied Physics, 137(13), 135104. https://doi.org/10.1063/5.0255569

Dennington, R., Keith, T., Millam, J. 2009. GaussView, Version 5. Semichem Inc., Shawnee Mission, KS.

Esfandiarpour, R., Zamanian, F., Badalkhani-Khamseh, F., Hosseini, M. R. 2022. Carbon dioxide sensor device based on biphenylene nanotube: A density functional theory study. Computational and Theoretical Chemistry, 1218, 113939. https://doi.org/10.1016/j.comptc.2022.113939

Fan, Q., Yan, L., Tripp, M. W., Krejčí, O., Dimosthenous, S., Kachel, S. R., Chen, M., Foster, A. S., Koert, U., Liljeroth, P., Gottfried, J. M. 2021. Biphenylene network: A nonbenzenoid carbon allotrope. Science, 372(6544), 852–856. https://doi.org/10.1126/science.abg4509

Genç, F., Dalgic Senturk, S., Kandemirli, F. 2025. Potential Application of Al-Doped Carbon Nanotubes for Tretinoin: A Theoretical Study. Cumhuriyet Science Journal, 46(2), 319–328. https://doi.org/10.17776/csj.1646890

Hariharan, P. C., Pople, J. A. 1973. The influence of polarization functions on molecular orbital hydrogenation energies. Theoretica Chimica Acta, 28(3), 213–222. https://doi.org/10.1007/BF00533485

Hohenberg, P., Kohn, W. 1964. Inhomogeneous Electron Gas. Physical Review, 136(3B), B864–B871. https://doi.org/10.1103/PhysRev.136.B864

Hudspeth, M. A., Whitman, B. W., Barone, V., Peralta, J. E. 2010. Electronic Properties of the Biphenylene Sheet and Its One-Dimensional Derivatives. ACS Nano, 4(8), 4565–4570. https://doi.org/10.1021/nn100758h

Kohn, W., Sham, L. J. 1965. Self-Consistent Equations Including Exchange and Correlation Effects. Physical Review, 140(4A), A1133–A1138. https://doi.org/10.1103/PhysRev.140.A1133

Lu, T., Chen, F. 2012. Multiwfn: A multifunctional wavefunction analyzer. Journal of Computational Chemistry, 33(5), 580–592. https://doi.org/10.1002/jcc.22885

Lu, T. 2024. A comprehensive electron wavefunction analysis toolbox for chemists, Multiwfn. The Journal of Chemical Physics, 161(8), 082503. https://doi.org/10.1063/5.0216272

Momma, K., Izumi, F. 2011. VESTA 3 for three-dimensional visualisation of crystal, volumetric and morphology data. Journal of Applied Crystallography, 44(6), 1272–1276. https://doi.org/10.1107/S0021889811038970

Parr, R. G., Pearson, R. G. 1983. Absolute hardness: companion parameter to absolute electronegativity. Journal of the American Chemical Society, 105(26), 7512–7516. https://doi.org/10.1021/ja00364a005

Parr, R. G., von Szentpály, L., Liu, S. 1999. Electrophilicity Index. Journal of the American Chemical Society, 121(9), 1922–1924. https://doi.org/10.1021/ja983494x

Reed, A. E., Weinstock, R. B., Weinhold, F. 1985. Natural population analysis. The Journal of Chemical Physics, 83(2), 735–746. https://doi.org/10.1063/1.449486

Ren, K., Shu, H., Huo, W., Cui, Z., Xu, Y. 2022. Tuning electronic, magnetic and catalytic behaviors of biphenylene network by atomic doping. Nanotechnology, 33(34), 345701. https://doi.org/10.1088/1361-6528/ac6f64

Scalmani, G., Frisch, M. J. 2010. Continuous surface charge polarizable continuum models of solvation. I. General formalism. The Journal of Chemical Physics, 132(11), 114110. https://doi.org/10.1063/1.3359469

Tomasi, J., Mennucci, B., Cammi, R. 2005. Quantum Mechanical Continuum Solvation Models. Chemical Reviews, 105(8), 2999–3094. https://doi.org/10.1021/cr9904009

Zhao, Y., Truhlar, D. G. 2008. The M06 suite of density functionals for main group thermochemistry, thermochemical kinetics, noncovalent interactions, excited states, and transition elements: two new functionals and systematic testing of four M06-class functionals and 12 other functionals. Theoretical Chemistry Accounts, 120(1-3), 215–241. https://doi.org/10.1007/s00214-007-0310-x

PERFORMANCE ASSESSMENT OF CO_2 ADSORPTION ON PRISTINE AND DOPED BIPHENYLENE NANOTUBES USING DFT AND INTEGRATED AHP–TOPSIS

Selin Yalcin[1], Simge Sude Dalgic[2], Serap Senturk Dalgic[3], Dilek Kuzalic Burucu[4], Fatma Kandemirli[5]

[1] Industrial Engineering Department, Faculty of Engineering and Architecture, Istanbul Beykent University, Istanbul, Türkiye

[2] Industrial Engineering Department, Faculty of Engineering and Natural Sciences, Bahcesehir University, Istanbul, Türkiye

[3] Department of Physics, Faculty of Science, Trakya University, Edirne, Türkiye

[4] Electrical and Electronic Engineering Department, Faculty of Engineering and Architecture, Istanbul Beykent University, Istanbul, Türkiye

[5] Biomedical Engineering Department, Faculty of Engineering and Architecture, Kastamonu University, Kastamonu, Türkiye

ABSTRACT

The development of efficient adsorbent materials for CO_2 capture is essential for reducing industrial carbon emissions and improving carbon-capture process efficiency. In this study, density functional theory (DFT) calculations were performed to investigate CO_2 adsorption on pristine and Al-, Si-, and Zn-doped biphenylene nanotubes (BPNTs) under gas-phase and aqueous-environment conditions. The aqueous environment was represented using the IEFPCM implicit-solvent model. The effects of heteroatom doping on structural stability, adsorption behavior, regeneration characteristics, and electronic properties were evaluated. The adsorption configurations and the energetic and electronic descriptors obtained from the available molecular calculations were used to characterize the interactions between CO_2 and the nanotube surfaces. Recovery time was estimated to assess the regeneration characteristics of the investigated adsorbents. The obtained results were subsequently evaluated using integrated Analytic Hierarchy Process (AHP) and Technique for Order Preference by Similarity to Ideal Solution (TOPSIS) Multi-Criteria Decision-Making (MCDM) methods for comparative material selection. Five criteria, including adsorption distance, adsorption energy, recovery time, band-gap energy, and first hyperpolarizability, were considered in the decision-making process. These criteria represented CO_2-adsorbent interaction strength, regeneration capability, and electronic response. Their relative importance was determined using the AHP by aggregating expert assessments. The consistency analysis showed that the pairwise comparison structure was acceptable. The AHP results indicated that adsorption energy was the most influential criterion, followed by recovery time. The calculated criterion weights were incorporated into separate TOPSIS method for the gas and water phases. The TOPSIS evaluation indicated that Zn-doped BPNT ranked first under gas-phase conditions, whereas Al-doped BPNT achieved the highest rank in the water phase. These results demonstrated that the ranking of the investigated BPNTs varied depending on the environmental conditions. The integration of DFT-derived descriptors with AHP and TOPSIS provided a systematic framework for the comparative evaluation and selection of BPNTs for CO_2 adsorption.

Keywords: CO_2 capture; Biphenylene nanotubes; Density functional theory; AHP; TOPSIS; MCDM; Adsorbent selection; Carbon capture process optimization

INTRODUCTION

The biphenylene network contains four-, six- and eight-membered carbon rings. Its experimentally prepared two-dimensional network differs from the hexagonal lattice of graphene (Fan et al., 2021). Earlier calculations also examined the electronic properties of the sheet and its one-dimensional derivatives (Hudspeth et al., 2010). Curving this framework into a nanotube changes the local environment of its carbon atoms. Substitution by another element introduces a further change at the adsorption site.

Esfandiarpour et al. (2022) studied CO_2 adsorption on pristine, Al-doped and Si-doped biphenylene nanotubes. They found stronger adsorption for the Al-substituted structure and considered its electronic sensing response. Their work provides a direct comparison for the present calculations. The additional Zn model and the gas–water comparison extend the set of adsorption environments considered here.

Related nanotube studies show how dopants affect different adsorbates. Genç et al. (2025a) examined formaldehyde on Zn-doped carbon nanotubes. Genç et al. (2025b) compared tretinoin adsorption on Al-doped nanotubes in gas, water and n-octanol. Şentürk Dalgıç (2025) analysed the local N–Si interaction between imiquimod and a Si-doped nanotube. These studies combine structural and electronic results with an examination of the contact region. Their adsorption mechanisms depend on the adsorbate and cannot be assumed for CO_2.

Adsorption strength alone does not determine the preference for a reusable adsorbent. Strong binding favours retention but can delay release. The analytic hierarchy process (AHP) assigns weights through pairwise comparisons (Saaty, 1977). The technique for order preference by similarity to an ideal solution (TOPSIS) then ranks alternatives using those weights (Hwang and Yoon, 1981). Turan and Özkan (2025) applied multicriteria methods to amine-based solid sorbents for CO_2 capture. Here, AHP–TOPSIS is applied to molecular descriptors calculated for four nanotube hosts.

The comparison uses adsorption distance, adsorption energy, estimated recovery time, frontier orbital gap and static first hyperpolarizability. Optimized geometries, frontier orbitals and selected electron-density maps support the interpretation. Gas and implicit water are evaluated separately. The aim is to identify how the preferred host changes when the dielectric environment and the relative importance of binding and release are considered.

MATERIAL AND METHOD

Molecular models and calculations

The pristine biphenylene nanotube (BPNT) model contained 48 carbon atoms and eight terminating hydrogens. One carbon atom was replaced by Al, Si or Zn to form $C_{47}H_8M$. A single CO_2 molecule was added to each host. The four complexes were optimized in the gas phase and in implicit water, giving eight 59-atom systems. The same substitution site was used throughout.

Calculations employed M06-2X with the 6-31G(d) basis set in Gaussian 09 (Zhao and Truhlar, 2008; Hariharan and Pople, 1973; Rassolov et al., 1998; Frisch et al., 2009). Water was represented by the integral-equation-formalism polarizable continuum model, IEFPCM (Cancès et al., 1997). The complexes were neutral. Pristine, Si and Zn systems were restricted singlets; Al systems were unrestricted doublets. Harmonic frequency calculations gave no imaginary frequencies for the eight optimized complexes. They therefore correspond to local minima for the configurations examined.

The electronic adsorption energy was calculated from the optimized complex and separately optimized fragments:

$$E_{ads}=E_{complex}-E_{host}-E_{CO_2} \quad (1)$$

The zero-point-corrected adsorption energy, $E_{ads,0}$, was obtained by applying the same difference to the electronic energy plus zero-point energy. Negative values indicate stabilization relative to the separated fragments. Each fragment reference used the same environment as its complex. No counterpoise correction was applied. The reported values therefore retain basis-set superposition error.

The recovery-time indicator was estimated at 298.15 K:

$$\tau = \frac{1}{\nu_0} \exp\left(\frac{|E_{ads,0}|}{k_B T}\right) \quad (2)$$

The attempt frequency ν_0 was 3×10^{12} s^{-1}, and k_B was $8.617333262 \times 10^{-5}$ eV K^{-1}. $E_{ads,0}$ was expressed in eV in Eq. (2). This estimate substitutes the binding-energy magnitude for a desorption barrier. No transition state was calculated. The resulting times are model indicators rather than measured regeneration rates.

Electronic response and interaction maps

The frontier orbital gap was defined as $E_g = \varepsilon_{LUMO} - \varepsilon_{HOMO}$. Separate α and β gaps were obtained for the open-shell Al complexes. The larger within-channel gap, $\max(E_{g,\alpha}, E_{g,\beta})$, was used as the single TOPSIS descriptor. The other systems were closed shell. These values describe finite molecular clusters and are not periodic band gaps.

Static first hyperpolarizability was calculated from the Cartesian response tensor:

$$\beta_0 = \sqrt{\beta_x^{\,2} + \beta_y^{\,2} + \beta_z^{\,2}} \quad (3)$$

Here $\beta_x = \beta_{xxx} + \beta_{xyy} + \beta_{xzz}$, $\beta_y = \beta_{xxy} + \beta_{yyy} + \beta_{yzz}$ and $\beta_z = \beta_{xxz} + \beta_{yyz} + \beta_{zzz}$. The conversion was 1 atomic unit = 8.6393×10^{-33} esu. The values are molecular static responses. They do not represent a bulk optical susceptibility or an experimental CO_2 uptake.

Reduced density gradient and noncovalent interaction (RDG/NCI) maps were used to inspect the contact region (Johnson et al., 2010). Their colour assignment follows $\mathrm{sign}(\lambda_2)\rho$, where λ_2 is the second eigenvalue of the density Hessian. The electron localization function (ELF) describes spatial localization on a scale from 0 to 1 (Becke and Edgecombe, 1990). Selected two-dimensional ELF sections were compared with the interaction surfaces. The maps were used for interpretation and were not entered into TOPSIS.

Charge-density difference (CDD) was defined as $\Delta\rho = \rho_{complex} - \rho_{host} - \rho_{CO_2}$. Fragment geometries were fixed at their positions in the optimized complex. CDD isosurfaces were displayed at $|\Delta\rho| = 0.0004$ a.u.

Criterion weights and ranking

Three reciprocal pairwise-comparison matrices were aggregated by taking the geometric mean of their corresponding entries. Each column of the group matrix was normalized. The row averages gave the weights in Table 1. Consistency was evaluated from the mean componentwise ratio of Aw to w. The group consistency ratio was 0.08293, below the adopted 0.10 threshold (Saaty, 1977).

Table 1. Criteria, preference directions and AHP weights.

Criterion	Descriptor	Preference	Weight (%)
K_1	Minimum distance	Minimum	11.50
K_2	Adsorption energy	Minimum	52.02
K_3	Recovery time	Minimum	27.26
K_4	Adopted orbital gap	Minimum	5.97
K_5	First hyperpolarizability	Maximum	3.25

The distance criterion was the shortest atom-pair separation between CO_2 and the host. Minimizing the signed adsorption energy favours stronger binding. Minimizing recovery time favours faster release. Recovery time is derived from adsorption energy, so these two criteria are coupled. Hyperpolarizability adds a preference for electric response.

The gas and water decision matrices were normalized separately. For alternative i and criterion j, vector normalization and weighting gave

$$r_{ij}=\frac{x_{ij}}{\sqrt{\Sigma_i x_{ij}^2}}, v_{ij}=w_j r_{ij} \quad (4)$$

The positive ideal contained the minimum weighted values for K_1–K_4 and the maximum for K_5. The negative ideal used the opposite values. Euclidean distances D^+ and D^- were calculated from these two ideals. The closeness coefficient was

$$C_i=\frac{D_i^-}{D_i^+ + D_i^-} \quad (5)$$

Alternatives were ranked by decreasing C_i (Hwang and Yoon, 1981). Recovery times entered the normalization directly, without a logarithmic transformation. Because each environment has its own ideal solutions, a gas-phase coefficient and a water coefficient are not a common absolute performance scale.

Weight sensitivity was tested by changing each criterion weight by ±20% of its base value, one at a time. The other weights were rescaled proportionally to keep their sum equal to one. This produced ten scenarios in each environment.

RESULTS AND DISCUSSION

Optimized structures and adsorption

Figure 1 compares the eight optimized structures. Al and Zn form the shorter contacts with a CO_2 oxygen atom. Pristine BPNT and the Si-substituted host retain more distant adsorption geometries.

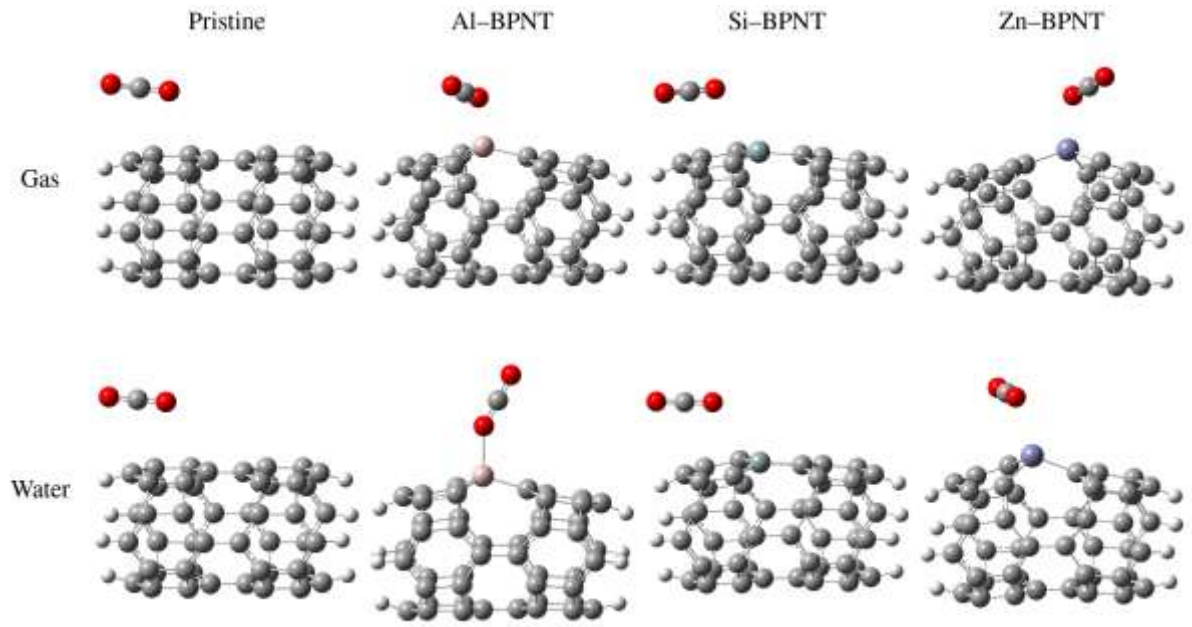

Figure 1. Optimized BPNT–CO_2 complexes. Gas-phase structures are in the upper row and implicit-water structures in the lower row. Columns show pristine, Al, Si and Zn hosts.

The Al–O distance decreases from 2.097 Å in the gas phase to 2.019 Å in water. The Zn–O bond distance changes in the opposite direction, increasing from 2.256 to 2.489 Å. For aqueous Si-BPNT, the shortest interfragment distance is 3.065 Å between carbon atoms; its Si–O distance is 3.164 Å. The minimum-distance definition therefore matters when comparing the four adsorption sites.

CO_2 remains nearly linear in every optimized complex. The largest bending occurs for gas-phase Al-BPNT–CO_2, where the O–C–O angle is 176.55°. The adsorbate remains molecular in all eight structures. Table 2 gives the five descriptors used in the decision analysis.

Table 2. Calculated descriptors for the gas (G) and implicit-water (W) complexes.

Complex	d_{min} **(Å)**	$E_{ads,0}$ **(eV)**	**τ (s)**	E_g **(eV)**	**β₀ (10^{-30} esu)**
G Pristine	3.033	−0.1616	1.795×10^{-10}	2.5238	3.599
G Al	2.097	−0.5313	3.190×10^{-4}	2.7437	24.978
G Si	3.104	−0.2067	1.038×10^{-9}	2.5255	19.075
G Zn	2.256	−0.4160	3.584×10^{-6}	2.4581	74.800
W Pristine	3.063	−0.0973	1.468×10^{-11}	2.5361	18.657
W Al	2.019	−0.5856	2.641×10^{-3}	2.7883	48.990
W Si	3.065	−0.1692	2.413×10^{-10}	2.5874	63.252
W Zn	2.489	−0.1042	1.921×10^{-11}	2.5965	289.909

Al has the most negative $E_{ads,0}$ in both environments (Figure 2). Its binding strengthens from −12.252 to −13.505 kcal mol^{-1} in water, consistent with its shorter oxygen contact. Gas-phase Zn binds more strongly than Si and pristine BPNT. In water, however, the Zn value becomes much less negative, changing from −9.593 to −2.402 kcal mol^{-1}. The longer Zn–O distance accompanies this loss of stabilization.

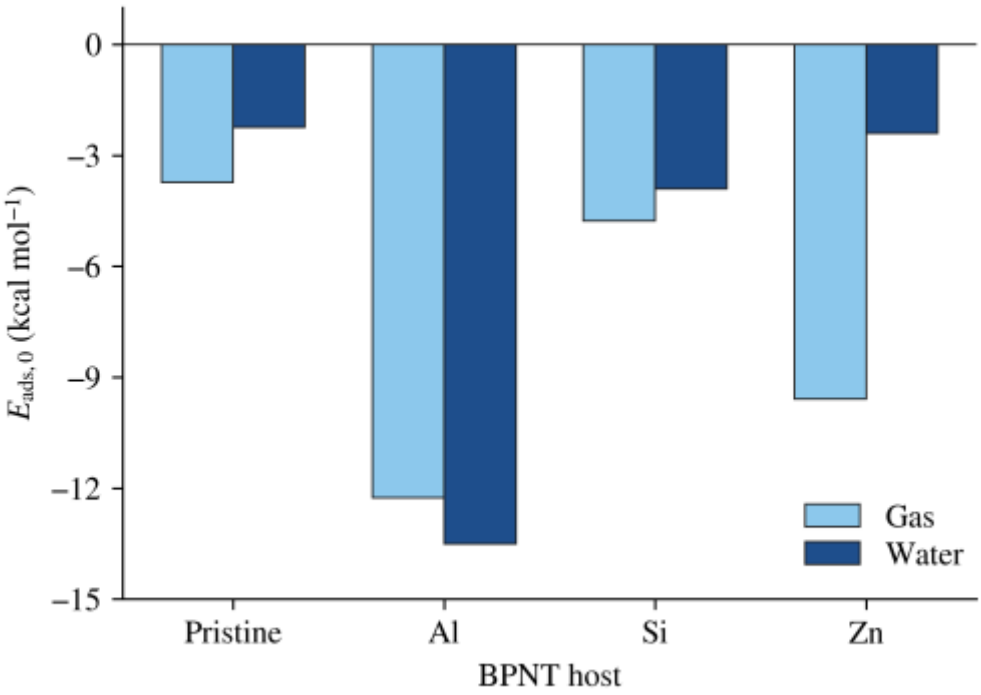

Figure 2. Zero-point-corrected adsorption energies. Gas is shown in light blue and implicit water in dark blue. Values use separately optimized fragment references.

Pristine and Si-BPNT also bind less strongly in water, but their changes are smaller than that of Zn. The adsorption-energy order is Al > Zn > Si > pristine in the gas phase. It changes to Al > Si > Zn > pristine in water, where the order denotes decreasing binding strength. The solvent response is therefore specific to the substituted site.

Recovery time follows the binding-energy magnitude exponentially. Al has the longest estimate in both environments: 3.190×10^{-4} s in the gas phase and 2.641×10^{-3} s in water. Gas-phase Zn gives 3.584×10^{-6} s. The much shorter aqueous estimates for the other hosts follow their weaker calculated binding. These small values should not be read as experimentally achievable device switching times.

For the hosts shared with Esfandiarpour et al. (2022), the gas-phase binding order agrees: Al > Si > pristine.

Orbital gaps and first hyperpolarizability

Zn has the smallest gas-phase gap, 2.4581 eV. Pristine and Si-BPNT have similar values near 2.52 eV. Al gives α and β gaps of 2.6936 and 2.7437 eV; the latter enters Table 2. In water, the Al gaps are 2.7202 and 2.7883 eV. The β gaps enter TOPSIS.

Pristine BPNT has the smallest aqueous gap, 2.5361 eV. The Si and Zn gaps increase to 2.5874 and 2.5965 eV. These changes modify the electronic criterion but receive a relatively small weight in TOPSIS. A smaller molecular gap alone does not establish a measurable conductivity response.

The Al electronic trend differs from the earlier BPNT–CO_2 calculation. Esfandiarpour et al. (2022) reported a gap decrease after adsorption. For the present finite model, the Al α gap increases from 2.654 to 2.694 eV. Agreement in adsorption strength therefore does not establish agreement in sensing response. Cluster size, the basis set and the open-shell orbital treatment remain relevant to this comparison.

The first hyperpolarizability follows a different order from adsorption strength. Gas-phase Zn has the largest β_0, 74.800×10^{-30} esu, followed by Al, Si and pristine BPNT. Water increases β_0

for all four systems. Zn reaches 289.909 × 10^{-30} esu, while Si exceeds Al in the aqueous comparison. The Zn structure thus retains a large electric response even when its CO_2 binding becomes weak.

Selected interaction regions

Figures 3 and 4 show the CDD isosurfaces for the eight complexes. The maps locate electron-density redistribution around CO_2 and the neighbouring nanotube framework. They do not quantify the net charge transferred between the fragments.

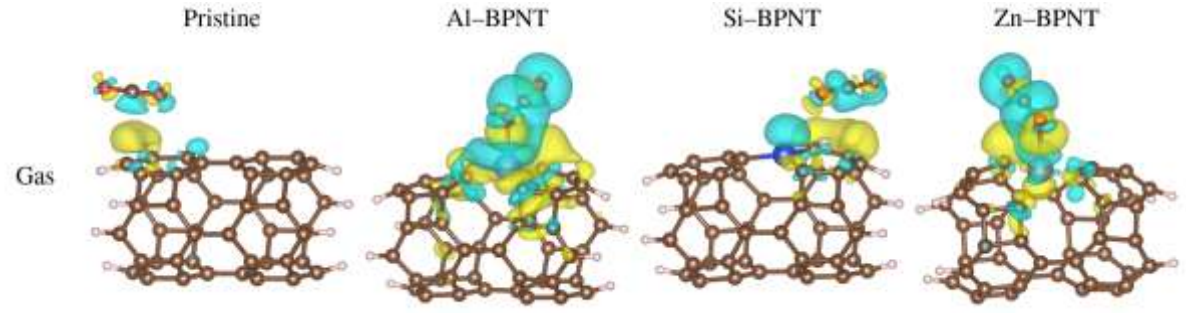

Figure 3. Charge-density-difference isosurfaces in the gas phase at $|\Delta\rho|$ = 0.0004 a.u. Panels show pristine, Al, Si and Zn hosts from left to right.

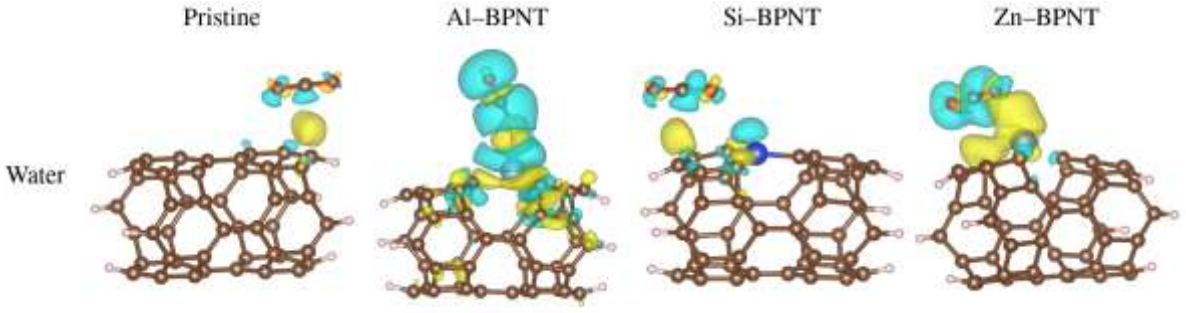

Figure 4. Charge-density-difference isosurfaces in implicit water at $|\Delta\rho|$ = 0.0004 a.u. Panels show pristine, Al, Si and Zn hosts from left to right.

Figure 5 compares gas-phase Zn and aqueous Al, the leading alternatives under the base weights. In the Zn RDG/NCI surface, the contact contains green and blue regions. These are consistent with a low-density interaction that includes an attractive contribution near the dopant. The aqueous Al surface also shows an attractive contribution near CO_2, together with a small repulsive region around the local framework.

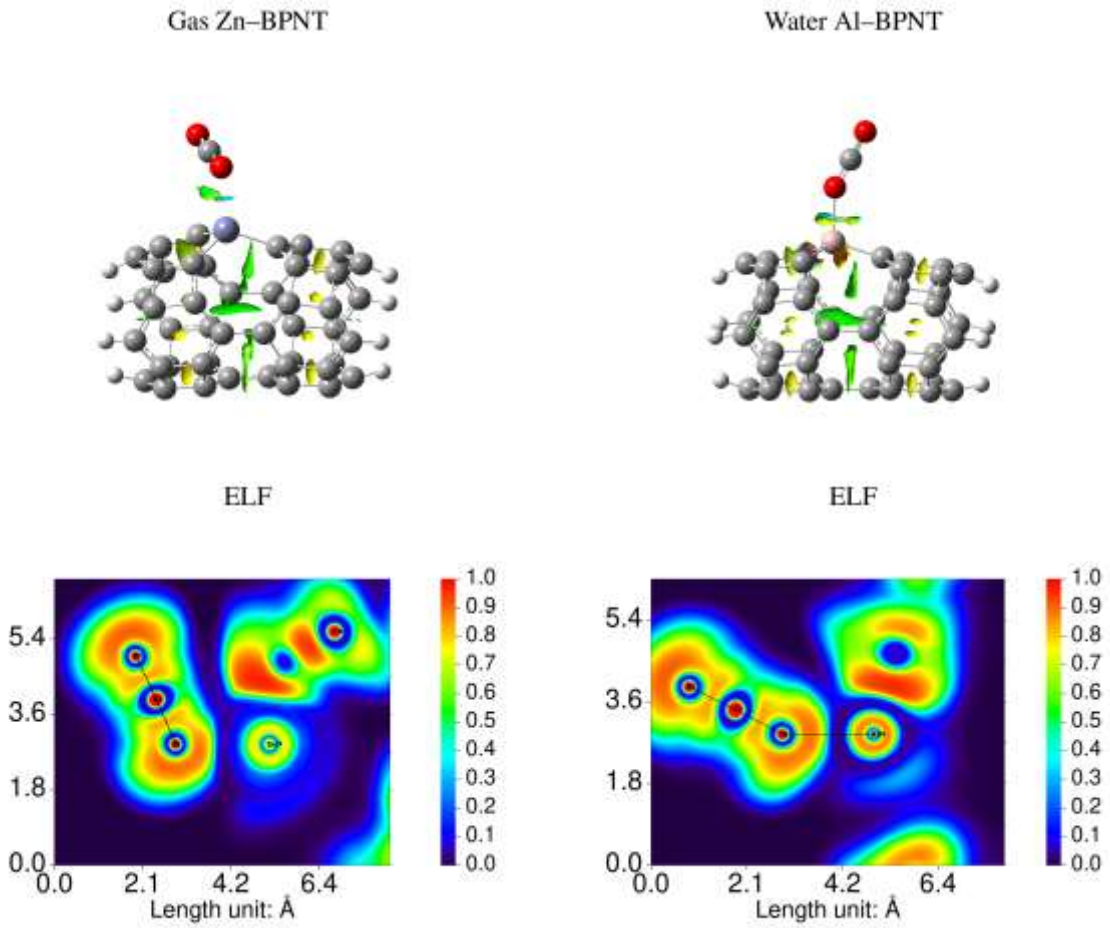

Figure 5. RDG/NCI surfaces (upper panels) and ELF sections (lower panels) for the gas Zn and aqueous Al complexes. In RDG/NCI, blue indicates attractive and red repulsive regions; green marks weak interactions. ELF uses a 0–1 scale. The original section extents are retained.

The ELF sections contain regions of high localization around the constituent atoms. The interfragment region is less localized than these atomic regions. This pattern is consistent with polarized adsorption contacts rather than a uniformly localized electron pair between the fragments. A two-dimensional section does not establish an ELF basin population or a complete bond topology (Becke and Edgecombe, 1990).

The intraring NCI features belong to the nanotube framework and are distinct from the CO_2–host contact (Johnson et al., 2010).

AHP–TOPSIS ranking

Adsorption energy and recovery time account for 79.28% of the total weight. Their opposing preference directions dominate the selection. Al benefits from its strong binding and short contact, but its longer estimated release time lowers its score. Table 3 and Figure 6 show the resulting rankings.

Table 3. TOPSIS closeness coefficients and ranks under the base weights.

Host	**Gas C_i**	**Gas rank**	**Water C_i**	**Water rank**
Pristine	0.5043	3	0.4008	4
Al	0.4938	4	0.5975	1
Si	0.5385	2	0.4453	2
Zn	0.7978	1	0.4068	3

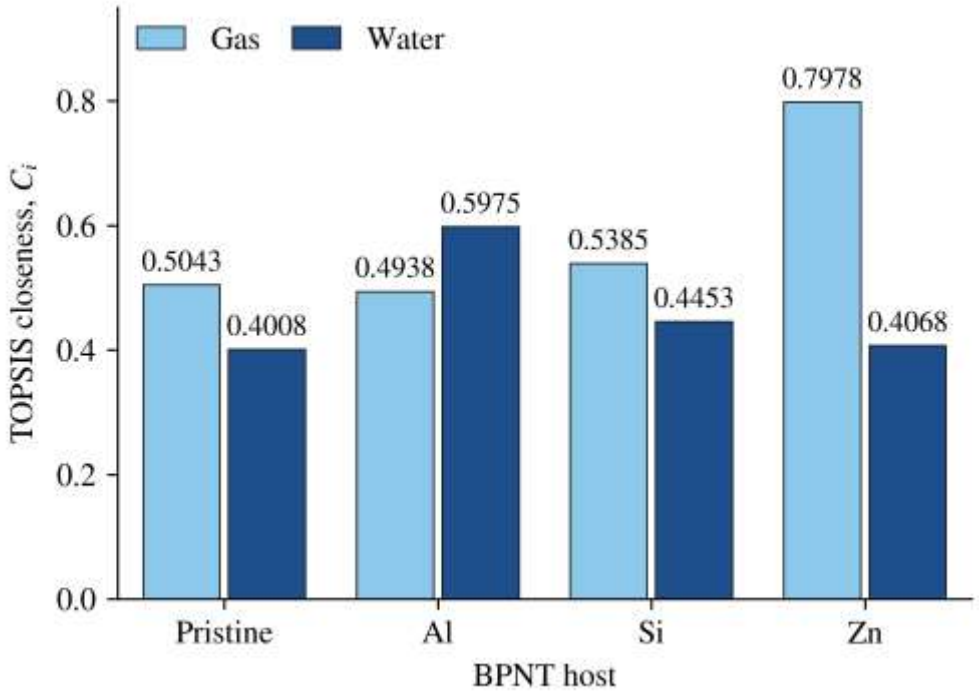

Figure 6. TOPSIS closeness coefficients. Gas is shown in light blue and implicit water in dark blue. Each environment is normalized independently; a larger coefficient is preferred within that environment.

The gas-phase order is Zn > Si > pristine > Al. Zn combines substantial binding with a shorter recovery estimate than Al. It also has the smallest adopted gap and the largest β_0. Al ranks fourth despite having the strongest adsorption. This position follows from the selected balance between retention and release.

The aqueous order is Al > Si > Zn > pristine. Al retains strong binding while Zn loses much of its adsorption stabilization. The high aqueous Zn hyperpolarizability contributes only weakly because of its small criterion weight. Al therefore becomes the preferred alternative under the same weights used for the gas-phase comparison.

Zn remains first in all ten gas-phase weight perturbations. In water, Al remains first in nine scenarios. Reducing the adsorption-energy weight by 20%, from 0.5202 to 0.4162, places Si first. A finer scan locates the Al–Si crossover near a weight of 0.442. The aqueous preference therefore depends more on the weight assigned to adsorption energy.

An acceptable AHP consistency ratio checks the coherence of the pairwise judgements; it does not validate the quantum-chemical method. TOPSIS compares the available alternatives against the selected criteria rather than estimating absolute capture performance.

The implicit-water calculation represents dielectric polarisation. It contains no explicit solvent molecules and cannot describe competitive water adsorption. The finite clusters also provide no adsorption capacity, gas selectivity or repeated-cycle measurements.

CONCLUSIONS

Al substitution yields the strongest calculated CO_2 adsorption in the gas phase and in implicit water. Its shorter aqueous Al–O contact is associated with stronger binding. Zn shows the greatest solvent-induced weakening, although it has the largest first hyperpolarizability in both environments. Adsorption strength and electric response therefore indicate different host preferences.

The five-criterion evaluation ranks Zn first in the gas phase and Al first in water under the base AHP weights. Gas-phase Zn remains first across the range of tested weight changes. The aqueous result is less stable, and Si becomes preferred when the adsorption-energy weight is sufficiently reduced. Verification with explicit environments and adsorption measurements is needed before assigning capture or regeneration performance.

REFERENCES

Becke, A. D.; Edgecombe, K. E. (1990). A simple measure of electron localization in atomic and molecular systems. The Journal of Chemical Physics, 92(9), 5397–5403. https://doi.org/10.1063/1.458517

Cancès, E.; Mennucci, B.; Tomasi, J. (1997). A new integral equation formalism for the polarizable continuum model: Theoretical background and applications to isotropic and anisotropic dielectrics. The Journal of Chemical Physics, 107(8), 3032–3041. https://doi.org/10.1063/1.474659

Esfandiarpour, R., Zamanian, F., Badalkhani-Khamseh, F., and Hosseini, M. R. (2022). Carbon dioxide sensor device based on biphenylene nanotube: A density functional theory study. Computational and Theoretical Chemistry, 1218, 113939. https://doi.org/10.1016/j.comptc.2022.113939

Fan, Q., Yan, L., Tripp, M. W., Krejčí, O., Dimosthenous, S., Kachel, S. R., Chen, M., Foster, A. S., Koert, U., Liljeroth, P., and Gottfried, J. M. (2021). Biphenylene network: A nonbenzenoid carbon allotrope. Science, 372(6544), 852–856. https://doi.org/10.1126/science.abg4509

Frisch, M. J., et al. (2009). Gaussian 09, Revisions E.01 and A.02. Gaussian, Inc., Wallingford, CT. https://gaussian.com/g09citation/

Genç, F., Dalgic Senturk, S., S.; Kandemirli, F. (2025a). Density Functional Theory Investigation on The Interaction of Formaldehyde with Zn Doped (6,0) SWCNT for Sensor Applications. Bitlis Eren Üniversitesi Fen Bilimleri Dergisi, 14(4), 2552–2561. https://doi.org/10.17798/bitlisfen.1754990

Genç, F., Dalgic Senturk, S., Kandemirli, F. (2025b). Potential Application of Al-Doped Carbon Nanotubes for Tretinoin: A Theoretical Study. Cumhuriyet Science Journal, 46(2), 319–328. https://doi.org/10.17776/csj.1646890

Hariharan, P. C.; Pople, J. A. (1973). The influence of polarization functions on molecular orbital hydrogenation energies. Theoretica Chimica Acta, 28, 213–222. https://doi.org/10.1007/BF00533485

Hudspeth, M. A., Whitman, B. W., Barone, V., and Peralta, J. E. (2010). Electronic Properties of the Biphenylene Sheet and Its One-Dimensional Derivatives. ACS Nano, 4(8), 4565–4570. https://doi.org/10.1021/nn100758h

Hwang, C.-L.; Yoon, K. (1981). Multiple Attribute Decision Making: Methods and Applications—A State-of-the-Art Survey. Springer, Berlin, Heidelberg. Lecture Notes in Economics and Mathematical Systems, 186. https://doi.org/10.1007/978-3-642-48318-9

Johnson, E. R.; Keinan, S.; Mori-Sánchez, P.; Contreras-García, J.; Cohen, A. J.; Yang, W. (2010). Revealing Noncovalent Interactions. Journal of the American Chemical Society, 132(18), 6498–6506. https://doi.org/10.1021/ja100936w

Rassolov, V. A.; Pople, J. A.; Ratner, M. A.; Windus, T. L. (1998). 6-31G* basis set for atoms K through Zn. Journal of Chemical Physics, 109(4), 1223–1229. https://doi.org/10.1063/1.476673

Saaty, T. L. (1977). A scaling method for priorities in hierarchical structures. Journal of Mathematical Psychology, 15(3), 234–281. https://doi.org/10.1016/0022-2496(77)90033-5

Senturk Dalgic, S. (2025). Investigation of the N-Si Dative Bond at the atomistic level in drug carrier/drug delivery nanosensor applications of Si-CNTs. Journal of Materials and Electronic Devices, 2(1), 33–41. https://dergi-fytronix.com/index.php/jmed/article/view/324

Turan, E.; Özkan, A. (2025). Prioritization of amine-based solid sorbents for post-combustion CO2 capture using different multi-criteria decision-making tools. International Journal of Environmental Science and Technology, 22, 9129–9140. https://doi.org/10.1007/s13762-024-06181-8

Zhao, Y.; Truhlar, D. G. (2008). The M06 suite of density functionals for main group thermochemistry, thermochemical kinetics, noncovalent interactions, excited states, and transition elements: two new functionals and systematic testing of four M06-class functionals and 12 other functionals. Theoretical Chemistry Accounts, 120(1–3), 215–241. https://doi.org/10.1007/s00214-007-0310-x

A THEORETICAL STUDY OF THIOPHENE ADSORPTION ON BIPHENYLENE NANOTUBES: DFT INVESTIGATION

Serap Senturk Dalgic[1], Habibe Hasan Nuri[2], Seyfettin Dalgic[1], Dilek Kuzalic Burucu[3], Fatma Kandemirli[4]

[1] Trakya University, Faculty of Science, Department of Physics, Edirne, Turkey

[2]Electric, Electronic and Automation Engineering Dept., Technical University of Sofia, Faculty of Engineering and Pedagogika, Sliven, Bulgaria, bsbhabibeozgur@gmail.com

[3]Electric and Electronic Engineering Dept.. Faculty of Engineering & Architecture, Beykent University, Turkey.

[4]Biomedical Engineering Department. Faculty of Engineering & Architecture, Kastamonu University, Kastamonu, Turkey.

Corresponding author e-mail: dserap@yahoo.com

ABSTRACT

In this study, the adsorption behaviour of thiophene molecules on pristine and metal-doped biphenylene nanotubes (BP-NTs and metalBP-NTs) was investigated using density functional theory (DFT) calculations. The Al-, Si- and Zn-doped BP-NTs were considered. The structural, electronic, and energetic properties of the thiophene/BP-NT and thiophene/metal-doped BP-NT systems were examined to elucidate how different dopant atoms influence the interaction mechanism between thiophene and the nanotube surface. Different configurations, corresponding adsorption energies, equilibrium geometries, charge transfer, and electronic structure were also studied. The results reveal that thiophene adsorption on pristine BP-NT is relatively weak, whereas substitutional doping with Al, Si and Zn significantly modifies the adsorption characteristics of the nanotube. In particular, dopant atoms create active adsorption sites and enhance interactions between the thiophene molecule and the Biphenylene nanotube (BPNT) surface, changing adsorption energy and charge redistribution. Furthermore, electronic structure analysis shows that thiophene adsorption induces noticeable changes in the density of states (DOS) and the electronic properties of doped nanotubes. Among the investigated systems, Al-, Si-, and Zn-doped BPNTs exhibit different sensitivities to thiophene, indicating that the nature of the dopant plays a crucial role in controlling adsorption properties. These findings suggest that doped BPNTs have considerable potential as detecting and sensing materials for thiophene.

Keywords: Thiophene, Biphenylene nanotubes, Sensors, DFT

INTRODUCTION

Thiophene is an organosulfur compound found in petroleum-derived fuels. Researchers investigate thiophene adsorption as a potential approach to reduce fuel sulfur content. Thiophene adsorption is important, particularly for fuel desulfurization. To understand catalyst behaviour, thiophene adsorption onto metal surfaces or catalysts can occupy active sites and

influence catalytic reactions. Therefore, studying thiophene adsorption is important for understanding catalyst-poisoning mechanisms.
To investigate adsorption mechanisms, thiophene interacts with a surface via physisorption or chemisorption; understanding its adsorption energy, molecular orientation, and electronic structure provides valuable insight into molecule–surface interactions.
For sensor applications, thiophene interactions with metal, metal oxide, or carbon-based surfaces can contribute to the development of sensors for detecting sulphur-containing compounds.
The electronic properties of thiophene are important. Because thiophene contains a π-electron system, its adsorption onto metals and two-dimensional materials can induce charge transfer and alter the electronic structure. These effects make thiophene adsorption relevant to molecular electronics and sensing applications.
In some studies, there is particular interest in the interaction between thiophene and carbon-based nanostructures, such as fullerenes, carbon nanotubes (CNTs) and graphene sheets, and thiophenes (Nogueira et al., 2007; Denis et al., 2010; Al-Sawaff, Z. H., 2021; Al-Sawaff, Z. H., 2022; Farhami, N, 2022, Dalgic Senturk et al. 2023, Dalgic Senturk et al. 2025) .
To the best of our knowledge, no theoretical data are available on thiophene adsorption onto BP-NTs. Therefore, theoretical studies of the interaction between BP-NTs and thiophenes are needed.
In this study, we used recently developed BP-NT structures (Dalgic Senturk et al., 2026) to investigate the interaction between thiophenes and alternative CNTs, including BP-NTs.

MATERIAL AND METHOD

In this study, DFT was utilised to investigate the adsorption of thiophene on BP-NTs using the Gaussian 09W package (Frish et al., 2009) and visualised in Gauss View (Dennington et al., 2008).

The pristine BPNT model comprises 48 carbon atoms and eight hydrogens terminating the open ends. Replacing one framework carbon at the selected site with Al, Si, or Zn gives $C_{47}H_8M$ (M = Al, Si or Zn). All models are neutral. We treated pristine, Si- and Zn-BPNT as restricted singlets, while Al-BPNT, with 303 electrons, as an unrestricted doublet.

We optimised the first thiophene and pristine/doped BP-NTs independently. The complexes were formed by positioning the active atoms at various sites on the BP-NTs. We performed all geometry optimisations, frequency, and single-point (SP) calculations using the M062X functional with the 6-31G(d) level of theory.

Recent studies have shown that the M062X/6-31G(d) method is preferred for molecular interactions because it performs better than traditional functionals [8, 19-21]. In this context, the M062X/6-31G(d) method is considered to provide more reliable results for accurately describing weak/non-covalent interactions and for including long-range corrected energy. The adsorption energies (E_{ads}) of thiophene on pristine and doped BP-NTs without any correction have been calculated by the following formula:

$$E_{ads} = E_{complex(Thiophene\ /BP-NTs)} - \left(E_{Thiophene} + E_{BP-NTs}\right) \quad (1)$$

Where $E_{Thiophene}$ and $E_{BP\text{-}NTs}$ are the isolated energies of the thiophene and pristine and doped BP-NTs, respectively. The total energy of the Thiophene/BP-NT complexes after optimisation is represented by $E_{complex}$ (Thiophene/BP-NTs). The basis-set superposition error (BSSE) correction to the Eads, obtained by the counterpoise (CP) method, is denoted Eads (BSSE).

The Molecular Orbital (MO) analysis was complemented by density of states (DOS) calculations performed with the GaussSum software (O'Boyle et al. 2008). To determine the sensing mechanism of the BP-NTs, the variation in the Eg bandgap due to the adsorption process of thiophene is taken into account by:

$$\%\Delta E_g = \left(\frac{Eg2-Eg1}{Eg1}\right) x100 \quad (2)$$

Where the Eg1 and Eg2 values correspond to the Eg values of BP-NTs and complex structures which are composed from thiophene and BP-NTs, respectively. Both % ΔEg and %ΔΦ values represent the percentage changes in bandgap and work function of the complexes relative to BP-NTs, respectively, and are listed in Table 2. The %ΔΦ value can be determined using the same logic as for band gap energies, as shown in Eq. (2).

RESULTS AND DISCUSSION

The thiophene molecule and pristine and doped BP-NTs optimised with the M062X functional level and the 6-31G(d) basis set are shown in Figure 1 and Figure 2, respectively. Frequency analyses confirmed that the optimised thiophene and BP-NT structures are stable, as no imaginary frequencies were observed.

Figure 1. The optimized structures of Thiophene

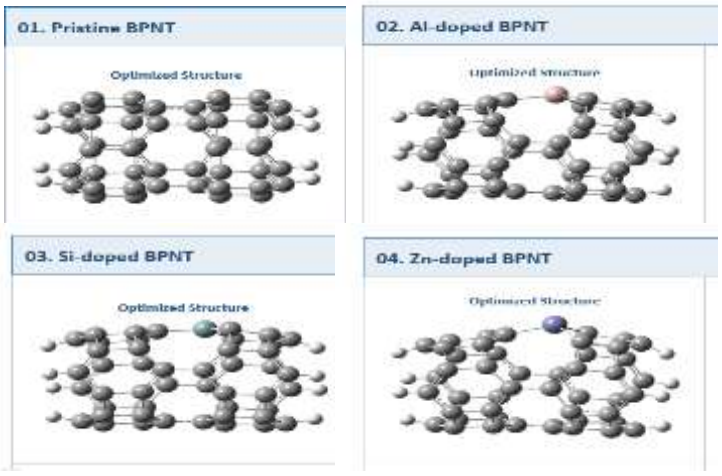

Figure 2. The optimised structures of BP-NTs

To investigate thiophene adsorption behaviour, we considered several initial orientations and adsorption positions on pristine and doped BP-NT surfaces. Figure 3 shows the optimised representative configurations for pristine BP-NT, Al-BPNT, Si-BPNT, and Zn-BPNT,

designated as Complexes 1–4, respectively. The structural analysis considered both weakly bound and more strongly interacting configurations. The calculated adsorption, interaction, and deformation energies provide a quantitative basis for comparing how different dopant atoms affect thiophene–BP-NT interactions.

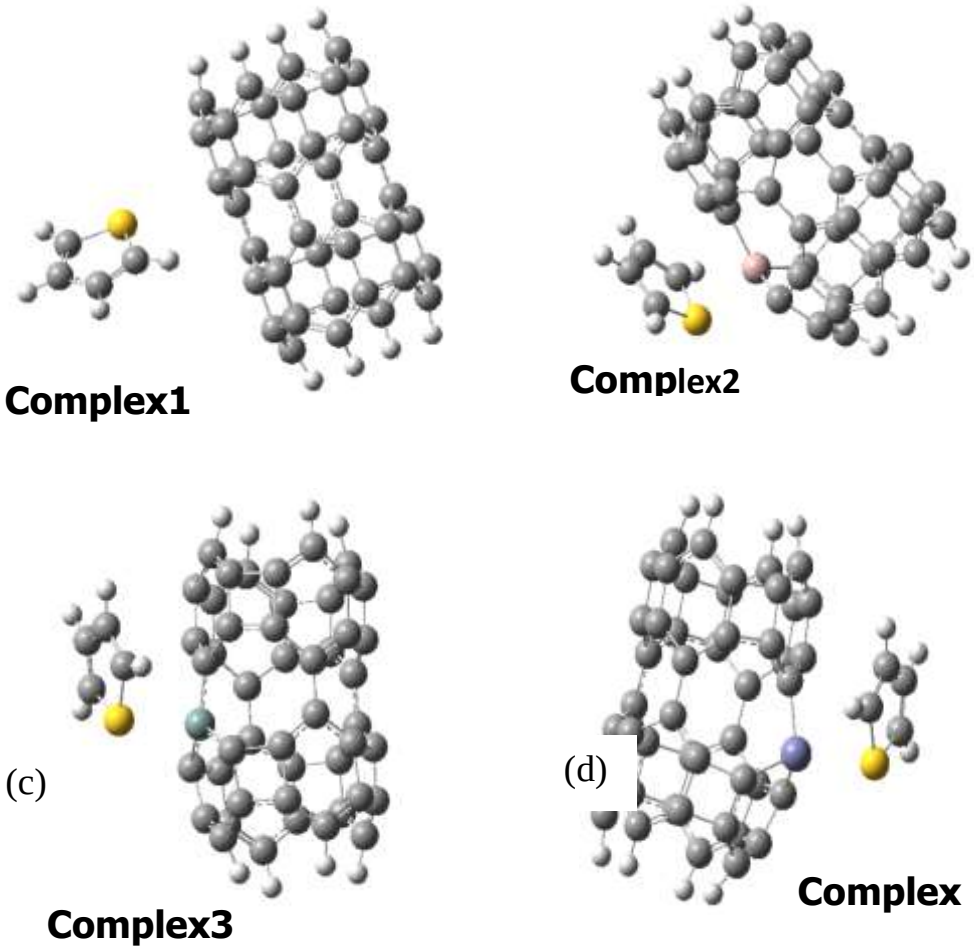

Figure 3. The optimized geometries of the complex structures composed of thiophene with BP-NTs a) Pristine BP-NT (complex1), b) Al-BPNT (complex2) c) Si-BPNT (complex3) d) Zn-BPNT (complex4).

The investigation of the adsorption process, the interaction, and deformation energies are also calculated (refer to Dalgic Senturk, 2023).

The complexes shown in Figure 3 are identified as having positive frequencies in the single-point (SP) calculations. Four complexes, from both physisorption and chemisorption categories, are presented here. The calculated energetic parameters are summarised in Table 1. Table 1 presents the bond distances, along with the calculated, without BSSE-corrected, adsorption, interaction, and deformation energies in kcal/mol for the gas phase. For pristine BP-NT, the adsorption energy of thiophene is −4.115 kcal/mol, while the corresponding interaction energy is −4.014 kcal/mol and the deformation energy is only 0.100 kcal/mol. The relatively small adsorption energy indicates that thiophene interacts weakly with the pristine BP-NT surface. The small deformation energy further indicates that the adsorption process produces only a minor structural perturbation of the individual components.

Substitutional doping yields markedly different behaviour. For Al-doped BP-NT, the adsorption energy decreases to −18.079 kcal/mol, with an interaction energy of −20.175 kcal/mol and a deformation energy of 2.096 kcal/mol. Thus, replacing a carbon atom with Al markedly increases the magnitude of the thiophene–nanotube interaction relative to the pristine system. The larger deformation energy also indicates that structural relaxation of the interacting components contributes more significantly to the final complex than in pristine BP-NT. For Si-BPNT, the calculated adsorption energy is −10.705 kcal/mol, whereas the interaction and deformation energies are −13.161 kcal/mol and 2.455 kcal/mol, respectively. The interaction is therefore stronger than that calculated for pristine BP-NT but weaker than that obtained for Al-BPNT. The larger deformation contribution compared with pristine BP-NT suggests that Si substitution also modifies the local geometry and electronic environment around the adsorption site.

Table 1. Bond distances (Å), adsorption energy (Eads) without BSSE, interaction energy (Eint), deformation energy (Edef) for the complexes, the change in enthalpy (ΔH) and Gibbs Free energy (ΔG). (All energies are in kcal/mol).

Structure	d (Å)	Eads (kcal/mol)	Eint	Edef	ΔH	ΔG
complex1	3.101	-4.115	-4.014	-0.100	**-3.296**	>0
complex2	2.532	-18.079	-20.175	2.096	-17.364	-6.766
complex3	2.552	-10.705	-13.161	2.455	-10.170	>1.324
complex4	2.619	-14.878	-16.226	1.347	-14.171	-3.483

The Zn-doped BPNT exhibits an adsorption energy of −14.878 kcal/mol, an interaction energy of −16.226 kcal/mol, and a deformation energy of 1.347 kcal/mol. The magnitude of the Zn-associated adsorption energy is substantially larger than that of pristine BP-NT and lies between the Al- and Si-doped systems in the calculated series. These results demonstrate that substitutional metal doping creates adsorption environments that interact more strongly with thiophene than the undoped BP-NT surface. Overall, the calculated adsorption energies indicate that substitutional doping substantially alters the interaction strength. Across the investigated systems, values range from approximately −4.1 to −18.1 kcal/mol, showing that the dopant's chemical nature strongly influences thiophene adsorption. The corresponding interaction energies follow the same general trend, confirming that enhanced adsorption is associated with changes in the underlying molecule–surface interaction rather than structural deformation alone.

Deformation energies should also be considered when interpreting adsorption energies. The pristine BP-NT complex has the smallest deformation energy, whereas the doped systems show larger values. In particular, Si-BPNT has a deformation energy of 2.455 kcal/mol, followed by Al-BPNT (2.096 kcal/mol) and Zn-BPNT (1.347 kcal/mol). < intermolecular interactions and the structural relaxation required to accommodate thiophene at the modified adsorption site.

The calculated enthalpy changes further support the differences observed across the systems. The calculated values are −3.296 kcal/mol for thiophene/pristine BP-NT, −17.364 kcal/mol for thiophene/Al-BPNT, −10.170 kcal/mol for thiophene/Si-BPNT, and −14.171 kcal/mol for thiophene/Zn-BPNT. The substantially more negative enthalpy changes observed for the Al-,

Si-, and Zn-doped systems indicate that substitution alters the energetic environment experienced by thiophene. The Al-containing system shows the largest magnitude of calculated enthalpy change, followed by Zn and Si. This trend aligns with the adsorption-energy results and indicates that metal substitution can significantly alter the thermodynamic driving force for thiophene–BP-NT association. The reported Gibbs free-energy values also differ between the systems. For the Al-doped complex, the calculated value is −6.766 kcal/mol, whereas the Zn-doped system gives −3.483 kcal/mol. For pristine BP-NT, the reported value is >0, and the Si-doped system also reports>1.324 kcal/mol.

These values indicate that energetic and thermodynamic descriptions are not interchangeable. Although the doped systems exhibit substantially stronger electronic interactions with thiophene, the calculated free-energy values are also affected by the thermodynamic treatment. Therefore, adsorption and interaction energies provide the clearest direct comparison of molecule–surface binding strength, whereas the reported Gibbs free energies should be interpreted in the context of the study's computational thermodynamic convention.

Electronic Properties and Quantum Molecular Descriptors

To determine the electrical and electronic properties of BP-NTs /doped-BPNTs and the Thiophene/BP-NTs- doped-BPNTs complexes, and the sensing capabilities of BP-NTs for thiophene, the Molecular Orbital Energies of HOMO and LUMO, the HOMO–LUMO energy band gap (Eg), Fermi level energy EF, work function Φ, hardness (η), and electrophilicity (ω) have been calculated and tabulated in Table 2. The pristine BP-NT has an Eg of 2.54 eV and a work function of 4.02 eV. Substituting a carbon atom with M=Al, Si, or Zn alters both quantities, indicating that the M-BPNT framework's electronic structure is sensitive to dopant type.

Table 2. HOMO energy (HOMO) in eV, LUMO energy (LUMO) in eV, HOMO/LUMO energy gap (Eg), work function (Φ), hardness (η), and electrophilicity (ω) of the complexes. %Δ Eg and %ΔΦ indicate the percentage change in bandgap and work function (Each complex was compared with its corresponding nanotube reference: pristine BPNT for complex 1, Al–BPNT for complex 2, Si–BPNT for complex 3, and Zn–BPNT for complex 4)

	BPNT	Al–BPNT	Si–BPNT	Zn–BPNT	complex1	complex2	complex3	complex4
HOMO	-5.29	-5.23	-5.35	-5.03	-5.31	-4.89	-5.06	-4.84
LUMO	-2.76	-2.49	-2.85	-2.58	-2.79	-2.18	-2.42	-2.35
Eg	2.54	2.74	2.50	2.45	2.52	2.71	2.63	2.48
%ΔEg					-0.79	1.09	5.20	1.22
Φ	4.02	3.86	4.10	3.81	4.05	3.53	3.74	3.59
%ΔΦ	-	-	-	-	0.75	-8.55	-8.78	-5.77
η	1.27	1.37	1.25	1.22	1.26	1.35	1.32	1.24
ω	6.39	5.44	6.72	5.93	6.52	4.61	5.31	5.20
EF	-4.02	-3.86	-4.10	-3.81	-4.05	-3.53	-3.74	-3.59
μ (-X)	-4.02	-3.86	-4.10	-3.81	-4.05	-3.53	-3.74	-3.59

In Table 2, Pristine BP-NT exhibits an Eg of 2.54 eV and a work function of 4.02 eV, while Al–BPNT, Si–BPNT, and Zn–BPNT exhibit Eg values of 2.74, 2.50, and 2.45 eV, respectively. Their corresponding work functions are 3.86, 4.10, and 3.81 eV. For Al–BPNT, the HOMO–LUMO gap increases to 2.74 eV (a 7.87% rise relative to pristine BPNT), while the work

function decreases from 4.02 to 3.86 eV (−3.98%). Si substitution slightly decreases Eg from 2.54 to 2.50 eV (−1.57%) and increases Φ to 4.10 eV (+1.99%). In the Zn-doped system, the HOMO–LUMO gap decreases to 2.45 eV (−3.54%), while the work function decreases to 3.81 eV (−5.22%).

The calculated HOMO–LUMO gaps for Complexes 1–4 are 2.52, 2.71, 2.63, and 2.48 eV, respectively. For Complex 1, the Eg decreases from 2.54 eV for pristine BPNT to 2.52 eV after complex formation, a reduction of 0.02 eV (0.79%). In contrast, Complex 2 shows a decrease in Eg from 2.74 eV for Al–BPNT to 2.71 eV, a reduction of 0.03 eV (1.09%). Complex 3 shows an increase in Eg from 2.50 eV for Si–BPNT to 2.63 eV, an increase of 0.13 eV (5.20%). Finally, Complex 4 exhibits a slight decrease in Eg from 2.45 eV for Zn–BPNT to 2.48 eV, corresponding to an increase of 0.03 eV (1.22%).

The work function provides complementary information on the electronic response. Complex 1 exhibits an increase in Φ from 4.02 eV for pristine BPNT to 4.05 eV, corresponding to a 0.75% increase. For Complex 2, the work function increases from 3.86 eV for Al–BPNT to 3.53 eV, corresponding to an 8.55% decrease. Complex 3 shows a decrease in Φ from 4.10 eV for Si–BPNT to 3.74 eV, corresponding to an 8.78% decrease. For Complex 4, the work function decreases from 3.81 eV for Zn–BPNT to 3.59 eV, corresponding to a 5.77% decrease.

These results indicate that the dopant's electronic influence is not uniform. Al substitution primarily increases frontier-orbital separation, whereas Zn substitution simultaneously decreases both Eg and Φ. Si–BPNT remains close to pristine BPNT in energy gap but exhibits the highest work function among the four isolated nanotube systems. Thus, the dopants establish distinct electronic environments prior to molecular adsorption, which must be considered when interpreting subsequent adsorption-induced changes.

To evaluate the electronic effect of adsorption, each complex was compared with its own corresponding nanotube reference. Complex 1 is associated with pristine BPNT, Complex 2 with Al–BPNT, Complex 3 with Si–BPNT, and Complex 4 with Zn–BPNT. This reference scheme allows the changes induced by molecular adsorption to be evaluated independently for each system.

These results demonstrate that adsorption does not produce a uniform change in the HOMO–LUMO gap. Complexes 1 and 2 show slight reductions in Eg relative to their corresponding nanotube references, whereas Complexes 3 and 4 show increases. The magnitude of these changes is relatively small, with the largest variation observed for Complex 3. This indicates that the effect of adsorption on the frontier-orbital separation depends on the electronic structure of the underlying nanotube and the specific adsorption configuration. The work-function results indicate that molecular adsorption produces a more pronounced response in Φ than in Eg for several of the systems. In particular, Complexes 2 and 3 exhibit substantial reductions in work function relative to their corresponding nanotube references, whereas the change for Complex 1 is small. Complex 4 also shows a noticeable reduction in Φ. These changes indicate modifications of the surface electronic potential associated with molecular adsorption.

The results therefore demonstrate that the electronic response of BPNT to molecular adsorption is strongly dependent on both the dopant and the adsorption environment. In particular, the pronounced work-function changes observed for the Si-containing and pristine BPNT complexes indicate substantial modifications of the surface electronic potential, whereas the Zn-containing system shows that adsorption can partially modify the electronic characteristics

introduced by metal substitution. These findings provide a consistent electronic-structure basis for further investigation of metal-doped BPNTs as adsorption-responsive nanomaterials.

Density of States (DOS) Analyses

From a materials perspective, the calculated above results indicate that pristine and doped BP-NTs should not be expected to respond identically to thiophene. The relatively weak interaction calculated for pristine BP-NT contrasts with the considerably stronger interactions obtained following Al, Si, and Zn substitution. In addition, adsorption modifies the electronic structure of the doped nanotubes, as demonstrated by the frontier-orbital and DOS analyses. Figure 5 compares the gas DOS spectra of Al-BPNT and Thiophene/Al-BPNT. Figure 6, presented the gas DOS spectra of Thiophene/Zn-BPNT.

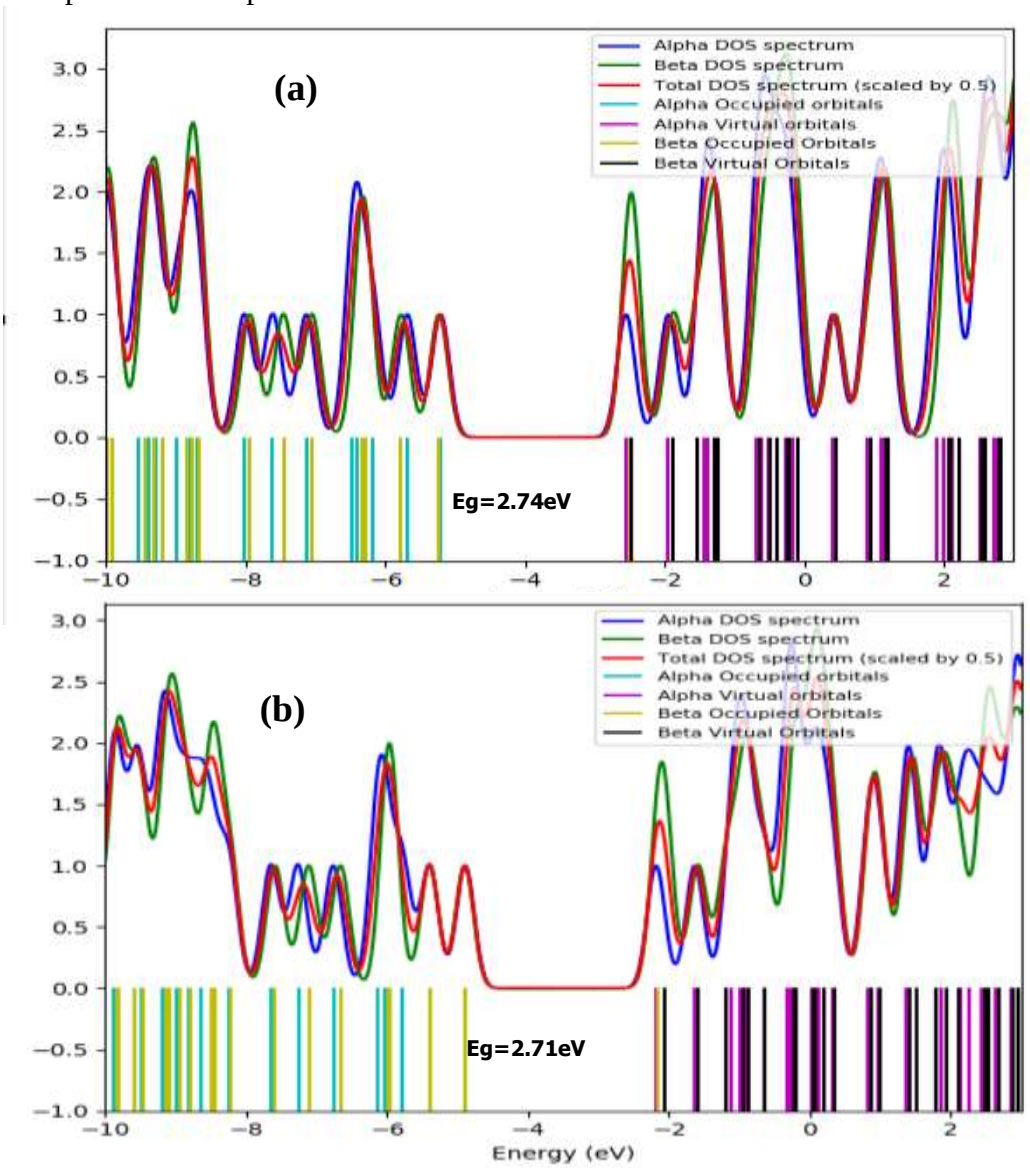

Figure. 5: DOS spectra of (a) Al-BPNT. The red Al curve is 0.5(DOS_α + DOS_β); the marked gap is the beta gap. (b) Thiophene/Al-BPNT (complex2)

For the Al-BPNT system, the DOS spectrum of the isolated Al-BPNT shows a distinct distribution of occupied and virtual electronic states, with a calculated energy gap of 2.74 eV. After thiophene adsorption, forming complex 2 (Thiophene/Al-BPNT), the DOS profile changes, and the energy gap decreases slightly to 2.71 eV. This relatively small reduction

indicates that thiophene adsorption perturbs the electronic structure of Al-BPNT without causing a dramatic collapse of the electronic gap. The change is consistent with electronic interaction between the adsorbed thiophene molecule and the doped nanotube. Thus, the Al dopant provides an electronically active adsorption environment in which thiophene adsorption produces a measurable redistribution of the available electronic states. The DOS spectra also preserve distinguishable contributions associated with the spin channels in the Al-containing system. The Al-BPNT DOS was therefore treated by considering the alpha and beta contributions, with the reported Al curve corresponding to 0.5(DOSα + DOSβ), while the indicated gap corresponds to the beta channel. This feature is important when interpreting the electronic response because the interaction cannot be described solely by the total density of states without considering the individual electronic contributions.

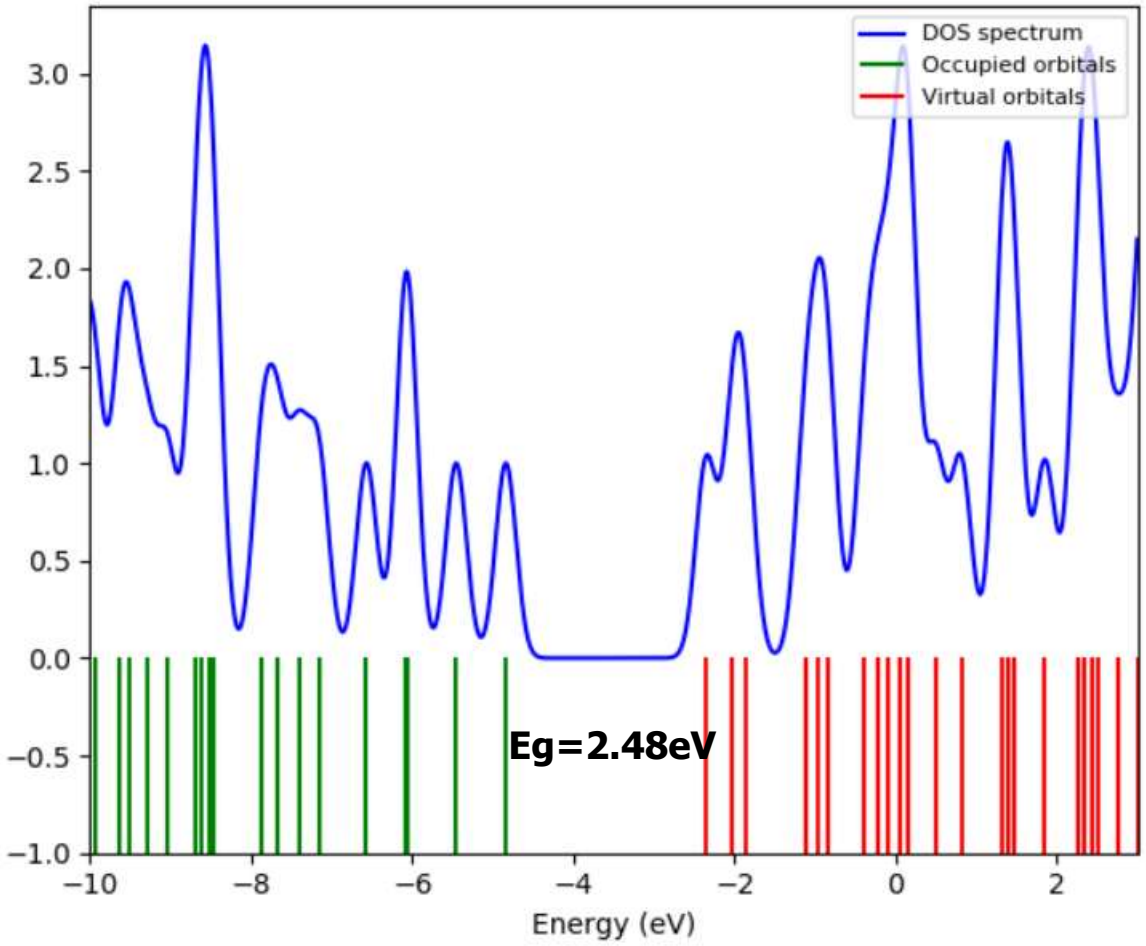

Figure. 6: DOS spectra of Thiophene/Zn-BPNT.

A similar electronic perturbation is observed in the Zn-doped system. The DOS spectrum of Thiophene/Zn-BPNT shows an energy gap of 2.48 eV. This substantially smaller gap than in isolated Al-BPNT indicates that Zn substitution creates a different electronic environment around the adsorption site.

The DOS distribution of the Zn-containing complex therefore shows that Zn incorporation modifies the electronic states available near the frontier region and that these states contribute to the electronic response to thiophene adsorption.

The DOS results should be interpreted alongside the calculated adsorption energies and charge-transfer characteristics. The stronger interactions observed for the metal-doped BP-NTs indicate that metal substitution introduces electronically active sites that interact more effectively with thiophene than the pristine nanotube. The DOS analysis provides an electronic-structure explanation for this behaviour: adsorption is accompanied by changes in the distribution and separation of occupied and unoccupied states. These changes are particularly relevant for understanding the response of the doped nanotubes, as the electronic structure near the frontier region determines how sensitively the material responds to molecular adsorption.

CONCLUSIONS

This work investigated thiophene adsorption on pristine and doped biphenylene nanotubes. Table I indicates that thiophene is physically adsorbed onto biphenylene nanotube surfaces. Thus, Al-biphenylene nanotubes and Zn-biphenylene nanotubes are candidates for use as electrochemical sensors for thiophene, and others are suitable for detection.

The DFT results demonstrate that substitutional Al, Si, and Zn doping significantly modifies thiophene adsorption on BP-NTs. The calculated adsorption energies, interaction energies, deformation energies, frontier-orbital properties, and DOS changes collectively show that the dopant atom plays an important role in determining the strength and electronic consequences of thiophene adsorption. The results thus provide a computational foundation for further investigation of doped BP-NTs in applications involving sulfur-containing molecular detection. The original paper likewise identifies the doped BP-NT systems as candidates for thiophene detection.

The DOS analysis demonstrates that **metal substitution and thiophene adsorption act cooperatively to modify the electronic structure of BP-NTs.** For Al-BPNT, thiophene adsorption changes the calculated gap from 2.74 to 2.71 eV, whereas the Thiophene/Zn-BPNT system exhibits a gap of 2.48 eV. These changes, together with the stronger adsorption calculated for the doped systems, support the conclusion that Al, Si, and Zn substitution creates electronically differentiated adsorption environments.

These results provide a theoretical basis for considering metal-doped BP-NTs as candidate materials for thiophene detection. However, the present calculations describe molecular adsorption on finite BP-NT models and therefore primarily establish the interaction and electronic-response characteristics of the systems. Experimental sensor performance, selectivity, response time, regeneration under operating conditions, and long-term stability would require separate investigation.

REFERENCES

Al-Sawaff, Z. H., Dalgic, Senturk, S., Kandemirli, F., 2021. Theoretical study of the adsorption of BMSF-BENZ drug for osteoporosis disease treatment on Al-doped carbon nanotubes (Al-CNT) as a drug delivery vehicle. European Journal of Chemistry, 12(3), 314–322. https://doi.org/10.5155/eurjchem.12.3.314-322.2143

Al-Sawaff, Z. H., Senturk Dalgic, S., Najim, Z. A. , Othman, S. S., Kandemirli, F., 2022, A comparative Density Functional Theory study of BMSF-BENZ Chemisorption on Zn12O12, Al12P12 nanocages, Physics and Chemistry of Solid State, **23**, 120. https://doi.org/10.15330/pcss.23.1.120-133

Dalgic Senturk S., Al-Sawaff, Z. H., Dalgic, S., Kandemirli, F. 2023, A comparative DFT study on Al- and Si-doped single-walled carbon nanotubes (SWCNTs) for Ribavirin drug sensing and detection, Materials Science and Semiconductor Processing. **158**, 107360. https://doi.org/10.1016/j.mssp.2023.107360

Dalgic, Senturk S., Burucu, D. K., Dalgic, S., Kandemirli, F. 2025, A comparative DFT study on the interaction of Aldara drug molecule with SiC and Si-carbon nanotubes. Journal of Applied Physics, 137(13), 135104. https://doi.org/10.1063/5.0255569

Denis, Pablo A. I., Federico, 2010, Thiophene adsorption on Single Wall Carbon Nanotubes and graphene, Journal of Molecular Structure: THEOCHEM 957 114–119, https://doi.org/10.1016/j.theochem.2010.07.020

Dennington, R. D., Keith, T. A., Millam, J. M., 2008 GaussView 5.0.8, Gaussian Inc.

Farhami, N. 2022, A Computational study of Thiophene Adsorption on Boron Nitride Nanotube, 2, 148-157., **https://doi.org/10.22034/jaoc.2022.154821**

Frisch, M. J., et al. (2009). Gaussian 09, Revisions E.01 and A.02. Gaussian, Inc., Wallingford, CT. https://gaussian.com/g09citation/

Genç, F., Dalgic Senturk, S., S.; Kandemirli, F. (2025a). Density Functional Theory Investigation on The Interaction of Formaldehyde with Zn Doped (6,0) SWCNT for Sensor Applications. Bitlis Eren Üniversitesi Fen Bilimleri Dergisi, 14(4), 2552–2561. https://doi.org/10.17798/bitlisfen.1754990

Genç, F., Dalgic Senturk, S., Kandemirli, F. (2025b). Potential Application of Al-Doped Carbon Nanotubes for Tretinoin: A Theoretical Study. Cumhuriyet Science Journal, 46(2), 319–328. https://doi.org/10.17776/csj.1646890

Lu, T., Chen, F. 2012. Multiwfn: A multifunctional wavefunction analyser. Journal of Computational Chemistry, 33(5), 580–592. https://doi.org/10.1002/jcc.22885

Lu, T. 2024. A comprehensive electron wavefunction analysis toolbox for chemists, Multiwfn. The Journal of Chemical Physics, 161(8), 082503. https://doi.org/10.1063/5.0216272

Nogueira, A.F., Lomba, B.S. , Soto-Ovideo, M.A., Duarte Correia, C.R. , Corio, P. , Furtado, C.A., Hummelgen, I.A. ,2007, Polymer Solar Cells Using Single-Wall Carbon Nanotubes Modified with Thiophene Pedant Groups,J. Phys. Chem. C 111 18431. https://doi.org/10.1021/jp074979n

O'Boyle N.M., Tenderholt A.L, Langner K.M Cclib. 2008, A library for package-independent computational chemistry algorithms, J. Comput. Chem., **29**, 839. https://doi.org/10.1002/jcc.20823

RELATIONSHIPS BETWEEN SOIL STRUCTURE AND CARBON DIOXIDE EMISSIONS

Coşkun GÜLSER [1], Füsun GÜLSER [2]*

[1] Ondokuz Mayıs University, Faculty of Agriculture, Department of Soil Science and Plant Nutrition, Samsun, Türkiye
**e-mail: cgulser@omu.edu.tr*

[2] Van Yüzüncü Yıl University, Faculty of Agriculture, Department of Soil Science and Plant Nutrition, Van Türkiye
e-mail: fgulser@yyu.edu.tr

ABSTRACT

Soil structure is the most dynamic physical factor directly governing atmospheric carbon dioxide (CO_2) emissions through aggregate development, pore size distribution, and gas diffusion capacity. The CO_2 released from the soil is essentially a product of microbial decomposition (heterotrophic respiration) and root respiration (autotrophic respiration). Soil structure controls this release with two basic protective barriers consisting of aggregation and porosity. In aggregation or physical conservation, the stable structure of micro aggregates (<250 µm) in particular stabilizes organic carbon by trapping it in narrow pores inaccessible to microbial enzymes and oxygen. Mechanical interventions, such as intensive tillage, break down these aggregates, releasing carbon and causing sudden bursts of CO_2. The macro and micro-pore network of the soil determines the rate of gas exchange through the regulation of gas diffusion. In conclusion, sustainable agricultural practices that preserve soil structure, such as no-till cropping, cover crop use, and organic fertilization, enhance the soil's capacity to act as a carbon sink by increasing bio-glucosides like glomalin and aggregate stability, thereby minimizing CO_2 emissions that contribute to global warming.

Key words: Soil, structure, porosity, carbon dioxide, emission.

INTRODUCTION

Mitigating global climate change and reducing greenhouse gas emissions constitute one of the most critical focal points of modern environmental and agricultural sciences. As frequently emphasized in the reports of the Intergovernmental Panel on Climate Change (IPCC), terrestrial ecosystems play a dual role in the global carbon (C) cycle, acting both as a massive sink and a potential source (IPCC, 2023).

Global soils represent the largest dynamic terrestrial carbon pool, storing approximately three times the amount of carbon found in the atmosphere and four times that of aboveground biomass (around 1500–2400 Pg C) (Lal, 2004; Batjes, 2016). Consequently, even minor percentage fluctuations within the soil carbon pool possess the potential to exert a multiplier effect on atmospheric carbon dioxide (CO_2) concentrations and global warming trends. The relationship between soil structure and CO2 emissions is a critical issue regarding the global carbon cycle and sustainable agriculture

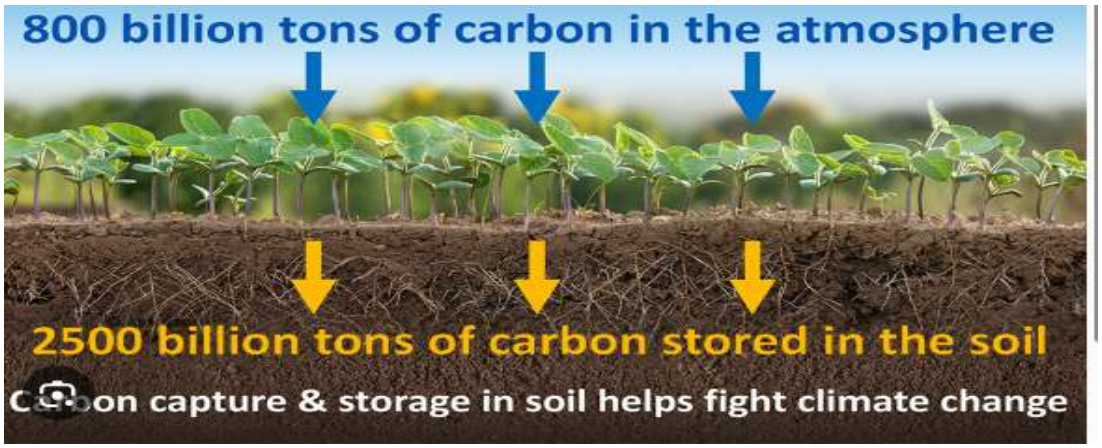

Fig. 1. Carbon in the soil plays a huge role in combating climate change
https://drearth.com/resources/article/fertilizer-nutrient-information-copy/

Fig. 2. Soil Carbon Sequestration https://www.azocleantech.com/article.aspx?ArticleID=1655

Physical properties such as soil aggregates, porosity, and gas diffusion directly govern the respiration activities of microorganisms and roots. Soil structure consists of the arrangement of aggregates formed by the combination of primary mineral particles (sand, silt, clay) with organic binding agents, fungal hyphae, and root exudates and the pore network situated between these arrangements (Tisdall and Oades, 1982). On the other hand, CO_2 emission is a result of root respiration (autotrophic) and microbial decomposition (heterotrophic) (Schlesinger ve Andrews, 2000). The rate and magnitude of these processes are directly controlled by soil structure which the most dynamic physical property of soil as well as by climatic factors such as soil temperature and moisture (Six et al., 2004). This review discusses how soil structure shapes CO_2 emissions through aggregation dynamics and pore-size distribution mechanisms, the effects of anthropogenic structural degradation on emission kinetics, and the potential of

sustainable soil management strategies to transform soil from a carbon source into a stable carbon sink.

The Role and Mechanisms of Soil Structure on CO_2 Emissions

Soil structure influences CO_2 emissions through aggregate stability and pore size distribution**.** Aggregates are classified into macro aggregates (>250 µm) which are generally held together by roots and fungal hyphae and are more sensitive to management and micro aggregates (<250 µm) which are more persistent and responsible for the long-term stabilization of soil organic carbon (SOC) (Tisdall and Oades, 1982). The narrow pore structure of micro aggregates entraps organic matter, making it inaccessible to microbial enzymes and oxygen (O_2). This physical barrier prevents heterotrophic microorganisms from utilizing carbon as a substrate, consequently minimizing CO_2 production (Lal, 2004). The macro pore and micro pore network of the soil governs the rate of gas exchange (gas permeability). In loose and well-aggregated soils, O_2 influx and CO_2 diffusion are rapid, thereby supporting aerobic respiration (Smith et al., 2003). However, when soil becomes severely compacted or water-saturated, gas diffusion is virtually halted. In these anoxic environments, while aerobic CO_2 production is suppressed, anaerobic processes are activated, leading to the emission of greenhouse gases with much higher global warming potentials, such as methane (CH_4) and nitrous oxide (N_2O) (Davidson and Janssens, 2006, Ball, 2013).

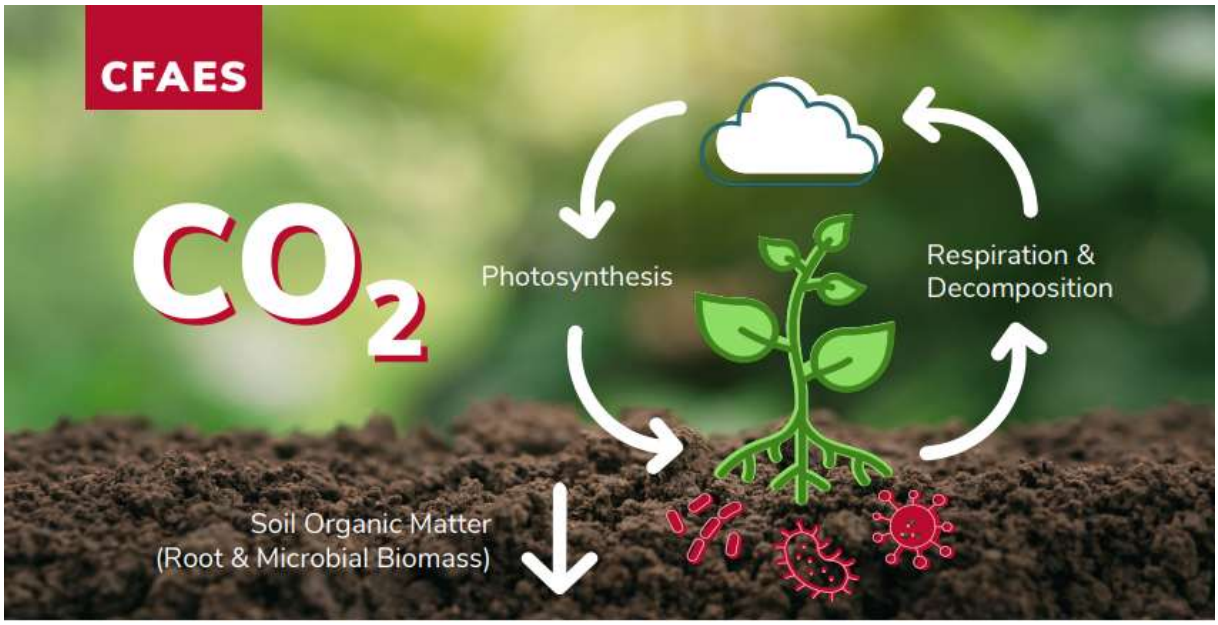

Fig. 3. The soil carbon cycle and the role of soil organic matter in carbon (https://carbon.osu.edu)

The Effect of Tillage on Aggregate Breakdown and CO2 Emission

Anthropogenic interventions such as intensive tillage, overgrazing, and monoculture production lead to the structural degradation of aggregate stability (Reicosky, 1997). The mechanical shear forces applied to the soil by tillage implements lead to the direct disruption of macro aggregates (>250 µm), which are particularly unstable (Beare et al., 1994), and result in the release of carbon-rich micro aggregates and free light fraction organic matter. Since vegetation and the stubble layer are removed in tilled soils, the direct impact of raindrops on the bare soil (splash effect) physically disperses the aggregate structure (Al-Kaisi & Licht, 2005). Furthermore, as tilled dry soil rapidly becomes saturated with water, the compression of air within aggregate pores causes micro-explosions (slaking) and the disintegration of aggregates (Zaher et al.,

2005). Fungi play a crucial role in binding aggregates together through their hyphae and glomalin, a stable glycoprotein they secrete (Wright & Upadhyaya, 1998). Intensive tillage physically disrupts fungal (Arbuscular Mycorrhizal Fungi - AMF) networks, significantly reducing new aggregate formation and aggregate stability (Helgason et al., 1998). When soil aggregates break down, stable organic carbon fractions, which have long been protected inside the aggregates, are suddenly exposed to a macroscopic influx of oxygen and thus become readily consumable substrates for heterotrophic microorganisms (Balesdent et al., 2000). This leads to massive emission waves from agricultural soils into the atmosphere, referred to as CO_2 bursts (Ellert and Janzen, 1999).

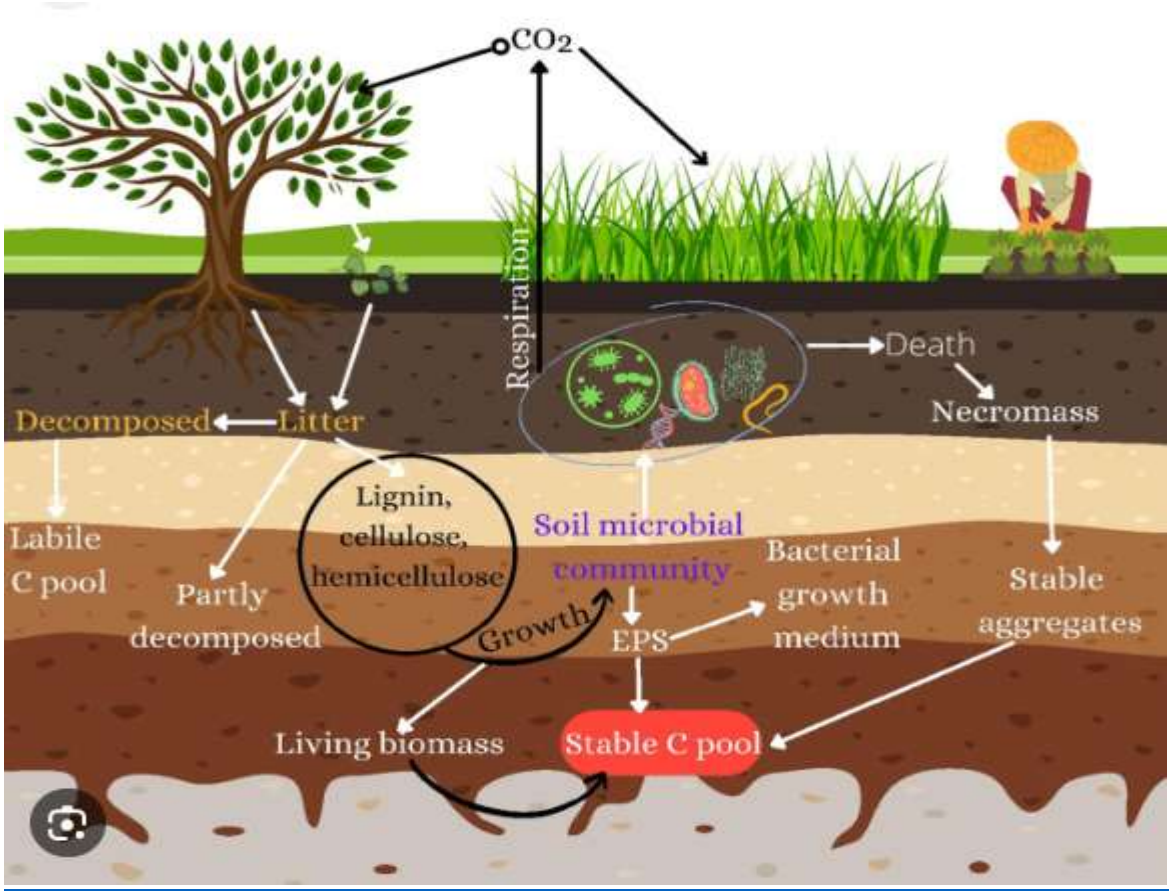

Fig. 4. Conceptual diagram of soil organic carbon formation and stabilization through plant residues and microbial processes. https://www.sciencedirect.com/science/article/pii/S0048969722000171

Sustainable Soil Management and Increasing Carbon Sinks

It has been reported that if global soil carbon stocks were increased by 0.4% annually, total human-induced annual CO2 emissions could be offset (Rodrigues et al., 2017). Achieving this goal depends on the global adoption of sustainable management practices. Sustainable agricultural practices that preserve and improve soil structure are the most effective tools for increasing the soil's carbon sequestration capacity. Conventional tillage mechanically disrupts macro aggregates, making carbon-rich micro aggregates vulnerable to microbial decomposition (Beare et al., 1994). In contrast, conservation or no-till practices maintain aggregate stability and prevent mechanical fragmentation. Since the soil structure remains undisturbed, fungal hyphae and organic binding agents such as glomalin are preserved (Wright and Upadhyaya, 1998). This ensures the physical protection of carbon within the soil matrix and allows carbon to remain locked in the soil for extended periods, thereby minimizing CO_2 emissions (Six et

al., 2002). Cover crops promote macro aggregate formation through their root systems and fungal hyphae. By blocking the physical impact of raindrops (splash effect) and wind erosion, they prevent the transport and loss of carbon-rich topsoil (Al-Kaisi & Licht, 2005). They stabilize microbial activity and prevent carbon loss through erosion. Keeping the soil covered with vegetation throughout the year ensures a continuous input of carbon. Furthermore, they contribute directly to microbial biomass and stable carbon fractions via root exudates (Paustian et al., 2016). Organic fertilizers such as compost and farm yard manure introduces humic substances and glomalin that a biotic glue produced by arbuscular mycorrhizal fungi into the soil and suppresses carbon emissions by maximizing aggregate stability (Wright and Upadhyaya, 1998). For example compost accelerates the formation of humic substances (humification) by supporting soil microbial activity and aggregation. Biochar obtained through the pyrolysis of biomass in an environment without oxygen consists of highly stable carbon that can remain in the soil without decomposing for hundreds or even thousands of years (Lehmann, 2007). When perennial plants and deep-rooted species are incorporated into the system instead of monoculture farming, deep-rooted plants transport carbon to the subsoil layers. Due to microbial activity and low oxygen levels, carbon in these subsoil layers is sequestered for a much longer period (centuries) compared to surface layers (Lorenz & Lal, 2005). Integrating trees into agricultural lands maximizes both above-ground (woody biomass) and below-ground carbon stocks simultaneously (Nair et al., 2009).

CONCLUSIONS

Soil structure is not just a mechanical support unit, but a biophysical filter that balances the global carbon budget. It plays a central role in regulating soil carbon dynamics and CO_2 emissions by mediating the accessibility of soil organic carbon (SOC) to microbial decomposers, the diffusion and transport of CO_2 and other gases within the soil, and the distribution and cycling of root and microbial respiration. Enhancing aggregate stability and optimizing porosity are highly effective in reducing CO_2 emissions by keeping the heterotrophic respiration rate under control. Sustainable agricultural management strategies directly contribute to the fight against global warming by transforming the soil from a carbon source into an active carbon sink.

REFERENCES

Al-Kaisi, M. M., & Licht, M. A. (2005). Soil carbon dioxide emissions in relation to tillage, crop residue, and sulfur micro-climate. *Soil and Tillage Research, 80*(1-2), 141-158.

Balesdent, J., Chenu, C., & Balabane, M. (2000). Relationship of soil organic matter dynamics to physical protection and tillage. *Soil and Tillage Research, 53*(3-4), 215-230.

Ball, B. C. (2013). Soil structure and greenhouse gas emissions: A synthesis of 20 years of experimentation. *European Journal of Soil Science, 64*(3), 357-373.

Batjes, N. H. (2016). Harmonized soil property values for broad-scale applications (WISE30sec) with estimates of global soil carbon stocks. *Geoderma, 269*, 61-68.

Batjes, N. H. (2016). Total carbon and nitrogen in the soils of the World. *European Journal of Soil Science, 47*(2), 151-163.

Beare, M. H., Cabrera, M. L., Hendrix, P. F., & Coleman, D. C. (1994). Aggregate-protected and unprotected organic matter pools in conventional and no-tillage soils. *Soil Science Society of America Journal, 58*(3), 787-795.

Davidson, E. A., & Janssens, I. A. (2006). Temperature sensitivity of soil carbon decomposition and feedbacks to climate change. *Nature, 440*(7081), 165-173.

Ellert, B. H., & Janzen, H. H. (1999). Short-term reactive carbon dioxide fluxes from agricultural soils after tillage. *Soil Science Society of America Journal, 63*(1), 212-222.

Helgason, B. L., Walley, F. L., & Germida, J. J. (1998). Fungal and bacterial abundance in long-term no-till and intensive till soils. *Soil Biology and Biochemistry, 31*(3), 397-410.

IPCC. (2023). *Climate Change 2023: Synthesis Report. Contribution of Working Groups I, II and III to the Sixth Assessment Report of the Intergovernmental Panel on Climate Change*. IPCC, Geneva, Switzerland.

Lal, R. (2004). Soil carbon sequestration impacts on global climate change and food security. *Science, 304*(5677), 1623-1627.

Lehmann, J. (2007). A handful of carbon. *Nature, 447*(7141), 143-144.

Lorenz, K., & Lal, R. (2005). The depth distribution of soil organic carbon in relation to land use and management. *Soil and Tillage Research, 83*(1), 14-21.

Ramachandran Nair, P. K., Mohan Kumar, B., & Nair, V. D. (2009). Agroforestry as a strategy for carbon sequestration. *Journal of plant nutrition and soil science, 172*(1), 10-23. Paustian, K., et al. (2016). Climate-smart soils. *Nature, 532*(7597), 49-57.

Reicosky, D. C. (1997). Tillage-induced CO_2 emissions from soil. *Soil and Tillage Research, 41*(1-2), 105-115.

Rodrigues, C. I. D., Brito, L. M., & Nunes, L. J. (2023). Soil carbon sequestration in the context of climate change mitigation: A review. *Soil Systems, 7*(3), 64.

Schlesinger, W. H., & Andrews, J. A. (2000). Soil respiration and the global carbon cycle. *Biogeochemistry, 48*(1), 7-20.

Six, J., Bossuyt, H., Degryze, S., & Denef, K. (2004). A history of research on topsoil aggregation and soil organic matter turnover: A review. *European Journal of Soil Science, 55*(4), 629-641.

Six, J., Feller, C., Denef, K., Ogle, S., de Moraes Sa, J. C., & Albrecht, A. (2002). Soil organic matter, biota and aggregation in temperate and tropical soils-Effects of no-tillage. *Agronomie, 22*(7-8), 755-775.

Smith, K. A., Ball, T., Conen, F., Dobbie, K. E., Massheder, J., & Rey, A. (2003). Exchange of greenhouse gases between soil and atmosphere: Interactions of soil physical factors and biological processes. *European Journal of Soil Science, 54*(4), 779-791.

Tisdall, J. M., & Oades, J. M. (1982). Organic matter and water-stable aggregates in soils. *Journal of Soil Science, 33*(2), 141-163.

Wright, S. F., & Upadhyaya, A. (1998). A survey of glomalin, a novel glycoprotein produced by arbuscular mycorrhizal fungi, on aggregates from diverse soils. *Plant and Soil, 201*(1), 43-52.

Zaher, H., Caron, J., & Parent, L. E. (2005). Aggregate stability index under wet-dry cycles. *Soil Science Society of America Journal, 69*(6), 1663-1673.

EFFECTS OF BIOCHAR AND POTASSIUM SOLUBILIZING BACTERIA APPLICATIONS ON WHEAT DEVELOPMENT, POTASSIUM CONTENT, AND SOIL PH AND EC

FERİT SÖNMEZ[1], YASİN SÖNMEZ[1], FÜSUN GÜLSER[2]

[1] Bolu Abant İzzet Baysal University, Faculty of Agriculture, Department of Seed Science and Technology, Bolu-Türkiye
[2] Van Yüzüncü Yıl University, Faculty of Agriculture, Department of Soil Science and Plant Nutrition, Van-Türkiye

ABSTRACT

This study was conducted to investigate the effects of potassium solubilizing bacteria (KSB) and different doses of biochar applications on growth parameters of wheat (*Triticum aestivum* L.), plant potassium content, and soil pH and electrical conductivity (EC). The experiment was carried out in a controlled climate chamber for 45 days under a photoperiod of 16 hours light (25°C) and 8 hours dark (20°C) with 60-70% relative humidity. The experiment was arranged in a completely randomized factorial design with three replications, consisting of two main factors: KSB application (non-inoculated control and KSB-inoculated) and four different biochar doses (0%, 1%, 2%, and 4%). Seeds were inoculated by immersion in bacterial suspension at approximately 10^8 CFU mL^{-1} for 30 minutes, while control seeds were treated with sterile distilled water. Each pot contained 2 kg of air-dry soil, and all pots received basal fertilization of 200 mg N kg^{-1} as ammonium sulfate and 80 mg P_2O_5 kg^{-1} as triple superphosphate, with no additional potassium fertilizer applied. At the end of the experiment, plant height (PH), plant fresh weight (PFW), plant dry weight (PDW), dry leaf weight (DLW), dry root weight (DRW), number of spikes (NS), plant potassium content, and soil pH and EC values were determined. the findings showed that KSB application significantly increased plant height by 6.2%, plant fresh weight by 15.8%, plant dry weight by 16.0%, and plant potassium content by 7.9%. Biochar application, particularly at the 4% dose, provided increases of 20.3% in plant height, 43.1% in dry leaf weight, and 43.2% in dry root weight, while causing a 23.7% decrease in plant potassium content. Analysis of variance results revealed that KSB × biochar interaction had highly significant ($p<0.01$; $p<0.001$) effects on plant fresh weight, plant dry weight, number of spikes, dry leaf weight, and dry root weight. While both KSB and biochar applications individually and in interaction had significant effects on soil pH, only KSB × biochar interaction was found to be significant for EC. In conclusion, it was determined that optimum dose ratios that would minimize potassium adsorption need to be determined in the combined application of biochar and KSB, and that long-term field trials using different biochar types and different KSB species are needed.

Keywords: Biochar, potassium solubilizing bacteria, *Triticum aestivum*, plant development

INTRODUCTION

Wheat (*Triticum aestivum* L.) is one of the staple food sources for the world's population and ranks among the strategic crops with the largest cultivation area in global cereal production. Sustainable increase in wheat production is of great importance to meet the food needs of the growing population. However, intensive agricultural practices lead to problems such as imbalanced use of nutrients in soils, loss of organic matter, and deterioration of soil quality. In this context, developing alternative methods that reduce chemical fertilizer use while preserving

soil health and improving plant nutrition has become a critical necessity for sustainable agriculture.

Potassium (K) is one of the three essential macro-nutrients required for healthy plant development. Potassium, which plays vital roles in physiological processes such as enzyme activation, protein synthesis, photosynthesis, water regulation, and osmotic control in plants, also directly determines product quality and yield (Marschner, 2012). Although total potassium content in soils is generally high, most of this potassium is trapped in the crystal structure of primary minerals such as feldspar and mica and is not in a soluble form directly available to plants (Sparks, 1987). Only 1-2% of soil potassium exists in plant-available forms (soluble and exchangeable K). This situation necessitates the development of alternative strategies to make potassium available to plants.

In recent years, the use of organic soil amendments has become increasingly widespread to enhance soil fertility and improve plant nutrition. Biochar, one of these amendments, is a carbon-rich, porous material produced through pyrolysis of organic materials under oxygen-limited or oxygen-free conditions (Lehmann, 2007). Biochar has the potential to improve physical, chemical, and biological properties of soils due to its high surface area, porous structure, high cation exchange capacity, and chemical functional groups (Lehmann et al., 2011). Numerous studies have reported that biochar applications increase soil water holding capacity, improve aeration, raise pH in acidic soils, and enhance nutrient retention (Chan et al., 2007; Atkinson et al., 2010). However, the effects of biochar on nutrients may vary significantly depending on application dose, feedstock type, pyrolysis temperature, and soil properties. Notably, findings also suggest that high-dose biochar applications may reduce nutrient availability to plants by adsorbing some nutrients through cation exchange capacity (Glaser et al., 2002; Bruun et al., 2012).

Potassium solubilizing bacteria (KSB) are microorganisms that live in the rhizosphere and can convert insoluble potassium minerals in soil into soluble forms available to plants. These bacteria belong to various genera, primarily *Bacillus*, *Pseudomonas*, *Paenibacillus*, *Rhizobacter*, and *Agrobacterium*, and their potassium solubilization mechanisms include production of organic acids (citric acid, malic acid, oxalic acid, gluconic acid, etc.), exopolysaccharide synthesis, and siderophore production (Sheng and He, 2006; Zhang and Kong, 2014). These microorganisms facilitate the release of potassium from mineral structures through acidification and chelation in the root zone. Research has shown that KSB inoculation significantly increases dry matter production and potassium uptake in wheat (Zahedi, 2016; Etesami et al., 2017). Furthermore, KSB applications are known to contribute directly to plant growth not only by enhancing potassium availability but also by producing plant growth-promoting hormones (indole-3-acetic acid, gibberellins) and activating biocontrol mechanisms against pathogens (Meena et al., 2014).

The combined use of biochar and KSB applications has the potential to create synergistic effects for sustainable agriculture. The porous structure of biochar can provide a protected habitat for microorganisms, facilitating their long-term survival and maintenance of metabolic activities in soil (Quilliam et al., 2013; Thies and Rillig, 2009). Additionally, biochar's surface chemistry and nutrient supply capacity can directly or indirectly influence microbial activity. However, current knowledge regarding biochar-KSB interactions is limited, and studies examining the effects of different biochar doses on KSB efficacy in wheat are needed.

The primary objective of this study is to investigate the effects of different doses of biochar and potassium solubilizing bacteria applications on wheat growth parameters, plant potassium content, and soil pH and EC values. Specifically, the study aims to: (i) determine the effect of KSB inoculation on wheat growth and potassium nutrition, (ii) evaluate the effects of increasing biochar doses on wheat growth and potassium dynamics, (iii) examine KSB × biochar interactions, and (iv) assess changes in soil pH and EC resulting from the applications. The

findings are expected to contribute to the development of optimal strategies for the combined use of biochar and KSB applications in wheat cultivation.

MATERIALS AND METHODS

Experimental Site and Conditions

The experiment was conducted in a controlled climate chamber for 45 days. The climate chamber was maintained at a photoperiod of 16 hours light (25°C) and 8 hours dark (20°C) with 60-70% relative humidity. Temperature, humidity, and lighting were regularly monitored and kept constant throughout the experiment.

Plant Material

Wheat (*Triticum aestivum* L.) seeds were used as plant material. Seeds were subjected to surface sterilization before applications, and healthy, uniformly sized seeds were selected for use in the experiment. Twenty wheat seeds were sown in each pot, and no thinning was performed following germination.

Experimental Design

The experiment was arranged in a completely randomized factorial design with three replications in a controlled climate chamber. The study included two main factors. The first factor was potassium solubilizing bacteria (KSB) application at two levels: non-inoculated control group [KSB(-)] and potassium solubilizing bacteria inoculated group [KSB(+)]. The second factor was biochar application consisting of four different doses: 0% (control), 1%, 2%, and 4%. Each treatment combination was tested in three pots. Accordingly, the total number of experimental units was 2 (KSB level) × 4 (biochar dose) × 3 (replication) = 24 pots. Pots were randomly positioned within the climate chamber to minimize variation caused by environmental conditions, and pot positions were periodically changed throughout the experiment. This approach aimed to reliably test differences among treatments while minimizing experimental errors.

Potassium Solubilizing Bacterial Culture and Seed Inoculation

For inoculation, wheat seeds were first surface sterilized by treatment with 70% ethanol (2 minutes) and 0.1% sodium hypochlorite (1 minute) solutions. Subsequently, seeds were rinsed three times with sterile distilled water. For KSB(+) application, seeds were immersed in prepared bacterial suspension (10^8 CFU mL^{-1}) for 30 minutes. For KSB(-) control application, seeds were kept in sterile distilled water for the same duration. Following inoculation, all seeds were air-dried under sterile conditions and sown immediately after drying.

Soil Preparation and Fertilization

The soil used in the experiment was air-dried, passed through a 2 mm sieve, and homogenized. Each pot was filled with 2 kg of air-dry soil. Soil samples were analysed prior to the experiment to determine certain physical and chemical properties.
All pots received basal fertilization of 200 mg N kg^{-1} soil as ammonium sulfate ($(NH_4)_2SO_4$) and 80 mg P_2O_5 kg^{-1} as triple superphosphate (TSP, 44% P_2O_5). No additional potassium fertilizer was applied. Fertilizers were homogeneously mixed with the soil.

Irrigation and Experimental Maintenance

Throughout the experiment, pots were regularly irrigated with distilled water to maintain 70% of field capacity, determined by gravimetric method. Irrigation was controlled by weighing, and leaching from pots was prevented. Pot positions were regularly changed throughout the experiment to minimize variation from environmental conditions.

Harvest and Measurements

Harvest was performed on day 45 of the experiment. Various morphological and physiological parameters were measured to evaluate plant development during harvest. Plant height was measured with a ruler from the soil surface to the plant tip, determined individually for all plants in each pot, and averaged. For plant fresh weight determination, harvested plants were cleaned of soil residues and weighed on a precision balance, with total fresh weight recorded per pot. For plant dry weight determination, fresh plant samples were dried in an oven at 65°C until constant weight and subsequently weighed on a precision balance to obtain dry weight values. For dry leaf weight and dry root weight determination, dried plants were separated into leaves and roots, and these parts were weighed separately and recorded in grams. For plant count per pot, the total number of emerged plants in each pot was counted and expressed as number. All measurements were performed in triplicate, and averages of the obtained data were calculated and used in statistical analyses.
Potassium analysis of plant samples was performed according to the method described by Kacar and İnal (2008). Dried plant samples were subjected to dry ashing, dissolved in appropriate acid solution, and potassium concentrations were determined using ICP-OES (Inductively Coupled Plasma Optical Emission Spectrometry). Results were expressed as percentage (based on dry weight).

Soil pH and Electrical Conductivity (EC) Analyses

Soil samples were collected from each pot after harvest. Soil pH was determined in soil-water suspension prepared at 1:2.5 (soil: distilled water) ratio using a pH meter. Electrical conductivity (EC) measurements were performed in the same suspension using an EC meter according to the method described by Kacar (1994). Both analyses were conducted in triplicate, and average values were calculated.

Statistical Analysis

Obtained data were subjected to analysis of variance (ANOVA) using SPSS (Statistical Package for Social Sciences) software. Differences among treatments were compared using LSD (Least Significant Difference) test at $\alpha=0.05$ significance level. ANOVA results were evaluated according to significance levels of $p<0.05$, $p<0.01$, and $p<0.001$.

RESULTS

ANOVA results for all parameters examined in the study are presented in Tables 1 and 2, while means and Duncan grouping for treatment effects on growth criteria, plant potassium content, and growing medium pH and EC contents are presented in Table 3.
As shown in Table 1, potassium solubilizing bacteria application had statistically significant effects on plant height ($p<0.05$), plant fresh weight ($p<0.05$), plant dry weight ($p<0.05$), and root fresh weight ($p<0.05$). In contrast, the effect of KSB application on root dry weight was found to be non-significant.

Table 1. Analysis of variance values for effects of potassium solubilizing bacteria (KSB) and biochar applications on plant growth criteria

Source	df	PH	PFW	PDW	RL	RFW	RDW
KSB	1	4.60 *	5.35 *	8.04 *	25.00 **	4.87 *	3.07 ns
Biochar	3	8.03 **	13.02**	11.26**	4.41 *	9.06 **	7.98 **
KSB × Biochar	3	2.42 ns	1.90 ns	3.00 öd	14.44 **	6.57 **	4.94 **

* ,**: Significant at p<0.05, p<0.01 respectively; ns: Non-significant. PH: Plant Height, PFW: Plant Fresh Weight, PDW: Plant Dry Weight, RL: Root Length, RFW: Root Fresh Weight, RDW: Root Dry Weight.,

As shown in Table 1, biochar application had statistically significant effects on plant height (p<0.01), plant fresh weight (p<0.05), plant dry weight (p<0.01), root fresh weight (p<0.01), and root dry weight (p<0.01). The KSB × biochar interaction showed highly significant effects on root length (p<0.001), root fresh weight (p<0.01), and root dry weight (p<0.01). The interaction effect was found to be non-significant for plant height, plant fresh weight, and plant dry weight.

Table 2. Analysis of variance values for effects of potassium solubilizing bacteria (KSB) and biochar applications on plant potassium, soil pH, and EC values

Source	**Df**	**Potassium**	**pH**	**EC**
KSB	1	6.25 **	129.39 **	0.49 ns
Biochar	3	14.36 **	21.18 **	7.62**
KSB × Biochar	3	1.06 ns	0.30 ns	1.13 ns

*, **: Significant at p<0.05, p<0.01 respectively; ns: Non-significant

When Table 2 is examined, it is seen that KSB application had highly significant effects on plant potassium content (p<0.05) and soil pH (p<0.001), whereas its effect on soil EC was non-significant. Biochar application created significant effects on plant potassium content (p<0.001), soil pH (p<0.01), and EC (p<0.01). The KSB × biochar interaction was found to be non-significant for plant potassium content, soil pH, and EC.

As shown in Table 3, potassium solubilizing bacteria application generally provided positive and statistically significant increases in the examined growth parameters of wheat. With KSB application, plant height increased by 6.2% from 31.08 cm to 33.00 cm compared to the control group. Plant fresh weight increased by 15.8% from 4.152 g to 4.808 g compared to the control group. Similarly, plant dry weight increased by 16.0% from 0.419 g to 0.486 g with KSB application. Root fresh weight increased by 13.0% with KSB inoculation, rising from 1.540 g to 1.740 g. The increase in root dry weight was determined to be statistically non-significant. KSB application also had a positive effect on plant potassium content, increasing it by 7.9% from 1.825% to 1.970%. In contrast, the effect of KSB application on root dry weight was not found to be statistically significant. Root dry weight was recorded as 0.138 g in the control group and 0.152 g in the KSB application. These findings reveal that potassium solubilizing bacteria significantly promotes vegetative growth and potassium nutrition of wheat, but this effect does not occur at the same level in all plant organs. The fact that KSB application provided particularly pronounced increases in above-ground parts suggests that in addition to the bacteria's potassium solubilizing capacity, other plant growth-promoting mechanisms (hormone production, nutrient solubilization, etc.) are also effective.

Table 3. Means and Duncan grouping for effects of potassium solubilizing bacteria (KSB) and biochar applications on plant growth criteria, plant potassium content, soil pH, and EC

Treatments	PH	RL	PFW	PDW	RFW	RDW	Potassium	pH	EC
	cm		g, plant^{1}				%		µS cm^{-1}
Potassium Solubilizing Bacteria (KSB)									
KSB(-)	31.08 B	17.33 B	4.152 B	0.419 B	1.540 B	0.138	1.825 B	7.12 B	570
KSB(+)	33.00 A	19.42 A	4.808 A	0.486 A	1.740 A	0.152	1.970 A	7.27 A	558
Biochar, %									
0	28.67 C	19.17 A	3.474 C	0.397 B	1.385 C	0.118 C	1.611C	7.15 B	508C
1	31.67 B	18.33 AB	4.113 BC	0.411 B	1.462 C	0.134 BC	1.860 B	7.17 B	547B C
2	33.33 AB	18.83 A	4.438 B	0.434 B	1.731 B	0.157 AB	2.007A B	7.17 B	576 AB
4	34.50 A	17.17 B	5.896 A	0.568 A	1.982 A	0.169 A	2.112A	7.28 A	625 A

A, B, C: Means followed by the same letters are not statistically different. PH: Plant Height, RL: Root Length, PFW: Plant Fresh Weight, PDW: Plant Dry Weight, RFW: Root Fresh Weight, RDW: Root Dry Weight.

Soil pH value increased from 7.12 to 7.27 with KSB application (2.1% increase), while EC decreased from 570 µS cm⁻¹ to 558 µS cm⁻¹ (2.1% decrease). Soil pH varied with biochar applications, with the highest pH value of 7.28 measured in the 4% biochar application, corresponding to a 1.8% increase compared to the control group. The 1% and 2% biochar applications did not cause significant changes in pH. Soil EC values showed a notable increase parallel to increasing biochar doses. Compared to the control group (0% biochar, 508 µS cm⁻¹), EC increased by 7.7% to 547 µS cm⁻¹ with 1% biochar, by 13.4% to 576 µS cm⁻¹ with 2% biochar, and by 23.0% to 625 µS cm⁻¹ with 4% biochar. These findings demonstrate that increasing biochar doses linearly increase soil EC values (Table 3).

As biochar application doses increased, different trends in parameter changes were determined depending on the dose. A regular increase in plant height was observed with increasing biochar dose. Plant height, which was 28.67 cm in the control group (0% biochar), reached 31.67 cm with 1% biochar, 33.33 cm with 2% biochar, and 34.50 cm with 4% biochar application. The 4% biochar application provided a 20.3% increase compared to the control group. The highest value was obtained from the 4% biochar application.

When biochar applications were examined, significant changes in plant fresh weight were observed depending on increasing biochar doses. Plant fresh weight was measured as 3.474 g in the control group (0% biochar), while it was determined as 4.113 g (18.4% increase) with 1% biochar, 4.438 g (27.7% increase) with 2% biochar, and 5.896 g (69.7% increase) with 4% biochar. The highest plant fresh weight was obtained with 4% biochar application. A similar trend was observed for plant dry weight. Plant dry weight, which was 0.397 g in the control group, was measured as 0.411 g (3.5% increase) with 1% biochar, 0.434 g (9.3% increase) with 2% biochar, and 0.568 g (43.1% increase) with 4% biochar. The highest plant dry weight was determined with 4% biochar application, while no statistically significant difference was found between the control group and 1% and 2% biochar applications. However, the 4% biochar application was statistically superior to all other doses (Table 3).

Biochar application caused significant increases in root fresh weight. The lowest value was determined in the control group (1.385 g), while it increased to 1.982 g with a 43.1% increase in the 4% biochar application. The 1% biochar application (1.462 g) was similar to the control, while 2% biochar (1.731 g) and 4% biochar applications gave significantly higher values (Table 3).

As shown in Table 3, root dry weight significantly increased with increasing biochar doses. Root weight, which was 0.118 g in the control group, increased to 0.134 g with 1% biochar, 0.157 g with 2% biochar, and 0.169 g with 4% biochar. A 43.2% increase was determined in the 4% biochar application compared to the control group. A significant increase in plant potassium content was observed with increasing biochar dose. Potassium content, which was 1.611% in the control group, increased to 1.860% with 1% biochar, 2.007% with 2% biochar, and 2.112% with 4% biochar. A 23.7% increase occurred in the 4% biochar application compared to the control group.

As indicated in the ANOVA table (Table 1), KSB × biochar interaction had highly significant effects on root length ($p<0.001$), root fresh weight ($p<0.01$), and root dry weight ($p<0.01$). This indicates that the effect of KSB application varies depending on biochar dose and that the combinations of the two applications should be evaluated together. The interaction effect on plant height was found to be non-significant.

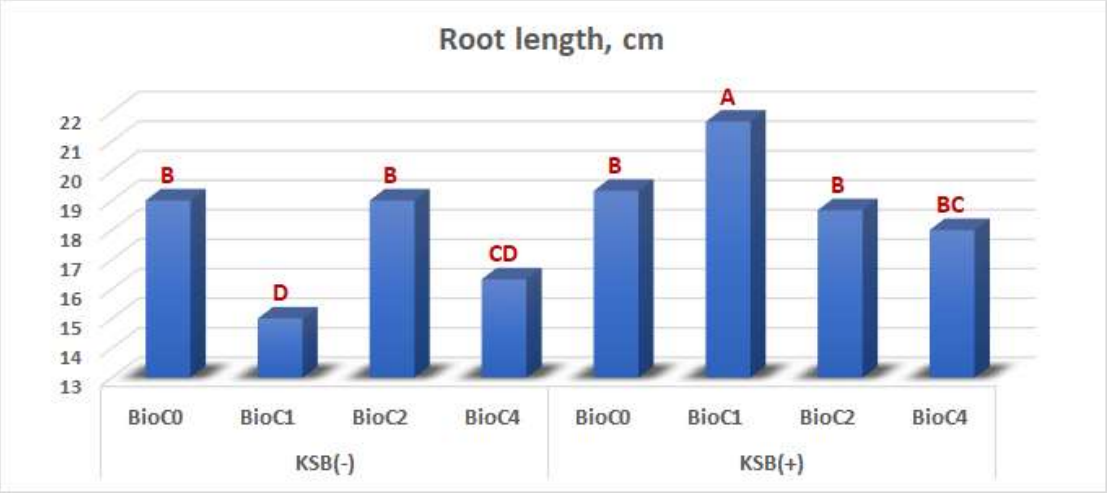

Fig. 1. Effect of potassium solubilizing bacteria (KSB) and biochar interaction on root length, BioC0, 0% Biochar; BioC1, 1% Biochar; BioC2, 2% Biochar; BioC4, 4% Biochar.

The KSB × biochar interaction was found to be statistically significant for root length ($p<0.001$). The highest root length was observed as 21.67 cm in the KSB(+) × BioC1 treatment, while the lowest value was determined as 15.00 cm in the KSB(-) × BioC1 treatment. KSB(+) application increased root length by 44.4% at the BioC1 dose, while in the KSB(-) group, BioC1 application showed a 21.1% decrease compared to the control. At high biochar doses (BioC4), root length showed a decreasing trend in both KSB applications.

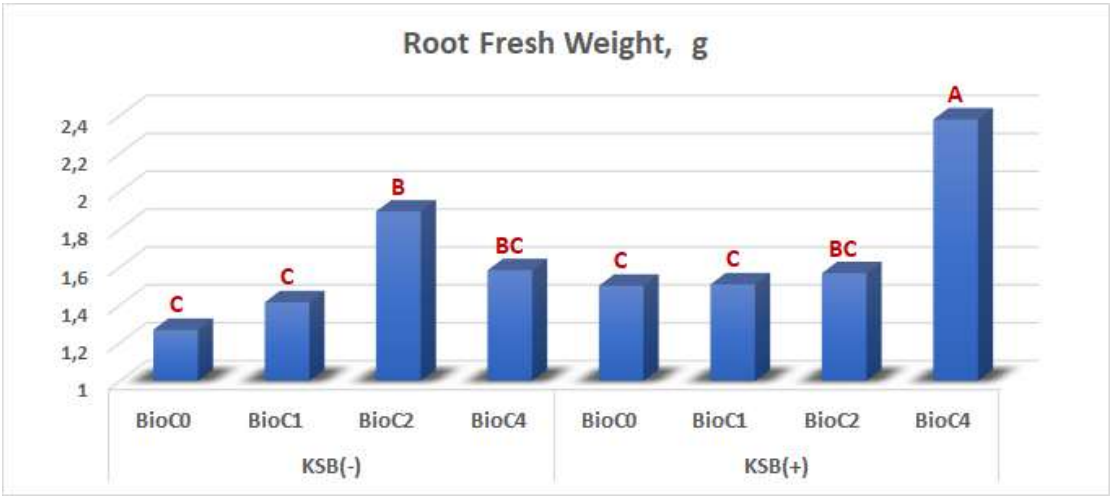

Fig. 2. Effect of potassium solubilizing bacteria (KSB) and biochar interaction on root fresh weight, BioC0, 0% Biochar; BioC1, 1% Biochar; BioC2, 2% Biochar; BioC4, 4% Biochar.

As shown in Figure 2, The KSB × biochar interaction was found to be statistically significant for root fresh weight ($p<0.01$). The highest root fresh weight was measured as 2.380 g in the KSB(+) × BioC4 treatment, while the lowest value was determined as 1.269 g in the KSB(-) × BioC0 treatment. KSB(+) application at the BioC4 dose increased root fresh weight by 87.5% compared to the KSB(-) × BioC0 control group. While increasing biochar dose showed an increasing effect on root fresh weight in KSB(-) applications, the highest increase was obtained in the KSB(+) × BioC4 treatment.

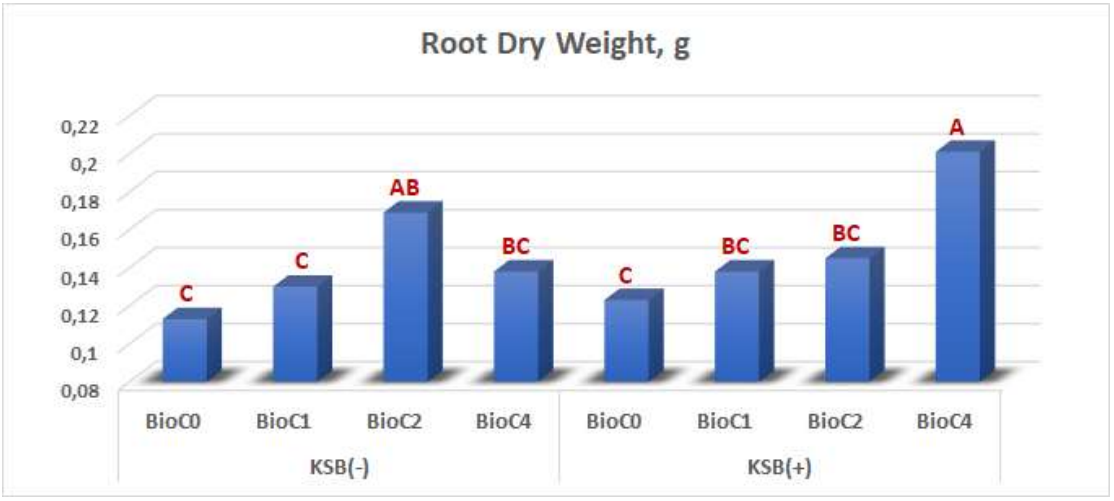

Fig. 3. Effect of potassium solubilizing bacteria (KSB) and biochar interaction on root dry weight, BioC0, 0% Biochar; BioC1, 1% Biochar; BioC2, 2% Biochar; BioC4, 4% Biochar.

The KSB × biochar interaction was found to be statistically significant for root dry weight ($p<0.01$). The highest root dry weight was obtained as 0.201 g in the KSB(+) × BioC4 treatment, while the lowest value was measured as 0.113 g in the KSB(-) × BioC0 treatment. The KSB(+) × BioC4 treatment provided a 77.9% increase compared to the control group, while the highest value in the KSB(-) group was observed as 0.169 g in the BioC2 treatment. The use of KSB application with 4% biochar caused significant increases in root dry weight.

DISCUSSION

Effects of Potassium Solubilizing Bacteria Application on Plant Growth and Potassium Uptake

In this study, potassium solubilizing bacteria (KSB) application was determined to have significant and positive effects on plant height, fresh and dry weight, dry leaf weight, and plant potassium content in wheat. The fact that KSB application provided increases of 6.2% in plant height, 15.8% in plant fresh weight, and 16.0% in plant dry weight is consistent with the plant growth-promoting effects of these microorganisms.@

The findings obtained are consistent with previous studies in this field. Zahedi (2016) reported that *Bacillus* species potassium solubilizing bacteria increased dry matter yield in wheat by up to 20%. Similarly, Sheng and He (2006) reported that potassium solubilizing bacteria solubilize fixed potassium by secreting organic acids (primarily citric, malic, and oxalic acids) in the rhizosphere, thereby significantly increasing potassium uptake by plants. This mechanism explains the 7.9% increase in plant potassium content observed with KSB application.

The positive effects of KSB application on plant growth are not limited to potassium solubilization activity. These bacteria can also contribute to plant growth through multiple mechanisms including production of plant growth-promoting hormones (particularly indole-3-acetic acid - IAA), reduction of ethylene stress through 1-aminocyclopropane-1-carboxylate (ACC) deaminase activity, improvement of iron uptake through siderophore production, and phosphate solubilization (Meena et al., 2014; Etesami et al., 2017). Therefore, the growth increases observed with KSB application may be a result of both direct improvement in potassium nutrition and other plant growth-promoting properties of the bacteria.

However, KSB application was determined not to have a statistically significant effect on root dry weight and spike number. This suggests that the effect of KSB does not occur at the same level in different plant organs, and that the application period (45 days) may have been insufficient to create significant differences in parameters such as root development and generative organ formation. In particular, differences in carbon and nutrient distribution between vegetative and generative growth may cause bacterial effects to manifest at different levels in different organs.

Effects of Biochar Application on Plant Growth, Potassium Uptake, and Soil Properties

In our study, biochar application, particularly at the 4% dose, provided significant increases of 20.3% in plant height, 43.1% in dry leaf weight, and 43.2% in dry root weight. These plant growth-promoting effects of biochar applications are consistent with findings widely reported in the literature.

Lehmann et al. (2011) stated that biochar increases soil water holding capacity, improves aeration, and creates a more suitable environment for root development due to its porous structure. The significant increase in root weight observed with 4% biochar application in this study is an important finding supporting this mechanism. The surface area and porosity of biochar may allow roots to spread over a larger area within the soil and access a greater volume for nutrient uptake.

Chan et al. (2007) expressed that biochar increases the nutrient retention capacity of soils through cation exchange capacity (CEC), thereby improving plant nutrition by reducing nutrient losses, especially in systems where leaching is intensive. Atkinson et al. (2010) also reported that biochar application increases soil aggregate stability and improves soil structure, emphasizing that these physical improvements contribute positively to plant root development and consequently plant growth.

However, the 23.7% decrease in plant potassium content with increasing biochar dose is a quite remarkable and unexpected finding in this study. High-dose biochar application may have reduced potassium availability to plants by adsorbing potassium ions from the soil solution onto

its surface. Biochar, especially when pyrolyzed at high temperatures, can have high cation exchange capacity, and this increases the retention of cations such as K^+, Ca^{2+}, and Mg^{2+} (Glaser et al., 2002; Mukherjee et al., 2011). Negatively charged functional groups on the biochar surface (carboxyl, phenolic hydroxyl, carbonyl, etc.) can electrostatically attract and retain potassium ions. At high doses, biochar can limit potassium uptake by plants by increasing this adsorption effect. Bruun et al. (2012) also stated that biochar application may reduce the uptake of some nutrients by plants and that this may be related to the adsorption mechanism.

The high rate of increase in plant biomass with biochar application may have remained behind the increase in potassium uptake, leading to a relative decrease in potassium concentration in tissues. This is known as the "dilution effect," commonly encountered in plant nutrition. For example, while dry leaf weight increased by 43.1% and dry root weight by 43.2% with 4% biochar application, the increase in potassium uptake did not reach these rates, resulting in a decrease in potassium concentration in tissues. The dilution effect occurs particularly during rapid growth periods when nutrients are diluted within cell walls and protoplasm, and it is also one of the main reasons for the decrease in nutrient concentrations as plants age (Marschner, 2012).

According to ANOVA results, biochar application has a highly significant effect on soil pH ($p<0.01$). Considering that the biochar used in this study is alkaline in character, it can be assumed that it increased soil pH. Changes in soil pH can indirectly affect potassium availability to plants. At high pH values, the surface charges of soil colloids may change, and the amount of potassium in exchangeable form may decrease. Additionally, pH increase may affect microbial activity and organic matter mineralization, thereby altering potassium cycling. However, since potassium availability is generally influenced more by soil mineralogy and cation exchange systems than by pH, this effect may be less determining compared to adsorption and dilution.

In the study, biochar application alone was determined not to have a statistically significant effect on soil EC. This finding indicates that biochar does not directly change soil salinity as an inert material, but when applied together with KSB, it affects EC through interaction. This suggests that the effects of biochar on salinity occur largely indirectly through microbial activity and changes in soil chemistry.

KSB × Biochar Interaction

The fact that KSB × biochar interaction was found to be highly significant for plant fresh weight ($p<0.001$), plant dry weight ($p<0.01$), number of plants per pot ($p<0.001$), root fresh weight ($p<0.01$), and root dry weight ($p<0.01$) in the ANOVA reveals that the effects of the combined use of the two applications differ from their simple sums and indicates the presence of synergistic or antagonistic interactions.

Interactions between biochar and KSB can be explained by various mechanisms:

1. **Habitat Provision:** The porous structure of biochar can serve as a protected habitat for microorganisms, allowing KSB populations to survive longer in soil and maintain their metabolic activities (Quilliam et al., 2013; Thies and Rillig, 2009). This may lead to increased effectiveness of KSB and greater contribution to plant growth. Biochar pores help maintain population densities by protecting bacteria from predators (protozoa, nematodes) and adverse environmental conditions (drought, extreme temperatures).
2. **Nutrient Supply:** Biochar may contain carbon sources and mineral nutrients that microorganisms can utilize. This may increase the metabolic activity and potassium solubilization capacity of KSB (Liang et al., 2010). Labile carbon fractions on the biochar surface can provide energy sources for microorganisms, positively affecting population dynamics and enzymatic activities.

3. **Chemical Environment Modification:** Biochar can affect the working environment of KSB by changing soil pH, ionic strength, and forms of nutrients. For example, changes in soil pH with biochar application may affect bacteria's organic acid production and potassium solubilization efficiency. Additionally, the amount of potassium adsorbed by biochar may determine whether the potassium solubilized by bacteria can be taken up by plants.
4. **Root Development Modulation:** Root development promoted by biochar can increase bacterial-plant interactions by expanding the colonization area of KSB in the rhizosphere. A more developed root system provides a larger colonization surface for KSB, and this may increase the amount of root exudates, thereby promoting bacterial activity.

However, the non-significant KSB × biochar interaction on plant potassium content ($p>0.05$) suggests that biochar's potassium adsorption may be more dominant than bacteria's potassium solubilization activity. In other words, biochar's potassium retention capacity may have limited KSB's potassium solubilization effect, and changes in plant potassium content occurred largely depending on biochar dose.

Quilliam et al. (2013) reported that biochar application significantly changes rhizosphere microbial community structure and can promote the activity of some bacterial groups while suppressing others. This finding indicates that biochar may have strain-specific effects on KSB and that interactions may occur at different levels in studies with different strains.

Effects on Soil pH and EC

In the study, KSB and biochar were found to have highly significant effects on soil pH both individually and in interaction. The decrease in soil pH with KSB application can be evaluated in relation to organic acid production by bacteria. Similarly, the effect of biochar application on pH varies depending on biochar's specific chemical structure and alkaline or acidic character. While the biochar used in this study was expected to show a pH-increasing (alkaline) effect, absolute measurement of soil pH values is necessary to determine exactly in which direction it causes change.

The significant effect of KSB × biochar interaction on soil EC ($p<0.01$) reveals that combined applications may produce unpredictable results on salinity and therefore caution should be exercised in practical applications. Electrical conductivity is an indicator of total ion concentration in soil solution, and excessive salinity is an important factor negatively affecting plant development. Biochar and KSB applications may cause increases or decreases in EC by changing ion balance. Detailed analysis of soil solution ion composition is needed to better understand the mechanisms underlying these effects.

CONCLUSION

In this study, the effects of potassium solubilizing bacteria (KSB) and different doses of biochar applications on wheat growth parameters, plant potassium content, and soil pH and electrical conductivity (EC) were investigated. The findings obtained showed that both applications significantly promoted plant growth, but biochar application in particular may cause unexpected negative effects on potassium nutrition.

Potassium solubilizing bacteria application provided statistically significant increases in plant height, fresh and dry weight, and plant potassium content in wheat. These findings are consistent with the study by El-Egami et al. (2024), who reported that potassium uptake significantly increased in wheat plants inoculated with *Bacillus circulans* and yield increases were achieved even under saline soil conditions. Similarly, Chen et al. (2018) reported that biochar application promotes the development of potassium solubilizing bacteria populations

in soils and this accelerates the decomposition of especially 2:1 type potassium-containing minerals, thereby increasing plant potassium uptake. Furthermore, Jiang et al. (2024) showed that bacterial strains applied together with biochar significantly increased plant biomass and nutrient uptake and increased the diversity and abundance of beneficial bacterial groups belonging to the families Bacillaceae and Paenibacillaceae in the rhizosphere. This supports that the positive effects of KSB application on plant growth are not limited to potassium solubilization activity but also contribute to plant nutrition by positively shaping rhizosphere microbial communities. However, the fact that KSB application did not create a statistically significant effect on root dry weight and spike number in this study suggests that bacterial effects do not occur at the same level in different plant organs and that the 45-day experimental period may have been insufficient to create significant differences in these parameters.

Biochar application, particularly at the 4% dose, provided significant increases in parameters such as plant height, dry leaf weight, and dry root weight. These findings are partially consistent with the review study by Bilias et al. (2023), who stated that biochar application may promote plant potassium uptake through indirect mechanisms by increasing potassium retention capacity through properties such as cation exchange capacity, porosity, and specific surface area in soil. It is thought that biochar promotes root development and increases water holding capacity by improving the physical properties of soil through its porous structure and high surface area. However, a serious decrease of 23.7% occurred in plant potassium content at the same dose. This unexpected finding can be explained by factors such as high-dose biochar application reducing potassium availability to plants by adsorbing potassium ions from the soil solution onto its surface, the high rate of increase in plant biomass with biochar application remaining behind the increase in potassium uptake, leading to dilution of potassium concentration in tissues (dilution effect), and/or biochar indirectly affecting potassium uptake mechanisms by changing soil pH. On this subject, Bilias et al. (2023) emphasized that the effects of biochar applications on soil potassium availability show significant differences depending on the type of feedstock from which biochar is produced, pyrolysis temperature, and soil properties, and that biochar produced at low pyrolysis temperatures (<500°C) has higher water-soluble and exchangeable potassium fractions. This suggests that the properties of the biochar used in our study may have led to potassium adsorption. Additionally, the significant effect of biochar application on soil pH ($p<0.01$) indicates that this change may indirectly affect potassium uptake mechanisms.

ANOVA results showed that KSB × biochar interaction had highly significant effects on plant fresh weight, plant dry weight, spike number, dry leaf weight, and dry root weight. This indicates that the effects of the combined use of the two applications differ from their simple sums and that biochar modulates the living environment and metabolic activity of KSB by changing rhizosphere conditions. Chen et al. (2018) reported that biochar application promotes potassium solubilizing bacteria development in both soil types and this is associated with changes in soil pH and water-soluble potassium. Furthermore, in the study by Li et al. (2025) examining the effects of different fertilizer regimes and biochar applications on rhizosphere microbial communities, it was emphasized that biochar application promotes specific microbial communities and offers a promising option for sustainable agricultural practices. However, the non-significant interaction effect on plant potassium content suggests that biochar's potassium adsorption may be more dominant than bacteria's potassium solubilization activity.

While KSB and biochar applications were found to have highly significant effects on soil pH both individually and in interaction, only KSB × biochar interaction was found to be significant for EC value. This finding reveals that the effects of biochar and KSB applications on soil salinity are not independent of each other and may produce unpredictable results when applied together.

Based on the results obtained from this study, it is of great importance to determine optimum dose ratios in field conditions that will minimize potassium adsorption and maximize KSB

efficacy in cases where biochar and KSB will be used together. Since the 4% biochar dose in this study provided high biomass production but caused significant decrease in potassium content, it is recommended to try lower doses (e.g., 1-2%) or biochar types produced from different feedstocks. As stated by Bilias et al. (2023), the potassium supply potential of biochar largely depends on feedstock type and pyrolysis conditions. Additionally, detailed analysis of potassium fractions (soluble, exchangeable, mineral) before and after application in soils treated with biochar will enable better understanding of biochar's effects on potassium dynamics. KSB application should be considered as part of an integrated nutrient management strategy to reduce chemical fertilizer use, especially in soils where potassium is present at sufficient levels but not in available form. Previous studies have shown that KSB application can provide similar yield increases when used with half the dose of chemical potassium fertilizers. Practitioners should consider the initial potassium status of soils, physicochemical properties of biochar, and local climatic conditions when recommending biochar and KSB combinations.

For future research, these findings obtained under controlled climate chamber conditions need to be verified with long-term field trials under different soil, climate, and agricultural practices. Chen et al. (2018) stated that the effects of biochar applications on plant potassium uptake vary depending on soil type, and that biochar effects last longer especially in soils rich in 2:1 type potassium-containing minerals. Comparative investigation of the effects of biochar types produced from different feedstocks (wood, agricultural wastes, animal manure, grape pomace, coffee husk, hazelnut shell, etc.) and at different pyrolysis temperatures is recommended. Bilias et al. (2023) emphasized that potassium-rich biomasses are promising resources for biochar production but are not yet widely used. Detailed investigation of the interactions of potassium solubilizing bacteria belonging to different species and strains with different biochar types will allow identification of the most successful combinations. Mechanistic studies such as biochar's potassium adsorption kinetics, KSB's organic acid production profile, and effects on root exudation will enable better understanding of the physiological and chemical processes underlying the observed effects. Investigation of the effects of biochar application on rhizosphere microbial community structure and functional gene activity using metagenomics, metatranscriptomics, and other advanced molecular methods will make significant contributions to elucidating biochar-KSB-plant triple interactions at the molecular level. Investigation of the persistent effects of biochar and KSB applications in different growing periods and different crop rotation systems is of critical importance for long-term sustainability. Furthermore, cost-effectiveness analyses of biochar and KSB applications and economic feasibility studies at different farm scales will be a critical evaluation criterion for the adoption and dissemination of these practices by farmers in practice. Finally, modeling the effectiveness of biochar and KSB applications under climate change scenarios can guide the determination of future agricultural production strategies.

In conclusion, although the combined use of biochar and potassium solubilizing bacteria in wheat cultivation is a promising approach within the scope of sustainable agricultural practices, optimum dose, application time, and methods need to be studied in detail under field conditions. This study makes significant contributions to the knowledge in this field and provides a valuable foundation for future research.

ACKNOWLEDGEMENT

This study was supported by Bolu Abant İzzet Baysal University Scientific Research Projects Coordination Unit under project number 2025-ÖĞP-026. The authors thank Bolu Abant İzzet Baysal University for the financial and technical support provided during the conduct of the study.

REFERENCES

1. Atkinson, C. J., Fitzgerald, J. D., & Hipps, N. A. (2010). Potential mechanisms for achieving agricultural benefits from biochar application to temperate soils: A review. Plant and Soil, 337(1-2), 1-18. https://doi.org/10.1007/s11104-010-0464-5
2. Bilias, F., Kalderis, D., Richardson, C., Barbayiannis, N., & Gasparatos, D. (2023). Biochar application as a soil potassium management strategy: A review. Science of the Total Environment, 858, 159782.
3. Bruun, E. W., Ambus, P., Egsgaard, H., & Hauggaard-Nielsen, H. (2012). Effects of slow and fast pyrolysis biochar on soil C and N turnover dynamics. Soil Biology and Biochemistry, 46, 73-79. https://doi.org/10.1016/j.soilbio.2011.11.019
4. Chan, K. Y., Van Zwieten, L., Meszaros, I., Downie, A., & Joseph, S. (2007). Agronomic values of greenwaste biochar as a soil amendment. Australian Journal of Soil Research, 45(8), 629-634. https://doi.org/10.1071/SR07109
5. Chen, F., Liu, Y., Nie, X., Xue, C., & Wang, L. (2018). Effects of biochar application on soil potassium dynamics and crop uptake. Journal of Plant Nutrition and Soil Science, 181(5), 635-643.
6. El-Egami, H. M., Hegab, R. H., Montaser, H., El-Hawary, M. M., & Hasanuzzaman, M. (2024). Impact of Potassium-Solubilizing Microorganisms with Potassium Sources on the Growth, Physiology, and Productivity of Wheat Crop under Salt-Affected Soil Conditions. Agronomy, 14(3), 423.
7. Etesami, H., Emami, S., & Alikhani, H. A. (2017). Potassium solubilizing bacteria (KSB): Mechanisms, promotion of plant growth, and future prospects – A review. Journal of Soil Science and Plant Nutrition, 17(4), 897-912. https://doi.org/10.4067/S0718-95162017000400005
8. Glaser, B., Lehmann, J., & Zech, W. (2002). Ameliorating physical and chemical properties of highly weathered soils in the tropics with charcoal – A review. Biology and Fertility of Soils, 35(4), 219-230. https://doi.org/10.1007/s00374-002-0466-4
9. Jiang, Z., Li, Q., Peng, F., & Yu, J. (2024). Biochar Loaded with a Bacterial Strain N33 Facilitates Pecan Seedling Growth and Shapes Rhizosphere Microbial Community. Plants, 13(9), 1226.
10. Kacar, B. (1994). Toprak analizleri. Ankara Üniversitesi Ziraat Fakültesi Eğitim ve Araştırma Vakfı Yayınları, No: 3, Ankara.
11. Kacar, B., & İnal, A. (2008). Bitki analizleri. Nobel Yayın Dağıtım, Ankara.
12. Lehmann, J. (2007). Bio-energy in the black. Frontiers in Ecology and the Environment, 5(7), 381-387. https://doi.org/10.1890/1540-9295(2007)5[381:BITB]2.0.CO;2
13. Lehmann, J., Rillig, M. C., Thies, J., Masiello, C. A., Hockaday, W. C., & Crowley, D. (2011). Biochar effects on soil biota – A review. Soil Biology and Biochemistry, 43(9), 1812-1836. https://doi.org/10.1016/j.soilbio.2011.04.022
14. Li, K., Rahman, S. U., Rehman, A., Li, H., Hui, N., & Khalid, M. (2025). Shaping rhizocompartments and phyllosphere microbiomes and antibiotic resistance genes: The influence of different fertilizer regimes and biochar application. Journal of Hazardous Materials, 486, 137052.
15. Liang, B., Lehmann, J., Sohi, S. P., Thies, J. E., O'Neill, B., Trujillo, L., Gaunt, J., Solomon, D., Grossman, J., Neves, E. G., & Luizão, F. J. (2010). Black carbon affects the cycling of non-black carbon in soil. Organic Geochemistry, 41(2), 206-213. https://doi.org/10.1016/j.orggeochem.2009.09.007
16. Marschner, P. (2012). Marschner's mineral nutrition of higher plants (3rd ed.). Academic Press.

17. Meena, V. S., Maurya, B. R., & Verma, J. P. (2014). Does a rhizospheric microorganism enhance K^+ availability in agricultural soils? Microbiological Research, 169(5-6), 337-347. https://doi.org/10.1016/j.micres.2013.09.003
18. Mukherjee, A., Zimmerman, A. R., & Harris, W. (2011). Surface chemistry variations among a series of laboratory-produced biochars. Geoderma, 163(3-4), 247-255. https://doi.org/10.1016/j.geoderma.2011.04.021
19. Quilliam, R. S., Glanville, H. C., Wade, S. C., & Jones, D. L. (2013). Life in the 'charosphere' – Does biochar in agricultural soil provide a significant habitat for microorganisms? Soil Biology and Biochemistry, 65, 287-293. https://doi.org/10.1016/j.soilbio.2013.06.004
20. Sheng, X. F., & He, L. Y. (2006). Solubilization of potassium-bearing minerals by a wild-type strain of Bacillus edaphicus and its mutants and increased potassium uptake by wheat. Canadian Journal of Microbiology, 52(1), 66-72. https://doi.org/10.1139/w05-117
21. Sparks, D. L. (1987). Potassium dynamics in soils. Advances in Soil Science, 6, 1-63. https://doi.org/10.1007/978-1-4612-4682-4_1
22. Thies, J. E., & Rillig, M. C. (2009). Characteristics of biochar: Biological properties. In J. Lehmann & S. Joseph (Eds.), Biochar for environmental management: Science and technology (pp. 85-105). Earthscan.
23. Zahedi, H. (2016). Effect of potassium solubilizing bacteria on growth and yield of wheat under different levels of potassium application. Journal of Plant Nutrition, 39(11), 1621-1629. https://doi.org/10.1080/01904167.2016.1143496
24. Zhang, C., & Kong, F. (2014). Isolation and identification of potassium-solubilizing bacteria from tobacco rhizospheric soil and their effect on tobacco plants. Applied Soil Ecology, 82, 18-25. https://doi.org/10.1016/j.apsoil.2014.05.002

PHOSPHORUS FİXATİON CAPACİTY İN SELECTED SOİLS OF THE ISHËM RİVER BASİN, CENTRAL ALBANİA

Fatos Huqi[1], Xhuljo Sema[1], Vjola Bakillari[1], Eugen Skura[1], Seit Shallari[1], Ilir Kristo[1], Fatbardh Sallaku[1]*

Department of Environment and Natural Resources, Faculty of Agriculture and Environment, Agricultural University of Tirana, Tirana, Albania

**Corresponding author e-mail:* fhuqi@ubt.edu.al

ABSTRACT

Phosphorus fixation influences both fertilizers use efficiency and the potential transfer of phosphorus from soil to surface waters. However, phosphorus-fixation behavior in Albanian river basin soils remains poorly documented. This study assessed phosphorus fixation in topsoil (0–30 cm) from the Ishëm River Basin and examined its relationship with selected soil properties. Two grams of soil were equilibrated in duplicate with 20 mL of KH_2PO_4 solution prepared in 0.01 M $CaCl_2$, supplying 0, 25, 50, 100, 200 and 500 mg P kg^{-1} soil. Samples were shaken for 24 h at approximately 24 °C, and phosphorus remaining in solution was measured colorimetrically by the Murphy–Riley method. The selected soils exhibited total phosphorus levels ranging from 182.81 to 662.65 mg P kg^{-1}, organic matter contents from 0.94% to 4.66%, and clay contents from 5.16% to 62.48%. Fixed phosphorus was calculated as added phosphorus minus phosphorus remaining at equilibrium. Across all P additions, adsorption ranged from 38.31% to 98.99%. Soils with higher clay and organic matter contents retained a greater proportion of added phosphorus, following logarithmic relationships with clay content ($R^2 = 0.962$) and organic matter content ($R^2 = 0.622$). These patterns indicate that total P content alone does not dictate fixation behavior, which is strongly governed by soil texture and organic matter content. These preliminary findings provide an essential baseline for improving phosphorus-fertilizer management and assessing phosphorus mobility in the Ishëm River Basin.

Keywords: Phosphorus fixation, Ishëm River Basin, soil texture, organic matter, adsorption capacity

INTRODUCTION

Phosphorus (P) is an essential macronutrient that supports plant growth, energy transfer and crop production. Although soils may contain considerable amounts of total P, only a small proportion is present in the soil solution and immediately available for plant uptake. When mineral fertilizers or organic materials are added to the soil, the soluble phosphate they release reacts with soil constituents, reducing its concentration and mobility. These reactions affect fertilizer-use efficiency and can promote the long-term accumulation of P in agricultural soils (Asomaning, 2020; Ning et al., 2022).

The removal of phosphate from the soil solution is commonly described as P fixation or sorption. Sorption initially involves the adsorption of phosphate onto reactive mineral surfaces, whereas subsequent reactions can convert adsorbed P into more stable or precipitated forms. Phosphorus retention therefore has a dual agronomic and environmental role. Strong fixation can reduce P availability to crops and increase fertilizer requirements. In contrast, soils with low retention capacity, or soils in which sorption sites have become progressively saturated, may be more susceptible to P mobilisation and transfer through runoff, erosion or drainage

(Ning et al., 2022; Kamali et al., 2023). Understanding soil P-retention capacity is consequently important for both fertilizer management and the control of nutrient losses to surface waters.

Phosphorus-fixation capacity varies considerably among soils because it is controlled by interacting physical and chemical properties. Clay minerals and iron and aluminium oxides provide reactive surfaces for phosphate adsorption, particularly in acidic and highly weathered soils. In neutral and alkaline soils, reactions involving calcium and carbonate minerals may become increasingly important. Soil pH, texture, organic matter, parent material and previous P inputs can therefore influence both the amount and strength of P retention (Asomaning, 2020; Oyebanjo et al., 2022; Kamali et al., 2023). The role of organic matter is particularly complex. Organic compounds can compete with phosphate for sorption sites or block reactive mineral surfaces, but they can also influence P retention indirectly through interactions with metal oxides, soil aggregation and organo-mineral complexes. Consequently, neither total P nor an individual soil property can independently describe P-fixation behaviour.

Previous studies in Albania have shown considerable variation in P fixation among soils with contrasting physicochemical properties. Huqi et al. (2021) examined selected soils from different regions of Albania and found differences in the retention of added P, which were related to clay content, organic matter, and soil pH. A subsequent study of greenhouse soils with contrasting cultivation histories and initial P contents also revealed substantial variation in P retention. In that study, the proportion of added P that was fixed generally decreased as the amount of P applied increased, whereas soils with lower initial P contents tended to retain a greater proportion of the applied phosphorus (Huqi et al., 2023). Together, these studies provided an initial basis for understanding P-fixation behaviour in Albanian soils; however, they focused on individual soils and agricultural production systems rather than examining soils within a river-basin context.

This approach is particularly relevant to the Ishëm River Basin, where agriculture, dense settlements and other human activities affect a connected soil–water system. Recent monitoring across five tributaries in the basin reported elevated TP concentrations (Huqi et al., 2025). Topsoil P can reach rivers attached to eroded particles or dissolved in surface runoff, depending on soil properties, land use, hydrology and topography (Dong et al., 2021). Strong P retention may reduce P-use efficiency and promote soil P accumulation, requiring careful fertilizer management. Assessing P retention can therefore support soil-fertility management and help identify potential nutrient pressures on surface waters.

Despite earlier studies of selected Albanian soils, information on P-fixation behaviour in the Ishëm River Basin remains limited. This study provides a preliminary assessment of selected topsoils differing in clay, organic matter and total P content. Soils richer in clay and organic matter were expected to retain more of the added P, while total P alone was not expected to explain differences in P fixation among soils. The study therefore quantified the fixation of added P in selected topsoils (0–30 cm) and examined its relationship with key soil properties. The findings provide an initial basis for assessing P availability and mobility and supporting integrated soil and water management in the basin.

MATERIALS AND METHODS

Soil sampling and preparation

Three topsoil samples were collected from selected locations within the Ishëm River Basin, Central Albania. The samples were identified as Soil A (Krujë), Soil B (Larushk), and Soil C

(Lanabregas). All samples were collected from the 0–30 cm soil layer. Following collection, the samples were air-dried at room temperature, gently disaggregated, homogenized, and passed through a 2-mm sieve before laboratory analysis.

Physicochemical soil analyses

Physicochemical characterization of the prepared soil samples was conducted in the laboratory of the Faculty of Agriculture and Environment, Agricultural University of Tirana, Tirana, Albania. Soil pH was measured in a 1:5 soil-to-water suspension according to ISO 10390:2021, while electrical conductivity (EC) was determined in a 1:5 aqueous soil extract according to ISO 11265:2025. Soil organic matter was determined by the potassium dichromate oxidation method described by Walkley and Black (1934). Total nitrogen (TN) was determined using the modified Kjeldahl method according to ISO 11261:1995. Following sample digestion, total phosphorus (P-tot) in the resulting solution was determined using the ammonium molybdate spectrometric method according to ISO 6878:2004. Soil particle-size distribution was determined by the hydrometer method following the principles of ISO 11277:2020.

Phosphorus-fixation experiment

The phosphorus-fixation experiment was performed using a modified batch-equilibration procedure adapted from Ahmed et al. (2008). Two grams of each soil sample were placed in 50-mL centrifuge tubes, and each treatment was prepared in duplicate. Phosphorus solutions containing 0, 2.5, 5, 10, 20, and 50 mg P L^{-1} were prepared by dissolving potassium dihydrogen phosphate (KH_2PO_4) in 0.01 M $CaCl_2$. A 20-mL aliquot of each solution was added to the soil samples, resulting in a soil-to-solution ratio of 1:10 and corresponding P additions of 0, 25, 50, 100, 200, and 500 mg P kg^{-1} soil.

The soil suspensions were shaken for 24 h at approximately 24 °C and 144 rpm. After equilibration, the samples were centrifuged at 5,000 rpm for 15 min, and the resulting supernatants were passed through 0.45-µm syringe membrane filters. Phosphorus remaining in the equilibrium solution was measured colorimetrically at 880 nm using the molybdenum-blue method of Murphy and Riley (1962). A zero-P treatment containing soil and 0.01 M $CaCl_2$ without added phosphorus was included for each soil to account for phosphorus released naturally during equilibration.

The amount of P adsorbed by each soil was calculated as the difference between the amount of P added and the amount remaining in the equilibrium solution, after correction for P measured in the zero-P treatment. Adsorbed P was expressed as mg P kg^{-1} soil, while percentage P adsorption was calculated relative to the amount of P added.

RESULTS AND DISCUSSION

Physicochemical properties of the selected soils

Selected physicochemical properties of the three studied soils are presented in Table 1.

Table 1. Physicochemical properties of the selected soils.

Code	pH	EC µS cm^{-1}	Organic Matter %	Total Phosphorus mg kg^{-1}	Total Nitrogen mg kg^{-1}	Clay %	Silt %	Sand %
Soil A	7.70	83.20	1.90	182.81	2010.04	62.48	27.16	10.36
Soil B	6.81	26.20	0.94	265.15	1020.33	5.16	20.64	74.20
Soil C	7.59	110.95	4.66	662.65	2953.05	31.62	23.72	44.66

The selected soils differed mainly in texture, organic matter and total P content. Soil A had the highest clay content (62.48%) and the lowest total P content (182.81 mg P kg^{-1}), whereas Soil B was predominantly sandy (74.20%) and had the lowest organic matter content (0.94%). Soil C had the highest organic matter (4.66%) and total P contents (662.65 mg P kg^{-1}). These contrasting properties may influence P fixation because clay minerals and associated Fe and Al oxides provide reactive sites for phosphate retention, while organic matter may modify this process through interactions with mineral surfaces (Asomaning, 2020; Kamali et al., 2023).

Phosphorus remaining after equilibration

The amount of P remaining in the equilibrium solution after the 24-h equilibration period is presented in Table 2.

Table 2. Phosphorus remaining after equilibration in the selected soils at different P-addition levels.

Added P (mg P kg^{-1} soil)	P remaining after equilibration (mg P kg^{-1} soil)		
	Soil A	**Soil B**	**Soil C**
25	0.759	1.453	0.326
50	0.683	3.580	0.503
100	1.270	16.639	1.613
200	2.703	69.045	6.6387
500	23.340	308.442	49.089

Phosphorus remaining in solution generally increased with increasing P addition, although the response differed among the soils (Table 2). Differences were relatively small at the lower P additions but became more pronounced at higher levels. At 500 mg P kg^{-1}, the equilibrium solution of Soil B contained 308.44 mg P kg^{-1}, compared with 23.34 mg P kg^{-1} for Soil A and 49.09 mg P kg^{-1} for Soil C. This indicates that Soil B had a substantially lower P-retention capacity under high P loading. A similar increase in equilibrium-solution P with increasing P addition has been associated with the progressive occupation and reduced availability of soil P-binding sites (Ahmed et al., 2008).

The relationship between added P and P remaining after equilibration was further evaluated using linear regression (Table 3).

Table 3. Linear regression equations relating added P to P remaining after equilibration.

Soil	Regression equation	R^2 Value
Soil A	y = 0.0491x - 2.8334	0.9272
Soil B	y = 0.667x - 36.9	0.9768
Soil C	y = 0.1059x - 6.9008	0.9453

Linear regression showed strong positive relationships between added P and P remaining after equilibration (R^2 = 0.927–0.977). The higher slope observed for Soil B suggests that a greater proportion of the added P remained in solution as P addition increased, indicating lower P retention compared with the other soils.

Phosphorus adsorbed to soil after treatment with added P

The amounts of P adsorbed by the selected soils at different P-addition levels are presented in Table 4.

Table 4. The amount of Adsorbed – P to soil after treatment with Added – P in solution

Added P (mg P kg^{-1} soil)	Adsorbed P (mg P kg^{-1} soil)		
	Soil A	**Soil B**	**Soil C**
25	24.241	23.546	24.674
50	49.316	46.419	49.496
100	98.730	83.360	98.386
200	197.297	130.954	193.361
500	476.660	191.557	450.910
Mean	**169.25**	**95.17**	**163.37**

Adsorbed P increased with increasing P addition in all three soils (Table 4). Differences among the soils were relatively small at the two lowest addition levels but became more pronounced as P addition increased. At 500 mg P kg^{-1}, Soil A adsorbed 476.660 mg P kg^{-1} and Soil C adsorbed 450.910 mg P kg^{-1}, compared with only 191.557 mg P kg^{-1} in Soil B. Across all P-addition levels, mean adsorbed P followed the order Soil A (169.25 mg P kg^{-1}) > Soil C (163.37 mg P kg^{-1}) > Soil B (95.17 mg P kg^{-1}). The lower adsorption by Soil B is consistent with its sandy texture and low clay and organic matter contents, whereas the greater adsorption by Soils A and C may be associated mainly with their higher clay contents and differences in organic matter (Asomaning, 2020; Kamali et al., 2023).

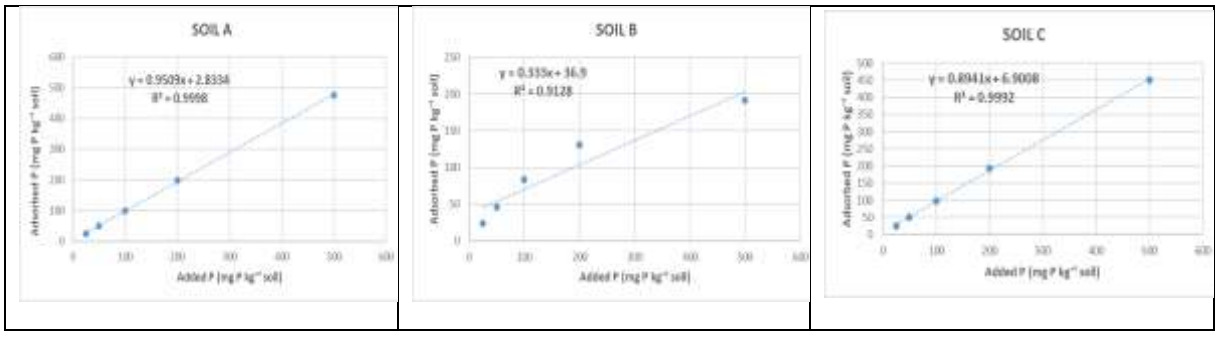

Figure 1. Relationships between added P and adsorbed P in the selected soils. Linear regression equations and R^2 values are shown in each panel.

Changes in the amount of P adsorbed with added P were examined for each soil. The regression analysis showed that there is a linear relationship between the amount of P added to the solution and the amount of P adsorbed from soil at the time of equilibrium in all studies soils.

The relationships between Added – P and percentage of Adsorbed – P in selected soils.

The percentage of the added P adsorbed to the soil is shown in Table 5.

Table 5. Adsorbed P as a percentage of the added P in solution

Added P (mg P kg^{-1} soil)	Adsorbed – P as % of Added – P in solution		
	Soil A	**Soil B**	**Soil C**
25	96.96	94.184	98.696
50	98.63	92.838	98.992
100	98.73	83.360	98.386
200	98.65	65.477	96.681
500	95.33	38.311	90.182
Average	**97.66**	**74.834**	**96.587**

The percentage of added P adsorbed remained high in Soil A and Soil C, averaging 97.66% and 96.59%, respectively. In contrast, adsorption in Soil B decreased from 94.18% to 38.31% as P addition increased, resulting in a lower mean adsorption of 74.83%.

Relationships between mean adsorbed phosphorus and selected soil properties

The relationships between mean adsorbed P and selected properties of the three soils were examined. Mean adsorbed P was calculated as the average amount adsorbed by each soil across the five P-addition levels, ranging from 25 to 500 mg P kg^{-1} soil. Soil organic matter and clay content were considered, and their relationships with mean adsorbed P are presented in Figure 2.

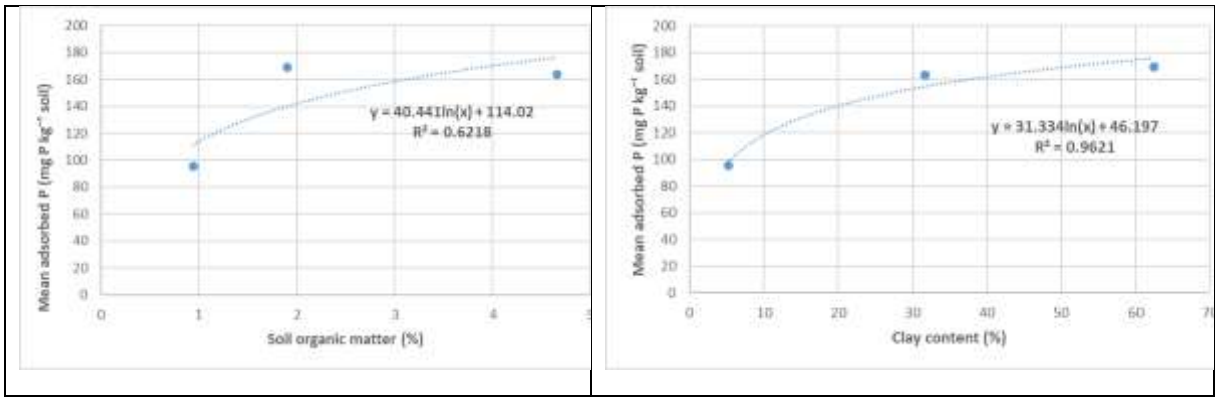

Figure 2. Relationships between mean adsorbed P and (a) soil organic matter and (b) clay content in the selected soils.

CONCLUSIONS

The selected soils exhibited substantial differences in P adsorption, with 38.31–98.99% of added P adsorbed after 24 h of equilibration. Although the amount of adsorbed P increased with increasing P addition in all soils, the proportion adsorbed varied considerably. Soils A and C maintained high mean adsorption percentages of 97.66% and 96.59%, respectively. In contrast, Soil B had a lower mean adsorption of 74.83%, which decreased to 38.31% at the highest P-addition level. This indicates that Soils A and C retained added P more effectively, whereas Soil B showed lower retention under high P loading.

Mean adsorbed P showed a stronger relationship with clay content ($R^2 = 0.962$) than with organic matter ($R^2 = 0.622$). Within the three studied soils, mean adsorbed P showed a stronger descriptive association with clay content than with organic matter; however, additional soils are required to confirm this pattern. The results also indicate that total P content alone cannot adequately explain soil P-retention behaviour. Although these findings are based on only three soils and should be considered preliminary, further studies involving additional soils are needed to better understand P adsorption. Nevertheless, the present results provide a useful baseline for developing soil-specific phosphorus-fertilizer strategies that balance fertilizer-use efficiency with the potential risk of P mobility in the Ishëm River Basin.

Acknowledgments

This research was carried out within the framework of the AMORE AL project. The project is funded by Austrian Partnership Programme in Higher Education and Research for Development (APPEAR) and supported by BOKU University, TU Wien and Karlsruhe Institute of Technology. The authors would like to express their sincere gratitude to all project partners and associated institutions for their valuable support, data provision and technical contributions.

REFERENCES

Ahmed, M. F., Kennedy, I. R., Choudhury, A. T. M. A., Kecskés, M. L., & Deaker, R. (2008). Phosphorus adsorption in some Australian soils and influence of bacteria on the desorption of phosphorus. Communications in Soil Science and Plant Analysis, 39(9–10), 1269–1294. https://doi.org/10.1080/00103620802003963

Asomaning, S. K. (2020). Processes and factors affecting phosphorus sorption in soils. In G. Z. Kyzas & N. K. Lazaridis (Eds.), Sorption in 2020s (pp. 1–16). IntechOpen. https://doi.org/10.5772/intechopen.90719

Dong, B., Qin, T., Wang, Y., Zhao, Y., Liu, S., Feng, J., Li, C., & Zhang, X. (2021). Spatiotemporal variation of nitrogen and phosphorus and its main influencing factors in Huangshui River Basin. Environmental Monitoring and Assessment, 193, Article 292. https://doi.org/10.1007/s10661-021-09067-1

Huqi, F., Skura, E., Bakillari, V., Sema, Xh., Sallaku, F., Shallari, S., & Kristo, I. (2021). Phosphorus fixation capacity in some selected soils in Albania. In Proceedings of the 3rd International Conference on Agriculture and Life Sciences (ICOALS III) (p. 390). Agricultural University of Tirana. ISBN 978-9928-07-746-2. Proceedings

Huqi, F., Skura, E., Bakillari, V., Sema, Xh., Sallaku, F., Shallari, S., & Kristo, I. (2023). Phosphorus fixation capacity in some greenhouse soils in Albania. In Proceedings of the 4th International Conference on Agriculture and Life Sciences (ICOALS 4) (p. 363). Agricultural University of Tirana. ISBN 978-9928-3635-10. Proceedings

Huqi, F., Bakillari, V., Sema, X., Skura, E., Shallari, S., Kristo, I., & Sallaku, F. (2025). Assessment of total phosphorus emissions in the Ishëm River Basin, Central Albania. In *Proceedings of the 5th International Conference on Agriculture and Life Sciences of Albania 2030 (ICOALS 5)* (pp. 545–548). Agricultural University of Tirana.

International Organization for Standardization. (1995). Soil quality—Determination of total nitrogen—Modified Kjeldahl method (ISO Standard No. 11261:1995). https://www.iso.org/standard/19239.html

International Organization for Standardization. (2004). Water quality—Determination of phosphorus—Ammonium molybdate spectrometric method (ISO Standard No. 6878:2004). https://www.iso.org/standard/36917.html

International Organization for Standardization. (2020). Soil quality—Determination of particle size distribution in mineral soil material—Method by sieving and sedimentation (ISO Standard No. 11277:2020). https://www.iso.org/standard/69496.html

International Organization for Standardization. (2021). Soil, treated biowaste and sludge—Determination of pH (ISO Standard No. 10390:2021). https://www.iso.org/standard/75243.html

International Organization for Standardization. (2025). Environmental solid matrices—Determination of the specific electrical conductivity (ISO Standard No. 11265:2025). https://www.iso.org/standard/85887.html

Kamali, B., Mahdavi Mazdeh, A., Sotoodehnia, A., & Wohnlich, S. (2023). Study of phosphorus adsorption behaviour of soils of the Qazvin Plain, NW Iran. Soil Science Annual, 74(3), Article 183657. https://doi.org/10.37501/soilsa/183657

Murphy, J., & Riley, J. P. (1962). A modified single solution method for the determination of phosphate in natural waters. *Analytica Chimica Acta, 27*, 31–36. https://doi.org/10.1016/S0003-2670(00)88444-5

Ning, J., Yao, J., Wang, R., Li, Y., Li, M., Shen, J., Chen, Y., Zhu, S., Wang, S., Luo, J., Li, T., Zeng, R., & Ai, S. (2022). Phosphorus status and adsorption characteristics of perennial vegetable-cultivated soils in South China. PLOS ONE, 17(4), Article e0264189. https://doi.org/10.1371/journal.pone.0264189

Oyebanjo, O., Ekosse, G.-I., & Odiyo, J. (2022). Phosphorus sorption in soils and clay fractions developed from different parent rocks in Limpopo Province, South Africa. Sustainability, 14(14), Article 8528. https://doi.org/10.3390/su14148528

Walkley, A., & Black, I. A. (1934). An examination of the Degtjareff method for determining soil organic matter, and a proposed modification of the chromic acid titration method. *Soil Science, 37*(1), 29–38. https://doi.org/10.1097/00010694-193401000-00003

ASSESSMENT OF MYCOTOXIN CONTAMINATION IN FEED COMMODITIES FOR DAIRY-PRODUCING ANIMALS: EVIDENCE FROM ALBANIA

Marjeta Daja[1], Dritan Topi[1],

Gabrijela Tavchar[2], Janja Babič[2], Breda Jakovac Strajn[2]

[1]Department of Chemistry, Faculty of Natural Sciences, University of Tirana, Blvd Zog 1, 1016 Tirana, Albania

[2]Veterinary Faculty, Institute of Food Safety, Feed and Environment, University of Ljubljana, Gerbičeva 60, 1000 Ljubljana, Slovenia

Corresponding author: dritan.topi@unitir.edu.al

ABSTRACT

The occurrence of mycotoxins in rye, barley, and wheat bran in Albania was investigated. Twenty-four mycotoxins—including aflatoxins (B1, B2, G1, and G2), deoxynivalenol (DON), 15-acetyl DON, 3-acetyl DON, mycophenolic acid, penicillic acid, zearalenone (ZEA), fumonisins (FB1, FB2), ochratoxin A (OTA), roquefortine C, HT-2, T-2, gliotoxin, neosolaniol, cyclopiazonic acid, diacetoxyscirpenol (DAS), tenuazonic acid, tentoxin, alternariol, and alternariol methyl ether—were analyzed using liquid chromatography-tandem mass spectrometry. Samples were collected from feed-producing facilities. At least one mycotoxin was detected in 75.0% of analyzed samples (9/12), with barley exhibiting the highest incidence (71.4%), followed by rye and wheat bran. Toxins produced by the Alternaria genus were most prevalent, while Fusarium toxins were less common; only DON was identified in one sample. Alternaria toxins—tenuazonic acid (75.0%), tentoxin (22.5%), alternariol (8.33%), and alternariol methyl ether (8.33%)—were the most abundant among analyzed mycotoxins. Deoxynivalenol (DON) was the only Fusarium toxins detected in wheat bran (33.3%), while mycotoxins from the genera Aspergillus and Penicillium were not detected. The occurrence of mycotoxins in feed ingredients was lower than previously reported for maize grown in Albania, with concentrations remaining below maximum levels where applicable. However, the presence of Alternaria toxins highlights the necessity for enhanced monitoring of raw materials, and preventive measures throughout the cereal supply chain.

Keywords: feed, rye, barley, wheat bran, mycotoxins, aflatoxin, deoxynivalenol, fumonisins, LC-MS/MS, Albania

INTRODUCTION

Mycotoxins are low-molecular-weight secondary metabolites produced by filamentous fungi (Costa et al., 2019; Gurikar *et al.*, 2023). Fungal spoilage of agricultural commodities can contaminate food and feed (Stroka and Gonçalves, 2019). The main producing fungal genera are Aspergillus, Penicillium, Fusarium, and Alternaria (Pinton et al., 2025), which grow in the field and during storage under inappropriate conditions (Kępińska-Pacelik & Biel, 2021).

Mycotoxin contamination is a global threat and will become more significant due to climate change and the globalization of the food and feed market (Altomare, Logrieco, Gallo, 2021). All over the world, more than 1000 mycotoxins have been identified, yet less than 20 are regulated (Pinton et al., 2025). Market globalization of agricultural commodities has increased awareness of mycotoxin contamination, with AFs being most distinguished for their public health implications and agro-economic significance (Altomare, Logrieco, Gallo, 2021).

European Commission has established maximum levels (ML) in food (European Commission, 2023; European Commission, 2024), where, for unprocessed cereals intended for human consumption or as an ingredient in foodstuffs other than maize, the ML is 2 µg/kg for AFB1 and 4 µg/kg for the sum of AFs, while in maize the ML is 5.0 µg/kg for AFB1 and 10.0 µg/kg for the sum of AFs. The ML of AFB1 is 0.02 mg/kg in feed, 0.01 mg/kg in complementary and complete feed, except feed for dairy animals, piglets and young poultry animals where ML is 0.005 mg/kg (European Commission, 2011).

Tabela 1. EU Maximum Levels in feed materials for main mycotoxins

Mycotoxin	Feed material (mg/kg)	Compound feed	Notes
Aflatoxin B1	0.02	(Cereal, oilseed, maize)	Strictet for dairy animals (carry over into milk)
Deoynivaleno (DON)	8-12	Cereal, maize, soybeans	Horses highly sensitive
Zearalenone	2-3	Maize, cereals	Pigs most sensitive
Ochratoxin A	0.25	Cereals, cereal products	Cats extremely sensitive
Fumonisins (B1 and B2)	60	Maize, maize products	Horses most sensitive
T-2 and HT-2- toxin	0.25-0.5	Cereals, cereal products	Cats excluded due to extreme sensitivity

Aflatoxins (AFs) are produced mainly by *A. flavus* and *A. parasiticus* (Cary et al., 2018; El-Sayed et al., 2022). The growth of aflatoxigenic-producing fungi depends on crop and soil types, as well as climate conditions (Sudan et al., 2026). Aflatoxin contamination of cereals is associated with poor storage conditions and field contamination. Post-harvest spoilage may occur due to inappropriate moisture content and storage temperatures. Natural aflatoxins include aflatoxin B1 (AFB1), aflatoxin B2 (AFB2), aflatoxin G1 (AFG1), aflatoxin G2 (AFG2) (CAST, 2003). AF contamination of foods and feedstuffs is global, but groundnuts, maize, and cottonseeds are reported to be at higher risk of contamination and, consequently, a major source of exposure (Akpoghelie et al., 2025).

Fusarium species are among the most well-known toxigenic fungi, particularly in temperate regions, and can cause severe reductions in crop yield through various plant diseases (Munkvold et al., 2019). The most distinguished Fusarium mycotoxins are zearalenone (ZEA), fumonisins (FBs), T-2 toxin, HT-2 toxin, neosolaniol (NEO), diacetoxyscirpenol (DAS), deoxynivalenol (DON), and its 3-acetyl (3-AcDON) and 15-acetyl (15-AcDON) derivatives (Leite et al., 2021; El-Sayed et al., 2022).

Alternaria toxins naturally occur on food and feed that are contaminated with Alternaria species, and alternariol, alternariol monomethyl ether, tenuazonic acid, altertoxins, and tentoxin are the most present. Some of these mycotoxins are carcinogenic, toxic, and mutagenic. The limited evidence on toxigenic effects has dictated no established maximum levels for this group of mycotoxins (Nagda & Meena, 2024).

The fate of different mycotoxins during cereal treatment processes, such as sorting, cleaning, debranning, and thermal processing, can significantly reduce mycotoxin concentrations (Bullerman and Bianchini, 2007). In contrast, milling processes result in repartitioning of mycotoxins in different milling fractions (Tibola et al., 2015).

Exposure to these compounds is a major threat to human and animal health and is associated with different acute or chronic mycotoxicoses (Awuchi et al., 2022).

Mycotoxin occurrence in barley and rye

Among cereals, maize and wheat are the most important in terms of production quantity and are consequently the most studied for mycotoxin contamination. Occurrence of aflatoxins in barley was mainly reported from Europe and the Mediterranean region (Binder et al., 2007), Spain (Ibanez-Vea et al., 2012), Serbia (Kos et al., 2014) and Slovenia (Babič et al., 2021), occurrence of aflatoxins in rye was reported from Europe during the period 2007-2012 (EFSA, 2013), Serbia (Kos et al., 2014) and Poland (Kosicki et al., 2020)

This study aimed to provide insight into the presence of twenty-four mycotoxins produced by four fungal genera: Alternaria (tenuazonic acid, tentoxin, alternariol, alternariol methyl ether), Fusarium (DON, 3-acetyl-DON, 15-acetyl-DON, ZEA, FB1, FB2, T-2, HT-2, DAS, and NEO), Aspergillus (aflatoxins B1, B2, G1, and G2), and Penicillium (mycophenolic acid, cyclopiazonic acid, roquefortine C) in two main cereal commodities produced in Albania, maize and wheat, both used as food and feed. This study represents the first report on the presence of these mycotoxins in crop commodities from Albania.

MATERIALS AND METHODS

Sample characterization

Barley, rye, and wheat bran were sampled from local feed distributors in Albania. The sampling procedure was carried out in accordance with Commission Regulation (EC) No 401/2006 (European Commission, 2006) on sample collection.

Standards and Chemicals

Single standards of ZEA, FB1 and FB2 (Romer Labs, Tulln, Austria) mixed with trichothecene standard solution in acetonitrile (DON, 3-AcDON, 15-AcDON, T-2, HT-2, DAS and NEO) produced by Trilogy (Washington, MO, USA); both stock standard solutions and the mixed working standard solutions were prepared in acetonitrile and stored in amber glass vials at –20°C. Aflatoxin standards (AFB1, AFB2, AFG1 and AFG2) were purchased from Romer (Union, MO, USA). Stock standard solutions were prepared in acetonitrile, and the mixed working standard solution was prepared with acetonitrile, methanol, acetic acid (Sigma-Aldrich, Steinheim, Germany), and ammonium acetate (Merck, Darmstadt, Germany), all of

p.a. or LC-MS grade purity. Deionized water was prepared using a Milli-Q system (Millipore, Bedford, MA, USA).

Deionized water was prepared using a Milli-Q system (Millipore, Bedford, MA, USA). The extraction solution was a mixture of acetonitrile and deionized water in an 84:16 (v/v) ratio. For the final sample solution, a mixture of deionized water and methanol in an 80:20 (v/v) ratio was used. Mobile phase components A and B were deionized water and methanol, both containing 0.2 g of ammonium acetate and 5 mL of acetic acid per liter.

Aflatoxin extraction

For simultaneous determination of aflatoxins (AFB1, AFB2, AFG1 and AFG2), a procedure consisting of the extraction of mycotoxins from ground cereal samples with the acetonitrile-deionized water mixture and liquid chromatography-tandem mass spectrometry (LC-MS/MS) was used. Sample preparation and mycotoxin determination were performed according to analytical procedures described elsewhere (Driehuis, Spanjer, Scholten, & Te Geffel, 2008; Lattanzio, Della Gatta, Suman, & Visconti, 2011; Rasmussen, Storm, Rasmussen, Smedsgaard, & Nielsen, 2010). 10 g of a sample was shaken with 100 mL of an acetonitrile-deionized water mixture (84+16) for 1 hour using a linear shaker IKA HS 501 digital (IKA Labortechnik, Staufen, Germany). 4 mL of the filtered extract was evaporated under vacuum to dryness using the system Syncore Polyvap (Büchi, Flawil, Switzerland). The dry residue was reconstituted with 0.5 mL of a methanol-deionized water mixture (80+20). 10 µl of the solution was injected into the LC-MS/MS system (Acquity UPLC H Class system coupled with a triple-quadrupole instrument, Waters).

Fusarium and Alternaria toxins extraction procedure

For the simultaneous determination of mycotoxins (DON, 3-AcDON, 15-AcDON, ZEA, FB1, FB2, T-2, HT-2, DAS, and NEO), a procedure described in detail by Topi et al. (60) was applied. The procedure consisted of extracting mycotoxins from ground cereal samples and determining them by LC-MS/MS. Specific MS/MS parameters related to the determined mycotoxins (retention times, ionization mode, and monitored transitions) are given in Table 7.

Table 1. Retention times of Fusarium toxins, ionization mode, and monitored transitions.

Analyte	Ionization mode	Retention time (min)	Precursor ion (m/z)	Quantifier ion (m/z)	Qualifier ion (m/z)
DON	ESI+	3.14	297.3	203.1	249.1
3-AcDON	ESI+	5.00	339.1	203.1	137.0
15-AcDON	ESI+	5.00	339.1	136.9	261.1
DAS	ESI+	7.06	384.3	307.2	247.2
HT-2	ESI+	8.91	442.4	215.1	263.2
T-2	ESI+	10.27	484.4	185.1	215.2
ZEA	ESI-	11.30	317.2	131.0	174.9
FB1	ESI+	10.20	722.4	334.2	352.2
FB2	ESI+	12.70	706.4	318.2	336.2

LC-MS/MS analysis

The chromatographic separation was performed on a Zorbax Eclipse Plus C18 Rapid Resolution HD column (2.1 x 100 mm, 1.8 µm; Agilent). The mobile phase consisted of two components mixed in gradient mode. Component A consisted of deionized water (995 ml), acetic acid (5 ml), and ammonium acetate (0.2 g), and component B consisted of methanol (995 ml), acetic acid (5 ml), and ammonium acetate (0.2 g). The initial eluent composition was 95% A and 5% B. The proportion of component B was linearly increased to 40% within 4 min and further to 70% within the next 8 min. The composition was held for 4 min, and then component B was increased to 90% in 1.5 min. The proportion of component B was held at 90% for 2.5 min, then returned to 5% over 1 min. The composition was held for 4 min. The mobile phase flow rate was 300 µL/min, and the chromatography column temperature was 40 °C. MS/MS analysis was carried out using electrospray ionization (ESI), and the triple-quadrupole mass spectrometer was operated in multiple reaction monitoring (MRM) mode. The capillary voltage was 3,4 kV, desolvation temperature 500 ºC, ion source temperature 150 ºC, and collision cell voltage 20 V. Other LC-MS/MS parameters as well as the limits of detection (LOD), limits of quantification (LOQ), and recoveries obtained within the validation process for single mycotoxins are given in Table 2. The Limit of detection (LOD) of single analytes was determined based on the signal-to-noise ratio of 3:1. As LOQ, a value of 2.5 times LOD was selected. LOD and LOQ were 0.20 µg/kg and 0.40 µg/kg, respectively, for every single aflatoxin.

Table 2. Retention times, the m/z precursor ion, the m/z monitored product ions, LOD, LOQ, and the recovery of aflatoxins (AFB1, AFB2, AFG1 and AFG2).

Analyte	Retention time (min)	Precursor ion (m/z)	Quantifier ion (m/z)	Qualifier ion (m/z)	LOD (µg/kg)	LOQ (µg/kg)
AFB1	5.25	313.2	213.2	241.1	0.6	2.0
AFB2	4.75	215.2	243.2	259.1	0.6	2.0
AFG1	2.92	329.1	214.8	199.9	0.6	2.0
AFG2	5.33	331.1	189.0	285.1	0.6	2.0

Method Validation

The Limit of detection (LOD) of single analytes was determined at a signal-to-noise ratio of 3:1. A value 3.3 times the LOD was selected as the Limit of quantification (LOQ). The recoveries and precision were tested using maize and wheat samples spiked with *Fusarium* toxins at the concentration levels of 50, 100 and 500 □g/kg.

The linearity of the method was tested in the concentration range 50–500 □g/kg using matrix-matched standard solutions analyzed in triplicate. Good linearity was demonstrated for all analytes, with correlation coefficients exceeding 0.997. The accepted LOD and LOQ for all single Fusarium toxins were 15 (g/kg) and 50 (g/kg), respectively. The mean recoveries of single toxins in maize at the tested concentration levels ranged from 90% to 117%. In wheat, recoveries ranged from 87% to 112%, except for DON, which was 124%. The reproducibility expressed as RSD_R was less than 16% for all *Fusarium* toxins in maize and ≤30% for all *Fusarium* toxins in wheat. The reproducibility and mean recoveries of the toxins were in line

with the criteria set out in Commission Regulation (EC) No 401/2006 and its amendments, except for DON, which slightly exceeded the required value.

RESULTS AND DISCUSSIONS

Contamination of barley and rye

In the investigated barley samples, no aflatoxin contamination was detected (Table 3). Aflatoxin G2 was detected in one barley sample. Aflatoxin occurrence in barley has been reported mainly in European countries (Kow et al., 2025). AFB1 in barley from the Czech Republic was reported in 87% of samples, with mean and maximum values of 2.1 and 4.0 □g/kg, respectively (Sedmikova *et al*., 2001). The AFB1 incidence in barley samples from northern regions of Spain during 2007-2008 was found in 100%, and the mean value was 0.11 □g/kg, while the mean value of the sum of AFs was 0.12 □g/kg (Ibanez-Vea *et al*., 2012). In conclusion, our findings on AFB1 contamination are in accord with reports from Europe and the Mediterranean region (Pleadin *et al*., 2024).

Table 3: Occurrence of mycotoxin contamination in rye and barley samples

	Parameter	**Sum of AFs**	**AFB1**	**AFB2**	**AFG1**	**AFG2**
Barley	No. positive/Total samples	0/5	0/5	0/5	0/5	0/5
Rye	No. positive/Total samples	1/2	0/2	0/2	0/2	1/2
Rye	% of positive samples	50.0	0.0	0.0	0.0	50.0
Rye	Min-Max (□g/kg)	0.61	n.d	n.d	n.d	0.61
Rye	No. samples above 2 □g/kg		0			
Rye	No. samples above 4 □g/kg	0				

N.B. Results expressed for 12% moisture content.

Occurrence of aflatoxin G2 in one barley sample with an uncommon presence of 0.61 □g/kg. This situation was similar to that of wheat samples from the same region of Korça. Rye is cultivated and used in modest amounts in Albania compared to other cereal grains. Data on AFB1 Occurrence reported in rye samples come mainly from Europe. In the EFSA report, during the period 2007□2012 was not found AF contamination in a total of 57 analyzed samples (EFSA, 2013). Occurrence of aflatoxins in rye from the region indicates that they were not found in rye samples from Serbia (Kos *et al*., 2014), while they were found at elevated levels (4.56 □g/kg) in samples from Romania (Gagiu *et al*., 2018).

Results indicate the presence of four Alternaria toxins in barley samples: tenuazonic acid, tentoxin, alternariol and alternariol methyl ether, while in rye and wheat bran two toxins were detected: tenuazonic acid and tentoxin. The most prevalent was tenuazonic acid, with an incidence of 71.4% and a maximum value of 0.22 mg/kg.

The highest incidence (100%) was observed in wheat bran, while occurrence was the second-most-contaminated feed commodity, with a maximum of 0.088 mg/kg.
The rye commodity presented an incidence of 50%, and a maximum occurrence of 0.022 mg/kg.
Based on the dataset for the Occurrence of Alternaria toxins in barley, rye, and wheat bran feed commodities, both the variability of contamination and the potential risk to animal exposure are evident.
Barley crop showed the highest contamination frequency, with 71.4% of samples positive for tenuazonic acid (TeA) and the same proportion positive for the sum of Alternaria toxins. The mean TeA concentration (0.1458 mg/kg) was notably higher than in rye and wheat bran, with values ranging from 0.0832 to 0.227 mg/kg. Tentoxin, alternariol, and alternariol methyl ether were each detected in only one sample (14.3%), but their presence indicates a broader spectrum of Alternaria metabolites. The relatively high median values suggest that barley is a significant contributor to Alternaria toxin exposure in feed.
Rye crop exhibited lower contamination levels, with only 50% of samples positive for TeA and tentoxin, and no alternariol or alternariol methyl ether detected. Concentrations were minimal (mean TeA 0.022 mg/kg; tentoxin 0.006 mg/kg), reflecting limited fungal activity or effective post-harvest handling. The absence of alternariol derivatives may indicate either lower fungal colonization or differences in substrate susceptibility compared to barley and wheat bran.
Wheat bran resulted contaminated with TeA, with all samples positive (100%). The mean concentration (0.061 mg/kg) was lower than in barley but higher than in rye. Tentoxin was detected in two-thirds of samples (66.7%), though alternariol and its methyl ether were absent. The average sum of Alternaria toxins was 0.0693 mg/kg, with a maximum of 0.092 mg/kg. This suggests that wheat bran is a consistent carrier of TeA, possibly due to its high nutrient content and surface area that favor fungal growth.

Comparative Insights

Tenuazonic acid was the most prevalent toxin across all commodities, confirming its dominance among Alternaria metabolites in feed.
Barley seed showed the broadest toxin profile, with occasional detection of alternariol and alternariol methyl ether, while wheat bran was consistently contaminated but with a narrower spectrum. Rye appeared least affected, both in frequency and concentration, suggesting species-specific resistance or lower fungal colonization.

Implications

The findings emphasize the need for routine monitoring of Alternaria toxins in feed, particularly in barley and wheat bran, which demonstrated higher contamination rates. Although concentrations were relatively low compared to regulated mycotoxins (e.g., aflatoxins, DON), the co-occurrence of multiple Alternaria metabolites raises concerns about additive or synergistic toxic effects (Lin, Jia, Wu, 2023). Given the absence of EU maximum levels for Alternaria toxins in feed, these results contribute valuable baseline data for risk assessment and may support future regulatory considerations.

Table 4. Alternaria toxin occurrence in barley and rye grain.

	Tenuazonic acid	**Tentoxin**	**Alternariol**	**Alternariol methyl ether**	**Alternariol methyl ether**	**Σ Alternaria toxins**	**Σ Alternaria toxins**
Barley							
No. samples	7	7	7	7	7	7	7
No. positive sample (%)	5 (71.4%)	1 (14.3%)	1 (14.3%)	1 (14.3%)	1 (14.3%)	5 (71.4%)	5 (71.4%)
Mean (mg/kg)	0.1458		0.071.0	0.062.0	0.062.0	0.1738	0.1738
Median (mg/kg)	0.1522		0.071	0.062	0.062	0.1564	0.1564
Min-Max (mg/kg)	0.0832 – 0.227	0.007	0.071	0.062	0.062	0.0832-0.2922	0.0832-0.2922
Rye	**Rye**	**Rye**	**Rye**	**Rye**	**Rye**	**Rye**	**Rye**
No. of samples	2	2	2	2	2	2	2
No. positive sample (%)	1 (50%)	1(50%)	0%	0%	0%	1 (50%)	1 (50%)
Mean	0.022	0.006	n.d	n.d	n.d	0.014	0.014
Median	0.022	0.006	n.d	n.d	n.d	0.014	0.014
Min-Max	0.022	0.006	0	0	0	0.028	0.028
Wheat bran	**Wheat bran**	**Wheat bran**	**Wheat bran**	**Wheat bran**	**Wheat bran**	**Wheat bran**	**Wheat bran**
No. samples	3	3	3	3	3	3	3
No. positive sample (%)	3(100.0%)	2(66.7%)	0.0%	0.0%	0.0%	0.0%	3(100.0%)
Mean	0.061	0.0125					0.0693
Median	0.072	0.0125					0.0888
Min-Max	0.027 - 0.084	0.005 - 0.020					0.027-0.092

The Occurrence of Fusarium toxins and other metabolites produced by Aspergillus and Penicillium species was also investigated in the analyzed feed samples. Target compounds

included DON, 15-acetyl-DON, 3-acetyl-DON, mycophenolic acid, penicillic acid, zearalenone (ZEA), fumonisins (FB1, FB2), ochratoxin A (OTA), roquefortine C, HT-2, T-2, gliotoxin, neosolaniol, cyclopiazonic acid, and diacetoxyscirpenol (DAS). Among all these toxins, contamination was evidenced only in a single sample for DON, while the remaining analytes were not detected. This finding is in accordande with previous publication on mycotoxin occurrence (Topi et al., 2023).

Conclusions

This study provides new insights into the occurrence of twenty-four mycotoxins, analyzed by liquid chromatography coupled with tandem mass spectrometry, in selected feed commodities (barley, rye, and wheat bran) cultivated and used in Albania.

Alternaria toxins revealed the highest incidence, with tenuazonic acid (TeA) as the most prevalent metabolite, detected in all wheat bran samples and in the majority of barley samples, while rye showed lower contamination levels. These findings confirm that TeA is the dominant Alternaria toxin in feed, with barley and wheat bran representing consistent sources of contamination.

No aflatoxin B1 contamination was detected in the barley samples analyzed, although aflatoxin G2 was found in one barley sample at 0.61 μg/kg. This uncommon occurrence is consistent with sporadic findings reported in wheat from the same region. Rye samples analyzed in this study did not show aflatoxin contamination, in agreement with international reports.

Screening for Fusarium toxins (DON, 15-acetyl-DON, 3-acetyl-DON, zearalenone, fumonisins FB1 and FB2, HT-2, T-2) and for metabolites of Aspergillus and Penicillium (ochratoxin A, mycophenolic acid, penicillic acid, roquefortine C, gliotoxin, cyclopiazonic acid, diacetoxyscirpenol, neosolaniol) revealed contamination only in a single sample for DON. The low incidence of these regulated mycotoxins indicates that, under the conditions studied, Alternaria toxins are the primary concern for contamination.

Overall, the results highlight the importance of monitoring non-regulated mycotoxins such as Alternaria metabolites, which were consistently present in barley and wheat bran. Although aflatoxin contamination was limited in this dataset, its occurrence in barley confirms the need for vigilance, given the established risk in European contexts. The absence of significant Fusarium and Aspergillus toxins suggests that contamination pressure in the studied region is currently low. Nevertheless, continued surveillance is essential to ensure feed safety and to support future regulatory considerations for Alternaria toxins.

Acknowledgment

This study did not receive financial support.

REFERENCES

Akpoghelie, P.O., Edo, G.I., Gaaz, T.S., Oghenekome Akpoghelie, E., Iwanegbe, I., Oghenewogaga Owheruo, J., et al. (2026). Mycotoxins in food and agriculture: from occurrence

to economic consequences. *Archives of Microbiology*, 208, 4. https://doi.org/10.1007/s00203-025-04559-x

Altomare, C., Logrieco, A. F., Gallo, A. (2021). Mycotoxins and Mycotoxigenic Fungi: Risk and Management. A Challenge for Future Global Food Safety and Security, In: Encyclopedia of Mycology, Editor(s): Ó. Zaragoza, A. Casadevall, Elsevier, 64-93, DOI: 10.1016/B978-0-12-819990-9.00032-9.

Awuchi, C.G., Ondari, E.N., Nwozo, S., Odongo, G.A., Eseoghene, I.J., Twinomuhwezi, H., et al. (2022). Mycotoxins' Toxicological Mechanisms Involving Humans, Livestock and Their Associated Health Concerns: A Review. Toxins (Basel),14(3), 167. doi: 10.3390/toxins14030167.

Babič, J., Tavčar-Kalcher, G., Celar, F. A., Kos, K., Knific, T., & Jakovac-Strajn, B. (2021). Occurrence of Alternaria and Other Toxins in Cereal Grains Intended for Animal Feeding Collected in Slovenia: A Three-Year Study. Toxins, 13(5), 304. DOI: 10.3390/toxins13050304

Binder, E.M., Tan, L.M., Chin, L.J., Handl, J., Richard, J. (2007). Worldwide Occurrence of mycotoxins in commodities, feeds and feed ingredients. Animal Feed Science and Technology, 137, 3–4, 265-282, doi: 10.1016/j.anifeedsci.2007.06.005.

Bullerman, L. B. & Bianchini, A. (2007). Stability of mycotoxins during food processing. *International Journal of Food Microbiology*, 119, 1–2, 140-146, doi: 10.1016/j.ijfoodmicro.2007.07.035.

Cary, J.W., Gilbert, M.K., Lebar, M.D., Majumdar, R., Calvo, A.M. (2018). Aspergillus flavus Secondary Metabolites: More than Just Aflatoxins. *Food Saf (Tokyo*). 6(1), 7-32. doi: 10.14252/foodsafetyfscj.2017024.

Commission Regulation (EU) 2023/915 of April 25, 2023 on maximum levels for certain contaminants in food and repealing Regulation (EC) No 1881/2006 (Text with EEA relevance). C/2023/35, OJ L 119, 5.5.2023, pp. 103–157.

Commission Regulation (EU) 2024/1022 of April 8, 2024 amending Regulation (EU) 2023/915 as regards maximum levels of deoxynivalenol in food. C/2024/2079, OJ L, 2024/1022, 9.4.2024.

Commission Regulation (EU) 2024/1038 of April 9, 2024 amending Regulation (EU) 2023/915 as regards maximum levels of T-2 and HT-2 toxins in food. C/2024/2135,OJ L, 2024/1038, 10.4.2024.

Costa, J., Rodríguez, R., García-Cela, E., Medina-Vayá, Á., Magan, N., Lima, N., Battilani, P., & Santos, C. (2019). Overview of fungi and mycotoxin contamination in Capsicum pepper and in Its derivatives. Toxins. https://doi.org/10.3390/toxins11010027

EFSA CONTAM Panel (EFSA Panel on Contaminants in the Food Chain), 2013. Scientific Opinion on risks for animal and public health related to the presence of nivalenol in food and feed. EFSA Journal 2013; 11(6):3262, 119 pp. doi:10.2903/j.efsa.2013.3262

El-Sayed, R. A., Jebur, A. B., Kang, W., El-Demerdash, F. M. (2022). An overview of the major mycotoxins in food products: characteristics, toxicity, and analysis. Journal of Future Foods, 2/2, 91-102, doi:10.1016/j.jfutfo.2022.03.002.

European Commission. (2006). Commission Recommendation 2006/576/EC of August 17, 2006 on the presence of deoxynivalenol, zearalenone, ochratoxin A, fumonisins, T-2 and HT-2 toxin in products intended for animal feeding. Official Journal of the European Union, L 229, 7–9.

European Commission. (2006). Commission Regulation (EC) No 401/2006 of February 23, 2006 laying down the methods of sampling and analysis for the official control of the levels of mycotoxins in foodstuffs. *Official Journal of the European Union*, L 70, 12–34.

European Commission. (2013). Commission Recommendation 2013/165/EU of March 27, 2013 on the presence of T-2 and HT-2 toxin in cereals and cereal products. Official Journal of the European Union, L 91, 12–15.

European Commission. (2026). Commission Recommendation (EU) 2026/1801 of July 24, 2026 on the presence of deoxynivalenol, zearalenone, ochratoxin A, fumonisins, T-2 and HT-2 toxins in products intended for animal feeding. Official Journal of the European Union, L 180, 1–15.

Gagiu, V., Mateescu, E., Armeanu, I., Dobre, A. A., Smeu, I., Cucu, M. E., Oprea, O. A., Iorga, E., & Belc, N. (2018). Post-Harvest Contamination with Mycotoxins in the Context of the Geographic and Agroclimatic Conditions in Romania. *Toxins*, 10(12), 533, doi:10.3390/toxins10120533

Gurikar, C., Shivaprasad, D.P., Sabillón, L., Nanje Gowda, N.A., Siliveru,K. (2023). Impact of mycotoxins and their metabolites associated with food grains. Grain & Oil Science and Technology,6, 1, 1-9, doi: 10.1016/j.gaost.2022.10.001.

Ibáñez-Vea, M., González-Peñas, E., Lizarraga, E., López de Cerain, A. (2012). Co-occurrence of mycotoxins in Spanish barley: A statistical overview. Food Control, 28, 2, 295-298, doi: 10.1016/j.foodcont.2012.04.046.

Institute of Geosciences. (2026). Monthly Climatic Bulletin. Department of Meteorology, Polytechnic University of Tirana. Retrieved July 26, 2026, from https://www.geo.edu.al/Services/Department_of_Meteorology/Monthly_Climatic_Bulletin

Kępińska-Pacelik, J., & Biel, W. (2021). Alimentary Risk of Mycotoxins for Humans and Animals. Toxins, 13(11), 822. https://doi.org/10.3390/toxins13110822

Kos, J., Radić, B., Lešić, T., Anić, M., Jovanov, P., Šarić, B., Pleadin, J. (2024). Climate Change and Mycotoxins Trends in Serbia and Croatia: A 15-Year Review. *Foods*, 13(9), 1391. https://doi.org/10.3390/foods13091391

Kosicki,, R., Twarużek, M., Dopierała, P., Rudzki, B., Grajewski, J. (2020). Occurrence of Mycotoxins in Winter Rye Varieties Cultivated in Poland (2017-2019). *Toxins* (Basel). 12(6):423. doi: 10.3390/toxins12060423.

Kow, R., Er, B., Khoo, J, Chan, JSH, Aung, KT. (2025). Analysis of Reported Aflatoxin Levels in the EU's Rapid Alert System for Food and Feed (RASFF) Notifications. Foods, 14(18), 3250. doi: 10.3390/foods14183250.

Leggieri, M.C., Toscano, P., Battilani, P. (2021). Predicted Aflatoxin B1 Increase in Europe Due to Climate Change: Actions and Reactions at Global Level. *Toxins*, 13, 292, https://doi.org/10.3390/toxins13040292

Leite, M., Freitas, A., Sanches Silva, A., Barbosa, J., Ramos, F. (2021). Maize food chain and mycotoxins: A review on occurrence studies. Trends in Food Science & Technology, 115, 307-331, doi: 10.1016/j.tifs.2021.06.045.

Lin, H., Jia, B. & Wu, A. (2023). Cytotoxicities of Co-occurring alternariol, alternariol monomethyl ether and tenuazonic acid on human gastric epithelial cells. Food and Chemical Toxicology 171. https://doi.org/10.1016/j.fct.2022.113524

Mato, L., Damani, Z., Spahiu, J., Halimi, E., Seiti, B., & Topi, D. (2024). High prevalence of mycotoxigenic fungi and Aflatoxin B1 contamination in corn and wheat grains grown to Albania: implications for food safety. *Journal of Food Quality and Hazards Control*, 11/1, 59-68

Milićević, D. & Pleadin, J. (2022). Mycotoxins incidence in southeastern European countries: Implication on the food supply chain. In: Fang, C. & Gurinović, M. (Eds.), Sustainable and nutrition-sensitive food systems for healthy diets and prevention of malnutrition in Europe and Central Asia (Chapter 3, pp. 109–141). Food and Agriculture Organization of the United Nations (FAO). September 2022.

Munkvold, G.P., Arias, S., Taschl, I., Gruber-Dorninger, C. (2019). Mycotoxins in Corn: Occurrence, Impacts, and Management, in Corn (Third Edition), Eds: Sergio O. Serna-Saldivar, AACC International Press, 235- 287, doi:10.1016/B978-0-12-811971-6.00009-7.

Nagda, A. & Meena, M. (2024). Alternaria mycotoxins in food and feed: Occurrence, biosynthesis, toxicity, analytical methods, control and detoxification strategies. *Food Control*, 158, 110211, doi:10.1016/j.foodcont.2023.110211

Pinton, P., Terciolo, C., Payros, D., Oswald, I. P. (2025). Mycotoxin hazard: the European view. *Current Opinion in Food Science*, 63, 101306, doi: 10.1016/j.cofs.2025.101306.

Pleadin, J., Kos, J., Radić, B., Vulić, A., Kudumija, N., Radović, R., Janić Hajnal, E., Mandić, A., & Anić, M. (2023). Aflatoxins in Maize from Serbia and Croatia: Implications of Climate Change. *Foods*, 12(3), 548. https://doi.org/10.3390/foods12030548

Sdogati, S., Pacini, T., Bibi, R., Caporali, A., Verdini, E., Orsini, S., Ortenzi, R., & Pecorelli, I. (2024). Co-Occurrence of Aflatoxin B1, Zearalenone and Ochratoxin A in Feed and Feed Materials in Central Italy from 2018 to 2022. *Foods*, 13(2), 313. https://doi.org/10.3390/foods13020313

Stroka, J., Anklam, E. (2002). New strategies for the screening and determination of aflatoxins and the detection of aflatoxin-producing molds in food and feed. *Trends in Analytical Chemistry*, 21, 90–95.

Stroka, J., Gonçalves, C. (2019). Mycotoxins in Food and Feed: An Overview. In: Encyclopedia of Food Chemistry, Eds: L.Melton, F. Shahidi, P. Varelis, Academic Press, 401-419, https://doi.org/10.1016/B978-0-08-100596-5.21801-5.

Sudan, J., Verma, A., Bashir, S., Rawat, M., Batool, A., Pathak, H., Zargar, S.M., Masi, A. (2026). Chapter 1 - Introduction to aflatoxin status in crops, in: Aflatoxin Management in Crops, Eds: S. M. Zargar, J. Sudan, H. Pathak, A. Masi, Academic Press, 1-18, doi:10.1016/B978-0-443-33863-2.00002-3.

Tahiri, A., Risto, J., Mato, L., Cani, A., Topi, D. (2025). Occurrence of Aflatoxin M1 in Milk Consumed in Tirana, Albania, and Health Risk Assessment in Different Population Groups. *Toxins*, 17, 315. https://doi.org/10.3390/toxins17070315.

Tibola, C.S., Cunha Fernandes, J.M., Guarienti, E.M., Nicolau, M. (2015). Distribution of Fusarium mycotoxins in wheat milling process. *Food Control*, 53, 91-95, doi: 10.1016/j.foodcont.2015.01.012.

Topi, D., Babič, J., Jakovac-Strajn, B., & Tavčar-Kalcher, G. (2023). Incidence of Aflatoxins and Ochratoxin A in Wheat and Corn from Albania. *Toxins* (Basel), 15(9), 567. doi:10.3390/toxins15090567.

Topi, D., Babič, J., Pavšič-Vrtač, K., Tavčar-Kalcher, G., & Jakovac-Strajn, B. (2021). Incidence of Fusarium Mycotoxins in Wheat and Maize from Albania. *Molecules*, 26(1), 172. https://doi.org/10.3390/molecules26010172

Topi, D., Damani, Z., Babič, J., Jakovac-Strajn, B., Tavčar-Kalcher, G. (2024). The Presence of Some Minor Aspergillus and Penicillium Unregulated Mycotoxins in Main Cereals Cultivated in Albania. *Molecules*, 29, 5292. https://doi.org/10.3390/molecules29225292..

Topi, D., Tavčar-Kalcher, G., Pavšič-Vrtač, K., Babič, J., & Jakovac-Strajn, B. (2019). Alternaria mycotoxins in grains from Albania: alternariol, alternariol monomethyl ether, tenuazonic acid and tentoxin. *World Mycotoxin Journal*, 12(1), 89-100. https://doi.org/10.3920/WMJ2018.2342

RESEARCH ON THE INFLUENCE OF THE MANAGEMENT SYSTEM ON MILK PRODUCTION IN SAANEN GOATS

Dorina NADOLU[1], Laura MARINICĂ[2],Andreea Hortanse ANGHEL[1,2], Camelia Zoia ZAMFIR[1], Oana Corina PREȘA[1], Cristian-Vasile ILISIU[1],*

[1]Research and Development Institute for Sheep and Goat Breeding, Palas, Constanța, Romania
[2]Ovidius University of Constanta, Faculty of Natural Sciences and Animal Sciences, Romania

Corresponding author e-mail: lauralaviniamarinica@gmail.com*

ABSTRACT

Dairy goat farming is a significant sector of modern animal husbandry, and methods to enhance productive performance are a current priority in the context of optimizing resource use and increasing sustainability in the industry. Saanen dairy goats are distinguished by their high production potential and adaptability to various farming systems. This study analyses the milk production of two Saanen goat farms involved in purebred improvement programs over a three-year period, comparing two farming systems: traditional (pasture-based) and intensive (permanent housing). Milk yield was estimated using the Fleischmann formula (accounting for the kid-rearing period), and statistical analysis was performed using a paired two-sample t-test for means. Significant differences ($p<0.001$) in average milk production were observed over the three years for the pasture-raised group; yields increased progressively from 737.31 ± 186.11 kg in the first lactation to 856.07 ± 180.90 kg in the second and 929.44 ± 224.89 kg in the third, while the average lactation length decreased from 315.6 days to 307.3 days. Consequently, total milk production was primarily driven by the goats' increasing productive capacity, with average daily yields of 2.34 kg/day in the first lactation, 2.79 kg/day in the second, and 3.02 kg/day in the third. Milk production in the intensively managed goat group increased significantly from one lactation to the next, alongside an extension of the lactation period and an increase in average daily yield. Goats raised under the intensive system achieved higher production levels than those in the traditional system starting from the very first lactation (836.4 kg vs. 737.3 kg), with the differences becoming even more pronounced in subsequent lactations (1,198.6 kg and 1,236.2 kg vs. 856.1 kg and 929.4 kg, respectively). These results suggest that intensive management, through the control of nutrition and husbandry conditions, facilitates a fuller expression of the genetic potential of Saanen goats.

Keywords: Saanen goats, milk production, management system

INTRODUCTION

Goat farming is a livestock sector undergoing continuous development, driven by the species' adaptability, the nutritional value of its milk, and growing interest in efficient production systems. Population growth, urbanization, and rising incomes in certain regions of the world have led to an increasing demand for food sources, with animal-derived protein playing a key role—thereby boosting interest in the development and intensification of the livestock sector (Dida F.M. et al., 2025).

Amidst current concerns regarding resource optimization and increased sustainability in livestock farming, the choice of production system can significantly influence animal performance. Intensifying livestock production entails the construction of housing and facilities for storing feed and manure, as well as the acquisition of energy- or fuel-consuming machinery, factors viewed as contributing to a larger carbon footprint. Conversely, intensive livestock farming is considered more efficient in terms of emissions per unit of output, owing to improved feed conversion and animal productivity (Gerber et al., 2011). However, traditional systems are regarded as more eco-friendly and more effective at reducing greenhouse gas emissions (Parsad R et al., 2025; Kerven C, 2024). Furthermore, regarding grazing, goats offer the advantage of utilizing rugged, marginal land unsuitable for arable crops, thereby avoiding competition with land used for human food production (Van Zanten et al., 2018).

Milk is an excellent source of protein and other nutrients; goat milk, in particular, is preferred due to its favourable organoleptic and nutritional properties, making it suitable for sensitive consumers, including children and individuals with allergies or lactose intolerance (Castro N. et al., 2023). Goat milk is characterized by higher digestibility compared to milk from other animal species, owing to the smaller diameter of its fat globules (Zhao L. et al., 2022). Rich in medium-chain fatty acids, oligosaccharides, essential amino acids, and easily absorbable minerals (Verma A.K., 2025), goat milk is often considered a functional food.

Saanen goats are robust animals with a calm temperament that adapt very well to various rearing methods, particularly intensive systems. The Saanen breed is one of the most widespread breeds specialized for milk production, valued for its high productive potential, adaptability to diverse geographical regions and climates (E.B. Mawussi et al., 2024; O.T.L.F. Offoumon et al., 2023), and ability to thrive under different farming conditions. Consequently, a comparative analysis of productive performance based on the rearing system can provide valuable insights for optimizing management in dairy goat farms.

Against this background, this study aims to evaluate the productive performance of Saanen goats raised under traditional (extensive) and intensive systems, highlighting the specific characteristics and advantages of each system analysed.

MATERIAL AND METHOD

The study was conducted at two Saanen goat farms involved in milk production improvement programs and managed under two different systems: intensive and traditional. The herds at both farms originated from a core group of goats imported from the Poitiers region of France. Females in their first lactation were selected from the herds, and their milk production was monitored over the first three lactation years. Two groups were thus formed: the ST group (traditional system), consisting of 30 goats, and the SI group (intensive system), consisting of 40 goats.

The farm managed under the traditional system is located in the sub-mountainous zone of the Western Carpathians at an altitude of 700 m, an area characterized by productive pastures available for an extended period of the year. Vegetation growth is favoured by the cool, humid climate, which ensures a supply of lush, succulent grass. The local vegetation consists of a mixture of grasses (*Dactylis glomerata, Festuca pratensis, Lolium perenne*), legumes (*Medicago falcata, Trifolium repens*), and other medicinal plants (*Plantago lanceolata, Achillea millefolium, Taraxacum officinale*), as well as varied shrubby vegetation, such as bilberry, cowberry, and dwarf juniper, ensuring a diverse and substantial diet for 7–9 months of the year. During the winter, the goats are kept in loose housing and fed mountain hay, supplemented with 500 g of a barley, corn, and pea mixture. Reproduction in mountain farm

goats (traditional system) is influenced by climatic factors; it occurs earlier in years characterized by short, mild summers (temperatures of 17–20°C) and a cool, rainy autumn, compared to years with longer, hotter summers (22–28°C) and low precipitation.

The Saanen goats raised under an intensive farming system belong to a farm located in Dobrogea, a region characterized by a pronounced temperate-continental, semi-arid climate, with summer temperatures ranging from 26°C to 34°C. Under these conditions, the goats are kept exclusively in a permanent loose-housing system within shelters equipped with artificial ventilation. Feeding follows a strictly established schedule, with rations tailored to the animals' age, physiological status, and milk production levels. At this intensive-system farm, lactating goats are grouped according to lactation number (first-lactation vs. multiparous goats) and milk yield (1.5–2 kg, 2–3 kg, 3–4 kg, and over 4 kg/day). Specifically, lactating goats received 2.5 kg of alfalfa (split into two feedings) and a pelleted feed based on corn, barley, bran, and sunflower meal, containing 15.5% crude protein and fed in variable amounts (1.5–2.8 kg, depending on milk yield) split into three feedings, along with straw provided ”ad libitum”. Wheat straw was used for bedding in the pens due to its superior capacity for absorbing liquid manure. In this intensive system, manure removal was automated and performed every three weeks to maintain an optimal microclimate, specifically, keeping ammonia levels minimal and preventing overheating and excessive humidity. Goats in both farming systems (ST and SI) had access to fresh water ad libitum, provided via troughs in the traditional system and automatic drinkers in the intensive system. Salt licks and mineral blocks were also provided. (Molasses Licking Blocks, 5 kg, ROMVAC).

In both farms, reproduction was achieved through controlled mating during the breeding season (September–October). Concentrating matings within a short timeframe and stimulating fertile estrus were accomplished through herd management, specifically, by housing males separately from the does at a distance that prevented visual or olfactory contact. Each year, starting in early September, olfactory and visual stimulation was induced by keeping males in the presence of females for one to two hours daily, both morning and evening. In the traditional farm, teaser bucks wore protective aprons and were allowed to roam freely among the does, whereas in the intensive farm, bucks were led along the aisles between the female pens. In this way, the "male effect" triggered and relatively synchronized estrus in the females, resulting in a concentrated mating and, consequently, a concentrated kidding season.

Kidding was followed by a suckling period that varied from year to year depending on the kids' physical development and, above all, the farmer's priority regarding whether to retain the offspring for herd replacement or to market the milk. After weaning, the goats were milked mechanically, ensuring complete and hygienic milking twice daily, using mobile milking units equipped with ”Melasty milk meters” (SC Expert Moldova Trading SRL) for gravimetric milk measurement. Milk production monitoring, specifically, recording a goat's milk yield—was carried out on a scheduled control day by recording the quantity of milk obtained during the two daily milkings. The monitoring took place over five consecutive months, with an interval of 28–34 days between checks (official method A4) (ICAR, 2018; Sargent, 1968).

The total milk yield per goat was determined by applying the Fleischmann formula with the standard interval method:

$$MY = I_0M_1 + I_1*\frac{(M_1 + M_2)}{2} + I_2*\frac{(M_2 + M_3)}{2} + I_{n-1}*\frac{M_{n-1} + Mn}{2} + I_nM_n$$

where:

M_1, M_2, M_n are the weights in kilograms, given to one decimal place, of the milk yielded in the

24 hours of the recording day.
I_1, I_2, I_{n-1} are the intervals, in days, between recording dates.
I_0 is the interval, in days, between the lactation period start date and the first recording date. I_n is the interval, in days, between the last recording date and the end of the lactation period.

Correlations between the parameters monitored in the study (mean, standard deviation, minimum and maximum values) were calculated using Excel functions, and the statistical assessment of differences between parameters within each farming system was performed using the "t-Test: Paired Two-Sample for Means." Statistical differences regarding the monitored parameters, specifically gestation length, total milk yield, and average daily production, between the two farming systems were evaluated for each lactation rank using the "t-Test: Two-Sample Assuming Unequal Variances."

RESULTS AND DISCUSSION

The group of 30 Saanen goats, managed under a traditional system, showed a progressive increase in average milk yield: from 737.31 ± 186.11 kg in the first lactation to 856.07 ± 180.90 kg in the second, and to 929.44 ± 224.89 kg in the third (Table 1). A comparison of yields using the paired-sample t-test revealed statistically significant differences between all analysed lactations: lactation I vs. lactation II ($p = 0.00002$), lactation II vs. lactation III ($p = 0.00033$), and lactation I vs. lactation III ($p < 0.000001$). The results demonstrate a significant increase in milk yield as the animals age and reach productive maturity, with the yield in the third lactation being 26.05% higher than in the first.

Table 1

Evolution of milk production in Saanen goats raised under a traditional system during the first three years of lactation

Year	Specification	Average	STD DEV.	MIN.	MAX.
2023 L1	Lactation length (days)	315.57	15.06	279	333
	Total milk/lactation (kg)	737.31	186.11	466.23	1174.28
	Average kg/day	2.34	0.59	1.54	3.58
2024 L2	Lactation length (days)	309.60	28.16	286	448
	Total milk/lactation (kg)	856.07	180.90	613.47	1217.18
	Average kg/day	2.79	0.66	1.96	4.13
2025 L3	Lactation length (days)	307.30	19.29	266	330
	Total milk/lactation (kg)	929.44	224.89	535.35	1360.12
	Average kg/day	3.02	0.71	1.67	4.73

L1 – lactation in primiparous animals,
L2 – second year of lactation,
L3 – third year of lactation.

The average total milk yield and average daily yield obtained from Saanen goats raised in Romania's temperate zone exceed the yields obtained under grazing conditions in humid tropical regions, where reported yields for the first three lactations were 603.1 liters (primiparous goats), 626.6 liters (2nd lactation), and 648.5 liters (3rd lactation), with daily yields of 1.7 liters, 2.6 liters, and 2.7 liters, respectively (Offoumon et al., 2023).

Lactation duration (in days) showed no significant differences across the three consecutive years, although a slight decrease in the number of days was observed (Graph 1):
315.6 days for the first lactation, 309.6 days for the second, and 307.3 days for the third;

statistical comparison across the three lactation years yielded p-values > 0.05: p = 0.2842 (lactations 1 and 2), p = 0.6940 (lactations 2 and 3), and p = 0.0749 (lactations 1 and 3).

Graph 1. Correlation between lactation length and average annual milk production in Saanen goats raised under a traditional system

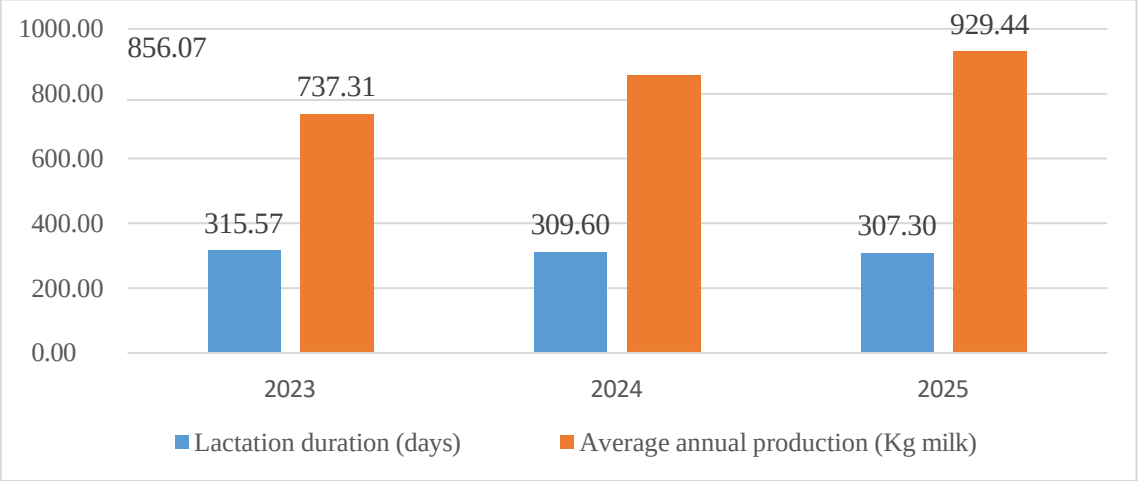

The long lactation period observed in this study, compared to the 266.8 days reported by Mioc et al. (2008), can be attributed to the quality of the alpine pasture and favoured by a long autumn with moderate rainfall. Lower lactation lengths have been reported for Saanen goats raised on pasture in tropical regions: 171.25 days for the first lactation, 193.18 days for the second, and 214.41 days for the third (E.B. Mawussi et al., 2024), highlighting the influence of environmental factors on milk production in traditional extensive farming systems.

Consequently, the increase in average annual production among goats in the traditional group was driven by the animals' enhanced productive capacity, linked to body growth and physiological and hormonal maturation—rather than by changes in the duration of lactation (A. Kasap et al., 2026).

Average daily milk production over the three consecutive years showed significant increases (p > 0.05), with values of 2.34 ± 0.59 kg/day for primiparous goats, 2.79 ± 0.66 kg/day for the second lactation, and 3.02 ± 0.71 kg/day for the third lactation.

In the intensive system, milk production among the 40 Saanen goats increased significantly from one lactation to the next, alongside an extension of the lactation period and an increase in average daily production (Table 2). Total milk production values were 836.36 ± 184.50 kg for primiparous goats, 1,198.63 ± 132.16 kg for the second lactation of the same goats, and 1,236.19 ± 142.13 kg for the third lactation. The paired-sample t-test revealed highly statistically significant differences: between the first and second lactations ($p < 0.000001$), between the second and third lactations ($p = 0.0062$), and between the first and third lactations ($p < 0.000001$). The results indicate a marked increase in production between the first and second lactations (+43.3%), followed by a smaller, weakly statistically significant increase ($p = 0.006$, $p < 0.05$) between the second and third lactations (+3.13%).

Milk production increased by approximately 47.8% between the first and third lactations, highlighting the superior capacity of Saanen goats to realize their productive potential under intensive farming conditions.

The results of the present study are superior in terms of total milk yield compared to a sample of 670 intensively farmed Saanen goats in Croatia, which showed a production of

697.59 kg for primiparous goats (K. Zeljić Stojiljković et al., 2025), and to a yield of 727.9 kg obtained in New Zealand (M. Scholtens et al., 2020). Higher values were reported for a herd of 3,434 intensively farmed Saanen goats in Canada, which recorded an average total milk yield of 921 kg during the first lactation (E. Massender et al., 2022), while M. Teissier et al. (2024) report an average total yield of 1,119 kg of milk.

Table 2. Evolution of milk production in Saanen goats raised under an intensive system during the first three years of lactation

Year	Specification	Average	STD DEV.	MIN.	MAX.
2023 L1	Lactation length (days)	285.28	19.04	265	318
	Total milk/lactation (kg)	836.36	184.49	540.54	1195.91
	Average kg/day	2.93	0.62	1.86	4.48
2024 L2	Lactation length (days)	322.48	10.76	296	333
	Total milk/lactation (kg)	1198.63	131.71	931.62	1537.86
	Average kg/day	3.72	0.39	3.02	4.63
2025 L3	Lactation length (days)	307.05	13.37	293	337
	Total milk/lactation (kg)	1236.19	142.16	966.85	1555.00
	Average kg/day	4.03	0.47	3.22	5.15

L1 – lactation in primiparous animals,
L2 – second year of lactation,
L3 – third year of lactation.

Primiparous goats recorded the shortest average lactation duration (285.28 ± 19.04 days), while the longest duration was observed during the second lactation (322.48 ± 10.76 days); during the third lactation, the duration decreased slightly to 307.05 ± 13.37 days. Statistically significant differences ($p < 0.000001$) in average lactation duration were observed across the three years. Notably, although the average duration of the third lactation decreased compared to the second, milk yield increased by 3.13%, as illustrated in Graph 2.

Graph 2. Correlation between lactation length and average annual milk yield in Saanen goats raised under an intensive system

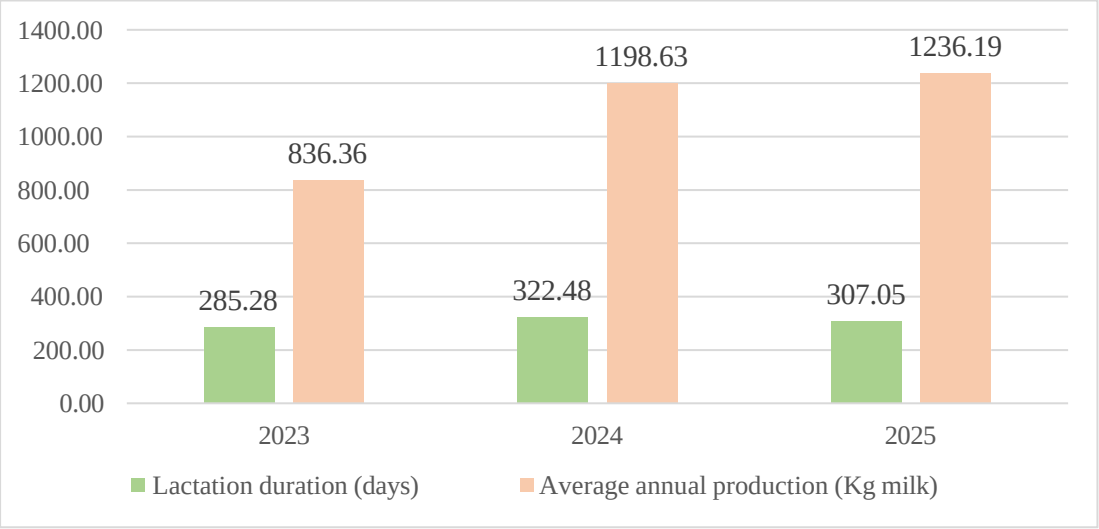

The controlled management conditions, specifically the microclimate and nutrition characteristic of the intensive system practiced at this farm, enabled a better expression of the productive potential inherent to the Saanen breed. This is further demonstrated by the evolution of average daily milk yield over the three-year period: it rose from 2.9 ± 0.62 kg/day for primiparous goats to 3.72 ± 0.39 kg/day in the second lactation and 4.03 ± 0.47 kg/day in the third lactation, with differences being highly statistically significant across all comparisons (L1/L2, L2/L3, L1/L3; $p < 0.000001$).

These results demonstrate, as was the case with the group managed under the traditional system, a continuous improvement in the animals' productive capacity as they reach physiological maturity.

To clearly highlight the influence of the two management systems used for Saanen goats at the two farms, the monitored parameters were compared, and performance differences were determined for each stage of lactation (Table 3).

Table 3. A summary overview of milk production indicators for Saanen goats raised under traditional and intensive systems.

Indicator	Traditional system	Intensive System	The Difference Intensive–Traditional	p
Average total production L1 (kg)	737.31	836.36	99.05 (13.43%)	0.0307
Average total production L2 (kg)	856.07	1198.63	342.56 (40.02%)	< 0,000001
Average total production L3 (kg)	929.44	1236.19	306.75 (33.01%)	< 0,000001
Lactation duration I (days)	315.57	285.28	-30.29 (9.59%)	< 0,000001
Lactation duration II (days)	309.60	322.48	12.88 (4.16%)	0.023
Lactation duration III (days)	307.30	307.05	-0.25 (0.08%)	0.9517
Average daily production L1 (kg)	2.34	2.93	0.59 (25.21%)	0.0001
Average daily production L2 (kg)	2.79	3.72	0.93 (33.33%)	< 0,000001
Average daily production L3 (kg)	3.02	4.03	1.01 (33.44%)	< 0,000001

A comparative analysis of the productive performance of Saanen goats from the two farms, managed under a traditional system (based on grazing) and an intensive system (permanent housing), categorized by lactation rank, reveals differences between the systems regarding total milk yield, average daily yield, and lactation length.

For primiparous goats, the average milk yield (per lactation) was 737.31 kg in the traditional system and 836.36 kg in the intensive system. The 99.05 kg difference, representing a 13.43% advantage for the intensive system, was statistically significant ($p = 0.0307$); this trend persisted through the subsequent two lactations, albeit with a smaller margin of difference.

Differences in total average yield (per lactation) between the management systems became more pronounced during the second lactation: the yield rose to 856.07 kg in the traditional system and to 1,198.63 kg in the intensive system, resulting in a highly statistically significant difference ($p< 0.000001$) of 342.56 kg (or 40.02%) in favour of the intensive system.

By the third lactation, average milk yield increases more significantly in goats raised under the intensive system, reaching 1,236.19 kg compared to 929.44 kg in the traditional system, with the difference of 306.75 kg (33.01%) being statistically highly significant ($p < 0.000001$).

In both farming systems, milk yield increases with successive lactations, though the magnitude of this increase is greater in the intensive system. This trend can be attributed to the physiological and, by extension, productive maturation of the goats; furthermore, the farming system, microclimate conditions, and nutrition allow for varying expressions of the Saanen breed's productive potential.

Regarding lactation duration, it is evident in both systems that a higher total milk yield is not solely the result of a greater number of milking days. Thus, the higher milk yield obtained from goats in the intensive system compared to the traditional system is not consistently associated with a longer lactation period. In the first lactation, the average duration was actually significantly shorter in the intensive system (285.28 days) than in the traditional system (315.57 days), a difference of 30.29 days ($p < 0.000001$). Consequently, the superior milk yield of primiparous goats in the intensive system, which was 13.43% higher than that of goats in the traditional system, cannot be attributed to a longer lactation duration. During the second lactation, the situation changes: the lactation period was 322.48 days in the intensive system compared to 309.60 days in the traditional system, with the difference of 12.88 days (4.16%) being statistically significant ($p = 0.023$). However, this difference is insufficient to explain the 40.02% higher total milk production in the intensive system, given that the lactation period is only 4.16% longer.

The fact that a longer milking period does not necessarily result in higher milk yield is evident during the third lactation; the average lactation duration for goats raised under the two systems was roughly equal, 307.30 days in the traditional system and 307.05 days in the intensive system, with a statistically insignificant difference ($p = 0.9517$) of only 0.25 days.

Under these conditions, the intensive system recorded a total yield 33.01% higher than that of the traditional system. The lack of a direct correlation between lactation duration and milk yield is clearly supported by the average daily yield, which was significantly higher in the intensive system across all three lactations. Primiparous goats in the intensive system recorded a daily yield of 2.93 kg/day, compared to 2.34 kg/day in the traditional system, representing a 25.21% advantage ($p = 0.0001$). During the second lactation, the values were 3.72 kg/day versus
2.79 kg/day, with the difference rising to 33.33% ($p < 0.000001$). In the third lactation, daily yield reached 4.03 kg/day in the intensive system compared to 3.02 kg/day in the traditional system, a superiority of 33.44% ($p < 0.000001$).

Average daily production is the indicator that best illustrates the advantage of raising Saanen goats under an intensive system; this is evident during the first lactation, where goats in the intensive system achieve higher total production despite a shorter lactation period, and during the third lactation, where production is 33.01% higher even though lactation duration is nearly equal between the two farming systems. In the current context, with increasing emphasis on reducing GHG emissions from livestock farming systems, the issue of pasture-based versus indoor (stabled) rearing continues to be a subject of research, yielding controversial results.

In the current context of increasing emphasis on reducing GHG emissions from livestock farming systems, the issue of pasture-based versus confinement-based systems remains a subject of ongoing research, with results proving controversial. For instance, Dida
F.M. et al. (2025) cite Flysjö et al. (2011), Belflower et al. (2012), and O'Brien et al. (2014), who reported that pasture-based and confinement systems have similar carbon footprints when grassland carbon sequestration is excluded from the analysis; conversely, Capper et al. (2009)

and Gerber et al. (2011, 2013) argue that intensive milk production systems generate lower greenhouse gas emissions per unit of milk produced, owing to superior feed efficiency and higher productivity.

CONCLUSIONS

Milk production performance, specifically total average production and average daily production, in Saanen goats is influenced by the farming system from the very first lactation; intensive systems yield higher production levels compared to traditional farming methods. Saanen goats, a breed specialized for milk production and highly adaptable to environmental conditions, effectively utilize natural resources (such as alpine pastures); however, they inevitably expend energy traversing greater distances to forage and adapt to the natural environment, which limits their productive performance. Under stabling conditions, characterized by limited movement, feeding tailored to physiological stage and production levels, and a controlled, optimal microclimate, Saanen goats raised in Romania are able to fully realize the breed's inherent productive potential.

REFERENCES

Castro, N.; Suarez-Trujillo, A.; Gonzalez-Cabrera, M.; Hernandez-Castellano, L.E.; Argüello, A.,2023, Goat Lactation Research as a Gateway for the Development of the Dairy Goat Industry, Anim. Front. No 13, 108–111

Dida F.M., Garcia S.C., Gonzale L.A., 2025, Greenhouse gas emissions of confinement- and pasture-based dairy farms: Implications for mitigation, J. Dairy Sci., Vol. 108, Issue 10, p11026-11040, https://doi.org/10.3168/jds.2025-26566

Gerber, P., T. Vellinga, C. Opio, H. Steinfeld., 2011, Productivity gains and greenhouse gas emissions intensity in dairy systems. Liv est. Sci. 139:100–108. https://doi.org/10.1016/j.livsci.2011.03.012

Kasap, A., Mulc, D., Špehar, M., Držaić, V., Prpić, Z., Jurković, D., Barać, Z. și Mioč, B. (2026). Impactul vârstei la prima împerechere asupra producției de lapte pe viață la caprele alpine: echilibrarea câștigurilor timpurii și eficiența pe parcursul vieții. *Agricultură* , *16* (6), 687. https://doi.org/10.3390/agriculture16060687

Kerven, C., 2024, Contribution of Goats to Climate Change: How and Where? Pastor. Res. Policy Pract., vol. 14, 13988, doi: 10.3389/past.2024.13988

Mawussi EB, Assah AK, Kulo EA (2024). Reproduction and milk production performance of Saanen dairy goat in Southern Togo (West Africa). Adv. Anim. Vet. Sci., 12(6):1028-1033. DOI | https://dx.doi.org/10.17582/journal.aavs/2024/12.6.1028.1033 ISSN (Online) | 2307-8316

Miller, B.A.; Lu, C.D. Current Status of Global Dairy Goat Production: An Overview. Asian-Australas. J. Anim. Sci. 2019, 32, 1219–1232

Mioc B, Prpić Z, Vnučec I, Barać Z, Sušić V, Samaržija D, Pavić V (2008). Factors affecting goat milk yield and composition. Mljekarstvo Dairy, 58(4).

Offoumon, OTLF, Assanı Seıdou, A., Sannı Worogo, Sh, Soule, F., Assobga, B., Gbangboche, Ab, & Alkoıret Traore, I. (2023). Factors influencing milk production of Saanen, Maradi Red, and Saanen x Maradi Red cross goats in the Sudanian-Guinean zone of northern Benin. *Annales De l'Université De Parakou - Série Sciences Naturelles Et Agronomie* , *13* (1), 121–128. https://doi.org/10.56109/aup-sna.v13i1.127

Parsad, R., Ahlawat, S., Bagiyal, M., Arora, R., Gera, R., Chhabra, P., Sharma, U., Singh, A, Climate Resilience in Goats: A Comprehensive Review of the Genetic Basis for Adaptation to Varied Climatic Conditions. Mamm. Genome, 36, 151–161

Scholtens, M.; Lopez-Villalobos, N.; Lehnert, K.; Snell, R.; Garrick, D.; Blair, H.T. Advantage of Including Genomic Information to Predict Breeding Values for Lactation Yields of Milk, Fat, and Protein or Somatic Cell Score in a New Zealand Dairy Goat Herd. Animals 2020, 11, 24.

Teissier, M., Brito, L.F., Schenkel, F.S., Bruni, G., Fresi, P., Bapst, B., Robert-Granie, C., Larroque, H., 2024, Genetic Parameters for Milk Production and Type Traits in North American and European Alpine and Saanen Dairy Goat Populations. JDS Commun., 5, 28–32.

Van Zanten, H. H. E., M. Herrero, O. Van Hal, E. Röös, A. Muller, T. Garnett, P. J. Gerber, C. Schader, I. J. M. De Boer. 2018, Defin ing a land boundary for sustainable livestock consumption. Glob. Change Biol. 24:4185–4194. https: / / doi .org/ 10 .1111/ gcb .14321.

Verma, A.K.; Singh, T.P.; Rajkumar, V., Chatli, M.K., Kushwah, T., Nanda, P.K., Curros, B., Lorenzo, J.M., Das, A.K., Goat Milk: A Versatile Dairy Alternative with Unique Health Benefits and Functional Properties. Food Rev. Int. 2025, 1–36,

https://doi.org/10.1080/87559129.2025.2479122

Zhao, L., Wang, J., Mao, X., 2022, Composition and Interfacial Properties Play Key Roles in Different Lipid Digestion Between Goat and Cow Milk Fat Globules In Vitro, Food Chem, 374, 131538

Zeljić Stojiljković, K., Mićić, N., Bogdanović, V., Đedović, R., Pihler, I., Stojiljković, N. și Stanojević, D. (2025). Evaluarea genetică a trăsăturilor de producție de lapte în populația sârbă de capre Saanen. *Animals* , *15* (20), 3008. https://doi.org/10.3390/ani15203008.

***FAO. Crops and Livestock Products; Food and Agriculture Organization of the United Nations: Rome, Italy, 2024. Available online: https://www.fao.org/faostat/en/#data/QCL

***ICAR- The Global Standard for Livestock Data, 2018, Section 16 - Guidelines on recording performance of dairy ewes and dairy goats, Version February, 2018.

HUMIC ACID-BASED BIO STIMULATION ENHANCES GROWTH AND EARLY DEVELOPMENT OF TRITICUM DURUM UNDER SEMI-ARID CONDITIONS IN EASTERN ALGERIA

A. Kemmouche[1,2], R. Ghallab[3], O. Bahi[3], I. Khen[1], A. Kentour[4]

[1]Ecole Nationale Supérieure de Biotechnologie (ENSB), Taoufik Khaznadar [2]Laboratoire de Conception et Application de Molécules Bioactives (CamBio) [3]Ecole Nationale Polytechnique de Constantine (ENPC), Malek Ibn Nabi
[4]Institut Technique des Grandes Culture (ITGC Constantine)

ABSTRACT

Humic substances are known for their benefits to improve soil quality, and consequently improve plants' growth. A study was carried out at the Technical Institute of Vaste Cultures (ITGC El-Khroub) in Constantine, using Triticum Durum Wheat known as "Wahbi", of Algerian origin as a plant material. The experimental trial is a randomized complete block design with 4 replications, consisting of 5 treatments: (**T0**: Control soil with no treatment, **T1**: Urea 46% at a dose of 133kg/Ha, **T2**: Humic acid at a dose of 1 L/Ha, **T3**: Humic acid at a dose of 1.5 L/Ha and **T4**: Humic acid at a dose of 2 L/Ha).The use of humic acid has shown an efficiency on all the studied parameters: number of plants per square meter, number of grains per ear, length of ears with and without awns, plant height, thousand grain weight (tgw), number of ears per square meter and yield per hectare. The R software was used for statistical calculations. The optimum HA dose of T3 resulted in a 62.73% increase in yield over the control soil, with improvements in grain number, ear length and plant height. The use of humic acid shown better effect on the plant growth parameters compared to Urea 46%, even at low doses. Statistical analysis using ANOVA demonstrated significant differences among the treatments for most agronomic parameters ($p < 0.05$), confirming the robust impact of humic acid applications compared to the control and urea treatments across yield and growth-related traits.

INTRODUCTION

Durum wheat is the second most important crop of wheat and the tenth most important crop in the world. It has a crucial importance in ensuring food safety of populations (Mohammadi et al., 2023). Humic Acid is one of the most important organic acids, known for its benefits to plants growth (Sallume et al., 2023). It is resulting from the decomposition of the organic matter and contains a combination

(Al Fayyadh et al., 2020). The use of humic substances to enhance the yield of Durum wheat production has made the subject of several recent studies around the world (see, for example, Pacuta, 2021; Mutlu & Tas, 2022; Sallume, 2023; Arambam, 2024).

Arambam. (2024) reported that humic acid has greater potential impacts on various agronomic parameters and soil properties, by increasing the intake of nutrients, strengthening the structure of the soil, reducing stress, and encouraging biological activity. The study carried out by Mutlu & Tas. (2022) revealed that foliar application of (1.5, 2.5, 3.5 and 4.5 L/Ha) humic acid at heading increased photosynthesis activity of plants. Sharma et al. (2023) mentioned that the addition of humic acid to the 100 percent recommended dose of fertilizers increases all the growth parameters of wheat significantly. The present work aims at studying the effect of humic acid at low doses (1, 1.5 and 2 L/Ha) on growth parameters of Triticum Durrum Wheat, known as "Wahbi", of Algerian origin, applied on an agricultural land in Constantine- Algeria.

MATERIALS AND METHODS

Site Localisation and Characteristics

The experiment was carried out during the 2023-2024 agricultural season at the Technical Institute of Vaste Cultures (ITGC) in El Khroub, Constantine, located at BP 35, El Baaraouia, El Khroub (7MCC+WWX). The station is located in the sub-humid bioclimatic zone with mild winters, characterised by a rainy season from October to May, followed by a dry season from June to September. This region also has a wide range of temperatures, with average values ranging from 0.45°C in March to 45.26°C in June, indicating a temperate climate with mild winters and warm summers, which favours resilient plant species such as cereals.

Figure 1. Site Location

Application of Humic Acid on Durum Wheat

The plant material used is a variety of durum wheat (Triticum durum) known as "Wahbi", of Algerian origin, developed by the ITGC of Constantine in 1986. The experimental design is a randomised complete block design with 4 replications, consisting of 5 treatments. Each plot or block is 1.2m x 5m, which corresponds to a size of $6m^2$.The study focuses on a single variable, the "fertilisation element", with a series of treatments and doses applied to evaluate their effectiveness. T0: control with no treatment, T1: Urea 46% at a dose of 133kg/Ha, T2: HA at a dose of 1 L/Ha, T3: HA at a dose of 1.5 L/Ha and T4: HA at a dose of 2 L/Ha. These treatments were applied every fifteen days starting from 60 days after seeding with applications scheduled for days 60, 75, 90, 105, and 120.

The following parameters were studied to evaluate the effect of different doses of HA on DURRUM Wheat growth: number of plants per square meter, number of grains per spike, spike length, plant height, thousand grain weight (tgw), spike number per square meter and yield per hectare.

Data Analysis

Statistical analysis was performed on the original untransformed data. A two-way analysis of variance (ANOVA), including F-value and p-value for all parameters, was performed using R statistical software. The least significant difference (LSD) multiple comparison post hoc test was used to compare means when ANOVA indicated significant differences.

RESULTS AND DISCUSSION

Physicochemical Properties of Soil

Soil physicochemical properties are basic indicators of soil nutrient content and characteristics (Meena et al., 2020). Soil samples were analysed for their physicochemical properties, the results of which are presented in Table 1. As research has demonstrated that HA affects the physicochemical properties of soil (Zhao et al., 2022), analysis was conducted both before and after applying HA at different concentrations.

The soil pH values remained within the optimal range (6.5–8.5) both prior to and following humic acid (HA) application, indicating consistently slightly alkaline conditions (Dandwate,

2020). HA functioned as a buffering agent, effectively stabilizing soil pH by mitigating fluctuations in acidity, thereby enhancing nutrient availability in alkaline soils. Electrical conductivity (EC) values were stable and consistently below salinity thresholds, demonstrating that HA application did not adversely impact soil salinity (Dandwate., 2020).

Table 1. Physico-chemical Properties of Soil Samples

Parameter	T0	T1	T2	T3	T4
pH	8.34	8.28	8.42	8.32	8.45
EC (dS/m)	0.19	0.30	0.18	0.22	0.17
O.C%	1.53	1.48	1.60	1.67	1.75
O.M%	2.65	2.57	2.77	2.89	3.03
N %	2.40	2.47	2.42	2.45	2.51
C/N	1.10	1.04	1.14	1.17	1.20

Significant increases in soil organic carbon (O.C%) and organic matter (OM) were observed with HA treatments, particularly at higher application rates (T3 and T4), elevating the soil fertility status to high and very high categories as per established classifications (Hazelton & Murphy, 2007; Addis & Abebaw, 2014). These findings suggest that HA contributes to enhanced carbon sequestration and improved soil quality, likely through the augmentation of humic substances (Pettit., 2015). Conversely, urea alone (T1) was associated with a slight reduction in organic carbon content, despite increasing nitrogen availability.

Nitrogen content exhibited a modest but consistent increase corresponding with HA application rate, reaching maximum levels at the highest HA dose, indicative of improved nitrogen retention or bioavailability. Additionally, the carbon-to-nitrogen (C/N) ratio displayed a progressive increase with HA treatment, underscoring the role of HA in promoting organic matter stabilization and long-term soil fertility by facilitating balanced nutrient cycling.

In summary, HA application exerted a beneficial influence on soil physicochemical properties

by enhancing organic matter content, nutrient status, and pH buffering capacity without

detrimental effects on salinity. These improvements collectively support the establishment of healthier soil conditions conducive to sustainable crop productivity (Lato et al., 2023).

Soil texture was also studied, showing that the soil type is “Silty Clay” with 2.56% of sand, 46.15% of silt and 56.41% of clay.

Study of Growth Parameters

Parameters such as plant density, grain and spike numbers, spike length, plant height, thousand grain weight, and crop yield were compared in the diagrams below (Figure 2), and summarised in table 2. Statistical analysis was carried out on the raw data using two-way ANOVA (reporting F and p-values). Where significant differences were found, means were compared by the LSD post hoc test, following the approach of Mutlu & Tas (2022).

At the onset of treatment application, the number of wheat plants per square meter was uniform across all treatments, including the control group. Statistical analysis confirmed no significant differences in initial plant density ($p > 0.05$), as expected, since this measurement was taken before any treatments could exert their effects. This baseline uniformity validated the experimental design and ensured that subsequent variations in measured traits resulted from the treatments themselves, rather than pre-existing differences in plant establishment. The application of humic acid demonstrated a marked impact on the number of grains per spike. While the control (T0) and urea treatment (T1) produced similar results, treatments with humic acid (T2, T3, and T4) led to a substantial increase, with T2 and T3 showing the greatest enhancements. ANOVA results revealed statistically significant differences between treatments ($p < 0.05$), emphasizing the efficacy of humic acid, particularly at certain dosages, in promoting reproductive productivity in wheat.

Spike length, was positively influenced by humic acid application. The longest spikes were observed in T2 (1 L/Ha). The control and urea treatments lagged behind, indicating a clear benefit from humic acid supplementation. Statistical analyses highlighted significant inter-treatment differences ($p < 0.05$), reinforcing the role of humic acid particularly at moderate doses in stimulating spike elongation and potentially improving grain-setting capacity.

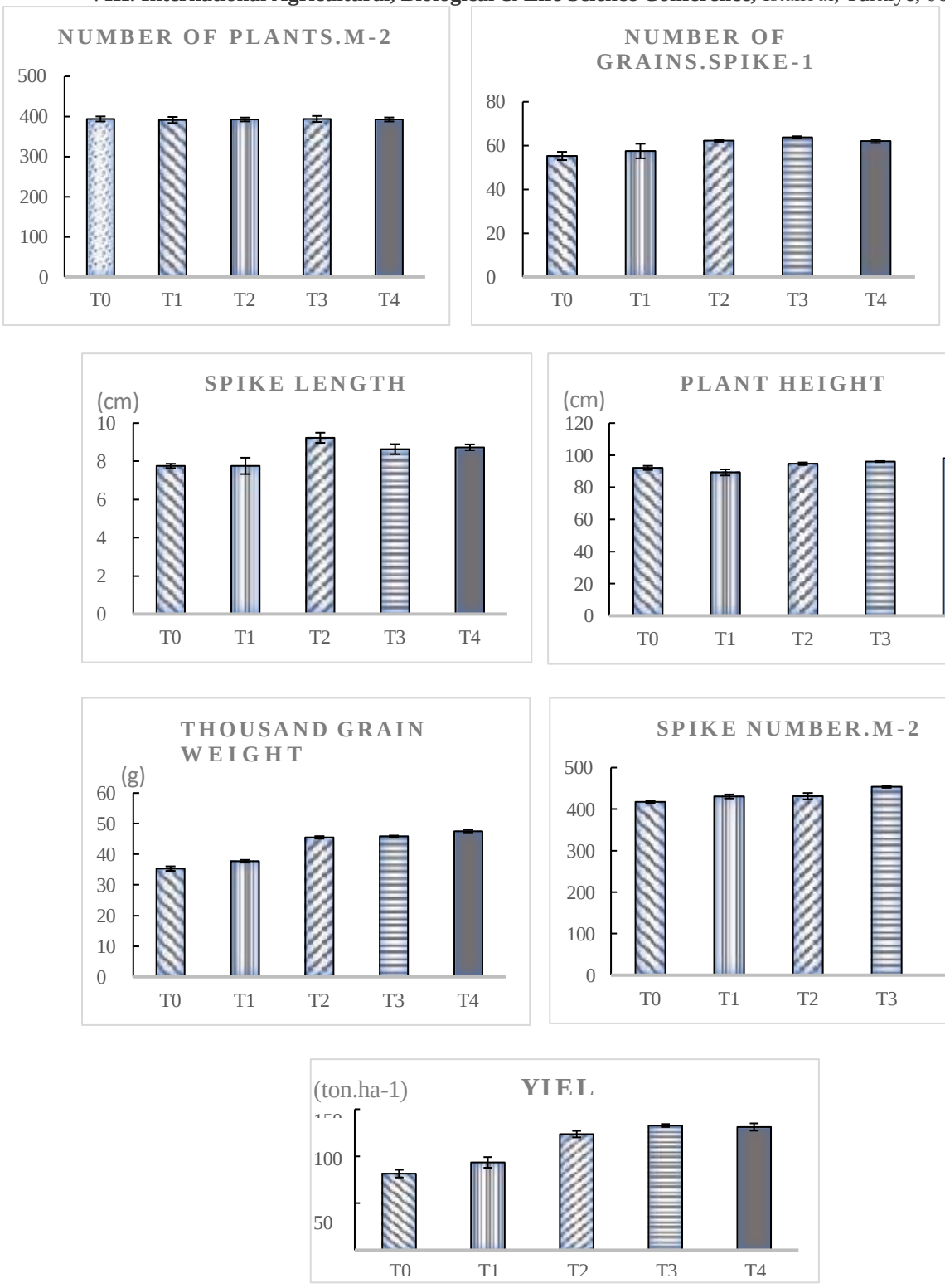

Figure 2. The Impact of Treatments on Major Yield and Growth Parameters in Wheat

Table 2. Comparative Analysis of Major Yield and Growth Parameters in Wheat Under Five Distinct Treatments: Means, Variance, and Statistical Significance

Parameter	**T0**	**T1**	**T2**	**T3**	**T4**	**ANOVA F-value**	**LSD Value**	**Pr > F**	**Notes**
Number of plants m^{-2}	393.8±6.3	391.3±7.5	392.5±4.8	393.8±7.5	392.5±5.0	0.125	—	0.971	No letter groups
Number of grains/spike	55.3±1.9 (C)	57.5±3.3 (D)	62.3±0.5 (B)	63.8±0.5 (B)	62.0±0.8 (A)	16.45	1.71	$2.33e^{-5}$	Groups: A–D
Spike length (cm)	7.76±0.11(C)	7.76±0.43(C)	9.23±0.27(A)	8.63±0.26(B)	8.75±0.15(B)	23.35	0.40	$2.7e^{-06}$	Groups: A–C
Plant height (cm)	92.1±1.3 (B)	89.3±1.9 (B)	94.7±0.8 (A)	96.0±0.3 (A)	98.0±0.7 (A)	36.23	2.67	$1.53e^{-7}$	Groups: A–B
1000 grain weight (g)	35.3±0.7 (D)	37.7±0.5 (C)	45.5±0.4 (B)	45.8±0.3 (B)	47.6±0.4 (A)	519.5	0.72	$6.94e^{-16}$	Groups: A–D
Spike number. m^{-2}	417.5±2.4 (D)	430.5±4.8 (C)	431.3±7.5 (C)	454.0±2.7 (A)	444.5±8.2 (B)	21.71	8.52	$1.88e^{-06}$	Groups: A–D
Yield (t/ha)	81.4±4.1 (D)	93.4±5.7 (C)	123.5±3.5 (B)	132.7±1.5 (A)	131.1±3.9 (A)	140.4	5.97	$1.08e^{-11}$	Groups: A–D

Treatments incorporating humic acid resulted in increased plant height compared to both the control and urea-only applications. Whereas urea alone produced a slight reduction in stature relative to the control, the addition of humic acid (T2, T3, T4) promoted notable height gains. The most pronounced increase was recorded at the 2 L/ha application rate (T4). Statistical grouping further delineated the humic acid treatments as significantly superior in this trait ($p < 0.05$), demonstrating its role in enhancingvegetative growth.

Grain weight exhibited substantial improvement in response to humic acid treatments. The greatest thousand grain weights were recorded in T4, followed closely by T3 and T2, while T1 and T0 showed comparatively lower values. The statistical analysis ($p < 0.05$) confirmed the superiority of humic acid treatments, suggesting that they effectively promote grain filling and improve overall grain quality.

The density of spikes per unit area, a key yield determinant, was most favourably impacted by the 1.5 L/ha humic acid treatment (T3), which yielded the highest spike number. T4 and T2 also facilitated notable increases, whereas

T1 and the control (T0) showed significantly lower spike densities. The observed differences were statistically significant ($p < 0.05$), underscoring the ability of humic acid to enhance reproductive efficiency and maximize productive tillering. Yield comparisons revealed striking advantages conferred by the humic acid treatments. Treatments T3 and T4 achieved the highest yields, with T3 narrowly outperforming T4. Both were followed by T2, which also showed a marked improvement over the control and urea-only treatments. The differences in yield were highly significant ($p < 0.05$), and the application of humic acid, especially at 1.5–2 L/ha, resulted in yield increases of over 60%compared to the untreated
control, highlighting its agronomic value.

CONCLUSION

The comparative evaluation of different treatments across seven key growth parameters (number of plants per square meter, number of grains per spike, spike length, plant height, thousand grain weight (tgw), spike number per square meter and yield per hectare) in wheat demonstrates the pronounced and consistent benefits of humic acid applications. When applied at appropriate rates, humic acid significantly enhances plant growth, reproductive development, and final yield, outperforming both the control and urea-only treatments in every measured trait. These results strongly advocate for the integration of humic acid into wheat cultivation practices, as it offers a promising strategy for unlocking higher productivity and improved crop performance under field conditions.

The humic acid treatment at 1.5 L/ha (T3) emerged as the most efficient approach for optimizing wheat growth and productivity across seven key agronomic parameters. Specifically, T3 achieved the highest number of grains per spike, averaging 63.75. Plant height was also significantly enhanced under T3, surpassing both the control and urea treatments. Furthermore, the thousand grain weight reached 45.84 grams, while the spike number per square meter peaked at 454, marking the densest spike population recorded. Most notably, T3 delivered the highest grain yield, producing 132.66 tons per hectare, which represents a substantial increase compared to all other treatments. Collectively, these findings underscore the superior efficacy of humic acid at 1.5 L/ha in promoting wheat development and yield, highlighting its potential as a valuable agronomic strategy for sustainable crop improvement.

REFERENCES

Al-Fayyadh, D. Z., Hasson, A. A., Hussein, A. K., & Hassan, R. K. (2020). Effect of humic acid spray on growth characteristics of wheat varieties. Journal of Life Science and Applied Research, 1(1), 13-24.

Arambam, S. (2024). Effect of humic acid on growth, yield and soil properties in rice: A review. *Int. J. Plant Soil Sci*, *36*(6), 26-35.

Mohammadi, R., Cheghamirza, K., Geravandi, M., & Zarei, L. (2023). Durum wheat (Triticum turgidum L. var. durum Desf.) landraces and their potential for enhancing agro-physiological characteristics and stability performance in breeding programs. *Crop & Pasture Science*, *75*(1), CP22408.

Mutlu, A., & Tas, T. (2022). Foliar application of humic acid at heading improves physiological and agronomic characteristics of durum wheat (Triticum durum L.). *Journal of King Saud University-Science*, *34*(8), 102320.

Pačuta, V., Rašovský, M., Michalska-Klimczak, B., & Wyszyński, Z. (2021). Grain yield and quality traits of durum wheat (Triticum durum Desf.) treated with seaweed-and humic acid-based biostimulants. *Agronomy*, *11*(7), 1270.

Pettit, R. E. (2015). Organic matter, humus, humate, humic acid, fulvic acid and humin: Their importance in soil fertility and plant health. Alpha Agri.

Sallume, M. O., Mahdi, L. E., Alani, A. R., Farhan, K. J., & Al-Dulaim, K. H. (2023, December). Effect of spraying humic acid and different types of zinc fertilizer on some growth and yield traits of wheat. In *IOP Conference Series: Earth and Environmental Science* (Vol. 1252, No. 1, p. 012073). IOP Publishing.
Sharma, G., Tripathi, L. K., Tyagi, D. B., Nehal, N., & Chaurasiya, R. Effect of Humic acid on the Growth Attributes of Wheat (Triticum aestivum L.) Crop in sandy loam soil of Gwalior region of Madhya Pradesh, India.
Zhao, K., Yang, Y., Peng, H., Zhang, L., Zhou, Y., Zhang, J., ... & Luo, L. (2022). Silicon fertilizers, humic acid and their impact on physicochemical properties, availability and distribution of heavy metals in soil and soil aggregates. Science of the total environment, 822, 153483

THE CYTOTOXIC EFFECT AND WOUND HEALING POTENTIAL OF ROSE OIL ON HUMAN KERATINOCYTE CELL LINE (HACAT)

İrem DEMİR[1], Nurdan SARAÇ[1]

[1] [1]Department of Biology, Faculty of Science, Muğla Sıtkı Koçman Unıversity, Muğla, Türkiye

Corresponding author e-mail: iremdemir@posta.mu.edu.tr

ABSTRACT

The present study was conducted to evaluate the in vitro cytotoxic effect and wound healing potential of rose (*Rosa damascena*) oil on the human keratinocyte cell line (HaCaT).HaCaT cells were exposed to rose oil at concentrations ranging from 312.5 to 10,000 µg/mL, and cell viability was assessed using the MTT assay. Additionally, the wound healing capacity of the oil was determined through an in vitro scratch (wound closure) assay. The MTT assay results revealed that keratinocyte viability exhibited a concentration dependent response following oil treatment. Cell viability ranged from 18.32% at the highest tested concentration (10,000 µg/mL) to values exceeding 100% at concentrations of 2,500 µg/mL and lower, reaching a maximum of 120.30% at 312.5 µg/mL Notably, rose oil demonstrated a pronounced proliferative effect at lower and moderate concentrations, suggesting that it actively supports cell viability within this concentration range. In the scratch assay, the oil exhibited considerable wound healing activity, as evidenced by enhanced cell migration and closure of the denuded area. Given its capacity to promote cell regeneration and facilitate wound repair, this natural product holds promise for diverse therapeutic and industrial applications. In conclusion, rose oil may be regarded as a potential natural agent for wound healing, with possible utility in both medical and cosmetic formulations. Further investigations, including mechanistic studies and in vivo evaluations, are warranted to fully elucidate its bioactive potential and safety profile.

Keywords: Rose oil, HaCaT, cytotoxicity, wound healing, MTT

INTRODUCTION

The genus *Rosa* comprises over 200 species; however, only a limited number of these are utilized for commercial-scale essential oil production (Gudin, 2000). Among them, the Damask rose (*Rosa damascena* Mill.), a member of the Rosaceae family, stands out as a commercially significant and widely recognized aromatic plant. A variety of products derived from its flowers—including rose oil, rose concentrate, rose extract, and rose hydrosol—are extensively employed in the medical, dietary, cosmetic, and healthcare sectors (Umezu et al., 2002; Lohani et al., 2013).

The essential oil obtained from Damask rose flowers via steam distillation exhibits a remarkably rich chemical profile. Its principal constituents include monoterpene alcohols such as citronellol, geraniol, nerol, and phenylethyl alcohol, alongside various aliphatic hydrocarbons (Baydar & Baydar, 2005). The synergistic interaction among these components confers upon the oil a broad spectrum of biological activities, including anti-inflammatory, antimicrobial, antioxidant, and wound-healing properties (Boskabady et al., 2011; Mahboubi, 2015).

Re-epithelialization, a crucial phase in the wound healing process, involves the migration of keratinocytes from the wound margins to cover the injured area. Consequently, in vitro models that assess cell viability and migration using human keratinocyte cell lines, such as HaCaT, are widely employed in the development of novel therapeutic agents (Rheinwald & Green, 1975; Liang et al., 2007). In this regard, previous studies have reported that various extracts and fractions of *R. damascena* exert proliferative and anti-inflammatory effects on keratinocyte cells.

The present study was therefore designed to investigate the in vitro cytotoxic effects and wound healing potential of *R. damascena* (Isparta rose) oil on the HaCaT human keratinocyte cell line. The effects of different concentrations of rose oil on cell viability were assessed using the MTT assay, while its wound healing capacity was evaluated through an in vitro wound closure assay. It is anticipated that the findings will contribute to the understanding of this natural product's potential applications in medical and cosmetic fields and will provide a foundation for future mechanistic and in vivo investigations.

MATERIAL AND METHOD

Cell Line

The human keratinocyte cell line HaCaT used in this study was obtained from a commercial source.

Determination of Cytotoxic Activity

The cytotoxic activity of commercially available rose oil on HaCaT keratinocyte cells was assessed using the 3-(4,5-dimethylthiazol-2-yl)-2,5-diphenyltetrazolium bromide (MTT) colorimetric assay (Mossman, 1983). Cells were counted using the trypan blue exclusion method and seeded into 96-well microplates at a density of 1×10^4 cells per well in 200 µL of Dulbecco's Modified Eagle Medium (DMEM). The plates were incubated at 37°C for 24 hours in a humidified atmosphere containing 5% CO_2 to allow cell attachment. Following incubation, the culture medium was removed, and the cells were treated with rose oil at various concentrations (10,000–312.5 µg/mL) dissolved in dimethyl sulfoxide (DMSO) for 24 hours. At the end of the treatment period, the wells were emptied, washed with 100 µL of Dulbecco's Phosphate-Buffered Saline (D-PBS), and then 100 µL of fresh DMEM containing 10 µL of MTT solution (5 mg/mL in PBS, final concentration 0.5 mg/mL) was added to each well. The plates were further incubated for 3 hours at 37°C under 5% CO_2 and 98% humidity. After this incubation, the medium was removed, 100 µL of DMSO was added to each well, and the plates were shaken at room temperature for 25 minutes. Absorbance was then measured at 540 nm (Abdul Ghafoor et al., 2022; Yeniocak et al., 2025). The percentage of inhibition was calculated using the following equation:

$$\% \text{ Inhibition} = 100 - [100 \times (\text{Sample}_{abs}) / (\text{Control}_{abs})]$$

Determination of Wound Closure Effect

The wound closure effect of rose oil was evaluated using the scratch (wound closure) assay method (Justus et al., 2014). HaCaT cells (5×10^5) were seeded into 6-well plates and cultured in DMEM supplemented with 10% fetal bovine serum (FBS) and 1% antibiotic

solution under standard conditions. Once the cells reached an appropriate confluency, a linear scratch was created in each well using a 10-µL pipette tip. The wells were then washed with D-PBS to remove cellular debris. Subsequently, the cells were treated with rose oil at the IC_{30} concentration. DMSO (the solvent for rose oil) and cells cultured in DMEM alone (cell control) served as control groups. Images of the scratched areas were captured using a Leica IL microscope to monitor and estimate cell migration.

Statistical Analysis

Data are expressed as mean ± standard deviation (SD) from at least three independent experiments. Concentration-inhibition data were analyzed using R software (version 4.5.2) (R Core Team, 2024). A four-parameter logistic model (LL.4) was fitted to the data using the "drc" package (Ritz et al., 2015), and IC_{30} values were subsequently calculated. Model fitting and visualization were performed using the "ggplot2" package (Wickham, 2011).

RESULTS AND DISCUSSION

The concentration-inhibitory graph of rose oil on human keratinocyte cells is shown in Figure 1.

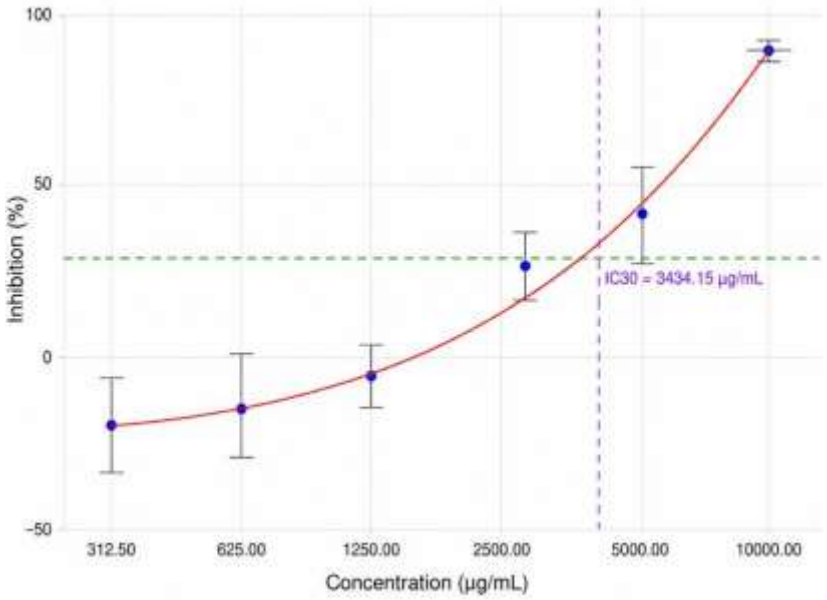

Figure 1. The inhibitory effect of rose oil on HaCaT cells. Data points represent mean inhibition percentages. Error bars would mean ±SD from three independent experiments.

The lowest inhibitory effect of rose oil on HaCaT cells was observed at 312.50 µg/mL, whereas the highest inhibition was detected at 10000 µg/mL.

The wound closure effect of rose oil at the IC_{30} concentration on HaCaT cell migration is presented in Figure 2. Images were captured at 0, 4, and 24 hours, and the wound closures were compared with those of the control group.

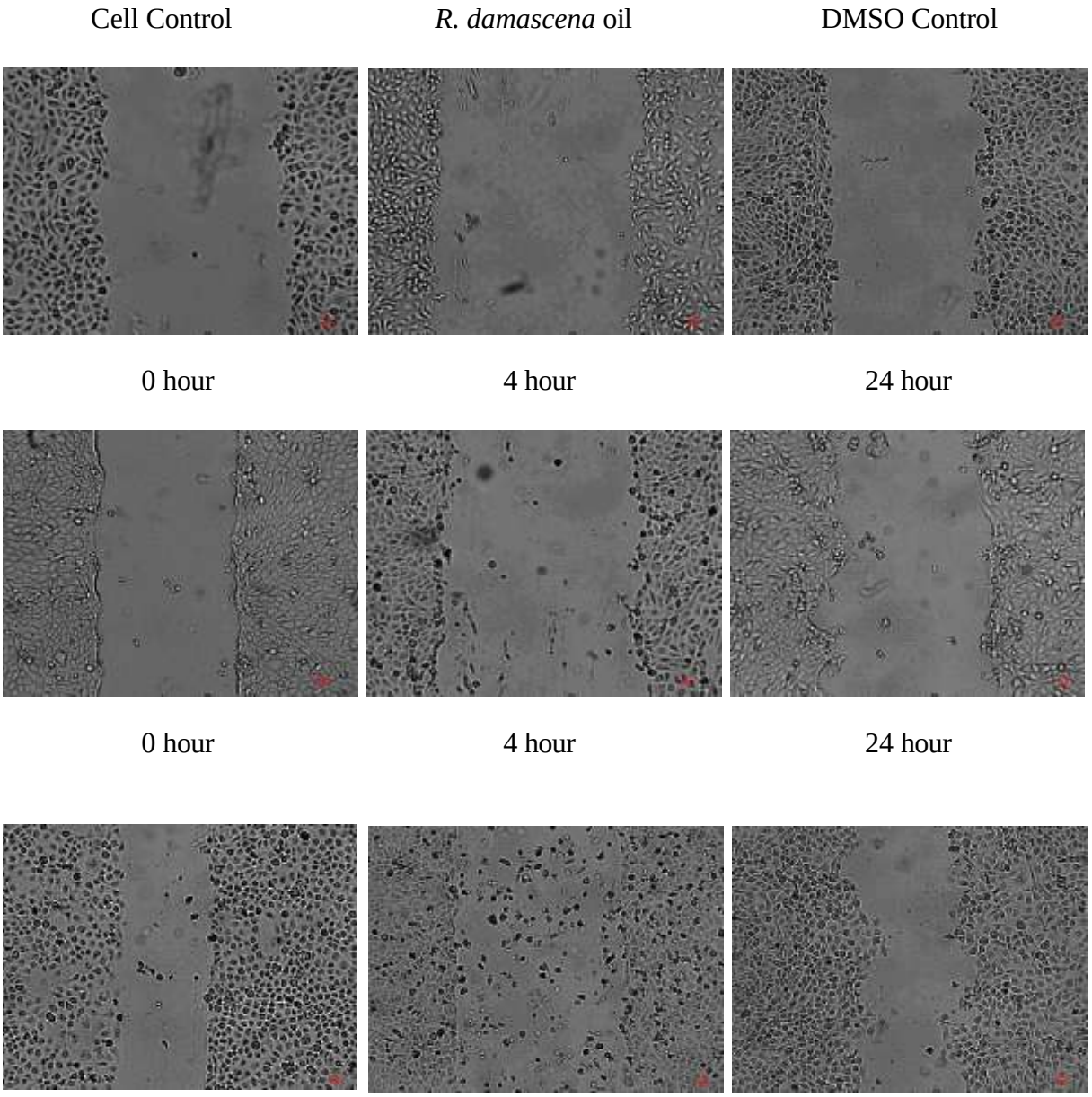

Figure 2. The images from each well of the scratched areas in HaCaT cells

To evaluate the wound closure effect, three main groups were established: a rose oil-treated cell group, a solvent control group (DMSO), and an untreated cell control group. Measurements were performed at three different time points (0, 4, and 24 hours). The 0-hour measurements served as the baseline, the DMSO control group was used to distinguish any potential effects of the solvent alone, and the cell control group allowed for the observation of time-dependent effects of the essential oil by referencing natural cell behavior. As a result, no significant change was observed in the rose oil-treated group at 4 hours compared to the control groups; however, a distinct trend was noted at 24 hours. In the cell control group, similar levels were maintained across all time points.

CONCLUSIONS

In conclusion, the present study demonstrated that *Rosa damascena* (Isparta rose) oil exhibits concentration-dependent cytotoxic activity against HaCaT keratinocytes, with the highest inhibitory effect observed at 10000 µg/mL. Moreover, at the IC_{30} concentration, the oil showed a notable wound closure effect at 24 hours, suggesting a potential wound-healing modulatory role. These findings indicate that Damask rose oil may serve as a promising natural candidate for topical applications in dermatology and cosmetic formulations. However, further in vivo studies and detailed mechanistic investigations are required to fully elucidate its therapeutic efficacy and safety profile**.**

REFERENCES

Abdul Ghafoor, N., Galatali, S., Yeniocak, S., Kaya, E., Sarac, N., & Ugur, A. (2022). Investigating anticancer potency of in vitro propagated endemic *Thymus cilicicus* Boiss. & Bal. extract on human lung, breast, and prostate cancer cell lines. *Biologia, 77*, 3229-3239. https://doi.org/10.1007/s11756-022-01168-7

Baydar, H., & Baydar, N. G. (2005). The effects of harvest date, fermentation duration and Tween 20 treatment on essential oil content and composition of industrial oil rose (Rosa damascena Mill.). Industrial Crops and Products, *21*(2), 251-255. https://doi.org/10.1016/j.indcrop.2004.04.004

Boskabady, M. H., Shafei, M. N., Saberi, Z., & Amini, S. (2011). Pharmacological effects of Rosa damascena. Iranian Journal of Basic Medical Sciences, *14*(4), 295-307.

Gudin, S. (2010). Rose: genetics and breeding. Plant Breed. Rev, 17, 159-189.

Justus, C. R., Leffler, N., Ruiz-Echevarria, M., & Yang, L. V. (2014). In vitro cell migration and invasion assays. *Journal of Visualized Experiments, 88*, e51046. https://doi.org/10.3791/51046

Liang, C. C., Park, A. Y., & Guan, J. L. (2007). In vitro scratch assay: A convenient and inexpensive method for analysis of cell migration in vitro. Nature Protocols, *2*(2), 329-333. https://doi.org/10.1038/nprot.2007.30

Lohani, H., Andola, H. C., Chauhan, N. K., Gwari, G., & Bhandari, U. (2013). Volatile constituents of rose water of damask rose (Rosa damascena Mill.) from Uttarakhand Himalayas. Medicinal Plants - International Journal of Phytomedicines and Related Industries, *5*(2), 102. https://doi.org/10.5958/j.0975-6892.5.2.016

Mahboubi, M. (2016). Rosa damascena as holy ancient herb with novel applications. Journal of Traditional and Complementary Medicine, *6*(1), 10-16. https://doi.org/10.1016/j.jtcme.2015.09.005

Mosmann, T. (1983). Rapid colorimetric assay for cellular growth and survival: Application to proliferation and cytotoxicity assays. *Journal of Immunological Methods, 65*(1-2), 55-63. https://doi.org/10.1016/0022-1759(83)90303-4

R Core Team. (2024). *R: A language and environment for statistical computing* [Computer software]. R Foundation for Statistical Computing. https://www.R-project.org/

Rheinwald, J. G., & Green, H. (1975). Serial cultivation of strains of human epidermal keratinocytes: The formation of keratinizing colonies from single cells. Cell, *6*(3), 331-343.

Ritz, C., Baty, F., Streibig, J. C., & Gerhard, D. (2015). Dose-response analysis using R. *PLOS ONE, 10*(12), e0146021. https://doi.org/10.1371/journal.pone.0146021

Umezu, T., Ito, H., Nagano, K., Yamakoshi, M., Oouchi, H., Sakaniwa, M., & Morita, M. (2002). Anticonflict effects of rose oil and identification of its active constituents. Life Sciences, *72*(1), 91-102. https://doi.org/10.1016/S0024-3205(02)02197-5

Wickham, H. (2011). ggplot2. *WIREs Computational Statistics*, *3*(2), 180–185. https://doi.org/10.1002/wics.147

Yeniocak, S., Galatalı, S., Demir, İ., Uğur, A., Saraç, N., & Kaya, E. (2025). Investigation of biological activities of in vitro grown *Sesamum orientale* plant extract on the cell cultures: Wound healing and antiproliferation. *Advances in Traditional Medicine, 25,* 233-246. https://doi.org/10.1007/s13596-024-00791-w

EFFECT OF ORGANIC WASTE on SOIL MECHANICAL PROPERTIES and WORKABILITY

Coşkun GÜLSER

Ondokuz Mayıs University, Faculty of Agriculture, Soil Sciece and Plant Nutrition Department, Samsun Türkiye

Corresponding author email:cgulser@omu.edu.tr

ABSTRACT

Soil mechanical properties are useful to people interested in land planning, construction and maintenance projects, along with agricultural soil management. Atterberg limits describe the soil consistency under the different soil moisture contents. The objective of this study was to determine the effects of tobacco waste (TOW) application on Atterberg limits of a clay soil. Tobacco waste was incorporated to a clay field at four different doses (0, 2, 4, and 6 %) with three replications. After eight months, soil samples were taken from field and analyzed for liquid limit (LL), plastic limit (PL) and plasticity index (PI). The index of consistency (Ic) was calculated to evaluate optimum soil moisture contents for soil workability. Increasing the application doses of TOW increased LL and PL values and decreased PI value in the field. According to control treatment, while the highest increments for liquid and plastic limits were statistically determined with the highest application rate. Increasing TOW application doses increased soil moisture levels at 0,75, 1,00 and 1,30 of Ic values. It was determined that clay soil can be cultivated at higher soil moisture contents without structural damage compare with the control treatment. Using agricultural waste as a soil conditioner helps to soil structural development and allow soil workability at higher soil moisture contents.

Key words: Soil cultivation, Atterberg limits, consistency index, clay soil.

INTRODUCTION

Atterberg limits developed for engineering purposes evaluate soil engineering properties. They are useful to planning, construction and maintenance projects, along with soil management systems. Atterberg limits describe the soil mechanical properties under the different soil moisture contents. If water is added to dry soil, the moisture content at which the soil becomes plastic is the plastic limit (PL). If more water is added, the moisture content at which the soil changes from plastic to a fluid state is the liquid limit (LL). Plasticity index (PI) is the moisture content between plastic and liquid limit (Baumgarti, 2002). Soil moisture content is one of the most important factors for tillage operation. The optimum water content for tillage defined as the water content at which tillage produces the greatest proportion of small aggregates (Dexter and Bird 2001). The plastic limit is generally regarded as the most suitable moisture content for soil cultivation and seedbed preparation (Kirchhof, 2002).

Soil workability is related with soil moisture condition. Baumgartl (2002) indicated that index of consistency (Ic) value defines consistency condition of a soil at any given soil moisture content. Many studies showed that optimum soil moisture contents near the field capacity are highly related with index of consistency values of soils (Gülser et al., 2009; Gülser et al., 2010; Gülser, 2023). Gülser and Candemir (2006) found that optimum soil moisture contents near field capacity for workability would not have structural deformation in soil series of Ondokuz Mayis University Campus area. In this study, the effects of tobacco waste application on Atterberg limits and soil workability were investigated in a clay soil under field conditions.

MATERIAL AND METHODS

Tobacco waste (TOW) was mixed within 0 - 20 cm of a clay soil depth as four different doses (0, 2, 4, and 6 %) with three replications in a randomized block design at the Experimental Field of Agricultural Faculty in Ondokuz Mayıs University, Samsun. Some chemical and physical characteristics of the soil were determined in soil samples taken from 0 to 20 cm depth of the field as follows; particle size distribution by hydrometer method (Day, 1965), soil reaction, pH, in the 1:1 (w:v) soil water suspension by pH meter, electrical conductivity (EC_{25^oC}) in the same soil suspension by EC meter, organic matter content by Walkley-Black method (Jackson, 1962) and exchangeable cations by ammonia acetate extraction (Kacar, 1994). After eight months, soil samples were taken from each plot for chemical and mechanical analyses. Liquid limit, plastic limit and plasticity index values of the soil samples were determined according to Black (1965). The results can be summarized as follows; the textural class of soil is clay, neutral in pH, high in organic matter, none saline according to EC value (Soil Survey Staff., 1993) (Table 1).

Table 1. Some physical and chemical properties of the soil

Sand, %	18,94	NH_4OAc extractable	
Silt, %	24,82	K, cmol/kg	1,15
Clay, %	56,23	Na, cmol/kg	0,21
EC_{25^oC}, mmhos cm^{-1}	0,65	Ca, cmol/kg	34,87
PH	6,95	Mg, cmol/kg	8,13
Organic matter, %	3,85		

Statistical analysis of the results was done by standard analysis of variance, pairs of mean values compared by Duncan test and correlations among the Atterberg limits and soil properties estimated using the SPSS 17.0 package programme.

RESULTS AND DISCUSSION

Liquid limit values increased with increasing the application rates of TOW application (Figure 1). Liquid limit values varied between 62,5% for the control and 66,0% for the highest application dose of TOW. Increments in LL values for 4% and 6% doses of TOW were determined as significantly different from control treatment ($P<0,01$). Arthur et al. (2020) investigate the effect of rice straw biochar on the Atterberg limits and found that 30 t/ha treatment increased plastic limit (27%) and liquid limit (20%) significantly compared to the control ($P<0,05$). They

concluded that there is potential for increased optimum water content at tillage and increased workability after biochar application.

Plastic limit values also increased with increasing the application rates of TOW application (Figure 2). Plastic limit values varied between 35,8% for the control and 44,0% for the highest application dose of TOW. Increments in PL values for all doses of TOW were determined as significantly different from control treatment (P<0,01).

Plasticity index, which is the difference between LL and PL, was also significantly reduced by the TOW application (p<0.01). Plasticity index varied from 26,7% for the control to 21% for the lowest dose of TOW (Figure 3). All application doses of TOW significantly decreased the PI values compared to the control application.

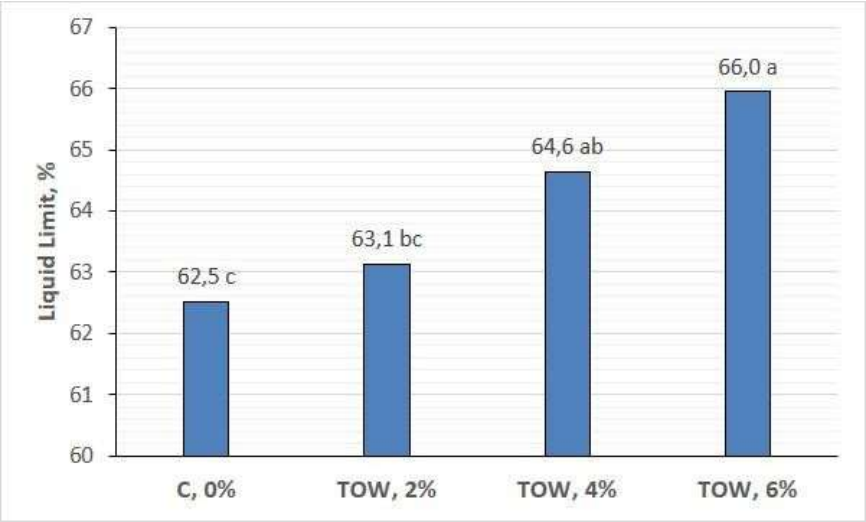

Figure 1. Changes in liquid limit values at the different tobacco waste (TOW) doses (P<0.01).

.

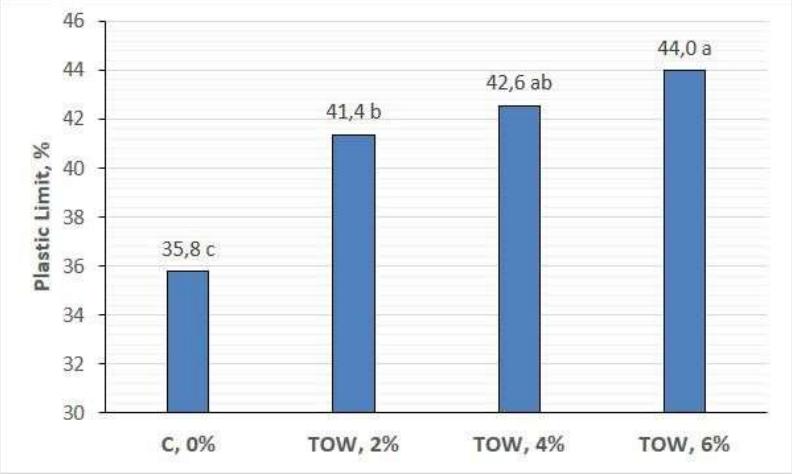

Figure 2. Changes in plastic limit values at the different tobacco waste (TOW) doses (P<0.01).

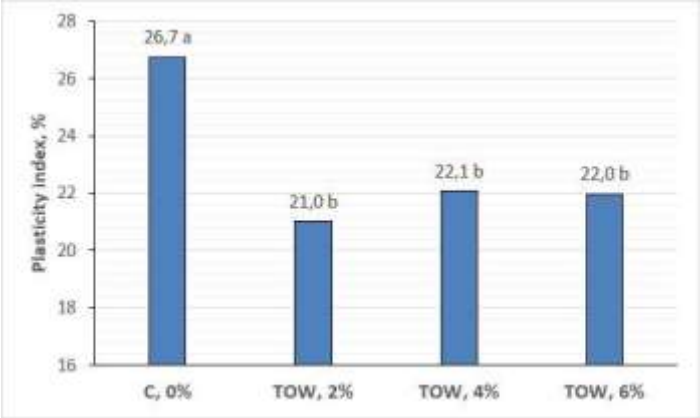

Figure 3. Changes in plasticity index values at the different tobacco waste (TOW) doses (P<0.01).

Percentage changes in the LL, PL and PI with different application dose of TOW treatments according to the control are given in Figure 4. While application doses increased from 2% to 6%, percentage increments in LL and PL over the control also increased. The highest dose of TOW showed the highest percent increase in LL (6%) and PL (23%) over the control. However, percentage changes in PI according to control reduced with all doses of TOW treatment. The lowest decrease in PI (21%) was obtained with 2% of TOW application.

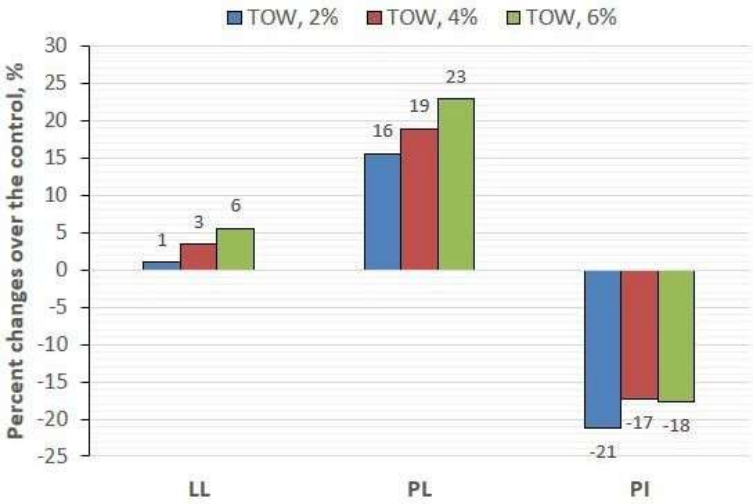

Figure 4. Percent changes in the LL, PL and PI with different doses of tobacco waste.

Descriptive statistic for the effects of TOW treatment on pH, EC, organic C and exchangeable cations is given in Table 2. While TOW application decreased soil pH slightly, all the other soil properties increased with the TOW application. Many studies reported that organic matter addition to soils improve most soil physical and chemical properties such as, soil water content, total porosity, soil organic C, EC, exchangeable cations (Gülser et al., 2008; Gülser and Candemir, 2012; Gülser and Candemir, 2015; Demir and Gülser, 2021; Mawalla and Gülser, 2025a; Mawalla and Gülser, 2025b; Demirkaya et al., 2025; Ay et al. 2026).

Table 2. Descriptive statistical results for the effects of tobacco waste (TOW) on some soil chemical properties

	Treatment	Minumum	Maximum	Mean	Std. Deviation
pH (1:1)	Control	6,95	7,10	7,01	0,076
	TOW	6,75	7,00	6,87	0,087
EC, dS/m	Control	0,46	0,88	0,69	0,213
	TOW	1,27	3,23	1,98	0,734
OC, %	Control	2,24	2,52	2,37	0,136
	TOW	2,52	5,13	3,75	0,830
K, cmol/kg	Control	0,64	1,66	1,12	0,515
	TOW	1,20	3,67	2,54	0,821
Na, cmol/kg	Control	0,20	0,21	0,21	0,006
	TOW	0,04	0,68	0,15	0,197
Mg, cmol/kg	Control	6,82	9,44	8,13	1,311
	TOW	9,97	13,11	12,03	1,035
Ca, cmol/kg	Control	34,62	35,14	34,88	0,262
	TOW	36,71	41,96	40,40	1,810

The relationships among the Atterberg limits and the soil properties are given in Table 3. The positive correlations among soil OC and Atterberg limits indicate that increasing application rates of TOW increased LL and PL. However, soil OC content had a significant negative relationship with PI. Kirchhof (2002) reported that soil organic matter has a high absorptive capacity for water and increases the Atterberg limits, but tends to have a little effect on the plasticity index. Demiralay and Güresinli (1979) found that LL, PL and PI were significantly correlated with organic matter (OM) contents of soils and these limits increased with increasing OM content. Plasticity index gave the significant negative correlations with PL. When the increase in PL was higher than the increase in LL due to TOW application, plasticity index decreased.

Soil pH had significant negative correlations with LL and PL while EC had significant positive correlations with LL and PL. Type of exchangeable cation in soil has an important effect on Atterberg limits. Kirchhof (2002) reported that divalent cations tend to increase Atterberg limits of soils due to their position in the lyotropic series. Generally, LL and PL had significant positive correlations with exchangeable Ca, Mg and K contents. Atanur (1973) found that PL of montmorillonit clay increased with the cation type in the following order: Na<H<Mg<Fe<Ca<K. In this study, PI significantly decreased with increasing divalent exchangeable cations (Ca, Mg) in the soil.

Table 3. The relationships among the limits and the soil properties

	PL	PI	OC	pH	EC	Ca	Mg	K	Na
LL	0,738**	-0,330	0,745**	-0,696*	0,833**	0,759**	0,385	0,890**	-0,482
PL		-0,881**	0,821**	-0,754**	0,800**	0,914**	0,739**	0,783**	-0,230
PI			-0,625*	0,565	-0,534	-0,745**	-0,763**	-0,470	-0,017
OC				-0,842**	0,834**	0,846**	0,489	0,866**	-0,331
pH					-0,801**	-0,820**	-0,554	-0,802**	0,483
EC						0,795**	0,630*	0,927**	-0,331
Ca							0,735**	0,877**	-0,527
Mg								0,609*	-0,148
K									-0,502

** Correlation is significant at 1% level, * Correlation is significant at 5% level.

Mueller et al. (2003) compared the data of water retention, Atterberg limits, and Proctor compaction tests to select a methodology for estimating the maximum gravimetric soil water content for optimum tillage with preventing soil structural damage. They found that maximum soil water content for optimum tillage of cohesive soils was at a consistency index of 1.15 and 90% of the plastic limit value. The soil moisture contents at different index of consistency (Ic) values were calculated for different TOW application doses (Table 3). Optimum gravimetric soil water content for tillage operation of clay soil varied between 31,8% and 42,5% for control treatment and between 40,7% and 49,5% for 6% dose of TOW treatment. Gülser et al. (2009) studied mechanical properties and workability of soils in the field of Karadeniz Agricultural Research Institute. They reported that moisture contents for soil workability at 1,15, 1,00 and 0,75 of index of consistency (Ic) were 33,2%, 39,2% and 49,50%, respectively. They concluded that soil tillage can be operated without structural damage at the 40,4% of field moisture capacity in the experimental station field.

Table 3. The lower and upper soil gravimetric water contents for optimum soil workability

Treatments	**Ic: 0,75**	**Ic: 1,0 (PL)**	**Ic.1,15 (0,9*PL)**	**Ic: 1,30**
0% TOW	42,5	35,8	31,8	27,7
2% TOW	47,4	41,4	39,0	35,8
4% TOW	48,1	42,6	39,3	25,9
6% TOW	49,5	44,0	40,7	37,4

If the soil has the optimum water content for workability, tillage produces the greatest proportion of small aggregates. Dexter and Bird (2001) reported that the optimum water content for tillage was 90% of the water content at the PL. The range of water contents for tillage increases with increasing TOW application dose. Increases in the PL limit can be desirable for tillage in an early spring when soil has high moisture content. However if soil shows high plasticity index, tilling the soil when it is wet causes structural damage and muddy condition instead of friable condition in soil (Demiralay and Güresinli, 1979). TOW treatment decreased the plasticity index with increasing PL according to control.
As a result, TOW application into clay soils has a benefit to tilling soil at higher moisture content without structural damaging and having friable condition in soil. The results of this study indicate that manure application in to a clay soil allows for field operations at high moisture contents depends on the application doses.

REFERENCES

Arthur, E., Oppong Danso, E., Beiranvand, M., Pouladi, N., Yakubu, A., Abenney-Mickson, S., & Sabi, E. B. (2020). Rice straw biochar effects on Atterberg limits and aggregate characteristics of an Acrisol in Ghana. *Archives of Agronomy and Soil Science*, *66*(13), 1861-1872.

Atanur, A. 1973. Kireç stabilizasyonu ve yol yapımındaki tatbikatı. Bayındırlık Bakanlığı Karayolları Genel Müd. Yayın No:208.

Ay, Abdurrahman, Salih Demirkaya, Elif Öztürk ay, Ömer Taş, Gürkan Bilir, Coşkun Gülser, Rıdvan Kizilkaya, Rahila Islamzade, and Deniz Ekinci. (2026). The effectiveness of biochar in mitigating copper toxicity: the impacts of dose and particle size on soil properties and plant physiology. BMC Plant Biology.

Baumgarti, T., 2002. Atterberg Limits. Encyc.of Soil Sci. Marcel Dekker Inc. pp:89-93.

Black, C.A. (Editor-in-Chief), 1965. Methods of Soil Analysis.Part I.ASA, Madison WI. Day, P.R., 1965. Particle fractionation and particle size analysis. p. 545-567 in C.A.
Black, ed. Methods of soil analysis.Agronomy No:9, Part I ASA., Madison WI.
Demir, Z., Gülser, C. 2021. Effects of rice husk compost on some soil properties, water use efficiency and tomato (Solanum lycopersicum L.) yield under greenhouse and field conditions. Communications in soil science and plant analysis, 52(9), 1051-1068.
Demiralay, İ. ve Y.Z. Güresinli, 1979. Erzurum Ovası topraklarının kıvam limitleri ve sıkışabilirliği üzerinde bir araştırma. Atatürk Ün. Zir. Fak., Ziraat Der. 10(1-2):77-93.
Demirkaya, S., Ay, A., Gülser, C., & Kızılkaya, R. (2025). Enhancing clay soil productivity with fresh and aged biochar: A two-year field study on soil quality and wheat yield. Sustainability, 17(2), 642.
Dexter, A.R., Bird, N.R.A.2001.Methods for predicting the optimum and the range of soil water contents for tillage based on the water retention curve.Soil Til.Res. 57:203-212. Gülser C., İç, S., Candemir, F., Demir, Z. 2008. Effects of rice husk application on mechanical properties and cultivation of a clay soil with and without planting. In International Meeting on Soil Fertility Land Management and Agroclimatology.
Turkey (pp. 217-223).
Gülser, C. 2023. Effect of soil tillage on soil organic matter in a clay field. Agricultural Sciences/Agrarni Nauki, 15(38).
Gülser, C., Candemir, F. 2012. Changes in penetration resistance of a clay field with organic waste applications. Eurasian Journal of Soil Science, 1(1), 16-21.
Gülser, C., Candemir, F. 2015. Effects of agricultural wastes on the hydraulic properties of a loamy sand cropland in Turkey. Soil Science and Plant Nutrition, 61(3), 384-391. Gülser, C., Dengiz, O., İç, S., Demir, Z., Selvi, K.Ç. 2010. Some mechanical properties and workability of Aşağı Aksu Basin soils. In Proceedings of the International Soil Science Congress on Management of NaturaResources to Sustain Soil Health and
Quality. R. Kizilkaya, C. Gulser, O. Dengiz (pp. 26-28).
Gülser, C., F. Candemir, 2006. Some mechanical properties and workability of Ondokuz Mayıs University Kurupelit Campus Soils. J.of Fac.of Agric. OMU, 2006, 21 (2): 213-217.
Gülser, C., Selvi, K. Ç., & İç, S. (2009). Some mechanical properties and workability of soils in a Karadeniz Agricultural Research Institute Field. Tarım Makinaları Bilimi Dergisi, 5(4), 423-428.
Jackson, M.L., 1962. Soil Chemical Analysis. Prentice Hall Inc.Eng. Cliffs. U.S.A.
Kacar, B., 1994. Bitki ve toprağın kimyasal analizleri III. Toprak analizleri.Ankara Üniv.
Ziraat Fak. Eğitim Araş. ve Gel.Vakfı Yay., No:3 Ankara.
Kirchhof, G.,2002.Plastic properties.Encyc.of Soil Sci.Marcel Dekker Inc. pp:1005-1007.
Mawalla, D. E., & Gülser, C. (2025a). Using agricultural originated biochars to improve chemical properties of an acid soil and wheat yield. Discover Soil, 2(1), 82.
Mawalla, D. E., & Gülser, C. (2025b). The Influence of Biochars Derived from Different Agricultural Wastes on Water Use Efficiency and Wheat Yield in Two Contrasting Textural Soils. Journal of Agriculture and Ecology Research International, 26(5), 150-156.
Mueller, L., Schindler, U., Fausey, N. R., & Lal, R. (2003). Comparison of methods for estimating maximum soil water content for optimum workability. Soil and Tillage Research, 72(1), 9-20.
Soil Survey Staff, 1993. Soil Survey Manuel. USDA Handbook No:18 Washington

FROM THE BRONTLAND REPORT TO FOOD SECURITY IN THE SUSTAINABLE DEVELOPMENT GOALS

Ahmet NAYIR

Beykent University, Faculty of Engineering and Architecture, Electrical and Electronics Engineering Department, Ayazağa Mahallesi, Hadim Koruyolu Cd. No:19, İstanbul/ Turkiye

Corresponding author e-mail: : ahmetnayir@beykent.edu.tr

ABSTRACT

The world today produces more food per capita than ever before in human history. Amidst this abundance, millions of people lack sufficient nutrition to sustain a fully productive working life. There are places where very little agriculture is done; there are places where many people cannot afford to buy food. The fifth chapter of the Brontland Report, published in 1987, addresses the potential for food security and its sustainability. The Sustainable Development Goals, developed in 2015, emphasized food security. This study examines food security through the annual reports of the Sustainable Development Goals, based on the Brontland Report. There are large areas for increases in food production in both industrialized and developing countries, parallel to climate change. These areas can be increased through global collaborative efforts.

Keywords: Food Security, Brontland report, Sustainable development goals, SDG, Our future,

INTRODUCTION

After rising sharply in the wake of the COVID-19 pandemic, global hunger and food insecurity remained persistently high and almost unchanged for three years. In 2023, about 733 million people faced hunger, and 2.33 billion people experienced moderate to severe food insecurity. Despite progress, 148 million children under age 5 suffered from stunting in 2022. If current trends persist, one in five children under age 5 will be affected by stunting in 2030. In 2022, almost 60 per cent of countries worldwide faced moderately to abnormally high food prices due to the spillover effects of conflicts, such as disrupted supply chains. Achieving zero hunger requires intensified efforts to transform food systems so they are sustainable, resilient and equitable. Moreover, accelerating improvements in diets, nutrition, health and hygiene is crucial to meeting the target of halving the number of children suffering from chronic undernutrition. Hunger, food insecurity and malnutrition remain prevalent, calling for intensified efforts Food insecurity is not just a problem today.

Climate change includes long-term changes in Earth's climate that have occurred previously. The current increase in global temperatures is caused by human activities, particularly the burning of fossil fuels since the Industrial Revolution. Fossil fuel burning, deforestation, and some agricultural and industrial practices release greenhouse gases. These gases absorb some of the heat radiated by Earth's sunlight, warming the lower atmosphere. Carbon dioxide, the primary gas responsible for global warming, has increased in concentrations by approximately 50% since the pre-industrial era, to levels not seen for millions of years. Climate change is hindering poverty reduction, and disasters result in millions of households becoming poor or remaining trapped in poverty. Ending poverty requires a wide-ranging approach that combines comprehensive social protection systems, inclusive economic

policies, investments in human capital, measures to address inequality and climate resilience, and international cooperation and partnership.

The concept of sustainable development was first officially used in 1987 in the report titled "Our Common Future" (Brundtland Report) published by the World Commission on Environment and Development (WCED) under the chairmanship of the Norwegian Prime Minister Gro Harlem Brundtland. Accordingly, sustainable development was defined as "meeting the needs of the present without compromising the ability of future generations to meet their own needs".

Our Common Future, From One Earth to One World
An Overview by the World Commission on Environment and Development

I. The Global Challenge
1. Successes and failures
2. The Interlocking Crises
3. Sustainable Development
4. The Institutional Gaps
II. The Policy Directions
1. Population and Human Resources
2. Food Security: Sustaining the Potential
3. Species and Ecosystems: Resources for Development
4. Energy: Choices for Environment and Development
5. Industry: Producing More with Less
6. The Urban Challenge
III. International Cooperation and Institutional Reform
1. The Role of the International Economy
2. Managing the Commons
3. Peace, Security, Development, and the Environment
4. Institutional and Legal Change
4.1 Getting at the Sources
4.2 Dealing with the Effects
4.3 Assessing Global Risks
4.4 Making Informed Choices
4.5 Providing the Legal Means
4.6 Investing in our Future

At the same time, there is a widespread sense of frustration and inadequacy in the international community about our ability to address and effectively deal with vital global issues. The truth is compelling and should not be easily dismissed. Since answers to fundamental and serious concerns are not readily available, there is no alternative but to continue trying to find them.

Meeting humanity's goals and aspirations responsibly will require the active support of all of us. Scientists are drawing our attention to urgent but complex problems affecting our survival: a warming globe, threats to Earth's ozone layer, deserts depleting agricultural land. We respond by demanding more details and blaming institutions ill-equipped to address them. Environmental degradation, once seen primarily as a problem of wealthy nations and a side effect of industrial prosperity, has become a survival issue for developing nations. It is part of a downward spiral of interconnected ecological and economic decline that has trapped many of the poorest nations. Despite official hopes expressed on all sides, no identifiable trend, no program, or policy today offers any real hope of narrowing the widening gap between rich and poor nations. In this article, current food security is investigated with the Brantland report and sustainable development goals. Chapter 5 of the Brantland report deals with food safety. The subheadings are listed below.

Our Common Future, Chapter 5: Food Security: Sustaining The Potential

I. Achievements
II. Signs of Crisis
1. Impact of Subsidies
2. Neglect of the Small Producer
3. Degradation of the Resource Base
3.1 Loss of Soil Resources
3.2 Impact of Chemicals
3.3 Pressure on Forests
3.4 Advancing Deserts
III. The Challenge
IV. Strategies for Sustainable Food Security
1. Government Intervention
2. A Global Perspective
3. The Resource Base
3.1 Land Use
3.2 Water Management
3.3 Alternatives to Chemicals
3.4 Forestry and Agriculture
3.5 Aquaculture
4. Productivity and yields
4.1 The Technological Base
4.2 Human Resources
4.3 Productivity of Inputs
5. Equity
5.1 Land Reforms
5.2 Subsistence Farmers and Pastoralists
5.3 Integrated Rural Development
5.4 Food Availability Fluctuations
V. Food for the Future

Our Common Future is not a prediction of increasing environmental degradation, poverty, and hardship in an increasingly polluted world amid dwindling resources. Instead, it posits a new era of economic growth based on policies that sustain and expand the environmental resource base. It is the belief that such growth is absolutely essential to alleviate the deepening poverty in many developing countries. Agricultural policies in nearly all countries focused on increasing production. Despite this, consistently increasing global agricultural production by 3% per year by the mid-1980s proved much more difficult than in the mid-1950s. Furthermore, production records were offset by the outlook. Chemical fertilizers and pesticides have played a significant role in increasing production since World War II, but clear warnings have been issued against over-reliance on them. Nitrogen and phosphate leaching from excessive fertilizer use is damaging water resources, and this damage is spreading. Forests are vital for maintaining and improving the productivity of agricultural land. Desertification results from a complex mix of climatic and anthropogenic influences. Human influences over which we have greater control include the rapid growth of both human and animal populations, harmful land-use practices, unfavorable trade conditions, and civil conflict. This visualization shows the total land used for agriculture (which is a combination of cropland and grazing land) over the long term, measured in hectares. In the following Figure (Figure 1), you can find disaggregated data on cropland land change over time.

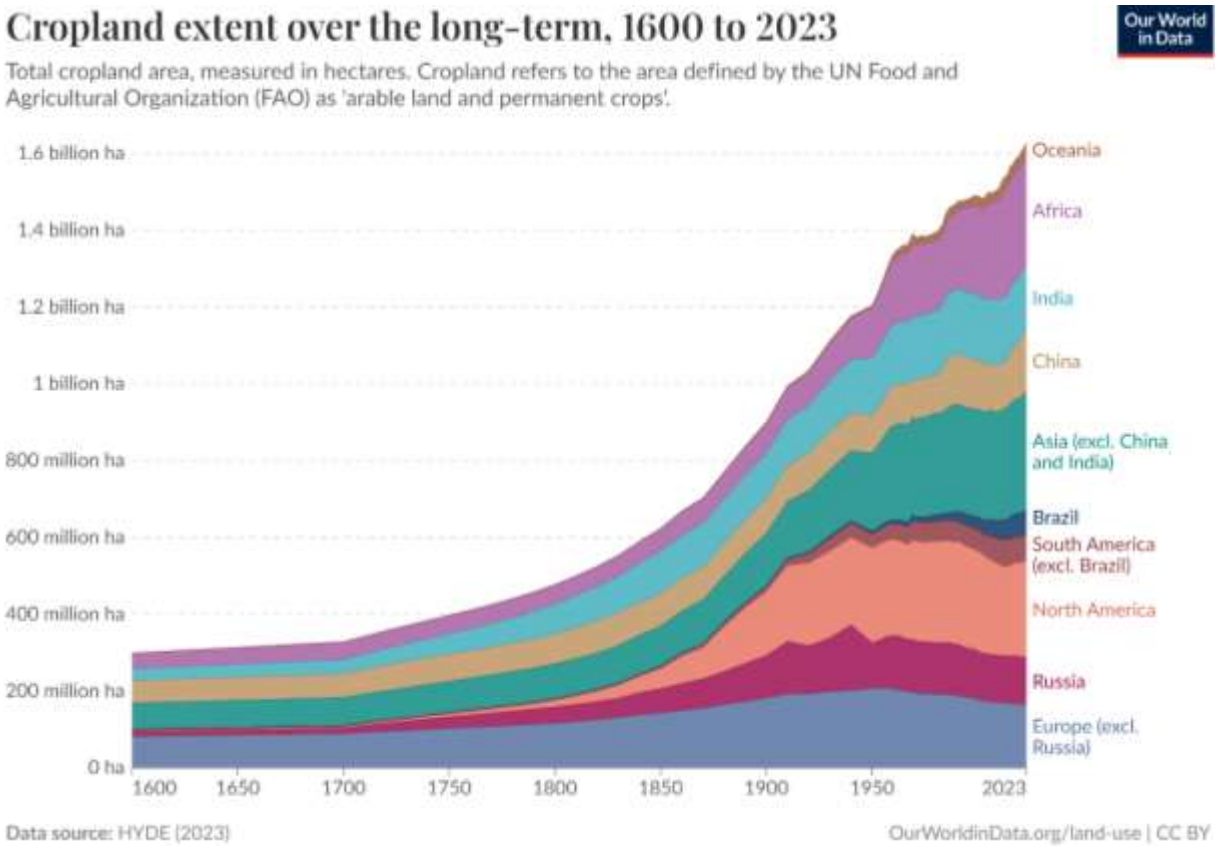

Figure 1: The total land used for agriculture over the long term

Global trends highlight the ongoing challenges for biodiversity and forests, despite their critical role as the planet's life-support systems. Despite significant progress in sustainable forest management, global forest area continues to decline, primarily due to agricultural expansion. There is also a growing global commitment to biodiversity conservation, as reflected in the adoption of the Kunming-Montreal Global Biodiversity Framework (2022). Addressing urgent environmental challenges—including climate change, biodiversity loss, pollution, desertification, and deforestation—and their underlying drivers and linkages, requires intensified and accelerated efforts at the local, national, and global levels and a comprehensive and integrated approach.

The UN Sustainable Development Goals

Sustainable development can be understood as primarily a process and as implying practical goals or desirable outcomes, such as the UN Sustainable Development Goals (SDG) being developed in 2015 (Figure 2). The 2030 Agenda for Sustainable Development, adopted by all United Nations Member States in 2015, provides a shared blueprint for peace and prosperity for people and the planet, now and into the future. At its heart are the 17 Sustainable Development Goals (SDGs), which are an urgent call for action by all countries - developed and developing - in a global partnership. They recognize that ending poverty and other deprivations must go hand-in-hand with strategies that improve health and education, reduce inequality, and spur economic growth – all while tackling climate change and working to preserve our oceans and forests. EU Missions aim to lead the way by bringing concrete solutions to achieve the SDG targets. They have ambitious targets and will deliver tangible results by 2030. The five EU Missions are:

Adapting to Climate Change: Supporting at least 150 European regions and communities to become climate resilient by 2030

Cancer: Working with Europe's Beat Cancer Plan to improve the lives of over 3 million people by 2030 through prevention, treatment, and solutions for longer and better lives
Restoring our Oceans and Waters by 2030
100 Climate-Neutral and Smart Cities by 2030
A Land Deal for Europe: 100 living laboratories and lighthouses to lead the transition to healthy lands by 2030
They are putting research and innovation in a new role, combining them with new forms of governance and cooperation, and engaging citizens.

Figure 2: The UN Sustainable Development Goals (SDG)

The Sustainable Development Goals targets on food and land systems are particularly off track. The Sustainable Development Reports (SDR) 2024 offer new FABLE pathways to support sustainable food and land systems.

By 2030, 600 million people worldwide will still be hungry, obesity is rising globally, and greenhouse gas emissions from Agriculture, Forestry, and Other Land Use (AFOLU) represent almost a quarter of annual global greenhouse gas emissions. The new FABLE pathways brought together more than 80 local researchers from 22 countries to assess how 16 targets on food security, climate change mitigation, biodiversity conservation, and water quality can be achieved by 2030 and 2050. Continuing current trends widens the gap with the targets on climate change mitigation, biodiversity, and water quality. Meeting the commitments already made by countries would improve the situation, but these remain largely insufficient. Significant progress can be made, but this will require several key changes:
1) Avoid overconsumption beyond recommended levels and limit animal protein consumption through dietary changes consistent with cultural preferences;
2) Invest in improving productivity, particularly for crops and areas with strong demand growth; and
3) Implement inclusive, robust, and transparent monitoring systems to halt deforestation. Our sustainable pathway prevents deforestation of up to 100 million hectares by 2030 and 100 Gt of CO_2 emissions by 2050. Additional measures will be needed to avoid trade-offs related to on-farm employment and water pollution from over-fertilizer application, and, in particular, to end hunger.

Government Intervention

Government intervention in agriculture is the rule in both industrial and developing countries, and it is here to stay. Public investment in agricultural research and extension services, assisted farm credit and marketing services, and a range of other support systems have

all played parts in the successes of the last half-century. In fact, the real problem in many developing countries is the weakness of these systems. Protecting and expanding agriculture's resource base will increase production and productivity. However, specific measures are needed to make inputs more efficient. This can best be achieved by strengthening the technological and human resource base for agriculture in developing countries.

Technological Base

Bringing together traditional and modern technologies offers opportunities to improve nutrition sustainably and increase rural employment. Biotechnology, including tissue culture techniques, technologies for preparing value-added products from biomass, microelectronics, computer science, satellite imagery, and communications technologies, are all leading technologies that can improve agricultural productivity and resource management. The technological transformation of traditional agriculture will be difficult without a concerted effort to develop human resources. Efforts to promote literacy should focus on functional literacy, encompassing the efficient use of land, water, and forests. Despite women's critical role in agriculture, their access to education and representation in research, extension, and other support services are crucial. The use of renewable energy is becoming increasingly important due to the dwindling availability of fossil fuel resources, rising costs, and environmental concerns. Recently, interest in solar energy as a renewable energy source has been growing. Electricity generation and cost analysis using solar panels in agricultural fences is supported by scientific studies.

CONCLUSIONS

Agricultural production can only be sustainable in the long term if the soil, water, and forests on which it depends are not degraded. Redirecting public intervention, as proposed, will provide a framework for this. Improvements in water management are essential to increase agricultural productivity and reduce land degradation and water pollution. Critical issues relate to the design of irrigation projects and water use efficiency. Many countries, especially developing countries, can and should increase yields through increased use of chemical fertilizers and pesticides. However, countries can also increase yields by helping farmers use organic nutrients more efficiently. Therefore, governments should encourage increased use of organic plant nutrients to complement chemical fertilizers. Protecting and expanding agriculture's resource base will increase production and productivity. However, specific measures are needed to make inputs more efficient. This can best be achieved by strengthening the technological and human resource base for agriculture in developing countries. Applying the concept of sustainable development to efforts to achieve food security requires systematic attention to the regeneration of natural resources.

This requires a holistic approach focused on ecosystems at the national, regional, and global levels, coordinated land and water use, and careful planning of forest exploitation. Recently established agricultural systems have contributed significantly to reducing hunger and raising living standards. These systems require agricultural systems that focus on people as much as technology, resources as much as production, and the long term as much as the short term. Only these systems can meet the challenges of the future.

REFERENCES

https://sdgs.un.org/goals

https://climate.ec.europa.eu/index_en

https://en.wikipedia.org/wiki/Climate_change

https://sdgtransformationcenter.org/

The Sustainable Development Goals Report, 2024

Sachs, J.D., Lafortune, G., Fuller, G. (2024). The SDGs and the UN Summit of the Future. Sustainable Development Report 2024. Paris: SDSN, Dublin: Dublin University Press.

HYDE (2023) – with minor processing by Our World in Data. "Cropland extent over the long-term" [dataset]. PBL Netherlands Environmental Assessment Agency, "History Database of the Global Environment 3.3" [original data]. Retrieved September 7, 2025 from https://archive.ourworldindata.org/20250903-083611/grapher/cropland-use-over-the-long-term.html (archived on September 3, 2025).

Elif Türkboyları, Ahmet Nedim Yüksel, Meeting The Energy Needs In Livestock Enterprises With Hybrid Renewable Energy Systems And Its Environmental Effects, VI. International Agricultural, Biological & Life Science Conference, Edirne, Turkey, 18-20 September 2024, pp-1836-1846

Dinçer Akal, Taşkın Tez, Electricity generation and cost analysis using solar panels in agricultural fences**,** VI. International Agricultural, Biological & Life Science Conference, Edirne, Turkey, 18-20 September 2024, pp-1913-1919

Taşkın Tez, Dinçer Akal, Ozan Akı, İlhan Umut, Technical and cost analysis of inverter selection for a farmhouse solar energy system**,** VI. International Agricultural, Biological & Life Science Conference, Edirne, Turkey, 18-20 September 2024, pp-1898-1905

STRUCTURAL MODELING OF COMBINE HARVESTER CUTTERBAR SERRATED KNIFE SECTIONS USING A STEPWISE FUNCTIONALLY GRADED MATERIAL APPROACH

Serhan KARAMAN GENÇ

Trakya University, Faculty of Engineering, Department of Mechanical Engineering, Edirne, Türkiye
Corresponding author e-mail: serhankaraman@trakya.edu.tr

ABSTRACT

Serrated knife sections used in combine harvester cutterbars are critical components responsible for efficient crop cutting during harvesting operations. Owing to continuous reciprocating motion and repeated cutting loads, these components are exposed to severe mechanical stresses, localized stress concentrations, edge wear, and progressive cutting edge dulling, which eventually reduce harvesting efficiency and service life. Conventional knife sections are generally manufactured from homogeneous steel, making it difficult to simultaneously achieve the high hardness required at the cutting edge and the toughness needed around the mounting holes to resist impact and fracture. In this study, a stepwise functionally graded material (FGM) approach **was proposed** as an alternative structural design concept for combine harvester serrated knife sections. The proposed model **was designed** to provide enhanced hardness in the cutting region while maintaining improved toughness in the mounting region through a gradual variation of material properties represented by a stepwise configuration. A three-dimensional model of the existing knife geometry was established, and homogeneous and stepwise functionally graded material models were developed. Their structural behaviors were comparatively evaluated under identical loading conditions using the finite element method. The numerical results showed that both FGM configurations reduced the maximum deformation compared with the homogeneous 75Cr1 reference model. The Layered Graded model provided the most balanced global structural response, reducing maximum deformation by approximately 5.4% and total strain energy by approximately 5.5%, while limiting the increase in maximum von Mises stress to approximately 1.2%. These findings demonstrate that not only the WC content but also its geometric distribution plays an important role in the structural response of the knife section.

Keywords: Combine harvester, Serrated knife section, Functionally graded material (FGM), Finite element analysis (FEA), Structural modeling.

INTRODUCTION

The efficiency of the cutting process in combine harvesters used for cereal harvesting is an important factor in reducing crop losses, increasing harvesting capacity, and ensuring the reliability of the cutting system. Serrated knife sections in the cutterbar system are key components that cut plant stems through reciprocating motion and are subjected to repeated mechanical loading during operation (Song et al., 2016; Wang et al., 2022). In addition to plant material, the interaction of the cutting edges with dust, soil, and other abrasive particles encountered during harvesting may lead to progressive wear and dulling of the cutting surfaces (Jankauskas et al., 2024). Studies on combine harvester cutting components have shown that the mechanical properties of the blade material, as well as cutting-edge hardness and geometry, have a significant influence on wear behavior. In particular, cutting-edge hardness and

geometry have been reported as important parameters governing wear behavior (Jankauskas et al., 2024).

Achieving high wear resistance together with sufficient toughness and structural strength represents an important material-selection challenge in the design of cutting components. Although increasing cutting-edge hardness is advantageous in terms of wear resistance, imparting high hardness to the entire component may increase the risk of brittle behavior under impact and bending loads (Jankauskas et al., 2024; Xu et al., 2021). Comparative studies on combine harvester knife sections have shown that abrasive wear alters the cutting-edge geometry and consequently deteriorates cutting performance, while blades with different hardness levels and geometric characteristics exhibit different wear behavior (Jankauskas et al., 2024). Surface-hardening and coating approaches aimed at combining a hard, wear-resistant working region with a tougher load-bearing structure have also been investigated for agricultural cutting components (Xu et al., 2021; Xu et al., 2022). These approaches highlight the need for different mechanical characteristics in different regions of a single knife section.

Functionally graded materials (FGMs) enable spatially varying material properties within a component through controlled changes in composition or microstructure (Saleh et al., 2020). In contrast to the sharp material interfaces that may occur in conventional composites, a controlled variation in properties can enable different mechanical and functional requirements to be addressed within the same structure (Saleh et al., 2020; Martínez-Pañeda, 2019). This approach offers particular potential for applications requiring the integration of a surface with high hardness and wear resistance and a more ductile and tougher load-bearing region within a single component. FGM structures can be designed with continuously varying properties or modeled in a stepwise manner using successive regions with different compositions (Saleh et al., 2020). Various approaches based on spatially varying material properties have been developed for implementing functional gradation in finite element models. In particular, Martínez-Pañeda focused on the finite element implementation of functionally graded materials (Martínez-Pañeda, 2019).

The use of tungsten carbide (WC) in steel- and iron-based matrices has been widely investigated in metal-matrix composites intended for applications requiring high hardness and wear resistance. WC reinforcement has been shown to significantly influence the hardness, strength, and tribological properties of iron-based composites, and composites containing different WC fractions have been successfully produced (Chen et al., 2020; Zhao et al., 2023). In particular, substantial increases in hardness have been reported in steel-based systems containing relatively high WC fractions, although the resulting hardness–toughness balance must also be considered. Chen et al. experimentally investigated WC-reinforced iron-based composites, whereas Zhao et al. examined the hardness–toughness balance in steel-matrix systems containing WC (Chen et al., 2020; Zhao et al., 2023).

The application of WC reinforcement to agricultural cutting components is also of particular interest. A highly wear-resistant silage knife exhibiting self-sharpening behavior was developed using a Ni–WC-based laser-cladded layer, and subsequent research demonstrated the potential of WC-containing hard phases for preserving the cutting edges of agricultural cutting components (Xu et al., 2021; Xu et al., 2022). These findings indicate that WC-based hard phases are applicable not only to general industrial wear-resistant systems but also directly to cutting components used in agricultural machinery. The study by Xu et al. specifically aimed to develop a long-service-life agricultural knife with enhanced wear resistance (Xu et al., 2021).

More recent studies have also demonstrated the feasibility of producing WC–steel systems directly in a functionally graded configuration (Moreira et al., 2025). A functionally graded WC-reinforced stainless-steel composite was produced, exhibiting a marked improvement in abrasive wear resistance in WC-rich regions. Similarly, manufacturing approaches based on controlled variation of WC content have demonstrated the feasibility of

creating graded hard-phase distributions in iron- and steel-based matrices (Chen et al., 2020; Moreira et al., 2025; Li et al., 2026).

In this study, a steel–WC-based stepwise functionally graded material approach is proposed for the structural design of serrated knife sections used in combine harvester cutterbars. By gradually reducing the WC fraction from the cutting edge toward the mounting region, the design aims to promote high hardness and wear resistance in the cutting region while retaining the comparatively tougher characteristics of the steel matrix in the mounting region. Based on the geometry of an existing knife section, homogeneous steel and stepwise FGM models are developed, and their structural responses under identical loading conditions are compared using the finite element method. The study thereby aims to provide a fundamental numerical assessment of the applicability of a stepwise material gradation approach to the structural design of combine harvester cutting components.

MATERIALS AND METHODS

Material Selection

Combine harvester cutting blades are subjected not only to repeated cutting loads during operation but also to contact with plant material, soil, and hard foreign objects. Therefore, in addition to providing sufficient mechanical strength, the blade material should exhibit high hardness and wear resistance at the cutting surfaces. In this study, 75Cr1 (1.2003) steel was selected as the base material of the knife section and as the homogeneous reference material. 75Cr1, specified according to DIN EN 10132, is a low-alloy, high-carbon tool steel. According to Thyssenkrupp, its nominal chemical composition ranges are 0.70–0.80 wt.% C, 0.25–0.40 wt.% Si, 0.65–0.80 wt.% Mn, and 0.30–0.40 wt.% Cr, with the material designation 1.2003 **(Thyssenkrupp Steel Europe AG, 2024)**. Based on the density of 7.85 kg/dm³ reported by Walzwerke Einsal, a density of 7850 kg/m³ was assigned to 75Cr1 in the numerical model **(Walzwerke Einsal GmbH, n.d.)**.

In addition to the mechanical characteristics provided by 75Cr1 as the metallic matrix, tungsten carbide (WC) was selected as the hard reinforcement phase to enhance the potential hardness and wear resistance, particularly in the serrated cutting regions. WC, as a hard ceramic phase, has been reported to improve the wear resistance of metal-matrix systems, while increasing WC content can significantly affect their mechanical and tribological properties **(Xu et al., 2021; Chen et al., 2020; Zhao et al., 2023; Moreira et al., 2025)**. However, it should be considered that increasing the hard-phase fraction may involve a trade-off with other mechanical properties, particularly the hardness–toughness balance. WC is a carbide phase with a hexagonal crystal structure and is characterized by high elastic stiffness. Although the elastic behavior of single-crystal WC is anisotropic, high elastic modulus values have been reported for polycrystalline WC. In the present study, **E = 722 GPa** and **ν = 0.197** were adopted as the input elastic properties of WC **(Golovchan and Litoshenko, 2010)**. Similar micromechanical studies have employed values of approximately **E = 707.7 GPa** and **ν = 0.197** for WC, further supporting its high elastic stiffness on the order of 700 GPa **(Tkalich et al., 2017)**.

For the micromechanical homogenization calculations performed in this study, E = 210 GPa, ν = 0.30, and ρ = 7850 kg/m³ were used for the 75Cr1 matrix, while E = 722 GPa, ν = 0.197, and ρ = 15,800 kg/m³ were adopted for the WC phase. The density of 75Cr1 was based on manufacturer data (Walzwerke Einsal GmbH, n.d.), whereas its Young's modulus and Poisson's ratio were adopted as engineering values for the isotropic elastic modeling of the steel matrix. The elastic properties of WC were based on literature data (Golovchan and Litoshenko, 2010; Tkalich et al., 2017). The fundamental material properties of 75Cr1 steel and the WC phase used in the numerical modeling are summarized in Table 1.

Table 1. Fundamental material properties of 75Cr1 steel and the WC phase used in the numerical modeling.

Property	**75Cr1 (1.2003)**	**WC**
Density, ρ (kg/m³)	7850	15 800
Young's modulus, E (GPa)	210	722
Poisson's ratio, ν	0.30	0.197
C (wt.%)	0.70–0.80	—
Cr (wt.%)	0.30–0.40	—
Mn (wt.%)	0.65–0.80	—
Si (wt.%)	0.25–0.40	—

Stepwise FGM Definition and Micromechanical Homogenization

For the stepwise functionally graded material model, 75Cr1 steel was used as the matrix and WC as the reinforcement phase. Previous studies have demonstrated that steel–WC composites can be produced with different WC contents and that increasing the WC fraction can enhance particularly the hardness and wear resistance of these materials (Xu et al., 2021; Chen et al., 2020; Zhao et al., 2023; Moreira et al., 2025). Accordingly, in addition to the homogeneous 75Cr1 reference material (0 vol.% WC), two equivalent composite material levels containing 10 and 20 vol.% WC were defined. The upper limit of 20 vol.% WC was selected considering literature data demonstrating the experimental feasibility of producing steel-matrix composites with WC contents up to this level (Zhao et al., 2023).

In the FGM model, 0 vol.% WC (homogeneous 75Cr1 steel) was assigned to the mounting region, 10 vol.% WC to the transition region, and 20 vol.% WC to the cutting region. Thus, a stepwise FGM structure was represented in which the WC content gradually decreased from the cutting edge toward the mounting region.

The equivalent elastic properties of the 75Cr1–WC composite regions were determined using the Mori–Tanaka micromechanical homogenization method, based on the material properties of the 75Cr1 matrix and WC reinforcement phase. The effective Young's modulus and Poisson's ratio were calculated using the Mori–Tanaka approach, while the density was determined using the linear rule of mixtures based on the volume fractions of the constituent phases. In this way, the influence of increasing WC content on the effective Young's modulus and Poisson's ratio was accounted for micromechanically, whereas the density values were determined from the corresponding phase volume fractions. In this approach, the WC phase was assumed to be a homogeneously dispersed, isotropic reinforcement phase within the steel matrix.

The equivalent material properties obtained for 0, 10, and 20 vol.% WC were defined as separate material cards in ANSYS Engineering Data and subsequently used in the finite element analyses. The resulting effective material properties are presented in Table 2.

Table 2. Effective material properties of 75Cr1–WC compositions used in the finite element analyses.

Material Description	WC Volume Fraction (%)	Density, ρ (kg/m³)	Young's Modulus, E (GPa)	Poisson's Ratio, ν
75Cr1	0	7850	210.000	0.30000
75Cr1–10WC	10	8645	234.934	0.29174
75Cr1–20WC	20	9440	262.851	0.28343

Blade Segment Geometry and Numerical Model

In this study, the structural behavior of a commercial serrated knife section used in a combine harvester cutterbar was investigated using the finite element method. The principal geometric dimensions of the knife section were determined from the actual component, and its three-dimensional solid model was created in **SolidWorks**. The model includes the serrated cutting edges, the main body region, and the mounting holes used to attach the knife section to the cutterbar mechanism. The model dimensions were defined as **75 mm in base width, 83.5 mm in overall height, and 2.5 mm in thickness.**

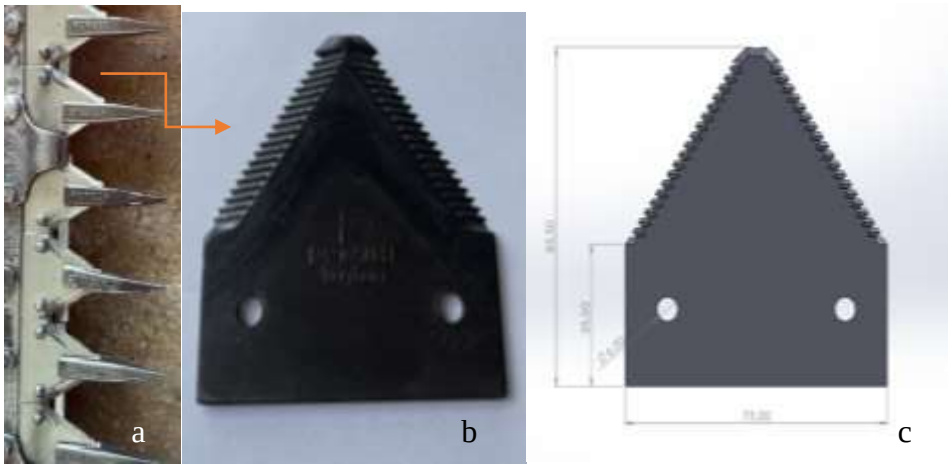

Figure 1. Investigated combine harvester knife section: (a) actual knife sections mounted on the cutterbar, (b) individual knife section, and (c) CAD model with its principal dimensions.

The developed three-dimensional model was imported into ANSYS Workbench in STEP format, and the finite element analyses were performed using ANSYS Mechanical. The geometric dimensions and external boundary conditions were kept identical for all models to enable a direct comparison of the effects of material distribution and gradation geometry on the structural response. Accordingly, one homogeneous reference model (Homogeneous 75Cr1) and two different stepwise functionally graded material models (Edge-Following Graded Model and Layered Graded Model) were developed.

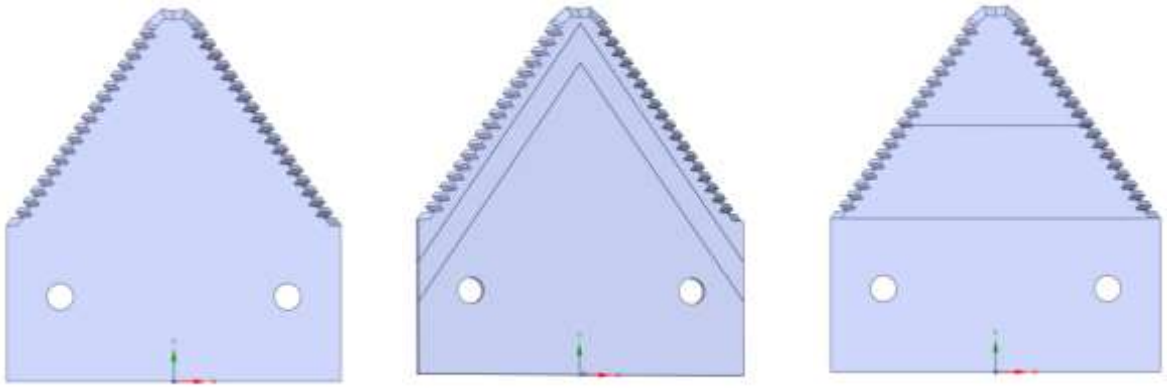

a b c

Figure 2**.** Investigated material configurations: (a) Homogeneous 75Cr1, (b) Edge-Following Graded Model, and (c) Layered Graded Model.

Homogeneous 75Cr1 – Reference Model**:** In the first model, the entire knife section was defined as homogeneous 75Cr1 steel. This configuration was used as the reference model for evaluating the structural effects of the FGM configurations.

Edge-Following Graded Model**:** In this FGM configuration, the material distribution was designed to follow the actual cutting geometry of the knife section. While the main body was maintained as 75Cr1 steel, the WC content was increased to 10 vol.% toward the cutting region and further increased to 20 vol.% in the outermost serrated cutting region. The main concept underlying this configuration was to localize the WC-rich material near the cutting surface, where frictional contact and wear are expected to occur, rather than distributing it throughout the entire component. The literature on cutting tools indicates that wear behavior depends on several parameters, including tool geometry, contact conditions, material properties, and friction, while the FGM concept enables different functional requirements to be addressed in different regions of a component. Therefore, the Edge-Following model does not represent a direct wear simulation. Instead, it represents a function-oriented FGM design in which the WC-rich region, with its potential for increased hardness and wear resistance, is strategically positioned along the cutting edge.

Layered Graded Model: In the second FGM configuration, the same 0, 10, and 20 vol.% WC levels were maintained; however, the material regions were arranged in a layered/regional distribution rather than directly following the cutting-edge geometry. This configuration was designed to investigate the effect of gradation geometry on the structural response while maintaining the same material constituents and WC volume fractions.

By evaluating the Edge-Following and Layered models together, the study aimed to investigate the influence of not only WC content but also the geometric distribution of the WC-rich regions on deformation, stress distribution, and strain-energy storage.

Finite Element Analysis Conditions

The finite element mesh for all models was generated by considering the geometric partitioning and material regions. A finer mesh was employed in critical geometric regions to adequately capture the stress gradients around the serrated cutting surfaces, material transition regions, and mounting holes. Depending on the geometric partitioning, the investigated models contained between **44,534 and 58,000 nodes** and between **19,486 and 29,231 elements**. A global element size of **1.5 mm** was adopted, with local mesh refinement applied where necessary (**Figure 3**).

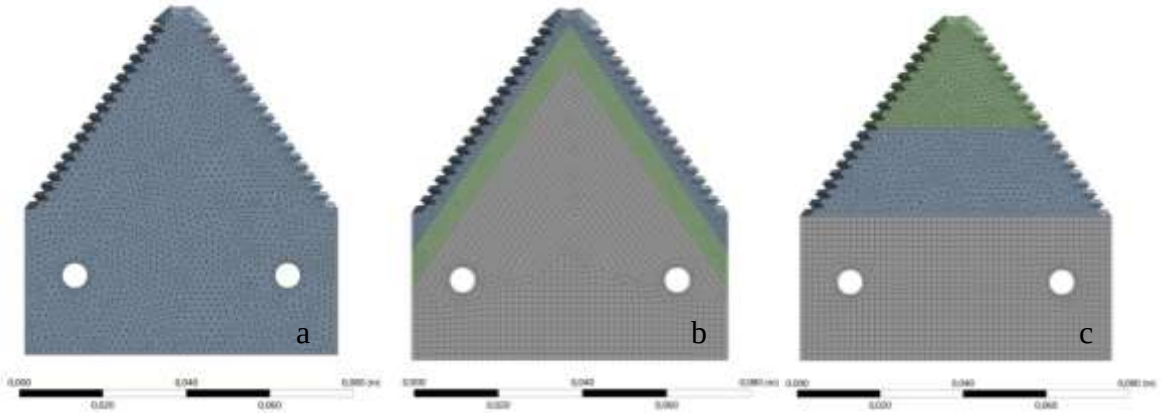

Figure 3. Finite element meshes and local mesh refinements of the investigated models: (a) Homogeneous 75Cr1, (b) Edge-Following Graded Model, and (c) Layered Graded Model.

In the FGM models, adjacent material regions were modeled to form a mechanically continuous structure, thereby ensuring load transfer between the regions. To represent the mechanical attachment of the knife section to the combine harvester cutterbar, a Fixed Support boundary condition was applied to the two mounting holes (Figure 4).

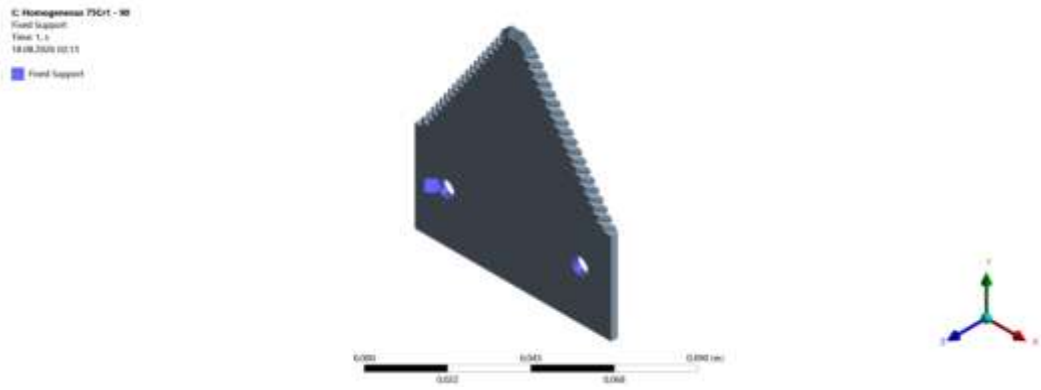

Figure 4**.** ANSYS view of the finite element model showing the two mounting holes subjected to the Fixed Support boundary condition.

Fully constraining the mounting holes represents an idealized approximation of the actual attachment conditions. Since this idealization may induce localized stress concentrations around the holes, the spatial distribution of stress throughout the model was also considered when evaluating the maximum stress values.

Under actual operating conditions, combine harvester knife sections may experience localized contact with stones and other hard foreign objects in addition to cutting plant material. Rather than modeling the actual time-dependent impact behavior associated with such contacts, an equivalent static local pressure approach was adopted in the present study to compare the relative effects of different loading intensities on the investigated material configurations.

The pressure was applied to five adjacent serrated surfaces in the cutting region (Figure 5). The area of each selected surface was approximately 4.28 mm², resulting in a total effective loading area of approximately 21.4 mm².

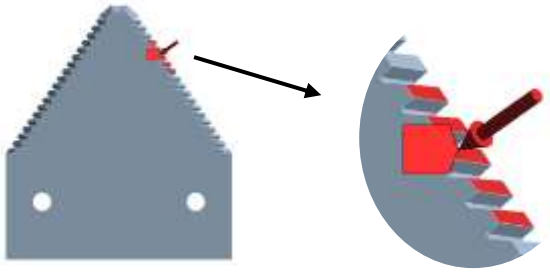

Figure 5. Application of the equivalent static local pressure to five adjacent serrated surfaces in the cutting region of the blade segment.

To compare the behavior of the material configurations under different loading intensities, three equivalent static local pressure levels of 30, 60, and 90 MPa were applied. The corresponding approximate equivalent forces were calculated using the pressure–area relationship and are presented in Table 3.

Table 3. Equivalent static local pressure levels and corresponding forces applied to the cutting region.

Pressure (MPa)	Effective Area (mm^2)	Approximate Equivalent Force (kN)
30 MPa	21.4 mm^2	0.642 kN
60 MPa	21.4 mm^2	1.284 kN
90 MPa	21.4 mm^2	1.926 kN

These pressure levels were used as equivalent static loading levels to compare the effects of increasing load intensity on different material configurations over the same local contact area. The same solution procedure was applied to all three material configurations at pressure levels of 30, 60, and 90 MPa, resulting in a total of nine analysis cases. For each analysis, the structural response parameters Total Deformation, Equivalent (von Mises) Stress, Maximum Principal Stress, and Strain Energy were obtained. The Homogeneous 75Cr1 model was taken as the reference for all comparisons. The relative changes in the structural response parameters of the FGM models were expressed as percentage changes with respect to the corresponding values of the homogeneous reference model. Negative values indicate a reduction relative to the reference model, whereas positive values indicate an increase.

RESULTS AND DISCUSSION

The structural behavior of the serrated knife section used in a combine harvester cutterbar was compared among a reference model consisting of homogeneous 75Cr1 steel and two functionally graded material (FGM) designs. To evaluate the influence of WC reinforcement distribution within the blade geometry on the structural response, two different material configurations, namely the Layered Graded Model and the Edge-Following Graded Model, were investigated. All models were subjected to surface pressures of 30, 60, and 90 MPa under identical boundary conditions, and the maximum total deformation, maximum equivalent (von Mises) stress, maximum principal stress, and total strain energy were compared. The values obtained from the analyses are presented in Table 4.

Table 4. Structural response of homogeneous and functionally graded blade segment models under different equivalent local pressure levels.

Model	Pressure (MPa)	Max. Deformation (mm)	Max. von Mises Stress (MPa)	Max. Principal Stress (MPa)	**Total Strain Energy (J)**
Homogeneous 75Cr1	30	1.3900	757.95	1088.6	0.20095
Homogeneous 75Cr1	60	2.7801	1515.9	2177.2	0.80381
Homogeneous 75Cr1	90	4.1701	2273.8	3265.8	1.8086
Edge-following graded	30	1.3347	861.06	1275.4	0.19259
Edge-following graded	60	2.6695	1722.1	2550.9	0.77037
Edge-following graded	90	4.0042	2583.2	3826.3	1.7333
Layered graded	30	1.3152	767.25	1146.5	0.19000
Layered graded	60	2.6304	1534.5	2293.0	0.75999
Layered graded	90	3.9456	2301.8	3439.5	1.7100

For all three models, the deformation and stress values increased approximately linearly as the applied pressure increased from 30 to 90 MPa. For example, in the homogeneous model, the maximum deformation increased from 1.3900 mm at 30 MPa to 2.7801 mm at 60 MPa and 4.1701 mm at 90 MPa. Similarly, the maximum von Mises stress values were 757.95, 1515.9, and 2273.8 MPa, respectively. The same trend was observed for both FGM designs.

In contrast, the total strain energy did not increase linearly with the applied load but exhibited an approximately quadratic dependence on pressure. For example, in the Layered Graded Model, the total strain energy increased from 0.190 J at 30 MPa to approximately four times this value (0.760 J) at 60 MPa and approximately nine times this value (1.710 J) at 90 MPa. This behavior is consistent with the expected energy response of the models under the adopted linear elastic material assumption.

The percentage changes obtained for the FGM models relative to the homogeneous 75Cr1 reference model are summarized in **Table 5**. Under the investigated linear elastic loading conditions, deformation and stress magnitudes scaled linearly with the applied pressure. Consequently, the percentage changes exhibited by the FGM models relative to the homogeneous reference model remained nearly constant at **30, 60, and 90 MPa**. Therefore, rather than repeating the percentage changes separately for each load level in **Table 5**, a single representative value is presented for each FGM configuration. Overall, both gradation approaches reduced the **maximum deformation** and **total strain energy**, whereas their effects on the maximum stress values varied depending on the **geometry of the material distribution**.

Table 5. Percentage changes in the structural response of FGM models relative to homogeneous 75Cr1.

Model	Max. Deformation Change (%)	Max. von Mises Stress Change (%)	Max. Principal Stress Change (%)	**Total Strain Energy** Change **(%)**
Edge-following graded	−3.98	+13.60	+17.16	−4.16
Layered graded	−5.38	+1.23	+5.32	−5.45

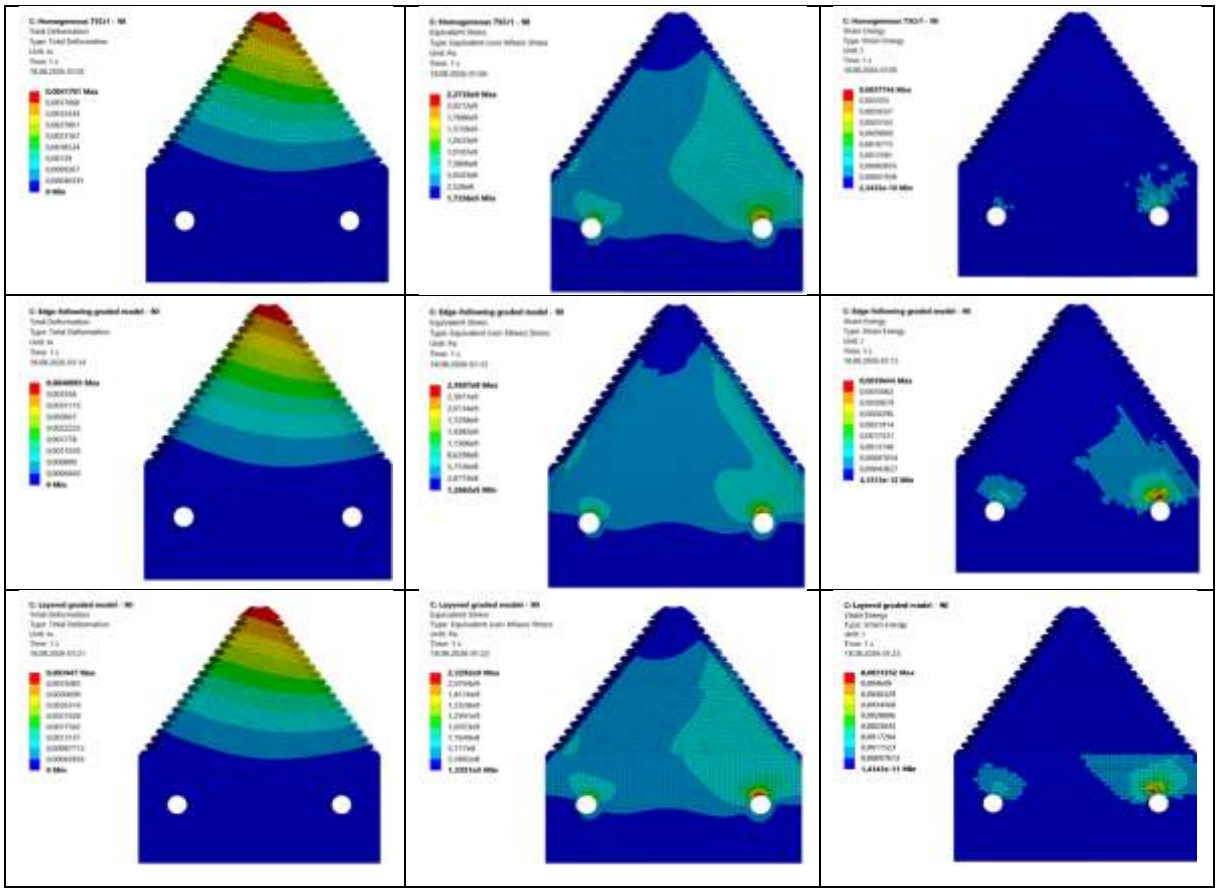

Figure 6. Total deformation, equivalent (von Mises) stress, and strain energy distributions of the blade segment models under an equivalent local pressure of 90 MPa: homogeneous 75Cr1 (top row), Edge-following graded (middle row), and Layered graded (bottom row).

The corresponding deformation, equivalent stress, and strain energy distributions for the investigated material configurations at 90 MPa are presented in Figure 6. One of the most pronounced effects of the FGM implementation was observed in the total deformation response. Compared with the homogeneous 75Cr1 model, both graded models exhibited lower maximum deformation at all loading levels.

At a pressure of 30 MPa, the maximum deformation was 1.3900 mm for the homogeneous model, compared with 1.3347 mm for the Edge-Following Graded Model and 1.3152 mm for the Layered Graded Model. The same relationship was maintained at the 60 and 90 MPa loading levels. Relative to the reference model, the Edge-Following design reduced the maximum deformation by approximately 4.0%, whereas the Layered design achieved a reduction of approximately 5.45%. These results indicate that the regions with increased elastic

modulus resulting from higher WC content contributed to an increase in the global stiffness of the knife section. However, not only the WC content but also the geometric arrangement of the reinforced regions influenced the global stiffness. The Layered model exhibited the lowest deformation at all loading levels, indicating that, under the investigated loading and boundary conditions, the layered gradation was more effective in limiting the overall bending deformation of the knife section. In terms of maximum von Mises stress, the FGM models exhibited a different trend from that observed for deformation. The Layered model produced maximum equivalent stress values very close to those of the homogeneous model. At 30 MPa, the maximum equivalent stress was 757.95 MPa for the homogeneous model and 767.25 MPa for the Layered model, corresponding to a difference of only approximately 1.23%. The same relative difference was maintained at the 60 and 90 MPa loading levels. In contrast, the maximum equivalent stresses in the Edge-Following model were approximately 13.6% higher than those in the homogeneous model. For example, at the 90 MPa loading level, the maximum equivalent stress increased from 2273.8 MPa in the homogeneous model to 2583.2 MPa in the Edge-Following model.

This finding demonstrates that the use of an FGM does not necessarily result in a reduction in the maximum local stress. Spatial variations in material stiffness alter the load-transfer paths and local stress distribution within the component. In particular, in the Edge-Following design, the high-stiffness WC-rich regions following the outer cutting geometry of the knife section resulted in higher localized stress levels in certain regions. Therefore, the performance of the Edge-Following design should not be evaluated solely on the basis of the maximum von Mises stress. The primary objective of this configuration is to position the WC-rich material close to the serrated cutting edges, where its functional properties are required, while maintaining regions with lower WC content in the mounting and main body regions. Accordingly, rather than representing a strategy aimed solely at minimizing global stress, the Edge-Following design represents an approach in which the material distribution is geometrically tailored to the mechanical and tribological requirements of the cutting edge.

The maximum principal stress results exhibited a trend similar to that observed for the von Mises stress. Compared with the homogeneous 75Cr1 model, the maximum principal stress was approximately **5.3% higher** in the Layered model and approximately **17.2% higher** in the Edge-Following model. At the **90 MPa** loading level, the maximum principal stress was calculated as **3265.8 MPa** for the homogeneous model, **3439.5 MPa** for the Layered model, and **3826.3 MPa** for the Edge-Following model. These values represent numerical stress magnitudes calculated within the framework of the linear elastic model and should not be interpreted as physical strength values under conditions in which the actual yielding or damage limits of the material may be exceeded.

Examination of the stress contours revealed that the high-stress regions were concentrated particularly around the mounting holes and in regions involving geometric and material transitions. It should be noted that the **Fixed Support** idealization applied to the mounting holes may increase localized stress concentrations in these regions. Therefore, the maximum stress values were evaluated not solely on the basis of individual peak values but also in conjunction with the stress distribution in the cutting region and the overall structural response.

The total strain energy results further support the global stiffness behavior of the FGM designs. Compared with the homogeneous model, the total strain energy decreased by approximately **4.2%** in the Edge-Following model and by approximately **5.45%** in the Layered model. At a pressure of **90 MPa**, the homogeneous model stored **1.8086 J** of strain energy, whereas the corresponding values were **1.7333 J** for the Edge-Following model and **1.7100 J** for the Layered model. The fact that the Layered model exhibited both the lowest maximum deformation and the lowest total strain energy supports its characterization as the configuration with the highest global elastic stiffness among the three models.

The reduction in strain energy should not be interpreted directly as indicating greater **impact-energy absorption**. Under the same loading conditions, lower elastic energy storage primarily reflects a stiffer structural response within the framework of the present linear elastic model. A meaningful comparison of actual impact-energy absorption or damage tolerance would require additional modeling of **plastic deformation, fracture or damage mechanisms, and dynamic material behavior.**

Considering the results as a whole, the **Layered Graded Model** exhibited the most balanced global structural response under the investigated linear elastic loading conditions. Compared with the homogeneous 75Cr1 model, this configuration reduced the maximum deformation and total strain energy while limiting the increase in maximum von Mises stress to a relatively small level. Although the **Edge-Following Graded Model** exhibited more pronounced increases in the maximum stress values, it provided a functionally tailored material distribution by allowing the WC-rich region to directly follow the serrated cutting-edge geometry, thereby addressing the mechanical and tribological requirements of the cutting region. Overall, the results demonstrate that the mechanical response of the FGM design depends not only on the WC content but also significantly on the **geometric distribution of the reinforcement phase within the knife section.**

CONCLUSIONS

In this study, the structural behavior of serrated knife sections used in combine harvester cutterbars was numerically investigated using a functionally graded WC reinforcement approach within a 75Cr1 steel matrix. In addition to the homogeneous 75Cr1 reference model, Layered Graded and Edge-Following Graded designs representing different geometric distributions of WC-rich regions were developed and compared using the finite element method under equivalent local pressure levels of 30, 60, and 90 MPa.

The following main conclusions were drawn:

- For all three models, the maximum deformation, equivalent von Mises stress, and maximum principal stress increased approximately linearly with the applied pressure, whereas the total strain energy varied approximately with the square of the pressure. This behavior is consistent with the load–response relationship expected from a linear elastic solution.
- Both FGM configurations reduced the maximum deformation compared with the homogeneous 75Cr1 model. The Edge-Following Graded Model showed an approximately 4.0% reduction, whereas the Layered Graded Model showed an approximately 5.45% reduction in maximum deformation.
- Among the investigated designs, the Layered Graded Model provided the most balanced global structural performance. Compared with the homogeneous model, it reduced the maximum deformation by approximately 5.45% and the total strain energy by approximately 5.45%, while limiting the increase in maximum von Mises stress to approximately 1.2%.
- Although the Edge-Following Graded Model reduced the maximum deformation and total strain energy by approximately 4.0% and 4.2%, respectively, its maximum von Mises and maximum principal stresses increased by approximately 13.6% and 17.2%, respectively, compared with the homogeneous model. This result indicates that the geometric arrangement of high-stiffness WC-rich regions can significantly influence local stress concentrations.
- Nevertheless, the Edge-Following approach enables the WC-rich material to be positioned along the serrated cutting edge. Therefore, this design is important not only

in terms of the global structural response but also in terms of the functional placement of WC-rich regions at the cutting edges where high hardness and wear resistance are required.

- The relative differences among the models remained nearly unchanged at 30, 60, and 90 MPa, indicating that, within the investigated linear elastic range, the relative mechanical effect of the FGM design was governed primarily by the material distribution and gradation geometry rather than by the applied load level.

Overall, the results indicate that WC-reinforced functional gradation in combine harvester knife sections offers potential as a design strategy for balancing the high stiffness, hardness, and wear-resistance requirements of the cutting region with the mechanical requirements of the body and mounting regions through spatially tailored material design. However, increasing the WC fraction alone was found to be insufficient; the geometric distribution of the reinforcement phase was identified as a critical design parameter affecting structural performance. Among the investigated configurations, the Layered Graded design was more advantageous in terms of global elastic behavior, whereas the Edge-Following configuration provided an alternative FGM design strategy for the functional placement of WC-rich regions along the cutting edge.

The present study was conducted within the framework of linear elastic static structural analysis. Therefore, the high localized stresses obtained should not be interpreted as direct indicators of the actual damage or fracture behavior of the material. Future studies should incorporate the elastoplastic behavior of the 75Cr1–WC system, realistic impact loading, fracture/damage criteria, wear behavior, and experimental validation. Optimization of the WC distribution and transition geometry would also be important for evaluating the performance of the proposed FGM knife designs under actual operating conditions.

REFERENCES

Chen, H., Gu, D., Kosiba, K., Lu, T., Deng, L., Xi, L., Kühn, U. (2020). Achieving high strength and high ductility in WC-reinforced iron-based composites by laser additive manufacturing. Additive Manufacturing, 35, 101195.

Golovchan, V.T., Litoshenko, N.V. (2010). The stress–strain behavior of WC–Co hardmetals. Computational Materials Science, 49(3), 593–597.

Jankauskas, V., Abrutis, R., Žunda, A. (2024). Wear and Damage Study of Straw Chopper Knives in Combine Harvesters. Machines, 12(11), 789.

Li, G., Li, Y., Wang, Y. (2026). Microstructure and high-temperature tribological properties of WC/Fe functionally graded coating fabricated by laser directed energy deposition. Tribology International, 218, 111744.

Martínez-Pañeda, E. (2019). On the Finite Element Implementation of Functionally Graded Materials. Materials, 12(2), 287.

Moreira, A.B., Ribeiro, L.M.M., Vieira, M.F. (2025). Functionally Graded WC-Reinforced Stainless-Steel Composites via Casting: Microstructure and Wear Performance. Journal of Composites Science, 9(9), 495.

Saleh, B., Jiang, J., Fathi, R., Al-hababi, T., Xu, Q., Wang, L., Song, D., Ma, A. (2020). 30 Years of functionally graded materials: An overview of manufacturing methods, applications and future challenges. Composites Part B: Engineering, 201, 108376.

Song, Z., Song, H., Yan, Y., Li, Y., Gao, T., Li, F. (2016). Optimizing design on knife section of reciprocating cutter bars for harvesting cotton stalk. Transactions of the Chinese Society of Agricultural Engineering, 32(6), 42–49.

Thyssenkrupp Steel Europe AG. (2024). precidur® 75Cr1 – Tool Steel, Material No. 1.2003, based on DIN EN 10132. Product Information, Version 11/2024.

Tkalich, D., Cailletaud, G., Yastrebov, V.A., Kane, P.-A. (2017). A micromechanical constitutive modeling of WC hardmetals using finite-element and uniform field models. Mechanics of Materials, 105, 166–187.

Walzwerke Einsal GmbH. (n.d.). Material Datasheet 1.2003 – 75Cr1 (1075 + Cr). Material Database.

Wang, W., Lv, X., Yi, Z. (2022). Parameter Optimization of Reciprocating Cutter for Chinese Little Greens Based on Finite Element Simulation and Experiment. Agriculture, 12(12), 2131.

Xu, L., Song, Z., Li, M., Li, F., Guo, J., Gao, M. (2021). Self-Grinding Silage Knife Strengthened with Ni–WC Alloy Prepared by Laser Cladding. Applied Sciences, 11(21), 10236.

Xu, L., Li, M., Song, Z., Li, F., Guo, J., Gao, M. (2022). WC-High Entropy Alloy Reinforced Long Life Self-Grinding Silage Knife Prepared by Laser Cladding. Nanomaterials, 12(6), 1013.

Zhao, M., Jiang, X., Guan, Y., Yang, H., Zhao, L., Liu, D., Jiao, H., Yu, M., Tang, Y., Zhang, L. (2023). Enhanced Hardness-Toughness Balance Induced by Adaptive Adjustment of the Matrix Microstructure in In Situ Composites. Materials, 16(12), 4437.

NEW RECORDS OF *ANEMONE BLANDA* SCHOTT & KOTSCHY IN ALBANIA

Dhimiter Peci[1], Nehat Collaku[2], Ilma Lili[3], Alfred Mullaj[1]*

[1]Research Center of Flora and Fauna, Faculty of Natural Sciences, University of Tirana, Albania

[2]Department of Forestry, Faculty of Forestry Science, Agriculture University, Tirana, Albania

[3]Department of Informatics, Faculty of Natural Sciences, University of Tirana, Albania

Corresponding author e-mail: dhimiter.peci@fshn.edu.al

ABSTRACT

Anemone blanda Schoot & Kotschy is a perennial geophyte of the Ranunculaceae family, it is northeastern Steno Mediterranean species of Balkan Peninsula. It is native and registered in the Albanian National Herbarium and in Flora of Albania v.1, as grown in a single locality, Bzhet/ Malesi e Madhe, in Northern Albania. According to IUCN categories this species is classified as endangered EN (A1B) and listed in National Red List. During field surveys in March 2026 on two protected areas of Dajti and Qafshtama Mountain, two new records of the species were discovered at the distance of 161 km and 144 km from the previously known site, respectively. The current findings comes from *Fagus sylvatica* and mixed *Fagus sylvatica* , *Pinus nigra* and *Erica carnea* communities, on calcerous well drained substrat, where typical ecological conditions of mountain belt of Dajti and Qafe-Shtama were favorable for this species growth. In this contribution, new data concerning the distribution of native species *A. blanda* in Albania are presented. These findings extend the known range of *A. blanda* in the country and suggest that the species may be more widespread than previously documented, contributing to more comprehensive mapping of rare and endangered species within Albania

Keywords: *Anemone blanda*, Albania, distribution range, national park

INTRODUCTION

Anemone blanda Schott &Kotschy is a perennial herbaceous geophyte with a tuberous underground rootstock of Ranunculaceae family. The flowing stems are erect, simple and relatively slender, generally reaching 5-30 cm in height. Basal leaves are usually one or two, long petiolate and deeply divided into three main segments, which are further lobed, the leaves are glabrous, particularly on the lower surface. The involucral leaves are stalked and deeply divided, resembling the basal foliage. Flowers are solitary, terminal and conspicuous borne above the foliage. The perianth consist of numerous petaloid segments, usually blue to violet-blue, although paler or white forms may occur. The perianth segments are glabrous and narrowly oblong to elliptic. Numerous stamens surround the central group of carpels. Following flowering numerous small achenes develop, forming a characteristic fruiting head. The species is a spring-flowering geophyte occurring in open rocky habitats, grasslands and pastures, scrum land, forest cleaning and forest margines. Its native through Southeastern Europe and Western Asia. (Paparisto et al., 1988). The specie is currently accepted as Anemone blanda Schott & Kotschy. and is considered native to Albania, with a natural distribution from Southeastern Europe through the Caucasus and Western Syria (POWO 2026)

According to Albanian National Herbarium *Anemone blanda* is reported only in a small area in the district of Malesia e Madhe in the North of Albania. The vegetation of its location, Bzhete area in the Shkrel region of Northern Albania, is characteristic of a sub-Mediterranean to Mediterranean influenced calcareous landscape, with a mosaic of woodland, open rocky habitat and shrubland. The area is developed mainly in limestone substrates, shallow soils and roadside habitats at approximately 550m above sea level (Colacino 2023). The woody vegetation includes elements of thermophilous oak woodland and Mediterranean-type shrub vegetation. In the region *Quercus trojana* and *Juniperus oxycedrus* have been recorded at approximately 450m above sea level, indicating the presence relatively dry open woodland and shrub communities adapted to calcareous substrate (Colacino 2023). These communities form a heterogeneous vegetation with open grassy and rocky microsite which provide suitable condition for *Anemone blanda*. According to Vangjeli et al., 2000 the ecological characteristic of this area consists with the broader vegetation where Mediterranean shrubs thermophilous oaks and open rocky land form an important component of the vegetation landscape. The occurrence of *Anemone blanda* in such open calcareous environments is also consistent with species flowering in rocky slopes, scrubs and forest margins (Rak 2015). In the figure 1 is presented the distribution of this species in Europe.

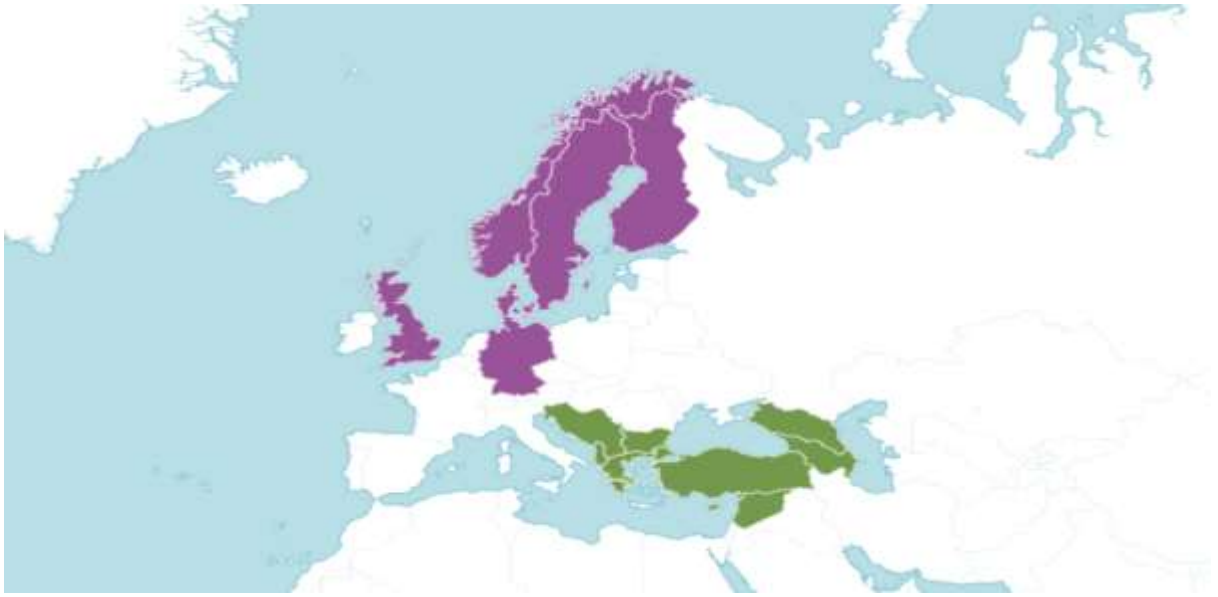

Figure 1. POWO 2026. The distribution of Anemone blanda Scott & Kotschy in Europe

MATERIAL AND METHOD

The surveys were conducted on two National Natural Parks included in the list of protected areas mountain of Dajti dhe Qafshtame in the central Albania, to investigate the flora composition under protected criteria. The trips were carried out during spring 2026. The plants were collected in flowering stage and a voucher of each representative population was deposited in National Herbarium under the Research Center of Flora and Fauna, Albania.

The plants were taxonomically identified using Albanian flora and taxonomic keys guidelines. During the sample collection data for the sites where the new records of *Anemone blanda* were recorded, including geographical coordinates and elevation using GPS system, the associated vegetation, habitat characteristics such as substrate, slope, exposure and associated species were recorded for each locality.

RESULTS AND DISCUSSION

Anemone blanda new records were found into two new not previously reported localities in Dajti and Qafshtama Mt.. The localities are given in the figure 2

Locality 1- Mt Dajti

Number of Populations: 3

Size of the populations: approximately 25 individuals per m^2

Population 1 Geographical coordinates:N 41^0 21'41'' E 19^0 54'47'', elevation 1080 m a.s.l

Population 2 Geographical coordinates: N 41^0 21'42'' E 19^0 54'19'', elevation 1100 m a.s.l

Population 3 Geographical coordinates: N 41^0 21' 53'' E 19^0 54'26'', elevation 1050 m a.s.l

Locality 2- Mt Qafshtama

Number of Populations: 2

Size of the populations: approximately 10-15 individuals per m^2

Population 1 Geographical coordinates: N 41^0 31' 11'' E 19^0 53' 52'', elevation 1220 m a.s.l

Population 2 Geographical coordinates: N 41^0 31' 06;; E 19^0 53' 46'', elevation 1190 m a.s.l

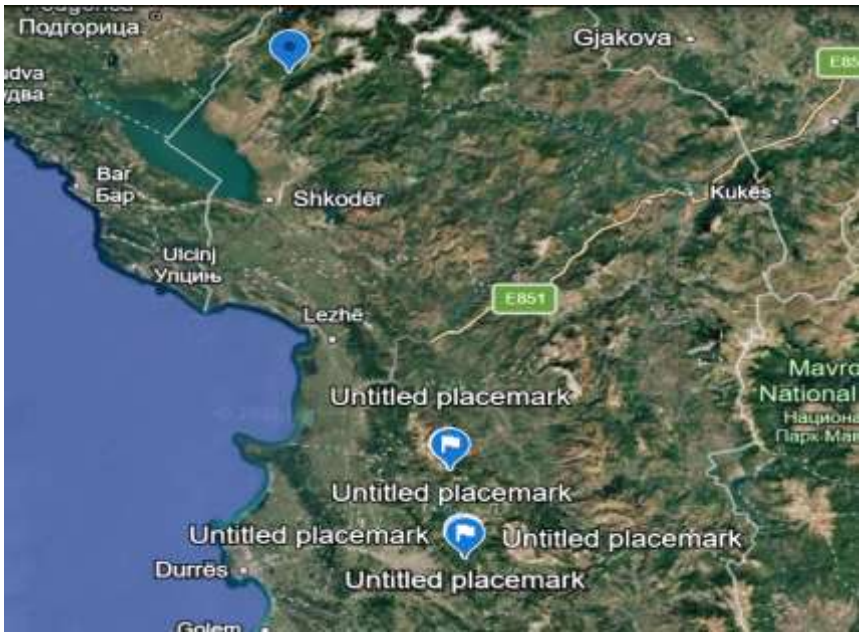

Figure. 2 Distribution map showing the previously known locality and the two new localities of Anemone blanda in Albania.

Habitat characteristics

Fagus sylvatica L represents one the main component of montane forest vegetation in Albania. The distribution of beech forest is closely associated with increasing altitude, lower temperature and more mesic environmental conditions. In Albania *Fagus sylvatica* forest occur across relatively broad altitudinal range, forming both pure stands and mixed communities with other tree species (FAO 2004; Fanelli et al., 2020).

The populations of *Anemone blanda* found in the Dajti and Qafshhtama mountain areas occur in mixed montane *Fagus sylvatica* forests with *Pinus nigra* and *Erica carnea*, mainly on calcareous, well-drained and heterogeneous mountain soils (Fig. 3 |A, B).

A- *Anemone blanda* in Qafshtama

B- Anemone blanda population in Dajti Mountain

Figure 3. Anemone blanda collected at Qafshatama and Dajti and their new habitats

At both localities, *Anemone blanda* occurs in montane beech forest communities dominated by Fagus sylvatica, where *Pinus nigra* and *Erica carnea* occur as important associated species. These communities are developed on calcareous substrates (on Mt Dajti) and serpentine substrate (on Mt. Qafshtama), generally on mountain slopes with well drained

moderately deep and humus rich soils. The habitats are characterized by cool and relatively humid microclimatic conditions, particularly during winter and early spring, followed by dry summer.

In Dajti Mountain forest vegetation had a district altitudinal zonation. According Kalajxhiu et al (2012), from 13 woodland communities identified five of these were assigned to the Order *Fagetalia sylvaticae* highlighting the importance of beech forest within the montane vegetation of Dajti. The composition and distribution of these communities are influenced by a combination of geological substrate, soil characteristic, altitude, topography, anthropogenic disturbance and overgrazing.

The beech forest in Dajti National Park is dominated by *Fagus sylvatica*, while the composition of shrubs and herbs layer varies according to local ecological conditions. This forest occurs mainly between 1000-1500 m above sea level, particularly on northern and northwestern slopes, where Fagus sylvatica is associated with other montane forest element (Mecaj &Muharremaj 2002).

A phytosociological assessment of beech forest in Albania demonstrated considerable ecological differentiation within *Fagus sylvatica* community. There are identified several ecological types, including thermos-basophilous, meso-basophilous and acidophilous beech forest as well as communities characterized by the association of *Corylus avellana* and *Ostrya carpinifoli*a with *Fagus sylvatica*. This indicates that in Albania beech forests do not constitute a homogeneous vegetation unit, but rather a complex of communities differentiated by topographic, climatic and edaphic conditions (Fanelli et al 2020)

Qafshtama National Park provides an additional example of the ecological differentiations of montane forest vegetation in Albania. The upper vegetation belt between 1400-1700m above sea level is characterized by beech forest and coniferous formations, dominated by *Pinus nigra*. The coexistence between them, together with substrate, exposure and soil moisture contribute to the heterogenous forest mosaic. The ecological relationship between beech and black pine is particularly relevant for understanding the vegetation structure of Qafshtama. *Pinus nigra* occupy dry and exposed faces, whereas *Fagus sylvatica* requires more mesic conditions. The variation in exposure, substrate and soil moisture may contribute to the spatial differentiation of these forest communities. The vegetation is therefore characterized by a mosaic of *Fagus sylvatica* forest, scattered *Pinus nigra*, and patches of *Erica carnea*, together with a diverse spring herbaceous layer. Other associated species recorded include *Ostrya carpinifolia*, *Acer pseudoplatanus*, *Fraxinus ornus*, *Helleborus odorus*, *Galanthus nivalis*, *Crocus* spp., *Primula vulgaris* and *Viola* spp. (Fanelli et al 2020).

CONCLUSIONS

Anemone blanda is a rare and endangered specie in Albania, previously known from one location in Bzhet Malesia e Madhe. The field survey conducted in March 2026 identified two new locations of the specie in the protected areas of Dajti Mountain and Qafshtama Mountain. These findings significantly extend the previously known distribution range of *Anemone blanda* in Albania with two new localities located approximately 161 km and 144 km from the previously recorded site. The species was found mainly in *Fagus sylvatica* and mixed *Fagus sylvatica-Pinus nigra-Erica carnea* communities, on calcareous and well drained substrates. The discovery of these two localities suggests that *A. blanda* may have wider distribution in Albania than previously documented. Additional field survey and monitoring are recommended to determine the population size, distribution, ecological requirements and conservation status of the species. These two new records provide additional data crucial for the conservation and more accurate mapping of this rare and endangered plant species in Albania.

REFERENCES

FAO (2004). Global Forest Resources Assessments 2000: Main Report. FAO Forestry Paper 140. Rome: Food and AgricultureOrganization of the United Nations. https:/www.fao.org.

Fanelli, G., De Santis, M.,Gjeta, E., Mullaj,A.,& Atore F., 2020. Phytosociological classification of beech and hazel forests in Albania. Plant Sociology, 57(2), 1-20.

Kalajnxhiu A., Mullaj A., Hoda P. 2012. Phytosociological study of the forest vegetation of Dajti Mountain in Albania. Biodiversity and Conservation, 21, 1-18

Mecaj N., & Muharremaj S., (2002) Dajti National Park; Natural Values and Management considerations. Academy of Sciences of Albania.

Paparisto K., Demiri M., Mitrushi I., Qosja Xh. 1988. Flora e Shqiperise, Vol.1 Akademia e sShkencave te Shqiperise, Qendra e Kerkimeve Biologjike, Tirane 457f.

POWO 2026. Anemone blanda Schott. & Kotsch. Plants of the World Flora Online, Royal Botanic Garden, Kew.

Kak L 2015. Anemone blanda Scott & Kotsch- Balkan Anemone. Botany.cz.

Colacino 2023. Contribution to the bryophyte flora of Albania.

Vangjeli J., Ruci B.,Mullaj A., Xhulaj M. 2000. Flora e vegetacione in Albania. Cahiers Options Mediterraneennes, 53: 51-66.

STUDY OF THE INFLUENCE OF BIOPRODUCTS ON THE GROWTH AND PRODUCTIVE QUALITIES OF GREENHOUSE CUCUMBERS

Boyan Arnaoudov

Agricultural Academy, "Maritsa" Vegetable crops research Institute, Plovdiv, Bulgaria
e-mail: huan_veron@abv.bg

Abstract

The experimental work was carried out in an unheated Venlo-type glasshouse at the Maritsa Vegetable Crops Research Institute (VCRI) in Plovdiv, Bulgaria, using the greenhouse cucumber cultivar Defense F_1. The objective of the research was to evaluate the effects of innovative biological agents and their combinations with conventional chemical tools on the vegetative growth and productive qualities of vegetable crops from the Cucurbitaceae. The results demonstrated that the highest biometric parameters were achieved by plants grown under sole soil treatment with an experimental strain of B. thuringiensis (Var. 5) or when combined with subsequent foliar inoculation of newly isolated endophytic bacteria (Var. 6). In Variant 6, the main stem growth rate reached 3.86 cm/24 h, and the leaf formation rate peaked at 0.64 leaves/24 h. The same variant (Var. 6) exhibited strong synergistic interaction, generating the highest total yield of 16697 kg/da and the maximum volume of first-class production (9578 kg/da). Conversely, the sole application of the conventional chemical nematicide Velum Prime (Var. 1) resulted in the lowest total yield (13789 kg/da), while its combined application with B. thuringiensis (Var. 3) significantly reduced the volume of premium-grade fruits to 7398 kg/da. These findings underscore the high potential of the studied biological products as viable alternatives to synthetic chemical protection within integrated pest management (IPM) systems.

Keywords: Cucumis sativus, Bacillus thuringiensis, endophytic bacteria, greenhouse production, synergistic effect, integrated pest management (IPM), crop yield.

INTRODUCTION

The cultivation of crops from the Cucurbitaceae family is traditional in Bulgaria, which determines their significant economic role. In Bulgaria, cucumbers rank second in terms of economic importance within the structure of greenhouse vegetable production (Velkov and Pevicharova, 2016), despite being a crop highly sensitive to a wide spectrum of phytopathogens and pests (Lebeda et al., 2007).

For many years, increasing and maintaining high yields in the agricultural sector relied predominantly on conventional chemical pesticides. Despite their undeniable initial efficacy, intensive and uncontrolled chemical application has led to serious ecological and agronomic problems. Among these, the acquisition of rapid resistance by pests, secondary infestations due to disruptions in the natural biocenotic balance, and the mass destruction of beneficial entomophages and antagonists stand out most prominently (Parveen & Rashtrapal, 2024). Residual amounts of chemical substances in the produce pose severe risks to public health and environmental pollution. This necessitates the urgent implementation of reliable, cost-effective, and environmentally friendly solutions (Akello et al., 2001).

Integrated Pest Management (IPM) is a modern holistic approach that combines prevention, diagnostics, the breeding of resistant varieties, and judicious biological control with the aim of maintaining pest populations below the economic injury level (EIL), without seeking the complete and destructive elimination of species within the agrobiocenosis (Akello et al.,

2009). A key element in this strategy is the use of entomopathogenic microorganisms and plant growth-promoting bacteria.

In the course of a long coevolution, spore-forming bacteria such as B. thuringiensis Berliner have developed the capability to synthesize highly specific crystalline parasporal proteins (Cry toxins), which possess a potent insecticidal spectrum against economically important pests, including soil nematodes, without harming the remaining fauna (De Maagd et al., 2003; Vilcinskas, 2010). Modern "omics" technologies further reveal innovative mechanisms of action for these bioagents, transforming them into a cornerstone of modern organic agriculture (Ruiu et al., 2013).

Although entomopathogenic bacteria have historically been viewed primarily as biocontrol agents, they are increasingly defined in contemporary scientific literature as multifunctional plant growth-promoting rhizobacteria (PGPR). Numerous studies have established that, in addition to direct insecticidal and nematicidal effects, strains of *B. thuringiensis* can induce systemic resistance (ISR) in plants, improve phosphorus solubilization, and synthesize phytohormones. Due to their complex polyvalent mechanism of action, products based on *B. thuringiensis* significantly reduce the risk of resistance development. While their sole application is effective, researchers such as Morris (1972), Seleena et al. (1999), and Musser et al. (2006) indicate that their combined or rotational treatment with moderate doses of conventional plant protection products can induce a synergistic effect.

The objective of this study was to determine the influence of innovative biological agents and their combinations with conventional chemical products on the vegetative growth and productive traits of greenhouse cucumbers.

MATERIAL AND METHODS

The experiment was conducted in an unheated Venlo-type glasshouse at the Maritsa Vegetable Crops Research Institute (VCRI) in Plovdiv, Bulgaria, using the greenhouse cucumber cultivar Defense F_1. The trial was laid out using the long-plot method in 3 replications with a planting density of 2.16 plants/m². The crop was grown according to standard cultivation technology with vertical training of the main stem and removal of its growing tip upon reaching the support wires (2 m).

Experimental Conditions:

Sowing: 01.04; Transplanting: 23.04; Harvesting period: 02.06. to 25.06.

The experimental design consisted of 6 variants with differentiated or combined soil and foliar treatments **(Table 1).**

Table 1. Experimental variants of the study

№	Soil treatment	Foliar treatment
1.	Velum Prime	
2.	Velum Prime	Endophytic bacteria
3.	Velum Prime + *Bacillus thuringiensis*	
4.	Velum Prime + *Bacillus thuringiensis*	Endophytic bacteria
5.	*Bacillus thuringiensis*	
6.	*Bacillus thuringiensis*	Endophytic bacteria

Applied Products and Treatments:

Seedling stage:

Simargal and a Bacillus thuringiensis-based formulation active against nemato

des.

Soil, pre-transplanting:

Simargal, a Bacillus thuringiensis-based formulation, and StimAK (amino acid fertilizer).

During vegetation:

Simargal, StimAK P, StimAK (foliar application), and endophytic bacteria.

Experimental Parameters and Assessments:

1. Microclimatic parameters: Recorded daily at 08 00 h and 14 00 h using minimum-maximum thermometers, soil thermometers at a 10 cm depth, digital hygrometers, and a lux meter for solar radiation.

2. Soil agrochemical status: Evaluated at the beginning and end of the vegetation period using a 1:2 (v/v) water extract to determine pH, electrical conductivity (EC), nitrogen (ion-selective method), phosphorus (spectrophotometrically), as well as calcium and magnesium (complexometrically).

3. Biometric analysis: Weekly measurements of the main stem growth rate (cm/24 h) and the leaf formation rate (leaves/24 h).

4. Yield and quality: Harvest data was recorded three times per week, with produce graded by quality class (Class I and Class II) and average fruit mass measured (kg). The collected data were subjected to statistical analysis to determine the significance of the differences (Sig.).

RESULTS AND DISCUSSION

Microclimatic Factors

The experimental work was carried out in an unheated Venlo-type glasshouse with limited environmental control capabilities. Consequently, the microclimatic parameters closely followed the dynamics of external weather conditions and were further influenced by the cultivated crop itself.

Light Conditions

During the morning hours of the first half of the vegetation period, the average illumination values inside the greenhouse remained below the optimal light requirement thresholds. In the afternoon hours of the months with peak solar intensity, the illumination levels approached the requirements of the crop, reaching average monthly values between 29508 and 33132 Lux. To protect the plants, the incoming solar radiation flux was artificially limited from mid-May onwards using a commercial greenhouse shading agent **(Fig. 1).**

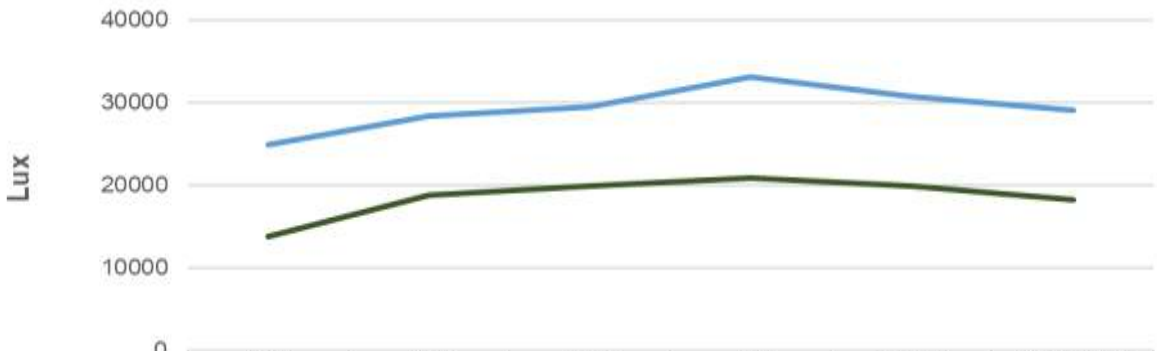

	April	May	June	July	August	September
08.00h	13833.3	18850.0	19871.8	20925.0	19944.4	18248.5
14.00h	24925.0	28333.3	29508.2	33131.6	30666.7	29000.0

Figure 1. *Greenhouse illumination (Lux), monthly averages.*

Temperature Conditions

The average minimum temperature in April was 12.1 °C. The recorded values for this microclimatic parameter decreased to 9.7 °C in May. Subsequently, these values increased through June (15.2 °C) and July (17.1 °C), after which this upward trend systematically reversed, resulting in average minimum temperatures of 16.3 °C and 14.1 °C in August and September, respectively. In the morning hours (08 00 h), the average monthly air temperature gradually increased by 2.0 to 2.5 °C each month until July, reaching its maximum value of 20.1 °C, followed by a decline at a similar rate during the final two months of vegetation. As the day progressed (14 00 h), temperature values fluctuated within the range of 28.0 to 31.8 °C. The average maximum air temperature during the reporting period did not exceed 33.3 °C, which was recorded in July. The low minimum temperatures during the first two months of vegetation exerted an unfavorable influence on plant growth and development (***Table 2***).

Table 1. *Temperature conditions*.

	April		May		June		July		August		September	
Avg. Min. T °C	12.1		9.7		15.2		17.1		16.3		14.1	
Avg. Max.T°C	37.3		31.6		33.3		30.1		32.3		32.9	
	8^{00}h	***14^{00}h***	***8^{00}h***	***14^{00}h***	***8^{00}h***	***14^{00}h***	***8^{00}h***	***14^{00}h***	***8^{00}h***	***14^{00}h***	***8^{00}h***	***14^{00}h***
Avg. Air T °C	14.6	30.6	16.0	28.0	18,6	31.8	20.1	28.7	18.0	31.1	15.8	28.8
Avg. Soil T °C	20.8	23.9	17.9	20.8	20.9	23.2	20.9	22.7	21.3	22.0	21.4	22.5

Relative Humidity

During the vegetation period, air humidity was regulated through ventilation, irrigation, and refreshing overhead sprinkling. Despite the implementation of these measures, intensive ventilation combined with high temperatures caused the relative air humidity to drop below the optimal threshold for cucumbers (80% – 85%).

During the first month of the vegetation period, the average morning air humidity (08 00 h) was 75.0 %, while throughout the remainder of the reporting period, the humidity within the same time frame fluctuated between 52.7 % and 67.8 %. Throughout the entire vegetative cycle, the values of this microclimatic parameter decreased significantly in the afternoon hours, ranging from 42.2 % to 65.5 % (***Fig. 2***).

The recorded data for the microclimatic factors indicate that during the first half of the experimental period, the low spring temperatures and air humidity exerted a certain limiting effect on the optimal development of the plants; however, they did not compromise the execution of the trial.

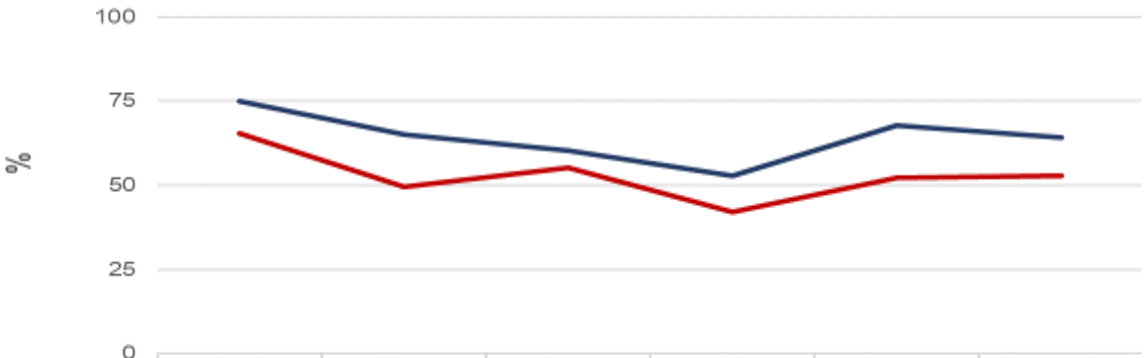

	April	May	June	July	August	September
08.00h	75.0	65.1	60.4	52.7	67.8	64.2
14.00h	65.5	49.5	55.1	42.2	52.2	52.9

***Figure 2**. Humidity inside the greenhouse in %.*

Nutrient Regime

The experiment was conducted under a uniform fertilization background tailored to the standard technology for greenhouse cucumber cultivation. To maintain an optimal nutrient regime based on agrochemical analysis recommendations, a basal application of 30 kg/da triple superphosphate and 40 kg/da potassium sulfate was performed. From April 11th to August 14th, the plants were fertigated weekly with 3.50 kg/da each of ammonium nitrate and potassium sulfate, after which the application rate was increased to 5.00 kg/da until the end of the vegetation period.

Growth Manifestations

The experimental data reflect a clear differentiation between the effects of the bioagents and the chemical variant on the vegetative development of the plants (Table 2).

The most intensive growth rate of the main stem was recorded under the sole soil application of *B. thuringiensis* (3.89 cm/24h) and its combination with endophytic bacteria (3.86 cm/24h). These values significantly exceed those obtained in the variant with Velum Prime application (3.03 cm/24h). The recorded differences in the parameters of this indicator among the remaining variants range from 3.38 cm/24h (Velum Prime + *B. thuringiensis*) to 3.69 cm/24h (Velum Prime + *B. thuringiensis* + endophytic bacteria), but they are not statistically supported.

The synergistic effect is even more pronounced regarding the leaf formation rate, where the variant combining *B. thuringiensis* and endophytic bacteria reaches the highest values of 0.64 leaves/24h.

The retardation of growth processes in the Velum Prime variant could be attributed to a phytotoxic or temporary inhibitory effect on the root microflora caused by the chemical active ingredient (fluopyram). Conversely, the stimulating effect exerted by *B. thuringiensis* confirms that this entomopathogen, in addition to its pesticidal properties, possesses traits of a plant growth-promoting rhizobacterium (PGPR). As noted by Francis et al. (2024), metabolites and bioformulations based on *B. thuringiensis* act as potent biostimulants, facilitating water uptake and cell elongation under stress conditions.

The interaction between *B. thuringiensis* and autochthonous endophytic bacteria (*B. thuringiensis* + endophytic bacteria) further catalyzes the process of leaf formation. This effect aligns with studies on modern cucumber hybrids, which establish that enriching the plant microbiome with bacteria from the genus *Bacillus* leads to a corresponding and sharp increase in stem length and leaf number (Prasad et al., 2024). Endophytic bacteria successfully colonize the internal tissues of the host, optimizing the physiological balance (homeostasis) of phytohormones and antioxidant defense.

Table 2. *Biometric parameters of greenhouse cucumbers cultivar Defense F_1.*

VARIANT	***Stem Height***		***Growth Rate***	***Number of Leaves***		***Leaf Formation Rate***
	cm. ***Initial***	*cm.* ***Final***	*cm/24h*	*Leaf No.* ***Initial***	*Leaf No.* ***Final***	*Leaf No. /24h*
1. Velum Prime	136.1	221.1	***3.03 b***	18.0	28.9	***0.39 c***
2. Velum Prime Endophytic bacteria	131.9	227.6	***3.42 ab***	18.6	31.2	***0.45 ab***
3. Velum Prime + B. thuringiensis	133.2	228.0	***3.38 ab***	17.7	31.0	***0.47 ab***
4. Velum Prime + B. thuringiensis Endophytic bacteria	125.3	228.8	***3.69 ab***	17.7	30.9	***0.47 ab***
5. B. thuringiensis	134.1	242.9	***3.89 a***	18.3	32.6	***0.51 b***
6. B. thuringiensis Endophytic bacteria	126.6	234.8	***3.86 a***	15.8	33.7	***0.64 a***

Productive Qualities and Yield Structure

The results for total and fractional yields demonstrate a distinct statistical fragmentation, distributed into clear statistical significance groups (***Fig. 1***).

Statistical analysis of the values representing first-class production categorized the data into four groups. The first group includes plants grown with soil application of *B. thuringiensis* and foliar treatment with endophytic bacteria, which achieved the highest values at 9578 kg/da. The second group consists of cucumbers treated with *B. thuringiensis* alone at 8739 kg/da. In the third group, values ranged from 7398 kg/da (Velum Prime + *B. thuringiensis*) to 7738 kg/da (Velum Prime + endophytic bacteria). The statistical group with the lowest value comprised the Velum Prime standalone variant at 6343 kg/da.

The values for second-class production are clearly differentiated into three significance groups. Cucumbers grown with a combined soil application of Velum Prime and *B. thuringiensis* kg/da, significantly outperforming the other variants. The lowest measurement for this parameter was recorded in plants treated via soil with *B. thuringiensis* alone (6722 kg/da). The remaining variants fell into a single significance group, with data falling within the range of 7098 kg/da (Velum Prime + *B. thuringiensis*) to 7446 kg/da (Velum Prime).

Regarding the total yield parameter, the collected data are even more sharply fragmented statistically, with differences between every single variant proved significant. The maximum total yield volume was obtained from cucumbers treated with *B. thuringiensis* and subsequent inoculation with endophytic bacteria at 16697 kg/da. The lowest values for this investigated indicator were observed in plants grown with soil-applied Velum Prime at 13789 kg/da. Among the remaining variants, recorded values fluctuated from 14496 kg/da (Velum Prime + *B. thuringiensis*) to 15918 kg/da (Velum Prime + *B. thuringiensis* + endophytic bacteria).

The experimental data regarding the productive traits of the cucumbers demonstrate a clear differentiation of fractional and total yields depending on the applied treatment schemes.

The highest total yield reported in the *B. thuringiensis* + endophytic bacteria variant is most likely a consequence of the dual application of both biological agents. This outcome is supported by the findings of Yuan et al. (2022), who demonstrated that the co-inoculation of

rhizospheric bacteria and intra-species endophytes induces a synergistic effect that optimizes the nutrient and water regimes. This optimization enables the plant to set and develop a significantly larger number of fruits.

The standalone soil application of *B. thuringiensis* and its combination with endophytes achieved the highest first-class yield values. These data confirm the scientific hypothesis of Francis et al. (2024) that *B. thuringiensis* metabolites act as potent physiological stimulants facilitating cell elongation and water homeostasis. Consequently, a higher percentage of the fruits possess high market quality, avoiding deformation or remaining underdeveloped under the influence of abiotic or biotic stress.

Within the yield structure, the lowest results for both total yield and first-class production were observed under the standalone application of the chemical nematicide Velum Prime. However, when this product is combined with bioproducts (Variants 2, 3, and 4), total yield increases substantially. The yield reduction observed under the standalone use of Velum Prime (fluopyram) can be explained by its mode of action as a succinate dehydrogenase inhibitor (SDHI). This temporarily exerts a negative impact on the energy metabolism of the root system or disrupts the balance of the beneficial autochthonous microflora (Massoud et al., 2021). The yield increase in Variants 2, 3, and 4 is most likely due to the added bioproducts, which successfully assist in overcoming this pesticide stress, thereby restoring rhizospheric homeostasis and recovering the productive potential of the crop.

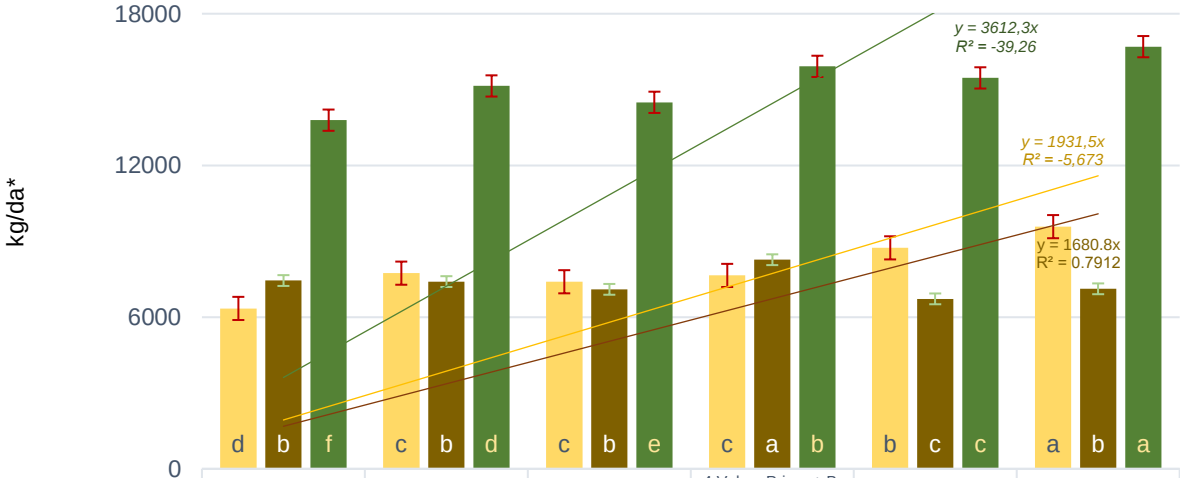

	1. Velum Prime	2. Velum Prime + Endophytic bacteria	3.Velum Prime + B. thuringiensis	4.Velum Prime + B. thuringiensis + Endophytic bacteria	5. B. thuringiensis	6.B. thuringiensis + Endophytic bacteria
I-st Quality Yield (kg/da)	6343	7738	7398	7648	8739	9578
II-nd Quality (kg/da)	7446	7405	7098	8270	6722	7119
TOTAL YIELD (kg/da)	13789	15143	14496	15918	15461	16697

* *da=ha*$^{-1}$

Figure 1. *Structure and distribution of yield by quality.*

Regarding the parameter of average fruit mass for first-class production, only the cucumbers treated with *B. thuringiensis* stood out with a lower value of 0.260 kg. For the remaining variants, the obtained data fell within the range of 0.275 kg (Velum Prime + *B. thuringiensis*) to 0.287 kg (Velum Prime + *B. thuringiensis* + endophytes).

No significant differences were recorded in the average mass of second-class fruits. Their values fluctuated between 0.265 kg (Velum Prime + *B. thuringiensis* + endophytes) and 0.287 kg (Velum Prime + *B. thuringiensis* + endophytes).

The calculated average fruit mass based on the total yield did not differ substantially among the individual variants. Exceptions were observed in cucumbers treated with *B. thuringiensis* (0.263 kg), which possessed a significantly lower mass compared to the variants treated with

Velum Prime + endophytic bacteria (0.284 kg) and Velum Prime + *B. thuringiensis* + endophytic bacteria (0.284 kg). The data obtained from the remaining plants varied between 0.270 kg (Velum Prime + *B. thuringiensis*) and 0.270 kg (Velum Prime). The results recorded for the individual variants were analogous to those of the parameter reflecting the average fruit mass of first-class production, where the registered differences were primarily between the aforementioned variants (***Table 5.***).

The data obtained for the average fruit mass under the sole application of *B. thuringiensis* (Var. 5) are of particular interest; this treatment induced high fruit set but reduced the average fruit mass to 0.260 kg. However, when *B. thuringiensis* was combined with endophytic bacteria (Var. 6), the average fruit mass increased substantially, reaching 0.281 kg. This physiological compensation can be explained by the findings of Kaya et al. (2026), who reported that inoculation with plant growth-promoting rhizobacteria (PGPR) in greenhouse production increases the accumulation of nitrogen and phosphorus in the leaves, balancing the shoot-to-root biomass ratio, which subsequently improves fruit nourishment.

Table 5. *Average fruit mass by quality class in greenhouse cucumbers.*

ВАРИАНТ	***I-во качество*** кг	***Sig.***	***II-во качество*** кг	***Sig.***	***ОБЩ ДОБИВ*** кг	***Sig.***
1. Velum Prime	0.279	a	0.275	n.s.	0.277	ab
2. Velum Prime + *Endophytic bacteria*	0.286	a	0.283	n.s.	0.284	a
3.Velum Prime + *B. thuringiensis*	0.275	a	0.265	n.s.	0.270	ab
4.Velum Prime + *B. thuringiensis* + *Endophytic bacteria*	0.287	a	0.287	n.s.	0.287	a
5. B. thuringiensis	0.260	b	0.267	n.s.	0.263	b
6. *B. thuringiensis* + *Endophytic bacteria*	0.281	a	0.266	n.s.	0.275	ab

The obtained results reflecting the share of first-class production relative to the total yield volume show a nearly equitable distribution among most treatments. The percentage distribution of first-class production relative to the total yield was highest in cucumbers grown under soil treatment with the *B. thuringiensis* - based bioproduct alone (Var. 5) at 56.52%, and when followed by inoculation with endophytic bacteria (Var. 6) at 57.37%. Conversely, the share of first-class fruits fell below half of the total yield in the variants treated with Velum Prime standalone at 46.00% and Velum Prime + *B. thuringiensis* + endophytic bacteria at 48.05%. These results are illustrated in ***Figure 2***.

The proven increase in both total and fractional yields under the influence of single-strain or combined endophytic inoculants aligns with contemporary global scientific literature. In a study by Singh et al. (2026) on open-field cucumbers, it was demonstrated that seed inoculation with endophytic bacterial strains of *Bacillus sp.* and *Microbacterium sp.* leads to a sustainable and statistically significant increase in the number and average mass of fruits per plant throughout the entire vegetation period. The present data confirm these findings under greenhouse conditions as well, demonstrating that Variant 6 successfully increases the share of premium-grade production to 57.37%.

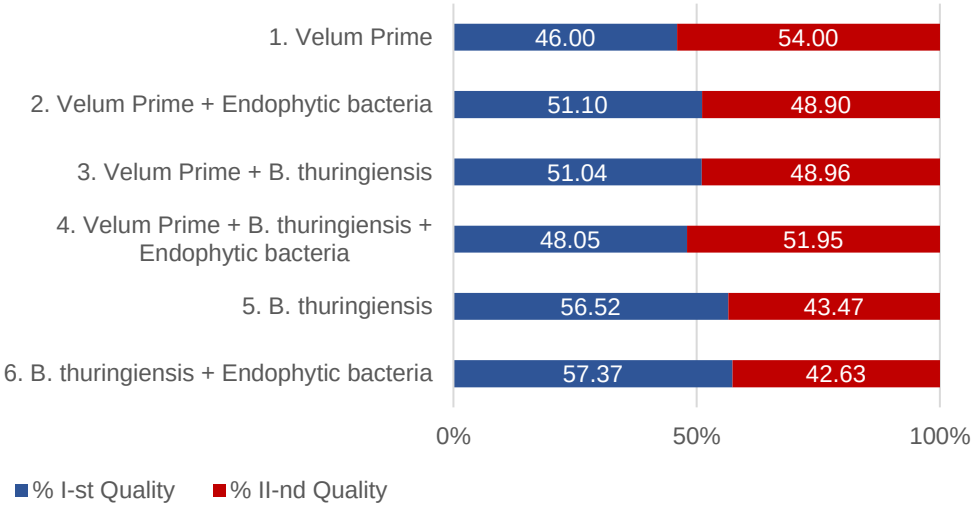

Figure 2. *Percentage distribution of production by quality relative to the total yield in greenhouse cucumbers.*

CONCLUSIONS

The application of the *B. thuringiensis* - based bioproduct (both standalone and combined) exerts a potent biostimulatory effect on the growth of greenhouse cucumbers. The treated plants exhibit the fastest main stem growth rate (3.89 cm/24 h and 3.86 cm/24 h, respectively), which confirms its PGPR properties.

The combined inoculation of greenhouse cucumbers with *B. thuringiensis* and autochthonous endophytic bacteria induces a significant synergistic effect on vegetative growth, which exerts a particularly strong influence on the leaf formation rate, reaching a maximum of 0.64 leaves/24 h.

Overcoming chemical stress: The standalone application of the conventional chemical nematicide Velum Prime exerts an inhibitory effect that suppresses growth processes (3.03 cm/24 h and 0.39 leaves/24 h) and results in the lowest total yield (13789 kg/da). Integrating biological agents into the chemical background exerts a positive impact and assists in recovering the productive potential of the crop, with the total yield increasing to 15918 kg/da.

The highest values of first-class production (9578 kg/da) and total yield (16697 kg/da) are formed under the combined use of B. thuringiensis and endophytic bacteria. This variant also achieves the maximum relative share of premium-grade production relative to the total yield (57.37%).

The combined application of *B. thuringiensis* and endophytic bacteria increases the average mass of first-class fruits (0.281 kg) compared to the standalone inoculation with *B. thuringiensis*. In the standalone *B. thuringiensis* variant, a higher fruit-setting intensity is established, which exceeds the plant's capacity to nourish them, consequently leading to a proven lowest average fruit mass (0.260 kg).

The application of Velum Prime or its combination within the three-component scheme impairs the commercial quality structure. These are the only variants in the study where the share of first-class production relative to the total yield falls below half (46.00% and 48.05%, respectively). In all other variants involving the application of bioproducts and endophytes, the percentage distribution of first-class production successfully exceeds 50%.

REFERENCES

1. **Akello, J., Dubois, T., Coyne, D., & Hillnhutter, C. (2001).** *Beauveria bassiana* as an endophyte in tissue cultured banana plants: A novel way to combat the banana weevil *Cosmopolites sordidus*. *Acta Horticulturae*, 828, 129–138.
2. **Akello, J., Dubois, T., Coyne, D., & Kyamanywa, S. (2009).** The effects of *Beauveria bassiana* dose and exposure duration on colonization and growth of tissue cultured banana (*Musa* sp.) plants. *Biological Control*, 49(1), 6–10.
3. **De Maagd, R. A., Bravo, A., Berry, C., Crickmore, N., & Schnepf, H. E. (2003).** Structure, diversity, and evolution of protein toxins from spore forming entomopathogenic bacteria. *Annual Review of Genetics*, 37, 409–433.
4. **Francis, A., Thompson, J., Roberts, M., & Garcia, L. (2024).** Encapsulation efficiency and survival of plant growth-promoting microorganisms in an alginate-based matrix for slowed and efficient delivery. *ResearchInBio*, 359, 102–115.
5. **Francis, A., Subramanian, S., Mosa, K. A., & Smith, D. L. (2024).** Metabolites and bioformulations based on *Bacillus thuringiensis* act as potent biostimulants facilitating water uptake and cell elongation under stress. *Journal of Plant Growth Regulation*, 43(2), 115–128.
6. **Kaya, M., Yilmaz, O., Demir, E., Aslan, H., & Kurt, S. (2026).** Enhancing cucumber production through compost and plant growth-promoting rhizobacteria (*Pseudomonas fluorescens* and *Bacillus* spp.) in protected environments. *Soil & Crop Science*, 142, 1129–1141.
7. **Lebeda, A., Ryder, E. J., Grube, R., Doležalová, I., & Křístková, E. (2007).** Lettuce (*Asteraceae*; *Lactuca* spp.). In *Genetic Resources, Chromosome Engineering, and Crop Improvement, Vegetable Crops* (Vol. 3, pp. 377–472). CRC Press.
8. **Massoud, M. A., El-Aziz, A. A., Khalil, M. S., & Darwesh, O. M. (2021).** Biological performance of certain bio-agents, fluopyram and fosthiazate against *Meloidogyne* spp. on guava trees (*Psidium guajava* L.). *Alexandria Science Exchange Journal*, 42(4), 789–797.
9. **Morris, O. N. (1972).** Susceptibility of some forest insects to mixtures of commercial *Bacillus thuringiensis* and chemical insecticides. *The Canadian Entomologist*, 104(9), 1419–1425.
10. **Musser, F. R., Nyrop, J. P., & Shelton, A. M. (2006).** Integrating biological and chemical controls in decision making. *Journal of Economic Entomology*, 99(5), 1538–1549.
11. **Parveen, S., & Rashtrapal, S. (2024).** Chemical pest control and its impacts on natural predator communities in agroecosystems. *Journal of Agricultural Ecology*, 12(2), 45–58.
12. **Prasad, R., Kumar, A., Sharma, V., Singh, S., & Yadav, P. (2024).** Growth enhancement and changes in bacterial microbiome of cucumber plants inoculated with endophytic bacterial species. *Letters in Applied Microbiology*, 78(4), 215–228.
13. **Ruiu, L., Satta, A., & Floris, I. (2013).** Emerging entomopathogenic bacteria for insect pest management. *Bulletin of Insectology*, 66(2), 181–186.
14. **Seleena, P., Lee, H. L., & Chiang, Y. F. (1999).** Compatibility of *Bacillus thuringiensis* serovar *israelensis* and chemical insecticides. *Journal of Vector Ecology*, 24(2), 216–223.
15. **Singh, K., Mishra, S., Choudhary, R., Patel, N., & Joshi, A. (2026).** Plant growth-promoting endophytic bacteria enhance growth and yield of cucumber (*Cucumis sativus* L.): A two-year field validation of single-strain inoculants. *Postharvest Biology and Technology*, 212, 112–124.
16. **Velkov, N., & Pevicharova, G. (2016).** Effects of cucumber grafting on yield and fruit sensory characteristics. *Zemdirbyste-Agriculture*, 103(4), 405–410.
17. **Vilcinskas, A. (2010).** Coevolution between pathogen-derived proteinases and proteinase inhibitors of host insects. *Virulence*, 1(3), 206–214.
18. **Yuan, J., Zhao, M., & Huang, Q. (2022).** *Bacillus* for plant growth promotion and stress resilience: Interaction mechanisms and bioformulation strategies. *Plants*, 11(19), 2482.

BİOACCUMULATION MECHANISMS AND OXIDATIVE STRESS-MEDIATED TOXIC EFFECTS OF PER- AND POLYFLUOROALKYL SUBSTANCES (PFAS)

Bahar İkizoğlu [1], İlayda Reyhan Kundakçı [2]

[1] Süleyman Demirel University, Faculty of Engineering and Natural Sciences, Department of Environmental Engineering, Isparta, Turkey
[2] Yıldız Technical University, Department of Molecular Biology and Genetics, Turkey
Corresponding author e-mail: baharikizoglu@sdu.edu.tr

ABSTRACT

Per- and polyfluoroalkyl substances (PFAS), which cannot be metabolized due to their strong carbon–fluorine bonds, can stay in the human body for years because of their long biological half-lives and lead to bioaccumulation. Because of their high chemical stability and resistance to biological breakdown, they are called “forever chemicals.” These compounds attach to albumin and other carrier proteins, are transported through the bloodstream, and enter cells via carrier proteins, building up in various tissues, mainly in the liver.

PFAS exposure causes toxicity mainly through oxidative stress at the cellular level. By disrupting mitochondrial function, PFAS increase the production of reactive oxygen species (ROS) while suppressing antioxidant defenses such as superoxide dismutase, catalase, and the glutathione system, thereby reducing overall antioxidant capacity. As a result, cells struggle to counteract the increased ROS, disrupting redox balance and leading to oxidative stress. This stress results in DNA damage, lipid peroxidation, and changes in cell structure. Studies have shown that PFAS compounds such as PFOS, PFOA, PFNA, and PFHxS cause DNA strand breaks, elevate biomarkers of oxidative and nitrosative stress, and trigger inflammatory responses. The liver is the primary target, where PFAS accumulation disrupts lipid metabolism, promotes inflammation, and causes liver toxicity. Furthermore, the nervous system and developmental processes are negatively impacted through PFAS-induced oxidative stress. PFAS also activate PPARα and related pathways, alter fatty acid metabolism, increase peroxisomal oxidation, and enhance the internal oxidative load.

This study examined the bioaccumulation mechanisms of PFAS, the processes involved in oxidative stress development, and the toxic effects resulting from these mechanisms. It assessed cellular uptake, bioaccumulation features, stages of oxidative stress, and PFAS impacts on DNA damage, lipid peroxidation, hepatotoxicity, neurotoxicity, and developmental toxicity based on current literature. The findings demonstrate that PFAS are important environmental pollutants posing a serious risk to human health due to their bioaccumulation and oxidative stress-related toxicity mechanisms. Consequently, developing strategies to reduce PFAS exposure and further exploring their toxicity mechanisms are recommended.

Keywords: PFAS, oxidative stress, bioaccumulation, reactive oxygen species (ROS), toxicity.

1. INTRODUCTION

Per- and polyfluoroalkyl substances (PFAS) are synthetic organofluorine compounds that have been widely used in industrial and commercial applications since the 1940s (Yurtsever et al., 2025, Tancreda et al., 2025, İkizoglu, 2024). Due to their water-, oil-, and stain-repellent properties, as well as their high thermal and chemical stability, they are commonly used in firefighting foams, food packaging, textile products, non-stick coatings, cosmetics, and various industrial processes. The strong carbon-fluorine bonds in their structures largely prevent their

degradation in the environment and biological systems, leading these compounds to persist for a long time and earning them the nickname "forever chemicals". PFAS can be transported over large areas through water, soil, and air, bioaccumulate throughout the food chain, and accumulate in various organs - particularly the liver - in humans (Ding et al., 2025). Recent studies have shown that PFAS exposure is associated with various adverse health effects, including liver toxicity, immune system disorders, endocrine disruptions, reproductive and developmental issues, and certain types of cancer. For these reasons, PFAS are now considered among the priority pollutants concerning environmental and public health (İkizoglu et al., 2024, Taibl et al., 2022, Ding et al., 2025, Behr et al., 2019).

Reactive oxygen species (ROS) are reactive derivatives of oxygen that naturally occur in mitochondria during cellular metabolism. ROS, which include molecules such as superoxide radical ($O_2^{\bullet -}$), hydroxyl radical (•OH), hydrogen peroxide (H_2O_2), and singlet oxygen ($^1O_2$), play crucial roles in many biological processes such as cellular signal transduction, immune response, stem cell signaling, fat cell metabolism and differentiation (adipogenesis), and regulation of inflammation under normal conditions. Oxidative stress results from an imbalance between the production and accumulation of reactive oxygen species (ROS), which is an essential cellular regulatory mechanism in biological systems, and the detoxification of these reactive molecules (Gundacker et al., 2022). When ROS accumulate excessively due to insufficient antioxidant defenses, they can oxidize macromolecules such as DNA, proteins, and lipids, leading to cellular damage and toxicity (Wielsøe et al., 2014, Ding et al., 2025). To manage rising ROS levels, cells have evolved defense mechanisms that include oxidative stress biomarkers such as Total Antioxidant Capacity (TAC), DNA damage, and ROS production (Wielsøe et al., 2014). This protective system, which includes various antioxidant mechanisms like superoxide dismutase (SOD), catalase (CAT), and the glutathione system, plays a vital role in minimizing the effects of ROS from abnormal mitochondrial oxidative respiration (Valle et al., 2025).

Figure 1. Oxidative stress mechanism caused by excessive production of reactive oxygen species (ROS)

2. The Role of PFAS Exposure in Causing Oxidative Stress

The primary mechanism by which PFAS induces oxidative stress is increased mitochondrial ROS production. PFAS disrupts the electron transport chain in mitochondria, which reduces ATP production, causes electron leakage, and leads to the formation of ROS such as superoxide and hydroxyl radicals through leaked electrons reacting with molecular oxygen (O_2). Another mechanism involves the suppression of antioxidant defense systems. The activity of enzymes like SOD (superoxide dismutase), catalase, and the glutathione system, which help the cell remove ROS under normal conditions, decreases with PFAS exposure. This weakens the cell's

defenses against rising ROS levels. In fact, PFOA has been shown to significantly reduce Total Antioxidant Capacity (TAC) in HepG2 cells (Gundacker et al., 2022, Wielsøe et al., 2014). The third mechanism involves the activation of the PPARα signaling pathway. Studies have shown that PFOS and PFOA increase peroxisomal fatty acid oxidation by activating PPARα, leading to additional H_2O_2 production and a greater intracellular oxidative load (Gundacker et al., 2022, Behr et al., 2019, Rosen et al., 2017).

Studies conducted on human hepatoma cells (HepG2) have shown that PFOA (Perfluorooctanoic acid) exposure significantly reduces total antioxidant capacity (TAC). This indicates that PFOA weakens the liver cells' protective defenses, leading to an imbalance between increased ROS production and inhibited antioxidant mechanisms, thereby causing heightened oxidative stress and cellular damage. Conversely, the lack of significant change in TAC levels for the other six PFAS compounds suggests that different PFAS types may have varying oxidative stress potentials (Wielsøe et al., 2014, Behr et al., 2019). Similarly, while PFNA prevents oocyte maturation by disrupting mitochondrial functions, PFOS and PFOA increase fatty acid oxidation by activating the PPARα signaling pathway and boost ROS production by upregulating genes involved in peroxisomal fatty acid oxidation, such as ACOX1. This creates an oxidative burden in the cell that antioxidant defenses cannot adequately counter (Rosen et al., 2017). Under normal conditions, antioxidant defenses like SOD (superoxide dismutase), catalase, and the glutathione system neutralize ROS and maintain cellular redox balance. However, PFAS exposure inhibits these enzymes, reduces TAC, and hampers the cell's defense capability (Behr et al., 2019). A study among adults in Taiwan found a positive correlation between linear PFOS levels, a type of PFAS, and biomarkers of DNA oxidative and nitrosative stress, such as 8-hydroxy-2-deoxyguanosine (8-OHdG) and 8-nitroguanine (8-NO2Gua). The findings indicate that increased PFOS exposure has an oxidative and nitrosative impact on DNA, with higher PFOS levels correlating with significantly increased urinary 8-OHdG and 8-NO2Gua levels (Lin et al., 2020). Laboratory studies have demonstrated that PFAS exposure induces oxidative stress by raising ROS production and disrupting redox homeostasis, leading to lipid peroxidation, DNA damage, reduced antioxidant capacity, and cytotoxicity (Tancreda et al., 2025, Taibl et al., 2022). These effects negatively impact liver function, metabolism, and the immune system. Oxidative damage resulting from the failure of cellular antioxidant defenses to counteract the increased ROS load is associated with various diseases, including atherosclerosis, heart attacks, chronic inflammatory diseases, central nervous system disorders, age-related diseases, and cancer (Wielsøe et al., 2014).

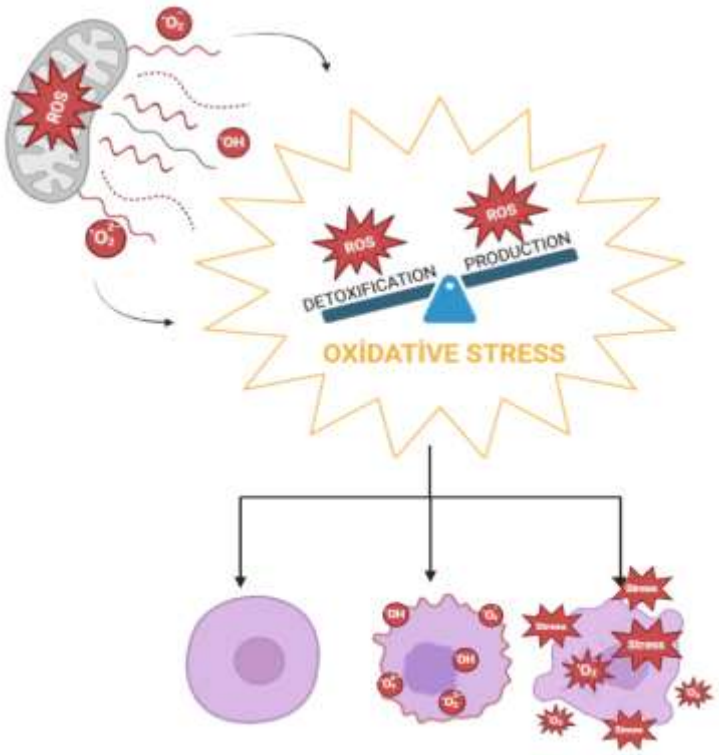

Figure 2. Schematic illustration of the oxidative stress mechanism and the resulting cellular damage caused by excessive reactive oxygen species (ROS) production

3. Bioaccumulation Mechanisms of PFAS

PFAS bioaccumulate because of their high chemical stability, as the carbon–fluorine (C–F) bonds in their structure are among the strongest in nature, and because they cannot be metabolized or biodegraded in the body (Yurtsever et al., 2025, Connolly et al., 2025, Behr et al., 2019).

Since PFAS bind to blood proteins, they cannot easily pass through the cell membrane by passive diffusion because of their amphiphilic structure. They are transported through the bloodstream by binding to carrier proteins such as albumin, fatty acid-binding proteins, organic anion transporters (OAT), and ABC transporters, and are taken into the cell through this transport. This process facilitates the circulation and bioaccumulation of PFASs in the organism (Zhao et al., 2017). PFHxS has long half-lives of approximately 8.8 years, PFOS approximately 5.4 years, and PFOA approximately 2.3–3.8 years; this shows that these compounds can stay in the body for many years and, because of their long biological half-lives, they can circulate in the organism for an extended period and cause bioaccumulation (Wielsøe et al., 2014).

The reason they bioaccumulate mainly in the liver is that all blood passes through it, and PFAS are strongly retained there by binding to albumin. However, although the liver attempts to eliminate PFASs through metabolism, it cannot effectively remove these compounds (Connolly et al., 2025, Zhao et al., 2017, Forsthuber et al., 2020). In a study conducted on zebrafish, F-53B, a PFOS alternative, has been reported to accumulate mostly in the ovaries (gonads) of female zebrafish and then in the liver. It has also been reported that in men, it accumulates most in the liver, least in the brain, and its toxic effects (vacuolization and oxidative stress) are mainly observed in liver tissue (Wu et al., 2019). Studies have shown that ROS levels increase proportionally with higher doses of PFHxS and PFUnA; it has been reported that although antioxidant systems such as SOD2 and HSP70 are activated as short-term stabilizers, oxidative

stress becomes inevitable as the effects of PFAS persist in the long term (Wielsøe et al., 2014, Valle et al., 2025).

4. Toxic Effects of PFAS Mediated by Oxidative Stress

The analysis of DNA damage caused by the toxic effects of PFAS through oxidative stress has shown that excessive ROS production damages DNA bases, leading to double-strand breaks, increasing levels of DNA damage biomarkers such as 8-OHdG and 8-NO_2Gua. Specifically, PFOS, PFOA, PFNA, and PFHxS cause DNA breaks in HepG2 cells. Additionally, it has been reported that PFAS exposure dose-dependently increases DNA strand breaks and worsens genotoxic effects (Wielsøe et al., 2014, Eriksen et al., 2010).

Regarding lipid peroxidation, cell membrane integrity is compromised as ROS oxidize membrane lipids, leading to an increase in lipid peroxidation biomarkers, such as 8-iso-$PGF_2\alpha$. It has also been reported that PFAS exposure may influence birth weight in pregnant women, due to the strong link between PFOS levels and this biomarker. As lipid peroxidation progresses, cell membrane permeability increases, causing deterioration of cellular functions and loss of cell integrity (Taibl et al., 2022, Gundacker et al., 2022, Behr et al., 2019).

Regarding liver toxicity, it is known that the liver is the primary site of PFAS accumulation, and that excessive ROS production—which occurs when PFAS activates PPARα and increases peroxisomal fatty acid oxidation—disrupts lipid metabolism, leading to fatty liver, inflammation, hypertrophy, and necrosis. This process raises serum ALT and AST levels, forming the basis of chronic hepatotoxicity. It has also been reported that increases in pro-inflammatory cytokines like IL-6 and IL-1β worsen hepatic inflammation and heighten the risk of long-term fibrosis (Yurtsever et al., 2025, Tancreda et al., 2025, Connolly et al., 2025, Behr et al., 2019, Rosen et al., 2017).

Regarding neurotoxicity, the FTOH (fluorotelomer alcohol) compound disrupts the actin cytoskeleton by increasing intracellular ROS production and may cause structural damage to neurons. It has also been shown that PFAS worsen inflammation by raising levels of cytokines such as IL-6 and IL-1β, making nerve cells more vulnerable to oxidative damage. It is reported that disruption in actin polymerization contributes to negative effects on neuronal functions by weakening the integrity of the cytoskeleton. This process is considered a fundamental mechanism behind the slowing of fetal growth and the development of disorders (Ding et al., 2025, Connolly et al., 2025).

Regarding fetal and developmental effects, prenatal PFAS exposure is associated with low birth weight, growth retardation, and issues in fat cell development. It has been reported that PFAS causes abnormal differentiation of pre-adipocytes by increasing ROS production and activating PPARγ, AKT, and MAPK pathways, which negatively impacts birth weight by disrupting fetal adipose tissue development. This process is considered one of the main mechanisms behind slowed fetal growth and the development of developmental disorders (Gundacker et al., 2022, Connolly et al., 2025, Behr et al., 2019, Rosen et al., 2017).

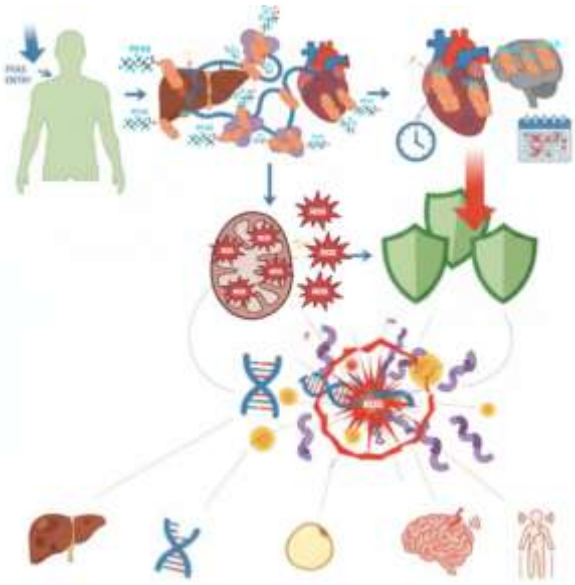

Figure 3. Schematic illustration of bioaccumulation, oxidative stress, and toxic effects from PFAS exposure

Overall, oxidative stress caused by PFAS exposure and DNA damage is considered one of the main mechanisms behind the toxic effects impacting multiple organs and systems, including lipid peroxidation, hepatotoxicity, neurotoxicity, and developmental toxicity.

5. Comparison of PFAS Types' Potential to Induce Oxidative Stress

The oxidative stress-inducing potential of PFAS types varies with chain length and isomer structure. Based on chain length, PFOA, which has the shortest chain length (C8) among perfluorinated carboxylic acids (PFCA), is the only PFCA that significantly affects the three oxidative stress parameters tested: DNA damage, ROS production, and Total Antioxidant Capacity (TAC) reduction. In contrast, longer chain PFCAs such as PFDA, PFUnA, and PFDoA did not produce a significant increase in DNA damage (Wielsøe et al., 2014).

Regarding isomer structure, a study of Taiwanese adults found a positive correlation between linear serum PFOS levels and 8-OHdG and 8-NO_2Gua, biomarkers of oxidative and nitrosative DNA stress. The study also noted that this relationship varies depending on the PFOS isomer (Lin et al., 2020).

5. CONCLUSION AND RECOMMENDATIONS

Per- and polyfluoroalkyl substances (PFAS) are significant pollutants that remain in the environment and living organisms because of their high chemical stability, non-biodegradability, and long biological half-lives. Their entry into cells through albumin and other carrier proteins, along with their accumulation in various tissues—especially the liver—form the basis of the toxic effects of these compounds.

Literature findings indicate that PFAS exposure increases reactive oxygen species (ROS) production by impairing mitochondrial functions, inhibiting antioxidant defenses such as superoxide dismutase, catalase, and the glutathione system, and disrupting cellular redox homeostasis, which leads to oxidative stress. Additionally, activation of PPARα-mediated signaling pathways and heightened peroxisomal fatty acid oxidation further elevate the intracellular oxidative load, amplifying toxicity mechanisms.

PFAS-induced oxidative stress causes significant biological effects that impact multiple organs and systems, including DNA damage, lipid peroxidation, hepatotoxicity, neurotoxicity, and

developmental toxicity. It is known that the ability to generate oxidative stress varies among PFAS types based on their chain length and isomer structure, with compounds like PFOA and linear PFOS potentially showing more pronounced oxidative effects.

In conclusion, it is crucial to consider bioaccumulation properties and oxidative stress mechanisms together when assessing the toxic effects of PFAS on human health. Developing regulatory strategies to reduce PFAS exposure, expanding environmental monitoring efforts, and increasing in vitro, in vivo, and epidemiological research to explore the molecular toxicity mechanisms of various PFAS compounds will significantly contribute to a better understanding of their long-term impacts on the environment and public health.

REFERENCES

Behr, A., Plinsch, C., Braeuning, A., & Buhrke, T. (2019). Activation of human nuclear receptors by perfluoroalkylated substances (PFAS). Toxicology in Vitro, 62, 104700. https://doi.org/10.1016/j.tiv.2019.104700

Connolly, J. C., Ishihara, Y., Sawaya, E., Whitfield, V., Garrity, N., Sohata, R., Tsymbal, M., Lundberg, A., La Merrill, M. A., DeWitt, J. C., Ehrlich, A. K., & Vogel, C. F. A. (2025). Per- and polyfluoroalkyl substances (PFAS) enhance cholesterol accumulation and dysregulate inflammatory responses in macrophages. Cardiovascular Toxicology, 25(10), 1455–1470. https://doi.org/10.1007/s12012-025-10048-w

Ding, X., Xu, N., Zhang, W., & Wang, P. (2025). Integrated microfluidic three-organ chip for real-time toxicity analysis of fluorotelomer alcohols in the gut–vascular–nerve axis. Lab on a Chip, 25(23), 6170–6176. https://doi.org/10.1039/d5lc00631g

Eriksen, K. T., Raaschou-Nielsen, O., Sørensen, M., Roursgaard, M., Loft, S., & Møller, P. (2010). Genotoxic potential of the perfluorinated chemicals PFOA, PFOS, PFBS, PFNA and PFHxA in human HepG2 cells. Mutation research, 700(1-2), 39–43. https://doi.org/10.1016/j.mrgentox.2010.04.024

Forsthuber, M., Kaiser, A. M., Granitzer, S., Hassl, I., Hengstschläger, M., Stangl, H., & Gundacker, C. (2020). Albumin is the major carrier protein for PFOS, PFOA, PFHxS, PFNA and PFDA in human plasma. Environment international, 137, 105324. https://doi.org/10.1016/j.envint.2019.105324

Gundacker, C., Audouze, K., Widhalm, R., Granitzer, S., Forsthuber, M., Jornod, F., Wielsøe, M., Long, M., Halldórsson, T. I., Uhl, M., & Bonefeld-Jørgensen, E. C. (2022). Reduced Birth Weight and Exposure to Per- and Polyfluoroalkyl Substances: A Review of Possible Underlying Mechanisms Using the AOP-HelpFinder. Toxics, 10(11), 684. https://doi.org/10.3390/toxics10110684

İkizoglu B. (2024). PFOA and PFOS Pollution in Surface Waters and Surface Water Fish. Water, 16, 2342. https://doi.org/10.3390/ w16162342

Lin, C. Y., Lee, H. L., Hwang, Y. T., & Su, T. C. (2020). The association between total serum isomers of per- and polyfluoroalkyl substances, lipid profiles, and the DNA oxidative/nitrative stress biomarkers in middle-aged Taiwanese adults. Environmental research, 182, 109064. https://doi.org/10.1016/j.envres.2019.109064

Rosen, M. B., Das, K. P., Rooney, J., Abbott, B., Lau, C., & Corton, J. C. (2017). PPARα-independent transcriptional targets of perfluoroalkyl acids revealed by transcript profiling. Toxicology, 387, 95–107. https://doi.org/10.1016/j.tox.2017.05.013

Taibl, K. R., Schantz, S., Aung, M. T., Padula, A., Geiger, S., Smith, S., Park, J. S., Milne, G. L., Robinson, J. F., Woodruff, T. J., Morello-Frosch, R., & Eick, S. M. (2022). Associations of per- and polyfluoroalkyl substances (PFAS) and their mixture with oxidative stress biomarkers during pregnancy. Environment international, 169, 107541. https://doi.org/10.1016/j.envint.2022.107541

Tancreda, G., Campisi, L., Sarti, M., Pozzo, L., & Vornoli, A. (2025). Perfluoroalkyl Substances (PFAS) and Lipid Metabolism in Experimental Animal Models: A Scoping Review on the Mechanisms Behind the Induced Hepatotoxicity. Current Issues in Molecular Biology, 47(11), 944. https://doi.org/10.3390/cimb47110944

Wielsøe, M., Long, M., Ghisari, M., & Bonefeld-Jørgensen, E. C. (2014). Perfluoroalkylated substances (PFAS) affect oxidative stress biomarkers in vitro. Chemosphere, 129, 239–245. https://doi.org/10.1016/j.chemosphere.2014.10.014

Wu, Y., Deng, M., Jin, Y., Liu, X., Mai, Z., You, H., Mu, X., He, X., Alharthi, R., Kostyniuk, D. J., Yang, C., & Tu, W. (2019). Toxicokinetics and toxic effects of a Chinese PFOS alternative F-53B in adult zebrafish. Ecotoxicology and Environmental Safety, 171, 460–466. https://doi.org/10.1016/j.ecoenv.2019.01.010

Valle, E. M. A., Sultan, A., Konig, I., Cabello, C. Q., de Oliveira, H. P. M., Codognoto, L., & Martyniuk, C. J. (2025). Toxicity Assessment of Mixture Effects of Insecticides and Perfluorinated Chemicals (PFAS) in Zebrafish (Danio rerio): A Case Study with Chlorpyrifos and Perfluorohexanoic Acid (PFHxA). Journal of applied toxicology: JAT, 10.1002/jat.4980. Advance online publication. https://doi.org/10.1002/jat.4980

Yurtsever, M. (2025). Çevredeki Per ve Polifloroalkil Madde (PFAS) Kirliliği: Tarihçesi, Kaynakları, Analizi, Riskleri ve İlgili Düzenlemeler. Recep Tayyip Erdoğan Üniversitesi Fen Ve Mühendislik Bilimleri Dergisi, 6(1), 403–427. https://doi.org/10.53501/rteufemud.1536329

Zhao, W., Zitzow, J. D., Weaver, Y., Ehresman, D. J., Chang, S. C., Butenhoff, J. L., & Hagenbuch, B. (2017). Organic Anion Transporting Polypeptides Contribute to the Disposition of Perfluoroalkyl Acids in Humans and Rats. Toxicological sciences : an official journal of the Society of Toxicology, 156(1), 84–95. https://doi.org/10.1093/toxsci/kfw236

THE EFFECT OF MURASHIGE AND SKOOG MEDIA STRENGTHS ON *IN VITRO* SHOOT AND ROOT REGENERATION FREQUENCIES OF BAMBARA GROUNDNUT (*Vigna subterranea* (L.) VERDC.) GENOTYPES

Prince-Charles KULEKEY [1], Çiğdem ULUBAŞ SERÇE [1], Allah Bakhsh JOIYA [2]*

[1] Niğde Ömer Halisdemir University, Faculty of Agricultural Sciences and Technologies, Department of Plant Production and Technologies
[2] National Centre of Excellence in Molecular Biology, Faculty of Sciences, University of the Punjab, Lahore, Pakistan
**Corresponding author e-mail: princecharleskulekey@gmail.com*

ABSTRACT

Bambara groundnut *(Vigna subterranea (L.) Verdc.)* is a vital indigenous African leguminous crop valued for its drought tolerance, adaptability to poor soils, and nutritional composition. Despite its valuable agricultural importance, the crop remains under-utilized because of inadequate regeneration systems and limited genetic enhancement programs. The development of efficient *in vitro* regeneration protocols is hence crucial for genetic transformation, germplasm conservation, and rapid multiplication of Bambara groundnut. The optimization of basal medium composition is crucial for developing efficient regeneration systems in *V. subterranea,* precisely for applications involving genetic transformation and micropropagation. This study investigated the effects of different strengths of Murashige and Skoog (MS) medium on the shoot and root frequencies of five Bambara groundnut landraces (Ci1–Ci5). Explants were cultured on MS media at 1×, ¾×, ½×, and ¼× strengths, and regeneration responses were evaluated. Data were analysed using ordinary two-way analysis of variance (ANOVA) in GraphPad Prism. Shooting frequency was significantly influenced by genotype ($F_{4, 40} = 76.63$, $P < 0.0001$) and MS medium strength ($F_{3, 40} = 600.2$, $P < 0.0001$), whereas their interaction was not significant ($F_{12, 40} = 1.095$, $P = 0.3903$). Rooting frequency was significantly affected by genotype ($F_{4, 40} = 95.80$, $P < 0.0001$), MS medium strength ($F_{3, 40} = 581.0$, $P < 0.0001$), and their interaction ($F_{12, 40} = 2.636$, $P = 0.0107$). Full-strength (1×) MS medium promoted optimal shoot induction, whereas half-strength (½×) MS medium enhanced root formation. Among the genotypes, Ci2 consistently exhibited superior regenerative performance. These findings provide vital insights for the development of efficient *in vitro* regeneration protocols for *V. subterranea* enhancement programs.

Keywords: GraphPad Prism, Bambara groundnut, *Vigna subterranea*, MS medium strengths, shoot regeneration, root induction, tissue culture.

INTRODUCTION

Bambara groundnut (*Vigna subterranea* (L.) Verdc.) is an indigenous African leguminous crop that has attracted increasing agricultural and scientific interest because of its outstanding resilience to harsh climatic conditions and its potential contribution to sustainable food production (Tan et al., 2020; Chelangat et al., 2023). The crop is well adapted to low-fertility soil and drought-prone regions where many conventional leguminous crops fail to perform satisfactorily (Mayes et al., 2019). Its ability to produce stable and high-quality yields under water-limited conditions highlights that it's an essential climate-resilient crop with significant potential to advance food and nutritional security, particularly in sub-Saharan Africa and other semi-arid regions (Nhamo et al., 2022). In addition to their adaptability, Bambara groundnuts are highly nutritious, containing substantial amounts of protein, dietary fiber, minerals,

carbohydrates, healthy lipids, and essential amino acids, making it a vital source of affordable plant-based nutrition (Maphosa et al., 2022; Pasipanodya et al., 2025). Furthermore, its nitrogen-fixing ability enhances soil fertility improvement, making it an essential component of sustainable cropping systems.

Despite these important characteristics, Bambara groundnut remains one of the world's most under-researched and underutilised leguminous crops (Majola et al., 2021). Compared with major legumes such as common bean, soybean, and cowpea, relatively little progress has been made in genetic improvement (Tan et al., 2020). Conventional breeding exploits are hindered by the crop's predominantly limited genetic variability, low natural hybridization rates, self-pollinating reproductive system, and the lengthy breeding cycles required to develop improved cultivars (Bilali et al., 2024). The limitations have slowed the development and improvement of varieties possessing enhanced yield potential, improved nutritional quality, disease resistance, and tolerance to abiotic stresses (Kunene et al., 2024). Consequently, there is increasing interest in integrating modern biotechnological strategies, including genetic transformation and CRISPR/Cas-mediated genome editing, into Bambara groundnut enhancement programs (Mubaiwa et al., 2018).

The success of these advanced breeding strategies depends basically on the availability of reliable and efficient *in vitro* regeneration systems (Maren et al., 2022). Plant regeneration through tissue culture depicts a critical prerequisite for genetic transformation because transformed cells must retain the capability to regenerate into complete, fertile plants (Youngstrom et al., 2024; Maren et al., 2022). Likewise, genome-editing technological systems require efficient regeneration protocols to recover altered tissues into viable plants for subsequent investigation, evaluation, and breeding (Altpeter et al., 2016; Wu et al., 2024). Hence, the development of a reproducible regeneration system is considered one of the most important foundations for functional genomics, transgenic research, molecular breeding, and large-scale micropropagation of Bambara groundnuts.

Among the factors influencing successful *in vitro* regeneration, the composition of the culture media plays a pivotal role in facilitating organogenesis and overall plant developmental growth (Biswas et al., 2024). The mineral nutrients provided in the culture media directly influence osmotic balance, cellular metabolism, enzyme activity, nutrient uptake, and the differentiation of cultured tissues (Jung et al., 2021). Murashige and Skoog (MS) medium remains the most widely utilized medium for plant tissue culture because of its comprehensive mineral composition and its ability to support regeneration in a broad range of plant species (Holmes et al., 2021). However, the optimal concentration of MS salts is highly species-dependent and may also vary among genotypes, explant types, and developmental stages (Sokolov et al., 2014). Consequently, determining the appropriate nutrient concentration is essential for maximizing regeneration efficiency.

Previous investigations have demonstrated that full-strength MS medium generally provides sufficient micro- and macronutrients to facilitate rapid shoot induction, multiplication, and vigorous vegetative growth (Biswas et al., 2024; Jung et al., 2021). Nonetheless, excessive concentrations of salt may inhibit root formation, reduce root elongation (Jung et al., 2021), or induce physiological stress in regenerating tissues. Conversely, reducing MS salt concentration often improves rooting by reducing ionic toxicity and lowering osmotic pressure, thereby facilitating healthier root initiation and elongation (Biswas et al., 2024). Several studies involving legumes and other plant species have reported improved rooting performance on diluted MS or half-strength media, although the optimal nutrient concentration often depends on the culture conditions and genotype (Biswas et al., 2024; Jung et al., 2021).

Because Bambara groundnut exhibits considerable genotypic variation in its *in vitro* response (Mongomaké et al., 2009), regeneration protocols optimized for one landrace may not necessarily be suitable for others. Having insight into how different genotypes respond to variations in nutrient concentration is henceforth crucial for developing robust regeneration

systems that can be broadly utilized across breeding materials. Such optimisation not only enhances the efficiency of tissue culture but also facilitates effective downstream applications covering genetic transformation, genome editing, rapid multiplication and conservation of elite germplasm of improved genotypes.

In light of these considerations, the present study was conducted to investigate and quantify the effects of different MS medium strengths on the shooting and rooting responses of five Bambara groundnut landraces (Ci1–Ci5). Specifically, full-strength (1×), three-quarter-strength (¾×), half-strength (½×), and quarter-strength (¼×) MS media were evaluated to determine their effects on root and shoot regeneration frequencies. The findings of the study are expected to contribute to the optimisation of genotype-independent regeneration techniques and protocols, providing an essential platform for future applications of CRISPR/Cas genome editing, genetic transformation, and other advanced biotechnological improvement techniques in Bambara groundnut genotypes.

MATERIALS AND METHODS

Plant Material and Culture Conditions

Five Bambara groundnut landraces (Ci1, Ci2, Ci3, Ci4, and Ci5) (Figure 1) from the Northern part of Ghana (Upper East Region) were explored in this study. Embryonic axes were cultured on MS media prepared at four different strengths: full, three-quarter, half, and quarter. Cultures were maintained under controlled environmental conditions conducive to *in vitro* regeneration. The pH of all the media was adjusted to 5.6 with 0.1 N NaOH or 0.1 N HCl after addition of the growth regulators, prior to the addition of 0.25% agar (Duchefa). The media were autoclaved at 121°C for 30 min. All the cultures were maintained in a growth chamber at 25 ± 2°C, under a 12 h light period and constant 70% relative humidity. The fluorescent tube light flux (100 µEm-2S-1) was provided by warm white.

Figure 1. Characteristics of the five Bambara groundnut landraces used in this study. Ci1 (cream); Ci2 (cream-red); Ci3 (black-cream); Ci4 (black); and Ci5 (red)

Establishment of Regeneration System

At the beginning of the experiment, seeds were surface-sterilized with 70% (v/v) ethanol for 30 s, then treated with 10% (w/v) sodium hypochlorite for 30 min, followed by 3-4 rinses in

sterile distilled water. The seeds were soaked in sterile distilled water for 72 hrs in total obscurity. After this step, the seed coat was removed under aseptic conditions, and the embryonic axes were excised from the cotyledons and cultured on full-, three-quarter, half-, and quarter-strength MS medium (1962) supplemented with 30 g/l sucrose without vitamins and hormones (Figure 2). Cultures were incubated for 3 weeks, and epicotyl segments were cut from the seedlings and used for the induction of adventitious shoots. Epicotyls were cut into 2 cm fragments. The explants were vertically cultured on a basal initiation medium containing full MS salts (1962), vitamins B5 as established by Gamborg et al. (1968), and 30 g/l sucrose supplemented with different BAP concentrations (0.5, 1, and 2 mg/l) (Figure 3) to promote shoot regeneration.

Figure 2. Surface sterilization (A and B); removal of the embryonic axis (C) from mature seeds to obtain *Vigna subterranea* (L.) *in vitro* seedlings as starting material. (C and D) An embryonic axis isolated from a Bambara groundnut seed was placed on MS medium without a growth regulator. (E, F, and G) Development of the embryonic axis into a plantlet on MS0 after 3 weeks of culture

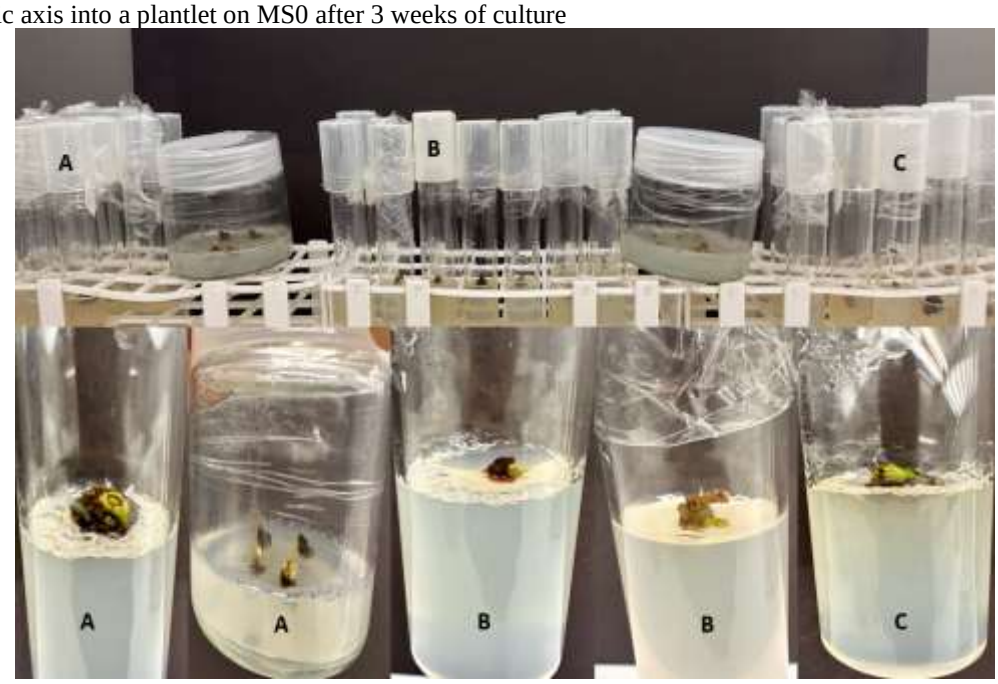

Figure 3. Shows the Bambara groundnut *in vitro* regeneration system using epicotyl as explants (from Ci2). A represents 0.5 mg/l; B is 1 mg/l and C is 2 mg/l of BAP concentrations.

Experimental Design

The investigation was premised on a completely randomized design with three replicates per media strength. Rooting and shooting frequencies were measured and recorded as percentages of embryonic axes producing roots and shoots, respectively.

Statistical Analysis

Data on embryonic axes developing into full plants were analysed utilizing ordinary two-way ANOVA in GraphPad Prism, considering Bambara groundnut landraces and different MS medium strengths as the main factors. Differences were considered statistically significant at $P < 0.05$.

Results and Discussion

Effect of Genotype and MS Medium Strength on Shooting Frequency in Bambara Groundnut

The shooting response of five Bambara groundnut genotypes (Ci1–Ci5) was significantly influenced by different strengths of the MS basal medium. The percentage of embryonic axes producing shoots varied considerably among the different MS concentrations analysed (Table 1). In general, shoot induction decreased progressively as MS salt concentration decreased. Shooting frequency decreased progressively as MS salt concentration decreased. The highest shoot initiation frequencies were observed on full-strength MS medium, whereas quarter-strength MS medium showed the lowest responses (Figure 4). Two-way ANOVA depicted significant influence of Bambara genotype ($F_{4, 40} = 76.63$, $P < 0.0001$) and different MS medium strengths ($F_{3, 40} = 600.2$, $P < 0.0001$) on shooting frequency. Nevertheless, the interaction between MS strength and genotype was not significant ($F_{12, 40} = 1.095$, $P = 0.3903$), indicating that all genotypes responded similarly to changes in MS strength. MS media strength contributed 83.35% of the total variation, while genotype accounted for only 14.19%. Full-strength MS medium significantly enhanced shoot formation and development, consistent with previous reports that full-strength salt concentration enhances shoot initiation by maintaining and facilitating nutrient balance (Jung et al., 2021; Biswas et al., 2024).

Table 1. Displays the statistical ANOVA analysis on shoot frequency

Two-way ANOVA (Alpha)	**Ordinary** 0.05				
Source of variation	**% of total variation**	**P value**	**P-value summary**	**Significant?**	
Interaction	0.6083	0.3903	Ns	No	
Row factor	14.19	<0.0001	****	Yes	
Column factor	83.35	<0.0001	****	Yes	
ANOVA table	**SS**	**DF**	**MS**	**F (DFn, DFd)**	**P value**
Interaction	90.23	12	7.519	F (12, 40) = 1.095	P=0.3903
Row factor		4	526.2	F (4, 40) = 76.63	P<0.0001
Column factor		3	4122	F (3, 40) = 600.2	P<0.0001
Residual		40	6.867		
Total		59			

Table 2. Shows shooting frequency (%) under different MS medium strengths.

Genotype	1× MS	¾× MS	½× MS	¼× MS
Ci1	65.0 ± 1.4	57.5 ± 1.25	45.0 ± 1.45	27.5 ± 1.2
Ci2	75.0 ± 1.5	67.5 ± 1.35	52.5 ± 1.3	32.5 ± 1.25
Ci3	60.5 ± 1.2	52.5 ± 1.25	42.0 ± 1.15	25.0 ± 1.35
Ci4	55.0 ± 1.3	48.0 ± 1.2	37.5 ± 1.25	20.0 ± 1.15
Ci5	70.0 ± 1.35	63.0 ± 1.25	50.0 ± 1.3	30.0 ± 1.3

Values expressed as mean ± SEM, n = 3.

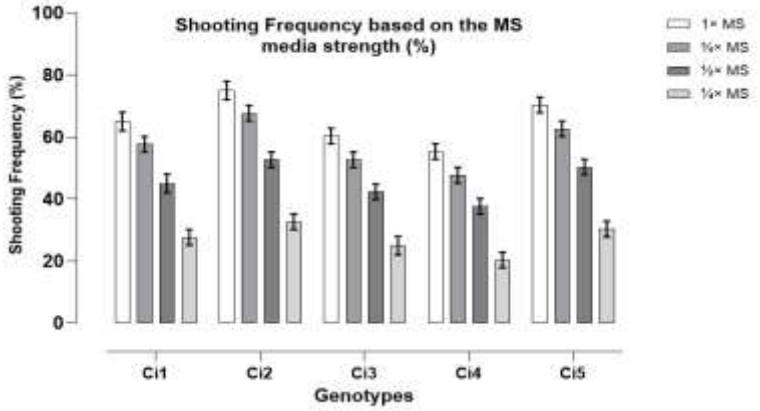

Figure 4. Shows shooting frequency (%) based on the MS medium strength

Effect of Genotype and MS Medium Strength on Rooting Frequency in Bambara Groundnut

The rooting response of five Bambara groundnut genotypes (Ci1–Ci5) was significantly influenced by different strengths of the MS basal medium. The percentage of embryonic axes producing roots varied considerably across the different MS concentrations, as statistically analysed (Table 4). In general, root induction increases progressively as the MS salt concentration is reduced to half MS, then starts to decrease at quarter MS. Rooting frequency exhibited the opposite trend to that of shoot frequency. Root induction increased as MS salt concentration decreased from full MS to half MS, after which a decline was observed at quarter MS (Figure 5). Two-way ANOVA indicated significant effects of genotype ($F_{4, 40} = 95.80$, $P < 0.0001$), MS medium strength ($F_{3, 40} = 581.0$, $P < 0.0001$), and their interaction ($F_{12, 40} = 2.636$, $P = 0.0107$). MS medium strength accounted for 79.31% of the total variation, while genotype accounted for only 17.43% (Table 3). Half-strength MS medium significantly enhanced root formation and development, supporting previous reports that reduced salt concentrations enhance root initiation by lowering osmotic stress and facilitating nutrient balance (Jung et al., 2021; Biswas et al., 2024).

Table 3. Displays the statistical ANOVA analysis on rooting frequency

Two-way ANOVA (Alpha)	Ordinary 0.05				
Source of variation	**% of total variation**	**P value**	**P-value summary**	**Significant?**	
Interaction	1.439	0.0107	*	Yes	
Row factor	17.43	<0.0001	****	Yes	
Column factor	79.31	<0.0001	****	Yes	
ANOVA table	**SS**	**DF**	**MS**	**F (DFn, DFd)**	**P value**
Interaction	228.8	12	19.06	F (12, 40) = 2.636	P=0.0107
Row factor	2772	4	692.9	F (4, 40) = 95.80	P<0.0001
Column factor	12609	3	4203	F (3, 40) = 581.0	P<0.0001
Residual	289.3	40	7.233		
Total	15899	59			

Table 4. Rooting frequency (%) under different MS medium strengths.

Genotype	1× MS	¾× MS	½× MS	¼× MS
Ci1	42.0 ± 0.9	57.0 ± 1.0	83.0 ± 1.05	65.0 ± 1.0
Ci2	49.0 ± 0.8	66.0 ± 0.85	95.0 ± 1.0	75.0 ± 0.9
Ci3	38.0 ± 1.0	52.0 ± 0.8	73.0 ± 1.1	60.0 ± 0.95
Ci4	36.0 ± 0.75	51.0 ± 1.15	70.0 ± 0.9	54.0 ± 1.25
Ci5	47.0 ± 0.7	60.0 ± 0.75	90.0 ± 0.95	72.0 ± 0.9

Values expressed as mean ± SEM, n = 3.

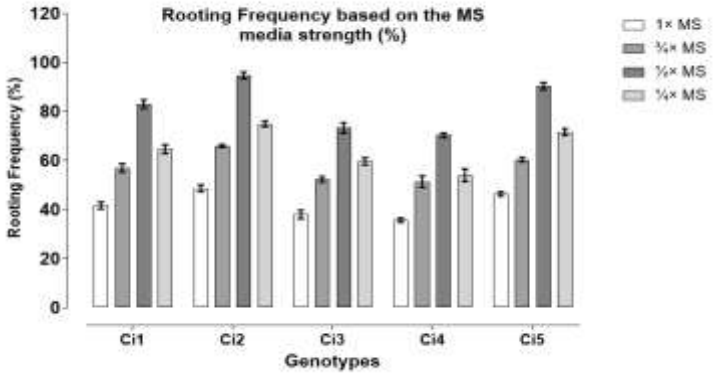

Figure 5. Shows rooting frequency (%) based on the MS medium strength

CONCLUSION

MS medium strength plays a pivotal role in regulating *in vitro* regeneration in Bambara groundnut. Full-strength MS medium is recommended for shoot induction, whereas half-strength MS medium is more suitable for root induction. Genotypic variation significantly influences regenerative responses, with Ci2 emerging as the most responsive genotype. Furthermore, the consistently higher responses observed in genotypes Ci2 and Ci5 highlight the importance of genotype selection in developing efficient regeneration systems for Bambara groundnut improvement studies. The results illustrated the contrasting effects of MS medium strength on shoot and root regeneration in Bambara. Full-strength MS medium was optimal for shoot induction and development, likely because it provides sufficient nutrients to support active cell division and shoot growth. Conversely, half-strength MS medium significantly

enhanced root formation and development, supporting previous reports that reduced salt concentrations enhance root initiation by lowering osmotic stress and facilitating nutrient balance. The significant genotype effects realized in both shoot and root frequency analyses signify that regenerative competency is partially under genetic control. Ci2 consistently exhibited the highest frequencies of shoot and root formation, indicating superior morphogenetic potential. In contrast, Ci4 displayed comparatively lower regenerative responses.

The absence of a significant genotype-medium- interaction for shoot-induction frequency indicates that a common shoot-induction and development protocol may be applicable widely across Bambara groundnut genotypes. However, the significant interaction observed during rooting indicates that genotype-specific optimisation may be necessary to facilitate and maximise rooting efficiency. These findings contribute to the development of efficient regeneration systems that can support future studies in micropropagation, genetic transformation, and CRISPR/Cas-mediated enhancement of Bambara groundnut. The utilization of GraphPad Prism software ensured reliability and scientific validity by enabling accurate statistical analysis of the experimental data. The software provided a clear and transparent interpretation of treatment and interaction effects, thereby amplifying the conclusions drawn from the experiment.

Acknowledgments

The authors acknowledge the Tissue Culture and Plant Biotechnology Laboratory of Ayhan Şahenk Agricultural Faculty of Niğde Ömer Halisdemir University for providing facilities for this study.

Conflict of Interest

The authors declare no conflict of personal interest.

REFERENCES

Altpeter, F., Springer, N. M., Bartley, L., Blechl, A., Brutnell, T., Citovsky, V., Conrad, L. J., Gelvin, S., Jackson, D., Kausch, A., Lemaux, P. G., Medford, J. I., Orozco-Cárdenas, M., Tricoli, D., Van Eck, J., Voytas, D., Walbot, V., Wang, K., Zhang, Z. J., & Stewart, C. N. (2016). Advancing Crop Transformation in the Era of Genome Editing [OPEN]. *Plant Cell, 28*, 1510-1520. https://doi.org/10.1105/tpc.16.00196

Bilali, E. H., Kiébré, Z., Nanema, R., Guimbo, I. D., Rokka, V., Gonnella, M., Tietiambou, S. R. F., Dambo, L., Nanema, J., Grazioli, F., & Acasto, F. (2024). Mapping Research on Bambara Groundnut (Vigna subterranea (L.) Verdc.) in Africa: Bibliometric, Geographical, and Topical Perspectives. *Agriculture*. https://doi.org/10.3390/agriculture14091541

Biswas, P., Kumari, A., & Kumar, N. (2024). Impact of salt strength on in vitro propagation and rebaudioside A content in Stevia rebaudiana under semi-solid and liquid MS media. *Scientific Reports, 14*. https://doi.org/10.1038/s41598-024-70899-1

Chelangat, M., Muturi, P., Gichimu, B., Gitari, J., & Mukono, S. T. (2023). Nutritional and Phytochemical Composition of Bambara Groundnut (Vigna subterranea [L.] Verdc) Landraces in Kenya. *International Journal of Agronomy*. https://doi.org/10.1155/2023/9881028

Holmes, J., Lung, S., Collyer, D., & Punja, Z. (2021). Variables Affecting Shoot Growth and Plantlet Recovery in Tissue Cultures of Drug-Type Cannabis sativa L.. *Frontiers in Plant Science, 12*. https://doi.org/10.3389/fpls.2021.732344

Jung, W., Chung, I., Kim, S.-H., Chi, H.-Y., Yu, C., & Ghimire, B. (2021). Direct Shoot Organogenesis from Lycium chinense Miller Leaf Explants and Assessment of Genetic Stability Using ISSR Markers. *Agronomy*. https://doi.org/10.3390/agronomy11030503

Kunene, S., Gerrano, A., & Odindo, A. (2024). Stability and performance of Bambara groundnut (Vigna subterranea (L.) Verdc.) genotypes in different South African environments. *South African Journal of Plant and Soil, 41*, 83 - 94. https://doi.org/10.1080/02571862.2024.2420109

Majola, N. G., Gerrano, A., & Shimelis, H. (2021). Bambara Groundnut (Vigna subterranea [L.] Verdc.) Production, Utilisation and Genetic Improvement in Sub-Saharan Africa. *Agronomy*. https://doi.org/10.3390/agronomy11071345

Maphosa, Y., Jideani, V., & Maphosa, L. (2022). Bambara groundnut production, grain composition and nutritional value: opportunities for improvements. *The Journal of Agricultural Science, 160*, 448 - 458. https://doi.org/10.1017/s0021859622000521

Maren, N., Duan, H., Da, K., Yencho, G. C., Ranney, T., & Liu, W. (2022). Genotype-independent plant transformation. *Horticulture Research, 9*. https://doi.org/10.1093/hr/uhac047

Mongomaké, K., Hilaire, K. T., Daouda, K., Michel, Z., Justin, K. Y., & Ochatt, S. J. (2009). In vitro plantlets regeneration in Bambara groundnut [Vigna subterranea (L.) Verdc.(Fabaceae)] through direct shoot bud differentiation on hypocotyl and epicotyl cuttings. *African Journal of Biotechnology, 8*(8), 1466.

Mubaiwa, J., Fogliano, V., Chidewe, C., Bakker, E., & Linnemann, A. (2018). Utilization of bambara groundnut (Vigna subterranea (L.) Verdc.) for sustainable food and nutrition security in semi-arid regions of Zimbabwe. *PLoS ONE, 13*. https://doi.org/10.1371/journal.pone.0204817

Mayes, S., Ho, W. K., Chai, H., Gao, X., Kundy, A. C., Mateva, K., Zahrulakmal, M., Hahiree, M. K. I. M., Kendabie, P., Licea, L., Massawe, F., Mabhaudhi, T., Modi, A., Berchie, J., Amoah, S., Faloye, B., Abberton, M., Olaniyi, O., & Azam-Ali, S. (2019). Bambara groundnut: an exemplar underutilised legume for resilience under climate change. *Planta, 250*, 803 - 820. https://doi.org/10.1007/s00425-019-03191-6

Nhamo, L., Paterson, G., Van Der Walt, M., Moeletsi, M., Modi, A., Kunz, R., Chimonyo, V., Masupha, T., Mpandeli, S., Liphadzi, S., Molwantwa, J., & Mabhaudhi, T. (2022). Optimal production areas of underutilized indigenous crops and their role under climate change: Focus on Bambara groundnut. https://doi.org/10.3389/fsufs.2022.990213

Pasipanodya, J. T., Horn, L. N., Togarepi, C., Sibiya, J., Musango, R., & Achigan-Dako, E. (2025). Exploring farmer perspectives on Bambara groundnut [Vigna subterranea (L.) Verdc]: production constraints, preferred varietal traits and implications for varietal development in northern Namibia. *Frontiers in Sustainable Food Systems*. https://doi.org/10.3389/fsufs.2025.1520677

Sokolov, R., Atanassova, B., & Iakimova, E. (2014). Physiological Response of In Vitro Cultured MAGNOLIA SP. to Nutrient Medium Composition. *Journal of Horticultural Research, 22*, 49-61. https://doi.org/10.2478/johr-2014-0006

Tan, X., Azam-Ali, S., Von Goh, E., Mustafa, M., Chai, H., Ho, W. K., Mayes, S., Mabhaudhi, T., Azam-Ali, S., & Massawe, F. (2020). Bambara Groundnut: An Underutilized Leguminous Crop for Global Food Security and Nutrition. *Frontiers in Nutrition, 7*. https://doi.org/10.3389/fnut.2020.601496

Wu, M., Chen, A., Li, X., Li, X., Hou, X., & Liu, X. (2024). Advancements in delivery strategies and non-tissue culture regeneration systems for plant genetic transformation. *Advanced Biotechnology, 2*. https://doi.org/10.1007/s44307-024-00041-9

Youngstrom, C., Wang, K., & Lee, K. (2024). Unlocking regeneration potential: harnessing morphogenic regulators and small peptides for enhanced plant engineering. *The Plant Journal, 121*. https://doi.org/10.1111/tpj.17193

INFLUENCE OF SUMMER MICROBIOLOGICAL POLLUTION ON THE DISTRIBUTION OF ANTIBIOTIC-RESISTANT *ESCHERICHIA COLI* IN THE VJOSA RIVER BASIN.

Kerol Saçaj[1*], Etleva Hamzaraj[2], Brikena Parllaku[2], Selin Saçaj[2]

[1]Department of Biology, Faculty of Technical and Natural Sciences, University Ismail Qemali Vlore.
[2]Department of Biology, Faculty of Natural Sciences, University of Tirana, Tirana, Albania.
**Corresponding Author: kerol.sacaj@univlora.edu.al*

ABSTRACT

The Vjosa River basin is increasingly exposed to faecal contamination derived from agricultural runoff, livestock activity, rural settlements, and tributary inflows. At the same time, environmental *Escherichia coli* isolated from the basin has shown high levels of antibiotic resistance, including marked resistance to β-lactam antibiotics and a high multidrug-resistant (MDR) fraction. This study develops an integrated interpretation of one-year microbiological monitoring data from thirteen stations along the Vjosa River and its tributaries, with a particular focus on the summer period as a critical window for contamination and antimicrobial resistance risk. Faecal coliforms/*E. coli* proxy and intestinal enterococci were analysed monthly from October 2024 to October 2025, and summer microbial loads were linked with previously determined antibiotic resistance patterns in environmental *E. coli* isolates. Since station-specific and month-specific antimicrobial susceptibility data were not available in the microbiological spreadsheet, resistant *E. coli* burdens were estimated by applying reported resistance prevalences to the observed microbial concentrations. The annual mean faecal coliform/*E. Coli* proxy concentration was 183.6 MPN/100 mL, while the summer mean was 163.4 MPN/100 mL. The highest summer microbial loads were observed at stations S-13-GJO, S-16-KDQ, S-17-GJK, and S-15-DRI, indicating spatially concentrated contamination pressure. The estimated MDR *E. coli* burden was highest at these same locations, especially S-13-GJO. The results suggest that summer faecal pollution can function as a seasonal amplifier of antibiotic-resistant E. coli distribution in the Vjosa River basin by increasing the abundance of bacterial hosts exposed to environmental selection pressures. These findings support the need for coordinated summer monitoring of microbiological pollution, antibiotic resistance, wastewater inputs, and agricultural runoff in the Vjosa River National Park.

Keywords: Antibiotic resistance; *Escherichia coli*; faecal contamination; multidrug resistance; summer season; Vjosa River; water quality.

1. INTRODUCTION.

Freshwater rivers are important ecological corridors and essential resources for agriculture, recreation, irrigation, and local communities. However, they may also act as pathways for the transport of faecal microorganisms and antibiotic-resistant bacteria when catchments are affected by wastewater discharge, livestock pressure, and agricultural runoff [5, 7, 18]. The Vjosa River is one of the most ecologically important river systems in Southeast Europe. Still, its basin receives inputs from rural settlements, tributaries, cultivated land, and livestock areas, creating conditions in which microbiological pollution can vary markedly in space and time.

Faecal indicator bacteria, particularly *Escherichia coli* and intestinal enterococci, are widely used to assess the sanitary status of surface waters because they indicate recent faecal input and

the presence of potential pathogens [1,3,11,12]. In parallel, antibiotic-resistant *E. coli* is increasingly recognized as a relevant environmental and public health indicator because it can reflect the combined effects of faecal pollution, antibiotic residues, and horizontal gene transfer in aquatic systems [4, 6, 16, 17]. Previous antimicrobial susceptibility analysis of environmental E. coli from the Vjosa River reported resistance to Cephalothin, Amoxicillin, Oxytetracycline, and Trimethoprim, with approximately 70% of isolates classified as multidrug-resistant [13].

Seasonality is a key factor in the interpretation of both microbial contamination and antimicrobial resistance risk. Summer conditions may increase water temperature, reduce river discharge, and lower dilution capacity, while also coinciding with tourism, irrigation, agricultural activity, and livestock presence near riverbanks. These conditions can increase faecal indicator concentrations and may indirectly increase the environmental burden of resistant *E. coli* by increasing the total pool of bacterial hosts entering and persisting in the river system [2,5,8,9,10,14].

This study aimed to create an integrated assessment linking summer microbiological pollution with the expected distribution of antibiotic-resistant *E. coli* in the Vjosa River basin. Specifically, the study aimed to: (i) evaluate monthly and summer patterns of faecal indicator bacteria; (ii) identify summer microbial hotspots; (iii) estimate the seasonal and spatial burden of antibiotic-resistant E. coli using previously reported resistance prevalences [4, 6, 15, 16, 17]; and (iv) propose a conceptual framework for summer-driven amplification of antimicrobial resistance risk in riverine environments.

2. MATERIALS AND METHODS.

2.1 Study area and sampling design

The study was based on microbiological monitoring data collected from thirteen sampling stations located along the Vjosa River and its major tributaries. The selected stations represented different hydrological sectors of the basin, including upstream, midstream, downstream, and tributary-influenced environments. Monitoring was carried out throughout a complete annual cycle from October 2024 to October 2025. Particular attention was given to the summer period (June-September 2025), which is characterized by higher temperatures, lower dilution capacity, and increased anthropogenic pressures, conditions that may promote both faecal contamination and the dissemination of antibiotic-resistant *Escherichia coli* [2, 5, 8, 9, 17].

2.2 Microbiological indicators.

Microbiological assessment focused on faecal coliforms/*E. coli* proxy and intestinal enterococci. For each station and month, replicate Most Probable Number (MPN) results were averaged and expressed as MPN/100 mL. These values were used to evaluate monthly patterns, summer averages, and spatial hotspots of contamination. The use of *E. coli* and enterococci as faecal indicators follows standard microbiological water-quality interpretation [1, 3, 5, 11, 12, 18].

2.3 Antibiotic resistance data and estimation of resistant *E. coli* burden.

Antibiotic resistance data were obtained from a parallel investigation conducted on environmental Escherichia coli isolates collected from the same monitoring network within the Vjosa River basin (figure1) [19]. That study reported resistance prevalences of 75% for Cephalothin, 55% for Amoxicillin, 35% for Oxytetracycline, and 3% for Trimethoprim, while approximately 70% of the isolates were classified as multidrug-resistant (MDR). To investigate the relationship between seasonal microbiological contamination and antimicrobial resistance, the observed bacterial concentrations recorded during the summer monitoring period were integrated with the reported resistance profiles. This approach allowed the assessment of potential spatial and temporal patterns linking elevated faecal contamination with the distribution of antibiotic-resistant E. coli within the river basin.

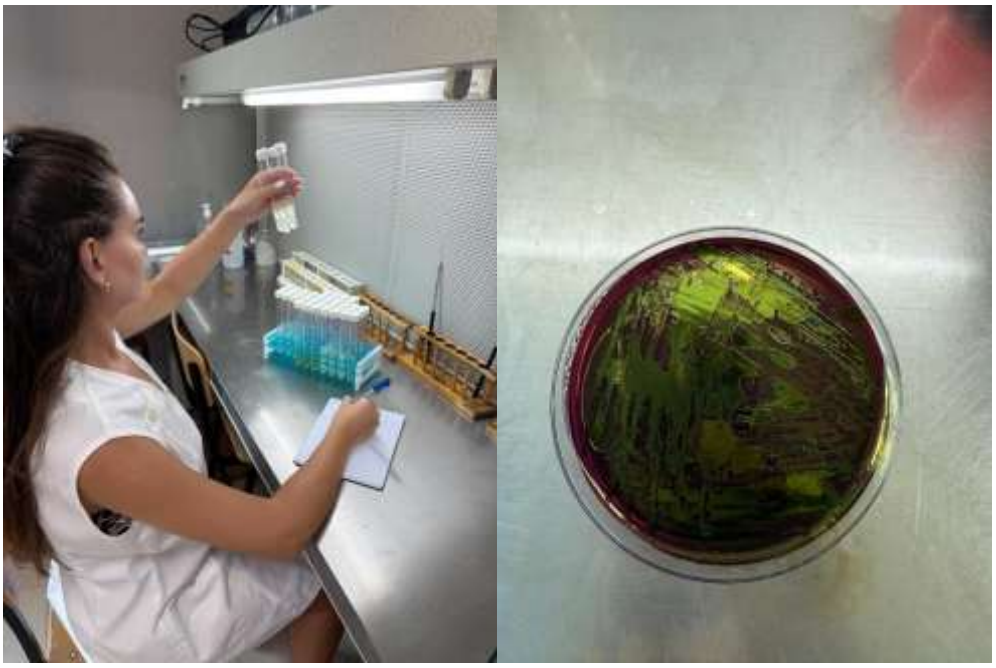

Figure 1. Laboratory procedures for microbiological analysis and isolation of Escherichia coli from water samples collected in the Vjosa River basin.

2.4 Data analysis and graphical outputs.

Data were organised by month, station, and microbial indicator. Monthly means were calculated across all stations, while summer station means were calculated using June, July, August, and September 2025. Hotspots were identified as stations with the highest summer faecal indicator concentrations and the highest estimated MDR burden. Six original figures were generated: monthly microbiological trends, summer station means, a faecal coliform/E. coli proxy heatmap, estimated monthly antibiotic-resistant *E. coli* burden, estimated summer MDR burden by station, and the relationship between summer microbial load and estimated MDR burden.

2. RESULTS.

3.1 Monthly variation of faecal indicator bacteria.

Across the complete monitoring period, the annual mean faecal coliform/E. coli proxy concentration was 183.6 MPN/100 mL, while the annual mean intestinal enterococci concentration was 136.4 MPN/100 mL. Monthly faecal coliform/E. coli proxy values varied considerably, with elevated values in October 2024 (234.9 MPN/100 mL), February 2025 (215.7 MPN/100 mL), and August 2025 (210.0 MPN/100 mL). During the summer period, August showed the highest faecal coliform/E. coli proxy mean, indicating a critical month for microbiological pressure.

As illustrated in Figure 2, both faecal coliform/E. coli **proxy concentrations and intestinal enterococci exhibited noticeable temporal fluctuations throughout the monitoring period. The highest bacterial concentrations were generally recorded during warmer months, particularly in late summer, suggesting that elevated temperatures and reduced river discharge may favour the persistence and accumulation of faecal microorganisms** [2, 5, 8, 9]**. In contrast, lower concentrations were observed during several cooler monitoring periods, reflecting more favourable dilution conditions and reduced environmental stress** [2, 5]**. The seasonal pattern presented in Figure 2 highlights the importance of summer conditions in shaping microbiological water quality within the Vjosa River basin. The simultaneous increase of both faecal indicator groups during the summer months suggests enhanced**

faecal inputs and a greater risk of environmental contamination [7, 8, 9, 11]**. These findings support the hypothesis that seasonal factors play a significant role in the distribution of faecal bacteria and may contribute to the increased occurrence of antibiotic-resistant** Escherichia coli **during periods of elevated microbiological pollution** [4, 6, 16, 17]**.**

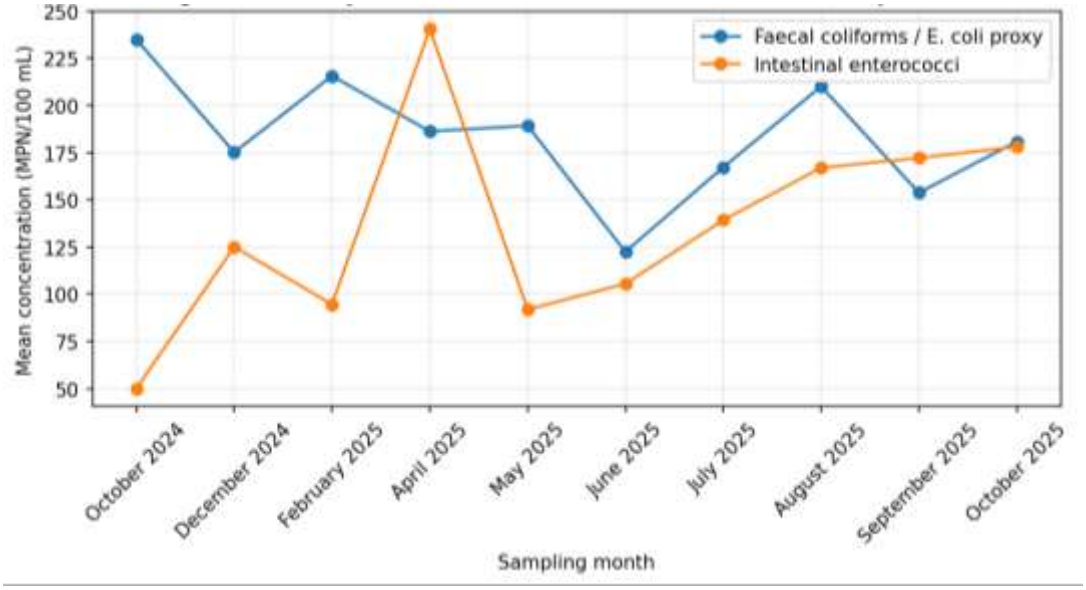

Figure 2. Monthly variation of faecal indicator bacteria in the Vjosa River basin.

3.2 Summer microbial hotspots

The mean summer faecal coliform/E. coli proxy concentration was 163.4 MPN/100 mL, while intestinal enterococci averaged 146.0 MPN/100 mL. The highest summer faecal coliform/E. coli proxy loads were observed at S-13-GJO (333.0 MPN/100 mL), S-16-KDQ (206.4 MPN/100 mL), S-17-GJK (188.0 MPN/100 mL), and S-15-DRI (184.6 MPN/100 mL). These stations can be interpreted as summer microbiological hotspots, most likely reflecting the influence of tributary inputs, nearby settlements, agricultural land use, and livestock-related faecal sources [7, 8, 9, 10].

As shown in Figure 3, the spatial distribution of faecal indicator bacteria was not uniform across the Vjosa River basin. Several stations exhibited substantially higher bacterial concentrations than the basin average, indicating localized sources of faecal pollution and increased environmental pressure. The most contaminated sites were generally associated with tributary confluences and areas affected by human activities, where surface runoff, livestock grazing, and untreated wastewater discharges may contribute additional microbial loads to the river system [5, 7, 8, 9]**. Station S-13-GJO displayed the highest summer contamination level, exceeding 330 MPN/100 mL, and clearly stands out as the principal microbiological hotspot of the study area. Elevated concentrations recorded at S-15-DRI, S-16-KDQ, and S-17-GJK further suggest that downstream and tributary-influenced sectors are particularly vulnerable to faecal pollution during the summer season. The pattern illustrated in Figure 3 indicates that local environmental conditions, combined with anthropogenic pressures, strongly influence the spatial distribution of microbial contamination** [5, 8, 9]**.**

The identification of these hotspot locations is particularly important because areas characterized by persistent faecal contamination may also favour the maintenance and dissemination of antibiotic-resistant bacteria [4, 6, 14, 16, 17]**. Consequently, the stations exhibiting the highest bacterial concentrations during summer represent priority sites**

for future microbiological surveillance and antimicrobial resistance monitoring within the Vjosa River basin [4, 16, 17].

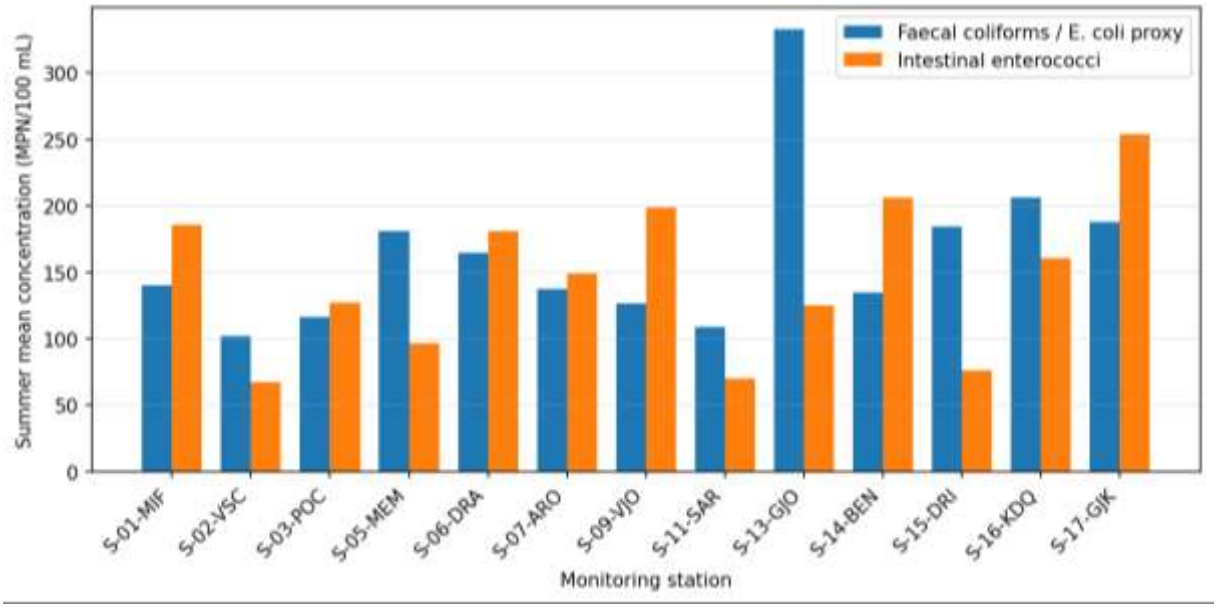

Figure 3. Summer microbiological contamination across monitoring stations.

3.3 Estimated monthly antibiotic-resistant *E. coli* burden.

When the reported resistance percentages were applied to the monthly faecal coliform/E. coli proxy concentrations, the estimated burden of resistant E. coli followed the same temporal pattern as microbiological contamination. Cephalothin-resistant and MDR E. coli showed the highest estimated burdens because their reported resistance prevalences were 75% and 70%, respectively. August 2025 represented the strongest summer month for estimated resistant burden, supporting the hypothesis that warm-season faecal contamination may amplify the environmental distribution of resistant E. coli *[4, 6, 16, 17]*. **As illustrated in Figure 4, the estimated abundance of antibiotic-resistant** E. coli **increased during periods characterized by elevated microbiological contamination. Months exhibiting higher faecal indicator bacteria concentrations also showed a greater estimated burden of resistant bacteria, suggesting a close relationship between faecal pollution and antimicrobial resistance dynamics within the river system [4, 6, 13, 15, 17]. This pattern was particularly evident during the summer season, when environmental conditions favored bacterial persistence and accumulation [2, 5, 17]. The highest estimated resistant burden occurred during August, coinciding with one of the periods of greatest microbiological pressure observed throughout the monitoring program. Elevated temperatures, reduced river flow, and increased anthropogenic activities during summer may enhance the introduction, survival, and dissemination of resistant bacteria originating from agricultural runoff, livestock operations, and domestic wastewater sources [6, 10, 14, 16, 17].**

Figure 4 further demonstrates that resistance associated with Cephalothin and multidrug-resistant (MDR) E. coli **consistently represented the largest proportion of the estimated resistant bacterial population. These findings suggest that seasonal peaks in faecal contamination may contribute not only to increased bacterial abundance but also to a greater environmental reservoir of antibiotic-resistant microorganisms [4, 6, 15, 16, 17]. Consequently, summer conditions appear to play an important role in shaping the temporal distribution of antimicrobial resistance within the Vjosa River basin [4, 16, 17].**

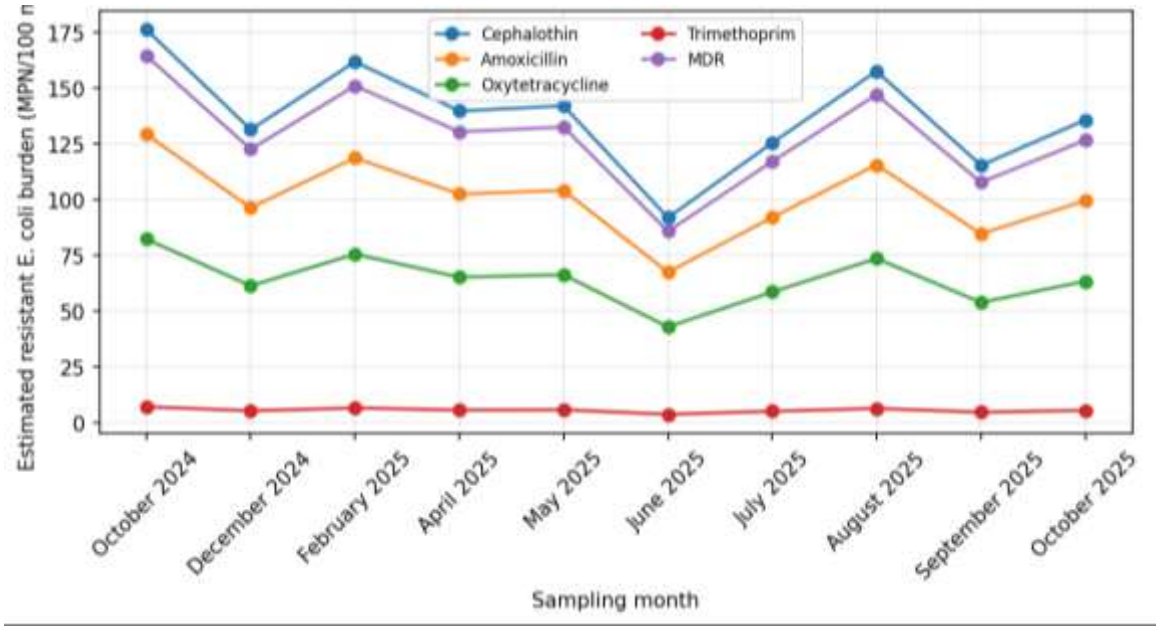

Figure 4. Estimated monthly antibiotic-resistant *E. coli* burden based on observed microbial concentrations and reported resistance prevalences.

3.5 Estimated summer MDR *E. coli* hotspots.

The estimated summer MDR E. coli burden was highest at S-13-GJO (233.1 MPN/100 mL), followed by S-16-KDQ (144.5 MPN/100 mL), S-17-GJK (131.6 MPN/100 mL), and S-15-DRI (129.2 MPN/100 mL). These results suggest that the same locations showing high summer faecal contamination may also represent priority areas for antimicrobial resistance surveillance [4, 16, 17]. **As shown in Figure 5, the spatial distribution of the estimated MDR** E. coli **burden was highly uneven across the Vjosa River basin. A limited number of stations accounted for a disproportionately large share of the estimated resistant bacterial load, indicating the presence of localized antimicrobial resistance hotspots. The most affected stations corresponded closely to those previously identified as microbiological contamination hotspots, highlighting a strong association between faecal pollution and the potential dissemination of multidrug-resistant bacteria** [4, 6, 13, 15, 16, 17]**.**

Station S-13-GJO exhibited by far the highest estimated MDR burden, clearly distinguishing it as the principal hotspot during the summer season. Elevated values recorded at S-15-DRI, S-16-KDQ, and S-17-GJK further indicate that tributary-influenced sectors and areas subjected to greater anthropogenic pressure may provide favorable conditions for the persistence and spread of resistant microorganisms [5, 8, 9, 17]**. Agricultural activities, livestock farming, wastewater inputs, and diffuse runoff are likely to contribute to the introduction of both faecal bacteria and antimicrobial resistance determinants into the aquatic environment** [6, 8, 10, 14, 16, 17]**.**

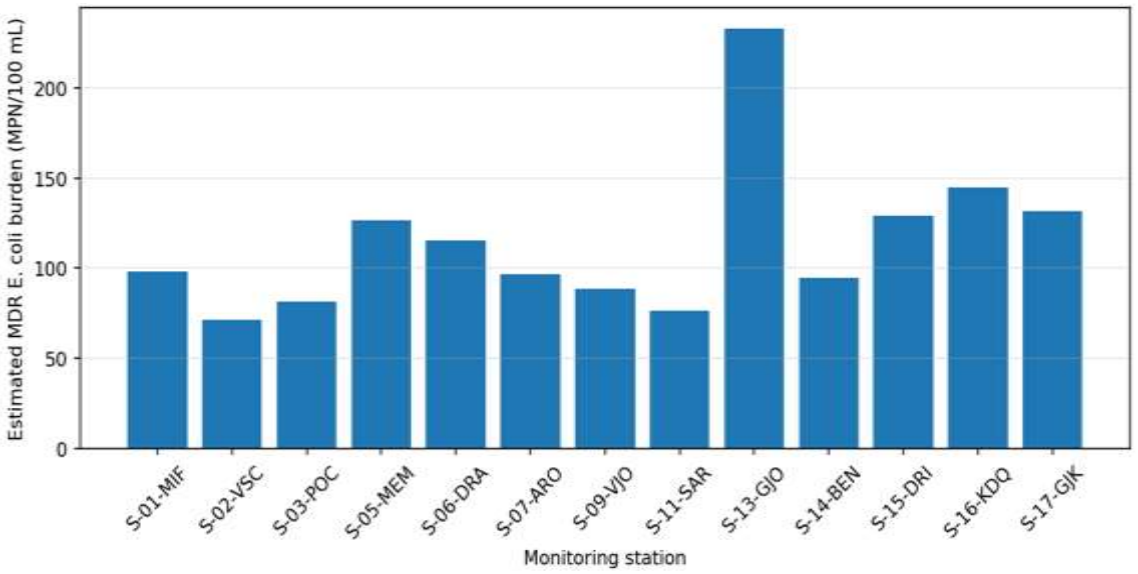

Figure 5. Estimated summer MDR *E. coli* burden by monitoring station.

3.6 Relationship between summer microbial load and estimated MDR burden.

The relationship between summer faecal coliform/E. coli proxy concentration and estimated MDR burden was direct because MDR burden was calculated from the observed microbial load and the reported 70% MDR prevalence. Although this relationship is therefore model-derived, it is useful for identifying where high microbial pollution would be expected to translate into the greatest environmental burden of resistant E. coli [4, 6, 15, 16, 17]. As illustrated in **Figure 6**, stations characterized by elevated summer microbial concentrations also exhibited the highest estimated MDR burden. The strong positive association observed across monitoring stations suggests that areas experiencing greater faecal contamination may act as important environmental reservoirs for multidrug-resistant bacteria [4, 6, 13, 15, 16, 17]. **Figure 6 clearly demonstrates that the most contaminated stations, particularly S-13-GJO, S-16-KDQ, S-17-GJK, and S-15-DRI, were also associated with the highest estimated MDR loads. This pattern indicates that microbiological pollution and antimicrobial resistance are closely interconnected processes within the Vjosa River basin [4, 6, 14, 16, 17]. Although the MDR estimates are based on the reported resistance prevalence rather than direct station-specific susceptibility testing, the observed trend provides valuable insight into the potential distribution of resistant bacteria under summer conditions.**

The results further suggest that seasonal increases in faecal contamination may contribute to the expansion of environmental reservoirs of antibiotic-resistant E. coli [4, 6, 16, 17]. **Elevated bacterial concentrations increase the likelihood that resistant strains originating from wastewater discharges, livestock activities, and agricultural runoff will persist and spread throughout the river system [6, 8, 10, 14, 16, 17]. Consequently, locations with consistently high microbial loads may represent priority areas for antimicrobial resistance monitoring and mitigation measures [4, 16, 17].**

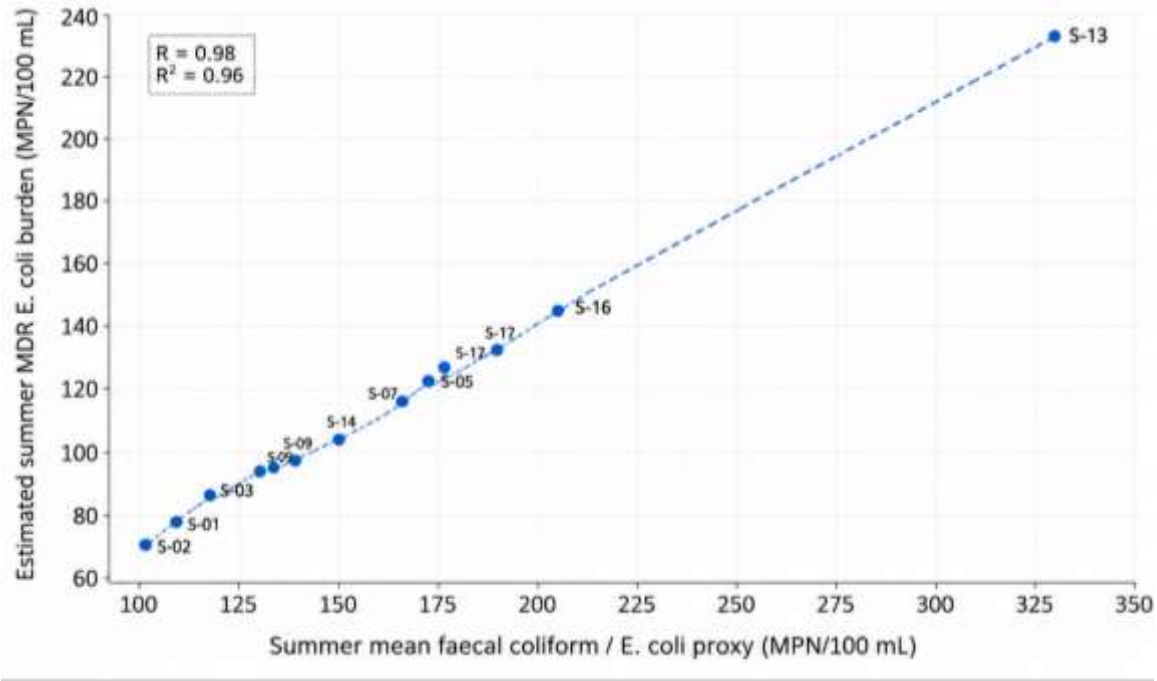

Figure 6. Relationship between summer microbial load and estimated MDR *E. coli* burden.

3. DISCUSSION.

The integrated analysis indicates that summer microbiological pollution can act as an important driver of antibiotic-resistant *E. coli* distribution in the Vjosa River basin. The mechanism is not necessarily that temperature directly creates resistance, but rather that summer conditions can increase the abundance and persistence of faecal bacteria. When faecal inputs contain resistant strains, a higher microbial load increases the absolute number of resistant E. coli cells transported through the river system [2, 4, 5, 6, 17].

The strongest summer hotspot identified in this analysis was S-13-GJO, followed by S-16-KDQ, S-17-GJK, and S-15-DRI. These stations overlap with locations previously described as microbiological and antimicrobial resistance concern areas in the Vjosa basin. Such overlap supports the interpretation that local sources, including tributary inflows, livestock activity, untreated or insufficiently treated wastewater, and agricultural runoff, may simultaneously contribute faecal microorganisms, antibiotic residues, and resistant bacteria [6, 8, 9, 10, 14, 16, 17].

The estimated resistant-burden approach provides a practical method for linking microbiological monitoring with antimicrobial resistance data when full isolate-level temporal susceptibility data are not available. The highest estimated values were obtained for Cephalothin-resistant and MDR E. coli because these categories had the highest reported resistance prevalences. This indicates that β-lactam resistance and multidrug resistance should be priority targets in future surveillance [4, 6, 13, 16, 17].

However, the analysis must be interpreted carefully. The resistance percentages used here were applied uniformly across months and stations. Therefore, the figures represent estimated risk burdens rather than direct measurements of resistant *E. coli* at each station and month. A stronger future study should combine monthly *E. coli* isolation, station-specific susceptibility testing, antibiotic-residue analysis, and hydrological measurements [1, 4, 16, 17]. This would allow direct statistical testing of whether summer temperature, reduced discharge, and faecal contamination significantly increase the prevalence of resistant and MDR isolates.

Despite this limitation, the results are useful for management because they identify summer as a critical monitoring period and highlight stations where microbial contamination and estimated resistance burden converge. These locations should be prioritized for wastewater control, livestock runoff reduction, and repeated antimicrobial resistance screening [4, 16, 17, 18].

4. CONCLUSION

This study created a new integrated interpretation linking summer faecal contamination with the potential distribution of antibiotic-resistant E. coli in the Vjosa River basin. The results show that microbial pollution is spatially concentrated during the summer period, with S-13-GJO, S-16-KDQ, S-17-GJK, and S-15-DRI representing the most important hotspots. When previously reported resistance prevalences were applied to observed microbiological concentrations, the highest estimated MDR E. coli burdens occurred at the same hotspot stations. These findings suggest that summer faecal contamination may amplify antimicrobial resistance risk by increasing the absolute load of resistant *E. coli* entering and persisting in the river. Routine summer monitoring should therefore combine faecal indicator bacteria, antibiotic susceptibility testing, hydrological measurements, and source-tracking approaches to support evidence-based management of the Vjosa River National Park [1, 4, 16, 17, 18].

6. REFERENCES.

1. APHA. *Standard Methods for the Examination of Water and Wastewater*. 23rd ed. Washington, DC: American Public Health Association; 2017.
2. Blaustein R.A, Y. Pachepsky, R.L. Hill, D.R. Shelton, G. Whelan, Escherichia coli survival in waters: Temperature dependence, Water Research, Volume 47, Issue 2, 2013, Pages 569-578, ISSN 0043-1354, Cabral JPS.
3. Byappanahalli MN, Nevers MB, Korajkic A, Staley ZR, Harwood VJ. Enterococci in the environment. Microbiol Mol Biol Rev. 2012 Dec;76(4):685-706. doi: 10.1128/MMBR.00023-12. PMID: 23204362; PMCID: PMC3510518.
4. Berendonk, T., Manaia, C., Merlin, C. *et al.* Tackling antibiotic resistance: the environmental framework. *Nat Rev Microbiol* **13**, 310–317 (2015). https://doi.org/10.1038/nrmicro3439
5. Cabral, J. P. S. (2010). Water Microbiology. Bacterial Pathogens and Water. International Journal of Environmental Research and Public Health, 7(10), 3657-3703. **https://doi.org/10.3390/ijerph7103657**.
6. Fernando Baquero, José-Luis Martínez, Rafael Cantón, Antibiotics and antibiotic resistance in water environments, Current Opinion in Biotechnology, Volume 19, Issue 3,2008, Pages 260-265, ISSN 0958-1669.
7. G. Katharine . Field, Mansour Samadpour, Fecal source tracking, the indicator paradigm, and managing water quality, Water Research, Volume 41, Issue 16, 2007, Pages 3517-3538, ISSN 0043-1354,
8. Garcia-Armisen T., P. Servais, Respective contributions of point and non-point sources of E. coli and enterococci in a large urbanized watershed (the Seine river, France), Journal of Environmental Management, Volume 82, Issue 4,2007, Pages 512-518, ISSN 0301-4797.
9. Servais P, Tamara Garcia-Armisen, Isabelle George, Gilles Billen, Fecal bacteria in the rivers of the Seine drainage network (France): Sources, fate and modelling, Science of The Total Environment, Volume 375, Issues 1-3,2007, Pages 152-167, ISSN 0048-9697.
10. Jamieson, Rob & Gordon, Robert & Sharples, K.E. & Stratton, Glenn & Madani, A.. (2002). Movement and persistence of fecal bacteria in agricultural soils and subsurface

drainage water: A review. Canadian Biosystems Engineering / Le Genie des biosystems au Canada. 44. 1.1-1.9.

11. Payment, P. and Locas, A. (2011), Pathogens in Water: Value and Limits of Correlation with Microbial Indicators. Groundwater, 49: 4-11. **https://doi.org/10.1111/j.1745-6584.2010.00710.x**
12. Tallon, P., Magajna, B., Lofranco, C. *et al.* Microbial Indicators of Faecal Contamination in Water: A Current Perspective. *Water Air Soil Pollut* 166, 139–166 (2005). **https://doi.org/10.1007/s11270-005-7905-4**.
13. **Thomas A Edge** and **Stephen Hill**. 2005. Occurrence of antibiotic resistance in *Escherichia coli* from surface waters and fecal pollution sources near Hamilton, Ontario. *Canadian Journal of Microbiology*. **51**(6): 501-505. **https://doi.org/10.1139/w05-028**.
14. Jose Luis Martinez, Environmental pollution by antibiotics and by antibiotic resistance determinants, Environmental Pollution, Volume 157, Issue 11, 2009, Pages 2893-2902, ISSN 0269-7491.
15. Pruden, Amy & Pei, Ruoting & Storteboom, Heather & Carlson, Ken. (2006). Antibiotic Resistance Genes as Emerging Contaminants: Studies in Northern Colorado †. Environmental science & technology. 40. 7445-50. 10.1021/es060413l.
16. Karkman A, Thi Thuy Do, Fiona Walsh, Marko P.J. Virta, Antibiotic-Resistance Genes in Waste Water, Trends in Microbiology, Volume 26, Issue 3,2018, Pages 220-228, ISSN 0966-842X.
17. Wellington EH, Alistair BA Boxall, Paul Cross, Edward J Feil, William H Gaze, Peter M Hawkey, Ashley S Johnson-Rollings, Davey L Jones, Nicholas M Lee, Wilfred Otten, Christopher M Thomas, A Prysor Williams, The role of the natural environment in the emergence of antibiotic resistance in Gram-negative bacteria, The Lancet Infectious Diseases, Volume 13, Issue 2,2013, Pages 155-165, ISSN 1473-3099.
18. WHO. *Guidelines for Drinking-water Quality*. 4th ed. Geneva: World Health Organization; 2022.

LINKING SUMMER WATER QUALITY DYNAMICS TO FAECAL CONTAMINATION HOTSPOTS IN THE VJOSA RIVER (ALBANIA).

Kerol Saçaj[1*], Etleva Hamzaraj[2], Brikena Parllaku[2], Selin Saçaj[2]

[1]Department of Biology, Faculty of Technical and Natural Sciences, University Ismail Qemali Vlore.
[2]Department of Biology, Faculty of Natural Sciences, University of Tirana, Tirana, Albania.
**Corresponding Author: kerol.sacaj@univlora.edu.al*

ABSTRACT

The Vjosa River represents one of the last free-flowing river systems in Europe and supports a wide range of ecological functions and biodiversity. Despite its ecological importance, seasonal variations in water quality, particularly during summer, may significantly influence microbial contamination patterns. This study investigates the relationship between summer physicochemical conditions and faecal contamination dynamics across selected monitoring sites of the Vjosa River and its major tributaries. Water quality assessment focused on the summer period (June-September 2025), when elevated temperatures, reduced river discharge, increased agricultural activities, and intensified recreational use create favorable conditions for bacterial proliferation. The study evaluates the influence of temperature, dissolved oxygen, electrical conductivity, total dissolved solids, and pH on the distribution of *Escherichia coli* and intestinal enterococci. Particular attention was given to contamination hotspots previously identified in Poçem, Sarandoporo, Gjorm, Drino, and Kardhiq. Results indicate that the summer season represents the most critical period for microbiological deterioration of river water quality. Elevated temperatures and reduced dilution capacity were associated with increased concentrations of faecal indicator bacteria, while dissolved oxygen showed an inverse relationship with microbial abundance. The findings highlight the importance of seasonal monitoring and provide valuable information for the management and protection of the Vjosa River ecosystem.

Keywords: *Escherichia coli*, faecal contamination, intestinal enterococci, physico-chemical parameters, summer season, Vjosa River, water quality.

1. INTRODUCTION

Rivers are dynamic freshwater ecosystems whose ecological condition is strongly influenced by seasonal fluctuations in hydrological, physical, chemical, and biological processes. Among these seasonal variations, the summer period is often associated with significant changes in water quality due to increased temperatures, reduced water discharge, and intensified anthropogenic pressures. Such conditions may alter the ecological balance of aquatic systems and favor the development and persistence of microbial contaminants [2,14,15]. The Vjosa River, extending from the Pindus Mountains in Greece to the Adriatic Sea in Albania, is recognized as one of Europe's last large free-flowing rivers. Its ecological importance is reflected in its high biodiversity, diverse habitats, and fundamental role in supporting local communities through irrigation, agriculture, recreation, and ecosystem services. Although the river remains relatively unfragmented compared to many European river systems, increasing human activities within the watershed have introduced new environmental pressures affecting

water quality. Microbiological contamination has become an important environmental concern in freshwater ecosystems worldwide [4,16]. Faecal indicator bacteria such as *Escherichia coli* and intestinal enterococci are widely used to assess microbial water quality because their presence is closely linked to faecal pollution originating from human and animal sources [3,7,18]. Elevated concentrations of these microorganisms may indicate the presence of pathogenic bacteria, viruses, and protozoa that can affect both the environment and public health [4,16,20]. Previous investigations along the Vjosa River have demonstrated spatial differences in microbial contamination, with several tributaries and downstream sectors showing higher concentrations of faecal indicator bacteria than upstream locations. However, most studies have focused on annual monitoring patterns, while limited attention has been paid to the seasonal mechanisms that control microbial dynamics. Summer conditions deserve particular attention because they coincide with increased tourism, agricultural activity, livestock presence near riverbanks, and reduced river flow, all of which may enhance bacterial accumulation and survival [2,14,15]. Temperature is considered one of the principal environmental drivers influencing microbial growth and persistence in aquatic ecosystems. Higher water temperatures can accelerate bacterial metabolism and prolong survival under favorable conditions [2]. Simultaneously, reduced river discharge during summer decreases dilution capacity, allowing contaminants to become more concentrated within the water column [9,17]. Other physico-chemical parameters, including dissolved oxygen, electrical conductivity, total dissolved solids, and pH, may further influence microbial distribution and reflect broader environmental changes occurring within the watershed [8,19]. Understanding the interactions between physico-chemical conditions and microbial contamination is essential for identifying areas vulnerable to environmental degradation. Such information provides valuable scientific support for water management strategies, public health protection, and biodiversity conservation within the Vjosa River National Park [5,19,20]. Therefore, the main objective of this study is to investigate the relationships between summer water quality dynamics and faecal contamination hotspots along the Vjosa River. Particular emphasis is placed on evaluating how temperature, dissolved oxygen, conductivity, and total dissolved solids influence the distribution of *Escherichia coli* and intestinal enterococci during the summer season. Furthermore, the study aims to identify the most vulnerable locations and assess the environmental factors contributing to elevated microbial contamination during periods of increased ecological pressure.

2. MATERIALS AND METHODS

2.1 Study Area and Sampling Design

The present study focused exclusively on the summer season in order to investigate the influence of physico-chemical conditions on microbiological water quality in the Vjosa River. Sampling was conducted between June and September 2025 at thirteen monitoring stations distributed along the main channel of the river and its major tributaries. The selected stations covered upstream (Figure 1), midstream, and downstream sections, providing a representative overview of environmental conditions throughout the watershed.

Special attention was given to sites previously identified as microbiological contamination hotspots, including Poçem, Sarandoporo, Gjorm, Drino, and Kardhiq. These locations are influenced by different anthropogenic activities such as agriculture, livestock farming, rural settlements, and seasonal tourism, all of which may contribute to variations in microbial water quality [7,9,14,17]. Water samples were collected monthly according to the recommendations of ISO 19458 for microbiological water quality assessment [11]. At each station, samples were obtained from a depth of approximately 30-50 cm below the water surface using sterile sampling bottles. Following collection, samples were immediately stored in insulated containers at approximately 4°C and transported to the laboratory for analysis within six hours [11].

Figure 1. Sampling stations located along the Vjosa River main channel and its tributaries (GIS-generated)

2.2 Physico-Chemical Analysis

Physico-chemical measurements were performed in situ during each sampling campaign using a calibrated multiparameter probe. The parameters monitored included water temperature, dissolved oxygen, pH, electrical conductivity, and total dissolved solids. These variables were selected because of their direct influence on microbial survival, growth, and distribution within freshwater ecosystems [2,4,16]. Water temperature was considered a particularly important factor due to its role in regulating bacterial metabolic activity and reproduction rates [2]. Dissolved oxygen was measured as an indicator of ecosystem condition and organic matter decomposition processes, while electrical conductivity and total dissolved solids were used to evaluate mineral content and possible inputs from agricultural runoff and wastewater discharges [8,9,17]. Measurements of pH were included to assess the suitability of environmental conditions for microbial persistence [4,16].

2.3 Microbiological Analysis

Microbiological assessment focused on the determination of *Escherichia coli* and intestinal enterococci, two internationally accepted indicators of faecal contamination in surface waters [3,7,18,19]. Enumeration of both bacterial groups was carried out using the Most Probable Number (MPN) method following standardized laboratory procedures [12,13]. Serial dilutions were prepared for each sample, and bacterial concentrations were expressed as MPN per 100 mL of water (Figure 2).

The use of *E. coli* as a primary faecal indicator is widely recognized due to its strong association with recent faecal contamination from human and animal sources [7,18]. Intestinal enterococci were analyzed as a complementary indicator because of their greater persistence under environmental stress conditions and their relevance in recreational water quality assessment [3,18,19]. All microbiological analyses were conducted immediately after sample arrival at the laboratory to minimize potential changes in bacterial abundance [11].

Figure 2. Microbiological analysis of water samples in the laboratory.

2.4 Statistical Analysis

Descriptive statistical analyses were performed to evaluate temporal and spatial variations in both physico-chemical and microbiological parameters during the summer season. Mean values, minimum values, maximum values, and standard deviations were calculated for all variables. Seasonal trends were assessed through comparisons among sampling stations and sampling months. To investigate the relationships between environmental conditions and microbial contamination, correlation analyses were performed between physico-chemical variables and faecal indicator bacteria. Particular emphasis was placed on evaluating the influence of temperature, dissolved oxygen, electrical conductivity, and total dissolved solids on the abundance of *Escherichia coli* and intestinal enterococci. These factors have been reported to influence bacterial survival and distribution in aquatic environments [2,4,16]. Pearson correlation coefficients and linear regression analyses were applied to identify significant relationships and determine the environmental factors most strongly associated with summer microbial contamination. Furthermore, contamination hotspot analysis was conducted using the average summer concentrations of faecal indicator bacteria. Sites exhibiting consistently elevated bacterial concentrations throughout the monitoring period were classified as hotspots and further evaluated in relation to local environmental pressures and surrounding land-use activities [7,9,14,17].

3. RESULTS AND DISCUSSION

3.1 Relationship Between Summer Temperature and Faecal Contamination

Water temperature exhibited considerable variation during the summer monitoring period and represented one of the most influential environmental factors affecting microbial water quality [2,4]. Elevated temperatures recorded during the summer months created favorable conditions for the persistence and proliferation of faecal indicator bacteria [2,14]. The relationship between water temperature and *Escherichia coli* concentrations is presented in Figure 3.

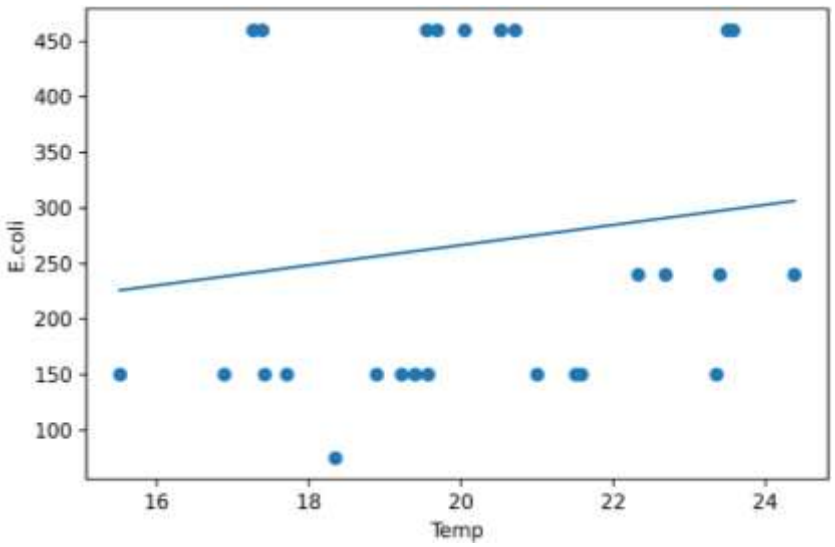

Figure 3. Relationship between water temperature and *Escherichia coli* concentrations during the summer monitoring period.

The results indicate a positive association between increasing water temperature and *E. coli* abundance [2]. Higher temperatures enhance bacterial metabolic activity and may prolong bacterial survival under favorable environmental conditions [2,4]. During periods of reduced river discharge, elevated temperatures also reduce the water's dilution capacity, allowing faecal contaminants to accumulate in the water column [9,17]. Similar observations have been reported in several Mediterranean river systems, where summer warming is frequently associated with increased microbiological contamination levels [2,9,17].

3.2 Influence of Dissolved Oxygen on Microbiological Water Quality

Dissolved oxygen is widely recognized as an important indicator of ecological condition and organic matter decomposition processes in freshwater ecosystems [4,8,16]. The relationship between dissolved oxygen and E. coli concentrations is shown in Figure 4.

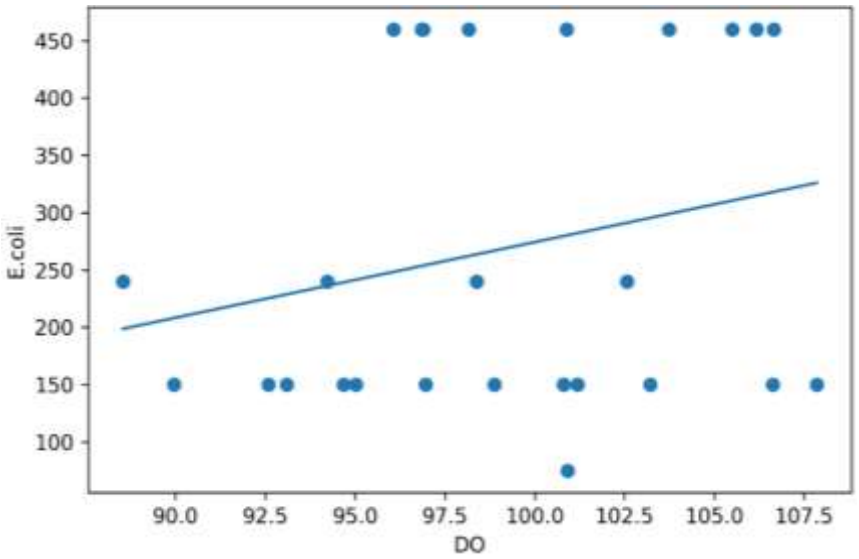

Figure 4. Relationship between dissolved oxygen and *Escherichia coli* concentrations during the summer season.

The analysis suggests an inverse relationship between dissolved oxygen levels and faecal contamination [4,16]. Sites exhibiting lower dissolved oxygen concentrations generally presented higher bacterial counts [17]. This pattern may be associated with increased organic matter inputs and microbial decomposition processes, which consume oxygen while simultaneously

providing favorable conditions for the survival of faecal bacteria [4,17]. Reduced oxygen availability during warm summer periods may therefore serve as an indicator of ecological stress and an increased risk of contamination [8,16].

3.3 Electrical Conductivity and Microbial Contamination

Electrical conductivity reflects the concentration of dissolved ions in water and may indicate the influence of agricultural runoff, wastewater inputs, and other anthropogenic activities [8,9,17]. The relationship between conductivity and *E. coli* concentrations is presented in Figure 5.

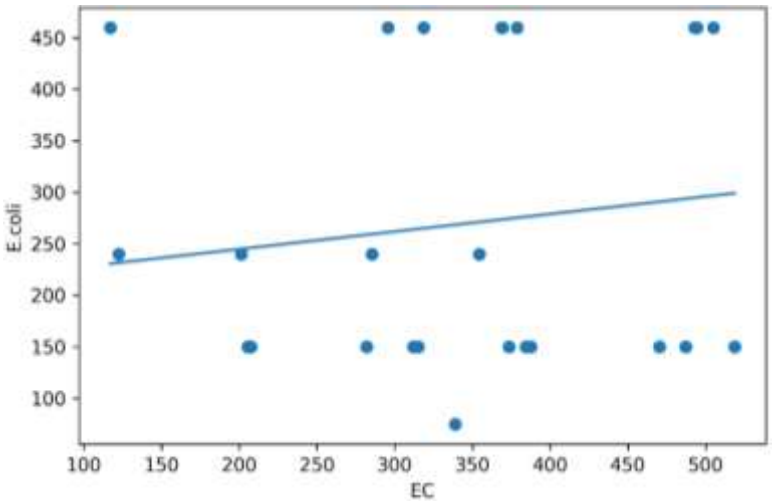

Figure 5. Relationship between electrical conductivity and *Escherichia coli* concentrations during summer.

Variations in conductivity were associated with differences in microbiological water quality among monitoring stations [9,17]. Locations characterized by elevated conductivity values frequently corresponded to areas influenced by human activities and tributary inputs [8,9]. Although conductivity itself does not directly affect bacterial growth, it may serve as an indirect indicator of contamination sources contributing both nutrients and faecal microorganisms to the river system [7,9,17].

3.4 Total Dissolved Solids and Faecal Indicator Bacteria

Total dissolved solids (TDS) provide additional information regarding the concentration of dissolved substances transported within the aquatic environment [8,17]. The relationship between TDS and *E. coli* concentrations is illustrated in Figure 6.

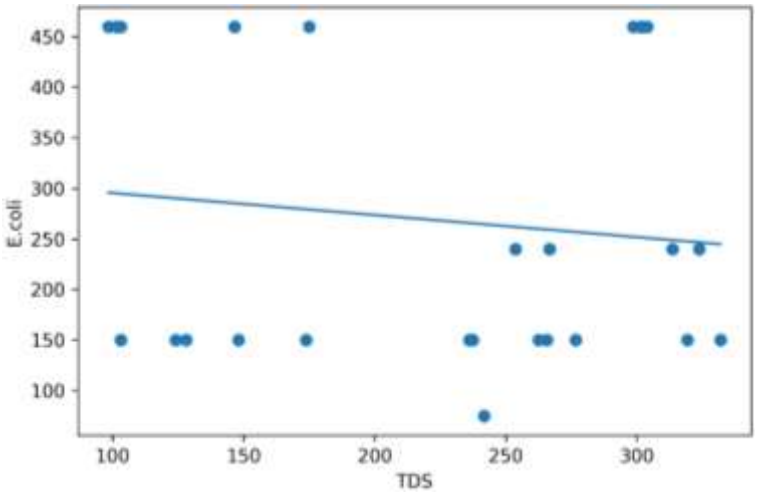

Figure 6. Relationship between total dissolved solids and *Escherichia coli* concentrations during the summer period

The results indicate that stations with higher TDS values often exhibited increased concentrations of *E. coli* [9,17]. This pattern suggests that dissolved materials transported by agricultural runoff, livestock activities, and domestic wastewater inputs may contribute to the introduction and persistence of faecal bacteria in the aquatic environment [7,9,14,17]. During the summer months, reduced river discharge and increased evaporation can further concentrate dissolved substances, enhancing the observed relationship between TDS and microbiological contamination [2,17].

Although TDS does not directly promote bacterial growth, it reflects environmental conditions and potential pollution sources that may influence microbial water quality [8,16]. Therefore, elevated TDS values can serve as an additional indicator of areas more vulnerable to faecal contamination within the Vjosa River basin [7,9,18].

3.5 Correlation Between Physico-Chemical and Microbiological Parameters

To better understand the interactions among environmental variables and faecal contamination indicators, a correlation analysis was performed using all summer monitoring data. The resulting correlation matrix is presented in Figure 7.

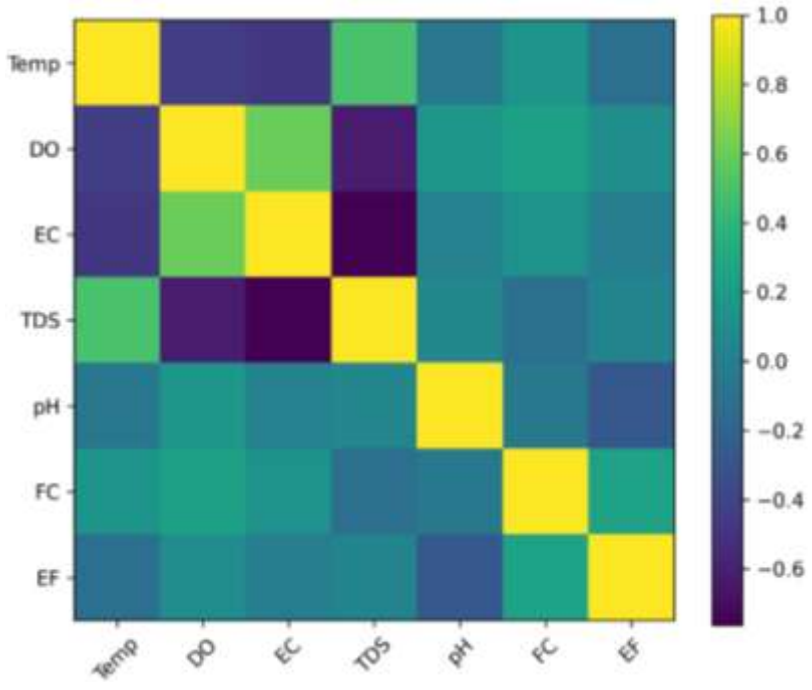

Figure 7. Correlation matrix showing relationships among summer physico-chemical and microbiological parameters.

The results indicate that water temperature was generally positively associated with *E. coli* concentrations, suggesting that warmer summer conditions favor bacterial survival and persistence [2,4]. In contrast, dissolved oxygen showed a negative relationship with microbial contamination, with lower oxygen levels often corresponding to higher bacterial counts [4,16,17]. Electrical conductivity and total dissolved solids exhibited moderate positive associations with faecal indicator bacteria, indicating the potential influence of agricultural runoff, livestock activities, and other anthropogenic sources [7,9,14,17]. These findings suggest that both natural seasonal conditions and human pressures contribute to the observed patterns of microbiological contamination [4,7,17].

Overall, the correlation analysis highlights temperature, dissolved oxygen, conductivity, and TDS as important factors influencing the spatial and temporal distribution of faecal contamination in the Vjosa River during the summer season [2,4,8,16].

3.6 Identification of Summer Faecal Contamination Hotspots

Spatial analysis of *E. coli* concentrations revealed substantial differences among monitoring stations throughout the summer period. To visualize these variations, a heatmap was developed using monthly bacterial concentrations recorded at each site (Figure 8).

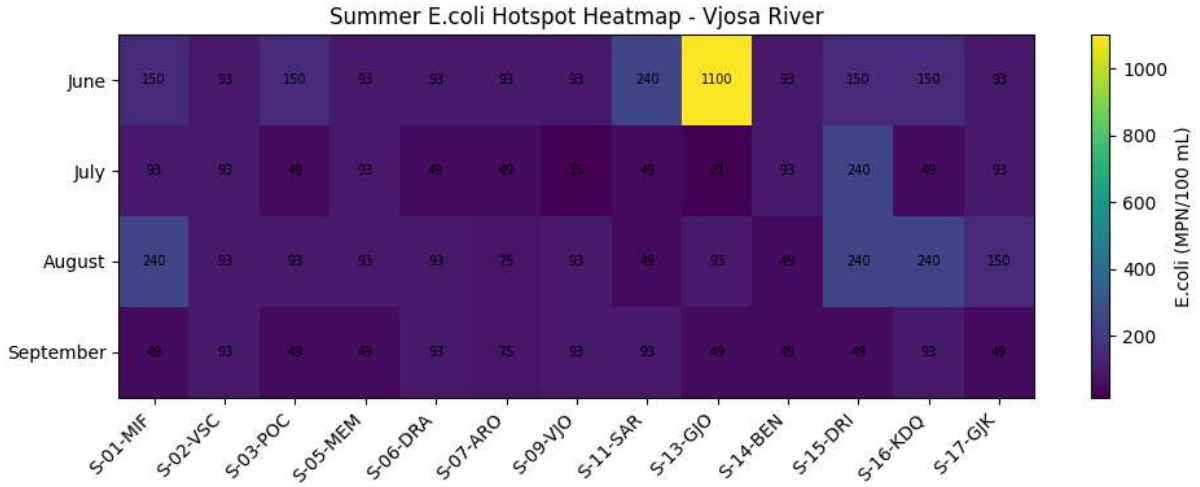

Figure 8. Summer heatmap of *Escherichia coli* concentrations across monitoring stations in the Vjosa River basin.

The heatmap clearly identifies several locations characterized by elevated microbiological contamination. The highest concentration recorded during the study period occurred at station S-13 GJO in June, reaching approximately 1100 MPN/100 mL. Elevated values were also observed at stations S-01 MIF, S-15 DRI, and S-16 KDQ during August, indicating increased microbiological pressure during peak summer conditions. These areas can therefore be considered microbiological hotspots within the Vjosa River basin and deserve particular attention in future monitoring and management programs [8,19].

The spatial distribution of contamination suggests that local anthropogenic pressures, including agricultural activities, livestock presence, tributary inputs, and human settlements, may significantly influence microbial water quality at these locations [7,9,14,17].

3.7 Seasonal Trend of *E. coli* During Summer.

To evaluate the temporal evolution of faecal contamination, average *E. coli* concentrations were calculated for each summer month. The resulting seasonal trend is shown in Figure 9.

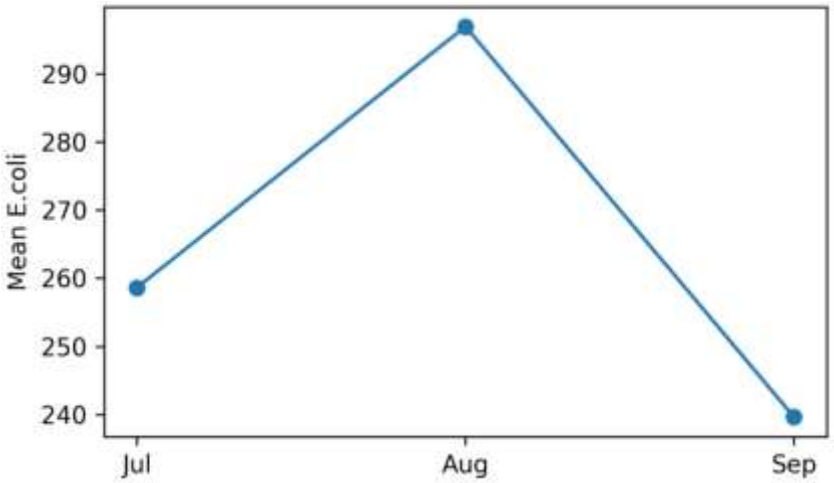

Figure 9. Average summer trend of *Escherichia coli* concentrations in the Vjosa River basin.

The temporal analysis indicates that microbiological contamination varied considerably throughout the summer season. Higher bacterial concentrations were generally observed during the warmest periods, reflecting the combined effects of elevated temperatures, reduced river discharge, and increased anthropogenic activity [2,9,14,17]. Toward the end of the summer period, bacterial concentrations tended to decrease, suggesting improved dilution conditions and reduced environmental stress [2,17].

Overall, the results demonstrate that summer represents the most critical period for microbiological water quality in the Vjosa River [2,4]. The combined influence of hydrochemical conditions and human pressures contributes to the formation of contamination hotspots and highlights the importance of seasonal monitoring for effective river management and ecosystem protection [5,8,19,20].

5. CONCLUSIONS

This study investigated the relationship between summer physico-chemical conditions and microbiological water quality in the Vjosa River basin, with particular emphasis on the identification of faecal contamination hotspots during the warmest period of the year. The results demonstrated that summer represents the most critical season for microbiological deterioration of water quality, highlighting the strong influence of environmental conditions on the distribution and persistence of faecal indicator bacteria [2,4,17]. The analysis revealed that water temperature plays a significant role in shaping microbial dynamics during summer. Elevated temperatures, combined with reduced river discharge and lower dilution capacity, created favorable conditions for the survival and accumulation of *Escherichia coli* and other faecal indicators [2,9,17]. In contrast, dissolved oxygen generally exhibited an inverse relationship with bacterial abundance, suggesting that sites experiencing greater ecological stress were more vulnerable to microbiological contamination [4,16,17].

Electrical conductivity and total dissolved solids also contributed to the observed spatial variability in bacterial concentrations. Higher values of these parameters were frequently associated with areas influenced by agricultural activities, tributary inflows, and human settlements, indicating that anthropogenic pressures remain important drivers of water quality degradation within the watershed [7,9,14,17]. The hotspot analysis identified several monitoring stations characterized by elevated concentrations of faecal indicator bacteria during the summer period. Particularly high contamination levels were observed at stations S-13 GJO, S-15 DRI, and S-16 KDQ, while additional microbiological pressure was detected at other locations influenced by tributary inputs and surrounding land-use activities. These findings demonstrate that faecal contamination is not uniformly distributed throughout the river system but is concentrated in specific sectors where environmental and anthropogenic factors interact [7,9,17].

The correlation analysis further confirmed that summer hydrochemical conditions are closely linked to microbiological water quality [2,4,16]. The combined effects of increased temperature, reduced oxygen availability, and changes in dissolved substances contribute to the formation of contamination hotspots and influence the spatial distribution of faecal indicator bacteria across the basin [2,9,17]. Overall, the findings of this study emphasize the importance of seasonal monitoring programs focused specifically on summer conditions [5,8,19]. Understanding the interactions between physico-chemical parameters and microbial contamination is essential for protecting aquatic ecosystems, safeguarding public health, and supporting sustainable management strategies within the Vjosa River National Park [19,20].

Future investigations should expand seasonal monitoring efforts, incorporate hydrological variables, and evaluate the contribution of specific pollution sources in order to improve the understanding of contamination processes and support evidence-based conservation and water management policies in the Vjosa River basin [5,19,20].

5. REFERENCES

1.APHA (2017). *Standard Methods for the Examination of Water and Wastewater* (23rd ed.). American Public Health Association, Washington, DC.

2. Blaustein R.A., Y. Pachepsky, R.L. Hill, D.R. Shelton, G. Whelan, Escherichia coli survival in waters: Temperature dependence, Water Research, Volume 47, Issue 2,2013, Pages 569-578, ISSN 0043-1354.

3. Byappanahalli MN, Nevers MB, Korajkic A, Staley ZR, Harwood VJ. 2012. Enterococci in the Environment. Microbiol Mol Biol Rev 76:. https://doi.org/10.1128/mmbr.00023-12.

4. Cabral JP. Water microbiology. Bacterial pathogens and water. Int J Environ Res Public Health. 2010 Oct;7(10):3657-703. doi: 10.3390/ijerph7103657. Epub 2010 Oct 155.

5. European Environment Agency (2021). *Bathing Water Quality in Europe 2020*. Publications Office of the European Union, Luxembourg.

6.Edge, T. A., & Hill, S. (2005). Occurrence of antibiotic resistance in *Escherichia coli* from surface waters and fecal pollution sources near Hamilton, Ontario. Canadian Journal of Microbiology, 51(6), 501-505.

7. Field Katharine G., Mansour Samadpour, Fecal source tracking, the indicator paradigm, and managing water quality, Water Research, Volume 41, Issue 16,2007, Pages 3517-3538, ISSN 0043-1354,7.

8. Francy, D.S., Brady, A.M.G., Carvin, R.B., Corsi, S.R., Fuller, L.M., Harrison, J.H., Hayhurst, B.A., Lant, J., Nevers, M.B., Terrio, P.J., and Zimmerman, T.M., 2013, Developing and implementing predictive models for estimating recreational water quality at Great Lakes beaches: U.S. Geological Survey Scientific Investigations Report 2013-5166, 68

9. Garcia-Armisen T, P. Servais, Respective contributions of point and non-point sources of *E. coli* and enterococci in a large urbanized watershed (the Seine river, France), Journal of Environmental Management, Volume 82, Issue 4,2007, Pages 512-518, ISSN 0301-4797,9.

10. Isabelle George, Philippe Crop, Pierre Servais, Fecal coliform removal in wastewater treatment plants studied by plate counts and enzymatic methods, Water Research, Volume 36, Issue 10, 2002, Pages 2607-2617,

11. ISSN 0043-1354, 10. ISO 19458 (2006). *Water Quality-Sampling for Microbiological Analysis*. International Organization for Standardization, Geneva.

12.ISO 7899-1 (2014). *Water Quality-Detection and Enumeration of Intestinal Enterococci*-International Organization for Standardization, Geneva.

13.ISO 9308-2 (2014). *Water Quality-Enumeration of Escherichia coli and Coliform Bacteria*-International Organization for Standardization, Geneva.

14. Jamieson, Rob & Gordon, Robert & Sharples, K.E. & Stratton, Glenn & Madani, A.. (2002). Movement and persistence of fecal bacteria in agricultural soils and subsurface

drainage water: A review. Canadian Biosystems Engineering / Le Genie des biosystems au Canada. 44. 1.1-1.9.

15. Muirhead, Richard & Collins, Rob & Bremer, Phil. (2006). Interaction of Escherichia coli and Soil Particles in Runoff. Applied and environmental microbiology. 72. 3406-11. 10.1128/AEM.72.5.3406-3411.2006.

16. Payment, P. and Locas, A. (2011), Pathogens in Water: Value and Limits of Correlation with Microbial Indicators. Groundwater, 49: 4-11.

17. Servais Pierre, Tamara Garcia-Armisen, Isabelle George, Gilles Billen, Fecal bacteria in the rivers of the Seine drainage network (France): Sources, fate and modelling, Science of The Total Environment, Volume 375, Issues 1-3,2007, Pages 152-167,

18. Tallon, P., Magajna, B., Lofranco, C. et al. Microbial Indicators of Faecal Contamination in Water: A Current Perspective. Water Air Soil Pollut 166, 139-166 (2005). https://doi.org/10.1007/s11270-005-7905-4

19.USEPA (2012). *Recreational Water Quality Criteria*. United States Environmental Protection Agency, Washington, DC.

20. WHO (2022). *Guidelines for Drinking-water Quality* (4th ed., updated). World Health Organization, Geneva.

CONTROL OF FUNGAL DISEASES IN GREENHOUSE CUCUMBERS THROUGH A FUNGICIDE TREATMENT SCHEME

Nataliya Karadzhova & Boyan Arnaoudov*

Maritsa Vegetable Crops Research Institute, 4003 Plovdiv, Bulgaria
Agricultural Academy, 1373 Sofia, Bulgaria
**E-mail: scorpioo_cb@abv.bg*

ABSTRACT

The article presents the results of a study evaluating the efficacy of a fungicide treatment scheme against aerogenic fungal diseases in greenhouse cucumbers. The experimental work was carried out in 2025 at the Maritsa Vegetable Crops Research Institute, Plovdiv, in an unheated steel-glass greenhouse using the cucumber cultivar 'Defense F1', transplanted during the second decade of April. Phytosanitary monitoring indicated that the primary fungal diseases affecting the crop in 2025 were downy mildew (*Pseudoperonospora cubensis*) and powdery mildew (*Erysiphe cichoracearum*). Regular preventive treatments with fungicides containing the active substances metalaxyl, folpet, and cymoxanil at standard application rates delayed the onset of downy mildew by 21 days. Subsequent curative treatments demonstrated high efficacy, reducing the downy mildew infection pressure from its peak of 18.33% down to a final baseline of 10.00%, achieving an overall curative and protective efficacy of 79.54%. Furthermore, incorporating azoxystrobin- and penconazole-based fungicides into the treatment scheme effectively suppressed powdery mildew, keeping it at zero through June and early July, with a final disease index of 12.08% at the end of the harvesting cycle. The evaluated scheme of prophylactic and curative fungicide treatments proved highly effective against economically important aerogenic diseases (downy mildew and powdery mildew) in greenhouse cucumbers and can be successfully recommended as part of the plant protection system in the commercial growing technology for this crop.

Keywords: greenhouse cucumbers, downy mildew, powdery mildew, treatment scheme model, fungicidal effect

I. INTRODUCTION

Greenhouse production of cucumbers (*Cucumis sativus* L.) is continuously exposed to the risk of economically significant pathogens, among which downy mildew (*Pseudoperonospora cubensis* Berk. et M. A. Curtis) and powdery mildew (*Erysiphe cichoracearum* DC.) are the most dangerous. The specific microclimate within protected environments - high air humidity, moderate temperatures, and leaf wetness - creates optimal conditions for rapid spore dissemination and epiphytotic disease development. Recent epidemiological studies emphasize that modern greenhouse systems face accelerated polycyclic infection cycles under such conditions, significantly increasing disease pressure (Mirzwa-Mróz et al., 2024; Savory et al., 2011).

The taxonomy, physiological race differentiation, and host-pathogen interactions - particularly regarding *Podosphaera xanthii* and *Erysiphe cichoracearum* - have been extensively documented, highlighting the increasing genetic variability among cucurbit cultigens and specific pathogen races (McCreight, 2006; Lebeda & Sedláková, 2004; Braun et al., 2002). Furthermore, monitoring resistance shifts to fungicides in regional pathogen populations underscores the necessity of structured, multi-application integrated pest management (IPM)

programs (Lopez-Ruiz et al., 2010; Ojiambo et al., 2015). Adapting advanced breeding and protection strategies to specific microclimatic conditions remains crucial for maintaining plant health and durability in protected cultivation (Liu et al., 2019; Lebeda et al., 2010).

In modern agricultural practice, the chemical method remains the primary and most reliable tool for rapidly controlling the infection background upon reaching critical economic thresholds. However, the high adaptability of target pathogens and the intensive, repeated use of single-site inhibitors create an escalating risk of resistance buildup and reduced field performance (Liang et al., 2022). To mitigate these risks and manage resistance effectively, contemporary plant protection strategies rely on meticulously timed, combined fungicide schemes. These frameworks integrate systemic and translaminar active substances with specific biochemical modes of action - such as phenylamides (FRAC 4, affecting nucleic acid synthesis), strobilurins / QoI inhibitors (FRAC 11, disrupting mitochondrial respiration at the Qo site), and triazoles / DMI inhibitors (FRAC 3, inhibiting sterol biosynthesis) - coupled with broad-spectrum, multi-site contact protectants including phthalimides and cyanoacetamide-oximes (CAA). This strategic integration ensures a dual-action mechanism: systemic components provide internal eradication during early latent infection stages, while multi-site contact barriers prevent spore germination on the leaf surface, averting rapid resistance selection. Deploying such structured chemical frameworks is vital for safeguarding the yield potential and physiological stability of high-yielding greenhouse hybrids, such as cv. 'Defense F1'.

The aim of this study is to determine the biological efficacy of combined preventive and curative fungicide schemes against downy mildew and powdery mildew in greenhouse cucumbers of the 'Defense F1' variety.

MATERIAL AND METHODS

The experiments were conducted under conditions in steel-glass greenhouses following established methodology for pesticide efficacy testing.

Plant Material - An indeterminate hybrid cucumber variety, 'Defense F1', was used, cultivated under soil technology with the maintenance of an optimal microclimate (temperature range of 22–26 °C and relative air humidity of 75–85%).

Transplanting date - April 24, 2025.

Fungicide Treatments - A total of 11 foliar fungicide applications were performed throughout the growing season at weekly intervals (Table 1).

Recording and Analysis - The degree of attack (disease index in %) was dynamically monitored through periodic phytopathological assessments using a 10-point rating scale, conducted immediately before and after each respective fungicide treatment. Statistical processing was performed via linear regression analysis in Microsoft Excel to establish the correlation dependency between the treatment time (reporting dates) and the spread of pathogens.

The biological efficacy of the curative treatments against downy mildew was calculated relative to the maximum peak infection background using the general formula:

$$\text{Efficacy (\%)} = \frac{\text{I(peak)} - \text{I(obs)}}{\text{I(peak)}} * 100$$

Where:

- I(peak) is the maximum recorded disease severity index,
- I(obs) is the disease severity index observed on the respective post-treatment evaluation date.

Efficacy Calculation for Powdery Mildew: The biological efficacy or suppression level was determined based on the dynamics of the disease index relative to the untreated control and critical economic thresholds throughout the active harvest period.

Table 1. Schedule of fungicide treatments against downy mildew and powdery mildew in greenhouse cucumbers (cv. 'Defense F1')

Treatment Date	Fungicide	Active Ingredient	Concentration / Rate
17.05.2025	Ridomil Gold Combi 45 WG	Metalaxyl-M 48.5 g/kg + Folpet 400 g/kg	300 g/da
24.05.2025	Ridomil Gold Combi 45 WG	Metalaxyl-M 48.5 g/kg + Folpet 400 g/kg	300 g/da
30.05.2025	Cymbal 45 WG	Cymoxanil 450 g/kg	25 g/da
07.06.2025	Cymbal 45 WG	Cymoxanil 450 g/kg	25 g/da
14.06.2025	Quadris 25 SC + Topaz 100 EC	Azoxystrobin 250 g/l + Penconazole 100 g/l	75 ml/da + 35 ml/da
21.06.2025	Quadris 25 SC + Topaz 100 EC	Azoxystrobin 250 g/l + Penconazole 100 g/l	75 ml/da + 35 ml/da
28.06.2025	Topaz 100 EC	Penconazole 100 g/l	50 ml/da
05.07.2025	Trunfo	Azoxystrobin 250 g/l	80 ml/da
12.07.2025	Cymbal 45 WG	Cymoxanil 450 g/kg	25 g/da
19.07.2025	Trunfo	Azoxystrobin 250 g/l	80 ml/da
26.07.2025	Trunfo	Azoxystrobin 250 g/l	80 ml/da

RESULTS AND DISCUSSION

The monitoring of aerogenic diseases in greenhouse cucumbers of the 'Defense F1' cultivar during the 2025 growing season demonstrated high biological efficacy and reliable crop protection through the implementation of structured, integrated preventive and curative fungicide schemes (Table 2).

1. Dynamics and Control of Downy Mildew (*Pseudoperonospora cubensis*)

The implementation of early preventive treatments using systemic and contact active ingredients (metalaxyl-M, folpet, and cymoxanil) successfully established a protective barrier in the initial phases of crop development. The first five treatments maintained the disease index within minimal limits (from 0.00% to 0.42%) until mid-June. The first symptoms of downy mildew were recorded on June 11 (48 days post-transplanting) in the form of single local spots with an index of 0.42%.Under the influence of favorable microclimatic conditions in the greenhouse, infection pressure increased during the second half of June and early July, reaching its peak on July 12 with a disease attack index of 18.33%. The inclusion of curative treatments with azoxystrobin, penconazole, and cymoxanil demonstrated a strong therapeutic effect, limiting the spread of the pathogen and reducing the final disease index to 10.00% by July 31. Regression analysis of downy mildew dynamics shows an upward linear trend for the entire period, described by the equation $y = 1.61x - 4.36$, with a high coefficient of determination ($R^2 = 0.687$) confirming the strong dependence between time (reporting dates) and the development of the disease under the influence of the applied scheme. These findings corroborate the conclusions of recent epidemiological studies regarding the necessity of multi-site rotational schemes to suppress polycyclic infection waves in enclosed cultivation systems (Ojiambo et al., 2015; Mirzwa-Mróz et al., 2024).

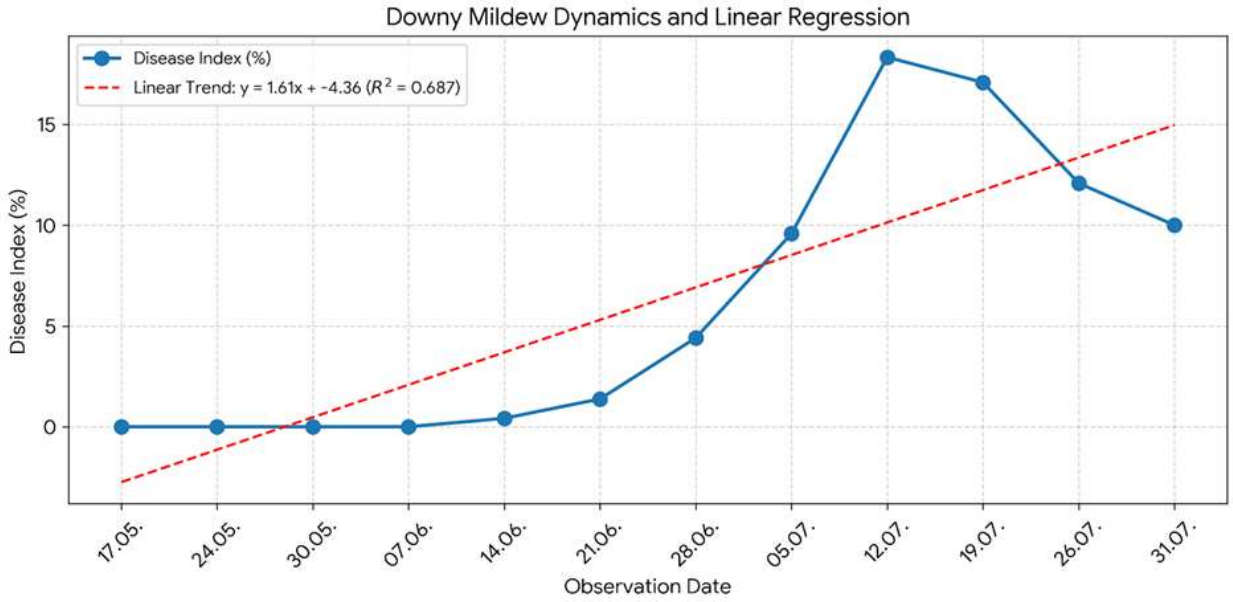

Figure 1. Dynamics of downy mildew (*Pseudoperonospora cubensis*) development in cucumber crops of the 'Defense F1' variety during the 2025 growing season.

2. Dynamics and Control of Powdery Mildew (*Erysiphe cichoracearum*)

The incorporation of dedicated powdery mildew fungicides based on the active ingredients azoxystrobin (QoI inhibitor) and penconazole (DMI inhibitor)—administered through consecutive applications of Quadris 25 SC, Topaz 100 EC, and Trunfo—demonstrated exceptional preventive capacity. The application schedule successfully extended the incubation and latency period of powdery mildew in the greenhouse cucumbers by approximately one month. Initial symptoms of powdery mildew only appeared in mid-July (specifically on July 12) as isolated spots with a minimal attack index of 0.41%.Despite the natural accumulation of inoculum towards the end of the vegetation cycle, disease development was effectively checked, reaching a final severity of 12.08% at the conclusion of the harvest period on July 31 (Table 2). Regression analysis of powdery mildew dynamics shows a moderate linear trend towards the end of the period, described by the equation $y = 0.79x - 3.17$, where the coefficient of determination ($R^2 = 0.536$) confirms the stable character of infection accumulation following the appearance of the first symptoms.Comparing these trends with broader greenhouse pathology findings, the observed one-month incubation delay aligns with the protective thresholds reported by Cohen et al. (2018) and McGrath (2001), confirming that structured DMI and QoI alternation effectively restrains conidial dispersal during critical fruit-setting stages. The combined utilization of systemic demethylation inhibitors and strobilurins ensured prolonged suppression of secondary spore dissemination during the critical vegetative phase.

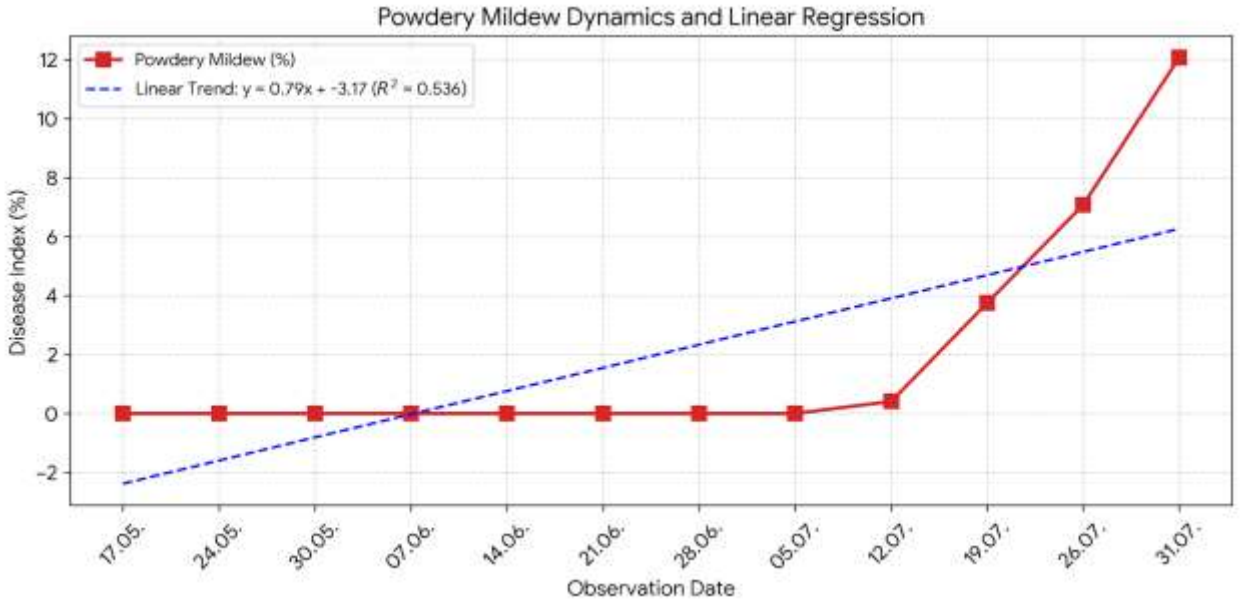

Figure 2. Dynamics of development of powdery mildew *Erysiphe cichoracearum* in cucumber *Defense F1* variety during the 2025 growing season.

Table 2. Development of aerogenic diseases in greenhouse cucumbers (cv. 'Defense F1') grown under an integrated plant protection system, 2025.

No.	Observation Date / Treatment	Fungicide Applied	Downy Mildew (%)	Efficacy (%)	Powdery Mildew (%)	Efficacy (%)
I.	**Preventive Treatments**					
1	17.05.	Ridomil Gold Combi 45 WG	0,00	n.a.	0,00	n.a.
2	24.05.	Ridomil Gold Combi 45 WG	0,00	n.a.	0,00	n.a.
3	30.05.	Cymbal 45 WG	0,00	n.a.	0,00	n.a.
4	07.06.	Cymbal 45 WG	0,00	n.a.	0,00	n.a.
5	14.06.	Quadris 25 SC + Topaz 100 EC	0,42	n.a.	0,00	n.a.
II.	**Curative Treatments**					
6	21.06.	Quadris 25 SC + Topaz 100 EC	1,38	n.a.	0,00	n.a.
7	28.06.	Topaz 100 EC	4,41	n.a.	0,00	n.a.
8	05.07.	Trunfo	9,58	n.a.	0,00	n.a.
9	12.07.	Cymbal 45 WG	18,33	n.a.	0,41	n.a.
10	19.07.	Trunfo	17,08	6,82	3,75	n.a.
11	26.07.	Trunfo	12,08	34,10	7,08	n.a.
12	31.07.	Final observation	10,00	45,44	12,08	n.a.
—	**Final / Summary**	—	**10.00[2]**	**79,54[3]**	**12.08[2]**	n.a.

Note: Transplanting date: April 24, 2025

*[1] **n.a. (not applicable):** Fungicide efficacy was not calculated during periods of zero or escalating infection parameters prior to the establishment of the maximum disease pressure, as mathematical evaluation requires a declining baseline post-treatment.*

*[2] **Final Severity:** The summary values for disease percentages represent the final recorded infection status at the end of the commercial harvesting cycle (July 31).*

*[3] **Overall Curative Capacity:** The value of 79.54% reflects the cumulative reduction of the downy mildew infection pressure from its peak of 18.33% to the final baseline of 10.00%, combined with the 3-week developmental delay achieved during the preventive phase.*

3. General Evaluation and Resistance Management

The applied schedule of consecutive preventive and curative treatments demonstrated robust performance against both economically significant pathogens. By alternating active substances with distinct biochemical modes of action and FRAC groups, the scheme effectively managed the infection background while mitigating the selection pressure for resistance buildup, safeguarding the physiological stability of greenhouse cucumbers. The proposed schedule of fungicide treatments for the cucumber crops is presented in Table 3.

Table 3. Recommended schedule of fungicide treatments for the control of downy mildew and powdery mildew in greenhouse cucumbers.

Treatment Info		Downy Mildew		Powdery Mildew	
No.	Treatment Date	Product & Active Ingredient	Concentration (%)	Product & Active Ingredient	Concentration (%)
1	17.05.	Ridomil Gold Combi 45 WG (metalaxyl + folpet)	0.30	-	-
2	24.05.	Ridomil Gold Combi 45 WG (metalaxyl + folpet)	0.30	-	-
3	30.05.	Cymbal 45 WG (cymoxanil)	0.25	-	-
4	07.06.	Cymbal 45 WG (cymoxanil)	0.25	-	-
5	14.06.	Quadris 25 SC + Topaz 100 EC (azoxystrobin + penconazole)	0.06 + 0.02	Quadris 25 SC + Topaz 100 EC (azoxystrobin + penconazole)	0.06 + 0.02
6	21.06.	Quadris 25 SC + Topaz 100 EC (azoxystrobin + penconazole)	0.06 + 0.02	Quadris 25 SC + Topaz 100 EC (azoxystrobin + penconazole)	0.06 + 0.02
7	28.06.	-	-	Topaz 100 EC (penconazole)	0.02
8	05.07.	Trunfo (azoxystrobin)	0.08	Trunfo (azoxystrobin)	0.08
9	12.07.	Cymbal 45 WG (cymoxanil)	0.25	-	-
10	19.07.	Trunfo (azoxystrobin)	0.08	Trunfo (azoxystrobin)	0.08
11	26.07.	Trunfo (azoxystrobin)	0.08	Trunfo (azoxystrobin)	0.08

Conclusions:

1. Preventive treatments of cucumbers with fungicides based on the active ingredients metalaxyl, folpet, and cymoxanil (applied at standard concentrations of 0.3% and 0.25% following a schedule of two consecutive sprayings with Ridomil Gold Combi 45 WG, followed by two treatments with Cymbal 45 WG at one-week intervals) delayed the development of downy mildew (*Pseudoperonospora cubensis*) by three weeks.
2. The subsequent integration of curative treatments using scheduled fungicidal applications demonstrated strong therapeutic control, successfully reducing the downy mildew disease index from its peak of 18.33% down to 10.00% by the end of July.
3. Fungicides based on the active ingredients azoxystrobin and penconazole, applied at standard concentrations as consecutive sprays during the period of active harvesting, successfully extended the incubation and latency period of powdery mildew (*Erysiphe cichoracearum*) in greenhouse cucumbers by approximately one month, keeping the final disease severity at 12.08% on July 31.

4. The combined schedule of preventive and curative fungicide treatments implemented in the experiment demonstrated high biological efficacy against economically important aerogenic diseases (downy mildew and powdery mildew) in greenhouse cucumbers. It can be successfully recommended as an essential component of the integrated pest management system within the cultivation technology for this crop.

REFERENCES

Braun, U., Cook, R. T. A., Inman, A. J., & Shin, H. D. (2002). The taxonomy of the powdery mildew fungi. In R. R. Bélanger, W. R. Bushnell, A. J. Dik, & T. L. W. Carver (Eds.), *The powdery mildews: a comprehensive treatise* (pp. 13-55). APS Press, St. Paul, MN.

Cohen, Y., Rubin, A. E., & Galperin, M. (2018). Efficacy of new fungicides for controlling downy mildew and powdery mildew in greenhouse crops. *Plant Disease*, 102(4), 789–798. doi.org

Lebeda, A., & Sedláková, B. (2004). Species spectrum, pathogenic variability and fungicide resistance in cucurbit powdery mildew. *Rostlinolékař*, 15(6), 15-19.

Lebeda, A., & Sedláková, B. (2010). Fungicide resistance in cucurbit powdery mildew fungi. In H. Thajuddin (Ed.), *Fungicides* (pp. 221-242). InTech. doi.org

Liang, Q., Wei, L., Xu, B., Liu, J., Zhang, S., & Liu, L. (2022). Induction of resistance of *Podosphaera xanthii* (hull-less pumpkin powdery mildew) to triazole fungicides and its resistance mechanism. *PLoS ONE*, 17(2), e0263068. doi.org

Liu, L. L., Liang, Q. L., Zhang, A. Q., & Zhang, H. (2019). Sensitivity of hull-less pumpkin powdery mildew to five kinds of triazole fungicides. *Journal of Yangzhou University (Agricultural and Life Science Edition)*, 40(2), 101–106.

Lopez-Ruiz, F. J., Pérez-García, A., Fernández-Ortuño, D., Romero, D., de Vicente, A., & Torés, J. A. (2010). Resistance to single-site fungicides in field and greenhouse populations of plant pathogens: Current perspectives. *Pest Management Science*, 66(5), 481–493. doi.org

McCreight, J. D. (2006). Cucurbit powdery mildew: Genotypic and phenotypic characterization of *Podosphaera xanthii* races. *Proceedings of Cucurbitaceae 2006*, 319–326.

McGrath, M. T. (2001). Fungicide resistance in cucurbit powdery mildew: experiences and challenges. *Plant Disease*, 85(3), 236-245. doi.org

Mirzwa-Mróz, E., Witkowska, M., & Schollenberger, M. (2024). Epidemiology and population dynamics of *Pseudoperonospora cubensis* in protected cultivation systems. *Journal of Phytopathology*, 172(1), 45–58. doi.org

Ojiambo, P. S., Holmes, G. J., Keeney, W., & Thomas, A. (2015). Managing polycyclic epidemics in enclosed systems: The role of multi-component rotational fungicide programs. *Phytopathology*, 105(8), 1032–1044. doi.org

Savory, E. A., Granke, L. L., Quesada-Ocampo, L. M., Varbanova, M., Hausbeck, M. K., & Day, B. (2011). The oomycete *Pseudoperonospora cubensis*: Biology, ecology, and control strategies. *Molecular Plant Pathology*, 12(3), 217–226. doi.org

ACOUSTIC METAMATERIALS FOR LOW-FREQUENCY SOUND ABSORPTION: RESONANCE MECHANISMS, DESIGN APPROACHES, AND CURRENT TRENDS

TUNAHAN PAMUKCU[1], NILHAN URKMEZ TASKIN[2],

[1,2]Trakya University, Engineering Faculty, Turkey

ABSTRACT

Effectively controlling low-frequency sounds is one of the most challenging problems in acoustic engineering due to their long wavelengths. Traditional porous sound-absorbing materials perform well in the mid and high frequencies thanks to energy dissipation mechanisms based on viscous and thermal losses, but they require high material thicknesses to provide effective sound absorption at low frequencies. This creates significant limitations, especially in engineering applications where volume and weight constraints exist. Acoustic metamaterials developed in recent years offer an alternative approach to traditional materials in controlling low-frequency sounds thanks to their properties based on local resonance and subwavelength structural design principles. In this study, acoustic metamaterials developed for low-frequency sound absorption are evaluated based on a comprehensive literature review. First, the historical development and theoretical foundations of acoustic metamaterials are discussed, and then Helmholtz resonators, membrane-type metamaterials, local resonance-based structures, and hybrid metamaterial systems are examined in terms of their working principles, advantages, and limitations. Furthermore, the possibilities offered by additive manufacturing technologies for the production of complex metamaterial geometries were evaluated, and the effects of geometric parameters, resonance characteristics, and material properties on sound absorption performance were compared in line with findings reported in the literature. The studies examined show that low-frequency sound absorption performance depends significantly not only on material properties but also on cell geometry, resonator configuration, and multi-scale structural design parameters. In conclusion, the potential of acoustic metamaterials to offer high-performance and compact solutions in low-frequency noise control has been demonstrated; current research trends, key challenges encountered, and future research requirements have been evaluated.

Key words: nanofertilizers, food quality, nanotechnology, nutrient uptake, plant nutrition.

INTRODUCTION

Today, with rapid urbanization, increasing industrialization, and the development of transportation systems, noise pollution has become an environmental problem with significant impacts on human health and quality of life. A significant portion of the noise produced by transportation vehicles (automotive, aviation, and railway systems), industrial machinery, and mechanical systems within buildings consists of low-frequency components. Low-frequency sounds (generally in the 20–500 Hz range), due to their long wavelengths and high propagation capabilities, are among the most difficult acoustic components to both isolate and dampen.

The main challenge in controlling low-frequency noise is that these waves have large wavelengths. The wavelength of an acoustic wave propagating in a free medium is determined by the inverse relationship between the speed of sound and frequency. For example, a sound wave at a frequency of 100 Hz has a wavelength of approximately 3.4 m, and for such waves to be effectively dampened, conventional acoustic materials need to have similar thicknesses.

This creates significant limitations in terms of volume, weight, and cost in engineering applications.

Traditional sound-absorbing materials are generally porous or fibrous structures that dampen sound energy through viscous friction and thermal losses. While these materials are quite effective in the mid and high frequency ranges, they do not perform adequately at low frequencies (Cummer et al., 2016). The main reason for this is that low-frequency waves are transmitted directly within the material without sufficient energy loss. Furthermore, increasing the thickness of these materials to improve their effectiveness creates significant disadvantages in practical applications. To overcome these limitations, acoustic metamaterials have become a significant research area in acoustic engineering over the last two decades. Metamaterials are artificially designed materials that can exhibit physical properties not found in natural materials and generally have periodic or quasi-periodic internal structures. The most important characteristic of these materials is that their acoustic behavior largely stems from their internal geometry rather than their chemical composition (Ma et al., 2016).

One of the most striking features of acoustic metamaterials is their ability to exhibit unusual parameters such as negative effective density and negative modulus. These properties allow for the complete blocking or anomalous redirection of wave propagation in specific frequency ranges. In this context, metamaterials offer great potential not only for sound absorption but also for advanced acoustic applications such as sound redirection, focusing, and isolation (Maa et al., 1998). The working principle of metamaterials is largely based on the resonance phenomenon. In particular, the local resonance mechanism makes it possible to create band gaps much smaller than the wavelength. This provides a critical advantage in terms of controlling low-frequency sounds. In addition, different resonance-based systems such as Helmholtz resonators, membrane-based structures, and microperforated panels are also widely used in the development of acoustic metamaterials (Maa et al., 1998; Fang et al., 2006).

Recent studies have focused on developing hybrid structures that use different resonance mechanisms together to improve the performance of metamaterials. In such systems, broadband sound absorption is achieved by combining structural elements with different resonance frequencies. Furthermore, the development of 3D printing technologies has made it possible to produce metamaterials with complex internal geometries, significantly accelerating research in this field. However, there are still significant problems to be solved regarding the integration of acoustic metamaterials into practical applications. These include factors such as production costs, scalability, mechanical strength, and sensitivity to environmental conditions. Discrepancies between numerical modeling and experimental results are also a significant research issue. This study aims to comprehensively examine the theoretical foundations, resonance mechanisms, and design approaches of acoustic metamaterials for low-frequency sound absorption. It also evaluates current developments in the literature, revealing existing trends and research gaps in this field. In this context, the study aims to provide a systematic perspective for both academic research and engineering applications.

Historical Development and Theoretical Foundations of Acoustic Metamaterials

The concept of acoustic metamaterials was developed inspired by electromagnetic metamaterials. The first significant studies in this field are based on the principle of local resonance. Liu et al. (2000) showed that a negative effective mass density could be obtained in certain frequency ranges with a structure consisting of coated spheres embedded in an elastic matrix (Liu et al., 2000). This work was a turning point in the field by demonstrating that wave propagation could be controlled at low frequencies. Following this, Fang et al. (2006) showed that a negative effective volume modulus could be obtained using Helmholtz resonator arrays (Fang et al., 2006). This development revealed that not only the density but also the compressibility properties of acoustic metamaterials could be controlled. Subsequent studies

have focused on membrane-based systems and hybrid structures. Yang et al. (2008) demonstrated that strong sound absorption at low frequencies can be achieved through masses placed on the membrane (Yang et al., 2008). Mei et al. (2012) introduced the concept of "acoustic dark metamaterials" with very high absorption coefficients (Mei et al., 2012).

Wave propagation in acoustic metamaterials is defined by effective medium parameters:

$$\nabla^2 p - \frac{\rho_{eff}}{K_{eff}} \frac{\partial^2 p}{\partial t^2} = 0$$

Here, ∇^2 represents the Laplace operator, p represents the acoustic pressure (Pa), ρ_{eff} represents the effective density (kg/m^3), K_{eff} represents the effective volume modulus (Pa), and t represents time (s). Due to the nature of acoustic metamaterials, these effective parameters are frequency-dependent and can exhibit negative values in certain resonance frequency ranges. When the effective density or effective volumetric modulus is negative, the wave number becomes complex. As a result, wave propagation cannot occur in the medium, and sound waves are exponentially attenuated, leading to the formation of acoustic bandgaps. Physically, this unusual behavior stems from the dynamic interaction between the resonant elements integrated into the metamaterial skeleton and the incoming sound waves (Ma et al., 2016).

Low-Frequency Sound Absorption and Resonance Mechanisms

Effectively damping low-frequency sounds is considered one of the most challenging problems in acoustic engineering. The main reason for this is that low-frequency waves have long wavelengths. For a planar wave propagating in free space, the wavelength is defined by the relationship:

$$\lambda = \frac{c}{f}$$

where λ is the wavelength (m), c is the speed of sound (m/s), and f is the frequency (Hz). As can be seen from the equation, the wavelength increases rapidly as the frequency decreases. This situation requires the characteristic dimensions of classical sound-absorbing materials to increase in order to function effectively. In traditional porous materials, sound absorption relies on the damping of acoustic energy through viscous friction and thermal losses. However, this mechanism is only effective in frequency ranges where the wavelength is comparable to the pore size of the material. At low frequencies, the acoustic wave is transmitted without undergoing sufficient phase change within the material, and therefore absorption does not occur (Cummer et al., 2016). This problem is also directly related to acoustic impedance mismatch. For a surface to provide maximum sound absorption, its surface impedance must be equal to the air impedance. Surface impedance is expressed as:

$$Z = R + jX$$

Here, R represents the resistance (dissipative component), and X represents the reactive component. At low frequencies, the reactive component becomes dominant, leading to increased reflection.

Acoustic metamaterials solve this problem differently than classical approaches. Thanks to the resonant elements they contain, these structures can provide effective impedance matching even at low frequencies. In particular, mechanisms such as local resonance and Helmholtz resonance allow for high absorption to be achieved with structures much smaller than the wavelength (Ma et al., 2016).

Helmholtz Resonance

Helmholtz resonators are one of the most fundamental and widely used structures for low-frequency sound absorption. In this system, the air column in the neck is modeled as the effective mass, and the air in the cavity as a spring. At the resonance frequency, the air in the neck moves back and forth while the air in the cavity compresses and expands. During this process, sound energy is stored within the system and damped due to viscous losses. Figure 1 shows a schematic representation of the Helmholtz resonator.

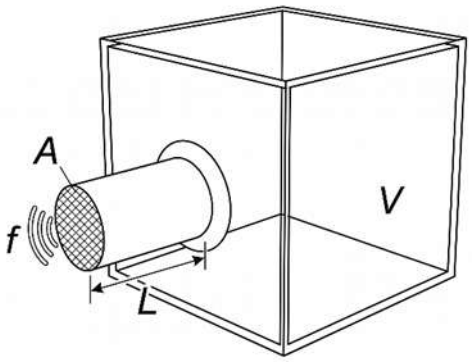

Fig. 1: Schematic representation of a Helmholtz resonator.

The resonance frequency (f, Hz) of a Helmholtz resonator is expressed by the equation:

$$f = \frac{c}{2\pi}\sqrt{\frac{A}{VL}}$$

In this equation, c represents the speed of sound (m/s), A represents the cross-sectional area of the resonator neck (m^2), V represents the volume of the inner chamber (m^3), and L represents the effective length of the neck (m).
The most significant disadvantage of classic Helmholtz resonators is their relatively narrow band. Therefore, in some studies, bandwidth is increased by using multiple resonator arrays, cells with different volumes, and stepped geometry designs (Fang et al., 2006).

Local Resonance Mechanism

Local resonance arises from the vibration of microstructural elements within metamaterials. These systems are generally described using mass-spring models. The resonance frequency depends on the mass and stiffness parameters of the system. The most important feature of this mechanism is its ability to create a low-frequency band gap without the need for Bragg scattering. This completely prevents wave propagation. This feature provides a significant advantage, especially in vibration and sound insulation applications (Liu et al., 2000).

Membrane-Based Resonance

Membrane-type metamaterials achieve low-frequency resonance through masses placed on thin and flexible surfaces. In these systems, the resonance frequency depends on the membrane tension, surface density, and added mass parameters. Figure 2 shows a schematic representation of a membrane-based resonator.

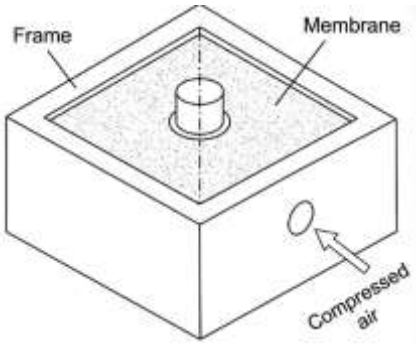

Fig. 2: Schematic representation of membrane-based resonator.

The most important advantage of membrane systems is that high performance can be achieved with very thin structures. However, the performance of the system is quite sensitive to environmental conditions (temperature, stress change, etc.) (Yang et al., 2008).

Hybrid and Multiple Resonance Systems

The narrow band of single-resonance systems is a significant limitation for engineering applications. Therefore, hybrid systems have been developed in recent years. In these systems, Helmholtz resonators, membrane structures, and porous materials are used together to achieve broadband absorption. In such systems, different resonance frequencies are superimposed to provide high absorption over a wide frequency range. This approach is considered one of the most effective design strategies in the current literature (Tang et al., 2017). The combination of porous materials and resonance-based structures offers significant advantages in terms of both bandwidth and absorption performance (Tang et al., 2017). Porous structures provide broadband damping through viscous and thermal losses, while resonance-based systems generate high absorption at low frequencies. Combining these two mechanisms allows for the creation of more balanced acoustic systems operating over a wider frequency range.

Manufacturing Methods and Design Approaches

The performance of acoustic metamaterials largely depends on their geometric design. Therefore, manufacturing technologies play a critical role in the development of these structures. In particular, additive manufacturing methods, which have developed in recent years, have made it possible to produce metamaterials with complex internal geometries. Internal channels, convex resonators, multi-cavity systems, and periodic cellular structures, which are difficult to manufacture with traditional methods, can be produced with high precision thanks to 3D printing technologies (Ma & Sheng (2016); Tang et al., (2017)). Polymer-based materials such as PLA, ABS, and photopolymer resins are widely preferred in experimental studies due to their advantages such as low cost, ease of production, and geometric flexibility. A significant portion of metasurface and Helmholtz resonator-based structures developed especially for low-frequency sound absorption are produced using additive manufacturing methods (Jimenez et al., (2016); Tang et al., (2017)). These advancements in manufacturing technologies have enabled the development of acoustic metamaterials not only on a laboratory scale but also for engineering applications. However, the effect of manufacturing precision on resonance frequencies is quite significant. Especially in low-frequency systems, even small changes in geometric parameters can significantly alter acoustic performance. Therefore, manufacturing tolerances have become one of the fundamental parameters to consider in metamaterial design. Numerical modeling methods are also an indispensable part of the metamaterial design process. The finite element method (FEM) is

widely used in the analysis of acoustic wave propagation, resonance behavior, and absorption performance (Jimenez et al., 2016). FEM-based analyses offer a significant advantage, particularly in optimizing structures with complex geometries before experimental manufacturing. Thanks to these methods, numerous design variables such as resonator dimensions, channel geometries, cavity volumes, and membrane parameters can be systematically evaluated. In addition, parametric design and topology optimization methods have become an important research area in metamaterial engineering in recent years. Thanks to these approaches, optimum geometries that will provide maximum absorption in a specific frequency range can be obtained. Optimizing multiple resonance mechanisms is of great importance, especially in studies targeting broadband low-frequency absorption (Tang et al., 2017).

Another notable development in recent years is the use of artificial intelligence and data-based optimization methods in metamaterial design. Instead of the traditional trial-and-error approach, it has become possible to determine optimum structures in a wide parameter space in a shorter time using machine learning algorithms and artificial neural networks. Yan et al. (2024) showed that the machine learning-supported design approach in acoustic metamaterials developed for low-frequency sound absorption yielded high-accuracy results (Yan et al., 2024). Such methods significantly accelerate the design process, especially in complex multi-parameter systems.

Recently, the combination of complex cellular structures such as TPMS (Triply Periodic Minimal Surface) geometries with acoustic metamaterials has attracted attention. These types of structures offer advantages such as low density and high mechanical strength, as well as increased acoustic energy absorption capacity due to their large internal surface area. Furthermore, the ability to produce these geometries using 3D printing technologies presents significant potential for the development of multifunctional acoustic structures in the future.

Current Literature Review

In recent years, studies in the field of acoustic metamaterials have focused particularly on solving the problem of low-frequency sound absorption. A significant portion of these studies focuses on the development of classical resonance mechanisms, the creation of hybrid structures, and the achievement of broadband absorption.

A review of the literature after 2020 shows that the most common approach for low-frequency sound absorption is the combined use of multiple resonance mechanisms. For example, Ji et al. (2020) demonstrated that metasurface structures created by combining multiple resonator cells can provide high absorption in a very low frequency range such as 20–100 Hz. In this study, broadband absorption was achieved thanks to the interaction of resonator cells of different sizes. In more recent studies, hybrid and multifunctional metamaterials are coming to the forefront. Yang et al. (2025) developed systems that provide both mechanical strength and broadband low-frequency sound absorption using carbon fiber reinforced composite metastructures. It has been stated that these structures offer advantages, especially in applications requiring lightness and load-bearing capacity.

Similarly, the series-parallel arrangement metamaterial structure developed by Zhuang et al. (2024) was designed with a combination of convex channels and Helmholtz resonators. In this study, a very high sound absorption coefficient of 0.97 on average in the 130–145 Hz range was obtained and validated both numerically and experimentally.

Geometric optimization and structural innovation are also important research topics in recent years. Hou et al. (2025) achieved an absorption of over 0.90 on average in the 510–970 Hz range by designing a metamaterial consisting of cylindrical voids at different depths. In the study, finite element method and impedance tube experiments were used together. In addition, thin-film based metamaterials are emerging as an important alternative for low-frequency

applications. Xu and Chen (2024) investigated the effect of parameters such as porosity, strain, and thickness on absorption performance in silicon-based thin-film metamaterials and showed that optimum parameter combinations are critical at low frequencies.

Another approach that has recently attracted attention is active and tunable metamaterials. Hedayati et al. (2024) achieved broadband low-frequency absorption using Helmholtz resonator-based active metamaterials and demonstrated the frequency tunability of the system.

Finally, artificial intelligence-supported design methods have also begun to appear in the literature. Yan et al. (2024) achieved high-accuracy predictions in low-frequency metamaterial design by combining impedance-based optimization and artificial neural networks.

Table 1 provides a summary of studies conducted on this topic.

Table 1: Literature review

Author (Year)	Structure Type	Frequency Range	Max. Absorption (α)	Method	Key Feature
Ji et al. (2020)	Metasurface (multi-cell)	20–100 Hz	~0.93	Experiment + Analysis	Low frequency, broadband
Zhuang et al. (2024)	Helmholtz + channel	130–145 Hz	0.97	Experiment + FEM	Series-parallel structure
Xu & Chen (2024)	Thin film	<500 Hz	High	FEM + Experiment	Parametric optimization
Hedayati et al. (2024)	Active resonator	Broadband	High	Experiment	Tunable system
Yan et al. (2024)	AI-assisted structure	220–550 Hz	High	Experiment + Model	Artificial intelligence design
Yang et al. (2025)	Composite metastructure	Low frequency	Broadband	Experiment	Lightweight + durable
Hou et al. (2025)	Cylindrical cavity	510–970 Hz	>0.90	Experiment + FEM	3D printing validation

CONCLUSION AND FUTURE PERSPECTIVES

This study comprehensively examines the effects of acoustic metamaterials on low-frequency sound absorption. Theoretical and experimental studies in the literature clearly demonstrate that metamaterials offer significant advantages over classical acoustic absorbing materials. One of their most important advantages is the ability to achieve high sound absorption performance with structures having thicknesses much smaller than the wavelength, particularly through resonance-based mechanisms. However, a review of existing studies in the literature reveals that acoustic metamaterials still have some fundamental limitations. Chief among these is the inherently narrow band nature of single-resonance systems. Although Helmholtz resonators, membrane systems, and local resonance-based structures can achieve high

absorption coefficients at certain frequencies, this performance is generally limited to a specific frequency range. This can be insufficient to meet the need for broadband noise control in real engineering applications. Multi-resonance and hybrid systems, developed to overcome this limitation, are gaining increasing importance in the literature. These systems, obtained by using structural elements with different resonance frequencies together, can provide high absorption over a wide frequency range. However, in such designs, new engineering problems arise, such as the interaction of resonances with each other, impedance matching, and manufacturing complexity. Therefore, there is a need for optimization between performance increase and design complexity.

In terms of manufacturing technologies, it is seen that additive manufacturing (3D printing) methods play an important role in the development process of acoustic metamaterials. These technologies enable the production of structures with complex internal geometries with high precision. However, the effects of material properties (e.g., viscoelastic behavior in polymer-based materials) on acoustic performance are not yet fully understood. This can lead to discrepancies between experimental results and numerical models.

Another development that has attracted attention in recent years is active and tunable metamaterials. These systems allow the dynamic modification of resonance frequencies using piezoelectric elements, smart materials, or external control mechanisms. Thus, adaptive acoustic control becomes possible in variable noise environments. However, issues such as the energy requirements, control complexity, and long-term stability of such systems are still open to investigation. In addition, artificial intelligence and machine learning-based design approaches are creating a new paradigm in metamaterial engineering. Compared to traditional trial-and-error methods, data-driven optimization techniques enable faster and more effective solutions in a multidimensional design space. These methods are expected to be used more widely in the future, especially in complex problems such as low-frequency sound absorption. From a future perspective, the main research directions in the field of acoustic metamaterials can be summarized as follows:

- Development of multi-resonant structures providing broadband low-frequency absorption
- Making active and adaptive metamaterials energy-efficient and stable
- Solving cost and scalability problems in production processes
- Minimizing the differences between numerical modeling and experimental results
- Development of multifunctional (acoustic, mechanical, thermal) metamaterial designs

In particular, the combination of porous structures with metamaterials stands out as a very promising research area for future studies. Such hybrid structures can simultaneously provide both broadband damping based on viscous losses and resonance-based low-frequency control. In this context, complex geometries that can be produced with 3D printing technologies (e.g., TPMS structures), when combined with acoustic metamaterials, enable the development of new generation engineering materials that can optimize both structural and acoustic performance. Such studies hold great potential not only for academic research but also for industrial applications such as automotive, aerospace, and building acoustics. In conclusion, while acoustic metamaterials offer a powerful alternative for solving the low-frequency sound absorption problem, significant engineering challenges remain to be addressed in this field. In the future, it is expected that these problems will be overcome and metamaterials integrated into large-scale applications through interdisciplinary approaches, advanced manufacturing technologies, and data-driven design methods.

REFERENCES

1. Cummer, S. A., Christensen, J., & Alù, A. (2016). Controlling sound with acoustic metamaterials. *Nature Reviews Materials, 1*(3), 16001. DOI: 10.1038/natrevmats.2016.1
2. Ma, G., & Sheng, P. (2016). Acoustic metamaterials: From local resonances to broad horizons. *Science Advances, 2*(2), e1501595. DOI: 10.1126/sciadv.1501595
3. Liu, Z., Zhang, X., Mao, Y., Zhu, Y. Y., Yang, Z., Chan, C. T., & Sheng, P. (2000). Locally resonant sonic materials. *Science, 289*(5485), 1734–1736. DOI: 10.1126/science.289.5485.1734
4. Fang, N., Xi, D., Xu, J., Ambati, M., Srituravanich, W., Sun, C., & Zhang, X. (2006). Ultrasonic metamaterials with negative modulus. *Nature Materials, 5*(6), 452–456. DOI: 10.1038/nmat1644
5. Yang, Z., Mei, J., Yang, M., Chan, N. H., & Sheng, P. (2008). Membrane-type acoustic metamaterial with negative dynamic mass. *Physical Review Letters, 101*(20), 204301. DOI: 10.1103/PhysRevLett.101.204301
6. Mei, J., Ma, G., Yang, M., Yang, Z., Wen, W., & Sheng, P. (2012). Dark acoustic metamaterials as super absorbers for low-frequency sound. *Nature Communications, 3*, 756. DOI: 10.1038/ncomms1758
7. Maa, D. Y. (1998). Potential of microperforated panel absorber. *Journal of the Acoustical Society of America, 104*(5), 2861–2866. DOI: 10.1121/1.423870
8. Jiménez, N., Huang, W., Romero-García, V., Pagneux, V., & Groby, J. P. (2016). Ultra-thin metamaterial for perfect and quasi-omnidirectional sound absorption. *Applied Physics Letters, 109*(12), 121902. DOI: 10.1063/1.4962328
9. Tang, Y., Ren, S., Meng, H., Xin, F., Huang, L., Chen, T., Zhang, C., & Lu, T. J. (2017). Hybrid acoustic metamaterial as super absorber for broadband low-frequency sound. *Scientific Reports, 7*, 43340. DOI: 10.1038/srep43340
10. Ji, J., Zhang, X., & Cheng, Y. (2020). Low-frequency broadband acoustic metasurface absorbing panels. *Frontiers in Mechanical Engineering, 6*, 586249. DOI: 10.3389/fmech.2020.586249
11. Zhuang, H., Cui, H., & Hu, H. (2024). Low-frequency sound-absorbing metamaterial based on a series-parallel arrangement structure. Journal of Low Frequency Noise Vibration and Active Control, 43(1), 371–382. https://doi.org/10.1177/14613484231195277
12. Xu, J., & Chen, C. (2024). Low-frequency attenuation signal absorption performance of thin-film acoustic metamaterials. Acta Acustica, 8. https://doi.org/10.1051/aacus/2024066
13. Hedayati, R., & Lakshmanan, S. P. (2024). Active Acoustic Metamaterial Based on Helmholtz Resonators to Absorb Broadband Low-Frequency Noise. Materials, 17(4). https://doi.org/10.3390/ma17040962
14. Yan, X., Liang, Q., Feng, J., He, J., Fu, R., Li, D., & Chen, T. (2024). Design and manufacture of low-frequency acoustic absorption metamaterials with enhanced coupling characteristic. Virtual and Physical Prototyping, 19(1). https://doi.org/10.1080/17452759.2024.2383297
15. Hou, Z., Zhang, K., Zhou, Z., Zheng, Y., Wang, J., & Wang, L. (2025). Low and medium frequency acoustic absorption properties of acoustic metamaterials with irregular cylindrical cavities. Scientific Reports, 15(1). https://doi.org/10.1038/s41598-025-24387-9
16. Yang, Y., Liu, S., Li, Y., Gao, T., Pan, Y., Li, Y., & Jin, Y. (2025). Broadband low-frequency sound absorption of multifunctional composite metastructure. Science China Technological Sciences, 68(2). https://doi.org/10.1007/s11431-023-2644-7

AGBIOL 2026 CONFERENCE STUDENT ORGANIZING TEAM

#	NAME

1. Emrah Akpınar
2. Metin Burak Tatlıses
3. Deniz Kızılkaya
4. Selinay Demir,
5. Mutlu Şen
6. İlayda Küçük Tekinalp
7. Serhat Kayan
8. Neslihan Yılmaz
9. Öyküm Ural
10. Selin Buzcu
11. Nisa Sena Güler
12. Begüm Kurt
13. Yaren Akkoç
14. Mustafa Daşman
15. Serhat Parlak
16. Berk Aydın
17. Mehmet Efe Tanrıverdi
18. Burcu Ersoy Kara

OUR SPONSORS

PLATINUM SPONSOR

TRAGEN RD CO Ltd

www.tragen.gen.tr
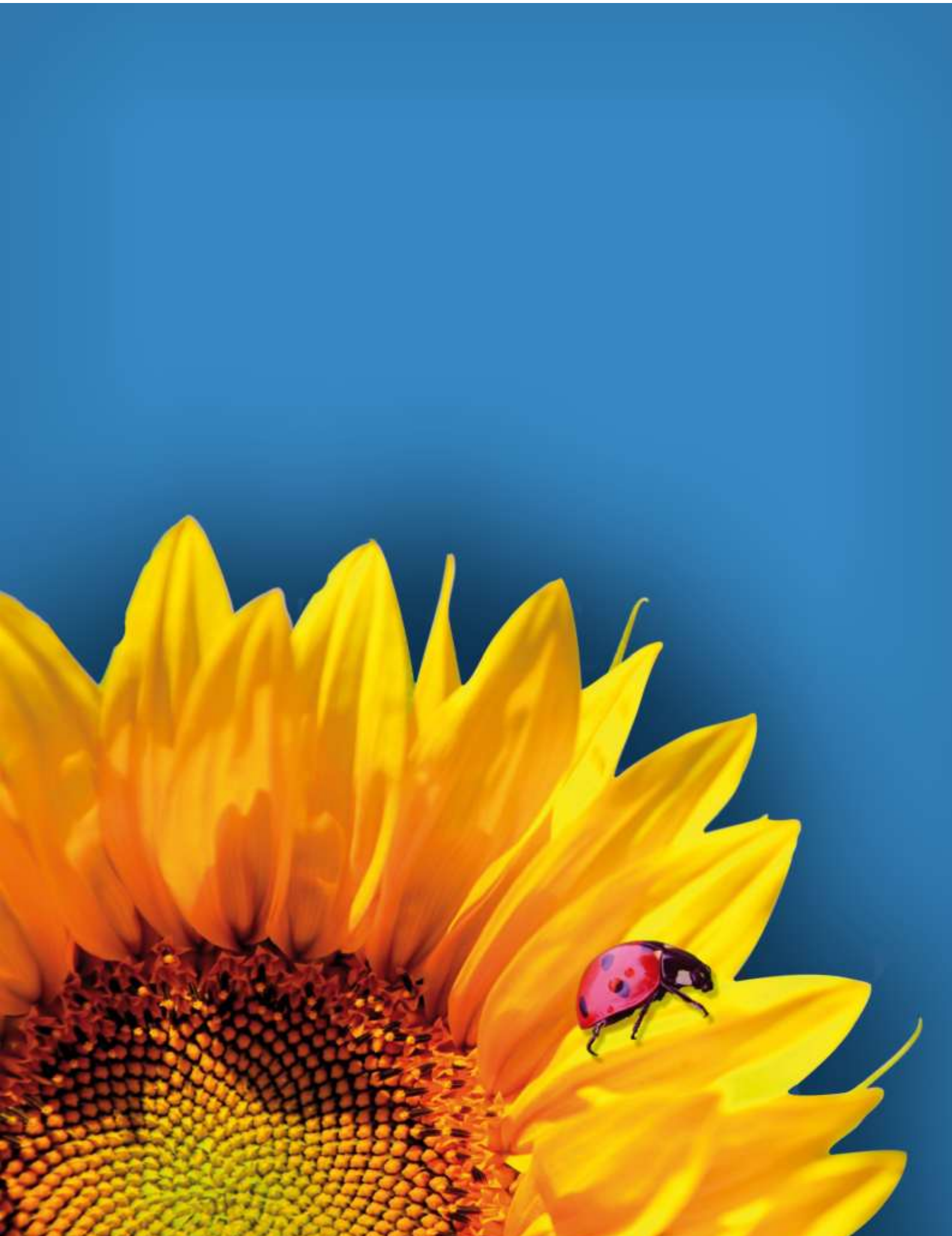
We get support from TUBITAK